NINTH SYMPOSIUM

(INTERNATIONAL)

ON

COMBUSTION

At Cornell University
Ithaca, New York
August 27 to September 1, 1962

Organized by
THE COMBUSTION INSTITUTE

1963

ACADEMIC PRESS  New York and London

United Kingdom Edition
Published by
ACADEMIC PRESS INC. (LONDON) LTD.
BERKELEY SQUARE HOUSE, LONDON, W. 1

Library of Congress Catalog Card Number 55-9170

PRINTED IN THE UNITED STATES OF AMERICA

PREFACE

The Ninth Symposium (International) on Combustion was held at Cornell University, Ithaca, New York, August 27 to September 1, 1962, under the auspices of the Combustion Institute. Registration was in excess of 600, with more than 100 attending from Australia, Belgium, Canada, France, Germany, Great Britain, Hungary, Israel, Italy, Japan, Netherlands, Spain and Sweden.

Over 200 papers were submitted for consideration, of which 121 were placed on the program and 108 printed in the Proceedings.

Two Discussions (*Detonations*, organized by Dr. D. R. White, General Electric Research Laboratory; *Fundamental Flame Processes*, organized by Dr. W. H. Avery, APL/The Johns Hopkins University) occupied 4 half-day sessions each. Preprints of all Discussions papers were available several weeks prior to the Symposium.

Three Colloquia (*Modeling Principles*, organized by Professor D. B. Spalding, Imperial College; *Reactions and Phase Changes in Supersonic Flow*, organized by Professor P. P. Wegener, Yale University; *Reciprocating Engine Combustion Research*, organized by Professor E. S. Starkman, University of California) occupied 2 or 3 half-day sessions each.

Contributed Papers in many areas of the combustion field were presented in 10 half-day sessions. Comments on nearly every paper are included in the Proceedings.

Two Plenary Lectures were given at the Inaugural Meeting by Dr. T. M. Sugden (University of Cambridge) and Dr. F. T. McClure (APL/The Johns Hopkins University) who spoke with wit and erudition about "Electricity and Flames" and on "Sounds Inside Rockets." They were preceded by Provost Dr. S. Atwood who welcomed the audience to Cornell University and by Dr. B. Lewis, the President of The Combustion Institute.

Awards for exceptional contributions to combustion research were made at the Symposium banquet on the recommendation of the Awards Subcommittee (Mr. A. J. Nerad, Chairman). Professor W. Jost (University of Göttingen) received the Sir Alfred Egerton Gold Medal from Dr. G. von Elbe for "distinguished, continuing and encouraging contributions to the field of combustion." Professor F. P. Bowden presented to Professor George B. Kistiakowsky (Harvard University) the Bernard Lewis Gold Medal for "brilliant research in the field of combustion, particularly on detonation phenomena." Mr. A. J. Nerad presented the Silver Combustion Medal to Dr. Tucker Carrington (National Bureau of Standards) for "an outstanding paper presented at the Eighth International Combustion Symposium, 1960."

The organization of the symposium would have been impossible without the contributions of a large number of members of various subcommittees. The 98 members of the Papers Subcommittee (Dr. W. G. Berl, Chairman) were responsible for the formulation of the technical program and the selection and refereeing of the Contributed Papers. A Steering Committee, which included among its members the Chairmen of the Discussions and Colloquia and Chairmen of previous Papers Subcommittees, met in Washington twice to arrange organization details. The Cornell University Subcommittee (Professor D. G. Shepherd, Chairman) carried out the innumerable tasks of a friendly host, provided admirable lecture room facilities and an always-busy coffee and tea bar. A book exhibit on the History of Combustion was also arranged. A social hour in the Big Red Barn and a Barbecue on the Alumni Field provided opportunities for friendly get-togethers. A Ladies Program under Mrs. D. G. Shepherd and Mrs. H. J. Loberg and a post-symposium tour to Harvard and M.I.T., organized by Professor G. C. Williams, complemented these activities.

Mr. M. P. L. Love was Chairman of the effective Finance Subcommittee. Lecture tours for overseas scientists were arranged by Dr. B. M. Sturgis. Mr. N. P. W. Moore (Secretary of the British Section of The Combustion Institute) and later, Professor W. G. Parker, his successor, arranged the complex Group Flights.

Dr. W. G. Berl (APL/The Johns Hopkins University) was responsible for editing the Proceedings. The collecting and typing of the comments and replies were capably done by Mrs. G. Fristrom and Mrs. M. Cole (APL/The Johns Hopkins University). The preparation of the manuscripts for preprinting and for the Proceedings was efficiently handled by Mr. E. Kohn (APL/The Johns Hopkins University), while the reworking of hundreds of illustrations was in the hands of

Mr. J. W. Grabenstein (APL/The Johns Hopkins University). The publication date was advanced greatly by the cooperation of Mr. M. Klatzkin (Mono of Maryland, Inc.) whose staff set the type for this book. The Academic Press was most helpful in this complex publishing venture.

The Combustion Institute gratefully acknowledges the generous hospitality extended by Cornell University and the major financial support afforded by:

U. S. Army Research Office
Contract No. DA-36-034-ORD-3534RD

National Aeronautics and Space Administration,
Grant NsG245-62

National Science Foundation
Grants NSF-G21074 and NSF-G21506

and the contributions received from:

AeroChem Research Laboratories, Inc.
American Electric Power Service Corporation.
American Gas Association.
American Oil Company.
Atlantic Research Corporation.
AVCO Corporation—Lycoming Division.
Bethlehem Steel Company.
The Boeing Company.
C. F. Braun & Company.
California Research Corporation.
Canadian Industries Limited.
Caterpillar Tractor Company.
Champion Spark Plug Company.
Chrysler Corporation.
Cities Service Research and Development Company.
Columbia Gas Systems Service Corporation.
Combustion and Explosives Research, Inc.
Combustion Engineering, Inc.
Con-Gas Service Corporation.
Consolidation Coal Company.
Cummins Engine Company, Inc.
Curtiss-Wright Corporation.
Douglas Aircraft Company, Inc.
E. I. du Pont de Nemours & Company, Inc.
The Ensign-Bickford Company.
Esso Research and Engineering Company.
Ethyl Corporation.
Factory Mutual Engineering Division.
Fenwal Incorporated.
Flame Research, Inc.
The Fluor Corporation, Ltd.
Food Machinery and Chemical Corporation.
Ford Motor Company.
The Garrett Corporation.
General Dynamics Corporation.
General Electric Company.
General Motors Corporation.
Gulf Research & Development Company.
Hauck Manufacturing Company.
Hercules Engine Division, Hupp Corporation.
Hercules Powder Company.
International Harvester Company.
Koppers Company, Inc.
The Arthur D. Little Foundation.
Lockheed Propulsion Company.
Lone Star Gas Company.
The Lummus Company.
Monsanto Chemical Company.
National Airoil Burner Company.
National Fire Protection Association.
North American Aviation, Inc.
Oil Insurance Association.
Owens-Corning Fiberglas Corporation.
Phillips Petroleum Company.
Pittsburgh Plate Glass Company.
The Pure Oil Company.
Richfield Oil Corporation.
Rohm & Haas Company.
Shell Development Company.
Socony Mobil Oil Company, Inc.
Solar Aircraft Company.
The Standard Oil Company (Ohio).
Sun Oil Company.
Texaco Inc.
Thiokol Chemical Corporation.
The Travelers Insurance Company.
Union Oil Company of California.
United Aircraft Corporation, Pratt & Whitney Aircraft Division.
United States Steel Corporation.
United Technology Corporation.
Westinghouse Electric Corporation.

THE COMBUSTION INSTITUTE

A nonprofit professional society, incorporated in 1954, to promote the science and application of combustion and to disseminate knowledge in this field.

Officers

President	Bernard Lewis
Vice President	Hoyt C. Hottel
Treasurer	Stewart Way
Assistant Treasurer	Bernard M. Sturgis
Secretary	Glenn C. Williams

Executive Office

Union Trust Building, Pittsburgh 19, Pennsylvania
Mrs. Helen G. Barnes, *Executive Secretary*

Board of Directors

Dr. William G. Agnew	General Motors Research Laboratories
Dr. David Altman	United Technology Corporation
Dr. William H. Avery	APL/The Johns Hopkins University
Mr. William J. Bennet	The Marquardt Corporation
Dr. J. S. Clarke	Joseph Lucas, Limited
Dr. Louis Deffet	Centre des Recherches pour L'Industrie des Produits Explosifs
Dr. Newman A. Hall	Commission on Engineering Education
Dr. Amos G. Horney	Office of Scientific Research, USAF
Professer Hoyt C. Hottel	Massachusetts Institute of Technology
Professor Wilhelm Jost	University of Göttingen
Dr. Bernard Lewis	Combustion and Explosives Research, Inc.
Dr. J. P. Longwell	Esso Research and Engineering Company
Mr. J. B. Macauley	US Department of Defense
Mr. A. J. Nerad	General Electric Research Laboratory
Dr. Walter T. Olson	Lewis Research Center, NASA
Professor Bruce H. Sage	California Institute of Technology
Dr. Bernard M. Sturgis	E. I. du Pont de Nemours & Company, Inc.
Dr. Stewart Way	Westinghouse Research Laboratories
Professor Glenn C. Williams	Massachusetts Institute of Technology

Western States Section

Dr. Robert S. Levine, *Chairman*	Rocketdyne
Prof. Ernest S. Starkman, *Vice-Chairman*	University of California
Dr. M. Wesley Rigg, *Treasurer*	Office of Naval Research
Mr. Gilbert S. Bahn, *Secretary*	The Marquardt Corporation

The Combustion Institute Committee

United States

Dr. David Altman, *Chairman*	United Technology Corporation
Dr. Richard D. Geckler	Aerojet-General Corporation
Dr. Amos G. Horney	Office of Scientific Research, USAF
Dr. J. P. Longwell	Esso Research and Engineering Company
Dr. Walter T. Olson	Lewis Research Center, NASA
Professor Glenn C. Williams	Massachusetts Institute of Technology

1962 SYMPOSIUM SUBCOMMITTEES

Papers Subcommittee

Dr. Walter G. Berl, *Chairman*, APL, The Johns Hopkins University.
Dr. W. G. Agnew, General Motors Research Center.
Dr. W. H. Avery, APL, The Johns Hopkins University.
Dr. C. Beckett, National Bureau of Standards.
Mr. W. J. Bennet, Marquardt Corporation.
Dr. A. L. Berlad, Convair Scientific Research Laboratory.
Professor M. Boudart, University of California.
Professor F. P. Bowden, University of Cambridge.
Mr. S. L. Bragg, Rolls-Royce Ltd.
Dr. S. R. Brinkley, Jr., Combustion and Explosives Research, Inc.
Dr. H. P. Broida, National Bureau of Standards.
Dr. J. H. Burgoyne, Imperial College of Science and Technology.
Dr. H. F. Calcote, AeroChem Research Laboratories, Inc.
Professor A. B. Cambel, Northwestern University.
Dr. H. M. Cassel, U. S. Bureau of Mines.
Dr. J. S. Clarke, Joseph Lucas, Ltd.
Professor M. A. Cook, University of Utah.
Dr. R. E. Duff, Institute for Defense Analyses.
Dr. G. L. Dugger, APL, The Johns Hopkins University.
Professor H. W. Emmons, Harvard University.
Dr. Marjorie W. Evans, Stanford Research Institute.
Professor J. A. Fay, Massachusetts Institute of Technology.
Professor J. Fenn, Princeton University.
Dr. S. N. Foner, APL, The Johns Hopkins University.
Mr. W. L. Fons, U. S. Forest Service.
Dr. R. Friedman, Atlantic Research Corporation.
Dr. R. M. Fristrom, APL, The Johns Hopkins University.
Dr. D. Garvin, National Bureau of Standards.
Professor A. G. Gaydon, Imperial College of Science and Technology.
Dr. R. D. Geckler, Aerojet-General Corporation.
Professor I. Glassman, Princeton University.
Dr. A. S. Gordon, U. S. Naval Ordnance Test Station.
Professor P. Gray, The University of Leeds.
Professor A. V. Grosse, Temple University.
Dr. F. Hill, APL, The Johns Hopkins University.
Professor H. C. Hottel, Massachusetts Institute of Technology.
Dr. W. H. Jones, Institute for Defense Analyses.
Mr. B. Karlovitz, Combustion and Explosives Research, Inc.
Dr. W. E. Kaskan, General Electric Space Research Center.
Dr. F. Kaufman, Ballistic Research Laboratories.
Professor L. N. Khitrin, USSR Academy of Sciences.
Professor T. Kinbara, Sophia University, Tokyo.
Dr. P. H. Kydd, General Electric Research Laboratory.
Professor P. Laffitte, University of Paris.
Dr. R. S. Levine, Rocketdyne.
Dr. B. Lewis, (ex officio), Combustion and Explosives Research, Inc.
Dr. J. W. Linnett, Queen's College, Oxford.
Dr. J. P. Longwell, Esso Research and Engineering Company.
Dr. F. T. McClure, APL, The Johns Hopkins University.
Professor F. E. Marble, California Institute of Technology.
Dr. G. H. Markstein, Cornell Aeronautical Laboratory.
Professor C. J. Marsel, New York University.
Dr. F. J. Martin, General Electric Research Laboratory.
Dr. J. F. Masi, Office of Scientific Research, USAF.
Dr. C. C. Miesse, Westinghouse Electric Corporation.
Professor P. S. Myers, University of Wisconsin.
Mr. A. J. Nerad, General Electric Research Laboratory.
Professor J. A. Nicholls, University of Michigan.
Dr. P. Nichols, Aerojet-General Corporation.
Dr. W. T. Olson, Lewis Research Center, NASA.
Professor A. K. Oppenheim, University of California.
Professor H. B. Palmer, Pennsylvania State University.
Professor W. G. Parker, College of Advanced Technology, U.K.
Professor S. S. Penner, California Institute of Technology.
Professor G. Porter, Sheffield University.
Dr. E. W. Price, U. S. Naval Ordnance Test Station.
Dr. D. J. Rasbash, Joint Fire Research Station, U.K.
Dr. R. Roberts, Office of Naval Research.

Mr. A. Rothrock, National Aeronautics and Space Administration.
Professor N. W. Ryan, University of Utah.
Dr. A. C. Scurlock, Atlantic Research Corporation.
Dr. E. H. Seymour, Reaction Motors Division, Thiokol.
Professor K. I. Shchelkin, USSR Academy of Sciences.
Dr. K. E. Shuler, National Bureau of Standards.
Professor D. B. Spalding, Imperial College of Science and Technology.
Professor E. S. Starkman, University of California.
Dr. T. M. Sugden, University of Cambridge.
Professor M. Summerfield, Princeton University.
Dr. C. P. Talley, Texaco Experiment, Incorporated.
Dr. P. H. Thomas, Joint Fire Research Station, U.K.
Dr. R. Thompson, Rocketdyne.
Professor M. W. Thring, Sheffield University.
Professor A. R. Ubbelohde, Imperial College of Science and Technology.
Dr. R. W. Van Dolah, U. S. Bureau of Mines.
Dr. G. von Elbe, Atlantic Research Corporation.
Dr. H. Gg. Wagner, University of Göttingen.
Professor A. D. Walsh, University of St. Andrews.
Dr. S. Way, Westinghouse Research Laboratories.
Professor P. P. Wegener, Yale University.
Dr. F. Weinberg, Imperial College of Science and Technology.
Dr. A. A. Westenberg, APL, The Johns Hopkins University.
Professor F. A. Williams, Harvard University.
Professor G. C. Williams, Massachusetts Institute of Technology.
Dr. H. Wise, Stanford Research Institute.
Dr. H. G. Wolfhard, Reaction Motors Division, Thiokol.
Professor M. J. Zucrow, Purdue University.
Professor E. E. Zukoski, California Institute of Technology.

Finance Subcommittee

Mr. M. P. L. Love, *Chairman*, Shell Oil Company.
Mr. J. M. Campbell, General Motors Corporation.
Mr. A. L. Haynes, Ford Motor Company.
Dr. W. E. Kuhn, Texaco Incorporated.
Mr. A. J. Nerad, General Electric Research Laboratory.
Dr. B. M. Sturgis, E. I. du Pont de Nemours & Company.

Awards Subcommittee

Mr. A. J. Nerad, *Chairman*, General Electric Research Laboratory.
Dr. N. A. Hall, Commission on Engineering Education.
Dr. A. G. Horney, Office of Scientific Research, USAF.
Dr. B. Lewis (ex officio), Combustion and Explosives Research, Inc.
Professor R. N. Pease, Princeton University.
Dr. E. H. Seymour, Reaction Motors Division, Thiokol.
Professor D. G. Shepherd, Cornell University.
Professor G. C. Williams, Massachusetts Institute of Technology.

Lecture Tours

Dr. B. M. Sturgis, *Chairman*, E. I. du Pont de Nemours & Company.

Nominations Subcommittee

Dr. N. A. Hall, *Chairman*, Commission on Engineering Education.
Professor H. C. Hottel, Massachusetts Institute of Technology.
Mr. J. B. Macauley, US Department of Defense.
Mr. A. J. Nerad, General Electric Research Laboratory.
Dr. B. M. Sturgis, E. I. du Pont de Nemours & Company.
Dr. S. Way, Westinghouse Research Laboratories.

Cornell University Subcommittee

Professor D. G. Shepherd, *Chairman*
Professor H. N. McManus, Jr., *Vice Chairman*
Professor B. Conta
Professor C. O. Mackey
Members of Thermal Engineering Staff

Ladies Program

Mrs. H. J. Loberg, Mrs. D. G. Shepherd } *Co-Chairmen*

CONTENTS

DISCUSSION ON FUNDAMENTAL FLAME PROCESSES

COLLOQUIUM ON CHEMICAL REACTIONS AND PHASE CHANGES IN SUPERSONIC FLOW

COLLOQUIUM ON MODELING PRINCIPLES

COLLOQUIUM ON RECIPROCATING ENGINE COMBUSTION RESEARCH

LIST OF AUTHORS

11

INTRODUCTION

W. G. BERL*

The Ninth Symposium (International) on Combustion, the latest in the series of highly successful symposia held since the war, continues the aim of The Combustion Institute to supply a forum for presenting and discussing outstanding papers in combustion research and technology. In this Introduction the Chairman of the Papers Subcommittee traditionally is given an opportunity to sum up the highlights of the meeting.

A symposium is to be judged on its content and form. Its success depends on whether it was host to new concepts or helped in the destruction of long-established prejudices and on how well it communicated these events to its audience.

Technical Program

Perhaps the most significant and exciting advances have taken place in one of the oldest and "simplest" areas of the combustion field—the premixed laminar flame. On the basis of a number of papers presented at the Symposium, it is fair to say that statements deploring the "insuperable complexities" of even the simplest real flame systems have become outdated by events.

The theory of the laminar flame was formulated by Hirschfelder and Curtiss, Lewis and von Elbe, Zeldovich, and others, several years ago. To apply it to any actual system, however, it is necessary to know reaction mechanisms, rate constants, and transport properties. Largely due to spectacular advances in the availability of such data, it has now become possible to apply the theory to realistic combustion reactions (in particular, the hydrogen–oxygen reaction). By a variety of methods—explosion limits (Baldwin, pp. 184, 667), shocks (Nicholls, p. 488), atom reactions in flow systems (Kaufman, p. 659; Clyne, p. 211), and flame studies—a comprehensive list of rate data for important elementary reaction steps is being acquired. While a complete analytical description of the behavior of the hydrogen–oxygen flame has not been wholly successful as yet (Dixon-Lewis, p. 576), most encouraging progress has been made in characterizing the kinetically controlled chemical changes during nozzle expansion (Westenberg, p. 785), and the ignition and reaction of hydrogen in air at high flow velocities (Momtchiloff *et al.*, p. 220; Buswell *et al.*, p. 231). This ability to predict complex reaction behavior from basic data is of great significance *per se*, and aids in the estimation of performance potential in rockets and hypersonic ramjets, where experimental work, unguided by theory, would be prohibitively difficult and unrewarding.

The understanding of hydrocarbon flames has been substantially advanced thanks to the detailed investigation of their structure. Despite the large number of possible reaction steps, the long-awaited use of such flames as "reaction vessels" in which meaningful kinetic measurements can be made has now become reality. The initial attack of methane by hydroxyl radicals (Fristrom, p. 560) and of higher hydrocarbons by atoms and radicals (Fenimore and Jones, p. 597) was disentangled satisfactorily from subsequent reactions and has provided rate constants at temperatures inaccessible by other methods. Direct determination of atom and radical profiles (Wagner, p. 572) gives promise that the reasons for the effectiveness of "inhibitors" and "promoters" will become understandable.

While the dominant processes in flames are being successfully attacked, several other problems have received substantial clarification, *viz.*, the electrical properties of hydrocarbon flames, transport processes at high temperature and subtle effects due to the existence of nonequilibrium species. There is now substantial agreement about the nature of the "primary" ionized radical in hydrocarbon–oxygen flames which undergoes subsequent rapid exchange reactions (Sugden, p. 607). Identification of ionized species in various flames is progressing (Calcote, p. 622; Padley *et al.*, p. 638), although no quantitative rate or concentration measurements have been attempted. Negative ions, too, have been identified (van Tiggelen, p. 634; Knewstubb, p. 635). The neutralization of these charged species during nozzle expansion is of considerable significance in determining the electrical properties of combustion exhaust streams (Bray, p. 770).

In the field of transport properties (diffusion

* Chairman of Papers Subcommittee and Editor of Proceedings.

coefficients, thermal conductivities, etc.), essential in the interpretation of flames with steep concentration and temperature gradients, extension of the kinetic theory to the interaction of polyatomic and polar gases (Mason and Monchick, p. 713; Brokaw and O'Neal, p. 725) promises to close the gap of estimating these properties at temperatures where experimental work is most difficult. Applying the analysis to "dusty" gases containing small solid particles (Waldman, p. 723) will give valuable insights into thermomechanical effects in flames. Heterogeneous recombination reactions of free radicals have also been investigated with promising new techniques (Wise, p. 733).

A few remarks are in order regarding new developments in kinetics. Nonequilibrium vibrational and electronic effects in flames are responsible for some of the characteristic radiation properties of flames (Garvin and Broida, p. 678; Thrush, p. 177) and are of particular concern in those cases where rapid reactions are proceeding in sequence (Benson, p. 760). Efforts are under way (Greene *et al.*, p. 669) to supplement conventional kinetic measurements with experiments in crossed molecular beams where the energy states of the reacting species are known with good accuracy.

In a quite different area, the field of combustion instability, notable progress is evident, heralded by the "round-table" of the Eighth Symposium on this subject. A number of papers (Ryan, p. 328; Watermeier *et al.*, p. 311; Horton and Price, p. 303; Wood, p. 335), address themselves to the measurement of characteristic propellant constants whose knowledge is of importance for predicting the amplifying-damping behavior of the solid-gas combustion reaction. As demonstrated by the paper of Hart (p. 993) the theoretical understanding and prediction of phenomena have outdistanced the capabilities of the experimentalist—a rare event in combustion.

Several Contributed Papers deserve special mention among a multitude of stimulating contributions. The paper by Potter and Anagnostou (p. 1) shows that in diffusion flames, too, the interaction between theory and experiment can produce valuable insights. Their opposed-jet flame should provide a useful tool for many systems that cannot readily be investigated by conventional techniques. Wolfhard's study of the boron hydride–hydrazine flame (p. 127) is as novel in the nature of the reactants as it is complex in its behavior. The studies of Gilbert and Marxman (p. 371) on solid–gas (hybrid) combustion illuminate with great skill a particularly intricate and potentially useful propulsion situation. The kinetic scheme for the ignition of hydrogen–oxygen mixtures sensitized by nitrogen dioxide at the lean and rich limits is worked out in detail by Ashmore and Tyler (p. 201). The fluid dynamics of the transition to detonation in an explosive gas is presented with great clarity by Oppenheim *et al.* (p. 265).

In their Introductions the Chairmen of the Discussions and Colloquia have effectively summarized the highlights of the sessions and the problems which face the investigators. One cannot but be impressed by the subtleties of the detonation propagation and ignition processes (Bowden, p. 499), the sophisticated knowledge accumulated in the investigation of nozzle flow, the difficulties of combustion scaling (Spalding, p. 833; Thomas, p. 844) and the determination shown in refining the concepts of engine combustion (Starkman, p. 1005).

Organization

A major modification in procedure was the organization of two Discussions on the subjects of *Detonations* (Dr. D. R. White) and *Fundamental Flame Processes* (Dr. W. H. Avery). The intent was to give detailed consideration to several areas of combustion research where significant progress had been made in recent years and where vigorous comments from the audience could be expected. By preprinting the papers several weeks prior to the Symposium (over 400 copies of each Discussion were distributed), restricting the authors to a brief review of the highlights of their papers, requesting specific comments from particularly qualified discussors, and giving ample time to discussions from the floor, it was possible to reach the objective of presenting developments in proper perspective. The numerous thoughtful comments in the Proceedings are indicative of the spirited give-and-take during these sessions.

A somewhat different approach was taken in the organization of three Colloquia on subjects having strong interaction with engineering applications (*Modeling Principles*, Professor D. B. Spalding; *Chemical Reactions and Phase Changes in Supersonic Flow*, Professor P. P. Wegener; *Reciprocating Engines Combustion Research*, Professor E. S. Starkman). They were patterned along more conventional lines of choosing particular subjects for their current timeliness but without the benefit of preprinted papers. It was thought (erroneously, as it turned out), that these topics might be less easy to discuss at length. One would hope that, in the future, preprinting can be done whenever an active field is being looked at in some detail. In this respect, the feat of the organizers of the Seventh Symposium of preprinting all papers remains unequaled.

The Discussions and Colloquia occupied approximately half of the program, the remainder being given over to Contributed Papers in many areas of the combustion field. Their content is indicative of the areas of research in which emphasis is placed at present.

A few comments need to be made about the time scales which were involved. There is a conflict between the desires of the authors for late manuscript deadlines but an early publication date, the necessity of detailed technical review of papers prior to their acceptance for publication and the time-consuming mechanics of publishing. In the case of the Discussions and Colloquia the Chairmen accepted the editorial responsibilities for reviewing papers, suggesting revisions, etc. For preprinting, the Discussion papers were directly reproduced from manuscript as received. The manuscript deadline (April 15, 1962) gave ample time for this, followed by review and revision prior to the Symposium. The Colloquia papers, with a tentative May 1 deadline, also were subject to refereeing.

For the Contributed Papers the following method was adopted: Informative abstracts were requested by February 1, 1962 and reviewed rapidly by the Papers Subcommittee. The authors were informed by March 1 whether their papers were accepted for presentation at the Symposium. Deadlines for submission of final manuscripts were set for May 1, 1962, followed by review by the Papers Subcommittee who applied customary rigorous refereeing standards. Authors were then asked to revise their manuscripts by August 15, 1962. Thus, acceptance by abstracts provided authors with an additional two to three months for writing their final papers.

The response of the audience and speakers in submitting their comments and replies in writing was most gratifying. The sessions chairmen made the final editorial selections, eliminating those comments which in their judgment did not contribute greatly to the illumination of the subject.

No Round-Tables or Invited Review Papers were scheduled since it was felt that the Discussions and Colloquia and the Introductions to them would fill their functions. However, two delightful Plenary Lectures (*Sounds Inside Rockets* by F. T. McClure and *Electricity and Flames* by T. M. Sugden), purposely designed to be instructive while not wholly technical, were given. A large audience listened in rapt attention. With the consent of the speakers, their remarks are not included in the Proceedings.

These carefully considered plans would not have succeeded without the help and assistance of many persons. Foremost, thanks are due to the more than 200 authors who made the creative effort to present the results of their investigations. They had to run a heavy gauntlet of deadlines, referees and revisions. While fewer papers are published than in the past several Symposia, the product of numbers times quality is as high or higher than ever before. We were guided in this by the publishing motto of Gauss: *"Pauca Sed Matura."*

The Chairmen of the Discussions and Colloquia had a free hand to select the particular ways in which to develop the topics assigned to them, to invite speakers and discussors, to referee the papers and to select contributed comments. With their own small advisory panels, they carried out these tasks with great skill and devotion.

A large, efficient and helpful Papers Subcommittee offered valuable advice and comments on the program, reviewed abstracts of Contributed Papers, and refereed the final manuscripts. Fifty-nine members remained active to the end as authors, discussors or session chairmen. Of particular help in the early stages was the advice of Professor A. R. Ubbelohde and Dr. J. W. Linnett who shared their experiences as organizers of Faraday Society Discussions and the plea of Professor A. G. Gaydon that summaries be supplied with all printed papers.

Conclusions

Symposia of the type recorded in these Proceedings have lately been criticized. It is said that they cannot and should not compete with informal discussions, called only at a time of need, where work in progress is discussed in a critical manner before a small audience of experts without the requirements of manuscript deadlines and paper reviews, nor should they interfere with publication of papers in widely read, well-edited and refereed journals as soon as the research work is completed. The contents of symposia proceedings all too frequently remain locked up in increasingly expensive and inaccessible books or are published again elsewhere. To these criticisms are added the organization costs in both time and money, and the publication problems connected with the sudden influx of a large number of manuscripts from a widely dispersed group of contributors.

In defense of symposia, it is worthwhile to look at some of the shortcomings of the informal discussions and of journal publication. Almost by definition the informal discussions must be severely restricted in attendance and confined to narrow topics. Since there is no permanent record of the subjects that are discussed, the conclusions and controversies do not reach a wide audience. While often extremely stimulat-

ing and effective, this combination of limited attendance and lack of permanent record has serious drawbacks. Neither the interested "outsider" who wishes to enter the field nor the young contributors who are at the beginning of their careers will be exposed to the excitement of the give-and-take of a lively discussion. Publication in professional journals, on the other hand, suffers from the handicap of dispersal and fragmentation, particularly if the subject is one inviting contributions from several disciplines. In addition, the papers are not illuminated further by thoughtful comments or discussions, nor is it possible to indicate the present state of development by appropriate introductory surveys. This has led to a wide-spread frustration with "keeping up" with the current literature and discerning the direction in which progress is made or where unresolved difficulties remain.

Thus, valuable service can be performed by symposia if they emphasize those features that cannot be met otherwise. As international meeting places they provide effective means for supplying the framework for sharing common experiences. In their printed proceedings over the years the state and direction of the research effort are clearly mirrored. If scheduled at reasonably regular intervals, both the contributors and planners become accustomed to a "style" of procedures which is well understood by the participants. The proceedings become useful repositories of papers of permanent value. A carefully planned program will attract novel and first-rate work, justifying the publication delay of some contributions in awaiting the date of the symposium.

A strict editorial policy on the quality of the papers, particularly of those accepted for publication, is essential. Most important, time for discussions and space for the inclusion of significant comments in the proceedings must be provided. Preprinting of the more challenging papers and circulation of manuscripts is vital, as is the presence of competent discussors and of chairmen who know how to make a discussion fruitful. If these essentials are met, the limitations—the paper deadlines, the complex organization, the bulky proceedings and the expense connected with rapid publication—become bearable. These were the guidelines by which the Ninth Symposium (International) on Combustion was carried out.

February 1963

Turbulent Gas Flames

Chairman: Mr. B. Karlovitz (*Combustion and Explosives Research*)
Vice Chairman: Prof. M. W. Thring (*University of Sheffield*)

FLAME STRENGTH OF PROPANE-OXYGEN FLAMES AT LOW PRESSURES IN TURBULENT FLOW

EVELYN ANAGNOSTOU AND A. E. POTTER

The apparent flame strength, a unique combustion measurement described previously by Potter and co-workers, was investigated for the system propane-oxygen in turbulent flow at low pressures. The dependence of flame strength on pressure and on burner diameter was determined at Reynolds numbers ranging from 2000 to 10,000, for pressure between 0.17 and 0.85 atm and burner diameters ranging from 0.398 to 0.635 cm. The results were compared with those predicted by a theory developed recently by Spalding, according to which the flame strength should vary directly with burner diameter and the pressure dependence of the flame strength should be the same as the reaction order when the Reynolds number of the flow is sufficiently high. The results of this study show that the theoretical predictions are correct, provided that the Reynolds number is over 2000.

This study shows that, under proper conditions, flame strength is a useful and meaningful measurement for characterising fuel-oxidant systems. It differs from other flame properties in that it is independent of transport properties. Its most important use may be in studying fuel-oxidant systems which are difficult to mix.

Introduction

In order to study reactive fuel-oxidant combinations not easily handled as premixed systems, a unique combustion measurement, the apparent flame strength, has been described[1,2] which uses two opposed jets, one of fuel and one of oxidant. The basis for this measurement was the theoretical work of Spalding[3] and Zeldovich.[4] They showed that there was a maximum flow of fuel and oxidant into the reaction zone of a diffusion flame. When this value was exceeded, the flame would go out. In the opposed-jet diffusion flame, as the mass flows of fuel and oxidant are increased, a critical flow is reached at which the flame is extinguished in an area surrounding the jet axis. The average mass flow of fuel and oxidant at the jet axis when this occurs is defined as the apparent flame strength. This is not the same quantity as Spalding's flame strength[3] but is related to it. In the body of this paper flame strength and apparent flame strength will be used interchangeably to denote the average mass flow at the flame breaking point, the quantity of references 1 and 2.

In the early theories of Zeldovich and Spalding, mass transport by diffusion alone was considered and convective flow was neglected. This was a major omission, since the diffusion flame can only be extinguished by the application of forced convection. Recently, Spalding[5] included convective flow in his theory. When he compared the theory with the experimental results of Potter *et al.*[1,2] he found that the experimental results did not agree with theory with respect to the dependence of the flame strength on the diameter of the burner and on the pressure. On further analysis Spalding deduced that the actual flows in these experiments did not closely resemble the idealized flow, which was that of a jet impinging on a flat plate perpendicular to it. In order for his theory to hold, the Peclet number (i.e.,

$C_{p,\infty}\rho_\infty UD/\lambda_\infty$ or Reynolds number $\times$ Prandtl number) for the fuel jet should be greater than 1000 and a value of several thousand would be desirable.[5] A high Peclet number infers a high Reynolds number since the Prandtl number for nonpolar gases (e.g. propane) is about 0.7. The earlier work of Potter and his co-workers[1,2] was done mainly with laminar flows and so these data did not fit the requirement for the theory. Therefore, the disagreement between theory and experiment is not surprising.

The present paper reports measurements of the pressure and burner diameter dependence of propane-oxygen flames at high Reynolds numbers where Spalding's theory is expected to be valid. In addition, the maximum heat-release rate calculated from flame strength is compared to the rate calculated from laminar flame properties.

Experimental

Apparatus. A sketch of the apparatus, which is basically similar to that described in references 1 and 2, is shown in Fig. 1. Tubes of various inner diameters could be interchanged in the burner through the O-ring seal at the base. The burners were cooled with nitrogen gas which exhausted into the containing chamber. The burners were surrounded by a glass chimney plugged with transite at the bottom and supported rigidly by holders which were adjustable in several ways to insure alignment of the jets. The apparatus was enclosed in a large chamber with a viewing port, and the chamber was connected to a vacuum system through a scrubber containing soda lime. The pressure was maintained using two Beech-Russ pumps of 100 cfm capacity; a plenum chamber smoothed out pressure changes. The pressure was measured with a differential mercury manometer.

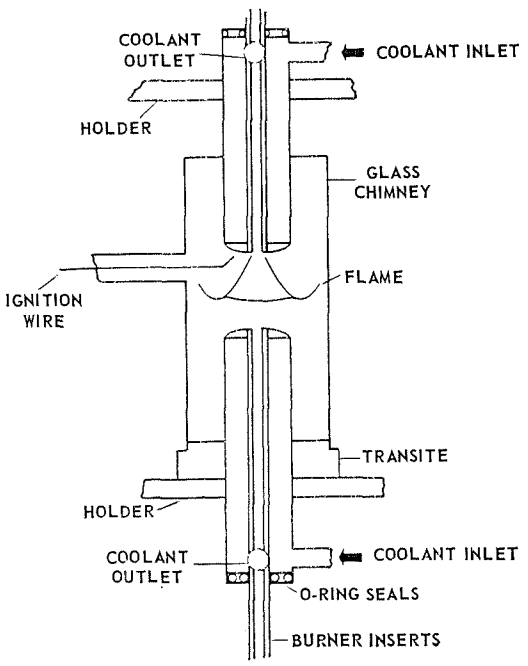

FIG. 1. Burner assembly.

Procedure. The system was first evacuated and then filled with nitrogen to approximately the pressure desired. The pressure could then be maintained during a run by adjusting both the valve to the vacuum system and the nitrogen inlet valve. The fuel and oxidant were separately metered with critical flow orifices; ignition was accomplished using a spark from a molybdenum wire, embedded in the glass chimney, across to the top burner.

The measurements were made either by setting the pressure and increasing the fuel and oxidant flow or by setting the flows and slowly lowering the pressure, until a hole appeared in the flame around the jet axis. During these operations, the flame was kept midway between the two jet tubes. The hole appeared very abruptly at a flow rate or pressure reproducible to within $\pm 5\%$. The measurements at very high Reynolds numbers were generally made by lowering the pressure at fixed flow rate, since the flames at high Reynolds numbers easily blew off with slight increases in flow rate, and were difficult to restabilize. At lower Reynolds numbers, when both techniques could be used, they gave the same results. The flame strength reported was calculated as follows: the mass flow rate at the instant of flame "breaking" was divided by the burner area to give the average mass flow rate per unit area. This was done for both the fuel and oxidant jets. The average mass flows were then multiplied by an appropriate factor to give the mass flow rate at the jet axis. This factor is 2.0 for laminar flow and 1.22 for turbulent flow. The resulting values for the fuel and oxidant jets were averaged to yield the final flame strength value. For hydrocarbon-oxygen flames the oxidant and fuel flow rates do not differ by more than 10%.

The Reynolds numbers referred to thus far and later on in the paper are in all cases the Reynolds numbers for the propane flow. The Reynolds numbers for the oxygen flow were approximately three-eighths of those of the fuel. Even in those cases where the oxygen Reynolds number was greater than 2000, the mass flows of fuel and oxidant at the jet axis were nearly equal only when the oxygen flow was assumed to be laminar. This assumption was used for all data

even though the Reynolds number for the oxygen flow was as high as 2800.

The appearance of the turbulent diffusion flames was similar to that of flames in the laminar region[1] except at the highest Reynolds numbers. As mentioned earlier, these flames were unsteady; they also tended to be smoky and to blow out rather easily.

Results and Discussion

Table 1 lists the flame-strength data along with burner diameter, Reynolds number, fuel and oxidant mass flows, and flame strengths corrected to a 0.462-cm diameter burner. This last quantity takes into account the dependence of flame strength on burner diameter which is discussed in the next section. Also included is a datum from reference 2, recalculated using the new burner diameter dependence.

Diameter Dependence of Apparent Flame Strength. The measured flame strengths depend on the diameter of the burner. This effect was determined at two pressures, 0.33 and 0.285 atm (9.9 inches and 8.6 inches Hg respectively) and for burner diameters from 0.398–0.635 cm. These data were at fuel Reynolds numbers ranging

TABLE 1

Flame strength data for turbulent propane-oxygen flames

Pressure (atm)	Burner diameter (cm)	Flame strength (gm/cm³sec)	Flame strength (corr. to 0.462-cm burner)	Fuel Re number ($\times 10^3$)	Mass flow at extinguishment (gm/sec)	
					Fuel	Oxidant
0.291	0.635	1.12[a]	0.815	6.81	0.272	0.187
0.331	0.635	1.46[a]	1.05	8.85	0.353	0.247
0.169	0.635	0.400	0.292	2.49	0.0995	0.0655
0.313	0.635	1.41	1.03	8.74	0.348	0.233
0.331	0.635	1.51[a]	1.10	9.85	0.393	0.237
0.261	0.635	0.724	0.526	4.61	0.184	0.117
0.167	0.635	0.375	0.273	2.17	0.0865	0.0657
0.285	0.619	1.07[a]	0.800	6.91	0.269	0.161
0.331	0.619	1.49[a]	1.11	9.07	0.367	0.225
0.338	0.619	1.49[a]	1.11	9.44	0.353	0.233
0.334	0.546	1.19[a]	1.00	6.28	0.220	0.145
0.285	0.546	0.915[a]	0.774	5.29	0.185	0.101
0.282	0.546	0.901[a]	0.762	5.29	0.185	0.0982
0.288	0.462	0.750[a]		3.12	0.091	0.071
0.285	0.462	0.738[a]		3.20	0.093	0.068
0.292	0.462	0.764[a]		3.58	0.1042	0.0647
0.482	0.462	2.58		11.2	0.325	0.236
0.454	0.462	2.28		10.0	0.291	0.207
0.420	0.462	1.80		8.0	0.232	0.160
0.331	0.462	1.005[a]		4.51	0.131	0.089
0.331	0.462	1.05[a]		5.09	0.148	0.087
0.246	0.462	0.517		2.10	0.0610	0.0497
0.242	0.462	0.513		2.17	0.0630	0.0484
0.331	0.398	0.876[a]	1.02	2.93	0.0733	0.0641
0.288	0.398	0.650[a]	0.755	2.03	0.0508	0.0498
0.382	0.321	0.920	1.32	2.76	0.0555	0.0406
0.346	0.321	0.743	1.07	2.10	0.0423	0.0342
0.478	0.321	1.37	1.95	4.60	0.0928	0.0539
0.846	0.168	2.18	6.00	3.02	0.0318	0.0291
0.975	0.168	3.51	9.66	Ref. (2)		

[a] Data for Fig. 2.

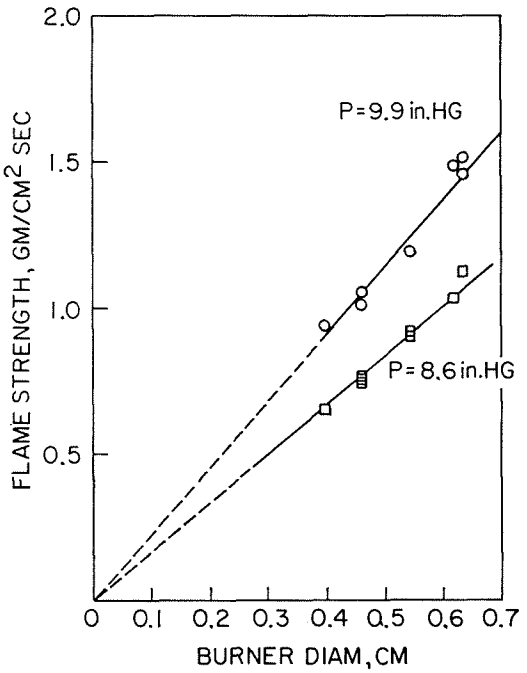

FIG. 2. Dependence of flame strength on burner diameter at 2 pressures for the propane-oxygen system.

from 2030–9850. The results are shown in Fig. 2. Lines going through the origin have been drawn through the data. The data fit the lines to within ±5%, which is the over-all precision of the measurements. The indication, then, is that the flame strength is directly proportional to the burner diameter. This is precisely what Spalding's theory[5] predicts.

TABLE 2

Effect of Reynolds number on flame strength

Pressure (atm)	Burner diameter (cm)	Flame strength (corrected to 0.462-cm burner)	Reynolds number (×10³)
0.331	0.635	1.05	8.85
0.331	0.635	1.10	9.85
0.331	0.619	1.11	9.07
0.331	0.462	1.00	4.51
0.331	0.462	1.05	5.09
0.331	0.398	1.02	2.93

Effect of Reynolds Number on the Apparent Flame Strength. The theory predicts that the transport properties of the gaseous jets should have no effect on the flame strength. Hence, the flame strength is expected to be independent of Reynolds number (at least, above $Re = 2000$ where the theory applies). This is found to be the case, as shown in Table 2, where the flame strength at constant pressure, and constant (corrected) jet diameter is given for Reynolds numbers ranging from 2.93 to 9.07×10^3.

Pressure Dependence of Apparent Flame Strength. Figure 3 shows the effect of pressure on the apparent flame strength of the propane-oxygen

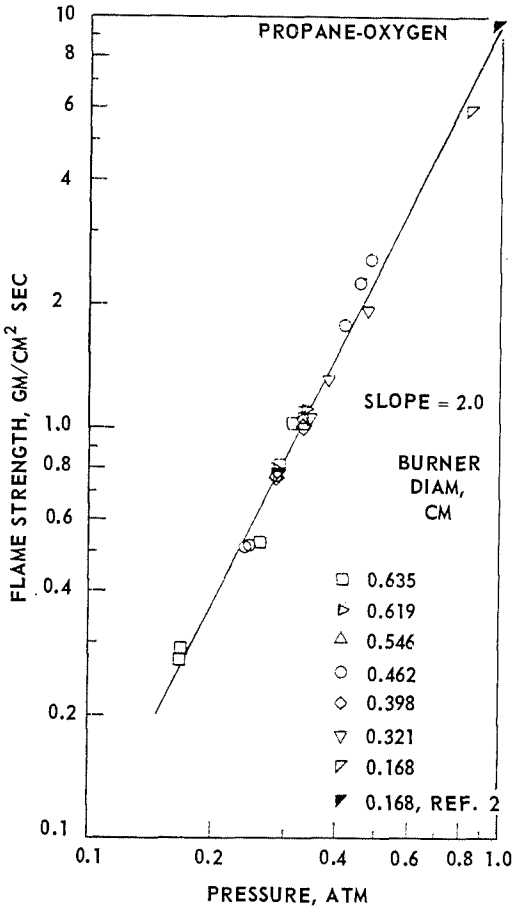

FIG. 3. Pressure dependence of flame strength.

system. Since there is an effect of burner diameter, the data must be referred to a single diameter. Most of the data are for a 0.462-cm burner covering a pressure range of 0.24 to 0.48 atm. The data for the other burner diameters have been converted to this diameter, using the diam-

eter dependence established in Fig. 2, to extend the pressure range of the correlation at both the high and low end. The least-squares slope of the line drawn through the data is 2.0.

The slope should be close to the order of the reaction since, according to Spalding, the apparent flame strength is directly proportional to the maximum reaction rate in the flame. The slope of 2.0 agrees well with the reaction order of 2.1 found from quenching distance experiments.[6]

Calculation of Maximum Heat Release Rate. It is possible to calculate a maximum heat release rate using the value of the flame strength extrapolated to 1 atm.

From Spalding's theory,[5] the maximum volumetric reaction rate is

$$\dot{m}'''_{fu,\max} = \frac{\rho}{\rho_\infty}\frac{\rho_\infty U_{\text{ext}}}{D}\frac{m_{fu,\infty}\Omega_{st}^2}{2\bar{\psi}_{st} f_{st}}$$

By multiplying $\dot{m}'''_{fu,\max}$ by the heat of combustion of propane, one obtains the volumetric heat release

$$\dot{q}'''_{\max} = 5.4 \times 10^4 \text{ cal/cm}^3 \text{ sec}$$

This value should be multiplied by a correction factor between 1.5 and 3 which accounts for viscous and density effects on the jet velocity.[5]

Bittker and Brokaw[7] have reported a method of determining chemical space heating rates using properties of the laminar flame. Their equation is

$$\dot{q}'''_{\max} = \frac{F}{K[\Gamma(n+1)]}\left(\frac{E}{RT_f}\right)\left(\frac{T_f - T_0}{T_f}\right)\left(\frac{n}{e}\right)^n \times \left(\frac{C_p}{2\lambda}\right)\left(\frac{p}{RT_0}\right) U_f^2 \, \Delta H_v$$

The value of $\dot{q}'''_{\max}$ obtained from this equation is 170×10^4 cal/cm³ sec.

The discrepancy between these two values is somewhat greater than one order of magnitude. The reason for this difference is not now apparent, but may be revealed in further theoretical studies.

Conclusion

It has been shown that the opposed-jet diffusion flame yields apparent flame strength data which corroborate Spalding's theory,[5] if the precaution is taken to keep the flows high enough to conform to the idealized flow, which is that of a jet impinging on a flat plate perpendicular to it. The method can now be extended to other systems of interest (for example, those using fluorine or chlorine as an oxidizer) with some assurance that it is a true measure of maximum reaction rate in the flame.

Nomenclature

C_p	Heat capacity at constant pressure
$C_{p,\infty}$	Heat capacity of the fuel at constant pressure
D	Diameter of the burner
E	Activation energy
e	Base of natural logarithms
F	Conversion factor
f_{st}	Mass fraction
ΔH_v	Volumetric heat of combustion
K	Correction factor
$m_{fu,\infty}$	Mass fraction of fuel in the fuel-bearing stream
$\dot{m}'''_{fu,\max}$	Maximum volumetric reaction rate
n	Reaction order
p	Pressure
R	Gas constant
T_f	Flame temperature
T_0	Initial temperature
U	Jet velocity far upstream of the impingement region
U_f	Burning velocity
Γ	The gamma function
λ	Thermal conductivity
λ_∞	Thermal conductivity of the fuel
ρ	Density
ρ_∞	Density of the fuel
$\rho_\infty U_{\text{ext}}$	Flame strength
$\bar{\psi}_{st}$	Average flame reaction rate at stoichiometric
Ω_{st}	A function of f_{st}, indicative of the burning rate in the flame at stoichiometric

References

1. Potter, A. E. and Butler, J. N.: ARS Journal *29*, 54 (1959).
2. Potter, A. E., Heimel, S., and Butler, J. N.: *Eighth Symposium (International) on Combustion*. Baltimore, Williams and Wilkins, 1962.
3. Spalding, D. B.: Fuel *33*, 253 (1954).
4. Zeldovich, Y. B.: Zhur. Eksp. i Teoret. Fiz. *19*, 119 (1949); trans. as NACA Tech. Memo. 1296 (1951).
5. Spalding, D. B.: ARS Journal *31*, 763 (1961).
6. Anagnostou, E. and Potter, A. E.: Combustion and Flame *3*, 453 (1959).
7. Bittker, D. A. and Brokaw, R. S.: ARS Journal *30*, 179 (1960).

Discussion

PROF. M. W. THRING (*University of Sheffield*): Does the paper indicate that the theory predicts a reaction rate per unit volume differing by a factor of 40 from the observed value? If so the agreement in relative effects of pressure and diameter is a less powerful verification of the theory than if the predicted reaction rate were of the right order of magnitude.

MISS E. ANAGNOSTOU (*NASA*): The paper does not predict a reaction rate per unit volume differing by a factor of 40 from the observed value. It does predict a reaction rate smaller by a factor of 40 than a rate calculated using a method based on Semenov's flame theory. This is disappointing but since we have compared theory with theory the result is inconclusive.

A proper test of reaction rates per unit volume from the opposed jet is to compare the calculated values with measured ones. This has been done previously by Spalding, who noted agreement within an order of magnitude between maximum space-heating rates observed in the stirred reactor and those calculated from opposed jet data for hydrocarbon-air flames.

NINTH SYMPOSIUM (INTERNATIONAL) ON COMBUSTION

MIXING AND FLOW IN DUCTED TURBULENT JETS

H. A. BECKER, H. C. HOTTEL, AND G. C. WILLIAMS

The aerodynamic flow pattern of a confined, turbulent jet can differ profoundly from that of a free jet, most pronouncedly so in the massive recirculation of downstream gases which occurs under the operating conditions of many industrial furnaces. This paper reports on a study of furnace mixing patterns as represented in the cold by a round jet of oilfog-marked air issuing axially into a cylindrical duct fed by a uniform stream of clear air. Investigation of the fields of mean and fluctuating concentration was made possible by applying the recently developed scattered light technique of illuminating the space-point of interest with a strong light beam and measuring the intensity of 90°-scattered light. The technique has been refined to the point where the signal can be representative of a cubical volume element as small as 0.5 mm on a side.

Emphasis was on the aerodynamic flow regime in which appreciable recirculation occurs. A mapping of the field of mean velocity was made with impact tubes. Velocity fluctuations were not measured as such, but indirect evidence was obtained from a mapping of the field of mean static-pressure defect in the jet. The sol-scattered-light technique itself yielded the fields of mean concentration of nozzle fluid, $\bar{\gamma}$, and r.m.s. fluctuating concentration, $(\overline{\gamma'^2})^{\frac{1}{2}}$; lateral and longitudinal correlation coefficients and spatial scales of concentration fluctuations; and the wave-number spectrum of concentration fluctuations.

Introduction

The problem of a turbulent jet as it issues into a confined, cocurrent stream has been but scantily studied. In fact, the nature of turbulence properties, which is basic to the aerodynamics of furnaces, has been wholly neglected until very recently. This paper is therefore a study of the simple generic example of a round jet which discharges axially into a cylindrical duct fed by a uniform stream whose entrance momentum relative to that of the jet varies from zero to moderately high values.

The turbulent jet in a cocurrent, constant-velocity stream was early analyzed by Squire and Trouncer.[1] The investigations by Forstall and Shapiro,[2] and Landis and Shapiro[3] of a round jet in a cylindrical duct were conducted under conditions approximating those of Squire and Trouncer's theory; the uniform stream fed to the duct greatly exceeded the entraining power of the jet. These conditions, however, differ from those often prevailing in furnaces, since it is common to find that the entrainment capacity of a furnace-flame jet is partly or even wholly filled by the recirculation of downstream gases. This recirculation was first examined in an approximate analysis by Thring and Newby[4] and subsequently in investigations by the International Flame Research Foundation. The theory of confined jets has been developed by Curtet[5,6,7] who, with Craya,[8] enunciated the criterion governing the similarity of fully turbulent, incompressible, confined jet flows. Curtet[5,6,7,9] has also investigated experimentally the velocity fields of several confined jets.

The present work is a study, within the regime in which recirculation occurs, of the effect of the Craya-Curtet similarity parameter on turbulent mixing patterns in axisymmetrical constant-density confined-jet flows. The fields of the axial component of mean velocity, the mean static pressure, and the mean and the turbulently fluctuating components of the concentration of a species marking the jet-nozzle fluid are mapped. The marking species is an oil fog of which the point concentration was sensed by the scattered-light technique developed by Rosensweig.[10] The concentration fluctuations were characterized by their r.m.s. (root-mean-square) value and were, moreover, analyzed spectrally; extensive measurements were also made of the spatial correlation of concentration fluctuations.

The great volume of the results limits the present scope to the fields of mean velocity and mean concentration. The results on concentration fluctuations will be published elsewhere.

Similarity

It is well known that fully turbulent constant-density jets in infinite stagnant atmospheres are

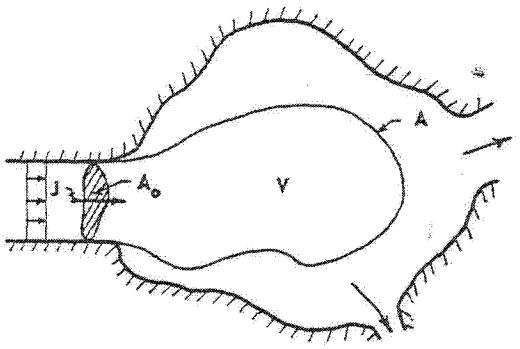

FIG. 1. A confined-jet system with the initial conditions (i) entering stream uniform, (ii) jet-source momentum flux cocurrent with the entering stream.

aerodynamically similar, except in the region immediately surrounding the jet source. Confined jets introduce additional parameters. To develop a similarity criterion for confined jets, from a more general approach than that of Craya and Curtet, consider an arbitrarily shaped enclosure containing one inlet opening and any number of outlet openings (Fig. 1). The entering fluid stream is nonturbulent and uniform; located within it is the cocurrent point source of a turbulent jet. Since the only variation possible between geometrically similar systems of this type is in the relative strengths of the jet source and the uniform feed stream, similarity must hinge on the constancy of some parameter which defines the ratio of these strengths.

In Fig. 1, A_0 is a control plane sectioning the uniform feed stream at right-angles to its motion at a point just *downstream* of the jet source, J, and A is a surface bounding with A_0 an arbitrary control volume V inside the enclosure. The conservation of fluid volume in steady flow requires that

$$-\int_{A_0} \mathbf{n}\cdot\mathbf{u}\, dA_0 = \int_A \mathbf{n}\cdot\mathbf{u}\, dA, \qquad (1)$$

where $\mathbf{n}$ is the unit vector normal to an element of surface. Further, formulation of the steady state dynamic equilibrium gives

$$-\int_{A_0} (\rho\mathbf{n}\cdot\mathbf{u}\,\mathbf{u} + p\mathbf{n})\, dA_0$$

$$= \int_A (\rho\mathbf{n}\cdot\mathbf{u}\,\mathbf{u} + p\mathbf{n})\, dA - \int_V \rho\mathbf{g}\, dV \qquad (2)$$

In a constant-density, incompressible flow weight forces and absolute pressure level have no effect on turbulent mixing; to eliminate them, let

$$p_{f,0}{}^* = (p - \rho\mathbf{g}\cdot\mathbf{x} + \tfrac{1}{2}\rho\mathbf{u}\cdot\mathbf{u})_{f,0}, \qquad (3)$$

where subscript $_{f,0}$ denotes evaluation in the uniform feed stream at plane A_0. Noting that in a constant-density system

$$\int_V \rho\mathbf{g}\, dV = \int_{A_0} \rho\mathbf{g}\cdot\mathbf{x}\,\mathbf{n}\, dA_0 + \int_A \rho\mathbf{g}\cdot\mathbf{x}\,\mathbf{n}\, dA, \qquad (4)$$

Equation (2) reduces to

$$-\int_{A_0} (\rho\mathbf{n}\cdot\mathbf{u}\,\mathbf{u} - \tfrac{1}{2}\rho\mathbf{u}_{f,0}\cdot\mathbf{u}_{f,0}\mathbf{n})\, dA_0$$

$$= \int_A (\rho\mathbf{n}\cdot\mathbf{u}\,\mathbf{u} + (p - p_{f,0}{}^* - \rho\mathbf{g}\cdot\mathbf{x})\mathbf{n})\, dA \qquad (5)$$

If aerodynamic drag at the enclosure walls is negligible, than the left-hand sides of Eqs. (1) and (5) are the only configurations of independent variables entering into analysis of the fluid motion. Let u_k and u_d be called the kinematic-mean and the dynamic-mean inlet velocities; u_d is that uniform entering velocity which produces a force equal to the excess of the true stream thrust at A_0 over the stagnation pressure-area force of the induced stream.

$$u_k = -(1/A_0) \int_{A_0} \mathbf{n}\cdot\mathbf{u}\, dA_0$$

$$u_d{}^2 = -(1/A_0) \left| \int_{A_0} (\mathbf{n}\cdot\mathbf{u}\,\mathbf{u} - \tfrac{1}{2}\mathbf{u}_{f,0}\cdot\mathbf{u}_{f,0}\mathbf{n})\, dA_0 \right| \qquad (7)$$

It follows that similarity of confined, constant-density, fully turbulent, point-source jets in such geometrically similar systems depends uniquely on the characteristic velocity ratio u_k/u_d.

The confined-jet similarity parameter m derived by Craya and Curtet is the unique function of u_k/u_d

$$m = (u_d{}^2 - \tfrac{1}{2}u_k{}^2)/u_k{}^2 \qquad (8)$$

The difference $u_d{}^2 - \frac{1}{2}u_k{}^2$ is a measure of the nonuniformity of the momentum-flux distribution at the system inlet; it is zero for a uniform distribution. Let $u_0{}^* = \sqrt{(u_d{}^2 - \frac{1}{2}u_k{}^2)}$. The present study has shown that $u_0{}^*$ is the characteristic system velocity to which the performance of a confined jet is most closely scaled; i.e., it is that normalizing velocity which minimizes the dependence of the normalized velocity field on the similarity criterion. The most efficient form of the similarity criterion itself is $u_k/u_0{}^* = 1/\sqrt{m}$. Since Craya and Curtet discovered the rigorous confined-jet similarity principle, we have named $u_k/u_0{}^*$ the Craya-Curtet number and denote it by Ct.

The physical significance of Ct as a criterion of flow regime for axisymmetrical jet flows in cylindrical ducts is easily appreciated. For point-source jets Eq. (7) gives

$$u_d^2 = (i_s/\pi\rho r_w^2) + \tfrac{1}{2}u_{f,0}^2, \qquad (9)$$

hence

$$Ct = \frac{u_k}{\sqrt{(i_s/\pi\rho r_w^2) + \tfrac{1}{2}u_{f,0}^2 - \tfrac{1}{2}u_k^2}} \qquad (10)$$

For a cylindrical enclosure, u_k is the space-mean velocity. The ideal point source of a jet is defined as one which supplies a finite flux of momentum, i_s, but zero flux of mass. With such a source, $u_{f,0} = u_k$. If i_s is finite, but $u_{f,0}$ is zero, then $Ct = 0$. This is the case of total recirculation, since the jet is supplied with no fresh entrainment fluid. On the other hand, if i_s is zero while $u_{f,0}$ is finite, $Ct = \infty$ and the flow is uniform throughout the duct. Experiment shows that recirculation is limited to $Ct < \frac{3}{4}$. With finite sources, account must be held of the source characteristics. For an ideal, circular nozzle, the initial velocity distribution is

$$u = u_{f,0}, \qquad r_s < r < r_w$$
$$u = u_s, \qquad 0 \leq r < r_s,$$

where u_s is the uniform nozzle velocity. Here

$$Ct = \frac{u_k}{\sqrt{(u_s^2 - u_{f,0}^2)r_s^2/r_w^2 + \tfrac{1}{2}u_{f,0}^2 - \tfrac{1}{2}u_k^2}} \qquad (11)$$

and

$$u_k = (u_s - u_{f,0})r_s^2/r_w^2 + u_{f,0}. \qquad (12)$$

Hence, when $u_s = u_{f,0}$, $u_k = u_{f,0}$ and $Ct = \infty$. However, when $u_{f,0} = 0$, $Ct = (r_s/r_w)/(1 - \frac{1}{2}r_s^2/r_w^2)$, and $Ct = 0$ is approached only as $r_s/r_w \ll 1$. For a given ratio r_s/r_w, Ct is a unique criterion of dynamic similarity. For jet-type flows, i.e., $0 \leq u_{f,0} < u_s$, Ct lies in the range $(r_s/r_w)/(1 - \frac{1}{2}r_s^2/r_w^2)^{\frac{1}{2}} \leq Ct < \infty$. The condition $u_{f,0} > u_s$ describes wake-type flows and generates imaginary values of Ct, but is of no present interest; $u_{f,0} < 0$ is not an initial condition.

Squire and Trouncer[1] early predicted that similarity of axisymmetrical jets in uniform constant-velocity streams should depend uniquely on the velocity ratio u_s/u_f (they only considered ideal flow–nozzle sources). Forstall and Shapiro[2] and Landis and Shapiro,[3] influenced by Squire and Trouncer's analysis, concluded that in their experimental range of $u_s/u_{f,0}$, $\frac{1}{4} < u_s/u_{f,0} < \frac{3}{4}$, similarity of axisymmetrical ducted jets depends only on $u_s/u_{f,0}$, and not on r_s/r_w. Actually ducted jets can closely approach Squire and Trouncer's conditions only at very high values of Ct. Thring and Newby,[4] on the other hand, made a reasonable hypothesis for small values of Ct; i.e., in regimes in which recirculation occurs a ducted jet should, to a first approximation, have the same entrainment properties as a free jet in a stagnant atmosphere. They concluded that similarity ought to depend on $\sqrt{(\pi\rho u_k^2 r_w^2/i_s)}$. This parameter has considerably more general validity than do Thring and Newby's intuitive arguments in deriving it; it is exactly the reciprocal of Ct for an ideal point-source jet. Craya and Curtet[5] were, however, the first to develop rigorously the general similarity principle of confined jets.

Mixing Zones of a Ducted Jet

Turbulent mixing in an ideal ducted jet occurs in three fairly distinct zones. The true jet-mixing zone in which the jet grows laterally, is upstream, and ends when the jet reaches the duct wall. In the next zone lateral gradients in the mean velocity are dissipated. Finally there is a zone in which the remaining turbulence is dissipated. In reality all three zones may be blurred and the final one wholly obscured by the growth of a wall boundary layer, ultimately to a fully developed pipe flow.

The velocity field in the jet mixing zone has certain well-defined characteristics: The flow through the duct can be regarded as the superposition of a *jetting stream* with a bell-shaped radial velocity profile on a laterally uniform *ground stream* (Fig. 2). That portion of the ground stream between the edge of the jet and the duct wall will be called the *free stream*. The uniform stream supplied to the duct at entrance is the *feed ground stream*.

The jetting stream grows until it reaches the duct wall at which point the free stream vanishes and entrainment ceases. Consequently a confined jet has a finite entrainment capacity. When the feed ground stream flow falls short of the entrain-

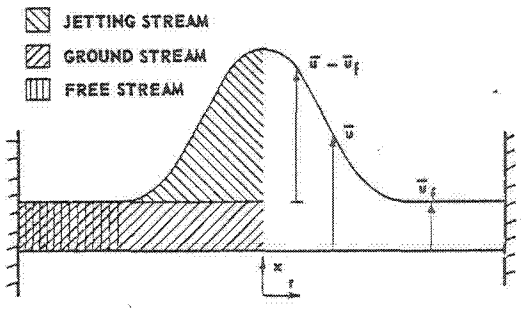

FIG. 2. The radial velocity distribution in a ducted jet represented as the superposition of a jetting stream and a uniform ground stream.

ment capacity of the jet, the balance is satisfied with recirculated fluid. Recirculation defines a *recirculation eddy* about whose eye the recirculatory flow revolves. Since its source lies in the region of maximum development of the jet, the free stream in the recirculatory zone is massively turbulent. It is convenient to speak of the downstream-directed portion of the free stream as the *feed free stream* and of the upstream-directed portion as the *recirculatory free stream*, though their boundary is considerably diffused by the turbulence of the latter.

Apparatus and Methods

The duct was a transparent Plexiglass cylinder 125 cm long and 19.7 cm inside diameter. The jet source was an essentially ideal flow nozzle of 0.635 cm throat diameter and 2.41 cm upstream inside diameter. The uniform feed ground stream entering the duct was ambient air inspired by the jet. The inspiration rate was limited by aerodynamic resistances (Tyler sieves and perforated plates) fitted over the duct inlet. A rounded entry section was provided. The duct outlet opened abruptly into the atmosphere.

Experiments were carried out at a nozzle velocity of 130 m/sec, excepting a few in which the effect of nozzle Reynolds number was investigated.

Mean velocities were measured with sharp-lipped, thin-walled cylindrical impact tubes. The effects of probe Reynolds number and probe diameter were investigated and eliminated from the results. The velocity measured by such a probe evidently[11] lies between the simple-mean velocity $\bar{u}$ and the r.m.s. velocity $(\overline{u^2})^{\frac{1}{2}}$. For simplicity, the measured mean velocities will be treated as simple-mean values, but the possible error in this interpretation should be kept in mind.

Concentration of an oil fog marking the source fluid (air) was measured by the sol-scattered-light technique of Rosensweig.[10] In this technique, a narrow beam of light is shone through the mixing field. Light scattered at right-angles to the beam is gathered by a lens and focused on a diaphragm containing a slit oriented normal to the direction of the beam. The slit permits light from a short segment of the beam to illuminate a multiplier phototube behind the diaphragm. Thus an electrical signal is generated proportional to the space-average concentration of aerosol in the volume of space defined by the cross section of the beam and the width of the slit. In the present work this volume was as small as 0.5 mm in length and diameter, and the signal represented truly the point value of fog concentration.

Mechanical traversing devices were used which permitted radial position in the duct to be measured within 0.02 mm and axial position within 0.2 mm. A Prandtl-type micromanometer permitted measurement of small dynamic pressures to an accuracy of ± 0.01 mm of water. Manometers and voltmeters were damped to provide time constants of 2 sec or 10 sec for accurate time-averaging of signals.

The Radial Profile of the Jetting Velocity

The jetting velocity is the excess, $\bar{u} - \bar{u}_f$, of the mean axial component of velocity inside the jet over its value, $\bar{u}_f$, in the free stream outside the jet (Fig. 2). At a given axial position, the jetting velocity is characterized by its radial maximum, $\bar{u}_m - \bar{u}_f$, which occurs on the jet axis of symmetry. The radial confine of the jet is characterized by some representative radius, here taken as the radius $r_{u/2}$ at which $\bar{u} - \bar{u}_f = \frac{1}{2}(\bar{u}_m - \bar{u}_f)$. Consequently the radial profile of the jetting velocity can be represented in the normalized form

$$U/U_m = f(R/R_{u/2})$$

where

$$U/U_m = (\bar{u} - \bar{u}_f)/(\bar{u}_m - \bar{u}_f)$$

and

$$R/R_{u/2} = r/r_{u/2}.$$

The velocity profile at the jet nozzle was, within the accuracy of the experiment, perfectly rectangular. The course of the transition from such an initial profile to the bell-shaped jetting-velocity profile of a fully developed, turbulent jet is well known and will not be described, although full measurements were made.[11] Interest here is in the fully developed jetting flow whose characteristics are independent of the nature of the source. Full development was closely approached about eight nozzle diameters downstream of the nozzle mouth. Beyond here and within the jet-mixing zone, the normalized profile of the mean jetting velocity was essentially self-preserving (i.e., invariant with respect to downstream position), as illustrated by Fig. 3.

Radially, the fully developed jet divided into two zones. The fully turbulent core extends to about $R = R_{u/2}$. Within it the velocity profile has a universal form, unvarying with Craya-Curtet number in the experimental range $0 < Ct < 1.2$ and the same for confined axisymmetrical jets as for free jets (free jets will be treated in another paper). From about $R = R_{u/2}$ to about $R = 2.3R_{u/2}$ is a variably turbulent annulus whose characteristics vary with the Craya-Curtet number and differ for

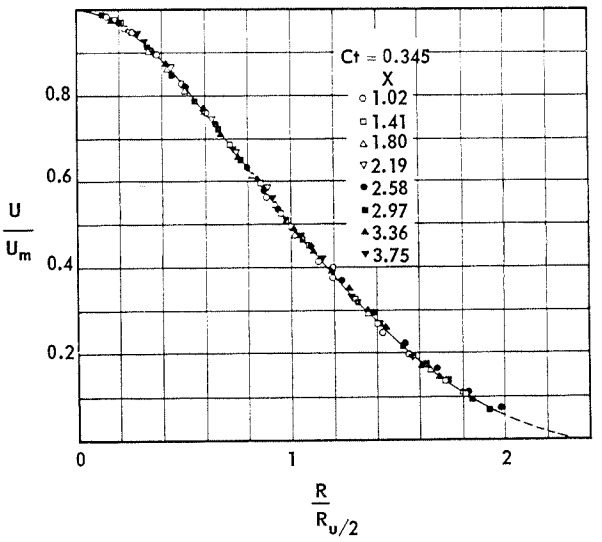

FIG. 3. The radial profile of the jetting velocity at $Ct = 0.345$.

free and confined jets. In zones without recirculation, this annulus is a region of intermittent turbulence.

A plot of ln $(-\ln U/U_m)$ vs. ln $(R/R_{u/2})$ was invariably linear up to at least $R = 1.2R_{u/2}$, giving

$$U/U_m = \exp\{-(\ln 2)(R/R_{u/2})^a\} \quad (13)$$

Experimental values of the exponent a ranged from 1.79 to 1.86 and showed no systematic dependence on Ct. An average value of $a = 1.82$ represents all the data quite accurately.

Up to $R = 0.8R_{u/2}$, Eq. (13) with $a = 1.82$ is, in the value of U, practically indistinguishable from

$$U/U_m = \{1 + (\sqrt{2} - 1)(R/R_{u/2})^2\}^{-2} \quad (14)$$

For a free jet in a stagnant free stream this velocity distribution function signifies a radially constant eddy viscosity μ_E. For a ducted jet in the range $0 < Ct < 1$ the predicted μ_E is constant up to about $R = R_{u/2}$.

In the variably turbulent annulus, the velocity distribution in a ducted jet depends on Ct. At $R > R_{u/2}$ and in regimes with little or no recirculation ($Ct > \frac{1}{2}$), the present data are well portrayed by

$$U/U_m = \{1 - (1 - 2^{-\frac{1}{2}})(R/R_{u/2})^b\}^2 \quad (15)$$

Values of b ranged from 1.45 to 1.55, but the average value $b = \frac{3}{2}$ is generally good. This distribution function gives the jet a finite radial limit located, for $b = \frac{3}{2}$, at $R = 2.27R_{u/2}$. In recirculatory zones the turbulence of the free stream erases the sharp jet edge: at $Ct = 0.033$ (the condition for zero induction of ground-stream feed in the present system), Eq. (13) with $a = 1.82$ is applicable at all values of R. Thus, in a recirculating ducted jet the transition from nonturbulent to turbulent free-stream flow with downstream distance is accompanied by departures from self-preservation at the edges of the jet. These departures are, however, rather small. The dominant factor affecting the velocity profile is Ct. When recirculation is extensive (Ct small), the massively turbulent recirculation free stream penetrates the nonturbulent feed free stream throughout the jet-mixing zone, thereby erasing the greater part of the possible dependence of the velocity profile on downstream position.

In the region of inflection of the velocity profile, the relation between U and R is essentially linear in a range $0.6 < R/R_{u/2} < 1.1$ or greater.

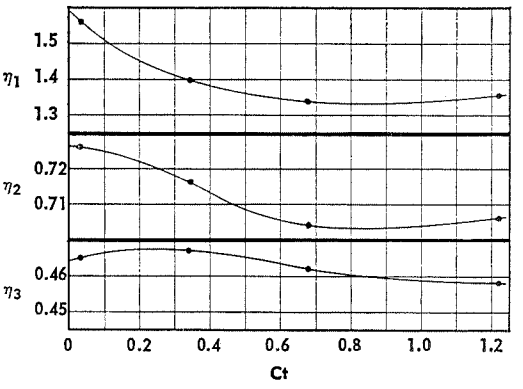

FIG. 4. The Craya-Curtet number dependency of the velocity profile shape factors η.

The slope here was

$$\left[\frac{\partial(U/U_m)}{\partial(R/R_{u/2})}\right]_{\partial^2 U/\partial R^2=0} = 0.645 \pm 0.005$$

Average values of the profile shape functions η (see the Nomenclature section for definitions) for different values of Ct were obtained by graphical integration from plots of U/U_m, and $(U/U_m)^2$, and $(U/U_m)^3$ vs $(R/R_{u/2})^2$. They are shown as functions of Ct in Fig. 4. Curtet and Ricous' data[9] for $Ct = 2.77$ give $\eta_1 = 1.25$, $\eta_2 = 0.68$, and $\eta_3 = 0.455$.

The Radial Growth of the Jet

A set r_n of characteristic jet radii is defined by

$$r_n^2 = \int_0^\infty (U/U_m)^n \, dr^2, \qquad (16)$$

where r_1 may be termed the "volume-flux radius," r_2 the "momentum-flux radius," and r_3 the "kinetic-energy-flux radius." Another useful set $r_{\alpha u}$ is defined by

$$r = r_{\alpha u} \quad \text{at} \quad \bar{u} - \bar{u}_f = \alpha(\bar{u}_m - \bar{u}_f), \qquad (17)$$

where α is a fraction between zero and unity.

In analyzing jet behavior, it is expedient to select one characteristic jet radius as primary and to replace all others with it multiplied by an appropriate proportionality factor. There are strong arguments here favoring a member of the set $r_{\alpha u}$ pertaining to that region of the fully turbulent core where velocity is linear in radial position. Following the commonest precedent, the primary characteristic jet radius was taken to be the velocity half-radius, $r_{u/2}$.

The normalized velocity half-radius is shown in Fig. 5 as a function of the normalized downstream distance with Ct as a parameter. The curve $Ct = 0.673$ is evidently identical with that for a free jet in a stagnant free stream: Comparison with literature data[12–15] indicates this, and the congruity of the concentration half-radii (see below) would seem to prove it conclusively. The radial growth law for $Ct = 0.673$ is

$$R_{u/2} = 0.084X. \qquad (18)$$

In the neighborhood of the jet source (where $U_m \gg U_f$), the radial growth of a confined jet is expected to approach asymptotically that of a free jet in a stagnant free stream. Hence the first term in a power series representation of $R_{u/2}$ is $0.084X$. It was found that in the regime of recirculatory flows ($0 < Ct < 0.7$)

$$R_{u/2} = 0.084X\{1 + (X/X_r)^{5/3}\}, \qquad (19)$$

$$X_r = 4.07 \exp(3.54\, Ct). \qquad (20)$$

The data for the highest Craya-Curtet numbers presently studied, $Ct = 1.00$ and $Ct = 1.22$, do not obey Eq. (19) exactly but are well correlated by

$$R_{u/2} = 0.0813X. \qquad (21)$$

Axial Decay of Jetting Velocity

The optimum choice of a characteristic value of the jetting velocity is unambiguous: $\bar{u}_m - \bar{u}_f$ is the only logical possibility.

The reciprocal of the normalized value of $\bar{u}_m - \bar{u}_f$ is shown in Fig. 6 as a function of the normalized downstream distance with Ct as

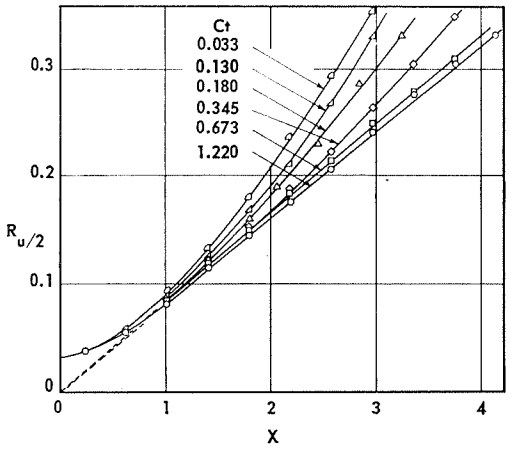

FIG. 5. The axial growth of the velocity half-radius.

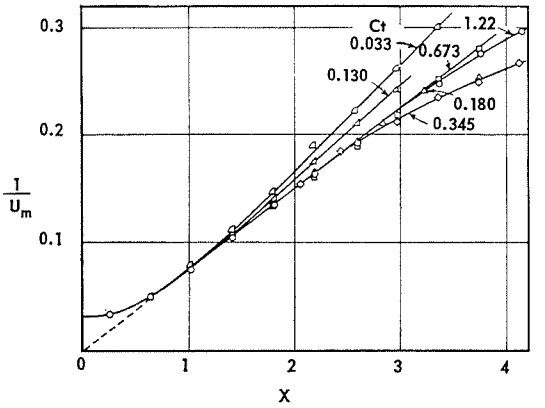

FIG. 6. The axial decay of the radial maximum of the jetting velocity.

parameter.* The curves are quite similar to those in Fig. 5, and the curve for $Ct = 0.673$ is again identical with that for a free jet. The data are for the most part well correlated by

$$1/U_m = 0.0725X\{1 + (X/X_u)^{5/3}\}, \quad (22)$$

$$X_u = 5.95 \exp(3.54Ct), \quad (23)$$

but some deviation from this relation occurs at high values of X with $Ct = 0.180$ and 0.345.

The data of Curtet and Ricou[7] formally obey Eq. (22) at values of Ct up to five; hence the full range of validity of the equation is $0 < Ct < 5$.

The Effect of Jet Reynolds Number

The effect of the jet Reynolds number was investigated at a Craya-Curtet number of 1.22. At the standard nozzle Reynolds number of $Re_s = 54000$, the laws of the jet were (see section on The Radial Growth of the Jet)

$$R_{u/2} = 0.0813X \quad (24)$$

$$U_m R_{u/2} = 1.122 \quad (25)$$

while at $Re_s = 18500$

$$R_{u/2} = 0.053 \quad (26)$$

$$U_m R_{u/2} = 1.126 \quad (27)$$

The radial velocity profile was unaffected. The insignificant change in $U_m R_{u/2}$ shows that the jetting momentum flux was constant. It can be shown that the observed change in the rate of radial growth of the jet consequently signifies a proportional change in the total shear stress $\rho\overline{u'v'} - \mu\, \partial\bar{u}/\partial r$.

Spalding and Ricou[16] have studied the entrainment law of the free jet issuing into a stagnant free stream. At sufficiently high Reynolds number, the entrainment rate was constant. The ratio of the jetting flow at a given Reynolds number to the flow at very high Reynolds number is (noting conservation of axial momentum flux), $R_{u/2}/(R_{u/2})_{Re_s \to \infty}$. Figure 7 shows that the Reynolds number effect decays to insignificance by $Re_s = 30{,}000$. Since the present experiments were, excepting the one just discussed, conducted at $Re_s = 54{,}000$, they pertain to the regime of sufficiently high Reynolds numbers in which the effect of viscosity on the

* The origin of x is at the virtual point source of the fully developed jet. The origin was located from the data for $Ct = 0.673$ by extrapolating to zero ordinate the linear (see Figs. 3 and 5) relation between $R_{u/2}$ or $1/U_m$ and distance from the jet nozzle. The virtual point source lay 4.5 nozzle radii downstream of the nozzle mouth.

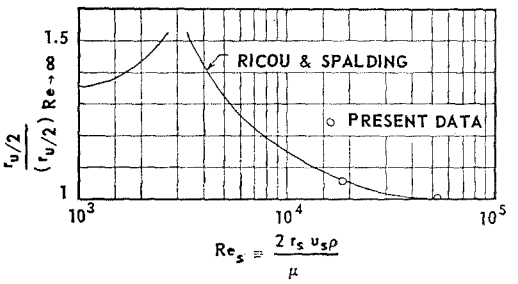

FIG. 7. The Reynolds number dependency of the velocity half-radius.

mean jetting flow is insignificant (the jet turbulence itself[17] attains a constant structure only at Reynolds numbers exceeding 10^6).

Axial Variation of the Free-Stream Velocity

Given the field of the jetting velocity of an axisymmetrical ducted jet, the axial variation of the free-stream velocity follows from the continuity equation

$$\eta_1 U_m R_{u/2}^2 + U_f = Ct, \quad (28)$$

wall boundary layer neglected.

The experimental values of U_f for the annulus between the wall boundary layer and the jet edge are shown as a function of X in Fig. 8

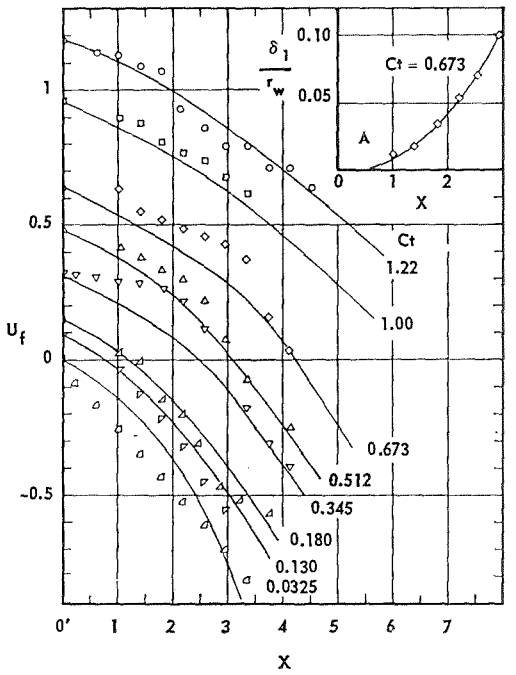

FIG. 8. The axial evolution of the free-stream velocity.

and compared with the values calculated from Eq. (28) using Fig. 5 and Eqs. (22) and (19) for the values of η_1, U_m, and $R_{u/2}$. At $Ct = 0.345$, 0.512, and 0.673 the divergence between the measured and calculated values of U_f is due to the wall boundary layer, but at $Ct = 0.0325$, 0.130, and 0.180 it is mainly ascribable to the error in measuring U_f in a highly turbulent recirculatory flow.

The effect of the wall boundary layer on the mean flow is accounted for by writing Eq. (28) in the form

$$\eta_1 U_m R_{u/2}^2 + (1 - \Delta_1)^2 U_f = Ct, \quad (29)$$

where Δ_1 is the normalized displacement thickness of the boundary layer. Values of U_f calculated from this equation using the experimental values of Δ_1 agree well with the directly measured U_f's at $Ct = 0.345$, 0.512, and 0.673. The great boundary layer thickness in the feed free stream at these Ct's is attributable to intensely adverse pressure gradients; boundary layer separation occurred near the upstream edge of the recirculatory flow. Since boundary layer development here is primarily dependent on the pressure field of the ducted jet, it should be effectively modelled by Ct.

Recirculation

The occurrence of recirculation, marked by negative free-stream velocities, is plainly evident in Fig. 8.

The recirculation eddy has the following well-defined characteristics: Its statistical upstream edge lies where $U_f = 0$. In general, the edge of the recirculatory (upstream-directed) flow is defined by the surface $\bar{u} = 0$. The normalized axial component of the recirculatory flow is

$$Q_r = -\int_{r_{u=0}}^{r_w} \bar{u}\, dr^2 \Big/ u_0^* r_w^2 \quad (30)$$

The maximum of Q_r represents the volumetric flux of fluid around the recirculation eddy, Q_{eddy}. The eye of the eddy, around which this flow revolves, is located where $\bar{u} = 0$, $Q_r = Q_{eddy}$. The complete statistical envelope of the eddy is difficult to determine exactly, but if the flow is treated one-dimensionally the radial coordinates r of the envelope are defined by

$$\int_r^{r_{\bar{u}=0}} \bar{u}\, dr^2 = -\int_{r_{u=0}}^{r_w} \bar{u}\, dr^2 \quad (31)$$

Some of the above features of the eddy are illustrated by Fig. 9.

From a plot of Q_r as a function of X and Ct, the axial maxima of Q_r give

$$Q_{eddy} = 0.32 - 0.43Ct. \quad (32)$$

Figure 10 shows the statistical locations of the eye and the upstream edge of the eddy as functions of Ct. Also shown is the approximate downstream limit of the eddy, estimated as the point where $R_{u/2} = \frac{1}{2}$. Figure 11 shows the mean boundaries of the recirculatory flow.

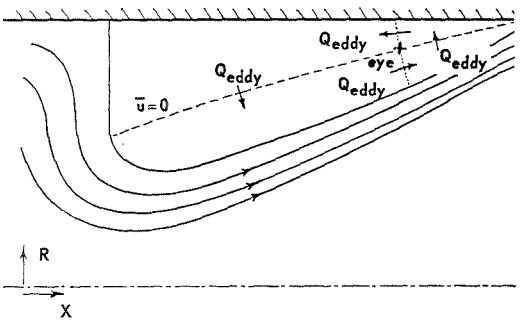

FIG. 9. Some features of the recirculation eddy.

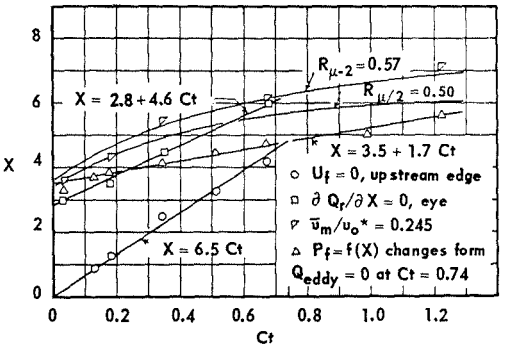

FIG. 10. The Craya-Curtet number dependency of the axial location of various features of the recirculation eddy.

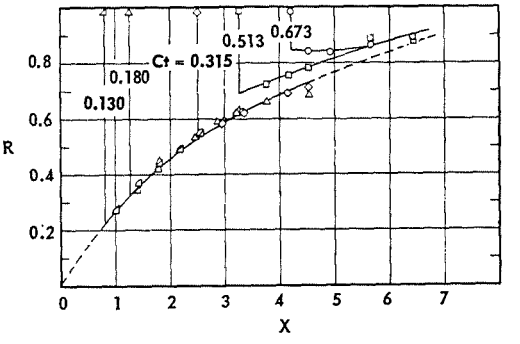

FIG. 11. The mean boundaries of the recirculatory flow, i.e., the surfaces over which $\bar{u} = 0$.

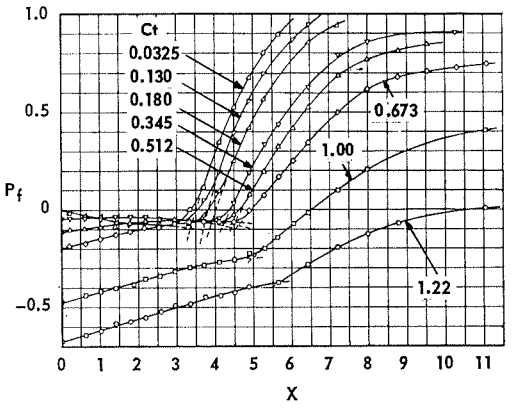

FIG. 12. The axial evolution of the static pressure at the duct wall.

Axial Variation of Static Pressure

The axial variation of the mean static pressure (measured at the duct wall) should reflect changes in mixing regime. In particular, one expects a change in the law of static pressure variation between the jet mixing zone and the succeeding zone of dying gradients in the mean velocity, and the intersection of the two laws should identify the point at which the free stream effectively vanishes and entrainment ceases.

Figure 12 bears out this expectation. The points of jet extinction thus deduced are shown as a function of Ct in Fig. 10. They lie, for the most part, considerably nearer the eye of the recirculation eddy than do the points resulting from the approximation that $R_{u/2} = \frac{1}{2}$ here.

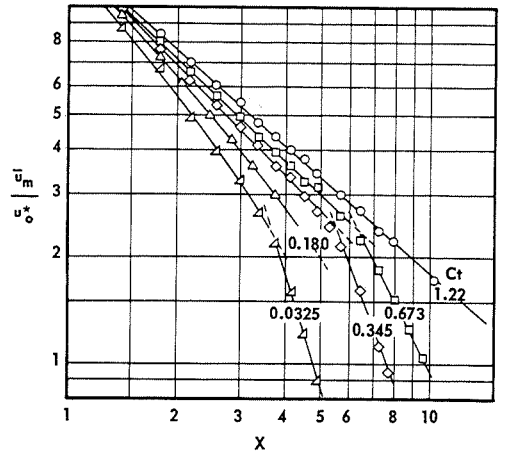

FIG. 13. The axial decay of the radial maximum of the mean velocity.

Post-Jet-Mixing Zone

Complete investigation of the mean velocity field in the post-jet-mixing zone was possible only at the higher Craya-Curtet numbers, since only then were velocities generally high enough to be measurable.

Figure 13 shows the axial decay of the radial maximum of the mean velocity. In flow with recirculation there is a marked change in the velocity decay rate at about $\bar{u}_m/u_0^* = 0.24$; this change signals the beginning of the post-jet-mixing zone insofar as $\bar{u}_m$ is concerned. The values of $X(\bar{u}_m/u_0^* = 0.24)$ correspond exactly with $X(R_{u/2} = 0.57)$, Fig. 10. Extrapolation of

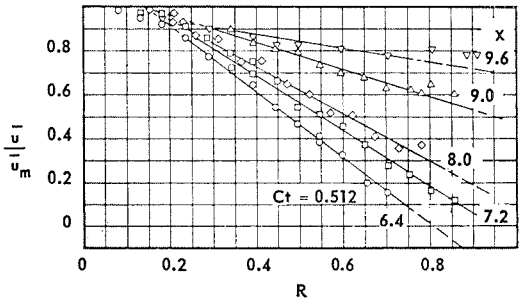

FIG. 14. Radial velocity profiles in the post-jet-mixing zone at $Ct = 0.512$.

the data in Fig. 13 to $\bar{u}_m/u_k = 1$ gives for the point at which gradients in the mean velocity effectively disappear

$$X(\bar{u}_m/u_k = 1) = 6 + X(\bar{u}_m/u_0^* = 0.24) \quad (33)$$

Figure 14 shows typical radial velocity profiles for the post-jet-mixing zone. A simple, quite satisfactory velocity distribution function is

$$\bar{u}/\bar{u}_m = 1, \quad R < 0.14$$

$$\bar{u}/\bar{u}_m = 1 - (R - 0.14)[(\partial\bar{u}/\bar{u}_m)/\partial R], \quad R > 0.14, \quad (34)$$

where for values of Ct between 0.345 and 1.22

$$(\partial\bar{u}/\bar{u}_m)/\partial R = 0.195[X(\bar{u}_m/u_k = 1) - X]/Ct, \quad R > 0.14. \quad (35)$$

Radial Profile of the Jetting Component of Mean Concentration

The field of the jetting component, $\bar{\gamma} - \bar{\gamma}_f$, of the mean concentration, $\bar{\gamma}$, of a species (here an oil fog) marking the jet-source fluid is similar to that of the jetting velocity.

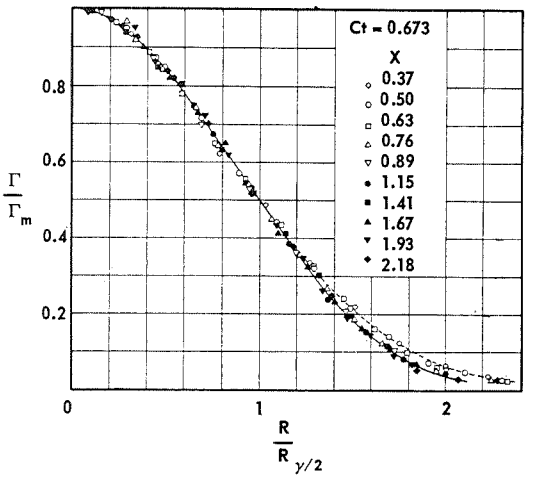

FIG. 15. The radial profile of the jetting concentration at $Ct = 0.673$.

Figure 15 shows a typical normalized radial profile of the jetting concentration. The profiles differed slightly, but consistently, from the jetting velocity profile. The fully turbulent core can be represented by

$$\Gamma/\Gamma_m = \exp\{-(\ln 2)(R/R_{\gamma/2})^a\} \quad (36)$$

The exponent a varied slightly with $R/R_{\gamma/2}$ in ducted operation of the jet:

$R/R_{\gamma/2}$	0.2	0.3	0.4	0.5	0.6–1.0
a	2.00	1.97	1.95	1.92	1.90

In unconfined (free) operation of the jet, the exponent was radially constant and slightly smaller: $a = 1.85$. The data of Landis and Shapiro[3] on a ducted jet at high values of Ct (between 3 and 25) give $a = 2.0$.

The linear intermediate region of the concentration profile extends over the range $0.5 < R/R_{\gamma/2} < 1.2$. The value found for the slope of the profile here was

$$\left[\frac{\partial(\Gamma/\Gamma_m)}{\partial(R/R_{\gamma/2})}\right]_{\partial^2\Gamma/\partial R^2=0} = 0.66 \pm 0.01.$$

In the variably turbulent annulus, the concentration profile was not self-preserving, but except at $Ct = 1.22$ the departures were generally no worse than in Fig. 15. The concentration edge of the jet was considerably more diffuse than the velocity edge, and no simple distribution function has been found which fits all of the variably turbulent annulus. However, for Ct greater than 0.345, the distribution

$$\Gamma/\Gamma_m = \{1 - (1 - 2^{-\frac{1}{2}})(R/R_{\gamma/2})^b\}^2$$

with $b = \frac{3}{2}$ gives a good average fit in the region $1 < R/R_{\gamma/2} < 1.8$. At values of Ct smaller than 0.345, the data for the edge of the jet were not accurate enough (owing to recirculation) to exhibit clearly any special characteristics.

Important characteristic radii for the theory of the jetting concentration field, analogous with the radii r_n for the velocity field (see Eq. (16), are

$$r_\gamma^2 = \int_0^\infty (\Gamma/\Gamma_m)\, dr^2 \quad (37)$$

$$r_{\gamma,1}^2 = \int_0^\infty (\Gamma U/\Gamma_m U_m)\, dr^2 \quad (38)$$

Average values of the shape factors $\eta_\gamma = r_\gamma^2/r_{u/2}^2$ and $\eta_{\gamma,1} = r_{\gamma,1}^2/r_{u/2}^2$ are 2.10 and 0.845, respectively.

Concentration Half-Radius

The concentration half-radius of the fully developed jet was in a constant ratio with the velocity half-radius, giving $\eta_{\gamma/2} = r_{\gamma/2}^2/r_{u/2}^2 = 1.50$. Such a proportionality is expected theoretically for a self-preserving flow, and the reciprocal of $\eta_{\gamma/2}$ approximates the eddy Schmidt number.[11]

Unconfined (free) operation of the jet gave

$$r_{\gamma/2} = 0.103(x + 2r_s), \quad (39)$$

identical with the result for confined operation at $Ct = 0.673$. Hence, in part, the conclusion in the sections on Radial Growth of the Jet and on Axial Decay of Jetting Velocity is that at $Ct = 0.673$ the mean-jetting-flow properties of the ducted jet are essentially identical with those of a free jet in a stagnant free stream.

The constant $2r_s$ in Eq. (39) signifies that the virtual origin of $r_{\gamma/2}$ was two nozzle radii upstream of the virtual origin of $r_{u/2}$.

Axial Decay of Jetting Concentration

Arguments like those in the section on Similarity of Confined Jets indicate that the performance of a confined-jet-mixing system is closely scaled to the characteristic concentration

$$\gamma_0^* = 1/A_0 u_0^* \int_{A_0} (\gamma - \gamma_{f,0})\, u\, dA. \quad (40)$$

For the present system (in which $\gamma_{f,0}$ was zero).

$$\gamma_0^* = j_s/\pi u_0^* r_w^2 = \gamma_s u_s r_s^2/u_0^* r_w^2 \quad (41)$$

When the field of the mean velocity and the shape factors η are known, the radial maximum of the jetting concentration is given by the equation of the conservation of marking species:

$$\eta_{\gamma,1}\Gamma_m U_m + \eta_\gamma \Gamma_m U_f + Ct\Gamma_f = 1. \quad (42)$$

The present data satisfied this equation within the accuracy of the experiment.

The data on the free jet give

$$\bar{\gamma}_m x = 6.18 j_s \sqrt{(\rho_s/i_s)}.$$

Free-Stream Concentration

Since the marking species was supplied only in the jet-source fluid, the free-stream concentration was nonzero only in zones of recirculation. The free-stream concentration was, to good approximation, radially uniform.

Figure 16 shows the normalized free-stream concentration $\Gamma_f Ct$ as a function of X and Ct. Linear extrapolation of the data for $Ct = 0.212$ and 0.345 to $\Gamma_f = 0$ and $\Gamma_f Ct = 1$ gives 2.2 duct radii as the effective length of the recirculation zone with respect to variations in mean concentration.

Consider the following ultimately idealized picture of recirculation: Fluid of normalized concentration $\Gamma_f Ct = 1$ recirculates from far downstream. Ideally

$$\Gamma_f Ct = 1, \quad X > X(U_f = 0) \quad (43)$$
$$\Gamma_f = 0, \quad X < X(U_f = 0)$$

Actually, the recirculated fluid comes from the jet itself, mostly from the region where the jet nears the duct wall, and is highly turbulent. Turbulent mixing between the edges of the jet and the recirculated fluid and massive penetration of the feed free stream by eddies of that fluid nullify Eq. (43). The eddy has (see section on Axial Variation of the Free Stream Velocity) a statistical velocity edge at $U_f = 0$, but the concentration edge is exceedingly diffuse. The reciprocal of $d(\Gamma_f Ct)/dX$ at the point where $\Gamma_f Ct = \frac{1}{2}$, 2.2 in value at $Ct = 0.212$, and 0.345, is a measure of the spatial scale of the large concentration eddies associated with the recirculatory motion.

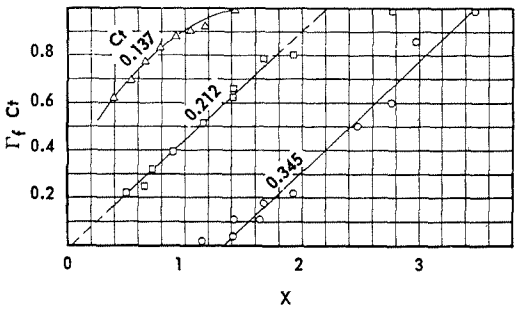

FIG. 16. The axial evolution of the free-stream concentration.

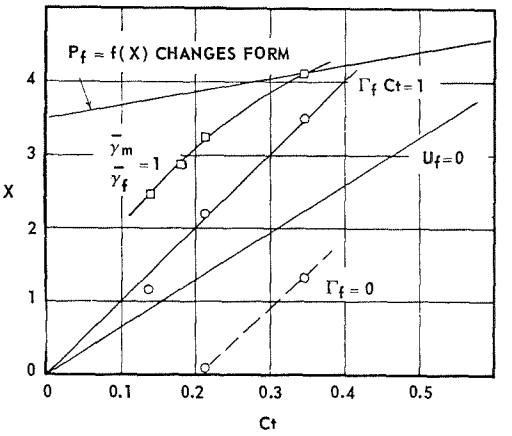

FIG. 17. The Craya-Curtet number dependency of the axial location of various features of the recirculatory flow.

The intercepts $X(\Gamma_f = 0)$, $X(\Gamma_f Ct = 1)$, $X(U_f = 0)$, and $X(\bar{\gamma}_f/\bar{\gamma}_m = 1)$ are shown as functions of Ct in Fig. 17; the last was obtained by extrapolating the relation (not shown) between $\bar{\gamma}_f/\bar{\gamma}_m$ and X to unit ordinate. Also shown is the point at which, according to the axial pressure variation, the free stream vanishes. The intercept $X(\gamma_f/\gamma_m = 1)$ represents the point at which concentration gradients effectively disappear. It is evident that in regimes of heavy recirculation the erasure of concentration gradients is accomplished within the jet-mixing zone, i.e., before the jet reaches the duct wall. Hence the only process occurring in the post-jet-mixing zone is the straining of concentration eddies to ever-decreasing volume-to-surface ratio until they are finally dissipated by particle diffusion of the observed species.

Summary

The isothermal, constant density fields of mean velocity and mean concentration of a turbulent round jet discharging down the axis of a cylindrical duct have been mapped and analyzed.

1. Up to the position where the jet reaches the duct wall the flow acts as the superposition of a jetting flow on a radially uniform ground flow.

2. Similarity of geometrically similar systems requires constancy of the ratio of the initial strengths of the ground stream and the jet. This

ratio is measured by a parameter we have named the Craya-Curtet number.

3. The field of the jetting velocity is described by semi-empirical functions giving the velocity half-radius of the jet, the radial maximum of the jetting velocity, and the self-preserving radial profile of the jetting velocity.

4. The field of the jetting component of the concentration of a species (here an oil fog) marking the jet-source fluid is described analogously.

5. The velocity half-radius of the jet is 0.82 times the concentration half-radius. The square of this ratio, 0.67, represents the turbulence Schmidt number.

6. At small values of the Craya-Curtet number, the initial ground-stream flow into the duct falls short of the entrainment need of the jet. The deficiency is made up by fluid recirculated from downstream. Such recirculation is of great practical importance, e.g., in furnaces. The properties of the recirculation eddy are described: the locations of the eye and the boundary of the eddy, the magnitude of the circulation of fluid around the eddy, and the concentration pattern within the eddy.

7. The velocity field in the post-jet-mixing zone downstream of the position where the jet reaches the duct wall is described.

Nomenclature

Subscripts

f	Value in the free stream
m	Radial maximum
0	Initial value (value at $x = 0$)
s	Value at the jet source
w	Value at the enclosure wall

Dimensional Variables

A	Surface or area
g	Acceleration due to gravity
i_s	Source flux of axial momentum
j_s	Source flux of species marking source fluid
p	Pressure
$p_{f,0}{}^*$	Characteristic pressure for confined-jet system; see Eq. (3)
r	Radial cylindrical coordinate
$r_{u/2}$	Velocity half-radius of jet
$r_{\gamma/2}$	Concentration half-radius of jet
r_1	Volume-flux radius of jet
r_2	Momentum-flux radius of jet
r_3	Kinetic-energy-flux radius of jet
r_γ	Concentration radius of jet
$r_{\gamma,1}$	Marking-species-flux radius of jet
$\mathbf{u}$	Velocity vector
u	Magnitude of the axial component of $\mathbf{u}$
$u_0{}^*$	Characteristic mean velocity for a confined-jet system; see third section
u_k	Kinematic-mean velocity of streams entering a confined-jet system
u_d	Dynamic-mean velocity of streams entering a confined-jet system
x	Axial cylindrical coordinate
γ	Concentration of species marking the source fluid
$\gamma_0{}^*$	Characteristic mean concentration for a confined-jet system; see Eq. (40)
δ_1	Displacement thickness of boundary layer
ρ	Fluid density
μ	Fluid viscosity

Dimensionless Variables

a, b	Exponents in the radial distribution functions of velocity and concentration
Q_r	Normalized axial component of recirculatory flow; see Eq. (30)
R	r/r_w
Δ_1	δ_1/r_w
U	$(\bar{u} - \bar{u}_f)/u_0{}^*$
Γ	$(\bar{\gamma} - \bar{\gamma}_f)/\gamma_0{}^*$
η_n	$r_n{}^2/r_{u/2}{}^2$
η_γ	$r_\gamma{}^2/r_{u/2}{}^2$
$R_{u/2}$	$r_{u/2}/r_w$
X	x/r_w
U_m	$(\bar{u}_m - \bar{u}_f)/u_0{}^*$
Γ_m	$(\bar{\gamma}_m - \bar{\gamma}_f)/\gamma_0{}^*$
$\eta_{\gamma,1}$	$r_{\gamma,1}{}^2/r_{u/2}{}^2$
$\eta_{\gamma/2}$	$r_{\gamma/2}{}^2/r_{u/2}{}^2$
$R_{\gamma/2}$	$r_{\gamma/2}/r_w$
U_f	$\bar{u}_f/u_0{}^*$
Γ_f	$\bar{\gamma}_f/\gamma_0{}^*$
p_f	$(p_f - p_{f,0}{}^*)/u_0{}^{*2}$

Dimensionless Parameters and Constants

n	Integer index or exponent
$\mathbf{n}$	Unit vector normal to an element of surface
Ct	Craya-Curtet number; see third section
Re_s	$2r_s u_s \rho/\mu$, jet-nozzle Reynolds number

ACKNOWLEDGMENTS

This work was supported by the Office of Ordnance Research of the U. S. Army and its successor, the U. S. Army Research Office (Durham); Contract No. DA-19-020-ORD-4549, OOR Project No. 2013, DA-599-01-004 Ordnance Basic Research BR-01(TB2-0001), and Grant No. DA-ARO(D)D-31-124-G8, Grant No. DA-ORD-31-124-61-G55, Project No. 2013-E. H.A.B. has also received personal support from the National Research Council of Canada.

REFERENCES

1. SQUIRE, H. B. and TROUNCER, J.: Round Jets in a General Stream. A.R.C. Technical Report, R and M No. 1974, 1944.
2. FORSTALL, W. and SHAPIRO, A. H.: J. Appl. Mech. *17*, 399 (1950).
3. LANDIS, F. and SHAPIRO, A. H.: Proc. Heat Transfer and Fluid Mech. Inst., Palo Alto, Cal., p. 133 (1951).
4. THRING, M. W. and NEWBY, M. P.: *Fourth Symposium (International) on Combustion*, p. 789. Williams and Wilkins, 1953.
5. CURTET, R.: Compt. rend. *244*, 1450 (1957).
6. CURTET, R.: Combustion and Flame *2*, 383 (1958).
7. CURTET, R.: Sur l'ecoulement d'un jet entre parvis. Publications Scientifiques et Techniques de l'Air, No. 359 (1960).
8. CRAYA, A. and CURTET, R.: Compt. rend. *241*, 621 (1955).
9. CURTET, R. and RICOU, F.: Effects de Turbulence sur des Construction Hydrauliques. Ninth Congres de L'A.I.R.H. Dubrovnik, 1961.
10. ROSENSWEIG, R. E. HOTTEL, H. C., and WILLIAMS, G. C.: Chem. Eng. Sci. *15*, 111 (1961).
11. BECKER, H. A.: Concentration Fluctuations in Ducted Jet-mixing. Sc.D. thesis in the Department of Chemical Engineering, M.I.T., 1961.
12. TAYLOR, J. F., GRIMMETT, H. L., and COMINGS, E. W.: Chem. Eng. Prog. *47*, 175 (1951).
13. POLYAKOV, E. I.: Soviet Phys.-Tech. Phys. *5*, 1173 (1961).
14. HINZE, J. O. and VAN DER HEGGEZIJNEN, B. G.: Appl. Sci. Res., Hague *A1*, 435 (1949).
15. CORRSIN, S.: Investigation of Flow in an Axially Symmetrical Heated Jet of Air. N.A.C.A. Wartime Report W–94, 1943.
16. RICOU, F. P. and SPALDING, D. B.: J. Fluid Mech. *11*, 21 (1961).
17. HINZE, J. O.: *Turbulence*. McGraw-Hill, 1959.

Discussion

PROF. M. W. THRING (*University of Sheffield*): I consider the experimental work in this paper excellent, but I do not feel that the theoretical treatment throws new light on the matter. The "intuitive picture" of Thring and Newby given at the Fourth Symposium that the coefficient required from experiment to explain flow pattern mixing and recirculation for a small diameter enclosed jet could be equated to the angle of spread or turbulent diffusion coefficient of a high Reynolds number free jet has been shown by later experimental work and the more detailed theory of Craya and Curtet to give a close approximation to a time description of the system. It has the advantages that the similarity law for a nonisothermal system can be derived at once from the concept of the equivalent nozzle diameter and that a physical meaning can be given to all the zones.

DR. H. A. BECKER (*Massachusetts Institute of Technology*): Craya and Curtet derived the rigorous similarity criterion for confined jets, using the classical method of determining what dimensionless parameters arise when the boundary conditions are used to put the governing equations into dimensionless form. We advocate the parameter of Craya and Curtet but prefer to use it in the form of the square root of its reciprocal, the parameter we have named the Craya-Curtet number and denote by *Ct*. We have shown how *Ct* can be derived for most general systems, thereby underlining the conditions of its validity. With recirculation and when the ratio of nozzle size to duct size is very small, the parameters of Craya and Curtet and of Thring and Newby are essentially equivalent, but under other conditions the latter parameter is quite inadequate. The intuitive hypothesis underlying the Thring-Newby parameter contains no recognition of the system dynamics; when a force balance is brought into consideration, the concept of an equivalent nozzle diameter becomes superfluous; all that is important about the nozzle is the fluxes of mass and momentum issuing from it.

In reply to Mr. Karlovitz we feel that the sol-scattered light method is our best hope of studying the turbulence properties of flames and are planning work in this direction. We will begin with a free-jet turbulent diffusion flame. Appropriate aerosols must be found to tag the nozzle (fuel) gas. A dc mercury arc lamp will be used as the light source and the light scattered will be examined in the ultraviolet region of the spectrum in order to escape the flame radiation. It will be possible to measure the mean concentration of nozzle fluid (unburnt basis), the r.m.s. concentration fluctuation, the spectrum of concentration fluctuation, and spatial correlation coefficients.

DR. A. E. PENGELLY (*United Steels Research, England*): Dr. Williams said that, should a suitable aerosol be available, he would extend his measurements of mixing, using light scattering methods to do investigations in combusting gas flames.

I suggest that iron oxide fume might be used for this purpose: I refer to the type of fume involuntarily generated in oxygen steelmaking processes.

This fume is chemically stable and would relatively easily be produced on a small scale.

In connection with investigations into radiation pyrometry in, and fume nuisance from steelmaking we have had occasion to compute light scattering functions for this fume together with the accumulation of other required data. We have measured size distribution and found them to be relatively invariant. It should be possible to find a quite strong response in a wave band which would avoid CO_2 and H_2O emissions. To a first approximation the fume is gray in the visible region for relatively low concentrations.

TURBULENT FLAME STUDIES IN TWO-DIMENSIONAL OPEN BURNERS

J. H. GROVER, E. N. FALES, AND A. C. SCURLOCK

The newly devised techniques for studying the effects of turbulence on homogeneous gas flames in two-dimensional open burners through the determination of (1) the mean flow field in the neighborhood of the flame front, (2) the position of the mean flame front and the root-mean-square displacement of the mean flame front, (3) the local turbulent flame velocity, and (4) the position of the instantaneous flame front have been refined and extended to several conditions of flow, turbulence, air–fuel ratio, and burner size. This technique has also been extended to study the growth of wrinkles in the instantaneous flame front by high-speed photography. The experimental results obtained indicate the following: (1) For all of the conditions investigated the effect of turbulence on the flame is only to wrinkle and extend the surface of the flame front. (2) The ratio of the local turbulent flame velocity to the laminar flame velocity, S_T/S_L, can be correlated, as indicated in the previously presented theory of Scurlock and Grover, with the dimensionless time parameter, $S_L t/l_2$ (where t is the time of exposure of the flame element to the turbulence and l_2 is the Eulerian scale of turbulence), and the dimensionless turbulence intensity in the approach flow v_0'/S_L (where v_0' is the turbulence intensity). (3) S_T/S_L can be correlated with the root-mean-square displacement of the mean flame front, $(\overline{Y^2})^{\frac{1}{2}}$. These results also verify that a useful technique has been developed for studying the effects of turbulence on flames.

Introduction

In a previous paper by the authors,[1] a new technique for studying the effect of turbulence on flames was described and discussed. The work being presented herein is a continuation and application of this technique to several conditions of flow, turbulence, and air–fuel ratio. This technique has also been extended to study by high-speed photography the growth of wrinkles in the instantaneous flame front.

As was pointed out in a previous review of the status of experimental turbulent-flame studies,[2] the existing experimental results for turbulent flames propagating in homogeneous mixtures (as distinguished from turbulent diffusion flames) were inadequate to obtain an understanding of the mechanism of turbulent flame propagation. It was not even possible from the data to resolve the conflicting concepts of the turbulent flame being essentially only a wrinkled laminar flame as proposed by Damköhler[3] or a diffuse reaction zone as proposed by Summerfield *et al.*[4]

Most of the earlier studies with turbulent flames were concerned with the over-all effects of turbulence on the entire flame brush, and have not attempted to follow the local development of the flame at various distances from the stabilizer. In 1953, Scurlock and Grover[5] outlined their concept of the role of eddy diffusion, and thus of flame exposure time, on the development of the turbulent flame, and recognized that a better understanding of turbulent flames could be achieved from analysis of measurements of local turbulent flame velocity versus distance from the stabilizer under various conditions of turbulence, mixture composition, and flow. It has been the purpose of the present investigation to obtain these measurements and to follow the growth of wrinkles in the flame front through the use of the two-dimensional open burner.

Description of Apparatus

A two-dimensional open burner that was employed in this investigation is shown schematically in Fig. 1. Both a 1-by-3-inch and a 2-by-6-inch burner were used. The long sides of the burners are open. Transparent confining walls extend along the short sides of the burners (the front and back of the burner). These serve to constrain the flow, causing it to be essentially two-dimensional and making it possible to view and photograph the flame. A detailed description of the 1-by-3-inch burner and the associated apparatus are given in the previous paper.[1]

Turbulence in the burner was generated by a four-mesh or an eight-mesh screen placed normal

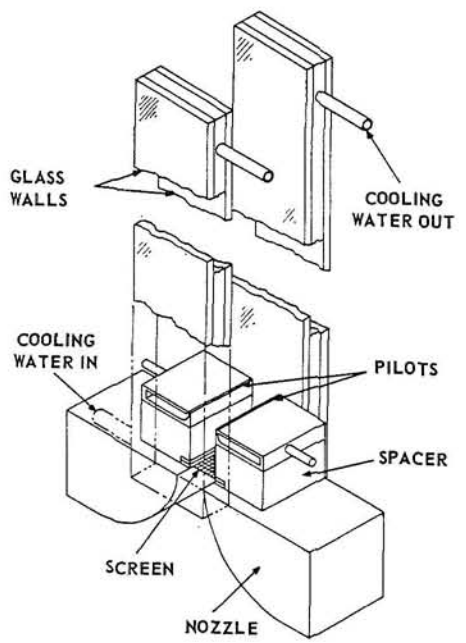

FIG. 1. Schematic of two-dimensional open burner.

to flow in the nozzle throat. These screens are of stainless steel with a ratio of mesh width to wire diameter of 5:1. To generate less random disturbances, a pair of either 0.05- or 0.025-inch stainless steel rods were placed normal to the flow in the nozzle throat. These rods were placed parallel to the long axis of the burner, each halfway between the center line of the burner and the edge.

In addition to the previously described[1] single flash-tube exposures of the magnesium oxide particles in the flow, multiple, short-duration photographs of the particles for following the growth of wrinkles in the instantaneous flame were obtained by an entirely different method. Illumination for about 0.02 second was provided by two banks of eight No. 5 flash bulbs. The particles were photographed with a high-speed Eastman camera at 1600 frames per second. This provides about 30 consecutive pictures which is sufficient to follow a flame element from its inception at the pilot until it disappears at the flame tip.

Review of Previous Results

The previously reported experimental results[1] will be reviewed briefly to give a more thorough understanding of the experimental techniques. All of the previous work was conducted with stoichiometric natural gas-air flames in the 1-by-3-inch burner. The main results were obtained with a flow velocity at the entrance to the burner of 20 ft/sec and with a four-mesh screen in the nozzle throat.

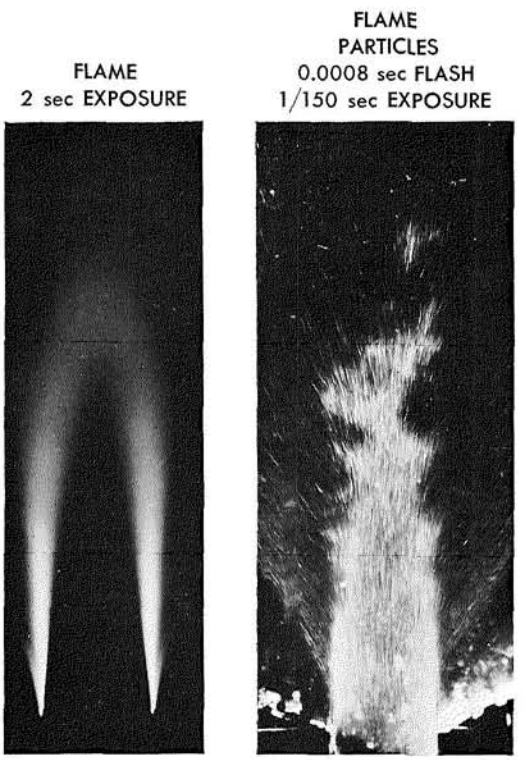

FIG. 2. Photographs of flame and flow in two-dimensional open burner. (Stoichiometric natural gas-air mixture; approach velocity, 20 ft/sec; four-mesh screen 2 inches upstream of burner rim.)

An example of both 2-second time exposures of the flame and single flash exposures of the particles that were obtained is shown in Fig. 2. On the left is a time exposure with the flame as the sole source of light, and on the right a flash-tube exposure with 1-micron magnesium oxide particles in the flow.* The particles appear in the picture as short dashes indicating the local instantaneous direction of the flow. The instantaneous boundary between burned and unburned gases, which was shown to be the actual flame front, is clearly visible. The presence of a continuous, sharply defined flame front in this and

* Gilbert, Davis, and Altman[6] concluded that 1-micron particles would correctly trace the streamline direction through a propane-air flame. It is thus believed safe to assume that the magnesium oxide particles follow the flow in these flames with at least the precision to which the direction of the particles is measured.

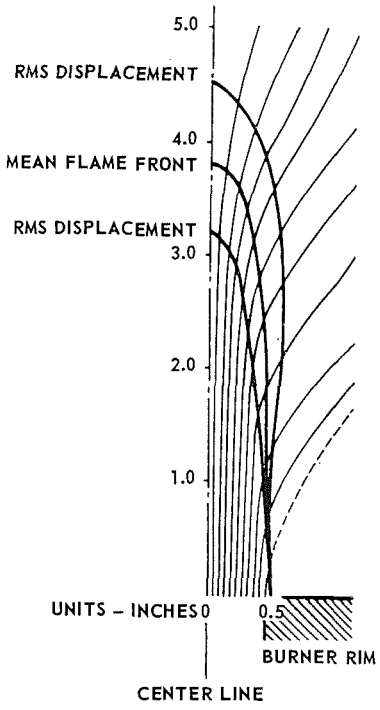

FIG. 3. Mean flow lines, mean flame front, and root-mean-square displacement of the mean flame front. (Stoichiometric natural gas-air flame with inlet flow velocity of 20 ft/sec and four-mesh screen 2 inches upstream of burner rim.)

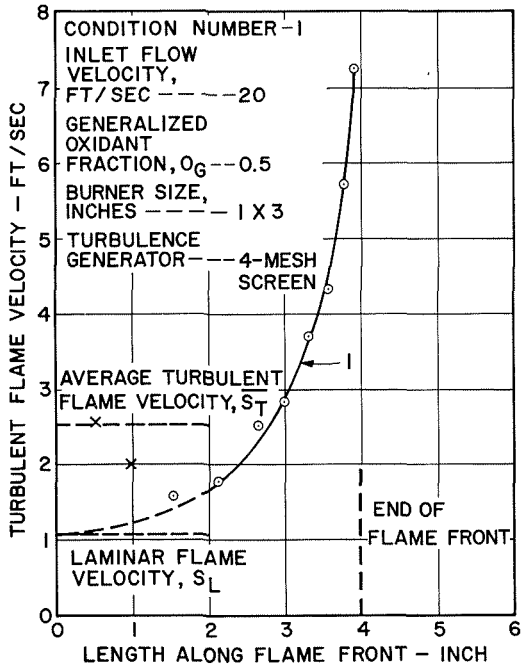

FIG. 4. Turbulent flame velocity versus flame length.

similar photographs lends support to the wrinkled flame concept of turbulent flame propagation.

From the two types of photographs shown in Fig. 2, the mean flame front and the flow lines into the flame were obtained. These mean flow lines, with the mean flame front superimposed, are shown in Fig. 3. From the flow lines and the mean flame front the local turbulent flame velocity, S_T, was determined as a function of distance measured along the flame front from the burner rim as is shown in Fig. 4.

Experimental Results

The range over which the parameters could be varied was limited because of the size of the burner and the nature of the experiments, but was adequate to indicate the relative effect of the various parameters studied. Listed below are the parameters which were varied and the values used.

1. Velocity of flow at entrance to burner: 20 and 40 ft/sec.
2. Disturbance generators: 4- and 8-mesh screens with a mesh-to-wire diameter ratio of 5:1; 200-mesh screen; a pair of 0.05-inch rods; and a pair of 0.025-inch rods.
3. Air-natural gas ratio: O_G = 0.5 (stoichiometric), 0.453 (rich), and 0.599 (lean).*
4. Burner size: 1-by-3-inch and 2-by-6-inch.

Data were obtained at twelve different conditions. These various run conditions are given in Table 1. Condition number 1 was the standard condition.

For each of the twelve conditions listed in Table 1, at least two 2-second time exposures and a set of 20 flash-tube exposures were obtained using the technique described above. From these time and flash-tube exposures, four distinct types of data were obtained for each condition. From the 2-second time exposures, the position of the mean flame front and the root-mean-square displacement of the mean flame front were determined. From the flash-tube exposures, the outline of the instantaneous flame front and the direction of flow into and through the flame front were determined. These last two types of data are independent of each other and both are independent of the data from the 2-second time exposures. As discussed in the previous paper,[1] the two types of measurements

* O_G is the generalized oxidant fraction and is defined as

$$\frac{\text{air–fuel ratio}}{\text{air–fuel ratio} + \text{stoichiometric air–fuel ratio}}$$

TABLE 1

Conditions of flow, disturbance generator, air–fuel ratio, and burner size

Condition number	Inlet velocity (ft/sec)	O_G	Burner size (inches)	Turbulence generator
1	20	0.5	1 × 3	4-Mesh screen
2	40	0.5	1 × 3	4-Mesh screen
3	20	0.5	1 × 3	8-Mesh screen
4	40	0.5	1 × 3	8-Mesh screen
5	20	0.453	1 × 3	4-Mesh screen
6	20	0.599	1 × 3	4-Mesh screen
7	20	0.5	2 × 6	4-Mesh screen
8	40	0.5	2 × 6	4-Mesh screen
9	20	0.5	1 × 3	Two 0.05-inch rods
10	20	0.5	1 × 3	Two 0.025-inch rods
11	20	0.5	1 × 3	200-Mesh screen
12	20	0.5	1 × 3	200-Mesh screen and two 0.05-inch rods

from the time exposures were checked against the outline of the instantaneous flames, and the agreement was good. This provided confidence for three of the four types of data from the still pictures, and also for the outline of the instantaneous flame fronts obtained from the high-speed motion pictures. Unfortunately, no experimental check was possible on the flow-direction data and the method of determining the mean flow lines from these data.

Using the mean flow lines and the position of the mean flame front (for each condition a plot similar to Fig. 3 was prepared) the local turbulent flame velocity along the mean flame front was calculated for eleven of the twelve conditions.* The results for conditions number 1, 2, 3, 4, 6, 7, and 8 are shown in Figs. 4 through 10.

For condition number 1 (approach velocity of 20 ft/sec, stoichiometric flame, four-mesh screen, and 1-by-3-inch burner) several runs were made. The curve shown in Fig. 4 is the best obtained for that condition, and is believed to represent most accurate values of the local turbulent flame velocity for this condition obtainable by this technique. The curves of Figs. 5 through 10 usually represent the results from only a single run of 22 camera exposures at each condition.

There is considerable scatter in the results shown in Figs. 5 through 10. There are several factors which limit both the precision and accuracy of the local turbulent flame velocity de-

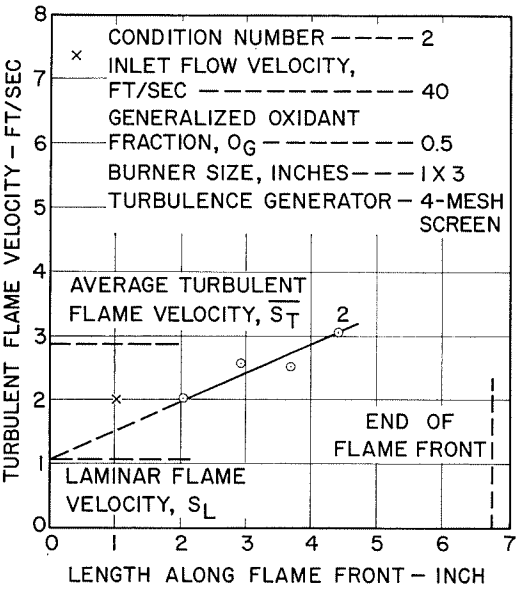

FIG. 5. Turbulent flame velocity versus flame length.

* For the run made with the fuel-rich mixture (condition number 5), the line of maximum brightness of the flame front as obtained from densitometer traverses of a 2-second time exposure does not give the position of the mean flame front of the primary combustion. Comparison of the line of maximum brightness with the mean flame front obtained from the flash-tube photographs indicates that the maximum brightness occurs a considerable distance after the true mean flame front. This is probably due to secondary combustion taking place beyond the primary flame front with the emission of additional light. This erroneous displacement of the mean flame front resulted in values of S_T/S_L that are lower than the true values. Thus, the results for the rich flame of condition number 5 were not used.

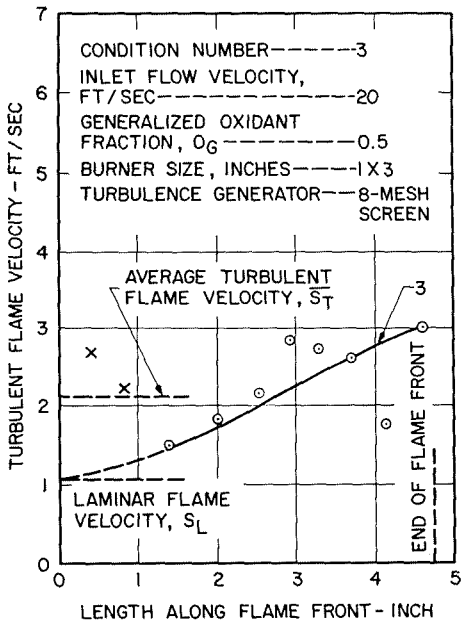

FIG. 6. Turbulent flame velocity versus flame length.

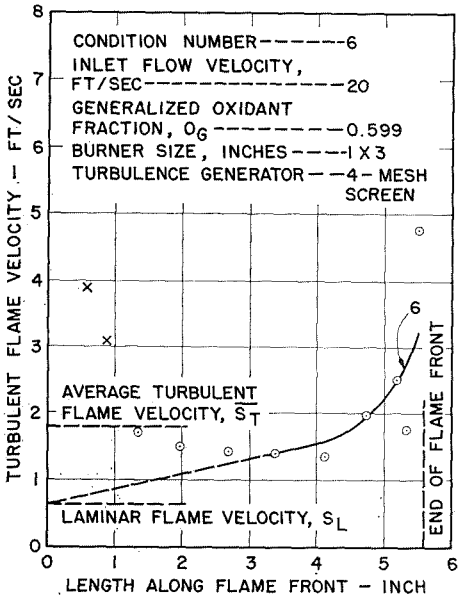

FIG. 8. Turbulent flame velocity versus flame length.

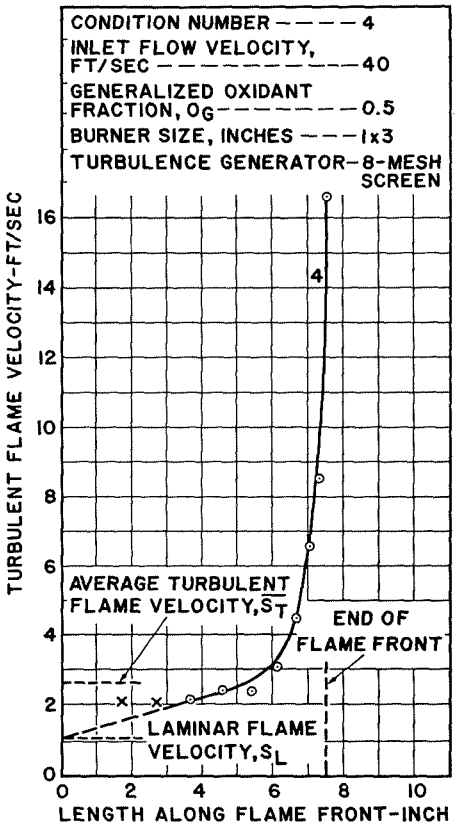

FIG. 7. Turbulent flame velocity versus flame length.

terminations and contribute to the scatter of the data. These are:

1. The direction of the particles in the flow field can only be determined to within a few degrees of angle.

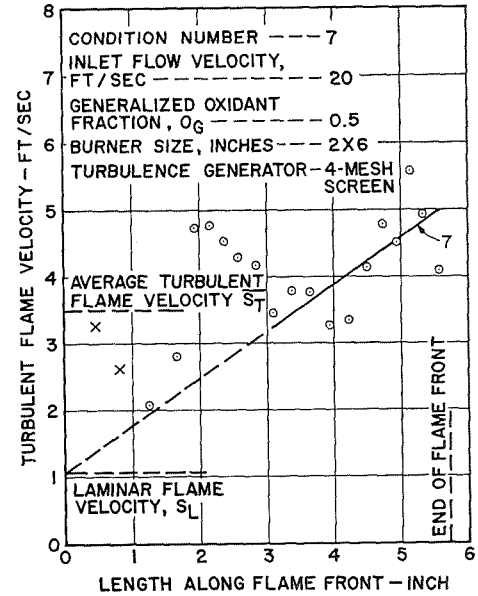

FIG. 9. Turbulent flame velocity versus flame length.

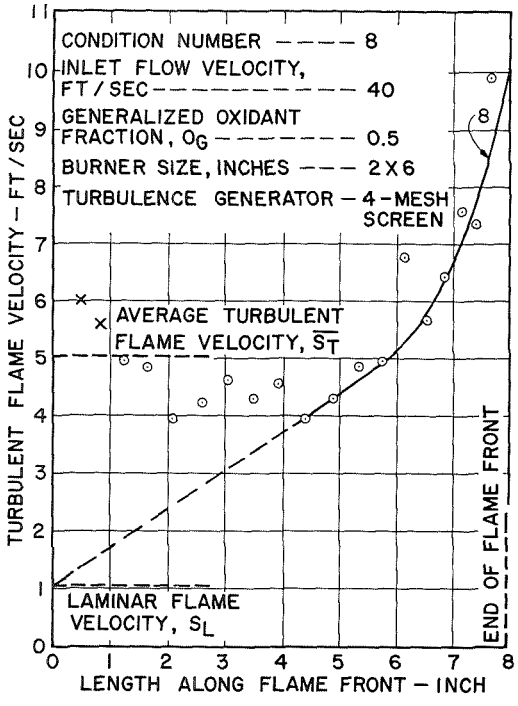

FIG. 10. Turbulent flame velocity versus flame length.

2. The particles do not appear to follow the flow near the burner rim.*

3. It is difficult to determine the exact location of the position of the mean flame front in the vicinity of the flame tip. These factors all limit the confidence that can be placed in these curves, particularly in the regions near the burner rim and the tip of the flame. However, the accuracy of the data is believed to be sufficient to indicate general trends.

In addition to the local turbulent flame velocity versus flame length, three other experimentally determined results are given in Figs. 4 through 10. These are: (1) the total length of the mean flame front from the burner rim to the flame tip; (2) the value of the average turbulent flame velocity, $\overline{S_T}$, (averaged over the entire flame†); and (3) the laminar flame velocity, S_L, for the natural gas-air flame used for the run.

* For this reason the values for the turbulent flame velocity for two stream tubes nearest the burner rim are shown as × rather than ○ in Figs. 4 through 10 and were not used in drawing the curves.

† This result is of interest in comparing the results of this study with those of previous investigators who only measured a single average value of the turbulent flame velocity for each condition. This average turbulent flame velocity is simply the ratio of burner width-to-total flame length times the flow velocity at the inlet of the burner.

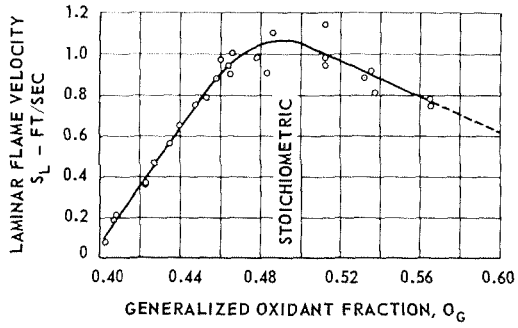

FIG. 11. Laminar flame velocity of natural gas-air mixtures.

The laminar flame velocity was determined by the angle method‡ using a 1-by-$\frac{5}{16}$-inch nozzle burner. The results are shown in Fig. 11.

In addition to the position of the mean flame front, the root-mean-square displacement $(\overline{Y^2})^{\frac{1}{2}}$ of the mean flame front from its mean position was obtained from the 2-second time exposures. These values are given in Table 2 for various distances along the flame front for each of the twelve conditions studied (see Table 1 for these conditions). The height of the tip of the mean flame for each of these conditions is also given in Table 2.

The final type of experimental data is the outline of the instantaneous wrinkled flame front. These outlines are obtained from both the still flash-tube exposures and the high-speed motion pictures. A typical flash-tube exposure for each of the twelve conditions studied is shown in Fig. 12. These photographs all show the outline of instantaneous flame front as the boundary between the high and low concentration of magnesium oxide particles. To facilitate analysis of these photographs, an outline tracing of each photograph has been made and is shown in Fig. 13.

From these photographs and tracings, several measurements of the instantaneous wrinkled flame front have been made. One measurement is the distance above the burner rim at which wrinkles first appear in the instantaneous flame front; up to this point the flame velocity should be essentially the laminar flame velocity. A second measurement is the minimum height of the continuous flame front. This height represents

‡ A description and discussion of this method is given by Linnett.[8]

TABLE 2

Flame height and root-mean-square displacement of mean flame front

Condition number	Flame height (inches)	Root-mean-square displacement of mean flame front, $(\overline{Y^2})^{\frac{1}{2}}$ (inches)										
		Length along flame front (inches)										
		1.2	1.6	2.0	2.5	3.0	3.5	4.0	4.5	5.0	5.5	6.0
1	3.9	0.05	0.08	0.12	0.16	0.21	0.28	—	—	—	—	—
2	6.6	0.04	0.06	0.07	0.09	0.12	0.15	0.19	0.22	0.25	0.29	0.36
3	4.7	0.06	0.09	0.12	0.17	0.22	0.28	—	—	—	—	—
4	7.4	0.05	0.06	0.07	0.10	0.13	0.15	0.18	0.21	0.25	0.31	0.34
5	—	—	—	—	—	—	—	—	—	—	—	—
6	5.5	0.06	0.08	0.09	0.12	0.16	0.18	0.22	—	—	—	—
7	5.4	0.07	0.12	0.18	0.25	0.34	0.42	0.47	0.58	—	—	—
8	7.8	0.09	0.11	0.14	0.19	0.24	0.29	0.34	0.42	0.46	0.49	0.52
9	4.8	0.04	0.06	0.09	0.14	0.21	0.26	0.32	—	—	—	—
10	5.4	0.05	0.07	0.08	0.11	0.16	0.25	0.33	—	—	—	—
11	6.7	0.03	0.03	0.04	0.05	0.06	0.09	0.11	0.14	0.17	0.22	—
12	4.7	0.04	0.05	0.08	0.11	0.14	0.18	0.23	—	—	—	—

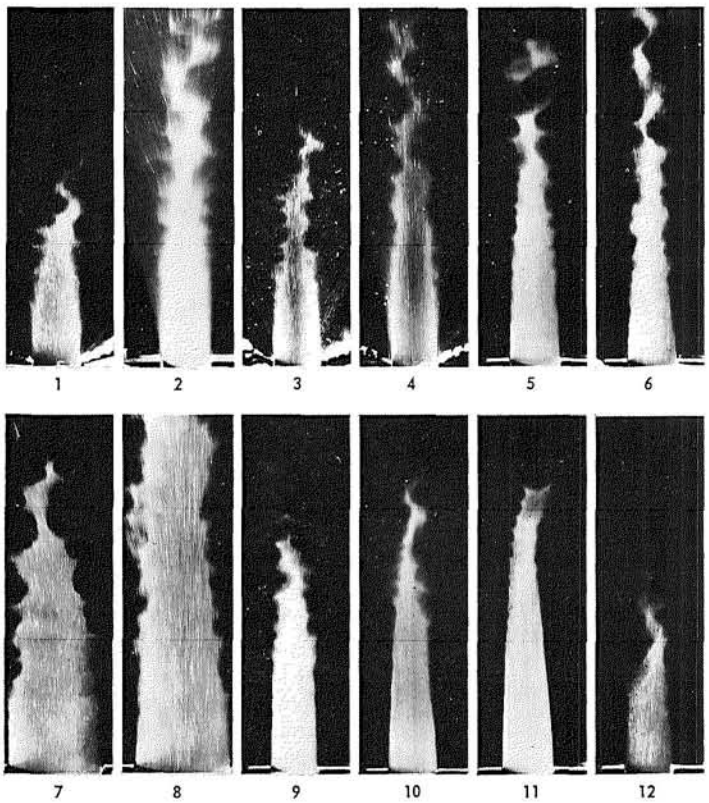

FIG. 12. Instantaneous flash-tube photographs of flames for twelve different conditions.

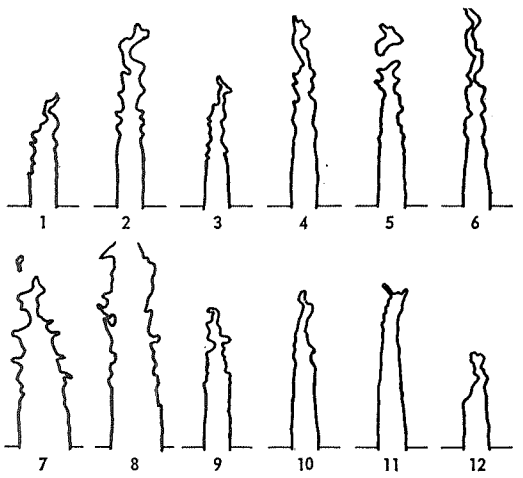

FIG. 13. Flame front outlines traced from flash photographs of Fig. 12.

the minimum flame-tip height. Above this point, islands of unburned gas are sometimes present. Although the occurrence of these islands is not in contradiction to the theoretical model proposed by Scurlock and Grover,[5] their presence has not been considered in the quantitative effect of turbulence on flames.

A third measurement that was obtained from the outlines of the instantaneous wrinkled flame front tracings is the average width of the base of the wrinkles. This measurement is taken as the dimension that characterizes the size of the wrinkles in the flame front for each condition.

TABLE 3

Measurements of instantaneous flame front

Condition number	Unwrinkled flame length (inches)	Minimum continuous flame height (inches)	Average width of wrinkle base (inches)
1	0.8	4.2	0.28
2	1.1	6.5	0.27
3	1.0	4.6	0.23
4	0.9	6.7	0.31
5	0.9	5.7	0.28
6	0.7	7.0	0.28
7	0.5	6.3	0.42
8	0.9	8.7	0.37
9	1.4	4.7	0.27
10	1.8	5.5	0.23
11	1.9	5.8	0.26
12	1.1	3.6	0.23

These results are given in Table 3 for the twelve conditions studied.

High-speed motion pictures of illuminated particles were obtained for condition number 1 (the standard condition). From these high-speed pictures the growth of the wrinkles in the flame front can be followed by enlarging the individual frames of the motion picture film and tracing the outline of the flame front. A series of five such outlines is shown in Fig. 14, where every third frame is shown. The time interval between tracings is 1.88 milliseconds. To facilitate the following of particularly prominent wrinkles in the flame front, inclined lines have been shown that pass through the same wrinkles in successive tracings.

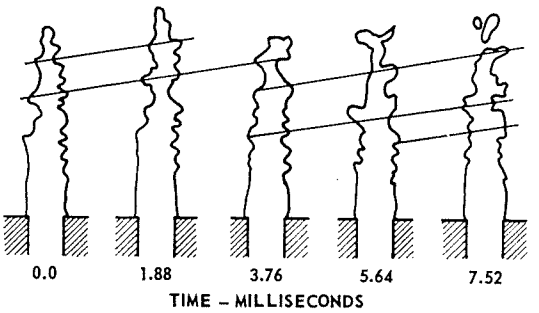

FIG. 14. Change in outline of instantaneous flame front from high-speed motion pictures. (Stoichiometric natural gas-air flame with inlet flow velocity of 20 ft/sec; and four-mesh screen 2 inches upstream of burner rim.)

Discussion of Results

Before discussing the detailed effects of the various parameters, it should be pointed out that the over-all effects of turbulence as shown by the turbulent flame velocity results of Figs. 4 through 10 confirm the results of earlier investigators,[3,9,10] who found that the turbulent flame velocity increased with increasing turbulence. This is more readily apparent from the average values of turbulent flame velocity than from the local turbulent flame velocity points.

The scatter of the data within runs is, unfortunately, usually as great as the variation of the local turbulent flame velocity points from run to run. This large scatter makes it difficult to determine the exact values of the local turbulent flame velocity along the flame front length, and also hard to compare the results of one run with another. The results as shown in these figures cannot be compared with the theory[5] directly because the theory correlates the ratio of the local

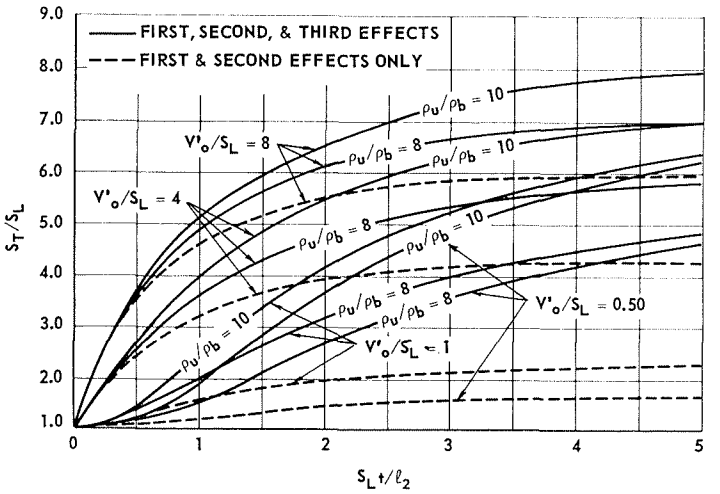

FIG. 15. Plots of S_T/S_L versus $S_L t/l_2$ under several different conditions calculated including all three effects.

turbulent flame velocity to the laminar flame velocity, S_T/S_L, with a dimensionless time parameter, tS_L/l_2, where t is the time of exposure of the flame element to the turbulence, rather than flame front length. The theoretical curves of S_T/S_L versus $S_L t/l_2$ for several values of v_0'/S_L, where v_0' is the turbulence intensity in the approach flow, for density ratios of eight and ten, and with and without the presence of flame-generated turbulence predicted by Scurlock and Grover[5] are shown in Fig. 15.

Comparison of Turbulent Flame Velocity Results with Time. The results of one run have been

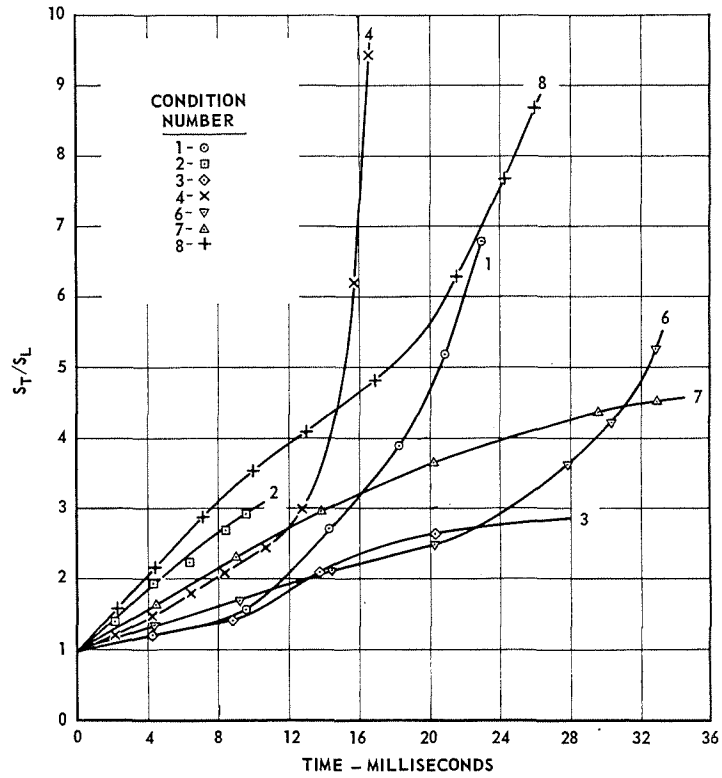

FIG. 16. S_T/S_L versus time.

compared with those of other runs using the theoretical concept of the importance of time of exposure of a flame element to the turbulence developed by Scurlock and Grover.[5] As a first step in doing this, the experimental results shown in Figs. 4 through 10 have been replotted in Fig. 16 as S_T/S_L versus time, using the same method as was described in the previous paper.[1]

The first two runs to be compared are those for conditions number 1 and 2. Both runs were made using the same air-fuel ratio (same S_L) and the same screen (same l_2). Thus, curves 1 and 2 of Fig. 16 are on the same dimensionless time, $S_L t/l_2$, basis and can be compared with each other. The only difference in the conditions for those two runs was an approach flow velocity of 20 ft/sec for curve 1 and 40 ft/sec for curve 2. Thus, a comparison of these two runs should indicate the effect of turbulence intensity, since for a given screen and distance downstream of the screen, the absolute turbulence intensity is proportional to the mean flow velocity. Using the relation of Dryden *et al.*[7] for turbulence behind screens in cold flow, average turbulence intensities of 1 and 2 ft/sec were predicted for conditions number 1 and 2, respectively. These turbulence intensities correspond to values of the dimensionless parameter, v_0'/S_L, of one and two, respectively. Curve 2, for condition number 2 ($v_0'/S_L = 2$), is consistently much higher than curve 1, for condition number 1 ($v_0'/S_L = 1$), which is in general agreement with the theory (see Fig. 15). Also, the shapes of the initial portions of both curves 1 and 2 correspond to the shapes of the theoretical curves, with the initial slope of the curve being much higher for the condition of higher turbulence intensity.

The next parameter studied was the screen size. Two runs in the 1-by-3-inch chamber were made with an eight-mesh screen. Condition number 3 was with an eight-mesh screen and an inlet flow velocity of 20 ft/sec, and condition number 4 was with an eight-mesh screen and an inlet flow velocity of 40 ft/sec. The approximate predicted[7] values of the turbulence scale and intensity produced by the eight-mesh screen for cold flow at the average downstream distance of the flame is 0.03 inch and 3 per cent, respectively. This compares with values of 0.05 inch and 5 per cent for the four-mesh screen. To compare the results for the eight-mesh screen with those for the four-mesh screen using the dimensionless time parameter, $S_L t/l_2$, the results were replotted in Fig. 17 as S_T/S_L versus $S_L t/l_2$ for conditions number 1, 2, 3, and 4, using $S_L = 1.06$ ft/sec, $l_2 = 0.05$ inch for conditions number 1 and 2, and $l_2 = 0.03$ inch for conditions number 3 and 4.

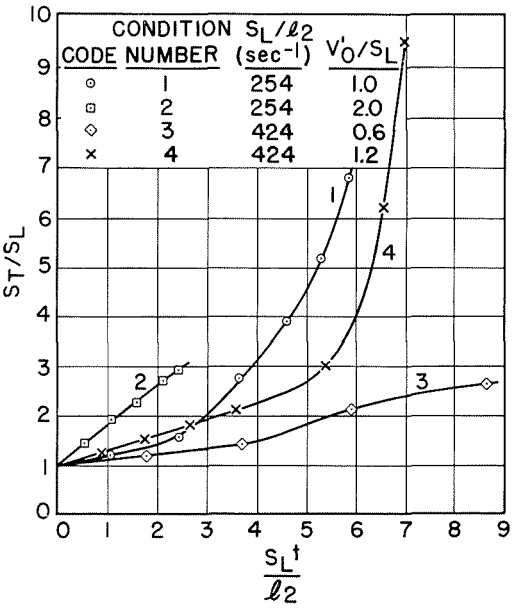

FIG. 17. S_T/S_L versus $S_L t/l_2$.

At both 20 ft/sec and 40 ft/sec inlet flow velocities, the dimensionless flame velocity for eight-mesh screen conditions (conditions number 3 and 4) is always much lower than the corresponding values for the respective four-mesh screen conditions (conditions number 1 and 2). The most interesting comparison is that between the curves for conditions number 1 and 4. Although these runs are for different screens (four- and eight-mesh, respectively), the turbulence intensity differs only by 20 per cent, and thus the curves S_T/S_L versus $S_L t/l_2$ should be approximately the same. Considering the approximation made and the low precision of the measurements, the agreement between the curves for conditions number 1 and 4 is good.

In comparing the four curves of Fig. 17 with the theoretical curves of Fig. 15, two important differences stand out. One is that higher values of S_T/S_L are obtained experimentally than were predicted from the theoretical considerations, even when flame-generated turbulence was taken into account. The second important variation of the experimental results with the predicted curves is that the experimental values of S_T/S_L show no tendency to leveling off, indicating that either the dimensionless time required for the experimental values of S_T/S_L to approach an asymptote is much greater than the value of five for the dimensionless time required by the theoretical curves or that the end effects (interaction of the two approaching flame fronts) greatly increase the effective flame velocity and

masks any tendency to reach an asymptotic value.

The third parameter studied was air-fuel ratio. Although two runs were made in which an air-fuel ratio of other than stoichiometric was used, one a rich mixture ($O_G = 0.453$) and one a lean mixture ($O_G = 0.599$), only the data for the lean mixture were good. The main effect of this parameter is to control the laminar flame velocity. As is shown in Fig. 10, the laminar flame velocity for the lean mixture is 0.63 (the stoichiometric value is 1.06). A secondary effect of this parameter is to control the ratio of the densities of the unburned-to-burned gases ρ_u/ρ_b. The value of ρ_u/ρ_b for the lean mixture is 6.01 (the stoichiometric value is 7.63). The dimensionless turbulent flame velocity versus time results for the lean run is shown as curve 6 of Fig. 16.

In order to compare the results for the lean flame (condition number 6) with those of the stoichiometric flames (conditions number 1 and 2) the results for these three conditions have been plotted as S_T/S_L versus S_Tt/l_2 in Fig. 18. The results of these three runs show a trend of increasing v_0'/S_L which is in agreement with the theoretical results of Fig. 15. There is an additional parameter which is ρ_u/ρ_b that is slightly lower for condition number 6 (6.01) than for conditions number 1 and 2 (7.62). The theoretical effect of this variable is to permit slightly less flame-generated turbulence and might result in slightly lower values of S_T/S_L for condition number 6 than would be obtained otherwise. This agrees with the experimental values for condition number 6 being slightly lower than a direct interpolation of the other two curves would indicate.

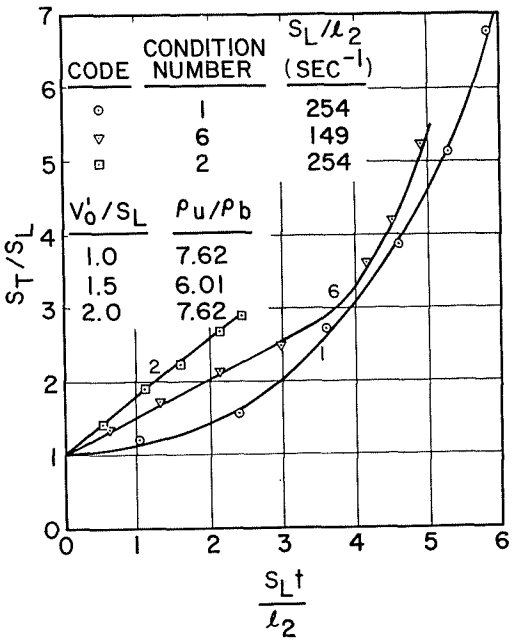

FIG. 18. S_T/S_L versus S_Lt/l_2.

The final parameter which was varied in this study of turbulent flame velocity as a function of time was the size of the burner. Two runs were made with a 2-by-6-inch burner. These runs were made to permit greater times of exposure of a flame element to the turbulence and to determine if the size of apparatus (burner dimensions) affected the results. The results of these two runs are given as curves 7 and 8 in Fig. 16. These conditions are identical to those of curves 1 and 2, respectively, of Fig. 16 except for the burner size, and can thus be compared directly on the same time basis.

There is considerable discrepancy between curves 1 and 7 (conditions number 1 and 7, respectively) which are both for inlet flow velocities of 20 ft/sec. Curve 7, for the 2-by-6-inch burner, is initially higher, then lower, than is curve 1, for the 1-by-3-inch burner. However, referring to the original results for the 2-by-6-inch burner (Fig. 9), there is considerable scatter of data and not much weight is given to this lack of agreement between the results for conditions number 1 and 7.

There is very good agreement between curves 2 and 8 (conditions number 2 and 8, respectively) which are both for inlet flow velocities of 40 ft/sec. As would be expected from the theoretical consideration, the two curves fall very close together. Once again, however, there is no tendency for curve 8 to reach an asymptote.

Comparison of Turbulent Flame Velocity with Root-Mean-Square Displacement Flame Front. Another type of comparison of the experimental results of this study that can be made on the basis of the theoretical concepts of Scurlock and Grover[5] is a correlation of S_T/S_L with $(\overline{Y^2})^{\frac{1}{2}}$. Such a correlation is particularly desirable because all of the theoretical curves were based on Eq. (1)

$$S_T/S_L = [1 + C_1(\overline{Y^2}/l_2^2)]^{\frac{1}{2}} \qquad (1)$$

which relates S_T/S_L to $(\overline{Y^2})^{\frac{1}{2}}$ through the Eulerian scale of turbulence, l_2, and a constant C_1, which was assumed to have a value of four.

The experimental values of S_T/S_L are plotted against $(\overline{Y^2})^{\frac{1}{2}}$ in Fig. 19 for conditions number 1, 2, 3, 4, 6, 7, and 8. Also shown in Fig. 19 are the two curves of S_T/S_L versus $(\overline{Y^2})^{\frac{1}{2}}$ that are obtained from Eq. (1) assuming C_1 to be 4 and l_2 to be 0.05 and 0.03 inch which are the values for flow behind four- and eight-mesh screens as obtained from the relation of Dryden *et al.*[7]

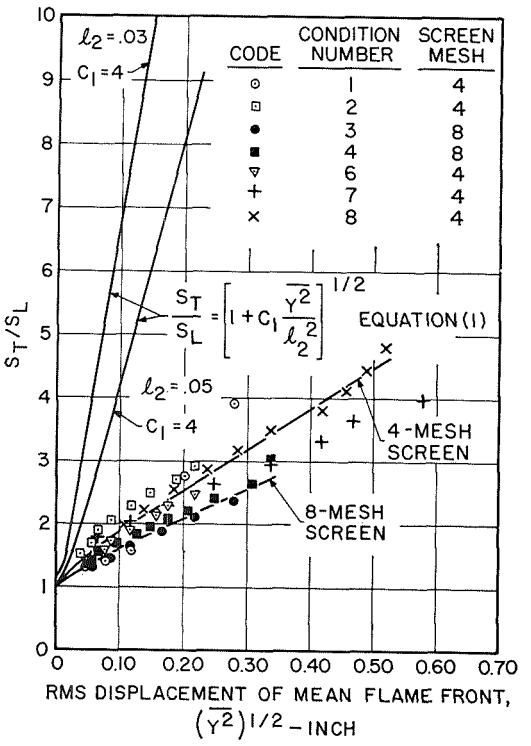

FIG. 19. S_T/S_L versus root-mean-square displacement of mean flame front.

The experimental results shown in Fig. 19 do not fall on the two theoretical lines predicted by Eq. (1) using a value of 4 for C_1 and the cold flow value of l_2. These data all fall far below the theoretical curves. These results confirm the earlier conclusions[1] that either C_1 is much less than 4, or the base of the wrinkles in the flame is much larger than the assumed value of 4 (l_2), or the model on which Eq. (1) is based needs to be revised.

Although the data do not correlate with the previously predicted curve, they do show a definite increase of S_T/S_L with increasing $(\overline{Y^2})^{\frac{1}{2}}$. Also, the results for the two runs with the eight-mesh screen (conditions number 3 and 4) fall below the others which are all for a four-mesh screen. In an attempt to obtain a correlation of the results shown in Fig. 19, a line has been drawn through the data for the runs with a four-mesh screen and another for the data for the runs with the eight-mesh screen. These lines are nearly straight, showing a tendency for S_T/S_L to increase with the first power of $(\overline{Y^2})^{\frac{1}{2}}$. This result, together with the fact that the line for the eight-mesh screen lies below rather than above that for the four-mesh screen, indicates that Eq. (1) needs revision.

Wrinkle Size. Indications of the size of the wrinkles in the instantaneous wrinkled flame front were obtained from the flash-tube exposures exemplified by the photographs of Fig. 12 and tracing of Fig. 13. These are the average width of the base of the wrinkles, and are listed in Table 3. Since these wrinkles, by their very nature, are not of uniform size, shape, and frequency, measurements of them are somewhat subjective and difficult to make, and thus lack precision.

The values in Table 3 for the average width of the base of the wrinkles show little variation from run to run and practically no tendency to correlate with any of the variables studied. There is no effect of velocity, screen size, or air-fuel ratio. Even for conditions number 9, 10, 11, and 12, where a pair of rods and/or a 200-mesh screen was used to generate the flow disturbances there was no change in the average width of the base of the wrinkles, although the initiation of wrinkle formation did not occur until a greater distance downstream of the burner rim. The only variable that had any tendency to affect the wrinkle width was burner size. For the 2-by-6-inch burner, the size of the wrinkle was slightly larger than for other runs; but the difference is not great and may be due to the longer exposure time of the flame elements to the turbulence for this burner.

Although there is little difference in wrinkle size from run to run, there is considerable variation within a flame front. In general, for all conditions the wrinkles expand with increasing distance from the burner rim.

High-Speed Motion Pictures. Only the standard condition (condition number 1) has been studied using high-speed motion pictures. The outlines of the instantaneous flame fronts obtained for this condition are shown in Fig. 14. This sequence of flame fronts shows the individual wrinkles in the flame to move upward with the expected velocity of 20 ft/sec. This sequence also shows the process whereby unburned gas is pinched off to form islands in the burned gas.

Conclusions

From these results the following conclusions have been made.

1. All the experimental conditions of this investigation verify the concept that the effect of turbulence on flames is only to wrinkle and extend the surface of the flame front. The flash-tube photographs show the instantaneous flame front (as denoted by the change in concentration of

suspended particles) to be a thin wrinkled continuous boundary between unburned and burned gases. The experimental measurements and the propagation of wrinkles in the high-speed motion picture all substantiate this conclusion.

2. The results indicate that the ratio of the local turbulent flame velocity to the laminar flame velocity, S_T/S_L, can be correlated with the dimensionless time parameter, $S_L t/l_2$, and the dimensionless turbulence intensity in the approach flow v_0'/S_L. Since such a correlation was predicted by Scurlock and Grover[5] based on a wrinkled flame front model, the results lend further support to the general validity of the physical picture of the mechanism of turbulent flame propagation which underlies the theory.

3. Although the basic dimensionless parameters derived by Scurlock and Grover[5] had been verified, the results do not correspond to their theoretical curves. Also, although an experimental correlation of S_T/S_L with $(\overline{Y^2})^{\frac{1}{2}}$ is obtained, this correlation is not that predicted by Eq. (1). Thus, this equation and possibly the model on which it is based needs to be revised, taking into account the nearly constant width of wrinkle bases.

4. A useful technique has been developed and verified for determination for a turbulent flame of the mean flow field in the neighborhood of the flame, the mean flame front, the root-mean-square displacement of the mean flame front, the local turbulent flame velocity, and the position of the instantaneous flame front. Also, a technique has been developed for following the formation and growth of wrinkles in the instantaneous flame front.

References

1. Grover, J. H., Fales, E. N., and Scurlock, A. C.: ARS Journal *29*, 275 (1959).
2. Scurlock, A. C. and Grover, J. H.: Experimental Studies of Turbulent Flames, *Selected Combustion Problems*, Advisory Group for Aeronautical Research and Development, NATO, p. 214. Butterworths Scientific Publications, 1954.
3. Damköhler, G.: Z. Elektrochemie *46*, 610 (1940); English Translation: NACA Tech. Memo. 1112, 1947.
4. Summerfield, M., Reiter, S. H., Kebely, V., and Mascolo, R. W.: Jet Propulsion *25*, 377 (1955).
5. Scurlock, A. C. and Grover, J. H.: *Fourth Symposium (International) on Combustion*, p. 645. Williams and Wilkins Co., 1953.
6. Gilbert, M., Davis, L. and Altman, D.: Jet Propulsion *25*, 26 (1955).
7. Dryden, H. L., Schubauer, G. B., Mock, W. C., Jr., and Skramstad, K. H.: NACA Report 581, 1937.
8. Linnett, J. W.: *Fourth Symposium (International) on Combustion*, p. 20. Williams and Wilkins Co., 1953.
9. Bollinger, L. M. and Williams, D. T.: The Effects of Turbulence and Flame Speed of Burner Type Flames, NACA Tech. Note 1707, 1949; also, *Third Symposium on Combustion, Flame and Explosion Phenomena*, p. 176. Williams and Wilkins Co., 1949.
10. Wohl, K., Shore, L., von Rosenberg, H., and Weil, C. W.: *Fourth Symposium (International) on Combustion*, p. 630. Williams and Wilkins Co., 1953.

Discussion

Dr. F. J. Weinberg (*Imperial College, England*): My question concerns the definition of the relevant instantaneous flame contour which underlies this kind of burning velocity analysis.

Some time ago we completed a study[1] of turbulent flames which was identical in aims to the one presented, in that we also set out to develop methods to measure local burning velocities. Our methods, however, were optical and our conclusions somewhat different. We developed three groups of optical techniques[2]—one to record the randomness of orientation of the turbulent flame front, another to measure the time-mean distribution of hot products, and a third to delineate the instantaneous flame front. It is the latter—a modified schlieren method—I wish to compare with the authors' technique for obtaining flame front contours.

Schlieren records of turbulent flames have an important property which seems to have been overlooked hitherto. The schlieren image is the locus of maximum ray deflection and it therefore occurs at points where the flame is tangential to the light beam. If the beam is parallel, all the sin θ in $S_u = v \sin\theta$ (S_u = burning velocity, v = flow velocity, θ = angle between flame and vector) lies in the plane of the record and can be measured. It is important to realize that the contours in records such as Fig. 1 are not plane sections through the flame but loci of points for which the above condition is satisfied. It means that we have been able to deduce S_u from

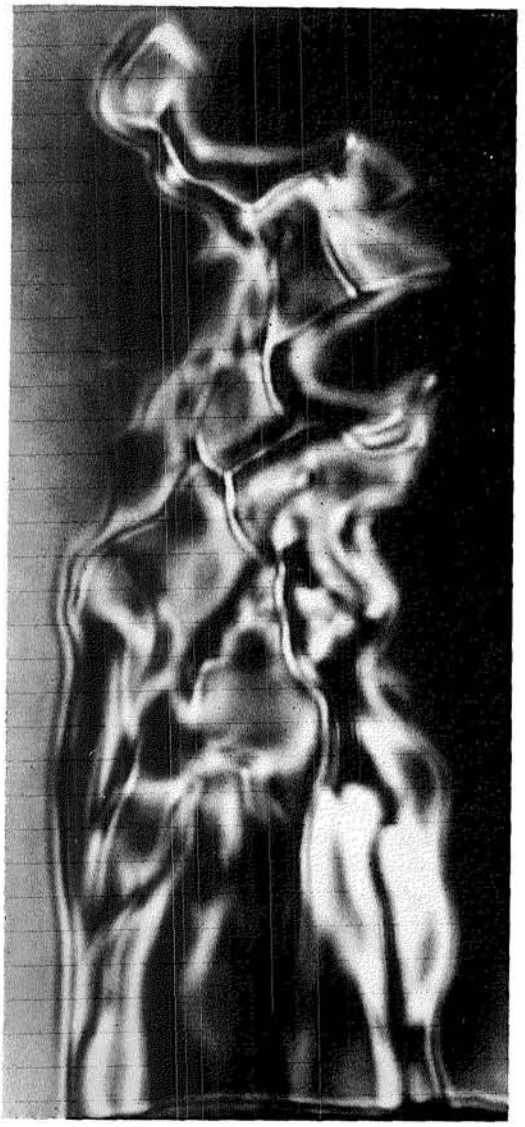

FIG. 1. Instantaneous schlieren photograph of turbulent flame (10^{-6} sec, approximately).

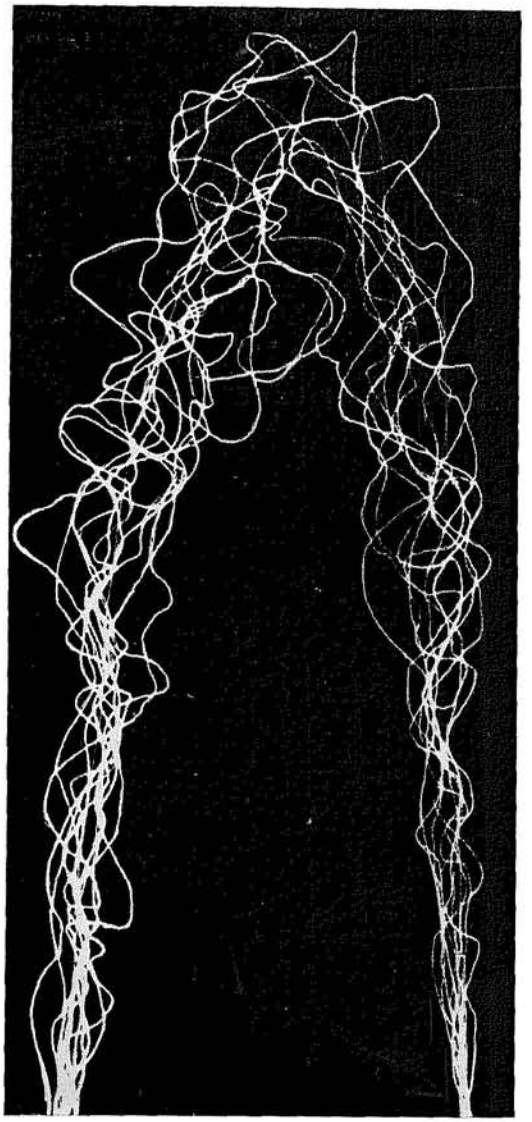

FIG. 2. Superimposed contours of instantaneous flame boundaries.

particle track velocities and sin θ. The latter is equal to (annular element of burner radius)/(corresponding element of length along contour). The mean values of length along the flame were obtained using a large number of instantaneous schlieren contours —as in Fig. 2. We found that the burning velocity of each element is greater than that of the corresponding laminar flame and we were able to explain the discrepancy in terms of the difference between the concave and convex curvatures—which is shown clearly in Fig. 3 and had been predicted theoretically by Karlovitz.[3]

It will be evident that we have been measuring a different kind of contour from that in Dr. Grover's paper. There, a plane section was obtained in each case, and then averaged. This means that sin θ generally had a component at right angles to the record and this ought to lead to low burning velocities. The authors actually used areas, and the point I am trying to make then becomes more obscure. It amounts to cutting a "landscape of steep peaks and gradual valleys" by a large number of vertical planes and trying to construe the typical contour by averaging the sections. Obviously the proba-

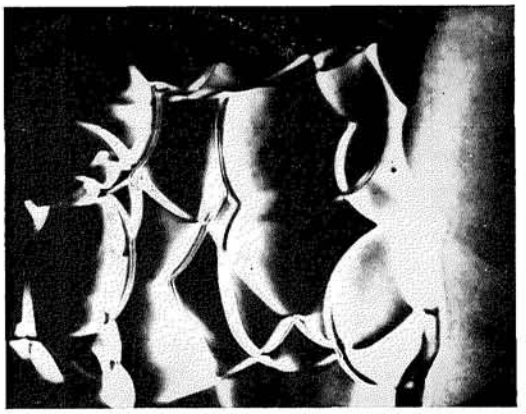

FIG. 3.

bility of cutting valleys is vastly greater than that of encountering peaks. Consider random vertical sections through even a right circular cone. The average section will be most like the conic obtained by sectioning the cone half-way between axis and edge. The result will have a broad (almost correct) base, but a greatly reduced peak.

REFERENCES

1. FOX, M. D. and WEINBERG, F. J.: Proc. Roy. Soc. (London) *A268*, 222 (1962); also ARL–62–337.
2. FOX, M. D. and WEINBERG, F. J.: Brit. J. Appl. Phys. *11*, 269 (1960).
3. KARLOVITZ, B., DENNISTON, D. W., and WELLS, F. E.: J. Chem. Phys. *19*, 541 (1951).

TURBULENT MASS TRANSFER AND RATES OF COMBUSTION IN CONFINED TURBULENT FLAMES

N. M. HOWE, JR., C. W. SHIPMAN, AND A. VRANOS

Measurements of time-mean reaction rate and of coefficients of turbulent mass transfer throughout the combustion zone of confined turbulent flames are reported. The flames studied were of homogeneous, stoichiometric mixtures of propane and air and were stabilized on cylindrical flameholders in a 3 × 1-inch duct. Combustor inlet velocities of 60, 100, and 175 ft/sec were used. The primary data consisted of a complete mapping of static and impact pressures, and of chemical composition throughout the zone studied. Densities, velocity components, and mass fractions of the various species could be computed from these data. Reaction rates were obtained by means of the appropriate material balance equation. Turbulent mass transfer coefficients were obtained by means of a material balance equation applied to a radioactive tracer injected from a simulated line source upstream of the combustion zone.

The composition data show that with negligible error the combustion zone may be considered as an inhomogeneous mixture of burned and unburned gas. The turbulent mass transfer coefficients increase with increasing feed velocity, and the values are about one to two orders of magnitude greater than the molecular diffusivities. The generation of turbulence by the shear in the combustion zone is clearly shown. The rates of oxygen consumption (lb_m/ft^3 sec) at constant composition are dependent on location in the combustion zone, indicating a strong influence of the character of the flow, and the failure of a "stirred reactor" model of the burning zone. Maximum reaction rates are found to be about one order of magnitude lower than the overall reaction rates in laminar flames, and of the same order of magnitude as the overall rates found in open turbulent flames. The rates of reaction tend to increase with increasing feed velocity.

Introduction

The problem of quantitative treatment of turbulent flame propagation in homogeneous fuel-air mixtures has been attacked by many competent investigators. Generally speaking, turbulent flames of this type have been characterized by a burning velocity or spreading rate,[1–6] or a volumetric heat release rate.[7] Most of the theoretical development has been concerned with relationships between the character of the turbulence and the burning velocity,[1,4,8] the character of the turbulence being described in terms of the parameters of the statistical theory of turbulence. Some rather ingenious methods have been used to attempt measurement of the turbulence parameters within the flame.[9] All of this work has emphasized the interplay between the progress of the reaction and the aerodynamics of the flow field. Studies of radiation from turbulent flames have been made.[10,11] Studies of spreading rates of flames of homogeneous air–fuel mixtures burning in ducts[3] have shown that turbulence generated by the flow patterns caused by the flame has apparently greater importance than normally expected turbulence of the feed stream or turbulence generated by the flameholder. Somewhat more detailed studies of the reaction zone in ducted flames have been made.[10,12] It is the purpose of this paper to report the results of measurements of reaction rates and mass transfer coefficients made within the burning zone of homogeneous mixtures of propane and air under conditions where the flow pattern is developed primarily by the combustion process. The ultimate objective in accumulating such data is to relate the quantities so found to the patterns of the flow which must be, at least in part, responsible for them. Exploratory work describing the method was published by Barbor *et al.*[13]

In principle, the method of measurement consists of obtaining experimentally a complete mapping of composition, density, and velocity (time mean quantities) throughout the flame so that these quantities may be substituted into the material balance equation for the species whose reaction rate is to be determined, *viz*:

$$-\rho \mathbf{u} \cdot \nabla \chi_j + \nabla \cdot (\varepsilon \nabla \chi_j) = -Q_j \qquad (1)$$

where only time mean quantities are involved. Logically, this equation may be taken as the definition of Q_j (or $\mathcal{E}$ if Q_j is zero). $\mathcal{E}$ must be determined by application of the equation to a chemically inert substance; with the reasonable assumption that, where the major contributor to diffusive flux is turbulence, $\mathcal{E}$ is independent of the species being transferred.

Experimental

The 3 by 1-inch rectangular combustion chamber was $16\frac{7}{8}$ inches in overall length. Cylindrical flameholders were placed $12\frac{1}{8}$ inches from the downstream end of the combustor midway between the 1-inch walls with axes normal to the flow. The homogeneous, stoichiometric, propane–air mixture was fed to the chamber through a plenum chamber and nozzle so that the velocity profile at the combustor inlet was uniform. The turbulence intensity at inlet was estimated to be less than 0.3 per cent. The combustor exhausted to the atmosphere. Since the chamber was not long enough to cause development of boundary layers of significant thickness on the walls, the flame itself was responsible for development of the flow patterns. Figure 1 is a schematic of the experimental apparatus. The co-ordinate system used in computation is also shown.

Primary measurements were impact and static pressure and chemical compositions as functions of position within the burning zone of the flames. The water-cooled, stainless-steel probes were $\frac{1}{4}$ inch in outside diameter, 0.020 inch in inside diameter, and were inserted into the combustor from the downstream end. Velocity calculations were made by the usual pitot-static formula,

$$u = (2g_c\Delta p/\rho)^{\frac{1}{2}}$$

and this velocity was used for the time mean x-velocity in all calculations. Samples for determining composition were withdrawn through the impact probe at local stream velocity to insure representative sampling.[14] Elementary heat transfer considerations[15] show that samples would be cooled from 2200°K to 1000°K in about 24×10^{-6} seconds. Final chemical analyses for hydrocarbons, CO, CO_2, H_2, O_2, and N_2 were made by means of a Beckman GC–1 chromatograph using silica gel and molecular sieve (type 5A) columns and dried samples. Total analyses checked within 1 per cent, with a precision for individual species of 0.1 per cent. For purposes of estimating compositions a Beckman oxygen analyzer was used. Water content of samples was computed by hydrogen balance. Sample analysis was well within the precision of the feed stream metering by ASME standard orifice meters.

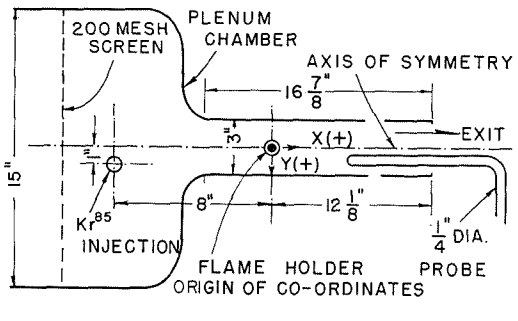

FIG. 1. Schematic of apparatus.

For measurements of rates of turbulent diffusion, a radioactive tracer (Kr^{85}) was injected into the feed stream from a line source in the plenum chamber 8 inches upstream from the combustor entrance and 1 inch below the centerline. The copper "line source" was $\frac{1}{8}$ inch in outside diameter. For some data at 60 ft/sec inlet velocity, the tracer was injected into the wake of the flameholder. Samples withdrawn from the combustor were counted directly by means of a Tracerlab Model TGC–5A detector tube and a Tracerlab SC–90 scaler. Spot checks showed that there was no effect of the tracer injection on any of the other measurements mentioned above and established effective uniformity of the line source.

Flames were studied for inlet velocities of 60, 100, and 175 ft/sec; flameholders were 0.1, 0.1, and 0.2 inch in diameter, respectively. In all cases two-dimensionality of the region studied was confirmed by spot checks.

Data Treatment and Discussion

A. Composition Data. It was mentioned above that samples were withdrawn at local stream velocity. Since local stream velocity was found from a knowledge of the impact pressure, the static pressure, and the density, and since the density was determined from a knowledge of the composition, a trial and error procedure was used to determine the final analysis.

Figure 2 shows a typical set of composition profiles, and Fig. 3 is a set of oxygen composition profiles for the 100 ft/sec flame. It was found that all of the composition data from all positions in all three flames could be correlated by plotting mole fractions of any species in any location against oxygen mole fraction for that location. The correlation is shown in Figures 4a, 4b, and 4c (overlapping points have been omitted). The scattering of the data is well within the precision of the measurements. This correlation made

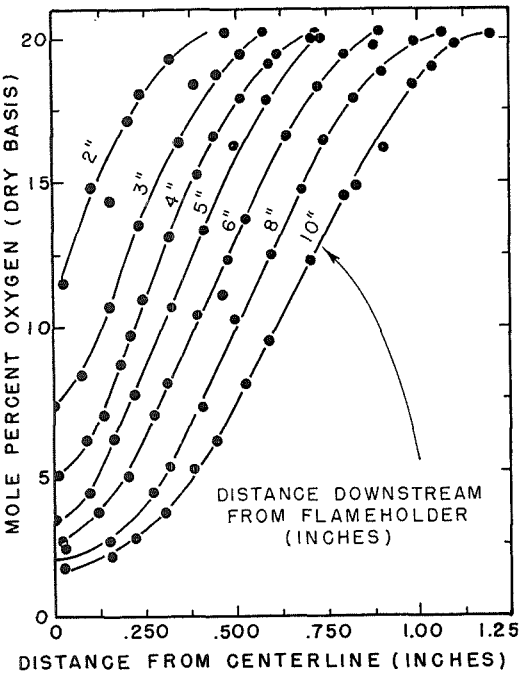

FIG. 3. Oxygen concentration profiles (100 ft/sec inlet velocity).

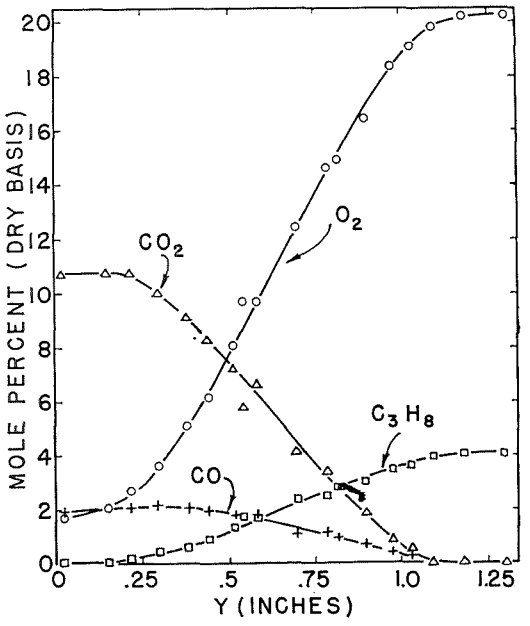

FIG. 2. Composition profiles (100 ft/sec flame, × = 10 in.).

possible fairly accurate preliminary composition and density estimates by means of oxygen analysis alone, facilitating the trial and error procedure indicated above.

It is to be noted that the only "partially burned" species found were carbon monoxide and hydrogen. It is possible that because of the analytical techniques used, polar compounds (aldehydes and acids) could have been missed, but since the analyses accounted for 99 per cent or better of the sample, such materials were certainly present in amounts less than 1 per cent. Analysis of liquids (water) condensed from samples showed no aldehydes.

Equilibrium carbon monoxide and hydrogen for adiabatic combustion of stoichiometric propane–air mixtures are 1.55 and 0.12 mole per cent (dry gas), respectively. It is clear that the amounts of CO reported herein are in excess of the equilibrium amount while the H_2 is less than predicted from equilibrium. The hydrogen deficiency can be explained by slow quenching in the probe. There are several possible reasons for "excess carbon monoxide": (1) carbon monoxide burns out slowly in the flame itself; (2) separation by molecular diffusion as hypothesized by Wohl,[6,16] or (3) small inhomogenieties in the feed mixture. At present there is no conclusive way of deciding which, if any, of these possibilities is responsible, but it is noted that (2) and (3) should result in excess hydrogen. In any event, the departures from the equilibrium amounts are so small as to be negligible for engineering calculations.

On the basis of the correlation shown in Fig. 4 and the absence of significant amounts of partially burned materials, it seemed legitimate to consider the flame to be made up of completely burned and completely unburned gases. Density computations were based on this model with the

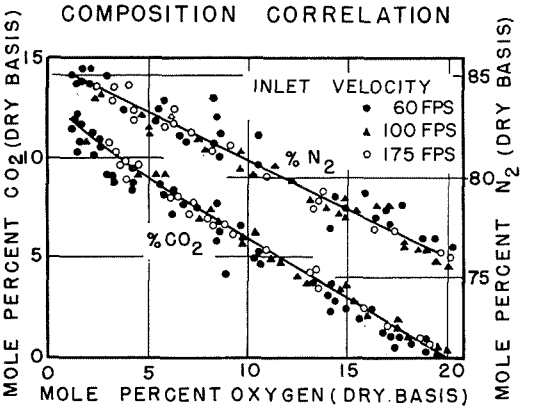

FIG. 4a

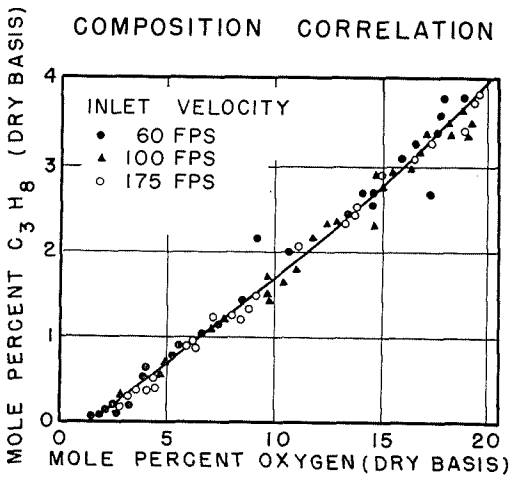

FIG. 4b

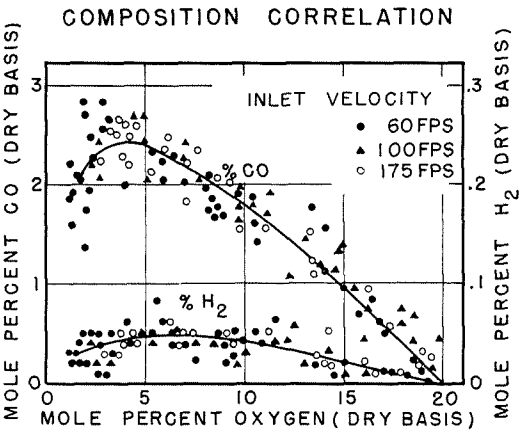

FIG. 4c

FIG. 4. Correlation among CO_2, C_3, H_2, and CO.

assumptions that the burned part was at its adiabatic flame temperature and the unburned part was at feed temperature. (Kinetic energy terms were of negligible importance in the energy balance.) The density at any point was then taken as the reciprocal of the mass average specific volume. For a few cases density was calculated assuming the mixture to be uniform in temperature; differences between results so obtained and those obtained as described above were as much as 12 per cent, but since the homogeneous assumption requires the existence of propane far above temperatures where it is known to decompose rapidly, this latter assumption was rejected as unrealistic.

The correlation shown in Fig. 4, since it applies to all positions within the flame, and since, as will be shown later, the turbulent diffusion coefficient varies throughout the burning zone, implies that the mechanism of the burning process is independent of the character of the turbulence, at least for the range of variables studied so far. The results of the composition measurements would indicate the validity of a model of the turbulent burning zone consisting of hot, burned gas and cold, unburned gas separated by burning zones like the laminar combustion wave. That is, like the wrinkled flame model. However, it seems unlikely that a single, wrinkled flame sheet would be adequate because average wrinkle depths of an inch or greater would be required in some regions of the flames. It will be necessary to make allowance in the model for the "tearing" of the flame front and dispersal of flame elements through the burning zone.

B. Diffusion Data. As indicated earlier, the coefficients of turbulent mass transfer were found by solution of the material balance equation for the krypton, *viz*:

$$-\frac{\partial}{\partial x}(\rho u_x \chi_K) - \frac{\partial}{\partial y}(\rho u_y \chi_K) - \frac{\partial}{\partial x}(J_{Kx}) - \frac{\partial}{\partial y}(J_{Ky}) = 0 \quad (2)$$

Numerical solution of Eq. (2) requires knowledge of the velocity components. Since the impact pressure is insensitive to tube azimuth for angles between flow and probe axis of 5 degrees or less, it was assumed that, as a first approximation, the

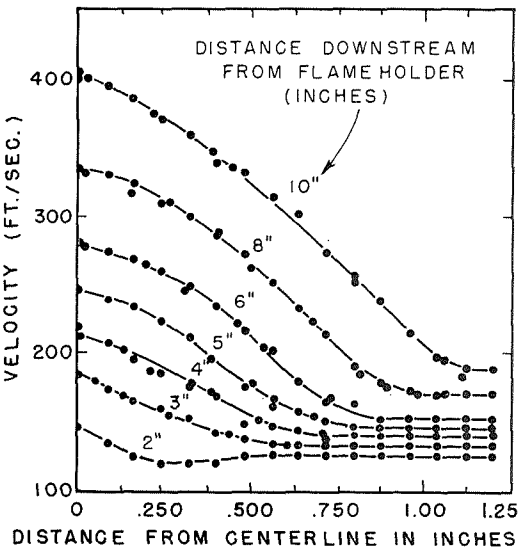

FIG. 5. Velocity profiles (100 ft/sec inlet velocity).

velocity obtained from impact pressures was the longitudinal or x-velocity component. Figure 5 is a typical set of velocity profiles. The shear produced by the flame is apparent, and the region where the flow pattern is influenced by the flameholder is also clear.

Lines of mean flow (lines bounding fixed mass flux, or "streamlines") were determined by finding at each x-position values of y_s such that

$$\int_{y_w}^{y_s} \rho u_x \, dy = \text{constant} \qquad (3)$$

for selected values of the constant. Integration of the continuity equation with respect to y between the centerline of the combustor, where $u_y = 0$ and one of the streamlines ($y = y_s$) gives:

$$\int_0^{y_s} \frac{\partial}{\partial x}(\rho u_x)\, dy + \int_0^{y_s} \frac{\partial}{\partial y}(\rho u_y)\, dy = 0 \qquad (4)$$

By virtue of the identity,

$$\frac{\partial}{\partial x}\int_0^{y_s} \rho u_x \, dy = \int_0^{y_s} \frac{\partial}{\partial x}(\rho u_x)\, dy + \left[\rho u_x \left(\frac{\partial y_s}{\partial x}\right)\right]_{y=y_s} \qquad (5)$$

and the lower limit on the second term as stated above, Eq. (4), becomes

$$\frac{\partial}{\partial x}\int_0^{y_s} \rho u_x \, dy - \left[\rho u_x \left(\frac{\partial y_s}{\partial x}\right)\right]_{y=y_s} + [\rho u_y]_{y_s} = 0 \qquad (6)$$

Because of the definition of y_s, the first term of Eq. (6) is zero, and

$$u_y = u_x \left(\frac{\partial y_s}{\partial x}\right) \qquad (7)$$

The results showed that the maximum angle between the probe axis and the mean flow lines was 3 degrees, verifying the assumption that the impact pressure was an indication of the x-component of velocity. No corrections were made for the fact that the tip of the probe was in a stream of steep velocity and density gradients because the method of correcting for the latter effect is not known. The integrated mass fluxes at all longitudinal positions were compared with the metered mass flux, and deviations were less than 2.5 per cent. Figure 6 is a set of the "streamlines obtained." Smooth curves through the density and velocity data were used in all calculations.

The mean flow lines determined as described above were joined to a potential flow net upstream from the flameholder in order to determine the position for injection of the radioactive tracer. The dot-dash line in Fig. 6 is the locus of the maximum tracer mass fraction and indicates the accuracy of the streamline determination. The lines of constant oxygen fraction indicate the location of the flame in the flow field.

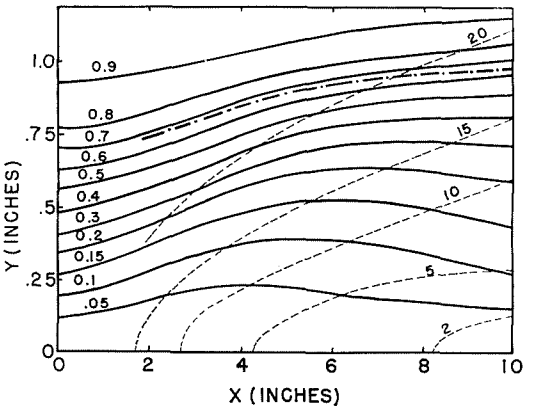

FIG. 6. Streamlines (100 ft/sec flame); ——, mass flow fraction; — - —, O_2 mole per cent (dry); —·—·, from Kr^{85}.

Profiles of tracer count were converted to values proportional to mass fraction in order to obtain the diffusion coefficients. A typical set of profiles of tracer composition is shown in Fig. 7. The smooth curves through the data were used in subsequent calculations.

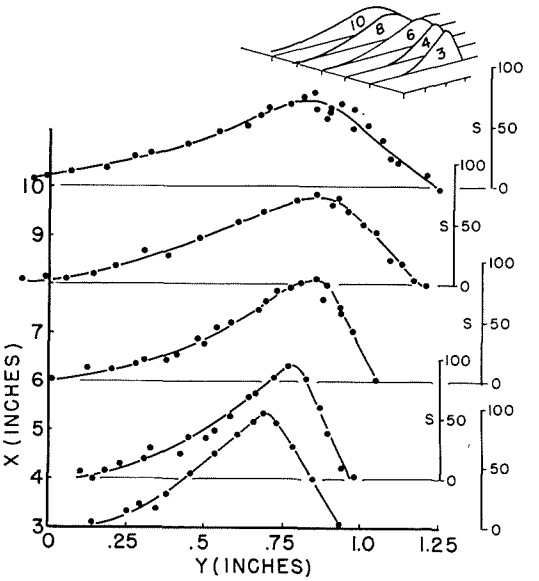

FIG. 7. Tracer count profiles (mass basis, 100 ft/sec flame).

In order to avoid multiple differentiation of the data, solution of Eq. (2) was accomplished by an integral technique. Equation (2) was integrated with respect to y between the wall ($y = y_w$) where u_y and J_{Ky} were identically zero and a streamline passing through the point of interest ($y = y_s$) with the preliminary assumption that the longitudinal diffusive flux, J_{Kx}, is negligible;

$$-\int_{y_w}^{y_s} \frac{\partial}{\partial x}(\rho u_x \chi_K)\, dy - \int_{y_w}^{y_s} \frac{\partial}{\partial y}(\rho u_y \chi_K)\, dy - [J_{Ky}]_{y=y_s} = 0 \quad (8)$$

Use of the identity:

$$\frac{\partial}{\partial x}\int_{y_w}^{y_s} \rho u_x \chi_K\, dy = \left[\rho u_x \chi_K \left(\frac{\partial y_s}{\partial x}\right)\right]_{y=y_s} + \int_{y_w}^{y_s} \frac{\partial}{\partial x}(\rho u_x \chi_K)\, dy \quad (9)$$

with Eq. (8) yields

$$-\frac{\partial}{\partial x}\int_{y_w}^{y_s} \rho u_x \chi_K\, dy + \left[\rho u_x \chi_K \left(\frac{\partial y_s}{\partial x}\right)\right]_{y=y_s} - [\rho u_y \chi_K]_{y=y_s} = [J_{Ky}]_{y=y_s} \quad (10)$$

Comparison of the second and third terms with Eq. (7) shows them to be equal and opposite in sign, and therefore:

$$-\frac{\partial}{\partial x}\int_{y_w}^{y_s} \rho u_x \chi_K\, dy = [J_{Ky}]_{y=y_s} \quad (11)$$

The data were then integrated numerically (by Simpson's rule), and the first term of Eq. (11) was obtained by numerical differentiation of the results. The turbulent mass transfer coefficient was then found from the defining relation:

$$\mathcal{E} = -J_{Ky}/(\partial \chi_K/\partial y) \quad (12)$$

The assumption that $\mathcal{E}$ is a scalar then permitted an estimate of J_{Kx}, *viz*:

$$J_{Kx} = -\mathcal{E}(\partial \chi_K/\partial x) \quad (13)$$

In principle, such determinations would permit iteration to an accurate result, but J_{Kx} was in every case found to be less than 1 per cent of J_{Ky} so that iteration was not necessary. It is recognized that the assumption that $\mathcal{E}$ is a scalar is probably in error. However, there is at present no reasonable experimental method for separating its components. Further, the principal diffusive flux is in the y-direction, and the error is not serious.

At this point it is necessary to justify the use of the gradient of mass fraction as the driving force for diffusion, which results in a transfer coefficient of the dimensions

$$(\text{mass})/(\text{length})\,(\text{time}).$$

Possible substitutes for the driving force are the gradients of mass concentration, mole concentration, mole fraction, or partial pressure. Because the nitrogen in the flame is substantially inert, its mass fraction is unaltered by the combustion process, while its mass concentration,

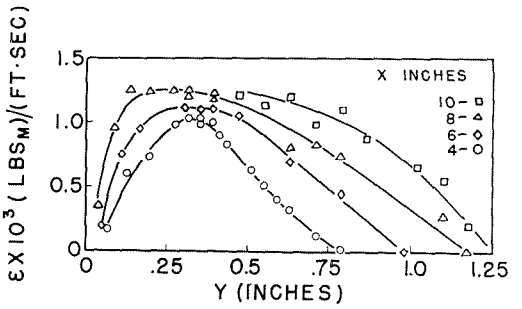

FIG. 8a

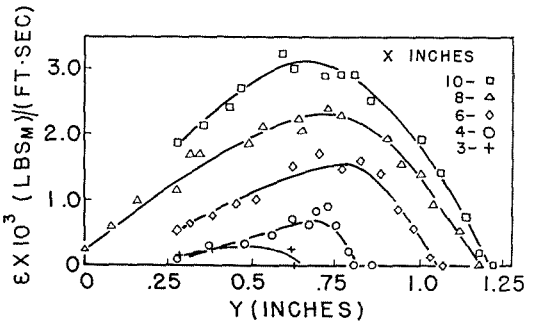

FIG. 8b

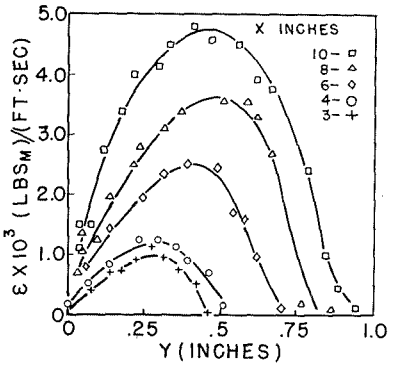

FIG. 8c

FIG. 8. Turbulent mass transfer coefficients; a, 60 ft/sec flame; b, 100 ft/sec flame; c, 175 ft/sec flame.

mole concentration, mole fraction, and partial pressure are changed because of the change in number of moles on reaction. Had mass transfer been responsive to any of the alternative gradients, a variation in mass fraction of nitrogen due to diffusion would have been found. The data show that the mass fraction of nitrogen is uniform throughout the flames, justifying the driving force used.

The turbulent mass transfer coefficients obtained as described above are shown in Figures 8a, 8b, and 8c. While there is some scattering of the data about the smooth curves, the results seem fairly consistent. For purposes of orientation: (1) The maxima of the curves in Fig. 8 range from 0.3×10^{-3} to 4.8×10^{-3} lb_m/ft sec. (2) The maximum value of the coefficient of molecular diffusion of nitrogen in the same units is about 0.6×10^{-4}. (3) Turbulent mass transfer coefficients calculated from the data of Forstall and Shapiro[17] on mixing of co-axial, nonreacting jets are in the range of $0 < \varepsilon < 4 \times 10^{-4}$.[18] (However, the Forstall-Shapiro data are not directly comparable because of a difference in boundary conditions on the flow field.)

It should be emphasized that the feed stream to the combustor is essentially laminar, and that any turbulence in the flames studied must be caused by the combustion process. The velocity profiles show clearly the shear generated by the flame, and the turbulence found is undoubtedly due principally to this shear. That the turbulence produced in these flames is significant is evidenced by the fact that the maximum values of the coefficient are significantly greater than those obtained for co-axial jet mixing. Variations of ε with time for several streamlines in one flame are shown in Fig. 9. The increase with time for all streamlines reflects the production of turbulence.

To our knowledge, there have been no previous measurements of turbulent mass transfer coefficients within flames of this type. Barbor *et al.*[13] computed turbulent momentum transfer coefficients, and the assumption of a turbulent Schmidt number near unity with their data yields values of about the same order of magnitude as in the present work, but the pattern of behavior is different and the values are generally higher—variations attributable to differences in flameholder design and combustor geometry.

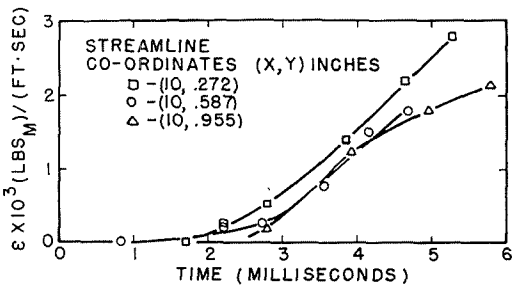

FIG. 9. Time variation of turbulent mass transfer coefficient (100 ft/sec flame).

Westenberg[19,20] has deduced values of turbulence intensity in flames of burners of the same type as those discussed herein from measurements of helium diffusion. He reports values of turbulence intensity which are roughly constant through the flame except on the centerline of the burner where the values were quite low. Since the inlet turbulence intensity even for Westenberg's "low turbulence flame" is about an order of magnitude greater than for the present case, it seems probable that the turbulence intensities in the flames discussed herein vary significantly.

Prudnikov[21] has measured diffusion on the axis of a similar flame and found that the intensity of turbulence decreases as one moves downstream from the flameholder to approach a value approximately the same as that found by Westenberg. If low intensity and low values of turbulent mass transfer coefficient are related, the present results on the axis of symmetry are in substantial agreement with both Prudnikov and Westenberg. The latter author attributed the low centerline values to the viscous damping caused by the high kinematic viscosity. Prudnikov states simply that the decrease noted is a violation of Scurlock's predictions.[3] It is emphasized that Scurlock's predictions were based on the generation of turbulence by shear. In the absence of shear, turbulence will always dissipate, and the low values on the axis are probably due primarily to lack of shear in this region.

It is interesting that the values of ε at any cross section increase with increasing feed velocity, and the increase is nearly linear. Such an increase is consistent with the observation that the rate of flame spreading as measured by luminosity is substantially independent of feed velocity.[3,5] The assumption that the lateral spreading of the flame and the interdiffusion of reactants and products are related is consistent with the model of the turbulent combustion process indicated by the composition data: i.e. the combustion zone is a region of burned and unburned gas separated by relatively thin flames, probably very like laminar flames.

C. Reaction Rate Data. The rates of oxygen consumption (lb_m/ft^3sec) were determined by direct substitution of the smoothed results previously described into the material balance equation for

oxygen, *viz*:

$$-\rho u_x \frac{\partial \chi_{O_2}}{\partial x} - \rho u_y \frac{\partial \chi_{O_2}}{\partial y} + \frac{\partial}{\partial x}\left(\varepsilon \frac{\partial \chi_{O_2}}{\partial x}\right) + \frac{\partial}{\partial y}\left(\varepsilon \frac{\partial \chi_{O_2}}{\partial y}\right) = -Q_{O_2} \tag{14}$$

Initially the first two terms in Eq. (14) were determined and plotted. The third and fourth terms in the equation were then applied to smooth curves through the initial results. Necessary derivatives were obtained by numerical differentiation using the Douglass-Avakian method.[22] The diffusion term was as much as 12, 23, and 40 per cent of the reaction rate term for the 60, 100, and 175 ft/sec flames, respectively.

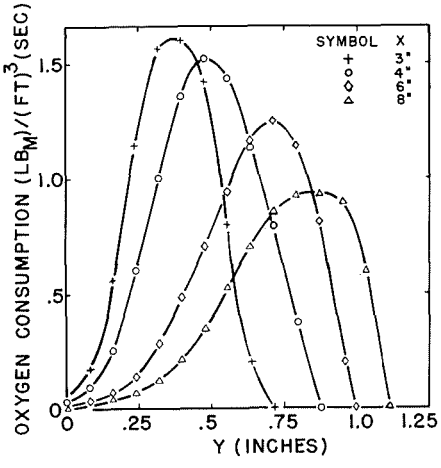

FIG. 10a

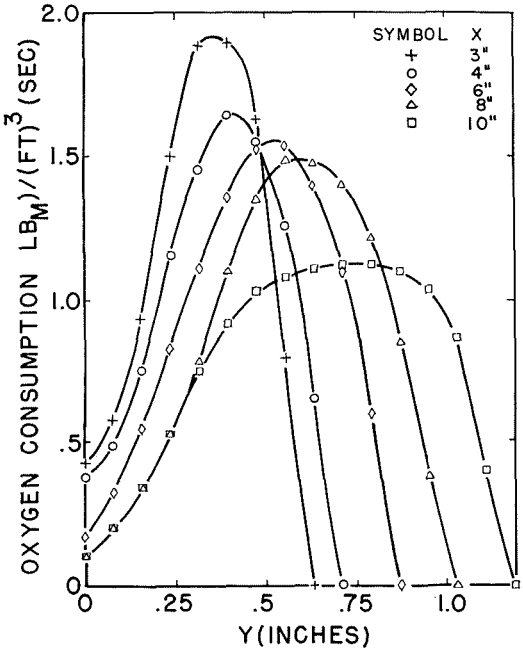

FIG. 10b

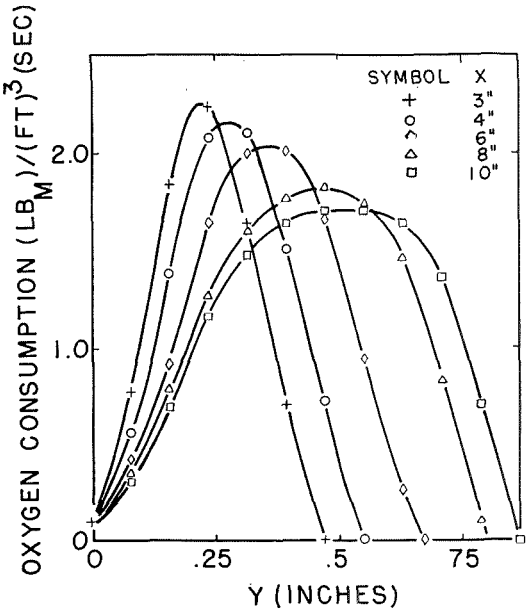

FIG. 10c

FIG. 10. Reaction rate profiles; a, 60 ft/sec flame; b, 100 ft/sec flame; c, 175 ft/sec flame.

Figures 10a, 10b, and 10c are profiles of reaction rates. The general characteristic of these curves, decreasing maximum with increasing distance downstream from the flameholder, has been observed previously.[13] The general broadening of the combustion zone is consistent with the thickening of the luminous zone observed visually. Comparison of the data for the three flames shows that while there is some increase of reaction rate with increasing feed velocity, the increase is less than proportionate. This means that while, as pointed out above, the mass transfer coefficient rises to keep pace with the increased feed rate, thus making the rate of spreading of the flame nearly independent of the feed rate, the reaction rate apparently does not keep pace, and, as observed, the burning zone thickens. It is noted that at the two higher feed rates, there is a measurable reaction rate in the center of the flame. As shown in Fig. 12 there is significant unburned fuel on the centerline of the burner. Hence, a knowledge of the spreading rate of flames of this type is clearly an insufficient

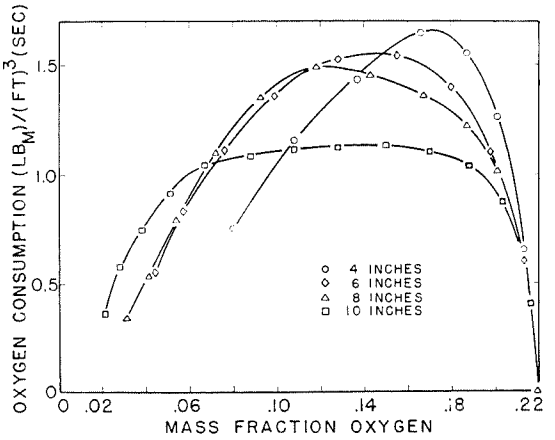

FIG. 11. Reaction rate profiles (100 ft/sec flame).

measure of the burning rate. In all three flames burnout of carbon monoxide is taking place in the center of the duct.

A second representation of the reaction rate data is shown in Fig. 11 where the reaction rates for the 100 ft/sec flame are plotted against mass fraction oxygen. This latter plot shows that the reaction rate is a function of position as well as composition, indicating (1) that the flow pattern influences the reaction rate, and (2) that in the range studied, chemical kinetics are not controlling, i.e. a stirred reactor concept of the burning zone is not valid, as would be expected because the shear in these flames is low compared with that in the so-called stirred reactor.

With one exception[13] there are no data in the literature directly comparable with those reported herein. The reaction rates obtained in the present work for 60 ft/sec inlet velocity are comparable with those of Barbor *et al.*[13] The maximum values of the present data are 5 to 10 per cent of the overall reaction rates of a laminar flame of the same mixture [(density) (laminar burning velocity)/(flame thickness)], variations being due to inclusion or exclusion of estimated thicknesses of the preheat zone in laminar flames; and are 10 to 15 per cent of the overall values as reported by Longwell and Weiss[23] and by Schneider.[24] Overall reaction rates indicated by the data of Petrein *et al.*[12] for a ducted flame and by Simon and Wagner[7] for open flames are the same order of magnitude as in the present results.

Scurlock's data[3] indicate two regimes: one at low velocities where the rate of spreading as indicated by the luminosity is dependent on the feed velocity, the other at higher inlet velocities (above 130 ft/sec) where the rate of spreading is substantially independent of the feed velocity. The streamlines and spreading characteristics of the flames studied in this work show a different character at 60 and 100 ft/sec inlet velocities than for the 175 ft/sec inlet velocity—the spreading being more nearly linear at the highest velocity.

Finally, it is noted that there has been some discussion of an appropriate model of the turbulent flame based upon relationships between fractional oxygen consumption and locus of maximum luminosity (see, e.g., ref. 10). While the present data do not contribute specifically to such a discussion, Fig. 11 shows that the maximum reaction rate at any cross section does not appear at any fixed composition, and the argument appears to be academic.

It is necessary to note for consideration of these data that the range of the data does not include complete combustion of the feed stream. The total fractions of the oxygen burned in the three flames were 27.8, 18.8, and 14.8 per cent for the 60-, 100-, and 175-ft/sec flames, respectively. Problems of equipment size and stability have prevented extending the results to higher fractional completion of the combustion.

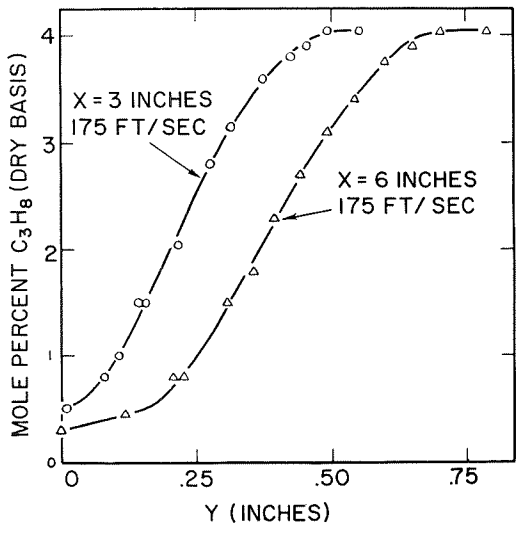

FIG. 12. Profiles of propane content.

Conclusions

The results of this study show that for the range of variables so far investigated:

(1) It is possible to obtain meaningful and interpretable values of the turbulent mass transfer coefficients and reaction rates in the turbulent flame. It is emphasized that the data have been obtained and processed without prejudice as to the best characterization of the flame and without a choice of model of the combustion process. The

results may be examined with respect to any model.

(2) The character of the flame is strongly influenced and controlled by the character of the flow rather than by the kinetics of molecular scale processes.

(3) The shear generated by the confined flame itself can generate turbulence comparable with or greater than that found in jet mixing.

(4) For the range of variables studied the composition in the burning zone can be related to the oxygen content alone, and samples obtained may be regarded as made up of burned and unburned gas. Thus, a modified wrinkled flame model appears to be valid, but a single wrinkled flame sheet would have wrinkles of an inch or more in depth. This means that there must be some tearing of the flame front.

(5) Indications are that the turbulent diffusion coefficient increases roughly in proportion to feed velocity, while the volumetric reaction rate does not increase as rapidly. These facts are consistent with the notion that while the spreading of the flame would be nearly independent of feed velocity, the fractional completion of combustion in a given volume of the combustor would decrease with increased feed rate.

It should perhaps be emphasized that the method of attack on the problem of turbulent combustion described herein by-passes knowledge of parameters describing the flow in terms of the statistical theory of turbulence. Practically speaking, since for engineering purposes application of the statistical description of the turbulence must be related to the boundary conditions, this by-passing is not a shortcoming but an advantage because it eliminates an extremely difficult measurement.

The next task is to relate the results reported here to the patterns of the flow and the properties of the system, to develop a model of the process. Such relationships, valid for most of the range of the present data, have been developed[25,26] and will be presented in a later paper.

Nomenclature

$\mathcal{E}$	Turbulent mass transfer coefficient [lb_m/ft sec]
J_{jx}	x-Component of diffusive flux of species j
J_{jy}	y-Component of diffusive flux of species j
Q_j	Rate of production of species j [lb_m/ft^3 sec]
S	Quantity proportional to mass fraction of Kr^{85} [counts/min lb]
$\mathbf{u}$	Velocity vector
u_x	x-Component of velocity vector
u_y	y-Component of velocity vector
x	Longitudinal distance from flameholder
y	Lateral distance from flameholder
y_s	Value of y corresponding to a streamline [cf. Eq. (3)]
y_w	Value of y at combustor wall
χ_j	Mass fraction of species j
ρ	Density [lb_m/ft^3]

Acknowledgment

This work was supported by National Science Foundation Grant NSF G–11275. Mr. Vranos was supported in part by a fellowship from the Stauffer Chemical Company. Mr. Howe was supported by a National Science Foundation Co-operative Fellowship.

References

1. Karlovitz, B., Denniston, D. W., Jr., and Wells, F. E.: J. Chem. Phys. *19*, 541 (1951).
2. Richmond, J. K., Singer, J. M., Cook, E. B., Oxendine, J. R., Grumer, J., and Burgess, D. S.: *Sixth Symposium (International) on Combustion*, p. 303. Reinhold, 1957.
3. Williams, G. C., Hottel, H. C., and Scurlock, A. C.: *Third Symposium on Combustion and Flame and Explosion Phenomena*, p. 21. Williams and Wilkins, 1949.
4. Scurlock, A. C. and Grover, J. H.: *AGARD, Selected Combustion Problems, Fundamentals and Aeronautical Applications*, p. 215. Butterworths, 1954.
5. Zukoski, E. E. and Wright, F. H.: *Eighth Symposium (International) on Combustion*, p. 933. Williams and Wilkins, 1962.
6. Wohl, K., Shore, L., von Rosenberg, H. E., and Weil, C. W.: *Fourth Symposium (International) on Combustion*, p. 620. Williams and Wilkins, 1953.
7. Simon, Dorothy M. and Wagner, P.: Ind. Eng. Chem. *48*, 129 (1956).
8. Richardson, J. M.: *Proceedings of the Gas Dynamics Symposium on Aerothermochemistry*, p. 169. Northwestern University, Evanston, Illinois, 1956.
9. Karlovitz, B., Denniston, D. W., Jr., Knapschaefer, D. H., and Wells, D. E.: *Fourth Symposium (International) on Combustion*, p. 613. Williams and Wilkins, 1953.
10. Wohl, K. and collaborators: *Sixth Symposium (International) on Combustion*, p. 333. Reinhold, 1957.
11. John, R. R. and Summerfield, M.: Jet Propulsion *27*, 169 (1957).
12. Petrein, R. J., Longwell, J. P., and Weiss, M. A.: Jet Propulsion *26*, 81 (1956).
13. Barbor, R. P., Larkin, J. D., von Rosenberg, H. E., and Shipman, C. W.: A.I.Ch.E. Journal *5*, 37 (1959).

14. LEEPER, C. K.: Sc.D. thesis, Mass. Inst. Technol., Cambridge, Mass. (1954). See also HOTTEL, H. C. and WILLIAMS, G. C.: "Experimental Techniques," *High Speed Aerodynamics and Jet Propulsion*, Vol. XI, p. 62. Princeton University Press, 1960.
15. MCADAMS, W. H.: *Heat Transmission*, 3rd ed., p. 238. McGraw-Hill, 1954.
16. WOHL, K. and SHORE, L.: Ind. Eng. Chem. *47*, 828 (1955).
17. FORSTALL, W., JR. and SHAPIRO, A. H.: J. Appl. Mech. *17*, 399 (1950); Trans. A.S.M.E. *72*, (1950).
18. HOWE, N. M., Jr. and SHIPMAN, C. W.: to be published.
19. WESTENBERG, A. A.: J. Chem. Phys. *22*, 814 (1954).
20. WESTENBERG, A. A. and RICE, J. L.: Combustion and Flame *3*, 459 (1959).
21. PRUDNIKOV, A. G.: *Seventh Symposium (International) on Combustion*, p. 575. Butterworths, 1959.
22. MICKLEY, H. S., SHERWOOD, T. K., and REED, C. E.: *Applied Mathematics in Chemical Engineering*, 2nd ed., pp. 25–28. McGraw-Hill, 1957.
23. LONGWELL, J. P. and WEISS, M. A.: Ind. Eng. Chem. *47*, 1634 (1955).
24. SCHNEIDER, G.: Sc.D. thesis, Mass. Inst. Technol., 1961.
25. HOWE, N. M., JR.: Ph.D. thesis, Worcester Polytechnic Inst., 1962.
26. VRANOS, A.: Ph.D. thesis, Worcester Polytech. Inst., 1962.

Discussion

DR. S. L. BRAGG (*Rolls-Royce, England*): Figure 11 of the paper shows that the volumetric reaction rate is virtually independent of composition. This implies that the flow into an elementary volume of the combustion zone is not mixed (for reaction rate theory shows that the heat release rate in such a mixture would depend critically on combustion), but consists of a stream of slugs of unburned and burned combustibles. If we assume that combustion takes place at the interfaces between these slugs, at a local volumetric heat release rate equal to that in a laminar flame, then the measured average rate should yield a figure for the surface:volume ratio and thus the scale of the turbulence.

These ideas could be checked by running tests at constant Reynolds number with a model of double the size of the prototype. The scale of turbulence should then be found to be double its previous value and if local reaction kinetics were not significant the mean volumetric reactions rate at a point, which depends on a surface:volume ratio, would be reduced to one-half its previous value.

PROF. C. W. SHIPMAN (*Worcester Polytechnic Institute*): Dr. Bragg's suggestion of a model to relate volumetric reaction rate to the size of the slugs of burned or unburned gas is the basis of some work already done by the authors. However, the resulting surface:volume ratio should not be confused with the scale of the turbulence, for as a slug of unburned gas flows through the system, it will be reduced in size both by burning and by the shear in the mean flow. The effect of burning is shown by the dropping off of the reaction rates at low oxygen concentrations (Fig. 11). Thus, the surface:volume ratio will probably give a scale which is too small.

With respect to the tests on a larger prototype, we feel this would be a worthwhile experiment. One should bear in mind, however, that the present results apply to a region of developing shear, where the flame has not yet reached the wall; and the behavior is more likely related to that development rather than the overall size of the system. One would expect the prototype experiment to be of more value for regions farther downstream.

PROF. J. J. BROEZE (*Technological University, Delft*): The very interesting paper by Howe, Shipman, and Vranos, dealing with higher degrees of turbulence, may indicate that there is a limit to which the flame front wrinkling theory would apply, as the reaction rate is found to lag at high flame velocities. As long as it does apply, one has clearly to deal with the propagation mechanism of laminar flame, which is heat conductance plus radical diffusion (in relay race fashion). This mechanism leads to the formulation of a layer of reacting material which is so heavily impregnated with radicals as to be actually autonomous. This means that, under conditions of high shear, chunks may be torn out of this layer, losing contact with the flame front but because of this autonomy continuing the reaction by themselves. However, such a reaction in an isolated area is no longer the same as the normal propagating flame reaction but may resemble more the building up of flame from a self-ignition reaction, and it is conceivable that this would take more time and thereby explain the author's findings.

This leads me to make a request of the authors, namely to consider the possibility of extending their work with hydrocarbons of equal normal flame velocity but different autoignition properties. Theoretically *n*-heptane versus one of the more complex isoheptanes might be ideal but for practical

purposes a good pair of commercial products may be found such as naphtha or light kerosene and isooctane. Also, variations of inlet temperature might be enlightening.

PROF. C. W. SHIPMAN: The authors would like to thank Professor Broeze for his interesting suggestion. The process of rupture of the flame front which he describes has been and continues to be of some concern to us. However, we have so far found no partial oxidation products in the gas samples (other than those expected in the normal post-combustion zone) and thus have no evidence of such rupture. We must, of course, also consider the possibility that the quenching rates in our probe (estimated at 50×10^6 °K/sec) are too slow to enable us to detect the phenomenon. Further it would seem that rupture of the wrinkled flame, which has already taken place in the flame studies so far, will take place perpendicular to the plane of the burning wave more often than parallel to it, and our subsequent development of a model to describe the reaction rates has considered this.

Professor Broeze's comment is interesting from another point of view. No theoretical models of turbulent combustion so far developed accounts for the observed fact that turbulence can extinguish the flame. Rupture of the burning zone as described by Professor Broeze, but at a slightly different plane may supply the necessary mechanism.

Laminar Gas Flames

Chairman: Dr. R. M. Fristrom (*APL/Johns Hopkins University*)

Vice Chairman: Prof. C. S. Tarifa (*Madrid*)

FURTHER STUDY ON FLAME STABILIZATION IN A BOUNDARY LAYER: A MECHANISM OF FLAME OSCILLATIONS

W. S. WU AND T. Y. TOONG

In this paper a mechanism of flame oscillation is proposed in an attempt to explain the often-sought flame oscillation phenomena in a boundary layer and also to bring together with a unified theory the two distinct types of flame stabilization in a boundary layer. These types are: (1) the steady flame observed by Hottel *et al.* and (2) the oscillating flame observed by Gross, Ziemer, and Turcotte.

This proposed hypothesis postulates that the oscillation phenomenon of the flame in a boundary layer is caused by the instability of the boundary layer flow. The adverse pressure gradient immediately upstream of the flame nose in the boundary layer and the heat transfer to the unburned mixture from the solid boundary make the boundary-layer flow highly unstable. This instability, combined with the basic principles of flame stabilization and propagation, sets off the oscillation.

A comparison of the experimental conditions with the existing boundary-layer stability theory indicates that the boundary layer in the experiments is in the unstable region. Evidences are provided to support the theory.

A further study of the oscillation characteristics of the flame was made by means of high-speed motion pictures. It shows that the oscillating pattern of the flame repeats itself exactly and the advance speed and the oscillation frequency of the flame become higher when the plate temperature increases, while the retreat speed remains constant. The advance speed remains constant when the amplitude of oscillation is changed. Furthermore, the steady flame observed by Hottel *et al.* was also obtained by the authors at a very low-plate temperature and flow velocity. All these phenomena can be fully explained by the proposed hypothesis.

As discussed, some of the present results agree with the observations of previous investigators, but some do not.

The proposed hypothesis is further employed to examine and alleviate some of the doubts concerning the use of the equilibrium theory to correlate oscillating-flame data by a group of parameters. It is found that though the reason for choosing these parameters is different from that of the previous investigators, our results are quite similar. The correlation is readily explained qualitatively by the steady-flame theory.

Introduction

Many studies have been made of flame stabilization in a boundary layer because of its relatively simple model and the existence of an established boundary layer theory to assist in the analysis. However, the results of these studies are not generally comparable, due to differences in emphasis and experimental conditions.

Gross[1] first reported the possibility of flame stabilization in a boundary layer over a flat plate. Hottel, Toong, and Martin[2] investigated

the same problem in a boundary layer adjacent to a slender water-cooled rod placed in a combustible stream with its axis parallel to the flow direction. Later, Ziemer and Cambel[3] studied stabilization in a laminar boundary layer next to a heated plate, and Turcotte[4] also studied stabilization in a turbulent flow. Hottel, Toong, and Martin succeeded in obtaining steady flames, while Gross, Ziemer and Cambel, and Turcotte observed oscillating flames. Gross reported a regular pattern of oscillations with a definite frequency and amplitude, while Ziemer *et al.* reported a random pattern with no explanation as to how their experimental results were related to the equilibrium theory of flame stabilization. Turcotte proposed a continuous ignition theory for flame stabilization, while Ziemer and Hottel used Bunsen-flame stabilization theory.

This paper presents the results of a critical study needed to bring together the different observations in a single hypothesis which will explain the mechanism of flame oscillations. This hypothesis is further used to justify the application of the steady-flame stabilization theory to correlate oscillating-flame data.

Description of Apparatus

The apparatus consists of a test section, a calming section, and a fuel-air mixing section. The exhaust gases from the test section are removed from the laboratory through an overhead hood.

The metered fuel (ethanol) is first vaporized through a steam-heated heat exchanger (Fig. 1), mixed with filtered, metered air to give a desired mixture, and then preheated in a steam-jacketed tank to a desired temperature. The uniform mixing of fuel and air is achieved by ejecting vaporized fuel through numerous pinholes perpendicular to the air stream.

From the mixing tank, the mixture flows through a diffuser and a straightening-calming section and reaches the air-film introducing section. Here, two sheets of air film are introduced in parallel to the mixture stream at a carefully matched stream velocity, to minimize mixing with the main stream. The sandwiched stream then passes immediately through a converging nozzle and a test section into the atmosphere. These two air films separate the quartz windows of the test section from direct contact with the mixture and hence prevent the boundary layers on the windows from affecting the flame.

Figure 2 shows the one-square-inch test section, formed by a heated flat plate, two quartz side walls, and a top wall. The plate temperature distribution is measured by nine thermocouples and can be controlled by adjusting the current through thirty-two quartz-insulated

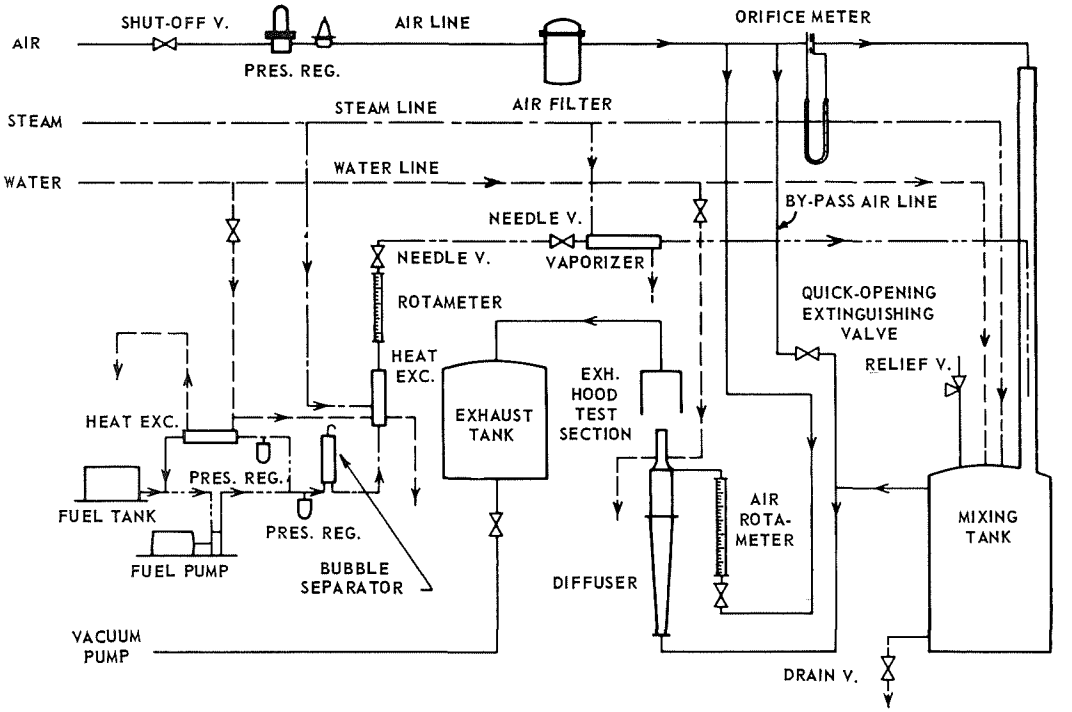

FIG. 1. Schematic diagram of apparatus.

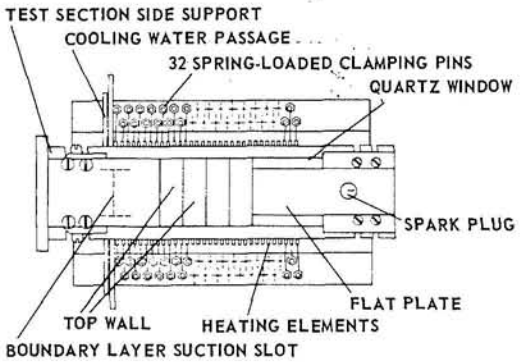

FIG. 2. Test section assembly.

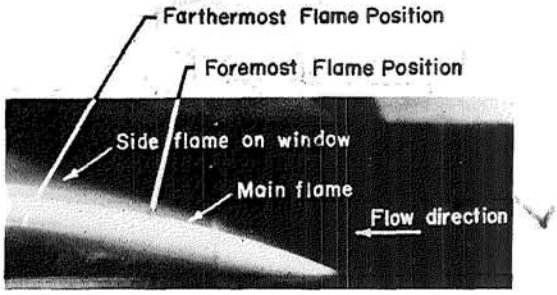

FIG. 3. Side flame and main flame in test section.

heating elements embedded in the stainless-steel flat plate. The plate is carefully designed to maintain a nearly constant transverse temperature distribution. A 0.006-inch suction slot is provided at the leading edge of the plate to ensure the generation of a new boundary layer.

The mixture temperature was measured by a double-shielded calibrated thermocouple probe which was retracted during the test. The double shielding reduced error caused by radiation from the hot plate.

Oscillating Flames

Observed Phenomena

In the study of flame stabilization in boundary layers, the authors, like other investigators[1,3,4] observed various types of oscillating flame and also experienced extreme difficulties in eliminating the oscillation. To ensure that these oscillations were not caused by inaccuracy of the measuring instruments or by faulty design of the apparatus, special attention was paid to the design of the apparatus and to the calibration of the measuring instruments. Before the installation of the air-film introduction section, a three-dimensional flame was observed in the test section. The flame was closely attached to the wall of the test section and advanced and retreated along the two adjacent corners, alternately one at a time. When the temperature of the heated plate was high, the flame always chose the pair of corners formed by the heated plate and the quartz windows. Introducing air jets along the corners through a fine (0.030-inch O.D.) hypodermic tube eliminated the alternating advancement of the flame along the corner. However, two side flames attached to the quartz windows still oscillated with the main flame (Fig. 3). The introduction of air films further eliminated the side flames but did not eliminate the oscillation. When the air-film velocity was matched with that of the mixture, the flame front became strictly two-dimensional across the test section and was "stabilized" in the boundary layer adjacent to the heated wall. The high-frequency oscillations persisted; their presence was revealed by the appearance of two distinct bright lines (Fig. 3) at the extreme positions occupied by the flame.

When the air-film velocity was mismatched with the mixture velocity, the development of turbulent mixing caused by the shear flow was clearly observed from the shape of the flame sheet. Since the turbulence caused a higher burning velocity, the two mixing regions formed two ridges on the flame sheet. The ridges developed with the growth of the mixing zone, finally met each other, and filled the full width of the test section.

During this study the (common) occurrence of acoustic oscillation in a combustion chamber was at first suspected as the cause of these flame oscillations. However, an approximate calculation of the fundamental natural frequency of the system yielded a value which was several times larger than the observed oscillation frequencies. Experiments also showed that the oscillation was not influenced by such variables as the geometry of the exhaust hood. Other possible external disturbances also were suspected, such as vibration of the air compressor, vacuum pump, etc. These possibilities were also ruled out by experimentation.

Also considered was the possibility that a steady mode of propagation existed at a certain position along the heated plate, but that the ignition mechanism used in these experiments forced the flame into an oscillating mode. In this study the flame was ignited by a spark plug located at the trailing edge of the heated plate. As the mixture was ignited, the flame propagated upstream to the foremost position of the oscil-

lating mode, possibly creating a disturbance sufficient to cause oscillation. However, experiments designed to investigate this line of argument have disproved the hypothesis that the flame would be stable either if ignition were initiated at the position of the stable mode, or if the oscillation amplitude were reduced to a certain level.

The failure of many extensive experiments aimed at eliminating the flame oscillation and the observation of certain characteristics of the oscillation indicate that the oscillation might possibly be an inherent feature of this type of flame stabilization (in the sense that the flame does stay in the boundary layer) under the experimental conditions. It is similar to a flow behind a cylinder which will always oscillate owing to alternately shed eddies on each side, and which does not lend itself to a potential-flow solution.

A Mechanism of Flame Oscillations

If oscillation is assumed to be inherent to the type of stability studied, what mechanism causes this oscillation?

The hypothesis proposed here is based on boundary-layer instability. As is well known, a flame acts like a porous object in a flow. According to the equilibrium theory of flame stabilization, the flame front in a boundary layer must have a blunt-nose shape. The unburned mixture approaching the nose is retarded, deflected to the side, and finally passed through the front and burned. This is because the pressure in the region immediately upstream of the nose is higher than the free-stream pressure. According to the boundary-layer instability theory, this adverse pressure gradient, upstream of the flame, and the high temperature of the flat plate make a laminar flow highly unstable. This instability leads to the growth of disturbances and to eventual transition to turbulence.

Once the flow is turbulent or on the verge of becoming turbulent, the increase in burning velocity causes the flame to advance toward the leading edge of the flat plate. This advancement results in further increase of the adverse pressure gradient in front of the flame nose, lowering the stability limit of the boundary layer so that the flame keeps advancing. On the other hand, several other factors are also changing as the flame advances. First, the Reynolds number at the position of the flame is decreasing and the corresponding velocity gradient at the wall is increasing. Second, the ratio between quenching distance and thermal boundary-layer thickness becomes larger as the flame approaches the leading edge of the plate. This fact leads to a lower hump of the burning velocity profile, caused by the thermal boundary layer of the unburned mixture as the flame advances.[5,11] When these factors balance the increase of burning velocity caused by transition and turbulence, the advance stops. As soon as the flame stops, the pressure gradient in front of the flame is no longer the same as when the flame was advancing. The decrease of the pressure gradient increases the boundary-layer stability limit, thus changing turbulent flow to laminar flow with a result of decreased burning velocity; hence the flame retreats. This retreat continues until the Reynolds number corresponding to the flame position increases sufficiently so that turbulence is once again generated. The turbulence makes the flame again move toward the leading edge of the flat plate.

Supporting Evidences

In the present investigation, four series of data were obtained under the conditions that the undisturbed free-stream velocity (U_∞) varied from 4 to 17 ft/sec and that the ratio of the wall to free-stream temperature (T_w/T_∞) of each series was 2.11, 1.82, 1.55, and 1.14. Each of these experiments showed a definite pattern of oscillation. Let us first examine the stability limit of each.

Schlichting and Ulrich have made a theoretical study of the stability limit of a boundary layer under the influence of streamwise pressure

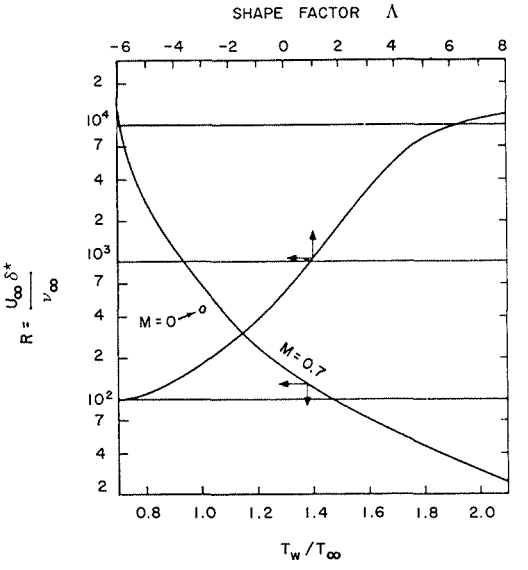

FIG. 4. Stability limit of flow in a boundary layer due to heating effect and pressure-gradient effect. (From *Boundary Layer Theory*, by H. Schlichting. Copyright 1960. McGraw-Hill Book Company, Inc.)

gradient.[6] Lees and Lin have studied the effect of heat transfer from wall to gas on the stability limit.[7,8] Their investigations demonstrate that the critical Reynolds number above which instability appears is greatly affected by either the adverse pressure gradient or by the temperature of the heated wall (Fig. 4). However, no solution is available which takes into account both of these factors at the same time. The solutions of Lees and Lin are for a free-stream Mach number of 0.7 and cover a range of T_w/T_∞ from 0.7 to 1.25. Also, one point corresponding to T_w/T_∞ equals 1 and M equals 0 gives a lower critical Reynolds number (Fig. 4) than that for which $M = 0.7$. When their solutions are extrapolated to the values of T_w/T_∞ used in our study, three out of the four series in the experiments give a Reynolds number beyond the theoretical stability limit. However, to use their solution as a guide for the flow stability of our experiment is extremely conservative because their solutions are for $M = 0.7$ and these authors do not consider the effect of the adverse pressure gradient upstream of the nose of the flame. Therefore, it is highly probable that the experiments in the fourth series correspond also to an unstable region.

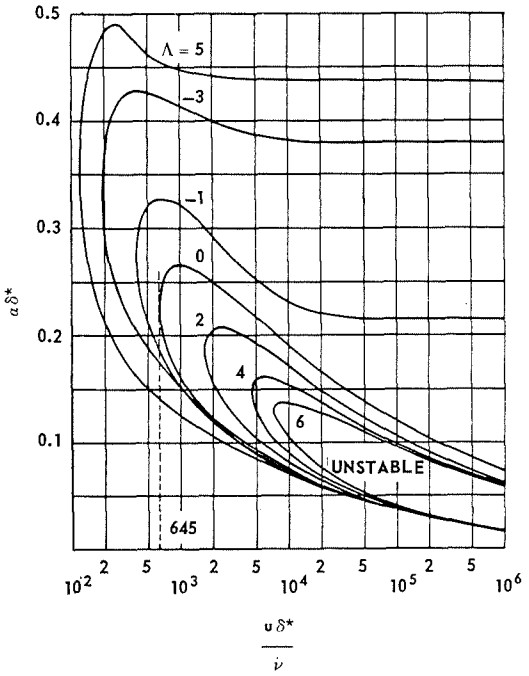

FIG. 5. Curves of neutral stability for a boundary layer with pressure gradient. (From *Boundary Layer Theory*, by H. Schlichting. Copyright 1960. McGraw-Hill Book Company, Inc.)

In considering the effect on the stability limit of pressure gradient or shape factor Λ, it is known that there are two kinds of neutral stability curves (Fig. 5). The first type is that in which both branches of the stability curves (for all velocity profiles with a decreasing pressure or $\Lambda > 0$) tend to approach zero as the Reynolds number approaches infinity, as was the case for the flow over a flat plate ($\Lambda = 0$). The second type, called frictionless instability, is characterized by a velocity profile with a point of inflection. This often corresponds to a velocity profile with an adverse pressure gradient ($\Lambda < 0$). For this kind of instability, a finite region of wavelength exists at which disturbances are always amplified when the Reynolds number exceeds a critical value.

L. B. Dumont[9] shows in his report that the velocity profile immediately upstream of the flame is not only highly distorted but also possesses a point of inflection. A comparison of the velocity profile at separation ($\Lambda = -12$) with the velocity profile obtained by Dumont indicates the considerable effect of the flame on the stability limit of the boundary layer.

For the present case, no stability solution which considers the effects of both temperature and the adverse pressure gradient is available for a more precise estimation of the critical Reynolds number, or stability limit. However, according to the postulated mechanism, there should be a steady flame if the Reynolds number corresponding to the flame position is low enough. This was indeed observed when U_∞ was equal to 4.06 ft/sec, T_w was equal to 92°F, and T_∞ was equal to 118°F. Under these conditions the flame stood still at X equals 0.688 inch (from the suction slot) and its corresponding length Reynolds number, R_x, was 1266. This steady flame is difficult to obtain in this apparatus, because there was no provision for cooling of the flat plate. (Note that the steady flame reported in the paper by Hottel *et al.* was obtained by the use of a water-cooled solid boundary.)

It is difficult to provide further detailed and quantitative proof of the boundary-layer stability. For instance, the stability solution for the present configuration (that is, for a compressible boundary layer with constant wall temperature and a pressure gradient due to a porous obstacle) is a difficult problem. Solution of the unsteady boundary-layer flow with an oscillating porous obstacle is also difficult. Experimentally, the ordinary method of detecting turbulence, namely hot-wire anemometry, is no longer practical because the flame would burn up the fine wire and the probe would not physically be able to follow the fast-oscillating flame. The Schlieren technique also is not applicable, because the

region of transition and turbulence is expected to be very small and the strong density gradient of the flame front would overshadow the minute disturbances which are present immediately upstream of the flame tip. (This is indeed the case, as demonstrated by Schlieren pictures.)

Nevertheless, instead of an elaborate theoretical analysis or an involved experiment, a relatively simple experiment has been performed to provide further supporting evidence. A turbulent flow is created by using a wire. This wire is placed on the flat plate perpendicular to the flow direction downstream of the oscillating flame. The wire is then moved slowly upstream, and as soon as the flame touches the wire, it immediately attaches itself to the wire and no longer oscillates. As the wire moves farther upstream, the flame first remains attached to it, then develops a tendency to detach itself from the wire, and finally jumps back to a position about $\frac{3}{8}$ inch to $\frac{1}{2}$ inch downstream of the wire. The most interesting phenomenon is that the flame is very steady at this point when the wire is immediately upstream of it. This evidence clearly demonstrates that the oscillation mechanism is destroyed due to the presence of this wire. If the wire is moved farther upstream, localized turbulence is damped out due to a low Reynolds number in that region, and the flame begins to oscillate again. Wires of different sizes have been tried, and the same general phenomenon was observed. With a wire smaller than a certain size, however, it is harder to produce the steadily detached flame, and even if it is produced, it readily starts to oscillate. This observation may be explained again by the fact that insufficient turbulence is generated by a smaller wire.

The previously mentioned alternatively advancing and retreating flame along two adjacent corners of the combustion tunnel was first observed without using the air film. The frequency of the oscillation increased as the plate temperature increased. When the frequency of oscillation became very high, the oblique intersection lines moved so fast that they appeared to be two crossed lines on the plate. Conversely, when the plate temperature is lowered to a certain level, the flame no longer seems to have a particular preference for the pair of adjacent corners composed by the heated plate and quartz windows, but never chooses a pair of diagonally opposite corners. In this case the boundary layer in the corners can become turbulent or separated due to an adverse pressure gradient more easily than can a two-dimensional boundary layer, because the shear stress at each corner is zero. The postulated hypothesis can immediately be applied to explain such oscillations, though it does not explain the fact that the flame takes alternatively adjacent corners. Without offering a satisfactory answer to this question, let it be mentioned here that the alternatively oscillating pattern is quite similar to that observed by J. Nikuradse[10] on flow in a divergent channel. Possible similarities between the fundamental oscillating mechanisms in these two cases have not been thoroughly studied.

High-Speed Motion Pictures

High-speed motion pictures, taken under various conditions, provide insight into these oscillation phenomena. Most of these motion pictures were taken at approximately 1000 frames per second. The precise film speed was indicated by the timing markers on one side of the film.

These films yielded data on three major areas of interest. The first area involved the flame propagation when the mixture was just ignited. The second area pertained to the relationship between oscillation amplitude and the advance and retreat speeds of flames for each cycle of oscillation at the same U_∞, T_∞, and T_w. The third area related the effect of plate temperatures on the advance and the retreat speeds. By studying consecutive frames of the film strips, the relationships between the flame anchoring point and time were obtained and plotted. A typical plot of these curves is given in Fig. 6,

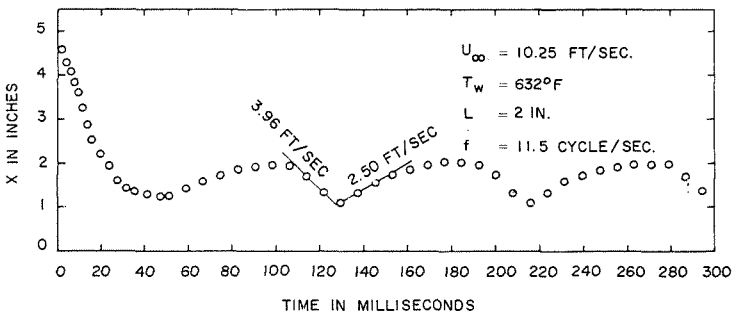

FIG. 6. Flame position versus time.

TABLE 1

Flame oscillation characteristics under different conditions

Case	T_w (°F)	U_∞ (ft/sec)	Adv. speed (ft/sec)	Retreat speed (ft/sec)	Osc. freq. (cps)	X_{min} (inches)	X_{max} (inches)	Osc. ampl. (inches)	L (inches)
1	632	10.25	3.96	2.50	11.49	1.10	2.00	0.90	2.0
2	632	10.25	4.06	2.81	8.33	1.33	2.80	1.53	3.0
3	632	10.25	4.16	3.22	6.13	1.10	4.10	3.00	4.0
4	829	10.31	6.67	3.50	12.5	0.50	2.00	1.50	4.5
5	413	4.10	1.47	1.30	19.8	0.41	0.66	0.25	2.0

and the characteristics of these curves are summarized in Table 1.

When the mixture is ignited, the flame propagates (Fig. 6) from the trailing edge toward its "stabilized" position at a relatively high speed of 16.8 ft/sec. This speed far exceeds the burning velocity of a stoichiometric ethanol-air mixture, since the wall temperature is only 623°F. After the flame has reached its "stabilized" position, the oscillation pattern is immediately established and repeats itself exactly at each cycle, unlike the ordinary second-order oscillation system which usually overshoots when it is underdamped. The flame is clearly seen to be propagating through the boundary layer. The experimental conditions corresponding to Fig. 6 were U_∞ equals 10.25 ft/sec, T_w equals 632°F, and a stoichiometric mixture was used. The oscillation frequency was 11.49 cycles/sec, the advance speed was 3.96 ft/sec, and the retreat speed was 2.50 ft/sec.

To carry out the second goal of this study, the length of the top wall was changed to vary the oscillation amplitude. Interestingly, when the length of the top wall is changed to 3 and 4 inches, the advance speed remains nearly constant when the amplitude of oscillation is changed (see Table 1). According to the previously stated instability theory of flame oscillation, the advance speed indeed should be independent of oscillation amplitude because transition and turbulence are the basic cause of the flame advancement. As long as the intensity of the turbulence remains the same, the increase of the burning velocity should be the same.

Another motion picture taken under the same conditions shows that the oscillation pattern is clearly reproducible at each run.

To achieve the third purpose, a motion picture was taken with a higher plate temperature. Compare case 4 with case 3 in Table 1. The advance speed and the frequency became higher when the plate temperature was higher, while the retreat speed remained approximately constant. According to the proposed theory, the flame retreat is simply due to "wash-away" by the free stream. When either the length of the top wall or the flow pattern in the free stream remains the same, the retreat speed should be the same. Conversely, when the top wall is shortened, the resulting flow divergence in the free stream reduces the free-stream velocity. Thus, the wash-away speed or the retreat speed is reduced, as can be seen from Table 1.

Flame oscillation at a low-plate temperature was also studied. However, at low-plate temperature the flame cannot be kept in the test section at the same free-stream velocity (10.3 ft/sec). Another motion picture was taken with U_∞ equal to 4.10 ft/sec, and T_w equal to 413°F. The advance speed shows a lower value than that for T_w equals 632°F. The fact that the advance speed became lower when the plate temperature was lower may be explained again by the instability theory. It is known that the higher the plate temperature, the lower the stability limit. Thus, turbulence can be generated more readily, or the intensity of the turbulence may be higher at higher plate temperatures. Therefore, the advance speed becomes higher when T_w is higher.

The oscillation pattern obtained from the high-speed movies agrees with Gross' description that "the flame front appears to dart down through the boundary layer, dragging the rest of the flame with it. It then stops near the leading edge and washes back toward the trailing edge." The words "dart," "dragging," and "washes back" also seem to best describe the present observed oscillating motion, although the ratio of advance velocity to retreat velocity is not four to one, and the frequency is not 25 ± 5 cps, as Gross observed. These differences may be caused by various factors such as different kinds of fuel used, temperature profile of the plate, free stream-mixture flow velocity, etc.

Gross mentioned that 600°F plate temperature

was sufficient for oscillation to take place and water-cooling of the plate stopped the oscillation and caused the flame to stabilize itself along the rear edge of the plate. The authors observed the oscillation at a much lower plate temperature than 600°F. At the same time, we also realized the fact that Gross' plate length was shorter, his mixture velocity was higher, and different kinds of fuel were used.

The present experiment shows that the oscillation has a definite pattern for each set of conditions and repeats itself exactly at each cycle. This fact disagrees with Ziemer's observations that a frequency variation of an individual cycle (from 14 to 30 cycles/sec) appears to be random and that the amplitude variation (from $\frac{1}{2}$ to 2 inches) does not seem to correlate with the frequency. He also found that the ratio of the average advance velocity to the average retreat velocity of the flame front varies randomly from 0.5 to 2.0. He states that this ratio does not seem to be influenced by the frequency.

In the present investigation, the advance velocity of the flame tip is independent of the amplitude of oscillation and is increased with plate temperature, while the retreat velocity depends on the top-wall length. The flame oscillation is not believed to be an ordinary linear spring-mass type. These facts can all be explained by the proposed theory of oscillation and may thus serve as further evidence for supporting this theory.

Flame-Holding Characteristics

A New Interpretation of the Selection of Stability Parameters

Previous investigators have often treated the flame stability in a boundary layer by an equilibrium theory[11] and have also correlated the experimental data by it, even though the observed flame may be oscillating. An attempt is made here to examine and allay some of the doubts concerning the use of the equilibrium theory to correlate oscillating-flame data.

The equilibrium theory of flame stabilization postulates that the flame always attempts to seek a position along the flat plate where the mixture-velocity profile is tangent to the burning-velocity profile. If both of these profiles are steady, a definite position exists at which the flame would be stabilized. In this case, the correlation among aerodynamic, heat transfer, and chemical characteristics would be most logically accomplished through the use of the wall temperature, free-stream velocity, flame-stabilized position, fuel-air ratio, or any other convenient variables which may be derived therefrom. This is the method of correlation that Hottel *et al.*[2] and Ziemer *et al.*[3] have used in their analyses. Now if an oscillating flame is examined on the basis of the postulated instability mechanism, it is realized that $X_{\min}$ represents a position at which the increased burning velocity due to transition or turbulence is finally balanced by the steepened velocity gradient at the wall and by the more pronounced quenching effect of the flat plate. This characteristic quantity, $X_{\min}$, is then used as one of the parameters to correlate the flame-holding characteristics. In fact, good experimental correlation is achieved by using $X_{\min}$ with U_∞ and T_w as variables and holding T_∞ constant. Though the reason that these parameters have been chosen is different from that of the previous investigators', our final result is quite similar.

Correlation between Stability Parameters

Four series of data corresponding to T_w equals 829, 632, 431, and 203°F, and T_∞ equals 147, 144, 128, and 127°F, respectively, have been collected, screened, and organized[5] and are shown in Fig. 7. The curves in Fig. 7 show a consistent trend of variation as predicted by the equilibrium theory; however, they do not agree with the observation by Hottell *et al.*[3] that the boundary velocity gradient $(\partial u/\partial y)_w$ immediately upstream of the flame is independent of the free-stream velocity. Figure 8 shows a definite trend of increasing $(\partial u/\partial y)_w$ as U_∞ increases. (The velocity gradient at the wall in Fig. 8 is calculated on the basis of compressible fluid flow at a very

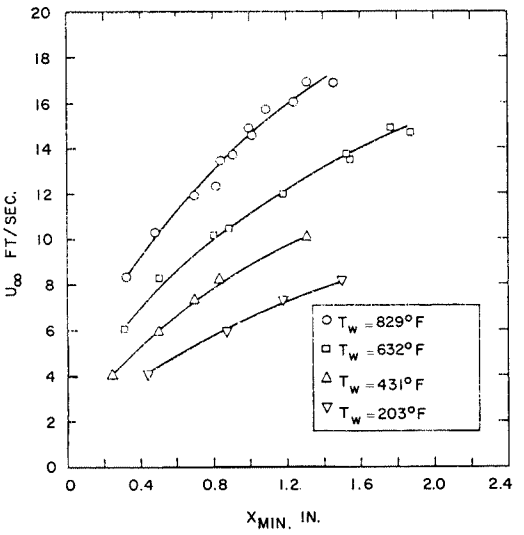

FIG. 7. Relation between free-stream velocity and flame position.

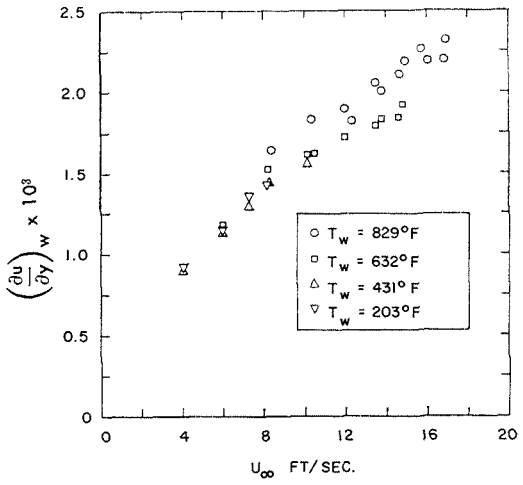

FIG. 8. Relation between velocity gradient at wall and free-stream velocity.

small Mach number adjacent to a heated plate.) This disagreement can be explained by the following reasoning, as discussed also in references 5 and 12.

If we observe the fact that the quenching effect of the plate on the flame is not a strong function of X, the distance from the leading edge, we may treat the quenching distance as independent of X. On the other hand, the thermal boundary layer is growing as flow moves downstream. As the burning velocity increases when the unburned mixture temperature increases, the peak of the burning-velocity profile will increase as the distance from the leading edge increases. Now, as the quenching distance is assumed to be constant and, as the peak of the burning-velocity profile increases with X, $(\partial u/\partial y)_w$ must be higher as the flame moves downstream with increasing U_∞, because the mixture-velocity profile is required to be tangent with the burning-velocity profile.

Another interesting fact also indicated in Fig. 8 is that at the same free-stream velocity, $(\partial u/\partial y)_w$ becomes smaller for a lower plate temperature (although this relationship is somewhat obscured by experimental error due to difficulty in controlling the mixture temperature). Again, the lower plate temperature causes a lower peak of the burning velocity and hence $(\partial u/\partial y)_w$ is smaller than that of a higher plate temperature case.

Conclusions

After an extensive investigation which includes careful control of instrumental and experimental error and elimination of any possible extraneous factors which might cause flame oscillations, it is concluded that the observed oscillation of a flame stabilized in a boundary layer next to a heated plate is an inherent characteristic of this type of flame stabilization.

The proposed mechanism of flame oscillation explains all the observed oscillation phenomena and characteristics. We have also given evidences to support the theory without contradiction.

The study of high-speed motion pictures showed that the advance speed is almost independent of the oscillation amplitude and increases as the plate temperature increases. The retreat speed is merely the "wash-away" speed and is nearly independent of the plate temperature. These facts give full support to the proposed theory, which therefore appears to be a sound one.

Using the proposed theory in interpreting the correlation of flame-holding characteristics, we found that, though our reasons for choosing the parameters are different from those of the previous investigators, our final result is quite similar.

Nomenclature

L	Top wall length
M	Mach number
R_δ	Reynolds number based on boundary layer thickness
R_x	Reynolds number of flame position based on X
T	Temperature
T_w	Temperature of the heated plate
T_∞	Free-stream mixture temperature in test section
U	Free-stream velocity
u	Stream velocity
U_∞	Undisturbed free-stream velocity
X	Linear distance from the leading edge of the heated plate
$X_{\min}$	Foremost position of the oscillating flame
$X_{\max}$	Farthermost position of the oscillating flame
δ	Boundary-layer thickness
y	Linear distance, normal to solid boundary
δ^*	Displacement thickness
Λ	Shape factor defined as $(\delta^2/\nu)(dU/dx)$
ν	Kinematic viscosity
α	Wave number, defined as $\alpha = 2\pi/\lambda$
λ	Wavelength of disturbance

ACKNOWLEDGMENTS

This study was sponsored by the National Science Foundation under grant numbers G–3274 and G–7039.

REFERENCES

1. GROSS, R. A.: Jet Propulsion *25*, 288 (1955).
2. HOTTEL, H. C., TOONG, T. Y., and MARTIN, J. J.: Jet Propulsion *27*, 28, 48 (1957).
3. ZIEMER, R. W. and CAMBEL, A. B.: Jet Propulsion *28*, 592 (1958).
4. TURCOTTE, D. L.: J. Aerospace Sci. *27*, 509 (1960).
5. WU, W. S.: Flame Stabilization and Propagation in Boundary Layer, Sc.D. Dissertation, M. E. Dept., Massachusetts Institute of Technology, Cambridge, Mass., May 1959.
6. SCHLICHTING, H. and ULRICH, A.: Zur Berechnung des Umschlages laminar-turbulent, Jahrbuch d. dt. Luftfahrtforschung, I, 8 (1942). (Memorial Lecture 1940 of the Lilienthalgesellschaft für Luftfahrtforschung, Flugzeugbau.) Complete text in Bericht S 10 of the Lilienthal-Gesellschaft.
7. LEES, L. and LIN, C. C.: Investigation of the Stability of the Laminary Boundary Layer in a Compressible Fluid, NACA Tech. Note 1115 (1946).
8. LEES, L.: The Stability of the Laminar Boundary Layer in a Compressible Flow, NACA Tech. Note 1360 (1947), and NACA Rep. No. 876 (1947).
9. DUMONT, L. B.: Flow Field in the Region of a Laminar Flame, M.I.T. unpublished note.
10. NIKURADSE, J.: Untersuchungen über die Strömungen des Wassers in konvergenten und divergenten Kanälen, Forschungsarbeiten des VDI, No. 289 (1929).
11. TOONG, T. Y.: Flame Stabilization in Boundary Layers, *Combustion and Propulsion, Third AGARD Colloquium*, p. 581. Pergamon Press, 1958.
12. TOONG, T. Y., KELLY, J. R., and WU, W. S.: This volume, p. 59.

FLAME PROPAGATION IN LAMINAR BOUNDARY LAYERS

1950 5

T. Y. TOONG, J. R. KELLY, AND W. S. WU

This paper presents the results of an experimental program aimed at providing a critical test of the equilibrium theory of flame stabilization in boundary layers previously proposed by the senior author. Using schlieren photography and a particle-track technique, the characteristics of a two-dimensional flame stabilized on a cylindrical rod and propagating into a laminar boundary layer adjacent to a flat plate are investigated.

The results presented include the velocity distribution of the unburned mixture in the free stream, the velocity profile in the boundary layer, and the experimental burning-velocity profiles for three different plate temperatures. The latter profiles are compared with the adiabatic profiles computed on the basis of a previous theoretical analysis, and the effect of quenching due to the presence of the flat plate is discussed.

The steps which lead to the experimental burning-velocity profiles are carefully examined and compared with available theoretical results. In each case the comparison adds weight to the experimental findings.

Finally, it is shown that the burning-velocity profiles are indeed affected by the growth of the thermal boundary layer when the flat plate is heated, and that these profiles assume shapes postulated in the theoretical study of the mechanism of flame stabilization. Quantitatively, the flame-holding characteristics of a smooth surface predicted by the use of these measured profiles agree with reported experimental results.

Introduction

In an earlier paper[1] by the senior author, a mechanism has been postulated for the stabilization of a flame in a laminar boundary layer of a steady stream of a combustible gas flowing over a smooth surface. In this case, the stabilization is realized when the tendency for the flame to propagate at the local burning velocity is in stable equilibrium with the fluid motion. Although there is good agreement between the flame-holding characteristics predicted by this theory and those measured in experiments,[2,3] a critical test of the validity of the postulated mechanism is still desirable. Such a test requires the knowledge of the variation of the burning velocity in the boundary layer. A program which includes both theoretical and experimental investigations was thus initiated to determine this burning-velocity profile.

The results obtained in the theoretical phase of this program have been reported.[4] They include two parts: The effects on the burning velocity of an adiabatic flame due to a change in the temperature of the unburned mixture, and the effects on the flame structure and the burning velocity due to quenching from a heat sink.

In the experimental program, the characteristics of a two-dimensional flame stabilized on a cylindrical rod and propagating into a laminar boundary layer adjacent to a flat plate[5] are now further investigated by using schlieren photography and a particle-track technique. The present paper presents the results obtained in this program, compares them with those obtained in the theoretical study, and further justifies the validity of the postulated mechanism of flame stabilization in boundary layers.

Experimental

Apparatus. A detailed description of the experimental apparatus and a discussion of experimental error have been given in Wu's thesis.[5] The test section of the combustion tunnel is 1 inch square and 4 inches long. A flat plate, which serves as one of the walls of the test section, is heated externally to a uniform temperature by 32 electrical heating elements. The temperature of the plate is measured by eight thermocouples embedded in it. A suction slot is provided in the plate just downstream of the entrance to the test section, and the plate is cooled upstream of this slot. Thus, both the velocity and thermal boundary layers begin to grow at the slot. The other three walls of the test section are transparent so that photographic techniques can be employed to study the flow field and the flame. The two side

78

walls of the tunnel are provided with air films to minimize three-dimensional effects.

The flame holder is a cylindrical nichrome rod, 0.061 inch in diameter, mounted in the central plane of the test section, parallel to the heated wall, and normal to the flow of a combustible mixture. This is heated electrically to ignite the mixture.

Test Conditions. A stoichiometric mixture of ethanol and air was used throughout the experiments, and all tests were conducted at atmospheric pressure. Results have been obtained for three conditions of the plate temperature for a mixture velocity of about 5.5 ft/sec at the entrance of the test section. The exact temperature conditions and entrance velocities are tabulated with the final burning-velocity profiles in Fig. 4. (It is to be noted that all photographs were taken immediately after ignition to minimize any effect on the initially uniform wall-temperature distribution due to the presence of the flame.)

Schlieren Photographs. Ideally, burning-velocity measurements should be made along the unburned boundary. Broeze[6] and Linnett,[7] among others, have pointed out the advantages of the use of a schlieren flame front for burning-velocity measurements. It is preferred because it represents the unburned boundary more closely than a visible flame front does. For this reason, schlieren photographs are used for this study.

Particle Track Technique. The velocity field upstream of the flame is determined by a particle-track technique. Particles of a diatomaceous earth (Johns-Manville Celite 502) of the order of 15 μ in diameter are dried, mechanically agitated, and injected into the combustible mixture upstream of the test section. As they pass through the test section, they are illuminated by intense stroboscopic light and photographed. The flash frequency is approximately 5000 per second with a duration of 2 μsec. The rate of travel of the slit of a focal-plane shutter is adjusted so as to follow the image of the particles across the film. In this manner, long tracks can be recorded without overexposure by the flame.

To facilitate measurements, the particle-track photograph is superimposed onto a simultaneous schlieren and direct photograph by matching the visible flame fronts. An example is shown in Fig. 1. The upstream and the downstream edges of the dark band in the photograph (barely discernible along the lower wing) represent, respectively, the schlieren and the visible flame fronts.

Discussion of Results

Detailed measurements have been made on 27 particle tracks and the results are typified by three tracks taken from Fig. 1. These tracks, labeled $P1$, $P2$ and $P3$, are shown in Fig. 2(a). The distance x is measured downstream from the plane of the stabilizer. Note that $P1$ always remains in the free stream and that $P3$ enters the boundary layer (as determined from schlieren photographs) far upstream of the stabilizer. The track labeled $P2$ is an intermediate track which enters the thermal boundary layer at x equals 0.6 inch. The interpretation of the particle behavior will be discussed below in two separate sections, depending on whether or not the particle remains outside of the boundary layer.

Free-Stream Velocity. Measurements on tracks

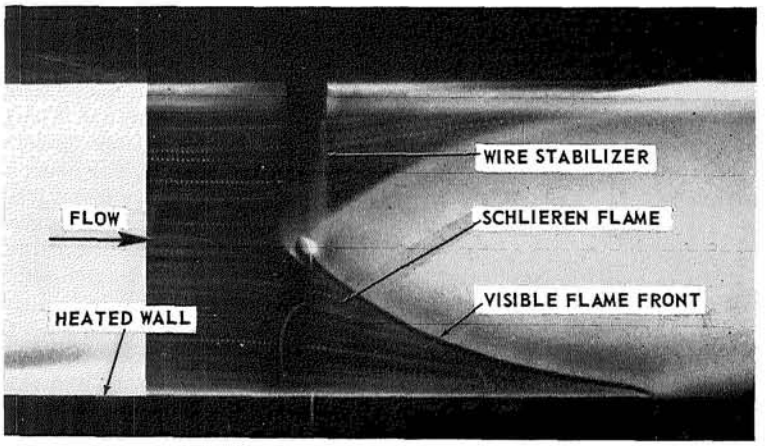

FIG. 1. Particle-track photograph of typical flame superimposed on simultaneous schlieren and direct photograph, T_w = 429°F, T_∞ = 130°F, u_0 = 5.97 ft/sec.

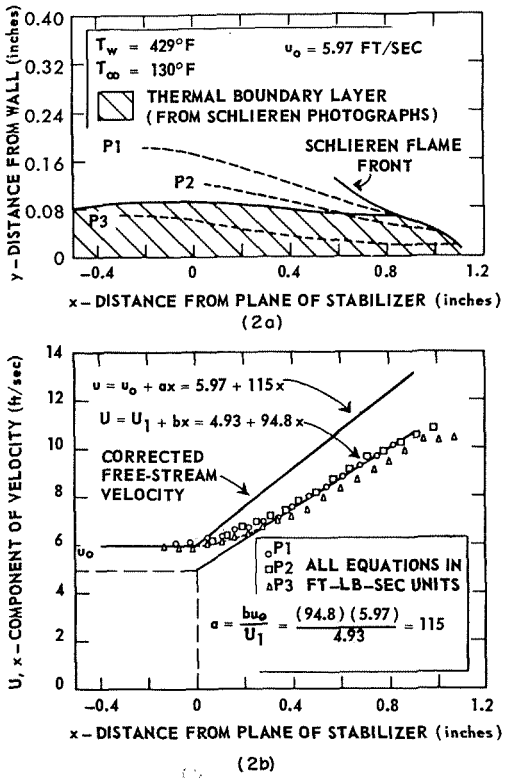

FIG. 2. Particle paths and velocity histories for three representative particles.

such as $P1$, which remain outside of the boundary layer, reveal that U, the x-component of particle velocity, is independent of y in the free stream except in a small region around the wire stabilizer. Upstream of the stabilizer, all particles in the free stream shown in a given photograph have equal and constant velocities, and their value, designated as u_0, should be very close to the stream velocity. Downstream thereof, the free stream accelerates due to flame spreading and the particles lag behind the stream due to their inertia. Adequate corrections must therefore be made to the measured particle velocities to obtain the stream velocities. In this region, since the x-component of the particle velocity is observed to be independent of y, Stokes' law can be used to find the x-component of the stream velocity.

Figure 2(b) shows a plot (versus x) of the x-component of the particle velocity for track $P1$. It is noted that the particle-speed gradient gradually increases until it approaches a constant value. This behavior is typical for all particles which remain in the free stream, unless they enter the flame before attaining the final gradient. According to Stokes' law, this finding suggests that u, the x-component of the free-stream velocity, should also have a constant gradient, upstream of the flame front and at a sufficiently large distance downstream of the flame holder. In other words, when x is large,

$$U = U_1 + bx \qquad \text{(for a particle)} \tag{1}$$

$$u = u_1 + ax \qquad \text{(for a fluid stream)} \tag{2}$$

By the use of Stokes' law:

$$U(dU/dx) = k(u - U) \tag{3}$$

It can further be shown that

$$\frac{u}{U} = \frac{u_1}{U_1} = \frac{b + k}{k} = \frac{a}{b} \tag{4}$$

Wu[5] has indeed found support for Eq. (2) by computation on the basis of the analysis of Williams *et al.*[8] In fact, he found that Eq. (2) is valid in the *entire* free-stream region downstream of the stabilizer, with u_1 equal to u_0, which is the stream velocity measured upstream of the stabilizer. Thus, for a given set of values of b and U_1 determined from a particle track such as $P1$, Eqs. (4) and (2) can be used to compute the values of a, k, and u.

That the above correction scheme is adequate for the determination of reliable stream velocities from particle behavior is further justified by the following facts:

1. The computed values of k correspond to particle equivalent diameters, which fall near the middle of the size distribution given by the manufacturer.
2. The values of a, computed from tracks such as $P1$ obtained in a given experiment, agree within 2% and their average is only 6% lower than the value computed by Wu.[5]
3. The measured response of a given particle agrees very well with that predicted on the basis of Stokes' law for a stream velocity distribution represented by Eq. (2). [A typical comparison is shown in Fig. 2(b), where the dashed curve represents the predicted response for track $P1$, which remains in the free stream.]

Boundary-Layer Velocity. The particle motion inside the boundary layer is very complex due to the presence of the opposing effects of flame spreading, which tends to increase the velocity, and of viscosity, which tends to decrease the velocity because the particles move closer to the wall as they move downstream. As the stream velocity in the boundary layer is undoubtedly dependent on both x and y, it would indeed be very difficult to compute the stream velocity by the use of Stokes' law on the basis of the particle

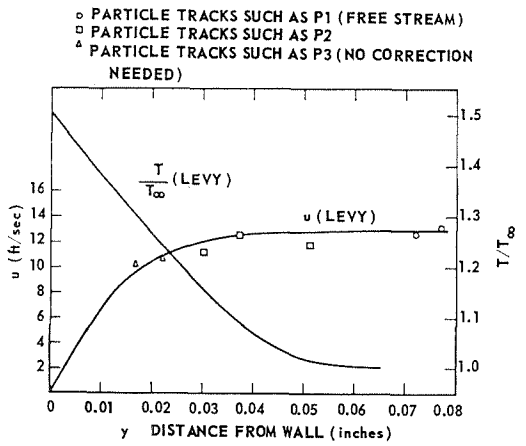

FIG. 3. Typical experimental velocity profile (corrected) at x equals 0.8 of an inch compared with a theoretical profile after Levy,[9] for T_w equals 429°F, and the Levy temperature profile.

behavior.* However, a somewhat crude (though quite reliable) correction scheme can be used to obtain the stream velocities by properly interpreting the particle behavior.

Several observations have been made to help formulate such a correction scheme. First, as illustrated by $P3$ in Fig. 2(b), particles can be found which eventually reach a constant velocity in the x-direction. It is reasonable to assume that for these particles, no correction is needed, and the measured particle velocity in the x-direction can be taken to be equal to the stream velocity in this direction. Secondly, for tracks like $P2$, the velocity gradient decreases after the particles get into the boundary layer. It is thus reasonable to expect that the correction needed here would be smaller than that required should the particles remain in the free stream. Thirdly, for tracks like $P2$, which enter the flame front at a small angle, the burning velocity is only weakly dependent on the stream speed and thus errors introduced in the correction scheme have very small effect on the final result.

The above observations indicate that much weight should be given to the velocities measured from tracks like $P3$ (which enter the flame front almost at its tip near the wall). This is further justified by Fig. 3, which shows a typical comparison of the boundary-layer velocities predicted by Levy's analysis[9] for the particular free-stream velocity distribution and those corrected from particle-track measurements. It is to be noted that points which represent particle tracks such as $P3$ do lie very close to the predicted curve.

The above observations also indicate that the correction scheme for tracks like $P2$ need not be elaborate and that the corrections needed should be smaller than that required if the particles had remained outside of the boundary layer. To the first approximation, it is assumed that the correction needed is proportional to the ratio of the normal distance (from the wall) of the particular particle under consideration to the corresponding velocity boundary-layer thickness. (In other words, the full free-stream correction would be made if the particle were at the outer edge of the boundary layer.) That this approximation is good is indicated in Fig. 3, which contains three such corrected points, denoted by squares. (Similar agreement is observed for other cases, for which Fig. 3 is an example.)

The above correction scheme for tracks like $P2$ can be used in the region upstream of the position where the boundary layer and the flame meet. ($x \approx 0.8$ of an inch, for the case shown in Fig. 2.) Downstream of this position, there is no longer an identifiable free stream. However, as the extent of this downstream region is rather small, very little error is introduced if the same correction scheme is extended thereto. Some assurance that this scheme is quite reliable is obtained when the corrected stream velocities at the schlieren flame front are found to lie on a smooth and well-behaved curve, which passes through points representing tracks like $P3$ (which do not require any velocity correction) and which is tangent to a curve representing the free-stream velocities at the flame front.

Burning-Velocity Profiles. The burning velocity, S_u, is determined as usual by finding the component of the mixture velocity which is normal to the chosen flame front. Let α be the angle between the x axis and a given particle path at the flame front; β, the angle between the x axis and the tangent to the flame front; and u_f, the x-component of the stream velocity at the flame

* To further complicate the particle motion, the reviewers have pointed out other possible effects, such as thermomechanical effect, Magnus effect, electrostatic effect on charged particles, and interaction between particle rotation and particle translation through variable drag. It would be interesting to carry out a detailed study of each of these effects. However, it is felt that these effects are rather unimportant in this study, because (*a*) none of the particles considered here comes closer than 25 diameters from the wall and thus the wall effect would be negligibly small at such a "large" distance, (*b*) the transverse velocity gradient which might lead to Magnus effect is small due to the low stream velocity used, and (*c*) the number of the particles used is extremely small and thus they are many diameters apart.

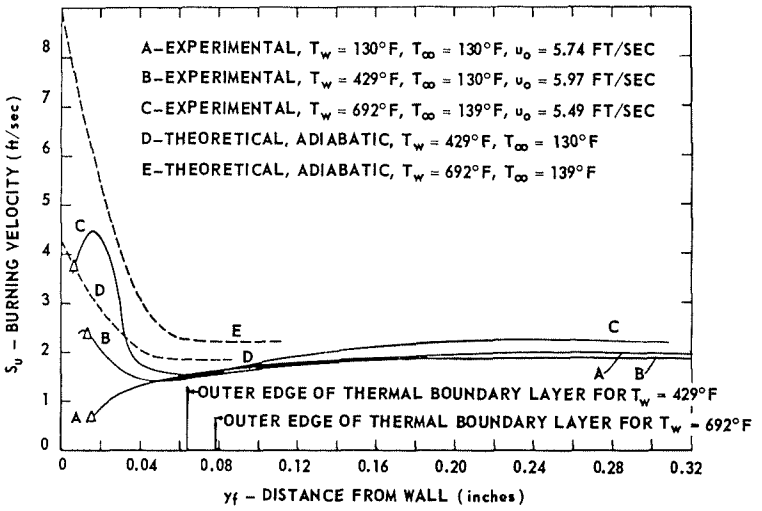

FIG. 4. Burning-velocity profiles for three different wall temperatures.

front. Then, the burning velocity is given by

$$S_u = u_f \frac{\sin(\beta - \alpha)}{\cos \alpha} \tag{5}$$

Corrections for the measured values of α are not deemed necessary for three reasons: (*a*) the particle tracks have very small curvature as they approach the flame; (*b*) only the smallest particles are used for the measurement of α; and (*c*) the quantity $\sin(\beta - \alpha)/\cos \alpha$ in Eq. (5) has a weak dependence on α because of its compensating effect in the numerator and the denominator. Therefore, small errors in measuring α have very small effect on the computed values of the burning velocity.

Curves A, B, and C in Fig. 4 are the burning-velocity profiles computed on the basis of the schlieren flame fronts for three values of the wall temperature. For curve A, the wall temperature, T_w, is equal to the mixture temperature at the entrance of the test section, T_∞. For curve B, derived from the photograph in Fig. 1, $T_w/T_\infty = 1.51$, and for curve C, $T_w/T_\infty = 1.92$.

As expected, the burning velocity at large distances from the wall is constant and agreement between the three curves is reasonably good. The free-stream temperature is slightly higher for curve C, and this is believed to account for part of the discrepancy. The burning velocity for all three curves begins to fall (due to quenching) at about y_f equals 0.22 of an inch, which is in good agreement with the quenching distance reported in the literature.

When $T_w = T_\infty$, the only effect which tends to change the burning velocity is due to quenching. As y_f decreases, the burning velocity falls more and more rapidly. However, when the wall is heated, the effect of increased unburned mixture temperature in the boundary layer tends to raise the burning velocity. The outer edges of the thermal boundary layers for T_w equal to 429°F and T_w equal to 692°F are shown in Fig. 4.† When the mixture temperature begins to rise with decreasing y_f, the effect of quenching at the flame is somewhat offset for some distance for curves B and C, and the burning velocity rises. As expected, the rise is steeper for curve C (higher wall temperature). This continues until the effect of quenching again dominates the behavior of the curves, and the burning velocity falls for $y_f < 0.013$ inch. For $y_f < 0.010$ inch, the schlieren flame front cannot be determined from the photographs of Fig. 1. Thus, the burning-velocity curve corresponding to this case (where T_w = 429°F) cannot be extended to this region. The curves for the other wall temperatures must be terminated for the same reason. Each of the three experimental curves A, B, and C in Fig. 4 is marked by one data point near the wall. These points, each from a particle track such as *P*3, represent the closest (to the wall) experimental measurement of velocity for each case. The

† It is to be noted that the quenching distance is greater than the observed thermal boundary-layer thickness upstream of the flame. Since the schlieren pictures do not show any density gradient in a region within the quenching distance but outside of the thermal boundary layer, one can conclude that the quenching effect does not take place upstream of the flame but rather takes place downstream of and/or along the flame.

shape of each curve for smaller values of y is based on extrapolated velocity profiles.

The behavior of curves B and C is consistent with the theoretical adiabatic profiles calculated by the method of reference (4) in conjunction with the Levy temperature profiles (Fig. 3). This is shown by curves D and E which describe the behavior of the calculated adiabatic burning velocity. Again note the steeper rise in the burning velocity with increasing wall temperature.

Conclusion

The measured burning-velocity profiles are indeed affected by the growth of the thermal boundary layer next to the heated plate, and they assume the shapes postulated in the theoretical study of the mechanism of flame stabilization.[1] The flame-holding characteristics of a smooth surface predicted by the use of the measured profiles also agree quite well with the experimental results reported.[3] The predicted values of the velocity gradient at the wall, at which equilibrium between the fluid motion and flame propagation is attained, are in order-of-magnitude agreement with the measured values. More accurate comparisons cannot be made, however, because the flow field for the case of a flame stabilized in a boundary layer differs from that considered in this report.

Acknowledgment

The work reported here was supported by a research grant (NSF–G7039) from the National Science Foundation.

References

1. Toong, T. Y.: *Combustion and Propulsion, Third AGARD Colloquium*, p. 581. Pergamon, 1958.
2. Ziemer, R. W. and Cambel, A. B.: Jet Propulsion, *28*, 592 (1958).
3. Wu, W. S. and Toong, T. Y.: This volume, p. 49.
4. Chen, T. N. and Toong, T Y.: Combustion and Flame, *4*, 313 (1960).
5. Wu, W. S.: Sc.D. thesis, Massachusetts Institute of Technology, 1959.
6. Broeze, J. J.: *Third Symposium on Combustion, Flame and Explosion Phenomena*, p. 146. Williams & Wilkins Co., Baltimore, 1949.
7. Linnett, J. W.: *Fourth Symposium (International) on Combustion*, p. 20. Williams & Wilkins Co., Baltimore, 1953.
8. Williams, G. C., Hottel, H. C., and Scurlock, A. C.: *Third Symposium on Combustion, Flame and Explosion Phenomena*, p. 21. Williams & Wilkins Co., Baltimore, 1949.
9. Levy, S.: J. Aero Sci., *21*, 459 (1954).

ON THE STRUCTURE OF PREMIXED AND DIFFUSION LAMINAR SPHERICO-SYMMETRICAL FLAMES

P. PÉREZ DEL NOTARIO AND C. SÁNCHEZ TARIFA

Premixed and diffusion laminar spherico-symmetrical flames are studied by means of a non-adiabatic model which considers variable temperature at infinity. The flame is supposed to be maintained by a porous sphere through which the gaseous mixture or one of the reactant gases is injected.

Stationary conditions are assumed and chemical kinetics of the process is approximated by means of an overall reaction rate.

Solution of the problem is achieved by means of an approximate analytical method. Flame temperature, mass flow per unit area at the flame surface, thickness and radius of the flame and temperature at the sphere surface are given as functions of the mass flow. The influence of the main parameters of the process: temperature at infinity, dimensionless ratio of the activation energy to the heat of reaction and sphere radius is also considered.

Some experimental results for diffusion flames are also given in the paper.

Introduction

The study of flames by means of spherico-symmetrical models presents several advantages in comparison with the studies performed by using one-dimensional models, especially for nonadiabatic cases.

Nonadiabatic conditions are natural in spherical flames owing to the heat transfer from the flame towards its surrounding atmosphere. On the contrary, nonadiabatic cases have to be introduced rather artificially in one-dimensional flames. Furthermore, truly one-dimensional flames are difficult to observe because of the lateral heat losses which cannot be avoided and because it is very difficult to produce a fluid motion absolutely perpendicular to the flame front.

A large number of studies have been performed on spherical flames in connection with droplet combustion. However, most of them referred to the diffusion flame of a fuel droplet burning in air, and such flames were studied disregarding chemical kinetics by assuming an infinitely fast reaction rate. There are a few studies on the decomposition spherical flame of monopropellant droplets[1,2] and on the combustion of fuel droplets considering finite chemical kinetics.[3,4]

On the contrary, there are very few studies on the theory of laminar spherical flames of the premixed type in which only gaseous species are involved in the process, and there are no studies, as far as we know, on diffusion spherical flames.

Spalding[5] has studied a premixed spherical flame in which the gases emerge from a point source. The study is restricted to the adiabatic case and the reaction rate is considered to be only a function of the temperature. Several analytical and analog solutions are given.[6,7]

Westenberg and Favin[8] have studied a premixed spherical laminar flame supported by a porous sphere. They studied only the adiabatic case and for a particular set of values of the principal parameters of the process.

The adiabatic case, in which the reaction products are supposed to extend indefinitely at the flame temperature, is the simplest one. Its interest lies in the possibility of comparing the results obtained with those of one-dimensional flames, but it seems very difficult to make an experimental model in which such conditions could be approximately reproduced.

At the Instituto Nacional de Técnica Aeronáutica, Madrid, Spain, a research program on spherical flames is being conducted and a résumé of the results so far obtained are given in this paper.

Such results have been published in full in ref. 9. The theoretical program comprises the general study of both premixed and diffusion flames, and the theoretical model of the process has been selected in such a form that their conditions can be experimentally reproduced. The mixture or one of the gases is assumed to emerge from a porous sphere, which prevents chemical reaction within it due to a quenching effect. The study includes the analysis of the influence of the main parameters of the process such as temperature at infinity, activation energy, heat of reaction, sphere diameter, etc.

The experimental program comprises the obser-

vation of diffusion and premixed butane-air and hydrogen-oxygen-nitrogen flames. Results for diffusion flames are given in the paper, as well as a qualitative comparison between theoretical and experimental results.

Fundamental Assumptions

The model of the process will be based on the following assumptions:

1. The flame is supposed to be maintained by a porous sphere through which the mixture or one of the gases is injected. It is assumed that chemical reaction does not take place within the sphere, and that chemical reaction goes to completion at infinity, where the temperature and composition of the atmosphere are given.

2. Stationary conditions will be considered, pressure will be taken constant and the process will be assumed to have spherical symmetry. Therefore, free convection effects are disregarded.

3. Only reactant species and reaction products will be considered. The influence of radicals is only exerted through the chemical kinetics of the process. This chemical kinetics will be approximated by means of an over-all reaction rate of any form, which may be deduced from the actual chemical kinetics of the process.[1,3]

4. The heat exchange through radiation between the hot gases and the porous sphere will be disregarded. For nonluminous flames this heat exchange is not important, and for luminous flames such exchange of radiant heat is small as compared to the heat transmitted through conduction, if the flame is close to the sphere surface.

On the other hand, the radiant heat exchange between the sphere at T_s and the surroundings at T_∞ will be taken into account.

5. Gases and their mixtures are assumed to be perfect gases. Mean values for the specific heats and thermal conductivities will be taken.

General Equations and Boundary Conditions

According to the foregoing assumptions the fundamental equations of the process and boundary conditions are as follows:

1. Continuity.

$$\frac{\dot{m}}{4\pi r^2}\frac{d\epsilon_i}{dr} = w_i \tag{1}$$

2. Energy.

$$\dot{m}\left[-(\epsilon_3 - \epsilon_{3s})q_r + \bar{c}_p(T - T_0) + \frac{4\pi r_s^2}{\dot{m}}\sigma(T_s^4 - T_\infty^4)e_s\right] - 4\pi r^2\bar{\lambda}\frac{dT}{dr} = 0 \tag{2}$$

3. Diffusion.

$$\sum_j \frac{Y_j}{M_j}\left[\frac{\dot{m}\bar{c}_p}{4\pi r^2\bar{\lambda}}\left(\frac{\epsilon_j}{Y_j} - \frac{\epsilon_i}{Y_i}\right)\mathfrak{L}_{ij} - \frac{1}{Y_i}\frac{dY_i}{dr} + \frac{1}{Y_j}\frac{dY_j}{dr}\right] = 0 \tag{3}$$

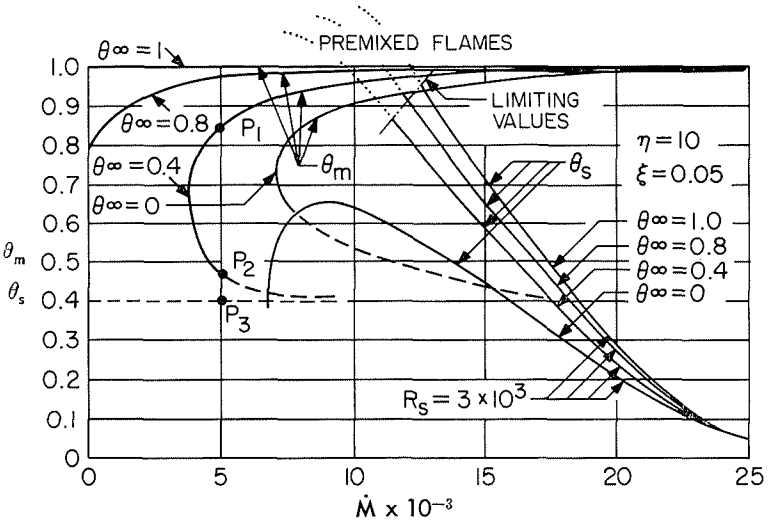

FIG. 1. Flame temperatures and temperatures at the sphere surface for premixed flames.

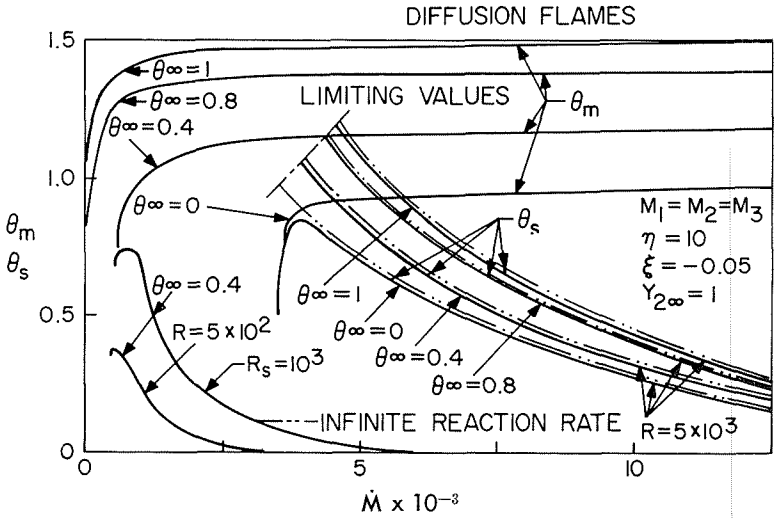

FIG. 2. Flame temperatures and temperatures at the sphere surface for diffusion flames.

4. Boundary conditions.

$$r = r_s \begin{cases} \epsilon_{1s} = 1 \\ \epsilon_{2s} = \epsilon_{3s} = 0 \end{cases}$$

$$r = \infty \begin{cases} T = T_\infty \\ Y_{1\infty} = 0 \rightarrow \epsilon_{1\infty} = 0 \\ Y_2 = Y_{2\infty} = 1 - Y_{3\infty} \end{cases} \qquad (4)$$

Solution of the system gives functions $\epsilon_i(r)$, $Y_i(r)$ and $T(r)$ for given values of the mass flow $\dot{m}$ and sphere radius r_s. An expression of the reaction rate w_i as a function of mass fractions and temperature should also be given.

Solution of the system is accomplished by means of an approximated analytical method which is developed in ref. 9.

Theoretical Results

Results are fully discussed in ref. 9. They have been obtained by taking a first order over-all reaction rate for premixed flames and a second order over-all reaction rate for diffusion flames. In the present work only some of the more significant results, especially in connection with experimental values, will be discussed.

Dimensionless maximum flame temperature θ_m and dimensionless temperature* at the sphere surface θ_s are represented in Figs. 1 and 2 for premixed and diffusion flames as functions of the dimensionless mass flow $\dot{M}$ for several values of the temperature at infinity θ_∞. It may be seen that flame temperatures depend considerably on mass flow and on θ_∞ at low values of $\dot{M}$ for both types of flames, but they do not depend on the sphere size.

For premixed flames, when $\dot{M}$ is large all curves tend towards $\theta_m = 1$, which is the temperature corresponding to the adiabatic case. On the other hand, for diffusion flames at large values of $\dot{M}$ all results tend towards those obtained by taking an infinitely fast reaction rate. This is the Burke and Schumann hypothesis for studying diffusion flames disregarding chemical kinetics, and in ref. 9 it is shown that such a hypothesis gives the asymptotic values of those obtained considering finite chemical kinetics.

When the temperature at infinity is small and in the region of small values of the mass flow three values of θ_m appear for each value of $\dot{M}$ in both types of flames. These values correspond to three mathematical solutions of the problem, such as P_1, P_2, P_3 (Fig. 1). The actual physical existence of solutions P_2 and P_3, which correspond to combustion processes taking place at low temperature through a wide reaction zone,[9] seems doubtful. Therefore, the results suggest that for nonadiabatic cases and when θ_∞ is small there exist minimum values of the mass flow under which combustion is not possible. This result is independent of the size of the sphere and the minimum value would also exist although the flame were originated from a point source.

Temperatures θ_s at the sphere surface are also shown for both types of flames in Figs. 1 and 2

* Temperatures θ_m and θ_s are practically proportional to actual temperatures T_m and T_s, because parameter ξ is usually very small (See Nomenclature and ref. 9).

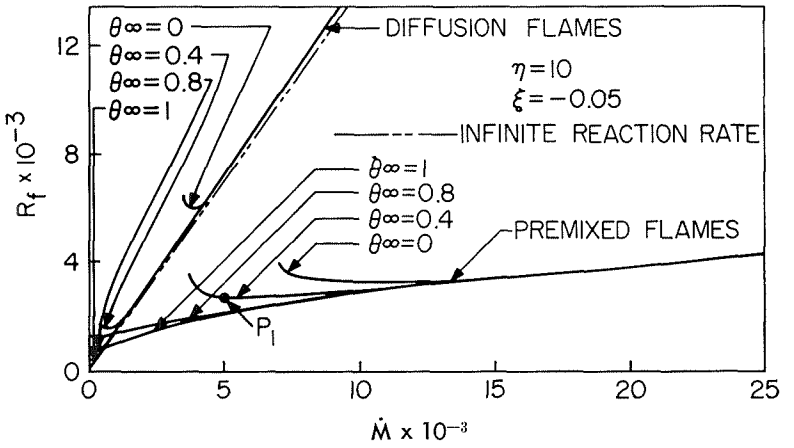

FIG. 3. Flame radius for premixed and diffusion flames.

as functions of the mass flow $\dot{M}$. These temperatures also depend on the sphere radius as shown in Fig. 2.

All curves $\theta_s = f(\dot{M})$ have a maximum value but in some curves the maximum does not appear because results are limited by the condition that the reaction zone must be located outside of the flame. Temperature θ_s increases rapidly until it reaches its maximum value and then it decreases slowly, tending towards zero.

Results for flame location are shown in Fig. 3. It may be seen that premixed flames are considerably closer to the sphere surface than diffusion flames.

Flame radius is practically independent of the sphere size, and its value decreases as the mass flow decreases. Therefore, for a given sphere radius there exists a minimum value of the mass flow under which the flame cannot be maintained, since the reaction zone should be located within the sphere. This minimum value is not related to the minimum value of the mass flow which was deduced from chemical kinetics considerations and it may have larger or smaller values depending on the sphere size and on the flame characteristics.

Experimental Results

An experimental investigation on diffusion and premixed spherical flames recently has been initiated. Diffusion flames have been studied by burning in air, butane gas, and hydrogen injected through different sized ceramic spheres.

Flames were not spherical due to free convection, except for very small values of the mass flow. Flame diameter was taken as the flame width measured at the mean horizontal plane of the sphere.

Flame temperatures and temperatures at the sphere surface were measured by means of small Pt-Pt-Rh thermocouples. These temperatures were corrected for radiation errors.

Flame temperature was taken as the maximum temperature at the aforementioned mean horizontal plane. This maximum value was obtained by displacing horizontally the thermocouple until a maximum temperature was reached. Temperatures at the sphere surface were measured at the same plane, inserting a half of the thermocouple bead within the sphere. These temperatures at the sphere surface were almost constant at different points on the lower hemisphere, but they were smaller at the upper hemisphere.

Experimental results are shown in Figs. 4 and 5. A good qualitative agreement between theoretical and experimental results could not be expected due to the disturbing influence of free convection.* However, the laws of variation of flame temperature and temperature at the sphere surface as functions of the mass flow are in excellent agreement with those predicted theoretically (curves $\theta_m = f(\dot{M})$ and $\theta_s = f(\dot{M})$ for $\theta_\infty = 0$ of Fig. 2). The influence of the sphere size on θ_s also agrees very well with the theoretical results (Figs. 2, 4, and 5).

In the region close to the minimum values of the mass flow the flame temperature was a function of the sphere radius. In such a region the flame is located very close to the sphere surface, and combustion might be altered by the proximity of the sphere, since part of the reaction zone should be located within the sphere. This effect might explain the discrepancy between theoretical

* In order to avoid free convection effects, combustion of air and oxygen within hydrogen[2] will be studied.

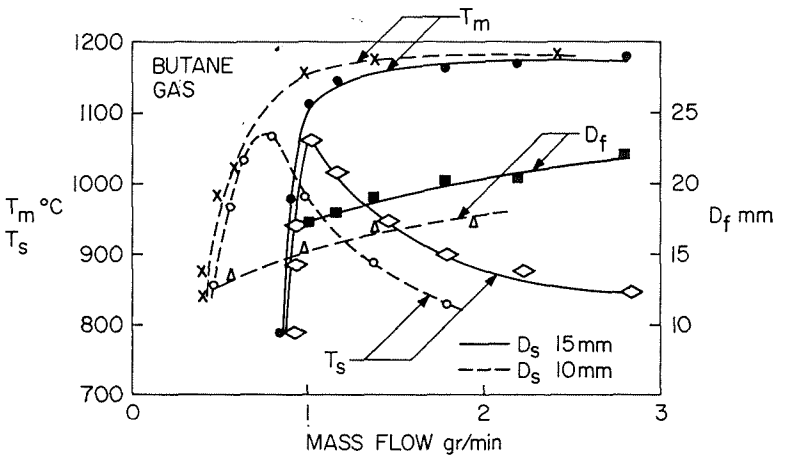

FIG. 4. Butane gas-air diffusion flame. Experimental results.

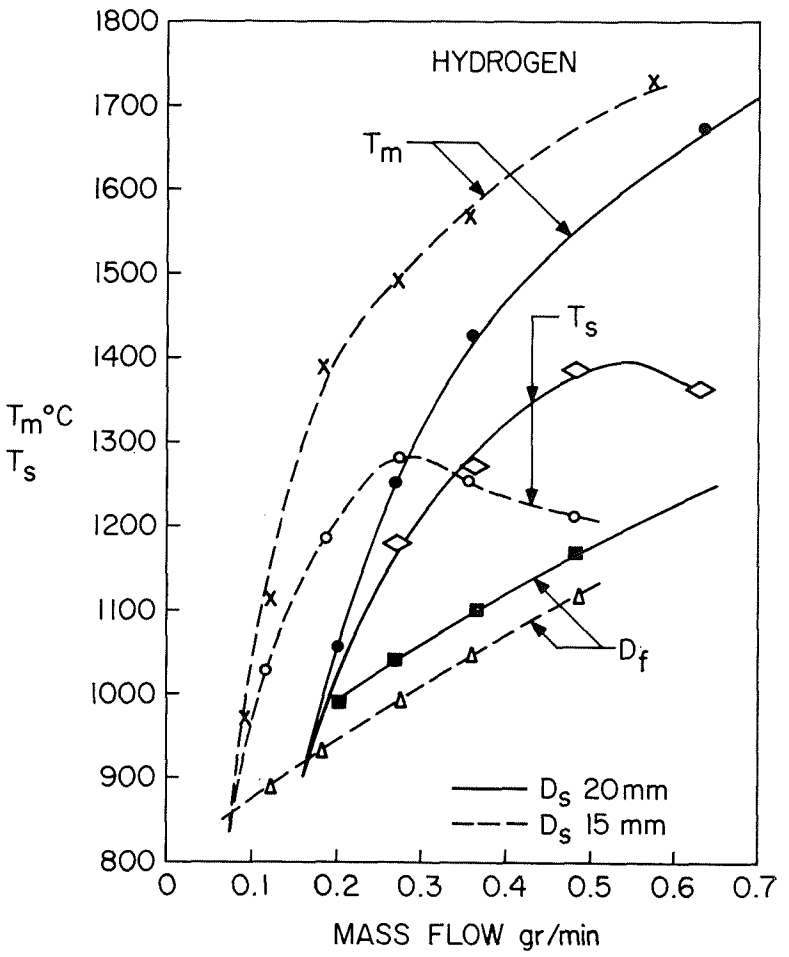

FIG. 5. Hydrogen-air diffusion flame. Experimental results.

and experimental results or else they might be produced by a free convection effect.

Finally, flame diameters increased with mass flow in a form similar to that obtained theoretically, but depending on the sphere radius. This result could be expected because the influence of free convection on such a variable is particularly important.

Nomenclature

$\bar{c}_p$	Average value of the specific heats for the mixture
D	Diameter
e_s	Sphere emissivity
$\dot{m}$	Mass flow injected through the sphere
M_j	Molecular weight
$\dot{M}$	Dimensionless mass flow
q_r	Heat of reaction
r	Radius
R	Dimensionless radius
T	Absolute temperature
w_i	Reaction rate
Y_i	Mass fraction
ϵ_i	Ratio of flux of mass of species i to total mass flow
$\bar{\lambda}$	Average value of thermal conductivities for the mixture
$\mathcal{L}_{ij}$	Lewis–Semenov number
θ	$(\bar{c}_p/q_r)\,T + \xi$, dimensionless temperature
ξ	$\frac{1}{q_r}\left[\frac{4\pi r_s^2}{\dot{m}}\sigma(T_s^4 - T_\infty^4)e_s - \bar{c}_p T_0\right]$, dimensionless parameter
η	Dimensionless ratio of the activation energy to the heat of reaction
σ	Stefan Boltzmann constant

Subscripts

i, j	Reactant species
1	Gaseous reactant from the porous sphere
2	Gaseous reactant surrounding the sphere
3	Reaction products
f	Flame front
s	On the sphere surface
∞	At infinity
m	Maximum value of temperature
0	Initial conditions of the gas injected through the sphere

Acknowledgment

The research reported in this document has been sponsored in part by the Office of Scientific Research, OAR through the European Office, Aerospace Research, United States Air Force.

References

1. Sánchez Tarifa, C. and Pérez del Notario, P.: Instituto Nacional de Técnica Aeronáutica. AFOSR TN 58–1038, 1958.
2. Sánchez Tarifa, C., Pérez del Notario, P., and García Moreno, F.: *Eighth Symposium (International) on Combustion*. Williams and Wilkins, 1962.
3. Sánchez Tarifa, C., Pérez del Notario, P., and García Moreno, F.: Instituto Nacional de Técnica Aeronáutica. AFOSR TN 62–25, 1961.
4. Sánchez Tarifa, C. and Pérez del Notario, P.: Instituto Nacional de Técnica Aeronáutica. AFOSR TN 59–975, 1960.
5. Spalding, D. B.: Combustion & Flame, *4*, 51 (1960).
6. Spalding, D. B. and Jain, V. R.: Combustion & Flame, *5*, 11 (1961).
7. Spalding, D. B., Jain, V. R., and Lamain, M. D.: Combustion & Flame, *5*, 19 (1961).
8. Westenberg, A. A. and Favin, S.: Combustion & Flame, *4*, 161 (1960).
9. Pérez del Notario, P. and Sánchez Tarifa, C.: Instituto Nacional de Técnica Aeronáutica. AFOSR Grant AF–EOAR 62–90, 1962.

Discussion

Dr. D. E. Rosner (*AeroChem Research Laboratories*): For the same reactant mass flow rate three distinct steady state solutions have been obtained. According to Professor Tarifa's comment, however, only one has any physical significance. In the theory of nonadiabatic reactors three distinct steady state solutions are frequently found, of which the two extreme ones represent systems which are statically stable (physically attainable) and the intermediate solution represents a system which is statically unstable (and therefore physically unattainable). In these cases the stable solution which is realized in practice depends upon the direction or method of attainment, and hysteresis effects are observed. Is it not possible that a similar situation exists for the laminar spherical flame system treated here? Could you elucidate the grounds on which you rule out the physical existence of two of the three steady state solutions?

Prof. C. S. Tarifa (*National Institute of Technological Aeronautics, Madrid*): I do agree with Dr. Rosner's comment regarding the stability of the intermediate solution. We studied such stability for

the case of the premixed spherical flame of a monopropellant droplet and we found that the flame was unstable.

Regarding the third solution, it corresponds to a theoretical combustion taking place at very low temperature (practically at ambient temperature) and through an extremely wide reaction zone. Flames of such type do not have physical existence. They have a mathematical existence due to the Arrhenius law which gives reaction rates different from zero for any value of the temperature.

DR. R. B. ROSENBERG (*Institute of Gas Technology*): The question of the existence of a maximum temperature in the flame holder has been raised. We have observed the same phenomenon in the study of a circular, porous plate flame holder. We measured temperatures both by use of thermocouples and the sodium line reversal technique. This temperature maximum apparently is indicative of the mechanism of flame stabilization on this type of flame holder.

A THEORETICAL STUDY OF SOME PROPERTIES OF LAMINAR STEADY STATE FLAMES AS A FUNCTION OF PROPERTIES OF THEIR CHEMICAL COMPONENTS

E. S. CAMPBELL, F. J. HEINEN, and L. M. SCHALIT

18507

This paper combines results of three different types of studies in an attempt to begin developing a mathematical and physical understanding of (1) how certain flame properties depend upon the characteristics of the flame gases, and (2) the significance of some approximations which have been introduced into flame theories. The types of studies are: (a) the construction of the functional form of the general asymptotic solutions to the hydrodynamic equations for laminar steady state flames as a function of the distance; (b) construction of different methods of solving the equation systems; (c) numerical studies of these equations for both hypothetical and real flames. The most important numerical sources of the ideas presented in this paper are four systems with the following kinetic schemes:

Scheme (A) (1) heat + X + A $\rightleftarrows$ B + X
(2) B + A $\rightleftarrows$ C + B + heat

Scheme (B) A simplification of the $H_2 - Br_2$ scheme:
(1) heat + X + A $\rightleftarrows$ 2B + X
(2) B + A $\rightleftarrows$ C + B + heat

Scheme (C) $H_2 - Br_2$ system

Scheme (D) $O_3 - O_2$ system*

The essential aspects of a "free radical" for flame kinetics are assumed to be: (1) In the presence of a free radical a chemical reaction can proceed with a comparatively low activation energy. (2) The formation of a free radical requires a comparatively high activation energy. (3) Radical recombination involves a comparatively low activation energy. In this sense, the species B carries out the function of a free radical for the hypothetical schemes A and B.

Finally, certain problems encountered in numerical integrations and comparative usefulness of some procedures are considered. Specific attention is devoted to the sensitivity of the calculation to starting values.

Form of the General Asymptotic Solution; the Significance of Eigenvalues

The flame equations and boundary conditions for a one-dimensional steady state flame proposed by Hirschfelder and Curtiss[1] will be used. In this model, the dependent variables are chosen as the temperature and a linearly independent set of mole fractions and fractional mass flow rates.

G_α The fractional mass flow rate for species $\alpha = m_\alpha n_\alpha v_\alpha / M$ (1a)

M The total mass flow rate $= \sum_\beta n_\beta m_\beta v_\beta$ (1b)

n_β The concentration of species β in g mole/cc (1c)

m_β The molecular weight of species β in g/g mole (1d)

v_β The velocity of species β with respect to a laboratory coordinate system in cm/sec (1e)

X_α The mole fraction of species α (2)

T The absolute temperature (3)

The independent variable is chosen as the

* There has been only a preliminary study of scheme B. The study of the ozone-oxygen system is in progress.

distance along the Z axis of a Cartesian coordinate system.

For brevity, let $\mathbf{u} = \langle u_1, \cdots, u_n \rangle$ denote an n-dimensional vector whose components are the set of dependent flame variables and F_j the Z derivative of u_j. The F_j are assumed to be independent of Z and to depend only upon $\mathbf{u}$, so that

$$du_j \mid dZ = F_j(\mathbf{u}). \tag{4}$$

These differential equations are to be solved for a domain (Z_c, ∞) subject to the boundary conditions:

Hot Boundary: An asymptotic approach to chemical, thermal and diffusion equilibrium as $Z \longrightarrow \infty$:

$$\lim_{Z\to\infty} F_j(\mathbf{u}) = 0. \tag{5a}$$

Cold Boundary (mathematical idealization of a flame holder at Z_c):

$G_\alpha(Z_c)$: specified by measurements on the premixed fuel gas

$$(dT/dZ)_{Z_c} > 0 \; * \tag{5b}$$

Thus the general solution at the hot boundary should be expected to contain L arbitrary parameters to permit one to fit the cold boundary values for the L linearly independent G_α. Due to the difficulty in developing solutions to differential equations whose boundary conditions are specified by Eq. (5a) for the improper point at infinity, it has been conventional to transform the independent variable from Z to one of the dependent flame variables. An appropriately scaled reduced temperature, t, has been found to be most suitable.[3a,b]

Then the equations are

$$du_j/dt = F_j/F_t \tag{6a}$$

$$t = (T - T_m)/T_m \tag{6b}$$

$$T_m = \lim_{Z\to\infty} T(Z) \tag{6c}\,\dagger$$

Since

$$\lim_{T\to T_m} F_T(\mathbf{u}) = 0,$$

T_m is a singular point of the system. Moreover, the simple requirement that the one-sided derivatives exist and are continuous at T_m, restricts the system to a single eigenvalue, the total mass flow rate, M.[4] For this reason, one can expect that the exact solution to the flame equations lies in this restricted class of solutions for the differential equations in t only when there is one linearly independent G_α. The mathematical details of the general solution required when there is more than one linearly independent G_α will be discussed elsewhere. Only those features pertinent to the eigenvalue discussion will be included here.

Consider a transformation, $w = f(Z)$ which carries the neighborhood of the point at infinity into the neighborhood of a finite point, w_0. Most $f(Z)$ give differential equations in w which do not have solutions of a simple form. A function which does give tractable equations is suggested by standard solutions to linear homogeneous equations subject to the boundary conditions of Eq. (5a):

$$w = \exp(\alpha Z), \alpha < 0$$

$$du_j/dw = F_j(\mathbf{u})/(\alpha w). \tag{7}$$

It can be shown[3c] that the equations in w can have solutions with finite limits for the derivatives as $w \longrightarrow 0$ only if α is a root of the characteristic equation,

$$\left| (\partial F_j/\partial u_k) - \alpha \delta_k{}^j \right| = 0$$

$$\delta_k{}^j = 0 \quad \text{if} \quad j \neq k, \; 1 \quad \text{if} \quad j = k. \tag{8}$$

Although, it has been found,[3c] that the w equations do not give as convenient single eigenvalue solutions as the t equations, they can be used to give general solutions of the form:

$$u_j(w) = \sum_{\mathbf{n}} d_j(\mathbf{n}) \prod_{j=1}^{c} (r_j{}^{n_j} w^{n_j \beta_j}) \tag{9a}$$

where

$$w = \exp(\alpha_1 Z) \tag{9b}$$

$$\beta_j = \alpha_j/\alpha_1 \tag{9c}$$

α_j: a negative root of Eq. (8) (9d)

c: number of negative roots of Eq. (8) (9e)

$\mathbf{n} = \langle n_1, \cdots, n_c \rangle$, a vector whose components are nonnegative integers (9f)

$d_j(\mathbf{n})$: constants determined uniquely by the form of the differential equations (9g)

$r_1, \cdots, r_c$: c arbitrary parameters (9h)

* These boundary conditions have been discussed from various points of view (see, e.g., refs. 1 and 2a). Whereas it has been asserted that the mole fractions are discontinuous at Z_c, the discontinuity must be physically negligible if the mathematical model is to be a good approximation to a physical flame. It is easy to prove rigorously that a discontinuity must exist for any flame with all unit Lewis numbers. This will be discussed in a subsequent article.

† This presupposes that T is a monotone-increasing function of Z. This appears to be true for simple flames in the absence of heat losses to the surroundings and radiation.

In all cases which have been studied, c, the number of negative roots of Eq. (8) has just been L, the number of linearly independent G_α. Since it has been proven that one r_j serves only as a scale factor in the distance Z, the remaining $(L - 1)r_j$ and M together form a set of L arbitrary parameters required for a general solution.

Significance of the Eigenvalues in the General Solution

Solutions With Fewer Than L Eigenvalues; Significance of M

It is desirable to determine when adequate approximations can be constructed without using all of the eigenvalues. Such approximations not only eliminate the work required to determine the eigenvalues, but also lead to some understanding of their role in the more general solution. The results of numerical studies on systems with kinetic schemes A, C, and D will be used for this purpose.

The kinetic steady state for a species α is defined by the condition,

$$R_{\alpha,c} = R_{\alpha,p} \tag{10}$$

where $R_{\alpha,c}$, $R_{\alpha,p}$ represent the rate of consumption and production of α, respectively. The relative deviation from the steady state,

$$d_\alpha = (R_{\alpha,c} - R_{\alpha,p})/R_{\alpha,c}, \tag{11a}$$

is a useful parameter for the study of free radical systems. Conventionally, the steady state approximation,

$$d_\alpha = 0, \tag{11b}$$

has been used as an algebraic equation to replace the differential equation for X_α. Even when this approximation is too crude, provided that d_α is not too large, it has been shown that the solution of the exact multi-eigenvalue problem can be replaced by the solution of a sequence of successive approximating equations. At each stage in the sequence, the pair of differential equations for each such G_α and X_α is replaced by an algebraic equation system. Whereas the differential equations presume that starting values for X_α and G_α are known, the algebraic equations do not require such starting values and it is therefore unnecessary to know an eigenvalue for such a G_α.*

* The mathematical formulation and the results of specific calculations are being submitted for publication elsewhere. The approximation may not be carried through an arbitrarily large number of successive levels. The convergence can be described as asymptotic in the sense that the error will increase if too many levels are used.

This conclusion has been tested by two types of checks in numerical studies of the free radical scheme (A) for which the two linearly independent G_α can be chosen as $G_{\text{fuel}} = G_{\text{A}}$ and $G_{\text{free radical}} = G_{\text{B}}$.

Check 1. The Taylor series expansion for single-eigenvalue solutions in t was constructed about the singularity at $t = 0 (T = T_m)$. When the solution was extended to all remaining T by the method of successive approximations, the values of the flame variables at the point of juncture of the two solution methods agreed to eight digits (within probable rounding error).

Check 2. The asymptotic convergence of the successive approximations was compared with multi-eigenvalue solutions described in Appendix I. In general, the two agreed within the expected error.

Thus, if there are L linearly independent G_α and N d_α which are not too large, only $(L - N)r_j$ are required for solution by the method of successive approximations. For this reason, it seems useful to think of M as that one of the L parameters which is to be used to adjust $G(Z_c)$ for one of the major fuel components.

Use of the r_j in More General Solutions

In order to understand the relation between the general solution (9) to the w equations and the single-eigenvalue solutions to the Eqs. (6) in t, note first that previous studies suggest that the general solution can be used only for a fraction of the flame. Therefore, the question about the relation between the two solutions becomes, "What is the difference between starting values predicted at some temperature, T_1, off the hot boundary?" The first point is that in those cases studied thus far, examination of the $d_j(\mathbf{n})$ of Eq. (9) has shown that the relative change in starting values for a component which approximately satisfies the steady state condition [Eq. (11b)], is at least an order or two of magnitude greater than the relative change for a component which does not.* The discrepancy in free radical values appears as follows. As previously noted under *Check 1*, for sufficiently small deviations, d_α, the values obtained from the method of successive approximations agree closely with those produced by the single eigenvalue Taylor Series expansions. The very fact that the successive approximation scheme is independent of input free radical values, suggests the result shown by calculations: With increasing d_α the scheme fails to converge* closer and closer to the hot bound-

* It is interesting to note that in the hot region of an O_2–O_3 flame, the single eigenvalue solution makes O_3 obey the steady state condition more closely than the free radical.

ary. Ultimately, it can no longer be used to extend the single eigenvalue series solution. Then the discrepancy between the starting values predicted by the single eigenvalue series and the correct solutions increases steadily with d_α.

The use of the r_j to provide the required changes in free radical starting values and the sensitivity of M to changes in the starting values (or, equivalently, to changes in the r_j) is to be discussed elsewhere.

Relation Between M and the Properties of the Fuel

Extensive studies of scheme (A) can be used as a test case to investigate the relation between M and the fuel properties. The numerical parameters used, the simplifying assumptions, and the form of the flame equations are summarized in ref. 5. For this discussion of kinetics and diffusion, the significant parameters are: the Lewis number for the pair (α, β),

$$\delta_{\alpha\beta} = (nCD_{\alpha\beta})/\lambda; \qquad (12a)$$

a function of M (and therefore an eigenvalue),*

$$\mu_2 = (m^2\lambda k_2')/(M^2C); \qquad (12b)$$

and

$$\omega = k_2'/k_1'; \qquad (12c)$$

where:

k_2' is any function of temperature which is a common multiplicative factor for the forward and reverse specific rates for reaction (2); (13a)

k_1' is defined for reaction (1) as k_2' is for reaction (2); (13b)

λ is the coefficient of thermal conductivity in cal deg^{-1} cm^{-1} sec^{-1}; (13c)

C is heat capacity in cal/g mole, assumed the same for all species; (13d)

m is the mass in g/g mole assumed the same for all species. (13e)

For simplicity, the pre-exponential factor for the specific rates has been chosen to be the same for forward and reverse reactions so that k_2' and k_1' are taken to be those pre-exponential factors.

* In this paper μ_2 is used in place of the parameter used by ref. 5: $\mu = \mu_2/\omega = (m^2\lambda k_1')/(M^2C)$. The use of μ_2 seems desirable since the flame properties are more strongly affected by the properties of the main combustion reaction than by those of the free radical reaction.

Furthermore, the temperature dependence of these factors has been assumed to be the same so that

$$\omega = k_2'/k_1' = \text{constant} \qquad (14)$$

Finally, $\lambda k_2'$ has been assumed to be constant so that μ_2 will be independent of temperature.

It is important to note that the equilibrium constants for reactions (1) and (2) of Scheme A are independent of ω and that an increase in ω corresponds to a proportional increase in both the forward and reverse specific rates of the main combustion reaction compared with those for the free radical reaction. As is to be expected, as the main combustion reaction becomes more rapid with respect to the free radical reaction, the latter becomes ever less able to follow the changes in concentration produced by the former and the deviation from the kinetic steady state increases. Thus, for qualitative extrapolation to other flame systems, an increase in ω is to be viewed as an increase in deviation from the kinetic steady state produced by increasing the main combustion rates compared with free radical rates.

Since the ratio of two Lewis numbers is just the ratio of the binary diffusion coefficients, the effect of changing the binary diffusion coefficients has been investigated by using three sets of Lewis numbers.

Set 1. All Lewis numbers equal one

$$\delta_{AB} = \delta_{BC} = \delta_{AC} = 1 \qquad (15)$$

Hirschfelder[6] has proven that the enthalpy per gram is constant throughout the flame $\leftrightarrow$ all Lewis numbers are unity.* Since this reduces the number of differential equations which must be integrated by providing an algebraic equation between the mole fractions and temperature, and since it simplifies the remaining equations, Spalding[7] has called this "normal diffusion."

Set 2. "Heavy free radicals."† The Lewis numbers involving the free radical, B, are taken to be smaller than δ_{AC}:

$$\delta_{AB} = \tfrac{1}{2}; \quad \delta_{BC} = \tfrac{2}{3}; \quad \delta_{AC} = 1. \qquad (16)$$

Set 3. "Light free radicals."† The Lewis numbers involving the free radical, B, are taken to be

* This proof makes the usual approximation of ignoring terms in kinetic energy in the equation of energy balance and also terms in thermal diffusion.

† Although these values for δ would not be expected for species with the same mass, it seemed desirable to ignore this inconsistency in order to make a test of diffusion using this simple equation system.

TABLE 1

The total mass flow rate as a function of ω and of the diffusion coefficients[a]

	$10^2[\mu_2(\omega)]^{-\frac{1}{2}} \sim M$			$[\mu_2(\omega = 1)/\mu_2(\omega)]^{\frac{1}{2}}$		
	Set 1	Set 2	Set 3	Set 1	Set 2	Set 3
1	1.4779	1.4761	1.4890	1.0000	1.0000	1.0000
20	1.4864	1.4776	1.6082	1.0058	1.0010	1.0800
50	1.4985	1.4783	1.7678	1.0139	1.0015	1.1872
100	1.5151	1.4788	1.9245	1.0252	1.0018	1.2924
300	1.5593	1.4812	1.9676	1.0550	1.0035	1.3214
600	1.5894	1.4813	—	1.0755	1.0036	—
1000	1.6054	—	—	1.0863	—	—

[a] For definition of ω, and Sets 1, 2, 3, see Eqs. (12c), (15), (16), and (17), respectively.

much greater than δ_{AC}:

$$\delta_{AB} = 20/3; \qquad \delta_{BC} = 10; \qquad \delta_{AC} = 1. \quad (17)$$

As a first step in interpreting the results given in Table 1, consider the steady state approximation. If the approximation were valid, then the parameter ω would not appear in the equation system and μ_2 would be the same for all ω:

$$M[C/(\lambda k_2' m^2)]^{\frac{1}{2}} = \mu_2^{-\frac{1}{2}} = \text{constant}. \quad (18)$$

Since μ_2 is the eigenvalue determined by the cold boundary value on G_A, the form of Eq. (18) shows that the effect of increasing ω [i.e., of increasing deviations from the steady state] is shown better by tabulating the value of $\mu_2^{-\frac{1}{2}} \sim M$ rather than M itself.

Furthermore, for the particular equilibrium constants chosen, the steady state is a fairly good approximation for $\omega = 1$($|\, d_B \,|$ is in general less than: set 1, 0.4%; set 2, 0.2%; set 3, 4%). Therefore, the ratios $[\mu_2(\omega = 1)/\mu_2(\omega)]^{\frac{1}{2}}$, have been included to show the relative change.

The following general observations can be made:

Obs. (1) Asymptotic approach of μ_2 to a limiting value. For each of the three sets of diffusion parameters used, as ω increases M increases from its steady state value and appears to approach a limiting value asymptotically. Table 2 compares these μ_2 with those obtained by Klein.[2a,8a,9] Klein's values are based on a neat parameter expansion in powers of ω. Unfortunately, lack of careful estimation of the limits of convergence of his expansion has led to the assumption that μ_2 continues to decrease with increasing ω. It is apparent that his values are good for $\omega \leq 100$ and subject to increasingly serious error for $\omega \geq 300$.

Obs. (2) Qualitative variations of $\mu_2^{-\frac{1}{2}}$ with binary diffusion coefficients. Consider a free radical which is formed in a reaction involving one of the fuel molecules. To begin the argument, suppose the steady state approximation [0 = net rate = (rate production − rate consumption)] were exact. Since as T increases, the fuel concentration will, in general, decrease* slowly compared with the increase in specific rate for free radical formation, one should expect the rate of free radical formation (and, therefore, the mole fraction) to rise to a maximum and decrease to its limit as the flame approaches the hot boundary. Diffusion will tend to introduce greater

TABLE 2

Comparison of values of $\mu_2(\omega) \times 10^{-3}$ [a]

ω	Klein	This study
1	4.5886	4.5783
20	4.5358	4.5260
50	4.4632	4.4535
100	4.3607	4.3561
300	3.9531	4.1130
600	2.7155	3.9583
1000	1.1229	3.8800

[a] For definition of $\mu_2(\omega)$ see Eq. (12b).

* Locally, a fuel mole fraction can increase. For example, for a hydrogen-bromine flame, diffusion causes X_{H_2} to pass through a maximum in the vicinity of the cold boundary.[4]

TABLE 3

Deviations from the kinetic steady state, d_B [a]

	$\omega = 1$		$\omega = 300$		$\omega = 1000$
$t \times 10$	Set 2	Set 3	Set 2	Set 3	Set 1
−0.06	$+5.33 \times 10^{-5}$	$+2.32 \times 10^{-4}$	$+1.70 \times 10^{-2}$	$+8.17 \times 10^{-2}$	$+8.22 \times 10^{-2}$
−1.03	$+9.39 \times 10^{-6}$	-1.17×10^{-3}	-2.90×10^{-2}	-3.08×10^{-1}	-1.91×10^{-1}
−1.51	-3.21×10^{-4}	-4.37×10^{-3}	-1.00×10^{-1}	-4.45×10^{-1}	-3.43×10^{-1}
−1.91	-5.94×10^{-4}	-6.55×10^{-3}	-1.42×10^{-1}	-4.78×10^{-1}	-4.14×10^{-1}
−2.55	-8.35×10^{-4}	-6.78×10^{-3}	-1.68×10^{-1}	-3.94×10^{-1}	-4.23×10^{-1}
−3.51	-3.61×10^{-4}	$+4.64 \times 10^{-2}$	-9.69×10^{-2}	-2.93×10^{-2}	-2.05×10^{-1}
−4.15	-6.04×10^{-4}	$+2.11 \times 10^{-2}$	$+2.24 \times 10^{-2}$	$+2.91 \times 10^{-1}$	$+6.09 \times 10^{-2}$
−4.79	$+2.01 \times 10^{-3}$	$+4.37 \times 10^{-2}$	$+1.93 \times 10^{-1}$	$+5.93 \times 10^{-1}$	$+3.72 \times 10^{-1}$
−6.07	$+5.77 \times 10^{-3}$	$+1.02 \times 10^{-1}$	$+6.23 \times 10^{-1}$	$+9.43 \times 10^{-1}$	$+8.69 \times 10^{-1}$
−7.51	$+1.20 \times 10^{-2}$	$+1.93 \times 10^{-1}$	$+9.69 \times 10^{-1}$	$+9.99 \times 10^{-1}$	$+9.99 \times 10^{-1}$
−8.23	$+1.45 \times 10^{-2}$	$+2.27 \times 10^{-1}$	$+9.99 \times 10^{-1}$	—	$+1.00 \times 10^{0}$
−8.47	$+1.36 \times 10^{-2}$	$+2.13 \times 10^{-1}$	$+1.00 \times 10^{0}$	—	$+1.00 \times 10^{0}$

[a] For definitions of d_B and t see Eqs. (11a), and (6b), respectively.

uniformity in the free radical concentration. This will lead to deviation from the steady state with a negative net rate near the hot and cold boundaries and a positive net rate at intermediate temperatures. Suppose the binary diffusion coefficients involving free radicals are increased (decreased) compared with the coefficients for other pairs of species. This increase (decrease) should lead toward greater (lesser) uniformity in free radical mole fraction and, therefore, to an increase (decrease) in deviation from the kinetic steady state. This is the result obtained by this and by other studies.[8c,11b]

The effect upon M of an increase in deviation from the kinetic steady state depends upon the kinetic scheme. In Observation (1), it has been seen that a variation in kinetic parameters to increase the deviation led to an increase in M. This suggests the result actually found: An increase (decrease) in the binary diffusion coefficients involving a free radical leads to an increase (decrease) in M. This is the qualitative variation predicted by Spalding[7a,10a] for certain rates and also by diffusional theories of flame propagation. Conversely, when Giddings and Hirschfelder studied first and second order chain breaking schemes,[8b,11] an increase (decrease) in deviation from the kinetic steady state led to a decrease (increase) in M. Moreover, these authors report a variation in M of two per cent and less with a twofold variation in diffusion coefficients. Table 3 shows a larger variation.

Obs. (3) Adequacy of the steady state approximation. For this model, the data of Table 1 show that the accuracy of the approximation $M \cong M$ (steady state) [i.e., $\mu_2^{-\frac{1}{2}} \cong \mu_2^{-\frac{1}{2}}$ (steady state)] improves as the binary diffusion coefficients involving the free radical B are decreased with respect to δ_{AC} and becomes increasingly poorer as they are increased.

Prediction of M

Spalding and Adler[7,10,12,13] have developed neat, simple methods for predicting flame speeds in certain cases. Their basic theory assumes that the reaction rate is an explicit function of temperature. This will be true if: (a) there are $(N + 2)$ chemical species present and N are free radicals, assumed to obey steady state conditions; (b) all Lewis numbers are unity. As noted following Eq. (15), in this case the equation (enthalpy/g = constant) gives the necessary additional equation relating the mole fractions. For this case of all Lewis numbers of unity, their theory gives a relation between the temperature centroid, τ_c and a parameter $\lambda_{\text{Spalding}}$.*

* In Eqs. (19) and (20), Spalding's symbolism has been altered to conform to that of this paper. His (k, H = heat released/g, $\dot{m}_A'''$ = rate of consumption of the fuel A in g/cc, G, λ, c) have been replaced by (λ, Q = heat released/g mole; R = rate of consumption of A in g mole/cc; M, $\lambda_{\text{Spalding}}$, $\hat{c}$). Also, factors which cancel in the numerator and denominator have been omitted.

TABLE 4

Prediction of M [a]

				$\lambda_{\text{Spalding}}$					
	τ_c			Set 1		Set 2		Set 3	
ω	Set 1	Set 2	Set 3	c	S	c	S	c	S
1	0.701	0.701	0.696	0.276	0.264	0.277	0.264	0.270	0.260
50	0.693	0.698	0.645	0.270	0.257	0.274	0.261	0.215	0.211
100	0.687	0.695	0.619	0.264	0.251	0.272	0.259	0.191	0.186
300	—	0.688	0.603	—	—	0.262	0.252	0.179	0.171
600	0.656	0.681	—	0.233	0.222	0.250	0.246	—	—

[a] τ_c, $\lambda_{\text{Spalding}}$, ω and Sets 1, 2, 3 are defined by Eqs. (19), (20), (12c), (15), (16), and (17), respectively. The letters c and S designate $\lambda_{\text{Spalding}}$ computed by Eq. (20) and by Spalding's centroid formula,[7,10] respectively.

$$\tau_c \equiv \left(\int_0^1 \tau\lambda R d\tau\right) \Big/ \left(\int_0^1 \lambda R d\tau\right) \quad (19a)$$

$$\tau = (T - T_u)/(T_b - T_u) \quad (19b)$$

T_b, T_u are the temperatures of burned and unburned gas, respectively; (19c)

λ is the coefficient of thermal conductivity; (19d)

R is the rate of consumption of one of the fuel species per unit volume.* (19e)

$$\lambda_{\text{Spalding}} = \left(Q \int_0^1 \lambda R d\tau\right) \Big/ (\hat{c}^2 M^2) \quad (20a)$$

$\hat{c}$ is specific heat in cal/g, assumed the same for all species. (20b)

Special models are used to extend their method to some cases with Lewis numbers different from unity.

The effect of the assumption of the kinetic steady state and of unit Lewis numbers has been discussed in the preceding section. Although in the absence of these assumptions, the reaction rate is not an explicit function of temperature, τ_c and $\lambda_{\text{Spalding}}$ have been computed *a posteriori* to check the relation between the two parameters as a function of deviation from the kinetic steady state and of the variation of the Lewis numbers. Since the flame of scheme (A) is not the same as any of the special models used, the value of $\lambda_{\text{Spalding}}$ computed from Spalding's original equation (based on equations for unit Lewis number for all species) has been included in Table 4, for comparison.

* See footnote at bottom of preceding page.

APPENDIX I

Multiple Eigenvalue Solutions

Consider the problem of continuing the integration starting at some reduced temperature, t_1, off the hot boundary, $t = 0$. When d_α is too small, standard methods of point-by-point integration fail due to subtraction in computing R_α[14,15] in the differential equation:

$$dG_\alpha/dt = (m_\alpha R_\alpha)/MF_t \quad (I.1a)$$

$$dt/dz = F_t \quad (I.1b)$$

where R_α is the rate of production of α in g mole/cc.

However, when d_α increases, standard methods can be applied provided *accurate* starting values are known. As noted in the section on use of r_j the starting values predicted by single eigenvalue solutions are much poorer for a component which approximately obeys a steady state condition than for one which does not. In favorable cases the values for the latter *may* be sufficiently accurate, or, one may be able to correct them (this was the case for scheme A). To show how the starting values can be determined for a species which does approximately follow the steady state condition, consider scheme A. Four differential equations in the fractional mass flow rates and mole fractions of the fuel A and of the free radical B had to be integrated as functions of temperature. In place of $X_B(t_1)$ and $G_B(t_1)$ as input, it seemed to be more convenient (*vide infra*) to use

$R_B(t_1)$ and $(dR_B/dt)_{t_1}$. The solution was determined iteratively in the following steps:

Step I. Estimate $R_B(t_1)$ and for this estimate determine an approximation for the $(dR_B/dt)_{t_1}$ required in integrating toward $t(Z_c)$ in the fashion described below.

As should be expected, the boundary condition $G_B(Z_c) = 0$ does not select a unique pair of starting values, $[R_B(t_1), (dR_B/dt)_{t_1}]$. Instead, there is an interval of possible values $R_B(t_1)$. For a given $R_B(t_1)$, an error in $(dR_B/dt)_{t_1}$ could be recognized as follows. All free radical flames which have been studied have had the same qualitative maxima and minima shown in Fig. 1.

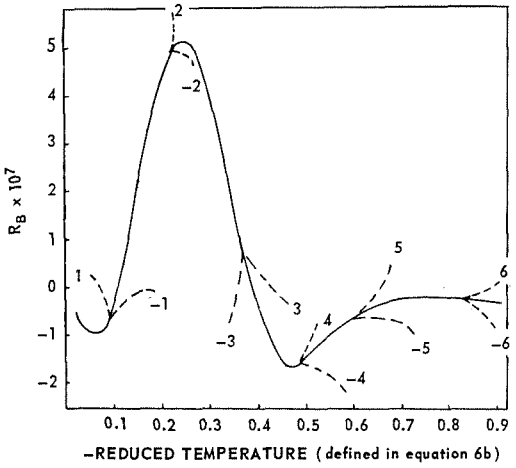

FIG. 1. Curves for the free radical reaction rate as a function of starting values.

Moreover, it was possible to estimate a curve from the steady state solution. Then, if $(dR_B/dt)_{t_1}$ < correct value (> correct value), R_B would diverge positively (negatively).* This made it possible to recognize an error without integrating to $t(Z_c)$.

Step II. For the same $R_B(t_1)$ determine an approximation for $(dR_B/dt)_{t_1}$ required in integrating toward the hot boundary. Use the sort of reasoning described in Step I.

Step III. If the two values for $(dR_B/dt)_{t_1}$ do not agree, use the sign of the discrepancy to determine whether $R_B(t_1)$ must be increased or decreased.

Repeat steps I, II for the new approximation to $R_B(t_1)$.

The validity of the solutions has been subjected to the following tests:

1. comparison with integrations using different interval sizes;

2. comparison with integrations using different methods involving different rounding and truncation errors;

3. comparison of integrations from t_1 to t_2 with reversed runs from t_2 to t_1;

4. comparisons with the method of successive approximations for that range of d_α for which both are applicable.

* These inequalities depend upon the fact that t decreases from t_1 to $t(Z_c)$.

ACKNOWLEDGMENTS

This research was supported by the Propulsion Research Division of the Air Force Office of Scientific Research under Contract AF 49(638)-169 with New York University.

REFERENCES

1. HIRSCHFELDER, J. O., CURTISS, C. F., and BIRD, R. B.: *Molecular Theory of Gases and Liquids*, pp. 698, 748–51, 765. John Wiley and Sons, New York, 1954.
2. KLEIN, G.: Phil. Trans. *249*, 389–415; (a) 396–7; (b) 407–8 (1957).
3. HIRSCHFELDER, J. O. and CAMPBELL, E. S.: Analytical Power Series Solutions to the Flame Equations, University of Wisconsin CM-784 (1953): (a) p. 50; (b) p. 96; (c) p. 37–8, 48.
4. CAMPBELL, E. S.: *Sixth Symposium on Combustion*, pp. 213–222, cf. pp. 219–20. Reinhold Publ. Corp., New York, 1956.
5. CAMPBELL, E. S., HIRSCHFELDER, J. O., and SCHALIT, L. M.: *Seventh Symposium on Combustion*, pp. 332–8. Butterworths Publ., London, 1959.
6. HIRSCHFELDER, J. O.: Phys. Fluids *3*, 109 (1960).
7. SPALDING, D. B.: Combustion and Flame *1*, 296–307, (a) p. 306 (1957).
8. GIDDINGS, J. C. and HIRSCHFELDER, J. O.: *Sixth Symposium on Combustion*, (a) pp. 210; (b) pp. 210–11; (c) pp. 204–5. Reinhold Publ. Corp., New York, 1957.
9. KLEIN, G.: A Simple Ideal Non-branching Chain Reaction Flame, University of Wisconsin, Report Squid 2, February, 1955, cf. p. 70, 88.
10. SPALDING, D. B.: Combustion and Flame *1*, 287–95, (a) pp. 293–4 (1957).
11. GIDDINGS, J. C. and HIRSCHFELDER, J. O.: J. Phys. Chem. *61*, 738–743 (1957); (a) pp. 738, 743; (b) pp. 740–2.
12. ADLER, J.: Combustion and Flame *3*, 389 (1959).
13. ADLER, J. and SPALDING, D. B.: Combustion and Flame *5*, 123 (1961).
14. CAMPBELL, E. S.: MTAC 11 (1957) 229–33.
15. CAMPBELL, E. S.: A Method for Integrating A Set of Ordinary Differential Equations Subject To A Type of Numerical Indeterminacy, University of Wisconsin Report CM-847, July, 1955, cf. Appendix A.

Discussion

PROF. J. F. WEHNER (*Johns Hopkins University*): The identification of the eigenvalues of a multiple reaction flame as mass fluxes of the independent species points to the possibility of a new basis for fundamental flammability limits. A limitation on the fluxes in the cold gases can be transformed into composition limits in these gases taking into account the discontinuity at the flameholder if necessary. This limit corresponds to the limit of flame propagation or as it is often described, the flammability limit.

Perturbation theory and the heat loss hypothesis can then be put aside as bases for fundamental limits. However, the heat loss hypothesis and convection effects may in some cases constitute practical limits of flame propagation.[1]

The composition eigenvalues need to be determined for a real flame. Professor Campbell's work[2] on the hydrogen-bromine flame suggests that the 50% mixture which he considered is not flammable. Calculations on the ozone flame show that it is a single eigenvalue problem for a composition observed to support a flame, although it has sufficient independent species to be a double eigenvalue problem.[3]

PROF. E. S. CAMPBELL (*New York University*): Professor Wehner's suggestion that the multi-eigenvalue solution should be used to investigate flammability limits would appear to be feasible for the simplest cases and should be pursued. This paper has discussed conditions under which a single eigenvalue solution is an adequate approximation to the solution of the exact multi-eigenvalue problem. With regard to the ozone-oxygen system, studies now in progress do not agree with some conclusions of the calculations he mentions and judgment should be held in temporary abeyance. The earlier hydrogen-bromine studies were, of course, restricted to single eigenvalue solutions. This system is sufficiently simple that it would be possible to study multi-eigenvalue solutions to test his suggestions.

REFERENCES

1. LEWIS, B. and VON ELBE, G.: *Combustion, Flames, and Explosions of Gases*, p. 310, 2nd edition. Academic Press, New York, 1961.
2. CAMPBELL, E. S.: *Sixth Symposium on Combustion*, p. 213. Reinhold, New York, 1957.
3. HIRSCHFELDER, J. O., CURTISS, C. F., and CAMPBELL, D. E.: *J. Phys. Chem. 57*, 403 (1953).

High Temperature Spectroscopy

Chairman: Dr. H. P. Broida (*U.S. Bureau of Standards*)

Vice Chairman: Dr. H. G. Wolfhard (*Reaction Motors*)

ABSORPTION SPECTRA AT HIGH TEMPERATURES. I. THE ULTRAVIOLET SPECTRA OF SHOCK-HEATED, *CIS*- AND *TRANS*-1,2-DICHLOROETHYLENE

S. H. BAUER, HELEN KIEFER, AND N. C. ROL

Absorption spectra were taken of *cis*- and *trans*-1,2-dichloroethylene between 37,000 cm^{-1} and 43,000 cm^{-1}, over the temperature range 800°–1055°K. These gases were highly diluted with argon (97%) and shock-heated. Photographic $[I_\tau(\lambda)]$ and oscilloscope $[I_{\lambda 2537}(t)]$ recordings were made with a resolution of 3–10 μsec.

A curve for the ground state electronic energy vs. torsional angle was plotted using the assigned torsional frequencies for the *cis*- and *trans*-forms, and an assumed barrier height of 62 kcal. The large shift toward longer wavelengths observed for the low frequency limits of the continua recorded for both compounds can be qualitatively accounted for as arising from population changes in the upper torsional vibration levels of the ground (N) electronic state. A theory is outlined for exploiting such data for the estimation of the shape of the upper (V) state as a function of the angle between the planes of the CClH planes.

Preliminary spectra taken by Dr. Carl Aten of benzene vapor and of perfluorobenzene from about 700° to 1900°K are also presented. For the latter compound the integrated absorption coefficients change with temperature, as predicted by Albrecht. However, for benzene, the coefficients show a very sharp increase at about 1100°K which cannot be accounted for in this way. This suggests that the B_{2u} state is perturbed by predissociation.

Introduction

As a consequence of the very rapid heating of a gaseous sample by a shock wave, a heating which is homogeneous and free from disturbing wall effects, it is possible to observe chemical changes in such a sample as they develop with time. Thus, one can study separately a sequence of steps, provided sufficiently rapid instrumentation is used. An interesting exploitation of this technique is the recording of molecular spectra of a gas at a temperature so high that under normal conditions the sample would decompose. It is now possible to record an absorption spectrum $[I_\tau(\lambda)/I_0(\lambda)]$ in about 5 μsec using a very intense short-duration flash (half-time, 2 μsec) triggered at a specified instant (τ) following passage of the shock. In contrast, pyrolysis and isomerization reactions at comparable temperatures require much longer periods before they progress to an appreciable extent.

There is a twofold need for these investigations. Since pyrolytic and combustion studies of necessity place materials at high temperatures at which the reaction times are of the order of milliseconds, both absorption and emission spectra must be used to identify the products formed and to measure the rates of attrition of the reactants. However, characteristic spectra change with temperature, often to an unpredictable extent. Second, very few molecular spectra have been recorded of samples at high temperatures, so

that there is little experimental basis for testing the few theoretical analyses which have been made of the dependence of molecular spectra on temperature.

This is a report on the high temperature ultraviolet absorption spectra of *cis*- and *trans*-1,2-dichloroethylene (between 37,000 cm^{-1} and 43,000 cm^{-1}) and of preliminary data on the spectrum of benzene. These substances were selected for our first studies because they show, respectively, large shifts in position of their UV bands and a large increase in the absorption coefficient with a rise in temperature.

Experimental Procedures and Results

Commercial samples of *cis*- and *trans*-1,2-dichloroethylene were purified by fractional distillation. The *trans*-isomer, as used in our experiments, had a boiling point range between 47.1° and 47.4°C at 745 mm Hg; the range of the *cis*-isomer was 59.9° to 60.3°C. Vapor-phase chromatograms at 36°C showed sharp peaks with very weak subsidiary peaks. We estimated that each sample contained no more than 1% of its isomer species and much less than that of any other impurity. The purified isomers were kept frozen at liquid nitrogen temperatures, and distilled, as needed, into a 12-liter flask where they were diluted with pure argon to a concentration of 3%. Sufficient time was allowed for complete mixing.

The experiments were performed in a $1\frac{1}{2}$ inch (I.D.) round shock tube. The driver section was 35.5 inches; the experimental section 127.8 inches long. Diaphragms were of 0.008 inch brass shimstock scribed to a depth of 0.0015 inches. The driver gas was helium, and pressure ratios across the diaphragm were of the order of 220 psi to 40 cm of the sample gas. Incident shocks were used exclusively. Shock arrival times at four stations were recorded with thin strip platinum resistance gauges on an oscilloscope raster; there was a slight attenuation in the shock speed. The temperatures and densities immediately behind the incident shocks were computed using one-dimensional ideal shock tube theory; allowance was made for the dependence of the heat capacity of the dichloroethylene on the temperature. It was assumed that the sample attained full vibrational equilibrium at the shock temperature but there was no chemical reaction.[1] Table 1 is a summary of shock conditions for those runs in which the complete spectrum was photographically recorded during the first 20–50 μsec after passage of the shock.

Two types of spectra were recorded. During the early experiments an intense mercury flash, of approximately 4 msec duration, was set off just prior to passage of the shock past the observation windows. A monochrometer, set on the Hg λ2537 line monitored the absorption of the gas as a function of time $[I_\lambda(t)/I_0]$. Typical oscillogram records for short and long sweep

TABLE 1

Summary of shock conditions

Run No.	Isomer	Shock speed (mm/μsec)	Initial pressure driven gas (mm Hg)	Incident shock temp. (°K)	Isomer conc. (moles/liter)
19	*Cis*	0.820	453	845	2.150×10^{-3}
21	*Cis*	0.841	332	875	1.527
22	*Cis*	0.892	255	950	1.170
23	*Cis*	0.958	205	1055	1.079
24	*Trans*	0.958	201	1055	1.069
25	*Trans*	0.892	259	950	1.207
26	*Trans*	0.826	343	855	1.684
27	*Trans*	0.910	259	980	1.348
28	*Trans*	0.910	259	980	1.348
29	*Cis*	0.910	259	980	1.333
30	*Cis*	0.802	407	820	1.913
31	*Trans*	0.805	405	825	1.933
32	*Trans*	0.865	323	910	1.611
33	*Cis*	0.859	323	905	1.633

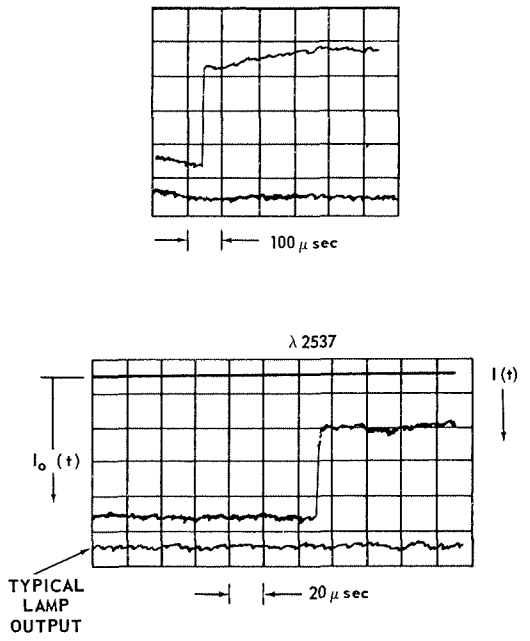

FIG. 1. Oscillograms for 3% *trans* in Ar; p_1 = 242 mm; T[shock (incident)] = 1085°K.

times are shown in Fig. 1. From these it is evident that the initial compression and heating brought about an appreciable increase in absorption at 2537 Å. This remained constant for a period which depended on the shock temperature. Eventually the gas decomposed (isomerization, dehydrohalogenation, and the formation of a variety of molecular fragments) so that an increase in absorption resulted. These oscillograms demonstrate, however, that there is sufficient time preceding the decomposition during which spectra of the heated original compound could be recorded. The magnitude of the initial jump immediately following passage of the shock was used to determine the absorption coefficient of the sample at λ 2537 for each of the shock temperatures. Seventeen such determinations were made. The corresponding points are plotted in Figs. 2 and 3. Note that $\epsilon = \log_{10}(I_0/I)/lc$ with l = 3.810 cm, and c is given in moles/liter. These values correlated well with the absorption coefficients determined photographically, and were included in the empirical extrapolations presented below.

The second set of spectra were taken with a short duration flash in argon (mean half-time 10 μsec) triggered to go off immediately after passage of the shock past the observation windows. The total light output was recorded photographically with a medium quartz Hilger spectrograph. It was demonstrated that the light output for a well-prepared, properly conditioned lamp was reproducible. On each plate seven additional discharges were recorded, in the absence of gas in the shock tube, through a set of neutral filters which had been previously calibrated and found to transmit 63.3, 57.5, 29.0, 13.6, 8.93, and 2.34% of the incident light. Eastman Kodak number O–III spectrographic plates were used.

Each of the eight strips on the plate was microphotometered. For closely spaced wavelengths a densitometric curve was plotted and the fraction

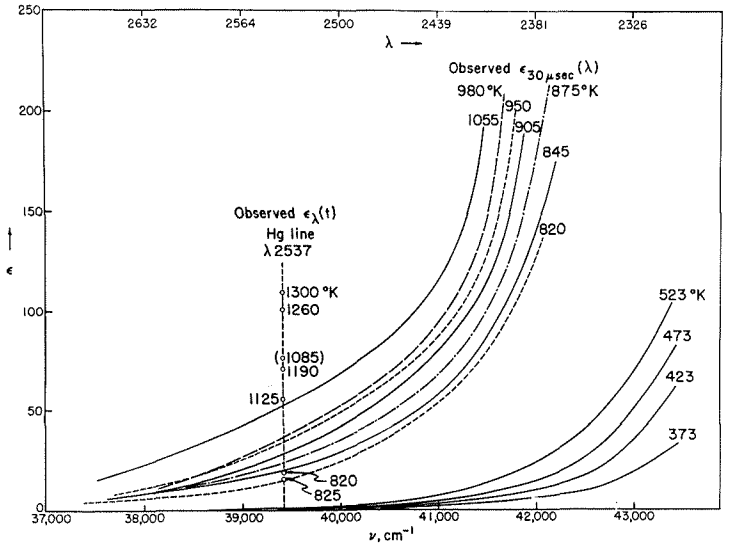

FIG. 2. Absorption coefficients as a function of the frequency for *cis*-1,2-dichloroethylene.

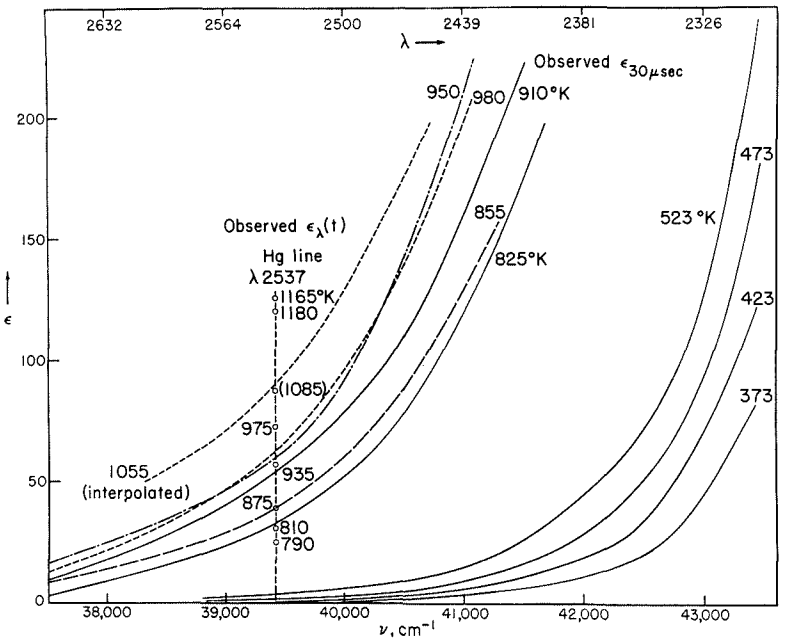

FIG. 3. Absorption coefficients as a function of the frequency for *trans*-1,2-dichloroethylene.

of light transmitted by the sample at each wavelength was deduced. The absorption coefficients as defined above were then computed and plotted as a function of frequency. These data, smoothed and combined with the low temperature data, are shown in Figs. 2 and 3. It was found empirically, both for the *cis*- and *trans*-isomers, that to a reasonable approximation the logarithm of the absorption coefficient versus the reciprocal of the temperature at a constant frequency gave a straight line. The arbitrarily chosen frequencies were, for the *cis*-compound: 38, 820, 39,420, and 41,150 cm^{-1}; for the *trans*-isomer: 38,820, 39,420, and 40,500 cm^{-1}. The degree of consistency may be judged from Fig. 4.

Theory—Background

For the dichloroethylenes at room temperature, the equilibrium constant for isomerization is[2,3]:

$$K_{eq}(300°K) = C_{trans}/C_{cis} = 0.647$$

At elevated temperatures the rate of isomerization increases to a measurable degree and the equilibrium constant approaches unity. The early kinetic studies[4] suggested that the isomerization occurs by a unimolecular process with an activation energy $E = 41.9$ kcal/mole, and $\log A = 12.7$. This parallels the conversion kinetics observed for a number of other *cis-trans*-isomerizations in which the proposed mechanism is the accumulation of sufficient torsional energy in the double bond, leading to large amplitudes of vibration, sufficient to overcome the barrier between these geometric isomers. However, it has recently been shown that for the 1,2-dichloroethylene the isomerization probably proceeds by a free-radical chain mechanism[5] with an activation energy 32 ± 2 kcal/mole. In addition to the *cis-trans*-isomerization, 1,2-dichloroethylene also dehydrohalogenates at sufficiently high temperatures.[6] Whatever the actual mechanisms for the thermal and photochemical isomerizations prove to be, in the present context the salient point is that interconversion would occur whenever the torsional amplitude exceeded some critical magnitude, had the free-radical processes not been rapid enough. An estimate of the activation energy for the unimolecular process is necessary so that we may sketch the shape of the ground state electronic energy as a function of the angle about the C═C bond.

The activation energies reported for *cis-trans*-isomerizations about ethylenic bonds range from 41.6 kcal/mole for methyl *cis*-cinnamate[7] to 61.3 kcal/mole for *cis*-1,1′-dideuteroethylene.[8] The most recent data for the gas phase butene-2 isomerization also give 62 kcal/mole[9,10,11] for the barrier height separating the *cis*- and *trans*-isomers. The minima of the valleys (at $\theta = 0$ and π) must be drawn in as parabolas with curvatures which match the torsional frequencies as

derived from infrared and raman data: 406 cm^{-1} for the *cis* and 227 cm^{-1} for the *trans*.[3] It is interesting to note that in butene-2, even though the reduced moment about the C═C axis is quite different from that in $C_2H_2Cl_2$, the corresponding frequencies are 402 cm^{-1} and 240 cm^{-1}.[12] For both species the force constant restraining deviations from planarity for the *cis*-configuration is almost twice that for *trans*-, in spite of the fact that *cis*-butene-2 is less stable than *trans*- by about $\frac{1}{2}$ kcal, whereas *cis*-dichloroethylene is more stable than *trans* by 445 kcal/mole. Clearly, a function of the form $\frac{1}{2}V_0(1 - \cos 2\theta)$ used for ethylene[13] cannot express these differences. Finally, if one assumes that the anharmonicity factors for the two isomers are comparable, he is forced to draw a smooth curve, as shown in Fig. 5, the maximum of which is somewhat closer to the *cis*-configuration.

The characteristic $\pi \longrightarrow \pi^*$ absorption by the double bond in ethylene has been studied both experimentally and theoretically. In recent papers on the vacuum ultraviolet absorption spectra of ethylene and fully deuterated ethylene[13] the total absorption was analyzed in terms of a superposition of a Rydberg sequence and a $V(^1B_{1u})$—$N(^1A_{1g})$ sequence of bands. The strong continuum and long wavelength toe ($l\lambda t$) appear to be an upper state progression of the C═C stretching vibration with a superposed structure due to the torsional oscillations about the C═C bond. The complete visible and ultraviolet spectra of the 1,2-dichloroethylenes were first reported in 1935[14]; maxima occur at 1850 Å for the *cis* and 1950 Å for the *trans*. Olson and Maroney[2] recorded the spectra of the chloroethylenes over the temperature range 373–523°K. It was suggested[14] that these absorptions resulted in C—Cl bond disruption. Wijnen[15] recently showed that in the photolysis of *cis*-1,2-dichloroethylene two primary photochemical steps occur, one of which produces Cl_2, and another HCl. However, Lacher *et al.*[16] argued that the initial absorption occurs to the excited V state. Indeed, further investigation may show that subsequent radiationless transitions to two unstable states produce the dissociation products cited. We shall assume that the absorption continuum as recorded in this experiment is due primarily to the $V \leftarrow N$ transition, with perhaps some $R \leftarrow N$ contribution.[17]

Interpretation of the High T Effect

It is proposed here that the excitation of one of the π electrons in the double bond leads to an excited state in which, in the most stable configuration, the two CHCl groups are oriented with their planes perpendicular to each other, as for ethylene; i.e., that the substitution of chlorine atoms does not markedly change the character of the $V \leftarrow N$ transition, although this substitution does shift the absorption peaks to longer wavelengths. The spectral shift is presumed to be due to a resonance between the π electrons in the double bond and the nonbonding d electrons of the chlorine atoms. The extension of the band system toward the visible in the form of a $l\lambda t$ is due to transitions from vibrationally excited levels of the ground electronic state. When the temperature of the sample is raised, the population of the higher torsional levels in the N state increases. Since high quantum numbers are reached the oscillators approach classical behavior, such that maxima in the probability distribution functions with angle appear at the corresponding classical maximum amplitudes. By the Franck-Condon condition, electronic transitions occur near the limiting angles given by the potential energy curves. Thus, the energy separation between the N and V states decreases (shift toward lower frequencies) for absorptions from the higher vibrational levels. A similar explanation was given by Potts[18] for the reduction of the intensity of the "shoulders" on the long wavelength end of the UV absorption spectra of several olefines when measurements were made at low temperatures in glasses.

As was indicated above, this is a highly simplified account, due to the possible presence of three complicating factors:

(a) The torsional motion is not fully separable from the CClH wagging modes.[3]

(b) There may be a small superposed continuum originating from the $R \leftarrow N$ transition, and additional perturbations due to possible predissociations.

(c) Only in zero order is it correct to factor the electronic and nuclear transition moments. In first order, the integrated absorption over an electronic band increases with rising temperature due to increased coupling between the electronic and nuclear wave functions, when the larger amplitudes of the latter introduce large distortions in the molecular framework.[19] Indeed, this is the basis for the large effect of temperature on the observed spectrum of benzene (see below).

To deduce the shape of the V curve as a function of the torsional angle from data such as that reported here, one must either correct the recorded spectrum for these contributions or select a region where these are minimal. We propose that at each temperature the very end of the $l\lambda t$ is such a region. Of course, the shape of the N curve must be given. Then, define the absorption

coefficient μ_ν,

$$\mu_\nu = 1/nl \ln I_0(\nu)/I(\nu) \qquad (1)$$

The coefficient is thus given in units of cm^2 per molecule, where n is the number of molecules per cm^3, and l is the path length in cm. The observed absorption coefficient is due to a superposition of a sequence of bands originating from a number of vibrational levels in the lower state. Designate the lower levels by α and the upper levels by i. One may therefore express the absorption coefficient at any specified frequency as a sum over transition probabilities and populations:

$$\mu_\nu = \sum_{i,\alpha} A_{i\alpha}(n_\alpha/n) f_{i\alpha}(\,|\,\nu_{i\alpha} - \nu\,|\,,\ \beta\cdots) \qquad (2)$$

The inherent transition probability $A_{i,\alpha}$ is an overlap integral over the vibrational wave functions as they depend on the torsional angle, for the lower and upper states (ψ_α, ψ_i); $A_{i,\alpha}$ is independent of the temperature. On the other hand, the population of the lower level, n_α, depends exponentially on the temperature. Now, the shape factor for the band, $f_{i\alpha}$, which is dependent on temperature due to the changes in the population among rotational levels associated with each of the vibrational states, is only weakly dependent, whereas the population ratio is given by a Boltzmann distribution:

$$n_\alpha/n = \exp(-\epsilon_\alpha/kT)/Q, \qquad (3)$$

where

$$\epsilon_\alpha = h\nu_0(\alpha + \tfrac{1}{2}) - h\nu_0 x(\alpha + \tfrac{1}{2})^2;$$
$$Q = \sum_\alpha \exp(-\epsilon_\alpha/kT)$$

and ν_0 is the fundamental torsional frequency.

The required overlap integrals have not yet been evaluated. When this is accomplished it will be possible to partition the observed coefficient among the contributing torsional levels, and then deduce the effect of temperature on the population of the uppermost detectable level. Qualitatively, if one assumes that at any specified temperature the $I\Delta t$ is essentially due to a single transition from the uppermost level in the N state, and that the V state has no θ dependence (flat), he finds that at about 900°K, $\alpha_{cis(\max)}$ is about 17 and $\alpha_{trans(\max)}$ is about 30. However, consideration of limits of detectability indicate that these maximal values should be about 10 and 18, respectively. In turn, this requires that the V curve fall with increasing θ as θ recedes from zero, and rise with increasing θ as it approaches π; i.e., V has maxima at $\theta = 0$ and π, in conformity with theory.[13]

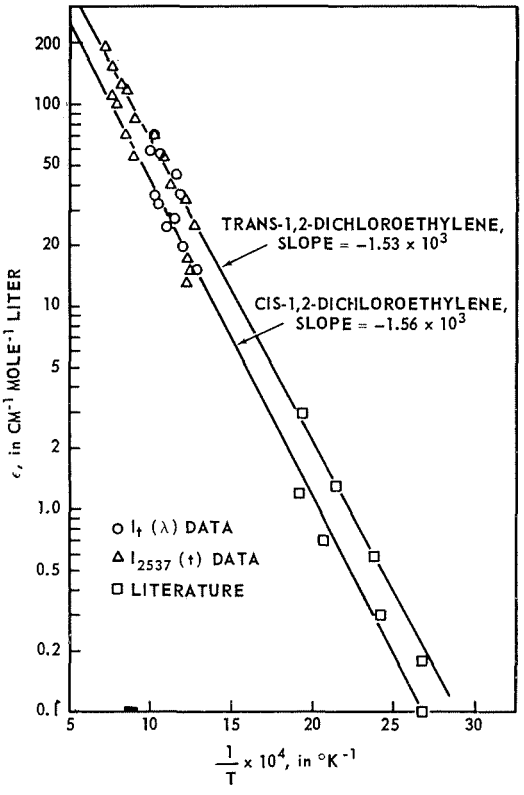

FIG. 4. Absorption coefficients as a function of $1/T$ (at ν = 39,420 cm^{-1}).

A satisfactory explanation for the linear relation observed between log ϵ_ν and $1/T$, has yet to be found. Indeed, it may be fortuitous that, in Eq. (2), the temperature dependence of the partition function, which appears in the denominator of n_α, and that of $f_{i\alpha}$ very nearly cancel for the few transitions which contribute appreciably to the absorption coefficient at a given ν. The sum over the Boltzmann factors of the adjacent n_α's will then show the simple exponential dependence of Fig. 4, with a slope roughly equal to $\langle\alpha\rangle h\nu_0/k$.

Preliminary Results on C_6H_6 and C_6F_6

Absorption spectra over the wavelength interval 2700–2100 Å of shock-heated benzene-argon and perfluorobenzene-argon mixtures (1.7–9%) were taken by Dr. Carl Aten. He used a slightly modified technique with which it was possible to check whether each shock was well formed, and to estimate precisely the interval in time after passage of the shock over which the absorption spectra were recorded. He also measured $I_{2537}(t)/I_{2537}{}^0$, and covered the temperature range

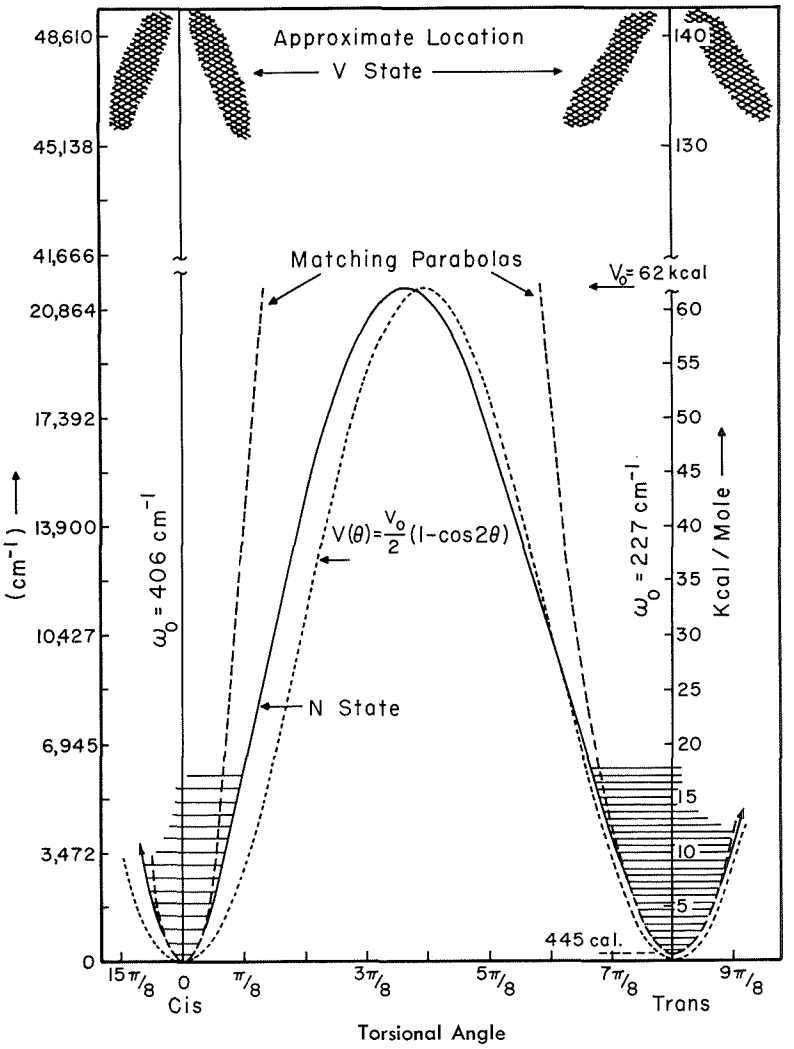

FIG. 5. Dependence of the electronic energy on the angle between the planes of the two CClH groups. The solid curve (N) was drawn to match the parabolas at $\theta = 0$ and α and to simulate a $(1 - \cos 2\theta)$ shape at its maximum. The latter was shifted slightly toward the *cis*-configuration to equalize the anharmonicity factors for the two forms. The approximate location of the V state is indicated by the hatched regions. It was deduced from a rough analysis of the location of the $l\lambda t$ and its shift with temperature. (The vibrational levels should be drawn as slowly converging.)

from about 600°K to 1900°K. Up to about 650°K, the general features of the benzene spectra agreed with previously published data.[20] The transition involved is $B_{2u} \leftarrow A_{1g}$ which is symmetry forbidden. However, nontotally symmetric vibrations in the ground state suitable perturb the electronic wave function to provide a small transition moment. As the temperature is slowly raised, the intensities of the bands originating in the ground vibrational levels steadily decrease whereas those which came from the first excited vibrational levels first increase and then decrease. On further increase of temperature the structure in the spectrum is lost and is replaced by a continuum.

At the higher temperatures (above 700°K) the integrated absorption coefficients as previously reported on the basis of measurements made

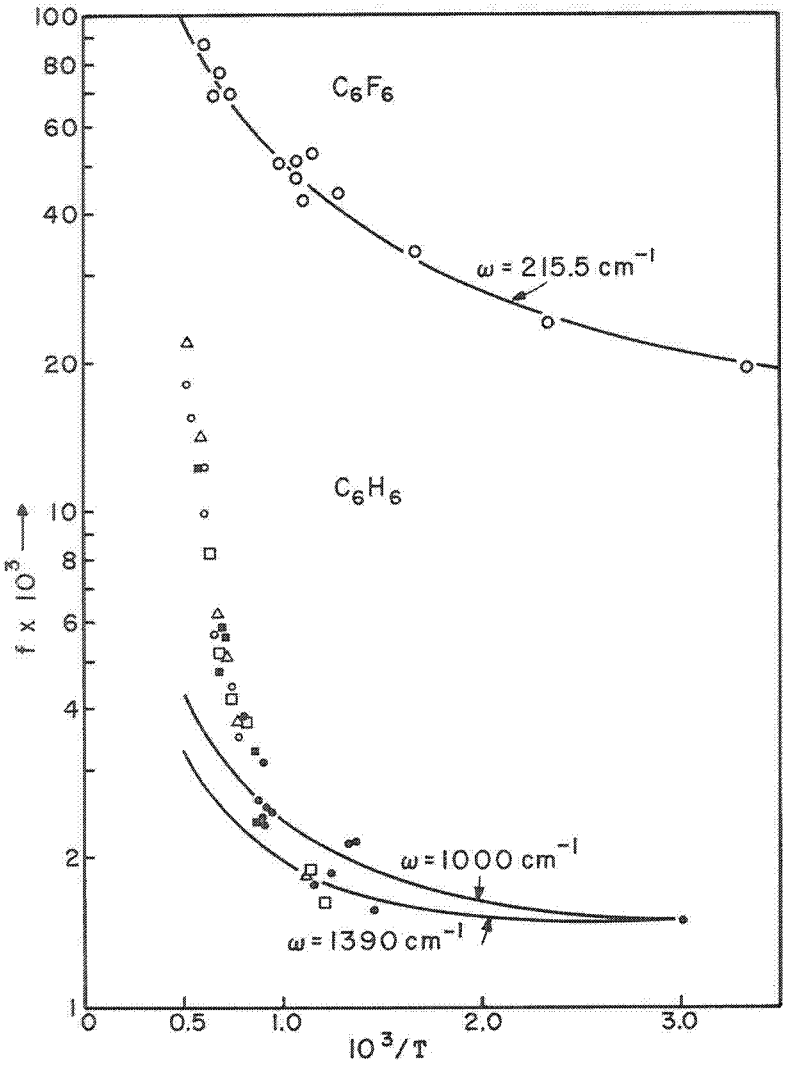

FIG. 6. Integrated absorption coefficients over the ${}^1B_{2u}$—${}^1A_{1g}$ bands for benzene and perfluorobenzene (Carl Aten). The curves were fitted to the function $f = f_0 \coth(\theta/2T)$ with $\theta = 1.439\alpha$, as indicated. For the benzene data: ●, as measured photometrically, from $I_T(\lambda)$ curves. ■, 8.8%, as measured photoelectrically. □, 5.0%, as measured photoelectrically. ○, 2.6%, as measured photoelectrically. △, 1.7%, as measured photoelectrically.

with the absorber flowing through a hot tube are many times those found by Dr. Aten, indicating that the benzene spectra were masked by decomposition products. At about 850°K another band began to overlap the high frequency end of the $B_{2u} \leftarrow A_{1g}$ transition. Presumably this was the $B_{1u} \leftarrow A_{1g}$ which is centered around 50,000 cm^{-1}. It is also forbidden and could be expected to show a temperature dependence similar to that of $B_{2u} \leftarrow A_{1g}$. To obtain the integrated coefficient for the latter, the upper integration limit was kept at 42,200 cm^{-1} in the hope that the mutual overlap of the toes will approximately cancel.

Data for C_6H_6 and C_6F_6 are summarized in Fig. 6 in which the integrated coefficients are plotted vs. $1/T$. The curves are "best fits" according to a relation derived by Albrecht.[19] Thus, were a single vibrational mode (ω) to provide the major contribution, then

$$f(T) = f_0 \coth(\theta/2T), \qquad (4)$$

where $\theta = 1.439\,\omega$. For C_6F_6, the reasonable frequency 215.5 cm^{-1} appears to be satisfactory; for C_6H_6 points up to 1100°K fall between $\omega = 1000$ cm^{-1} and 1390 cm^{-1}. Above that temperature the very sharp increase precludes a fit with any theory. It should be emphasized that the coefficients used were extrapolated to zero time, so that these are affected to a minimal extent by decomposition. The only explanation open at present is that, when the vibrational modes in the upper electronic state are highly excited, predissociation adds further perturbations and thus induces a higher transition moment.

Acknowledgments

We aknowledge with thanks the aid of Dr. Wing Tsang who helped in the recording of the data, and of several discussions with Dr. John Kiefer regarding the theoretical interpretations. This work was supported by the Department of the Air Force, Wright Air Development Center, under Contract No. AF33(616)-6694.

References

1. Fogg, P. G. and Lambert, J. D.: Proc. Roy. Soc. (London) *A232*, 537 (1955).
2. Olson, A. R. and Maroney, W.: J. Am. Chem. Soc. *56*, 1320 (1934).
3. Pitzer, K. S. and Hollenberg, J. L.: J. Am. Chem. Soc. *76*, 1493 (1954).
4. Jones, J. L. and Taylor, R. L.: J. Am. Chem. Soc. *62*, 3480 (1940).
5. Steel, C.: J. Phys. Chem. *64*, 1588 (1960).
6. Goodall, A. M. and Howlett, K. E.: J. Chem. Soc. *1956*, 2640.
7. Kistiakowsky, G. B. and Smith, W. R.: J. Am. Chem. Soc. *57*, 269 (1935).
8. Rabinovitch, B. S. *et al.*: J. Chem. Phys. *23*, 315, 2439 (1955).
9. Rabinovitch, B. S. and Michel, K. W.: J. Am. Chem. Soc. *81*, 5065 (1959).
10. Cundall, R. B. and Palmer, T. F.: Trans. Faraday Soc. *57*, 1936, 2226 (1961).
11. Lifshitz, Assa and Bauer, S. H.: unpublished shock tube data.
12. Kilpatrick, J. E. and Pitzer, K. S.: J. Research Natl. Bur. Standards *38*, 191 (1947).
13. (a) Wilkinson, P. G. and Milliken, R. S.: J. Chem. Phys. *23*, 1895 (1955); (b) Wilkinson, P. G.: Can. J. Phys. *34*, 643 (1956).
14. Mahncke, H. E. and Noyes, A. W., Jr.: J. Chem. Phys. *3*, 536 (1935).
15. Wijnen, M. H. J.: J. Am. Chem. Soc. *83*, 4109 (1961).
16. Lacher, J. R., Hummel, L. E., Bohmfolk, E. F. and Pork, J. D.: J. Am. Chem. Soc. *72*, 5486 (1950).
17. Walsh, A. D.: Trans. Faraday Soc. *41*, 35 (1945).
18. Potts, W. J., Jr.: J. Chem. Phys. *23*, 65 (1955).
19. Albrecht, A. C.: Cornell University, private communication.
20. Almasy, F. and Laemmel, H.: Helv. Chim. Acta. *34*, 462 (1951).

SPECTRA OF ALKALI METAL-ORGANIC HALIDE FLAMES

WILLIAM J. MILLER AND HOWARD B. PALMER

An experimental survey has been made of the emission from flames of a number of halides burning in potassium and sodium vapor. There appear to be no previous reports in the literature of emission from such flames, other than characteristic alkali metal atomic radiation. Results of the present study show that these flames emit, in addition to atomic line spectra, a complex array of molecular band spectra. A continuum is also observed in several of the flames. Interpretation of unusual C_2 excitation in haloform-K systems has produced added evidence for the importance of the reactions, $2CH \rightarrow C + CH_2$ and $C + CH \rightarrow C_2 + H$, as a mechanism for producing excited C_2. An analogous interpretation of the C_2 emission in CCl_4–K and –Na flames has yielded evidence supporting the value, $D_{C-Cl} = 51$ kcal, in the CCl radical. Energy transfer processes are important in these flame systems. Although there are several unanswered questions about the spectra, it is felt that these reaction systems may lend themselves to a useful study of electronic and vibrational energy transfer.

Introduction

The study of sodium diffusion flames, pursued over a period of about 15 years by Polanyi, Bawn, Warhurst, and others,[1,2,3] has received little attention recently. Notable exceptions are the papers by Reed and Rabinowitch.[4] These flames can be a means of preparing a wide variety of free radicals from the corresponding halides. With Tingey and Skell[5] we are undertaking studies of some reactions of radicals generated. The results of spectroscopic observations of light emission from flames of this type are reported here.

Surprisingly, the literature examined does not mention sodium diffusion flame luminescence other than characteristic atomic emission. Gaydon[6] summarizes the emission from flames of H and O atoms with several organic halides, noting for example that the $H + CCl_4$ flame produces bands of CH, C_2, CCl, C_3, and a violet continuum. This type of system represents the closest approach to the present work that has been discussed in the literature.

Apparatus and Method

The flames are inverted Polyanyi flames in the sense that halides are allowed to enter an atmosphere of alkali metal vapor (usually potassium). This arrangement is employed because most of the halides have been multiple halogenated and the inverted flame guarantees complete reaction.

The reaction vessel is a one-liter Pyrex bulb with a protuberance on the bottom for the metal bath, a sidearm with quartz window for spectroscopic observations, and inlet-outlet arrangements at the top. The vessel is completely enclosed in a furnace except for the sidearm and the top head. The latter is equipped with a water jacket and a glass wool trap to prevent metal vapor, metal halide, or carbon particles from entering the product-trapping portion of the flow system. Halides are carried (usually by an inert gas stream) through an inlet tube that ends in the center of the reaction chamber. With proper adjustment of furnace temperature, halide flow rate, and system pressure, an almost spherical flame (Fig. 1) of convenient size forms around

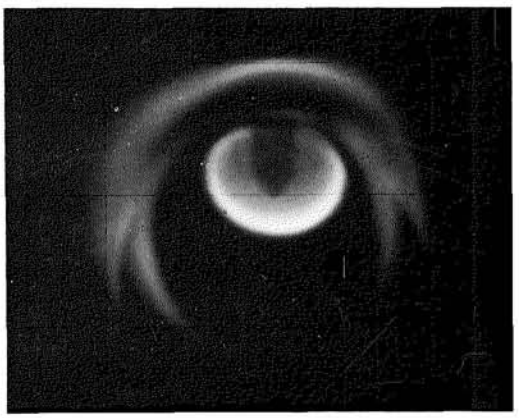

FIG. 1. Photograph of a diffusion flame of C_2Cl_4 burning in potassium vapor. Extraneous light is reflected from the wall of the viewing sidearm.

the inlet. Flames remain steady over periods of hours, with occasional attention.

A narrow thermocouple well runs through the reaction zone. Temperatures measured along the well reach steady values promptly, after reaction has begun. Spectra taken with and without the thermocouple well reveal no differences. The spectrograph employed is a Hilger E517/518 F/4 Raman instrument with quartz and glass optics. The spectra reported here have all been taken with glass optics, using Eastman Kodak Superpan Press or 103aF plates. For the present use as a survey instrument, the spectrograph has been adjusted so that the violet and red ends are in good focus, which means that the middle region is somewhat out of focus in all the plates. Wave lengths have been determined with the aid of Hg and Fe lines, measurements being made with a traveling microscope and a scanning-recording densitometer. Reaction product analyses are performed by standard gas-chromatographic methods.

The starting materials for the reactions have all been reasonably pure. These include K, Na, Cl_2, CF_4, CCl_4, C_2Cl_4, $CHCl_3$, $CHBr_3$, $CFCl_3$, CH_2Br_2, CH_3I, CH_3Cl, and CH_2CHCH_2Cl. The potassium seems always to be slightly contaminated with sodium, but this has not been a source of difficulty. The carrier gases have included He (99.99 per cent), N_2 (99.996 per cent), and Ar (99.998 per cent). When the halide is a liquid (e.g. CCl_4), a bubbler is used to introduce it into the carrier gas. Provision is made for adding carrier gas to the exit stream from the bubbler, to change the halide:carrier ratio. Typical ratios used have been 1:8. Most of the work has employed He as the carrier.

The pressure in the reaction system is controlled by the balance between gas admission rate and effective pumping speed, the former being regulated with a needle valve. Typical partial pressures of halide have been 200 to 400 microns Hg. Total pressures have ranged between a few hundred microns and several mm Hg. Potassium achieves a vapor pressure appropriate to these conditions at temperatures in the neighborhood of 350° to 400°C. Hence 400°C represents a characteristic vessel temperature.

Spectrograph slit widths used necessarily have been somewhat dependent upon the brightness of the flames. The range of slit widths is approximately 25 to 150 microns.

Experimental Results

Although product analysis shows that reaction occurs in all systems tried, singly- or doubly-halogenated compounds have not produced enough emission for the recording of spectra, even with a wide slit and an exposure of several hours. This group of (at most) weakly emitting systems includes CH_3I–K, CH_3Cl–K, CH_2Br_2–K, CH_2CHCH_2Cl–K, and, as an exception to the previous comment, CF_4–K. The systems that have yielded spectra include Cl_2–K, CCl_4–K, CCl_4–Na, C_2Cl_4–K, $CFCl_3$–K, $CHCl_3$–K, and $CHBr_3$–K.

Several of these spectra are shown in Figs. 2

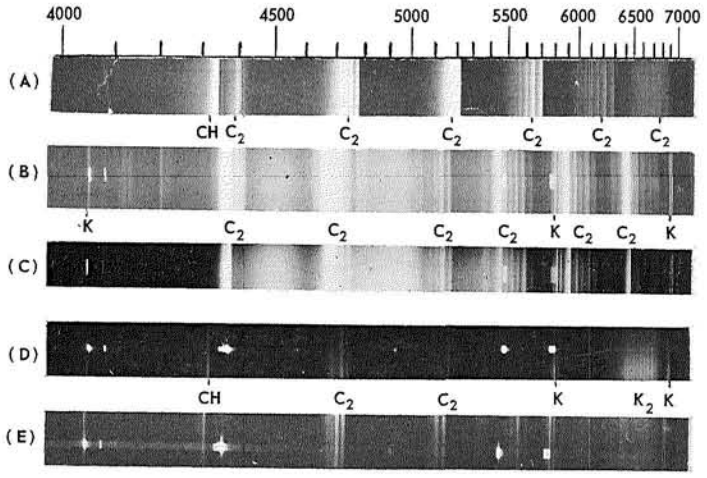

FIG. 2. Flame spectra. (A) Natural gas-air bunsen flame with added $CHCl_3$. (B) CCl_4–K, He carrier. CCl_4:K ratio 1:8; 50 μ slit, 75 min exposure. (C) $CFCl_3$–K, He carrier. $CFCl_3$:He ratio 1:8; 50 μ slit, 30 min exposure. (D) $CHCl_3$–K, He carrier. $CHCl_3$:He ratio 1:8; 75 μ slit, 240 min exposure. (E) CHB_3–K, He carrier. $CHBr_3$:He ratio 1:8; 75 μ slit, 240 min exposure.

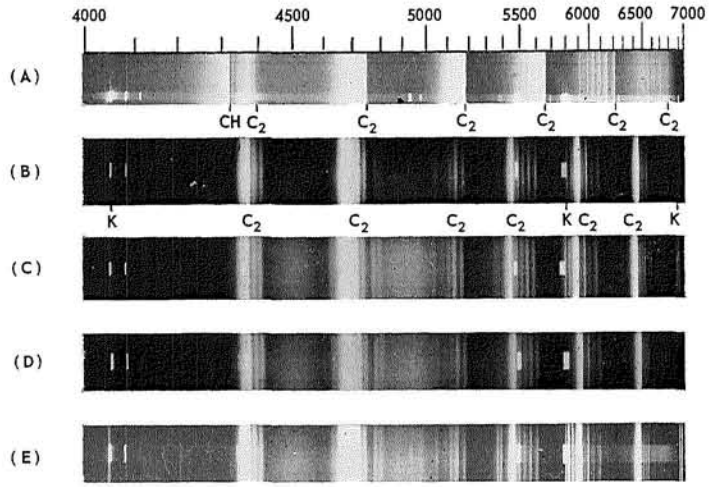

FIG. 3. Flame spectra. 50 μ slit in all cases. (A) Natural gas-air flame with added $CHCl_3$. (B) CCl_4–K, no carrier gas, 60 min exposure. (C) CCl_4–K, He carrier. CCl_4:He ratio 1:8; 75 min exposure. (D) CCl_4–K, N_2 carrier. CCl_4:N_2 ratio 1:2; 75 min exposure. (E) CCl_4–K, Ar carrier. CCl_4:Ar ratio 1:8; 75 min exposure.

and 3. The Cl_2–K spectrum is omitted because it shows only a weak continuum plus K atomic lines, while the C_2Cl_4–K spectrum, also omitted, shows a continuum with several intensity maxima, plus extremely weak K radiation. The C_2Cl_4–K continuum is identical to that in the $CFCl_3$–K spectrum. The CCl_4–Na spectrum also is not included because, with the exception of stronger Na lines, it is identical to the spectrum from CCl_4–K.

For comparison, a spectrum from a natural gas-air bunsen flame containing $CHCl_3$ is shown in Fig. 2. This shows C_2 Swan bands and CH bands that are characteristic of normal hydrocarbon-air flames. It is immediately obvious that the C_2 intensity distributions in all of the potassium diffusion flames are abnormal. They appear the more so when it is remarked that the temperature rise in the flames, as measured in the thermocouple well, is never more than 20° to 30°C. Even allowing for some thermal loss along the well, it is clear that these flames are very cool and the emission is, therefore, entirely chemiluminescent. The luminous zone temperature surely does not exceed 500°C in any of the flames.

Adiabatic flame temperature calculations for these reactions indicate that the low temperatures require incomplete reaction in the sense that there must be large radical concentrations present, and solid alkali halides and solid carbon must not be forming in the luminous zone, but rather later, in cooler regions or on the walls. Indeed, if solid carbon were forming, the calculations show that its formation would produce self-heating such that black-body radiation would be observed. Radical and alkali metal radiation losses may contribute to maintaining a low temperature. We have no quantitative information on this point.

Product analyses have been carried out for the reaction systems, CH_3I–K, CH_3Cl–K, and $CHCl_3$–K. In the first two, carbon is not formed and the only trapped product of any consequence is ethane. With $CHCl_3$, however, solid carbon is formed (but not in the luminous zone), and there is a wide distribution of trapped hydrocarbon products. The dominant one is C_2H_4; C_2H_2 and propylene are present in secondary quantity; and minor amounts of several other olefinic and saturated species are also captured. The prominence of C_2H_4 is at first surprising, and proves to be of help in postulating reactions responsible for the chemiluminescence.

Description of the Spectra

The main features of the spectra may be summed up as follows.

C_2: $CHCl_3$ in a bunsen flame gives well-defined Swan bands having a normal intensity distribution. $CHCl_3$–K and $CHBr_3$–K diffusion flames both give preferential excitation to $v' = 1$ and 2 of the upper state. $CFCl_3$–K gives preferential excitation to $v' = 6$ and 7. Weak transitions from $v' = 8$ are also observed. CCl_4–K and CCl_4–Na give identical intensity distributions, with preferential excitation generally found to $v' = 7$ and 8. The $\Delta v = 0$ bands appear weak relative to the others, particularly with $CFCl_3$ and CCl_4. Rota-

tional energy distribution appears to be broader in all cases than that in the bunsen flame.

C_3: Weak intensity maxima that are observed in the 3950–4100 Å region in CCl_4–K may be C_3.

CH: Weak 4312 Å (0, 0) radiation, plus some rotational fine structure, is observed in $CHCl_3$–K and $CHBr_3$–K.

K_2: There appears to be radiation in the near red system of K_2 in all cases (when K is used). The bands are clearest in $CHCl_3$–K, where they are not obscured by C_2. They are very weak in pure CCl_4–K (no carrier gas).

K: Lines are observed up to a K excitation level of about 32,000 cm^{-1}, or 91.5 kcal, in most spectra. The exception is C_2Cl_4–K, from which there is only a hint of K radiation.

Continua: Emission from C_2Cl_4–K appears to be almost entirely continuous (150 micron slit), with maxima at about 4100, 4500, 4900, 5400, and 5700 A. The identical continuum underlies the bands in $CFCl_3$–K and, less strongly, in CCl_4–K.

Unidentified bands: Several diffuse bands in the region between about 4050 and 4250 Å have not been adequately identified in CCl_4–K (or Na) spectra. An additional pair of unidentified bands occurs at 4780 and 4803 Å in CCl_4–K. The most important of the unidentified bands in the short wave length region lies at 4198 Å. It corresponds well with the (1, 2) band of the CN violet system, and there *is* a very diffuse band at about the right spot for the (0, 1) transition, but there is no other support for assigning it to CN. Two or three of the bands around 4100 to 4150 Å agree reasonably well with computations for the (7, 4), (8, 5), and (9, 6) transitions of the C_2 Swan system, but we are reluctant to make this assignment because the (6, 3) cannot be observed. No suggestions can be even tentatively put forward at this time for the 4780 and 4803 Å bands.

Carrier gas effects: The type of C_2 excitation is not affected by the nature or quantity of the carrier gas. Experiments are not exact enough to judge whether or not carrier gas affects the C_2 light yield. It is clear, however, that there are carrier gas effects upon the potassium radiation. In CCl_4-K systems, all of the K atomic lines are reduced markedly in intensity when N_2 is used as a carrier gas instead of He or Ar. K_2 is stronger when there is a carrier than when there is none. The nature of the carrier, i.e., noble gas or N_2, makes no obvious difference. K_2 seems relatively strongest in the haloform-K systems.

Discussion

It is interesting to find that the emission from Polanyi-type flames is much richer than the atomic radiation reported in earlier literature. One hopes to go further than this observation, seeking an explanation of the emission and perhaps gleaning from its features some significant information concerning molecular energetics. The C_2 excitation is the most obvious feature of special interest and will be dealt with first.

Since the excitation in haloform-K spectra (preferentially to $v' = 1$ and 2 of the $A\,^3\pi_g$ state) does not vary from $CHCl_3$ to $CHBr_3$, it may be concluded that the halogen plays no role in the excitation mechanism. Drawing upon the results for CCl_4, where the dilution ratio had no effect upon the preferred v' values, it seems quite certain that the excitation occurs directly as a result of a single elementary reaction step that does not involve a halogen. It would appear likely that the reaction involves CH. However, this probability must be reconciled with the prominence of C_2H_4 in the products.

Assuming that the most likely source of C_2H_4 is CH_2 radicals, we are led to the suggestion that CH_2 originates in the reaction, $2\,CH \rightarrow C + CH_2$. This is not a new suggestion. The reaction is exothermic and there are no spin conservation problems. We then examine the reaction, $C + CH \rightarrow C_2 + H$. If the C and CH have been thermalized by the time they collide, then this reaction will produce about 61 kcal, or about 21,300 cm^{-1}, of excess energy. If this energy all appears in the C_2 radical, it is almost exactly the right quantity to excite it to $v' = 1$ of the $A\,^3\pi_g$ state. Figure 4 is a semi-quantitative drawing of

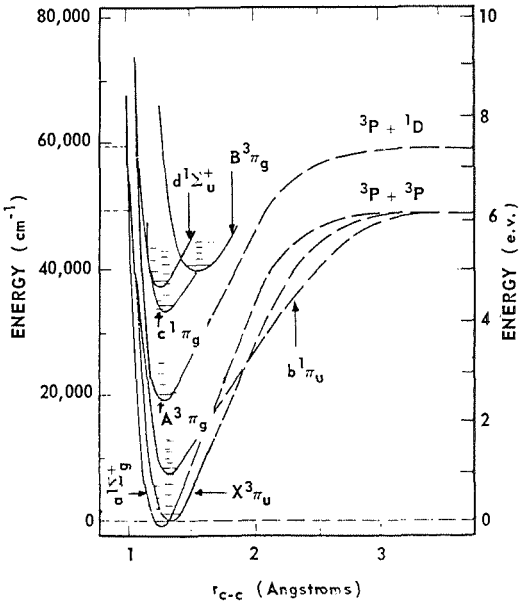

FIG. 4. Potential diagram of lower states of C_2. Notations on the several potentials follow Herzberg.[7]

the lower state potentials for C_2. It is taken largely from Herzberg,[7] but is revised to conform with the establishment of the $a\ ^1\Sigma_g^+$ state as the ground state by Ballik and Ramsay[8] and the correct value for the dissociation energy (141 ± 2 kcal) established by Inghram and co-workers.[9]

Although the H atom may carry off some of the reaction energy as translational energy, the agreement between the energetics of reaction and the observed C_2 excitation is rather striking, so we are satisfied that the explanation is essentially correct. One notes the implication that the reactions, $2\ CH \rightarrow C_2H_2$ and $2\ CH \rightarrow C_2 + H_2$, exothermic as they are, are both nonetheless much less probable than the disproportionation reaction forming C and CH_2.

In the CCl_4–K and Na reactions, excitation in a single reaction step is again indicated. Since the observed excitation in these two systems is the same, the step does not involve the alkali metal atom. By analogy to the probable event in haloform systems, let us examine the reaction, $C + CCl \rightarrow C_2 + Cl$. The observed excitation ($v' = 7$ and 8) corresponds to the range of energies, 30,700 to 32,100 cm^{-1}, or 87.7 to 91.8 kcal. Calling this 90 ± 2 kcal, and assuming that all of the excess energy from the reaction has gone into C_2 electronic-vibrational excitation, we compute $D_{C-Cl} = 51 \pm 2$ kcal in the CCl radical. Although there is no accepted value for D_{C-Cl} in CCl reported in the literature, 51 kcal happens to be the best estimated value, as quoted (from Gaydon) in the JANAF tables.[10] The present results appear to provide considerable support for this figure.

The C_2 excitation in $CFCl_3$–K is so like that from CCl_4 that no real distinction appears possible. Actually, the excitation mechanism discussed would predict the same preferential excitation as found in CCl_4–K. The reason is that the reaction step, $C + CF \rightarrow C_2 + F$, is only 27 kcal exothermic,[10] so this will not contribute to peculiar Swan band intensities. This also explains why one does not observe emission from CF_4–K. One does expect, however, that the reaction, $CFCl_3 + K \rightarrow CCl_3 + KF$, which is some 12 kcal exothermic,[11] will occur readily with a low activation energy, along with $CFCl_3 + K \rightarrow CFCl_2 + KCl$. Moreover, we estimate the reaction, $CFCl_2 + K \rightarrow CCl_2 + KF$, to be about 23 kcal exothermic, so it also should take place easily. The end result is that CCl radicals will be produced in quantity, hence the same excitation mechanism can operate as in CCl_4.

With large production of CCl_2 radicals from CCl_4 and CCl_3F, it is not surprising that a part of the emission (*viz.*, the continuum) from these is the same as that from C_2Cl_4–K. The absence of C_2 emission in the latter case indicates that no reaction can produce it in the $A\ ^3\pi_g$ state. The almost total absence of K emission from C_2Cl_4–K is surely significant also, and may provide a clue as to the origin of the continuum, which presumably arises in a radiative recombination process. However, we have not been able to find a logical hypothesis for the responsible process.

CH emission from the haloforms is weak, as noted. Nevertheless, it is present, and represents some 66 kcal of excitation energy. In the absence of oxygen, one is hard put to find a chemi-excitation mechanism for CH. Possibly it should be attributed to a trace of air in the vacuum system; but, particularly in view of the very high K atom excitations observed, the possibility of CH excitation by energy transfer should not be ruled out.

That energy transfer processes are operating is evident from the quenching of K atom radiation by added N_2, and its strength in the presence of He and Ar.[12] The means by which K atoms gain excitation energies as high as 91.5 kcal are not clear. In the CCl_4 systems, the preferential excitation of C_2 is almost exactly right for exciting K to this energy by an energy exchange; but the 91.5 kcal level is also observed, weakly, in the haloform-K spectra. Here, it seems necessary to postulate successive excitations. The most logical mechanism for these is resonant absorption, rather than collisional transfer.

K_2 radiation probably arises from collisional stabilization of recombined K atoms, one of which is excited, in the $B\ ^1\pi_u$ state. The principal evidence for this is that in the lowest pressure system, *viz.*, pure CCl_4–K (no carrier), K_2 radiation is weakest.

Conclusions

A number of new spectroscopic observations have been possible by examining radiation from alkali metal-organic halide flames. Interpretation of unusual C_2 excitation in haloform–K systems in a logical manner has produced added evidence for the importance of the reactions, $2\ CH \rightarrow C + CH_2$ and $C + CH \rightarrow C_2 + H$, as a mechanism for producing excited C_2. An analogous interpretation of the C_2 emission in CCl_4–K and Na flames has yielded evidence supporting the value, $D_{C-Cl} = 51$ kcal in the CCl radical.

Energy transfer processes are important in these flame systems. Although there are several unanswered questions about the spectra, with further study these reaction systems may lend themselves to a useful study of electronic and vibrational energy transfer.

ACKNOWLEDGMENTS

This work was supported principally by the National Science Foundation, and partially by Project Squid, Office of Naval Research, Contract Nonr 1858(25), NR–098–038.

REFERENCES

1. BEUTLER, H. and POLANYI, M.: Z. physik. Chem., *1B*, 3 (1928).
2. BAWN, C. E. H. and MILSTED, J.: Trans. Faraday Soc., *35*, 889 (1939).
3. EVANS, M. G. and WARHURST, E.: Trans. Faraday Soc., *35*, 593 (1939).
4. REED, J. F. and RABINOWITCH, B. S.: J. Phys. Chem., *61*, 598 (1957).
5. TINGEY, G. and SKELL, P. S.: unpublished work, Dept. of Chemistry, The Pennsylvania State University, University Park, Pa.
6. GAYDON, A. G.: *The Spectroscopy of Flames*, Chapman and Hall, London, 1957.
7. HERZBERG, G.: *Spectra of Diatomic Molecules*, p. 454, Van Nostrand, New York, 1950.
8. BALLIK, E. A. and RAMSAY, D. A.: J. Chem. Phys., *31*, 1128 (1959).
9. DROWART, J., BURNS, R. P., DEMARIA, G., and INGHRAM, M. G.: J. Chem. Phys., *31*, 1131 (1959).
10. JANAF Thermochemical Data, The Dow Chemical Co., Midland, Mich.
11. SEMENOV, N. N.: *Some Problems in Chemical Kinetics and Reactivity*, translated by M. Boudart. Princeton Univ. Press, Princeton, N. J., 1958.
12. LAIDLER, K. J.: *The Chemical Kinetics of Excited States*, Oxford University Press, 1955.

Discussion

DR. B. A. THRUSH (*University of Cambridge*): Why does Prof. Palmer prefer the reaction C + CH → C_2^* + H to the more exothermic CH + CH → C_2^* + H_2 as a source of excited C_2 in flames where CH is produced?

PROF. H. B. PALMER (*Pennsylvania State University*): Our preference for the reaction, C + CH → C_2^* + H is based upon three points, none of which constitutes a proof. They are: (1) The major product recovered is C_2H_4. We cannot see any more probable way to obtain this than through combination of CH_2 radicals resulting from the reaction, 2CH → C + CH_2. This reaction also produces C atoms. Their most probable fate will be to react with CH, so we are confident that this reaction occurs. Some careful measurements of the absolute yields of products should permit us to state just how important the alternative reaction, 2CH → C_2^* + H_2, in fact is. (2) The preferred reaction can account strikingly well for the observed excitation of C_2^*. (3) An analogous reaction in the K–CCl_4 system seems to account well for the observed C_2^* excitation there. In this system, there is much less chance for the reaction, 2CCl → C_2^* + Cl_2, to occur than there is for reaction between two CH radicals in the K–CHX_3 systems. The most probable fate of a CCl radical is a reactive encounter with a K atom rather than with another CCl. If reaction between two CCl radicals caused the emission, it should hence be weaker than emission brought about by reaction between two CH radicals; but much stronger emission is observed.

As to why the reaction, 2CH → C + CH_2, should be faster than 2CH → C_2^* + H_2, we are reluctant to speculate. The first is an atom abstraction while the second is more complicated. Applying rough rules for estimating activation energies, the first might be of the order of 10 kcal or less, while the second might be 20 kcal or more. It also appears that steric or entropy requirements should favor the first reaction.

SPECTRAL EMISSIVITY OF THE 4.3 μ CO_2 BAND AT 1200°K

U. P. OPPENHEIM

Under certain conditions the emission (or absorption) of spectral bands of molecules in the gaseous state may be described with the help of the "statistical" model. The present study deals with application of this model to the 4.3 μ band of CO_2 at a temperature of 1200°K. A simple method was employed for correlating the observed emissivity with the experimental parameters of the gas (pressure, optical depth, etc.). Use was made of curves of growth for every frequency in the band. Experimental emissivities were obtained by heating CO_2 in cells of different length in an electrical furnace. Good quantitative agreement was found with experimental results of other workers. It is shown that Lambert-Beer's law is not obeyed and that the statistical model predicts the emissivity correctly over wide ranges of pressure and optical depth.

Introduction

Recently a number of spectroscopic studies have been made of the infrared radiation emitted by molecules present in the exhaust plumes of rockets and jet engines.[1,2] Quantitative infrared emission data are of particular interest since they furnish direct information on the temperature and composition of the emitting gases. From a knowledge of these parameters basic information about the chemical and physical processes occurring during combustion may be derived.

The experimental difficulties in studying infrared emission from flames and exhaust gases are mostly due to temperature gradients and local inhomogeneities which occur in the gases. In order to obtain the radiation properties of the constituent gases under well-defined conditions it is advisable to study them statically in closed vessels. Conditions in the flame (apart from those of flow) may then be simulated by changing the composition, temperature, pressure, and optical depth of the gas in the vessel. Studies of CO_2,[3] CO,[4] and H_2O,[5] heated in closed vessels up to about 1200°K have been reported by various authors. It is usually preferred to study the gas in absorption rather than in emission.

Although many measurements of spectral and total band absorption have been reported, large discrepancies have often been found between results for a given band of the same molecular species. The main problem here is not one of experimental error but one of finding the correct laws governing the emission of radiation. Because of thermal excitation at elevated temperatures very large numbers of spectral lines contribute to a single band and this results in a rather complicated dependence of the emitted radiation on pressure, path length, composition, and temperature of the emitting gas. It has been found that the simple Lambert-Beer absorption law usually does not hold and certain "band models" have been invented[6,7] for correlating the observed absorption with the experimental parameters of the gas. A careful selection of an appropriate band model is necessary for a prediction of absorption which is to be valid over a wide range of the parameters. Such a selection is not possible without a thorough study of the absorption under widely varying conditions of pressure, path length, etc. It is the purpose of the present study to show how for a certain band the selection of the model was carried out and how its validity was tested. It will be shown that the "statistical" model may be applied to the 4.3 μ band of CO_2 at a temperature of 1200°K. As a result the absorption of CO_2 at this temperature over wide ranges of pressure and optical depth may be represented as a unique function of certain spectroscopic parameters. Satisfactory agreement is found between the present experimental results and previously published data for this band.

Theoretical

A detailed description of existing band model theories for the representation of molecular band absorption has been given by Plass.[6,7] The calculations presented by Plass expressed the band absorption as an infinite family of curves which depended on various theoretical parameters. Each of these curves showed the dependence of the fractional transmission of the band on the amount of absorbing gas when the gas was kept at constant total pressure, or the depend-

ence of transmission on total pressure when the amount of gas was kept constant. These curves implied that the absorbing gas was to be pressurized by an inert gas, a procedure which introduces the effects of foreign gas broadening in a rather undefined manner. In what follows we shall describe a somewhat different method of presenting the data using at first only pure gases, thereby avoiding both the multiplicity of absorption curves and the experimental necessity of mixing the absorbing gas with a foreign gas. From the various models described by Plass we shall discuss only the statistical model, since this model is often appropriate at high temperatures, when very large numbers of lines contribute to a given band.

According to Mayer[8] and Goody[9] a "disordered" band is one in which the position and intensity of the lines are distributed at random, there being no correlation between line position and line intensity. The average line spacing of n lines in the interval under consideration is assumed to be d cm^{-1}. If the number of lines is allowed to approach infinity, while keeping the line spacing constant, the statistical model gives a simple expression for the mean fractional absorption $\bar{A}_\nu$ at the center of the band:

$$\bar{A}_\nu = 1 - \exp\left[-\bar{W}_{sl}/d\right] \qquad (1)$$

where

$$\bar{W}_{sl}(\bar{S}, \gamma, p, l) = \int_0^\infty W_{sl}(S, \gamma, p, l)\, P(\bar{S}, S)\, dS$$

Here $\bar{W}_{sl}$ is the average value of the equivalent width W_{sl} over the distribution of line strengths, S is the integrated intensity of a line, γ the semi-half-width of the line, p the pressure of the absorbing gas (assuming a pure gas), and l the absorbing path length. $P(\bar{S}, S)\,dS$ is the probability that a line has an integrated intensity between S and $S + dS$. $\bar{S}$ indicates a mean line intensity which occurs in the intensity distribution function $P(\bar{S}, S)$. It should be noted that $\bar{A}_\nu$ represents the fractional absorption at the frequency ν, after averaging over all possible arrangements of the lines in the band. Thus, while it is impossible to predict the actual absorption A_ν, the statistical model allows us to calculate $\bar{A}_\nu$ which is an average value of A_ν for the whole band. While A_ν is a rapidly varying function of frequency, $\bar{A}_\nu$ is a constant which represents the smoothed out value of the fractional absorption in the whole band. From the experimental point of view a similar smoothing process is carried out by the observation of the spectrum with an instrument of finite spectral slit width. It is seen that if d is small compared to the spectral slit width, the observed value of A_ν will approach $\bar{A}_\nu$ very closely. In an actual experiment this is borne out by the fact that the fractional absorption is independent of slit width. It is clear that before the statistical model may be applied to spectral measurements the independence of A_ν of the slit width has to be established.

For an observed disordered band we may calculate $\bar{A}_\nu$ at any frequency (i.e., not only at the center of the band) by assuming that this frequency is at the center of an infinite disordered band of given $P(\bar{S}, S)$. By varying $\bar{S}$ with frequency we may calculate $\bar{A}_\nu$ for each frequency in the band with the help of Eq. (1). It is seen that $\bar{W}_{sl}$ and d are in this case frequency dependent quantities. We shall indicate all frequency dependent quantities by a subscript ν.

For Lorentz lines we have[10]

$$W_{sl,\nu} = W_{sl} = \int_0^\infty \left[1 - \exp\left(-k_\nu p l\right)\right] d\nu$$

$$= 2\pi\gamma f(x)$$

with

$$f(x) = x \exp(-x)\left[I_0(x) + I_1(x)\right]$$

where k_ν is the spectral absorption coefficient and I_0 and I_1 are the Bessel functions of imaginary argument. The dimensionless parameter x is given by

$$x = Sl/2\pi\gamma$$

If a pure gas is used $W_{sl,\nu}$ depends linearly on pressure and we may write

$$W_{sl,\nu} = W_{sl,\nu}^0 \cdot p$$

where $W_{sl,\nu}^0$ is the equivalent width per unit pressure. From the definition of $\bar{W}_{sl}$ it follows that we may also write

$$\bar{W}_{sl,\nu} = \bar{W}_{sl,\nu}^0 \cdot p$$

and Eq. (1) now becomes

$$\bar{A}_\nu = 1 - \exp\left[-(\bar{W}_{sl,\nu}^0/d_\nu)p\right] \qquad (2)$$

It follows from Eq. (2) that

$$-\ln(1 - \bar{A}_\nu)/p = \bar{W}_{sl,\nu}^0/d_\nu$$

Since $\bar{W}_{sl,\nu}^0$ and d_ν are independent of pressure it is seen that a plot of $-\ln(1 - \bar{A}_\nu)$ against pressure results in a straight line through the origin. However, this by itself does not constitute proof of the validity of the statistical model, since the simple Lambert–Beer law[10]

$$A_\nu = 1 - \exp\left[-k_\nu p l\right]$$

also results in a similar linear plot for

$$-\ln(1 - A_\nu)$$

against p. In the latter case, however, the value of k_ν is independent of the path length l. In the case of the statistical model on the other hand the dependence of $\bar{W}_{sl,\nu}{}^0/d_\nu$ on l is quite pronounced and it is this departure from Lambert-Beer's law which makes it possible to distinguish between the various absorption laws which govern the absorption of molecular bands.

Without much loss of generality[6] we shall assume that the probability function $P(\bar{S}, S)$ is given by $P(\bar{S}, S) = \delta(S - \bar{S})$, where δ denotes the Dirac delta function. In this case all lines are equally intense and we have $\bar{W}_{sl,\nu} = W_{sl,\nu}$. Equation (2) becomes

$$\bar{A}_\nu = 1 - \exp\left[-(W_{sl,\nu}{}^0/d_\nu)p\right] \qquad (3)$$

The dependence of $W_{sl,\nu}{}^0$ on optical path length is given by the well-known curves of growth.[10] It is interesting to note that according to Eq. (3) the absorption at a given frequency is determined by $W_{sl,\nu}{}^0/d_\nu$, which assumes the role of a spectral absorption coefficient multiplied by a length. It also follows from Eq. (3) that if the present statistical model is valid for a certain band, a logarithmic plot of $-\ln(1 - A_\nu)/p$ against l should follow the curve of growth, for pure Lorentz lines. Once this plot is fitted to the curve of growth, the validity of the present statistical model has been proved. Since $W_{sl,\nu}{}^0$ is determined by two parameters only ($S_\nu{}^0$ and $\gamma_\nu{}^0$, defined respectively by the relations $S_\nu{}^0 = S_\nu/p$ and $\gamma_\nu{}^0 = \gamma_\nu/p$) the fractional absorption A_ν is seen to be fully determined by the parameters $S_\nu{}^0/d_\nu$ and $\gamma_\nu{}^0/d_\nu$, which may be read off the curve of growth.

The following procedure is found useful in determining the basic parameters $S_\nu{}^0/d_\nu$ and $\gamma_\nu{}^0/d_\nu$. The absorption spectrum of a given band is recorded, using a pure gas in a cell of fixed length filled to an arbitrary pressure. With the help of Eq. (3) the value of $W_{sl,\nu}{}^0/d_\nu$ is derived for as many values of the frequency as is required. This procedure is repeated for a number of different cell lengths and the resulting values of $W_{sl,\nu}{}^0/d_\nu$ for each selected frequency are plotted against l on a log-log scale. By fitting these plots to a graph of the curve of growth in the usual manner, values of $S_\nu{}^0/d_\nu$ and $\gamma_\nu{}^0/d_\nu$ are obtained. It is also possible to derive the quotient of these two parameters from the position of the curve and to obtain x_ν/l which is more convenient to use in practical calculations:

$$x_\nu/l = S_\nu{}^0/2\pi\gamma_\nu{}^0$$

Once the above quantities have been established experimentally, the value of $\bar{A}_\nu$ can be predicted for any value of pressure and optical path.

The values of x_ν/l and $\gamma_\nu{}^0/d_\nu$ may also be used to predict the fractional absorption of gas mixtures, provided $\gamma_\nu{}^0$ is corrected to include the effect of foreign gas broadening. In calculating x_ν/l it should be noted that for a gas mixture

$$x_\nu' = (p/p_t)x_\nu$$

where p and p_t are the partial and total pressure respectively. In computing $W_{sl,\nu}{}^0$ for gas mixtures x' has to be substituted for x.

Application to the ν_3 Fundamental of CO_2

As an example of the foregoing considerations we have measured and analyzed the 4.3 μ band of CO_2 at a temperature of 1200°K. This band which is centered at 2349 cm^{-1}, has recently been studied extensively at temperatures of 1200°K and higher. In these studies the gas was heated in a number of ways: by placing it in a furnace,[3,11,12,13] by heating it in a shock tube,[14] and by observing it in the exhaust jet of a supersonic burner.[2] Apart from these experimental studies Plass[15] has made an extensive theoretical calculation of the spectral emissivity of the band for temperatures between 1200–2400°K. There is a general lack of agreement between the various results, which sometimes differ by a factor of two or more. Since the data measured by these authors were not suitable for the type of representation suggested in the present paper, it was decided to make a new series of measurements and to correlate them with the help of curves of growth in the manner outlined before.

In order to have thermal equilibrium in the gas sample, it was decided to heat it in a furnace to the desired temperature. Pure copper absorption cells with sapphire or magnesium oxide windows were filled with CO_2 and heated in a tube furnace to 1200°K. The entire optical path outside the absorption cell was flushed with dry nitrogen until the atmospheric absorption band of cold CO_2 disappeared. A Perkin-Elmer Model 12G infrared spectrometer was employed to record the spectra, using a spectral slit width of 2–3 cm^{-1}. A more detailed account of the experimental procedure will be given elsewhere.

The lengths of the cells used were 1.24, 5.74, 30.0, 93.35, and 150.5 mm. A longer cell of 250 mm was also employed, but the pressures needed for this cell were so low (less than 40 mm Hg) that the effect of Doppler broadening became noticeable and the absorption no longer obeyed Eq. (3). Data from this cell were therefore not included in the present study. The gas was introduced at a series of different pressures and the absorption spectrum was recorded for each pressure. Three to six spectra with different pressures

were recorded for each cell length. An increase or decrease of the slit width did not change the spectrum in a noticeable way, in agreement with observations of other authors.[3,14]

The recorded spectra were analyzed in the following way. From each absorption curve the pressure independent quantity $-\ln(1-A_\nu)/p$ was derived for a selected number of frequencies, and plotted against ν. In most cases the values of $W_{sl,\nu}{}^0/d_\nu$ for a given frequency coincided within $\pm 5\%$, while the pressures varied over a factor of 4 or 5. A smooth curve was then drawn through the resulting points. Five such curves resulted from the five cell lengths employed.

The frequency range over which the absorption occurred extended between 2200–2400 cm^{-1}. About 20 different frequencies were selected in this range and curves of growth were constructed by plotting log $W_{sl,\nu}{}^0/d_\nu$ against log l. With a few exceptions the points could be fitted to the Ladenburg–Reiche curve. Values of x_ν/l and $2\pi\gamma_\nu{}^0/d_\nu$ were read off the curves and plotted against frequency. The resulting curves are shown in Fig. 1.

Assuming the validity of the statistical model the spectral fractional absorption $\bar{A}_\nu$ may now be calculated from the curves in Fig. 1 for any desired value of the pressure and optical path. The only restriction seems to be that the pressure has to be larger than 40 mm Hg, in order to avoid the effects of Doppler broadening. For a given value of l the curve of x_ν/l determines the value of x_ν. The tabulated values of $f(x)$[16] may then be used to obtain $f(x_\nu)$, which, after multiplication by $(2\pi\gamma_\nu{}^0)/d_\nu$, produces $W_{sl,\nu}{}^0/d_\nu$. The desired value of the pressure is then inserted in Eq. (3) and $\bar{A}_\nu$ is calculated.

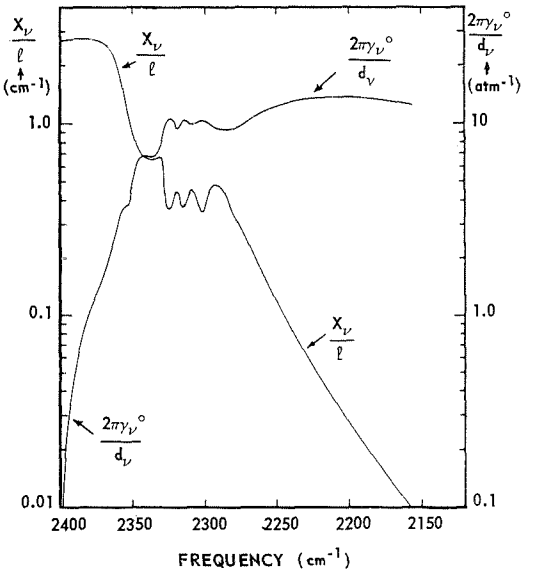

FIG. 1. The frequency dependence of the parameters x_ν/l and $(2\pi\gamma_\nu{}^0)/d_\nu$ for the 4.3 μ band of CO_2 at a temperature of 1200°K. The length is measured in centimeters, $\gamma_\nu{}^0$ is measured in cm^{-1} atm^{-1} (at 1200°K), x_ν is dimensionless, and d_ν is given in units of cm^{-1}. The ordinate scale for $(2\pi\gamma_\nu{}^0)/d_\nu$ is 10 times larger than the corresponding scale for x_ν/l.

Comparison with Other Experimental Work

Most workers who measured CO_2 absorption or emission for the 4.3 μ band at elevated temperatures assumed the validity of Lambert–Beer's law. As was explained above Lambert–Beer's law predicts a linear dependence of

TABLE 1

Comparison of experimental results of k_ν obtained by different authors by the application of Lambert-Beer's law to the 4.3 μ band of CO_2 at a temperature of 1200°K[a]

Author	Heating method	Temperature (°K)	Path length (cm)	Broadening gas	p/p_t	k_ν (cm^{-1} atm^{-1})
Tourin[3]	Furnace	1273	12.7	CO_2	1.00	1.09
Steinberg and Davies[14]	Shock tube	1230	7.62	N_2	0.05	2.9
Ferriso[2]	Supersonic burner	1200	3.12	Exhaust gases	0.13–0.26	2.6
Babrov[11]	Furnace	1273	12.7	N_2	0.0293	2.7
					0.0585	2.4
					0.117	2.1

[a] All data are for a wavelength of 4.4 μ.

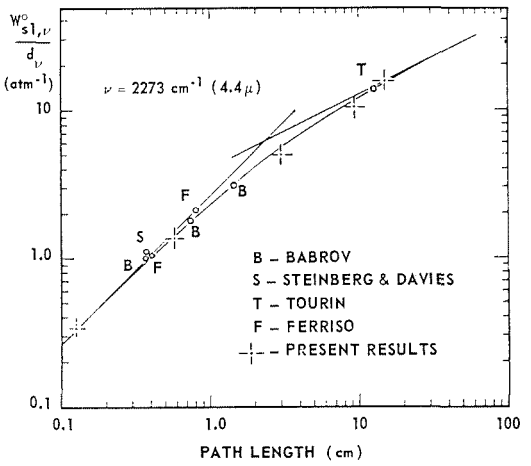

FIG. 2. The curve of growth at 4.4 μ for the 4.3 μ band of CO_2 at a temperature of 1200°K. Present experimental results are indicated by crosses. Circles represent measurements of other authors (as indicated in the drawing). Data were taken from Table 1.

$-\ln(1 - A_\nu)$ on pressure, and this dependence was indeed found to hold by most authors. However, when a value of the spectral absorption coefficient was derived from these straight line plots no agreement was found between values obtained from different laboratories where different cell lengths were used. Table 1 summarizes some of the results obtained at a wavelength of 4.4 μ. Reference to this table shows the large variation observed for the spectral absorption coefficient k_ν.

Assuming the validity of the statistical model for the 4.3 μ band of CO_2 it is possible to reconcile all these results by introducing Eq. (3) as the correct absorption law instead of Lambert–Beer's law. As an example, the curve of growth found by us at 4.4 μ is shown in Fig. 2. We have also calculated the values of $W_{sl,\nu}{}^0/d_\nu$ from the data of Tourin, Steinberg and Davies, Ferriso and Babrov at this wavelength and plotted these values in Fig. 2. Reference to Fig. 2 shows that all points fall very near to the curve of growth. The agreement between these results and ours is the more remarkable, since many of the data were taken with gas mixtures and under completely different conditions of heating and of spectral resolution.

Comparison with Plass's Calculations

Plass[15] has carried out machine calculations of the emissivity of the ν_3 fundamental of CO_2 at temperatures between 1200°K and 2400°K. The spectroscopic parameters which Plass used were taken from empirical data observed at room temperature. Quantum mechanical considerations[17] were used to compute the intensities and the number of rotational and vibrational lines which contributed to the emission of the band at various temperatures. Plass computed basic curves of $S_\nu{}^0/d_\nu$ and of $(2\pi\gamma_\nu{}^0 S_\nu{}^0)/d_\nu{}^2$ in the frequency range of interest. From these curves the spectral emissivity was derived for a number of values of the experimental parameters.

In order to compare our results with those of Plass we have computed the quantity

$$(2\pi\gamma_\nu{}^0 S_\nu{}^0)/d_\nu{}^2$$

and compared it with Plass's results at 1200°K. Another comparison was made between our results for $S_\nu{}^0/d_\nu$ and those obtained by Plass. It was found that in both cases Plass's values were lower than ours, thereby producing too low values of fractional absorption (or emissivity).

ACKNOWLEDGMENTS

The author is indebted to Mr. Y. Ben Aryeh for his assistance in planning and carrying out many of the measurements and calculations. Valuable technical help was given by Mr. T. Andrashi.

REFERENCES

1. FERRISO, C. C.: *Eighth Symposium (International) on Combustion*, p. 275. Williams and Wilkins Co., Baltimore, Maryland, 1962.
2. FERRISO, C. C.: *High Temperature Infrared Emission and Absorption Studies*, General Dynamics—Astronautics, September, 1961.
3. TOURIN, R. H.: J. Opt. Soc. Am. *51*, 175 (1961).
4. OPPENHEIM, U. P.: J. Appl. Phys. *30*, 803 (1959).
5. TOURIN, R. H.: J. Opt. Soc. Am. *51*, 799 (1961).
6. PLASS, G. N.: J. Opt. Soc. Am. *48*, 690 (1958).
7. PLASS, G. N.: J. Opt. Soc. Am. *50*, 868 (1960).
8. MAYER, H.: *Methods of Opacity Calculations*. Los Alamos, LA–647, Oct. 31, 1947.
9. GOODY, R. M.: Quart. J. Roy. Meteorol. Soc. *78*, 165 (1952).
10. BENEDICT, W. S., HERMAN, R., MOORE, G. E., and SILVERMAN, S.: Can. J. Phys. *34*, 830 (1956).
11. BABROV, H. J., HENRY, P. M., and TOURIN, R. H.: *Methods for Predicting Infrared Radiance of Flames by Extrapolation from Laboratory Measurements*. The Warner and Swasey Co., Flushing, N. Y., October 1961.
12. EDWARDS, D. K.: J. Opt. Soc. Am. *50*, 617 (1960).
13. BEVANS, J. T., DUNKLE, R. V., EDWARDS, D. K., GIER, J. T., LEVENSEN, L. L., and OPPENHEIM, A. K.: J. Opt. Soc. Am. *50*, 130 (1960).

14. STEINBERG, M. and DAVIES, W. A.: J. Chem. Phys. *34*, 1373 (1961).
15. PLASS, G. N.: J. Opt. Soc. Am. *49*, 821 (1959).
16. KAPLAN, L. D. and EGGERS, D. E.: J. Chem. Phys. *25*, 876 (1956).
17. PENNER, S. S.: *Quantitative Molecular Spectroscopy and Gas Emissivities*, p. 115. Addison-Wesley Publishing Co., Inc., Reading, Mass., 1959.

Discussion

DR. R. H. TOURIN (*Warner Swasey Company*): I should like to underscore this excellent paper with a few supplementary remarks, based on recent measurements in our laboratory. Dr. Oppenheim's paper explains the apparent discrepancies among the measurements made by various people on the infrared absorption of hot CO_2 in the 4.3 μ region. We have been much concerned with these discrepancies. They cannot be explained on the basis of variations in optical-path length; in particular, the measurements of Tourin, Steinberg and Davies, and Babrov, Henry, and Tourin, which were all for a path of 12.7 cm. We found that plots of logarithm reciprocal transmittance ln $(1/\tau)$ versus optical depth ρl are always straight lines through the origin when the ratio of absorbing (infrared-active) gas in a mixture to the total pressure is constant, but the slopes of such straight-line plots depend upon both pressure ratio and optical path. Hence a family of curves, each a straight line through the origin, can be obtained by varying either pressure ratio or optical path as a parameter, for the same range of values ρl. We have done both experimentally. Clearly the slopes of such plots are not unique absorption coefficients in the sense of the Beer-Lambert law. Both types of variation—with pressure ratio and optical-path length—can be explained quantitatively with the aid of Dr. Oppenheim's formulation.

Details of the experiments and applications to flame-gas analysis have been published.[1,2] We have also developed a graphical technique for predicting CO_2 radiation, based on the same "band-model" approach used by Dr. Oppenheim.[3]

REFERENCES

1. TOURIN, R. H. and BABROV, H. J.: J. Chem. Phys. *37*, 581 (1962).
2. PENZIAS, G. J. and TOURIN, R. H.: *Combustion and Flame, 6*, 147 (1962).
3. BABROV, H. J. and TOURIN, R. H.: *J. Quant. Spectros. and Rad. Transf.*, submitted for publication (1962).

THE EMISSIVITY OF LUMINOUS FLAMES

R. G. SIDDALL AND I. A. McGRATH

The results of previous experimental work on extinction coefficients have been expressed in the form $K_\lambda = k \cdot \lambda^{-\alpha}$, where k is independent of the wavelength (λ) of the incident radiation. This paper describes the results of an experimental investigation into the values of α corresponding to soot layers deposited from a small laminar diffusion flame, on optically ground rock salt discs. The fuels used in the flame included amyl acetate, gas oil, petrotherm, towns gas, and some hydrocarbon gases. Extinction curves were obtained for each soot layer by means of an infrared spectrometer. The results are: (i) The variation of α with λ may be approximated by $a + b \ln \lambda$ in some cases, and by a parabola in λ in others; (ii) The "mean" α for any soot [obtained as the slope of the best-fit straight line to the results plotted in the form of graphs of $\ln \cdot \ln (I_0/I_L)$ against $\ln \lambda$] appears to be independent of the mean soot particle size; (iii) α appears to be definitely correlated with the carbon to hydrogen ratio of the soot.

In the second part of the paper a theoretical method is described, based upon the Mie theory, which permits the prediction of the variation of α with λ for any material at any temperature, provided that the optical properties of the material are known. The theory demonstrates that α is independent of particle size. An illustrative calculation is carried out for baked electrode carbon at 2250°K. For this case: (i) α is approximately constant for wavelength in the visible spectrum; (ii) α is given within 3% by the equation $\alpha = 0.906 + 0.283 \ln \lambda$ for the range $1\ \mu < \lambda < 10\ \mu$; (iii) as $\lambda \rightarrow \infty$, α tends to an absolute maximum of 2.

The method is extended to give a single curve from which the monochromatic emissivity of a cloud of particles of the specified material may be found for any wavelength and concentration of material. From this curve the variation of total emissivity with particle concentration may be found by numerical integration.

Introduction

The solid carbon particles which are formed in a flame as a result of the incomplete combustion of hydrocarbons prove extremely desirable from the point of view of the heat transfer characteristics of the flame. Their presence causes an increase in flame emissivity and an associated increase in the rate at which heat can be transferred from the flame to its surroundings. However, the exact prediction of the emissivity resulting from the presence of carbon particles has proved extremely complicated. Experimental investigations carried out by various workers in an attempt to solve the problem of prediction of luminous emissivity have led to some inconclusive and contradictory results. The work described in this paper constitutes an attempt to resolve some of the anomalies by providing further experimental evidence, and a theoretical method which throws light on the experimental work and provides a basis for the calculation of luminous emissivity.

Previous Work on Extinction Coefficients

It has been found that when a parallel beam of radiation passes through a system of particles there is an exponential attenuation of the beam. This can be expressed mathematically in the form

$$I_L/I_0 = \exp(-K_\lambda \cdot L) \qquad (1)$$

where I_L is the intensity of the beam after traveling a distance L through the system of particles, I_0 is the intensity at $L = 0$, and K_λ is a constant depending upon the wavelength of the radiation and having the dimensions of reciprocal length. K_λ is commonly called the extinction coefficient of the system (sometimes called "turbidity" in optical measurements of particle size). Equation (1) has the same form as Lambert's law for a homogeneous medium and Beer's law for a solution. Becker[1] has shown that both soot suspended in flames and soot deposited from a flame onto glass exhibit the same variation of K_λ with wavelength. For small particles (<600 Å) at large wavelengths ($>2\ \mu$)

scattering can be ignored in comparison with absorption and K_λ becomes the absorption coefficient.

Rossler and Behrens[2] measured I_L and I_0 for soot layers of various thicknesses with radiation in the visible spectrum and plotted their results in the form of graphs of $\ln \cdot \ln (I_0/I_L)$ against $\ln \lambda$. The approximate linearity of the resulting curves led them to the conclusion that

$$K_\lambda \propto \lambda^{-\alpha} \tag{2}$$

α being the numerical value of the slope of the straight lines. The value of α was found to be independent of layer thickness but dependent on the fuel from which the soot was formed. Their results indicated α values between 0.65 and 1.43.

Pepperhoff[3] carried out similar experiments and also found α to be a constant for soot from a given fuel, independent of wavelength, in the visible spectrum. He suggested that the difference in α values for various soots was due to the differences in the particle diameters of the soots produced from various fuels. His results indicated that α reached a maximum of 2 at a particle diameter of 100 mμ and that the α versus diameter curve was symmetrical about that point, falling to $\alpha = 0$ at 200 mμ.

Naeser and Pepperhoff,[4] and Pepperhoff and Bahr[5] extended this work to include radiation in the infrared region and found that whilst a constant α value was satisfactory in the visible spectrum, a better approximation to the results in the infrared region was given by $\alpha = a - b \ln \lambda$, a and b being determined from the experimental results.

The above results can be summarized in the form: (i), α is independent of wavelength in the visible spectrum; (ii), $\alpha = a - b \ln \lambda$ in the infrared region; (iii), α is independent of layer thickness; (iv), α depends upon the fuel from which the soot is formed; (v), some authors suggest that (iv) can be made more specific and in fact say that α depends on particle size.

No theoretical predictions of the dependence of α on wavelength and particle size have been reported by previous workers and the work described later in this paper represents an attempt to remedy this deficiency. In addition, experimental evidence on the variation of α has been obtained to provide a basis of comparison with both the new theoretical work and previous experimental work. This experimental work is described in the next section.

Experimental Determination of α

Values of α have been found from experimental measurements on soot layers. Each soot layer was produced by holding an optically ground rock salt disc in a small laminar diffusion flame. The fuels used in the flame were selected to produce soot of various particle diameters and C/H ratios, and included amyl acetate, gas oil, petrotherm, benzene, towns gas, and some hydrocarbon gases. After the soot layer had been formed the disc was placed in an infrared spectrometer and an extinction curve, upon which was superimposed the absorption peaks of carbon dioxide and water vapor, was obtained. With each fuel soot layers of different thickness were produced and tested.

Dependence of α on Wavelength. A representative value of α for any run can be obtained by plotting $\ln \cdot \ln (I_0/I_L)$ versus $\ln \lambda$ and fitting the "best-fit" straight line. The slope of this line gives a "mean" value of α. Some of the experimental results subjected to this treatment are shown in Fig. 1. The corresponding mean α values are given in Table 1. It can be seen from Fig. 1 that the results exhibit approximate linearity over short wavelength ranges. The marked S-shape of the curves when viewed over the whole wavelength range considered suggests considerable variation of α with λ and that the use of the mean α values may give misleading results. Therefore, the experimental results were used to find individual α values for each of the experimental points. Equations (1) and (2) can be combined in the form

$$I_L/I_0 = \exp (-k \cdot \lambda^{-\alpha} \cdot L) \tag{3}$$

where k is the proportionality constant of Eq. (2). On taking logarithms twice and considering the form of the result when $\lambda = 1$, Eq. (3) can be rearranged as

$$\alpha = \frac{[\ln \cdot \ln (I_0/I_L)]_{\lambda=1} - \ln \cdot \ln [I_0/I_L]}{\ln \lambda} \tag{4}$$

This equation has been used to find the variation of α with λ for each of the sets of results shown in Fig. 1. In each case $[\ln \cdot \ln (I_0/I_L)]_{\lambda=1}$ was found by interpolation. The types of variation found are illustrated in Figs. 2 and 3. Variation as shown in Fig. 2 can be represented approximately by an equation of the form $\alpha = a + b \ln \lambda$, where a and b are positive constants. Linear variation of α with $\ln \lambda$ can only be used for short wavelength ranges for the curves of Fig. 3. A parabolic representation would be necessary to describe the variation over the whole of the range considered. It can be seen from Figs. 2 and 3 that the measured α values lie between 0.65 and 1.65.

Dependence of "Mean" α on Particle Size. Soot particle sizes were measured by means of an

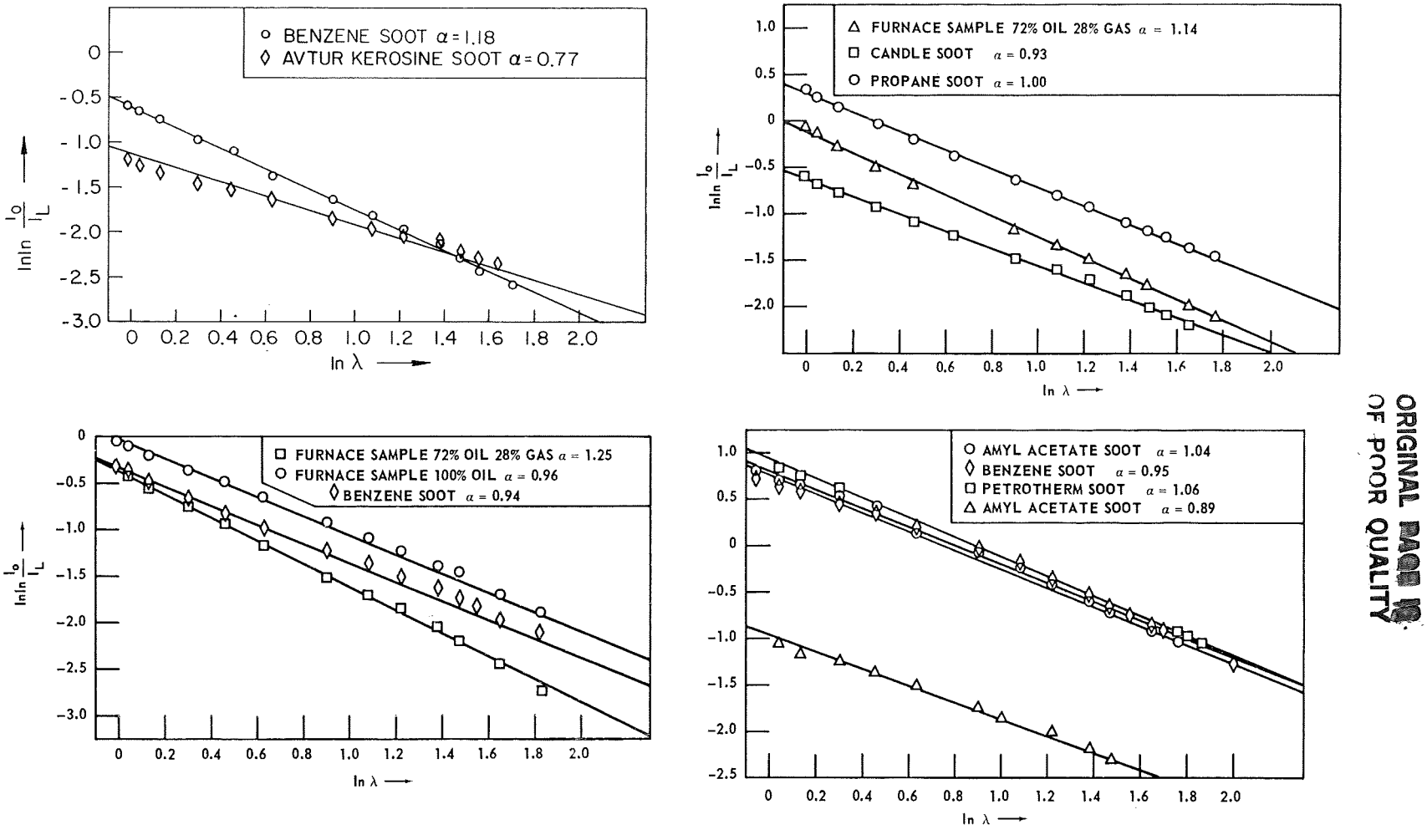

FIG. 1. Plots of ln·ln (I_0/I_L) versus ln λ together with best-fit straight lines for experimental results—slope gives a mean α value.

TABLE 1

Mean α values corresponding to Fig. 1

Source of soot		Mean α
Amyl acetate	1	0.89
Amyl acetate	2	1.04
Avtur kerosine		0.77
Benzene	1	0.94
	2	0.95
Candle		0.93
Furnace samples	1	0.96
	2	1.14
	3	1.25
Petrotherm		1.06
Propane		1.00

electron microscope and a mean particle size estimated for each soot sample from the measured diameters of a large number of particles (using micrographs of some 350,000 times magnification). In each case the size distributions were very similar and the particle sizes, except for soots from towns gas and methane, were generally found to be of the order of 400–600 Å. In contrast to the results of Naeser and Pepperhoff,[4] there appeared to be no definite correlation between α and the mean particle diameter. It should however be stressed that the range of measured mean diameters was small and the demonstrated lack of correlation is therefore far from conclusive.

Dependence of "Mean" α on the Carbon-to-Hydrogen Ratio of the Soot. As the experimental results suggest that the mean α is independent of particle size the dependence of α on the carbon to hydrogen ratio of the soot was investigated. The carbon to hydrogen ratio of each soot was determined by burning the carbon to CO_2 and the hydrogen to H_2O. No accurate microapparatus was available for the CO_2 and H_2O determinations but nevertheless the results as shown in Fig. 4 indicate a definite correlation between the mean α and the C/H ratio. Millikan[6] working simultaneously and independently has obtained similar results but with less scatter.

As neither the new nor the previous experimental work on extinction coefficients produces sufficiently conclusive results to permit the accurate prediction of α values (and thereby the prediction of monochromatic emissivity) for different materials and conditions an attempt has been made to provide a theoretical basis for the calculation of α for any given material under specified conditions. This is described in the next section.

Theoretical Determination of α

On the basis of the Mie theory Hawksley[7] showed that the extinction of radiation by a small absorbing sphere is given by the expression

$$E = \frac{24 \cdot \pi \cdot x}{\lambda} \cdot \frac{n_1^2 \cdot n_2}{[(n_1^2 + n_1^2 n_2^2)^2 + 4(n_1^2 n_2^2 + 1)]} \qquad (5)$$

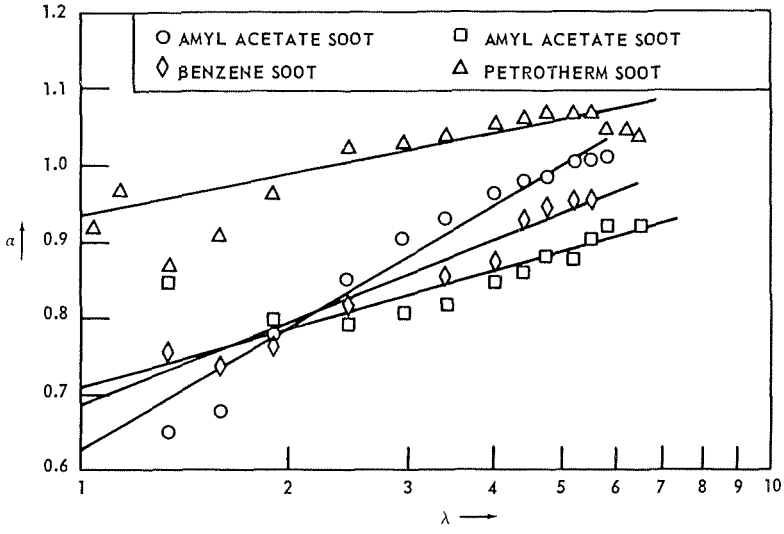

FIG. 2. Experimental values of α plotted against λ (log scale) for cases in which α varies approximately linearly with ln λ.

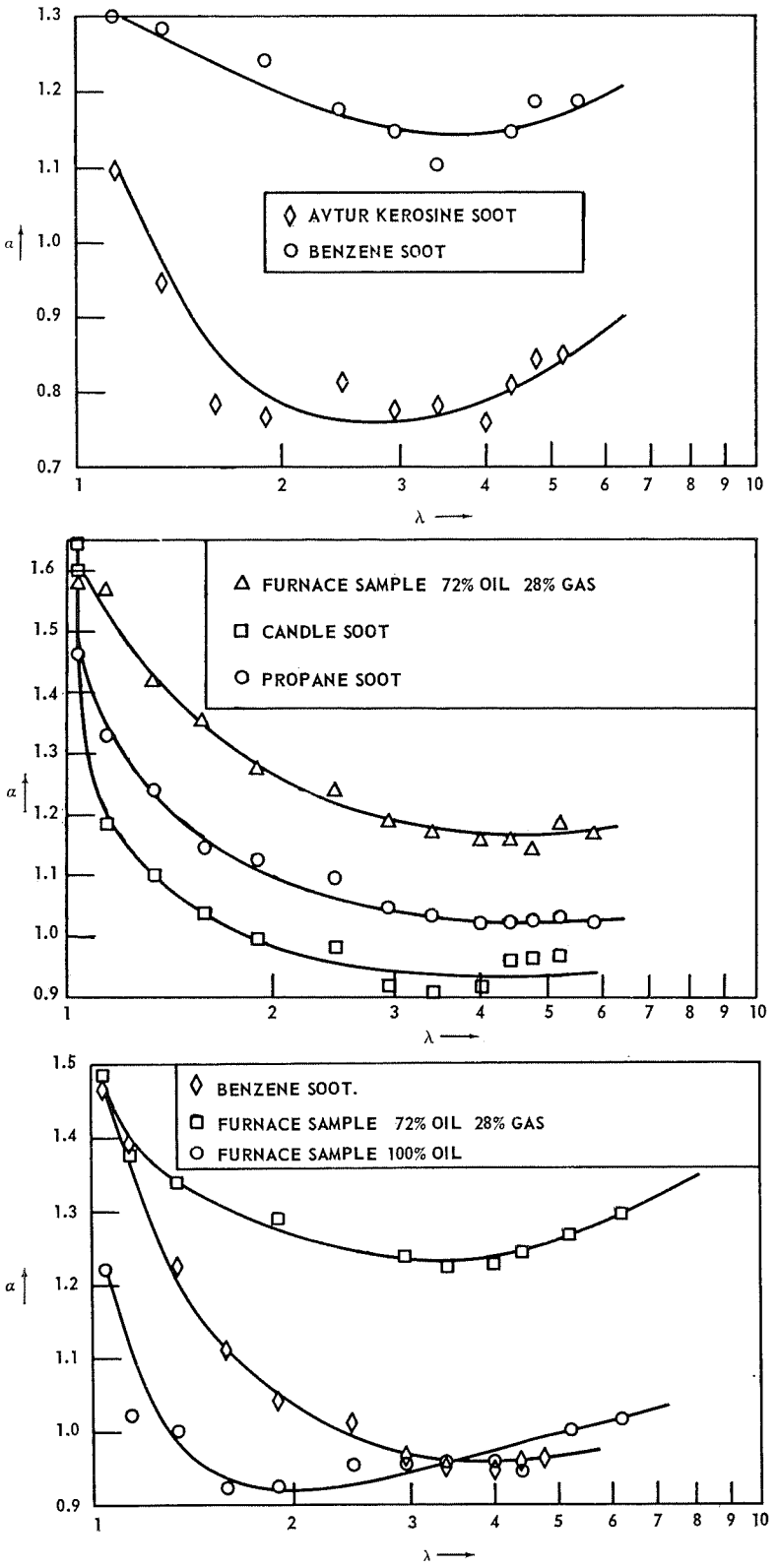

FIG. 3. Experimental values of α plotted against λ for cases in which α does not vary linearly with ln λ.

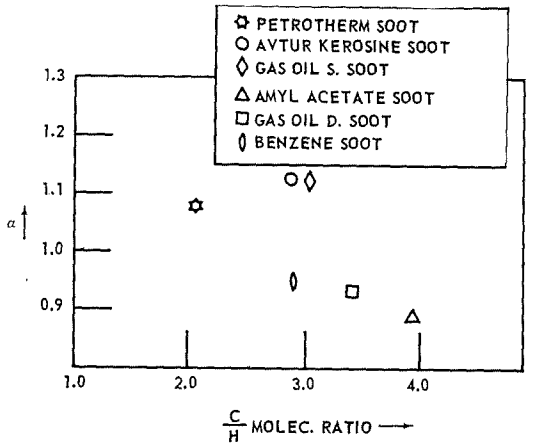

FIG. 4. Experimental values of mean α plotted against the C/H ratio of the soot.

if $\pi x/\lambda \ll 1$, where x is the particle diameter, and n_1 and n_2 are related to the complex refractive index (m) of the particle by means of the equation

$$m = n_1(1 - in_2) \tag{6}$$

n_1 and n_2 depend upon the wavelength of the incident radiation, the material of the sphere, and the temperature of the sphere. The determination of n_1 and n_2 as functions of λ for a specific material and temperature is illustrated in the Appendix.

When dealing with a specific case Eq. (5) can be written in the form

$$E = \frac{24\cdot\pi\cdot x}{\lambda}\cdot f(n_1^2, n_2) = 24\cdot\pi\cdot x\cdot\frac{F(\lambda)}{\lambda} \tag{7}$$

For a flame or soot layer containing particles of uniform size the extinction coefficient can be related to the extinction of a single particle by means of the equation

$$K_\lambda = E\cdot N\cdot A. \tag{8}$$

provided that the aperture of the beam of radiation is large compared with the particle diameter. In Eq. (8) N is the average number of particles per unit volume and $A(=\pi x^2/4)$ is the projected area of a single particle. Combination of Eqs. (7) and (8) leads to the result

$$K_\lambda = 36\cdot\pi\cdot c\cdot[F(\lambda)/\lambda] \tag{9}$$

where c is the average volume of particles per unit volume of the cloud $[=(N\cdot\pi\cdot x^3)/6$ in this case$]$.

When particles of nonuniform size are present Eq. (8) must be modified. Suppose in this case that $g(x)$ is the fraction of the total number of particles with diameter less than or equal to x. The average number of particles per unit volume with diameter between x and $(x + dx)$ is then $N\cdot g'(x)\cdot dx$, and the contribution to the extinction coefficient by these particles is $E\cdot N\cdot g'(x)\cdot dx\cdot\pi\cdot(x^2/4)$. In this case the extinction coefficient is therefore given by the equation

$$K_\lambda = \int_{x=0}^{x=\infty} E\cdot N\cdot g'(x)\cdot\pi\cdot\frac{x^2}{4}\cdot dx \tag{10}$$

The average volume of particles per unit volume of cloud is

$$c = \frac{\pi\cdot N}{6}\int_{x=0}^{x=\infty} x^3\cdot g'(x)\cdot dx \tag{11}$$

Combination of Eqs. (7), (10), and (11) finally leads to the result

$$K_\lambda = 36\pi\cdot c\cdot[F(\lambda)/\lambda]$$

which is identical with the result for particles of uniform size.

The empirical form for the extinction coefficient suggested by experimental work is

$$K_\lambda = k\cdot\lambda^{-\alpha} \tag{12}$$

Equations (9) and (12) can be equated to give a theoretical equation for α. From Eqs. (9) and (12)

$$k\cdot\lambda^{-\alpha} = 36\pi\cdot c\cdot[F(\lambda)/\lambda] \tag{13}$$

The two unknowns in this equation are k and α. When $\lambda = 1$, Eq. (13) simplifies to give

$$k = 36\cdot\pi\cdot c\cdot F(1) \tag{14}$$

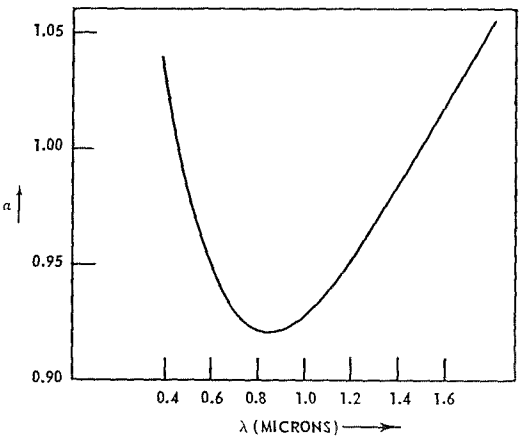

FIG. 5. Calculated variation of α with λ for baked electrode carbon at 2250°K.

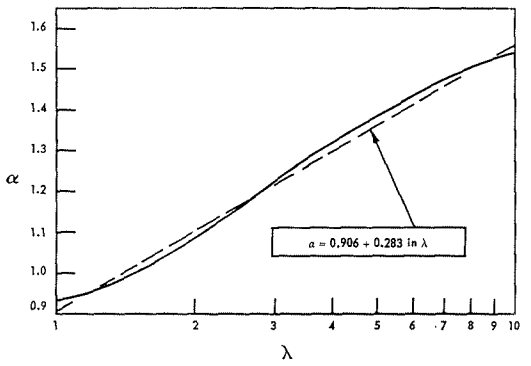

FIG. 6. Calculated variation of α with ln λ, together with best-fit straight line—illustrating linear variation of α with ln λ for 1 $\mu < \lambda < 10$ μ for the case in question.

Substituting from Eq. (14) into Eq. (13) and rearranging finally leads to the following expression for α

$$\alpha = 1 + \frac{\ln [F(1)/F(\lambda)]}{\ln \lambda} \qquad (15)$$

From this equation it follows that α depends solely on the material and temperature of the particles, and the wavelength of the incident radiation. It is absolutely independent of particle size. Equation (15) has been used to calculate the variation of α with λ for the specific case under consideration. The result is shown in Figs. 5 and 6. For this case the following conclusions can be drawn: (i), α is approximately constant in the visible spectrum; (ii), α varies approximately linearly with ln λ over the range 1 $\mu < \lambda < 10$ μ. The best-fit straight line is superimposed on the calculated curve in Fig. 6. This variation is similar to the experimental results of Fig. 3 in that α increases linearly with ln λ in the infrared region, i.e., $\alpha = a + b \ln \lambda$, not $\alpha = a - b \ln \lambda$. Inspection of the formulas used to calculate α shows that

$$\lim_{\lambda \to \infty} \alpha = 2.$$

This result is true whatever the particular optical constants used in the calculation of n_1 and n_2.

The method of calculation described in this section can be used to draw up an α- versus λ-curve for any material at any temperature provided the optical properties necessary for the calculation of n_1 and n_2 are known.

Determination of the Emissivity of a Cloud of Particles

If a cloud (or layer) of particles is suspended in a medium which does not interfere with or contribute to the incident radiation, then the monochromatic emissivity (ϵ_λ), if assumed equal to its absorptivity, may be defined by means of the equation

$$\epsilon_\lambda = (I_0 - I_L)/I_0 \qquad (16)$$

Substitution from Eq. (1) leads to the result

$$\epsilon_\lambda = 1 - \exp(-K_\lambda \cdot L) \qquad (17)$$

Two possible forms of K_λ are given by Eqs. (9) and (12). The corresponding equations for ϵ_λ are

$$\epsilon_\lambda = 1 - \exp\{-36\pi \cdot c \cdot L \cdot [F(\lambda)/\lambda]\} \qquad (18)$$

and

$$\epsilon_\lambda = 1 - \exp\{-[36\pi F(1)] \cdot c \cdot L \cdot \lambda^{-\alpha}\} \qquad (19)$$

Equation (18) has been used to calculate the variation of ϵ_λ with λ for baked electrode carbon at 2250°K. To avoid the necessity for drawing a series of curves corresponding to various values of cL, Eq. (18) may be rearranged in the form

$$\frac{-cL}{\ln (1 - \epsilon_\lambda)} = \frac{\lambda}{36\pi F(\lambda)} \qquad (20)$$

This equation is used to draw up a curve of $-cL/\ln (1 - \epsilon_\lambda)$ against λ, which is shown in Fig. 7. For given values of λ and cL the value of ϵ_λ may be found. It is possible to draw up similar curves for other materials at other temperatures. This method of calculation of ϵ_λ needs only values of cL and not size distributions as used by Stull and Plass.[8] In fact the results of Stull and Plass could have been correlated with cL irrespective of the distribution of sizes chosen.

Equation (18) can be used to calculate the

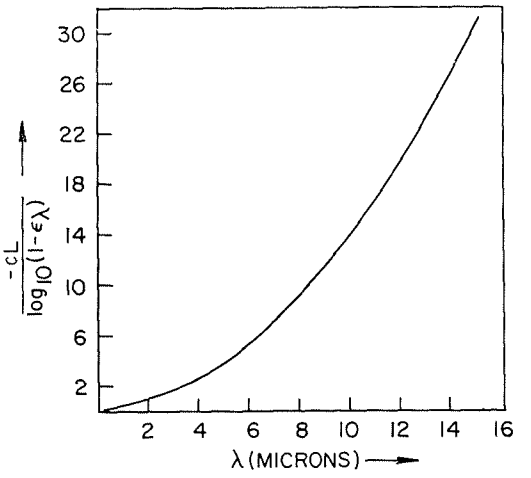

FIG. 7. Calculated variation of $-cL/\log_{10}(1 - \epsilon_\lambda)$ with λ for baked electrode carbon at 2250°K.

variation of total emissivity (ϵ) of a cloud with cL by making use of the relationship

$$\epsilon = \frac{1}{W_B}\int_{\lambda=0}^{\lambda=\infty} W_{B\lambda}\cdot\epsilon_\lambda\cdot d\lambda \qquad (21)$$

where $W_{B\lambda}$ is the monochromatic emissive power of a black body at wavelength λ, and W_B the total emissive power of a black body. Numerical integration of Eq. (21), with ϵ_λ found from Eq. (18), permits the calculation of the curve of ϵ versus cL. The calculation has not been carried out for the case in question.

Finally, if the suspending medium plays a significant part in the radiation interchange, it must be accounted for in calculating an over-all emissivity for the cloud. If ϵ_G is the emissivity of the suspending medium then the total over-all emissivity (ϵ_T) is given by the equation

$$\epsilon_T = \epsilon + \epsilon_G(1 - \epsilon) \qquad (22)$$

where ϵ is found from Eq. (21).

Conclusions

Previous experimental work on the determination of extinction coefficients has led to empirical equations of the form $K_\lambda = k\cdot\lambda^{-\alpha}$. The present experimental investigation, which has been confined entirely to the infrared region, leads to several conclusions regarding α.

(i) It appears impossible to specify a general but simple form for the variation of α with λ which will be true for all materials. In some cases the results may be represented approximately by an equation of the form $\alpha = a + b\ln\lambda$, whereas in other cases it would be necessary to use a general polynomial (a quadratic may be satisfactory) of the form $\alpha = a + b\lambda + c\lambda^2 + \cdots$. In these cases the form $a \pm b\ln\lambda$ could be used over short wavelength ranges of the order of $1 - 2\ \mu$ without any serious error.

(ii) Mean α values appear to be independent of particle size but appear to show a definite correlation with the C/H ratio of the soot.

A simplified theoretical method for the estimation of α (and hence ϵ_λ) for any given set of conditions leads to a curve of α against λ for a particular case. From the curve it appears that a constant α value is satisfactory for wavelengths in the visible region, whereas the expression $\alpha = a + b\ln\lambda$ satisfactorily represents the variation of α with λ over the range $1\ \mu < \lambda < 10\ \mu$, for the case considered. Consideration of the method of calculation leads to the conclusion that an absolute maximum for α is 2.

The theoretical method permits the drawing up of a single curve representing the variation of the monochromatic emissivity of a cloud of particles with wavelength. The curve is independent of the size distribution of the particles in the cloud. Numerical integration on the basis of this curve permits the calculation of the variation of total emissivity with the volume of particles present. The methods described are being used to draw up total emissivity against cL curves for different materials under different conditions.

Appendix: Determination of F(λ)

Stull and Plass[8] derived relationships for n_1 and n_2 based upon the experimental measurements of Senftleben and Benedict.[9] The general forms of these relationships are

$$n_1^2 - n_1^2n_2^2 = 1 + \frac{e^2}{m\epsilon_0}\cdot\sum_j \frac{n_j(\omega_{0j}^2 - \omega^2)}{(\omega_{0j}^2 - \omega^2)^2 + \omega^2 g_j^2} - \frac{e^2}{m\epsilon_0}\cdot\frac{n_c}{(\omega^2 + g_c^2)} \qquad (23)$$

and

$$2n_1^2n_2 = \frac{e^2}{m\epsilon_0}\cdot\sum_j \frac{n_j\cdot\omega\cdot g_j}{(\omega_{0j}^2 - \omega^2)^2 + \omega^2 g_j^2} + \frac{c^2}{m\epsilon_0}\cdot\frac{n_c g_c}{\omega(g_c^2 + \omega^2)} \qquad (24)$$

where n_c = number of conduction electrons/unit volume; g_c = damping constant for conduction electrons; n_j = number of bound electrons in jth state/unit volume; ω_{0j} = natural frequency of jth state; g_j = damping constant for jth state; e = charge on electron; m = mass of electron; ϵ_0 = electric inductive capacity in vacuum; ω = circular frequency of incident radiation. Stull and Plass obtained values of the constants in these equations from the work of Senftleben and Benedict. These constants apply to baked electrode carbon at a temperature of 2250°K. If the constants are found for other materials at other temperatures then Eqs. (23) and (24) can be used to calculate the variation of n_1 and n_2 with λ. The method of manipulation of these equations is illustrated below. If Eqs. (23) and (24) are written in the form

$$n_1^2 - n_1^2n_2^2 = \theta(\omega) \qquad (25)$$

$$2n_1^2n_2 = \phi(\omega) \qquad (26)$$

then manipulation finally leads to the following equations for n_1 and n_2

$$n_1 = \sqrt{\frac{\phi(\omega)}{2n_2}} \qquad (27)$$

and

$$n_2 = \sqrt{\left[\frac{\theta(\omega)}{\phi(\omega)}\right]^2 + 1} - \frac{\theta(\omega)}{\phi(\omega)} \qquad (28)$$

These equations have been used to draw up curves of n_1 and n_2 against λ for baked electrode carbon at 2250°K.

The function $F(\lambda)$ was defined in the text by means of the equation

$$F(\lambda) = \frac{n_1^2 n_2}{[(n_1^2 + n_1^2 n_2^2)^2 + 4(n_1^2 - n_1^2 n_2^2 + 1)]} \qquad (29)$$

The calculated values of n_1 and n_2 are then used to draw up the curve of $F(\lambda)$ against λ.

References

1. Becker, A.: Ann. Phys. *28*, 1017 (1909).
2. Rossler, H. and Behrens, F.: Optik. *6*, 145 (1950).
3. Pepperhoff, W.: Optik. *8*, 354 (1951).
4. Naeser, G. and Pepperhoff, W.: Kolloid Z. *125*, 33 (1952).
5. Pepperhoff, W. and Bahr, A.: Archiv. Eisenhütten. *23*, 335 (1952).
6. Millikan, R. C.: General Electric Co., N. Y., Report No. 60 RL2530C, (1960).
7. Hawksely, P. G. W.: B.C.U.R.A. Bulletin *XVI*, Nos. 4 & 5, 134 (1952).
8. Stull, V. R. and Plass, G. N.: J. Opt. Soc. Am. *50*, 121 (1960).
9. Senftleben, H. and Benedict, E.: Ann. Phys. *54*, 65 (1917); *60*, 297 (1919).

Discussion

Dr. R. C. Millikan (*General Electric Research Laboratory*): The conclusion that particle size (within limits) does not determine the α-value of a soot deposit is in agreement with our own study in the visible and UV region. It can be added that α-values measured *in situ* agree with those measured upon a soot deposit caught from the flame on a cool plate. However, catching the deposit on a heated plate often yields different α-values for soot from a given flame. This means that the α-value is a parameter of soot, sensitive to its time-temperature history. The fact that one can obtain identical α-values measured *in situ* and from a deposit is evidence that soot can be extracted from a flame without undergoing change, at least with respect to its α-value, and any properties related thereto. The carbon-hydrogen ratio of the soot appears to be one such related property.

THE THERMAL RADIATION THEORY FOR PLANE FLAME PROPAGATION IN COAL DUST CLOUDS

ROBERT H. ESSENHIGH AND JOSEPH CSABA

The Nusselt radiation theory of steady state propagation of a plane flame through a dust cloud has been extended to take into account: a finite temperature difference between the particles and air; and, a finite preignition zone (implying finite ignition time or distance).

The dust cloud is assumed to be monodisperse, formed by the suspension of finely ground coal in air. As the ignition temperature of coal dust is believed to be the coal decomposition temperature, this is a constant, independent of the ambient conditions, and it therefore effectively decouples the preignition and flame zones; this means that the preignition zone can be treated independently of the flame. The dust in the preignition zone is assumed to be heated by radiation from the flame alone; conduction is neglected. Part of the radiant heat absorbed by the particles is then lost by conduction to the surrounding gas. The gas temperature therefore lags that of the particles. Because of this heating, however, the gas expands with the consequence that the gas density and the dust concentration (and therefore the radiation-attenuation coefficient) all drop.

The system as specified is governed by two simultaneous ordinary differential equations, and analytical solutions for the respective rise of the particles and gas temperatures have been found. In the limiting case, when the particle temperature reaches ignition, the solution for the particle temperature provides an expression for the flame speed.

Introduction

Flames propagating in combustible mixtures can be grouped in three categories: (1) plane flames, (2) jet flames, and (3) explosion flames. The mechanism of propagation is strongly influenced by flame category but depends mainly on the type of fuel; the mechanism in dust flames of all categories is generally believed to be thermal.

Thermal theories of flame propagation are based on the assumption that flame speed is determined by the "rate of ignition"—the rate at which the unburned fuel-air mixture ahead of the flame is raised to its "ignition temperature" by heat transferred to it from the flame. The possible mechanisms of heat transfer are, of course, conduction, convection, and radiation, but the predominating mode of transfer in dust flames appears to be determined largely by the flame category. Calculations indicate that conduction is relatively unimportant in all three flame types, being largely swamped in most cases by either convection and/or radiation. Convection is important or dominant in the enclosed jet and explosion flames (types 2 and 3): In the jet flame it is the forced convection of recirculation generated by jet entrainment; in the moving explosion flame it is believed to be the intense form of forced convection characterized as turbulent exchange. Only in the plane flame system can radiation be treated as the dominant factor.

The radiation theory for propagation of plane flames in dust clouds was originated by Nusselt.[1] With modifications (cf. Traustel[2]) it has now been in existence for nearly 40 years, but its experimental substantiation is still unsatisfactory because, until recently, the flame systems against which the theory was tentatively tested were of the recirculating-jet, or the turbulent-explosion type. As the flame speeds in these convecting systems were generally in the region of 10 m/sec or more, unless the experimental system was very small (ignition distance less than 10 cm), they were something like an order of magnitude greater than the expected values as predicted by the plane flame theory; the factor of disagreement was therefore high and its source was obscure. Only in the last decade have experimental systems been developed that generate acceptably plane flames, burning at speeds within the predicted order of magnitude of about 1 m/sec. This, in our opinion, has now justified a more detailed study of the thermal radiation theory of plane flame propagation; and the purpose of this paper is to present the results of our extended analysis. The analysis has already been checked, tentatively but satisfactorily, against experimental measurements in one of the plane flame furnaces; these data are to be published in due course.

This extended analysis takes into account both a finite preignition zone and a finite temperature difference between the dust particles and air;

this also introduces the previously unknown influence of ignition time on the value of that optimum dust concentration at which the peak flame speed is generated. The number of assumptions on which the analysis is based is still considerable; the intention is to eliminate these progressively in due course by the use of fast calculators, but only as and when the closer approximations are justified by higher experimental accuracy in the flame speed and associated measurements.

Flame Model

The system as idealized for analysis is the standard model of a flame with a flat vertical flame front, with invariant properties in the y and z planes at any x; though burning in the negative x direction, the flame is assumed to be maintained stationary at the origin as a consequence of the motion of the cloud which is traveling in the positive x direction with increasing velocity, v. The dust cloud is assumed to emerge from a bank of water-cooled burners at initial velocity, temperature, and dust concentration, respectively: v_0, T_0, and D_0. The burners are assumed to be water-cooled so that it may also be assumed that any thermal flux reaching the plane of the burners is then absorbed by the water cooling and not by the cloud inside the burners. The burners are located at a distance L_i up stream (negative x) from the flame front so, by definition, L_i is the ignition distance, and the time required for the dust cloud to travel that distance is the ignition time, t_i. Both these parameters change with variation in other conditions so that, to preserve the flame front at the origin, which is convenient mathematically, the axes are assumed to move with the flame front as this latter changes its real physical position relative to the fixed burners.

As the cloud approaches the flame front, the absorption of heat causes it to heat up and expand so that the air and dust densities drop while the cloud velocity rises; also, because the heat transfer in the first instance is predominantly by radiation to the dust, which then loses heat by conduction to the ambient air, there is a temperature differential between the dust and air (see Fig. 1).

In Fig. 1 the cloud element of width η has a gas temperature that has risen from the initial temperature T_0 to T_g. The element is heated by a thermal flux that enters at intensity I and leaves at intensity $(I - \delta I)$; this is true in a steady state system whatever the mechanism of heat transfer. The changes in cloud volume, velocity, and density, are dependent on the gas temperature, not on the particle temperature, and are given by

$$\text{cloud volume} \qquad \eta = \eta_0(T_g/T_0) \qquad (1a)$$

$$\text{cloud velocity} \qquad v = v_0(T_g/T_0) \qquad (1b)$$

$$\text{dust density} \qquad D = D_0(T_0/T_g) \qquad (1c)$$

$$\text{air density} \qquad \rho = \rho_0(T_0/T_g) \qquad (1d)$$

It is assumed here that net relative motion between the particles and the dust can be neglected. In the analysis to follow, a number of other

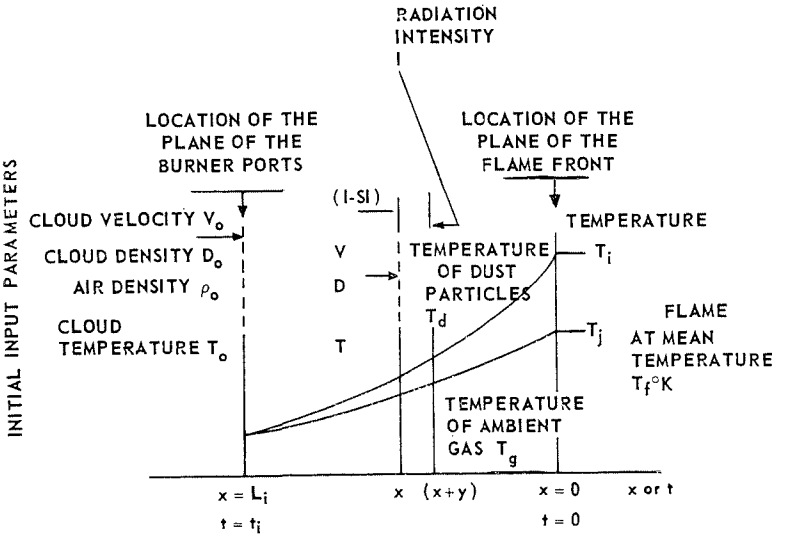

FIG. 1. Diagrammatic representation of a cloud element in the preignition zone. Temperature curves of dust and ambient gas are also shown.

assumptions are either stated explicitly or implied. They are mostly the standard assumptions, but as their number is not always appreciated they have been listed for convenience in the Appendix so that the assumptional basis of the theory, and its magnitude, is clearly understood. Their number and validity also become important now that there is a realistic possibility of taking them into account by numerical computation.

Equations

For the model as described and illustrated in Fig. 1, three differential equations governing the behavior of the system are required: (1) that for the heat transfer by radiation from the flame to the dust; (2) that for the loss of heat by conduction from the particles to the ambient gas; and (3) that for the rate of rise of the gas and particle temperatures.

Radiation Transfer. In Fig. 1 the radiation intensity incident on the element η is I so, for an attenuation coefficient k, we have

$$dI/dx = +kI \tag{2a}$$

All quantities are positive in this equation since I decays in the negative x direction. The absorption coefficient k may be related to the particle size (of radius a), and to particle density (by number n_d); we assume that the fractional absorption of monotropic radiation passing through a very thin element of the cloud is the ratio: projected solid area of particles to total area of containing element. We then have for the absorption coefficient

$$k = \pi a^2 n_d \tag{3a}$$

$$= 3D/4a\sigma \tag{3b}$$

where D is the dust cloud concentration; this is related to the solid particle density σ by

$$D = (4/3)\pi a^3 \sigma n_d \tag{4}$$

This introduces assumptions (1) and (2) (see Appendix); namely that the particles are spherical and monodisperse.

This standard analysis of radiation absorption by particulate clouds was not used by Nusselt[1]; he used a probability argument to establish a view factor for a single particle, and then summed for many particles. This, however, is cumbersome as the resulting equation for absorption by a mass of particles then had to be solved numerically whereas, as shown below, Eq. (2) in a slightly different form can be solved analytically.

Particle–Gas Conduction. For a particle at temperature T_d surrounded by gas at a temperature T_g the total rate of heat transfer in a quiescent system (Nusselt number 2) is

$$q = 4\pi a^2 \lambda (T_d - T_g)/a \tag{5}$$

where λ is the thermal conductivity of the gas. The restriction of quiescence is based on assumptions (4) and (5) (see Appendix) of zero relative motion between the particles and gas.

Since there are n particles exchanging heat with unit gas volume at density ρ and constant pressure specific heat c_p, then

$$dT_g/dt = (4\pi a n \lambda/\rho c_p)(T_d - T_g) \tag{6a}$$

$$= (4\pi\lambda/a\rho c_p)(T_d - T_g) \tag{6b}$$

the second form being obtained by elimination of n. This statement neglects the heat capacity of the boundary layer, thus introducing assumption (7) (Appendix). Eq. (6b) is Nusselts original equation for the temperature rise of the gas, and it incorporates the implicit assumption (6) that the volume occupied by the dust in the cloud is negligible.

Energy in the Cloud. The energy absorbed from the radiation by the dust particles, and partly transmitted to the ambient gas, is δI. This raises both the particles temperature and the gas temperature by small but different increments. By a simple heat balance between the absorbed radiation and the temperature rises of the two components, we then get

$$dI/dx = Dc_d(dT_d/dt) + \rho c_p(dT_g/dt) \tag{7a}$$

$$= kI \quad \text{from Eq. (2a)} \tag{7b}$$

Time Functions. The differential equations above are a mixture of functions in both space and time, but as they have to be solved simultaneously it is convenient to reduce them all to time functions. As the system is a steady state we may write

$$d/dx = (d/dt)(dt/dx) = (1/v)(d/dt) \tag{8}$$

whence Eq. (2a) becomes

$$dI/dt = (kv) \cdot I \tag{2a}$$

$$= m \cdot I \tag{2b}$$

where m is the time-attenuation coefficient, given by

$$m = kv = 3D_0 v_0/4a\sigma \tag{9}$$

derived by substitution and rearrangement from Eqs. (3b) and (1). Hence, m is a constant, independent of x and t.

Similarly, Eqs. (6b) and (7) become

$$dT_g/dt = (4m\alpha/av_0)(T_d - T_g) \tag{6c}$$

where α is the thermal diffusivity $(\lambda/\rho_0 c_p)$, and Eq. (7) becomes

$$(m/v_0) \cdot I = (D_0 c_d)(dT_d/dt) + (\rho_0 c_p)(dT_g/dt) \tag{7c}$$

Solutions

Radiation Attenuation. Because the time-attenuation coefficient m is independent of space and time, Eq. (2c) may now be integrated independently. Taking limits: $I = I$ at $t = t$; and $I = I_f$ at $t = 0$ we get

$$I = I_f e^{mt} \tag{10}$$

Since t is inherently negative by formulation of the problem, the equation shows that the radiation intensity therefore decays exponentially with time away from the flame front, running into the cloud towards the burner array.

The attenuation with *distance* through the cloud on the other hand will only approximate to an exponential because, as the expansion of the cloud on heating makes it accelerate, its change in position with time is nonlinear.

Temperature Functions; General Solutions. The two differential equations now to be solved simultaneously are (6c) and (7c). Writing

$$4m\alpha/av_0 = K \tag{11}$$

and substituting for I in Eq. (7c) we have

$$dT_g/dt = K(T_d - T_g) \tag{6d}$$

and

$$(m/v_0) I_f e^{mt} = D_0 c_p (dT_d/dt) + (dT_g/dt)(\rho_0 c_p) \tag{7d}$$

The solutions to these equations may be written

$$T_d - T_0 = \frac{I_f\{(e^{mt} - e^{mt_i}) - (e^{-nt} - e^{-nt_i}) e^{(m+n)t_i}(m/n)[1 - n/K]/[1 + m/K]\}}{v_0[D_0 c_d + \rho_0 c_p/(1 + m/K)]}$$

$$T_g - T_0 = \frac{I_f[(e^{mt} - e^{mt_i}) - (e^{-nt} - e^{-nt_i}) e^{(m+n)t_i}(m/n)]}{v_0\{D_0 c_d[1 + m/K] + \rho_0 c_p\}} \tag{12a, b}$$

where the coefficients m and K are given by Eqs. (9) and (11); and

$$n = (1 + \rho_0 c_p/D_0 c_d)(3\alpha D_0/a^2\sigma) \tag{13}$$

m is a function of velocity; n is not; both are inherently positive.

These solutions were obtained by inspection, although the probable forms were indicated by the special solutions given below. The boundary limits taken were:

at $t = t_i$; $T_d = T_g = T_0$;

at $t = t$; $T_d = T_d$; $T_g = T_g$

Special Solutions. Certain special cases are now considered to illustrate the influence of different components in the general solution; these were also helpful originally in providing indications of the form of the general solutions above. There are two groups to be considered: the infinite system ($t_i = \infty$) in which the distance between burner array and flame front is assumed to be infinite, and the finite system. For each system the following cases are considered: (1) that $T_d = T_g$, as a consequence of the heat transfer between particles and gas being assumed infinitely fast; (2) that T_g remains constant, (a) because the heat loss from the dust is assumed to be infinitely slow and no air heats up; and (b) because the heat capacity of the air is assumed to be infinitely large; and finally (3) no special assumptions are made.

So that the various solutions can be more easily compared they have been set out in Table 1. The exponential term in n that appears in these solutions in cases (2b) and (3) of the finite system, is clearly the term governing the heat transfer from the dust to the air; this interpretation was substantiated by solving the equation for the heat loss from the dust to the air alone.

Flame Speed

The use of the above equations to predict flame speed is now possible, though flame speed must first be defined.

Flame speed is most clearly defined in the case of a moving flame and a stationary cloud; in such a case the flame speed is the rate of displacement of the flame front relative to the cold stationary cloud, and to the container walls. If the cold cloud is now blown forward at such a speed that the flame front is brought to rest, the flame speed is now defined by the input speed of the cold cloud, and *not* as defined by Nusselt[1] as the hot cloud speed at the flame front; in the plane flame system, the flame speed therefore coincides with the burning velocity. The speed relative to the hot cloud in the plane flame coincides in direction with the flame speed, but in magnitude is higher

TABLE 1

Special solutions of heat transfer equations.

A. Infinite system ($t_i = \infty$)

(1) $T_d = T_g$ Infinite heat transfer rate from dust to air

$$T - T_0 = \frac{I_f e^{mt}}{v_0[D_0 c_d + \rho_0 c_p]} \tag{14a}$$

(2) T_g, constant

(a) Heat transfer from dust to air assumed zero; no air heats up

$$T_d - T_0 = I_f e^{mt}/v_0 D_0 c_d \tag{15a}$$

(b) Heat capacity of air assumed infinite

$$T_d - T_0 = I_f e^{mt}/v_0[D_0 c_d + \rho_0 c_p/(m/K)] \tag{16a}$$

(3) $T_d \neq T_g$ No special assumptions made

$$T_d - T_0 = \frac{I_f e^{mt}}{v_0[D_0 c_d + \rho_0 c_p/(1 + m/K)]} \tag{17a}$$

$$T_g - T_0 = \frac{I_f e^{mt}}{v_0[D_0 c_d(1 + m/K) + \rho_0 c_p]} \tag{17b}$$

B. Finite system

(1) $T_d = T_g$ Infinite heat transfer rate from dust to air

$$T - T_0 = \frac{I_f(e^{mt} - e^{mt_i})}{v_0[D_0 c_d + \rho_0 c_p]} \tag{14b}$$

(2) T_g, constant

(a) Heat transfer from dust to air assumed zero; no air heats up

$$T_d - T_0 = I_f(e^{mt} - e^{mt_i})/v_0 D_0 c_d \tag{15b}$$

(b) Heat capacity of air assumed infinite

$$T_d - T_0 = \frac{I_f[(e^{mt} - e^{mt_i}) - (e^{-nt} - e^{-nt_i})]}{v_0[D_0 c_d + \rho_0 c_p/(m/K)]} \tag{16b}$$

(3) $T_d \neq T_g$ No special assumptions made

General solutions: Eqs. (12a, b)

than the flame speed because it has to match the velocity of the cold cloud speed *plus* the additional effect of the thermal expansion towards the flame.

At the flame front the particle temperature has just reached the ignition temperature T_i, so writing s as the flame speed in place of the cold cloud speed v_0, and rearranging Eq. (12a) we have

$$s = \frac{I_f(1 - e^{+mt_i})}{(T_i - T_0)\{D_0 c_d + \rho_0 c_p/[1 + m/K]\}} \times \left[1 + \frac{(1 - e^{-nt_i})[1 - n/K]m}{(1 - e^{mt_i})[1 + m/K]n}\right] \tag{18}$$

TABLE 2

Special solutions of flame speed equations

A. Infinite system ($t_i = \infty$)

(1) $T_d = T_g$ Infinite heat transfer rate from dust to air

$$s_0 = I_f/(T_i - T_0)(D_0 c_d + \rho_0 c_p) \tag{19a}$$

(2) T_g, constant

(a) Heat transfer from dust to air assumed zero; no air heats up

$$s_0 = I_f/(T_i - T_0)(D_0 c_d) \tag{20a}$$

(b) Heat capacity of air assumed infinite

$$s_0 = I_f/(T_i - T_0)[D_0 c_d + \rho_0 c_p/(m/K)] \tag{21a}$$

(3) $T_d \neq T_g$ No special assumptions made

$$s_0 = I_f/(T_i - T_0)[D_0 c_d + \rho_0 c_p/(1 + m/K)] \tag{22}$$

B. Finite system

(1) $T_d = T_g$ Infinite heat transfer rate from dust to air

$$s = \frac{I_f(1 - e^{mt_i})}{(T_i - T_0)(D_0 c_d + \rho_0 c_p)} \tag{19b}$$

(2) T_g, constant

(a) Heat transfer from dust to air assumed zero; no air heats up

$$s = I_f(1 - e^{mt_i})/(T_i - T_0) D_0 c_d \tag{20b}$$

(b) Heat capacity of air assumed infinite

$$s = \frac{I_f[(1 - e^{mt_i}) - (1 - e^{-nt_i})]}{(T_i - T_0)[D_0 c_d + \rho_0 c_p/(m/K)]} \tag{21b}$$

(3) $T_d \neq T_g$ No special assumptions made

General solutions: Eq. (18)

This may be compared with the equation proposed by Cassel *et al.*[3] for burning velocity.

As before, particular solutions can be deduced for the special systems described above, and these have been set out in Table 2; for reasons to be given later the values of s at infinite t_i are written as s_0.

Discussion

Experimental Background. Before discussing the consequences of the flame speed equations some brief outline of the experimental devices used to get flame speed data will help to place the theory in perspective.

The first of all plane flame systems in which recirculation was positively eliminated was a vertical tube device, with top dust feed, developed by Jones and White[4] to study moving flames; but, although they reported satisfactory propagation of flame, both with bottom open-end and top closed-end ignition, they were interested only in measuring limit concentrations, not in flame speeds. The first detailed measurements of speed in plane dust flames are therefore believed to be those made in a copy[5] of the Jones and

White apparatus; the dust used was from cork, a carbonaceous material that can apparently be regarded as a very low rank coal,[6] and the flame speeds were in the range: 0.35 to 1.1 m/sec. As the vertical containing tube was Pyrex of only 3-inch diameter, the lateral heat loss possibly represented a substantial thermal load on the flame; the system has therefore been criticized on the grounds that, although recirculation was eliminated, true one-dimensionality may not have been achieved because the thermal load could generate a temperature distribution across the flame. This objection was largely satisfied in the next system developed; this was the furnace used to get the data (to be reported in due course) against which the theory in this paper is being tested. The furnace was of refractory insulating brick, about 9 ft high, 6-inch internal cross section, and 3-inch walls, with a cone-shaped top to contain the jet and so eliminate recirculation; the dust and air were introduced and mixed at the cone apex. The design of this system was based explicitly on the horizontal cone-furnace used by Taffanel and Durr[7] for flame speed measurements; this cone method for flame speeds was first proposed by Gouy,[8] and early users included Michelson[9] and Mache.[10] This furnace also served in effect as the prototype for the larger one-dimensional flame furnace already reported in the literature.[11,12,13] One other plane flame system exists: the stationary flame device built by Cassel *et al.*[3b] using a Mache-Hebra burner; the flame length in this is about 10 cm (compared with up to 1.5 m in the moving flames; about 2 m in the smaller cone furnace; and 4 to 5 m in the larger cone furnace.[11,12,13]

Influence of Particle–Gas Temperature Difference. It is clear from Tables 1 and 2, with Eqs. (12) and (18), that much of the complexity of the temperature and flame speed solutions is a consequence of the temperature difference between particles and gas. This temperature difference carries two physical implications: firstly, the implied assumption that the volatiles still ignite at the moment of evolution (see Appendix: point 9), in spite of the lower gas temperature; and secondly, that there is an effective reduction in the thermal capacity of the cloud.

In fact it seems unlikely that the volatiles will always ignite at the moment of evolution, but the impression from photographic and other evidence[5,14] is that, when the volatiles are eventually ignited downstream from the flame front, the flame then flashes rapidly back upstream to the evolution point or flame front. The net effect then is that of immediate ignition; this, however, is a point that we hope to test experimentally in a current experimental project.

The magnitude of the temperature difference effect is of interest. This may be deduced from a thermal capacity factor β given from Eq. (12a) by

$$\beta = 1/(1 + m/K) \tag{23a}$$

$$= 1/(1 + av_0/4\alpha) \quad [\text{from Eq. (11)}] \tag{23b}$$

The value of this factor lies between 0 and 1. These limits are obtained at the extreme values of (1) either the input speed v_0 (i.e., the flame speed) at infinity and zero, or, (2) at values of thermal diffusivity (α) at zero and infinity. The direct physical meaning of this capacity factor β is that it represents the fractional heat input into the air as a consequence of this only heating up to the gas temperature T_g instead of to the particle temperature, T_d. As a net, or effective, physical meaning it can also be looked at in two other ways: (i) it is as though all the air heats up to the particle temperature T_d, but its effective heat capacity is only a fraction β that of its true value; or (ii) it is as though only the fraction of air, β, heats up to T_d, though that fraction then exerts its true heat capacity.

Values of β have been calculated to get an order of magnitude. For particles of 25 and 5 microns radius, taking v_0 as 1 m/sec, and α as 0.25, the respective values for β were 0.8 and 0.95. This means in effect that respectively 80 per cent and 95 per cent of the air is heated to the particle temperature; or alternatively that all the air is so heated, but having reduced heat capacity by the percentages given.

With such close approximations to full heating it does seem reasonable therefore to neglect the over-all effect of temperature differential, at least at a first approximation. It follows also that the additional terms involving exp $(-nt)$ in the temperature and flame speed expressions can also be neglected within the same limits of accuracy, as we shall do in the remaining sections.

Flame Position. The flame has been assumed to stabilize at the plane where the burning velocity and the (hot) cloud speed at the moment of ignition are equal and opposite. The ignition time and the cold cloud speed (or flame speed) under these conditions are then related by the flame speed Eq. (18). Adopting the approximations described in the previous section we may use the simplified expression

$$s = v_0 = \frac{I_f(1 - e^{+mt_i})}{(T_i - T_0)(D_0c_d + \rho_0c_p)} \tag{19b}$$

From this equation it is clear that, other things being equal, the ignition time—unexpectedly—is a dependent parameter that is determined within certain limits by the independent param-

eter v_0. Increasing v_0 will increase t_i, and hence increase also the ignition distance L_i, so that the flame front is blown further and further away from the burners. The theoretical limit to this is when the flame front has receded to infinity. This is achieved by a limiting input velocity that is not itself infinite; as shown by the Eq. (19b) the relationship between v_0 and t_i is approximately a (1 − exp)—only approximately so because the decay parameter m is itself a function of v_0 [Eq. (9)].

It is self-evident that the ignition distance is likely to increase as the input velocity increases, but it is less obvious why the ignition time will also do this. The specific ignition energy is a constant (other things being invariant), being given by $(T_i - T_0)(D_0 c_d + \rho_0 c_p)$; so, for a given fraction of radiant energy absorbed between the flame front and burners [given by $(1 - e^{+mt_i})$], it might seem intuitively that the ignition time should be an invariant with input velocity, instead of increasing as it does. The physical reason for this increase seems to be as follows: assume first that t_i remains constant as v_0 increases; so, clearly, the ignition distance will also increase. Discounting the effect of the variable decay parameter, m, the shape of the radiation profile otherwise remains unchanged; but because it now extends through a greater length of cloud, this means (as a simple integration shows) that the *mean* radiation density or flux drops. For the cloud then to absorb the necessary specific ignition energy in such a field of reduced radiation density it requires more time: the ignition time, therefore must also rise.

Another unexpected factor is the existence of a lower limit to both ignition time and distance. It might be thought perhaps that, as the approach velocity of the cold dust cloud tended to zero, the flame front would approach as close as we please to the burner while still allowing sufficient time for the necessary absorption of heat. However, for small values of t_i we may expand the exponential of Eq. (19b) to its first two terms and, substituting then for m, we get

$$(t_i)_L = (4a\sigma/3I_f)(T_i - T_0)[c_d + c_p(\rho_0/D_0)] \tag{24}$$

which is independent of input velocity v_0. By Eq. (19b) there is also a limiting input velocity to give this limiting ignition time; so there must also be, in that case, a low limit to the ignition distance.

Two other important factors that affect ignition distance are: cloud density D_0; and input temperature T_0. The effect of cloud density is complex, and to determine its effect requires detailed calculation from the equations because D_0 appears both in the denominator of the equation and in the absorption coefficient m. The effect of temperature as preheat, however, is clear: by Eq. (19b) the ignition time must drop, as we would expect, as T_0 or the preheat increases; this also reduces $(t_i)_L$.

Ignition Time and Distance. Values of the ignition times and distances under limiting conditions have considerable physical significance.

For the lower limit of ignition time, consider a particle of 5 microns radius, influenced by a black body flame at 1500°C and heated by this flame to ignition at 300° above the input temperature T_0. From Eq. (24) the minimum ignition time at a stoichiometric concentration is 150 to 200 millisec (which as observed before can be reduced by preheat). The minimum velocity for dust clouds is when dropping under gravity. Measured values for such clouds[15] are about 50 cm/sec for the usual particle size distribution found in P.F. clouds; so the minimum ignition distance must be about 10 cm. This means that plane flames, of coal-in-air, ignited only by back radiation from the flame are unlikely to stabilize in a distance less than about 10 cm from the burner. Cassel *et al.*[3b] stabilized their graphite flames in less distance than this but their particle sizes and cloud velocities were smaller, and they also estimated that the conductive heat transfer contribution was as high as 40 per cent of the total. It is questionable, therefore, whether the behavior of such small flames can be usefully or reliably extrapolated to predict or interpret the behavior of large ones (see also Appendix: point 10).

This figure of 10 cm can now be compared with the effective "infinite" distance. Quite clearly, if the exponential term of Eq. (19b) is small, say less than 0.01, the ignition distance is effectively infinite. Once again values have been calculated for particles of 5 microns radius at a stoichiometric concentration; for these, the "infinite" ignition time is found to be $\frac{1}{2}$ to 1 sec at input speeds of 50 to 100 m/sec. The ignition distance is therefore about 1 meter. This point was only appreciated after the completion of our experiments (yet to be reported) but, as it happened, the ignition distance was about 90 cm throughout so that the absorption distance was close to the "infinite" requirement.

If this is true of the cloud it is also true of the radiating flame itself which will only behave substantially as a black body if it is more than about 1 meter or so thick; indeed measurements of the emissivity even across the 2 meters of the IJmuiden furnace have shown values down to 0.5 (due substantially to ash) in the tail of the flame. It is clear then that this is another factor

that must vitiate the usefulness of studies on small flames of 0.1 m thickness or thereabouts, whether plane or jet,[3,16–20] as methods of elucidating large flame behavior (though such small flame studies can, of course, have considerable intrinsic interest and value of their own).

Flame Speed. The flame speed is given by the general Eq. (18); the approximate form to be used as the basis for the discussion in this section is Eq. (19b), based on the assumption that the gas–particle heat exchange is fast, and which may be written

$$v_0 = s = s_0(1 - e^{+mt_i}) \qquad (25a)$$

where the limiting value s_0 is given by Eq. (19a) (Table 2).

Now it has already been shown above (section on Influence of Particle Gas Temperature Difference) that, of the parameters in this equation, the dependent one is t_i, and the independent one (between two limits) is v_0. Because, therefore, of the relation between v_0 and s, it follows that flame speed is also an independent parameter and, within certain limits, also within our arbitrary control. What, however, is not within our control is the upper limiting or "infinite" flame speed, s_0; this is a fundamental parameter determined solely by the combustion conditions and behavior, and will be referred to as the fundamental flame speed. As this fundamental measurement can only be made directly on reasonably large flames, of about one meter ignition distance (by the calculations of the previous section), this explains why it was so important that the ignition distance in our experiments should have approached this value.

The fundamental flame speed, s_0, varies with cloud concentration, flame temperature, and input temperature (T_0), as shown by Eq. (19a). The variation of s_0 with cloud concentration is of hyperbolic form in the fuel-rich range from the stoichiometric concentration upwards; below the stoichiometric, the position has still not been elucidated because of the involved relationship with flame temperature. Just how flame temperature varies with concentration is still largely undetermined, so far as inclusion in any theory is concerned, although the additional work on combustion mechanism[21–24] (that is another part of this general program) is directed partly towards elucidation of this relationship. In general, however, we expect to find the peak flame temperature to exist at the stoichiometric concentration, dropping away on both sides of this in either the air-rich or the fuel-rich direction. On the fuel-rich side this may be partially offset by the increased surface area of the dust causing an increase in the rate of heat release; this could reduce the proportional heat losses due to thermal load and so maintain the flame temperature against the rising heat capacity of the dust cloud. In this connection we may note that the measured expansion factor in the cork dust flames,[5] which estimates the flame temperature, was substantially constant over a wide range of fuel-rich concentrations. However, the net effect of concentration in general will probably be to steepen the flame speed curve, as calculated from a constant flame temperature (constant I_f), on either side of the stoichiometric.

The influence of the third factor, input temperature (T_0) or preheat, is also self-evident. As T_0 rises, ($T_i - T_0$) drops, and the flame speed will rise; this has particular relevance, as will be explained below, to stabilization of jet flames.

If the ignition time or distance is not either infinite, or effectively so, flames can still be stabilized at speeds below the value of the fundamental speed, s_0. To see the qualitative effect of reducing t_i or L_i it is convenient to introduce the approximation of writing L_i for ($v_0 t_i$). The attenuation coefficient, m, which is a function of v_0, may then be replaced by k_0, where

$$k_0 = 3D_0/4a\sigma \qquad (3c)$$

This is independent of v_0. We then have also

$$s = s_0(1 - e^{+k_0 L_i}) \qquad (25b)$$

The variation of flame speed with dust concentration is illustrated graphically in Fig. 2. These values have been calculated for two particle sizes, 5 and 25 microns radius (diameter 10 and 50 microns), assuming a radiation flux from a black body flame at 1500°C. Of particular interest here, of course, is the effect of different values of the ignition distance. This figure shows that the exponential ignition-distance term creates a peak in the flame speed curve which is displaced in the fuel-rich direction, away from its expected position at the stoichiometric concentration. As the ignition distance is reduced, the peak flame speed drops in value and moves progressively fuel-rich: This is believed to be particularly significant in relation to jet flames. In our experiments, the peak appeared at a concentration of about 0.15 g/liter, which is about 1.5 times that of the stoichiometric. In contrast, the moving cork-dust flames[5] showed very flat peaks at 5 to 7 times the stoichiometric: This phenomenon requires closer examination but is believed to be quite possibly due to the preferential ignition and combustion of an increasing proportion of fines.

Jet and Explosion Flames. By comparison with the plane flames, the recirculating-jet and turbulent-explosion flames are markedly more complex. There is not even an approximate working solu-

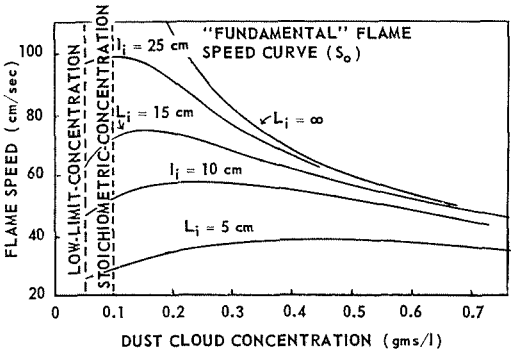

(a)

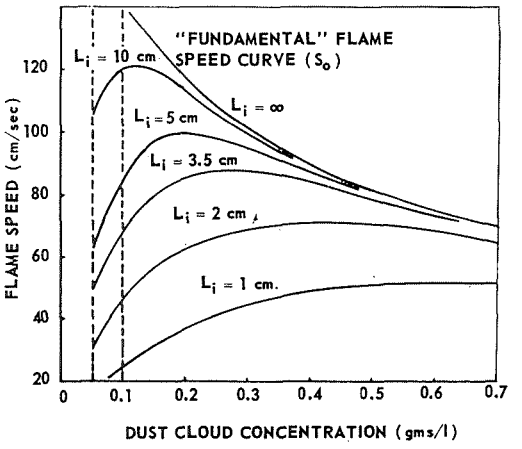

(b)

FIG. 2. Variation of flame speed with dust concentration showing the influence of finite ignition distance (L_i) on the value of the fundamental speed, s_0. (a) Particle radius, 25 microns. (b) Particle radius, 5 microns.

tion to either system yet in existence; however, the plane flame solution does provide by contrast quite a lot of useful information, at least about the jet flame.

The jet flame is, of course, three-dimensional with marked recirculation, due to entrainment that increases with the jet momentum, and its flame speed is at least an order of magnitude greater than that of the plane flame. The value of the recirculation in stabilizing the flame has been regarded as questionable,[25] and it is often assumed that marked increase in flame speed, and therefore improved stability, can only be achieved by the use of refractory wall sections round the burners to increase the radiation intensity; in industrial plants this is usually referred to as "ignition" refractory. If, however, the burner is surrounded by such refractory area that it matches the flame area seen by the cloud (and this would be a lot), then at the *same* temperature and emissivity as the flame, the radiant flux to the dust cloud would only be doubled. By Eq. (18) the flame speed also would only be doubled, but as we require a factor of 10 or more, it is clear that the direct influence of the refractory on either the flame speed or flame stability is small. If, however, we assume that hot combustion products drawn back from the flame by recirculation are mixed in with the incoming fuel jet, this "preheat" then in effect raises the initial temperature, T_0. If $(T_i - T_0)$ is initially 300°, then raising T_0 by 270° reduces the difference to 30°, and by Eq. (18) this increases the flame speed by a factor of 10. Now, if the mass of gas recycled from the flame is at 1500°C, and it then shares its heat completely with the fuel jet, the mass required is only about 20 per cent that of the fuel jet. By volume at flame temperature this would be 120 per cent of the fuel jet. Since measurements[26] have now shown that the percentage recirculation in the experimental IJmuiden furnace can be as high as 300 per cent, it is clear that recirculation is entirely capable of accounting for the difference in flame speeds between the plane and the jet flame; in the jet flame it means that 90 to 95 per cent of the ignition heat is supplied by recirculation. Experimentally, support for this view is provided by some observations made by Beér[12] on the one-dimensional furnace. This furnace was fitted with gas burners to inject a fully burned stoichiometric mixture of towns gas and air into the stabilizing cone, about half-way up it; these burners were intended to simulate an artificial recirculation effect. The injected quantity of combustion products was about 150 per cent of the primary cloud, and their effect was to increase the flame speed by at least a factor of 3. The flame front was then observed to be stabilized at the gas injection ports so that any further potential increase in flame speed could not be observed by this method; the result, however, was in line with expectation. If there were any effects caused by the oxygen vitiation due to the injection of combustion products, these were never observed.

What also becomes clear from this analysis is the probable function of the so-called "ignition" refractories. When ignition is unstable and can be improved by the addition of refractory round the burners, its probable function is to cut down the convective heat loss of the recirculating products to the cold water-wall. The effect of such a thermal load on the recirculation products would also seem to be important in very small jet flames[16–20] which in general could only be stabilized in the presence of a continuous ignition source such as a surrounding gas flame or electrical heating of the furnace walls.

The most important factor in jet flames, how-

ever, is the existence of the prevailing belief that the peak flame speed in coal dust flames occurs at a concentration 2 to 5 times that of the stoichiometric. Almost certainly the origin of this belief is based on the widely quoted set of flame speed curves published by de Grey,[27] and evidently interpretively derived from the dozen or so experimental values obtained by Taffanel and Durr[7] from a single coal. The industrial importance of this, if correct, is its value as the basis of de Grey's principles of burner design.[27] According to these, the primary burner should carry the optimum fuel-air mixture that will generate the peak flame speed; this will generate the most stable flames and provide the maximum (and therefore the most economical) utilization of combustion space. Unfortunately, the de Grey curves have never been substantiated; indeed, on the contrary they have been heavily criticized by Orning.[28] Certainly our *a priori* expectations would place the peak flame speed at a concentration close to that of the stoichiometric, as found now in our plane flame experiments, and as also implied in some explosion propagation experiments.[29] It may be, however, that the answer to this is to be found in the ignition-distance factor as shown by Fig. 2. If there is 300 per cent recirculation in the furnace, the minimum ignition time as calculated from Eq. (24) is reduced, by this effective preheat, from 200 millisec to about 10, which is about the value measured in the IJmuiden furnace.[30] Limiting input conditions for a horizontal burner are determined primarily by the minimum conveying velocity of about 60 ft/sec that must be exceeded to keep the dust in suspension. It would seem then that this may have created such ignition conditions that the ignition time or distance was low, and the consequence was that the exponential factor of Eq. (25b) created a flame speed peak in the fuel-rich region. This proposition now requires testing by experimental investigation.

Conclusions

The theoretical system analyzed is that of a plane flame front propagating through a monodisperse and premixed dust cloud, formed by the suspension of finely ground coal in air. The propagation mechanism is assumed to be the radiant heating to ignition of the dust cloud contained between the flame front and the burners. The specification of coal dust implies that the ignition temperature, being the coal decomposition temperature, is constant and independent of the ambient conditions. The flame front is assumed to stabilize where the burning velocity and the hot cloud speed are equal and opposite. The conclusions of the analysis are that:

(1) Flame speed can be defined as the *cold* cloud speed required to hold the flame stationary at some suitable plane, and is identical to burning velocity in this experimental system.

(2) The fundamental flame speed, s_0, is that obtained when the ignition time or distance is infinite.

(3) The fundamental flame speed is given by the general Eq. (22); if heat transfer between the particles and gas is fast it may be written approximately as

$$s_0 = I_f/(T_i - T_0)(D_0 c_d + \rho_0 c_p) \quad (19a)$$

(4) The fundamental flame speed is expected to peak at the stoichiometric concentration; it has a normal value of the order of 1 m/sec; in the fuel-rich region the value drops with increasing dust concentration, but it increases with rise in input temperature or preheat.

(5) With reduced input velocity of the dust cloud the flame speed drops and is then controllable by adjustment of the input velocity; the flame front then adjusts to a position from the burners such that the ignition time or distance is finite. Ignition time and distance are the dependent parameters, being related to the independently controllable flame speed by

$$s = s_0(1 - e^{mt_i}) \quad (20a)$$

$$\cong s_0(1 - e^{k_0 L_i}) \quad (20b)$$

(6) As ignition time or distance is allowed to drop so does the flame speed; and the position of the flame speed peak (optimum concentration) moves progressively fuel-rich.

(7) Flame speed in enclosed jet flames is increased as a consequence of "preheat" by the recycled combustion products; calculations based on the effect of preheating indicate that this recirculation can increase the flame speed by at least an order of magnitude (factor of 10 or more). Recirculation then supplies 90 to 95 per cent of the heat required for ignition. The effect of "ignition" refractory round burners is not so much to increase the radiant flux to the dust cloud as to maintain the temperature of the recirculating flow.

(8) Peak flame speeds in jet flames are usually believed to occur at high fuel-rich concentrations; if this is true, as has yet to be confirmed experimentally, it is probably a consequence of fuel injection speeds or recirculation preheats being such as to create low ignition times, so that the peak flame speed migrates into the fuel-rich region.

Nomenclature

a	Particle radius
c_d	Specific heat of dust
c_p	Constant pressure specific heat of ambient gas
D	Dust cloud concentration
I, I_f	Radiation intensity: at any x-plane; and at the flame front
k, k_0	Radiation space attenuation coefficient: space variant; and invariant
K	Convection coefficient parameter ($= 4m\alpha/av_0$)
L_i	Ignition distance
L_f	Flame length
m	Radiation time-attenuation coefficient
n_d	Numerical particle density (number per unit volume)
n	Convection attenuation coefficient
q	Rate of heat transfer (cal per unit area per unit time)
s, s_0	Flame speed: dependent speed; fudamental speed
T, T_d, T_g T_i, T_f	Temperature: any (general); of a dust particle; of the ambient gas; of particle ignition; mean flame
t	Time
t_i, $(t_i)_L$	Ignition time; limiting ignition time
v, v_0	Velocity of dust cloud: at any x-plane; and at input
x	Distance
α	Thermal diffusivity ($=\lambda/\rho_0 c_p$)
β	Thermal capacity factor
ϵ', ϵ	Emissivity: of the flame; and of a unit element of the flame
η, η_0	Volume of an element of the dust cloud: at any x-plane; and at input
λ	Thermal conductivity of the ambient gas
σ	Solid particle density
ρ, ρ_0	Air density: at any x-plane; and at input

Appendix

The assumptions that the developed theory is based on are listed here for reference and critical evaluation; now there is a possibility of detailed numerical solution by computer, the nature and magnitude of the approximations is no longer largely academic.

We have assumed that:

(1) The dust is composed of spherical particles of coal; this is the standard assumption[1] that ignores shape factor.

(2) There is no particle size distribution; inclusion of a size distribution must be considered in due course but at this stage would only obscure the physical picture being developed.

(3) Conduction from the flame through the gas is negligible; this again is a standard assumption[1] that is probably true to within a 10 per cent accuracy for fairly large flames. Incorporation of this factor in the system as described here would appear to preclude the possibility of an analytical solution; however, it is quite amenable to numerical solution by analog computer. The program for this has already been set up and we hope to calculate the effect of this factor in due course.

(4) There is no net relative motion between particles and air (i.e., no progressive displacement of one with respect to the other as assumed in the section on Equations). This is quite possibly true; conclusions based on Stoke's Law, as in Kisligs[31] or in Long and Murray's[32] analysis, are now thought to have been demonstrated[15] as inapplicable when considering high dust concentrations.

(5) Local relative motion between individual particles and the ambient gas (micromixing) is negligible; this is of doubtful validity but, lacking precise information relating to this particular system, it is currently the best assumption to make.

(6) The volume occupied by the dust is entirely negligible compared with the gas volume; since the porosity of the cloud varies from unity to about 0.9985 over the entire inflammable range this is acceptable.

(7) The thermal capacity of the boundary layer around each particle is small so that the temperature excess of this above the mean ambient gas temperature, due to the temperature gradient, is small. This is questionable; it could be significant but has never been calculated. The real temperature gradient extends far beyond the boundaries of the Nusselt "fictitious" or effective film, of thickness equal to the particle radius; and with interparticle distances of only 30 diameters or less, the effect could be appreciable.

(8) The thermal conductivities and specific heats are invariant over the temperature range concerned; this again is not true but is accurate enough as a reasonable assumption to get an analytical solution. Here again this can be included in the analysis for numerical calculation by computer.

(9) The ignition temperature is fixed, independent of conditions; this again is a standard assumption but one that has been strongly criticized. For coals, however, it is our opinion that the "ignition" temperature is the coal decomposition temperature. The basis of this

opinion is the evidence provided by the interpretation of analyses of carbonized coals; these[33,34] show that the decomposition temperature is fairly clearly defined and rises steadily with coal rank. Since ignition in the dust flame starts in the evolved volatiles, with a rapid temperature rise at this point, it seems reasonable to equate the decomposition temperature with ignition temperature; the validity of this identification is currently being investigated experimentally. If true it operates as a decoupling factor between the preignition and the flame zones (as assumed in this paper).

(10) The flame may be regarded as a gray body of *average* temperature T_f, so the intensity of the radiant heat flux, I_f, at the flame front is given by

$$I_f = \epsilon' \sigma T_f^4$$

where the flame emissivity ϵ' is related to flame length (L_f), and to specific mean emissivity of an element of the flame (ϵ), by

$$\epsilon' = 1 - \exp(-\epsilon L_f)$$

This factor becomes important in flames less than 100 cm thick.[3,16–20] The assumptions of mean temperature and emissivity can only be eliminated by the use of the detailed kinetic equations for the reaction, and the use of computers for solution; again these necessary equations have been set up for computer solution.

Acknowledgments

This work formed part of a program on combustion phenomena in pulverized coals carried out for the Electricity Supply Research Council at the Department of Fuel Technology and Chemical Engineering, University of Sheffield, England.

We have pleasure in acknowledging provision of financial support for this work and permission to publish from the E.S.R.C.

References

1. Nusselt, W.: V.D.I. *68*, 124 (1924).
2. Traustel, S.: Feuerungstechnik *29*, 1, 25, 49 (1941).
3. (a) Cassell, H. M., Das Gupta, A. K. and Guruswamy, S.: *Third Symposium (International) on Combustion*, p. 185, Wisconsin, 1948. Williams and Wilkins, 1949. (b) Cassel, H. M., Liebman, I. and Mock, W. K.: *Sixth Symposium (International) on Combustion*, p. 602, New Haven, 1946. Reinhold Publishing Corp., 1957.
4. Jones, E. and White, A. G.: Conference on *Dust in Industry*, p. 129, Leeds, 1948. Society of the Chemical Industry (London, 1948).
5. (a) *1953 Annual Report of the Joint Fire Research Organization*, p. 23. H.M.S.O., 1954. (b) Essenhigh, R. H. and Woodhead, D. W.: Combustion and Flame *2*, 365 (1958).
6. Essenhigh, R. H.: Fuel *36*, 395 (1957).
7. Taffanel, J. and Durr, A.: *Fifth Series of Experiments on the Inflammation of Coal Dusts.* Comité Central des Houillères de France, Paris, August 1911.
8. Gouy, G.: Ann. Chim. Phys. *18*, 27 (1879).
9. Michaelson, W.: Ann. Physik *37*, 1 (1889).
10. Mache, H.: Ann. Chim. Phys. *46*, 527 (1907).
11. Beér, J. M., Thring, M. W. and Essenhigh, R. H.: Combustion and Flame *3*, 557 (1959).
12. Beér, J. M.: Ph.D. thesis. University of Sheffield, 1960.
13. Thring, M. W. and Beér, J. M.: *Proceedings of the 1960 Conference on Anthracite*: Bulletin of the Mineral Industries Experiments Station, Pennsylvania State University; No. 75 (1961) p. 25.
14. Thring, M. W. and Hubbard, E. H.: Conference: on *Flames and Industry*, London, 1957, paper 1, p. A1. Institute of Fuel, London, 1958.
15. Essenhigh, R. H.: *General Discussion on The Physical Chemistry of Aerosols*, Bristol, 1960, p. 145. Faraday Society, London, 1961.
16. Long, V. D.: Ph.D. thesis. Imperial Coll. of Science & Technology, London, 1956.
17. Burgoyne, J. H. and Long, V. D.: Conference on *Science in the Use of Coal*, Sheffield, April 1958, paper No. 28, p. D16. Institute of Fuel, London, 1958.
18. Hattori, H.: *Sixth Symposium (International) on Combustion*, p. 590. Reinhold, 1957.
19. Ghosh, B., Basu, D. and Roy, N. K.: *Ibid.* p. 595.
20. McCann, C. R. and Orning, A. A.: Paper presented at the A.S.M.E. 1961 (Nov.) Annual Meeting; Session on Furnace Performance Factors (No. 61–WA–302; to be published).
21. Essenhigh, R. H.: *Second Conference on Pulverized Fuel*, London, 1957, paper 2, p. B1. Institute of Fuel, London, 1958.
22. Essenhigh, R. H. and Thring, M. W.: Conference on *Science in the Use of Coal*, Sheffield, April, 1958, paper 29, p. D21. Institute of Fuel, London, 1958.
23. Essenhigh, R. H.: J. Inst. Fuel *34*, 239 (1961).
24. Beér, J. M. and Essenhigh, R. H.: Nature *187*, 1106 (1960).
25. Long, V. D.: Conference on *Science in the Use of Coal*, Sheffield, April, 1958, p. E53. Institute of Fuel, London, 1958.
26. Beér, J. M.: Private communication, 1961.
27. de Grey, A.: Rev. de Métall. *19*, 645 (1922).
28. Orning, A. A.: *Chemistry of Coal Utilization*, Vol. II, p. 1549. Chapman & Hall, London, 1947.

29. ESSENHIGH, R. H. and PERRY, M. G.: Conference on *Science in the Use of Coal*, Sheffield, April 1958, p. D1. Institute of Fuel, London, 1958.
30. International Flame Research Foundation: *Report on the First Performance Trial with Pulverized Coal*; August, 1956.
31. KISLIG, F.: Thesis: Eidgenössische Technische Hochschule. Zurich: Rosch, Vogt; Bern, 1950.
32. LONG, V. D. and MURRAY, W. L.: Safety in Mines Research Establishment: Research Report No. 145 (H.M.S.O., 1958).
33. FRANKLIN, R. E.: Conference on *Ultra-Fine Structure of Coals and Cokes*; (B.C.U.R.A., London, 1944).
34. ESSENHIGH, R. H.: Conference on *Science in the Use of Coal*, Sheffield, April 1958, p. A73. Institute of Fuel, London, 1958.

Discussion

DR. R. G. SIDDALL (*Sheffield University*): The solution to simultaneous differential Eqs. (6d) and (7d) was "obtained by inspection." This "solution by inspection" is, however, unnecessary and prone to error and the method of analytical solution which should have been used is shown below.

Equation (7d) can be integrated directly with respect to time to give

$$D_0C_dT_d + \rho_0c_p \cdot T_g = (I_f/v_0)e^{mt} + A \qquad (1)$$

where A is a constant of integration whose value is to be determined directly from the boundary conditions. The conditions chosen by the author are $T_d = T_g = T_0$ at $t = t_i$. Substitution of these values into Eq. (1) leads to the following value for A

$$A = (D_0C_d + \rho_0c_p)T_0 - (I_f/v_0)e^{mt_i} \qquad (2)$$

Combination of Eqs. (1) and (2) leads to a simple relationship between T_d, T_g, and t which is about impossible to obtain by combination of the two solutions (12a, b) which are quoted in the paper. This relationship is

$$D_0C_d(T_d - T_0) + \rho_0c_p(T_g - T_0) = (I_f/V_0)(e^{mt} - e^{mt_i}) \qquad (3)$$

This equation can be used to test the justification of the assumption $T_d = T_g$ which is used in some solutions later in the paper and will indicate under what conditions this assumption is permissible.

On substituting solution (1) into the differential (6d) and rearranging, the following simple first order differential equation in T_g is obtained.

$$\frac{dT_g}{dt} + \phi T_g = \frac{K}{D_0c_d}\left[\frac{I_f}{v_0}e^{mt} + A\right] \qquad (4)$$

where

$$\phi = K\left(\frac{\rho_0c_p}{D_0c_d} + 1\right) \qquad (5)$$

Multiplying through by the integrating factor $e^{\phi t}$ and then integrating leads to the result

$$T_g = \frac{K}{D_0c_d}\left[\frac{I_f}{v_0}\cdot\frac{1}{(m + \phi)}e^{mt} + \frac{A}{\phi}\right] + Be^{-\phi t} \qquad (6)$$

where B is a constant of integration which is found by substitution of the boundary conditions. The resulting value of B is

$$B = e^{\phi t_i}\left\{T_0 - \frac{K}{D_0c_d}\left[\frac{I_f}{v_0(m + \phi)}e^{mt_i} + \frac{A}{\phi}\right]\right\} \qquad (7)$$

where A is given by Eq. (2). Substitution for A and B into Eq. (6) finally leads to the following equation for T_g

$$T_g - T_0 = \frac{KI_f}{v_0D_0c_d(m + \phi)}\left[(e^{mt} - e^{mt_i}) + (me/\phi)(m + \phi)t_i(e^{-\phi t_i} - e^{-\phi t})\right] \qquad (8)$$

Inspection of the author's constant n shows that $\phi = n$. So that the final solution, in terms of the constant used in the paper is

$$T_g - T_0 = \frac{KI_f}{v_0D_0c_d(m + n)}\left[(e^{mt} - e^{mt_i}) + (me/n)(m + n)t_i(e^{-nt} - e^{-nt_i})\right] \qquad (9)$$

This expression is to be compared with Eq. (12b) of the paper, the only difference being the plus sign before the second term in the square bracket.

The expression for T_g in Eq. (9) may finally be substituted into Eq. (1) to give the corresponding equation for T_d.

PROF. R. H. ESSENHIGH (*Pennsylvania State University*): As the final result is the same it checks the validity of the solution by inspection. As Dr. Siddall points out, his Eq. (3) provides additional information not otherwise easily obtainable. His contribution is welcome and appreciated.

DR. J. L. LAUER (*Sun Oil Company*): I am worried about the "decomposition = ignition" temperature as one point on the temperature scale. As decomposition is gradual, the temperature must go through a

range and furthermore, a concentration gradient around the particles will be established. I also would like to call attention to some of our observations with high-boiling petroleum residues. Motion picture studies have shown that droplets consisting of liquid + solid particles would break up into fragments during burning. Fragmentation would take place in spurts. Semisolids like asphaltenes would break up similarly and decompose much more rapidly during and after fragmentation.

PROF. R. H. ESSENHIGH: The point raised by Dr. Lauer about equating decomposition with ignition temperature is important, and we are in fact currently developing a research program to test the proposition experimentally. However, in the light of present knowledge I think that the proposition is acceptable as the most reasonable assumption to make at the present time. If it is not exactly true I think that in all probability it will prove to be effectively true: If volatiles that are generated at the flame front are carried downstream but not yet burning, eventually they will ignite and flame will flash back to their point or plane of evolution. This would appear to be the pattern as shown up by short exposure and time exposure photographs of the flame front.

So far as petroleum burning is concerned, behavior is superficially similar, but differences are important. Volatiles evolved from coal particles are channeled by the solid carbon matrix of the solid residue into irregular jets that issue with considerable force. This helps to break up any boundary layer with attendant concentration gradients, and promotes uniform mixing in the space between the particles. Also, the temperature is not held down, as it is in liquid drops until the lowest boiling point fraction has evaporated (unless the drop becomes superheated), so the temperature rise of a coal particle can be far more rapid than that of a liquid drop. The onset of volatile evolution from a coal particle is much more precisely determined, and evolution in quantity then takes place with a relatively small temperature rise.

If coal particles are heated too fast they can fragment, presumably because of pressures generated by too rapid generation of volatiles that cannot escape fast enough in the normal manner. In the single particle studies that I have carried out, this only happened with large particles (above about 1 mm). In flames, the steeper temperature gradient may promote fragmentation of much smaller particles but the evidence indicating that this is what is happening is still uncertain.

Fragmentation of liquid drops may be a different phenomenon. If heavy hydrocarbons crack to form a carbon residue inside the drop, this residue can absorb radiation that otherwise would have been transmitted. The residue is then able to heat up faster than the surrounding liquid. This means that the surrounding liquid must either boil or superheat. If it first superheats and then flashes into vapor, this could provide the driving force for exploding the drop into fragments.

Reaction Kinetics I

Chairman: Prof. M. Boudart
(*University of California*)

Vice Chairman: Dr. A. L. Berlad
(*General Dynamics*)

FLAME CHARACTERISTICS OF THE DIBORANE-HYDRAZINE SYSTEM

M. VANPÉE, A. CLARK, AND H. G. WOLFHARD

Premixed flames of diborane-hydrazine have been stabilized at low pressures and a number of their characteristics (stability region, burning velocity, reaction products, light emission) have been established. The flame could only be stabilized at pressures below 50 mm Hg because of adduct formation occurring at higher pressures. The main features of the flame are a high burning velocity (5 m/second), a low reaction temperature (≃1100°C) and the absence of any light emission other than a continuum from solid particles. The data support the view that originally a gaseous adduct is formed between diborane and hydrazine that grows by polymerization and dehydrogenation to form the final solid products of the flame.

Introduction

Exotic flames are of interest from a theoretical point of view as their properties can differ markedly from those of flames that have historically received extensive study. The diborane-hydrazine flame reaction is thus of special interest because it has unusual products, solid BNH_x and gaseous H_2, and a high reaction rate despite a low molar heat release and adiabatic flame temperature (actual temperature <2000°K).

Further, the flame is experimentally challenging because at 1 atmosphere premixed flames cannot be obtained.[1,2] Condensed phase adducts of explosive properties form as soon as diborane mixes with hydrazine, collapsing the flow and precluding a flame. However by working at low pressure, adduct formation (or condensation) can be delayed sufficiently to permit establishing a true premixed flame.

This paper describes the conditions under which a premixed flame was obtained. The flame characteristics such as burning velocity, spectrum, and combustion products were measured and analyzed. Finally the kinetics of the diborane-hydrazine flame are considered and reviewed in the light of the experimental results.

Experimental

Low Pressure Feed and Combustion System

Flames were obtained at 0.5 to 70 mm Hg, in the vacuum vessel shown in Fig. 1. Compared with earlier low-pressure flame apparatus[3] the present system had a very large (14 inches diameter × 48 inches length) combustion chamber and the pumping capacity was of the order of 600 cubic feet per minute. The vacuum system contains, in addition, a ballast tank of 500 cubic feet capacity which when evacuated can act as a pump, bypassing the mechanical pump so that corrosive gases do not damage it.

Figure 1 also shows the all-glass hydrazine flow system. Steady hydrazine vapor flows up to 4 grams/minute were obtained from a 3-liter flask, containing 300 to 500 grams of hydrazine, maintained at 110°C to obtain the needed vapor pressure. The flask was in an underground shelter adjacent to the laboratory. Diborane (refriger-

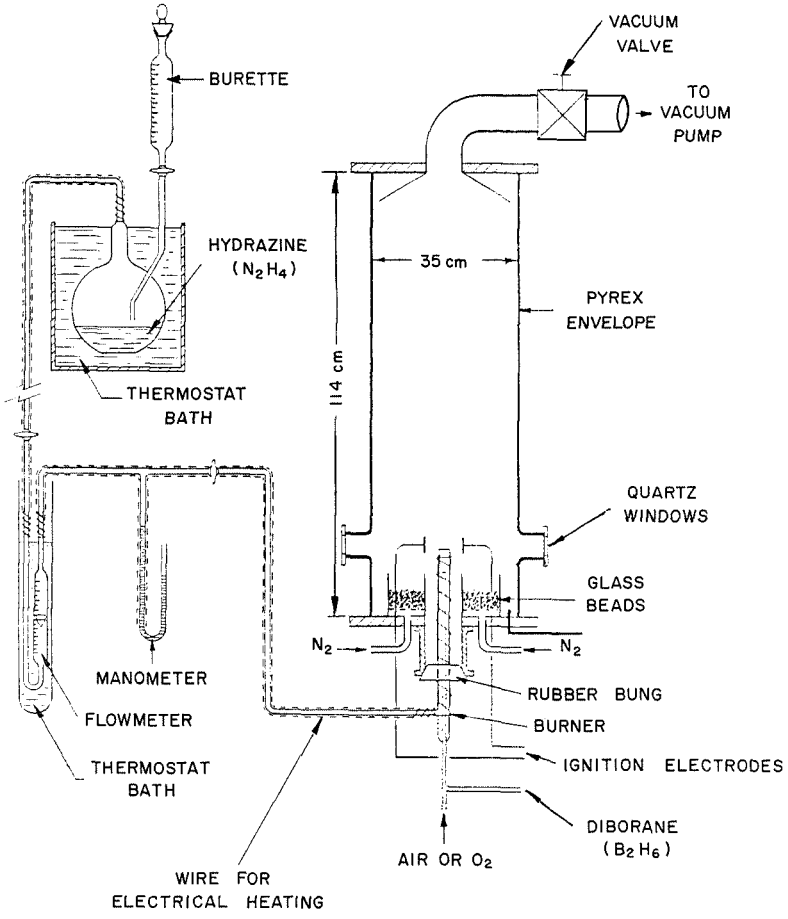

FIG. 1. Low pressure burner and hydrazine flow system.

ated) was also stored in, and fed from, this shelter. The hydrazine line was kept above 100°C by a heating wire around the tubing. The rotameter was thermostated at 98°C. Nitrogen, air, oxygen, and diborane were flow-rated through separate rotameters. All rotameters were calibrated at working pressure.

The flame was ignited by the discharge of a 2 kw transformer between two electrodes located above the burner. It was necessary, especially during ignition, to flow nitrogen or argon inside the low pressure vessel as an inert atmosphere to prevent explosions in the pump. To get uniform flow, these gases were introduced through a layer of glass beads.

Hydrazine was obtained from the Olin Mathieson Chemical Corporation. Our analysis indicated 96.7 per cent N_2H_4, 2.1 per cent NH_3, remainder water. Diborane (96 per cent) was from the Callery Chemical Co. Other gases (N_2, O_2, air) were obtained in commercial cylinders at 99.8 per cent purity.

Burning Velocity Measurements

Burning velocities were obtained at pressures from 2 to 7 mm Hg on a Pyrex bunsen burner of 28 mm diameter.

Burning velocities were calculated as the volumetric gas flow divided by the area of the reaction zone, the latter being computed graphically from a direct photograph of the flame. No attempt was made to make these measurements more accurate than ±10 per cent as the rather unstable nature of the flame itself did not afford greater accuracy.

Analysis of Reaction Products

Gaseous and solid reaction products of a flame at 2.7 mm Hg on a 55 mm diameter burner were sampled and analyzed.

The samples were taken through a quartz probe, collected in a pre-evacuated 500 cc flask to a final pressure of 1.5 to 2.0 mm Hg, and

analyzed with a mass spectrometer. Originally, the diameter of the probe opening was 300 microns but rapid plugging of the orifice by the solid products prevented proper sampling, so that an opening of 1 mm was used. The probe was positioned 1.5 cm above the apex of the reaction zone. No attempt was made to withdraw samples from the reaction zone itself. Solid products were collected on a wire mesh screen also at 1.5 cm above the reaction zone. The solids were analyzed by chemical elemental analysis, infrared absorption, and X-ray diffraction.

Mole Ratio of Gaseous Product to Reactant

Reactant–product mole ratio was determined by measuring the rate of pressure rise in a constant volume as the flame burned. The volume comprised the 500 cubic foot ballast tank, reaction vessel, and connecting vacuum line. The flame was operated between 1.5 and 4 mm Hg in an argon atmosphere on a 55 mm burner. The total volume flow was about 0.5 standard cubic feet per minute. The flame was maintained for a period up to 3 minutes, with an accompanying pressure rise in the system of about 1 mm Hg as measured with a modified McLeod gage.

No temperature correction was made as the flame gases cooled very rapidly to ambient in the ballast tank.

Spectrography of the Flames

Spectra were taken with a Hilger F/4 Raman spectrograph, using both quartz and glass optics.

Flame Temperature Measurements

The color temperature of the flame was determined by comparing its brightness to that of a calibrated tungsten strip filament lamp. The intensity of the flame and tungsten lamps were measured separately throughout the visible region with a Farrand Monochromator using an RCA 1P28 photomultiplier tube as detector. The radiation curves obtained were recorded on an x–y plotter.

Results

Stabilization of the Premixed Flame

Considerable difficulties were experienced in stabilizing a premixed diborane-hydrazine flame. When the reactants come into contact at room temperature they form a white solid explosive adduct of low vapor pressure. This compound condenses even at low pressure at the wall of the burner and no flame can be obtained under these circumstances. Fortunately this deposit can be reduced by heating the burner wall to above 150°C. However, at these wall temperatures another difficulty is encountered as the system approaches spontaneous ignition. Thus it was found necessary to heat the burner to just the correct temperature; this had to be found by experience.

The burner consisted of two concentric tubes as shown in Fig. 1. The diborane is fed through the inner tube that is recessed within the larger

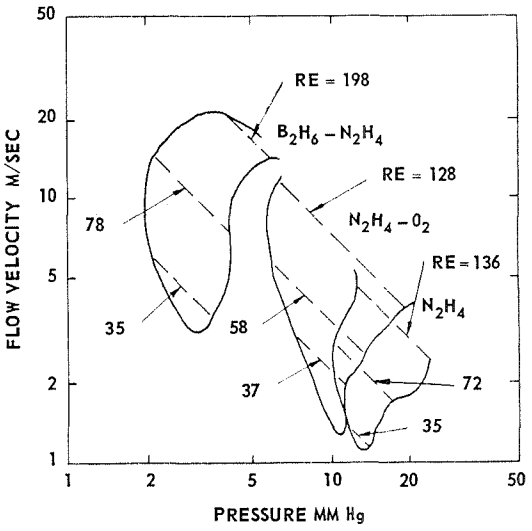

(a)

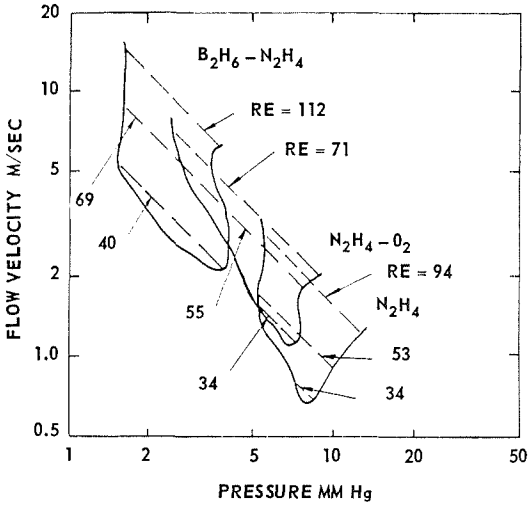

(b)

FIG. 2. Stability regions for the flames of B_2H_6–N_2H_4, N_2H_4–O_2, and N_2H_4.

a. Burner diameter—55 mm.
b. Burner diameter—28 mm.

tube carrying the hydrazine. By reducing the length of the burner section in which the gases mix, stable flames could be obtained. The short mixing length was long enough to premix the gases (at the low pressures used) yet short enough to prevent adduct formation (or condensation) and self-ignition.

Figures 2a and 2b show the stability regions of stoichiometric diborane-hydrazine flames (mole ratio $N_2H_4/B_2H_6 = 1$) on 55 mm and 28 mm diameter burners. Figure 2 shows also, for comparison, the stability region of the hydrazine-oxygen and hydrazine decomposition flames as obtained on the same burners. The average gas linear velocity within the burner is plotted against pressure in the chamber. A flame is stable only inside an area which is limited on the low pressure side by the "blow-off" and on the high pressure side by the "strike-back." These two limits join at a minimum velocity, where the flame has the appearance of a flat disc. It can be seen that the stability region on the smaller burner (28 mm) has a tendency to close up with increasing flow rates; for Reynolds numbers higher than 200 self-ignition occurred inside of the burner. With still smaller burners (and higher pressures) the stability region could not be determined as, at the higher pressures required to stabilize the flames, the flame could not be operated safely due to adduct accumulation in the burner. In general, it was observed that the total area of the stability region is very sensitive to small changes in experimental conditions. For instance in our effort to duplicate the B_2H_6–N_2H_4 curve represented in Fig. 2b only the lower part of the curve could be reproduced. For Reynolds number higher than 40 self-ignition occurred. It must finally be noted that no flame could be stabilized unless inert gas was bled into the combustion chamber.

Flame Structure

a. Premixed Flames. With reactants entirely free of oxygen the only indication of the B_2H_6–N_2H_4 flame is a red plume of hot gases similar to a hydrocarbon flame containing carbon particles. This flame anchors on the burner above a cone which represents a nonvisible reaction zone. If, however, traces of oxygen are present a single bluish zone forms below the onset of the reddish radiation. When adduct formation is not completely suppressed on the burner wall, solid adduct particles are occasionally swept into the flame where they explode giving an impression similar to the spark from a grinding wheel.

b. Diffusion Flames. Circular diffusion flames were obtained with two concentric tubes of equal height. With diborane in the inside tube a flame with multiple zones as shown in Fig. 3 was obtained. The region directly above the burner did not emit light unless traces of oxygen were present, which then caused a bluish radiation. Following this dark region was a bright yellow zone that became slowly red as the gases and particles cooled down further away from the burner. Most of the light emitted by the flame is from this luminous zone.

A third zone of greenish-yellow color was often observed above the annulus carrying the N_2H_4 flow. This was the decomposition flame of hydrazine, which of course can exist independent of the presence of diborane. On decreasing the pressure the hydrazine decomposition flame dies out. This, however, does not affect the diffusion flame which continues to burn without prior decomposition of hydrazine.

Burning Velocities

a. Diborane-Hydrazine. Burning velocities could not be measured in the oxygen-free flame as the reaction zone was not clearly identified. Since small amounts of air did not seem to influence burning velocities these were measured in the presence of traces of air and the inner surface of the blue cone was taken for calculation of the burning area. A temperature of 120°C was assumed for the premixed gases due to the preheating caused by the hot burner walls. All burning velocity measurements were done with the same burner wall temperature. This includes the measurements for B_2H_6–N_2H_4–O_2, N_2H_4–O_2, and N_2H_4 decomposition flames discussed below.

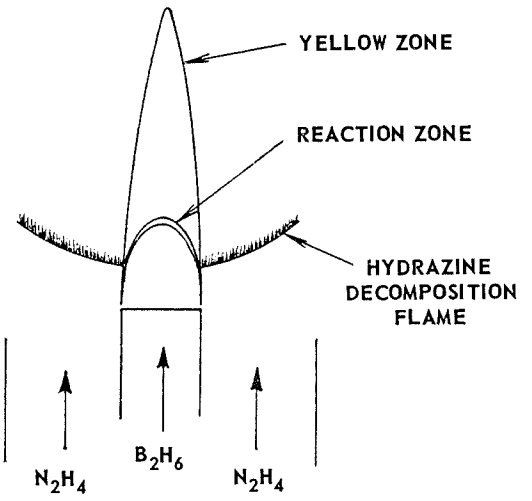

FIG. 3. Structure of diborane-hydrazine diffusion flame.

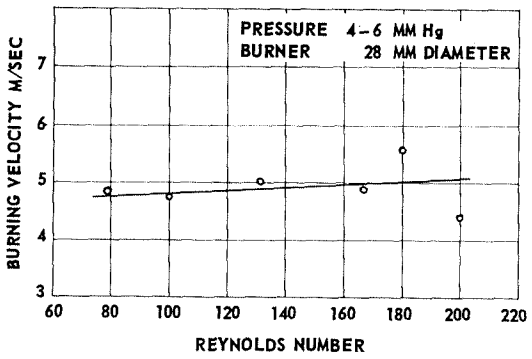

FIG. 4. Effect of Reynolds number on burning velocity of stoichiometric diborane-hydrazine flames.

TABLE 1

Comparison of burning velocities

Flame	Burning velocity (m/s)	Reynolds number	Pressure (mm Hg)
$N_2H_4 + O_2$	2.36	161	10
N_2H_4 (decomposition)	1.86	125	15
$N_2H_4 + B_2H_6$	5.0	167	5

Thus all burning velocity measurements reported are comparable as the same preheating was used throughout. As the flame could be stabilized only at low flows in the burner, for which quenching effects could become important, the influence of the Reynolds number on burning velocity was investigated. The results for stoichiometric flames are given in Fig. 4. The burning velocity shows a normal tendency to increase with the Reynolds number, but this increase seems rather small and a mean value of 5.0 meters per second is deduced for the burning velocity of the stoichiometric flame.

The effect of the hydrazine/diborane ratio on burning velocity is shown in Fig. 5. The effect is obscured by the scatter of the experimental points. The maximum burning velocity seems to occur slightly below stoichiometric, i.e., at N_2H_4:B_2H_6 = 0.9. For N_2H_4:B_2H_6 less than 0.5 and greater than 1.3, no flame could be established.

b. Hydrazine-Oxygen and Hydrazine Decomposition Flames. The burning velocities of these flames were determined on the 28 mm burner for comparison with the diborane-hydrazine system. The results for stoichiometric flames are listed in Table 1.

c. Three Component System: $B_2H_6/N_2H_4/O_2$. Some burning velocity measurements were also made on the three component system: $B_2H_6/N_2H_4/O_2$. Figure 6 shows the effect of air and oxygen on the diborane-hydrazine stoichiometric mixture. The burning velocity increases continuously as air or oxygen is added. There is, however, an indication of a plateau in the curves which corresponds to a condition where the diborane-oxygen reaction becomes the predominant one.

Figure 7 shows the effect of introducing diborane into the hydrazine-oxygen flame. With the first addition of diborane the burning velocity increases considerably.

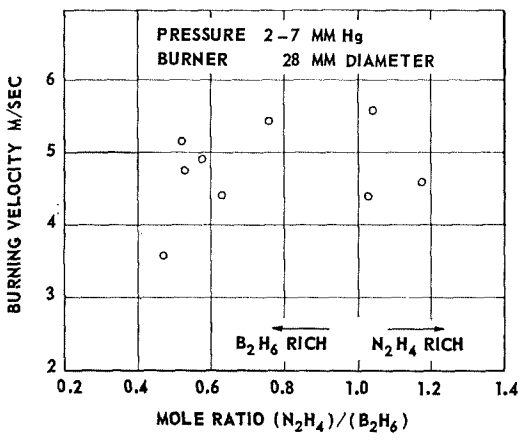

FIG. 5. Burning velocity of diborane-hydrazine flames.

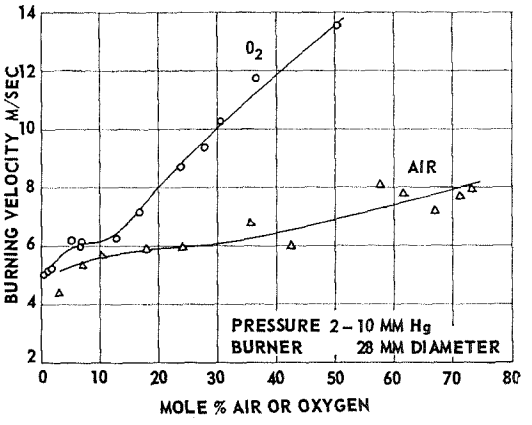

FIG. 6. Effect of air and oxygen addition to diborane-hydrazine system. Mole ratio $(N_2H_4)/(B_2H_6)$ = 1.

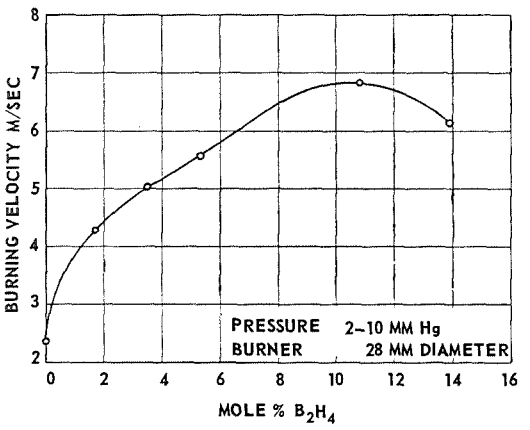

FIG. 7. Effect of diborane addition to hydrazine-oxygen system. Mole ratio $(N_2H_4)/(O_2) = 1$.

Analysis of Combustion Products

a. Gaseous Products. Figure 8 gives the results of the gas analysis for various mole ratios of hydrazine to diborane. When the flame is rich in diborane the only component in the gaseous flame products is hydrogen. Very close to a mole ratio of one, ammonia and nitrogen appear in the products with the mole per cent of ammonia rising almost immediately to about 8 per cent, and that of nitrogen to 2 per cent. No traces of unreacted hydrazine or diborane could be detected in the range of mole ratios investigated. Two runs with results not clearly fitting into the general trend are marked by open circles.

All flames were operated in an atmosphere of argon. At the low pressures used this gas diffuses into the flame. About 1 per cent of argon is present in the gaseous products when the probe is located at 1 cm above the burner. This amount increases to 10 per cent for a probe location of 4.7 cm above the burner, which corresponds roughly to 1.5 cm above the apex of the reaction zone.

b. Solid Products. Elemental analyses of the solid products for various N_2H_4/B_2H_6 mole ratios are shown in Table 2.

The solid products always contain an appreciable amount of hydrogen. The ratio of boron to nitrogen is dependent on the mole fraction of the initial diborane-hydrazine mixture. For flames rich in diborane, the B/N ratio is as high as 4. Since a mole ratio of $N_2H_4:B_2H_6 = 0.5$ was the most diborane-rich that could be burned a B/N ratio of 2 should be a maximum as no nitrogen was found in the gaseous products. This raises the possibility that the screens used for collecting the solid did not give a representative sample. On the hydrazine-rich side the data indicate a B/N ratio close to one.

The solid from diborane-rich flames appeared as a dust-like material, brownish-black in color. This solid easily released its hydrogen content when a match was held close to it. A pale flame could be seen that consumed this hydrogen. The remaining solid was then of pure white color. Sometimes but not always this flame had a green color indicating that boron contributed to the combustion. The product of the hydrazine-rich flame was pure white, powdery and also less abundant.

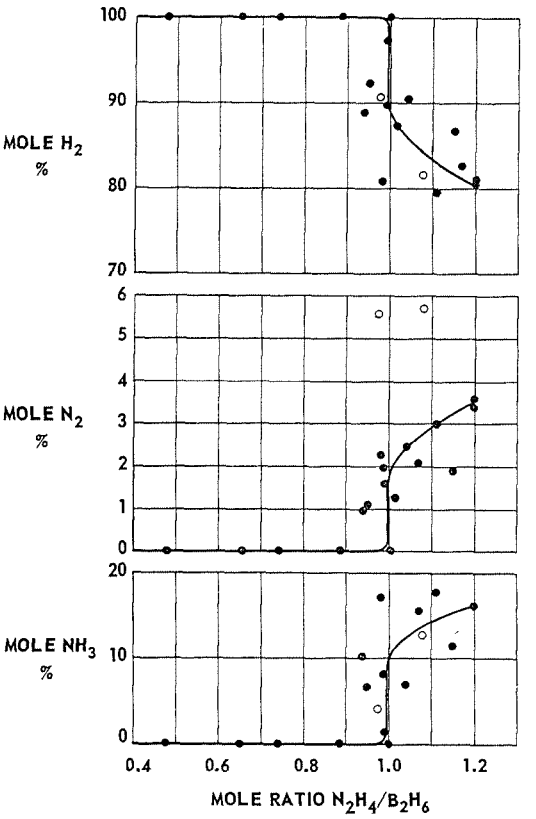

FIG. 8. Gas composition of products of diborane-hydrazine flame.

The major features of the infrared absorption spectrum are the two broad absorption bands at 7.0 μ and at 12.5 μ similar to those in the spectrum of pure boron nitride. There are also frequencies which correspond to the B–H (4.0 μ) and N–H (2.9 μ) stretching modes. The relative intensities of the absorption bands did not change markedly with the N_2H_4/B_2H_6 ratio of the original mixture. Therefore, the high B/N ratio found for the solid products of the diborane-rich

TABLE 2

Composition of solid products collected from the diborane-hydrazine flame

Mole ratio N_2H_4/B_2H_6	Weight per cent B	N	H	Mole ratio B/N
0.48	73.2	22.9	3.82	4.14
0.53	55.0	40.3	4.72	1.77
0.85	44.6	49.8	2.83	1.23
0.88	57.0	40.8	1.80	1.81
0.98	53.1	44.5	2.37	1.54
1.00	41.1	56.8	2.66	0.94
1.00	57.0	40.1	2.90	1.84
1.25	41.6	55.2	3.62	0.976
1.26	42.3	53.9	3.90	1.075
1.30	41.3	56.8	2.32	0.94

flame must be associated with the presence of a substance which does not absorb in the infrared, presumably elemental boron.

X-ray diffraction patterns were taken from two samples, one from a diborane-rich flame, the other one from a hydrazine-rich flame. In the diffraction pattern of the hydrazine-rich sample there was a very diffuse band at 4.5 Å indicative of very small crystallites with small subsidiary peaks at 2.75, 4.27, 4.43, and 4.93 Å. The diborane-rich sample did not contain these 4 smaller peaks but only the main diffuse band. The nature of these peaks is obscure. No peaks due to BN were found.

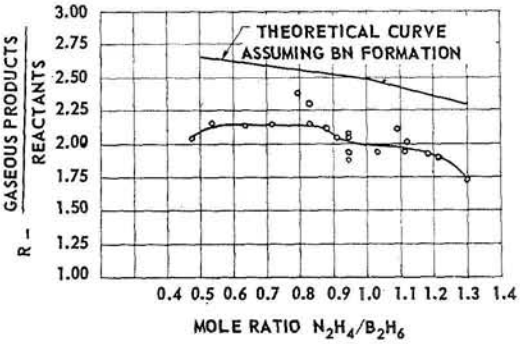

FIG. 9. Ratio of gaseous products to reactants versus mole ratio.

Mole Ratio of Gaseous Product to Reactant

The mole ratio (R) of the gaseous products of the flame to the initial reactant was determined as a function of the mole ratio of hydrazine to diborane. The results are shown in Fig. 9, where the experimental curve is compared with a theoretical curve assuming the formation of only BN, B_{solid}, and gaseous products. It will be seen that the experimental values are about 20 per cent lower than the theoretical ones. This result is in agreement with the observation that the solid product of the flame is not pure BN but a B–N–H compound only partially dehydrogenated. From the values of R and from the pressure, temperature, and composition of the flame gases it is possible to calculate the total mass of solid products contained per unit volume

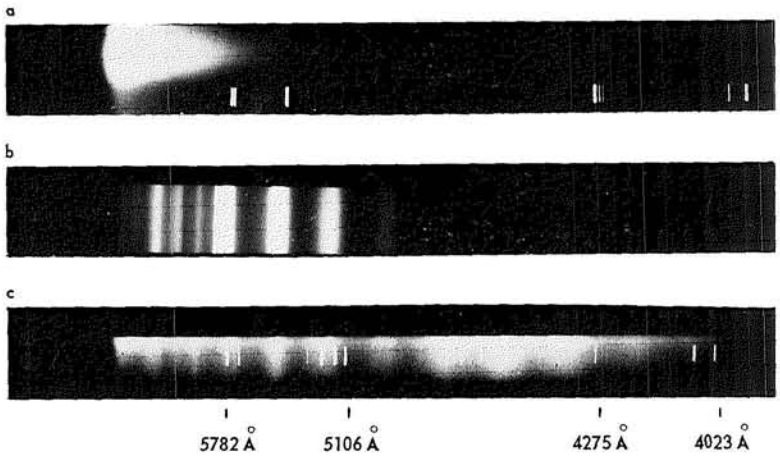

FIG. 10. Spectrum of boric acid fluctuation bands and hydrazine-diborane flame. a.Hydrazine-diborane flame 5-min. exposure and HgCd spectra. b. Boric acid in H_2-air flame at 1 atm. c. Hydrazine-diborane flame with trace of air and Cu spectra.

of flame. This number changes very little with N_2H_4/B_2H_6 ratio.

Spectroscopic Observations

a. Premixed Flames. The dominant feature of the spectrum (Fig. 10a) is a continuum from solid particles. This radiation starts above an invisible cone where the reactions leading to solid particles occur. The intensity of the light emitted increases considerably as the diborane content increases from stoichiometric to the diborane-rich limit.

For flames rich in hydrazine a very weak emission characteristic of the ammonia α band system is superimposed on the continuum. Traces of air premixed with the diborane and hydrazine cause a bluish radiation to be emitted in the reaction zone (Fig. 10) due to the B_2O_3 fluctuation bands. Their intensity distribution is rather unusual. The blue and red bands are emitted with nearly equal intensity, whereas normally the red and green bands predominate in this system giving the radiation the characteristic green color. The difference can clearly be seen in Figure 10.

Figure 10c shows the spectrum of the blue glow of the reaction zone of the diborane-hydrazine flame at about 3 mm Hg with a trace of air. Figure 10b shows the same bands emitted from a hydrogen-oxygen flame at 1 atmosphere with boric acid introduced into the flame. The intensity distribution in the H_2-air flame is the one normally observed both in emission and absorption.[4] Tentatively, to explain the unusual character of our spectrum, it is assumed that the B_2O_3 molecule is formed in a vibrationally excited state. At low pressure randomization is not achieved before the molecule emits, thus permitting the observation of this anomalous vibrational distribution.

b. Diffusion Flames. Diffusion flames of diborane and hydrazine emit mainly continuous radiation from solid particles as in premixed flames. At relatively high pressure (>10 mm Hg) when the hydrazine maintains a separate decomposition flame zone with the particular burner geometry used, there is a tendency for the diborane to react with the products of decomposition rather than with the original molecule. In this case ammonia α bands can be seen together with the continuum.

A very weak emission due to BH could also be identified when the flow of diborane was in excess of that of hydrazine.

Flame Temperature

A color temperature of a low-pressure premixed diborane-hydrazine flame could be found by comparing the intensities of the continuous radiation of the flame over the visible wavelength range to that of a tungsten strip filament of known temperature. It has already been noted that the brightness of the flame increases considerably with the diborane-hydrazine ratio. For stoichiometric flames the brightness was so low that no reliable measurement could be made. Therefore measurements were obtained from a flame at $N_2H_4:B_2H_6 = 0.74$. For this flame the continuum emitted as a gray body with a color temperature of 1085°C. The emissivity of small particles usually increases with decreasing wavelength. Thus the color temperature of this flame is an upper bound for the true flame temperature. Assuming the color temperature to represent the true flame temperature, the ratio of absolute intensities of flame and tungsten strip lamp represents approximately the emissivity of the flame. Thus a value of 0.05 was found for the emissivity of the flame at $\lambda = 0.57$ microns. For flames of N_2H_4/B_2H_6 ratios greater than 0.74, light intensities were measured alone as no reliable color temperature could be obtained. The brightness of the stoichiometric flame was found to be approximately 6 times lower than that of the flame considered above.

The emissivity of dispersed carbon particles has been recently calculated by V. R. Stull and G. N. Plass[5] on the basis of the Mie theory of scattering. It appears from this work that only a slight change of emissivity is to be expected from a change in particle size (50 Å to 5000 Å) if the total amount of solid per unit flame volume remains constant. Because in the diborane-hydrazine flame this quantity does not vary appreciably with the mixture ratio it is suggested that the increased light emitted from the rich diborane-hydrazine flame is partially associated with the presence of boron particles. This picture is in agreement with the analytical results suggesting strongly that elemental boron was present in the products of flames rich in diborane.

Discussion

The hydrazine-diborane flame system has so far received little attention. The only published work is due to Berl and Wilson,[1] who burned a diffusion flame of gaseous hydrazine and diborane on a multichannel burner at 1 atmosphere. They sampled solid products from the flame and observed their infrared absorption. The absorption curve is in every detail identical with the one found in this investigation from the solid products of a low-pressure premixed flame that will be discussed below.

In analyzing the results of this investigation one has to realize the experimental difficulties in

burning this flame. This affected the reproducibility of our results. Data are therefore not as accurate as one would wish and this is especially so for the analysis of the solids and gaseous products of the flame.

We assumed at the beginning of this investigation that one possible reaction mechanism would be decomposition of the hydrazine and subsequent reaction of diborane with the hydrazine decomposition intermediates such as NH_2 and NH. This assumption is not tenable as it can not explain the surprisingly high burning velocity of the hydrazine-diborane flame compared with the hydrazine decomposition flame, despite the lower actual flame temperature of the former.

We assume now that originally a gaseous adduct is formed between diborane and hydrazine that grows by polymerization and dehydrogenation to form the finally observed solid products of the flame. This mechanism is analogous to that by which solid carbon particles are known to form in an acetylene decomposition flame, and the analogy extends to similarities in the supporting data.

The experimental evidence will now be reviewed with this working hypothesis in mind. The high flame speed precludes as noted a N_2H_4 decomposition step, but does not in itself suggest a detailed alternate mechanism. The adduct formation appeared to produce little heat so that the main energy release was due to subsequent steps. These are believed to be polymerization and release of hydrogen with exothermic formation of the B–N bond and H_2. The large heat conductivity of hydrogen, which is the only gas present within the flame zone, will help to increase burning velocity. The small initial influence of oxygen added to the stoichiometric flame indicates that this reaction mechanism is originally little disturbed until the influence of the large additional heat release from H_2O and B_2O_3 formation becomes noticeable.

In the flame there is growth of solid particles. At flame temperature continuous radiation from these particles can be expected and is observed. Hydrazine does not decompose prior to adduct formation, inasmuch as bands due to NH_2 and NH are absent. Only in the hydrazine-rich flame was weak radiation from these bands observed. The reaction zone is therefore not normally marked by light emission due to intermediate compounds so characteristic of most flames, such as in the hydrocarbon-oxygen flame where C_2 and CH emission is prominent. Again the analogy to the acetylene decomposition flame is striking as the latter flame has also only continuous radiation and does not emit the C_2 and CH bands.

It is not surprising that small amounts of oxygen will lead to the emission of the boron-oxide fluctuation bands. This emission was greatly welcome as it helped to mark the otherwise very diffuse flame boundary for burning velocity measurement. The anomalous intensity distribution within these bands needs further study and especially comparison with the band emitted by the diborane-oxygen flame.

The analysis of the gaseous products of the flame showed at least for diborane-rich mixtures a gratifyingly simple result, with hydrogen being the sole product. The analysis of the solids, however, showed that dehydrogenation is far from complete. This shows up in many ways. The amount of hydrogen released in relation to the amount of diborane and hydrazine consumed is deficient by 20 per cent. The solid on the hydrazine-rich side has an over-all composition of BNH_x with x having values between 0.5 and 1.0 for different mixture ratios. On the diborane-rich side additional elementary boron is probably present, increasing the B to N ratio with x varying between 0.5 and 2.0. These solids do not seem to have crystallized into a B–N graphitic structure and are still mainly in an amorphous state as evidenced by the X-ray diffraction pattern. The small peaks actually observed beside the broad and ill-defined band do not coincide with the pattern for pure BN. Finally the measured color temperature of 1360°K was about half the theoretical adiabatic flame temperature for quantitative reaction at the same mixture strength ($N_2B_4/B_2H_6 = 0.74$).

We expect that the deficiency in the completeness of BN formation is partly but not completely due to the low pressure at which this flame has been burned. Unfortunately premixed flames at higher pressure do not seem to be possible. Thus the question of whether BN forms into larger crystals at higher pressure cannot be resolved at this time. The B–N bond is, however, present in large amounts as evidenced by the infrared absorption spectra.

The hydrazine-rich flame is, of course, expected to have gaseous products of nitrogen and ammonia in addition to hydrogen as excess hydrazine will form these products. Unexpected is the sudden stepwise appearance of N_2 and NH_3 at the stoichiometric point. This may point to a change in reaction mechanism that cannot, however, be further specified.

Inconclusive evidence also prevails as far as the higher total light emission from diborane-rich flames is concerned. From the measurement of total gaseous products of the flame it is clear that the ratio of solid to gaseous products does not vary greatly for different mixture strengths. Nevertheless only small amounts of solids from the hydrazine-rich flame were collected on the

screens in contrast to the diborane-rich flame where accumulation was copious. Thus particle size may be smaller for hydrazine-rich flames and the particles are not trapped by the screen. As noted before, particle size does not affect the emissivity of light greatly for constant mass of solids per unit volume. It has, therefore, tentatively to be assumed that the amount of elementary boron contained in the particles influences greatly the emissivity leading to stronger light emission from diborane-rich flames.

In conclusion, it can be stated that at least some features of this flame are now understood. The flame forms adducts that polymerize and dehydrogenate into solids. At least for diborane-rich flames hydrogen is the only gaseous product as predicted by thermodynamic considerations. The formation of solid BN is not complete as not all hydrogen is released and BN formation does not proceed into a well-ordered graphitic structure, although on a molecular basis B–N bonds are present as evidenced by infrared absorption.

ACKNOWLEDGMENTS

The authors wish to acknowledge the contribution of Clyde Poulin on the experimental work of the gas sampling analysis.

Research was supported by the Office of Naval Research, through a Project Squid Subcontract [Prime Contract NOnr 1858(25)].

REFERENCES

1. BERL, W. G. and WILSON, W. E.: Nature *191*, 380 (1961).
2. VANPÉE, M., WOLFHARD, H. G., and CLARK, A. H.: Western States Section, The Combustion Institute 1961 Fall Meeting. WSS/CI Paper 61–22 (1961).
3. WOLFHARD, H. G.: Z. tech. Physik *24*, 206 (1943).
4. SOULEN, J. R., STHAPITANONDA, P., and MARGRAVE, J. L.: J. Phys. Chem. *59*, 132 (1955).
5. STULL, V. R. and PLASS, G. N.: Publication No. U–503, Aeronutronic, Newport Beach, Calif., May, 1959.
6. LAUBENGAYER, A. W., MOEWS, JR., P. C., and PORTER, R. F.: J. Am. Chem. Soc. *83*, 1337 (1961).

Discussion

DR. W. E. WILSON (*APL, The Johns Hopkins University*): I would like to mention some related work that has been done on a B_2H_6–N_2H_4 flame at one atmosphere using a multidiffusion burner. Both reactants were diluted with argon and hydrazine was always in excess. In contrast to Dr. Wolfhard's premixed, low pressure flame, our BN reaction goes essentially to completion. The solid contains only a few tenths of a per cent of bound hydrogen. The flame temperature is at least 80% of theoretical; if reasonable losses are assumed it is about 95%.

To establish the flame, a N_2H_4 decomposition flame is first stabilized; argon is added until the N_2H_4 flame is almost blown off. When B_2H_6 is added the flame jumps back to the burner surface. This indicates, in agreement with Dr. Wolfhard, that the B_2H_6 must react with the N_2H_4 prior to its decomposition. Similarly in an opposed jet flame no BN reaction occurs unless the N_2H_4 decomposition flame is blown off prior to addition of B_2H_6.

We have had considerable difficulty with analysis of the solids formed in these flames. It would appear that there is a reaction with water vapor, perhaps liberating ammonia and forming borates. Hence the analytical technique should be critically evaluated.

Several other systems in which BN may be formed from B_2H_6 have been investigated: with NH_3 there is no flame reaction, only adduct is formed; with N_2O, boron oxides and acids are the only products; however, with NO it is possible to obtain some BN as a product.

MAGNESIUM-OXYGEN DILUTE DIFFUSION FLAME

GEORGE H. MARKSTEIN

The Polanyi dilute-diffusion-flame method has been applied to the magnesium-oxygen system. Diffusion flames were obtained at pressures of a few mm Hg by carrying magnesium vapor in an argon stream into an atmosphere of oxygen-argon. Photographic photometry was used to measure reaction rates. The data favor a unimolecular rate law, independent of oxygen concentration, but scatter too much to exclude with certainty a bimolecular reaction of first order in oxygen concentration. Based on an estimated flame temperature of 1000°K, the unimolecular rate constant, averaged over all runs, was 2.5×10^3 sec^{-1}, and the average bimolecular rate constant was 4×10^{11} cm^3 mole^{-1} sec^{-1}.

The emission spectrum of the flame consisted of continuum radiation with a broad maximum in the blue and narrower maxima in the near ultraviolet and the red. The spectrum of surface luminescence of MgO deposits growing in the flame zone consisted of a continuum in the blue resembling the broad maximum of the flame spectrum. On the basis of the spectroscopic evidence and of thermodynamic arguments, it is suggested that, at least at low pressures and temperatures, only a small amount of gaseous MgO, sufficient for nucleation of MgO particles, is formed in the flame, while most of the oxidation takes place as a heterogeneous reaction on growing oxide particles. The proposed heterogeneous mechanism is compatible with a unimolecular rate law and with the order of magnitude of the measured unimolecular rate constant.

Introduction

Interest in metal combustion processes[1,2] has been stimulated recently by the use of metal additives in propellants. Many current studies[3,4] have therefore been performed under conditions simulating those in propulsion systems. These investigations have provided considerable insight into the complicated interplay of the processes of vaporization, conductive and radiative heat transfer, diffusion, and chemical reaction, which participate in the burning of metals. For this very reason, however, the kinetics and mechanisms of metal-combustion reactions are as yet almost entirely unknown, since in the great majority of recent studies the chemical effects were obscured by many other factors.

To obtain information on reaction kinetics, one must select experimental conditions under which the chemical effects have a dominant influence. Among the methods that satisfy this condition, Polanyi's "dilute diffusion flame" technique[5–9] appeared especially attractive, since it had been originally developed and successfully employed for studying the reactions of alkali metals. In the present investigation, this method has been adapted for the study of the magnesium-oxygen system, which was chosen for initial work because of the relatively high vapor pressure of magnesium. It was also anticipated that the reaction mechanism should be comparatively simple, since in this system only one oxide species, MgO, has been observed in the gas phase by spectroscopic[10] and mass-spectrometric[11] methods. This is also the only species that is regarded as important in the condensed phase.[12] Previous studies of magnesium combustion have been concerned with determination of spectra and flame temperatures, as well as of burning times of magnesium ribbons, but have not yielded kinetics data.[13–15]

Experimental

Preliminary work showed that a diffusion flame of magnesium vapor burning in an oxygen atmosphere at pressures of a few mm Hg could be obtained without difficulty. The magnesium vapor was carried into the oxygen by a stream of argon issuing from an orifice in an electrically heated boron nitride crucible. A standard glass bell jar assembly served as combustion chamber in this exploratory work. An inherent difficulty became apparent from the outset: A deposit of magnesium oxide formed near the orifice of the vaporizer and in the course of about 10 minutes closed the orifice off, thus limiting severely the time interval during which the flame could be maintained under constant conditions. Attempts to eliminate this difficulty completely were un-

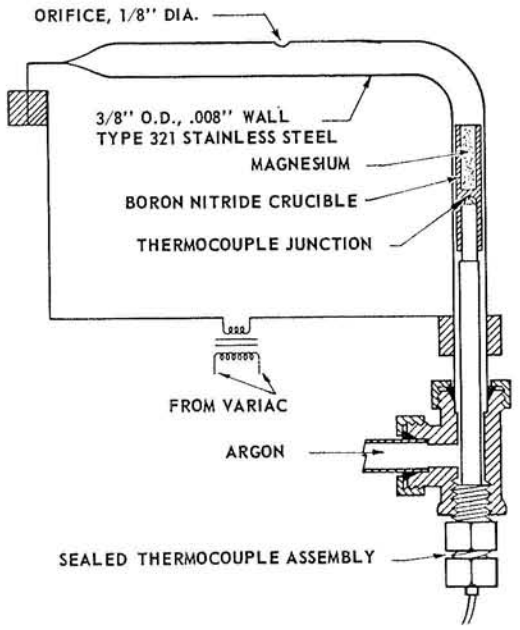

FIG. 1. Schematic of vaporizer.

successful, but subsequently its severity was greatly reduced by diluting the oxygen atmosphere with argon. Moreover, removal of the MgO deposit from the boron nitride crucible after each run was difficult, but with the present vaporizer, described below, deposit removal presented no serious problem.

The apparatus developed on the basis of the exploratory work consisted of a stainless steel chamber of 12-inch i.d. and 20-inch height. Four viewing ports were placed 90° apart around the circumference of the chamber and 10 inches from its bottom. Flat glass windows were used for photographic photometry, and flat quartz windows for spectrographic runs.

The flows of oxygen and argon into the chamber, and of argon carrier gas into the vaporizer, were controlled by needle valves and metered with rotameters. Commercial cylinder gases, passed over Drierite but otherwise not purified, were used. The gases were continuously removed from the chamber through an exhaust port in the top plate by means of a mechanical vacuum pump. A Cartesian manostat (Model No. 10, Emil Greiner Co., New York) was inserted between the chamber and the pump for the purpose of maintaining the chamber pressure constant. The exhaust from the vacuum pump could be passed through a moving-soap-film device (Bubble-O-Meter, Temple City, California), which was used for calibrating the individual rotameters, as well as for determining the total gas flow.

The design of the vaporizer underwent several changes during the exploratory work. The final version, shown in Figs. 1 and 2, consisted of a Joule-heated stainless-steel tube of the shape and dimensions given in Fig. 1. The magnesium metal is contained in a boron nitride crucible supported on top of a protective tube, which forms part of the thermocouple assembly. The crucible fits this tube loosely, and was removed after each run for weighing and refilling, in order to determine the total magnesium consumption. An iron-constantan thermocouple was used. Stainless steel was employed for all parts of the vaporizer that heat up during a run, including the electrical leads to the tube, the Tee, the thermocouple assembly and the tube feeding argon to the Tee. Lava sealant was used in the thermocouple gland (Conax Corp. No. XTG-24-A2). As shown in Fig. 2, the vaporizer was mounted on the bottom plate of the chamber. This plate was suspended with counterweights and was lowered between runs for refilling the vaporizer.

An $f/14$ medium quartz spectrograph was used in the spectroscopic runs. Flame-emission spectra, and spectra of surface luminescence of MgO deposits, were photographed on Kodak 103a-F plates, while 103-F plates were used for absorption spectroscopy. A spherical mirror of 18-inch focal length was employed for projecting a 1:1 image of the flame on the spectrograph slit. In order to increase the depth of the flame zone viewed by the spectrograph, a vaporizer with a

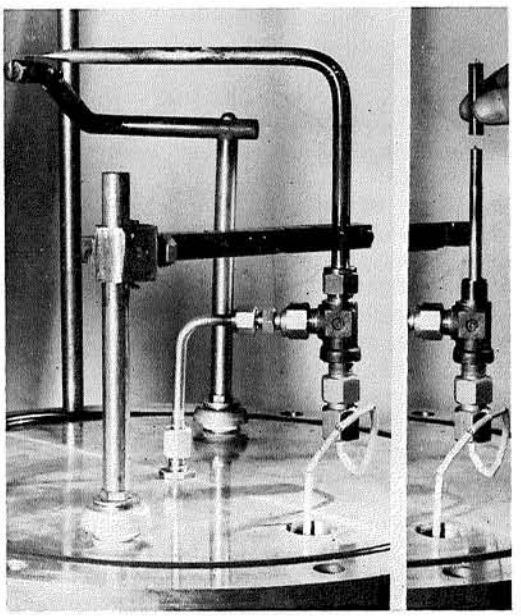

FIG. 2. Photographs of vaporizer. Left: assembled; right: thermocouple and boron nitride crucible.

slit orifice of 1-inch × 1/16-inch size was used in the spectroscopic work, instead of the vaporizer with circular orifice.

The method of photographic photometry[8,9] was used for deriving reaction-rate data from the distribution of light emitted by the flame. The technique of Rapp and Johnston,[9] which is based on relative values of emission intensity and thus does not require step-wedge calibration of the film, was adopted for the present work.

The theory of this method, discussed in detail in ref. 9, is based on the following assumptions: 1. The local radiation intensity is proportional to the local rate of a significant reaction step. Instead of the usually postulated bimolecular rate law, the more general expression $kC_N C_A^n$ may be assumed for this reaction step, where k is the rate constant, C_N and C_A are the concentrations of nozzle and atmosphere reactants, respectively, and n is the order of the reaction with respect to atmosphere reactant, which may be different from unity. 2. For sufficiently large distances from the nozzle orifice, the flow term is negligible compared with the diffusion and reaction terms, and the flame has therefore spherical symmetry for large enough radii. 3. The concentration of atmosphere reactant C_A is regarded as constant. (An analysis of the effect of atmosphere depletion is presented in ref. 16).

With these assumptions, the radial distribution of nozzle reactant is given by

$$C_N = (A/r) \exp(-\omega r), \qquad (1)$$

where A is a constant for radii r large compared to the orifice radius, and

$$\omega^2 = kC_A^n/D_N. \qquad (2)$$

In the latter expression, D_N is the diffusion coefficient of nozzle reactant. Since the reaction rate and therefore the radiation intensity are proportional to C_N, the light-intensity distribution on the flame photographs is obtained by integrating the expression (1) along the light paths. The result of the integration[8,9] can be expressed in terms of zero-order modified Bessel functions of the second kind, and may be approximated for sufficiently large radii by

$$I = \text{const.}\, r^{-\frac{1}{2}} \exp(-\omega r). \qquad (3)$$

By taking a series of photographs of the flame with constant aperture and various exposure times, the value of ω can be determined under the further condition that the photographic reciprocity law is satisfied. For this purpose, microphotometer traces of the photographs through the flame center are taken. If the expression (3) is satisfied, the values of r corresponding to constant film transmission for various exposure times τ should give a straight line of slope $-\omega$, when $\log(r^{\frac{1}{2}}/\tau)$ is plotted versus r.

In the present work, exposure times between 0.5 sec and 2 min were used. The photographs were taken on Kodak Royal Ortho film with an $f/4.5$ lens. The red-insensitive film was chosen to minimize background fogging due to scattering of thermal radiation emitted by the vaporizer.

An oxygen transducer[17] was used for recording the oxygen concentration in the pump exhaust flow during the photometric runs. The instrument was calibrated before and after each run by exposing it to the atmosphere. Since its output is proportional to the oxygen partial pressure, and the exhaust flow was essentially at atmospheric pressure, the readings gave directly the oxygen mole fraction in the flow. Owing to the consumption of oxygen by the flame, the O_2 reading dropped off shortly after the start of combustion and levelled off at a lower value after about 10 min. This long delay was primarily due to the large volumes of the chamber and of other parts of the apparatus between the chamber and the pump exhaust. After the flame was extinguished by turning off the heating current, the oxygen reading rose again, and attained a constant value after a similar delay. The final reading usually differed from the value before combustion by less than 4 per cent. Runs in which the difference was appreciably larger were discarded. The computation of the reaction rates was based on the oxygen mole fraction established in the presence of the flame. From the total gas flow and the difference between the oxygen mole fractions in the absence and presence of flame, the rate of oxygen consumption was computed.

The formation of deposits was studied by inserting suitable targets into the flame zone. Rapid insertion and removal of the targets was accomplished by mounting them on a rod that could be moved axially past an O-ring seal in a flange that replaced one of the windows.

Results

Appearance of the Flame. The flame became visible as a faint luminosity surrounding the vaporizer orifice, when the temperature of the vaporizer reached about 600°C. The intensity of the radiation increased appreciably when the vaporizer temperature was raised further. The color of the flame appeared uniformly pale-blue throughout the combustion zone. Occasionally, particularly at high vaporizer temperatures and pressures above about 4 mm Hg, the flame seemed to have a central zone of higher luminosity distinctly separated from the surrounding region of radially decreasing radiation. However, the ex-

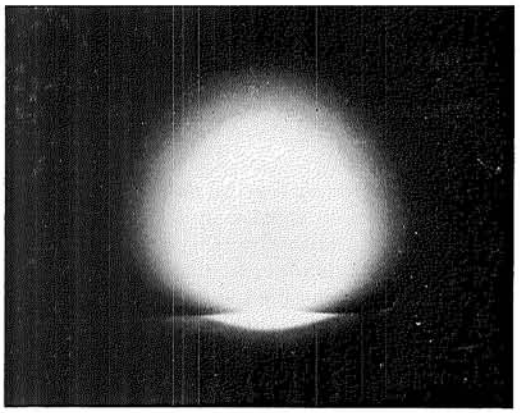

FIG. 3. Photograph of $Mg-O_2$ dilute diffusion flame.

istence of this visually observed zone was not confirmed by the flame photographs. A typical flame photograph, taken as one of a series for a photometric run, is shown in Fig. 3. The flame zone is seen to deviate only slightly from spherical shape, so that application of the photometric method[9] appeared justified. The size of the flame zone decreased with increasing pressure and with increasing oxygen concentration, and increased with increasing vaporizer temperature, i.e., increasing magnesium concentration.

Combustion Products. The magnesium oxide formed in the diffusion flame collected as a fluffy translucent white layer on all surfaces within the combustion chamber, except on those in the immediate vicinity of the flame. This deposit could be wiped off easily and was readily soluble in dilute acids. Figure 4 shows an electron micrograph of the deposit collected on an electron-microscope specimen screen placed into the combustion chamber. The structure of the deposit resembles that of carbon formed in rich hydrocarbon flames[18,19] and that of many other

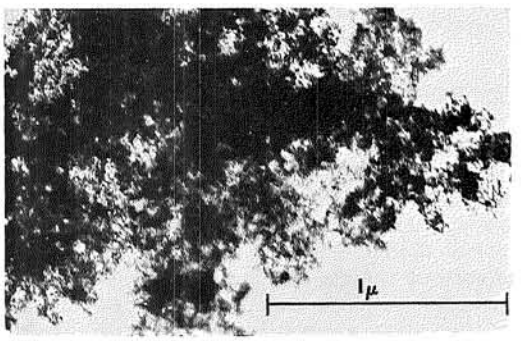

FIG. 4. Electron micrograph of magnesium oxide smoke formed in the flame.

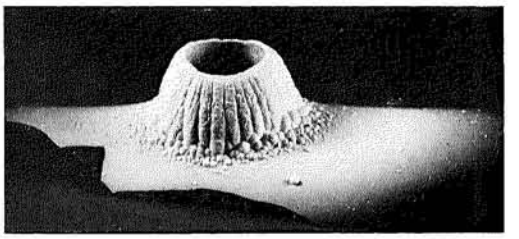

FIG. 5. Magnesium oxide deposit formed around the vaporizer orifice.

"smokes."[20] The size of the individual particles is estimated to be of the order of 0.01 μ.

A magnesium oxide deposit of entirely different structure accumulated on the surface of the vaporizer around the orifice, and on any other surface placed close enough to the orifice. This deposit formed a dense, hard layer, which, as already mentioned, adhered strongly to the materials used in earlier versions of the vaporizer (boron nitride in the first, and inconel in later designs). It dissolved only slowly even in concentrated hydrochloric or nitric acids. Fortunately, the deposit separated spontaneously from the stainless-steel tube used in the present vaporizer, after the heating current was turned off at the termination of each run. Figure 5 shows a typical deposit formed during one of the photometric runs. Comparison of the weight of the deposits and the weight of the magnesium consumed during a run showed that between about 25 and 35 per cent of the magnesium appeared in the deposit. The percentage varied presumably because of variations of flame geometry, which determined the portion of the reacting gases that impinged on the tube surface.

The inner diameter of the deposit that grew around the orifice was not simply determined by

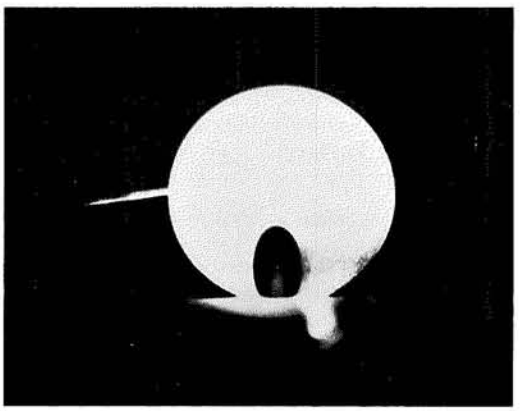

FIG. 6. Deposit with dark central region formed on boron nitride disc inserted vertically into flame.

the diameter of the orifice, but varied with oxygen concentration, chamber pressure, and vaporizer temperature in a manner similar to the variation of flame size. For high oxygen concentration, high pressure and low vaporizer temperature, the deposit grew conically inward and closed the orifice off after a few minutes. For conditions at the other extreme, the oxide formed a cylinder whose inner diameter exceeded that of the orifice appreciably (the diameter ratio exceeded 1.6 in some runs). In the latter case, a thin deposit formed on the tube in the annular region between the orifice and the cylinder, but the bulk of the oxide deposit grew outside this region.

The growth of the deposit was accompanied by a surface luminescence which could be particularly well observed when the vaporizer temperature and/or the chamber pressure were reduced until the flame radiation just disappeared. The color of the luminescence was a light blue of somewhat more saturated hue than that of the flame emission. In the presence of the diffusion flame, the rim of the deposit emitted, instead of the luminescence, fairly bright thermal radiation indicating a temperature in excess of that of the vaporizer.

The growth of a hard magnesium oxide deposit, and the associated luminescence, were also observed on targets introduced into the flame zone. However, within a central region of the flame a black or dark-brown deposit formed instead of the white layer in the surrounding region. Figure 6 shows this sharply separated dark area deposited on a boron nitride disc that was inserted into the flame with its vertical surface slightly behind the flame axis. The surface luminescence was absent in the dark region. The small area of lighter color within the dark region was found to consist of magnesium metal. It was therefore suspected that the dark deposit was formed by finely divided magnesium dispersed in MgO. To test this hypothesis, the dark layer was deposited on a BN disc provided with two electrodes. It was found that a current of a few μA passed through the dark deposit when a potential of about 1 kV was applied. The current did not increase when the deposit was heated, indicating metallic rather than semiconducting properties.

The elongated shape of the dark area indicates some deviation from spherical symmetry, which is due to the influence of carrier-gas flow and thus becomes unimportant for larger distances from the orifice. The size of the dark area was of the same order as the inner diameter of the deposit at the orifice, and varied in a similar manner with oxygen concentration, chamber pressure, and vaporizer temperature.

Instead of the dark area, a central region free from deposit formed on a microscope cover glass inserted vertically into the flame; this region was surrounded by cylindrical deposits that grew horizontally on both sides of the glass, as shown in Fig. 7.

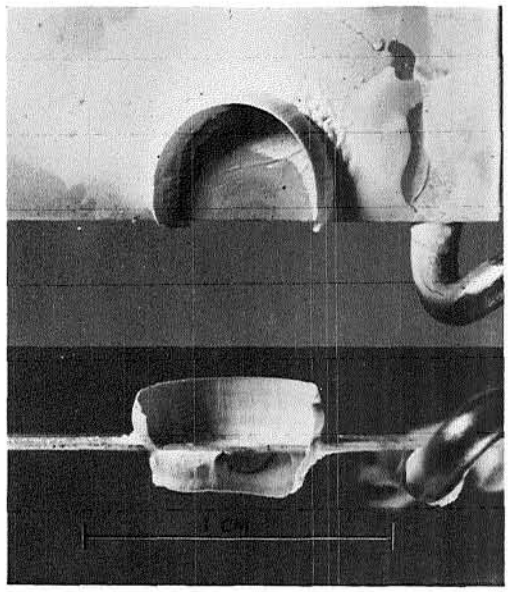

FIG. 7. Deposit formed on microscope cover glass inserted vertically into the flame. Seen from front (top) and from below (bottom).

Spectroscopic Results. The emission spectrum of the dilute diffusion flame is shown at the top of Fig. 8. It consists entirely of continuum radiation, with a broad maximum at about 4500 Å and narrower maxima at about 3900, 6000, 6500, and 6900 Å. None of the well-known features of the spectrum of magnesium flames burning at higher pressures[13,15] were present. The spectra of the flame of a magnesium ribbon burning in air at atmospheric pressure, shown for comparison on Fig. 8, contain the MgO band at about 5000 Å, the bands at 3700 and 3820 Å now attributed partly to MgO and partly to MgOH,[21] and a number of magnesium lines, including the self-reversed resonance line at 2852 Å, visible on the spectrum taken with longer exposure.

The spectrum of the luminescence that appeared on the surface of magnesium oxide deposits growing in the flame zone is shown in the second band from the top on Fig. 8. For the purpose of obtaining this spectrum, a microscope glass slide was used as target for deposit formation and the chamber pressure (0.5 mm Hg) and vaporizer temperature were set low enough so that no flame radiation was visible. The spectrum is seen to contain a broad continuum, rather similar to the blue continuum of

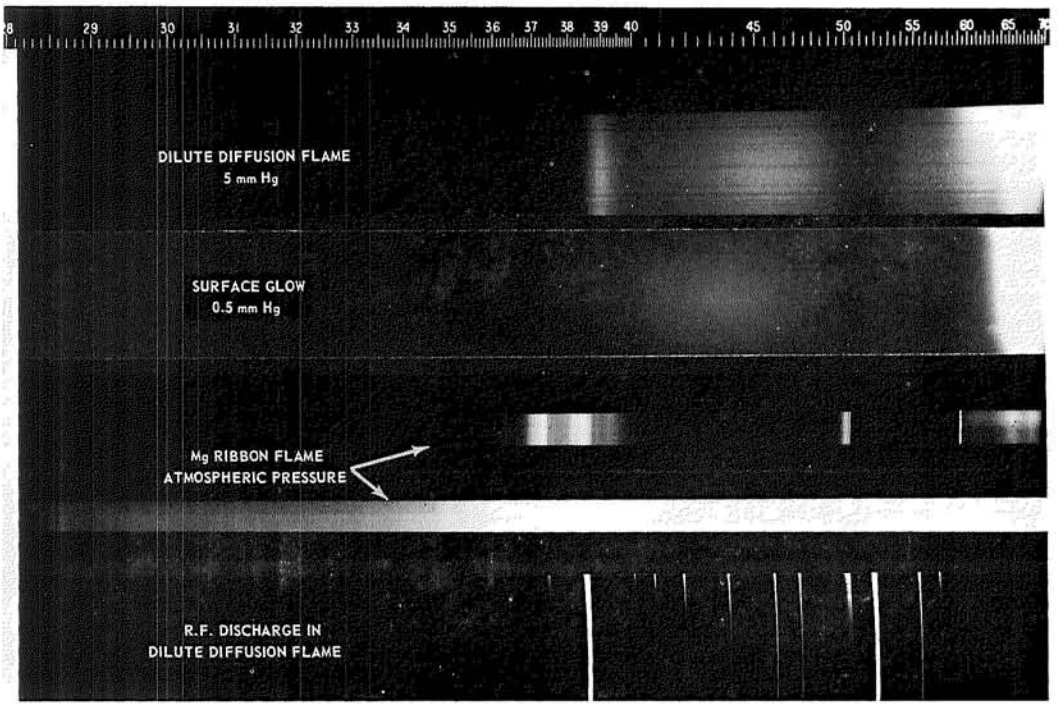

FIG. 8. Emission spectra.

the flame spectrum, but with the location of maximum intensity shifted to about 4300 Å. Thermal radiation emitted by the vaporizer and scattered by the MgO deposit caused the heavy exposure visible above 6000 Å and prevented observation of any luminescence that may have been present in the red portion of the spectrum.

During the exploratory work, it had been observed that a bright green radiation was excited in the flame by electrical discharges. The nature of this radiation seemed of some interest and therefore the spectrum of the radiation excited by a radio-frequency discharge through the flame was photographed. The spectrum, shown at the bottom of Fig. 8, shows the magnesium triplets at about 3830 and 5180 Å as the most prominent features, as well as several other magnesium lines and, rather faintly, the MgO band. Since this spectrum was taken with the preliminary setup in the glass bell jar, the resonance line at 2852 Å could not be observed.

A xenon-filled flash tube was used as a continuum light source in attempts to obtain absorption spectra of the flame. The only feature that appeared in absorption was the magnesium resonance line, which was also completely extinguished when the line spectrum from a magnesium hollow-cathode lamp was passed through the flame. In view of the complete extinction, the application of the lifetime method[6] for determining reaction rates does not appear promising for this flame.

Photometric Runs. The experimental conditions and the results of the runs using photographic photometry are listed in Table 1. The oxygen partial pressures were computed from the oxygen mole fractions measured by the oxygen transducer in the pump exhaust flow in the presence of the flame; as mentioned before, these constant readings were established with some delay after combustion started. The rates of oxygen consumption were determined, as mentioned, from the difference of oxygen readings without and with combustion. The rates of magnesium consumption, determined from the initial and final weights of the crucible and the durations of the runs, agreed well with the rates of oxygen consumption. However, the accuracy of the measurements of either the oxygen or the magnesium consumption rate is probably not better than ± 10 per cent, because the oxygen rate was determined as a small difference of two readings, while the duration of the run included the time of approach to constant temperature of the vaporizer after the start of combustion.

The ranges over which the experimental conditions could be varied were determined by

TABLE 1

Experimental conditions and results of photometric runs

Pressure, p (mm Hg)	O_2 partial pressure, p_{O_2} (mm Hg)	Vaporizer temperature (°C)	Rate of O_2 consumption $\times 10^5$ (moles/min)	ω (cm^{-1})	Unimolecular rate constant, $k_1 \times 10^{-3}$ (sec^{-1})	Bimolecular rate constant, $k_2 \times 10^{-11}$ ($cm^3 mole^{-1} sec^{-1}$)
2.10	1.095	652	18.4	2.49	3.27	1.86
2.20	0.177	628	11.7	2.71	3.70	13.00
2.60	0.246	644	17.2	2.35	2.35	5.96
2.60	0.390	644	22.0	2.49	2.64	4.22
2.75	0.456	667	29.2	2.12	1.81	2.48
2.90	0.248	620	8.6	2.18	1.82	4.56
2.90	0.522	632	9.6	2.54	2.46	2.94
2.95	0.233	646	16.4	1.87	1.31	3.51
4.50	0.313	660	16.9	2.67	1.75	3.50
4.50	0.500	623	6.0	3.41	2.86	3.56
4.55	0.425	661	21.5	2.51	1.53	2.25
4.95	0.305	647	10.8	3.57	2.85	5.84
4.95	0.910	643	12.0	3.57	2.85	1.95
6.90	0.302	666	15.1	3.42	1.88	3.87
6.90	1.562	690	35.4	3.92	2.47	0.98
7.40	0.400	645	8.6	4.92	3.62	5.65
7.45	0.393	673	16.5	3.46	1.78	2.82
9.40	0.861	640	8.1	5.58	3.67	2.65

various factors. The useful range of pressure was limited by the requirement of obtaining a flame of suitable size. To satisfy the condition of excess atmosphere reactant, the oxygen partial pressure could not be reduced below a certain value, while the rate of growth of deposit at the vaporizer orifice imposed an upper limit on oxygen partial pressure.

Unavoidably, particularly for runs with high oxygen partial pressure, the growth of deposit caused some change of flame geometry during the course of a run. In order to minimize systematic errors caused by these gradual changes of flame geometry, the photographs were taken with random sequence of exposure times, and a few exposures were repeated in each run to detect such gradual changes. Runs in which the changes were excessive were eliminated. The majority of the runs yielded very satisfactory straight-line plots of $\log (r^2/\tau)$ versus r for constant film transmission (see Experimental). Plots for 50 per cent and 70 per cent transmission were prepared for all runs and gave values of ω that differed for each run at most by 5 per cent. The listed values are the averages obtained from these two plots.

In order to convert the ω values into rate constants, the oxygen concentration C_{O_2} and the diffusion coefficient D_{Mg} of the nozzle reactant must be known [see Eq. (2)]. This requires in turn a knowledge of the temperature in the flame zone. As yet, no attempt has been made to measure this temperature. In view of the formation of MgO deposits on all surfaces introduced into the flame zone, the use of fine-wire thermocouples undoubtedly would not yield the true temperature of the gas phase. Owing to the dilution with inert gas and the low pressure, the flame temperature is too low, on the other hand, for using the line-reversal method in the visible part of the spectrum. In the absence of any accurate knowledge of flame temperature, it was estimated that it would exceed that of the vaporizer only slightly, and therefore the values of D_{Mg} and C_{O_2} were determined for the arbitrarily chosen temperature of 1000°K.

The binary diffusion coefficient of magnesium in argon was computed from kinetic theory,[22] using values of the Lennard-Jones parameters σ and ϵ listed in a recent compilation.[23] The result, for 1000°K, was $D_{MgAr} = 1108/p$ cm^2/sec, where p is the pressure in mm Hg. (The error incurred by using the binary coefficient, rather than the expressions for ternary mixture, was estimated to be less than 3 per cent for the highest oxygen concentration used).

Equation (2) also contains the reaction order n with respect to oxygen concentration. One should be able, in principle, to determine n from the ω values measured within a range of oxygen partial pressures. Since the diffusion coefficient is proportional to p^{-1}, the slope of a logarithmic plot of ω^2/p vs. p_{O_2} should yield the order n and thus enable computation of the rate constant according to Eq. (2). However, the present results were found to scatter too much on such a plot for reliable determination of reaction order. If all runs are regarded as equally reliable, the data seem to favor a value of n considerably less than unity, not excluding the value $n = 0$, which is suggested by the heterogeneous reaction mechanism presented in the Discussion. However, if the two runs at the extreme of the range of p_{O_2}(p_{O_2} = 0.177 and 1.562, respectively) are regarded as less reliable and are omitted, the rest of the data admit larger values of n, including $n = 1$.

In view of this uncertainty of the reaction order with respect to oxygen concentration, both a unimolecular rate constant k_1, corresponding to $n = 0$, and a bimolecular rate constant k_2, corresponding to $n = 1$, were computed. Substituting the expression for the diffusion coefficient D_{MgAr}, and that for the oxygen concentration,

$$C_{O_2} = p_{O_2}/RT, \tag{4}$$

into Eq. (2), one obtains the following relations for these rate constants:

$$k_1 = 1108\omega^2/p \text{ sec}^{-1}, \tag{5}$$

and

$$k_2 = 6.90 \times 10^{10}\omega^2/p\ p_{O_2} \text{ cm}^3\text{mole}^{-1}\text{sec}^{-1}. \tag{6}$$

In these expressions, the pressures are in mm Hg, and, as stated earlier, a temperature of 1000°K was arbitrarily assumed.

These rate constants are listed in Table 1; their average values are $k_1 = 2.5 \times 10^3$ sec^{-1}, and $k_2 = 4.0 \times 10^{11}$ cm^{3}mole^{-1}sec^{-1}, respectively. Individual values of k_1 differ from the average by less than ±50%. The scatter of the k_2 values is much larger, if one retains the two runs at the extremes of p_{O_2}; even if one omits these two runs, the scatter of k_2 is still somewhat in excess of ±50%. The variations of either k_1 or k_2 do not show any systematic trends with vaporizer temperature or with rate of oxygen consumption.

Discussion

While the rate data shown in Table 1 do not exhibit trends that, by themselves, would allow conclusions regarding a reaction mechanism, fairly convincing arguments in favor of a specific mechanism can be advanced when the rate measurements are confronted with the results of thermodynamic analysis. These arguments are further reinforced by the spectroscopic results, combined with the observation of the tendency for growth of deposits of MgO in the flame zone in a surface reaction accompanied by luminescence. In view of the low pressure, it appears safe to exclude all three-body processes from the mechanism, as far as homogeneous reactions in the gas phase are concerned. Thus, the initial step should be the bimolecular reaction

$$\text{Mg(g)} + \text{O}_2 \rightarrow \text{MgO(g)} + \text{O}, \qquad \Delta H_0^\circ = 28.0 \text{ kcal.} \tag{I}$$

However, the concentration of gaseous MgO formed by this endothermic reaction must remain small, as can be seen from the values of the equilibrium constant $K = p_{MgO}p_O/p_{Mg}p_{O_2}$, computed using current thermodynamic data,[12] and shown in Table 2. Moreover, a rough estimate of the activation energy of reaction (I) shows that its rate constant would be about five orders of magnitude smaller than the experimental bimolecular constant k_2.

Neither the reaction of magnesium atoms with oxygen atoms, nor the recombination of oxygen atoms to molecules, would seem to be of importance at low pressure, since they would require three-body collisions. The possibility for occurrence of the bimolecular reaction

$$\text{O} + \text{Mg}_2 \rightarrow \text{MgO} + \text{Mg} \tag{II}$$

exists, but this reaction seems unimportant, since, unlike the alkali metals, the alkaline-earth metals have not been observed to form appreciable concentrations of diatomic molecules in the vapor phase.

The possibility of other reaction steps occurring in the gas phase is thus essentially exhausted after reaction (I) has occurred. However, in

TABLE 2

Equilibrium constant of reaction (I)

T(°K)	500	1000	1500	2000	2500
$p_{MgO}p_O/p_{Mg}p_{O_2}$	6.2×10^{-12}	1.1×10^{-5}	1.3×10^{-3}	1.5×10^{-2}	6.5×10^{-2}

view of the very small equilibrium vapor pressure of condensed magnesium oxide, the small concentration of MgO vapor formed by reaction (I) corresponds to large supersaturation, and nucleation of oxide particles must therefore set in rapidly.[24] The observed tendency for growth of oxide deposits suggests that the nuclei will continue to grow as a consequence of heterogeneous reaction of magnesium vapor and oxygen on their surface. The absence of atomic and molecular spectra in the flame radiation, and the similarity of the blue continuum emitted by the flame to the spectrum of the surface luminescence of growing MgO deposits, strongly support the conclusion that most of the oxidation takes place as a heterogeneous reaction on the surface of growing oxide particles.[25]

One may regard the free-energy change ΔF_{III}° of the stoichiometric over-all reaction

$$\mathrm{Mg(g)} + \tfrac{1}{2}\mathrm{O_2} \rightarrow \mathrm{MgO(s)},$$
$$\Delta H_0^{\circ} = -178.0 \text{ kcal} \qquad \text{(III)}$$

as determining the tendency for occurrence of the surface reaction. Indeed, for given partial pressures p_{Mg} and p_{O_2}, the equilibrium partial pressure p_{MgO} corresponding to stoichiometric reaction differs from the vapor pressure $(p_{MgO})_{eq}$ in equilibrium with condensed MgO, and defines a supersaturation

$$S = p_{MgO}/(p_{MgO})_{eq} = p_{Mg}p_{O_2}^{\frac{1}{2}} \exp\left(-\Delta F_{III}^{\circ}/RT\right), \qquad (7)$$

which may be regarded as a measure of the driving force of the surface reaction. The exponential factor of the above expression is given in Table 3, which demonstrates the magnitude of this driving force.

The similarity between the spectra of flame emission and of surface luminescence suggests that the photometrically determined reaction rate is that of the postulated heterogeneous reaction, rather than that of any gas-phase reaction step. Furthermore, as long as the condition of excess oxygen concentration is satisfied, the surface reaction should obey the unimolecular rate law, independent of oxygen concentration, which is favored by the experimental data. The details of the reaction may be visualized as follows[26]: Owing to the oxygen excess, many more oxygen molecules than magnesium atoms will collide with the particle surface in unit time. The surface will therefore normally be covered by a monatomic layer of oxygen atoms, which will react with arriving Mg atoms with high collision efficiency. On the sites where Mg atoms have reacted, a clean oxide surface is temporarily formed, which will be able to dissociate arriving O_2 molecules, so that the monatomic oxygen layer is continuously re-established.

The rate of oxide formation will thus depend only on the collision frequency of Mg atoms with the particle surface, in agreement with a unimolecular rate law. However, the reaction rate will be proportional not only to Mg concentration but also to particle surface area per unit volume. Since the particles grow in the flame zone as they move radially outward, their surface area increases with radial distance r. Thus, the differential equation that determines flame structure becomes nonlinear, and the distribution of Mg concentration cannot agree exactly with Eq. (1). Corresponding deviations from linearity should appear on the plots of log $(r^{\frac{1}{2}}/\tau)$ vs. r for the photometric runs, but were not observed in the present work. However, the absence of nonlinearity of the plots does not exclude the proposed mechanism, since the deviations from linearity may be too small to be noticeable, particularly since the measurements are restricted to outer regions of the flame zone, where the growth of surface area with radial distance should be slow.

A rough estimate showed that particle diameters of 0.01 μ or less would provide adequate surface area per unit volume to yield a unimolecular rate of the measured order of magnitude, provided the collision efficiency is close to unity. It seems very difficult, however, to determine whether reaction (I), followed by nucleation, could create a sufficient number of particles to support the proposed mechanism, or whether other (possibly heterogeneous) starting reactions may be required.

Similar heterogeneous mechanisms have been proposed recently for the formation of carbon from acetylene[27] and of nickel from nickel carbonyl,[28] and they might be a common feature of reactions in which solid products are formed

TABLE 3

Exponential factor of Eq. (7)

T(°K)	500	1000	1500	2000	2500
$\exp(-\Delta F_{III}^{\circ}/RT)$	5×10^{66}	5×10^{27}	6×10^{15}	3×10^{8}	4×10^{4}

from gaseous reactants. However, while the above argument seems quite convincing for low pressures and correspondingly low temperatures, it becomes less decisive at atmospheric or higher pressures and high flame temperatures. The quite different spectrum of the magnesium flame at atmospheric pressure shows that the reaction mechanism may indeed be considerably more involved. The proposed heterogeneous mechanism will probably continue to participate to some extent, but should become increasingly less important as the flame temperature approaches the theoretical upper limit given by the boiling point of the oxide.[2]

In view of the suggested importance of the surface reaction, the observations on formation of surface deposits are of considerable interest. The luminescence that accompanies the surface reaction is presumably closely related to the "candoluminescence" observed on oxides, including MgO, exposed to other flame gases.[29,30,31] The appearance of a dark deposit in the central region of the flame (Fig. 6) might provide information on composition of the flame gases and on kinetics, if its nature would be known. If the deposit consists of finely divided magnesium metal, the sharp boundary of the dark area could be explained by the phase rule, which allows coexistence of Mg(s) and MgO(s) for given temperature only at a prescribed composition of the gas phase. Thermodynamic analysis shows that this composition should correspond to vanishingly small oxygen concentration. The absence of luminescence within the dark region and the dependence of its size on oxygen concentration support the view that the dark deposit is related to oxygen depletion. However, the boundary does not seem to correspond to total depletion, since some oxide is still deposited in the dark region.

Acknowledgments

The author gratefully acknowledges many valuable suggestions by Dr. S. H. Bauer, Dr. A. L. Myerson, and Dr. G. Rudinger; participation in the spectroscopic work by Mr. H. Thompson; evaluation of the flame photographs by Miss M. J. Williams; design of apparatus by Mr. V. F. Napierski and its construction by Mr. C. S. Bardo and Mr. J. G. Bennett; preparation of the electron micrograph by Mr. F. E. Hanlon; and valuable advice regarding photographic technique by Mr. J. W. Baxtresser and Mr. E. J. Schifferli.

This work was sponsored by Project SQUID which is supported by the Office of Naval Research, Department of the Navy, under Contract Nonr 1858(25) NR-098-038. Reproduction in full or in part is permitted for any use of the United States Government.

References

1. Grosse, A. V. and Conway, J. B.: Ind. Eng. Chem. *50*, 663 (1958).
2. Glassman, I.: Am. Rocket Soc. Preprint 938–59 (1959).
3. *Solid Propellant Rocket Research,* Chapter C, pp. 253–291. M. Summerfield, Ed. Academic Press, New York (1960).
4. Friedman, R. and Maček, A.: Combustion and Flame *6*, 9 (1962).
5. Polanyi, M.: *Atomic Reactions.* Williams and Norgate, London (1932).
6. Bawn, C. E. H: Annual Reports on the Progress of Chem. *39*, 36 (1942).
7. Garvin, D. and Kistiakowsky, G. B.: J. Chem. Phys. *20*, 105 (1952).
8. Garvin, D., Gwyn, P. P., and Moskowitz, J. W.: Can. J. Chem. *38*, 1795 (1960).
9. Rapp, D. and Johnston, H. S.: J. Chem. Phys. *33*, 695 (1960).
10. Brewer, L. and Porter, R. F.: J. Chem. Phys. *22*, 1867 (1954).
11. Porter, R. F., Chupka, W. A. and Inghram, M. G.: J. Chem. Phys. *23*, 1347 (1955).
12. National Bureau of Standards Report No. 6484, July 1959.
13. Scartazzini, M.: Compt. rend. *230*, 97 (1950).
14. Coffin, K. P.: *Fifth Symposium (International) on Combustion*, p. 267. Reinhold, New York (1955).
15. Brzustowski, T. A. and Glassman, I.: Report No. 586, Dept. of Aeronautical Engineering, Princeton University, October 1961.
16. Smith, F. T.: J. Chem. Phys. *22*, 1605 (1955).
17. Neville, J. R.: Rev. Sci. Instr. *33*, 51 (1962); See also *ibid.*, p. 144. Instrument manufactured by Chemtronics, Inc., San Antonio, Texas.
18. Van der Held, E. F. M.: *Seventh Symposium (International) on Combustion*, p. 554, Butterworths, London (1959).
19. Singer, J. M. and Grumer, J.: *ibid.*, p. 559.
20. Harvey, J., Matthews, H. I., and Wilman, H.: Discussions Faraday Soc. No. 30, p. 113 (1960).
21. Brewer, L. and Trajmar, S.: J. Chem. Phys. *36*, 1585 (1962).
22. Hirschfelder, J. O., Curtiss, C. F., and Bird, R. B.: *Molecular Theory of Gases and Liquids*, p. 539. Wiley & Sons, New York (1954).
23. Svehla, R. A.: NASA TR R-132 (1962).
24. Frenkel, J.: *Kinetic Theory of Liquids*, Chapter 7. Oxford University Press, New York (1946).
25. This heterogeneous mechanism was proposed by H. M. Cassel during a discussion at the Fourth Meeting, JANAF–ARPA–NASA Thermochemical Panel, Aeronutronic, July 1961.

26. MYERSON, A. L.: private communication.
27. TESNER, P. A.: Discussions Faraday Soc. No. 30, p. 170 (1960); *Eighth Symposium (International) on Combustion*, p. 627. Williams & Wilkins, Baltimore (1962).
28. CALLEAR, A. B.: Proc. Roy. Soc. (London) *A265*, 71 (1961).
29. MINCHIN, L. T.: Trans. Faraday Soc. *35*, 163 (1939).
30. ARTHUR, J. R. and TOWNEND, D. T. A.: *Energy Transfer in Hot Gases*, p. 99. National Bureau of Standards Circular 523, March 1954.
31. GORBAN', A. N. and SOKOLOV, V. A.: Optika i Spektr. *5*, 713 (1958); Optics and Spectr. *7*, 164 (1959); SOKOLOV, V. A., GORBAN', A. N., and NAZIMOVA, N. A.: Optics and Spectr. *11*, 144 (1961).

Discussion

PROF. A. D. WALSH (*University of St. Andrews, Dundee, Scotland*): I was a little surprised by the statement that the only gas phase reaction that need be considered was

$$Mg(g) + O_2 \rightarrow MgO(g) + O \qquad (1)$$

In view of the fact that the energy of activation of this reaction must be at least 28 kcal/mole, could a third-order reaction (of zero activation energy)

$$Mg(g) + O_2 + M \rightarrow MgO_2(g) + M \qquad (2)$$

be faster than reaction (1), in spite of the low pressure used?

DR. G. H. MARKSTEIN (*Cornell Aeronautical Laboratory*): In reply to Dr. Walsh's question, the proposed reaction was not considered because it postulates a species, $MgO_2(g)$, that has not been observed experimentally (see refs. 10, 11, and 21 of the paper). I agree that this reaction would be appreciably faster than reaction (I) of the paper. However, the measured rate constant would still be about three orders of magnitude too large, and, moreover, the three-body reaction would require ω to be proportional to p rather than to $p^{\frac{1}{2}}$; the latter pressure dependence is borne out by the data.

Although the proposed reaction thus does not agree with the measured rates, it may very well determine the rate of formation of MgO particles.

PROF. I. GLASSMAN (*Princeton University*): In support of Dr. Markstein's answer to Dr. Avery's question as to the possible existence of Mg_2 vapor and consequently, the feasibility of other reaction routes we[1] could not find any bands that we could attribute to Mg_2 in spectrograms we have taken of magnesium ribbons in oxygen-inert gas atmospheres at pressures which are relatively high compared to those of Markstein's experiments. A typical spectrogram we have taken is shown in the accompanying figure, which gives the results of burning magnesium in air at a total pressure of 75 mm Hg. This particular spectrogram is chosen from the many we have taken of a pressure range of 60 mm Hg to 30 atm because the lines and bands are not obscured by the background continuum from condensed MgO that we obtain in our experiments at the higher pressures. On the spectrogram, which has first and second order spectra superimposed, the green system of MgO bands (4900–5007 Å) is marked and one can clearly observe the characteristic broadened and self-absorbed profile of the Mg resonance line at

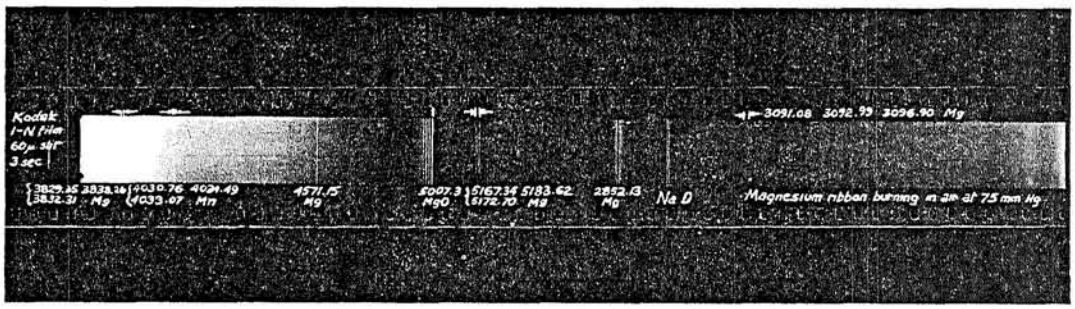

2852 Å, which one obtains when Mg vapor exists at varying temperatures in the flame.[1,2]

Thus even at 75 mm Hg total pressure MgO vapor can be present in appreciable amounts in Mg flames and the heterogeneous kinetic route discussed by Markstein does not necessarily have to be the major one with overall reaction at higher pressures.

REFERENCES

1. BRZUSTOWSKI, T. A. and GLASSMAN, I.: *Spectroscopic Investigation of Metal Combustion.* Princeton University Aero Eng. Lab. Report No. 586, 1961.
2. MAVRODINEANU, R. and BOITEUX, H.: *L'Analyse Spectrale Quantitative par la Flamme.* Masson, Paris, 1954.

STUDIES OF THE COMBUSTION OF DIMETHYL HYDRAZINE AND RELATED COMPOUNDS

PETER GRAY AND MALCOLM SPENCER

Spontaneous ignition studies are here reported on hydrazine and (unsymmetrical) dimethyl hydrazine. This paper is part of a general program on the combustion of endothermic fuels.

1. Hydrazine systems: $N_2H_4 + NO$; $N_2H_4 + N_2O$. The work on hydrazine concerns the $N_2H_4 + NO$ and $N_2H_4 + N_2O$ systems. Particular aims are to establish the modes of reaction, to investigate the critical conditions for ignition, and to investigate the possible thermal character of the explosion.

In mixtures with nitric oxide there is either slow reaction or explosion. The stoichiometric mixture ($N_2H_4 + 2NO$) is the most ignitible. The influence of inert diluents and comparison with $N_2H_4 + O_2$ suggests that explosion is thermal in character. The ready ignition is correlated with the postulated reactivity of nitric oxide towards radicals such as NH and NH_2.

In mixtures with nitrous oxide, explosion appears to be *initiated* as if nitrous oxide were merely a diluent although the nitrous oxide does not survive the flame.

2. Dimethyl hydrazine systems: $Me_2NNH_2 + O_2$. There is very little previous published work on dimethyl hydrazine (DMH) combustion. The conditions for DMH to undergo spontaneous ignition both in decomposition and in oxidative combustion have been examined. Distinct modes of oxidation exist. They include strong explosions, weak ignition, chemiluminescent oxidation, and slow reaction; in addition, multiple ignitions have been observed. Qualitatively, the combustion differs markedly from that of the superficially analogous mono-, di-, and trimethyl amines although there are resemblances to the ethylamines.

Introduction

Hydrazine and dimethyl hydrazine are examples of endothermic compounds which can support a flame in decomposition as well as in oxidation. Such systems are of interest for several reasons: Decomposition flames are chemically the simplest combustions known; their study broadens knowledge of flame systems (the vast majority of experiments relate to the chemically complex but narrower field of hydrocarbon combustion); and such compounds have attracted attention technically as high energy fuels.

Previous work has included studies of hydrazine in slow and explosive decomposition, in slow oxidation[1] and explosive combustion[2] supported by oxygen. In addition measurements have been made on laminar flame propagation both in decomposition, and in oxidation supported by oxygen,[3] nitric oxide,[3,4] or nitrous oxide.[3] There appears to be rather little published work on dimethyl hydrazine other than Bamford's[5] spark ignition experiments.

For this study the work on hydrazine is an investigation of the spontaneous ignition of hydrazine + nitric oxide and hydrazine + nitrous oxide mixtures. The particular aims are to establish the modes of reaction, to investigate the mechanism of ignition by examining the critical conditions for ignition, and especially to investigate the role of self-heating in this thermal reaction.

Dimethyl hydrazine (DMH) is considerably more complex. It is the aim of this work to establish the conditions for DMH to undergo spontaneous ignition in decomposition and to discover whether in oxidation it behaves in a simple manner (as do mono-, di-, and trimethylamine[6]) or shows complex "cool flame" phenomena (as do di- and triethylamine[6]). In fact several distinct modes of ignition are observed. The conditions for their occurrence, their chemical characteristics (mass spectrometric analyses have been used to characterize reaction products), and the role in them of self-heating are clarified.

Experimental

Procedure

The critical pressure limits of spontaneous ignition were determined by measuring the total pressure of reaction mixture necessary for ignition on admission to a hot vessel; the apparatus

was a modification of that described by Gray and Yoffe.[7]

A silica vessel of 4.5 cm internal diameter, 350 cm^3 capacity, and 330 cm^2 surface was used. The vessel was cleaned with hot concentrated nitric acid and distilled water before use. The apparatus could also be used to follow changes of pressure in a reacting system, although it was not suitable for accurate determinations of rate constants because the dead space was not negligible.

Materials

Concentrated hydrazine, containing approximately 98 per cent N_2H_4 by weight, was dehydrated by refluxing for 2–3 hours over fused caustic soda in an atmosphere of nitrogen at 120 mm Hg, followed by distillation under similar conditions. It was distilled and stored *in vacuo*. Iodate analysis[8] showed 99.8 to 100.1 per cent w/w.

Commercial unsymmetrical dimethyl hydrazine, obtained from Lights' Ltd., was purified by fractional vacuum distillation.

Nitric oxide was prepared by reducing sodium nitrite with acidic ferrous sulfate solution. Impurities were removed by passing the gas over pellet caustic soda, phosphorous pentoxide, and by fractional vacuum distillation from caustic soda. The product, stored at −180°C, boiled as an "ice blue" liquid.

Other gases were obtained from cylinders. The oxygen, nitrous oxide, hydrogen, and "white spot" oxygen-free nitrogen were supplied by British Oxygen Gases Ltd. Argon of 99.99 per cent purity was supplied by Saturn Industrial Gases Ltd. Airco helium of 99.99 per cent purity was imported. The anhydrous ammonia was a product of Imperial Chemical Industries.

Results

Combustion of Hydrazine—Nitric Oxide Mixtures

Composition Dependence of the Pressure Limit for the Spontaneous Ignition of $NO + N_2H_4$ *Mixtures.* The variation with composition of the pressure limit for spontaneous ignition in a silica vessel has been investigated between 652° and 392°C (Fig. 1). At both temperatures, the stoichiometric mixture ($N_2H_4 + 2NO$) is the most readily ignited. After the explosion of such a mixture, the measured pressure increase was about 33 per cent, in accord with the equation for complete oxidation:

$$N_2H_4 + 2NO \rightarrow 2N_2 + 2H_2O$$

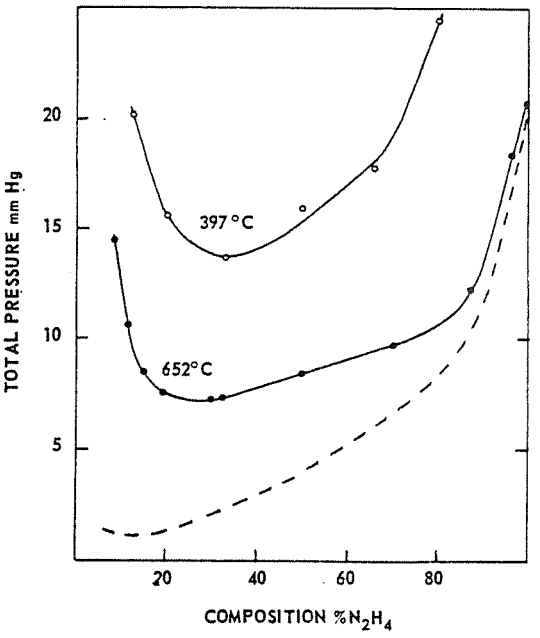

FIG. 1. Spontaneous ignition of hydrazine-nitric oxide mixtures; dependence of the pressure limit on composition. Dashed line shows the variation of partial pressure of N_2H_4 with composition at 652°C.

Explosions in hydrazine-rich mixtures were accompanied by a bright yellow flash. In rich mixtures (33 to 80 per cent N_2H_4) the pressure increase suggests that all the nitric oxide is reduced and the excess hydrazine is decomposed to N_2 and H_2. Ammonia is formed in very rich mixtures as the decomposition flame of hydrazine eventually supplants the combustion flame.

In hydrazine-lean mixtures the luminosity was relatively low. Chemical analysis[3] revealed the decomposition of excess nitric oxide.

Temperature Dependence of the Pressure Limit for the Spontaneous Ignition of $NO + N_2H_4$ *Mixtures.* The dependence on temperature of the limiting total pressure for ignition of a stoichiometric mixture ($N_2H_4 + 2NO$) was examined from 343 to 652°C (Fig. 2). The ignition pressures of a rich mixture ($N_2H_4 + NO$) were approximately 10 per cent higher.

At temperatures above 365°C induction periods of less than one second separated the admission of stoichiometric mixtures to the reaction vessel from explosion. Explosion was rarely audible at the limit. At temperatures below 365°C ignition delays in excess of 2 seconds were observed. The explosion limit was less reproducible at lower temperatures.

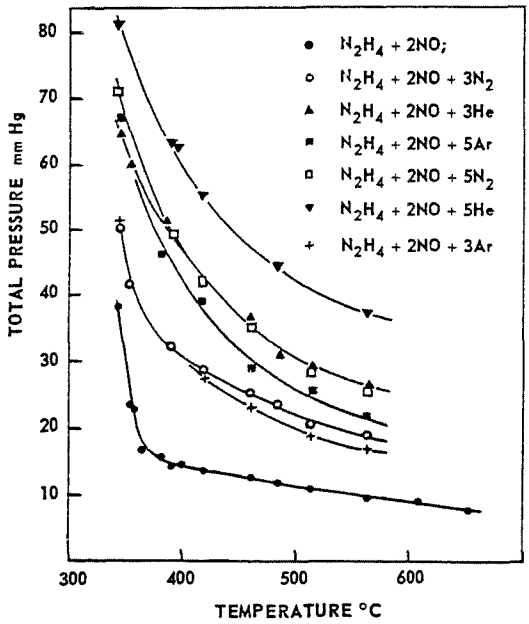

FIG. 2. Spontaneous ignition of hydrazine-nitric oxide mixtures; dependence of the pressure limit on temperature, and influence of inert gases.

Influence of Diluents on the Pressure Limits for the Spontaneous Ignition of $NO + N_2H_4$ *Mixtures.*

The effect on the explosion limit of added diluents has been examined. Figure 2 shows the variation with temperature of the explosion limit for mixtures of composition $N_2H_4 + 2NO + 3X$ and $N_2H_4 + 2NO + 5X$ where X is He, Ar, N_2. The addition of argon, nitrogen, and helium raises the limiting total pressure for explosion.

Combustion of Hydrazine–Nitrous Oxide Mixtures

Mixtures of hydrazine with nitrous oxide were ignited in the silica vessel at 685 and 652°C. Figure 3 shows the variation with mixture composition of the pressure limits for ignition at these temperatures. The composition–pressure curve does not have the familiar U-shape associated with second-order reaction in binary mixtures: The partial pressure remains approximately constant. The rate of reaction thus does not depend on the partial pressure of N_2O, and the primary role of N_2O may be that of a diluent. The pressure increase on ignition, however, indicates that N_2O as well as N_2H_4 must suffer extreme decomposition so that N_2O may be involved in subsequent oxidation. Complete oxidation in stoichiometric mixtures is represented by:

$$2N_2O + N_2H_4 \rightarrow 3N_2 + 2H_2O$$

$$\Delta H = -177.5 \text{ kcal/mole}$$

Tests for the Ignition of the Decomposition Products of Hydrazine with Nitric and Nitrous Oxides

In order to establish that all the ignitions observed were the consequence of primary processes (e.g. direct interaction between hydrazine and nitric oxide), and did not result merely from secondary oxidations of the products of hydrazine decomposition (H_2 and NH_3), blank experiments were carried out. The four mixtures $H_2 + NO$, $NH_3 + NO$, $H_2 + N_2O$, $NH_3 + N_2O$ were each admitted to the vessel at 652°C. In no case was ignition observed; even the thermal reaction was slight. These results are in accord with previous work on these systems.[9–12]

Spontaneous Ignition of Pure Dimethyl Hydrazine

Like hydrazine, pure unsymmetrical dimethyl hydrazine (DMH) will undergo spontaneous ignition. The luminosity of the ignition, semi-transparent and whitish in color, was slightly weaker than that of ignitions in DMH-rich mixtures with oxygen. The pressures required were:

Temperature (°C)	420°	443°	484°	514°
Pressure (mm Hg)	48.5	28.9	12.4	5.7

The addition of argon facilitated ignition.

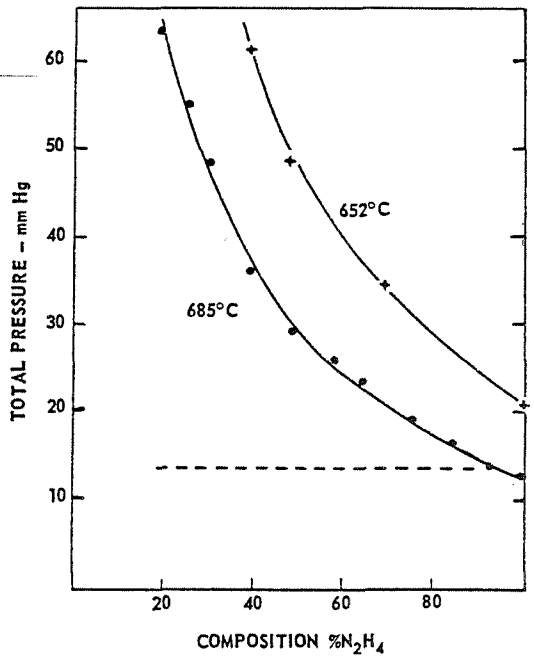

FIG. 3. Spontaneous ignition of hydrazine-nitrous oxide mixtures; dependence of pressure limit on composition. Dashed line shows the mean partial pressure of N_2H_4 at 685°C.

Analysis has identified only the simple products. Those of *slow* decomposition were mainly nitrogen and methane. In *explosive* decomposition however, other products including H_2, NH_3, and HCN were found.

Spontaneous Ignition of Mixtures of Dimethyl Hydrazine with Oxygen

The explosive combustion of mixtures of dimethyl hydrazine with oxygen is complex. According to the pressure, composition, and temperature, oxidation may be either (1) a *slow reaction*, unaccompanied by light emission, (2) a very feebly *chemiluminescent reaction*, (3) a *weak ignition*, or (4) a *violent, audible explosion* accompanied by an intense flash. Furthermore, there are possibilities within regions (3) and (4) of multiple ignitions. For example, a mixture containing 33 per cent of DMH, at 420°C, at a total pressure of 40 mm Hg gave a single intense white ignition. The same mixture at the same temperature but at a pressure of 41 mm Hg gave two successive ignitions.

The *vigorous explosion* was found in all mixtures from 15 to 45 per cent DMH, the critical pressure limit tending to a minimum near the center of this composition range. The *weak ignitions* were observed in mixtures which were either too rich or too lean in DMH for strong explosion to occur. The *chemiluminescent reaction* was seen (under conditions too mild for strong explosion or weak ignition) in mixtures containing from 14 to 62 per cent DMH.

In oxidation, H_2 was found in the products of strong explosion, weak ignition, and chemiluminescent reaction. The products of weak ignition are similar to those of the decomposition flame but include water (and possibly CO). The products of strong explosion were fairly simple including H_2O, N_2 and smaller amounts of the oxides of nitrogen and carbon. Slow oxidation and chemiluminescent reaction give products differing from those of strong explosion only in the greater concentration of large molecules (up to about mass number 80) present.

Composition Dependence of the Pressure Limits for the Spontaneous Ignition of O_2 + DMH *Mixture at* 514°C. At 514°C the vigorous explosion was examined in mixtures from 20–40% DMH. The minimum pressure for strong ignition (Fig. 4) occurred at a composition close to DMH + $2O_2$. At approximately this composition the intense flash changed, with decreasing DMH content, from white to a more audible pink ignition. The addition of inert gas raised the total pressure for ignition. At higher pressures, and within the composition limits for a single strong explosion, multiple ignitions were observed. A bright pink or white explosion was followed half a second later by one or more silent whitish ignitions, occupying the whole of the vessel. These latter ignitions, which were similar to the "weak ignitions," occurred at 0.3 second intervals.

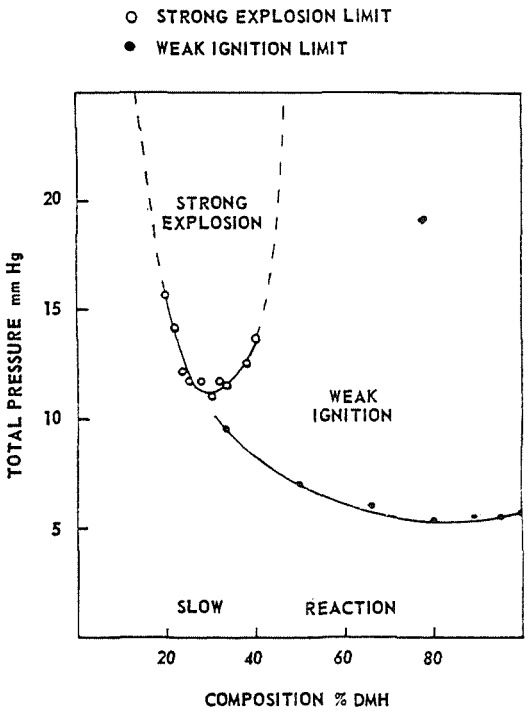

FIG. 4. Spontaneous ignition of DMH-oxygen mixtures at 514°C; dependence of the pressure limit on composition.

Weak ignition was seen in mixtures containing more than 32 per cent DMH. The ignitions were silent, semi-transparent, and white. The limit showed an apparent minimum corresponding to 4DMH + O_2. The addition of inert diluents (argon, nitrogen, and helium) raised the total pressure limit for ignition, the general form of the limit being preserved. Multiple "weak ignitions" were observed at higher pressures. The first ignition was strongest and was followed by similar ignitions at less than half second intervals.

Composition Dependence of the Pressure Limit for the Spontaneous Ignition of O_2 + DMH *Mixtures at* 420°C. At 420°C, the oxidation of DMH by oxygen showed more complex features. Figure 5 maps the ignition limits for the three fundamental ignition processes which can occur in the system. The boundary associated with the region of strong explosion showed two close but quite distinct lobes (minima), one at 30 per cent corre-

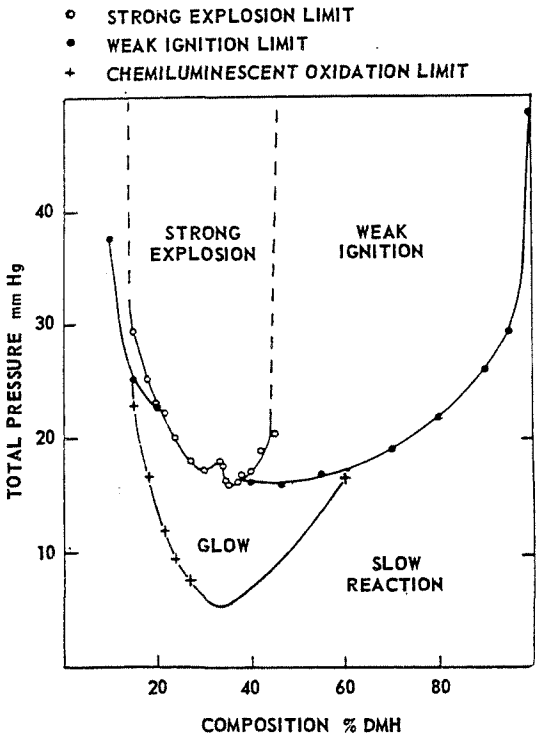

FIG. 5. Spontaneous ignition of DMH-oxygen mixtures at 420°C; dependence of the pressure limit on composition.

sponding to the strong pink explosion and one corresponding to the white explosion at 35 per cent DMH. The shape of the pressure limit for multiple ignitions emphasized the double-minima shape of the single ignition limit, and the addition of nitrogen to DMH-oxygen mixtures produced two isolated regions of explosion at elevated pressures.

The shape of the weak ignition limit was quite different at 420°C from that at 514°C. The minimum pressure for ignition now occurred in leaner mixtures (Fig. 5). The ignitions were observed in mixtures containing between 10 and 20 per cent DMH and more than 39 per cent DMH. The pressure limit for multiple weak ignitions was examined. The addition of nitrogen was observed to raise the total pressure limit for ignition of both the single and multiple ignitions.

Chemiluminescent oxidation of DMH was observed at 420°C under conditions too mild for strong explosion. It occurred between 14 and 62 per cent DMH (Fig. 5). The addition of the inert diluents argon, nitrogen, and helium lowered the partial pressure of DMH + O_2 necessary for chemiluminescence.

Influence of Temperature and Inert Diluent on the Pressure Limit for the Spontaneous Ignition of O_2 + DMH *Mixtures.* The variation with temperature from 514°C to 300°C of the limiting total pressure for explosion in a mixture of DMH + $2O_2$ was examined (Fig. 6). Induction periods varying from 2 seconds at 353°C to 8 seconds at 300°C were observed to occur with some explosions. Below 380°C, the character and occurrence of explosion was markedly dependent on the speed of entry of the gases into the reaction vessel. The addition of argon, nitrogen, and helium in mixtures DMH + $2O_2$ + 3X raised the total pressure limit for ignition.

Figure 7 shows the effect of temperature upon the pressure for weak ignition in a mixture 4DMH + O_2. This was studied between 514° and 380°C. The addition of inert diluents in mixtures 4DMH + O_2 + 12X(X = Ar, N_2, He) raised the total pressure for this ignition. The results, plotted as partial pressures of DMH in the ignition mixture, show that argon and nitrogen facilitate weak ignition. Helium makes it more difficult.

Chemiluminescent oxidation was observed between 420° and 307°C. The results are less reproducible above 400°C, and at higher pressures. The luminosity appeared a few seconds after

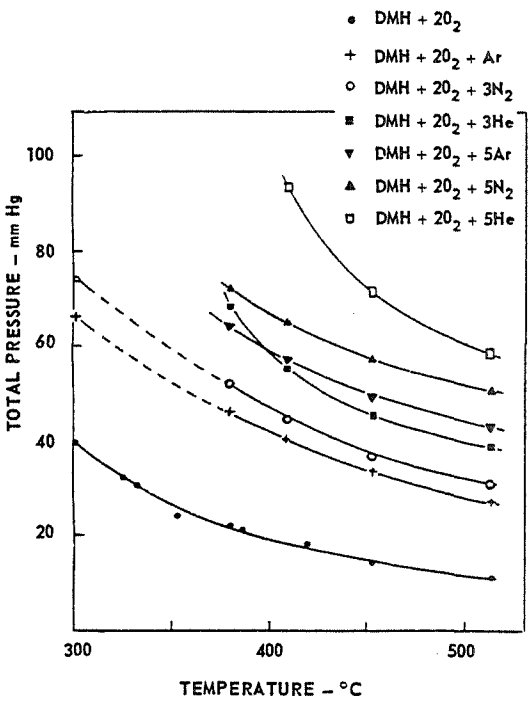

FIG. 6. Strong explosion of DMH + $2O_2$; dependence of the pressure limit on temperature and the influence of inert gases.

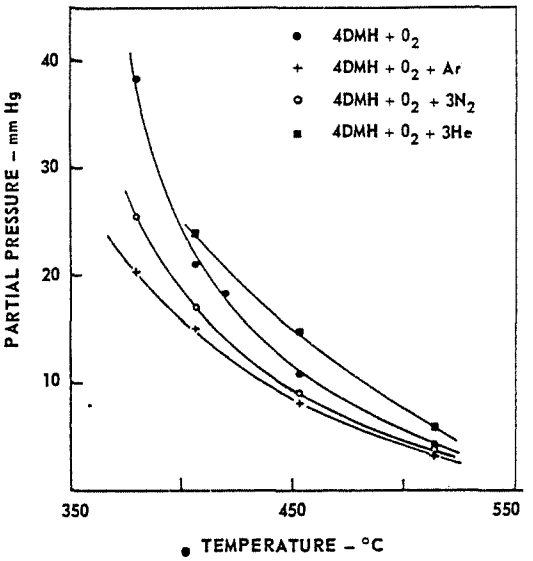

FIG. 7. Weak ignition of 4DMH + O_2; dependence of the pressure limit on temperature and the influence of inert gases.

admission of the reactants to the hot vessel and persisted for 5 to 6 seconds as a blue glow. The rate of pressure change in the first 10 to 15 seconds was about four times greater in the mixture DMH + $2O_2$ than in the mixture DMH + $2N_2$; it fell off rapidly with time. Figure 8 shows the

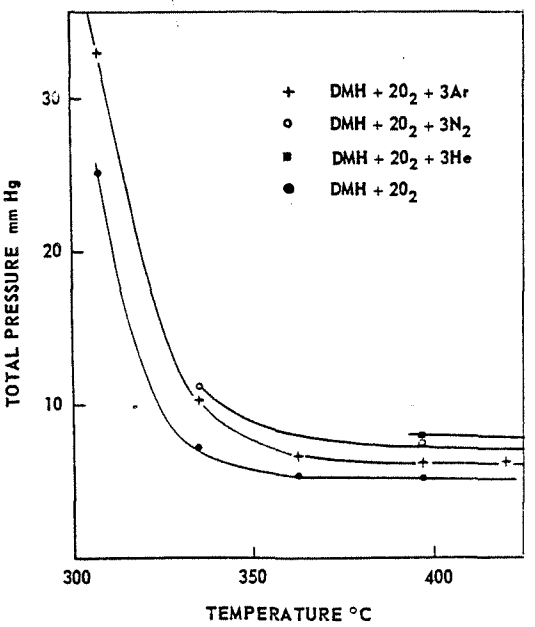

FIG. 8. Chemiluminescent reaction of DMH + $2O_2$; dependence of the pressure limit on temperature and the influence of inert gases.

temperature-dependence of the luminescent reaction. Luminescence was also observed in mixtures DMH + $2O_2$ + 3X (where X = Ar, N_2 or He) at lower partial pressures of DMH + $2O_2$.

Discussion

Results are discussed in two sections. The first is concerned with hydrazine oxidation; the second with dimethyl hydrazine in decomposition and oxidation.

Spontaneous Ignition of Hydrazine with Nitric Oxide

Only two modes of reaction are observed over the whole range of composition and temperature studied: slow thermal oxidation and explosive combustion. The temperature-dependence of the explosion limit is simple (Fig. 2). That the observed ignitions are the consequence of direct interaction between the reactants is shown by the evidence of "blank" experiments in which

TABLE 1

Minimum ignition temperatures (°C)

	NO	O_2	N_2O
NH_3	800[a]	1070	1000
N_2H_4	335	400	670

[a] Wolfhard and Strasser[14]; flow system.

mixtures of nitric oxide with ammonia or hydrogen (the decomposition products of hydrazine) do not ignite, and the lengthy half lives of the hydrazine decomposition.[13] These observations exclude the possibility of prior pyrolysis of hydrazine to stable products. The pressure increase accompanying the oxidation of hydrazine with nitric oxide indicates that reaction to N_2 and H_2O is complete:

$$N_2H_4 + 2NO \rightarrow 2N_2 + 2H_2O$$

$$\Delta H = -181.5 \text{ kcal/mole}$$

For nonstoichiometric mixtures, the reactant in excess, whether this is hydrazine or nitric oxide, is decomposed.

The spontaneous ignition of NO + N_2H_4 may be usefully compared with that of related systems. Table 1 summarizes the approximate minimum ignition temperatures of binary stoichiometric fuel oxidant mixtures at 50 mm Hg total pressure.

A nitric oxide-hydrazine mixture ignites far more readily than does one of nitric oxide plus ammonia. Ordinarily however, ammonia is considered to be very reactive towards nitric oxide[14]; this is the case relative to hydrocarbons (such as methane) which are believed to require the prior decomposition of nitric oxide to its elements before explosive oxidation can occur. The reactivity of ammonia towards nitric oxide is ascribed to the formation of NH_2 and NH radicals. Their reaction with NO has been proposed[15] to explain the low intensity of the NH_2 band emission from the ammonia nitric oxide flame.

$$4NH_3 + 6NO \rightarrow 5N_2 + 6H_2O$$

$$\Delta H = -432 \text{ kcal/mole}$$

If the ability to furnish NH_2 radicals is the necessary condition for the efficient reduction of NO, it is natural that hydrazine, which readily decomposes to NH_2 radicals,[16] should be more reactive than ammonia.

$$N_2H_4 \rightarrow 2NH_2 \qquad \Delta H = 60 \text{ kcal/mole}$$

When nitric oxide is compared with oxygen as a supporter of the combustion of hydrazine, two contrasts emerge. First, the spontaneous ignition of $N_2H_4 + 2NO$ is somewhat easier than that of $N_2H_4 + O_2$ (Table 1). This may be a further manifestation of the reactivity of nitric oxide with amino radicals, or of the greater heat release of the reaction with nitric oxide. Secondly, the ignition limit with nitric oxide is simple whereas that with oxygen shows two distinct modes of ignition.[2] One is a strong explosion which resembles that found with nitric oxide; the other, a weak delayed ignition, is due to the explosion of hydrogen formed in a side reaction. Delayed ignition is not possible when nitric oxide is the supporter of combustion.

The mechanism of the spontaneous ignition of $NO + N_2H_4$ mixtures may now be examined and the extent to which self-heating can account for the observed behavior assessed.

It is known that spontaneous ignition in $O_2 + N_2H_4$ occurs by a self-heating mechanism.[2] Oxidation supported by NO is even more exothermic and unlike O_2, N_2 cannot participate in branching reactions. Thus the same interpretation is expected to apply to this system. The addition of helium, of high thermal conductivity, raises the pressure limit for ignition, showing the existence of self-heating. If a unique interpretation is to be offered for the mechanism of ignition, it should be possible to explain quantitatively (1) the composition dependence of the pressure limit for ignition, (2) the temperature dependence of the limit, and (3) the influence of inert diluents upon ignition. However, in the absence of adequate isothermal kinetic measurements on the homogeneous reaction a detailed test is not possible.

The results of a simple thermal theory[17] of explosion are summarized by the relation:

$$\ln \frac{P_{N_2H_4}{}^m P_{NO}{}^n}{T^{m+n+2}} = \frac{E}{RT} + \ln \frac{2R\sigma}{QEAKr^2} \quad (1)$$

where m and n are the orders of reaction with respect to hydrazine and nitric oxide; r is the radius of the vessel treated as an infinite cylinder; R is the gas constant; Q is the heat of reaction (cal/mole); E is the activation energy; σ is the thermal conductivity of the mixture (cal/sec cm deg); A is the frequency factor; and K is a "rate" constant.

For the composition dependence of the ignition pressure, Eq. (1) predicts that the ratio

$$P_{N_2H_4}{}^m P_{NO}{}^n/\sigma$$

should be constant. This ratio has been calculated (Table 2) for two cases assuming $m = 1$ and $n = 1$ or 2. The thermal conductivities were calculated by the method of Lindsay and Bromley.[18]

TABLE 2

Values of the ratio $P_{N_2H_4}{}^m P_{NO}{}^n/\sigma$

	$P_{N_2H_4}P_{NO}/\sigma$	$P_{N_2H_4}P_{NO}{}^2/\sigma$
14% N_2H_4	1.183×10^5	1.22×10^6
50% N_2H_4	1.902×10^5	1.059×10^6
90% N_2H_4	4.49×10^5	1.309×10^6

In both cases some fluctuation of values is observed, but those values calculated for a second-order dependence on NO are more nearly constant. Many of the known reactions of nitric oxide are third order. However, those reactions in which the N–O bond is broken appear to have more complex kinetics; for example, the rate of slow oxidation of ammonia by nitric oxide shows a half power dependence on the concentration of NO. For $N_2H_4 + NO$ mixtures it is not possible to establish conclusively the order of reaction without further isothermal kinetic studies.

The thermal theory of explosion applied to a reaction obeying the Arrhenius law permits an effective activation energy to be obtained from the temperature-dependence of the ignition pressure. In the case of $N_2H_4 + NO$, a plot of $\log P/T^x$ (where $x = 2$ for a second-order reaction and 1.66 for a third-order reaction) against

$1/T$ is not linear. Thus E varies and the reaction is complex.

From thermal theory, if $P = P_{N_2H_4} + 2P_{NO}$ Eq. 1 simplifies so that for the addition of inert gas to a third-order reaction the ratio $P/\sigma^{\frac{1}{2}}$ should be constant. This is approximately the case.

Inert gas	none	Ar	N_2	He
$P/\sigma^{\frac{1}{2}}$	180	170	180	200

The experimental results agree qualitatively with the predictions of thermal theory and suggest that self-heating is the principal agent leading to explosion. Short radical chains are almost certain to exist in the system and their presence may well account for the lack of agreement between experiment and theory.

Dimethyl Hydrazine

Dimethyl hydrazine is, of course, less simple than hydrazine itself and might have been expected to resemble dimethylamine in combustion characteristics, or to bear the same relation to hydrazine as does dimethylamine to ammonia. In fact, its behavior is considerably more complex, for in combustion the three methylamines[6] show only slow reaction or vigorous explosion whereas dimethyl hydrazine combustion displays in addition, multiple ignitions, weak ignitions, and chemiluminescence (resembling the "cool" flames reported in di- and triethylamine combustion.[6] In the following discussion, attention is given only to the salient features of the new observations reported here: In any case, a unique interpretation cannot be put on all the modes of reaction discovered.

Spontaneous Ignition of Pure Dimethyl Hydrazine.

When dimethyl hydrazine decomposes thermally, methane and nitrogen are the major products.

$$(CH_3)_2NNH_2 \rightarrow 2CH_4 + N_2$$

$$\Delta H = -92.2 \text{ kcal/mole}$$

In spontaneous ignition (which is accompanied by a pressure increase of 85 to 100 per cent) mass spectrometric analysis confirms that methane and nitrogen are the major products and shows the formation of smaller amounts of hydrogen, ethane, ammonia, and some HCN. Such stoichiometry suggests the intervention of free radical processes, although branching chains are extremely unlikely and ignition is almost certainly thermal in origin. The simple form of the ignition limit, the form of a graph of log P/T^3 against $1/T$, and the influence of added argon are in accord with this interpretation. At 484°C, the quotient P_{DMH}/σ which on a thermal explosion theory should depend only on temperature, has the value 8.0×10^4 in pure DMH and 7.0×10^4 in the threefold diluted mixture DMH + 3Ar. The agreement is moderately good.

As with hydrazine, initiation of reaction is quite likely to occur by N–N bond fission. Though the thermochemical data leave much to be desired, this step seems likely to be endothermic by some 55 kcal/mole.[19]

$$(CH_3)_2NNH_2 \rightarrow N(CH_3)_2 + NH_2$$

$$\Delta H = 55 \text{ kcal/mole}$$

The effective activation energy $E = 27$ kcal/mole, derived from a graph of log P/T^3 against $1/T$, suggests that the step above is not the rate-determining one. The same situation occurs in the spontaneous ignition of hydrazine.

Spontaneous Combustion (Strong Explosion) of Dimethyl Hydrazine Plus Oxygen. The minimum pressure required for ignition occurs near DMH + $2O_2$. The fact that with oxygen DMH explodes much more readily than does a stoichiometrically equivalent artificial ethane-hydrazine mixture, together with the observation that induction periods before explosion are much shorter than are half-lives for DMH decomposition, confirm direct reaction between fuel and oxidant as the origin of explosion.

Complete oxidation is very exothermic[20]:

$$(CH_3)_2NNH_2 + 4O_2 = 2CO_2 + 4H_2O + N_2$$

$$\Delta H = -472.6 \text{ kcal/mole}$$

Mass spectrometric studies of the slow reaction of DMH + $2O_2$ indicate that N_2, CO, and H_2O are the principal products and H_2, CH_4, and NH_3 are formed in smaller amounts. Other unidentified products exist, some having mass numbers greater than that of the parent molecule. The products of strong explosion are less complex.

Thus a simple reaction path is not expected and radicals are probably involved. However, the exothermicity and the simple T-dependence of the pressure limit lead one to expect a considerable thermal contribution to explosion. Some support is lent to this view by the raising of the ignition limit by inert-diluents, more quantitatively by the approximate constancy of $P/\sigma^{\frac{1}{2}}$,

Inert gas	Ar	N_2	He	None
$10^{-3}\ P/\sigma^{\frac{1}{2}}$ (at 514°C)	1.8	1.87	1.65	1.57

and by the linearity of log P/T^2 against $1/T$. However, around the explosion boundary at 514°C, $P_{N_2H_4}P_{NO}/\sigma$ is not constant and a wholly thermal origin to explosion cannot be postulated.

The multiple (strong and weak) ignitions are more characteristic of higher hydrocarbons than of hydrazine oxidation. It is surprising that they are not found in dimethylamine oxidation.

Weak Ignition and Chemiluminescent Ignitions in Mixtures of Dimethyl Hydrazine with Oxygen

Weak ignitions and chemiluminescence (though different from each other) are the principal phenomena which are not paralleled by methylamine oxidation. Their occurrence here, although similar to that in di- and triethylamine oxidation, disposes of the possibility that such phenomena are confined to molecules with carbon–carbon bonds in them.

Weak ignition is most readily observed in very rich (4DMH + $1O_2$ at 514°C) mixtures and resemblances to spontaneous ignition in decomposition are therefore not surprising. These include the appearance, and the product analyses. All the products of decomposition are present, some in slightly increased amounts; some water and carbon monoxide are also found. The temperature-dependence of the weak ignition limit in a 4DMH + $1O_2$ mixture is simple. Both this and the quantitative effect of inert gases are in accord with a thermal mechanism.

Chemiluminescence, occurring in the mixture DMH + $2O_2$ at temperatures from 300 to 400°C, has qualitative resemblances to the "cool flames" of hydrocarbon combustion and alkyl nitrate[7] decomposition. Mass spectrometry shows that it resembles slow oxidation in the similarity of its reaction products; only small amounts of hydrogen are found, together with water, ammonia, methane, and nitrogen. Chemiluminescence appears not to be a precursor of ignition (whether weak or strong). It is markedly facilitated by all the inert diluents and self-heating cannot be of primary importance. It appears to be a true feature of oxidation since it has not been observed in pure decomposition and since in the mixture DMH + $2O_2$ the rate of reaction in the initial stages (i.e. while chemiluminescence is occurring) is considerably greater than in DMH + $2N_2$.

The occurrence of chemiluminescence in this system in the absence of any hydrocarbon groups more complex than methyl is remarkable.

References

1. Bowen and Birley: Trans. Faraday Soc., *47*, 580 (1951); Winning: J. Chem. Soc. *1954*, 926.
2. Gray and Lee: *Fifth Symposium (International) on Combustion*, p. 692. Reinhold, 1955.
3. Gray and Lee: *Seventh Symposium (International) on Combustion*, p. 61. Butterworths, 1959.
4. Bamford: Trans. Faraday Soc., *35*, 1239 (1939).
5. Bamford: Trans. Faraday Soc., *36*, 1036 (1940).
6. Cullis and Khokhar: Combustion and Flame *4*, 265 (1960).
7. Gray and Yoffe: Proc. Roy. Soc. (London), *A200*, 114 (1949).
8. Penneman and Audrieth: Ind. Eng. Chem. (Anal. Ed.) *20*, 1058 (1948).
9. Graven and Poole: J. Am. Chem. Soc. *83*, 283 (1961).
10. Melville: Proc. Roy. Soc. (London), *A142*, 524 (1933).
11. Destriau: J. Chimie Physique *56*, 936 (1959).
12. Rozlovskii: Zhur. Fiz. Khim. *30*, 1444 (1956).
13. Lee: Thesis, Cambridge, 1955.
14. Wolfhard and Strasser: J. Chem. Phys., *28*, 172 (1958).
15. Wise and Frech: J. Chem. Phys., *22*, 1463 (1954).
16. Szwarc: Proc. Roy. Soc. (London), *A198*, 267 (1949).
17. Frank-Kamenetksii: Acta Physicochim. U.R.S.S., *10*, 365 (1939).
18. Lindsay and Bromley: Ind. Eng. Chem., *42*, 1508 (1950).
19. Gowenlock, Pritchard-Jones, and Majer: Trans. Faraday Soc., *57*, 23 (1961).
20. Aston: J. Am. Chem. Soc., *74*, 2484 (1952).

Discussion

Dr. H. M. Cassel (*Bureau of Mines, Pittsburgh*): I would like to know whether or not the experiments permit a conclusion regarding a relation between length of induction period and activation energy. Of course, very short ignition delays may result from superheating.

Dr. M. Spencer (*University of Leeds*):

(a) *Hydrazine + Nitric Oxide.* Ignition delays larger than 2 seconds have not been observed in this system. Bearing in mind the uncertainty of the instant of entry of gas into the reaction vessel, the measured induction periods are too small and the possible errors in them too large to make an attempt at correlating induction periods with activation energy worthwhile.

(b) *DMH decomposition flame.* No induction periods.

(c) DMH + O_2. No induction periods were observed for weak ignition in such mixtures.

Induction periods were observed at the lower temperatures for strong explosion in DMH + $2O_2$ mixtures. The results for a quartz vessel (reported at the Symposium) are somewhat limited. However, studies in Pyrex vessels have extended to slightly lower temperatures. Here induction periods are larger and a correlation energy might be possible with activation, but only when more activation energy data are available.

At the moment much kinetic data needs to be collected for the N_2H_4 + NO and DMH + O_2 systems, concerning the reactions occurring immediately prior to ignition.

Every effort has been made to eliminate the possibility of the superheating of gases entering the reaction vessel.

THERMAL DECOMPOSITION OF WOOD IN AN INERT ATMOSPHERE

A. F. ROBERTS AND G. CLOUGH

The thermal decomposition of wood has up to now been represented by an overall first order reaction with a definite heat of reaction.[1] There is now sufficient experimental evidence to show that such a treatment is too simple, since values obtained for activation energy and heat of reaction vary with experimental conditions.[2,3]

The present paper describes a series of experiments in which cylinders of wood were decomposed under controlled heating conditions in an atmosphere of nitrogen in a furnace. During each experiment, the specimen was weighed continuously and its temperature was measured at several points. Data were analyzed in terms of the above theory to examine its validity and shortcomings.

Introduction

A knowledge of the rate of thermal decomposition of wood under different heating conditions is essential to a detailed understanding of the growth of fires. However, methods of calculating rates of decomposition still await adequate experimental confirmation. Owing to the complexity of the reactions involved, it has become customary to treat this process in terms of an overall reaction, expressed as an equation of a given order, and to assign to it a single heat of reaction.

Experiment suggests that these simplifications are not always justified. Evidence for a variation in activation energy with temperature,[2] and of heat of reaction with reaction rate has been reported,[3] while Thomas and Bowes[4] have recently shown that discrepancies between data on self heating and on self ignition of fiber-board can be partially explained by the presence of more than one exothermic reaction. There is therefore a need for a more detailed examination of the processes involved.

Much of the information that exists at present has come from experiments on the self ignition of materials derived from wood, such as fiber-board and sawdust. A typical experiment consists in finding, for a pile of material at a given ambient temperature, the critical size at which the heat generated by exothermic reaction can no longer be dissipated and a thermal ignition occurs.

Experiments of this type are limited in scope: The temperature range which can be covered is limited by the rapid decrease of critical size with temperature, and each experiment gives only a critical condition which must be interpreted in terms of a somewhat complicated theory. A critical condition would occur whether this theory were valid or not and it is only by studying the variation of a critical parameter with temperature that the required information is obtained.

Bamford, Crank, and Malan[1] combined the equations for heat conduction in a solid with those for heat generation by a first order reaction and solved them by a finite difference method, for the conditions of a series of experiments which they performed. In their experiments boards of various thicknesses were heated on both sides by flames, and their surface and center temperatures were measured. The values of activation energy, velocity constant, and heat of reaction which gave the best agreement between experimental and calculated values of the center temperature were then determined.

The present experiments follow this approach, but in addition:

(i) Specimens were weighed continuously;
(ii) the temperature of the specimen was measured at several points;
(iii) the heating conditions were capable of independent variation;
(iv) the composition of the atmosphere surrounding the specimen was controlled.

Experimental

Preparation of Specimens. Cylinders of beech of approximately 1 cm radius were turned and divided into two sections of approximate lengths 10 cm and 5 cm. On the face of separation of the longer of the two sections five holes were drilled along a single diameter to a depth of 2.5 cm,

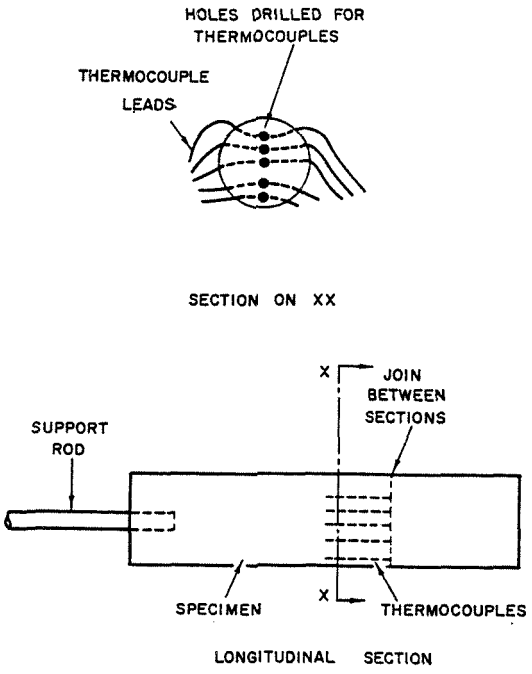

FIG. 1. Preparation of specimen.

parallel to and at different distances from the axis (see Fig. 1).

A 30 s.w.g. Chromel/Alumel thermocouple was inserted to the full depth of each of these holes and grooves were made in the end face so that the thermocouple leads could be laid flat without projecting beyond this face. The smaller section was then glued to this face, with the axes carefully aligned and the original orientation of the two sections restored. The adhesive used was a phenol-resorcinol-formaldehyde resin which remained adhesive at temperatures over 450°C.

After reassembly a sixth thermocouple was attached, to the surface, in line with the others.

The specimens were prepared in this way to ensure that the junctions of the thermocouples lay along a diameter of the cylinder, approximately equidistant from each end, and that the leads of the thermocouples could be made to leave along isothermal paths. Preliminary work had shown that these precautions were necessary to avoid end effects, the effects of any slight asymmetry in the heating conditions, and errors due to conduction of heat along the thermocouple leads.

Experimental Arrangement. The general layout of the apparatus is shown in Fig. 2.

The specimen was supported along the axis of the furnace by a steel rod which formed part of a continuous weighing system accurate to within 0.2 grams; losses in weight of the specimen were detected by increases in tension in the spring of the spring balance, while movement of the specimen due to elongation of this spring was compensated for by the proximity switch and motor.

The furnace used for the experiments had a zone of uniform heating 40 cm long; this was sufficient to render conditions uniform along the length of the specimens. When the furnace was switched on its temperature rose by 20°C/min to a preset control temperature which it maintained to within ±5°C. The ends of the furnace were sealed as shown in Fig. 2. Nitrogen was passed continuously into the furnace, and samples

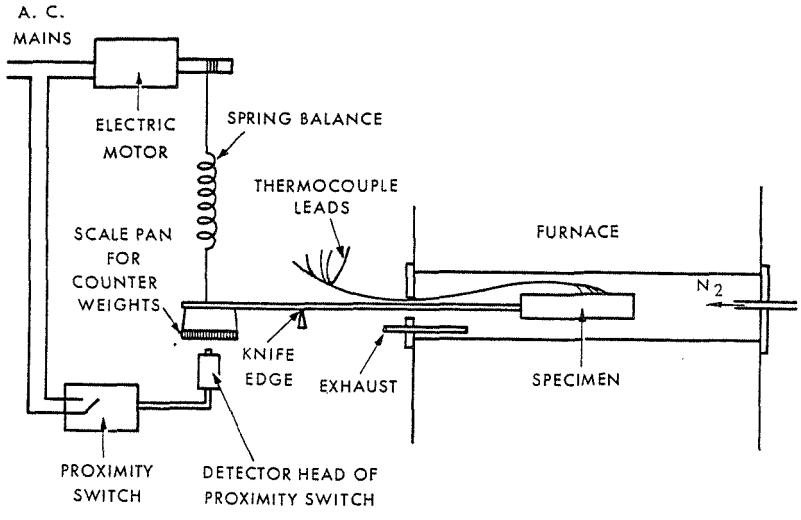

FIG. 2. General layout of apparatus.

from the atmosphere of the furnace showed less than 2 per cent oxygen with this arrangement.

Experimental Procedure. The specimen was prepared and inserted into the cold furnace, as described above. A furnace control temperature was selected and the furnace switched on.

Throughout the experiment the reading of each thermocouple was recorded at 30 second intervals and the weight of the specimen at 15 second intervals. Measurements continued until 5 minutes after the weight of the decomposed specimen had become constant. The furnace was then switched off and the specimen allowed to cool in an atmosphere of nitrogen. Its final weight, when checked on an analytical balance, agreed with that given by the continuous weighing system to within 0.2 grams.

Results

Some of the more significant features of each experiment are summarized in Table 1.

The experimental weight/time data for each experiment are given in Fig. 3. The differences between the curves demonstrate how sensitive is the behavior of wood to changes in the heating conditions.

The surface and center-temperature/time records for each experiment are given in Fig. 4; exothermic reactions within the specimens cause the center temperature to rise above the surface temperature. The temperature records enabled graphs of temperature against distance from surface to be plotted at 1 minute intervals. Curves of this type are shown in Fig. 5, which covers the period of greatest activity of experiment 3. The effects of the exothermic reactions on the temperature distribution are clearly illustrated; the rate of rise of the center temperature is very much greater than that of the surface temperature in the period 19–22 minutes, and the earlier temperature pattern is inverted.

Calculations Based on Results. In considering the data obtained from the above experiments the following assumptions were made:

(1) The thermal decomposition of wood can be represented by an overall first order reaction and

(2) the rate of heat release in the exothermic reactions is proportional to the rate of weight loss.

The cross section of the cylindrical specimens was, for the purpose of computation, considered as four annuli and a central disc of equal area; average temperatures and surface-temperature gradients were calculated for each section at 1 minute intervals throughout the period covered by the temperature record. Each section was sufficiently small for variations of conditions across it to be neglected.

The Overall Kinetics of the Reaction. For a specimen of uniform temperature decomposing according to a first order reaction law, the rate of weight loss would be given by

$$-dw/dt = (w - w')k \exp(-E/RT) \quad (1)$$

where w = weight of specimen at time t, w' = final weight of specimen, k = velocity constant, E = activation energy, R = gas constant, T = absolute temperature. Separating the variables in Eq. (1) and integrating

$$\ln \frac{w - w'}{w_0 - w'} = -k \int_0^t \exp(-E/RT)\, dt \quad (2)$$

where w_0 = initial weight of specimen.

TABLE 1

Summary of experiments

	Experiment No.				
	1	2	3	4	5
Equilibrium furnace temperature (°C)	375	305	435[a]	325	275
Maximum temperature achieved by specimen (°C)	445	353	505	394	282
Initial weight of specimen (moisture free) (g)	30.1	27.8	25.0	24.2	22.9
Final weight of specimen (g)	9.3	14.6	7.0	9.6	18.0
(Final weight/initial weight) × 100 (per cent)	30.9	52.5	28.0	39.7	78.6
Maximum rate of weight loss (mg/sec)	92	26	193	40	8
Radius of specimen (cm)	1.06	1.07	1.00	1.00	1.00
Length of specimen (cm)	14.5	13.0	14.0	14.0	13.5

[a] Furnace temperature at time of maximum wood temperature. It was still rising.

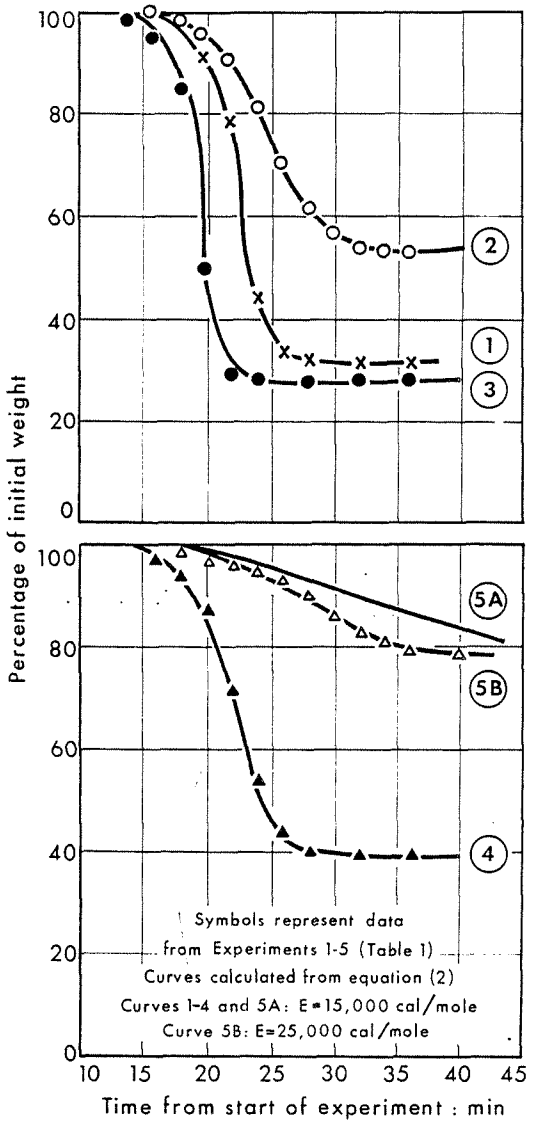

FIG. 3. Experimental weight/time data and calculated curves.

Since, in the experiments, the temperature of the specimens was not uniform, Eq. (2) was applied separately to each of the five hypothetical sections into which the specimen was divided (temperature variations across these sections were negligible). Denoting w, w', w_0 and T corresponding to the ith section by w_i, w_i', $w_{0,i}$ and T_i, and assuming $w_i' = w'/5$, $w_{0,i} = w_0/5$, Eq. (2) can be written

$$\ln \frac{w_i - w_i'}{w_{0,i} - w_i'} = -k \int_0^t \exp\,(-E/RT_i)\, dt \quad (2a)$$

also

$$w = \sum w_i \quad (2b)$$

Equations (2a) and (2b) were applied to the data for experiment 1 by (1) assuming a value for E, (2) evaluating the integral in (2a) for each annulus at $t = 23$ minutes (the time by which half the eventual weight loss had occurred), then (3) choosing a value for k so that the calculated value of w agreed with the experimental value; (4) values of w_i, and hence w, were then calculated for different times throughout the period of significant weight loss.

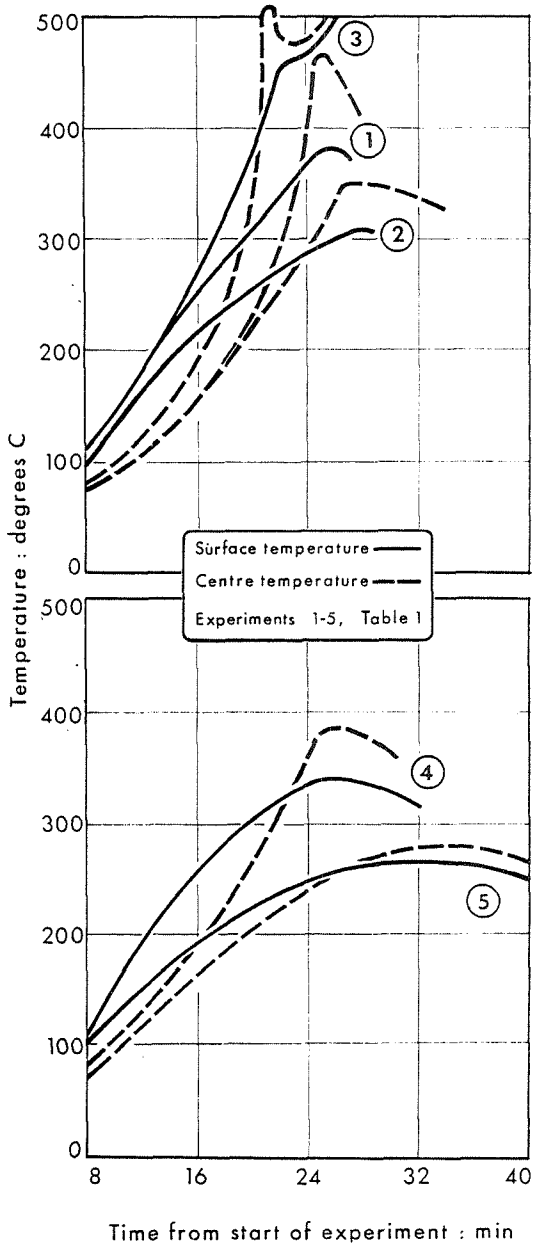

FIG. 4. Experimental temperature/time curves.

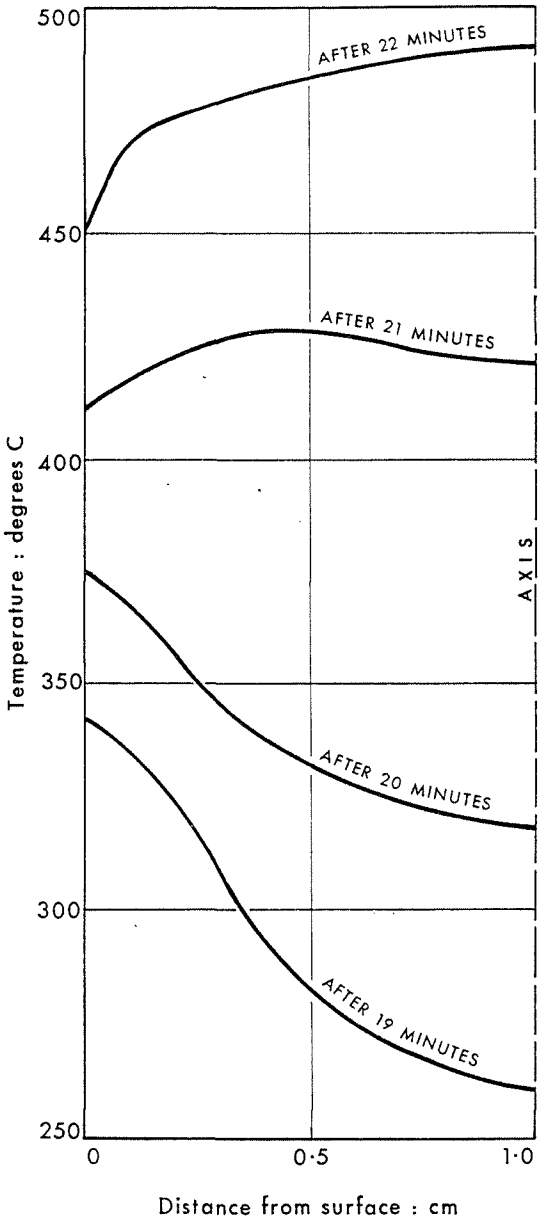

FIG. 5. Variation of temperature distribution within specimen during period of maximum activity (experiment 3).

The following values of activation energy were used to evaluate the data for experiment 1.

E = 30,000 cal/mole ($k = 2.6 \times 10^{10}$ min^{-1})

E = 12,000 cal/mole ($k = 6.5 \times 10^{3}$ min^{-1})

E = 15,000 cal/mole ($k = 9.1 \times 10^{4}$ min^{-1})

The calculated weight/time curves are plotted in Fig. 6, together with the experimental data: it can be seen that a value of E = 15,000 cal/mole gives the best agreement.

Curves of w against time which were calculated from the temperature data of experiments 1–5, assuming E = 15,000 cal/mole and $k = 9.1 \times 10^4$ min^{-1}, are plotted with the experimental values in Fig. 3. For the first four experiments the agreement is satisfactory; but for the fifth better agreement was obtained assuming E = 25,000 cal/mole and $k = 2.6 \times 10^9$ min^{-1}.

The Heat of Reaction. If one considers a cylindrical surface of radius r within a cylinder of length l then one can write the equation for a heat balance within this surface as

$$\int_0^t 2\pi r l \kappa \left(-\frac{\partial T}{\partial r}\right) dt + (w_0 - w_r) q = \int_{T_0}^{T} w_r c \, dT \quad (3)$$

where T = temperature at time t; T_0 = initial temperature; κ = thermal conductivity; c = specific heat; q = heat of reaction, cal/gm of weight loss; and subscript r relates to quantities within a surface of radius r.

A number of comments must be made on this heat balance:

1. When the equation is applied to the outer surface of the specimen the first term may be in error because the specimen is heated by radiation.

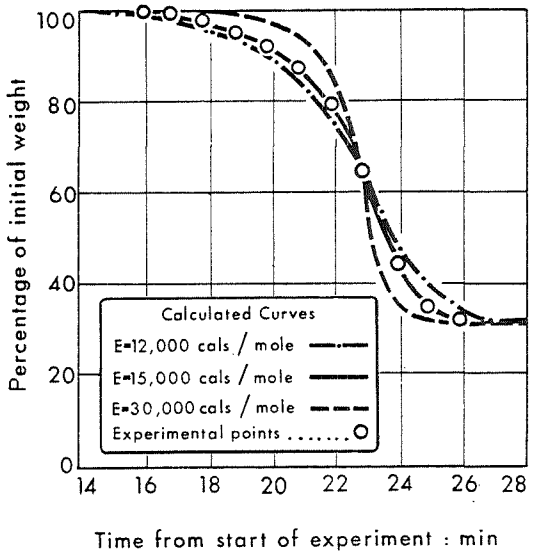

FIG. 6. Calculated weight/time curves for different activation energies. (Data from experiment 1.)

The radiation is absorbed in a thin zone near the surface rather than at the surface, but no allowance will be made for this effect.

2. The thermal conductivity is affected by two factors, namely, the increasing porosity of the wood as thermal decomposition proceeds, and the increasing temperature. As a first approximation κ will be taken as constant in time.

3. The wood shrinks as decomposition proceeds. However, the product $r(\partial T/\partial r)$ is not affected by uniform shrinkage, provided that $\partial T/\partial r$ is determined from a graph plotted on the original distance scale.

4. The second term makes use of a single heat of reaction which does not vary as the reaction proceeds.

5. It is assumed that volatile matter leaves the specimen without transferring heat to or from the solid residue through which it passes.

6. It will be assumed that c is constant at 0.33 throughout each experiment.

The experimental data allow

$$\int_0^t (-\partial T/\partial r)\, dt$$

and

$$\int_{T_0}^{T} w_r c\, dT$$

to be evaluated for values of t over the complete range of the temperature records, and for each of the five values of r corresponding to the outer surfaces of the five annuli considered earlier. (The values of w_r used are calculated values).

When the second integral is plotted against the first a curve is obtained of the form shown in Fig. 7. It is now possible to account for the effects of self heating by subtracting values of $(w_0 - w_r)q$ from

$$\int_{r_0}^{r} w_r c\, dT$$

and thus constructing a family of curves for different values of q.

From Eq. 3 it follows that the slope of these curves is related to κ. Since κ is changing only slowly with time, the curve corresponding to the best estimate of q should, near the maximum value of

$$\int_0^t (-\partial T/\partial r)\, dt,$$

show no open or closed loop. This is most nearly so in experiment 2 for $q = 75$ cal/gm (this curve has been omitted in Fig. 7 for the sake of clarity).

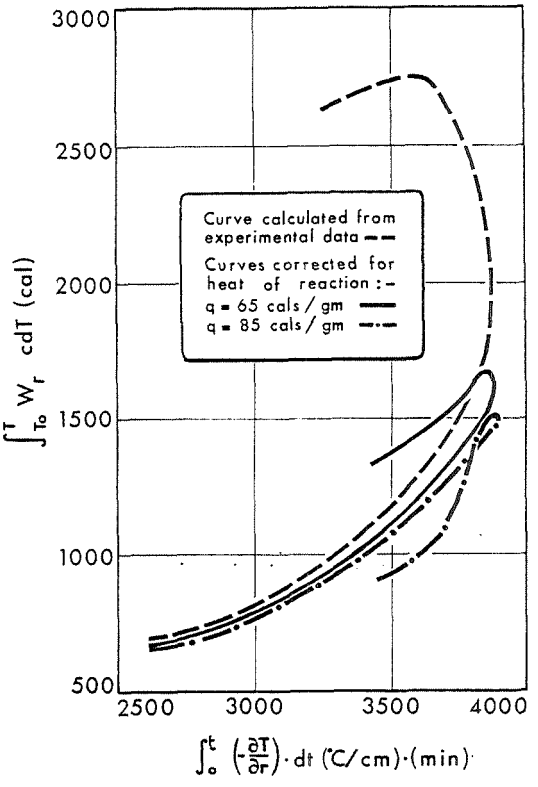

FIG. 7. Determination of the heat of reaction. (Experiment 1, data for complete cylinder.)

This procedure, while not very precise, does permit values of q to be estimated within ± 10 cal/gm. Values of q, obtained in each of the experiments, for the volumes within the five cylindrical surfaces, are given in Table 2.

TABLE 2

Values of q (cal/gm)

	Experiment No.				
	1	2	3[a]	4	5
Cylinder 1 (innermost)	70	80	—	75	75
Cylinder 2	70	80	—	60	130
Cylinder 3	55	80	—	55	210
Cylinder 4	70	80	—	60	250
Cylinder 5 (complete specimen)	75	80	—	70	280

[a] Insufficient data obtained to determine q.

Discussion

a. The Overall Kinetics of the Decomposition Reactions. For the first four experiments, in which weight losses exceeded 47.5 per cent and maximum wood temperatures exceeded 350°C, values of 15,000 cal/mole for E and 9.1×10^4 min^{-1} for k were used in calculating each weight/time curve, and the agreement between calculation and experiment over a wide range of conditions is encouraging. For the fifth experiment however, with a weight loss of 21 per cent and a maximum wood temperature of 282°C, the above values gave rise to a calculated curve differing widely from the experimental curve. Much better agreement was obtained with values of 25,000 cal/mole for E and 2.6×10^9 min^{-1} for k. It is clear, therefore, that the early stages of the reaction differ from the later ones, and it can be assumed that a reaction with an activation energy of 25,000 cal/mole predominates at lower temperatures and proceeds to completion, whereupon a reaction with an activation energy of 15,000 cal/mole becomes important. The transition between these two types of behavior must be investigated further.

At this stage it is interesting to consider values for activation energy obtained in self ignition experiments. A recent paper by Thomas and Bowes[4] considers data from three different sources (their own experiments and those of Gross and Robertson,[5] and Mitchell[6]) for the self ignition of wood fiber board. These data were obtained in the range 110–315°C and could be correlated by using an activation energy of 25,000 cal/mole. Thus, the data from the one experiment of the present series which lay completely within this temperature range were satisfied by the same value for the activation energy as the self ignition experiments.

The kinetics equation used by Bamford, Crank, and Malan[1] and Thomas and Bowes[4] makes use of a quantity corresponding to the percentage loss of weight during thermal decomposition of wood, which is taken to be constant, irrespective of any variation in heating conditions. However, in the present experiments (in which the specimens were maintained at an elevated temperature for at least 1 hour after the last detectable weight change) it was found that the percentage loss of weight depended on the heating conditions, as can be seen from Table 1.

This dependence points to a disadvantage of Eq. (1), which incorporates the final weight of the specimen, inasmuch as it is not necessarily known in advance what this final weight will be. Equation (1) is therefore suitable for analyzing data already obtained, but not for making *a priori* calculations of the behavior of wood in circumstances where the final weight of the wood can not be predicted; for instance, where it is known that the maximum temperature of the wood will not exceed 350°C (say).

More experimental data and a modification of the conventional kinetics equation are therefore needed to deal with this situation.

b. The Heat of Reaction. The method used to determine the heat generated by reaction is not sufficiently accurate to establish whether the heat of reaction is constant with time in a particular region. It does, however, give an average value which is probably accurate to within ±10 cal/gm, and the variation of this average value with position and with experimental conditions can be investigated. The data in Table 2 show that for experiments 1, 2, and 4 there is not sufficient evidence to say that the heat of reaction varies systematically with position or with the final percentage loss of weight. An average value of 70–75 cal/gm, expressed in terms of grams of weight lost, is derived from these experiments.

The heats of reaction for experiment 5, just as the reaction kinetics data, are completely different from those of the other experiments. The heat of reaction is very much greater except at the center of the cylinder, than in the other experiments, and there is a systematic increase of heat of reaction with distance from the surface. The values given in Table 2 are average values for cylinders of varying radii; values for each annulus can be calculated from these, and are given in Table 3.

The heat of reaction therefore increases rapidly

TABLE 3

Values of q for each annulus (experiment 5)

Inner radius of annulus (cm)	0	0.45	0.63	0.77	0.89
Outer radius of annulus (cm)	0.45	0.63	0.77	0.89	1.00
Heat of reaction (cal/gm)	75	185	370	370	400

with distance from the axis and then becomes approximately constant.

It has been suggested by Akita[7] that the primary decomposition of wood has a very low heat of reaction and that the main cause of heat generation in decomposing wood is a secondary decomposition of volatile matter, possibly catalyzed by the solid residue. If this were so, it could provide an explanation of the various differences observed, because the heat of reaction would increase with increasing residence time of volatile matter in the solid prior to evolution. Thus, under gentler heating conditions the expulsion of volatile matter once formed would be less rapid and more time would be available for a secondary decomposition. Similarly, volatile matter created near the axis of the specimen would have to travel outwards through partially decomposed regions and more secondary reaction would take place in the surface layers than near the center.

Various values have been quoted for the heat of reaction of the thermal decomposition of wood. Thomas and Bowes[8] quote data corresponding to a rate of heat generation of 8 cal/gm min at 250°C (referred to grams of total substance). Kinbara and Akita[8] quote data corresponding to a value of 7.9 cal/gm min on the same basis, derived from self ignition experiments. The present data gave a value of heat generation at 250°C of 7.2 cal/gm min for $q = 400$ cal/gm of weight lost. Thomas and Bowes[4] quote a value of $q = 80$ cal/gm of initial weight which, allowing for the 5:1 ratio between initial weight and weight lost, agree very well with the results from experiment 5. In the present context it is considered preferable to express heats of reaction in terms of weight lost rather than initial weight.

Thus the experiment in the same temperature region as that of the self ignition experiments, experiment 5, again gives results in good agreement with the published values for such experiments. Experiments at higher temperatures show marked differences of behavior.

Conclusions

The present investigation shows that data on the thermal decomposition of wood can be analyzed in terms of an overall first order reaction with a single heat of reaction. The analysis makes use, however, of the final weight of the specimen and, since the percentage loss of weight varies with the maximum temperature achieved by the specimen, the final weight is not known *a priori*. More experimental data and a modified form of the kinetics equation are needed to obviate this difficulty.

Two quite distinct sets of results were obtained. An experiment in which the wood temperature did not exceed 280°C gave values for activation energy and heat of reaction which agreed with those obtained by other workers in self ignition experiments within the same temperature range. The other experiments carried out at higher temperatures gave values which were self consistent but which differed widely from the above results. It is concluded that in lower temperature experiments an initial reaction of activation energy 25,000 cal/mole predominates, whereas in higher temperature experiments this reaction is rapidly completed and a further reaction of activation energy 15,000 cal/mole becomes important. Differences in heat of reaction could arise if secondary rather than primary decomposition were the main cause of heat generation.

Further experiments will therefore be performed to examine the transition between the two types of behavior observed and to examine more complicated but more realistic kinetics equations, and the factors affecting the heat of reaction.

Acknowledgments

The illustrations to this paper are British Crown Copyright and are reproduced by permission of Her Britannic Majesty's Stationery Office.

The paper is published by permission of the Ministry of Power.

References

1. Bamford, C. H., Crank, J., and Malan, D. H.: Proc. Camb. Phil. Soc. *42*, 166 (1946).
2. Browne, F. L.: Forest Products Laboratory, U.S. Dept. of Agriculture Report No. 2136 (1958).
3. Byram, G. H.: *Thermal properties of forest fuels.* U.S. Dept. of Agriculture Forest Service, Division of Fire Research, Oct. 1952.
4. Thomas, P. H. and Bowes, P. C.: Brit. J. Appl. Phys. *12*, 222 (1961).
5. Gross, D. and Robertson, A. F.: J. Research, Nat. Bur. Standards *61*, 413 (1958).
6. Mitchell, N. D.: Quart. Nat. Fire Prot. Assoc. *45*, 165 (1951).
7. Akita, K.: Bull Fire Prev. Soc. Japan *5*, 43 (1956).
8. Kinbara, T. and Akita, K.: Combustion and Flame *4*, 173 (1960).

Discussion

DR. P. H. THOMAS (*Fire Research Organization, England*): I should like to ask Dr. Roberts two questions:

(1) At what oven temperature would one have to include heat transfer due to the passage of volatile materials through the wood?

(2) What numerical values do the data give for the thermal conductivity of wood?

DR. A. F. ROBERTS (*Safety in Mines Research Establishment, England*): (1) No experimental evidence was obtained concerning the magnitude of any heat transfer between volatiles and wood during the passage of the former through the latter. The analysis of the temperature data is based on the assumption that the volatile matter leaves at its temperature of formation. However, any effect of this process would be most marked in the outer regions of the specimen and for the four experiments at higher temperatures there were no systematic differences between values obtained for heat of reaction in the innermost and outermost annuli. It would be of interest to know more about the importance of this process but I have not yet found out how to obtain such information in our type of experiment.

(2) Until appreciable decomposition has occurred the slope of curves such as that shown in Fig. 7 gives a value for the thermal conductivity of wood equal to published values. As decomposition proceeds this slope changes, but no effort was made to calculate values of thermal conductivity in this region; when decomposition was complete and the specimen started to cool another straight line portion of the curve was obtained. This gave a value for the thermal conductivity of the residue which was less by a factor of 2 than published values for charcoal. However, by this time considerable shrinkage and cracking of the wood had occurred, and the thermocouple positioning was no longer accurately known; these data are not therefore accurate.

PROF. R. H. ESSENHIGH (*Pennsylvania State University*): (1) In writing out the equation to be tested, that is thought to govern the decomposition kinetics, is not the equation quoted the differential at constant temperature, i.e., $(\partial w/\partial t)_T$? The full differential in a rising temperature system would then be

$$\frac{dw}{dt} = \left(\frac{\partial w}{\partial t}\right)_T + \left(\frac{\partial w}{\partial T}\right)_t \cdot \frac{\partial T}{\partial t}$$

Is the author satisfied that the method he has used to test the equation adequately takes into account the influence of a rising temperature?

(2) Is the author satisfied that the physical model implied by his rate equation is in fact adequate and realistic? A rate proportional to weight w, or weight difference $(w - w')$ implies a volume reaction. Experimentally, pyrolyzing solids that are homogeneous are known to be area (surface) reactions, not volume reactions. A volume reaction in wood is applicable only if the material is approximated by a set of discrete volumes, distributed throughout the solid, with adequate pore space for the volatiles' escape. In that case, however, the volatiles' escape may well be the determining (slow) rate-controlling process with the actual decomposition being relatively fast. This is known to be quite possible and in some instances probable, i.e., in coals. In coals, it is also known that gaseous diffusion is frequently, if not invariably, an activated process. In the wood decomposition this would account for two activation energies, either because of an increased pore size, or because of the production at higher temperature, of smaller and/or more mobile molecules.

DR. A. F. ROBERTS: (1) In these experiments the temperature is a known function of time. Calculations are based on the use of a stepwise approximation to this known continuous function, each step consisting of an isothermal period of short duration followed by a small discontinuous temperature rise. The errors involved in such an approximation are small.

(2) I agree that the rate equation used implies a reaction occurring throughout a homogeneous volume rather than a surface reaction. It is my opinion that the model of thermal decomposition occurring throughout the solid at a rate depending on the local temperature is more realistic in the case of wood, than a model of a decomposition front proceeding into the solid with decomposition products on one side and unaffected wood on the other.

The point about volatile escape is an interesting one. In the experiments the percentage loss of weight of the specimen, hence the final structure, varied widely. Nevertheless, an experiment yielding a residue in which the original grain of the wood was still clearly apparent gave identical values for activation energy to an experiment in which the residue was amorphous and heavily fissured. A single value of activation energy applies over a wide range of temperature and porosities. The transition between the two values of activation energy is quite sharp and does not correspond to any marked change in structure.

ISOTOPIC CARBON AS A TRACER IN COMBUSTION RESEARCH

C. F. CULLIS, A. FISH, AND D. L. TRIMM

Several researches are described in which the solution of combustion problems has been facilitated by the use of carbon-13 and carbon-14 tracer methods. One of the widest applications is in the elucidation of the mechanism of formation of combustion products and some work is described in which the position of the isotopic carbon has been determined in the principal products formed from [2-C^{14}] and [4-C^{14}]-2-methyl-but-2-enes. Another use is in the determination of the most probable points of oxidative attack of fuel molecules and in this connection 2-methylpentane has been labeled specifically in all its skeletal positions and the isotopic enrichment of the final combustion products has been measured. The technique of isotopic labeling has also been applied to discover which component of a mixed fuel is responsible for the formation of a given product; thus measurement of the activity of the carbon deposits formed from samples of gasoline containing each constituent labeled in turn with carbon-14 gives quantitative information about their deposit-forming tendency. The role of additives in fuel + oxygen systems may be elucidated by labeling either the additive or the fuel. If the additive is an intermediate combustion product, the origin of certain of the other intermediate and final products may be found; some work is described in which the mechanism of formation of certain products has been investigated by addition of [1,3-C^{14}]-acetone to isobutane + oxygen mixtures. Another example of the power of tracer techniques is their use in the determination of the actual rates of formation and consumption of intermediates (as opposed to their net rate of accumulation) even when these two processes occur concurrently and work is discussed from which it has been possible to calculate the rates of certain elementary reactions occurring during the combustion of paraffins and olefins. Determination of the rates of competing processes has also been effected by the use of fuels and additives labeled with isotopic carbon; measurement of the total isotopic concentrations in the products enables their relative rates of formation from a given labeled intermediate to be determined irrespective of their concurrent production by other routes. Finally consideration is given to possible further applications of isotopic carbon in combustion research.

Introduction

A number of recent investigations has shown that isotopic tracer techniques can assist in the solution of combustion problems which will not yield to more conventional methods of attack. The purposes of this paper are to indicate the range of these problems and the wide varieiy of combustion systems and regimes where this technique has proved to be of value and also to point the way to possible further applications of isotopic tracers in this field.

Generally speaking the most widely used fuels are hydrocarbons and in studies of their combustion it is possible to use labeled carbon, hydrogen, or oxygen. In this paper attention is restricted to systems in which labeled carbon (either carbon-13 or carbon-14) has been used, since much of the most significant information has been obtained in this way. The combustion systems to which carbon-labeling methods have been applied fall into two broad groups. In the first, the reaction of a binary (fuel + oxygen) mixture is studied, the fuel itself being labeled, usually in one specific skeletal position. In the second, a third component, which may or may not be a combustion product, is also present and the part played by this additive may be elucidated if either the additive or the fuel is labeled. Each method can yield valuable information about a number of different combustion problems. An attempt is made here to enumerate and classify some of these problems and to illustrate their solution by discussion of suitable examples chosen from a wide variety of combustion regimes, including slow oxidation, cool flames, explosive combustion, and the more particular case of engine testing.

Fuel Plus Oxygen Systems

The Mechanism of Product Formation

The route by which a particular combustion product is formed may often be elucidated if the fuel molecule is labeled with carbon-13 or carbon-

14 in a particular skeletal position and the concentration and site of the labeled isotope in this product is then determined. The fate of a given carbon atom is thus "traced" throughout the combustion reaction. This is perhaps the most obvious and widest use of isotopic carbon in combustion research and examples may readily be cited of applications of this technique in studies of slow combustion, of cool and hot flames, and of catalytic combustion.

Byrko, Kryuglakova, and Lukovnikov[1] reported one of the earliest studies of a slow combustion reaction involving the use of labeled carbon. The mode of production of formaldehyde during oxidation of [2-C^{14}]-propane was studied in order to test the validity of Semenov's postulate[2] that this aldehyde was formed from the *n*-propyl radical rather than from the isopropyl radical and was derived predominantly from the terminal positions. Radioassay of the formaldehyde formed from [2-C^{14}]-propane showed that 77% of this product did indeed arise from the end groups of the fuel molecule.

Cullis, Hardy, and Turner determined the origin of carbon monoxide[3] and of the ketones[4] formed by the slow combustion of 2-methylpentanes labeled with C^{14} in each skeletal position in turn. Carbon monoxide was found to be derived principally from the 3- and 4-positions while the 2-carbon atom of 2-methylpentane was shown to become the 2-carbon atom of acetone. This leaves little doubt that the mechanism of production of acetone is:

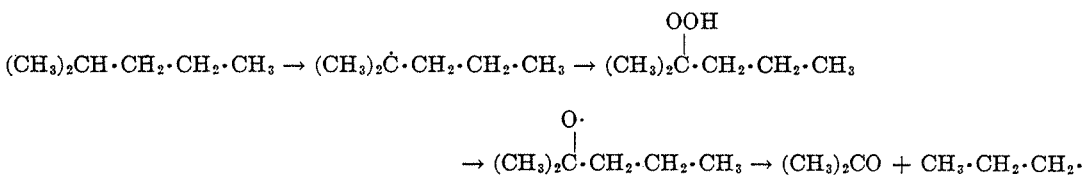

As would be expected, small quantities of methyl *n*-propyl ketone were also produced by breakdown of the above alkoxy radical. The origin of the considerable amounts of methyl ethyl ketone formed is less obvious. Tracer experiments showed however that the 2- and 3-carbon atoms of the hydrocarbon molecule became the carbonyl and CH_2 groups respectively of this ketone while the 4-carbon atom was not incorporated. The mechanism of formation of methyl ethyl ketone therefore appears to involve the following rearrangement reaction of an intermediate alkylperoxy radical:

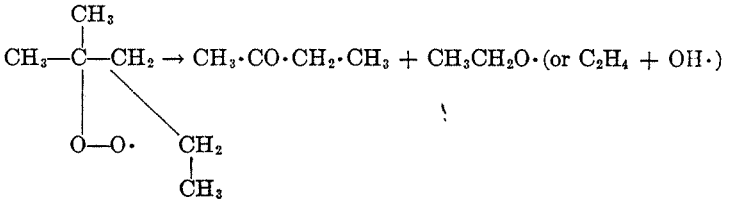

The slow combustion of [2-C^{14}]- and [4-C^{14}]-2-methyl-but-2-enes has been extensively studied by Cullis, Fish, and Turner.[5] Determinations of the specific activities of, and sites of carbon-14 in, the major products (acetone, acetaldehyde, methyl isopropyl ketone, and methanol) and the minor products (methyl ethyl ketone, propionaldehyde, isopropyl alcohol, and *tert*-butyl alcohol) derived from the olefin labeled in turn in each position—together with kinetic and analytical data for the oxidation of the inactive olefin[6]—have shown that the two generally postulated mechanisms of olefin oxidation operate concurrently. Hydrogen abstraction followed by hydroperoxylation leads to methyl isopropyl ketone while oxygen addition at the double bond forms in turn biradicals and a cyclic peroxide which is the precursor of acetone and acetaldehyde. Acetaldehyde is further oxidized to methanol and carbon oxides. Furthermore, simple rearrangements (by hydrogen or methyl transfer) of the peroxy monoradicals and biradicals produced by these modes of attack provide a consistent explanation of the formation of the minor products:

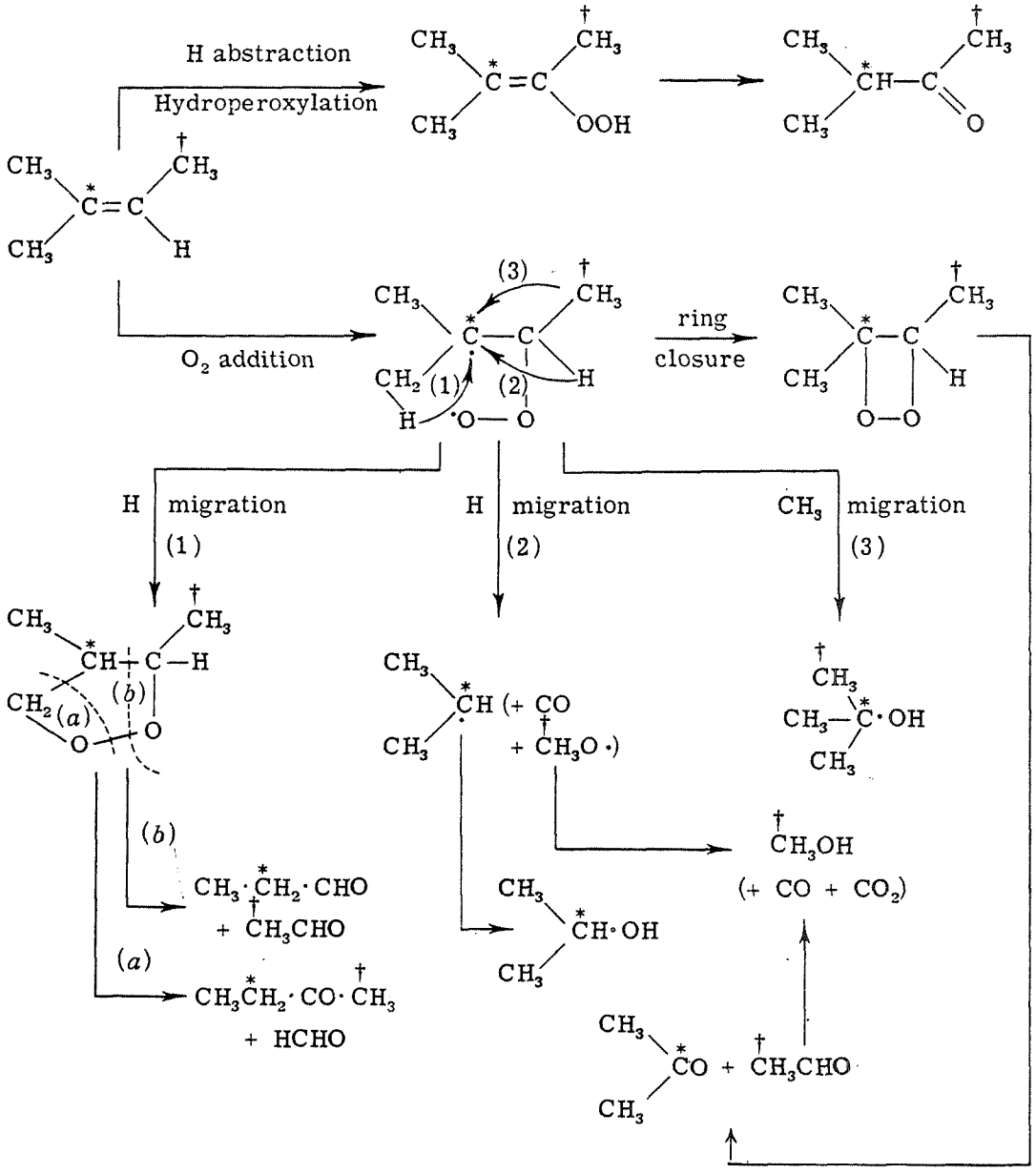

The mechanism of product formation under cool-flame conditions has been studied by Neiman and his co-workers with the aid of C^{14}-labeled fuels. Measurement of the activities of the acetaldehyde, formaldehyde, carbon monoxide, and carbon dioxide formed by the cool-flame combustion of [1-C^{14}]-*n*-butane[7] has shown that the formaldehyde is derived about equally from each carbon atom, while the mechanism of production of acetaldehyde is specific, the carbonyl group being derived from the 2- and 3-carbon atoms. In the same way, studies of the combustion of [1-C^{14}]-, [2-C^{14}]-, and [3-C^{14}]-*n*-pentane[8] have shown that the 2-carbon atom (and not the 1-carbon atom) is the major source of formaldehyde. It is evident therefore that destructive oxidation of the hydrocarbon chains does not occur in stepwise fashion. Similar work on the oxidation of [1-C^{14}]- and [2-C^{14}]-acetaldehyde has also been reported[9] and a combustion mechanism has been derived on the basis of the results obtained.

Ferguson and Yokley[10] have studied the cool-flame oxidation of [2-C^{13}]-propane, the products

being analyzed by gas-liquid chromatography and their isotopic composition being determined by mass spectrometry. The passage of a cool flame through an equimolar propane + oxygen mixture at 318°C produced propylene, propylene oxide, propionaldehyde, isopropyl alcohol, acetone, ethane, ethylene, ethylene oxide, acetaldehyde, methane, methanol, formaldehyde, carbon monoxide, and carbon dioxide. All these products were analyzed and the isotopic compositions showed that all the C_3 products contained the original propane skeleton with the exception of ca. 20% of the acetone which, it was suggested, must have been produced by the complete breakdown and reassembly of the carbon chain. This postulate is however contrary to the results of Porter and Benson[11] on the decomposition of di-*tert*-butyl peroxide in the presence of C^{14}-carbon monoxide. The C_2 products of the cool flame combustion of [2-C^{13}]-propane were all intact fragments of the parent hydrocarbon molecule with the exception of ca. 20% of the ethane. Methane and methyl alcohol were derived from the end groups while formaldehyde and carbon oxides were of mixed origin, the former being produced predominantly from the terminal positions and the latter from the 2-carbon atom. Oxidative attack thus appears to occur most frequently at the central skeletal position.

Ferguson[12] has also studied flame processes with the aid of carbon-13 as a tracer. The mechanism of the production of the excited C_2 radical in C^{13}-acetylene + oxygen flames has been investigated by spectroscopic determination of the relative concentrations of $C^{12}C^{12}$, $C^{12}C^{13}$, and $C^{13}C^{13}$. The observed values show that the species C_2 is not formed directly either from the acetylene molecule or from the particles produced by its direct polymerization. Most of the bonds in C_2 radicals are evidently formed in the reaction zone by the random recombination of C_1 fragments. Shock-tube techniques have also been used to study the production of C_2 radicals from C^{13}-acetylene + oxygen mixtures at temperatures of the order of 3500°K[13]; the results agree with those obtained at lower temperatures.

The isotopic composition of the soot formed in the closed bomb explosion flames of [1-C^{13}]-propane[14] has shown that this does not arise preferentially from a C_2 fragment of the fuel. Thus if the soot is formed by the commonly postulated mechanism via acetylene,[15] this latter intermediate cannot be a simple degradation product of the fuel. Isotopic analysis of the residual acetylene confirmed this. It was shown too that under flame conditions carbon monoxide and methane are derived equally from the three different skeletal positions in propane.

Fuels labeled with carbon-14 have also been used in studies of the oxidation of olefins over heterogeneous catalysts.[16–19] The great majority of these experiments have however involved the use of additives and they will therefore be considered, as a group, in a later section of this paper.

Point of Attack

A knowledge of those positions in a fuel molecule at which initial oxidative attack takes place preferentially is of prime importance in the elucidation of the detailed mechanism of combustion processes. Conventional analytical data rarely give reliable information about the relative probabilities of attack at different skeletal positions, since any results obtained in this way are weighted in favor of those products which are resistant to further oxidation. However, by the labeling in turn of each carbon atom in a given fuel molecule and measurement of the isotopic enrichment of each of the final combustion products, it is possible to estimate the relative extents of initial oxidation at the different carbon atoms. In this way the preferred point of attack has been determined for the slow combustion of 2-methylpentane,[3,4] which contains primary, secondary, and tertiary C—H bonds. Carbon monoxide and various ketones are the principal stable oxidation products. The former product was shown to be derived to an appreciable extent from all the carbon atoms in the paraffin molecule, while the latter compounds arose exclusively from initial attack at the 2-carbon atom, which became the carbonyl group of each ketone.

The total amounts (expressed as moles per 100 moles of initial oxygen) of stable products (carbon monoxide + ketones) formed by attack at each skeletal position were as follows:

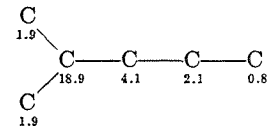

and these figures reflect the relative frequencies of initial oxidation at each position. The most frequent point of attack is thus the tertiary C—H group, in agreement with the predictions of Walsh.[20] On the other hand, it is well known that an increase in the number of tertiary centers in a hydrocarbon molecule of given carbon content decreases the over-all susceptibility to oxidation.[21] The tracer results described help to solve this paradox. Attack at the tertiary C—H group leads to the formation of stable ketonic products while initial oxidation at secondary or primary centers gives rise to aldehydes which are effective chain-branching agents and can therefore cause extensive oxidation of fresh molecules of the original hydrocarbon. Thus, although the most *frequent* point of attack in the slow combustion

of hydrocarbons is a tertiary center, secondary centers are nevertheless the most *effective* points of attack.

Combustion of Mixed Fuels

The technique of isotopic labeling may be applied in order to determine which component of a mixed fuel is responsible for the formation of one or more given products. Thus Shore and Ockert[22] used carbon-14 to determine the effect of the composition of gasoline on the formation of combustion chamber deposits. A few parts per million of one of the constituents labeled with carbon-14 were added to the gasoline which then underwent combustion in a single cylinder engine. The carbonaceous deposit formed was completely oxidized by a wet method, and gas counting of the resulting carbon dioxide enabled the specific activity of the carbon to be compared with the specific activity of the fuel. The ratio of these specific activities provides a direct and reproducible measure of the deposit-forming tendency of the particular constituent in question and the method has the advantage that addition of the labeled fuel does not unbalance the gasoline composition. Aromatics were found to deposit about three times as much carbon as paraffins, and the behavior of olefins was intermediate between those of the other two fuels. The relative deposit-forming tendencies of individual aromatics were dependent on their boiling points according to the relationship:

$$\log_{10} \frac{\text{specific activity of deposit}}{\text{specific activity of fuel}} \propto \text{b.p. of labeled component}$$

Moreover, single-ring aromatics, fused-ring aromatics, and fused aromatic-alicyclics (e.g., indane) all fell on the same straight line, suggesting that in an aromatic hydrocarbon each carbon atom has an equal tendency to form deposits, irrespective of its molecular environment. This finding is consistent with a mechanism of deposit formation involving liquefaction of the fuel followed by carbonization. The tendency of a gasoline to deposit carbon in an engine can be calculated from weighted averages of the activity ratios of its components, the weights being determined by composition analyses. Such measurements have shown that the "bottom" 1.73% of a gasoline can produce as much as 65% of the carbonaceous part of an engine deposit, and it is concluded that careful control of the higher-boiling fraction is needed to give a clean-burning gasoline.

The tendency of an engine lubricant to deposit carbon was also determined, leaded benzene being used as the fuel and C^{14}-benzene as an additive. The deviation from unity of the specific activity ratio (deposit:fuel) gave a measure of that fraction of the deposit formed from the lubricant; its value was found to be ca. 8%.

Sechrist and Hammen[23] have used similar techniques (with C^{14}-labeled benzene or toluene as fuels) to demonstrate the differing tendencies to form deposits of various classes of lubricant. Synthetic lubricants of the polyalkylene glycol type gave much lower deposit weights than petroleum-based lubricants. Comparison of the activities of cylinder head and piston crown deposits showed that each lubricant tended to deposit carbon preferentially on the piston, as would be expected from temperature considerations.

Several radiotracer studies of the nature of the surface films formed on metal engine parts by lubricants have been reported and the use of C^{14}-labeled long-chain fatty acids and their salts (e.g., tridecanoic acid[24]) has proved effective. A further use of C^{14}-labeling in engine research is illustrated by the work of Cooper[25] who has investigated the distribution of fuel containing C^{14}-labeled lead tetraethyl to each cylinder of a carburetted V8 engine which was fitted with special sampling valves to facilitate the removal of small samples of the combustion gases from each cylinder.

Fuel Plus Oxygen Plus Additive Systems

The Role of Additives

The part played by a compound X in the combustion of a fuel Y to a product Z may be elucidated by the addition of X to the fuel + oxygen system, either X or Y being labeled. The additives whose mode of action has been studied in this way may be divided into two classes according to whether on the one hand they are intermediate products of the combustion of Y or on the other they have an accelerating or inhibiting influence on the combustion of Y.

X is an Intermediate Combustion Product. Let us consider the reaction system:

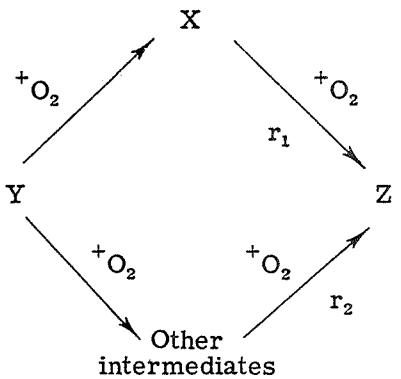

in which the rate of formation of Z from X is r_1 and that from the other intermediates is r_2.

If a small concentration of C^{14}-labeled additive, $[X^*]$, is introduced into the system and if the activities of X and Z are denoted by a_x and a_z respectively, then if $[X^*] \ll [X]$, it follows that:

$$[Z^*] \ll [Z] \tag{1}$$

and

$$a_x = [X^*]/[X]; \qquad a_z = [Z^*]/[Z] \tag{2}$$

Now $d[Z]/dt = r_1 + r_2$ so that:

$$d[Z^*]/dt = r_1^* = r_1 a_x \tag{3}$$

From Eq. (2),

$$\frac{da_z}{dt} = -\frac{[Z^*]}{[Z]^2}\frac{d[Z]}{dt} + \frac{1}{[Z]}\cdot\frac{d[Z^*]}{dt}$$

$$= -\frac{a_z}{[Z]}\cdot\frac{d[Z]}{dt} + \frac{1}{[Z]}\cdot\frac{d[Z^*]}{dt}$$

and from Eq. (3),

$$\frac{da_z}{dt} = -\frac{a_z}{[Z]}(r_1 + r_2) + \frac{a_x r_1}{[Z]}$$

i.e.,

$$\frac{da_z}{dt} = \frac{r_1}{[Z]}\left[a_x - a_z\left(\frac{r_1 + r_2}{r_1}\right)\right]$$

If a small amount of inactive Z is added initially, $a_z = 0$ when $t = 0$ and a_z will at first increase, pass through a maximum, and subsequently decrease. At the maximum, $da_z/dt = 0$, so that:

$$a_x/a_z = (r_1 + r_2)/r_1$$

Measurements of the variation with time of a_x and a_z and determination of the value of a_x/a_z when a_z is a maximum thus enables r_2/r_1 to be calculated. If $r_2 = 0$, i.e., if Z is produced solely by a mechanism involving X, then the a_x/t curves intersect when a_z is a maximum. If $r_2 \neq 0$, a_x is always greater than a_z and the curves do not intersect.

These principles have been applied by Neiman and his co-workers to several combustion systems. It has been shown for example that during the slow combustion of methane, carbon monoxide is formed solely by further oxidation of formaldehyde[26] but only 25% of the carbon dioxide is produced via carbon monoxide.[27] Similarly addition of [1-C^{14}]-acetaldehyde to *n*-butane + oxygen[28] and propylene + oxygen[29] systems has shown that the carbon oxides produced by the passage of a cool flame are formed both from the carbonyl group of acetaldehyde and by other routes; thus with propylene, some 30% of the carbon monoxide and some 50% of the carbon dioxide are produced via acetaldehyde. In the same way, studies of the cool-flame combustion of propylene in the presence of added [2-C^{14}]-acetaldehyde[30] have shown that 75% of the methanol formed originates from the methyl group of acetaldehyde; on the other hand, addition of C^{14}-methanol indicates that less than 5% of the formaldehyde arises by further oxidation of the methanol, and it is therefore believed that the formaldehyde arises mainly from breakdown of $CH_3O_2\cdot$ radicals. The addition of C^{14}-carbon monoxide and inactive carbon dioxide to *n*-butane + oxygen[31] and propylene + oxygen[29] systems has shown that $a_{z_{max}} \ll a_x$, only 3–4% of the carbon dioxide being derived from carbon monoxide.

A somewhat similar approach has been used by Trimm,[32] who has elucidated the mechanism of the formation of methyl ethyl ketone from isobutane under both slow combustion and cool-flame conditions. It has been suggested[33] that this compound arises from further reactions of acetone which is a major product of the oxidation of isobutane:

$$CH_3\cdot CO\cdot CH_3 \xrightarrow[-H]{+CH_3} CH_3\cdot CO\cdot CH_2\cdot \xrightarrow{+CH_3} CH_3\cdot CO\cdot CH_2\cdot CH_3$$

Alternatively, methyl ethyl ketone could be formed, for example, by the intramolecular rearrangement of *tert*-butyl peroxy-radicals:

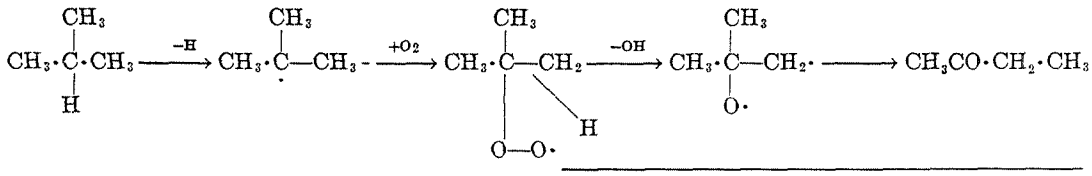

Trimm has indeed shown that, although methyl ethyl ketone is under certain conditions a product of the combustion of acetone, the methyl ethyl ketone formed by the slow oxidation of isobutane in the presence of 1,3-C^{14}-acetone has in fact an activity less than one-third of that of the acetone, thus proving the dominance of the intramolecular mechanism.

Some similar studies of the effect of added 1-C^{14}-acetic acid on the oxidation of acetaldehyde[34]

have shown that some carbon dioxide is derived from the carbonyl group of this acid and that it thus does not all arise by breakdown of radicals derived from aldehydes and peroxy acids.

Ferguson[14] has examined the role of carbon monoxide in the formation of carbon from hydrocarbon flames by introducing C^{13}-carbon monoxide into these flames. The carbon collected was found not to contain any excess of carbon-13 and the only gaseous product which was enriched was carbon dioxide.

The role of additives in the metal- and metal oxide-catalyzed oxidation of C^{14}-ethylene has been investigated by Margolis and Roginskii. The additives used were acetaldehyde[16,18,19] and ethylene oxide[17,19] and it was shown that, although aldehydes were important intermediates in the silver-catalyzed oxidation, these compounds did not play a significant part in the oxidation over vanadium pentoxide or other semiconductors. An interesting discovery was that the vanadium pentoxide-catalyzed oxidations of acetaldehyde and ethylene oxide exhibit the phenomenon of "mutual induction".[17] A novel mechanism involving ionized oxygen, peroxides, and alkoxides was postulated to account for the oxidation of ethylene over certain semiconductors.[19]

The nature of processes occurring in metal-catalyzed oxidations has been further studied by Neiman[35] who, using a flow system, added C^{14}-labeled acetone to a 3% acetone/20% isopropyl alcohol/air mixture immediately after it had left the silver catalyst. The acetone was attacked and radioactive isopropyl alcohol was produced. It is thus evident that desorption of active radical species from the catalyst takes place and that reaction can continue in the absence of the initial catalyst.

X is a Catalyst. The addition of cyclohexane to benzene makes it possible to obtain appreciable yields of phenol by homogeneous oxidation at temperatures of about 600°C.[36] Donald and Darlington[37] have however carried out the oxidation with C^{14}-benzene and have shown that the cyclohexane merely acts as a promoter and is not itself converted to phenol, since the specific activity of the phenol formed is the same as that of the initial benzene.

Neiman and his co-workers[30] introduced C^{14}-labeled azomethane as an additive during studies of the slow combustion of propylene. The C^{14}-methyl radicals thus produced were found to react to give labeled formaldehyde and methyl alcohol and it was therefore concluded that methyl radicals were probably the precursors of these products of the uncatalyzed oxidation of propylene.

A similar technique was applied to elucidate the inhibiting action of styrene and the accelerating effect of acetophenone on the slow combustion of *n*-hexane.[34] By use of [1-C^{14}]-styrene it was shown that the side chain was detached from the benzene ring and ultimately converted to reaction products while introduction of acetophenone labeled with carbon-14 in the carbonyl group led to the production of active carbon dioxide; this indicates that both the inhibitor and the accelerator are decomposed in the course of the reaction.

Rates of Formation and Destruction of Intermediates

The net rate of accumulation (r_a) of a given intermediate product, X, in a combustion system may be determined directly from conventional analytical data but the separate rates of formation (r_f) and destruction (r_d) cannot be found in this way. If, however, a C^{14}-labeled intermediate is introduced into the system in very low concentration, $[X^{*}]$, its activity is given by:

$$a_x = [X^{*}]/[X]$$

from which it follows that:

$$\frac{da_x}{dt} = \frac{1}{[X]}\frac{d[X^{*}]}{dt} - \frac{[X^{*}]}{[X]^2}\frac{d[X]}{dt}$$

But:

$$d[X]/dt = r_a = r_f - r_d$$

and as $r_f^{*} = 0$,

$$d[X^{*}]/dt = -r_d^{*} = -r_d \cdot a_x$$

Thus:

$$\frac{da_x}{dt} = \frac{-r_d a_x}{[X]} - \frac{a_x}{[X]}(r_f - r_d) = \frac{-a_x r_f}{[X]}$$

so that:

$$r_f = -[X]\frac{d(\ln a_x)}{dt}$$

Measurements of the variation with time of [X] and a_x therefore make it possible to calculate r_f and hence r_d.

In this way, Neiman and his co-workers have determined by addition of ca. 1% of [1-C^{14}]-acetaldehyde the separate rates of formation and destruction of this compound in the cool flames of both *n*-butane[28,38] and propylene.[26] It was shown that in the former system acetaldehyde is both formed and destroyed throughout the reaction, r_f being particularly high during passage of the cool flame. First-order velocity constants and energies of activation for the decomposition of acetaldehyde were also calculated. During oxida-

tion of propylene, both r_f and r_d exhibit sharp maxima in the cool-flame region and the values of r_f obtained in this way are in good agreement with those calculated from the combustion mechanism postulated by Shtern and Polyak.[39,40]

Rates of Competing Reactions

It is generally possible, in simple systems, to determine the relative rates of two competing processes:

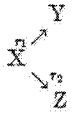

by measurement of the change with time of the concentrations of Y and Z. In combustion processes, however, a large number of concurrent reactions usually occur and the products Y and Z may also be formed from precursors other than X. The reactions resulting in conversion of X to Y and of X to Z may be *isolated* however if X is isotopically labeled, e.g., with carbon-14. Then if A_Y and A_Z are the total activities of Y and Z

$$r_1/r_2 = dA_Y/dA_Z$$

In this way Neiman and Serdyuk[29] were able, by use of [1-C^{14}]-acetaldehyde, to estimate the different competing fates of acetyl radicals during the slow combustion of propylene. Here the two concurrent processes in question are:

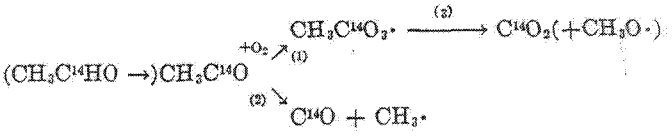

Provided that (1) is slower than (3) and if r_1 and r_2 and k_1 and k_2 are the rates and velocity constants respectively for the correspondingly numbered reactions, then:

$$\frac{r_1}{r_2} = \frac{k_1[O_2]}{k_2} = \frac{dA_{CO_2}}{dA_{CO}}$$

so that the relative rates of the two competing processes may readily be calculated if the total activities of the two carbon oxides are separately determined.

This treatment explains at least in part why the ratio of carbon monoxide to carbon dioxide in the products of hydrocarbon combustion is so highly variable.

Future Developments

Although isotopic carbon has already found numerous and diverse applications as a tracer in combustion research, there appears to be a large number of unsolved problems in this field where its use would be of considerable value. A selection of these is given below.

Hitherto, the application of isotopic carbon to the determination of the mechanism of the formation of combustion products has yielded mainly qualitative information. However, now that the separate rate of formation and destruction of intermediates can be found, the individual rate constants and hence the activation energies of many of the constituent radical reactions could also profitably be determined. There is also a considerable need for further applications of tracer techniques to the study of competing reactions, where such methods have so far only been used in a few systems.

Although too the use of isotopic carbon has thrown some light on the mode of action of promoters of gaseous oxidation reactions, there seems to be a pressing need for similar applications to the study of inhibition, the mechanism of which is in some cases still obscure.

Another field in which tracer methods may be usefully applied is that of fast reactions. Indeed, such methods have been used in studying the cracking of ethane at 800–900°C in a turbulent reactor, and have enabled velocity constants and activation energies—both for the over-all process and for individual stages—to be determined from a single series of runs.[41] Similar methods could be profitably used for the study of fast combustion reactions.

Finally one of the least understood factors which exert a considerable influence on combustion reactions is the surface of the containing vessel. In many cases the walls of the reaction vessel in such systems become coated with a carbonaceous deposit, the formation of which influences the rate of subsequent combustion. The introduction of labeled carbon into this surface film and the "tracing" of its fate during combustion reactions carried out in its presence might well throw light on the way in which the surface participates in the reaction.

C-3

ACKNOWLEDGMENT

The authors would like to thank Mr. H. L. West, of Esso Research Limited, for drawing to their attention some of the work described in this paper.

REFERENCES

1. BYRKO, V. M., KRYŬGLAKOVA, K. E., and LUKOVNIKOV, A. F.: Doklady Akad. Nauk S.S.S.R. *108*, 1093 (1956).
2. SEMENOV, N. N.: Uspekhi Khim. 20, (1951).
3. CULLIS, C. F., HARDY, F. R. F., and TURNER, D. W.: Proc. Roy. Soc. (London) *A244*, 573 (1958).
4. CULLIS, C. F., HARDY, F. R. F., and TURNER, D. W.: Proc. Roy. Soc. London *A251*, 265 (1959).
5. CULLIS, C. F., FISH, A., and TURNER, D. W.: Proc. Roy. Soc. (London) *A267*, 433 (1962).
6. CULLIS, C. F., FISH, A., and TURNER, D. W.: Proc. Roy. Soc. (London) *A262*, 318 (1961).
7. NEIMAN, M. B. and FEKLISOV, G. I.: Doklady Akad. Nauk S.S.S.R. *91*, 877 (1953).
8. NEIMAN, M. B., LUKOVNIKOV, A. F., and FEKLISOV, G. I.: *Symposium on Chemical Kinetics, Catalysis and Reactivity.* p. 184. Moscow, 1955.
9. NEIMAN, M. B. and FEKLISOV, G. I.: Doklady Akad. Nauk S.S.S.R. *90*, 583 (1953).
10. FERGUSON, R. E. and YOKLEY, C. R.: *Seventh Symposium (International) on Combustion*, p. 113. London, Butterworths Scientific Publications, 1959.
11. PORTER, G. B. and BENSON, S. W.: J. Am. Chem. Soc. *75*, 2773 (1953).
12. FERGUSON, R. E.: J. Chem. Phys. *23*, 2085 (1955).
13. FAIRBAIRN, A. R.: *Eighth Symposium (International) on Combustion*, p. 304. Baltimore, Williams & Wilkins, 1962.
14. FERGUSON, R. E.: Combustion and Flame, *1*, 431 (1957).
15. PORTER, G.: *Fourth Symposium on Combustion*, p. 248. Baltimore, Williams & Wilkins, 1953.
16. MARGOLIS, L. YA. and ROGINSKII, S. Z.: Doklady Akad. Nauk S.S.S.R. *96*, 311 (1954).
17. MARGOLIS, L. YA. and ROGINSKII, S. Z.: Doklady Akad. Nauk S.S.S.R. *96*, 549 (1954).
18. MARGOLIS, L. YA. and ROGINSKII, S. Z.: Bull. Acad. Sci. U.S.S.R. Div. Chem. Sci. 271 (1956).
19. MARGOLIS, L. YA. and ROGINSKII, S. Z.: Problemy Kin. i Kat., Akad. Nauk. S.S.S.R. *9*, 107 (1956).
20. WALSH, A. D.: Trans. Faraday Soc. *42*, 269 (1946).
21. CULLIS, C. F. and HINSHELWOOD, C. N.: Discussions Faraday Soc. *2*, 117 (1947).
22. SHORE, L. B. and OCKERT, K. F.: Soc. Automotive J. *65*, 18 (1957).
23. SECHRIST, C. N. and HAMMEN, H. H.: Ind. Eng. Chem. *50*, 341 (1958).
24. GEMANT, A.: J. Phys. Chem. *54*, 569 (1950).
25. COOPER, D. E.: *Symposium on Applications of Radioactivity in Petroleum Research and Refinery Operations.* Boston, Tracerlabs Inc., 1956.
26. NEIMAN, M. B., ANTONOVA, I. N., KUZMIN, V. N., MOSHKINA, R. I., NALBANDYAN, A. B., and FEKLISOV, G. I.: Izvest. Akad. Nauk. S.S.S.R. Otdel Khim. Nauk. 789 (1955).
27. MOSHKINA, R. I., NALBANDYAN, A. B., NEIMAN, M. B., and FEKLISOV, G. I.: Bull. Acad. Sci. U.S.S.R. Div. Chem. Sci. 821 (1957).
28. NEIMAN, M. B. and FEKLISOV, G. I.: Zhur. Fiz. Khim. *30*, 1126 (1956).
29. NEIMAN, M. B., EFRAMOV, V. YA., SERDYUK, N. K., and LUKOVNIKOV, A. F.: Bull. Acad. Sci. U.S.S.R., Div. Chem. Sci. 397 (1956).
30. NEIMAN, M. B., EFRAMOV, V. YA., and SERDYUK, N. K.: Kin. i Kataliz. *1*, 345 (1960).
31. NEIMAN, M. B. and LUKOVNIKOV, A. F.: Zhur. Fiz. Khim. *29*, 1410 (1955).
32. TRIMM, D. L.: unpublished work.
33. BOSE, A. N.: Trans. Faraday Soc. *55*, 778 (1959).
34. GAL, D., KENDE, I., DUTKA, F., and GUCZI, L.: Magyar. Kem. Folyoirat *65*, 249 (1959); *Seventh Symposium (International) on Combustion*, p. 128. London, Butterworths Scientific Publications, 1959.
35. NEIMAN, M. B.: International J. Appl. Radiation, *3*, 20 (1955).
36. DENTON, W. H., DOHERTY, M. C., and KRIEBLE, R. H.: Ind. Eng. Chem. *42*, 777 (1954).
37. DONALD, M. B. and DARLINGTON, M. E.: Industrial Chemist. *34*, 8 (1958).
38. NEIMAN, M. B. and FEKLISOV, G. I.: Zhur. Fiz. Khim. *28*, 1235, 1737 (1954).
39. SHTERN, V. YA. and POLYAK, S. S.: Zhur. Fiz. Khim. *27*, 341, 631, 950 (1953).
40. SHTERN, V. YA. and POLYAK, S. S.: Doklady Akad. Nauk. S.S.S.R. *95*, 1231 (1954).
41. BRODSKII, A. M., KALIENKO, R. A., and LAVROSKII, K. P.: Zhur. Fiz. Khim. *34*, 192 (1960).

Discussion

DR. W. E. FALCONER (*National Research Council, Canada*): To determine the most probable points of oxidative attack on 2-methylpentane, Cullis and coworkers have assumed that the carbon monoxide yield from the decomposition of primary and secondary hydroperoxides, and the sum of carbon monoxide yield plus carbonyl yield from tertiary hydroperoxides is representative of initial attack at primary, secondary, and tertiary C—H bonds, respectively. While it is reasonable that carbon-

oxygen bonds formed at the position of initial hydrogen abstraction do persist to the final products which are isolated, carbon monoxide may also be formed in other reactions. In view of the uncertainties concerning the over-all mechanism of the low-temperature oxidation of hydrocarbons, does the additional formation of carbon monoxide from the further oxidation of fragments, such as methyl and other alkyl radicals formed from the initially attacked species, not complicate the quantitative evaluation of the point of initial attack using this method?

DR. A. FISH (*Imperial College, London*): The figures given in the paper are total amounts of carbon monoxide plus ketones. The carbonyl group of each ketone formed (acetone, butanone, and pentan-2-one) is derived from the tertiary center of the fuel molecule (as shown by degradation of these products). The figures given for each other skeletal position are exclusively carbon monoxide; no ketonic carbonyl groups are derived from these positions.

If some of the carbon monoxide is formed by oxidation of fragments such as CH_3, and CH_3-CH_2CH_2, I agree that the tracer results will suggest frequencies of initial attack at the secondary and primary centers which are slightly too great. The experimental results for tertiary center cannot however be substantially affected as ketones labeled in the position found cannot be formed by oxidation of these fragments and little carbon monoxide is derived from the tertiary position.

Any errors in the quantitative treatment arising from this source then, will cause the experimentally found ratios of frequency of attack at the tertiary position to frequencies at the secondary and primary positions to be less than the true ratios. The conclusion that the tertiary position is by far the most frequent point of attack therefore holds. Indeed, the relative frequency of attack at the tertiary position may be slightly greater than our results suggest.

DR. F. J. WRIGHT (*Esso Research and Engineering*): I wonder if Dr. Fish could elaborate on his reasons for investigating whether acetone could be the intermediate leading to methyl ethyl ketone in the oxidation of isobutane. It seems to me that acetone is a most unlikely candidate, since it has been shown that ketones are highly resistant to oxidation. Indeed, it is the fact that tertiary hydrocarbons can form ketones which can only be further oxidized with difficulties, which makes the tertiary hydrocarbons more resitant to oxidation although, as you have pointed out yourself the tertiary carbon is the most susceptible position of attack.

DR. A. FISH: I agree with Dr. Wright that previous work indicates that acetone is unlikely to be further oxidized to an appreciable extent during the slow oxidation of hydrocarbons. However, it has been suggested as recently as 1959 (reference 33 in this paper) that methyl ethyl ketone can arise by the oxidation of acetone. As the amounts of acetone formed in the slow- and cool-flame oxidations of isobutane are very large (compared with the amounts of other products) the further oxidation of even a small proportion (ca. 1%) of the acetone could account for the small quantities of methyl ethyl ketone formed. For this reason, an investigation of acetone as a possible intermediate was made. As stated in the paper, the results of these studies showed that for the greater part the methyl ethyl ketone was produced by routes not involving acetone.

Reaction Kinetics II

Chairman: Dr. F. Kaufman (*Ballistic Research Laboratory*)

Vice Chairman: Prof. P. Laffitte (*Sorbonne, Paris*)

THE KINETICS OF THE CARBON MONOXIDE FLAME BANDS

M. A. A. CLYNE AND B. A. THRUSH

The intensity I_c of the carbon monoxide flame bands observed in the low-temperature reaction of O with CO was found to have similar kinetics to those of the O + NO and H + NO emissions,

$$I_c = I_{0c}[O][CO],$$

where I_{0c} depended upon the *nature* but not on the *pressure* of the carrier gas used as third body. I_{0c} and the rate constant k_{1c} for overall combination of O and CO were found to be much less at 293°K than I_{0a} and k_{1a} (the analogous quantities in the O + NO reaction), but while k_{1a} and I_{0a} showed small negative temperature coefficients, I_{0c} was found to have a positive Arrhenius activation energy of +3.7 kcal/mole. Extrapolated values of I_{0a} and I_{0c} at $1/T = 0$ were similar.

Most of the excited CO_2 molecules formed in the third order combination process are quenched collisionally rather than radiatively. The absence of any effect upon the value of I_{0c} when the third body used is in a triplet state (O_2) shows that a spin reversal reaction is not rate determining. The observation of similar pre-exponential factors for I_{0a} and I_{0c} shows that the emission process in the O + CO reaction does not involve spin reversal. It is considered that the flame band emission is due to a transition from an excited singlet state to the (singlet) ground $^1\Sigma_g^+$ state of CO_2. Molecules in this excited singlet state are formed by a rapid radiationless transition from the triplet state of CO_2 in which they are initially formed. The low value observed for I_{0c} is then due to the presence of an energy barrier in forming the excited triplet and singlet state, and not to the spin-forbidden nature of the overall combination reaction.

Introduction

The carbon monoxide flame bands are one of the most characteristic emission systems encountered in combustion processes. These bands have not been analyzed, but the large amount of evidence that they are due to electronically excited CO_2 formed in the combination reaction O + CO has been discussed by Gaydon.[1] One of the most important pieces of evidence is Broida's and Gaydon's observation of this system in emission during the reaction of oxygen atoms with carbon monoxide in a low-pressure flow system at room temperature.[2] Such a system is very convenient for studying the kinetics of the process and for a comparison of them with related chemiluminescent combination reactions such as H + NO, O + NO and O + SO.

Investigations of the kinetics of the H + NO[3,4] and O + NO[4,5,6] reactions have shown that the intensity (I) of the HNO or NO_2 emission which accompanies the third order combination reaction,

$$X + NO + M \rightarrow XNO + M \qquad (1)$$

obeys the kinetic law

$$I = I_0[X][NO] \qquad (2)$$

In these reactions, I_0 and the third order rate constant k_1 show similar small negative temperature coefficients. The quantity I_0 is found to be independent of the pressure of the carrier gas which provides the bulk of the third bodies [M] but to depend on the nature of the third body.[4,6] This can be simply explained by a mechanism of the type

$$X + NO + M \rightleftharpoons XNO^* + M \quad (3)$$

$$XNO^* \rightarrow XNO + h\nu \quad (4)$$

$$XNO^* + M \rightarrow XNO + M \quad (5)$$

with $k_4 \ll k_5[M]$ under the experimental conditions. It can be shown that this scheme leads to the expression

$$I_0 = k_3k_4/k_5$$

where k_3 is the net rate constant for recombination via the electronically excited state.[6] In the case of the O + NO reaction where the ratio k_4/k_5 can be obtained from fluorescence data, k_3 is found to be half the total rate of combination to form NO_2.

Investigations of this type on the CO flame bands can provide information about the mechanism of the reaction involved, which differs from those cited above, in that the overall process is spin forbidden.

$$O(^3P) + CO(^1\Sigma^+) \rightarrow CO_2(^1\Sigma_g^+)$$

Experimental

The experiments were carried out in a 28 mm diameter Pyrex flow tube approximately 1 meter long. This tube was immersed in liquid in an insulated trough which could be held at temperatures between 200°K and 350°K. Oxygen atoms were produced by a radio-frequency discharge, and to ensure proper equilibration, the discharge products travelled 30 cm down the tube before entering the reaction zone. Measurements of the emission intensity were made with a 9558B photomultiplier cell, which observed a 5 cm length of the downstream end of the reaction zone through double Pyrex windows. When fitted with the Chance OX1 filter used to measure the CO flame band emission, the photocell sensitivity extended from 3200 to 3900 Å.

The reaction zone was 60 cm long and incorporated four evenly spaced mixing jets through which reactants could be introduced to give four different reaction times.[7] Total pressures between 0.8 and 3.0 mm were used with linear flow velocities between 1 and 10 m/sec. Oxygen atom concentrations were determined by titration with NO_2,[5] these concentrations being between 0.3 and 3.0% for O + O_2 mixtures. In experiments using Ar, He or Ne carriers, approximately 1% of oxygen was added to the inert gas passing through the discharge and the products contained very little molecular oxygen. Oxygen atoms in a nitrogen carrier were produced by passing pure nitrogen through the discharge and then adding the stoichiometric quantity of nitric oxide according to the nitrogen atom titration reaction[7,8]

$$N(^4S) + NO(^2\Pi) = N_2(^1\Sigma^+) + O(^3P)$$

NO and NO_2 were prepared and purified in the usual manner. Other gases were obtained from commercial cylinders and purified, particular care being taken to remove impurities such as iron carbonyl from the carbon monoxide used. Gas flows were controlled with needle valves and measured with capillary flow meters. Pressures were measured with spiral or McLeod gauges or with silicone oil manometers.[7]

Results

Figures 1 and 2 show the variation of the CO flame band intensity (I_c) with carbon monoxide concentration and with oxygen atom concentration. For these experiments, an oxygen carrier with a total pressure of 1.7 mm at 293°K was used, and conditions were such that there was negligible O atom decay between the point of mixing and the photomultiplier cell. These figures demonstrate clearly that the glow intensity is proportional to the concentrations of O atoms and of CO, i.e.

$$I_c = I_{0c}[O][CO]$$

Table 1 gives values of $I_c/[O][CO]$ for total pressures between 0.86 and 2.69 mm. It can be

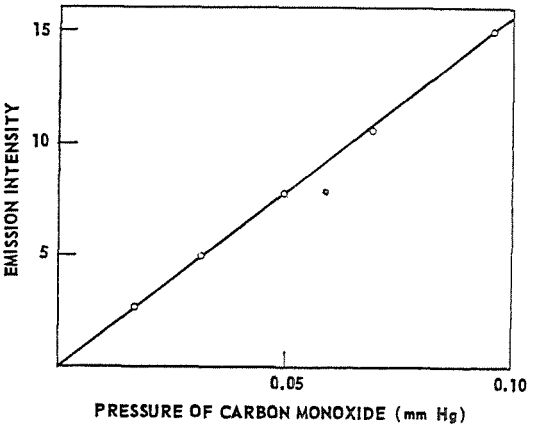

FIG. 1. Dependence of I_c on [CO] for constant [O] at 293°K and 1.69 mm total pressure.

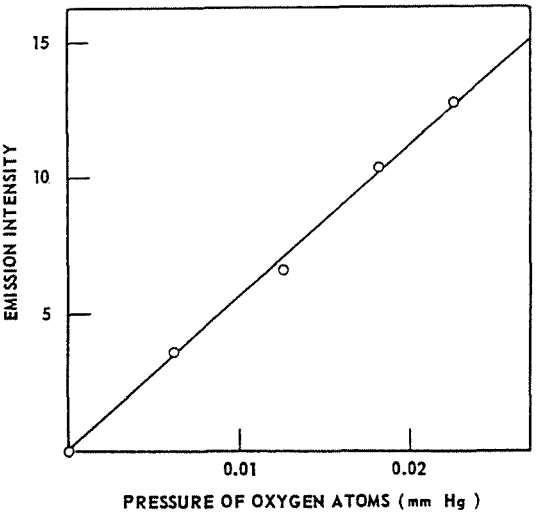

FIG. 2. Dependence of I_c on [O] for constant [CO] at 293°K and 1.69 mm total pressure.

seen that I_{0c} is independent of the pressure of [M] over this range. For measurements of the absolute intensity of the CO flame band emission, the photocell was calibrated with the air-afterglow emission using Fontijn's and Schiff's values of its spectra distribution and absolute emission intensity between 4000 and 6200 A.[9] On the basis of experiments with different filters it was concluded that 60% of CO flame band emission lay between 3200 and 5000 Å. Measurements were made of the ratio of the photocurrents I_{0a}' and I_{0c}' due to the O + NO and O + CO emissions observed respectively with filters 61 and OX1. I_{0c} was then given by

$$\frac{I_{0c}}{I_{0a}} = \frac{I_{0c}'}{I_{0a}'} \times \frac{q_a}{q_c},$$

where I_{0a} is the absolute value of the air afterglow emission intensity and q_a, q_c are the fractions detected of incident quanta in the O + NO and O + CO emissions, respectively. In this way a value of I_{0c} over the whole wavelength range of $6 \times 10^6 \exp[(-3700 \pm 500)/RT]$ cm^3 mole^{-1}

TABLE 1

Variation of I_c with total pressure [M] at 293°K

Total pressure (mm Hg)	I_c/[CO] (arbitrary) units)	[O] (mm Hg)	I_c/[O][CO] ($\times 10^2$)
0.86	3.59	0.0095	3.8
1.05	4.00	0.0092	4.3
1.26	4.77	0.0109	4.4
1.69	6.34	0.0142	4.4
2.16	6.28	0.0170	3.6
2.69	4.39	0.0133	3.3

TABLE 2

The dependence of the emission constant (I_0) and third order rate constant (k_1) on the nature of M at 293°K[a]

	The O + NO reaction[6]		The H + NO reaction[4]		The O + CO reaction	
	$I_{0a} \times 10^{-7}$[b]	$k_{1a} \times 10^{-16}$[b]	$I_{0b} \times 10^{-5}$[b]	$k_{1b} \times 10^{-16}$[b]	$I_{0c} \times 10^{-3}$[b]	$k_{1c} \times 10^{-16}$[b]
O_2	4.0 ± 0.2	2.7 ± 0.3	—	—	12.0 ± 0.8	<0.003
N_2	—	3.1 ± 0.4	—	—	11.2 ± 0.8	—
H_2	—	—	4.3 ± 0.3	1.48 ± 0.15	—	—
A	4.0 ± 0.1	2.7 ± 0.3[c]	3.2 ± 0.3	0.87 ± 0.15	8.0 ± 0.8	—
Ne	—	—	2.0 ± 0.4	0.72 ± 0.10	5.6 ± 1.0	—
He	5.0 ± 0.1	1.8 ± 0.3	2.4 ± 0.2	0.66 ± 0.10	5.6 ± 0.8	—

[a] The errors quoted in this table are the standard errors of the relative values of I_0 and k_1 and not of the absolute values of these quantities.

[b] Units of I_0 cm^3 mole^{-1} sec^{-1}; units of k_1 cm^6 mole^{-2} sec^{-1}.

[c] Data from ref. 5.

sec^{-1} for M = O_2 was determined. An extrapolation of this expression to flame temperatures gives a value of I_{0c} in fair agreement with that obtained from studies of carbon monoxide flames.[15]

In none of the experiments was it possible to measure the rate of the overall reaction

$$O + CO + M \rightarrow CO_2 + M \qquad (1c)$$

An upper limit for k_{1c} is shown in Table 2, which gives emission constants (I_0) and third order rate constants (k_1) for the H + NO, O + NO and O + CO reactions with a variety of third bodies.

Discussion

The results show that the intensity of the CO flame band emission at pressures between 0.8 and 3.0 mm can be represented by the equation

$$I_c = I_{0c}[O][CO]$$

where the constant I_{0c} depends on the *nature* but not on the pressure of the carrier gas used. As in the H + NO and O + NO reactions this behavior of I_0 shows that the rate-determining processes in the formation and removal of excited CO_2 molecules both involve the carrier gas (M),

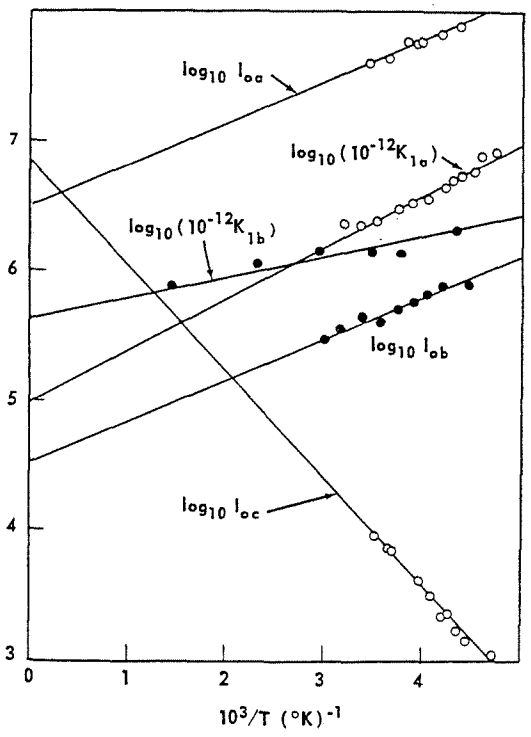

FIG. 3. Arrhenius plots for k_1 and I_0.

but that the pressure dependences cancel out

$$CO + O + M \rightleftharpoons CO_2 + M \qquad (3c)$$

$$CO_2 \rightarrow CO_2 + h\nu \qquad (4c)$$

$$CO_2 + M \rightarrow CO_2 + M \qquad (5c)$$

In this scheme $I_{0c} = k_{3c}k_{4c}/k_{5c}$ if $k_{5c}[M] \gg k_{4c}$, where k_{3c} is the *net* rate constant for combination into the excited state which emits.

Figure 3 is an Arrhenius plot of the I_0 values and third order rate constants for the O + NO + O_2, H + NO + H_2, and O + CO + O_2 reactions. It can be seen that while the spin-allowed combination reactions O + NO and H + NO and their associated light emission show small negative temperature coefficients which can be represented by negative activation energies of 1.0 to 1.5 kcal, the emission associated with the spin-forbidden O + CO reaction exhibits a positive activation energy of 3.7 kcal. Its extrapolated I_0 value for $1/T \rightarrow 0$ is close to that for the O + NO reaction where half the recombination occurs via the electronically excited state of NO_2 responsible for the air afterglow emission,[4] which is an allowed transition.

Further evidence that the low value of I_{0c} is due largely to this energy barrier and not to a slow spin-reversal step is produced by the similarity of the I_{0c} value for O_2 to that for N_2 and A. Since O_2 has a triplet ground state, it would be expected to accelerate a process in which spin-reversal was rate determining. It follows that the rate of reaction (3c) is not controlled by a spin-reversal process, and that the bulk of the emission observed does not involve a change of multiplicity.

The banded nature of the emission spectrum shows that the emitting state has a potential minimum, and the activation energy of I_{0c} must be due to the presence of an energy barrier in the combination reaction (3c) by which this state is reached. The predominant paths for depopulation of the radiating state will be collisional quenching and collision-induced redissociation. The increase in the rate of the latter process relative to the former at higher temperatures is thought to be responsible for the small negative temperature coefficient observed for I_{0a} and I_{0b} in the O + NO and H + NO reactions.[4,6] Since redissociation must also be considered in the O + CO reaction, the height of the energy barrier in this reaction is taken to be equal to the difference between the logarithms of the temperature coefficients of I_{0c} and those of I_{0a} and I_{0b}; this yields a barrier height of 5 kcal/mole. Thus the maximum energy available for emission is 125 + 5 = 130 kcal. The energy of the largest quanta observed is 90 kcal and it follows that the lower state to which the

emission occurs must lie not more than 40 kcal/mole above the ground state of CO_2. No such low-lying electronic state of CO_2 has been detected spectroscopically, nor is one expected on the basis of molecular orbital theory.[10]

It follows that the emission occurs to excited vibrational levels of the ground state of CO_2. It has been shown above that an allowed transition without change in multiplicity is involved. If this interpretation is correct, the CO flame band emission must correspond to a detectable transition in the absorption spectrum of CO_2. The first absorption spectrum of CO_2 with adequate intensity has its maximum at 1475 Å[11] while the maximum emission intensity occurs at 4000 Å. The wide energy spread both of this absorption spectrum and of the CO flame band emission indicates that the transitions involve a change of configuration, and molecular orbital considerations shows that the excited state of this transition is a bent $^1B_2$ or $^1A_2$ state derived from $^1\Delta_u$. Making the very reasonable assumption that this state has the same bending force constant and bond angle (134°) as the ground state of NO_2 the Franck–Condon principle would predict that the strongest transitions in emission and absorption would occur to levels with bending vibrational energies of 35 and 70 kcal/mole, respectively. The sum of these energies (105 kcal) agrees well with the difference between the energies of the observed maximum intensities, which is 120 kcal. It can therefore be concluded that most of the CO flame band emission comes from a $^1B_2$ or $^1A_2$ state of CO_2 which has a minimum excitation energy of about 110 kcal. For convenience, it will be assumed that the excited singlet state involved is $^1B_2$, as the transition $^1A_2 \leftrightarrow {}^1\Sigma_g^+$ is forbidden except with the excitation of the asymmetric stretching vibration. The discussion would be unaffected if it were the $^1A_2$ state, owing to the expected similarity of the bond angles.

The mechanism of formation of the excited singlet state is of interest. Avramenko and Kolesnikova gave a value of

$$4 \times 10^{17} \exp(-3500/RT) \text{ cm}^6 \text{ mole}^{-2} \text{ sec}^{-1}$$

for the rate constant of the overall combination reaction,[12] while a value of 3.7 kcal/mole for the activation energy of this reaction has also been reported.[16] Although the Russian work predicts a higher rate constant than the upper limit detectable in Kaufman's work and ours, it shows that the energy barrier exists for all combinations of O (^3P) + CO ($^1\Sigma^+$) and not only for light emission.

Since the electronic states of CO_2 which arise from O (^3P) + CO ($^1\Sigma^+$) are triplets, the mechanism by which excited CO_2 molecules reach the $^1B_2$ state must be such that spin-reversal is not rate determining. If all these triplet states were unstable, crossing into the singlet state must occur at the same time as stabilization by a third body. Spin reversal would then be part of the rate-determining process and a low transmission coefficient and a specific effect of M = O_2 would be expected. If, however, the combination O (^3P) + CO ($^1\Sigma^+$) yielded a stable triplet state via a potential maximum, the rate of formation of molecules in this state rather than their rate of crossing into the excited singlet state, could be rate determining. CO_2 would be expected to have such a triplet state ($^3B_2$) lying about 20 kcal below the excited singlet ($^1B_2$) state, both from molecular orbital considerations and by analogy with CS_2 and SO_2 where such states have been observed.[13] Radiationless crossing to the singlet state from the higher vibrational levels of the triplet state in perturbations would be much faster than radiation by or collisional quenching of the excited singlet state. This phenomenon is observed in the H + NO reaction, where the radiating HNO ($^1A''$) molecules are formed by radiationless crossings from a $^3A''$ state formed by

$$H(^2S) + NO(^2\Pi) + M \rightarrow HNO(^3A'') + M.$$

The mechanism of the CO flame band emission can therefore be represented by:

$$O(^3P) + CO(^1\Sigma^+) + M \rightleftharpoons CO_2(^3B_2) + M$$

$$CO_2(^3B_2) \rightleftharpoons CO_2(^1B_2)$$

$$CO_2(^1B_2) \rightarrow CO_2(^1\Sigma_g^+) + h\nu$$

$$CO_2(^1B_2) + M \rightarrow CO_2(^1\Sigma_g^+) + M$$

The corresponding potential curves are represented diagrammatically in Fig. 4.

The probability of the radiative transition ($^3B_2 \rightarrow {}^1\Sigma_g^+$) is less than 10^{-4} of that from ($^1B_2 \rightarrow {}^1\Sigma_g^+$). The former process can be neglected for those CO_2 molecules which have energies where crossing between the excited triplet and singlet states can occur. Rapid vibrational quenching of the $^3B_2$ state would yield molecules which have too low an energy to cross to the $^1B_2$ state, and which would show slower collisional electronic quenching. These metastable molecules would have long enough lives to contribute appreciably to the CO flame band emission, at longer wavelengths.

Gaydon's spectrum of the SO_2 afterglow[14] (which we have recently shown to be associated with the SO + O reaction) shows bands known to originate from the low lying triplet state of SO_2, but they appear from the published spectrum

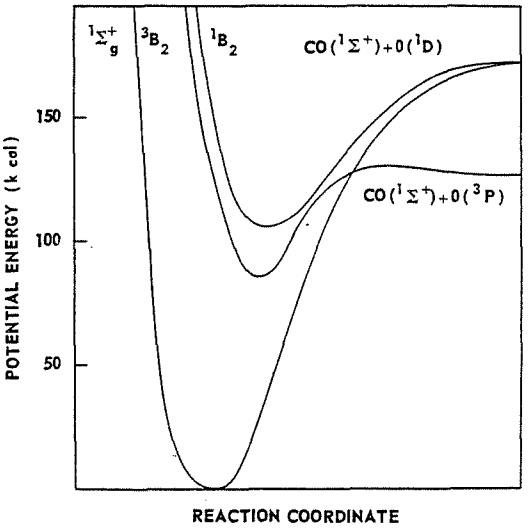

FIG. 4. Diagrammatic potential curves for the O + CO reaction.

to contribute less than 10% of the total intensity. The proportions of triplet–singlet emission might well be lower in the O + CO reaction, as a violation of the spin selection rule would occur less readily for CO_2 than for SO_2.

The energy barrier to combination in the O + CO system is related to that observed both in the unimolecular and bimolecular decompositions of the isoelectronic molecule N_2O:

$$N_2O(^1\Sigma^+) \rightarrow N_2(^1\Sigma^+) + O(^3P)$$

In this case the barrier height of the combination process is 20 kcal while the heat of reaction is 40 kcal, as compared with 125 kcal for O + CO. Although it has not been possible to determine the absolute rate constant for the O + CO reaction, the kinetics of the emission process show that apart from its activation energy, this should be a normal third order reaction. Bimolecular radiative combination could only make a small contribution, owing to the very low concentration of excited CO_2 which could be in equilibrium with CO + O at energies above that of the barrier to recombination. It is believed that the great complexity of the emission spectrum is due to emission from many vibrational levels of the $^1B_2$ state of CO_2 lying below the energy barrier, the intensity distribution being governed by the relative rates of vibrational and electronic quenching and by the energy removed by the third body in the stabilization process.

REFERENCES

1. GAYDON, A. G.: *The Spectroscopy of Flames*, Chapman and Hall, Ch. 6 (1957).
2. BROIDA, H. P. and GAYDON, A. G.: Trans. Faraday Soc., *49*, 1120 (1953).
3. CLYNE, M. A. A. and THRUSH, B. A.: Trans. Faraday Soc., *57*, 1305 (1961).
4. CLYNE, M. A. A. and THRUSH, B. A.: Discussions Faraday Soc. *33*, 139 (1962).
5. KAUFMAN, F.: Proc. Roy. Soc. (London), *A247*, 123 (1958).
6. CLYNE, M. A. A. and THRUSH, B. A.: Proc. Roy. Soc. (London) *A269*, 404 (1962).
7. CLYNE, M. A. A. and THRUSH, B. A.: Proc. Roy. Soc. (London), *A261*, 259 (1961).
8. KISTIAKOWSKY, G. B. and VOLPI, G. G.: J. Chem. Phys., *27*, 1141 (1957); *28*, 665 (1958).
9. FONTIJN, A. and SCHIFF, H. I.: *Chemical Reactions in the Lower and Upper Atmosphere*, Stanford Research Institute (1961).
10. MULLIKEN, R. S.: Canad. J. Chem., *36*, 10 (1958).
11. INN, E. C. Y., WATANABE, K., and ZELIKOFF, M.: J. Chem. Phys., *21*, 1648 (1953).
12. AVRAMENKO, L. I. and KOLESNIKOVA, R. V.: Izvest. Akad. Nauk. S.S.S.R., 1562 (1959).
13. DOUGLAS, A. E.: Canad. J. Phys., *36*, 147 (1958).
14. GAYDON, A. G.: Proc. Roy. Soc. (London), *A146*, 901 (1934).
15. KASKAN, W. E.: Combustion and Flame, *3*, 39 (1959).
16. MAHAN, B. H. and SOLO, R. B.: A.C.S. Meeting, March 1961, Abst. R62.

Discussion

PROF. S. W. BENSON (*University of Southern California*): Dr. Thrush's very interesting results should be compared with those of Mahan and Solo who reported for a very similar system a bimolecular rate of CO_2 formation. For Dr. Thrush's system the rate would be termolecular.

DR. B. A. THRUSH (*University of Cambridge*): We think that the rate of CO_2 formation would be termolecular under our conditions, the reaction involving an activation energy similar to that for light emission.

DR. R. R. BALDWIN (*Hull University*): I should like Dr. Thrush to clarify one point in his paper. The convincing evidence he presents that the process responsible for light emission is termolecular clashes with the view expressed by Avramenko and Kolesh-

nikova that O + CO occurs by a bimolecular reaction: This clash could have been resolved by suggesting that only a relatively small part of the CO_2 formed is via the reaction responsible for light emission and that there is another bimolecular process forming CO_2. However, since Dr. Thrush used the activation energy obtained by Avramenko and Kolesnikova to support his termolecular scheme, I assume he does not take this view, and would be glad if he would confirm this.

DR. B. A. THRUSH: On the basis of our experiments, we consider that all the O (^3P) + CO ($^1\Sigma^+$) reaction involves an energy barrier. We think that recombination via the electronic states responsible for light emission makes an appreciable contribution to the total rate of combination. Some recombination must also occur via states which do not radiate significantly.

Avramenko and Kolesnikova appear to have carried out all their experiments at one pressure. Since all known atom + diatomic molecule combination reactions are third order in this pressure range, we have interpreted their data in terms of a third order rate constant. This view is supported by the mechanism of the light emission process.

THE SELF-INHIBITION OF GASEOUS EXPLOSIONS

R. R. BALDWIN, N. S. CORNEY, P. DORAN, L. MAYOR, AND R. W. WALKER

In discussing the conditions under which branched-chain reactions, either of the linear branching or quadratic branching type, can give rise to isothermal explosion, it is usually assumed that the initial values of the parameters (e.g. initiation rate, branching factor, termination constants) determine whether the system is stable or explosive. If, however, a reaction product can inhibit the reaction, substantial modification of the explosion condition may result. Two types of mechanism are discussed, one with linear branching and one with quadratic branching, which illustrate this point. In the case of linear branching, it is shown that the original isothermal limit may be modified to a chain-thermal boundary. Thus, whereas ethane, propane, and butane inhibit the second-explosion limit of H_2 and O_2 by direct chain-terminating reactions with H, OH, and O, methane and neopentane can inhibit only via their reaction products (formaldehyde in the case of methane, aldehydes and olefins in the case of neopentane). Such products are formed in significant concentrations only after the uninhibited explosion boundary has been crossed and incipient explosion is developing. A variety of evidence supports the view that the character of the explosion changes from the original isothermal chain-branching explosion to a chain-thermal explosion with these two hydrocarbons. The second type of inhibiting mechanism, applicable when quadratic branching occurs, is exemplified by the self-inhibition of the H_2/O_2 reaction, as shown by the effect of withdrawal rate on the second limit.

Introduction

Reactions proceeding by a chain mechanism may become explosive by either of two possible processes:

(*a*) *Thermal Explosion*

Here the primary cause of the explosion is the self-heating of the reaction system. Basic conditions that must be satisfied are that the reaction must be exothermic and the activation energy must be finite. The reaction starts at a moderate rate, evolving heat; to dispose of this heat, the temperature of the gas rises above its surroundings. Under certain conditions, this temperature rise may be quite small, and the system stabilizes. Under other conditions, this rise in temperature may cause a considerable increase in reaction rate so that more heat is evolved in unit time, and a further temperature rise occurs. Repetition of this spiral process indefinitely gives the thermal explosion. Factors influencing the critical rate that leads to explosion include the activation energy and heat of reaction, the vessel diameter and gas conductivity (which influence conduction of heat to the walls), and the specific heat of the gas (which determines how much heat is used up in raising the gas temperature). Precise formulation of the boundary condition has been attempted by a number of authors.[1–6]

(*b*) *Isothermal Explosion*

The word isothermal emphasizes that the primary cause of the explosion is the kinetic feature of the reaction that causes the concentration of chain centers to increase in a continuous and exponential manner with time. There are two subdivisions in this category:

(*i*) *Linear branching mechanisms.* Here only linear (first-order) reactions of chain centers are involved, the development of the concentration of chain centers, n, with time t being governed by the equation:

$$dn/dt = \theta + fn - gn - \gamma n \qquad \text{(i)}$$
$$= \theta + \phi n$$

where θ, fn, gn, γn are the rates of initiation, chain-branching, gas-phase termination, and surface destruction,* respectively. The net branching factor $\phi = (f - g - \gamma)$, and the explosion boundary is defined by the condition $\phi = 0$. The $n - t$ relationships for the three situations ϕ negative, ϕ zero, and ϕ positive, are shown in Fig. 1.

(*ii*) *Quadratic branching mechanisms.* Here branching is possible at a rate proportional to the square of the chain center concentration.

* More precise discussions of surface termination have been given elsewhere.[7–9]

Equation (i) now becomes:

$$dn/dt = \theta + \phi n + Fn^2 \qquad \text{(ii)}$$

and explosion is possible not only when ϕ is positive, but also when ϕ is negative, provided $4\theta F > \phi^2$. The corresponding situations to Fig. 1 may be shown by two diagrams, Fig. 2A being the plot of $dn/dt - n$, and Fig. 2B the plot of $n - t$. In curve 1, $dn/dt = 0$ at S, and the concentration of chain centers becomes constant at this value. In curve 3, dn/dt is always positive and the chain center concentration increases continuously with time. Curve 2 represents the boundary condition. The corresponding $n - t$ relations are shown in Fig. 2B.

It is generally assumed in discussing both slow reaction and explosion that θ, ϕ, and F are defined only by the initial conditions. Thus, both the short induction periods preceding explosion of H_2/O_2 mixtures[10] and the long induction periods in hydrocarbon oxidation have been analyzed on the assumption of a constant value of ϕ throughout the induction period. This paper discusses some examples in fairly simple systems where this assumption is not true, and where the changing value of ϕ as the reaction develops produces substantial modification in the explosion condition.

I. Inhibition of the H_2/O_2 Reaction by Methane

The reason why the methane-inhibited H_2/O_2 reaction provides an illustration of the above phenomenon can be understood by reviewing briefly the inhibiting action and mechanism of

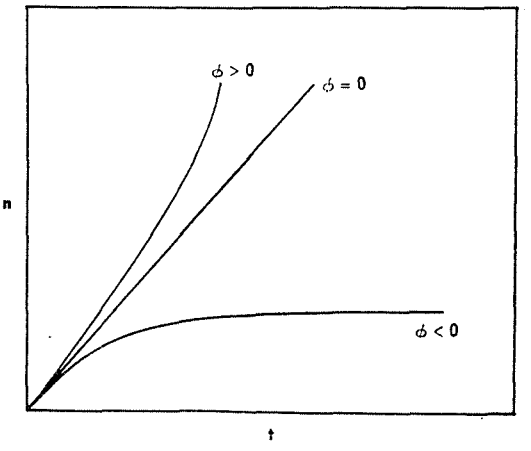

FIG. 1. Chain center concentration (n)–time (t) relationships with linear branching and linear chain termination.

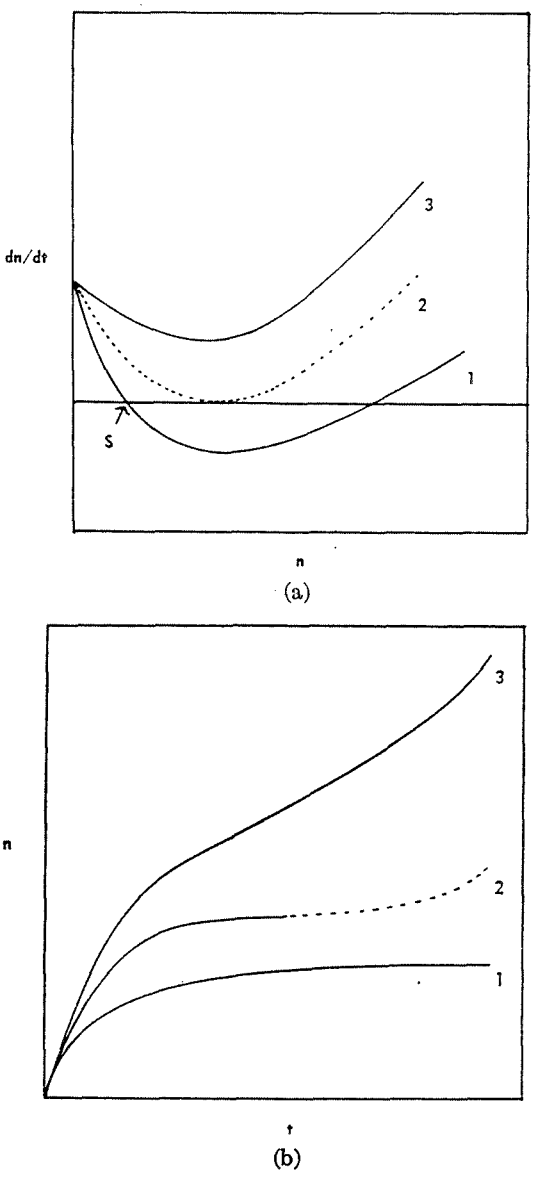

FIG. 2. (a) $dn/dt - n$ relationship with quadratic branching. (b) n–t relationship with quadratic branching; n = concentration of chain centers, t = time.

inhibition in the case of ethane, propane, and n- and i-butane. These hydrocarbons from ethane to butane exert a very similar inhibiting action on the H_2/O_2 reaction,[11–14] the characteristic feature being that as the concentration of hydrocarbon is increased, the explosion limit is reduced in an almost linear manner down to the junction of the first and second limits. Because of this linear relationship, the efficiency of inhibition can be conveniently assessed in terms of $i_{\frac{1}{2}}$, the

mole fraction of inhibitor required to halve the uninhibited limit; $i_{\frac{1}{2}}$ is almost proportional to y, the mole fraction of O_2, is much less dependent on the mole fraction of H_2, x, and is effectively independent of vessel diameter. Assuming an isothermal boundary, defined by $\phi = 0$, the main features of the inhibition can be accounted for by adding reaction (14) to the simplest mechanism, involving reactions (1)–(5a), which describes the second limit of the H_2/O_2 system.

$$H + RH = H_2 + R \qquad (14)$$

$$OH + H_2 = H_2O + H \qquad (1)$$

$$H + O_2 = OH + O \qquad (2)$$

$$O + H_2 = OH + H \qquad (3)$$

$$H + O_2 + M = HO_2 + M \qquad (4)$$

$$HO_2 \xrightarrow{\text{surface}} \text{destruction} \qquad (5a)$$

Assuming that reaction (14) leads to chain termination, this mechanism gives the relations:

$$\frac{P_2 - P}{P_2} = \frac{k_{14}i}{2k_2y}; \quad i_{\frac{1}{2}} = \frac{k_2y}{k_{14}} \qquad \text{(iii)}$$

P_2, P are the uninhibited and inhibited limits, respectively, and i is the mole fraction of hydrocarbon. Minor features of the inhibition can be accounted for by adding reaction (15) or the kinetically equivalent reaction (13).

$$OH + RH = H_2O + R \qquad (15)$$

$$O + RH = OH + R \qquad (13)$$

$i_{\frac{1}{2}}$ is then given by:

$$\frac{1}{i_{\frac{1}{2}}} = \frac{k_{14}}{k_2y} + \frac{2k_{15}}{k_1x + k_{15}i_{\frac{1}{2}}} \qquad \text{(iv)}$$

In the case of ethane, it has been shown[13] that the variation of $i_{\frac{1}{2}}$ over a wide range of mixture composition can be interpreted precisely by Eq. (iv) if it is assumed that every alkyl radical is destroyed without continuing the chain. This evidence, as well as studies of the inhibition of the first limit,[13] shows that reactions (21a) and (16a) are negligible compared with reaction (20a), and that reaction (19a) can, at most, be only of minor importance. This latter conclusion is supported by the high yields of ethylene[15] obtained when ethane is oxidized in a flow system at these temperatures. The similar inhibition features obtained with propane, *n*- and *i*-butane are attributed to the fact that reactions similar to (20a), producing the unreactive HO_2 radical, are predominant in these cases also.

$$C_2H_5 + O_2 = C_2H_4 + HO_2 \qquad (20a)$$

$$C_2H_5 + O_2 = CH_3CHO + OH \qquad (19a)$$

$$C_2H_5 + H_2 = C_2H_6 + H \qquad (16a)$$

$$C_2H_5 = C_2H_4 + H \qquad (21a)$$

There is no doubt that the uninhibited second limit is isothermal in character; in particular,

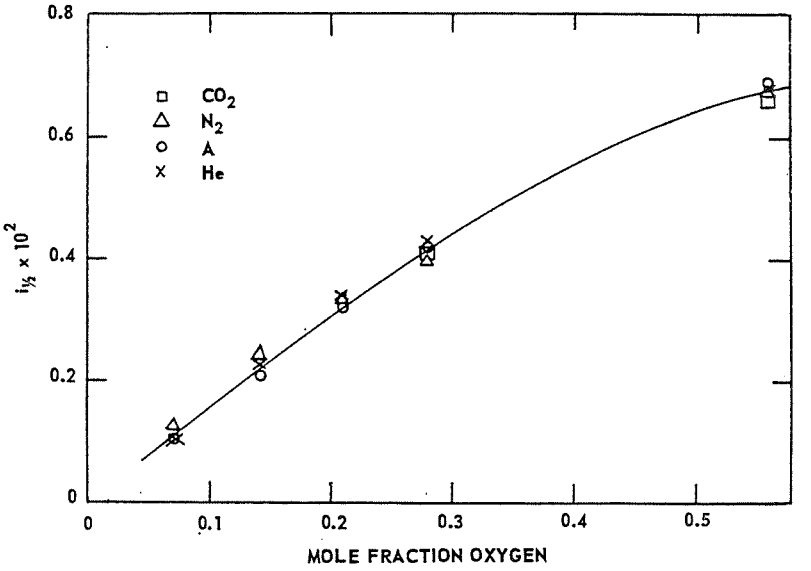

FIG. 3. Effect of inert gas on inhibiting action of ethane; 35 mm diameter KCl-coated vessel at 540°C, H_2 = 0.28 mole fraction

the relative effects of helium and argon on the second limit agree exactly[8] with the ratio of their collision frequencies in reaction (4) and there is no evidence for any abnormal effect of helium resulting from its high thermal conductivity. Confirmation of the isothermal nature of the inhibited limit in the presence of ethane comes from studies of the effect of different inert gases.[16] According to Eq. (iv), which is based on an isothermal boundary condition, i_4 for a given H_2–O_2 mixture should be independent of inert gas. Figure 3 shows the effect of the four inert gases, helium, argon, nitrogen, and carbon dioxide for a series of mixtures in which the mole fraction of O_2 varied from 0.07–0.56, the mole fraction of H_2 being constant at 0.28 and the remainder of the mixture (apart from the trace of ethane) being the one inert gas added. The fact that i_4 is independent of inert gas is particularly striking in view of the wide variation (60–180 mm Hg at 540°C) in the uninhibited limit resulting from the different inert gas coefficients in reaction (4).

With methane, a reaction analogous to (20a) will produce the reactive CH_2 radical and cannot, therefore, be regarded as a chain termination process; moreover, no evidence for this reaction has been found, reaction (19) being generally accepted.

$$CH_3 + O_2 = HCHO + OH \qquad (19)$$

Since an OH radical is produced, no direct chain termination can result. It is thus not surprising that the inhibition features with methane differ spectacularly from those with ethane and the higher hydrocarbons.[11,17] At first sight, no inhibition by methane would be expected. However, the formaldehyde formed in reaction (19) has been shown to be an extremely effective inhibitor and explosion may be prevented if the formaldehyde concentration builds up sufficiently before the explosion develops.

The situation may be generalized by supposing that a reactant R forms an intermediate I by reaction with a chain center. This intermediate I is destroyed by reaction with chain centers and some fraction at least of these reactions do not produce further chain centers. Suppose the reaction mixture is subjected to conditions where the net branching factor ϕ is initially positive. The differential equations for the center concentration n and the intermediate I then become:

$$dn/dt = \theta + \phi n - A[\mathrm{I}]n \qquad (v)$$

$$d[\mathrm{I}]/dt = B[\mathrm{R}]n - C[\mathrm{I}]n \qquad (vi)$$

If all reactions destroying the intermediate also remove a chain center, $A = C$. From (vi), the stationary concentration of intermediate $= B[\mathrm{R}]/C$. If $\phi > AB[\mathrm{R}]/C$, dn/dt is always positive and an isothermal explosion occurs. If $\phi < AB[\mathrm{R}]/C$, dn/dt is negative when the equilibrium concentration of intermediate is reached, and isothermal explosion is impossible. Since dn/dt is initially positive, however, the n–t curve must pass through a maximum, as shown diagrammatically in Fig. 4. The resultant maximum reaction rate may be sufficient to cause a thermal explosion. The striking feature about this mechanism is that the inhibited boundary can become thermal in character, in contrast to the isothermal nature of the uninhibited limit.

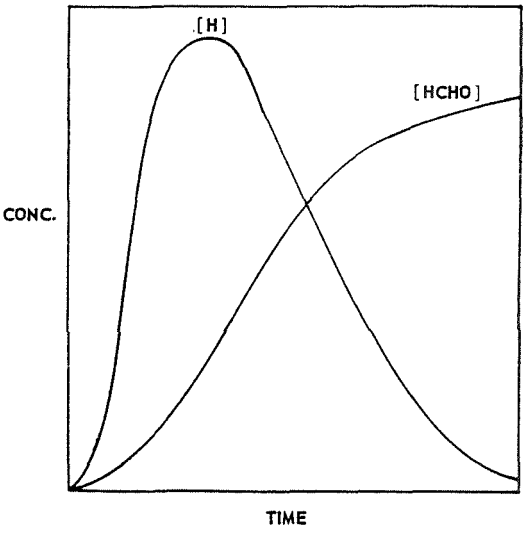

FIG. 4. Sketch of concentration–time relationships given by Eqs. (v) and (vi).

The main features of the inhibition of the H_2/O_2 reaction by methane have been discussed elsewhere[16,17] and only a summary of the main points, and the evidence supporting a thermal boundary, will be given here.

(a) Increasing amounts of methane have little effect on the second limit until a critical concentration i_c is reached, when explosion is suddenly and completely suppressed. The contrast between the behavior of methane and ethane is shown in Fig. 5.

(b) The value of i_c increases almost linearly with increasing mole fraction of O_2. As in the case of ethane, this suggests a competition between the hydrocarbon and oxygen for the same chain carrier, H.

(c) Here i_c is more markedly dependent on the mole fraction of H_2 than in the case of ethane. Initially i_c increases almost linearly with increasing x, then passes through a maximum, and decreases as x is further increased. Such a

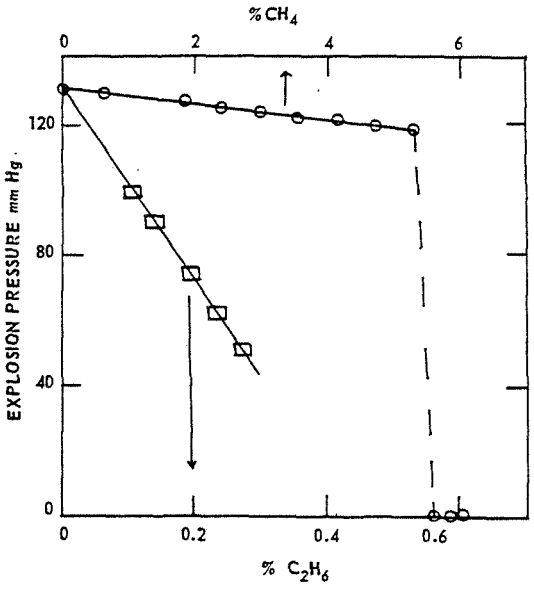

FIG. 5. Comparison of inhibiting action of methane and ethane; 35 mm diameter KCl-coated vessel at 540°C, H_2 = 0.28, O_2 = 0.14 mole fraction.

relationship could result from the combination of a chemical effect in which i_c increases continuously with x, and a physical effect in which the increased conductivity in mixtures of high H_2 content makes thermal explosion more difficult, so that less inhibitor is required.

(d) The value of i_c increases as the vessel diameter increases, with a less than first power relationship. While this could be interpreted in terms of an inefficient surface termination process, this possibility is excluded by the observation that i_c is effectively the same in both clean and KCl-coated Pyrex vessels; it is extremely unlikely that the inefficiency of these two surfaces should be identical. A thermal mechanism, however, provides a simple explanation of the diameter dependence without an accompanying surface dependence; the less than first power relationship can be attributed to the importance of specific heat and convection contributions, in addition to conduction.

(e) Although no significant reaction occurs in mixtures maintained above the explosion boundary for up to 5 minutes, analysis of completely inhibited mixtures withdrawn from the reaction vessel without explosion shows that significant reaction has occurred. This is consistent with the burst of reaction indicated in Fig. 4.

(f) Normal explosions in large diameter vessels are accompanied by a violent kick in the Hg level of the manometer used to follow the pressure in the reaction vessel; with methane concentrations just greater than i_c, a small kick is observed which disappears as the methane is further increased. This again is consistent with the burst of reaction evident in Fig. 4. Further support is provided by the detection of small temperature rises (using a centrally located thermocouple in a glass sheath) in mixtures with methane concentrations just greater than i_c when the pressure falls just below the uninhibited limit. Similar evidence comes from the observation of a faint glow, presumably a consequence of the temporary high concentration of radicals, in certain mixtures with methane concentrations just greater than i_c; these glows disappear if the methane concentration is increased slightly.

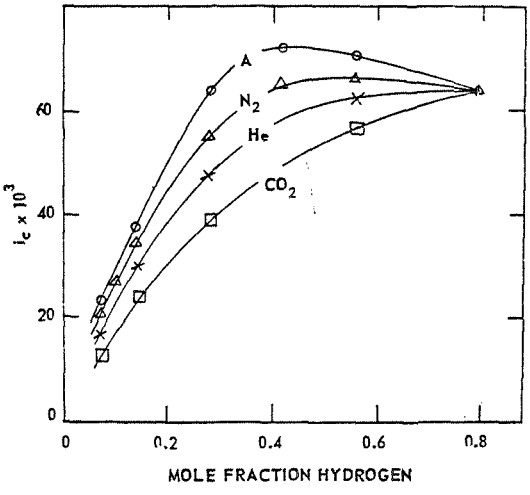

FIG. 6. Effect of inert gas on inhibiting action of methane; 35 mm diameter KCl-coated vessel at 540°C, O_2 = 0.14 mole fraction.

(g) The most direct evidence for a thermal boundary comes from the effect of the inert gases He, A, N_2, and CO_2. If the boundary is isothermal in character, inert gases should either have no effect (as with ethane), or should have an effect determined directly by their influence on ϕ. This could arise either through their ability to reduce diffusion of chain centers to the wall, in which case the order of effectiveness should be $CO_2 > N_2 > A > He$, or through their ability to take part in activating (e.g. $H_2O_2 + M = 2OH + M$) or deactivating collisions (e.g. $H + O_2 + M$), in which case the order of effectiveness is again likely to be $CO_2 > N_2 > A > He$.* If, however, the explosion has thermal

* This is the order given by Ritchie[18] for a number of reactions; however, in both the decomposition of NO_2Cl[19] and in the reaction $H + O_2 + M = HO_2 + M$, He lies between N_2 and A.

character, the specific heat and conductivity of the gas mixture will also influence the boundary. Because of its high conductivity, helium may become particularly effective in suppressing explosion, and the order of effectiveness may become $CO_2 > He > N_2 > A$. Figure 6 shows the variation of i_c with mole fraction of H_2, the mole fraction of O_2 being 0.14, and the remainder of the mixture being one of the four inert gases. The order of effectiveness is entirely consistent with a thermal explosion boundary.

The inhibiting action of methane on the H_2/O_2 reaction thus provides an example of a "degenerate" inhibition, where the inhibitor itself exerts no direct inhibiting action, but under conditions where the explosion begins to develop, the inhibitor gives rise to products that may suppress the developing explosion.

II. Inhibition of the H_2/O_2 Reaction by Neopentane

The peculiar inhibiting features found with methane arise because the methyl radical is unable to undergo the chain termination reaction forming an olefin and HO_2. Such a reaction requires a C—H bond adjacent to the carbon atom at which the free valency exists. Neopentane is the next simplest hydrocarbon which is incapable of giving such a radical. Two alternative reactions are possible for the neopentyl radical formed in the primary inhibition process:

(a) Fission at the C—C bond to give *i*-butylene and a methyl radical which then undergoes reaction (19), regenerating an active chain center. Although no direct inhibition is possible, olefins have been shown to be efficient inhibitors so that this sequence forms two products capable of inhibiting the reaction, and a methane-type inhibition would be expected.

$$(CH_3)_3C—CH_2 = (CH_3)_2C=CH_2 + CH_3$$

(b) Reaction with O_2 to give an aldehyde:

$$(CH_3)_3C—CH_2 + O_2 = (CH_3)_3C—CHO + OH$$

Although no direct inhibition occurs, the aldehyde could inhibit through the following reaction sequence:

$$(CH_3)_3C—CHO + \text{center X} = (CH_3)_3C—CO + XH$$

$$(CH_3)_3C—CO = (CH_3)_3C + CO$$

$$(CH_3)_3C + O_2 = (CH_3)_2C=CH_2 + HO_2$$

A methane-type inhibition would again be expected.

Studies with neopentane confirm that the inhibition is similar to that obtained with methane, particularly in the following respects:

(i) Increasing addition of neopentane has little effect on the limit until a critical concentration is reached when explosion is completely suppressed; the critical concentration is about one-fiftieth of that with methane;

(ii) i_c is dependent on vessel diameter;

(iii) i_c is dependent on inert gas, the order for increasing i_c being CO_2, He, N_2, A. This order confirms the thermal nature of the boundary.

III. Inhibition of the H_2/O_2 Reaction by Ethane, Propane, and Butane

In KCl-coated vessels at 540°C, the inhibiting action of ethane is independent of withdrawal rate over a wide range, and is almost independent of the mixing time, prior to withdrawal, over the range 20 sec to 5 min. In clean Pyrex vessels at 500°C, the limit is again almost independent of mixing time. However, although the inhibited limit is independent of withdrawal rate over a

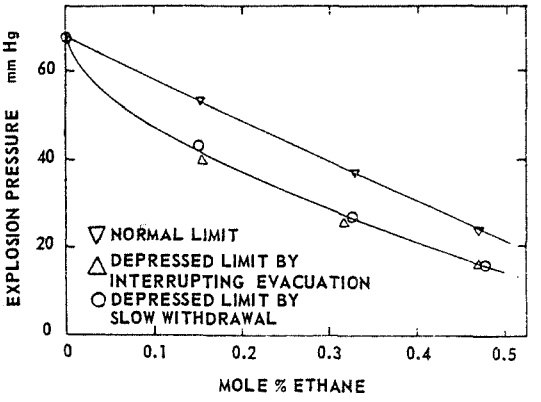

FIG. 7. Normal and depressed limits in inhibition by ethane; 23 mm diameter Pyrex vessel at 500°C, $H_2 = 0.80$, $O_2 = 0.14$ mole fraction.

certain range, further reduction in withdrawal rate suddenly gives a "depressed" limit, which remains roughly constant as the withdrawal rate is further reduced. Typical results for the "normal" and "depressed" limits for a mixture containing 0.80 mole fraction H_2 and 0.14 mole fraction O_2 in a 23 mm diameter vessel are shown in Fig. 7. The "depressed" limit can also be obtained by interrupting the evacuation for a period of several minutes at a pressure just above the normal boundary, and then continuing the rapid evacuation. In KCl-coated vessels, depressed limits are only obtained by using inconveniently slow withdrawal rates, but can be

obtained by this "interrupted evacuation" technique.

These depressed limits are almost certainly due to the formation of ethylene, which has been shown to be a more efficient inhibitor than ethane. The fact that depressed limits are more easily obtained in Pyrex vessels, where quadratic branching plays a significant role, suggests that the self-inhibition mechanism here may be similar to that described in the next section, rather than to that described for methane.

Although depressed limits were only obtained with difficulty in KCl-coated vessels with ethane, they were obtained much more easily with propane, *n*- and *i*-butane; with some mixtures, normal limits could only be obtained by using freshly coated vessels. Tests have shown that propylene is a more efficient inhibitor than propane[20]; the butylenes have not been examined. The increased tendency to obtain depressed limits with propane may be due partly to the fact that propylene is a more efficient inhibitor than ethylene, and partly to the increased rate of propane oxidation which is likely because of the lower C—H bond strength.

While the isothermal nature of the "normal" inhibited limit has been shown by inert gas tests, it has not yet been possible to make similar studies on the depressed limits.

IV. Self-Inhibition of the H_2/O_2 Reaction

Perhaps the simplest case of self-inhibition arises where only two reactants, H_2 and O_2, are involved. In KCl-coated vessels, the second limit is normally independent of withdrawal rate over a very wide range. In clean Pyrex vessels, the limit is markedly dependent on withdrawal rate, as shown in Fig. 8. With mixtures of high O_2 content, decreasing the withdrawal rate has little effect until a critical rate is reached, when explosion is completely suppressed. With mixtures of lower O_2 content, the limit is gradually reduced as the withdrawal rate is reduced below a critical value. Since this phenomenon is only significant in Pyrex and boric-acid–coated vessels, where quadratic branching occurs, it appears to be connected in some way with the quadratic branching process.

The only feasible inhibitor is H_2O, which is an extremely efficient third body in the reaction $H + O_2 + M = HO_2 + M$. The formation of H_2O as the explosion boundary is crossed cannot be shown using the withdrawal method, because the pressure change due to H_2O formation is masked by the pressure decrease due to withdrawal. If, however, the boundary is approached by raising the temperature, formation of H_2O can be detected. A mixture (0.28, 0.14 mole fractions of H_2, O_2, respectively) was prepared in the reaction vessel at 480° and 500 mm Hg pressure, and the pressure then reduced to 86 mm Hg, at which pressure the ignition temperature is 490°C. The mixture was then heated at about 2°C/min, the pressure being followed on a sensitive Bourdon gauge. Between 480° and 490°C, the pressure rose gradually as expected from thermal expansion. At 490°C, the mixture

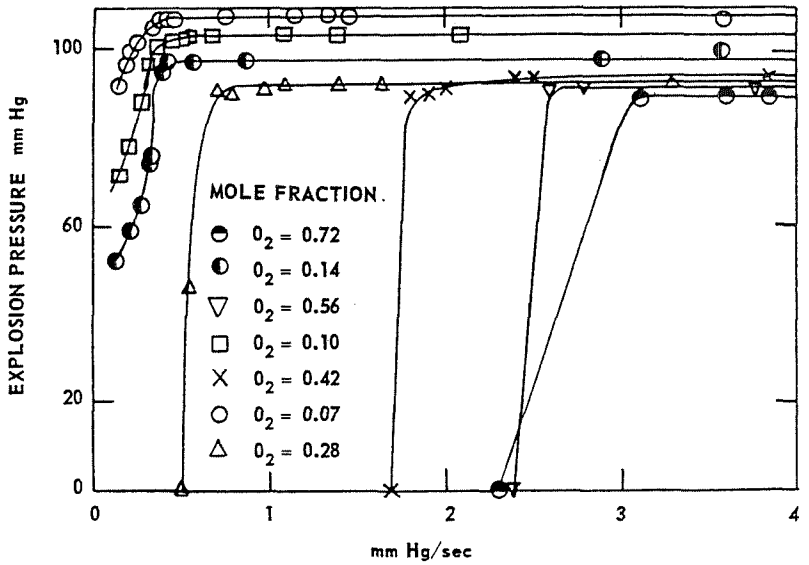

FIG. 8. Effect of withdrawal rate on second limit of H_2/O_2 reaction; 35 mm diameter Pyrex vessel at 500°C, H_2 = 0.28.

did not explode, but no further pressure increase occurred up to 505°C. From the difference between the observed pressure at 505°C and that calculated for thermal expansion, 3.9% of H_2O had been formed. At a constant temperature of 505°C, the mixture was withdrawn fairly rapidly. Explosion occurred at 80 mm Hg, as compared to the normal uninhibited limit of 112 mm Hg at this temperature. From the known inhibiting effect of H_2O, this drop of 32 mm Hg indicates the formation of 4.1% of H_2O, in good agreement with that estimated from pressure change.

The fact that this phenomenon is only significant in Pyrex and boric-acid–coated vessels, where quadratic branching occurs, suggests that it is connected with the quadratic branching process. While, therefore, the type of inhibition mechanism obtained with methane, where formaldehyde is the effective agent, could also be visualized with H_2O as the effective inhibitor, it appears that this type of inhibition is negligible.* From the discussion of quadratic branching already given (Fig. 2A), the concentration n_e of chain centers at the boundary is obtained by writing $d(dn/dt)/dt = 0$, giving $n_e = -\phi/2F$ (ϕ is negative). As a result of this concentration, there is a definite rate of H_2O formation, so that ϕ decreases (becomes more negative) at a definite rate. If this rate of decrease of ϕ exceeds the rate at which ϕ is increasing due to the withdrawal process, then the system will remain just outside the explosion boundary throughout the withdrawal process, and no explosion will occur.

To apply the above formal treatment to a precise interpretation of critical withdrawal rates requires a precise chemical mechanism for the slow reaction between H_2 and O_2. While this is not possible for clean Pyrex vessels and for vessels freshly coated with boric acid, it has been possible to give a precise interpretation of the kinetics in aged boric-acid–coated vessels. Although this mechanism was developed to interpret results in the pressure range 200–600 mm Hg, it can be extrapolated to predict the reaction rate at the explosion boundary; from this rate, and the known inhibiting efficiency of H_2O, the critical withdrawal rate can be predicted. The calculations are rather sensitive to small errors but Fig. 9 shows that the critical withdrawal rates can be predicted to within 30% over a range of mole fractions of O_2. The treatment also predicts that the critical withdrawal rates should be independent of diameter, in agreement with the experimental results. A full discussion of this treatment has been given elsewhere.[21]

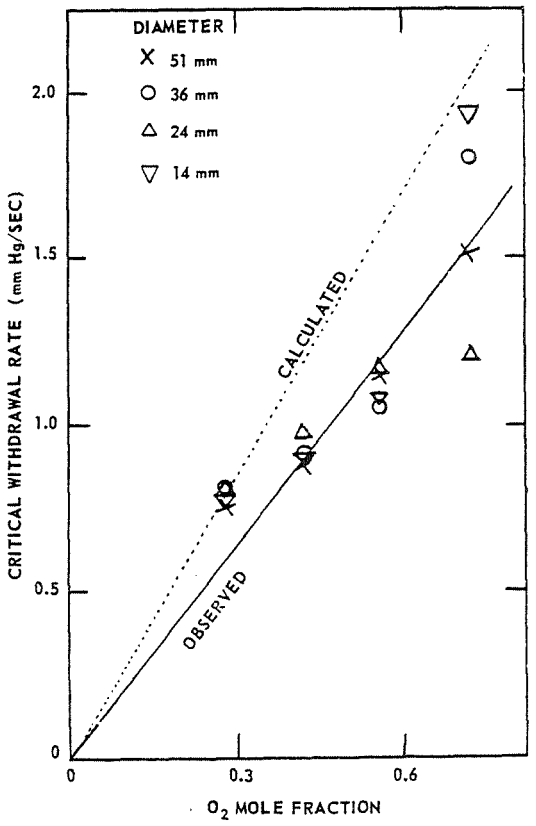

FIG. 9. Comparison of calculated and experimental critical withdrawal rates. Aged boric-acid–coated vessels at 500°C, H_2 = 0.28 mole fraction.

Conclusion

Four cases have been discussed in which the explosion boundary condition has been considerably modified by the inhibiting action of products formed by reactions occurring in the immediate vicinity of the boundary. Under such conditions the system cannot be treated as though the net branching factor ϕ remains constant. The H_2/O_2 reaction sensitized by NO_2 appears to be another case where ϕ varies continuously throughout the induction period preceding slow reaction or explosion.[22] All four cases discussed involve the H_2/O_2 reaction, and this has the advantage that since the mechanism of this reaction is well-established, a precise interpretation can be obtained for the peculiar features shown by these self-inhibition cases. It is remarkable that such self-inhibition is possible

* Small effects of very slow withdrawal rates, particularly noticeable at extreme mixture compositions in KCl-coated vessels, may be attributed either to a methane-type mechanism, or to a small contribution from quadratic branching even in KCl-coated vessels.

even in the H_2/O_2 system which is continuously branching, and it seems likely that such effects may operate in other systems where only intermittent branching occurs. The oxidation of hydrocarbons is a particular case where care is needed in assessing the role of intermediates such as peroxides, aldehydes, and olefins, and their effect on the constancy of the net branching factor. The marked inhibiting action of reaction products on the cool flame of diethyl ether[23] confirms the view that self-inhibition phenomena may operate in at least some cases.

Acknowledgments

Part of this work was carried out under support from the Air Force Office of Scientific Research, OAR, through the European Office, Aerospace Research, United States Air Force. A grant from the Shell Company, from the Preston Education Committee to L. Mayor and D.S.I.R. support for P. Doran, are gratefully acknowledged.

References

1. Semenoff, N. N.: *Chemical Kinetics and Chain Reactions*. Oxford, 1935.
2. Frank-Kamenetskii, D. A.: Zhur. Fiz. Khim. *13*, 738 (1939).
3. Frank-Kamenetskii, D. A.: Acta Physiochim. U.R.S.S. *10*, 365 (1939).
4. Frank-Kamenetskii, D. A.: Acta Physiochim. U.R.S.S. *16*, 357 (1942).
5. Frank-Kamenetskii, D. A.: Acta Physiochim. U.R.S.S. *20*, 729 (1945).
6. Gray, P.: *Seventh Symposium (International) on Combustion*, p. 425. Butterworths, 1959.
7. Semenoff, N. N.: Acta Physiochim. U.R.S.S. *18*, 93 (1943).
8. Lewis, B. and von Elbe, G.: *Combustion, Flames and Explosions of Gases*. Academic Press, New York, 1951.
9. Baldwin, R. R.: Trans. Faraday Soc. *52*, 1337 (1956).
10. Kowalski, A. A.: Phys. Z. Sowjet. *4*, 723 (1933).
11. Baldwin, R. R., Corney, N. S. and Simmons, R. F.: *Fifth Symposium (International) on Combustion*, p. 502. Reinhold, 1955.
12. Baldwin, R. R. and Simmons, R. F.: Trans. Faraday Soc. *51*, 680 (1955).
13. Baldwin, R. R. and Simmons, R. F.: Trans. Faraday Soc. *53*, 955, 964 (1957).
14. Baldwin, R. R. and Walker, R. W.: Unpublished work.
15. Gray, J.: J. Chem. Soc. *1953*, 741.
16. Baldwin, R. R., Booth, D., and Walker, R. W.: Trans. Faraday Soc. *58*, 60 (1962).
17. Baldwin, R. R., Corney, N. S., and Walker, R. R.: Trans. Faraday Soc. *56*, 802 (1960).
18. Ritchie, M.: J. Chem. Soc. *1937*, 857.
19. Volpe, M. and Johnston, H. S.: J. Am. Chem. Soc. *78*, 3903 (1956).
20. Baldwin, R. R. and Melvin, A.: Unpublished work.
21. Baldwin, R. R., Doran, P. and Mayor, L.: Trans. Faraday Soc. 1962 (accepted for publication).
22. Ashmore, P. G. and Levitt, B. P.: *Seventh Symposium (International) on Combustion*, p. 45. Butterworths, 1959.
23. Cheney, D. E.: Ph.D. thesis, St. Andrews University, 1962.

A SHOCK TUBE STUDY OF IGNITION OF METHANE-OXYGEN MIXTURES

T. ASABA, K. YONEDA, N. KAKIHARA, AND T. HIKITA

Ignition of methane-oxygen mixtures was studied by use of the shock tube. Data on ignition delay suggested that two different mechanisms exist, depending upon the methane content; first, for lean mixtures, the branching chain mechanism at relatively low temperatures governs the reaction during the induction period; and second, for rich mixtures, the thermal chain mechanism governs the reaction at high temperatures.

For rich mixtures, the controlling reaction is considered to be the second order reaction between methane and oxygen with an activation energy of about 55 kcal.

For lean mixtures, it is suggested the ignition is of the branching chain type and the activation energy is found to be about 21 kcal

In discussing the branching chain mechanism, oxygen atoms are considered to be important chain carriers. As the concentration of methane increases, methane molecules deactivate oxygen atoms. This may be the reason why the branching chain reactions do not occur in the rich region.

Introduction

Chemical kinetics during the induction period or ignition delay is of great interest in view of the mechanism of ignition or growth of explosions, as shown by Schott,[1] Strehlow,[2] and Kistiakowsky *et al.*[3] Oxidation or combustion of methane has been extensively studied by many researchers under conditions of low pressures and relatively low temperatures and the reaction mechanism has been elucidated almost completely.[4] However, only a few papers dealing with ignition of methane at higher temperatures and pressures are available at present[5–9] and the mechanism is not yet uniquely determined.

Reliable data on ignition delay are provided by the shock tube technique[10] which makes use of the reflected shock wave as a reaction volume under such condition that the reaction in the incident shock can be neglected.

The present work was undertaken to investigate the ignition of methane-oxygen mixtures at high temperatures and pressures by means of the shock tube and to get information concerning the chemical kinetics during the induction period.

Experimental

Apparatus. The shock tube used was of the CAL type reported by Glick *et al.*[11] The fundamental

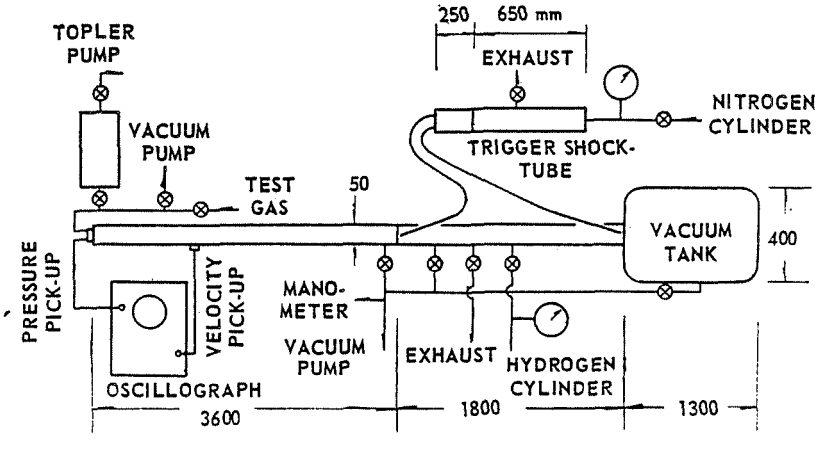

FIG. 1. Schematic diagram of shock tube and associated instrumentation.

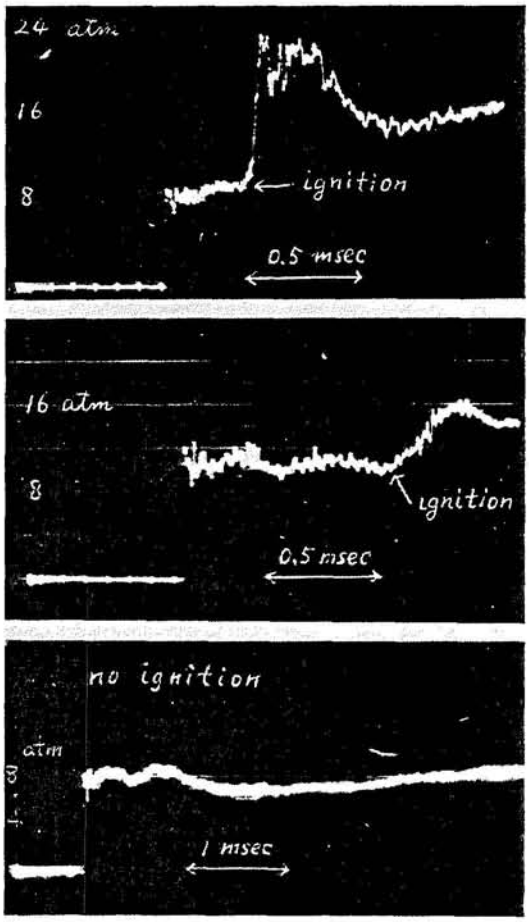

FIG. 2. Examples of pressure records.

properties of the shock tube have been reported elsewhere.[12] The configuration and associated instrumentation are schematically shown in Fig. 1. The vacuum tank was used only in case of gas sampling for gas chromatographic or mass-spectroscopic analysis of products. The first pressure transducer of barium titanate acted as the trigger for the oscillograph and the second one indicated the pressure curve. Sometimes a photomultiplier was attached to the end plate in place of the pressure transducer for comparison with the pressure records. A transparent acrylate pipe was used to observe the ignition process occurring near the end plate by means of streak photographs.

Procedure. Test gases were taken from commercial cylinders, introduced into the evacuated storage tank and mixed with a rubber bulb. The mixture was introduced into the evacuated test section at a definite pressure. The purity of methane was 98 per cent with 2 per cent air. Most experiments were carried out with various compositions of methane and oxygen. Runs were also made with methane-air, methane-oxygen-argon, and methane-oxygen with added small amounts of formaldehyde.

Hydrogen was used as the driver gas and several sheets of cellophane were used as the diaphragm which was punctured by a plunger operated by the trigger shock tube. The pressure ratio of test gas to driver gas was controlled so as to give a reflected shock pressure of around 7 atm and so that the main reaction would take place behind the reflected shock.

The temperature behind the reflected shock was calculated from the observed value of the incident shock velocity and the reflected shock pressure. The thermodynamic data were mainly taken from Rossini's tables[13] and the specific heats of methane at high temperatures were calculated from the vibration frequencies, assuming the vibrational relaxation of methane and oxygen to be established immediately after the reflection of the shock.[11]

The ignition delay was measured on the oscillogram as the time interval between the instant of the reflection of shock at the end plate and the origin of the apparent pressure rise. Here the ignition delays of methane-oxygen mixtures could be obtained in the range of 0.1–1.5 msec within a precision of 0.05 msec in the region of 800–2000°K and 7 ± 3 atm.

Results

Examples of pressure oscillograms are given in Fig. 2. The first slow rise of pressure is considered to indicate the ignition occurring near the end

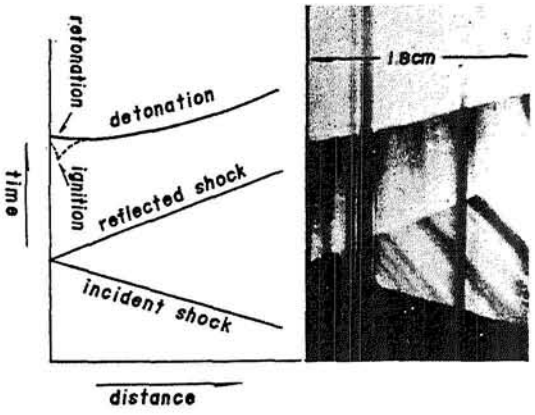

FIG. 3. An example of streak photograph showing the wave phenomena near the end plate of the shock tube.

TABLE 1

Experimental conditions employed for measurement of ignition delay

System	Composition range of tested gas	State behind the reflected shock wave		Measurable range of ignition delay (msec)
		Temperature (°K)	Pressure (atm)	
CH_4:O_2	10:90–60:40	800–2000	7 ± 3	0.1–1.5
CH_4:Air	5:95–20:80	1200–2200	10 ± 3	0.1–1.5
CH_4:O_2:A	9:11:80–15:5:80	1400–2200	10 ± 3	0.1–1.5

plate and the subsequent sharp rise of pressure to indicate the retonation wave emitted from the point of onset of detonation. This is confirmed from the streak photograph taken through a paraxial slit on the acrylate pipe as shown in Fig. 3. Here the wall effect may be negligible since little variation in ignition delay time was observed when the end plate was coated by potassium chloride or sodium tungstate.

Data on the ignition delay obtained from the photomultiplier records are almost the same as those from the pressure records for lean mixtures, but for rich mixtures no good photomultiplier data could be obtained. Hence the pressure records were used to measure the ignition delays of rich mixtures.

The experimental conditions employed are listed in Table 1. Some of the data are compared with those reported by other authors[5,6,7,9,14,15] in Fig. 4, although the experimental conditions differed in the studies cited.

The relation between the logarithm of ignition delay and the reciprocal of temperature is nearly expressed by a straight line for each mixture. These data were replotted as a graph giving the

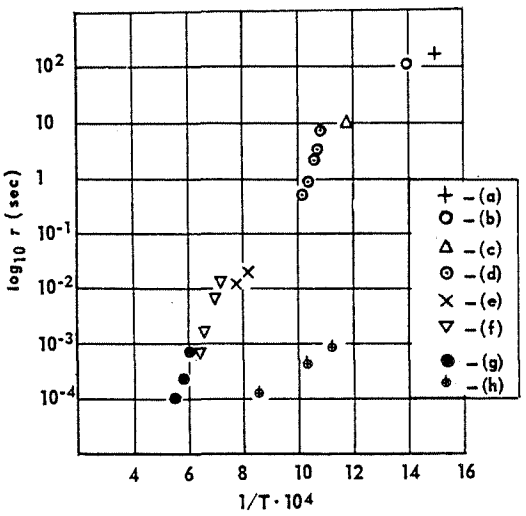

FIG. 4. Ignition delay data of methane due to different authors: (a) Bone and Gardner[14]; $2CH_4 + O_2$, 1 atm (closed vessel). (b) Newitt and Gardner[15]; $CH_4 + O_2$, 1 atm (flow method). (c) Vanpée and Grard[9]; $2CH_4 + O_2$, 1 atm (closed vessel). (d) Coward[5]; CH_4 in air, 1 atm (concentric tube). (e) Mullins[6]; CH_4 in air, 1 atm (concentric tube). (f) Skinner and Ruehrwein[7]; CH_4:O_2:A = 6:4:90, 5 atm (shock tube). (g) Present authors; CH_4:air = 15:85, 16 atm (shock tube). (h) Present authors; CH_4:O_2 = 30:70, 9 atm (shock tube).

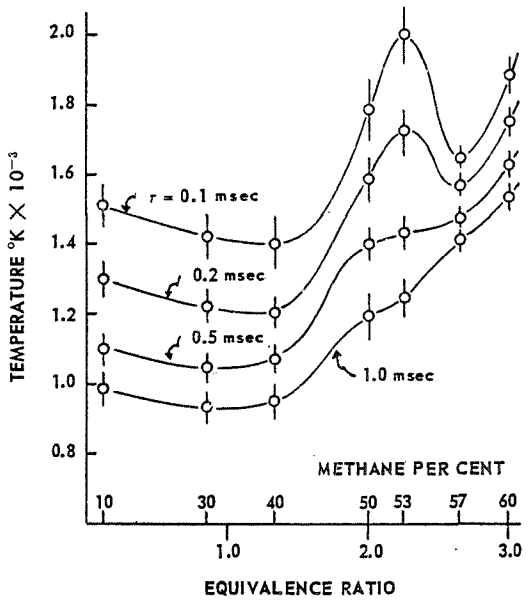

FIG. 5. Examples of contour-line of definite ignition delay as functions of temperatures and methane per cent in methane-oxygen mixtures.

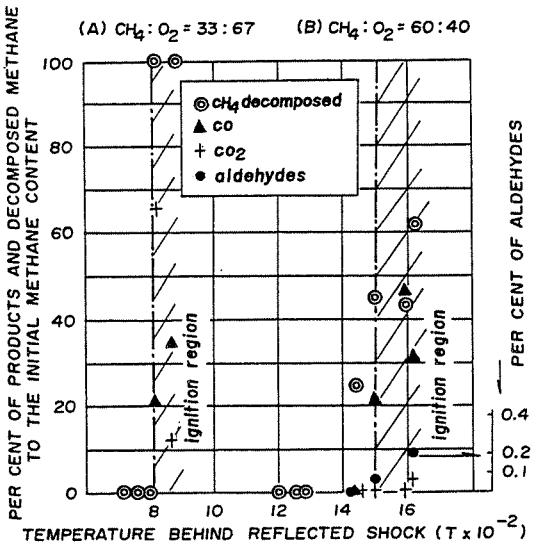

FIG. 6. Gas analysis data of shocked gas before or after ignition. The occurrence of ignition was judged from pressure records. Sometimes ignition was followed by rapid quenching. Test gas: (A) $CH_4:O_2$ = 33:67; (B) $CH_4:O_2$ = 60:40. Pressure: 7 ± 2 atm.

contour-lines with definite values of ignition delay as functions of temperatures and methane contents, as shown in Fig. 5. Scatter of the data is mainly due to the variations in the reflected shock pressures.

Gas-chromatographic analyses of the products of shocked gas, with or without ignition, were performed in a single-pulse shock tube where the vacuum tank was used for rapid quenching of the products. The result is shown in Fig. 6. Some aldehydes were detected in the combustion and decomposition products of the methane-rich mixture, while in the case of lean mixtures containing less than 50 per cent methane only a trace of aldehydes could be found.

Discussion

The curves shown in Fig. 5 are of special interest in connection with chemical kinetics of the oxidation of methane. The contour-line of ignition delay shows that in the range of methane-rich mixtures a considerably higher temperature is needed to produce ignition with a definite delay. A characteristic maximum can be clearly seen for shorter delay ignition. This last fact may suggest that two different mechanisms exist, depending upon the methane content.

For oxidation of methane at relatively low temperatures, say below 700°K, the following scheme has been proposed by Enikolopyan.[16]

$$CH_4 + O_2 \rightarrow CH_3 + HO_2; \quad \Delta H = 55 \text{ kcal}, E = 55 \text{ kcal} \quad (a)$$

$$CH_3 + O_2 \rightarrow CH_2O + OH; \quad \Delta H = -50\ , E = 20 \quad (b)$$

$$OH + CH_4 \rightarrow CH_3 + H_2O; \quad \Delta H = -15\ , E = 8 \quad (c)$$

$$CH_2O + O_2 \rightarrow CHO + HO_2; \quad \Delta H = 32\ , E = 32 \quad (d)$$

$$CHO + O_2 \rightarrow CO + HO_2; \quad \Delta H = -20 \quad (e)$$

$$HO_2 + CH_4 \rightarrow CH_3 + H_2O_2; \quad \Delta H = 11\ , E = 11 \quad (f)$$

Here, reactions between aldehyde and radicals and reactions at wall surface were omitted because of their low contribution to the kinetics under the conditions of the shock tube.

Assuming the time derivatives of concentrations [OH], [CHO] and [HO_2] are zero, we get

$$d[CH_3]/dt = 2k_a[CH_4][O_2] + 2k_d[O_2][CH_2O] \quad (1)$$

Integration yields

$$[CH_3]_\tau = 2k_a[CH_4]_0[O_2]_0\tau + \int_0^\tau 2k_d[O_2][CH_2O]dt \quad (2)$$

When it is assumed that $[CH_4]_\tau \doteqdot [CH_4]_0$ and $[O_2]_\tau \doteqdot [O_2]_0$, where subscript 0 or τ denotes the value at time zero or τ (the ignition delay time), respectively.

Case A: Rich Mixtures. If it is assumed that the controlling reaction for the methane-rich mixtures is reaction (a), the second term in the right-hand side of Eq. (2) may be ignored. Then, inserting the Arrhenius expression for k_a,

$$k_a = b \exp(-E_a/RT),$$

we have

$$\log[CH_4]_0[O_2]_0\tau = E_a/RT + \log\{[CH_3]_\tau/2b\} \quad (3)$$

Although $[CH_3]_\tau$ is unknown, we put this quantity to be nearly constant and examined the relation using the observed values of τ and calculated values of concentrations of oxygen and methane at initial conditions in reflected shock waves. The result is shown in Fig. 7. For the rich region containing more than 53 per cent of methane in

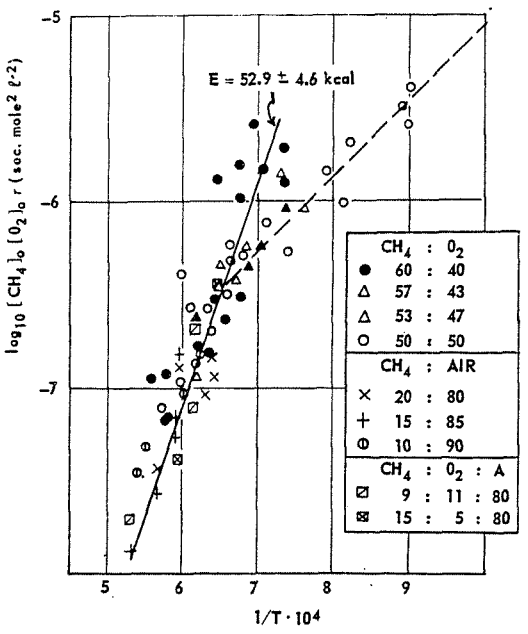

FIG. 7. Dependence of ignition delays and concentrations $[CH_4]_0[O_2]_0$ on temperatures for the case of rich mixtures.

methane-oxygen mixtures, the plots form a straight line, although some scattering of the points is observed. The data for methane-air (10:90), (15:85), (20:80) and methane-oxygen-argon mixtures (9:11:80), (15:5:80) also fall on the same line. This may suggest that the assumption, $[CH_3]_\tau$ = constant, is justifiable. From the slope of this line, the activation energy is found to be 52.9 ± 4.6 kcal with a confidence level of 70 per cent by the least square method. This value is in line with the energetics of reaction (a) and renders support to the assumptions made at the beginning.

Hence for the methane-rich case, the controlling factor is considered to be the second order reaction between methane and oxygen. This reaction will be followed by autocatalytic chain reactions and the branching chain reaction will not play any important role. The explosion will be of the thermal type as suggested by Skinner.[7]

Results of gas analysis also support this idea. As seen for 60 per cent methane-oxygen in Fig. 6, a considerable amount of methane was decomposed before ignition and also after ignition followed by rapid quenching. This fact favors the thermal ignition mechanism and not the branching chain mechanism.

Gas analysis for methane-air mixtures showed a similar tendency.

Case B: Lean Mixtures. Data for equimolar methane-oxygen mixtures lie on the straight line only when the temperature is high enough and begin to deviate greatly as temperature decreases, as can be seen in Fig. 7. Plots for the case where the methane content is less than 50 per cent form a grouping different from this straight line. It should be noted that the runs with lean mixtures were made at relatively low temperatures because of their high reactivity.

Consequently it should be considered that another reaction is controlling for ignition of lean mixtures.

The second term in the right-hand side of Eq. (2) represents the contribution of the degenerate branching chain reaction where accumulation of formaldehyde is required to produce ignition. However, it should be remembered that this theory was presented in connection with the reaction at low temperatures (less than about 700°K).

In the present experiment making use of the single-pulse shock tube the quantity of aldehydes produced in lean mixtures before ignition was found to be far less than that produced in rich mixtures. So it was considered that in this case formaldehyde would be rapidly oxidized without accumulation.

Making use of the assumed reaction mechanism, we get

$$d[CH_2O]/dt = k_b[O_2][CH_3] - k_d[O_2][CH_2O] \tag{4}$$

According to the above stated idea, Eq. (4) was assumed to be zero and inserted into Eq. (1).

$$d[CH_3]/dt = 2k_a[CH_4][O_2] + 2k_b[O_2][CH_3] \tag{1}'$$

For lean mixtures the second term in the right-hand side of Eq. (1)′ was supposed to be controlling as is usually the case in chain branching ignition. Hence, neglecting the first term, the integration yields

$$[CH_3]_\tau = [CH_3]_0 \exp(2k_b[O_2]_0\tau) \tag{5}$$

Inserting the Arrhenius expression in k_b and assuming $[CH_3]_\tau$ = constant as done previously, we get

$$\log [O_2]_0\tau = E_b/RT + \text{const.} \tag{6}$$

Plots of $\log [O_2]_0\tau$ versus $1/T$ for lean mixtures containing less than 40 per cent methane fall nearly on a straight line as shown in Fig. 8, which gave the activation energy of 20.6 ± 1.9 kcal with the confidence level of 70 per cent by the least square method. Thus the first term of

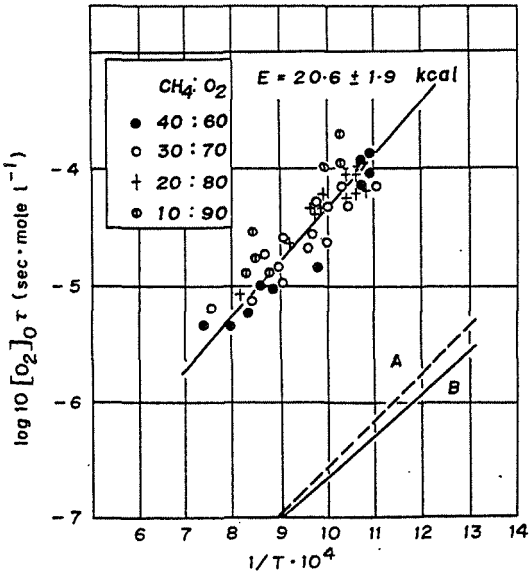

FIG. 8. Dependence of ignition delays and concentration $[O_2]_0$ on temperature for the case of lean mixtures. Dashed line A: Schott and Kinsey's data for H_2–O_2. Line B: Gardiner's data for C_2H_2–O_2.

Eq. (1)′ for which the activation energy was about 53 kcal can not be the controlling factor for this case.

In Fig. 8, reference lines reported by Schott and Kinsey[1] for dilute mixtures of hydrogen and oxygen in argon and by Gardiner,[17] for acetylene and oxygen in xenon were shown. Although the slope is essentially the same as that obtained in this experiment, the absolute value of $\log_{10}[O_2]_0\tau$ is two orders of magnitude smaller. This may be ascribed to the pressure effect as well as to the difference in the reaction mechanism.

Gas analysis data render further support by the fact that little indication of methane decomposition was found during the induction period and ignition was produced abruptly, this being the feature of branching chain explosion.

Two different mechanisms for different ranges of methane content were proposed and explained tentatively with the aid of experimental results. However, some difficulties remain.

According to the theory proposed by Enikolopyan, the oxidation of formaldehyde in reaction (d) requires an activation energy of 32 kcal, while in the present experiment the apparent activation energy for lean mixtures was about 20.6 kcal. However, it should be pointed out that reaction (d) was applicable for the reaction at low temperatures. Under such high temperatures and pressures as were employed in this work, the oxidation of formaldehyde might proceed through a reaction with less activation energy than 21 kcal. If not so, reaction (b) can not be rate determining.

The effect of formaldehyde addition to rich mixtures is shown in Fig. 9, which shows that formaldehyde has little effect. In lean mixtures, as shown in Fig. 10, some promoting effect of formaldehyde exists at low temperatures and some retarding effect at higher temperatures. Hence, it is concluded that formaldehyde produces no major effect upon ignition. From this, the following consideration is introduced.

Harding and Norrish[18] suggested that, besides reaction (d), reaction (g) would also be possible:

$$CH_2O + O_2 \rightarrow HCO_2H + O; \qquad \Delta H = 0,\ E = 21 \text{ kcal} \quad \text{(g)}$$

As an alternative to reaction (g), the reaction (h) may also be considered.[19]

$$CH_2O + O_2 \rightarrow H_2 + CO_2 + O; \qquad \Delta H = -10.4 \text{ kcal} \quad \text{(h)}$$

These reactions (g) and (h) will have activation energies of about 21 kcal which is of the same order as that of reaction (b). Accordingly, if re-

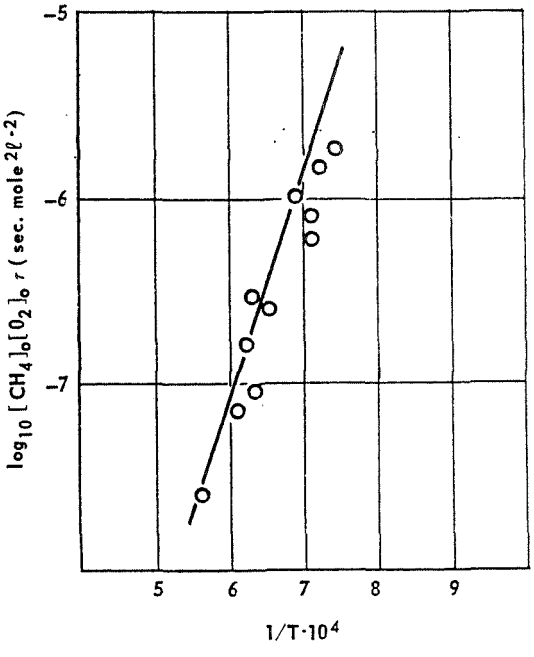

FIG. 9. Effect of formaldehyde on ignition delay data for the case of rich mixtures, the composition being CH_4:O_2:CH_2O = 60:40:1.45. Solid line represents the data for the case where no aldehyde was added.

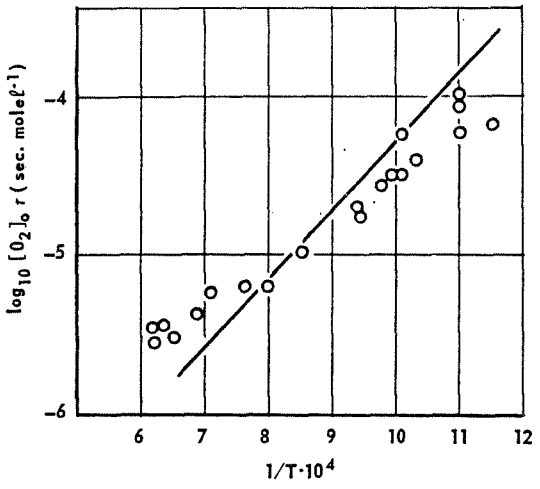

FIG. 10. Effect of formaldehyde on ignition delay data for the case of lean mixtures, the composition being $CH_4:O_2:CH_2O$ = 40:60:1.45. Solid line represents the data for the case where no aldehyde was added.

action (g) or (h) can be adopted instead of reaction (d), the difficulty concerned with the activation energy of formaldehyde oxidation will disappear. Here reaction (h) seems favorable and will be adopted in the later treatment.

The reason why the controlling reaction changes with methane content must be explained. For this, the inhibiting action of methane should be taken into account. Such an inhibiting action of methane has been conceived for hydrogen-oxygen mixtures by Baldwin *et al.*[20] and by Levy,[21] for carbon monoxide-oxygen by Hoare *et al.*[22] and for methane-oxygen by Vanpée *et al.*[9] and by Hoare *et al.*[8] As radicals in question which will be deactivated due to the existence of methane molecules, hydrogen atoms were proposed by Baldwin *et al.*, hydrogen atoms and hydroxyl radical by Hoare *et al.* and oxygen atoms by Vanpée *et al.*

Among these, oxygen atoms were considered to be favorable in this case and the following mechanism was adopted:

Oxygen atoms produced by reaction (h) will react with methane as shown in reaction (i) which has received support.[19]

$$O + CH_4 \rightarrow CH_2 + H_2O;$$

$$\Delta H = -50 \text{ kcal}, E = 8.1 \text{ kcal} \quad \text{(i)}$$

Reaction (i) should occur in both rich and lean mixtures.

Then the chain-ending reaction will follow, in the case of rich mixtures, through a path as shown reaction (j), proposed by Vanpée *et al.*[9]

$$CH_2 + CH_4 + M \rightarrow C_2H_6 + M;$$

$$\Delta H = -65.3 \text{ kcal} \quad \text{(j)}$$

In the case of lean mixtures chain branching reactions such as reaction (k) will follow instead of reaction (j).

$$CH_2 + O_2 \rightarrow HCO + OH;$$

$$\Delta H = -32 \text{ kcal} \quad \text{(k)}$$

The fact that the result of mass spectroscopic product analysis showed the existence of traces of ethane and butane in addition to carbon monoxide and carbon dioxide, prior to the ignition of lean mixtures, provides support for the occurrence of reaction (j).

Against the idea above proposed, the existence of oxygen atoms has been questioned by Gaydon[23] and Fabian and Bryce.[24] However, it should be pointed out that oxygen atoms will act at very low concentrations. Further experiments are required.

In accordance with the above considerations, reactions (h) to (k) were adopted instead of reaction (d).

Then stationary state method yields

$$\frac{d[CH_3]}{dt} = 2k_a[CH_4][O_2] + \frac{2k_bk_h[O_2]^2}{k_i[CH_4][M] + k_h[O_2]}[CH_3] \quad (6)$$

which was derived under the assumption that the time derivatives of radical concentrations [OH], [HO_2], [HCO], [CH_2], and [CH_2O] were zero.

For the case where $[CH_4][M]k_i \ll [O_2]k_h$, Eq. (6) is reduced to Eq. (1)′. While for the case of methane-rich mixtures, the second term in right-hand side of Eq. (6) may be negligible as above stated.

Thus, it was concluded that Eq. (6) was the final expression applicable to the whole range of mixtures. For rich mixtures, the first term in the right-hand side of the equation gives the predominant effect in ignition, while for lean mixtures the second term becomes important.

Summary

Ignition of methane-oxygen mixtures was studied by use of the shock tube. Data on ignition delays were plotted on a graph giving the contour-lines of definite ignition delays as functions of temperatures and methane contents. The contour-lines suggested that two different mechanisms exist, depending upon the methane content; first, for lean mixtures the branching chain mechanism at relatively low temperatures gov-

erns the reaction during the induction period; and second, for rich mixtures the thermal chain mechanism governs the reaction at high temperatures.

The reaction scheme was written along the line of Enikolopyan's theory proposed for the degenerately branched chain mechanism of methane oxidation. However, in order to fit the experimental results obtained here, some alterations of the scheme were required.

For rich mixtures, the controlling reaction is considered to be the second order reaction between methane and oxygen with an activation energy of about 55 kcal. This is supported by the experimental results and the ignition in this region is concluded to be of thermal nature.

On the other hand, for the case of lean mixtures it is suggested that the ignition is of the branching-chain type and the activation energy for the case is found to be about 21 kcal. To explain this value, the mechanism of oxidation of formaldehyde has been considered. In discussing the branching chain mechanism, oxygen atoms are considered to be important chain carriers. It is suggested that oxygen atoms are deactivated by reacting with methane molecules as the concentration of methane increases. This may be the reason why the branching chain reactions do not occur in the rich region and why the ignition needs high temperatures where the thermal mechanism is predominant.

Results of gas analysis using the single pulse shock tube technique support the above considerations.

Acknowledgments

This work was supported by scientific research funds of the Japanese Educational Ministry. The authors are grateful to Drs. K. Akita and H. Miyama for their discussions and to Mr. Y. Kanai for experimental assistance.

References

1. Schott, G. L. and Kinsey, J. L.: J. Chem. Phys., *29*, 1177 (1958).
2. Strehlow, R. A. and Cohen, A.: Amer. Chem. Soc. Meeting, March 21–30, 1961.
3. Bradley, J. N. and Kistiakowsky, G. B.: J. Chem. Phys., *35*, 264 (1961).
4. Lewis, B. and von Elbe, G.: *Combustion, Flames and Explosions of Gases*, p. 90. Academic Press Inc. (1961).
5. Coward, H. F.: J. Chem. Soc., 1382 (1934).
6. Mullins, B. P.: Fuel, *32*, 343 (1953).
7. Skinner, G. B. and Ruehrwein, R. A.: J. Phys. Chem., *63*, 1736 (1959).
8. Hoare, D. E. and Walsh, A. D.: *Fifth Symposium (International) on Combustion*, p. 467. Reinhold Publishing Corp. (1955).
9. Vanpée, M. and Grard, F.: *ibid.*, p. 484.
10. Strehlow, R. A. and Cohen, A.: J. Chem: Phys. *30*, 257 (1959).
11. Glick, H. S., Squire, W., and Hertzberg, A.: *Fifth Symposium (International) on Combustion*, p. 393. Reinhold Publishing Corp. (1955).
12. Hikita, T., Asaba, T., and Yoneda, K.: J. Chem. Soc. Japan, Industrial Chemistry Section, *64*, 1920 (1961).
13. Rossini, H. D.: *Selected Values of Physical and Thermodynamic Properties of Hydrocarbons and Related Compounds*. Carnegie Press (1953).
14. Bone, W. A. and Gardner, J. B.: Proc. Roy. Soc., *A154*, 279 (1936).
15. Newitt, D. M. and Gardner, J. B.: Proc. Roy, Soc., *A154*, 329 (1936).
16. Enikolopyan, N. S.: *Seventh Symposium (International) on Combustion*, p. 157. Butterworths (1959).
17. Gardiner, W. C., Jr.: J. Chem. Phys., *35*, 2252 (1961).
18. Harding, A. J. and Norrish, R. G. W.: Nature. *163*, 797 (1949).
19. Steacie, E. W. R.: *Atomic and Free Radical Reactions*, Vol. 2. Reinhold Publishing Corp. (1954).
20. Baldwin, R. R., Corney, N. S., and Simmons, R. F.: *Fifth Symposium (International) on Combustion*, p. 502. Reinhold Publishing Corp. (1955).
21. Levy, A.: *Fifth Symposium (International) on Combustion*, p. 495. Reinhold Publishing Corp. (1955).
22. Hoare, D. E. and Walsh, A. D.: Trans. Faraday Soc., *50*, 37 (1954).
23. Gaydon, A. G.: Trans. Faraday Soc., *42*, 295 (1946).
24. Fabian, D. J. and Bryce, W. A.: *Seventh Symposium (International) on Combustion*, p. 150. Butterworths Sci. Pub. (1959).

Discussion

Dr. B. J. Tyler (*University of Cambridge*): Is there any outside evidence for the chain-breaking reaction

$$CH_2 + CH_4 + M \rightarrow C_2H_6 + M \quad ?$$

Prof. T. Hikita (*University of Tokyo*): For example, Vanpée and Grard (ref. 9) stated this reaction may be possible, and moreover we found traces of C_2H_6 and C_4H_{10} mass-spectrographically in the pre-ignition products.

THE NATURE AND CAUSE OF IGNITION OF HYDROGEN AND OXYGEN SENSITIZED BY NITROGEN DIOXIDE

P. G. ASHMORE AND B. J. TYLER

This paper explains the evidence that ignitions in mixtures of hydrogen, oxygen, and nitrogen dioxide are isothermal near some ignition boundaries and thermal near others. It also examines a reaction scheme that can account for the two types of ignition, for the occurrence of ignition limits, and for the induction periods.

The ignitions or slow reactions occur after induction periods in which nitrogen dioxide is converted to nitric oxide by a chain reaction with hydrogen. The lengths of the induction periods are fully explained by the kinetics of this reaction.

At the end of the induction period there are rapid changes in the NO_2 concentration, leading to ignition or to a slow pressure change. These changes and the changes in the total pressure during this time have been studied in detail. With low sensitizer pressures there is direct evidence of a substantial temperature rise before ignition or slow reaction, supported by indirect evidence obtained by variation of the thermal conductivity, changes of the vessel diameter, and studies of the rate of the slow reaction. In contrast, at higher sensitizer pressures there is little evidence of thermal effects before the onset of the main reaction.

The separate experimental studies of the ignitions and of the slow reactions are correlated to give a simple condition determining the position of the limits.

The kinetic scheme, based on the branching reactions of the H_2–O_2 system, accounts for the transition from thermal to near isothermal ignitions by a change from quadratic termination by HO_2 to linear termination by OH.

Introduction

As a result of an extensive study of ignitions and slow reactions in mixtures of hydrogen, oxygen, and nitrogen dioxide, it is now possible to identify the factors that control the occurrence of ignition limits in this system. It has long been known[1] that ignitions occur at about 360°C if the initial pressure p_0 of nitrogen dioxide lies between lower and upper "sensitizer limits," whereas slow combination of hydrogen and oxygen occurs when p_0 lies outside these limits. The ignitions and slow reactions are preceded by induction periods of some seconds duration in which no change of pressure occurs. More recently, photometric studies[2,3] have shown that the nitrogen dioxide is removed during the induction period. The rate of removal increases sharply at the end of the induction period, when p_{NO_2} reaches "p_e," and if p_0 lies within the sensitizer limits, ignition follows when p_0 reaches "p_i." It was also shown that if p_0 lies above the upper limit, the acceleration declines and p_{NO_2} reaches a stationary value "p_s." A preliminary study[3] of p_e, p_i, and p_s at values of p_0 near the upper sensitizer limit, showed that p_e fell as p_0 was increased, and suggested that the upper limit occurred when p_s exceeded the value that p_i would have to reach. It also appeared that p_s was established because of opposing reactions that form and remove NO_2, *viz.* $2NO+O_2 \rightarrow 2NO_2$ (12) and $NO_2+H_2 \rightarrow NO+H_2O$ (14), reaction (14) occurring by a chain mechanism throughout the induction period. Later work has shown that the reverse of reaction (12) has also to be taken into account for an accurate description of p_s at higher values of p_0, where a truly catalyzed combination of hydrogen and oxygen occurs.[4] It has also been shown that a stationary value of p_{NO_2} is reached below the lower limit and it has been possible to identify the reactions responsible for maintaining p_s in this region.[5]

Detailed studies[6] of the rates of the slow reactions just outside the two limits, and of changes in the total pressure and in p_{NO_2} after p_e is reached, have given some extremely interesting information about the nature of the ignitions. In particular, it appears that ignitions just below the upper limit may be nearly isothermal branched-chain ignitions, whereas ignitions near the lower limit have some pronounced "thermal" characteristics. The purpose of this paper is to

explain the evidence for these interpretations of the ignitions and to suggest a reaction scheme that can account for the two types of ignition and for the occurrence of ignition limits.

Experimental Procedure

The apparatus used was a conventional vacuum system and has been described in detail elsewhere.[6] The reactions were carried out in plane-ended, cylindrical vessels, 20 cm long, with internal diameters from 9 to 34 mm. The vessels were heated in an electrical furnace, and temperatures were measured by a thermocouple with the hot junction sited midway along the vessel. The absolute accuracy of the measurement was within ±0.7°C, and no part of the vessel differed by more than 1.5°C from the temperature at the central point.

A modified form[6] of a double-beam photometer[3] was used to record continuously the concentration of nitrogen dioxide in the reaction vessel. Pressure changes were recorded automatically by a modified Bourdon spoon gauge.[7] The reactant mixtures were premixed at room temperatures.

Nitric oxide was prepared by the action of dilute sulfuric acid upon a saturated solution of sodium nitrite and was purified by distillation. Nitrogen dioxide was prepared by reacting nitric oxide with excess of oxygen and was separated by passing the products through a trap in dry ice-acetone. Dried cylinder hydrogen, oxygen, and nitrogen were used. A gift of a sample of helium from the Mond Laboratory, Cambridge, is gratefully acknowledged.

Experimental Results

The experimental work described in this paper was carried out at 360°C, and all pressures are quoted as millimeters of Hg at 360°C. The symbols defined below are used to refer to the nitrogen dioxide pressures at which certain events occur during an experiment: p_0, the initial sensitizer pressure; p_e, the pressure of NO_2 at which there is an acceleration in the rate of its removal, defining the end of the induction period; p_i, the pressure of NO_2 at which the ignition occurs; p_s, the final stationary pressure of NO_2 (below p_e) that is reached in runs outside the ignition region.

Changes in Total Pressure and in p_{NO_2} during Individual Experiments. Prior to the end of the induction periods there were no detectable changes of pressure (to within 0.05 mm) in any experiments except for a few with very long induction periods, of some minutes, when changes of about 0.2 mm were observed, these changes being gradual with no increase in rate as p_e was approached.

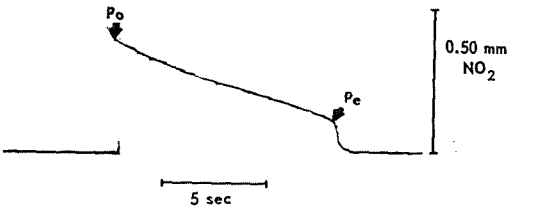

FIG. 1. Pen recorder trace of NO_2 concentration during an induction period before explosion; 150 mm $2H_2 + O_2$; 0.40 mm NO_2; 34-mm quartz vessel; 360°C.

The changes observed in nitrogen dioxide concentration during the course of an experiment are illustrated in Fig. 1. The end of the induction period is marked by the rapid increase in the rate of removal of nitrogen dioxide, closely followed by ignition or the slow pressure decrease characteristic of the reaction between hydrogen and oxygen. The events at the end of the induction period are resolved on the oscilloscope traces shown in Fig. 2. The thick curves show the removal of nitrogen dioxide, the thin curves the

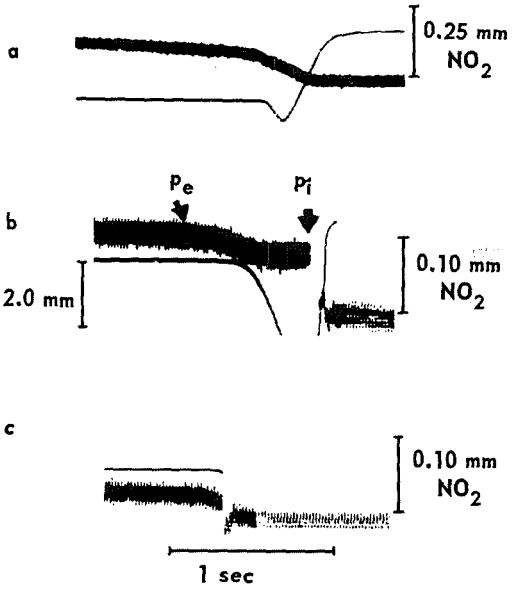

FIG. 2. Oscilloscope records of changes in the NO_2 concentration (thick lines, decrease downward) and total pressure (thin lines, increase downward). (a) Slow reaction; 150 mm $2H_2 + O_2$; 0.38 mm NO_2; 15-mm quartz vessel. (b) Explosion; 300 mm $2H_2 + O_2$; 0.14 mm NO_2; 34-mm quartz vessel. (c) Explosion; 100 mm $2H_2 + O_2$; 0.60 mm NO_2; 34-mm quartz vessel.

changes in pressure; 2a refers to a slow reaction and 2b to an ignition. In 2a, the faster removal of nitrogen dioxide when p_e is reached soon declines and p_{NO_2} levels out to a finite stationary value p_s. In 2b, the onset of ignition is shown by the breaks in both traces. However, there are marked differences in the transitions from p_e to p_i at the extreme ends of the ignition region, and in the pressure-time curves outside the two limits. Near the lower limit, the increased rate of removal of nitrogen dioxide after p_e rapidly dies away, and the concentration of nitrogen dioxide is steady, or changes extremely slowly, for periods as long as 1 sec. During this time the pressure increases rapidly and the mixture eventually explodes. This behavior is illustrated in Fig. 2b.

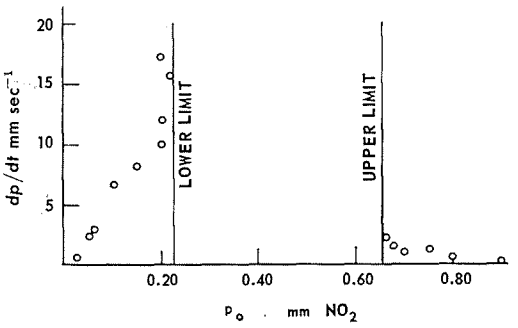

FIG. 3. Rates of pressure change outside the ignition limits; 100 mm $2H_2 + O_2$; 20-mm quartz vessel; 360°C.

Just outside the lower ignition limit there is a similar acceleration in the rate of removal of nitrogen dioxide and a similar decline, but a truly steady concentration p_s is reached; there is again a pressure rise or pulse, followed by the fall in pressure corresponding to the formation of water vapor, as in Fig. 2a.

In contrast to this, near the upper limit the faster removal of nitrogen dioxide is maintained between p_e and p_i, and the time between p_e and p_i is much shorter (Fig. 2c). Outside the upper limit, the pressure pulse typical of the lower limit was rarely observed, and it was then much smaller. In addition, the rate of the slow reaction within a run fell off much more rapidly at the upper than at the lower limit. The maximum rates observed as close as possible to the limits were much slower at the upper limit than at the lower, as shown in Fig. 3.

The Variation of p_e and p_i with p_0, Total Pressure P_T, Reactant Pressure P_R, Vessel Diameter, and Thermal Conductivity. When the sensitizer pressure p_0 is varied, keeping other factors constant, p_e rises at first, passes through a maximum, and

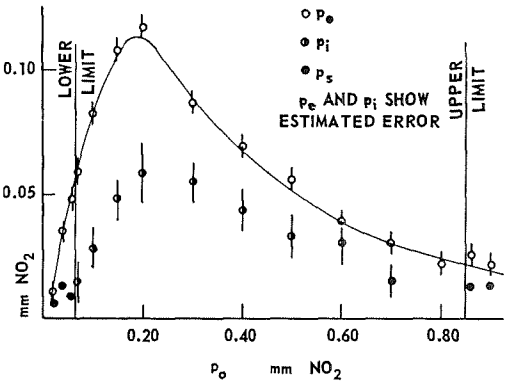

FIG. 4. Plots of p_e, p_i, and p_s against p_0; 100 mm $2H_2 + O_2$; 34-mm quartz vessel; 360°C (p_e and p_i show estimated errors).

falls as the upper limit is approached. This behavior is illustrated in Fig. 4. The values of p_i follow a similar pattern, and at both limits are close to the values of p_s observed in the slow reactions just outside the limits.

The effects on p_e and p_i of varying the total pressure of a mixture of constant composition is shown in Fig. 5. The values of p_s at high total pressures are also shown, and it can be seen that p_i and p_s are nearly coincident at the boundary of ignition. Increasing the reactant pressure, $P_R = 2H_2 + O_2$, at constant p_0 causes p_e to rise, but the rate of increase is not maintained at high P_R (Fig. 6).

The effect of varying only the vessel diameter was investigated using aged quartz vessels of 9, 15, 20, and 34 mm internal diameter. A KCl-coated Pyrex vessel of a diameter of 34 mm was also used. With the three larger vessels the values of p_e in equivalent experiments were identical within the experimental errors. In the 15-mm

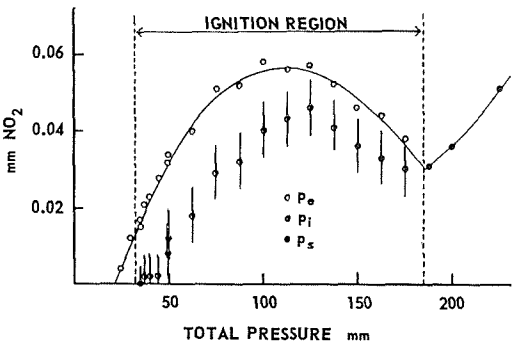

FIG. 5. Plots of p_e, p_i, and p_s against the total pressure; H_2:O_2:p_0 = 133:67:1; 34-mm quartz vessel; 360°C (p_i shows estimated error).

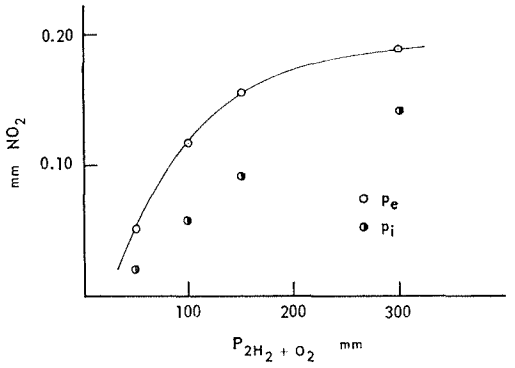

FIG. 6. Plots of p_e and p_i against the reactant pressure ($P_{2H_2+O_2}$); 0.20 mm NO_2; 34-mm quartz vessel; 360°C.

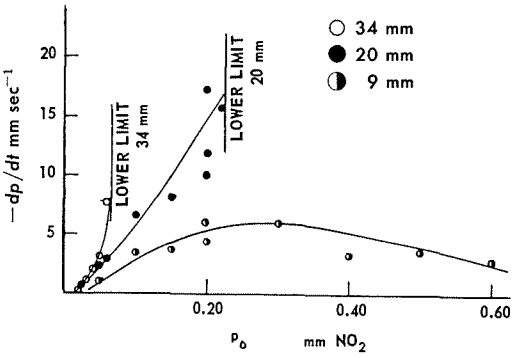

FIG. 7. Variation of rate with initial sensitizer pressure; 100 mm $2H_2 + O_2$; 360°C; 9, 20, and 34 mm diameter quartz vessels.

vessel the values of p_e were about 10% higher at all initial sensitizer pressures, and not until the smallest vessel was used was there any significant fall in the values of p_e. This pattern was followed at each of the three reactant pressures fully investigated, i.e., with 50, 100, and 150 mm of $2H_2 + O_2$. Due to the greater experimental errors in determining p_i, as shown in Fig. 4, the trends are less certain; in the cases where significant changes were detected p_i decreased as the vessel diameter was decreased.

In contrast to the lack of effect of changes of vessel diameter on p_e, the lower sensitizer limit was higher, and the upper limit was lower, in vessels of smaller diameter. The relative change in the lower limit was much greater than in the upper, as shown in Table 1. It was also found that the maximum rate outside the lower limit was appreciably higher in smaller diameter vessels (Fig. 7).

The thermal conductivity of the mixture was varied by using mixtures with an excess of inert gas present, and exchanging nitrogen and helium while keeping their total pressure constant. In this way any changes in the effect of the gases present on three-body recombination reactions were minimized, and changes could be attributed to the effect of changes in the thermal conductivity. It was found that p_e was affected very little by changes in the proportions of the two gases, being about 20% higher in experiments with only helium present than in experiments with only nitrogen present. This change in conductivity had very little effect on the position of the upper limit. With 100 mm of $2H_2+O_2$ the limit in the 34-mm vessel changed from 0.31–0.32 to 0.30–0.31 mm when 200 mm of nitrogen were replaced by 200 mm of helium. In contrast, the same exchange of gases raised the lower sensitizer limit from 0.06–0.07 mm to 0.12–0.13 mm, and

TABLE 1

Variation of the Limit Positions with Reactant Pressure and with Vessel Diameter

		$2H_2 + O_2$ (mm)					
		Lower limit			Upper limit		
Vessel type	Diam. (mm)	50	100	150	50	100	150
Pyrex (KCl)	34	0.08–0.09	0.05–0.10	—	0.65–0.70	0.80–0.90	—
Quartz	34	0.07–0.08	0.06–0.07	0.07–0.08	0.66–0.68	0.84–0.86	0.90–0.92
Quartz	20	0.36–0.37	0.22–0.23	0.18–0.20	0.69–0.70	0.65–0.66	0.70–0.72
Quartz	15	N.E.[a]	N.E.	0.38–0.39	N.E.	N.E.	0.52–0.54
Quartz	9	N.E.	N.E.	N.E.	N.E.	N.E.	N.E.

[a] N.E. indicates that no explosions occurred at that particular combination of reactant pressure and vessel diameter. The limit positions are given in millimeters of NO_2 bracketing the limit.

also substantially increased the maximum rate of reaction outside the lower limits from 5.6 mm/sec to 18.5 mm/sec.

The Relation between p_i and p_s at the Explosion Limits. It has been suggested previously that the upper sensitizer limit was due to the value of p_i, which was shown to fall as the upper limit was approached with p_0 increasing, reaching a value below p_s and so being effectively unattainable.[3] The more detailed evidence now available shows that this is true at the lower limit as well as at the upper. This is most conveniently demonstrated at comparatively high reactant pressures (200–300 mm of $2H_2+O_2$) and correspondingly high values of p_s, as shown in Fig. 8. Attention may also be drawn to the similar trends in Fig. 5 at an ignition boundary found on increasing the total pressure.

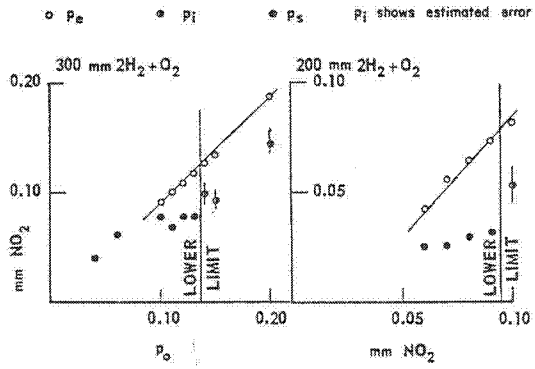

FIG. 8. Plots of p_e, p_i, and p_s against p_0 at lower limit; 200 and 300 mm $2H_2 + O_2$; 34-mm quartz vessel; 360°C; (p_i shows estimated error).

Discussion

Factors Affecting p_e. There is no evidence that the removal of nitrogen dioxide during the induction period before p_e is reached is due to anything other than an isothermal reaction between hydrogen and nitrogen dioxide. The near-constancy of p_e when substantial changes are made in the diameter of the vessel, or in the conductivity of the mixtures, all support this view. The small changes in p_e that occur when the conductivity is changed by replacing nitrogen by helium could be due[6] to changes in the rate of the reaction $H + O_2 + M \rightarrow HO_2 + M$ (4). This reaction will become important relative to the reaction $H + NO_2 \rightarrow OH + NO$ (9) towards the end of the induction periods when p_{NO_2} is low, as nitrogen is somewhat more efficient than helium as M.

A critical examination of results like those shown in Fig. 2 shows that the pressure pulse observed before slow reactions does not begin before p_e, i.e., does not precede the accelerated removal of nitrogen dioxide. Allowance was made in this examination for the time lag of the Bourdon spoon gauge, determined experimentally.[7]

Thus it may be concluded that the accelerated removal of nitrogen dioxide at p_e is not due to thermal effects.

The acceleration might be due to changes in the rates of one or more of the reaction steps in the hydrogen-nitrogen dioxide chain reaction, e.g., an increase in the chain initiation or propagation steps, or a decrease in the termination steps. However, there is no known method by which any of these changes could operate so quickly in an isothermal system, and it has been concluded[6] that the acceleration is brought about by an increase in chain center concentration due to branching reactions.

The concentration of chain centers, n, in such a system changes with the rate of initiation θ, the positive branching fn, the linear termination gn, and the quadratic termination δn^2, according to the equation

$$dn/dt = \theta + (f - g)n - \delta n^2$$
$$\equiv \theta + \phi n - \delta n^2$$

If the quantity $\phi = (f - g)$, called the net branching factor, is negative the reaction behaves like a nonbranching chain reaction. This probably occurs during the induction periods. If ϕ increases during the induction periods, because of the removal of nitrogen dioxide and the appearance of nitric oxide, then a sudden increase in the center concentration would occur when ϕ passes through zero and becomes positive, provided that δ is not too large. Thus an acceleration of the form observed at p_e could occur if the changes in concentration of nitrogen dioxide and nitric oxide cause ϕ to pass through zero. This has been taken[6] as the condition necessary to define p_e when the chosen kinetic scheme is analyzed later.

The Transition from p_e to p_i. Although the system is isothermal until p_e is reached, there is much evidence that a substantial temperature rise may occur before slow reaction or ignition. These effects are most marked near the lower limit.

The most remarkable effect is the pressure rise (or pulse) that is recorded both before the slow pressure decrease in experiments outside the lower sensitizer limit, and also before the main pressure rise which accompanies ignition above the lower limit (Fig. 2). The magnitude of the pressure rises (e.g., 2.5 mm in 150 mm of $2H_2 + O_2$ with p_0 equal to 0.07 mm of NO_2 in

the 34-mm quartz vessel) is far too great to be associated with any conceivable reaction involving a pressure rise or to be due directly to an increase in the concentration of chain centers. The only acceptable conclusion is that it is due to a temperature rise in the system, and in the example quoted above it corresponds to an average increase in the whole reaction vessel of about 10°C. The increase in temperature at the center of the vessel is likely to be larger, perhaps as much as 2.5 times as large.[8] It was the observation of these pressure pulses that led Norrish and his co-workers[9] to the conclusion that these sensitized ignitions are chain-thermal in character.

There is further evidence to support this hypothesis of thermal ignition near the lower limit. The maximum rates of pressure decrease outside the lower limit are extremely high, often between 10 and 20 mm/sec. Also the maximum rate near the lower limit changes with the vessel diameter, being greater in smaller vessels. The limit position is dependent upon the thermal conductivity of the reacting mixture, and also the maximum rate outside the lower limit is greater in the mixtures of greater thermal conductivity. These facts are in complete agreement with the predictions of the thermal ignition theory.[8]

In contrast, these features of thermal ignitions are much less marked at the upper limits. Only occasionally was there a detectable pressure pulse before the slow reactions outside the upper limits, and the pulse, and the maximum rate of subsequent pressure drop near the limit, are both much smaller than at the lower limit. The effect of vessel diameter on the upper limit is less marked than on the lower, and although there were some changes in both the position of the limits and the maximum rates with changes in thermal conductivity, the effects were proportionately much less than at the lower limits.

It is therefore concluded that the ignitions near the lower limit are controlled by thermal factors, but those near the upper limits are little affected by thermal factors, and can be treated as isothermal. This extreme contrast between the ignitions at the two limits applies completely only when the limits are well separated, as in Fig. 4. When they converge, for example in very small vessels or at very low or high reactant pressures, the distinction is less valid.

The Position of the Ignition Limits. It is now clear that the suggestion of Ashmore and Levitt[3] that the upper limit occurs when p_i lies below p_s is basically correct. It is clear that the same criterion applies to the lower sensitizer limit (Figs. 4 and 8) and that it can be applied to changes of total pressure (Fig. 5) as well as to changes of p_0.

By studying separately the variations of p_s and of p_i with factors such as the reactant pressure, the addition of inert gases, and the sensitizer pressure, it is possible to account for the observed changes of limit position.

The kinetics of the reactions that control p_s were studied[5] with reactant pressures that are sufficiently high to be above the closed ignition region which is a well-established feature.[1,6,10] of these systems. It appears that p_s is independent of the vessel diameter, and is also independent of the pressure of nitric oxide present (and hence of p_0) provided that p_0 lies below about 1 mm. The occurrence of a stationary state for p_s in this region is attributed to a balance between reaction (9), which removes nitrogen dioxide, and reactions (4) and (7) which form it.

$$H + NO_2 \rightarrow OH + NO \qquad (9)$$

$$H + O_2 + M \rightarrow HO_2 + M \text{ (slow)} \qquad (4)$$

$$HO_2 + NO \rightarrow OH + NO_2 \text{ (fast)} \qquad (7)$$

This scheme predicts that p_s should conform to the equation

$$p_s = \frac{\sum k_{4,M}[M]}{k_9}[O_2]$$

where M represents *any* gas present, including O_2. The experimental variation of p_s with $[O_2]$ and with $[M]$, and the absence of any effect of p_0, are in agreement with this equation. Moreover, the relative values of $k_{4,M}$ which were obtained from the study[5] of p_s are in excellent agreement with published values[11] when account is taken of later revisions.[12] It may safely be assumed, therefore, that p_s is independent of p_0, provided that p_0 lies below about 1 mm, and increases as P_T^2 when the total pressure is altered with mixtures of constant composition. At higher values of p_0 the reactions

$$2NO + O_2 \underset{(-12)}{\overset{(12)}{\rightleftharpoons}} 2NO_2$$

become increasingly important and eventually dominate the free radical reactions.[3,4] The effect of this is to make p_s increase at high values of p_0. However, in the regions of sensitized ignitions, p_s can be taken as independent of p_0, and to increase as P_R^2 for mixtures of $2H_2 + O_2$ in the absence of inert gases.

Using these results, and the experimental variation found for p_i with p_0 (Fig. 4) and with P_R (Fig. 6) it is possible to account for the

position of the ignition limits under different conditions. Perhaps the most striking demonstration of this can be given by the derivation of the closed region of ignition mentioned previously.

The experimental variations of p_i and p_s with p_0 and with P_R are shown schematically in Fig. 9. It can readily be seen that sections of the p_i curves at chosen values of P_R give curves of p_i versus p_0 shown in 9a, in keeping with Fig. 4. Figure 9b also shows a curve for p_s against P_R, this being independent of p_0 as discussed above. The points of intersection of the p_i, p_s curves in Fig. 9b lead, as illustrated in 9c, to a closed boundary, and the condition that $p_i > p_s$ for ignition to occur shows that ignition will occur inside this closed boundary. Not only the existence, but also the general shape, of this boundary are in agreement with published results.

Although this simple condition is fulfilled in examples tested, and the ignition boundary

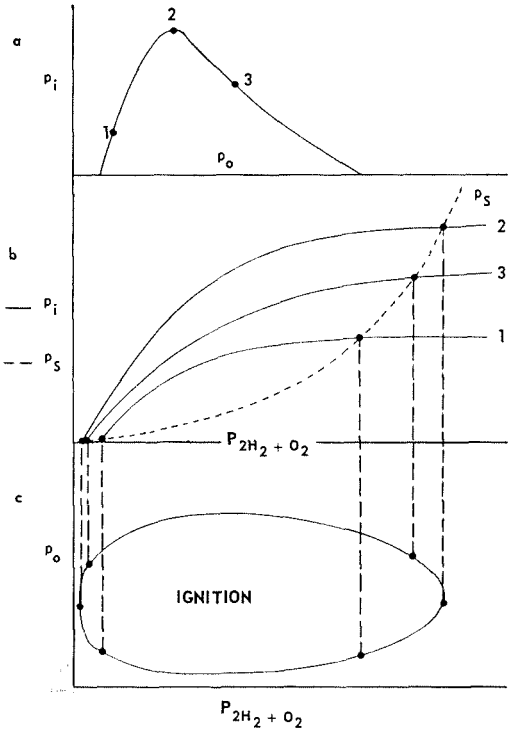

FIG. 9. Illustration of factors controlling the ignition limits and the closed ignition region. (a) p_i against p_0, derived as vertical section of 9(b). (b) p_i against $P_{2H_2+O_2}$ at three different initial sensitizer pressures, as indicated in 9(a). p_s is independent of p_0. (c) p_0 against $P_{2H_2+O_2}$, showing closed ignition region. Correspondence of p_i and p_s in 9(b) determines the limit position.

appears to be defined by the condition $p_i = p_s$ in all the larger vessels, the values of p_i just inside the lower sensitizer limit in smaller vessels is significantly higher than the values of p_s just outside the lower limit. Where there is a considerable thermal contribution to the rates of reaction before ignition, therefore, it may be necessary for p_s to lie below the appropriate value of p_i and in addition the rate of heat production after p_e is reached must attain a certain minimum value.

The Kinetic Scheme. Several possible kinetic schemes have been examined in detail.[6] The scheme which provides the most satisfactory explanation of the observed results is set out below. A significant feature of the scheme is that, apart from reaction (7), all of the reactions proposed are known to occur in other systems. This applies in particular to the branching reactions chosen, reactions (1) and (2). In contrast to earlier suggestions[10] it has not proved necessary to postulate an alternative branching reaction involving nitric oxide. Instead, reaction (7) has proved adequate. The occurrence of reaction (7) is strongly supported by the detailed study[5] of p_s, and by work[13] on the H_2O_2/NO system.

$$H + O_2 \rightarrow OH + O \quad (1)$$

$$O + H_2 \rightarrow OH + H \quad (2)$$

$$OH + H_2 \rightarrow H_2O + H \quad (3)$$

$$H + O_2 + M \rightarrow HO_2 + M \quad (4)$$

$$HO_2 \rightarrow \text{removed on the wall} \quad (5)$$

$$HO_2 + HO_2 \rightarrow H_2O_2 + O_2 \quad (6)$$

$$HO_2 + NO \rightarrow OH + NO_2 \quad (7)$$

$$O + NO_2 \rightarrow NO + O_2 \quad (8)$$

$$H + NO_2 \rightarrow OH + NO \quad (9)$$

$$OH + NO_2 + M \rightarrow HNO_3 + M \quad (10)$$

$$OH + NO + M \rightarrow HNO_2 + M \quad (11)$$

$$2NO + O_2 \rightarrow 2NO_2 \quad (12)$$

$$2NO_2 \rightarrow 2NO + O_2 \quad (-12)$$

$$H_2 + NO_2 \rightarrow HNO_2 + H \quad (13)$$

This scheme, and several others, were analyzed assuming stationary state conditions for the free radicals present, with the further assumption that the stationary state broke down when $p_{NO_2} = p_e$, i.e., that ϕ passes through zero at p_e. From the analyses expressions for ϕ could be

derived which were set equal to zero when $p_{NO_2} = p_e$, and the resulting equations were examined to see how p_e varied with factors such as p_0, P_R, changes of reactant composition, addition of inert gases, and so on. The scheme presented is the one that accounts most satisfactorily for the trends in p_e. Not only can the trends be described qualitatively, but by using the values that are known for many of the velocity constants, and by assuming reasonable values of the others, the changes of p_e can be predicted quantitatively,[6] and the fit with the experimental data is quite good. It is hoped to publish this analysis.

It seems very likely that similar fits for p_i could be made by setting ϕ equal to some positive quantity, since the variations of p_i follow those of p_e so closely. It is not certain, however, that there would be a unique value for ϕ, for it seems possible that the transition from isothermal branched-chain ignitions to thermal ignitions would require corresponding changes in the critical value of ϕ.

The relation between the kinetic scheme and the events during and at the end of the induction periods will now be explained.

During the induction periods, nitrogen dioxide is removed by the chain steps (9) and (3), the chains being initiated by reaction (13) and terminated by reactions (10) and (11) provided that the value of p_0 is not too low. If p_0 is very low, reaction (4) competes with (9) and the chains may be terminated by reactions (5) or (6). The effect of this is to decrease the rate of removal of NO_2, and so increase the length of the induction periods, at very low values of p_0. At higher values of p_0, reactions (9) and (7) become more important, and the rate of removal of NO_2 increases towards the values characteristic of the H_2–NO_2 reaction with oxygen acting only as an inert gas M in reactions (10) and (11). At higher values of p_0, however, the concentration of NO_2 has to fall to lower values to reach p_e, and the length of the induction periods will increase again; quantitative agreement between predicted and observed lengths of the induction periods has been found in this region.[3] Thus the existence of a minimum[1] in the plot of induction period against p_0 can be explained. In addition, the effects of changing reactant concentration and of adding inert gases can be satisfactorily explained by the observed kinetics of the reaction between hydrogen and nitrogen dioxide, as explained previously.[3]

During the induction period, the branching reaction (2) is not important because oxygen atoms are removed by the fast reaction (8). This reaction becomes less effective as nitrogen dioxide is converted to nitric oxide; simultaneously, there is a further reduction in the rate of termination via reactions (4) and (5) or (6), because the nitric oxide converts HO_2 to HO by reaction (7). Both these effects cause ϕ to increase during the induction periods. Reactions (10) and (11) have been shown to have similar rate constants,[14] and so their effect on termination, and hence on ϕ, is constant as NO replaces NO_2. Thus at the beginning of the induction periods ϕ is large and negative, and approaches zero towards the end of the induction periods.

Of the two termination reactions for HO_2, it seems likely that reaction (6) is more important. Firstly, apart from the smallest vessel, the value of p_e was substantially independent of diameter. As the termination reactions must occur in the expression for ϕ, and hence in that for p_e, it appears that reaction (5) cannot be of major importance, except perhaps in very small vessels. Secondly, the adoption of reaction (6) accounts for the thermal effects found at the lower limits, and also for the need for a double criterion of ignition in smaller vessels. If the main termination reaction at low p_0 is (6) rather than (5) or (10) or (11), the chains are quadratically terminated. It is impossible[1] to get a purely isothermal ignition in such a reaction, as there is a limiting concentration of radicals for all values of ϕ. Thus in addition to ϕ passing through zero at an NO_2 pressure lying above p_s, which by itself would satisfy an isothermal criterion of ignition, it is necessary for the rate of reaction to reach a critical value and there is need for a p_i as well as a p_e. The critical rate will be greater in vessels of smaller diameter or in mixtures of greater thermal conductivity.

With mixtures near the upper limit the nitric oxide concentration at p_e is much greater than near the lower limit. As a result, HO_2 is converted to OH by reaction (7), and the ratio $[HO_2]/[OH]$ falls. Thus reaction (11) becomes more important than (6) as a terminating step, and its rate is further enhanced by the higher values of p_0 and hence of p_{NO}.

Thus there is a gradual transition as p_0 is increased from mainly quadratic termination to mainly linear. With this transition, ignitions will change from purely thermal to near isothermal. This accounts for the observations that as the upper limit is approached (*a*) p_i and p_e become more nearly coincident, (*b*) there is less evidence of a pressure pulse before ignition, and (*c*) p_i more accurately approaches p_s. Moreover, as ϕ is negative above the upper limit, the rate of the slow reaction is governed by the values of θ and ϕ, and so can take quite different values from the rates below the lower limit, which are governed by ϕ and δ.

There is an alternative, but less probable,

explanation of the different phenomena. It is based on isothermal conditions for the limits (i.e., $\dot{\phi}$ = zero at the limits) with the assumption that ϕ varies more slowly with changes in p_0 (i.e., in p_{NO}, since p_a is constant) at the lower than at the upper limit. Then faster rates could be observed near the lower limits than near the upper, since in practice finite changes must be made in p_0 from run to run. These faster rates would produce thermal effects, irrespective of the final isothermal criterion for ignition. However, the quantitative analyses of the schemes considered do not allow ϕ to change more slowly at the lower limit. In addition, in cases where there is good evidence for isothermal limits, as in the glow limits of phosphorus, the rates just outside the limits are exceedingly slow.

Thus the simplest logical explanation of the whole phenomenon requires quadratic termination such as reaction (6) provides.

The rise and fall of p_e as p_0 is varied can be simply explained on the reaction scheme proposed. At low p_0 the branching depends upon reaction (2), reduced by reaction (8), and the termination upon (6), reduced by (7). The quantitative treatment[6] shows that a relatively large increase in p_{NO_2} [with consequent reduction by (8) of branching] is compensated by a smaller increase in p_{NO} reducing termination via (7). Thus when p_0 is increased, only a part of the additional sensitizer need be converted to nitric oxide to restore the previous balance of branching and termination, e.g., at ϕ equal to zero. Hence p_e *increases* with p_0 at low values of p_0, as observed in Fig. 4.

The fall in p_e as p_0 increases further is explained by the transition from quadratic to linear termination. As p_0 approaches the upper limit there is an increased rate of termination by (11), which has, as already explained, replaced (6). This increase in termination would reduce ϕ, and to restore the balance the nitrogen dioxide must decrease further to reduce the effect of reaction (8) on the branching step (2). Eventually p_e and p_i, which are becoming more nearly coincident as p_0 is increased, fall below p_a and the upper limit is reached.

References

1. Dainton, F. S. and Norrish, R. G. W.: Proc. Roy. Soc. (London) *A177*, 393 (1941).
2. Ashmore, P. G. and Levitt, B. P.: *Advances in Catalysis and Related Subjects*, Vol. IX p. 367. Academic Press, 1957.
3. Ashmore, P. G. and Levitt, B. P.: *Seventh Symposium (International) on Combustion*, p. 45. Butterworths, 1958.
4. Ashmore, P. G. and Tyler, B. J.: J. Catalysis *1*, 39 (1962).
5. Ashmore, P. G. and Tyler, B. J.: Trans. Faraday Soc. *58*, 1108 (1962).
6. Tyler, B. J.: Ph.D. dissertation, University of Cambridge (1961).
7. Tyler, B. J.: J. Sci. Instrum. *39*, 111 (1962).
8. Benson, S. W.: J. Chem. Phys. *22*, 46 (1954).
9. Foord, S. G. and Norrish, R. G. W.: Proc. Roy. Soc. (London) *A152*, 196 (1935).
10. Ashmore, P. G.: Trans. Faraday Soc. *51*, 1090 (1955).
11. Lewis, B. and von Elbe, G.: *Combustion, Flames and Explosions of Gases*, Academic Press, 1951.
12. Baldwin, R. R. and Brooks, C. T.: Trans. Faraday Soc. *58*, 1782 (1962).
13. Tyler, B. J.: Nature *195*, 279 (1962).
14. Ashmore, P. G. and Levitt, B. P.: Trans. Faraday Soc. *53*, 945 (1957).

Hydrogen-Oxygen Reaction

Chairman: Dr. G. L. Dugger
(APL, The Johns Hopkins University)

Vice Chairman: Prof. I. Glassman
(Princeton University)

RATES OF SOME ATOMIC REACTIONS INVOLVING HYDROGEN AND OXYGEN

M. A. A. CLYNE

Reactions of ground state oxygen and hydrogen atoms produced by an rf electric discharge were studied in a flow system at pressures of about 1 mm Hg. Hydroxyl radicals and oxygen atoms are generated in the H + NO_2 reaction and measurements of the rate of removal of oxygen atoms in this system led to a value for the rate constant k_3 of the rapid reaction

$$O + OH \rightarrow H + O_2 \qquad (3)$$

of $3 \pm 1 \times 10^{13}$ $cm^3mole^{-1}sec^{-1}$ at 293°K and 265°K.

The reaction of H with O_2 in the presence of an argon carrier was found to have over-all third order kinetics at 293°K,

$$H + O_2 + Ar \rightarrow HO_2 + Ar \qquad (7)$$

and under these conditions k_7 was found to be $1.2 \pm 0.3 \times 10^{16}$ $cm^6mole^{-2}sec^{-1}$. This rate constant is similar in magnitude to that of the analogous combination reaction,

$$H + NO + Ar \rightarrow HNO + Ar.$$

The rate of reaction of oxygen atoms (in the absence of O_2) with molecular hydrogen was measured between 409° and 733°K. Assuming the slow primary step (−4)

$$O + H_2 \rightarrow OH + H \qquad (-4)$$

to be followed by the rapid reaction

$$O + OH \rightarrow O_2 + H$$

a value of $k_{-4} = 1.2 \times 10^{13} \exp[(-9200 \pm 600)/RT]$ $cm^3mole^{-1}sec^{-1}$ was determined in this temperature range.

Introduction

Until recently, there have been few reliable data for the rate constants of the propagation and branching steps in the chain reaction between oxygen and hydrogen. However, the rate constant of the chain propagation reaction

$$OH(^2\Pi) + H_2 \rightarrow H_2O + H(^2S) + 14 \text{ kcal/mole} \qquad (6)$$

has been redetermined recently,[1] while in this

work values of the rate constants k_3 and k_{-4} are reported:

$$OH(^2\Pi) + O(^3P) \rightarrow H(^2S) + O_2 + 17 \text{ kcal/mole} \quad (3)$$

$$O(^3P) + H_2 \rightarrow OH + H(^2S) - 1 \text{ kcal/mole} \quad (-4)$$

Reaction (−4) and the reverse of reaction (3) are branching steps in the hydrogen + oxygen reaction. Direct information regarding the rate of the reaction

$$H(^2S) + O_2 + Ar \rightarrow HO_2 + Ar \quad (7)$$

has been obtained in this work.

Experimental

Ground state hydrogen atoms and oxygen atoms (0.2–2% of total flow) were produced by an electrodeless electric discharge at 18 Mc/sec in mixtures of the molecular gas (1%) with argon (99%) or in the pure molecular gas. Partially dissociated gas from the discharge was pumped into a 28 mm internal diameter Pyrex flow tube having four backward-facing inlet jets along its length for the admission of reactants. Reactant flows were regulated by needle valves and were measured with calibrated capillary flowmeters. For experiments at temperatures up to 800°K a similar quartz flow tube enclosed in a furnace was employed. Pressures in the flow tubes were 1–4 mm Hg measured on a McLeod gauge and silicone fluid manometer. Pressure gradients at 1 mm Hg total pressure and 150 μmole/sec total flow along the 100 mm length of the reaction tube were less than 0.03 mm Hg. The total pressure p in the flow tube was controlled by a large stopcock downstream from the mixing inlets. The reaction time t could be altered by variation of the distance x along the flow tube between the reactant admission inlet and the observation point, $t = xAp/RT\sum F$, where A is the cross-section area of the tube and $\sum F$ is the total flow rate.

Two photomultiplier cells, an RCA 1P28 and an EMI 9558B, were used to measure the intensity of light emitted normally from a short section of reaction tube. The 1P28 tube fitted with a Wratten 61 filter was used for the measurement of the intensity of emission of the green-gray air afterglow spectrum ($O + NO + M \rightarrow NO_2 + M + h\nu$) from 4900 to 5800 Å. The 9558B cell had a superior red sensitivity to that of the 1P28 and when fitted with a Wratten 88A filter had a sensitivity range from about 7350 to 8000 Å. It was therefore used for the measurement of the intensity of the strong (000, 000) band of HNO at 7625 Å emitted in the reaction of H with NO.[9,14] Measurements of the emission intensities from the O + NO and H + NO systems were used for the determination of the concentrations of oxygen atoms and hydrogen atoms, respectively. In systems containing O as well as H in the presence of nitric oxide, the air afterglow emission made a small contribution to the near infrared signal observed by the 9558B photomultiplier cell, and a small correction was made for this effect as described previously.[2] The photocells were operated at potentials of 800–950 V (1P28) and 850–1400 V (9558B) respectively, supplied by stabilized power sources. The isothermal-wire calorimeter described previously[4] was used in some experiments for the determination of hydrogen atom concentrations.

The Kinetic Method

Hydrogen atoms and oxygen atoms were generated in these experiments by means of an electrodeless electric discharge in a mixture of the molecular gas with 99% argon. The rates of elementary reactions involving H or O atoms can be determined directly from measurements of the rates of removal of atomic species from the flow system. In this work the rates of reaction of atoms (A) were determined by measurement of the atom concentrations remaining at a fixed point in the flow system when equal amounts of reactant (R) were introduced at each of the four inlet jets in turn. If recombination second order in [A],

$$A + A + M \rightarrow A_2 + M \quad (9)$$

is much slower than the reactions

$$A + \text{wall} \rightarrow \tfrac{1}{2}A_2 \quad (10)$$

$$2A + R \rightarrow \text{products} \quad (11)$$

the rate of reaction of atoms determined in this way is equal to the rate of reaction (11) and is independent both of the first order surface decay and of the initial concentrations of atoms at the inlets. This can be demonstrated in the following manner. The rate of reaction of atoms is of the form

$$-d[A]/dt = a[A]^2 + b[A]$$

where $a = 2k_9[M]$ and $b = 2k_{11}[R] + k_{1c}$.

On integration we obtain

$$\ln\left(\frac{[A]}{[A]_0}\right) - \ln\left(\frac{a[A] + b}{a[A]_0 + b}\right) = -bt$$

where $[A] = [A]_0$ when $t = 0$.

Reactant is added at time $t = t_1$, at which point $[A] = [A]_1$, and the atom concentration $[A]_3$ is then measured further downstream after a further reaction time t_2; $[A]_2$ is the concentration of atoms at the point of observation (reaction time $t_1 + t_2$) when no reactant is added. We then have the following relations:

$$\ln\left(\frac{[A]_1}{[A]_0}\right) - \ln\left(\frac{2k_9[M][A]_1 + k_{10}}{2k_9[M][A]_0 + k_{10}}\right) = -k_{10}t_1;$$

$$\ln\left(\frac{[A]_2}{[A]_0}\right) - \ln\left(\frac{2k_9[M][A]_2 + k_{10}}{2k_9[M][A]_0 + k_{10}}\right) = -k_{10}(t_1 + t_2);$$

$$\ln\left(\frac{[A]_3}{[A]_1}\right) - \ln\left(\frac{2k_9[M][A]_3 + k_{10} + 2k_{11}[R]}{2k_9[M][A]_1 + k_{10} + 2k_{11}[R]}\right) = -(k_{10} + 2k_{11}[R])t_2;$$

and therefore

$$\ln\left(\frac{[A]_3}{[A]_2}\right) - \ln\left[\left(\frac{2k_9[M][A]_3 + k_{10} + 2k_{11}[R]}{2k_9[M][A]_1 + k_{10} + 2k_{11}[R]}\right) \times \left(\frac{2k_9[M][A]_1 + k_{10}}{2k_9[M][A]_2 + k_{10}}\right)\right] = -2k_{11}[R]t_2.$$

Providing that $k_{10} + 2k_{11}[R] \gg 2k_9[A][M]$ and $k_{10} \gg k_9[M] \times ([A]_1 - [A]_2)$, this equation reduces to the simple form

$$\ln ([A]_3/[A]_2) = -2k_{11}[R]t_2.$$

The condition for reaction (9) to be much slower than reactions (10) or (11) was easily fulfilled by working with low concentrations of atoms. The method was very useful for the determination of the rates of third order combination reactions, such as the H + NO + M reaction[14] and the H + O_2 + M system described here, since the measurements give the required third order rate constants without involving large corrections for concomitant atomic recombination processes.

Results

Reaction of OH *with* O. Hydroxyl radicals in the electronic ground state were generated by addition of NO_2 to a stream of atomic hydrogen and argon from the discharge.[2,3] Measurements of the red HNO and green NO_2 (air afterglow) emission intensities I_b and I_a were made at various points downstream from the NO_2 inlet. Nitric oxide was thus produced stoichiometrically in the rapid reaction (1),[2]

$$H + NO_2 \rightarrow OH + NO \qquad (1)$$

and since NO is not removed from the system,[4,5] $I_a/[NO_2]_0$ and $I_b/[NO_2]_0$ are proportional to [O] and [H], respectively.[4,5] The two emission intensities were also measured in NO + O + Ar and NO + H + Ar mixtures, respectively, with simultaneous measurement of the corresponding oxygen atom and hydrogen atom concentrations. In this way measurements of $I_a/[NO_2]_0$ and $I_b/[NO_2]_0$ gave directly the absolute atom concentrations in the H + NO_2 system. Figure 1 shows the variation of [O] and [H] with concentration of added nitrogen dioxide, $[NO_2]_0$, for a constant reaction time of 0.03 sec. [H] was found to be a linear function of $[NO_2]_0$ and thus NO_2 titration to the critical extinction of the HNO emission provides a method for the estimation of H atoms in H + Ar systems.[2] Under the conditions of the author's experiments, the reaction

$$OH + OH \rightarrow H_2O + O \qquad (2)$$

[followed by the rapid reaction

$$O + OH \rightarrow H + O_2 \qquad (3)]$$

has proceeded almost to completion between the NO_2 inlet and the photomultiplier observation point. Reaction (3) regenerates hydrogen atoms and thus for each H atom initially present, critical removal of H occurs when $\frac{3}{2}NO_2$ molecules have been introduced into the system. It follows that the NO_2 titer in these circumstances is equal to $\frac{3}{2}$ of the concentration of hydrogen atoms present in the absence of NO_2.

The initial concentration of hydroxyl radicals

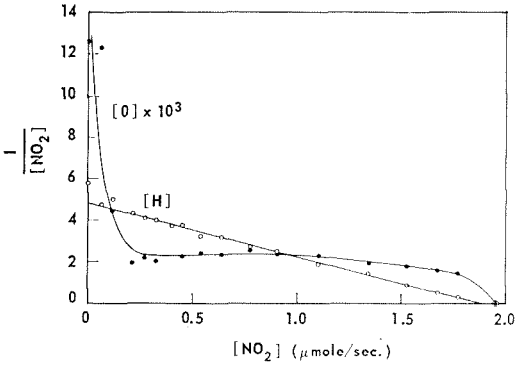

FIG. 1. The variation of [H] and [O] with concentration of added NO_2 ($[OH]_0$) at 293°K and 1.09 mm Hg total pressure. Reaction time 0.03 sec.

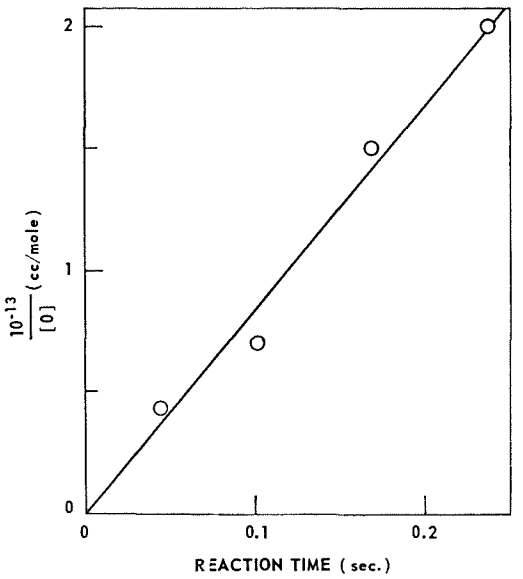

FIG. 2. Oxygen atom decay plot at 1.29 mm Hg total pressure and 293°K.

$[OH]_0$ is equal to the concentration of NO_2 added, $[NO_2]_0$, when atomic hydrogen is in excess. Figure 1 shows that for constant reaction time, $[O]$ is independent of $[NO_2]_0 = [OH]_0$ over a wide range of $[OH]_0$. The concentrations of oxygen atoms observed are of the order of 10^{-5} to 10^{-6} mm Hg, while those of H are about 10^{-2} mm Hg. For constant reaction time, $[O]$ was found to be independent of total pressure. The decay of $[O]$ along the tube was measured at total pressures of 1.09 to 2.23 mm Hg. Plots of $1/[O]$ against reaction time t were linear, with slopes independent of total pressure and of $[OH]_0$. A typical oxygen atom decay plot is shown in Fig. 2. The slopes of these plots and the absolute values of $[O]$ were unaffected by a tenfold increase in the hydrogen atom concentration in the system. It is evident that $[O]$ decays at a rate proportional to $[O]^2$ by means of a process which does not involve H in rate-determining steps,

$$-d[O]/dt = k'[O]^2.$$

The mean value of k' at 293°K was found to be 9×10^{13} $cm^3mole^{-1}sec^{-1}$ and a similar value was obtained in experiments at 265°K.

The possible reactions for the production of ground state oxygen atoms are

$$H + OH \rightarrow O + H_2 + 1 \text{ kcal/mole} \quad (4)$$

and

$$OH + OH \rightarrow H_2O + O + 15 \text{ kcal/mole} \quad (2)$$

The former reaction must be excluded as a rate-determining step since $[O]$ and k' were found to be independent of $[H]$; in addition, the magnitude of the rate of this reaction calculated from the rate constant k_{-4} of the reverse reaction[6] is much less than the rate of reaction (2) in the author's experiments. Removal of O can occur by means of

$$O + NO_2 \rightarrow NO + O_2 \quad (5)$$

and

$$O + OH \rightarrow O_2 + H \quad (3)$$

The rate of reaction (5) would be expected to be much less than that of reaction (3) under conditions where appreciable concentrations of H are present, since NO_2 is then predominantly removed by the faster reaction (1). It is therefore considered that oxygen atoms are generated by reaction (2), and removed by reaction (3); the influence of reaction (5) only becomes appreciable when $[H]$ is small, as shown by the tailing of the oxygen atom plot in Fig. 1 near the titration endpoint.

On this basis, assuming a steady state concentration of oxygen atoms,

$$[O] = k_2[OH]/k_3$$

and

$$-d[OH]/dt = 3k_2[OH]^2,$$

$$1/[OH] = 1/[OH]_0 + 3k_2t.$$

It follows that $[O]$ is given by the expression

$$[O] = \frac{k_2}{k_3(1/[OH]_0 + 3k_2t)} \quad (I)$$

For a typical reaction time of 0.05 sec and $[OH]_0 = 10^{-2}$ mm Hg, $3k_2t$ is very much greater than $1/[OH]_0$,[1] and hence (I) reduces to the simple form of Eq. (II):

$$[O] = 1/3k_3t \quad (II)$$

consistent with the observed second order removal of $[O]$. The observed lack of dependence of $[O]$ and k' upon $[OH]_0$ and total pressure (for constant t) are in agreement with Eq. (II), which shows that $k' = 3k_3$. Values of k_3 determined at 293°K and 265°K were $3 \pm 1 \times 10^{13}$ $cm^3mole^{-1}sec^{-1}$.

Within the experimental error of the observations, the data are consistent with Eq. (II), which is based upon the assumption of a steady state concentration of oxygen atoms. The validity of this assumption can be tested by a comparison of the calculated rate of production of oxygen atoms, $k_2[OH]^2$, with the observed *net* rate of removal of oxygen atoms, $k'[O]^2$, which is the

difference between $k_2[OH]^2$ and $k_3[OH][O]$. For a steady state assumption to be a good approximation, this difference must be considerably smaller than the value of the individual terms $k_2[OH]^2$ and $k_3[OH][O]$. A typical observed *net* rate of removal of oxygen atoms was $\sim 1 \times 10^{-12}$ mole cm^{-3} sec^{-1}, while the value of $k_2[OH]^2$ calculated from Kaufman and Del Greco's data[1] under the same conditions was about 1×10^{-10} mole cm^{-3} sec^{-1}. It follows that the steady state assumption for [O] is a good approximation in this kinetic study.

Reaction of H *with* O_2. It has been shown that the rate constant k_3 is of the order of 0.1 of the bimolecular collision frequency between OH and O at room temperature. The reverse reaction (−3) thus has an activation energy of around 17 kcal/mole,

$$H + O_2 \rightarrow HO + O - 17 \text{ kcal/mole} \quad (-3)$$

as found by Schott and Kinsey.[7] Reaction (−3) can therefore be neglected as a rate-controlling step in the flow experiments at 293°K with H + O_2 systems. However, the addition of O_2 to H + Ar mixtures under such conditions at 1–2 mm Hg total pressure led to removal of hydrogen atoms. The nature of this reaction was investigated in the following manner. The reaction time between H and O_2 was varied by addition of the same oxygen flow ($[O_2] \gg [H]$) at each of four inlets along the reaction tube, [H] being measured at a downstream fixed point, the phototube housing. A small amount of nitric oxide was added to the reaction products 3 cm before the 9558P photomultiplier cell housing, and the photocurrent I_b due to the HNO emission was measured. $I_b/[NO]$ was then proportional to [H].[4] The small amount of added nitric oxide was found to have a negligible effect on the rate of removal of hydrogen atoms from the system. Plots of $\log_{10}(I_b/[NO])$ against t obtained in this way were accurately linear, with slopes proportional to $[O_2]$, as shown in Fig. 3.

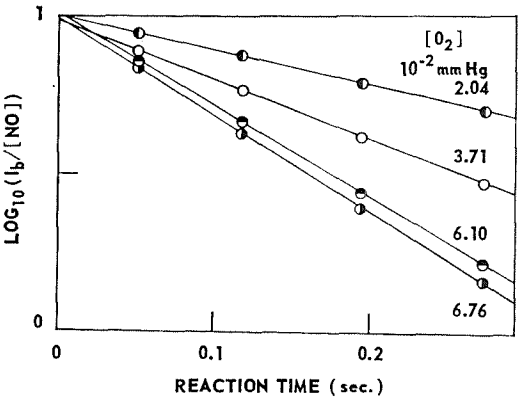

FIG. 3. Kinetics of the H + O_2 + M reaction at 1.64 mm Hg total pressure and at 293°K. Flow rates: Ar, 141 μmole/sec; H, 0.5 μg-atom/sec; H_2, 0.2 μmole/sec; O_2, 1.8–5.8 μmole/sec.

The quantity

$$\frac{1}{[O_2]} \frac{d}{dt} \ln (I_b/[NO]) \qquad \text{(III)}$$

was found to be proportional to total pressure [M] from 1.01 to 2.42 mm Hg, as shown in Table 1. The rate of reaction of hydrogen atoms in this system is therefore given by

$$-d[H]/dt = k''[H][O_2][M]$$

and the rate-controlling reaction in the H + O_2 system is

$$H + O_2 + M \rightarrow HO_2 + M \qquad (7)$$

It is known that the steady state concentration of HO_2 in such systems is very small,[8] and it is reasonable to suppose that reaction (7) is followed by one of the rapid reactions 8 a, b or c:

$$H + HO_2 \rightarrow H_2O + O \qquad (8a)$$

$$H + HO_2 \rightarrow OH + OH \qquad (8b)$$

$$H + HO_2 \rightarrow H_2 + O_2 \qquad (8c)$$

TABLE 1

The variation of (III) with total pressure at 293°K

Total pressure (mm Hg)	[M] (mole cm^{-3})	(III) (cm^{3}mole^{-1}sec^{-1})	(III)/[M] (cm^{6}mole^{-2}sec^{-1})
1.01	5.56×10^{-8}	1.43×10^9	2.6×10^{16}
1.20	6.57	1.84	2.8
1.48	8.11	2.20	2.7
1.82	10.00	2.23	2.2
2.42	13.30	2.46	1.9

On this basis,

$$-d[\mathrm{H}]/dt = 2k_1[\mathrm{H}][\mathrm{O}_2][\mathrm{M}],$$

and a value of $k_1 = 1.2 \pm 0.3 \times 10^{16}$ $\mathrm{cm^6 mole^{-2}\,sec^{-1}}$ for M = Ar at 293°K was obtained.

Reaction of O *with* H_2. The rate of removal of oxygen atoms in the O + H_2 system was measured and used to determine k_{-4}. This method can only be reliably employed when O_2 is absent from the system, since reaction (7) and subsequent reactions of HO_2 must be considered to contribute to oxygen atom removal in the presence of molecular oxygen. Ground state oxygen atoms in the absence of O_2 were generated by addition of the stoichiometric quantity of nitric oxide to nitrogen atoms in a stream of active nitrogen,[6]

$$\mathrm{N}\ (^4S) + \mathrm{NO}\ (^2\Pi) \rightarrow \mathrm{N_2}\ (^1\Sigma) + \mathrm{O}\ (^3P).$$

Hydrogen atoms are a product of the O + H_2 reaction and thus a method for the measurement of oxygen atom concentrations in the presence of H must be employed for following the reaction. A fixed-position 1P28 photomultiplier cell was used to measure the intensity of the air afterglow emission from the reaction products to which a known small amount of nitric oxide had been added just before the photomultiplier. When this phototube was fitted with a green transmission filter (Wratten No. 61) the HNO emission (due to the radiative combination of H with NO) made a negligible contribution to the total photocurrent (I_a), which was therefore proportional to [O][NO]. Ln[O] measured in this way was found to be proportional to reaction time t and to $[H_2]$ when excess hydrogen was added to the stream of oxygen atoms at temperatures between 409° and 733°K. Typical data are shown in Fig. 4; $(1/[H_2])\{d(\ln[O])/dt\}$ was independent of total pressure between 1.71 and 2.77 mm Hg. The absence of any significant dependence upon total pressure is not surprising, since the only third order reaction which could be important is forbidden by the spin correlation rule:

$$\mathrm{O}\ (^3P) + \mathrm{H_2}\ (^1\Sigma) + \mathrm{M} \rightarrow \mathrm{H_2O}\ (^1A) + \mathrm{M}.$$

The kinetic data can be represented by the equation

$$-d[\mathrm{O}]/dt = k'''[\mathrm{O}][\mathrm{H_2}].$$

The equilibrium constant of reaction (4) is around unity, but since the final concentration ratio $[H]/[H_2]$ was typically 0.1–0.2, the reverse reaction (4) can be neglected in comparison to reaction (−4) as a rate-determining step.

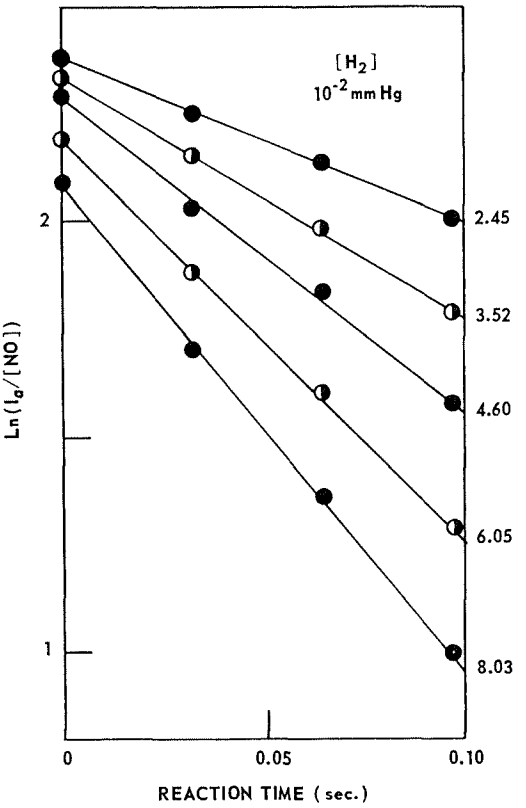

FIG. 4. Kinetics of the O + H_2 reaction at 2.19 mm Hg total pressure and at 441°K. Flow rates: N_2, 197 μmole/sec; O, 0.3 μg-atom/sec; H_2, 2.2–7.3 μmole/sec.

Reaction (−4),

$$\mathrm{O} + \mathrm{H_2} \rightarrow \mathrm{OH} + \mathrm{H} \qquad (-4)$$

can be followed by any of the three reactions (2), (3), or (6). The relative magnitudes of k_2, k_3, and k_6. [see ref (1) and this work] show that reaction (3),

$$\mathrm{O} + \mathrm{OH} \rightarrow \mathrm{O_2} + \mathrm{H} \qquad (3)$$

is predominant for OH removal under the author's conditions. In these circumstances, k_3 is much greater than k''', and hence

$$-d[\mathrm{O}]/dt = 2k_{-4}[\mathrm{O}][\mathrm{H_2}].$$

Therefore k_{-4} could be evaluated from the experimentally determined values of k''' and a value of

$$k_{-4} = 1.2 \times 10^{13}$$

$$\exp(-9200 \pm 600)/RT\ \mathrm{cm^3 mole^{-1} sec^{-1}}$$

was determined in the temperature range 409 to

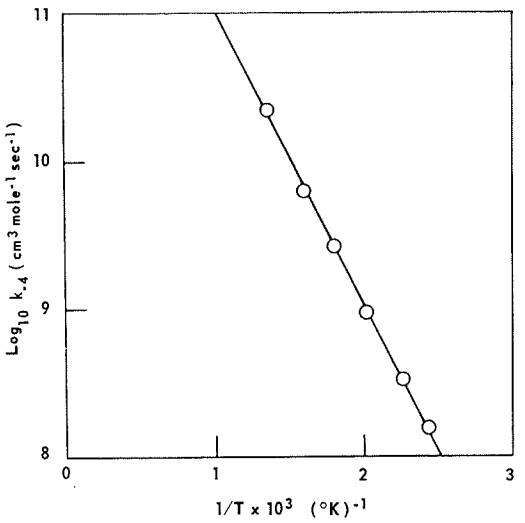

FIG. 5. The variation of k_{-4} ($cm^3 mole^{-1} sec^{-1}$) with temperature from 409°K to 733°K.

733°K. Figure 5 shows a plot of $\log_{10} k_{-4}$ against $1/T$.

Discussion

It has been shown that the rate constant of the reaction

$$O + OH \rightarrow H + O_2 \qquad (3)$$

is $3 \pm 1 \times 10^{13}$ $cm^3 mole^{-1} sec^{-1}$ at 293°K. The activation energy of reaction (3) is therefore near zero. This conclusion is in agreement with long extrapolations from Schott and Kinsey's[7] values of k_{-3}, and with the activation energy $E_{-3} = 17 \pm 1$ kcal/mole found by Voevodskii.[10] The present value for k_3 at 293°K is within a factor of 3 of that reported by Del Greco and Kaufman.[1] The high value obtained for k_3 ($\sim$0.1 of the bimolecular collision frequency) shows that O and OH cannot coexist in significant concentrations for appreciable periods of time. Products of a discharge in moist oxygen would therefore be expected to contain H as well as O but not hydroxyl. Kinetic studies (such as those of Avramenko *et al.*) in which a discharge in water vapor is used as a source of OH are thus open to criticism.

The activation energy of 9.2 ± 0.6 kcal/mole found for reaction (−4) is significantly different from that determined by Harteck and Kopsch[11] (6 ± 1 kcal/mole) and Azatyan *et al.*[12] (11.7 ± 0.7 kcal/mole) but in fair agreement with the value of 7.7 kcal/mole obtained by Fenimore and Jones.[13] However, the expressions for k_{-4} obtained by the last two groups of workers can be extrapolated to 700°K, yielding values within a factor of 5 of those obtained in the present work. In the work of Harteck and Kopsch,[11] the amounts of water were measured which were produced when hydrogen reacted with oxygen atoms contained in oxygen from an electric discharge. It is doubtful whether the extent of water formation under these conditions is a valid measure of the extent of reaction (−4), since water may also be formed by means of reaction (7) followed by the fast step (8a). In addition, most of the OH produced in reaction (−4) would be removed by reaction (3) rather than by reaction (6) under the experimental conditions used. The difference between the values of E_{-4} reported by the author and by the Russian workers[12] could be removed by the assumption in the latter work of a slightly different temperature coefficient for the surface recombinations of atomic species.

In this work it has been shown that formation of HO_2 requires participation by a third body M,

$$H + O_2 + M \rightarrow HO_2 + M \qquad (7)$$

The observed over-all third order kinetics show that, under the author's conditions, reaction of HO_2 with H (reaction 8) is faster than dissociation of HO_2 (reaction −7). The rate constant $k_7 = 1.2 \pm 0.3 \times 10^{16}$ $cm^6 mole^{-2} sec^{-1}$ for M = Ar at 293°K is similar to that of the reaction

$$H + NO + M \rightarrow HNO + M$$

at 293°K.[14] Several values of k_7 at room temperature (for M = H_2) have been reported previously, but since these vary from 4×10^{14} [see ref. (15)] to about $10^{18} cm^6 mole^{-2} sec^{-1}$, [see ref. (16)], reliance can only be placed on the determinations of k_7 at elevated temperatures, which are in fair agreement with one another. The value found in the present work for k_7 at 293°K is somewhat greater than most of those obtained from studies in the $H_2 + O_2$ system at higher temperatures. Voevodskii and Kondratiev,[17] for example, have deduced a value of $k_1 = 4.3 \times 10^{15}$ $cm^6 mole^{-2} sec^{-1}$ for M = H_2 at about 800°K. These data, taken in conjunction with the author's results at 293°K, suggest that reaction (7) may have a small negative activation energy similar to that of −0.6 kcal/mole found for the H + NO + M reaction.[14] This possibility is now being investigated and further experiments are to include a study of the dependence of k_7 upon the nature of the third body.

REFERENCES

1. DEL GRECO, F. P. and KAUFMAN, F.: Discussions Faraday Soc. *33*, 128 (1962).

2. Clyne, M. A. A. and Thrush, B. A.: Trans. Faraday Soc. *57*, 2176 (1961).
3. Del Greco, F. P. and Kaufman, F.: J. Chem. Phys. *35*, 1895 (1961).
4. Clyne, M. A. A. and Thrush, B. A.: Trans. Faraday Soc. *57*, 1305 (1961).
5. Kaufman, F.: Proc. Roy. Soc. (London) *A247*, 123 (1958).
6. Clyne, M. A. A. and Thrush, B. A.: Nature *189*, 135 (1961).
7. Schott, G. L. and Kinsey, J. L.: J. Chem. Phys. *29*, 1177 (1958).
8. Foner, S. N. and Hudson, R. L.: J. Chem. Phys. *23*, 1974 (1955).
9. Clement, M. J. Y. and Ramsay, D. A.: Canad. J. Phys. *39*, 205 (1961).
10. Voevodskii, V. V.: Dokl. Akad. Nauk S.S.S.R. *44*, 308 (1944).
11. Harteck, P. and Kopsch, U.: Z. physik. Chem. *B12*, 327 (1931).
12. Azatyan, V. V., Voevodskii, V. V., and Nalbandyan, A. B.: Kinetika i Kataliz *2*, 340 (1961).
13. Fenimore, C. P. and Jones, G. W.: J. Phys. Chem. *65*, 993 (1961).
14. Clyne, M. A. A. and Thrush, B. A.: Discussions Faraday Soc. *33*, 139 (1962).
15. Avramenko, L. I. and Kolesnikova, R. V.: Izv. Akad. Nauk S.S.S.R. 1971 (1961).
16. Burgess, R. H. and Robb, J. C.: Chem. Soc. (London), Special Publication No. 9, p. 167, 1958.
17. Voevodskii, V. V. and Kondratiev, V. N.: *Progress in Reaction Kinetics*, Vol. 1, p. 47. Pergamon Press, London (1961).

Discussion

Dr. F. Kaufman (*Ballistic Research Laboratories, Aberdeen Proving Ground*): In another paper in this volume, Dr. Del Greco and I have measured the rate constant, k_3, for $O + OH \rightarrow O_2 + H$ in a similar, though faster flow system by following the rate of decay of OH when O and OH are mixed. Our value for k_3 near 300°K is $(1.1 \pm 0.4) \times 10^{13}$ cm^3 mole^{-1} sec^{-1}, about a factor of three smaller than Dr. Clyne's. It should be pointed out that in Dr. Clyne's steady state decay of the O atoms generated by reaction (2) [O] is extremely small, of the order of 10^{-5} mm Hg, and that both the application of the air afterglow in the measurement of such traces of O and the importance of competing processes such as $O + NO + M \rightarrow NO_2 + M$ followed by reaction (1) must be carefully considered.

Dr. M. A. A. Clyne (*University of Cambridge*): Although the concentration of atomic oxygen is small, use of the air afterglow for its measurement is a very sensitive method. Removal of atomic oxygen by $O + NO + M$ and by other third order homogeneous processes could possibly be important in the experiments at the higher pressure used in this work (2.2 mm Hg) but not at the lower pressure of 1.1 mm Hg. This is confirmed by the observation that for constant reaction time, [O] was independent of the amount of nitric oxide present in the system, as shown in Fig. 1. A small correction (−10%) to my value of k_3 should probably be made to allow for surface combination of oxygen atoms. In view of the different methods used by Kaufman and Del Greco and by us, the agreement between our respective values of k_3 seems satisfactory.

Dr. R. R. Baldwin (*University of Hull, England*): I would like to point out an important consequence of the value given by Dr. Clyne for his reaction (7), $H + O_2 + M = HO_2 + M$.

The value of k_7 at temperatures around 500°C can be obtained by combining measurements on the second limit M_2 of the H_2/O_2 reaction, which is given by $[M_2] = 2k_{-3}/k_7$, with estimates of k_{-3}.

$$H + O_2 = OH + O \qquad (-3)$$

A new estimate of k_{-3} has recently been made[1] by using the inhibiting action of formaldehyde on the H_2/O_2 reaction to obtain k_{14}/k_{-3}, and combining this with independent determinations of k_{14}.

$$H + HCHO = H_2 + HCO \qquad (14)$$

The value obtained is consistent with independent estimates by Baldwin[2] and by Semenov,[3] and the mean value of 0.6×10^7 liter mole^{-1} sec^{-1} at 540°C is considered accurate to within 50%. From second limit measurements, $2k_{-3}/k_7 = 72$ mm Hg ($M = H_2$), giving $k_7 = 0.84 \times 10^{10}$ liter^2 mole^{-2} sec^{-1} ($M = H_2$), or 0.17×10^{10} with argon as M.

Previously, the only estimates of K_7 at room temperature are those made by Hoare and Walsh[4] from the results of Robertson[5] and Patrick and Robb,[6] lower limits for k_7 being 2.9×10^{11} and 1.8×10^{11} liter^2 mole^{-2} sec^{-1}, respectively; consistent with these is the value of 6.3×10^{11} given by Burgess and Robb[7] as a result of further studies of the Hg-photosensitised H_2/O_2 reaction. As pointed out by Walsh, these estimates ($M = H_2$ in

all cases) imply a negative activation energy for reaction (7) of 3–5 kcal/mole. Support for this value comes firstly from the temperature coefficient of the photochemical reaction studies by Burgess and Robb, from which they deduce that $E_7 = -4.8$ kcal/mole; secondly, Warren[8] finds that the most accurate value for the temperature coefficient of the second limit of the H_2/O_2 reaction corresponds to $(E_{-3} - E_7) = 20$ kcal/mole. Since evidence from a variety of sources suggests $E_{-3} = 16$–17 kcal/mole, a negative value of 3–4 kcal/mole is suggested for E_7.

The new value of 1.2×10^{10} liter^2 mole^{-2} sec^{-1} (M = argon) given by Clyne provides further information on this negative activation energy, though the value ($E_7 = -(2$–$3)$ kcal/mole) is slightly less than previous estimates.

References

1. Baldwin, R. R. and Cowe, D. W.: Trans. Faraday Soc. *58*, 1768 (1962).
2. Baldwin, R. R.: Trans. Faraday Soc. *52*, 1344 (1956).
3. Semenov, N. N.: Acta Physicochim. U.S.S.R. *20*, 290 (1942).
4. Hoare, D. E. and Walsh, A. D.: Trans. Faraday Soc. *53*, 1102 (1957).
5. Robertson, A. J. B.: Discussions Faraday Soc. *17*, 98 (1954).
6. Patrick, C. R. and Robb, J. C.: Discussions Faraday Soc. *17*, 98 (1954).
7. Burgess, A. R. and Robb, J. C.: Trans. Faraday Soc. *54*, 1008 (1958).
8. Warren, D. R.: Proc. Roy. Soc. (London) *A211*, 86 (1952).

KINETICS IN HYDROGEN-AIR FLOW SYSTEMS. I. CALCULATION OF IGNITION DELAYS FOR HYPERSONIC RAMJETS

I. N. MOMTCHILOFF, E. D. TABACK, AND R. F. BUSWELL

An analytical method of estimating auto-ignition delay time based on dissociation and recombination rates of gases has been developed. In this analytical method, the one-dimensional gas-dynamics equations are combined with reaction-kinetics equations to formulate a set of $(n + 5)$ simultaneous, nonlinear-first-order differential equations, where n is the number of species considered. These equations describe the behavior of a mixture of reacting gases flowing supersonically down a duct. A computer program has been evolved and used to solve these equations for the particular case of hydrogen-air mixtures. The ignition delay periods obtained through this program are in good agreement with the limited amount of experimental data available for hydrogen and air.

Introduction

The intake of a conventional ramjet engine is designed to produce subsonic flow at the inlet to the combustor. For hypersonic vehicles, however, it seems that there are advantages to be gained by so designing a ramjet that flow is supersonic throughout.[1,2,3,4] Such a design involves the concept of supersonic combustion. One parameter which must be evaluated in the design of a supersonic combustion system is the ignition delay period.

If a mixture of fuel and air is suddenly raised above its ignition temperature, a significant heat release does not occur immediately but after a finite time, commonly called the ignition delay period. The design length of a supersonic combustion chamber depends upon both the length required to mix the fuel and air, and the length required to complete the reaction, the latter being comprised of an ignition delay length and a reaction length. An indication of the importance of ignition delay can be formed from the fact that, in a typical case, a delay of one millisecond can represent a length of some 15 feet.

For a number of reasons, hydrogen is often considered as the fuel for ramjets for hypersonic vehicles. Information on delay periods for hydrogen-air systems is not plentiful. Although static temperatures and pressures can, to a certain extent, be controlled by intake design, an accurate knowledge of the dependence of delay period on these and the equivalence ratio is mandatory before a proper balance can be drawn among all the design considerations.

An experimental investigation would be the most satisfactory way to resolve the problem. Such an investigation, however, would have been both expensive and technically difficult. Previous theoretical studies have been limited to deriving an overall rate of ignition from the limited experimental data available or to examination of the rate constant data for the various reactions. The latter technique involves the selection of what appears to be the predominating reaction and assuming that it controls the overall rate. A more accurate representation of the combustion process could be obtained by simultaneous solution of the chemical kinetic rate equations for major reactions with the gas dynamics equations. The resulting theoretical analysis has led to the evolution of a computer program capable of predicting delay periods throughout the range of interest. The objectives of this investigation were:

(1) To derive the simultaneous differential equations governing the progress of a number of reactions occurring in a combustible mixture of air and hydrogen flowing down an adiabatic, frictionless duct.

(2) To evolve a computer program capable of solving these equations with acceptable accuracy.

(3) To test the accuracy of this procedure in a number of cases, particularly in relation to experimentally determined delay periods.

(4) To estimate delay periods over a wide range of operating conditions.

This paper presents the results of this investigation.

Analysis

General Considerations. Consider an elemental volume forming part of an air stream, and let it

be near the surface of separation between the air and a stream of hydrogen which is being injected into it. Let the flow ratios and static temperatures of the streams be such that, on mixing, the mixture would ignite spontaneously. Assume that the composition of each stream is the equilibrium composition corresponding to the stream static pressure and temperature. Let enough hydrogen, both atomic and diatomic, cross the surface of separation and enter the elemental air volume to make the local equivalence ratio fall between the flammability limits.

Now consider the history of that elemental volume as it moves downstream. Assuming that the air and hydrogen are injected with a small relative velocity and that the cross-sectional area of the duct does not change abruptly, there will be no appreciable change in pressure or temperature until the reaction rate begins to increase rapidly, with a corresponding increase in static temperature and pressure. The local equivalence ratio will change as the mixing process continues, but it will be shown that equivalence ratio has a relatively small effect on the length of the delay period for mixtures near stoichiometric. This sequence of events can then be represented by the model consisting of hydrogen and air that is instantaneously mixed and allowed to flow down a duct. Although in this model the air and hydrogen were both individually in equilibrium, the instantaneously formed mixture is not. Changes in the constitution of the mixture will now take place and the formation of species such as OH and H_2O will begin to occur. Many reactions can be written to describe what could or does take place. Only by very sophisticated experiments could one firmly establish which of these are important. For any analysis one must assume the reactions which occur and compute the progress of these as the mixture flows down the duct. At some point the exothermic reactions would predominate and the temperature would begin to rise. As the reaction rates (on the average) increase with temperature, the rate of temperature rise increases. As the final "flame" temperature is approached, however, the rate of temperature rise decreases and the temperature and composition tend to final equilibrium values. This only applies to a constant area duct. A duct of continually varying cross section would not allow a unique set of equilibrium conditions to be reached, since the temperature and pressure will continually vary due to the area change.

Basic Assumptions. In this analysis the following assumptions are made:

(1) The fuel and air are instantaneously mixed at the duct entrance.
(2) The gases obey the perfect-gas laws.
(3) One-dimensional gas dynamics treatment is applied to analyze the supersonic flow along an adiabatic, frictionless duct.
(4) Radiation, which is very small from hydrogen-air flames, is neglected.

Derivation of Equations. Consider the equations which govern the physical model previously mentioned and its associated assumptions.

Three conservation equations—mass, energy, and momentum—may be enumerated:

$$\textit{Mass:} \qquad \dot{m} = \rho v A \tag{1}$$

$$\textit{Energy:} \qquad H_0 = H + v^2/2g_0J \tag{2}$$

$$\textit{Momentum:} \qquad v\frac{dv}{dx} + \frac{g_0}{\rho}\frac{dp}{dx} = 0 \tag{3}$$

The duct cross-sectional area may be presented as a function of axial distance along the duct:

$$A = A(x)$$

The equation of state may also be written:

$$p = \rho TR \sum (\gamma_i/W_i)$$
$$= \rho TR \sum \sigma_i$$

The enthalpy is given by:

$$H = \sum h_i\sigma_i$$

where

$$h_i = \int_{Tb}^{T} C_{pi}\,dT + H_{fi}^{b}$$

From these equations, the following first-order, nonlinear differential equations can be derived (see Appendix):

$$T' = \frac{A'/A - \sum \sigma_i'/\sum \sigma_i - J\sum h_i\sigma_i'(g_0/v^2 - \rho/p)}{J\sum \sigma_i C_{pi}(g_0/v^2 - \rho/p) + 1/T}$$

$$H' = \sum h_i\sigma_i' + \sum \sigma_i C_{pi}T'$$

$$v' = -g_0JH'/v$$

$$p' = -\rho vv'/g_0$$

$$\rho' = -\rho(A'/A + v'/v)$$

where the primes denote differentiation with respect to x.

Let n be the total number of chemical species such as M_i in the gas mixture of which the first n_a are atomic species and the remaining $(n - n_a)$ are molecular species. The jth chemical reaction taking place in the mixture can be formally written as:

$$\sum_{i=1}^{n} \alpha_i{}^{j'} M_i \underset{k_b{}^j}{\overset{k_f{}^j}{\rightleftharpoons}} \sum_{i=1}^{n} \alpha_i{}^{j''} M_i$$

The $(n - n_a)$ differential continuity equations for the molecular species are given by:

$$\rho \frac{D\sigma_i}{Dt} = \sum_{j=1}^{N} (\alpha_i{}^{j''} - \alpha_i{}^{j'}) X^j$$

where

$$X^j = k_f{}^j \prod_{i=1}^{n} (\rho\sigma_i)^{\alpha_i j'} - k_b{}^j \prod_{i=1}^{n} (\rho\sigma_i)^{\alpha_i j''}$$

In the case of steady, one-dimensional flow, the term $\rho D\sigma_i/Dt$ reduces to $\rho v\, d\sigma_i/dx$.

The n_a atomic continuity equations are given by:

$$\Gamma_i = \sigma_i + \sum_{q=n_a+1}^{n} (\beta_{iq}\sigma_q).$$

These equations can be differentiated to give:

$$\sigma_i{}' = -\sum_{q=n_a+1}^{n} (\beta_{iq}\sigma_q{}')$$

where primes denote differentiation with respect to x.

The equilibrium constant for the jth reaction is defined as:

$$K_c{}^j = \prod_{i=1}^{n} (\rho\sigma_i)^{(\alpha_i j'' - \alpha_i j')}$$

This is the equilibrium constant based on mole concentrations; it is related to the more usual one based on partial pressure or fugacity by the equation:

$$K_c{}^j = K_p{}^j (RT)^{-\sum_{i=1}^{n} (\alpha_i j'' - \alpha_i j')}$$

where $K_p{}^j$ is the equilibrium constant based on partial pressure.

It is assumed that the forward and backward rates obey the relation:

$$K_c{}^j = (k_f{}^j/k_b{}^j)$$

This is a reasonable assumption for bimolecular reactions but is probably not very good for three-body reactions.[5]

These relations were used to compile $(n + 5)$ first-order, nonlinear differential equations; n_a of these are the atomic continuity equations, $(n - n_a)$ are the molecular continuity equations, and the remaining five are the equations for temperature, enthalpy, pressure, velocity, and density evolved from the gas dynamics and state equations. Solutions of the equations for any given initial conditions can be obtained by standard numerical methods utilizing a digital computer.

Reactions Selected. The general equations must now be applied to a specific set of reactions. The selection of the reactions to be considered is a difficult matter; even the selection of the species to be considered is not straightforward and when these have been chosen there are a large number of reactions that could be considered.

On the advice of Dr. T. M. Sugden, of the Physical Chemistry Department of Cambridge University, and Dr. J. P. Appleton of the University of Southampton, the following reactions were selected:

$j = 1$ $\quad H_2 + OH \xrightarrow{k_f{}^1} H_2O + H$

$j = 2$ $\quad H + O_2 \xrightarrow{k_f{}^2} OH + O$

$j = 3$ $\quad H_2 + O \xrightarrow{k_f{}^3} OH + H$

$j = 4$ $\quad H + H + M \xrightarrow{k_f{}^4} H_2 + M$

$j = 5$ $\quad H + OH + M \xrightarrow{k_f{}^5} H_2O + M$

$j = 6$ $\quad O + O + M \xrightarrow{k_f{}^6} O_2 + M$

$j = 7$ $\quad NO + M \xrightarrow{k_f{}^7} N + O + M$

$j = 8$ $\quad N_2 + O \xrightarrow{k_f{}^8} NO + N$

$j = 9$ $\quad O_2 + N \xrightarrow{k_f{}^9} O + NO$

$j = 10$ $\quad O_2 + N_2 \xrightarrow{k_f{}^{10}} 2NO$

M in the three-body reactions is taken to represent all the molecules in the system. Its mass fraction is taken as 1 and its molecular weight as the mean molecular weight of the mixture.

Thus, the species considered in the program are O, H, O_2, H_2, OH, H_2O, N_2, N, and NO.

Thermodynamic and Chemical Kinetic Data. In order that the physical parameters used in the calculation may be represented with acceptable accuracy up to 6000° Rankine, a base tempera-

ture of 1800° Rankine was chosen. Heats of formation at 1800° Rankine were used. The specific heats at constant pressure were represented by relations of the type:

$$C_p = A_c + B_c(T - T_b) + C_c(T - T_b)^2$$

Values of C_p, K_p, $H_f{}^b$ were taken from reference 6. The expressions for C_p and K_c derived from the listed values are valid in the range 1800–6000° Rankine.

The forward rate constants $k_f{}^j$ were in the form:

$$k_f = D \cdot T^E \cdot \exp(F/T)$$

The equilibrium constants $K_c{}^j$ were in the form:

$$K_c = D_c \cdot T^{Ec} \cdot \exp(F_c/T)$$

$k_b{}^j$ is given by $k_b = k_f/K_c$.

The rate constants used are here quoted in units more familiar to physical chemists. Temperature is in degrees Kelvin.

$k_f{}^1 = 4.2 \times 10^9 \times T^{.5} \exp(-10/RT)$	liters/mole sec[7,8]
$k_f{}^2 = 5.64 \times 10^{10} \exp(-15.1/RT)$	liters/mole sec[9]
$k_f{}^3 = 1.2 \times 10^{10} \exp(-9.2/RT)$	liters/mole sec[10]
$k_b{}^4 = 10^{18} \times T^{-1.5} \exp(-103.2/RT)$	liters/mole sec[11] adjusted to agree with[5]
$k_b{}^5 = 2 \times 10^{19} \times T^{-1.5} \exp(-114.7/RT)$	liters/mole sec[11] adjusted to agree with[5]
$k_f{}^6 = 18.5 \times 10^{10} T^{-.5}$	liters^2/mole^2 sec[12]
$k_b{}^7 = 1.43 \times 10^9 (T/4500)^{-1.5}$	liters^2/mole^2 sec[13]
$k_f{}^8 = 6.71 \times 10^{10} (4500/T)^{-.5} \exp(-38000/T)$	liters/mole sec[14]
$k_f{}^9 = 6.8 \times 10^9 (4500/T)^{-.5} \exp(-3120/T)$	liters/mole sec[15]
$k_f{}^{10} = 2.7 \times 10^{10} \exp(-53800/T)$	liters/mole sec[16]

Computer Program. The numerical integration method chosen was that of Runge–Kutta, incorporating modifications by Gill.[17] Since it is known that the rate equations become unstable near equilibrium,[18] it was decided to attempt to minimize this difficulty by using a double precision facility which, when required, doubles the number of digits used in computation. An IBM 7090 was used.

Discussion

Comparison with Experimental Delay Time. Although the analytical procedure developed is capable of calculating the progress of the reaction from initiation to completion and the amount of recombination during expansion, the preliminary results reported here are primarily concerned with the ignition delay or induction period. As a first check on the validity of the procedure, reactions, and rates used, the calculated ignition delay times were compared with the existing experimental data. The primary variable affecting ignition delay time is the initial mixture temperature. In order to show a simple comparison between the theoretical and experimental effect of temperature on ignition delay, the comparison was restricted to hydrogen-air mixtures at an equivalence ratio of 1.0 and 1-atmosphere pressure. Thus, only the experimental data at these conditions or the data which could be reliably extrapolated to these conditions were used in the comparison.

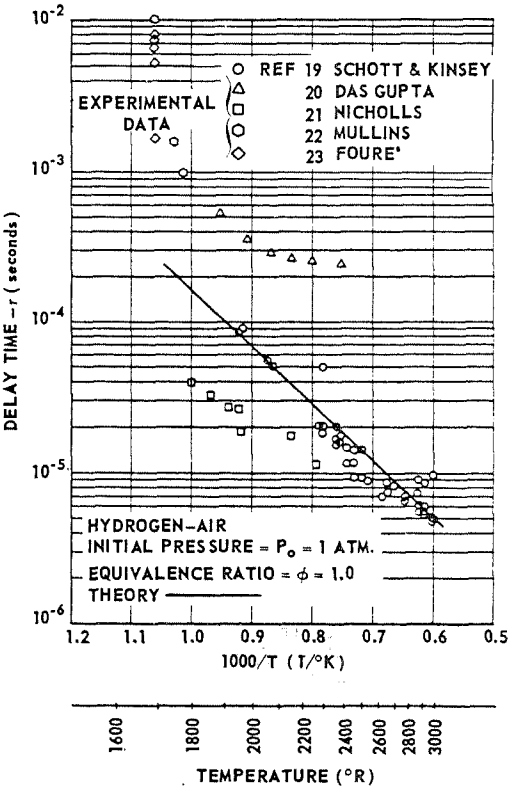

FIG. 1. Comparison of experimental and theoretical ignition delay time.

The comparison between the theoretical and experimental effect of temperature on ignition delay is shown in Fig. 1. The shock tube data of Schott and Kinsey was obtained with hydrogen-oxygen appreciably diluted with argon in order to lengthen the induction period. Since their results indicate that the delay time varies inversely with the oxygen concentration, the data has been adjusted to the partial pressure of oxygen for a stoichiometric hydrogen-air mixture at one atmosphere pressure. The agreement between the theoretical results and experimental data of Schott and Kinsey[19] is exceptionally good. While the slopes are similar for the other two sources of experimental data in the temperature range of interest, Das Gupta[20] and Nicholls,[21] the levels are different. Nicholls, whose measured delay times for hydrogen-air mixtures passed through a stabilized normal shock are very small, expressed some concern about the accuracy of his results due to possible errors in measurement of temperature, delay distance, and fuel-air ratio as well as errors in the method of data reduction. The data of Das Gupta were obtained with a subsonic flow rig rather than a shock tube and the delay time reported includes the time to physically mix the fuel and air. The separation of the mixing time from the overall delay times reported would tend to lower Das Gupta's values and is necessary before a valid comparison can be made.

At temperatures below 1700° Rankine only a representative amount of the available experimental data is shown. A more complete summary of these data can be found.[24] The experimental results in this low temperature range are from bomb and flame experiments and include physical mixing effects, such as those included in the results of Das Gupta,[20] and probably are affected by wall quenching effects and surface reactions. Similar conclusions have been stated by others, e.g., Drell and Belles.[25] It is therefore not surprising that the theoretical ignition delay times are appreciably less than the experimental values at low temperatures. Further analytical and experimental work is required to resolve this problem.

Aside from the major differences in experimental techniques, the various experimenters have also used different criteria for measuring the delay time depending upon their test techniques. Schott and Kinsey[19] assumed the delay to be equivalent to the time required for the hydroxyl radical concentration to reach the threshold of experimental detection, (10^{-6} mole/liter). Das Gupta[20] measured the pressure variation along the combustion tube length by a series of pressure probes and assumed that the ignition point was represented by the intersection of the initial and maximum pressure slopes. Nicholls[21] used a schlieren sodium emission photographic technique to establish the separation between the shock wave and combustion zone, from which the delay times were computed.

In the theoretical analysis as well as the experimental work there is no positive definition of the point at which ignition occurs. Therefore the theoretical ignition delay was calculated using the following criteria representative of the various test techniques: (a) time for the hydroxyl radical concentration to reach 10^{-6} mole/liter, (b) an interpolation procedure based on the location of the intersection of the slopes of the initial and maximum temperature rise, (c) time required to reach a temperature 5 per cent higher than the initial temperature, and (d) the point at which the slope of the temperature versus time reached $10^{6°}$ Rankine/second. Although each criterion provides a different curve (Fig. 2), the general trends are similar and the differences are not large enough to account for the differences in the experimental data. Since any criterion is an arbitrary decision, it was decided to use the hydroxyl concentration criterion[19] to be consistent with what is believed to be the most reliable experimental data.

As a further check on the validity of this analytical procedure, the theoretical effect of equivalence ratio and pressure were compared with the experimental results at various temperatures. The equivalence ratio has a very

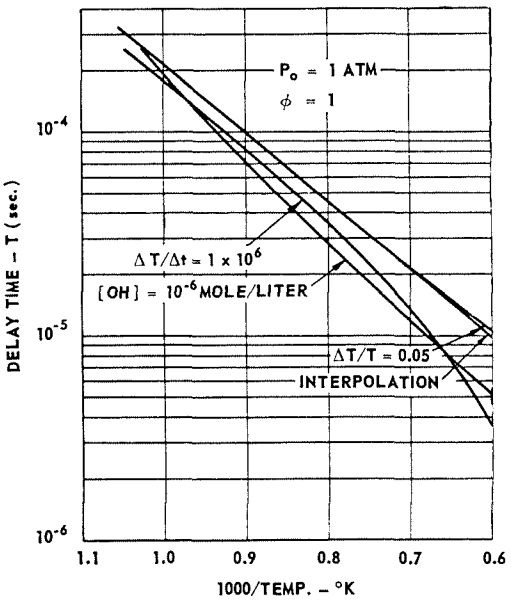

FIG. 2. Effect of ignition delay criteria on theoretical ignition delay time.

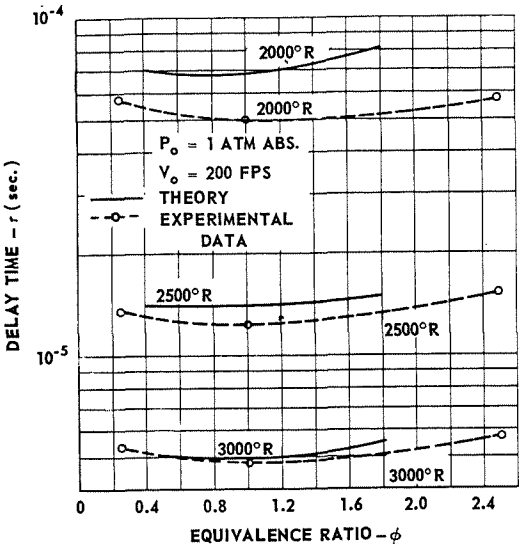

FIG. 3. Effect of equivalence ratio.

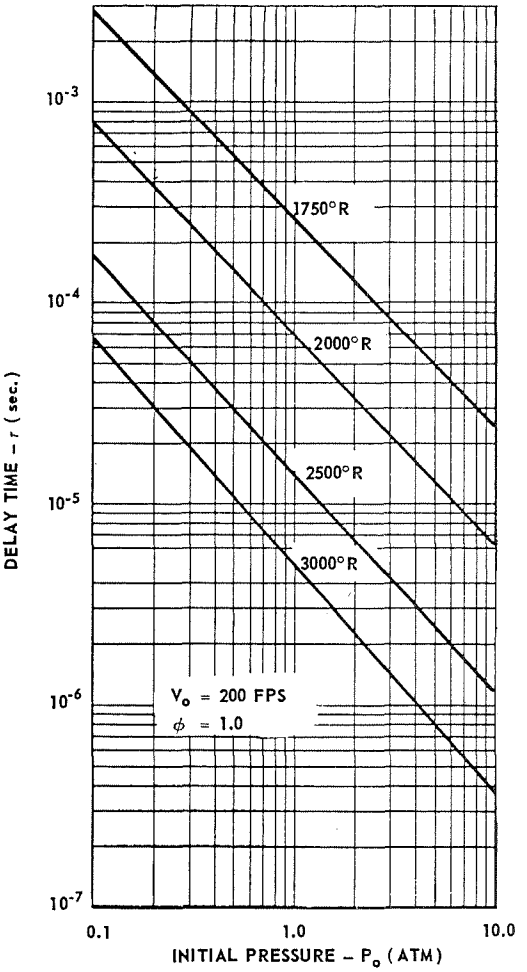

FIG. 4. Effect of pressure.

slight effect on the theoretical ignition delay time with the minimum delay occurring near the stoichiometric mixture ratio (Fig. 3). Schott and Kinsey[19] indicated that at a constant temperature the ignition delay time is inversely proportional to the oxygen concentration for all equivalence ratios. This implies that the delay time should increase slightly as the equivalence ratio increases. However, inspection of their data revealed systematic differences in the value of oxygen concentration times delay time for the three equivalence ratios tested (0.250, 1.0, 2.50). The experimental results shown in Fig. 3 are for the published data with these systematic differences taken into account. Although the experimental values of Das Gupta[20] are high due to the inclusion of the mixing time, he reported that there was no large or consistent effect of equivalence ratio.

The theoretical ignition delay time increases with decreasing pressure (Fig. 4). The slopes of the theoretical curves, which vary from 1.03 to 1.11, are consistent with the data of Schott and Kinsey which indicate a slope of 1.0. The slopes of the experimental results of Das Gupta vary from less than one to greater than one with an average slope of about 0.9.

A possible source of error in the theoretical prediction of delay time is the accuracy of the rate constant data. This is a complicated matter since an error in the rate of one reaction may or may not have a vital effect on the computed delay times, depending upon the importance of that reaction. A discussion on the effect of the accuracy of rate constant determination will be found in ref. 18. Most rates used in this work are believed to be correct within a factor of two or three. The correlation between the computed and experimental values would seem to corroborate this view. However, before the computed values can be considered an accurate representation of actual conditions, further investigation of the reaction mechanism, and rate constant data in the range of interest is necessary.

Concentration Profiles. The computational procedure contributes to an understanding of the combustion process by providing complete reaction profiles (Fig. 5) for the system under consideration. In the past, the progress of the combustion process has been estimated by examination of the relative magnitude of the rate constants. The present procedure allows the importance of the minor reactions to be assessed. It should also be interesting and useful for

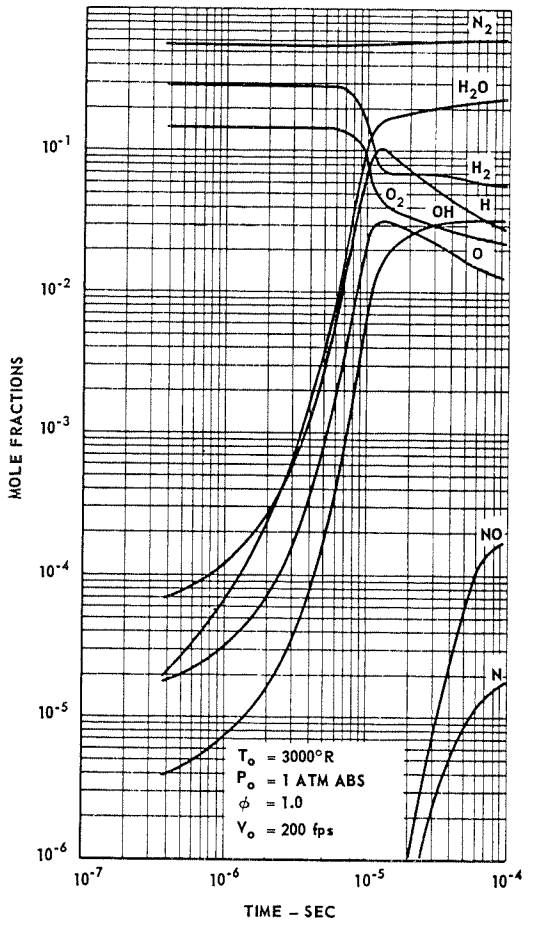

FIG. 5. Typical concentration profiles.

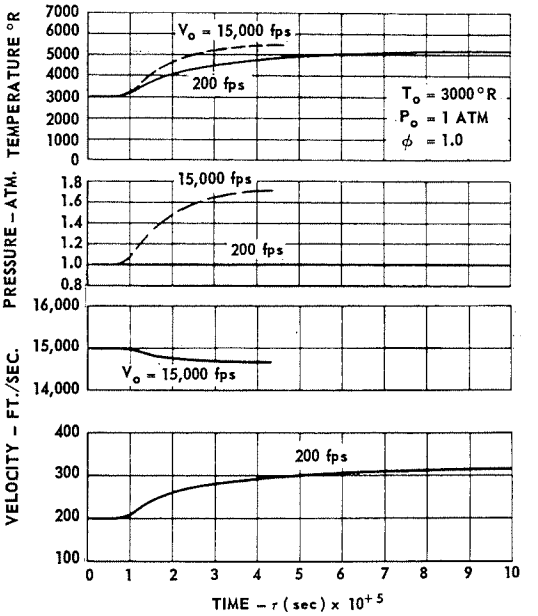

FIG. 6. Effect of initial velocity.

investigating the region below 1700° Rankine where the experimental data indicate there may be a shift in the reaction of major importance. This region has not been studied in detail as yet due to the long computation time involved.

The reaction profiles for a typical set of initial conditions (Fig. 5) are characterized by the presence of several distinct regions. The first stage consists of the formation of small concentrations of atoms and hydroxyl radicals capable of initiating the chain-branching mechanism. At the end of this initial period the chain-branching mechanism sets in due to the simultaneous action of reactions 1, 2, and 3. During the remainder of the reaction, the product species increase exponentially with time, until significant quantities of H_2 and O_2 are consumed and the rates of the forward and reverse reactions become comparable. During this period the temperature increases slowly (Fig. 6). Particularly conspicuous is the excess of O and H atoms at the end of the induction period. It has been pointed out[19] that an overshoot in atom and radical concentration is a property of the chain-branching mechanism.

It is interesting to note the behavior of the H_2O and H concentrations during the latter portion of the induction period. Assuming the OH and O atoms to be steady-state intermediates, the stoichiometry of the chain may be written as:

$$3H_2 + O_2 \rightarrow 2H_2O + 2H$$

This predicts that the rates of formation of H_2O and H are the same, as are observed in the reaction profiles of Fig. 5. The remainder of the reaction is characterized by the relatively slow recombination of the excess species. It should be noted that, as anticipated, the nitrogen reactions are comparatively unimportant below 4000° Rankine.

Effect of Velocity. The time variation of temperature, pressure, and velocity for typical subsonic and hypersonic reacting flows in constant area ducts are shown in Fig. 6. With subsonic flow the progress of the combustion process is accompanied by an increase in temperature, a reduction in static pressure and an acceleration of the stream. For supersonic flow the temperature rise is accompanied by an increase in static pressure and a reduction in velocity. Linked with these changes is the time required for the combustion process to reach completion. It was noted

earlier that an increase in pressure is accompanied by a reduction in delay time due to an increase in the rate of reaction. Hence for the same initial static pressure and temperature the supersonic stream should approach equilibrium more rapidly than the subsonic stream, as shown in Fig. 6. Although the time required for complete reaction is shorter in supersonic flow the length is longer due to the higher velocities. The ignition delay time is essentially independent of stream velocity since ignition occurs at such an early stage of the combustion process that the difference in state properties is negligible.

Ignition Delay Lengths for Hypersonic Ramjets. One of the areas where ignition delay time is of considerable interest at present is for hypersonic ramjets utilizing supersonic combustion, in which even a short ignition delay time may represent a long length. Ignition delay lengths were calculated for a range of flight Mach numbers for a typical supersonic combustion ramjet with a fixed geometry inlet at representative flight altitudes. The ignition delay length (Fig. 7) increases rapidly at the lower flight Mach numbers. Previous curves on effect of temperature and pressure on delay time can be used to estimate effect of lower altitude or increased inlet diffusion on delay length. The

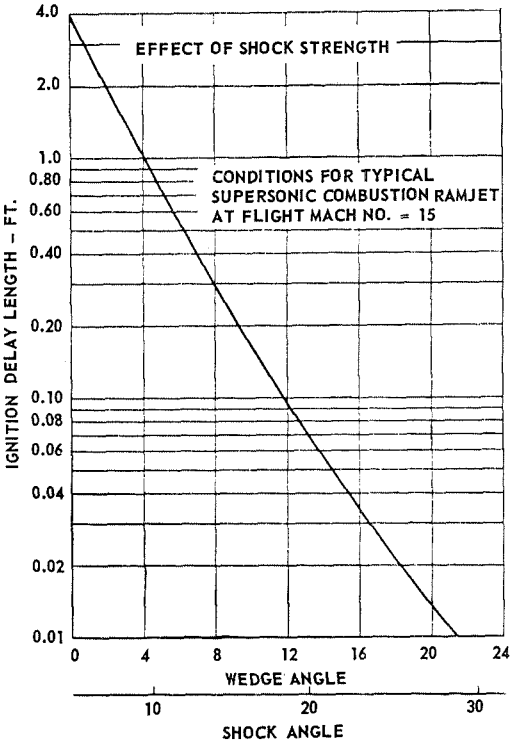

FIG. 8. Effect of shock strength.

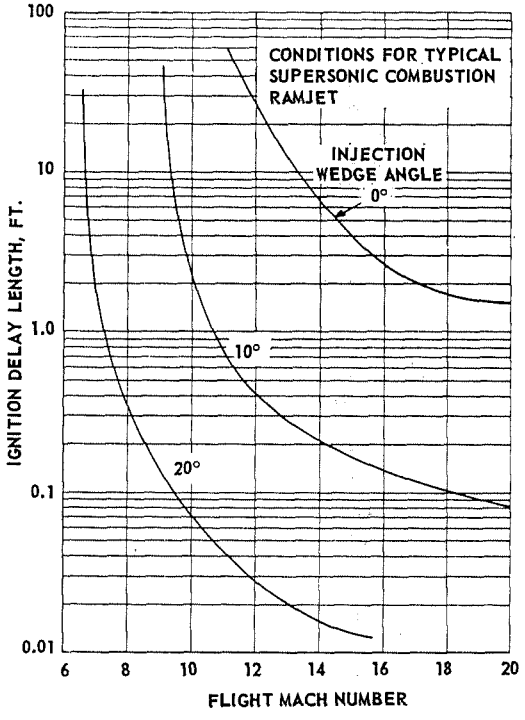

FIG. 7. Ignition delay length.

actual delay length which will occur in an engine will depend not only on flight altitude, inlet design, and efficiency, but also on the manner in which fuel is injected and fuel-air mixing occurs. Detailed consideration of these practical engine effects was beyond the scope of this work, but the reaction analysis presented is a basic tool necessary to estimate the delay time for any particular situation. To illustrate how this analysis may be combined with the fluid dynamic equations, ignition delays were estimated assuming that the fuel injection created a shock equivalent to that from a wedge. As shown in Figs. 7 and 8, at the conditions in a hypersonic ramjet even relatively weak shocks will decrease the ignition delay by an order of magnitude. The effect of the mixing process, boundary layers, etc. on local flow conditions and thus reaction ratio must be evaluated before the actual importance of ignition delay can be determined. At most it will be of concern only at the lower flight speeds and will depend upon the design details of the engine.

As suggested by Fig. 6, the capability of the basic procedure for estimating the time and length required to complete the reaction and the amount of recombination during the expansion will be of equal or greater importance in the

analysis of hypersonic ramjet performance. With minor modifications to adjust the composition of the initial mixture, the procedure also provides a method of estimating the differences between the simulated air, often used in testing at hypersonic velocities, and air.

ACKNOWLEDGMENTS

The authors gratefully acknowledge the contributions of Dr. K. N. C. Bray and Dr. J. P. Appleton of the University of Southampton, Dr. T. M. Sugden of Cambridge University, and the assistance of personnel at IBM Data Center, London, England.

REFERENCES

1. WEBER, R. J. and MACKAY, J. S.: NACA, TN 4386 (1958).
2. MCLAFFERTY, G. N.: ARS Journal *30*, 1019 (1960).
3. DUGGER, G. L.: *Fourth AGARD Combustion and Propulsion Symsosium.* Pergamon, 1961.
4. MORDELL, D. L. and SWITHENBANK, J.: *Second International Congress of Aeronautical Sciences.* Pergamon, 1960.
5. SUGDEN, T. M.: Private communication, (June, 1961).
6. JANAF Thermochemical Tables.
7. SEMENOV, N. N.: *Some Problems of Chemical Kinetics and Reactivity.* Pergamon, 1959.
8. AVRAMENKO, L. I. and LORENTOA, R. V.: Zhur. Fiz. Khim. *24*, 207 (1950).
9. KARMILOVA, L. V. et al.: Zhur. Fiz. Khim. *32*, 1193 (1958).
10. CLYNE, M. A. A. and THRUSH, B. A.: Nature *189*, 56 (1961).
11. DUFF, R. E.: J. Chem. Phys. *28*, 1193 (1958).
12. MATTHEWS, D. L.: Phys. Fluids *2*, 170 (1959).
13. WRAY, K. L. et al.: *Eighth Symposium (International) on Combustion*, p. 328. Williams and Wilkins, 1962.
14. DAVIDSON, N.: AVCO Res. Lab. Rept. No. 32, (1958).
15. VINCENTI, W. G.: Stanford University Department of Aeronautical Engineering Report No. 101 (1961).
16. KAUFMAN, F. and KELSO, J. P.: J. Chem. Phys. *23*, 1072 (1955).
17. RALSTON, A. and WILF, H. S.: *Mathematical Methods for Digital Computers.* John Wiley and Sons, 1960.
18. BRAY, K. N. C. and APPLETON, J. P.: AASU Report No. 166, Department of Aeronautics and Astronautics, University of Southampton, England, (1961).
19. SCHOTT, G. L. and KINSEY, J. L.: J. Chem. Phys. *29*, 1177 (1958).
20. DAS GUPTA, N. C.: McGill University Department of Mechanical Engineering Report No. SCS 36, (1961).
21. NICHOLLS, J. A.: Stabilization of Gaseous Detonation Waves with Emphasis on the Ignition Delay Zone, Ph.D. Thesis, University of Michigan, January 1960.
22. MULLINS, B. P.: NATO AGARD AG5/P2, 16–31 (1952).
23. FOURÉ, C.: Recherché Aeron. 33 (1954).
24. PATCH, R. W.: ARS Journal *31*, 46 (1961).
25. DRELL, I. L. and BELLES, F. E.: NACA Report 1383 (1958).

Nomenclature

A	Duct cross-sectional area function [sq ft]
A_c	Specific heat function coefficient [Btu/lb-mole-°R]
B_c	Specific heat function coefficient [Btu/lb-mole-(°R)^2]
C_c	Specific heat function coefficient [Btu/lb-mole-(°R)^3]
C_p	Specific heat at constant pressure [Btu/lb-mole-°R]
D	Forward rate constant coefficient
D_c	Equilibrium constant coefficient
E	Forward rate constant coefficient
E_c	Equilibrium constant coefficient
F	Forward rate constant coefficient
F_c	Equilibrium constant coefficient
g_0	Inertial constant [lbf/lbm]
H	Enthalpy of mixture [Btu/lb]
H_0	Stagnation enthalpy [Btu/lb]
H_{fi}^b	Heat of formation of ith constituent at enthalpy base temperature T_b [Btu/lb-mole]
h_i	Enthalpy of ith component [Btu/lb-mole]
i	Species index
J	Mechanical equivalent of heat [ft-lb/Btu]
j	Reactions index
K_c^j	Equilibrium constant based on concentration [none or cu ft/lb-mole]
K_p^j	Equilibrium constant based on fugacity or partial pressure [none or sq ft/lb]

k_b^j	Backward rate constant [cu ft/lb-mole-sec or $ft^6/(lb\text{-}mole)^2\text{-}sec$]
k_i^j	Forward rate constant [cu ft/lb-mole-sec or $ft^6/(lb\text{-}mole)^2\text{-}sec$]
M	Symbol representing all constituents
M_i	Chemical formula of ith species
$\dot{m}$	Mass velocity [lb/sec]
N	Total number of reactions
n	Total number of species
n_a	Number of atomic species
p	Static pressure [psf]
P_0	Initial static pressure [atm]
R	Universal gas constant [lb-ft/lb-mole-°R]
T	Static temperature [°R]
T_b	Enthalpy base temperature [°R]
T_0	Initial static temperature [°R]
t	Time [sec]
v	Velocity [fps]
V_0	Initial velocity [fps]
W_i	Molecular weight [lb/lb-mole]
X^j	Net rate parameter [lb-mole/cu ft-sec]
x	Distance from inlet [ft]

Greek Letters

$\alpha_i^{j'}, \alpha_i^{j''}$	Stoichiometric coefficients of the ith species in the jth reaction, reactants and products respectively
β_{iq}	Number of atoms of the ith atomic species in the qth molecular species
γ_i	Mass fraction of ith constituent
Γ_1	Atomic continuity parameter—oxygen [lb-mole/lb]
Γ_2	Atomic continuity parameter—hydrogen [lb-mole/lb]
ρ	Density [lb/cu ft]
σ_i	Concentration; mass fraction divided by molecular weight [lb-mole/lb]
τ	Ignition delay time [sec]
ϕ	Equivalence ratio = $\dfrac{\text{mass of fuel/mass of mixture}}{\text{(mass of fuel/mass of mixture) at stoichiometric}}$

Appendix

Derivation of General Equations

Gas Dynamics Equations

Conservation: *Mass*

$$\dot{m} = \rho v A \tag{1}$$

Energy

$$H_0 = H + v^2/2g_0J \tag{2}$$

Momentum

$$\frac{vdv}{dx} + \frac{g_0dp}{\rho dx} = 0 \tag{3}$$

Area:

$$A = A(x) \tag{4}$$

State:

$$p = \rho TR\Sigma\sigma_i \tag{5}$$

$$h_i = \int_{T_b}^{T} C_{pi}dT + H_{fi}^b \tag{6}$$

$$H = \Sigma h_i\sigma_i \tag{7}$$

Differentiating Eq. (5) with respect to x and denoting derivatives by primes:

$$p' = TR\Sigma\sigma_i\rho' + \rho R\Sigma\sigma_iT' + \rho RT\Sigma\sigma_i' \tag{8}$$

Similarly, from (1):

$$A'/A + v'/v + \rho'/\rho = 0 \tag{9}$$

Equations (3) and (9) may now be used to substitute for p' and ρ' in (8)

$$-\rho vv'/g_0 = -\rho TR\Sigma\sigma_i(A'/A + v'/v) + \rho R\Sigma\sigma_i T' + RT\sigma_i' = -p(A'/A + v'/v + pT'/T + p\Sigma\sigma_i'/\Sigma\sigma_i$$

Or:

$$(\rho v/pg_0 - 1/v)v' = A'/A - T'/T - \Sigma\sigma_i'/\Sigma\sigma_i \tag{10}$$

An expression for v' can be obtained by combining (2), (6), and (7):

$$v' = -(g_0J/v)(\Sigma h_i\sigma_i' + \Sigma\sigma_i C_{pi}T') \tag{11}$$

This expression can now be substituted in Eq. (10):

$$T' = \frac{A'/A - \Sigma\sigma_i'/\Sigma\sigma_i - J\Sigma h_i\sigma_i'(g_0/v^2 - \rho/p)}{J\Sigma\sigma_i C_{pi}(g_0/v^2 - \rho/p) + 1/T} \tag{12}$$

Differentiating (6) and (7) with respect to x, H' becomes:

$$H' = h_i\sigma_i' + \Sigma\sigma_i C_{pi}T' \tag{13}$$

Similarly, from (2):

$$v' = -(g_0J/v)H' \tag{14}$$

Rearranging (3) gives:

$$p' = -(\rho v/g_0)v' \tag{15}$$

Solving (9) for ρ' gives:

$$\rho' = -\rho(A'/A + v'/v) \tag{16}$$

It will be noticed that the expression for T' [Eq. (12)] can be evaluated in terms of the variables σ_i, p, t, v and x, using Eqs. (4), (5), and (6) and the reaction kinetics equations for σ_i'. Eqs. (13) to (16) can then be evaluated in turn.

KINETICS OF HYDROGEN-AIR FLOW SYSTEMS. II. CALCULATIONS OF NOZZLE FLOWS FOR RAMJETS

V. J. SARLI, A. W. BLACKMAN, AND R. F. BUSWELL

The performance of exhaust nozzles through which highly dissociated gases are accelerated depends greatly on the degree to which these gases are chemically recombined during the expansion process. An analytical method for calculating the extent of recombination for a specified nozzle contour has been developed from a combination of the chemical kinetic, gas dynamic, and state equations. A computer program has been evolved and used to solve these equations for hydrogen-air combustion products. The solution of these equations leads to the determination of concentrations, temperatures, pressures, and velocities as a function of time or distance for the combustion process and nozzle expansion. To illustrate the use of the computer program, the extent of recombination of hydrogen-air combustion products in a convergent-divergent exhaust nozzle, having a throat diameter of 6.18 inches was calculated for combustion chamber entrance conditions of pressure 3000 psf, temperature 2000°R, velocity 200 ft/sec, and an equivalence ratio equal to one. The results indicate that the flow freezes at an area ratio of approximately 1.1 in the nozzle convergent section.

Introduction

In recent years a great deal of interest has been shown in the evaluation of the effect of combustion and recombination rates on the over-all efficiency of propulsion systems for hypersonic vehicles.[1,2,3] It is well known that a relatively large proportion of the chemical energy released from combustion can be used to dissociate chemical species into atomic species and radicals. When the combustion products are expanded through a supersonic nozzle, the chemical energy absorbed in dissociating the combustion products is not available for conversion to kinetic energy unless the absorbed energy is first made available to the gas mixture through recombination of the dissociated species. Maximum energy release which produces maximum nozzle thrust is attained when the dissociated gases are in equilibrium at every station in the exhaust nozzle. The success or failure of certain propulsion schemes, such as the hypersonic ramjet, is greatly dependent on the degree to which combustion and the subsequent expansion approach equilibrium.[4] Thrust differences between frozen and equilibrium expansion as great as 75% at a flight Mach number of 9 and 200% at Mach 10 are indicated.[5] The degree to which chemical equilibrium is approached during the expansion process is dependent on the rate processes of the individual reactions in the recombination scheme and residence time of the gases in the nozzle.

Recent comprehensive reviews of chemical nonequilibrium effects have been reported by Vincenti[6] and by Bray and Appleton.[7] It is pointed out that the nature of the flow process can be determined by numerical analysis, provided the necessary kinetic data are available. Because of the laborious calculations that must be performed when a recombination scheme involving a multireaction mechanism which interacts with the gas dynamic process is considered, it is not surprising that solutions to these problems are lacking except in simplified forms. The simplified models consider a single nonequilibrium reaction or a single nonequilibrium process in which one reaction controls the rate behavior of multicomponent mixtures[8,9]. In addition to the single reaction process, studies have been reported which consider criteria for determining if a reaction departs from equilibrium.[7,10] For a single reaction system or for a single nonequilibrium process which is assumed to control, the criteria can be used to specify an equilibrium and frozen region. The nature of the flow in the transition region, however, is not defined. Of greater difficulty is the application of the criteria to a multireaction system. This difficulty arises when each reaction departs from equilibrium at a different station. A comprehensive discussion of the extension of this technique to multireaction systems is presented by Bray and Appleton.[7] Until exact solutions are performed for multireaction systems, the approximate solutions in

which a single reaction is assumed to control remains questionable because of the complex interaction of all the species.

Two recent studies have been reported which present exact solutions for nonequilibrium expansions of air with coupled chemical reactions.[6,11] Difficulty in each case is encountered at the entrance to the nozzle where the species are at equilibrium because of the singularity in each of the kinetic equations at this point. In order to avoid the singularity problems, a perturbation solution is used until the species are sufficiently removed from equilibrium. Integration can proceed from this point using the kinetic differential equations along with the gas dynamics equations.

In addition to the analytical studies, recent experimental work has been reported for hydrogen-air combustion products expanding through a supersonic exhaust nozzle.[5] Deviations from equilibrium were observed. The attempt to correlate an over-all recombination equation and rate with experimental data applying Bray's sudden freezing technique showed only qualitative agreement and the need for more exact calculation schemes.

The objective of this study was to develop a computer program for calculating the recombination of hydrogen-air combustion products expanding through a supersonic exhaust nozzle. Also, it was desirable to develop the program for use in conjunction with a program for computing ignition-delay and combustion reaction times as described in the preceding paper. The total program could then be used to determine composition and process profiles in the combustion chamber and supersonic nozzle.

Analytical Method

It is logical to assume that gases leaving a combustion chamber and entering an exhaust nozzle are not at equilibrium conditions because these conditions exist only for 100% combustion efficiency which is approached but usually not completely attained. Hence, it is desirable to establish the nonequilibrium conditions at the nozzle entrance based on the degree of equilibrium attained in the combustion chamber. In the procedure described herein, the conditions at the nozzle entrance are calculated by establishing the time-dependent ignition and reaction characteristics in the combustion chamber. The nozzle entrance conditions can be calculated as near-equilibrium conditions or conditions consistent with a specified fraction of maximum temperature rise. The progress of the combustion products concentration and the flow characteristics can be followed in the constant-area duct or combustion chamber as the fuel and oxidizer react. As the final "flame temperature" is approached, the rate of temperature rise decreases and the temperature and composition tend toward final equilibrium values. Since the approach to equilibrium is time dependent, the combustion chamber calculations are terminated when an arbitrarily small temperature-distance or temperature-time slope is attained. At this juncture the calculations are continued for a variable-area duct or nozzle. The nozzle entrance conditions are therefore near equilibrium. Any number of near-equilibrium conditions for the nozzle entrance can be simulated by this technique. This process also can simulate the conditions for combustion chamber efficiencies.

In this scheme for calculating the nature of the flow, it is never necessary to eliminate a reaction which may become insignificant due to the sudden "freezing" of certain species; nor is it necessary to preferentially deal with fast or slow reactions. Each reaction is continuously weighted according to its contribution to the flow process. An analysis of this type computes a complete history of the gaseous mixture between the inlet to the combustion chamber and the exit of the exhaust nozzle. Also, since complete chemical equilibrium is avoided everywhere in the analysis, the mathematical difficulties due to singularity in each of the reaction kinetic equations are eliminated.

The generalized equations which govern the nature of nozzle flows are formulated with the following basic assumptions:

1. The gases are fully mixed.
2. The gases are assumed to obey the ideal gas laws.
3. The flow is steady, one-dimensional, laminar, adiabatic, and frictionless.
4. Equilibrium between the internal degrees of freedom of all species is maintained.
5. Radiation effects are assumed small and are therefore neglected.

The formulation of the generalized mass, energy, momentum, state, and kinetic equations is standard for calculations of this type and is presented in the preceding paper. In addition to these equations, an additional equation must be included to allow for a specified variation of area.

The convergent and divergent nozzle contour can be expressed as

$$A = A_1 + A_2x + A_3x^2 \qquad (1)$$

where A_1, A_2, and A_3 are arbitrary constants separately specified for the convergent and divergent sections and x is the distance measured

from the nozzle entrance for the convergent section and from the throat for the divergent section.

Reaction Mechanism and Thermodynamic Data. The recombination model is represented by 10 reactions involving 9 species. The species are O, H, O_2, H_2, OH, H_2O, N, N_2, and NO. The selection of the reactions to be considered in the recombination scheme is a difficult matter. Although the species listed above are believed to be the important species, others could be written for the hydrogen-air system at equilibrium. Several of the above will be present in such small quantities that they may be thermodynamically unimportant. However, kinetically the species may be extremely important because of their role in reactions which involve thermodynamically important species.

Even when agreement exists on the mechanism, the specific reaction rates are open to question. The effects of different third bodies and temperatures are lacking in the majority of reactions which are likely to be important in the study of nonequilibrium nozzle flows. Although accuracy of the reaction-rate data is not of a high order, it is still worthwhile to perform "exact" calculations which may be improved as better data become available.

The reactions considered include most of the reactions reported in recent ignition-delay studies involving hydrogen-oxygen[12,13] and air dissociation-recombination studies.[11,14,15] Since the ignition calculations reported in the preceding paper involve the dissociation and recombination of hydrogen-air within the temperature range of interest for nozzle recombination, it was assumed that the same mechanism could be applied to recombination in the exhaust nozzle.

The kinetic data are the same as reported in the preceding paper. The thermochemical data utilized for these calculations are values from JANAF thermochemical tables.[16]

Calculation Procedure. The nonlinear differential equations were integrated for the proposed reaction mechanism and specific nozzle contour by a Runge-Kutta technique incorporating modifications by Gill.[17] This technique is employed by most workers in this and similar fields.[6,13] An IBM 7090 digital computer was used. Unlike the ignition delay calculations the integration at the nozzle entrance and the early phases of the convergent section can be relatively slow. The near-equilibrium conditions and coupled interaction of temperature and composition gradients of the complex mixture contributes to the difficulty. This can be seen from the generalized rate equations:

$$\rho V \sigma_i' = (\alpha_i{}^{j''} - \alpha_i{}^{j'})(R_f{}^j - R_b{}^j) \qquad (2)$$

$$R_f{}^j = k_f{}^j \prod_{j=1}^{N} (\rho\sigma_i)^{\alpha_i j'} \qquad (3)$$

$$R_b{}^j = k_b{}^j \prod_{j=1}^{N} (\rho\sigma_i)^{\alpha_i j''} \qquad (4)$$

As the jth reaction approaches equilibrium, the term in parentheses approaches zero. However, the flow can never be in a state of equilibrium if the derivatives of the flow variables are finite. If the values of $R_f{}^j$, the forward rate parameter, and $R_b{}^j$, the reverse rate parameter, are large relative to the value of their difference, the nature of the flow is near equilibrium. For near-equilibrium conditions, $R_f{}^j - R_b{}^j$ is almost indeterminant, and to avoid loss of accuracy the interval size for step-by-step integration must be very small. If there are many reactions which are near equilibrium and depart from this state at different stages in the nozzle, a small interval size may be required everywhere in the nozzle and consequently the machine time may be quite long. Nevertheless, numerical integration of the finite reaction-rate equations, the state equations, and the fluid dynamic equations can be accomplished if the conditions are away from equilibrium. The extent that the conditions must be away from equilibrium is dependent on machine accuracy. In order to reduce further the difficulties at near-equilibrium conditions, a double-precision facility was used which, when required, doubled the number of digits carried in the computation. It is readily seen that starting the recombination calculations at equilibrium conditions would increase the difficulties.

Another difficulty which is encountered is in the region of the throat of a converging-diverging nozzle. A singularity point exists in the flow equations between the converging and diverging sections of the nozzle. This is seen from the following equation (derived in the preceding paper) which relates the temperature gradient, composition gradients, and other process variables.

$$T' = \frac{(A'/A) - (\sum\sigma_i'/\sum\sigma_i) - J\sum h_i\sigma'[(g_0/v^2) - (\rho/p)]}{J\sum\sigma_i c_{pi}[(g_0/v^2) - (\rho/p)] + 1/T} \qquad (5)$$

In order for the temperature gradient to remain negative throughout the exhaust nozzle, the sign of the summation of the terms in the numerator must be opposite to that of the summation of the terms in the denominator. In the convergent and divergent sections the sign of the denominator must change from positive to negative when the numerator changes from negative to positive. This implies that the numerator and denominator

TABLE 1

Adjacent values between convergent and divergent sections

	A (ft²)	v (ft/sec)	p (lb/ft²)	T (°R)	ρ (lb/ft³)
Convergent	0.208561	3433.7	1657.1	4491.2	0.005672
Divergent	0.208579	3452.3	1645.8	4484.9	0.005641

pass through a zero point simultaneously and thus T' is undefined at some point between the subsonic and supersonic flow regimes. For nonequilibrium flow with heat release the sonic point should occur downstream of the throat. The difficulties encountered near the sonic points have been avoided by selecting an inlet area to the divergent section on the basis of continuity at the end of the convergent section.

In order to estimate the values of the properties at the divergent section of the exhaust nozzle, it was convenient to extrapolate the temperature, pressure, and velocity through the critical region to give the initial values for the divergent section. The procedure was carried out by utilizing the pressure, temperature, velocity, and density gradients when the Mach number defined by

$$M_f = v/\{[\sum\sigma_i c_{pi}/\sum\sigma_i(c_{pi} - R)](g_0 RT)(\sum\sigma_i)\}^{\frac{1}{2}} \quad (6)$$

equaled one. The gradients of the variables were calculated at each increment during the normal course of the integration. The extrapolation through the critical region was performed by determining the velocity consistent with a second Mach number defined by

$$M_p = v/(p'/\rho')^{\frac{1}{2}} \quad (7)$$

The pressure and density gradients, p' and ρ', can be calculated close to M_f equal to 1.0 and the corresponding Mach number M_p can de determined. The value of M_p for the start of the divergent section was arbitrarily increased to a value slightly greater than one. It was assumed that the ratio p'/ρ' at M_f near 1 is unchanged through the critical region. The distance over which the extrapolation was performed was estimated as $\Delta x = \Delta v/(v')$ where Δv represents the change in velocity and v' the velocity gradient across the critical region. In this case the distance through which the extrapolation was performed was approximately 10^{-5} ft.

The corresponding changes in the other variables through the critical region were determined as the product of the gradients for each variable and the incremental distance determined above. The area at the start of the divergent section of the nozzle was fixed by the continuity equation. From this point the integration of the kinetic, flow, and state equations was resumed with the area profile specified for the divergent section. The temperature gradient at the start of the divergent section remains negative if the signs of the numerator and denominator of Eq. (5) change within the critical region.

Table 1 indicates the values of the variables calculated across the critical region.

Although the above method is not rigorous theoretically, the results of the numerical calculations should be unaffected. When the throat size is fixed, the problem becomes more difficult for it is necessary to determine the unique mass flow by iteration until the solution satisfies the conditions that temperature, pressure, and density decrease and velocity increases along the nozzle. When it is necessary to consider only the divergent portion of the nozzle (as in the case of a supersonic combustion ramjet), any supersonic mass flow rate will allow a unique solution without iteration.

Results and Discussion

Analytical results for recombination of hydrogen-air combustion products in a supersonic nozzle are presented in Figs. 1–4 to illustrate the output of the computational scheme. For these calculations the constants for Eq. (1) are specified as shown in the tabulation below.

Constant	Convergent section	Divergent section
A_1	1.0000	0.2086
A_2	−1.8820	0.0010
A_3	1.0120	1.0120

Beyond the point where the divergent area-distance slope was equivalent to 15° (beyond an area ratio, $A/A^* = 1.35$), the divergent section expanded at a constant slope. The results which are presented represent one completed run for which the nozzle inlet conditions are near equilib-

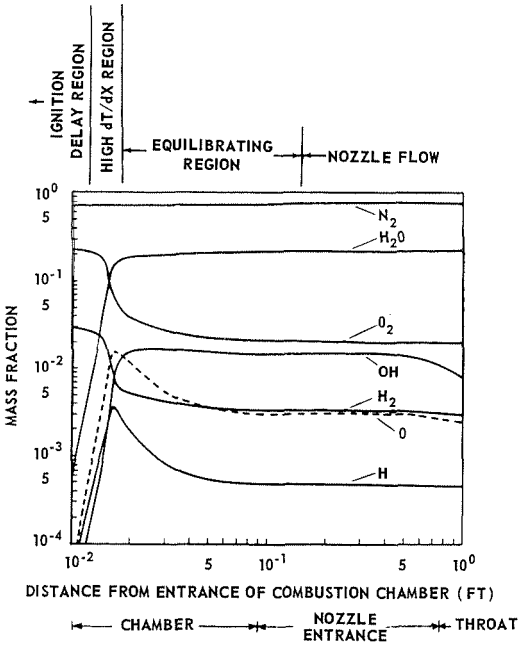

FIG. 1. Composition profile for hydrogen-air combustion products in subsonic combustor. $\phi = 1$, $T_{ci} = 2000°R$, $p_{ci} = 3000$ psf, $v_{ci} = 200$ ft/sec, $A_c = 1$ ft^2.

rium for an initial hydrogen-air equivalence ratio, ϕ of 1.0, initial temperature, T_{ci} of 2000°R, initial pressure, p_{ci} of 3000 psf, and initial velocity, v_{ci} of 200 ft/sec. The near-equilibrium nozzle inlet conditions were calculated by solving the state, kinetic, and fluid dynamics equations in a constant-area chamber of 1 square ft. After the ignition-delay and rapid temperature-rise region, the combustion-chamber calculations were terminated at a temperature-distance slope of 200° per ft and the nozzle calculations begun. The

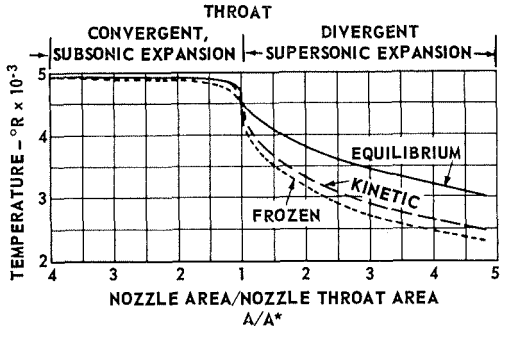

FIG. 2. Variation in nozzle temperature distribution for equilibrium, frozen, and kinetic flow (same flow conditions as Fig. 1).

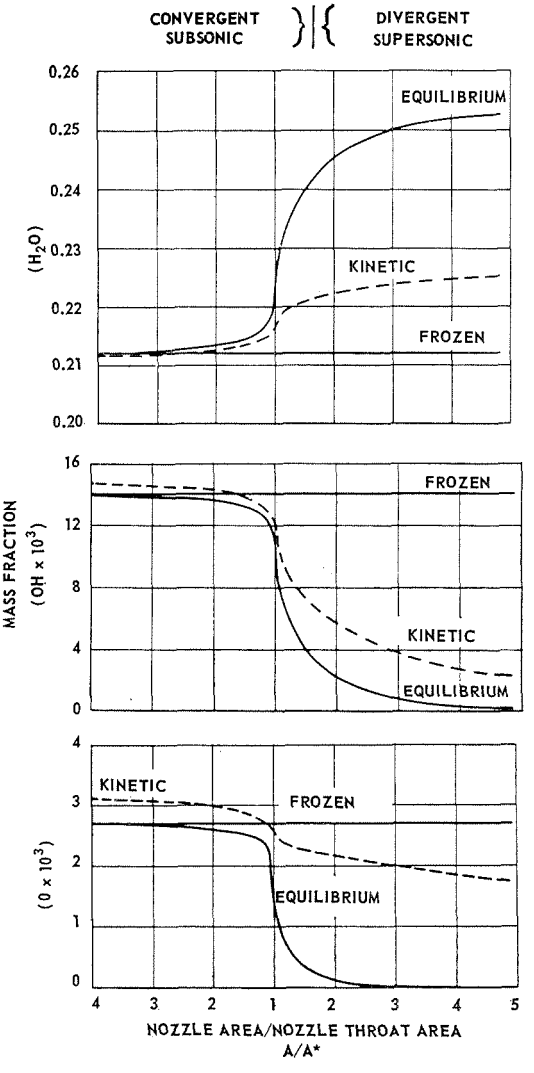

FIG. 3. Composition profile: mass fraction H_2O, OH, O versus nozzle area/nozzle throat area; equilibrium, kinetic, and frozen flow (same flow conditions as Fig. 1).

conditions at the nozzle entrance were characterized by temperature, pressure, and velocity of 4960°R, 2969 psf, and 443.1 ft per sec, respectively. The composition profiles in Fig. 1 show that the compositions are changing slowly at the nozzle entrance, indicating that near-equilibrium conditions exist. The profiles for NO and N are not shown because their values are very small for the scale used in Fig. 1.

Figure 2 illustrates the temperature profiles for equilibrium, frozen, and kinetic flow in the nozzle. The chemical equilibrium and frozen equilibrium solutions were calculated by a sep-

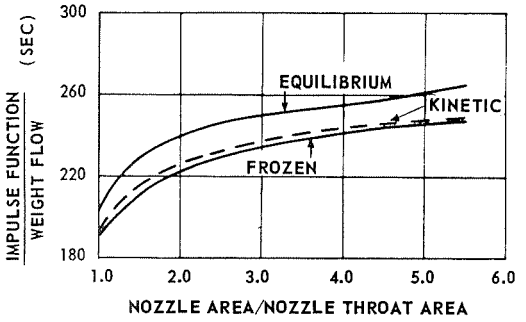

FIG. 4. Impulse function, $pA\ (1 + \gamma M^2)$, divided by nozzle weight flow versus nozzle area ratio (same flow conditions as Fig. 1).

arate machine program.[18] Since the reaction was still in progress toward equilibrium at the entrance to the nozzle, the temperature rose minutely during the early stages of subsonic expansion, then it remained nearly constant as reaction and expansion effects nearly balanced, until the expansion effect strongly dominated just ahead of the throat $(A/A^* \rightarrow 1)$. The kinetic flow curve departs from equilibrium near the nozzle throat. After the throat, it is closer to the frozen curve than the equilibrium one, about one-fourth of the way between them. This is not surprising for the relatively low values of chamber pressure and nozzle area assumed here. For higher chamber pressures and larger nozzles, the kinetic temperature would be expected to rise further toward the equilibrium temperature.

Some composition profiles are presented in Fig. 3 to show the variation between the frozen, kinetic, and equilibrium flow. The near-equilibrium water composition at the nozzle entrance and the subsequent increase in water composition as recombination progresses in the nozzle can be seen. The character of the kinetic flow curve for water with respect to its position between frozen and equilibrium is similar to that of the temperature curve, because the water composition at the nozzle entrance is slightly less than the composition for equilibrium conditions. Species such as OH and O, which attained their peak concentrations during the ignition-delay period and dropped off during the equilibration process (Fig. 1), are present at higher than equilibrium concentrations at the nozzle entrance as shown in Fig. 3. Beyond the throat, OH approaches equilibrium much faster than O, because OH equilibration is not dependent on slow third-body reactions.

The results of the kinetic flow computations, the comparative equilibrium flow, and frozen flow calculations which are expressed as an impulse function divided by the weight flow of the gas mixture are shown in Fig. 4. The impulse function is defined as $F = pA(1 + \gamma M^2)$. The impulse values of Fig. 4 do not consider the inlet momentum and therefore are not representative of ramjet performance. About 15% recovery of the impulse-function difference between frozen and equilibrium conditions is indicated. This low recovery however does indicate the importance of pressure in design consideration of ramjets. At higher chamber pressures the recovery could be considerably higher.

In addition to the concentration profiles which indicate the degree that each species is away from equilibrium, some measure of the divergence from equilibrium can be gained from forming for

TABLE 2

Ratio of equilibrium constant and concentrations, K_c/R_c, for various reactions in hydrogen-air system in nozzle[a]

	Flow	Subsonic		Supersonic	
	A/A^*	4[b]	1.827	1.728	6.75
	T (°R)	4960	4920	3481	2239
1.	$H_2 + OH \rightleftharpoons H_2 + H$	1.01^{0}	1.01^{0}	1.01^{0}	1.37^{0}
2.	$H + O_2 \rightleftharpoons OH + O$	1.04^{0}	1.03^{0}	9.42^{-1}	6.94^{-1}
3.	$H_2 + O \rightleftharpoons OH + H$	9.55^{-1}	9.58^{-1}	8.82^{-1}	1.13^{0}
4.	$H + H + M \rightleftharpoons H_2 + M$	2.53^{-4}	2.37^{-4}	4.07^{-3}	1.68^{5}
5.	$H + OH + M \rightleftharpoons H_2O + M$	3.28^{-4}	2.87^{-4}	5.54^{1}	2.08^{6}
6.	$O + O + M \rightleftharpoons O_2 + M$	7.89^{-4}	6.98^{-5}	0.43^{0}	2.52^{6}

[a] Exponents are powers of 10.
[b] Nozzle entrance.

each reaction the ratio of the equilibrium constant to the corresponding concentration ratios. At equilibrium the ratio of the equilibrium constant, K_c, and the corresponding concentration ratio for each reaction, R_c, equals one. At various stations along the nozzle the concentrations of the species are not at equilibrium and the ratio of K_c and R_c is not equal to one. The value of the ratio approaches or departs from one for each reaction as the concentration of the species for the reaction proceeds towards or moves away from equilibrium. The computed values of these ratios at several positions along the nozzle are tabulated in Table 2. It is noted that the ratios for reactions 1, 2, and 3 are very nearly at equilibrium in the subsonic flow and do not depart from equilibrium appreciably up to the area ratio 1.728 in the divergent section. Reactions 4, 5, and 6 are considerably removed from equilibrium, because they are slow three-body reactions. The equilibrium constants of these reactions increase much faster than the corresponding concentration ratios. This indicates a rapid approach to equilibrium, followed by rapid freezing of the three-body reactions, which occurs between area ratios of 1.827 in the convergent section and 1.728 in the divergent section.

The determination of the freezing point by application of Bray's criteria[7] for a multireaction system is not practical for a complex mechanism when the species are involved in more than one reaction. However, the area ratio at which probable gross freezing occurred was approximated by determining the area ratio on the equilibrium temperature profile from which frozen equilibrium expansion resulted in a temperature profile coincident with the kinetic flow temperature curve. The over-all freezing point in this case was estimated to occur at a subsonic area ratio, A/A^*, of 1.1. This result is in reasonable agreement with the experimental results of Lezberg and Lancashire[5] who report the freezing point for the expansion of hydrogen-air combustion to occur very close to the nozzle throat.

The exact nonequilibrium solution for the nozzle inlet conditions presented in this study required approximately 2 hr of machine time. Approximately 1 hr and 45 min were expended in reaching the throat. Experience indicates that the computation time is reduced considerably when the velocity of the flow is high. At a higher velocity a larger increment size can be tolerated in the integration without considering a larger increment of reaction time. The reaction-time interval is an important criteria which determines the computation time. The computation time for a length of divergent nozzle when only a supersonic flow calculation is necessary should be considerably shorter relative to an equivalent length convergent-divergent nozzle with subsonic entrance conditions.

Concluding Discussion. The calculation procedure discussed herein can be used to compute the extent of exhaust nozzle recombination for selected exhaust nozzle contours and selected recombination rate constants. Accuracy of the results is of course dependent on the accuracy of the rate constants utilized. Extension of the calculations to reacting systems other than hydrogen-air can be easily accomplished. The procedure should be useful in determining the effect of exhaust nozzle contours and combustion-chamber flow conditions on the extent of recombination and in defining the accuracy and utility of less complicated methods of determining exhaust nozzle recombination for multireaction systems such as that described in reference 7.

Nomenclature

A	Duct cross sectional area function
A^*	Throat cross sectional area
ci	Chamber inlet
g_0	Inertial constant
h_i	Enthalpy of ith component
i	Species index
J	Mechanical equivalent of heat
j	Reaction index
K_c^j	Equilibrium constant based on concentrations
K_p^j	Equilibrium constant based on partial pressures or fugacity
k_b^j, k_f^j	Forward and backward rate constant
M	Mach number
$\dot{m}$	Mass flow
p	Static pressure
p_{ci}	Static pressure at combustor entrance
R	Universal gas constant
R_c	Concentration ratios as in equilibrium constant
R_b^j	Backward rate parameter
$k_f^j \prod_{j=1}^{N} (\rho\sigma_i)^{\alpha_i j'}$	
R_f^j	Forward rate parameter
$k_b \prod_{j=1}^{N} (\rho\sigma_i)^{\alpha_i j''}$	
T	Static temperature
T_{ci}	Static temperature at combustor entrance
v	Velocity
v_{ci}	Velocity at combustor entrance
x	Distance from inlet

$\alpha_i^{j'}, \psi_i^{j''}$	Stoichiometric coefficient of the ith species in the jth reaction, reactants, and products, respectively
β_{iq}	Number of atoms of ith atomic species in the qth molecular species
Γ_i	Atomic continuity parameter
γ	Specific heat ratio
ρ	Density
σ	Concentration: mass fraction divided by molecular weight
ϕ	Equivalence ratio

References

1. Weber, R. J. and MacKay, J. S.: An Analysis of Ramjet Using Supersonic Combustion. NACA TN. 4386, 1958.
2. Dugger, G. L.: Comparison of Hypersonic Ramjet Engines with Subsonic and Supersonic Combustion. *4th AGARD Combustion and Propulsion Colloquium*. Pergamon, 1960.
3. Drake, J. A.: Hypersonic Ramjet Development. *4th AGARD Combustion and Propulsion Colloquium*. Pergamon, 1960.
4. Olsen, W. T.: Recombination and Condensation in Nozzles. *2nd International Congress in the Aeronautical Sciences*. Pergamon, 1961.
5. Lezberg, E. A. and Lancashire, R. B.: Expansion of Hydrogen-Air Combustion Products Through a Supersonic Exhaust Nozzle; Measurements of Static-Pressure and Temperature Profiles. *4th AGARD Combustion and Propulsion Colloquium*. Pergamon, 1960.
6. Vincenti, W. G.: Calculations of the One-Dimensional Nonequilibrium Flow of Air Through a Hypersonic Nozzle-Interim Report. Stanford University, Dept. of Aeronautical Engineering Report No. 101, January 1961.
7. Bray, K. N. C. and Appleton, J. P.: Atomic Recombination in Nozzles: Methods of Analysis for Flows With Complicated Chemistry. University of Southhampton, A.A.S.U. Report No. 166, April 1961.
8. Hall, J. G. and Russo, A. L.: Studies in Chemical Non-Equilibrium in Hypersonic Nozzle Flows. Cornell Aero. Lab., Report No. AD–1118–A–6, 1959.
9. Reynolds, T. W. and Baldwin, L. V.: One Dimensional Flow with Chemical Reaction in Nozzle Expansion. Symposium on Thermodynamics of Jet and Rocket Propulsion, Amer. Inst. Chem. Engrs., Kansas City, May 17–20, 1959.
10. Penner, S. S.: *Chemistry Problems in Jet Propulsion*. Pergamon, 1957.
11. Eschenroeder, A. Q., Boyer, D. W., and Hall, J. G.: Exact Solutions for Nonequilibrium Expansions of Air With Coupled Chemical Reactions, Cornell Aeronautical Laboratory, Inc., Report No. AFOSR 622, May 1961.
12. Schott, G. L. and Kinsey, J. L.: J. Chem. Phys. *29*, 1172 (1958).
13. Duff, R. E.: J. Chem. Phys. *28*, 1193 (1958).
14. Wray, K., *et al.*: *Eighth Symposium (International) on Combustion*. Williams and Wilkins, 1962.
15. Davidson, N.: Rates of Selected Reactions Involving Nitrogen and Oxygen. Avco Res. Lab. Res. Rept. No. 32, 1958.
16. Stull, D. R., *et al.*: *JANAF Interim Thermochemical Tables*, Vol. 1 and 2. Dow Chemical Company, Midland, Michigan, December 1960.
17. Ralston, A. and Wilf, H. S.: *Mathematical Methods for Digital Computers*. Wiley, 1960.
18. McMahon, D. G. and Roback, R.: Machine Computation of Chemical Equilibrium in Reacting Systems. Paper presented at the Fall Meeting, Western States Section of the Combustion Institute, Los Angeles, November 2–5, 1959.

Discussion

Dr. H. S. Pergament (*General Applied Science Laboratory*): I would like to point out that the reaction time (i.e., the time from the end of the ignition delay period to a near equilibrium state) is, in many practical cases, the predominating factor in determining the length of a combustion chamber. Using an analysis and corresponding digital program similar to that developed by the authors, we have found that at low pressures (approximately 0.2 atm) and high initial temperatures (approximately 3000°R) the reaction time is approximately an order of magnitude greater than the ignition delay time for stoichiometric burning. It should also be mentioned that the results of the complete program have indicated that the reaction time is increasingly proportional to roughly the square of the pressure. This is not surprising since the reaction period is controlled by the three-body recombination reaction.

In regard to the problem of the expansion of H_2–air products in a supersonic nozzle, our results have shown that the proximity to a near-equilibrium expansion is strongly dependent upon the pressure level for nozzle inlet temperatures in the range of 5000°R. For example, at an initial pressure of 3.0 atm and an expansion ratio of about 100 in a conical

nozzle, the flow is close to equilibrium throughout the entire nozzle, while for an inlet pressure of about 0.2 atm freezing is noted almost immediately. These effects seem to be relatively independent of the nozzle inlet velocity (as long as it is supersonic).

For the range of conditions investigated above (with the nozzle inlet velocity ranging from 10,000 fps to 25,000 fps), the time required to complete the calculation on an IBM 7090 digital computer was also found to be strongly dependent on the pressure level. That is, for near-equilibrium flow, the composition gradients are large, thus requiring a small step size (and thus a long running time) for reasonable accuracy. For near-frozen flow the running time is quite short (about 2 minutes) for the case listed above with an inlet pressure of 0.2 atm and a pressure ratio of 100 in a conical nozzle.

MR. E. D. TABACK (*Pratt & Whitney*): The computer program used by Pratt & Whitney Aircraft is capable of estimating the reaction time. However, reaction times were not reported at this time since our primary interest was the verification of the validity of the procedure and of the proposed reactions and rate constants by comparing computed delay times with existing experimental data. For a typical case (see Fig. 6) the reaction time is approximately an order of magnitude greater than the delay time. There are many factors to be considered for estimating the actual chamber length required for a supersonic ramjet. As indicated in the paper, the inlet conditions are of particular importance. An investigation of these effects was, however, beyond the scope of the paper.

DR. E. M. BULEWICZ (*University of Cambridge*): The reasons for the particular choice of chemical reactions considered are not very clear. Reactions like (7) and (10) are very endothermic (e.g., 150 and 45 kcal/mole, respectively) and require considerable activation energies. Thus the amounts of NO and N atoms formed in the system will be very small and hardly likely to affect the overall rate of radical recombination—unless the temperature of the system is very much higher (at least 3000°K) than that of a burner flame of comparable composition (not more than 2300°K).

If the concentration of NO is appreciable, the recombination rate will be affected, but through a catalytic mechanism,

$$NO + H \rightarrow HNO$$

$$H + NO + H \rightarrow H_2 + NO.$$

The addition of about 1% of NO to the burned gases of a hydrogen-air flame can increase the observed radical recombustion rate by a factor of 2.[1,2]

DR. G. R. SALTER (*McGill University*): Calculations on the performance of hypersonic ramjet engines, which I have recently completed indicate that a high degree of recombination is necessary for the attainment of any net thrust at all.

The engine considered had a double oblique shock intake diffusing the flow to approximately $\frac{1}{3}$ of the free stream Mach number. This was followed by constant area combustion of hydrogen (equivalence ratio = 1.0) with an assumed 100% combustion efficiency. Isentropic expansion of the combustion products followed, down to an exit pressure of twice ambient pressure.

A minimum acceptable recombination efficiency was defined as

$$(\eta_R)_{\min} = [(h_f - h_a^*)/(h_f - h_e)]_s$$

where h_f = frozen exit enthalpy, h_e = equilibrium exit enthalpy, and h_a^* = the enthalpy that would result in zero net thrust. By net thrust I refer to the conventional net thrust, that is, neglecting external drag. Considering this point, the 100% combustion efficiency and the isentropic nozzle flow, the high values of $(\eta_R)_{\min}$ calculated would seem to indicate that we must strive for more energy conversion than is at present expected. The above investigation was carried out for two typical flight paths—one for cruise and one for boost.

DR. G. L. DUGGER (*Applied Physics Laboratory, The Johns Hopkins University*): In connection with Mr. Salter's remarks, I would like to say, first, that if his $(\eta_R)_{\min}$ criterion permits a ramjet to go to speeds near Mach 20 (as he suggested), this is no mean accomplishment in itself, and, second, there may be other modes of operation which will permit a ramjet to go to orbital speeds if desired. One such possibility, proposed by Breitwieser of the NACA (now NASA) in 1958[3] is fuel-rich operation, which tends to reduce static temperatures and hence dissociation in the combustor. With very rich operation, a desirable mass addition effect, coupled with the desirable reduction in mean molecular weight of the products, further aids thrust production. More efficient air diffusion (relative to the two-shock inlet cited by Salter) followed by fuel-rich supersonic combustion (beginning at a Mach number approximately $\frac{1}{3}$ the flight Mach number) should produce useful thrusts to very high speeds, even with exhaust flow frozen at the combustor exit composition.

DR. E. T. CURRAN (*Wright-Patterson Air Force Base*): Regarding Dr. Salter's comments on the effect of recombination efficiency on the performance of the supersonic-combustion ramjet engine, I would like to point out that, for this engine system, the designer has more freedom to overcome the nozzle-recombination problem than was formerly the case with the conventional subsonic-combustion engine.

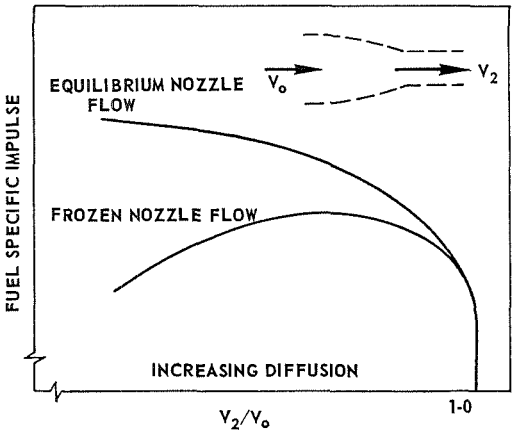

Note: Diagram is for a given flight Mach No., fixed intake efficiency, and constant expansion ratio.

FIG. 1. Supersonic-combustion ramjet engine. Effect of diffusion on specific impulse.

This is because the amount of diffusion accomplished in the supersonic-combustion engine can be controlled over wide limits, whereas in the conventional ramjet engine the flow is always ultimately diffused to subsonic velocities. The fuel-specific impulse of the supersonic-combustion engine can be plotted as a function of the amount of diffusion as shown in Fig. 1. It is apparent that the potential losses associated with frozen flow in the nozzle increase as the amount of diffusion increases, i.e., as the temperature at entry to the combustion chamber rises. It follows that the significance of such nozzle-flow losses depends markedly on the intake design and operating condition: thus by utilizing a low amount of diffusion the degree of dissociation can be reduced. Of course a certain minimum amount of diffusion is required, at any given flight condition, in order to achieve conditions at the combustor entry which will yield high combustion efficiencies. In summary it is stressed that the engine designer is able to overcome some of the adverse chemical-kinetic effects by careful choice of engine operating conditions.

REFERENCES

1. BULEWICZ, E. M. and SUGDEN, T. M.: *Studies of Oxygen Atoms at High Temperatures*, p. 81. The Chemical Society Special Publication No. 9, 1958.
2. SUGDEN, T. M., BULEWICZ, E. M., and DEMERDACHE, A.: Some Observations on Oxides and Hydrides of Nitrogen and Sulfur in Flame Gases Containing Atomic Hydrogen, Atomic Oxygen, and Hydroxyl Radicals, in *Chemical Reactions in the Lower and Upper Atmosphere*. Interscience, 1961.
3. BREITWIESER, R.: Addendum to Minutes of 23rd Meeting of Bumblebee Propulsion Panel, APL/The Johns Hopkins University, TG-63-47A, 1959.

CATALYSIS OF RECOMBINATION IN NONEQUILIBRIUM NOZZLE FLOWS

A. Q. ESCHENROEDER AND J. A. LORDI

The effects of a chemically active additive were investigated for nonequilibrium expansions of a dissociating gas. Numerical solutions were obtained in order to assess the catalytic influence of free radicals formed by bonding between the additive element and atoms of the dissociating gas. High-enthalpy nozzle flows of hydrogen with small quantities of carbon addition were studied over a range of equilibrium reservoir conditions appropriate to nuclear and electrothermal rocket operation. A chemical kinetic model consisting of eight species and twelve reaction steps evolved from studies of composition histories based on various finite-rate reaction schemes. Through two-body abstraction and association reactions between hydrogen atoms and hydrocarbon species, more of the energy in hydrogen dissociation is released than would kinetically be available in the absence of carbon. In some cases, this effect counterbalances the increased molecular weight so that the specific impulse of the system exceeds that of pure hydrogen in finite-rate nonequilibrium flows.

Introduction

It has been suggested[1] that dissociation of the working substance in a nuclear or electrically heated rocket could increase the equilibrium specific impulse by large amounts at a given temperature if a sufficiently low chamber pressure were employed. In practice, departures from chemical equilibrium limit the specific impulse of thermal rockets by withholding chemical energy which would otherwise be converted to directed kinetic energy in the expansion process. Where the differences between frozen and equilibrium specific impulses are greatest (i.e., at low densities) the performance of hydrogen rockets most nearly approaches the frozen levels.[2,3] As can be seen from Fig. 1, at a fixed reservoir temperature the specific impulse approaches the equilibrium curve with increasing reservoir pressure. Since the equilibrium curve descends steeply over a corresponding pressure range, the finite-rate specific impulse curve goes through a maximum value. Therefore, there is an optimum reservoir pressure above which the suppression of dissociation limits the performance, and below which nonequilibrium losses reduce the impulse. Methods of recovering additional energy by recombination have been sought. Presently, the region of significant frozen-flow losses is of interest for low thrust, upper-stage rockets. Increasing the scale[2,3] and decreasing the expansion rate[2] do not provide practical solutions to the problem because of size limitations and viscous losses, respectively.

In the present work the influence of an additive upon the extent of atom recombination is investigated for nonequilibrium nozzle flows of hydrogen. The choice of an additive element is based on its ability to form hydrogen-bearing radicals or compounds with the propellant gas such that rapid, two-body chain reactions produce molecules faster than three-body recombination reac-

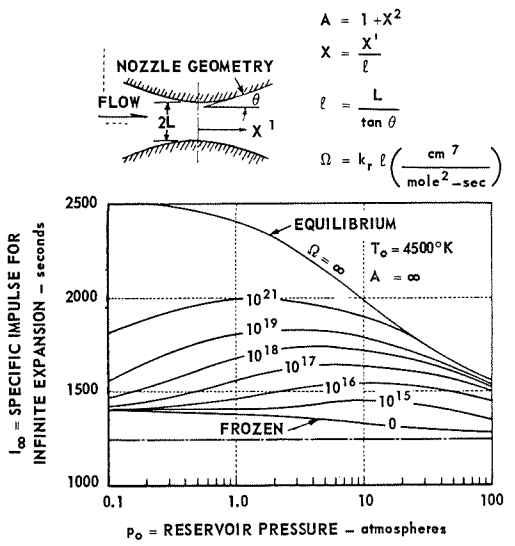

FIG. 1. The influence of chemical nonequilibrium on the specific impulse of a hydrogen rocket nozzle with infinite expansion (reference 2).

tions. At low densities, the slow exothermic path is

$$H + H + M \rightarrow H_2 + M \qquad (I)$$

and the rapid paths are represented by

$$H + R \rightarrow RH \qquad (II)$$

$$H + RH \rightarrow R + H_2 \qquad (III)$$

where R is a radical of sufficient complexity to permit the two-body recombination reaction (step II). In the terminology of homogeneous gas phase catalysis, R is the catalyst and RH is the intermediate.[4] The reaction chain represented by steps (II) and (III) may be considered to be autocatalytic because products of the reactions enter the order of the expression for hydrogen atom removal. Inevitably, the additive element will have a greater atomic mass than hydrogen so that the specific impulse is reduced by increasing the effective molecular weight while it is enhanced by decreasing the ultimate frozen-dissociation fraction. Because of the hydrogenous compounds and radicals they form, carbon, oxygen, nitrogen, and boron appear to be likely possibilities as additive elements.

As a first step in the systematic investigation of possible additives, numerical solutions of nonequilibrium nozzle flows are obtained for dilute carbon-hydrogen systems by means of a program for the IBM 704 computing machine. This program, which has been described in a previous paper,[5] is written to solve exactly the equations governing the quasi-one-dimensional expansions of a multicomponent mixture undergoing coupled, reversible, chemical reactions. Equilibrium reservoir conditions are assumed and transport effects are neglected.

The reaction and species models are chosen by comparing absolute reaction rates near equilibrium. Reactions having negligible rates are eliminated, and species participating in these reactions are also eliminated unless they are involved in reactions having significant rates. By the use of thermochemical data reported in the literature[6,7] equilibrium composition distributions are obtained for isentropic expansions over the range of conditions treated in references 3 and 4. The equilibrium computational procedurei is an isentropic modification of the Brinkley method.[9] Rate constants based on experimental results and on theoretical estimates are employed for the absolute rate estimates. Successive truncations of the system of species and reactions are carried out to determine a reasonable initial model for nonequilibrium flow solutions.

Results of numerical solutions for nozzle flows are presented to show the dependences of catalytic effects upon reservoir temperature, reservoir pressures, C/H ratio, and steric factors for the estimated reaction rate constants. Concentration and reaction-rate histories show the detailed action of the catalysis. The validity of a highly simplified kinetic scheme is examined. Performance comparisons are made on the basis of frozen hydrogen atom concentration and specific impulse.

Chemical Kinetic Model

Equilibrium Studies. It has been demonstrated[7] by extensive equilibrium calculations for a 57-species model that various generalizations can be made regarding the composition of carbon-hydrogen systems in the temperature range 500–5000°K. For a wide range of C/H ratio, the stable hydrocarbons (e.g., methane, ethane, and ethylene) are present in negligible quantities above 1500°K. Acetylene (C_2H_2) and the ethynyl radical (C_2H) assume significant roles in the high temperature composition. Since the present work deals with dilute systems, the concentrations of many of the carbon-rich compounds considered in reference 7 may be neglected.

In order to choose a workable but adequate set of species, the equilibrium composition must be examined for typical reservoir conditions of interest. Four conditions having considerable differences between frozen and equilibrium specific impulse[3] are as follows: (*a*) 3500°K, 0.1 atm; (*b*) 3500°K, 1.0 atm; (*c*) 4500°K, 1.0 atm; (*d*) 4500°K, 10 atm. Based on extrapolations of the results of reference 7 to low C/H ratios, an equilibrium model of the following 17 species is a reasonable first choice: H_2, H, C_2H_2, C_2H, C_3H, CH_2, C_4H, C_3, C, C_4H_2, C_3H_2, CH_3, C_2, CH, C_3H_3, C_2H_3, and C_2H_4. Earlier studies[2,3] show that the freezing region occurs above 1500°K for the nozzle flows of interest. Therefore, most of the familiar low-temperature stable species (e.g., CH_4, C_2H_6, etc.) are omitted. Subsequent computations of catalyzed nonequilibrium flows, which are reported below, demonstrate the validity of such an assumption. Chemical freezing precludes the activity of any mechanism which might form the stable compounds.

For the adiabatic expansion process, infinite rate, equilibrium, composition histories were computed by the method of reference 8 to determine the shifts of species mass-concentrations in an idealized nozzle flow. Over a major portion of each equilibrium expansion, acetylene (C_2H_2) plays the major role among the species containing carbon. Table 1 shows mass concentrations obtained from such calculations at the sonic throat condition for reservoir state (*d*) and a C/H ratio of 0.02, which is the largest additive level considered here. The four most important

TABLE 1

Comparison of equilibrium composition at sonic conditions for 17-, 8-, and 4-species models[a]

Species	Mass concentration (moles i/gm of mixture)		
	17-Species model	8-Species model	4-Species model
H_2	0.2202	0.2198	0.2222
H	0.3485	0.3490	0.3487
C_2H_2	0.9930×10^{-3}	0.1100×10^{-2}	0.1699×10^{-2}
C_2H	0.3684×10^{-2}	0.4097×10^{-2}	0.6250×10^{-2}
C	0.1659×10^{-2}	0.1763×10^{-2}	
C_2	0.1987×10^{-3}	0.2225×10^{-3}	
CH	0.3445×10^{-3}	0.3662×10^{-3}	
CH_2	0.2893×10^{-2}	0.3058×10^{-2}	
CH_3	0.2643×10^{-4}		
C_3H	0.3289×10^{-3}		
C_4H	0.5065×10^{-4}		
C_3H_2	0.7551×10^{-5}		
C_4H_2	0.1284×10^{-5}		
C_2H_3	0.9854×10^{-6}		
C_3H_3	0.2516×10^{-6}		
C_2H_4	0.4828×10^{-7}		

[a] $T_0 = 4500°K$, $p_0 = 10.0$ atm, C/H = 0.02.

carbonaceous species (C_2H, CH_2, C, C_2H_2) are grouped in magnitude at this condition. Also shown in Table 1 is the effect of including only H, H_2, C, C_2, CH, CH_2, C_2H, and C_2H_2. This reduction to eight species increases C_2H and C_2H_2 each by about 10%. The hydrogen concentrations are practically unaffected. Further reduction to the four species H, H_2, C_2H, and C_2H_2 brings about 1% increases in the hydrogen species and 50% increases in the two remaining hydrocarbon species. The eight and four species results are shown to illustrate the interaction of the simultaneous mass action relationships. However, the final choice of a minimal species model must be deferred until absolute reaction rates are compared in nonequilibrium flows.

In order to examine trends, 16 equilibrium expansion solutions were obtained among the set of four reservoir conditions (*a–d*), five C/H ratios (0–0.02), and two species models (8 and 17). Only a brief summary will be undertaken here because of space limitations. At the representative reservoir state (*c*) the most important species (aside from H and H_2) are C and CH_2 followed by the group CH, C_2H, and C_2H_2. Both C_2H and C_2 increase sharply with increasing (C/H) ratio. From a comparison of the 1-atm reservoir states (*b*) and (*c*), it is found that CH_2, C_2H, and C_2H_2 increase with decreasing temperature at the expense of C-atoms. The concentration of CH radical is not as sensitive to temperature as those just cited. Comparison of the 3500°K cases (*a*) and (*b*) shows that C and C_2 decrease sharply with increasing pressure because of a general increase in saturation of the hydrocarbon radicals. At 4500°K, acetylene appears to be more sensitive to pressure than any other species. For a tenfold pressure decrease the acetylene mass concentration decreases by approximately a factor of 20. In the isentropic expansions, the temperature dependence of acetylene dominates over the pressure dependence; i.e., acetylene always increases to a plateau level throughout an equilibrium expansion process.

Reaction Kinetic Studies. Before any simplification of all the possible reactions in the 17-species model can be made, the significant chemical degrees of freedom must be established. Reactions which are considered may be grouped into two classes: (1) association of atoms or radicals and (2) abstraction of atoms or radicals. An 18 × 18 array including a zero row and a zero column can be generated for determining all possible elementary reaction steps. Each position is filled by possible steps arising from collisions between a row-species molecule and a column-species molecule. The zero row and the zero column allow for unimolecular decompositions. At first sight, this seems to be a formidable procedure; however, immediate reductions become apparent upon the construction of the array.

TABLE 2

Chemical kinetic model[a,b]

i	Reaction	A_i	η_i	E_i	Source
1	$H + H + H \rightleftharpoons H_2 + H$	3.5×10^{17}	−0.5	0	10, 11, 12
2	$H + H + M \rightleftharpoons H_2 + M$	7.0×10^{17}	−0.5	0	10, 11, 12
3	$H + C + H \rightleftharpoons CH + H$	1.0×10^{17}	−0.5	0	Estimated
4	$H + C + M \rightleftharpoons CH + M$	2.0×10^{16}	−0.5	0	Estimated
5	$H + CH \rightleftharpoons CH_2$	(A) 4.5×10^{11} (B) 4.5×10^{12}	0.5		Estimated
6	$H + CH_2 \rightleftharpoons CH + H_2$	(A) 4.5×10^{11} (B) 4.5×10^{12}	0.5	2.5×10^4	Estimated
7	$H + C_2H \rightleftharpoons C_2H_2$	(A) 4.5×10^{11} (B) 4.5×10^{12}	0.5	0	Estimated
8	$H + C_2H_2 \rightleftharpoons C_2H + H_2$	(A) 4.5×10^{11} (B) 4.5×10^{12}	0.5	1.5×10^4	Estimated
9	$H + C_2H_2 \rightleftharpoons C_2H_3$	(A) 9.0×10^{9} (B) 9.0×10^{10}	0.5	1.5×10^3	14
10	$H + C_2H_3 \rightleftharpoons C_2H_2 + H_2$	(A) 4.5×10^{11} (B) 4.5×10^{12}	0.5	2.0×10^3	Estimated
11	$H + C_2 \rightleftharpoons C_2H$	(A) 4.5×10^{11} (B) 4.5×10^{12}	0.5	0	Estimated
12	$H + C_2H \rightleftharpoons C_2 + H_2$	(A) 4.5×10^{11} (B) 4.5×10^{12}	0.5	3.5×10^4	Estimated
13	$H + C_2 \rightleftharpoons CH + C$	(A) 4.5×10^{11} (B) 4.5×10^{12}	0.5	1.0×10^4	Estimated
14	$H + CH \rightleftharpoons C + H_2$	(A) 4.5×10^{11} (B) 4.5×10^{12}	0.5	5.0×10^3	Estimated

[a] The forward rate constant for the ith reaction is given by $k_{Fi} = A_i T^{\eta_i} \exp(-E_i/RT$ ($cm^6mole^{-2}sec^{-1}$, i = 1–4; $cm^3mole^{-1}sec^{-1}$, i = 5–14) for T in °K.

[b] M denotes any species but H.

Product species excluded from the seventeen-member set are not permitted, the regions on either side of the diagonal are redundant, and allowance for reverse reactions effects a twofold collapse of the system. A further simplification is imposed, both from steric considerations and from ordering rules permitted by the assumption of C/H $\ll$ 1. This simplification is the omission of steps involving no hydrogen atoms or molecules.

With the selection of 33 elementary steps obtained by the reduction of the 18 $\times$ 18 array, the absolute forward reaction rates must be compared in order to truncate further the 17 $\times$ 33

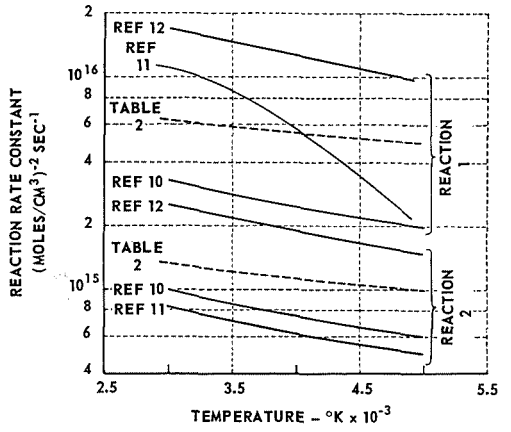

FIG. 2. Specific reaction-rate constants for three-body hydrogen atom recombination as functions of temperature.

kinetic matrix in a rational manner. Such a comparison for typical conditions (sonic throat, case *d*) near equilibrium permits a reduction to a 9×14 matrix by eliminating unimportant reactions and species. The 14 reactions chosen are listed in the second column of Table 2. Determination of the reaction rates from experiment and from collision theory is discussed in the succeeding paragraphs.

Association Reactions. The kinetic data employed for three-body hydrogen atom recombination are obtained by averaging the results of three series of shock-tube results reported in the literature.[10,11,12] Figure 2 shows three experimental curves and the selected average for H and H_2 each acting as a third body. The temperature dependences were chosen to be weaker than the experimental ones shown so that reasonable agreement with room temperature experiments could be obtained. The third-body efficiency of H_2 is assumed to approximate that for all other third-body species. The forward rate constant for the ith reaction is given in general form as

$$k_{F_i} = A_i T^{\eta_i} \exp(-E_i/RT)$$

where A_i, η_i, and E_i are constants and T is the absolute temperature. Although some objection has been raised to relating forward to reverse rates through the equilibrium constant,[13] this procedure is employed in the present work. Such an approximation is consistent with the assumption of vibrational equilibration which is also incorporated in the analytical statement of the problem.[5] Table 2 contains a summary of the (A_i, η_i, E_i) values used in the complete finite-rate calculations. The data for reactions (1) and (2) are the same as those used for the averaged curves shown in Fig. 2. Under the assumptions of an inverse square-root temperature dependence and zero-activation energy, A_3 is estimated to be 10^{17} on the basis of the experimental hydrogen-rate data. A_4 is taken to be $0.2A_3$ by analog with the ratio between reactions (1) and (2).

Hydrogen atom plus free-radical association reactions of the class exemplified by $i = 5$, 7, 9, and 11 (see Table 2), are assumed to proceed via second-order kinetics because the products are triatomic or larger. Hence, redistribution of internal energy in the product species may obviate the need for a third body to remove excess energy. This assumption is provisional in order to illustrate possible catalytic effects. Taken as pairs, reactions (5, 6), (7, 8), (9, 10), and (11, 12), are examples of the chain scheme shown as (II, III) in the Introduction. Actually, the pair (13, 14) is a variant of the scheme because the recombination of C + H [reactions (3) and (4)] is most probably a three-body process. Also, this pair is significant because of the importance of free carbon atoms in all cases considered here.

The rate constants governing binary reactions were obtained from theoretical estimates to a great extent. Experimental information was introduced wherever possible either in a direct fashion or by analog. A total of nine (H-atom + R-radical) association reaction steps were considered including the four appearing in the final selection (Table 2). These constitute steps (II) in the parallel catalytic chains described above. Zero-activation energies are assumed for each association reaction except for $i = 9$(R = C_2H_2) in Table 2. The value of 2 kcal/mole for E_9 is based on experimental data,[14] which are discussed in the next paragraph. For R = CH, CH_2, and C_2H, steric factors of 10^{-2} are assigned in applying collision theory, while for R = C_3, C_3H, C_4H, C_3H_2, and C_2H_3 the steric factors are assumed to be 10^{-1}. In Table 2 the set of A_i values for these reactions labeled (A) are based on these steric factors, while those labeled (B) are based on ten times these steric factors. None of the reactions for the latter set of R-groups appears in Table 2. The choice of steric factors depends on the size and structure of the product species. Actually, some of the steps may require a third body to enter the collision complex and carry energy away by recoil. This is especially true for R = CH in this class of reaction.

Review of Experiments on Catalyzed Recombination. Experimental studies of acetylene addition in streams of hydrogen atoms (produced by discharge, hot filament, or photo processes) have demonstrated catalysis of atom recombination in low-temperature systems. The results of this

work have been collected and compared in order to provide values for high-temperature rate constants in the present analysis. Before continuing the presentation of the values employed, it is useful to digress briefly in an examination of these experiments. Early observations of the reactions of hydrogen atoms with acetylene appear in the German literature,[15,16] however, it was not until 1935 that serious investigation was devoted to the detailed mechanism of catalytic recombination. In that year, Geib and Steacie[17] reported studies of reacting deuterium atoms with acetylene in order to determine the fate of the atomic species. They reasoned first that the chain

$$C_2H_2 + D \rightarrow C_2H + HD$$
$$C_2H + D_2 \rightarrow C_2HD + D$$

regenerates H and is, therefore, noncatalytic to recombination. The two possibilities which they proposed were:

$$C_2H_2 + D \rightarrow C_2H + HD$$
$$C_2H + D \rightarrow C_2HD$$

or

$$C_2H_2 + D \rightarrow C_2H_2D$$
$$C_2H_2D + D \rightarrow C_2HD + HD$$

Since the presence of the quasi-molecule C_2H_2D could react to form stable $C_2H_2D_2$, and no such species was found in the products, they later reasoned that the first chain must dominate the catalysis of recombination. In an experiment some years later, LeRoy and Steacie[17] contended that reactions of H_2 with the vinyl radical (C_2H_3) were significant only in the case of H-atoms produced in low concentrations by mercury photosensitized decomposition because only under these conditions were ethane and butane produced. With H-atoms produced in a discharge at higher concentration, the hydrogen analog to the first chain shown above was thought to dominate since the stable products were not produced. This was justified either because of a lack of H_2 or a lack of vinyl radical. In 1948, Tollefson and LeRoy[18] investigated the ($H + C_2H_2$) reaction using H-atoms produced by thermal decomposition of H_2 on a hot filament. This method was believed to produce atoms more nearly at thermal equilibrium with the background gas in the flow system. Small amounts of hydrogenated products were detected (e.g., ethane, ethylene, butane). Dingle and LeRoy,[14] using the same technique for atom production, took the position that neither

$$H + C_2H_2 \rightarrow H_2 + C_2H \qquad (8F)^*$$

* Reaction numbers refer to Table 2.

nor

$$H + C_2H_2 \rightarrow C_2H_3 \qquad (9F)$$

should be ruled out as a possibility for the ($H + C_2H_2$) reaction. For the one that was operating (which remained undetermined) they report an activation energy in the vicinity of 1.5 kcal/mole and a steric factor of 4×10^{-4}. The temperature range studied was below 1000°K. Shortly after the appearance of reference 14, Stepukhovich and Timonin[19] proposed a theoretical method of computing steric factors for processes like reaction (9). In a paper which followed,[20] these same workers applied the method to reaction (9F) and obtained a steric factor of approximately 10^{-3}. Reaction (8F) is endothermic by 12 kcal/mole according to the thermochemical data of references 6 and 7; therefore, it is not possible for this reaction to have an activation energy of less than this amount. Thus, strong arguments can be advanced in light of the results in references 6, 7, 19, and 20 that the rate data reported by Dingle and LeRoy are for reaction (9F) and not (8F). In Table 2, the coefficient A_9 in set (A) is computed from a steric factor of 4×10^{-4} and an activation energy of 1.5 kcal/mole is assigned. This steric factor is lower than the others used because reaction (9) involves the attack of a stable molecule by a hydrogen atom. The rate constant for reaction (8) must be estimated theoretically along with those for the other hydrogen-abstraction reactions.

Abstraction Reactions. It appears that no direct experimental measurements are available for the hydrogen-abstraction reactions of interest here. These reactions are steps of the form given by (III) in the catalytic chains. The only hope of using experimental results for steric factors is by drawing analogs with data on reactions of H-atoms with simple stable hydrocarbons. Results of many early experiments are of little value here because in much of the data reduction steric factors of 10^{-1} were arbitrarily assumed, and activation energies were computed from observed reaction rates. Modern work is carried out over a range of temperatures permitting the determination of the activation energy independently by means of an Arrhenius plot. The steric factor for

$$H + CH_4 \rightarrow CH_3 + H_2$$

has been estimated by Benson[21] to be 0.019 on the basis of various experimental results. An earlier review by Steacie[22] concludes that the experimental evidence then available tended to indicate a steric factor of 10^{-4}. The probable value based on Eyring's transition state theory[23]

for an (atom + polyatomic molecule) collision is nearer 10^{-2} according to the tabulation in reference 21. This same theory gives values of order 10^{-1} for (atom + diatomic molecule) collisions and of order 1 for (atom + atom) collisions. For binary association of methyl radicals reference 21 gives 0.5 as an experimental value. Thus, it appears as if the (radical + radical) collision is more like (atom + atom) than (atom + molecule). None of these data relate directly to the (atom + radical) collisions arising in high-temperature systems.

For all of the hydrogen-atom abstraction reactions in the present work a steric factor of 10^{-2} is employed for the set of A_i designated (A) and 10^{-1} for the set designated (B). Nonequilibrium flow results for set (A) are compared with those for set (B) later in the paper in an effort to bracket the probable range of rates. For the activation energy of exothermic abstraction reactions, 6% of the broken-bond energy is used in accordance with Hirschfelder's procedure.[24] Bond energies are determined by forming energy balances with the heats of formation given in references 6 and 7. In cases of endothermic reactions, activation energies are taken to be the energy of reaction plus 3 to 5 kcal/mole. In the original set of (H + RH) reactions, R was taken to be C_2H, C, C_2, C_3, CH, C_3H, C_4H, CH_2, C_2H_2, C_3H_2, and C_2H_3. After the absolute rates were compared for the throat conditions shown in Table 1 (17-species model), reactions (6), (8), (10), (12), and (14) (see Table 2) were selected. Reaction (13) is a carbon abstraction, and its rate constant is calculated according to the same rules.

Six reactions of the class

$$H_2 + R \rightleftharpoons RH_2 \qquad \text{(IV)}$$

were considered in the original 33-member set, but were eliminated because of their small rates. Hence, none appears in Table 2. To form these steps R is considered to be C_2H_2, C_2H, C_3H, C, C_2, or CH. For the first three R-groups, the experimental values of Skinner[25] may be utilized indirectly. These results show the activation energy of

$$C_2H_4 \rightarrow C_2H_2 + H_2$$

to be 46 kcal/mole. This reaction is endothermic by 40 kcal/mole, giving a reverse-reaction activation requirement of 6 kcal/mole. By analog, the reactions (IV F) for R = C_2H and C_3H are assigned activation energies of 6 kcal/mole. The pre-exponential is estimated by assuming a steric factor of 10^{-3}. For R = C, C_2, or CH, the activation energy is estimated to be 28% of the broken-bond energy,[24] and a steric factor of 10^{-3} is used.

Summary of Procedure Used in Determining the Model. In summarizing the methods of establishing the chemical kinetic model, it is observed that a 3-stage process of elimination has been followed:

(1) By extrapolating results[7] for a 57-species equilibrium model to low (C/H) ratio, a reduction to 17-species is made. The cutoff point is determined by observing magnitude groupings of species concentrations. The location of the cutoff point in a ranked list of groups is arbitrary.

(2) The possible reaction steps involving the 17 species are reduced from a few hundred to 33 in number. Order of magnitude and probability arguments are invoked in this stage.

(3) The 17 × 33 species-reaction matrix is truncated to 9 × 14. Comparison of absolute reaction rates at conditions of interest permits the further elimination of both species and reactions. Estimates of specific rate constants must be made in this stage.

The process of elimination yields a set of species and reactions which is well within the capabilities of the computing machine code[5] used for nonequilibrium flows. It will be shown in the next section that further reductions of the 9 × 14 model are possible. The catalytic effect will be demonstrated over a range of parameters with an 8 × 12 model. The validity of a 4 × 4 kinetic model will be studied for describing the thermodynamics and hydrogen atom kinetics of nonequilibrium nozzle flows.

Nonequilibrium Expansion Solutions

The study of recombination catalysis in nozzle flows can be carried out using the kinetic model developed in the previous section. Integration of the fully coupled species, mass, momentum, and energy conservation equations is necessary in such an investigation. The pertinent analytical and numerical techniques developed at Cornell Aeronautical Laboratory are reviewed first in this section. After an 8-species × 12-reaction mechanism is established by numerical solutions, the results of further nozzle-flow solutions are presented and discussed. Sample plots of reaction and species behavior are analyzed to demonstrate the role of catalysis in the system. Next, the influences of (C/H) ratio, reservoir conditions, and steric factors are studied. Finally, the utility of a 4-species × 4-reaction kinetic model for describing the essential features of the flow is investigated.

Method of Solving the Coupled Conservation Equations. The analytical and numerical approach to

the nonequilibrium nozzle-flow problem is briefly reviewed here because complete details of the equations and their solution have been described elsewhere.[5] In formulating the equations, a quasi-one-dimensional flow which is free from transport effects is assumed. Reverse reaction-rate constants are related to forward rate constants through the equilibrium constant in the source terms appearing in the species equations. Substitution of algebraic expressions for conservation laws and state equations yields one differential equation in addition to the species conservation relationships. Before these equations can be directly integrated, however, initial values must be provided in the nonequilibrium regime. This need arises because of the singular nature of the species source terms in the early portions of the expansion. The condition of chemical equilibration at the reservoir state results in small differences between large absolute reaction rates in these terms. A singular perturbation technique is used to obtain the needed initial values from equilibrium solutions, which are started at large area ratios in the subsonic region.

The additional requirement of critical flow poses problems for flows departing from equilibrium in the subsonic region because the mass flow is not known *a priori* for a fixed nozzle geometry. An inverse method based on a prescribed density distribution and mass flow is constructed to overcome these difficulties. Since density and mass flow are each relatively insensitive to chemical nonequilibrium these boundary values are determined from an equilibrium flow solution obtained for the desired area distribution. A new area distribution is computed in the inverse procedure thereby providing a consistency check with the geometry originally assumed. Even for extremely early freezing, this approach has never given a throat area more than 10% different from that assumed. Comparison at the throat is the most stringent check that can be devised because this is the point of greatest disagreement. After a loop procedure to place the forward integration on the supersonic solution curve, the direct solution is obtained; i.e., the specified area distribution replaces the density distribution as a boundary value. The direct procedure may be followed throughout if departures from equilibrium are small through the entire subsonic region.

In the present calculations, an axisymmetric hyperbolic nozzle geometry (Fig. 1) is adopted with $l = 1$ cm. The scale parameter l is defined as the throat radius L divided by the tangent a of the semi-angle θ of the asymptote cone. The area distribution is given by $A = 1 + x^2$ where area A is normalized by throat area, and distance downstream from the throat x is normalized by l.

Further Reduction of Kinetic Model from (9×14) *to* (8×12). Based on reaction rates, the vinyl radical and its associated reactions ($i = 9$ and 10) could have been omitted before undertaking numerical solutions. The importance of this radical through its coupling with acetylene kinetics, however, merits its further consideration in light of the available experimental evidence.[14–18] Two nozzle-flow solutions were carried out for a (C/H) atom ratio of 10^{-3} at reservoir state (a). One solution was obtained for the 9×14 model shown in Table 2, and another, for an 8×12 model resulting from the omission of C_2H_3, reaction (9), and reaction (10). Rate constants were chosen from group A. No discernible differences appeared to the third significant figure in the concentrations of the eight species. This would seem to be another example in the kinetics of chain reactions where one mechanism dominates at low temperature and another at high temperature. In the case considered, low-temperature experiments[14–18] and theory[6,7,20,21] point to the chain mechanism

$$H + C_2H_2 \rightarrow C_2H_3 \qquad (9F)$$

$$H + C_2H_3 \rightarrow C_2H_2 + H_2 \qquad (10F)$$

as the main contributor in recombination catalysis. However, the calculations show that the chain

$$H + C_2H \rightarrow C_2H_2 \qquad (7F)$$

$$H + C_2H_2 \rightarrow C_2H + H_2 \qquad (8F)$$

is responsible at high temperatures despite the higher activation energy (15 kcal/mole) for step (8F). Evidently a combination of circumstances brings about this shift in mechanism. First, there is a sufficient fraction of energetic particles at high temperature to drive reaction (8F), and second, the lifetime of C_2H_3 formed by (9F) is short because of its instability at elevated temperature. This fact can be seen from the equilibrium solutions. On the other hand, C_2H and C_2H_2 are relatively abundant at high temperature. The comparison, therefore, justifies the adoption of an 8×12 model including the eight species H, H_2, C_2H_2, C_2H, CH_2, CH, C, and C_2 participating in reactions (1–8) and (11–14).

Catalytic Effects in Nozzle Flows. An examination of specific reaction rates and species concentrations is useful for attaining some further insight into the catalytic action as it affects nozzle flows. Figure 3 shows a plot of the significant net elementary reaction rates as functions of area ratio

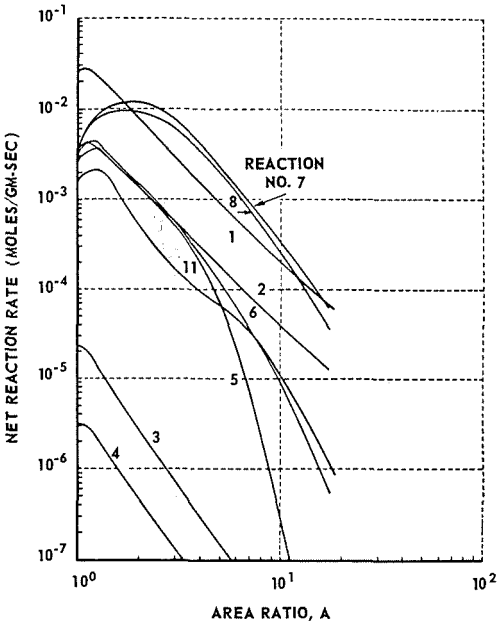

FIG. 3. Net reaction rates as functions of area ratio for nonequilibrium nozzle flow. $T_0 = 4500°K$, $p_0 = 10.0$ atm, C/H = 0.01, $l = 1.0$ cm, and (8 × 12) A kinetic model.

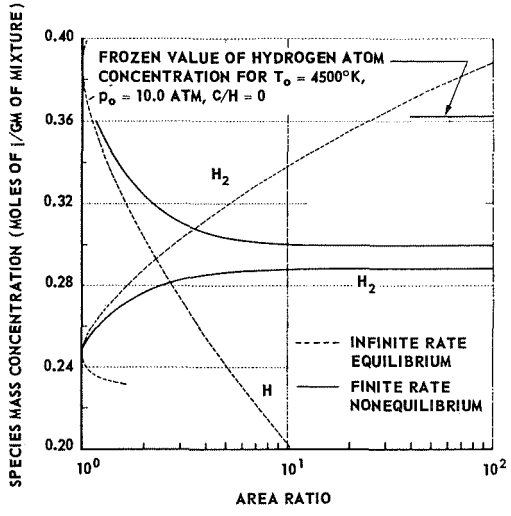

FIG. 4a. Species mass concentrations as functions of area ratio for nozzle flows. $T_0 = 4500°K$, $p_0 = 10.0$ atm, C/H = 0.01, $l = 1.0$ cm, and (8 × 12)A kinetic model.

for a system expanding from reservoir state (d) with a (C/H) ratio of 10^{-2}. For this solution, rate constants from set (A) were used. Immediately downstream from the throat, the first three-body association reaction ($i = 1$) dominates as the hydrogen atom removal mechanism. As this reaction decreases in rate, the acetylene chain-reaction rates ($i = 7, 8$) increase and overtake it. The other two-body chains, which contribute to a lesser degree, go through rate maxima and decrease rapidly. Farther downstream, the acetylene rates go through their maxima and decrease more rapidly than the three-body rates. Finally, all two-body rates are once more below the three-body rates. The rapid descents in the cases of binary association reactions are due to a dissipation of radical concentration, and those characterizing the abstraction reactions are governed by the exponential temperature dependence of rates which takes over at low temperature regardless of concentration.

The examination of catalytic action is completed by studying the variations of species concentrations with area ratio for the same expansion process. Figures 4a and 4b show plots of this information. The use of mass concentration, expressed here in gram-moles of species j per gram of mixture, removes the expansive contribution leaving the chemical reaction contribution. The

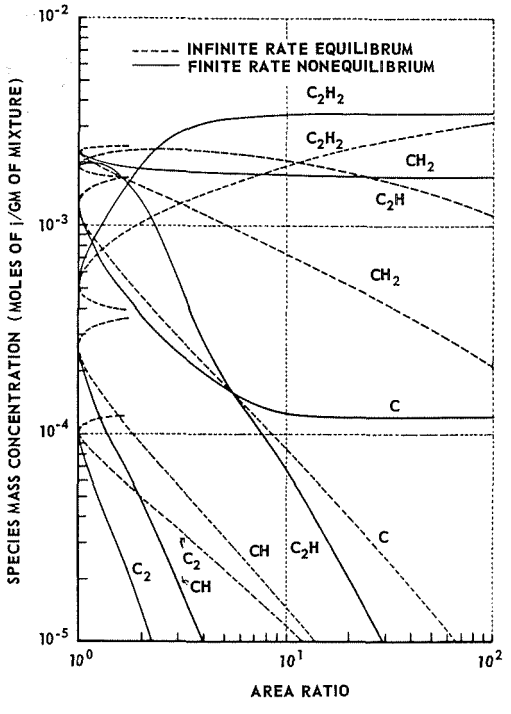

FIG. 4b. Species mass concentrations as functions of area ratio for nozzle flows. $T_0 = 4500°K$, $p_0 = 10.0$ atm, C/H = 0.01, $l = 1.0$ cm, and (8 × 12) A kinetic model.

two are combined in the conventional volumetric concentration expressed in moles j per cubic centimeter. Figure 4a shows the comparison between equilibrium and nonequilibrium histories of hydrogen species concentrations. Significant departures from equilibrium do not occur until the flow is supersonic. Hence, in the freezing region (the range between near-equilibrium and near-frozen flow) the system is receiving the maximum benefit from the fast-chain reactions as indicated by Fig. 3. The asymptotic frozen level of H-atoms is shown on Fig. 4a for an uncatalyzed system expanding from the same reservoir condition. Comparison of the solution curve with this level shows the relatively sizable reduction brought about by 1% carbon addition. The corresponding hydrocarbon and carbon radical species variations are plotted on Fig. 4b. It may be observed that the acetylene overshoots equilibrium and becomes level. Evidently, this occurs at the expense of the other species which descend below the equilibrium curves. The explanation of this behavior lies in the temperature histories. The freezing process leads to a greater cooling rate than would be experienced with equilibrium flow; therefore at a given area ratio the temperature of the nonequilibrium flow is considerably below that of an equilibrium flow at the same area ratio. The hydrocarbon and carbon species are nearly following quasi-equilibria among themselves. The quasi-equilibria are maintained via rapid two-body paths which follow local temperature variations dictated by hydrogen freezing, the energetically dominant process. Lowering the temperature raises the quasi-equilibrium acetylene concentration and lowers the others. Carbon-atom concentration finally becomes an exception as reactions (13R) and (14R) freeze ("R" refers to reverse reactions). In each reaction, the disappearance of a carbon atom requires a moderate activation energy. The other reactions freeze downstream.

With the establishment of the mechanism underlying the catalytic action, the influence of various parameters on catalytic effectiveness will now be considered. The sensitivity of chemical and thermodynamic behavior to the (C/H) ratio is of central interest. Table 3 contains a summary of results illustrating this dependence. The second column shows that even one part in a thousand of carbon atoms effects a 2% reduction in the ultimate frozen level of hydrogen atoms. For reaction rates from set (A), the frozen hydrogen atom concentration bears a rough relationship to (C/H) ratio such that each per cent carbon addition reduces the frozen atom level by about 16%. This rule is valid for reservoir conditions (d) and for the $l = 1$ cm nozzle. For rates from set (B), the influence coefficient becomes greater, giving a 42% reduction for 1% additive and 56% for 2% additive.

The thermodynamic influence is reflected in the comparisons of specific impulse for infinite expansions shown in Table 3. A monotonic decrease in performance with carbon addition occurs when rates in set (A) are assumed. Increases in molecular weight counterbalance the energy recovery benefits in all of these cases. Note that the relative decreases approximately follow those in the equilibrium flow values shown in the right-hand column of Table 3. However, the decreases are not as rapid as those in the frozen-flow results which reflect principally the reduction due to increased molecular weight. If the radical reaction steric factors are increased from 0.01 to 0.1, the specific impulse passes

TABLE 3

Catalytic effects on hydrogen rocket performance[a]

C/H (atom fraction)	Frozen concentration of hydrogen atoms for finite-rate flows (moles j/gm of mixture)		Specific impulse at infinite expansions (sec)			
				Finite reaction-rate flow		
	Rates in set (A)	Rates in set (B)	Fully frozen flow	Rates in set (A)	Rates in set (B)	Equilibrium flow
0	0.3625	0.3625	1326	1503	1503	1972
0.001	0.3551	0.3368	1318	1500	1523	1963
0.002	0.3486	0.3127	1311	1496	1550	1953
0.01	0.2999	0.2107	1269	1473	1605	1884
0.02	0.2515	0.1587	1203	1444	1584	1807

[a] (8 × 12) Kinetic model, $l = 1.0$. Influence of C/H ratio. $T_0 = 4500°K$, $p_0 = 10$ atm.

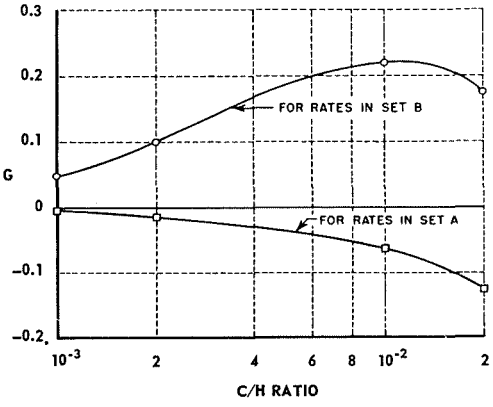

FIG. 5. Percentage of available impulse gain obtained, G, as a function of C/H ratio. $T_0 = 4500°K$, $p_0 = 10.0$ atm, $l = 1.0$ cm, and (8 × 12) A kinetic model.

through a maximum in the vicinity of (C/H) equals 10^{-2}. This behavior is shown in the column based on the rates in set (B). The maximum value represents an optimization between catalytic activity and molecular weight.

A graphical presentation of a performance parameter is shown in Fig. 5. The parameter, G, is a measure of the percentage of the available specific impulse gain which is brought about by carbon addition. This gain factor is computed from the expression

$$G = \frac{I_{nc} - I_{np}}{I_{ep} - I_{np}}$$

where I_e is the infinite expansion specific impulse for equilibrium flow and I_n is the infinite expansion specific impulse for finite-rate nonequilibrium flow. The subscript p denotes pure hydrogen and c denotes catalyzed hydrogen. The top curve in Fig. 5 displays the (C/H) ratio optimization of impulse gain referred to above. This curve is based on rate set (B) with the steric factors of 10^{-1} for atom-radical reactions. The lower curve shows the dominant effect of increased molecular weight.

Table 4 shows the influence of catalysis for (C/H) equals 10^{-3} and rate set (A) at the four reservoir conditions considered. Relative reductions in frozen hydrogen atom concentrations at each temperature indicate that the catalysis is more effective at higher pressure levels. Increased amounts of hydrocarbon species and higher collision number combine to bring about such an effect. For the same reason, the effectiveness is greater at lower temperature for a given pressure. This is seen by comparing results for reservoir states (b) and (c). The specific impulse decrease is greatest at reservoir state (c)

TABLE 4

Catalytic effects on hydrogen rocket performance[a]

		Frozen concentration of hydrogen atoms for finite-rate flows (moles j/gm of mixture)	
T_0 (°K)	p_0 (atm)	C/H = 0	C/H = 0.001
(a) 3500	0.1	0.6740	0.6655
(b) 3500	1.0	0.2681	0.2633
(c) 4500	1.0	0.8188	0.8096
(d) 4500	10.0	0.3625	0.3551

	Specific impulse at infinite expansions (sec)					
	Fully frozen flow		Finite-rate flow		Equilibrium flow	
T_0 (°K)	C/H = 0	C/H = 0.001	C/H = 0	C/H = 0.001	C/H = 0	C/H = 0.001
(a) 3500	1184	1178	1186	1182	2106	2097
(b) 3500	1132	1127	1155	1152	1593	1586
(c) 4500	1373	1365	1435	1427	2396	2385
(d) 4500	1326	1318	1503	1500	1972	1963

[a] (8 × 12) Kinetic model, $l = 1.0$. Influence of reservoir conditions.

TABLE 5

Comparison of (4 × 4) and (8 × 12) kinetic models for describing hydrogen rocket performance[a]

	Frozen hydrogen atom concentration for finite-rate flow (moles j/gm of mixture)		Specific impulse at infinite expansion (sec)					
			Fully frozen flow		Finite-rate flow		Equilibrium flow	
	Kinetic model		Kinetic model		Kinetic model		Kinetic model	
C/H	(4 × 4) B	(8 × 12) B	(4 × 4) B	(8 × 12) B	(4 × 4) B	(8 × 12) B	(4 × 4) B	(8 × 12) B
0.01	0.2042	0.2107	1259	1269	1608	1605	1877	1884
0.02	0.1536	0.1587	1204	1203	1584	1584	1799	1807

[a] Influence of C/H ratio. $T_0 = 4500°K$, $p_0 = 10.0$ atm, $l = 1.0$.

compared with all others. Frozen and equilibrium flow values are also shown in Table 6 for reference purposes.

Evaluation of a (4 × 4) *Chemical Kinetic Model.* In many cases a highly simplified chemical mechanism can serve as an adequate means for describing gross features of a flow which is influenced by a rather complex coupled reaction system. This is the basis of the so-called "global" reaction-rate equations employed in combustion theory.[26] For the catalysis of hydrogen recombination at the conditions of interest, an examination of rates and species (see Figs. 3 and 4b) suggests the selection of 4 reactions [(1), (2), (7), (8)] and 4 species (H, H_2, C_2H, C_2H_2). This restricts the system to catalysis by the chain involving ethynyl radical (C_2H) as the

TABLE 6

Comparison of (4 × 4) and (8 × 12) kinetic models for describing hydrogen rocket performance[a]

		Frozen concentration of hydrogen atoms for finite-rate flow (moles j/gm of mixture)	
		Kinetic model	
T_0 (°K)	p_0 (atm)	(4 × 4) A	(8 × 02) A
3500	0.1	0.6649	0.6655
3500	1.0	0.2625	0.2633
4500	1.0	0.8073	0.8096
4500	10.0	0.3530	0.3551

	Specific impulse at infinite expansion (sec)					
	Fully frozen flow		Finite-rate flow		Equilibrium flow	
$T°$ (°K)	(4 × 4) A	(8 × 12) A	(4 × 4) A	(8 × 12) A	(4 × 4) A	(8 × 12) A
3500	1178	1178	1183	1182	2095	2097
3500	1126	1127	1154	1152	1586	1586
4500	1366	1365	1431	1427	2383	2385
4500	1319	1318	1503	1500	1962	1963

[a] Influence of reservoir conditions. C/H = 0.001, $l = 1.0$.

catalyst and acetylene as the intermediate. As shown in Table 1, such a reduction has the effect of lumping all hydrocarbon species under equilibrium conditions. The nonequilibrium species histories (Fig. 4b) indicate that the simplification may not be as serious as it seems because the production of acetylene rapidly exhausts the supply of other hydrocarbons. Therefore, the utility of the 4 × 4 model may be better for nonequilibrium flows than it is for equilibrium flows.

The validity of the approximation has been examined at two (C/H) ratios for rates from set (B). Table 5 shows the comparisons between the (4 × 4) results and the (8 × 12) results for reservoir condition (*d*). Deviations of the order of 3% appear in the frozen H-atom concentrations at each of the two (C/H) ratios, indicating that the simplification still gives a reasonable description of the catalyzed hydrogen kinetics. Since the chemical energy frozen in the flow is sensitive to hydrogen atom level, it is necessary to investigate the effect on nozzle thermodynamics. For this purpose, specific impulse values are also compared in Table 5. The agreement in impulse values given by the two models is remarkably good. The approximation improves at higher (C/H) ratio. From the viewpoint of frozen energy, the shift in hydrocarbon composition resulting from the truncation of the kinetic model is closely counterbalanced by that in frozen hydrogen concentration. Note that neither the frozen nor equilibrium flow values agree as well as those for finite-rate flow.

The uniformity of the approximation at different reservoir states is illustrated in Table 6. It should be observed that rate set (A) was used for this comparison. For a fixed reservoir temperature the approximation improves somewhat at higher pressure and at a fixed reservoir pressure, it is approximately uniform with temperature. Again, excellent agreement is obtained among the specific impulse values. However, the equilibrium and frozen-flow comparisons are slightly better, in general, than the finite-rate comparisons.

The simplification of the (8 × 12) kinetic model to a (4 × 4) kinetic model gives an adequate description of the hydrogen concentration and the gross thermodynamics of catalyzed hydrogen flows in nonequilibrium expansions. Obviously, detailed behavior of the hydrocarbon species included is not described accurately in the near-equilibrium portions of the flow.

Concluding Remarks

The catalysis of recombination in high-enthalpy nozzle flows of hydrogen can be accomplished by the addition of small amounts of carbon to the system. Although the asymptotic frozen concentration of hydrogen atoms is always reduced, the specific impulse of a hydrogen rocket may not always be increased. Opposing tendencies arise between the larger molecular weight and the catalyzed energy release caused by carbon addition. For conservative estimates of the pertinent radical-atom reaction rates (based on steric factors of 10^{-2}), the molecular weight penalty overrides the enhancement of energy conversion from chemical modes to active modes. However, if the steric factors of these reaction steps approach 10^{-1}, an optimum (C/H) ratio exists such that substantial increases in specific impulse may be realized. The over-all effects of catalysis may be described extremely well by the use of a reaction model involving only the species H, H_2, C_2H, and C_2H_2.

The accuracy of any calculations such as these presented here is limited by the uncertainties in reaction-rate constants for specific elementary steps. The available hydrogen atom recombination rate data disagree by substantial amounts as shown in Fig. 2. Specific information on the atom-radical rates at high temperatures is practically nonexistent. It is amply demonstrated by the variation of steric factors over a factor of 10 that the success of catalytic recombination in improving rocket performance depends strongly on the efficiency of detailed kinetic steps. The accuracy of the (4 × 4) model points to the possibility that experimental studies of the acetylene chain [reactions (7) and (8)] at high temperature could increase our confidence in performance calculations to a great extent. A significant corollary to these findings is the warning that great care must be exercised in controlling gas-purity levels in nozzle kinetics experiments with this system.

Since the feasibility of gas-phase catalysis of recombination has been demonstrated for the case of carbon addition, other compounds, for example, oxygen, nitrogen, or chlorine, should be considered. Preliminary studies have been initiated for the use of trace amounts of oxygen.

Acknowledgments

The authors wish to thank Mr. A. Hertzberg for suggesting this problem, and Dr. J. G. Hall for his helpful discussions during the course of the work. The authors also wish to express their appreciation for the suggestions of Professor Simon H. Bauer of Cornell University in the studies of reaction kinetics and thermochemistry. The contribution of Mr. Duane B. Larson, Systems Research Department, Cornell Aeronautical Laboratory, in carrying out the machine computations is gratefully acknowledged.

This work was sponsored by the National Aeronautics and Space Administration under Contracts NAS 5-670 and NASr-109.

References

1. Sanger-Bredt, I.: Astronautica Acta *3*, 241 (1957). (Available in English translation as NASA TT F-1.)
2. Hall, J. G. and Russo, A. L.: *Kinetics, Equilibria, and Performance of High Temperature Systems*, p. 219. Butterworths, 1960.
3. Hall, J. G., Eschenroeder, A. Q., and Klein, J. J.: ARS Journal *30*, 188 (1960).
4. Frost, A. A. and Pearson, R. G.: *Kinetics and Mechanism*, Chapter 9. John Wiley & Sons, 1953.
5. Eschenroeder, A. Q., Boyer, D. W., and Hall, J. G.: Phys. Fluids *5*, 615 (1962).
6. Cowperthwaite, M. and Bauer, S. H.: J. Chem. Phys. *36*, 1743 (1962).
7. Duff, R. E. and Bauer, S. H.: J. Chem. Phys. *36*, 1754 (1962).
8. Boyer, D. W., Eschenroeder, A. Q., and Russo, A. L.: Cornell Aeronautical Laboratory Report No. AD-1345-W-3, 1960.
9. Brinkley, S. R., Jr.: J. Chem. Phys. *15*, 113 (1947).
10. Rink, J. P.: J. Chem. Phys. *36*, 262 (1962).
11. Sutton, E. A.: Dissertation, Cornell University, 1961.
12. Patch, R. W.: J. Chem. Phys. *36*, 1919 (1962).
13. Pritchard, H. O.: J. Phys. Chem. *65*, 504 (1961).
14. Dingle, J. R. and LeRoy, D. J.: J. Chem. Phys. *18*, 1632 (1950).
15. Bonhoffer, K. F. and Harteck, P.: Z. physik. Chem. *A139*, 64 (1928).
16. Wartenberg, H. von and Schuttze, G.: Z. physik Chem. *B2*, 1 (1929).
17. LeRoy, D. J. and Steacie, E. W. R.: J. Chem. Phys. *12*, 369 (1944).
18. Tollefson, E. L. and LeRoy, D. J.: J. Chem. Phys. *16*, 1057 (1948).
19. Stepukhovich, A. D. and Timonin, L. M.: Zhur. Fiz. Khim. *26*, 145 (1952).
20. Stepukhovich, A. D.: Doklady Akademii Nauk USSR *92*, 127 (1953).
21. Benson, S. W.: *Foundations of Chemical Kinetics*. McGraw-Hill, 1960.
22. Steacie, E. W. R.: *Atomic and Free Radical Reactions*. Reinhold, 1954.
23. Glasstone, S., Laidler, K. J., and Eyring, H.: *The Theory of Rate Processes*. McGraw-Hill, 1941.
24. Hirshfelder, J. O.: J. Chem. Phys. *9*, 645 (1941).
25. Skinner, G. B.: J. Phys. Chem. *64*, 1028 (1960).
26. Emmons, H. W.: J. Aero. Sci. *25*, 730 (1958).

Discussion

Dr. R. E. Duff (*Lawrence Radiation Laboratory*): Some time ago a cursory examination was given to this problem and a few "back of an envelope" calculations were made which were also based on the pioneering work of Hall. In a sense the results were even more pessimistic than those presented by Dr. Eschenroeder. Since it was not possible to do detailed kinetic calculation as presented here an effort was made only to demonstrate the potential gains in rocket performance which recombination catalysis might provide. Two conclusions were apparent: (1) If considerations are restricted to finite nozzle expansion ratios of 100 or even 10,000 the specific impulse gain is much smaller than an infinite expansion ratio calculation would indicate, and (2) for a finite expansion nozzle the addition of the order of 1% by volume of a perfect catalyst with the molecular weight of C_2H_2 leads to no increase in specific impulse. The increase in molecular weight under these conditions compensates for the enthalpy added to the flow by recombination.

Dr. A. Q. Eschenroeder (*Cornell Aeronautical Laboratory*): In the numerical solutions obtained for the nozzle flow of a carbon-hydrogen system the molecular weight was found to counterbalance the catalysis effect when a steric factor of 10^{-2} is used for the hydrogen atom–hydrocarbon radical reaction steps. However, as discussed in detail in the written version of the paper, using a steric factor of 10^{-1} for these reaction steps did provide a specific impulse gain, indicating that the impulse gain is critically dependent on these reaction-rate constants. These two steric factors represent an estimate of the range of possible values.

The choice of complete expansion rather than a finite exit area as a basis of comparison in our numerical solutions has no influence whatever on the effective increase in the recombination rate constant providing the mixture is nearly frozen at exit conditions. Also, for the cases in which an impulse gain was obtained for finite expansion, roughly the same percentage of the available impulse gain was realized for all area ratios downstream of the freezing region. It is true that the actual impulse gain at finite area ratios is lower because the impulse for pure hydrogen, equilibrium flow, and hence the available impulse gain is lower at finite-area exit

conditions. For example, in the case for which the optimum impulse gain at infinite expansion was obtained using the 10^{-1} steric factors (T_0 = 4500°K, p_0 = 10.0 atm, and C/H = 0.01) the impulse gain at A/A^* = 100 is 50 seconds out of a possible 210 seconds or approximately 24% of the available gain. The corresponding values of specific impulse at A/A^* = 10^4 are essentially the same as the infinite expansion values. Therefore, the conclusions of our paper are not dependent on the selection of any particular area ratio downstream of the freezing region.

DR. G. R. SALTER (*McGill University*): The nozzle throat considered in the analysis is a hyperbolic type. Dr. Appleton of the University of Southampton has shown that for the maintenance of equilibrium, a bell-shaped nozzle should be considered. Do you think that, by combining a bell-shaped nozzle and the addition of a catalyst, more specific impulse could be achieved?

DR. A. Q. ESCHENROEDER: In theory, certainly an increase of specific impulse could be achieved by proper contouring of the nozzle in addition to recombination catalysis. As in the case of Dr. Appleton's calculations, however, the actual implementation of this idea would depend on additional gasdynamic considerations such as boundary layer growth and three-dimensional effects. Size and weight limitations would also enter any complete engineering analysis of nozzle design for a given application. The scope of the present work was limited to the study of recombination catalysis.

DR. T. M. SUGDEN (*University of Cambridge*): I should like to express a general doubt as to whether the rate constant of bimolecular recombination of H with a molecule X, as part of a catalytic process, could be at all fast unless X were a more elaborate molecule than is likely either to survive the previous treatment of the gases or to be formed in the nozzle. In such circumstances a three-body process might be more probable. I would refer in particular to the catalytic effect of NO in H recombination, described by Bulewicz, Demerdache, and Sugden ["Chemical Reactions in the Upper and Lower Atmosphere," Interscience, 1961]. The appropriate mechanism is

$$NO + H + M \rightarrow HNO + M$$

$$HNO + H \rightarrow H_2 + NO$$

with M a third body. The rate of this about doubles the rate of H recombination when 1% of nitric oxide is used. The effect is quite a large one, since in the flame studies referred to, the reaction

$$H + OH + M \rightarrow H_2O + M$$

with a rate constant 20 times that of

$$H + H + M \rightarrow H_2 + M$$

is proceeding at least as fast as the latter process, and often a good deal faster.

The outstanding need at the moment seems to me to be for more laboratory studies of single processes.

DR. A. Q. ESCHENROEDER: In the present work, the reservoir conditions of T_0 = 4500°K and p_0 = 10 atm were selected for the example. For a C/H ratio of 10^{-2}, the solution of the simultaneous mass action laws shows that nearly one-half of all the carbon is combined as C_2H at sonic throat conditions. Thermodynamic properties given in reference 7 were employed. The onset of nonequilibrium flow occurs immediately downstream from the throat (see Fig. 4a). Hence, the possibility of two-body association of H with C_2H (as suggested in references 14 and 22, for example) to yield C_2H_2 cannot be discounted in the consideration of catalytic reaction steps. A significant feature of catalysis via binary reactions in nozzle flows is the persistence of reaction rates in expanded portions of the flow (see Fig. 3, comparing reactions 1 and 7 for example).

The suggested reaction mechanism involving nitric oxide as an additive will be examined in future theoretical studies. As stated in the concluding remarks of our paper, we agree heartily with Dr. Sugden's final comment pointing up the need for further experimental studies of specific reaction steps.

DR. D. E. ROSNER (*AeroChem Research Laboratories, Inc.*): In view of the possibility of catalysis, the fact that the specific impulse of a rocket propulsion device can vary by more than a factor of 2 depending upon the kinetics of reassociation processes seems to raise some interesting control possibilities. Dr. S. A. Gordon, Dr. A. Fontijn, and I have tentatively concluded that the injection of small amounts of ("positive" and/or "negative") catalysts would provide an excellent means of continuously varying thrust level and direction. In the latter case this would be accomplished by simply introducing the catalyst asymmetrically in the nozzle inlet region. The accompanying change in wall pressure distribution in only one sector of the nozzle would produce the desired turning moment. Techniques of this type would be attractive in that large effects could be produced by controlling trace quantities of catalyst; i.e., one is taking advantage of "trapped" energy already present in the system, regulating its rate of release by literally turning a valve. I wonder if Dr. Eschenroeder could comment on the feasibility of thrust level control in the light of his calculation? Despite its obvious computational difficulty, could he be persuaded to look into the thrust vectoring problem?

DR. A. Q. ESCHENROEDER: Comparing the two applications which Dr. Rosner mentioned, I believe that the thrust level control is the more promising one. Our computing machine code is presently written for quasi-one-dimensional flows in the absence of transport effects: Rather complicated extensions would be required to compute the thrust-vectoring problem. A better approach might be to utilize the present results in a streamtube-type analysis where the two-dimensional nature of thrust-vectoring is limited to first-order terms in the equations of motion. This may provide estimates of the effect without resort to machine computation. In the immediate future, our studies will be directed toward learning more about recombination catalysis through further theoretical studies and through experimental investigations.

ENERGY TRANSFER FROM HYDROGEN-AIR FLAMES

ROY A. COOKSON AND JOHN K. KILHAM

An experimental procedure is devised by which the heat flux is measured in and near the reaction zone of lean hydrogen-air flames, which are burned on a porous disc burner. A conductivity-type heat flow meter is used which has an isothermal sheath surrounding the probe. It is found that in the region of the reaction zone the heat flux is much greater than that predicted from ordinary convection alone. Calculations are made by means of a heat transfer equation which includes terms for the diffusion and recombination of the various labile species present in the flame. The concentrations of the active species present are calculated from quasi-equilibrium considerations with reference to the amount of OH present in the flame gases. The concentrations of OH, and hence the other species, necessary to produce the high rates of heat transfer measured, are determined and are found to be approximately of the order of the concentrations which have been reported in the literature. The receiving surface of the heat flow meter is treated with catalytic and noncatalytic materials. Since the surface treatment influences the heat flux only to a small extent the bulk of the recombination appears to take place in the gas phase.

Introduction

In his work on heat transfer from flames and flame gases, Kilham[1] showed that the heat flux from a hydrogen-air flame to a body placed in the flame gases in the vicinity of the reaction zone could not be attributed to ordinary convection alone. He calculated the rate of heat transfer due to convection by means of an expression which had been verified for the conditions prevailing. The experimental results were found to exceed those calculated by a considerable amount near the reaction zone. It was also shown that this excess decreased as the distance from the reaction zone increased. Thus Kilham's results indicated that there was some mechanism of energy transfer in or near the reaction zone other than convection. He conjectured that a large part of the excess heat transfer was due to the exothermic recombination of atoms and radicals; the recombination taking place either heterogeneously or homogeneously.

A conclusion similar to that of Kilham was reached by Ziebland,[2] after he had carried out a series of experimental observations on the heat transfer from combustion gases to the cooled walls of rocket engines.

More recently Geidt *et al.*,[3] investigated the heat transfer from an oxyacetylene flame to a flat plate and postulated that recombination of hydrogen atoms, either in the gas phase or on the solid surface, enhanced the heat transfer rates predicted by simple convection theory from 30 to 90 per cent. These authors also attempted to differentiate between the effects of surface recombination and recombination occurring in the gas phase. To do this they compared heat transfer rates to a flat plate of ingot iron first uncoated and then coated with porcelain. They found the difference in heat flux to be negligible.

In the present investigation, we have developed an experimental technique by which the heat flux from the flame and flame gases can be measured. Measured values of the heat flux have then been compared with values predicted by recent theory for gases containing active species.

Experimental Method

The hydrogen-air mixtures were burned on a 2 inch diameter porous bronze burner of the now conventional Botha and Spalding[4] design. The porous disc burner has the advantage of producing flat uniform flames with flow perpendicular to the flame surface. The flame so produced has great stability since it depends upon the profile of the disc for position. In a case such as the study of heat transfer from flames in which there are a great number of variables, the simplification of the geometry of the flame is itself a great advantage.

Flame Temperature Measurement. The flame and flame gas temperatures were measured by means of platinum/platinum 13 per cent rhodium thermocouples. In order to allow for the effects of the thermocouple wire diameter and radiation from the thermocouple, the method suggested by

Nicholls[5] was used. In this method the temperature is measured by a series of diminishing diameter thermocouples and an extrapolation to zero diameter is made.

A complete investigation was made of the variation of flame temperature with composition and vertical distance above the flame front. Although this "map" of flame temperature versus composition and displacement was made, an independent temperature reading was taken whenever the heat flux was measured.

To overcome the well-known catalysis of hydrogen atom recombination on platinum, the thermocouples were coated with silica using the method described by Kaskan[6] involving their immersion in a flame in which hexamethyldisiloxane is burned.

Heat Flow Meter. Heat transfer rates from the flame were measured by a conductivity-type heat flow meter as shown in Fig. 1. This type of meter consists of a uniform rod along which heat is conducted. One end of the rod is presented to the source of heat and the other is maintained at a constant temperature by a coolant, in this instance water. Thermocouples are fixed in the rod at a known distance apart to determine the temperature gradient down its length. In the steady state the temperature gradient along the probe is directly proportional to the heat flux, if the thermal conductivity of the rod is constant for the range of temperatures to which it is subjected. A radiation shield surrounding the rod so as to leave a small annular space reduces the radial heat loss by radiation. It also reduces the convection down the sides of the rod.

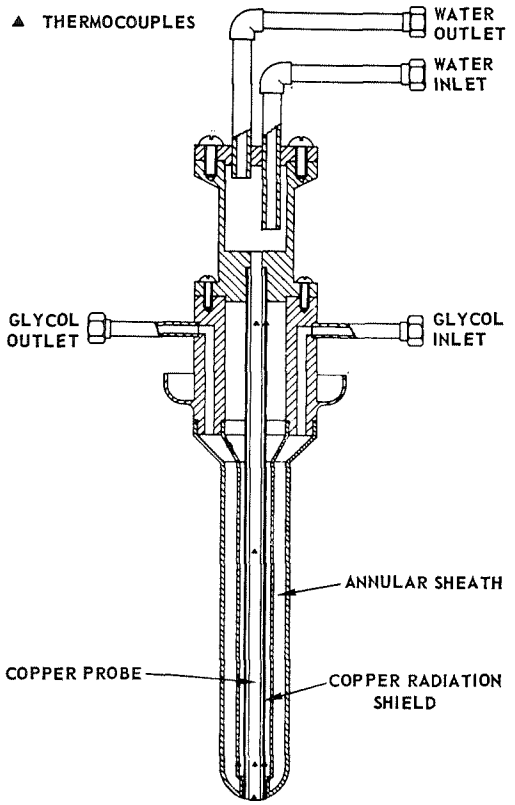

FIG. 1. Heat flow meter.

A hollow annular sheath surrounds the rod and shield, this sheath being kept at a constant temperature by means of a coolant which is pumped between the walls. Since it was undesirable to have water vapor condensing on the exterior walls of the meter a coolant which gives a surface temperature greater than 100°C is required. Ethylene glycol proved to a good choice of coolant with a boiling point well above that of water.

To obtain a calibration of the meter in actual values of the heat received a black body furnace was used, that is, the meter was directed at a radiation source of known temperature and from simple radiation laws the amount of heat falling on the receiving surface of the probe was calculated. In the black body furnace used for the calibration, the radiating element consisted of a spherical cavity in a silica brick which was heated in a nichrome wound tube furnace. In this way, the probe could be positioned so that the receiving surface became integral with the wall of the spherical cavity. Since the area of the receiving surface was small compared with the total furnace surface area, black body conditions could be said to hold. Heat conduction from the furnace wall to the probe was avoided by maintaining the surrounding sheath at a constant temperature. A platinum/platinum 13 per cent rhodium thermocouple was cemented into the furnace wall to indicate the radiating temperature. This temperature was compared with that given by an optical pyrometer and in the lower temperature range a small correction factor was applied. The meter was calibrated in this manner for three different conditions of the receiving surface: (a) platinum coated, (b) oxide coated, and (c) untreated copper.

Results

It was found that flame temperature readings, for the central portion of the flame, were steady for a distance of approximately 3.0 cm, above the burner. They were also found to be laterally uniform until quite near the edge of the flame. This would seem to indicate that the combustion products in the central portion of the flame were unaffected by recirculation or turbulence at dis-

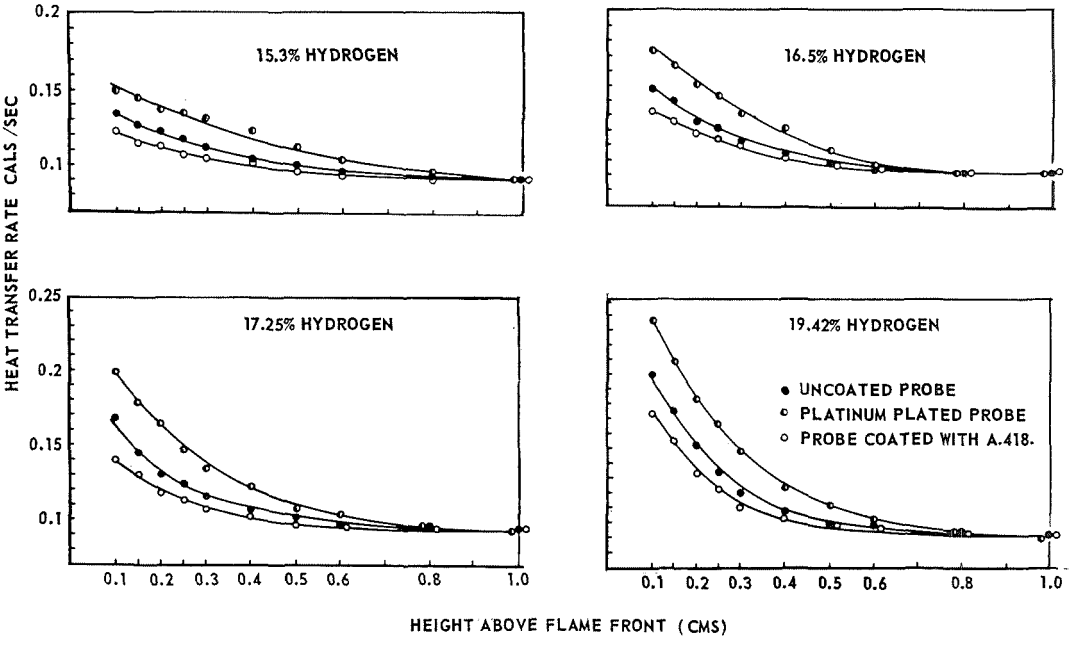

FIG. 2. Variation of heat flux with height above flame front.

tances of less than 3.0 cm, above the burner. Since the maximum height at which the heat flux readings have been considered is 1.0 cm, this will be seen to be well within the region of steady conditions.

The development of a cellular flame at hydrogen-air mixtures less than 13.5 per cent set a lower limit to the operation of the burner while the heat conducting properties of the sintered bronze disc made it difficult to burn flames richer than 22 per cent hydrogen-air. The investigation was, therefore, restricted to the range of values between 15 per cent and 20 per cent hydrogen-air mixtures.

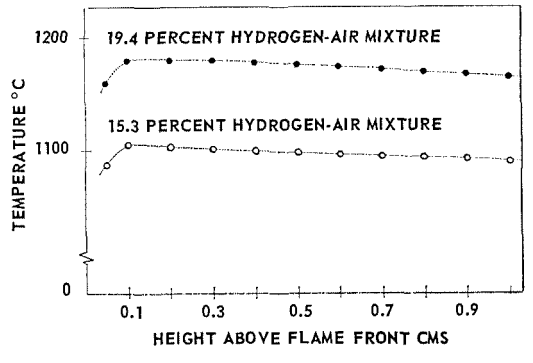

FIG. 3. Variation of flame temperature with height above flame front.

Heat flux readings for four different hydrogen-air mixtures at varying heights above the flame front, using three conditions of the receiving surface are shown in Fig. 2.

A plot of flame gas temperature against vertical height above the flame front is given in Fig. 3 for two of the mixture compositions. The temperature values are those obtained by extrapolating to zero thermocouple diameter.

Heat Transfer from a Gas Containing Dissociated Species

In order to predict the heat flux from a flame to a solid body placed within it an expression of the following form is required

$$\dot{q} = -k\,\partial T/\partial y + \sum_{i}^{n} \rho\alpha_i V_i Q_i \qquad (1)$$

which includes a chemical energy term due to the diffusion and recombination of species i in addition to the conduction contribution.

Sibulkin[7] has derived the following expression for the convective heat transfer to the stagnation point of a blunt body of revolution.

$$\dot{q}_s = 0.763\ (\mathrm{Pr})^{-0.6}(\rho_e\mu_e[\partial U_e/\partial x]_s)^{0.5}(h_e - h_w) \qquad (2)$$

Several workers[8,9,10] have extended the theory to include the effects of dissociation in the gas

phase and subsequent atom recombination on the solid surface. The following form was derived analytically by Rosner.[10]

$$\dot{q}_s = 0.763\ (\mathrm{Pr})^{-0.6}[\rho_e\mu_e(\partial U_e/\partial x)_s]^{0.5}(h_e - h_w) \times \left[1 + \Phi\,[(\mathrm{Le})^{0.6} - 1]\,\frac{\alpha_e Q}{h_e - h_w}\right] \quad (3)$$

This correlation equation was derived by Rosner for the case of a binary mixture of atoms and molecules. It can however be extended to deal with the situation in which there are several active species provided that a Lewis number is calculated for each species.

$$\dot{q}_s = 0.763\ (\mathrm{Pr})^{-0.6}[\rho_e\mu_e(\partial U_e/\partial x)_s]^{0.5}(h_e - h_w) \times \left[1 + \sum_i^n \Phi_i\,[(\mathrm{Le}_i)^{0.6} - 1]\,\frac{\alpha_{i,e} Q_i}{h_e - h_w}\right] \quad (4)$$

The catalysis-diffusion function Φ_i can be calculated if the mass transfer coefficient and the rate constant for the surface atom recombination are known. For the present investigation, however, the receiving surface was first coated with platinum and later with a known catalysis inhibitor.* Thus it was assumed that the value of the catalysis-diffusion function for the platinum surface was unity and that Φ_i for the oxide coating would be less than unity. It is unlikely, however, that Φ_i will be the same for all of the active species.

Figure 1 shows that the tip profile of the heat flow meter is hemispherical and that the receiving surface of the copper probe is at the stagnation point of the hemisphere. The value of $(\partial U_e/\partial x)_s$ for a sphere in an ideal fluid is given by Sibulkin[7] as $3U_e/D$. However, a slightly lower value is obtained experimentally for a hemisphere-cylinder in a real gas.

The thermodynamic and transport properties used in these calculations were taken in the main from refs. 11 and 12. The mixture viscosities were calculated from the expression derived by Wilke.[13] The thermal conductivities of the mixtures were calculated from the simple form suggested by Penner[14] which has been found to be accurate for cases in which the thermal conductivities of the components are similar. For the density and the "frozen" specific heat, simple weighted forms were used.

In order to obtain the Lewis number $(\rho c_p D_{i-\mathrm{mix}})/k$ for each of the labile species a knowledge is required of the diffusion coefficients $D_{i-\mathrm{mix}}$ of each component into the mixture. There is unfortunately a dearth of information with regard to the diffusion coefficients of atoms and radicals. For the present investigation it was assumed that the species taking part in the recombination energy transfer would be the hydrogen atom H, molecular hydrogen H_2, the hydroxyl radical OH, and atomic oxygen. The binary diffusion coefficients for each of these labile species into each of the major components of the combustion products can be calculated from Chapman-Enskog theory. However, a knowledge is first required of the various collision parameters. Many of the latter are available in the literature, but when applicable diffusion coefficients were to be found, they were used. The parameters for atomic hydrogen were derived by substituting experimental diffusion coefficients given by Amdur[15] into the Chapman-Enskog expression using the Lennard-Jones potential. A slightly modified form is required when one of the components is polar, but the calculation for the diffusion of one polar component into another, as with OH into H_2O, has not been dealt with in the literature so far. In the present investigation the diffusion coefficients for OH were assumed to be the same as those for atomic oxygen.

The combining law used to calculate the over-all diffusion coefficients required to determine the Lewis number was that given by Wilke.[16] This expression

$$D_{i-\mathrm{mix}} = \Big[\sum_{k,\,i\neq k} (x_k/D_{ik})\Big]^{-1}$$

is an approximation for the case in which i is a trace component, based upon the Stefan-Maxwell diffusion equations which has been verified experimentally by several workers.[17–19]

The over-all diffusion coefficients obtained as well as the resulting Lewis numbers are given in Table 1.

Accurate determination of the local concentration α_i of atoms and radicals is unfortunately not possible from present knowledge. Many workers have reported concentrations of some particular species which are in excess of those expected from equilibrium considerations. Laminar flame theory predicts atom and radical concentrations higher than the equilibrium values. In this respect it is possible to adopt the quasi-equilibrium approach suggested by Kaskan.[2]. He postulated that although the respective free radical concentrations were not consistent with thermodynamic equilibrium, they would be in equilibrium with each other. He assumed that the relationship between the amounts of H, O, OH, and H_2 could be expressed by the use of an appropriate set of quasi-equilibrium constants. Although values for some of these constants are not available in the literature they can be expressed in terms of the more usual equilibrium constants relevant to the

* National Bureau of Standards Oxide Coating A418.

TABLE 1

Multicomponent diffusion coefficients (cm^2/sec) and Lewis numbers for the diffusion of labile species into the combustion products

	19.42% Hydrogen-air				15.3% Hydrogen-air			
	380°K		1450°K		380°K		1380°K	
Species	$D_{i\text{-mix}}$	Le_i	$D_{i\text{-mix}}$	Le_i	$D_{i\text{-mix}}$	Le_i	$D_{i\text{-mix}}$	Le_i
O	0.486	1.64	4.504	1.65	0.477	1.62	4.076	1.61
H	1.681	5.67	12.746	4.87	1.654	5.52	12.430	4.71
H_2	1.547	5.21	12.155	4.64	1.514	5.05	11.768	4.48

hydrogen-oxygen reaction. Thus by assuming a given value for one of the concentrations the corresponding values of the other concentrations can be calculated.

Table 2 gives the mole fractions of the reaction products for various assumed concentrations of OH in the 19.42 per cent and 15.3 per cent hydrogen-air flames.

Since the values of the heats of reaction Q_i are known it is now possible to evaluate the heat flux expected for certain assumed values of the concentrations of the OH radical. It must be

TABLE 2

Mole fractions of reaction products calculated from quasi-equilibrium consideration

19.42% Hydrogen-air flame

	Concentration of OH molecules per $cm^3 \times 10^{-16}$				
Component	0.998	1.96	2.44	2.91	3.36
O_2	0.0794	0.0995	0.0805	0.0806	0.0815
N_2	0.7035	0.6924	0.6884	0.6861	0.6773
H_2O	0.2121	0.2098	0.1945	0.1863	0.1738
OH	0.0020	0.0039	0.0048	0.0058	0.0067
O	0.0012	0.0045	0.0078	0.0117	0.0165
H_2	0.0014	0.0050	0.0081	0.0114	0.0150
H	0.0006	0.0055	0.0103	0.0181	0.0292

15.3% Hydrogen-air flame

	Concentration of OH molecules per $cm^3 \times 10^{-16}$				
	1.05	2.01	2.52	3.02	3.29
O_2	0.1084	0.1077	0.1073	0.1067	0.1061
N_2	0.7221	0.7139	0.6962	0.6919	0.6796
H_2O	0.1628	0.1518	0.1507	0.1264	0.1133
OH	0.0020	0.0038	0.0048	0.0057	0.0062
O	0.0016	0.0087	0.0152	0.0228	0.0301
H_2	0.0012	0.0052	0.0085	0.0116	0.0137
H	0.0019	0.0089	0.0173	0.0350	0.0507

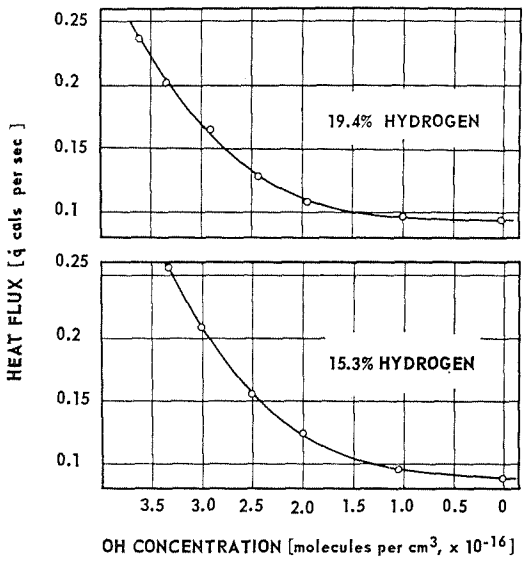

FIG. 4. Calculated heat flux for various hydroxyl radical concentrations.

remembered that the $\alpha_{e_i} Q_i$ product appears also in the enthalpy of the external flow h_e. Thus the calculated value of $h_e - h_w$ will increase with increasing concentrations of the labile species.

The finally calculated values of the heat flux $\dot{q}_s$ for each assumed value of OH concentrations, are given in Fig. 4.

Discussion

Figure 2 shows that the measured heat transfer rates are reasonably constant at distances greater than approximately 1.0 cm from the flame front. Nearer than this the heat flux increases as the distance decreases. From Fig. 3 however, it can be seen that there is no such marked increase in the flame gas "temperature." The results would appear therefore to confirm Kilham's conclusion that convection was not the only mechanism of energy transfer in the region near to the reaction zone. If this added mechanism is the exothermic recombination of the molecular fragments, then the heat transfer at distances greater than 1.0 cm above the flame front would appear to be attributable to combustion products in which the labile species are no longer present in significant concentrations. These asymptotic values of heat flux are seen to agree closely with the values calculated from Eq. (4) for the condition when each α_i is zero, given in Fig. 4. In this special case Eq. (4) reduces to Sibulkin's original form.

Dixon-Lewis,[21] among others, has shown that the energy transfer by dissociation and subsequent recombination will not add to the total energy flux if the Lewis number is unity, provided that the difference between the "undissociated" gas temperature and the wall temperature is used in calculating the heat flux. However, calculations made by the authors have shown that the high diffusion rates of the various molecular fragments through the gas mixture lead to Lewis numbers considerably greater than unity (Table 1).

If the maximum measured heat transfer rates for the 19.42 per cent and 15.3 per cent hydrogen-air flames as given by Fig. 2 are projected onto Fig. 4, it is possible to read off the amount of OH and hence of the other labile species, necessary to give such heat transfer rates. Thus for the richer and weaker flames respectively, the maximum measured heat transfer rates correspond to theoretical hydroxyl radical concentrations of approximately 3.5×10^{16} and 2.5×10^{16} molecules per cm^3. These amounts are equivalent to mole fractions of 0.7 per cent and 0.5 per cent and the corresponding mole fractions calculated for hydrogen atoms from quasi-equilibrium considerations are approximately 3 per cent and 1.7 per cent, respectively. Unfortunately, there are very few measured concentrations with which these values may be compared. Kaskan[20] has measured OH concentrations in a lean hydrogen-air flame which are of an order of magnitude less than those given above. However, Kaskan also measured OH concentration in rich hydrogen-air flames which were lower than those reported by Padley and Sugden.[22] Padley and Sugden gave concentrations of between 0.5 per cent and 1 per cent mole fraction for OH and between 1 per cent and 3 per cent for hydrogen atoms for approximately the same temperature range as that covered by this investigation. It would seem possible, therefore, that Kaskan's technique gave consistently low values and that the concentrations calculated here are near to the actual concentrations present.

From Fig. 2 it would appear that the heat transfer rate was affected by the condition of the receiving surface, unlike the work reported by Geidt *et al.*[3] The difference in the heat flux is quite small, however, and would seem to indicate that the bulk of the recombination takes place in the gas phase. Rosner[23] has discussed this condition and has shown that Eq. (4), which was based upon the assumption that there was no gas phase recombination, will probably still be applicable.

The above work is continuing at Leeds and it is expected that several gas mixtures will be dealt with in addition to rich hydrogen-air flames.

Nomenclature

c_p	Specific heat at constant pressure
$D_{i-\mathrm{mix}}$	Multicomponent diffusion coefficient of component i
D	Body diameter
h	Enthalpy
k	Coefficient of thermal conductivity
Le_i	Lewis number $(\rho c_{p_f} D_{i-\mathrm{mix}})/k$ of component i
M	Molecular weight
Pr	Prandtl number $(c_{p_f}\mu)/k$
p	Absolute pressure
Q_i	Heat of recombination of component i
$\dot{q}$	Heat flux
T	Absolute temperature
U	Free steam velocity
V_i	Diffusion velocity of component i
x	Distance along surface measured from stagnation point
x_i	Mole fraction of component i
y	Coordinate perpendicular to gas–solid interface
α_i	Mass fraction of component i
μ	Dynamic viscosity
ρ	Density
Φ_i	Catalysis-diffusion function of component i

Subscripts

e	Outer edge of boundary layer
s	Stagnation point
w	Wall (gas/solid interface)
f	Chemically frozen

Acknowledgments

The investigation described in this paper formed the subject of a thesis presented at the University of Leeds.[24] The authors wish to thank the Joint Research Committee of the Gas Council, Great Britain, and the University of Leeds for permission to publish the results. Thanks are also extended to Dr. D. E. Rosner of AeroChem Research Laboratories, Princeton, New Jersey for many helpful discussions and useful suggestions.

References

1. Kilham, J. K.: Gas Research Board (London) Communication GRB 47, 1949.
2. Ziebland, H.: Explosives Research and Development Estab. Tech. Memo No. 13/M/56, 1956.
3. Geidt, W. J., Cobb, L. L. Jr., and Russ, E. J.: A.S.M.E. Publication 60–WA–256, 1960.
4. Botha, J. P. and Spalding, D. B.: Proc. Roy. Soc. (London) *A225*, 71 (1954).
5. Nicholls, H. L.: Phys. Rev. *10*, 234 (1900).
6. Kaskan, W. E.: *Sixth Symposium (International) on Combustion*, p. 134. Reinhold, 1957.
7. Sibulkin, M.: J. Aero. Sci. *19*, 570 (1952).
8. Fay, J. A. and Riddell, F. R.: J. Aero. Sci. *25*, 85 (1958).
9. Goulard, R. J.: Jet Propulsion *28*, 737 (1958).
10. Rosner, D. E.: ARS Journal *29*, 215 (1959).
11. Hilsenrath, J., *et al.*: Natl. Bur. Standards Circular 564, 1955.
12. Hirschfelder, J. O., Curtiss, C. F. and Bird, R. B.: *Molecular Theory of Gases and Liquids*. Wiley, 1954.
13. Wilke, C. R.: J. Chem. Phys. *18*, 517 (1950).
14. Penner, S. S.: *Chemical Reactions in Flow Systems*. Butterworth, 1955.
15. Amdur, J.: J. Chem. Phys. *4*, 339 (1936).
16. Wilke, C. R.: Chem. Eng. Prog. *46*, 95 (1950).
17. Fairbanks, D. and Wilke, C. R.: Ind. Eng. Chem. *42*, 471 (1950).
18. Walker, R. E., DeHaas, N. and Westenberg, A. A.: J. Chem. Phys. *32*, 1314 (1960).
19. Wise, H.: J. Chem. Phys. *31*, 1414 (1959).
20. Kaskan, W. E.: Combustion and Flame *2*, 286 (1958).
21. Dixon-Lewis, G.: Gas Council (London) Research Communication GC 58, 1958.
22. Padley, P. J. and Sugden, T. M.: Proc. Roy. Soc. (London) *A248*, 262 (1958).
23. Rosner, D. E.: AeroChem. Res. Lab. Publication ARL 99, Part 1, 1961.
24. Cookson, R. A.: Thesis, University of Leeds, 1960.

Discussion

Dr. P. J. Padley (*Cambridge University*): Since the values of (H) and (OH) in the system are deduced to be up to about one per cent (or more) each in the total burned flame gas concentration, it seems somewhat surprising that the measured flame temperature shows no dependence on height above the reaction zone. P. J. Padley and T. M. Sugden: [Proc. Roy. Soc. (London) *A248*, 256 (1958)] have shown that recombination of radical concentrations of the order suggested by Dr. Kilham's results and in similar systems, should lead over the first millisecond after primary combustion to a measurable temperature rise, which can itself be used to provide quantitative evidence about radical disequilibrium.

Detonation and Transition to Detonation

Chairman: Dr. L. Deffet (*Brussels*)

Vice Chairman: Dr. S. R. Brinkley, Jr. (*Combustion and Explosives Research, Inc.*)

ON THE GENERATION OF A SHOCK WAVE BY FLAME IN AN EXPLOSIVE GAS

A. J. LADERMAN, P. A. URTIEW, AND A. K. OPPENHEIM

This paper provides experimental, as well as theoretical, proof that a laminar flame can generate a shock front quite early in the course of its initial acceleration. The flame at this stage of the process is wrinkled laminar, and it propagates at a velocity which is only a few times larger than the normal burning speed. However, no mechanism other than the break-up of the flame front into a cellular structure is necessary for this purpose, nor was it observed.

Introduction

The fact that the transition from slow burning to detonation is, to a large extent, governed by the action of shock waves, is today well known.[1,2,3,4] The most intricate problem in this respect is posed by the question: How do the shock waves originate?

The belief most prevalent in the literature[5,6] is that, in order to generate detonation, the combustion zone has to become first distributed in space either by the action of turbulence or by breaking down into separate combustion pockets, providing thus a sufficiently large increase in flame front area to render the combustion process an "explosive" character. Basically such a property of a combustible mixture should be exhibited most unequivocally by the facility it has in generating shock waves. However, except for the analytical inquiries of Boa-Teh Chu[7,8] who investigated the mechanism of pressure wave generation by the flame, and of Jones,[9] who demonstrated under what circumstances shocks are formed in a compression wave preceding a highly idealized piston model of a flame, very little has been done so far to explore this phenomenon. It is for the purpose of elucidating this question that the present paper is offered.

Experimental Evidence

The experiments were performed with stoichiometric hydrogen–oxygen mixtures, initially at NTP, in a rectangular $1 \times 1\frac{1}{2}$ in. cross-section detonation tube. Optically flat windows were fitted on both sides of the $1\frac{1}{2}$ in. deep channel, providing an unobstructed view from wall to wall across the 1 in. width of the tube. The ignition was performed either by electric-spark discharge or by a hot-wire glow-plug, most of the observations reported here having been obtained with the latter. The optical observations have been made by means of the streak schlieren and instantaneous interferometer techniques. This was accomplished using an 18 in. mirror Z type schlieren system and an 8 in. Mach-Zehnder interferometer. Simultaneously with these observations, pressure measurements were made by means of a quartz piezo-electric, PZ-6 Kistler transducer.

Figure 1 is the interferogram of the flame at the instant when it first touches the sidewalls.

FIG. 1. Interferogram of flame contacting sidewalls.

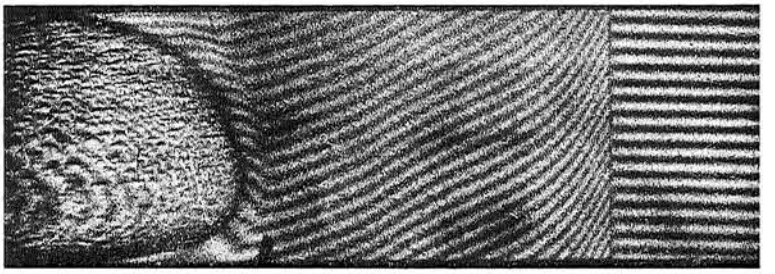

FIG. 2. Interferogram of flame-shock system.

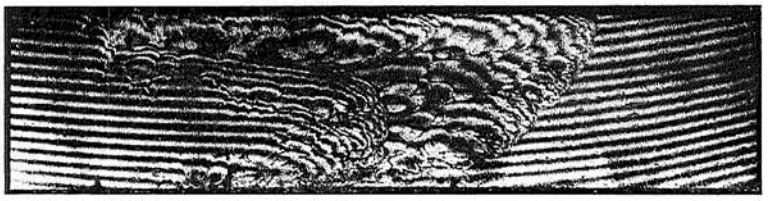

FIG. 3. Interferogram of a turbulent flame.

The full 1 in. width of the flow field is completely included in the interferogram. The spiral wire that formed the glow-plug is clearly discernible near the left end of the tube. It should be noted that at this instant the flame has not yet contacted the windows which are $1\frac{1}{2}$ in. apart. The pressure increase shifts the fringes downward. The flame has the characteristic laminar dome-like appearance with some evidence of a pressure wave ahead, exhibited by the direction of the fringes.

Figure 2 shows the interferogram obtained 0.3 milliseconds later. A fully developed shock wave is here clearly evident at a distance of only 3 cm ahead of the flame front. The shock appears as if it had been formed at the leading edge of a collapsing pressure wave. The dome of the flame front, which is in the middle of the tube, is recorded on the interferogram as the line associated with a sharp change in the slope of the fringes, producing an apparent rarefaction. The edge of the interaction between the flame and the boundary layer at the sidewalls manifests itself as a dark thick line followed by a highly turbulent regime where the fringes are broken down into an irregular pattern.

In contrast to Fig. 2, Fig. 3 demonstrates a typical interferogram of a turbulent flame. The flame front acquires then the well-known[4,6] characteristic "tulip" shape, due to the onset of turbulence in the boundary layer that promotes a much higher rate of the combustion process at the sides than in the middle.

Figure 4 is a streak schlieren photograph of the same process as that observed in Figs. 1 and 2. Time 0 corresponds to the instant of Fig. 1. The pressure wave appears now as a dark zone ahead of a sharply delineated flame front which is followed by streaks made by the wrinkles of the flame at the side boundaries. The collapsing pressure wave forms a shock wave which accelerates somewhat faster than the flame. Also visible as light streaks are the contact discontinuities formed by the collapsing pressure wave when the shock wave is generated.

Figure 5 represents the pressure record obtained simultaneously with the schlieren photograph of Fig. 4 while the transducer was situated at a distance of approximately 23 cm from the closed end, its exact position being denoted by the vertical white line on the photograph.

The pressure record is transformed, as shown

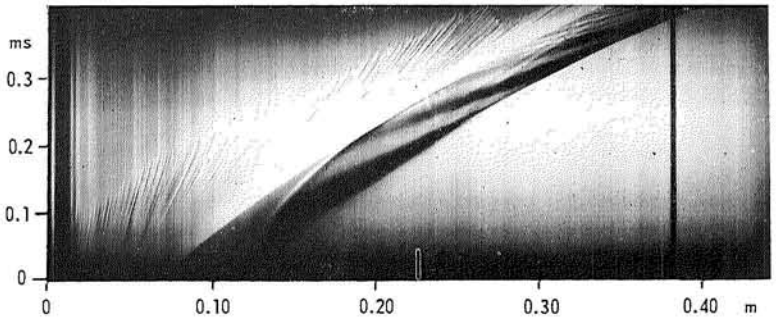

FIG. 4. Streak schlieren photograph. The flame front appears as the bright curved line, while dark areas ahead of it represent the pressure wave. Vertical white line at bottom of the photograph indicates position of pressure transducer.

in Fig. 6, into a space profile for comparison with the interferogram. This is done by taking advantage of the fact that when the pressure record is taken, the pressure wave is simple Riemannian, i.e. isentropic. Furthermore, the thermodynamic behavior of the hydrogen-oxygen mixture is considered to be adequately described by a perfect gas with a specific heat ratio $\gamma = 1.4$, while the local velocity of sound in the undisturbed medium at normal temperature is $a_0 = 537$ m/sec. Under these circumstances the relationship between the pressure ratio, p/p_0 and the slope of the characteristics, $u + a$, plotted in Fig. 5 is given by the simple expression[7]:

$$\frac{p}{p_0} = \left[\tfrac{5}{6} + \tfrac{1}{6}\left(\frac{u+a}{537}\right)\right] \qquad (1)$$

The wave pattern deduced in this manner from the pressure record bears a close resemblance to that exhibited on the schlieren record of Fig. 4. The shock wave which is formed at about 25.5 cm from the closed end has a Mach number of approximately 1.5. Since the characteristics of a simple wave are lines of constant state, knowledge of their traces in the time–space domain (world-lines) is sufficient for the deduction of the pressure–space profile. Such a profile, plotted for the instant of 0.235 milliseconds, corresponding to the interferogram record, is shown in the upper diagram of Fig. 6.

The fringe shift in Fig. 2 expresses the change in refractive index. In the absence of chemical reaction the latter is directly proportional to density which, for the isentropic, simple wave, is

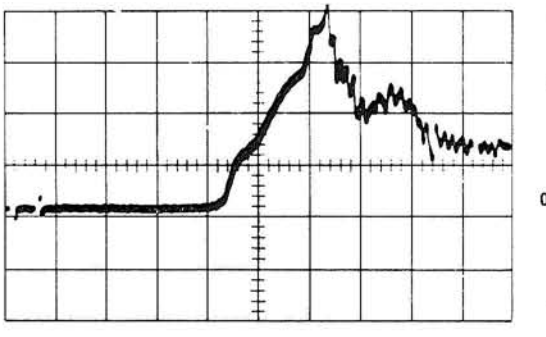

FIG. 5. Pressure transducer record obtained simultaneously with schlieren photograph of Fig. 4. Horizontal scale: 1 cm = 50 μsec from left to right. Vertical scale: 1 cm = 26 psi.

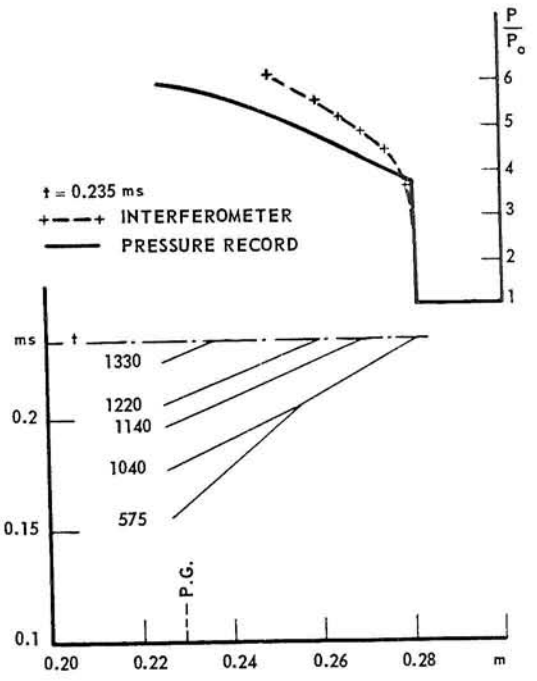

FIG. 6. Transformation of pressure–time history into a space profile. Numbers adjacent to world-lines indicate wave velocities in m/sec.

exponentially related to pressure. This then leads to the following relation between the pressure ratio p/p_s and the fringe shift, l:

$$\frac{p}{p_s} = \left[1 + \frac{\lambda}{(n_s - 1)w}\left(\frac{l}{D}\right)\right]^{\gamma} \qquad (2a)$$

where $D = 1.55$ mm is the fringe spacing, $w = 3.81$ cm is the width of the test section, $\lambda = 5510$ Å is the wavelength of light, $\gamma = 1.4$ is the specific heat ratio, $n_s = 1.000338$ is the index of refraction of the unreacted medium, and subscript s denotes conditions immediately behind the shock wave, determined from normal shock wave relations for $M = 1.50$. Substitution of numerical values into Eq. (2a) yields

$$\frac{p}{p_s} = (1 + 0.275l)^{1.4} \qquad (2b)$$

The pressure profile evaluated according to the above from the interferogram record of Fig. 2 is shown in the upper diagram of Fig. 6 in comparison with that deduced from the pressure measurement. The agreement between the two pressure profiles should be considered sufficiently close to warrant our contention regarding the nature of the wave-dynamic processes observed on the interferogram of Fig. 2.

This provides then an experimental proof that

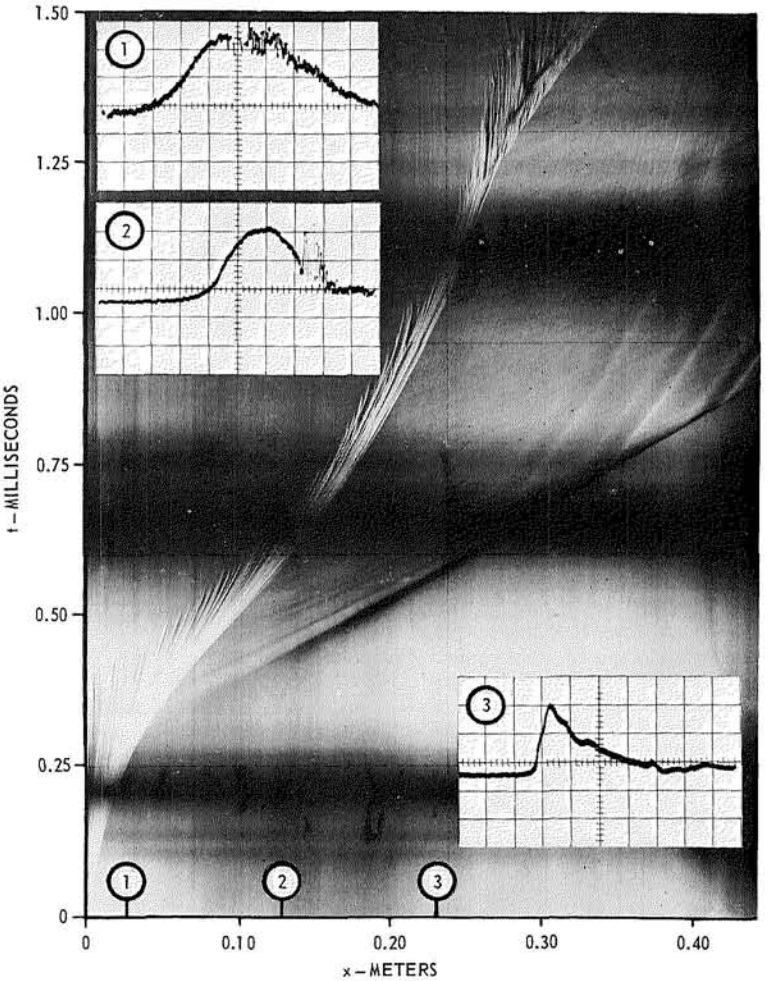

FIG. 7. Schlieren photograph of initial flame acceleration following ignition by spark discharge in a stoichiometric hydrogen-oxygen mixture. Pressure records at positions 1, 2, 3, shown as inserts. Vertical scale: 1 cm = 5.2 psi for insert (1), 10.4 psi for inserts (2) and (3). Horizontal sweep: 1 cm = 100 μsec for inserts (1) and (2), 200 μsec for insert (3), from left to right. (Reprinted from Reference 10).

a shock wave of strength corresponding to Mach number of 1.5 has been formed indeed by an accelerating, wrinkled, laminar flame.

Theory

The theory of the formation of the shock wave is developed most clearly with reference to the case where the ignition process is tractable right from its inception. Such an insight has been obtained in our experimental program only when ignition was performed by an electric spark discharge.

Figure 7, reprinted from Reference 10, demonstrates the streak schlieren photograph and pressure transducer records of such an experiment performed in our $1\frac{1}{2} \times 1$ in. detonation tube with a stoichiometric mixture of hydrogen-oxygen initially at NTP. Simultaneously obtained frame photographs revealed that the flame expanded initially in the form of a hemisphere whose surface was quite smooth until it contacted the sidewalls. The mode of its propagation was then undoubtedly laminar with some evidence of cellular structure which was reflected in about a fivefold increase of the normal burning speed.

The results of Fig. 7 have been interpreted by us[10] on the basis of a theoretical model, suggested originally by Chu,[8] where the flame is represented, in effect, by an equivalent, plane heater. When the relative flame velocity and the particle velocity are small compared to local speed of sound, the derivative of the pressure in the wave, p, with respect to the rate of heat release per unit flame frontal area, ω, can be expressed then as

$$\frac{dp}{d\omega} = \frac{\gamma_2 - 1}{(\gamma_2/\gamma_1)a_1 + a_2} \tag{3}$$

where γ is the specific heat ratio, a the local speed of sound, and subscripts 1 and 2 refer, respectively, to states immediately ahead of and behind the flame. For the flame, the requirement of energy equivalence yields:

$$d\omega/dA_f = \rho_1 Sq/A_t \tag{4}$$

where A_f is the flame surface area, A_t its effective frontal area specified here by the cross section of the detonation tube, ρ is the density, S the relative flame velocity (normal burning speed), and q the heat released per unit mass. The compression wave and flame acceleration computed on the basis of Eqs. (3) and (4) have been shown to be in good agreement with experimental results.[10]

The theory is now extended to determine the position where the shock wave is formed in the simple (isentropic) wave ahead of the flame. For this purpose Eq. (3) is first simplified by taking $a_2 = [m - (\gamma_2/\gamma_1)]a_1$ so that

$$\frac{dp}{d\omega} = \frac{\gamma_2 - 1}{ma_1} \tag{5}$$

where m is assumed constant, adjusted to match the results obtained by numerical analysis based on Eq. (3). The approximation of Eq. (5) is sufficiently accurate within the regime of interest with $m = 4$. Combining Eqs. (4) and (5), with the equation of motion for the wave process

$$du_1/dp_1 = a_1/\gamma_1 p_1$$

and the isentropic relation

$$\frac{p_1}{p_0} = \left(\frac{\rho_1}{\rho_0}\right)^{\gamma_1} = \left[1 + \left(\frac{\gamma_1 - 1}{2}\right)\frac{u_1}{a_0}\right]^{2\gamma_1/(\gamma_1 - 1)}$$

yields:

$$\frac{d(u/a_0)}{dA_f} = \frac{\gamma_2 - 1}{\gamma_1}\frac{\rho_0 Sq}{mA_t a_0 p_0}\left[1 + \left(\frac{\gamma_1 - 1}{2}\right)\frac{u_1}{a}\right]^{-2} \tag{6}$$

which is easily integrated to give:

$$\frac{u_1}{a_0} = \frac{2}{\gamma_1 - 1}[(1 + K_1 A_f)^{\frac{1}{2}} - 1] \tag{7}$$

where

$$K_1 = \tfrac{3}{2}\left(\frac{\gamma_1 - 1}{\gamma_1}\right)\frac{\gamma_2 - 1}{mA_t}\frac{\rho_0 Sq}{a_0 p_0}$$

Since the detonation tube was rectangular in cross section, the flame contacted the metal walls before reaching the windows. After that the flame was still considered to expand as a hemisphere, but its surface area was now represented by the area of the hemisphere less the area of the spherical segments intercepted by the walls. Consequently for $x_f < w/2$:

$$A_f = 2\pi x_f^2 = 6.28 x_f^2$$

while for $w/2 < x_f < d/2$

$$A_f = 2\pi x_f^2 - 2\pi x_f h = \pi w x_f = 7.97 x_f$$

where x_f is the radius of the flame front, $h = x_f - (w/2)$, $w = 2.54$ cm being the width, and $d = 3.81$ cm, the depth of the tube.

Equation (7) then becomes:

$$\left.\begin{aligned}\frac{u_1}{a_0} &= \frac{2}{\gamma_1 - 1}\left[(1 + 2\pi K_1 x_f^2)^{\frac{1}{3}} - 1\right] \qquad x_f < 1.27 \text{ cm} \\ &= \frac{2}{\gamma_1 - 1}\left[(1 + w\pi K_1 x_f)^{\frac{1}{3}} - 1\right] \qquad 1.27 < x_f < 1.91 \text{ cm}\end{aligned}\right\} \tag{8}$$

Since $2\pi K_1 x_f^2$ and $w\pi K_1 x_f$ are much smaller than unity, the terms in the brackets can be expanded into a power series. Furthermore, neglecting terms of second order leads to a maximum error of only 5%. We arrive then at the following simple expressions for the equivalent piston motion of the flame:

$$\left.\begin{aligned}u_1 &= 2K_2 x_f^2 \qquad x_f < 1.27 \text{ cm} \\ &= wK_2 x_f \qquad 1.27 < x_f < 1.91 \text{ cm}\end{aligned}\right\} \tag{9}$$

where $K_2 = 2\pi a_0 K_1/3(\gamma_1 - 1)$

It appears immediately from the above that the acceleration of the piston is never constant but increases in both cases and consequently, as it was demonstrated by Jones,[9] the shock wave will be formed inside the collapsing pressure wave rather than at its leading edge.

We proceed now to evaluate the onset of the shock wave. The flame world-line (its trace in time–space) is found from Eq. (9) and the expression for its absolute velocity:

$$dx_f/dt = S + u_1 \tag{10}$$

For $x_f < 1.27$ cm it is then:

$$\left.\begin{aligned}t_{\mathrm{I}}(x_f) &= \frac{1}{(2K_2 S)^{\frac{1}{2}}} \tan^{-1} x_f (2K_2/S)^{\frac{1}{2}} \\ \text{while for } 1.27 < x_f < 1.91 \text{ cm} \\ t_{\mathrm{II}}(x_f) &= t_{\mathrm{I}}(w/2) + \frac{1}{wK_2} \ln \frac{S + wK_2 x_f}{S + (w^2 K_2/2)}\end{aligned}\right\} \tag{11}$$

where $t_{\mathrm{I}}(w/2) = t_{\mathrm{I}}\ (1.27) = 190\ \mu\text{sec}$.

For a simple compression wave propagating into a perfect gas with $\gamma_1 =$ constant the equation of the world-line is:

$$x = \left[a_0 + \left(\frac{\gamma_1 + 1}{2}\right)u\right]t + f(u) \tag{12a}$$

To evaluate $f(u)$ we make use of Eqs. (11) and (8), the first permitting to eliminate t and the second allowing to express x, at $x = x_f$ in terms of u.* For the initial period when $x_f < 1.27$ cm we obtain:

$$f(u) = \left(\frac{\chi(u)}{2\pi K_1}\right)^{\frac{1}{2}} - \frac{1}{(2K_2 S)^{\frac{1}{2}}}\left[a_0 + \left(\frac{\gamma_1 + 1}{2}\right)u\right]\tan^{-1}\left(\frac{K_2\chi(u)}{\pi S K_1}\right)^{\frac{1}{2}} \tag{12b}$$

where

$$\chi(u) = \left[1 + \left(\frac{\gamma_1 - 1}{2}\right)\frac{u}{a_0}\right]^3 - 1$$

Consequently, within the simple wave:

$$x = \left[a_0 + \left(\frac{\gamma_1 + 1}{2}\right)u\right]\left[t - \frac{1}{(2K_2 S)^{\frac{1}{2}}}\tan^{-1}\left(\frac{K_2\chi(u)}{\pi S K_1}\right)^{\frac{1}{2}}\right] + \left(\frac{\chi(u)}{2\pi K_1}\right)^{\frac{1}{2}} \tag{13}$$

A shock wave should occur when $(\partial x/\partial u)_t = 0$. Equation (13) yields for this condition:

$$t = \left(\frac{2\pi K_1}{\chi(u)}\right)^{\frac{1}{2}} \frac{3}{4\pi K_1 a_0}\left(\frac{\gamma_1 - 1}{\gamma_1 + 1}\right)\left[1 + \left(\frac{\gamma_1 - 1}{2}\right)\frac{u}{a_0}\right]^2 \left\{\frac{a_0 + [(\gamma_1 + 1)/2]u}{S[1 + (K_2/S\pi K_1)\chi(u)]} - 1\right\}$$
$$+ \left(\frac{1}{2SK_2}\right)^{\frac{1}{2}} \tan^{-1}\left(\frac{K_2\chi(u)}{S\pi K_1}\right)^{\frac{1}{2}} \tag{14}$$

* Note that although Eq. (11) is approximate, Eq. (8) is exact.

which with (13) defines the locus of points in the time–space domain where the shock wave may be formed.

Similarly for $1.27 < x_f < 1.91$ cm, combining Eqs. (8), (11), and (12) leads to the following expression for the flow ahead of the flame:

$$x = \left[a_0 + \left(\frac{\gamma_1 + 1}{2}\right)u\right]\left[t - t_I\left(\frac{w}{2}\right) + \frac{1}{w\pi K_2}\ln\frac{S + (K_2/K_1)\chi(u)}{S + (w^2K_2/2)}\right] + \frac{\chi(u)}{\pi w K_1} \tag{15}$$

The locus of $(\partial x/\partial u)_t = 0$ is now given by:

$$t = t_I\left(\frac{w}{2}\right) + \frac{2}{w\pi K_2(\gamma_1 + 1)}\left[1 + \left(\frac{\gamma_1 - 1}{2}\right)\frac{u}{a_0}\right]^2\left\{\frac{a_0 + [(\gamma_1 + 1)/2]u}{S + (K_2/K_1)\chi(u)} - 1\right\}$$
$$+ \frac{1}{w\pi K_2}\ln\frac{S + (K_2/K_1)\chi(u)}{S + (w^2K_2/2)} \tag{16}$$

For a stoichiometric hydrogen-oxygen mixture in our $1 \times 1\frac{1}{2}$ in. cross-section detonation tube

$p_0 = 14.7$ psia $\quad \gamma_1 = 1.40$

$a_0 = 537$ m/sec $\quad A_t = 9.7$ cm^2

$\rho_0 = 0.03$ lb/ft^3 $\quad m = 4$

while good agreement with experimental results has been obtained in Reference 10 when the remaining parameters had the following values:

$S = 50$ m/sec

$q = 3160$ BTU/lb

$\gamma_2 = 1.20$

Therefore, the constant coefficients in Eqs. (13) through (16) are:

$K_1 = 70.63$ m^{-2} $\quad K_2 = 198{,}600$ (m-sec)$^{-1}$

The results of the analysis are demonstrated in Fig. 8. The flame world-line is shown by the heavy solid line starting at the origin, while the straight thin solid lines emanating from the flame front represent the simple wave generated during the acceleration process. The characteristics C_1, C_2, and C_3 have values of $u + a = 537$ m/sec, 612 m/sec, and 649 m/sec and represent, respectively, the sound waves generated at $x_f = 0$, $x_f = 1.27$ cm, and $x_f = 1.91$ cm. The C_2 characteristic separates the simple wave obtained

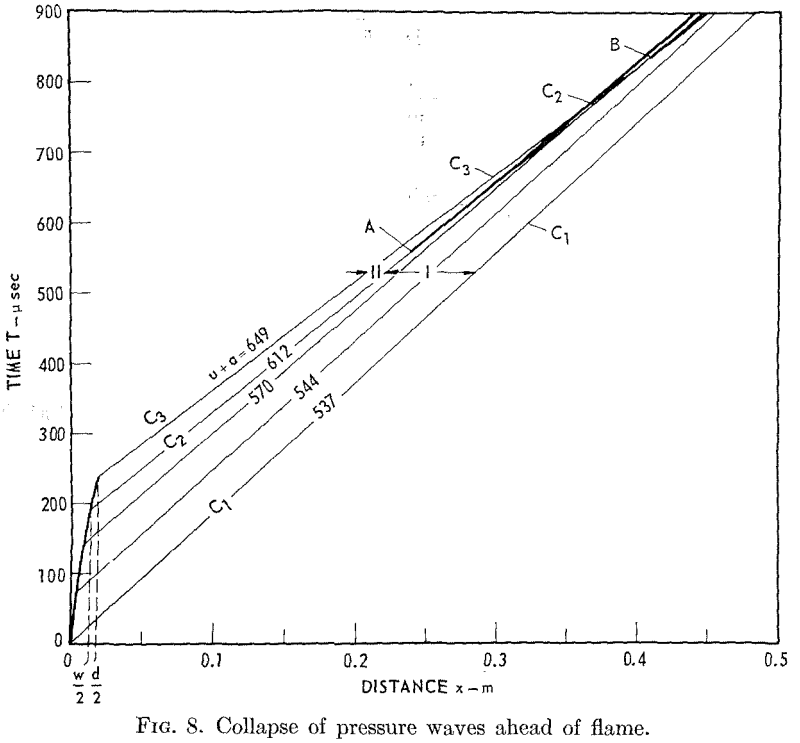

FIG. 8. Collapse of pressure waves ahead of flame.
(Wave velocities in m/sec.)

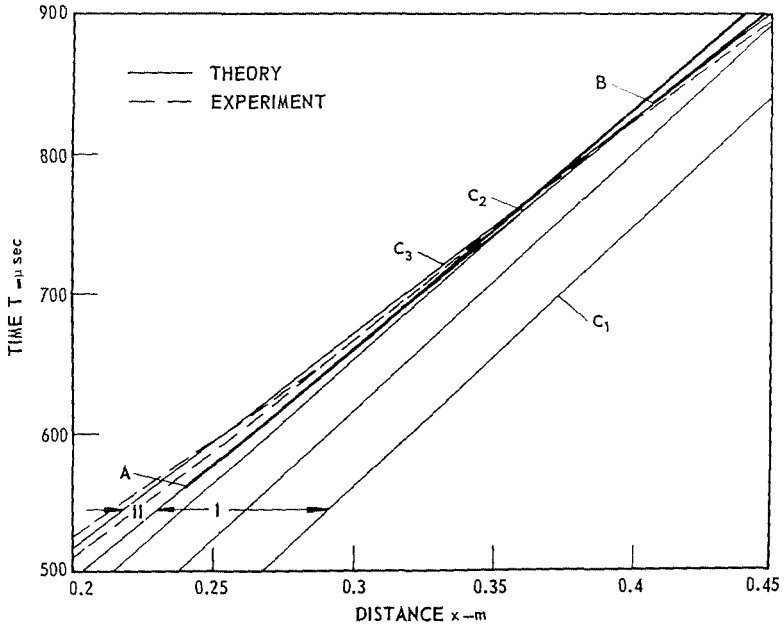

FIG. 9. Locus of shock wave formation points.

when $A_f \propto x_f^2$, i.e. for $x_f < 1.27$ cm, from that which occurs when $A_f \propto x_f$, i.e. for $1.27 < x_f < 1.91$ cm. For later reference these flow regimes are denoted as regions I and II, respectively.

The locus of points where $(\partial x/\partial u)_t = 0$ is shown in Fig. 8 by solid diagonal lines that originate at point A for region I and at point B for region II. For clarity the space–time diagram of these loci is reproduced to a larger scale in Fig. 9. Since the characteristics C_2, which passes through point A, and C_3, which passes through point B, lie to the right of the loci of points where $(\partial x/\partial u)_t = 0$ points A and B represent the location where shock waves are formed in regions I and II, respectively, while the remainder of the loci has no physical significance.

In both cases the shock waves will lie to the right of the characteristics which pass through the point of their formation. Both shock waves will increase in strength at a relatively slow rate and, after traversing the simple waves which precede them, they can attain, at most, a Mach number of 1.08. In particular, the shock wave which originates at point A will, to a first approximation, precede in time the extension of the characteristic C_2 by some 10 sec, when in the tube both reach the section of x_B. The expected shock wave path should lie therefore very close to the C_2 characteristic.

The dashed line shown in Fig. 9 represents the experimentally observed shock wave path replotted from the schlieren record of Fig. 7 for comparison with our analytical result. Pressure measurements shown in Fig. 7 verify our result that the shock reproduced in Fig. 9 is indeed the first one to occur in the simple wave ahead of the flame and that it was formed in the interior of the wave rather than at its leading edge.

Finally, to complete the historical description of the growth of the shock wave, a series of pressure profiles obtained from Fig. 9 at a number of time instants, has been plotted in Fig. 10. The discontinuity in the slope at earlier times corresponds to the boundary line between the two simple waves of regions I and II. Later this becomes obscured by the shock wave formed in region I.

To sum up, our studies of the formation of pressure waves by an accelerating flame have been extended to include the formation of shocks. It has been demonstrated that at the initial stage

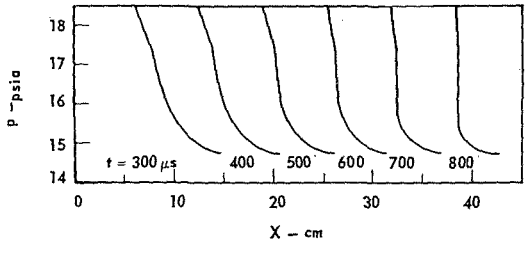

FIG. 10. Pressure profiles depicting formation of shock wave.

of the development of the process, shock waves are formed by laminar flames which exhibit a certain amount of cellular structure but are still far from breaking down into a turbulent brush. Furthermore, the acceleration of the flame is usually sufficiently intense (its value increasing with time) to promote the formation of the shock inside the simple wave generated by the flame, rather than at its leading edge. Both the experimental evidence and the theory indicate that shock waves are fully formed quite early and surprisingly close to the front of the accelerating flame.

Nomenclature

A_f	Flame surface area
A_t	Cross sectional area of detonation tube
a	Velocity of sound
D	Fringe spacing
d	Depth of detonation tube
$f(u)$	Function of u defined by Eq. (12a)
h	$x_f - (w/2)$
K_1	Constant defined by Eq. (7)
K_2	Constant defined by Eq. (9)
l	Fringe shift
m	Constant $= (a_2/a_1) + (\gamma_2/\gamma_1)$
n_s	Index of refraction
p	Pressure
q	Heat release per unit mass of mixture
S	Relative flame velocity
t	Time
t_{I}	Time measured along flame front world-line for $x_f < w/2$
t_{II}	Time measured along flame front world-line for $x_f > w/2$
u	Particle velocity
w	Width of detonation tube
x	Space coordinate
x_f	Radius of the flame front
γ	Specific heat ratio
λ	Wavelength
ω	Rate of heat release per unit flame frontal area
ρ	Density
$\chi(u)$	Function of u defined by Eq. (12b)

Subscripts

0	Denotes initial undisturbed state
1	Denotes state immediately ahead of flame
2	Denotes state immediately behind flame
S	Denotes state immediately behind shock wave

References

1. Evans, M. W. and Ablow, C. M.: Chem. Rev. *129*, 129 (1961).
2. Oppenheim, A. K. and Stern, R. A.: *Seventh Symposium (International) on Combustion*, pp. 837–850, Butterworths Scientific Publications, London, 1959.
3. Adams, G. K. and Pack, D. C.: *Seventh Symposium (International) on Combustion*, pp. 812–819, Butterworths Scientific Publications, London, 1959.
4. Salamandra, G. D., Bazhenova, T. V. and Naboko, I. M.: *Seventh Symposium (International) on Combustion*, pp. 851–855, Butterworths Scientific Publications, London, 1959.
5. Brinkley, S. R. and Lewis, B.: *Seventh Symposium (International) on Combustion*, pp. 807–811, Butterworths Scientific Publications, London, 1959.
6. Martin, F. J. and White, D. R.: *Seventh Symposium (International) on Combustion*, pp. 856–865, Butterworths Scientific Publications, London, 1959.
7. Chu, Boa-Teh: *Fourth Symposium (International) on Combustion*, pp. 603–612, The Williams and Wilkins Co., Baltimore 1953.
8. Chu, Boa-Teh: NACA TN 3683, October, 1956.
9. Jones, H.: Proc. Roy. Soc. (London) *A248*, 333–349 (1958).
10. Laderman, A. J. and Oppenheim, A. K.: Proc. Roy. Soc. (London) *A268*, 153–180 (1962).

Discussion

Prof. A. K. Oppenheim (*University of California, Berkeley*): For those who are interested in what happens to the shock wave whose formation was described in our paper, it might be worth adding that we have traced the later events and our first results have been recently published [Oppenheim, A. K., Laderman, A. J., and Urtiew, P. A.: Combustion and Flame, *6*, 193 (1962)]. The interesting feature observed then is the generation of spin. It appears that it is, in effect, the result of a point explosion that occurs at the boundary of our tube somewhere in the turbulent reaction zone that follows a system of precursor shocks. Instantaneous Schlieren photographs taken across the whole cross section of the tube reveal the exact nature of the oscillatory process which, on streak Schlieren records, gives the appearance of streaks usually associated with the phenomenon of spin.

Dr. S. R. Brinkley, Jr. (*Combustion and Explosives Research*): The photographs referred to by Oppenheim of the volume explosion in the turbulent

flame just prior to the transition to detonation would appear to afford confirmation of the suggestion made by Brinkley and Lewis in their paper at the Seventh Symposium. It was then suggested that such a volume explosion in the highly turbulent flame zone is probably the usual event immediately prior to the transition and is an essential part of the mechanism of the transition.

PROF. A. K. OPPENHEIM: With reference to the comment of Dr. Brinkley, we report indeed our observations and our experimental verification of the hypothesis put forward by him and Lewis and we stated this, in fact, in our Combustion and Flame paper.

DR. L. F. JESCH (*Sun Oil Company*): One of the oscillograms showing the pressure history was interpreted to have a peak value of ~100 psi. How was the system calibrated to give dependable values? Can the natural frequency of the crystal affect the accuracy and reproducibility of the measurement at sudden pressure rises? Our experience teaches that we can depend on the crystal pressure transducers only for the time of arrival measurement but not for numerical pressure values.

DR. A. J. LADERMAN (*University of California Berkeley*): The performance of the transducer used in our experiments was subjected to careful evaluation to assure accurate determination of pressure. For the range of pressures encountered during the flame acceleration process, the transducer was shock tube calibrated both prior to and after the experimental program. A shock isolation mount reduced the "ringing" to a small percentage of the useful signal. As a further check, pressures were deduced from the photographic observations. Since the pressure wave was isentropic, the pressure was related to the slope of the characteristics which could be observed on the Schlieren records. Pressures determined in this manner were in full agreement with the shock tube calibration. Furthermore, it should be noted that since the reported pressures resulted from a continuous compression process rather than a shock wave, the frequency of the phenomena was considerably lower than the natural frequency of the crystal.

SPHERICAL DETONATIONS OF ACETYLENE-OXYGEN-NITROGEN MIXTURES AS A FUNCTION OF NATURE AND STRENGTH OF INITIATION

H. FREIWALD AND H. W. KOCH

The spherical detonation of mixtures of acetylene–oxygen–nitrogen was investigated by means of self-luminosity photography and by pressure–time measurements near the detonation. The gaseous mixtures were contained in transparent rubber balloons of different sizes. The detonation was initiated in the balloon center by flame, electric spark, hot wire, exploding wire, or the detonation of a small quantity of lead azide, or mercury fulminate–Tetryl with or without a PETN booster. In addition a "linear" gaseous detonation in a tube was transformed to a spherical one and was studied as a function of tube diameter and mixture composition.

Generally the detonation region increased with increasing ignition energy. With 7 gm PETN the spherical detonations of near-stoichiometric rich mixtures were initiated even with 75% nitrogen, e.g., with more nitrogen than is contained in the corresponding fuel-air mixture. With spark ignition one always observed an ignition delay and a deflagration preceding the spherical detonation. The consecutive shock waves produced by the spherical detonation and by reflections were also investigated.

Introduction

Although detonations of gaseous mixtures in tubes have been known for a long time the existence of self-sustained spherical detonations in the gaseous phase was experimentally proved about 10 years ago by Manson and Ferrie,[1] Freiwald and Ude,[2] and Zeldovich, Kogarko, and Simonov.[3] In 1923 Laffitte[4] observed spherical detonation waves in mixtures of $CS_2 + 3O_2$ but recorded these waves over rather short distances (10 to 13 cm) and initiated the detonation by relatively powerful detonators of 1 gm of mercury fulminate. There was some doubt regarding the character of a self-sustained detonation wave (see Jost[5]).

While composition ranges of flammability of mixtures of many hydrocarbons with air and with oxygen are well known[6] these limits are completely lacking for spherical detonations, with exception of some data in references 1, 2, and 3.

Experimental

The gases used in this investigation were of normal purity and used without further purification. The composition was generally known to $\pm 1\%$.

The gases were filled at normal pressure into thin-walled, transparent rubber balloons of different sizes (15–500 liters). The overpressure in the inflated balloons was 3–4 cm of water.

The ratio of fuel to oxygen is expressed by $\lambda =$ (ratio of actual quantity of oxygen in the mixture/stoichiometric quantity of oxygen); the "atmosphere" of the mixture is expressed as $O_2/O_2 + N_2$ without including the fuel.

In the investigation of spherical detonations and its composition limits self-luminosity photography was used employing streak camera, Kerr cell shutter, and high-speed camera. We also investigated the consecutive shock waves produced by the spherical detonation by means of a condenser microphone placed near the detonation.

The detonations were initiated in the balloon center by flame, red-hot wire, exploding wire, electric spark, impact of a flying projectile, by the detonation of lead azide, electric detonators and boosters, and by a "linear" detonating mixture in a tube.

Examples of Spherical Gaseous Detonations and Related Shock Waves

The spherical detonation of an acetylene-oxygen mixture in a rubber balloon, initiated by a pressed pellet of 0.2 gm of lead azide, and taken with a Kerr cell shutter, is shown in Fig. 1. The photograph was taken 36 μsec after the initiation

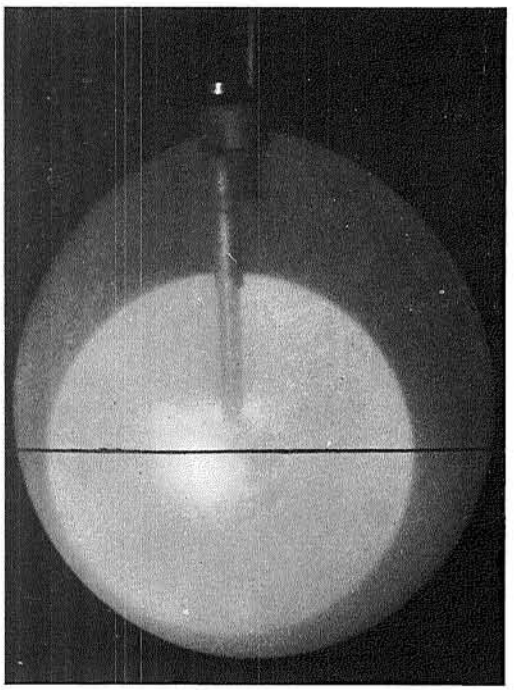

FIG. 1. Kerr cell shutter photograph of spherical detonation of 21.6 liters $C_2H_2 + O_2$ in a rubber balloon. Initiation: 0.2 gm of Pb N_6; 36 μsec after initiation.

and shows clearly the spherical detonation wave and its propagation through the gas mixture.

A typical streak camera record of the spherical detonation of $C_2H_2 + 2.5O_2 + 2.5N_2$ in a rubber balloon is shown in Fig. 2. The gaseous detonation was initiated at time A by the detonation of 0.2 gm of lead azide. The detonation shock wave is partially reflected on the balloon envelope and runs concentrically towards the balloon center where it is reflected at time B. The air and the lead vapor in the balloon center are heated by the converging shock waves. One can see the converging and diverging shock wave as a luminous cross on the film at time B. At time C one sees the originating second shock wave (combustion products shock wave). In detonations of spherical solid explosives the detonation center is normally covered by nontransparent combustion products.[7] The originating second shock wave is—perhaps for the first time—easily recorded by streak camera records in spherical gaseous detonations.[2,8]

The second shock wave is partially reflected on the spherical boundary of combustion products. It moves back to the center and reaches it at the time D.

The velocities of the waves are: detonation velocity from A 2075 m/sec, reflected shock wave at B 1370 m/sec, combustion products shock wave originating in C 930 m/sec, reflected shock wave at D 1010 m/sec. The scatter in these results is about $\pm$30–50 m/sec, depending on the sharpness of the wave record. This sharpness is decreased by the thin wall of the rubber balloon.

The velocity of the reflected shock wave at B depends on the relatively high detonation velocity. The velocity of the wave at D as a converging and diverging wave has a distinctly higher velocity than the products shock wave at C.

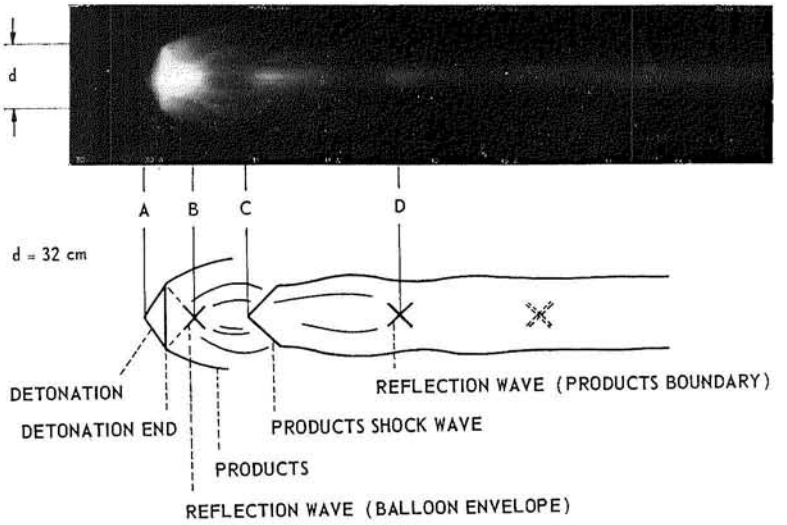

FIG. 2. Streak camera record of spherical detonation of 16 liters of $C_2H_2 + 2.5O_2 + 2.5N_2$; $\lambda = 1$; 50% O_2 in "atmosphere." Initiation: 0.2 gm of Pb N_6.

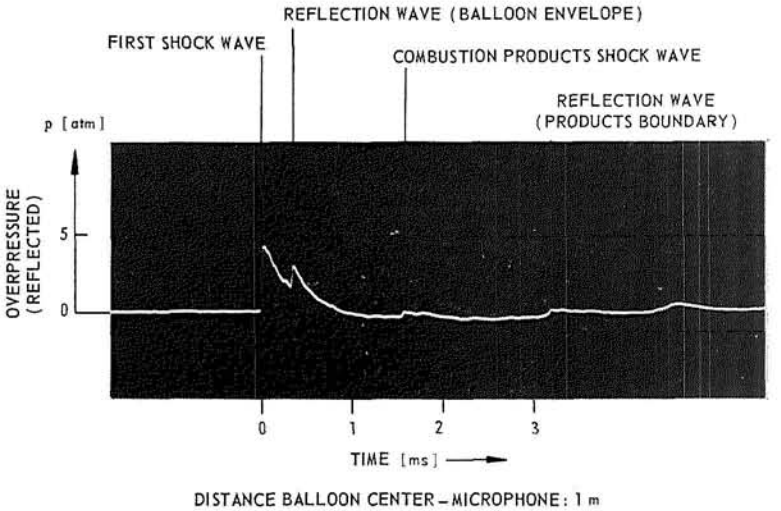

FIG. 3. Pressure–time record near to detonation of 184 liters of acetylene–air mixture (25% C_2H_2). Distance balloon center to microphone: 1 m.

On high-speed camera records one sees similar consecutive changes of brightness in the balloon center due to converging and diverging waves. The same sequence of shock waves was observed by recording the pressure as a function of time[9] (Fig. 3). The "reflected" pressure was recorded by a condenser microphone[7] situated 1 m distance from the balloon center. Behind the first air-shock wave one sees the shock wave reflected on the balloon envelope and at the center (point B in Fig. 2) and the wave reflected on the boundary of combustion products and in the center (point D in Fig. 2).

The sequence of shock waves is independent of the nature of the gaseous mixture and was observed with mixtures of hydrogen, ethylene, and propane with oxygen and nitrogen. The time of the occurrence of shock waves and of luminous phenomena produced by them depends only on the geometry of the balloon.

The maximum reflected pressure of the first shock wave as a function of the acetylene concentration in mixtures of 51 gm of acetylene with air are shown in Fig. 4.

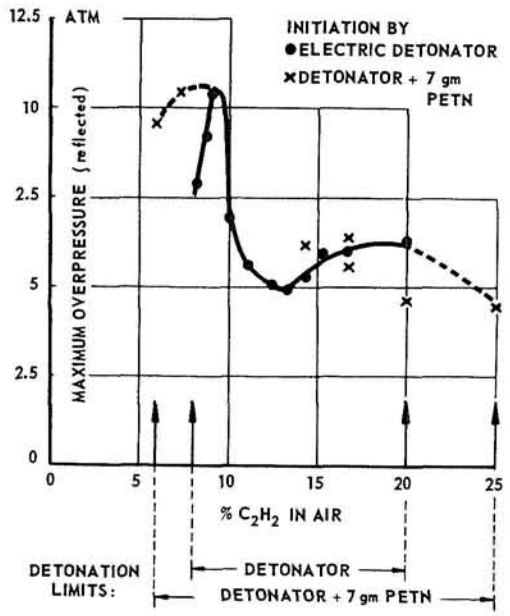

FIG. 4. Maximum (reflected) pressure of the shock wave of spherical detonation of C_2H_2–air mixtures as function of C_2H_2 percentage for different initiation. Fifty-one grams of (46 liters) C_2H_2. Distance balloon center to microphone: 1 m.

Composition Regions of Spherical Detonation

Ignition by Flame. With a commercial igniter producing a flame jet of 10 to 15 cm length one obtains a spherical detonation of C_2H_2–O_2 mixtures in the range from 16% (v/v) C_2H_2 to 54% C_2H_2 corresponding to λ between 2.3 and 0.34 (Fig. 5). In the C_2H_2–O_2–N_2 mixture a spherical detonation occurs up to a maximum nitrogen content of 33% in approximately stoichiometric mixtures. Manson[1] found narrower limits in C_2H_2–O_2 mixtures (25–50% C_2H_2) probably due to a weaker igniter flame.

Ignition by Electric Spark. An electric spark was used between tungsten electrodes with a gap dis-

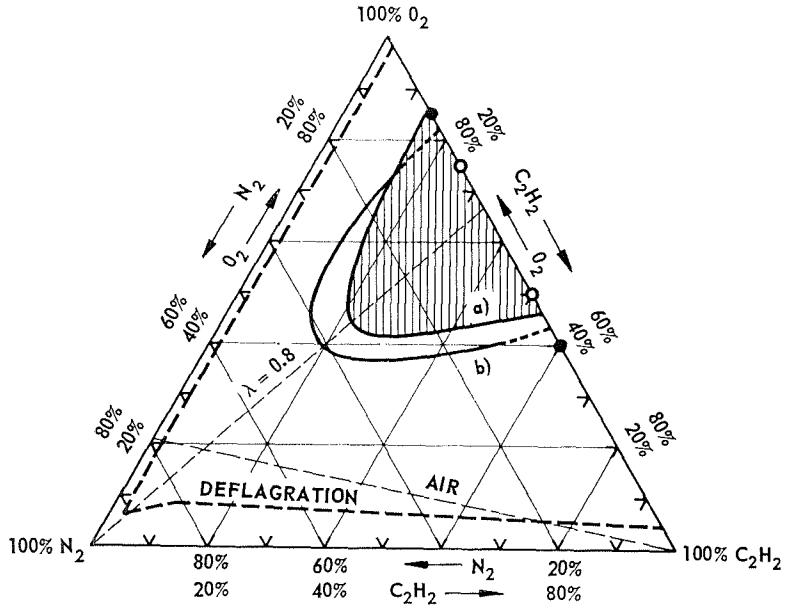

FIG. 5. Composition regions of spherical detonations of C_2H_2–O_2–N_2 mixtures. Ignition: (a) by igniter flame jet; (b) by electric spark, energy: 4.5 joules. Results of Manson[1]: ○ to curve (a); ● to curve (b); energy 12 joules.

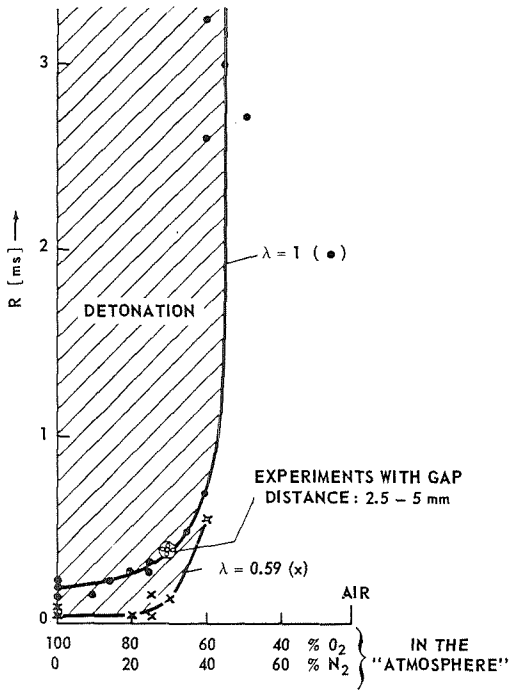

FIG. 6. Delay of spherical detonation of C_2H_2–O_2–N_2 mixtures after ignition by electric spark (4.5 joules) as a function of the composition of the "atmosphere."

tance from 2.2 to 5 mm.[10] The electrodes were mounted in the balloon center. The stored energy of the 1 μ F-condenser charged to 6 kV was 18 joules, but only 25% of the spark energy was effective in the spark as determined by calorimetry.[11] The limits of spherical detonations initiated by a spark of 4.5 joules energy were from approximately 18 to 57% C_2H_2 in the C_2H_2–O_2 mixture (Fig. 5). Curve b in Fig. 5 shows the spark ignition results with a maximum of 40.5% N_2 at $\lambda = 0.8$ in the three-component system.

In the case of initiation by electric spark a deflagration always precedes the spherical detonation propagating with a velocity of about 100–300 m/sec. The time delay from the spark to beginning of detonation depends on the gas mixture composition (Fig. 6). In a fuel-rich mixture ($\lambda = 0.59$) the delays are shorter than in the stoichiometric mixture. The delay of 0.1 m/sec with stoichiometric C_2H_2–O_2 mixture is in reasonable agreement with the results of Bollinger, Fong, and Edse[12] who determined a detonation induction distance of 2 cm for the same mixture in a 15-mm I.D. tube ignited by a melting 0.005-inch copper wire. The results of Kistiakowsky and Kydd[13] of the detonation delay of a mixture of 40% C_2H_2, 40% O_2, and 20% Ar at the head of a 10-cm diameter tube agree well with our results.

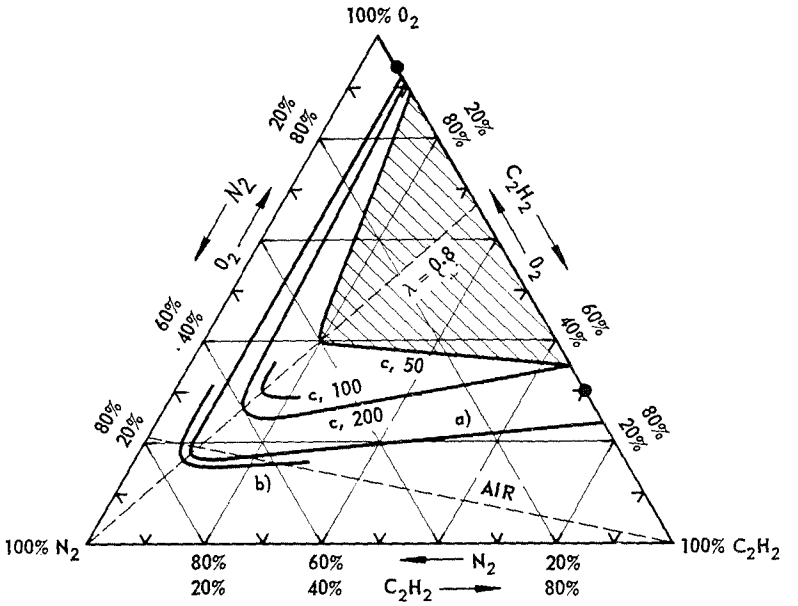

FIG. 7. Composition regions of spherical detonations of C_2H_2–O_2–N_2 mixtures. Initiation: by (a) electric detonator; (b) electric detonator and 7 gm PETN booster; (c) 50, 100, 200 mg Pb N_6. Results of Manson[1]: ●, electric detonator.

The electrode gap length has no influence on the time delay (Fig. 6).

Initiation by Detonation. The ranges of spherical detonation of ternary mixtures initiated by a detonation depend strongly on the strength of this initial detonation. We used small pressed pellets of lead azide from 50 to 200 mg, detonator No. 8 containing 0.4 gm of mercury fulminate and 0.8 gm of tetryl in a thin copper cap, and a booster of 7 gm of PETN (Fig. 7).

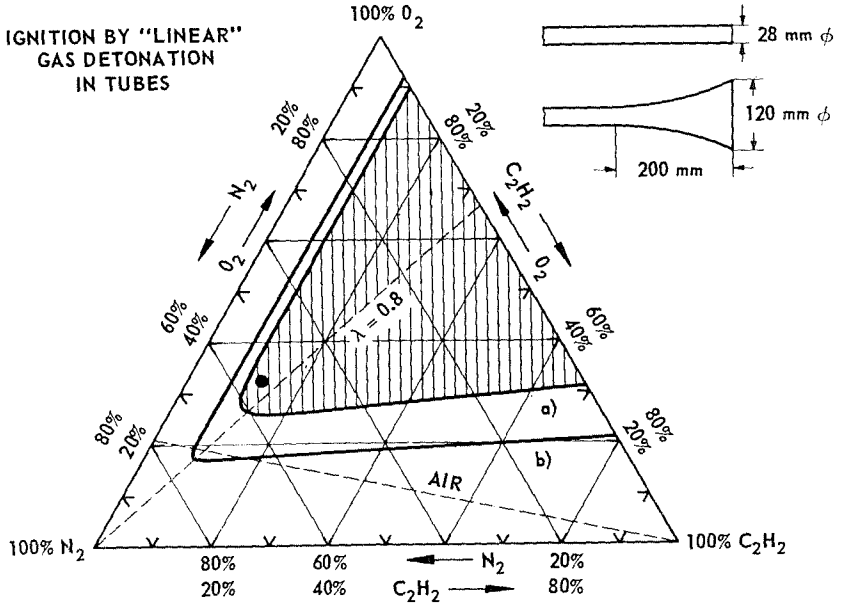

FIG. 8. Composition regions of spherical detonation of C_2H_2–O_2–N_2 mixtures. Ignition by transformation of linear gaseous detonation in a spherical one. ●, result of Zeldovich[3]; $\lambda = 1$; critical diameter, 28 mm.

Initiation by "Linear" Gas Detonation. "Linear" detonations of gaseous mixtures propagating in a tube are able to transform into spherical detonations.[10] There is a critical transformation diameter for each mixture. For a linear gas detonation in a 28-mm diameter tube ending in the balloon center, the composition region for transformation in spherical detonation (Fig. 8) is nearly the same as that of the 0.2 gm PbN_6 initiation (Fig. 7). Our results agree very well with those of Zeldovich[3] who determined the critical diameter for stoichiometric mixtures of acetylene and oxygen with increasing addition of nitrogen.

If the tube with an inside diameter of 36 mm is enlarged at the tube end in the balloon center, to a diameter of 120 mm the domain of spherical detonation of C_2H_2–O_2–N_2 mixtures is expanded (Fig. 8) so that it is nearly identical with that of the detonator initiation.

Ignition by Flying Projectile. The impact of a rifle bullet flying at 300–800 m/sec against the thin wall of the inflated rubber balloon is able to produce a spherical detonation. A bullet piercing transparent paper of 0.03 mm (800 m/sec) or an aluminum foil of 0.05 mm thickness (300 m/sec) initiates a spherical detonation of a fuel-rich ($\lambda = 0.59$) C_2H_2–O_2–N_2 mixture with 20.3% N_2 after a very short delay.

Ignition by Red-Hot Wire. For a thermal ignition source we used a 0.13 mm diameter red-hot resistance wire (1 cm length; 0.8 ohm). Contrary to results of other authors[1] we succeeded in igniting a spherical detonation of 350 liters of C_2H_2–O_2 from 15 to more than 35% C_2H_2 without much preceding deflagration.

Ignition by Exploding Wire. An "exploding" wire produces a local increase of temperature and a shock wave, similar to an electric spark. A 40 μ diameter copper wire of 10-mm length (0.1 ohm) was "exploded" by discharging a 64 μF-condenser charged to 450 V. The composition region of spherical detonation of C_2H_2–O_2–N_2 mixtures ignited by the 6.5 joules exploded wire is somewhat larger than the domain for the 4.5 joule spark (Fig. 5 curve b). Generally an exploding wire seems to be more effective in ignition of spherical gaseous detonations than an electric spark of the same energy.

Discussion of the Results. Influence of Ignition Energy on Detonation Limits

The results demonstrate the influence of ignition energy on the detonation limits, as shown distinctly in the ternary mixtures by the maximum nitrogen content. The regions of spherical detonation characterized by this maximum nitrogen content in near-stoichiometric acetylene rich mixtures ($\lambda = 0.8$) as a function of ignition energy are shown in Fig. 9. The ignition values from detonation yield a continuous curve, tending with increasing ignition energy asymptotically to a nitrogen content of about 77% at 10^5 joules.

The results of ignition by "linear" gas detonation are inserted in the curve. In this way we can determine the ignition energy of gaseous detonations propagating in tubes in the absence of deflagration (the ignition delay being less than 10 μsec and most probably only a few microseconds.)[3]

The curve was extrapolated to a value of 10

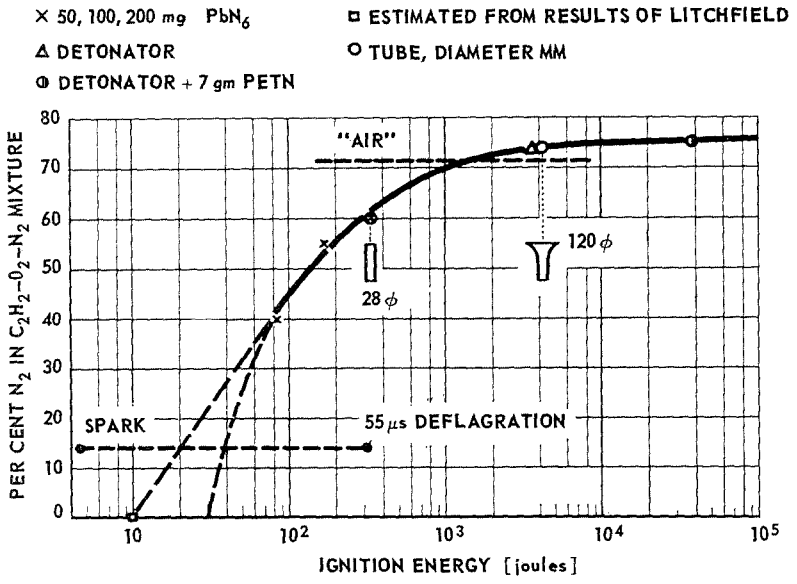

FIG. 9. Maximum nitrogen content in spherical detonations of C_2H_2–O_2–N_2 mixtures as a function of ignition energy; $\lambda = 0.8$.

joules and 30 joules at $N_2 = 0$. The 10 joules value is estimated from results[14] with exploding wire ignition in H_2–O_2 mixtures (13 joules) and ethylene–oxygen (8.7 joules). The 30 joules value is derived from a fit to the curve in Fig. 9.

$$\left(\frac{p_\infty}{p_\infty - p}\right)^n = \frac{\ln x}{\ln x_0}$$

where p = % N_2, $p_\infty = 77\%$, x = energy in joules. Plotting $\ln [p_\infty/(p_\infty - p)]$ versus $\ln \ln x$ we find $n = 3$, with $p = 0$, x_0 is about 30 joules.

For spark ignition one finds ignition delays of at least 50 μsec, even for C_2H_2–O_2 mixtures with a spark energy of about 5 joules. This ignition delay probably decreases with increasing ignition energy. In Fig. 9 we inserted the spark ignition data of a ternary mixture with 14% N_2 and a spark energy of 4.5 joules. This value differs from the extrapolated curves. The spark is followed by deflagration for 55 μsec with a velocity of about 300 m/sec. The combustion energy of the acetylene burned during the delay time is about 310 joules. This energy, will initiate ternary mixtures with 60% N_2 in direct initiation by detonation. This result indicates that only those ignition methods are comparable which produce a detonation without an intermediate state of deflagration.

References

1. Manson, N. and Ferrie, F.: *Fourth Symposium (International) on Combustion*, p. 486. Williams and Wilkins, 1953; Manson, N.: Rev. Inst. Franç. Pétrole. Ann. Comb. Liquid. *9*, 133 (1954).
2. Freiwald, H. and Ude, H.: Compt. rend. *236*, 1741 (1953); Freiwald, H. and Ude, H.: Z. Elektrochem. *61*, 663 (1957).
3. Zeldovich, Y. B., Kogarhko, S. M., Simonov, N. N.: Zhurnal Tekhnickeskoi Fiziki *26*, 1744 (1956); translated in Soviet Phys.—JETP. *1*, 1689 (1957).
4. Laffitte, P.: Compt. rend. *177*, 178 (1923); Ann. Phys. *10*, Ser. IV, 645 (1925).
5. Jost, W.: *Explosions-und Verbrennungsvorgänge in Gasen*, p. 185, Springer, 1939.
6. Coward, H. F. and Jones, G. W.: *Limits of Flammability of Gases and Vapors*. Bur. of Mines, Bull. 503, Washington, 1952.
7. Schardin, H.: Communs. Pure and Appl. Math. *VII*, 223 (1954).
8. Freiwald, H.: Z. Elektrochem. *65*, 711 (1961).
9. Freiwald, H. and Ude, H.: Explosivstoffe *7*, 251 (1959).
10. Freiwald, H. and Ude, H.: Compt. rend. *241*, 736 (1955); Z. Elektrochem. *59*, 910 (1955).
11. Boulay, J. and Freiwald, H.: *LRSL* Note Technique 18a/57.
12. Bollinger, L. E., Fong, M. C. and Edse, R.: ARS Journal *31*, 588 (1961).
13. Kistiakowsky, G. B. and Kydd, P. H.: J. Chem. Phys. *23*, 271 (1955).
14. Litchfield, E. L.: Phys. Fluids *5*, 114 (1962).

Discussion

Prof. N. Manson (*University of Poitiers, France*): I think that it might be of interest to bring to your attention the fact that Professor Laffitte performed some experiments on spherical detonations as early as 1924 (Annales de Chemie, Paris). I would like to ask Dr. Freiwald what is the accuracy of his measurements of detonation velocity?

Dr. H. Freiwald (*German-French Research Institute, France*): We know very well the experiments of Professor P. Laffitte [Compt. rend. *177*, 178 (1923); Ann. Phys. *10*, Ser. IV, 645 (1925)] with mixtures of $CS_2 + 3O_2$ in a glass balloon of 21 cm diameter. The mixture was initiated in the balloon center by 1 gm of mercury fulminate. Because of the effect of the relatively strong shock waves from the initiator there was some doubt about the existence of a really self-sustained spherical detonation in the mixture. Also from the theoretical point of view a spherical detonation in gases was believed to be impossible at that time.

In the case of initiation of spherical detonation by "linear" detonation we found the delay time to be less than the limit of time resolution of our smear camera (10 μsec). Zeldovich mentioned delay times of 1 to 2 μsec for the C_2H_2–O_2–N_2 mixtures used in our experiments.

Dr. W. E. Gordon (*Combustion and Explosives Research Inc.*): Concerning the secondary shock waves appearing in the microphone-pressure records in Dr. Freiwald's paper, I draw attention to the work of Brode [Brode, H. L., Phys. Fluids *2*, 217 (1959)] on the origin of such a sequence of shocks. Brode's integration of the hydrodynamic equations shows that expansion of an initially uniform sphere of compressed gas must give rise, in addition to an outward-facing shock wave, to an inward-facing shock. The latter implodes on the center, and subsequently is reflected, after outward movement, at the contact surface. As a result there is an indefinite number of pulsations of decreasing amplitude, as the pressure records in this case demonstrate.

DIRECT ELECTRICAL INITIATION OF FREELY EXPANDING GASEOUS DETONATION WAVES

E. L. LITCHFIELD, M. H. HAY, AND D. R. FORSHEY

Electrical initiation of freely expanding detonation waves has been demonstrated for three gaseous systems. It has been shown that a well-defined minimum stored-energy requirement exists for a given experimental system.

Both spark discharges and exploding-wire discharges are discussed as initiation sources, and exploding-wire discharge is shown to produce detonation from smaller stored energies in the systems investigated. In each instance, the existence of a composition, or a range of compositions, requiring discharge of a minimum energy for initiation of freely expanding detonation waves has been established.

Typical experimental data have been presented for mixtures of oxygen with the individual fuels ethylene, hydrogen, and propane. The data indicate that initiation of detonation in hydrogen systems requires more energy than in ethylene systems, but less than in propane systems. The pressure dependence of the stored energy required for initiation of detonation is quite complicated; in some instances the pressure sensitivity is large, and in other instances it disappears. Whenever a marked pressure effect exists, increasing the initial pressure decreases the required initiation energy.

Introduction

This Bureau of Mines study concerns the direct initiation of freely expanding gaseous detonation waves by electric discharge. "Direct initiation" means the production of the detonation wave as a direct and immediate consequence of the electric discharge, without introduction of extraneous chemical initiators and without the aid of artifices such as turbulence-producing grids. The detonable mixtures are contained within spherical reaction vessels, but the developing waves have no knowledge of the presence of the walls until the detonation impinges upon them. Thus, development to this stage occurs as though the walls were not present, hence the term "freely expanding."

This work is an extension of the pioneering endeavors of Manson and Ferrie,[1] Freiwald and Ude,[2] and Zel'dovich, Kogarko, and Simonov.[3] The initial demonstration of the detonation wave by Laffitte[4] and by Manson and Ferrie,[1] and the initial postulate of a minimum energy consideration by Zel'dovich and others[3] are explicitly acknowledged.

The acetylene-oxygen-inert system successfully used by the other authors has not been investigated here. Rather, the electrical initiation of detonation has been extended to mixtures of oxygen with the individual fuels ethylene, hydrogen, and propane.

The previous investigators worked entirely with spark discharges. In this study some investigations with spark discharges are reported, but the principal concern is with initiation by exploding-wire discharges.

Experimental Procedures

Gas mixtures were prepared with gases taken from commercial cylinders and used without further treatment. Composition was calculated from partial pressures; mixing was accomplished within the reaction vessel. Two spherical reaction vessels were used: a 1-liter bomb of about 12-cm diameter and a 14-liter bomb of about 30-cm diameter. Pressure-time histories were observed at the walls of the vessels with piezoelectric transducers (rise times of 1 and 3 μsec) whose outputs were displayed as an oscilloscope trace.

Electrical energy was stored on a capacitor, and discharges were usually accomplished with a three-element triggered spark gap, although hydrogen thyratrons have been used on occasion. The switch was necessary in the exploding-wire work and was retained in the spark work for reasons of convenience and similarity.

Wire composition, diameter, and length, switch characteristics, and electrode geometry are all quite important in determining the stored energy required for initiation of freely expanding detonations. However, in any given experimental

circumstance there are ranges of wire length and diameter over which there is little effect upon the stored energy required to produce detonation.

Experimental Results and Discussion

The results contained in this paper were derived from pressure-time histories at the bomb walls. This technique has been used for observation because of the desirability of the spherical vessels and the difficulties involved in achieving both strength and optical instrumentation in such vessels.

Figure 1 indicates, with some simplification, the criteria for interpretation of detonation. These three pressure-time histories were obtained from mixtures of 30% ethylene + 70% oxygen contained in the 14-liter bomb at an initial pressure of $\frac{1}{4}$ atm. The sweep rate is $\frac{1}{2}$ msec per major division and the auxiliary sweep corresponds to the deflection anticipated from a pressure increase of 200 psi. Discharge of the electrical energy was triggered approximately one-half of a major division from the edge of the graticule scale.

Figure 1a is a normal combustion record initiated by spark discharge of about 40 mjoules stored energy. This energy is 10^3 times the minimum energy for initiation of deflagration but is of a magnitude ordinarily employed for such purposes as burning velocity studies. Time from initiation of discharge to development of peak pressure is about 2.75 msec and corresponds to a mean wave velocity of about 54 m/sec over the bomb radius. The pressure rise of about 60 psi corresponds roughly to a sixteenfold increase.

Figure 1b corresponds to Fig. 1a except that a stored energy of 8.7 joules was discharged through a 30-mm length of 0.003 inch copper wire to provide initiation. Shock waves are evident ahead of the main combustion wave, and transient peak pressures are somewhat higher than in Fig. 1a; the propagation time has been reduced by about 50%. Thus, this 200-fold increase in stored energy has produced some acceleration of the combustion processes but the processes are still those of a deflagration. The apparent negative pressure developed at the latter times is the result of transducer heating by the combustion wave and seems to be partially a radiative effect.

Figure 1c corresponds to Fig. 1b except for a 4.5% increase in the stored energy used for initiation. This slight increase in stored energy results in an increase in transit velocity by more than twelvefold and a significant increase in the peak pressure is observed. The mean velocity of the wave in Fig. 1c is supersonic, and no shocks are observable ahead of the main wave. This record is considered to indicate detonation. The radiative effect upon the transducer is again apparent, although less than in Fig. 1b.

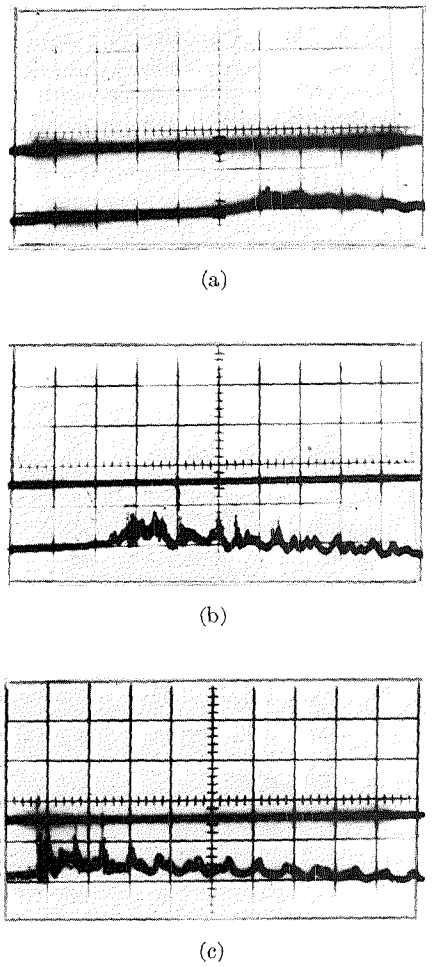

(a)

(b)

(c)

FIG. 1. Pressure-time histories at bomb walls for mixtures of 30% C_2H_4 + 70% O_2 at initial pressures of $\frac{1}{4}$ atm and initiated with different stored energies. Sweep rates are $\frac{1}{2}$ msec per major division and the auxiliary sweep corresponds to a deflection of 200 psi. (a) "Normal" deflagration, spark initiated, stored energy is approximately 40 millijoules. (b) "Accelerated" deflagration, exploding-wire initiated, stored energy is 8.7 joules. (c) Detonation, conditions identical to (b) except stored energy is 9.1 joules.

It is emphasized that all pressure effects at the

bomb walls in Fig. 1 are due to consumption of combustible within the reaction vessel. The maximum stored energy utilized does not produce observable (on this scale) pressure at the bomb walls if discharged into noncombustible atmospheres.

With the possible exception of some of the work on hydrogen–oxygen mixtures, stored energy is the controlling variable for production of detonation in a given gas mixture composition and pressure, and range of wire parameters. For a given set of wire parameters the energy limit for the occurrence of detonation is sharp and reproducible to about 1%.

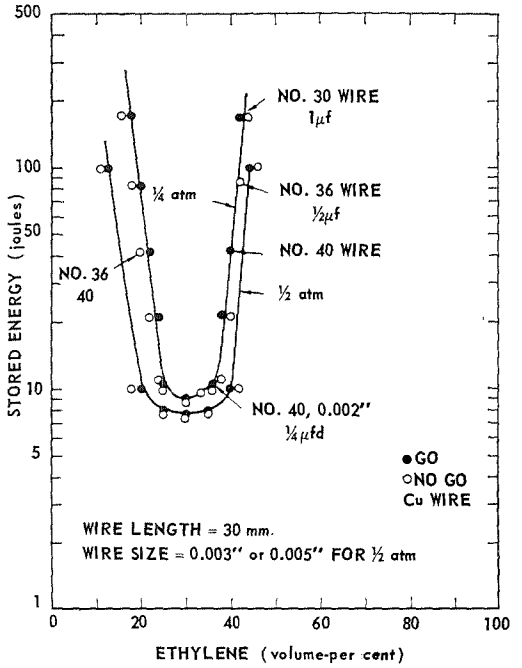

FIG. 2. Stored energy required for exploding-wire initiation of detonation as a function of volume per cent of ethylene in mixtures of ethylene and oxygen at initial pressures of $\frac{1}{4}$ and $\frac{1}{2}$ atmospheres.

There are circumstances under which transition from deflagration to detonation occurs. Such transitions that have been observed occur only after interaction with the vessel walls or in the presence of inhomogeneities in the gas mixture. A transition is not counted as a detonation in this investigation.

In Fig. 2, the minimum stored energy observed to detonate $\frac{1}{4}$ and $\frac{1}{2}$ atm ethylene-oxygen mixtures is plotted against mixture composition. Figure 3 contains similar data for propane-oxygen mixtures at initial pressures of $\frac{1}{2}$ and 1 atm. Figure 4 contains data for initiation of hydrogen-oxygen mixtures with both spark and exploding-wire sources.

Changing the initial pressure may produce either quite large or negligible changes in the stored energy required for initiation of detonation. At the minimum energy composition, the energy required to detonate propane-oxygen is unaffected by a change in initial pressure from $\frac{1}{2}$ to 1 atm. For the minimum energy composition of ethylene-oxygen, a change in initial pressure from $\frac{1}{4}$ to $\frac{1}{2}$ atm produces a small (15%) reduction in the stored energy required to produce detonation. At other compositions the energy

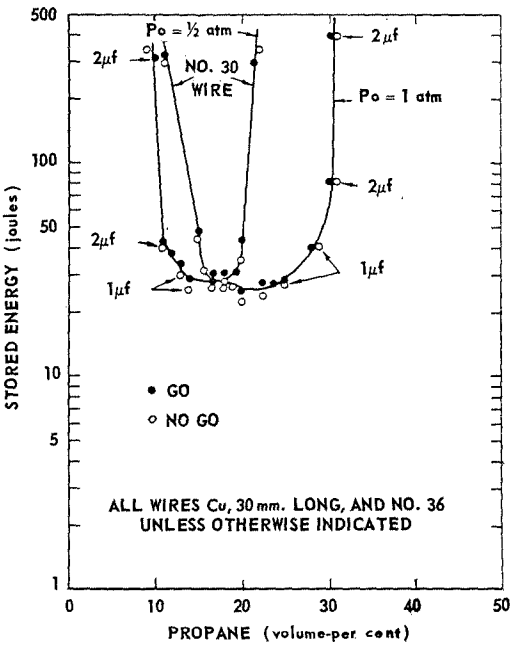

FIG. 3. Stored energy required for exploding wire initiation of detonation as a function of volume per cent of propane in mixtures of propane and oxygen at initial pressures of $\frac{1}{2}$ and 1 atm.

reduction with increased pressure may be relatively large—c.f., it is 1,000% for the mixture containing 21.5% propane. For both the propane and the ethylene mixtures, the range of compositions that may be detonated with given stored energy is significantly increased by doubling the initial pressure. The increase is especially spectacular in the case of the propane-oxygen mixture.

Other data, not contained in the figures, indicate significantly different behaviors below the pressures of the data in Figs. 2, 3, and 4, re-

spectively. For the minimum energy composition of ethylene-oxygen, two points at pressures of $\frac{1}{4}$ and $\frac{1}{6}$ atm and fitted by a relationship of the form p^n have given $n \cong -3$. For propane-oxygen, $n \cong -5$ from two points at pressures of $\frac{1}{2}$ and $\frac{1}{3}$ atm. For hydrogen–oxygen mixtures, $n = -3$ over the range between $\frac{1}{2}$ and 1 atm.

Figure 4 shows the relationship between stored energy for detonation and composition for hydrogen-oxygen mixtures at an initial pressure of 1 atm. Data are shown from both spark and exploding-wire initiation sources, and the effect of composition is similar. The stored energy requirements for spark initiation exceed those for exploding-wire initiation by the ratio 82:12.5 at the minimum initiation-energy composition. The ratio is quoted in terms of the observed energies. Other data, not contained in the figures, show the corresponding ratios for ethylene plus 3 oxygen to be 46.5:10.5 and 12.5:8.0 at initial pressures of $\frac{1}{4}$ and $\frac{1}{2}$ atm.

In all investigations the stored energy requirements for spark initiation have been in excess of the stored energy requirements for exploding-wire initiation. There is no apparent simple relationship between the two stored energies. The relatively larger "efficiency" of the exploding wire is assumed to be associated with a greater efficiency of energy transfer to the gas but no definite knowledge is presently available.

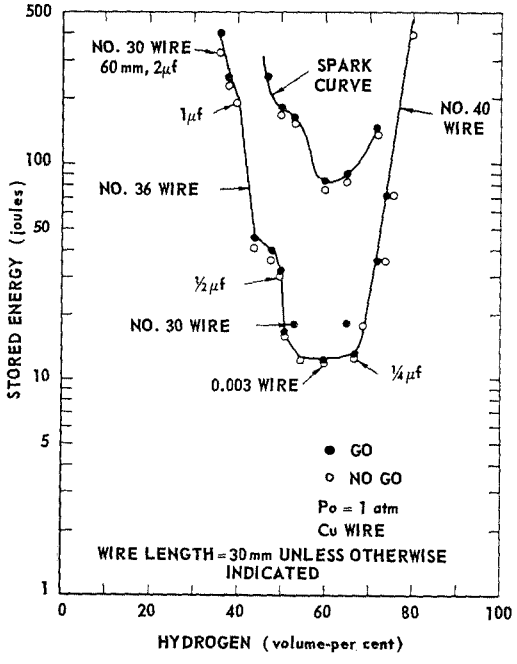

FIG. 4. Stored energy required for spark and exploding-wire initiation of detonation as a function of volume per cent of hydrogen in mixtures of hydrogen and oxygen at initial pressure of 1 atm.

Stored energy seems to be the controlling experimental variable. In this experimental arrangement, not all of the stored energy is delivered to the wire, and it is reasonable to assume that not all energy delivered to the wire will be transferred to the gas. As the concept of energy delivered to the gas is probably one of the fundamental concepts in this investigation of detonation initiation, it is appropriate to inquire whether any information on this subject is contained in the data presented here.

Three conclusions of qualitative and semiquantitative nature can be drawn: (1) that the steeply rising portions of the curves in Figs. 2 and 3 are a reflection of the behavior of the gas and are not a reflection of energy transfer characteristics from wire to gas; (2) that the ratio of energies actually delivered to the minimum energy compositions of the gas mixtures ethylene-oxygen/propane-oxygen is not more than the corresponding ratio of stored energies, i.e., ethylene is indeed more sensitive to initiation of detonation than is propane; (3) that energies delivered to the gas for initiation of the $\frac{1}{2}$- and 1-atm propane mixtures are equal and further that the flat portion of the 1-atm propane data is representative of an approximately constant initiation sensitivity over this range of compositions.

Investigations of the type described here are presently being conducted with other fuel gases. Optical studies of the detonation initiation process are also in progress.

ACKNOWLEDGMENT

This work was sponsored in part by Project SQUID, which is supported by the Office of Naval Research, Department of the Navy, under contract Nonr 1858(25) NR-098-038. Reproduction in full or in part is permitted for any use of the U. S. Government.

REFERENCES

1. MANSON, N. and FERRIE, F.: *Fourth Symposium (International) on Combustion*, pp. 486–94. Williams & Wilkins, Baltimore, 1953.
2. FREIWALD, H. and UDE, H.: Z. Elektrochem. *29*, 910 (1955).
3. ZEL'DOVICH, Y. B., KOGARKO, S. M. and SIMONOV, N. N.: Soviet Phys.—JETP *1*, 1689 (1956).
4. MULLINS, B. P. and PENNER, S. S.: *Explosions, Detonations, Flammability and Ignition*, AGARD, p. 67. Pergamon Press, London, 1959.

Discussion

DR. A. MACEK (*Atlantic Research Corporation*): We have been doing work on the initiation of spherical detonation in near-stoichiometric hydrogen-oxygen mixtures to which we add up to 10% of a third gas. The manner of initiation—by means of exploding wires—and of pressure measurement is quite similar to that described by Litchfield. In pure hydrogen-oxygen mixtures our minimum initiation energies are 10 to 11 joules, which is only slightly lower than the value reported by Litchfield. It is also interesting to note that the effect of dilution by nitrogen in the acetylene-oxygen mixture shown by Freiwald is similar to our results obtained with the hydrogen-oxygen system: addition of 10% nitrogen, in either case, increases the minimum initiation energy by a factor of 2 (very roughly).

We found in our work that when a given mixture is initiated by an amount of energy considerably in excess of the minimum so that detonation is formed relatively long before it reaches the wall, the record of pressure at the wall corresponds roughly to the reflected steady-state detonation pressure. If, however, the initiating energy is near the minimum, the pressure at the wall can be much higher. We believe that the effect is the result of the temporarily overdriven detonation in its nascent stage described by Brinkley and Lewis in the Seventh Combustion Symposium. I wonder if either Dr. Freiwald or Mr. Litchfield has observed such an effect.

DR. H. FREIWALD (*German-French Research Institute, France*): We did not find any overshooting detonation velocities in the case of ignition of spherical detonations of C_2H_2–O_2–N_2 mixtures by electric spark, but the precision of our measurements of detonation velocity was limited by the transparency of the envelope of the rubber balloons.

MR. E. L. LITCHFIELD (*U. S. Bureau of Mines*): We have not actually worked with acetylene-oxygen systems. Dr. Freiwald has simply taken a conservative number from our work and applied it to his. We certainly believe his estimate to be conservatively high.

With regard to measured pressure characteristics, we are not prepared to discuss the extent to which we have quantitative confidence in the transducer records.

THE GROWTH AND DECAY OF HOT SPOTS AND THE RELATION BETWEEN STRUCTURE AND STABILITY

T. BODDINGTON

Explosions frequently occur in condensed phase explosives as a consequence of the sudden formation of localized regions of high temperature known as hot spots or temperature spikes.[1] Hot spots may be produced under impact conditions or by irradiation with light, neutrons, and fission fragments or by the arrival of a shock wave at an impedance discontinuity. In spite of their obvious importance hot spots have received little theoretical consideration, probably because the relevant equations are rather intractable. This paper deals with two methods of estimating the critical conditions for explosion to occur. The first method involves an approximate analytical approach and has the advantage of demonstrating the relative importance of the numerous parameters involved. The second method, an exact machine solution of the same problem, gives results in good agreement with those derived from the analytical method. Growth to explosion is shown to depend on the magnitude of a single dimensionless criterion. Finally we consider the dependence of the explosive character of a solid upon its electronic structure.

Growth and Decay of Hot Spots

We shall regard the evolution of a hot spot as a purely thermal problem in which mass flow can be ignored. With this viewpoint explosion occurs if self-heating within the hot spot exceeds the rate at which heat is conducted into its surroundings, the subsequent growth and propagation of a flame being taken for granted once the material within the hot spot "explodes."

In the absence of an exact knowledge of the nature of a hot spot we assume that its temperature profile is initially rectangular and that it corresponds to a slab, cylinder, or sphere at an elevated temperature T_s within an infinite, homogeneous, isotropic explosive mass at an ambient temperature T_0. The radius of the cylinder or sphere and the half-width of the slab will be denoted by a. We assume that the explosive concentration n follows an Arrhenius rate law

$$\frac{\partial n}{\partial t} = -n\nu \exp\,(-E/RT) \qquad (1)$$

and that the activation energy E, the pre-exponential factor ν, the heat capacity c, the density σ, the exothermicity q, and the thermal conductivity κ are all constant. The equation expressing conservation of energy is

$$\sigma c \frac{\partial T}{\partial t} = \kappa \,\mathrm{divgrad}\, T - q\frac{\partial n}{\partial t} \qquad (2)$$

and the initial conditions are

$$\left.\begin{aligned} T &= T_s \quad \text{for} \quad |r| < a \\ T &= T_0 \quad \text{for} \quad |r| > a \end{aligned}\right\} \quad \text{at} \quad t = 0 \qquad (3)$$

where r is the distance from the center of the hot spot. The conditions for explosion should arise naturally from the solutions of Eqs. (1) and (2) with the initial condition (3).

Analytical Solution

For simplicity reactant consumption is ignored in this section so that n is equal to σ throughout the pre-explosion period. Equations (1) and (2) thus give

$$\sigma c \frac{\partial T}{\partial t} = \kappa \,\mathrm{divgrad}\, T + q\sigma\nu \exp\,(-E/RT) \qquad (4)$$

I II III

This equation cannot be integrated directly but the form of the initial conditions enables us to introduce simplifying approximations.

By dropping term II from Eq. (4) we obtain an equation corresponding to an adiabatic hot spot and this can be integrated approximately[2] to give

$$t = t_\infty(1 - e^{-\theta}) \qquad (5)$$

where

$$t_\infty = \frac{cRT_s^2 \exp\,(E/RT_s)}{q\nu E}$$

$$\theta = \frac{E}{RT_s^2}(T - T_s)$$

According to Eq. (5) the temperature increases slowly at first and then at, say, θ equals 1, rises

very rapidly. The temperature increase at the end of the induction period is given by

$$T - T_s = RT_s^2/E$$

Now typically $T_s \sim 1000°K$, $E \sim 40$ kcal/mole and $T_0 \sim 300°K$, so the temperature increase ($\sim 50°C$) is small compared with the temperature drop at the edge of a hot spot ($\sim 700°C$) even towards the end of the pre-explosion period. Thus the heat loss from a reactive hot spot is nearly the same as that from the corresponding inert hot spot (for which $q = 0$). This approximation was first used by Rideal and Robertson.[3]

The decay of an inert hot spot is governed by the Fourier equation obtained by dropping term III from Eq. (4) to give

$$\partial U/\partial \tau = \nabla_\rho^2 U \qquad (6)$$

with the initial conditions

$$\left.\begin{aligned} U = U_0 = T_s - T_0 \quad &\text{for} \quad |\rho| < 1 \\ U = 0 \quad &\text{for} \quad |\rho| > 1 \end{aligned}\right\} \text{ at } \tau = 0 \qquad (7)$$

where $U = T - T_0$; $\tau = \kappa t/\sigma c a^2$; $\nabla_\rho^2 \equiv (\partial^2/\partial\rho^2) + (k/\rho)(\partial/\partial\rho)$; $\rho = r/a$; and k is 0, 1, 2 for a slab, cylinder, or sphere, respectively. The solutions of Eq. (6) with condition (7) are given by

$$\begin{aligned} U/U_0 &= \tfrac{1}{2}(\operatorname{erf} v + \operatorname{erf} u) && k = 0 \\ &= \int_0^\infty J_1(k)\, J_0(k\rho)\, \exp(-k^2\tau)\, dk && k = 1 \\ &= \tfrac{1}{2}(\operatorname{erf} v + \operatorname{erf} u) \\ &\quad + \frac{1}{\rho}\sqrt{\frac{\tau}{\pi}}\left[\exp(-u^2) - \exp(-v^2)\right] && k = 2 \end{aligned}$$

where $u = (1 + \rho)/2\sqrt{\tau}$; $v = (1 - \rho)/2\sqrt{\tau}$. Thus for $k = 0$, 1, or 2 $U < \frac{1}{2}U_0$ if $|\rho| > 1$ and we can neglect reaction rates outside the hot spot.

The temperature gradient at the hot-spot boundary ($|\rho| = 1$) is given by

$$\left(\frac{\partial T}{\partial r}\right)_{r=a} = \frac{1}{a}\left(\frac{\partial U}{\partial \rho}\right)_{\rho=1} = -\frac{T_s - T_0}{2a\sqrt{\pi}} \cdot \tau^{-\frac{1}{2}} \cdot f$$

where

$$\begin{aligned} f &= 1 - \exp(-1/\tau) && k = 0 \\ &= 1 - 3\tau/4 + 0(\tau^2) && k = 1 \\ &= 1 - 2\tau + (1 + 2\tau)\exp(-1/\tau) && k = 2 \end{aligned}$$

We show below that we are concerned with times such that τ is less than 10^{-2}. Thus the approximation

$$\left(\frac{\partial T}{\partial r}\right)_{r=a} \simeq -\frac{T_s - T_0}{2a\sqrt{\pi}} \cdot \tau^{-\frac{1}{2}} \qquad (8)$$

is valid to within a few per cent.

We are now in a position to solve Eq. (4). Integrating over the volume of the hot spot we obtain

$$V\sigma c \frac{\partial \bar{T}}{\partial t} = \kappa \int_A \int \operatorname{grad} T \cdot dA + Vq\sigma\nu \exp(-E/RT_*) \qquad (9)$$

where A denotes the surface $|r| = a$ and $\bar{T}$ and T_* are mean temperatures given by

$$\bar{T} = V^{-1} \int\int_v\int T\, dV$$

$$\exp(-E/RT_*) = V^{-1} \int\int_v\int \exp(-E/RT)\, dV$$

Assuming that $T_* = \bar{T} = T$ and noting that $A/V = (k + 1)/a$ we can combine Eqs. (8) and (9) with the Frank-Kamenetskii exponential approximation[4] to give

$$\tau_\infty \frac{d\theta}{d\tau} = e^\theta - \epsilon\tau^{-\frac{1}{2}} \qquad (10)$$

where

$$\tau_\infty = \frac{\kappa R\, T_s^2 \exp(E/RT_s)}{q\sigma\nu E a^2}$$

$$\epsilon = \frac{k + 1}{2\sqrt{\pi}} \cdot \frac{\kappa(T_s - T_0)\exp(E/RT_s)}{q\sigma\nu a^2}$$

Our initial condition becomes $\theta = 0$ at τ equals 0. The ordinary differential Eq. (10) can be integrated directly giving

$$x = (1 - \phi)e^y + \phi(1 + y) \qquad (11)$$

where

$$x = e^{-\theta}$$

$$y = \Delta\tau^{\frac{1}{2}}$$

$$\Delta = 2\epsilon/\tau_\infty = \frac{k + 1}{\sqrt{\pi}} \cdot \frac{E}{RT_s^2}(T_s - T_0)$$

$$\phi = \tau_\infty/2\epsilon^2 = \frac{2\pi}{(k + 1)^2} \cdot \frac{q\sigma\nu a^2 R}{\kappa E}\left(\frac{T_s}{T_s - T_0}\right)^2 \exp(-E/RT_s)$$

Equation (11) describes the temperature evolution of any hot spot in terms of the dimensionless measure of temperature x and the dimensionless measure of time y. In physical terms y is

proportional to the square root of the time since inception and x is inversely proportional to the rate of heat evolution within the hot spot. The parameter ϕ is of considerable importance, as. can be seen from an examination of Eq. (11). We see that

$$x' = dx/dy = (1 - \phi)e^y + \phi,$$

$$x'' = d^2x/dy^2 = (1 - \phi)e^y,$$

and

$$x = x' = 1, \qquad x'' = 1 - \phi$$

at y equals 0. Obviously the nature of the temperature evolution depends upon the value of ϕ. We distinguish five cases which are of interest to us.

Case 1: $\phi = 0$, corresponding to an inert hot spot. Equation (11) becomes $x = e^y$ or $\theta = -\Delta\tau^{\frac{1}{2}}$. This is an approximate solution of the Fourier equation. The temperature falls steadily.

Case 2: $0 < \phi < 1$, corresponding to a hot spot of low radius. We see that $x'' > 0$, $x' > 1$, $x > 1 + y$. The temperature declines steadily but is always greater than that of the corresponding inert hot spot. No explosion occurs.

Case 3: $\phi > 1$, corresponding to a hot spot of large radius. x'' is now negative and

$$x' > 0 \quad \text{for} \quad 0 < y < \ln [\phi/(\phi - 1)],$$

$$x' < 0 \quad \text{for} \quad y > \ln [\phi/(\phi - 1)].$$

The temperature falls at first but then increases, finally leading to explosion. Physically we expect an initial fall in the mean temperature since the rate of self heating is finite while the rate of heat loss is initially infinite for our idealized temperature distribution.

Case 4: $\phi = 1$, corresponding to a critical hot spot. Equation (11) becomes $x = 1 + y$. The temperature falls steadily and no explosion occurs.

Case 5: $\phi = \infty$, corresponding to an adiabatic hot spot. This case is included for the purpose of comparison. The approximate solution for the adiabatic case is obtained by setting ϵ equal to 0 in Eq. (10) to give $\tau_\infty(d\theta/d\tau) = e^\theta$ or $\tau/\tau_\infty = 1 - e^{-\theta}$ which we may write as $x = 1 - \frac{1}{2}\phi y^2$ where the reduced time y is that appropriate to a hot spot characterized by the value ϕ. The temperature becomes infinite at y equals $(2/\phi)^{\frac{1}{2}}$.

The variation of x with y for various values of ϕ is given in Fig. 1. The dotted curve is the locus of the maxima in x (minima in θ) for $\phi > 1$ and is given by $x = y(1 - e^{-y})^{-1}$.

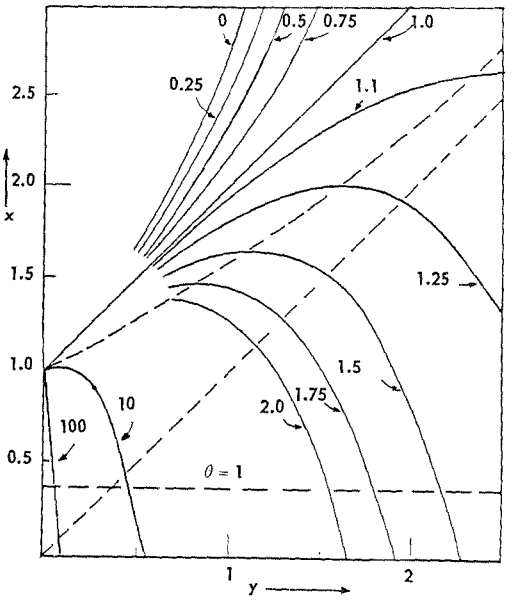

FIG. 1. Evolution of a hot spot as a function of the parameter ϕ. Curves given by $x = (1 - \phi)e^y + \phi(1 + y)$ are all tangential to the line $x = (1 + y)$ at y equals 0. Dashed curve is the locus of the maxima in x for $\phi > 1$. Explosion occurs at θ equals 1.

Explosion Times. The time taken by the hot spot to reach infinite temperature (τ_{ex}, y_{ex}) is given by

$$(1 - \phi) \exp (y_{ex}) + \phi(1 + y_{ex}) = 0 \quad (12)$$

Table 1 shows some values of y_{ex}, y_{ad} (the corresponding adiabatic explosion time), and τ_{ex}/τ_∞ for various values of ϕ. The reduced adiabatic explosion time at the critical temperature is

TABLE 1

The Dimensionless Explosion Time as a Function of the Criterion ϕ

y_{ex}	y_{ad}	τ_{ex}/τ_∞	ϕ
0.01	0.00997	1.006	2.10^4
0.1	0.097	1.062	2.10^2
1.0	0.725	1.905	3.80
2.0	1.090	3.37	1.68
4.0	1.344	8.86	1.11
10.0	1.410	50.3	$1 + 5.10^{-3}$
20.0	1.414	200	$1 + 5.10^{-6}$

given by

$$\tau_\infty = 2/\phi_{cr}\Delta^2 = \frac{2\pi}{(k+1)^2}\left(\frac{RT_s}{E}\right)^2\left(\frac{T_s}{T_s - T_0}\right)^2 \simeq 5.10^{-3}$$

and therefore a hot spot which is ca. 5° supercritical ($\phi \simeq 1.1$) explodes after a time given by $\tau_{ex} \simeq 5.10^{-2}$. Since Eq. (10) is valid for $\tau < 3.10^{-2}$ it is reasonably valid throughout the pre-explosion period for a near-critical hot spot.

Validity of the Solution. Most of the assumptions and approximations implicit in the derivation of Eq. (10) are demonstrably reasonable for the conventional explosives provided that (1) $E/RT_s \gtrsim 20$, (2) $|\theta| < 2$ or $0.13 < x < 7$, and (3) $\tau \lesssim 3.10^{-2}$ or $y \lesssim 4$.

These three conditions are satisfied in cases of interest to us. However the assumption that $\bar{T} \simeq T_*$ is difficult to justify. Reasonable estimates of the temperature profile at the end of the induction period suggest that $T_* - \bar{T}$ can be ca. 15° at this stage although zero initially. Thus the error incurred should not be serious.

The results of the numerical method described below indicate that Eq. (10) is substantially correct.

Numerical Solution

The basic equations for a spherical hot spot have been solved exactly with allowance for reactant consumption and without the use of Frank-Kamenetskii's exponential approximation. Our procedure is to replace Eqs. (1) and (2) by their infinite difference equivalents using the Crank-Nicolson finite difference scheme.[5] These equations are then solved numerically using a high-speed digital computer. The machine is supplied with the necessary parameters and provides the temperature and concentration profiles in the neighborhood of the hot spot as a function of time. The critical conditions for explosion are found by trial and error. Using the idealized rectangular temperature distribution the critical conditions so obtained for $600°K < T_s < 1300°K$ are given by $0.2 < \phi_{cr} < 0.35$ and the explosion times are given by Eq. (12) to within 6% provided that $\phi > 1.2$. Figure 2 shows the evolution of the temperature profile corresponding to a spherical hot spot in RDX (where $a = 5\ \mu$ and $T_s = 417°C$). The hot spot, which is just supercritical, develops in quasi-adiabatic fashion near the center but reaction is quenched by a "cold wave" moving inwards, so that only the central portion explodes. A hot spot is critical when the "cold wave" just succeeds in quenching the reaction at $r = 0$.

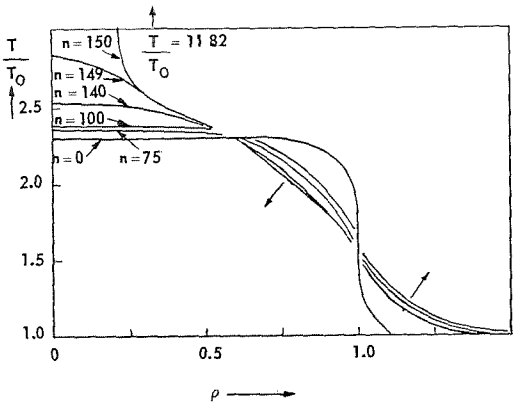

FIG. 2. Evolution of a nearly critical hot spot in RDX. $a = 5\ \mu$, $T_s = 417°C$. The time since inception is given by $t = n \cdot \delta t$ where $\delta t = 2.53 \times 10^{-2}$ μsec. Explosion time equals 3.8 μsec (arrows indicate direction of increasing n).

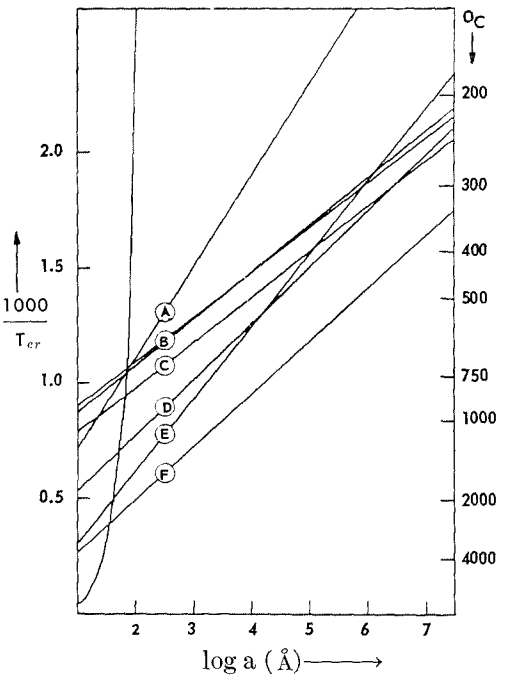

FIG. 3. Critical temperature as a function of hot-spot size for some common explosives. Straight lines are for $k = 0$ and should be displaced to the right by the amounts 0.301, 0.477 for $k = 1, 2$ respectively. A: AgN_3; B: HMX, PETN (greatest slope); C: RDX; D: tetryl; E: ethylenedinitramine; F: ammonium nitrate. The steep curve represents decay of a thermal spike caused by a fission fragment (corrected to k equals 1).

Only the spherical case ($k = 2$) has been studied numerically but the critical conditions found agree closely with the condition where $\phi = 1$. Because of the strong temperature dependence of ϕ the critical temperatures predicted by the analytical and the numerical methods are in excellent agreement for a wide range of hot-spot sizes.

The Critical Condition for Explosion. The critical hot-spot size, a_{cr}, is given by writing the condition $\phi = 1$ in the form

$$a_{cr} = a_0(k + 1)(1 - T_0/T_s) \exp (E/2RT_s)$$

where $a_0^2 = \kappa E/2\pi q\nu R\sigma$ is a constant for a given explosive. Since T_0/T_s usually lies in the range 0.2 to 0.5 we may use the approximation $1 - T_0/T_s \simeq \exp (-5T_0/4T_s)$ in order to estimate critical temperatures. We then find

$$T_{cr} = (2T_a - 5T_0)/4 \ln \frac{a}{(k + 1)a_0} \quad (13)$$

where T_a is the Arrhenius temperature, E/R. Figure 3 shows the variation of reciprocal temperature with log a for planar hot spots in some common explosives under the critical conditions given by Eq. (13). The corresponding critical conditions for k equals 1 or 2 are obtained by displacing the straight lines in Fig. 3 to the right by an amount $\log_{10} 2$ or $\log_{10} 3$, respectively. Allowing for experimental error, all the data quoted by Bowden and Yoffe[1] fit condition (13).

It is interesting to observe that the critical conditions for explosion do not depend upon the value of the heat capacity of the explosive.

Impact Sensitivity. If we assume that in a well-standardized "drop hammer" impact sensitivity test hot spots are formed which have a size roughly equal to the half-thickness ($a*$) of the sample, and that their temperatures are given by a frequency curve which is independent of the explosive used, then we expect the observed order of sensitivity to be the same as the order of the critical hot-spot temperatures at $a \simeq a*$. Examination of the ordinates of Fig. 3 between a equals 0.1 mm and a equals 1 mm shows that this oversimplified model does indeed correctly forecast the order of impact sensitivities.

Fission Fragment Bombardment. Bowden and Singh[6] have shown that the common explosives are not initiated by this mechanism, nor by irradiation with α-particles and slow neutrons. Simple calculations show that high-speed fission fragments generate more intense temperature spikes in solids than those formed by α-particles or neutrons. A typical (100 MeV) fragment from U^{235} generates a cylindrical spike which has a gaussian temperature profile of intensity ca. 2000 eV/Å. The way in which this spike decays is shown by the steep curve in Fig. 3 (a is the radial distance of the temperature profile inflection, T is the temperature at $r = 0$). The spike becomes subcritical for all the common explosives after ca. 10^{-10} sec, although it is supercritical before this. We conclude that, inasmuch as our idealized model is applicable, no thermochemically significant reactions can occur in this short time and thus no explosion occurs.

The Relation between Structure and Stability

This section of the paper considers some recent work of A. D. Yoffe and his co-workers in my laboratory.[7] They are attempting to show the general relationship between the electronic structure and the stability of explosive substances. For simplicity only the azides are discussed here.

It is now accepted that in a number of the inorganic azides the initial step in the decomposition by heat and light is the formation of an

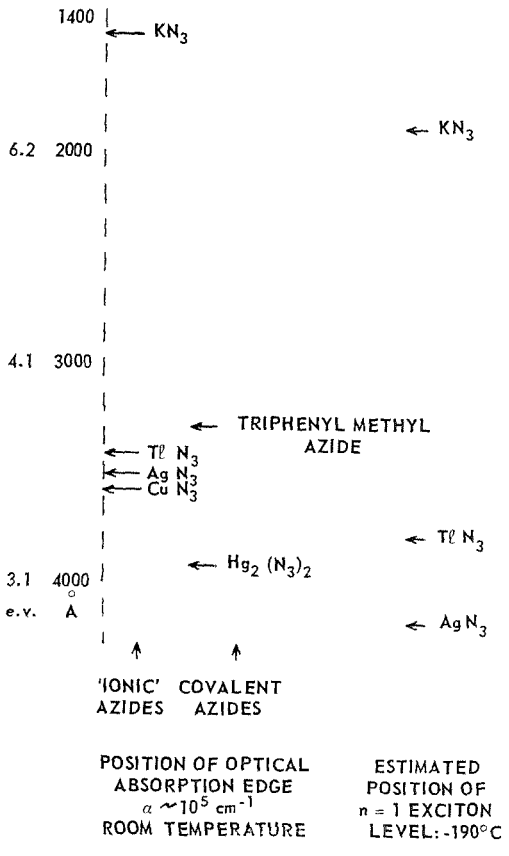

FIG. 4. Absorption spectra of some azides.

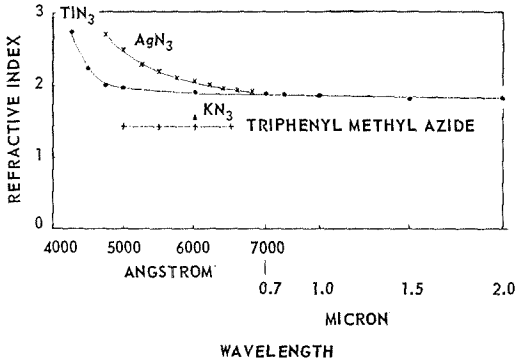

FIG. 5. Refractive index. Wavelength curves of monovalent azides at room temperature using unpolarized light.

azide radical by the promotion of a valence electron to the conduction band of the solid. Two azide radicals can then react exothermically to form nitrogen ($\Delta H = -232$ kcal mole^{-1}), and the metal ions liberated can aggregate to form electron traps capable of capturing any fresh electrons promoted to the conduction band.

The size of the azide group precludes the rapid diffusion of N_3 radicals in the solid lattice so that reaction occurs at the crystal surface and perhaps at imperfections. The rate-limiting process is the production of a free electron from an azide ion or an exciton. A study of the absorption spectrum of a solid azide enables us to calculate the optical energy required for these basic processes. The thermal (activation) energy can then be found from the ratio of the high and low frequency dielectric constants.[8] Figure 4 gives a schematic summary of measurements on absorption spectra and Fig. 5 gives the results of refractive index measurements. The ignition characteristics of a series of azides are given in Table 2. As the ionization potential of the metal increases the

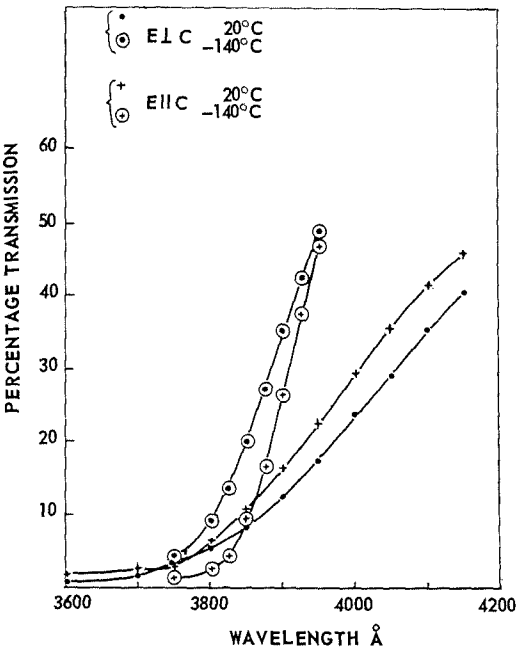

FIG. 6. Dichroism in single crystals of thallium azide, 5 μ thick.

gap between the valence and conduction bands decreases and the azide becomes less stable. Thus KN_3 is relatively stable while CuN_3 is very sensitive. The absence of photoconductivity in KN_3 indicates a large gap between the $n = 1$ exciton band and the conduction band in accordance with the observed stability, although Deb (private communication) has recently obtained evidence for photoconductivity with this compound.[9] When the ionization potential exceeds 8 eV the azides lose their "ionic" character altogether and the covalently bonded azide group is no longer symmetric. The first step in the de-

TABLE 2

Explosion Characteristics of Some Inorganic Azides

Compound	Ionization potential of of metal (eV)	Thermal ignition temperature (°C)	Optical ignition energy (joules)	Propagation velocity of film ca. 0.1-mm thick	Photo-conduction	Thermal dissociation energy of $n = 1$ exciton (eV)
KN_3	4.32	—	—	—	No	0.9
TlN_3	6.07	475	92	1480	Yes	0.3
AgN_3	7.54	475	39	2170	Yes	0.33
CuN_3	7.72	210	12	2720	No	ca. 0.35
$Hg_2(N_3)_2$	10.44	400	164	3000	No	—

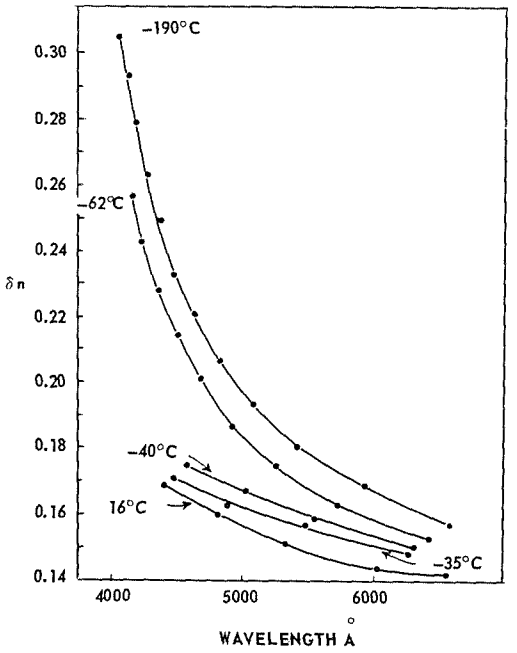

FIG. 7. Birefringence in thallium azide as a function of temperature.

composition is now the fission of the longest N—N bond[10] and the required activation energy *increases* with ionization potential. Thus CuN_3 is more sensitive than $Hg_2(N_3)_2$ which in turn is more sensitive than the organic azides.

We see that we can account for the stability of a simple series such as the azides by the study of their optical and electrical properties. Most of the data available at present, however, refers to measurements made between liquid helium and room temperatures. Figures 6 and 7 indicate that a significant variation in properties occurs in this temperature range.[11] Measurements of dichroism, birefringence, and differential thermal analysis suggest that at −30°C thallium azide undergoes a change to a more complicated structure. Silver azide also undergoes a phase change at 190°C.[12] A study of the high-temperature properties of the azides must be made in order to further our knowledge of the decomposition process.

Some consideration must also be given to liquid-phase reactions. In molten explosives the mobility of the species is high and fast bulk reactions occur. Although some solids do not melt prior to explosion, e.g., oxalates and acetylides, a molten phase is usually necessary before self heating leads to explosion.

REFERENCES

1. BOWDEN, F. P. and YOFFE, A. D.: *Initiation and Growth of Explosion in Liquids and Solids.* Cambridge University Press, 1952.
2. GRAY, P. and HARPER, M. J.: Trans. Faraday Soc. *55*, 581 (1959).
3. RIDEAL, E. K. and ROBERTSON, A. J. B.: Proc. Roy. Soc. (London) *A195*, 144 (1949).
4. FRANK-KAMENETSKII, D. A.: *Diffusion and Heat Exchange in Chemical Kinetics* (Moscow, 1947); English translation: Princeton University Press (1955).
5. CRANK, J. and NICOLSON, P.: Proc. Camb. Phil. Soc. *43*, 50 (1947).
6. BOWDEN, F. P. and SINGH, K.: Proc. Roy. Soc. (London) *A227*, 22 (1954).
7. EVANS, B., GRAY, P., and YOFFE, A. D.: Chem. Revs. *59*, 515 (1959).
8. MOTT, N. F. and GURNEY, R. W.: *Electronic Processes in Ionic Crystals.* Oxford University Press, 1948.
9. DEB, S. K.: J. Chem. Phys. *35*, 2122 (1961).
10. DEB, S. K. and YOFFE, A. D.: Proc. Roy. Soc. (London) *A256*, 514, 528 (1960).
11. YOFFE, A. D.: Unpublished work.
12. BARTLETT, B. E., TOMPKINS, F. C., and YOUNG, D. A.: Proc. Roy. Soc. (London) *A246*, 197 (1958).

A CORRELATION OF IMPACT SENSITIVITIES BY MEANS OF THE HOT SPOT MODEL

MORTON H. FRIEDMAN

It is generally accepted that explosions of most impact-sensitive materials are thermal in origin. The mechanism of impact initiation presumably involves the formation of small regions of high temperature within the reactant.[1] These "hot spots" may serve as nuclei from which grow the more gross phenomena—decomposition, deflagration and detonation. The phenomenon of impact explosion may be treated as a two-step process. First, the hot spot is formed in the explosive; second, exothermic reaction within the hot spot leads to sustained deflagration and/or detonation. Exothermic reaction is considered first, and critical hot spot size is determined by computer integration as a function of hot spot and ambient temperatures and the properties of the reactant. It is assumed in the analysis that the sample is infinitely large, heat flow is one dimensional, reactant consumption and heat losses are negligible, and exothermicity and all physical properties are constant. The validity of the last four assumptions is examined and generally established. The closed form equation for critical hot spot size is applicable when the hot spot temperature is between 400° and 9000°K and when the activation energy for decomposition lies between 5 and 60 kcal/mole.

Based on several assumptions regarding the mechanism of hot spot formation, an impact sensitivity correlation is derived, presented graphically, and used to predict the sensitivities of 16 explosives, propellants, and recently synthesized organic compounds. The correlation predicts experimental sensitivities to 40% and indicates the degree to which impact sensitivity is affected by the several thermal and kinetic properties of explosive materials.

Introduction

Hot spots can be produced in many ways by impact. In liquids, hot spots may be formed by the adiabatic compression of minute gas bubbles, or, more likely, by the partially adiabatic compression of spray-filled bubbles.[2] Gas may be entrapped in a solid by the rapid mechanical crushing attendant upon impact. A particle of grit, rubbing against either another particle or the sample container, may become hot enough to initiate an explosion. Under severe conditions, the heat generated by the shearing of liquid or molten layers may be sufficient to cause explosion. Hot spots have also been attributed to tribochemical effects.[3] Therefore, hot spots, although a convenient intermediate in models of impact initiation, can vary widely in physical nature depending on the state, purity, and physical properties of the substance in which they are formed.

Homogeneous Hot Spot Model

Regardless of the physical nature of the hot spot, it is likely that such factors as high-temperature decomposition rate and exothermicity, which determine whether or not a given hot spot will grow or decay, rank similarly in importance regardless of the exact nature of the hot region. For this reason, the hot spot model described here was used.

Consider an infinitely large homogeneous sample of explosive, at temperature T_1. If reactant consumption and heat losses to the surroundings are negligible, and if the heat of reaction of the material is independent of temperature, then, for any hot spot formed in the material, there exists a critical hot spot size. If this value is exceeded, the temperature at the center of the hot spot will rise monotonically. If the hot spot is of subcritical size the central temperature will first rise and then fall toward the ambient temperature.

Under the above assumptions the differential equation which determines the dependence of temperature on time at any point in the explosive when heat is transferred by conduction alone is

$$C\rho \frac{\partial T}{\partial t} = k\nabla^2 T + \rho Q Z \exp\left(-\frac{E}{RT}\right) \quad (1)$$

where C = heat capacity
ρ = density
T = absolute temperature
t = time
k = thermal conductivity
Q = heat evolved by decomposition
Z = frequency factor
E = energy of activation
R = gas constant.

To simplify the initial problem of determining the critical hot spot size as a function of hot spot and ambient temperatures and the properties of the explosive, the hot spot is postulated to be a two-dimensionally infinite slab of thickness $2d$ imbedded in an infinite mass of reactant. Equation (1) then becomes

$$C\rho \frac{\partial T}{\partial t} = k \frac{\partial^2 T}{\partial x^2} + \rho Q Z \exp\left(-\frac{E}{RT}\right) \qquad -\infty \leq x \leq \infty \quad (2)$$

with the boundary conditions

$$T(x,0) = T_0(\,|x| < d)$$
$$= T_1(\,|x| > d) \quad (3)$$

where x = distance
T_0 = hot spot temperature.

Integration of the Heat Sensitivity Equation

Two digital computer programs were written to find critical hot spot sizes from Eq. (2). The first of these programs used a method described by Goheen,[4] which treats the hot spot as a temperature perturbation; the second employed a second-order finite difference approximation to the sensitivity equation. Both of the computer programs operated not on the variables indicated in Eq. (2), but rather on the dimensionless variables given by Eqs. (4)

$$\theta = \frac{RT}{E} \quad (4a)$$

$$\tau = \frac{RQZ}{CE} t \quad (4b)$$

$$\xi = x \sqrt{\frac{R\rho QZ}{kE}} \quad (4c)$$

The dimensionless parameters corresponding to T_0, T_1 and d are, respectively, θ_0, θ_1 and a. The results of the integrations are given in Table 1. If $T_1 = 300°$K, these results correspond to hot spot temperatures of 400° to 9000°K and activation energies between 5 and 60 kcal/mole.

TABLE 1

Critical dimensionless hot spot half-widths

Dimensionless hot spot temperature θ_0	Dimensionless ambient temperature θ_1	$\text{Log}_{10} a_{cr}$ (See note [a])
0.05	0.01	3.53
0.10	0.01	1.62
0.20	0.01	0.82
0.30	0.01	0.47
0.03	0.02	6.18
0.04	0.03	4.39
0.06	0.03	2.82
0.08	0.03	2.04
0.10	0.075	1.37
0.15	0.075	0.89
0.20	0.075	0.65
0.16	0.12	0.66
0.24	0.12	0.45
0.34	0.12	0.35–0.43

[a] This is the just-subcritical radius. The true value of log a_{cr} lies less than 0.01 above the given value.

Analytical Correlation of Results

The utility of an analytical correlation of the results presented in Table 1 is evident. Such a correlation can be used to predict values of the critical hot spot size for cases other than those given above without necessitating further computer work. In addition, such an analysis can lead to the development of equations to predict the impact sensitivities of potential explosive and propellant ingredients. To determine the form of the correlation, it is first necessary to construct a mathematically convenient model whose behavior is similar to that of the hot spot simulated on the computer.

Denote the dimensionless temperature at the center of the hot spot by θ^*. For any combination of values of θ_0, θ_1 and a, plots of θ^* versus time exhibit one of three forms. For $a < a_{cr}$, θ^* rises to a maximum value, θ^*_{peak}, at a time, τ_{peak}, and then falls toward θ_1. When a is slightly greater than a_{cr} (the just supercritical case), θ^* rises continuously, exhibiting an inflection at θ^*_{inf} and τ_{inf}. The inflection temperatures and times for the just-supercritical case are quite close to the peak values for the corresponding just-subcritical case. When a exceeds a_{cr} by more than a

small amount, θ^* rises continuously without exhibiting an inflection.

In evaluating a model to represent the behavior of θ^* with time, it is most important that this model be accurate up to the inflection point; after inflection, which could be said to take place when $t = 0$ for highly supercritical cases, the course to explosion is evident. Observation of the results of the computer integration for just-supercritical cases yields the following conclusions:

1. The space-average heat generation rate within the hot spot changes relatively little prior to inflection.
2. Before the inflection point is reached, not much heat is generated outside the hot spot.

From these observations, two assumptions were made regarding the rate of heat evolution in the vicinity of the hot spot; first, that the region external to the hot spot is unreactive; and second, that heat is generated at a constant rate, B, within the hot spot. The solution of this initial value problem is, for $|\xi| < a$,

$$\theta = B\tau\left(1 - 2i^2\,\mathrm{erf}\,\frac{a-\xi}{2(\tau^{\frac{1}{2}})} - 2i^2\,\mathrm{erf}\,\frac{a+\xi}{2(\tau^{\frac{1}{2}})}\right) + (\theta_0-\theta_1)\left(1 - \tfrac{1}{2}\,\mathrm{erf}\,\frac{a-\xi}{2(\tau^{\frac{1}{2}})} - \tfrac{1}{2}\,\mathrm{erf}\,\frac{a+\xi}{2(\tau^{\frac{1}{2}})}\right) + \theta_1 \tag{5}$$

When $x = 0$, Eq. (5) reduces to

$$\theta^* = (\theta_0 - \theta_1)\,\mathrm{erf}\,\frac{a}{2(\tau^{\frac{1}{2}})} + \tau B\,\mathrm{erf}\,\frac{a}{2(\tau^{\frac{1}{2}})} + B(\tau/\pi)^{\frac{1}{2}}a\exp(-a^2/4\tau) - \tfrac{1}{2}Ba^2\,\mathrm{erf}\,\frac{a}{2(\tau^{\frac{1}{2}})} + \theta_1. \tag{6}$$

The derivative of θ^* with respect to τ is obtained formally.

$$d\theta^*/d\tau = -(\theta_0 - \theta_1)\,\frac{a}{2\tau(\pi\tau)^{\frac{1}{2}}}\exp(-a^2/4\tau) + B\,\mathrm{erf}\,[a/2(\tau^{\frac{1}{2}})]. \tag{7}$$

Making the substitution $\phi = a^2/4\tau$,

$$\frac{d\theta^*}{d\tau} = C_1\phi^{\frac{3}{2}}e^{-\phi} + B\,\mathrm{erf}\,\sqrt{\phi} \tag{8}$$

where

$$C_1 = \frac{4(\theta_0 - \theta_1)}{a^2(\pi)^{\frac{1}{2}}}. \tag{9}$$

According to this analysis, the criterion for stability should be a function of B and $(\theta_0 - \theta_1)/a^2$. From plots of Eq. (8) with C_1/B as parameter, it can be seen that $d\theta^*/d\tau$ shows no nontrivial zero unless C_1 is sufficiently negative. Nontrivial zeros correspond to local maxima on the θ^*–τ plot. The computer solution of Eq. (2) indicates that once $d\theta^*/d\tau$ goes negative, no explosion obtains, even for a zero order reaction. The value of C_1 was found which would just cause $d\theta^*/d\tau$ to have a zero. This critical value of C_1 is

$$C_{1\mathrm{cr}} = -2.2B. \tag{10}$$

Then, letting B equal the nondimensional heat release rate at θ_0, solving for a in Eq. (9), and letting the factor of 1.012 equal one

$$a_{\mathrm{cr}} = (\theta_0 - \theta_1)^{\frac{1}{2}}\exp\left(\frac{1}{2\theta_0}\right) \tag{11}$$

Equation (11) and the computed values of a_{cr} are shown in Fig. 1. Agreement is good. The above correlation can easily be used to predict critical hot spot sizes in other geometries without further computer work.

Reactant Consumption Prior to Explosion

The validity of the assumptions that the exothermic reaction is zero order and that the heat capacity, thermal conductivity and density are constant depends largely on whether much of the explosive or propellant is consumed before explosion. To estimate the maximum conversion of the reactant, the degree of reaction at the center of the hot spot will be considered since, for any unstable case, the temperature history here will be hottest and the most reaction will

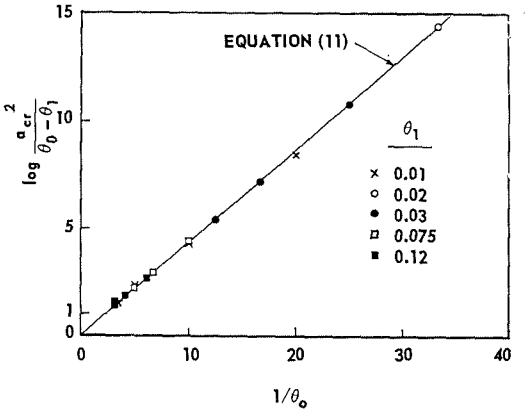

FIG. 1. Generalized plot of critical hot spot size.

have taken place at any time. The just-supercritical case will be considered because, for any pair of initial temperatures, this case requires the greatest degree of reaction at the center to achieve a given central temperature. The conversion at the inflection point will be found because, after inflection, self-heating in the hot spot region becomes nearly adiabatic, and increased conversion will confer stability to no greater extent than is observed in bomb tests.

It can easily be shown that the conversion at a point ξ at a time τ is given by

$$f(\xi, \tau) = \frac{CE}{RQ} \int_0^{\tau} \exp\left(-\frac{1}{\theta(\xi, \tau')}\right) d\tau' \quad (12)$$

where f = fractional conversion.

If we assume an ambient temperature of 300°K, the selection of a value of θ_1 implies a value for E/R. The maximum conversion to inflection is given by

$$f^* = CI^*/Q \quad (13)$$

where

$$I^* = \frac{E}{R} \int_0^{\tau_{inf}} \exp\left(-\frac{1}{\theta^*(\tau')}\right) d\tau'$$

Table 2 gives some values of I^* for several just-supercritical cases. From these results, it can be seen that the conversion at inflection increases as the hot spot temperature rises. The effect of energy of activation on conversion is negligible. Taking a typical value of 5×10^{-4} °K^{-1} for C/Q, a maximum conversion of 1%–8% is indicated. When high-temperature hot spots are produced in materials with large heat capacities or low heats of explosion, reactant depletion and reaction order may have to be considered; in general, however, reactant consumption may be neglected.

TABLE 2

Conversion integrals for selected just-supercritical cases

Dimensionless hot spot temperature θ_0	Dimensionless ambient temperature θ_1	I^* (degrees K)[a]
0.04	0.03	39
0.20	0.075	160
0.08	0.03	157
0.16	0.12	25
0.24	0.12	125

[a] See Eq. (13).

Further analysis of the computer results yields the following conclusions:

1. The times to explosion obtained from the computer integration agree with those found experimentally from impact sensitivity studies.
2. Variations in heat capacity, thermal conductivity, density, and heat of explosion in the period after hot spot formation, due to either reactant depletion or temperature change, have little effect on hot spot stability.
3. Only a minor fraction of the heat flux through the explosive can be attributed to thermal radiation.

Impact Sensitivity Correlation

To study the practical implications of the hot spot model with regard to impact sensitivity, it is first necessary to restate Eq. (11) in dimensional form

$$d_{cr} = \sqrt{\frac{k(T_0 - T_1)}{Z\rho Q}} \exp\left(\frac{E}{2RT_0}\right)$$

$$= F\sqrt{T_0 - 300}\ 10^{0.10928E/T_0} \quad (14a)$$

where $F = \sqrt{k/Z\rho Q}$ and T_1 is taken to be 300°K. Assume that the number of hot spots formed by a given impact is the same in all materials, that they are formed in all species with the same efficiency of energy transfer, and that the energy in a hot spot under impact is proportional to the drop height, h, raised to an empirical power, n. Then,

$$d^3(T_0 - T_1) = D_1 h^n \quad (15)$$

where D_1 is a proportionality constant which may include volumetric heat capacity. The value of n depends on the means of energy transfer from the impacting hammer to the sample. If the hot spot size is fixed, the "drop height" of an explosive corresponds to that value of h which generates a hot spot of temperature $T_{0_{cr}}$, where $T_{0_{cr}}$ is defined implicitly by Eq. (14a). Equation (14a) can be rewritten as

$$d_{cr} = \sqrt{\frac{k(T_0 - T_1)}{V(T_0)}} \quad (14b)$$

where $V(T_0)$ = volumetric rate of heat evolution at the hot spot temperature, cal/sec cc. Impact sensitivity may be related through Eq. (14b) to rate constants for decomposition, times to explosion, and other easily measured phenomena, rather than more basic properties such as heat of

reaction, frequency factor, and energy of activation. In the present study, Eq. (14a) will be used.

Substituting Eq. (15) into (14a), taking the decimal logarithm, and rearranging,

$$\log F + \tfrac{1}{2}n \log h - \log d + \log \sqrt{\frac{D_1}{d^3}} + \frac{0.10928E}{300 + (D_1 h^n/d^3)} = 0 \quad (16)$$

Equation (16) is the first to include the hot spot size as an independent variable determining sensitivity. As hot spot sizes cannot yet be predicted or measured accurately, the terms in d were replaced by constants, giving the final correlation equation:

$$\log F + \tfrac{1}{2}n \log h + \frac{0.1093E}{300 + D_2 h^n} + D_3 = 0 \quad (17)$$

where n, D_2 and D_3 are parameters of the correlation.

To find the best values of n, D_2 and D_3, the observed impact sensitivities of nine COHN explosives, four propellants, one sensitive inorganic compound, and two sensitive classified compounds were correlated by Eq. (17). The index of sensitivity was the 50% drop height, in cm, as measured on the Explosives Research Laboratory Machine with Type 12 tools and sandpaper.[5,6] The best values of the parameters are those which minimize the logarithmic standard error defined below:

$$S_{\log} = \sqrt{\frac{D}{N - M}} \quad (18)$$

where $S_{\log}$ = logarithmic standard error

$$D = \sum_i w_i \left[\log \frac{H_i}{h_i}\right]^2$$

N = number of species correlated
M = number of parameters fitted
i = counter ranging over those compounds whose experimental and predicted 50% drop heights are not both below 6 cm or over 50 cm
H_i = experimental drop height, ith component
h_i = predicted drop height, ith component
w_i = normalized statistical weight, ith component

The standard error is defined in this fashion to allow the correlation to best fit the experimental data between 6 and 50 cm. The terms "very sensitive" (less than 6 cm) and "insensitive" (greater than 50 cm) are treated qualitatively rather than quantitatively.

The final correlation is

$$0.287 \log h + \log F + \frac{0.1093E}{300 + 22.9h^{0.574}} + 0.297 = 0 \quad (19)$$

TABLE 3

Final sensitivity correlation

Compound	O.I. exptl.	O.I. predicted	H (cm)	h (cm)
Q	1	1	>50	72
TNT	2	2	>50	50
Ammonium perchlorate	3	3	44	45
Tetryl	4–6	10	36	17
Composite propellant 1 (Cl)	4–6	5	34	43
Cyclotol	4–8	8	32	29
Double-base propellant (DB)	6–10	11–12	28	15
HMX	6–10	7	27	31
RDX	7–11	6	24	34
DINA	7–11	9	23	19
Composite propellant 2 (C2)	9–11	4	21	44
PETN	12	11–12	12	15
Nitroglycerine	13+	13	<6	7
Classified compound 1 (S1)	13+	14–15	<6	4
Classified compound 2 (S2)	13+	16	<6	1
Perchloric anhydride	13+	14–15	<6	4

Equation (19) predicts the experimental sensitivities of the sixteen diverse exothermic materials with a logarithmic error of estimate of 0.158; that is, the correlation is accurate to a factor of 1.4. In view of the numerous approximations involved in the development of Eq. (17) from the heat sensitivity equation, such agreement is quite satisfactory.

The results of the final correlation are in Table 3.

The results of an impact test are of greatest value in ordering the impact sensitivities of a series of materials rather than in providing insensitivity "numbers." For this reason, the results in Table 3 are considered not only in terms of drop heights, but also in terms of "order of insensitivity" (O.I.) values. The determination of the predicted O.I. values is straightforward; experimental drop heights are assumed to be accurate to ± 5 cm so that experimental O.I. values are sometimes known only approximately. It is probably unwise to credit the correlation with enough inherent accuracy to justify extensive rationalization of its poor prediction of the sensitivities of the propellants, tetryl and RDX. However, the following brief remarks may be made:

1. Composite propellants: The physical nature of these materials may enhance the formation of hot spots and the fuel-oxidizer interfaces at which they are formed have a higher-than-average specific energy content.

2. Tetryl: Wenograd's photographic studies[7] indicate that impact explosions in tetryl propagate with difficulty.

3. Double-base propellant: The desensitization of nitroglycerine by admixture with nitrocellulose does not appear explicable on kinetic grounds.

4. RDX: If a different set of reported decomposition kinetics is used, the predicted drop height of RDX is 25 cm.

Discussion

Although Eq. (19) does correlate quite well the experimental sensitivity data on a diverse collection of materials, it is essential that the user of the correlation be aware of the inherent limitations of the formula. Equation (19) is, in essence, an empirical best fit of a collection of sensitivity data to a correlational form derived by applying suitable assumptions (i.e. constant hot spot size) to an approximate analytical treatment (assuming one-dimensional heat transfer, constant generation rate in the hot spot) of a model (hot spot) proposed to correlate with reality. Many assumptions were made in deriving Eq. (17), but the most questionable is that the hot spot temperature can be simply related to impact energy. Neither the efficiency of conversion of impact energy to hot spot energy, nor the size or number of hot spots formed under impact, need be the same for all materials, yet this is necessarily assumed, for lack of pertinent data, in the derivation of Eq. (16). The quality of the final correlation measures the degree to which thermal and kinetic properties determine sensitivity; the unexplained variance is largely due to the invalidity of the physical assumptions imposed by our ignorance of the complete physical picture. For these reasons, D_2 and D_3, which include the assumed constant hot spot size in their definition, have physical significance only if the size, number and efficiency of formation of hot spots do not vary among the species being correlated.

Another feature of the correlation which limits its physical significance arises from the definition of standard error. It is frequently difficult to define deviation such that its minimization affords the most physically significant values of the best fitting constants, and there is no doubt that, by truncating the range of quantitative interest of the correlation, the best values of D_1, D_2, and n found are not the values which relate most closely to reality.

Equation (17) was derived from Eq. (16) by assuming that the sizes of the initiating hot spots in each material studied were all identical. This "mean" hot spot size can be computed from the best fit parameters.

$$d_{avg} = 10^{-D_3}\sqrt{D_2} \tag{20}$$

Substitution of the best values of D_2 and D_3 into Eq. (20) yields a value for d_{avg} of 2.4 cm! This is not a surprising consequence of the assumption that d is constant; in fact, if Eq. (16) holds, the absurd height of the value of d_{avg} is in fact further proof that the hot spot size cannot be assumed to be the same in all materials.

The sizes of hot spots in similar materials probably do not vary widely. The sensitivities of TNT, cyclotol, HMX, DINA, and PETN were correlated by Eq. (17); the standard error was defined by

$$S_{log} = \sqrt{\frac{D^1}{N - M}} \tag{21}$$

where

$$D_1 = \sum_{i=1}^{N}\left(\log\frac{H_i}{h_i}\right)^2$$

When the best values of D_2 and D_3 yielded by this run were substituted into Eq. (20), a more

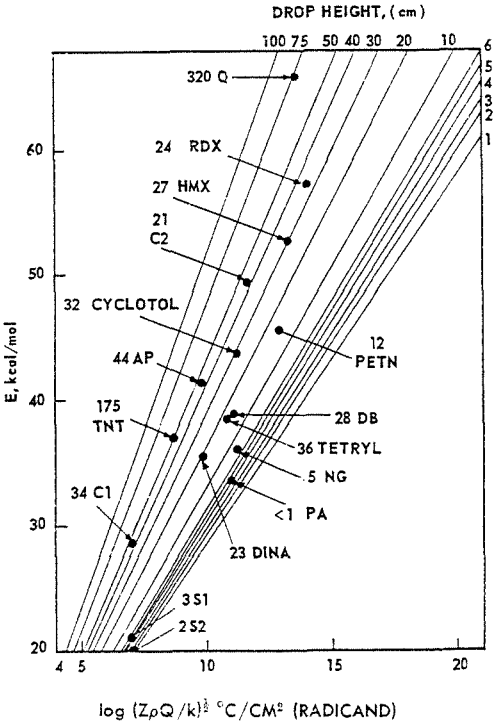

FIG. 2. Impact sensitivity correlation.

reasonable hot spot size, 0.03 cm, was obtained. Further work is planned to estimate d for each material of interest and to use Eq. (16) to predict impact sensitivity.

Inspection of Eq. (19) reveals that "isosensitive" curves are linear on a plot of log F versus E. Such a plot is given as Fig. 2. The factors comprising F affect sensitivity most markedly when E is small, and *vice versa*. The experimental points for each of the 16 correlated species are on the plot.

ACKNOWLEDGMENT

The author is deeply grateful to Dr. G. B. Rathmann for having suggested this investigation and for many instructive and stimulating discussions during its course.

REFERENCES

1. BOWDEN, F. P., *et al.*: Proc. Roy. Soc. (London) *A188*, 291 (1947).
2. JOHANSSON, C. H. *et al.*: Proc. Roy. Soc. (London) *A246*, 160 (1958).
3. AFRICANO: *Advances in Cryogenic Engineering* p. 543. Plenum Press, 1960.
4. GOHEEN, H. E.: J. Math. and Phys. *28*, 107 (1949).
5. GROSS, D. and AMSTER, A. B.: *Eighth Symposium (International) on Combustion*, p. 728. Williams & Wilkins, 1960.
6. KAMLET, M. J.: Naval Ordnance Laboratory Report 6126, 1958.
7. WENOGRAD, J.: Naval Ordnance Laboratory Report 6767, 1960.

Discussion

DR. J. BOUCART (*Explosives Research Center, Belgium*): About two years ago we made a study on sympathetic detonation in air for several safety explosives. In this case the acceptor cartridge may be initiated by the detonation products from the donor cartridge. We first studied the initiation of a coarse classical NH_4NO_3/NaCl/nitroglyceroglycol explosive.

According to the view of Scholl the energy necessary for initiation is:

$$E = \tfrac{2}{3}\pi a^3 \epsilon$$

where ϵ = energy/unit mass; a = thickness of the reaction zone in this cartridge.

For the explosive tested, the thickness of the reaction zone was 2.1 mm (measured on X-ray photographs) corresponding to a hot spot of approximately 18 mm³, and the minimal initiation energy ranged between 2 and 4 cal.

On the other hand, using the rotating-mirror camera and high-speed photography, it was shown that for certain safety explosives initiation may occur by impact of one particle projected by the initiating cartridge. The dimension of those particles (2–3 mm in diameter) and also their kinetic energy (2–3 cal) are in good agreement with the other results.

DR. J. ALSTER (*Picatinny Arsenal*): In line with Dr. Boddington's comment regarding the various assumptions employed in the solution of the complete heat conduction equation

$$\frac{\delta T}{\delta t} = \frac{k}{\rho c}\frac{\delta^2 T}{\delta x^2} + \frac{QZ}{c}\exp(-E/RT)$$

where k = thermal conductivity; ρ = density; c = specific heat; Q = heat of decomposition; Z = pre-exponential factor; E = activation energy which is

obtained via the isothermal decomposition experiment. I wish to point to a pertinent study by Dr. F. Stein of Picatinny Arsenal. In treating the well-known case of one-dimensional heat flow into a crystal of explosive taken as a semi-infinite solid with one face maintained at a constant elevated temperature, Dr. Stein determined the effect of error in parameters k, ρ, Q, Z, and E on the computed ignition delay time. It turns out that not only does the delay time depend more strongly on E than on any of the other parameters (as expected from the nature of the exponential term in that heat generation function) but it is indeed extremely sensitive to E. For example a 20% error in E when $E = 46$ kcal/mole more than doubles the computed delay time over a considerable range of temperature chosen for the hot face. Often, however, E is not known to better than $\pm 5\%$ and then only for a range of temperatures some 100°C or more below the experimentally determined minimum temperature of ignition.

Consider further that the exponential term essentially represents a first-order decomposition process which many explosives actually do not follow. In fact, there is considerable variation in the decomposition pattern of different explosives.

All this seems to suggest a need for incorporating into the conduction equation a heat generation function which more realistically reflects the specific decomposition behavior of the explosive in question. It might even be possible to arrive at a nonexponential function which is not critically affected by error in any decomposition parameter such as E.

DR. M. H. FRIEDMAN: I certainly agree that more refined kinetic data would be a valuable asset toward understanding impact sensitivity. However, I think the results obtained at Picatinny are somewhat misleading in this respect, because, in practice, errors in E are accompanied by compensating errors in Z. Ultimately, values of activation energy are obtained from plots of the logarithm of the rate constant, k', or some similar parameter, such as explosion time, versus reciprocal temperature. Suppose such a plot to be made and an activation energy E_1 and frequency factor Z_1 obtained (Case 1 on the figure). Now superimpose a random error on the data (Case 2). The new line through the data may exhibit an activation energy 5% or more higher than E_1 but Z_2 also exceeds Z_1, so that both lines describe the rate constant k_2' with similar accuracy over the experimental temperature range. As indicated in the paper, critical hot spot size and, in an implicit manner, impact sensitivity, relate directly to the heat evolution rate per unit volume rather than to E or Z per se. The variation of Boddington's criterion with activation energy directly, apart from its presence in the Arrhenius form of the heat evolution rate, is very weak, and can essentially be neglected. It does become clear, however, that errors in E can have a considerable effect on calculated critical criteria and times to explosion if the Arrhenius plots are extrapolated beyond the experimental temperature range.

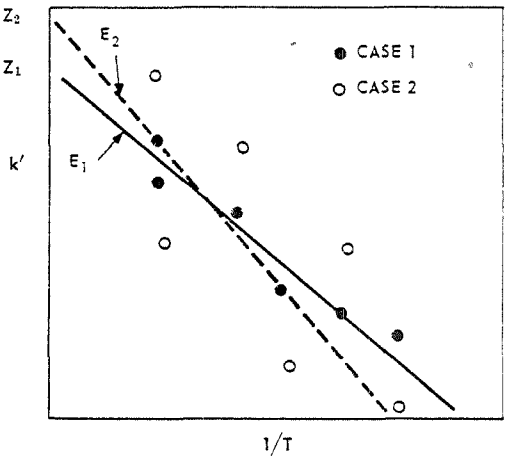

In view of the demonstrated danger implicit in extrapolation of an Arrhenius plot, and the importance of V (T_0) rather than E or Z per se, and Dr. Alster's note that Arrhenius plots are not necessarily representative of the decomposition process, we are presently trying to obtain plots of k' versus T over a wide temperature range, thus obviating the need for interpolation. We represent $k'(T)$ by whatever form provides the best fit, without restricting ourselves to the Arrhenius form. We hope in this way to bypass some of the difficulties pointed out by Dr. Alster and gain a better understanding of the behavior of sensitive materials.

DR. T. BODDINGTON (*University of Cambridge*): It is interesting to compare Friedman's explosion criterion with my criterion $\phi = 1$. If we consider the quantity R, which is the ratio of the initial heat evolution rate due to chemical reaction within the hot spot to an effective rate of heat loss due to conduction

$$R = \frac{Vq\sigma\nu \exp(-E/RT_s)}{kA(T_s - T_0)/a}$$

we see that Friedman's criterion is $R_f = 1$ while the criterion $\phi = 1$ is equivalent to

$$R_b = \frac{k+1}{2\pi}\frac{E(T_s - T_0)}{RT_s^2}$$

$$= \left[\frac{k+1}{2\pi}\right]\left[(T_s - T_0)\left(\frac{\partial \ln k_1}{\partial T}\right)\right] \approx 3$$

where k_1 is the first-order rate constant.

Because of the strong temperature dependence of the exponential the two criteria predict critical temperatures which are in good agreement despite derivations which are quite dissimilar. Under critical conditions Friedman's criterion requires the equality of the initial heat evolution and loss rates while my criterion requires that their ratio be a function of geometry (the term $(k + 1)/2\pi$) and of the extent to which conduction cooling "quenches" chemical reaction. The latter is expressed by the term

$$(T_s - T_0)\left[\frac{\partial \ln k_1}{\partial T}\right]_T = (T_s - T_0)\left(\frac{1}{k_1}\frac{\partial k_1}{\partial T}\right)_{T_s}$$

which is seen to be a good measure of the influence of the temperature drop at the edge of the hot spot on the value of the first-order rate constant.

Dr. M. H. Friedman: Dr. Boddington's comparison of our results is most interesting and satisfying, particularly inasmuch as we approximated the solution of the sensitivity equation in very different ways. I might note here that the agreement between our solutions extends to cylindrical and spherical geometries as well as the linear.

This agreement is not surprising, however. Boddington made assumptions which could be justified *a posteriori* and I made different approximations based on the observed computer output. Under these conditions, our solutions, at least within their individual ranges of applicability, necessarily were good fits to the computer results.

I am not certain that there is any significance to the ratio of Boddington's result to mine. Its form may well be a fortuitous result of difference in our analytical approaches. From inspection of the differences between the results of my computer integration and Eq. (11), there appears to be no systematic error upon varying either activation energy or hot spot temperature.

Combustion Instability

Chairman: Prof. H. W. Emmons (*Harvard University*)

Vice Chairman: Dr. R. Thompson (*Rocketdyne*)

DYNAMIC CHARACTERISTICS OF SOLID PROPELLANT COMBUSTION

M. D. HORTON AND E. W. PRICE

This paper describes the experimentally determined response of a solid propellant combustion zone to normally incident, one-dimensional pressure waves. A self-excited, side-vented, tubular burner in which end-burning grains are used is the experimental vehicle.

During a firing in this burner, the early growth period of the oscillations and also the decay are exponential with time. The exponential growth and decay constants are used to calculate the acoustical admittance of the combustion zone and these admittances are reported as a function of pressure (200 to 1,600 psi) and frequency (500 to 3,500 cps) for four different propellants. The experimental results are also reported in terms of the fractional increase in energy content of a wave reflecting from a combustion zone.

Because the oscillations have exponential growths and decays, observations made during these portions of a firing might be expected to have relevance to a theory, such as that of Hart and McClure, which is mathematically linear. Accordingly, the experimental results are compared in a tentative and general way with this theory and the comparison shows that the experimental admittances are somewhat larger than the theoretical predictions. In the treatment of the experimental data, the mean flow field in the burner is neglected, and the rather questionable assumption is made that the damping of the oscillations in the burner is the same during the decay period (after the propellant is consumed) as it was during the rise. Because of these approximations, the results must be regarded as a little uncertain at this time.

Introduction

In solid propellant rockets it is often observed that the combustion chamber pressure oscillates with a frequency and spatial distribution typical of the acoustic modes of the combustion chamber. This behavior is known to be associated with combustion oscillations which supply the acoustic energy to drive the gas oscillations. Such behavior is referred to as "oscillatory combustion."

The problems imposed by oscillatory combustion have long commanded the attention of rocket development engineers who have necessarily been preoccupied with the short range goal of control rather than the elusive goal of understanding. However, the prohibitive cost of trial-and-error development methods with very large rockets led to a substantially increased research effort as the most economical means of forestalling delays in development programs.

The principal technical goal of research in high frequency combustion instability is the characterization of transient combustion behavior in the presence of acoustic disturbances. This is reflected in the recent analytical efforts to characterize combustion behavior in terms of the

acoustic admittance of the combustion zone.[1] Experimentally, a rocket motor is a very poor medium for research on combustion instability because of the geometrical complexity of the acoustic behavior. Most of the recent advances in the understanding of transient combustion behavior have followed from the development of propellant burners designed to exhibit oscillatory combustion under conditions of minimum complexity and maximum control.[2,3,4] This paper is concerned with the use of a one-dimensional burner for study of the acoustic power radiated by a solid propellant combustion zone which is subjected to normally incident pressure waves in the acoustic frequency range. Data are presented for several propellants and the results compared with theoretical predictions.

A detailed review of the theories which treat oscillatory burning is beyond the scope of this paper but a brief survey of them will be made. A pioneer theory was developed by Grad[5] who treated a tubular burner, assumed an elementary time-lag model for transient combustion response to pressure perturbations, and concluded that the most unstable mode of the chamber was a so-called "spiral mode." Cheng[6] derived a similar theory based on a more sophisticated combustion time-lag model. Shinnar and Dishon[7] considered heat transfer across a boundary layer as the basis for their theory, and Smith[8] also developed a theory derived from heat transfer considerations. The most comprehensive theory thus far developed is that of Hart and McClure,[1] who consider the physical processes taking place in the combustion zone and a particular model of this combustion zone. A more recent theory which treats low frequency oscillatory burning was developed by Dennison and Baum.[9]

From an experimentalist's point of view, perhaps the most noticeable feature of the above theories is that they are very difficult to examine experimentally. This is so because most of the theories predict only stability or nonstability and not the degree of stability. In this respect the theory of Hart and McClure is distinctive in that the theoretical results are presented in terms of a characterization of the combustion behavior which seems amenable to experimental determination.

Experimental

In the experimental program, a 1.5 inch inside diameter, side-vented tubular chamber was used as the burner. The burner, which is described in ref. 4 and illustrated in Fig. 1, employed opposed, end-burning, 0.25-inch thick and 1.4-inch outside diameter grains. A wide variety of burner tubes was constructed so that the first mode longitudinal frequencies ranged between 250 and 3500 cycles per second. A surge tank rather than a nozzle was used for establishing the desired operating pressure so that the problems associated with the venting of the combustion gas were minimized.

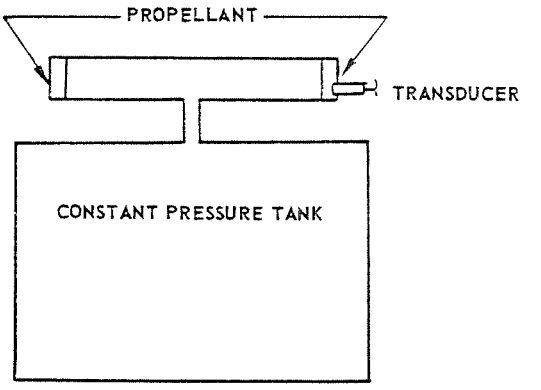

FIG. 1. Schematic of burner system.

A great deal of care was taken in the loading and assembly of the burner so that fair reproducibility was obtained. After the grains were fastened into the ends of the burner tubes with epoxy resin, the front surfaces of the grains were coated with a pyrotechnic igniter paste (Thiokol X-225), and a resistance wire coated with a ball of the igniter material was glued to the burner wall slightly away from the front of each grain. The motor was then assembled in such a manner that any void between the rear surface of the propellant and the endplate was filled with grease. A transducer was screwed into an endplate so that the pressure sensitive diaphragm was in contact with the rear surface of the propellant. The leads to the resistance wire were passed out through the gas port and connected to a power source, then the burner was mounted on a surge tank which was subsequently pressurized with nitrogen. A 24 volt dc voltage was used to fire the igniter and initiate each run.

Several pressure records are made from each firing but the most significant one is a galvanometer oscillograph trace of the first longitudinal mode pressure oscillations, an example of which is shown in Fig. 2. Note that this record could logically be divided into several time regimes: A, the ignition transient; B, a period of exponential growth; C, a transitional and steady amplitude period; and D, the exponential decay which occurs after the propellant is consumed.

To show that a transducer placed in contact with the rear surface of the grain would experience the same pressure oscillation as the front surface of the grain, it was necessary to compare

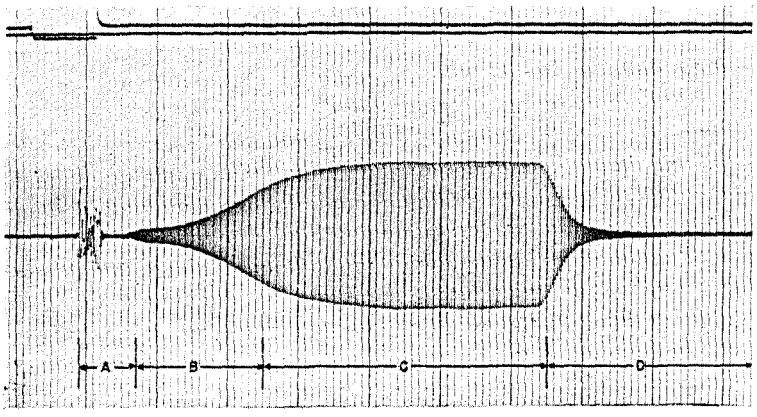

FIG. 2. Record of pressure oscillations.

the oscillations at these two locations. Such a comparison did show that so long as the grain is short (its length must be a small fraction of the wavelength of the oscillations in the solid) the maximum amplitude of the pressure oscillations is correctly measured by a transducer in contact with the rear propellant surface.

Theory

While the oscillations are growing or decaying exponentially, it is possible to use two treatments of the data to characterize the combustion driving of the oscillations. In the first method we note that the average oscillatory energy density in a standing wave[10] is

$$E_\rho = \frac{p_m^2}{4\rho c^2} \tag{1}$$

Therefore if we neglect the proportionately small amount of this energy which is in the propellant, the oscillatory energy content per unit end area of the burner cavity is

$$E = \frac{p_m^2}{4\rho c^2} l \tag{2}$$

When the amplitude of the oscillations is changing exponentially as

$$p_m = p_0 e^{\alpha t} \tag{3}$$

the rate of energy accumulation in this unit area of the burner is

$$\frac{dE}{dt} = \frac{l\alpha p_0^2 e^{2\alpha t}}{2\rho c^2} \tag{4}$$

If the rather logical assumption is made that the acoustic damping was the same after burnout when the oscillations decayed as it was during their growth, then the rate at which energy is being fed into the oscillations by a unit area of the combustion surface is the sum of the accumulation rate and the decay rate measured at the same amplitude. Application of Eq. (4) to the two situations shows that

$$dE_c/dt = E_\rho(\alpha_1 + \alpha_2)l \tag{5}$$

In this equation, α_1 is the exponential growth constant and $-\alpha_2$ is the decay constant. The fractional increase in acoustic energy in the burner per unit area of combustion during one cycle of the oscillations is then

$$\frac{\tau}{E}\frac{dE_c}{dt} = \frac{2l(\alpha_1 + \alpha_2)}{c} \tag{6}$$

and the group $[2l(\alpha_1 + \alpha_2)]/c$ is a good and convenient variable which represents the response of the combustion zone to a normally incident pressure wave.

A second treatment of the data is based on the presumption that the existence of exponential growth and decay periods for the oscillations provides justification for assuming that data taken from these portions of a firing will be relevant to theories which are formulated upon linear mathematics. Accordingly, it is possible also to use these growth and decay rates to calculate the real part of the specific acoustic admittance of the combustion zone.

Hart and McClure[1] first reported that, theoretically, the admittance is

$$Y = -\frac{V}{P}\left(\frac{\mu}{\epsilon} - \frac{1}{\gamma}\right) \tag{7}$$

and more recently,[11] for the burner in question, it was represented as being

$$Y = -\frac{V}{P}\left(\frac{\mu}{\epsilon} + \frac{1}{\gamma} - \sigma\right) \tag{8}$$

The factor σ represents the amplification function for the nozzle in a side-vented burner and rigorously should not be represented as part of the acoustic admittance. However, when the mean flow in the burner is neglected, the nozzle amplification can be artifically accounted for by the inclusion of the σ in the admittance equation. Watermeier[12] showed that if the mean gas flow in the burner is neglected the real part of the admittance can be evaluated experimentally by the use of an end burner which employs a grain at only one end, and the expression

$$Y_r = -\frac{l}{\rho c^2}(\alpha_1 + \alpha_2). \tag{9}$$

For an end burner which uses a grain at each end, the value is

$$Y_r = -\frac{l}{2\rho c^2}(\alpha_1 + \alpha_2) \tag{10}$$

We can call the real part of the groups $[(\mu/\epsilon) - (1/\gamma)]$ and $[(\mu/\epsilon) - (1/\gamma) + \sigma]$, the "reduced specific acoustic admittance" y and by using the mass conservation law determine that

$$y = -\frac{\rho g_c l(\alpha_1 + \alpha_2)}{2c^2 \rho_s r} \tag{11}$$

This expression is very useful as it provides a scale upon which the Hart-McClure theory can be weighed.

Discussion of Results

The experimental results of the program are presented in Figs. 3–10. In Figs. 3–6 are shown plots of $[2l(\alpha_1 + \alpha_2)]/c$ as a function of frequency and pressure for four propellants. The propellants used were, respectively, a polysulfide-ammonium perchlorate composite (T-35), a polybutadiene acrylic acid copolymer-ammonium perchlorate composite (R.C.), a double base (JPN), and a mesa-type double base (X-14). Figs. 7–10 are plots of the reduced specific acoustic admittance y as a function of the same variables.

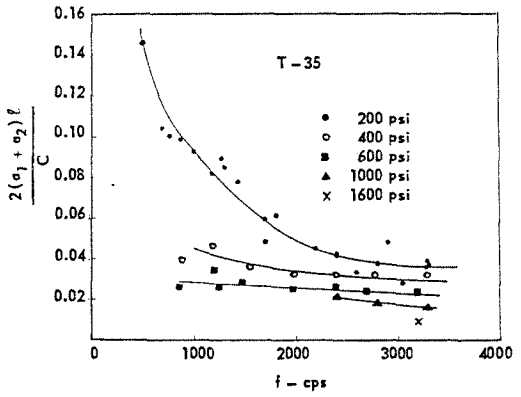

FIG. 3. Fractional increase per cycle of acoustic energy in a standing wave being driven by a unit area of combustion surface as a function of frequency. The propellant used (Thiokol T-35) was a polysulfide-ammonium perchlorate composite.

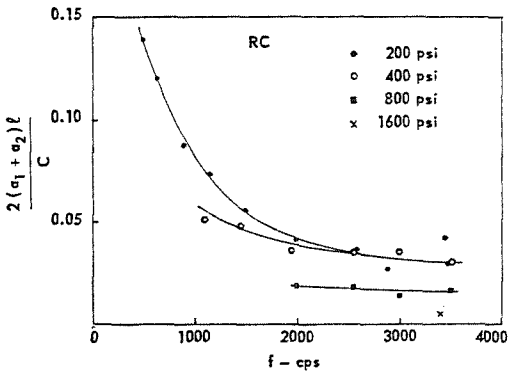

FIG. 4. Fractional increase per cycle of acoustic energy in a standing wave being driven by a unit area of combustion surface as a function of frequency. The propellant used (R.C. or Utah "F") was a polybutyl acrylic acid copolymer-ammonium perchlorate composite.

It is difficult to make many generalizations about the data although some can be made. For the composite propellants, the driving increases with decreasing frequency and pressure. The same is true for the double base propellants at low pressures while at higher pressures the driving is strongest at some intermediate frequency, then decreases as the frequency either

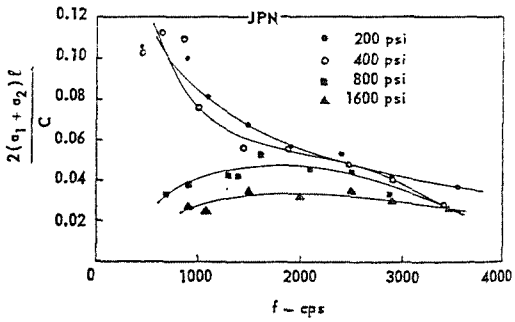

FIG. 5. Fractional increase per cycle of acoustic energy in a standing wave being driven by a unit area of combustion surface as a function of frequency. The double-base propellant used was JPN.

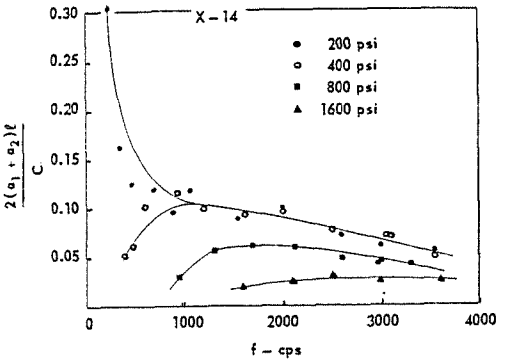

FIG. 6. Fractional increase per cycle of acoustic energy in a standing wave being driven by a unit area of combustion surface as a function of frequency. The mesa-type, double-base propellant used was X-14.

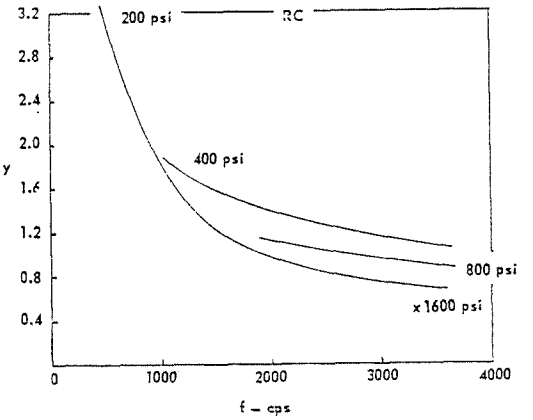

FIG. 8. The real part of the reduced specific acoustic admittance as a function of frequency for a polybutyl acrylic acid copolymer-ammonium perchlorate propellant (R.C. or Utah "F").

increases or decreases. The frequency of most severe driving decreases with decreasing pressure.

The mesa-burning propellant is unique with respect to the other propellants in one aspect. For each pressure tested above 200 psi there was a definite cut-off frequency below which the propellant did not drive oscillations in the burner. This frequency decreased with decreasing pressure. For all of the other propellants, there were no cut-offs but only limits established by the accuracy of the method. The experimental scatter is much larger at lower frequencies because of the difficulty inherent in taking the values of the slopes. The maximum scatter is probably $\pm 20\%$ at higher frequencies and as much as $\pm 40\%$ at low pressures and low frequencies. Inasmuch as attempts to take data at lower frequencies would have produced data which scattered by as much as $\pm 50\%$, it was felt that the effort was not justified.

In order to compare the experimental values of y with the theoretical ones, a theoretical plot of y is also given in Fig. 9. The theoretical value of y is calculated by the use of Eq. (8) and the data taken from ref. 1, Fig. 4. The data were taken from Fig. 4 not because JPN is believed to

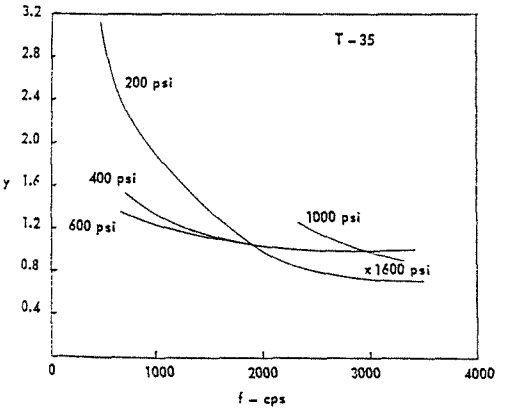

FIG. 7. The real part of the reduced specific acoustic admittance as a function of frequency for a polysulfide-ammonium perchlorate propellant (Thiokol T-35).

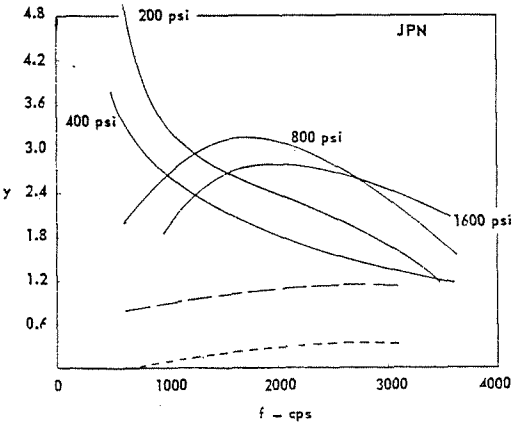

FIG. 9. The real part of reduced specific acoustic admittance as a function of frequency for the double-base propellant JPN. Solid lines are experimental plots. Dashed lines are representative theoretical curves from the theory of Hart and McClure. The lower dashed line is calculated from the inappropriate Eq. (7), and the upper dashed line is calculated from Eq. (8).

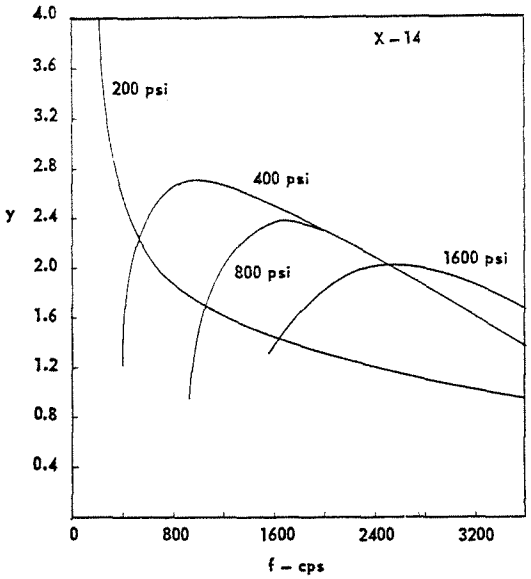

FIG. 10. The real part of the reduced specific acoustic admittance as a function of frequency for the mesa-type, double-base propellant X–14.

be similar to the hypothetical propellant of Fig. 4, but because these theoretical values of y are some of the largest yet reported. The experimental values of y are generally much larger than the theoretical ones and this comparison is the one most favorable to the theory.

A general comparison between the Hart-McClure theory and the experimental results shows that neither the magnitude of the experimental y nor the trends with frequency and pressure are more than qualitatively explained. The theory does, however, correctly predict the general shape of the higher pressure curves for the double-base propellants.

There are uncertainties in both the above comparison and the experimental method. The calculation of the theoretical y values is not rigorous because the value of σ is unknown but assumed to be 0.8 and the use of $1/\gamma$ is an approximation. By far the largest uncertainty in the experimental technique is the measurement of the α_2. There are reasons for doubting that the damping is truly the same after burnout as it was during the growth of the oscillations, and also the decay of the oscillations is only approximately exponential. Nevertheless, the authors feel that the experimental results are quite accurate. Insofar as doubt is related to the comparison of experiment and theory, the values of y obtained for the 800 psi JPN series are twice as large as the theoretical ones even if α_2 is treated as being zero.

An explanation for the discrepancy between the theory and experiment might be that Hart and McClure use what is perhaps an oversimplified model for the combustion zone, as the measurements of Heller and Gordon[13] indicate that the combustion zone contains two exothermic reaction zones as contrasted to the single one considered in the model. Furthermore, these authors do not include chemical reaction in their treatment while there is good evidence[13] that a chemical induction zone is a significant feature in the combustion of double-base propellants. It is possible that the inclusion of these features into the combustion zone model would make the problem mathematically intractable, however.

A similar comparison between the data and other theories is not easily accomplished because the other theories are presented in rather cumbersome forms.

There is a difference by a factor of about ten in the y values as calculated from Eq. (11) and those calculated by the method given in ref. 14. The discrepancy seems to be due to the fact that the method given by ref. 14 relies on rather accurate determination of various constants and these constants cannot be measured to the required degree of accuracy.

From a theoretical standpoint, the measurement of the acoustic admittance of the combustion zone is valuable because it permits the evaluation of transient combustion theories. The practical significance of the measurement is that if a rocket designer also had data for the acoustic damping of the particular rocket, he could calculate the degree of stability or instability the motor would exhibit.

To test the possibility that these one-dimensional driving data may be used to calculate the stability of three-dimensional motors, an attempt was made to predict the stability of a side-vented, tubular JPN burner. It was assumed that, at a given frequency, the driving of the tubular propellant surface was the same as in the one-dimensional situation at equivalent acoustical pressures. The damping was assumed to be proportional to the gas volume in the burners and the damping appropriately reduced from the end-burner data. The local surface driving was integrated over the length of the burner, the damping accounted for, and the exponential growth rate constant (α_1) for the first longitudinal mode in the tubular burner was predicted to be 570 sec^{-1}. When the constants were measured from two tubular burner shots they were found to be 730 and 790 sec^{-1}. The agreement is considered to be remarkable in view of all the uncertainties that exist in the method. If this type of calculation were made for every mode in a rocket motor then one should be able to predict

stability characteristics with a fair degree of accuracy.

Summary

The exponential growth and decay rate data from the first mode longitudinal oscillations in an end-burning test configuration are used to calculate the acoustic admittance of the burning solid propellant surface and also the fractional increase in energy of a wave reflected from the surface.

In general, the admittances are larger than predicted by the Hart-McClure theory and the low frequency values especially are much larger. The uncertainties in both the comparison and the experimental results necessarily make the comparison somewhat tentative, but the comparison is probably valid to a fair degree of approximation.

It is hoped that the present results will act as a stimulant to both theoreticians and experimentalists and encourage them to make such improvements as are necessary to bring about the agreement between theory and experiment.

Nomenclature

c Speed of sound in the gas
E Acoustic energy content of a unit area of burner
E_c Oscillatory energy radiated by a unit area of combustion surface
E_ρ Acoustic energy density
g_c Gravitational conversion factor
l Length of gas phase in burner
P Mean chamber pressure
p_m Maximum acoustic pressure
p_0 Amplitude of growth period pressure oscillations at arbitrary time zero
t Time
V Flame velocity of the combustion zone
Y The specific acoustic admittance of the combustion zone
Y_r Real part of Y
y The real part of $[(\mu/\epsilon) - (1/\gamma)]$ or $[(\mu/\epsilon) + (1/\gamma) - \sigma]$
α_1 Exponential growth rate constant
$-\alpha_2$ Exponential decay rate constant
γ The ratio of the specific heats of the combustion products
μ/ϵ Propellant response function
ρ Gas density
σ A factor related to the compressional process of the combustion zone
τ The period of the oscillations

Acknowledgment

This research was sponsored by Special Projects Office of the U. S. Navy Bureau of Naval Weapons.

References

1. Hart, R. W. and McClure, F. T.: J. Chem. Phys. *30*, 1501 (1959).
2. Price, E. W. and Sofferis, J. W.: Jet Propulsion *28*, 190 (1958).
3. Brownlee, G. W. and Marble, F. E.: An Experimental Investigation of Unstable Combustion in Solid Propellant Rocket Motors, *Solid Propellant Rocket Research* (edited by M. Summerfield), p. 455. Academic Press, 1960.
4. Horton, M. D.: ARS Journal *31*, 1596 (1961).
5. Grad, Harold: Communs. Pure and Appl. Math. *2*, 79 (1959).
6. Cheng, Sin-I.: Jet Propulsion *24*, 27, 102 (1954).
7. Shinnar, R. and Dishon, M.: ARS Preprint 1040–60 (1960).
8. Smith, A. G.: A Theory of Oscillatory Burning of Solid Propellants Assuming a Constant Surface Temperature, *Solid Propellant Rocket Research* (edited by M. Summerfield), p. 375. Academic Press, 1960.
9. Dennison, M. R. and Baum, E.: ARS Journal *31*, 1112 (1961).
10. Kinsler, L. C. and Frey, A. R.: *Fundamentals of Acoustics*. John Wiley and Sons, Inc., New York, 1950.
11. Personal communication from Dr. F. T. McClure, Applied Physics Laboratory, Johns Hopkins University, Silver Spring, Maryland, April 1962.
12. Personal communication from Leland Watermeier, Ballistics Research Laboratory, Aberdeen Proving Ground, Maryland, March 1962.
13 Heller, C. A. and Gordon, A. S.: J. Phys. Chem. *59*, 773 (1955).
14. Horton, M. D.: ARS Journal *32*, 644 (1962).

Discussion

DR. L. A. DICKINSON (*CARDE, Canada*): Could the authors outline the contribution of the upper harmonics to the interaction of the oscillations with the propellant burning surface?

DR. M. D. HORTON (*U. S. Naval Ordnance Test Station, China Lake*): Experimentally, the small amount of harmonic content in the oscillations has no observable effect upon the driving of the first mode oscillations by the combustion zone. Theoretically, this should be so because if the oscillations are truly in the linear regime, the different modes are orthogonal and no interaction between modes is possible.

VIRTUAL SPECIFIC ACOUSTIC ADMITTANCE MEASUREMENTS OF BURNING SOLID PROPELLANT SURFACES BY A RESONANT TUBE TECHNIQUE

R. STRITTMATER, L. WATERMEIER, AND S. PFAFF

A resonant tube technique was used to measure the virtual specific acoustic admittance at the surface of a burning solid propellant. Only the real part of the complex admittance is presented because of its importance in determining the acoustic power generating capacity of a burning propellant.

A cast double-base propellant, ARP, was investigated. Results are given in the frequency range from 3500 to 13,500 cps and in the mean chamber pressure range from 310 to 1030 psi.

The theory that forms the basis for the analysis of data is given together with approximate working equations. These equations are very accurate in the frequency range in which data is presented. A single longitudinal mode is assumed in the analysis of data. Frequency analysis of taped pressure records shows this to be an acceptable assumption since the harmonic content is small (~4%) for those portions of the records that are used to measure growth and decay rates.

The initial web (dimension perpendicular to the burning surface) of the propellant samples was varied. In all cases studied, the web was small compared with the quarter wavelength. Effects of the web dimension on the experimental results are discussed.

Introduction

This experiment originated late in 1960 from the theoretical work of Hart and McClure[1] on unstable combustion in solid rocket propellants. In their work the response of the combustion process to small harmonic pressure oscillations was determined. By assuming that the thickness of the burning and induction zones is small compared with the wavelength of sound, a simple connection is made between the combustion response and the specific acoustic admittance of the burning zone-product gas boundary. To the experimentalist this work is important since the physical constants of the unstable combustion process were thereby directly related to a quantity that might be determined by many of the conventional surface-admittance measurement techniques. A significant feature of the complex surface admittance is that the sign of the real part determines whether a wave will be attenuated at reflection or reflected with increased amplitude. Therefore the contribution to stability or instability associated directly with propellant combustion is determined by the real part of the surface admittance of a burning propellant.

A single end burning resonant tube technique was adopted for measurement of the surface admittance of burning propellants after consideration of various methods. Similar one-dimensional burners have been in use for combustion instability studies by other groups for some time.[2,3] The resonant tube technique for measurement of surface admittance is presently being used by other agencies as well as BRL, namely, the Naval Ordnance Test Station and the University of Utah. Some results of the investigation at NOTS were recently reported in the open literature.[4]

Experimental Approach and Apparatus

The basic experimental apparatus consists of a combustion chamber or tube and a large surge tank as shown in Fig. 1. The combustion chamber is a steel block with cylindrical internal geometry. The cylinder or tube is $1\frac{3}{16}$ inches in diameter and can be varied in length from $1\frac{1}{4}$ to 5 inches by using different end plates. The ends of the tube are closed by steel plates, one of which receives the propellant sample. The propellant samples are circular tablets of varying thicknesses which are held rigidly in a depression in one end plate. These end plates are designed so that the internal geometry of the chamber at ignition is the same for all thicknesses of propellant at the same nominal frequency. The product gases are ejected radially through an orifice into a 4-cubic foot tank. The orifice is located at the midpoint

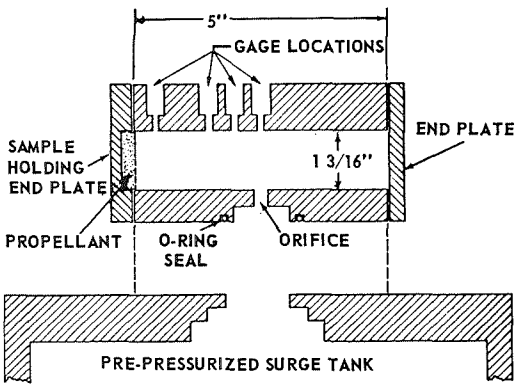

FIG. 1. Cross sectional sketch of combustion chamber and constant-pressure tank.

of the tube length. The chamber is designed to permit simultaneous pressure measurements at several locations along its length. Two transducers were used for the results presented here—one at the midpoint of the chamber length opposite the orifice and another very close to the propellant surface.

The entire system is prepressurized with nitrogen to the desired operating level.

Instrumentation

The chamber pressure variations are recorded by two Kistler type No. 401 piezoelectric pressure transducers with their associated Model 568 Universal charge amplifiers. Their signals are fed into a Model 502 Tektronix dual beam oscilloscope. The scope signal is recorded on film by a General Radio 35-mm camera. The output of the pressure transducer next to the burning surface is brought into an Ampex tape recorder as well as to the dual beam oscilloscope. A Bruel-Kjaer Frequency Spectrum Analyzer is used to reduce the tape records.

Theory

The physical system to be described is the flowing, hot, propellant gas within a cylindrical tube. One end of the tube is closed rigidly by a steel cap. The other end is formed by a burning solid propellant surface which when ignited was perpendicular to the axis of the tube. The propellant is inhibited on the circular periphery to try to keep the burning surface in the original plane. The hot-product gases flow from the tube radially through a short orifice, located at the middle of the tube length, into the large constant pressure tank.

In addition to the conventional assumptions of acoustics the following assumptions are made to set down a tractable description of the above system.

1. The possibility of transverse mode excitation is small and these modes are neglected.
2. The change in tube length due to the regression of the burning surface is neglected.
3. The effect of the mean gas flow is neglected.
4. All damping mechanisms can be combined into one bulk gas damping effect which is proportional to the first power of the acoustic velocity. The damping coefficient is denoted by R.
5. The product gases are homogeneous with the mean gas density given by ρ and the velocity of sound denoted by C.
6. The boundaries of the tube are all rigid except at one end ($x = l$) where the action of propellant combustion on acoustical phenomena can be described by giving the acoustic admittance of the burning zone-product gas boundary in accord with the theory of Hart and McClure.[1]

Under these assumptions the fundamental equation governing gas motion within the tube is the damped wave equation for acoustic displacement (ψ) which can be written:

$$\frac{\partial^2\psi}{\partial t^2} + 2k\frac{\partial\psi}{\partial t} - C^2\frac{\partial^2\psi}{\partial x^2} = 0 \qquad (1)$$

where $k = R/2\rho$. The origin of the axial coordinates (x) is coincident with the steel-capped end and x equals l is the coordinate of the propellant surface. The boundary conditions are $\psi = 0$ at $x = 0$ and

$$\eta = \rho C\frac{u}{p}\bigg|_l = -\frac{(\partial\psi/\partial t)}{C(\partial\psi/\partial x)}\bigg|_l \qquad (2)$$

where η is a complex constant. This constant is termed the acoustic admittance ratio and is defined as the ratio of the specific acoustic admittance of the surface to the characteristic admittance of the product gas. Acoustic velocity is denoted by u. Acoustic pressure is denoted by p, and can be expressed as

$$p = -\rho C^2(\partial\psi/\partial x) \qquad (3)$$

An attempt will be made to identify the pressure oscillations observed with a solution of the following form:

$$Af(x)e^{-ibt} \qquad (4)$$

Substitution of Eq. (4) in Eq. (1) gives:

$$-b^2f(x) - 2kibf(x) - C^2f''(x) = 0 \qquad (5)$$

where primes denote partial differentiation with respect to x.

Try $f(x)$ of the form Ae^{rx}. Substitution for

$f(x)$ in Eq. (5) gives

$$-b^2 - 2ikb - C^2r^2 = 0$$

thus

$$r = \pm\frac{i}{C}\sqrt{b^2 + 2ikb} = \pm g \qquad (6)$$

$\psi = 0$ at x equals 0, therefore,

$$f(x) = A[e^{gx} - e^{-gx}] \qquad (7)$$

Using this form for $f(x)$ the admittance boundary boundary condition, expressed in Eq. (2), at $x = l$ gives

$$\eta = \frac{ibf(x)}{Cf'(x)} = \frac{ib}{Cg}\left[\frac{e^{gl} - e^{-gl}}{e^{gl} + e^{-gl}}\right] = \frac{ib}{Cg}\tanh gl \qquad (8)$$

Substituting for g from Eq. (6) gives

$$\eta = \left(\sqrt{1 + \frac{2ik}{b}}\right)^{-1}\tanh\frac{ilb}{C}\sqrt{1 + \frac{2ik}{b}} \qquad (9)$$

Estimated theoretical and experimental values of k indicate that both the real and imaginary parts of the ratio k/b are very small ($\sim 10^{-3}$) in the frequency range reported in this report. An approximation can be used to simplify Eq. (9) which gives

$$\eta = \left(1 + \frac{ik}{b}\right)^{-1}\tanh\frac{il}{C}(b + ik) \qquad (10)$$

Observation of Eq. (4) reveals that the imaginary part of b gives a real exponent of e and therefore determines the exponential rise or decay of amplitude of ψ. Also, the real part of b is 2π times the frequency. These two quantities are easily determined by experiment from pressure measurements.

Use of Eq. (3) gives for the imaginary part of b

$$\text{Im}\,(b) = \frac{\partial}{\partial t}(\ln P) \qquad (11)$$

where P is the exponential envelope of the pressure (p) while the propellant is burning and the real part of b

$$\text{Re}\,(b) = 2\pi\nu \qquad (12)$$

where ν is the frequency.

When the propellant burns out and a steel end plate forms the second-end boundary condition the bulk damping constant determines the exponential decay[7] and

$$\text{Im}\,(b) = \frac{\partial}{\partial t}(\ln P_a) = -k \qquad (13)$$

where P_a is the exponential envelope of the pressure (p) after the propellant burns out. The error incurred by evaluating k at a slightly different frequency than the frequency during burning is neglected here.

It is believed that the best method for determining the natural frequency ($\pi C/l$) of the tube is to carefully plot frequency versus time through burnout of the propellant and measure the frequency shift at the time of burnout. It is assumed here that the new mode is established very fast (a few periods) and will therefore show up as a fast change in frequency approaching a discontinuity at burnout. The frequency shift is then applied to the measured frequency ν during burning to determine the rigid end damped-tube frequency (ν_d) from which the natural frequency can be computed by the following formula[7]

$$\pi C/l = (4\pi^2\nu_d^2 + k^2)^{\frac{1}{2}} \qquad (14)$$

Limited frequency versus time plots show percentage frequency shifts at burnout to be small (a few per cent).

Substitution from Eqs. (11), (12), (13), and (14) into Eq. (9), expanding the complex radical, rationalizing, expanding the hyperbolic tangent of a complex number, and rationalizing again gives η.

The expansion has not been performed to calculate the results presented in this report because an approximate form which simplifies computation is available as follows:

Theory and experiment indicate that the imaginary part of the argument of the hyperbolic tangent in Eq. (10) is a number very close to π, i.e., the combined effect of damping and boundary condition has a small effect on the undamped, rigid end fundamental frequency for the data given in this report. With this assumption, and neglecting the small number k/b, Eq. (10) can be written

$$\eta = -\tanh\{l[\text{Im}\,(b) + k]/C\} + i\frac{\tan[l\,\text{Re}\,(b)/C]}{\cosh^2\{l[\text{Im}\,(b) + k]/C\}} \qquad (15)$$

This approximate form of Eq. (9) is very accurate for the frequency range reported in this paper. However, additional study would be necessary to justify its use at low frequencies. Substituting Eqs. (11) and (13) into Eq. (15) gives for the real part of the admittance ratio

$$\text{Re}\,(\eta) = -\tan h\left\{l/C\left[\frac{\partial}{\partial t}(\ln P) - \frac{\partial}{\partial t}(\ln P_a)\right]\right\} \qquad (16)$$

The real part of the specific acoustic admittance Re (Y) is obtained by dividing Re (η) given in Eq. (16) by ρC.

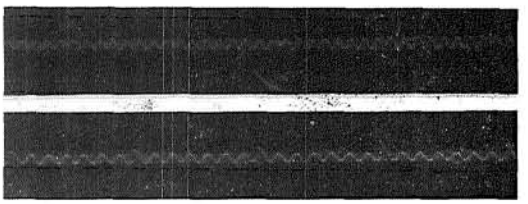

FIG. 2. Typical record showing acoustic field growth (during burning) and decay (after burnout) close to propellant surface within the cylindrical combustion chamber. The chamber is $2\frac{1}{4}$ inches long and the oscillation is the first characteristic mode (8100 cps). The average oscillatory amplitude is 2.5 psi. The time markers, superimposed on the trace, are 1 msec apart.

The mathematical development for propellant burning at both ends ($\eta_0 = \eta_l$) is similar to the single end burner given above. The argument of the hyperbolic tangent turns out to be half the value given in Eq. (8) for the double-end case.

Results and Conclusions

From the records obtained it appears that the first characteristic mode obscures all others for peak-to-peak amplitudes less than 40 psi. Tape analysis revealed that the higher harmonic content was less than 4% during the build-up and decay of oscillatory pressure amplitude where measurements are obtained. Figure 2 shows a typical record. The initial pressure was 500 psi in the experiment where this record was obtained. The mean pressure rise during burning was small (~15 psi).

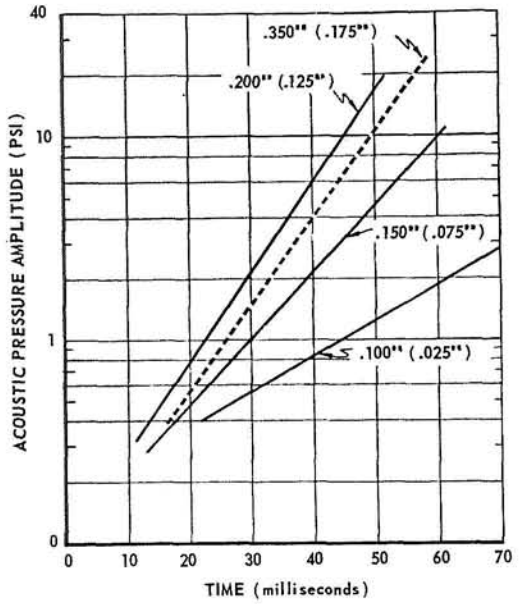

FIG. 3. Acoustic pressure amplitude versus time, during burning, for various thicknesses of ARP propellant. The mean pressure is 515 psi and the frequency is 8100 cps.

The growth curves of ln P versus time are presented in Fig. 3 for various initial thicknesses (webs) of propellant to illustrate a point to be considered in establishing propellant geometry for experiments of this type. Each curve represents an average of a few experiments at the given conditions. The corresponding decay curves of ln P_a versus time have been drawn for the above experiments. The extreme variation with web of the quantity $\partial/\partial t(\ln P_a)$ is small compared to change in $\partial/\partial t(\ln P)$ for the various webs shown in Fig. 3. For this reason the pressure-decay data were not considered significant and are not presented here. The nominal value of $\partial/\partial t(\ln P_a)$ for these runs is 38 sec^{-1}. The data given in Fig. 3 were obtained in a chamber of initial length 2.200 inches (fundamental longitudinal mode ~8100 cps). The time scale of Fig. 3 originates at the onset of discernible oscillations. The lag from ignition until the onset of oscillations is the same for all webs (~130 msec). The initial web of the propellant is given above each curve. The dimension in parenthesis is the estimated thickness (web) at the time of onset of oscillations. Since l has the same value for all webs at the onset of oscillations attention will be directed to the effect of the web on the $\partial/\partial t(\ln P)$ term in Eq. (16) and therefore on Re (Y). The theory of Hart and McClure[1] shows that Re (Y) is sensitive to changes in surface temperature (T_0). It is possible that this effect is evident in Fig. 3 where, at the small webs, the propellant provides very little in the way of insulation and the active surface feels the presence of the steel end plate and lowers T_0. In the particular example given in the above reference, Re (Y) is doubled for a 60°K increase in T_0 at 8000 cps.

All this points out that a minimum sample thickness must be specified if various experimental results are to be compared with each other and with present theory without making rather difficult temperature corrections. The experiments also point out that an acceptable approach to thermal equilibrium conditions must be obtained before measurements are made on the burning propellant. When measurements are to be obtained at a frequency where a propellant is very unstable, some means must be provided to damp self-excited oscillations until the acceptable approach to equilibrium occurs. Otherwise, oscillations are out of the linear range before this near-equilibrium condition exists.

For propellants that are only slightly unstable in resonant tubes of this type no damper is needed. For more active ones such as ARP a perforated propellant tablet or a valve is needed to control the damping. To this end a perforated (11 $\frac{1}{8}$-inch diameter holes) tablet of propellant of the same diameter as the tube and 0.150 of an inch thick was rigidly positioned in the tube about $\frac{1}{3}$ the length of the tube from the steel-capped end. A 0.350 inch thick tablet of the same propellant was pushed in the recess in the steel end plate, and this was rigidly attached to the other end of the tube.

The perforated slab removed the fundamental oscillations (8200 cps) as it burned. At burnout of the perforated slab the fundamental oscillation appeared and was amplified. Measurements were then made on the monotone increase in pressure amplitude of the acoustic field of the cavity. This information is given by the dashed line on Fig. 3. The value of $\partial/\partial t(\ln P)$ obtained from this experiment was accepted as the one obtained under conditions most nearly duplicating those assumed in the Hart-McClure theory. Results obtained in this way were used to compute Re (Y). Figure 4 gives a plot of Re (Y) versus frequency for ARP propellant at various pressures. The quantity computed, Re (Y), from measurements made in the far zone of the product gas includes effects other than those assumed in the isentropic mechanics of acoustic theory.[5] There is also the effect of sources of sound at locations other than the combustion zone i.e., steel walls and nozzle.[6] Because these effects are present to some degree in the measurements and computations made to determine Re (Y), this quantity is termed the real part of the *virtual* specific acoustic admittance of the propellant surface.

Acknowledgments

The authors wish to acknowledge Dr. W. C. Taylor for helpful discussions on this work. Mention must also be made of Mr. J. E. Cole and Mr. J. D. Dykstra for their help and cooperation.

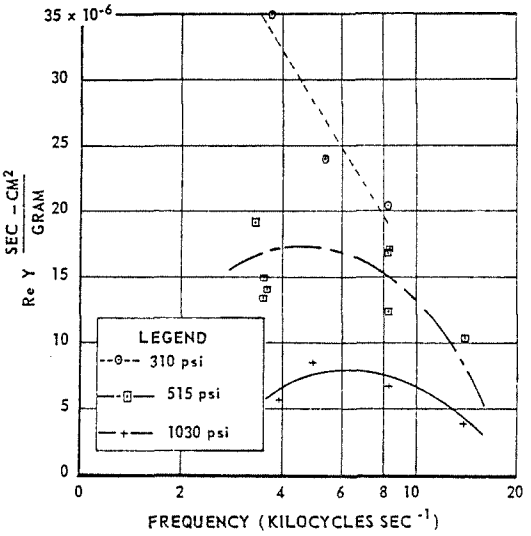

FIG. 4. Real part of the virtual specific acoustic admittance versus frequency of ARP propellant at various mean pressures.

References

1. HART, R. W. and MCCLURE, F. T.: J. Chem. Phys., *30*, 1501 (1959).
2. PRICE, E. W.: Am. Rocket Soc., *Progress in Astronautics and Rocketry* vol. 1, p. 597; *Solid Propellant Rocket Research* (M. Summerfield, ed.) Academic Press Inc., New York, 1960.
3. RYAN, N. W.: Panel Discussion, *Eighth Symposium (International) on Combustion*, p. 924. The Williams & Wilkins Company, Baltimore, 1962.
4. HORTON, M. D.: ARS Journal, *32*, 644 (1962).
5. HART, R. W. and CANTRELL, R. H.: Applied Physics Laboratory, Johns Hopkins University, Report TG 335–11 (1962).
6. Discussions in meeting with R. W. Hart, F. T. McClure, E. W. Price, M. D. Horton, N. W. Ryan, R. Cantrell, A. Baer, and R. Coates at University of Utah, May, 1962.
7. MORSE, P. M. and FESHBACH, H.: *Methods of Theoretical Physics*, vol. I, p. 137. McGraw-Hill, (1953).

Discussion

Comments relevant to this paper can be found on pp 333–334.

AN EXPERIMENTAL STUDY OF THE ALUMINUM ADDITIVE ROLE IN UNSTABLE COMBUSTION OF SOLID ROCKET PROPELLANTS

L. A. WATERMEIER, W. P. AUNGST, AND S. P. PFAFF

Composite-double base rocket propellant slabs which contained different concentrations and particle sizes of aluminum were burned in a transparent-walled chamber. The chamber was exhausted to the atmosphere. The slabs were ignited in cigarette fashion and burned under ambient nitrogen pressures of 200–900 psi. Experimental runs were made under steady flow conditions and under oscillating conditions with a siren rotating over the exhaust port.

Motion pictures were taken of the burning process at high framing rates. Data on droplet burning and concentrations in various regions above the propellant surfaces were obtained from individual frames of the film.

The rate of growth and rate of burning or evaporation of the aluminum droplets on the surface and in the flame zone are discussed. Agglomeration of aluminum on the propellant surface was appreciable and was a function of chamber pressure and initial aluminum concentration. As droplets of aluminum left the surface, they vibrated at frequencies near those predicted by the Rayleigh assumption for liquid droplets. Concentration measurements did not support the postulation that this process could be a factor in low frequency combustion instability, however.

A low frequency variation of the measured mass flux of aluminum above the propellant surface was found. It is concluded that this is probably a major contributor to low frequency phenomena reported in firings of some highly aluminized propellant systems. It also provides a partial explanation for low frequency luminosity variations reported by some investigators.

Introduction

Interest in the combustion of metal powders has increased considerably over the last few years. Much of this interest has been motivated by the inclusion of metals, aluminum in particular, in solid propellant formulations.[1] These metals act as combustion instability suppressants and as sources of additional energy. For a few years powdered aluminum occupied the unique position of being probably the best cure for unstable combustion when added to solid rocket propellants. This position has recently been challenged and it is now feared that aluminum may actually contribute to or cause low frequency combustion instability, in some cases, rather than cure it. It seemed to us that observations of aluminum agglomeration on burning double base propellant surfaces by Angelus of ABL and on composite propellant surfaces made by our group at BRL[2] might be quite significant in this problem. Therefore a series of experiments was conducted in the Interior Ballistics Laboratory to further investigate the possible role of aluminum in low frequency instabilities. The approach used was to burn individual propellant slabs in a windowed chamber at high pressures and to photograph the combustion process. The propellants contained different percentages and different particle sizes of aluminum. The results of these experiments are given in this paper. Some of the data on droplet burning have been treated in the manner of liquid droplet evaporation which has been used in investigations of liquid propellant systems.

Experimental Apparatus

The propellant slabs were burned in a windowed chamber. It was exhausted to the atmosphere either through a vent plate or through a slotted wheel (siren). The chamber is made of brass and is a parallelepiped measuring approximately $1\frac{1}{4} \times 4\frac{1}{4} \times 1\frac{3}{4}$ inches internally. The windows which form the sides of the chamber are made of $\frac{3}{4}$ inch thick plastic. An elevator was used to maintain the propellant burning surface at a particular level in the chamber during a run.

Pressure gauges (Dynisco and Dynagauge) were located at the burning surface level and at the end of the test chamber. These pick-ups recorded chamber pressure variations at their respective locations during an experimental run.

They were recorded on an oscillograph recorder and on magnetic tape.

Nitrogen was used to raise the chamber pressure to the desired operating level and was used as an inhibitor as it flowed past the nonburning sides of the propellant slab. The flow was maintained by four pressurized tanks attached to a manifold. The manifold was connected to a pressure reducing valve and thence to a flow rate meter, a line with a critical orifice, and the elevator housing. A diffusion plate in the test chamber provided for laminar flow past the sides of the propellant sample.

High speed motion pictures (2000 to 4500 pictures per second) of the burning surfaces and flame zones of the slabs were taken through the test chamber windows. A Fairchild 16 mm Motion Analysis camera was used. Lens systems yielding magnifications up to 2.5:1 were used. This magnification was further enhanced for film reading purposes by using a Kodak Contour projector with ratios up to 100:1. Both color and black and white film were used. Neutral density filters were incorporated on occasions. Front and rear lighting was furnished when needed by prefocused 300-watt flood lamps.

Experimental Approach

Technique. The technique used in these experiments consisted of burning $\frac{1}{4} \times \frac{3}{4} \times 1\frac{1}{4}$ inch slabs of propellant, cigarette fashion, in a limited pressure range simulating rocket chamber conditions. The pressure range investigated was 200 to 900 psi. The slabs were ignited on the $\frac{1}{4} \times \frac{3}{4}$ inch edge and were burned in an upright position in the test chamber. A hot wire–combustible paste ignition system was used. Inked lines were placed on the sides of the slab as standard distance references. Supplementary standards were provided by wires projecting from the chamber walls. The slabs were photographed during the burning process and measurements were made subsequently from the film. Fiducial timing dots were placed along the sides of the film by a generator. The dots provided millisecond time references. Pressure records were made during each run and time–pressure relationships were compared with phenomena observed on the motion picture film.

In some experimental runs, the siren was pulled over the vent hole approximately one or two seconds after ignition. Pressure waves or variations normal to the burning surface of the propellant were introduced in this manner. Observations could then be made on aluminum droplet behavior under steady and under oscillating conditions.

Propellants. The propellants chosen for this study were of the type using nitrocellulose-nitroglycerin-ammonium perchlorate-aluminum. Some information concerning the propellant lots investigated is shown in Table 1. The aluminum was obtained from two different companies, namely, Alcoa and Reynolds. It was incorporated in the propellants in 2, 10, and 20 per cent by weight fractions. Three different ranges of particle sizes were used: 5–8 microns, 20 microns, and 43–143 microns. The calculated equilibrium flame temperatures varied from approximately 2950°K to 3650°K dependent upon the percentage of

TABLE 1

Lot numbers of the propellants used together with the types of aluminum and equilibrium flame temperatures at the pressure indicated

	Type and diameter of Al				
Per cent by weight of Al, T_F(°K), and P_C(psi)	REY 28 XD Flake (<5 μ)	REY 400 (5 ± 2 μ)	REY 120 (20 ± 5 μ)	ALCOA 140 (6–8 μ)	ALCOA 101 (43–143 μ)
2% 2954°K (100 psi) to 3135°K (1000 psi)	220	217	211	226	223
10% 3178°K (100 psi) to 3397°K (1000 psi)	221	218	212	227	224
20% 3386°K (100 psi) to 3657°K (1000 psi)	222	219	229	228	225

aluminum and upon the chamber pressure. The flame temperatures were essentially constant over the pressure range studied for each of the three percentages, however.

Experimental Results and Analysis

Approximately 250 firings were made. The data obtained gave information on both surface and flame zone events.

Surface Phenomena, Melting, and Agglomeration. The aluminum appeared to melt on the propellant surface in all the cases observed. In many instances it started to burn or vaporize there. This was in evidence as smoke, vapor, or flame trails projecting from the droplet on the surface upward into the flame zone (Fig. 1). In frame to frame observations from the motion pictures, tiny droplets of aluminum could be seen forming on the propellant burning surface as a result of melting. The droplets usually did one of two things: (a) they grew in diameter as they rolled around on the surface, picked up or coalesced with other droplets and then rose into the flame zone or (b) they remained fixed in place for a few milliseconds, grew only a slight bit in diameter, and then were released into the flame zone. The rolling motion and diameter growth on the surface is thought to be strong evidence of surface agglomeration. In some instances, especially at high pressures and with high initial aluminum concentration, the propellant burning surface would appear to be almost covered with a blanket of molten aluminum. As many of the droplets were ready to leave the surface, they would cling momentarily by a cord or thread of molten metal and then be released (Fig. 1).

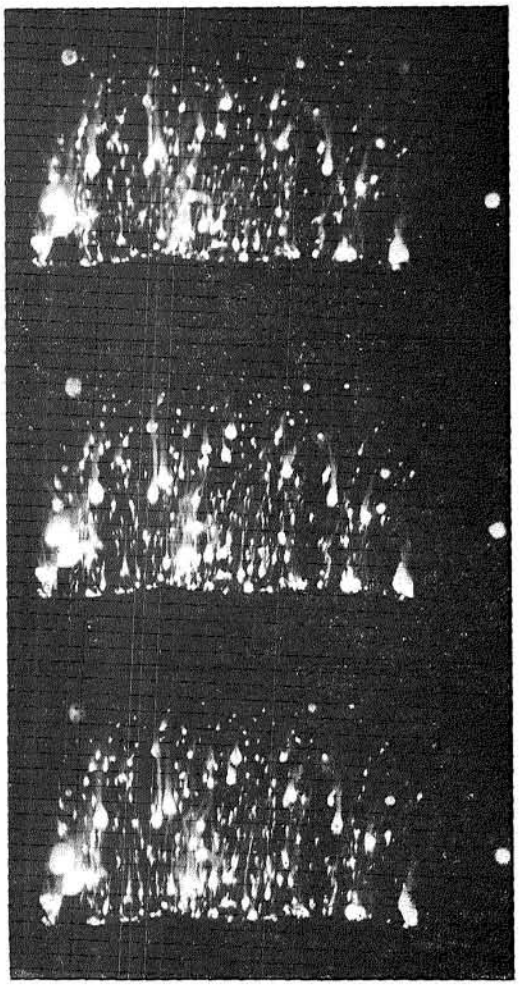

FIG. 1. Consecutive frames (3800/sec) from film of propellant lot 225 burning at 200 psi. Note vapor trails from the droplets and surface formation of agglomerates

Droplet Growth and Evaporation Above the Surface. As the droplets left the propellant burning surface, they assumed a semi-spherical shape, in most instances, with a vapor trail preceding them (Fig. 2). They grew in diameter until they reached a certain level above the burning surface. At this level they would start to decrease in diameter (Fig. 3). The rates of decrease of droplet diameters were increased under the influence of siren pulsing at 1100–1300 cps. The level above the surface at which the diameters started to decrease was not appreciably affected by the siren pulsing, however.

The propellant burning surface was assumed to be near a velocity antinode[2] in the chamber as the siren-driven oscillations were introduced. The pressure gauges located in the walls at this level verified the assumption to some extent. It is questionable, however, whether this condition actually exists near the burning surface since the surface itself may act as a local end plate.

It is postulated that the droplet growth phenomena above the surface could be, among other things, a result of (a) meteoric pelting of large liquid droplets by small particles which are beyond the resolution of the optical system, (b) ignition above the surface with an apparent diameter growth due to the formation of a flame envelope, or (c) hollow spheres or droplets which are inflating like balloons as the vapor pressure inside increases with temperature. The experimental evidence seems to lend more support to (a) or (b) as will be discussed in succeeding sections.

The distances above the surface at which the droplets started to evaporate or decrease rapidly

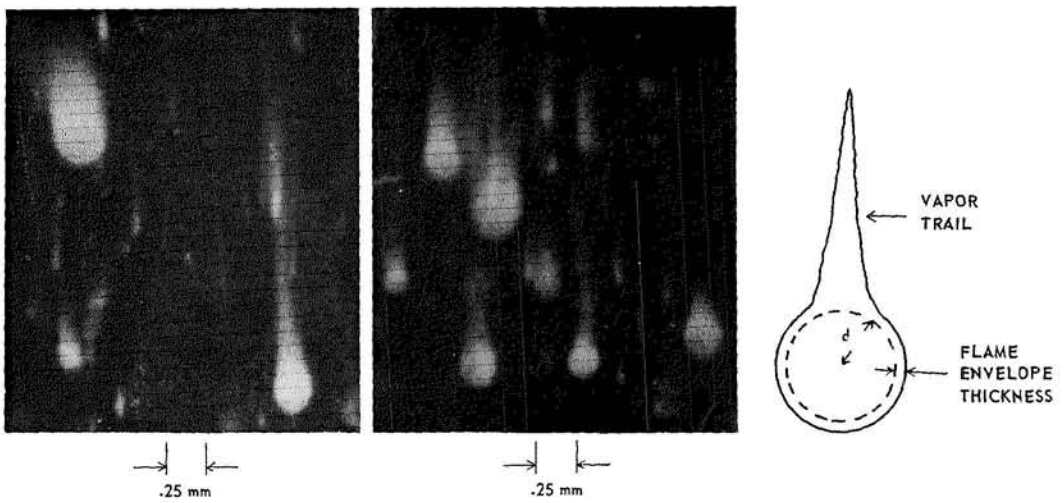

FIG. 2. Enlargement of burning droplets showing the vapor trails. The schematic drawing illustrates the flame envelope surrounding the liquid droplet. The envelope thickness varied from approximately $0.02d$ at 800 psi to $0.15d$ at 200 psi as determined by silhouette lighting.

are plotted vs. chamber pressure in Fig. 4. The particle diameters shown were arbitrarily divided into two ranges, i.e. 200–400 microns and 400–800 microns. The plot exhibits a profile which is expected until it reaches the higher pressures. There are at least two possible ways of explaining this discrepancy. In one case, the hot flame zone would be expected to recede from the surface at low pressures and come closer to it at high pressures. At low presures the droplets move far from the surface before appreciable evaporation takes place. At intermediate pressures, the droplets start evaporating closer to the surface. At the higher pressures, combined effects of increased mass flow rate of the product gases and an oxide insulation or protective layer on the droplets are probably evident as the droplets are carried further from the surface before starting to decrease in size. One thing must be kept in mind, however. The growth mechanism is probably present the entire time during which our data are taken so the point at which the diameter starts decreasing takes on more significance. It means that the evaporation or burning rate has overcome this gain mechanism and has, indeed, exceeded it by a significant amount. Some typical

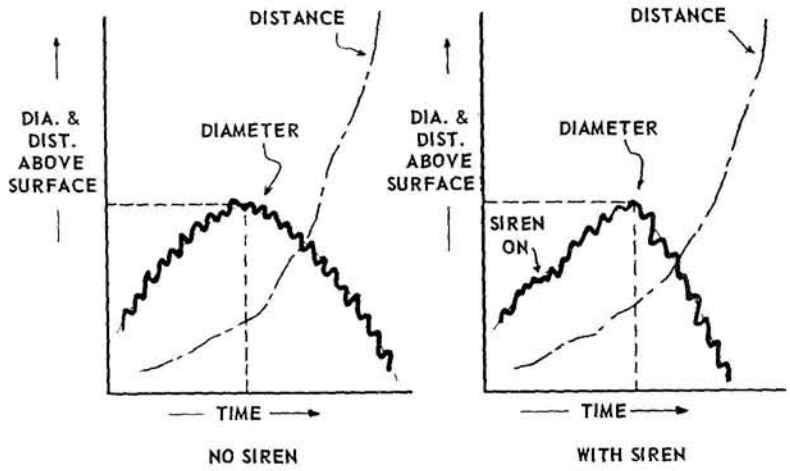

FIG. 3. Typical plots of droplet diameter and distance above the propellant surface as functions of time.

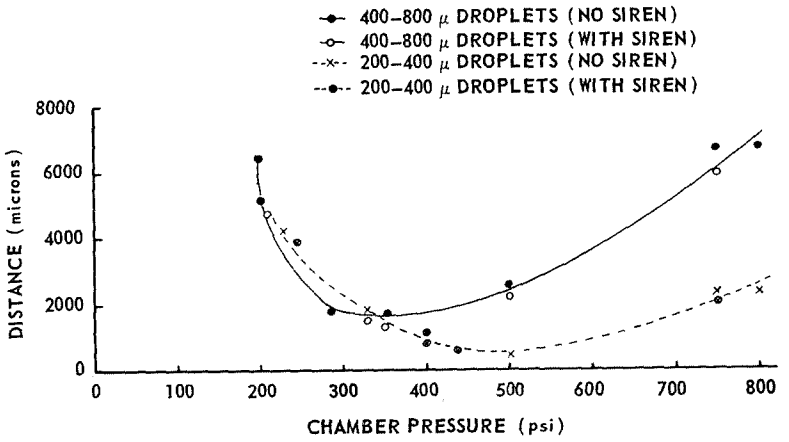

FIG. 4. Plot of chamber pressure vs. distance above the burning propellant surface at which the droplets started decreasing in diameter. Siren pulsation had little or no influence on these distances.

growth and decay rate data are shown in Table 2. Calculations were made on aluminum droplet histories by treating them in the manner of Miesse,[3] Schuyler,[4] and Goldsmith and Penner[5] for burning fuel droplets in a flowing medium. On the basis of the computed histories and the measured values, it appears that the data in Table 2 were obtained in temperature regions approximating 0.7 to 0.9 of the theoretical flame temperatures.

Another possible explanation for the distance vs. chamber pressure plot data would be based on the assumption that the reaction zone was extremely thin in all cases and that there is essentially a constant temperature throughout the measurable field. This assumption is not too bad considering the previous discussion. Then a strong controlling factor on the evaporation rate would be the concentration of the aluminum vapor. In other words, near the surface where there would be a large vapor concentration at some pressures the evaporation rate would be

TABLE 2

Typical experimental growth and decay rates of droplets at various chamber pressures

	Droplet growth			Droplet decay			Distance above propellant surface when decrease started (cm)
Chamber pressure (psi)	Diameter expansion (cm)	Time for expansion (sec × 10^3)	Surface area growth rate (cm^2/sec)	Diameter decrease (cm)	Time for decrease (sec × 10^3)	Surface area decrease rate (cm^2/sec)	
200	0.0510→0.0670	21.5	0.276	0.0670→0.0560	27.9	0.152	0.58
225	0.0400→0.0475	28.0	0.074	0.0475→0.0380	29.5	0.087	0.42
300	0.0238→0.0283	5.2	0.142	0.0283→0.0169	2.24	0.723	0.22
325(w/siren)	0.0400→0.0595	6.08	1.003	0.0595→0.0145	4.32	2.421	0.16
400	0.0285→0.0351	8.30	0.159	0.0351→0.0235	4.96	0.431	0.10
400(w/siren)	0.0240→0.0333	13.84	0.121	0.0333→0.0167	3.05	0.562	0.11
500	0.0350→0.0545	14.93	0.367	0.0545→0.0273	5.35	0.872	0.08
500(w/siren)	0.0273→0.0633	24.44	0.419	0.0633→0.0100	7.52	1.632	0.06
750	0.0272→0.0363	13.50	0.135	0.0363→0.0195	13.50	0.218	0.23
750	0.0575→0.0675	28.85	0.136	0.0675→0.0625	4.70	0.435	0.66

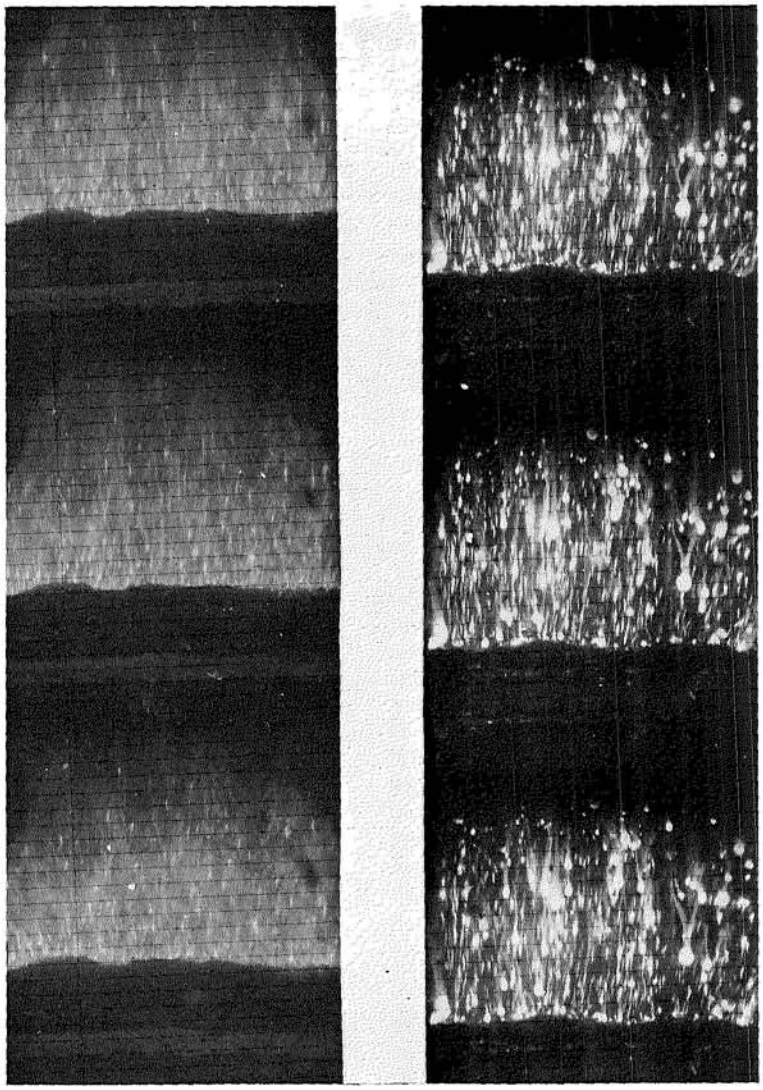

FIG. 5. Enlargements of consecutive frames from film of burning propellant. On the left, lot 217 burning at chamber pressure of 390 psi. The framing rate was 2800 fps. On the right, lot 219 burning at chamber pressure of 405 psi. The framing rate was 3000 fps.

low and the droplet would travel further from the surface before decreasing appreciably in size. This mechanism, then, would hinge more on vapor concentration and less on temperature considerations. This type of phenomenon has been discussed by Burgoyne and Cohen[6] on effects of drop size on flame propagation in liquid aerosols. They maintain that the mechanism of flame propagation is completely transformed within the droplet diameter range of 7 to 55 microns. Below 10 microns, the suspension behaves as a vapor; above 40 microns, the drops burn individually with one drop igniting adjacent ones. This process, they claim, leads to increased burning rates for the larger drops. Figure 5 shows consecutive frames from film of burning propellants containing 2 per cent and 20 per cent of aluminum, lots 217 and 219, respectively. The flame zone, in comparison appears to be transformed from one of a diffusion or vapor flame in the 2 per cent composition to a zone of droplet burning in the 20 per cent composition. Therefore, the aluminum vapor theory may be quite applicable.

Droplet Vibrations. In all experimental runs in which the burning aluminum droplet histories could be traced, oscillations of the major and minor dimensions of the ellipsoidal droplets were observed. Measurements of frequency and amplitude were made. The vibration frequencies ranged from 500 to 1100 cps for droplets with mean diameters (average of major and minor dimensions) of 200 to 700 microns. The magnitude of the diameter variations was often quite large, i.e., 50 to 100 per cent. Vibrations of smaller droplets were discernible but the frequencies approached the photographic framing limits so these data were not analyzed. The frequency of vibration and amplitude of the oscillations were dependent upon particle diameter and chamber pressure.

When siren pulsations were introduced, the larger droplets (>200 microns) would assume a vibration frequency close to the siren frequency. Their evaporation or burning rate would also be increased as was already discussed.

Two approaches were used to compute the natural vibration frequencies of the droplets in an undisturbed medium, i.e., no siren pulses introduced. In the first case, it was assumed that (a) the aluminum was molten on the burning propellant surface, and (b) it left the surface as liquid droplets which were set into vibration by the release from the surface. This vibratory motion did not damp out but continued with the surface tension of the liquid acting as a restoring force. Using Rayleigh's analysis[7] for the period of oscillation of droplets, the following relationship was obtained

$$\tau = (3\pi m/8\sigma)^{1/2} = 0.785\ (\rho/\sigma)^{1/2}\ (d)^{3/2}$$

where τ = period of vibration, m = mass of the droplet, σ = surface tension of the liquid, ρ = liquid density, and d = diameter of the droplet. Values of 2.2 grams/cm^3 and 250 dynes/cm were assumed for ρ and σ, respectively, in all cases. These approximate values were assumed for a temperature near the boiling point of aluminum (2823°K). The vibration frequencies of droplets ranging from 50 to 1000 microns in diameter were computed. These frequencies varied from 39000 to 400 cps, respectively.

In the second approach to theoretical vibration frequencies, it was assumed that (a) the aluminum melted on the surface and formed vapor filled bubbles which were ejected into the flame zone, and (b) the bubbles oscillated with the periodicity controlled by the properties of the wall and the enclosed vapor. Therefore, vibration frequencies of hollow, flexible spheres were computed according to the method of Morse and Feshbach.[8] Although the major and minor dimension variations we measured did not indicate symmetric vibrations, we assumed that this would provide a close enough approximation to the actual case. So their equations for symmetric vibrations were used as

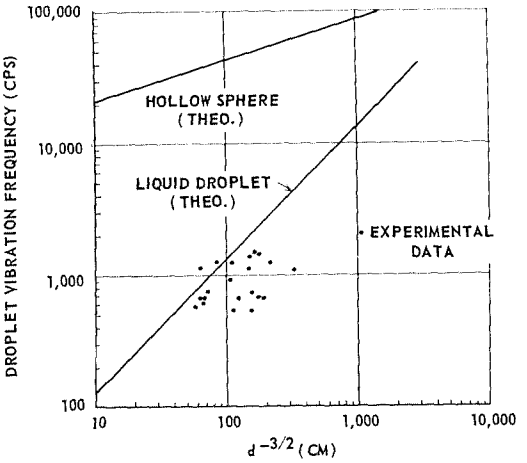

FIG. 6. Plot of droplet vibration frequencies vs. (diameter)$^{-\frac{3}{2}}$. The straight lines indicate theoretical values based on either hollow sphere or liquid droplet assumptions at the boiling point temperature of pure aluminum.

$$\omega_{os} = \pi\gamma_{os}\ c/a$$

If the membrane is the restoring factor and controls the motion, they show that the lowest natural frequency will be

$$\pi\gamma_{01} \simeq \left(\frac{3\rho a}{\rho_s h}\right)^{1/2}\left[1 + \left(\frac{2Eh}{3\rho\ c^2 a}\right)\right]$$

where ρ = density of gas inside sphere, a = equilibrium sphere radius, ρ_s = wall density, h = wall thickness, c = sound velocity, and E = modulus of elasticity. Frequencies of the order of 30000 to 120000 cps were obtained for droplets whose diameters ranged from 1000 to 50 microns, respectively. Wall thicknesses were varied from less than 5 per cent to about 99 per cent of the droplet radius.

The theoretical vibration frequencies were several orders higher than those measured experimentally. We assumed therefore that the droplets under observation were not hollow. A comparison of some of the experimental values obtained and the frequencies computed from these two methods are shown in Fig. 6. Adjustments in the surface tension of the droplets could alter the relationships shown, of course.

Evidence of some hollow particles was found collected on cooler portions of the chamber, however. Photomicrographs of some of the residue

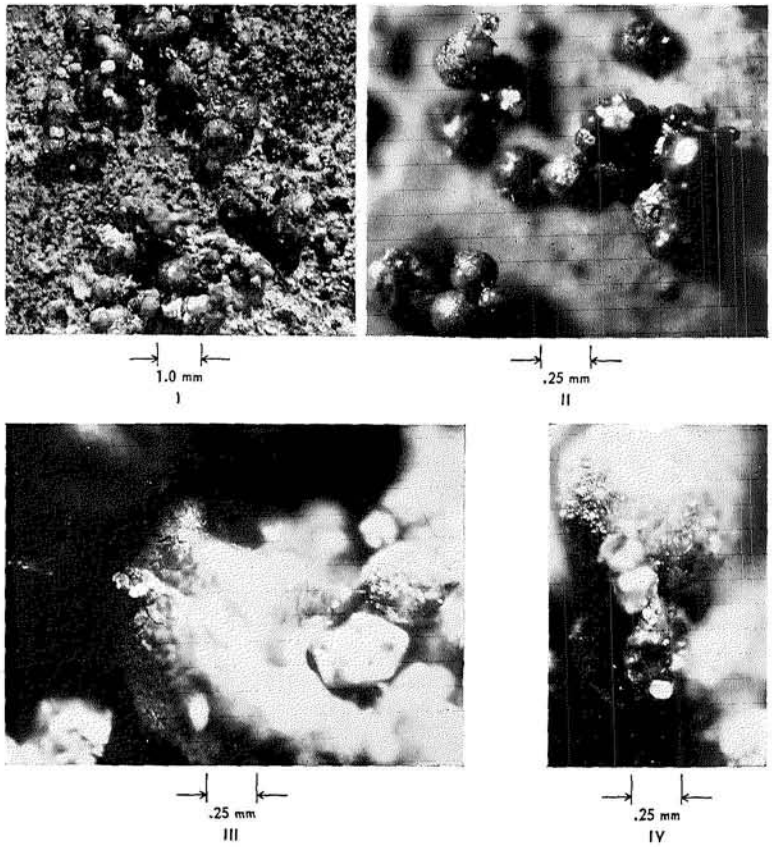

FIG. 7. Photomicrographs of solidified residue collected in the test chamber from the burning aluminized propellants. Photo I shows many particles with holes in them. Photos II and III are enlargements of individual particles. Photo IV shows a particle that has apparently deflated after expelling enclosed gas.

are shown in Fig. 7. It is thought that if the amount of hollow droplets formed is significant, this process must occur at a distance further from the surface than we can observe in our film, namely, 1.6 cm.

Zone Concentrations and Aluminum Mass Flux. Measurements were made of size and distribution of visible droplets in various zones above the propellant surfaces. All data reported in this section were taken from runs in which siren pulses were not introduced. The data were obtained by placing the film in the Kodak projector and marking off zones of ~200 micron thicknesses vertically above the surface. Then measurements were made in each zone over a series of frames. An approximate volume basis was established using the propellant thickness as the third dimension. Corrections were made for such things as (a) deviation from a vertical plane, (b) obscuring of smaller particles by larger ones, and (c) depth of field or focus effects.

Figure 8 is a plot summarizing the data obtained on all lots 211 through 229. It shows the percentage of particles in a thin zone above the surface with diameters in the same range as the original particle sizes. The percentage is shown as a function of pressure and aluminum concentration in the propellant. The percentage of particles with diameters greater than the original particle size is highest at the low pressures and high aluminum concentrations in the propellants. This phenomena, we believe, is an indication of the amount of agglomeration and meteoric pelting taking place in the thin zone next to the surface. Apparently at high pressures and low initial aluminum concentrations, the opportunity for agglomeration or pelting after the aluminum melts is reduced.

Some measurements made in thicker zones

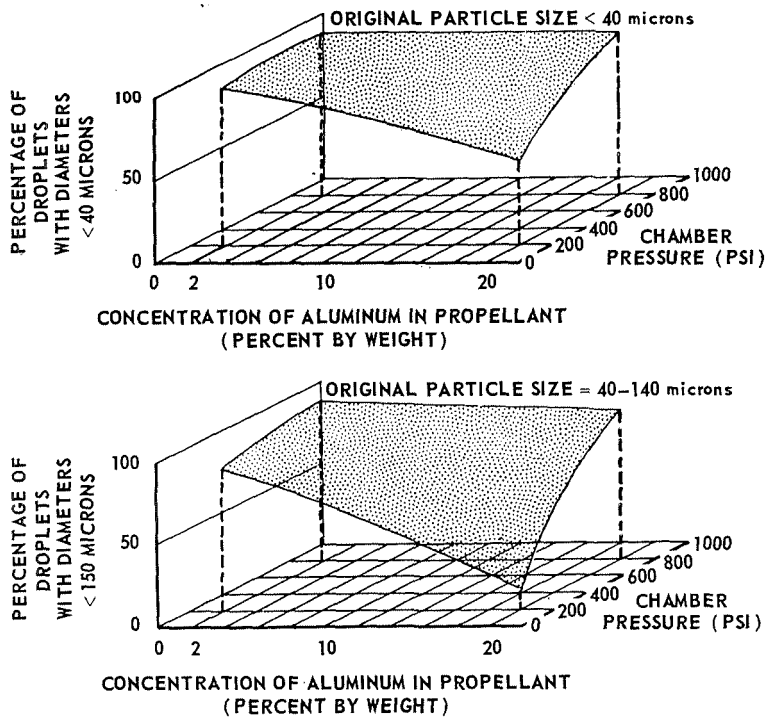

FIG. 8. Plot of percentage of particles with diameters in the same range as the original particle sizes. Measurements were made in a zone 200 microns in height above the burning surface of the propellant. This is plotted as a function of pressure and concentration. The lower plot represents lots 223, 224, and 225; the upper plot represents all other lots.

above the surface are shown in Fig. 9. In general these findings verify those made in zones near the surface by reflecting the results of phenomena that have occurred there.

Aluminum mass flux determinations were made based on visible particles in the motion pictures. The framing rate was such that most larger droplets were essentially stopped for frame to frame measurements. A fairly accurate determination of the velocities of the various sized droplets could then be made. The simple relationship was used of

$$\text{Total Mass Flux} = \sum m_i v_i$$

where m_i and v_i were the total mass and velocity of the ith species, respectively.

In most instances mass flux variations of a low frequency nature (300–700 cps) were observed in the thin zones above the surface. The variations were often quite large but the mean value was lower than the calculated aluminum mass evolution rate from the propellant surface. This discrepancy is to be expected since all of the aluminum particles are not visible on the film. The important factor brought out by these measurements is not the absolute values of the burning particle flux (probable error ±10 per cent) but the fact that it is varying significantly at a low frequency. This phenomena may be a key point in luminosity variations reported by other investigators.[9]

Conclusions

The following conclusions are drawn from the experimental results:

1. Agglomeration of aluminum on the burning surface of a double base-composite propellant is appreciable. It appears to be a function of chamber pressure and initial aluminum concentration in the propellant. In cases observed where it almost covers the surface as a molten blanket, it would probably alter the acoustic admittance of the burning surface.

2. The vibration or oscillation of liquid droplets above the propellant burning surface is a measurable phenomenon. It is concluded that even though the majority of the droplets measured were vibrating in the low frequency range

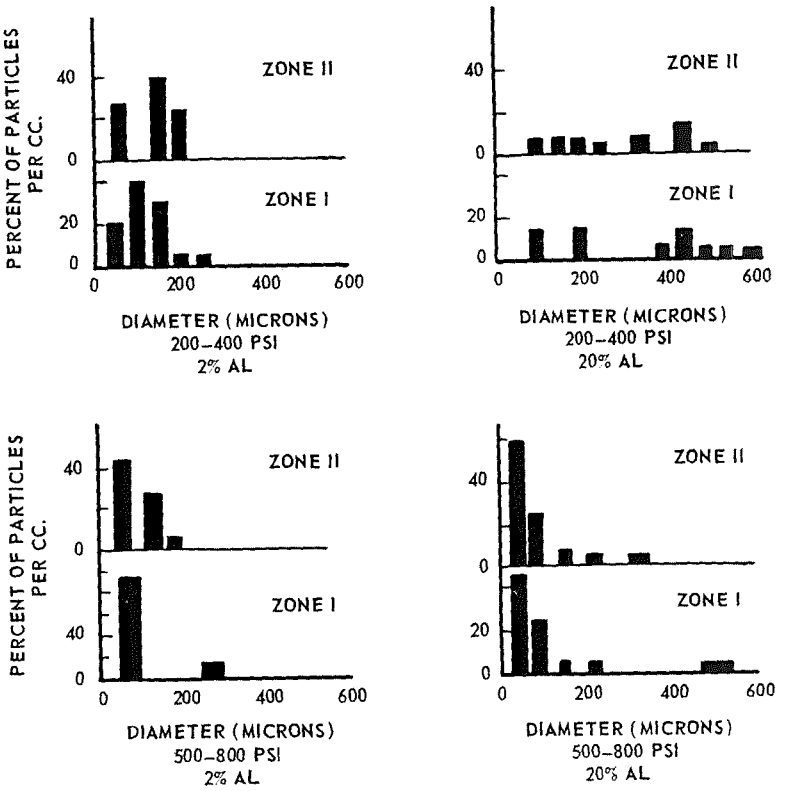

FIG. 9. Plots of particle diameters and concentrations in thick zones above the propellant surfaces. They are shown as a function of pressure and initial aluminum concentration. Zone I = 1750 microns high; Zone II = 3500 microns high.

(<1000 cps), this is not a major contributor to low frequency pressure oscillations. Concentration profiles taken above the surface support this postulate.

3. Most of the droplets in zones up to 3.5mm thick above the propellant surfaces were apparently liquid rather than hollow spheres with liquid walls.

4. Measurements show that appreciable droplet evaporation or burning may occur at a relatively large distance above the surface. It is postulated that this is a vapor controlled process. Siren pulsation increased the evaporation rate of the droplets but did not affect the distance above the surface at which it became controlling.

5. The mass flux of aluminum above the propellant surface varied with time at a low frequency. It is concluded that this could be a major contributor to low frequency chamber oscillations measured in some highly aluminized propellant systems.

ACKNOWLEDGMENTS

The authors are indebted to Mr. Richard Strittmater, Mr. Eugene Bonhage, Dr. Richard Jones, and Mr. James Cole of the Interior Ballistics Laboratory for their help and discussions during the course of this program.

REFERENCES

1. GLASSMAN, I.: *Progress in Astronautics and Rocketry*, Vol. 1, p. 253. *Solid Propellant Rocket Research* (M. Summerfield, ed.) Academic Press, 1960.
2. WATERMEIER, L.: *An Experimental Study of Combustion Instability in Solid Rocket Propellants—Part II*, Ballistic Research Laboratories Report 1116 (September, 1960); and ARS Journal *31*, 564 (1961).
3. MIESSE, C. C.: Jet Propulsion *24*, 237 (1954).
4. SCHUYLER, F. L.: *Combustion Instability; Liquid Stream and Droplet Behavior—Part I Experimental and Theoretical Analysis of Evaporating Droplets.* WADC Technical Report 59–720 (September 1960).
5. GOLDSMITH, M. and PENNER, S. S.: Jet Propulsion *24*, 245 (1954).
6. BURGOYNE, J. and COHEN, L.: Proc. Roy. Soc. (London) *A225*, 375 (1954).

7. LORD RAYLEIGH: *Theory of Sound*, II, 373 (1945).
8. MORSE, P. and FESHBACH, H.: *Methods of Theoretical Physics*, Vol II., p. 1470. McGraw-Hill, 1953.
9. SHANFIELD, H., *et al.*: Study of Resonance Behavior in Solid Propellants, Quarterly Reports, NAVORD Contract 17945, Task 2, Aeronutronic (1961–1962).

Discussion

DR. H. SHANFIELD (*Aeronutronic Division, Ford Motor Company*): In connection with assumptions on the origin of aluminum agglomeration on solid propellant surfaces, it is important to take accurate account of the temperature–time history of individual aluminum particles at the propellant surface. This will be a strong function of initial particle size as well as pressure, since the latter influences the flame zone thickness. Since agglomeration proceeds by growth of small particles to large ones on the surface, particles must first melt and then reside sufficiently long on the surface to coalesce with one or more partners. A plausible assumption for the final ejection mechanism of the agglomerated particles is that they finally rise in temperature sufficiently to vaporize material on which they rest, resulting in expulsion. Obviously low concentrations of aluminum may fail to agglomerate simply because the number density of potential partners on the surface is low, and this probably accounts for such observations at the 2% aluminum level. This hypothesis suggests a critical size above which agglomeration is possible and below which particles will not do so. The data presented by the author on the size of burning globules as a function of pressure and distance above the propellant surface can very likely be rationalized in terms of the physical picture described.

PROF. H. W. EMMONS (*Harvard University*): In comparing the experimental frequency of oscillation with those computed for "solid" and hollow spheres showing good agreement with the former, the same mode was not computed in each case. For the hollow sphere a pure radial mode was used in which the restoring force is largely internal gas pressure while for the deforming modes surface tension is the only restoring force. The comparison should be made with the same mode in both cases.

MR. L. A. WATERMEIER (*Aberdeen Proving Ground*): This is no doubt true in a rigorous treatment of the situation. We felt we could understand reasons for liquid droplets deforming in the manner observed in our movies on the basis of displacement of mass with surface tension restoring forces. It was more difficult to comprehend a similar mechanism for hollow spheres. We did feel that the alternate compression and decompression of the enclosed gases would be a large factor, however. So the point that Prof. Emmons brings up is, in our estimation, difficult to approach but would probably yield computed values closer to those for the liquid droplets and closer to the measured values.

DR. K. P. MCCARTY (*Hercules Powder Company*): The thickness (distance across the burning surface) of the propellant samples in this work was $\frac{1}{4}$ inch. Past experience has shown that aluminum combustion in samples of this size can be considerably different than with larger samples. This marked scale effect was reported by Dr. B. Brown in the Eighth Symposium. With this in mind the aluminum combustion in larger samples or in rocket motor firings might be expected to be quite different. The motion pictures show a comparatively small amount of radiation from oxide products as compared with the central aluminum particles indicating very poor combustion. Much greater combustion efficiency would be expected with larger samples and with rocket motors. This comment is intended more as a warning to use extreme care in applying the results of this work to rocket motor performance than as a criticism of the present work.

MR. L. A. WATERMEIER: I believe Dr. W. Wood of Rohm & Haas has shown in some experiments that the thickness criteria noted by Dr. McCarty is not as critical as he is pointing out. As to Dr. McCarty's comments on extreme care in applying the results of this work to rocket motor performance, I do not believe that such an application was advocated in this paper, at least, not intentionally. Scaling effects certainly are a factor in all laboratory experiments as we all know.

DR. W. A. WOOD (*Rohm and Haas Company, Redstone Arsenal*): In response to Dr. McCarty's questions regarding effects of sample size (area) on the observed microscopic deflagration behavior of aluminized propellants, we have conducted two kinds of studies in which the sample size was widely varied without appreciably influencing the nature of the results sought. One of these investigations involved determination of the distance from the propellant surface at which ignition of aluminum occurred; the sample surface ranged from 2 to 50 mm diameter. The other study involved measurement of the distribution of aluminum particles at a plane in the deflagration zone and employed cylindrical samples from 6 to 38 mm in diameter. Both studies were done with ammonium perchlorate-containing plastisol nitrocellulose composite formulations at 500 psi. In both cases the results were essentially insensitive to changes in deflagrating area.

DR. G. J. PENZIAS (*Warner and Swasey Company*): I am particularly interested in the apparent thickness of the reaction zone, which the authors measured to be on the order of 800–3000 μ. We have recently obtained a similar result in time-resolved measurements of the infrared radiation and temperatures of solid propellant flames in an optical strand burner. The spectral radiant emittance and spectral emissivity of the flame were measured as a function of time at various wavelengths in the infrared bands of CO_2 and H_2O. The ratio of spectral emittance to spectral emissivity is equal to the Planck function, from which the temperature can be calculated [TOURIN, R. H.: *Temperature, Its Measurement and Control in Science and Industry*, C. M. Herzfeld, ed., Vol. III, Part 2, Chap. 43 (Reinhold, New York, 1962)]. The instrument is focused directly above the propellant strand. As the strand starts to burn, the burning surface moves away from the point of observation; therefore the temperature-time record obtained can be converted to temperature-distance information, since the strand burning rate is known.

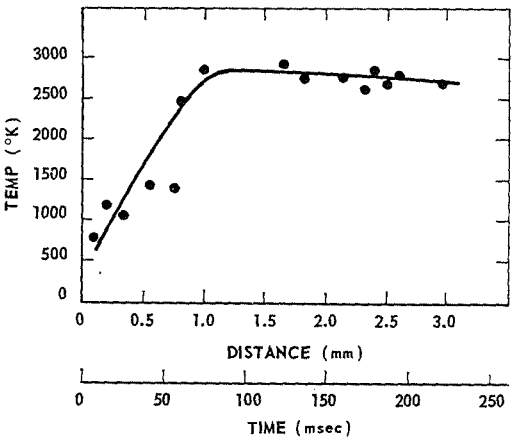

The figure shows typical results of measurements made at 4.50 μ, which corresponds to the radiation emitted by the CO_2 formed in the reaction. The propellant used was Arcite 368, a composite-type ammonium perchlorate propellant, burned at 800 psig in nitrogen atmosphere. As can be seen, the temperature rises rapidly with time, and after a distance of approximately 0.8 mm, reaches a maximum which is close to the theoretical adiabatic temperature of the propellant. The temperature then slowly starts to fall as the burned gases cool due to interactions with the surrounding nitrogen. The time or distance to reach this high-temperature flame zone can be thought of as the reaction zone, and is in agreement with the results presented here.

PARTICIPATION OF THE SOLID PHASE IN THE OSCILLATORY BURNING OF SOLID ROCKET PROPELLANTS

N. W. RYAN, R. L. COATES, AND A. D. BAER

An experimental study of the interaction between the solid and gas phases during oscillatory burning of solid propellants has been undertaken with the objective of exploring the validity of the complex theory describing the phenomenon. The apparatus employed was a side-vented, cylindrical vessel with an end-burning propellant grain closely fitted in one end and provision for maintaining the burning zone at a fixed position. Pressure oscillations both at the gas-zone end plate and beneath the grain were recorded.

Energy dissipation in the solid propellant, isolated from other losses in the system, was determined from the growth rate constants of the amplitudes of pressure oscillation for grains of varying lengths. The efficiency of acoustical energy or absorption by the grain was found to be maximum when the oscillations are at frequencies close to the natural frequency of the grain. These results confirm the description of oscillatory burning by the acoustical theory in its broad generalizations.

Introduction

The practical interest in oscillatory burning of rocket propellants derives largely from its association with severe combustion irregularities, though it is not always found in such bad company. Where they occur together, suppression of oscillatory burning results in elimination of the more serious irregularities. Thus, whether the one is a cause or merely a concomitant symptom of the other, it is believed that a basic understanding of the more tractable, oscillatory burning, will lead to preventives or cures for the more harmful, irregular burning.

In an excellent discussion of oscillatory burning, R. W. Hart[1] summarized the state of knowledge on the subject in 1960. His remarks and those of others on the same occasion indicated that the principal emphasis in research is being guided by the acoustical theory of oscillatory burning put forth by R. W. Hart and F. T. McClure and their associates.[2,3] The essential premise of the theory is that the combustion zone serves as a broad-band amplifier for oscillations in the natural frequencies of the composite gas cavity-solid propellant acoustical system. Because of the complex, nongeneralizable influences of hardware and geometrical configuration on the phenomenon as it is encountered in rocket practice, research attention has been directed toward those critical, relevant properties of propellant and its combustion that can be isolated in laboratory apparatus.

The work here reported concerns isolating the effects of propellant participation in the oscillatory burning. Observations amply confirm the broad features of the acoustical theory and demonstrate that the behavior of the solid can be described.

Apparatus and Propellant

The key apparatus used in the study is a 1.5-inch-diameter cylindrical, side-vented burner. A closely fitted grease-lubricated cylindrical grain is placed in one end. The grain is burned at the free end, gas being vented midway between the burning surface and the closed end of the gas column. The grain is backed by a piston which is advanced at the rate necessary to maintain the burning surface at a fixed position ($\pm\frac{1}{8}$ inch), thus fixing the gas-phase geometry during a firing. The burner is a modification of the one-dimensional burner first developed at the University of Utah.[4] It has the virtue of sustaining only axial acoustic modes in the gas phase, often only the fundamental, thus simplifying greatly the analysis of experimental results.

Pressure transducers are mounted in the flanged end of the gas cavity, opposite the burning surface, and in the piston face at the base of the propellant grain. The transducer signals are recorded with oscilloscopes and a tape recorder. From these recordings, measurements are made of oscillation frequency and amplitude, the rates of growth of the pressure oscillations, and the phase angle between the two pressure signals.

In some experiments, short grains are mounted

at both ends of the chamber. In these runs, the piston is left in a fixed position, and both pressure signals are obtained from beneath propellant.

The propellant used was mixed, cast, and cured at the test facility under rigidly controlled conditions. A simple composition of PBAA-epoxy binder, ammonium perchlorate oxidizer, and copper chromite burning rate catalyst (18/80/2 wt per cent) was selected for exhaustive study.

Illustrative Results

Figures 1 and 2 illustrate the kinds of information obtained from an experiment, in this case the burning of a grain initially 5 inches in length with a gas column maintained at $4\frac{1}{8}$ inches in length. The grain was brought to a temperature of 60°C before it was ignited. Strong oscillations made their appearance shortly after ignition, died out after about 4.5 seconds, and resumed after about 6.5 seconds for another 6 seconds. Also plotted on Fig. 1, as functions of time to the scale established by the pressure traces, are phase angle between solid-end and gas-end signals and the ratio of solid-end to gas-end pressure oscillation amplitudes. The constancy of the mean pressure testified to the constancy of burning rate, so that the instantaneous length of unburned grain is proportional to time to burn-out.

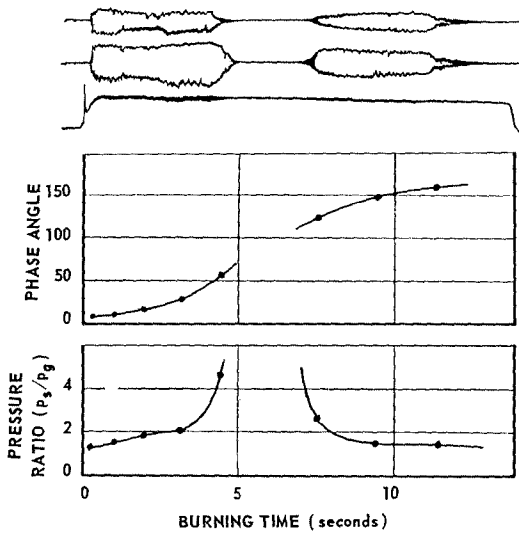

FIG. 1. Results from the firing of a 5-inch grain, preconditioned at 60°C, with a $4\frac{1}{8}$-inch gas column. Oscilloscope traces show oscillating pressure at gas end (top) and beneath grain (center, max. amplitude 20 psi peak to peak) and mean chamber pressure (bottom). The phase angle by which the signal beneath the grain leads the signal at the gas end and the ratio of the signal amplitudes (p_s/p_g) are also shown.

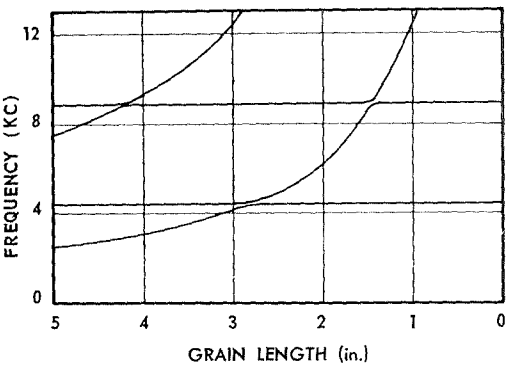

FIG. 2. Idealized acoustic modes for the firing shown in Fig. 1. Speed of sound 4,150 ft/sec in solid, 3,000 ft/sec in gas.

The gross features of the experimental observations can be explained readily in terms of acoustic theory applied to a two-component, one-dimensional elastic system, bounded by rigid walls at the extreme ends of the two phases. The theory in this application is set forth clearly by Hart, Bird, and McClure,[3] and will not be reproduced here.

Figure 2 is an idealized frequency-solid length mode map drawn for the experiment depicted on Fig. 1. The gas quasi-modes are horizontal lines drawn assuming a pressure antinode at the phase boundary; the curved solid quasi-modes are drawn assuming a pressure node at the phase boundary. As the ratio of acoustic impedances (solid to gas) is very large (1900), the composite system modes follow quasi-modes very closely except where these intersect. The intersection of the first gas quasi-mode and the first solid quasi-mode was located at the critical propellant grain length for which interpolation of the phase angle curves of Fig. 1 gives a phase angle of 90 degrees. This length, 2.9 inches, is a quarter wave length in the solid at the observed frequency of 4400 cps. These numbers establish the speed of sound in the solid as 4250 feet per second and thus supply all the information needed for construction of the idealized mode map.

In the experiment of Fig. 1, the only significant frequency observed was close to 4300 cps, so that it is inferred that only the second (first period of oscillation) and first (second period of oscillation) composite modes were, at their respectives times, active. The transition from the second to the first composite mode was attended by the momentary disappearance of oscillations. When the grain length was in the neighborhood

of the critical value, the phase interface was located close enough to a pressure node that the combustion process could not supply acoustical energy at a sufficient rate to balance energy losses.

The solid-phase resonance condition approached as the grain burned to the critical length is reflected in the ratio of oscillating pressure amplitudes, the amplitude in the solid greatly exceeding that in the gas even though the absolute values of both amplitudes were diminishing. Under these conditions the acoustical coupling between the phases was such as to result in effective pumping of energy from the gas phase into the solid. The consequent increased energy dissipation in the solid contributed to the damping processes.

General Results

Figure 3 presents results from the experiment of Fig. 1 and two other experiments to show the ratio of pressure amplitudes and phase difference as functions of reduced length, which is the ratio of grain length to critical grain length. These represent a degree of generalization of the results shown on Fig. 1.

An important parameter that does not appear on Fig. 1 is the growth constant, $d \ln p/dt = \alpha$, measured at the first onset of oscillations for those runs in which the ignition transient was short. It has been determined for each run in several series. Within a series the initial length of grain was varied from run to run, the series differing with respect to assigned length of gas column. For the runs shown, initial propellant temperature was 30°C. The values of the growth

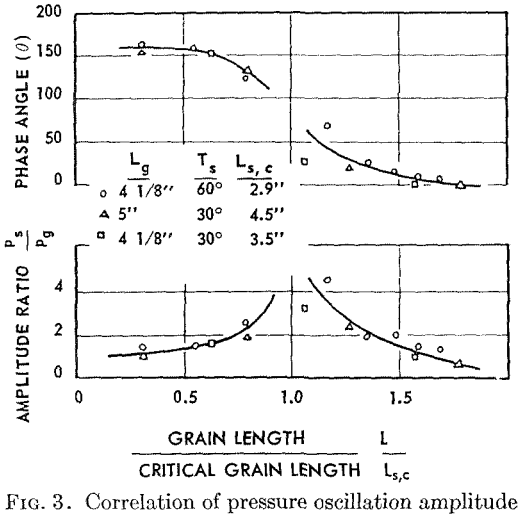

FIG. 3. Correlation of pressure oscillation amplitude ratio and phase angle with grain length for three firings. Pressure, 200 psi.

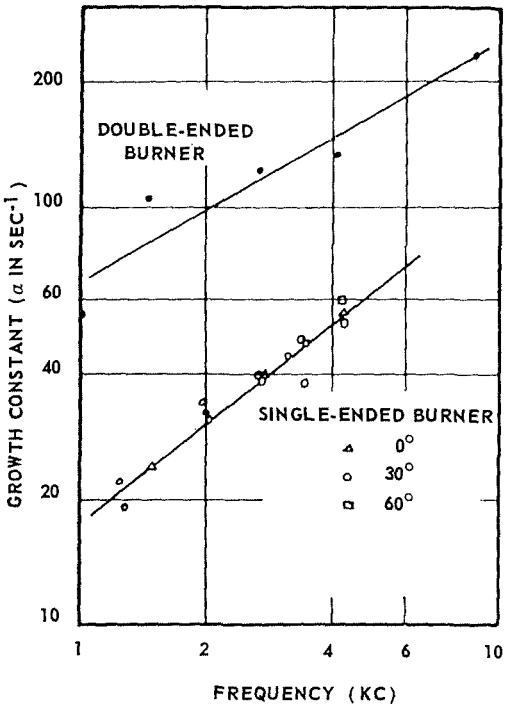

FIG. 4. Variation of the rate of growth of pressure oscillations with frequency ($d \ln p/dt = \alpha$) for both single and double-ended burners. Pressure, 200 psi.

constant, determined for grains much shorter than the critical length, has been found to be inversely related to mean pressure level, dropping to small values at chamber pressure above 300 psi, apparently approaching a maximum at about 150 psi.

On Fig. 4 which applies only to short grains, α is plotted against frequency, which is determined by length of gas column. It is found that $\alpha/f^{0.8} =$ constant is a good representation of the data at the three temperatures for the single-ended burner, i.e., propellant in only one end. That this relationship is apparently not temperature dependent, whereas the visco-elastic properties of the solid are, leads to the supposition that the small propellant charge is not an important contributor to the losses. Under these conditions, α is determined altogether by combustion zone amplification and gas phase (homogeneous, surface, and nozzle) losses. This observation validates the assumption made by Horton[5] that solid losses in short test samples may be neglected.

Also displayed on Fig. 4 is a line for a double-ended burner (short burning grains in both ends), showing, for a given frequency, an α more than twice the value for the single-ended burner. A simplified analysis shows that α represents the difference between the acoustic amplification due

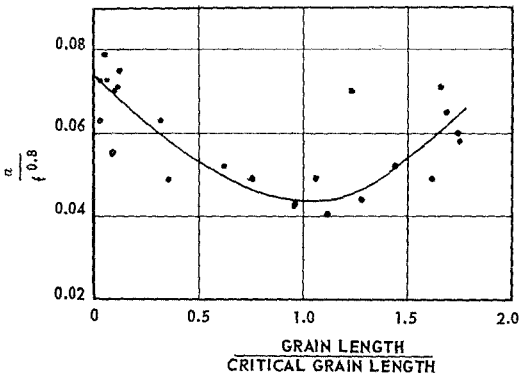

FIG. 5. Variation of the rate of growth of oscillations with initial grain length ($T_s = 30°$). Pressure, 200 psi

to combustion and the damping which is characteristic of the gas-filled chamber. The difference between the double-ended value and twice the single-ended value, assuming that the amplification is simply proportional to burning-surface area, is therefore primarily a function of the characteristic damping of the two systems. The damping is different in the two systems chiefly because of the effects of the nonhomogeneous gas in the "cold" end of the single-ended system.

On Fig. 5 the effect of grain length on oscillation growth is shown as a reduced (but dimensional) α vs. reduced grain length ($L_s/L_{s,c}$). The choice of $\alpha/f^{0.8}$ to represent the growth constant is suggested by Fig. 4, and is motivated purely by correlational convenience. The data of Fig. 5 were all obtained with grains conditioned to 30°C. Data taken at 0° and 60°C are somewhat scattered but, in the neighborhood of the critical length α values are greater than the corresponding value for 30°C. With respect to Fig. 5, it should be mentioned that in some series of tests, grains originally at or near the critical length did not exhibit oscillatory burning after ignition. For these, the value of α was zero or less and the two branches of the curve dipped sharply downward. The curve is to be regarded as poorly defined for lengths near the critical length.

Discussion

It is felt that, at this stage of experimentation, the most fruitful philosophy of interpretation is to argue inductively from results at hand. The greatest profit is seen in supplying the sorely missed experimental bridge from the elaborate acoustical theory now in vogue to the working generalizations useful to engineering practice.

It has already been noted that the growth constants measured for short grains, Fig. 4, apparently are free of contributions due to losses in the solid. It is speculated that if corrections were made for the gas-zone losses, the residual α could be correlated with frequency by

$$\alpha \propto f^m,$$

where m is less than unity, perhaps $\frac{1}{2}$. As m is not unity, it is inferred on dimensional grounds that the α, f relationship must involve another characteristic time parameter, constant for all the experiments here reported, a grain temperature-insensitive characteristic of the combustion process.

That the growth constant for grains near the critical length is less than for short grains is attributed to losses in the solid. There is, however, another contribution to the reduced growth constant. Consider a grain ignited at a length such that initial oscillations are in the second system mode, very nearly the first gas quasi-mode. (See Fig. 2.) As the grain burns down to the critical length, the frequency increases; the pressure antinode moves away from the interface into the gas phase. As a consequence, the combustion zone at the interface receives a reduced signal to amplify, and the pressure increment is correspondingly less. This reduced increment is seen in relation to the full oscillation amplitude at a true antinode, where the pressure measurement is made, and thus is reported, wrongly, as a reduced constant.

A quantitative estimate of this effect can be made as follows: For short grains, the antinode is very close to the interface:

$$\frac{\Delta p}{p_b} = \frac{\Delta p}{p_g} = \frac{\alpha_s}{f}$$

For the long grains, frequency the same,

$$\frac{\Delta p}{p_b} = \frac{p_g}{p_b}\frac{\Delta p}{p_g} = \frac{p_g}{p_b}\frac{\alpha_1}{f}$$

where α_1 and α_s are measured at the gas-zone end plate. In these equations Δp is the pressure increment per cycle, p_b and p_g are oscillating pressure amplitudes at the interface and the gas end plate. If it is assumed that $\Delta p/p_b$ is the same in the two cases,

$$\frac{\alpha_1}{\alpha_s} = \frac{p_b}{p_g} = \cos\left(\frac{\Delta f}{f}\pi\right),$$

where Δf is the shift in frequency from the gas quasi-mode value closely approximated for short grains. Observed frequency shifts are all well within 10 per cent of the quasi-mode value, so that

$$\frac{\alpha_1}{\alpha_s} > \cos\frac{\pi}{10} = 0.95$$

As the observed values of this ratio, Fig. 5, are often less than 0.7, reduction in α cannot be accounted for by displacement of the pressure antinode.

The sole remaining plausible explanation is that energy is more effectively transferred from the gas to the solid as the critical length is approached. The net rate of energy absorption by and dissipation in the solid ($\dot{E}_s$) is estimated from

$$\dot{E}_s = 2E_g(\alpha_s - \alpha_1)$$

when α's are compared at the same frequency and the same acoustic energy density in the gas (E_g). The same quantity may be equated to the time rate of increase of internal energy in the propellant:

$$\dot{E}_s = \rho c_v R(dT/dt)$$

where R is the ratio of gas volume to propellant volume. Thus the time rate of increase of temperature throughout the propellant grain can be calculated.

For reasonable values of parameters—frequency, 3600 cps; α values, from this frequency and readings from Fig. 5 at reduced lengths of 0 and 0.8, of 52 and 32 sec^{-1}; acoustic energy density of the gas, for 10 psi amplitude, of 15 ft-lb per cu ft; ρc_v of about 60 Btu/(cu ft, °C); R of 1—the above equations give

$$\dot{E}_s = 600 \text{ ft-lb. per sec per cu ft of gas}$$

$$dT/dt = 0.013°\text{C per sec}$$

These figures show that the propellant temperature rise in the experiments reported here was certainly less than 0.5°C. An extension of the calculation shows, however, that the temperature rise in the solid may be significant in a rocket. If, for a propellant similar to that discussed here, the pressure amplitude were 100 psi and the α difference 20 sec^{-1}, the corresponding rate of temperature rise in the bulk of the propellant would be of the order of 1.3°C per sec. This space-average rise, not impressive in itself, may be alarming as indicating the possibility of much greater local values. The spectre of disruptive mechanical stress may have as a partner the spectre of excessive local internal heating.

Conclusion

The results presented above confirm the description of oscillatory burning by the acoustical theory in its broad generalizations. The results isolate the effects of solid participation in the oscillations and permit a close estimation of the rate of energy dissipation in the solid from experimentally measured oscillation growth constants. The solid proves to be an effective absorber of energy from the gas phase when the oscillation frequency approaches the resonant values for the solid. Sharp discrimination near transition from the second to the first system modes (high Q) is not indicated, solid participation being pronounced when the frequency impressed on the solid is half the quasi-mode value.

Nomenclature

E_g	Energy density in the gas phase
$\dot{E}_s$	Energy dissipation rate in the solid per unit volume of gas
f	Frequency of oscillations
L_s	Propellant grain length; $L_{s,c}$, critical value
p	Pressure; amplitude of oscillation, as used in text
R	Ratio of solid volume to gas volume
T	Temperature
t	Time
α	Oscillation growth constant, $d \ln p/dt$, measured at gas end; α_s for short grains, α_1 for long grains

Subscripts

b	Refers to burning surface
g	Refers to gas
s	Refers to solid (except with α)

ACKNOWLEDGMENT

This work was performed under Air Force—ARPA sponsorship, Contract AF 49(638)-1074, ARPA No. 24-61.

REFERENCES

1. HART, R. W.: *Eighth Symposium (International) on Combustion*, p. 904. Williams and Wilkins, Baltimore, 1962.
2. HART, R. W. and MCCLURE, F. T.: J. Chem. Phys. *30*, 1501 (1959).
3. HART, R. W., BIRD, J. F., and MCCLURE, F. T.: *Progress in Astronautics and Rocketry*, Vol. I: *Solid Propellant Rocket Research*. (M. Summerfield, ed.) Academic Press, New York, 1960.
4. HORTON, M. D.: Ph.D. thesis, University of Utah, 1961.
5. HORTON, M. D.: ARS Journal *32*, 644 (1962).

General Discussion

DR. M. D. HORTON (*U. S. Naval Ordnance Test Station*): The question has been asked how the measurements in the papers by Horton, Strittmater, and Ryan compare. The two figures show the data for the three papers in a comparative way.

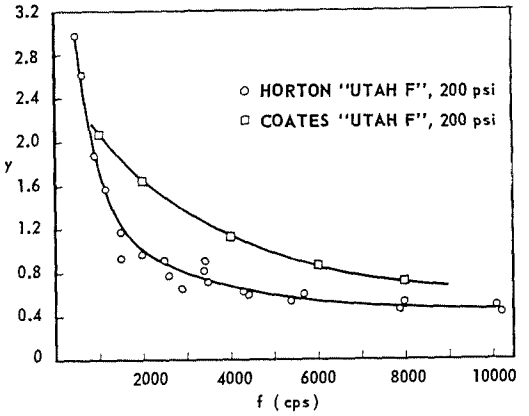

FIG. 1. Comparative values of the reduced specific acoustic admittance of the "Utah F" propellant as a function of frequency. The data obtained by Dr. Coates are reported in his unpublished University of Utah Ph.D. thesis.

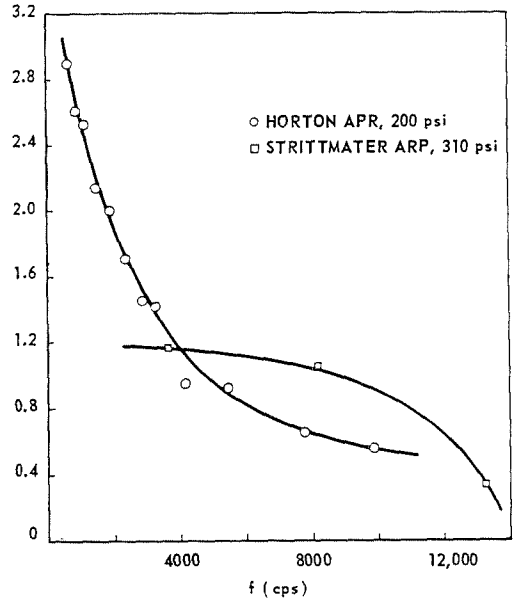

FIG. 2. A comparison between the values of the reduced specific acoustic admittance of ARP double base propellant as obtained by NOTS and BRL. The difference in test pressures may account for the discrepancy between the sets of data.

DR. R. J. PRIEM (*NASA/Lewis Research Center*): What is the variation in growth rate constant with time or amplitude in each run? If there is a variation in growth rate constant at what point does one measure the growth rate constant? How does one explain the fact that the wave amplitude reaches an equilibrium where the damping must equal the driving? It would appear that second order effects are required to explain the equilibrium. If second order effects are important at equilibrium then it would appear that second order effects at lower amplitudes would be important.

PROF. N. W. RYAN (*University of Utah*): The growth constant values reported were measured at the initial part of the oscillation growth period, where the acoustic pressure–time relationship is in fact exponential. As defined, the growth constant implies that gains and losses effective at low acoustic pressure amplitudes—the first order effects—are linear in the sense that they can be represented either by linear terms in the wave equation or by constant acoustic admittances at the phase boundaries. Second order (nonlinear) effects that are not active at low acoustic pressures are invoked to explain the "equilibrium" acoustic pressure. It may be pointed out that the second order loss effect can be quite small compared to a first order effect and yet very significant, because it detracts from a small difference between large first order gain and loss effects.

DR. L. A. WATERMEIER (*Ballistic Research Laboratories*): The problem of ignition is by no means small. Experiments at BRL indicate that the application of an igniter paste on the propellant surface must be done with great care. This particular point is even more important than bits of wire remaining in the chamber after ignition. Dr. Ryan's group has apparently overcome this problem by using a hot gas ignition.

DR. H. SHANFIELD (*Aeronutronic*): Recently the Applied Physics Laboratory, The Johns Hopkins University, published an analysis of the acoustic characteristics of the "T" rocket motor configuration. They conclude, in part, that the placement of the exhaust nozzle at the center leads to a source for acoustic excitation of the burning propellant. In what manner does this influence the calculations of specific acoustic admittance in these experiments?

DR. M. D. HORTON: In the text of the paper by Horton et al., the amplification function of the exhaust port is accounted for by the inclusion of the

factor σ in Eq. (8) which artificially describes the acoustic admittance of the combustion zone as being

$$Y = -\frac{V}{P}\left(\frac{\mu}{\varepsilon} - \frac{1}{\gamma} + \sigma\right).$$

Because the value of σ is about $1/\gamma$, the values of the reduced specific acoustic admittance as reported are equal to the "response function" of the combustion zone.

DR. R. STRITTMATER (*Ballistic Research Laboratory*): The regions of the combustion chamber near the nozzle may appear as sources of sound. Because of this effect negative values of the burning surface admittance are obtained that are too large in absolute magnitude. The results of the theoretical analysis by APL, now that they are available, should be used to isolate the burning surface effect in "T" motors for it is this effect alone that is needed when making gain–loss analyses for a general sort of rocket motor configuration.

PROF. N. W. RYAN: The APL analysis shows that in the region of the centrally located vent, flow energy may be converted to acoustic energy in the odd modes of oscillation. It is not known if, in the experiments reported, circumstances were favorable for this conversion. The effect has been ignored in the calculation of acoustic admittance. Partial justification, *a posteriori*, comes from a preliminary comparison of results from two different kinds of experiments in which the vent effects are believed to be very different. The acoustic admittance values calculated are in good agreement.

DR. L. F. JESCH (*Sun Oil Company*): Professor Ryan describes a chamber in which the solid is moved as it burns to maintain position of its front. Strittmater *et al.*, however, make an assumption that regression is negligible and set the initial and boundary conditions accordingly. Is it justified to set this boundary condition fixed?

DR. R. STRITTMATER: It would be desirable to advance the solid at the same rate it burns in our experiment, as is described in Professor Ryan's paper, if this could be done without detrimental side effects. Some consideration and rough calculations, however, show that the effect of the regression on the results presented in our paper is small and can therefore be neglected. This can be shown as follows: In the self-excited tube technique for determining the admittance the gains must exceed the losses, otherwise no measurement can be obtained. Experiment indicates that the losses, as characterized by the decay of the natural logarithm of the pressure envelope after burnout ($\partial \ln P_a/\partial t$) will have a minimum value of the order of 10 sec^{-1}. Simple harmonic standing wave theory indicates that the relative energy change rate is twice this value. Therefore the acoustic power capability of the combustion process must be such that the energy in the acoustic field of the cavity would be increased by a factor of 20 each second if the gain equal loss condition is met and a measurement is obtained.

Even for a fast burning propellant (1 inch/sec) in the shortest chamber (1.3 inch) used, the reduction rate of acoustic energy density in the chamber due to the addition of volume by regression of the surface is 0.77 sec^{-1}. Thus, under these extreme conditions we conclude from energy considerations, that neglecting the regression could affect results by $\sim$4%, i.e., $0.77/20 \sim .04$. For the results reported in our paper this figure would be considerably smaller (less than 1%).

There is also the effect of the changing fraction of the wave length from the burning surface to the measuring location (gage site) in the side of the tube, as the surface regresses. Calculations have shown the error involved in neglecting this effect is small ($\sim$1%).

In some cases it is possible that the sum of these effects may introduce significant error. In these cases either the propellant must be moved to present a fixed boundary or the mathematical treatment must be extended to include the time dependent boundary condition.

It is also of interest to note that the fractional change in frequency due to regression in one period of oscillation is small ($\sim 10^{-4}$) and therefore interference effects should be virtually nonexistent.

OSCILLATORY BURNING OF SOLID COMPOSITE PROPELLANTS

W. A. WOOD

Analytical consideration of the interaction of an oscillatory pressure disturbance with the burning zone of a composite propellant leads to the conclusion that acoustic waves induce periodic variations in the ratio of the mass release rates of composite propellant components that give rise to harmonic composition and adiabatic flame temperature fluctuations in the gases above the propellant. These mass-release-rate, composition, and flame-temperature fluctuations may make large contributions to the amplification of acoustic waves by burning composite propellants. The magnitudes of these contributions to the admittance are particle-size-dependent and decrease as the ratio of particle burning time to oscillation period decreases.

In contrast to homogeneous propellants, the amplification tendency of composite propellants is not expected to be a strong function of the burning rate pressure index of the over-all propellant. On the other hand, composition and flame-temperature contributions to the admittance may obtain for double-base propellants at high frequencies.

Experimental work shows that bands of varying luminosity are released from the burning surfaces of propellants that are burned under the influence of an oscillatory pressure. The release of these bands can be related to composition and temperature fluctuations in the gases, but as yet not unambiguously.

Introduction

Oscillatory combustion and combustion instability problems associated with solid rocket propellants have existed since the early days of modern rocket technology. The fact that the subject has warranted discussion at two consecutive Combustion Symposia is in itself witness that the problems persist. At the last Symposium[1,2] a number of hypotheses concerned with the interaction of solid propellant combustion zones with acoustic disturbances were reviewed and compared. For the most part these hypotheses were based on response properties expected of homogeneous propellants and did not deal specifically with problems that stem from the heterogeneity of composite-type propellants.

Composite propellants consist of oxidizer and additives embedded in a continuous binder phase, usually a polymeric fuel. Owing to the nature of preparation of these propellants, the oxidizer particles are distributed randomly throughout the binder. Since at least two discrete phases having different regression characteristics are present, these propellants may not be expected to respond to acoustic disturbances as do homogeneous propellants of the type described by Hart and McClure.[3]

Approaches to the composite problem have been made by Cheng,[2] who considers a two-component system with each component assigned an arbitrary response function, and Barrère,[4] who applies distributed reaction time lags to a Green-type theory.[5] The present discussion advances the multi-component picture to include the effects of time-dependent variations in the composition of the flame zone brought about by differences in the regression rates of the individual components of the propellant and the implications of their subsequent effects on the acoustic admittance of the burning zone.

Response at Low Frequencies

The surface and flame-zone properties of a composite propellant burned under the influence of a very-low-frequency acoustic disturbance can be represented adequately by a series of steady-state (constant-pressure) models that span the pressure range of the acoustic disturbance.

During steady-state burning of one face of a semi-infinite slab of composite propellant the ratio of the mass release rate of oxidizer to that of the binder, $\dot{w}_o/\dot{w}_b$, is equal to the ratio of the weight fractions of these components, W_o/W_b, incorporated in the propellant. The mass release rate of a component may be expressed in terms of its condensed phase density, ρ, its surface area, S, and its instantaneous regression rate, r, to give

$$\frac{\dot{w}_o}{\dot{w}_b} = \frac{S_o\rho_o r_o}{S_b\rho_b r_b} = \frac{W_o}{W_b} \qquad (1)$$

If the propellant is burned under the influence of a very-low-frequency acoustic disturbance, both the surface area and regression rate will adjust so that Eq. (1) will be satisfied at all times.

Response at High Frequencies

The response of a composite propellant to high-frequency disturbances cannot be represented by a series of steady states. However, some insight into the problem may be obtained through examination of the general stoichiometry relationship expressed by Eq. (1).

At high frequencies only the burning rates of the constituents will respond to the pressure fluctuations[3]; their surface areas will be invariant. The sample surface may exhibit irregularities comparable in size to the larger oxidizer particles incorporated in the propellant, or roughly 20–200 microns. The burning rates of oxidizer and binder are generally less than 1 cm per second at 500–1000 psi pressure; hence, during the period of a half-cycle of an imposed acoustic oscillation, the surfaces of each regress by approximately (5×10^3/frequency in cps) microns (or 0.5 μ at 10^4 cps) or less. At high frequencies these regression distances are small compared to the surface irregularities and the surface areas of both oxidizer and binder should remain essentially constant throughout a cycle.

If a small change in pressure, dP, due to the acoustic disturbance, effects changes dr_o and dr_b in the regression rates, then the following equation results for stoichiometric flow:

$$\frac{S_o\rho_o(r_o + dr_o)}{S_b\rho_b(r_b + dr_b)} = \frac{S_o\rho_o r_o}{S_b\rho_b r_b} \tag{2}$$

Elimination of terms leads to

$$d \ln r_o = d \ln r_b \tag{3}$$

From Eq. (3) it is readily seen that stoichiometric flow will occur only in the unique case in which the relative changes in the regression rates of the oxidizer and binder are equal, i.e., their pressure responses are identical. In general this similarity of burning rate response of the components is not expected since they may differ considerably in their chemical and physical natures, and their surfaces will be subjected to different temperature and environmental regions of the propellant combustion zone. As a result of these differences, nonstoichiometric flow should obtain and give rise to time-dependent fluctuations in composition and adiabatic flame temperature of the gases above the propellant surface.

Of importance in most rocket work are the conditions under which burning goes from stoichiometric to nonstoichiometric and the magnitude of surface and composition effects on the admittance of a propellant. In line with this, a quasi-steady-state analysis of the interaction of a composite propellant burning zone with an acoustic disturbance is presented in the following section. Although this analysis will break down at moderate frequencies, it points out many essential features of the problem.

Response of a Composite Propellant Combustion Zone to a Acoustic Disturbance

The reaction of a boundary to an acoustic disturbance may be presented in terms of the specific acoustic admittance at the boundary. An acoustic disturbance incident from the gas side (positive x side) on a boundary will be reflected with increased intensity if the real part of the admittance at the boundary is negative and attenuated if positive.[3,6] The admittance is given by $Y = -dV_x/dP$ where P is the pressure at the boundary and V_x the normal velocity of the gas into the boundary. The problem, therefore, lies in deriving an expression to relate the gas velocity at the combustion zone boundary to the acoustic pressure at the boundary.

A model representative of the burning of an ammonium perchlorate-containing plastisol nitrocellulose propellant has been set up whose principal assumptions are:

1. The combustion of the propellant is considered a three-step process. The first two steps are independent volatilization and primary combustion of (i) the binder and (ii) the oxidizer. The third step is comprised of secondary combustion reactions between oxidizer and binder primary combustion products.

2. Linear regression rates of the surfaces of both the oxidizer and the binder are considered independent of the secondary combustion reactions. These rates are each represented by a burning rate law of the form $r = LP^q$ where L and q are constants and P the pressure.

3. The binder surface remains planar; therefore, its average surface area is constant. The regression rate of the binder is set equal to that of the propellant. It will be shown later that these restrictions may be relaxed without seriously affecting the results.

4. Oxidizer particles are spherical and deflagrate in a narrow zone adjacent to the solid propellant surface. The rate of release of these particles into this deflagration zone is governed by the regression rate of the solid propellant surface.

5. Combustion reactions between oxidizer and binder decomposition products are rapid compared to the period of the pressure oscillation.

6. Only surface-average properties are con-

sidered. Compositional fluctuations within the propellant are small and random.

At any time during the deflagration of a composite propellant the total mass flow rate, $\dot{w}$, may be expressed as

$$\dot{w} = \dot{w}_b + \dot{w}_o \tag{4a}$$

$$= \dot{w}_b + \dot{w}_{o,s} + \dot{w}_o - \dot{w}_{o,s} \tag{4b}$$

$$= S_b C P^n \rho_b + S_{o,s} B P^m \rho_o + (S_o - S_{o,s}) B P^m \rho_o \tag{4c}$$

where $\dot{w}_{o,s}$ and $S_{o,s}$ are the mass flow rate and oxidizer surface area required to give stoichiometric burning of the binder, CP^n is the regression rate of the binder (and propellant surface), and BP^m is that of the oxidizer. The first two terms of Eq. (4c) represent the steady-state mass flow rate of the propellant and may be replaced by $S_p C P^n \rho_p$ where S_p is the cross-sectional area of the propellant over which S_b, S_o, and $S_{o,s}$ are determined and ρ_p is the density of the composite propellant.

If the combustion products follow ideal gas behavior then the gas velocity may be written as

$$V = \frac{KT}{S_p M P}\left[S_p C P^n \rho_p + (S_o - S_{o,s}) B P^m \rho_o\right] \tag{5}$$

where M and T are the molecular weight and temperature of the gases and K is the gas constant.

In order to determine the admittance, all variables of Eq. (5) must be expressed as functions of time. This is facilitated by imposition of a sinusoidal pressure fluctuation, of small amplitude ϵ, normal to the propellant surface. The pressure fluctuation will be written in the form

$$P = \bar{P}(1 + \epsilon \exp -i\omega t) \tag{6}$$

Surface-Area Relationships. The surface area, S_o, of all deflagrating oxidizer particles at some time t_c may be obtained by integration over the interval τ (where τ is the burning time of a particle that terminates combustion at t_c) of the product of the surface area at t_c of particles released from the propellant surface at prior time t_f and the rate of release of particles at t_f:

$$S_o = \int_{t_c-\tau}^{t_c} [4\pi R^2] \times [N S_p C \bar{P}^n (1 + \epsilon \exp -i\omega t_f)^n]\, dt_f \tag{7}$$

R is the radius at t_c of a particle released at t_f, N is the number of oxidizer particles per unit volume of composite propellant, and

$$C\bar{P}^n(1 + \epsilon \exp -i\omega t_f)^n$$

is the burning rate of the propellant at time t_f.

R may be determined from the following equation

$$R = R_i - \int_f^{t_c} B P^m dt \qquad t_c - t_f \leq \tau \tag{8}$$

$$= 0 \qquad t_c - t_f > \tau$$

Equations (7) and (8) may be solved analytically, omitting higher-order terms of ϵ, in the following manner. Integration of Eq. (8) gives

$$R = \frac{R_i}{\bar{\tau}}(t_f - t_c - \bar{\tau}) - \frac{m\epsilon}{i\omega}[\exp(-i\omega t_f) - \exp(-i\omega t_c)] \tag{9}$$

where $\bar{\tau} \equiv R_i/B\bar{P}^m$ = average burning time of a particle.

The variable limit $t_c - \tau$ of Eq. (7) may be replaced by a constant limit $t_c - \bar{\tau}$ since Eq. (7) has the form

$$\int_{(t_c-\tau)}^{t_c} f(t_f)\, dt_f = \int_{(t_c-\bar{\tau})}^{t_c} f(t_f)\, dt_f + \int_{(t_c-\bar{\tau})+(\bar{\tau}-\tau)}^{t_c-\bar{\tau}} f(t_f)\, dt_f$$

and, by the mean-value theorem, this may be expressed as

$$(\tau - \bar{\tau}) f(t_c - \bar{\tau}) + \int_{t_c-\bar{\tau}}^{t_c} f(t_f)\, dt_f$$

Consequently Eq. (7) reduces to

$$S_o = \int_{t_c-\bar{\tau}}^{t_c} [4\pi R^2] \times \{N S_p C \bar{P}^n [1 + \epsilon \exp(-i\omega t_f)]^n\}\, dt_f \tag{10}$$

since

$$[4\pi R_i^2]\{N S_p C \bar{P}^n [1 + \epsilon \exp(-i\omega t_f)]^n\}[\tau - \bar{\tau}] = 0 \qquad \text{at } t_f = t_c - \bar{\tau}.$$

Integration of Eq. (10) yields

$$S_o = \bar{S}_o\left[1 + \frac{3\epsilon \exp(-i\omega t)(m-n)}{i} \times \left(\frac{1}{\omega\bar{\tau}} - \frac{2i}{\omega^2\bar{\tau}^2} - \frac{2i}{\omega^3\bar{\tau}^3} + \frac{2\exp(i\omega\bar{\tau})}{\omega^3\bar{\tau}^3}\right)\right] \tag{11}$$

where

$$\bar{S}_o = \frac{4\pi N S_p C \bar{P}^n R_i^3}{3B\bar{P}^m}$$

Here the subscript has been dropped from t_c since t_c may have any preassigned value.

The oxidizer surface area $S_{o,s}$ required for stoichiometric burning at time t is calculated from the oxidizer surface area which would exist under a constant pressure equal in magnitude to the instantaneous pressure; i.e., $S_{o,s}$ is $\bar{S}_o$ evaluated at P rather than at $\bar{P}$. Therefore

$$S_{o,s} = \frac{4\pi N S_p C P^n R_i^3}{3BP^m} \tag{12}$$

and for small values of ϵ may be written

$$S_{o,s} = \bar{S}_o[1 - (m - n)\epsilon \exp(-i\omega t)] \tag{13}$$

The relationship between S_o and $S_{o,s}$ is made clear by consideration of the variation of S_o with time at various values of $\omega\bar{\tau}$. S_o is given by the real part of Eq. (11) which is

$$S_o = \bar{S}_o[1 + 3\epsilon(m - n)\beta]$$

where

$$\beta = -\cos\omega t\left[\frac{2}{\omega^2\bar{\tau}^2}\left(1 - \frac{\sin\omega\bar{\tau}}{\omega\bar{\tau}}\right)\right] - \sin\omega t\left[\frac{1}{\omega\bar{\tau}} - \frac{2}{\omega^3\bar{\tau}^3}(1 - \cos\omega\bar{\tau})\right].$$

At low values of $\omega\bar{\tau}$, i.e., at low frequencies or short particle burning times (small particle sizes), the cosine term predominates. As $\omega\bar{\tau} \to 0$ the instantaneous oxidizer surface area, S_o, approaches the surface area required for stoichiometric burning, $S_{o,s}$, since $\beta \to -\frac{1}{3}\cos\omega t = \mathrm{Re}[-\frac{1}{3}\exp(-i\omega t)]$. In this limiting case the composite propellant behaves as a homogeneous propellant. As $\omega\bar{\tau}$ increases the oxidizer surface area cannot adjust fast enough to maintain stoichiometric burning. In the limit, as $\omega\bar{\tau} \to \infty$ the oxidizer surface area remains constant. Here $\beta \to 0$ and the instantaneous surface area, S_o, approaches the surface area, $\bar{S}_o$, that obtains under constant pressure conditions at the pressure $\bar{P}$. How the oxidizer surface area fluctuations vary between these limits is shown in Fig. 1.

The difference between the instantaneous oxidizer surface area and that required for stoichiometric burning is of importance since fluctuation of this difference $(S_o - S_{o,s})$ gives rise to corresponding fluctuations in composition and temperature of the burning zone above the propellant surface. This difference function, given by

$$S_o - S_{o,s} = \bar{S}_o(m - n)\epsilon \exp(-i\omega t)\psi, \tag{14}$$

where

$$\psi = 1 + \frac{3}{i}\left(\frac{1}{\omega\bar{\tau}} - \frac{2i}{\omega^2\bar{\tau}^2} - \frac{2}{\omega^3\bar{\tau}^3} + \frac{2\exp(i\omega\bar{\tau})}{\omega^3\bar{\tau}^3}\right),$$

vanishes as $\omega\bar{\tau} \to 0$ and approaches a maximum value as $\omega\bar{\tau} \to \infty$. The nature of this difference

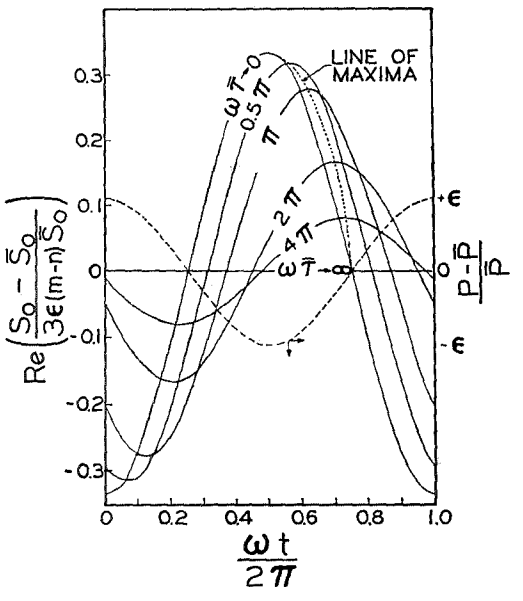

FIG. 1. Form of the deviation of the instantaneous oxidizer surface area from its mean over one pressure cycle.

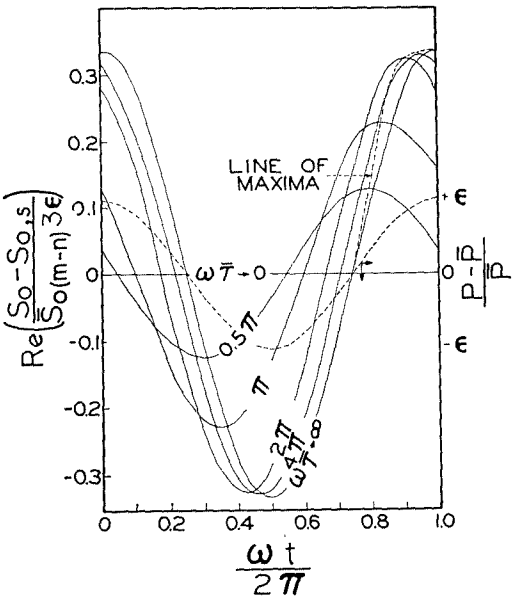

FIG. 2. Form of the deviation of the instantaneous oxidizer surface area from the stoichiometric requirement over one pressure cycle.

function is shown in Fig. 2, in which

$$\mathrm{Re}\,[(S_o - S_{o,s})/3\epsilon(m-n)\bar{S}_o]$$

is plotted versus $\omega t/2\pi$.

Molecular Weight and Temperature Fluctuations. Compositional fluctuations that arise when $S_o \neq S_{o,s}$ give rise to variations in M and T that may be expressed as

$$M = M_s\left[1 + \left(\frac{\partial \ln M_s}{\partial W_o}\right)dW_o\right] \tag{15}$$

and

$$T = T_s\left[1 + \left(\frac{\partial \ln T_s}{\partial W_o}\right)dW_o\right] \tag{16}$$

where M_s and T_s are the molecular weight and temperature for stoichiometric burning at $P = \bar{P}$.

The pressure oscillation will also produce variations in M and T; however, changes of M will in many cases be small and here will be neglected. Following Hart and Cantrell,[7] the temperature fluctuation due to the acoustic wave may be written as $T_s\theta \exp(-i\omega t)$, where $T_s\theta$ is the temperature fluctuation due to a pressure variation $\bar{P}\epsilon$ when burning is stoichiometric. Since only small fluctuations are considered the effects of composition and pressure changes will be considered independent of each other and Eq. (16) expands to

$$T = T_s\left[1 + \theta \exp(-i\omega t) + \left(\frac{\partial \ln T_s}{\partial W_o}\right)dW_o\right] \tag{17}$$

Consideration of only small fluctuations permits dW_o to be written as

$$dW_o = W_b\frac{\dot{w}_o - \dot{w}_{o,s}}{\dot{w}_o + \dot{w}_b} = W_b\frac{\bar{S}_o(m-n)\epsilon \exp(-i\omega t)\psi BP^m\rho_o}{S_pCP^n\rho_p + \bar{S}_o(m-n)\epsilon \exp(-i\omega t)\psi BP^m\rho_o}$$

Setting $\partial \ln M_s/\partial W_o$ and $\partial \ln T_s/\partial W_o$ as constants ϕ and κ, respectively, and substituting the foregoing expressions in Eqs. (15) and (17) gives

$$M = M_s\left[1 + \phi W_b\frac{\bar{S}_o(m-n)\epsilon\psi BP^m\rho_o \exp -i\omega t}{S_pCP^n\rho_p + \bar{S}_o(m-n)\epsilon\psi BP^m\rho_o \exp -i\omega t}\right] \tag{18}$$

$$T = T_s\left[1 + \theta \exp(-i\omega t) + \kappa W_b\frac{\bar{S}_o(m-n)\epsilon\psi BP^m\rho_o \exp -i\omega t}{S_pCP^n\rho_p + \bar{S}_o(m-n)\epsilon\psi BP^m\rho_o \exp -i\omega t}\right] \tag{19}$$

Determination of the Admittance. Since all variables of Eq. (5) are now expressible as functions of time, the admittance may be determined. Substitution for $(S_o - S_{o,s})$, M, and T from Eqs. (14), (18), and (19), respectively, followed by expansion of the resultant expression and retension only of terms to first order in ϵ gives the gas velocity

$$V = \frac{KT_s}{S_pM_sP}\{S_pCP^n\rho_p[1 + \theta \exp(-i\omega t)] + [1 + W_b(\kappa - \phi\{1 + \theta \exp -i\omega t\}) + \theta \exp -i\omega t][\bar{S}_o(m-n)\epsilon\psi BP^m\rho_o \exp -i\omega t]\} \tag{20}$$

The admittance,

$$Y = -dV/dP = -(dV/dt)(dt/dP),$$

may be determined from Eq. (20). For those cases in which the thickness of the combustion zone is small compared with the wavelength of the oscillation

$$Y = -\frac{KT_s}{S_pM_s\bar{P}^2}\{S_pCP^n\rho_p[(\theta/\epsilon - 1) + n + \Sigma_1] + \bar{S}_o(m-n)\rho_oB\bar{P}^m\psi \times [1 + W_b(\kappa - \phi) + \Sigma_2]\} \tag{21}$$

where Σ_1 and Σ_2 are terms that contain θ and ϵ in their numerators only. The term $\theta/\epsilon - 1$ will generally lie between -1 (the value proposed by Summerfield *et al.*[8] for the limiting low-frequency case where $dT/dP = 0$) and $-1/\gamma$ (the value obtained by Hart and McClure[3] for the isentropic limiting case where

$$dT/dP = [1 - 1/\gamma]T/P,$$

with $\gamma = c_p/c_v$). Hence $\theta < \epsilon(1 - 1/\gamma) \approx 0.2\epsilon$. As ϵ approaches zero both Σ_1 and Σ_2 approach zero and Eq. (21) becomes

$$Y = (\bar{V}/\bar{P})[(1 - \theta/\epsilon) - n - \xi] \tag{22}$$

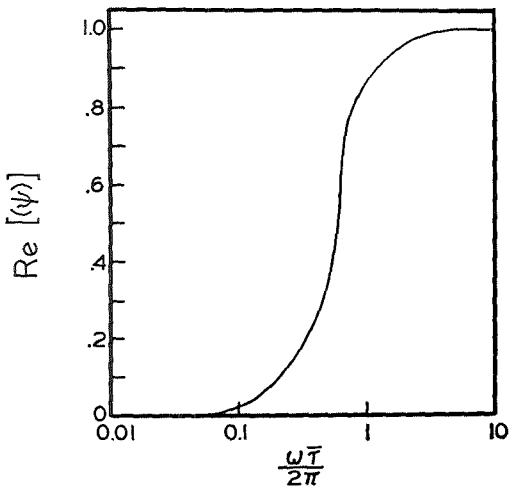

FIG. 3. Real part of ψ as a function of the acoustic frequency and average particle burning time.

where

$$\bar{V} = \frac{KT_s}{M_s\bar{P}} C\bar{P}^n\rho_p$$

and

$$\xi = W_o[m - n][1 + W_b(\kappa - \phi)]\psi$$

The sign of ξ, the contributions to the admittance by fluctuations in oxidizer surface area, gas composition, and flame temperature is of importance, since an acoustic disturbance will be amplified if Re $[Y]$ is negative and attenuated if Re $[Y]$ is positive. The term $[1 + W_b(\kappa - \phi)]$ will generally be positive for high-energy oxidizers currently employed in solid propellants. Re $[\psi]$ varies from +1 (large values of $\omega\bar{\tau}$) to zero (small values of $\omega\bar{\tau}$) as shown in Fig. 3. Consequently the sign of Re $[\xi]$ is determined by the difference between the pressure exponents of the regression rate relations of the constituents. If $m > n$ the amplification tendency of the propellant will be increased and if $m < n$ it will be decreased.

It is possible to make an order-of-magnitude estimation of the effect of ξ on the admittance. Sibbett[9] has found values of $B = 0.007$ cm/sec-atm. and $m = 1.2$ for ammonium perchlorate. Values of other constants for a typical ammonium perchlorate-containing plastisol nitrocellulose propellant are $n = 0.6$, $\gamma = 1.2$, $W_o = 0.35$, $\kappa = 1.03$, and $\phi = 0.53$. Using these values along with values of Re $[\psi]$ from Fig. 3, one obtains the results shown in Table I for a sample case at a mean pressure of 1000 psig fluctuating at 1000 cycles per second. These calculations show that ξ may make a significant contribution to the admittance and that a decrease in $\omega\bar{\tau}$ may effect a change in sign of the real part of the admittance. These results are especially important since perturbations in the burning rates of the solid components due to composition-induced temperature fluctuations and to acoustic oscillation-induced temperature and radiation fluctuations are not included and should in many cases cause an increase in Re $[\xi]$.

It is pertinent to point out that a decrease in R_i and, consequently, in $\omega\bar{\tau}$ (where ω is held constant) will not necessarily lead to a reduction in the amplification tendency of a burning propellant. The real part of ξ is relatively insensitive to changes of $\omega\bar{\tau}$ if $\omega\bar{\tau} > 2\pi$, whereas $\bar{V}$ may increase considerably with an oxidizer particle size decrease and thus lead to an increased value of $|\text{Re}[Y]|$.

Effect of Variable Binder Surface Area. Up to this point, the binder has been assumed to exhibit a flat surface and to have the same regression rate as the propellant. This restricts the interpretation of the results since individual effects of binder and propellant burning proper-

TABLE 1

Example of effect of oxidizer particle size or acoustic frequency on the dimensionless admittance

$\omega\bar{\tau}/2\pi$	R_i (microns)	Re (ξ)	Dimensionless admittance: Low-frequency limit [1-n-Re (ξ)]	Dimensionless admittance: Isentropic limit [(1/γ)-n-Re (ξ)]
2.7	30	0.28	+0.12	−0.05
1.8	20	0.27	+0.13	−0.03
0.9	10	0.23	+0.17	0.0
0.45	5	0.13	+0.27	+0.10

ties on the admittance are indistinguishable. In order to estimate the potential contribution of the binder, the admittance function has been rederived for the case in which the binder and the propellant have different regression rates and in which the binder is assigned a fluctuating-surface-area function.

In this case both binder and oxidizer are assumed to burn as particles and the binder, oxidizer, and propellant regression rates are given by DP^y, BP^m, and CP^n, respectively. Analysis of this example by the procedures already demonstrated leads to the expression

$$Y = (\bar{V}/\bar{P})[(1 - \theta/\epsilon) - n - \xi_{o,b}] \quad (23)$$

where

$$\bar{V} = (KT_s/M_s\bar{P})C\bar{P}^n\rho_p$$

$$\xi_{o,b} = (y - n)(W_b\psi_b + W_o\psi_o) + W_o[1 + W_b(\kappa - \phi)] \times [(m - n)\psi_o - (y - n)\psi_b]$$

and ψ_o and ψ_b are values of ψ for the oxidizer and binder, respectively.

As $\omega\bar{\tau}_o$ and $\omega\bar{\tau}_b$ approach zero, ψ_o and ψ_b approach zero and the admittance equation reduces to that for a homogeneous propellant.

$$Y = (\bar{V}/\bar{P})[(1 - \theta/\epsilon) - n] \quad (24)$$

At high values of both $\omega\bar{\tau}_o$ and $\omega\bar{\tau}_b$, ψ_o and ψ_b both approach 1 and the admittance is given by

$$Y = (\bar{V}/\bar{P})[(1 - \theta/\epsilon) - W_b y - W_o m - W_o W_b(\kappa - \phi)(m - y)] \quad (25)$$

This relationship shows that the sign of the admittance depends strongly on regression rate pressure exponents y and m of the binder and the oxidizer and that the burning rate pressure exponent of the propellant, n, enters only through the term $\bar{V}$. This result is noteworthy in view of the fact that heretofore no correlation between n and the extent of instability shown by propellants has been reported, although theoretical treatments of homogeneous propellants indicate there should be such a correlation.

Discussion. The model used here neglects several factors that can become important during oscillatory burning of composite propellants.

Time-dependent fluctuations in heat and mass transfer and in the rates of chemical reaction and gaseous diffusion in the propellant combustion zone are not included. At low frequencies, chemical reaction and gaseous diffusion times should be small compared with the oscillation period and consequently cause only small deviations from steady-state behavior. The theoretical treatment of Hart and McClure[3] indicates that, at low frequencies and low amplitudes, heat and mass transfer processes in homogeneous propellants approach their steady-state values. For composite propellants, we expect a similar behavior; however, deviations from steady-state behavior may appear at lower frequencies than those expected of homogeneous propellants.

The effects which may ensue from the acoustic oscillation on the instantaneous flame temperature and on the radiant heat exchange between the gases and the propellant have been neglected. The former should increase in significance with increase in dP/dt ($dP/dt = -i\omega\bar{P}\epsilon \exp -i\omega t$); hence, it should increase with increase of either frequency or oscillation amplitude. Radiation effects are geometry dependent; however, in motors with large cavities they should increase with increase in amplitude and decrease in frequency. At high frequencies and short wavelengths the propellant surface sees only an average gas temperature, whereas, at low frequencies, the surface sees a gas temperature that varies in phase with the pressure. While the influence of instantaneous variations in gas composition on the flame temperature has been considered in the model, the potential effects of such changes in composition and temperature on the regression rates of binder and oxidizer have not been included, and may alter the calculated results in either a positive or negative direction.

At high amplitudes and/or high frequencies there is a possibility that the compression-induced temperature variations will couple with those arising from changes in gas composition, resulting in appreciable fluctuations in gas-phase reactions and in the regression rates of the constituent solids. Since dP/dt maxima precede those of P by 90° and the composition-induced flame temperature fluctuations for the case calculated are either in phase with or lead the pressure waves, the coupling of the two thermal effects would result in increased reaction and regression rates as pressure increased, followed by decreased rates as pressure decreased.

In omitting the interaction of the gas composition and flame temperature fluctuation with the regression rates of the propellant constituents, the indicated method of calculating stoichiometric effects on the admittance becomes independent of the burning zone thickness as long as this is small relative to the acoustic wavelength. The acoustic perturbations in turn are considered sufficiently small that the thermodynamic properties of the combustion zone vary linearly with respect to composition. Although high-speed motion pictures indicate particle burning as far as 1 cm from the propellant surface, the

wavelength of the acoustic oscillation at, say, 1000 cps is 120 cm.

On the other hand, calculation of the amplitudes of thermal fluctuations that arise from compositional variations in the gases may be considerably in error because the thickness of the particle-burning zone is, in general, larger than the "wavelengths" associated with these thermal fluctuations. These wavelengths are strongly dependent on frequency, propellant regression rate, and chamber pressure. As an example, a propellant burning at $1\frac{1}{2}$ cm/sec at 1000 psi exhibits a thermal "wavelength" of 0.3 to 0.4 cm at 1000 cps.

Since most deviations from the constant-pressure regression rate relationships discussed above become more important at high frequencies, the model should be more representative of composite propellant burning at low rather than at high frequencies. Even at high frequencies, however, composition and temperature effects are expected.

Although the present treatment deals with true composite (i.e., polyphase) propellants the same arguments may be applied, at least hypothetically, to so-called homogeneous propellants, in which during deflagration a liquid zone is predicated,[10] from which the constituents may volatilize at rates that have different pressure indices. If each of N components is assigned a mass vaporization rate of the form LP^q gm sec^{-1} cm^{-2}, where q is a constant and L is determined from stoichiometric relationships that must exist under constant-pressure deflagration, then the admittance is given by the equation

$$Y = (\bar{V}/\bar{P})\{(1 - \theta/\epsilon) - \sum_{j=1}^{N}[W_j q_j - (\kappa_j - \phi_j)(1 - W_j)(W_j)(q_j - q_N)]\} \quad (26)$$

where

$$\kappa_j - \phi_j = \frac{\partial \ln T_s}{\partial W_j} - \frac{\partial \ln M_s}{\partial W_j}$$

Consider JPN propellant, a double-base formulation[11] containing about 51% nitrocellulose (NC), 43% nitroglycerin (NG), 3% diethyl phthalate (DEP), and 1% ethyl centralite (EC). Values of κ_j and ϕ_j may be determined graphically from theoretical curves of T_s and M_s as functions of W_j. The $\kappa - \phi$ differences for EC, DEP, NG, and NC, are 0.7, 0.6, 0.4 and 0.1, respectively; these are the same order of magnitude as the value of 0.5 estimated for the composite propellant example.

Experimental

Experiments have indicated the existence of thermal waves in the combustion zone above a propellant surface. Streak photographs taken of the gaseous region above propellant samples burning under the influence of imposed acoustic oscillations show the periodic release of luminous bands of gases parallel to the propellant surface varying in intensity in regular fashion.

Apparatus. A schematic diagram of the experimental apparatus is shown in Fig. 4. A modified T-motor[12] was used as an acoustic driver. This motor generates acoustic oscillations primarily in the fundamental longitudinal mode across the arms of the T, the frequency of which may be varied by changing this length. The sample propellant, an ammonium perchlorate–containing plastisol nitrocellulose type, was a 1.8-inch-diameter cylindrical waver approximately $\frac{1}{4}$ inch thick. The windows of the sample section were formed from $\frac{1}{2}$-inch-thick Herculite or $\frac{3}{8}$-inch-thick colorless synthetic sapphire. The photographs were taken with a Beckman and Whitley Dynafax high-speed framing camera, modified for operation as a streak camera. The acoustic pressure was measured by means of a strain-gauge transducer located near the propellant surface and oriented parallel to the direction of the gas flow. Correspondence between the pressure traces and the streak photographs was obtained by means of an exploding wire that simultaneously put a spot on the film and effected a discontinuity in the pressure trace.

Results. Streak photographs (Fig. 5) show two distinct patterns of radiant energy emission. The first is an oscillation in the over-all luminosity of the gases, of frequency equal to that of the driver pressure. From correlation of the pressure and streak traces, it has been found that this radiant oscillation is in phase with the acoustic oscillation within $\pm 20°$ at 500 cps. The second pattern is evidenced by the release of bands of varying luminosity, parallel to the propellant surface. Since this release occurs at the same frequency as the acoustic oscillation the separation of bands of similar intensity can be related directly to the deflagration rate of the propellant, the average pressure, and the frequency and amplitude characteristics of the imposed acoustic oscillation. The phase relationship between the emergence of the luminous bands and acoustic pressure appears to change with experimental conditions. Data at 500 and 200 cps, at average chamber pressures of 400 and 800 psi, for an ammonium perchlorate–containing plastisol nitrocellulose composite propellant, indicate that the release of luminous bands from the propellant surface generally precedes the pressure maximum, by approximately 180°, and that the phase difference decreases with increase in frequency and decrease in pressure.

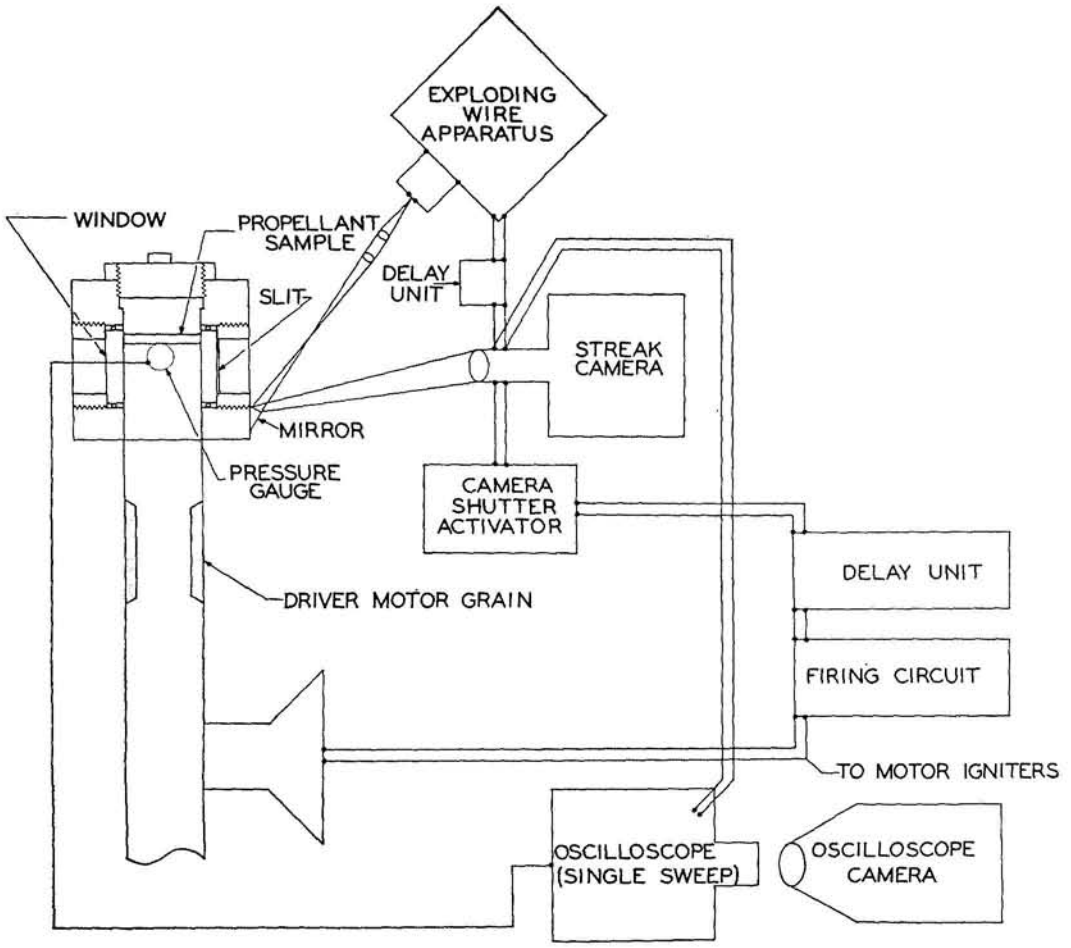

FIG. 4. Schematic of apparatus for observing propellant combustion in a T-motor.

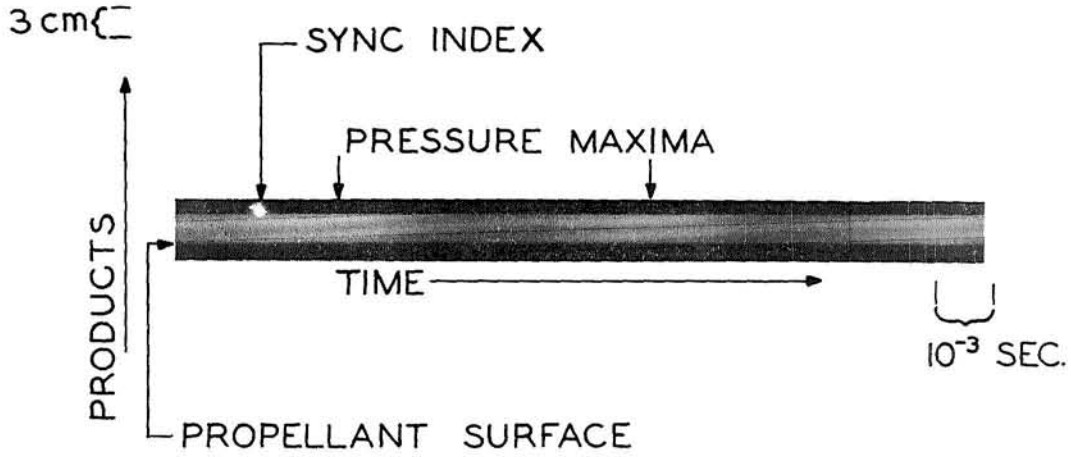

FIG. 5. Typical streak photograph of the gaseous region above a propellant sample burned under oscillatory burning conditions.

Discussion. There are at least three explanations for bands of varying luminosity in the gases above a propellant that is burned under the influence of an oscillatory pressure fluctuation. The first involves the release of strata of gases of varying composition and temperature discussed earlier. Either an increase in average pressure or a decrease in frequency reduces the burning time of ammonium perchlorate particles relative to the period of an imposed oscillation and results in increased phase lags between the thermal and pressure waves. The second involves particle release from the surface. Coupling of the propellant burning rate to the acoustic pressure can lead to an oscillatory rate of particle release and consequently give luminous bands in the gases above the surface corresponding to particle concentration gradients. The third, postulated by Summerfield *et al.*,[8] is based upon the difference in pressure–volume work done by the acoustic oscillation on propellant combustion products having flame temperatures independent of pressure. This mechanism gives rise to thermal waves that are 180° out of phase with the pressure at low frequencies.

At the present time it is not possible to separate the individual contributions of the three mechanisms of luminous band formation described above. At 200 cps the phase relationship of luminous band release to pressure is close to that predicted from the pressure-volume work mechanism. The decrease in lead of luminous band release to pressure with increase in frequency and decrease of average pressure, however, could result from either composition-temperature or particle-release mechanisms or from a combination of the two.

Acknowledgments

This program was conducted under Contract DA-01-021-ORD-12024 with the Office of the Chief of Ordnance, administered by the Army Ordnance Missile Command. The author wishes to extend special acknowledgment to Dr. R. H. Cantrell of the Applied Physics Laboratory, The Johns Hopkins University, for suggesting the method of analytical integration of the surface-area equations.

References

1. Panel Discussion: Solid Propellant Combustion Instability, *Eighth Symposium (International) on Combustion*, p. 904. Williams and Wilkins, 1962.
2. Cheng, S. I.: *ibid*, p. 81.
3. Hart, R. W. and McClure, F. T.: J. Chem. Phys. *30*, 1501 (1959).
4. Barrère, M. and Bernard, J. J.: see reference 1, p. 886.
5. Green, L., Jr.: Jet Propulsion *28*, 386 (1958).
6. Morse, P. M.: *Vibration and Sound*, p. 367. McGraw-Hill, 1948.
7. Hart, R. W. and Cantrell, R. H.: *The Johns Hopkins University Applied Physics Laboratory Report TG-335-11*, April 1962.
8. Summerfield, M., Waesche, R. H. W., and Wenograd, J.: *Aeronautical Engineering Report No. 564-b*. Princeton Univ., Dec. 20, 1961.
9. Sibbett, D. J. and Lobato, J. M.: *Investigation of the Mechanism of Combustion of Composite Solid Propellants, Aerojet General Corporation, AFOSR-TR-60-64*, 1960.
10. Lewis, B., Pease, R. N., and Taylor, H. S.: *Combustion Processes*, Vol. II of *High Speed Aerodynamics and Jet Propulsion*, p. 532. Princeton Univ. Press, 1962.
11. Wimpress, R. N.: *Internal Ballistics of Solid-Fuel Rockets*, p. 4. McGraw-Hill, 1950.
12. Wood, W. A.: *Rohm & Haas Company Quarterly Progress Report No. P-61-7*, Oct. 3, 1961, (Conf.). For original description see Price, E. W. and Sofferis, J.: Jet Propulsion *28*, 109 (1958).

Discussion

Prof. H. Emmons (*Harvard University*): Dr. Wood's theory supposes oxidizer particles which burn as spheres. If both oxidizer and fuel particles were present would the ψ functions show two positions of rapid rise and the resultant burning show two regions of rapid admittance change?

Dr. W. A. Wood (*Rohm & Haas*): The case in which both oxidizer and binder burn as particles has been included in the written text. The frequency-average particle burning time ψ is a function of $(\omega\bar{\tau})$ only and may be used for either binder or oxidizer. If $\bar{\tau}_b$ differs sufficiently from $\bar{\tau}_o$ then the admittance will show two regions of rapid change.

Combustion Involving Solids

Chairman: Dr. D. Altman (*United Technology Corp.*)

Vice Chairman: Dr. P. Nichols (*Aerojet-General Corp.*)

ON THE ANALYSIS OF LINEAR PYROLYSIS EXPERIMENTS

W. NACHBAR AND F. A. WILLIAMS

Linear pyrolysis experimental data have been used as surface boundary conditions in the analytical treatment of solid propellant combustion problems. The surface boundary conditions required for the analysis are functional relationships between normal regression velocity, gaseous reactant density, total pressure, temperature, and possibly derivatives of these quantities as well, evaluated at the interface between condensed and gaseous phases during combustion. Available experimental data indicates that a relation based upon equilibrium conditions prevailing at the interface is not generally valid. There are available for many substances, however, hot-plate linear pyrolysis data which give an explicit relation between regression velocity of the condensed phase and a measured hot-plate temperature. This hot-plate temperature has been assumed to be also the temperature at the interface. However, this assumption is thought in some cases to be questionable. In addition, the use of such a rate law in combustion analysis would imply that the total pressure and the gaseous reactant partial pressures or densities, which are greatly different for the pyrolysis test as compared to the combustion, have a negligible effect on the rate. This implication again is questionable.

The present paper seeks to answer in part these questions on the validity of using linear pyrolysis data. A one-dimensional hot-plate linear pyrolysis experiment is proposed which uses a porous heated plate in place of the present impervious plate. The proposed experiment, having simpler fluid dynamics than present hot-plate experiments, is capable of a reasonably precise analytical description. The analysis is carried out for a general case and is then specialized to simple and chainlike surface gasification processes. Conditions are developed to determine whether the surface process is either a rate process or is one of near-equilibrium. A description is presented of the possible use of data from the proposed pyrolysis experiments to compute the accommodation coefficient and the vacuum sublimation rate as functions of surface temperature. With this information, the surface boundary condition for a given material will then be specified. The pyrolysis rate of potassium chloride is calculated as an example of the use of the derived formulas.

If fluid dynamic effects are not too important in the present experiments, and in some respects it is estimated that they are not, interpretation from the results of this analysis serves present pyrolysis data as well. Interpretations are carried out for a number of compounds which have interest in propellant combustion studies. From published data on ammonium perchlorate, for example, revised values are estimated for the heat of sublimation, for the activation energy in linear pyrolysis, and for the difference between the hot-plate temperature and the surface temperature in linear pyrolysis.

Introduction

Schultz *et al.*[1–6] have reported experiments in which hot-plate pyrolysis techniques are used to measure the linear regression rates of solids undergoing surface heating. These experiments have yielded pyrolysis rate data for many different materials at pressures and temperatures approaching (but not yet equaling) pressures and temperatures encountered in solid propellant rockets. These data are of practical importance in helping to predict, for example, the deflagration rate of pure ammonium perchlorate,[7–12] and thereby in promoting further understanding of the factors controlling the burning rate of composite solid propellants containing ammonium perchlorate. It has also been proposed[13] to use pyrolysis data for actual rocket propellants (if such data is available) to predict burning rates.

The pressure is sufficiently high in these pyrolysis experiments so that the continuum equations of fluid mechanics may be applied to the gas adjacent to the solid. The geometry of the gas flow is so complicated, however, that unquestionable interpretations of the significance of the measurements appear to be difficult to obtain. Consequently, it is of interest to investigate the possibility of modifying these experiments in order to yield data which can be interpreted more easily.

In the present paper there is suggested a modified hot-plate linear pyrolysis experiment which should not be difficult to perform. A mathematical analysis of this experiment is carried out under simplifying assumptions which, in the main, do not appear to be unduly restrictive. However, the reader's attention is directed to the following assumptions made in this analysis. Except for the mathematically thin, plane surface in contact with the hot gas, the condensed phase is assumed here to be in a uniform phase and to be homogeneous. (We will refer in particular to the solid phase in our discussion.) Both gaseous and condensed phases are assumed to exhibit no chemical reaction. These assumptions may not be valid for certain materials under all conditions. There may occur in the solid energetic bulk chemical reactions, at temperatures less than the surface temperature, which transform one solid-phase state into another solid-phase state.[14] There may also occur, as in ammonium perchlorate, for example, a partial decomposition of the solid into a reactant gas plus a solid residue. The plane surface in this latter case is more exactly a layer of finite thickness in which the two phases exist simultaneously. These mechanisms may be important if the linear regression rate of the solid is sufficiently small. There appears to be no essential difficulty, however, in extending the present analysis to the more complex cases where these assumptions are relaxed. The usefulness of such an extension in particular cases will depend upon whether the kinetics of the condensed-phase reactions and the degree of nonhomogeneity are known.

Conditions under which the surface process is either a rate process or is one of near-equilibrium are determined for the modified experiment from our analysis, and interpretations of the significance of the measurements are given for these two limiting cases. The pyrolysis rate of potassium chloride is computed as an example. The mathematical simplicity of the system described here provides a strong incentive to construct such an apparatus for measuring regression rates. A degree of similarity of the present model to the previous hot-plate linear pyrolysis experiments also makes it possible to draw some conclusions concerning the previous measurements.

The Modified Experiment

It is suggested that the impervious hot plate used in previous pyrolysis experiments be replaced by a porous hot plate. If suitable shielding can be provided to prevent gas from escaping without passing through the porous plate, then the flow would be approximately one-dimensional, and the arrangement would appear as illustrated in Fig. 1. The solid is assumed to be converted to gas at x equals 0, and the gas flows through the porous plate at x equals l, where l is the normal distance between the surface and the inner face of the porous plate. Steady-state conditions are assumed. For convenience in the analysis, the solid is considered to be semi-infinite. At x equals $-\infty$, the solid has a density ρ_π and a velocity v_π directed towards the interface, which remains stationary.

In analyzing this experiment, the gas-phase and the interface conditions will be considered in that order. The momentum conservation equation is considered in the Appendix. The solid sample is assumed to be homogeneous and nonreactive for $x < 0$.

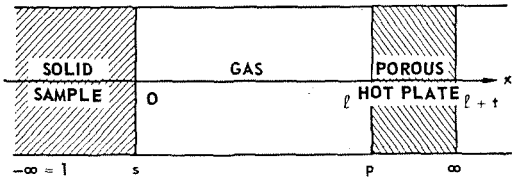

FIG. 1. Schematic diagram of modified pyrolysis experiment.

The one-dimensional, steady-state equations on $0 < x < l$ for conservation of total mass, mass of species K (in the absence of gas-phase chemical reactions), and energy of a mixture of N species of ideal gases are, respectively[15]:

$$\rho v = \dot{m} = \rho_\pi v_\pi = \text{constant} \tag{1}$$

$$\dot{m}\frac{dY_K}{dx} = \frac{d}{dx}\left(\rho D \frac{dY_K}{dx}\right), \quad K = 1, \cdots, N \tag{2}$$

and

$$\dot{m}\frac{dH}{dx} = \frac{d}{dx}\left(\rho D \frac{dH}{dx}\right) \tag{3}$$

Equation (2) implies that the binary diffusion coefficients of all pairs of chemical species are equal. Equation (3) relies upon this assumption, the approximation that the Lewis number is unity ($\lambda = \rho D \bar{c}_p$), and the assumption that either the mass diffusivity equals the effective coefficient of viscosity ($\eta = \rho D$) or the kinetic energy is negligible in comparison to the thermal plus chemical energy:

$$([\tfrac{1}{2}v^2(R_1/R_3)] \ll h)$$

It is to be noted $\bar{c}_p$, λ, and ρD may depend upon both T and Y_K in this formulation. When the energy flux at $x = -\infty$ is equated to the energy flux at $x = 0+$, and when the conditions $T = T_i$ and $(dH/dx) = 0$ are imposed at $x = -\infty$, the equation

$$\dot{m}[h_\pi(T_i) + (R_1/R_3)\tfrac{1}{2}v_\pi^2] = \dot{m}\left[\sum_{K=1}^{N} Y_{K,s}h_K(T_s) + (R_1/R_3)\tfrac{1}{2}v_s^2\right] - [\rho D(dH/dx)]_s \tag{4}$$

is obtained. This relation is a boundary condition for Eq. (3), and it is written as

$$\left(\rho D \frac{dH}{dx}\right)_s = \dot{m}J \tag{5}$$

Conservation of mass across the phase interface requires that the net flux (i.e., mass per unit area per second) of species K leaving the surface to be equal to $\dot{m}\epsilon_K$, which is the mass flux of species K produced in the gasification process. The ϵ_K's are the mass flux fractions of species K in the decomposition of the solid, and they are determined by the over-all stoichiometry of the gasification process. With this boundary condition at x equals 0, the following integrals of Eq. (2) are obtained

$$\dot{m}Y_K - \rho D(dY_K/dx) = \dot{m}\epsilon_K, \quad K = 1, \cdots, N \tag{6}$$

Denoting the boundary values of Y_K and H at x equals l as Y_p and H_p, one finds the solutions to Eqs. (3), (5), and (6) to be

$$H(\xi) = H_p - J[\exp(\xi_p) - e^{\xi}] \tag{7}$$

and

$$Y_K(\xi) = Y_{K,p}\exp(\xi - \xi_p) + \epsilon_K[1 - \exp(\xi - \xi_p)], \quad K = 1, \cdots, N \tag{8}$$

where

$$\xi \equiv \dot{m}\int_0^x [dx/\rho D] \tag{9a}$$

$$\xi_p \equiv \dot{m}\int_0^l [dx/\rho D] \tag{9b}$$

While the experimenter often has direct control over the plate temperature T_p, the values of $Y_{K,p}$ [which are needed along with T_p to determine H_p and Y_p in Eqs. (7) and (8)]* will basically be determined by a permeability P_K of the porous plate of species K and by the partial pressure $p_{K,\infty}$ of species K on the downstream side of the plate. A reasonable phenomenological expression is obtained by assuming that the mass flux $\dot{m}\epsilon_K$ for each species is proportional to the pressure difference across the plate for each species, *viz.*

$$\dot{m}\epsilon_K = \frac{P_K}{t}\left(\frac{Y_{K,p}\bar{W}_p p_p}{W_K} - p_{K,\infty}\right) \quad K = 1, \cdots, N \tag{10}$$

Here p_p is the total pressure at $x = l$, t is the thickness of the porous plate, and the first term inside the bracket is the partial pressure p_K of the species K at $x = l$. The mass-average molecular weight of the gases at $x = l$ is $\bar{W}_p$:

$$\bar{W}_p = \left[\sum_{K=1}^{N} (Y_{K,p}/W_K)\right]^{-1}$$

Equation (10) can be put into a convenient, nondimensional form by introducing a characteristic pressure p^*, defined as

$$p^* \equiv t\sum_{K=1}^{N} (\epsilon_K/P_K) \Big/ \int_0^l \frac{dx}{\rho D}, \tag{11}$$

and a ratio σ, which is a measure of p_p and which is defined as

$$\sigma = p^*/p_p \tag{12}$$

* Strictly speaking, either v_p must also be measured or the momentum equation (see Appendix) must be solved in order to determine completely the constants in Eq. (7). However, the kinetic energy will usually be negligibly small.

In view of these definitions and of Eq. (9b), Eq. (10) is written as

$$\frac{\bar{W}_p}{W_K} Y_{K,p} = \sigma \left[\frac{(\epsilon_K/P_K)}{\sum_{J=1}^{N} \epsilon_J/P_J} \xi_p + \frac{p_{K,\infty}}{p^*} \right] \qquad K = 1, \cdots, N \quad (13)$$

Although only $N - 1$ of the $Y_{K,p}$ are linearly independent, the N relations in Eq. (13) are independent, since summing Eq. (13) over all N species gives the nontrivial equation

$$1 = \sigma \left(\xi_p + \frac{p_{,\infty}}{p^*} \right) \quad (14)$$

where $p_{,\infty}$ is the total pressure maintained on the downstream side of the plate, *viz.*

$$p_{,\infty} = \sum_{K=1}^{N} p_{K,\infty} \quad (15)$$

A general boundary condition at the solid surface is now obtained for each of the species evolved in the gasification of the solid. Let the species numbering be so ordered that, if M is an integer, $0 < M \leq N$, then the first M species in the gas are evolved from the decomposition of the solid. Consequently, $K = M + 1, \cdots, N$ denotes the chemically inert species in the pressurizing gas which are present at the surface through diffusion. If $M = N$, there are no inert species. It follows that $\epsilon_K = 0$, by definition, for the inert species $K = M + 1, \cdots, N$. The general boundary condition for the evolved species is obtained by equating the net surface mass flux $\dot{m}\epsilon_K$ of each species to the difference between the vacuum sublimation rate w_K, which is the mass flux of the species leaving the surface, and the mass flux of the species entering the surface,[16–19]

$$\dot{m}\epsilon_K = w_K - \alpha_K Y_{K,s}(\rho c_K)_s \qquad K = 1, \cdots, M \quad (16a)$$

$$\epsilon_K = 0 \qquad K = M + 1, \cdots, N \quad (16b)$$

Here α_K is a surface accommodation coefficient for species K,

$$c_K = [(R_3 T_s)/(2\pi W_K)]^{\frac{1}{2}} \quad (17)$$

is the average velocity of molecules of species K (of the ideal gas mixture) in the $-x$ direction at the surface, and

$$\rho = p\bar{W}/(R_2 T) \quad (18)$$

according to the ideal gas law. In general, the w_K and α_K may be functions of T_S, p_S, and all the $Y_{K,s}$'s for complex surface processes. Equation (16a) may be written in the nondimensional form

$$\xi_p \epsilon_K = \beta_K(\omega_K - Y_{K,s}), \qquad K = 1, \cdots, M \quad (19)$$

where

$$\beta_K \equiv \alpha_K(\rho c_K)_s \int_0^l [dx/(\rho D)] \quad (20)$$

$$\omega_K \equiv w_K[\alpha_K(\rho c_K)_s]^{-1} \quad (21)$$

From Eq. (19) it follows that, in general, the surface process with respect to any evolved species K will be a rate process, similar to that encountered in vacuum vaporization or sublimation experiments[19–21] if the following condition holds:

$$(Y_{K,s}/\omega_K) = 1 - (\xi_p \epsilon_K/\omega_K \beta_K) \ll 1 \quad (22)$$

At the opposite extreme, near-equilibrium conditions will prevail for an evolved species K at the surface if $(Y_{K,s}/\omega_K) \sim 1$, that is, if

$$(\xi_p \epsilon_K/\omega_K \beta_K) \ll 1 \quad (23)$$

General Equations for Determination of Pyrolysis Rate

The simple geometry of the modified pyrolysis experiment, and the simplifying assumptions which have been made in the analysis, allow the temperature and concentrations at each point of the gas to be expressed in an elementary form by Eqs. (7) and (8). The constants or parameters appearing in these equations must be determined uniquely with the use of the boundary conditions, however, in order to determine a unique solution. In order to do this, certain of the parameters must be known either from predetermined physical properties or from measurements taken during the pyrolysis experiment. Which of the parameters fall into this class is somewhat arbitrary. We will assume at first that the unknown parameters are:

$$\{Y_{K,p}\}, \{Y_{K,s}\}, \{\epsilon_K\}, T_s, \sigma, \xi_p \quad (24)$$

The notation $\{(\ )_K\}$ stands for the set $(\ )_K$, $K = 1, \cdots, N$. Since there are $3N + 3$ unknown parameters in group (24), then the same number of independent equations must exist to determine them. Evaluating Eqs. (7) and (8) at ξ equals 0 gives $N + 1$ of these equations, *viz.*

$$Y_{K,s} = Y_{K,p} \exp(-\xi_p) + \epsilon_K[1 - \exp(-\xi_p)] \qquad K = 1, \cdots, N \quad (25)$$

$$H_s = H_p - J[\exp(\xi_p) - 1] \quad (26)$$

Note that the identity

$$\sum_{K=1}^{N} \epsilon_K = 1$$

is implied by the summation of Eqs. (25) from $K = 1$ to $K = N$.

Equations (13), (16b), (19), (25), (26) and the two identities

$$\sum_{K=1}^{N} Y_{K,s} = \sum_{K=1}^{N} Y_{K,p} = 1 \qquad (27)$$

constitute a set of $(3N + 3)$ transcendental equations to determine the unknown parameters in (24). For this problem it is assumed that $\{P_K\}$, $\{W_K\}$, and t are predetermined constants for an experiment, that l, p_S, $\{p_{K,\infty}\}$, T_i, and T_p are parameters measured in the experiment, and that $\bar{c}_p$, ρD, J, $\{\beta_K\}$, and $\{w_K\}$ are known functions of these parameters and of the parameters in group (24). If all of this information is given, then one could, for instance, compute the pyrolysis rate v_π expected in a pyrolysis test as a function of the plate temperature T_p and the downstream pressure $p_{,\infty}$. A numerical example of such a computation is given in one of the following sections.

The application of the hot-plate, linear-pyrolysis test results to practical problems which have been its chief motivation is not nearly so straightforward, however. An important practical problem is to obtain, for solid propellant constituents, the data which enter into the general surface conditions, Eqs. (16), so that these equations can be used to compute propellant deflagration rates from a combustion theory. If $\{w_K\}$ and $\{\alpha_K\}$ are known functions, however, as was implied in the paragraph just preceding, then it would not be necessary, for application to this particular combustion problem at least, to perform the pyrolysis test. The necessary parameters for the general surface conditions, Eqs. (16), would be determined already. However, the central difficulty of this problem is that the data necessary to evaluate Eqs. (16) for propellant constituents are not usually available, and especially not for the range of surface temperatures obtained in deflagration. To apply Eqs. (16) to the propellant combustion problem, we should ideally like to be able to calculate from the linear pyrolysis data the vacuum sublimation rates $\{w_K\}$ and the surface accommodation coefficients $\{\alpha_K\}$ as functions of T_S, p_S, and $\{Y_{K,S}\}$. Data from previous pyrolysis experiments[1–6] (i.e., v_π as function of T_p for fixed $p_{,\infty}$) has not been applied to the calculation of these functions, however. Such application would appear to be generally quite difficult to perform in an unequivocal way because of the complicated geometry of the gas flow. The modified pyrolysis experiment suggested in the present paper has certain advantages in this application, and this will be demonstrated in the following sections.

Simple, Chainlike Surface Processes

The equations which are developed in the preceding two sections are now reduced to a much simpler set by the introduction of the following additional assumptions.

a. The surface process is simple, that is, the α_K and w_K are functions only of T_s (i.e., independent of p_s and $\{Y_{K,s}\}$).

b. The surface process is chainlike, meaning that parallel, competing surface reactions do not occur. A consequence of this assumption is that the ϵ_K are constants—independent of T_s, p_s, and $\{Y_{K,s}\}$—and each ϵ_K will be assumed to have a known value.

c. The molecular weights of the gaseous species are all equal to a common molecular weight $\bar{W}$.

d. Changes in kinetic energy are neglected in comparison to changes in thermal energy to a first approximation (higher approximation can be computed through integration of the momentum equation).

e. The isobaric heat capacities of all species are equal to an average value of the mixture heat capacity $\bar{c}_p$ between T_s and T_p.

Let the process indicated in (*b*) above be represented by

$$M_\pi(c) \rightleftarrows \sum_{K=1}^{M} \nu_K' M_K(g) \qquad (28)$$

The ν_K''s are the fixed number of moles of species K produced per mole of solid; as a consequence of (*b*) and (*c*) above,

$$\epsilon_K = \nu_K' \left[\sum_{K=1}^{M} \nu_K' \right]^{-1}$$

Consider Eq. (28) in equilibrium at a fixed T_s; let $p_{K,e}$ be the equilibrium partial pressure of species K, and let p_e be the total equilibrium pressure of all evolved species:

$$p_e = \sum_{K=1}^{M} p_{K,e}$$

As a consequence of the chainlike assumption (*b*),

$$p_{K,e} = \epsilon_K p_e \qquad K = 1, \cdots, M, \qquad (29)$$

the enthalpy difference $\Delta Q(T_s)$ corresponding to Eq. (28) is, per unit mass of solid,

$$\Delta Q(T_s) = \sum_{K=1}^{M} \epsilon_K h_K(T_s) - h_\pi(T_s)$$

Hence, the Van't Hoff equation for the equilibrium (28) is written as

$$d\left[\ln \prod_{K=1}^{M} (p_{K,e})^{\nu_K'}\right] = W_\pi \, \Delta Q \, dT_s/(R_1 T_s^2) \tag{30}$$

The chainlike assumption means $d(\nu_K') = 0$, $K = 1, \cdots, M$. Since mass conservation requires

$$W_\pi = \bar{W} \sum_{K=1}^{M} \nu_K'$$

then the following integral of Eq. (30) expresses p_e as a function of T_s only:

$$p_e(T_s) = p_e(T_r) \exp\left[-\int_{T_s}^{T_r} \frac{\bar{W} \, \Delta Q}{R_1 T^2} \, dT\right] \tag{31}$$

Here T_r is an arbitrary reference temperature at which p_e is known.

These results are now applied to Eqs. (19). The quantities β and ω, which are functions only of T_s [cf., Eqs. (17), (18), (20), (21), (31), and assumption (a)], are defined as

$$\beta(T_s) = \frac{p_e}{p_s}\left[\sum_{K=1}^{M} (\epsilon_K/\beta_K)\right]^{-1} \tag{32}$$

$$\omega(T_s) = \frac{p_s}{p_e} \sum_{K=1}^{M} \omega_K \tag{33}$$

The summation of Eqs. (19) over $K = 1, \cdots, M$ then gives the equation

$$\xi_p = \beta\left(\omega - \frac{Y_s p_s}{p_e}\right) \tag{34}$$

where Y, defined as

$$Y \equiv \sum_{K=1}^{M} Y_K$$

is the total mass fraction of the evolved species. But $Y_s p_s$ in Eq. (34) is the partial pressure of the evolved species at the surface. For fixed T_s, ξ_p (or $\dot{m}$) varies only with $Y_s p_s$, and as $Y_s p_s \to p_e$, the equilibrium requirement is $\xi_p \to 0$. It must therefore follow (under the assumptions already made) that $\omega(T_s) \equiv 1$ for all T_s. Using this result, together with Eqs. (17), (18), (21), and (33), we find the following equation to hold:

$$\left[\frac{R_2^2 T_s}{2\pi R_3 \bar{W}}\right] \sum_{K=1}^{M} \frac{w_K(T_s)}{\alpha_K(T_s)} = p_e(T_s) \tag{35}$$

Returning now to the development of a simplified set of equations, we find it convenient, as a consequence of assumptions (d) and (e), to define the nondimensional parameter τ,

$$\tau \equiv \frac{H_p - H_s}{J} = \frac{\bar{c}_p(T_p - T_s)}{\Delta Q(T_s) + h_\pi(T_s) - h_\pi(T_i)} \tag{36}$$

as a measure of T_s. The last equality in Eq. (36) can be derived from Eqs. (5), (25), and (26). For typical endothermic surface reactions, it is usually the case that $\tau \ll 1$. It is the case in many of the pyrolysis experiments reported previously.

The first two of the following set of equations are obtained by summing Eqs. (13) and (25) from $K = 1, \cdots, M$; the third is obtained from Eq. (34); the fourth from Eq. (14) and the fifth from Eq. (26).

$$Y_p = \sigma[\xi_p + (p_{M,\infty}/p^*)] \tag{37a}$$

$$1 - Y_s = (1 - Y_p) \exp(-\xi_p) \tag{37b}$$

$$\xi_p = \beta[1 - (Y_s p_s/p_e)] \tag{37c}$$

$$1 = \sigma[\xi_p + (p_{,\infty}/p^*)] \tag{37d}$$

$$\tau = \exp(\xi_p) - 1 \tag{37e}$$

In Eq. (37a),

$$p_{M,\infty} \equiv \sum_{K=1}^{M} p_{K,\infty}$$

Equations (37a, b, c, d) may be combined to eliminate Y_p and Y_s; the result is the equations

$$\xi_p + \frac{p_{,\infty}}{p^*} - \frac{p_p}{p_s}\frac{p_e}{p^*}\left(1 - \frac{\xi_p}{\beta}\right) = \left(\frac{p_{,\infty} - p_{M,\infty}}{p^*}\right) \times \exp(-\xi_p) \tag{38a}$$

$$p_p/p^* = \xi_p + (p_{,\infty}/p^*) \tag{38b}$$

An approximate solution of the preceding equations is now obtained in order to discuss the physical aspects of these results. It is now assumed that $\tau \ll 1$, and so it follows from Eq. (37e) that

$$\tau \simeq \xi_p \ll 1 \tag{39}$$

As a first approximation we set p_s equal to p_p (see Appendix). Then, neglecting terms which are of higher order than the first power of τ, Eq. (38a) may be shown to take the following form; it is understood that p_e and β are evaluated at the plate temperature T_p in this expression:

$$\xi_p = \frac{p_e - p_{M,\infty}}{[p^* + p_{,\infty} - p_{M,\infty} + p_e(\beta^{-1} + A)]} \tag{40}$$

where

$$A \equiv \frac{\bar{W} \, \Delta Q(T_p)}{\bar{c}_p R_1 T_p^2}\left[\sum_{K=1}^{M} \epsilon_K h_K(T_p) - h_\pi(T_i)\right]$$

For simplicity of presentation, we will neglect A as small compared to β^{-1}, and we will also neglect $p_{M,\infty}$ with respect to both p_e and $p_{,\infty}$.

The limiting criteria for the surface process (cf. Eqs. (22) and (23)) are $(\xi_p/\beta) \sim 1$ for a rate

process and $(\xi_p/\beta) \ll 1$ for a near-equilibrium process. We may then write from Eq. (40):

$$(\xi_p/\beta) = [1 + (p^* + p_{,\infty})(\beta/p_e)]^{-1} \quad (41)$$

The limiting criteria are therefore

$$(p^* + p_{,\infty})(\beta/p_e) \ll 1$$

for a rate process, and $(p^* + p_{,\infty})(\beta/p_e) \gg 1$ for a near-equilibrium process. An expression for (β/p_e) follows from Eqs. (17), (18), (20), and (32); again for simplicity, we restrict attention to the case $M = 1$:

$$\frac{\beta}{p_e} = \alpha \sqrt{\frac{R_3 W_1}{2\pi (R_2)^2 T_s}} \int_0^l \frac{dx}{\rho D} \quad (42)$$

In most present pyrolysis experiments,[1–6] experimental conditions are approximately equivalent to setting $p^* + p_{,\infty}$ equal to $p_{,\infty}$ equal to 1 atm. Surface temperatures are assumed to be in the range $300°\text{K} \lesssim T_s \lesssim 900°\text{K}$, and for reasonable ρD and $W_1(\rho D \approx 5 \times 10^{-4}$ g/cm sec, $W_1 \approx 75$ g/mole) it follows from Eq. (42) that

$$\frac{\beta}{p_e \alpha l} = 5 \times 10^3 \ (\text{cm}^{-1})$$

within a factor of 10. Since it is expected that one mean free path $\sim 10^{-5}$ cm, it is therefore estimated that 10^{-5} cm $\leq l \leq 10^{-2}$ cm, and it follows that

$$0.05\alpha \leq (p^* + p_{,\infty}) \frac{\beta}{p_e} \leq 50\alpha$$

Hence, for simple, chainlike surface processes with $\tau \ll 1$, the surface process will probably be near equilibrium for α equals 1 and a rate process for $\alpha < 0.01$.

We now discuss the determination of accommodation coefficients and vacuum sublimation rates, of substances for which these functions are not known, by means of the modified hot-plate, linear-pyrolysis test proposed in this paper. For this purpose we restrict attention to simple, chainlike surface processes for which $M = 1$, and base this discussion on the simplified set of Eqs. (41) and (42). There are to be varied at our disposal in this experiment the dimensions and porosity of the hot plate, which are incorporated into the characteristic pressure p^*, the pressure $p_{,\infty}$ maintained on the downstream face of the hot plate, the hot-plate temperature T_p, and possibly also the sample spacing l.

It is proposed that suitable ranges of values for these parameters be found so that, on any one given material, two series of tests may be performed: one has the surface process for the test series as a rate process; the other has the surface process as near-equilibrium. From Eq. (41) and the subsequent discussion, it follows that, in the rate process $\beta \cong \xi_p$, while in the equilibrium process $p_e \cong (p^* + p_{,\infty})\xi_p^{-1}$. Hence, if $\dot{m}$ is measured as a function of T_p, then we determine $p_e(T_s)$ in the surface-equilibrium test series, and we determine $\beta(T_s)$ in the surface rate-process test series. Using this data we can determine $\alpha(T_s)$ from Eq. (42) and $w(T_s)$ from Eq. (35).

Pyrolysis Rate of Potassium Chloride

As an example of the application of the preceding analysis we shall consider KCl, one of the few materials whose properties are sufficiently well known to permit an *a priori* calculation of the pyrolysis rate. Sublimation of KCl is a simple chainlike surface process (reference 23). In Fig. 2, the theoretical pyrolysis rate is plotted as a function of the plate temperature T_p for various values of l.

The computation was made from Eq. (40) with $p^* + p_{,\infty}$ equal to 1 atm, $p_{M,\infty}$ equal to 0, and T_i equal to 300°K. Here (references 23, 24,

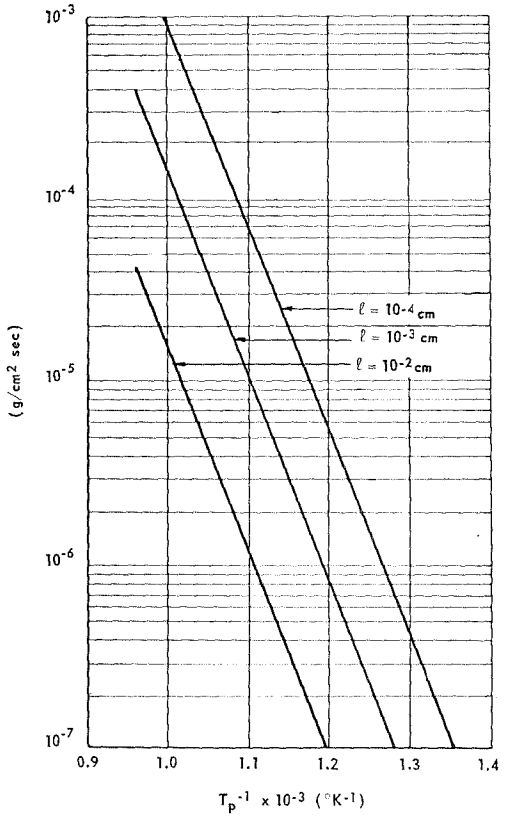

FIG. 2. Linear pyrolysis rate of potassium chloride.

and 25) $\bar{c}_p = 0.117$ cal/gm°K, $h_\pi(T_s) - h_\pi(T_i) = 0.166(T_s - T_i)$ cal/gm, $\Delta Q = 693$ cal/gm, $\rho D = 5 \times 10^{-4}$ gm/cm sec, $\alpha = 0.63$, and $p_e = 6.4 \times 10^7 \exp(-26{,}070/T_s)$ atm. The computations were completed only for T_s less than the melting point (1049°K). The results imply that surface equilibrium exists (provided $l > 10^{-5}$ cm). Since it was always found that $T_p - T_s < 5$°K, Eq. (40) is actually valid here, and a pyrolysis rate measurement yields the equilibrium sublimation pressure.

Remarks on the Interpretation of Pyrolysis Experiments on Ammonia Salts

Schultz and co-workers have reported linear-pyrolysis rate measurements for NH_4Cl,[1,2] NH_4NO_3,[5] and NH_4ClO_4,[6] and have given consistent interpretations of their results on the basis of absolute reaction-rate theory.[1,5,26] These interpretations rely upon the assumption that the surface process is an unopposed rate process (i.e., surface conditions are far from equilibrium). Our previous analysis of the surface process indicates that, under certain conditions, surface equilibrium may be approached in these experiments. In this section, we apply some of our preceding results to the interpretation of these pyrolysis-rate measurements, and we suggest an alternative hypothesis, concerning the nature of the surface process, which leads to a simple explanation of the pyrolysis results whether the surface process is near or far from equilibrium. Since our preceding results were derived for a modified pyrolysis experiment, we will find it necessary in the following discussion to consider the extent to which the results that we use are applicable to the previous pyrolysis experiments.

Difference between Plate Temperature and Surface Temperature. In the previous interpretations of the pyrolysis experiments it has been assumed that the plate and surface temperatures are approximately equal in order to compute activation energies for the surface process. It appears reasonable that in the pyrolysis experiments heat is transferred from the hot plate to the solid surface across the gas film by a conduction process which is essentially one-dimensional. If this is the case, then the difference between the plate temperature T_p and the surface temperature T_s can easily be estimated in terms of the observed pyrolysis rate. The appropriate one-dimensional heat conduction equation has, in fact, been solved in Eq. (7), and the result is given by Eq. (37e), since the pyrolysis rates are so small that kinetic energy and viscous dissipation are negligible. It can be shown that Eq. (37e), with τ given by Eq. (36), relies upon none of the aspects of our preceding model except the heat-transfer equation.

The pyrolysis results,[2,5,6] are

$$\dot{m}/\rho_\pi = 120 \exp\left[-13{,}500/(R_1 T_p)\right] \text{ cm/sec} \quad (629°\text{K} < T_p < 807°\text{K}) \quad (43a)$$

for NH_4Cl,

$$\dot{m}/\rho_\pi = 120 \exp\left[-7100/(R_1 T_p)\right] \text{ cm/sec} \quad (453°\text{K} < T_p < 573°\text{K}) \quad (43b)$$

for NH_4NO_3, and

$$\dot{m}/\rho_\pi = 4600 \exp\left[-20{,}000/(R_1 T_p)\right] \text{ cm/sec} \quad (753°\text{K} < T_p < 903°\text{K}) \quad (43c)$$

for NH_4ClO_4.

Since ρ_π is 1.527 gm/cm³ for NH_4Cl, 1.725 gm/cm³ for NH_4NO_3, and 1.95 gm/cm³ for NH_4ClO_4, Eqs. (43) imply that $\dot{m}$ never exceeds 0.35 gm/cm² sec. Utilizing the reasonable values that $\rho D = 5 \times 10^{-4}$ gm/cm sec and $l = 10^{-4}$ cm, we find

$$\xi_p \equiv \dot{m} \int_0^l \left[dx/(\rho D)\right] \ll 1,$$

whence Eq. (39) is valid. With the reasonable estimate $\bar{c}_p = 0.2$ cal/gm°K, the dimensional form of Eq. (39) becomes

$$(T_p - T_s) = \dot{m}\left[\Delta Q + h_\pi(T_s) - h_\pi(T_i)\right] \quad (44)$$

where use has been made of Eq. (36).

The quantity in the square brackets in Eq. (44) may be computed from the relations

$$\Delta Q = \Delta H / W_\pi \quad (45)$$

and

$$h_\pi(T_s) - h_\pi(T_i) = c_{p,\pi,1}(T_t - T_i) + \Delta h_t + c_{p,\pi,2}(T_s - T_t) \quad (46)$$

where ΔH is the enthalpy change in the gasification of one mole of the salt, T_t is a temperature at which a phase transition of the sample occurs, Δh_t is the heat of transition per unit mass, and $c_{p,\pi,1}$ and $c_{p,\pi,2}$ are the heat capacities of the sample below and above the transition temperature, respectively. For NH_4Cl,[25,27–29] $W_\pi = 53.5$ gm/mole, $T_t = 457.6$°K (a solid phase transition), $\Delta h_t W_\pi = 1000$ cal/mole, $c_{p,\pi,1} W_\pi = 20.1$ cal/mole °K, and $c_{p,\pi,2} W_\pi = 22.3$ cal/mole °K; for NH_4NO_3 (references 25, 29, 30), $W_\pi = 80$ gm/mole, $T_t = 442.8$°K (melting), $\Delta h_t W_\pi = 1300$ cal/mole, $c_{p,\pi,1} W_\pi = 43.5$ cal/mole °K, and $c_{p,\pi,2} W_\pi = 38.5$ cal/mole °K; for NH_4ClO_4,[25] $W_\pi = 117.5$ gm/mole, $T_t = 513$°K (a solid phase

transition) but since heat of transition data and heat-capacity data appear to be absent, it will be assumed that $\Delta h_t \approx 0$, $c_{p,\pi,1} \approx c_{p,\pi 2} \approx 0.5$ cal/gm °K; and $T_i = 300$°K in all cases. Utilizing this data and Eqs. (43)–(46), one can solve for $(T_p - T_s)$ as a function of T_p for all three salts, provided ΔH values are known.

Using the values of ΔH given in Eqs. (48) (based on our alternative hypothesis concerning the surface process) we find that $(T_p - T_s)$ varies from 1°K at T_p equals 629°K to 14°K at T_p equals 807°K for NH_4Cl, from 9°K at T_p equals 453°K to 80°K at T_p equals 573°K for NH_4NO_3, and from 3°K at T_p equals 753°K to 40°K at T_p equals 903°K for NH_4ClO_4. Thus, the assumption $T_p \approx T_s$ is approximately valid for NH_4Cl, invalid for NH_4NO_3, and poor for NH_4ClO_4. It is interesting that the variation in $(T_p - T_s)$ is such that the experimental checks employed indicate that the approximation $T_p \approx T_s$ is valid; e.g., $(T_p - T_s)$ is relatively small at the melting point of NH_4NO_3, so that the break in the pyrolysis curve would occur at a value of T_p near the melting point.

If the larger ΔH values in Eqs. (47) (which are usually assumed to hold) are used instead of those in Eqs. (48), then the calculated values of $(T_p - T_s)$ are roughly doubled; it is clear that they must increase since the term $\dot{m}\Delta H/W_\pi$ enters on the right-hand side of Eq. (44). The estimate of $\rho D\bar{c}_p$ used in this calculation should not be wrong by more than a factor of 5 and therefore cannot substantially modify our conclusion. Varying l does not alter the conclusion; if l is increased the estimate of $(T_p - T_s)$ increases [see Eq. (37e)], while when l is decreased free molecule heat conduction sets in and the estimate of $(T_p - T_s)$ changes very little. The result that $(T_p - T_s)$ increases substantially as T_p increases for NH_4NO_4 and NH_4ClO_4 appears to be inescapable. A theoretical analysis by Cantrell,[31] in which a thin-film lubrication theory was used to account for the non-one-dimensional flow effects in pyrolysis experiments, also supports the contention that $(T_p - T_s)$ is not small.

The main effect of the difference $(T_p - T_s)$ is to modify the computed activation energy for the interpretation corresponding to Eqs. (47), and to modify the ΔH values for the interpretation corresponding to Eqs. (48). For NH_4Cl, NH_4NO_3, and NH_4ClO_4, respectively, the corrected activation energies would be roughly 14 kcal/mole, 30 kcal/mole, and 30 kcal/mole and the corrected heats of sublimation would be very roughly 14 kcal/mole, 25 kcal/mole, and 25 kcal/mole.

Alternative Interpretation of Pyrolysis Experiments. Other investigators have assumed that in the pyrolysis of ammonia salts the over-all surface process is one of dissociation,[2,5,6] *viz.*,

$$NH_4Cl(s) \rightarrow NH_3(g) + HCl(g) \qquad \Delta H = 40.3 \text{ kcal/mole} \quad (47a)$$

$$NH_4NO_3(l) \rightarrow NH_3(g) + HNO_3(g) \qquad \Delta H = 39.8 \text{ kcal/mole} \quad (47b)$$

and

$$NH_4ClO_4(s) \rightarrow NH_3(g) + HClO_4(g) \qquad \Delta H = 56 \text{ kcal/mole} \quad (47c)$$

This hypothesis is supported by some evidence for dissociation in vacuum sublimation experiments.[1,5,14,26–28,30] The ΔH values listed here are obtained mainly from equilibrium vapor-pressure measurements,[27–30] except in the case of NH_4ClO_4 for which ΔH must be calculated from the heats of formation since no vapor-pressure measurements exist.

In the pressure and temperature range of the pyrolysis experiments, it may be true that either (1) the equilibrium composition is one with a negligible amount of dissociation, or (2) dissociation occurs in a gaseous process, the rate of which is small compared with the rate of escape of the gas from the film between the plate and the sample. In either of these cases, the over-all surface process would be sublimation to the associated vapor. If the surface processes are simple chainlike processes such as that encountered in KCl sublimation, then our previous analysis suggests that the temperature dependence of the pyrolysis rate would determine the heat of sublimation regardless of the importance of the fluid-transfer processes. The restriction to simple chainlike surface processes can be removed if surface equilibrium prevails in the pyrolysis experiments.

When the correction for $T_p \neq T_s$ is neglected, Eqs. (43) would then imply that

$$NH_4Cl(s) \rightarrow NH_4Cl(g) \qquad \Delta H = 13.5 \text{ kcal/mole} \quad (48a)$$

$$NH_4NO_3(l) \rightarrow NH_4NO_3(g) \qquad \Delta H = 7.1 \text{ kcal/mole} \quad (48b)$$

and

$$NH_4ClO_4(s) \rightarrow NH_4ClO_4(g) \qquad \Delta H = 20 \text{ kcal/mole} \quad (48c)$$

respectively, in the temperature ranges indicated in Eqs. (43). Although these conclusions seem reasonable because of the similarity between our proposed modified pyrolysis experiment and the experiments of Schultz and co-workers, the present conclusions lack the rigor of those in the previous subsection.

Finally, we shall briefly discuss each material

separately, pointing out arguments for and against the hypotheses leading to the processes given in Eqs. (48).

NH_4Cl: Since the pyrolysis data[2] yields the same activation energy as the vacuum sublimation data[27] and the low-pressure equilibrium appears at present almost certainly to involve entirely dissociated NH_4Cl in the gas,[28] our interpretation will be valid only if hypothesis (2) of one of the previous paragraphs holds true. The large effect of H_2O in catalyzing the decomposition,[28] and the absence of H_2O from the dried NH_4Cl samples used in the pyrolysis experiments,[1] make it probable that the gas-phase dissociation is slow.

NH_4NO_3: In pyrolysis NH_4NO_3 melts before gasification, and a change in the mechanism of gasification at the melting point causes the break in the experimental pyrolysis curve.[5] Since there exists some evidence that in equilibrium the gas is completely dissociated,[30] hypothesis (2) seems more plausible than (1) for the temperature range of the pyrolysis experiments.

NH_4ClO_4: In spite of the large amount of recent work on NH_4ClO_4, [for example, *The Eighth International Symposium on Combustion*, Williams and Williams Co., Baltimore, 1962, and also other papers of the present symposium] there appears to be no conclusive experimental information to eliminate hypothesis (1) or (2). A number of investigators (e.g., reference 14) have cited experimental evidence which is consistent with the assumption of dissociated vapor at equilibrium, but all of this evidence is equally consistent with the hypothesis of associated vapor. Since Galwey and Jacobs[32] concluded from theoretical considerations that the equilibrium vapor should exhibit a tendency toward association, hypothesis (1) may be valid. If Eq. (48c) is correct, then the pyrolysis experiments provided the first determination of any thermodynamic property of undissociated $NH_4ClO_4(g)$.

ACKNOWLEDGMENT

This research was supported by the Air Force Office of Scientific Research, Office of Aerospace Research, under Contract AF 49(638)-412.

Nomenclature

c_K	$[(R_3T)/(2\pi W_K)]^{\frac{1}{2}}$, average velocity of molecules of species K in the $-x$ direction [cm/sec]
$c_{p,K}$	Specific heat at constant pressure of gaseous species K [cal/gm °K]
$\bar{c}_p$	$\sum_{k=1}^{N} c_{p,K} Y_K$, mass-average specific heat at constant pressure of gas mixture [cal/gm °K]
D	Binary diffusion coefficient [cm²/sec]
H	$h + (v^2/2)(R_1/R_3)$, total stagnation enthalpy per unit mass [cal/gm]
h	$\sum_{K=1}^{N} h_K Y_K$, total enthalpy per unit mass [cal/gm]
h_K	Total enthalpy per unit mass of gaseous species K [cal/gm]
h_π	Total enthalpy per unit mass of solid [cal/gm]
J	$\sum_{K=1}^{N} Y_{K,s} h_K(T_s) - h_\pi(T_i) + \frac{1}{2}(R_1/R_3) \times (v_s^2 - v_\pi^2)$ [cal/gm]; see Eq. (5)
l	Thickness of gas film [cm]
M	Total number of gaseous chemical species evolved from the solid
$M_\pi(c)$	Chemical symbol for solid
$M_K(g)$	Chemical symbol for gaseous species K
$\dot{m}$	Mass flux per unit area [gm/cm² sec]
N	Total number of gaseous chemical species
P_K	Permeability of porous hot plate to gaseous species K [gm/cm sec atm]
p	Total pressure [atm]
p^*	$t \sum_{K=1}^{N} (\epsilon_K/P_K) \Big/ \int_0^l (dx/\rho D)$; characteristic pressure
p_e	$\sum_{K=1}^{M} p_{K,e}$ [atm]
$p_{K,e}$	Partial pressure of species K at surface equilibrium [atm]
p_K	Partial pressure of species K [atm]
$p_{M,\infty}$	$\sum_{K=1}^{M} p_{K,\infty}$ [atm]
p_π	A constant in the momentum equation [atm]: see Appendix
R_1	Universal gas constant, 1.986 [cal/mole °K]
R_2	Universal gas constant, 82.06 [atm cm³/mole °K]
R_3	Universal gas constant, 8.317×10^7 [gm(cm/sec)²/mole °K]
T	Temperature [°K]
t	Thickness of the porous plate [cm]
v	Mass-average velocity [cm/sec]
W_K	Molecular weight of species [gm/mole]
$\bar{W}$	$\left[\sum_{K=1}^{N} Y_K/W_K\right]^{-1}$; mass-average molecular weight
w_K	Mass of molecules of species K leaving a unit area of surface per second [gm/cm² sec]
x	Spatial coordinate [cm]

Y_K Mass fraction of gaseous species K

Y $\sum_{K=1}^{M} Y_K$, total mass fraction of gases evolved from solid

α_K Surface accommodation coefficient for species K (dimensionless)

β $p_e \left[p_s \sum_{K=1}^{M} (\epsilon_K/\beta_K) \right]^{-1}$

β_K $\alpha_K(\rho c_K)_s \int_0^l [dx/(\rho D)]$, ratio of a characteristic diffusion time to a characteristic recondensation time for species K

ϵ_K Mass flux fraction of species K

ΔQ $\sum_{K=1}^{M} \epsilon_K h_K(T_s) - h_\pi(T_s)$

η $(4/3)\mu + \kappa$, effective viscosity coefficient [gm/cm sec]

κ Coefficient of bulk viscosity [gm/cm sec]

λ Thermal conductivity of the gas [cal/cm sec °K]

μ Ordinary (shear) viscosity coefficient [gm/cm sec]

ν_K' Stoichiometric coefficients for surface process, Eq. (28)

ξ $\dot{m} \int_0^x [dx/(\rho D)]$, dimensionless spatial coordinate

ξ_p $\dot{m} \int_0^l [dx/(\rho D)]$, dimensionless mass flow rate

ρ Density [gm/cm^3]

σ $\equiv p^*/p_p$; dimensionless measure of pressure at upstream face of porous hot plate

τ Dimensionless surface temperature; see Eq. (36)

ω Dimensionless forward surface gasification rate; see Eq. (33)

ω_K $w_K/[\alpha_K(\rho c_K)_s]$, dimensionless forward surface gasification rate of species K

Subscripts

e Surface equilibrium

i At upstream boundary of solid ($x = -\infty$)

K Integer index used only to denote chemical species

p At upstream face of porous hot plate

r Reference condition at which equilibrium vapor pressure is known

s At solid-gas interface

π In solid

∞ At downstream face of porous hot plate

References

1. Schultz, R. D. and Dekker, A. O.: Aerojet-General Corporation, *The Absolute Thermal Decomposition Rates of Solids: Part I, The Hot-Plate Pyrolysis of Ammonium Chloride and the Hot-Wire Pyrolysis of Polymethylmethacrylate (Plexiglas IA)*. Technical Note No. 2, U. S. Air Force Office of Scientific Research Contract No. AF 18(600)–1026, Azusa, November 1954.
2. Bills, K., *et al.*: The Linear Vaporization Rate of Solid Ammonium Chloride. Technical Note No. 10, U. S. Air Force Office of Scientific Research Contract No. AF 18(600)–1026, Azusa, July 1955.
3. Schultz, R. D. and Dekker, A. O.: *Fifth Symposium (International) on Combustion*, pp. 260–267. Reinhold, New York, 1955.
4. Barsh, M. K., *et al.*: Rev. Sci. Instr. *29*, 392 (1958).
5. Schultz, R. D., Green, L. Jr. and Penner, S. S.: Studies of the Decomposition Mechanism, Erosive Burning, Sonance and Resonance for Solid Composite Propellants, *Combustion and Propulsion, Third AGARD Colloquium*, pp. 367–420. Pergamon Press, New York, 1958.
6. Anderson, W. H. and Chaiken, R. F.: Aerojet-General Corporation, On the Detonability of Solid Composite Propellants, Part I. Technical Memorandum No. 809, Azusa, January 1959.
7. Friedman, R., Nugent, R. G., Rumble, K. E. and Scurlock, A. C.: *Sixth International Symposium on Combustion*, pp. 612–618. Reinhold, New York, 1957.
8. Friedman, R., Levy, J. B. and Rumble, K. E.: Atlantic Research Corporation, *The Mechanism of Deflagration of Ammonium Perchlorate*. AFOSR TN–59–173, AD No. 211–313, Alexandria, Va., February 1959.
9. Levy, J. B. and Friedman, R.: *Eighth International Symposium on Combustion*, pp. 663–672. Williams and Wilkins Co., Baltimore, 1962.
10. Johnson, W. E. and Nachbar, W.: *Eighth International Symposium on Combustion*, pp. 678–689. Williams and Wilkins Co., Baltimore, 1962.
11. Adams, G. K., Newman, B. H. and Robins, A. B.: *Eighth International Symposium on Combustion*, pp. 693–705. Williams and Wilkins Co., Baltimore, 1962.
12. Arden, E. A., Powling, J. and Smith, W. A. W.: Combustion and Flame *6*, 21 (1962).
13. Rosen, G.: J. Chem. Phys. *32*, 89 (1960).
14. Bircumshaw, L. L. and Phillips, T. R.: J. Chem. Soc. *1957*, 4741.

15. PENNER, S. S.: *Chemistry Problems in Jet Propulsion*, pp. 234–241. Pergamon, New York, 1957.
16. KNUDSEN, M.: Ann. Physik *28*, 75 (1909).
17. KENNARD, E. H.: *Kinetic Theory of Gases*, pp. 60–71. McGraw-Hill, New York, 1938.
18. PLESSET, M. S.: J. Chem. Phys. *20*, 790 (1952).
19. BROOKFIELD, K. J., *et al.*: Proc. Roy. Soc. (London) *A190*, 59 (1947).
20. KNUDSEN, M.: Ann. Physik, *47*, 697 (1915).
21. WYLLIE, G.: Proc. Roy. Soc. (London) *A197*, 383 (1949).
22. KENNARD, E. H.: *Kinetic Theory of Gases*, pp. 320–324. McGraw-Hill, New York, 1938.
23. SCHULTZ, R. D. and DEKKER, A. O.: Aerojet-General Corporation, *The Absolute Thermal Decomposition Rates of Solids: Part III, The Vacuum Sublimation Rate of Ionic Crystals*. Technical Note No. 7, U. S. Air Force Office of Scientific Research Contract No. AF 18(600)–1026, Azusa, July 1955.
24. BRADLEY, R. S. and VOLANS, P.: Proc. Roy. Soc. (London) *A217*, 508 (1953).
25. National Bureau of Standards, Circular 500, 1952.
26. SCHULTZ, R. D. and DEKKER, A. O.: Aerojet-General Corporation, *The Absolute Thermal Decomposition Rates of Solids: Part IV, Transition-State Theory of the Linear Rates of Exchange and Decomposition of Crystalline Ammonium Chloride*. Technical Note No. 8, U. S. Air Force Office of Scientific Research Contract No. AF 18(600)–1026, Azusa, July 1955.
27. SPINGLER, H.: Z. Physik. Chem. *B52*, 90 (1942).
28. RODEBUSH, W. H. and MICHALEK, J. C.: J. Am. Chem. Soc. *51*, 748 (1929).
29. LUFT, N. W.: Ind. Chemist *31*, 502 (1955).
30. FEICK, G.: J. Am. Chem. Soc. *76*, 5858 (1954).
31. CANTRELL, R. H. JR.: *Gas Film Effects in Linear Pyrolysis of Solids*. Ph.D. thesis, Harvard University, Cambridge, May 1961.
32. GALWEY, A. K. and JACOBS, P. W. M.: J. Chem. Soc. *1959*, 837.

Appendix

The Momentum Equation

In the gaseous region, the one-dimensional momentum equation is

$$\dot{m}\frac{dv}{dx} + \frac{R_3}{R_2}\frac{dp}{dx} - \frac{d}{dx}\left(\eta\frac{dv}{dx}\right) = 0 \qquad (49)$$

the first integral of which is

$$\left(\frac{R_3}{R_2}\right)p + \dot{m}v - \eta\frac{dv}{dx} = \left(\frac{R_3}{R_2}\right)p_\pi = \text{constant} \qquad (50)$$

Equations (1), (18), and (50) determine the distributions of p, ρ, and v in the gas in terms of the composition and temperature distributions studied in the main body of the paper.

The evaluation of the constant p_π in Eq. (50) depends upon the experimental arrangement. If the gas layer alone supports the solid (in which case l is not known *a priori*), then it can be shown that p_π is the axial compressive stress in the solid, which equals the atmospheric pressure plus any additional pressure applied to the cold end of the solid sample in order to increase "thermal contact" with the porous hot plate. On the other hand, if the solid is supported in such a way that the spacing l is fixed (e.g., by means of a specially designed sample holder, or by protuberances on the surface of the sample, as appears to be the case in the previous pyrolysis experiments), then the gas-phase equations given in the main body of the text determine p_π. An interesting consequence of these observations arises when

$$\dot{m}v - \eta(dv/dx) \ll (R_3/R_2)p \qquad (51)$$

Equations (50) and (51) imply, approximately,

$$p = p_s = p_p = p_\pi \qquad (52)$$

In the discussion at the end of the section entitled Simple, Chainlike Surface Processes, it is assumed that Eqs. (51) and (52) are valid first approximations for an integral of Eq. (50). The dimensional form of Eq. (38b) is written for this case as

$$\dot{m} = (P_1/t)(p_\pi - p_{,\infty}) \qquad (53)$$

If p_π is not measured, as in the second experimental arrangement discussed above, then it is determined through Eq. (53) by measurements of $\dot{m}$ and $p_{,\infty}$ (provided that Eq. (52) is valid). If p_π is easily measured, as in the first experimental arrangement, then we might ask whether this measurement could replace the more difficult measurement of l for this arrangement. Unfortunately, it cannot. In this case, $\dot{m}$ and p_π, both easily measured quantities, satisfy Eq. (53) as a redundant equality independent of l. It would still be necessary to measure l for this first experimental arrangement in order to carry out the calculations indicated in the section mentioned above.

Discussion

DR. D. J. SIBBETT (*Aerojet-General Corporation*): The analysis of linear pyrolysis experiments by Dr. Nachbar and Prof. Williams indicates very nicely the critical factors and limitations of the technique.

It is obviously of paramount importance in the interpretation of data collected by this method that the measured experimental temperature be identifiable with surface temperature. Recently in the course of a study of the rates of sublimation of the four ammonium halides, evidence was obtained which confirms this identity.

In these experiments the rates of vacuum sublimation of the ammonium halides were determined gravimetrically by use of the quartz balance at low temperatures and by the linear pyrolysis technique at high temperatures. Surface temperatures during the gravimetric determinations were obtained from dual sets of experiments. In one set, rates of sublimation and the temperature of a thermowell in the quartz balance wall were obtained simultaneously. In the second set, thermowell temperatures and sample surface temperatures were correlated to give temperature corrections which were applied to the rate measurements. Linear pyrolysis temperatures were measured directly.

The figure, which is a plot of the rates of sublimation of ammonium bromide between 153 and 574°C is a typical example of these data. Rates, which are indicated on a logarithmic scale on the ordinate, have been converted to linear regression units (cm/sec). Data from 153 to 227°C were obtained gravimetrically; those at higher temperatures were obtained by use of the linear pyrolysis or "hot-plate" method. For all four halides, NF_4Fl, NH_4Cl, NH_4Br, and NH_4I, the data took the same form.

The figure demonstrates that: 1, The vacuum sublimation data are consistent with the linear pyrolysis data and give an Arrhenius plot with a single apparent activation energy value. 2, At very high rates, a departure from linearity was observed which corresponds to the range of conditions in which meaningful temperature measurements fail. However, by increasing the loading force between the stand and the hot plate, which decreases the thickness of the gaseous layer, the linear plot can be extended. This effect is demonstrated by the two sets of data at the upper limits of the rate measurements.

From these data, it has been concluded: 1, The temperatures measured by the nonporous hot-plate apparatus are valid measures of the surface temperature in these experiments. 2, Linear pyrolysis measurements are determinations of the rates of sublimation of the ammonium halides. That is, a single reaction mechanism appears to be operating over the entire temperature range.

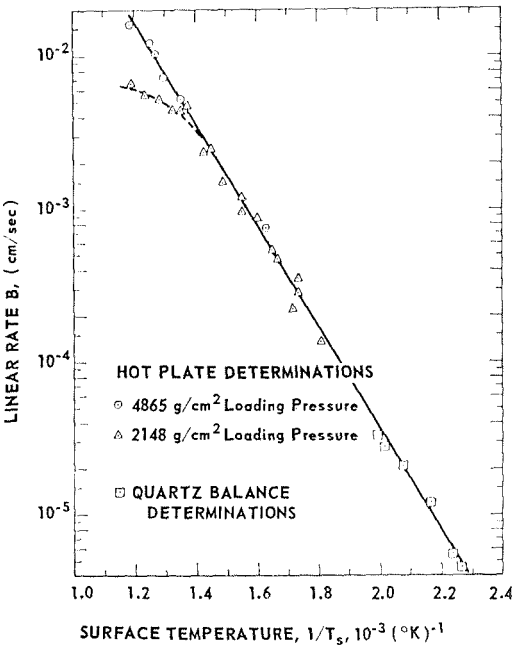

FIG. 1. Rates of sublimation of ammonium bromide.

Application of the linear pyrolysis technique requires experimental or theoretical analysis of the processes involved at the hot interface in order to establish the meaning of the measured temperature. Within these limitations it has proven a very useful tool.

PROF. F. A. WILLIAMS (*Harvard University*): The only ammonium halide that we have considered is NH_4Cl, and, as indicated in the paper, we agree with Dr. Sibbett that the difference between the plate temperature and the surface temperature is negligible in this case. We found significant differences only for NH_4NO_3 and NH_4ClO_4.

DEFLAGRATION CHARACTERISTICS OF AMMONIUM PERCHLORATE AT HIGH PRESSURES

O. R. IRWIN, P. K. SALZMAN, AND W. H. ANDERSEN

The deflagration characteristics of pure ammonium perchlorate (AP) strands have been investigated by means of a closed-bomb strand burning technique at pressures from 1000 to 23,000 psi. The data are in general agreement with vented-chamber AP burning-rate data of other investigators at pressures from 1000 to 5000 psi. At pressures above 5000 psi (the pressure limit of previously reported studies) a marked increase in pressure dependence of the linear burning rate occurs.

It is postulated that the observed increase in burning rate results from an increased burning surface area, i.e., surface break-up, under the action of the very high pressures existing in the closed bomb. The action of pressure, or stress, upon the burning surface can produce shearing giving rise to increased burning area by forming new cracks and pores or by enlarging existing cracks and pores. It appears reasonable that the rate at which such cracks can propagate in a material under an applied stress will be determined by the mechanical properties of the material. The crack growth process has therefore been analyzed in terms of a theory, due to Eyring, which relates creep and fracture to fundamental atomic and molecular properties of a material.

A geometrical model is presented which considers the accelerated burning process as a development of micro-cracks that form into conically-shaped burning surfaces, the area of which depends upon the pressure. The model is in good agreement with the experimental burning-rate data and with the pressure versus time data for individual burning-rate experiments at pressures above 5000 psi.

Introduction

This paper summarizes the present status of an investigation currently being conducted in these laboratories to determine and interpret the influence of very high pressures on the deflagration rate of pure ammonium perchlorate (AP).

Friedman and co-workers[1–3] have studied the burning rate of pressed pure AP (ρ = 1.91 grams/cc; $\rho_{crystal}$ is 1.95 grams/cc) in a vented strand burner at pressures up to 5000 psi. They found a lower pressure limit for deflagration of about 300 psi, and an upper pressure limit of about 4000 psi for bare strands of dimensions 4 × 4 × 38 mm at ambient temperature. It was found possible to increase the upper pressure limit to at least 5000 psi (the pressure limit of the equipment) if the strands were wrapped in asbestos. The upper pressure limit was attributed to convective (edge) heat losses from the burning strand; it was concluded that this limit may be modified or eliminated by suitable changes in the sample geometry or insulation. The lower pressure limit was attributed to radiative heat losses from the burning surface. It was found that the pressure exponent for both the bare and insulated strands is essentially unity at pressures below 1500 psi and decreases to about 0.4 at 5000 psi. Sibbett and Lobato[4] have measured the burning rate of pressed AP strands by an end-to-end burning technique in a window bomb. The pressure exponent was found to be essentially unity over the pressure range of 50 to 1500 psi.

Experimental

Strands of essentially pure AP (~99.5 weight per cent) were prepared by pressing unground AP which had an average (50 per cent point) particle size of about 200 microns (as determined by Micromerograph) in a die. Strands of dimensions 4 × 4 × 38 mm and a density of 1.9 grams/cc were obtained utilizing an Atlantic Research Corporation-type strand mold at 100,000 psi[1]; cylindrical strands of $\frac{5}{8}$ inch diameter by 1-$\frac{1}{2}$ inch length and density 1.92 grams/cc were obtained utilizing a three-piece split vertical die at 80,000 psi. The strands were prepared for burning by drilling 0.018 inch diameter holes in them at $\frac{1}{2}$ inch intervals (starting $\frac{1}{4}$ inch from one end), and inserting electrical timing wires ($\frac{1}{2}$ ampere lead fuse wire) through the holes to provide burning-rate timing signals. When insulating and restricting coatings were used on the strands, they were applied before drilling of the holes. Ignition of the strands was usually accomplished by means of a 9-mil Nichrome wire and a $\frac{1}{4}$ inch diameter wafer

of JPN propellant cemented to the top of the strand with a drop of Duco cement. All strands were burned in an unvented bomb in a nitrogen atmosphere at ambient temperature. To determine strand burning rates at pressures above 2000 psi (nitrogen cylinder pressure), the chamber was first pressurized to 2000 psi with nitrogen, then water was pumped into the chamber until the chamber volume had been sufficiently reduced to give the desired pressure. The average burning rate and average burning pressure for each $\frac{1}{2}$-inch increment were determined from simultaneous tracings of fuse-wire break-time and bomb pressure on a recording oscillograph.

Results

The burning rate of bare, unrestricted 4 × 4 × 38 mm AP strands was determined in the closed bomb at pressures of 3000, 3500, and 4000 psig. The results are in agreement with the Crawford-bomb burning-rate curve of Friedman for similar strands. The upper pressure limit for deflagration of these strands was found to be approximately 4000 psi.

Again in agreement with Friedman, it was found that the 4 mm square strands could be burned at pressures above 4000 psig if they were first insulated by a loose-fitting wrapping of asbestos paper and ignited with a hot wire–JPN pellet combination. However, the measured burning rates were considerably below those obtained by Friedman. Attempts to provide better strand insulation by the use of close-fitting insulating jackets fabricated of glass cloth or Micarta resulted in burning rates which were as much as 50 times greater than Friedman's values. Restriction of the sides of the strands with materials such as Acryloid, Krylon, or Pliobond, and the use of smaller JPN pellets, or a hot wire alone, for ignition failed to eliminate this "flash" type of burning when the strands were also tightly confined in, but not bonded to, an insulating coating. Flashing was considerably reduced, however, when the strands were restricted with Pliobond and wrapped with asbestos while the final Pliobond coating was still tacky. These results suggest that a tight, unbonded confinement may provide narrow channels which direct the flame along the sides of the strands, breaking the timing fuse wires prematurely. Apparently, meaningful burning-rate data for insulated, restricted strands in the closed bomb can be obtained only if these narrow channels between the restricting coating and the strand, and/or the insulation, are eliminated. In view of the difficulty of eliminating these channels at the corners of AP strands of square cross section, further studies were confined to the use of cylindrical strands.

Bare $\frac{5}{8}$-inch diameter cylindrical AP strands were burned at pressures of 2000, 3000, and 4500 psig. A progressive decrease in burning rate with increasing pressure was found, in agreement with Friedman's data for bare strands of 4 mm square cross section. The more gradual decrease in burning rate of the cylindrical strands in comparison to square strands is apparently the result of a smaller relative heat loss because of the greater ratio of burning surface area to peripheral heat loss area as indicated by Friedman.

When the Pliobond restricting coating and asbestos insulation were used on the cylindrical strands, the burning rate increased with increasing pressure and was determined satisfactorily from 1000 to 23,000 psig. In contrast to the somewhat erratic burning behavior of the insulated, restricted strands of 4 mm square cross section, burning-rate data for the similarly prepared cylindrical strands showed relatively little scatter over the entire pressure range (Fig. 1). The validity of the burning-rate data obtained by the fuse-wire method was checked by means of a thermocouple technique. In this method the burning rate is calculated from an oscillograph record of the time of flame-front

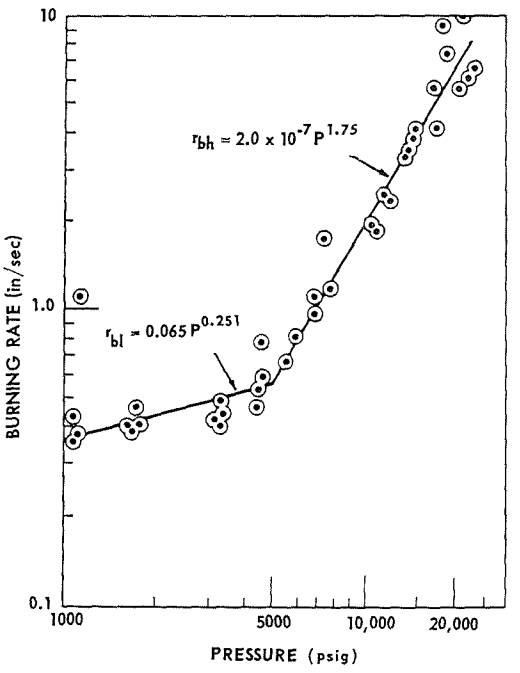

FIG 1. Effect of pressure on closed-bomb burning rate of insulated, restricted cylindrical ammonium perchlorate strands.

passage across thermocouples spaced at $\frac{1}{2}$ inch intervals along the side of a strand. Data obtained in this way are in substantial agreement with the results of the fuse-wire technique.

Discussion

Friedman and co-workers[1–3] and Sibbett and Lobato[4] showed that the linear burning rate of AP obeys a linear pressure dependence up to about 1500 psi under constant pressure (vented) conditions. That is, the pressure exponent n in the empirical burning-rate expression $r_b = cP^n$ is near unity which suggests that the rate is controlled in this pressure range by a second-order gas-phase reaction. The thermal layer theory of Chaiken[5] predicts a linear pressure dependence for pure AP at moderate pressures and indicates that at sufficiently high pressures the pressure exponent should thereafter decrease. Burning rate theories for double base propellants[6] also imply that the pressure exponent should decrease with increasing pressure at very high pressures, as does the Summerfield theory[7] for solid composite propellants, and the theory of Johnson and Nachbar[8] for ammonium perchlorate.

In the present investigation, the burning rate studies were not conducted at constant pressure, but rather in a closed bomb wherein the pressure continually increased as the burning proceeded. The average linear burning rate of each $\frac{1}{2}$ inch increment of a strand was computed over a finite time interval and correlated with an average pressure in the interval to give the burning rate curve shown in Fig. 1. At pressures of about 1000 to 5000 psig the results are consistent with published burning rate data obtained under constant-pressure conditions[3,4] in that the pressure exponent remains below unity. A least-squares fit of the data in this case gives the expression $r_{bl} = 0.065P^{0.251}$ inches/sec. However, above this pressure region the pressure dependence increases sharply and obeys the expression $r_{bh} = 2.0 \times 10^{-7}P^{1.75}$ inches/sec. It is not known whether this change in pressure dependence occurs abruptly at one particular pressure or occurs smoothly over some small but finite pressure region.

Some possible effects which might cause a sharp increase in burning rate above 5000 psi are (a) a premature breaking of the timing fuse wires by flash-burning along the surface of the strands, (b) a change in the general burning-rate law (i.e., a change in the deflagrative mechanism), or (c) an increase in the actual burning surface area.

Flashing (case a) as a possible mechanism was discounted by comparing the gasification rate calculated from pressurization rate data using the equation

$$\frac{dm}{dt} = \frac{1}{b_0}\frac{dP}{dt} \tag{1}$$

where b_0 is a constant, with the gasification rate computed from the fuse wire data and sample geometry. These values were found to agree with an average absolute error of 17 per cent.

If a change in the general burning-rate law (case b) occurs, the conservation of mass is given by:

$$dm/dt = \rho S_0 r_{bh} \tag{2}$$

where ρ is the sample density and r_{bh} is the linear burning rate in the high pressure region. If a change in the actual burning area (case c) occurs, and the local burning is proceeding "normally," the conservation of mass is given by $dm/dt = \rho S r_{bl}$ where r_{bl} is in this case the linear burning rate in the low pressure region extrapolated to high pressures, or by:

$$dm/dt = \rho S_0 v \tag{3}$$

where v may be considered physically as the flame-front velocity. Equations (2) and (3) are indistinguishable in terms of the mechanism involved since they both predict the same function for the high pressure rate. Sufficient evidence is not available to show unequivocally which of the choices apply in the present case.

If a change takes place in the normal burning mechanism (or rate-controlling steps) at high pressures it might involve either the solid or gas phase. The normal solid surface decomposition of deflagrating AP has been considered to involve an endothermic reaction giving rise to gaseous perchloric acid and ammonia.[1–3] It has also been assumed to involve simultaneously an endothermic dissociative sublimation of the mosaic AP crystals to gaseous perchloric acid and ammonia, and an exothermic decomposition of the intermosaic (defect-lattice) material—the overall surface reaction being endothermic[9,10] and dependent on the (unknown) rate of the transition from the orthorhombic to the cubic crystalline phase of AP. The decomposition rate of the intermosaic material (exothermic reaction) is faster than the sublimation rate of the mosaic material (endothermic reaction) for orthorhombic crystals, and slower than the sublimation rate for cubic crystals. This latter assumption is also supported by the thermal decomposition studies of AP by Bircumshaw and Newman,[11] Bircumshaw and Phillips,[12] and Galwey and Jacobs.[13] Therefore there exists the possibility that at a sufficiently high pressure (and corresponding surface temperature) the

surface reaction mechanism may become exothermic or considerably less endothermic than the reaction under normal burning conditions. However, this possibility does not seem too likely in that the normal thermal surface regression rate law is roughly adequate to explain the grain-burning detonation of pure AP where the temperatures and pressures involved are considerably greater than in the present high-pressure burning case.[9,14] A knowledge of the crystalline phase-transition kinetics will be necessary for a final evaluation of the influence of the solid surface reactions on the burning behavior of AP at very high pressures. There is little direct information available at present to evaluate the possible change in mechanism (or rate-determining step) of the gas-phase kinetics at high pressures.

The general similarity of the present results with those obtained previously on other combustible systems suggests that an increased surface area available for instantaneous deflagration (above that of the cross-sectional area of the sample) may be responsible for the abnormal (increased) burning rate at high pressures. Taylor[15] found that the burning rate of relatively low-density (porous) RDX, PETN, and HMX increases sharply above a certain pressure. The result was attributed to flame penetration into the porous material (due to pressure gradients) when the normal burning rate becomes sufficiently high to prevent buildup of molten explosive over the pore openings. The transition pressure is thus a function of pore size, pressure gradient, and molten film thickness. Paulson and co-workers[16] found that the substitution of a part or all of the AP oxidizer by $KClO_4$ in a propellant reduces or eliminates the change in pressure exponent at high pressures (Fig. 2). Since potassium chloride, which is an end product in the thermal decomposition of $KClO_4$, is a liquid from about 800 to 1500°C, it might be expected to be effective in preventing abnormal burning by forming a molten layer on the burning surface. However, the effect cannot be attributed with certainty to the presence of a molten layer since there are other decomposition characteristics of $KClO_4$ which may also play a role. Whittaker and co-workers[17] studied the burning rate of liquid bipropellants and found that the rate increased sharply above certain pressures (fixed by the composition). They attributed the effect to the onset of turbulence and liquid breakup, with a consequent large burning liquid surface area. Wachtell, McKnight, and Shulman[18] observed similar effects above certain pressure levels in the closed-bomb burning-rate curves of solid explosives and propellants. They attributed the effect to a cracking or crazing of the burning

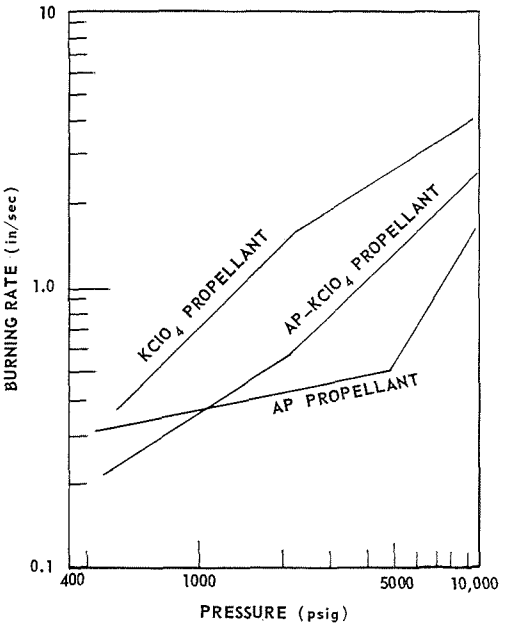

FIG. 2. Effect of oxidizer composition on the closed-bomb burning rate of polyurethane propellants.

surface under the action of the rapidly increasing pressure in the bomb. On the other hand, they found that the burning rate in a vented (constant-pressure) strand burner remained "normal." This apparent effect of pressurization rate on abnormal burning merits further investigation because of its importance in the development of a model of burning. In the present study, attempts to duplicate the constant-pressure (i.e., zero dP/dt) conditions of Wachtell and co-workers failed. However, experiments were performed in which an AP propellant (see Fig. 2) was burned under conditions of increasing and decreasing pressure where dP/dt passed through zero. In all cases the results were in agreement with the closed-bomb curve of Fig. 2 (i.e., the burning rate did not remain "normal").

A simple geometrical model of burning accompanied by stress-induced formation of new burning surface area is presented. The treatment, while approximate, is useful as a starting point for a more exact investigation. Basic assumptions of the model (Fig. 3) are:

1. The pressure (static and/or dynamic) of the burning gases above the propellant surface can produce shearing in the surface due to the nonhomogeneous nature of the propellant. The shear process, which may be strongly influenced by the surface temperature of the propellant, gives rise to increased burning area (above that of the sample cross section) by forming new

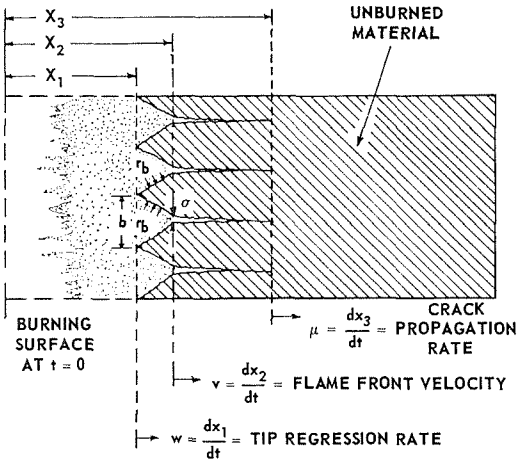

FIG. 3. Schematic of model of accelerated burning.

cracks and pores, or by enlarging existing cracks and pores. In the present case the gas flow into these cracks is considered to be fast (or proportional to the shear rate) so that crack propagation (i.e., the generation of new surface area) is the rate-controlling process. This is in contrast with an earlier model of porous burning proposed by Andersen and Chaiken[9] in which the burning surface area was assumed to be proportional to the chamber pressure, i.e., new burning surface was generated by gas penetration into existing pores.

2. Flame cannot penetrate into pores with a diameter less than the reaction zone thickness of the flame.

3. The distribution and number of cracks is regular and remains constant.

4. Conically shaped burning surfaces are produced by gas penetration into growing cracks.

5. Burning area variations take place only with variations in the height of the cones ($X_2 - X_1$). The base of the cones, b, remains fixed.

6. The propagating crack tips are also conically shaped with base, σ.

7. The base of the burning cone is much larger than the base of the cracking cone (i.e., $b \gg \sigma$).

If a differential time change of the situation in Fig. 3 is considered, the following may be established geometrically:

$$\frac{\sigma/2 + k\,dX_3}{dX_3 + X_3 - X_2} = \frac{\sigma/2}{dX_3 - dX_2 + X_3 - X_2} \quad (4)$$

where $k\,dX_3$ is the rate at which the base of the cracking cone is assumed to open. Neglecting higher order terms, this leads to a differential equation $k(X_3 - X_2)\,dX_3 = \sigma\,dX_2/2$, whose solution is:

$$X_2 = X_3 - \frac{\sigma}{2k}\left[1 - \exp\left(\frac{-2k}{\sigma} X_3\right)\right] \quad (5)$$

Differentiating this with respect to time gives:

$$v = \mu\left[1 - \exp\left(\frac{-2k}{\sigma} X_3\right)\right] \quad (6)$$

and for $X_3 \geq 3$ mm and $k > 10^{-3}$, $v \simeq \mu$ within 1 per cent.

The creep rate of a material at a fixed temperature and subject to stress has been related to certain fundamental constants of the material by Eyring[19] and is given by:

$$\text{creep rate} = \frac{1}{L_0}\frac{dL}{dt} = \frac{L}{L_1} Z \exp\left(\frac{-E}{RT}\right) \times 2 \sinh\left(\frac{\beta' P'}{RT}\right)$$

where T is the temperature, P' is the shear stress, E is the activation energy for the process in the absence of an applied stress and the rest of the terms are defined in ref. 19. The crack propagation rate may be assumed directly proportional to the creep rate, giving:

$$\mu = K \frac{L}{L_1} Z \exp\left(\frac{-E}{RT}\right) 2 \sinh\left(\frac{\beta' P'}{RT}\right) \quad (7)$$

where K is a proportionality constant. Since shear stress may be expressed in terms of a tensile or compressive stress, Eq. (7) may be rewritten as $\mu = 2\alpha \sinh \beta P$ where the conversion factor between gas pressure (i.e., tensile stress) and shear stress is combined with β'/RT to give β and α is a combination of the other constants. Since $v \simeq \mu$:

$$v \simeq 2\alpha \sinh \beta P \quad (8)$$

Because $2\alpha \sinh \beta P \simeq \alpha \exp \beta P$ when $\beta P > 1.5$, α and β may be estimated by plotting the best-fit line through the high pressure data on semi-log paper. This gives $\alpha = 0.35$ and $\beta = 1.59 \times 10^{-4}$. Equation (8) is then plotted on Fig. 4 along with the burning-rate data and the best-fit line for r_{b1} from Fig. 1. When $P < 4500$ psig the linear burning rate (i.e., r_{b1}) is clearly greater than the crack propagation rate predicted by Eq. (8) at that pressure. Therefore no cracking and consequently no burning area increase takes place. When $P > 4500$ psig the cracking rate exceeds r_{b1} so that the burning area (and hence the burning rate) increases sharply. The observed sharp increase in burning rate above 4500 psig is thus explained by the geometrical model.

The combination of r_{bl} and Eq. (8) is clearly in very good agreement with the burning rate data for AP over the whole pressure range. The applicable expressions are:

$$r_{bl} = 0.065P^{0.251}; \qquad 1000 < P < 4500 \text{ psig}$$

$$r_{bh} = v = 0.70 \sinh (1.59 \times 10^{-4}P); \qquad 4500 < P < 23000 \text{ psig}$$

Also, from Fig. 3, the general equation for burning area for pressures above 4500 psig may be developed as follows: Geometrically

$$S = (N\pi b/2)[(\tfrac{1}{2}b)^2 + (X_2 - X_1)^2]^{\frac{1}{2}} \quad (9)$$

where N is the number of cracks in the cross section and b is the base of the burning cone. Solving Eq. (9) for $(X_2 - X_1)$ and differentiating with respect to time gives:

$$v - w = \frac{\sqrt{S_0}}{2\sqrt{N}} \frac{R}{(R^2 - 1)^{\frac{1}{2}}} \frac{dR}{dt} \quad (10)$$

where $R = S/S_0$ and S_0 is the original cross-sectional area of the strands. It can be shown geometrically that the regression rate is given by $w = r_{bl}R$ where r_{bl} is the low pressure burning rate extrapolated to values of pressure greater than 4500 psig and is in the form $r_{bl} = cP^n$. Substituting this and Eq. (8) into Eq. (10) gives:

$$2\alpha \sinh \beta P - cP^n R = \frac{\sqrt{S_0}}{2\sqrt{N}} \frac{R}{(R^2 - 1)^{\frac{1}{2}}} \frac{dR}{dt} \quad (11)$$

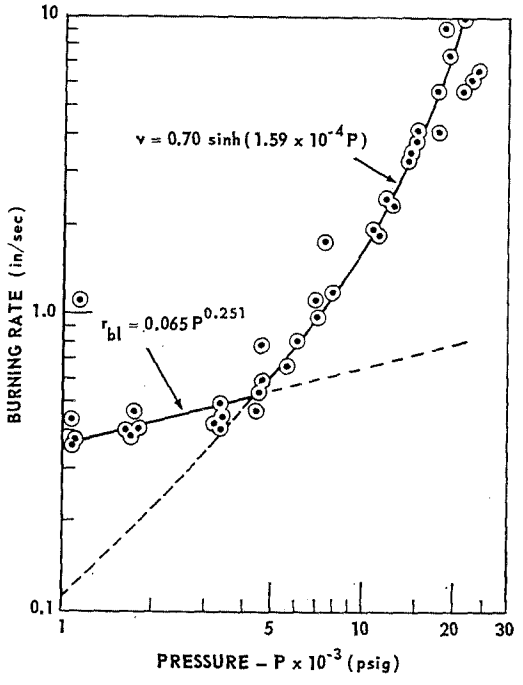

FIG. 4. Comparison of derived accelerated burning expression with experimental data.

which is the differential equation relating surface area and pressure to time. We are only interested in the solution to Eq. (11) that describes the increase of burning area above the normal (i.e., $R > 1$). From Fig. 4 this can only occur when $2\alpha \sinh \beta P > cP^n$.

If constant pressure conditions are assumed (i.e., a vented bomb), Eq. (11) can be solved directly. Since the factor $R/(R^2 - 1)^{\frac{1}{2}}$ is essentially unity for $R \geq \frac{3}{2}$, Eq. (11) may be integrated from $\frac{3}{2}$ to R and 0 to t to give:

$$S = S_0\left[\frac{2\alpha \sinh \beta P}{cP^n} - \left(\frac{2\alpha \sinh \beta P}{cP^n} - \tfrac{3}{2}\right) \times \exp\left(-\frac{2\alpha\sqrt{N}}{\sqrt{S_0}} cP^n t\right)\right] \quad (12)$$

The transient term of the solution in the present case dies out rapidly giving a steady-state solution (for $t \geq 0.03$ sec) of:

$$S = S_0\left[\frac{2\alpha \sinh \beta P}{cP^n}\right], \qquad P > 4500 \text{ psig} \quad (13)$$

Noting Eq. (8) and that $r_{bl} = cP^n$ this becomes $S = S_0 v/r_{bl}$ which indicates how the burning area varies with the flame-front velocity and is to be expected as seen from combining Eq. (3) with $dm/dt = \rho S r_{bl}$. Since Eq. (13) shows that the steady-state burning area is a unique function of pressure, it will also apply to conditions of changing pressure, e.g., a closed bomb. Because of this, area variations are independent of time derivatives of pressure for the present model.

From the model, the pressure vs. time relation can be computed as follows. Combining Eq. (1) and the conservation equation gives $dP/dt = b_0 \rho S r_{bl}$ and from Eq. (13) and $r_{bl} = cP^n$ this becomes:

$$dP/dt = 2\alpha b_0 \rho S_0 \sinh \beta P \quad (14)$$

Integrating from P_0 to P and 0 to t gives:

$$\tanh (\beta P/2) = \tanh (\beta P_0/2) \exp (2\alpha b_0 \beta S_0 t) \quad (15)$$

Equation 15 was shown to closely fit the original oscillograph traces of pressure versus time. This result provides further support for the validity of the model.

Additional calculations based on this model show that the maximum burning cone height $(X_2 - X_1)$ at 20,000 psig is 0.5 mm and the cracking cone height is less than or equal to 0.5 mm if $k > 10^{-3}$. This indicates that the cracking zone is less than 1 mm from the regression tips.

The agreement between the experimental data and the equations derived from the geometrical model does not prove conclusively the validity of the postulated mechanism. Nevertheless, the general approach appears to warrant further investigation since it emphasizes the possible significance of the mechanical properties of a propellant on its deflagration characteristics. The above treatment has ignored many well-known points which should be taken into consideration in more exact treatments. Among these may be mentioned the difference in the crack pressure and the chamber pressure which has been discussed by Artz and Cramer,[20] the gas penetration (permeability) process, the time dependence of the pressure in the crack and the required conditions for nonsteady runaway cracks.

Acknowledgment

This work was supported by the Special Projects Office, Bureau of Weapons, Department of the Navy, under contract NOrd 18487, Task 1.

The authors wish to express their appreciation for the encouragement given to them during the course of this work by Dr. L. Zernow, Director of Research, and Mr. D. V. Paulson, Head, Propellant Physics Department and to Mr. R. D. Erickson for his excellent experimental work. The permission of D. V. Paulson, G. L. Roark, R. B. Christensen, A. Gaylord, and R. D. Erickson of the Ordnance Division to use Fig. 2 is also gratefully acknowledged.

References

1. Friedman, R., Nugent, R. G., Rumbel, K. E., and Scurlock, A. G.: *Sixth Symposium (International) on Combustion,* pp. 612–618. Reinhold, New York, 1957.
2. Friedman, R., Levy, J. B., and Rumbel, K. E.: The Mechanism of Deflagration of Pure Ammonium Perchlorate. AFOSR TN 59–173, Atlantic Research Corp., February 1959.
3. Levy, J. B. and Friedman, R.: Further Studies of Pure Ammonium Perchlorate Deflagration, *Eighth Symposium (International) on Combustion,* pp. 663–672. Williams and Wilkins, Baltimore, 1962.
4. Sibbett, D. J. and Lobato, J. M.: Report No. 0263–01–4, Aerojet-General Corp., Azusa, California, December 1959.
5. Chaiken, R. F.: Combustion and Flame *3,* 285 (1959).
6. Geckler, R. D.: The Mechanism of Combustion of Solid Propellants, *Selected Combustion Problems,* pp. 289–339. Butterworths, London, 1954.
7. Summerfield, M., Sutherland, G. S., Webb, M. J., Taback, H. J., and Hall, K. P.: Burning Mechanism of Ammonium Perchlorate Propellants, *Solid Propellant Rocket Research,* pp. 141–182. Academic Press, New York, 1960.
8. Johnson, W. E. and Nachbar, W.: Deflagration Limits in the Steady Linear Burning of a Monopropellant with Application to Ammonium Perchlorate, *Eighth Symposium (International) on Combustion,* pp. 678–689. Williams and Wilkins, Baltimore, 1962.
9. Andersen, W. H. and Chaiken, R. F.: ARS Journal *31,* 1379 (1961).
10. Chaiken, R. F. and Anderson, W. H.: The Role of Binder in Composite Propellant Combustion, *Solid Propellant Rocket Research,* pp. 227–244. Academic Press, New York, 1960.
11. Bircumshaw, L. L. and Newman, B. H.: Proc. Roy. Soc. *A227,* 115, 228 (1954).
12. Bircumshaw, L. L. and Phillips, T. R.: J. Chem. Soc. 4741 (*1957*).
13. Galwey, A. K. and Jacobs, P. W. M.: J. Chem. Soc. 837 (*1959*); Proc. Roy. Soc. *A254,* 455 (1960).
14. Andersen, W. H. and Pesante, R. E.: Reaction Rate and Characteristics of Ammonium Perchlorate in Detonation, *Eighth Symposium (International) on Combustion,* pp. 705–710. Williams and Wilkins, Baltimore, 1962.
15. Taylor, J. W.: Trans. Faraday Soc. *58,* 561 (1962).
16. Paulson, D. V., Roark, G. L., Christensen, R. B., Gaylord, A. and Erickson, R. D.: Aerojet-General Report No. 0253–01–307–4, July 1960.
17. Whittaker, A. G., Williams, H., Rust, P. M. and Skolnik, S.: Burning Rate Studies, Part 1. NAVORD Rpt. 1999, NOTS No. 599, China Lake, Calif., Nov. 1952; Williams, H., Whittaker, A. G., and Rust, P. M.: *Ibid.,* Part 2, NAVORD Rpt. 1999, NOTS No. 1085, March 1955.
18. Wachtell, S., McKnight, C. E., and Shulman, L.: Establishment of Improved Standards for Classification of Explosives and Propellants. Report No. 1; A Method for Determination of Susceptibility of Propellants and Explosives to Undergo Transition from Deflagration to Detonation. Picatinny Arsenal Technical Report DB–TR: 3–61, June 1961.
19. Glasstone, S., Laidler, K. J., and Eyring, H.: *The Theory of Rate Processes,* pp. 477–551. McGraw-Hill, New York, 1941.
20. Artz, G. D. and Cramer, S. B.: Runaway Phenomena in Ultrahigh Burning Rate Propellant. Paper presented at the Western States Section Meeting of the Combustion Institute, April 1961.

Discussion

DR. R. FRIEDMAN (*Atlantic Research Corporation*): Direct observations of pressed brittle propellant combustion in our laboratories have occasionally revealed spalling phenomena, consistent with the authors' proposal that crack propagation may be induced by combustion. The authors propose, however, that the crack formation is induced by a shearing force associated in some unspecified manner with the high pressure. The mechanics of this is not clear to me. An alternate means by which stress may be induced is by thermal expansion of the not-quite-homogeneous pressed solid as the combustion temperature wave propagates into it. The steepness of this temperature gradient increases with burning rate and hence with ambient pressure. The phase transition of ammonium perchlorate at 240°C, also leading to stresses, will probably be involved here. The distance from the surface to the 240°C isotherm may be critical.

In brief, will the authors comment on this possible relation between the temperature wave and crack formation?

DR. O. R. IRWIN (*Aerojet-General Corporation*): The remarks of Friedman are certainly apropos of the present paper, and we have previously considered some of them in more detail in Aerojet Report 025301, January 1960. From a fundamental point of view both mechanical stress and temperature are always involved in any nonhomogeneous strain or shear process, and it makes little difference mathematically whether the stress originated by thermal or hydrostatic means. From the viewpoint of controlling the phenomenon, however, one must ascertain whether the shear stress leading to crack formation results directly from the hydrostatic chamber pressure, or whether the chamber pressure (by its effect on the burning rate) influences the thermal gradient in the burning surface, which in turn produces the stresses leading to cracking. The data available do not allow an unambiguous choice of these alternatives, particularly in attempting to reconcile the "abnormal" deflagrative behavior of various materials. Insofar as our mathematical treatment is involved it appears to make little difference which viewpoint is chosen since we have related shear stress to chamber pressure by an arbitrary constant. However, the possibility of thermal stresses rather than hydrostatic stresses playing the dominant role in a brittle material like ammonium perchlorate is attractive, particularly in view of the observations of Bowden and coworkers on cracking accompanying the deflagration of crystals at low pressures. However, even here one must remember that the pressure in pores, fissures, etc., may possibly differ appreciably from the measured pressure.

It seems reasonable that the thermal stresses produced during the orthorhombic to cubic phase transition of ammonium perchlorate may possibly be involved in the change of the burning rate pressure exponent in the present case. However, a large variety of deflagrative materials have also been observed to undergo a similar change at sufficiently high pressures, and hence in many instances a crystalline phase change does not seem to be a controlling factor.

A SIMPLE THEORY OF SELF-HEATING AND ITS APPLICATION TO THE SYSTEM AMMONIUM PERCHLORATE AND CUPROUS OXIDE

P. W. M. JACOBS AND A. R. TARIQ KUREISHY

The approximations usually made in theories of self-heating are discussed briefly. It is pointed out that kinetic experiments close to the critical ignition state yield results for the fractional decomposition α as a function of time t which depart from the kinetic law applicable at lower temperatures. Nevertheless, these $\alpha(t)$ curves can be analyzed to yield *effective* rate constants which depend on the temperature of the surroundings (T_0) rather than on the temperature of the reactant (which is, of course, a function of time).

A theory of self-heating is developed using these effective rate constants and this is applied to the calculation of ignition times and self-heating curves. Results are in good agreement with experiment.

Introduction

The differential equation governing the temperature, as a function of time and position, in a solid undergoing an exothermic chemical reaction is

$$Cm(\partial T/\partial t) = V\lambda\nabla^2 T + Qm_0(\partial\alpha/\partial t) \quad (1)$$

where C is the heat capacity at constant pressure (cal deg^{-1} gm^{-1}), m the mass of reactant (in grams) at time t (sec), T the temperature (°K), V the volume of reactant (cm^3), λ the thermal conductivity (cal cm^{-1} deg^{-1} sec^{-1}), ∇^2 the Laplacian operator, Q the heat of reaction (cal gm^{-1}), and α the fractional decomposition at time t. The reaction rate is given by

$$\partial\alpha/\partial t = k[F'(\alpha)]^{-1} = A \exp(-E/RT)\,[F'(\alpha)]^{-1} \quad (2)$$

where k is the rate constant (sec^{-1}) and A and E are the usual Arrhenius parameters, the kinetic equation describing the progress of the reaction being written in the form

$$F(\alpha) = kt \quad (3)$$

$F'(\alpha)$ in Eq. (2) denotes $\partial F(\alpha)/\partial\alpha$.

Analytical solutions to Eq. (1) may only be obtained by making certain approximations. These approximations are connected (*a*) with the reduction in the number of independent variables on which $T(x, y, z, t)$ depends and with the boundary conditions at the surface of the reactant, (*b*) with the form of the kinetic law assumed for $F(\alpha)$, and (*c*) with the simplification of the exponential term in the Arrhenius law.

Frank-Kamenetskii[1] assumed essentially that the surface temperature of the reactant T_s was equal to that of the surroundings T_0 and integrated Eq. (1) subject to this boundary condition, assuming a steady-state temperature distribution within the reactant.[2–5] The results of this analysis are usually expressed in terms of the maximum value of a dimensionless parameter, δ, for which a steady-state solution is possible. This parameter is defined by the relation

$$\delta = \frac{Qm_0}{\lambda V}\frac{E}{RT_0^2}r_0^2 k(T_0) \quad (4)$$

where m_0 is the initial mass of reactant and r_0 is the significant geometrical dimension of the reactant (half-thickness of slab, etc.).

At the other extreme lies the assumption of Semenov[6] that the temperature inside the reactant is uniform at a value $T > T_0$ and that there is a discontinuity at the boundary where T falls sharply to T_0. The heat-conduction term on the right-hand side of Eq. (1) must therefore be replaced by the heat-loss term $-\chi S(T - T_0)$ where S is the surface area and χ the heat-transfer coefficient. This approximation will evidently apply when $\chi \ll \lambda/r_0$ while the Frank-Kamenetskii approximation, $T_s = T_0$, will hold when $\chi \gg \lambda/r_0$. Real cases will be in between these two extremes. Using the most general form for the boundary conditions,

$$\chi(T_s - T_0) + \lambda\,(dT/dx)_s = 0 \quad (5)$$

and the linear rate law $d\alpha/dt = k$, Thomas[7] showed that the critical condition for the steady state is still given by Eq. (1) but that the Frank-

Kemenetskii values for δ are too high if self-cooling is important.

The similarity in form between this result [Eq. (4)] and Semenov's equation

$$(E/RT_0^2)Qm_0k = V\chi(\kappa + 1)/r_0e \qquad (6)$$

permits the use of the assumption of uniform temperature,[8,9] provided that the true heat-transfer coefficient χ is replaced by an effective transfer coefficient χ' given by

$$\chi' = \frac{e\delta}{\kappa + 1}\left(\frac{\lambda}{r_0}\right) \qquad (7)$$

In Eqs. (6) and (7) κ is a constant which defines the geometrical form of the reactant, being 0 for a semi-infinite slab, 1 for a semi-infinite cylinder, and 2 for a sphere. Thomas[8] has shown further that, just as χ' should replace χ when thermal conduction alone is important, $(\lambda/r_0) \gg \chi$, so the intermediate case [Eq. (5)] corresponds to the heat-transfer coefficient χ'' given by

$$1/\chi'' = 1/\chi + 1/\chi' \qquad (8)$$

The importance of Thomas' contribution as far as our work is concerned is that it entitles us to use the assumption of uniform temperature without serious error, provided an empirically determined heat-transfer coefficient is employed.

Almost all the early work in this field limited consideration to the linear kinetic law $\partial\alpha/\partial t = k$; this corresponds to a zero-order reaction. Allowing for the consumption of reactant greatly increases the mathematical complexity of the problem. Rice *et al.*,[10] Todes and Melentiev,[11,12] and Gray and Harper[13] have tackled the problem numerically while Frank-Kamenetskii[14] and Thomas[15] have preferred to obtain analytical solutions at the expense of some approximations.

The Effective Rate-Constant Approximation

In all these theories it is implied that the kinetic parameters A and E (values of which will have to be substituted in the equations when the theories are applied to real problems) are known from measurements made at temperatures sufficiently low for self-heating to be negligible. Such measurements will result in the determination of the true rate law $F(\alpha) = kt$ and numerical values for the rate constant k. It has been our experience, however, that substantial self-heating is found[16] at temperatures well below those at which ignition can occur. One cannot be sure, therefore, of the value of k or even that the rate law found is the correct one, unless it is demonstrated that the kinetic measurements are not accompanied by self-heating.

From extensive measurements of the rate of decomposition of mixtures of NH_4ClO_4 and Cu_2O we have found that the kinetics of the reaction conform to the exponential law

$$\alpha = \alpha_0' \exp(kt) \qquad (9)$$

and that this rate law holds both for the pre-ignition kinetics and for temperatures below that at which ignition occurs. k is an "effective rate constant" in that, whatever the form of the true rate law, the reaction rate at any instant is given by the derivative of Eq. (9) with k a function of T_0 only, despite the fact that the temperature of the reactant is varying with time. The increase in reaction rate during any one decomposition, due to varying T, has been allowed for by a change in the isothermal rate law to the (empirical) exponential law. The justification for the use of effective rate constants lies in the applicability of the Arrhenius equation to $k(T_0)$. This is shown, for example, by Fig. 1 for mixtures containing 4.56 mole % Cu_2O.

With the Semenov assumption of uniform temperature (which we know from Thomas' work to be justifiable provided χ refers to an effective heat-transfer coefficient), Eq. (1) becomes

$$Cm(dT/dt) = -\chi S(T - T_0) + Qm_0(d\alpha/dt) \qquad (10)$$

Total derivatives are written since T is not a function of position and the reaction rate is to be obtained from an effective rate law in which α is a function of (t, T_0) but not of the instantaneous temperature T. The heat-loss term has so far been written in the conventional manner as $-\chi S(T - T_0)$ where S, the surface area, should clearly depend on α. However, heat is abstracted from the reactant mass by the gaseous products and, in the self-heating experiments,[16] by conduc-

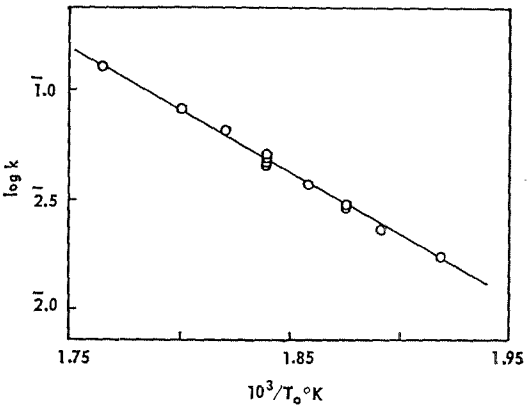

FIG. 1. Test of the Arrhenius equation for effective rate constants, k, found from the exponential law, Eq. (9); $-\log \alpha_0' = 7.78$; $E = 26.0$ kcal/mole.

tion up the thermocouple leads. As it is not possible to decide how the total heat loss is divided between these three contributions, it seems a better approximation to write $-H(T - T_0)$ for the first term on the left-hand side of Eq. (10) and to regard H as approximately constant. With this change, and the usual substitution for the relative excess temperature,

$$\theta = (T - T_0)E/RT_0^2,$$

Eq. (10) becomes

$$(1 - \alpha)(d\theta/dt) = -(H/Cm_0)\theta + (QE/CRT_0^2)(d\alpha/dt) \quad (11)$$

on recalling that $m = m_0(1 - \alpha)$. On substituting for $d\alpha/dt$ from the empirical rate law

$$d\alpha/dt = k\alpha,$$

Eq. (11) becomes

$$d\theta/d\alpha = \{-(a\theta/\alpha) + b\}(1 - \alpha)^{-1} \quad (12)$$

where

$$a = H/Cm_0k \quad \text{and} \quad b = QE/CRT_0^2 \quad (13)$$

are constants for constant T_0. When α is small, a solution of Eq. (12) is

$$\theta = b\alpha/(1 + a) \quad (14)$$

which shows that θ should also be an exponential function of t. Equation (14) is limited in its applicability to the range in which the kinetic equation $d\alpha/dt = k\alpha$ holds, i.e., to the accelerator part of the reaction.

The induction times can be obtained from Eq. (14) by substituting for α and setting a prescribed limit on θ. Before doing this, however, some comment on the relation of this work to that of Merzhanov and Dubovitskii[17,18] would seem appropriate. Equation (12) may be transcribed to

$$b^{-1}(d\theta/d\alpha) = 1 - (a\theta/b\alpha), \qquad \alpha \ll 1 \quad (15)$$

The left-hand side of Eq. (15) is the ratio of the rate of accumulation of heat to its rate of supply by the chemical processes involved. The second term on the right-hand side is the ratio of the rate of heat loss to its rate of supply. Neglect of this term ($a = 0$) clearly corresponds to the assumption of adiabatic conditions. Merzhanov and Dubovitskii assume that the left-hand side of Eq. (15) is small in comparison with unity and postulate that, under these conditions, the system will adopt a quasi-stationary state in which "the principal role in the nonisothermal reaction process is played by the isothermal alteration in the velocity." In contrast, in our approximate theory, there is no requirement that $a\theta/b\alpha = a/(1 + a)$ shall tend to unity. Numerical values for a turn out to be 0.40 at 540°K and 0.17 at 560°K. This is roughly the temperature range studied over which ignition occurred. For our system, therefore, it seems that the Merzhanov and Dubovitskii assumption of a quasi-stationary state would not be justified except, possibly, well below the explosion limit.

In contrast, our assumption of an isothermal rate law, $(1/\alpha)\, d\alpha/dt = k(T_0)$, is based on experimental evidence. All that the theory requires is that k shall be a single-valued function of T_0 and independent of t. The empirical fact that k obeys the Arrhenius equation (see Fig. 1) is the justification for calling k an "effective rate constant."

Calculation of Ignition Times

Ignition will occur when the relative self-heating temperature exceeds a particular value of θ, say $\theta = n$. The corresponding ignition time obtained from Eq. (14) and (9) is

$$t_n = (1/k \ln\{n(1 + a)/b\alpha_0'\} \quad (16)$$

As a appears only in the factor $1 + a$ inside the logarithmic term its influence on the final values of t_n is rather small. We may term the ignition time t_n^0 calculated from Eq. (16) with $a = 0$, the zero-order approximation. Reasons will shortly be given in support of the value 0.01 cal deg^{-1} min^{-1} for H. Using this value, and the values 312 cal/gm for Q and 0.34 cal/gm deg for C, t_n, and t_n^0 were calculated from Eq. (16). With $n = 1$, t_n and t_n^0 differed by only $2\frac{1}{2}\%$ at 540°K and by 1% at 560°K. The plot of log t_n is shown in Fig. 2 as a function of T_0^{-1}. The lines for $n = 1$ and $n = 2$ were in good agreement with the experimental data. The line for $n = 30$ is also shown in Fig. 2 to illustrate the relative

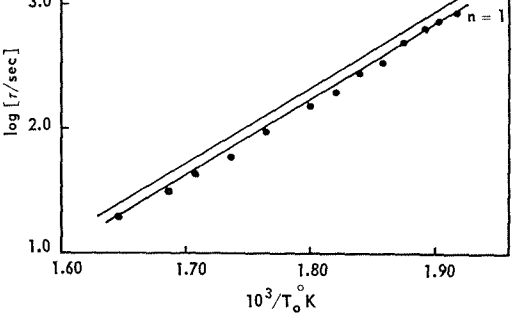

FIG. 2. Ignition times as a function of T_0^{-1}. Lines show calculated values; points are experimental results.

insensitivity of log t_n to the chosen value for n, if it is greater than 1. Zero-order calculations are not shown since they differ but little from the first-order plots.

Calculation of Self-Heating Temperatures

Experimentally determined values of θ are shown by the points in Fig. 3. These were fitted to curves calculated from Eq. (14) by choosing suitable values of $\alpha_0'/(1 + a)$ but using the experimental values of k and E found from the kinetic experiments. Since the $\theta(t)$ curves at various temperatures (T_0) should be satisfied by unique values of H and α_0', values of $1/(1 + a)$

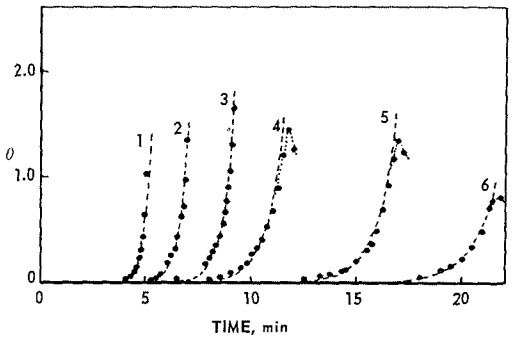

FIG. 3. The relative excess temperature θ as a function of time for pellets of NH_4ClO_4 containing 4.56% of Cu_2O. Points represent experimental values. Dashed lines are the best fit of Eq. (14). (1) 271.2°C; (2) 266.8°C; (3) 263.6°C; (4) 253.4°C; (5) 250.4°C; (6) 245.8°C. Five minutes has been added to the time scale for curve (6) for the sake of clarity.

were calculated for a set of arbitrary values of H and the corresponding values of α_0' were found. These are shown in Fig. 4 in the form of plots of $-\log \alpha_0'$ versus H. These curves should show a common point of intersection. That they do not do so is due to uncertainties in the (unsmoothed) values of k used in the calculation. The only triple intersection lies close to $H = 0.01$ cal deg^{-1} min^{-1}, the corresponding value of $-\log \alpha_0'$ being in good agreement with the kinetically determined value, 7.78. A set of theoretical self-heating curves have been calculated using this value of H and the kinetic values of α_0' and k (see Fig. 1). The results for four typical runs (including both the best and the worst fit) are shown in Fig. 5. On the whole the agreement is rather encouraging. The shape of the self-heating curves is well reproduced and the discrepancies in the induction periods are only in one instance as large as 25%. It should be borne in

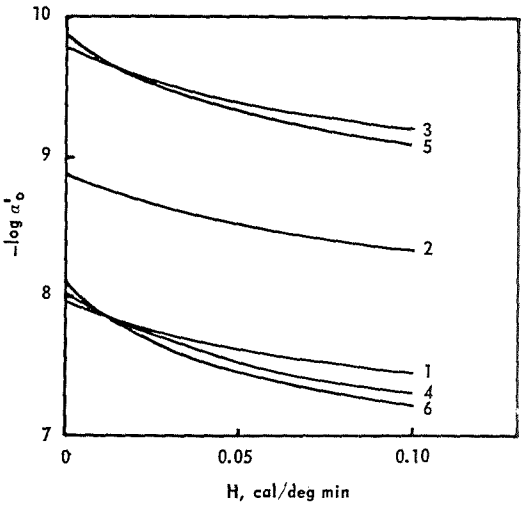

FIG. 4. The isotherms show the values of H and $-\log \alpha_0'$ required to give the best fit to the self-heating curves shown in Fig. 3.

mind that the reproducibility in the experimental ignition times is only ±10%.

The Critical State

The condition that self-heating shall result in an explosion is that $d\theta/dt$ shall always be positive, i.e., that

$$d\alpha/dt > ak\theta/b \qquad (17)$$

The condition for nonexplosion is that $d\theta/dt$ shall be zero for $0 < \alpha < 1$ (i.e., for $d\alpha/dt \neq 0$). Equation (11) then yields

$$d\alpha/dt = ak\theta/b \qquad (18)$$

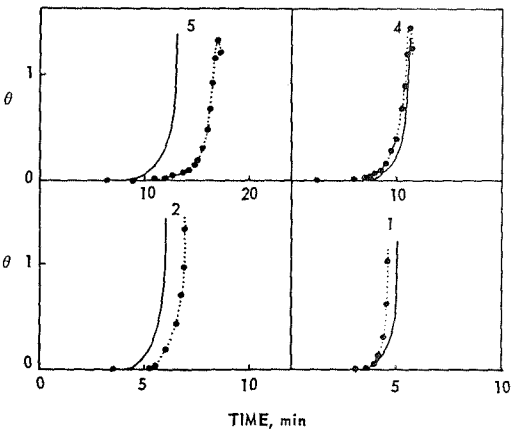

FIG. 5. Comparison of theoretical self-heating curves with experimental data. Only kinetic information has been used in the calculation of these curves from Eq. (14). Temperatures as for Fig. 3.

as the condition for nonignition. Clearly a kinetic equation fitted only to the acceleratory period of the reaction cannot predict a critical state except for the physically uninteresting situation $a \gg 1$. Although our kinetic results were not fitted beyond the acceleratory stage (because the runs usually ended in an explosion) it is possible to account approximately for the deceleratory stage of the reaction by writing

$$d\alpha/dt = k\alpha(1 - \alpha) \qquad (19)$$

On combining Eqs. (19) and (18) and using the physically realistic assumptions that, when explosion just fails to occur, $d\theta/dt = 0$ when $\alpha \simeq 0.5$, $\theta \simeq 1$, we are able to calculate a value for H from the experimental values of k, m_0, and T_0 which correspond to the critical state. The result is $H = 0.012$ cal deg^{-1} min^{-1} in satisfying agreement with the previous value.

References

1. Frank-Kamenetskii, D. A.: *Diffusion and Heat Exchange in Chemical Kinetics*. University Press, Princeton, U.S.A., 1956.
2. Frank-Kamenetskii, D. A.: Acta Physicochimica U.R.S.S., *16*, 357 (1942).
3. Harris, E. J.: Proc. Roy. Soc. (London), *A175*, 254 (1940).
4. Rice, O. K.: J. Chem. Phys., *8*, 727 (1940).
5. Chambré, P. L.: J. Chem. Phys., *20*, 1795 (1952).
6. Semenov, N. N.: Z. Physik, *48*, 571 (1928).
7. Thomas, P. H.: Trans. Faraday Soc., *54*, 60 (1958).
8. Thomas, P. H.: Trans. Faraday Soc., *56*, 837 (1960).
9. Gray, P. and Harper, M. J.: Trans. Faraday Soc., *55*, 581 (1959).
10. Rice, O. K., Allen, A. O., and Campbell, H. C.: J. Am. Chem. Soc., *57*, 2212 (1935).
11. Todes, O. M. and Melentiev, P. B.: Zhur. Fiz. Khim., *13*, 1594 (1939).
12. Todes, O. M. and Melentiev, P. B.: Zhur. Fiz. Khim., *14*, 1026 (1940).
13. Gray, P. and Harper, M. J.: *Reactivity of Solids*, p. 283. Elsevier, Amsterdam, 1960.
14. Frank-Kamenetskii, D. A.: Zhur. Fiz. Khim., *20*, 139 (1946).
15. Thomas, P. H.: Proc. Roy. Soc. (London), *A262*, 192 (1961).
16. Jacobs, P. W. M. and Kureishy, A. R. Tariq: J. Chem. Soc., *1962*, 556.
17. Merzhanov, A. G. and Dubovitskii, F. I.: Proc. Acad. Sci. U.S.S.R., *120*, 427 (1959).
18. Merzhanov, A. G. and Dubovitskii, F. I.: Zhur. Fiz. Khim., *34*, 1062 (1960).

Discussion

Dr. A. B. Amster (*Stanford Research Institute*): As the authors indicate, the mathematical treatment of the self-heating system requires the introduction of restrictive assumptions. These relate to the geometry, the chemical kinetics, or the boundary conditions. Consequently, the significance of experimental studies and the applicability of results to other real situations is, at best, difficult and tenuous.

This paper meets head on the problem of obtaining information from which ignition delays can be predicted. In defining and confirming the validity of the concept of "effective rate constant" it is possible to avoid the necessity of assuming zero-order or, under some circumstances, first-order kinetics. By utilizing Thomas' model troublesome aspects of heat transfer rates are avoided. In independent experiments, internally consistent values are obtained for the arbitrary parameters and reasonable values are predicted for the induction periods. This is an encouraging aspect of this semi-empirical heuristic approach.

A question has been asked regarding the alternate assumptions that ignition occurs in the solid phase or occurs in the gaseous phase and propagates to the solid. I shall not become involved in the kinetic problem but should like to reiterate that no assumption is made as to the nature of the kinetics or the phase in which the reaction occurs. So long as the "effective rate constant" behaves as if it were a true rate constant and so long as the heat is evolved within the geometrical boundaries of the solid sample, the requirements are met.

The experiments reported involve the reaction, nonisothermally and nonadiabatically, of the solid samples. These conditions invite the application of Semenov's unrealistic condition as modified and made useful by Thomas. An alternative approach which avoids this problem is to study self-heating adiabatically.

Such an approach also has the value of exposing the kinetics to more direct study. I am pleased to say that we are arranging with Professor Jacobs for the authors to furnish some of their samples for use in our adiabatic apparatus. The comparison will be interesting.

I should like to raise a point regarding this paper and others presented on the development of hot spots. Our mathematical and computing precision far exceed that with which we are able to conduct our experiments, and accordingly I, for one, question the wisdom of continuing to develop more refined computing systems while, at the same time, the precision of the kinetic and thermodynamic data remains so limited.

TURBULENT BOUNDARY LAYER COMBUSTION IN THE HYBRID ROCKET

G. MARXMAN AND M. GILBERT

In this paper an effort has been made to survey recent theoretical and experimental work related to several aspects of the hybrid combustion process. It has been found that hybrid combustion is controlled by the rate at which heat can be delivered to the fuel surface, rather than by the surface reaction rates. By assuming the combustion occurs in a turbulent boundary layer, a regression rate equation has been developed. This formula is based on the procedures used in other relatively recent studies of heat transfer in reacting boundary layers.

Two important factors in this equation are the position of the flame in the boundary layer, and the effective heat of gasification. A simple analysis provides an estimate of the flame position when the boundary layer is turbulent. It is found that for a Plexiglas–oxygen system, the flame height above the surface should be approximately in the range of 10% to 20% of the boundary layer thickness, depending on operating conditions. The surface gasification process is also discussed.

The boundary layer nature of the combustion process leads one to anticipate that combustion may occur at a fuel-rich mixture ratio. This has been observed experimentally, and the boundary layer combustion model suggests a means of improving the combustion efficiency. This has also been proven experimentally.

The regression rate equation predicts the existence and location of the minimum regression rate in a special case where the nonlinear ballistics problem can be treated by an approximate method. This provides a considerable confidence in the underlying assumptions. A theoretical estimate of the regression rate agrees reasonably well with the observed experimental data. However, much experimental and theoretical work is still needed to clarify the influence of the parameters in the equation, and to provide a description of the internal ballistics under general operating conditions.

Introduction

The "hybrid" rocket engine is a potentially important propulsion technique, because it shows promise of combining many of the advantages of both liquid and solid rockets. The configuration of the hybrid engine is basically similar to that of a solid rocket, except that the solid propellant of the latter is replaced by a solid fuel. A vaporized oxidizer streams axially through the core of the solid fuel, and after ignition the gas phase combustion of the oxidizer and fuel provides the heat necessary to vaporize the fuel. Combustion is then self-sustaining, and the combustion products are raised to a high temperature.

This paper gives a partial account of recent progress in studies of the boundary layer combustion process in the hybrid engine. Several fundamental aspects of the combustion mechanism are discussed in an effort to indicate the important variables and to clarify the behavior associated with hybrid engines. Some experimental results which highlight features of the model are briefly discussed.

Hybrid Combustion Model

The combustion model for the hybrid engine is similar to that of a turbulent diffusion flame, where the flame zone is established within the boundary layer. In the hybrid system, fuel enters the boundary layer as a result of the sublimation process at the wall surface, while oxidizer is fed into the boundary layer from the main stream. Combustion occurs when a suitable mixture ratio has been achieved. This suggests a model for the hybrid combustion process wherein the flame zone is treated, to a first approximation, as a discontinuity in the temperature gradient and composition profiles, as illustrated in Fig. 1.

According to this model the boundary layer comprises two zones, one above the flame where the temperature gradient and velocity gradient are opposed in direction, and one below the flame where the gradients are in the same direction. The zone below the flame is the effective boundary layer for heat transfer to the wall, while both zones together form the boundary layer for momentum transfer.

The formulation of a hybrid combustion theory

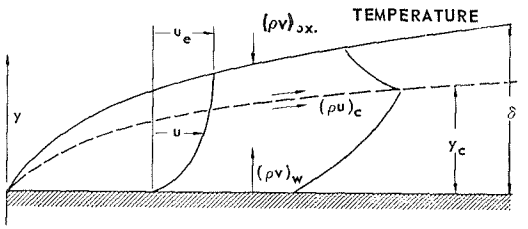

FIG. 1. Boundary layer combustion model.

requires consideration of the process of heat transfer from the flame to the wall, since the regression rate is proportional to this heat flux:

$$\rho_f \dot{r} = (\rho v)_w = \dot{Q}_w/\Delta H \qquad (1)$$

where ρ_f = density of solid fuel; $\dot{r}$ = linear regression rate of fuel surface; $(\rho v)_w$ = gas phase mass flux of fuel at the fuel surface; $\dot{Q}_w$ = heat transfer per unit area to the wall; ΔH = effective heat of gasification of the solid fuel. The effective heat ΔH is the total energy required to gasify a unit mass of solid fuel originally at the internal temperature of the solid grain. If the fuel were Plexiglas, for example, ΔH would include the sensible heat needed to raise the solid fuel from the steady-state internal temperature to the sublimation temperature at the surface, the energy required for depolymerization, and the ordinary latent heat of sublimation for the monomer. Other fuel materials would have similarly unique total heats of gasification.

During the past decade there has been great interest in heat transfer through a chemically reacting boundary layer such as that which occurs when a very hot gas flows over a surface. Several investigators of this problem have considered the influence of mass addition at the wall (frequently called "blowing"), as is found when there is surface ablation, for example. A comprehensive account of the present understanding of convective heat transfer through the reacting boundary layer with mass addition is given by Lees.[1] The hybrid combustion process falls within this general category of heat transfer problems, and the relatively recent studies in this area provide the foundation for an analytical treatment of hybrid combustion.

It has been found[1] that if the gas mixture comprises two groups of components, where the components in each group have molecular weights of the same order and similar collision cross sections, then the gas may be replaced by an effective binary mixture, in which each group acts as a single component from the standpoint of diffusion. If in addition the Lewis number Le = 1 when the boundary layer is laminar, and if Reynolds' analogy is valid when the boundary layer is turbulent, an important simplification is possible. The heat flux is then independent of both the transport mechanism and the magnitudes of reaction rates in the gas, and it is described by an equation formally identical to that for a pure, nonreacting gas:

$$\dot{Q} = -(k/\bar{C}_p)(\partial h/\partial y) \qquad (2)$$

where k = thermal conductivity appropriate to laminar or turbulent flow; $\bar{C}_p$ = mean specific heat; h = sum of sensible (thermal) and chemical (heat of formation) enthalpies; y = coordinate normal to the surface.

With the heat flux given by this equation, a Stanton number C_H can be defined in the usual way. In the present case, the Stanton number is defined in terms of the mass flux and enthalpy at the flame, because this leads to a convenient, separate parameter u_e/u_c which relates the regression rate to the flame position. This parameter, in turn, can be related to the independent operating variables of the system quite easily, as shown in the next section.

Thus, the Stanton number is defined by:

$$\dot{Q}_w = \left(\frac{k}{\bar{C}_p}\frac{\partial h}{\partial y}\right)_w = C_{H_0}\frac{C_H}{C_{H_0}}\rho_c u_c (h_{c_s} - h_{w_g}) \qquad (3)$$

where C_{H_0} = Stanton number in the absence of blowing; $\rho_c u_c$ = axial mass flux at the combustion layer; h_{c_s} = stagnation enthalpy at the flame; h_{w_g} = enthalpy at the wall in the gas phase. The reduction in heat transfer to the wall caused by blowing is accounted for by the ratio C_H/C_{H_0}. When the boundary layer is turbulent, surface ablation can result in a value as low as about 0.2 for this ratio.[2] With the much greater surface mass addition found in hybrid combustion, C_H/C_{H_0} may be somewhat less than 0.2.

In a boundary layer without combustion or blowing, the transition from laminar to turbulent flow occurs when the Reynolds number (based on the distance from the leading edge) is 10^5–10^6. The presence of ordinary evaporation, as when the gas stream flows over water, may reduce the transition Reynolds number to 10^4.[3] This effect is greatly magnified in the hybrid system, due to the combustion and extensive fuel sublimation at the surface. Therefore, the hybrid boundary layer is expected to be turbulent over most of its length. It follows that the Stanton number can probably be evaluated by using the semiempirical turbulent boundary layer theory, if Reynolds' analogy is valid with chemical reactions and blowing. This is the approach taken in the earlier turbulent boundary layer heat transfer studies surveyed by Lees,[1] where it has given satisfactory results.

If Le = Pr = 1 (Pr = Prandtl number = $\bar{C}_p\mu/k$), Reynolds' analogy holds across the entire boundary layer and is expressed by the equation:

$$-\frac{\dot{Q}}{\partial h_s/\partial y} = \frac{\tau}{\partial u/\partial y} \tag{4}$$

where $\dot{Q}$ = heat flux; τ = shear stress. A relation between the Stanton number and the friction coefficient, consistent with the hybrid combustion model, is obtained by taking $\dot{Q}/\dot{Q}_w = \tau/\tau_w$, integrating from the wall to the flame (inasmuch as the zone below the flame is the effective boundary layer for heat transfer to the wall) and multiplying by $1/\rho_c u_c$:

$$\dot{Q}_w/\rho_c u_c(h_{c_s} - h_{w_g}) = \tau_w/\rho_c u_c^2$$

or:

$$C_H = \tfrac{1}{2}C_f(\rho_e u_e^2/\rho_c u_c^2) \tag{5}$$

where C_H is defined by Eq. (3) and C_f = local skin-friction coefficient = $\tau_w/(\rho_e u_e^2/2)$.

The upper limit, or boundary, on this integration is the lower edge of the reaction zone or flame. The combustion reactions occur in a thin zone just above this boundary, while the integration is confined to the boundary layer zone between this boundary and the fuel surface. In this region there are no reactions, or the reactions are so slow as to be negligible. From the standpoint of the integration the upper boundary, or flame, is seen as a source for heat and combustion products, and a sink for gaseous fuel. The assumptions Le = Pr = 1 and $\dot{Q}/\dot{Q}_w = \tau/\tau_w$ are required only in the domain of the integration, where from the boundary layer momentum and energy equations they can be shown to be entirely compatible. No assumptions regarding the details of the actual reaction zone are implied or necessary, and this is important. For example, it is unlikely that Reynolds' analogy is valid within the thin reaction zone itself, although it is probably quite acceptable in the nonreacting zones of the boundary layer above and below the flame.

According to the postulated model for hybrid combustion the friction coefficient is approximately the same as that for an ordinary boundary layer with equivalent blowing, because the velocity profile is practically unchanged. For the turbulent boundary layer with no blowing, the friction coefficient is given by the well-known empirical formula:

$$C_{f_0} = 2C\ \mathrm{Re}_x^{-0.2}\ \mathrm{Pr}^{-\frac{2}{3}} \tag{6}$$

Thus, for the hybrid when Pr = 1,

$$C_{H_0} = C\ \mathrm{Re}_x^{-0.2}\ (\rho_c/\rho_c)\,(u_c/u_c)^2 \tag{7}$$

where C = function of mainstream Mach number $\approx$ 0.03 for the low Mach numbers expected in the hybrid; $\mathrm{Re}_x = (\rho_c u_c x)/\mu$ (Reynolds number referred to distance x from leading edge).

Equations (3) and (7) together describe the convective heat transfer from the flame to the fuel surface. Normally this is expected to be the primary mechanism of heat transfer, but in some cases radiation may make a significant contribution. If, for example, a gray body radiation term is added to the convective heat transfer, then according to Eq. (1) the regression rate for the case of a turbulent boundary layer is given by:

$$\dot{r} = \frac{CG\ \mathrm{Re}_x^{-0.2}}{\rho_f}\frac{C_H}{C_{H_0}}\frac{u_c}{u_c}\frac{(h_{c_s} - h_{w_g})}{\Delta H} + \frac{\sigma\epsilon_w(\epsilon_g T_c^4 - \alpha_g T_w^4)}{\rho_f\,\Delta H} \tag{8}$$

where $C \approx 0.03$; $G = \rho_e u_e$; σ = Stefan–Boltzmann constant; ϵ_w = emissivity and absorptivity of the wall; ϵ_g = emissivity of gas at T_c; α_g = absorptivity of gas at T_w or T_{mean} in boundary layer; T_c = flame temperature; T_w = wall temperature.

Equation (8) is regarded as a basic framework for a theory of hybrid combustion. However, it is still necessary to determine the behavior of the various parameters appearing in the equation before the theory can be considered as complete. Under many practical operating conditions radiative heat transfer to the fuel surface is likely to be small relative to the convective contribution; therefore the most important of these parameters are the blowing coefficient C_H/C_{H_0}, the velocity ratio u_e/u_c (which is determined by the flame position in the boundary layer), and the effective gasification heat ΔH. The integral technique of boundary layer theory can be applied to the hybrid combustion model to evaluate C_H/C_{H_0} and u_e/u_c, but this will not be discussed in the present paper. A relatively crude estimate of the flame position and the ratio u_e/u_c is presented below, and the sublimation process underlying the gasification heat ΔH is considered.

The Flame Position in the Boundary Layer

Evaluation of the parameter u_e/u_c in Eq. (8) requires that the flame position and velocity profile in the hybrid boundary layer be determined. A first approximation to the location of the flame relative to the momentum boundary layer and the ratio u_e/u_c can be obtained through a relatively simple calculation, based on the combustion model represented in Fig. 1.

For this analysis reactions are considered to be confined to a "flame sheet" of negligible thickness, at an elevation y_c above the fuel surface. The flame zone is expected to be well above the laminar sublayer, and it is assumed that Reynolds' analogy is valid in the boundary layer zone above the flame. These assumptions lead to the important simplification that the concentration profiles can be represented as linear functions of the velocity profile in the region above the flame, provided this is compatible with the boundary conditions.[1] According to the model, the change in the velocity profile due to the presence of a combustion zone is negligible, as a first approximation, but the influence of surface mass addition must be considered.

There have been several reasonably successful attempts to extend the "mixing length" technique of turbulent thin film theory so that it gives the velocity profile with blowing.[4–8] In all cases this procedure begins with the following equation, which is obtained from the boundary layer momentum equation and is valid near the wall[1]:

$$\tau = (\mu + \rho\epsilon)(du/dy) \approx \tau_w[1 + B(u/u_e)] \quad (9)$$

where τ is the shear stress; μ is the viscosity coefficient; ϵ is the turbulent exchange coefficient; τ_w is the shear stress at the wall; and B is the $(\rho v)_w/(\rho_e u_e C_f)/2$. In the mixing length method a suitable function of u and y is substituted for ϵ in this equation, which is assumed to hold across the entire boundary layer, and integration yields a velocity profile. Unfortunately, the profile equations obtained this way are usually somewhat inconvenient for present purposes. A form more suitable for this analysis can be obtained through a slightly different approach.

By defining $\phi = u/u_e$ and $\eta = y/\delta$ Eq. (9) can be written in the dimensionless form:

$$d\phi/d\eta = \left[\frac{\tau_w\delta/u_e}{\mu + \rho\epsilon}\right](1 + B\phi)$$
$$= f(y, B)(1 + B\phi) \quad (10)$$

It is clear that when $B = 0, f(y, 0) = (d\phi/d\eta)_{B=0}$. When there is no surface mass addition, the velocity profile in a turbulent boundary layer can be described adequately by the empirical relation:

$$\phi = \eta^n \quad (11)$$

where $n \approx 1/7$ when the Reynolds number (based on axial grain position) $\mathrm{Re}_x \lesssim 10^6$.[9] Therefore,

$$(d\phi/d\eta)_{B=0} = n\eta^{n-1} \quad (12)$$

It will be assumed that in Eq. (10) $f(y, B) = An\eta^{n-1}$, where $A = A(B)$ and $A(0) = 1$. Furthermore, as a first approximation the correction term due to blowing can be written $B\phi \approx B\eta^n$. This suggests the following equation as an approximate description of the velocity profile with blowing:

$$d\phi/d\eta = An\eta^{n-1}(1 + B\eta^n) \quad (13)$$

After integrating Eq. (13), the constant A and the integration constant are evaluated by imposing the boundary conditions $\phi(0) = 0$ and $\phi(1) = 1$. The solution is:

$$\phi = \frac{\eta^n[1 + (\frac{1}{2}B)\eta^n]}{1 + \frac{1}{2}B} \quad (14)$$

As required in the formulation, Eq. (14) reduces to Eq. (11) when there is no blowing. This approach should provide a first approximation to the profile distortion caused by blowing and has the important advantage of a simple, closed form.

In principle, oxidizer is delivered to the flame by both convection and diffusion. However, the convective flow is expected to be practically tangential to the flame sheet; furthermore, the convective flux of oxidizer is proportional to the mass fraction of oxidizer, which is small near the flame where oxidizer is being consumed. In contrast, the diffusion current is proportional to the mass fraction gradient, and at the flame this gradient is large in the direction normal to the flame sheet. It follows that the flux of oxidizer into the flame is ordinarily diffusion-controlled, and the convective flux is negligible. Therefore, if Reynolds' analogy is valid the following relation describes the oxidizer mass flux at the flame:

$$|(\rho v)_{ox}|_c = |\rho_c(\epsilon + D)_c(\partial K_{ox}/\partial y)_c|$$
$$= [O/F](\rho v)_w \quad (15)$$

where: $[O/F]$ = oxidizer-to-fuel mass ratio at which combustion occurs; D = molecular diffusion coefficient; K_i = mass fraction of species i.

This expression defines the flame position as that point in the boundary layer where the oxidizer mass flux, given by the left-hand side of the equation, and the fuel flux $(\rho v)_w$ meet in the proportions required for combustion to occur. Ideally, this mass fraction of oxidizer to fuel would be near the stoichiometric mixture ratio, but there is evidence that hybrid combustion occurs at a fuel-rich mixture ratio. This is discussed further in a later section of this paper.

It is assumed in Eq. (15) that all fuel leaving each unit area of the solid surface $(\rho v)_w$ reaches the flame and is consumed in the combustion reaction. Also, gradients in the axial direction are neglected relative to gradients normal to the fuel surface, which is consistent with the boundary layer character of the flow.

It can be shown that a small fraction of the fuel leaving the grain surface fails to reach the flame, remaining instead in the boundary layer zone below the flame. For simplicity this fuel loss can be accounted for by using an "effective" $[O/F]$ in Eq. (15).

As a first approximation the turbulent exchange coefficient ϵ is assumed to have the same behavior as in a boundary layer without combustion or blowing. According to the mixing length hypothesis of Prandtl[10]:

$$\epsilon = C'y^2(du/dy) \tag{16}$$

where C' = empirically determined constant = 0.16.[11]

Equations (14) and (16) can be combined to obtain an expression for ϵ in terms of y (or η). Furthermore, the assumption that the oxidizer mass fraction profile is a linear function of the velocity profile provides the following equation for the mass fraction in the boundary layer zone above the flame:

$$K_{ox} = K_{ox_e}\left[\frac{\eta^n[1 + (\frac{1}{2}B)\eta^n] - \eta_c{}^n[1 + (\frac{1}{2}B)\eta_c{}^n]}{1 + \frac{1}{2}B - \eta_c{}^n[1 + (\frac{1}{2}B)\eta_c{}^n]}\right] \tag{17}$$

Therefore:

$$\left(\frac{dK_{ox}}{dy}\right)_e = \frac{K_{ox_e}}{\delta}\frac{n\eta_c{}^{n-1}(1 + B\eta_c{}^n)}{\{1 + \frac{1}{2}B - \eta_c{}^n[1 + (\frac{1}{2}B)\eta_c{}^n]\}} \tag{18}$$

With the combustion process occurring within the boundary layer, it is expected that a controlling factor in determining the flame characteristics, including its location, will be the rate at which oxidizer can be delivered from the main stream to the flame. This suggests that the flame will be well above the laminar sublayer, so that at the flame the molecular diffusivity $D \ll \epsilon$ and can be neglected. If in addition $\rho_c/\rho_e \approx T_e/T_c$, Eqs. (14), (15), (16), and (18) can be combined to yield the following relation for the position of the flame relative to the boundary layer thickness:

$$\frac{\eta_c{}^{2n}(1 + B\eta_c{}^n)^2}{(1 + \frac{1}{2}B)\{1 + \frac{1}{2}B - \eta_c{}^n[1 + (\frac{1}{2}B)\eta_c{}^n]\}} \approx \frac{[(\rho v)_w/\rho_e u_e][O/F]T_c/T_e}{n^2C'K_{ox_e}} \tag{19}$$

With the relative flame position determined by this equation, the parameter $u_e/u_c \equiv 1/\phi_c$ in Eq. (8) can be obtained from Eq. (14).

It is not possible to calculate precisely the value of the right-hand side of Eq. (19) for a given hybrid configuration. In general, the empirical constant C' will not be the same for the hybrid boundary layer as for an ordinary turbulent boundary layer, although it should have a similar value. Furthermore, the friction coefficient C_f (and therefore B), the mixture ratio $[O/F]$, and the temperature ratio T_c/T_e are not precisely known for the hybrid. However, it is probably possible to estimate the right-hand side of Eq. (19) to within a factor of two, or perhaps better. Fortunately, this is sufficient to provide useful information, because it locates the flame within reasonably narrow limits.

For typical hybrid operation with a Plexiglas fuel, where $[O/F] \sim 1$, $K_{ox_e} \sim 1$, $T_c/T_e \sim 2$, and $(\rho v)_w/\rho_e u_e \sim 0.005$ the right-hand side of Eq. (19) is approximately 3 to 3.5, assuming $n = 1/7$. If $5 \lesssim B \lesssim 15$, this corresponds to $\eta_c = y_c/\delta \approx 0.15$ and from Eq. (14), $u_c/u_e \approx 1.7$. For a given value of $(\rho v)_w/\rho_e u_e = B \cdot C_f/2$, the flame position η_c is a relatively insensitive function of B, according to Eq. (19). This is important, because a small change in $(\rho v)_w/\rho_e u_e$ may correspond to a large change in B; i.e., C_f decreases as $(\rho v)_w$ increases so that B usually varies much more than the product $B \cdot C_f/2$.

An examination of Eq. (8) (neglecting radiation) indicates that $\rho_f \dot{r}/G = (\rho v)_w/\rho_e u_e$ varies approximately as $(Gx/\mu)^{-0.2}$. This relatively weak dependence suggests that over a fairly wide range of operating conditions, the flame position relative to the boundary layer thickness will not change drastically for a given fuel and oxidizer. For example, if G is increased by a factor of 3, η_c should decrease by about 20%. Due to the surface fuel addition G increases with x, and it follows that η_c should also decrease slowly with x, i.e., as $(Gx)^{-0.2}$. Allowing for the uncertainty in evaluating the right-hand side of Eq. (19), the analysis indicates that in normal operation with a Plexiglas-oxygen system $0.10 \lesssim y_c/\delta \lesssim 0.20$, while $2 \lesssim u_e/u_c \lesssim 1.5$ over most of the grain length where the boundary layer is thin relative to the port radius. Schlieren studies of the boundary layer have been initiated to check the validity of these conclusions. Preliminary results show very good agreement between the predicted and observed behavior.

Effective Heat of Gasification

The important characteristics of the gasification process at the fuel surface may be clarified by considering the specific case of a Plexiglas-type polymer. The corresponding surface reactions are:

$$\text{Polymer}(s) \rightarrow \text{monomer}(l) \quad +\Delta H_1 \tag{20}$$

$$\text{Monomer}(l) \leftrightharpoons \text{monomer}(g) \quad +\Delta H_2 \tag{21}$$

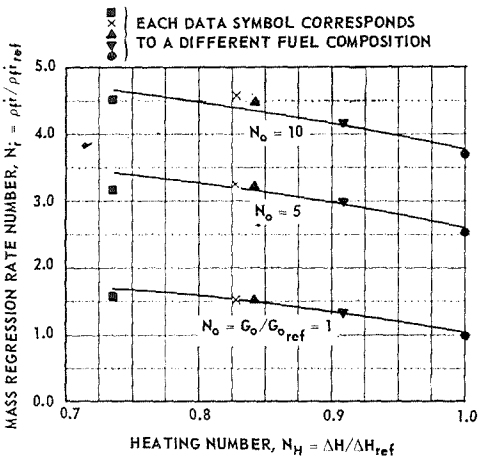

FIG. 2. Influence of effective heat of gasification on fuel flux.

where ΔH_1 is the heat of decomposition per unit mass; ΔH_2 is the heat of vaporization per unit mass.

The vaporization equilibrium (21) is established very rapidly. The decomposition rate (20) is a function of the surface temperature T_s and normally will control the over-all flux into the gas phase. Therefore, a simple view of the process is that steady-state combustion is established when the surface is heated to a temperature T_s such that the solid phase decomposition rate equals the net gasification rate given by Eq. (1). Usually the activation energy for decomposition is great enough so that large changes in the regression rate correspond to a relatively small variation in T_s.

For this process ΔH in Eq. (1) is:

$$\Delta H = \Delta H_1 + \Delta H_2 + C_f'(T_s - T_o) \quad (22)$$

where C_f' = heat capacity of solid fuel; T_o = steady-state internal temperature of fuel. Ordinarily the thermal diffusivity of the fuel is very low. Combined with the high regression rate, this leads to a rapid exponential decay of the temperature with distance from the surface; therefore, T_o is essentially the ambient temperature.

Figure 2 shows the average mass regression rate as a function of the total heat of gasification for some fuel formulations. The regression rate and heat of gasification are expressed as dimensionless numbers, in terms of arbitrarily chosen reference values; $N_r = (\rho\dot{r})_f/(\rho\dot{r})_{f\,ref}$ and $N_H = \Delta H/\Delta H_{ref}$. The data were obtained in a burner with gaseous oxygen flowing over fuel slabs about 1 inch wide, 3 inches long, and $\frac{5}{8}$ of an inch thick. The pressure was in the range of 400 to 500 psi. Total burning times were 5–10 sec. Three values of the oxygen mass flux G_0 (based on the initial port area) were used—($N_0 = G_0/G_{0\,ref}$). Figure 2 shows the type of inverse dependence of mass regression rate on ΔH predicted by Eq. (1). Furthermore, $\rho_f\dot{r}\,\Delta H$ is roughly constant, which implies that $\dot{Q}_w$ is nearly constant throughout this limited $\dot{r}$ range.

Combustion Mixture Ratio

It was mentioned in connection with Eq. (15) that hybrid combustion usually does not occur at the stoichiometric mixture ratio; also, in calculating the numerical example in the section entitled *The flame position of the boundary layer*, it was assumed that $O/F \approx 1$, which is half of the stoichiometric O/F ratio. The over-all mixture ratio (based on the total mass flow of oxidizer and fuel) has been observed to be fuel-rich rather than stoichiometric. This may be expected because the boundary layer diffusion process restricts the transport of oxidizer from the main stream to the flame. This leads to a decidedly fuel-rich local mixture ratio at the boundary layer flame zone.

If one considers the opposing concentration gradients of fuel and oxidizer as they exist in the hybrid burner, it is seen that for the reaction zone to be stoichiometric (as in true diffusion flames) the flame front must be established close to the midpoint of the boundary layer, or even near the free stream boundary. On the other hand, the flame can be established close to the surface, in the "buffer" zone of the boundary layer, only if the oxygen-deficient mixture near the wall has a high reaction rate.

Preliminary measurements have shown that the flame temperature is quite low and that the flame is close to the surface. This is consistent with a locally fuel-rich flame (rather than a stoichiometric flame with part of the fuel passing through unburned, for example, which would also result in a fuel-rich over-all mixture ratio). Furthermore, from an analysis of the combustion products the local mixture ratio has been calculated as $O/F \approx 1$ for Plexiglas-oxygen, where the stoichiometric value is 2.[12] Equation (19) predicts the flame position in good agreement with experimental measurements when it is assumed that $O/F = 1$; on the other hand, the sensitivity of Eq. (19) to O/F is such that for $O/F = 2$ the calculated flame height relative to the boundary layer thickness would be more than two times as great as the observed relative position. Therefore, all available evidence consistently supports the conclusion that a locally

fuel-rich reaction zone is controlling the hybrid burner.

Because the flame is within the boundary layer, as in the combustion model, the oxidizer cannot be entirely depleted until the boundary layer completely fills the port, i.e., the turbulent flow is essentially fully developed. Some distance downstream of the point where this happens the flame will form a conical apex at the center of the port, and all oxidizer will then have been consumed. An ordinary, fully developed, turbulent flow is achieved in 40 to 100 diameters. Nearly the same length should be required in the hybrid, because the relative importance of boundary layer thickening due to blowing diminishes downstream, where the boundary layer is already very thick.

It is interesting to compare these observations with typical experimental results. The stoichiometric mixture ratio for an oxygen-Plexiglass system is (oxygen/Plexiglas) = 2. Given the oxygen mass flux G_0 and the fuel mass regression rate $(\rho\dot{r})_f$, the L/D ratio at which all oxygen would be depleted if combustion were stoichiometric all along the grain can be calculated from the following equation:

$$\dot{w}_{ox}/\dot{w}_f = \frac{G_{ox}\pi D^2/4}{(\rho\dot{r})_f \pi D L} = 2$$

For typical experimentally observed values of G_0 and $(\rho\dot{r})_f$ this relation shows that a stoichiometric mixture ratio would deplete the oxygen in somewhat less than 30 diameters. However, all the oxygen cannot enter the boundary layer flame zone in less than 40 to 100 diameters, as previously explained. It follows that the observed combustion must occur at a mixture ratio which is fuel-rich. Experimental measurements have shown that the over-all mixture ratio in the Plexiglas-oxygen system is, in fact, about half the stoichiometric value, i.e., $O/F \approx 1$ instead of 2. Similar results were obtained by others.[12]

This result suggests that the combustion efficiency could be improved by disrupting the core flow at the end of the grain and forcing the unused oxidizer to mix rapidly with the fuel-rich products in the boundary layer. This has been done experimentally, and the performance increased by as much as 30%, reaching nearly the theoretical limit. Practically no additional mixing length was required after the flow was disrupted, because the high-temperature, partially burned mixture reacted almost instantaneously with the excess oxidizer.

Internal Ballistics

It has been observed experimentally that the regression rate has a minimum at some axial position in a circular port configuration. It has been noted[12] that this minimum seems to correspond to a length Reynolds number in the range 3×10^5 to 3×10^6, and the minimum was attributed to transition from a laminar to a turbulent boundary layer. However, this explanation does not seem entirely satisfactory. Although transition occurs in this Reynolds number range in a boundary layer without blowing, the extensive mass addition and combustion in the hybrid boundary layer should cause transition at a much lower Reynolds number. Furthermore, Eq. (8) does not necessarily indicate that the regression rate must increase with x in a turbulent boundary layer. It is quite possible for the regression rate to continue decreasing with x after transition, although the rate of decrease should be less than in a laminar boundary layer.

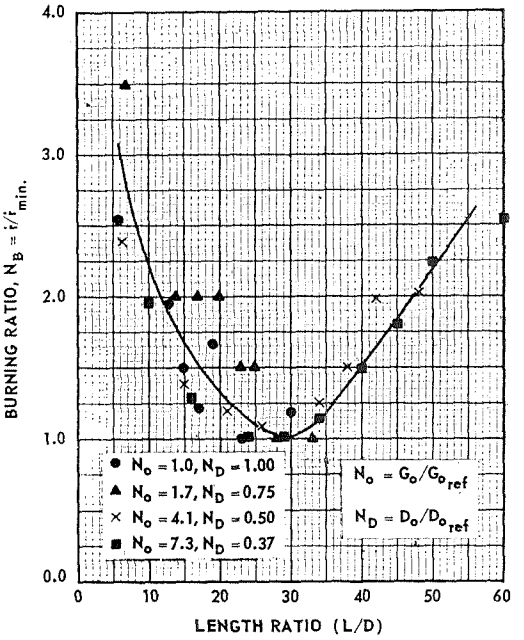

FIG. 3. Regression rate as a function of axial position.

On the other hand, Eq. (8) does predict that there will be a minimum regression rate somewhere in the turbulent boundary layer. Due to the fuel addition G increases with x, while $Re_x^{-0.2}$ decreases. At some point these effects have a crossover, and this corresponds to the minimum regression rate.

An internal ballistics analysis based on Eq. (8) has been performed for the special case where the burning time is short, so that the total change in web thickness during burning is small relative to the initial port radius. It was assumed that Eq. (8) is valid over the entire grain length,

i.e., that transition occurs at a very low Reynolds' number. This analysis yields the following approximate equation for the location of the minimum regression rate in an oxygen-Plexiglas system:

$$(x/L)_{\dot{r}=\min} \approx [2.8\ \mathrm{Re}^{1/5}/(L/D_o)]^{1.25} \quad (23)$$

where $\mathrm{Re} = (G_0 L)/\mu$; L = grain length; D_0 = initial port diameter.

This equation indicates that if $\mathrm{Re} = 10^5$, the minimum regression rate will just be attained at the end of a tube with $L/D_0 \approx 28$. If the grain is longer, the regression rate will have a minimum upstream of the end of the grain.

Figure 3 shows the experimentally determined regression rate as a function of axial position for four different values of G_0 and D_0. The oxidizer mass flux is expressed in terms of the dimensionless ratio $N_0 = G_0/G_{0\,\mathrm{ref}}$, where $G_{0\,\mathrm{ref}}$ is an arbitrarily selected reference value. Similarly, the port diameter and regression rate are given in terms of the dimensionless numbers $N_D = D_0/D_{0\,\mathrm{ref}}$ and $N_B = \dot{r}/\dot{r}_{\min}$, respectively. The agreement between the results and Eq. (23) seems to indicate that the boundary layer is turbulent over most of the grain length, so that transition occurs at $\mathrm{Re} \ll 10^5$. Furthermore, Eq. (8) apparently adequately describes the combustion process in the turbulent boundary layer.

The limiting assumptions underlying Eq. (23) make it impossible to apply this equation to long-duration runs. However, it can be shown that the minimum regression rate will tend to move upstream with time, which agrees qualitatively with experimental results for 60-sec and 120-sec runs.[12]

Calculation of the Regression Rate

From Eq. (8) a quantitative estimate of the regression rate for the Plexiglas-oxygen system can be made. The radiative term is neglected for this system, based on experiments not reported here due to space limitations. It was found that over a wide range of pressure, at constant mass flux, and Reynolds number, the optical opacity of the gases and the absorptivity of the tube wall were sufficiently small to preclude a significant radiative contribution.

A calculation shows that for this system $h_s - h_w/\Delta H \approx 5$. Although C_H/C_{H_0} has not been measured at the high blowing rates considered here, an extrapolation of available data[2] indicates that $C_H/C_{H_0} \approx 0.1$. Taking $u_e/u_c = 2$, a Reynolds number of 10^5, and a value of G_0 corresponding to $N_0 = 4.1$ in Fig. 3, Eq. (8) gives $N_B = 1.2$ (referring to the appropriate $\dot{r}_{\min}$ for that G_0). A comparison with Fig. 3 shows this to be reasonably close to measured values for these conditions. Over a wide range of G_0 and Re Eq. (8) gives results which agree within a factor of two or better with experimental values.

Nomenclature

A	Constant [Eq. (13)]
B	Blowing parameter $= 2(\rho v)_w/\rho_e u_e C_f$
C	Constant [Eq. (7)]
C'	Constant [Eq. (16)]
C_f	Friction coefficient $= 2\tau/\rho_e u_e^2$
C_f'	Heat capacity of solid fuel
C_H	Stanton coefficient
$\bar{C}_p$	Mean specific heat of gas mixture
D	Port diameter; molecular diffusion coefficient
D_0	Initial port diameter before burning
G	Mass flux in main stream $= \rho_e u_e$
G_0	Mass flux in main stream at $x = 0$
ΔH	Effective heat of gasification of the solid fuel
h	Enthalpy
K_i	Mass fraction of species i
k	Effective thermal conductivity of gas mixture
L	Total length of grain
Le	Lewis number $= \rho D \bar{C}_p/k$
n	Exponent, usually 1/7 [Eq. (11)]
O/F	Oxidizer-to-fuel mass ratio at combustion zone
Pr	Prandtl number $= \bar{C}_p\mu/k$
Q	Heat flux
Re	Reynolds' number $= G_0 L/\mu$
Re_x	Reynolds' number $= \rho_e u_e x/\mu$
$\dot{r}$	Linear regression rate
T	Temperature
T_s	Surface temperature
u	Axial velocity component
v	Velocity component normal to fuel surface
$\dot{w}$	Mass flow
x	Coordinate along fuel surface in direction of flow
y	Coordinate normal to fuel surface

Greek Symbols

α_g	Absorptivity of gas [Eq. (8)]
δ	Boundary layer thickness
ϵ	Turbulent exchange coefficient; emissivity [Eq. (8)]
η	y/δ
μ	Viscosity coefficient
ρ	Mass density
σ	Stefan-Boltzmann constant
τ	Shear stress
ϕ	u/u_e

Subscripts

c	Combustion zone
e	Edge of boundary layer (main stream)
f	Fuel
g	Gas phase
i	Species i
min	Minimum
0	No blowing; at $x = 0$
ox	Oxidizer
ref	Reference value
s	Stagnation condition; surface
w	Wall

ACKNOWLEDGMENTS

The authors are grateful for permission to use experimental data supplied by Messrs. Allen Holzman, Donald Matthews, Raymond Muzzy, Thomas Scortia, and Peter Stang. The aforementioned and Dr. David Altman provided enlightening discussion. Research was performed under sponsorship of Advanced Research Projects Agency, Dept. of Defense, under Bureau of Weapons, Dept. of the Navy, Contract NOw 61-1000-c.

REFERENCES

1. LEES, L.: *Combustion and Propulsion, Third AGARD Colloquium* p. 451. Pergamon, 1958.
2. LEADON, B. M. and SCOTT, C. J.: J. Aero. Sci. *23*, No. 8, 798 (1956).
3. PERRY, J. H. (editor): *Chemical Engineers' Handbook, 3rd Edition* 545 (1950).
4. RANNIE, W. D.: Jet Propulsion Laboratory, Progress Report, No. 4-50 (1947).
5. CROCCO, L.: J. Amer. Rocket Soc. *22*, No. 6, 331 (1952).
6. DORRANCE, W. H. and DORE, F. J.: J. Aero Sci. *21*, No. 6, 404 (1954).
7. RUBESIN, M. W.: NACA TN 3341 (1954).
8. DENISON, M. R.: J. Aero. Sci. *28*, No. 6, 471 (1961).
9. SCHLICHTING, H.: *Boundary Layer Theory*, p. 431. Pergamon Press, 1955.
10. PRANDTL, L.: ZAMM *5*, 136 (1925).
11. SCHLICHTING, H.: *loc. cit.*, p. 406.
12. Rocketdyne: Research in Hybrid Combustion Summary Report, December 1, 1960–November 30, 1961, (30 January 1962), Contract Nonr 3016(OO).

Discussion

DR. T. HAUSER (*Rocketdyne*): We are engaged in a very similar program at Rocketdyne, but have confined our pressures to about 1 atmosphere. Dr. Marxman's mechanism for the reactions on the surface has ignored certain basic facts which have considerable influence on the mechanism which can occur, and subsequently on one of your basic assumptions. The facts are these:

(a) The rates of pyrolysis for PMMA as reported by National Bureau of Standards show that the surface temperatures must be greater than 300°C, in view of the relative reaction times, etc.

(b) As has been reported, our measurements are within crude agreement with this minimum.

(c) PMMA starts to soften about 110°C.

(d) If Methylmethacrylate monomer could exist in the liquid state at its boiling point, it would boil at about 100°C (compare to B.P. for methyl acrylate at about 80°C, which polymerizes rapidly at that temperature). Thus the reaction at the surface can be written:

$$\text{PMMA (l)} \rightarrow \text{Products (g)}$$

where the products are a mixture of monomer, dimer, fragments, etc. (Some charring is seen to occur on the surface in our experiments.)

This is no longer an equilibrium process but a kinetically controlled chemical reaction process. The rate $\dot{r}$ will be influenced by the heat flux, of course, but a direct, simple proportionality is not possible. Both the kinetic parameters and the heat flux must be taken into account. For example, higher heat fluxes will produce higher surface temperatures, which in turn increase $\dot{r}$, but also the heat conducted into the fuel and away from the surface increases and some heat is used up in raising the temperature of the pyrolizing layer.

We agree with the statement that our flows produce turbulence over the entire axial length. In fact our minima in $\dot{r}$ vs. axial length (Z) were essentially caused by the apparatus; modifications have corrected this. We have found that the instantaneous $\dot{r}$ values continually decrease throughout our firings and that the initial $\dot{r}$ vs. Z has no minimum but $\dot{r}_0$ steadily increases with Z. After about 30 seconds the $\dot{r}$ vs. Z appears to be about constant, but the average rates still show the initial effects. Thus it is possible to explain the observed variations by transient conditions and reactions in the initial stages of the run. In view of the short run times and small burning surfaces employed by United Technology Corporation, it is suggested that the above phenomena may offer an alternative explanation for the observed results. These areas admittedly require further investigation, which is going on at present at Rocketdyne.

DR. G. A. MARXMAN (*United Technology Corporation*): The basic facts listed by Dr. Hauser are

well known, of course, and they have not been ignored in developing the treatment presented in the paper.

Most materials suitable for use as solid fuels in a hybrid engine are characterized by a relatively large activation energy for depolymerization, while the vaporization process proceeds essentially in equilibrium, i.e., with a high reaction rate. In this situation, which is the one considered in the paper, an increase in heat transfer to the fuel surface will result in a corresponding increase in the regression rate with very little change in the surface temperature. Because of the high activation energy, a very large change in the gasification rate can be accomplished with a small temperature adjustment at the burning surface. Measurements with PMMA show that the surface temperature remains at about 600°K over a wide range of regression rates, which is in agreement with the mechanism just described. Such a process is definitely controlled by the heat flux to the fuel surface, and reaction kinetics play a minor role.

On the other hand, we do not wish to imply that a kinetically controlled process can never occur in the hybrid. If the solid material has a relatively low activation energy, an appreciable change in the surface temperature will be required for a variation in the regression rate. In this case, both the heat flux and the reaction kinetics at the surface are important. For example, if a twofold increase in the heat flux to the surface is insufficient to provide the temperature change required for a corresponding increase in the regression rate, the process is kinetically controlled. This situation may arise in some cases, particularly in the "reverse hybrid," wherein the oxidizer is solid and the fuel gaseous.

The depth to which the temperature "wave" due to surface heating penetrates the grain in steady-state operation is on the order of $K_f/\dot{r}$, where K_f is the thermal diffusivity of the solid fuel, and $\dot{r}$ is the regression rate. In PMMA with typical regression rates this penetration depth is small relative to the distance burned in 1 second, i.e., $\dot{r}$. Thus, the solid fuel is subjected to temperatures exceeding 100°C for a very short time near the surface, and little softening is expected. We have taken motion pictures of the PMMA surface in hybrid operation and there was no evidence of appreciable softening or flowing on the surface.

With materials having a greater thermal diffusivity, or with lower regression rates (as when the hybrid is throttled for an appreciable period), the softening and liquefaction of the surface may become more important. This problem is under investigation at UTC.

With regard to the position of minimum $\dot{r}$, it is important to note that Fig. 3 may be misleading if one does not keep in mind that it depicts the ratio of the average local regression rate to the minimum regression rate over times of the order of several seconds. In the initial few seconds of burning the regression rate may vary by as much as a factor of three over the grain length, as Fig. 3 shows. However, this is a transient effect, and after steady state operation has been established the total variation of regression rate over the grain length is much less. Equation (8), which assumes steady state operation, predicts that the regression rate should vary by about 25% over a length of 50 diameters (excluding the first five diameters). This is entirely in agreement with the observed behavior for longer burning times, where steady state operation definitely has been established.

The important point is that the axial position of the minimum regression rate can be shown to shift very little during the transient period. Therefore it is possible to use the steady state regression rate law [Eq. (8)] to predict the position of minimum $\dot{r}$ for short burning times, although the presence of transient effects makes it impossible to predict the detailed behavior of $\dot{r}$ vs. z without modifying the equation. If this is the case, it is advantageous to make the comparison of predicted and observed positions of minimum $\dot{r}$ during the transient period, because the minimum is then quite pronounced, as Fig. 3 shows. After steady operation is achieved the curve shown in Fig. 3 would become much flatter, as explained above, and the locus of minimum $\dot{r}$ would be harder to determine experimentally.

The transient behavior just mentioned is associated with the establishment of the steady-state temperature profile in the fuel grain just after ignition. In addition, the ballistics analysis shows that the variation of $\dot{r}$ with z for a given G_0 will become more pronounced as the initial port diameter is reduced. Therefore, to provide an easily measurable locus of minimum $\dot{r}$ the data for Fig. 3 were confined not only to short burning times, as explained above, but also to very small tube diameters. In most practical applications where similar values of G_0 are used, the initial port area will be much greater. The overall variation of $\dot{r}$ with z will then fall quickly to less than 25 per cent over 50 diameters, as mentioned above, but if the L/D is great enough a minimum will still be observed.

The primary purpose of Fig. 3 was to demonstrate that the present analysis leads to a correct prediction of the observed effects on grain shape with hybrid combustion. The thermal lag (or transient) analysis, the ballistics analysis, and experiments which describe these effects will be discussed in detail in a future paper.

DR. T. Y. TOONG (*Massachusetts Institute of Technology*): In determining the combustion-zone position in the boundary layer, the authors used the following expression:

$$\rho_c(\epsilon + D)\ (\partial K_{ox}/\partial y)_c = (O/F)\ (\rho v)_w$$

They seem to imply that the entire mass flux of fuel vapor at a given position of the surface would be burned at the flame at the same axial position. This is at odds with the observation for the laminar case [TOONG, T. Y.: Combustion and Flame *5*, 221 (1961)] that the local combustion rate at the flame is always smaller than the local evaporation rate at the same axial position.

It seems to me that some modification should be made in the expression for the boundary-layer velocity distribution to account for density variation due to combustion.

DR. G. A. MARXMAN: As Professor Toong suggests, in the turbulent boundary layer as well as in the laminar case the gasification rate at a given axial position is greater than the fuel consumption rate in the flame at the same point. Our calculations have shown that approximately 10% of the fuel flows axially in the boundary layer zone below the flame rather than diffusing across this zone to the flame. This fuel loss is no greater than the present uncertainty in the actual O/F ratio at the flame. Therefore, for simplicity, Eq. (15) was written in terms of the total gasification rate and an effective O/F ratio. The effective (O/F) must account for the fuel loss between the wall and the flame as well as the actual combustion mixture ratio. At present it is not possible to calculate the latter to within 10% accuracy, but if this value can be established with greater accuracy it may become desirable to account for the fuel loss more explicitly.

It was our intention to keep the present flame-height analysis as simple as possible, and owing to the uncertainties in some of the related parameters no correction for the effect of density variation on the velocity profile was included. In our more recent analysis, to be reported at a later date, this effect is considered.

DR. R. S. LEVINE (*Rocketdyne*): There is much in this paper that bears on how to obtain efficient hybrid propulsion, especially the information that combustion near the grain is fuel rich, and that the gases must therefore be mixed subsequent to initial combustion. However, if one considers a practical hybrid rocket with a cylindrical fuel grain of reasonable length-to-diameter ratio, using liquid oxidizer, there are two regions where the analysis used cannot be expected to apply.

The first region is near the head end of the grain, where the processes involving liquid impingement on the surface will predominate, and these will be quite different, in controlling the rate of fuel and oxidizer contact, from the processes in the boundary layer at the leading edge of a flat plate that sees only parallel gas flow.

The second region will be that far enough downstream in the tubular grain so that turbulence from the opposite wall will have migrated to the surface in question. The Reynolds number describing the flow will then have to be based on the channel diameter, not the distance from the leading edge of the grain; and the transport equations adjusted accordingly.

DR. G. A. MARXMAN: The authors recognize that the analysis presented in the paper does not apply at the head end of a grain in a practical hybrid engine where injection effects predominate, particularly with liquid injection. In fact, it seems unlikely that any simple analytical approach can adequately describe the complex phenomena introduced by injection. Instead, a semi-empirical study of injection processes will probably be necessary. However, in a hybrid rocket of practical dimensions the injector-dominated region will probably be, of necessity, short relative to the total grain length, and it was the object of the present paper to provide a simple model capable of describing the combustion process over nearly all of the fuel grain. The analysis was not intended to be taken as a complete description of the entire combustion process, including all localized effects.

We assume that the second region referred to by Dr. Levine is that zone far downstream where the boundary layer has thickened sufficiently to fill the tube. No major change in the analysis is required in that region, because the governing process is still heat transfer from the flame, (which apparently remains relatively near the surface) through the portion of the boundary layer between the flame and the surface, and into the fuel surface. Experimental results with long tubes seem to corroborate this viewpoint. The main complication which arises in this region is the variable boundary condition at the "edge" of the velocity boundary layer (i.e., at the centerline of the tube). Upstream of this region conditions at the edge of the velocity boundary layer are independent of axial position, because there is a core flow of oxidizer. After the entire cross section has become turbulent the temperature and composition at the centerline vary with axial position.

In grains that are excessively long, a further effect arises out of the fact that the hot core gas will cause vaporization of the fuel beyond that required for efficient combustion, with attendant drop in temperature and performance.

DR. LEON GREEN JR. (*Lockheed Propulsion Company*): The authors are to be commended for their opening attack upon a complex problem, following the model of hybrid combustion proposed by Moutet and Barrère [Contribution a l'Étude de la Combustion les Fusées a Lithergol ou Hybrides,

Advances in Aeronautical Sciences, pp. 465–496. Pergamon Press, 1961]. This model, shown in their Fig. 1, depicts the situation near the upstream edge of the fuel surface, where the oxidizer concentration in the "external" flow is high and the rate of combustion or fuel surface regression is limited by the rate of diffusion of oxidizer into the boundary layer, where it produces a thin combustion zone close to the surface and thus a sharp discontinuity in the temperature gradient within the boundary layer. It seems reasonable to assume that Reynolds' analogy, which hypothesizes that the length scales of the processes for turbulent transport of mass, momentum, and energy are identical, holds even though the heat release at the flame renders the temperature and velocity profiles dissimilar. However, it appears that, in their integration of Eq. (4) expressing this analogy across the thin zone beneath y_c (10 to 20% of the total thickness δ), the authors have overlooked the fact that the fluid shearing stress at the flame position y_c is not insignificant, whereas the heat flux at this point is zero. Thus the assumption of constant sheer stress and heat flux or proportionality between the two required for integration of Eq. (4) would not appear appropriate to the combustion model of Fig. 1. Thus the integrated shear-stress term should involve a difference $(\tau_w - \tau_c)$ rather than τ_w alone. To neglect τ_c is equivalent to integrating one side of the analogy expression (the momentum-transport term) across the entire boundary layer and the other only to the flame, and the validity of the analysis as it now stands is thus open to question.

An assumption basic to the analysis is that the Lewis number of the boundary-layer gas is unity. However, the region adjacent to the surface consists of almost pure fuel, and if the fuel is hydrogen rich (as it should be for optimum performance) the effects due to deviations of Lewis number from unity may be significant. This question requires further investigation.

Finally, it should be noted that the combustion model of Fig. 1 is not good in the vicinity of the downstream end of the fuel surface, where the oxidizer is depleted; the combustion zone is weak or nonexistent, and the fuel regression rate is no longer controlled by oxidizer diffusion but by surface pyrolysis. In this region a regime of fully developed pipe or channel flow prevails and the dominant heat-transfer mechanism is that of turbulent transport of purely sensible enthalpy from the core. A complete theory of hybrid rocket combustion must provide a description of the transition between the fore-end and aft-end regimes, and the task appears formidable. However, the present authors have pointed the way, and further refinement of this first step is eminently desirable.

DR. G. A. MARXMAN: Because Reynolds' analogy is so frequently used in studies of heat transfer in turbulent flows, only the essential points of its application to the hybrid boundary layer model were included in the paper. Dr. Green's first comment may be based on an incorrect interpretation of our use of the analogy. Perhaps this point can best be clarified by presenting an alternative derivation of Eq. (5) which is entirely equivalent to the integration of Eq. (4) in the paper.

As is pointed out in the paper, it is consistent with Reynolds' analogy as applied in the present treatment to assume that Le = Pr = 1. When this is true it can be shown that the enthalpy is linearly related to the velocity profile,[8] so that:

$$\partial h/\partial y = (h_c - h_w)\frac{\partial(u/u_c)}{\partial y} = \frac{h_c - h_w}{u_c}\frac{\partial u}{\partial y}$$

Equation (4) then becomes:

$$Q/(h_c - h_w) = \tau/u_c$$

This expression is valid at any point between the flame and the wall. In particular, at the wall it becomes identical with Eq. (5) after multiplication by $(1/\rho_c u_c)$.

This derivation of the relation between C_H and C_f for the hybrid shows that neither the shear stress nor the heat flux at the flame has been neglected in the treatment given in the paper, because no such assumption has been made in the present derivation, which leads to the same result. In fact, in integrating Eq. (4) as in the paper, it is not necessary to make any statement regarding the shear stress at the integration limit, regardless of where the integration stops in the boundary layer, as long as Reynolds' analogy is valid throughout the region of integration.

In the present treatment the integration of Eq. (4) stops just at the bottom edge of the combustion zone, where Q is the total heat flux leaving the flame and directed toward the surface, and is therefore not zero. On the other hand, there may be a point at the center of the thin combustion zone where $\tau \neq 0$ but $Q = 0$ (since heat is transferred from the flame in both normal directions). If the integration were carried to this point Eq. (5) would not be correct, presumably because Reynolds' analogy breaks down within the combustion zone. Dr. Green's comment implies that he may have had this situation in mind. Although this may be a legitimate point in general, it does not apply to the present case, in which the flame is treated as a boundary on the integration acting as a heat source.

As Dr. Green suggests, the presence of a substantial mass fraction of hydrogen will cause the Lewis number to deviate appreciably from unity.

However, because the temperature falls off rapidly from the flame to the wall it seems likely that the gaseous fuel will not dissociate into its elements until it is practically at the combustion zone. In this case the Lewis number should be nearly unity over most of the boundary layer, except in the immediate vicinity of the flame, where this assumption does not apply in the analysis. The magnitude of the correction for the case when Le $\neq 1$ can be inferred from ref. 1. This effect is sufficiently small that its inclusion in the present treatment is unwarranted, because there are greater uncertainties in some of the empirical parameters such as C'.

Dr. Green's final comment has previously been discussed in connection with a similar point raised by Dr. Levine, and no further discussion is required.

AN AEROTHERMOCHEMICAL ANALYSIS OF EROSIVE BURNING OF SOLID PROPELLANT

HIROSHI TSUJI

In a solid propellant rocket of a side burning type, the flow rate of the hot combustion gases parallel to the burning surface is approximately proportional to the distance from the leading edge of the propellant. In the present paper, therefore, the erosive burning of the solid propellant is analyzed by the boundary-layer approximation in aerothermochemistry for the case where the velocity, u_∞, of the hot combustion gas stream outside the boundary layer increases linearly with the distance, x, from the leading edge of the propellant, i.e., $u_\infty = Gx$, and the effects of the hot gas stream on the burning rate of the propellant are examined.

Introduction

It is well known that the burning rate of the solid propellant increases above its normal value with an increase in velocity of the hot combustion gases parallel to the burning surface. This phenomenon, which plays an important role in high performance rocket engines, is called erosive burning. In the case in which the hot combustion gases flow along the surface of the propellant, the greater part of the combustion reaction may be considered to occur within the boundary layer developed over the surface of the propellant. Therefore, this phenomenon can be analyzed as a boundary-layer problem of the reactive gases.

Governing Equations

The present analysis is made for the two-dimensional model, because the axially symmetrical boundary-layer equations can be reduced to the two-dimensional form by using the so-called Mangler transformation.[1] The flow field is schematically shown in Fig. 1. Let the origin of the coordinate be at the leading edge of the decomposing surface of a burning solid propellant, and the x and y axes be along and perpendicular to the surface, respectively. The hot combustion gases of temperature T_∞ and density ρ_∞, outside the boundary layer, flow at a velocity u_∞ parallel to the x axis.

The following assumptions are made for the analysis:

1. The solid propellant decomposes (sublimates) into the premixed stoichiometric combustible gases and the laminar flame is formed within the boundary layer.

2. The surface temperature T_w and the mass burning rate $\rho_s v_s$ are constant along the surface of the propellant.

3. Within the solid propellant ($y < 0$), chemical reactions are negligible and the specific heat c_s and the density ρ_s are constant.

4. The mixture gases behave like a perfect gas.

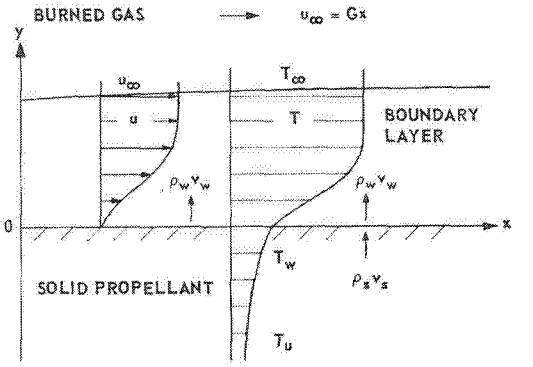

FIG. 1. Schematic diagram of the boundary layer over the solid propellant.

5. The specific heat c_p at constant pressure is the same for all gaseous species and constant.

6. The Prandtl number $\sigma(= c_p\mu/\lambda)$ and the Schmidt number $S\,(= \mu/\rho D)$ of gaseous mixtures are constant and equal, so that the Lewis number $\mathrm{Le}(= \sigma/S)$ is 1.

7. A one-step unopposed global chemical reaction which follows any-order reaction kinetics with the temperature dependence according to the Arrhenius rate law is considered.

8. The system is in quasi-steady state.

Under assumptions (2) and (3), the equation of heat conduction within the solid propellant is

$$c_s\rho_s v_s \frac{dT}{dy} = \frac{d}{dy}\left(\lambda_s \frac{dT}{dy}\right) \quad \text{for} \quad y < 0 \tag{1}$$

and the boundary conditions are

$$T \to T_u \quad \text{as} \quad y \to -\infty,$$
$$T = T_w \quad \text{at} \quad y = 0. \tag{2}$$

On integrating, we find

$$T = T_u + (T_w - T_u) \exp\left[c_s\rho_s v_s \int_0^y dy/\lambda_s\right]. \tag{3}$$

The steady laminar boundary-layer equations of reactive gases may be written as follows:
Global continuity equation

$$\frac{\partial(\rho u)}{\partial x} + \frac{\partial(\rho v)}{\partial y} = 0. \tag{4}$$

Momentum equation

$$\rho u \frac{\partial u}{\partial x} + \rho v \frac{\partial u}{\partial y} = -\frac{dp_\infty}{dx} + \frac{\partial}{\partial y}\left(\mu \frac{\partial u}{\partial y}\right)$$
$$= \rho_\infty u_\infty \frac{du_\infty}{dx} + \frac{\partial}{\partial y}\left(\mu \frac{\partial u}{\partial y}\right). \tag{5}$$

Energy equation

$$\rho u \frac{\partial c_p T}{\partial x} + \rho v \frac{\partial c_p T}{\partial y} = \frac{\partial}{\partial y}\left(\frac{\mu}{\sigma}\frac{\partial c_p T}{\partial y}\right) + u\frac{dp_\infty}{dx}$$
$$- \sum_i w_i \Delta h_i + \mu\left(\frac{\partial u}{\partial y}\right)^2. \tag{6}$$

Diffusion equation for each species

$$\rho u \frac{\partial Y_i}{\partial x} + \rho v \frac{\partial Y_i}{\partial y} = \frac{\partial}{\partial y}\left(\frac{\mu}{\sigma}\frac{\partial Y_i}{\partial y}\right) + w_i. \tag{7}$$

Equation of state

$$p = \rho R T \sum_i Y_i/m_i. \tag{8}$$

Let us consider in this paper only one-step forward chemical reaction of arbitrary complexity represented by the equation

$$\sum_{j=1}^{n} \nu_j' M_j \to \sum_{j=1}^{n} \nu_j'' M_j, \tag{9}$$

in which ν_j' and ν_j'' are the stoichiometric coefficients for the reactants and the products respectively; M_j stands for the jth chemical species; and n is the total number of different chemical species which take place in the reaction. According to the law of mass action, the net rate of production per unit volume of the ith chemical species, w_i, due to the chemical reaction represented by Eq. (9) is given by the expression

$$w_i = m_i(\nu_i'' - \nu_i') k \prod_{j=1}^{n} (\rho Y_j/m_j)^{\nu_j'}. \tag{10}$$

The specific reaction rate coefficient k is given by the classical Arrhenius equation

$$k = b \exp\left[-E/RT\right], \tag{11}$$

in which b is the so-called frequency factor and E the activation energy for the reaction.

Instead of the diffusion Eq. (7) for each species, we use the following equation for the present analysis.

$$\rho u \frac{\partial \Gamma_i}{\partial x} + \rho v \frac{\partial \Gamma_i}{\partial y} = \frac{\partial}{\partial y}\left(\frac{\mu}{\sigma}\frac{\partial \Gamma_i}{\partial y}\right)$$
$$+ \frac{\partial}{\partial y}\left[\mu(1 - \sigma^{-1})\frac{\partial}{\partial y}\left(\frac{u^2}{2}\right)\right]$$
$$+ \frac{\partial}{\partial y}\left[\mu(S^{-1} - \sigma^{-1})\frac{\partial}{\partial y}(q_i Y_i)\right], \tag{12}$$

in which Γ_i and q_i are defined by

$$\Gamma_i = c_p T + \tfrac{1}{2}u^2 + q_i Y_i, \tag{13}$$

and

$$q_i = \frac{\sum_i \Delta h_i m_i(\nu_i'' - \nu_i')}{m_i(\nu_i'' - \nu_i')}, \tag{14}$$

respectively. Equation (12) is derived from Eqs. (5), (6), (7), and (10).

The boundary conditions of these governing equations are as follows:

$$\begin{aligned} &\text{at } y = 0: \\ &u = 0, \quad v = v_w, \quad T = T_w, \\ &Y_i = Y_{iw} \quad (\text{i.e., } \Gamma_i = \Gamma_{iw}), \\ &\text{as } y \to \infty: \\ &u \to u_\infty,\ T \to T_\infty, \\ &Y_i \to Y_{i\infty} \quad (\text{i.e., } \Gamma_i \to \Gamma_{i\infty}). \end{aligned} \tag{15}$$

As is well known, however, in the boundary layer problem with foreign gas injection, Y_{iw} cannot be specified independently of v_w. In general, the velocity v_i in the y direction of the ith species is composed of a diffusion velocity

$$-(D/Y_i)(\partial Y_i/\partial y)$$

and a convection velocity v, i.e.,

$$\rho Y_i v_i = -\rho D(\partial Y_i/\partial y) + \rho Y_i v. \tag{16}$$

It is reasonable to put the physical condition that there is to be no net flow of the combustion products through the surface of the propellant. Therefore, v_{iw} is 0 and the relation

$$\rho_w D_w (\partial Y_i/\partial y)_w = \rho_w Y_{iw} v_w \qquad (17)$$

exists for these combustion products. The resulting convection velocity v_w at the surface of the propellant is the velocity associated with the momentum equation and, therefore, Eq. (17) gives the relationship between the injection velocity and the concentration of the combustion product at the surface, i.e., Y_{iw} is determined when the injection velocity is specified. If the concentrations of the combustion products are determined, those of the combustible species at the surface of the propellant are easily obtained.[2]

Moreover, the boundary conditions [Eq. (15)] must be supplemented with the condition of energy balance at the surface of the propellant, i.e.,

$$\left(-\lambda \frac{\partial T}{\partial y}\right)_w = \left(-\lambda_s \frac{dT}{dy}\right)_w + \rho_s v_s H_s, \qquad (18)$$

in which H_s is the heat of decomposition (sublimation) for the propellant surface and it is positive (negative) for exothermic (endothermic) gasification of the propellant. Recalling the solution (3) for the temperature within the solid, the condition (18) becomes

$$\left(\lambda \frac{\partial T}{\partial y}\right)_w = \rho_s v_s \{c_s(T_w - T_u) - H_s\}. \qquad (19)$$

Analysis

Transformation of Equations. Now we assume that $\rho\mu$ = const. ($= \rho_\infty \mu_\infty$) throughout the flow field and introduce a change of variables that combines the Levy transformation and the Dorodnitzyn-Howarth transformation,[3,4] i.e.,

$$\xi = \int_0^x \mu_\infty \rho_\infty u_\infty \, dx$$

and (20)

$$\eta = \frac{\rho_\infty u_\infty}{2(\xi)^{\frac{1}{2}}} \int_0^y \frac{\rho}{\rho_\infty} dy.$$

Moreover, we introduce the stream function ψ, which is defined by the usual relations

$$\rho u = \partial\psi/\partial y$$

and (21)

$$\rho v = -(\partial\psi/\partial x)$$

as well as the following dimensionless variables

$$\psi = \xi^{\frac{1}{2}} f(\eta), \qquad \Gamma_i = \Gamma_{i\infty} g(\eta),$$
$$\frac{T - T_w}{T_\infty - T_w} = \theta(\eta), \qquad Y_i = Y_i(\eta), \qquad (22)$$

in which $\Gamma_{i\infty} = c_p T_\infty + (u_\infty^2/2) + q_i Y_{i\infty}$ is constant independent of x. On the other hand, T_∞ is not constant and decreases as u_∞ increases. However, it may be considered to be approximately constant, because $c_p T_\infty \gg u_\infty^2/2$. From the equation of state, ρ/ρ_∞ is given by

$$\frac{\rho}{\rho_\infty} = \left[\frac{T}{T_\infty}(\eta) \sum_i Y_i(\eta)/m_i\right]^{-1} \cdot \sum_i Y_{i\infty}/m_i, \qquad (23)$$

and it becomes a function of η alone. By the use of the above transformation, the governing equations are reduced to their "locally similar" form, i.e., Eqs. (4) and (5) yield

$$f''' + ff'' + 2M\left(4\frac{\rho_\infty}{\rho} - f'^2\right) = 0 \qquad (24)$$

where

$$M = (\xi/u_\infty)(du_\infty/d\xi),$$

Eq. (12) gives

$$\frac{g_i''}{\sigma} + fg_i' + \frac{u_\infty^2}{4\Gamma_{i\infty}}[(1 - \sigma^{-1})f'f'']' + \left[(S^{-1} - \sigma^{-1})\frac{q_i}{\Gamma_{i\infty}} Y_i'\right]' = 0, \qquad (25)$$

Eq. (6) gives

$$\frac{\theta''}{\sigma} + f\theta' - \frac{4\xi}{\mu_\infty \rho_\infty^2 u_\infty^2} \cdot \frac{\sum_i w_i \Delta h_i}{c_p(T_\infty - T_w)(\rho/\rho_\infty)} - \frac{u_\infty^2}{c_p(T_\infty - T_w)} \cdot 2M \cdot \frac{f'}{\rho/\rho_\infty} + \frac{u_\infty^2}{4c_p(T_\infty - T_w)} f''^2 = 0, \qquad (26)$$

in which primes denote differentiation with respect to η. The condition (19) of energy balance at the surface of the propellant is reduced to

$$\frac{\theta_w'}{f_w} = \frac{-\sigma[c_s(T_w - T_u) - H_s]}{c_p(T_\infty - T_w)}. \qquad (27)$$

The condition (17) becomes

$$(dY_i/d\eta)_w \cdot 1/Y_{iw} = -Sf_w. \qquad (28)$$

Solution of Momentum Equation. In the present problem in which $\rho_w/\rho_\infty \gg 1$, the term containing the velocity or pressure gradient in the mo-

mentum equation (24) is small and has only a small effect on the velocity profile. The effect on the concentration and enthalpy profiles is even smaller, so that an excellent first approximation for these profiles is obtained by dropping the pressure gradient term altogether.[3,4] This approximation is quite accurate for surface-heat transfer rate at values of ρ_w/ρ_∞ as low as 2.0.[5]

Under the assumptions mentioned above and for $u_\infty = Gx$, the momentum equation (24) becomes

$$f''' + ff'' = 0, \tag{29}$$

and the boundary conditions are

at $\eta = 0$:

$$f' = 0, \qquad f = f_w = -\frac{\rho_w v_w}{(\rho_\infty \mu_\infty G/2)^{\frac{1}{2}}}. \tag{30}$$

as $\eta \to \infty$:

$$f' \to 2.$$

Therefore, complete similar solutions can be obtained. The solutions of this equation have been reported in several references and recently in more detail by Emmons and Leigh for a range of injection rates, f_w.[6]

Solution of Equation of Total Enthalpy for Each Species. In Eq. (25), the third and fourth terms can be neglected, because the kinetic energy is very small compared to the total enthalpy for each species, i.e., $u_\infty^2 \ll \Gamma_{i\infty}$, and the Lewis number has been assumed to be 1. Therefore, Eq. (25) is also reduced to the ordinary differential equation,

$$g_i'' + \sigma f g_i' = 0, \tag{31}$$

and the boundary conditions are

at $\eta = 0$:

$$g_i = g_{iw},$$

as $\eta \to \infty$: (32)

$$g_i \to 1.$$

The solution which satisfies the boundary conditions is

$$g_i = g_{iw} + (1 - g_{iw}) \frac{\int_0^\eta (f'')^\sigma d\eta}{\int_0^\infty (f'')^\sigma d\eta}. \tag{33}$$

Substituting Eq. (33) into Eq. (28) and using Eq. (27), the value of g_{iw} for the species of combustion products can be determined, i.e.,

$$g_{iw} = \frac{\sigma f_w[c_p T_w - \{c_s(T_w - T_u) - H_s\}] - \Gamma_{i\infty}(f_w'')^\sigma \Big/ \int_0^\infty (f'')^\sigma d\eta}{\Gamma_{i\infty}\left[\sigma f_w - (f_w'')^\sigma \Big/ \int_0^\infty (f'')^\sigma d\eta\right]}, \tag{34}$$

in which

$$\begin{aligned} \Gamma_{i\infty} &= c_p T_\infty + q_i Y_{i\infty} \\ &= c_p T_\infty - \{(\textstyle\sum_i \nu_i'' m_i)/\nu_i'' m_i\} q Y_{i\infty} \\ &= c_p T_\infty - q, \end{aligned} \tag{35}$$

because

$$Y_{i\infty} = \nu_i'' m_i / \textstyle\sum_i \nu_i'' m_i$$

for the species of combustion products. Here q is the heat of reaction in the gaseous mixtures, and the relation

$$q = c_p(T_\infty - T_w) + c_s(T_w - T_u) - H_s, \tag{36}$$

holds for burning of the solid propellant. Therefore, g_{iw} becomes 1, and it is concluded that Γ_i is constant throughout the flow field. The concentration distribution across the boundary layer then becomes

$$Y_i = \frac{\nu_i' m_i}{\sum_i \nu_i'' m_i} \cdot \frac{c_p(T_\infty - T_w)(1 - \theta)}{q} \tag{37}$$

for the combustible species, and

$$Y_i = \frac{-\nu_i'' m_i}{\sum_i \nu_i'' m_i}\left[\frac{c_p(T_\infty - T_w)(1 - \theta)}{q} - 1\right] \tag{38}$$

for the species of combustion products.

Solution of Energy Equation. The energy equation (26) is the only governing equation which remains yet to be solved. The last two terms of this equation can be neglected, because the kinetic energy is very small compared to the thermal enthalpy, i.e., $u_\infty^2 \ll c_p(T_\infty - T_w)$. Therefore, Eq. (26) becomes

$$(\theta''/\sigma) + f\theta' - ABb \exp[-E/RT] \times (\rho/\rho_\infty)^{-1} \prod_{j=1}^{n} \left(\frac{\rho}{\rho_\infty} Y_j\right)^{\nu_j'} = 0, \quad (39)$$

in which

$$\left.\begin{aligned} A &= \frac{4\xi\rho_\infty{}^{n*}}{\rho_\infty{}^2\mu_\infty u_\infty{}^2} = 2\rho_\infty{}^{n*-1}/G, \\ B &= \frac{\sum_i \Delta h_i m_i(\nu_i'' - \nu_i')}{c_p(T_\infty - T_w)\prod_{j=1}^{n}(m_j)^{\nu_j'}} \\ &= \frac{-q\sum_i m_i\nu_i''}{c_p(T_\infty - T_w)\prod_{j=1}^{n}(m_j)^{\nu_j'}}, \\ n^* &= \sum_{j=1}^{n}\nu_j' \quad \text{(reaction order)}. \end{aligned}\right\} \quad (40)$$

Because ρ_∞ is a function of ξ, the parameter A is also a function of ξ except the case where $n^* = 1$. Therefore, in order to obtain the solution of this equation for any order chemical reaction, it is unavoidable to put the assumption that A is approximately constant for the limited range of ξ. The boundary conditions of this equation are

at $\eta = 0$:

$$\theta = 0, \theta_w' = \frac{-\sigma[c_s(T_w - T_u) - H_s]f_w}{c_p(T_\infty - T_w)}, \quad (41)$$

as $\eta \to \infty$:

$\theta \to 1$.

The energy equation (39) is a nonlinear second-order ordinary differential equation for the temperature. However, the temperature has to satisfy three boundary conditions at the outer edge of the boundary layer and at the surface of the propellant. Therefore, we have to solve an "eigenvalue" problem in which the only parameter to be determined is f_w. By solving this eigenvalue problem, the relation between the parameter A and the burning rate v_s of the solid propellant can be obtained, because

$$\rho_s v_s = \rho_w v_w = -(\rho_\infty\mu_\infty G/2)^{\frac{1}{2}} f_w. \quad (42)$$

Finally, the burning rate of the solid propellant can be obtained as a function of the velocity gradient of the hot gas stream along the surface of the propellant.

If the velocity gradient G is very large and hence A is very small, the chemical-reaction term in equation (39) can be neglected and the solution of this equation becomes

$$\theta = \int_0^\eta (f'')^\sigma d\eta \Big/ \int_0^\infty (f'')^\sigma d\eta. \quad (43)$$

This solution also gives the temperature distribution across the boundary layer in the case of ablation without chemical reaction within the boundary layer, i.e., in the case in which $b = 0$. Substituting Eq. (43) into the energy balance equation (27) at the surface of the propellant, we obtain

$$\frac{(f_w'')^\sigma}{\int_0^\infty (f'')^\sigma d\eta} \cdot \frac{1}{f_w} = \frac{-\sigma[c_s(T_w - T_u) - H_s]}{c_p(T_\infty - T_w)}, \quad (44)$$

from which f_w is determined.

The present analysis has been carried out for the case where the surface temperature T_w of the decomposing (sublimating) propellant is constant independent of the burning rate. When the decomposing mechanism of the solid propellant is described in terms of an Arrhenius-type pyrolysis law,[7]

$$v_s = a \exp[-qn_s/c_s T_w], \quad (45)$$

in which a is the prefactor of the pyrolysis law and n_s the index for the surface decomposition, then the burning rate and the surface temperature are determined as functions of the velocity gradient of the hot gas stream by solving Eqs. (39) and (45) simultaneously.

Numerical Examples

As examples, the numerical calculations have been carried out for the case of the first-order chemical reaction represented by the equation

$$M_1 \to M_2 + M_3 + \cdots, \quad (46)$$

and for the case of the second-order chemical reaction represented by the equation

$$M_1 + M_2 \to M_3 + M_4 + \cdots \quad (47)$$

for the gaseous mixtures.

As mentioned above, in the case of the first-order chemical reaction, the parameter A in Eq. (39) becomes constant independent of ξ, and the complete similar solution for the temperature can be obtained. Equation (39) is reduced to

$$(\theta''/\sigma) + f\theta' + Ab(1-\theta) \times \exp\left[\frac{-E/R}{T_w + (T_\infty - T_w)\theta}\right] = 0. \quad (48)$$

This equation has been solved numerically with the aid of the electronic digital computer Burroughs Datatron 205 of National Aeronautical Laboratory. The values of parameters assumed in this numerical calculation are as follows:

$$\begin{aligned} E &= 45 \text{ kcal/mole} \\ T_\infty &= 2600°\text{K} \\ T_u &= 300°\text{K} \\ q &= 800 \text{ cal/gr} \\ H_s &= -(200 - 0.07\ T_w) \text{ cal/gr} \\ c_p &= 0.27 \text{ cal/gr, }°\text{K} \\ c_s &= 0.34 \text{ cal/gr, }°\text{K} \end{aligned} \quad (49)$$

For the convenience of numerical calculation, we have assumed $\sigma = 1$. Figure 2 shows the relations between the parameter Ab and the eigenvalue f_w for $T_w = 600°\text{K}$, 800°K, and 1000°K. As is well known, the limiting case of $f_w = -1.23849$ corresponds to the condition that the boundary layer with gas injection blows away.[6]

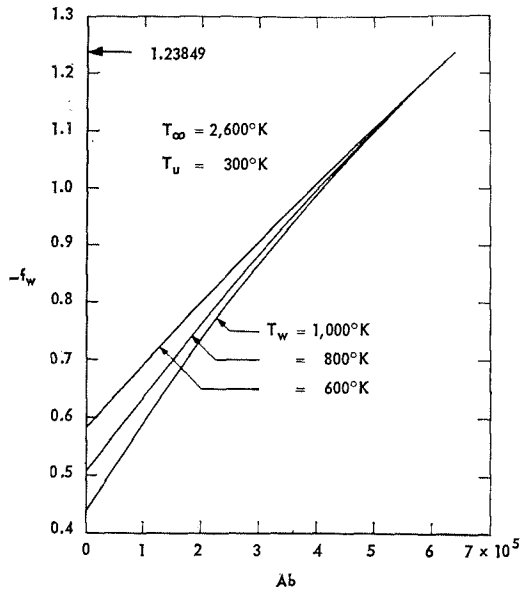

FIG. 2. Relations between the parameter Ab and the eigenvalue f_w for the first-order chemical reaction.

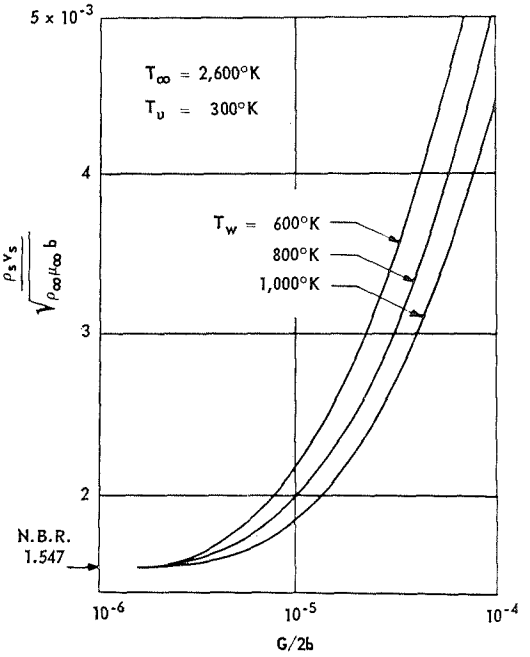

FIG. 3. Relations between the velocity gradient of the hot gas stream and the burning rate of the solid propellant for the first-order chemical reaction.

The dependence of the burning rate of the solid propellant upon the velocity gradient of the hot gas stream outside the boundary layer is shown in Fig. 3 in which $\rho_s v_s/(\rho_\infty \mu_\infty b)^{\frac{1}{2}}$ is plotted against $G/2b$, the parameter being T_w. The value indicated by an arrow shows the normal burning rate of the solid propellant in the case without hot gas stream along the surface of the propellant. This value has been determined independently by solving the equations in the case without hot gas stream (see Appendix). The results obtained in the present analysis on the erosive burning show that as the velocity gradient of the hot gas stream becomes zero, the burning rate tends to the normal burning rate in the case without hot gas stream, and that the burning rate increases with the velocity gradient. Moreover, it is found that as the velocity gradient becomes large and the thickness of the boundary layer becomes very thin, the effects of the chemical reaction within the boundary layer can be neglected and the erosive burning can be treated as the problem of ablation without chemical reaction within the boundary layer.

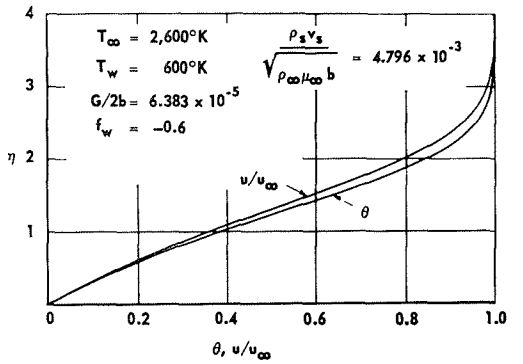

FIG. 4. The velocity and temperature distributions across the boundary layer: $f_w = -0.6$, $T_w = 600°K$, the first-order chemical reaction.

The velocity and temperature distributions across the boundary layer in the case in which $f_w = -0.6$ and $T_w = 600°K$ and in the case in which $f_w = -1.0$ and $T_w = 600°K$ are shown in Figs. 4 and 5, respectively. In the case in which the velocity gradient is small, the velocity boundary layer is thick and the flame reaction occurs in the inner part of the boundary layer. When the velocity gradient becomes large, however, the flame reaction occurs in the whole region of the boundary layer.

In the case of the second-order chemical reaction, Eq. (39) is reduced to

$$\frac{\theta''}{\sigma} + f\theta' + \frac{Ab}{m}\cdot\frac{c_p(T_\infty - T_w)}{q} \times \frac{(1-\theta)^2}{(T_w/T_\infty) + [1 - (T_w/T_\infty)]\theta} \times \exp\left[\frac{-E/R}{T_w + (T_\infty - T_w)\theta}\right] = 0, \quad (50)$$

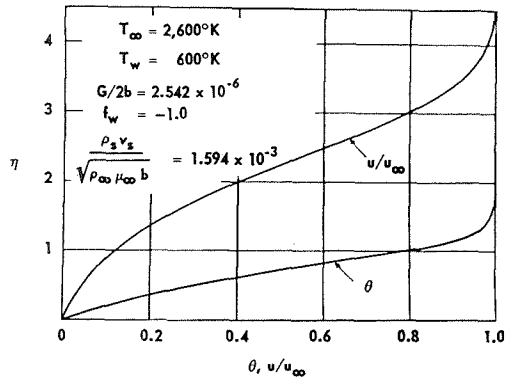

FIG. 5. The velocity and temperature distributions across the boundary layer: $f_w = -1.0$, $T_w = 600°K$, the first-order chemical reaction.

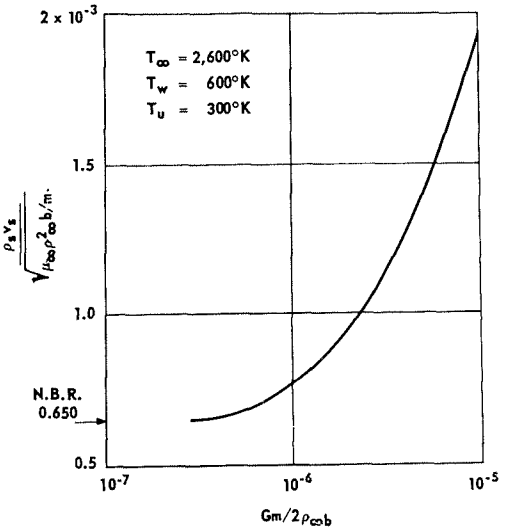

FIG. 6. Relation between the velocity gradient of the hot gas stream and the burning rate of the solid propellant for the second-order chemical reaction.

in which $m = m_1 + m_2$ and $\sum_i Y_i/m_i$ is assumed to be approximately constant. This equation has also been solved numerically for the values of the parameters given in Eq. (49). The dependence of the burning rate of the solid propellant upon the velocity gradient of the hot combustion gas stream outside the boundary layer is shown in Fig. 6 in which $\rho_s v_s/(\mu_\infty \rho_\infty{}^2 b/m)^{\frac{1}{2}}$ is plotted against $Gm/2\rho_\infty b$. The value indicated by an arrow shows the normal burning rate of the solid propellant. It has been also confirmed that the burning rate increases with the velocity gradient.

Conclusions

In the present paper, the erosive burning of the solid propellant has been analyzed by the boundary-layer approximation in aerothermochemistry for the case where the velocity of the hot combustion gas stream outside the boundary layer increases linearly with the distance from the leading edge of the propellant.

In the investigations about the erosive burning which have been conducted by many authors, the relation between the stream velocity outside the boundary layer and the burning rate has been examined. According to the boundary-layer theory, however, it is well known that the velocity and temperature distributions across the boundary layer depend on the thickness of the boundary layer as well as the stream velocity. The thickness of the boundary layer is a function of u_∞ and x,

so that the erosive burning rate is also a function of u_∞ and x. Therefore, it is not appropriate to consider the velocity u_∞ as the only governing parameter for the erosive burning.

It has been found in the present analysis, however, that the similar solutions of the boundary-layer equations can be obtained approximately in the case in which $u_\infty = Gx$ and the velocity gradient of the hot combustion gas stream, G, is the only governing parameter. As the results of analysis, it was confirmed that as G becomes zero, the burning rate tends to the normal burning rate in the case without hot gas stream, and that the burning rate increases with G.

Nomenclature

D	Diffusion coefficient of gas mixtures
Δh_i	Standard heat of formation of ith species
m_i	Molecular weight of ith species
p	Pressure
R	Universal gas constant (1.9872 cal/°K, mole)
T	Local temperature of solid propellant or gas mixtures
T_u	Initial temperature within the interior of propellant
u	Velocity component in x direction
v	Velocity component in y direction
Y_i	Mass concentration of ith species
ρ	Local density of gas mixtures
μ	Viscosity of gas mixtures
λ	Thermal conductivity of gas mixtures
λ_s	Thermal conductivity of solid propellant

Acknowledgment

The author would like to express his sincere thanks to Dr. N. Hayasi of National Aeronautical Laboratory who kindly prepared the programs for the Burroughs Datatron 205 and carried out the numerical calculations.

References

1. Mangler, W.: ZaMM *28*, 97 (1948).
2. Tsuji, H.: Aero. Res. Inst., Univ. Tokyo, Report No. 365, 1961.
3. Levy, S.: J. Aero. Sci. *21*, 459 (1954).
4. Lees, L.: Jet Propulsion *26*, 259 (1956).
5. Lees, L.: *Combustion and Propulsion, Third AGARD Colloquium* p. 451. Pergamon, 1958.
6. Emmons, H. W. and Leigh, D.: Combustion Aero. Lab., Harvard Univ., Interim Tech. Report No. 9, 1953.
7. Rosen, G.: J. Chem. Phys. *32*, 89 (1960).

Appendix

Burning Rate of Solid Propellant. An analysis to determine the normal burning rate of solid propellant can be carried out under the same assumptions made for the analysis of the erosive burning. By transformations of variables, the energy equation to be solved is reduced to

$$(\theta''/\sigma) - \theta' - cBb \exp\left[-E/RT\right] \times (\rho/\rho_\infty)^{-1} \prod_{j=1}^{n} \left(\frac{\rho}{\rho_\infty} Y_j\right)^{\nu_i'} = 0, \quad (51)$$

in which

$$\theta = (T - T_w)/(T_\infty - T_w),$$

$$\eta = \frac{\rho_w v_w}{\mu_\infty} \int_0^y \frac{\rho}{\rho_\infty}\, dy,$$

$$c = \mu_\infty \rho_\infty{}^{n*}/(\rho_w v_w)^2, \quad (52)$$

$$Y_j = \frac{\nu_j' m_j}{\sum_j \nu_j'' m_j} \cdot \frac{c_p(T_\infty - T_w)}{q} (1 - \theta)$$

for combustible species. The boundary conditions are

at $\eta = 0$:

$$\theta = 0, \qquad \theta_w' = \frac{\sigma[c_s(T_w - T_u) - H_s]}{c_p(T_\infty - T_w)}, \quad (53)$$

as $\eta \to \infty$:

$$\theta \to 1.$$

This equation is also a nonlinear second-order ordinary differential equation for the temperature. However, the temperature has to satisfy three boundary conditions [Eq. (53)]. Therefore, we have to solve an "eigenvalue" problem in which the only parameter to be determined

is c. By solving this equation, the burning rate of the solid propellant v_s can be obtained, because

$$\rho_s v_s = \rho_w v_w = (\mu_\infty \rho_\infty{}^{n*}/c)^{\frac{1}{2}}. \quad (54)$$

Equation (51) is the same form as Eq. (39) in the case in which $f = -1$. Equation (51) is reduced to

$$(\theta''/\sigma) - \theta' + cb(1-\theta) \times \exp\left[\frac{-E/R}{T_w + (T_\infty - T_w)\theta}\right] = 0 \quad (55)$$

in the case of the first-order chemical reaction, and to

$$\frac{\theta''}{\sigma} - \theta' + \frac{cb}{m}\cdot\frac{c_p(T_\infty - T_w)}{q} \cdot\frac{(1-\theta)^2}{(T_w/T_\infty) + [1 - (T_w/T_\infty)]\theta} \times \exp\left[\frac{-E/R}{T_w + (T_\infty - T_w)\theta}\right] = 0 \quad (56)$$

in the case of the second-order chemical reaction for the gaseous mixtures. The burning rates obtained by solving Eqs. (55) and (56) are shown by an arrow in Figs. 3 and 6, respectively.

Discussion

DR. LEON GREEN, JR. (*Lockheed Propulsion Company*): The author has presented an elegant analysis of an interesting problem. However, it is doubtful that the problem as formulated here bears much resemblance to the situation prevailing in actual erosive-burning owing to several questionable assumptions, the first of which is that of laminar boundary-layer flow. At the axial-flow stagnation point of a side-burning propellant grain the gas velocity is normal to the surface, and the boundary-layer approximations do not become valid until the flow has proceeded several channel diameters downstream. By the time this point has been reached and a boundary layer can be defined, the strong destabilizing action of the rapid mass transfer from the wall will have ensured its being turbulent. Another assumption made at the outset is that the mass burning rate is constant along the surface of the propellant, even though the variation in this quantity constitutes the very object of erosive burning studies. Such a procedure is conventional in cases where only small perturbations from a mean value are of interest, but seems inconsistent in the present case where the burning rate can increase strongly under conditions of high velocity. The assumption that the rate-limiting step is a gas-phase chemical reaction is also questioned, since various investigations have indicated that the rate-controlling step is one of surface pyrolysis.

Perhaps as a consequence of the above assumptions, the analysis arrives at a conclusion which conflicts with experience; i.e., that, for a situation involving a constant streamwise velocity gradient, $u_\infty = Gx$, the gradient "... is the only governing parameter." Such a velocity distribution is a good approximation to that prevailing in conventional side-burning solid propellant rocket motors, yet in the erosive-burning experience with such motors of which the writer is aware, the dominent parameter is velocity per se (either linear or mass velocity, or reduced forms thereof), with the streamwise gradient having little if any effect. Finally, it is worth noting the existence of an interesting phenomenon which will probably require explanation by a complete "aerothermochemical" theory of erosive burning; namely, that of negative erosion or reduction of burning rates at low parallel gas velocities. Such behavior was first noticed with double-base propellants but has recently been reported by Canadian investigators using composite, polyurethane-base formulations [L. A. Dickinson and F. Jackson: "Combustion in Solid Propellant Rocket Engines," Fifth AGARD Combustion & Propulsion Colloquium, Braunschweig, 9–13 April 1962].

DR. H. TSUJI (*University of Tokyo*): The four points raised by Green are summarized with the responses below:

Q. In the actual erosive burning situation the boundary layer is not defined until several channel diameters downstream from the fore-end, by which time it is turbulent.

A. I also think that the flow becomes turbulent in the actual erosion-burning situations. If the analysis for the case of laminar boundary layer can be made, the analytic method can be easily extended to the case of turbulent boundary layer by using μ_T (turbulent viscosity), λ_T (turbulent thermal conductivity), D_T (turbulent diffusion coefficient), etc., instead of μ, λ, D, etc., respectively. Therefore, this study was conducted as the first step to analyze the erosive burning by the boundary layer theory.

Q. Assumption of constant $\rho_w v_w$ at the start is not consistent with predictions of large increases in $\rho_w v_w$ by theory.

A. This theory does not satisfy all actual condi-

tions. For the convenience of the analysis, the system is assumed to be in a quasi-steady state. If the solution of the equations can be obtained under these assumptions, the assumption of constant $\rho_w v_w$ is not inconsistent with the predictions of large increases in $\rho_w v_w$ by theory.

Q. Velocity gradient is of no effect in actual situations. High velocity flow produces strong erosion with zero or negative gradient. The model does not explain negative erosion experienced in some propellants at low velocities.

A. This is an analysis of erosive burning. The author contends that the erosive burning rate depends on the velocity U_∞ as well as the thickness of the boundary layer (i.e., the boundary layer characteristic at any section depends not only on the velocity U_∞ but also on the distance x from the fore-end, according to the boundary layer theory). However, in the case of $U_\infty = Gx$ and $\rho_w v_w$ = constant, the boundary layer characteristics depend on G only (i.e., G is the only parameter for the boundary layer characteristics). The present analysis was made for this special case. If it is necessary to analyze the erosive burning with zero or negative gradient, the analysis for U_∞ = constant or $U_\infty = U_{\infty 0} - Gx$ can be made. However, in these cases, the analysis becomes rather complicated and $\rho_w v_w$ becomes the function of two parameters (i.e., U_∞ and x).

Q. The rate-controlling step is probably surface pyrolysis (a function of surface temperature) rather than gas-phase reaction.

A. It is considered also in this paper that the rate-controlling step is probably surface pyrolysis. The burning rate and the surface temperature are determined as functions of G by solving the energy equation (39) and the pyrolysis law (45).

Although the model is necessarily oversimplified for analytical treatment, the mathematical development appears to be consistent with the model assumptions.

PRECEDING PAGE BLANK NOT FILMED

Miscellaneous Studies

Chairman: Dr. S. Way (*Westinghouse*)

Vice Chairman: Prof. J. A. Nicholls (*University of Michigan*)

DRAG COEFFICIENTS OF INERT AND BURNING PARTICLES ACCELERATING IN GAS STREAMS

C. T. CROWE, J. A. NICHOLLS, AND R. B. MORRISON

The effects of burning and acceleration on the drag coefficients of particles suspended and accelerating in gas streams were studied in a Reynolds number range extending from 250 to 1600.

The model chosen for the analytical study was a spherical particle with mass flux through the surface to simulate burning. The governing equation was the integrodifferential representation of the tangential equation of motion of a thin boundary layer on a sphere. The solutions indicated that burning and acceleration tend to reduce the drag coefficient. The fractional reduction was found to be a function of the ratio of mass flux from the surface to that in the free stream f for the burning particle and the acceleration modulus Ac for the accelerating particle.

The effects of burning and acceleration were studied experimentally by subjecting burning particles (gunpowder) and nonburning particles to the convective flow behind a shock wave in a shock tube. The variation in particle size and displacement with time were obtained by photographing particle shadows with a high speed framing camera and concentrated light source. The particle density, the shock wave velocity, and the atmospheric conditions together with the photographic data provided sufficient information to calculate the particle's drag coefficient.

The analytical expressions predicted and experimental results verified that the particle drag coefficient was insensitive to burning and accelerative effects if $Ac \leq 10^{-2}$ and $f < 0.025$. When these conditions are met, other phenomena such as free stream turbulence, particle rotation, and roughness can create larger variations in the drag coefficient than the mechanisms considered in this study.

Introduction

The relatively large heats of formation of certain metal oxides has suggested their inclusion in solid propellant rocket fuels to improve the fuel density and specific impulse characteristics. Coupled with the improved chemical characteristics of the fuel, however, are the detrimental effects caused by the small metal oxide particles produced upon combustion. These small metal oxide particles, which are carried out with the exhaust gases, give rise to a specific impulse loss which is largely dependent on the gas-particle velocity and thermal lags.

The most fundamental parameter required to determine the gas-particle velocity lag—the particle drag coefficient—is itself a function of many parameters; its shape and orientation with respect to the flow, Mach number and Reynolds number based on the relative velocity between the particle and the gas, acceleration modulus, roughness, burning rate, and the relative turbulent intensity of the gas stream.

The possibility of a particle being in the molten state for a considerable portion of its trajectory suggests that the assumption of a spherical shape, due to surface tension forces, is reasonably valid. Obviously, a most extensive study would be re-

quired to study the effect of each of the above-mentioned parameters in detail. The present paper concerns itself with a spherical particle and the influence of Reynolds number, burning rate, and acceleration modulus. The Mach number and relative turbulence intensity are assumed small.

Particles in a rocket nozzle may experience Reynolds numbers extending from the Stokes's flow region (Re <2) to orders of a thousand. The largest particle Reynolds numbers occur in the throat region where the degree of particle velocity lag can largely determine the extent of performance loss. The present study will be restricted to the study of drag coefficients for Reynolds numbers greater than 200.

A limited number of experimental results have been reported for the drag coefficients of particles and droplets accelerating in gas streams. Ingebo[1] injected, with negligible entrance velocities, particles and droplets into a moving gas stream and recorded their velocity at various downstream stations. Hanson[2] performed essentially the same experiment, but recorded evaporation rates instead of velocities. Bolt and Wolf[3] injected burning kerosene drops into an essentially still air medium. Torobin and Gauvin[4] investigated the effect of turbulence by firing small metal spheres into a flow of known turbulent characteristics. Rabin *et al.*[5] subjected burning and nonburning fuel droplets to the convective flow behind a shock wave in a shock tube. These experimental results are shown in Fig. 1 together with the steady state experimental drag coefficient for a sphere.[6] Rather marked discrepancies in the experimental results are apparent.

Virtually no analytical results have appeared in the literature concerning the effects of burning or acceleration on a spherical particle's drag coefficient. Those analytical studies which have appeared[7,8] are confined to the study of accelerative effects in the Stokes's flow regime.

Experiments have been reported[9] which indicate an increased drag coefficient for a body accelerating into a stagnant medium. In these studies the velocity vector describing the motion of the medium with respect to the body and the body's acceleration vector were colinear but of opposite sense. For the case of a particle accelerating in a gas stream, however, these vectors are colinear but of the same sense.

The purpose of this study is the attainment of analytical and experimental values of drag coefficients which are valid for burning particles accelerating in a gas stream.

Equation of Motion for a Particle with Mass Flux Through the Surface

The equation of motion for a burning (or evaporating) particle differs from that of a nonburning particle by a term which accounts for

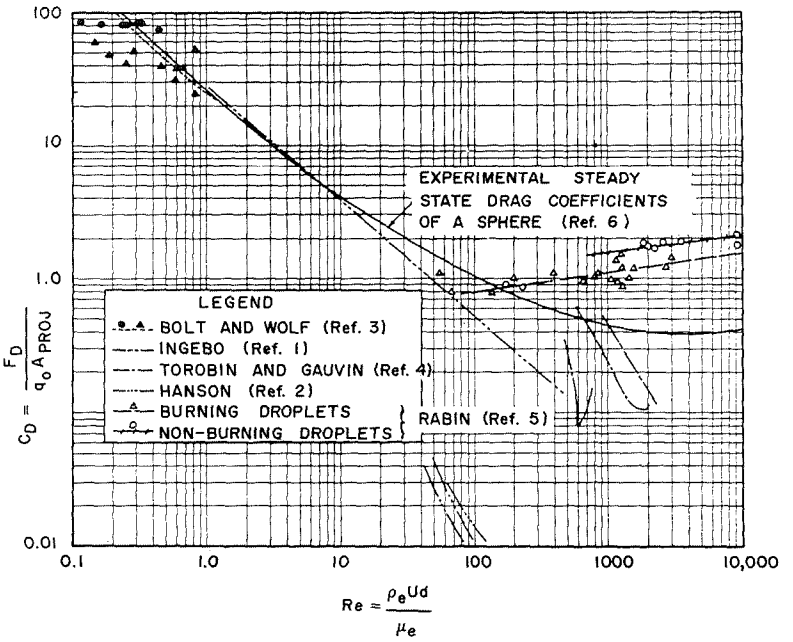

FIG. 1. Summary of experimental data for particles accelerating in a gas stream as obtained by various investigators.

the inertial force contributed by the mass flux from the surface.

Applying Newton's second and third laws to an arbitrarily shaped, rigid particle of mass m, the following equation of motion is obtained for a particle in continuum flow:

$$C_D(\rho_\infty/2) \mid \mathbf{u} \mid \mathbf{u}S_r + m\mathbf{f} = m\boldsymbol{\alpha} + \int_s (\rho u^2)\,\mathbf{n}\,dS \tag{1}$$

where C_D, ρ_∞, S_r, $\mathbf{n}$, $\mathbf{f}$, $\mathbf{u}$ and $\boldsymbol{\alpha}$ are the particle drag coefficient, free stream density, representative particle area, unit outward normal vector from particle surface, body force vector per unit mass, velocity vector of the medium with respect to the particle and the acceleration vector of the particle with respect to inertial space, respectively. For a nonburning particle or a particle for which ρu^2 is constant over the surface, the equation of motion is

$$C_D(\rho_\infty/2) \mid \mathbf{u} \mid \mathbf{u}S_r = m(\boldsymbol{\alpha} - \mathbf{f}) \tag{2}$$

Equation (2) has been used extensively for the determination of particle trajectories in rocket nozzles.[10,11,12]

In these studies the body force term is neglected and the drag coefficient employed is that for Stokes's flow or the experimentally determined drag coefficient for a sphere in steady flow.

Analytical Approach

The ensuing theoretical analysis is confined to the regime of continuum gas dynamics where the boundary layer thickness is small compared to the particle diameter. In essence, the problems are treated by rewriting the governing equations in integral form and solving the resulting equations to conform with the appropriate boundary conditions. This technique fails to give a detailed description of the flow field but serves to indicate the importance of the parameters involved.

Performing the conventional order of magnitude analysis on the continuity and momentum equations of gas dynamics assuming a thin boundary layer, retaining the significant terms, and rewriting the equations in spherical coordinates yields

$$\frac{1}{r^2}\frac{\partial}{\partial r}(\rho r^2 u_r) + \frac{1}{r\sin\theta}\frac{\partial}{\partial\theta}(\rho u_\theta \sin\theta) = -\frac{\partial\rho}{\partial t}$$

(continuity equation) (3)

and

$$\rho\partial V_\theta/\partial t + \frac{1}{r^2}\frac{\partial}{\partial r}(\rho u_r r^2 u_\theta) + \frac{1}{r\sin\theta}\frac{\partial}{\partial\theta}(\rho u_\theta^2 \sin\theta) + \frac{\partial}{\partial t}(\rho u_\theta) = \frac{-1}{r}\frac{\partial p}{\partial\theta} + \frac{1}{r^2}\frac{\partial}{\partial r}\left(r^2\mu\frac{\partial u_\theta}{\partial r}\right)$$

(tangential momentum equation). (4)

$$\frac{\Delta p}{p} = 0\left(\frac{\delta_r}{a}\right)$$

(normal momentum equation) (5)

where δ_v, a, V_θ, u_r, and u_θ are the velocity boundary layer thickness, sphere radius, tangential component of the velocity of the particle coordinate system with respect to inertial space, and the radial and tangential components of the surrounding gas velocity with respect to the particle, respectively. Integrating the above equations over r between the particle surface and the edge of the velocity boundary layer, substituting the continuity equation into the tangential momentum equation, and utilizing the thin boundary layer assumption results in

$$\left(\frac{\partial V_\theta}{\partial t} + U_e\frac{\partial}{\partial t}\right)\rho_e\int_0^{\delta_v}\left(\frac{\rho_e}{\rho} - 1\right)dg + \left(\frac{\partial}{\partial t} + \frac{1}{a}\frac{\partial}{\partial\theta}U_e\right)\rho_e U_e\int_0^{\delta_v}\left(1 - \frac{\rho u_\theta}{\rho_e U_e}\right)dg + \frac{1}{a\sin\theta}\frac{\partial}{\partial\theta}\sin\theta\rho_e U_e\int_0^{\delta_v}\frac{\rho u_\theta}{\rho_e U_e}\left(1 - \frac{u_\theta}{U_e}\right)dg - \frac{(\rho u_r)_s}{\rho_e U_e}\rho_e U_e^2 = \tau_s \tag{6}$$

where g, τ_s, $(\rho u_r)_s$, ρ_e and U_e are the radial distance measured from the particle surface, shear stress at the surface, radial mass flux at the surface, density, and tangential component of the gas velocity at the outer edge of the boundary layer, respectively. The conventional momentum and displacement thicknesses are easily recognized while the remaining integral could be called a "density" thickness and only appears with the existence of accelerating coordinate systems or temporal changes in the density distribution.

The three integrals are evaluated using a scheme reported by Covert[13] in which the variable of integration is changed from g to u_θ by employing

$$dg = (\mu/\tau)\,du_\theta. \tag{7}$$

Assuming:

$$\frac{\rho\mu}{\rho_e\mu_e}\frac{\tau_s}{\tau} = G(\eta) \quad \text{and} \quad \frac{\rho_e}{\rho} = F(\eta) \tag{8}$$

where $\eta = u_\theta/U_e$, the three integrals are evaluated as follows:

$$\int_0^{\delta_v} \frac{\rho u_\theta}{\rho_e U_e}\left(1 - \frac{u_\theta}{U_e}\right) dg = \frac{\mu_e U_e A}{\tau_s} \tag{9}$$

where

$$A = \int_0^1 G(\eta)\eta(1-\eta)\,d\eta$$

$$\int_0^{\delta_v}\left(1 - \frac{\rho u_\theta}{\rho_e U_e}\right) dg = \frac{\mu_e U_e B}{\tau_s}$$

where

$$B = \int_0^1 G(\eta)[F(\eta) - \eta]d\eta \tag{10}$$

$$\int_0^{\delta_v}\left(\frac{\rho_e}{\rho} - 1\right) dg = \frac{\mu_e U_e C}{\tau_s} \tag{11}$$

where

$$C = \int_0^1 G(\eta)[1 - F(\eta)]d\eta$$

In order to observe the dependence of the results on the particular form chosen for $G(\eta)$ and $F(\eta)$, consider the case of steady flow over a sphere with no mass flux through the surface. Substituting the above integrals into the equation of motion (6) and disregarding the unsteady and mass injection terms yields

$$a\tau_s = B\frac{dU_e}{d\theta}\frac{\rho_e U_e^2 \mu_e}{\tau_s} + \frac{A}{\sin\theta}\frac{d}{d\theta}\frac{\rho_e\mu_e U_e^3}{\tau_s}\sin\theta \tag{12}$$

Employing the classical incompressible velocity distribution for U_e, Eq. (12) can be integrated to give

$$C_f\sqrt{Re} = \left(\tfrac{3}{2}\right)^{\frac{1}{2}}\frac{2\sqrt{A}\sin^{4+(B/A)}\theta}{\left[\int_0^\theta \sin^{5+2(B/A)}\lambda\, d\lambda\right]^{\frac{1}{2}}} \tag{13}$$

where

$$Re = \frac{2a\rho_e U}{\mu_e}$$

and

$$C_f = \frac{\tau_s}{\frac{1}{2}\rho_e U^2}$$

For an unheated particle in a low Mach number flow, one may reasonably assume

$$\frac{\rho\mu}{\rho_e\mu_e} = 1 \quad \text{and} \quad \frac{\rho}{\rho_e} = 1 \tag{14}$$

and the solution will depend on the distribution of τ/τ_s. Considering three functional forms of τ/τ_s,

$\tau/\tau_s = 1$

$$(A = \tfrac{1}{6}, \qquad B = \tfrac{1}{2})$$

Case I (15a)

$\tau/\tau_s = \sqrt{1-\eta^2}$

$$(A = 0.215, \quad B = 0.571)$$

Case II (15b)

$\tau/\tau_s = 1 - \eta$

$$(A = \tfrac{1}{2}, \qquad B = 1)$$

Case III (15c)

yields the three solutions shown in Fig. 2. The more computationally complicated but accurate result of Tomotika[14] is shown for reference. The agreement of Case III and Tomotika's results near the forward stagnation point, together with the possibility of an increased skin friction due to the existence of free stream turbulence in a rocket nozzle,[15] suggest Case III is the most suitable shear stress distribution to be used in the analysis to follow.

The drag coefficient due to shear forces is determined by performing the integration

$$C_{D_f} = 2\int_0^{\theta_s} C_f \sin^2\theta\, d\theta \tag{16}$$

where θ_s is the angle of flow separation. The skin friction contribution beyond the separation point is neglected.

The form drag coefficient is determined by considering the pressure forces acting on a particle and is given by

$$C_{D_p} = \sin^2\theta_s[(1 - C_{p_w}) - (9/8)\sin^2\theta_s] \tag{17}$$

where the classical incompressible pressure distribution for a sphere and a constant pressure coefficient in the wake, C_{p_w}, have been assumed. The experimental results of Taneda[16] and Garner *et al.*[17] suggest the separation angle varies as

$$\theta_s = 180° - 35°\log_{10}(Re/3.26)$$

$$(80 < Re < 490)$$

$$\theta_s = 104° \qquad (Re \geq 490) \tag{18}$$

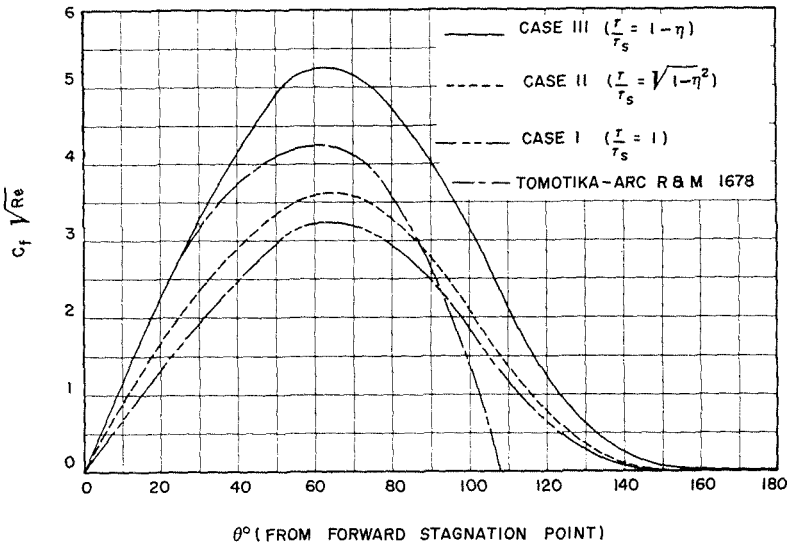

FIG. 2. Variation of skin friction over sphere surface.

while the experiments of Ermisch[18] indicate

$$C_{p_w} = -0.4 \tag{19}$$

The overall drag coefficient is found by summing the frictional and form drag coefficient. The drag coefficients resulting from the above analyses, together with the experimental steady state drag coefficient for a sphere,[6] appear in Fig. 3.

The existence of large temperature variations through the particle's boundary layer necessitates modification of the functional forms $G(\eta)$ and $F(\eta)$. Assume

$$\frac{T_s - T}{T_s - T_e} = \frac{u_\theta}{U_e} = \eta \tag{20}$$

This relationship is exact for a flat plate at zero

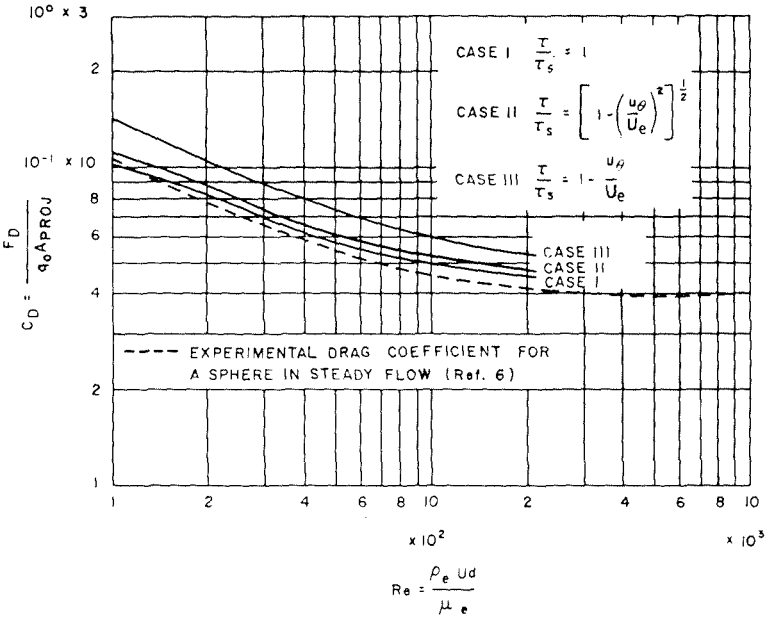

FIG. 3. Drag coefficients vs Reynolds number for three assumptions of shear distributions.

angle of attack in parallel flow at low velocities, provided the Prandtl number is unity. Although the present problem does not satisfy these conditions, the assumption should serve as a reasonable approximation. In addition, assume the viscosity variation with temperature can be expressed by

$$\frac{\mu}{\mu_e} = \left(\frac{T}{T_e}\right)^n \tag{21}$$

where n is to be chosen to conform as closely as possible with experimental evidence.

Utilizing the above assumptions for temperature and viscosity variation and the skin friction distribution corresponding to Case III results in

$$A = \frac{\bar{T}^{(1+n)} - (n+1)(\bar{T}-1) - 1}{n(n+1)(\bar{T}-1)^2} \tag{22a}$$

$$B = \frac{\bar{T}^{(1+n)} - \bar{T}}{n(\bar{T}-1)} \tag{22b}$$

$$C = \frac{\bar{T}^n - 1}{n} \tag{22c}$$

where $\bar{T} = T_s/T_e$.

The influence of particle burning is found by including the surface mass flux term in the governing equations. Employing the values of the integrals found above and the incompressible inviscid velocity distribution for U_e, the governing equation (6) can be written

$$\sin\theta \frac{d\beta^2}{d\theta} + 2\left(\frac{B}{A} + 3\right)\beta^2 \cos\theta = \frac{f\sqrt{Re}}{2A} + \frac{3}{8A} \tag{23}$$

where

$$\beta = \frac{9}{4}\frac{\sin\theta}{C_f\sqrt{Re}}$$

and

$$f = \frac{(\rho u_r)_s}{\rho_e U}$$

Strictly speaking, the values of A and B depend on the burning parameter f since the velocity distribution within the boundary layer will be influenced by the surface mass flux. However, small burning rates and the inherent crudeness of integral techniques suggest this refinement is not necessary in the present analysis.

Equation (23) can be solved in the vicinity of the forward stagnation point by assuming a series solution of the form

$$\beta = \sum_{j=0}^{\infty} G_j \frac{\theta^j}{j!} \tag{24}$$

This series converges for $\theta < \sqrt{2}$ and beyond this point conventional numerical integration methods are applicable.[19]

The above analysis can be used to predict the experimental results of the present study by

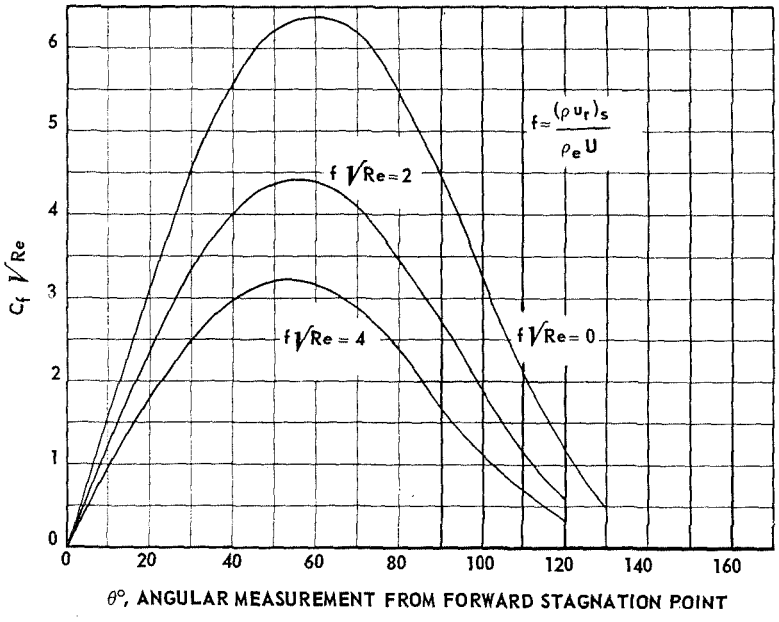

FIG. 4. Skin friction distribution over surface of burning sphere.

choosing $n = 0.8$ and $\bar{T} = 2$. The corresponding values of A and B/A are 0.472 and 3.96, respectively. However, for simplicity of computation, the value 0.5 will be retained for A while 4 will be used for the ratio B/A. Implicit in the application of Eq. (22) to the burning particle is the assumption of constant molecular weight of the gaseous mixture in the boundary layer. Solving Eq. (23) for the above conditions and assuming a constant burning rate over the surface results in the skin friction coefficient shown in Fig. 4.

The existence of a mass flux at the surface will modify the position of flow separation. The Karman—Polhausen technique for boundary layers[20] indicates separation will occur when

$$\frac{dp}{dx}\frac{\delta^*\Theta}{\mu_e U_e} \tag{25}$$

attains a certain value. Employing the classical inviscid pressure distribution for a sphere and the evaluations of the displacement and momentum thicknesses used above, the criterion for separation becomes

$$\frac{\sqrt{B}\,|\cos\theta_s|^{\frac{1}{2}}\sin\theta_s}{C_f\sqrt{Re}} = K \qquad (Re \geq 490) \tag{26}$$

Assuming separation occurs at $\theta_s = 104°$ for Case III with no mass flux at the surface, the constant K has the value 0.1725. For Reynolds numbers less than 490, it is assumed that the separation angle varies with the logarithm of the Reynolds number in the same way as indicated by Eq. (18), but translated to give the modified value at $Re = 490$.

Assuming the pressure coefficient in the wake region is not appreciably effected for burning rates considered in this study, sufficient information exists to evaluate the drag coefficient and the results appear in Fig. 5. A decrease in drag coefficient due to burning is apparent.

The effect of the particle's acceleration with respect to inertial space can be studied by including the unsteady terms in the governing equation. For the present study it is assumed that the particle undergoes a constant linear acceleration and the density integral remains invariant with time. Employing the classical incompressible velocity distribution for U_e, the governing equation can be written in the form

$$\frac{2}{3}\frac{B}{A}\frac{a}{U}\frac{1}{\sin\theta}\frac{\partial\xi^2}{\partial t} + \left[2\left(1+\frac{B}{A}\right)\frac{\cos\theta}{\sin\theta} - \frac{C}{A}\frac{2\alpha a}{U^2}\frac{4}{9\sin\theta}\right]\xi^2 + \frac{\partial\xi^2}{\partial\theta} = \frac{3}{8A}\sin^3\theta \tag{27}$$

where

$$\xi = \frac{9}{4}\frac{\sin^3\theta}{C_f\sqrt{Re}}$$

and

$$\alpha = \partial V/\partial t.$$

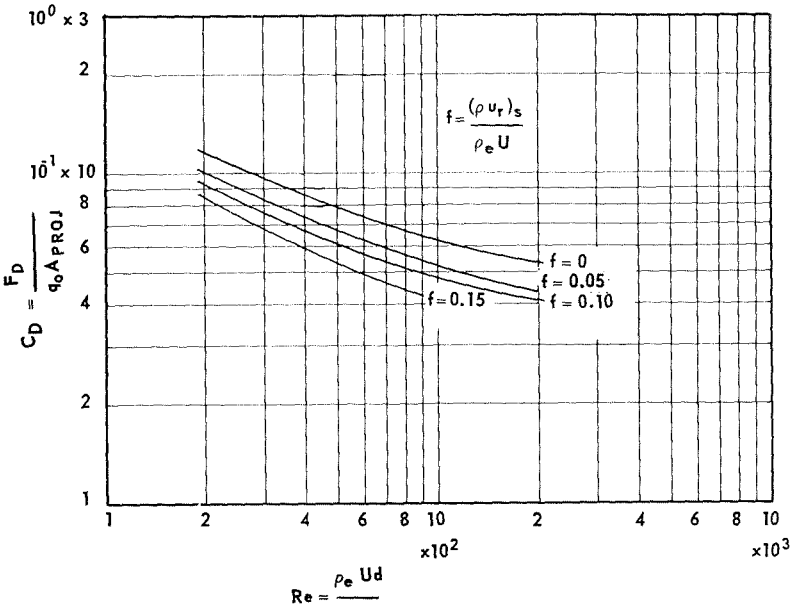

FIG. 5. Theoretical drag coefficient vs Reynolds number for a burning particle.

Employing the same conditions as used for the burning particle; namely, $n = 0.8$ and $\bar{T} = 2$, and assuming that the free stream velocity does not vary appreciably, Eq. (27) becomes

$$\frac{Ac}{\sin\theta}\frac{\partial\psi}{\partial\bar{t}} + \frac{3}{4}\frac{\partial\psi}{\partial\theta} = \frac{9}{16}\sin^2\theta \exp -\tfrac{2}{3}\bar{t} \quad (28)$$

where

$$\psi = \xi^2 \exp(-\tfrac{2}{3}\bar{t}) \sin^{10}\theta$$
$$\bar{t} = t\alpha/U$$
$$Ac = 2a\alpha/U^2$$

Employing the characteristic solution of the linear partial differential equation, it can be shown that

$$\left.\frac{C_f - C_{f0}}{C_{f0}}\right|_{\theta=\pi/2} \leq -\frac{\pi}{9}Ac$$

where

$$C_{f0} = C_f(Ac = 0) \quad (29)$$

indicating acceleration tends to reduce the skin friction coefficient.

The form drag is also influenced by acceleration. The pressure coefficient on the surface of an accelerating sphere can be expressed as[21]

$$C_p = -(\alpha a/U^2)\cos\theta + 1 - (9/4)\sin^2\theta \quad (30)$$

Assuming the pressure coefficient in the wake is unaffected by acceleration, the decrease in form drag due to acceleration becomes

$$C_{D_p} - C_{D_{p0}} = -(Ac/3)(1 - \cos^3\theta_s)$$

where

$$C_{D_{p0}} = C_{D_p}(Ac = 0) \quad (31)$$

Employing the result that $C_D = 0(1)$ for the range of Reynolds numbers considered in this study, it is possible to write

$$|\Delta C_D| = 0(Ac) \quad (32)$$

In conclusion, the effect of acceleration on the particle drag coefficient can be neglected for $Ac \leq 10^{-2}$.

The effect of both burning and acceleration is to reduce the particle's drag coefficient. The magnitude of the decrease is a function of the nondimensional burning rate f and acceleration modulus Ac.

Experimental Approach

The experimental setup had to be capable of providing sufficient data to determine drag coefficients and burning rates for accelerating particles. The schematic sketch in Fig. 6 illustrates the fundamental idea underlying the experimental setup. Particles were injected into a vertical shock tube above the test section and fell toward the testing region. A flame in the test section ignited the particles before a shock wave, coming from below, subjected them to a convective flow field accelerating them upwards. A high speed camera coupled with a concentrated light source took moving pictures of the particles from which acceleration and burning rate data were obtained. The occurrence of the shock wave had to be so timed that it encountered the particles shortly after they came into the field of view. This insured the largest particle acceleration and smallest velocity; a condition most attractive to the photographic technique.

The shock tube was 11 ft long and had an inside $\frac{1}{2}$ by $\frac{3}{8}$ inch rectangular cross section. The test section was located in the center portion while the driver section was attached at the bottom. The test section windows consisted of Pyrex glass etched to provide a reference line on the photographs for displacement measurements. The particles were ignited by a propane-air flame fed by two opposing jets installed in the test section wall. Two SLM pressure transducers located below the test section were used to measure the speed of the shock wave.

The shadowgraph technique was used to photograph the particles. A 100-watt Sylvania zirconium arc lamp coupled with a condensing lens supplied a sufficiently intense light to photograph particle shadows at high framing rates. The

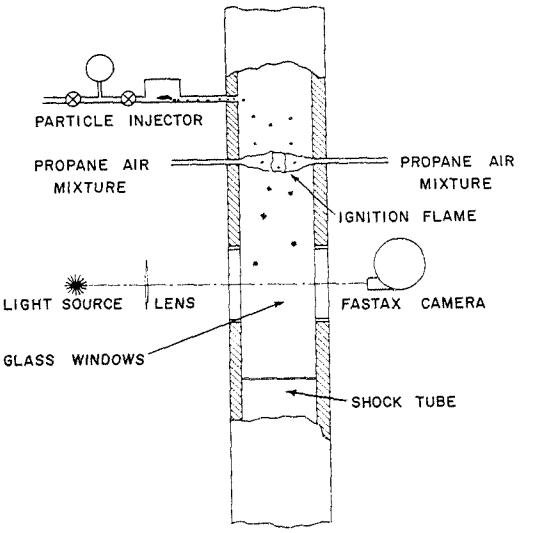

FIG. 6. Schematic diagram of experimental apparatus.

camera was a 16 mm Wollensak Fastax Camera fitted with extension tubes to provide a magnification of 1.174. The camera, in conjunction with a Wollensak "Goose," provided framing rates up to 7300 frames per second.

The particle injection system functioned by subjecting particles to a gust of air and blowing them into the tube.

The primary purpose of the study was to determine the drag coefficients of burning particles. However, a series of tests with nonburning particles was performed for comparison between the two cases. The two kinds of particles used were gun powder and glass beads. The gun powder consisted of military ball powder—Type C and Winchester Western 295 HP ball powder. The particles ranged from 100 to 250 microns in diameter. Photographs of them appear in Fig. 7.

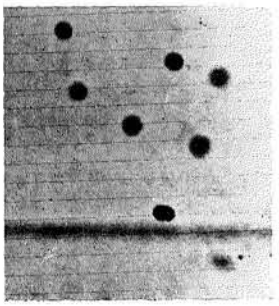

(A) GLASS BEADS

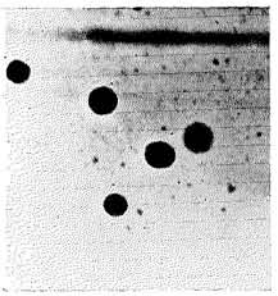

(B) 295 HP BALL POWDER

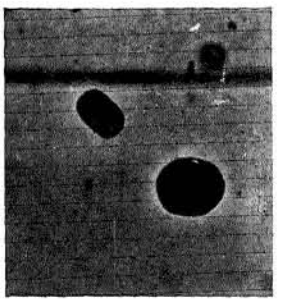

(C) MILITARY BALL POWDER-TYPE C

FIG. 7. Samples of particles used in experiments.

For purposes of data reduction it was assumed the glass beads and 295 HP powder were spherical in shape while an ellipsoidal shape was assumed for the military ball powder. The specific gravity of the particles ranged from 1.49 to 2.5.

The particle dynamics equation indicates six pieces of information are necessary to determine the drag coefficient of a burning particle; particle acceleration, mass, and size, relative velocity between the particle and gas, free stream density, and surface variation of burning rate. The magnitude of the integral in Eq. (1) may be estimated by choosing a simple model for a burning particle; namely, a flat disc normal to the flow. Employing conservative assumptions concerning the pressure distribution and burning rate dependence on pressure, it can be shown[19] that the contribution to the drag coefficient due to the momentum flux integral is negligible for the burning rates encountered in this study. Similarly, the gravitational body force can be neglected compared to the particle acceleration achieved in this study and the data reduction equation for a spherical particle simplifies to

$$C_D = \frac{4}{3}\frac{\rho_p}{\rho_\infty}\frac{d\alpha}{U^2} \tag{33}$$

where ρ_p and d are the particle density and diameter, respectively. It is interesting to note that the drag coefficient is proportional to the product of the acceleration modulus and particle-gas density ratio. The high speed motion pictures provided the particle's size, velocity, and acceleration. The wave speed and atmospheric conditions were used with the shock tube relationships to determine the gas velocity and density. The experimental results appear in Figs 8 and 9.

The vertical line associated with each experimental point represents the experimental probable error. The error in determining the convective flow velocity behind the wave was responsible for the majority of the probable error. For weak shock waves, one can show

$$\frac{\Delta u_g}{u_g} \cong \frac{1}{M-1}\frac{\Delta c_s}{c_s} \tag{34}$$

where Δ, u_g, c_s and M are the probable error operator, gas velocity behind the wave, wave speed, and shock wave Mach number, respectively. In the present experiment, the Mach number of the shock wave varied from 1.08 to 1.3. The wave speed error arose principally from the experimentally determined factor to account for wave attenuation between the location of measurement and the test section.

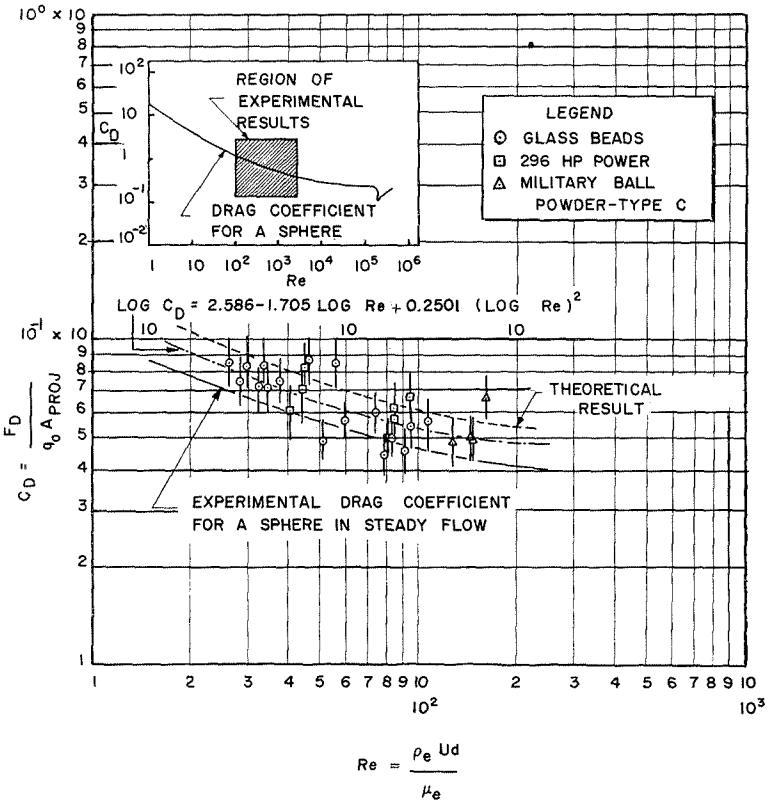

FIG. 8. Drag coefficient vs Reynolds number for nonburning particles.

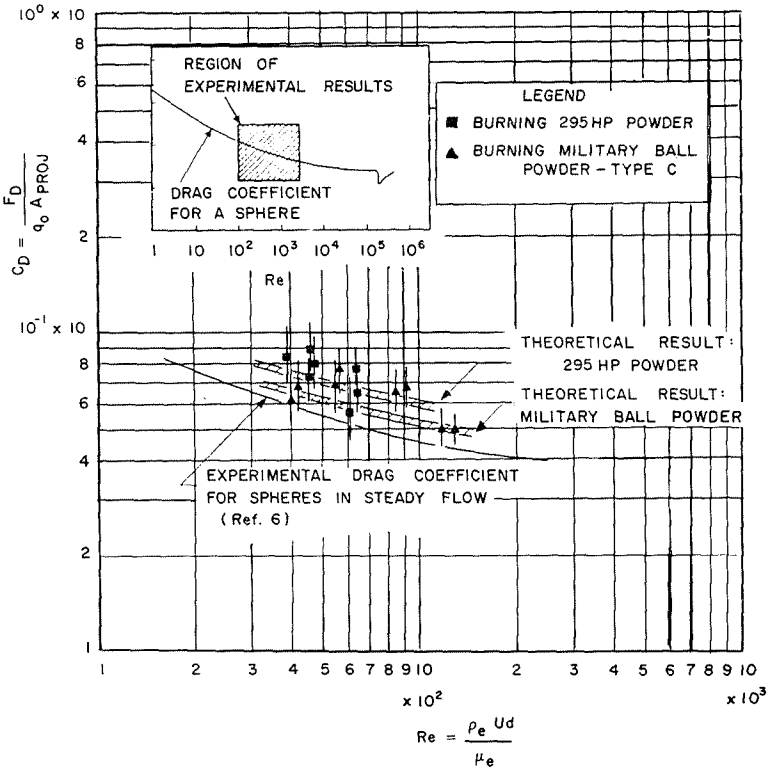

FIG. 9. Drag coefficient vs Reynolds number for burning particles.

Discussion and Conclusions

The experimental and analytical results appear in Figs. 8 and 9. The width of the theoretical curves for the burning particles is due to the nonuniformity in burning rates. The results generally indicate a larger drag coefficient than the standard steady state drag coefficient for sphere. This observation can be attributed to free stream turbulence, particle roughness factor, and particle rotations. In Fig. 8 the theoretical curve lies above the majority of the experimental results and this can be traced to the full velocity profile assumed in the analysis and large form drag associated with the simplified pressure distribution chosen. The acceleration modulus for the present studies was the order of 10^{-3}. Consequently, reduced drag coefficients due to accelerative effects were not detectable. Considering the relative crudeness of the analysis and the possible experimental errors, the agreement between the analytical and experimental results appears satisfactory.

The present experimental results agree very well with those of Torobin and Gauvin[4] in the subcritical Reynolds number range. Rabin's[5] experiments yielded larger drag coefficients than the present study and this can be attributed to liquid drop deformation towards a disc shape. It is believed that the noticeable low drag coefficients obtained experimentally by Ingebo[1] can be traced to a critical Reynolds number effect. Employing Torobin and Gauvin's results and Ingebo's experimental conditions, it can be shown analytically[19] that $C_D \propto Re^{-0.80}$ which corresponds closely with Ingebo's experimental findings. It is most difficult to determine the reasons for the very small drag coefficients obtained by Hanson.[2] Reference 19 indicates evaporation cannot account for such a large reduction in drag coefficient and the discrepancy is probably the result of the assumptions employed to determine the relative velocity between the drops and the gas.

Equation (33) indicates the acceleration modulus may be expressed as

$$Ac = \frac{3}{4}\frac{\rho_\infty}{\rho_p} C_D \qquad (35)$$

However, C_D is the order of one in the Reynolds number range considered in this study, it is possible to write

$$Ac = 0(\rho_\infty/\rho_p) \qquad (36)$$

For most practical nozzle problems, $Ac = 0(10^{-2})$ and accelerative effects can be neglected.

The mass flux associated with burning reduces the particle drag coefficient. However, the experimental and analytical results indicate the effects of particle burning will not be apparent for $f \leq 0.025$ since other effects such as turbulence, particle rotation, and roughness will be more dominant.

As a result of the present study, it appears the steady state drag coefficient for a sphere is applicable to particles found in rocket nozzles provided their Mach number, based on the relative velocity, is small. However, the experimentally determined result

$$\log_{10} C_D = 2.586 - 1.705 \log_{10} Re + 0.2501(\log_{10} Re)^2 \quad (200 \lesssim Re < 1600) \quad (M \simeq 0) \qquad (37)$$

would be appropriate should a more accurate drag coefficient be required.

Acknowledgments

This work was performed at the Aircraft Propulsion Laboratory of the University of Michigan and was supported by NASA grant NsG–86–60.

References

1. Ingebo, R. D.: NACA TN 3762 (1956).
2. Hanson, A. R.: University of Michigan, Ph.D. thesis (1951).
3. Bolt, J. A. and Wolf, L. W.: University of Michigan ERI Project No. 2253:3–6–P (1954).
4. Torobin, L. B. and Gauvin, W. H.: McGill University Technical Report No. 193 (1960).
5. Rabin, E., Schallenmuller, A. R., and Lawhead, R. B.: Rocketdyne AFOSR–TR–60–75 (1960).
6. *Chemical Engineers' Handbook.* J. Perry (ed.) (1941).
7. Basset, A. B.: *A Treatise on Hydrodynamics* (1888).
8. Pearcey, T. and Hill, G. W.: Australian J. Phys., *9*, 18 (1956).
9. Lunnon, R. G.: Proc. Roy. Soc. (London) *A110*, 302 (1926).
10. Gilbert, M., Davis, L., and Altman, D.: Jet Propulsion, *25*, 26 (1955).
11. Kliegel, J. R.: IAS Preprint No. 60–5 (1960).
12. Carrier, G. F.: J. Fluid Mech., *4*, 376 (1958).
13. Covert, E. E.: Mass. Institute of Technology Naval Supersonic Laboratory, TN 390 (1959).
14. Tomotika, S.: ARC R & M, No. 1678 (1935).
15. Hersch, M.: ARS Journal, *31*, 39 (1961).
16. Taneda, S.: Kyushu University, Res. Inst. for App. Mech., *4*, 99 (1956).
17. Garner, F., Jenson, V., and Kery, R.: Trans. Inst. Chem. Engr., *37*, 191 (1959).
18. Ermisch, H.: Ab. Aero. Inst. Tech. Hochschule, Aachen, *6*, 48 (1927).
19. Crowe, C. T.: University of Michigan, IP 544 (1961).
20. Schlichting, H.: *Boundary Layer Theory* (1955).
21. Milne-Thomson, L. M.: *Theoretical Hydrodynamics* (1957).

Discussion

DR. S. WAY (*Westinghouse Research Laboratories, Pittsburgh*): In the statement of the momentum equation for the particle, the body-force term was included, but the statement was made that it was generally unimportant. I would like to call attention to the possibility that under certain conditions electrostatic charges may accumulate on the particles and one must guard against this in studies of drag coefficient.

DR. C. T. CROWE (*United Technology Corporation*): In the equation describing the dynamics of the particle it is necessary to include the forces created by electrostatic forces when such forces are significant. However, these forces will not directly influence the particle's drag coefficient.

IGNITION OF MIXTURES OF COAL DUST, METHANE, AND AIR BY HOT LAMINAR NITROGEN JETS

JOSEPH M. SINGER

Ignition temperatures and limiting fuel concentrations of mixtures of coal dust, methane (firedamp), and air have been determined by the hot-gas jet ignition method. Ignition promoters and ignition suppressors were also incorporated into the hybrid mixtures and into the hot jet. This study was limited to use of a single coal having about 37 per cent volatile matter, ground to about 1–5 microns.

Hybrid mixtures containing coal dust and air in approximately stoichiometric balance for complete combustion required minimal methane concentrations for ignition at given temperatures.

Ignition temperatures and concentrations were decreased by addition of 90 per cent CO + 10 per cent H_2 to the hot jet. Ignition was inhibited when gaseous halogenated hydrocarbons were added to the hot jet or to the hybrid mixture. The inhibiting action of the additives investigated decreased in the following order: bromotrifluoromethane, methyl bromide, carbon dioxide, and water vapor. Our observations suggest that ignition suppressors adsorbed on inert dusts, incorporated into water-stemming cartridges, or into the explosive charge itself, will reduce the ignition hazard of detonation products from explosives.

General Considerations

Ignitibilities of systems of coal dust-air and methane-air have been investigated extensively. However, the ignition and combustion of "hybrid-mixture," three-component systems of coal dust-methane-air are rarely studied, although of great practical concern in coal mine safety. In the present investigation, the ignition of such mixtures by hot gases was chosen for study because of its analogy to the practical case of ignition of combustible coal mine atmospheres by detonation products from blasting shots. As far as is known, this is the first time that the method we have used has been applied to the ignition of solid-gas heterogeneous systems. We hoped among other things to obtain information on the ignition suppression effect of various solid and gaseous additives that would lead to recommendations for specific ignition inhibitors that could minimize explosion hazards in coal mines.

Hot-gas ignition, first used by Vanpée and Wolfhard[1] to study the ignition of gaseous mixtures by hot laminar jets, was modified for application to dust-gas mixtures. They have shown that the ignition of flammable methane-air mixtures by hot continuously flowing gas jets is, under some conditions, a special case of ignition. When the methane concentration is somewhat below the lower flammable limit, a luminous "flame" (pseudoflame) appears within the hot nitrogen ignition jet. This phenomenon is not observed with other fuel gas-air mixtures. A pseudoflame is inhibited by the slow increase of methane concentration into the flammable range and by halogenated hydrocarbons. Apparently, under some conditions, it is involved in the mechanism of hot-gas ignition of coal dust-methane-air as well as methane-air mixtures.

Experimental Procedures

The present approach to the study of heterogeneous combustion called for controlled dust concentrations in flowing gas systems. Only one coal-dust type and particle-size range was used. The coal dust was first reduced to approximately 1- to 5-micron particle size by a recirculating, centrifugal-type disintegrator. The coal composition in per cent by weight was: H_2 = 5.3, C = 77.3, N_2 = 1.5, O_2 = 6.4, ash = 7.8, S = 1.7; its proximate analysis in per cent by weight was: moisture = 2.4, volatile matter = 36.6, fixed carbon = 53.2, and ash = 7.8; its heating value was 14,630 Btu/lb, moisture- and ash-free. All gases except air were chemically pure grade.

Coal Dust Disperser Design

The disperser illustrated in Fig. 1 proved efficient. Flow rate and concentration of dust depend upon the size of the hypodermic tubing

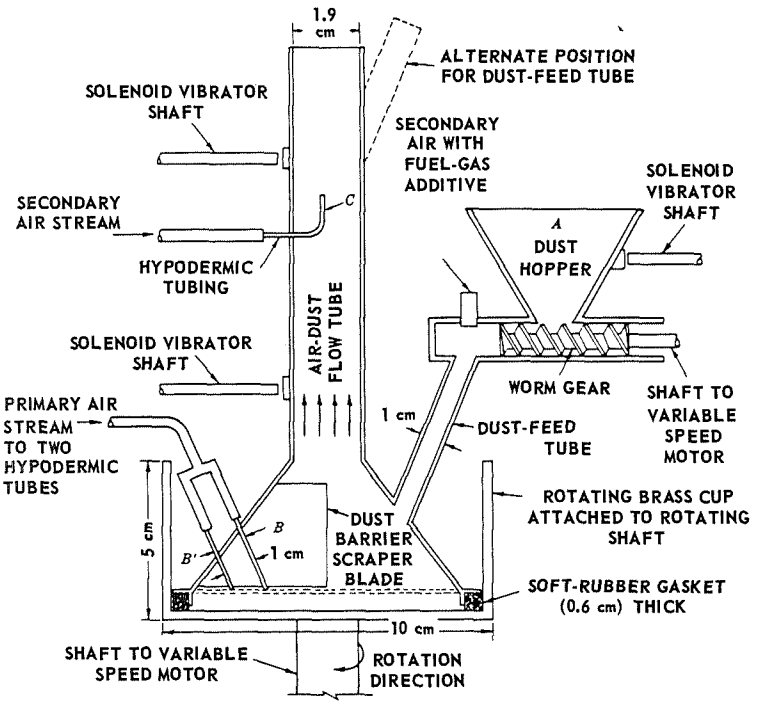

FIG. 1. Coal dust disperser.

69

that delivers air or other dust carrier to the dust chamber, and upon the amount of dust fed to the dust chamber from hopper A. In practice, air flows of approximately 300–400 cc/sec require driving pressures of 3 to 7 atm and hypodermic tubing ranging in size from B.S. gage No. 27 (0.031 cm) to No. 18 (0.102 cm). Carrier streams B, B′ are impelled at high momentum to the coal dust that has entered the dust cup from the hopper. Slight changes of concentration of the flowing dust cloud are achieved by varying the rotation speed of the bottom-cup surface. The exit tube leads dispersed dust and air to a manifold that branches to the explosion chamber through four symmetrically placed tubes of 2.5 cm diameter each. A separate air stream is injected through hypodermic tube C, which is centrally located in the manifold tube to facilitate movement of dust toward the explosion chamber. Feed tubes and manifold line are continuously vibrated during dust dispersion to prevent dust deposition of the tube walls.

Hot-Gas Ignition Apparatus

The hot-gas ignition apparatus is illustrated in Fig. 2. A stream of nitrogen flows through a vertical (60 per cent platinum, 40 per cent rhodium) wire-wound tubular ceramic furnace of 1.7 cm id and 100 cm long. To obtain a flat temperature profile* within the nitrogen stream at the exit port, the flow rate is maintained at 120 cc/sec STP (linear velocity at the axis of flow is 300 to 400 cm/sec, depending upon the temperature of the jet; Reynolds number is about 100). The flow of the methane–coal dust–air mixture surrounds the nitrogen stream and pseudoflame coaxially in the explosion chamber; the flowing mixture enters the chamber at the bottom through four inlet tubes of 2.5 cm diameter each. Dust concentrations are determined above the exit of flow nozzle A′ by a grab method, filtering the dust flow through a glass-wool cartridge for short periods and then measuring the weight gain. The explosion chamber is a heat-resistant glass tube 80 cm long, 14.5 cm ID, and 0.3 cm wall thickness.

In the ignition experiments, after steady nitrogen jet temperatures are established, methane† is added *rapidly* with uniform mixing to the flowing coal dust–air mixture in small increments to de-

* Temperature of the nitrogen jet is measured at the port axis of the furnace tube, using a 0.0125 cm diameter platinum–platinum, 10 per cent rhodium thermocouple, uncoated.

† Ethane was added to the methane in certain experiments. The ethane/methane ratio is included in all tables and figures.

termine the minimum methane concentration limit for ignition. This ignition technique differs from usual procedures in that the temperature is the independent variable and fuel concentration is the dependent variable. (In most ignition experiments the temperature is raised slowly until

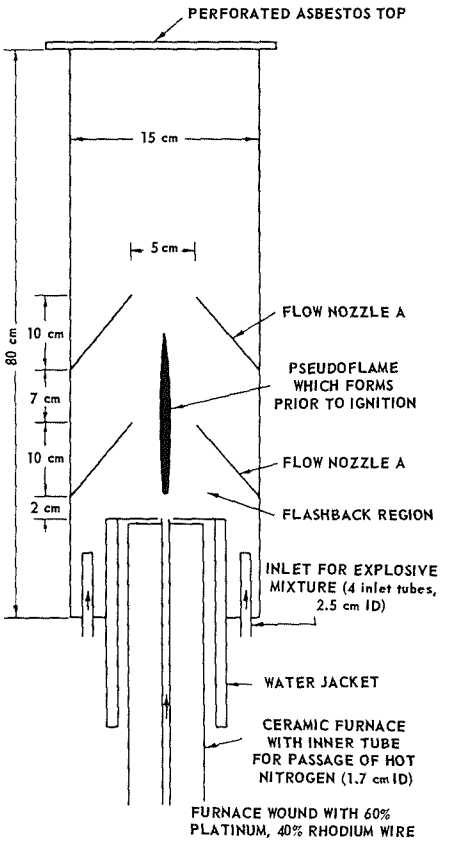

FIG. 2. Hot-gas ignition apparatus.

ignition occurs.) Ignition of the hybrid mixture is followed by flashback toward the inlet tubes; the resulting flame fills the bottom of the explosion chamber below nozzle A′ but does not extend upward above nozzle A. The total flow of the hybrid mixture is maintained at approximately 400 cc per sec, that is, at an average linear velocity of 20 cm per sec through the exit throat of nozzle A. The apparatus is limited to characteristic contact time periods that do not exceed 80–100 msec.*

* Ignition times of pulverized 6-micron coal-air in furnaces are usually less than 50 msec, according to Ghosh and Orning.[2]

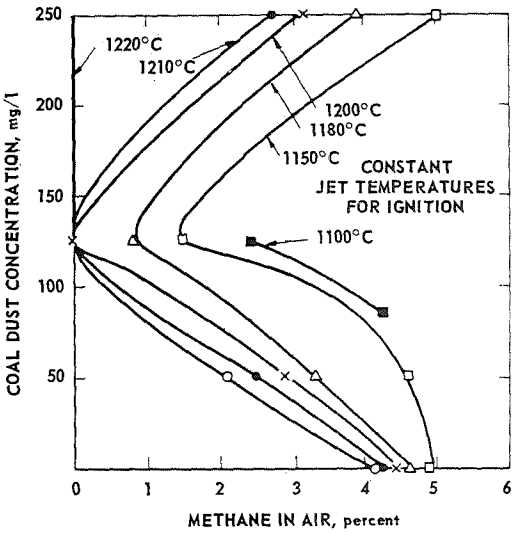

FIG. 3. Ignitibility of coal dust–(methane–ethane)–air by hot laminar nitrogen jets; ethane/methane ratio is 0.15.

Experimental Results and Discussion

Ignition of Hybrid Mixture

Nitrogen jet temperatures are given in Figs. 3 and 4 for the ignition of hybrid mixtures containing methane and four different coal dust concentrations (50, 86, 125, and 250 mg/liter). Coal dust concentration of approximately 125 mg/liter corresponds to a stoichiometric mixture with air.

These data indicate that hybrid mixtures containing the stoichiometric concentration of coal dust (125 mg/liter) require the least added methane for ignition at all hot-jet temperatures and that ignition temperatures are lower (at comparable fuel concentrations) when the hot jet contains 1.35 per cent of a 90 per cent CO + 10 per cent H_2 mixture; the added CO and H_2 serve to simulate the ignition hazard that may result from using under-oxygen-balanced explosives in mines.

As illustrated in Figs. 3 and 4, coal dust/methane ratios (slopes of the ignition lines) vary slightly with hot-gas jet temperature and with coal-dust concentration. For lean coal concentrations, less than 100 mg/liter, as the ignition temperature decreases, each percentage increment of methane becomes equivalent to a larger coal dust concentration increment; that is, the cooperative flammability of coal dust is less at low gas jet temperatures than at high ones. At gas jet temperatures between 1110° and 1220°C and approaching the stoichiometric coal dust concen-

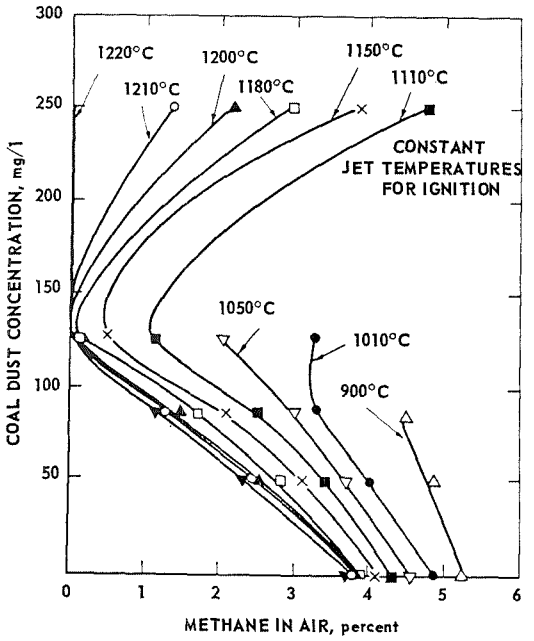

FIG. 4. Ignitibility of coal dust–(methane–ethane)–air by hot laminar nitrogen jets; ethane/methane ratio is 0.15; nitrogen jet contains 1.35 per cent (90 per cent CO + 10 per cent H_2).

trations from the lean side, the coal dust/methane ratio decreases, indicating greater cooperative flammability of coal dust. In this temperature range and above the stoichiometric coal dust concentration, more methane is required for ignition as the coal dust concentration increases and the hot-gas jet temperature decreases, the result of lack of oxygen for combustion and/or of thermal self-quenching. And finally for high nitrogen jet temperatures above 1220°C and coal dust concentrations above stoichiometric to at least 250 mg/liter, no additional methane is required for ignition.

Ignition Suppression Experiments

Pseudoflame Suppression. In the absence of halogenated hydrocarbon additives, *slow* methane addition to the flowing fuel–air mixture that envelops the pseudoflame inhibits the pseudoflame, causing it to rise in the nitrogen stream and finally disappear. Table 1 shows that the amount of methane required for pseudoflame suppression is decreased when bromotrifluoromethane is added to the hot nitrogen jet. Small quantities of additive are seen to be effective. Additional bromotrifluoromethane is required for pseudoflame suppression when 90 per cent

TABLE 1

Effect of bromotrifluoromethane (BTFM) on minimum methane concentration for suppression of pseudoflames when methane is added slowly to explosion chamber. No coal dust in fuel. Ethane concentration in methane is 13 per cent

Nitrogen jet temperature (°C)	Methane–ethane in explosion chamber (per cent in air)	In nitrogen jet	
		(90% CO + 10% H_2) (per cent)	BTFM (per cent)
1,118	4.1	0.0	0.0
1,118	3.4	0.0	0.04
1,118	2.5	0.0	0.08
1,118	(5.02)[a]	1.23	0.0
1,118	4.3	1.23	0.04
1,118	2.5	1.23	0.08
1,224	(5.5)	0.0	0.08
1,224	4.5	0.0	0.22
1,224	(5.5)	1.23	0.08
1,224	4.9	1.23	0.24
1,224	3.2	1.23	0.44

[a] Values in parentheses indicate ignition occurred.

TABLE 2

Effect of bromotrifluoromethane (BTFM) on minimum methane concentration for ignition of coal dust–methane–air when methane is added rapidly to explosion chamber. Coal dust concentration in explosion chamber is 100 mg/liter. Ethane concentration in methane is 13 per cent

	In explosion chamber		In nitrogen jet	
Nitrogen jet temperature (°C)	Methane-ethane, per cent in air for ignition	BTFM (per cent)	90% CO + 10% H_2 (per cent)	BTFM (per cent)
1,011	6.64	0.0	1.23	0.0
1,011	6.82	0.02	1.23	0.0
1,011	7.0	0.06	1.23	0.0
1,011	—[a]	0.07	1.23	0.0
1,011	5.8	0.08	1.23	0.0
1,011	6.9	0.16	1.23	0.0
1,011	—[a]	0.18	1.23	0.0
1,011	—[a]	0.0	1.23	<0.02
1,118	3.05	0.0	1.23	0.0
1,118	5.26	0.0	1.23	0.02
1,118	—[a]	0.0	1.23	0.04
1,118	4.63	0.0	0.0	0.0
1,118	—[a]	0.0	0.0	<0.02
1,207	2.26	0.0	1.23	0.0
1,207	3.05	0.0	1.23	0.04
1,207	5.0	0.0	1.23	0.08
1,207	5.8	0.0	1.23	0.17
1,207	—[a]	0.0	1.23	0.22
1,207	2.57	0.0	0.0	0.0
1,207	3.61	0.0	0.0	0.04
1,207	5.5	0.0	0.0	0.08
1,207	6.3	0.0	0.0	0.17
1,207	—[a]	0.0	0.0	0.18

[a] No ignition observed with methane addition.

CO + 10 per cent H_2 is added to the hot jet and when the temperature of the nitrogen stream is increased.

Ignition Suppression of Coal Dust–Methane–Air Mixtures. After the inhibitor is added to the hybrid mixture, or to the hot nitrogen jet, the amount of methane required for ignition of the coal dust–methane–air mixture is measured, adding the methane fuel *rapidly* to the hybrid mixture in the explosion chamber. Data were obtained for admixture of bromotrifluoromethane (Table 2) and methyl bromide (Table 3) to the hot nitrogen jet or to a hybrid mixture containing 100 mg/liter of coal dust. Similarly, in Table 4, data are given for admixtures of bromotrifluoromethane at a coal dust concentration of 250 mg/liter. The effect of bromotrifluoromethane is compared with the effect of water vapor and CO_2 on the ignitibility of hybrid mixtures of coal dust (100 mg/liter), firedamp, and air in Fig. 5. The foregoing shows that:

1. Bromotrifluoromethane inhibits ignition much more effectively than water vapor or CO_2, demonstrating the advantage of chemically active suppressors over inert gaseous suppressors. Carbon dioxide is slightly more effective than water vapor.

2. Less bromotrifluoromethane than methyl bromide is needed for equivalent ignition suppression (with or without CO and H_2 in the jet),

TABLE 3

Effect of methyl bromide on minimum methane concentration for ignition of coal dust–methane–air when methane is added rapidly to explosion chamber. Coal dust concentration is 100 mg/liter. Ethane concentration in methane is 13 per cent

	In explosion chamber		In nitrogen jet	
Nitrogen jet temperature (°C)	Methane-ethane, per cent in air for ignition	Methyl bromide (per cent)	90% CO + 10% H_2 (per cent)	Methyl bromide (per cent)
1,109	4.6	0.39	1.23	0.0
1,109	5.2	0.65	1.23	0.0
1,109	5.4	0.88	1.23	0.0
1,109	—[a]	0.90	1.23	0.0
1,208	3.5	0.0	1.23	0.74
1,208	5.9	0.0	1.23	1.24
1,208	—[a]	0.0	1.23	1.26
1,208	6.04	0.0	0.0	0.33
1,208	6.54	0.0	0.0	0.54
1,208	7.5	0.0	0.0	0.74
1,208	—[a]	0.0	0.0	0.76
1,200	6.7	1.5	0.0	0.0
1,200	—[a]	1.6	0.0	0.0
1,200	6.0	1.5	1.23	0.0
1,200	—[a]	1.9	1.23	0.0
1,200	8.1	0.86	1.23	0.0
1,200	9.3	0.86	1.23	0.0
1,200	—[a]	1.2	1.23	0.0

[a] No ignition observed with methane addition.

TABLE 4

Effect of bromotrifluoromethane (BTFM) on minimum methane concentration for ignition of coal dust–methane–air when methane is added rapidly to explosion chamber. Coal dust concentration in explosion chamber is 250 mg/liter. Temperature of jet is 1,230°C

	In explosion chamber		In nitrogen jet	
Methane, per cent in air for ignition	Ethane concentration, per cent in methane	BTFM (per cent)	90% CO + 10% H_2 (per cent)	BTFM (per cent)
0.0[a]	0.0	0.0	0.0	0.0
3.85	0.0	0.19	0.0	0.0
6.3	0.0	0.63	0.0	0.0
8.1	0.0	1.23	0.0	0.0
2.24	0.0	0.19	1.23	0.0
5.55	0.0	0.63	1.23	0.0
8.12	0.0	1.23	1.23	0.0
—[b]	0.0	1.24	1.23	0.0
3.72	0.0	0.0	0.0	0.17
—[b]	0.0	0.0	0.0	0.20
4.0	0.0	0.0	1.23	0.17
—[b]	0.0	0.0	1.23	0.23
3.04	1.6	0.0	1.23	0.23
—[b]	13.0	0.0	1.23	0.29

[a] Without BTFM, ignition occurs when methane is not in hybrid mixture.

[b] No ignition observed with methane addition.

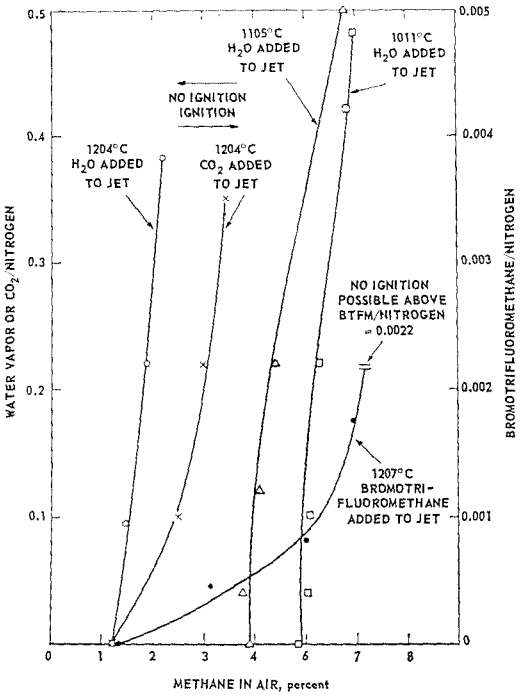

FIG. 5. Hot-gas ignition temperatures when water vapor, carbon dioxide, and bromotrifluoromethane are added to hybrid mixtures of coal dust, methane–ethane, and air. Ethane/methane ratio is 0.15. Nitrogen jet contains 1.35 per cent (90 per cent CO + 10 per cent H_2). Coal-dust concentration = 100 mg/liter.

as would be expected on the basis of the number of halogen and hydrogen atoms in each additive.

3. Halogenated hydrocarbons are more effective ignition inhibitors when added to the hot nitrogen jet than to the hybrid mixture, because of proximity and more direct involvement in the preignition reaction mechanism.

4. The concentration of halogenated hydrocarbon required to suppress ignition increases as the hot-gas jet temperatures rise.

The favorable ignition-suppression results obtained with halogenated hydrocarbons prompted another experiment in which the inhibitors bromine, methyl bromide, and bromotrifluoromethane were adsorbed on inert powders and added in this form to the hybrid mixtures. On the basis of preliminary adsorption and desorption rate experiments, in which each of the dusts silica gel, fireclay, or activated charcoal was impregnated at 1 atm, activated charcoal plus 28 per cent bromine was chosen as a stable ignition-suppressing system.

The effect of activated charcoal (with and without 28 per cent bromine) on the ignition of coal dust at 1228°C is shown in Table 5. The adsorbed bromine either completely prevents ignition or substantially increases the methane concentration required for ignition. It may be anticipated, based on previously described ignition-suppression experiments, that if the adsorbed systems were introduced in the hot nitrogen jet, increased inhibition efficiencies would result.

TABLE 5

Effect of activated charcoal (with and without 28 per cent adsorbed bromine) on minimum methane concentration for ignition of coal dust–methane–air when methane is added rapidly to the explosion chamber. Total dust concentration is 100 mg/liter. Dust composition is 50% coal dust and 50% activated charcoal. Nitrogen jet temperature is 1,228°C

Activated charcoal content	In explosion chamber		In nitrogen jet	
	Methane, per cent in air for ignition	Ethane concentration, per cent in methane	90% CO + 10% H_2 (per cent)	BTFM (per cent)
Without Br_2	7.72	0.0	0.0	0.0
With Br_2	—[a]	0.0	0.0	0.0
Without Br_2	5.52	13.0	0.0	0.0
With Br_2	8.8	13.0	0.0	0.0
Without Br_2	4.3	0.0	1.23	0.0
With Br_2	8.7	0.0	1.23	0.0
Without Br_2	4.2	10.0	1.23	0.0
With Br_2	7.7	10.0	1.23	0.0
Without Br_2	4.0	15.0	1.23	0.0
With Br_2	6.0	15.0	1.23	0.0
Without Br_2	—[a]	13.0	1.23	0.2
With Br_2	—[a]	13.0	1.23	0.04

[a] No ignition observed with methane addition.

Conclusions

Ignition temperatures and methane concentrations for ignition are found to be minimum for coal-dust concentrations approximately equal to the stoichiometric requirement for complete conversion. Ignition temperatures and concentrations are further decreased when 90 per cent CO plus 10 per cent H_2 is added to the hot jet.

Ignition can be prevented and ignition temperatures and methane concentrations for ignition are increased when gaseous halogenated hydrocarbons are added to the hot jet or to the hybrid mixture. The inhibiting action of the additives investigated decreases as follows: bromotrifluoromethane, methyl bromide, carbon dioxide, water vapor. Our observations suggest that ignition suppressors adsorbed on inert dusts, incorporated into water-stemming cartridges, or into the explosive charge itself would reduce the incendivity of gases from detonating explosives.

References

1. Vanpée, M. and Wolfhard, H. G.: Bureau of Mines Rept. of Inv. 5627, 1960.
2. Ghosh, B. and Orning, A. A.: Ind. Eng. Chem. *47*, 117 (1955).

Discussion on Detonations

(Organized by Dr. D. R. White)
(*General Electric Research Laboratory*)

Chairmen: Prof. J. A. Fay
(*M.I.T.*)
Prof. A. K. Oppenheim
(*University of California*)
Dr. R. E. Duff
(*University of California*)
Dr. Marjorie W. Evans
(*Stanford Research Institute*)

Vice Chairmen: Prof. F. P. Bowden
(*University of Cambridge*)
Prof. N. Manson
(*Poitiers*)
Dr. C. H. Johansson
(*Stockholm*)

INTRODUCTION

DONALD R. WHITE

Our aim in this Discussions meeting is to explore two topics: structure of detonation and initiation of detonation in the condensed phase.

In recent years as the detonation front has been probed experimentally with greater resolution, considerable evidence has accumulated to demonstrate that this flow phenomenon simply is not one-dimensional. Experimental definition and theoretical explanation of this structure is currently the central problem of gaseous detonation.

Those aspects of the behavior of detonation known as limit phenomena can be regarded as part of the structure problem. For example, working near the low pressure propagation limit for a self-sustaining detonation, one observes spin, a type of behavior discovered relatively early because of the gross perturbation upon planarity. Increasing the initial pressure of the experiment, one finds an increasing number of "hot spots" moving over the front, or multi-headed spin. Other evidence, direct and indirect, confirms that at higher pressures the phenomenon persists, but at reduced scale.

Alternatively, instead of increasing the initial pressure from a near-limit condition, one may supply more and more energy from an external source to produce a series of over driven detonations, all at the same initial pressure. Here it is observed that as the velocity increases above the Chapman-Jouguet value, the multiplicity of the disturbances in the detonation front increases, their scale correspondingly decreasing. This observed behavior is consistent with a disturbance phenomenon whose existence depends on an exothermal reaction behind the shock front and whose scale depends on the reaction zone thickness. The condition of exothermicity is of course no longer met for a sufficient degree of overdriving of the detonation.

The generality with which this non-one-dimensionality has been observed, apparently for all modes of initiation and at least most detonable mixtures, suggests that its source be sought within the properties of the shock-reaction zone structure itself. Analysis of the "laminar" detonation has occupied the attention of many in the past, and quite properly continues to do so, since such understanding may provide a point of departure for study of "turbulent" detonation. Other investigators are tackling directly the stability of the shock-reaction zone structure, and the difficulties are indeed formidable.

A characteristic feature of this turbulent structure is the existence of weak shock waves propagating transversely through the reacting mixture behind the primary shock front. These shocks must be maintained by the higher reaction rate

behind them as a result of the increased pressure and temperature. The minimum separation which must be maintained between two successive shock waves for them to be thus sustained must therefore increase with increasing reaction zone thickness. When this separation becomes of the order of the tube diameter, a propagation limit is observed. The analytical difficulty is evident when one considers that the three-shock interaction problem in an ideal gas remains unsolved.

It would indeed be of interest to produce a detonation in a tube in such a fashion that it remained laminar during the period of observation, and to study its properties. I would guess that the reaction zone would be appreciably thicker with a correspondingly greater influence of the tube walls on the detonation behavior.

Most gaseous detonation experiments are done in tubes, of course. Two papers are included here which discuss results obtained under significantly different circumstances. The transversely propagating shock waves may well be dependent for their continuing existence upon reflection from the tube wall. If so, then absence of walls in standing detonation experiments may be partially responsible for the apparently laminar structure observed. Similarly, if a recognizable detonation could be established using a liquid spray as a fuel, the "reaction zone" would be relatively thick and perhaps stable to this transverse type of disturbance, since the local rate of heat release by droplet burning would be less sensitive to changes in the local pressure and temperature.

Far fewer observations of the structure of detonation in the condensed phase have been reported, and for good reason. Such data as are available show that in the liquid phase a granularity similar to that in the gas phase exists. I anticipate that other work on structure in the condensed phase will be reported in the discussion periods.

Research in condensed phase detonation is, of course, much more difficult, both theoretical and experimental. In the selection of papers to be presented here, emphasis has been given to initiation. It is the hope of the organizing committee (the session chairmen and myself) that these papers, supplemented by the discussion, will provide a good picture of current ideas of condensed phase initiation, and perhaps point out some of the more fruitful directions for future work.

CONTRIBUTION TO THE THEORY OF THE STRUCTURE OF GASEOUS DETONATION WAVES

D. B. SPALDING

The paper presents exact solutions to the equations governing the distributions of temperature, velocity and pressure in a gaseous detonation wave, for the cases in which the dimensionless volumetric-reaction-rate w: (a) has a concentrated peak near the hot boundary but negligible values elsewhere; (b) obeys the law

$$w = n(\tau - \tau_C)\left\{\left(\frac{\tau - \tau_C}{\tau_H - \tau_C}\right)^{n-1} - \left(\frac{\tau - \tau_C}{\tau_H - \tau_C}\right)^{2n-2}\right\},$$

where n is a constant, τ is the dimensionless stagnation temperature, and subscript C denotes upstream conditions. Other exact solutions are also discussed. The methods used are analytical and graphical, requiring no high-speed computing facility. The gas is supposed to have a Lewis Number of unity and a Prandtl Number of $\frac{3}{4}$; for convenience its thermodynamic properties are supposed to be those of a perfect gas.

It is argued that, although the reaction-rate functions considered do not correspond to the chemical-kinetic properties of any particular detonating gas, studies of the kind presented permit clear perception of most of the important properties of real gaseous detonations.

Introduction

Theoretical analysis plays two distinct roles in applied science. The first is to provide quantitative predictions of the behavior of complex phenomena, based on the fundamental properties of the materials; the second is to improve the analyst's perception of the quantitative relations between the behavior and the properties by means of the study of simplified models. In the first case, the aim is to obtain the right numerical answer; in the second, it is more important to expose clearly to view the most significant interrelations, without the encumbrance of computational details. These differing purposes influence the way in which the analysis is executed: In the first role, elegance is not essential, and the results are obtained in numerical form; in the second, dimensionless quantities predominate, algebra is preferable to arithmetic, and graphical representation of results is desirable.

Generally speaking, the fundamental properties of chemically reacting systems require too elaborate a description, and are too imprecisely known, to have permitted combustion theory to achieve appreciable success in the first role. The present paper is accordingly of the second type, its particular purpose being to elucidate the way in which chemical-kinetic and transport properties influence the structure of a detonation wave in gases.

Most of the important facts about this phenomenon have already been uncovered by the pioneering work of Hirschfelder and others (see references 1, 2, 3, 15, and 16). The present contribution is intended to make these facts more generally accessible and understandable, partly by the presentation of new solutions to the equations.

The Problem

We shall consider the process of detonation in a gas of constant specific heat and mean molecular weight. Figure 1 shows a property diagram for such a gas, the ordinate and abscissa being, respectively, stagnation temperature T_s and velocity V, and the equation of state being that of air at moderate temperatures. The scales are logarithmic and the diagram carries curves of constant temperature T, nondimensional pressure p/mR, pressure divided by stagnation pressure p/p_s, and nondimensional momentum flux p_{mom}/mR, the latter having the significance of what are commonly called Rayleigh lines. Such a diagram is easily constructed from the equations of gas dynamics, which it would be inappropriate to introduce here. It should be noted when interpreting the quantities p/mR, etc., that, in a detonation wave, the "mass velocity" m is a constant throughout the wave; the gas constant R is also constant in our model gas.

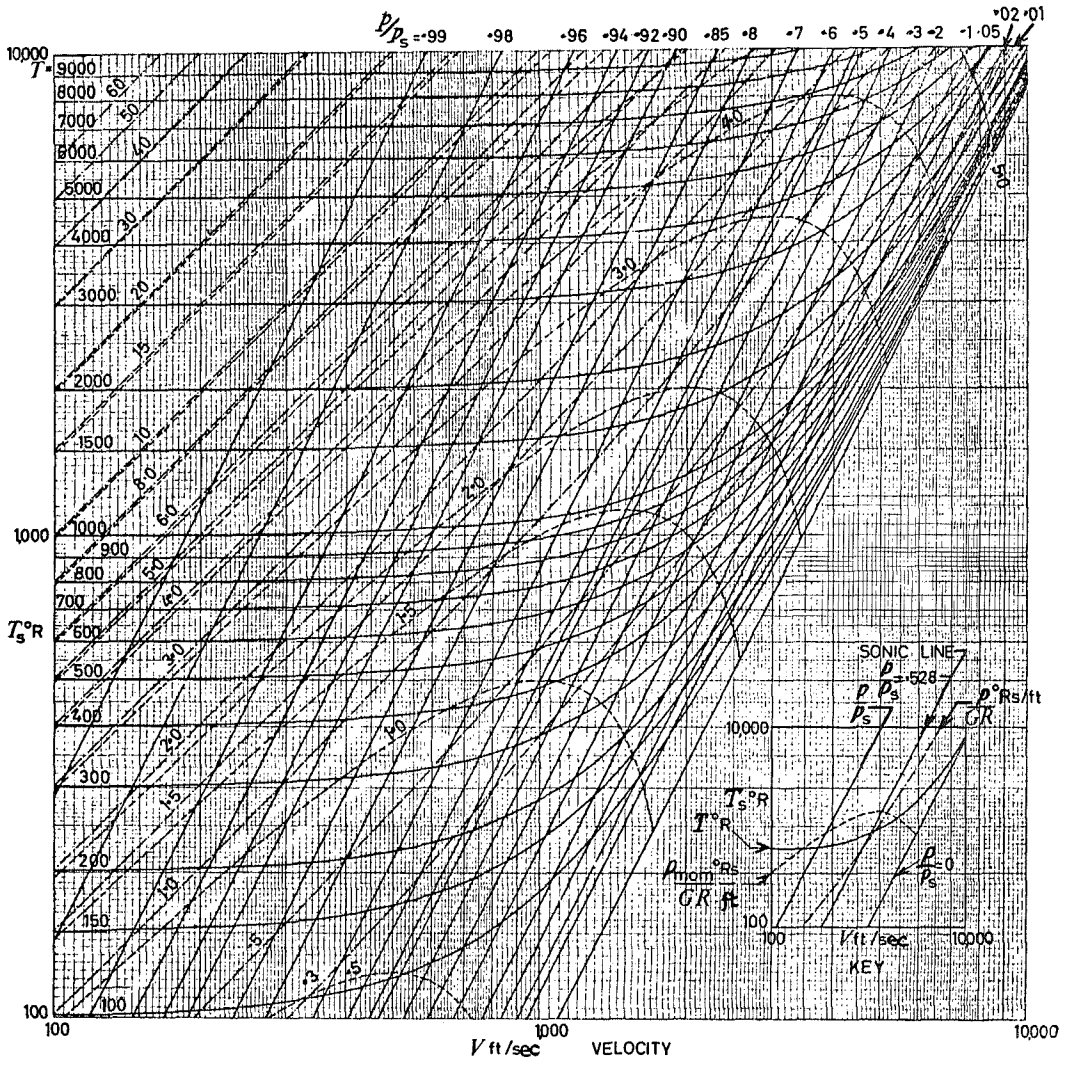

FIG. 1. Property diagram for flowing ideal gas with $\gamma = 1.4$ and $R = 1718$ ft^2/s^2 °R (ideal air)

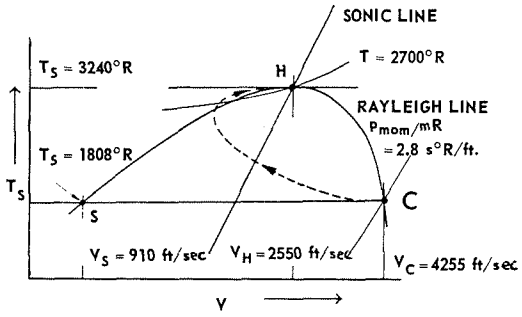

FIG. 2. A typical Chapman–Jouguet detonation represented on log T–log V diagram. C ≡ unburned condition; H ≡ burned condition; S ≡ von Neumann "spike." Broken line is possible path of gas passing through detonation wave.

It is well known that the laws of mechanics and thermodynamics applied to a detonation wave require that the upstream (cold) and downstream (hot) states lie on the same Rayleigh line; in addition, the downstream stagnation temperature $T_{s,H}$ exceeds the upstream value $T_{s,C}$ by an amount depending on the exothermicity of the reaction. Further, if the conditions giving rise to the detonation are of the Chapman–Jouguet (C–J) type, the downstream state point lies on the "sonic line" where $T_s = (\gamma + 1)V^2/2\gamma R$, γ being the specific heat ratio. Figure 2 illustrates this situation for a particular C–J detonation, the points C and H representing, respectively, the cold and hot gas states.

The question to be discussed is: What is the succession of states through which the gas passes

while traversing the detonation? Such a succession of states could be represented by a curve joining C and H on Fig. 2. Does the state-point simply travel along the Rayleigh line? Does it first move out horizontally to the left to point S (the von Neumann Spike) and then climb up the left-hand branch of the Rayleigh line? Or does it follow a path such as that indicated by the broken curve? Consideration of the p/mR lines of Fig. 1 shows that in the first of these three cases the pressure would rise continuously from C to H, in the second it would rise to a maximum at S and then fall again, while the third trajectory would exhibit an intermediate pressure variation. We shall want to be able to predict the variations of pressure and other quantities as functions of position within the wave.

Mathematical Theory

Equations. Since two properties suffice to characterize the state of the gas (for given m), we shall expect to have to solve equations for two dependent variables, for example T_s and V; there is a single independent variable, namely distance through the wave x. Since, however, distance cannot be influential *per se*, x only appears in differential form; it is consequently permissible to use the stagnation-temperature gradient as an alternative third variable. Of course, dimensionless forms of the variables are preferred.

The detailed derivation of the equations will not be presented here since it may be found elsewhere[1–4]; such derivation implies that, for a gas with a Lewis number of unity and a Prandtl number of $\frac{3}{4}$ (both "reasonable" values), we may write:

$$p\,(dp/d\tau) - p = -w \tag{1}$$

$$d\tau/du = p/(z - z_C) \tag{2}$$

where

$$\tau \equiv T_s/\gamma T_C \tag{3}$$

the nondimensional stagnation-temperature;

$$p \equiv (k/cm)\,(dT_s/dx) \tag{4}$$

the nondimensional stagnation temperature gradient;

$$w \equiv kW/\gamma T_C m^2 \tag{5}$$

the nondimensional reaction rate;

$$u \equiv V/(\gamma R T_C)^{\frac{1}{2}} \tag{6}$$

the nondimensional velocity;

$$z \equiv u(\gamma + 1)/2\gamma + \tau/u \tag{7}$$

the nondimensional momentum flux;

$k \equiv$ thermal conductivity of gas, which may vary with temperature;

$c \equiv$ specific heat of gas at constant pressure; and

$W \equiv$ reaction rate in the units of rate of increase of stagnation temperature per unit time.

Discussion of p, z, and w. Equation (4) shows that, when p has been obtained as a function of

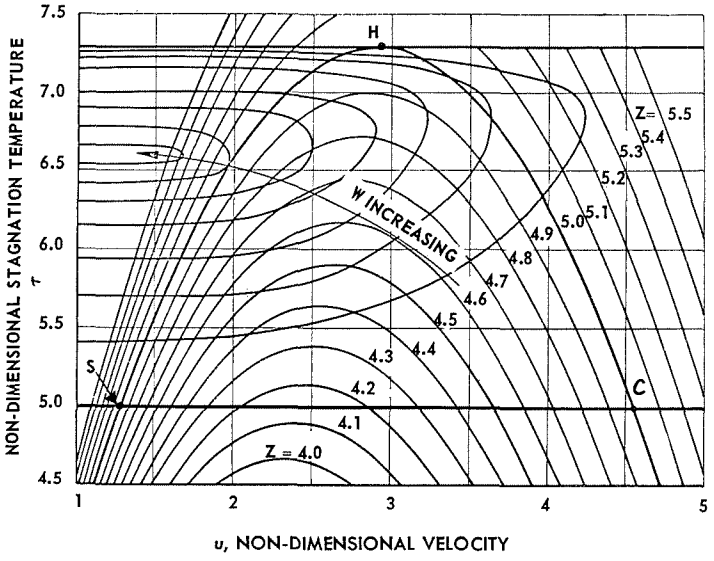

FIG. 3. Plot of z (τ, u) for gas of Fig. 1, with superimposed sketch of contours of constant dimensionless reaction rate w for the C–J detonation of Fig. 2.

stagnation temperature τ and velocity u, the variations of all properties with distance x can be obtained by means of a simple quadrature. For this reason we shall devote little further attention to x.

The quantity z, being the nondimensional form of the momentum flux, is constant along a Rayleigh line; it is a function of u and τ alone. Lines of constant z are drawn as inverted parabolae on Fig. 3, having τ as ordinate and u as abscissa. The $\tau \sim u$ plane is the nondimensional form of the $T_s \sim V$ diagram and will be extensively used below; for reasons which will appear, linear scales are now preferable to logarithmic.

For certain families of chemical reactions, namely those proceeding by means of a single step, reactions obeying the "stationary-state" hypothesis, and "explosive" chain-branching reactions, the reaction rate w can be expressed as a unique function of temperature and pressure when the Lewis number is unity.[5] From here onward we restrict attention to such reaction-kinetic systems. Accordingly, w can be expressed as a function of τ and u alone when the upstream conditions of the detonation wave are specified. Lines of constant w are sketched on Fig. 3, for a C–J detonation; w is zero in the upstream gas (because this is too cold to react appreciably) and in the downstream gas (because its reaction is complete); w is finite at high values of temperature between $\tau = \tau_C$ and $\tau = \tau_H$.

Appreciation of Mathematical Problem. We have to solve two simultaneous first order nonlinear differential equations, (1) and (2), given that w and z are known functions of τ and u and that the values of τ_C and u_C are specified. The problem is rendered somewhat difficult by the fact that the point C is a singular point on the $\tau \sim u$ plane since $p = 0$ and $z = z_C$ at the cold boundary. We may note however that the linkage between the two equations is slight: Eq. (2) could be integrated if p were known as a function of τ; thereafter Eq. (1) could be integrated.

Now, as was stated in the introduction, we are here concerned to obtain the maximum quantitative insight into the detonation process and not to predict the detonation structure for any particular reaction-kinetic scheme. It is therefore sensible to choose w functions which, while not being wholly unrealistic, permit the equations to be solved without numerical work. This practice has already been adopted with success in deflagration theory where only Eq. (1) has to be solved;[5] the technique used there was to choose $p(\tau)$ functions permitting Eq. (1) to be solved analytically. The same technique will be adopted below.

The Thin-Flame Model. The w-Function

One of the most fruitful ideas in flame theory has been the recognition that, when the activation energy of the reaction is very large, the volumetric reaction rate is practically zero except in the vicinity of the hot boundary; it was introduced by Zeldovich and Frank-Kamenetskii,[6] and has often been used subsequently.[5,7,8] If the constant-w contours of Fig. 3 are held to represent a mountain, the thin-flame model corresponds to a w-function representing a narrow steep ridge running immediately below $\tau = \tau_H$ and rising out of an otherwise flat plain.

The $p \sim \tau$ Solution. Far upstream of the detonation, the temperature gradient is zero; this is the reason why $p = 0$ at $\tau = \tau_C$. Our reaction-kinetic model ensures that $w = 0$ except when τ is very close to τ_H. We can immediately deduce that the $p \sim \tau$ relation satisfying Eq. (1) and the boundary condition is:

$$\begin{aligned} \tau_C \leqq \tau < \tau_H &: p = \tau - \tau_C \\ \tau = \tau_H \qquad &: p = 0 \end{aligned} \tag{8}$$

This relation is plotted in Fig. 4.

The $\tau \sim u$ Relation. On substitution of (8) into (2), the latter equation becomes:

$$d\tau/du = (\tau - \tau_C)/(z - z_C) \tag{9}$$

which is an equation in τ and u alone. It gives the slope of the solution curve which passes through each point on the plane and permits the curves themselves to be drawn by the following simple construction:

(a) Vertically below the point P through which the solution is to be drawn, find the point Q on the horizontal line $\tau = \tau_C$ (Fig. 5); then the length PQ equals $\tau - \tau_C$.

(b) On this same horizontal find the point R such that R lies to the left of Q a distance $z - z_C$,

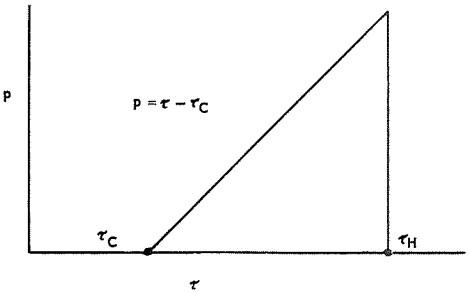

FIG. 4. Dimensionless plot of gradient of stagnation temperature p vs stagnation temperature τ for thin-flame model.

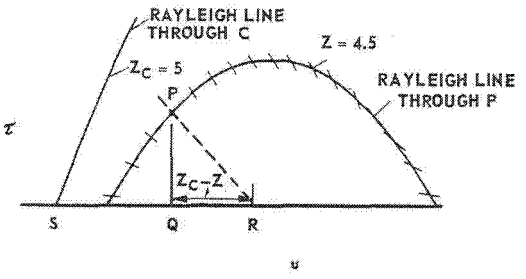

FIG. 5. Construction for drawing element of solution curve through arbitrary point p on τ–u plane for "thin-flame" detonation.

z being the value appropriate to the Rayleigh line through P. (N. B.: In Fig. 5, $z - z_C$ is negative, so R lies to the right of Q.)

(c) Draw a segment of the straight line PR extending a short distance to either side of P; this line satisfies Eq. (9) and so is a segment of the solution curve through P.

(d) Repeat the process for numerous points P on the $\tau \sim u$ plane and join them up smoothly by freehand curves. The result is the family of solution curves drawn on Fig. 6, for the C–J detonation in which $\tau_C = 5$ and $u_C = 4.552$. This choice of upstream condition is representative of hydrogen-air detonations.

When lines of constant z are provided beforehand, the solution curves of Fig. 6 can be drawn in an hour or two; there is certainly no need for a digital computer! The method is of course not restricted to C–J detonations.

Discussion of the Solution. We have now obtained *many* curves representing possible detonation structures; each one gives a relation between the velocity, pressure, temperature, and stagnation pressure. How can we decide which

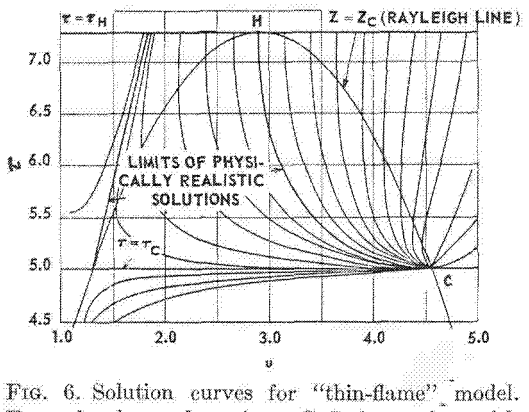

FIG. 6. Solution curves for "thin-flame" model. Example shown here is a C–J detonation with $\tau_C = 5.0$, $\tau_H = 7.292$, $Z_C = 5.0$.

one is the solution pertaining to a given detonation?

To answer this question, we first examine which curves satisfy the boundary conditions, i.e. which pass through both C and H. We then recall that, although many of the curves rise up to the line $\tau = \tau_H$, they cannot cross it; for along this line p falls to zero causing $d\tau/du$ to become zero *without change of sign*. Each $u \sim \tau$ curve is therefore completed by a segment of the line $\tau = \tau_H$ extending *to the right* from the point where the solution curve first hits this horizontal; if the "hitting-point" lies to the left of H, the solution curve is therefore completed by a horizontal line terminating at H. All solution curves starting from C and reaching the top horizontal to the left of H represent physically valid solutions.

Although we have now excluded from further consideration some of the solution curves of Fig. 6, many remain. Which is the "right" one? To answer this, we must reconsider Eq. (1) which, on integration between the limits τ_C and τ_H, yields:

$$\int_{\tau_H}^{\tau_C} w\, d\tau = \int_{\tau_C}^{\tau_H} p\, d\tau = \tfrac{1}{2}(\tau_H - \tau_C)^2 \qquad (10)$$

in the second line of which we have made use of the triangular $p \sim \tau$ relation of Fig. 4. The right-hand side of Eq. (10) has a known constant value, while the integral on the left-hand side represents the area of a vertical section cut through the w-mountain by the solution curve, when projected on to the left-hand border. Obviously, solution curves lying well to the left of the diagram pass through "high-altitude" regions, where the high temperature and pressure cause the reaction rate to be large; these are therefore the solutions which prevail at high detonation speed where m is large enough [see Eq. (5)] to permit Eq. (10) to be satisfied. Correspondingly the solutions farther to the right will occur when the reaction rate is lower relative to m.

There are many more physical lessons to be learned from the contemplation of Fig. 6 than space permits us to spell out here; one will have to suffice. The physically possible solutions are confined within the area indicated by the bold curves indicated there. If the reaction rates are either too large or too small to allow Eq. 10 to be satisfied by one of these solutions, *no "thin" flame can exist*. Usually the reaction rate is too low rather than too high; for if the latter limit were contravened, almost every collision between reactant molecules would have to lead to reaction, as Hirschfelder has shown.

More Realistic Reaction-Rate Functions

The $p \sim \tau$ Relation. The "thin-flame" model just considered is more realistic for deflagrations than for detonations; for reaction rates are almost invariably appreciable in the region on the $\tau \sim u$ plane to the left of the Rayleigh parabola. We therefore consider a family of $p \sim \tau$ relations which has previously been used in deflagration theory[5], which again permits analytical solution of Eq. (1), but which generates reaction-rate functions of realistic shape. The family is:

$$p = (\tau - \tau_C)\{1 - (\tau - \tau_C)^{n-1}/(\tau_H - \tau_C)^{n-1}\} \tag{11}$$

where n is a number which can be chosen freely. Substitution in Eq. (1) shows that the corresponding expression for w is:

$$w = n(\tau - \tau_C)\{[(\tau - \tau_C)/(\tau_H - \tau_C)]^{n-1} - [(\tau - \tau_C)/(\tau_H - \tau_C)]^{2n-2}\} \tag{12}$$

for which:

$$\int_{\tau_C}^{\tau_H} w\, d\tau = \tfrac{1}{2}\{(n-1)/(n+1)\}(\tau_H - \tau_C) \tag{13}$$

The realistic shape of the expression in Eq. (12) can be seen by inspection of the diagrams in reference 5.

The $u \sim \tau$ Solutions. Since Eq. (11) expresses p as a function of τ, Eq. (2) once again contains τ and u alone. It can be integrated graphically with only a slight modification to the construction described above: now the point Q must lie a distance $(\tau - \tau_C)\{1 - (\tau - \tau_C)^{n-1}/(\tau_H - \tau_C)^{n-1}\}$ rather than a distance $(\tau - \tau_C)$ below P; but the actual plotting of the curves takes scarcely any longer than before. Figure 7 contains curves plotted in this way for the case in which $n = 2$, other conditions being the same as for Fig. 6.

Inspection of Fig. 7 shows that the $u \sim \tau$ curves are now everywhere less steep than before; in particular, the sharp bend at the line $\tau = \tau_H$ is absent. However the general shape of the diagram is little changed and there is again only a limited group of solutions which pass through both points C and H.

Diagrams like Fig. 7 can, of course, be drawn for any desired value of n. When n is large (high-activation-energy reactions), the $u \sim \tau$ curves become similar to those of Fig. 6; when n is small, the physically satisfactory curves follow more closely the horizontal through C and the left-hand branch of the Rayleigh parabola. Once again, space limitations make it necessary to refrain from discussing all the physical implications of these facts. It should, however, be mentioned that, to make use of the solutions, it is necessary to choose n so that the reaction-rate expression w of Eq. (12) fits the profile of the actual w-mountain as closely as possible in the vicinity of the path taken over it by the $u \sim \tau$ curve. The n can have any value greater than unity, the lower values usually being most appropriate to detonations.

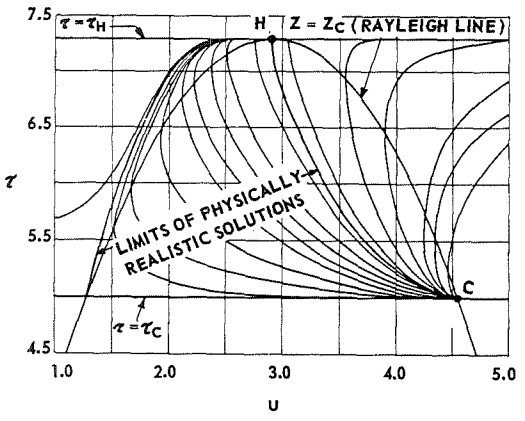

FIG. 7. Solution curves for "more realistic" model [Eq. (12), $n = 2$]. Example shown here is C-J detonation with same initial and final states as for Fig. 6.

Discussion

Other $p \sim \tau$ Relations. It is, of course, possible to evaluate exact solutions to the detonation equations, (1) and (2), starting from many other postulated $p \sim \tau$ relations. Thus one might follow Adams,[9] who postulated a constant value of p in the reaction region in an early study of monopropellant combustion; this leads to reaction-rate functions exhibiting a sharp peak at the hot boundary.[10] Another postulate permitting a particularly easy construction of the $\tau \sim u$ solution curves is illustrated in the top part of Fig. 8, where the slope of the right-hand linear portion can be varied at will; the corresponding reaction-rate function is shown in the bottom part of Fig. 8. Such $p \sim \tau$ distributions were employed by von Karman and Penner[14] as the basis of an approximate theory of deflagration and have subsequently been utilized by Curtiss, Hirschfelder, and Barnett,[3] under the name of the "ignition-temperature model," in exact digital-computer solutions of the detonation problem. The difficulty is, however, not to invent $p \sim \tau$ relations permitting solution, but to find ones which fit the actual w-functions reasonably well; the author believes that the family described in the preceding section 4 is as well-adapted to this purpose as any which have been studied so far.

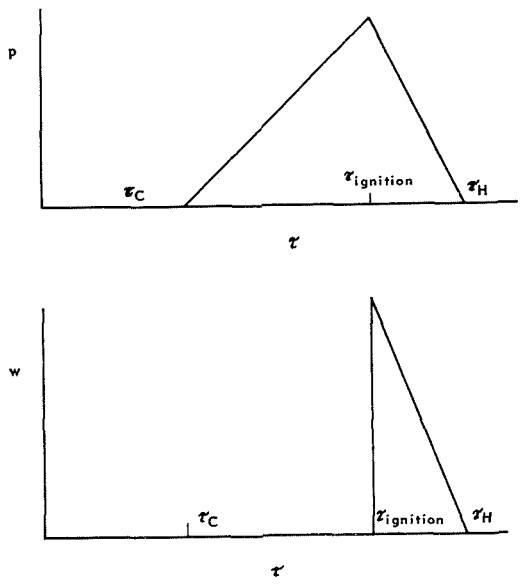

FIG. 8. Distribution of $p(\tau)$ and $w(\tau)$ for "ignition temperature" model.

Low-Reaction-Rate Solutions. A study of the above and other exact solutions leads to the conclusion that most detonating mixtures have reaction rates which are sufficiently low to cause the solution curves to lie very close to the left-hand branch of the Rayleigh parabola (if w is small at all τ, p must be small at all τ, so $d\tau/du$ is also small except where $z \approx z_C$). It is therefore reasonable, when faced with the problem of calculating the structure of a detonation wave *with prescribed kinetics* to assume that the $w \sim \tau$ relation is that for the left-hand branch of the parabola except where τ is close to τ_C. There is no space here to argue the matter in detail, but interested readers may care to verify that the following procedure then gives a good approximation to the exact solution:

(1) Integrate Eq. (1) numerically or graphically, using the $w \sim \tau$ relation just mentioned, from the hot boundary to a point where $p = \tau - \tau_C$.

(2) Construct the corresponding solution curves on the $\tau \sim u$ plane by the graphical procedure described, using the $p \sim \tau$ relation of (1) for $p > \tau - \tau_C$ and the curves of Fig. 6 for $p < \tau - \tau_C$. The curves of course join smoothly.

(3) Choose the curve of which

$$\int_{\tau_C}^{\tau_H} p \, d\tau = \int_{\tau_C}^{\tau_H} w \, d\tau$$

is the solution to the problem.

The resulting solution, when expressed in terms of temperature, velocity, and pressure distributions, will be found to correspond to a shock wave followed by a spontaneous-ignition flame, the latter approaching nearer to the former as the reaction rate increases. This is of course very close to the von Neumann–Döring–Zeldovich[11–13] model of detonation-wave structure; indeed it might be said that the main result of recent investigations into detonation-wave structure has been to confirm the physical validity of that model.

ACKNOWLEDGMENTS

The present paper is based on a more extensive report[4] written by the author at the University of California in Berkeley in 1960 as part of the work supervised by Professor A. K. Oppenheim under NASA Grant No. NSG–10–59. The author wishes to express his gratitude to Professor Oppenheim for many illuminating discussions on detonation phenomena, and to Miss M. P. Steele for her assistance with the diagrams.

REFERENCES

1. HIRSCHFELDER, J. O. and CURTISS, C. F.: J. Chem. Phys. *28*, 1130 (1958).
2. LINDER, B., CURTISS, C. F., and HIRSCHFELDER, J. O.: J. Chem. Phys. *28*, 1147 (1958).
3. CURTISS, C. F., HIRSCHFELDER, J. O., and BARNETT, H. P.: J. Chem. Phys. *30*, 470 (1958).
4. SPALDING, D. B.: *Contribution to the Theory of the Structure of Detonation Waves in Gases.* Internal Report of the Division of Aero. Sciences, University of California, Berkeley, 1960.
5. SPALDING, D. B.: Combustion and Flame *1*, 287, 296 (1957).
6. ZELDOVICH, Y. B. and FRANK-KAMENETSKII, D. A.: Zhur. Fiz. Khim. *12*, 100 (1938).
7. SPALDING, D. B.: Combustion and Flame *4*, 51 (1960).
8. ADLER, J. and SPALDING, D. B.: Proc. Roy. Soc. (London) *A261*, 53 (1961).
9. ADAMS, G. K.: private communication; see reference 10.
10. SPALDING, D. B. and JAIN, V. K.: Combustion and Flame *5*, 11 (1961).
11. VON NEUMANN, J.: Progress Report on Theory of Detonation Waves. Office of Sci. Res. and Dev. No. 549, May 4, 1942.
12. DÖRING, W.: Ann. Physik (Ser. 5) *43*, 421 (1943); Ann. Physik (Ser. 6) *5*, 133 (1949).
13. ZELDOVICH, Y. B.: Zhur. Eksp. i Teoret. Fiz. *10*, 542 (1940); Translated as NACA TM 1261 (1950).
14. VON KARMAN, T. and PENNER, S. S.: Fundamental Approach to Laminar Flame Propagation, in *Selected Combustion Problems.* Butterworths, London, 1954.
15. WOOD, W. W.: Phys. Fluids *4*, 46 (1961).
16. ADAMSON, T. C., JR.: Phys. Fluids *3*, 706 (1960).

DETERMINATION OF THE DETONATION WAVE STRUCTURE

A. K. OPPENHEIM AND J. ROSCISZEWSKI

In order to investigate the influence of transport properties on the coupling between the shock and deflagration that may occur in a steady, plane detonation wave, the structure of the wave has been determined for some specific cases by numerical analysis performed on an IBM 704 computer.

After a preliminary check with some representative cases of Hirschfelder and Curtiss,[1,2] the procedure was applied to detonation in dissociating ozone. Although the agreement with the solutions of Hirschfelder and Curtiss is not perfect, their contention concerning the strong coupling between the shock and deflagration has been essentially confirmed. The ozone computations included the consideration of the variation of transport properties with temperature and the change in the number of moles due to chemical reaction, while the rate of the reaction was described in terms of the best available data on kinetics. For this purpose the reaction rate has been expressed in terms of the quasi-steady-state approximation for the oxygen atom concentration which, with exception to the immediate vicinity of the hot boundary, represents quite accurately the exact chain reaction mechanism of the thermal decomposition of ozone.

On this basis the structure of the "laminar" detonation wave in ozone has been determined for three fundamental models: the coupled-wave, the von Neumann-Döring-Zeldovich model, and the decoupled deflagration wave. The results have been compared from the point of view of the approximation proposed by Spalding.[3] The validity of the continuum treatment has been checked by evaluating the variation throughout the wave of the average number of intermolecular collisions per molecule of product. It appears from this that, although the theory may not be realistic close to the hot boundary, it is certainly quite reasonable in the regime of coupling between the shock and deflagration—the primary objective of our inquiry.

In conclusion it is contended that only a thorough understanding of the so-called "laminar" wave structure can provide proper basis for the assessment of the effects of turbulence and other time dependent and multidimensional phenomena that may accompany the detonation process.

The Problem

Under the usual assumption of steady, one-dimensional flow and the essentially perfect gas behavior of reactants and products, the structure of the detonation wave is governed by the following equations[3]:

$$d\beta/d\chi = 1 - (\Gamma\Omega/m^2\beta)\omega(u, \chi) \qquad (1)$$

$$du/d\chi = [\chi - \chi_R(u)]/\gamma\beta u \qquad (2)$$

where the symbols have the following meaning:

$$\chi \equiv \frac{c_pT + (V^2/2)}{(c_pT)_c} \qquad (3)$$

is the nondimensional stagnation enthalpy,

$$\beta = d\chi/d\xi \qquad (4)$$

is the nondimensional stagnation enthalpy gradient,

$$d\xi \equiv (m/\Gamma)\, dl = (\Gamma_c/\Gamma)\, dx \qquad (5)$$

being the nondimensional space coordinate, with m representing the mass flow rate per unit area and

$$\Gamma = D\rho = \lambda/c_p = \tfrac{4}{3}\mu \qquad (6)$$

expressing the "transport" or "exchange coefficient"—a single quantity that, as a consequence of the assumption that Prandtl number is $\frac{3}{4}$ and Lewis number is 1, represents at the same time mass diffusion, thermal conductivity, and viscosity, while u is the nondimensional velocity or specific volume. Finally

$$\Omega = q/c_pT = \chi_h - \chi_c \qquad (7)$$

is the nondimensional heat release, the equation above representing in fact the over-all energy balance for the wave, while: $\omega(u, \chi)$ is the volumetric reaction rate expression and $\chi_R(u)$ is determined by the Rayleigh Line. For our purpose both these functions have to be given *a priori*.

The knowledge about the process is completed by the information on the composition of the

reacting mixture. This is obtained from the condition of constant total (i.e., thermal, dynamic, and chemical) enthalpy that results from our assumption concerning the Prandtl and the Lewis numbers. If the instantaneous composition can be expressed by a single parameter, for example, Y, the mass fraction of the product which changes from 0 to 1 in the course of the reaction, the constant total enthalpy condition, taking into account Eq. (7), yields simply:

$$Y = \frac{\chi - \chi_c}{\chi_h - \chi_c} \tag{8}$$

With the use of the equation of state, the above permits to determine $\omega(u, \chi)$ from the conventional form of $\omega = \omega(Y, T, p)$.

The problem lies in the solution of (1) and (2), subject to boundary conditions:

$$\text{at} \quad \chi = \chi_c \quad u = u_c \quad \beta = 0$$

$$\text{at} \quad \chi = \chi_h \quad u = u_h \quad \beta = 0, \tag{9}$$

where u_c, the Mach number of the detonation wave, and u_h, the volumetric contraction produced by the wave, are specified by the Rayleigh Line relations.

The Rayleigh Line

For a perfect gas the Rayleigh line equation is, in our coordinates,

$$\chi_R(u) = -[(\gamma + 1)/2]u(u - u_0) \tag{10}$$

an inverted parabola passing through $u = 0$ and $u = u_0$ on the $\chi = 0$ axis. In accordance with Eq. (7) of ref. 3:

$$u_0 = \frac{2}{\gamma + 1}\frac{\chi_c}{u_c} + u_c = \frac{2}{\gamma + 1}[\gamma u_c + u_c^{-1}] \tag{11}$$

the second equality above being the consequence of Eq. (3) from which it follows directly that

$$\chi_c = 1 + [(\gamma - 1)/2]u_c^2 \tag{12}$$

The Chapman-Jouguet condition, $M_h^2 = V_h^2/(\gamma - 1)c_pT_h = 1$, leads from Eq. (3) to:

$$\chi_h = [(\gamma + 1)/2]u_h^2 \tag{13}$$

which is satisfied at the peak of the $\chi_R(u)$ parabola, where according to (11),

$$u_h = \tfrac{1}{2}u_0 = [\gamma u_c + u_c^{-1}]/(\gamma + 1) \tag{14}$$

Finally, for the Chapman-Jouguet detonation, u_c is determined from the overall energy balance, (7), which with (12), (13), and (14) yields

$$u_c - u_c^{-1} = [2(\gamma + 1)\Omega]^{\frac{1}{2}} \tag{15}$$

Computations

For numerical computations, it is convenient to regard χ as the independent variable, this having been indeed already suggested in the form of our Eqs. (1) and (2). The major advantage of χ in this respect is that it varies monotonically in the domain of the solution. The computational procedure is then, in principle, quite straightforward: one evaluates the change in β from (1) and the change in u from (2). The main difficulty lies in the fact that both boundaries are nodal singularities where, for the physically correct solution, $du/d\chi$ is infinite.

In order to start from any boundary, one must therefore know the initial slope $\beta(\chi)$. Since at the boundaries both the numerator and denominator of the expression for $1 - (d\beta/d\chi)$ in Eq. (1) approach zero, one can apply for this purpose the l'Hospital rule, according to which:

$$\lim_{\beta \to 0}\left(1 - \frac{d\beta}{d\chi}\right) = \frac{\Gamma\Omega}{m^2}\frac{(d\omega/d\chi)_h}{(d\beta/d\chi)_h} \tag{16}$$

As indicated by Spalding[3] $d\beta/d\chi$ cannot be zero at the boundaries, while physical considerations imply that at the cold boundary $d\omega/d\chi$ must be essentially zero. Consequently

$$(d\beta/d\chi)_c = 1 \tag{16a}$$

while for the hot boundary Eq. (16) yields directly:

$$(d\beta/d\chi)_h = \tfrac{1}{2}\left\{1 - \left[1 + 4\frac{\Gamma\Omega}{m^2}\left(\frac{d\omega}{d\chi}\right)_{\chi=\chi_h}\right]^{\frac{1}{2}}\right\} \tag{16b}$$

With the known finite value of $d\beta/d\chi$ at the start, one has to guess only the value of u corresponding to the specified first step in χ, so that the solution will pass through the other boundary. It is also important to test the sensitivity of the solution to the value of $\delta\chi$, the step in the independent variable used for the computation. In our analyses, with $\Omega = \chi_h - \chi_c$ of an order of 10, it was demonstrated that $\delta\chi = 10^{-3}$ produced essentially the same results as $\delta\chi = 10^{-4}$ (see Figs 5 and 6). The computations were made starting from the cold, as well as from the hot end. The approach to hot boundary from below was, however, quite unstable, making the computation much more difficult than that corresponding to the reversed procedure when the cold boundary was approached from above. As a matter of practical convenience we recommend therefore the start from the hot boundary, in spite of having to solve in addition Eq. (16b)—actually a trivial task in comparison to that of having to hit the hot boundary from below.

Our solution is given by the functional relation

$\beta = \beta(\chi)$. According to (4) the nondimensional space coordinate is then:

$$\xi - \xi_0 = \int [\beta(\chi)]^{-1} d\chi \qquad (17)$$

while the physical coordinate can be obtained from (5) by the quadrature:

$$x - x_0 = \Gamma_c^{-1} \int \Gamma(\xi)\, d\xi \qquad (18)$$

since Γ, given usually as a function of temperature and composition, can now be expressed, with the use of the solution in the χ–u domain and Eq. (17), in terms of ξ alone. Finally the dimensional coordinate is simply $l = (\Gamma_c/m)x$.

The N-D-Z Model

A simple illustration of the solution is provided by the von Neumann–Döring–Zeldovich model which is based on the postulate that the shock is completely decoupled from the deflagration. Since such a solution serves as a convenient point of departure for our coupled wave solutions, it is here derived from our basic Eqs. (1) and (2) which now become decoupled by virtue of the model.

Under such circumstances we obtain directly the classical shock solution, since now, as a consequence of the assumption that Prandtl number is $\frac{3}{4}$, it follows that $\chi = \text{const} = \chi_c$. Equation (2) becomes then:

$$d\xi = (\gamma u\, du)/[\chi_c - \chi_R(u)] \qquad (19)$$

With Eqs. (10), (12), and (14) it can be shown that the denominator is simply:

$$\chi_c - \chi_R(u) = \frac{2}{\gamma+1}[(u-u_h)^2 - (u_c - u_h)^2]$$

$$= \frac{2}{\gamma+1}(u-u_c)(u-u_N) \qquad (20)$$

where $u_N = 2u_h - u_c = u_0 - u_c$ is the coordinate of the von Neumann spike.

Equation (19) upon integration gives therefore:

$$\xi - \xi_0 = \frac{\gamma}{\gamma+1}\left[\ln (u-u_c)(u-u_N) + \frac{2u_h}{u_c - u_N}\ln\left(\frac{u-u_c}{u-u_N}\right)\right]$$

$$= \frac{2\gamma}{\gamma+1}\left[\frac{u_c}{u_c-u_N}\ln(u_c-u) - \frac{u_N}{u_c-u_N}\ln(u-u_N)\right] \qquad (21)$$

In the classical N–D–Z model the deflagration is devoid of transport phenomena and proceeds along the Rayleigh Line. Consequently Eq. (1) reduces to:

$$d\chi/dx = (\Omega/m)\omega(u,\chi) \qquad (22)$$

while χ is related with u by the Rayleigh Line equation

$$\chi = -[(\gamma+1)/2]u(u-2u_h) \qquad (23)$$

according to which

$$d\chi = (\gamma+1)(u_h - u)\, du \qquad (24)$$

The structure of the wave is determined therefore by the quadrature:

$$x - x_0 = \frac{\gamma+1}{\Omega} m \int \frac{u-u_h}{\omega(u)}\, du \qquad (25)$$

Actually, as pointed out already by Hirschfelder and Curtiss,[1] the influence of transport properties on the deflagration can be evaluated quite simply; the structure is governed by Eqs. (1)–(8), as before, with different boundary conditions, namely:

at $\chi = \chi_h$ $u = u_h$ $\beta = 0$

at $\chi = \chi_c$ $u = u_N$ $\beta \neq 0$ (26)

The numerical solution is obtained in the same manner as for the coupled wave, but this time it must be started from the hot boundary, since the value of β at the von Neumann spike is not known *a priori*.

Specification of the Problem

Computations have been made for two representative cases of irreversible, unimolecular reactions which have been originally analyzed by Hirschfelder and Curtiss[1] (they will be referred to here as the H&C reactions) and for thermal decomposition of ozone. For the H&C reactions the expression for the volumetric reaction rate is

$$\omega = \frac{mk}{ua_c}(1-Y)\exp(-E^\ddagger/RT) \qquad (27)$$

so that, with (8), Eq. (1) becomes

$$\frac{d\beta}{d\chi} = 1 - \frac{\Lambda}{\beta}\frac{\chi_h - \chi}{u} \times \exp\left(-\frac{\epsilon}{\chi - [(\gamma-1)/2]u^2}\right) \qquad (28)$$

where for a Chapman-Jouguet detonation:

$$\Lambda = \frac{\Gamma k}{ma_c} = \frac{\gamma+1}{\gamma}\frac{\tau_0}{\Gamma^2 u_c(\gamma u_c^2 + 1)} \qquad (29)$$

and

$$\epsilon = E^{\ddagger}/RT_c = \tau_0^{-1} \tag{30}$$

while the Mach number of the wave is determined from the equation:

$$u_c - \frac{1}{u_c} = \left(\frac{2(\gamma^2 - 1)}{\gamma}\frac{\beta}{\tau_0}\right)^{\frac{1}{2}} \tag{31}$$

The right-hand expressions in Eqs. (29), (30), and (31) are given in terms of the notation used by Hirschfelder and Curtiss.[1] The two H&C reactions considered here have been specified in the above reference as follows:

κ^2	1	1
ω	0.0028	0.0045
τ_0	0.02	0.02
β	1.12	1.12

They will be denoted here by H&C 1 and H&C 2, respectively. For the purpose of our computations they are given as a consequence of (29), (30), and (31), in terms of the following parameters:

	H&C 1	H&C 2
Λ_H	159.043698	61.57543665
ϵ	50	50
u_c	7.23766	7.23766

both representing a Chapman–Jouguet detonation.

For the start of the computation from the hot end, the initial slope of β is evaluated from (16b) with

$$\frac{\Gamma\Omega}{m^2}\left(\frac{d\omega}{d\chi}\right)_{\chi=\chi_h} = \frac{\Lambda_H}{u_h} \times \exp\{-\epsilon/[\chi_h - \tfrac{1}{2}(\gamma - 1)u_h^2]\} \tag{32}$$

yielding for H&C 1:

$$(d\beta/d\chi)_h = -0.97974745$$

and for H&C 2:

$$(d\beta/d\chi)_h = -0.5002388$$

For the thermal decomposition of ozone we considered only the case of 100% initial O_3 concentration yielding undissociated O_2 at the Chapman–Jouguet state. Under the assumption of the quasi-equilibrium oxygen atom concentration, the reaction rate can be expressed then as follows:

$$\omega = \frac{2\rho^2 k}{M_3}\left(1 + \frac{Y}{2}\right)(1 - Y)\exp(-E^{\ddagger}/RT) \tag{33}$$

This time the variation of transport properties with temperature is taken into account by assuming $\Gamma = \Gamma_c(T/T_c)^{\frac{1}{2}}$. Eq. (1) becomes then:

$$\frac{d\beta}{d\chi} = 1 - \frac{\Lambda}{\beta}\frac{(\chi_h - \chi)(X + \chi)}{u^2}\theta^{\frac{1}{2}}\exp(-\epsilon/\theta) \tag{34}$$

where

$$\theta = \frac{T}{T_c} = \frac{X + \chi}{2\Omega}[\chi - \tfrac{1}{2}(\gamma - 1)u^2]$$

since

$$c_p/(c_p)_c = 1 + \tfrac{1}{2}Y = \frac{2\Omega}{X + \chi}$$

In the above, with $\Gamma_c = 2 \times 10^{-4}$ gm/cm sec., $k = 4.61 \times 10^{15}$ cm³/gm mole sec, $E^{\ddagger} = 24$ Kcal/gm mole (the latter two based on data of Benson and Axworthy[4]) $M_3 = 48$ gm/gm mole, $\gamma = 1.255$, for a Chapman-Jouguet detonation propagating into a mixture where the initial velocity of sound $a_c = 255.4$ m/sec ($T_c = 300°$K) at a Mach number $u_c = 7.20$, so that $\Omega = [u_c - u_c^{-1}]^2/2(\gamma + 1) = 11.0552$, we have

$$\Lambda \equiv \frac{\Gamma_c k}{M_3 a_c^2 \Omega} = 2.3618$$

$$X \equiv 2\chi_h - 3\chi_c = 14.5014$$

and

$$\epsilon = E^{\ddagger}/RT_c = 40.25$$

For the determination of the slope in β at the hot end Eq. (34) yields for the constant in Eq. (16b):

$$\frac{\Gamma\Omega}{m^2}\left(\frac{d\omega}{d\chi}\right)_{\chi=\chi_h} = \Lambda\frac{X + \chi_h}{u_h^2}\theta_h^{\frac{1}{2}}\exp(-\epsilon/\theta_h) \tag{35}$$

leading to

$$(d\beta/d\chi)_h = -0.6876897$$

Results and Conclusions

The results of our computations are presented in Tables 1–5 and Figs. 1–9.

Figure 1 shows the comparison between our results and those of Hirschfelder and Curtiss[1] in the χ–u plane. The discrepancy here is larger than in other coordinates, as indeed demonstrated in Fig. 3 where the corresponding differ-

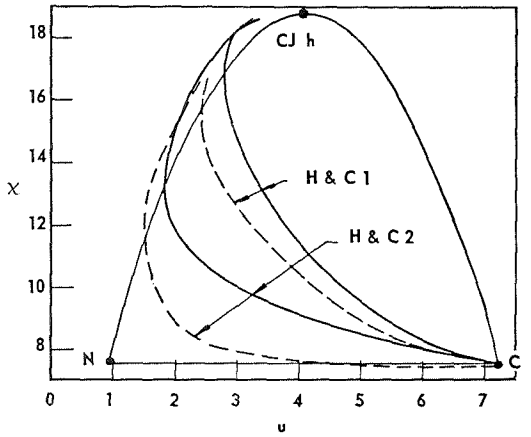

FIG. 1. Coupled wave for the H&C reactions in the χ–u plane.

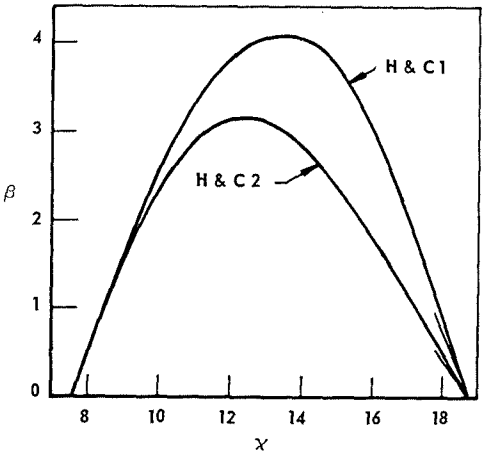

FIG. 2. Coupled wave for the H&C reactions in the β–χ plane.

TABLE 1

Coupled wave for the H&C 1 reaction

χ	β	u	θ	ξ
18.7486875	0.000000	4.082340	16.665500	$-\infty$
18.600000	0.173270	3.185000	17.331972	0.000000
18.399905	0.437926	3.037427	17.246760	0.696328
18.199811	0.696549	2.952060	17.110579	1.055581
17.999717	0.952000	2.893826	16.953038	1.300422
17.599528	1.447040	2.822355	16.603917	1.638620
17.199339	1.912991	2.788271	16.227632	1.878185
16.799150	2.342946	2.779717	15.833397	2.066752
16.198866	2.909932	2.802787	15.217015	2.295624
15.598583	3.373409	2.860630	14.575783	2.486601
14.998300	3.726208	2.947813	13.912199	2.655478
14.598111	3.897974	3.020615	13.457696	2.760405
13.997827	4.059434	3.150378	12.757317	2.911000
13.397544	4.106185	3.303949	12.033134	3.057764
12.797261	4.041119	3.481247	11.282475	3.204857
12.196977	3.868223	3.683221	10.501312	3.356403
11.796788	3.696078	3.832593	9.960792	3.462178
11.396599	3.481134	3.994877	9.401819	3.573676
10.996410	3.226250	4.171414	8.821424	3.693012
10.596221	2.934872	4.364153	8.215592	3.822970
10.196033	2.611144	4.575655	7.579055	3.967411
9.795844	2.260019	4.809392	6.904662	4.131932
9.393655	1.887287	5.070169	6.182428	4.325381
8.995466	1.499399	5.364864	5.397845	4.562747
8.595277	1.102864	5.703996	4.528431	4.872831
8.195088	0.702936	6.106017	3.534757	5.323833
7.994990	0.502666	6.341939	2.967566	5.659189
7.794976	0.302571	6.614880	2.325497	6.166819
7.594963	0.102472	6.959233	1.541198	7.249812
7.394949	−0.097628	7.280266	0.769764	—
7.547969	0.000000	7.237662	1.000000	∞

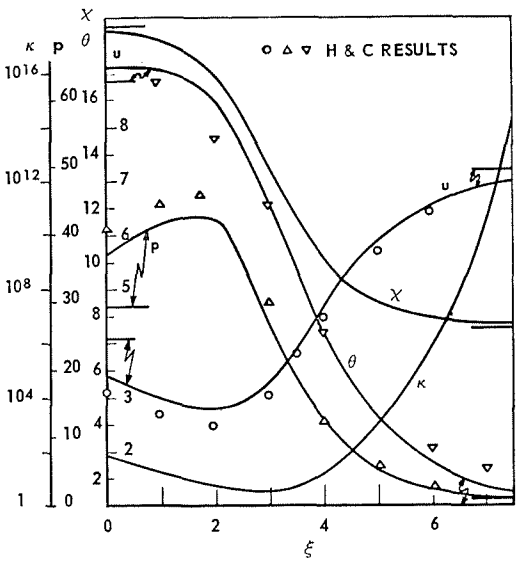

FIG. 3. Structure of coupled wave for the H&C 1 reaction.

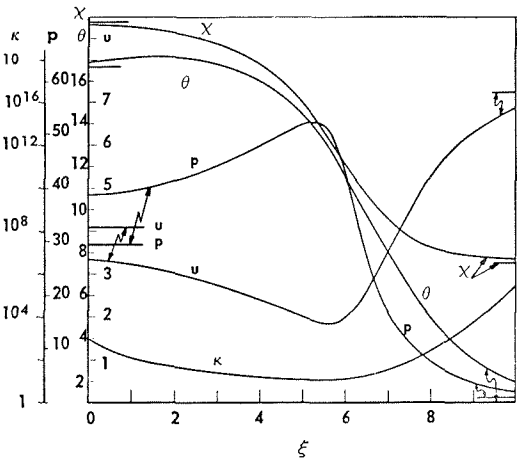

FIG. 4. Structure of coupled wave for H&C 2 reaction.

TABLE 2

Coupled wave for the H&C 2 reaction

χ	β	u	θ	ξ
18.7486875	0.000000	4.082340	16.665500	$-\infty$
18.600000	0.074380	3.328600	17.415033	0.00000
18.399014	0.223274	3.117939	17.184821	1.43437
18.198029	0.361348	2.978558	17.090053	2.13454
17.997044	0.500504	2.867148	16.970476	2.60480
17.595073	0.780033	2.688617	16.692490	3.24256
17.193102	1.057263	2.544404	16.384853	3.68318
16.590146	1.461133	2.366093	15.891346	4.16550
15.786204	1.963119	2.174462	15.196168	4.63725
15.384233	2.193039	2.093876	14.827194	4.83074
14.781277	2.504745	1.990600	14.286966	5.08739
14.148320	2.768482	1.910293	13.723168	5.31586
13.776350	2.912400	1.872202	13.339207	5.45728
13.173393	3.070934	1.845551	12.740636	5.65044
12.771422	3.131996	1.854411	12.342567	5.78791
11.766495	3.095026	2.012428	11.261262	6.10817
10.962554	2.843072	2.331079	10.284312	6.37757
10.359597	2.522110	2.709083	9.443206	6.60186
9.756641	2.098969	3.219947	8.461633	6.86270
9.354670	1.768308	3.642226	7.697444	7.07082
8.952699	1.406320	4.140256	6.810984	7.32487
8.550728	1.021322	4.731429	5.753426	7.67858
8.148757	0.623370	5.450472	4.436302	8.15723
7.746771	0.221605	6.390552	2.642877	9.19335
7.545774	0.020605	7.098907	1.247465	1.59091
7.547969	0.000000	7.2376623	1.000000	∞

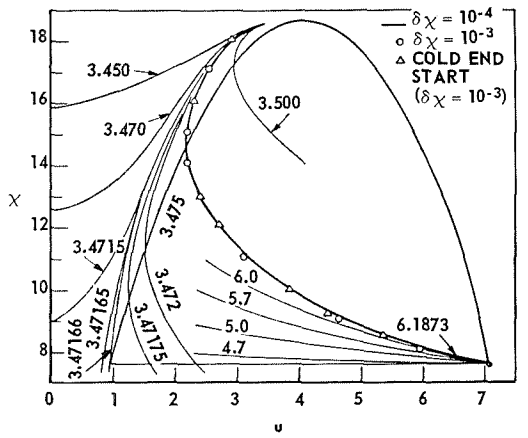

FIG. 5. Coupled wave for ozone in the χ–u plane. (Numbers denote initial values of $u(\chi = 18.6)$ and $u(\chi = 8)$ for curves starting from the hot and cold boundary, respectively).

ences in wave structure are less noticeable. Figure 2 gives the corresponding β–χ plots. They exhibit indeed the form of the approximation introduced by Spalding in ref. 3; the extent with which they adhere specifically to this approximation is discussed later in connection with Fig. 9. Figure 4 represents the wave structure in the case of the H&C 2 reaction demonstrating the effect that can be produced by a decrease of 61.3% in the transport coefficient–steric factor product, Γk.

Figure 5 is the χ–u diagram of solutions obtained for ozone. There has been a number of curves plotted here, depending on the initial value of $u(\chi = 18.6)$ for start at hot boundary, and $u(\chi = 8)$ for start at cold boundary, that have been used for the computation. They serve to demonstrate specifically the character of singularities in this domain as well as the sensitivity of the solution to the value of the assumed initial step in u. The final solution has

TABLE 3

Coupled wave for the ozone reaction

χ	β	u	θ	ξ	ξ	χ
18.664974	0.000000	4.0686868	11.035699	$-\infty$	$-\infty$	$-\infty$
18.600000	0.044631	3.475000	11.395632	0.000000	0.000000	0.000000
18.399905	0.143765	3.204380	11.485377	2.586516	2.584411	8.741526
18.199811	0.271141	3.037404	11.510212	3.589104	3.584606	12.133369
17.999717	0.408830	2.910828	11.510256	4.187715	4.181856	14.159827
17.599528	0.706112	2.718514	11.473182	4.926779	4.919284	16.660239
17.199339	1.023433	2.573543	11.407123	5.395898	5.387339	18.243619
16.799150	1.352206	2.459674	11.321897	5.735384	5.726014	19.385479
16.398961	1.684659	2.369967	11.221702	6.000142	5.990093	20.272170
15.798677	2.173084	2.274078	11.047415	6.312859	6.301920	21.312901
15.198394	2.624647	2.221431	10.846279	6.563469	6.551701	22.139453
14.798205	2.891228	2.210332	10.697161	6.708569	6.696252	22.613869
14.398016	3.120773	2.218962	10.535386	6.841629	6.828752	23.045575
13.797733	3.380095	2.270895	10.266629	7.025893	7.012135	23.637031
13.197449	3.521282	2.372400	9.961985	7.199353	7.184639	24.185665
12.597166	3.534739	2.526549	9.614317	7.368989	7.353196	24.713024
11.996883	3.420446	2.726323	9.213783	7.541100	7.524087	25.237358
11.396599	3.186248	3.005056	8.746909	7.722383	7.703917	25.776248
10.796316	2.845389	3.337367	8.194942	7.921124	7.900838	26.349352
10.396127	2.566762	3.597725	7.766831	8.068949	8.047174	26.762713
9.995938	2.252995	3.892952	7.278030	8.234994	8.211367	27.213012
9.795844	2.082611	4.055120	7.006336	8.327253	8.401308	27.715337
9.395655	1.728367	4.412826	6.396072	8.537537	8.630093	28.293199
8.995466	1.351276	4.823603	5.673230	8.798529	8.765921	28.622093
8.595277	0.960006	5.303790	4.794872	9.148053	9.106781	29.401440
8.195088	0.561444	5.885303	3.681396	9.686783	9.624691	30.465649
7.994990	0.361245	6.236327	2.984278	10.127875	10.038589	31.222143
7.794976	0.161154	6.662164	2.118235	10.935158	10.757406	32.371185
7.594963	−0.038946	7.319855	0.764059	11.960647	13.113231	35.447094
7.547969	0.000000	7.200000	1.000000	∞	∞	∞

TABLE 4

Deflagration in the N–D–Z model for ozone

χ	β	u	θ	x
18.664874	0.00000	4.0686868	11.035699	$-\infty$
18.464014	0.036819	3.647665	11.246590	0.000000
18.263029	0.082037	3.472434	11.287297	3.587711
18.062043	0.132985	3.338088	11.299706	5.498923
17.861058	0.188752	3.224867	11.297294	6.763028
17.459087	0.312742	3.034981	11.266143	8.407749
17.057116	0.451195	2.874927	11.212514	9.484514
16.052189	0.849337	2.546731	11.018258	11.084910
15.047262	1.304862	2.277699	10.764860	12.035362
14.042335	1.796805	2.044106	10.465138	12.689471
13.037407	2.300426	1.834808	10.123307	13.172190
12.032480	2.784342	1.643506	9.740026	13.577920
11.027553	3.208322	1.466228	9.313969	13.912853
10.022626	3.521835	1.300280	8.842400	14.210447
9.017699	3.664567	1.143731	8.321366	14.489623
8.414742	3.641041	1.053701	7.982908	14.653201
8.012772	3.571511	0.995146	7.745707	14.764469
7.811775	3.519306	0.966281	7.623468	14.821100
7.610777	3.455023	0.937682	7.498731	14.878679
7.409780	3.378414	0.909342	7.371435	14.937447

TABLE 5

Constant total enthalpy deflagration behind the shock in ozone

χ	β	u	θ	ξ	x
18.664874	0.000000	4.0686868	11.035699	$-\infty$	$-\infty$
18.660000	0.044631	3.471660	11.395632	0.000000	0.000000
18.399014	0.144979	3.194392	11.490857	2.578225	8.721776
18.198029	0.274381	3.020883	11.518554	3.572867	12.095678
17.997044	0.415146	2.887071	11.521626	4.165016	14.105623
17.595073	0.722837	2.677334	11.491520	4.892458	16.573681
16.992116	1.235016	2.436602	11.398418	5.525745	18.716811
16.389160	1.793916	2.243372	11.271861	5.929291	20.075810
15.585218	2.593629	2.028939	11.068092	6.300583	21.317201
14.982262	3.223579	1.889865	10.894387	6.508787	22.007267
13.977335	4.308964	1.686905	10.570480	6.777623	22.888412
12.972408	5.408729	1.510686	10.206209	6.985286	23.558022
11.967481	6.484543	1.355224	9.801717	7.154600	24.093761
10.962554	7.489787	1.217975	9.355075	7.298477	24.539210
9.957626	8.363673	1.099810	8.862595	7.425131	24.921598
9.555655	8.658741	1.059036	8.651560	7.472336	25.061285
8.952699	9.022767	1.007133	8.318465	7.540466	25.259747
8.550728	9.201825	0.980549	8.08444	7.584548	25.385982
8.148757	9.320226	0.962528	7.839897	7.627918	25.508353
7.947769	9.354072	0.957498	7.713346	7.649435	25.568350
7.746771	9.369751	0.955620	7.583739	7.670895	25.627693
7.545774	9.366503	0.957318	7.450895	7.692342	25.686485

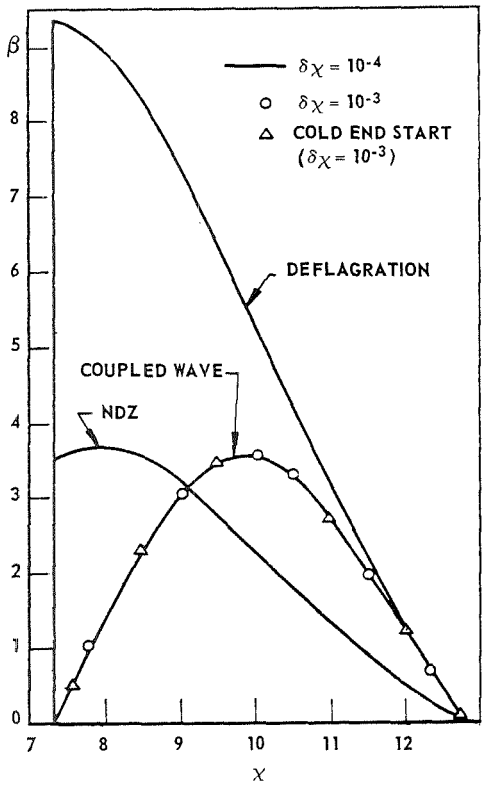

FIG. 6. Solutions for the ozone reaction in the β–χ plane.

been obtained with a 10^{-4} step in χ starting from the hot end; marked also on the diagram are some representative points corresponding to a 10^{-3} step in χ, and for the start from the cold end, in order to illustrate the agreement which has been attained in all these cases. The same is shown in the β–χ plot of Fig. 6 which describes dramatically the difference between the coupled detonation wave and the decoupled deflagrations, with and without the effect of transport properties taken into account. Finally, Figs. 7 and 8 show the structure of the detonation wave in ozone for the coupled wave and the N–D–Z model respectively.

In contrast to Figs. 3 and 4 the linear scale of the horizontal axis in Figs. 7 and 8 is that of the physical coordinate $x = (m/\Gamma_c)l$ which is obtained by integration of Eq. (18) on the basis of the solution $\theta = \theta(\xi)$. The values correspond to $p_c = 1$ atm; for other initial pressures the physical dimension is inversely proportional to p_c. With $\Gamma_c = 2 \times 10^{-4}$ gm/cm sec and $m = \gamma p_c(u_c/a_c) = 358$ (p_c/atm) gm/cm²sec the proportionality factor between l and x is: $\Gamma_c/m = 5.6 \times 10^{-6}$ (atm/p_c) mm.

Figure 9 presents the interpretation of our solutions in the light of the approximation introduced by Spalding in ref. 3. According to it the relationship between β and χ should resemble a function

$$\bar{\beta} = (\bar{\chi} - \bar{\chi}_c) - (\bar{\chi} - \bar{\chi}_c)^n \qquad (36)$$

where $\bar{\beta} = \beta/\Omega$ and $\bar{\chi} = \chi/\Omega$. Consequently a logarithmic plot of $[1 - (d\beta/d\chi)]$ versus $\bar{\chi} - \bar{\chi}_c$ should be a straight line whose slope is $(n - 1)$. Figure 9 is then such a plot based on data of Figs. 2 and 6. Indeed in the vicinity of the cold boundary the plots are quite linear, the value of the exponent in (36) being about 3.5 for all three coupled-wave solutions. However, starting from about 35% of the interval in χ between the cold and hot boundary, they deviate quite rapidly from the straight line dependence. Lines of constant n have been added as an aid in the interpretation of the variation of this parameter throughout the wave.

Of particular significance is the plot of κ in Figs. 3, 4, 7, and 8. It represents the variation that occurs throughout the wave process in the ratio of the reaction time t_r to the mean molecular collision time, t_c or in the average number of intermolecular collisions per one molecule of product formed by reaction. The collision time has been expressed for this purpose from the classical relation between the mean free path and viscosity yielding

$$\kappa \equiv \frac{t_r}{t_c} = \frac{8}{3\pi}\frac{p\rho}{\mu\omega} = 1.13\frac{p\rho}{\Gamma\omega} \qquad (37)$$

It should be noted that our value of this parameter is about half that of Wood[5] who based it on the rigid sphere model for thermal conduc-

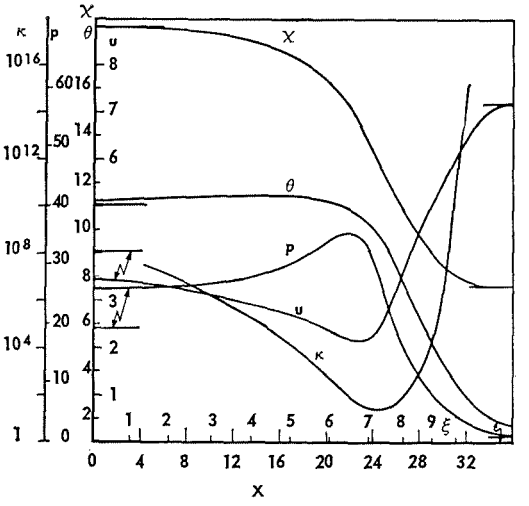

FIG. 7. Structure of coupled wave in ozone.

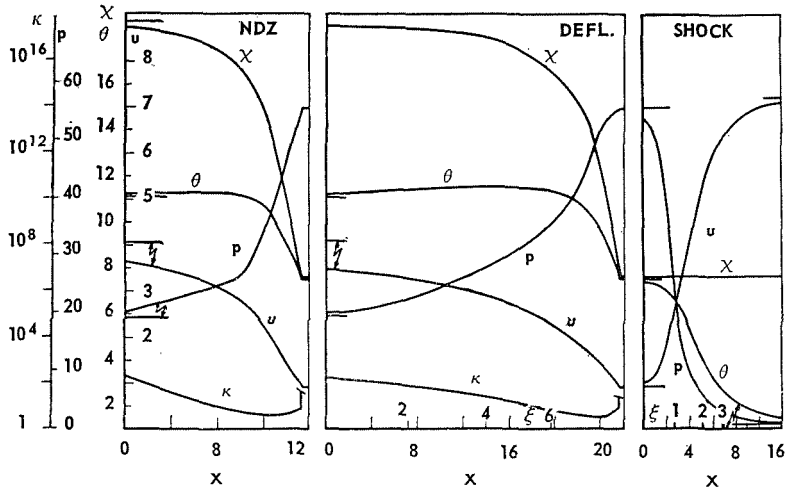

FIG. 8. Structure of uncoupled wave in ozone.

tivity; our results in this respect are therefore twice as conservative as his.

For the H&C reactions, with the help of Eqs. (1) and (28), we obtain for the evaluation of (37):

$$\kappa = 1.13 \frac{\Omega\theta \exp(\epsilon/\theta)}{\gamma\Lambda u(\chi_h - \chi)} \qquad (37a)$$

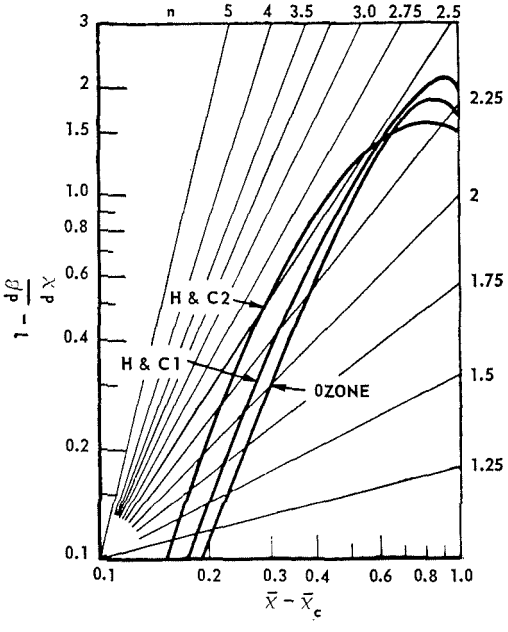

FIG. 9. Interpretation of solutions in the light of Spalding's approximation.

while for ozone, in accordance with (34):

$$\kappa = 1.13 \frac{\Omega\theta^{\frac{1}{2}} \exp(\epsilon/\theta)}{\gamma\Lambda(\chi_h - \chi)(X + \chi)} \qquad (37b)$$

It is of interest to note that in all cases analyzed by us, κ, starting from a high value at the cold boundary, approaches quickly a value of an order of 10 which it maintains for some time until, only in the immediate vicinity of the hot boundary equilibrium, it rises to infinity. For the H&C 1 reaction its minimum value in Fig. 3 is about twice as small as for H&C 2 in Fig. 4, essentially in accordance with the difference in the Γk product. For the ozone reaction, under the quasi-steady-state assumption of our theory which does not take into account the attenuating effect of oxygen recombination, the minimum value of about 10 collisions per molecule of oxygen formed as shown in Fig. 7, should be considered quite reasonable. Incidentally according to recent shock tube results of Jones and Davidson[6] the value of the steric factor appears to be an order of magnitude smaller than that used here. Consequently the minimum value of κ should be about 100, which is well within reasonable expectations.

In closing we would like to make the following comment. The advantage of our specific analysis is the fact that it takes into account the aerothermochemical effects with sufficient accuracy to render the results compatible with experimental evidence. Any deviations from the observed structure could be, therefore, considered in principle as a measure of some significant parameter governing the physics of the wave process. The most remarkable in this respect

turns out to be, not without surprise, the effect of the "transport coefficient," Γ. Moreover, its influence on the solution in the χ–u and β–χ planes is much smaller than in the straightforward transformation between ξ and the corresponding physical dimension, l.

The experimentally observed spatial structure of the wave may be reflected, therefore, much more in the value of Γ than in other parameters, as for instance those involved in the description of kinetics. In particular Γ may be regarded as a convenient, although admittedly somewhat oversimplified, measure of the effect of turbulence or any other time dependent and multidimensional phenomena, since the over-all "stretching" of the wave thickness due to their effects can be certainly taken into account by proper adjustment in its value.

Turbulence in detonation waves has been studied by White[7] who demonstrated the influence it can have on the properties of the Chapman–Jouguet state. However, in contrast to the essential, but relatively small modification in this respect, the effect of turbulence on "wave stretching" should be orders of magnitude larger. This throws then a special light on our study. Although today the investigation of the "turbulent" wave structure may very well be of the greatest significance to the understanding of detonation phenomena, it is only the intimate knowledge of the so-called "laminar" wave that can provide the correct point of departure for this purpose.

Nomenclature

c_p Specific heat at constant pressure
$E^\ddagger$ Energy of activation
k Steric factor
l Dimensional distance
m Mass flow rate per unit area
M Molar mass
n Exponent in Spalding's approximation (36)*
p Pressure
q Heat release per unit mass
R Gas constant
T Absolute temperature
u Nondimensional velocity or specific volume
V Velocity
x Nondimensional distance (ml/Γ_c)
Y Mass fraction of products
β Nondimensional stagnation enthalpy gradient (4)*
$\bar{\beta}$ $\equiv \beta/\Omega$
γ Specific heat ratio
Γ Transport or "exchange" coefficient (6)*
ϵ Nondimensional energy of activation
θ Nondimensional temperature (T/T_c)
κ Ratio of the reaction time to the mean intermolecular collision time or the average number of intermolecular collisions for one molecule of product formed by reaction (37)*
λ Conductivity
Λ Nondimensional transport coefficient ($\Gamma k/ma_c$)
μ Viscosity coefficient
ξ Nondimensional space variable (5)*
ρ Density
χ Nondimensional stagnation enthalpy (3)*
$\bar{\chi}$ $\equiv \chi/\Omega$
X $\equiv 2\chi_h - 3\chi_c$
ω Volumetric reaction rate
Ω Nondimensional heat release (7)*

Subscripts

c denotes cold boundary
h denotes hot boundary
0 Denotes the nonzero root of the Rayleigh parabola on the $\chi = 0$ axis
R Denotes the Rayleigh line

* Numbers in parentheses denote equations where the symbol is defined specifically.

Acknowledgments

The authors wish to express their appreciation to Professor D. B. Spalding for directing their attention to the advantages of the novel formulation of the problem that has been used in this work, and for the valuable incentive he provided in its execution. They would also like to acknowledge their gratitude to Mr. J. R. Bowen for helping them in establishing the most reliable description of reaction kinetics for the thermal decomposition of ozone.

This research was supported by the National Aeronautics and Space Administration under Grant No. NSG–10–59 and by the United States Air Force Office of Scientific Research of the Air Research and Development Command under Contract AF 49(638)–166.

References

1. Hirschfelder, J. O. and Curtiss, C. F.: J. Chem. Phys. *28*, 1130 (1958).
2. Hirschfelder, J. O. and Curtiss, C. F.: Propagation of Flames and Detonations, in *Advances in Chemical Physics*, Vol. III, pp. 59–129. Interscience Publishers, 1961.
3. Spalding, D. B.: *Ninth Symposium (International) on Combustion*, this volume. Academic Press Inc., 1962.
4. Benson, S. W. and Axworthy, A. E., Jr.: J. Chem. Phys. *26*, 1718 (1957).
5. Wood, W. W.: Phys. Fluids, *4*, 46 (1961).
6. Jones, W. M. and Davidson, N.: The Thermal Decomposition of Ozone in a Shock Tube. Paper presented at the 135th National Meeting of the American Chemical Society, Boston, Mass., April, 1959.
7. White, D. R.: Phys. Fluids, *4*, 465 (1961).

Discussion

DR. W. W. WOOD (*Los Alamos Scientific Laboratory*): The analysis by Hirschfelder and Curtiss (see references 1 and 2) of idealized ($A \rightarrow B$, first order Arrhenius kinetics, no back reaction, constant heat capacities, Pr = $\frac{3}{4}$, Le = 1, etc.) steady state Navier-Stokes detonations, modified by me[3] for the case of small reaction rates, was left incomplete as regards the case of very rapid reactions. Figure 1, a modification of Fig. 3 of reference 2, represents the existing interpretation of our analysis. Steady state strong (hot boundary Mach number $\kappa^2 < 1$) detonations were shown to exist in the shaded region of the figure, while weak ($\kappa^2 > 1$) detonations were shown to exist for values of the dimensionless rate parameter R lying on the curve R_u. For values of R above this curve, i.e., for very fast reactions, no steady state solutions were found.

As Hirschfelder and Curtiss indicated, and as Professor Spalding has mentioned, for such fast reactions the quasi-unimolecular reaction mechanism would be expected to become bimolecular, so that the physical significance of solutions for very fast first order kinetics is somewhat unclear. However, as Hirschfelder and Curtiss indicated, the changeover to a bimolecular mechanism has perhaps no marked effect as regards the coupling of the shock and reaction zones. Furthermore, even if nature abandons the unimolecular mechanism in such cases (it is doubtful if it really provides it for any realistic detonation in the first place), one can envisage performing a numerical integration of the time-dependent, one-dimensional hydrodynamic equations, for the flow produced by a piston which at time $t = 0$ moves at the constant speed U_P (relative to the reactants at rest) into a quiescent medium for which we prescribe such a fast first order reaction. It is clear that for suitable piston speeds the initial shock produced by the piston motion will initiate the reaction, and intuitively one might expect that the resulting long-time behavior would approach some sort of steady state flow. Here I would like to indicate that such a behavior can be predicted from the existing analysis if the steady state assumption is slightly relaxed to admit, in the region above the curve R_u in Fig. 1, two-wave solutions which are similar to the double-wave shock structures observed by Minshall[4] in iron, and which in the present case consist of a weak detonation followed by a slower moving shock.

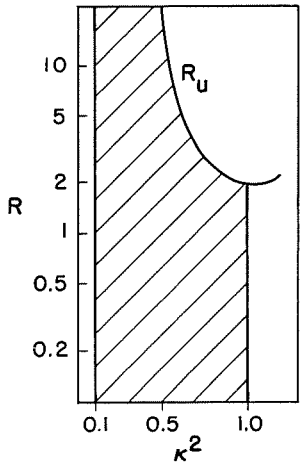

FIG. 1.

The dimensionless reaction-rate parameter R of Fig. 1 is given, in the notation of Hirschfelder and Curtiss, by

$$R = (k_0'\lambda_0/\rho_0 D^2 \overline{C}_p) \exp(-E^\ddagger/kT_\infty). \quad (1)$$

It will clarify our thinking if we consider an initial state with completely specific kinetic and thermodynamic properties (i.e., fixed values of the initial steric factor k_0', initial thermal conductivity λ_0, initial density ρ_0, activation energy $E^\ddagger$, etc.), and try to determine the nature of the flow as a function of the piston speed U_P. When the flow is truly steady (e.g. no rarefaction or Taylor wave is present) this piston speed coincides with the hot boundary mass velocity U of the steady state solution. This velocity is given in terms of the Hirschfelder–Curtiss variables by

$$U^2/c_0^2 = (u_0 - 1)^2(\kappa^2/\theta_0). \quad (2)$$

For a fixed initial state, u_0 and θ_0 in Eq. (2) depend on the hot boundary Mach number κ^2, so that U^2/c_0^2 (c_0 is the initial sound speed) is a function of κ^2. It increases monotonically as one moves up the detonation Hugoniot, beginning at the value 0 for the constant-volume detonation ($\kappa^2 = \infty$); at the C–J point, $\kappa^2 = 1$, we find

$$U^2/c_0^2 = U_{CJ}^2/c_0^2 = [2(\epsilon - 1)]/(\gamma + 1); \quad (3)$$

as one moves indefinitely up the strong detonation branch $U^2/c_0^2 \rightarrow \infty$ as $\kappa^2 \rightarrow (\gamma - 1)/2\gamma$. In the subsequent discussion we will take U as our independent variable instead of κ^2.

In Eq. (1), R depends for fixed initial state on the Mach number κ^2, and therefore on U, through the detonation velocity D and the hot boundary temperature T_∞. It is accordingly convenient to separate it into two factors, one of which depends only on the initial state:

$$\begin{aligned} R &= \Lambda_0 \tilde{R}, \\ \Lambda_0 &= k_0'\lambda_0/\gamma p_0 \overline{C}_p, \\ \tilde{R} &= (c_0^2/D^2) \exp(-E^\ddagger/kT_\infty). \end{aligned} \quad (4)$$

Similarly we define the eigenvalue Λ_u corresponding to the eigenvalue R_u of Fig. 1:

$$\Lambda_u = R_u/R. \tag{5}$$

The eigenvalue R_u, and consequently Λ_u, depends on κ^2 (i.e., on U/c_0), and the medium parameters γ, $\beta = Q/E^\ddagger$, and $\epsilon = 1 + Q/\bar{C}_pT_0$.

In Fig. 2 is shown the dependence of Λ_u on U/c_0 for the parameters of reference 1 ($\gamma = 1.25$, $\beta = 1.12$, $\epsilon = 12.2$), as determined by an iterative Runge–Kutta integration of Eqs. (1.10–1.12) of reference 3. The important feature is that Λ_u is found to increase monotonicly as one moves away from the C–J point in either direction along the detonation Hugoniot.

The nature of the flow produced by a given piston speed U_P is thus seen to depend upon the value of the parameter Λ_0 for the initial state, relative to the eigenvalue $\Lambda_u^{(C-J)}$ for the C–J detonation. If $\Lambda_0 < \Lambda_u^{(C-J)}$ then one has the classical situation, in which for $U_P > U_{C-J}$ the steady strong detonation with hot boundary mass velocity $U = U_P$ is produced; while if $U_P < U_{C-J}$ then the usual plausible extension[5] of the steady state analysis predicts a C–J detonation wave followed by a rarefaction wave, the latter reducing the mass velocity from the value U_{C-J} to the value U_P.

If $\Lambda_0 > \Lambda_u^{(C-J)}$ then the C–J detonation does not exist. Instead, if the value of Λ_0 corresponds to the value of $\Lambda_u(A) = \Lambda_u(A')$, A and A' being the points indicated in Fig. 2, then the situation is as follows. If $U_P > U(A')$ then the steady strong detonation wave in which the hot boundary mass velocity $U = U_P$ is produced. If $U_P < U(A)$, then by reasoning analogous to that referred to above for underdriven C–J detonations, one predicts a weak detonation wave with hot boundary mass velocity $U = U(A)$, followed by a slower moving rarefaction wave. In the intermediate range $U(A) < U_P < U(A')$ the same argument predicts a solution consisting of the same weak detonation

$$[U = U(A)],$$

followed by a slower moving shock wave which increases the mass velocity from $U(A)$ to U_P.

The present discussion of course leaves unanswered the question of the stability of these laminar flows to small perturbations.

If the reasonable values $k_0' = 10^{13}$ sec^{-1}, $\lambda_0 = 5\cdot10^{-5}$ cal cm^{-1} sec^{-1} deg^{-1}, $\bar{C}_p = \frac{1}{3}$ cal g^{-1} deg^{-1}, $\gamma = 5/4$, $p_0 = 1$ atm are substituted in Eq. (4), one obtains $\Lambda_0 \sim 1200$; the value of $\Lambda_u^{(C-J)}$ from Fig. 2 is $\sim$4600. Thus for the values quoted, the classical C–J strong detonation continuum mentioned above would be expected. However, a four-fold reduction in initial pressure would suffice to put such a system in the weak detonation, two-wave, strong detonation regime. I do not wish to overemphasize the physical significance of this particular calculation, in view of the highly idealized assumptions involved. However, the possibility of pseudo-steady-state solutions of the types described should perhaps be kept in mind in connection with more realistic calculations.

A more detailed account of the present analysis will probably be published elsewhere. I would like to mention my indebtedness to my colleague Dr. J. J. Erpenbeck, whose suggestion of a double-wave solution for a different problem led me to the present

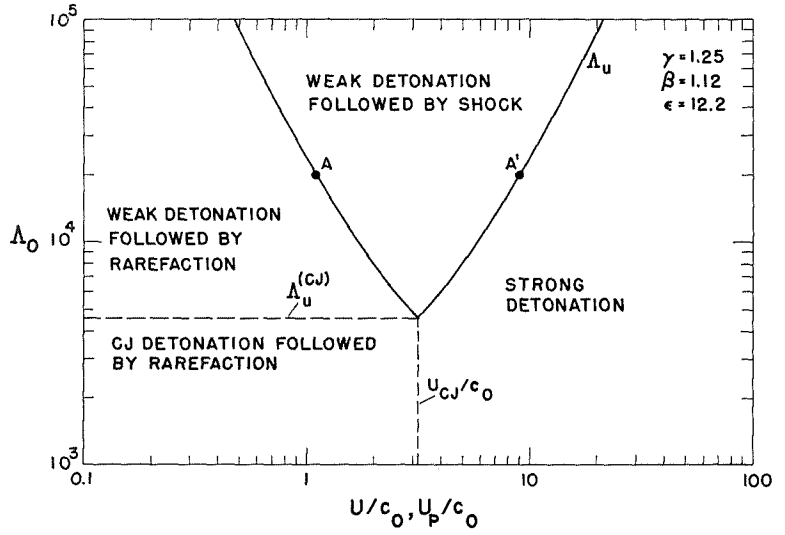

FIG. 2.

results. This work was performed under the auspices of the U. S. Atomic Energy Commission.

PROF. C. ADAMSON (*University of Michigan*): It is not clear that the results of this calculation prove that strong coupling does indeed exist between the shock and deflagration. Instead, as with the solutions presented by Hirschfelder and Curtiss, it is shown that for given values of the physical parameters, the solution of the equations shows a coupling effect. The point, of course, is how closely the physical parameters agree with a real physical case. In the discussion presented for the ozone detonation, it is mentioned that the steric factor found in most recent experiments appears to be an order of magnitude lower than that used in the calculations. Yet the amount of coupling between the shock and deflagration is very sensitive to the steric factor. In fact, a consideration of Figs. 1, or 3 and 4 of the paper, indicates that a decrease of 63% in the steric factor decreases the coupling significantly. A decrease by an order of magnitude could well make the coupling become negligible. Finally, it is quite possible that later experiments might result in different values for the steric factor as well as the other physical parameters.

Quite apart from the above considerations is a question which should be discussed before further calculations of this type are attempted. In all theoretical work in which the structure of the detonation wave has been studied, the Navier–Stokes equations have been used both in shock and in the reaction zone. For most detonation waves, the Mach number at which the wave propagates is 5 or above. Yet in the study of shock wave structure, it is well known that the Navier-Stokes equations are accurate only for relatively weak shocks with propagation Mach number no greater than 2. For strong shocks, near equilibrium theory simply does not describe the molecular transport of momentum and energy adequately. Hence, it should be born in mind that Navier–Stokes solutions to the coupling problem can give only qualitative results, at best, for the strong waves considered.

PROF. A. K. OPPENHEIM (*University of California*): I am in full agreement with Professor Adamson that indeed a strong coupling between the shock and deflagration is doubtful and the use of Navier–Stokes equations may not be entirely satisfactory. However I think that an attempt to evaluate exactly the extent of coupling that can be provided by transport properties is worthwhile. After all there is a difference between religion, the outcome of beliefs, and science, the code of knowledge. I am grateful to Professor Adamson for pointing out the marked difference of the steric factor on coupling. We are aware of this and we are continuing our work to investigate this very matter systematically. As to the Navier–Stokes equations, until we get a better formulation—perhaps from Professor Adamson himself—we are, albeit aware of their fundamental limitations, stuck with them. Actually they have been demonstrated to produce surprisingly accurate results for shocks propagating at even higher Mach numbers than 2.

DR. W. W. WOOD: Steady detonation solutions of the Navier–Stokes equations have been investigated in the case of arbitrary Prandtl number Pr and zero Lewis number Le by Friedrichs,[6] and for $\Pr = \frac{3}{4}$, $\mathrm{Le} = 1$ by Hirschfelder, Curtiss, and their co-workers,[7–10] Adamson,[11] Spalding,[12] and Wood.[13] The conclusion of these investigations was that the classical continuum of overdriven ("strong") detonation solutions, including the Chapman–Jouguet (C–J) solution, exists if the reaction rate is not *too large*. For any particular "weak" detonation a solution was found, but only for a corresponding *eigenvalue* of the reaction rate (the value being quite large, corresponding to a rather fast reaction). For still larger reaction rates no steady solutions were found; the author[14] has recently suggested that in these cases pseudo-steady, two-wave solutions exist. The object of the present note is to indicate that, contrary to a recent suggestion, no departure from the above-described behavior is likely to appear in the inviscid limit $\Pr \to 0$.

As our starting point we will take Eqs. (11)–(14) of Hirschfelder and Curtiss,[7] written in a slightly different notation[13] with the Prandtl and Lewis numbers inserted:

$$(4/3)\ \Pr\ \gamma\kappa^2 u R_1 (du/dt) = \theta - \theta_R(u) \tag{1}$$

$$R_1(d\theta/dt) = aG + \frac{\theta - 1}{\gamma} + \frac{\gamma - 1}{\gamma}(u - 1) - \tfrac{1}{2}[(\gamma - 1)\kappa^2](u - 1)^2 \tag{2}$$

$$R_1\ \mathrm{Le}\ (dx/dt) = x - G \tag{3}$$

$$dG/dt = -xr(\theta) \tag{4}$$

$$\theta_R(u) = \gamma\kappa^2 u(2u_m - u) \tag{5}$$

$$u_m = (\gamma\kappa^2 + 1)/2\gamma\kappa^2 \tag{6}$$

$$r(\theta) = \exp[(\theta - 1)/\tau_1\theta]. \tag{7}$$

In order to simplify the discussion we will set $\mathrm{Le} = 0$, remarking that on physical grounds one expects that in the limit $\mathrm{Le} \to 0$ the composition gradient dx/dt will remain finite, in which case Eq (3) shows that $x \to G$. In the subsequent discussion, then, we set

$$G = x. \tag{8}$$

In the limit $\Pr \to 0$, however, we may expect a more complicated behavior to appear. Namely, *shocks* are likely to form; that is, at certain points

in the flow one expects $du/dt \to \infty$ as $\mathrm{Pr} \to 0$, the dimensionless mass velocity u, as well as the density and pressure, developing jump discontinuities at these points. The dimensionless temperature θ, being governed by Eq. (2) for all Pr, is of course *not* expected to develop such discontinuities. For a discussion of the closely related problems of nonreactive shock structure in the inviscid limit, see Grad.[15] At points where du/dt remains finite, Eq. (1) shows that $\theta \to \theta_R(u)$ as $\mathrm{Pr} \to 0$. Rather than giving a detailed discussion of the limiting process $\mathrm{Pr} \to 0$, which entails a discussion of a three-dimensional vector field, we set

$$\theta = \theta_R(u), \tag{9}$$

and admit solutions in which θ and x are continuous while u may have a jump discontinuity. It is easy to show that Eq. (9) is equivalent to the familiar Rayleigh line relation of the standard p–v diagram.

Equation (9) can of course be solved for $u(\theta)$, and the four-dimensional (u, θ, x, G) system (1)–(4) reduced with the aid of Eq. (8) to a two-dimensional (θ, x) system. However, $u(\theta)$ is double-valued, and it is somewhat more convenient to substitute $\theta_R(u)$ for θ in Eq. (2), obtaining the two-dimensional (u, x) system

$$2\gamma\kappa^2 R_1(du/dt) = h(x, u)/(u - u_m), \tag{10}$$

$$dx/dt = -xr[\theta_R(u)], \tag{11}$$

where

$$h(x, u) = \tfrac{1}{2}(\gamma + 1)\kappa^2(u - 1)(u - f) - ax, \tag{12}$$

$$f = 1 + \frac{2(1 - \kappa^2)}{(\gamma + 1)\kappa^2}. \tag{13}$$

In Fig. 3 we have sketched the phase portrait of Eqs. (10)–(11) for the C–J case $\kappa = 1$; for the sake of clarity the separation between u_m and $u = 1$ has been exaggerated. The principal features are:

(1) the quasi-saddle point C at the intersection of $u = u_m$ and $h(x, u) = 0$;

(2) termination of integral curves on $u = u_m$ at points above C, origination at the points below;

(3) the integral curves in the triangular sector CR1 belong to a nodal fan tending to the C–J point 1;

(4) the presence of the separatrix integral curve S in sector QNC, and its continuation through C into point 1.

Let us consider the case of slow reaction rate (small R_1), and choose an ignition temperature T_{ig} slightly above T_0. Then, since diffusion is absent, the state point begins to react at a point I near 0 on $x = 1$, as indicated in Fig. 3. It will evidently remain near $x = 1$ and terminate on $u = u_m$ near

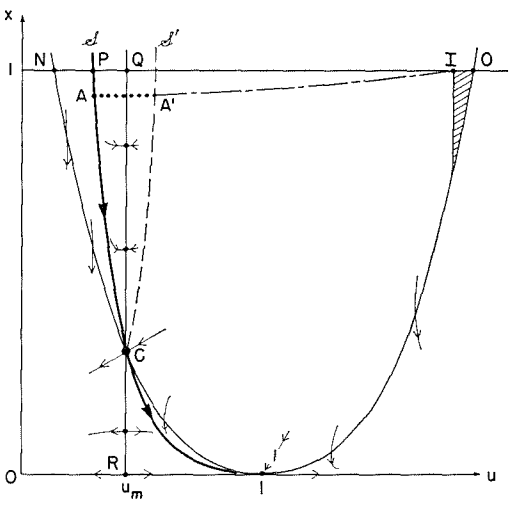

FIG. 3.

point Q, unless we introduce a jump discontinuity. The figure shows that a solution is obtained if a jump is introduced from the point A′, at which the integral curve from point I intersects the reflection S′ of separatrix S in the line $u = u_m$, to its source point A on S; note that according to Eqs. (5) and (9), $\theta(A) = \theta(A')$. The state point then moves along S until it reaches point C from which *two* integral curves depart; we choose the one in sector CR1, so that we reach the C–J point 1.

We believe that a detailed examination of the singular perturbation problem $\mathrm{Pr} \to 0$ indeed shows that Friedrichs' solution continues to exist in the limit and approaches the above solution IA′AC1. The latter exists in the limit of vanishing rate, at which it approaches the classical von Neumann solution.

For an intermediate range of large reaction rates, the integral curve from point I intersects $h(x, u) = 0$ below point C, and to the left of point 1, entering the sector $CR1$ and eventually reaching point 1. In this case no jump is required and point C is not encountered. For sufficiently large rates the C–J solution does not exist.

In the interval $\gamma^{-1} < \kappa^2 < 1$, a strong detonation exists (unless the reaction rate is too large), having essentially the behavior just described for the C–J case.

For $\kappa^2 < \gamma^{-1}$ point C lies in the physically meaningless region of negative x, so that the complication connected with the choice of its exit curve disappears. However, a jump A′A is now always necessary, until the reaction rate becomes so large that the solution no longer exists.

Finally, for any value $(\gamma - 1)/2\gamma < \kappa^2 < 1$ there is an eigenvalue R_1/κ^2) of the reduced reaction rate

R_1 for which the integral curve from point I reaches the weak detonation hot boundary point $u = f$, $x = 0$.

Thus, we see that detonation wave structure with $\mathrm{Pr} \to 0$ and $\mathrm{Le} \to 0$ is not qualitatively different from that found previously[6–14] for $\mathrm{Pr} \neq 0$, so far as the existence of the C–J detonation and the continuum of overdriven detonations is concerned.

This work was performed under the auspices of the United States Atomic Energy Commission.

DR. W. I. AXFORD (*Defense Research Board, Ottawa*): In principle we could solve all problems involving combustion waves and the like by using the appropriate exact equations, given a sufficiently large computer and enough time. In practice, however, we must proceed in two stages using suitable approximate equations as follows:

(1) Solve the "external" flow problem fully, treating the reaction zone (or its equivalent) as a discontinuity, but satisfying all external boundary conditions and allowing for the possible occurrence of shock waves (also treated as discontinuities).

(2) Having determined conditions on both sides of the reaction zone, solve for its structure. This entails transforming to a coordinate system moving with the discontinuity so that conditions can be assumed to be quasi-steady.

The solution as far as step (1) is certain to be indeterminate, since all possibilities of weak and strong detonations and deflagrations must be allowed for. A unique solution can only be found by completing step (2)—that is by sorting out which of the many possible solutions of the external flow problems involve reaction zones which have a real structure.

In combustion theory the situation is often confusing because the distinction between (1) and (2) is not always made clear, and also because the reactions that take place tend to be rather complicated. However a case has recently been discovered for which the complete solutions (1) and (2) can be carried out, hence providing an example of the propagation of a type of gas dynamic discontinuity which is at least instructive if not completely analogous to ordinary combustion. The discontinuity in this case is an "ionization front" (I.F.) which is produced when ionizing radiation is incident upon a mass of unionized gas. Ionization fronts occur when a newborn hot star irradiates the surrounding interstellar hydrogen–photons emitted at frequencies above the Lyman limit ionize and heat the neutral hydrogen and an expanding spherical nebula of hot ionized gas is thus formed around the star. The ionization front (corresponding to the reaction zone in ordinary combustion) separates regions of unionized and fully ionized gas (corresponding to unburned and burned gas, respectively), and the front itself must propagate according to Jouguet's rule.

Goldsworthy[12] has worked out part (1) of the solution for a number of different cases of I.F. propagation in which the flow pattern is "similar" or "self-preserving." Part (2) of the solution has been worked out by Axford[17] for two cases in which the radiation is assumed to come from a line source and the flow pattern has cylindrical symmetry. In the first case no recombination or cooling effects are considered so that both the ionized and unionized regions behave a a perfect gas with $\gamma = 5/3$ and each proton ionizes a fresh atom at the I.F. In the second case (which is more realistic) recombination and cooling effects are included and it is found that the ionized region must be treated as isothermal and only a small fraction of the ionizing photons ever reach the I.F. due to absorption by recombined atoms in the ionized region.

It is intuitively obvious that if a strong source radiates into low density surrounding, then the resulting I.F. will move out very rapidly, corresponding to a detonation. On the other hand a weak source radiating into high density surroundings will result in an I.F. which eats its way only slowly into the unionized gas, corresponding to a deflagration. If R is used to denote a suitable nondimensional form of the ratio (source strength to density of the surrounding unionized medium) then Goldsworthy finds in fact that for large values of R the I.F. can propagate as a weak detonation, while for small R the I.F. can propagate as a weak deflagration; for one particular intermediate value of R a strong detonation is possible. The flow pattern in the case of the weak detonation contains a shock in the ionized region, and in the case of the weak deflagration a shock moves ahead in the unionized region. The shock and the I.F. may be considered as moving together in the special case of the strong detonation. It is also possible however to have, for every value of R, an infinity of flow patterns in which the I.F. is a strong deflagration and shocks occur in both the ionized and unionized regions. The presence of these additional solutions produces an indeterminacy which is not resolved until part (2) is completed.

In the case in which recombination and cooling are neglected one does not have to embark on detailed calculations to see that the correct set of unique solutions for all values of R is obtained by ignoring the strong deflagrations. Since the reaction is entirely exothermic a strong deflagration would require a rarefaction shock to bring the solution from the subsonic to the supersonic branch of the Rayleigh line (see Fig. 4), and this is impossible. (The width of an I.F. is much greater than a mean free path and therefore it is permissible to consider

In the second case with recombination and cooling taken into account the results are not as obvious. For large values of R the I.F. is a weak detonation

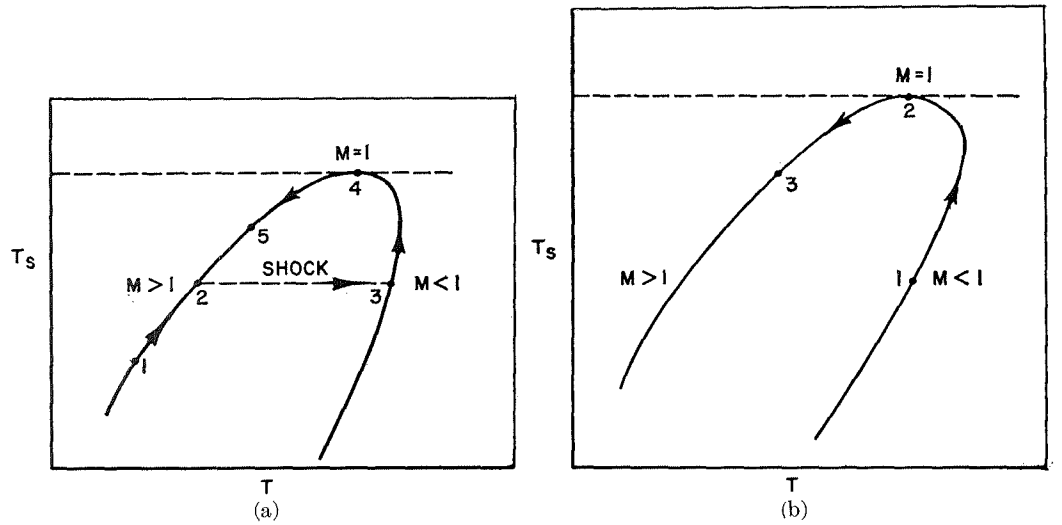

FIG. 4. Diagrams showing a form of the Rayleigh line, where T_s is the nondimensional stagnation temperature, T is the nondimensional temperature, and M the Mach number. The reaction processes are assumed to be such that T_s has a maximum at some point within the reaction zone. If this maximum value is equal to the maximum on the Rayleigh line then it is possible to change smoothly from $M < 1$ to $M > 1$. The solutions must follow the Rayleigh line except at shock waves which are transitions at constant T_s in the direction of increasing T. A weak detonation containing a shock is shown in (a), where the initial and final conditions are indicated by 1 and 5, respectively, the shock wave is $2 \rightarrow 3$ and 4 is a sonic point. A strong deflagration is shown in (b) where 1 and 3 are the initial and final conditions and 2 is a sonic point.

and for small values of R the I.F. is a weak deflagration as above. However in the intermediate range there are differences due entirely to the presence of the cooling process which can cause the reaction to be endothermic after being initially exothermic—that is, the stagnation temperature has a maximum somewhere in the interior of the reaction zone. In this case a smooth transition from subsonic to supersonic flow can take place provided the maximum stagnation temperature is equal to the value at the maximum of the Rayleigh line. It is easy to see that strong deflagrations can now occur and that the special condition on the stagnation temperature constitutes an over-determinacy within the reaction zone which compensates for the externally underdetermined flow pattern associated with strong deflagrations. Furthermore a weak detonation can now contain a shock since the flow can return smoothly to supersonic conditions— the position of the shock in the reaction zone is then determined by the requirement on the maximum stagnation temperature. The over-all picture then, is that as R decreases a shock appears in the weak detonation (internally) and gradually moves forward—eventually it becomes detached and moves ahead, causing the I.F. to become a strong deflagration; with further decrease of R the shock in the ionized region catches up and becomes absorbed in the I.F. which then becomes a weak deflagration—strong detonations do not occur in general.

Clearly the presence of a cooling process has a great influence on the character of I.F.'s and this is presumably true of gas dynamic discontinuities in general—this has also been remarked upon by Zeldovich and Kompaneets.[18] Furthermore the strong deflagration, if it can occur at all, is not indeterminate as the solution carried as far as step (1) would suggest—hence Hayes[19] proposal that the strong deflagration is "internally unstable" is incorrect.

White[20] has suggested that the turbulence commonly observed to be associated with detonating combustion waves is a feature of fundamental significance, and he has shown that weak detonations can be produced if turbulence is present. Since a detonating combustion wave must begin with a shock in general, the turbulence must somehow allow a smooth transition to occur from subsonic to supersonic flow in much the same manner as a cooling mechanism. The process is a little more complicated than described above, but its nature can be understood from the following argument. In a turbulent medium a larger fraction of the total energy is associated with translational motions of the mole-

cules than is normal. If the turbulence decays, then in suitable circumstances its energy is adiabatically transferred to molecular motions (and in particular to nontranslational degrees of freedom) so that the effective sound speed is reduced. By this means it is possible for a weak detonation to occur provided the turbulence induced in the reaction zone is sufficiently intense for the effective Mach number of the flow to become unity at some point. The detonation wave (considered as the ensemble of the initial shock. the reaction zone, and the zone of decaying turbulence) then has an "internal" Chapman–Jouguet point beyond which the flow can become supersonic as the turbulence decays. Presumably instabilities lead to exactly the right degree of turbulence to make the internal C–J point possible. The position of the shock is not disposable in this type of weak detonation wave, but this is compensated for by the fact that the Rayleigh line itself is variable, depending on the degree of turbulence at each point.

References

1. Hirschfelder, J. O. and Curtiss, C. F.: J. Chem. Phys. *28*, 1130 (1958).
2. Curtiss, C. F., Hirschfelder, J. O., and Barnett, M. P.: J. Chem. Phys. *30*, 470 (1959).
3. Wood, W. W.: Phys. Fluids *4*, 46 (1961).
4. Minshall, F. S.: *Metallurgical Society Conferences*, Vol. 9, p. 249. Interscience Publishers, New York, 1961.
5. Wood, W. W. and Salsburg, Z. W.: Phys. Fluids *3*, 549 (1960).
6. Friedrichs, K. O.: On the Mathematical Theory of Deflagrations and Detonations, NAVORD Report 79-46, 1946.
7. Hirschfelder, J. O. and Curtiss, C. F.: J. Chem. Phys. *28*, 1130 (1958).
8. Linder, B. Curtiss, C. F., and Hirschfelder, J. O.: J. Chem. Phys. *28*, 1147 (1958).
9. Curtiss, C. F., Hirschfelder, J. O., and Barnett, M. P.: J. Chem. Phys. *30*, 470 (1959).
10. Hirschfelder, J. O., Curtiss, C. F., and Barnett, M. P.: Phys. Fluids *4*, 262 (1961).
11. Adamson, Jr., T. C.: Phys. Fluids *3*, 706 (1960).
12. Spalding, D. B.: These Proceedings.
13. Wood, W. W.: Phys. Fluids *4*, 46 (1961).
14. Wood, W. W.: See Discussion of ref. 12.
15. Grad, H.: Communs. Pure and Appl. Math. *5*, 257 (1952).
16. Goldsworthy, F. A.: Phil. Trans. Roy. Soc. (London) *A253*, 277 (1961).
17. Axford, W. I.: Phil. Trans. Roy. Soc. (London) *A253*, 301 (1961).
18. Zeldovich, Ya. B. and Kompaneets, A. S.: *Theory of Detonation*. Academic Press, 1960.
19. Hayes, W. D.: *Fundamental of Gas Dynamics*. Princeton University Press, 1958.
20. White, D. E.: Phys. Fluids *4*, 465 (1961).

STRUCTURE AND STABILITY OF THE SQUARE-WAVE DETONATION

J. J. ERPENBECK

The structure of the square-wave limit of steady detonation is derived through the limiting behavior of a one-reaction detonation, having an Arrhenius rate constant, as the activation energy becomes large. In addition to the induction-zone and equilibrium-zone solutions, expressions are obtained to describe the reaction zone through which the chemical reaction proceeds.

The hydrodynamic stability of the square-wave detonation is also considered, with particular attention to the mode of propagation of disturbances through the induction zone. The recent analysis by Zaidel of the stability of the square-wave model (in which the reaction zone is taken to be a front of discontinuity) is found to be invalid in the sense that the reactivity of the fluid in the induction zone cannot be ignored for disturbances of a frequency commensurate with the length of this zone.

An additional difficulty, arising from the use of Rankine–Hugoniot conditions across the reaction front, is also pointed out. It is shown that the initial-value problem for the two-front stability equations has no solution of exponential order in the time. Although no attempt is made to decide upon whether the two-front stability problem is reasonable (in the sense of having a solution), the normal-modes (or Laplace time transform) approach is not valid.

It is observed that a more direct approach to the problem, whereby attention is focused at the outset onto the structure of the reaction "front", avoids both of these difficulties.

Introduction

In recent years, there has arisen a large body of experimental evidence[1] indicating that the assumptions of steady, one-dimensional flow commonly used in detonation theory are not always appropriate. The reaction zone, behind the initiating von Neumann shock, has appeared turbulent in certain instances, and careful measurements of various properties characterizing the reaction zone disagree with calculations based on the aforementioned assumptions.

From a theoretical point of view, it seems appropriate to investigate the question of the stability of steady, one-dimensional detonation waves to small disturbances. Should any disturbance grow with time, the steady flow is not expected to occur and is said to be unstable. Should the magnitude of every disturbance damp with time, the existence of the steady wave (under suitable boundary conditions) is possible.

Several investigations of stability have appeared recently. Shchelkin[2] has obtained a criterion for stability based upon certain intuitive considerations of the behavior of disturbances superimposed upon a square-wave model of steady detonation. Zaidel,[3] on the other hand, has obtained a stability criterion directly from the hydrodynamic-kinetic equations of reactive flow, but his analysis is specialized at the outset to the square-wave model. It is suggested[3] that Zaidel's criterion tends to support the conclusions of Shchelkin, but a complete elucidation of the consequences of this criterion has not as yet been reported.

Finally, the author[4] has presented a formal analysis of the stability question without reference to any specializing assumption on the nature of the detonating medium (other than the usual neglect of transport processes). The principal results of this analysis are given in the next section. There is obtained a general stability criterion which cannot, however, be applied to a specific system without a considerable amount of additional computation, apparently by numerical means. This necessity for numerical treatment arises from the fact that the flow variables in steady state detonations vary from point to point and this variation is reflected in the occurrence of nonconstant coefficients in a certain system of linear, homogeneous, differential equations of the stability theory.

In the present article, we investigate the stability of detonations in the square-wave limit. In particular, we consider the limiting behavior of a one-reaction detonation having an Arrhenius rate constant for large values of the activation energy. It is in just this limit that the square-wave model of Shchelkin and Zaidel arises. The section on Square-Wave Detonation Structure is concerned with the derivation of the asymptotic expressions for this steady flow.

The behavior of the stability equations in the square-wave limit is considered in the section on Stability Considerations. It is shown that the asymptotic form of these equations does not correspond to that employed by Zaidel. While the Zaidel analysis regards the steady flow as strictly uniform and nonreactive except across shock discontinuities at the von Neumann spike and the reaction front, the present results show that the reactivity of the fluid in the induction zone cannot be ignored for the values of certain stability parameters considered. We find that the high sensitivity of the reaction rate to the temperature implies a more complicated mode of propagation for the disturbances than the essentially nonreactive propagation used in this theory. Additional difficulties associated with the model calculation, arising in conjunction with the use of Rankine-Hugoniot conditions across the reaction front, are also pointed out.

The Discussion interprets the failure of the model-type calculation in terms of the time scale for growth or decay of disturbances. It is suggested that, on a time scale commensurate with the reaction-front thickness rather than the induction-zone length, a calculation of stability might be possible without recourse to specialized numerical procedures.

General Stability Analysis

In this section, we shall briefly review the general analysis of the detonation stability problem previously reported[4], and in addition present some qualitative discussion of the final stability criterion.

We consider a steady, one-dimensional detonation wave of so-called "normal" type, as described in general by Wood and Salsburg.[5] This consists of a quiescent medium into which a shock of velocity $D\mathbf{e}_x$ moves, followed by a reaction zone through which the chemical reactions excited by the shock are brought to equilibrium, the final equilibrium state being reached only asymptotically with distance from the shock. The question of stability is posed as the following initial-value problem: At the initial time, $t = 0$, let the steady flow variables* $\mathbf{q}(x) = (v, u_x, u_y S, \lambda)$ (where v is the specific volume, u is the mass velocity, S is the specific entropy, and λ is the set of progress variables for the n chemical reaction; $u_y = 0$) be perturbed at each spatial point (x, y) by a small amount $\tilde{\mathbf{q}}_0(x, y)$. Denoting by $\tilde{\mathbf{q}}(x, y, t)$ the subsequent values of the perturbations, we inquire into whether the magnitude of $\tilde{\mathbf{q}}$ becomes vanishingly small. Should every (sufficiently small) disturbance die out, the steady flow is said to be stable. If any disturbance grows in magnitude, the steady flow is unstable.

* For brevity, we include only two-dimensional disturbances.

The initial-value problem is solved in principle through the time-dependent hydrodynamic–kinetic equations of reactive flow, supplemented by the Rankine-Hugoniot equations across the shock discontinuity. The equations being nonlinear, there can be no hope of obtaining an exact solution. Therefore, we resort to the linearization technique of hydrodynamic-stability theory, whereby only terms of first order in the state perturbations $\tilde{\mathbf{q}}$ and shock-position perturbation $\tilde{\psi}(y, t)$ are retained in the two previously mentioned sets of equations. There result, then, the linear equations,

$$\partial\tilde{\mathbf{q}}/\partial t + \mathbf{A}_x(x)\cdot\partial\tilde{\mathbf{q}}/\partial x + \mathbf{A}_y(x)\cdot\partial\tilde{\mathbf{q}}/\partial y + \mathbf{B}(x)\cdot\tilde{\mathbf{q}} + \mathbf{g}_t(x)\,\partial\tilde{\psi}/\partial t + \mathbf{g}_y(x)\,\partial\tilde{\psi}/\partial y = 0, \quad (1)$$

$$\tilde{\mathbf{q}}(0_+, y, t) = \mathbf{Y}\cdot\tilde{\mathbf{q}}(0_-, y, t) + \mathbf{h}_t\,\partial\tilde{\psi}/\partial t + \mathbf{h}_y\,\partial\tilde{\psi}/\partial y, \quad (2)$$

in which the shock is fixed at $x = 0$, with $x > 0$ denoting the region behind the shock. The coefficient matrices and vectors are functions of the steady flow alone and are given (in part) in the Appendix. We note that the $\mathbf{A}$ matrices depend upon the flow variables themselves, with the matrix $\mathbf{B}$ dependent on both, (1) the gradients of the unperturbed flow, and (2) the thermodynamic derivatives of the entropy production and chemical rates, e.g., $(\partial\mathbf{r}/\partial v)_{S,\lambda}$.

The solution of the initial-value problem for these equations was the main task of the general theory. Therein, an expression for the Fourier-Laplace transform of $\tilde{\psi}$,

$$\xi(\tau, \epsilon) = \int_0^\infty dt \int_{-\infty}^{+\infty} dy \exp(i\epsilon y - \tau t)\tilde{\psi} \quad (3)$$

was obtained

$$\xi(\tau, \epsilon) = W(\tau, \epsilon)/V(\tau, \epsilon), \quad (4)$$

$$V(\tau, \epsilon) = \int_0^\infty \boldsymbol{\theta}(x, \tau, \epsilon)\cdot\mathbf{A}_x^{-1}(x)\cdot[\tau\mathbf{g}_t(x) + i\epsilon\mathbf{g}_y(x)]\,dx - \boldsymbol{\theta}(0, \tau, \epsilon)\cdot[\tau\mathbf{h}_t + i\epsilon\mathbf{h}_y].$$

The initial data are contained in $W(\tau, \epsilon)$, which is not displayed here. The vector function $\boldsymbol{\theta}$ is defined by the differential equations,

$$d\boldsymbol{\theta}/dx = -\mathbf{P}'(x, \tau, \epsilon)\cdot\boldsymbol{\theta}, \quad (5)$$

$$\mathbf{P}(x, \tau, \epsilon) = -\mathbf{A}_x^{-1}\cdot[i\epsilon\mathbf{A}_y + \tau\mathbf{I} + \mathbf{B}],$$

(the prime denoting the transpose matrix) sub-

ject to the condition of boundedness for Re $(\tau) > 0$,

$$\theta(x, \tau, \epsilon) = O(1), \qquad \text{as } x \to \infty. \qquad (6)$$

Since the time dependence of the shock distortion $\tilde{\psi}(y, t)$ is to be obtained from the inverse transform of $\xi(\tau, \epsilon)$ it is the singularities of $\xi(\tau)$ which will determine stability. Roots of V, $\tau_k(\epsilon)$, having positive real parts will contribute exponentially growing Fourier component of $\tilde{\psi}$, $\exp[\tau_k(\epsilon)t]$, while those with negative real parts will contribute exponential damping.

Essential to obtaining the roots of V is the solution $\boldsymbol{\theta}$ of Eqs. (5) and (6). Since the coefficient matrix $\mathbf{P}$ is ordinarily a function of x, whence no general prescription for obtaining solutions is available, numerical determination of $\boldsymbol{\theta}$ would appear necessary.

In addition to determining whether or not the steady flow is stable, the actual values of the roots of $V(\tau)$ are also important, for in the time-dependent, exponential components of $\tilde{\psi}$, the real part of τ_k is seen to be the inverse of a characteristic time for the system, the imaginary part being a time frequency. To estimate the magnitude of these quantities, we turn to the differential equations (5) to study the dependence of $\boldsymbol{\theta}$ (and hence V) on τ. The behavior of $\boldsymbol{\theta}$ is determined by the behavior of $\mathbf{P}$ with τ, whence the matrix sum,

$$\tau\mathbf{I} + i\epsilon\mathbf{A}_y + \mathbf{B},$$

is fundamental. Now in the general theory it was shown that for given ϵ, $V(\tau, \epsilon)$ has no roots for $|\tau|$ sufficiently large. That is, neither of the time constants, $1/\mathrm{Re}\ (\tau_k)$ and $1/\mathrm{Im}\ (\tau_k)$, can be small relative to *both* the spatial frequency *and* matrix $\mathbf{B}$. (Throughout, the magnitude of a matrix will refer to the maximum norm of its elements.) It can be similarly shown that if $|\tau|$ is of order ϵ while $\mathbf{B}$ is negligible, the nonconstancy of $\mathbf{A}_x$ and $\mathbf{A}_y$ can also be neglected (following from the fact that $\mathbf{B}$ contains the gradients of $\mathbf{A}_x$ and $\mathbf{A}_y$). Any roots of V for such values of τ and ϵ will be characteristic of a uniform, nonreactive flow and hence of the shock itself,[6] rather than the reactive flow. Therefore, disturbances of large spatial frequency ϵ (relative to $\mathbf{B}$) have no time constant of order $1/\epsilon$ of interest for detonation stability. Whether roots τ_k of the magnitude of $\mathbf{B}$ occur for such large ϵ is not known. In any case, we see that only for τ of order $\mathbf{B}$ are roots of V to be found which are characteristic of the reactive nature of the flow. It would appear more useful, then, to look for roots of V on the basis of the magnitude of the time scale $1/\tau$ relative to $\mathbf{B}$, rather than on the basis of spatial frequency ϵ.

Square-Wave Detonation Structure

In order to apply the results of the last section to a specific case, it is seen that the matrices $\mathbf{A}_x$, $\mathbf{A}_y$, and $\mathbf{B}$ which depend upon the unperturbed flow are required. Although in general the steady flow varies from point to point in a manner determined by the rate functions for the various chemical reactions, it is believed that this variation tends in practice to follow, more or less, the square-wave pattern, as sketched in Fig. 1. Since the main portion of the change in, say, the pressure occurs over a relatively narrow portion of the profile, this square-wave structure suggests the idealization whereby the steady flow is *uniform* within each of three zones with discontinuous changes across the shock and reaction fronts (see Fig. 1). As noted in the last section, the stability analysis for a steady flow which is uniform is greatly simplified from the general case. It will be our purpose to investigate the validity of this idealization.

Structure of square-wave type can be obtained analytically through consideration of a one-reaction detonation with an Arrhenius rate constant. In the limit of large activation energy, the steady state detonation equations will be shown to have a solution of the form displayed in Fig. 1. In addition, however, we shall obtain asymptotic expressions for the flow variables, which will be of importance in our consideration of stability in the square-wave limit.

We consider, then, a one-reaction detonation for which the rate equation is

$$d\lambda/dt = r = \exp(-E^{\ddagger}/RT) f(S, v, \lambda), \qquad (7)$$

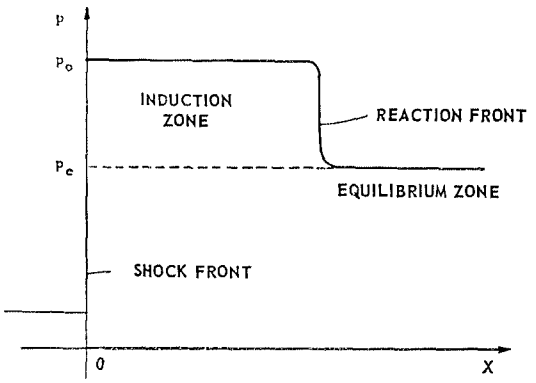

FIG. 1. Sketch of the pressure (p) profile for the square-wave model. Coordinate x measures distance from the shock; p_0 and p_e denote, respectively, the pressure behind the shock and the equilibrium pressure.

where f is a thermodynamic function, independent of the activation energy $E^\ddagger$. To obtain the steady state solution for any detonation velocity, we follow the usual procedure[5] of determining the thermodynamic and hydrodynamic variables as functions of the progress variable λ through the steady Rankine-Hugoniot relations which hold between all points in the steady flow. Thus, we assume the functions,

$$\begin{aligned} T &= T(\lambda), \\ S &= S(\lambda), \\ v &= v(\lambda), \\ u &= u(\lambda), \\ f &= f(\lambda), \end{aligned} \tag{8}$$

to be determined for all accessible values* of λ. These functions are, of course, double-valued, in accordance with the frozen subsonic and supersonic intersections of the Rayleigh line with the frozen-composition Hugoniots. In the sequel, we refer only to the subsonic branches of these functions. It is to be noted that the activation energy does not enter into these expressions.

For detonation velocities not less than the equilibrium Chapman-Jouguet value, the function f, appearing in the rate equation, will have at least one zero on the λ axis, i.e., the points of chemical equilibrium for the selected detonation velocity. We denote the high-pressure point by λ_e and assume that the solution of the rate equation, beginning at the shock with $\lambda = 0$, terminates at λ_e at an infinite distance from the shock.

We introduce, now, one additional assumption, namely that the temperature T is a monotonically increasing function of λ up to a maximum T_m at $\lambda_m < \lambda_e$, and is monotonically decreasing for $\lambda > \lambda_m$. However, we assume that $T_e > T_0$ (throughout this section, we shall use subscripts $_0$, $_m$, and $_e$ to denote evaluation at $\lambda = 0$, λ_m, and λ_e, respectively). This assumption, though to our knowledge not proved in general, appears not to be unreasonable, holding for an exothermic ideal-gas reaction.[7] In any case, it is expected that the asymptotic analysis which follows could be equally well applied under other conditions on $T(\lambda)$, with many of the structural features remaining unchanged.

Using the above assumptions, we examine the solution of the x-λ rate equation,

$$d\lambda/dx = \exp\left[-E^\ddagger/RT(\lambda)\right]\left[f(\lambda)/u(\lambda)\right], \tag{9}$$

asymptotically as $E^\ddagger$ becomes large. It is informative to make contact with the square-wave model at the outset and define an induction-zone length through the computation of x as a function of λ,

$$x(\lambda) = \int_0^\lambda \exp\,(E^\ddagger/RT)\,(u/f)\,d\lambda'. \tag{10}$$

For $\lambda = \lambda_e$, as implied earlier, the integral does not exist for any value of the activation energy, while (for fixed $E^\ddagger$) for λ $(0 < \lambda < \lambda_e)$, however, the integral on the right of Eq. (10) has a well-known asymptotic expansion[8] in $E^\ddagger$, independent of the value of the upper limit of the integral, *viz.*,

$$\begin{aligned} x(\lambda) &= (u/r\kappa)_0\left[1 + O(1/\kappa_0)\right], \\ \kappa &= aE^\ddagger/RT, \\ a &= d\ln T/d\lambda. \end{aligned} \tag{11}$$

Asymptotically in $E^\ddagger$, then, the reaction proceeds only in the neighborhood of the reaction front located at the "induction-zone length,"

$$x^* = (u/\kappa r)_0, \tag{12}$$

the extent of this neighborhood, relative to x^*, diminishing as $1/E^\ddagger$. The "induction time" can similarly be defined, through the asymptotic determination of $t(\lambda)$ from Eq. (7), to be

$$t^* = x^*/u_0. \tag{13}$$

It is to be remembered that κ, which appears frequently in the sequel, is proportional to $E^\ddagger$.

Induction-Zone Solution. We turn now to the determination of λ as a function of distance, considering first the induction zone lying between the shock and reaction fronts. For convenience, we introduce a reduced coordinate $z = x/x^*$ for which the rate equation becomes,

$$\begin{aligned} d\lambda/dz &= F, \\ F &= (fu_0/\kappa_0 f_0 u)\,\exp\left[E^\ddagger(1 - T_0/T)/RT_0\right]. \end{aligned} \tag{14}$$

The induction-zone solution is determined through the Taylor series expansion of $\lambda(z)$ about $z = 0$,

$$\lambda(z) = \sum b_i z^i. \tag{15}$$

The coefficients b_i are determined by repeated differentiation of Eq. (14) at $z = 0$, whereby it follows that,

$$b_i = \kappa_0^{-1}\left[1/i + O(1/\kappa_0)\right]. \tag{16}$$

Rearrangement of the convergent series, Eq. (15), to collect the leading terms in $E^\ddagger$, leads to

* Accessible values of λ are defined in reference 5 as those values for which the partial Hugoniot intersects the Rayleigh line.

the asymptotic result,

$$\lambda(z) = -\kappa_0^{-1} \ln (1 - z) + O(1/\kappa_0^2), \quad (17)$$

valid for all $z < 1$. Equation (17) represents the induction-zone behavior of λ in the square-wave limit.

Reaction-Zone Solution. The reaction proceeds, as we have seen, only in the neighborhood of $z = 1$. We designate this region as the reaction zone and consider now the nature of the solution therein. It turns out to be more convenient from this point on to compute z as a function of λ rather than the inverse.

From the differential equation (14), $z(\lambda)$ can be written as the integral,

$$z(\lambda) = z_m + \int_{\lambda_m}^{\lambda} F^{-1}(\lambda')\, d\lambda', \quad (18)$$

where z_m is defined through $x(\lambda_m)$, given by Eq. (10). The precise value of z_m is not determined by the analysis, although, of course, it differs from unity by a term of order $1/E^\ddagger$ [see Eq. (11)]. Yet $z(\lambda) - z_m$ will ordinarily be a more strongly decreasing function of $E^\ddagger$, so that in the following, the analysis shall provide asymptotic expressions for $z(\lambda) - z_m$, rather than for $z(\lambda)$ itself; indeed $z(\lambda)$ is asymptotically given by Eq. (11) to be unity.

The utility of selecting λ_m as the initial point for the integral Eq. (18) lies in the occurrence of the temperature maximum at this point. For the *exponential part* of the integrand has, for arbitrary λ, its greatest values (over the range of the integration) at the end point λ only when the integration path does not cross the point of maximum temperature. The integral can, then, be evaluated routinely,[8] provided $\lambda < \lambda_e$ and $\lambda \neq \lambda_m$, to be

$$z(\lambda) - z_m = -(a_0 T u f_0 / a T_0 u_0 f) \times \exp\left[-E^\ddagger (1 - T_0/T)/RT_0\right]\left[1 + O(1/\kappa f)\right] \quad (19)$$

where T, u, a, f, and κ are evaluated at λ.

The order expression for the remainder in this equation applies to a fixed value of λ within the stated range. It is seen, however, that, as λ approaches λ_m and λ_e, this order expression becomes (for fixed $E^\ddagger$) proportional to $1/\lambda - \lambda_m$) and $1/(\lambda - \lambda_e)$, respectively.* How near λ can be to each of these points, for the leading term in Eq. (19) to remain valid, must be investigated separately.

Near the point of maximum temperature, Eq. (19) loses its validity both because a is small and because the range of integration is small. To investigate the range of $\lambda - \lambda_m$ for which this result remains valid, it is necessary to transform the integration variable in Eq. (18) relative to $\lambda - \lambda_m$, so that a fixed range of integration is obtained. It can be shown, then, that the leading term in Eq. (19) remains dominant provided λ lies outside any ϵ_m-neighborhood of λ_m satisfying,

$$1/\epsilon_m(E^\ddagger) = o\left[(E^\ddagger)^{\frac{1}{2}}\right], \quad (20)$$

e.g.,

$$\epsilon_m = l_m(\ln E^\ddagger)/(E^\ddagger)^{\frac{1}{2}}.$$

Near the equilibrium point, the interval for the integration of Eq. (18) becomes constant as $\lambda - \lambda_e$ approaches zero. It can be shown then that Eq. (19) remains valid outside any ϵ_e-neighborhood for which $1/(\kappa f)$ approaches zero as $E^\ddagger \to \infty$, *viz.*,

$$1/\epsilon_e(E^\ddagger) = o(E^\ddagger). \quad (21)$$

It is of interest to observe that Eq. (19) predicts that $z(\lambda) \to z_m$, except for $\lambda = 0$ and λ_e. (It can, in fact, be readily shown that Eq. (19) includes the induction-zone solution, Eq. (17).) Even those λ near λ_e,

$$\lambda - \lambda_e = -\, l_e \ln E^\ddagger / E^\ddagger$$

[for which Eq. (21) is satisfied] "belong" to the reaction front. It will be seen later that those λ for which the flow is truely equilibrium are much closer to λ_e.

Near λ_m, it was seen that Eq. (19) is not valid. In order to find the behavior of the solution within this gap, we consider the Taylor series expansion,

$$z(\lambda) - z_m = F_m^{-1} \sum a_i (\lambda - \lambda_m)^i, \quad (22)$$

obtaining coefficients through straightforward differentiation of $1/F$,

$$a_1 = 1, \quad (23)$$
$$2a_2 = \left[d \ln (u/f)/d\lambda\right]_m,$$
$$a_{2n} = O\left[(E^\ddagger)^{n-1}\right],$$
$$a_{2n+1} = O\left[(E^\ddagger)^n\right].$$

For $|\lambda - \lambda_m| \leq \epsilon_i$, where ϵ_i satisfies

$$\epsilon_i(E^\ddagger) = o\left[(E^\ddagger)^{-\frac{1}{2}}\right], \quad (24)$$

Eq. (22) yields asymptotically,

$$z(\lambda) - z_m = (\lambda - \lambda_m) F_m^{-1}\left[1 + o(1)\right]. \quad (25)$$

* We restrict attention in the remainder of this section to detonation velocities greater than the equilibrium Chapman–Jourguet value. At the latter value, the assumed linear relation between f and $(\lambda - \lambda_e)$ is instead a quadratic one.

Within the inner part of the reaction zone, the rate is maximum and constant, with Eq. (24) defining the extension along the λ axis of the constant behavior.

The inner solution, Eq. (25), does not "fill" the gap in Eq. (19) [compare Eqs. (24) and (20)], so that a complete description has not been obtained. We shall not here attempt to remedy this deficiency.

Equilibrium-Zone Solution. Although the description of the reaction zone is also incomplete in that the rate is yet unbounded in $E^\ddagger$ at the equilibrium end of Eq. (19), the remainder of the detonation profile can be obtained through a single expression which we designate as the equilibrium-zone solution.

From the general theory of steady detonations,[5] the asymptotic behavior of $z(\lambda)$ as $(\lambda - \lambda_e)$ approaches zero (fixed $E^\ddagger$) is known to be that of a logarithmic singularity, namely

$$z(\lambda) \sim -k^{-1} \ln (\lambda - \lambda_e) \qquad (26)$$
$$k = -[F\, d \ln f/d\lambda]_e > 0.$$

It can be shown, however, that this result does not match the reaction-zone solution, Eq. (19), for at the boundary of the latter the first correction term to Eq. (26) is dominant in the limit of large $E^\ddagger$.

We derive now a generalization of Eq. (26) through the expression of the right-hand side of the rate Eq. (14) directly in terms of $(\lambda - \lambda_e)$. Using the power series expansions

$$1 - T_e/T = a_e(\lambda - \lambda_e)[1 + d(\lambda - \lambda_e) + \cdots]$$
$$f = (df/d\lambda)_e(\lambda - \lambda_e)[1 + b(\lambda - \lambda_e) + \cdots],$$
$$u = u_e[1 + c(\lambda - \lambda_e) + \cdots],$$

we obtain

$$F = -k(\lambda - \lambda_e)$$
$$\times \exp[\kappa_e(\lambda - \lambda_e)]\{1 + O[\kappa_e(\lambda - \lambda_e)^2]\}. \qquad (27)$$

For λ within the ϵ_e-neighborhood [see Eq. (21)] of λ_e,

$$\epsilon_e = l_e \ln E^\ddagger/E^\ddagger, \qquad (28)$$

the correction vanishes asymptotically in $E^\ddagger$. The rate equation can then be integrated in terms of the exponential integral,[9] yielding,

$$z(\lambda) - z_1 = -k^{-1}\{\mathrm{Ei}[-\kappa_e(\lambda_1 - \lambda_e)]$$
$$-\mathrm{Ei}[-\kappa_e(\lambda - \lambda_e)]\}[1 + o(1/\kappa_e)]. \qquad (29)$$

The initial point for the integration $z_1 = z(\lambda_1)$ is presumed to be determined through Eq. (19), at any point λ_1 for which Eq. (27) is valid. Equation (29), then, matches the reaction-zone solution, while carrying the solution to $\lambda = \lambda_e$. In the latter limit, the exponential integral has the logarithmic singularity of Eq. (26). The magnitude of the neighborhood of λ_e for which $z(\lambda)$ does not approach z_1 can also be seen from the logarithmic behavior of the Ei at zero. Since k increases exponentially with $E^\ddagger$, it is seen that $z(\lambda) \to z_1$ unless $(\lambda - \lambda_e)E^\ddagger$ becomes zero as the *exponential of an exponential in* $E^\ddagger$.

Stability Considerations

In this section, we investigate the form of the stability equations of the General Stability Analysis for the steady-state flow derived in the previous section. In particular, we are concerned with the determination of the relevance of the terms appearing in the differential equations (5), from which $\boldsymbol{\theta}(x, \tau, \epsilon)$ is to be determined. We shall discuss, then, the behavior of the matrices $\mathbf{A}_x$, $\mathbf{A}_y$, and $\mathbf{B}$ within the various zones of the steady solution. In addition, two-front stability analysis of Zaidel will be examined critically.

Before initiating the discussion, it is convenient to transform the General Stability Analysis equations to independent variables in which distance is measured in units of x^*, *and* time in units of t^*, Eqs. (12) and (13). Then Eqs. (5) become,

$$d\boldsymbol{\theta}/dz = -\mathbf{P}'(z, \tau, \epsilon)\cdot\boldsymbol{\theta}, \qquad (30)$$
$$\mathbf{P}(z, \tau, \epsilon) = -\mathbf{A}_x^{-1}\cdot[i\epsilon\mathbf{A}_y + \tau\,\mathbf{I} + \mathbf{B}],$$

where $\mathbf{A}_x$ and $\mathbf{A}_y$ are now $1/u_0$ times their former values and $\mathbf{B}$ has been increased by a factor t^*. The Fourier- and Laplace-transform parameters ϵ and τ are now x^* and t^*, respectively, times their former values.

Since the relative constancy of the matrices $\mathbf{A}_x$ and $\mathbf{A}_y$ is important, we compute their derivatives within each zone of the flow. Since $\mathbf{A}_x$ and $\mathbf{A}_y$ contain flow variables alone, e.g., u and v, it is observed that the gradient,

$$d\mathbf{A}_x/dz = (d\mathbf{A}_x/d\lambda)\,F, \qquad (31)$$

depends upon $E^\ddagger$ only through the rate F at the point in question.

The matrix $\mathbf{B}$, on the other hand, involves both the gradients themselves and the thermodynamic partial derivatives of the entropy production and the rate. The former terms are of order F, while the partial derivative terms are computed explicitly to have the form,

$$-\frac{x^*\phi_v}{u} = \left[\frac{\partial(\Delta F/T)}{\partial v}\right]_{s,\lambda} F + \frac{\Delta F}{T}\frac{x^* r_v}{u}, \qquad (32a)$$

$$\frac{x^* r_v}{u} = \frac{E^\ddagger}{RT^2}\left(\frac{\partial T}{\partial v}\right)_{s,\lambda} F + F\left(\frac{\partial \ln f}{\partial v}\right)_{s,\lambda}, \qquad (32b)$$

where ϕ is the entropy production, $-(\Delta F)r/T$, and ΔF (not to be confused with the reduced rate F) is the free energy increment. Similar expressions hold for the S and λ derivatives. These derivatives dominate the gradient terms of $\mathbf{B}$, for, away from equilibrium, the first term in Eq. (32b) is of order $E^\ddagger$ relative to F, while, at equilibrium, F vanishes, but the second term in Eq. (32b) is nonzero.

We turn now to the consideration of the various zones of the steady flow.

Induction Zone. Within this zone, we obtain the rate F through differentiation of Eq. (17),

$$F = RT_0/a_0E^\ddagger(1 - z). \tag{33}$$

Hence for $0 \leq z < 1$, $\mathbf{A}_x$ and $\mathbf{A}_y$ are constant to terms of order $1/E^\ddagger$, while $\mathbf{B}$ is, by virtue of Eq. (32), variable with z and of order 1 in $E^\ddagger$. Explicitly, one obtains,

$$\mathbf{B} = -(1 - z)^{-1}\mathbf{B}^{(o)}, \tag{34}$$

where $\mathbf{B}^{(o)}$ has nonzero elements in rows 4 and 5. Row 5 is found to have elements,

$$\begin{aligned}
\mathbf{B}_{51}{}^{(o)} &= a_0^{-1}(\partial T_0/\partial v)_{S,\lambda} \qquad (35)\\
\mathbf{B}_{52}{}^{(o)} &= \mathbf{B}_{53}{}^{(o)} = 0\\
\mathbf{B}_{54}{}^{(o)} &= a_0^{-1}(\partial T_0/\partial S)_{v,\lambda}\\
\mathbf{B}_{55}{}^{(o)} &= a_0^{-1}(\partial T_0/\partial \lambda)_{S,v}
\end{aligned}$$

while row 4 is $-(\Delta F/T)_0$ times row 5.

Consider now the sum of three matrices appearing in $\mathbf{P}$. It is observed that for τ and ϵ of order 1 in $E^\ddagger$, $\mathbf{B}$ is a nonnegligible part of $\mathbf{P}$ and $\mathbf{P}$ is *not constant*. The analysis of Zaidel[3] leads to roots τ for τ and ϵ of precisely the above magnitude but ignores $\mathbf{B}$ in the induction zone. Only for τ large relative to unity, say proportional to $E^\ddagger$, can $\mathbf{B}$ be ignored in this zone.

Equilibrium Zone. The equilibrium-zone solution derived in the Square-Wave Detonation section is of transitional type. At the head of the equilibrium zone, the flow is a continuation of the reaction zone, for the rate becomes infinite with $E^\ddagger$ and the reaction proceeds through small changes in z. For z any finite value larger than z_m, on the other hand, the flow becomes, for sufficiently large $E^\ddagger$, one of exponential decay to equilibrium. For present purposes, we shall consider only the latter part to constitute the equilibrium zone. The rate here is, of course, vanishingly small and $\mathbf{B}$ is dominated by the second terms in Eq. (32b). Thus $\mathbf{B}$ becomes

$$\mathbf{B} = -(u_e/u_0)(F/f)_e\mathbf{B}^{(e)} \tag{36}$$

where $\mathbf{B}^{(e)}$ has the nonzero elements,

$$\begin{aligned}
\mathbf{B}_{51}{}^{(e)} &= (\partial f/\partial v)_{S,\lambda}, \qquad (37)\\
\mathbf{B}_{54}{}^{(e)} &= (\partial f/\partial S)_{v,\lambda},\\
\mathbf{B}_{55}{}^{(e)} &= (\partial f/\partial \lambda)_{S,v},
\end{aligned}$$

all evaluated at $\lambda = \lambda_e$.

In the region $z > 1$, then, $\mathbf{P}$ is truely a constant matrix, the eigenvalues and eigenvectors of which determine $\boldsymbol{\theta}(z, \tau, \epsilon)$.

It is of interest to note the dependence of $\mathbf{B}$ on $E^\ddagger$ to be

$$\mathbf{B} = O\left\{\frac{1}{E^\ddagger}\exp\left[\frac{E^\ddagger}{RT_0}\left(1 - \frac{T_0}{T_e}\right)\right]\right\}. \tag{38}$$

Values of $\mathrm{Re}(\tau)$ of this order in $E^\ddagger$ correspond then to times t (in units of t^*) of the order one over this quantity, which, in turn, is of the magnitude of the relaxation time for small disturbances from equilibrium.

Reaction Zone. Within the reaction zone itself, $\mathbf{A}_x$ and $\mathbf{A}_y$ are not constant, varying with z at the rate F, which takes on values up to a maximum near z_m. $\mathbf{B}$ is again dominated by terms of order $E^\ddagger F$. In addition F varies rapidly with z except in the "inner" zone of the reaction front where it remains constant and maximum. The possibility of integrating Eqs. (30) through the reaction zone, for arbitrary values of τ, indeed seems remote.

Two-Front Model. The discontinuous nature of the solution across the reaction front has led Zaidel[3] to join solutions on either side through Rankine-Hugoniot shock relations, with the perturbation in the position of the reaction front being introduced as an additional unknown. Through a heuristic argument, this perturbation is expressed in terms of the perturbation in the shock position and the state variable perturbation between the two fronts. The final expression for $V(\tau, \epsilon)$ can be written in the form,

$$V = s_1(\tau, \epsilon)\exp\left[\mu(\tau, \epsilon)\right] + s_2(\tau, \epsilon) \times \exp\left[\nu(\tau, \epsilon)\right] + s_3(\tau, \epsilon). \tag{39}$$

Certain of the roots of V were examined by Zaidel, but another class of roots will be shown to exist, and to have serious implications with respect to the validity of the whole approach.

In order that $\xi(\tau)$ in Eq. (4) have an inverse Laplace transform, a necessary condition[10] is that there exists a right half-plane, $\mathrm{Re}(\tau) > \omega_0$, in which $\xi(\tau)$ is analytic. However, it will be demonstrated that Eq. (39) has zeroes in every right half-plane, whence ξ is not a Laplace transform. Thus the two-front stability problem, with the reaction front coupled to the shock

front by the Zaidel prescription, has no solution of exponential order in the time.* As to whether the initial-value problem (corresponding to that of the section on General Stability Analysis, but with the two fronts specified) is properly posed, it cannot be concluded, but the Laplace-transform (or normal-modes) approach to the problem is certainly not justified.

To demonstrate these ever-present roots of Eq. (39), it suffices to consider the one-dimensional form of V, obtained by setting $\epsilon = 0$. (The proof for arbitrary ϵ is not difficult.) For one-dimensional disturbances, Eq. (39) becomes (see ref. 3),

$$\epsilon^3 V = i\tau^3 L(\tau), \tag{40}$$

$$L(\tau) = a + b\tau + ce^{g\tau} + de^{h\tau},$$

with a, b, c, d, g, and h all real functions of the unperturbed flow, with g and h positive. For a given steady flow, all are fixed. The precise nature of these quantities is unimportant but without loss of generality, it is assumed that $h > g$ and that b and d are positive, the justification for the latter assumption being discerned from the argument which follows.

Separating L and τ into real and imaginary parts, we obtain,

$$\tau = \omega + i\sigma, \tag{41}$$

$$\text{Re } (L) = a + b\omega + ce^{g\omega} \cos g\sigma + de^{h\omega} \cos h\sigma,$$

$$\text{Im } (L) = b\sigma + ce^{g\omega} \sin g\sigma + de^{h\omega} \sin h\sigma.$$

In examining the roots of both the real and imaginary parts of L and their dependence on τ, it suffices to consider only values of ω sufficiently large that the exponential in $g\omega$ is small relative to that in $h\omega$. Then Re (L) is dominated by the final term on the right in Eq. (41), so that Re (L) has a root in the neighborhood of each root of $\cos h\sigma$,

$$\sigma_n = (n + \tfrac{1}{2})\pi/h. \tag{42}$$

With increasing ω, each root of Re (L) is then bounded in σ, approaching the limiting values σ_n.

A proof will now be sketched, showing that Im (L) has roots which vary continuously with ω so as to intersect a Re (L) root to the right of any ω_0, no matter how large. Define the locus Γ in the τ plane to contain the points,

$$\sigma = (d/b)e^{h\omega}. \tag{43}$$

For points above Γ, it is observed that Im (L) is dominated by the linear term in σ. Hence Im (L) is positive in this region, except in the neighborhood of those Γ-points $\tau_n{}^*$ for which the first and last terms of Im (L), Eq. (41), sum to zero, *viz.*,

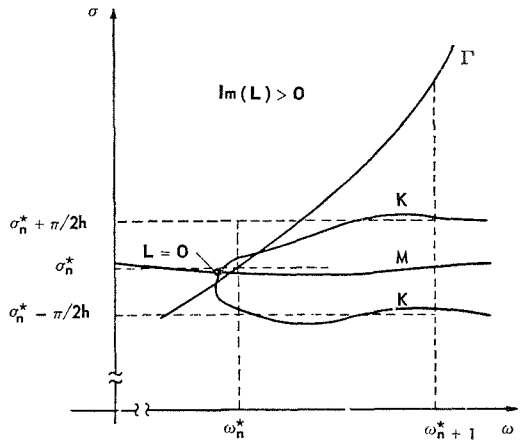

FIG. 2. The roots of L, Eq. (40), for large values of $\text{Re}(\tau) = \omega$, $\text{Im}(\tau) = \sigma$, are obtained from the intersection of curve K, on which $\text{Im}(L) = 0$, with curve M, on which $\text{Re}(L) = 0$.

$$\sigma_n{}^* = (2n + \tfrac{3}{2})\pi/h \tag{44}$$

$$\tau_n{}^* = \omega_n{}^* + i\sigma_n{}^*.$$

An enumerably infinite set of such points occur to the right of any ω_0. It is readily shown then that a locus K of roots of Im (L) passes through the neighborhood of $\tau_n{}^*$ with positive slope. With increasing ω, this curve is readily seen to lie above the line $\sigma = \sigma_n{}^*$ and, in fact, to approach asymptotically,

$$\sigma_n{}^{(1)} = \sigma_n{}^* + \pi/2h \tag{45}$$

With decreasing ω, on the other hand, the root is seen from Eq. (41) to remain above

$$\sigma_n{}^{(2)} = \sigma_n{}^* - \pi/2h, \tag{46}$$

and, therefore, to the right of Γ. It can then be shown that the curve K has the C-shape shown in Fig. 2, in which the lower branch approaches $\sigma_n{}^{(2)}$. Since the point of vertical slope, τ_n, satisfies

$$\text{Re } (\tau_n) > \omega_{n-1}{}^*,$$

it follows that the Re (L) root which approaches σ_{2n+1}, Eq. (42), crosses K, as illustrated in Fig. 2.

Discussion

It has been seen that the stability analysis of the square-wave model of Shchelkin and Zaidel breaks down on two counts. With regard to the

* In fact, the "generalization" of the theory of reference 4 to include the specification of a second "reaction" front, defined as the point of maximum rate, leads to precisely this same difficulty.

nonconstancy of $\mathbf{P}$ in the induction zone, it is important to reemphasize that this is only associated with values of τ (in units defined in the preceding section) of order unity in $E^{\ddagger}$. Regarded from the point of view of a shorter time scale (larger τ), the variation of $\mathbf{P}$ with distance vanishes.

The selection of a time scale for the square-wave model is, however, determined at the outset by the treatment of the reaction zone as a shock discontinuity, for then the structure of this zone is ignored and the only unit of time available is the time of flight from the shock front to the reaction front.

Even if the variation of $\mathbf{P}$ within the induction zone were taken into account, the improper behavior of V with τ remains for as τ becomes large, the V of Eq. (39) is obtained. In lieu of a proof that some roots of V are meaningful while others are extraneous, the two-front approach must be abandoned. Thus the task of determining V for τ commensurate with the induction-zone length appears hopeless, without numerical integration of the equations for $\boldsymbol{\theta}$ throughout the entire flow.

A change of approach is, however, suggested by the discussion of the General stability equations, which indicated that the largest value of τ for which $V(\tau, \epsilon)$ can vanish is for $\mathbf{B}$ nonnegligible relative to τ. If, then, the differential equations are solved for τ of the order of $\mathbf{B}_m$, rather than the minimum $\mathbf{B}$ as in the two-front approach, the difficulties of the model calculation are removed. Instead the differential equations must be solved through the generally difficult reaction zone, but the simplification that the rate is constant near the maximum rate point could conceivably lead to a tractable problem.

Acknowledgments

The author is deeply indebted to Dr. W. W. Wood of this laboratory and Professor Z. W. Salsburg of Rice University who investigated the stability of the square-wave model before the paper by Zaidel came to our attention. The proof of the existence of the improper roots of V in the model calculation is due to Dr. Wood. This work was performed under the auspices of the U. S. Atomic Energy Commission.

Appendix

The matrices and vectors of the differential equations of the second section are given here. The $\mathbf{A}$ matrices are (for perturbations given in the order v, u_x, u_y, S, λ),

$$\mathbf{A}_x = u\mathbf{I} + \mathbf{A}_2, \qquad \mathbf{A}_y = \mathbf{A}_3, \tag{A.1}$$

where $\mathbf{A}_i$ has nonzero elements,

$$(\mathbf{A}_i)_{1i} = -v, \qquad (\mathbf{A}_i)_{i1} = c_0^2/v, \qquad (\mathbf{A}_i)_{i4} = vp_S, \qquad (\mathbf{A}_i)_{i5} = vp_\lambda. \tag{A.2}$$

Here p denotes pressure, c_0 is the frozen sound speed, and subscripts S, v, or λ denote partial differentiation, holding the remaining two variables fixed.

The matrix $\mathbf{B}$ is,

$$\mathbf{B} = \begin{bmatrix} -u' & v' & 0 & 0 & 0 \\ p' - v(c_0^2/v)' & u' & 0 & vp_S' & vp_\lambda' \\ 0 & 0 & 0 & 0 & 0 \\ -\phi_v & S' & 0 & -\phi_S & -\phi_\lambda \\ -\mathbf{r}_v & \lambda' & \mathbf{0} & -\mathbf{r}_S & -\mathbf{r}_\lambda \end{bmatrix} \tag{A.3}$$

where $(')$ denotes differentiation with respect to x. The symbol ϕ denotes the entropy production, $-\boldsymbol{\Delta} F \cdot \mathbf{r}/T$. The $\mathbf{g}$'s are,

$$\mathbf{g}_t = -(\text{column 2 of } \mathbf{B}), \tag{A.4}$$

$$(\mathbf{g}_y)_3 = -vp', \tag{A.5}$$

with all other elements of $\mathbf{g}_y$ identically zero.

The vectors and matrix of the Rankine-Hugoniot relations are not given here. The reader is referred to the general theory[4].

References

1. See, for example: White, D. R.: Phys. Fluids *4*, 465 (1961).
2. Shchelkin, K. I.: J. Expt. i Theoret. Phys. (U.S.S.R.) *36*, 600 (1959); translation: Soviet Phys—JETP *9*, 416 (1959).
3. Zaidel, R. M.: Doklady Akad. Nauk S.S.S.R. *136*, 1142 (1961); translation: Proc. Acad. Sci. U.S.S.R., Phys. Chem. Sec., *136*, 167 (1961).
4. Erpenbeck, J. J.: Phys. Fluids *5*, 604 (1962).
5. Wood, W. W. and Salsburg, Z. W.: Phys. Fluids *3*, 549 (1960).
6. Erpenbeck, J. J.: Phys. Fluids *5*, 1181 (1962).
7. Doering, W. and Burkhardt, G.: *Contributions to the Theory of Detonations*, Technical Report No. F-TS-1227-IA (GDAM A9-T-46), Wright-Patterson Air Force Base, Dayton, Ohio, 1949, p. 187.
8. Erdelyi, A.: *Asymptotic Expansions*, pp. 36–39, Dover Publications, Inc., 1956.
9. Jahnke, A. and Emde, F.: *Tables of Functions*, pp. 1–3, Dover Publications, Inc., 1945.
10. Widder, D. V.: *The Laplace Transform*, p. 57, Princeton University Press, 1946.

Discussion

PROFESSOR J. A. FAY (*M.I.T.*): There is little doubt that the stability of the gaseous detonation wave is the major theoretical problem of the fluid mechanical aspects of the gaseous detonation wave. Considering the experimental evidence which has been accumulated within the past few years concerning the structure of the detonation front, the problem of stability appears to be more pertinent to the interpretation of these experiments than does the problem of the exact solution of the plane steady detonation front. It is therefore encouraging to see the attempts being made both in the USSR and the US to treat this problem.

I have proposed[1] a somewhat different approach to the problem of stability than that of the author which leads to a difference in our interpretation of Eq. (39). While the author treats the problem as an initial value problem to be solved through the use of the Fourier-Laplace transform and its subsequent inversion, I prefer to regard it in the classical manner of boundary layer instability theory. In this latter approach, for the perturbation to the basic flow, one assumes a sinusoidal disturbance in space in the direction parallel to the wave front, and seeks to determine an eigenfunction which describes the disturbance variation in a direction normal to the wave front and an eigenvalue for the complex time frequency. While there is a continuous spectrum of eigenfunctions and their associated eigenfrequencies, one tends first to look for those corresponding to neutral (that is, unamplified) disturbances, or those whose wavelength is comparable to the reaction zone thickness. While the determination of the eigenfunction and eigenvalues is straightforward, it is by no means trivial since it involves the solution of a nonlinear high order differential equation for which spurious solutions must be eliminated or avoided. However, the general pattern has been set by the analogous problem in viscous flow instability and perhaps should be used as a guide.

My interpretation of Eq. (39) is that this form is only suitable for frequencies comparable to the reciprocal of the induction time. The fact that this function has zeros for very large frequencies introduces a mathematical difficulty only if one insists on inverting a Laplace transform, but does not invalidate its usefulness as a representation for low frequencies. If one had originally posed the problem as indicated above, this difficulty would not arise when considering instabilities of moderate frequency. Since the high frequency perturbations are most likely to be stable, there does not seem to be much point in examining them in detail.

Even if the mathematical analysis of the square wave model is more tractable than the more general case, which remains to be seen, I have reservations concerning its appropriateness for the chemical systems with which one usually experiments. It would seem most likely that the initial stages of reaction involve two-body dissociative and exchange reactions which are relatively rapid, while the final stages involve three-body recombinative reactions which are relatively slow, at least for low pressures. This is certainly the nature of the relaxation process behind a strong shock wave and one should not expect great differences for the case of a strong detonation; that is, a near-stoichiometric mixture.

I agree wholeheartedly with the author's conclusion that a numerical solution to the problem will probably be required to settle many of these questions.

DR. J.J. ERPENBECK (*Los Alamos Scientific Laboratory*): The fact that Eq. (39) has "extraneous" roots τ_k with arbitrarily large real parts cannot be circumvented so simply as Professor Fay suggests. We agree, of course, that these large roots are physically meaningless, but with the occurrence of such behavior one is left with the problem of distinguishing whether a particular root (for example a $\mathrm{Re}(\tau_k) = 0$ "neutrally" stable root) is extraneous or not. There appears to be no way to make such an identification other than by performing the calculation without recourse to the model.

I would also like to point out that the square-wave detonation was investigated because of the possible simplification introduced into the stability analysis. Such a simple model cannot, of course, be expected to be generally suitable.

DR. P. KYDD (*General Electric Research Laboratory*): It seems to me that the author's model of the "square-wave" detonation is a very good one for the description of most of the common branched-chain combustion reactions which drive detonations. In these reactions there is characteristically a true chemical induction period during which the chain carrier concentration increases without releasing appreciable heat, followed by an extremely fast branching chain which generates large concentrations of free radicals, but in the case of $H_2 + O_2$ at least very little heat, and this in turn is followed by recombination of the radicals which release heat. Under conditions such that the recombination is fast relative to the induction period, not unreasonable at a high total pressure, the structure of the detonation wave will be "square" and this has been demonstrated theoretically by Duff and experimentally in shock waves through dilute combustible mixtures by Schott and Kinsey, and Kistiakowsky and Richards among others. Furthermore the length of the induction period depends on the chain

branching reaction $H + O_2 \rightarrow OH + O$ with an activation energy of 18 kcal per mole and thus is related in a particularly simple way to the temperature behind the shock. As a result this model is not only realistic, but convenient to use in studies of the stability of the wave.

PROF. D. F. HORNIG (*Princeton University*): The notion of a square wave is reasonable since in many systems, such as hydrogen-oxygen, the process is characterized by an isothermal induction period followed by heat releasing recombinations, which at high pressures are rapid.

To be sure it is a drastic simplification, but I think it may be even less realistic to use simple Arrhenius reaction rates which, except perhaps in systems like ozone, bear little relation to the real progress of the reaction.

PROF. A. K. OPPENHEIM (*University of California*): In reply to Professor Hornig I would like to throw nevertheless some doubt upon the applicability of the square-wave concept because of the inherent possibility of an oversimplification. I agree with Professor Hornig that it may be less realistic than the Arrhenius rate expression. However from the analysis we have made on the NDZ model of the detonation wave in ozone which, as contrasted to the one presented here, was not restricted to the quasi-steady-state assumption, but took into account the complete kinetic chain reaction scheme, it appears that the process is initially actually endothermic, the energy being used up for the creation of activated species (in this particular case the over-all dissociation producing atomic oxygen). Instead then of the induction period we obtain a regime of pressure and density increase before the conventional deflagration is set in. The process bears close relation in fact to the so-called von Neumann pathology.

PROF. BOA-TEH CHU (*Brown University*): It is evident that, for the linearization procedure employed by Dr. Erpenbeck to be valid, the perturbation must be "small." In practice, we are not interested in "infinitesimal" perturbations and this raises naturally the question as to how large a perturbation may be that it can still be regarded as "small."

Let us consider a sinusoidal perturbation of the type considered in the paper. The amplitude of the perturbation may be characterized in many equivalent ways. Let us characterize it by the displacement of an isothermal surface in the reaction zone. Here, the "reaction zone" is understood to mean the region where the concentration and temperature gradients are large. Referring now to Dr. Erpenbeck's paper, it is easy to see that his linearization procedure is still valid for a non-infinitesimal perturbation provided that the amplitude of the perturbation is small compared to both the wave length of the disturbance and the thickness of the reaction zone. The last condition is necessary because a displacement of the order of the magnitude of the reaction zone thickness produced by the perturbation may lead to a temperature change (at a fixed κ) of the order of the temperature rise across the reaction zone. It is on this second condition or restriction that we wish to make some comments.

It is certainly true that a stability analysis subjected to the two above stated restrictions still presents us with a mathematically meaningful problem and determines what one may call the "intrinsic" stability of the detonation wave. But is there really any physical significance in such a stability study when accidental disturbances in nature may have amplitudes of the order of the reaction zone thickness instead of being only a small fraction thereof? Furthermore, at an initial pressure of 1 atmosphere and at room temperature, the allowable displacement of an isothermal surface in the reaction zone (for Erpenbeck's analysis to be applicable) will be in the submicron range; it is, therefore, approaching the limit where a continuum theory may no longer be applied.

As pointed out earlier by Professor Fay the stability analysis proposed by Dr. Erpenbeck is similar to that for a laminar boundary layer and one may perhaps take advantage of this similarity. It is important, however, to remember that this similarity is quite limited because of the high gradients in the thin reaction zone. Except for the case of a vanishingly small perturbation, there is in fact a greater similarity between the stability of a detonation wave and the so-called generalized Helmholtz type instability in which the stability of a thin shear layer of small but nonzero thickness is in question. In such problems linearization may be achieved by introducing suitable coordinate systems which move with the thin region of transition, provided that the amplitude of perturbation is small compared to the wave length of the disturbance, even if it may be of the same order of magnitude of the reaction zone thickness.

DR. J. J. ERPENBECK: The orders of magnitude, given by Professor Chu, for the first neglected terms in the linearization, used in our analysis (see, ref. 4 of the paper), appear to be correct. Yet these magnitudes are of no special consequence with respect to the validity of the theory, over and above that implicit in any linear analysis.

In the first place, the validity of the continuum theory is not affected by the magnitude of the disturbances considered; the consideration of infinitesimal changes in physics is implicit in the use of differential and integral calculus.

The limitation of the analysis to infinitesimal disturbances, on the other hand, is a result of the

linearization, and in fact, must be imposed on any linearized theory, including that to which Professor Chu alluded at the end of his comments. However, the physical significance of the stability criterion which results from a linear analysis is not expected to be restricted to the infinitesimal domain.[2,3] Yet a mathematical theory of stability of partial differential equations to support this expectation does not, to our knowledge, exist, except perhaps in isolated instances.

References

1. Fay, J. A.: "Stability of Detonation Waves at Low Pressures," *Detonation and Two-Phase Flow*, pp. 3–16, ed. by S. S. Penner and F. A. Williams. Academic Press, 1962.
2. Lin, C. C.: *Theory of Hydrodynamic Stability*. Cambridge University Press, Cambridge, England, 1955.
3. Chandrasekhar, S.: *Hydrodynamic and Hydromagnetic Stability*. Oxford University Press, London, 1961.

REACTION ZONE AND STABILITY OF GASEOUS DETONATIONS

H. GG. WAGNER

Many experiments have been performed by various authors to measure the "thickness" of the reaction zone of gaseous detonations, i.e., the extension of the region where the main part of the chemical reaction takes place. These experiments have shown that at an initial pressure of 1 atmos the zone was too narrow to be resolved. Only in spinning detonations using modes close to the fundamental can one obtain a measure of the reaction time.

Both spin and the dependence of the detonation velocity on the flow of the burned gas seem to be closely related to the mechanism of stabilization of a detonation. If the reaction rate is increased, rather high modes of fundamental spin frequency can be detected, which seem to disappear in very long tubes. This indicates a rather strong coupling between the burned gas and the reaction zone, the source of energy. The energy involved in the spin vibrations was found to decrease with increasing mode (frequency roughly proportional to n^{-1}).

The dependence of the detonation velocity on the flow conditions in the burned gas, also obtained experimentally, points at the coupling between reaction zone and flow in the burned gas. The end of the zone, in which the energy release which propagates the detonation takes place, lies in a region where chemical reaction is not yet finished. Using the conditions for flow through Mach-number 1, while taking into consideration heat addition, change of the effective tube area by boundary layer and the influence of expansion waves from the wall etc., and applying it to the velocity deficit of the real detonation, one can get an estimate of the state of chemical reaction at the area where $M = 1$. This area seems to be rather sensitive to disturbances.

In order to investigate the chemical reaction in the main part of the reaction zone, low pressure detonations were used. In overdriven detonations, where the stabilization effects mentioned above are rather unimportant, the reaction zone was fairly smooth. The conditions of normal detonations had to be chosen very carefully in order to obtain regular signals. In some hydrocarbon–O_2 systems, density gradients were determined. In the system H_2–O_2–N_2 density gradients, temperatures, OH-concentrations etc. were measured. The temperatures at the "end of the reaction" zone agreed with calculated temperatures within the limits of experimental error. Density, temperature and OH-concentration distribution correspond in principle to the model of Doering, von Neumann and Zeldovich. The chemical reaction, immediately following the shock front in H_2–O_2–N_2 mixtures could be described using the known kinetic data of the H_2–O_2 reaction.

Many experiments have been performed by various authors in order to measure the "thickness" of the reaction zone of gaseous detonations, the extension of the region where the main part of the chemical reaction takes place. The information available today has been obtained by three different methods:[1]

(1) Calculations, using known kinetic data.

(2) Derivation of the quantity in question, using measurements of the macroscopic behavior of detonations (e.g., the dependence of the detonation velocity on the diameter of the tube, spin, etc.,) and applying an appropriate theoretical model.

(3) Direct investigation of the "reaction zone" by measuring density, density gradients, temperature, concentration of certain components, light emission or other quantities, which vary in the reaction zone.

As far as results are available values in the low pressure region agree within an order of magnitude.[2] This is rather satisfactory if one considers the errors involved in the different methods.

While methods (1) and (3) usually imply one-dimensional behavior of the detonation, method (2) is essentially based on the deviations from one-dimensional behavior and uses models of cylindrical symmetry. For example, the influence of the wall on the detonation by the forming of a boundary layer, turbulence, expansion waves traveling towards the tube axis and other ef-

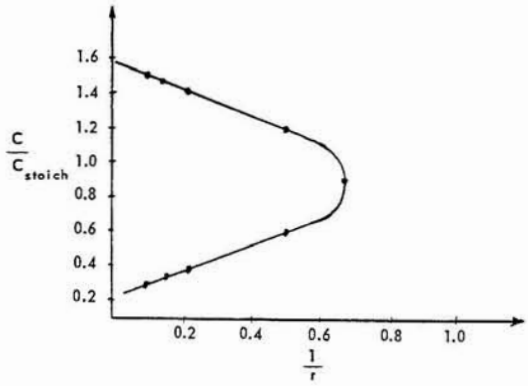

FIG. 1. Limits of detonability of CH_4–O_2 mixtures at normal pressure as a function of the tube radius r; c = concentration of CH_4 in vol %.

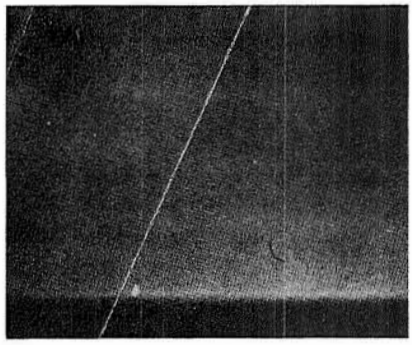

FIG. 2. Smear-camera picture of the front of a CO, H_2, O_2 detonation showing high frequency spin (about 20 times the fundamental mode).

fects are considered. Various models were applied to obtain a relation between the extension of the reaction zone and the velocity deficit of the detonation.[3–7] For the different models an expression of the form $\Delta D/D_\infty = a/r$ results (ΔD = velocity deficit, D_∞ = theoretical detonation velocity, r = tube radius, a is directly proportional to the extension of the reaction zone). Near the limits of detonability one should expect a stronger dependence of a on r. On the other hand, the limits of detonability which clearly are stability limits are approximately related to the tube radius by $C_{gr} = 1/r$. (C_{gr} = concentration at the limit.[8]) (Fig. 1).

These effects can be described using models with strict radial symmetry. However, we know that the processes taking place are more complex. From these experiments alone it is impossible to decide which model is to be preferred. Therefore, one may ask how the stability of a detonation with a velocity $D < D_\infty$ is really attained.

There are several experiments which could throw light on the situation.

(1) In the low pressure region where the reaction zone can be resolved, it normally shows a very irregular structure as shown by the excellent interferograms of White.[9] In order to obtain a rather smooth reaction zone, the detonation system has to be selected and adjusted extremely carefully.[10] Overdriven detonations show much less tendency to produce an irregular reaction zone.[9,10]

(2) If in spinning detonations the reaction rate is increasing (e.g., in the CO–O_2 system through the addition of more and more hydrogen) the spin frequency increases. The increase is too high to be explained by the change of the sound velocity in the burned gas. Spin frequencies of many megacycles can be obtained easily.[11] (Fig. 2.)

The pressure amplitude of the spin vibrations was found to decrease with an increasing number of spin modes. If n is the mode and Δp the pressure amplitude, we obtained $\Delta p \sim n^{-(1+\alpha)} (\alpha > 0)$. Therefore, the energy involved in the spin vibrations is roughly

$$E \sim (\Delta p)^2 n \approx 1/n$$

It too, decreases with increasing spin mode (or frequency in a given tube). Therefore, that part of the heat of reaction which is put into the spin vibrations decreases also.

(3) The velocity of a detonation depends on the flow in the burned gas.[12] Comparing the velocity of a detonation in a solid tube with the velocity in a tube which is destroyed a certain distance (l) behind the reaction zone, one finds the velocity of the detonation in the solid tube to be higher. In order to investigate this effect two equal detonation tubes (5 mm long) were mounted one above the other, coming out from a detonation tube of greater diameter, where the detonations were initiated. Part of one of the two tubes (50 cm long) was made of a specially prepared paper which was ruptured by the detonation at a certain distance behind the shock front of the detonation. This distance could be varied by changing the paper and its preparation. For the investigation stoichiometric city gas oxygen mixtures were used. The detonation in the two tubes were photographed together with a rotating drum camera. By an optical arrangement the rupture of the paper tube could be observed.

The high pressure in the detonation zone at first enlarges the area of the paper detonation tube. For the burned gas the paper tube acts as a nozzle. If one takes into account the increase of area due to the acceleration of the paper by the pressure one obtains

$$F/F_0 = 1 + \alpha 10^{-3} t^2.$$

F = real area; F_0 = initial area of the tube; t = time in μsec; α = factor depending on the mass of the paper ($\alpha \sim 1$). The time in which most of the chemical change takes place is less than 1 μsec in the detonations under consideration and, therefore, only the last part of the reaction zone may be influenced by the area increase.

The dependence of the velocity deficit on the length l is shown in Fig. 3. As long as l is not too short the increase in tube area acts very similarly to a boundary layer. The detonations start to fail when the velocity deficit is approximately 10% (or even lower in larger paper tubes).

In addition to the three experiments mentioned, we have to consider the fact that the chemical reaction is not completed in the zone between shock front and the effective Chapman-Jouguet state. Furthermore, the degree of completeness of chemical reaction varies within the cross section of the tube. With respect to a coordinate system fixed at the front of the detonation, the burned gas moves with a velocity which is higher than the sound velocity; therefore, the Mach number of gases coming from the shock front has to pass the value $M = 1$ in going from $M < 1$ to $M > 1$. How does this transition take place? Two possibilities should briefly be considered here.

In a stationary system the relation[13] holds.

$$\frac{1}{M}\frac{dM}{dx} = \frac{1}{1 - M^2} N \qquad (1)$$

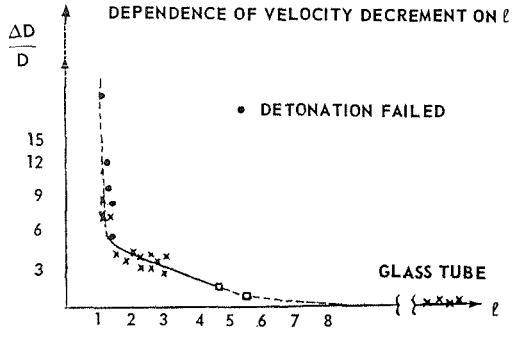

FIG. 3. Velocity decrement $\Delta D/D$, in per cent, of city gas oxygen detonations depending on l.

with

$$N = -\left[\left(1 + \frac{\kappa - 1}{2} M^2\right)\frac{d \ln F}{dx} - \frac{1 + \kappa M^2}{2}\frac{dq}{dx}\right]$$

where F = cross section; q = heat added; and κ = ratio of specific heats. In order to pass through $M = 1$ without an infinite derivative, dM/dx or dT/dx, N has to be zero and the derivative is given by $dM/dx = (dN/2dx)^{\frac{1}{2}}$. $N = 0$ means that the addition of heat by chemical reaction and by friction has to be compensated either by an increase of the effective tube area (e.g., due to boundary layer) or by an additional heat consuming process. (e.g., radiation or "turbulence").

Using this simplified stationary model one can describe the results of the experiments mentioned under point (3). In these experiments $d(\ln F)/dx$ is known. The velocity deficit can be used to calculate the corresponding reduction Δq of heat of reaction used for the propagation of the detonation through the relation $D \sim q^{\frac{1}{2}}$. Near equilibrium the equations describing the detonation process can be linearized and the value of dq/dx may be calculated. If one introduces this calculated dq/dx into Eq. (1), another value Δq_2 results. It was found that the two Δq values were at least in qualitative agreement. (It should be mentioned that the definition of M itself is not independent of the process taking place).

Another possibility to pass through $M = 1$ seems to be included in the nonstationary case and is suggested by the phenomenon of spin. A more realistic description of the situation around the zone with $M = 1$ has to be based on the corresponding differential equations.[14]

There seems to be a possibility of fulfilling the condition $M = 1$, at least as a time average, by introducing periodic variations of pressure and velocity.

During the initiation of a detonation, when the combustion due to flame propagation goes over into combustion initiated by shock wave, in most cases strong vibrations occur which interact with the reaction zone.[15] This means that vibrations as mentioned above and vibrations of the burned gas are present from the beginning. The vibrations in the burned gas are either attenuated by friction or supported due to their interaction with the reaction zone if their eigenfrequency is properly related to the chemical reaction process, resp. the mechanism mentioned above; if the vibrations of the burned gas and the "vibrations" necessary to fulfill $M = 1$ are in resonance. A similar phenomenon is well known from detonation spinning with relatively low frequency. The Chapman–Jouguet condition

in this case may be considered as a dynamic condition and the Chapman–Jouguet surface, the effective end of the reaction zone fluctuates around a mean value. These fluctuations influence the chemical reaction in the reaction zone. In addition, they may influence the shock front itself and therefore change the conditions for self-ignition immediately behind the shock front. This effect, however, becomes less important when the mode of the spin vibrations increases. Calculations made in order to check this model are not yet completed.

In overdriven detonations the flow does not have to pass through $M = 1$; at the "end of the reaction zone" the denominator in Eq. (1) does not become zero. Therefore, the reaction zone of overdriven detonations should show fewer irregularities than that of normal detonations. This was really observed.[9,10] If spin occurred during the initiation of overdriven detonations it seemed to disappear after some distance, especially if it had high frequency.

At the Combustion Symposium in Pasadena in 1960 we reported measurements in the reaction zone of gaseous detonations.[16] Results reported at that time were mainly based on measurements of density gradients by a schlieren method. In the meantime more extensive studies of the structure of the reaction zone were made by measuring the light emission, the temperature, and the change of OH-concentration. The absolute values of the induction times and the length of the reaction zone obtained by the different methods were not the same. However, if one takes into consideration that the methods used were sensitive to different quantities one can try to transform the results obtained with one method into values resulting from another method. For stable detonations this transformation establishes reasonable agreement among the values measured with the various methods.

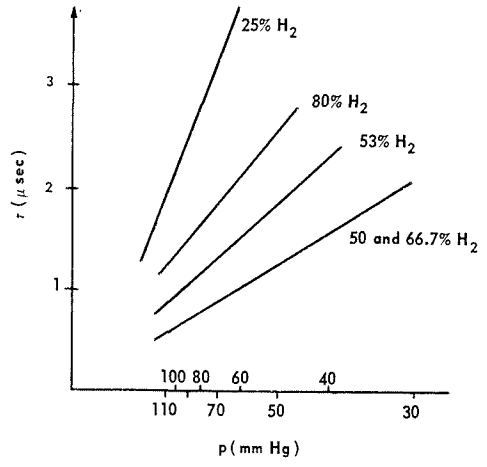

FIG. 4. Induction times in H_2–O_2 detonations as a function of pressure for various concentration (coordinate system at rest for all figures).

TABLE 1

Mixture	Detonation velocity, m/sec	Induction period, sec
$2H_2 + O_2 + N_2$	2290	1
$2H_2 + 2O_2$	2225	0.6
$2H_2 + O_2 + 3N_2$	1970	(2.6)
$2H_2 + 4O_2$	1875	1.2

As quantities characteristic of the reaction zone of a detonation we measured induction periods, representing the zone behind the shock front in which the change of the quantities under investigation was small compared with its change in the main part of the reaction zone. In addition, the length of the reaction zone was determined; it was defined as the distance between the shock front and that zone near the "end of the reaction zone" where the change of the quantity under investigation became too small to be measured.

Induction periods for H_2–O_2 detonations are plotted in Fig. 4 as functions of the reciprocal initial pressure. The fact that the results can be approximated by a straight line should be interpreted with caution with respect to the order of chemical reaction because the temperature along the straight line is not constant (but known). The influence of N_2 added to H_2–O_2 mixtures is shown in Table 1. Initial pressure $p = 90$ mm Hg. In addition, N_2 changes the detonation velocity and therefore the temperature behind the shock front and it influences the stability of the detonation. Nevertheless, the results obtained with the addition of nitrogen fit into the interpretation of the induction periods in pure H_2–O_2 mixtures, using the well-known mechanism of the H_2–O_2 system, the reactions $H + O_2 \rightarrow OH + O$ ($E_1 \sim 18$ kcal/mole); $O + H \rightarrow OH + H$ and $OH + H_2 \rightarrow H_2O + H$ ($E_{2,3} \sim 10$ kcal/mole).

The "length" of the reaction zone is shown in Fig. 5 for H_2–O_2 detonations as function of the initial pressure. Due to the fact that all measured quantities change very smoothly the "length" of the reaction zone is not well defined. The plotted curves, however, give an impression of the time in which the main part of the chemical reaction takes place.

In hydrogencarbon–oxygen detonations the definition of the extension of the reaction zone is easier than in H_2–O_2 detonations because the emission of C_2 and CH can be used as an addi-

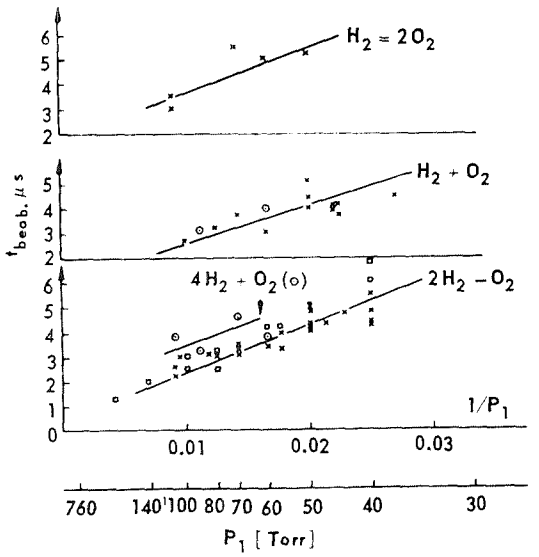

FIG. 5. Length of the reaction zone in μsec of H_2–O_2 detonations as a function of pressure.

tional source of information. Values for *n*-hexane–oxygen detonations are plotted in Fig. 6. The values are of the same order of magnitude as in H_2–O_2 detonations. In addition, the total reaction time is of the same order of magnitude as the (extrapolated) reaction time in flames of the same mixture burning at a pressure which corresponds to the pressure in the burnt gases of the detonation.

Induction times of benzene–oxygen and

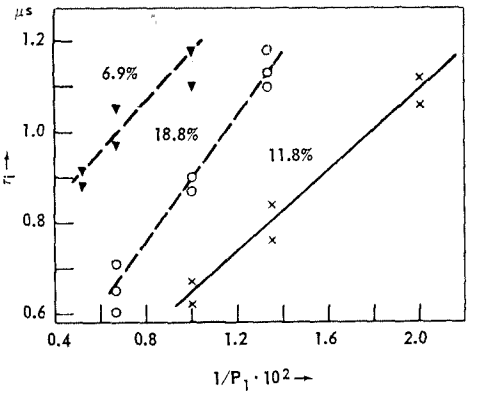

FIG. 7. Induction times for benzene–oxygen detonations as a function of pressure (*P* in mm Hg).

n-hexane–oxygen detonations are shown in Figs. 7, 8, and 9. In Fig. 9 some temperatures calculated from detonation velocities, assuming complete equilibrium behind the shock front are added. These values show how the temperature changes if pressure and concentration in the gas mixture are varied. The information obtained from the measurements of induction periods is not extensive enough to allow reasonable conclusions with respect to the kinetics of hydrocarbon oxidation under the conditions in a detonation. However, some time ago we measured the temperature dependence of the induction period for self-ignition in the same system using the rapid compression technique and shock waves. If these results are extrapolated to the

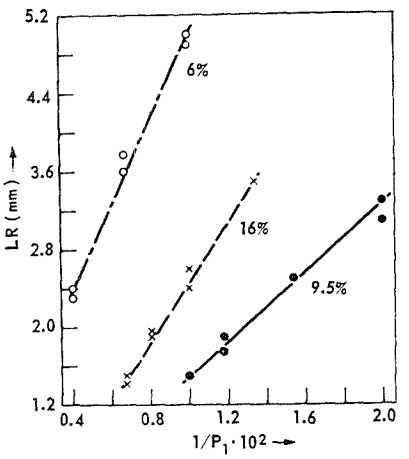

FIG. 6. Length of the reaction zone (in mm) of *n*-hexane oxygen detonations as a function of pressure (*P* in mm Hg).

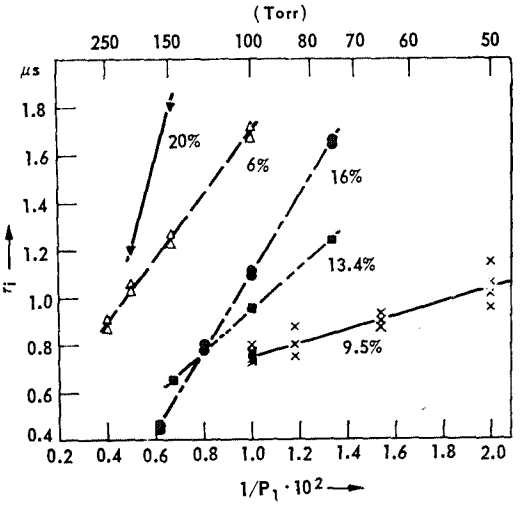

FIG. 8. Induction times for *n*-hexane–oxygen detonations as a function of initial pressure (*P* in mm Hg).

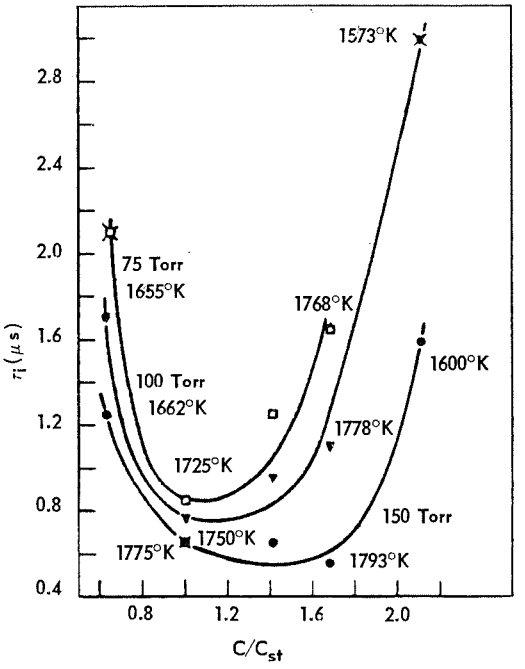

FIG. 9. Induction times for *n*-hexane–oxygen detonations as a function of the fuel concentration (c in vol %); ×'s are extrapolated.

conditions in detonations, induction periods result which in most cases are in agreement within a factor of less than two with the values obtained experimentally from detonations.

Besides the substances described above, other hydrocarbon-oxygen systems were investigated and the results were essentially the same as mentioned above except in the case of CH_4–O_2 detonations. In the CH_4–O_2 system stable detonations occurred very infrequently so that a unique interpretation of the signals was extremely cumbersome.[17]

REFERENCES

1. KISTIAKOWSKY, G. B., DUFF, R., JUST, TH., and WAGNER, H. GG.: *Fundamental Data Obtained From Shock Tube Results*. Pergamon, 1961.
2. JUST, TH.: Private communication, dissertation, 1959.
3. DOERING, W. and SCHON, G.: Z. Elektrochem. *54*, 233 (1950).
4. ZELDOVICH, IA. B. and KOMPANEETS, A. S.: Academic Press, London, 1960.
5. MANSON, N.: Z. Elektrochem. *61*, 586 (1957).
6. WAGNER, H. GG.: DVL-Colloquium, 1955.
7. FAY, J.: Phys. Fluids *2*, 283 (1959).
8. PUSCH, W. and WAGNER, H. GG.: Combustion and Flame (in press).
9. WHITE, D.: Phys. Fluids *4*, 465 (1961).
10. JUST, TH., *et al.*: Z. Elektrochem. *65*, 403 (1955); *64*, 501 (1960).
11. TOENNIES, P. and WAGNER, H. GG.: Z. Elektrochem. *59*, 7 (1955); *59*, 900 (1955).
12. HOMANN, K. H. and WAGNER, H. GG.: Tech. Sum. Report No. 2, AF 61 (514) 1142, 1960.
13. OSWATITSCH, K.: *Gasdynamik*. Springer, Wien, 1952.
14. KIRKWOOD, J. G. and WOOD, W. W.: J. Chem. Phys. *22*, 1915 (1954).
15. SCHULLER, W.: Dissertation, 1954.
16. JOST, W., JUST, TH., and WAGNER, H. GG.: *Eighth Symposium (International) on Combustion*. Williams and Wilkins, 1962.
17. PUSCH, W.: Diplomarbeit, 1960.

Discussion

DR. F. E. BELLES (*NASA, Cleveland*): The induction times τ observed when shock waves are driven into H_2–O_2-diluent mixtures correlate as log ($\tau[O_2]$) versus reciprocal temperature, where the temperature is calculated as that behind the normal shock. Both the temperature dependence and the magnitude of τ $[O_2]$ are governed by the rate of the reaction $H + O_2 \rightarrow OH + O$, and both can be predicted by Nicholls' theoretical expression.

In order to see whether the induction times measured by Wagner for free-running detonations deviate from this pattern, I have reduced his data to the appropriate form. The results agree well with the shock-tube data of Schott and Kinsey (and hence, also, with theory).

Consequently, stable detonation waves are not characterized by an unusually close degree of coupling between the reaction zone and the wave front, at least in H_2–O_2–N_2 mixtures.

DR. C. BROCHET (*University of Poitiers*): After Dr. Wagner's paper I want to mention one of the results found during our investigations of the influence of the wall on the detonation velocities.

As long as the detonation was stable (the concept of stable detonation that I use here is as defined in the paper of Manson *et al.*, presented at this Symposium) we confirmed that the relationship between the velocity and the reciprocal of the tube radius was indeed represented by a straight line.

However when the detonation became unstable

we did not find such a result because the deviation of the velocity measurements rapidly increased with decreasing pipe radius.

DR. R. E. DUFF (*Lawrence Radiation Laboratory*): In one respect the point of view expressed in Wagner's paper seems rather different from that taken by those more concerned with problems of detonation instability. It may be of some value to make this difference more explicit. This work shows that the structure of a "stable" detonation can be discussed satisfactorily in terms of the classical Döring, von Neuman, Zeldovich model even though weak, transverse perturbations are present. The perturbations do not seem to play an essential role in the initiation of the reaction. On the other hand Troshin and his co-workers seem to assert that the transverse and oblique waves existing on the shock front are essential to the propagation of the wave and that reaction initiation occurs in wave collisions or in turbulent slip discontinuities. These two positions are obviously quite different.

VIBRATORY PHENOMENA AND INSTABILITY OF SELF-SUSTAINED DETONATIONS IN GASES

N. MANSON, CH. BROCHET, J. BROSSARD, AND Y. PUJOL

A variation of one of the parameters (chemical composition, pressure, geometry of the container, etc.) of a self-sustained detonation involves a simultaneous modification of its structure (space between the shock wave and the flame) and its stability. However, despite the development of techniques for the observation of the structure and for measurement of the characteristics (velocity, etc.), it has not been possible to give an unambiguous definition of the stability and to specify the interaction between the shock wave and the combustion wave.

The purpose of the paper is to examine to what extent it is now possible to characterize: the stability of a self-sustained detonation, according to the results of propagation velocity measurements; the intrinsic instability, with the help of a scale of the vibratory phenomena frequencies; the coupling between the shock wave and the combustion wave, from the behavior of very unstable detonations, the self-sustained propagation of which is accompanied by a complete but momentary separation of the shock and the flame; the limits of formation of the self-sustained detonations, taking into account some instability parameters.

Introduction

It is now well known that during the first moments following its generation a detonation wave in a gaseous mixture contained in a pipe does not propagate with a constant velocity. Whatever the device used for generating the wave (another detonation, a powerful shock wave, a self-accelerated flame, or acceleration by means of various devices), its velocity during the first moments is higher than that observed after the detonation has run a further distance. The evolution of this velocity and the duration of this first phase depend upon the composition, pressure, and initial temperature of the mixture, upon the pipe dimensions, and, moreover, upon the device used for initiating the detonation. However, as the detonation runs away from its formation locus, the influence of the initiating device will attenuate and the detonation tends to become self-sustained and independent of the aforesaid initiating device.

For a long time it has been thought, in agreement with the classical Chapman–Jouguet theory, that the propagation velocity of a self-sustained detonation in a given mixture did not depend upon the traveled distance, and that the striae seen on some chronophotographic records (ordinary or schlieren) were specific for a particular type of waves (spinning detonation), but which propagate also with a constant velocity. However several investigations[1] have revealed that:

(1) the observed striae were due to the existence in gases of some transverse vibratory type of motions[2].

(2) the pipe diameter has an appreciable influence on the self-sustained detonation velocity[3]; and more recently[4,5] that:

(3) under some experimental conditions, this velocity could change notably with the traveled distance of the detonation;

(4) this variation sometimes was accompanied by a momentary but clear separation between the shock wave and the flame without any definitive destruction of the self-sustained detonation.

All these observations have raised with increased acuity the question of the validity limits of the Chapman–Jouguet theory, of the coupling mechanism between the shock wave and the flame, and of the idea of stability of the detonation wave.

The purpose of this paper is to contribute to the solution of these questions by analyzing the results of our observations on the self-sustained detonations in some mixtures,

$$C_3H_8 + X\,O_2 + Z\,N_2;\ 3 \leq X \leq 7,\ 0 \leq Z \leq 18.8,$$

and

$$C_2H_4 + X\,O_2 + Z\,N_2;\ 3 \leq X \leq 4,\ 0 \leq Z \leq 14.7$$

contained at ordinary temperature and pressure in long (25 to 30 m) pipes of 6 to 52 mm internal diameter.

After describing the experimental techniques and the main results of our observations[4–6] and computations,[7] we shall examine how and to what extent it is possible at the present time to characterize the stability, the intrinsic instability, the coupling between the shock wave and the flame, and the limits of self-sustained detonations.

Apparatus and Experimental Techniques

Mixtures. The mixtures were prepared in metal tanks (20, 40, or 400 liters capacity) with the usual precautions (drying of the gases with H_2SO_4 and P_2O_5; highly turbulent gas flow during the tank filling; waiting 2 to 3 hours between the filling and the use of the mixture). The proportions of components were deduced from their partial pressures, measured by either a water or mercury manometer. The deviation from ideal behavior of gases was taken into account (through suitable values of compressibility factors $z = pV/RT$) in order that the corresponding relative error of the detonation velocity would not exceed 0.1%. Two grades of propane were used: technical propane (TP) (sometimes containing up to 30% propylene C_3H_6) and pure propane (PP) (99.9%). The ethylene was 99% pure. Taking into account the various mixing operations, the combustible percentage in the mixture was known with an uncertainty of about 1% and the nitrogen content with an uncertainty of less than 0.5%.

Pipes for Velocity Measurements. Two series of stretched seamless steel pipes of an over-all length of 35 m were used for the velocity measurements: T_1, T_2, T_3, T_4 (12 mm, 20 mm, 36 mm, and 52 mm in diameter) and T_1', T_2', T_3' (14.6 mm, 28 mm, 44 mm in diameter). Measurements for some mixtures were also made in a steel pipe T_0, 6 m in length, 6 mm in diameter.

These pipes were filled (after they had been dried for five to ten minutes by a dry air flow) by passing through a volume of the experimental gas mixture, of at least twice their capacity. In all experiments, both ends of the pipes were shut before firing and the initial temperature and pressure conditions were $p_f = 1 \pm 0.0015$ atm, $T_f = 290 \pm 2°K$. The formation of the detonation wave was obtained via a flame initiated by an electric igniter and accelerated with a metal helical wire (1.5 m in length).

The velocity was measured by two or three pairs of ionization probes with time intervals recorded by 1/8 μsec electronic chronographs (Rochar A 809). The distance between two ionization probes actuating the same chronograph was $b = 500$ mm for the local velocity (D_l) measurements and, at least, 5 m for the average velocity (D_m) measurements. For every experimental mixture, a series of tests was performed to localize the locus of initiation of the detonation, after which, as a rule, the first pair of ionization probes was placed 2 or 3 m from that locus. The other pairs of probes were separated from the first by 1.5 m steps in the course of successive experiments.

Photographic Records. The photographic records were obtained for detonations propagating in a 20 mm diameter, 12 to 15 m length steel pipe, also fitted with 2 or 3 pairs of ionization probes for velocity measurements. This pipe could either include a section F_1 of an identical tube of 2.5 to 3 m in overall length and equipped with one side window, or another section F_2 of the same diameter, but fitted with two opposite optical glass windows, which, without changing the pipe section, permitted the use of a schlieren system. The position of those pipe sections was changed in the course of successive experiments, allowing the recording of the detonation waves at different distances from its formation locus. The camera had a 20 cm diameter drum (giving a film speed of 50 to 80 m/sec) and two Boyer 75/1.4 objectives provided with mirrors which made it possible to record on the same film the detonation wave, either in direct light only (over a 1.5 to 2 m distance in F_1) or simultaneously in direct and schlieren light (over a 40 cm distance in F_2). The Töpler-Foucault type schlieren system included two spherical mirrors (4 m in focal length), a horizontal knife, and a flash-lamp actuated by a photoelectric cell coupled to a thyratron. The light from the combustion front could be stopped down by a suitable field diaphragm, and one of the Boyer lenses was replaced by a 305/5.6 Gundlach lens.

Summary of Results

Detonation Velocity. Confirming and completing the observations of other investigators, our study of the local velocity D_l behavior in terms of the distance traveled by a self-sustained wave, and that of the average velocity D_m over the entire distance, has revealed that the relative deviation $\delta = \Delta D/\bar{D}$ (i.e., the maximum deviation ΔD of the D_l and D_m velocities divided by the average value $\bar{D}$ of these velocities)—considered as not significant when lower than 0.4%—tends to increase, with X and Z constant, as the diameter d of the tube diminishes; with X and d constant, Z increases; and with d and Z constant, X varies (increasing or diminishing according to the mixture strength).

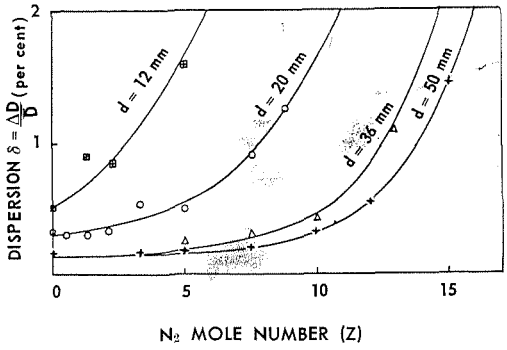

FIG. 1. Relative deviation δ vs nitrogen mole number Z. C_3H_8 (TP) + $5O_2$ + Z N_2; p_f = 1 atm; T_f = 298°K.

For instance (Fig. 1) in the case of the mixture C_3H_8 (TP) + $5O_2 + Z$ N_2, this relative deviation δ becomes larger than 0.4% for Z = 3.5 in the 20 mm pipe, for Z = 9 in the 36 mm pipe, and for Z = 10.5 in the 52 mm pipe. Consequently, X and Z being given, we could determine D_∞ with a precision of $\pm 0.2\%$ by extrapolating the D versus $(1/d)$ straight lines that were drawn from the values of the D_l and D_m velocities for which the relative deviation δ was 0.4% and in some cases by also taking into account the average values $\bar{D}$ of those velocities for which δ was less than 1%.

The comparison of the values of D_∞ with the values of D°_{th} computed from the Chapman–Jouguet theory with the help of the usual thermodynamic data,[8] and the assumptions of complete equilibrium and perfect gas law behavior of the burned gases shows that (Fig. 2 and Table 1) D_∞ is systematically 0.4 to 0.8% higher than D°_{th}. This result can be compared with that of White,[9] noting that:

(1) The characteristics computed by means of various techniques (semigraphic, or using an electronic computer) but with the same numerical data agree to within less than 0.3% for the velocity D°_{th} and to within 1.5 and 4%, respectively, for the density ρ_b and pressure p_b of the burned gases.[7]

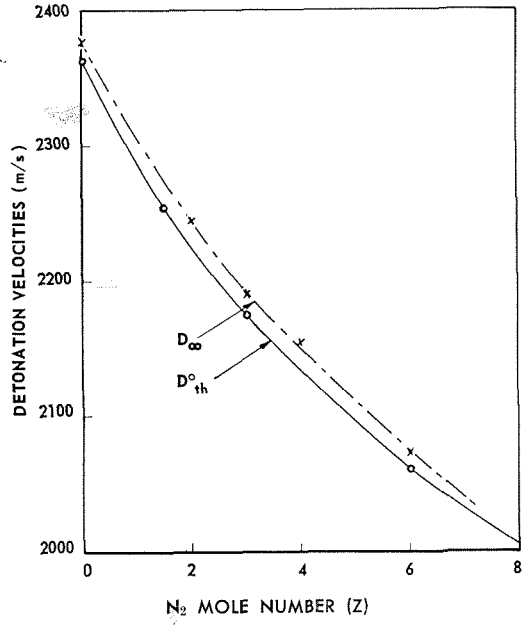

FIG. 2. Theoretical D°_{th} and observed D_∞ velocities as function of nitrogen mole number Z. C_3H_8 (PP) + $5O_2 + Z$ N_2; p_f = 1 atm; T_f = 298°K.

(2) If, instead of considering D°_{th}, we consider the velocity D_{th} that was computed with the same data, as D°_{th} but taking into account the deviation from the perfect gas law (as was done by Paterson[10] in the case of condensed explosives) we found that the difference between D_∞ and D_{th} is 0.2 to 0.5% lower than the difference between D_∞ and D°_{th}.[11]

Interpretation of Photographic Records. The records studied, in terms of the X and Z parameters, in the 20 mm diameter tube, have enabled us to make the following observations:

(1) As long as the relative deviation of the local (D_l) and average (D_m) velocities, is less

TABLE 1

Comparison of computed and measured detonation velocities

	C_3H_8 (PP) + X O_2				$C_2H_4 + 3O_2$
X	3	4	5	7	
D_∞ (m/sec)	2598	2480	2375	2213	2390
D°_{th} (m/sec)	2587	2470	2362	2201	2376
$(D_\infty - D^\circ_{th})/D_\infty$	0.004	0.004	0.005	0.005	0.006

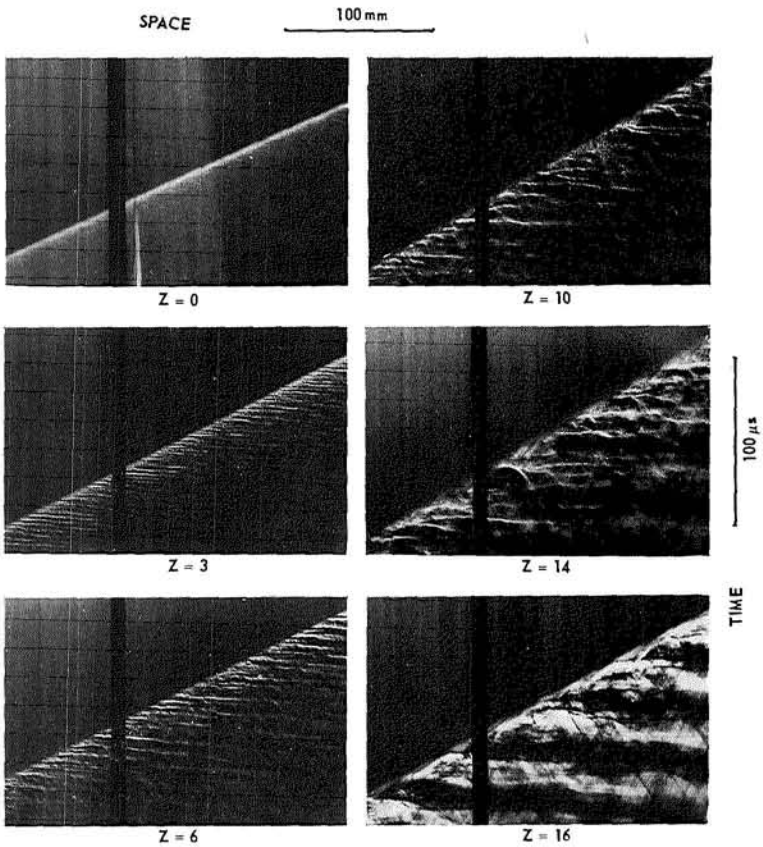

FIG. 3. Streak schlieren photographs of detonations showing instability evolution in $C_3H_8 + 5O_2 + Z\ N_2$ mixtures. $T_f = 298°K$; $p_f = 1$ atm; $d = 20$ mm.

than to 0.4–0.6%, the direct light records will not show any peculiarity, but the schlieren pictures reveal the existence in the burned gases of very high frequency (1 to 1.5 Mc/sec) vibratory phenomena, the frequency of which diminishes as Z increases, X being constant (Fig. 3).

(2) For increasing relative deviations of $\delta > 1\%$ the direct light records, and more clearly the schlieren records, show the appearance of some striae, the frequency of which is equal to the fundamental frequency of the transverse vibrations. Only the vibrations possessing the latter frequency can be seen on the records, when the deviation δ tends to become higher than 2%.

(3) When Z has a still higher value, the detonation decelerates and then gradually separates into a shock wave and a flame. Later we observe a sudden reformation of the detonation (Fig. 4), the phenomenon being repeated, roughly every 5 or 6 m, in a C_3H_8 (TP) $+ 5O_2 + 11.8N_2$ mixture.

It was also noticed that almost immediately after a reformation of the detonation (cf. photograph 2, Fig. 4), the striae, which at first had a very high frequency, tended stepwise towards the fundamental (first) mode transverse vibration, and that the latter became distinct a short time before a new dissociation took place between the shock wave and the flame.

Conventional Stability and Intrinsic Instability

When we want to summarize our knowledge of detonations, we are practically always referred to the Chapman–Jouguet wave as defined in the classical theory.

The characteristics of this wave are, in fact, a well-defined basis of comparison; but our inability to localize experimentally the surface which can be identified with the Chapman-Jouguet plane, allows us to consider only the detonation velocity.

The detonation velocity depends upon the pipe diameter. As theory does not take into ac-

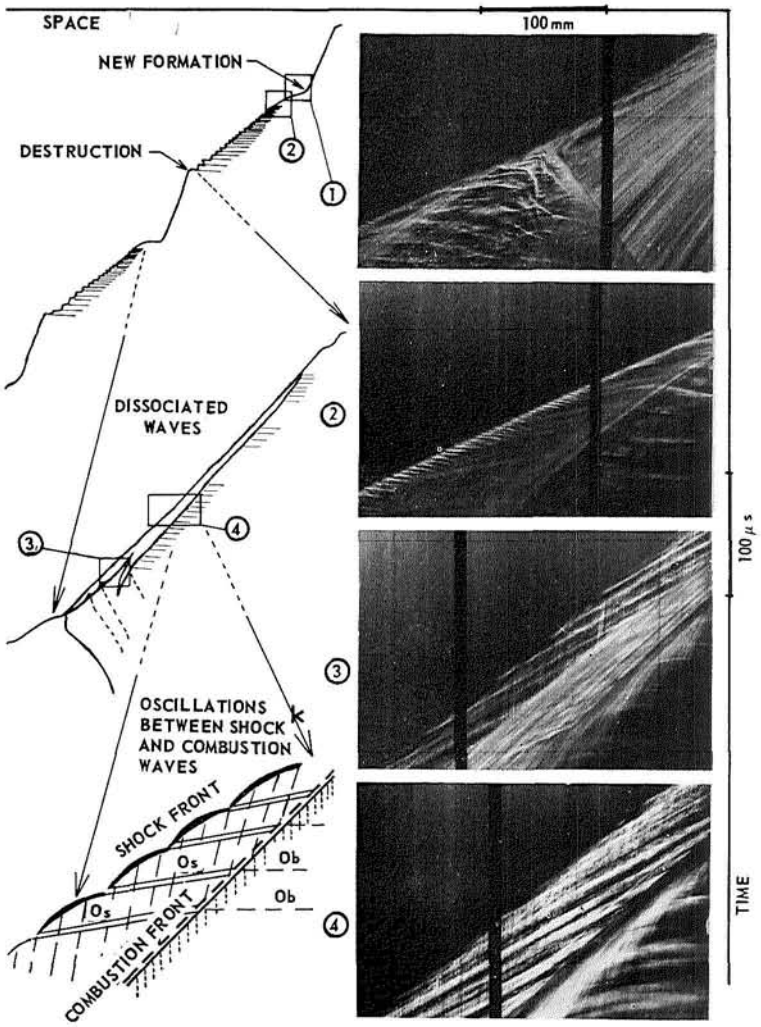

FIG. 4. Unstable detonation (different phases) in $C_3H_8 + 5O_2 + Z\,N_2$ (② and ④) and $C_2H_4 + 3.78\,O_2 + 14.2\,N_2$ (③ and ①) mixtures (p_f = 1 atm, T_f = 298°K).

count this factor, we are led to compare D_{th} values with the values of the experimental velocities D_∞ referred to the infinite diameter pipe. But these values D_∞ cannot be determined with equal accuracy, because the relative deviation corresponding to the measured D_l and D_m velocities in a given mixture also change with the pipe diameter (Fig. 1). As this variation of δ seems to be related to the instability of detonation, the comparison with the Chapman–Jouguet wave will finally be justified only for those detonations which are considered as "stable."

Since in our experiments it was possible to attain a relative deviation of 0.004, we have estimated that the self-sustained detonations for which the values D_l of local and D_m of mean velocities agree within about $\pm 0.2\%$ can be considered as "stable."

The arguments in favor of this statement can be found when examining the schlieren pictures. But it is clear that, in relating the idea of stability to one particular value δ^* of the dispersion ($\delta^* = 0.004$ in our case), we obtain a better basis for the comparison of D_∞ with D_{th}. Moreover, the comparison between the values of δ and a given δ^*, may provide a basis for a quantitative description of the degree of stability of the detonations.

Our choice of the value of reference δ^* (0.004) should not be considered as final because of improvement of the experimental techniques (use of gases of a higher purity, more precise deter-

mination of the composition of the mixtures). At the present time it seems difficult to measure the local velocities D_l with a lower relative deviation because of the intrinsic instability of the detonations. In fact, the existence of vibratory phenomena of more or less high frequency, proves that the gas flow and the combustion wave are not truly unidimensional and that, consequently, the relative deviation δ is not only due to the experimental techniques but also to the inherent nature of the phenomenon.

In assuming with Duff[12] that the vibratory phenomena are a manifestation of the intrinsic instability of the detonations in pipes, we can verify that there exists some parallelism between the variation of δ and this intrinsic instability. Indeed, as long as δ does not rise above 0.004, the frequency of the vibratory phenomena is high (1–1.5 Mc/sec). When it approaches the fundamental frequency δ becomes about 1 to 2%. Though unable to make precise measurements of the frequency (except when it is fundamental) our records confirm all of Edwards' observations[13] that for each of these frequencies it is possible to attribute a modal number of the transverse oscillation which diminishes when one of the parameters X, Z, or d (Fig. 3) changes in the corresponding way to diminish the stability. This modal number may be eventually used to define a scale of intrinsic instability.

The cause of this intrinsic instability and consequently the origin of the vibratory phenomena is, at present, unknown. They can be attributed to various phenomena such as transversal rarefaction waves, turbulence, timelags, etc., which may or may not be related to the presence of walls and their interaction. To understand each of these phenomena a more thorough knowledge of the nature of the coupling between the shock wave and the flame seems necessary. At present, to estimate the extent that a detonation can be considered as "stable" and consequently comparable with the Chapman–Jouguet wave, it is not only necessary to allow a highest value δ^* of the relative deviation of the local and average velocities, but also to ascertain that, even in larger diameter pipes, the vibratory phenomena always have a very high frequency (clearly greater than the fundamental frequency) independent of the traveled distance.

Coupling Between the Shock Wave and the Flame

The records (Fig. 3, 4) show that the coupling between the shock wave and the flame becomes weaker when the frequency of the vibratory phenomena approaches the fundamental frequency and the detonation becomes unstable.

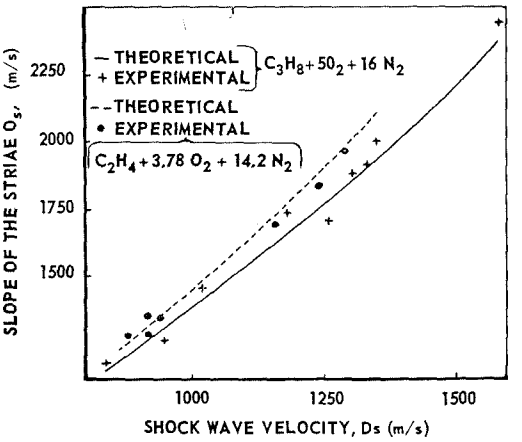

FIG. 5. Slope of the striae vs shock wave velocity D_s. Tube d = 20 mm.

In fact, this coupling in some mixtures becomes so weak that the shock and combustion waves separate. However, this separation is, momentary for the self-sustained detonations. Records (Fig. 4) of this phase show that the interaction between these two waves takes the form of a vibratory phenomenon with longitudinal and transversal components. Indeed, in assuming[14] that this complex vibratory motion is forced by the transversal vibrations in the gases behind the flame, we can compute the slopes of the oblique striae O_s. The comparison of these slopes to those measured on the records shows that they agree to ±5 to 8% and are functions of the velocity D_s of the shock wave (measured on the records to about ±4–5%) (Fig. 5).

The behavior of the shock wave and the flame indicates that these forced vibrations contribute towards the support of the shock wave by the flame. These vibrations seem to insure not only an energy transport from the flame to the shock wave but are also able to accumulate a sufficient amount of energy to generate one or several new flame fronts behind the shock wave and still ahead of the main (first) flame. The appearance of these new flames is followed by a new and strong association of the shock wave with a flame, the whole of this phenomenon plainly resembling the formation of the detonation by an accelerating deflagration.[15]

Thus it seems reasonable to presume that vibratory phenomena with a very high frequency should exist in the very thin gas layer, separating the shock wave from the flame front in the detonations that we have considered as "stable". A megacycle frequency is, in fact, compatible with the known[16] values of the stay-time of the gases in this layer.

Such an interpretation does not explicitly consider the effect of the wall surface. We have observed it, particularly in repeating some of Shchelkin's[17] and Guénoche's[18] experiments concerning the influence of a helical wire inserted in the pipe walls.[16] Our experiments were performed within a 20 mm diameter pipe with a 1.5 mm diameter helical wire, having the required characteristics (the distance between two turns of the helix equal to the wire diameter) for observing a detonation velocity that would be definitely lower than the velocity in "smooth" pipe. With the mixtures C_3H_8 (TP) + $5O_2$ + Z N_2 for instance, it appeared (Fig. 6) that (1) for $Z < 6$, i.e., for mixtures in which the detonation is "stable," the presence of the helical wire produces a decrease in the velocity that can reach 10%; (2) for $Z \simeq 8$, the helical wire causes the appearance of fundamental frequency striae, which for "smooth" pipes do not appear up to $Z \simeq 10$ to 12; (3) for $Z > 10$, the detonation is fully dissociated, and the distance between the shock wave and the flame is constant; likewise the velocities are about 40% less than the velocity measured in the "smooth" pipe.

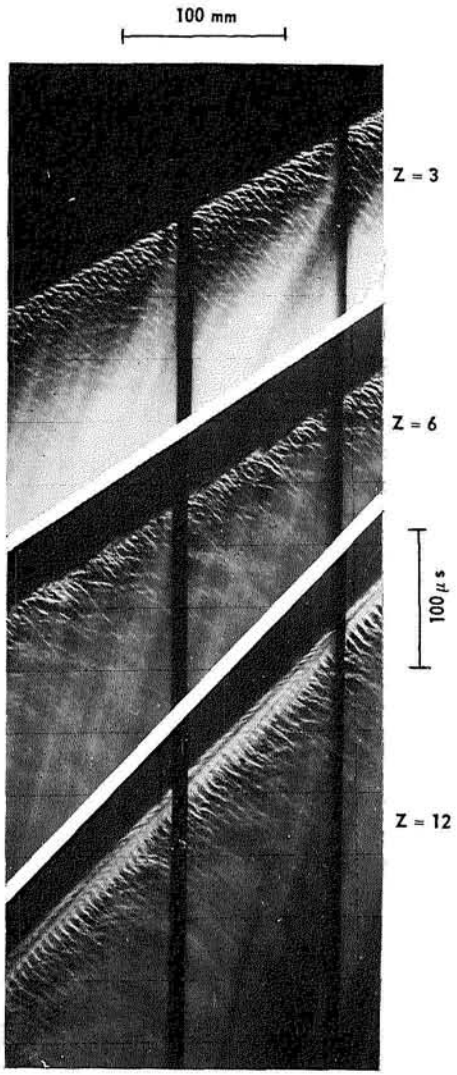

FIG. 6. Detonation waves in tube d = 20 mm with helical wire of 1.5 mm diameter and three turns per cm. C_3H_8 + $5O_2$ + Z N_2 mixtures.

The Limits

Generally, according to the parameter L ($L = X, Z, D, p_f, T_f$) one can conceive that there are two (or eventually just one) values L_i^* and L_s^* which characterize the limits of the domain where the formation of self-sustained detonations is possible. A pair of other values L_i, L_s of this same parameter will characterize, if they exist, the limits within which these detonations can be considered as "stable." But, while the definition of the first of these involves only the self-sustenance of the detonations, the definition of the latter involves a choice of a convention defining the "stability" of the detonation.

The necessity to distinguish between these two groups of limits was pointed out by Rivin and Sokolik.[19] They indicated that their experiments on the formation limits of detonations generated by self-acceleration of flames could not lead to the same results as those of the other investigators (Wendtland,[20] Laffitte and Breton[21]) who determined the limits within which a stable detonation could be propagated, the requisite conditions for its formation being achieved by the use of an appropriate initiating device.

To determine the limits, the initiation mode and the pipe length are of particular importance since, using a sufficiently energetic initiation mode, the propagation of a detonation over a shorter or longer distance can be observed although it is not necessarily self-sustained. The determination of the two groups of limits (L_i^*, L_s^*, and L_i, L_s) amounts to the determination of domains of existence of self-sustained detonations and of conventionally defined "stable" detonations.

From this point of view, the analysis of the results of the experiments allows us to indicate the general limits in terms of the pipe diameter d and the nitrogen mole Z number for the mixtures C_3H_8 + $5O_2$ + Z N_2 at ordinary temperature and pressure (Fig. 7). This figure shows the approximate limits of the domain of existence of self-sustained detonations, within which we have detonations considered as "stable" with the corre-

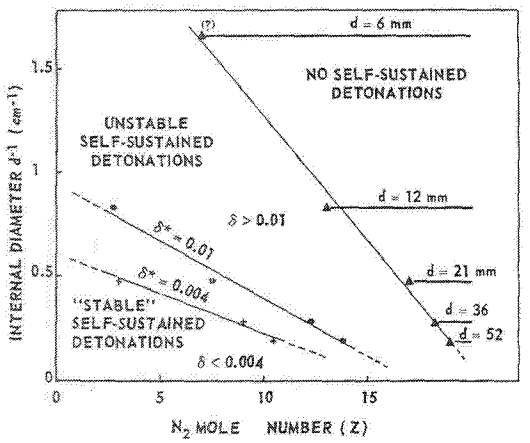

FIG. 7. Approximate limits of formation of self-sustained detonations in C_3H_8(T.P.) + $5O_2$ + Z N_2 (p_f = 1 atm, T_f = 298°K).

sponding relative deviations $\delta^* = 0.4\%$ and $\delta^* = 2\%$.

These limits can be determined with greater accuracy for small values of Z, but become quite difficult to determine for $Z > 18.8$. For this case it will be necessary to use pipes of much larger diameters and length than are used at the present time.

Conclusions

Summarizing the results of the analysis of the observations on self-sustained detonations we can conclude that:

(1) At the present time a self-sustained detonation can be considered as "stable" when the relative dispersion of the local and average velocities in 6 to 52 mm diameter pipe, having traveled a distance of about ten meters, is 0.004 and when the vibratory phenomena possess a high (~1 Mc/sec) constant frequency.

(2) The appearance of frequencies near the fundamental is an indication of a weakening of coupling between the shock wave and the flame.

(3) The vibratory phenomena which characterize the intrinsic instability of detonations may contribute closely to the aforementioned coupling.

(4) The specification of detonation limits must satisfy two criteria: (a) That the wave is self-sustained (the formation limits), and (b) that it is restricted by a given stability condition, such as vibration frequencies appreciably higher than those of fundamental mode, and the variation of the local velocities from the average does not exceed 0.2% (limits of "stable" waves).

REFERENCES

1. LEWIS, B. and VON ELBE, G.: *Combustion, Flames and Explosions of Gases*, 2nd ed. Academic Press, 1961.
2. MANSON, N.: Compt. rend. *222*, 46 (1946); FAY, J.: J. Chem. Phys. *20*, 942 (1952).
3. KISTIAKOWSKY, G. B., KNIGHT, H. T. and MALIN, M. E.: J. Chem. Phys. *20*, 876, 884 (1952).
4. BROCHET, CH., BROSSARD, J. and MANSON, N.: Compt. rend. *250*, 3949 (1959).
5. BROCHET, CH. and MANSON, N.: *Coll. Inter. du C.N.R.S. sur les Ondes de Detonation, 1961.* (In print by C.N.R.S., Paris.)
6. BROCHET, CH. and MANSON, N.: Compt. rend. *254*, 3992 (1962).
7. BROCHET, CH., BROSSARD, J., MANSON, N. and ROUZE, M.: Compt. rend. *255*, 1190 (1962).
8. ROSSINI, F. D. *et al.*: *Selected Values of Physical and Thermodynamic Properties of Hydrocarbons and Related Compounds*. Carnegie Press, Pittsburgh, 1953.
9. WHITE, D.: Phys. Fluids *4*, 465 (1961).
10. PATERSON, S.: Research (London) *1*, 221 (1948); TAYLOR, J.: *Detonation in Condensed Explosives*. Clarendon Press, Oxford, 1952.
11. PUJOL, Y. and MANSON, N.: To be published.
12. DUFF, R. E.: Phys. Fluids *4*, 1427 (1961).
13. EDWARDS, D. H., WILLIAMS, G. T. and PRICE, B.: *Coll. Inter du C.N.R.S. sur les Ondes de Detonation, 1961.* (In print by C.N.R.S., Paris.)
14. BROCHET, CH., LEYER, J. C. and MANSON, N.: Compt. rend. *253*, 621 (1961).
15. OPPENHEIM, A. K.: (private comm.)
16. WAGNER, H. GG.: AGARDograph *41*, 320 (1961). Pergamon Press.
17. SHCHELKIN, K.: Zhur. Eksp. i Teoret. Fiz. *10*, 283 (1940); Acta Physicochim. U.R.S.S. *20*, 303 (1945).
18. GUENOCHE, H. and LAFFITTE, P.: Compt. rend. *224*, 1224 (1947).
19. RIVIN, M. and SOKOLIK, A. S.: Acta Phys. Chimica U.R.S.S. *4*, 301 (1936); *ibid. 7*, 825 (1957).
20. WENDTLAND, R.: Z. phys. Chem. *110*, 637 (1924); *ibid. 116*, 227 (1924).
21. LAFFITTE, P. and BRETON, J.: Compt. rend. *199*, 146 (1934).
J. BRETON: Ann. Office Nat. Combust. Liq. *11*, 487 (1936).

Discussion

DR. R. E. DUFF (*Lawrence Radiation Laboratory*): I would like to mention work done several years ago which supports the reported observation of momentarily uncoupled shock and flame fronts which propagate as self-sustaining waves. At that time Dr. Knight and I published a note on the detonation behavior of pure acetylene gas. It was found that this gas would support a spinning detonation in relatively large tubes and a much slower wave in smaller tubes which was characterized by a large separation between the shock and the luminous zone. Subsequent, unpublished measurements of the wave velocity made by the Doppler radar technique have demonstrated that the slower mode is not stable. The velocity fluctuates with a wavelength of many meters over a wide velocity range. This type of propagation seems to correspond to the mode suggested long ago by Jost to explain spinning detonation. I suggest that the name "galloping detonation" might be an appropriate, suggestive one for this type of detonation propagation.

PROF. A. K. OPPENHEIM (*University of California*): As Professor Manson mentioned, his photographic records of the re-establishment of detonation wave bear an amazingly close resemblance to our schlieren photography of the formation of the detonation wave. The first publication of our observations is scheduled to appear in the forthcoming issue of *Combustion and Flame*. One may consequently infer that the gas-dynamic process of the reassociation of the reaction zone with the shock that occurs during the nonsteady ("galloping" as Dr. Duff suggested) detonation process is in fact identical with the phenomenon of coalescence that takes place at the origin of the detonation wave.

DR. H. GG. WAGNER (*University of Göttingen*): Dr. Manson has introduced a definition of stable detonation based on fluctuations of the detonation velocity. It may be, that part of the fluctuations reported by Dr. Manson is due to the fact that the front of a detonation which spins close to the fundamental mode is not always perpendicular to the axis of the tube, but fluctuates (e.g., J. Dove, Eighth Symposium on Combustion). Because the authors have measured the velocity using ionization gaps, this effect may have caused part of the fluctuations. In our own measurements of the influence of tube diameters on the limits of detonability the velocity deficit in tubes of smaller diameter compared with the velocity in tubes of larger diameter was really very small (about 1 per cent) as long as the detonation was stable and the tubes were sufficiently long. As soon as the velocity deficit increased the detonations started to fail. In long tubes the transition region between detonation and no detonation becomes a very narrow one. Therefore it might be that the curves in Fig. 1 of Manson's paper in fact are flatter in the flat part and steeper in the steep part.

The definition of a stable detonation will always be somewhat arbitrary. I would like to offer one which is different from that of Manson and which seems to be more closely related to the mechanism of detonation. We consider a detonation as a stable one when it travels over a very long distance with "count out" velocity and without visible separation between shock and reaction zone. This includes detonations spinning in the fundamental mode (at least partly, because there are detonations spinning in the fundamental mode which are out after some distance, while others are not; these two types can easily be separated experimentally). This definition is somewhat supported by an analogy; polyhedral flames exist in mixtures which under given conditions do not form stable flames with a plane flame front. However irregularities arising in the flame front are stabilized and a flame with larger area is formed which is perfectly stable. This means: Nature acts in a way that stability is obtained by using an additional process. A similar situation exists in spinning detonation. The reaction behind the main shock front does not like to start sufficiently fast. Therefore an additional effect, pressure and temperature rise due to spin, is needed in order to keep things going.

OPTICAL STUDIES OF THE STRUCTURE OF GASEOUS DETONATION WAVES

M. L. N. SASTRI, L. M. SCHWARTZ, B. F. MYERS, JR., AND D. F. HORNIG

The optical reflectivity method has been applied to the study of the initial stages of detonation waves in hydrogen-oxygen-argon mixtures.

Introduction

Two central problems have emerged concerning the structure of gaseous detonation waves: (a) whether the reaction zone is preceded by a more or less uncoupled shock wave as proposed by Zeldovich,[1] von Neuman,[2] and Doering,[3] or whether the two interact strongly[4]; and (b) whether the shock front is flat, indicating one-dimensional flow, at any pressures. The optical reflectivity method is the only one used thus far[5] which has sufficient resolution to detect and study the details of the initial compression and it also yields information on the second point at much higher pressures than other methods.[6]

Some time ago Levitt and Hornig observed[5] that when detonations in $H_2 + 3O_2$ mixtures passed through an intense beam of monochromatic light, a pulse which appeared to be reflected light from the initial shock front in the detonation wave could be detected. This phenomenon is analogous to that observed in the case of simple shock waves where it has proved very fruitful in studying their structure. The interpretation of the light signals from the detonation fronts as reflection seemed justified since the magnitude of the pulses as well as their dependence on angle of incidence and pressure was about that expected. Experiments in which the size of the exit aperture (and thus the degree of collimation of the beam) was varied led them to the conclusion that the initial shock front was smooth and planar at initial pressures of from one to three atmospheres, in contrast to the behavior observed by White,[6] for example, at lower pressures. We have now extended these observations, employing light of two wavelengths (4358 Å and 5790 Å) and a wider range of angles and initial pressures, and the situation appears considerably more complicated.

Experimental

The reflectivity method[7] is based on the fact that the reflectivity of a gas interface is given by the expression

$$R = (1 + \tan^4\theta)[F(2\cos\theta/\lambda)]^2, \quad (1)$$

where θ is the angle of incidence (and reflection), λ the wavelength of the incident light, and F the Fourier transform of the refractive index gradient,

$$F(2\cos\theta/\lambda) = \int_{-\infty}^{\infty} n^{-1}(dn/dx) \times \exp[-2\pi i(2\cos\theta/\lambda)]\,dx. \quad (2)$$

Equation (1) can be rewritten in the form,

$$R = \tfrac{1}{4}(1 + \tan^4\theta)\,(\Delta n)^2\,R'(\cos\theta/\lambda), \quad (3)$$

in which R' varies from one when λ is large compared to the scale of the phenomenon to zero when λ is small, and Δn is the index of refraction change during the shock compression, i.e.

$$\Delta n = (n_0 - 1)\,(\rho_1/\rho_0)\,(\Delta\rho/\rho_1). \quad (4)$$

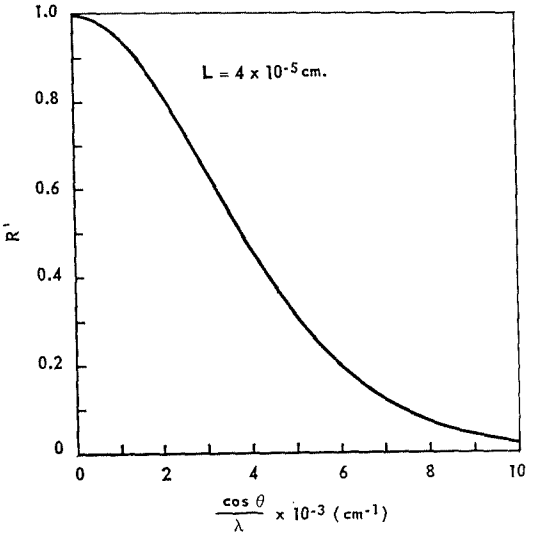

FIG. 1. Typical reflectivity for a simple shock wave of thickness L. For any other thickness, multiply abscissa by L/L'.

The subscript zero refers to NTP and one to the initial state of the unshocked gas; $\Delta\rho$ is the density change across the gas interface. The behavior of R' for a simple shock wave is illustrated in Fig. 1.

The experimental method employed, except for improvements in the efficiency of the optical system, was similar to that of Levitt and Hornig. The apparatus was calibrated with weak shocks in argon. The results obtained from measurements on $H_2 + 3O_2$ at an initial pressure of 20 psia are plotted in Fig. 2 as $R'(\Delta\rho/\rho_1)$,[2] the known variables having been eliminated by means of Eqs. (3) and (4). Although the magnitude of the "reflectivity" is close to that expected for reflection from the initial shock front, the data clearly do not fall on a single curve as expected from Eq. (3). Instead, the 4358 Å points form one curve and the 5790 Å points another.

In Fig. 3 the same results are plotted as total observed intensity, normalized against the argon reflections in calibration shots. The "scattering angle" is $2(\pi - \theta)$ in each case. The fact that in all of our experiments on $H_2 + 3O_2$ at 20 psia the 4358 Å signals were more than twice as intense as the 5790 Å signals clearly indicates that

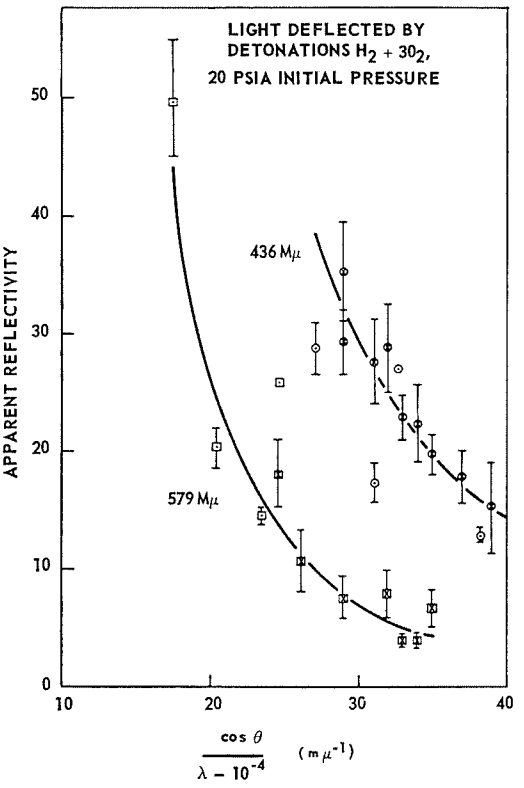

FIG. 2. Apparent reduced reflectivities, R' $(\Delta\rho/\rho_0)^2$, from detonations in $H_2 + 3O_2$ at 20 psia initial pressure. Circles represent data at 4358 Å and squares at 5790 Å. Dotted points are original older results and crossed points are recent results.

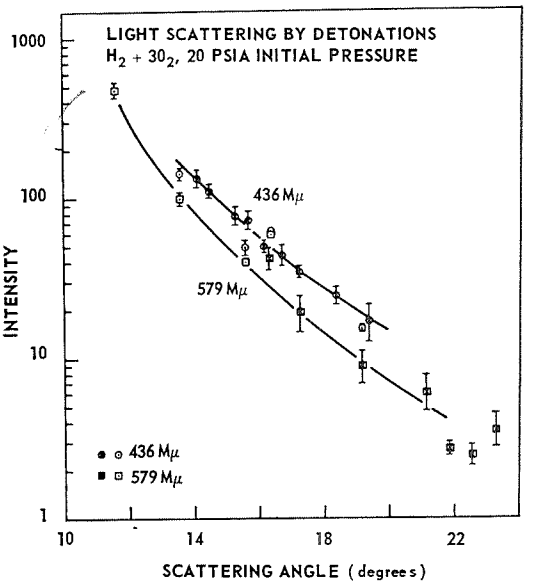

FIG. 3. Normalized scattering intensities from detonations in $H_2 + 3O_2$ at 20 psia initial pressure. Dotted points are older data and crossed points represent recent results.

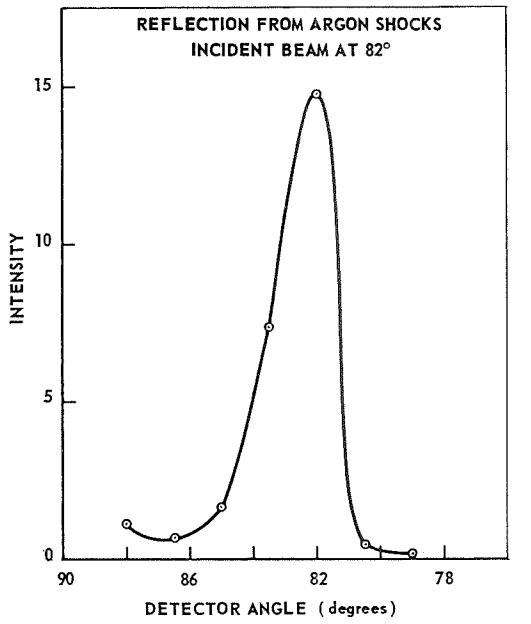

FIG. 4. Reflected intensity from argon shock with fixed incident beam as angle of observation is varied.

the phenomenon was not simple reflection and suggests a major contribution by light scattering instead.

To check on this conclusion we did further experiments in which the angle of incidence was kept constant while the angle of observation was varied. In the case of simple shock waves, as shown in Fig. 4, reflected light could be detected only when the angle of observation was equal to the angle of incidence to within 2°, which was the angular deviation in the collimation of the light beam in the optical system. Corresponding observations on detonations are given in Fig. 5; a signal was observed over a wide range of the angle of observation and there is no sign of a maximum at 16° which would have occurred if there had been reflection from a plane front at an angle of incidence of 82°. These results show clearly that either the major effect is scattering or that the reflection occurs from a rough or "bumpy" front. The intensity is a much more sensitive function of angle than would be expected for Rayleigh scattering, but it could, perhaps, be accounted for in terms of larger scattering centers. However, a "bumpy" reflecting surface might also yield a similar angular distribution of intensity. The reason is that the magnitude of the reflectivity varies as $1 + \tan^4 \theta$ and therefore increases very sharply as θ tends toward 90°.

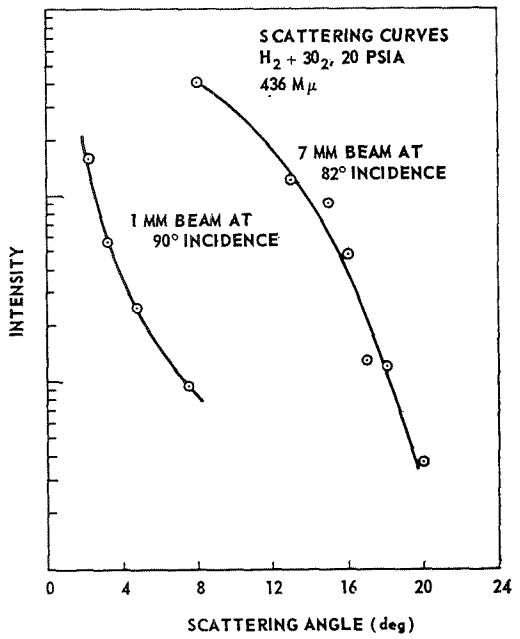

FIG. 5. Pulse intensity from detonations in $H_2 + 3O_2$ at 20 psia initial pressure as angle of observation is varied.

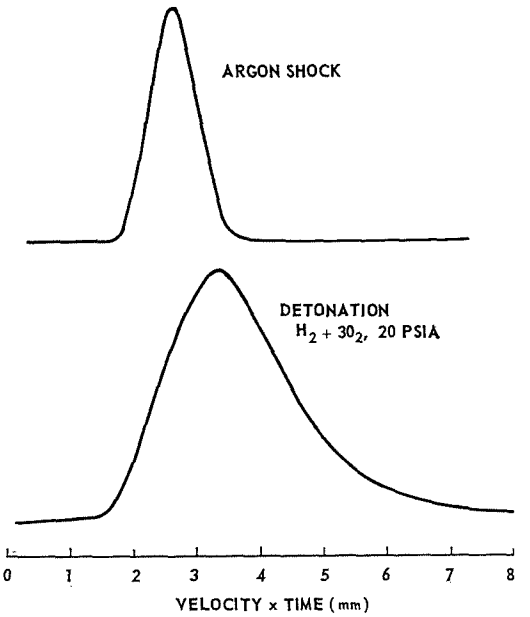

FIG. 6. Pulses observed from shock and detonation waves when illuminated with 1 mm wide incident beam at $\theta = 82°$.

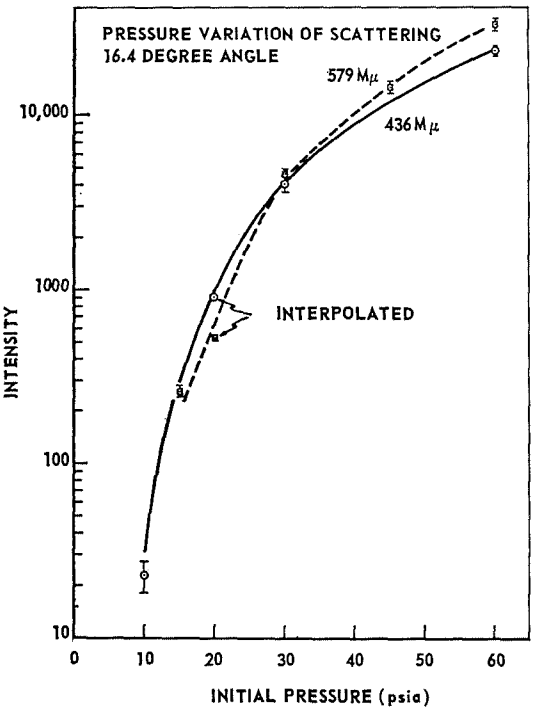

FIG. 7. Scattered intensity from detonations in $H_2 + 3O_2$ with angles of incidence and observation of 82° as initial pressure is varied. Interpolated points are taken from curves of Fig. 3.

Whatever their origin, the narrowness of the light pulses observed demonstrates that the signals originate in a narrow zone of the detonation wave. To determine the thickness of this zone, measurements of pulse duration were made with a 1.0 mm wide incident and observing slit system. Figure 6 shows the results obtained. The pulse width for the argon shock is that of the optical beam. The wider pulse from the detonation indicates that the signals originate in a zone approximately 2.5 mm thick. This zone may be thinner in any local portion of the detonation wave since it includes the effect of any curvature of the wave front.

Conclusions

We can therefore conclude that (a) at 20 psia the detonation front is neither plane nor smoothly curved, (b) the optical signal cannot originate in reflection alone but may arise predominantly from scattering, and (c) the optical signal originates in a zone less than 2.5 mm thick.

The situation is not yet entirely clear. Plots of signal strength vs. initial pressure at a constant scattering angle of 16° ($\theta = 82°$) (Fig. 7) seem to show that in going from 20 psia initial pressure to 60 psia, the 5790 Å signal becomes stronger than that at 4358 Å, apparently crossing over at about 30 psia. This suggests that the reflection component may become dominant at higher pressures but further experiments are needed before the relative roles of reflection and scattering can be determined.

References

1. Zeldovich, Y. B.: J. Exptl. Theoret. Phys. (U.S.S.R.) *10*, 542 (1940).
2. von Neuman, J.: OSRD Report No. 549, 1942.
3. Doering, W.: Ann. Physik *43*, 421 (1943).
4. Hirschfelder, J. O. and Curtiss, C. F.: J. Chem. Phys. *28*, 1130 (1958).
5. Levitt, B. and Hornig, D. F.: J. Chem. Phys. *36*, 219 (1962).
6. White, D. R.: Phys. Fluids *4*, 465 (1961).
7. Cowan, G. R. and Hornig, D. F.: J. Chem. Phys. *17*, 1008 (1951).

GENERAL DISCUSSION

DR. D. R. WHITE (*General Electric Research Laboratory*): Confusion is sometimes generated by use of the term "instability of detonation" to refer to different phenomena. On the one hand we have instability of propagation as studied so nicely by Manson *et al.* On the other hand we have instability of structure, by which we mean the apparent reluctance of a detonation front to possess a laminar, or one-dimensional, shock wave-reaction zone structure. This is the problem to which Erpenbeck has directed his attention, and which may be, if you will permit me, reflected in Hornig's observations.

The picture we are obtaining is that in general even detonations which propagate stably appear to have a non–one-dimensional structure.

As one changes the conditions of the experiment in such a fashion that the reaction zone thickens, the scale of the irregularities increases. As this scale becomes comparable with tube dimensions, spin is observed and we approach instability of propagation. Spin data are adequately correlated by the acoustic theory, but this tells us little about the origin of spin or why it is so commonly observed as to perhaps merit being called a "stable" phenomenon. It is the origin of this instability of structure which we are now investigating, and some of our ideas appear in the introductory remarks.

To rephrase them briefly the primary shock front is followed by an essentially thermoneutral induction period and then by an exothermic reaction zone. This induction period depends on the local gas temperature and density. A weak shock front propagating transversely will be followed by a higher-than-average reaction rate, the induction time will be reduced, and the exothermic reaction zone will move forward with respect to the primary shock front. This transverse wave is in essence a "stably" propagating "micro-detonation" wave. The minimum separation between two such transverse waves will be determined by the time required for the reaction zone to recede again from the shock front as the doubly shock-heated gas is swept out by gas processed only by the primary shock front. The result of course is a self-sustaining "stable" transverse structure whose scale depends (for a given mixture) on reaction zone thickness and whose amplitude may depend on the temperature sensitivity of the reaction rate. The triple shock configurations associated with this process are adequate to account for the density fluctuations which invariably appear in our interferograms of detonation in gases.

PROF. J. A. FAY (*M.I.T.*): There are two aspects of the structure of unstable detonation waves which deserve more experimental investigation. The first has to do with the occurrence of triple shock type configuration of the detonation front such as that which has been shown by Dr. White. The second problem is connected with the intensity of the "turbulent" fluctuations of the flow quantities in the combustion zone and their subsequent decay.

The existence of triple shock configurations during initiation or low modal number spin has been fairly well established. The principal question remaining is whether this phenomena persists at high pressures where the reaction zone is small compared with the tube diameter. One of the puzzling features of the structure of spinning detonations is that this shock structure always adjusts itself to propagate with the phase velocity of the acoustic vibrations of the product gases. At higher pressures where there appears to be no clearly defined frequency in the product gases, what will be the mode of propagation of these disturbances?

If the detonation front is unstable so that "turbulent" fluctuations of velocity, density etc., exist within the combustion zone, the intensity of these fluctuations ought to be determined. If the energy in these fluctuations is appreciable, it ought to effect the wave velocity and temperature. Even though it may not be possible to resolve the reaction zone for high pressure detonations, there ought to be some effects of these fluctuations downstream of the reaction zone since the viscous damping of turbulence would be quite small at the high Reynolds' number experienced in most detonation waves. The interferograms of White show a marked tendency for the intensity of the density fluctuations downstream of the reaction zone to be lower than that within the reaction zone, an effect which we have also noticed in our schlieren photographs. In this respect the "turbulence" appears to be quite different from that generated by a grid or screen placed normal to a flowing gas, where no decay in turbulence is experienced, except through viscous effects far downstream of the grid.

DR. D. R. WHITE: Our interferograms show large amplitude density fluctuations resembling those to be expected from compressible turbulence. A second contributing factor could be entropy variations in the product gas as a result of the shock strength varying from point to point over the detonation front. The state of the gas leaving the reaction zone could lie at various points up or down the equilibrium Hugoniot and, of course, the tangent property of the solution near the Chapman–Jouguet point results in rather large density changes for small changes in wave velocity. This effect may be accentuated in our optical observations if the square tube has imposed some regularity on this structure.

W. E. GORDON (*Combustion and Explosives Research, Inc.*): As more information is obtained by newly developed techniques, the picture emerges ever more strongly that the wave front in gaseous detonations in tubes almost always has three-dimensional features with various degrees of complexity. These range from the fundamental spin mode observed near the composition limits, to the multi-headed spins and highly turbulent reaction zones in richer mixtures. The question is: Do such three-dimensional effects always dominate? Are they, in fact, essential for the stability of detonation?

Some evidence obtained in our work at the University of Missouri[1,2] suggests that, in certain narrow regions of composition and pressure, mixtures of H_2–O_2–A, and O_3–O_2 may approach the NDZ model detonation. Figure 1 shows piezoelectric pressure records for various mixtures. It is seen that for the mixtures $2H_2 + O_2 + 13A$ and 17.3 mole per cent O_3 in O_2, spin (vibration) is virtually absent and sharp von Neuman "spikes" are in evidence. These records, the ones showing spin as well as the ones without spin,

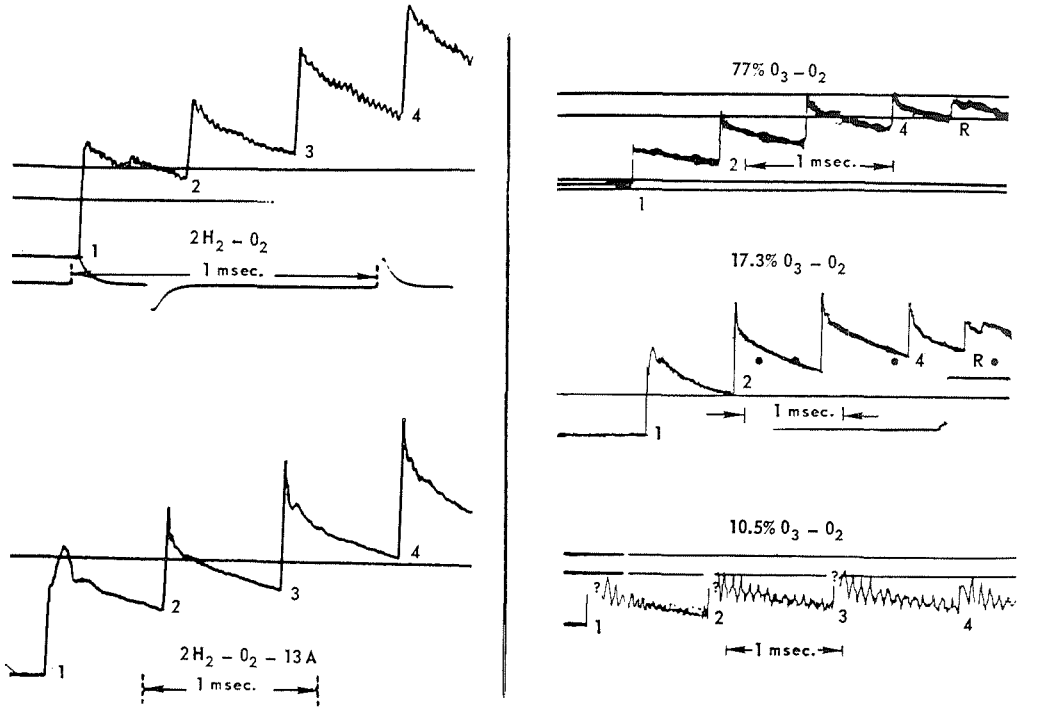

FIG. 1. The figures show oscilloscope records from four piezoelectric gauges placed at 1-meter intervals in the detonation tube. All gauges were connected to one channel; therefore, pressures are superimposed at succeeding intervals of time. Faint parts of the traces have been filled in with ink. Time scales are as indicated; pressure scales differ from gauge to gauge and record to record. The "smoothed" pressures, obtained by extrapolating the tail of the pressure contour back to the rise line, are comparable in magnitude with the theoretical C–J pressures, but always from 10% to 25% lower. On the other hand, the "spikes," where they are present, record pressures about 25% higher than the C–J values. The recorded peaks are, of course, reduced below the actual values because of the finite rise-time, which is in the range of 5 to 10 microseconds. It may be significant that the smoothed pressures are closer to the C–J values when the spike is present than when it is not.

were obtained with identical apparatus and with similar methods of initiation ($2H_2 + O_2$ driver).

It is likely that the regions in which these NDZ-like pressure traces are to be obtained will depend on the tube diameter, although this was always the same in our experiments (one inch). However, it is to be noted that these detonations were not overdriven, since the strength of the driver was studied over a wide range.[3] All evidence in these experiments supported the conclusion that the type of spin mode and the amplitude are intrinsic properties of gas composition and initial pressure (and, probably also, of tube diameter).

Although these data give no information on the presence or absence of turbulence in the reaction zone, they strongly suggest that the shock front is sometimes nearly planar and one-dimensional as prescribed by the NDZ model.

Dr. B. Lewis (*Combustion and Explosives Research Inc.*): This is a discussion of the cause of instability and shock generation in the detonation wave. I believe the instability to be a manifestation of the sudden ignition of a mass of gas that lies between the shock front and reaction zone behind it. The gas passing through the shock is heated and pressurized. Due to the slanting of the reaction front the induction period for ignition is transcended and the mass of gas referred to burns, giving rise to shocks, transverse and otherwise. Upon ignition the reaction front straightens out and the process is repeated resulting in pulsation. For a more detailed account of the suggested process I refer the reader to Lewis and von Elbe, "Combustion, Flame, and Explosion of Gases," Academic Press, 1951 and 1961.

Dr. S. R. Brinkley (*Combustion and Explosives Research Inc.*): Brinkley and Richardson,[4] in a discussion of possible quasi-steady detonation regimes showed that pulsating propagation is possible in one-dimensional systems under circumstances likely to exist in weak mixtures near the limit. It is felt that the description of the wave advanced in that paper provides a basis for the discussion of nonsteady propagation within the framework of classical theory.

Dr. F. W. Ruegg and Dr. W. W. Dorsey (*National Bureau of Standards*): Instability is evident in many schlieren pictures taken of the combustion region near a 20 mm spherical missile. The unstable detonations appear to be of two types. One type produces very regular and repetitive patterns from the front to far behind the missile. This is probably the result of a large amplitude acoustic oscillation that is driven by the Fame. A second type is probably due to surges which are connected with the way combustion is established as the missile enters the combustible gas. Although these patterns are repetitive, they do not display the symmetry and regularity of the acoustic oscillations, and generally the leading shock wave is more strongly affected by the surges.

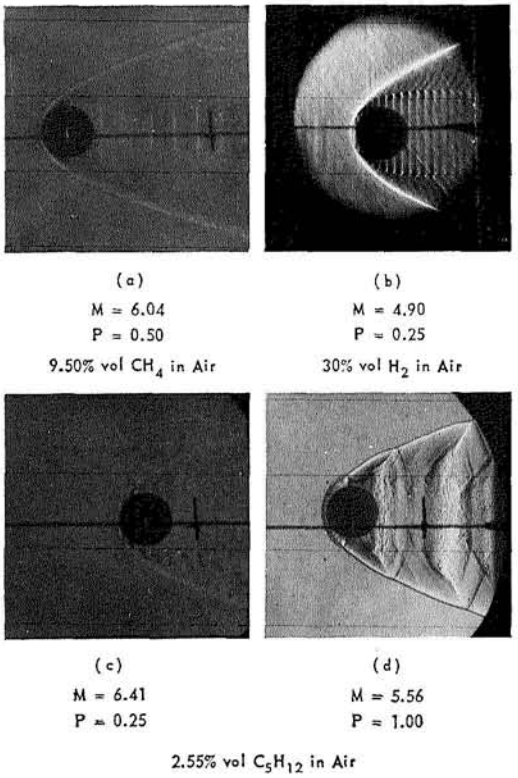

Fig. 2. Examples of unstable detonation near a hypervelocity missile. (a) $M = 6.04$; $P = 0.50$; 9.50% vol CH_4 in air. (b) $M = 4.90$; $P = 0.25$; 30% vol H_2 in air. (c) $M = 6.41$; $P = 0.25$; 2.55 vol % C_5H_{12} in air. (d) $M = 5.56$; $P = 1.00$; 2.55 vol % in air.

Figure 2 illustrates the various types of instabilities observed. Parts (a), (c), and (d) show combustion surges, while part (b) illustrates the effect of what is believed to be a strong acoustic oscillation. In this latter case, (b), waves propagate between the flame front and shock wave, and are there reflected and returned to the flame in proper phase to prevent damping of the disturbance. Range of Mach number, M, in the experiments is from four with hydrogen to seven in the pentane mixture. The observed distance, d, between surges varies by more than an order of magnitude. In this range of M the velocity of the shocked gas with respect to the missile can

vary by about only 35 per cent near the axis of flight where the wave is nearly normal to the axis. Thus distance, d, is approximately proportional to the period of the surges and oscillations, regardless of M.

In some instances the combustion appears intermittent, suggesting that ignition delay time may be an important part of the period of the surge. Ignition delay time, τ, is determined from the observed separation between the shock and combustion waves as described in ref. 5, and also by a technique described in ref. 6. While the times are well established for the hydrogen oxygen reaction, values used for pentane and methane are still tentative. Oxygen concentration, (O_2), mole liter^{-1}, accounts for the effect of pressure on the delay. A plot of d/R vs τ is presented in Fig. 3, where a linear relationship is obtained for pentane and possibly for hydrogen, but not for methane. A line labeled acoustic vibrations indicates the region in which the data for hydrogen at one-quarter atmosphere lie. The smaller values of d indicate a different oscillatory phenomenon.

The visible propagation of waves between the combustion and shock fronts of Fig. 2b suggests that acoustic waves at the front of the missile are responsible for the oscillations. Figure 4 shows a plot of d/R vs an approximate wave transit time between the combustion and shock

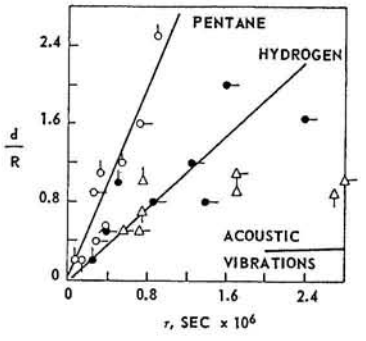

FUEL	SYMBOLS	C, ℓ. MOL^{-1} SEC^{-1}	T_a °K	PRESSURE
C_5H_{12}	o	1.43×10^6	23,000	1 ATM
H_2	•	1.60×10^4	8,570	½ ATM
CH_4	Δ	8.0×10^4	20,000	¼ ATM

$$\tau \times 10^6 = \frac{e^{T_a/T_2}}{c(O_2)}$$

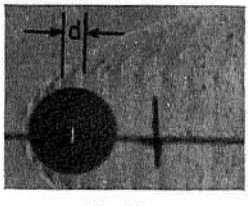

FIG. 3. Distance between combustion surges vs. ignition delay.

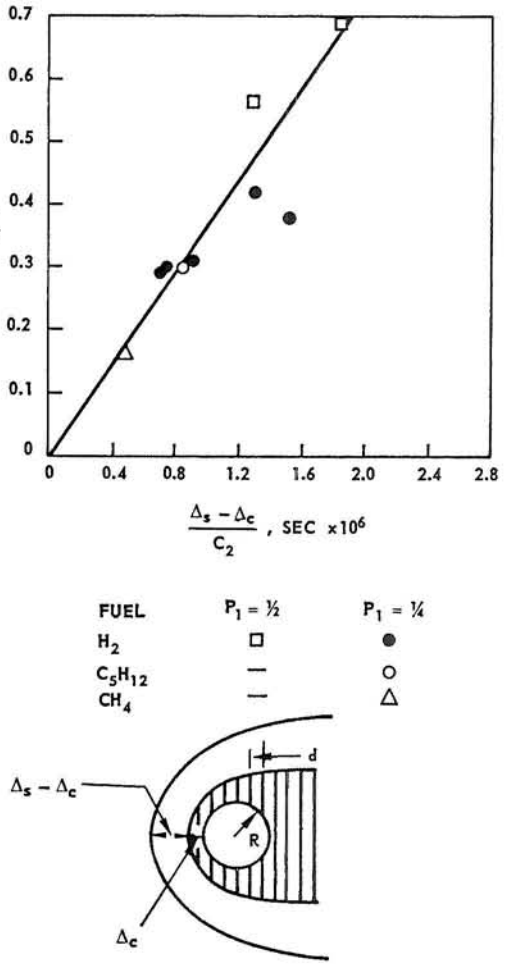

FIG. 4. Distance between acoustic oscillation vs. wave transit time between combustion and shock fronts.

fronts on the axis of flight. C_2 is the speed of sound there, and $\Delta_s - \Delta_c$ is the distance. A linear relationship indicates that the vibration is probably an acoustic effect. A more complete explanation would require an analysis involving a three-dimensional propagation of waves of finite amplitude with a time varying heat release.

DR. B. G. CRAIG (*Los Alamos Scientific Laboratory*): The evidence for turbulence in gas detonations presented by D. R. White[7] has generally been accepted. In the past year or so we have noted that some condensed explosive detonation phenomena can be explained by assuming that the detonation is not one-dimensional.

While engaged in reaction zone measurements we observed that shocked thin plates lost more

reflectivity than thick ones regardless of the actual pressure. To investigate this further we shocked thin aluminum foils (0.0003 inch thick) with nitromethane, water, and aqueous lead perchlorate and recorded specularly reflected light as a function of time and space with a smear camera. High magnification and resolution were used in order to observe small scale phenomena.

The photographs so obtained show some peculiar nonreflecting areas, presumably rough spots, which grow in size with time. Whatever is responsible for the nonreflecting areas is, by far, more prevalent in the case where the foil is driven by detonating nitromethane. The effect was not damped even when the length of the column of nitromethane was increased from one to six inches. A small reduction in the number of the nonreflecting areas could be obtained by initiating the nitromethane with a special booster system.

We have tentatively interpreted this data as evidence of turbulence of multidimensional flow in the detonation of condensed explosives. It is hoped that these comments will stimulate some of the audience to look for evidence of turbulence in condensed explosives.

DR. H. DEAN MALLORY and DR. W. S. MCEWAN (*U. S. Naval Ordinance Test Station*): In connection with the discussions of turbulence and other two-dimensional effects found behind the shock front in detonating gases, we should like to call attention to similar or perhaps related effects in the detonation of a homogeneous liquid system consisting of 18 molal hydrazine mononitrate (HMN) in hydrazine. This explosive was used because it is carbon free and it was hoped that its reaction products would be transparent and thus permit observation behind the reaction front. Nitromethane, which has been used by a number of investigators studying liquid explosives, was not useful under our experimental conditions since its products were opaque to our strongest backlight and this we believed was due to the presence of free carbon.

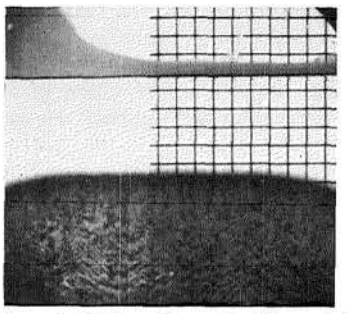

FIG. 5. Detonation of 18 molal HMN in hydrazine, $\frac{1}{4}$ inch thick charge, $\frac{1}{4}$ inch grid behind tank.

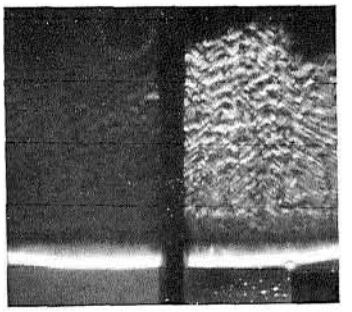

FIG. 6. HMN solution in divided tank, half of which was covered by tracing paper on tank back. Reduced brightness shows that backlight was transmitted.

Our experiments consisted of taking high speed photographs (0.15–0.20 μsec exposures) of liquid explosives in $6 \times 6 \times \frac{1}{4}$ inch "sheets." A "sheet" was contained in a tank having $1\frac{1}{2}$ inch thick Plexiglas front and back faces and backlighted with an explosive flash bomb. It was hoped that with clear reaction products, density gradients throughout the reaction zone could be observed. However, the appearance of strong turbulence, as seen in Fig. 5, prevented this. Indeed, the turbulence obscured the $\frac{1}{4}$ inch grid markers on the back surface of the tank. In experiments without backlight, proof of detonation was always obtained in later frames when a brilliant flash was observed at the liquid–air interface. This explosive is unusual in that no other detectable light is associated with its detonation. This can also be seen in Fig. 6 where a tank was divided by an aluminum separator. One division of the tank was covered with a tracing paper sheet on the back side which reduced the brightness showing that it was light from behind the tank, rather than in it, which was being transmitted.

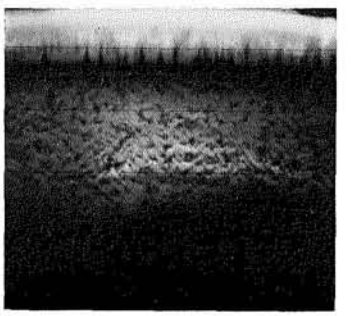

FIG. 7. Jets from free surface.

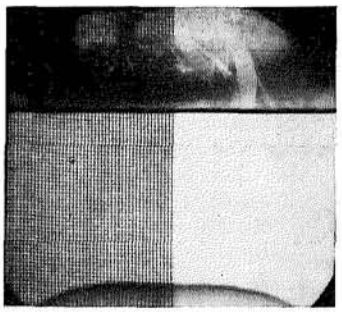

FIG. 8. Jets developed in failing detonation (6 molal HMN in hydrazine), screen wire grid. Turbulence is not developed behind pure shock front.

We believe the herringbone pattern in the wake of the wave can best be explained by initiation at individual sites. When the detonation wave reaches the free surface, small jet-like projections can be seen directly beneath the bright envelope leaving the surface (Fig. 7). Also, if the HMN is further diluted to 6 molal concentration, detonation seems to begin but does not propagate from a strong external shock. In this case, similar hair-like projections (opaque presumably from nitrogen oxides) can be seen extending for a short distance into the liquid (Fig. 8). From this, we postulate that detonation can start at discrete random points and spread spherically from these points. As the reacting spherical zones coalesce, the associated shock wavelets collide and cause reinitiation on a line midway between initial sites. As this process is repeated, lines of initiation tend to move at approximately 45° from the center line of the charge. Using plate glass confinement or thinner charges in Plexiglas, (the latter is seen in Fig. 9) strong turbulence is still observed but the patterns are more random. Thus, the herringbone pattern may, in part, be due to charge dimensions.

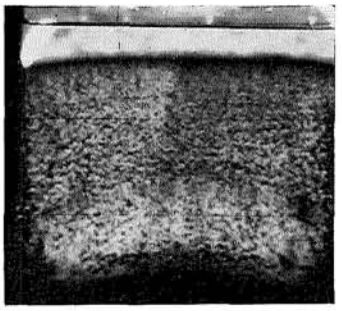

FIG. 9. Identical with subject of Fig. 5 except charge is $\frac{1}{8}$ inch thick. Turbulence is more random.

In conclusion we can say that we have seen what appears to be turbulence in the reaction products of a detonating homogeneous liquid which seems to have been generated at discrete points near or on the reaction front. The scale of this disturbance is similar to that which would be generated in a flow system by a mesh of from 25 to 200 squares per square centimeter.

DR. J. R. TRAVIS (*Los Alamos Scientific Laboratory*): When nitromethane is detonated in a tube near failure diameter or is diluted with an inert liquid, end-on smear camera records show dark regions crossing the bright field of the detonation light. We distinguish two types of behavior which are certainly related but the differences are quite recognizable. The first type is failures, single events due to rarefactions which temporarily quench detonation. The second type is apparently a set of stable waves which run back and forth across the detonation in a quasi-steady-state condition. These we call dark waves.

Several different observations have been made on these waves. First, in pure nitromethane there are:

1. Failures moving inward from the walls of a tube near failure diameter; i.e., Fig. 1 in the paper by Campbell *et al.*[8] These can be induced by grooves or holes in the walls, but large wall defects are not necessary to produce failures.
2. Detonation cutoff when the detonation wave expands from a well-confined region of diameter less than the failure diameter; i.e., Fig. 3 in ref. 8.
3. Any short radius divergent detonation shows failures; i.e., detonation starting from a shock interaction at a bubble. (See Figs. 13 and 14 in ref. 9). When nitromethane is diluted with acetone (~10 to 30% by volume) or toluene (~10 to 20%), one can observe the above phenomena as well as the following:
4. Quasi-steady-state dark waves, such as those shown in Fig. 2 of ref. 8.

These phenomena must be related but the cause of detonation quenching and reignition may not be the same in each case.

If the failure is large enough, i.e., if the detonation has been quenched for a long enough time, one observes the usual initiation behavior. Following the dark zone on an end-on smear camera picture is a region of low-level light, followed by a bright overshoot before the steady state intensity level is reached. Such evidence in the case of dark waves is not as clear largely because of camera resolution problems.

It is reasonable to suppose that the cause of failures of the kind described in 1, and 2, above

is a large drop in the pressure immediately behind the shock due to rarefractions from the unsupported edges.

The explanation for the cause of dark waves is still obscure. I believe the mechanism must involve stable perturbations existing near the front.

One interesting point in connection with dark waves is that their velocity is relatively constant (and equal to the velocity of cutoff) and is appropriate for sound velocity of nitromethane compressed to the value it would have immediately behind the shock wave.

Finally, I would like to make two specific comments relative to the experimental problem.

1. When photographing dark waves with a smear camera only a few of the total number of dark waves will register on the film at a particular writing speed, slit width, and magnification.

This can be shown both analytically and experimentally. For example, we have taken an end-on smear picture of the dark waves in a 25% acetone-nitromethane solution in which in effect the charge is observed simultaneously with slits perpendicular to each other. At the effective area of intersection, each slit should record the same event, but a detailed examination of the films shows no correlation between the two pictures of dark or light regions.

2. Failures in the detonation wave are related to the confinement of the charge. The two criteria which determine whether or not there will be failures are the shock impedence, $\rho_0 U_s$, and the time before a rarefaction from the outside wall can enter the charge.

A third condition is related to the smoothness of the walls. If the walls are sufficiently rough, pressure interactions can raise the local temperature sufficiently to lower the critical values of the first two criteria. For example, a wire screen lining a tube in which detonation would normally show large failures will reduce the number of failures dramatically.

DR. S. J. JACOBS (*Naval Ordnance Laboratory*): It seems to be there is little doubt of the existence of such waves moving across the detonation front. Unpublished smear camera records by Campbell have shown such herringbone patterns. I would be inclined to believe that their amplitude would not be high, perhaps a few kb above or below the norm. However for nitromethane a few kb could have a significant effect on the induction period and therefore the instability could continue to exist once it begins.

DR. B. B. DUNNE (*General Atomic*): Stimulated by a suggestion from Dr. D. R. White[10] we began looking into the possibility of detonation wave turbulence in condensed media. We now believe that we have fairly conclusive experimental evidence that there is indeed a complex turbulent structure in the flow immediately behind an overdriven detonation front, in both liquid and solid explosives. The results of this investigation imply that the flow behind a C–J detonation front, in such media, is also turbulent. Details of this work will be published shortly in the *Physics of Fluids*.

DR. F. E. ALLISON (*Ballistic Research Laboratories*): The pressure-sensitive electrical characteristics of sulphur[11,12] have been used for detecting large pressure gradients in the region between 80 and 200 kilobars. As shown in Fig. 10, the active element is a 0.005 inch thick sulfur disc embedded in a Teflon receptacle. Teflon was chosen because it is a good impedance match for sulfur. Since Teflon is a nonpolar insulator it is also free from spurious signals resulting from shock-induced displacement currents.[13] The resistivity of vacuum-melted sulfur is shown in Fig. 11 for different values of the shock strength. The calibration is based on the peak shock strength produced in an aluminum buffer plate by an explosive charge initiated with a plane wave lens. The peak pressure is varied by changing the thickness of the aluminum buffer plate. After calibrating a device suitable for detecting rapid changes in pressure, measurements were made which show the pressure profile of a detonation wave in a condensed explosive.[13,14]

Baratol (67–33) was chosen because the Chapman–Jouget pressure falls conveniently within the range covered by the sulfur detector. The pressure profile obtained from tests with 2 inch diameter baratol charges is illustrated in Fig. 12. The lower curve represents the pressure seen by the sulfur detector. The upper curve shows the time variation of the pressure in the detonating explosive. The pressure profile obtained from these tests indicates the presence of a von Neu-

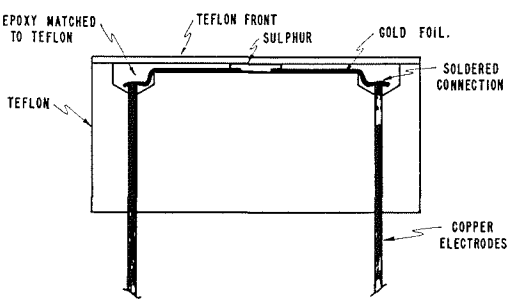

FIG. 10. Modified sulfur gauge.

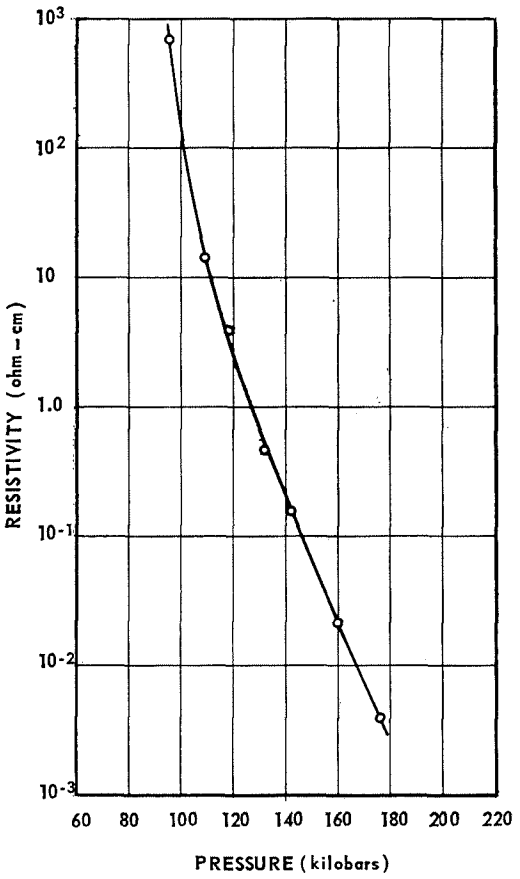

FIG. 11. Calibration curve—sulfur.

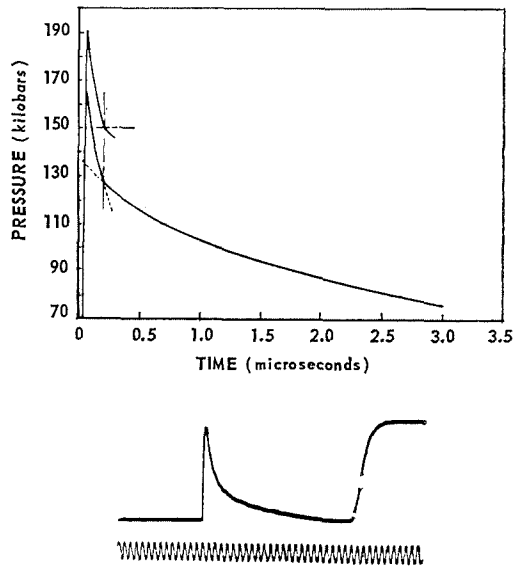

FIG. 12. Pressure profile—Baratol.

mann spike followed by a Taylor wave. The initial pressure of 190 kilobars is not the maximum since the pulse is limited by the rise time of the associated electronics and the pressure attenuation in the Teflon cover, which insulates the sulfur element from the ionized gases in the detonation front. The change in the pressure–time curve indicates a Chapman–Jouget pressure of about 150 kilobars and a reaction time of about 0.2 μsec.

Present efforts are directed toward improving the response and reproducibility of the pressure-sensitive sulfur element by using carefully ground single crystals. Also, questions associated with using a calibration curve based only on peak pressure data are being examined. Refinements in the technique may change quantative values slightly; however, the general characteristics of the pressure–time profile and the physical interpretation of these characteristics appear to be well established.

REFERENCES

1. GORDON, W. E., MOORADIAN, A. J., and HARPER, S. A.: *Seventh Symposium (International) on Combustion*, p. 752. Butterworth, 1959.
2. HARPER, S. A. and GORDON, W. E.: *Ozone*, Advances in Chemistry Series No. 21. American Chemical Society, 1959.
3. MOORADIAN, A. J. and GORDON, W. E.: J. Chem. Phys. *19*, 1166 (1951).
4. BRINKLEY, S. R., JR. and RICHARDSON, J. M.: *Fourth Symposium (International) on Combustion*, p. 450. Williams and Wilkins, 1952.
5. RUEGG, F. W. and DORSEY, W. W.: J. Research Natl. Bur. Standards *66C*, 51 (1961).
6. SCHOTT, G. L. and KINSEY, J. L.: J. Chem. Phys. *29*, 1177 (1958).
7. WHITE, D. R.: Phys. Fluids *4*, 465 (1961).
8. CAMPBELL, A. W., HOLLAND, A. W., MALIN, T. E., and COTTER, T. P., JR.: Nature *178*, 38 (1956).
9. CAMPBELL, A. W., DAVIS, W. E., and TRAVIS, J. R.: Phys. Fluids *4*, 498 (1961).
10. WHITE, D. R.: Private communication, September 1961.
11. ALDER, J. and CHRISTIAN, R. H.: Phys. Rev. *104*, 550 (1956).
12. JOIGNEAU, S. and THOUVENIN, J.: Compt. rend. *246*, 3422 (1958).
13. EICHELBERGER, R. J. and HAUVER, G. E.: *Solid State Transducers for Recording of Intense Pressure Pulses*. Les Ondes de Detonation, Editions du Centre National de la Recherche Scientifique, p. 363, 1962.
14. HAUVER, G. E.: *Third Symposium on Detonation*, p. 241. ONR Symposium Report ACR-52, Vol. 1, 1960.

THE ONSET OF DETONATION IN A DROPLET COMBUSTION FIELD

FRANK B. CRAMER

A sequence of events has been described which offers an explanation for the processes leading to the onset of detonation in a heterogeneous field of low volatility fuel droplets. While the gross pattern appears superficially similar to that occurring in premixed gases, the detailed mechanisms must be explained in terms of the physical behavior of the liquid component of the two-phase system.

The pressure ratios and shock velocity relations of both weak and strong shocks in this study fall very close to the values which are calculated for oxygen. That is, the gas phase into which these shocks are being driven is essentially pure oxygen at ambient temperatures. The highest concentration of fuel in this study was 0.20 volume per cent. The transport phenomena to produce fuel vapor at a rate sufficient to drive these detonation-like waves at the temperature differentials involved require specific surfaces which are orders of magnitude greater than the original spray presented. A type of mechanical shattering must be available which will produce enough of a less than 10-micron droplet mist to provide sufficient fuel vapor to continue to drive the detonation front. The effects of the predetonation, flame-driven flow field controls the time and magnitude of the onset of detonation through droplet shattering these flows impose.

Introduction

The development of very reliable large liquid rocket engines has been accomplished through a continuing advancement in the understanding of the basic mechanisms responsible for combustion instability. Studies of heterogeneous combustion in high Reynolds number flow fields[1] lead directly to the study of spray combustion in the presence of a travelling wave. The earlier phases of this work, reported at the 8th Symposium,[2] showed that sprays of very low volatility liquid fuels in gaseous oxidizers could be induced to generate and support high-amplitude, shock-like waves. This paper describes the processes which are occurring in this heterogeneous system leading up to the onset of a detonation-like phenomenon.

The Onset of Detonation in Premixed Gases

A review of the events leading to a detonation in a premixed gas and in the heterogeneous spray system illustrates a superficial parallelism of events. This apparent similarity must not be interpreted as an actual identity of events. There are actually a number of very critical heterogeneous phenomena controlling the onset of the detonation-like process in sprays.

Description of Conditions that Lead to the Onset of Detonation in a Droplet Spray Field

Experimental Apparatus and Techniques. Two, 2 × 96 inch, shock-tube devices were employed

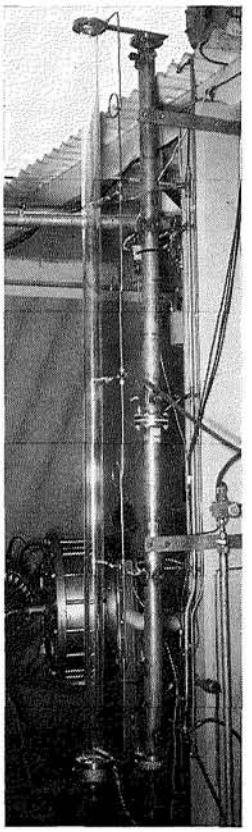

FIG. 1. Droplet spray shock tubes.

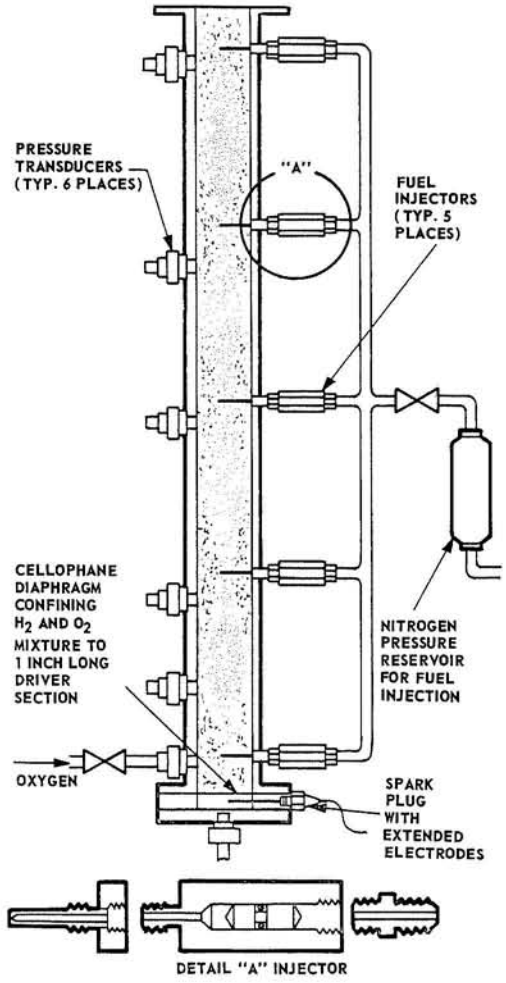

FIG. 2. Schematic of shock-tube installation.

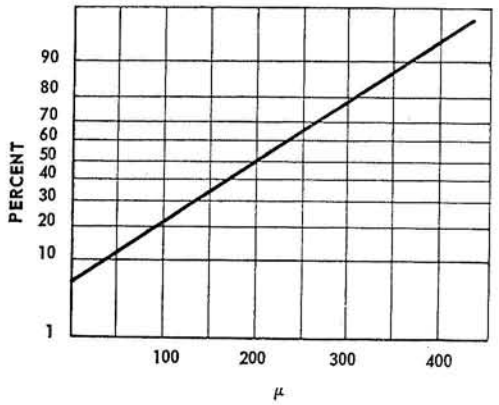

FIG. 3. Measured drop size vs normal accumulation ordinate.

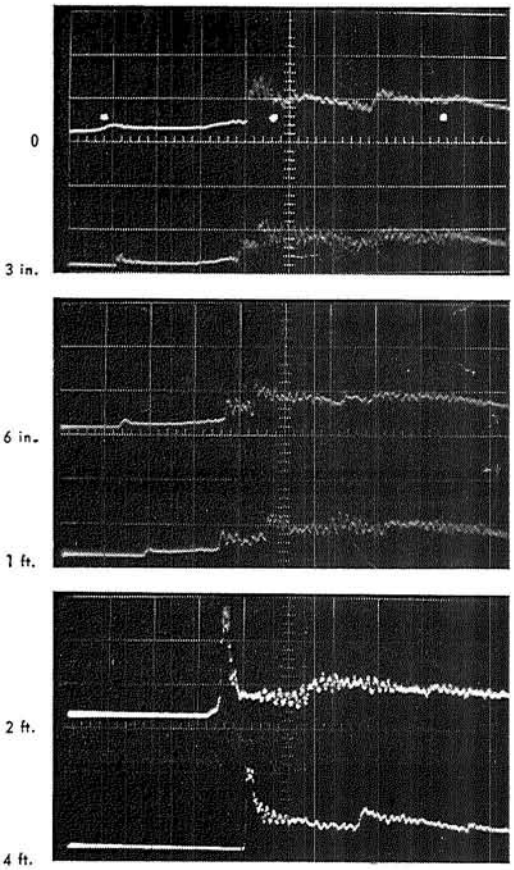

FIG. 4. Pressure record showing detonation. Injection to ignition delay, 0.200 sec; Fuel type, DECH; Fuel amount, 6 ml; Injection pressure, 150 psig; Oxygen pressure, ambient; Horizontal scale, ½ millisec/division; Vertical amplitude, 300 psi/division.

on this study, one of polyacrylate ester for photographic coverage, the other a stainless-steel tube for p–t–x records (Figs. 1, 2). Both tubes are equipped with five fuel injectors. Each of the central three injectors has an up and a down orifice. The end injectors each has a single inward oriented orifice. The orifice size is 0.0225 inch diameter. Fuel was expelled by movement of a small piston which was driven by gaseous nitrogen pressure. High-speed movies of the transparent tube showed a very uniform spray distribution throughout the tube in the period 100 to 300 milliseconds after injection with little fuel accumulation on the tube walls. The distribution follows a reasonably normal pattern (Fig. 3).

The steel tube was equipped with flush-mounted pressure pick-ups located at the outboard end of the driver section and on the side

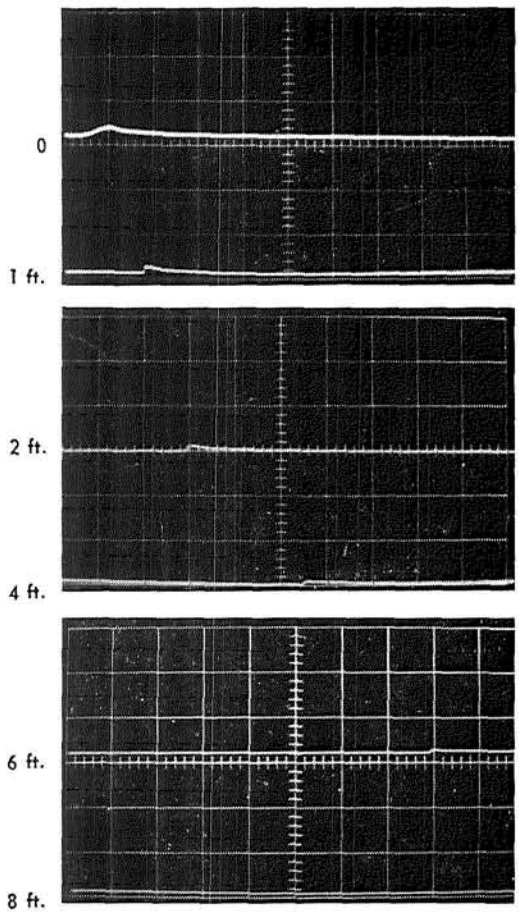

FIG. 5. Pressure record showing driver induced perturbation only. No fuel. Injector to ignition delay, 0.200 sec; Oxygen pressure, ambient; Horizontal scale, ½ millisec/division; Vertical amplitude, 200 psi/division.

of the main chamber at positions 3, 6, 12, 24, 48, 72, and 96 inches downstream of the position of the diaphragm. High response pressure pickups were employed, i.e. Photocon (325) and S.L.M. (601) pickups. The Photocon pickup signals were subjected to an electronic second order differential compensator (DADEE) and the S.L.M. signal was filtered for 100 kc ringing. The rise times of these output signals so treated are 20 and 15 microseconds, respectively. The corrected outputs of the pressure pickups were displayed on oscilloscopes to produce pressure–time histories of several locations in the tube (Figs. 4, 5). All of the oscilloscopes employed the same triggering signal for coordinated starts. The time base of the oscilloscopes was calibrated with a Tektronix "time base generator" so that each measured time could be assigned an exact time value.

The shock tube was filled with oxygen at one atmosphere pressure, while the one-inch long driver section was charged with a stoichiometric hydrogen–oxygen mixture. Fuel was injected into the tube, and after a preset delay the driver section was spark-ignited. The ignition impulse triggered the simultaneous start of all of the pressure recording oscilloscopes. The burning hydrogen-oxygen mixture consumes a one-mil cellophane membrane separating the driver chamber from the main chamber. This burning element behaves as "a hot gas piston", driving a pressure wave down the tube (Fig. 5). The burning time in the driver section is approximately 0.500 millisecond. Diethylcyclohexane (DECH) was the fuel most extensively employed in this study. Approximately 2.2 ml would have been the stoichiometric amount of fuel for the available volume. No detonations occurred when 2.0 or 2.5 ml of fuel were injected. When 3.0 and 3.5 ml were studied, there were no detonations in about 50 per cent of the cases. For 4.0 to 8.0 ml, a detonation consistently took place.

Discussion of Results

If the separating membrane disappears at the start of ignition, this system may be considered analogous to the burning gas driver section treated by Rieman characteristics by Rudinger.[3] The initial portions of the flow fields between the contact surface and the shock front were estimated (Fig. 6). The pressure histories in Fig. 5 are from a run with no droplets in the chamber.

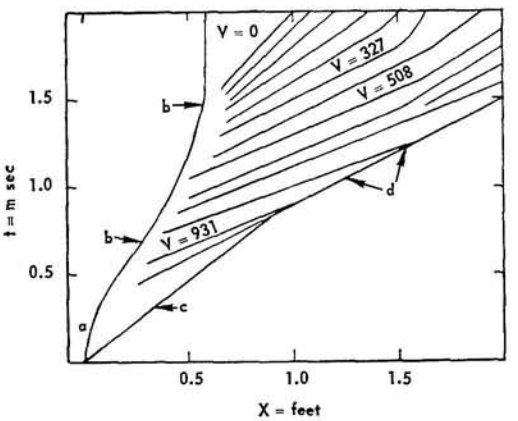

FIG. 6. Driver induced shock. a. Burning zone, b. contact surface, c. first forward pressure perturbation, d. shock front (gas velocities in ft/sec).

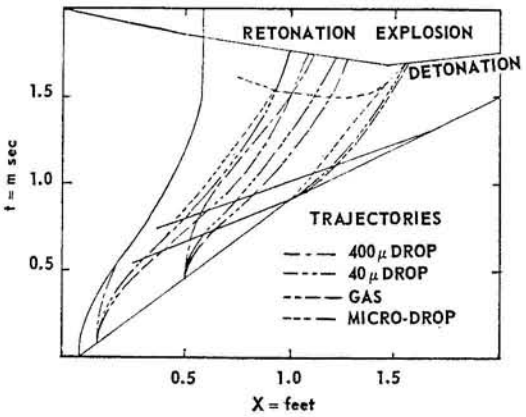

FIG. 7. Location of initial explosion. (Note droplet trajectories in the pre-explosion zone.)

An examination of the predetonation portion of the driven wave in Fig. 4, shows that the presence of droplets does not markedly impede or otherwise change its projected path. This is graphically presented in Fig. 7.

It is reasonable to consider that the flow field calculated from the tube without a spray charge will adequately describe the flow field to which the spray charge will be subject. In Figs. 4 and 7, it may be seen that a cataclysmic event occurs just short of the 2-foot measuring station and 2 milliseconds. The bulk of the initial explosions takes place in the region of the t–x plot between 1 and 2 feet, between 1 and 2 milliseconds. When conditions in the main chamber are marginal, the initial explosions are occasionally delayed. It is only on rare occasions that the initial onset occurs closer than 1 foot from the original diaphragm position.

At ignition, the injected fuel may be considered to be at rest. The gas drag has brought the spray field to an essentially stationary state. At ignition, the gases in the driver section expand, pushing the contact surface into the main chamber. This moving piston-like action generates forward-moving pressure wavelets pushing into the heterogeneous field. The heat release in the driver section accelerates, resulting in the downstream coalescence of these pressure perturbations to a shock front. There exists a time space period between ignition and the onset of explosion in which a heterogeneous droplet field is subjected to a transient variable flow field.

Droplet ballistics are described by Newton's Second Law of Motion, using empirically derived drag coefficients, such as:

$$dV_d/dt = (3C_D\rho_g V_r \mid V_r \mid)/4\rho_l D \qquad (1)$$

With both burning and nonburning drops, Rabin *et al.*,[4] observed that flattening of the droplets at high Reynolds numbers causes an increase in the apparent drag coefficient. Based on their data, a combination of expressions was derived to describe drag coefficients over a wide range of turbulence, namely:

$$C_D = 27\ \mathrm{Re}^{-0.84}, \qquad 0 < \mathrm{Re} < 80; \qquad (2a)$$

$$C_D = 0.271\ \mathrm{Re}^{0.217}, \qquad 80 < \mathrm{Re} < 10^4; \qquad (2b)$$

$$C_D = 2.0, \qquad \mathrm{Re} > 10^4. \qquad (2c)$$

Lambiris *et al.*,[5] showed these values to fit very well with the observed droplet trajectories in massed-droplet flows in a transparent rocket motor.

From these relations, the paths of three sets of droplets and the corresponding initially asso-

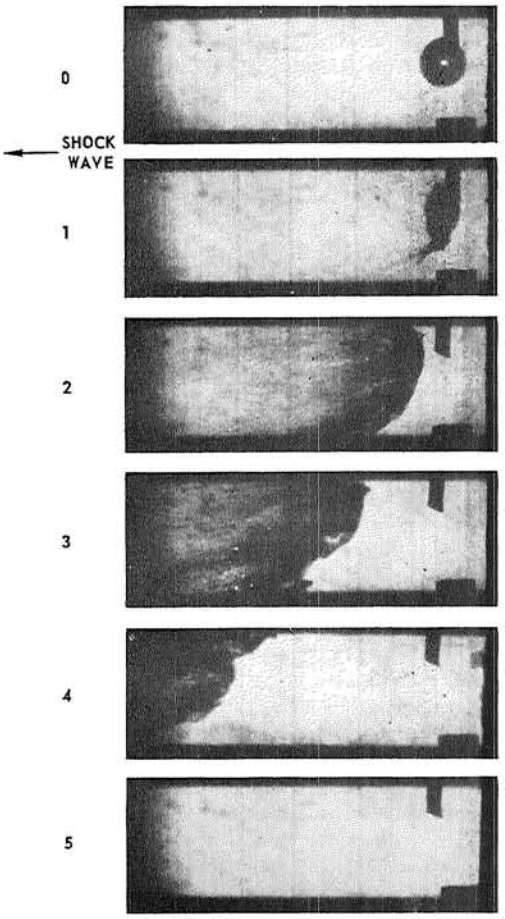

FIG. 8. Shear microdrop formation. Breakup of water droplet in high velocity air flow. Flow velocity, 760 ft/sec; Droplet diameter, 927 microns; frame rate, 12,700 frames/sec.

ciated gas particle path are shown in Fig. 7. It is seen that a substantial portion of the fine, high specific surface fraction of the droplet population is swept away from the contact surface of the hot burned gases of the driver region. In the precritical zone, the original distribution of droplet sizes is nearly restored. This balancing is the result of fine droplets which are swept in from upstream elements replacing those original fines which are swept downstream by the high relative gas velocities.

In addition to being displaced, droplets are also shattered by high relative velocity gas flows. Rabin,[4] showed that 1000-micron-diameter droplets would shatter with surface shear (Fig. 8) when abruptly subjected to flows of markedly greater than critical velocities. It appears that the sudden increase of relative gas velocity causes the shearing off of the surface layers before the body inertia of the drop will allow it to deform in response to this loading. Lambiris *et al.*,[5] found that it was necessary to assume delays to shattering of the order of one-half millisecond in their rocket chamber flow field to make their data self-consistent. Relative gas velocities as high as the value which shear shattered droplets were frequently found in rocket studies. In Lambiris' rocket chamber, however, these high relative gas velocities were not imposed abruptly, but took a few tenths of a millisecond for full maximum velocity differentials to occur. It would appear that when loading rates are sufficiently slow relative to the fundamental mechanical period of the droplet that the time to shatter is substantially increased.

The gas flows observed in Fig. 7 present two distinctly different types of gas drag loading. In the region between the contact surface and the collapse of the forward moving pressure perturbations into a shock front, the droplets are overtaken by gases with a gradual velocity build-up. Those droplets which are overtaken by the flow fields after shock wave formation will be subjected to a very abrupt gas drag loading with initial relative gas velocities of the order of 900 feet per second. This abrupt type of loading will result in surface-shear shedding of microdroplets which very rapidly assume the local gas velocity. This process can produce a substantial shower of microdroplets in the initial 100 microseconds (Fig. 8), however, nearly a millisecond at full gas velocity is required for complete droplet shattering to microdroplets.

The combustion region in the droplet field will be exposed to three different droplet population distributions as burning progresses downstream from the contact surface. The first zone is relatively free of fine droplets. This zone is followed by a zone with nearly the original size distribution of droplets. Finally (after 1 millisecond), the burning zone approaches the zone loaded with impact shear-produced microdroplets. At about the time the leading edge of the flame zone reaches this zone, the bulk of the large droplets in zones one and two (which is now a diffuse burning zone) will be shattering. Within a very brief period an order of magnitude larger droplet surface is formed.

A momentary explosion heat release is achieved which is capable of driving the flame front to the shock front. The detonation wave is apparently maintained by the burning of the shear-produced microspray immediately behind the shock front.

Quite frequently, the rapid shattering of larger droplets (above 50 microns) throughout the depth of the established flame zones will transiently result in a greater time rate release of heat than can be maintained by a thin flame front associated with the subsequent detonation front. This results in a velocity overshoot which must slow down to the level which can be driven by the heat release from the leading edge of the flame zone.

Nomenclature

C_D	Coefficient of drag
D	Drop diameter (microns)
Re	Reynolds number
u	Local gas velocity (feet per second)
V_d	Drop velocity
V_r	Relative velocity (drop to local gas) (feet per second)
ρ_g	Density of gas (pounds per cubic foot)
ρ_l	Density of liquid (pounds per cubic foot)
μ	Micron

Acknowledgments

An extensive amount of experimental and background data for this program was generated during the time that Mr. W. T. Webber was in charge of these studies.

The author wishes to acknowledge provocative stimulation provided from conversations with Dr. A. K. Oppenheim and Dr. A. Laderman.

This effort has been sponsored by the AFOSR, Office of Aerospace Research under Contract AF49(638)-817.

References

1. Cramer, F. B., Webber, W. T., and Lawhead, R. B.: WADC T.N. 57-426 (ASTIA AD 142255), 1957.

2. WEBBER, W. T.: *Eighth Symposium (International) on Combustion*. Williams and Wilkins, 1962.
3. RUDINGER, G.: *Wave Diagrams for Nonsteady Flow in Ducts*. Von Nostrand, 1954.
4. RABIN, E., SCHALLENMULLER, A. R., and LAWHEAD, R. B.: AFOSR 60–75, 1960.
5. LAMBIRIS, S., COMBS, L. P., and LEVINE, R. S.: *Fifth Colloquium of the Combustion and Propulsion Panel*, AGARD. Braunschweig, Germany, 1962.

STANDING DETONATION WAVES

J. A. NICHOLLS

It has long been realized that gaseous detonation waves are capable of propagating at high supersonic or even hypersonic velocities. This characteristic arises from the fact that the associated shock wave must elevate the unburned gas to a temperature sufficiently high that the chemical reactions can occur rapidly. The meaning of "rapidly" in this sense is that the length of the reaction zone must not be long compared to a characteristic dimension of the system. The usual method of studying such phenomena is through the use of flame tubes or shock tubes wherein the detonation wave propagates at the high velocities mentioned. In recent years a few groups have reported in the open literature the results of experiments directed to the study of standing or stabilized detonation waves (SDW). Such a wave can be attained (maintained stationary relative to laboratory coordinates) when a combustible mixture is accelerated to the appropriate velocity, pressure, and temperature conditions and then subjected to a shock wave. The ensuing complicated phenomena can vary somewhat between different experimental environments and from similar results obtained in shock tubes. Accordingly, it is well to be able to understand the reasons for these differences so that the shock-combustion wave can be better understood and thus the possible utility of the SDW technique evaluated. It is the purpose of this paper to examine the reported results on SDW as obtained in different facilities and compare them. Comparison will also be made with results obtained from shock tubes and a ballistic range. Towards this end it will be instructive to consider the ignition delay period, the effects of vibrational relaxation, and the importance of two-dimensional effects.

Experimental Facilities and Results

The experiments at the University of Michigan SDW facility[1–4] were effected by expanding high pressure, heated air through an axisymmetric convergent-divergent nozzle exhausting to the atmosphere. High pressure, unheated hydrogen was introduced at the throat and the gases mixed partially in the supersonic portion of the nozzle. Limited residence time and a dropping static temperature ordinarily precluded combustion in the nozzle. The nozzle was operated highly underexpanded and the familiar jet pattern shown in Fig. 1 was realized. A relatively small portion of the total mass flow passes through the Mach disc and hence the hydrogen/air ratio across the disc was quite uniform. The Mach number into the shock was high (4.5–6) so that the Mach number immediately downstream of the shock was low ($\simeq$0.4) and the static tempera-

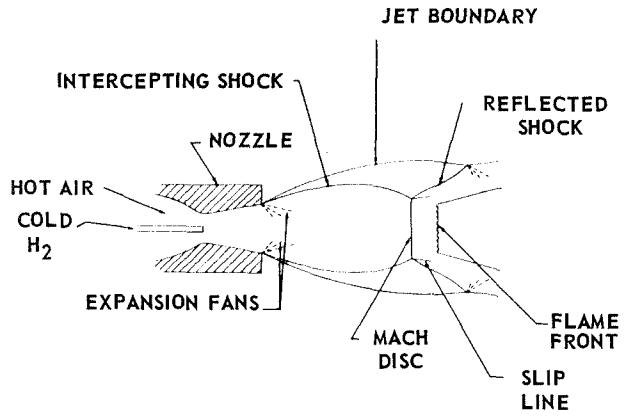

FIG. 1. Structure of underexpanded jet.

ture close to the stagnation temperature, this temperature being sufficiently high to "ignite" the mixture after a suitable ignition delay period. A number of experiments were conducted wherein the hydrogen-air ratio, the stagnation temperature, and the Mach number into the shock were varied. Note was taken of the shock wave position with and without combustion and the flame front position.

The supersonic combustion tunnel at Arnold Engineering Development Center (AEDC), which was originally designed, fabricated, and operated at Fairchild Engine Division, produces a shock pattern in the test section which is very similar to the underexpanded jet structure.[5,6] The normal shock is achieved in the two-dimensional Mach number 3.1 test section by the Mach reflection of two intersecting oblique shocks generated by wedges on the upper and lower tunnel surfaces. The hydrogen (heated to about 700°F) is introduced on the tunnel centerline either by an injector just upstream of the throat or right at the throat. Thus with the tunnel being two-dimensional there is neither truly two-dimensional nor axisymmetric flow at the normal shock location. The air is heated to 1200°F by an indirect fired heater and the rest of the heating is accomplished by the combustion of hydrogen in the plenum chamber of the tunnel.

Rhodes and Chriss[7] have reported on a series of experiments which were conducted in this facility. The experiments covered a range of hydrogen–air ratios and stagnation temperatures but at a fixed Mach number of 3.1. The use of the hydrogen injector upstream of the throat led to burning immediately downstream of the injector. The use of the throat injector eliminated this premature burning and then the phenomena observed in the test section were qualitatively identical to those observed at the University of Michigan.

A variation of the SDW technique is the ballistic range technique as has been reported by Ruegg and Dorsey.[8] This technique differs from the above in that the wave is maintained stationary relative to a projected nylon sphere rather than stationary relative to laboratory coordinates.* The three-dimensional geometry makes it difficult to compare these results to the previous ones but some attempt to do so will be made in a subsequent section.

A comparison of the general results obtained in the AEDC and UM facilities reveals the following:

(a) In both cases a certain minimum temperature is required before ignition occurs behind the shock.

(b) The shock wave and combustion zone are distinctly separated, this separation decreasing rapidly with increasing temperature.

(c) There is practically no influence of the presence of combustion on the shock wave except for a few isolated cases observed at UM wherein the shock was observed to move upstream slightly when combustion commenced.

Nicholls and Dabora[3] discussed the hydrodynamic and chemical kinetic considerations involved in generating SDW. As part of this discussion they invoked the explosion limit criteria to arrive at a predicted minimum temperature required to cause ignition behind the shock. With the pressure behind the shock taken as 1.3 atmospheres, which was the case in the UM experiments, the minimum temperature calculated ranged from about 1780°R for very lean mixtures to about 1850°R for rich mixtures. The UM experimental data appears to be in good agreement with these predictions although no systematic experimental investigation was undertaken to firmly establish this explosion limit variation with hydrogen-air ratio. Rhodes and Chriss[7] indicate that they first achieve ignition when the temperature reaches 1750°R. This temperature is somewhat below that indicated above but the difference is in the right direction when one considers that the pressure behind the shock at AEDC is 0.8 atmospheres. This lower pressure lessens the effect of the three-body chain-breaking reaction, $H + O_2 + M \rightarrow HO_2 + M$, which is involved in the explosion limit criteria. Of course, the temperature measurements in the two facilities are subject to some error which may account for the difference.

The separation between the shock and flame is attributable to the ignition time delay which is appreciable at the limited temperatures utilized in the UM and AEDC tests. If one invokes the criteria that the ignition delay distance be small compared to a characteristic dimension of the system, one arrives at a temperature of about 2050°R behind the shock in the case of the UM facility.[3] The results would not be too different for the AEDC facility. If one further requires that the reaction zone be essentially completed in this same relatively small distance, a temperature of a few hundred degrees higher would be required. As to the question of coupling between the shock and combustion zone, this should depend on the stagnation pressure loss across the shock as compared to that across the flame. In the case of high Mach numbers, such as are achieved in the UM facility, the stagnation pressure loss across the shock will far exceed that

* These spheres were fired at different Mach numbers into a stoichiometric mixture of hydrogen air maintained at a few different pressure levels.

across the combustion zone so that the shock will be perturbed little by the heat release. It was only at the higher temperatures with appreciable hydrogen content that sufficient energy was released near enough to the shock to force the shock slightly upstream into a region of lower Mach number, presumably to lower the stagnation pressure loss across the shock to accomodate that across the combustion zone. In the case of the AEDC facility the Mach number is much lower and hence more sensitivity of shock position to heat release would be expected. Evidently no coupling has been observed to date, however.

A more detailed comparison of the results obtained in the two facilities is presented in the following sections.

Hydrogen–Oxygen Ignition Delay. The experiments performed at the UM and AEDC have been limited in stagnation temperatures into the wave. Consequently, the static temperature behind the shock is not sufficiently high to yield "immediate" combustion and an ignition time delay zone results. In this zone the hydrodynamic variables remain essentially unchanged until the immediate vicinity of the "flame." It would appear, then, that the SDW is a convenient technique to facilitate the study of very short (microsecond range) ignition time delays. In this section as well as subsequent sections consideration will be given to such results already obtained and the factors that have influence on the observed results.

The hydrogen-oxygen-diluent ignition time delay has been studied quite extensively, theoretically as well as experimentally, by a number of investigators[2,4,9,10,11] and for the most part is quite well understood. For the temperature range 1100°–2000°K the pertinent reactions are:

$$H_2 + O_2 \xrightarrow{k_5} 2OH \qquad (V)$$

$$H + O_2 \xrightarrow{k_6} OH + O \qquad (VI)$$

$$H_2 + O \xrightarrow{k_7} OH + H \qquad (VII)$$

$$H_2 + OH \xrightarrow{k_8} H + H_2O \qquad (VIII)$$

wherein reaction V is the important initiation reaction to start the chain reaction of VI, VII, and VIII. Using a definition given by Nicholls,[2] we can write:

$$\tau = [2n_{O_2}(C)k_6]^{-1} \ln (n_{O_2}/n_{H_2} \cdot k_6/k_5) \qquad (1)$$

where: τ = ignition time delay; (C) = total concentration; n = mole fraction.

Many experiments were conducted in the UM facility using hydrogen–air mixtures wherein the distance between the normal shock wave and the visible flame front was measured. The data were reduced to yield ignition time delay versus temperature behind the shock. The details of these experiments and the methods of calibration are fully explained elsewhere.[2,3] Suffice it to say here that the hydrogen/air ratio was reasonably uniform over most of the Mach disc area and further this ratio has weak effect on ignition delay compared to the overpowering influence of temperature. It was estimated that the temperature was uncertain by about 40°K. The results of these experiments are shown in Fig. 2 along with a plot of Eq. (1) for stoichiometric hydrogen-air. The values used in the rate constants, $k = A \exp(-E/RT)$ were:

$$A_5 = 10^{14} \text{ (moles/cc)}^{-1} \text{ sec}^{-1}$$

$$E_5 = 7 \times 10^4 \text{ cal/mole}$$

$$A_6 = 10^{14} \text{ (moles/cc)}^{-1} \text{ sec}^{-1}$$

$$E_6 = 1.8 \times 10^4 \text{ cal/mole}$$

The data are plotted as $n_{O_2}(C)\tau$ versus reciprocal temperature in order to suppress the influence of mixture ratio.

Similar measurements on hydrogen-air were made by Rhodes and Chriss[7] and their results are also included in Fig. 2.

Ruegg and Dorsey[8] reduced their data on hydrogen–air in terms of the same parameter by measuring the separation on the axis of sym-

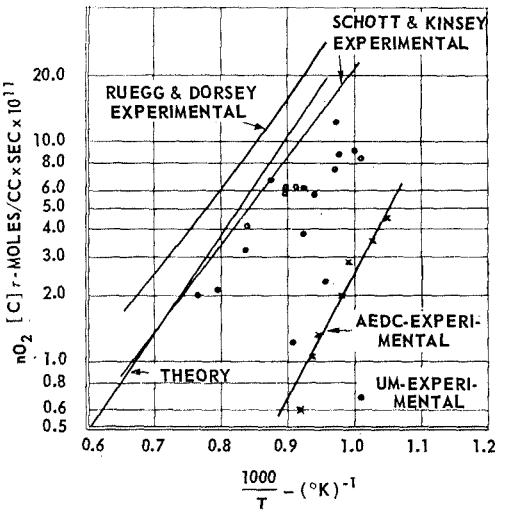

FIG. 2. Product of ignition time delay and oxygen concentration vs. reciprocal temperature, hydrogen-air.

metry between the detached shock and flame front ahead of the nylon sphere. They incorporated the assumption of a linear decrease in velocity with distance from the value immediately behind the shock to a value of zero at the sphere stagnation point in arriving at the experimentally determined ignition time delay. The experimental data was described by a best fit equation:

$$2.3 \log_{10}\{n_{O_2}(C)\tau \times [1 - 0.05(P/T) \exp (8570/T)]\} = (8570/T) - 23.49 \quad (2)$$

where (C) is in moles/liter, τ in seconds, P (the pressure immediately behind the shock) in atmospheres, and T (the temperature immediately behind the shock) in °K. The extra term, $0.05 (P/T) \exp (8570/T)$, arises from the fact that the experiments involved relatively high pressures behind the shock (up to about 10 atmospheres compared to approximately 1 atmosphere in the case of the UM and AEDC experiments). Consequently the authors considered a gas phase quenching reaction, $H + O_2 + I \rightarrow HO_2 + I$ (I an inert species), in correlating the data. Equation (2) is plotted in Fig. 2 with the pressure taken as 1 atmosphere.

It is interesting to include on this same figure the shock tube results of Schott and Kinsey.[10] Their equation for the best fit of their data is,

$$\log_{10}[(O_2)\tau] = -10.647 + (3966 \pm 625)(1/T) \quad (3)$$

wherein the units are the same as before. This equation is plotted in the figure.

Reference to Fig. 2 indicates that the results of Schott and Kinsey compare very favorably with the theoretical curve except for a rather small difference in slope, this slope being indicative of the activation energy of the rate-controlling reaction. In arriving at the theoretical Eq. (1), the order of magnitude of n_{O_2} and n_{H_2} was taken as unity, which allowed certain terms in the derivation to be dropped. Schott and Kinsey operated at values of n_{O_2} and n_{H_2} as low as 0.02 which is sufficiently low to account for some discrepancy between the two curves.

It can be noted that the UM results tend to be lower. This is believed to be attributable in part to two-dimensional effects as will be discussed in a later section.

The results from sphere tests of Ruegg and Dorsey are seen to be somewhat higher than the theoretical curve. The three-dimensional aspects of this problem make it difficult to evaluate the results as to a possible direction of correction. The AEDC tests indicate appreciably lower delay times than the other results presented. In a later section correction for two-dimensional effects will be seen to be in the wrong direction to explain this discrepancy. Probably one contributing factor is the nonuniform hydrogen distribution over the normal shock zone. Thus very lean mixtures in the outer portions of the shock mean higher mole fractions of oxygen which lead to shorter delay times. Another possible contributing factor stems from the fact that the higher temperatures were obtained by hydrogen preburning in the plenum chamber, thus leading to some chemical differences at the test section.

Vibrational Relaxation Effects. As is well known and is apparent from the foregoing, the temperature behind the shock portion of a detonation wave is of profound importance to ignition time delays and composition limits. There appears to be considerable doubt, however, as to whether the temperature actually realized in experiments is one corresponding to a vibrationally cold state or a state wherein vibration is equilibrated. Schott and Kinsey[10] believed that their ignition time delay measurements were subject to both extremes, dependent upon the particular mixture and experimental conditions. Patch[11] found that he could predict composition limits for hydrogen-oxygen-diluent systems much better by assuming a vibrationally cold condition.

In order to ascertain the sensitivity of the UM and AEDC experiments to vibrational excitation effects, a few calculations were made for the two limiting cases of (a) the vibrational relaxation time, ν, much greater than the ignition time delay, τ, and (b) $\nu \ll \tau$. A mixture of 20% (by volume) of hydrogen in air was used and the initial temperature taken as 291°K. A range of velocities into the shock were treated. The temperature behind the shock was calculated for the two cases; case (a) for no vibrational excitation and case (b) full vibrational excitation but assuming no dissociation. The temperatures thus determined were used in Eq. (1) to calculate the ignition time delay and thus compare the difference for vibrationally frozen and excited states. For these calculations it was not necessary to specify the pressure level in arriving at the temperatures but in arriving at the value for τ the pressure behind the shock was taken as 1 atmosphere in all cases. The results are shown in Fig. 3. For the cases considered and over the temperature range of validity of Eq. (1), the difference between the two cases ranges from about 30% to 60%. Unfortunately, the scatter of the experimental data and the uncertainty as to appropriate kinetic constants make it impossible to draw a conclusion regarding vibrational relaxation on

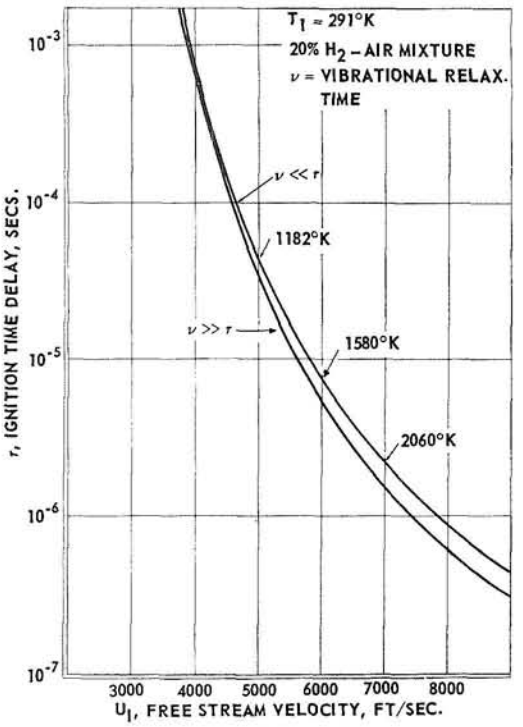

FIG. 3. Ignition time delay at different free stream velocities, with and without vibrational relaxation.

the basis of the SDW experiments. The effect should not be significantly different in the UM, AEDC, or Bureau of Standards experiments.

It should be noted that the lean mixture assumed in the calculations emphasizes the vibrational effect due to the high characteristic vibrational temperature of hydrogen. On the other hand, the characteristic vibrational temperature of oxygen is appreciably less than nitrogen so that the difference in τ for hydrogen-oxygen mixtures for the two cases of $\tau \ll \nu$ and $\tau \gg \nu$ would be greater than was shown here.

In view of the above it is believed that meaningful results regarding vibrational relaxation in detonation waves can be obtained for SDW experiments by judicious selection of operating conditions and refined instrumentation.

Two-Dimensional Effects in Gaseous Detonations. Early photographic investigation of gaseous detonation waves generated in flame tubes and shock tubes revealed the presence of nonuniform conditions behind the detonation wave. Such phenomena naturally make one wonder as to whether the propagation characteristics and detonation limits are not affected by this departure from one-dimensionality. Simplified analyses treating the viscous effects and heat transfer at the wall have been carried out by various investigators and correctly predicted the general trends but not the details. Rather recently, Fay[12] treated in some detail the influence of the boundary layer which is initiated at the shock wave in a tube and builds up through the reaction zone. The greater density in the boundary layer means that more mass flow passes through the boundary layer than would correspond to the geometric

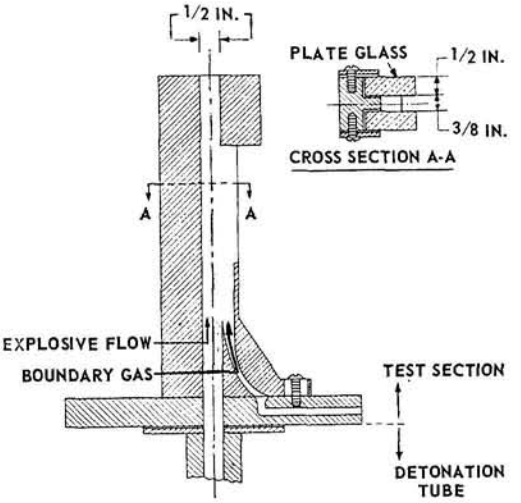

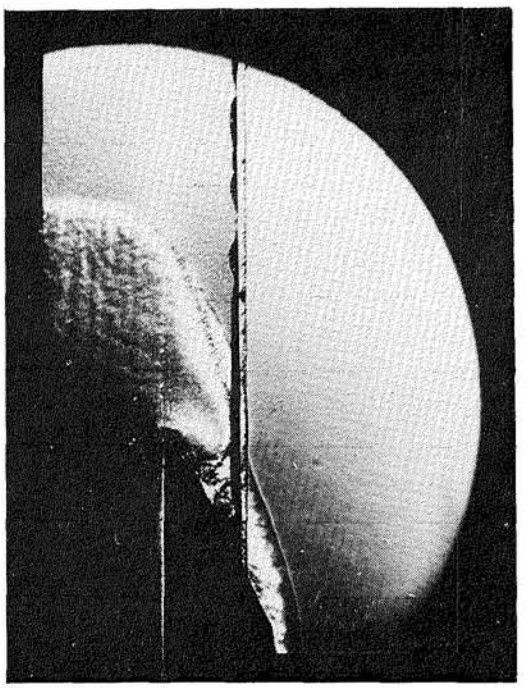

FIG. 4. Interaction of a hydrogen-oxygen detonation with an inert boundary gas. (a) Experimental set-up. (b) Schlieren photograph.

proportion. Thus the flow in the reaction zone is subject to an effect analagous to mass flow bleeding through the sides of the tube. Utilizing some experimental results on turbulent boundary layer growth and reaction zone thickness, Fay was able to show that this model predicted the correct effect of pressure and tube size on the velocity deficit; that is, the difference in velocity for a true one-dimensional case and the experimentally observed velocities.

Recently, some experiments and analyses have been effected at the University of Michigan Aircraft Propulsion Laboratory which enhance the two-dimensional effects in gaseous detonations. Sommers and Morrison[13,14] were interested in the lateral relief of combustion products of detonations in condensed explosives. The extremely high pressures behind such waves preclude the possibility of a rigid boundary and hence the properties of the container as well as those of the explosive enter into determining the detonation characteristics. The authors pointed out the significance of the ratio of acoustic impedance (product of density and speed of sound). They studied this experimentally by means of a gaseous analogy. An explosive gaseous mixture was caused to flow at low velocity into a three-sided tube wherein the fourth side was an inert gas flowing parallel to the explosive mixture at about the same velocity. A detonation was initiated in the explosive column which caused either oblique attached or detached shocks to be generated in the inert medium dependent upon the composition of the detonable medium and the inert gas used. Thus there was lateral relief on the detonation which caused the detonation to slow down, or in some cases, to be extinguished. A typical result, along with a schematic of the experimental apparatus, is shown in Fig. 4. The variation in velocity as a result of the lateral relief was measured.

Morrison and Cosens[15] considered the above results in establishing the geometry for a small workable model of a rotating detonation wave rocket motor. The hydrogen-oxygen detonation wave traversed an annular combustion chamber of rectangular cross section ($\frac{1}{2} \times 2$ inches) and about $7\frac{1}{2}$ inches in diameter. The combustion chamber was vented by an annular supersonic nozzle so that again the detonation wave experienced lateral relief. While the engine was operated for only a fractional part of a second many passes of the detonation wave were recorded and the velocity appeared constant at about 10,000 ft/sec. It was necessary, of course, to inject hydrogen-oxygen continuously in order that a fresh charge be available for each pass of the wave.

It is interesting and logical to apply the general ideas of the two-dimensional effects discussed above to the experimentally observed results on SDW. This discussion will be concerned with the results from the UM and AEDC facilities and hence will of necessity be limited to the influence of lateral relief on ignition delay time. This is so because the limitations of stagnation temperature in all of these experiments led to reaction zones far downstream where all knowledge of the flow field is pretty much in doubt.

The theoretical treatment of ignition time delay and the consequent predicted results are premised on the assumption that the flow parameters and molecular weight remain constant between the shock and flame front. Further, the raw experimental data obtained at UM were reduced to delay times by invoking the same assumptions. It can be seen from Fig. 2 that the UM experiments indicate shorter time delays relative to theoretical as the temperature level is lowered. The most palusible (if not only) explanation for this would appear to be lateral relief of the gases behind the normal shock causing deceleration to higher static temperatures and hence higher kinetic rates. It is the aim here to quantitatively assess this effect.

The main assumption to be made here is that the flow immediately behind the Mach disc diverges and that the angle of divergence remains constant for all ranges of ignition time delay. Thus the two-dimensional effect becomes that of finding the effect of increasing flow area on the theoretical delay distance. From the expression of the ignition delay time, Eq. (1), and the velocity behind the shock, the expression for the theoretical delay distance, Δx_t, is

$$\Delta x_t = \frac{RT_2}{2n_{O_2}P_2A_6} \exp\,(E_6/RT_2) \times \ln\,(n_{O_2}/\cdot n_{H_2}\cdot k_6/k_5) M_2(\gamma RT_2)^{\frac{1}{2}} \quad (4)$$

where M_2 is the Mach number behind the shock. Inasmuch as a change in area is assumed, the temperature and pressure and Mach number change with distance from the shock front. Thus Δx_t is a function of the three variables, P_2, T_2, and M_2. Taking the logarithm of Eq. (4) and differentiating we obtain

$$\frac{d(\Delta x_t)}{\Delta x_t} = \left(\frac{3}{2} - \frac{E_6}{RT_2}\right)\frac{dT_2}{T_2} - \frac{dP_2}{P_2} + \frac{dM_2}{M_2} \quad (5)$$

where the logarithm term of Eq. (4) has been taken as a constant. Since the flow is subsonic behind the shock, an area increase increases both the static temperature and the static pressure and decreases the Mach number and since $E_6/RT_2 > \frac{3}{2}$ in the range of temperature of

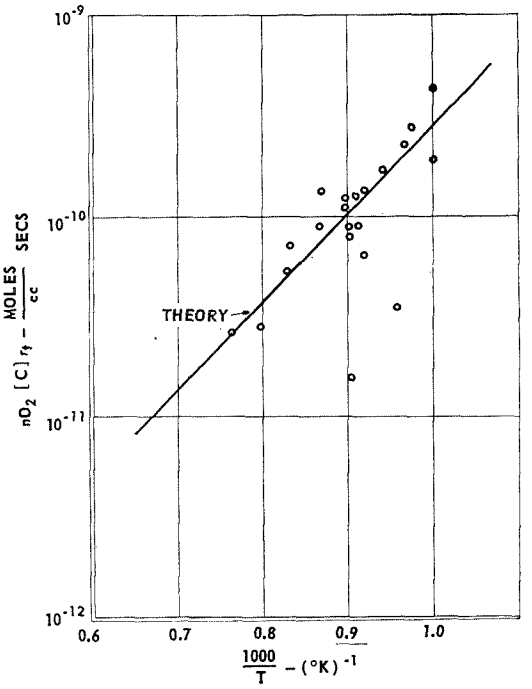

FIG. 5. University of Michigan ignition delay results with correction for two-dimensional effects.

interest here, an area increase reduces the delay distance.

Now, dT_2/T_2, dP_2/P_2 and dM_2/M_2 can be evaluated in terms of M_2 and dA/A by using influence coefficients.[16] Making the substitution we obtain

$$\frac{d(\Delta x_t)}{\Delta x_t} = \left[\left(\frac{3}{2} - \frac{E_6}{RT_2}\right)(\gamma - 1)M_2^2 - \gamma M_2^2 - \left(1 + \frac{\gamma - 1}{2} M_2^2\right)\right] \frac{1}{1 - M_2^2} \frac{dA}{A} \quad (6)$$

With the value of $E_6/RT_2 = 8.2$ corresponding to $T_2 = 1100°$K, it can readily be seen that $d(\Delta x_t)/\Delta x_t$ varies between $-1.945\ dA/A$ and $-1.05\ dA/A$ as M_2 varies between 0.4 and 0.1, so that as an average one can write

$$d(\Delta x_t)/\Delta x_t \simeq -1.5\ dA/A \quad (7)$$

This equation can be written in incremental form in terms of the experimental delay distance, Δx, the divergence angle, δ, and the Mach disc radius, r_d, as follows:

$$(\Delta x_t - \Delta x)/\Delta x_t \simeq 3\Delta x \tan \delta / r_d \quad (8)$$

when $\Delta x \tan \delta \ll r_d$. It shows that the fractional deviation between the theoretical and the experimental delay distances decreases with increasing radius of the Mach disc and decreasing delay distance. Thus the larger the scale of the experiment and the higher the temperature the better the agreement is between experiment and theory.

It remains now to evaluate tan δ. To do this, the results of the UM highest temperature run as indicated in Fig. 2, which seems to give the closest agreement with theory, are used. Admittedly, the values for the theoretical curve are not that well known to justify superimposing the two but it is the best we can do here to assess the two-dimensional aspects. Evaluating Δx_t from Eq. (8) and noting that $r_d = 0.25$ inch, tan δ is found to be 0.145 corresponding to $\delta = 8.25°$. Although this angle appears to be relatively large, it should be pointed out that the observed divergence angle of the flame is about twice this value, therefore $\delta = 8.25°$ is considered reasonable. With the value of δ thus obtained, it is possible to correct all the other experimental distances and thus evaluate τ_t, the corresponding theoretical time delay. Figure 5 shows a comparison between the corrected experimental results and theory and it can be seen that the agreement is extremely good. Most of the corrected experimental points lie within $\pm 25\%$ of the theoretical curve. Thus the above, admittedly somewhat crude, analysis indicates that two-dimensional effects are of importance in the case of longer delays and serve to explain the results observed.

The data obtained at AEDC could be analyzed in the same way in order to assess the sensitivity of measured ignition delays to two-dimensional effects. If one considers their standard run at a Mach number of 3.1 and stagnation pressure of 45 psia, the angle of the slip line behind the normal shock must be approximately 12° but with a slope such as to tend to accelerate the subsonic gases behind the shock. Thus the temperature will drop and the delays would be longer, just the opposite of the effect realized in the UM experiments. Reference to Fig. 2 reveals that the slope of the AEDC experimental data curve is appreciably steeper than would be true for the most likely activation energy (Schott has suggested $E_6 \simeq 17.5$ kcal/mole). This steepness could be a result of the two-dimensional effects although the evidence is too little to draw a firm conclusion. Also, the fact that the AEDC delays are appreciably shorter than the other investigators' results suggests that other factors, such as those mentioned earlier, may be influential.

Finally, let us look at two-dimensional effects insofar as they influence ignition delay distance in shock tube measurements. As mentioned earlier, the boundary layer buildup downstream of the shock causes the subsonic flow (relative to the shock wave) to see an effective area in-

crease and hence tends to decelerate with an attendant increase in temperature. The situation is qualitatively identical to the area relief behind the Mach disc in the UM experiments. In order to compare quantitatively it is necessary to know some details of the rate of boundary layer buildup. The approximate relation of Eq. (7) is still valid here and one needs the fractional area increase over the delay distance, Δx. Fay[12] has shown that Gooderum's[17] expression for the turbulent boundary layer thickness can be put in the form,

$$\delta^* = 0.22x^{0.8}(\mu_e/\rho_1 u_1)^{0.2}$$

where δ^* is the displacement thickness, Δx is the distance behind the shock in the steady flow coordinate system, μ_e is the viscosity at the outer edge of the boundary layer, and $\rho_1 u_1$ is the density velocity product into the shock wave. This can be written as,

$$\delta^* = 0.22x(1/\mathrm{Re}_x)^{0.2}$$

where,

$$\mathrm{Re}_x = \rho_e u_e x/\mu_e = \rho_1 u_1 x/\mu_e$$

Substitution of some typical values gives $\delta^* \simeq 0.03x$ so that $\tan \delta = 0.03$ and hence δ is of the order of 1.5–2° as compared to the 8° in the UM experiments. Then

$$(\Delta x_t - \Delta x)/\Delta x_t \simeq 3\Delta x \tan \delta/r_d = 0.09\Delta x/r_d$$

where r_d is now the radius of the shock tube. It follows that the errors to be incurred in the measurement of ignition time delays for hydrogen-oxygen systems in shock tubes are somewhat smaller than those realized in SDW when the size of the shock tube and Mach disc are of the same size. Correction for this effect would tend to steepen the slope of Schott and Kinsey's experimental curve.

The existence of appreciable two-dimensional effects in detonation waves causes the classification of such waves as to weak, strong, and Chapman–Jouguet detonation or merely as a shock induced combustion wave phenomenon to be somewhat ambiguous. Nicholls and Dabora[3] discussed this classification in interpreting their results on SDW. However, no attempt has been made in this paper to distinguish between shock induced combustion waves and detonation waves. Bragg[18] has proposed a consistent set of definitions for two-dimensional detonation waves that should prove useful. The problem of identification on SDW is in knowing how much of the chemical energy was actually released.

Conclusions

The experimental results obtained on SDW at the UM and AEDC have been presented and compared and have been found to be in good qualitative agreement. The minimum temperatures required to ignite the mixture behind the shock in the two facilities are quite close, the difference being explainable by a difference in pressure level behind the shock and some uncertainty in the temperature measurements. Limited stagnation temperatures have led to measureable ignition delay times in both facilities and consequently attention has been focused on this aspect. A consideration of the effects of vibrational relaxation (vibrationally cold or equilibrated) on ignition time delay indicates measureable differences between the two extremes but the scatter of the experimental results presented precludes a conclusion as to which limiting case was realized.

A correction for two-dimensional effects is seen to bring the UM delay data into substantial agreement with the shock tube measurements of Schott and Kinsey as well as with the theoretical predictions. Measurements made on nylon spheres fired into a quiescent mixture of hydrogen-air yielded ignition delay results comparable to these although a little on the high side. The AEDC measured delays are seen to be appreciably lower. This is believed to be largely the effect of nonuniform hydrogen-air ratio across the normal shock.

It was demonstrated that the errors incurred by two-dimensional effects on the ignition delay time for hydrogen-oxygen mixtures was smaller in shock tubes than in SDW experiments provided the scale of the two experiments were the same.

It is concluded that the SDW technique is of definite value to the study of certain types of problems provided the scale of the experiment is increased and extensive instrumentation is employed. Some of the advantages offered are:

(a) Steady flow system;

(b) There are not the usual lean and rich composition limits to contend with and investigations can extend continuously through these ranges;

(c) Ideal for studying appreciable ignition delay times that could not be obtained in detonations in shock tubes;

(d) By the nature of the experiment, good control of the operating conditions can be obtained;

(e) The high velocities behind the shock spread out the combustion process which should allow for reaction zone studies.

The main disadvantages would appear to be:

(a) the requirement of appreciable flows of heated fuel and oxidizer at initially high pressures that would be required for the larger scale experiments;

(b) the difficulty of ascertaining accurately the conditions into the shock wave; for some types of experiments this is not too critical, for others, such as the structure of the reaction zone, it would be essential to know the mixture ratio quite accurately;

(c) the equipment involved and method of operation make this technique more expensive operationally.

ACKNOWLEDGMENT

The author is indebted to many members of the Department of Aeronautical and Astronautical Engineering staff who were especially helpful in the preparation of this paper. Fruitful discussions were held with Professors R. B. Morrison and T. C. Adamson, Jr. Mr. E. K. Dabora was extremely helpful in evaluating two-dimensional effects and Mr. A. A. Ranger in evaluating vibrational effects.

The University of Michigan work reported was supported by AFOSR under Contract No. AF 49(638)-562 which has since terminated. The support of this agency is gratefully acknowledged.

REFERENCES

1. NICHOLLS, J. A., DABORA, E. K., and GEALER, R. L.: *Seventh Symposium (International) on Combustion*, p. 144. Butterworths, 1959.
2. NICHOLLS, J. A.: *Stabilization of Gaseous Detonation Waves with Emphasis on the Ignition Delay Zone*. Ph.D. thesis, Univ. of Michigan, 1960; also available as AFOSR TN 60-442, June 1960.
3. NICHOLLS, J. A. and DABORA, E. K.: *Eighth Symposium (International) on Combustion*. Williams and Wilkins, 1962.
4. NICHOLLS, J. A. *et al.*: *An Eexperimental and Theoretical Study of Stationary Gaseous Detonation Waves*. AFOSR 1764, October 1961.
5. GROSS, R. A.: *Design Report, Supersonic Combustion Tunnel*. AFOSR-TN-57-677, October 1957.
6. RUBINS, P. M.: *Installation of a Supersonic Combustion Tunnel*. AEDC-TN-60-162, September 1960.
7. RHODES, R. P. and CHRISS, D. E.: *A Preliminary Study of Stationary Shock Induced Combustion with Hydrogen-Air Mixtures*. AEDC-TN-61-36, July 1961.
8. RUEGG, F. W. and DORSEY, W. W.: J. Research Natl. Bur. Standards *66C*, 51 (1958).
9. DUFF, R. E.: J. Chem. Phys. *28*, 1193 (1958).
10. SCHOTT, G. L. and KINSEY, J. L.: J. Chem. Phys. *29*, 1177 (1958).
11. PATCH, R. W.: ARS Journal *31*, 46 (1961).
12. FAY, J. A.: Phys. Fluids *2*, 283 (1959).
13. SOMERS, W. P.: ARS Journal *31*, 1780 (1961).
14. SOMERS, W. P.: *The Interaction of a Detonation Wave with an Inert Boundary*. Ph.D. thesis, Univ. of Michigan, March 1961.
15. MORRISON, R. B. and COSENS, G. L.: ARS Journal (in press).
16. SHAPIRO, A. H.: *The Dynamics and Thermodynamics of Compressible Fluid Flow*, Vol. I, p. 228. Ronald Press, 1953.
17. GOODERUM, P. B.: NACA TN 4243, 1958.
18. BRAGG, S. L.: Combustion and Flame *5*, 390 (1961).

Discussion

DR. G. L. SCHOTT (*Los Alamos Scientific Laboratory*): The effect of vibrational relaxation on the ignition delay in hydrogen–oxygen mixtures may be more complicated than the text indicates. To be sure, a less than equilibrium vibrational energy in any diatomic component of a shocked gas results in an abnormally high translation–rotational temperature, and this may significantly shorten the ignition delay. However, there may be an opposing effect. The chemical reaction which controls the ignition delay is $H + O_2 \rightarrow OH + O$, and if O_2 is vibrationally cold, this reaction may proceed abnormally slowly, causing the ignition delay to be longer than in vibrationally equilibrated O_2. Evidence for this latter effect was found in the data of Schott and Kinsey.

MR. R. P. RHODES (*ARO Inc.*): The work which we have done at the Arnold Center (AEDC) agrees in general with the results of Mr. Nicholls. With regard to our ignition delay results we feel that there is some uncertainty in our measurements because of the lack of sharpness in our emission zones, but this will not account for the discrepancy between our data and that of Mr. Nicholls. One possible reason is that since we preheat the air by burning hydrogen, we may have small but significant quantities of OH radical in the mixture approaching the shock wave which could reduce the delay.

We take exception to the term "standing detonation wave" since our data indicate that the phenomena we see are simple shock waves followed by a combustion zone whose boundaries are not re-

stricted to constant area as in a detonation wave, but are controlled by the pressure field through which the combustion is taking place. In our case this is an accelerating flow field with a pressure drop through the combustion zone.

We have taken data by means of a sampling probe in the reaction zone which shows the degree of combustion as a function of distance behind the shock wave and indicates delays comparable to those which we reported from emission data. The result of our study of normal shock induced combustion may be found in "A preliminary study of shock induced combustion," Rhodes, R. P., Robins, P. M., and Chriss, D. E., AEDC TPR 62–78, May 1962.

DR. R. E. DUFF (*Lawrence Radiation Laboratory*): Have any measurements been made with high frequency response on standing detonations which can indicate whether or not instability phenomena analogous to those observed in free detonations exist in this case?

MR. R. P. RHODES: We have measured the intensity of the 4315 Å CH bands from an acetylene-air reaction initiated by an oblique shock wave. There appear to be large apparently random fluctuations in the intensity with frequencies from 20 to over 1000 cycles/second. These data are very recent and while they may reflect a factor inherent in the combustion process, they may also originate from disturbances outside the combustion zone.

PROF. J. A. NICHOLLS (*University of Michigan*): I know of no meaningful high frequency response measurements that have been made on standing detonations. Such measurements would certainly be in order if the experimental conditions were sufficiently clean. The fact that standing waves are contained by fluid boundaries rather than walls should shed light on the instability problem.

MR. C. L. SPINDLER (*U.S. Naval Ordnance Test Station*): Nicholls (in a paper in this volume) has compared the experimental observations of some recent standing detonation wave studies; comparison is also made with experimental observations of classical flame tube detonation waves. In general the paper is concerned with real gas phenomena and two-dimensional effects which result in deviations between experimental results and ideal theory. In this regard the paper is most adequate. However, the controlling boundary conditions for each detonation wave system have not been extensively compared either in this paper or elsewhere. In most instances these boundary conditions are apparent but in others apparent only to those closest to the subject. These boundary or controlling conditions must certainly be important in understanding differences in detonation wave phenomena. Accordingly the following brief discussion may help clarify these differences.

Presently it will be adequate to consider the detonation waves as highly idealized, one-dimensional, constant area processes consisting of a normal shock followed by a reaction or heat addition zone. The working fluid considered is a perfect gas with state properties represented by

$$P = \rho RT. \tag{1}$$

In Eq. (1) P is pressure, ρ is density, T is temperature, and R a gas constant. This working fluid obeys the constant area conservation equations of mass, momentum, and energy for a nonreacting (fixed composition) gas—the use of the nonreactive gas equations is justifiable since the reaction zone follows the shock front and consequently results determined for the shock wave will apply to the detonation wave as a whole. The respective conservation equations are:

$$\rho_0 v_0 = \rho_f v_f, \tag{2}$$

$$P_0 + \rho_0 v_0^2 = P_f + \rho_f v_f^2 \tag{3}$$

and

$$c_P T_0 + \tfrac{1}{2} v_0^2 + q = c_P T_f + \tfrac{1}{2} v_f^2, \tag{4}$$

where v is velocity, c_P is the constant specific heat capacity, and q is the specific heat addition. The subscripts 0 and f refer to conditions relative to the wave front, upstream and downstream, respectively. The three conservation equations must be satisfied by their nine variables; however, by use of the state equation, Eq. (1), they may be reduced to seven variables. Thus the boundary or control conditions must determine at least four of these variables if the phenomena are determinable for the remaining unknowns.

Three of the cases discussed by Nicholls will be considered: the classical flame tube detonation wave; the standing detonation wave, SDW, in a supersonic tunnel, such as the Arnold Engineering Development Center experiments; and a SDW produced in a free jet as investigated at the University of Michigan.

Consider the classical flame tube detonation: known values of ρ_0 or P_0, and q are apparent boundary conditions, but insufficient in quantity to solve the conservation equations, (2) through (4), explicitly. However, they are sufficient to determine the end state relationship between either ρ_f or P_f and v_f. By employing suitable thermodynamic arguments at this point, the well-known Chapman-Jouguet condition can be derived.

The second case for consideration is a SDW in a supersonic tunnel. In this detonation system the known boundary conditions, ρ_0, P_0, v_0, and q, are

obvious as well as sufficient to solve the three conservation Eqs. (2)–(4), explicitly for the remaining unknowns. However, if the wave is to maintain stability in relation to its coordinate systems, i.e., remain fixed, there is some maximum heat release, q_{max}, which the wave can tolerate. This stability point or heat release limit is dictated by the entropy consideration, discussed in the previous case, which requires that $v_f \leq a_f \cdot q_{max}$ is termined by solving the conservation equation for $q = q_{max}$ with the boundary condition ρ_0, P_0, and v_0, while letting $v_f = a_f$ together with the state relationship given by Eq. 5. Thus with the boundary condition of ρ_0, P_0, v_0, and q (known $q \leq q_{max}$) the properties of the SDW in a tunnel are completely determinable.

The final case for consideration here is the SDW in a hydrodynamic free jet which is characterized by the known boundary condition ρ_0^0, T_0^0, q, and P_f; the superscripts 0 refer to total or stagnation conditions. But, only two of these, P_f, and q, appear in our set of conservation equations. From the hydrodynamics of the free jet it is, however, possible to employ the adiabatic relationship between the initial static and stagnation state points as given by Eq. (5):

$$P_0/\rho_0^{\gamma} = P_0^0/(\rho_0^0)^{\gamma}. \tag{5}$$

It is also possible to develop an expression, Eq. (6), which relates the total and static energy properties of the initial gas state.

$$v_0 = [2c_P\,(T_0^0 - T_0)]^{\frac{1}{2}} \tag{6}$$

The conservation equations may thus be solved with the aid of Eqs. (5), (6), and the perfect gas law, Eq. (1). However, this case, as the preceding one, has a limiting q_{max} for maintaining stability. Values for q_{max} are determined in the same manner as described by the previous case but with the relevant boundary condition for the case under consideration. Thus the properties of the SDW in a free jet are also determined.

Although the previous considerations have necessarily been idealized and brief, it is hoped that they may add some insight into this aspect of the similarities and differences for various detonation wave phenomena.

THE INITIATION AND GROWTH OF EXPLOSION IN THE CONDENSED PHASE

F. P. BOWDEN

The Slow Decomposition of Explosive Crystals: Electron microscope studies show that the thermal decomposition of some explosive crystals, e.g., silver cyanamide, occurs primarily on the surface. With others, e.g., silver azide, the surface reaction is again important but there is evidence also for some decomposition within the crystal which can cause it to break up into many small fragments. There is also evidence that, for many of these explosives, an actual melting must occur—it is only in the molten phase that the reacting species have sufficient mobility for a rapid acceleration to take place.

The Effect of Fission Fragments and Nuclear Radiation: By choosing a crystal lattice which can be resolved in the electron microscope it has been possible to measure the extent of the damage with some precision. The damage depends upon the nature of the crystal and on other factors, but the track width may be approx. 100–120 Å. The disorder produced in the lattice and the holes and tunnels formed may be clearly seen. The damage may be interpreted on a thermal mechanism. The experiments at present suggest that even the intersection of two tracks would not produce explosion in an azide crystal. The intersection of three or more tracks within 10^{-11} sec is an unlikely event.

The Effect of Discontinuities in Promoting Shock Initiation: Recent experiments with single crystals emphasize the importance of very tiny defects in the initiation of explosion by weak shock waves and the part they play in the growth process. A perfect crystal of silver azide is not initiated by a shock but a defect only a few microns in size will start reaction. This reaction in small crystals (0.01 to 1 mm) is a fast burning. With crystals greater than 2 mm it may grow to detonation. The defects may be present initially or may be introduced by a precursor stress wave moving at sonic velocity through the crystal. When a shock wave of appropriate intensity passes over a crystal containing multiple defects it can initiate a deflagration at each so that the forward movement of the deflagration is coupled to the shock wave. In this way a "pseudo-detonation" is set up. There is evidence that appropriately shaped cavities in liquids and solids can give rise to the formation of tiny Munro jets of high velocity. These might aid initiation by concentrating and increasing the velocity of impact and by breaking up the explosive.

Introduction

The Chairman has pointed out, with his usual good sense, that the main function of a discussion paper is to provoke discussion. I would like to begin therefore by asking a few simple-minded questions about the initiation and growth of explosion in liquids and solids. I will not, of course, answer these questions—this gathering is much more able to do so—but I will, where relevant, mention some recent experiments which my colleagues and I have been making, and hope that others will do the same.

These may be grouped under three main headings: (1) The Slow Decomposition of Explosives; (2) The Effect of Fission Fragments; (3) The Role of Discontinuities in the Initiation and Growth of Explosion.

(1) *The Slow Decomposition of Explosive Crystals.* (i) What do we know about the physical changes which occur in an explosive crystal during its slow decomposition? When is the decomposition a surface reaction and when does it occur within the body of the crystal? How relevant is this behavior to their subsequent explosion and detonation?

Electron microscope studies show that the thermal decomposition of some explosive crystals, e.g., silver cyanamide, occurs primarily on the surface. With others, e.g., silver azide, the surface reaction is again important but there is evidence also for some decomposition within the crystal which can cause it to break up into many small fragments. There is also evidence that, for many of these explosives, an actual melting must occur—it is only in the molten phase that the

reacting species have sufficient mobility for a rapid acceleration to take place.

(ii) What is the relation between the electronic structure of an explosive molecule and its stability?

(2) *The Effect of Fission Fragments and Nuclear Radiation.* (iii) Can we explode explosives by bombardment with fission fragments, and if not, what effect do we expect it to have on them and on their subsequent performance?

Bombarding crystals with fission fragments provides a method of introducing a single burst of energy and it is possible to observe the effects directly by high resolution transmission electron microscopy. By choosing a crystal lattice which can be resolved in the electron microscope it has been possible to measure the extent of the damage with some precision. The damage depends upon the nature of the crystal and on other factors, but the track width may be approx. 100–120 A. The disorder produced in the lattice and the holes and tunnels formed may be clearly seen. The damage may be interpreted on a thermal mechanism. Rough estimates give values for approx. 700°–1000°C for the temperature at the edge of the track which last for times of the order of 10^{-11} sec. In addition, there will be heat liberated by the decomposition of the solid itself if it decomposes exothermally. We may expect the damage to be different for ionic, valence type, and molecular solids.

There is clear evidence that the subsequent thermal decomposition and stability of the crystal is profoundly affected by the fission fragments. With silver cyanamide this would appear to be due primarily to the increase in surface area by the formation of holes and tunnels in it.

The experiments at present suggest that even the intersection of two tracks would not produce explosion in an azide crystal. The probability of three or more tracks intersecting within 10^{-11} sec is extremely small.

(3) *The Effect of Discontinuities in Promoting Shock Initiation.* We know that discontinuities in an explosive such as cavities (either empty or filled with gas), foreign particles, cracks, and crystal imperfections will all increase the sensitivity to shocks of gentle or moderate intensity. We also know that bubbles, cavities, and particles are important in liquids.

(iv) What are the various mechanisms by which these different discontinuities (a) initiate the reaction and (b) assist its propagation?

(v) We know that the initiation at a discontinuity and its growth from that point is frequently a thermal process. What new information (both theoretical and experimental) have we about the limiting size of the hot spots?

(vi) We know that shock waves which are too weak to cause initiation may, if they reinforce one another, do so. How important is the reflection and reinforcement in sensitivity tests and in practice?

(vii) There is strong evidence that the fracture of the explosive and its disintegration into small fragments (or its dispersal as fine droplets of liquid) is of major importance in aiding both initiation and propagation. In initiation by gentle shock is there a "precursor" stress wave which "prepares" the explosive in this way? If we have a perfect crystal free from defects what shock intensity do we need to initiate reaction?

(viii) How important is the *shape* of the cavity: Are micro-Munro-jets formed and what effect do they have?

(ix) What about other mechanisms of initiation? Russian workers[27] have suggested that the heat of crystallization under pressure may be a cause of impact initiation in liquids. What additional evidence have we for this?

Is the initiation by shock always a thermal process or can it occur by a direct rupture of the molecule or other mechanism?

Our recent experiments with single crystals emphasize the importance of very tiny defects in the initiation of explosion by weak shock waves and the part they play in the growth process. A perfect crystal of silver azide is not initiated by a shock but a defect only a few microns in size will start reaction. This reaction in small crystals (100 microns to 1 mm or so) is a fast burning. With crystals greater than 2 mm it may grow to detonation.

The defects may be present initially or may be introduced by a precursor stress wave moving at sonic velocity through the crystal. When a shock wave of appropriate intensity passes over a crystal containing multiple defects it can initiate a deflagration at each so that the forward movement of the deflagration is coupled to the shock wave. In this way a "pseudo-detonation" is set up.

There is evidence that appropriately shaped cavities in liquids and solids can give rise to the formation of tiny Munro jets of high velocity. These might aid initiation by concentrating and increasing the velocity of impact and by breaking up the explosive.

These experiments help us to explain initiation of explosion by shocks of moderate intensity and also the propagation of low velocity detonation in thin films of compressed powders and of primary explosives pressed into cylinders of small diameter and heavily confined.

The Slow Decomposition of Explosive Crystals

Comprehensive investigations have been made of the kinetics of decomposition of explosive solids mainly by measurement of pressure–time curves and an interesting review of this has been given.[1]

Electron microscopy combined with electron diffraction has also proved a useful method for studying this slow decomposition of single crystals. Sawkill[2] has followed the decomposition of silver azide in some detail and shown how the silver atoms in the lattice collapse to form metallic silver crystals as the N_3 is removed. This appears to be primarily a surface process and it is there that the silver nuclei are formed. Nevertheless it has been shown that the crystals (particularly the thick ones) develop a color during decomposition and also crack and split along crystallographic planes. A crystal of silver azide which is heated under controlled conditions may split into numerous small fragments about a micron across. This shows that some decomposition is occurring, within the crystal, probably at localized defects. In this way a large surface area is created during the early phase of decomposition.

More recently Dr. Montagu-Pollock[3,4] has used transmission electron microscopy combined with electron diffraction to investigate the decomposition of thin crystals of silver cyanamide (Ag_2CN_2).

Figure 1a shows an undecomposed crystal of silver cyanamide. Such crystals give diffraction patterns consistent with the (100) orientation of the structure of silver cyanamide as determined by X-ray methods: This work gives a monoclinic unit cell containing four molecules, with $a = 7.26$, $b = 5.92$, and $c = 6.61$ Å, and with $\beta = 102°20'$. The space group is $P2_1/c$.

Figure 1b shows a crystal which has been heated for 2 min at 200°C *in vacuo*. A number of opaque specks can be seen at the edge of the crystal. Electron diffraction measurements show that these are single crystals of silver of random

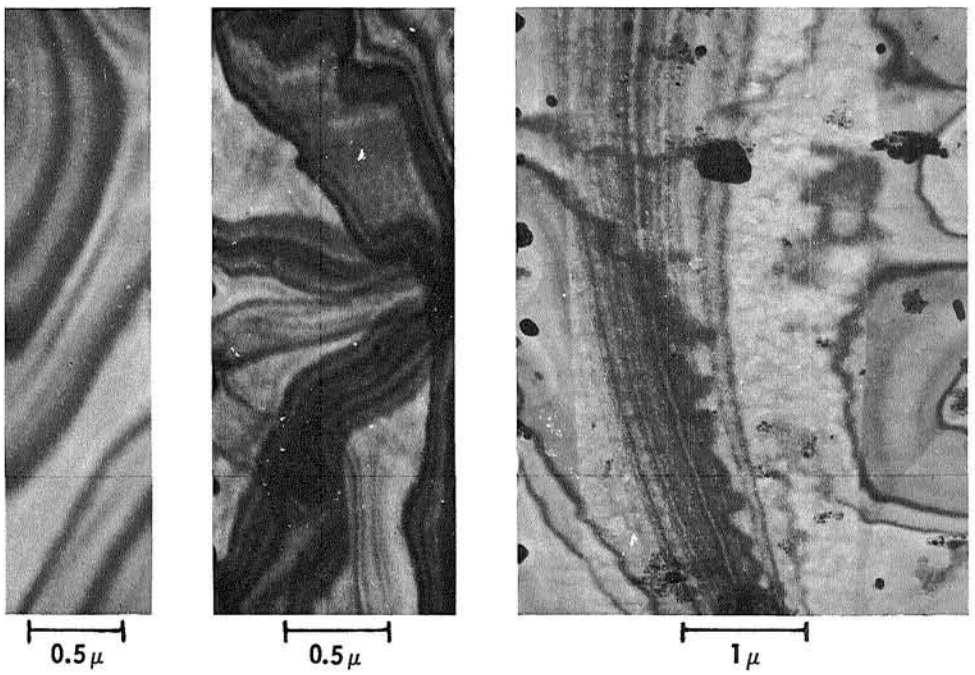

FIG. 1. (a) Undecomposed crystal of silver cyanide, about 300 Å thick. The dark bands are Bragg contours arising from slight elastic distortion. The crystal is highly perfect, but a decoration technique can reveal surface steps. (b) Crystal heated for 2 minutes at 200°C. Part of the surface has decomposed to an average depth of approx. 4 molecular layers. The silver produced has migrated over the surface of the crystal, and aggregated to form opaque specks. (c) Crystal heated for 8 hours at 200°C. Part of the surface has decomposed to a depth of approx. 100 Å. The silver whisker and specks are single crystals, of random orientation, and do not nucleate any visible decomposition in the adjoining silver cyanamide.

orientation. It would seem that the liberated silver is highly mobile and can migrate over the surface to sites of high surface energy on the crystal. These are frequently at the edge but may be elsewhere. These silver specks normally project from the crystal surface and, as they grow, develop more or less well-defined crystallographic faces; occasionally whiskers are seen; see Fig. 1c.

Nucleation, in the sense of decomposition spreading outwards from certain points, or from the silver nuclei, is not observed. Instead, the silver is liberated by an over-all surface decomposition, and diffuses to the aggregation sites; this was deduced from plots of the volume of silver per unit surface area of crystals against time at various temperatures, and confirmed by the observation that thermal decomposition was inhibited almost entirely if the crystals had previously been coated with a thin layer of carbon, evaporated on to the surface *in vacuo*. If the heating is continued for a sufficient length of time, the crystal is completely decomposed into crystalline silver and an amorphous layer which gives a diffraction pattern similar to that given by amorphous carbon (the possibility that some of this amorphous material may be formed by the polymerization of cyanogen is not ruled out).

There is no evidence from these experiments that the decomposition occurs preferentially at the silver nuclei. It is clear that the liberated silver is extremely mobile and that the thermal decomposition is essentially a surface process. If the temperature is raised the decomposition is of course more rapid and a large number of small silver nuclei are observed distributed widely over the surface. At higher temperatures still the crystal explodes.

Conclusion. The mechanism of slow decomposition is clearly important in enabling us to understand the transition to rapid burning and explosion. However, we do need measurements on the physical properties of explosive solids at elevated temperatures, particularly in the region of the melting point. If it is a surface reaction the behavior may be controlled by the state of subdivision of the solid and the area which is exposed. Some further evidence of the importance of surface area in the decomposition of silver cyanamide will be given below. If reaction is occurring throughout the crystal the initial rate may be determined by the nature and density of the dislocation and imperfections within it. With some explosives there is evidence that the crystal must actually melt—a liquid phase must be formed before the reacting species are sufficiently mobile to react at high speed.[26]

Structure and Stability of Solids. The stability of a solid to heat and light depends to a large extent on the activation energy necessary for decomposition. A knowledge of the kind of bonding in the solid is desirable since it determines whether decomposition develops by electron transfer mechanism or by bond fission. Dr. Yoffe has given some attention to this problem.[5–7] For the ionic solids such as the azides the ionization potential of the metal will determine the degree of ionic or covalent bonding in the solid. The electron energy levels of the simple azides have been estimated from measurements of a number of the physical, optical, and electrical properties of single crystals of the solids. He has shown that the activation energy for thermal decomposition is related to the gap between the full band and the conduction band of the solid. In the case of photochemical decomposition two mechanisms have been proposed. For wavelengths on the long wavelength side of the absorption edge, the activation energy for photochemical decomposition is related to the thermal energy required to dissociate optically formed excitons. The band gap decreases as the ionization potential of the metal increases and this explains in a simple way why the stability of azides decreases with increasing ionization potential. If the ionization potential of the metal is too high then a covalent solid either of the valence type or the molecular type is formed. Decomposition then develops by a bond fission mechanism and the stability can be greater than the corresponding ionic azides.

The Effect of Fission Fragments and Nuclear Radiation

We know that most of the metallic azides may be initiated by irradiation with light of sufficient intensity. The initial step appears to be a direct photochemical decomposition and this can then grow to an explosion by a thermal mechanism.[6,8,9] Irradiation of a crystal by an electron beam of high intensity will also cause explosion but this again is due to the rise in temperature. Kaufman[10] has investigated the change in thermal stability of explosives during γ-irradiation. Irradiation of the crystals of sensitive azides (such as lead azide and cadmium azide) with fission fragments of uranium, however, does not cause them to explode even if the crystals are preheated to approx. 280°C.[11] Irradiation with neutrons also fails to explode the crystals. These observations are consistent with the simple "hot spot" theory and with earlier experiments, which suggests that for a hot spot temperature of say 500°C the critical size for explosion to occur would be

approx. 10^{-5} cm. Crude calculations of the diameter of the hot spot (or rather hot cylinder) formed by the passage of the fission fragments through the crystal show that it should be considerably smaller than the critical size.

More recently we have attempted to make some direct observations of the damage produced in an explosive crystal and of the size of the track which is formed.[3] In Dr. Montagu-Pollock's experiments with silver cyanamide the crystals were placed in contact with thin foils of natural uranium and were irradiated in the Harwell BEPO reactor for periods of 1 min. to 10 hours at a pile factor of 12. The crystals were then examined by transmission electron microscopy.

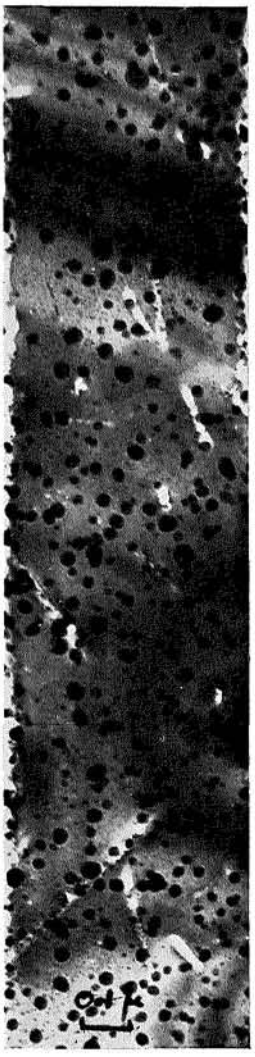

FIG. 2. Crystal irradiated with uranium fission fragments (neutron flux density of $7.2 \cdot 10^{13}$ nvt). At each bright area, material has been decomposed by a fragment. The dark areas are aggregated silver.

Figure 2 shows a typical result of the irradiation. The light dashes and dots show that where each fragment has penetrated the crystal and material has evaporated or diffused away from the track. The longest tracks represent paths of fragments travelling almost in the plane of the crystal, while dots indicate fragments that penetrated the crystal vertically. The mean track diameter is about 120 Å. The silver originally present in the volume occupied by a track has invariably diffused away from the track and accumulated as a silver nucleus elsewhere.

The greater part of the heat liberated by the passage of a fission fragment through a solid is due to ionization. Taking rough values of range and initial energy of a fragment in silver cyanamide to be 10 μ and 80 Mev. the energy released is about 900 ev/Å along a track. With the observed track radius of 60 Å, this gives a figure of about 2000°C (reached in about 5×10^{-11} sec) for the maximum temperature of a molecule at the wall of a track. This implies that this is the maximum instantaneous temperature that a molecule can reach without decomposing: but the figure of 2000°C is necessarily very crude, because of the assumptions made in the calculation. However, the width of each track is appreciably greater than that observed in the inert materials (see below) indicating that the damage may be greater when additional heat is liberated by the decomposition of the material. The heat liberated, however, is not enough to produce explosion; this is consistent with estimates of limiting hot-spot sizes.

The silver produced by the fission fragment diffuses away from the sites where it is liberated. It shows a high mobility similar to that observed with silver liberated by ordinary thermal decomposition.

The Effect of Irradiation on Subsequent Thermal Decomposition

Dr. M. J. Sole has studied the effect which neutron bombardment has on the thermal decomposition of crystals of silver cyanamide. The rate of chemical decomposition was measured in the temperature range 362°–391°C by determining the pressure of the evolved gases as a function of time. The behavior is complicated and the decomposition may be divided into four stages: (a) an initial fast surface reaction; (b) an acceleratory period; (c) a linear region; and (d) the decay period. In addition there is evidence that an intermediate product of uncertain composition is formed during the course of the reaction. The pressure–time curves may be inter-

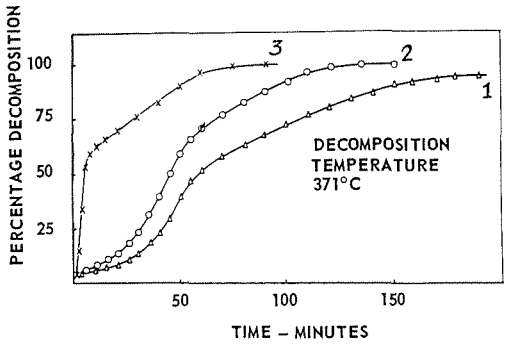

FIG. 3. Effect of neutron and fission fragment irradiation on the subsequent thermal decomposition of silver cyanamide crystals: curve 1, unirradiated; curve 2, after irradiation in B.E.P.O. for 150 hours (thermal neutron flux 6×10^{11} n/cm^2/sec); curve 3, after irradiation with fission fragments (sample intimately mixed with uranium oxide powder and irradiated as above—uranium oxide removed before thermal decomposition).

preted by considering the effect of simultaneous formation and decomposition of this intermediate.

Crystals of silver cyanamide were irradiated in three ways. Sample I received a γ-ray dose of 100 megarad from a Co^{60} source; sample II was irradiated in the Harwell reactor BEPO for 150 hours (thermal neutron flux 6×10^{11} n/cm^2/sec); sample III was irradiated in BEPO under the same conditions except that the crystals were intimately mixed with uranium oxide powder. Gamma irradiation produced no darkening of the crystals and the decomposition showed no departures from the unirradiated case (curve 1 of Fig. 3). Sample II was found to have undergone some slight decomposition as a result of the neutron irradiation as shown by the formation of silver which resulted in changes in the absorption spectrum. Figure 3 (curve 2) shows that the thermal decomposition is accelerated to some extent but that the general shape of the p–t curve is unchanged. On the other hand the crystals irradiated with fission fragments (sample III) showed marked deviations from the unirradiated case (curve 3 of Fig. 3) being particularly marked by the large and sudden burst of gas at the start of decomposition. Before decomposition these crystals showed considerable darkening and X-ray photographs have shown that this was due to the formation of polycrystalline silver. The b-lattice parameter as determined by the oscillation method showed no significant lattice expansion in this direction for either sample II or sample III. There was also no indication of spot broadening or asterism in either case.

Owing to the covalent nature of silver cyanamide the initial act in the thermal decomposition must involve bond rupture, as a result of thermally excited vibrations of the cyanamide radical. It thus differs from the inorganic azides where electronic excitation is the first step. It is therefore not surprising that γ irradiation, which is mainly ionizing, has no effect on decomposition rates. In the case of neutron irradiation in addition to ionization effects displacement processes are important and permanent damage will result from defect formation. At this stage it is not possible to identify the nature of the permanent defects involved but if silver atoms are primarily concerned damage will predominate along (100) planes where the silver atoms are close together and focusing collisions are more likely. In effect this will mean that the CN_2 groups in (010) planes are linked to adjacent planes by regions of disorder. The acceleration of the decomposition as a result of neutron irradiation is attributed to the fact that such damage will facilitate the propagation from plane to plane of the autocatalytic part of the decomposition which is considered to arise from a branching chain mechanism along planes of CN_2 groups.

In addition to the above effect fission fragments will produce a network of decomposition throughout the crystal as a result of the high temperatures liberated along the path of each fragment. The silver which is formed is mobile at these temperatures and migrates to the surface of the crystals. It would appear that the major effect of fission damage is simply to increase the effective surface area of the crystals by forming tunnels and holes in them. Experiments on the thermal decomposition of silver cyanamide in the form of a fine powder have shown that the initial burst is also greatly magnified because of the large surface area.

Direct Observation of the Damage to the Crystal Lattice

Various workers have examined the damage produced in comparatively stable materials such as mica,[12,13] uranium oxide,[14,15] and graphite[16] and tracks due to individual fission fragments can be seen. It should be possible if we choose an appropriate crystal to observe directly in the electron microscope the lattice disarray caused by the passage of a fission fragment and hence make a more precise determination of the nature and extent of the damage. Some years ago Menter[28] showed that it was possible to observe directly the lattice array in a crystal if the molecules composing it were sufficiently large and possessed the appropriate configuration. A suitable material for example is platinum phthalocyanine which crystallizes in the monoclinic form as long flat needles and with a large unit

cell (a_0 = 23.9 Å, b_0 = 3.81 Å, c_0 = 16.9 Å, β = 129.6°). It is this property in addition to the fact that the platinum atom, a heavy scatterer of electron waves, lies in the center of the molecule, which facilitates the direct observation of $(20\bar{1})$ lattice planes, separated by 11.94 Å, in the electron microscope. In a carefully aligned electron microscope with a nominal resolving power of "better than 10 Å," transmission electron micrographs of thin unstrained crystals of platinum phthalocyanine possess parallel fringes, the separation and direction of which correspond to $(20\bar{1})$ lattice planes in the crystal structure. It is a stable material and sublimes unchanged at about 500°C.

Figure 4 shows a transmission picture taken at comparatively low magnification (×160,000) of a crystal (a) before and (b) after irradiation with fission fragments. The crystal shows tracks and spots about 100 Å in diameter. These can be attributed unambiguously to individual fission fragments, since they do not appear in crystals irradiated with thermal neutrons only and since their number correlates with that calculated from dose considerations. The tracks, which are sometimes dashed and which sometimes have an alternating light and dark contrast, would appear to result from fission fragments which are travelling at an oblique angle, or almost parallel, to the plane of the crystal. The spots, however, have a light contrast on a dark background and these may be attributed to fission fragments travelling at a high angle or perpendicular to the plane of the crystal. We shall consider here the damage due to particles such as these which pass normally through crystals about 100 Å thick in a direction roughly parallel with the $(20\bar{1})$ planes.

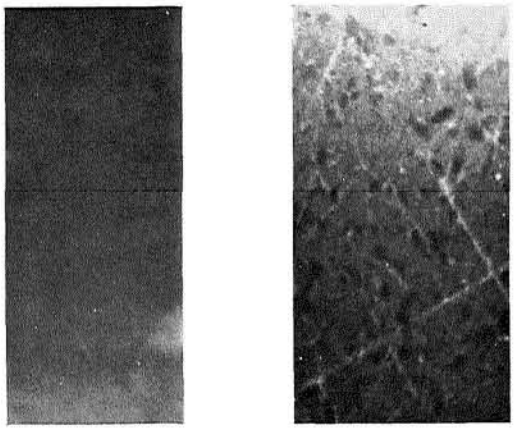

(a) (b)

FIG. 4. (a) Crystal of platinum phthalocyanine as seen at low magnification (approx ×160,000) in the electron microscope. No detail is visible. (b) Fission fragment bombarded crystal as seen at low magnification (approx. ×160,000). Tracks and spots are evident.

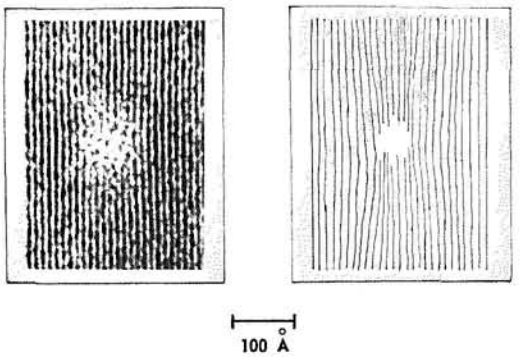

FIG. 5. High magnification (approx. ×1,500,000) photograph of a spot such as that seen in Fig. 4b. The molecular array is disordered over 7 rows of molecules. There is a marked inward curvature of the adjacent rows.

Figure 5 shows what can happen to the $(20\bar{1})$ fringes when the damage is in the main body of the crystal. This is taken at high magnification (×1,500,000): The dark parallel fringes are 11.9 Å apart and represent the regular array of the molecules in the lattice. A fission fragment has passed through the crystal. The regular lattice is disordered and there is a roughly circular diffuse region which extends over about 80 Å. Close to the edge of the diffuse region the $(20\bar{1})$ fringes curve inwards towards the disordered region: This is shown in the adjoining diagram.

When the fission fragment penetrates the crystal close to one of its parallel edges, the damage is very much greater in extent. This is illustrated in Fig. 6.

If we assume that fringe patterns obtained with platinum phthalocyanine crystals in the electron microscope represent in some measure the behavior of the $(20\bar{1})$ molecular planes (and for thin crystals the approximation is a good one), then certain conclusions can be drawn from the above observations.

Extent of the Damage. In the first instance, a measure of the extent of the damage due to a fast-moving fission fragment is obtained. In the body of the bombarded crystal the diameter of the damaged region caused by one nuclear fragment varies between 80 and 120 Å (that is, between 7 and 10 molecular planes). In Fig. 6, however, at a crystal edge, the appropriate figure is nearer 250 Å. The perfection of the $(20\bar{1})$ lattice planes is destroyed over this region

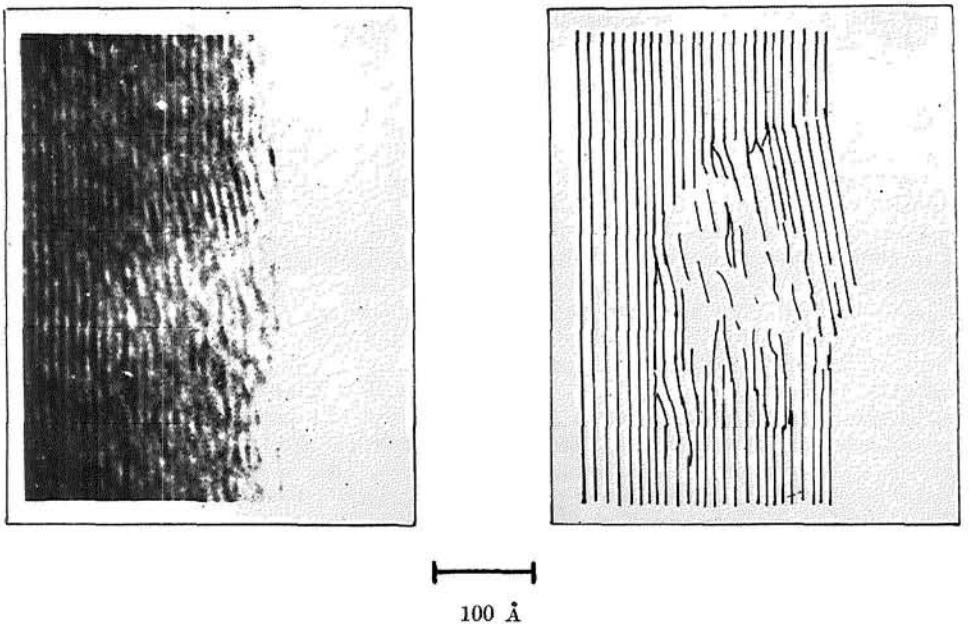

FIG. 6. High magnification (approx. ×1,300,000) photograph of the edge of a platinum phthalocyanine crystal after a fission fragment has passed through. The damage near an edge is more extensive than that observed in the body of the crystal.

and close to it there is evidence for a curvature of the molecular planes.

Nature of the Damage. The energy of a fission fragment at birth is about 100 Mev and the atomic weight may be anywhere between 72 and 161. Thus we are dealing with very fast moving particles (10^9 cm/sec) and the fragments have high charges (18 e). It can be deduced, using a value of 1.70 ev (Chadderton, L.T., unpublished work) for the low-energy limit of the main optical absorption band, that loss of energy by ionization exceeds that due to elastic collisions by a large factor. The production of primary knock-ons by Rutherford collisions accounts for only about one part in a thousand of the total loss of energy. In such circumstances we may consider the resulting excitation to be a purely thermal temperature spike; the damage arises from the rapid delivery of heat to the lattice by the moving particle. A temperature exceeding 1,000°C endures for times in the neighborhood of 10^{-11} sec, exact values depending on the thermal properties of the lattice. Since platinum phthalocyanine sublimes in air at temperatures above 500°C, it becomes evident that "evaporation" will occur along the length of the cylindrical track of the moving fragment and that recrystallization, if it takes place, is unlikely to be in perfect register with the undamaged lattice.

Other Crystals. The tracks produced in molybdenum trioxide under similar conditions are shown in Fig. 7. The fission fragments travelling through the crystal have produced tracks of an intermittent nature and some of the segments have a crystallographic shape. It is possible that the molybdenum atoms liberated by a high temperature decomposition in the track are able to

FIG. 7. Fission fragment tracks in molybdenum trioxide (approx. ×250,000). The moire patterns are due to overlying crystals.

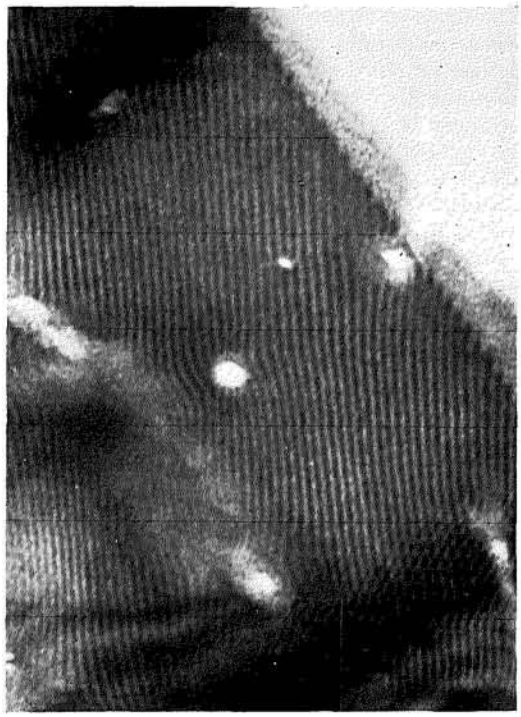

FIG. 8. Moire pattern of overlying crystals of molybdenum trioxide (approx. ×500,000). The white spots are "holes" made by fission fragments.

move away over the surface in an analogous manner to the silver mentioned earlier. The moire patterns which may be seen on the figure are due to interference between two overlying crystals (due to interference between the *a* and *c* directions). These moire patterns are shown more clearly in Fig. 8 and the white regions represent "holes" made by the fission fragments. Again an inward curving of the lattice planes adjacent to the track may be observed.

In molybdenum disulfide clearly defined tracks are again formed. These consist of a series of dislocation loops which move when the crystals are warmed or "annealed" in the electron beam.

With lead iodide the fission fragments produce a mass of dislocation loops of assorted sizes. They do not lie on a longitudinal track. They are probably due to a coagulation of highly mobile lattice defects. Under increased beam currents in the electron microscope the loops grow and coalesce—electrons and ions formed in the microscope create some point defects and these point defects travel to those dislocation loops already present due to fission fragment damage.

Conclusion. We see that by bombarding crystals with fission fragments it is possible to introduce single bursts of energy and to observe the effects directly in the electron microscope. Rough estimates give values of about 700–1000°C for the temperature at the edge of the track, this temperature lasting for times of the order of 10^{-11} sec. These estimates are of course based on a crude analysis of the energy liberated along the tracks.

The track width may be approx. 100–120 Å. It depends upon the nature of the crystal and on other factors but it has been possible to measure it with some precision particularly for crystals in which the lattice spacing can be resolved in the microscope. It is suggested that the damage can be interpreted in terms of thermal effects. The fragment causes ionization as it passes through the crystals and the recombination of electrons and positive ions liberates energy corresponding to the appropriate ionization potential. In addition there will be electron bombardment and heat liberated by decomposition if the solid decomposes in an exothermic manner. It is clear therefore that the damage and heating will vary according to the type of crystal and will be different for the ionic, valence type, and molecular solids. The electrical conductivity of the solid is also of major importance. These effects can be analyzed from a knowledge of the physical and chemical properties of the solids concerned. Irradiation with fission fragments can have a marked effect on the subsequent thermal stability of the explosive crystal. With silver cyanamide, for example, it makes the initial stages of thermal decomposition much more rapid. The effect can be attributed primarily to the increase in surface area by the formation of holes and tunnels in the crystals.

In considering the initiation of explosion by fission fragments we can speculate as to whether an explosion in an exothermic solid such as the azides will ever take place. The experiments at present suggest that even the intersection of two tracks will not initiate an explosion. The intersection of three tracks within 10^{-11} sec is a most unlikely event for fission fragment intensities which are being used at present.

The Effect of Discontinuities in Promoting Shock Initiation

Gentle Impact or Shock

For initiation by gentle impact or shock (e.g., shock pressure of a few kilobars), it would seem (from most of the experiments that we have done) that the mechanical energy of the impact must first of all be degraded into heat in a localized region of the solid or liquid and the explosion then grows by a normal chemical process. If small gas bubbles or voids are trapped

inside the liquid or solid then the gas is heated by adiabatic compression. Ideally the temperature rise is given by

$$T_2 = T_1(p_2/p_1)^{(\gamma-1)/\gamma}$$

where T_1 is the initial and T_2 the final temperature in the gas bubble and γ the ratio of the specific heats. Temperatures of the order of 500–1000°C are generated for times of the order of 10^{-5} to 10^{-4} sec when the compression ratio is about 20 to 1. These values are upper limits since the compression is not truly adiabatic and vapor and fine particles of the explosive must also be present inside the cavity. Foreign particles may also produce a localized hot spot. The size of these hot spots may be 10^{-5} to 10^{-2} cm in diameter.

Shock Waves of Moderate and High Intensity

A considerable amount of work has now been done with shocks of moderate and higher intensity, e.g., in the "gap test" and with detonating initiators. The results are beginning to fall into a pattern. It seems that if we have a homogeneous system, for example a liquid without gas bubbles, or a solid without defects, imperfections, or voids, then such a system is very insensitive to shocks of very high intensity. For example in bubble-free nitroglycerine shock waves with a velocity 3000–3500 m/sec and shock pressures of the order of 40 kilobars need not detonate the liquid. For nitromethane, pressure of the order of 85 kilobars is insufficient to initiate detonation in a homogeneous system. Similarly as Dr. Whitbread and others[17] have shown single crystals of RDX do not detonate during the passage of a shock wave but rather detonation starts from the end of the crystal remote from the "donor." We know that a shock wave of moderate intensity (pressure say 20 kilobars) on passing through the solid or liquid is sufficient to raise the temperature only by a few hundred degrees by adiabatic compression and this is below the thermal ignition temperature. If the shock wave is very intense (approx. 100 kb) then we may calculate that the temperature rise can be higher than 400°C and a thermal explosion leading to the usual stable detonation will result. The hydrodynamic calculations of Enig[18] and Hubbard and Johnson[19] apply to this homogeneous case.

With a nonhomogeneous liquid or solid the situation is different. If we compress powder to a pellet so that voids are present, or if we have foreign solid particles in the pellet then explosion and detonation can occur with moderately intense shock waves.[20,21] Detonation in a solid pellet may begin at a region well away from the surface where the shock wave originally entered. The shock wave may start a reaction in the solid which accelerates and builds up finally into a detonation after a time interval which depends on a number of factors. Again a thermal mechanism can be proposed for the initiation of explosion and detonation. Adiabatic compression of gas pockets (here the value of γ probably corresponds to monatomic gases), reflection of shock waves from inhomogeneities in the liquid or solid which can result in the intersection and reinforcement of shock waves, can all result in a high temperature in a localized region and these are all possible sources of initiation. In other words for a nonhomogeneous solid there is a distortion of the plane shock wave leading to localized regions of very high pressure and therefore of temperature. Since the reaction rate increases exponentially with temperature the result on over-all decomposition rate is higher than for the undisturbed wave.

The Initiation of Single Crystals by Shock of Moderate Intensity

We have been making some study of initiation in single crystals and I would like to mention here briefly some recent experiments by Dr. T. Boddington on the effect of shock waves of moderate intensity on small crystals of primary explosives. The single crystals are used as "Receptors" in what is essentially a gap test assembly. The barrier typically consists of a sheet of phosphor bronze with a thickness of 1/64 inch. The receptor crystals are usually in the form of long thin needles which may be up to 1 cm or so in length and the thickness may vary from 2 mm to 100 microns. The donor is a small amount of silver azide in contact with the other side of the plate and enclosed in plasticine. The shock pressures may be varied from a few kilobars to approx. 20 kilobars. The crystal may be surrounded by vacuum, by air, or by water.

Primary explosives: *Silver azide*. Figure 9 shows the typical behavior of a silver azide crystal which is free from defects and is surrounded by water. The shock passes through the barrier and enters the crystal. There is a delay of approx. 1 μsec before deflagration begins at the barrier interface (frame 4). This reaction continues in small crystals as a deflagration. The velocity is constant and depends upon the diameter of the crystal: it is not a detonation. The dark hemispherical shadow moving upwards is the shock wave travelling through the water and the pressure behind this is 13 kilobars. A weaker shock frequently fails to initiate deflagration either at the barrier or anywhere else. This is true of crystals which are devoid of visible imperfections.

If, however, the crystal contains small imper-

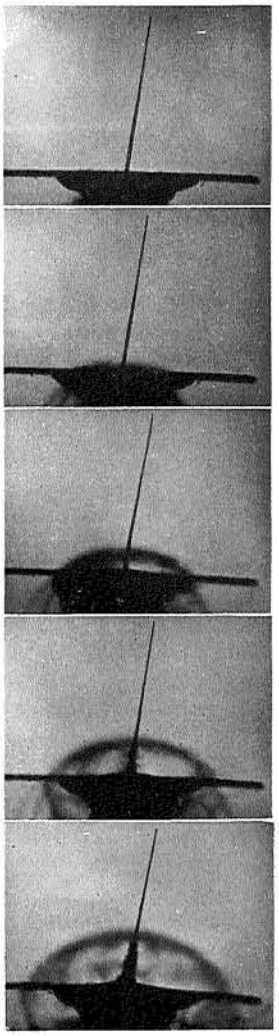

FIG. 9. Shock incident on silver azide crystal, length 15 mm. Interval between frames = 0.7 μsec. Water confinement. Deflagration is initiated at the barrier. Hemispherical shadow is the shock wave travelling through water.

fections the behavior is quite different. Examination of this crystal under the microscope shows that a number of small imperfections in the form of notches are present about half way along the crystal (Typical imperfections are shown at higher magnification in Fig. 10). The effect of these small imperfections is demonstrated quite clearly in the sequence shown in Fig. 11. Rapid deflagration is induced at each small discontinuity about half a microsecond after the arrival of the water shock (shock strength approx. 3.6 kb). The water shock produces no apparent effect while traversing the perfect sections of the crystal but causes initiation at each visible discontinuity. If the effective discontinuities are closely packed along the crystal length then initiation occurs almost continuously, so that a *deflagration is coupled to the water shock.* This "pseudo-detonation" is observable in Fig. 11 (frames 4 and 5). When no further discontinuities are available the deflagration form is left behind by the water shock and again propagates at its characteristic speed of approx. 800 m/sec (frames 6–9 of Fig. 11).

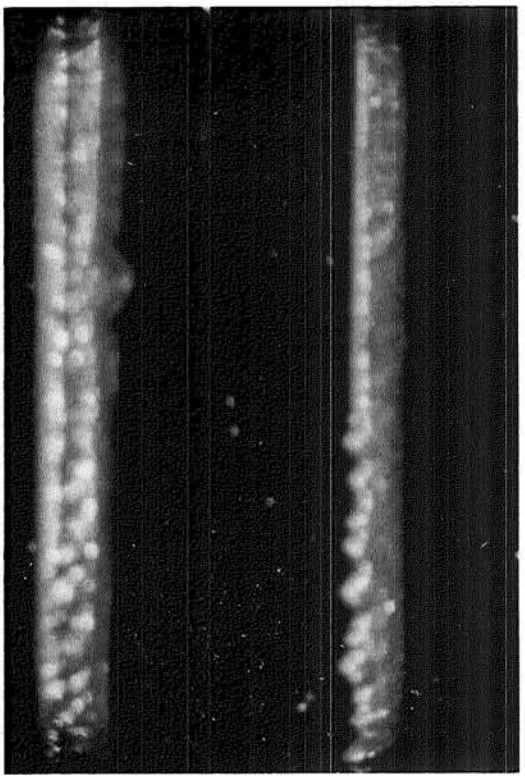

FIG. 10. Sensitivity sites in silver azide crystals. Left: a typical crystallographic "notch." Right: multiple discontinuities capable of propagating "pseudo-detonation." Diameter of crystal on the left = 100 μ.

Figure 12 is interesting. This crystal is initially free from defects. The shock enters the base of the crystal and there is evidence that it proceeds along it at sonic speed (approx. 2300 m/sec) and causes small "fractures" or imperfections to form. These can (with difficulty) be seen in frames 5–7 about two-thirds of the way along the crystal. The crystal initiates at the base about a microsecond after the passage of the shock and the deflagration spreads upwards at a speed of approx. 800 m/sec.

The main shock from the donor may be seen

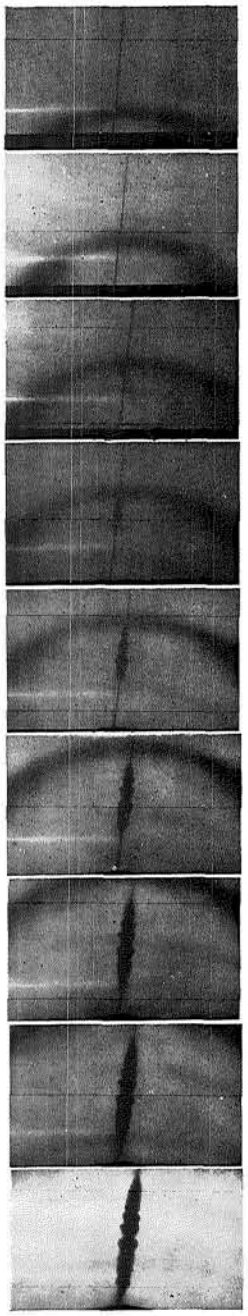

FIG. 11. "Pseudo-detonation" induced at multiple defects in silver azide crystal immersed in water. Interval between frames = 0.7 μsec, length of crystal = 9.8 mm, diameter = 110 μ.

travelling ahead through the water at approx. 1670 m/sec. As soon as it reaches the defects which have been formed in the crystal it initiates deflagration which propagates both forwards and backwards with its characteristic velocity of approx. 800 m/sec. (The subsidiary faint shocks in the water are generated by these deflagration heads.) The remaining frames in the series show the collision of the reaction heads, the interaction of the shocks, and the expansion of the reaction products.

Figure 13 shows the effect of inclining the crystal to the shock axis. Although the shock in the water is a very weak one (1.1 kb) the AgN_3 has undergone extensive deformation and cracking by frame 9. The crystal did not explode.

Silver azide crystals with water (or air) confinement do not exhibit a true detonation regime unless their thickness is greater than 2 mm. This regime of true detonation shows the characteristic product expansion cone and the wide-angle attached shock in the confinement. The propagation velocity is, for 2 mm crystals, 2900 m/sec and is constant.

Cavities and the Formation of Micro-Munro-jets

If the liquid or solid explosives contain bubbles, cavities, or voids of an appropriate shape we might expect them to act as microshaped charges and give rise to micro-Munro-jets when a shock passes over them. The possibility of this is illustrated by Fig. 14.

In these experiments[29] the liquid (water) projected rapidly from a small hole by the impact of a bullet. The hole was about 2 mm in diameter but smaller holes showed a similar effect. The shape and velocity of the liquid jet was very dependent on the curvature of its surface before impact. In Fig. 14a the liquid surface was nearly plane and the front of the jet which emerges is approximately so. There is some distortion but the main jet of liquid is moving with an approximate uniform velocity of 670 meters/sec. In Fig. 14b and c the liquid interface is concave (it might perhaps be regarded as one side of a spherical cavity). Two examples of the formation of micro-Munro-jets are shown. In each case the main jet is moving with approximately the same velocity as in Fig. 14a but it is now preceded by a Munro jet, moving at approximately 1.3 times and $2\frac{1}{2}$ times the speed of the main jet (Figs. 14b and 14c, respectively). In Fig. 14d the liquid surface is surrounded by a curved sheet of liquid which lags behind and which rapidly breaks up into a fine mist. We may expect that solids will behave in a similar way and we have observed this.

Conclusion. This section has emphasized the importance of tiny defects in the initiation of explosion by weak shock waves. It also demonstrates their importance in the growth process. A perfect crystal of silver azide is not initiated

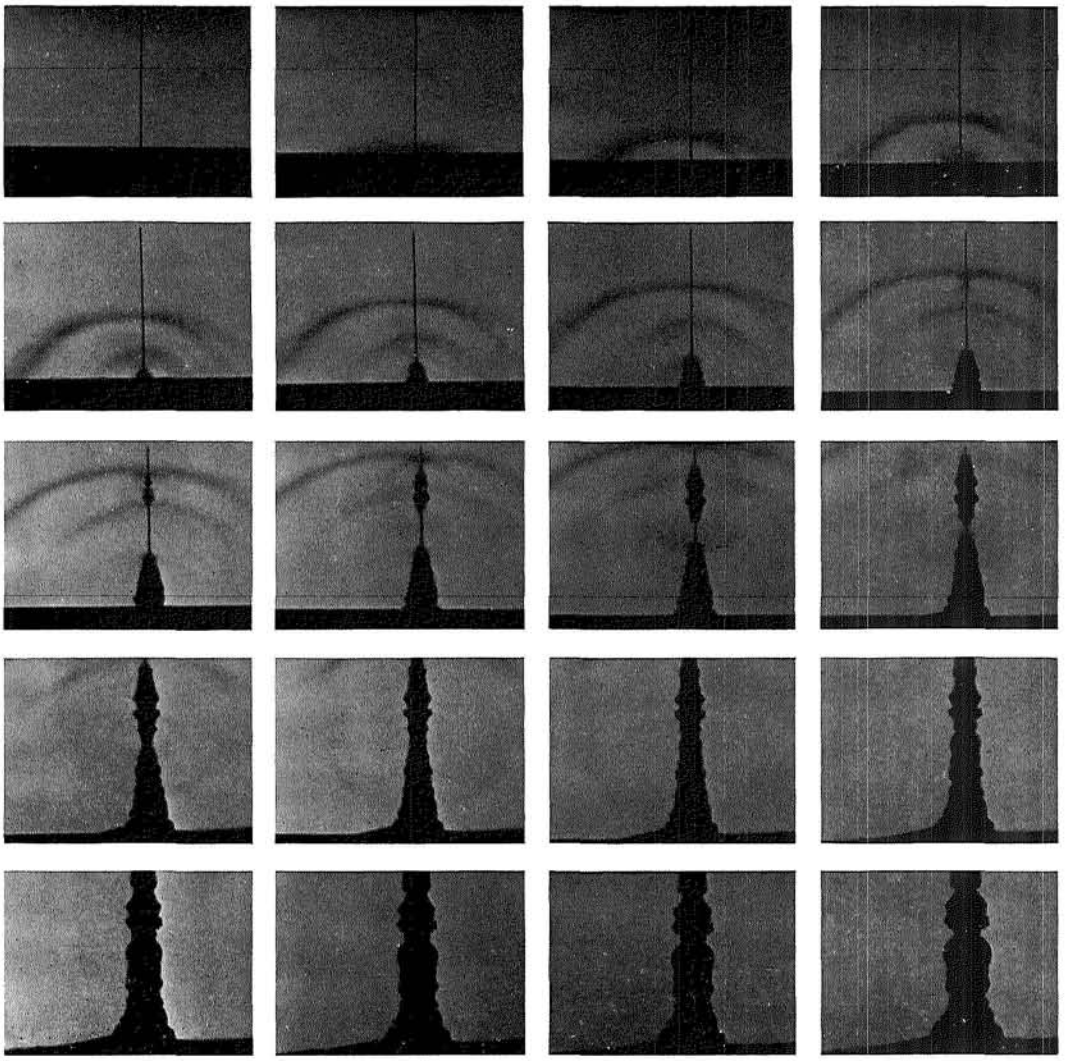

FIG. 12. The precursor sonic wave passing through the crystal has produced defects which are subsequently initiated by the water shock. Initiation has also occurred at the barrier. Crystal length = 11.9 mm, diameter = 120 μ. The framing interval is 0.7 μsec between frames 1–15 and 1.4 μsec between frames 15–20.

but a defect which may be only a few microns in size serves to start the reaction. With crystals of small diameter the reaction continues as a deflagration. Its velocity is dependent on size and for a crystal diameter of 200 microns it may be approx. 800 m/sec. Even though the velocity in thicker crystals may rise to 1600 m/sec. it is still a deflagration and not a detonation as we had previously supposed. This clears up an apparent anomaly in the behavior of primary explosives since this velocity is lower than that permitted by hydrodynamic theory.[22]

The defects responsible for initiation may be present in the crystal to begin with or they may be introduced by the passage of a stress wave along it. In these experiments this precursor stress wave is of course ahead of the water shock. When multiple defects are present the interaction of the multiple deflagrations may build up a shock wave and lead to the transition to a detonation. Detonation is not observed in these experiments unless the crystal diameter exceeds 2 mm.

A second and very interesting effect is observed when a shock wave passes along a crystal containing multiple defects. *As it passes each discontinuity it initiates a deflagration so that the forward movement of this deflagration is coupled*

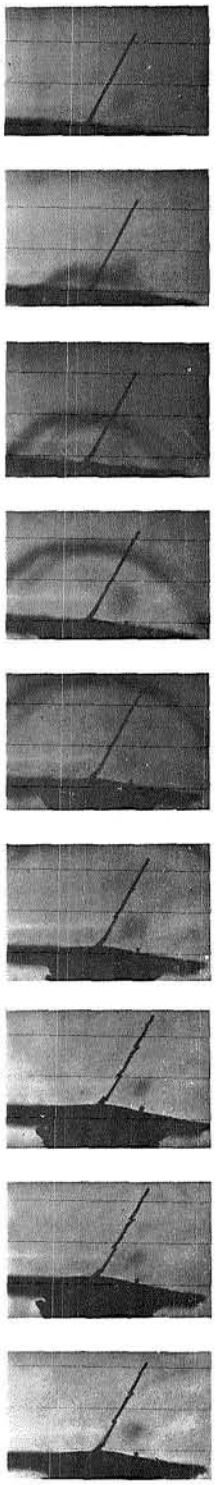

FIG. 13. Shock wave at oblique incidence causes extensive deformation of the crystal but is too weak to cause initiation.

to the shock wave and moves with it. In this sense a "pseudo-detonation" is set up. This is well illustrated by Fig. 11. It may have all the appearance of a stable low velocity detonation moving through the explosive but in reality the explosive is only burning. If no more discontinuities are present in the region ahead of the shock wave it will cease to propagate with a shock velocity and may die out.

These experiments help us to explain the initiation of explosion by shocks of moderate intensity and also the propagation of low velocity detonation in thin films of compressed powders and in primary explosives which are pressed in the form of cylinders of small diameter and heavily confined in metal tubes such as lead. We also see that, if the explosive contains small cavities these may lead to the formation of tiny Munro jets. The formation of these could aid initiation and propagation in two ways. Firstly by increasing the velocity of impact and secondly by breaking up the explosive into very fine particles so that its surface area is greatly increased in the critical region.[23–26] If two jets from the opposite sides of a cavity were to impinge the velocity of impact might be increased by a factor of ten or more. These observations suggest that further work might be done on the influence of the *shape* of the cavities and their effectiveness in initiating explosion. It would be interesting to hear what further experimental information is available about micro-Munro-jets of this type and whether there is any direct evidence that they can initiate explosion.

Direct Mechanical Rupture of Bonds in Explosive Solids

Another mechanism which has been suggested for the initiation of reaction in solids is the direct mechanical rupture of bonds resulting from the propagation of intense shock waves through the solid. Recently Dr. Field in this laboratory has made some direct measurements of the velocity with which cracks can propagate in hard solids. It is very high: For example with diamond the cracks can be propagated with a velocity of some 7200 m/sec. There is tetrahedral bonding in diamond and this means that C–C bonds are broken in times of the order of 2.1×10^{-14} sec and this is shorter than the vibration period in the unexcited state. It is clear therefore that the mechanical or "tribochemical" rupture of bonds in such crystals is a possibility and a thermal mechanism need not apply. With organic solids such as PETN however, the situation is different. The velocity of crack propagation is much lower (approx. 1500 m/sec) and further the solid is of the molecular kind. We may in fact separate

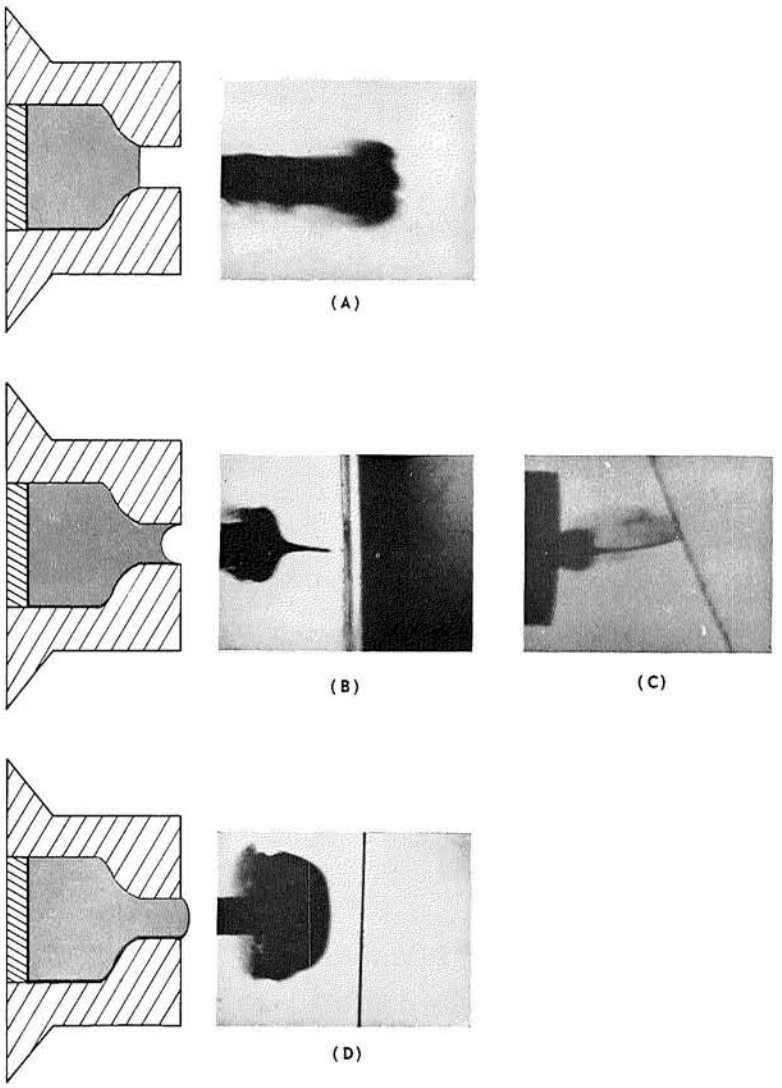

FIG. 14. Influence of shape of interface on the behavior under impact. If the interface is concave a micro-Munro-jet is formed. If it is convex a thin unstable umbrella is formed which rapidly disintegrates. The velocities of the jets are: (A)Main jet: 670 m/sec; (B)Main jet: 670 m/sec; Munro jet: 880 m/sec; (C)Main jet: 760 m/sec, Munro jet: 1,900 m/sec; (D)Main jet: 760 m/sec.

molecules of PETN rather than rupture bonds in the molecule itself. Further with such short molecules it is unlikely that the pressure profile is so sharp that a large pressure differential will occur along the length of the molecule. This of course will not apply to long chain polymers, where it is possible to rupture bonds directly.

We therefore conclude that it is unlikely that a "tribochemical" mechanism will apply to the decomposition of simple covalent explosives. It is also possible to argue from the electronic properties of the ionic solids such as the azides that the rapid break up of the crystal will not result in decomposition. The problem however is of some interest and would clearly repay further study.

ACKNOWLEDGMENTS

I thank Dr. T. Boddington, Dr. L. T. Chadderton, Dr. J. E. Field, Mr. M. McOnie, Dr. H. M. Montagu-Pollock, Dr. M. J. Sole and Dr. A. D. Yoffe for help and for permission to quote unpublished work.

REFERENCES

1. JACOBS, P. W. M. and TOMPKINS, F. C.: *Chemistry of the Solid State* (Garner, W. E., ed.), Chapter 7. Butterworths, 1955.
2. SAWKILL, J.: Proc. Roy. Soc. (London) *A229*, 135 (1955).
3. BOWDEN, F. P. and MONTAGU-POLLOCK, H. M.: Nature *191*, 556 (1961). See also BOWDEN, F. P. and CHADDERTON, L. T.: Nature *192*, 31 (1961); and Proc. Roy. Soc. (London) *A269*, 143 (1962).
4. MONTAGU-POLLOCK, H. M.: Proc. Roy. Soc. (London) *A269*, 219 (1962).
5. EVANS, B. L. and YOFFE, A. D.: Proc. Roy. Soc. (London) *A238*, 568 (1957).
6. EVANS, B. L. and YOFFE, A. D.: Proc. Roy. Soc. (London) *A250*, 346 (1959).
7. DEB, S. K. and YOFFE, A. D.: Proc. Roy. Soc. (London) *A256*, 514 (1960).
8. EGGERT, J.: Proc. Roy. Soc. (London) *A246*, 240 (1958).
9. COURTNEY-PRATT, J. S. and ROGERS, G. T.: Nature *175*, 632 (1955).
10. KAUFMAN, J. V. R.: Proc. Roy. Soc. (London) *A246*, 219 (1958).
11. BOWDEN, F. P. and SINGH, K.: Proc. Roy. Soc. (London) *A227*, 22 (1954).
12. SILK, E. C. H. and BARNES, R. S.: Phil. Mag. *4*, 970 (1959).
13. BONFIGLIONI, G., FERRO, A., and MOJONI, A.: J. Appl. Phys. *32*, 2499 (1961).
14. NOGGLE, T. S. and STIEGLER, J. O.: J. Appl. Phys. *31*, 2199 (1960).
15. BIERLEIN, T. K. and MASTEL, B.: J. Appl. Phys. *31*, 2314 (1960).
16. IZUI, K. and FUJITA, F. E.: J. Phys. Soc. Japan *16*, 1032 (1961).
17. ADAMS, G. K., HOLDEN, J., and WHITBREAD, E. G.: *31st International Congress on Industrial Chemistry*. Liege, 1958.
18. ENIG, J. W.: *Third Symposium on Detonation*. Princeton Univ., 1960.
19. HUBBARD, H. W. and JOHNSON, M. H.: J. Appl. Phys. *30*, 765 (1959).
20. CAMPBELL, A. W., DAVIS, W. C., and TRAVIS, J. R.: *Third Symposium on Detonation*. Princeton Univ., 1960.
21. CAMPBELL, A. W., DAVIS, W. C., RAMSAY, J. B., and TRAVIS, J. R.: *Ibid.*
22. EYRING, H., POWELL, R. E., DUFFEY, G. H., and PARLIN, R. B.: Chem. Revs. *45*, 69 (1949).
23. JOHANSSON, C. H. and others: Proc. Roy. Soc. (London) *A246*, 160 (1958).
24. ANDREEV, K. K.: Proc. Roy. Soc. (London) *A246*, 257 (1958).
25. BOWDEN, F. P. and YOFFE, A. D.: *Initiation and Growth of Explosion in Liquids and Solids*. Cambridge Univ. Press, 1952.
26. BOWDEN, F. P. and YOFFE, A. D.: *Fast Reactions in Solids*. Butterworths, 1958.
27. BOLKHOVITINOV, L. G.: Doklady Akad. Nauk, U.S.S.R. *130*, No. 5 (1960).
28. MENTER, J. W.: Proc. Roy. Soc. (London) *A236*, 119 (1956).
29. BOWDEN, F. P. and BRUNTON, J. H.: Proc. Roy. Soc. (London) *A263*, 433 (1961).

Discussion

PROF. F. P. BOWDEN (*University of Cambridge*): I would like to express my appreciation at being invited to take part in this symposium where so many scientists who are actively engaged in advancing our knowledge are present. In particular I must express my thanks to Dr. White and to Dr. Berl, and the members of the papers committee and organizing committee for the job they have done in arranging the session, in extracting the papers and in getting them distributed to us all in time. I am a member of the papers committee who has done very little work so I know what a remarkable job it was.

May I next take up a moment to make a mild grumbling noise mainly to clear the air in the discussion: Shortly before I left Cambridge Dr. Yoffe, who had read these preprinted discussion papers, asked why, when we have for many years been publishing experiments investigating the *different* ways in which discontinuities may initiate explosives, we are branded with only one of them. That is the adiabatic compression of gas spaces.

The position is really a very simple one. If we subject an explosive to a strong shock (say 100 kb pressure) no discontinuities are required: The adiabatic heating of the compressed explosive can initiate the reactions. For mechanical impact (pressures of, say, 1–2 kb), however, or for moderate shocks (say, pressures of 5–30 kb) this is no longer true. We need some mechanism for concentrating and localizing the shock energy so that it can give rise to local hot spots. For most explosives the temperature of the hot spot may need to be greater than 500°C and its diameter greater than 1000 Å.

We find that discontinuities may achieve their purpose in a variety of ways which are not mutually exclusive. At the Royal Society Discussion in 1957 we summarized some of these and perhaps I might reproduce this here.

The Initiation of Reaction in Solid and Liquid Explosives

"There is experimental evidence that, for materials which decompose exothermically, initiation may be

brought about in the following ways:

(1) by heat which raises the material to the ignition temperature;
(2) by impact or shock; this can act by:
  (a) an adiabatic heating of compressed gas spaces;
  (b) a frictional hot spot on the confining surface or on a grit particle;
  (c) intercrystalline friction of the explosive itself;
  (d) viscous heating of the explosive at high rates of shear;
  (e) heating of a sharp point when it is deformed plastically;
  (f) mutual reinforcement of gentle shock waves;
(3) by ultrasonic vibration;
(4) by electrons, α-particles, neutrons, and fission fragments;
(5) by light of sufficient intensity;
(6) by electric discharge;
(7) by 'spontaneous' initiation of a growing crystal."

You may note that under the heading of shock, one of the methods is the reinforcement of gentle shock waves. I had suggested this to Dr. Winning of duPont and in his letter to *Nature* of 1956 he describes this and his very elegant experiments showing that two gentle shock waves meeting could cause initiation although either separately was unable to do so.

Dr. Gurton in 1949 working in Cambridge showed that the effect of a shock in dispersing the explosive into fine particles or droplets could be a major factor in the initiation and growth of explosion. Dr. Rogers in 1955 showed that the flying particles from an exploding azide crystal could initiate explosion in a second crystal. If a device for focusing these flying particles were used (e.g., a convex mirror) they could produce initiation at distances up to 20 cm.

I mention these matters not because the History of Science is also holding a conference at Cornell but to simplify the discussion. These different mechanisms may each be effective under different experimental conditions. The most important of these are the *local* pressure of the initiating shock (and hence the local temperature it can generate) and the time for which it acts. In addition of course the scale of the effect, i.e., the actual size of the region which heated, is important.

For example there are the mechanisms we have been discussing this morning:

1. the adiabatic compression of gas bubbles;
2. the local distortion and the reinforcement of shock waves;
3. the dispersion of the explosive into fine particles;
4. the formation of micro-Munro jets.

We would consider that for mechanical impact and very gentle shocks where the pressure in the main shock front may be approx. 1 kb and the duration long (perhaps some milliseconds) 1, and 3, above could be particularly important. If the impact is very gentle the γ of the gas is significant; if it is intense, γ does not matter because any gas or vapor can produce a high enough temperature. For moderate shocks, however, where the pressures in the main shock may be, say 5–30 kb and the detonation short (perhaps microseconds) we may expect that all the methods can operate but that 2, 3, and 4 could be particularly important. These are the conditions which were obtained in Dr. Boddington's experiments and are, of course, those which occur in many gap tests. Boddington considers that the main role of the discontinuity in his single crystal is 2, that is the local distortion of the plane shock wave. For this reason I was particularly interested in Dr. Travis remarks describing the calculations made by Evans, Harlow, and Meixner of the temperature rise which could be produced in this way. I think we need to extend both experiments and theory here. Further consideration might also be given to the effect of the reinforcement of reflected shock waves.

J. R. Travis (*Los Alamos Scientific Laboratory*): Our studies of initiation of high-density solid explosives has convinced us that shock interactions at the wave front are primarily responsible for the generation of hot spots with subsequent release of energy to the front. We were led to this conclusion, in part, from experiments with liquid explosives. For example, roughening the initiating wave will result in a shorter induction time. Initiation will occur near a bubble ($\sim$ 1 mm dia.) at a much shorter time, and the time to initiation is relatively insensitive to the nature of the bubble (whether it is gas or a solid).

Some new developments along these lines might be worth pointing out. M. W. Evans, F. H. Harlow, and B. D. Meixner [Phys. Fluids *5*, 651 (1962)], have computed that the interaction of a shock wave with a bubble in nitromethane will produce a high temperature region, of volume approximately the same as that of the original bubble, downstream from the bubble. Mader has utilized this result and investigated the history of this kind of hot spot with the computational scheme outlined in my comment on the paper by G. K. Adams. He has presented the following results in an unclassified Los Alamos Report LA 2703:

"When a hydrodynamic hot spot has decomposed, it sends a shock wave into the undetonated ex-

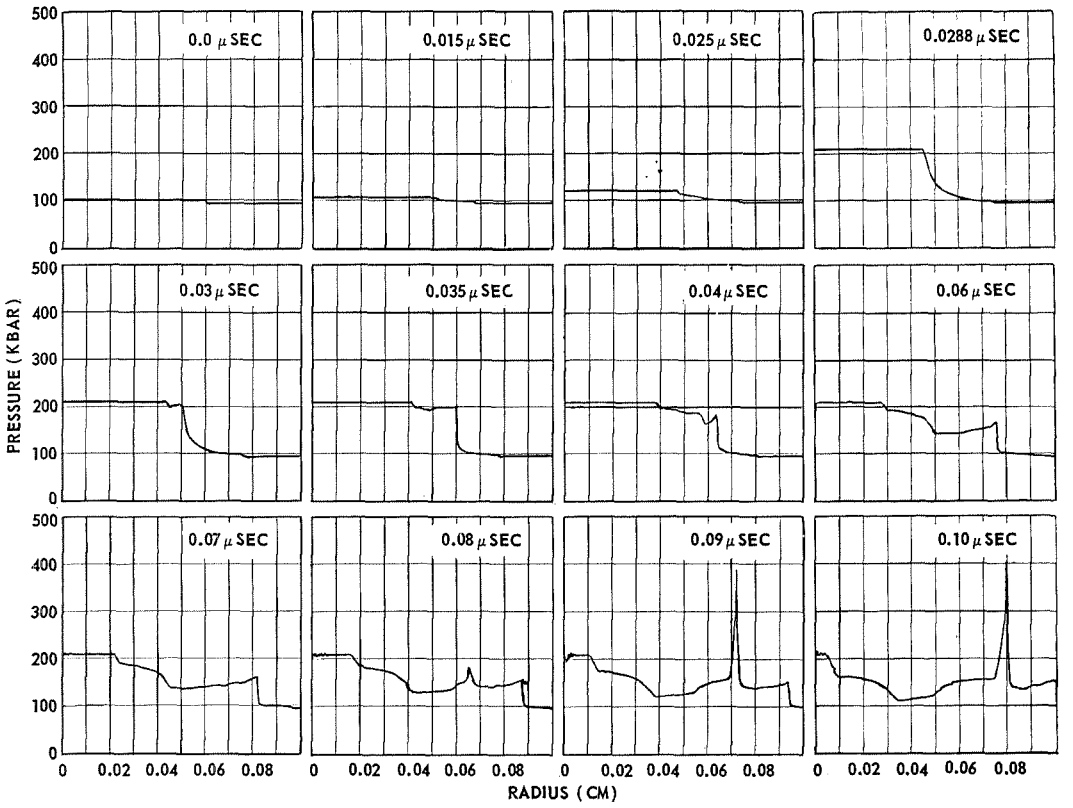

FIG. 1. Development of a detonation in shocked nitromethane (94.7 kbar, 1200°K) from a 0.06 cm radius spherical temperature hot spot (1404°K).

plosive which heats it. What occurs thereafter depends upon the initial strength of the shock wave and how well it is supported from the rear. Whether the explosion of the hot spot propagates to the rest of the fluid or not depends primarily on the initial size of the hot spot." Figure 1 shows the propagation of waves from a hot spot 0.6 mm in diameter (hot spot at 1400°K, nitromethane shocked to 1200°K by a 95 kbar shock).

We would like to suggest that hydrodynamic heating of this kind must be considered as important whenever shock interactions are expected and that this heating is independent of particular mechanisms such as shear or fracture.

The shock initiation of a nitromethane-carborundum slurry is an example where this is especially clear. The initiation behavior of the slurry is identical to that of a polycrystalline explosive, such as cyclotol. The slurry is composed of inert particles with the interstices filled with liquid, a situation in which hydrodynamic hot spots would be expected and some of the other mechanisms are not.

THE SHOCK-TO-DETONATION TRANSITION IN SOLID EXPLOSIVES

S. J. JACOBS, T. P. LIDDIARD, JR., AND B. E. DRIMMER

The development of a shock wave and its subsequent growth-to-detonation is considered to be a necessary step in the initiation of detonation in any explosive. Using this argument as a basis, it is logical to study in detail, the development of impulse-initiated detonations, to establish the dependence of the growth-to-detonation process on physical, chemical, and geometric variables which appear to be of importance. In this paper, experiments on shock initiation of cast and pressed explosives are discussed. Plane shocks developed by explosive plane-wave generators, and degraded to desired peak amplitudes by the use of intermediate layers of inert materials, were used to initiate detonation in the test explosive sample. The velocity of the shock in each sample was measured as a function of distance into the explosive and as a function of initial shock amplitude. Initial shock pressures ranged from 28 to 140 kilobars. Explosives discussed are TNT and various cyclotols. Both cast and pressed charges were used. In cast charges other than TNT the shock velocity remained essentially constant for a period of time, the length of which depended on the initial shock amplitude, and then rapidly accelerated to normal, steady state detonation velocity. In pressed charges it was found that in the rapid rise, the shock velocity temporarily exceeded the steady detonation value, but decayed thereafter to that of the normal steady detonation. In cast TNT the velocity was found to rise to a value intermediate to that of the initial shock and the final detonation, where it persisted for a time before growth to the normal detonation value. The over-all results can be explained by a hydrodynamic model in which pressure build-up, due to chemical reaction behind the shock, reinforces the shock front as it proceeds through the charge. On the other hand, the detailed results cannot be explained by thermal reactions in homogeneous domains, but require the concept of hot-spot initiation. In the discussion our findings will be compared with the work of others who have used various impact and gap-test configurations. Some of the problems and differences of opinion which have arisen in the interpretation of shock initiation will be discussed.

Introduction

It may be of historical interest to note that many years ago Cornell University was the scene of another discussion on the problems of shock-to-detonation transition. In 1945 a small group of scientists from the OSRD, the National Research Council of Canada, the Army, and the Navy met here to exchange ideas concerning detonation in explosives. Hertzberg[1] described to that group some interesting smear-camera records he had obtained concerning the initiation of detonation in solid and liquid explosives. At the same meeting he described a card-gap test which was probably the first of many to follow. Boggs[2] also presented a number of important, and at that time perplexing, experimental observations on the transition from shock to detonation. The work discussed in that meeting, and much of the work that followed suffered for lack of quantitative description of the forces and energies present in the incoming shock which cause a detonation to form.

After a lapse of over ten years, work began to be reported in the open literature which described in quantitative terms the build-up to detonation from shocks of known pressure amplitudes.[3–7] The list of papers has grown rapidly in more recent years.[8–15] In the majority of these papers the build-up to detonation has been attributed to an initiation of chemical reaction by either a uniform or a localized temperature rise associated with the adiabatic compression, followed by growth determined by the continued speed-up of the reaction once begun. An alternate hypothesis which postulates the development of high thermal conductivity behind the shock leading to a heat pulse has also appeared.[16–17] The latter hypothesis makes no clear distinction between the behavior of liquids and polycrystalline solids. The former, more prevalent, viewpoint supplies a framework for explaining differences in behavior: (a) between solids and liquids, (b) between solids formed by different techniques (such as by casting or by pressing), (c) due to geometric configurations of the medium under study, and

(d) due to spatial and temporal distribution of pressure and flow. The transition to detonation in a liquid explosive, when a plane step shock is induced in it, appears to be the simplest to explain in its physical aspects.[8,18–20] Here the temperature rise in a homogeneous compression seems sufficient to account for the build-up to detonation. The meager evidence from experiments on single crystals, carried out in such a way that rarefaction effects may be considered negligible, are in accord with this model.[9]

The response of polycrystalline solid explosives to the entering shock is not as clear as in the case of liquid explosives. Solid explosives are formed into a mass which contains numerous crystal entities, and both macroscopic and microscopic voids. When initiated by plane shocks of low shock amplitude, the dependence of build-up time on crystal size and void content makes it fairly evident that the low temperature rise calculated for a homogeneous compression cannot account for the observed transition. Thus a hot-spot mechanism of the type suggested by Bowden and others[21–23] is required. The confirmation of early work by Winning[7] and Marlow,[6] who reported that induced shocks with pressures as low as 20 kilobars would cause transition-to-detonation, has established important support of a mechanism centered around a relatively small number of initiation sites. Studies to show how a detonation develops when both the physical state of the explosive and the shock amplitude are varied, are beginning to lead to a better understanding of the nature, magnitude, and behavior of the initiation sites.

The shock-to-detonation transition has been studied at NOL by the use of a plane-wave system arranged in such a way as to make it possible to follow continuously the wave front within the shocked sample.[3,4] The experiments to be described have made it possible simultaneously to establish the initial pressure in the shock and to observe the growth-to-detonation as it develops. The observations are made on a wedge-shaped test sample, the wedge permitting observations without grossly affecting the one-dimensional flow in the region of interest. This is equivalent to the observation of growth *within* an explosive charge of much larger dimensions. Thus, the results appear to agree reasonably well with shock-initiation work on long cylinders of cross-sectional area comparable to the area of the face of the test wedge, provided: (a) the observations in the cylinder are made in the region of its axis (not on its exterior surface), and (b) the pressure–time histories of the entering shock are similar. The results of these experiments are in accord with the explanation that growth-to-detonation in polycrystalline solids is the result of pressure build-up from temperature-triggered chemical reaction spreading from localized sites.

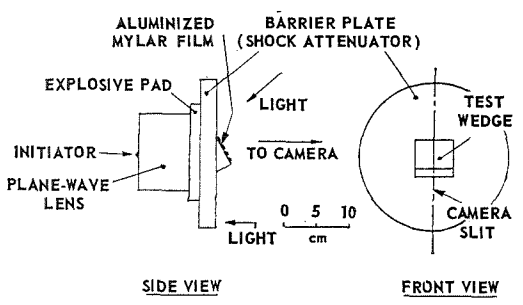

FIG. 1. Wedge-test arrangement.

Experimental

A typical set-up for generating 20 to 180 kilobar, plane shocks in the test specimen is illustrated in Fig. 1. In this example the 11 cm diameter plane-wave generator developed a detonation wave that was flat to ±0.3 mm over a diameter of 9 cm. A slab of explosive, 12.5 cm × 12.5 cm × 2.5 cm was placed between the generator and a 20 cm diameter disc of inert barrier, or shock attenuator. A sample of the test explosive, in the form of a 25° wedge (apex angle 90°) was then placed on the opposite face of the attenuator. (A thin film of silicone grease was generally placed between the attenuator and the test wedge to minimize the possibility of accidentally causing a hot spot by a small amount of entrapped air in the region.) In general the test wedges had faces 3.2 cm by 3.2 cm, and therefore were 1.4 cm high. For the less sensitive explosives, or where very low amplitude shocks were to be used, larger wedges were employed: faces 5 cm by 5 cm, and by changing to a 30° angle, were 2.6 cm high.

The different pressure levels in the test explosive wedge were obtained by varying the different components of the shock-generating system. Thus, the slab of explosive, between the plane-wave generator and the inert shock attenuator, was either cast Composition B, Baratol, or TNT; in addition, the thickness of this slab was increased to as much as 5 cm, as the need warranted. The attenuator was either solid brass, aluminum, or Plexiglas, or was made from 1 cm thicknesses of such materials in various laminated configurations, to produce the desired shock pressures.

The phase velocity of shock arrival along the wedge free surface was determined with a smear camera having a writing speed of 3.8 mm/microsecond. The arrival of the wave was recorded by the camera by using an aluminized Mylar film on

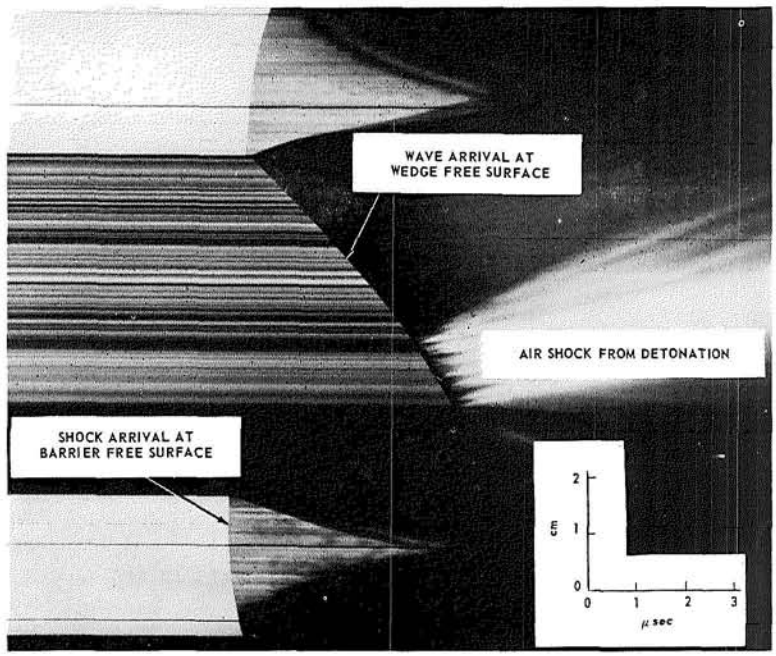

FIG. 2. Typical NOL wedge-test record.

the surface of the specimen, and reflecting light from an electrically exploded wire confined in a glass capillary. When the wave reached any point on the surface, the reflection from the Mylar mirror was abruptly reduced, as shown in Fig. 2, permitting precise determination of time vs distance of penetration of the shock into the wedge. Velocity of shock propagation was then obtained by graphical differentiation. The wedge angle was chosen to be as small as possible consistent with the desired height, so that rarefactions from the region previously shocked would not penetrate into the region behind the yet-unshocked portion of the wedge in time to affect the desired observations.

For each experimental arrangement the initial free-surface velocity of the attenuator, without the explosive sample, was determined by direct measurement in an identical lens-donor-attenuator system. Similar preliminary experiments determined that, at the center of the plate, over a diameter of 5 cm or more, the time-of-arrival of the shock was simultaneous to within 30 nanoseconds, while the free-surface velocity was constant to within $\pm 2\%$. The particle velocity in the attenuator, at the metal–specimen interface, is then given by the usual assumption that it was one-half the measured initial free-surface velocity. The shock Hugoniots for Plexiglas and for the Naval brass used in these experiments were obtained by direct measurement of shock and free-surface velocity by the methods described by Rice *et al.*,[24] and by Coleburn.[25] The Hugoniot for 24ST aluminum was taken from the report by Rice.[24]

Information Obtained

The explosives studied and their pertinent properties are listed in Table 1. The observed

TABLE 1

Explosive	State	Density gm/cm³
Composition B RDX/TNT/Wax; 59/40/1	Cast	1.71
Composition B–3 RDX/TNT 60/40 (Mean RDX particle size, 60–80 microns)	Cast	1.72
Cyclotol RDX/TNT; 75/25	Cast	1.73
Trinitrotoluene (TNT) (Microcrystalline)	Cast	1.58 1.62
Trinitrotoluene (Mean particle size: 40–80 microns)	Pressed	1.51 1.61 1.64

TABLE 2

Experimental constants for Eq. (1)
U and u (mm/microsecond)

Material	ρ_0	a	b	c
Naval brass	8.37	3.560	1.833	0
Plexiglas	1.18	2.710	1.568	−0.037
Lucite[a]	1.18	2.588	1.51	—
TNT	1.60–1.62	2.39	2.05	0
TNT (liquid)[b]	1.472	2.00	1.68	0
Composition B, B-3	1.72	2.71	1.86	0

[a] From reference 12.
[b] Garn, reference 30.

time-of-arrival of the shock disturbance at the wedge free surface was converted to a velocity–distance (U–S) curve within the wedge, by careful slope measurement of the smear-camera record, assuming plane-wave propagation inside the wedge. As shown below, the value of the observed shock velocity at zero wedge thickness was used with the Hugoniot data for the shock attenuator, to determine the initial pressure in the explosive. Hugoniots for the unreacted explosives were then constructed from these data, assuming that negligible chemical reaction had occurred at this zero wedge thickness during passage of the shock. Shock velocities at low pressure ($p < 2$ kb) were established from measurements made on the same explosives, using a simple aquarium method for shock transit-time observations.[26]

The shock Hugoniots for both the inert barriers and the nonreacting explosives are conveniently expressed by relating shock velocity (U) to particle velocity (u) in the simple form:

$$U = a + bu + cu^2, \qquad (1)$$

where a, b, and c are constants. When this equation is applied to the experimental data by the method of least squares, the value of the constant, c, is often so small, that in the region of interest, the U–u relation can generally be considered linear to acceptable accuracy. The values of a, b, and c in this equation are listed in Table 2 for a number of materials used in our work. Pressure, density, and energy jumps across the shock front are derived by the well-known hydrodynamic relations for a shock (assuming initial pressure negligible):

$$p = \rho_0 U u, \qquad (2)$$

$$\rho = \rho_0 U/(U - u), \qquad (3)$$

$$E - E_0 = p(v_0 - v)/2 = u^2/2, \qquad (4)$$

where p is pressure, ρ is density, E is specific energy, and v is specific volume (reciprocal of ρ). Subscript 0 refers to the unshocked state. The particle velocity in the nonreacting explosive was determined by boundary-value matching of p and u, as illustrated in Fig. 3, using the calibrated values of particle velocity and pressure in the barrier (at the barrier, test-explosive interface) and the observed shock velocity in the test explosive (at the same interface). In the figure, subscript e refers to states within the shocked explosive; subscript m refers to states, within the shocked metal barrier. In applying this method, the p–u curve for the reflected rarefaction (or shock) wave within the barrier (in this illustra-

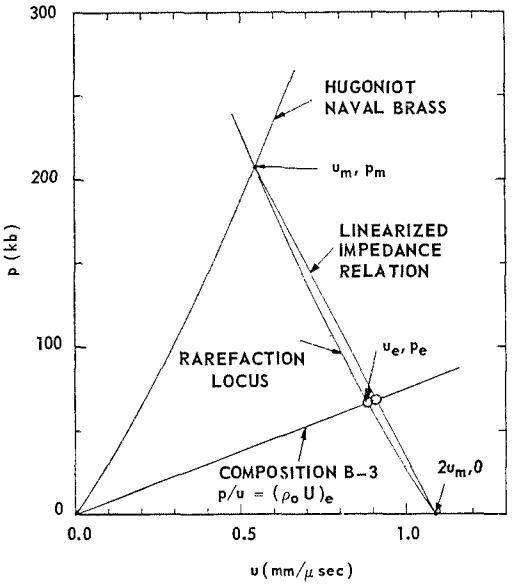

FIG. 3. Pressure-particle velocity diagram for determining shock pressure in the explosive.

tion, brass) is approximated by the reflection of the shock p–u curve for the barrier, about the line: u equal to $\frac{1}{2}$ the free surface velocity for the barrier in the given experiment. Since the pressure and the particle velocity across the interface must be continuous, the desired solution is the intersection of this rarefaction line, with the straight line for the explosive passing through the origin and having a slope

$$p/u = (\rho_0 U)_e \qquad (5)$$

where U is the measured shock velocity in the test wedge of explosive, at the barrier–wedge interface. In spite of the approximation involved, this method is a substantial improvement over the linearized impedance equation assumption often made, and previously used in this Laboratory.[3] The latter method leads to a larger systematic error in the pressure and particle velocity than the present approach.

Results

The experimental observations may be conveniently shown as graphs of shock velocity in the explosive sample as a function of distance traveled from the metal interface. Figs. 4 and 5 are typical of the results found at NOL. In Fig. 4, the results for the three cast cyclotols are shown for three initial shock amplitudes using brass attenuators. The first point to be noted is that the initial wave velocity increases as the brass plate thickness decreases. The initial values for the two Composition B types are the same for a given brass thickness. These velocities were converted to the pressures shown in Fig. 4. by the procedure previously described. The second feature of the curves is that the distance to build-up–to–detonation is a function of the initial pressure. Composition B–3 shows a shorter transition distance than Composition B at each pressure level. The difference most probably is due to an RDX particle-size effect. The curves of Fig. 4 are typical of the largest majority of records obtained in this Laboratory on over a hundred trials with a number of cast and plastic-bonded explosives at bulk densities in excess of 97% of theoretical maximum.

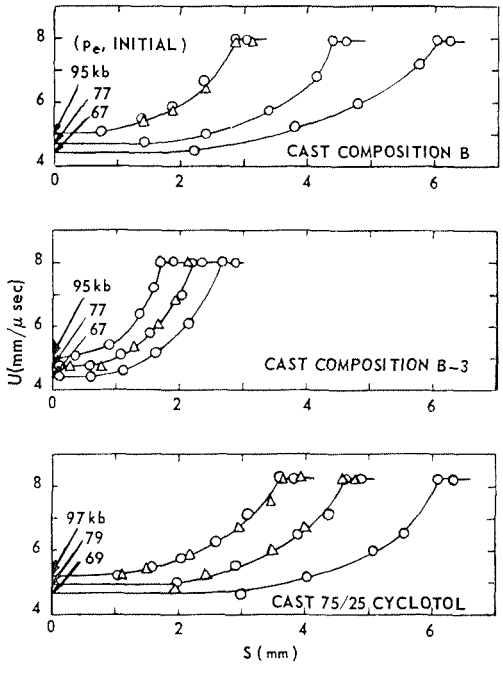

FIG. 4. Shock-velocity vs distance for 3 cyclotols (for each set of curves, reading from left to right the brass attenuator thickness was 0.5, 1.0, and 1.5 in.).

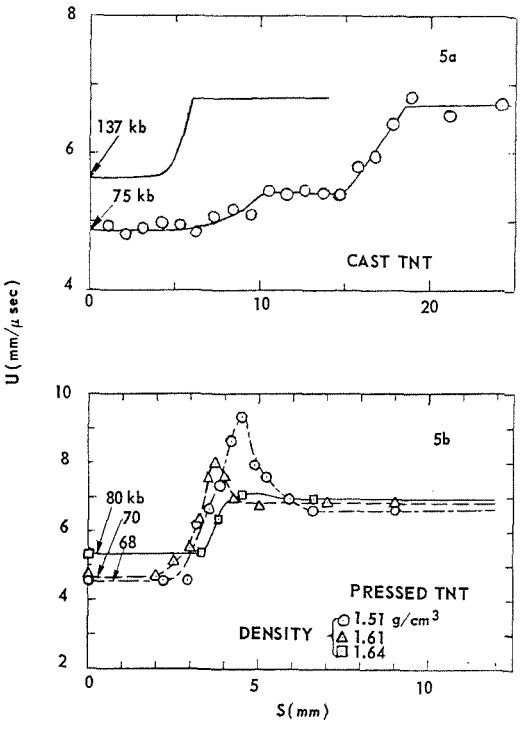

FIG. 5. Shock-velocity vs distance for several TNT charges.

TNT, when cast, exhibits a somewhat different shock propagation history. For initial pressures in the explosive below 100 kilobars our records consistently show evidence of what appears to be a leveling off of velocity in the neighborhood of 5.3 mm per microsecond, followed by a second rise, to normal detonation velocity, Fig. 5a. This type of observation has appeared too

frequently for us to attribute it to reading error. Majowicz[3] first observed this initial step, but failed to see the later transition-to-detonation because his wedge was only 14 mm in height. The final transition is seen to occur at greater distances in the pressure range shown in Fig. 5a. When the initial shock in the cast TNT exceeded 130 kilobars, the initial wave velocity exceeded this intermediate, plateau value and only one transition was observed, with a considerably shortened distance to detonation. For pressed TNT, the results for low initial shock pressure show new features, Fig. 5b. The observed initial shock velocity is out of line when compared with the results from cast TNT, being too high for a nonreactive shock. Furthermore, the transition-to-detonation occurs in a distance considerably shorter than in the case of cast TNT charges shocked by the same shock generator system. One may note that one of the curves in Fig. 5b involves a pressed charge at a density *higher* than that of the cast TNT, yet the growth distance to detonation is still only 4 mm as compared to 15 to 20 mm for the cast charges shocked in a similar manner. It is therefore quite clear that charge porosity *per se* is insufficient to describe the effect of physical state on the transition history. The effect of pressing, shown here for TNT, in shortening the transition distance is also present in the cyclotols and in other explosives. We may cite Composition B as an example: With a 1-inch brass barrier (initial p_e = 77 kilobars) pressed Composition B reached full detonation velocity in less than 2 mm, compared to 4 mm for the cast explosive.

The "overshoot" shown in the velocity–distance curve of pressed TNT, Fig. 5b, requires comment. In pressed explosives our camera records consistently have shown this irregularity, which we have interpreted as a transient rise to velocities in excess of the normal detonation rate. In some records the velocities appear to be as much as 50% over normal, but more frequently, as shown in Fig. 5b, the excess is about 20–30%. Such overshoots are entirely possible, we believe, on hydrodynamic grounds, depending on the nature of the reaction-rate profile behind the shock front. On the other hand the distance over which excess velocity has been observed in our records is small, of the order of 1–3 mm. While reading errors, made during measurements of phenomena rapidly changing over such small distances, are aggravated by the mathematical process of differentiation, careful examination of the photographs indicate that the records definitely exhibit such super-velocities. We believe therefore, that the photographic evidence of the overshoots is beyond reading error, although the magnitudes of the overshoots cannot be precisely determined. Campbell *et al.*[9] have also studied pressed charges. They have been quite emphatic that no overshoot had been detected in any of their experiments on pressed solids. We admit that there is room here for honest differences, and these may be due to differences in the two sets of experiments. More refinement of the experiments is needed to settle the question.

The transition distance vs initial shock amplitude within the explosive has now been determined for cast Composition B-3, over the range 30–130 kilobars. It has been found that a straight line very nearly fits the results if one plots the reciprocal of the distance against the initial pressure, as shown in Fig. 6. This line extrapolates to an infinite distance at p_e = 28 kilobars. This can be interpreted as an indication of the threshold pressure for initiating this explosive with the given shock generator. A cursory examination has been made of the rate of pressure decay behind the shock in the shock generator system used to obtain the data of Fig. 6. Our best estimate is that the pressure will fall to about 60% of peak in a time of 2 microseconds after passage of the shock into the explosive, in the absence of chemical reaction. This decay rate is comparable to that estimated to occur in the NOL gap test.[12] When Composition B-3 was tested in that gap experiment, the 50% point for detonation was found to require an initial peak pressure in the explosive of 20 kilobars. The closeness of the threshold shock pressures in the two experiments for the same explosive may be used to infer that the long cylinders will, near the sensitivity limit, show the same uniform initial velocity as we have found in the wedges at very nearly the same pressure level. The velocity would be near acoustic because at pressures in the neighborhood of 20 kilobars the shock wave velocity is near to the limiting acoustic value. Cachia and Whit-

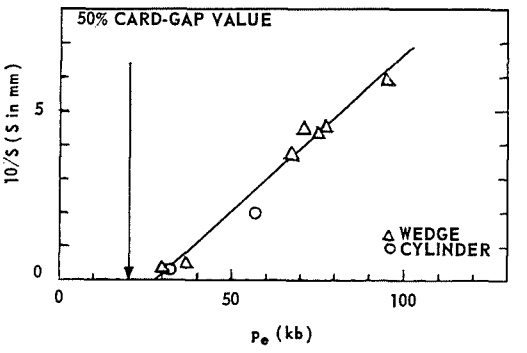

FIG. 6. Effect of input pressure (p_e) on distance (S) to steady-state detonations in cast composition B–3.

bread[5] have actually observed this initial "constant" velocity with ionization probes embedded in cylindrical charges at somewhat higher pressure levels (U = 4 mm/microsecond). The 50% gap experiment has shown a very sharp cutoff between "go" and "no-go" in Composition B. It now appears that the range between practically 0% probability of detonation build-up and practically 100% probability is about 1 to 2 kilobars in the donor shock. We could interpret this result to mean that in the constant velocity region the shock pressure is actually increasing by about this amount in the cases where a detonation is established.

Discussion

The clarification of the nature of the growth-to-detonation from a mechanical shock has required that quantitative measurements of the initial shock pressure be established. Since the first work at NOL we have mapped out (nonreactive) shock Hugoniots for a number of solid explosives; two are presented here. Our work has shown that both time and distance for growth-to-detonation is monotonely related to this initial shock amplitude. In 1956 an *ad hoc* theory was presented in a note by one of us[27] to relate the growth process to shock and reaction variables. It was pointed out in that note that the history of the build-up would probably depend not only on the initial shock amplitude but also on the nature of the rarefactions behind the initial shock. A subsequent paper by Majowicz and Jacobs[3] concluded that the build-up in experiments such as those presented here, must have involved a substantial induction period before any chemical reaction occurred, because the observed shock velocity was initially constant, insofar as we could determine. Our present position has changed in regard to this delay mechanism. It is now clear to us that our initial shock was followed by a rather steep pressure decay. In the presence of this rarefaction, the velocity of the leading shock in the explosive should have fallen by a measurable amount if it had not been supported by energy contributions from reactions which must have occurred shortly after passage of the shock. The absence of such a velocity decay indicates that the rate of the reaction closely behind the wave must be increasing as the shock progresses, so that ultimately, the reaction rate, increasing nonlinearly, causes the shock to build up very rapidly to a detonation.

There now have been reported a number of related studies by several groups to describe in quantitative terms, the growth-to-detonation in solids. Through these studies it is apparent that a unified picture is emerging. In discussing the problem we find important support in the work of Campbell *et al.*,[9] who used plane shocks as we did, but employed donor charges which were considerably larger, thus leading to a much slower decay of pressure behind the incident shock. Brown and Whitbread,[15] who studied initiation by the impact of disks made of several materials, showed quite clearly that the threshold for initiation depends on both the amplitude and duration of the initial shock within the explosive but not on the properties of the disk. Favier and Fauquignon[14] have also shown a dependence of the build-up distance on the pressure induced in the explosive irrespective of the attenuator composition. Similar findings have been reported by Sultanoff and Boyle[10] for shocks through various attenuating media including air, and for shocks induced by cylinder impact. Jaffe, Beauregard, and Amster[12] have established the relation between barrier thickness and shock peak pressure in a controlled gap-test experiment and have thereby established thresholds for initiation where the duration of the incident shock is somewhat longer than that of Brown and Whitbread.

If we confine our attention to cast and plastic-bonded explosives, the conclusion reached by Cachia and Whitbread[5] and by Campbell, Davis, Ramsay, and Travis[9] for build-up to detonation is, with minor modifications, the interpretation which we find acceptable. This may be stated as follows. The incident shock initiates a small amount of chemical reaction (in localized regions) with essentially no delay. The growth depends on the pressure effect due to the initial shock plus the pressure contribution due to the reaction. If the net pressure behind the wave increases, the leading shock will grow to a detonation. If it decreases the detonation will fail. The first point of complete reaction will depend on the reaction-time history experienced by the explosive layers after the shock has passed. If reactions in regions behind the shock are slowed down or stopped by adiabatic expansion or heat conduction, the detonation wave will probably form at or near the shock front, if it is formed at all. The extent of initial reaction and its subsequent growth in a given region will be strongly dependent on the shock amplitude entering that region.

Before exploring the mechanism further, we would like to point out a few facts and their implication concerning shock initiation of detonation near threshold pressures. It is now quite clear that detonations can be initiated in solid explosives by shocks with peak pressures between 20 and 40 kilobars, in cylindrical charges of 1- to 2-inch diameter or in comparable square charges.[6,7,10,12] By comparison, liquid nitromethane requires 86 kilobars, liquid TNT about 125 kilobars, and Dithekite 13 (HNO_3/nitro-

benzene/H_2O; 63/24/13) about 85 kilobars.[8] In these low density liquids, the average temperature rise at these pressures, in the neighborhood of 800° to 1000°C, appears quite adequate to account for transition to detonation by an initiation process involving homogeneous reaction kinetics. The hydrodynamic calculations made by Hubbard and Johnson,[18] Boyer,[19] and Enig,[20] clearly show a direct correspondence between what is observed experimentally and what is predicted from computer runs. In particular the rapid growth to a detonation behind the leading shock, the overshoot in velocity and pressure when this detonation overtakes the leading shock, and the subsequent decay to normal detonation, appear in both the experiments and in the computations. It is less clear that the temperature rise associated with a homogeneous compression can be sufficient to initiate reaction in solids at pressures of 80 kilobars, and at 20–30 kilobars such a possibility is out of the question. At 80 kilobars the Hugoniot energy jump given by Eq. (4) is 122 calories per gram for Composition B. If we assume that all of this energy is thermal and the specific heat is as low as 0.35 cal/gm/deg the temperature rise would be 350°C on the average. At 30 kilobars the Hugoniot energy is only 28 cal/gm and the average temperature rise using the above assumptions is 79°C. There is ample opportunity to consider the localizing of energy in microscopic regions (but large relative to molecular dimensions) within the solids under compression. Many workers following Bowden have noted the existence of small voids in solids, and have accepted the simple hypothesis that gas in such voids would get sufficiently hot under shock compression to supply the needed initiation temperature rise. This argument was tested by Cachia and Whitbread by comparing the 50% gaps for an explosive containing in its voids, various gases or a vacuum.[5] The same 50% point was found in every case. Is it not possible that the void act in other ways? We think the answer is yes.

A few of the possible ways for localizing energy are:

(1) Micro-roughness of the shock and shock-wave interaction (Campbell).
(2) Elastic–plastic changes behind the shock front with localized shear or fracture.
(3) Discontinuity of flow near voids leading to shear.
(4) Discontinuity of flow at grain boundaries.
(5) Spalling or spray into voids. (Johannson).
(6) Phase change under shock loading.
(7) Defects in the crystallites.

We do not have evidence to support unambiguously any of the above as the mechanisms. Our thinking has strongly learned to shock-produced microshear or microfracture at or near voids, as the path by which the explosive is locally ignited, but we do not yet know precisely how to characterize these variables.

In the paper by Campbell on initiation of solids,[9] evidence is cited to the effect that the explosive near the entering boundary reacts to only a small extent, transmits its excess pressure, and then apparently stops reacting. They state, on the basis of these experiments, that the explosive in that region not only fails to react to completion but also will not sustain further reaction when subjected to a second shock (as from the region where detonation finally is established). This argument is plausible, we believe, for some solid explosives in the wedge type experiment used by Campbell and by us. Two bits of information will be used to discuss this point. First, Boyer[28] has used a model to compute the transition to detonation in solid explosives in which two mechanisms for reaction are assumed to proceed simultaneously. One is an ignition reaction based on first order homogeneous reaction kinetics; the second is a surface burning reaction in which the Arrhenius terms contained in the equation are the same as in the ignition reaction. An arbitrary limit of 1% of the total mass is allowed to react according to the ignition mechanism. The computed result showed a shock velocity vs distance curve very similar to those shown in Fig. 4. The result also showed reaction to first go to completion at points in the explosive which were near the accelerating shock front. No basis is given for limiting the amount of material reacted by the ignition reaction to 1%. It is possible, however, that heat transfer from the reacted sites could, in fact, cause a limitation of reaction to this order of magnitude provided that the initial shock were not too strong. If it is assumed that localized reaction can quench after a very short time an explanation must still be found to account for failure to reignite and propagate a detonation backward after detonation is established in the forward direction. The following observation on detonation failure in preshocked solid explosives seems pertinent to this problem.

It has been established by repeated experiments in our Laboratory, that a steady state detonation in a sheet of EL-506C* between 0.05 and 0.24 inches in thickness, can be quenched if the detonation encounters a region in the explosive which is being compressed to a high density by a second shock wave having a peak pressure

* EL–506C is a pliable, sheet explosive, manufactured by E. I. duPont Co., containing approximately 70% PETN, and 30% inert material.

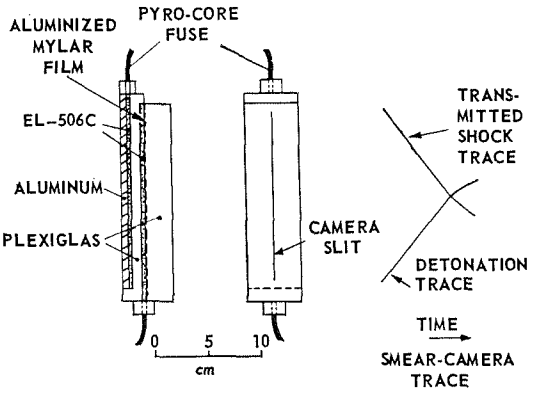

FIG. 7. Experimental set-up for detonation quenching by preshock and sketch of smear-camera trace.

between about 10 and 20 kilobars. In one series of experiments using the setup of Fig. 7, the explosive in two parallel layers separated by a plastic gap was initiated simultaneously at opposite ends. As both detonations propagated the bow shock behind the detonations moved toward the alternate layer of explosive. Each layer of explosive was thus compressed by a shock from the alternate layer of explosive. When a detonation reached the preshocked zone it was seen to fail very quickly in smear camera records. Undetonated explosive could be picked up later from the floor of the test chamber.† Other explosives have shown similar quenchout, e.g., cast HMX/TNT, HMX/Plastic. It is very likely that the shocked explosive reacted to some small degree because of the first shock, but then, not only was this reaction quenched in the manner suggested by Campbell, but also the explosive in this shocked, compressed state was unable to propagate a detonation already established in the unshocked region. These observations lead us to conclude that the hypothesis of Campbell can be valid under appropriate conditions. In the case of long cylinders shocked from one end, the retonation can be explained by the fact that rarefactions behind the growing shock (originating mainly at the cylinder sides), will return the explosive to a condition where it is again receptive to a build-up to detonation by a shock originating at the region where detonation is established. Some very interesting experiments described by Clay *et al.*[29] in which a shock in Composition B is found to grow to a detonation after passage through a preshocked zone also may find explanation in the observation of preshock quenching.

† Johannson[31] has described experiments on dynamites in which air shocks, leading a detonation, could cause the detonation to fail.

Summary

We have examined the growth-to-detonation from mechanical shock for TNT and three cyclotols. Both cast and pressed charges have been studied. Experiments have been conducted over a pressure range from 30 to 120 kilobars. In the cast charges the initial wave in the shocked specimen has the character of a nonreactive shock. The initial wave velocities in these charges have been used to compute the peak pressures behind these initial shocks. The build-up to detonation has been found to be sensitive to the RDX particle size in two cyclotols of very similar composition and density. The build-up to detonation has further been found to occur more rapidly in pressed charges than in cast charges of the same composition and density. These observations lead us to conclude that in this range of initial shock pressures, the initiation occurs at localized centers from which the reaction spreads. Before we can be sure that the hot-spot mechanism is the only mechanism for polycrystalline solids at higher shock pressures more information is needed in the higher range. In particular it will be necessary to develop an equation of state for solid explosives in which the temperature can be accurately defined. It remains a possibility in the higher range of pressures, between about 120 kilobars and the detonation pressure, that there may be competing processes going on. More or less homogeneous reaction may be taking place when the Hugoniot energy jump exceeds about 100 cal/gm, particularly if the activation energy can be decreased by compression as has been recently suggested by Teller.[32] It also remains for future work to establish the details of the process of localized initiation of reaction near the threshold limits of shock pressures, that is, in the range of pressures below 40 kilobars for most solid military explosives.

ACKNOWLEDGMENTS

The authors wish to acknowledge the painstaking work of J. Schneider, whose careful preparation and execution of the explosive tests permitted the development of the refined measurements reported herein.

This work was supported, in part, by the Atomic Energy Commission through the E. O. Lawrence Radiation Laboratory, Livermore, California.

REFERENCES

1. HERZBERG, G. and WALKER, G. R.: Optical Investigations of Initiation and Detonation, Nat. Res. Council, Canada, Project XR-84 (March 1945–August 1946). Also: Nature (London) *161*, 647 (1948).

2. Boggs, E. M., Messerly, G. H., and Strecker, H. A.: OSRD Report No. 5617, December 14, 1945.
3. Majowicz, J. M. and Jacobs, S. J.: Classified Naval Ordnance Laboratory Report, March 1958; *Also* Bull. Am. Phys. Soc. Ser. II, *3*, 293 (1958).
4. Jacobs, S. J.: ARS Journal *30*, 2, 151 (1960).
5. Cachia, G. P. and Whitbread, E. G.: Proc. Roy. Soc. (London) *A246*, 268 (1958).
6. Marlow, W. R. and Skidmore, I. C.: *ibid. A246*, 284 (1958).
7. Winning, C. H.: *ibid. A246*, 288 (1958).
8. Campbell, A. W., Davis, W. C., and Travis, J. R.: Phys. Fluids, *4*, 498 (1961).
9. Campbell, A. W., Davis, W. C., Ramsey, J. B., and Travis, J. R.: *ibid. 4*, 511 (1961).
10. Sultanoff, M. and Boyle, V. M.: ONR Symposium Report ACR–52, p. 520. September 26–28, 1960.
11. Kendrew, E. L. and Whitbread, E. G.: *ibid.* p. 574.
12. Jaffe, I., Beauregard, R. and Amster, A.: ARS Journal *32*, 22 (1962).
13. Travis, J. R., Campbell, A. W., Davis, W. R., and Ramsay, J. B.: Colloquium Report on *Les Ondes de Detonation*, 28 August–2 September 1961, Gif s/Yvette, Editions du CNRS, Paris (1961).
14. Favier, J. and Fauquignon, C. F.: *ibid.*
15. Brown, S. M. and Whitbread, E. G.: *ibid.*
16. Cook, M. A., Pack, D. H., Cosner, L. N., and Gey, W. A.: J. Appl. Phys. *30*, 1579 (1959).
17. Cook, M. A., Pack, D. H., and Gey, W. A.: *Seventh Symposium (International) on Combustion*, p. 820. Butterworths, 1959.
18. Hubbard, H. W. and Johnson, M. H.: J. Appl. Phys. *30*, 765 (1959).
19. Boyer, M. H. (and others): Study of Detonation Behavior, Pub. No. U 187, Aeronutronics Systems, Inc. (Ford Motor Co.) Navy Contract No. NOrd–17945, May 1958.
20. Enig, J. W.: see Reference 10, pp. 534–59.
21. Bowden, F. P. and Yoffe, A. D.: *Initiation and Growth of Explosion in Liquids and Solids.* Cambridge Univ. Press, 1952.
22. Andreev, K. K.: see Reference 5, pp. 257–67.
23. Johannson, C. H. and others: see Reference 5, pp. 160–167.
24. Rice, M. H., McQueen, R. G., and Walsh, J. M.: *Solid State Physics*, vol. 6, pp. 1–64, F. Seitz and D. Turnbull, editors. Academic Press, 1958.
25. Coleburn, N. L.: NavWeps Reports 6026, October 31, 1960.
26. Majowicz, J. M.: Unpublished data (Naval Ordnance Laboratory) (1958).
27. Jacobs, S. J.: Unclassified Note In Conference on Wave Shaping, Pasaden (June 5–7, 1956) sponsored by Picatinny Arsenal.
28. Boyer, M. H. (and others): Study of Detonation Behavior, Pub. No. U–369, Aeronutronics Systems, Inc. (Ford Motor Co.) Navy Contract No. NOrd–17945, Feb. 1959.
29. Clay, R. B., Cook, M. A., Keyes, R. T., and Stupe, O. K.: Bull. Am. Phys. Soc. Ser. II, *4*, 364 (1959).
30. Garn, W. B.: J. Chem. Phys. *30*, 819 (1959).
31. Johannson, C. H., Selberg, H. L., Persson, A., and Sjoelin, T.: *31st Int. Congress of Industrial Chemistry.* Liege, September 1958.
32. Teller, E.: J. Chem. Phys. *36*, 901 (1962).

Discussion

Dr. C. H. Johansson (*Stockholm, Sweden*): In transmission of detonation between coaxial cylindrical charges of pressed TNT with d = 21 mm through a cylinder of Al alloy with $l = l_m$ = 20 mm, we found that the receiver did not detonate behind the initiation plane approx. 8 mm from the end surface[1] (d is diameter and l_m maximum length for transmission of detonation). As this part had been preshocked to approx. 30 kilobars the result is in accordance with Campbell and Jacobs. In pressed PETN with d = 20 mm and $l = l_m$ = 29 mm the detonation propagated backwards from the initiation plane at the envelope surface but the core of the charge was left.

In another test with 2 cylinders of TNT having d = 21 mm, an aluminum cylinder was inserted having a length of 21 mm, a length which barely prevented the transmission of detonation. Both charges were initiated at their outer ends with a time difference of 8 μsec. The detonation wave of the last initiated charge (II) met the shock wave generated by the detonation of the opposite charge (I) approx. 13 mm from the end of charge II. The detonation proceeded in this case through the preshocked part without any observable disturbance. The detonation wave of charge II was, however, stopped when the length of the Al cylinder was l = 20 mm. The time difference was chosen so that the detonation wave met the oncoming shock wave from charge I just as the latter had turned over in detonation. Thus the steady state detonation of pressed TNT is quenched by preshocking only if the intensity of the shock wave is great enough to initiate detonation. The result of the interesting test performed by Jacobs *et al.*, using the set-up in Fig. 7 indicates that the steady state detonation of ex-

plosive E1–506C, like dynamite, is sensitive to pressure even when no reaction has occurred.

The decreased sensitivity of preshocked explosives may have several sources. If the intensity of the primary shock exceeds a limit value detonation is initiated due to the partial reaction in the most sensitive points. It is fairly obvious to assume that the explosive is less sensitive when these points are consumed. If the shock intensity is below the limit value at which initiation occurs it may be too small to ignite these points and preshocking does not influence the sensitivity of the explosive. Another point is that the increase in temperature at shock front compression is considerably lower if the compression is made in two stages and the heat losses will reduce the effect of the subsequent shock still more.

PROF. F. J. WARNER (*Royal College, Glasgow*): It was gratifying to see the overshoot shown in the velocity curve for pressed TNT. Some work on a holeburning model similar to the grain-burning model described in the paper by Jacobs, Liddiard, and Drimmer produced the same effect at roughly the same distance, and I spent some time trying to decide whether this was a genuine phenomenon or some hitherto unsuspected numerical instability. Because of the smearing out of the shock wave inherent in the use of finite differences, it is much easier in computation to determine the peak pressure of the explosive than the velocity of the shock wave. The two are related of course by the Rankine-Hugoniot jump conditions. Figure 1 shows the peak pressure plotted against time for an input shock of 100 kbars, and it can be seen that the pressure rises rapidly to over 700 kbars and falls almost as rapidly to the steady state value.

The model concerned had a burning equation of the form

$$Q(\partial f/\partial t) = \begin{cases} kp\, f_0^{\frac{2}{3}} \exp(-E/RT_g), & f < f_0 \\ kp\, f^{\frac{2}{3}} \exp(-E/RT_g), & f_0 \le f < 1 \\ 0, & f \ge 1, \end{cases}$$

where f_0 is some small but nonzero parameter. This corresponds to a solid explosive containing small spheres of gas, burning taking place at the gas/solid interface, so that initiation is performed by a hot-spot mechanism as suggested by Bowden. The parameter f_0 is required, otherwise the reaction would never start, but its value appears not to be critical. Indeed, in the first run on a "Mercury" computer the reaction was started by the automatic roundoff in the floating point arithmetic unit, and this showed very little change from a run with a proper parameter. One difference has been observed between my results and those in this

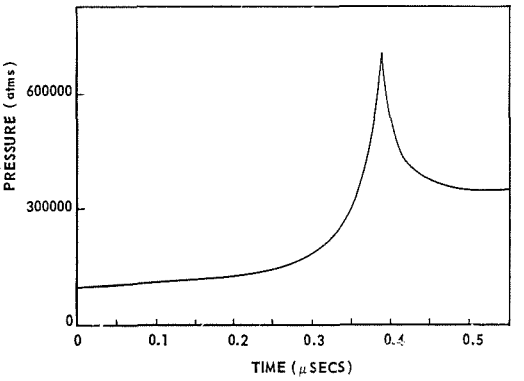

FIG. 1. Peak pressure—holeburning explosive.

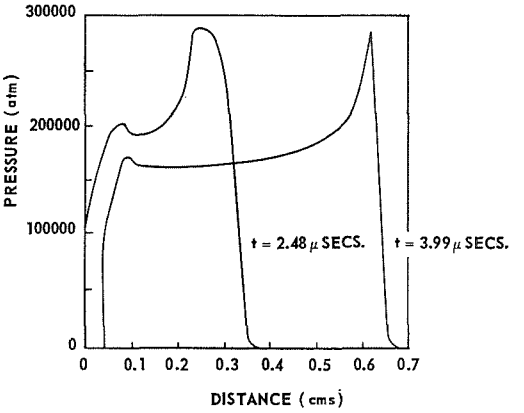

FIG. 2. Pressure profiles—holeburning explosive.

paper. The overshoot has always occurred in the computer runs, and the pressure has always risen to about the same value, while Fig. 5 of the Jacobs, Liddiard, and Drimmer paper would seem to indicate a variation in the overpressure with the magnitude of the initiating pressure pulse. This may be due to a change in the reaction mechanism, but equally it may be that the overpressure was just not observed because of the very small distance over which it occurs.

It appears that this overpressure is caused by the formation of a detonation wave just behind the initiating shock wave, and Fig. 2 shows the pressure profiles just before and just after the overpressure point. This contrasts with a homogeneous (liquid explosive) model where the detonation wave forms at the edge of the material, and also with a grain-burning (cast Composition B) model where the detonation wave forms at the shock front.

PROF. A. K. OPPENHEIM (*University of California*): With reference to the velocity and pressure overshoot that has been remarked upon on several occasions here, it might be of interest to note that there exists a proof[2] that if the deflagration is initially preceded by a shock, the detonation wave

cannot be established without an overshoot. The observation of the overshoot can be therefore considered indicative of the mechanism of the initiation process.

DR. J. R. TRAVIS (*Los Alamos Scientific Laboratory*): Dr. Jacobs *et al.*, report a large overshoot in the velocity at the point of transition from reactive shock to detonation for pressed TNT and other pressed explosives. As one of the authors of the paper referred to in their discussion (Jacobs' reference 9) I would like to restate our position. In our experiments on the initiation of liquid explosives, the presence of an overshoot velocity was an unmistakable phenomenon. Therefore, in our succeeding experiments with solid explosive wedges similar to those described in the paper under discussion, we expected to see an overshoot also. Several dozen experiments have convinced us that we can detect no overshoot for high density explosives, pressed or cast, initiated by a well-supported plane shock wave.

I do not intend to dispute their observation, but I would like to point out the difficulties in this kind of experiment. Of particular importance is uniformity of the charge density. Secondly, it is important that the initiating wave be flat, of constant pressure along the front, and have the same pressure profile behind the front at all points. Finally, the effect is a small one on the film. An x–t plot of even the largest overshoot shown in the authors' Fig. 5b is a bump of a few shakes ($\sim\pm 2$) from a smooth curve faired into straight lines representing the initial shock velocity and the final detonation velocity.

DR. S. J. JACOBS (*Naval Ordnance Laboratory*): The calculations by Warner showing the overshoot in the shock-to-detonation transition are interesting because they are the first machine calculations I have seen which show this effect. As these calculations show and as one must infer on hydrodynamic grounds, overshoot would not occur unless the pressure is higher at points behind the shock than at the shock front. Therefore, the establishment of the fact as to whether overshoot does or does not occur is an important point in determining what happens in real cases. I, for one, feel that the experiments need further checking to convince all concerned that the observations we have reported are due to the phenomenon and not to other causes. We will continue to look into the matter. In the cases where overshoot is absent it would appear that the shock must grow to detonation with maximal pressure always being at the shock front. It does not seem to me that it necessarily implies that reaction cannot go to completion at some points behind the plane at which detonation is finally established.

DR. J. B. RAMSAY (*Los Alamos Scientific Laboratory*): In the paper by Campbell *et al.* (Jacobs' ref. 9) on the initiation of solid explosives it was stated that the energy for the build-up of the shock wave to detonation was obtained directly at the front. I would like to review briefly what we consider are the significant experiments on this point. Mr. Whitbread of ERDE at Waltham Abbey (same as Jacobs' reference 13) and Mrs. Elizabeth Gettings of our laboratory have performed experiments in which they shocked solid explosives with thin "flying plates." This put a short duration shock into the explosive. In comparing the results obtained for the time of run to detonation vs. pressure for these experiments to our results which were obtained using flat, well-supported shocks, it was found that there was reasonable agreement. The only way in which this agreement can be obtained is if the energy which is driving the initiating shock is obtained very close to the shock front.

DR. FAUQUIGNON (*French Atomic Energy Commission*): This comment reports two types of observation about the existence of a retonation wave; the observations show also that this wave appears only after a quenching of the chemical reaction developed by the initiating shock. It is not our purpose to define the conditions in which this quenching may happen, probably when steep rear and lateral refractions are present.

In the first experiment we observe, after the shot, the deformation of a brass plate used as a gap in the gap-test experiment. In the classical case, where no retonation appears, there is only a shallow deformation, quite independent of the thickness of the plate. This is probably due to the shock generated at the section where detonation appears and propagating backwards, through the nonsupporting and partially reacting gases.

On the contrary, when retonation exists, we observe a large hole whose depth increases when the thickness of the plate increases. This can be interpreted by the fact that the thicker the plate the longer is the predetonation zone. Consequently the more important is the explosive supporting the retonation wave.

In the second type of experiments, we measured the electrical conductivity, simultaneously, at three sections of the predetonation zone. When no retonation is present we observe a long duration pulse, already studied by Los Alamos workers. On the contrary, in the retonation case, the conductivity developed by the initiating shock rapidly drops to zero, and, later on, we observe a second signal. This signal corresponds to a phenomenon propagating back towards the gap and can be attributed to the retonation wave. The amplitude of the signal is constant on the three oscillograms and the velocity of the corresponding wave is slightly below the normal detonation velocity.

DR. G. K. ADAMS (ERDE): I want to ask whether, in wedge type experiments, anyone has checked experimentally that the plane shock entering the wedge remains planar as it builds up in the explosive. We have found that if the entering front is tilted with respect to the explosive/barrier interface it rapidly loses its planarity in the explosive. Although this may not seriously affect the time or distance to the steady speed at the wedge surface it will distort the shape of the run-up curve. I should also like to know whether it has been found possible to superimpose shock speed/distance curves obtained with different wedge angles but constant initial shock pressure.

DR. J. R. TRAVIS. In regard to the tilt of the initiating wave in wedge experiments we have convinced ourselves that we have obtained waves with no tilt by experiments using electronic chronograph measurements. Very fine foils were mounted between blocks of explosives under enough static pressure to eliminate air between the blocks. Different pins are mounted at different heights across the block. As the reactive shock moves up the explosives, the pin foils are closed and the resulting signals recorded on the chronograph. The space–time history of the wave obtained in this way reproduces exactly that obtained from a wedge of the same explosive, boostered in the same way. It is necessary that the wave be flat with no tilt to get reasonable results from this type of electronic switch experiment.

REFERENCES

1. JOHANNSON, C. H. and SJOLIN, T.: Arkiv for Fysik, Svenska Vetenskapsakademien *21*, 185 (1962).
2. OPPENHEIM, A. K.: *Fourth Symposium (International) on Combustion*, p. 471. Williams and Wilkins, 1952.

SHOCK INITIATION OF GRANULAR EXPLOSIVES PRESSED TO LOW DENSITY

GLENN E. SEAY

The dependence of the shock initiation of pressed granular explosives on density of the pressing, interstitial gas in the pressing, grain size of the explosive, and characteristics of the initiating shock is discussed. The validity of applying the hydrodynamic equations for a homogeneous material to an inhomogeneous assembly of particles is examined. Various mechanisms for the initiation of granular explosives are compared in terms of current knowledge. Initiation of low density explosives is not satisfactorily explained by uniform shock heating of the pressing nor by shock heating of the interstitial gas, as has long been thought. It appears that initiation is dependent on minute shock interactions and resulting spalling and jetting, with initiation occurring in the fine particles of the spall or when the products of spalling or jetting are stagnated at the surface of an intact grain. Several experiments are suggested with plane wave constant pressure shocks replacing the complicated geometry of the usual gap sensitivity test. Other experiments are suggested for studying small scale details of proposed mechanisms of initiation.

Introduction

It has long been known that granular explosives pressed to a high density are more difficult to initiate by shock than the same explosive pressed to a low density. In one extreme case, a single crystal of PETN required about 112 kbar for initiation,[1] whereas PETN particles pressed to a density of 1.0 gram/cc ($\sim$ 56 per cent of crystal density) required only about $2\frac{1}{2}$ kbar for initiation.[2] These facts suggest that discontinuities in the explosive and/or interstitial gases must be of great importance in the initiation mechanism of the low density pressings.

It will be the purpose of this paper to review what is known about shock initiation of low density explosives and to define the problems that await solutions. Various experimental approaches will be reviewed along with a discussion of what has been learned. A brief description of proposed initiation mechanisms will follow with an attempt to evaluate the present status of each.

The Shock System

Very little quantitative research has been done on the initiation of low density pressed explosives by shock. Initiation of explosives by shocks has been studied most extensively by means of various gap sensitivity tests[3–5] in which the geometry is somewhat complicated. Usually such tests employ nonplanar shocks with large pressure gradients behind the front, and give results only in terms of the maximum thickness of some gap material which will allow transmission of a shock of sufficient strength to cause detonation of the explosive. Usually the criterion for "go—no go" is the presence of a dent in a witness block.[6] Occasionally considerable judgment is required in evaluating a "partial" or shallow dent. It has also been found that the use of different lengths of acceptor explosive can cause different results.

Gap tests have been made in which the initiating shock has been partially defined in the explosive itself.[6–8] In the most recent of these tests peak pressure into the explosive, shock curvature, and pressure gradient behind the front were evaluated to varying degrees. Even with these added precautions the results demonstrated the complicating influence of the gap-test geometry. It became clear, for example, that the gap must be thick enough to prevent reverberations from reinforcing the shock before initiation takes place; otherwise it is necessary to determine which reverberation is responsible for initiation. Also, the curvature of the wave changes more rapidly with gap thickness for thin gaps and the effect of this change in curvature has not been evaluated. As the gap thickness is changed, not only is the peak pressure in the explosive varied but the way in which the pressure varies behind the front is also changed. The initiation properties of different explosives are expected to depend on this pressure–time profile.

Controlled gap tests have been made with tetryl of two different particle sizes pressed to a

range of densities from 1.0 to 1.6 gram/cc. Two different gap materials, brass and Lucite, were used. It was found that the tetryl pressure at which 50 per cent of the charges detonated varied in about the same way with pressing density for the small particle size tetryl with both gap materials. The large particle tetryl at the lower densities, however, yielded two curves, differing both in magnitude and shape, depending on whether brass or Lucite was used for a gap material. It is not known whether this dependence on gap material is indicative of the large particle size tetryl having a "shock impedance" which is a function of the impedance of the gap material or whether the differences in wave curvature and pressure–time profile of the shock from a thin brass gap and a thicker Lucite gap is sufficient to cause the discrepancy in results. This is an example of how a precisely controlled gap test can fail to differentiate between the effects of the test geometry and the explosive being tested.

Before proceeding further, it should be emphasized that gap tests are an exceedingly valuable tool for sensitivity studies when a practical engineering answer or an ordering of the sensitivity of explosives to a given excitation is desired. The value of a gap test in selecting explosives for ordnance design purposes cannot be overestimated. The gap test is also an excellent research tool, particularly for survey programs and studies on small samples where some particular variable is being observed optically or electrically.

It seems, however, that if the purpose of an experiment is to study the mechanism by which an explosive is initiated by a shock, that the experiment should, if possible, be designed such that the shock can be completely described. Further, it seems that the shock should be of as simple a form as possible, i.e., a plane shock with a constant pressure behind the front—a step function of pressure. With such an idealized system the velocity of a shock in the explosive would either increase or remain constant. Complicated situations where the shock accelerates for a period of time and then finally fails to go to detonation are thus avoided. Certainly initiation and buildup are both extremely important processes, but is it not much more desirable to study them separately than to wonder whether a reaction was initiated and failed to buildup or was not initiated at all? Such experiments have been made with homogeneous explosives[1,9] and they have clearly demonstrated the shock-heating thermal mechanism of initiation for these materials. Similar experiments with high density solid explosives[10–12] have not yet resulted in complete understanding of the initiation mechanism. Some of these experiments suggest a velocity "overshoot" while others do not. This, however, may not be too surprising since some recent experiments with high density pressed explosives seem to yield results akin to those observed with homogeneous explosives for certain explosives and densities, and results akin to those observed with low density explosives for other explosives and densities.[13] Perhaps in high density solid explosives two different initiation mechanisms are competing: one in which energy is being fed to the front from all regions behind the shock, and the other where only regions near the front of the shock are contributing.

Low density, 1.0 gram/cc, pressed PETN has been studied in plane wave pressure-step type experiments.[2] The shocks entered PETN wedges from brass or Lucite plates. Shock pressures in the plates and depths at which the PETN was initiated were measured with a streak camera. It was found that a derived pressure of about $2\frac{1}{2}$ kbar in the PETN was barely sufficient for initiation. Experiments with various interstitial gases and low pressure air (50–100 μ) showed that the initiation process was independent of the interstitial gas. These experiments also showed that light from the detonation was independent of the interstitial gas or its absence. The depth at which initiation occurred, as a function of derived pressure, was the same for a shock entering from Lucite as for a shock entering from brass. In these experiments the explosive was characterized as to density, specific surface, and grain shape, but these parameters were not varied. A detailed history of the initiating disturbance was not obtained, but a reflection photography technique has since been developed for accomplishing this. A low density mirror material was tried on the surface of the PETN wedge, but this technique was abandoned because it gave misleading results for these low density pressings.

Hydrodynamics of Porous Materials

The term "derived pressure" as used above refers to the number obtained by treating the explosive sample as a homogeneous material and probably has little or nothing to do with the details of the mechanism of initiation.

The meaning of terms such as shock velocity, particle velocity, pressure, Hugoniot, etc., are at best vague when these terms are applied to a porous material. It is true that the velocity of a disturbance can be measured as it moves through such a material, but this observed disturbance must be the result of minute disturbances occurring at various voids, grain boundaries, etc. Numbers corresponding to particle velocity and

pressure can be obtained by using standard impedance match analysis methods; however, these numbers must be averages of some sort which tell very little about the state variables at discontinuity sites in the material. At the present time little is known concerning the gross character of a shock wave as it moves through a material composed of small regions of two or more materials with radically different sonic impedances and consequently even less is known about the details of such a shock.

Perhaps, before understanding the initiation process in porous explosives, it will be necessary to understand in more detail the phenomena associated with shocks in porous materials, both reactive and nonreactive.

Initiation Mechanisms

Several mechanisms may be considered for the shock initiation of low density pressed explosives. Uniform shock heating of the pressing can be eliminated immediately on the basis of the greatly increased sensitivity of heterogeneous explosives relative to homogeneous explosives. Probably the most universally accepted mechanism is that of shock heating of interstitial gases to a temperature necessary for ignition of grain surfaces.[14] Results with plane waves in low density PETN,[2] discussed above, and results of gap sensitivity tests made in England[6] seem to discredit the general applicability of this mechanism. Minute shock interactions have been given credit for the high temperature necessary for ignition. Since the process has been shown to be independent of the interstitial gas, such shock interactions would be expected to act on the interior of the grains or at contact points. If this is the case, then the high sensitivity of the materials suggests that secondary effects of such interactions might be more effective for initiation than the temperature at the site of the interaction. It has been suggested that the reaction might proceed in a fine powder formed by spalling or that this powder might initiate reaction on impact with the next grain.[6]

A similar mechanism has been recently proposed and studied by J. H. Blackburn and L. B. Seely, Jr.[15] This method depends on a secondary effect of minute shock interactions, namely jetting. It is proposed that material in jets resulting from shocked irregularities attains a very high temperature when stagnated against the next downstream grain which constitutes an essentially rigid barrier. This hypothesis developed from studies of the light observed during initiation and detonation of pressed granular explosives. In particular, it was shown that the light observed in these experiments was not due to the shocked interstitial gas because its intensity was not a function of the gas or the gas pressure ($P \leq 1$ atm). Also, the temperature attained in the detonation reaction was too low to account for the observed light. The light could be reduced both in duration and intensity by increasing the density of the pressing. This suggested that a large part of the light was being observed through a few layers of translucent grains. A detailed study of this phenomenon showed that light of the same nature could be observed from nonreacting granular materials. This light never lasted beyond the shock transit time in either the high explosive or nonreactive material.

Proposed Experiments

It is suggested that future work on this subject should be divided into two categories: (1) those experiments designed to provide macroscopic results and relationships with an accurately known shock and explosive system, and (2) those experiments designed to investigate the details of near-microscopic processes upon which certain of the proposed mechanisms of initiation depend.

Judging from past work, it appears that experiments of the first type can be useful in eliminating various possible mechanisms of initiation, e.g., shock heating of the interstitial gas. Also such experiments can provide valuable data, in terms of reproducible shocks, on the gross hydrodynamic and thermodynamic properties of low density pressed explosives. First priority in this group of experiments might be assigned to a study of the hydrodynamic properties of low density pressings of a nonreactive material which is otherwise similar to a particular explosive of interest. It has been the custom to assign pressure and particle velocity values according to a measured shock velocity in the explosive. If, however, the shock produces detonation, then the "initial" shock velocity must be obtained indirectly by extrapolating the velocity record back to the explosive-driver interface. This might be avoided if a complete pressure–volume Hugoniot relation could be determined for a similar but nonreactive material. Such a pressure–volume Hugoniot might also reveal whether the material is easily compressed to near crystal density and then abruptly becomes stiffer, or whether the crushing of grains coupled with grain motion and reorientation gives a smooth, slowly changing compressibility.

The question of the effect of interstitial gas seems to have been laid to rest for initial pressures of one atmosphere or less, but what of higher pressures? At what pressure does the interstitial gas begin to cushion the effect of

whatever mechanism is responsible for initiation? Possibly a granular explosive might be initiated in the same way as a homogeneous explosive if the interstitial material (obviously not a gas) had the same sonic impedance as the explosive grains. Perhaps, in this very special case initiation might even be independent of grain size and structure.

The dependence of shock initiation properties on grain size is still an unknown. If some process generated by shock interactions is responsible for initiation, then the number and size of the shock interactions and thus the initiation properties should depend on grain size. Grain size would be an important parameter in determining the way an initiated reaction builds up to detonation. Whether this buildup is described by the usual grain burning model[14] or requires additional details concerning shock interactions is an open question.

Probably the most obvious parameter for study in plane wave pressure-step experiments is the density of the pressed explosive. As already mentioned, some of the experiments with high density solid explosives suggest an initiation mechanism similar to that which prevails in homogeneous explosives. On the other hand, at very low densities it can be imagined that a reaction, even if weakly initiated, would not be accelerated because of the wide separation of the particles. This limit might occur at densities below settling density and experiments have yet to be designed to investigate this density region.

As pointed out earlier, in an idealized plane wave pressure-step experiment, the velocity of the disturbance in the explosive cannot decrease and must either remain constant or increase. Thus, using existing techniques for observing the shock as it builds up to detonation velocity, much can be learned about this buildup region without tolerating and attempting to explain complicated geometric effects.

Also in all of these experiments, a combination optical detection scheme can be used where a nonluminous disturbance is observed by reflected light and any luminous phenomena is observed directly. Observations of this sort led to the experiments[15] which yielded the "stagnation" model of initiation.

Plane wave "thin shock" experiments have been proposed by Lindstrom[13] for high density pressed explosives in order to investigate the hypothesis that, at high density, pressed explosives can begin to have some of the initiation properties of homogeneous explosives. Such "thin shock" experiments, applied to low density explosives could clarify the dependence of the initiation mechanism on processes occurring some distance behind the front of the shock. The "flying plate technique"[16] would be employed in order to establish a predictable pressure-time profile for a thin plane shock.

At the beginning of this section it was suggested that it would be desirable to investigate the details of near-microscopic processes upon which certain of the proposed mechanisms of initiation depend. This does not necessarily mean near-microscopic studies of such processes. Studies of shock interactions in random assemblies of grains, even large grains, of either explosive or nonreactive material, might provide more insight as to the number and strength of shock interactions occurring in a shocked pressing. Secondary effects of such interactions such as spalling, jetting, and stagnation, could also be observed and studied. This general approach has yielded much useful information in the case of studies of jetting and stagnation.[15]

Summary

The shock initiation of granular explosives pressed to low densities is a field in which little quantitative data is available and about which little is actually known. Most of the prevailing ideas have come from studies made on high density heterogeneous explosives. Perhaps studies of heterogeneous explosives in a low density region where the heterogeneities are most prominent would be more profitable, even for the purpose of understanding initiation in the high density region. Gap tests have yielded invaluable results for engineering and safety purposes; but, because of their geometrical complexity, they are not recommended for use in fundamental studies. A few experiments have been reported in which shocks with known properties have been used to initiate low density explosives. The results of these experiments are not confused by lack of knowledge of the geometric and hydrodynamic properties of the initiating shock. In this type of experiment the phenomena of initiation and buildup to detonation can be separated and evaluated individually.

In low density pressed explosives initiation is not the result of uniform shock heating of the pressing, nor can it be satisfactorily explained by shock heating of the interstitial gas—as has long been thought. Initiation seems to depend in some way on the discontinuities and resulting shock interactions. The shock interactions are believed to contribute to spalling, jetting, or some combination of these two phenomena. Perhaps initiation occurs in the fine particles of the spall or when the products of a jet or spalling are stagnated at the surface of the next downstream grain.

The experiments proposed here are of two

rather extreme types: those which observe gross effects of an accurately known shock, and those which examine in detail the possibly important near-microscopic processes.

ACKNOWLEDGMENTS

This work was performed under the auspices of the U. S. Atomic Energy Commission.

REFERENCES

1. CAMPBELL, A. W., DAVIS, W. C., and TRAVIS, J. R.: Phys. Fluids *4*, 498 (1961).
2. SEAY, G. E. and SEELY, L. B., JR.: J. Appl. Phys. *32*, 1092 (1961).
3. MURAOUR, H.: Mém. artillerie franç. *12*, 559 (1933).
4. EYRING, H., POWELL, R. E., DUFFEY, G. H., and PARLIN, R. B.: Chem. Revs. *45*, 138–142 (1949).
5. COOK, M. A., PACK, D. H., COSNER, L. N., and GEY, W. A.: J. Appl. Phys. *30*, 1579 (1959).
6. CACHIA, G. P. and WHITBREAD, E. G.: Proc. Roy. Soc. (London) *A246*, 268 (1958).
7. MARLOW, W. R. and SKIDMORE, I. C.: Proc. Roy. Soc. (London) *A246*, 284 (1958).
8. JOHNSON, J. O. and SEELY, L. B., JR.: Private communication.
9. HOLLAND, T. E., CAMPBELL, A. W., and MALIN, M. E.: J. Appl. Phys. *28*, 1217 (1957).
10. CAMPBELL, A. W., DAVIS, W. C., and RAMSAY, J. B.: Phys. Fluids *4*, 511 (1961).
11. MAJOWICZ, J. M. and JACOBS, S. J.: Initiation to Detonation of High Explosives by Shocks. Fluid Dynamics Division, American Physical Society, 10th anniversary meeting, Lehigh University, Bethlehem, Pennsylvania, November 25–27, 1957.
12. LIDDIARD, T. P., JR. and DRIMMER, B. E.: Bull. Am. Phys. Soc., Series II, 7 (1957).
13. LINDSTROM, I.: Private communication.
14. MAČEK, A.: Chem. Revs. *62*, 41 (1962).
15. BLACKBURN, J. H. and SEELY, L. B., JR.: Private communication.
16. RICE, M. H., MCQUEEN, R. G., and WALSH, J. M.: *Solid State Physics*, edited by F. Seitz and D. Turnbull, vol. 6, p. 17. Academic Press Inc., 1958.

Discussion

DR. J. F. WEHNER and DR. D. PRICE (*U.S. Naval Ordnance Laboratory*): "Thin shock" experiments using the "flying plate technique" which were proposed by Dr. Seay, have also been proposed at NOL and probably by several other groups. In principle, this technique forms the basis of an excellent method for determining what effects the duration and profile of the pressure pulse have on the ability of a shock to initiate detonation. The purpose of this comment is to point out that this conceptually simple experiment is difficult to implement.

While it is easy to drive thin plates explosively at sufficiently high velocities to obtain impact pressures above 100 kbar, maintaining an unbroken plate in a plane configuration is difficult. By confinement of the driver charge and plate, we have been able to drive a 20 mil plate 4 inches without fracture. However, the planarity at the end of flight was very poor; the curvature was greater than at the donor front. It is expected that the use of plane-wave generators of diameters much larger than those of the plates will produce the desired plane planarity. Without good planarity, the experimental design is invalidated.

These two difficulties arise when an explosive driver is used. A third limitation of this method is the loading of the test material by the detonation products; this can be avoided by careful design. There are, of course, other ways to drive the plate which may prove more advantageous in certain pressure ranges.

DR. C. H. JOHANNSON (*Stockholm, Sweden*): I should like to mention some calculations of H. L. Selberg[1] on a simple linear model of a charge with interstices. It consists of equidistant homogeneous plates of explosive, which have the same thickness and are oriented perpendicular to the detonation direction. The average density is assumed to be small compared with the plate density. Behind the detonation front a compact pile of plates is moving forward. If the impacts are inelastic the increase of the internal energy of the plates when one plate after another is connected at the front is approximately

$$E = (Q + c_v T_0)\,(\gamma^2 - 1)$$

Q is explosion heat; c_v, specific heat at constant volume; and $\gamma = c_p/c_v$. With $Q = 1200$ cal/g, $c_v = 0.4$ cal/g°K, $T_0 = 300$°K, and $\gamma = 1.2$ we get $\Delta E = 580$ cal/g and $\Delta T = 1450$°C.

The compression heat of the gas between the plates is small compared with ΔE. For atmospheric air it is only approx. 0.5 per cent of ΔE and it is rapidly given off due to the high temperature and the thin layers of the compressed gas. This may explain why the light emission is independent of the gas in the interstices.

Dr. Seay emphasizes the importance of a plane

shock with constant pressure in the gap test. In Sweden we have used a shooting test for a year or two to characterize the sensitivity to impact.[2] The projectile and the explosive sample are cylinders with plane end surfaces. We have found the test to be of great value in judging the properties of explosives with regard to safety in use, but I think it may also be usable for fundamental research. It has the advantages that it is simple to carry out and that all explosives can be included. As an example it may be mentioned that the critical velocity in meters per second with copper projectile is, for dynamite, about 100; phlegmatized PETN, 250; pure RDX, 360; pressed TNT, 530; AN-oil, 800; and cast TNT, 900. The test gives very reproducible results. An outstanding example is pressed TNT with 1.55 g/cm^3. In 20 tests no sample detonated below 535 m/sec while all detonated beyond 545 m/sec.

References

1. Stiftelsen Svensk Detonikforskning.
2. The test is based on investigations which have been carried out 1959–61 in cooperation between the Swedish Defence Research Institute, Nitroglycerin AB and the Swedish Research Foundation on Detonics.

THE INITIATION OF DETONATION IN SOLID EXPLOSIVES

F. J. WARNER

We consider the problem of transition from deflagration to detonation in a solid crystalline explosive. A mathematical model is set up for a semi-infinite block of explosive, and the partial differential equations resulting from a one-dimensional flow are integrated numerically, using an electronic computer.

The explosive is regarded as a homogeneous fluid so far as the hydrodynamic equations are concerned, but as a two-phase solid/gas system for the equation of state and equation of burning. This leads to the concept of two different temperatures coexisting in the system, solid explosive at one temperature burning to give gaseous detonation products at another temperature some three thousand degrees above the first. We assume that the explosive exists locally in the form of spheres and that the law of burning involves a pressure term.

Initiation is by a shock wave incident on the explosive, and in all the cases investigated, we find that the transmitted shock wave accelerates or decelerates steadily, and in the results quoted in the paper, the von Neumann spike can be seen building up out of the front of the initiating shock. This is in accord with experimental evidence on solid explosives, but is in sharp contrast with numerical results obtained by other workers and with experimental evidence on liquid explosives. It is believed that the differences are the result of the introduction of the pressure term into the law of burning.

Introduction

In this paper, we consider the problem of the transition from deflagration to detonation in a solid crystalline explosive. The one-dimensional partial differential equations relating to the motion of and chemical reaction in a detonating explosive are derived, and these equations have been integrated numerically using an electronic computer. The explosive is regarded as a homogeneous fluid so far as the hydrodynamic equations are concerned, but as a two-phase solid/gas system for the equation of state and equation of burning.

The equation of burning chosen for this investigation involves a pressure term, and the results obtained differ significantly from those obtained by other workers using the conventional Arrhenius law of burning. The detonation is assumed to have been initiated by a shock traveling into the explosive, the shock being caused by a piston pushing onto the surface of the explosive. In the later part of this work, the motion of the piston is stopped after a given time, and this causes a rarefaction wave to follow the shock which tends to damp down the detonation.

Main Equations

We consider our explosive as a semi-infinite block of material which is in the large homogeneous and has a constant specific heat, and we assume a one-dimensional flow. The coefficients of heat conduction, viscosity, and diffusion are taken as being negligibly small. This is justified as the transport effects are very much slower than the gas dynamic effects, a matter of milliseconds compared with microseconds. In order to simplify the equations computationally, we take a grid of a Lagrangian coordinate m, measured in grams. Equal intervals of m correspond originally to equal intervals of the space coordinate x, so that initially

$$m = x/v_0, \qquad t = t_0,$$

where v_0 is the initial specific volume in cc/gram, and the subsequent positions are given by

$$\partial x/\partial t = 10^{-6}u,$$

t being measured in microseconds, and u in cm/sec. This choice of a mass coordinate will occasionally lead to quantities in unfamiliar units, for example, a shock velocity measured in grams/microsec.

This gives the equation of continuity as

$$\partial v/\partial t = 10^{-6}(\partial u/\partial m)$$

and the equation of conservation of momentum as

$$\partial u/\partial t = -\partial p/\partial m,$$

p being in atmospheres (actually, p is in bars, but the difference is only one per cent). For the

homogeneous explosive, the energy equation is

$$C_v(\partial T/\partial t) = Q(\partial f/\partial t) - p(\partial u/\partial m),$$

where C_v is the specific heat in ergs/gram °K, Q is the quantity of heat liberated in burning in ergs/gram, and f is the fraction of explosive detonated.

We may assume the detonating explosive to exist in two distinct phases, solid unburned explosive at a temperature T_s and gaseous products at a temperature T_g. Now 1 gram of the aggregate contains f grams of gas and $(1 - f)$ grams of solid, so that the energy of the aggregate is given by

$$C_vT = fC_vT_g + (1 - f)\,C_vT_s,$$

that is, the average temperature is given by

$$T = fT_g + (1 - f)\,T_s. \tag{1}$$

We have assumed that neither the gas nor the solid is heat conducting, so that the gas can gain energy only by compression or the accretion of new gas, while the solid can gain energy only by compression and can lose energy only by ablation. This gives

$$C_v\frac{\partial(fT_g)}{\partial t} = C_vT_g\frac{\partial f}{\partial t} - fp\frac{\partial u}{\partial m}$$

for the gas and

$$C_v\,\partial\{(1 - f)\,T_s\}/\partial t = -C_vT_s(\partial f/\partial t) - (1 - f)p(\partial u/\partial m)$$

for the solid. Adding, we obtain

$$C_v(\partial T/\partial t) = C_v(T_g - T_s)(\partial f/\partial t) - p(\partial u/\partial m),$$

and by comparison with the energy equation for the homogeneous explosive, we see that

$$T_g - T_s = Q/C_v. \tag{2}$$

It is also possible to assume different specific volumes v_g, v_s for the two phases, but this is a matter properly taken up when considering the form of the equation of state.

If we now add a suitable equation of state and a law of burning, we obtain the full partial differential equations of the motion

$$\begin{aligned}
\partial v/\partial t &= 10^{-6}(\partial u/\partial m)\\
\partial u/\partial t &= -\partial p/\partial m\\
C_v(\partial T/\partial t) &= Q(\partial f/\partial t) - p(\partial u/\partial m)\\
\partial f/\partial t &= F(p, T, f)\\
p &= p(v, T)\\
\partial x/\partial t &= u
\end{aligned} \tag{3}$$

The set of Eqs. (3) forms a hyperbolic system of effectively fourth order, as the last equation in the set is merely one of definition of our coordinate system and takes no part in determining the motion. This set must have four sound speeds, and these are

$$m = 0 \text{ (twice)},$$

giving only possible contact discontinuities, and

$$\left(\frac{dm}{dt}\right)^2 = \frac{p}{C_v}\frac{\partial p}{\partial T} - 10^{-6}\frac{\partial p}{\partial v}.$$

The Rankine-Hugoniot conditions for the values of quantities across a finite discontinuity moving with instantaneous speed s grams/microsec fall out from this set as

$$\begin{aligned}
s[v] &= -10^{-6}[u]\\
s[u] &= [p]\\
s[C_vT + \tfrac{1}{2}u^2 - Qf] &= [pu]\\
s[f] &= 0
\end{aligned} \tag{4}$$

where $[w]$ denotes the change in the quantity w across the discontinuity, and for a shock advancing into stationary explosive at atmospheric pressure this gives

$$u_0 = 10^6s(v_1 - v_0) = (p_0 - 1)/s,$$

and a third equation which depends on the equation of state chosen. The fourth condition merely states that burning takes place over an interval much larger than the thickness of the shock. To obtain the Chapman–Jouguet conditions attained well to the rear of the shock we have to assume that burning takes place quickly over an interval of space much smaller than the distance between the shock and the point we are interested in, and set (4) becomes

$$\begin{aligned}
s[v] &= -10^{-6}u\\
s[u] &= [p]\\
s[C_vT + \tfrac{1}{2}u^2 - Qf] &= [pu]\\
[f] &= 1
\end{aligned} \tag{5}$$

Taken together with the Chapman–Jouguet condition, that the particles just at the fully burned point are moving at the local speed of sound with respect to the shock front, the two sets of Eqs. (4) and (5) give some information about the values of the variables in the steady state solution, referred to later as the Chapman–Jouguet solution, of the differential Eqs. (3), and this steady state solution is the one to which we expect our nonsteady solutions to be asymptotic. In order to obtain numerical information, however, we need to inquire into the form of the equation of state satisfied by our explosive.

The Equation of State and Choice of Parameters

We require a single equation of state to represent both the solid explosive and the gaseous detonation products, but with two such different materials we will not expect a very good fit. We take the specific heat C_v as being constant and equal for both phases, at a value of 0.3 cal/gram °K, that is at 1.2552×10^7 ergs/gram °K.

A very simple equation of state is that due to M. A. Cook (reference 1, p. 64) which is the modified Abel equation

$$p\{v - \alpha(v)\} = R_1 T,$$

where T_1 is the gas constant per gram and $\alpha(v)$ a function of the specific volume. From Cook's graph (*ibid.*) we may take a linear approximation to $\alpha(v)$ as

$$\alpha(v) = 0.5v + 0.2$$

whence the Abel equation of state becomes

$$p(v - b) = RT, \qquad (6)$$

where $b = 0.4$ cc/gram and $R = 2R_1$. If we assume the average molecular weight of the gaseous detonation products to be 30, then $R = 5.543$ cc bars/gram °K and $\gamma = 10^{-6}\, R/Cv + 1 = 1.442$. We take 1000 cal/gram, that is 4.184×10^{10} ergs/gram, as a typical value for Q. This is almost the same as the value of Q of a 40/60 RDX–TNT mixture, which is about 984 cal/gram. From the sets of Eqs. (4) and (5) we may now calculate the Chapman–Jouguet conditions, and the conditions at the shock of a steady detonation, and the values for an explosive of density 1.6 grams/cc are given in Table 1. The detonation velocity is of the same order of magnitude as the experimental value of 695000 cm/sec for TNT given by Robertson.[4] However, the temperature scale is rather distorted, and normal temperature is given as 0.04°K. This is not so serious as it appears at first sight, as the abnormally low temperatures occur at low pressures, and are associated with mainly solid explosive, while the equation of state has been fitted to the gaseous products, so that we would expect trouble at the end of the scale. Despite its bad fit, the modified Abel equation has been used for all the subsequent numerical calculations on account of its simplicity.

An equation of state suggested by some workers is that due to Tait,

$$(p + b)v - (p_0 + b)v_0 = R(T - T_0),$$

and Zovko and Macek[2] use this with $b = 100000$ bars, $R = 43.932$ cc bars/gram °K giving $\gamma = 4.5$. Table 2 gives the Rankine–Hugoniot jump relationships for both this equation and the modified Abel equation, and it can be seen that, while the Tait equation gives a better fit for the temperature at low pressures, it gives a zero temperature jump.

Since we already have a two-phase system, we might use one equation of state for the gaseous products and one for the unburned solid explosive. As 1 gram of the aggregate mixture consists of f grams of gas occupying fv_g cc and $(1 - f)$ grams of solid occupying $(1 - f)v_s$ cc, we have

$$v = fv_g + (1 - f)v_s.$$

The pressure must be the same under both equations of state, so that

$$p = p_s(v_s, T_s) = p_g(v_g, T_g)$$

and the equation linking T_s and T_g becomes, in its most general form,

$$C_{vg}T_g - C_{vs}T_s = Q$$

so that v_s, v_g, and (say) T_s can be eliminated to give

$$p = p(v, f, T_g)$$

as an over-all equation of state. It should be noted that if C_{vg} and C_{vs} are unequal, there cannot be said to be any unique "temperature" of the aggregate.

TABLE 1

Steady State Conditions, Abel Equation of State

	Gamma = 1.4416	R = 5.5430	B = 0.4		
	P	V	U	T	F
Initial values	1	0.6250	0	0.04	0
Values at shock	336 340	0.4407	249 160	2469.64	0
Values at C–J point	142 450	0.5469	105 530	3776.32	1

Detonation velocity = 1.3499 gm/μsec = 843 660 cm/sec

TABLE 2

R. H. Relations

Abel Equation of State

Gamma = 1.4416 R = 5.5430 V_0 = 0.6250 B = 0.4000

P	V	U	T	S
1	0.62500	0	0.04	0.00000
10	0.46207	1 211	0.11	0.00743
100	0.44287	4 246	0.77	0.02331
1 000	0.44091	13 561	7.38	0.07367
10 000	0.44072	42 926	73.46	0.23294
100 000	0.44070	135 758	734.21	0.73660
1 000 000	0.44069	429 308	7341.71	2.32933

Tait Equation of State

Gamma = 4.5000 R = 43.9320 B = 100 000 V_0 = 0.6250 T_0 = 288.00

P	V	U	T	S
1	0.62499	0	288.00	0.00000
10	0.62493	25	288.00	0.36187
100	0.62437	250	288.00	0.39657
1 000	0.61891	2 466	288.21	0.40506
10 000	0.57598	22 140	307.50	0.45162
100 000	0.45833	129 099	951.89	0.77459
1 000 000	0.40570	468 293	9023.58	2.13541

In the absence of any other information, let us assume that $C_{vg} = C_{vs} = C_v$, and that the equations of state for the two phases are of the modified Abel type

$$p_s(v_s - b_s) = R_s T_s$$

and

$$p_g(v_g - b_g) = R_g T_g \tag{7}$$

where $C_v = 1.2552 \times 10^7$, $R_g = 5.532$, and $b_g = 0.4$ from our previous considerations. Then R_s and b_s are linked by the form of the equation at normal temperature and pressure as

$$v_0 - b_s = 288\ R_s,$$

and we have one free parameter, either b_s or R_s, which we can fit by matching some other observable quantity. On performing the eliminations, we obtain as a combined equation of state

$$p\{v - fb_g - (1-f)b_s\} = \{fR_g + (1-f)R_s\}T + f(1-f)(R_g - R_s)Q/C_v.$$

The Chapman–Jouguet conditions depend very little on the solid phase parameters, which are not very well determined. This would seem to be about the most complicated equation of state attainable at the present time in the absence of further experimental evidence.

The Choice of the Law of Burning

It now remains for us to settle on a law for the burning of our explosive. The one used by most workers for homogeneous explosives is the pure Arrhenius law

$$Q(\partial f/\partial t) = Z(1-f)\exp(-E/RT) \tag{8}$$

where Z is the frequency factor and E the activation energy. This produces results which, as discussed later, are not in very good agreement with observations on detonating condensed explosives.

We may assume that our burning explosive mixture consists of solid grains of unburned explosive surrounded by hot gaseous detonation products, and we take these grains to be spherical. Burning takes place at the surface of each grain, so that the rate of burning is proportional to the surface area, that is, to $(1-f)^{\frac{2}{3}}$ and not to $(1-f)$. We introduce a pressure term into the

burning law so as to make the reaction more dependent on pressure than on temperature, and since the burning is taking place next to the hot gas and there is no transport of heat through the grain, we take the temperature in the Arrhenius term to be T_g and not T_s. Thus we have

$$Q\frac{\partial f}{\partial t} = kp^n(1-f)^{\frac{2}{3}} \exp\left\{\frac{-E/R}{T+(1-f)Q/C_v}\right\}.$$

For simplicity, in the first instance, we assume $n = 1$, and we take 10 000 °K as a typical value for E/R. Then the law of burning becomes

$$Q\frac{\partial f}{\partial t} = kp(1-f)^{\frac{2}{3}} \exp\left\{\frac{-10\,000}{T+(1-f)Q/C_v}\right\}, \tag{9}$$

where k is a parameter to be determined.

If we take the set of Eqs. (3) together with the equation of state (6) and the law of burning (9), we obtain as the full set of partial differential equations to be solved

$$\begin{aligned}
\partial v/\partial t &= 10^{-6}(\partial u/\partial m)\\
\partial u/\partial t &= -\partial p/\partial m\\
C_v(\partial T/\partial t) &= Q(\partial f/\partial t) - p(\partial u/\partial m):\\
Q(\partial f/\partial t) &= kp(1-f)^{\frac{2}{3}}\\
&\quad \times \exp\left\{\frac{-10\,000}{T+(1-f)Q/C_v}\right\} \qquad (10)\\
p(v-b) &= RT\\
\partial x/\partial t &= u.
\end{aligned}$$

The parameter k clearly acts as a scale factor, since if we double k and simultaneously halve the scales of t, m, and x, the equations are unaltered.

Under enclosed conditions, an integral of (10) exists and is expressible in closed form in terms of elementary functions, for if $\partial/\partial m \equiv 0$, then v, u, and x are all constant and the set of Eqs. (10) reduces to

$$\begin{aligned}
\partial T/\partial t &= (Q/C_v)(\partial f/\partial t)\\
\partial f/\partial t &= (kp/Q)(1-f)^{\frac{2}{3}}\\
&\quad \times \exp\left\{-\frac{10\,000}{T+(1-f)Q/C_v}\right\}\\
p &= RT/(v-b)
\end{aligned}$$

The first integrates up to

$$T = (Q/C_v)f + T_0,$$

where $T = T_0$ at $f = t = 0$, and on substituting this in the second and third and combining, we obtain a separable first order differential equation

$$\frac{df}{dt} = \frac{kR}{Q(v_0-b)} \exp\left\{\frac{-10\,000}{T_0+(Q/C_v)}\right\} \times (1-f)^{\frac{2}{3}}(T_0+fQ/C_v),$$

whose integral is

$$t = \frac{Q(v_0-b)}{2\beta kR[T_0+(Q/C_v)]} \exp\left\{\frac{10\,000}{T_0+(Q/C_v)}\right\} \times \left[\log\left\{\left(\frac{1-\beta^3}{1-\beta^3y^3}\right)\left(\frac{1-\beta y}{1-\beta}\right)^3\right\} + 2\sqrt{3}\tan^{-1}\frac{\sqrt{3}\beta(1-y)}{(2+\beta)+\beta y(1+2\beta)}\right] \tag{11}$$

where $y = (1-f)^{\frac{1}{3}}$ and

$$\beta^3 = (1 + C_vT_0/Q)^{-1}.$$

Most remarkably, the integral is finite at $f = 1$, that is, at $y = 0$.

Experimental observation gives that TNT at a pressure of 100 000 atmospheres burns completely in about 0.1 microsec, and if we put this in Eq. (11) we obtain k as 3.901×10^7 cc/gram sec. Table 3 gives a list of times for complete detonation computed for various input pressures, assuming that v_0 and T_0 are given by the Rankine–Hugoniot relations. This gives a time for complete combustion of 0.6 microsec at atmospheric pressure, which is obviously unreal even for the rather unreal situation of a completely confined explosive, and this points to one great

TABLE 3

Times for Complete Detonation for Confined Explosion

K = 3.9013391 cc/gm sec
R = 5.532 cc atm/gm deg
Q = 41 840 000 000 ergs/gm
CV = 12 552 000 ergs/gm°K
B = 0.4 cc/gm
V_1 = 0.625 cc/gm

P (atm)	T (microsec)
1	0.6328
10	0.6196
100	0.5195
1 000	0.4081
10 000	0.2795
100 000	0.1000
1 000 000	0.0062

difficulty in using a burning function that is everywhere smooth and continuous. For any law of burning like (8) or (9), there is a certain rate of burning at normal temperature and pressure, and after some finite time this burning will have released sufficient energy to have raised the temperature of our explosive to a point where burning will accelerate towards detonation. For this reason, we introduce an arbitrary pressure below which burning will not take place. In all numerical calculations. this was set at 1000 atmospheres, which is sufficiently far removed from detonation pressures so as to have a negligible effect on most of the results.

Results

The set of Eqs. (10) can be approximated by finite difference equations using Lax's difference scheme[3] and the resulting set of equations has been integrated numerically with various input pressure pulses and mesh lengths. This integration was performed initially on the DEUCE computer at Glasgow University, but the main bulk of the results was obtained on the "Mercury" computer at Manchester University.

The incoming energy required to initiate detonation is assumed to be provided by a piston driven into the explosive from the left, where the pressure at the left-hand edge of the explosive is given as a parameter of the particular case under study, and the other variables are derived from the Rankine–Hugoniot relations. This means that if there were no combustion a pressure pulse of given constant height would be propagated into the explosive. Where the input energy is required to be finite, the piston is stopped after a given time and the variables at the left edge revert instantly to normal, thus propagating a rarefaction wave into the explosive.

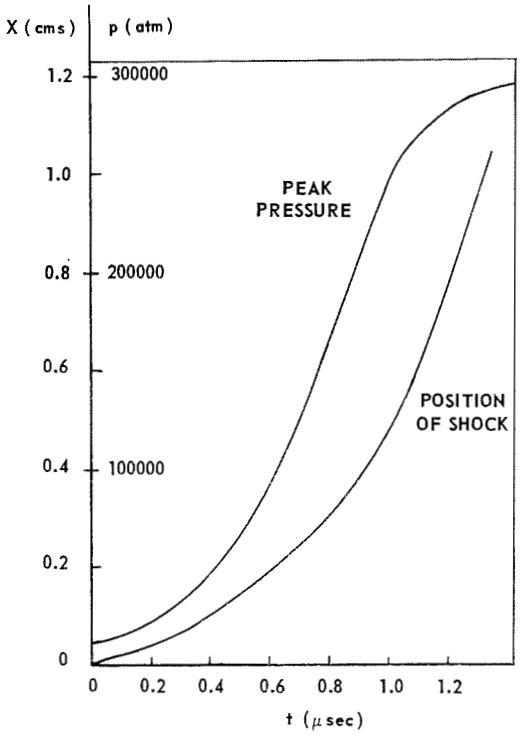

FIG. 1. Shock pressure and position, infinitely long pulse.

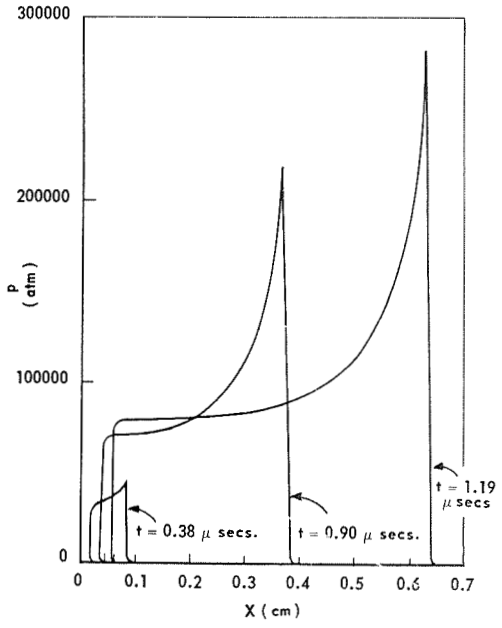

FIG. 2. Pressure profiles, infinitely long pulse.

In all the cases investigated, we find that the shock transmitted into the explosive accelerates or decelerates steadily. Moreover, the peak pressure never exceeds the calculated C–J value, that is, overshoot does not occur, even with an input pressure pulse of 100 000 atmospheres. This is in accord with experimental observations on condensed explosives,[7,8] but is in sharp contrast with numerical results obtained by other workers[2,5] and with experimental observations on liquid explosives.[6] The differences must be due to our use of the law of burning.[9]

A typical example of the behavior following the input of a pressure pulse of infinite duration is given in Figs. 1 and 2. The position of and pressure at the shock front is plotted against time in Fig. 1, and the smooth acceleration to detonation velocity and the smooth rise of pressure to the calculated C–J value can be clearly seen. Figure

2 shows the profiles of the pressure inside the explosive at three specific times, and here the von Neumann spike is seen building up. With such steady acceleration, a delay time cannot be measured to any great accuracy, but the delay until complete combustion is attained is quite short, of the order of a microsecond at most. Also, the vast disparity between delay times for pulses of only slightly different pressures is not found.

With a pressure pulse of finite duration, we have the experimental possibility of a failure to detonate. As already mentioned, this cannot

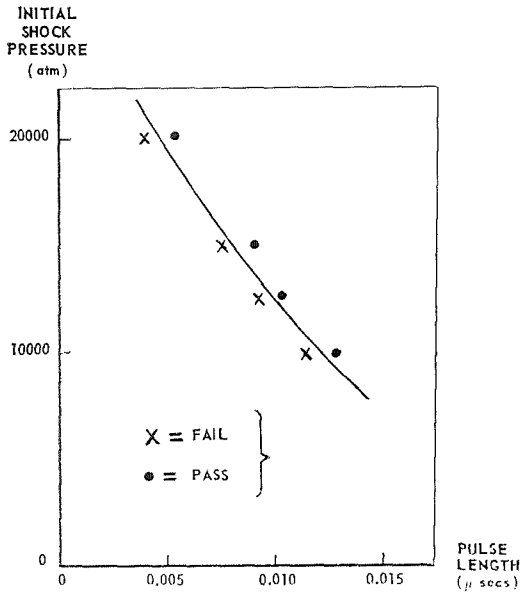

FIG. 3. Critical shock pressures.

happen in a theoretical system with a smooth and continuous law of burning, so we have to define what we mean by "failure." If we introduce an arbitrary pressure limit below which no burning takes place, then any pressure pulse which decays below this limit will fail to detonate. A critical pulse can be defined as that pulse which will just fail in infinite time. Unfortunately, this definition means that the parameters of a critical pulse will depend closely on just what pressure limit we set. This is illustrated in Fig. 3 which gives a plot of pressure height against pulse duration for various cases tried, together with an estimated curve for critical pulses. It must be appreciated that this curve is purely an estimate, and is subject to considerable error. This is because the peak pressure will in general not occur at a mesh point, so that our criterion of failure is affected by the size of the mesh and

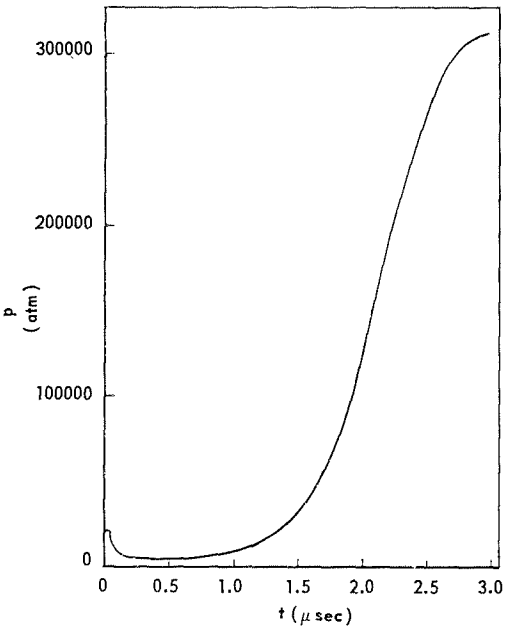

FIG. 4. Shock pressure, finite pulse.

our estimation of peak pressure. The determination is lengthy and involves several machine runs per point.

Figures 4 and 5 give the peak pressures and pressure profiles obtained in one case, with a pulse height of 20 000 atmospheres and a pulse length of 0.00617 microsec, which is just over the

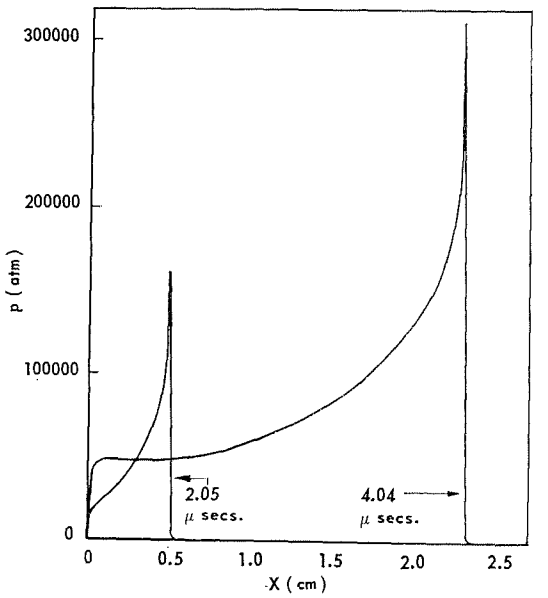

FIG. 5. Pressure profiles, finite pulse.

critical length at that pressure. The peak pressure drops when the rarefaction wave reaches the vicinity of the shock wave, and it remains low for a comparatively long time until the energy released by the burning of the explosive causes it to rise again and accelerate the shock to detonation velocity. The rise in peak pressure occurs much more abruptly here than for a shock of infinite duration, and the steepness of the gradient enables us to define a delay time as the time taken for the pressure to reach half the Chapman–Jouguet value. The case given in Figs. 4 and 5 had a delay time of 2.08 microsec, while a just-over-critical pulse of 10 000 atmospheres height and 0.0128 microsec duration had a delay time of 2.28 microsec, so it appears that the delay time is appreciably independent of the manner in which detonation is initiated. It must of course vary with the excess of energy input over the energy of a critical pulse, and we would also expect a marked variation with a variation in the pressure limit.

Conclusions

The results obtained above show that a law of burning containing a factor depending on pressure represents a solid explosive better than the usual Arrhenius law. We have only looked for solutions when the pressure index n is unity. The cases $n = 2$ and 3 and, possibly, nonintegral values of n need to be investigated next. The calculations have shown only too clearly some of the deficiencies in our knowledge of the equation of state; these require further experimental investigation both in the solid and gaseous phases of explosives.

Nomenclature

b	Covolume (cc/gram) or copressure (atm)
C_v	Specific heat (ergs/gram °K)
E	Activation energy
f	Fraction of explosive detonated
m	Mass coordinate (grams)
p	Pressure (atm)
Q	Heat liberated by burning explosive
R	Modified gas constant
R_1	Gas constant per gram (atm/gram °K)
s	Shock speed (gram/microsec)
t	Time (microsec)
T	Temperature (°K)
u	Velocity of a particle (cm/sec)
v	Specific volume (cc/gram)
x	Distance (cm)
Z	Frequency factor

Compound symbols

y	$(1 - f)^{\frac{1}{3}}$
β	$\dfrac{1}{(1 + C_v T_0/R)^{\frac{1}{3}}}$
γ	$10^{-6}R/C_v + 1$

Subscripts

0	Initial state
1	Shocked state
g	Gaseous phase
s	Solid phase

References

1. Cook, M. A.: *The Science of High Explosives.* Reinhold, 1958.
2. Zovko, C. T. and Macek, A.: Third Symp. Det. Report, ACR–52, vol. 2, p. 606, 1960.
3. Lax, P.: Communs. Pure and Appl. Math. *7*, 199 (1954).
4. Robertson, R.: J. Chem. Soc. *119*, 1 (1921).
5. Hubbard, H. W. and Johnson, M. H.: J. Appl. Phys. *30*, 765 (1959).
6. Campbell, A. W., Davis, W. C., and Travis, J. R.: Third Symp. Det. Report, ACR–52, vol. 2, p. 469, 1960.
7. Campbell, A. W., Davis, W. C., Ramsay, J. B., and Travis, J. R.: Third Symp. Det. Report, ACR–52, vol. 2, p. 499, 1960.
8. Cachia, G. P. and Whitbread, E. G.: Proc. Roy. Soc. (London) *A246*, 268 (1958).

Discussion

Dr. M. H. Boyer (*Aeronutronic*): The basic considerations and mathematical techniques discussed by Dr. Warner in treating the detonation problems are similar to those we have been using, with a few differences in detail.[1]

In the first place, one has to question whether or not the energies which exist in the charge can always be correctly regarded as "thermal." We have avoided the problem by expressing our equations in terms of total energy. However, at high density an appreciable portion of the energy may exist as potential energy of atomic or bond distortions. Under these conditions, the relation between energy density and reaction rate may be different

than the customary one between temperature and reaction rate. We are presently engaged in an experimental study of this question.

Our work made use of the Abel equation of state as has been adopted by Dr. Warner. However, this equation is somewhat in question for solids since it does not permit a finite volume at zero pressure except at zero energy. We have since changed to a solid equation of state based upon the Gruneisen theory of solids[2] which is similar to that of Tait, namely:

$$(P + \beta)v_s = (\gamma_s - 1)e_s + C$$

We feel that it more correctly represents behavior in the low pressure region. For the gas phase, we use the perfect gas equation

$$pv_g = (\gamma_g - 1)e_g.$$

Both γ_g and γ_s are treated as variable functions of v_g and v_s respectively. They are computed continuously by means of a relation derived from the data used by Cook in defining his variable covolume term, $\alpha(v)$. The term β is arbitrarily taken as a constant although this is not justified theoretically. We are presently engaged in a program to determine more correct functions for both γ and β from static pressure measurements at ultra-high pressure.

The most significant difference between Dr. Warner's work and ours resides in the formulation of the rate equations. We use a two-step rate process consisting of an ignition reaction which initiates and is followed by a grain burning process. The ignition reaction is assumed to involve a known fraction, F_1, of the charge material, and is described by an Arrhenius rate function. The grain burning equation is of the original Eyring form as shown in Dr. Warner's paper, except for some alterations affecting the pressure and energy dependence.

We have thought that the grain burning equation should show a pressure sensitivity at low pressure where it must approximate the strand burning laws for explosives, but that at pressures in the detonation range, it should become independent of pressure. Accordingly, we have used the following empirical pressure function to obtain such behavior

$$p/[(p/w) + 1]$$

where w is an arbitrary constant.

The exponential term of the grain burning equation is regarded as more correctly dependent upon the energy density on the gas side of the gas–solid interface rather than on the average gas energy density. Since the reaction is pictured as a stepwise process in which small increments of surface material react completely in succession, it is regarded as occurring at constant pressure as with a deflagration wave. The energy in the burned gas immediately adjacent to the interface is therefore given by

$$e_s + Q/\gamma_g$$

where e_s is the solid phase energy density and Q is the heat of reaction.

With these considerations the following are obtained for the two reaction rate laws:

Ignition:

$$df/dt = (1 - f)\, B \exp\,[A/(e_s + Qf)]$$

Grain Burning:

$$df/dt = (1 - f)^{\frac{2}{3}} B \frac{p}{(p/w) + 1} \exp \frac{A}{e_s + (Q/\gamma_g)}$$

We find that their use leads to a computed wave behavior analogous in most important respects to experimental observation.

DR. F. J. WARNER (*Royal College, Glasgow*): Dr. Boyer questions whether the energies of the charge are purely thermal. In this paper, we have assumed that they are, in order to keep the approach as simple as possible. However, any further development should take the distribution of energy into account. At the very high pressures involved, it is likely that the equations of state applicable will be those of plasma physics, and a magnetohydrodynamic set of equations will have to be used with all the complications that this entails.

REFERENCES

1. BOYER, M. H. and GRANDEY, R.: *Detonation and Two-Phase Flow.* Academic Press, 1961.
2. SLATER, J. C.: *Introduction to Chemical Physics,* Chap. XIII. McGraw-Hill, 1939.

THEORY OF INITIATION OF DETONATION IN SOLID AND LIQUID EXPLOSIVES

G. K. ADAMS

The experimentally observed differences in the growth of shock initiated detonation in liquid and in solid explosives are discussed with the object of deciding upon a reaction rate model for numerical calculations on the growth of reactive shock waves in granular solid explosives. It is suggested that while a strongly temperature dependent bulk reaction rate model is indicated for liquids and homogeneous solids, the behavior of granular solids indicates a reaction rate which is a function of the pressure behind the shock front and not of the average temperature.

A pressure dependent energy release rate is shown to result in the reaction building up at the shock front rather than at the explosive/barrier interface. Under this condition it is possible to attempt approximate analytical solutions of the reactive shock equations which illustrate the relation between the initial growth or failure behavior of the wave and the initial shock pressure, shock curvature, and the rate of energy release and its pressure dependence.

A pressure dependent energy release rate is shown to be a consequence of a grain burning model for the reaction process where the rate of propagation from ignition surfaces is assumed to be a function of the pressure and flame temperature of the products of reaction.

The problems in verifying this hypothesis are briefly discussed. In low bulk density explosive where the shock pressure is low enough for it to be possible to make independent measurements of burning rate and its over-all pressure dependence, it is difficult to make sufficiently precise measurements of shock pressure. In high density explosives where the shock pressure/distance to steady detonation relationship can be determined with some precision, the magnitude of the pressure is greatly in excess of those at which burning rate measurements can be made.

Introduction

The concept of initiation of detonation in explosives through conversion of the mechanical energy of the shock wave into thermal energy which activates chemical reaction was introduced many years ago for gaseous explosives[1,2] and was extended to liquid explosives by Ratner[3] and to granular solid explosives by Eyring and coworkers.[4] The latter assumed that reaction was initiated at points of contact on the surface of crystals where hot spots were produced by intercrystalline friction under the compression of the shock wave. Alternatively it has been assumed that ignition sources are produced by the adiabatic shock compression of interstitial gas.[5]

The effect of grain size on the detonation speeds and failure diameters of solid high explosives led Eyring to suppose that the reaction did not proceed homogeneously within the solid but by a burning or erosive process at the grain surface. The rate of energy release was assumed to be proportional to the area of burning surface and by analogy with chemical kinetic laws to an Arrhenius type function of the temperature of the decomposition products. However an approximate quantitative treatment of the steady detonation speed versus charge diameter problem, based upon this model, led to the conclusion that the apparent activation energy of the process was too small for it to be determined by chemical reaction rate but was of the order expected for a transport process.[4]

Until the last few years there have been few indications of a possibility of advance in the state of knowledge on the relation between the kinetics of the energy release process and the course of initiation of detonation by shock waves. The application of finite difference techniques to the solution of problems involving unsteady shock propagation in a chemically reactive medium, and improvements in experimental techniques for the observation of the properties of unsteady detonation phenomena have changed this situation. Hubbard and Johnson[6] computed the course of events following upon the passage of a finite duration shock pulse into a slab of explosive. The material flow was assumed to be restricted to one space dimension and the rate of energy release behind the shock front was taken

to vary with the temperature of the shocked explosive according to an Arrhenius type rate law with an activation energy of 40 kcal/mole. They found that, provided the duration of the pulse exceeded the adiabatic explosion time at the shock temperature, a detonation wave originating at the entry face at this time overtook the shock front from the rear. The computed initiation delays were compared with those found experimentally for a cast RDX–TNT explosive. Hubbard and Johnson note that their calculations indicate a much larger variation of time delay with shock strength than that found experimentally but ascribe this to inadequacy of their equation of state in the prediction of variation of shock temperature with shock strength. Campbell and co-workers[7] recognized that, although the Hubbard and Johnson results did not conform to the observed initiation behavior of solid explosives, they could be applied to their observations on initiation of detonation by shock waves in liquid explosives. They conclude from the order of magnitude agreement between calculated and observed initiation delay times and the sensitivity of the latter to shock strength *in liquid explosives*, that the thermal explosion resulting from a homogeneous chemical reaction in the bulk, was the appropriate model for liquid and homogeneous or nongranular, solids.

The major difficulty in confirming this hypothesis lies in the absence of precise information on either the temperature of the shocked explosive or on the chemical reaction rate at any given temperature at very high pressures (such data as is available has been obtained at atmospheric pressures).

In this paper we shall be mainly concerned with the problems of a formal energy release rate model for solid granular explosives.

Deductions from Experimental Observations

The assumption that, in the detonation of solid granular explosive composition, chemical reaction is initiated at hot spots produced at the crystal surfaces is of long standing. It appears to have been based on the lack of an alternative mechanism for obtaining grain temperatures sufficient to promote rapid chemical reaction in the initiation and propagation of low order detonations rather than by direct experimental evidence on the origin of the hot spots. Eyring and coworkers seem to have been the first to use the dependence of detonation velocity on grain size to develop a quantative theory of reaction zone length but their conclusion that the hot spots originated at contact points between the grains was based on limited evidence as to the effect of bimodel grain distribution on detonation velocity. Taylor[5] quotes experiments by Gurton on the effect of interstitial gas pressure on low order detonations as evidence for ignition by adiabatic compression of interstitial gases.

Although there is little evidence as to the physical nature of the initiation process in solids, the accumulated evidence for a fundamental difference between this process and that in liquids (or physically homogeneous solids) is very strong. This can be listed concisely as:

(a) Different orders of sensitivity shown by substance of similar chemical constitution but different physical state;

(b) A much larger range of nonideal detonation velocities found for granular solids than for homogeneous material;

(c) The failure diameters and shock sensitivities of granular solids are much less dependent on the initial charge temperature;

(d) The reactive shock in granular solids accelerates continuously in speed to the steady detonation value as opposed to a sudden onset of a detonation wave behind the initiating shock in liquids;

(e) The time required to reach steady detonation speed is much less sensitive to the initiating shock strength in granular solids than in liquids.

The first three of these are easily interpreted as indicating that the rate of energy release in the case of granular solids is much less affected by the temperature to which the bulk of the material is raised by compression in the shock wave. Indeed the higher sensitivity of a granular solid explosive compared with the same explosive in the liquid state, in spite of its lower compressibility, would seem to rule out bulk heating as the origin of chemical reaction in the granular solid. In order to understand the existence of a minimum shock strength for initiation of detonation or a minimum diameter for the propagation of steady detonation we need to assume some degree of increase in the rate of heat release by chemical reaction with increasing shock strength. It is not sufficient to assume that, for instance, there is some critical strength for ignition above which the rate is independent of shock strength. If one assumes that ignition is due to adiabatic heating of interstitial gas then the experiments of Seay and Seely[8] who varied the nature and pressure of the gas in low density PETN without affecting the growth of detonation must be interpreted as indicating that the ignition process is not the limiting one. If one assumes that intercrystalline friction or shock reflection at intercrystalline boundaries[7] is responsible for the creation of hot spots then although it becomes possible to argue that the number or effectiveness of such spots increases with increasing shock

strength it is difficult to envisage a way of confirming this experimentally or of developing a quantitative theory.

A more useful assumption is that the ignition process is not the factor of major importance in determining the variation of energy release rate with shock strength in a particular granular solid explosive composition even though it may determine the different sensitivities of different forms of that explosive. Kistiakowsky has suggested[9] that the conversion of chemical energy in the reaction zone of detonating solid explosives occurred through a grain burning process analogous to the burning of propellant grains in a gun. He points out that secondary explosives when ignited obeyed a similar law of increasing burning rate with pressure to that of propellants and that, if the rates were extrapolated to detonation pressures, the time of burning of the explosive crystals was not inconsistent with observed detonation reaction zone lengths. The application of this concept, i.e., pressure dependence of reaction time, to the growth of detonation waves appears to have been neglected. Eyring, in developing a theory of failure diameter, assumed the time of burning to be determined by the temperature of the reaction products not by their pressure. In order to fit the experimental data he concluded that the reaction time was nearly inversely proportional to the temperature, corresponding to a zero activation energy in his rate expression. It is easy to show that a similar degree of concordance is obtained if one assumes the reaction time to be inversely proportional to the pressure, i.e., inversely proportional to the square of the nonideal wave speed.

If we now assume that an increase in the energy release rate with increasing shock strength is a function of the pressure in the reacting medium rather than of temperature it becomes possible to see why the wave in the granular solid may accelerate continuously rather than be overtaken by a detonation originating behind it. We assume that the energy release rate can be written as a function of temperature *or* pressure and that these are uniform in a plane normal to the direction of motion of the shock. Changes in the temperature of a particle element due to chemical reaction in the subsonic flow behind the shock will be dissipated (by thermal conduction) very much more slowly than the resultant change of pressure. Under conditions of near steady flow a temperature dependent reaction rate will cause the reaction to build up along a particle path and to achieve its maximum value in the explosive element adjacent to the surface through which the shock entered the explosive. If the reaction is pressure dependent one would expect it to be more uniformly distributed behind the shock and to build up at the shock front if the shock pulse has a positive pressure gradient.

The Problem of a Reactive Shock Wave

The conditions for the growth of the wave can be more clearly seen if we write down the equations for the time rates of change of internal energy and pressure along a particle path in one-dimensional linear flow. Let E, p, and u represent the local values of internal energy, pressure, and particle velocity, respectively, at the point (x, t) and let $\dot{q}$ be the local heat release rate. Then

$$D \ln E/Dt = (\dot{q}/E) - (\gamma - 1)\, \partial u/\partial x \quad (1)$$

and

$$D \ln p/Dt = (\dot{q}/E) - \gamma\, \partial u/\partial x \quad (2)$$

where we have assumed an equation of state $p = (\gamma - 1)E\rho$.

The rate of change of both internal energy and pressure along a particle path are therefore determined by the heat release rate and the local gradient of particle velocity. Consider a near steady shock traveling into the explosive (x increasing) with initial and boundary conditions such that $\partial p/\partial x$ and $\partial u/\partial x$ are positive behind the front. Then it is clear from these equations that even when $D \ln p/Dt$ is negative $D \ln E/Dt$ can be positive. If $D \ln E/Dt$ is positive, $\partial E/\partial x$ is negative, and $\dot{q}$ is proportional to a high power of E the reaction rate will increase fastest at the explosive surface since the time rate of change of E along any other path corresponding to a speed S greater than the particle velocity, is less than that along the particle path

$$dE/dt = (DE/Dt) + (S - u)\, \partial E/\partial x$$

In the case of a reaction rate term which increases with a power of pressure such that $\dot{q}/E$ also increases then, assuming that the rear boundary condition imposes a positive pressure gradient, the rate of energy release must be a maximum at the head of the shock. We may therefore expect a pressure dependent energy release rate to result in the pressure building up most rapidly at the front and in a continuously changing shock speed.

In order to find the space-time history of the reactive shock wave and the condition for the wave to accelerate to the steady detonation state we need to integrate Eq. 1 and 2 together with the equation of motion

$$Du/Dt = -(\gamma - 1)\, E\, \partial \ln p/\partial x$$

In general this can only be achieved by numerical integration but it is useful to try to gain some

insight into the behavior of the system by seeking approximate solutions.

In the linear one-dimensional flow case the variation of parameters at any point behind the shock is determined by the local energy release rate and also by the local velocity gradient which is influenced not only by the rear boundary conditions but also by the energy release at other points in the wave. In the case of nonlinear flow there will also be a term due to the local divergence of the flow. We may seek situations where the development of the wave is dominated by the boundary conditions or by the divergence term.

Consider a spherically symmetric shock diverging from a point source in an inert medium and passing into an explosive at radius r_0. The acoustic impedance is assumed to be the same for inert and explosive so that the transmitted pressure is equal to the incident pressure. The properties of the incident wave can be determined from known similarity solutions. If the state equation is assumed to be of the form

$$p = (\gamma - 1)E\rho$$

the equations of motion and energy can be combined to give equations for the time rate of change of pressure and velocity along a path defined by $dr/dt = S$

$$\frac{d \ln p}{dt} + \frac{\gamma(S-u)}{a^2}\frac{du}{dt} = \gamma\left[\frac{(S-u)^2}{a^2} - 1\right]\frac{\partial u}{\partial r} - 2\gamma\frac{u}{r} + \frac{\dot{q}}{E} \quad (3)$$

where a is the local sound speed. Putting $S = U$ (shock speed), $u \pm a$ or u we obtain the time derivatives for points moving with the shock, along the characteristics defined by $dr/dt = u \pm a$ and along particle paths, respectively.

At the head of the shock the parameters are related by the Rankine-Hugoniot equations across the shock wave.

If we assume that the energy release rate $\dot{q}$ can be written in the form:

$$\dot{q} = kp^m, \qquad m > 1$$

and is greatest at the head of the shock we may try to approximate the development of the shock by an ordinary differential equation for the properties at the shock front. The problem lies in the velocity gradient term. An obvious first approximation which should be valid for the initial path of the wave in the explosive is to use the same function of u and r as is given by the solution for the nonreactive medium. In the case of $\gamma = 7$ this is particularly convenient since $\partial u/\partial r = u/r$.[10] It is clearly invalid for the later history of a wave which approaches the steady detonation speed since then the LHS of the equation approaches zero and the gradient term must become equal to the heat release term. It may be a reasonable approximation for the initial stages of spherically symmetric initiated detonation since the divergence term is comparable with the heat release term. The equation is particularly simple for a strong shock where $U/a_0 \gg 1$ and for $\gamma = 7$ when $\partial u/\partial r = u/r$. Putting $S = U = dr/dt$ and using

$$u = 2U/(\gamma+1), \qquad p = \rho_0 U u,$$
$$a^2 = \gamma U(U-u), \qquad E = E_0 p/p_0,$$
$$\dot{q} = kp^m \quad (4)$$

we obtain the rate of change of shock pressure with shock radius as:

$$d \ln p/dr = (2kp_0^{\frac{3}{2}}/3E_0U_0)p^{m-\frac{3}{2}} - (3/r) \quad (5)$$

Since p varies as U^2 this also gives the variation of shock speed with distance. It is exact in the inert medium where $k = 0$ and p and U vary as r^{-3} and $r^{-\frac{3}{2}}$, respectively. At the explosive–inert interface it defines critical values of the parameters at which the wave will start to grow in strength as it enters the explosive:

$$2kp_0^m/3E_0U_0 = 3/r_0 \quad (6)$$

If we regard this equation as defining a critical initial pressure $(p_0)_c$ and rewrite the differential equation in terms of $P = p/(p_0)_c$, $R = r/r_0$, and $n = m - \frac{3}{2}$, i.e.,

$$\tfrac{1}{3}(d \ln P/dR) = P^n - (1/R) \quad (5a)$$

the solutions passing through the point $P = P_0$, $R = 1$ are

$$P^{-n} = \left(P_0^{-n} + \frac{3n}{1-3n}\right)R^{3n} - \frac{3n}{1-3n}R, \qquad n \neq 0 \text{ or } \tfrac{1}{3} \quad (7)$$

The curve $P^{-n} = R$ is the locus of points of zero gradient which occur at values of R given by

$$R^{1-3n} = P_0^{-n}(1-3n) + 3n. \quad (8)$$

For $P_0 > 1$ [when $(d \ln P/dR)_0$ is greater than zero] $d \ln P/dR$ remains positive for all values of $R > 1$. Thus an initially accelerating wave continues to grow in speed.

If $P_0 < 1$ and the wave in the explosive is initially decelerating, its subsequent history depends upon the value of P_0 and of the exponent n. If $n = m - \frac{3}{2} > \frac{1}{3}$ then the wave will start to accelerate at a radius given by Eq. (8) for all values of $1 > P_0 > [(3n-1)/3n)]^{1/n}$. For values of the initial shock strength less than

this it will continue to fade as it propagates into the explosive. The range of initial shock strengths over which a detonation results after the wave travels into the explosive as a fading wave, decreases with increasing values of the reaction rate exponent, m. We see that the history of the process will depend not only on the parameter which determines the energy release rate but also on the rate of change of the rate with respect to that parameter. Failure is ensured if the losses due to the gradients behind the front and the divergence of the flow decrease less rapidly in the progress of the wave than the energy release rate.

Reaction Rate Models for Liquid and Solid Explosives

It is clear that the growth of the incident shock must depend not only on the functional dependence of heat release rate and the incident shock strength but also on the shape of the shock pulse and the curvature of the wave. One difficulty in interpreting or comparing experimental data is that no information is given on the shape of the pulse even in the extensive set of experiments on liquid and solid explosives made by Campbell and coworkers.[7] They did not use similar shock generating systems in the liquid and solid explosive experiments so that the pulse shapes were not necessarily similar in both sets of experiments. However it seems probable that in both sets the incident pressure pulse was nearly flat although slowly weakened by the Taylor wave expansion in the products of the donor charge. We may therefore assume that the difference in the observed behavior was due to different modes of heat release in the liquids and the granular solids. For the liquids the concept of a reaction rate strongly dependent on temperature would seem to be adequate providing we assume the velocity gradient at the interface was sufficiently small to allow the net time rate of change of temperature to be positive and the temperature gradient to be negative (i.e., the temperature to be higher at the interface than at points nearer to the shock front). The fact that they did not detect any change in the material velocity at the explosive/barrier interface during the time scale of their experiments would support this assumption.

Although the experimental data on the variation of time delay with shock strength, and the relation between the latter and shock temperature, are insufficient to enable the activation energy of the reaction process to be calculated, we may accept their conclusion that the activation energy of the thermal decomposition of nitromethane is adequate to account for the observed variation.

We have suggested that the different behavior of granular solid explosives can be understood if it is assumed that the energy release rate is pressure dependent rather than temperature dependent. The problem is to find a model which will give this result. Let us examine the consequence of assuming that the chemical reaction is in this case controlled not by a bulk reaction process but by a deflagration or burning process set up in a time which is much shorter than the time scale of the growth of the wave and originating at surfaces of temperature discontinuity in the solid. The rate of heat release will be proportional to the area of these surfaces and to the rate of propagation from them.

Elementary flame theory predicts that the rate of propagation is proportional to some power of the pressure of the order of unity and is also a function of final product temperature. The pressure dependence is the net result of the pressure variation of thermal diffusivity and of the specific reaction time determined by the effective reaction order of the rate-determining chemical process. The temperature dependence will be of the form $\exp -(A/2RT)$. This differs from that of the bulk reaction process in the factor two in the denominator and in that the temperature is given by the initial temperature plus the temperature rise due to reaction. Since the latter is in general 2000–3000°K then, even if the activation energy is the same as that of the bulk decomposition process, the sensitivity of the heat release rate to variations in initial temperature is reduced by about a factor of five or six. However more important in the development of the wave is the fact that this temperature, being that of the products of complete chemical reaction, is independent of the extent of chemical reaction except in so far as this determines the *mass average* internal energy and the pressure. (If we assume the pressure and velocity to be uniform the internal energy of the explosive and product phases at any space coordinate will differ by the enthalpy change due to complete chemical reaction.) Then the temperature of the reaction products which determine the heat release rate can be written as a function of the local pressure using the equation of state and the Hugoniot relations. Neglecting any variation in the area of burning surface with time, the heat release rate is then a function of pressure only. The over-all pressure dependence is then that due to the variation in rate at constant flame temperature plus that due to the variation in flame temperature produced by the shock compression and the expansion behind the front.

It should be possible to determine the pres-

sure and temperature coefficients of burning rate experimentally by conventional internal ballistic technique up to pressures of at least several kilobars. Then, if the Hugoniot curve for the solid explosive is known, the variation of internal energy and therefore of burning rate with shock pressure can be determined. Using this information in numerical integrations of the reactive shock equations, the computed development of the shock with time can be compared with experimental data on the growth of the shock into detonation.

The major difficulties are likely to be extrapolation of experimental burning rate/pressure/temperature relationships and the assumptions to be made as to the variation of the area of burning surface with time or with the fraction of explosive reacted. These suggest that the most fruitful field of application is to the shock initiation of detonation in low density pressings of fast burning colloidal propellant grains which can be initiated by shocks of the order of a few kilobars and where the surface area can be controlled.

It has not yet been possible to determine the shock pressures induced in low density materials with a sufficient degree of precision to make significant deductions on variation of the distance to detonation with shock pressure. Measurements with cast explosives suggest that this distance increases with about the reciprocal first power of the pressure.

In terms of a pressure dependent heat release rate model and linear one-dimensional flow this would indicate a burning rate varying with a power of pressure of between two and five halves depending on the form of the shock pressure/shock speed relationship. Although this is consistent with burning rate data in the range of 1 to 2 kilobars there is no justification for extrapolating this data to the tens of kilobars range appropriate to the initiation of cast explosives.

It is particularly difficult to justify any assumptions as to the variation in the area of burning surface with fraction reacted in such explosives since this must depend upon the physical nature of the ignition process. If the time to reach a maximum rate of energy release after the transit of the shock is small compared with the time scale of the growth of the wave this would be unimportant provided the area factor was not itself a function of shock pressure. Such problems can be determined only when experimental methods for the study of the wave structure become available.

References

1. Becker, R.: Z. Elektrochem. *23*, 40 (1917).
2. Wendlandt, R.: Z. physik. Chem. *116*, 227 (1925).
3. Ratner, S. B.: Acta Physicochim. U.R.S.S. *22*, 357 (1947).
4. Eyring, H., Powell, R. E., Duffey, G. H., and Parlin, R. B.: Chem. Revs. *45*, 69 (1949).
5. Taylor, J.: *Detonation in Condensed Explosives*, p. 173. Oxford University Press, 1952.
6. Hubbard, H. W. and Johnson, M. H.: J. Appl. Phys. *30*, 765 (1959).
7. Campbell, A. W., Davies, W. C., and Travis, J. R.: Phys. Fluids *4*, 489 (1961).
8. Seay, G. E. and Seely, L. B.: J. Appl. Phys. *32*, 1092 (1961).
9. Kistiakowsky, G. B.: *Third Symposium on Combustion, Flame and Explosion Phenomena*, p. 560. Williams and Wilkins, 1949.
10. Courant, R. and Friedrichs, K. O.: *Supersonic Flow and Shock Waves*, p. 424. Interscience, 1948.

Discussion

Dr. J. R. Travis (*Los Alamos Scientific Laboratory*): In regard to the fourth section of Dr. Adams' paper, I would like to summarize some recent calculational studies[1] by Charles Mader from Los Alamos on the initiation of detonation in physically homogeneous explosives. He has attempted to find complete numerical solutions to the equations of fluid dynamics for a reactive material. The following equations and conditions were used:

1. One-dimensional finite-difference form hydrodynamic equations;
2. ~500 finite-difference space zones with IBM 7090 computer;
3. Arrhenius first order reaction equation;
4. Best available equations of state for unreacted explosive and reaction products;
5. Initial and boundary conditions: plane shock wave. The rear boundary moves forward impulsively at the appropriate particle velocity for the desired shock pressure. When detonation begins, the wall is stopped.

Good agreement is obtained with the experimental results of Campbell, Davis, and Travis,[2] first, in the qualitative description of the initiation process and, second, in calculation of the hydrodynamic parameters.

The progress of the waves in initiation of nitromethane by a plane 92 kbar shock is shown in Fig. 1.

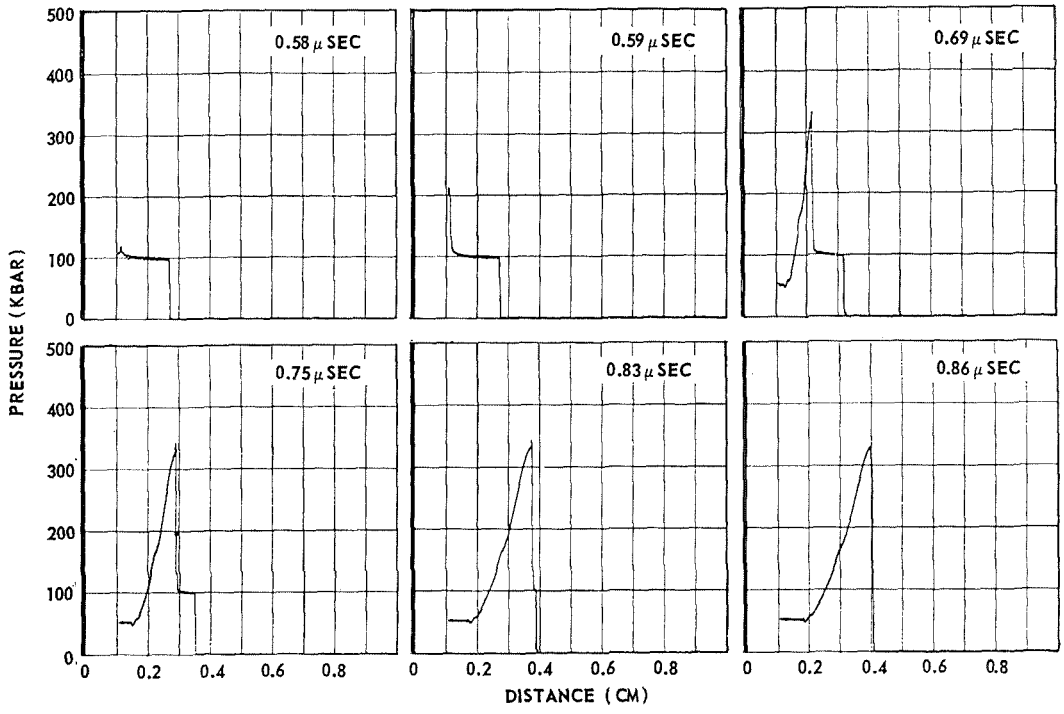

FIG. 1

DR. M. H. BOYER (*Aeronutronic*): Dr. Adams' paper emphasizes that the theoretical treatment of initiation and growth of detonation requires some means of representing the energy release processes. As he has indicated, this is a difficult problem and it is necessary to resort to the use of a simplified model which, one hopes, will be sufficiently close to reality to be useful, and at the same time capable of being used without presenting completely intractable mathematics.

We have also been concerned with the development of such a model and its use in predicting the detonation behavior of real systems. We divide the energy release process into two steps (three, in the case of composite propellants): an ignition reaction described by an Arrhenius rate law, and a following reaction represented by a surface regressive or grain burning rate law. This arrangement requires two parameters in addition to those normally appearing in these rate equations: a term, F_1, the fraction of the total charge material reacting via the ignition process, and a term, Z, which is the maximum regression distance of the surface burning process (i.e., the grain radius in the original grain burning concept).

The term F_1 relates to the physical nature of the ignition process. An interesting type of ignition occurs when there are pores or voids in the charge. It is found that if, upon passage of a shock over a porous material, the pores are compressed to zero volume, then the energy deposition in excess of that deposited by a shock of similar intensity in nonporous material is approximately proportional to the initial pore volume. This excess energy represents work done in collapsing the pore. It is associated with motion and viscous dissipation, and presumably is deposited in the vicinity of the pore. If the volume of material so affected is approximately equal to the pore volume, then the temperature rise will be twice that in bulk material. A hot spot approximately equal to the pore volume is therefore created; this logically becomes the volume of the ignition region, and it is concluded that in the initiation of porous explosives by such a mechanism, the parameter F_1 can be taken to be equal to the fractional porosity of the charge. It is to be noted that the foregoing arguments do not depend significantly upon the type, or even the presence of occluded gas.

This relation between porosity and the ignition process provides a reasonable interpretation of many widely observed characteristics of detonation waves. It is first necessary to realize that representation of the ignition reaction by an Arrhenius function means that the ignition reaction zone width is very narrow. Its energy contribution to support of the wave is therefore not seriously degraded by lateral expansions, even at small charge diameters. This

will be equally true of Taylor expansions behind the wave after a very short propagation distance. It follows that if a large fraction of the charge material is consumed in the ignition process, as would be the case, according to the previous argument, with loosely packed, porous charges (i.e., large F_1) one would expect a very short wave run-up to steady state and a small critical diameter. With a high density nonporous charge, the converse would be expected. Such behavior is in general accord with experiment.

The parameter Z has a similar effect upon the surface regressive process. A small Z provides a thin reaction zone width and consequently a short run-up distance and small critical diameter, whereas the converse is true with large Z. We have observed that computed waves in charges defined to have a large Z combined with a small value of F_1 will run for large distances at a velocity of about 4 mm/μsec before accelerating to steady state value. Since these waves were computed with one-dimensional geometry, the effect of lateral losses could not be ascertained, but it is believed that had such losses been present, these low velocity waves could have been indefinitely stabilized. Experimentally, it is reported that the condition of large grain size, high density, and small charge diameter is just that which results in stable low order detonation. The correlation is apparent.

The situation represented by a charge in which no centers of ignition are present is also of interest. Here one can think of the ignition reaction as the sole heat release process. However, an important distinction from the previous case exists, in that the heating due to pore collapse does not occur. The shock intensity required for ignition therefore should be approximately twice that of a porous charge of the same material.

The nonporous charge in which reaction occurs homogeneously as with a gas, and according to an Arrhenius rate law, is the problem treated by Hubbard and Johnson. Their work showed the occurrence of ignition behind the shock front, followed by a very rapidly moving reaction wave which overtakes the front. Such phenomena have been experimentally observed in gases, and occasionally in liquids where this type of ignition is most to be expected.

MR. G. K. ADAMS (*ERDE*): The burning rate functions used by Dr. Warner and Dr. Boyer are similar but assume that the difference in internal energy of initial and burned phase is given by the constant volume and constant pressure heat of reaction, respectively. In Warner's treatment this results from the assumption of uniform pressure and particle velocity in the two phases at any x plane. The use of the constant pressure by Boyer is more consistent with what one expects for a steady burning model but might be expected to require a different formulation of the energy and mass conservation equation.

DR. M. H. BOYER: Dr. Adams commented that use of constant pressure heat of reaction requires a velocity difference between solid and gas. This is not necessary. We assume a reaction unit partly solid and partly gas. Solid is converted to gas as a constant pressure process but the unit moves as a single entity.

REFERENCES

1. MADER, C. L.: The Hydrodynamic Hot Spot and Shock Initiation of Homogeneous Explosives. Unclassified Report LA–2703 (available from the Office of Technical Services, U.S. Dept. of Commerce, Washington 25, D. C.).
2. CAMPBELL, A. W., DAVIS, W. C., and TRAVIS, J. R.: Phys. Fluids *4*, 498 (1961).

Discussion on Fundamental Flame Processes

(Organized by Dr. W. H. Avery)
(APL/The Johns Hopkins University)

Chairmen: Dr. W. H. Avery
(APL/The Johns Hopkins University)
Dr. W. E. Kaskan
(General Electric Company)
Prof. J. Fenn
(Princeton University)
Dr. W. T. Olson
(NASA)

Vice Chairmen: Prof. W. G. Parker
(Birmingham)
Dr. S. N. Foner
(APL/The Johns Hopkins University)
Prof. G. Dixon-Lewis
(University of Sheffield)
Prof. C. F. Curtiss
(University of Wisconsin)

SOME REMARKS ON THE THEORY OF FLAME PROPAGATION

JOSEPH O. HIRSCHFELDER

The principal problems and the salient features of the theory of flame propagation are discussed in a qualitative manner.

The theory of flame propagation can be stated very succinctly. The detailed structure of a flame is determined by solving the equation of state and the hydrodynamical equations of change together with the boundary conditions which are experimentally imposed. The equations of change comprise[1]:

(1) The equation of continuity of each chemical species.
(2) The equation of motion.
(3) The equation of energy conservation.

In addition to these principal relations there are the auxiliary relations:

(4) The complete set of reaction rate equations in terms of the chemical reaction rate constants.
(5) The equations for the diffusion velocities in terms of the usual binary diffusion coefficients and the multicomponent thermal diffusion coefficients.
(6) The equation for the pressure tensor in terms of the coefficients of shear and bulk viscosity.
(7) The equation for the energy flux in terms of the coefficient of thermal conductivity.
(8) The equation for the radiation energy flux in terms of the absorption and emission spectra of the molecules and the radiation emitted or absorbed as a result of the chemical reactions.

Furthermore, there are the subsidiary relations which determine:

(9) The coefficient of viscosity for the multicomponent mixture.
(10) The coefficient of heat conductivity for the multicomponent mixture disregarding the effects due to chemical reactions (which are taken care of in the energy flux equation).

The boundary conditions should include heat transfer from the flame to the flameholder and to the surrounding medium. Chemical reactions may, or may not, occur on the surfaces of the combustion chamber.

There are a number of reasons why the theory of flame propagation is difficult:

(1) The principal equations of change form a

set of nonseparable nonlinear partial differential equations.

(2) The boundary conditions are difficult to satisfy both at the flameholder (where there are problems arising from back diffusion and from the heat transfer to the flameholder) and at the hot boundary (where the flame equation can almost, but usually not quite, be linearized).

(3) The sheer complexity of the hierarchy of equations is horrible to contemplate, even if we knew a suitable method of solving them on a high speed computing machine.

(4) For most practical flame systems we are lacking necessary input information such as the reaction kinetics and the values of the reaction rate constants.

(5) And last but not least, the intrepid theorist must be prepared to cope with convection, turbulence, or flicker.

Thus, if you are interested in determining *ab initio* the properties of a particular flame system, you would be wise to study it experimentally. However, the theory is very useful if you are interested in:

(1) The general features which are common to all flames.

(2) The differential effects expected when one makes small changes in the fuel, the combustion system, the ambient temperature, etc.

(3) The effects of scaling the combustion system.

(4) Or the effects of changing the ambient pressure.

For such applications, the problem and the equations are idealized so as to preserve the feature in question while rendering a less faithful description of other properties.

Most treatments of flame propagation are limited to steady state considerations of a flat flame such as could be produced experimentally with a very large bunsen burner. This has the advantage of reducing the flame equations to a set of simultaneous one-dimensional ordinary differential equations in which the flame velocity is an eigenvalue determined by the boundary conditions. Heat conductivity and diffusion must be included in any realistic treatment of flames. However, the essential features of the chemical kinetics can be idealized so as to make the mathematics a bit simpler. Unfortunately, the Arrhenius temperature dependence of reaction rate constants is somewhat hard to cope with and frequently it is replaced by a simpler functional form.

The one-dimensional steady state treatments are good for describing the nature of a reaction zone, or the effect of varying either the fuel or the ambient pressure. A one-dimensional steady state treatment can be used as the basis for a study of stability. However, such a treatment cannot be used to estimate the effects of varying the flameholder or the scale of the combustion system. We hope that satisfactory mathematical methods will soon make it possible to follow the variations with time of a hypothetical one-dimensional flame.

One of the most interesting features of research in flame propagation is that it has brought together a large number of scientists with a great variety of backgrounds: chemists, mathematicians, physicists, chemical engineers, mechanical engineers, aeronautical engineers, etc. These scientists come from all parts of the world and each group speaks a different language. It is the *language barrier* which has made it difficult for theoretical combustion researchers to climb upon the shoulders of others and advance as rapidly as they should. It is relatively easy for an American chemist to translate and to understand the works of his German or Russian colleagues. It is much more difficult for the American chemist to translate the work of an American aeronautical engineer. The aeronautical engineer is accustomed to using different types of approximations corresponding to different concepts and what he says is expressed in terms of different symbols. Thus it may take more than two days of hard work to understand and to transcribe into your own notation an idealized set of flame equations as given in some journal article. As a result, the experimental combustion research workers, who can understand each other, cooperate and work together very efficiently. But the theoreticians, who generally have not taken the time and the trouble to understand one another, have each developed independently and have little use for the works of others.

Since I, too, must plead guilty to not knowing enough about the work of my colleagues, the rest of this paper is devoted to a summary of the work of our group at the University of Wisconsin. I expect that the other speakers at this symposium will also talk about their own research.

In 1947 the Applied Physics Laboratory, The Johns Hopkins University, asked us to develop the theory of flame propagation on a rigorous basis. Their primary concern was the combustion in ram jets at pressures of the order of a few hundredths of an atmosphere. Which fuels would burn best, what size of combustion chamber would be required, and what sorts of problems in ignition and stability would be encountered? Since there was no empirical experience in this type of combustion, it seemed very desirable to obtain an *ab initio* theory which was not biased by known behavior at atmospheric pressure.

The first problem which we encountered was the development of the equations of change. These are based on the rigorous kinetic theory of gases. In Chapman and Cowling's treatise[2] the equations of change are given for a binary mixture of nonreacting monatomic gases. It is stated that the extension of these formulae to a multicomponent mixture is obvious and "no essentially different features are introduced when more than two gases are present." It took C. F. Curtiss and myself a year and a half to perform this *trivial* extension of the theory. Furthermore, it was necessary to include the effects of chemical reactions, internal degrees of freedom of the molecules, and radiative energy transfers. The equation of energy balance was particularly difficult to derive but our effort was repaid when we found errors in the previously accepted equations.

The second problem was to set up a mathematical model for a highly idealized flame system. Clearly we wanted to limit ourselves, at least in the beginning, to considerations of one-dimensional steady state flames for which the equations of change form a set of simultaneous ordinary differential equations. The model which we envisaged was a giant flat-flame bunsen burner. Radiative energy transfers were neglected. The hot boundary was taken to be an infinite distance above the flameholder. At the hot boundary, we supposed that complete thermal and chemical equilibrium would be attained. The real problem was to idealize the cold boundary conditions at the flameholder. Two difficulties arose. First, because of back-diffusion of the product gases into the mixing chamber, the chemical composition of the molecules entering the reaction chamber is ill-defined. Then, too, unless there is at least a small amount of heat transfer from the flame to the flame-holder, (1) the position of the flame with reference to the flameholder is undetermined, and (2) if the chemical reaction rates are not mathematically zero at the ambient temperature, then the flame velocity is not determined by the boundary conditions. For Arrhenius temperature dependence of the reaction rate constants, some infinitesimally small amount of chemical reaction takes place at even very low temperatures. Thus, our idealized flameholder has two properties:

(1) It serves as a porous plug permitting the reactant gases to pass through it freely but preventing the back-diffusion of the product gases.

(2) It serves as a heat sink with a small amount of heat transfer taking place from the flame to the flameholder.

With this idealized flameholder it is then possible to say that at the cold boundary the composition

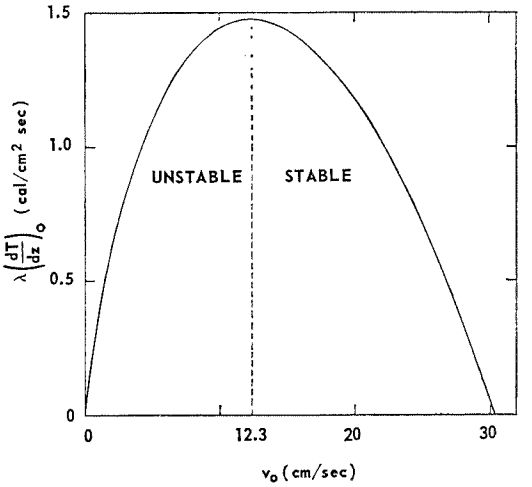

FIG. 1. The heat transfer to the flame holder, $\lambda(dT/dz)_0$, versus the flame velocity for a typical case. Note the minimum value of the flame velocity for stable flame propagation.

of the molecules entering the reaction chamber is the same as the composition of the reactant molecules in the mixing chamber and the average speed with which these molecules enter is equal to the flame velocity.

Somehow, our cold boundary conditions, especially the requirement for heat transfer to the flameholder, seemed to violate the intuition of a number of eminent authorities including Theodore Von Karman, Sol Penner, and Bernard Lewis. A rather interesting hassle developed. Howard Emmons came to our rescue with a set of heat transfer calculations which bolstered our arguments. Finally, the weight of the mathematical arguments overcame the intuitive feelings. Unfortunately, the vehemence of the discussions developed antagonisms which persisted for a long time.

Subsequently we found a curious result of our cold boundary conditions. Let us plot, as in Fig. 1, the heat transfer from the flame to the flameholder, $(\lambda\, dT/dz)_0$, as a function of the flame velocity, v_0. There is a maximum amount of heat transfer to the flameholder consistent with a steady state flame. For smaller amounts of heat transfer to the flameholder, the flame velocity is double valued. It is easy to show that the smaller of these two values corresponds to an *unstable* flame. Thus, there is a lower limit to the flame velocity of a stable steady state flame. An upper limit to the flame velocity corresponds to the gases at the hot boundary having a Mach number of unity. Usually, the flame velocity is very well determined and quite insensitive to the

heat transfer to the flameholder as long as it is varied through reasonable limits. Thus, in the example shown in Fig. 1, the ordinary flame velocity would be 30 cm/sec and to obtain any other value would require either unreasonably large or unreasonably small amounts of heat transfer.

Just from dimensional considerations, it is easy to see from the structure of the flame equations that if the chemical kinetics consists of only one step corresponding to an nth order reaction, the flame velocity varies as $p^{(n-2)/2}$ and the flame thickness varies as $p^{-n/2}$. Here p is the ambient pressure of the flame system. Thus the flame velocity for a unimolecular reaction system decreases with increasing pressure; the flame velocity for a bimolecular example is independent of pressure; and the flame velocity for a trimolecular reaction increases with pressure. The flame thickness should decrease with pressure regardless of the reaction order.

Once the equations of change and the boundary conditions had been determined, it was a simple matter to determine the properties of a hypothetical flame involving a single exothermic unimolecular reaction $A \rightarrow B$. This was accomplished in time for the Third International Combustion Symposium at Madison[3] in 1949. For this case, the flame equations boiled down to the solution of a single ordinary differential equation in which the assumed flame velocity was adjusted so as to satisfy the cold boundary conditions when the equation was integrated point by point from the hot boundary. Nowadays, with the use of high speed computing equipment and good formulae for the point by point integration of differential equations, such a problem would require a single mathematician an hour or so to code and a few minutes to run off on the giant brain. However, in 1949, we required a team of eleven girl mathematicians (most with a master's degree) a period of one to two months during which they were making the desk computers hum. High speed computing machines have two great advantages over desk machines. First, is the matter of accuracy—the chance of random errors in desk computations is very great and these errors are difficult to detect. Secondly, the high speed computers carry out iterative and cyclic procedures quickly and easily. This is important since most methods for numerical integration of differential equations involve iteration. It is doubly important since the best procedures for solving the flame equations as developed by Klein start with an approximate solution which gets progressively improved by carrying out an iterative cycle.[4]

The flame velocity for the $A \rightarrow B$ example is proportional to the square root of the reaction rate constant at the flame temperature. This result shows up very clearly in any one of the excellent approximations[5] which have been made to the structure of the $A \rightarrow B$ flame. Indeed, this dependence of the flame velocity on the square root of the high temperature reaction rate (for the principal reaction) is common to most flames.

Even in the $A \rightarrow B$ flames, diffusion plays an important role. The flame velocity decreases with increased diffusion. Thus, the flame velosity for a reasonable amount of diffusion (Lewis number$=1$) is about one-half what it would be for no diffusion. However, diffusion leads to a very big difference between x_A, the mole fraction of A, and G_A, the fraction of the mass rate of flow contributed by molecules of A. The value of x_A varies almost linearly with the temperature. However, G_A remains almost constant until the chemical reaction rate becomes large. Thus, the flame thickness based on x_A is much larger than flame thickness based on G_A. Experimentally, it is the chemical composition, rather than the mass fluxes, which is easy to determine.

We followed the hypothetical $A \rightarrow B$ flame with a treatment of a flame produced by the bimolecular dissociation of nitric oxide $2NO \rightarrow N_2 + O_2$. In this reaction only a very small amount of energy is released and our experimental colleagues were unable to produce such a flame. A few years later, Wolfhard succeeded in making a nitric oxide flame at very low pressures. However, for better or for worse, we have never discovered the accuracy of our theoretical predictions.

Flushed with the ease of solving the flame equations for systems involving one step of chemical reaction, we proceeded to consider practical flames which involved two or more chemical reactions. It did not take very long to discover that such flame systems are orders of magnitude more difficult to solve. However, in many cases, including chain-branching reactions such as the hydrogen-oxygen flame, a good first approximation to the properties of the flame are obtained[6] by assuming that all of the free radicals are in "pseudo-stationary" equilibrium with the reactants (and the number flux of the free radicals is zero). This has the effect of reducing the chemical kinetics to that of a one-step reaction. The resulting flame equations are then easy to integrate. However, a somewhat better approximation is obtained if we recognize that the "pseudo-stationary" concentration of the free radicals in the flame is not the same as for a static system. Thus, in a flame the equilibrium concentration of a free radical B is given by the solution to the equation

$$K_B = (M/nm_b)\, d(B)/dz - D\, d^2(B)/dz^2$$

Here K_B is the net rate of production of B by the chemical kinetics at the temperature in question, (M/nm_b) is the mass rate of flow of the flame gases divided by the density of the B, the D is the effective coefficient of diffusion of B, and z is the distance from the flameholder. The effect of the mass flow is to shift the maximum in the free radical concentration away from the flameholder toward the higher temperatures. The effect of the diffusion is to decrease the maximum concentration of the free radical and at the same time increase the concentration of the free radicals at the very low and again at the very high temperatures. Thus, the back diffusion of free radicals only occurs at very low temperatures. Such arguments tend to dispel the Tanford–Pease[7] purely diffusional theory of flame propagation. It was easy to develop the theory of flames involving chain reactions assuming such pseudo-stationary concentrations of the free radicals.

Depending on the values of the reaction rate constants there may be more than one pseudo–one-step chemical reaction which approximates the behavior of a multiple reaction flame system. For example, consider the case of a flame with the hypothetical chemical kinetics[8] corresponding to

$$A \underset{k_r}{\overset{k_f}{\rightleftharpoons}} B \xrightarrow{wk_f} C$$

Here A is the reactant species, B is the free radical, and C is the product. If $w \ll k_r/k_f$, then B is in "pseudo-stationary" equilibrium with A and the effective one-step reaction is $A \rightarrow C$. However, if $w \gg k_r/k_f$, then almost every time that a molecule of B is formed, it reacts to form C. The effective one-step reaction for this second case is $A \rightarrow B$. The surprising result of carrying out accurate numerical calculations for this flame system was that there is only a small range of parameters, around $w = k_r/k_f$, for which neither the first nor the second model provides a good approximation. Thus, in a complicated flame system, it may be useful to use a bit of ingenuity in selecting an appropriate idealized one-step chemical reaction to represent the kinetics.

In those rare cases where neither the chemical reactions can be idealized by an effective one-step reaction nor where the concentration of the free radicals is "pseudo-stationary," we must deal with the full sequence of flame equations. This leads to a number of mathematical difficulties. First, we see that the hot boundary conditions do not uniquely specify the flame solution for systems involving more than one chemical reaction even when we assume a value for the flame velocity. Second, for those flames where the "pseudo-stationary" approximation is not valid, we cannot linearize the flame equations in the vicinity of the hot boundary and start a point-to-point integration towards the cold boundary. And third, the equations of continuity for the free radicals are extraordinarily difficult to integrate.

The equation for the kinetics of formation and destruction of a free radical has a slowly varying principal solution and very rapidly varying transient solutions.[9] Equations of this type are called "stiff" because this behavior was first noted in connection with servomechanisms having a tight coupling between the driving and the driven member. The "pseudo-stationary" concentration of a free radical is, as we shall see, a first approximation to the principal solution. For example, let us consider tht formation of the hypothetical free radical B from the plentiful stable molecules A by the unimolecular reaction

$$A \underset{k_r}{\overset{k_f}{\rightleftharpoons}} B.$$

Thus,

$$d(B)/dt = k_f(A) - k_r(B). \qquad (1)$$

Letting $(B)_{eq} = k_f(A)/k_r$ and $y = (B)/(B)_{eq}$, the kinetics equation becomes

$$dy/dt = k_r(1 - y). \qquad (2)$$

Of course this equation has the solution

$$y = 1 + c \exp(-k_r t), \qquad (3)$$

where c is an arbitrary constant. However, since k_r is very large, Eq. (2) is extraordinarily difficult to integrate by the usual numerical point-to-point procedures. Integrating in one direction, the smallest rounding errors will throw one on to the transient solution; integrating in the opposite direction, one obtains hash as the result of over-stability. Such "stiff" equations are best integrated by an iterative procedure in which the differential equation is treated like an algebraic equation. Here the "pseudo-stationary" concentration serves as the first approximation. The nth approximation for y is then obtained by solving the kinetics equation in which the time derivative is taken of the $(n-1)$st approximation. This procedure is only asymptotically convergent. For "stiff" equations, this procedure converges to the principal solution (to the required precision). If the equation is not "stiff," this procedure usually does not lead to a solution. In practice, there are all degrees of "stiffness" and a particular equation may be "stiff" for only a limited range of the variables. Thus,

in integrating the flame equations we frequently obtained reasonable solutions for a considerable temperature range, then all of a sudden the solutions would go wild. In most cases this type of behavior was traceable to one or more of the equations becoming "stiff." In general, the forward extrapolation formulas behave best with respect to "stiffness" and they behave better the larger the integration interval

Klein[4] has developed a good iterative procedure for determining the structure of a complex flame system, given a good approximate solution. One type of approximate solution corresponds to assuming that the enthalpy remains constant throughout the flame and the free radicals have pseudostationary state concentrations.[10] With these assumptions, the flame equations are reduced to the equations corresponding to a single step of chemical reactions and can be solved. This solution can then be used as a starting point for the Klein iterative procedure. The assumption of constant enthalpy corresponds to assuming that all of the binary diffusion coefficients are equal to each other and equal to the ratio of the coefficient of thermal conductivity to the specific heat per unit volume of the flame gases.[11] In the $A \longrightarrow B$ flame, the enthalpy remains constant through the flame if the Lewis number is unity, a very reasonable value. In complex flames, the assumption of equal diffusion constants is generally unrealistic and the assumption of constant enthalpy is not very good.

The hydrogen-bromine flame is the most perplexing problem which we tackled. This involves the simultaneous chemical reactions:

$$X + Br_2 \rightleftarrows 2Br + X$$

$$Br + H_2 \rightleftarrows HBr + H$$

$$H + Br_2 \rightleftarrows HBr + Br$$

$$X + 2H \rightleftarrows H_2 + X$$

$$X + H + Br \rightleftarrows HBr + X$$

All of the reaction rate constants, thermodynamic properties, and transport coefficients for this system are either known or can be estimated fairly accurately. The hydrogen-bromine flame has been studied extensively in various laboratories. Thus, this should be an excellent problem. However, the solutions are complicated by the fact that at low temperatures the bromine atoms behave like free radicals, whereas at high temperatures it is the bromine molecules which have this property. Gradually, over a period of many years, the theoretical solution was approximated. I am sure that the hydrogen-bromine flame problem could be solved rather easily with today's giant computing machines using Klein's iterative procedure together with some of the improved techniques for numerical integrations.

The flame problems of the future will undoubtedly be much more complicated and realistic than any which have been tackled to date. Already Spalding and Weeks are trying to integrate time-dependent flame equations. Others are considering the propagation of spherical flames. And still others are considering the propagation of flames with complex three-dimensional geometry. Clearly, these are problems for the aerodynamicists and the applied mathematicians. With the help of clever numerical methods and giant computing machines, they will succeed in using mathematical flame experimentation to optimize fuels and combustion chambers. They will also succeed in predicting the optimum procedures for producing costly chemicals as a by-product of partial combustion or quenched flames. The theory of flames has passed into a new and much more practical phase.

Acknowledgments

For the past fifteen years Charles F. Curtiss and I have been working together as partners. In addition, the following people have been associated with our University of Wisconsin Naval Research (now Theoretical Chemistry) Laboratory and have made major contributions to our understanding of flame propagation (present occupations are given): R. Byron Bird, Prof. Chemical Engineering, Univ. Wis.; Ellen L. Spotz, Housewife, Philadelphia; H. Lowell Olson, Physicist, Appl. Phys. Lab.; J. W. Anderson, Chemical Engineer, Monsanto; Alfred Ingersoll, Dean, Engineering, Univ. So. Calif.; R. S. Fein, Chemical Engineer, Texas Oil; Ivan Weeks, Physicist, Livermore; Ray Friedman, Chemical Engineer, Atlantic Research; Edward N. Adams, Asst. Research Director, I.B.M.; John L. Magee, Prof. Chemistry, Notre Dame; Mary J. Henkel, Housewife, Los Alamos; Dorothy E. Campbell, Housewife, Dayton; Edwin S. Campbell, Prof. Chemistry, New York U.; Gerard Klein, Mathematician, Exeter, England; Thomas F. Schatzki, Chemist, Shell Development; J. Calvin Giddings, Prof. Chemistry, Univ. Utah; Alan McCone, Jr., Naval Lieutenant, Indianhead; and Agnessa Babloyantz, Chemist, University of Brussels. To these and many others, I am grateful.

This work was carried out at the University of Wisconsin Theoretical Chemistry Institute under Contract NOrd 15884 with the Naval Bureau Ordnance.

References

1. Hirschfelder, J. O. and Curtiss, C. F.: *Advances in Chemical Physics*, edited by

I. Prigogine. Vol. III, p. 59. Interscience Press, 1961.
2. Chapman, S. and Cowling, T. G.: *The Mathematical Theory of Non-Uniform Gases.* Cambridge University Press, 1939.
3. Hirschfelder, J. O. and Curtiss, C. F.: J. Chem. Phys. *17*, 1076 (1949); Hirschfelder, J. O., Curtiss, C. F., Hummel, H., Adams, E., II, Henkel, M. J., and Spaulding, W.: *Third Symposium on Combustion, Flame, and Explosion Phenomena*, pages 121, 127, and 135. Williams and Wilkins, 1949.
4. Klein, G.: Phil. Trans. Roy. Soc. (London) Ser. A, *249*, 389 (1957); see also Univ. of Wisconsin Naval Research Lab. Reports Squid–1 and 2 (1955).
5. Hirschfelder, J. O.: Phys. Fluids *2*, 565 (1959).
6. Giddings, J. C. and Hirschfelder, J. O.: J. Phys. Chem. *61*, 738 (1957); and *Sixth Symposium (International) on Combustion*, p. 199. Reinhold, 1957.
7. Tanford, B. C. and Pease, R. N.: J. Chem. Phys. *15*, 861 (1947).
8. Curtiss, C. F., Hirschfelder, J. O., and Taylor, M. H.: Phys. Fluids *4*, 771 (1961).
9. Hirschfelder, J. O.: J. Chem. Phys. *26*, 271 (1957).
10. Hirschfelder, J. O.: *First Iowa Thermodynamics Symposium* (April, 1953). Subsequently, Karman, T. von and Penner, S. S.: *AGARD Selected Combustion Problems*, p. 5. Butterworths, 1954.
11. Hirschfelder, J. O.: Phys. Fluids *3*, 109 (1960).

RADICAL CONCENTRATIONS AND REACTIONS IN A METHANE-OXYGEN FLAME

R. M. FRISTROM

A complete set of characteristic profiles is presented for a spherical methane–oxygen flame [$(CH_4) = 0.078$; $(O_2) = 0.92$; $P = 0.05$ atm]. The intensive properties which are presented as a function of radial distance include measured temperature, derived velocity, measured compositions of all of the stable species and measured and derived concentrations of the major free radical species.

The new type of information presented is the radical concentrations. Oxygen atoms were measured by a combination of microprobe sampling and chemical scavenging. Hydrogen atom concentrations were derived from the observed rate of oxygen reaction and confirmed by a preliminary scavenger sampling study. Hydroxyl radical concentrations were derived from the measured rate of carbon dioxide appearance and confirmed by direct measurement using the UV absorption. An upper limit has been set for methyl radical concentrations.

These data have been used to test various proposed mechanisms in this flame. Two alternative mechanisms are suggested. For the reaction $OH + CH_4 \rightarrow H_2O + CH_3$ the data suggests an activation energy of 6.5 kilocalories/mole and a frequency factor of 1.4×10^{-14} cc/moles/sec.

Introduction

Residence times in laboratory hydrocarbon–oxygen flames are short. The reactions involved are very fast and most of them appear to involve either atoms or free radicals.

The methane–oxygen flame, which is the simplest of the hydrocarbon series, involves some fifteen species for which over a hundred reactions can be written.* It is easy to reduce this number to perhaps fifty reactions which require serious consideration. Since the reactions are coupled, only certain combinations are mutually consistent. The observed concentrations of the intermediate species, particularly radicals, provide clues as to the dominant reactions. Specific mechanisms have been proposed for this flame by a number of authors.[1–3] The present work is an extension of the study by Westenberg and Fristrom,[2] using the new information presented here and recent work reported by Fenimore and Jones.[3]

* This estimate is the combination of fifteen species taken one or two at a time. It assumes that a pair of molecules can react in only one way and that under given conditions either the termolecular reactions or the equivalent bimolecular reaction will be dominant. This argument is valid for a given set of conditions, but if extremely wide conditions were considered the number would have to be increased to include the possibility of more than one product for a given reaction pair.

The appropriateness of a reaction can be tested by seeing if the observed concentrations and net species production rates give self-consistent kinetic constants. These constants can be compared with literature values from other types of chemical kinetic studies. This ideal can not always be realized because of the interference of competing reactions or reverse reactions, or because one of the species concentrations (usually a free radical) has not been measured. In the latter case, progress can be made if two reactions can be found which involve the missing species. The rates of these two competing reactions can be compared and kinetic constants can be derived for one reaction provided values are known for the other. In other cases one can take a known or assumed kinetic constant and derive a radical concentration profile necessary to give the observed reaction rate. The resulting profile can be tested for reasonableness and this technique can often be used to eliminate a reaction.

Experimental

A premixed spherical methane–oxygen flame [$(CH_4) = 0.078$, $(O_2) = 0.92$, $P = 0.05$ atm, $m_0 = 0.11$ g/sec] was used in this study. The apparatus is shown in Fig. 1. The materials were c.p. tank gases which were checked by analysis.

Characteristic Profiles

A one-dimensional flame can be described by a set of characteristic profiles giving temperature,

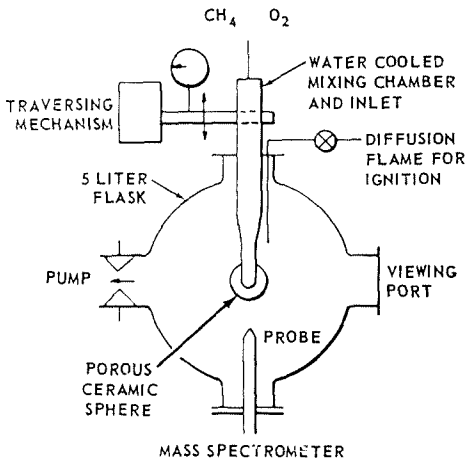

(a) Schematic diagram of spherical flame burner and associated equipment.

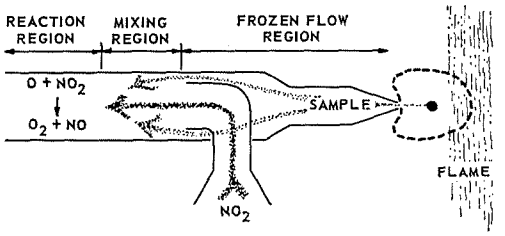

(b) Schematic diagram of scavenger probe.

FIG. 1. Apparatus.

gas velocity, and composition, as a function of distance (Fig. 2). Temperatures were measured with small silica coated Pt/Pt–10% Rh thermocouples. Compositions were derived by microprobe sampling followed by mass spectral analysis[4–6]; and velocities were calculated from the known mass flow, temperature, composition and radial position using Eq. (1).

$$v = 6.53(m_0 T/\bar{M} r^2) \qquad (1)$$

Here m_0 is the mass flow (g/sec); v the velocity (cm/sec); r the radial distance (cm); T the temperature (°K); M the molecular weight (g/mole). The subscript zero refers to inlet gas conditions. The superscript bar indicates an average.

Oxygen atom concentrations were measured by the scavenger sampling technique.[7] This method consists of microprobe sampling followed by rapid mixing of the sampled gases with a species which reacts quantitatively with the radical under study to give an analyzable product (Fig. 1b). It has been demonstrated that the reaction $NO_2 + O \rightarrow O_2 + NO$ gives a quantitative measure of oxygen atom concentration.[10] The technique is interfered with by H and OH which also can react with NO_2[8] so that the quantity actually measured is $[O + 1\frac{1}{2}H + \frac{1}{2}OH]$. In the primary reaction region these corrections can be made. In the recombination region the relation between the radical species can sometimes be estimated from equilibrium information,[9] so that the concentrations of all three radical species can

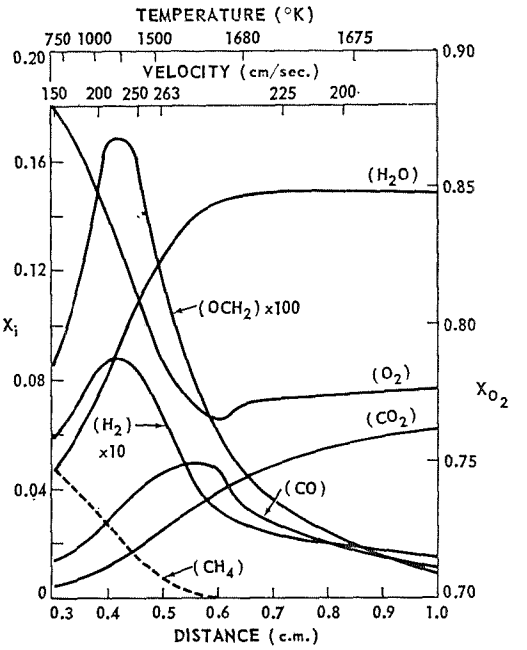

(a) Stable species (mole fraction versus distance from sphere surface, temperature, and velocity).

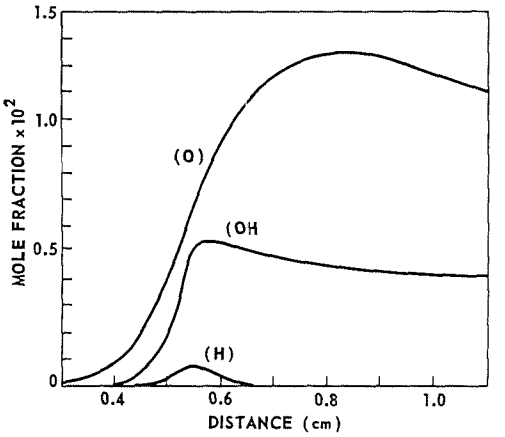

(b) Radical species (mole fraction versus distance).

FIG. 2. Characteristic profiles of a spherical flame; $(CH_4) = 0.078$; $(O_2) = 0.92$; $P = 0.05$ atm.

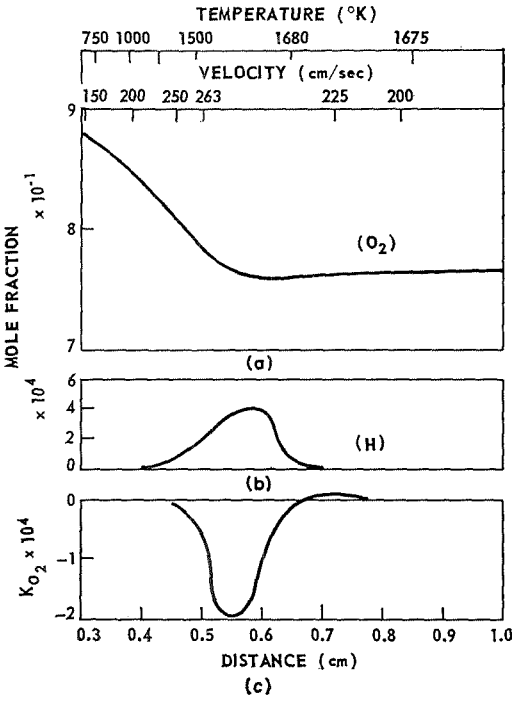

FIG. 3. Reaction of hydrogen atom with oxygen.

(a) O_2 concentration versus distance.
(b) H atom concentration versus distance [derived from Eq. (2)].
(c) Rates of oxygen consumption versus distance.

be inferred from the single measurement. Unfortunately, this latter simplification is not applicable to this flame.

Hydrogen atom concentration was measured directly using the scavenger reaction, $H + CCl_4 \rightarrow HCl + CCl_3$. The reaction was not quantitative under the conditions used[7,10]; however, they set a lower limit for maximum hydrogen atom concentration at 10^{-4} mole fraction. The estimate of hydrogen atom concentration given in Fig. 3 was obtained from Eq. (2) which assumes that all of the observed reaction of oxygen molecules is with hydrogen atoms.

$$(H) = \frac{-K_{O_2}}{N^2(O_2)k_{H-O_2}} \qquad (2)$$

where:

- () brackets indicate species concentration (mole fraction);
- N is the molar density (moles/cc);
- k_{ij} the rate constant for species i with species j (cc/moles/sec);
- K_i the observed rate of reaction of species i (mole/sec/cc);

Subscripts i, j, are species indices.

Hydroxyl radical concentrations were estimated from the rate of carbon dioxide formation (reaction 12, Table 1) using Eq. (3).[2]

$$(OH) = \frac{K_{CO_2}}{(CO)Nk_{OH-CO}} \qquad (3)$$

It is believed that the most probable mode of methyl radical disappearance in the sampling probe is by reaction with oxygen to form formaldehyde. This would mean that methyl radical concentration cannot exceed the observed formaldehyde concentration of 10^{-3} mole fraction. The absence of ethane in the sampled gases also argues for a low methyl radical concentration since the recombination of methyl radicals to form ethane is a very rapid reaction occurring on almost every collision around room temperature.[11]

The radical concentration profiles are presented in Fig. 2b.

Data Analysis

To facilitate analysis the temperature and composition data were reduced to equal distance increments using a least squares, second order, five point, running smoothing routine. Smoothed data points and first derivatives were tabulated at intervals of 0.02 cm. From these data rates of species production were calculated using Eq. (4). The smoothed data, calculated rates, and the standard deviation of the experimental data from the smoothed points are collected in Table 2. This method of analysis has been discussed in the literature.[2,4,12–14]

$$K_i = (m_0/4\pi r^2)\,dG/dr,$$
$$G = (M_i/\bar{M})(i)\left[1 - \frac{D}{v(i)}\frac{d(i)}{dr}\right] \qquad (4)$$

where G is fractional mass flux (dimensionless), and D is effective diffusion coefficient (cm^2/sec).

Discussion

The purpose of this study is to determine which elementary reactions are important in this flame and, if possible, to use the data to derive kinetic constants for the reactions. A number of the reactions seem well established and can be quantitatively accounted for. However, the picture is not completely clear and several apparently self-consistent interpretations might be made. For simplicity, this discussion will be restricted to reactions which can be considered irreversible. The other extreme where forward and reverse reactions are in equilibrium occurs in the radical recombination region and is a factor in rich flames.[3] The intermediate case where the back reaction is appreciable, but an equilibrium

TABLE 1

Reactions in the Methane–Oxygen Flame

Reaction	A_f (cc/moles/sec $\times 10^{14}$)	E_f (kcal/mole)	A_r (cc/moles/sec $\times 10^{14}$)	E_r (kcal/mole)	References
(1) $H + O_2 \rightleftarrows OH + O$	6	18	0.17	1.4	15, 19
(2) $H + CH_4 \rightleftarrows H_2 + CH_3$	2.5	11.5	—	10	1, p. 527; 3
(3) $OH + CH_4 \rightleftarrows H_2O + CH_3$	1.4	6.5	—	—	This work, 2, 3, 16
(4) $O + CH_4 \rightleftarrows OH + CH_3$	$<10^{-1}$	[8]	—	—	1, p. 601; 2, 3
(5) $O + CH_3 \rightleftarrows H + CH_2O$	~1	~0	—	—	1, 20
(6) $O_2 + CH_3 \rightleftarrows OH + CH_2O$	1	[1.5]	—	—	1, p. 612; 2
(7) $OH + CH_2O \rightleftarrows H_2O + HCO$	[3.5]	[1.5]	—	—	1, p. 594
(8) $O + CH_2O \rightleftarrows OH + HCO$	[1]	[<8]	—	—	This work, 1, p. 599
(9) $HCO \rightleftarrows H + CO$	[1]	26	—	—	1, p. 594
(10) $HCO + H \rightleftarrows H_2 + CO$	—	[5]	—	—	1, p. 594
(11) $HCO + OH \rightleftarrows H_2O + CO$	—	~0	—	—	2
(12) $CO + OH \rightleftarrows H + CO_2$	0.1	10	13	33	2, 16
(13) $H + H_2O \rightleftarrows OH + H_2$	10	25	2.5	10	18, 19, 21
(14) $O + O + M \rightleftarrows O_2 + M^*$	$\sim 10^{15}$ (cc^2/mole^2/sec)		$6 \times 10^{13}(117{,}000/RT)$	117	18, 22
(15) $O + NO + M \rightleftarrows NO_2 + M^*$	2×10^{16} [cc^2/mole^2/sec. (300°K)]				18
(16) $O + NO_2 \rightleftarrows O_2 + NO$	$>10^{12}$	~0	—		18
(17) $H + H + M \rightleftarrows H_2 + M^*$	2×10^{15} (cc^2/mole^2/sec. at 2000°K)				9

TABLE 2

Compositions and Net Rates of Species Production in the Spherical Flame

$[CH_4] = 0.078$; $[O_2] = 0.92$; $P = 0.05$ atm.

			Compositions[a] (mole fractions)								
r	T_0	v	$[CO_2]$	$[OCH_2]$	$[CO]$	$[H_2O]$	$[CH_4]$	$[H_2]$	$[NO]$	$[O_2]$	$[O]$
1.40	372	93	0.0019	0.0004	0.0061	0.0271	0.0647	0.0001	0	0.8948	0
1.50	665	145	0.0044	0.0008	0.0129	0.0465	0.0480	0.0052	—	0.8799	0.0001
1.60	1090	210	0.0113	0.0016	0.0278	0.0820	0.0266	0.0091	—	0.8397	0.0007
1.70	1540	263	0.0250	0.0012	0.0461	0.1275	0.0066	0.0066	0.0000	0.7852	0.0054
1.80	1666	253	0.0385	0.0006	0.0475	0.1476	0.0005	0.0032	0.0002	0.7578	0.0122
1.90	1680	230	0.0476	0.0003	0.0268	0.1478	0.0000	0.0023	0.0003	0.7624	0.0140
2.00	1679	207	0.0541	0.0002	0.0202	0.1478	—	0.0019	0.0004	0.7633	0.0147
2.10	1670	186	0.0586	0.0001	0.0146	0.1479	—	0.0016	—	0.7647	0.0145
2.20	1655	168	0.0620	0.00009	0.0108	0.1480	—	0.0014	—	0.7658	0.0137
2.40	1618	138	0.0659	0.00002	0.0064	0.1482	—	0.0011	—	0.7678	0.0119
2.60	1582	115	0.0677	0	0.0040	0.1486	—	0.0009	—	0.7695	0.0103
2.80	1557	98	0.0686	—	0.0026	0.1490	—	0.0007	—	0.7707	0.0089
3.00	1518	83	0.0691	—	0.0018	0.1494	—	0.0006	—	0.7717	0.0077
3.20	1485	71	0.0694	—	0.0013	0.1497	—	0.0005	—	0.7726	0.0065
3.70	1409	50	0.0698	—	0.0007	0.1505	—	0.0002	—	0.7743	0.0038
4.20	1335	37	0.0700	—	0.0002	0.1515	—	0	0.0004	0.7750	0.0020
		σ^b	0.01	0.13	0.05	0.04	0.05	0.26	—	0.009	0.05

Rates (moles/cc/sec)

r	T_0	v	K_{CO_2}	K_{OCH_2}	K_{CO}	K_{H_2O}	K_{CH_4}	K_{H_2}	K_{O_2}	K_O
			(10^{-5})	(10^{-6})	(10^{-5})	(10^{-5})	(10^{-5})	(10^{-5})	(10^{-6})	(10^{-5})
1.40	372	93	−0.041	−0.224	0.57	−0.40	−0.89	−0.138	1.84	−0.0059
1.50	665	145	−0.27	+0.10	−0.97	−2.59	+0.21	−1.08	27.47	−0.0618
1.60	1090	210	−1.12	2.81	−0.35	−3.72	0.41	4.96	55.56	−1.426
1.70	1540	263	+0.72	−0.15	4.01	10.8	−6.17	−0.045	−55.9	−0.303
1.80	1666	253	1.98	−1.01	6.45	5.42	−1.83	−2.89	−107.8	2.859
1.90	1680	230	1.08	−0.33	−4.19	1.13	−0.031	−0.43	9.56	0.457
2.00	1679	207	0.75	−0.13	−1.22	−0.12	−0.013	−0.097	−2.30	0.398
2.10	1670	186	0.50	−0.098	−0.73	+0.002	−0.006	−0.055	−1.71	0.192
2.20	1655	168	0.36	−0.071	−0.44	−0.0010	0	−0.041	−0.81	0.0310
2.40	1618	138	0.15	−0.003	−0.19	−0.0039	—	−0.0248	−1.29	0.0362
2.60	1582	115	0.070	0	−0.094	−0.0059	—	−0.0099	0.23	0.0379
2.80	1557	98	0.030	—	−0.047	−0.0015	—	−0.0079	0.12	0.0199
3.00	1518	83	0.014	—	−0.029	−0.0026	—	−0.0060	0.074	0.0128
3.20	1485	71	0.005	—	−0.012	−0.0019	—	−0.0055	0.110	0.0099
3.70	1409	50	0.002	—	−0.003	−0.0010	—	−0.0051	0.166	0.0151
4.20	1335	37	0.0010	0	−0.000	+0.0004	0	0	0.118	0.324

[a] Values obtained using running 5 point quadratic smoothing.

[b] Standard deviation $\sigma = \left[1/N \sum \left(\frac{[\text{Exp}] - [\text{Smooth}]}{[\text{Smooth}]}\right)^2\right]^{\frac{1}{2}}$ where N is number of observations, [Exp] is experimental value, [Smooth] is rate computed by smoothing routine.

TABLE 3

Self-Consistent Reaction Mechanisms

Mechanism 1

$$3O_2 + 3H \rightarrow 3OH + 3O$$
$$CH_4 + OH \rightarrow H_2O + CH_3$$
$$CH_3 + O \rightarrow OCH_2 + H$$
$$OCH_2 + OH \rightarrow H_2O + HCO$$
$$HCO \rightarrow CO + H$$
$$CO + OH \rightarrow CO_2 + H$$
$$O + O + M \rightarrow O_2 + M^*$$
$$\overline{CH_4 + 2O_2 \rightarrow 2H_2O + CO_2}$$

Mechanism 2

$$2O_2 + 2H \rightarrow 2OH + 2O$$
$$CH_4 + OH \rightarrow H_2O + CH_3$$
$$O_2 + CH_3 \rightarrow OCH_2 + OH$$
$$OCH_2 + O \rightarrow HCO + OH$$
$$HCO \rightarrow H + CO$$
$$CO + OH \rightarrow CO_2 + H$$
$$2OH \rightarrow H_2O + O$$
$$2O + M \rightarrow O_2 + M^*$$
$$\overline{CH_4 + 2O_2 \rightarrow 2H_2O + CO_2}$$

has not been reached, is usually restricted to a region just ahead of the final equilibrium zone.

The number of possible schemes is limited because not all combinations of reactions are compatible and a preliminary selection can be made by dividing the flame into several parts each of whose inlet and outlet fluxes are determined experimentally and must be satisfied. This means that there must be a reaction to account for every new species which flows out of the region (CO, CO_2, H_2O) and both forming and consuming reactions must be presented for species which appear transiently or go through a maximum (CH_3, OCH_2, H_2, H, O, OH, OCH_2).

A useful reaction scheme will account for a large part (hopefully better than 90%) of the reaction. Conservation considerations dictate that the integrated forward reaction rate for each of the individual steps must be equal to each other and the input flux of the initial species. Writing a dominant reaction scheme is based upon the reasoning that the probability of any two competing reactions having comparable rates is low. This is a reasonable assumption; although, as the number of steps required increases, the probability of accidental degeneracy of rates increases. Two self-consistent schemes are suggested in Table 3. These are probably not the only possibilities.

Hydrogen Atoms

The maximum concentration of H atoms is in excess of 10^{-4} mole fraction and lies just outside the primary reaction zone (luminous region). Hydrogen atom concentration was estimated using the assumption that oxygen disappears by reaction with hydrogen atoms. This might be high by a factor of two if methyl radicals also react with molecular oxygen.

The principle sources of H atoms in this flame are the reactions $CH_3 + O \rightarrow H + OCH_2$, $HCO \rightarrow H + CO$, and $CO + OH \rightarrow CO_2 + H$. Its principal mode of disappearance is reaction with oxygen. The reaction, $H + CH_4 \rightarrow H_2 + CH_3$, is minor in this flame but becomes more important as oxygen concentration is decreased and finally becomes dominant in rich flames. Hydrogen atoms also react with methyl radicals, formaldehyde, and carbon monoxide.

Oxygen Atoms

Oxygen atoms appear to be the most abundant radical in this flame; $[O]_{max} = 0.015$ (Fig. 4). This is a very reactive species and reactions have been reported with most of the reducing species. However, they seem to be generally less reactive than OH radicals, probably because the reactions are less exothermic and possess low steric factors. The negative flux of oxygen atoms (G_0) observed in the early part of this flame is due to the reaction of atoms which were not locally produced

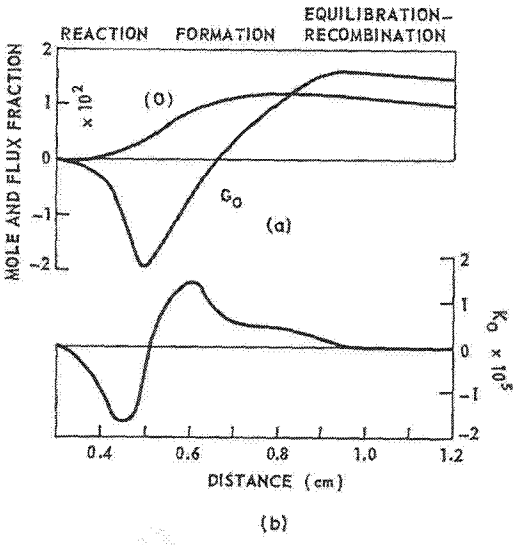

FIG. 4. Reaction of oxygen atoms.

(a) Mole fraction and flux fraction.
(b) Reaction (moles/cm³/sec).

but rather diffused from the higher temperature regions of the flame. This interesting phenomena points out one of the crucial differences between flames and homogeneous reactions. This behavior cannot be attributed to a surface reaction because a platinum thermocouple located on the flame holder shows no abnormal temperature rise. The reactant species is probably either methyl radical, formaldehyde or both. Reactions with methane, hydrogen, and carbon monoxide are negligible.

$O + OCH_2 \rightarrow OH + HCO$. The reactions of formaldehyde are a problem in this flame. Formaldehyde has been reported to undergo rapid reactions with most of the radicals present in the methane flame[1] and in addition there is a question whether part of the observed formaldehyde may be due to methyl radical combining with oxygen in the probe after sampling. The best present guess is that an appreciable part of the observed formaldehyde ahead of station 0.65 is methyl radical (see Table 4), but that beyond this point the major part of the observed formaldehyde is real. If this interpretation is correct it appears likely that the reaction of formaldehyde is primarily with oxygen atoms and it is possible to assign a rate constant. Contribution from the reaction $OH + OCH_2 \rightarrow H_2O + HCO$ cannot be excluded, but it definitely is not the dominant reaction since kinetic constants calculated using this assumption and OH concentrations estimated from the CO reaction showed wide variation.

$O + H_2 \rightarrow OH + O$ *and* $O + H_2O \rightarrow 2OH$. These reactions are too slow to be important in the primary reaction region. They are discussed in the section on recombination region.

TABLE 4

Rate Constant for Possible Reaction
$O + OCH_2 \rightarrow OH + HCO$

r (cm)[a]	T (°K)	$k(T) = \frac{K_{OCH_2}}{[CH_2O]\,[O]}$
1.6	1090	—
1.7	1540	(9.5)[b]
1.8	1666	(1.7)[b]
1.9	1680	0.129
2.0	1679	0.115
2.1	1670	0.077
2.2	1655	0.057

[a] Radial distance (cm).
[b] Region where part of CH_2O may be (CH_3).

Hydroxyl Radical

The OH radical is important in the methane flame; $[(OH)_{max} \sim 5 \times 10^{-3}]$, and can react with most of the reducing components in the flame (CH_4, CH_3, OCH_2, HCO, H_2, and CO). Its principal source is the reaction $H + O_2 \rightarrow OH + O$ with possible contributions from $O + OCH_2 \rightarrow OH + HCO$, and $O_2 + CH_3 \rightarrow OH + OCH_2$. It seems to be well established that in this flame the principle route of methane and carbon monoxide attack is by hydroxyl radical. It can also react with methyl radical, formaldehyde or HCO, but the present evidence favors the other reactions.

$OH + CO \rightarrow CO_2 + H$. The rate constant has been investigated by several authors[2,15,16] and there appears to be general agreement on the rate in the region of 1500–2000°K, although the separation of the rate between steric factor and activation energy is in doubt and estimates of activation energy vary by several kilocalories. This uncertainty is not important for present purposes. This is a fortunate situation because it offers a method of estimating OH radical concentration.

These calculated concentrations can be compared with experimental values determined by spectroscopic absorption on a flat flame of the same composition, pressure, and maximum temperature.* (See Table 5, Fig. 5.)

$OH + CH_4 \rightarrow H_2O + CH_3$. This is the dominant initial reaction in this flame (along with the hydrogen atom attack of oxygen). Reactions of CH_4 with H and O are not important. Since the present data covers a lower temperature range than previous studies of this laboratory,[2,12–14] it seems possible to combine these data to derive the activation energy and frequency factor (Fig. 5c). This estimate of the kinetic constant is essentially a comparison of the net rates of CO_2 and CH_4 assuming that they react with the same species, (OH).

$$k_{CH_4-OH} = \frac{-K_{CH_4}(CO)}{K_{CO_2}(CH_4)\,k_{CO-OH}} \qquad (5)$$

The results are in good agreement in absolute rate among themselves and with a recently reported study on flames with lower oxygen concentration.[3] The choice of activation energy differs from that of reference 3 and reference 16, but the difference is within the combined limits of error. The present value may be more reliable because more data is available. A least squares

* The author would like to thank Dr. H. Gg. Wagner of the Institut für Physikalische Chemie of the University of Göttingen, Germany, for this information and permission to publish it here.

TABLE 5

Maximum Radical Concentrations in Some Lean Methane–Oxygen Flames
$(CH_4) = 0.078$; $(O_2) = 0.92$

	[H]			[O]	[OH]		[CH_3]
	Calc.[a]	Calc.[b]	Exp.[c]	Exp[d]	Calc.[e]	Exp[f]	Exp[g]
0.05 atm. Flat $T_{max} = 1990°K$	3.5×10^{-4}	3.5×10^{-4}	—	—	1.5×10^{-2}	—	$<10^{-3}$
0.1 atm. Flat $T_{max} = 2000°K$	8×10^{-4}	3×10^{-3}	—	—	1.5×10^{-2}	—	$<10^{-3}$
0.05 atm. Spherical $T_{max} = 1680°K$	—	—	$>10^{-4}$	1.26×10^{-2}	5.5×10^{-3}	$(4.4 \times 10^{-3})^f$	$<10^{-3}$
0.1 atm. Spherical $T_{max} = 2000°K$	—	—	—	1×10^{-2}	—	—	—
0.1 atm. Flat $T_{max} = 1610°K$	—	—	—	—	—	$(3.83 \times 10^{-3})^f$	—

[a] Calculated from the rate of oxygen disappearance (Eq. 2, Table 2).
[b] Calculated for the rate of hydrogen disappearance at point of maximum flux (Eq. 2, Table 2).
[c] Scavanger sampling using reaction $H + CCl_4 \rightarrow HCl + CCl_3$ *Lower limit only.*
[d] Scavanger sampling using reaction $O + NO_2 \rightarrow NO + O_2$ corrected for [H] and [OH].
[e] Calculated from rate of carbon dioxide formation (Eq. 3).
[f] Spectroscopic measurements through courtesy of Dr. H. Gg. Wagner, Institut für Physikalische Chemie, Univ. of Göttingen, Germany.
[g] Upper limit set by formaldehyde concentration.

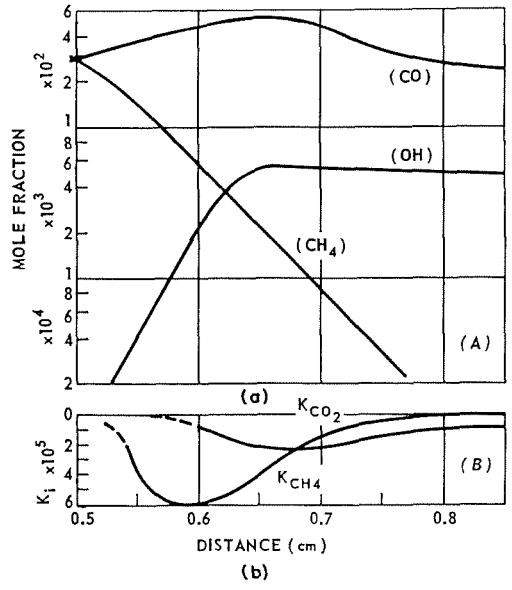

(a) Concentration of CH_4, CO, and OH [derived from Eq. (3)].
(b) Rates of CH_4 disappearance and CO_2 formation (moles/cm³/sec).

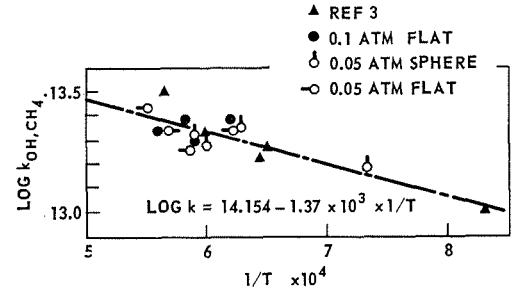

(c) Rate constants (cm³/moles/sec) for the reaction $OH + CH_4 \rightarrow CH_3 + H_2O$ versus $1/T$.

FIG. 5. Reaction of OH radicals.

fit was made of the data. The recommended constants are given in Table 2.

Methyl Radical

Methyl radical is an important intermediate in this flame. In lean flames it is a transient species; though appreciable amounts might be in equilibrium in the burned gases of rich flames. We have no direct experimental values for the concentrations although we suspect that an appreciable part of the observed formaldehyde may be methyl radicals which recombine with oxygen after sampling.

The upper limit for methyl radical concentration is approximately 10^{-3} mole fraction. Two reactions have been suggested to account for methyl radical disappearance in the methane flame.

$CH_3 + O_2 \rightarrow O_2CH_3 \rightarrow OCH_2 + OH$. This reaction was postulated by Westenberg and Fristrom[2] for this flame. It has been reported to be moderately rapid at room temperature[1] and the high concentration of oxygen favors the possibility.

$CH_3 + O \rightarrow OCH_3 \rightarrow H + OCH_2$. This reaction was suggested by Fenimore and Jones,[3] for flames with lower oxygen concentration than the present one. They believe that this reaction is rapid compared with the corresponding oxygen molecule reaction under all concentration conditions. The choice between these two possibilities requires more experimental study, particularly direct measurement of methyl radical concentrations.

The latter reaction is probably dominant in flames where excess molecular oxygen is not present since the concentration in the reaction zones of such flames is tenfold lower than the inlet value due to the effects of diffusion. In oxygen-diluted flames such as the present one, however, the question seems to be open since the argument given by Fenimore and Jones for excluding the molecular oxygen reaction is based on a rate constant which was estimated by assuming the methyl reaction is with oxygen atoms.

The provisional rate constants given in Table 2 are based on the integrated rate and an assumed methyl radical concentration of 10^{-3} M.F. The two values are mutually exclusive since one or the other reaction is likely to be dominant. The estimates do represent upper limits.

Radical Recombination Region

The direct measurement of oxygen atom concentrations has opened up the study of the radical recombination region (Fig. 6). Here the radicals and atoms formed in excess by branching reactions in the primary reaction zone are brought into thermal equilibrium. These reactions must be three-body since recombining radicals liberate sufficient energy for the dissociation of the recombined molecule. Unless it is stabilized by energy loss, the complex will decompose unimolecularly after a few vibrational periods. This period is about 10^{-13} sec for diatomic and simple polyatomic molecules. The usual mode of stabilization is by transfer of kinetic energy to a third molecule which because of the short lifetime of the collision complex must be a three-

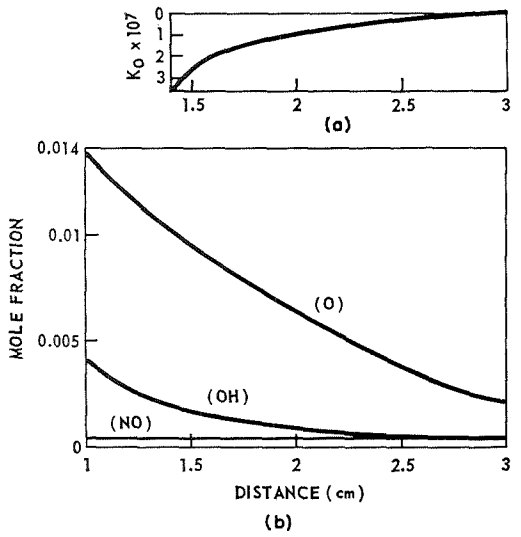

FIG. 6. Radical recombination region.

(a) Disappearance rate (moles/cm³/sec) of oxygen atoms.

(b) O and OH radical concentration versus distance.

body collision. Deactivation by light emission is usually an unimportant process and stabilization by distribution of the energy among many vibrational degrees only plays a role in complex molecules.

Because these reactions require rare three-body collisions they are generally much slower than bimolecular reactions. The ratio of three-body to two-body collisions is 0.001 at atmospheric pressure and falls off proportional to inverse pressure.

This difference in rate should result in a physical separation of the recombination region from the primary region, and indeed this is observed. Spatially separated reaction regions can only interact via transport processes which decrease in importance as spatial separation is increased. It would be expected that in very low pressure flames the two regions might be completely separated in the manner of the Smithells burner double flame.[17]

This spatial extension adds an interesting complication to the spherical flame. It is cooled by heat transfer to the walls of the flask so that it is not adiabatic. The maximum temperature is 300° lower than the adiabatic value and is reached even before the carbon monoxide reaction has been completed. The burning velocity as normally defined is not strongly affected (94 cm/sec for the flat flame at 400°K and 100 cm/sec for the spherical flame at 400°K). However, this is not the proper comparison because of the effects of curvature and the comparison should be made in the primary reaction zone (T = 1675°K). Here the effect is appreciable (spherical flame 164 cm/sec and flat flame 220 cm/sec), and it can be seen that the spherical flame is actually appreciably slower, as would be expected.

Sugden has pointed out that in the recombination region of a flame the three-body reactions are so slow compared with the two-body reactions that two-body reactions which exchange the identity of radicals[9] will maintain a pseudo-equilibrium between the species which is determined by the temperature alone. Thus, if one radical is in excess of thermal equilibrium all radicals are in excess, but their ratio is the same as determined in equilibrium calculations. Only the most rapid recombination reactions will be important since the radicals are readily interconverted. The situation in this flame appears to be more complex than that described by Sugden. In the present case the temperature is falling so rapidly that the initial excess of oxygen atoms (over both thermal equilibrium and the pseudo-equilibrium) over hydroxyl radical is never brought into equilibrium by the exchange reactions (see Table 6). The reaction responsible for oxygen atom disappearance is probably that with water to form OH radicals which are used up by reaction with carbon monoxide. If this interpretation is correct it may be possible to derive the rate of the reaction $O + H_2O \rightarrow 2OH$ but the situation will have to be clarified by direct experimental measurements on OH and H.

The recombination process is probably dominated by oxygen atom reactions since oxygen atom concentration is higher than that of both hydrogen atom and hydroxyl radical. In addition two of the fastest known recombination reactions involve oxygen atoms.†

$O + O + M \rightarrow O_2 + M^*$. This recombination is the fastest reaction in pure hydrocarbon oxygen systems, but the reported rates are too slow to account for the observed rate of oxygen atom disappearance in this flame.

$O + NO + M \rightarrow NO_2 + M^*$; $O + NO_2 \rightarrow NO + O_2$. This pair of reactions is some twenty times faster than the direct recombination reaction at room temperature. If they have the same or a lower temperature dependence the nitric oxide catalyzed recombination of oxygen atoms should be the dominant reaction wherever (NO) > 0.05 (O).

† These conclusions may be modified by the recent studies reported in this volume by Kaufmann and DelGreco which indicate that $2OH \rightarrow H_2O + O$ is a fast reaction.

TABLE 6

Comparison between Experimental Radical Concentrations and Equilibrium Calculations in the Radical Recombination Region, $r > 2$ cm

T (°K)	[H] Calc.	[H] Exptl.	[O] Calc.	[O] Exptl.	[OH] Calc.	[OH] Exptl.
1300	1.3×10^{-9}	—	6.9×10^{-7}	2×10^{-3}	3×10^{-5}	4×10^{-4}
1400	1.3×10^{-8}	—	3.7×10^{-6}	3.7×10^{-3}	8.9×10^{-5}	4.7×10^{-4}
1500	9.7×10^{-8}	—	1.6×10^{-5}	6.5×10^{-3}	2.3×10^{-4}	7×10^{-4}
1600	5.6×10^{-7}	—	5.6×10^{-5}	1.1×10^{-2}	5.3×10^{-4}	2.5×10^{-3}
1680	2.5×10^{-6}	—	1.5×10^{-4}	1.2×10^{-2}	1×10^{-3}	5×10^{-3}

In our flame nitric oxide was 4×10^{-4} mole fraction while O atoms ranged from 10^{-2} to 10^{-4} mole fraction. Thus the direct oxygen atom recombination would be important in the early recombination region while the nitric oxide recombination would be important in the later region. It seems likely that in air flames the nitric oxide catalyzed recombination would always be dominant while in oxygen diluted flames it would depend on the purity of the oxygen used. The characteristic greenish yellow glow which is associated with this reaction[18] has been observed in this and several other oxygen diluted flames. The experimentally observed NO is presumably derived from traces of nitrogen in the tank oxygen.

The importance of nitrogen oxides in oxygen atom recombination may explain some of the discrepancies between the high temperature and low temperature values measured for oxygen atom recombination.[18]

Summary

Although a number of questions still remain, the main outline of the dominant reactions in the methane flame appears to be fairly well established, and the dominant reaction scheme can be narrowed down to a choice between a few self-consistent systems. Further work should allow a choice between these competing possibilities.

Several of the reactions are well enough established so that the flame rate information can be used to determine kinetic constants.

Acknowledgments

The author would like to acknowledge the help of Mr. C. Grunfelder in obtaining these data, and Mr. S. Favin in the reduction of the data. He has had the benefit of a number of helpful discussions with Drs. A. A. Westenberg, W. G. Berl, and W. H. Avery.

This work was supported jointly by the Advanced Research Projects Agency and the U. S. Army Engineering Research and Development Laboratory (Ft. Belvoir) through contract NOw–62–0604–C with the Bureau of Naval Weapons.

References

1. Steacie, E. W. R.: *Atomic and Free Radical Reactions* (two volumes). Reinhold, 1954.
2. Westenberg, A. A. and Fristrom, R. M.: J. Phys. Chem. *65*, 591 (1961).
3. Fenimore, C. P. and Jones, G. W.: J. Phys. Chem. *65*, 2200 (1961).
4. Fristrom, R. M. and Westenberg, A. A.: Combustion and Flame *1*, 217 (1957).
5. Fristrom, R. M., Avery, W. H., and Grunfelder, C.: *Seventh Symposium (International) on Combustion*, p. 304. Butterworths, 1959.
6. Fristrom, R. M., Grunfelder, C., and Favin, S.: J. Phys. Chem. *64*, 1386 (1960).
7. Fristrom, R. M.: Scavenger Probe Sampling (in preparation).
8. Task R Quarterly Report No. 8, The Johns Hopkins University, Applied Physics Laboratory Report TG–331–8, Silver Spring, Md. (April 1961).
9. Bulewicz, E. M., James, C. G., and Sugden, T. M.: Trans. Faraday Soc. *54*, 1855 (1958).
10. Flame Inhibition Research Quarterly Report No. 2, The Johns Hopkins University, Applied Physics Laboratory Report TG–376–2 (May 1961).
11. Gomer, R. and Kistiakowsky, G. B.: J. Chem. Phys. *19*, 85 (1951).
12. Westenberg, A. A. and Fristrom, R. M.: J. Phys. Chem. *64*, 1393 (1960).
13. Fristrom, R. M., Grunfelder, C., and Favin, S.: J. Phys. Chem. *65*, 587 (1961).
14. Fristrom, R. M. and Westenberg, A. A.: *Eighth Symposium (International) on Combustion*, p. 438. Williams & Wilkins, 1962.
15. Fenimore, C. P. and Jones, G. W.: J. Phys. Chem. *63*, 1834 (1959).

16. AVRAMENKO, L. J. and LORETZO, R. V.: J. Phys. Chem. (USSR) *21*, 1135–42 (1947); Chem. Abstracts *42*, 2495 (1948).
17. GAYDON, A. G. and WOLFHARD, H. G.: *Flames*, p. 13. Chapman Hall Ltd., 1958.
18. KAUFMANN, F.: Reactions of Oxygen Atoms, in *Progress in Chemical Kinetics*, p. 3, edited by G. Porter. Pergamon, 1961.
19. SCHOTT, G. L. and KINSEY, J. L.: J. Chem. Phys. *29*, 1177–82 (1958).
20. FENIMORE, C. P. and JONES, G. W.: J. Phys. Chem. *65*, 1532 (1961).
21. FENIMORE, C. P. and JONES, G. W.: J. Phys. Chem. *62*, 693 (1958).
22. CAMAC, M. and VAUGHAN, A.: J. Chem. Phys. *34*, 460 (1961).

Discussion

DR. H. GG. WAGNER (*Göttingen University*): Extensive experimental investigations of the structure of the reaction zone of the laminar flames performed during the past few years has improved considerably our understanding of the flame propagation process. An important part of this work was done by Dr. Fristrom and his colleagues. It is therefore a great pleasure for me to be able to make a few remarks on his paper.

Dr. Fristrom mentioned that due to the low rate of recombination reactions at low pressure, the flame may be separated into two parts. This can be clearly seen from profiles of H_2–O_2 flames burning at a few millimeters of mercury. In these flames a stationary state is observed behind the main reaction zone (derivatives of concentrations and temperatures go to zero). The water concentration and the temperatures are far below the equilibrium value and the radical concentration is very high. This state can be described using the well-known chain and chain-branching reactions of the H_2–O_2 system (but no real recombination reaction) in a way that forward and reverse reactions have the same rate. In addition, the rate constants of these reactions can be evaluated using the measured profiles. The results are in fair agreement with those reported by Dr. Kaufman at this Symposium. As the total pressure is increased one can easily observe how recombination reaction becomes more and more important, and the existence of a peak in the concentration of radicals which are also present in the burned gases is observed. This peak-radical concentration seems to be of great importance for the understanding of the influence of inhibitors, the pressure dependence of flame velocity, and other flame properties.

One might expect that a maximum in the concentration of these radicals depends on the presence of a chain-branching reaction. Some calculations with the H_2–Cl_2 system, however, show that a peak radical concentration can exist in a system without branching reactions.

For the evaluation of the rate constants in Dr. Fristrom's paper the radical CH_3, among others, is of some importance. We have recently started some experiments which enable us to determine the concentration of radicals and stable products by taking samples immediately into the ionization chamber of a time-of-flight mass spectrometer. The profiles obtained from CH_4–O_2 flames are in principle in agreement with the measurements of Dr. Fristrom. The CH_4 disappears rather early in the flame. The maximum of the CH_3 concentration is close to the middle of the luminous zone and behind the maximum value of H_2CO, while C_2H_2 appears rather late in the reaction zone.

Figure 1, below, illustrates some preliminary results obtained in flames of different CH_4 concentration. (The final temperature of these flames was not the same.) The maximum concentration of CH_3

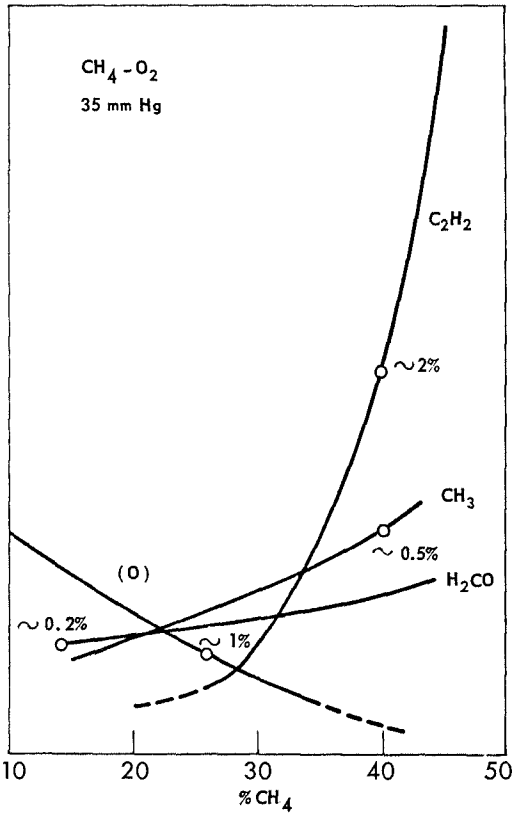

FIG. 1. Maximum concentration (in arbitrary units) of intermediates in methane–oxygen flames. Numbers on curves show approx. concentrations.

increases with increasing CH_4 content. The H_2CO concentration is less dependent on the CH_4 content. The O atom concentration decreases from lean to rich mixtures, while C_2H_2 strongly increases toward the rich side. Besides the species mentioned, many others could be detected. Though the method is not as accurate as other methods used by ourselves and by others it seems to provide useful information for the interpretation of flame processes.

DR. R. M. FRISTROM (*APL/The Johns Hopkins University*): Dr. Wagner has raised an interesting point on the relation between bimolecular flame reactions and the termolecular recombination reactions. Perhaps a few general comments on this problem would be in order.

Flame reactions can be divided into two general types—bimolecular and termolecular, i.e.,

$$A + B \rightarrow C + D$$

$$A + B + M^* \rightarrow AB + M^*$$

In many flames and the methane flame in particular, the initiating reactions are bimolecular while the terminating reactions are termolecular.

In a flame consisting of bimolecular reactions, distance structure scales as $1/P$. Such a flame when measured using a distance scale proportional to the mean free path is independent of pressure. In other terms, it requires a constant number of collisions to go to completion. This was first pointed out by Hirschfelder and Curtiss[1] and has been quantitatively checked on the initial portion of this flame.[2]

In the case of the termolecular reactions of the recombination region, the situation is different. For a given number of collisions required for completion, the required characteristic flame thickness will decrease as pressure is increased. This occurs because the ratio of three-body collisions to two-body collisions varies proportionally to $1/P$.

At high pressure the thickness of the recombination region will be small and transport processes will be important. At low pressure the thickness will become very large compared with corresponding bimolecular reactions and ultimately transport processes will become unimportant. The crossover point occurs at about 10 atm. In low pressure flames with apparatus of normal size, one deals primarily with the bimolecular reactions, and much of the recombination reactions occurs on the walls of the apparatus. This does not affect the measurement or analysis of flame structure data and is not a problem unless one is interested in the recombination reaction *per se*.

DR. T. M. SUGDEN (*University of Cambridge*): The question of the bimolecular recombination step has been raised. In hydrogen-air systems at least, all bimolecular steps of type $A + B \rightarrow C + D$ cannot lead to effective recombination because the number of free valencies cannot be reduced in this way, and the quantity $[H] + [OH] + 2[O] + 2[O_2]$ would be constant and equal to twice the original concentration of molecular oxygen.

It might be interesting to consider whether reactions which can occur in hydrocarbon flames, such as $CH + O_2 \rightarrow CO + OH$, might not be stable bimolecular recombination processes. In this example, the number of unpaired spins is reduced by two. The initial production of CH might, however, involve an increase in the number of free spins.

DR. R. M. FRISTROM: We have not considered this interesting reaction because no method is available at present to measure concentrations of CH. We have assumed it to be a trace species (below 10^{-6} mole fraction). If this is not the case, the reaction should receive serious consideration and studies of it in a simple system would be most desirable.

DR. R. R. BALDWIN (*University of Hull*): I would like to draw Dr. Fristrom's attention to some recent data given by Dr. Hoan of Dundee on the relative rates of the reaction

$$OH + CH_4 \qquad (3)$$

and

$$OH + CO, \qquad (12)$$

in which dissociating hydrogen peroxide was used as the source of OH radicals. The values of k_{12}/k_3 obtained decrease from 1.18 at 400°C to 0.29 at 650°C, with intermediate values at intermediate temperatures. The decrease corresponds to $E_3 - E_{12} \approx 7$ kcal/mole. The Arrhenius constants for reactions (3) and (12) given by Dr. Fristrom would make $k_3 > k_{12}$ at all temperatures, and the ratio k_{12}/k_3 ranging from 0.005 at 400°C to 0.01 at 650°C. These discrepancies suggest that Dr. Fristrom's combinations of Arrhenius parameters need modification, and a combination more suitable over a wide range could be obtained by combining his data with those of Dr. Hoan.

DR. R. M. FRISTROM: Dr. Hoan's study is new to me and I am looking forward to studying his paper. Hydrogen peroxide is a very treacherous source of OH since if any excess peroxide remains, the OH undergoes a very rapid quantitative reaction to form HO_2.[3]

$$OH + H_2O_2 \rightarrow H_2O + HO_2$$

DR. B. A. THRUSH (*University of Cambridge*): How does the presence of H atoms affect the scavenging of O atoms by NO_2? The reaction $H + NO_2 = NO + OH$ is much more rapid than

$O + NO_2 = NO + O_2$, and subsequently reactions such as the very rapid process $O + OH = H + O_2$ have to be considered.

DR. R. M. FRISTROM: As Dr. Thrush noted, the presence of hydrogen atoms does interfere with the determination of oxygen atoms. In this particular flame this is not a serious problem because of the low concentration of H atoms (0.004) relative to O atoms (0.015). The possible interference by OH would seem more serious. Our results are corrected for both of these interferences based on scavenger studies made in systems where these radicals were prepared by electric discharges.

DR. A. FONTIJN (*AeroChem Research Laboratories*): Scavenger probes of the general type described in Dr. Fristrom's paper may be extremely useful as atom detectors in very different environments as well. We have simultaneously developed a quartz scavenger probe for measuring local atom concentrations in supersonic plasmajets and have applied the technique to the quantitative determination of N atoms and excited N_2 molecules in Mach 3 streams of active nitrogen. We have used C_2H_4, NO, and NH_3 as scavenger gases and made use of product formation, scavenger gas destruction, or light titration end point to estimate the composition of the sampled gas. Further details concerning this application may be found in AeroChem TP–40 "Chemical Scavenger Probe Determinations of Atom and Excited Molecule Concentrations in Nonequilibrium Supersonic Streams of Active Nitrogen," by A. Fontijn, D. E. Rosner, and S. C. Kurzius. We subsequently hope to make a systematic comparison between scavenger probe results and catalytic detector measurements under identical discharge and flow conditions.

DR. R. M. FRISTROM: The scavenger probe technique was developed for studying radical concentrations. It combines microprobe sampling[4] with chemical scavenging.[5] The advantages are: (1) spatial resolution is high, (2) concentrations are determined in absolute rather than relative terms, and (3) it can be used in high temperature systems.

In a microprobe the sample is rapidly expanded adiabatically. This simultaneously reduces temperature and pressure and slows the flame reactions so the sample composition is frozen[6] close to the inlet conditions. Thus, sufficient time is available to allow the frozen sample to be mixed with a scavenger species which undergoes a quantitative reaction with the radical being studied to form a stable analyzable product. The initial radical concentration can then be deduced from its relation with this stable product.

For quantitative application the decompression, mixing, and scavenger reaction rates must be rapid compared with any other reactions which the radical can undergo; and the scavenger reaction must produce a unique product. The fast reaction $O + NO_2 \rightarrow O_2 + NO$ was used for O atom studies. The reliability of the method has been tested by comparing the results of scavenger probe sampling in an electric discharge with the more established technique of gas phase titration. The average deviation for a test set of comparisons was 4% and more than half of the dispersion was due to our titration technique.

In preliminary work, hydrogen atoms were studied using carbon tetrachloride and other

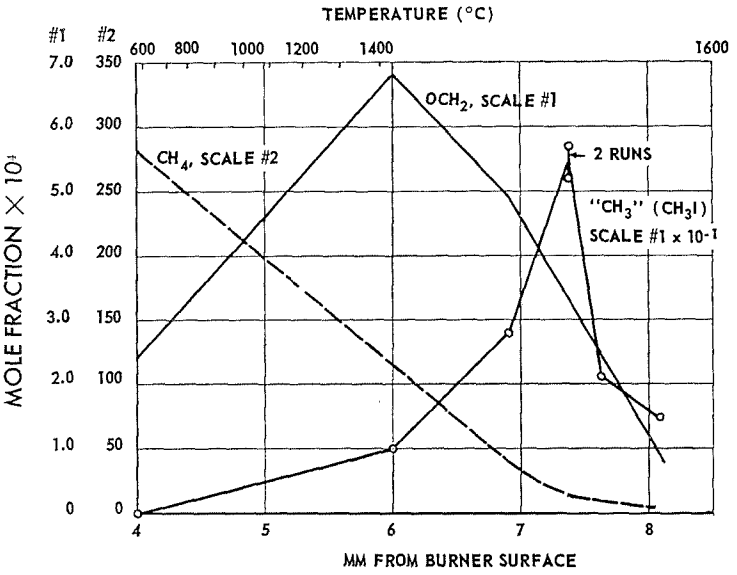

FIG. 2. Methyl radical concentration profile.

chlorinated hydrocarbons for scavenging. These results were reproducible and appeared proportional to H atom concentration, but the scavenging efficiency was only 20%.[7,8]

The scavenger probe used for flame studies is a standard quartz microprobe with a 100 micron orifice and a water-cooled body. Continuous flow sampling is used at a pressure level of 50 microns backed by a 6 liter per second diffusion pump, and isolated from the spectrometer inlet by a 3 ft section of 1 cm tubing. The scavenger gas is introduced at the base of the expansion section through a small Teflon tube. Results are independent of NO_2 concentration and sampling level.

Recently, Dr. Wilson and I have used this technique and an iodine scavenger to study the concentration of methyl radical in this methane–oxygen flame; preliminary results are shown in Fig. 2.

DR. L. S. ECHOLS (*Shell Oil Company*): In the sampling nozzle choked flow exists and presumably a shock pattern. How does one visualize this situation and its effects?

DR. R. M. FRISTROM: Choking flow does occur in the nozzle of the probes. Because of the large pressure drops employed (>10), supersonic flow might be expected and the gas is strongly cooled (simple adiabatic expansion considerations would predict a twenty-five–fold temperature drop). If such gas flow passes over an obstruction a strong shock would be expected. With complete recovery the gas would reach the inlet temperature, but no higher. In practice no shocks are observed in a probe when luminous gas from a discharge is sampled, and a thermocouple inserted in the probe registers a temperature much below the inlet temperature. This is because the ratio of mean free path to probe diameter is usually 5–10 and the boundary layer occupies most of the tube so that viscous losses drop the kinetic energy below the point where strong shocks can be observed.

DR. H. WISE (*Stanford Research Institute*): In the interpretation of the data, certain transport parameters are employed. What is the state of our knowledge on multi-component diffusion coefficients and their temperature coefficients?

DR. R. M. FRISTROM: In the data presented in this paper and most flame structure work, all species are treated as being traces in an oxygen carrier and binary diffusion coefficients are used. This results in errors which are of the order of 3% for this flame.[9] This is less than the error introduced by the neglect of thermal diffusion[9,10] and the errors introduced by the extrapolations required above 1200°K which is the upper limit of the experimentally determined diffusion coefficients[11] used for this study.

The rigorous multicomponent coefficients can be derived from a knowledge of all of the binary diffusion coefficients and the concentrations of the species.[12] For the fifteen components of this flame this would require a knowledge of over a hundred binary diffusion coefficients, only a fraction of which are known. The calculation is too cumbersome for present day use on systems of this complexity.

REFERENCES

1. HIRSCHFELDER, J. O., CURTISS, C. F., and BIRD, R. B.: *Molecular Theory of Gases and Liquids*, 765 ff. John Wiley and Sons, 1954.
2. WESTENBERG, A. A. and FRISTROM, R. M.: J. Phys. Chem. *65*, 591 (1961).
3. FONER, S. and HUDSON, R.: J. Chem. Phys. *36*, 2681 (1962).
4. FRISTROM, R. M.: *Experimental Methods in Combustion Research*, edited by J. Sugurue, Section 1.4. Pergamon Press, 1961.
5. STEACIE, E. W. R.: *Atomic and Free Radical Reactions*, vol. 1, p. 54. Reinhold, 1954.
6. BRAY, K. N. C.: J. Fluid Mech. *6*, 1 (1959).
7. FRISTROM, R. M.: *Scavenger Probe Sampling*, (in preparation).
8. FRISTROM, R. M.: Task R Quarterly, Report 8, p. 1, The Johns Hopkins University Applied Physics Laboratory Report TG–331–8, Silver Spring, Maryland, April 1961.
9. WESTENBERG, A. A. and FRISTROM, R. M.: J. Phys. Chem. *64*, 1393 (1961).
10. FRISTROM, R. M. and WESTENBERG, A. A.: Combustion and Flame *1*, 217 (1957).
11. WALKER, R. E. and WESTENBERG, A. A.: J. Chem. Phys. *32*, 436 (1960).
12. HIRSCHFELDER, J. O., CURTISS, C. F., and BIRD, R. B.: *Molecular Theory of Gases and Liquids*. John Wiley and Sons, 1954.

SOME OBSERVATIONS ON THE STRUCTURE OF A SLOW BURNING FLAME SUPPORTED BY THE REACTION BETWEEN HYDROGEN AND OXYGEN AT ATMOSPHERIC PRESSURE

G. DIXON-LEWIS AND A. WILLIAMS

The complete analysis of a flame structure consists of studying the variation of the temperature and all the composition parameters with distance y perpendicular to the flame front. By means of such analyses it is possible to investigate the mechanism and kinetics of the processes controlling the flame. However, for such investigations to have maximum effectiveness it is necessary to use the simplest flames consistent with the type of reaction mechanism. For this reason hydrogen–oxygen flames have for some time been studied in this laboratory as comparatively simple flames supported by a branched chain reaction system. The flame studied in this paper has an initial composition of 4.604 per cent oxygen, 18.83 per cent hydrogen and 76.56 per cent nitrogen. This flame is within the range of hydrogen–oxygen–nitrogen flames which can be stabilized at atmospheric pressure on an Egerton–Powling type of flat flame burner. For a matrix temperature of 336°K the theoretical flame temperature is 1078°K, and the burning velocity, measured by means of particle track techniques, is 9.2 cm/sec.[1] The flame burns as a flat disc with the reacting gases flowing in a direction normal to the plane of the reaction zone. This produces an approximately one-dimensional flow system, and thus simplifies the analysis.

In this paper the results of both an experimental and a theoretical investigation of the flame are described. These are combined in an attempt to give information about the flame mechanism. In the theoretical investigation the effects of alterations in some of the reaction and transport parameters on the flame have also been studied.

Conservation Equations

In addition to the burning velocity (which sets the time scale) it is necessary, in order to make a complete analysis of a flame, to know the temperature profile and the composition profiles of all the species present. For the one-dimensional system, let y be the distance coordinate in the direction of motion, and let H (in cal cm^{-2} sec^{-1}) represent the flow of heat liberated by the reaction across a plane normal to the y axis at distance y and time t. Then $\partial H/\partial y$ represents the volumetric heat release rate in cal cm^{-3} sec^{-1}. If the kinetic energy and pressure terms in the conservation equation are neglected for this slow burning flame, then the conservation of energy may be written as Eq. (1).

$$\rho \frac{\partial(c_p T)}{\partial t} = \partial/\partial y(\lambda\, \partial T/\partial y) - M \frac{\partial(c_p T)}{\partial y} + \partial H/\partial y \quad (1)$$

Here ρ is the density, T is the absolute temperature, M is the mass flow velocity, c_p is the specific heat at constant pressure, and λ is the thermal conductivity at temperature T.

In the experimental investigation a stationary flame was used. If now the system is referred to a set of coordinate axes which are fixed in space, then the time derivatives in Eq. (1) all vanish. Equation (1) may then be replaced by Eq. (2),

$$\begin{aligned} dH/dy &= d\{Mc_pT - \lambda(dT/dy)\}/dy \\ &= d\{M\bar{c}_p(T - T_u) - \lambda(dT/dy)\}/dy \end{aligned} \quad (2)$$

where $\bar{c}_p$ is the mean specific heat between T and T_u. Equation (2) gives the volumetric heat release rate in terms of the mass burning velocity, the thermal properties of the gas mixture, and values which may be derived from a measured temperature profile.

Similarly for each species in the mixture, if w_i is its weight fraction at distance y and time t, and its chemical rate of formation in mole cm^{-3} sec^{-1} is $[\partial n_i/\partial t]_{\text{chem}}$, then the conservation of species equation may be written as Eq. (3),

$$\rho(\partial w_i/\partial t) = \partial/\partial y(\rho D_i \partial w_i/\partial y) - M(\partial w_i/\partial y) + m_i[\partial n_i/\partial t]_{\text{chem}} \quad (3)$$

where D_i is the diffusion coefficient of species i in the mixture and m_i is the molecular weight. Strictly, the binary mixture form of the diffusion equation is not applicable to multicomponent mixtures, for which the exact forms are given by Hirschfelder, Curtiss, and Bird.[2] The much simpler binary form nevertheless gives a good approximation when i is present in only small amounts, a condition which applies fairly well to all the important reactive species in this flame. In this case the value of D_i in a mixture of i with A, B, $\cdots$, is given by

$$\frac{1}{D_i} = \frac{X_A}{\mathfrak{D}_{i-A}} + \frac{X_B}{\mathfrak{D}_{i-B}} + \cdots \quad (4)$$

where X represents mole fraction and the $\mathfrak{D}$'s represent the binary diffusion coefficients.

Again, for a stationary one-dimensional flame, Eq. (3) may be replaced by Eq. (5).

$$m_i[\partial n_i/\partial t]_{\text{chem}} = d\{Mw_i - \rho D_i(\partial w_i/dy)\}/dy = M\, dG_i/dy \quad (5)$$

Here G_i is the weight fraction of i in the mass rate of flow. Equations of the form of (3) and (5) may be set up for each species present in the flame, and the solution of the problem consists of satisfying the whole set of simultaneous equations.

The thermal conductivities of the mixtures encountered in the flame were calculated by the method of Lindsay and Bromley[3] from the conductivities of the pure constituents. For this purpose the composition was assumed to vary linearly with temperature. Even at the flame temperature of 1078°K little or no extrapolation of available data is needed. The sources of the data are given elsewhere.[4] Diffusion coefficients were calculated to be consistent with the appropriate sets of data of Walker and Westenberg,[5] and with the data of Wise[6] for H atoms in hydrogen.

Experimental Methods

The apparatus consists basically of a burner and fuel supplies, and methods of studying the flame. The burner used was of the Egerton–Powling type as modified by Dixon-Lewis and Isles.[7] The temperature of the gases entering the flame was measured by means of chromel–alumel thermocouples silver soldered to the top of the burner matrix. The temperature during the experiments was 336°K, and was low enough for catalytic oxidation inside the burner to be negligible. The hydrogen, oxygen, and nitrogen were drawn from cylinders, and the flow rates were carefully controlled and measured, after which the gases were thoroughly mixed before passing to the burner. Various chemical indicators could be added to the unburned, premixed fuels. Sodium chloride or other solutions, or heavy water, could be added in small amounts by means of a Collinson atomizer at a known steady rate. Small amounts of deuterium could also be metered and introduced.

In order to correlate the various profile measurements the plane of the schlieren maximum was used as the reference plane on the y axis. This is necessary since the flame itself is nonluminous.

Temperature profile measurements have been carried out using a suitably designed platinum/13 per cent rhodium–platinum thermocouple with its thermojunction made from 0.01 mm diameter wires butt-welded together and supported in a stirrup of somewhat thicker wires of the same material. The wires in the immediate neighborhood of the junction were then in an isothermal plane in the flame. Catalytic effects were eliminated by quartz coating.[8] Dixon-Lewis and Isles have shown that with such thermocouples any small distortions of the flame which may occur have a negligible effect on the profile.[9]

Corrections were applied to the thermocouple readings to allow for heat losses by radiation. The maximum correction was only 12°K in this flame, and the maximum measured temperature was only 6°K below the theoretical flame temperature. This small difference may be caused by radiation from the flame gases.

To determine the composition profiles the method principally used has been to withdraw samples of the gases from various positions in and near the flame by means of a quartz microprobe, and subsequently to analyze the samples. The probe itself consisted of 1 mm O.D. quartz tube drawn down to produce a 25 μ orifice. The analyses were carried out in different cases by gas chromatography, by mass spectrometry, and by volumetric methods.

Spectroscopic methods have been used in the study of radical concentrations, both in absorption for a preliminary estimate of hydroxyl radical concentration, and in emission when investigating hydrogen atom concentrations in the burned gas. In both cases a narrow vertical aperture was used, the light actually detected being restricted to that from a slice of flame 0.1 mm high at the flame center and 0.3 mm high at the edges. Detection was by a photomultiplier tube with quartz window. The light beam was chopped at 460 cps and the signal was amplified by means of a homodyne system and presented

on a chart recorder. Spatial scanning at the flame was effected by means of a calibrated thread and synchronous motor which raised the entire burner. To avoid difficulties due to schlieren effects the measurements were restricted to the burned gas and to the hotter parts of the flame.

Temperature Profile and Composition Profiles for Stable Species

Figure 1 shows the temperature profile for the flame under investigation while Fig. 2 gives the composition profiles for the stable species hydrogen, oxygen, and steam. Analysis of the temperature profile by the methods already outlined leads to the curve shown in Fig. 3 for the over-all heat release rate.

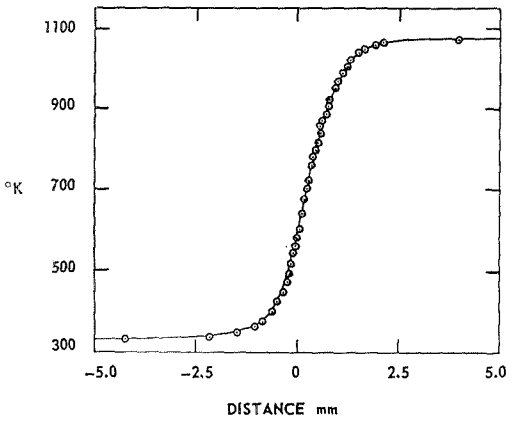

FIG. 1. Temperature profile for a hydrogen–oxygen–nitrogen flame with initial composition 4.604% oxygen, 18.83% hydrogen, and 76.56% nitrogen.

Measurement of Hydrogen Atom Concentration

In order to follow the hydrogen atom concentrations three methods have been used. First, the chemiluminescence when small amounts of sodium salts (about one part in 10^6) are added to the flame gases has been shown by Sugden and collaborators[10] to be due to excited sodium atoms formed by reactions (I) and (II). In the gases

$$H + H + Na = H_2 + Na^* \qquad (I)$$

$$H + OH + Na = H_2O + Na^* \qquad (II)$$

$$OH + H_2 \rightleftharpoons H_2O + H \qquad (III)$$

immediately behind the flame H and OH are present in concentrations much above their equilibrium value. If, however, it is assumed that reaction (III) is sufficiently rapid to maintain

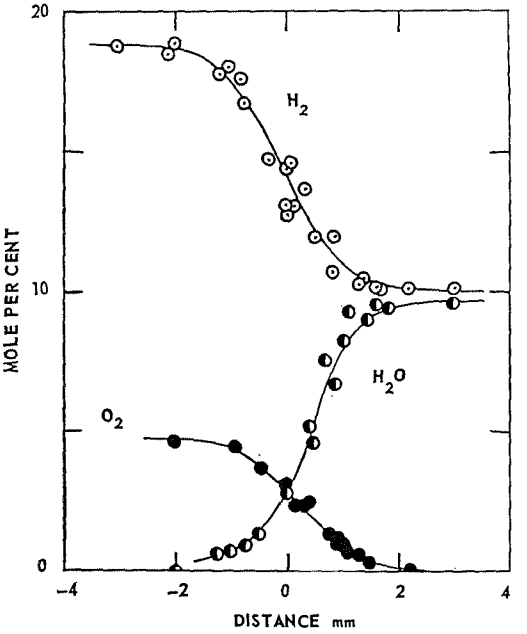

FIG. 2. The composition profiles of the stable molecular species.

the ratio [H]/[OH] at its equilibrium value while the general third order recombination reactions (IV) and (V) proceed, then the result is obtained that $[H] \propto I_{Na}^{\frac{1}{2}}$. Hence the decay of chemiluminescence in the burned gas may be used as a measure of relative hydrogen atom con-

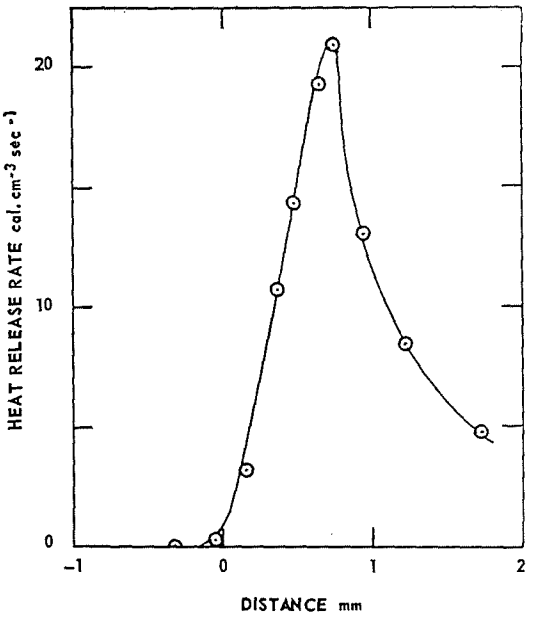

FIG. 3. The heat release profile.

centrations in this region. In these low temperature flames thermal emission from sodium is negligible.

$$H + H + M = H_2 + M \qquad (IV)$$

$$H + OH + M = H_2O + M \qquad (V)$$

Secondly, the reaction of H atoms with heavy water to form HD by reaction (VII) and associated reactions has been used to measure their relative concentrations in the burned gas region. In this method, which has been used by Fenimore and Jones,[11] small measured amounts (0.1 to 1 per cent) of heavy water are added to the gases

$$H + D_2 \underset{\frac{1}{2}k_6}{\overset{k_6}{\rightleftharpoons}} HD + D \qquad (VI)$$

$$H + D_2O \underset{\frac{1}{2}k_3}{\overset{k_7}{\rightleftharpoons}} HD + OD \underset{\frac{1}{2}k_7}{\overset{\frac{1}{2}k_3}{\rightleftharpoons}} DOH +$$

$$D \underset{k_3}{\overset{\frac{1}{2}k_7}{\rightleftharpoons}} D_2 + OH$$

entering the flame and the HD formation is followed by mass spectrometric measurement of the $[HD]/[H_2]$ ratios in samples withdrawn from the flame. If it is assumed (a) that H_2, D_2, and HD are always in equilibrium among themselves (since $k_6 \gg k_7$), (b) that rate constants are independent of isotopic species, and (c). that Eq (6) holds then it can be shown

$$k_3[OH][H_2] = k_7[H][H_2O] + [\partial(H_2O)/\partial t]_{chem} \qquad (6)$$

that $[\partial(HD)/\partial t]_{chem}$ is given by Eq. (7), where the subscript zero denotes initial concentrations corrected for the temperature rise.

In this work $[\partial(HD)/\partial t]_{chem}$ is obtained in mole cm^{-3} sec^{-1} by converting the mass fluxes of HD in Eq. (5) into molar fluxes. Figure 4 shows

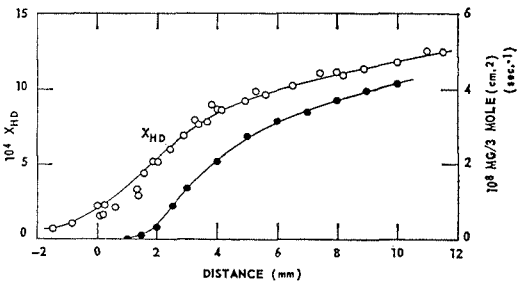

FIG. 4. The formation of HD by the reaction of hydrogen atoms with heavy water. X denotes mole fraction. $MG_{HD}/3$ is the molar flux of chemically formed HD.

the appropriate molar quantities. Since k_7 is not accurately known, this method again only gives

$$[\partial[HD]/\partial t]_{chem} = k_7[H][H_2]_0\left\{\frac{[D_2O]_0}{[H_2]_0} - \frac{[HD]}{2[H_2]}\right\} - \frac{[HD]}{2[H_2]}[\partial[H_2O]/\partial t]_{chem} \qquad (7)$$

relative H atom concentrations, in the form $k_7[H]$. Due to the comparatively high activation energy (approx. 20 kcal $mole^{-1}$) of the reaction between H and D_2O, this method is again only suitable for the burned gas region. In the post-flame gases $[\partial(H_2O)/\partial t]_{chem} = 0$, and if HD diffusion is ignored here Eq. (7) is that derived by Fenimore and Jones.[11]

In somewhat hotter flames than the present one it is possible to calibrate both the above methods by studying the processes concerned when the burned gas is in full equilibrium. In this low temperature flame this is not possible due to the low H atom concentration at equilibrium, and another approach is necessary in order to calibrate the system. The third approach is provided by adding measured traces of D_2 to the flame gases, a method which again has been used by Fenimore and Jones.[12] In the flame the exchange reactions (VI) and VIII) occur, together with oxidation of both D_2 and HD. The build up

$$D + H_2 \rightleftharpoons HD + H \qquad (VIII)$$

and subsequent decline of HD due to oxidation can again be followed by sampling and mass spectrometry. If $[D] = [H][HD]/2[H_2]$ and $[D_2] \gg [HD]^2/4[H_2]$, that is, if the reaction has not proceeded too far towards equilibrium, then the net rate of formation of HD is

$$[\partial[HD]/\partial t]_{chem} = k_6[H][D_2] - \frac{[HD]}{2[H_2]}[\partial[H_2O]/\partial t]_{chem} \qquad (8)$$

At the maximum value of $[\partial[HD]/\partial t]_{chem}$ the above inequality was satisfied. The maximum H atom concentration derived by this means was therefore assumed to coincide with the maximum chemiluminescent intensity, so that a calibration of the chemiluminescence profile in the burned gas is provided. The method depends, of course, on an accurate value for the rate constant of reaction (VI). Using the recent value of $k_6 = 6.1 \times 10^{11}$ cm^3 $mole^{-1}$ sec^{-1} at 1000°K obtained by Boato *et al.*,[13] together with an activation energy of 6.65 kcal $mole^{-1}$,[14] a maximum H atom concentration in the flame of 2.5×10^{-8} mole

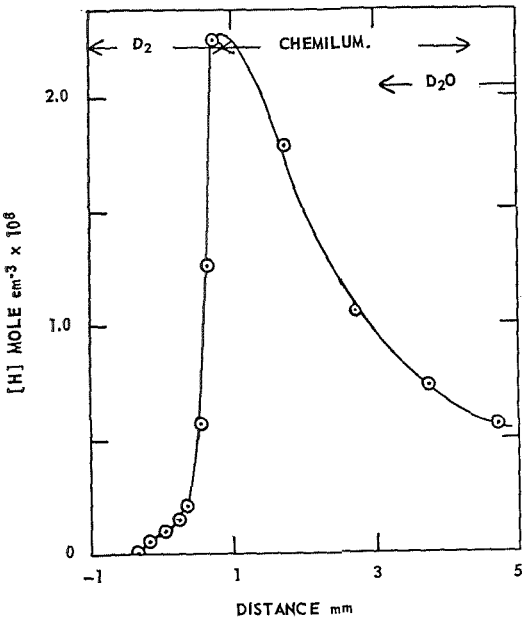

FIG. 5. The hydrogen atom concentration profile in the flame.

cm^{-3} at 900°K is obtained. The calibration of the chemiluminescence curves depends also on the equilibration of H and OH by reaction (III) throughout the chemiluminescent region. This will not be strictly true, and will tend to lead to low apparent values of the H atom concentration further out in the burned gas.

In order to fit the D_2O results into the scheme, the latter were scaled so that a position was found where they could be superimposed on the chemiluminescence profile. Figure 5 shows the complete H atom concentration profile, together with the range covered by the different methods. As a further product of the analysis a value is obtained for the rate constant of the reaction between H and D_2O at 1072°K. It is $k_7 = 5.0 \times 10^9$ cm^3 $mole^{-1}$ sec^{-1}. Due to the uncertainty already mentioned about the equilibration condition, this may be an upper limit for k_7.

Concentration of Hydroxyl Radicals

Hydroxyl radical concentrations in flames have been measured by absorption spectroscopy by both Kaskan[15] and by Bonne, Grewer, and Wagner.[16] Kaskan's method involves absorption by the broader ultra-violet absorption lines of the OH in the flame (0, 0 band at 3064 Å) of the narrow emission lines from a cooled water discharge lamp. This does not require such high spectrographic resolution as the more general method involving absorption from a continuous background as used by Bonne, Grewer, and Wagner. However, the strict applicability of Kaskan's method depends on the emission lines from the water discharge being sufficiently narrow, and this introduces some uncertainty. In the flame under consideration containing excess hydrogen, the OH concentration is low and the absorption small. Kaskan's method has been used to give preliminary results. The maximum OH concentration was found to be about 3×10^{-10} mole cm^{-3}.

Preliminary Kinetic Analysis

Burned Gas Region

In the burned gas region of the flame the establishment of full equilibrium proceeds by means of the third order reactions (IV) and (V), together with associated rapid reactions which tend to keep the [H]/[OH] ratio at its equilibrium value. In this region therefore the chemical rate of formation of H atoms is given by

$$[\partial[\mathrm{H}]/\partial t]_{\mathrm{chem}} = -k_a[\mathrm{H}]^2 \qquad (9)$$

where k_a is an apparent second order recombination constant for the particular gas composition. The diffusion Eq. (5) may therefore be written, for H atoms in the burned gas region,

$$-k_a \int [\mathrm{H}]^2\, dy = S_b[\mathrm{H}] - D_{\mathrm{H}} d[\mathrm{H}]/dy \qquad (10)$$

Here S_b is the linear flow velocity of the burned gas and [H] is the molar concentration. The constant k_a may therefore be found for the flame by means of a straight line plot. Alteration of the composition of the gases entering the flame to give different burned gas compositions having a common flame temperature enables k_a to be resolved into its six constituent third order constants. A preliminary analysis along these lines by Dixon-Lewis, Sutton and Williams[17] leads to values of the third order constants at 1072°K:

$$k_4^{\mathrm{N_2}} = k_4^{\mathrm{H_2O}} = 1 \times 10^{-32}\ \mathrm{cm^6/molecule^2/sec}$$

$$k_4^{\mathrm{H_2}} = 1.7 \times 10^{-32}\ \mathrm{cm^6/molecule^2/sec}$$

$$k_5^{\mathrm{N_2}} = k_5^{\mathrm{H_2O}} = 2.5 \times 10^{-31}\ \mathrm{cm^6/molecule^2/sec}$$

Consideration of Heat Release Profile

If it is assumed (a) that the maximum H atom concentration corresponds with the maximum rate of heat release, and (b) that the heat release is principally due to the recombination reactions, then the maximum heat release rate is found to be about 1.5 cal cm^{-3} sec^{-1}, compared with an experimental value of about 20 cal cm^{-3}

sec^{-1}. On pure reaction kinetic considerations, this discrepancy could be accounted for by assuming that the measured H atom concentrations are too low, by an order of magnitude. From Eq. (10), such a correction would involve a simultaneous reduction in k_a by a factor of 10, a result which is not in line with values of k_a obtained by Bulewicz and Sugden[18] and others (e.g., ref. 19). The alternative explanation is that the bulk of the heat release occurs by a mechanism other than the recombination. Because of this possibility, but primarily because of interest in the kinetic effect in flames, the expected properties of a few flames controlled by some variations of a simple hydrogen-oxygen reaction mechanism have been studied by numerical solution of the flame equations.

Manipulation and Solution of Flame Equations

The method used has been that proposed by Spalding[20] and by Adams and Cook,[21] and again used by Zeldovich and Barrenblatt.[22] It consists of setting up the time dependent heat conduction Eq. (1) and the diffusion equations of type (3), assuming an arbitrary initial set of temperature and concentration profiles, and then integrating by finite difference methods until the steady state profiles and propogation velocity are reached. The method is a powerful one for dealing with complex mechanisms. Details of the method itself will not be given here.

Kinetic Models Used

The main features of the hydrogen-oxygen reaction in static systems are now fairly well understood. The effect of many of the reactions in flames, however, is not known. For example, the simplest reasonable mechanism which could be assumed for a rich hydrogen-oxygen flame would be reactions (III), (IV), (IX), and (X).

$$OH + H_2 = H_2O + H \qquad (III)$$

$$H + O_2 = OH + O \qquad (IX)$$

$$O + H_2 = OH + H \qquad (X)$$

$$H + H + M = H_2 + M \qquad (IV)$$

Assuming reaction (IX) to be rate controlling in the oxygen deficient flame, reactions (III), (IX), and (X) may be combined to give:

$$H + O_2 \,(+3H_2) \xrightarrow{k_9} 2H_2O + 3H \qquad (IXa)$$

$$\Delta H_9 = -11.4 \text{ kcal mole}^{-1}$$

This over-all reaction does not liberate much energy, and the principal energy releasing reaction may be the H atom recombination reaction (IV), with $\Delta H_4 = -104.2$ kcal mole^{-1}.

Reactions (IX) and (IV) could provide a complete flame reaction mechanism. Unknown features of such a mechanism are the effect of the velocity constants k_9 and k_4 on the burning velocity and other features of the flame. In addition, in explosion limit work, an alternative reaction path via HO_2 formation is usually assumed as part of the basic mechanism. If it is further

$$H + O_2 + M = HO_2 + M \qquad (XI)$$

$$H + HO_2 = OH + OH \qquad (XII)$$

$$H + O_2 + M \,(+2H_2) \xrightarrow{k_{11}} 2H_2O + M + H; \qquad (XIa)$$

$$\Delta H_{11a} = -115.8 \text{ kcal mole}^{-1}$$

assumed that in the flame the HO_2 is rapidly removed by further reaction (XII) with H atoms, then the alternative cycle (XIa) is possible. Reactions (XIa) may be regarded as a chain-propagating cycle involving HO_2, whereby the heat releasing potential of the H atoms formed in the branching cycle (IXa) is increased. Further, reaction (XI) has virtually zero activation energy and hence, energetically, may occur in the cooler parts of the flame. Since oxygen is present in large concentration in this part of the flame, H atoms diffusing into this region may now alter the heat release pattern, and so also the other flame properties. Such effects may be important in our low temperature flame.

Another reaction which may follow HO_2 formation is reaction (XIII) which may result in a chain-breaking cycle (XIb).

$$HO_2 + HO_2 = H_2O_2 + O_2 \qquad (XIII)$$

$$H_2O_2 + H = H_2O + OH \qquad (XIV)$$

Hence

$$H + O_2 + M \,(+\tfrac{1}{2}H + \tfrac{1}{2}H_2) = H_2O + \tfrac{1}{2}H + M + \tfrac{1}{2}O_2 \qquad (XIb)$$

$$\Delta H_{11b} = -110.0 \text{ kcal mole}^{-1}$$

In all the composite reactions the important rate-controlling steps involve only H or O_2. Hence diffusion equations are only set up for these species, and suitable approximations are made when other concentrations are needed for third body effects.

The diffusion and transport properties of the mixtures appear in the equations in the forms $\lambda\rho/c_p$ and $D\rho^2$. Average values of these and other thermal constants are used, and assumed inde-

TABLE 1

Properties of Flames in Hydrogen–Oxygen–Nitrogen Mixtures, Showing Effects of Reaction Mechanism and Rate Constants, and of Diffusion of Hydrogen Atoms. Initial mole fractions: $X_{H_2} = 0.1883$, $X_{N_2} = 0.7656$, $X_{O_2} = 0.0460$. In all cases $c_p = 0.3085$ cal gram^{-1} °K^{-1}, and $(\lambda\rho/c_p)_m = (D_{O_2}\rho^2)_m = 2.37 \times 10^{-7}$ gram^2 cm^{-4} sec^{-1}

Run	$D_H\rho^2 \times 10^7$ (gram^2 cm^{-4} sec^{-1})	k_9	$k_4 \times 10^{33}$ (cm^6 molecule^{-2} sec^{-1})	$k_{11}^{H_2} \times 10^{32}$ (cm^6 molecule^{-2} sec^{-1})	S_u (cm sec^{-1})	$[H]_{max}$ (mole cm^{-3} $\times 10^8$)
1	13.4	A[a]	60[c]	0	6.0	6.5
2	13.4	A	6[d]	0	6.1	5.8
3	13.4	A	1.5	0	6.6	10.4
4	13.4	A	24	0	4.6	2.6
5	13.4	A	6	2.46[e]	86.4	5.1
6	2.37	A	6	0	8.5	10.8
8	13.4	A	12	0	5.5	4.1
10	13.4	A	12	2.46[f]	v. small	—
11	13.4	B[b]	12	0	14.1	8.3

[a] A $= 7 \times 10^{-10} \exp(-18\,000/RT)$ cm^3 molecule^{-1} sec^{-1}.
[b] B $= 2.8 \times 10^{-9} \exp(-18\,000/RT)$ cm^3 molecule^{-1} sec^{-1}.
[c] H_2O only effective third body.
[d] All molecules have same third body efficiencies in runs below this.
[e] Mechanism (XIa). H_2O assumed 8 times as efficient as H_2; N_2 half as efficient as third body.
[f] Mechanism (XIb). H_2O assumed 8 times as efficient as H_2; N_2 half as efficient as third body.

pendent of composition and temperature. D_H was given a value about five times that of D_{O_2}, except in one run where both were made equal in order to study the effect of H atom diffusion. In the finite difference form in which the equations are used, the form of the equations themselves indicates the dependence of burning velocity on thermal conductivity, namely $S_u \propto \lambda^{\frac{1}{2}}$.

The conditions used in a number of calculations are given in Table 1, together with steady state burning velocities and maximum H atom concentrations. Figures 6 and 7 show a few heat release profiles and H atom profiles. Clearly many of the burning velocities are sufficiently close to the experimental values to justify the study of these models.

The effect on the flame of varying the H atom recombination rate constant was first investigated. Assuming all molecules to be equally efficient third bodies, varying the recombination constant by a factor of 16 from 1.5×10^{-33} to 2.4×10^{-32} cm^6 molecule^{-2} sec^{-1} only reduces the burning velocity by about 30 per cent. Heat release profiles for runs 2 and 4 are shown in Fig. 6, and a hydrogen atom profile is shown in Fig. 7 for run 2. The maxima in both the heat release curves occurs at around 900°K, a property shared by the experimental profile.

The effect of reducing the diffusion coefficient of H atoms by a factor of between 5 and 6 is shown by a comparison of run 2 (large D_H) with run 6 (Table 1 and Fig. 7). The reduction in D_H *increases* both the burning velocity and

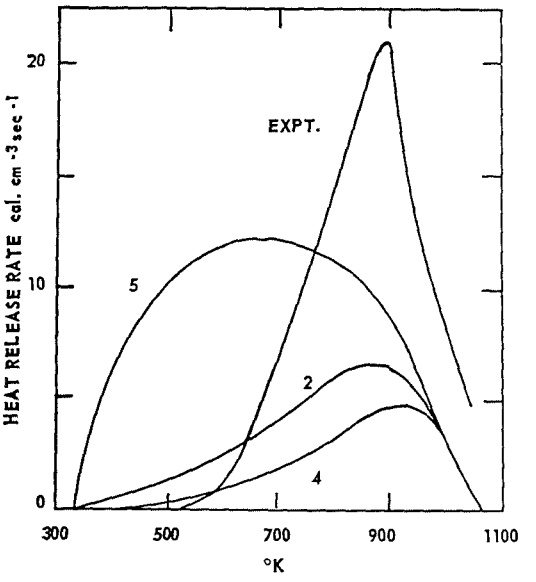

FIG. 6. Some calculated heat release profiles. Curve drawn for run 5 shows 0.1 actual values.

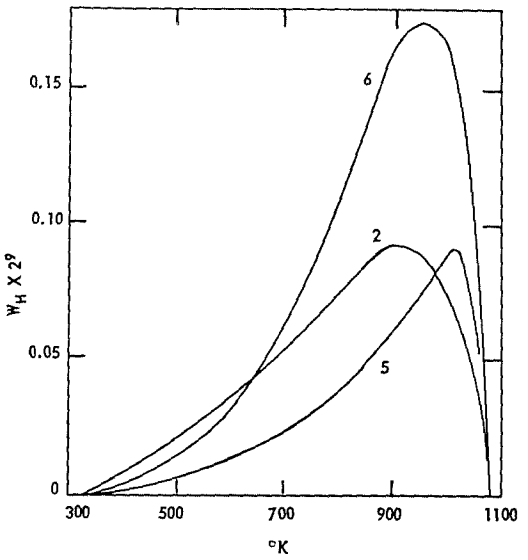

FIG. 7. Some calculated hydrogen atom concentration profiles. W_H is the weight fraction of hydrogen atoms.

the maximum H atom concentration. This is parallel with the effect obtained by Hirschfelder, Curtiss, and Campbell[23] for a flame supported by a unimolecular decomposition, and provides a further argument against the so-called "diffusion theories" of flame propagation. Clearly the flame is favored if H atoms can be kept in the high temperature chain-branching region.

Run 11 shows, as expected, that increasing the chain-branching rate constant increases the burning velocity. A fourfold increase in the branching increases S_u by a factor of about 2.5.

The HO_2 mechanisms(XIa) and (XIb), in the form in which they have been included, produced spectacular results. Mechanism (XIa) is equivalent to vastly increasing the reactivity of H atoms in all parts of the flame. The heat release pattern becomes entirely different in form, and the maximum H atom concentration moves towards higher temperatures as compared with the other runs. The burning velocity increases some 15 times. In contrast with this behavior, the chain-breaking mechanism (XIb) causes the burning velocity to fall to an insignificantly small value.

One further point about the profiles should be mentioned. The oxygen concentration becomes very small at about 900°K, where the maximum reaction rate and the maximum H atom concentration occur. The total enthalpy of the gases was therefore examined at a number of positions in one or two flames. It was found not to vary greatly through the flame (as would be expected since $\lambda\rho/c_p = D_{O_2}\rho^2$). In addition, however, it was found that in those flames with a low recombination constant, where diffusion of H atoms was most marked, there was a small enthalpy excess at each end of the flame, with a deficiency in the chain-branching region.

Comparison between Theory and Experiment

It has not yet been possible to reproduce the experimental flame by the numerical approach, although the level of agreement is reasonable. The main anomaly in the experimental flame appears to be as between heat release rate, H atom concentration, and recombination rate constant. The last two quantities are too small to account for the first in a simple manner. This could be due to some experimental problem, or alternatively it may be explicable by means of a more realistic reaction mechanism than has so far been used.

REFERENCES

1. DIXON-LEWIS, G. and WILLIAMS, A.: Combustion and Flame *4*, 383 (1960).
2. HIRSCHFELDER, J. O., CURTISS, C. F., and BIRD, R.: *Molecular Theory of Gases and Liquids*. Wiley, 1954.
3. LINDSAY, A. L. and BROMLEY, L. A.: Ind. Eng. Chem. (Industr) *42*, 1508 (1950).
4. DIXON-LEWIS, G. and ISLES, G. L.: *Eighth Symposium (International) on Combustion*, p. 448. Williams & Wilkins, 1962.
5. WALKER, R. E. and WESTENBERG, A. A.: J. Chem. Phys. *32*, 436 (1960).
6. WISE, H.: J. Chem. Phys. *34*, 2139 (1961).
7. DIXON-LEWIS, G. and ISLES, G. L.: Trans. Faraday Soc. *53*, 193 (1957).
8. KASKAN, W. E.: *Sixth Symposium (International) on Combustion*, p. 134. Reinhold, 1957.
9. DIXON-LEWIS, G. and ISLES, G. L.: To be published.
10. PADLEY, P. J. and SUGDEN, T. M.: *Seventh Symposium (International) on Combustion*, p. 235. Butterworths, 1959.
11. FENIMORE, C. P. and JONES, G. W.: J. Phys. Chem. *62*, 693 (1958).
12. FENIMORE, C. P. and JONES, G. W.: J. Phys. Chem. *63*, 1154 (1959).
13. BOATO, G., CARERI, G., CIMINO, A., MOLINARI, E., and VOLPI, G. G.: J. Chem. Phys. *24*, 783 (1956).
14. VAN MEERSCHEM: Bull. Soc. Chim. Belg. *60*, 99 (1951).
15. KASKAN, W. E.: Combustion and Flame *2*, 229 (1958).
16. BONNE, U., GREWER, TH., and WAGNER, H. G.: Z. phys. Chem. (Frankfurt) *26*, 93 (1960).

17. Dixon-Lewis, G., Sutton, M. M., and Williams, A.: Discussions Faraday Soc. *33*, 205 (1962).
18. Bulewicz, E. M. and Sugden, T. M.: Trans. Faraday Soc. *54*, 1855 (1958).
19. Steiner, H.: Trans. Faraday Soc. *31*, 623 (1935).
20. Spalding, D. B.: Phil. Trans. Roy. Soc. (London) *249*, 1 (1956).
21. Adams, G. K. and Cook, G. B.: Combustion and Flame *4*, 9 (1960).
22. Zeldovich, J. B. and Barrenblatt, G. I.: Combustion and Flame *3*, 61 (1959).
23. Hirschfelder, J. O., Curtiss, C. F., and Campbell, D. E.: *Fourth Symposium (International) on Combustion*, p. 190. Williams and Wilkins, 1953.

Discussion

Dr. Paul Kydd (*General Electric Research Laboratory*): The central problem posed in this paper is the lack of agreement between the rate of heat release obtained by differentiating the measured temperature profile and the same quantity deduced from the measured H atom concentration and the rate constant for H atom recombination. The maximum heat release is derived from the temperature profile at a point where its gradient is extremely steep, making the differentiation difficult; and the hydrogen atom concentration must be determined from the rate of the deuterium exchange reaction at a point where this method is losing its validity. The exchange rate constant is not without error and the atom concentration obtained must be squared and multiplied by the recombination rate constant which is also somewhat uncertain. In view of this, a discrepancy of a factor of ten in the two heat release rates is not at all surprising.

What is more serious is that the heat release and H atom profiles do not agree in shape as well as absolute magnitude. When the latter is squared as required by the proposed heat release mechanism and compared with the profile determined from the temperature, the temperature profile is more sharply peaked. If the latter is not in error, this can only be explained by a different mechanism than that proposed. Dr. Wagner's description of a hydrogen-oxygen flame at such a low pressure that no recombination was possible, and yet which still released enough heat to sustain itself suggests that the detailed stoichiometry and therefore heat release of the branching phase of the reaction may provide the answer. Certainly the calculations involving HO_2 or a change in the branching rate constant are not satisfactory as they either do not reproduce the burning velocity or fail to solve the discrepancy.

Prof. G. Dixon-Lewis (*University of Leeds*): It seems to us that perhaps Dr. Kydd has placed too much emphasis on the preliminary kinetic analysis outlined as the starting point for the theoretical section of the paper.

This preliminary analysis indicates the nonapplicability of the assumption that the major heat releasing process is the recombination reaction. The subsequent numerical solutions support this, and show that near the maximum heat release rate the less exothermic but much faster chain branching cycle provides the principal heat releasing step, when reasonable values are employed for the rate constants.

With regard to the accuracy of the experimental heat release profiles, similar measurements using the temperature profiles have been made on other flames with properties close to the one described in the paper. The heat release profiles all fall into a regular pattern, and indicate a lower limit for the maximum rate of about 18 cal cm^{-3} sec^{-1}. In addition, we have used D. B. Spalding's centroid rule in conjunction with our experimental profile in order to calculate the burning velocity of the flame. Granted that this contributes nothing about the detailed heat release profile, nevertheless the calculated 9.0 cm sec^{-1} as compared with the experimental 9.2 cm sec^{-1} argues well for its general correctness.

The H atom concentrations are also probably not too much in error, as evidenced also by the recombination rate constants obtained in reference 17. These are in reasonable agreement with literature values.

The picture that emerges from this work is that of a flame in which H atoms are produced very rapidly in the region of the maximum heat release rate. The majority of these diffuse out towards the hot and cold boundaries of the flame before recombining, so that in the region of the maxima in the profiles most of the heat release is associated with the branching cycle of reactions.

In assessing the contributions of HO_2 reactions, we would agree that as far as agreement with experiment is concerned these are not satisfactory. But then, the reaction mechanisms involving HO_2 as investigated in the paper are clearly oversimplified and unrealistic. Alteration of the branching constant clearly can be made to reproduce the burning velocity alone, whatever reaction mechanism is assumed, but, as pointed out in the paper,

some further kinetic analysis is necessary to obtain agreement with burning velocity and profiles.

DR. G. L. SCHOTT (*Los Alamos Scientific Laboratory*): The analysis of the heat release rate made by Dixon-Lewis and Williams provides a new avenue of insight into the chemical progress of the flame that was not pursued heretofore. In considering further the apparent discrepancy between the measured heat release rate and the recombination rate computed from the measured H atom concentration, it is instructive to compare the integral of the heat release profile with the total power which is chemically available from the flame. From Fig. 3,

$$\int_{-1\text{mm}}^{+2\text{mm}} (dH/dy)dy = 1.8 \text{ cal/sec/cm}^2,$$

and the crudely extrapolated contribution of the tail of the curve beyond $y = +2$ mm indicates

$$\int_{-\infty}^{+\infty} (dH/dy)dy \approx 2 \text{ cal/sec/cm}^2.$$

Now the velocity of the gas mixture into the flame is 9.2 cm/sec, measured at 1 atm and 291°K, so that the total input concentration is 4.2×10^{-5} mole/cm^3. Of this, the fraction 4.6×10^{-2} is the stoichiometrically limiting component, O_2. Burning of O_2 to H_2O will be complete at 1078°K, releasing 1.14×10^5 cal/mole of O_2. The product of these numbers, 2.0 cal/sec/cm^2, is the total chemical power per unit area of the flame. Thus, the approximate magnitude of (dH/dy) presented in Fig. 3 is confirmed, and it would seem that the difficulty probably lies in the assessment of the recombination rate. The consequences of energy transport by diffusion, and also the small area change of the flame, remain to be explored. These effects were included in the analysis of Fristrom *et al.*[1]

It would be possible, using the original data, to obtain a check on the H atom concentration (within the precision of the H_2 and H_2O data) by examining the conservation of hydrogen atoms using the methods of Fristrom.[1]

It would also be possible to determine the net progress of recombination, irrespective of the mechanism, using the relationship given recently by Kaskan.[2] The net rate of recombination in the flame is

$$\sum_{i=1}^{s} [\partial n_i/\partial t]_{\text{chem}}$$

moles/cm^3/sec, where the sum is over all species present. The net progress of recombination through the flame from the cold boundary to any point is the integral of this sum along y. From the final stoichiometry of oxygen consumption, we should expect

$$\int_{-\infty}^{+\infty} -\sum [\partial n_i/\partial t]_{\text{chem}}\, dy$$

to be $9.2 \times 4.2 \times 10^{-5} \times 4.6 \times 10^{-2} = 1.8 \times 10^{-5}$ moles/cm^2/sec, apart from the small effect of area change.

It is also interesting to note that Dixon-Lewis, Sutton, and Williams (reference 17 of the paper) find that N_2 and H_2O are of comparable efficiency as third bodies in the recombination reactions of H atoms with both H and OH. In reducing their rate data on these reactions, Bulewicz and Sugden (reference 18 of the paper) assumed the efficiency of H_2O to be very much greater than that of any other species in their system, which contained sizeable quantities of N_2.

PROF. G. DIXON-LEWIS: The integration of the heat release rate as performed by Dr. Schott is in fact a reversal of the final step in our derivation of the latter, and tells us nothing about the distribution of heat release rate. A similar argument would seem to apply to the comment regarding the net rate of recombination over the whole flame. We have not in the paper carried the analysis so far as to determine the terms $[\partial n_i/\partial t]_{\text{chem}}$ experimentally over the whole flame, since this involves extremely accurate knowledge of the diffusion characteristics throughout.

The suggested check on the H atom concentration profile in the particular flame would not be feasible, since we deal with H atom concentrations of the order of 0.1 mole per cent maximum.

DR. T. M. SUGDEN (*University of Cambridge*): I should like to raise three points concerned with recombination in these flames:

(1) The reactions $H + H + H_2O \rightarrow H_2 + H_2O$ and $H + OH + H_2 \rightarrow H_2O + H_2$ are indistinguishable in systems such as these where the balanced reaction $H_2 + OH \rightleftharpoons H_2O + H$ is set up. What assumption was made in obtaining a rate constant for the first of the above reactions?

(2) Was heat release from $H + OH + M \rightarrow H_2O + M$ taken into account in the calculations?

(3) In connection with rate constants for recombination, Dr. T. W. Rosenfeld and I have recently made measurements on hydrogen-rich flames at atmospheric pressure, but with temperatures in the region of 1500°K, i.e., well above that used by Prof. Dixon-Lewis. The results are in broad agreement with these presented by Prof. Dixon-Lewis. Atomic hydrogen was studied by the chemiluminescence of lead and thallium. Accuracy is not great enough, however, to make the results comparable enough to derive a meaningful activation energy.

In the earlier work of Dr. Bulewicz and myself, we made the assumption that H_2O was the only third body. This was only one of the possible points of view, and cannot be distinguished from the case of H_2 and N_2 having nearly equal effi-

ciencies, however large. The difficulty arises because of the relatively small range of relative concentrations of third bodies which has been obtained experimentally at any one temperature.

DR. P. J. PADLEY (*University of Cambridge*): I would like to draw Prof. Dixon-Lewis' attention to the paper by Padley and Sugden which he quotes, in which is given a very reasonable quantitative explanation of his temperature profiles over the first 1 millisecond or so after primary combustion, in terms predominantly of recombination of H and OH radicals in the reaction $H + OH + M \rightarrow HO_2 + M$. Since he, in agreement with earlier work by Bulewicz and Sugden, and Padley and Sugden, finds that reaction (V) is about twenty times as fast as reaction (IV), his omission to consider reaction (V) as a more likely means of radical destruction than reaction (IV) is surprising.

PROF. G. DIXON-LEWIS: We agree with Dr. Sugden regarding the indistinguishability of the two reactions mentioned. In the flames studied by us in reference 17 (of the paper) the ratio (H)/(OH) was very high (up to 500) in one or two of the flames, and the over-all effect in these most hydrogen-rich flames was therefore ascribed to the H atom recombination.

The heat release from $H + OH + M \rightarrow H_2O + M$ was not taken into account in the calculations presented in the paper. However, the equilibrium (H)/(OH) value even at the flame temperature is about 250, and the exploratory calculations showed at that time that the recombination rate did not have too much effect on at least the burning velocity. The effect of reactions involving OH has since been examined in more detail, and it turns out that our assumptions in this direction were completely justified for this flame.

DR. F. FINE (*NASA, Cleveland*): In an earlier investigation, Fenimore and Jones[3] determined a rate expression for the reaction $H + N_2O \rightarrow N_2 + OH$ based on the assumption that the value of (H) in the flame zone was constant throughout and equal to the value determined in the downstream zone. Their flames were stabilized at several pressures up to more than half an atmosphere and had maximum temperatures near 1750°K. To what extent does the observation of a sharp maximum in (H) within the flame zone vitiate their assumption?

PROF. G. DIXON LEWIS: In considering the assumption made by Fenimore and Jones regarding constancy of (H) over a large part of the flame, it must be noted that in addition to their working at lower pressures than ourselves, their values of (H) were about 50 times lower than our maximum value for their flame at 41 cm pressure, and 25 times lower at 12 cm. The combined effects of pressure and (H) are equivalent to decreasing the recombination rate for $H + H + M = H_2 + M$ by a factor of about four to five thousand. This would tend to produce constant (H) on the recombination side of the profile. Their flames also involved faster flows than ours, and this would enhance the effect. There would seem to us at present to be no difficulty in reconciling the assumption with our results.

REFERENCES

1. FRISTROM, R. M., GRUNFELDER, C., and FAVIN, S.: J. Phys. Chem. *65*, 58 (1961).
2. KASKAN, W. and SCHOTT, G. L.: Combustion and Flame *6*, 73 (1962).
3. FENIMORE, C. P. and JONES, G. W.: J. Phys. Chem. *63*, 1154 (1959).

THE STUDY OF THE STRUCTURE OF LAMINAR DIFFUSION FLAMES BY OPTICAL METHODS

T. P. PANDYA AND F. J. WEINBERG

This communication deals with progress made in the stabilization of flat diffusion flames and with the establishment of optical methods for the analysis of their structure at velocities up to blow-out.

The system has been considered theoretically to allow analysis for rate of heat release and correction for the effect of composition. Considerations of the magnitude of optical path gradients in such flames have led to the adaption of two types of optical method: one based on deflection mapping and the other on interferometry. The results presented include photographs of the flat diffusion flame, records of the distribution of flow velocities, and of refractive index and their interpretation.

Introduction

Methods based on refractive index measurement have proved to be well suited to the study of temperature distributions across flat premixed flames. This approach, which makes possible the *in situ* measurement of heat release rate and its distribution, is however limited at atmospheric pressure to near-limit mixtures. Unless recourse is taken to reduced pressures, it is impossible to study the structure of flames of burning velocities much in excess of 12 cm/sec—not to mention reactants too active to be premixed (which are becoming increasingly important in practice).

This communication reports on progress made in a project concerned with the stabilization of suitable diffusion flames and with the establishment of optical methods for the analysis of their structure at velocities up to blow-out.

The Flame

Experimental

In recent years, diffusion flames have been stabilized[1,2] in the counter-flow region of two directly opposed jets carrying individual reactants. The use, in such a system, of the flow rate of reactants at blow-out as a measure of reaction rate has been advocated. A flame of this type seemed, in principle, suitable for the present work, provided the following modifications could be implemented.

Firstly, for optical analysis, a flat flame surface of appreciable area is desirable. In order to achieve this, the reactant flow velocity distributions were rectified to approach constant and uniform values across the burner mouths. The method employed is analogous to that used in the "flat flame burner." The approach velocity distributions are first randomized by beds of glass beads and then streamlined by matrices of flame-trap material. The latter are constructed of adjacent plane and corrugated cupronickel strips spirally wound.

Secondly, the inert gas flow (e.g., the nitrogen of air) was always divided between the two jets in such a manner as to make volume flows equal, when the reactant supply rates are in stoichiometric ratio. This bestows kinetic, as well as aerodynamic advantages. The large difference in jet momenta involved at stoichiometric without this device, set a limit to flame flatness. As regards reaction velocity, the admixture of diluent makes possible the approach to blow-out conditions at conveniently low flow rates.

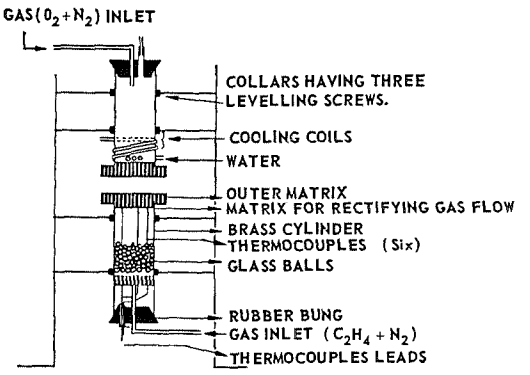

FIG. 1a. Opposed jet burner.

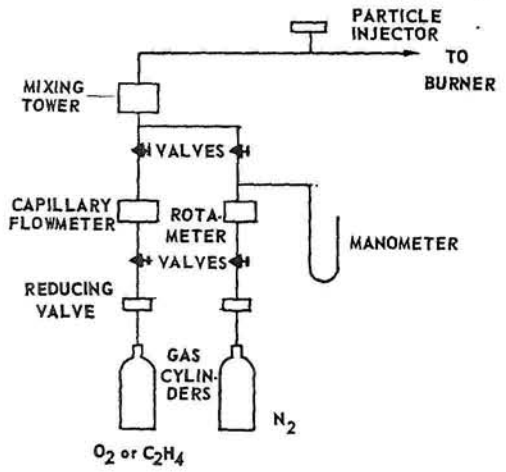

FIG. 1b. Flow delivery apparatus.

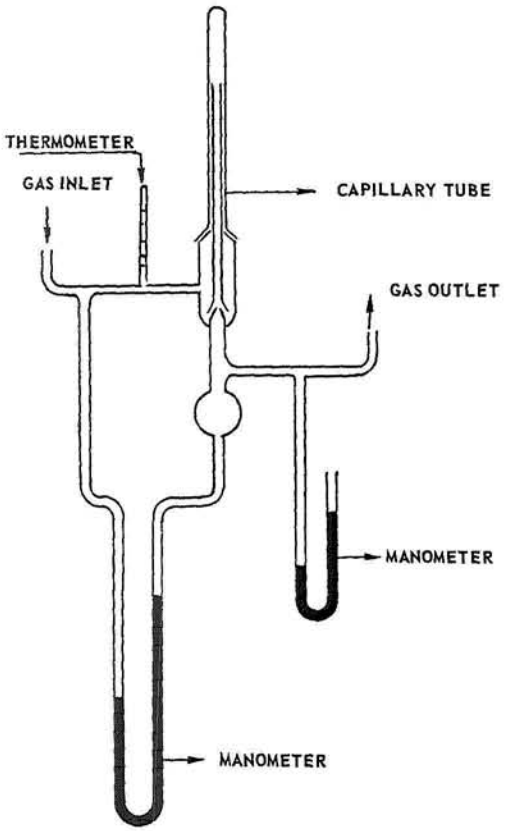

FIG. 1c. Capillary flow meter for measuring ethylene and oxygen flows.

Since the boundary between escaping hot products and the surrounding atmosphere gives rise to appreciable refractive index gradients, it seemed advisable to control it by streamlining the effluent also. Additional matrices were therefore wound on the outside of the vertical burner tubes.

In order to ascertain the approach stream temperatures and any variations in them across the burner mouths, six thermocouples were welded onto the downstream face of each matrix. The temperatures were controlled by water jackets around the burner tubes.

These measures proved successful and led to the stabilization of suitable flames. Figure 1 illustrates the layout of burner and flow systems. A photograph of the flame is shown in Fig. 2. The diameter of the luminous zone is about 8 cm.

FIG. 2. Flat counterflow diffusion flame.

The flow velocity patterns were ascertained by photographing particle tracks under interrupted Tyndall beam illumination. A typical record is shown in Fig. 3. The light source was a high pressure mercury arc operated by ac of 50 cps (i.e., 100 interruptions/sec). Matrix temperatures were of the order of 80°C and varied from their means by less than 5°C.

Theoretical

The system is axially symmetrical. Conservation equations can therefore be expressed in terms of z and r, the axial and radial coordinates respectively. (This is convenient for a general approach but is not necessarily the most suitable frame of reference. In particular cases it may be more convenient to resolve along, and at right angles to, lines of flow.) The generalized steady state equation for any gas property whose flow rate is F per unit area and whose rate of generation is q per unit volume, is

$$(1/r)(\partial/\partial r)(rF_r) + (\partial F_z/\partial z) - q = 0$$

where suffixes denote axes along which components of vectors are taken. For heat, the flow rate per unit area along any coordinate, p, is given, under conditions of laminar flow, by

$$F_p = -k(\partial T/\partial p) + \rho v_p H + R$$

where v, k, ρ, and H are, respectively, the local velocity, thermal conductivity, density, and enthalpy of the gas. R is the radiant energy flow rate, which is negligible in the absence of an

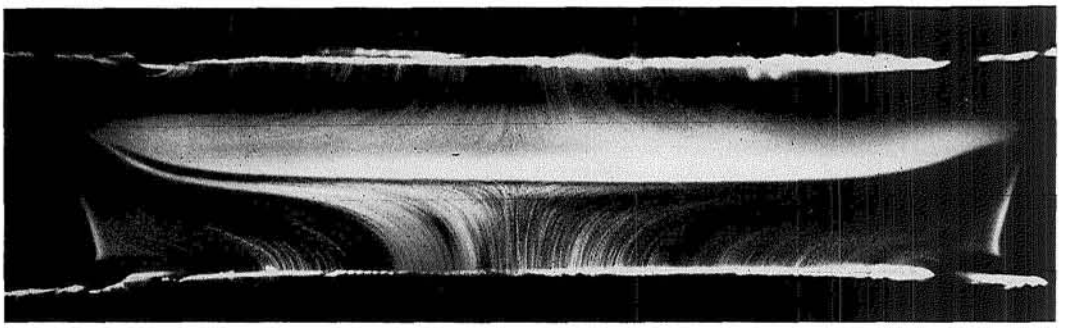

FIG. 3. Particle tracks in diffusion flame; ac-operated high pressure mercury arc (100 interruptions per second).

appreciable concentration of radiating and absorbing soot particles. Apart from this, only frictional terms will be neglected. The source term, q, becomes wQ, where w = rate of reaction and Q = heat of reaction, such that the product is the rate of heat release per unit volume. The full equation is therefore,

$$r^{-1}(\partial/\partial r)[-rk(\partial T/\partial r) + r\rho v_r H] + \partial/\partial z[-k(\partial T/\partial z) + \rho v_z H] - wQ = 0.$$

Away from zones of reaction, the equation must balance without the last term. Elsewhere, the differentials must be determined experimentally, in order to deduce heat release rate. It is worth noting that in the presence of appreciable pyrolysis a heat sink rather than a source term can appear on the fuel side.

Inspection of the heat conservation equation reveals that the deduction of local reaction rate, defined in terms of heat release, demands knowledge of the following data:

(1) The distribution of temperature in r and z. This is the primary function of the refractive index distribution measurement. It can be shown[3] that in flame systems, refractive index variation is occasioned mainly by changes in temperature. Secondary composition variations can be corrected for as indicated below. The method of refractive index measurement in this type of flame is detailed in a later section.

(2) The distribution of flow velocity in r and z. This is obtainable directly from photographs of particle tracks illuminated by an interrupted Tyndall beam. The light from a high pressure, AC-operated mercury arc is focused along a plane containing the burner axis. The particles are bentonite of mean diameter 4 microns. Larger agglomerates, which occur occasionally, can be identified and ignored on the photographs.

(3) Calculation of local values of thermal conductivity, density and enthalpy. In the case of the reactants under study, the major component in the variation of each of these parameters is temperature, which is known at every point. The remaining, composition-induced variation is due largely to diffusion. Only near the central zone of the flame is reaction likely to contribute appreciably. Calculation of composition effects can be based on theories[4,5,6] of diffusion flame structure. Such theories involve assumptions concerning interrelations between transport properties (in particular, equality of diffusion coefficient and thermal diffusivity). Because of the secondary importance of composition effects, it follows that these approximations are much less significant here than in the theories from which they derive. The same approach is involved in correcting the refractive index-temperature conversion for composition effects.

The Optical Method

Choice of Technique in Terms of Optical Path Gradient

The magnitude of the optical path gradient (which is the product of refractive index gradient and geometric path length in the flame—if the latter is constant) determines the steepness of the perturbations induced in an initially plane light wavefront by the test space. Two kinds of approach are available for determining the topography of the emerging wavefront. The methods of geometric optics—notably mapping the angles of deflection—are based on the concept of rays orthogonal to the emerging wavefront. They therefore record the *slope* of perturbations on the front and are most sensitive for large gradients, irrespective of the terminal values.

The methods of physical optics—notably interferometry—"shear" the wavefront, usually with an unperturbed one, producing fringes at fixed phase increments. They therefore record

absolute heights of the perturbations in the form of contour maps and are less suited to measuring steep variations, both because of consequent crowding of fringes and because of deflection effects which here become aberrations. In the analysis of "flat" premixed flames, deflection methods therefore become accurate[3,7] for large diameters. Interferometry has recently been successfully used[8] for a flat flame whose flat portion was relatively small.

The theory of diffusion flames suggests that, so long as blowout conditions are not approached, smaller refractive index gradients are to be expected. On the other hand, large geometric path lengths are again advisable, to guard against predominance of edge effects. It therefore seemed prudent to approach the problem without an *a priori* choice of only one method. The complementary nature of the techniques suggested, on the contrary, that one approach should be perfected from each, the deflection-mapping and the interferometric principles. This seemed desirable in view of the large range of conditions (e.g., flow velocities) that might be encountered and because it seemed quite possible that different approaches might be required even for different regions within the same flame.

Deflection Mapping

In previous deflection mapping studies of premixed flat flames,[7,9] the distorted shadows or images of slits placed before, and inclined at 45° to the flame, were recorded some distance beyond the flame. This method is convenient and accurate for the large angles of deflection caused by the large optical path gradients across these flames. If the method is to be extended to very much smaller optical path gradients, inaccuracies arise because of diffraction at the slits. Every criterion on the diffraction pattern which could be used to read the record, such as the central diffraction maximum, is defined by a given angle subtended at the slit. Thus the sensitivity of the method cannot be increased beyond a certain amount by increasing the displacement on the record per unit angle of deflection (e.g., by increasing the distance between test space and receptor). The width of the central diffraction maximum, for instance, will increase proportionately, and, by remaining a constant fraction of the displacement, will place an absolute limit on sensitivity. This difficulty is further aggravated if not only sensitivity, but also resolution in the test space, is to be increased. This can be achieved only by decreasing slit width and thereby increasing the diffraction-induced indeterminacy on the record.

If deflection mapping were to be extrapolated to optical path gradients very much smaller than those occurring in flat premixed flames, an alternative method of "marking the wavefront" would be advantageous. The principle of the "half-wave step"[10] seemed readily adaptable to present requirements. Parallel strips of magnesium fluoride film, half a wavelength thick, were evaporated onto an optically flat glass plate. The distances between adjacent strips were equal to each other and to the width of the strips. The equidistant steps so produced were used in the same manner as inclined slits in studies of premixed flames. At every step, the wavefront emerging on one side of the edge is π out of phase with the adjacent front. The destructive interference which takes place along the surface containing the step and perpendicular to the glass plate, results in a sharp dark line on a screen or photographic plate, as long as the latter is not too far removed from the half-wave step.

The "resolving power" of this device is compared with that of slits in Fig. 4. Both were placed in an accurately parallel light beam and the "shadow" recorded at a distance of 165 cm. The width of the slits shown lie between 0.049 and 0.123 cm and the wavelength of the light

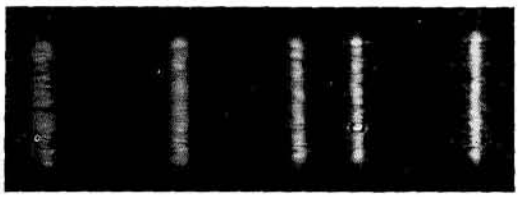

FIG. 4a. Slit diffraction patterns at 165 cm. Slit widths, left to right, are 0.49, 0.66, 0.90, 1.13, 1.23 mm.

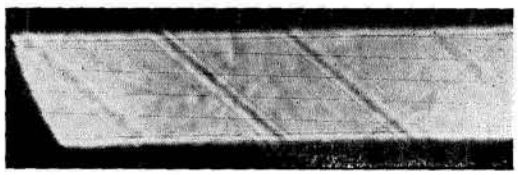

FIG. 4b. Half-wave step diffraction patterns at 165 cm.

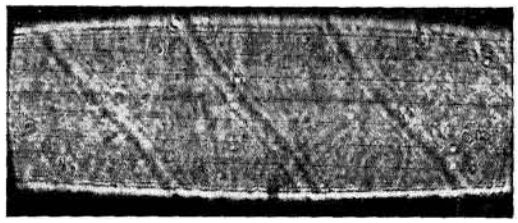

FIG. 5. Half-wave step diffraction patterns beyond flame.

was 5461 AU (green line of mercury). It will be seen that a very considerable improvement in accuracy results from the use of a grid of half-wave steps.

Figure 5 shows the distorted pattern of the half-wave grid after passage of the beam through the flat diffusion flame. Large deflections are observed in the immediate vicinity of the burner mouths. These are also responsible for the apparent increase in the distance between the burner mouths. This property of the deflection field of such diffusion flames has two undesirable consequences. Firstly, the angles of deflection are seen to fall to small magnitudes in the central zones, which are likely to prove the most interesting from the point of view of the flames' mechanism. Secondly, because the refractive index gradients extend right to the burner mouths, the undistorted shape of the grid cannot be ascertained readily from the distorted pattern. In the premixed flame, the refractive index gradient and hence deflection falls to zero on either side of the reaction zone, well before any solid boundary obscures the light beam. Consequently, the undistorted pattern can be construed[9] on the record by interpolation between the undeflected extremities, without requiring a superimposed "blank." The difficulty is aggravated, in the case of the diffusion flames by the necessity of recording the direction, as well as the magnitude, of deflection. The observed deflection pattern thus suggests that an interferogram of the diffusion flame would be valuable, at least as an auxiliary to the ray displacement record.

Interferometry

An interferometer for use in the present work must satisfy the following requirements in addition to those generally common to the study of refractive index fields: The transluminating beam must be collimated in all directions (i.e., the effective source must approximate to a point, not to a line), because the depth of the test space is too great to permit traversal at more than one angle. Furthermore, the interferometer must make possible the recording of fringes with the camera focused on the center of the test space, in order that the appreciably deflected "rays" may terminate on the corresponding points of the "image." This narrows the field very considerably.

The four-mirror Mach-Zehnder[11,12] interferometer is the one most commonly used for this kind of work. Its disadvantages from our point of view, are its very high initial cost and its difficulty of adjustment. The latter is inherent in any instrument based on beam reflection. Thus for mirrors 15 cm in extent and a wavelength of 5×10^{-5} cm, one "involuntary" fringe will appear for an angular misalinement of each mirror of 8×10^{-7} radians!

An interferometer based on much the same principle but employing four diffraction gratings[13] instead of mirrors, is free from these objections; it is both insensitive to misalinement and remarkably inexpensive. It is, however, wasteful of light and has hitherto been used only for non-luminous phenomena. Although the flat diffusion flame is found to be steady enough to permit extended exposure times, it is conceivable that the range of interest may include flames of appreciable luminosity and this interferometer was therefore not used.

The interferometer which appeared most suitable is that discovered by Kraushaar[14] during his attempts to extend a "Ronchi schlieren" system to gratings of greater line frequency. In this, the beam is split and recombined at points of focus by two fragments of a diffraction grating. The theory of the instrument has been developed subsequently.[15,3] It has been shown that the interferometer is insensitive to misalinement, provided[3] that the optical elements used are long-focus schlieren mirrors. Where these are already available, the instrument is also inexpensive. It is less wasteful of light than the four-grating interferometer though, of course, more so than the Mach-Zehnder interferometer.

The optical system used is illustrated schematically in Fig. 6. A circular field of view of diameter equal to the radius of the schlieren mirrors was employed. Thus the gratings should be blazed for maximum transmission in the zero and first orders and their spacings should be $\lambda/\sin(a/f)$, where (a/f) is the ratio of the mirrors' radius to their focal length and λ is the wavelength. (Apart from this relationship, however, the interferometer can be shown[15,3] virtually not to differentiate between wave-

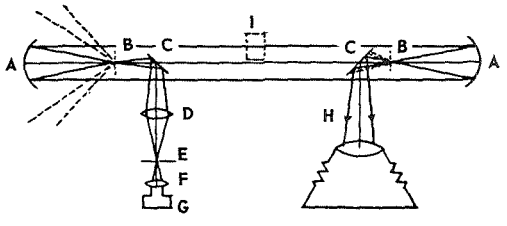

FIG. 6. Two grating interferometer. A—Schlieren mirrors, $f = 243$ cm, $2a = 20$ cm; B—plane transmission gratings 2000 lines/inch; C—front surface polished plane mirrors; D—convex lens of variable aperture; E—pin hole; F—condensing lens; G—M.V. arc; H—Camera focused on test space I.

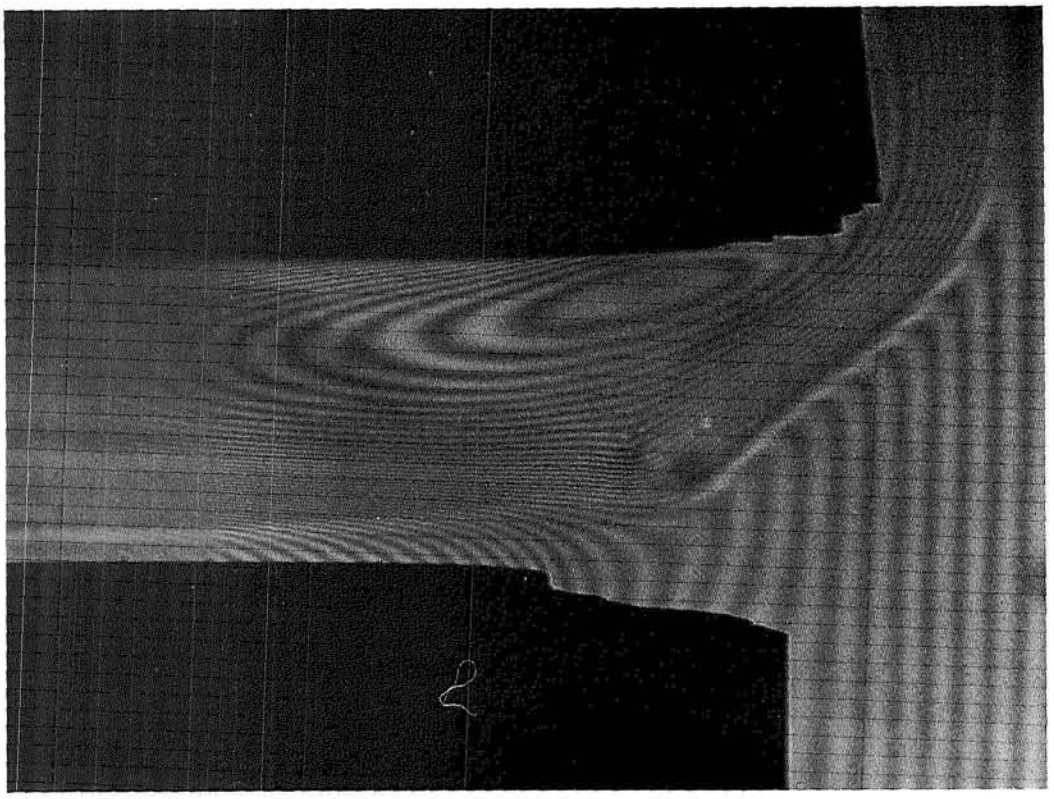

FIG. 7. Interferogram of part of diffusion flame.

lengths). With the (a/f) of 1/24 used, the grating displacement involved in going from 10 fringes/cm to the infinite fringe condition was approximately 2.5 cm.

Figure 7 shows an interferogram extending over half of a diffusion flame.

Analysis of Results

Assuming only radial symmetry, the test space was first divided into 10 "slices" by planes parallel to the burner mouths. Each slice was then divided into 25 annular rings, thus giving 250 elements, within each of which the refractive index was, in the first instance, assumed to be constant. Each slice was now treated independently by a method of numerical analysis: The optical path difference deduced from the interferogram for the outermost annulus was used to deduce the mean refractive index of that element. Considering next the beam which traverses the first and second, but not the third zone, the now calculable optical path due to the first zone was subtracted from the value recorded by the interferogram, to yield the optical path and hence the refractive index within the second annulus. This process was continued until the axis was reached. In some cases, the refractive index was observed to vary so steeply that a further subdivision of the "elements" seemed advisable. This treatment yielded the complete refractive index distribution.

The next step was the translation of the refractive index into a temperature distribution. While temperature is the main variable, the diffusion-induced variation in composition was also taken into account. As discussed above, this secondary dependence was calculated on the assumptions underlying the theories of diffusion flame structure, *viz.*, the equality of diffusion coefficients with the thermal diffusivity. Under these conditions it can be shown that the fractional change in composition is $(\tau - 1)/(\tau_b - 1)$, where τ denotes the ratio of temperature (°K) to its initial value (a parameter convenient in the calculation of refractive index) and the suffix b indicates the burned state.

One method of solution is the use of successive approximations. In this, the entire refractive index distribution is assumed, as a first approximation, to be due to temperature variation alone. The resulting temperature distribution is used to

compute the composition distribution, according to the above equation. The approximate temperature distribution is next corrected and the entire process is repeated until further variation is negligible.

Since, using the above relationship, the composition distribution can be expressed uniquely in terms of temperature, it is equally valid and more rapid to express the dual dependence analytically. Thus, in the law relating refractive index, $(1 + \delta)$, to temperature: $\delta = \delta_u/\tau$; δ_u refers to the mixture composition corresponding to τ and the suffix u denotes initial temperature. Adding the contributions of reactants (suffix r) and products (suffix p),

$$(\tau_b - \tau)\delta_u = (\tau_b - \tau)\delta_{r,u} + (\tau - 1)\delta_{p,u}$$

using this initial condition, it can be shown that

$$\tau = (\delta_{r,u} + x)/(\delta + x),$$

where

$$x = (\delta_{r,u} - \delta_{p,u})/(\tau_b - 1).$$

The flame portrayed in the interferogram in Fig. 7 was of C_2H_4, O_2, and N_2 in stoichiometric proportions. The approach volume flow rates were equal to each other and to 82.5 cc/sec. Thus the two approach molar compositions were $C_2H_4 + 10N_2$ and $3O_2 + 8N_2$. The mean approach temperatures were 75.6°C (top matrix) and 82.2°C (bottom matrix). Analysis of the interferogram yielded the temperature distribution shown in Fig. 8 in which are plotted approximate graphs of temperature against the radial co-ordinate in various planes between the burner mouths. At the flow rate employed, it appears that maximum temperatures are not attained until the gases approach the flame edge.

[*Note added in proof.* Recent work indicates that this is not typical for conditions away from blow-out.]

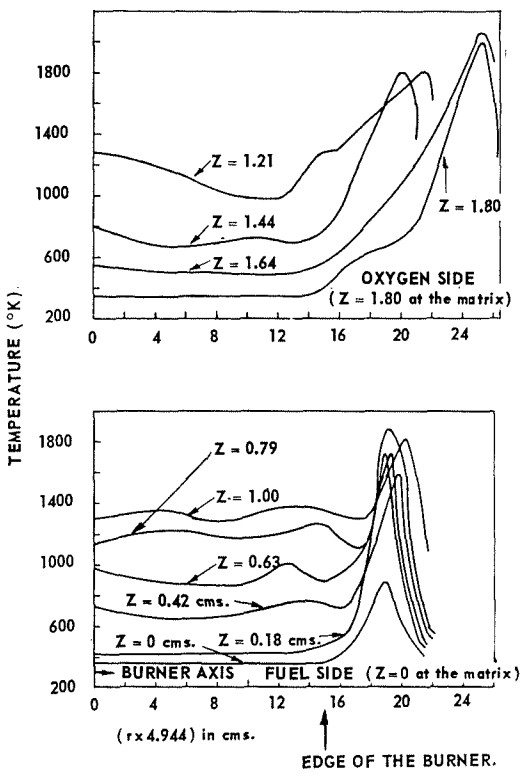

FIG. 8. Approximate temperature distribution in an opposed jet diffusion flame. (Gap = 1.80 cm).

Conclusions

1. A method of stabilizing large, flat diffusion flames in an equal-volume, counterflow regime has been established.
2. Instrumentation to measure the distribution of flow velocities and the approach stream temperatures has been set up.
3. Two optical methods, one based on deflection mapping and the other on interferometry, have been developed for the measurement of the distribution of refractive index and hence of temperature.
4. Their use is illustrated by a complete temperature map of a flame in two dimensions.
5. The approach for analyzing the flames' structures to deduce heat release rates is discussed. Results of such analyses will be published elsewhere.

REFERENCES

1. POTTER, A. E., HEIMEL, S., and BUTLER, J. N.: *Eighth Symposium (International) on Combustion*, p. 1027. Williams and Wilkins, 1962.
2. POTTER, A. E. and BUTLER, J. N.: ARS Journal, *29*, 54 (1959).
3. WEINBERG, F. J.: *Optics of Flames*. Butterworths, London, 1963.
4. FAY, J. A.: J. Aero Sci. *21*, 681 (1954).
5. ZELDOVICH, Y. B.: J. Tech. Phys. (Moscow) *19*, 119 (1949).
6. SPALDING, D. B.: Fuel *33*, 255 (1954); and ARS Journal *31*, 763 (1961).
7. LEVY, A. and WEINBERG, F. J.: *Seventh Symposium (International) on Combustion*, p. 296. Butterworths, 1959; Combustion and Flame *3*, 229 (1959).
8. SCHULTZ-GRUNOW, F. and WORTENBERG, G.: Int. J. Heat Mass Transfer *2*, 56 (1961).

9. BURGOYNE, J. H. and WEINBERG, F. J.: Proc. Roy. Soc. (London) *A224*, 286 (1954).
10. WOLTER, H.: *Handbuch der Physik*, Vol. 24, p. 555. Springer, 1956.
11. MACH, L.: Anz. Akad. Wiss. Wien (Math. Naturwiss.) *Kl. 28*, 223 (1891).
12. ZEHNDER, L.: Z. Instrumentenk. *11*, 275 (1891).
13. WEINBERG, F. J. and WOOD, N. B.: J. Sci. Instr. *36*, 227 (1959).
14. KRAUSHAAR, R.: J. Opt. Soc. Am. *40*, 480 (1950).
15. STERRETT, J. R. and ERWIN, J. R.: N.A.C.A. Tech. Note 2827 1952.

Discussion

H. G. WOLFHARD (*Thiokol Chemical Corporation*): The authors describe temperature measurements in flat diffusion flames using a modified interferometer. This allows the detailed plotting of a temperature map, which ultimately can be used to calculate reaction rates. This method is superior to Schlieren methods as temperature can be measured at low and high values and does not depend on temperature gradients. Two disadvantages, however, are apparent. The maximum temperature in the flame, on which reaction rates are finally based, will not be very accurate. This is due to the uncertainty of the composition and is also caused by the fact that density is proportional to $1/T$, thus at high temperatures the number of fringes will be smaller. In addition, the flame is not absolutely flat and corrections have to be applied for the curvature at the flame edge, again reducing the accuracy of the result, besides making this method rather tedious.

The purpose of this comment is to point out that temperature measurements by line reversal are not only practical but give reliable results and very good space resolution for temperature mapping. In flames as discussed by Dr. Weinberg the temperature gradients are not steep enough to deflect narrow beams of light. Sodium can be introduced into the flame locally, thus edge effects can be prevented.

The two figures give temperature measurements in vertical flat diffusion flames, the burner having two sections, each measuring 3.3 by 0.5 cm, one carrying the fuel, the other, air. It can be seen that

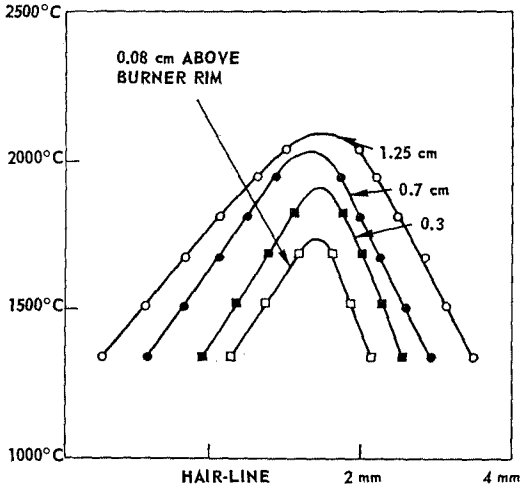

FIG. 2. H_2–air diffusion flame.

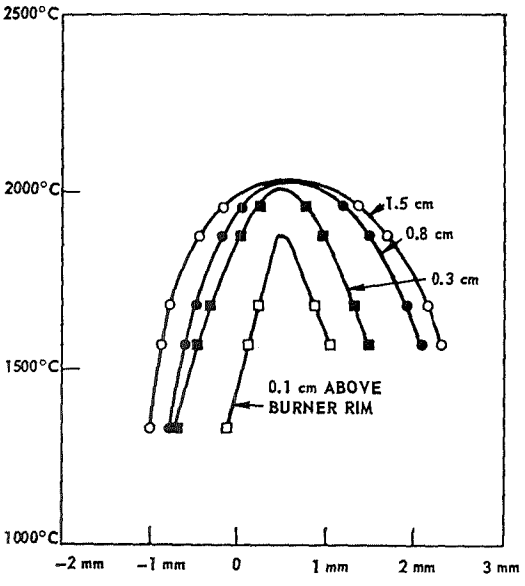

FIG. 1. C_2H_2–air diffusion flame.

the scattering of the reversal temperatures is very small and that various regions in the flame can be clearly distinguished. Of course, temperature measurements by reversal are only practical down to about 1300°C. Thus this method is not suggested to supersede Dr. Weinberg's method but to supplement it in the high temperature region.

There is nothing new in sodium line reversal. The point here is that this method is also useful for detailed temperature mapping and that it is possible to plot many temperature points within a distance of one millimeter by using very slender beams of light for temperature reversal.

DR. F. J. WEINBERG (*Imperial College*): We have already measured the maximum temperatures of these diffusion flames by line reversal (and, inci-

dentally, also by means of thermocouples). Sodium is not very suitable because its salts are insufficiently volatile for these low-temperature flames and chromium, introduced as chromyl chloride, was used.

Because of the finite angle subtended by the light beam at the center of the flame (where the source image is projected) such methods are not suited to the measurement of steep temperature gradients in large flat flames. Indeed, we found line reversal to occur over a range of temperatures at one position. It is, however, possible to deduce the maximum temperature of the range and when the interpretation of the interferogram is pegged to that value—rather than to room temperature—an extremely accurate temperature profile is obtainable.

PROF. L. WALDMANN (*Max Planck Institut für Chemie, Mainz*): A nonuniform gas mixture exerts a force on small suspended particles. The particle velocity due to the force by a temperature gradient and due to friction is $v = 0.14\ \lambda\ dT/p\ dx$, λ being the heat conductivity, p the pressure. For air at room temperature and 1 atm one finds $v = 3.4$ cm/sec for a temperature gradient of 10^4°C/cm. The particle velocity due to the force by a gradient of composition in a binary gas mixture with molecular masses $m_{1,2}$ and due to friction again is

$$v = -\delta m^{\frac{1}{2}}\ D\ d\gamma_1/\langle m^{\frac{1}{2}}\rangle\ dx,$$

where $\delta m^{\frac{1}{2}} = m_1^{\frac{1}{2}} - m_2^{\frac{1}{2}}$, and $\langle m^{\frac{1}{2}}\rangle$ means an average. For a mixture of hydrogen with a heavier gas in which the H_2-mole fraction drops from about 1 to about 0 at a distance of 1 mm, the particle velocity is $v = 10$ cm/sec.[1]

My question to Dr. Weinberg is whether these forces must be taken into account when interpreting the particle tracks in the diffusion flame in terms of the gas flow velocity.

DR. F. J. WEINBERG: These effects are relatively small at barometric pressures and for the flames we are discussing (as, indeed, the numerical value calculated by Prof. Waldmann indicates). Over the central regions of the diffusion flame studied, Fig. 8 of our paper shows that this velocity will barely exceed 1 cm/sec. A correction factor is readily calculable from our results.

The effect seems rather more perturbing in those studies of premixed flames where particle tracks were used for purposes other than the measurement of burning velocity. Considering the effect in the preheat zone alone,

$$\lambda(dT/dx) = \rho v c(T - T_0)$$

where ρ = density, v = flow velocity, c = mean specific heat, suffix 0 denotes standard state.

Thus the percentage error in v becomes

$$[14\rho c(T - T_0)/p]\% = [(14Mc/R)(1 - T_0/T)]\%$$

where R = gas constant and M, molecular weight. The maximum value of this, $(14Mc/R)\%$, seems unreasonably large; it would be valuable to have Dr.

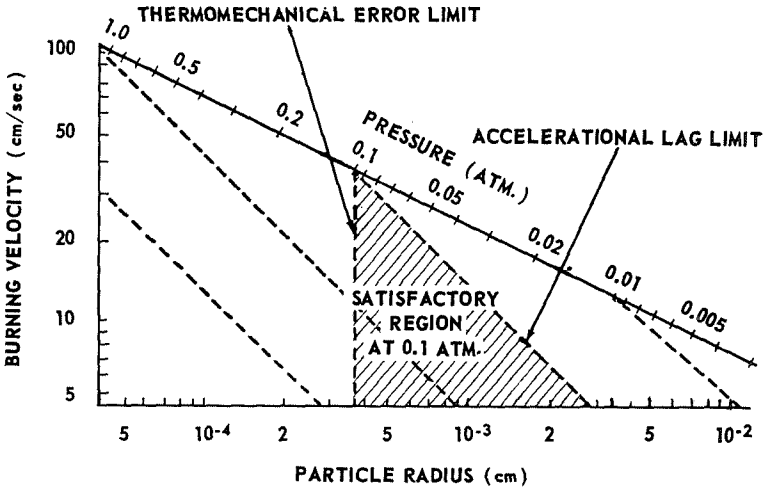

FIG. 3. Regions of quantitative applicability of particle track studies. Burning velocity (cm/sec) is plotted against particle radius (cm). The region for satisfactory particle track studies (error less than 3%) at 0.1 atm is cross hatched. To outline the region for any other pressure, locate the pressure on the diagonal axis. From this point drop a normal to the particle radius abcissa and run a line parallel to the pressure diagonals. (Figure II–7 of reference 3.)

Fristrom's view on this matter, since he used particle tracks in premixed flames in this capacity and has, no doubt, given the matter some thought.

DR. R. M. FRISTROM (*APL/Johns Hopkins University*): As Prof. Waldmann indicates, the thermomechanical effect can be a serious problem in particle track studies. The differences between Prof. Waldmann and Dr. Weinberg can perhaps be resolved by noting that the equation derived by Prof. Waldmann refers to particles which are small compared with the mean free path, while the particles used by Dr. Weinberg and Dr. Pandya were no doubt large compared with the mean free path. (In an atmospheric flame, mean free path ranges from 10^{-4} to 10^{-5} cm, where particles are usually $\sim 10^{-3}$ cm.) The thermomechanical effect for large particles is a factor of 4–5 smaller than estimated by the Waldmann–Einstein relation. (See Waldmann, reference 1, and also reference 2.)

The situation may be clarified by Fig. 3 which gives the rough relation between limits of error imposed by accelerational lag (calculated from Stokes law) and thermomechanical effect (using the relations of Prof. Waldmann for large particles, reference 2). An arbitrary acceptable error of 3% and an empirical relation between the thickness of the primary reaction zone, Eq. (1), were chosen.

$$L = 3P^{-1} v_0^{-1}, \tag{1}$$

where L is flame thickness (cm), P is pressure (atm), and v_0 is burning velocity (cm/sec). These calculations are rough and only apply directly to premixed hydrocarbon oxygen (or air) flames. They do, however, provide a rough guide in determining whether quantitative particle track studies can be made and what particle sizes should be used.

In relation to the velocity induced by a concentration gradient, it would seem that this could introduce serious errors if the products are of appreciably different molecular weight than the reactants. This means a change in mole number is necessary; otherwise, a first order cancellation occurs between the effects of the gradients of the products and reactants. The effect would also be reduced by the addition of a diluent.

DR. G. S. LONGABARDO (*Columbia University*): As a ray passes through a flame it is refracted toward the higher density region in both the r–θ plane and the Z direction. This results in two effects: the geometrical path, and hence the optical path length, differs from that of an unrefracted ray, and, if not considered, results in an error in fringe shift; the location of an image point in the interferogram is only an apparent one, being displaced as it is from its true location by an amount determined by the slope of the ray as it emerges from the flame and its distance at this point to the object plane.

Would Dr. Weinberg please comment on the magnitude of these corrections in his work and, if possible, make some remarks on what "temperature" is being measured?

DR. F. J. WEINBERG: It can be shown, either by calculation, or by direct measurement of our ray-deflection profiles, that the effects of refraction are negligible in our flames, so long as the receptor is focused on the center of the flame.

The temperature measured is translational. We are indeed comparing them with both line (chromium) reversal and thermocouple temperature in the zone of maximum temperature. The agreement is reasonable.

DR. B. FINE (*NASA, Cleveland*): If the Reynolds number of the opposed jets were sufficiently high that the flames were turbulent, would one expect the same sort of temperature distribution and flow pattern? In particular, is it not likely that opposed jet flames stabilized under the conditions of Potter and Anagnostou would show a much less sharp radial temperature profile because of increased mixing in the flame zone?

DR. F. J. WEINBERG: I should have thought that for hydrocarbon flames, the slower second stage of the reaction ($CO \rightarrow CO_2$) is always likely to be blown to the periphery, when blow-out conditions are approached. This would, of course, give rise to higher peripheral temperatures and the appearance of Potter and Anagnostou's flames at blow-out may be partly due to that effect. This, however, is speculation.

REFERENCES

1. WALDMANN, L.: *Rarefied Gas Dynamics*, edited by L. Talbot, p. 323. Academic Press, 1961.
2. SCHMITT, K. H.: Z. Naturforsch. *14A*, 870 (1959).
3. FRISTROM, R. M.: *Experimental Techniques for Flame Structure Studies*, Chapter II, APL/JHU BB Survey No. 300 (in preparation).

THE DECOMPOSITION OF ETHYLENE AND ETHANE IN PREMIXED HYDROCARBON–OXYGEN–HYDROGEN FLAMES

C. P. FENIMORE AND G. W. JONES

The experimental procedures used previously to study the breakup of CH_4 in flames are applied to C_2H_4 and C_2H_6. Composition and temperature profiles are obtained by probing low pressure, flat flames; the profiles are recast as reaction rates, and it is sought to express

$$-d[\text{hydrocarbon}]/[\text{hydrocarbon}]dt = k[\text{H}] + k'[\text{OH}] + k''[\text{O}]$$

and to estimate k, k', and/or k'' from the variation of the specific decay rate with [H], [OH], and [O]. The necessary radical concentrations can be inferred from $-d[O_2]/dt$ and $d[CO_2]/dt$ or from their equivalents if, as earlier work suggests, O_2 is consumed mostly by $H + O_2 \rightleftharpoons OH + O$ and CO_2 generated by $CO + OH \rightleftharpoons CO_2 + H$; and this is assumed true. The estimates of k, k', and k'' found in this way are expected to be correct to within a factor of about two.

In ethylene flames, the consumption of hydrocarbon is found to be due mostly to an attack by O atoms; $k'' \sim 3 \times 10^{10}$ liter mole^{-1} sec^{-1} at 1400° to 1860°K with little temperature dependence, in fair agreement with recent estimates at much lower temperatures. In the presence of much added H_2, transient CH_4 appears in the reaction zone in amounts which are quantitatively consistent with a formation of CH_3 radicals at the rate $k''[O][C_2H_4]$ and with the reaction $CH_3 + H_2 \rightleftharpoons CH_4 + H$ and $CH_3 + O \rightarrow \cdots \rightarrow CO + \cdots$, as previously deduced in CH_4 flames. This too is consistent with recent work at lower temperatures.

In ethane flames, an initial attack by O atoms is not important, and $k[H]$ or $k'[OH]$ predominates depending on the [OH]/[H] ratio in the reaction zone. For $H + C_2H_6$, $k \sim 1.4 \times 10^{11} \exp(-9.7$ kcal$/RT)$ liter mole^{-1} sec^{-1} in fair agreement with most estimates at lower temperatures, the activation energy being thought reliable to about ±2 kcal. For $OH + C_2H_6$, $k' \sim 3 \times 10^{10}$ at 1400° to 1600°K, but the temperature dependence has not been determined as well for k' as for k.

$-d[O_2]/dt$ and $d[CO_2]/dt$ in Hydrocarbon Flames

In flames of O_2–CO–H_2 mixtures, O_2 is consumed largely by reaction (1) and CO_2 generated by (2),

$$H + O_2 \underset{k_{-1}}{\overset{k_1}{\rightleftharpoons}} OH + O \qquad (1)$$

$$OH + CO \rightleftarrows CO_2 + H; \qquad (2)$$

and in hydrocarbon flames, it is probable that these reactions still play the same roles. Evidence that O_2 disappears mostly by (1) in several hydrocarbon flames was obtained[1] by estimating [H] and showing that $-d[O_2]/dt$ approximated to $k_1[H][O_2]$ as long as the reverse of (1) was negligible. This did not altogether exclude other reactions of O_2, to be sure, nor has conclusive evidence been obtained since then; although no case has been found in which it would seem forced to ascribe all of $-d[O_2]/dt$ to (1). The importance of (2) in hydrocarbon flames is generally accepted and is surely true if there is only one major path of CO_2 formation.

In CH_4 flames, furthermore, the roles suggested for reactions (1) and (2) are supported by more detailed studies. CH_3 radicals are thought to be formed by (3)[2,3] and (4),[3] and destroyed by O atoms in the incompletely understood (5),[4]

$$OH + CH_4 \rightarrow CH_3 + H_2O \qquad (3)$$

$$H + CH_4 \rightleftarrows CH_3 + H_2 \qquad (4)$$

$$CH_3 + O \rightarrow \cdots \rightarrow \text{eventually CO} + \cdots \qquad (5)$$

As far as is known, therefore, the CH_4 flame is an O_2–CO–H_2 flame fed by the breakup of CH_4, and the breakup neither consumes O_2 directly nor generates CO_2 directly.

The evidence just cited[1–4] suggests, and it is assumed true, that O_2 is consumed entirely by (1) and CO_2 generated by (2) in the C_2H_4 and C_2H_6 flames studied in this paper. Then it is shown that C_2H_4 reacts mostly by $O + C_2H_4 \rightarrow C_2H_4O^* \rightarrow \cdots$, where $C_2H_4O^*$ decomposes to

give a CH_3 radical and CO, and the CH_3 radical reacts subsequently as in CH_4 flames. The initial reactions of C_2H_6 do not involve O atoms, but are analogous to (3) and (4).

A Typical Experiment

It was not possible to interpret in a self-consistent fashion the decay of hydrocarbon by a hypothetical reaction with O_2; indeed, such an interpretation would contradict the hypothesis about reaction (1). The starting point, therefore, was to ask if the hydrocarbons could be destroyed by any of the probable reaction partners, H, OH, or O. To answer this question, composition, and temperature profiles were obtained by probing low pressure, flat flames on porous burners.[1,3] The profiles were corrected for diffusion and recast as reaction rates, and it was sought to express

$$-d[\text{hydrocarbon}]/[\text{hydrocarbon}]\,dt = k[H] + k'[OH] + k''[O]$$

and to estimate k, k', k'' from the variation of the specific decay rate with [H], [OH], and [O]. The following example shows how this was done for a C_2H_4 flame for which some profiles are plotted in the upper part of Fig. 1.

The necessary diffusion coefficients were obtained by assuming that any CO_2 found where $T < 1300°K$ had diffused from hotter parts of the flame. D_{CO_2} as calculated on this assumption was fitted to the equation $D_{CO_2} = AT^n$ cm^2 sec^{-1}; the parameters found $A = 7.5 \times 10^{-4}$, $n = 1.55$. D_{CO_2} at higher temperatures was taken by extrapolation, and D for other species taken from an inverse dependence on the square root of molecular weight. In other flames, the temperature range where CO_2 was supposed to be present only because of diffusion differed from that used for Fig. 1, but it was always a range in which most of the hydrocarbon had not yet reacted.

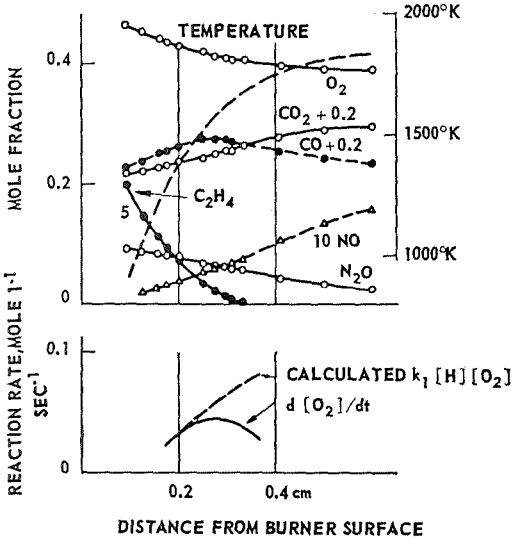

FIG. 1. Profiles through a flame of $C_2H_4 + 8.32\ O_2 + 1.45\ N_2O + 3.50$ Ar; burned at 3 cm of Hg pressure with a mass flow of 3.61×10^{-3} gm cm^{-2} sec^{-1}.

Then $-d[C_2H_4]/dt$ as calculated from Fig. 1 attained a maximum at 1520° and was still 75 per cent of this at 1620°. $-d[C_2H_4]/[C_2H_4]dt$ increased by a factor of 2.5 in this interval; so if the specific decay rate was proportional to [H], [OH], or [O], one or more of the radical concentrations must have increased also.

Radical concentrations were estimated from reactions (1) and (2) or from their equivalents, [H] and [OH] being correct relative to each other to perhaps 20 to 30 per cent, but [O] being less accurate. This estimate reflects the estimated relative accuracy in k_1, k_2, etc., which has been measured previously in terms of one another. A comparison of the k_1 with independent measurements, given in Table 3, suggests that the absolute radical concentrations might be wrong by a factor of about two.

The assumption that N_2O in Fig. 1 was consumed by reaction (6)[3,5]

$$H + N_2O \rightarrow N_2 + OH \qquad (6)$$

gave constant $[H] = 2.0 \times 10^{-7}$ mole liter^{-1} in the interval, 1520° to 1620°. Reaction (6) was convenient because it stayed irreversible everywhere through the flame. Its use was equivalent to the assumption that O_2 was consumed by (1); for early in any flame examined where the reverse of (1) was negligible, $-d[N_2O]/k_6[N_2O]\,dt$ was the same as $-d[O_2]/k_1[O_2]\,dt$.

Measurements of

$$d[CO_2]/dt = k_2[OH][CO] - k_{-2}[H][CO_2]$$

gave essentially constant $[OH] = 8 \times 10^{-7}$ mole liter^{-1}. The reverse of (2) was negligible in this example and small in all runs.

Measurements of

$$-d[O_2]/dt = k_1[H][O_2] - k_{-1}[OH][O]$$

[H] and [OH] being taken as above, gave $[O] = 6 \times 10^{-7}$ mole liter^{-1} at 1520° and 14×10^{-7} at 1620°. [O] depended on the difference,

$$k_1[H][O_2] - (-d[O_2]/dt);$$

since this was only 18 per cent of the calculated $k_1[H][O_2]$ at 1520° and 37 per cent at 1620°, as is shown at the bottom of Fig. 1, [O] could be considerably less certain than [H] or [OH].

It is certain that [O] increased, however; for otherwise the reverse of (1) could not have increased while [OH] remained constant. Also,

[O] could be estimated from the little NO generated by reaction (7)[6]

$$O + N_2O \rightarrow 2NO; \qquad (7)$$

and $[O] = d[NO]/2k_7[N_2O]dt$ agreed with that from (1) and had the same trend of increasing value. Reaction (7) could be used in this sample because NO is essentially inert in very lean flames; but NO is not inert in rich hydrocarbon flames, and (7) could not be used in general.

Thus, of the radical concentrations, neither [H] nor [OH] followed the increase in $-d[C_2H_4]/[C_2H_4]dt$; but [O] increased about 2.3 times as the specific decay rate increased by 2.5.

The Decomposition of Ethylene

Results from six flames are listed in Table 1; the first three were fuel-lean, the others fuel-rich. Transient CH_4 and C_2H_2 were formed in the rich flames and the CH_4 will be discussed below; but the C_2H_2 was ignored because it corresponded to only 1 and 3 per cent of the C_2H_4 fed in the two flames at 4 cm P. The hottest, and richest, run at 12 cm P gave a maximum yield of C_2H_2 equal to 17 per cent of the fuel and some of the C_2H_2 survived into the post-flame gas; but only an upper limit for [O] could be deduced for this run anyway, the last in Table 1, and no conclusions were based on it.

The question is whether an attack by OH, H, or O could account for the rate of decomposition of C_2H_4. The hypothetical process, OH + $C_2H_4 \rightarrow \cdots \rightarrow$ eventual decomposition, could account fairly well for the average consumption in each flame, but not for the increase of $-d[C_2H_4]/[C_2H_4]dt$ within individual runs; the failure excludes attack by OH as the chief reaction, although a smaller contribution of this process cannot be excluded.

The process, H + $C_2H_4 \rightarrow \cdots \rightarrow$ decomposition, could not account even for the average decay of the fuel. A rate constant smaller than 10^{10} liter mole^{-1} sec^{-1} at about 1700° would ensure the unimportance of this process in all runs except the last, and would not conflict with what is known of the reaction of H + C_2H_4 at much lower temperatures.[7]

A destruction by O atoms is most probable. The correlation of $-d[C_2H_4]/C_2H_4]dt$ with [O], as described for Fig. 1, was general; the rate constant in the last column of Table 1, 3×10^{10} liter mole^{-1} sec^{-1} with no marked dependence on

TABLE 1

Rate of Decay of C_2H_4 in Flames

Reactants				P		T Range
O_2/C_2H_4	H_2/C_2H_4	N_2O/C_2H_4	Ar/C_2H_4	(cm Hg)	CH_4, found/C_2H_4, fed*	(°K)
8.32	0	1.45	3.50	3	0	1520–1620
5.50	1.35	3.00	3.60	4	0.01	1720–1860
14.1	0	2.54	6.11	11	0	1380–1420
3.16	4.52	1.5	3.62	4	0.05	1670–1770
6.3	17.1	3.0	7.2	4	0.20	1220–1420
1.21	0	0.41	1.41	12	0.04	1880

$-d[C_2H_4] \times 10^{-4}/[C_2H_4]\,dt$ (sec^{-1})	Radical concentrations (mole liter$^{-1} \times 10^7$)			$k \times 10^{-10}$† (liter mole^{-1} sec^{-1})
	[H]	[OH]	[O]	
1.9–4.9	2	8.0	6–14	3.4
2.8–7.2	5	10.0	6–26	3.1
1.0–4.0	1.2	8.9	5–12	~2.7
2.3–7.5	16–20	5.0	7–22	3.5
0.7–1.2	27.0	5.5	3 ± 1	2 to 4
1.0	7.0	0.8	≤5.0	≥2.0

* Obtained by dividing the maximum CH_4/Ar in the reaction zone by C_2H_4/Ar fed.
† $k = -d[C_2H_4]/[C_2H_4][O]\,dt$.

temperature, agrees as well as should be expected with recent estimates by Cvetanović[8] and by Elias and Schiff.[9] Their values are quoted in Table 3, and their activation energy of 1.6 to 2.9 kcal mole^{-1} might easily be missed at flame temperatures.

Cvetanović[10] found that the attack of O atoms at 300° to 400°K was probably

$$O + C_2H_4 \xrightarrow{k_8} C_2H_4O^* \rightarrow CH_3 + HCO \quad (\text{or} + H + CO) \qquad (8)$$

where $C_2H_4O^*$ can be stabilized by transferring its energy to another molecule, but otherwise breaks up. Some support for this formulation was also found in flames; a mixture of $C_2H_4 + 32H_2 + 8.1O_2$ burned at 7 cm of Hg pressure gave a trace of substances early in the reaction zone which had the mass spectroscopic peaks of CH_3CHO and H_2CO. The substance or substances could be frozen out by liquid N_2, revaporized at room temperature, and could be largely removed from the sample by absorption on Ascarite.

It is reasonable that any $C_2H_4O^*$ which is stabilized in flames would still yield a CH_3 radical and CO on its decomposition, and therefore that CH_3 should be generated at about the rate of $-d[C_2H_4]/dt$. From the discussion of the CH_4 flame in the introduction, it is expected that such CH_3 would disappear by reaction (5) eventually, but also might form transient CH_4 by reversible reaction (4) if much H_2 were present,

$$H + CH_4 \underset{k_{-4}}{\overset{k_4}{\rightleftharpoons}} CH_3 + H_2$$

$$O + CH_3 \xrightarrow{k_5} \cdots \rightarrow CO + \cdots.$$

Table 1 shows indeed that more CH_4 was formed the greater the $[H_2]$; from a rich mixture

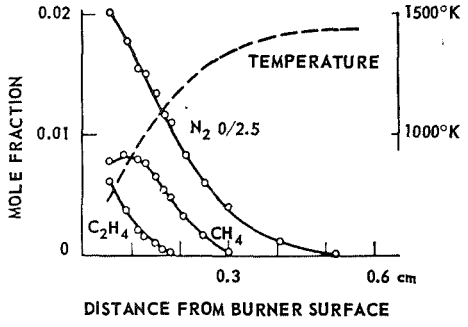

FIG. 2. Profiles through a flame of $C_2H_4 + 43.3\ H_2 + 8.80\ O_2 + 3.0\ N_2O + 7.0$ Ar; burned at 5 cm of Hg pressure with a mass flow of 3.16×10^{-3} gm cm^{-2} sec^{-1}.

of $C_2H_4 + 42H_2$, for which some traverses are shown in Fig. 2, a maximum yield of CH_4 was obtained equal to 46 per cent of the C_2H_4 fed, i.e., 23 per cent of the C atoms. When Fig. 2 was corrected for diffusion, $d[CH_4]/dt$ was found to equal zero at 1060°. The ratio $[CH_4]/[C_2H_4] = 8.4$ at this point can be shown in the following way to be compatible with reactions (4), (−4), (5), and (8).

When $d[CH_4]/dt =$ zero, the approximation

$$d(d[CH_4]/dt)/dt = d(k_{-4}[CH_3][H_2] - k_4[CH_4][H])/dt \sim k_{-4}[H_2]d[CH_3]/dt$$

is all right, the omitted terms being small; if so,

$$\frac{[CH_4]}{[C_2H_4]} = \frac{k_{-4}k_8[H_2]}{k_4k_5[H]}\left\{1 + \frac{d(d[CH_4]/dt)}{k_{-4}[H_2]d[C_2H_4]}\right\}$$

The equilibrium constant, $k_{-4}/k_4 \sim 0.2 \times \exp(-2/RT)$, is known relative to k_5,[4] and approximate values of the other constants are listed in Table 3. Also at 1060° in Fig. 2, $[H_2] = 4 \times 10^{-4}$ mole liter^{-1}, $[H] = 91 \times 10^{-7}$ mole liter^{-1}, $-d[C_2H_4]/dt = 0.019$ mole liter^{-1} sec^{-1}, and $d(d[CH_4]/dt)/dt \sim -410$ mole liter^{-1} sec^{-2}. Hence,

$$[CH_4]/[C_2H_4] \sim 5.4(1 + 0.8) = 10$$

as compared to 8.4 observed; so the transient CH_4 was compatible with (4), (−4), (5), and (8). In the same way, the smaller CH_4 in the flame of $C_2H_4 + 17.1H_2$ listed in Table 1 was compatible with these reactions.

To sum up: The destruction of C_2H_4 and the formation of transient CH_4 are consistent with the predominance of (8), and the k_8 obtained agrees as well as should be expected with recent literature values. A partial consumption of C_2H_4 by attack of OH is possible, but is not as important as (8). Very rich, and hotter, flames form considerable C_2H_2 and possess an additional complexity which has not been treated.

Experiments with Ethane Flames

N_2O was now omitted to avoid interfering with the mass spectroscopic analyses for C_2H_6; $[H]$, as estimated from $-d[O_2]/dt$ early in the reaction zones where the reverse of (1) was negligible, was assumed to persist into regions where $-d[O_2]/dt$ decreased because of the onset of (−1). The assumption was doubtlessly all right; it was certainly true in the C_2H_4 flames described in the last section.

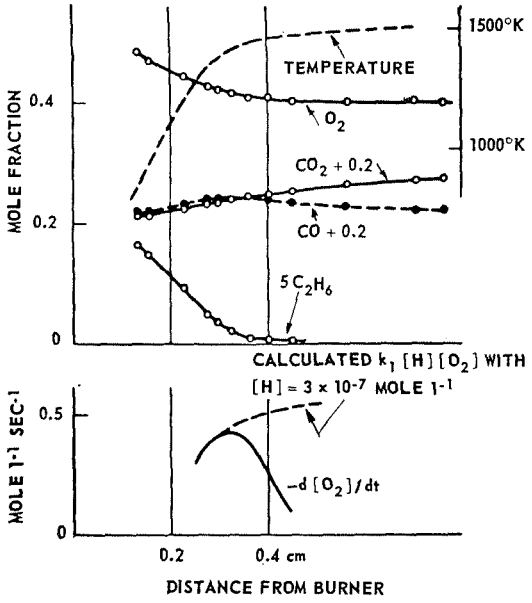

FIG. 3. C_2H_6 + 10.4 O_2 + 6.5 Ar; 3 cm of Hg pressure with a mass flow of 2.72 × 10^{-3} gm cm^{-2} sec^{-1}.

Figure 3 represents traverses through one flame and shows at the bottom of the figure how $-d[O_2]/dt$ was accounted for by $k_1[H][O_2]$ up to about 1420°, and how (−1) became important thereafter. [OH] was estimated as before and was almost constant at 1420° and 1460°, so the onset of (−1) should be ascribed mostly to an increase in [O].

C_2H_6 approached zero more slowly in Fig. 3 than C_2H_4 did in Fig. 1; when the specific decay rate was worked out, $-d[C_2H_6]/[C_2H_6]dt$ did not increase greatly as the fuel neared complete consumption. Since [O] increased in this region, it follows that C_2H_6 was not destroyed largely by O atoms. Either of the two reactions

$$OH + C_2H_6 \rightarrow C_2H_5 + H_2O \qquad (9)$$

$$H + C_2H_6 \rightarrow C_2H_5 + H_2 \qquad (10)$$

or both together would be consistent with the essentially constant [OH] and [H], however, and this was true of all the runs. The results are summarized in Table 2 where the average value of k_9 and k_{10} are listed which would be required to account entirely for $-d[C_2H_6]/dt$ by either (9) or (10).

From the required values of k_9 and k_{10}, it can be seen that if (9) was important in fuel-lean flames where [OH]/[H] was 1.0 to 3.3, it could not have been very important in rich flames too where [OH]/[H] was only 0.03 to 0.08, and conversely for (10). The most reasonable interpretation is that (9) and (10) were predominant in lean and rich flames, respectively. The constants selected in this way are plotted in Fig. 4, the lower curve giving separate estimates of k_{10} at 0.025 cm intervals through each rich flame, and the upper curve giving only the average k_9 from Table 2 because of the small temperature interval covered in each lean flame.

The estimate of k_9 was made in a more restricted temperature range than k_{10}, and E_9 and its associated pre-exponential factor are more uncertain than the corresponding quantities for k_{10}. For this reason, only an average value of k_9 is listed in Table 3, but this absolute value should be correct to about a factor of two; k_{10} would be too small if (10) had been reversible. But this is very unlikely; the values should scatter more if they reflect varying degrees of reversibility.

Previous measurements of k_{10}, listed in Table 3, give an activation energy of about 9 kcal and a steric factor of 0.1 to 1.0,[7] or alternately a smaller activation energy and a 100-fold smaller steric factor.[11] The flame value is consistent only with the larger steric factor, and a similar result was obtained before for the analogous k_4. The flame work asserts that the rate constants for H + RH → R + H_2, RH being CH_4 or C_2H_6, must have pre-exponential factors of order 10^{11} liter $mole^{-1}$ sec^{-1} at high temperatures.

Another comparison with previous work is possible. Since [H] was inferred from reaction (1), the quantity really measured was the ratio k_{10}/k_1, and this has already been estimated from shifts of the explosion limits of H_2–O_2 mixtures by additions of C_2H_6. Baldwin and co-workers[12] deduced k_{10}/k_1 = 68 at 793°K; Gorban and Nalbandian[13] found essentially the same, 40 at 753°; while the flame work, the ratio of the starred values in Table 3, extrapolates to k_{10}/k_1 = 52 at 773° and agrees therefore with estimates at lower temperatures. It is less satisfactory that over a 100° range, Gorban and Nalbandian found $E_1 - E_{10}$ = only 3.1 kcal $mole^{-1}$; for from flames, $E_1 - E_{10} \sim 8$ kcal. But the indirect

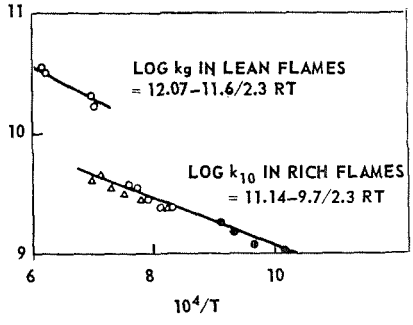

FIG. 4. Rate constants required to account for the destruction of C_2H_6 if this occurred entirely by irreversible reaction (9) or irreversible (10).

TABLE 2

Decay of C_2H_6 in Flames

Reactants			P	T	Required constants* (liter mole^{-1} sec^{-1} $\times 10^{-9}$)	
O_2/C_2H_6	H_2/C_2H_6	Ar/C_2H_6	(cm Hg)	(°K)	k_9	k_{10}
10.4	0	6.54	3	1440	20	67
5.0	0	6.4	3	1600	30	40
5.2	0	6.6	3	1600	30	31
7.3	0	6.6	3	1420	17	31
3.7	0	4.1	2	1610	36	35
4.55	6.3	0	5	1350	47	3.5
7.1	14.8	4.6	3	1260	51	3.0
12.0	46.5	6.9	5	1050	84	1.4

* Constants required to account for the consumption of C_2H_6 by reaction (9) entirely or by reaction (10) entirely.

evaluation from explosion limits assumes that C_2H_6 always consumes the same number of free valencies, and there is no evidence that such is the case. This is not to question the approximate validity of the low temperature interpretation, as Baldwin and co-workers examined it carefully at 793°, but only to suggest that it is not quantitatively invariant over a 100° range as Gorban and Nalbandian supposed.

The subsequent reactions of the C_2H_5 radicals, supposed to be formed in (9) and (10), have not been worked out in flames; nor is it clear how this can be done as well as was possible for CH_3, since $[C_2H_5]$ cannot be measured even roughly, as $[CH_3]$ was.

Discussion

Hydrocarbon flames are essentially O_2–CO–H_2 flames which are fed by the breakup of the hydrocarbon. The important reactions of the O_2–CO–H_2 flames are known, including approximate values of the rate constants, so the chief question remaining is the course of the breakup. Some understanding of this has now been attained in moderately low temperature CH_4 and C_2H_4 flames, although reaction (5), which plays an important role in both of these, is not yet understood. A plausible course of (5) is $O + CH_3 \rightarrow H + H_2CO$ followed by a facile destruction of H_2CO, but no test of this possibility has been made.

Only the initial reactions, (9) and (10), have been identified for C_2H_6, but it is probable that flames of this fuel too involve bimolecular, radical terminating reactions analogous to and even the same as (5). Although it was not discussed, considerable transient CH_4 was formed in rich C_2H_6 flames, and this suggests that (5) occurred in competition with the reverse of (4).

The work supports the old suspicion that low temperature oxidation mechanisms, involving reactions of hydrocarbon radicals with O_2, do not describe steady premixed flames. Doubtlessly an important reason is that reaction (1), with its 18 kcal mole^{-1} activation energy, is 1000 times faster at 1500° than at 700°K, but the reactions of hydrocarbon radicals with O_2 do not increase nearly so rapidly with increasing temperature.

Dependence of the Results on k_2

The value for k_2 was obtained by comparison of the reverse of reaction (2) with the analogous $H + H_2O \rightarrow H_2 + OH$. Kaufman and Del Greco's discharge work, reviewed in this volume, proves that the activation energy used for k_2 was too large, and that $E_2 = 6$ kcal mole^{-1} would be nearer the truth. If E_2 is decreased to 6 kcal but the absolute value of k_2 kept unchanged at 1350°K, the values of k_8 and k_9 in Table 3 do not change very much although the roughly determined activation energy indicated on Fig. 4 is lowered. The rate constant for $O + C_2H_4$ is still $k_8 = 2$ to 3×10^{10} liter mole^{-1} sec^{-1}, according to this paper. The activation energies for the reactions of $CH_4 + OH$ and $C_2H_6 + OH$ are the same, within experimental error, as for CO + OH, but the absolute rates are faster for the hydrocarbons. CH_4 reacts 15^2 or 22^3 times faster with OH than does CO, C_2H_6 reacts 34 times faster according to this paper.

TABLE 3

Reaction Rate Constants

$\log_{10} k(\text{liter mole}^{-1}\,\text{sec}^{-1}) = \log A - E(\text{kcal})/2.3RT$

Reaction	log A	E	T(°K)	Reference
1. $H + O_2 \rightarrow OH + O$	~10.3	15	770–820	14
	10.75	15.1	730–870	15
	11.78	18±3	1100–1500*	5
	log k_1= 9.15	at	1650	16
2. $OH + CO \rightarrow CO_2 + H$	10.35	10.3±3	1200–1350*	17
	log k_2~ 8.9	at	1950	2
4. $H + CH_4 \rightarrow CH_3 + H_2$	~11.5	12 to 13	500–800†	18
	~ 9.0	8	400–500‡	19
	~10.9	7.5 to 10.1	620–740§	20
	11.3	11.5±2	1300–1790*	3
5. $O + CH_3 \rightarrow \cdots \rightarrow CO + \cdots$	log k_5~10.3	at	1200–1900*	4
6. $H + N_2O \rightarrow N_2 + OH$	11.6	16.3±2	1260–1780*	5
7. $O + N_2O \rightarrow 2NO$	11.0	28±3	1400–1900*	6
8. $O + C_2H_4 \rightarrow C_2H_4O \rightarrow \cdots$	10.7¶	2.6 to 2.9	300–400	8
	10.04	1.6	220–460	9
	log k_5~10.5	at	1400–1860*	This work
9. $OH + C_2H_6 \rightarrow C_2H_5 + H_2O$	log k_5~10.4	at	1420–1610*	This work
10. $H + C_2H_6 \rightarrow C_2H_5 + H_2$	11.4	~9.0	300–580	7
	9.53	6.8	350–430‡	11
	11.1	9.7±2	990–1430*	This work

* These values, used or derived in this paper, are supposed to be self-consistent at flame temperatures. The errors in E should not change the absolute values of the constants at flame temperatures; for example, a decrease of 3 kcal in E at 1500° is to be compensated for by a decrease of 0.44 in log A. If the starred k_1 is extrapolated to the temperatures of the other three estimates, it predicts values 4.4 or 1.6 times larger than the independent estimates at 800°, and 2.0 times larger than that at 1650°; and this comparison suggests that the starred k might be wrong absolutely by a factor of about two.

† An approximate composite of older determinations.

‡ So small a log A is inconsistent with an important role for this reaction in flames.

§ In reference 20, E_4 reported as ~8 based on 5.4 kcal activation energy for $D + H_2 \rightarrow HD + H$. The broader range is written because the deuterium exchange might have E = 4.9 to 7.5 kcal.

¶ Ford and Endow[21] suggest an absolute value of k_8 from Cvetanović's relative measurements. Accepting this and Cvetanović's activation energy, one gets the log A written.

References

1. Fenimore, C. P. and Jones, G. W.: J. Phys. Chem. *63*, 1834 (1959).
2. Westenberg, A. A. and Fristrom, R. M.: J. Phys. Chem. *65*, 591 (1961).
3. Fenimore, C. P. and Jones, G. W.: J. Phys. Chem. *65*, 2200 (1961).
4. Fenimore, C. P. and Jones, G. W.: J. Phys. Chem. *65*, 1532 (1961).
5. Fenimore, C. P. and Jones, G. W.: J. Phys. Chem. *63*, 1154 (1959).
6. Fenimore, C. P. and Jones, G. W.: *Eighth Symposium (International) on Combustion*. Williams and Wilkins, 1962.
7. Darwent, B. de B. and Roberts, R.: Discussions Faraday Soc. *14*, 55 (1953).
8. Cvetanović, R. J.: J. Chem. Phys. *33*, 1063 (1960).
9. Elias, L., and Schiff, H. I.: Can. J. Chem. *38*, 1657 (1960).
10. Cvetanović, R. J.: J. Chem. Phys. *23*, 1375 (1955).
11. Berlie, M. R. and LeRoy, D. J.: Discussions Faraday Soc. *14*, 50 (1953).
12. Baldwin, R. R., Corney, N. S., and Simons, R. F.: *Fifth Symposium (International) on Combustion*, p. 502. Reinhold, 1955.
13. Gorban, N. I. and Nalbandian, A. B.: Doklady Akad. Nauk S.S.S.R. *132*, 1335 (1960).

14. BALDWIN, R. R.: Trans. Faraday Soc. *52*, 1344 (1956).
15. KARMILOVA, L. V., NALBANDIAN, A. B., and SEMENOV, N. N.: Zhur. Fiz. Khim. *32*, 1193 (1958).
16. SCHOTT, G. L. and KINSEY, J. L.: J. Chem. Phys. *29*, 1177 (1958).
17. FENIMORE, C. P. and JONES, G. W.: J. Phys. Chem. *62*, 1578 (1958).
18. STEACIE, E. R. W.: *Atomic and Free Radical Reactions*, p. 448. Reinhold, 1954.
19. MAJURY, T. G. and STEACIE, E. R. W.: Discussions Faraday Soc. *14*, 45 (1953).
20. KLEIN, R., MCNESBY, J. R., SCHEER, M. D., and SCHOEN, L. J.: J. Chem. Phys. *30*, 58 (1958).
21. FORD, H. W. and ENDOW, N.: J. Chem. Phys. *27*, 1277 (1957).

Discussion

DR. R. M. FRISTROM (*APL/The Johns Hopkins University*): The two major observations of this paper, (1) that the initial attack of ethane is by OH in lean flames and by H in rich flames, and (2) that the initial attack of ethylene is by oxygen atoms, adds to the number of fundamental reactions which have been studied in hydrocarbon flames by flame structure techniques. Initial reactions are known for a number of hydrocarbons including methane,[1,2,3] ethane,[4] ethylene,[4] and propane.[5] Acetylene and the higher hydrocarbons are yet to be elucidated but there is hope that before many symposia we will understand hydrocarbon oxidation in general mechanistic terms.

I would like to ask Dr. Fenimore if he found any ethane formed in this ethylene flame and if he feels that the reaction[6]

$$H + C_2H_4 \rightarrow C_2H_5$$

can be ruled out. This is a known reaction which is rapid at room temperature, and seems quite attractive in flame studies.

It should be emphasized, as Dr. Fenimore is no doubt aware, that obtaining poor correlation between radical concentration and reaction rate is not sufficient evidence to rule out a particular reaction, since this may mean that more than one radical is competing in the initial attack.

DR. C. P. FENIMORE (*General Electric Research Laboratory*): In answer to Dr. Fristrom's questions, we found no appreciable ethane in the ethylene flames, but a little could have escaped detection. The flames contained added N_2O which, with its decomposition products, would have obscured traces of ethane. The reaction $H + C_2H_4 \rightarrow C_2H_5$ would have been unimportant if its rate constant were about 10^{10} liter mole^{-1} sec^{-1}, the value extrapolated from Darwent and Robert's results at far lower temperatures. If Melville's tenfold larger rate were combined with Darwent and Robert's temperature dependence, a participation of $H + C_2H_4 \rightarrow C_2H_5$ in the decay of C_2H_4 could not be excluded. A partial destruction of C_2H_4 by OH and even by H if the larger rate constant were accepted, cannot be excluded. Our point is that a destruction principally by O atoms makes the best sense of the data and also agrees moderately well with the known reaction rate of $O + C_2H_4$ at lower temperatures.

DR. R. R. BALDWIN (*University of Hull*): I agree with Dr. Fenimore's concluding comment that low temperature oxidation mechanisms may not describe the chemical processes in flames. The correlation of low temperature and high temperature kinetic studies can be very valuable, however, and I should like to illustrate this with reference to the reaction

$$H + C_2H_6 = H_2 + C_2H_5. \qquad (10)$$

Estimates of the steric factors and activation energies of such reactions of H atoms with hydrocarbons have fluctuated considerably, since the first edition of "Atomic and Free Radical Reactions" by Steacie, in 1946. Dr. Fenimore prefers a high steric factor and high activation energy for (10), and this view can be supported by drawing in evidence from a wide range of temperatures. Four estimates of k_{10} are available:

(a) From the flame studies described by Dr. Fenimore and based on his previously determined value of $k_1(H + O_2 = OH + O)$.

(b) From studies of the inhibiting action of ethane on the H_2/O_2 reaction, which give the ratio k_{10}/k_1. The discrepancy between our results and those of Gorban and Nalbandian is less serious than appears from Dr. Fenimore's paper. Our value of 68 for k_{10}/k_1, quoted there, was based on the scheme given by Lewis and von Elbe for the second limit in KCl-coated vessels. Adoption of the simpler scheme that we now believe to operate gives a value of 38 at 813°K, in close agreement with the value of 40 given by Russian workers. We had previously used an extrapolation of the expression for k_{10} given by Berlie and LeRoy to obtain an estimate of k_1 at 813°K. It was noticeable at the time that this gave a lower value for k_1 than other estimates; this discrepancy would disappear if an activation energy

higher than the 6.8 kcal/mole, given by Berlie and LeRoy, were used. We have recently confirmed the higher estimate of k_1 by studies of the inhibiting action of formaldehyde on the H_2/O_2 reaction,[7] and the mean value of 0.6×10^7 liter mole^{-1} sec^{-1} at 813°K should be accurate to ±50%. It now seems more sensible to use this value with the ratio k_{10}/k_1 to estimate k_{10} at 813°K.

(c) From the values given by Berlie and LeRoy from a study of the direct reaction between H atoms and ethane over the temperature range 353–436°K.

(d) From the studies by Darwent and Roberts of the photolysis of D_2S in the presence of ethane. This gives the ratio of the velocity constants for the reaction of D atoms with D_2S and C_2H_6. The former reaction was evaluated relative to $D + H_2$, so that the absolute rate of $D + C_2H_6$ could be obtained. An improved interpretation of their results is possible, however, using the recent calculations of Shavitt[8] for the velocity constant of $D + H_2$.

These various values, at the extreme temperature range of each investigation, are given below.

Author	Temp. (°K)	k (liter mole^{-1} sec^{-1})
Fenimore and Jones	1000	1.05×10^9
	1500	5.4×10^9
Baldwin and Simmons	813	2.3×10^8
Berlie and LeRoy	353	2.1×10^5
	436	1.3×10^6
Darwent and Roberts	300	8.9×10^3
	600	3.9×10^7

The values give an extremely good log k–$1/T$ plot, the values of the Arrhenius parameters being: $\log_{10} A = 11.19 \pm 0.4$; $E = 9.9 \pm 1.0$ kcal/mole. The estimates of error are generous as they assume a possible 100% error in both high and low temperature values.

DR. F. J. WRIGHT (*ESSO Research and Engineering Company*): In his comments on the paper by Fenimore and Jones, Dr. Fristrom indicated that there existed a definite need for more information concerning the reaction of hydrocarbons with radicals such as O, H, and OH. This being also our own view, we have recently investigated the chemistry of the reaction of O atoms with several hydrocarbons such as propane, isobutane, neopentane, etc., using a flow system at 30°C and a titration technique for the production of O atoms. Using a variety of analytical tools, complete quantitative analysis of the reaction products has been obtained.

These studies have led us to the conclusion that the initial attack of the hydrocarbon by O atoms is not an abstraction of hydrogen to yield OH and one alkyl radical as is generally believed. Rather, we found that this initial step consists in the simultaneous displacement by an O atom of two groups on the parent hydrocarbon to yield either ketones or aldehydes. For instance, it is believed that the acetone which is the major reaction product formed from isobutane is produced by the replacement of CH_3 and H by an O atom without the intermediate formation of a *tert*-butoxy radical. Similarly, the acetone which is produced from neopentane also as the most abundant product results from the direct replacement of two CH_3 groups by one O atom. It appears from our work that there is a high probability for the 2 radicals (CH_3 or H) to become not as separate entities but combined as molecular species (H_2, CH_4 or C_2H_6). The details of the evidence and of the arguments which have led to this hypothesis will be published elsewhere. Suffice to say here that a mechanism involving hydrogen abstraction and the formation of alkoxy radicals as intermediates with which the reactive products are formed cannot account for the quantitative aspect of the product distribution and other experimental evidence that we have obtained.

We have also been able to calculate the rates of the reaction of O atoms with a number of saturated hydrocarbons. I hesitate to quote values at this moment, the work being still in progress. They are, however, of the same order of magnitude as those found by Cvetanović and by Schiff for *n*-butane. They are therefore quite low, several orders of magnitude lower, in fact, than the rates for the reaction of O atoms with olefins.

As an initiating reaction, an attack by O atoms on the parent hydrocarbon is thus even less favorable a reaction than the low rate constant would indicate, since, as our studies would indicate, there exists a high probability of formation of molecular products rather than free radicals. It is interesting to note that Fenimore and Jones, whose conditions are vastly different from those of our own work, have also reached this conclusion for ethane flames.

DR. F. J. WEINBERG (*Imperial College*): Concerning Dr. Fenimore's reference to our earlier work, we thought at the time that the concentration of any radical on which the over-all reaction rate were to depend, should have to pass through a maximum. I must confess that I still do not see how this can be avoided, since the radical concentration must eventually revert to a (lower) equilibrium association value.

DR. C. P. FENIMORE[9] Levy and Weinberg[9] deduced the local rates of heat evolution through lean C_2H_4–air flames a few years ago and considered the following question. If the rate of heat evolution, $\dot{q}$, was proportional to $[C_2H_4][x]k_0 \exp(-E/RT)$, where x was some unknown reaction partner, what must the profile of $[x]$ have been for various assumed E, it being supposed that $[C_2H_4]$ could be estimated from the temperature traverse with the use of $D_{C_2H_4} = \lambda/C_p\rho$. Their conclusions were that for large E (about 40 kcal), $[x]$ must have decreased far too rapidly as one went downstream through the reaction zone for x to have been O_2. For small E (5 kcal), $[x]$ must have increased through the reaction zone; and for intermediate E, $[x]$ must have gone through a minimum. The authors liked none of these results—but in fact, the combination of small E and $[x]$ increasing is what we find, and leads to the identification x = O atoms.

REFERENCES

1. WESTENBERG, A. A. and FRISTROM, R. M.: J. Phys. Chem. *65*, 591 (1961).
2. FENIMORE, C. P. and JONES, G. W.: J. Phys. Chem. *65*, 2200 (1961).
3. FRISTROM, R. M.: This volume, p. 560.
4. FENIMORE, C. P. and JONES, G. W.: This paper.
5. FRISTROM, R. M., AVERY, W. H., and WESTENBERG, A. A.: Institut Francais du Petrole et Annales des Combustibles Liquids, *13*, 544 (1958).
6. STEACIE, E. W. R.: *Atomic and Free Radical Mechanisms*, vol. 1, p. 439. Reinhold, 1954.
7. BALDWIN, R. R. and COWE, D. W.: Trans. Faraday Soc. *58*, 1768 (1962).
8. SHAVITT, I.: J. Chem. Phys. *31*, 1359 (1959).
9. LEVY, A. and WEINBERG, F.: Combustion and Flame *3*, 229 (1959).

SOME OBSERVATIONS ON THE MECHANISM OF IONIZATION IN FLAMES CONTAINING HYDROCARBONS

J. A. GREEN AND T. M. SUGDEN

Some new results using the mass spectrometric technique for studying positive ions in flames are reported. The great bulk of the ionization found in hydrogen flames is found to arise from traces of hydrocarbon impurity. Most of the work described deals with the ionization induced by addition of small amounts (about 1%) of acetylene to hydrogen–oxygen–nitrogen flames. A distinction between ions formed in the flame itself and those resulting from secondary reactions associated with the sampling system is drawn. The principal mechanism is found to be

$$CH + O \rightarrow CHO^+ + e^- \qquad k_1$$
$$CHO^+ + H_2O \rightarrow CO + H_3O^+ \qquad k_2$$
$$H_3O^+ + e^- \rightarrow H_2O + H \qquad k_3$$

k_3 is found to be 2.3×10^{-7} cm^3 sec^{-1}, and k_2 to be 7×10^{-9} cm^3 sec^{-1}. An estimate of k_1 of 3×10^{-12} cm^3 sec^{-1} is made. Thermochemical and structural considerations of possible primary ionization reactions are discussed.

Introduction

The past five years have been notable for a concerted attack on the problem of ionization in hydrocarbon flames by mass spectrometric means, instruments having been developed for this purpose by three separate groups, that of Calcote[1] in the United States, that of van Tiggelen[2,3,4] in Belgium, and that of Sugden[5–8] in England. All the instruments sample ionized gas directly from a flame, the most important differences between them being that Calcote's operates on flames at pressures of the order of 10^{-2} atm, van Tiggelen's at about 10^{-1} atm, while the Cambridge instrument has so far been applied to flames at atmospheric pressure.

The most significant point about the results is the fairly good agreement both on points of immediate fact, and on the type of reaction mechanism involved. The purpose of this paper is to present some new evidence in favor of a particular mechanism—that favored by Calcote[1]—which has also been discussed by Bascombe, Green, and Sugden.[8] This is

$$CH + O \rightarrow CHO^+ + e^-$$
$$CHO^+ + H_2O \rightarrow H_3O^+ + CO$$
$$H_3O^+ + e^- \rightarrow H_2O + H$$

for the main part of the reaction. A particular feature of the work to be presented is the use of hydrogen flames with controlled, small, amounts of hydrocarbon as additive. This has the advantage of making the source of ionization a controllable variable.

Experimental

The essential features of the mass spectrometric apparatus have already been discussed in some detail.[7] Briefly, the flame, burned with premixed gases at a 1.5 mm diameter Pyrex capillary tube, plays directly on to a water-cooled platinum foil about 0.002 inch thick, in which is pierced a hole of diameter in the range of 0.001–0.003 inch. Rapid pumping on the low pressure side of the foil maintains a pressure of about 10^{-3} mm Hg in the first chamber, about 3 cm long. The ions pass to a conventional 60° deflection magnetic analyzer via slits leading to further chambers maintained at about 10^{-5} and 10^{-6} mm Hg by additional pumping systems. Collimation is achieved by a system of electrostatic lenses in the various chambers.

Improvements since previous reports have been directed towards reproducibility and rapidity of measurement. These factors are tied together since the worst feature of the instrument, when used with hydrocarbons, is a drift on account of deposition of reaction products on the electrodes of the first chamber and the first slit.

The burner is held on the axis of two coaxial brass rings by three centering screws in each ring. This permits the flame to be centered accurately on the sampling hole in the platinum disc. The rings are mounted on a small sliding carriage, with a maximum traverse of about $\frac{1}{2}$ inch, controlled by a micrometer. This carriage is mounted on a much larger slide, with a traverse of about 5 inches. This slide is operated by a motor-driven screw of 1 mm pitch. The drive is obtained either from a dc motor, with reversing facilities, at a rate of about 2 inches/min, or, when correct positioning has been obtained, by a constant speed 1500 rpm ac motor coupled via a worm gear and an electromagnetic clutch. This latter motor synchronizes with the chart drive motor of a pen recorder, so that ion profiles can be plotted automatically. This is normally done over a distance of about 1 mm through the flame front at the tip of the reaction cone. An increase in working speed of about tenfold over manual operation is attained.

Another feature is the possibility of automatic, rather than manual, scanning of the final accelerating voltage over a portion of the range corresponding with about 4 mass units in the region of mass 20, and somewhat larger scans in higher mass regions. A 12-volt repetitive sawtooth signal is obtained either from a motor-driven potentiometer (period 10–60 sec) or from a time-base unit (period 20 sec or less). This is coupled to the mass spectrometer by a dc amplifier to give a scanning voltage amplitude of about 300 volts. The output from the detector of the mass spectrometer is fed either to an oscilloscope or to a pen recorder. Sweep periods of less than 20 sec are rarely used because of long time constants in the counting system. This device provides a marked improvement over manual scanning for limited ranges, and enables useful information to be obtained from small samples of relatively rare fuels (i.e., very pure or isotopically enriched).

The basic flame was obtained by burning premixed hydrogen, oxygen, and nitrogen, all from cylinders, with an unburned composition of $H_2/O_2/N_2 = 1.0/0.3/1.0$ (by volume). The primary reaction cone was about 3 mm in height, with a column of burned gas a few cm long. The burned gas just beyond the reaction zone had a sodium D line reversal temperature of 2300°K. The reaction zone (about 0.1 mm thick) became clearly visible on addition of 1% of acetylene to the fuel.

A feature of the present work was variation of the size of the input hole. This could be done rapidly by mounting platinum discs, each with a different sized hole, on separate front plates which were readily interchangeable. Further experimental points will be discussed as they arise.

Ionization in "Pure" Hydrogen Flames

Knewstubb and Sugden[7] have discussed at length the positive ions—principally H_3O^+ and its hydrates—which are obtained with a hydrogen-oxygen-nitrogen flame, using standard cylinder gases. Up to 10^9 ions cm^{-3} in the reaction zone were observed. On the basis of discussions at the 8th Combustion Symposium, and of the use of pure hydrogen as a nonionizing flame source for gas chromatographic detection, it was decided to see whether the ions observed arose from the presence of such impurities as would occur in cylinder gases—principally hydrocarbons and their derivatives. A significant point in this connection is the presence of small but distinct peaks at mass numbers 43, 59, and 77, which appear very strongly in pure hydrocarbon flames, and which cannot be given reasonable formulae unless carbon is included in them.

For this purpose the apparatus depicted in Fig. 1 was used. A is a precision steel tube about 70 cm long and 7 cm in diameter, closed at both ends, and containing a very light aluminum piston B. The piston is fitted to the tube so that it does not fall under its own weight when the closed tube is held vertically. A may therefore be filled with a mixture of combustible gas and oxidant through a valve at C, and B will remain at the top.

A tap (not shown) is operated so that the normal premixed supply to the burner is diverted through D, E being simultaneously opened to the burner. Thus the special supply of premixed gases from A passes to the burner through E, the piston B being driven down by the normal supply. At the end of the traverse of B, the normal supply is restored to the burner via D and E. Thus samples of special gas—e.g., very pure, or isotopically enriched—may be burned without the necessity of extinguishing and relighting the burner with consequent wastage. Valves at G and F give protection against striking back (which has not yet occurred). The cylinder holds sufficient supplies for about 20 sec of burning time.

Gas chromatography of cylinder hydrogen showed significant hydrocarbon peaks which became larger as the cylinder emptied. Experiments on electrical conductivity of diffusion flames with addition of small controlled amounts, up to 500 ppm, of acetylene to hydrogen fuel indicated that cylinder gas contained the equivalent of about 75 ppm of acetylene. The gas substitution apparatus of Fig. 1 was then run with

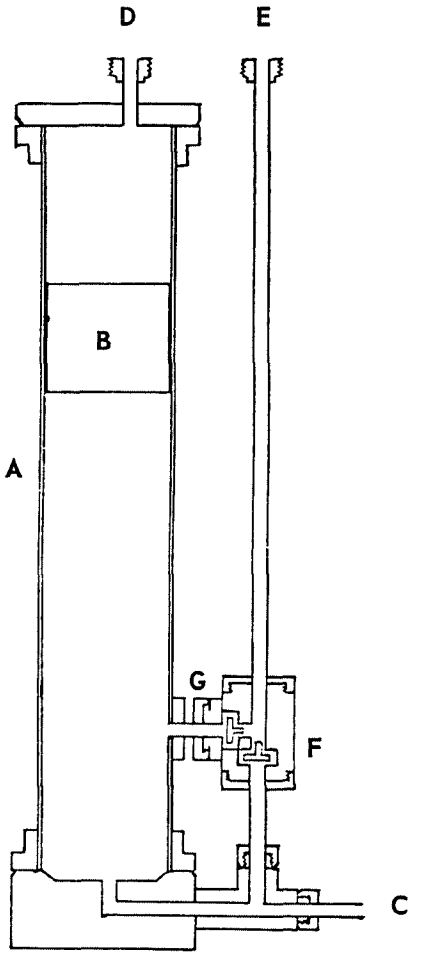

FIG. 1. Gas substitution system for burning mixtures of special fuels and oxidants. A, cylinder; B, aluminum piston; C, input valve; D leads to "normal" flame supply; E leads to burner; G and F, anti-"flash-back" valves.

purified hydrogen and air. The hydrogen was obtained by electrolysis of aqueous barium hydroxide using nickel electrodes. Air was purified by passing it over red-hot copper oxide, washing with 40% sodium hydroxide, and collecting over distilled, air-free, water. With these precautions, the ion count of H_3O^+ (by far the most abundant ion) registered by the mass spectrometer fell by a factor of 7 as compared with cylinder hydrogen and ordinary air.

It is considered that the residual ionization—equivalent to that of about 10 ppm of hydrocarbon—could arise from contaminants from the PVC connecting tubing, from the piston itself, or from indrawn ambient air around the flame. It is reasonable to draw the conclusion that the positive ions—presumably H_3O^+—observed in hydrogen flames are produced through the intervention of hydrocarbon impurities. A carbon-containing precursor is therefore to be expected.

Addition of Hydrocarbon to Hydrogen

It has been seen that, when a pure hydrocarbon is burned at atmospheric pressure, a bewildering array of positive ions is observed, which puts severe strains on deciding on reaction mechanisms.[6] Further, variations of the system by changing the hydrocarbon/oxygen ratio, for example, give simultaneous changes in composition, temperature, flame speed, and all other parameters of the flame. Some simplification should be achieved by using hydrogen as a basic fuel, adding to it controlled amounts of hydrocarbon sufficiently large to swamp the effects of adventitious impurities in the cylinder hydrogen, but small enough not to cause marked changes in the bulk properties of the flames. This enables the nature and quantity of the hydrocarbon additive to be used as separable variables, against a relatively constant background.

Hydrogen-oxygen-nitrogen flames as a basic system have the advantage of being rather well understood from the chemical standpoint. Large amounts of the radicals H, OH, and O are produced in the reaction zone, their concentrations in the burned gas right up to the zone being interrelated by the establishment of certain equilibria by rapid, reversible, bimolecular reactions[9]:

$$H_2 + OH \rightleftharpoons H_2O + H$$

$$H_2 + O \rightleftharpoons OH + H$$

$$O_2 + H \rightleftharpoons OH + O$$

H_2 and H_2O molecules are the bulk constituents, with N_2 diluent, for a fuel-rich flame. [H] and [OH] then considerably exceed [O], and the recombination of radicals in the burned gases towards full equilibrium is governed by

$$H + H + X \rightarrow H_2 + X$$

$$H + OH + X \rightarrow H_2O + X$$

where X is a third body. Flame photometric methods have been devised for measurement of [H] and [OH], and have been applied by Padley and Sugden[10] to obtain values in the region of emergence from the reaction zone. Observations on the NO–O "continuum" indicate that [O] is related to the concentrations of H and OH as would be expected from the above equilibria.[11]

A very useful advantage for the present work is the observation of Padley[12] that addition of

up to 1% of various hydrocarbons (including acetylene) to the hydrogen fuel does not materially affect the concentrations of H and OH near the reaction zone. It follows that [O] will be similarly unaffected. Combining Padley's observations with the most recent calibrations by Phillips[13], the maximum values of [H], [OH], and [O] reached in the reaction zone of the present hydrogen flame are 6×10^{16}, 2×10^{16}, and 1×10^{15} cm^{-3}, respectively.

Ions Detected on Addition of Acetylene to Hydrogen Flames

Figure 2 shows the maximum counts of positive ions up to mass 67 obtained when 1% of acetylene is added to the flame gas supply. The pattern is intermediate between those obtained with cylinder hydrogen with no hydrocarbon additive,[7] and with pure acetylene as fuel.[6] In particular mass numbers 19, 37, and 55 stand out, corresponding with the H_3O^+ ion (19) and its first two hydrates, although to a lesser extent than with the nominally pure hydrogen.

Identification is relatively easy although in some cases not without ambiguity. The following general points were of assistance:

1. All ions are based on C, H, O, and N, apart from the possibility of a trace of potassium impurity.

2. Masses 18 and 36 were very markedly reduced when argon was substituted for nitrogen in the flame gas supply, as was to some extent mass 26; this identifies them as NH_4^+, $NH_4^+ \cdot H_2O$, and (partially) CN^+.

3. Many ion peaks are explicable as isotopic satellites of their immediately lower mass neighbors, on the basis of natural concentrations of H^2, C^{13}, O^{17}, and O^{18}; such peaks are dotted in Fig. 2.

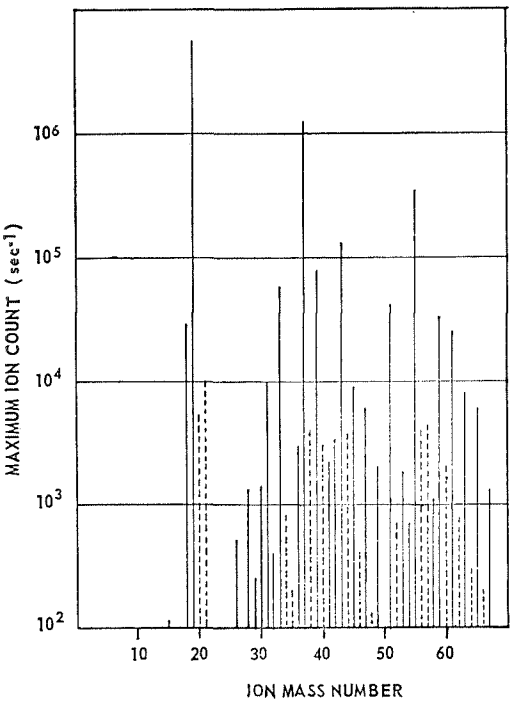

FIG. 2. Maximum ion counts in a flame of $H_2/O_2/N_2$ = 1.0/0.3/1.0 with 1% of acetylene in the fuel.

TABLE 1

Assignment of Formulae to Ion Peaks of Fig. 1

Mass No.	Formula	Mass No.	Formula
15	CH_3^+	43	$C_2H_3O^+$, $C_3H_7^+$
18	NH_4^+	45	$C_2H_5O^+$, CHO_2^+
19	H_3O^+	47	$C_2H_7O^+$, $CH_3O_2^+$
26	$C_2H_2^+$, CN^+	49	$CH_5O_2^+$
28	$C_2H_4^+$	51	$C_4H_3^+$
29	CHO^+, $(C_2H_5^+)$	53	$C_4H_5^+$, C_3HO^+
30	NO^+	54	$C_4H_6^+$, $C_3H_2O^+$
31	CH_3O^+	55	$H_3O^+ \cdot 2H_2O$
32	CH_4O^+	58	$C_2H_2O_2^+$, $C_3H_6O^+$
33	CH_5O^+, (HO_2^+)	59	$C_2H_3O_2^+$, $C_3H_7O^+$
36	$NH_4^+ \cdot H_2O$	61	$C_2H_5O_2^+$
37	$H_3O^+ \cdot H_2O$	63	$C_5H_3^+$, $C_2H_7O_2^+$
39	$C_3H_3^+$, (K^+)	65	$C_5H_5^+$
41	$C_3H_5^+$, C_2HO^+	67	$C_5H_7^+$, $C_4H_3O^+$
42	$C_2H_2O^+$, $C_3H_6^+$		

The assignment is given in Table 1. Where more than one formula is quoted in Table 1 there are ambiguities which arise because the basis of assignment does not lead to a unique result. The mass spectrometer does not have sufficient resolution to separate mass peaks of similar (integral) masses. There is, of course, no necessity for a mass peak to be unique to a particular ion in the flame. Some formulae have been omitted because of their chemical improbability, e.g., $C_2H_9O^+$ for mass 49. Others have been omitted because they correspond with substances of much higher ionization potential than substances of the same molecular weight. Thus $C_2H_4^+$ is preferred to CO^+, and CH_4O^+ is preferred to O_2^+. Where a second formula is quoted in parentheses it is distinctly a second preference. In the case of mass 29, CHO^+ is preferred to $C_2H_5^+$ since its profile through the flame front is very different from those of ions which must uniquely be hydrocarbons, e.g., CH_3^+ (15), $C_3H_3^+$ (39), $C_4H_3^+$ (51). For mass 33, CH_5O^+, the methyl derivative of

H_3O^+, is preferred to HO_2^+ because of the stability of H_3O^+ and of the rather high ionization potential of HO_2 (11.53 ev).

Investigations were not pursued beyond mass 67, although it is known that ions of greater mass occur,[6] because of what seemed to be unnecessary complication, and because it would seem likely that a mechanism involving production of primary positive ions of rather low molecular weight can operate, since considerable ionization occurs in low pressure flames.[1] The list of Table 1 is still a formidable one which fortunately can greatly be simplified by further experimental considerations.

"Flame Ions" and "Input System" Ions

Among the early features of the experimental results was the strong variation of the relative numbers of various ions. In particular, the 18/19 ratio (NH_4^+/H_3O^+) ranged from 10^{-1} to 10^{-3}. This was established as depending on the size of the input hole—small holes giving relatively more NH_4^+ ion, and relatively less H_3O^+. Examamination of other ion counts showed that a broad classification into those that behaved like NH_4^+ and those that behaved like H_3O^+ on reduction of hole size could be made.

In the class that are emphasized by small holes are notably the three known hydrates at masses 36, 37, and 55. These are molecules bound together by ion-dipole forces, which should not give bond strengths of more than 50 kcal/mole at the outside. Such ions could not be stable at flame gas temperatures. It is natural, therefore, to look for their formation in regions of lower temperature, i.e., in the boundary layer between the flame gases and the outer face of the platinum foil,[14] which will be about 0.1 mm thick, or in the gases expanding into the first chamber, which will have been cooled somewhat by contact with the walls of the hole. Decreasing the size of the hole will have the effect of allowing the boundary layer more effectively to extend across it, so that ions from the flame will have to pass through it, where they may be modified by reaction. A smaller hole will also give greater cooling of the gas passing through it.

One may therefore distinguish between "flame ions," which are produced homogeneously in the flame gases, and would be so in the absence of the sampling system, on the one hand, and on the other, "input system ions," produced in the boundary layer or first chamber by reactions of "flame ions" with neutral molecules. Counts of the former are decreased strongly by decreasing the hole size, while the latter may actually increase in number under these conditions. Table 2 shows the mass numbers which can firmly be put into one or the other category for the fuel system used here. The assignment of an ion to the "flame ion" group means that there is definite evidence for its production in the flame, and hence a complete mechanism must include it. Assignment of an ion to the "input system" group unfortunately does not mean that it cannot be produced in the simple flame as well. As pointed out above, however, some of the ions listed as "input system" types are most unlikely, for stability reasons, to be produced in the simple flame, and the point of view will be taken here that all ions in this class need not be considered in formulating a mechanism.

TABLE 2

Mass Numbers of Various Ion Types

Flame ions	Input system ions	Ions with no positive assignment
19	18	15
26	28	30
29	32	39
31	33	41
40	36	63
47	37	65
49	42	67
61	43	
	45	
	51	
	53	
	54	
	55	
	56	
	58	
	59	

Among the ions which show insufficient effect of hole size for distinct classification mass 39 is of interest. The difficulty arises because of contamination of the platinum with potassium, which has proved to be very difficult to eliminate, and which gives rise to a large 39 count with small input holes. Mass 40, however, which is reasonably explicable with large holes as a C^{13} isotopic

TABLE 3

Flame Ions

H_3O^+	$C_3H_3^+$
$C_2H_2^+$, CN^+	$C_2H_7O^+$, $CH_3O_2^+$
CHO^+	$CH_5O_2^+$
CH_3O^+	$C_2H_5O_2^+$

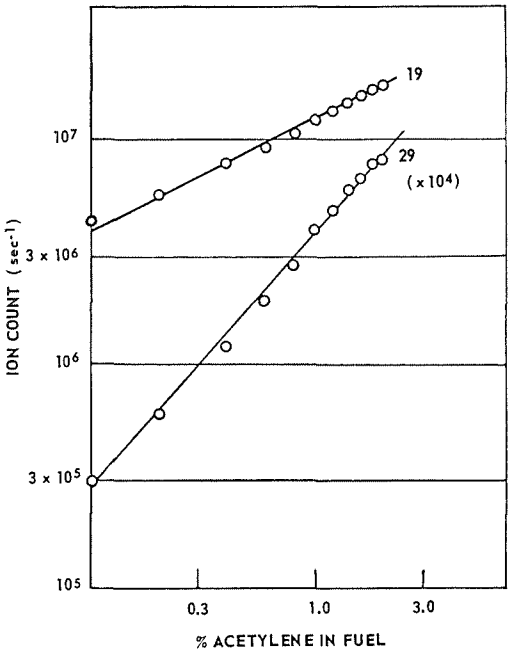

FIG. 3. Dependence of maximum counts of ions at mass 19(H_3O^+) and mass 29(CHO^+) on % acetylene in hydrogen fuel.

form of $C_3H_3^+$, is a flame ion, and hence C_3H_3 must be included in the list of ions to be discussed. These are set out in Table 3.

Effect of Variation of Amount of Additive

Figure 3 shows the effect of varying the amount of additive on the maximum counts of two ions—19 (H_3O^+), and 29 (CHO^+). The logarithmic plot has a slope of 1.1 for CHO^+ (or unity within experimental error), and 0.5 for H_3O^+. These experiments were all done with a relatively large input hole so as to give a minimum of interference by the sampling system. Similar plots for CH_3O^+ (31) and $C_3H_3^+$ (39) gave slopes of 1.6 and 2.1, respectively. Plots for the other flame ions of Table 3 are not yet available. Thus one may say, within experimental error that $[H_3O^+] \propto [C_2H_2]_0^{\frac{1}{2}}$, $[CHO^+] \propto [C_2H_2]_0$, $[CH_3O^+] \propto [C_2H_2]_0^{1\frac{1}{2}}$, and $[C_3H_3^+] \propto [C_2H_2]_0^2$, where $[C_2H_2]_0$ denotes the concentration of acetylene in the unburned gases. These indices are of great value in testing suggested mechanisms.

Ion Profiles and the Recombination Rate of H_3O^+

Figure 4 shows the profiles of two ions—19 and 29—through the flame front into the burned

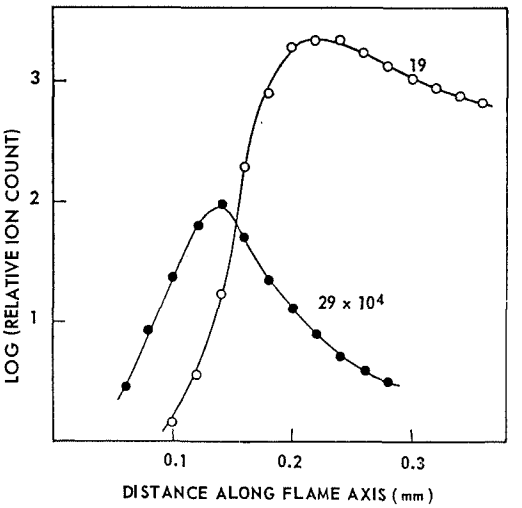

FIG. 4. Profiles of ion counts of mass 19(H_3O^+) and mass 29(CHO^+) through the flame front of a hydrogen flame with 1% acetylene.

gases obtained with a fairly large hole. Observa- of this kind on "input system" ions are not very helpful at this stage because of lack of precise knowledge of the history of such ions and thus of correlation of the position of the burner with the region of gas sampled. On the other hand, such profiles for "flame ions" should be meaningful if taken for large holes where the counts of these ions are not seriously depleted by input system effects.

The H_3O^+ ion is the only flame ion which persists downstream out of the immediate reaction zone, and is detectable with rapidly decreasing concentration for almost 2 mm. Under these conditions one may write $[H_3O^+] = [e^-]$, since experiments with the mass spectrometer show negative ions to be negligible. Disappearance of ions will then be by

$$H_3O^+ + e^- \rightarrow H_2O + H \qquad k_3$$

or possibly to give other products, and with equal concentrations of positive ions and electrons. H_3O^+ will follow a bimolecular decay law

$$1/[H_3O^+]_1 - 1/[H_3O^+]_2 = k_3(t_2 - t_1)$$

where t denotes time. Since the speed of the burned gases is known, the time scale may be converted into a distance scale. An absolute calibration of the detection system was made by spraying very dilute cesium chloride solution into the flame gas supply so as to deliver a known amount into the flame. The cesium is almost completely ionized, supplying therefore one Cs^+ ion for each added atom. On the basis of this calibra-

tion absolute values can be given to $[H_3O^+]$. Plots of $1/[H_3O^+]$ downstream of the reaction zone against distance can thus be made to yield values of the recombination rate constant k_3. Values of k_3 obtained in this way were found to depend on size of sampling hole since, as the hole becomes smaller, serious depletion of the H_3O^+ yield by hydrate formation occurs, giving too large a value of k_3. Extrapolation to infinite hole size, however, is short, and a final value of k_3 of $(2.2 \pm 1.0) \times 10^{-7}$ cm^3 sec^{-1} is obtained. This compares well with Calcote's value[1] of 2×10^{-7} cm^3 sec^{-1} for low pressure flames, and King's value[15] of 2.5×10^{-7} cm^3 sec^{-1} for a methane-air flame at 66 mm pressure.

The 29 profile differs from that of other flame ions (and most input system ions except hydrates) in not having a sharp cutoff on the downstream side. Some of these other ions are hydrocarbon ions, and it is this feature of mass 29 which supports the view, very important to the subsequent development, that it is CHO^+ rather than $C_2H_5^+$.

The Mechanism of Reaction

The general mechanism

$$B + C \rightarrow AH^+ + e^- \qquad k_1$$

$$AH^+ + H_2O \rightarrow H_3O^+ + A \qquad k_2$$

$$H_3O^+ + e^- \rightarrow H_2O + H \qquad k_3$$

is proposed to explain the formation of H_3O^+ via a precursor primary ion AH^+. The formulae of AH^+, B, and C are to be determined. The experiments with the substitution cylinder show that AH^+ must be carbon-containing, as therefore must be at least one of the molecules B or C.

The great excess of H_3O^+ among the flame ions shows that AH^+ must be a reactive intermediate, and application of steady state treatment to it yields

$$d[AH^+]/dt = 0 = k_1[B][C] - k_2[AH^+][H_2O]$$

At the maximum of the H_3O^+ profile, one may also put

$$d[H_3O^+]/dt = 0 = k_2[AH^+][H_2O] - k_3[H_3O^+]^2_{max}$$

since $[H_3O^+]_{max} = [e^-]$ (or very nearly).

$$[H_3O^+]_{max} = (k_1[B][C]/k_3)^{\frac{1}{2}}$$

$$[AH^+] = k_1[B][C]/k_2[H_2O]$$

Hence the intermediate must follow the rule $[AH^+] \propto [H_3O^+]^2_{max}$, and the only ion which has been examined which does this is CHO^+ (29): Its behavior must therefore be looked at more carefully. $[H_3O^+]_{max}$ for 1% acetylene is found to be 2.0×10^{11} cm^{-3}. Therefore

$$k_1[B][C] = 4.0 \times 10^{22} \times 2 \times 10^{-7} = 8 \times 10^{15}\text{cm}^{-3}\text{sec}^{-1},$$

where k_2 is the rate constant of a proton transfer reaction which should be exothermic if it is to produce H_3O^+ with the necessary efficiency. A survey of similar reactions by Trotman-Dickenson[21] leads to a suggestion of 10^{-8} cm^3 sec^{-1} for k_2, a value also chosen by Calcote,[1] and one which is confirmed by a rough determination described below. This leads to $[AH^+] = 8 \times 10^5$ cm^{-3}, taking $[H_2O]$ as 10^{18} cm^{-3}. Thus the ratio $[H_3O^+]_{max}/[AH^+]$ should be about 2.5×10^5, while the experimentally observed ratio is 4×10^5, which is very satisfactory. Thus $[CHO^+]$ fits well from a quantitative standpoint.

The product $[B][C]$ is observed to be proportional to $[C_2H_2]_0$, which makes it very unlikely that both B and C are carbon-containing. This would imply that one of them, say C, is a molecule normally to be found in hydrogen flames, the most likely candidates being the reactive radicals H, OH, and O. If this is so then B is CO, C, or CH, respectively. There is negligibile ionization in flames of hydrogen and carbon monoxide, and, using data from Gaydon[16] and from Field and Franklin,[17] the reaction $H + CO \rightarrow HCO^+ + e^-$ would be 176 kcal endothermic, and thus negligible. The reaction $C + OH \rightarrow CHO^+ + e^-$ is only 23 kcal endothermic, using 170 kcal/mole for the latent heat of sublimation of graphite, but in any case the evidence for appreciable atomic carbon in flames, except at very high temperature,[18] is slender. On the other hand the reaction $CH + O \rightarrow CHO^+ + e^-$ is thermoneutral, using the heat of formation of CH of 143 kcal/mole (i.e., the value based on $L(C) = 170$ kcal/mole), and further, CH is well known in electronically excited form as a reaction zone constituent, and the ground state has recently been detected in absorption experiments.[19] Padley[12] has shown that the CH emission from the reaction zone of hydrogen flames with small amounts of acetylene is directly proportional to the amount of additive, and it has already been pointed out that $[O]$ is hardly affected by the additive.

A rough estimate of k_1 of 3×10^{-12} cm^3 sec^{-1} for reactants CH and O has been obtained by Bascombe, Green, and Sugden[8] by considering the known rate constant of $NO^+ + e^- \rightarrow N + O$, which is an exothermic reaction, and equating the frequency factor of its reverse reaction, obtained by statistical thermodynamic calculation

of the equilibrium constant, with k_1. A very rough estimate of ground state [CH] of 10^{13} cm^{-3} (probably to within an order of magnitude in either direction) is based on consideration of the threshold of detectable absorption spectrum. Taking [O] = 10^{15} cm^{-3} from above, then k_1[B][C] is estimated to be 3×10^{16} cm^{-3} sec^{-1}, which is within a factor of 4 of that obtained in the present experiments.

The second reaction becomes

$$CHO^+ + H_2O \rightarrow CO + H_3O^+$$

and is exothermic to the extent of 34 kcal, if a heat of formation of 137 kcal/mole for H_3O^+ is used. This value is based on the very reliable measurement of the proton affinity of H_2O by Tal'rose and Frankevich[20] of 169 ± 2 kcal/mole. The heat of formation of 195 kcal/mole quoted by Field and Franklin is unreliable.[17] Thus the mechanism

$$CH + O \rightarrow CHO^+ + e^- \qquad k_1 \quad \Delta H \sim 0 \text{ kcal}$$

$$CHO^+ + H_2O \rightarrow CO + H_3O^+ \qquad k_2 \quad \Delta H = -34 \text{ kcal}$$

$$H_3O^+ + e^- \rightarrow H_2O + H \qquad k_3 \quad \Delta H = -145 \text{ kcal}$$

has been put on a firm quantitative basis. The revised thermochemistry strengthens the arguments in its favor already advanced by Calcote.[1]

The next section deals with possibilities of reaction of O atoms with other flame radicals R. It has proved impossible to find any reaction in which the molecules H, OH, HO_2 or O_2 in their ground states react with carbon-containing radicals in their ground states which remotely approaches thermoneutrality. There seems to be little reason for considering reactions involving electronically excited molecules, since their concentrations are always very low, when there is a thermoneutral reaction involving ground state molecules only.

Thermochemical and Structural Considerations of $R + O \rightarrow RO^+ + e^-$

The data given by Field and Franklin[17] show that, in general, radicals R with odd numbers of hydrogen atoms are about 40 kcal/mole easier to ionize than those with even numbers of these atoms. Table 4 lists the H-odd radicals up to an (arbitrary) limit of mass 65. The second column of this table shows the values of heat of formation of R with the addition of the heat of formation of atomic oxygen (59 kcal/mole). Heats of formation were derived from Field and Franklin,[17] a special point about CH being that the value

TABLE 4

Thermochemical Considerations of the Reaction $R + O \rightarrow RO^+ + e^-$

Radical R	Heat of formation of radical + 59 (kcal/mole)	Ion RO^+	Heat of formation of RO^+ (kcal/mole)
CH	202	CHO^+ (29)	203
CH_3	90	CH_3O^+ (31)	173
C_2H	(180)?	C_2HO^+ (41)	(200)?
C_2H_3	142	$C_2H_3O^+$ (43)	174
C_2H_5	83	$C_2H_5O^+$ (45)	165
C_3H	?	C_3HO^+ (53)	?
C_3H_3	143	$C_3H_3O^+$ (55)	(160)
C_3H_5	92	$C_3H_5O^+$ (57)	(150)
C_3H_7	79	$C_3H_7O^+$ (59)	136
C_4H	?	C_4HO^+ (65)	?
C_4H_3	?	$C_4H_3O^+$ (67)	?
CHO	59	CHO_2^+ (45)	150
CH_3O	50	$CH_3O_2^+$ (47)	(130)
C_2HO	59	$C_2HO_2^+$ (57)	(130)
C_2H_3O	49	$C_2H_3O_2^+$ (59)	(110)
C_2H_5O	41	$C_2H_5O_2^+$ (61)	(100)
CHO_2	?	CHO_3^+ (61)	?

TABLE 5

Structural Formulae of Radicals, R, and Ions, RO^+

Radical R	Positive ion RO^+
$\vdots CH$	$HC{\equiv}\overset{+}{O}$, $H\overset{+}{C}{=}O$
$\cdot CH_3$	$H_2{=}\overset{+}{C}{-}OH$, $H_2{=}C{=}\overset{+}{O}{-}H$
$\cdot C{\equiv}CH$	$\overset{+}{C}{\equiv}C{-}OH$, $O{=}C{=}\overset{+}{C}{-}H$
$H_2C{=}\dot{C}H$	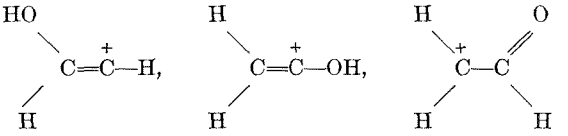
$\cdot C{\equiv}C{-}\ddot{C}H$, $:C{=}C{=}\dot{C}H$	$O{=}C{=}C{=}\overset{+}{C}H$, $\overset{+}{O}{\equiv}C{-}C{\equiv}CH$, $O{=}\overset{+}{C}{-}C{\equiv}CH$
$H_2\dot{C}{-}C{\equiv}CH$	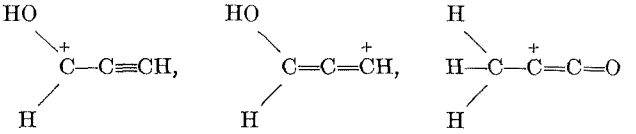
$H{-}\dot{C}{=}O$	$HO{-}\overset{+}{C}{=}O$, $H{-}\overset{+}{O}{=}C{=}O$, $HO{-}C{\equiv}\overset{+}{O}$
$H_2\dot{C}{-}OH$, $H_3C{-}\dot{O}$	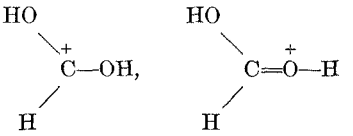
$H\dot{C}{=}C{=}O$, $H{-}C{\equiv}C{-}\dot{O}$	$HO{-}\overset{+}{C}{=}C{=}O$, $H{-}\overset{+}{O}{=}C{=}C{=}O$

based on 170 kcal/mole for the latent heat of sublimation of carbon was taken. The value for C_2H is a rough estimate of an upper limit assuming $D(HC \equiv C{-}H)$ to be 120 kcal/mole. The third column shows the ions RO^+ and heats of formation, where quoted without parentheses, from Field and Franklin.[17] The values in parentheses are rough estimates from data for related ions, and are not likely to be in error by more than 20 kcal/mole.

Table 4 shows at once that R molecules with one atom of oxygen are improbable sources of ions RO^+, since they give very endothermic reactions with O. Examination of Table 5, where representative structural formulae of R and RO^+ are set out, shows the kind of extra bonding achieved by the RO^+ formation. It is obvious that R molecules with two oxygen atoms can be ruled out. The examples of CH_3 and C_2H_3 in Tables 4 and 5 show that only very unsaturated hydrocarbon radicals need be considered. From a bonding point of view (Table 5) CH clearly scores over C_2H in stabilization by RO^+ formation. The radicals C_3H and C_3H_3 must clearly be left as possible sources, as must higher, heavily unsaturated radicals.

The only clear case of a very simple radical R which yields positive ions RO^+ by an almost thermoneutral reaction is, however, CH. Moreover, this radical is known to be present in the reaction zone, both in the ground state and electronically excited, which cannot at present be said for C_2H, C_3H, C_3H_3 or higher very unsaturated radicals, although the spectra of electronically excited C_2 and C_3 are known.[18] Thus, thermochemical and structural considerations lead directly to $CH + O \rightarrow CHO^+ + e^-$ as a primary ionization reaction.

The Behavior of Ions in the First Chamber and an Experimental Estimate of k_2

It is possible to arrive at a value of k_2 by considering the behavior of various ions in the first chamber of the mass spectrometer. Between the entrance hole and the slit leading to the second chamber is a hollow conical electrode with a hole in its apex[7] about 2 mm in diameter, directed axially along the analyzer with the apex pointing towards the entrance hole. This is usually maintained at a potential of about -150 volts relative to the platinum foil (ground), and serves to help to form and collimate the positive ion beam in an axial direction. The apex is about 1 cm from the entrance hole in the foil.

Figure 5 shows plots of four ion counts as the voltage on this conical electrode is varied. The collimating action is shown by the roughly linear variation of mass 19 (H_3O^+). A similar effect is shown by mass 18 (NH_4^+). This is an "input system" ion, and this result shows that it is made in the boundary layer outside the entrance hole—presumably by reaction of H_3O^+ with ammonia molecules generated by catalytic action at the platinum.

$$H_3O^+ + NH_3 \rightarrow H_2O + NH_4^+$$

Once in the first chamber, it is subject to the same collimation as H_3O^+ ions.

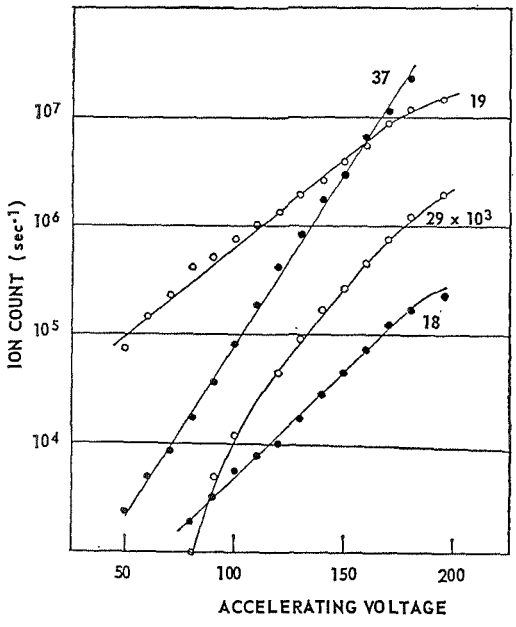

FIG. 5. Ion counts against accelerating voltage (negative) on the conical electrode in the first chamber of the mass spectrometer system, for a hydrogen flame with 1% acetylene.

The monohydrate of H_3O^+ at mass 37 shows a much steeper slope—roughly proportional to the square of the voltage. This suggests that it is made by attachment in the space between the entrance hole and the electrode.

$$H_3O^+ + H_2O \rightarrow H_5O_2^+$$

Higher accelerating voltages increase the chance of attachment by enhancing the retention of H_3O^+ and $H_5O_2^+$ ions in the nascent beam in the first chamber.

The CHO^+ ion (29) is of great interest here. At high accelerating voltages it behaves not very differently from H_3O^+ but falls away very rapidly at low voltages. It is suggested that this is caused by reaction of CHO^+ in the chamber with H_2O to give H_3O^+. On the basis of an estimated pressure of 10^{-1} mm Hg in the cloud of gas just inside the entrance hole the time for a CHO^+ ion to travel from the entrance to the apex of the first electrode, beyond which it is effectively collision-free, is 5×10^{-7} sec, when the electrode potential is -100 volts. Figure 5 suggests that this is about the half-life for reaction with H_2O in the chamber. Thus the half-life in the flame gas at atmospheric pressure is of the order of 10^{-10} sec. Since this gas contains about 10^{18} cm^{-3} molecules of H_2O, then

$$k_2 \sim [\ln 2/(10^{-10} \times 10^{18})] = 7 \times 10^{-9} \text{ cm}^3 \text{ sec}^{-1}$$

This is in agreement with the empirical estimate of 10^{-8} cm^3 sec^{-1} used above. A similar value has been used by Calcote.[1]

Other Flame Ions

The mechanism of production of the other flame ions of Table 3 deserves some consideration. Only one reasonable primary reaction has been found, and it is therefore natural to look for processes in which the other ions are derived from either CHO^+ or H_3O^+, preferably the latter because of its abundance. One should also, as far as possible, be restricted to neutral molecules which are either major constituents or known intermediates.

Thus, the equilibrium

$$CH_3O^+ + H_2O \rightleftharpoons H_3O^+ + CH_2O \quad (\Delta H \sim -4 \text{ kcal})$$

appears reasonable. The equilibrium constant of this reaction will be of order unity, and the ratio $[CH_3O^+]/[H_3O^+]$ is about 10^{-3} at the maximum of H_3O^+. This would imply a concentration of CH_2O molecules of about 10^{15} cm^{-3}, or about 0.02% of the total gases. Since formaldehyde is a known intermediate in oxidation at lower temperatures (cool flames), its presence in reaction zones to this extent is not improbable. As

it was consumed downstream the CH_3O^+ would rapidly be converted to H_3O^+.

Similarly, the $C_3H_3^+$ ion could be established from CH_3O^+ by the equilibrium

$$CH_3O^+ + C_2H_2 \rightleftharpoons C_3H_3^+ + H_2O \quad (\Delta H \sim -12 \text{ kcal})$$

involving unburned acetylene, or acetylene actually produced in the reaction zone. This reaction, with an equilibrium constant of about 10, and with $[C_3H_3^+]/[CH_3O^+] \sim 10$, would imply about 0.2% of acetylene in the reaction zone, which seems on the high side.

The above equilibria require that $[CH_3O^+] \propto [C_2H_2]_0^{1\frac{1}{2}}$, and $[C_3H_3^+] \propto [C_2H_2]_0^{2\frac{1}{2}}$, if both $[CH_2O]$ and $[C_2H_2] \propto [C_2H_2]_0$. The former requirement is in good agreement with observation, the latter not so good, the observed index being 2.1. Elucidation of the other flame ions must await further experiments, the number of reaction possibilities being large.

General Conclusions

Summarizing the evidence in favor of the primary ionization reaction proposed:

1. CHO^+ is observed to be a genuine "flame ion", the difference between its profile and that of known hydrocarbon peaks being sufficient to eliminate $C_2H_5^+$.
2. Thermochemical evidence, backed by structural reasoning, shows the reaction of CH with O to be about thermoneutral; the reaction is unlikely to involve significant energy of activation.
3. The count of CHO^+ is proportional to added acetylene, as is also $[CH^*]$ in the reaction zone, while $[O]$ is almost independent of the additive; it would seem probable that ground state CH shows the same dependence of CH^*.
4. The reaction of CHO^+ with water molecules is very exothermic and should proceed with ease; estimated rate constants for this reaction and that of the recombination of H_3O^+ with electrons lead to values of $[H_3O^+]/[CHO^+]$ in good agreement with experimental values.
5. Very approximate calculations of the rate constant for formation of CHO^+ from CH and O are in fair agreement with values inferred from the observations combined with rough estimates of the concentrations of CH and O.

Evidence against other primary reactions is:

1. Primary ionization reactions involving other radicals and molecules of the hydrogen flame with carbon-containing radicals are all too endothermic, if only ground state species are considered.
2. Even though such reactions can be made exothermic by use of electronically excited species, the low concentrations of such species makes the reactions improbable compared with the one proposed.
3. No other reaction R + O, except for rather improbable R for which there is no direct evidence in the flame, have even remotely the same thermochemical advantages as the proposed reaction.
4. No other flame ion has been found which gives a mechanism for subsequent H_3O^+ formation with the functional and quantitative agreement with the observations shown by CHO^+.

Acknowledgment

We wish to thank the Research Laboratory of the General Electric Company (Schenectady) for very generous financial assistance which has enabled this work to be carried out.

References

1. Calcote, H. F.: AeroChem Research Laboratories, Inc., Princeton, New Jersey, Report No. AFBMD–TR–61–54, ASTIA–AD 258 229, AeroChem TP–24, 1960.
2. Deckers, J. and van Tiggelen, A.: Combustion and Flame *1*, 281 (1957).
3. Deckers, J. and van Tiggelen, A.: *Seventh Symposium (International) on Combustion*, p. 254. Butterworth, 1959.
4. De Jaegere, S., Deckers, J., and van Tiggelen, A.: *Eighth Symposium (International) on Combustion*. Williams and Wilkins, 1962.
5. Knewstubb, P. F. and Sugden, T. M.: Nature *181*, 474 (1958).
6. Knewstubb, P. F. and Sugden, T. M.: *Seventh Symposium (International) on Combustion*, p. 247. Butterworth, 1959.
7. Knewstubb, P. F. and Sugden, T. M.: Proc. Roy. Soc. (London) *A255*, 1920 (1960).
8. Bascombe, K. N., Green, J. A., and Sugden, T. M.: *Joint Symposium on Mass Spectrometry, ASTM and Institute of Petroleum*. Pergamon Press, 1962.
9. Bulewicz, E. M., James, C. G., and Sugden, T. M.: Proc. Roy. Soc. (London) *A235*, 89 (1956).
10. Padley, P. J. and Sugden, T. M.: Proc. Roy. Soc. (London) *A248*, 248 (1958).
11. Bulewicz, E. M. and Sugden, T. M.: To be published.
12. Padley, P. J.: Ph.D. dissertation, Cambridge, 1959.
13. Phillips, L. F.: Ph.D. dissertation, Cambridge, 1960.
14. Kantrowitz, A.: Private communication, 1960.
15. King, I. R.: J. Chem. Phys. *27*, 817 (1957).

16. GAYDON, A. G. and WOLFHARD, H. G.: *Flames, Their Structure, Radiation and Temperature.* Chapman and Hall Ltd., 1960.
17. FIELD, F. M. and FRANKLIN, J. L.: *Electron Impact Phenomena.* Academic Press Inc., 1957.
18. GAYDON, A. G.: *The Spectroscopy of Flames.* Chapman and Hall, Ltd., 1957.
19. GAYDON, A. G., SPOKES, G. N., and VAN SUCHTELEN, J.: Proc. Roy. Soc. (London) *A256,* 323 (1960).
20. TAL'ROSE, V. L. and FRANKEVICH, E. L.: *Doklady Akad. Nauk S.S.S.R. 111,* 376 (1956).
21. TROTMAN-DICKENSON, A. F.: *Ann. Rept. Chem. Soc. (London) 55,* 36 (1958).

Discussion

DR. W. A. ROSSER (*Stanford Research Institute*): It is noteworthy that all three papers of this session propose the same reaction, Eq. (1), as a reaction which can produce ultimately the ions observed in hydrocarbon–O_2 flames.

$$CH + O \rightarrow CHO^+ + e^- \qquad (1)$$

It seems clear that the energy necessary for ionization results from the formation of a carbon-oxygen double bond with an energy ceiling of 256 kcal, the heat of dissociation of CO.

Professor Sugden's argument in support of Eq. (1) depends heavily on the experimentally determined relations summarized in the section on "Effect of Variation of Amount of Additive" of the paper. Because of the importance of the cited relations, I have several questions concerned with factors which might affect the apparent relation between maximum ion current and the concentration of C_2H_2 in the unburned gas. The first of these relates to the partition of observed ions into "flame" ions and "input system" ions. The procedure whereby ions of a given mass number were assigned to one or the other class is clear but not the extent to which the presence of input ions represents the loss of flame ions. Specifically, I would like to know whether this loss was considered in experiments which led to data such as shown in Fig. 3.

The second question concerns the statement at the end of the section on "Addition of Hydrocarbon to Hydrogen" that the "addition of up to 1% of various hydrocarbons to the hydrogen fuel does not materially affect the concentration of H and OH near the reaction zone." The reference cited (reference 12) is not readily available. Therefore, I hope the authors can amplify on the quoted statement. The reason for touching on this point is the observation[1] that low concentrations of CH_4 or C_2H_4 will noticeably reduce the flame speed of a H_2-air mixture similar in composition to that noted at the end of the section on "Experimental." I seek assurance that the flame chemistry has not been scrambled by the addition of C_2H_2.

In the section on "The Mechanism of Reaction," a brief steady state treatment of $[AH^+]$ and $[H_3O^+]$ leads to the relation

$$[AH^+] \propto [H_3O^+]^2_{max} \qquad (2)$$

From the derivation it is clear that the proportionality refers to the concentration of AH^+ at the point corresponding to $[H_3O^+]_{max}$. The conclusion that $AH^+ = HCO^+$ requires the proportionality

$$[AH^+]_{max} \propto [H_3O^+]^2_{max} \qquad (3)$$

which is not the same thing as Eq. (2) because HCO^+ and H_3O^+ peak at different points (see Fig. 4).

If, as claimed, Eq. (1) is the initial ion-producing reaction, then the origin of the CH radicals becomes as intriguing a problem as the origin of the ions themselves. Consider for instance the reactions recently proposed[2] to account for the kinetic behavior of shocked mixtures of C_2H_2, O_2, and diluent.

$$H + O_2 \rightarrow HO + O \qquad (4)$$

$$C_2H_2 + \{O, OH\} \rightarrow C_2H + \{OH, H_2O\} \qquad (5)$$

$$C_2H + C_2H_2 \rightarrow C_4H_2 + H \qquad (6)$$

To this list could then be added such reactions as

$$O + C_2H \rightarrow CO + CH \qquad (7)$$

$$O + C_4H_2 \rightarrow CO + C_3H_2 \qquad (8)$$

and then on to the ions CHO^+, H_3O^+, $C_2H_2^+$, $C_3H_3^+$, $C_4H_3^+$, etc. Such a reaction path is based on the radical C_2H, only one step removed from C_2H_2 but many steps removed from all the other hydrocarbons which also produce ions (e.g., Fig. 5 in the paper by Bulewicz and Padley, this volume, p. 643. How then can one account for the fact that hydrocarbons as diverse as CH_4, C_2H_2, and C_6H_6 give similar ion yields per carbon atom (see Fig. 5, Bulewicz and Padley, this volume, p. 643). Perhaps Eq. (1) is but one of several reactions which can produce ions. I am sure that Professor Sugden, and the authors of the other two papers, have considered the consequences of accepting Eq. (1) as the initial ion reaction and will be willing to comment thereon, even though it may require venturing into the quagmire of speculative kinetics.

DR. T. M. SUGDEN (*University of Cambridge*): In reply to the points raised by Dr. Rosser, I hope the following explanations will be satisfactory.

1. Direct accounting for all the "input system"

ions in terms of initial "flame" ions is difficult. However, when ammonia is added to the flame gas supply in small amounts, under experimental conditions such that "flame" ions predominate, the count of H_3O^+ (a flame ion) decreases by as much as the NH_4^+ ion (an input system ion) increases. This work, done in collaboration with Prof. H. I. Schiff, is to be published in the near future. The reaction is

$$H_3O^+ + NH_3 \rightarrow H_2O + NH_4^+.$$

2. The work of Padley on the effect of small amounts of hydrocarbon on radical concentration in hydrogen flames is in the course of publication. One per cent of acetylene (hydrocarbon used here) gives reduction in (H) and (OH) of the order of 10–20%, which should be of small account in the present work, i.e., not sufficient to refute the analysis.

3. We must apologize for not having stated that the whole CHO^+ profile varies linearly, and not only its maximum. This validates the use of the mechanism suggested, at the maximum of H_3O^+. Measurements of H_3O^+ at the maximum of CHO^+ are very difficult because of its rapid variation with position there.

4. I would rather not enter into the discussion of the mechanism of CH production at this stage, having no new ideas to offer. I would point out, however, that the reaction

$$C_2 + OH \rightarrow CO + CH$$

offers possibilities, as well as the suggested

$$C_2H + O \rightarrow CO + CH.$$

Prof. G. B. Kistiakowsky (*Harvard University*): Our investigations of the oxidation of acetylene in shock waves[3,4,5] have demonstrated a branching chain mechanism determined by the rate of the

$$H + O_2 \rightarrow OH + O \qquad (1)$$

reaction. The oxidation observed in the 1200–3000°K temperature range is accompanied by the emission of short UV radiation, since identified as the fourth positive band system of CO and ionization of the gas. Both rise exponentially and then decay, showing identical dependence on temperature and composition of the gas mixture. We believe, therefore, that very closely related reactions are responsible for both, for instance, the sequence

$$C_2H + O_2 \rightarrow CO_2 + HC \qquad (2)$$

$$HC + O \rightarrow HCO^* \qquad (3)$$

$$HCO^* \rightarrow H + CO^* \rightarrow H + CO + h\nu \qquad (4)$$

$$HCO^* \rightarrow HCO^+ + e^- \qquad (5)$$

Reactions (3) and (5) are the ones suggested by Dr. Sugden as the mechanism of ionization, but reaction (4) occurs at least an order of magnitude more frequently and, therefore, the sequence (3) and (4) is kinetically more important than (3) and (5).

Dr. T. M. Sugden: In relation to Prof. Kistiakowsky's remarks, I would like to mention the following result which we (Green, Larin, and Sugden) have obtained in recent months. There is a broad parallelism between maximum flame ionization and emission from CH* in the reaction zone when hydrocarbons (CH_4, C_2H_2, C_2H_4, C_2H_6, C_3H_8), as well as methyl alcohol, are added to a hydrogen flame. The relation is monotonic but not linear. Linearity is not expected from our mechanism, which indeed is possible with ground state CH, which need not be very closely related to CH* in all the circumstances.

As for the suggestion for testing the validity of the initial ionization step suggested, investigation in the hydrocarbon flame bands, which might well be produced by $CH + O + M \rightarrow CHO^* + M$, as well as on the chemiluminescence of additives such as iron in the ultraviolet at about 2000 Å, which we believe could be caused by $CH + O + Fe \rightarrow CHO + Fe^*$, should be considered.

Dr. H. F. Calcote (*AeroChem Research Laboratory*): It is most satisfying to see so much agreement not only in numerical constants derived from two different techniques, the mass spectrometer, and the Langmuir probe, but in actual interpretation of the phenomena in terms of elementary reactions.

In addition to these points of agreement noted by the authors, I would add one more. Where Green and Sugden found the rate of ion formation with 1% acetylene added to a H_2–O_2–N_2 flame to be 8×10^{15} ions/cc/sec, we found the rate of ion formation to be 2×10^{15} ions/cc/sec in a propane–O_2–N_2 flame.[6] Both flames were at 1 atm. As the pressure is decreased this rate also decreases.[7] Bascombe, Green, and Sugden (reference 8 of the paper) estimate the rate constant to be $k_1 = 3 \times 10^{-12}$ cc/sec. My estimate from collision theory was 5.4×10^{-11} cc/sec.

Green and Sugden's observation that the value of $\Delta H_f(CH) = 103$, which I had used from Field and Franklin's review (reference 17 of the paper), is low is certainly agreed to; the preferred value is 143. However, I would still prefer to hold open the question of the heats of formation of CHO^+ and H_3O^+. For CHO^+, Field and Franklin gave ~203 kcal/mole. A recent review by Bernecker and Long[8] gives 220 kcal/mole for $\Delta H_f(CHO^+)$.

For H_3O^+ Field and Franklin give 195 kcal/mole and Bernecker and Long give 207 kcal/mole. Green and Sugden use a value of 137 kcal/mole obtained from the proton affinity of H_2O^+. Both of the high

values are based on electron impact studies which may involve excess energy in the fragments. Bernecker and Long, however, point out that in seventeen randomly chosen polyatomic molecules, the ionization potentials by the impact method are only about 3.5 kcal/mole higher than those from photoionization. Majer, Patrick, and Robb[9] find that when the uncharged fragment, produced by electron impact, is more complex than a single atom, the appearance potentials may include excess energy. In studies on the acetyl radical ion, this excess energy was 5–9 kcal/mole. The measurements upon which the high values of $\Delta H_f(H_3O^+)$ are based included initial reactants $H_2 + O_2$, C_2H_5OH, and $HCOOC_2H_5$, so it is difficult to rationalize the difference between these values and 137 kcal/mole, which Green and Sugden use based on the proton affinity of H_2O. A difference of 58 to 70 kcal/mole is required. Certainly the correct value is still open to question.

The ion–molecule reaction $CHO^+ + H_2O \rightarrow CO + H_3O^+$ is exothermic by 34 kcal/mole using the data employed by Green and Sugden. Using Field and Franklin's values, I found this reaction to be endothermic by 25 kcal/mole.[7] With Bernecker and Long's values for CHO^+ and H_3O^+, the reaction is endothermic by 19 kcal/mole, and with Bernecker and Long's value for H_3O^+ and the other data used by Green and Sugden, the reaction is endothermic by 37 kcal/mole.

If the above reaction were not endothermic, my explanation[7] for the formation of NH_4^+ and H_2CN^+ ahead of the H_3O^+ peaks in van Tiggelen's experiments with the addition of NH_3 and HCN would not be valid.

We have all been defending various reaction mechanisms on the basis of ground state thermodynamics, but it may be well to remind ourselves of the hazards involved. The products may very well be in excited states and may involve excess energy causing all of our calculated heats of reaction to be low.

I prefer Green and Sugden's explanation of the formation of $C_3H_3^+$ via

$$H_3O^+ + CH_2O \rightarrow CH_3O^+ + H_2O$$

$$CH_3O^+ + C_2H_2 \rightarrow C_3H_3^+ + H_2O$$

to the mechanism I discussed in my paper (this symposium):

$$H_3O^+ + C_3H_2 \rightarrow C_3H_3^+ + H_2O$$

Fristrom and Westenberg[10] report, in a methane–oxygen flame, CH_2O to be present to 0.2%, which is more than sufficient for Green and Sugden's requirements of 0.02%. However, we find CH_3O^+ to be present only in extremely small concentrations, and van Tiggelen does not report it at all. Of course, the subsequent reaction with acetylene could be so fast that the steady state concentration of CH_3O^+ is negligible. Both mechanisms suffer in requiring hydrocarbon fragments in a lean flame to be about comparable to their concentration in a rich flame because we observe little difference in the magnitude of the $C_3H_3^+$ ion in rich and lean flames. More study is obviously required on the mechanism of producing $C_3H_3^+$.

DR. T. M. SUGDEN: We have used the heat of formation of H_3O^+ (137 kcal/mole) based on the value of the proton affinity of water obtained by Tal'rose and Frankevich (169 ± 2 kcal/mole). This latter was based on the reactions

$$H_2S^+ + H_2O \rightarrow HS + H_3O^+$$

$$C_2H_2^+ + H_2O \rightarrow C_2H + H_3O^+$$

Although the accuracy is probably not quite so high as the author claimed, nevertheless, it seems better to us than the electron impact data. Even if it were in error by as much as 30 kcal, which is very improbable, the reaction

$$H_2O + CHO^+ \rightarrow H_3O^+ + CO$$

would still be exothermic.

PROF. T. KINBARA (*Sophia University, Tokyo*): Dr. Sugden started with the equation $CH + O \rightarrow CHO^+ + e^-$. A hydrocarbon flame is divided into three regions—a green region from which mostly C_2 band is emitted, a blue region from which CH band is emitted mostly, and a faint purple region. This is clearly demonstrated in a low pressure flame. We used a concentric double tube as a burner, the hydrocarbon gas and the air being sent through the inner and the outer tubes, respectively. Diffusion takes place quickly at the top of the burner, and the flame thus obtained is very stable. The flame is a flat and thick flame. At the bottom of the flame, we could see the C_2 region of 2–3 mm thickness, and above this layer the CH region of 3–4 mm is observed, followed by the faint purple region.

We observed the ion concentrations at several points of the flame by the Langmuir probe method, and obtained the distribution of ion concentration in the flame. Our results show that the ion concentration, as we go upwards, increases gradually in the C_2 region, whereas it keeps constant or decreases in the CH region. This means that the ions are created in the C_2 region, and the ion production is likely connected with C_2 radicals rather than CH radicals. Of course, the green region is the one where excited C_2 radical predominates in number, and this does not necessarily mean the region where normal C_2 radicals predominate. CH radicals can predominate

in the C_2-region. However, I feel something unnatural in the theory that $CH + O \rightarrow CHO^+ + e^-$ is the first step of the combustion mechanism. Does Dr. Sugden think that the reaction $C_2 + OH \rightarrow CH + CO$ takes place before $CH + O \rightarrow CHO + e$?

DR. T. M. SUGDEN: The production of CHO^+ by $CH + O$ will depend on the profile of (O) as well as on that of (CH). Prof. Kinbara's observations on the distribution of C_2^* and CH^* in a diffusion flame are not inconsistent with the mechanism suggested.

REFERENCES

1. ASD–TR–61–717.
2. BRADLEY, J. N. and KISTIAKOWSKY, G. B.: J. Chem. Phys. *35*, 265 (1961); KISTIAKOWSKY, G. B. and RICHARDS, L. W.: J. Chem. Phys. *36*, 1707 (1962).
3. BRADLEY, J. N.: J. Chem. Phys. *34*, 748 (1961).
4. RICHARDS, L. W. and KISTIAKOWSKY, G. B.: J. Chem. Phys. *36*, 1701 (1962).
5. HAND, C. W.: J. Chem. Phys. *36*, 2521 (1962).
6. CALCOTE, H. F.: Combustion and Flame *1*, 385 (1957).
7. CALCOTE, H. F.: *Eighth Symposium (International) on Combustion*, p. 184. Williams and Wilkins, 1962.
8. BERNECKER, R. R. and LONG, F. A.: J. Phys. Chem. *65*, 1565 (1961).
9. MAJER, J. R., PATRICK, C. R., and ROBB, J. C.: Trans. Faraday Soc. *57*, 14 (1961).
10. FRISTROM, R. M. and WESTENBERG, A. A.: *Eighth Symposium (International) on Combustion*, p. 438. Williams and Wilkins, 1962.

ION AND ELECTRON PROFILES IN FLAMES

H. F. CALCOTE

It is shown how Langmuir probes can be used in flames to obtain not only the positive ion concentration but electron concentrations and electron temperatures. An internal method is presented for checking the results by comparing the wall potential calculated from the above three quantities with the observed wall potential. Satisfactory agreement between these two values in hydrocarbon air/or oxygen flames from 1.5 to 760 mm Hg increases the confidence in the use of Langmuir probes to obtain plasma profile properties in flames. The accuracy of positive ion and electron collision cross sections appears to be the major factor limiting the accuracy of the probe.

Detailed results are presented for a number of flames. The positive ion concentration always exceeds the electron concentration indicating the formation of negative ions. Electron temperatures exceed the gas temperature and do not decay as rapidly as might be expected.

A mass spectrometric technique for obtaining ion profiles of good spatial resolution is outlined and detailed profiles are presented for an acetylene–oxygen flame at 2.5 mm Hg. The ion CHO^+ peaks ahead of $C_3H_3^+$ which precedes H_3O^+. Many other ions are observed to peak at about the same position in the flame as $C_3H_3^+$. There are still problems, however, with respect to interpreting the results in terms of the first ion produced from neutral species and the sequence of ion molecule reactions which follows.

Introduction

It is generally agreed today that chemi-ionization[1–5] is the dominant ion producing mechanism in hydrocarbon–air or oxygen flames. There is even some accord that an important ion forming reaction is[6,7,9]

$$CH + O \rightarrow CHO^+ + e^-$$

However, evidence for this reaction is still not as conclusive as we would like. From flame ionization detectors in gas chromatography, we have learned that about one ion is produced for about every million carbon atoms in the combustion gases[8]; this is consistent with the rate of ion formation obtained by Langmuir probe studies.[9] Ionization flame detector studies for gas chromotography have also shown[8] that the rate of ion formation in a hydrogen–air flame is directly proportional to the hydrocarbon concentration over a concentration range of roughly 1 to 10^9. Detailed studies of ion precursors do not make clear why this should be so. Although mass spectrometric studies of ions in flames have done much to increase our understanding of ionization in flames, because of rapid ion–molecule reactions, they have still left doubts as to the primary ions produced from neutral species. Recombination measurements of flame ions are also vague on the point of whether the negative species is an ion or an electron.

There is therefore a need in hydrocarbon flames for more detailed flame profile studies of total positive ions, electrons, and individual positive and negative ions. In addition, the gas temperature and stable species profiles should be obtained in the same flame. We have embarked upon such a program, and this contribution represents a progress report. In previous work in this field either positive ion or electron concentrations have been measured. Positive ion concentrations have been obtained with Langmuir probes which give a high degree of spatial resolution but suffer from a bad reputation.[10,11,12] Microwave techniques have been used by others[6,27,28] for determining electron concentrations, but such experiments have the basic limitation of poor spatial resolution. We will show in this paper that Langmuir probes can be reliably used for obtaining both positive ion and electron concentrations. Electron temperature measurements in flames will also be presented. Results of detailed mass spectrometer profiles will be described for low pressure flames where, because of the flame thickness and the ion sampling technique employed, the spatial resolution is greatly improved.

Consistent with the invitation to present work in progress, it is not the intent of this paper to present a final piece of work with arguments for interpreting the data in terms of theoretical concepts but to outline the results of experiments in progress with the hope of stimulating discussion.

Langmuir Probe Studies

In the last symposium[9] we outlined the use of Langmuir probes to obtain positive ion concentrations; we will now discuss the use of the probe to obtain electron concentrations and electron temperatures and some of the problems involved. As our use of probes has continued and we have gained more confidence in them, it has become more and more evident that one of the main limitations is our lack of knowledge of collision cross sections of both positive ions and electrons. Incidentally, the electron collision cross section is also necessary for interpreting microwave techniques in terms of electron concentrations—it appears as collision frequency. We will therefore discuss how this problem can be handled in treating probe data and at the same time show how a self-consistency test can be applied to the probe data to increase confidence in the results obtained.

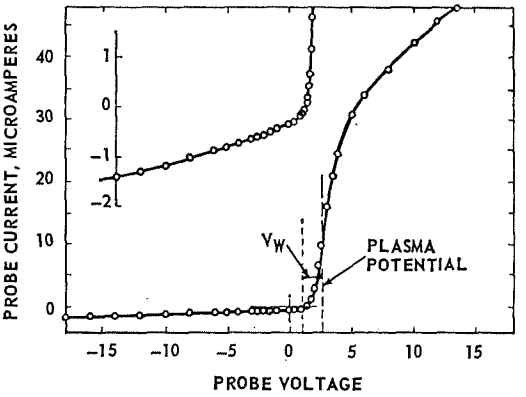

FIG. 1. Typical Langmuir probe curve in ethylene-oxygen flame, p = 2.6 mm Hg. (See Table 6.)

Small Probes

In our previous work relatively large probes were employed, frequently stretching across the flame, so that it was difficult to obtain saturation electron currents on the probe without saturating the other electrode, usually a screen over the entire flame. This difficulty arises because of the large mobility of free electrons with respect to positive ions. The currents (electron) to a positive probe are always much larger than currents (positive ions) to a negative probe (See Figs. 1 and 2). With large probes the large electron currents also produce excess drainage on the flame plasma, which affects the plasma being studied. We have been thwarted previously in attempts to build small probes because all electrical insulators become either semiconductors or thermal emitters at the elevated

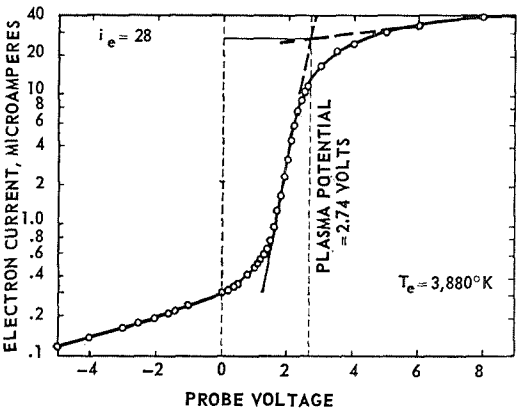

FIG. 2. Typical Langmuir probe curve for obtaining electron concentration and electron temperature (from Fig. 1).

temperatures of flames; considerable attention was therefore directed to the solution of this problem, and after many attempts a small water-cooled probe was developed and is shown in Fig. 3.

The insulating member, Fig. 3, is cooled by being in contact with a tube of material of good thermal conductivity, which is in turn cooled by circulating water. The cooling tube extends beyond the insulator to keep the tip of the insulator cool and, hence, a stagnant gas forms at the end. Several difficulties still must be recognized. The probe length is now not accurately known, but this can be checked by testing probes of varying lengths. The cooling effect on the gas and the effect on the ion sheath are difficult to assess, although the visual disturbance in the low pressure flames is negligible. They must also be evaluated by varying the probe length and diameter.

Interpretation of Probe Curves

In the last symposium[9] the equation was given for an ellipsoidal approximation to the equations

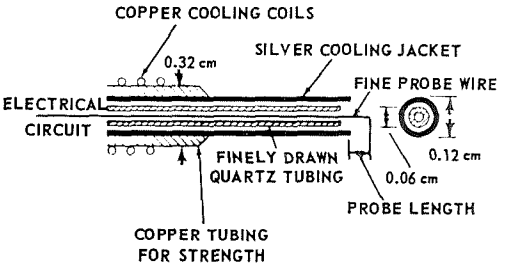

FIG. 3. Electrically and thermally insulated probe.

of Bohm, Burhop, and Massey[13] for calculating positive ion concentrations from probe currents, i.e., the cylindrical probe was approximated by an ellipsoid. A similar approximation can also be given for an infinite cylinder. These two equations can be written for either positive ions or electrons by substituting the appropriate quantities. For electrons they would read for a positive probe:

(1) ellipsoidal approximation;

$$n_e = \frac{j_e}{e}\left(\frac{2\pi m_e}{kT_e}\right)^{\frac{1}{2}}\left[1 + \frac{0.75Ld}{4\lambda_e B}\ln\left(\frac{X+B}{X-B}\right)\right] \quad (1)$$

(2) infinite cylinder approximation;

$$n_e = \frac{j_e}{e}\left(\frac{2\pi m_e}{kT_e}\right)^{\frac{1}{2}}\left[1 + \frac{0.75d}{2\lambda_e}\ln\left(\frac{L}{(d/2)+\lambda_e}\right)\right] \quad (2)$$

where:

j_e = electron current density at the plasma potential;
e = charge on electron;
k = Boltzman constant;
m_e = mass of electron;
T_e = electron temperature, obtained from the Langmuir probe data;
λ_e = electron mean free path;
d = probe diameter;
L = probe length;
$X = L + 2\lambda_e$; and
$B = [X^2 - (d + 2\lambda_e)^2]^{\frac{1}{2}}$.

For a negative probe Eqs. 1 and 2 must be multiplied by $\exp(-eV/kT_e)$ where V is the potential difference between the probe and the plasma potential and represents the barrier over which the electrons must diffuse. The plasma potential and the procedure for obtaining it are presented in Fig. 2.

The wall potential, V_w, is the potential, with respect to the plasma potential, at which the probe current is zero, Fig. 1. At this potential the positive ions reaching the wall are just balanced by the electrons and negative ions reaching the wall. It can be demonstrated that, unless the electron concentration is very much less than the negative ion concentration, the contribution of negative ions to the wall potential can be neglected. Then by equating $j_+ = j_e$ and letting $V = V_w$, the wall potential is given by:

$$V_w = \frac{kT_e}{e}\ln\left[\left(\frac{n_e}{n_+}\right)\left(\frac{T_e}{T_+}\frac{m_+}{m_e}\right)^{\frac{1}{2}}\frac{[+]}{[e^-]}\right] \quad (3)$$

where $[+]$ and $[e^-]$, sometimes called correction factors, are the respective bracket terms for positive ions and electrons from Eqs. (1) or (2).

The electron temperature can be obtained by writing either Eq. 1 or 2 for j_e to a negative probe:

$$j_e = n_e e\left(\frac{kT_e}{2\pi m_e}\right)^{\frac{1}{2}}[e^-]^{-1}\exp(-eV/kT_e) \quad (4)$$

On taking logarithms of both sides:

$$\ln j_e = \ln[n_e e(kT_e/2\pi m_e)^{\frac{1}{2}}[e^-]^{-1}] - (eV/kT_e) \quad (5)$$

Neglecting the weak temperature dependence of the first term on the right-hand side, this is the equation of a straight line:

$$\ln j_e = B - (e/kT_e)V. \quad (6)$$

Thus, a plot of $\ln j_e$ against the probe voltage, as in Fig. 2, yields through the slope, the electron temperature, T_e. Because the total current to the negative probe is:

$$j_{\text{total}} = j_+ + j_e \quad (7)$$

with appropriate signs the electron current may be obtained by extrapolating the approximately linear leg of the current to the negative probe in order to obtain the positive ion contribution at any particular voltage. The electron current is then obtained by subtracting the positive ion current from the meter or probe current.

Thus it is possible to extract from probe data:

1. The electron concentration from Eq. (1) or (2);
2. The positive ion concentration from Eq. (1) or (2) substituting positive ion values;
3. The electron temperature from the slope of $\ln j_e$ vs. V, Eq. (6);
4. The wall potential by the voltage difference between the plasma potential and the probe voltage (meter) at which the probe current (meter) is zero.

An internal check on the results is afforded by the observation that the first three quantities can be used in Eq. (3) to calculate the fourth. Thus the values of n_e, n_+, and T_e are used to calculate V_w by Eq. (3) and this value compared with the observed value of V_w. With the degree of independence of the various quantities, the restrictions imposed by the theory and the complexity of the experimental curves, agreement can hardly be considered as fortuitous. This agreement over a range of pressures and a range of the parameters involved justifies considerable confidence in the results. Experimental results will be presented in a later section.

One major stumbling block to the satisfactory interpretation of Langmuir probe data is the need for accurate knowledge of the mean free paths of positive ions and electrons, or more

basically, the need for accurate collision cross section data. As our work has progressed it has become more and more apparent that the differences between observed and calculated wall potentials were well within the choice of collision cross sections available in the literature. A brief discussion of this problem is thus warranted.

Mean Free Paths and Collision Cross Sections

The general equation for mean free path is[14]:

$$\lambda_i = \{\pi \sum_s [n_s S_{is}^2][1 + (m_i/m_s)^{\frac{1}{2}}]\}^{-1}$$
$$= \{\sum_s n_s Q_{is}[1 + (m_i/m_s)^{\frac{1}{2}}]\}^{-1} \quad (8)$$

where:

S_{is} = distance between centers of colliding species i and s, i.e., collision diameter for positive ions,
Q_{is} = collision cross section of species i colliding with species s;
m_i, m_s = masses of colliding particles i and s; and
n_s = number density of s species.

Because for electron collisions $m_e/m_s \ll 1$:

$$\lambda_e = (\sum_s n_s Q_{es})^{-1}. \quad (9)$$

Because for positive ions $m_i/m_s \approx 1$

$$\lambda_+ = (\sqrt{2} \sum_s n_s Q_{is})^{-1}. \quad (10)$$

The dominant ion in uncontaminated flames is H_3O^+, so the collision cross section of this ion with the various neutral components such as H_2O, CO_2, and N_2 is required. These data are not readily available and hence were estimated by assuming the additivity of molecular and ionic radii. The radii of neutral molecular species were taken from Hirschfelder, Curtiss, and Bird[15] except for H_2O, which was estimated to be 1.7 Å by comparison with other molecules. No value for H_3O^+ nor H_2O^+, which might be expected to be close, has been found. This value was therefore estimated from Pauling's data[16] to be 1.8 Å. Thus the collision diameters and cross sections for H_3O^+ with the products of combustion were estimated to be:

Collision	S	Q_+
$H_3O^+ + N_2$	3.6 Å	4.1×10^{-15} cm²
$H_3O^+ + O_2$	3.5	3.9
$H_3O^+ + CO_2$	3.8	4.5
$H_3O^+ + H_2O$	3.5	3.9

It is unfortunate that better values are not available. In previous work[1,9] we assumed S = 2.6 Å.

There are several sources of electron collision cross sections including actual measurement of the collision frequency in flames. Most of the electron collision cross sections are strongly electron temperature dependent and thus must be obtained as a function of electron temperature

TABLE 1

Measurements of Electron Collision Cross Sections in Flames

Conditions	Reference No.	Collision frequency (sec^{-1})	Collision cross section (10^{-15} cm²)
Acetylene–air flame			
760 mm Hg, 2480°K	28	2.6×10^{-11}	2.6
Acetylene–oxygen flame			
7.5 mm Hg, 2300°K	28	3.7×10^{9}	3.9
6–40 mm Hg, 2200°K	18	—	4
Acetylene–oxygen detonation			
76 mm Hg, 3500–4000°K	29	—	2.5
Coalgas–air flame			
760 mm Hg, 2200°K	30	8.8×10^{10}	8.4
Propane–oxygen flame			
760 mm Hg, 1800–2400°K	31	—	1.0

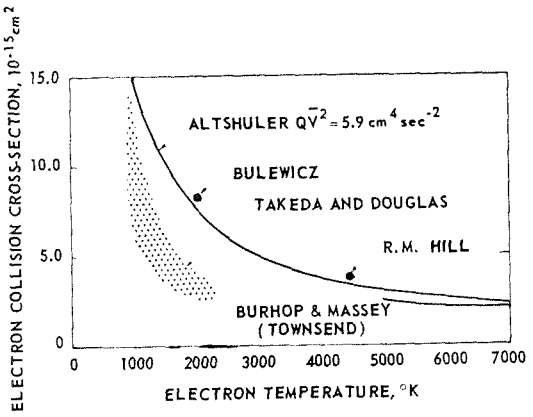

FIG. 4. Electron collision cross sections for water (see references 17 to 21).

in the flame. Some literature results in flames are summarized in Table 1. The collision cross sections when not given in the references have been calculated from:

$$Q_e = \nu/\bar{c}n_0 \qquad (11)$$

where:

ν = measured collision frequency;
n_0 = total number of molecules; and
$\bar{c}$ = mean electron velocity.

A more sophisticated means of obtaining the appropriate electron collision cross section would be to compute it from the components of the mixture. Water is usually a major product and has the largest cross section of the products of C, H, O, N flames. Literature values for H_2O are presented in Fig. 4. Values for CO_2, CO, and N_2 which have been used in reducing our data are presented in Table 2.

TABLE 2

Electron Collision Cross Sections Used in Calculations

Electron temperature (°K)	Collision cross sections (10^{-15} cm^2)		
	CO_2[a]	CO[a]	N_2[b]
2,000	1.7	1.1	0.85
3,000	1.4	1.1	0.95
4,000	1.1	1.1	1.0

[a] Data from reference 21, chap. 3 (Ramsauer and Townsend values), and reference 32.
[b] Data from reference 33.

Plasma Properties of Flames

The techniques of the previous section have been applied to a number of different flames, and the results are presented in this section.

TABLE 3

Plasma Properties of a Propane–Air Flame at 1 Atmosphere

Probe: Platinum
Length = 1.5 cm
Diam. = 0.063 cm

Equivalence ratio = 1.0
Gas temperature = 2270°K
Electron temperature = 2850°K
$n_0 = 3.23 \times 10^{18}$/cc

Cylindrical probe approximation used

$j_+ = 3.94 \times 10^{-8}$ amperes
$Q_+ = 4.15 \times 10^{-15}$ cm^2
$\lambda_+ = 5.26 \times 10^{-5}$ cm
$n_+ = 1.42 \times 10^{10}$ ions/cc

$j_e = 5.05 \times 10^{-6}$ amperes
$Q_e = 1.63 \times 10^{-15}$ cm^2
$\lambda_e = 1.90 \times 10^{-4}$ cm
$n_e = 2.42 \times 10^{9}$ electrons/cc

V_w (obs.) = 1.2 volts
V_w (calc.) = 1.20 volts

Sheath thickness (at −3.0 volts)

Parallel plate theory	0.036 cm
Cylindrical probe theory	0.035 cm
Simple current increase	0.031 cm

TABLE 4

Plasma Properties of a Propane-Air Flame at 33 mm Hg

Probe: Pt–40% Rh
Diam. = 0.025 cm
Length = 0.50 cm
$Q_+ = 4.11 \times 10^{-15}$ cm²

Equivalence ratio = 0.88
Gas temperature = 2100°K
Flow velocity = 182 cc/sec
$n_0 = 1.52 \times 10^{17}$ molecules/cc

Ellipsoidal probe approximation used

Distance from burner (cm)	Probe currents (10^{-8} amperes) i_+	i_e	T_e (°K)	Q_e (10^{-15} cm²)	Conc. (10^{-9} mole fraction) n_+/n_0	n_e/n_0	V_w (volts) Obs.	Calc.
0.34	0.77	150	2060	1.8	6.4	2.1	0.89	0.93
0.56	3.90	155	2400	1.7	32	2.0	0.68	0.76
1.02	1.95	142	2500	1.6	16	1.7	0.85	0.92
1.48	0.90	138	2700	1.6	7.4	1.5	1.1	1.2
2.40	0.52	133	2350	1.7	4.3	1.6	1.1	1.1
3.32	0.27	85	2350	1.7	2.3	1.1	1.1	1.2
4.01	0.22	74	2600	1.6	1.8	0.85	1.2	1.3

For a stoichiometric propane–air flame at 1 atmosphere the results are summarized in Table 3. The internal check via the wall potential is better than could be expected. Note that the electron temperature exceeds the adiabatic gas temperature, and the positive ion concentration is more than five times the electron concentration. If the ion sheath thickness around the negative probe is calculated by the usual theory described in Loeb[10] the two theoretical results reported in Table 3 are obtained. According to the simple picture upon which the Langmuir probe theory is based, the increase in current to the probe as it is made more negative is due to an increase in the positive ion sheath thickness, so that the area into which ions are diffusing is being increased. If the sheath thickness is zero at the plasma potential, then the sheath thickness at any voltage is

TABLE 5

Comparison of Data Reduced by Several Alternatives[a]

Distance from burner (cm)	Positive ion[b] Collision diameter (10^{-8} cm)	Probe theory	Correction factor	Positive ion conc. (10^9/cc)
0.34	3.6	Cylindrical	41	0.96
	3.6	Ellipsoidal	31	0.97
	2.6	Cylindrical	21	0.50
	2.6	Ellipsoidal	16	0.50
1.02	3.6	Cylindrical	41	2.4
	3.6	Ellipsoidal	31	2.5
	2.6	Cylindrical	21	1.3
	2.6	Ellipsoidal	16	1.3

[a] See Table 4 for experimental conditions.

[b] The collision diameter assumed prior to this report was 2.6×10^{-8} cm. The weighted average of the species involved gives 3.6×10^{-8} cm.

TABLE 6

Plasma Properties of an Ethylene–Oxygen Flame at 2.6 mm Hg

Varying composition

Probe: Pt–40% Rh
Diam. = 0.015 cm
Length = 0.159 cm

T_+ (assumed) = 2000°K
$n_0 = 1.22 \times 10^{16}$

Equivalence ratio	Maximum probe currents (10^{-6} amperes) i_+	i_e	T_e[a] (°K)	Max. conc. (10^{-7} mole fraction) n_+/n_0	n_e/n_0	V_w (volts) Obs.	Calc.
0.583	0.16	15	7800	3.0	0.74	2.7	3.0
0.708	0.19	16	8500	3.6	0.76	2.8	3.2
0.759	0.22	22	7800	4.2	1.1	2.7	3.0
0.831	0.23	20	9900	4.4	0.88	3.2	3.8
1.00	0.55	26	4330	10.4	1.7	1.5	1.4
1.03	0.48	28	3880	9.0	2.0	1.3	1.3

[a] At the distance of maximum ion mole fraction.

obtained simply from the ratio of current at the particular voltage to the positive ion current at the plasma potential. The value from this calculation is given as "simple current increase." The agreements are remarkable.

The results for a fuel lean propane–air flame at 33 mm Hg are summarized in Table 4. Again the electron temperature exceeds the adiabatic gas temperature, and the positive ion concentration is greater than the electron concentration. The internal check via the wall potential is satisfactory. The cylindrical probe approximation was used for the experiment in Table 3 and the ellipsoidal approximation for the experiment in Table 4 because of the relative probe lengths to diameters. Table 5 summarizes some results using combinations of the two different approximations in the probe theory, and the collision diameter assumed in our previous work[9] as well as that obtained by a weighted average of the major product species. The choice of approximation in the probe theory would appear to make little

TABLE 7

Plasma Properties of an Acetylene–Oxygen Flame at 1.5 mm Hg

Varying composition

Probe: Pt–40% Rh
Diam. = 0.015 cm
Length = 0.159 cm

T_+ (assumed) = 2,000°K
$n_0 = 7.29 \times 10^{15}$

Equivalence ratio	Maximum probe currents (10^{-6} amperes) i_+	i_e	T_e (°K)	Max. conc. (10^{-7} mole fraction) n_+/n_0	n_e/n_0	V_w (volts) Obs.	Calc.
0.418	0.26	40	3070	9.5	1.9	1.1	1.0
0.519	0.30	42	4030	9.5	4.7	1.9	1.9
0.550	0.48	52	4030	15.	4.9	1.6	1.6
0.640	0.50	21	4530	16.	7.1	1.7	1.7

TABLE 8

Plasma Properties of an Acetylene–Oxygen Flame at 1.5 mm Hg[a]

Distance[b] (cm)	Probe currents (10^{-6} amperes)		T_e (°K)	Conc. (10^{-7} mole fraction)		V_w (volts)	
	i_+	i_e		n_+/n_0	n_e/n_0	Obs.	Calc.
0.00	0.12	12	2320	4.0	1.9	0.97	0.91
0.788	0.30	24	3070	9.5	1.9	1.1	1.0
1.48	0.26	21	3380	8.4	2.7	1.1	1.3
2.42	0.22	18	3100	7.0	2.0	1.2	1.1
3.07	0.19	18	2650	6.1	2.1	0.98	0.98
3·74	0.21	16	3020	6.9	2.1	1.2	1.1
4.76	0.17	11	2260	5.4	1.8	0.97	0.82

[a] Equivalence ratio = 0.418. See Table 7 for experimental conditions.
[b] Measured from beginning of luminous zone.

difference in the results. However, the different choice of collision diameter leads to almost a factor of two differences in the results.

The results for an ethylene–oxygen flame at 2.6 mm Hg with varying equivalence ratios are recorded in Table 6. In the flame the electron temperatures are far in excess of the adiabatic flame temperature, and the positive ion concentration exceeds the electron concentration. At such low pressures the correction term in the probe theory reduces to 1. The same comments can be made for the acetylene–oxygen flame described in Tables 7 and 8.

The internal check through the wall potential certainly adds confidence to the validity of Langmuir probe data. The excess electron temperatures in the combustion zone, where electrons are being created, are no problem to explain. In chemi-ionization there may certainly be sufficient available energy to "kick" the electron out with an excess of kinetic energy. The persistence of these temperatures downstream of the combustion zone, where presumably electrons are no longer being created does, however, represent a problem. Although electron temperatures would be expected to decay relatively slowly

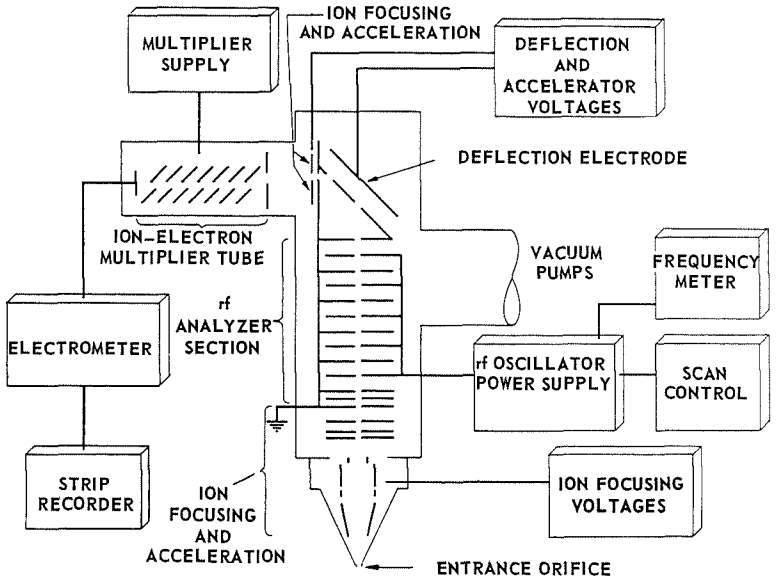

FIG. 5. Mass spectrometer circuit elements

because of inefficient momentum transfer to heavy molecules, the theoretical decay times[25] are expected to be measured in microseconds and not milliseconds. The explanation may lie in the high diffusion velocity of electrons, but this remains to be demonstrated.

The persistent excess of the positive ion concentration over the electron concentration indicates the presence of negative ions. Page[26] and Sugden[27] from microwave studies of electrons in flames deduced the presence of OH^-. This has, however, not yet been identified in mass spectrometric studies of flames.

Mass Spectrometer Studies

Although the Langmuir probe gives reasonably accurate data on total ion concentrations, this is insufficient to formulate a complete picture of the ion processes occurring in flames. The identity of the individual ions and knowledge of how they vary through the combustion wave are required. It has been shown by Knewstubb and Sugden[22] and by Deckers and Van Tiggelen[23] that many different ion species exist. Neither of their experimental systems was capable, how-ever, of obtaining ion profiles with any spatial resolution

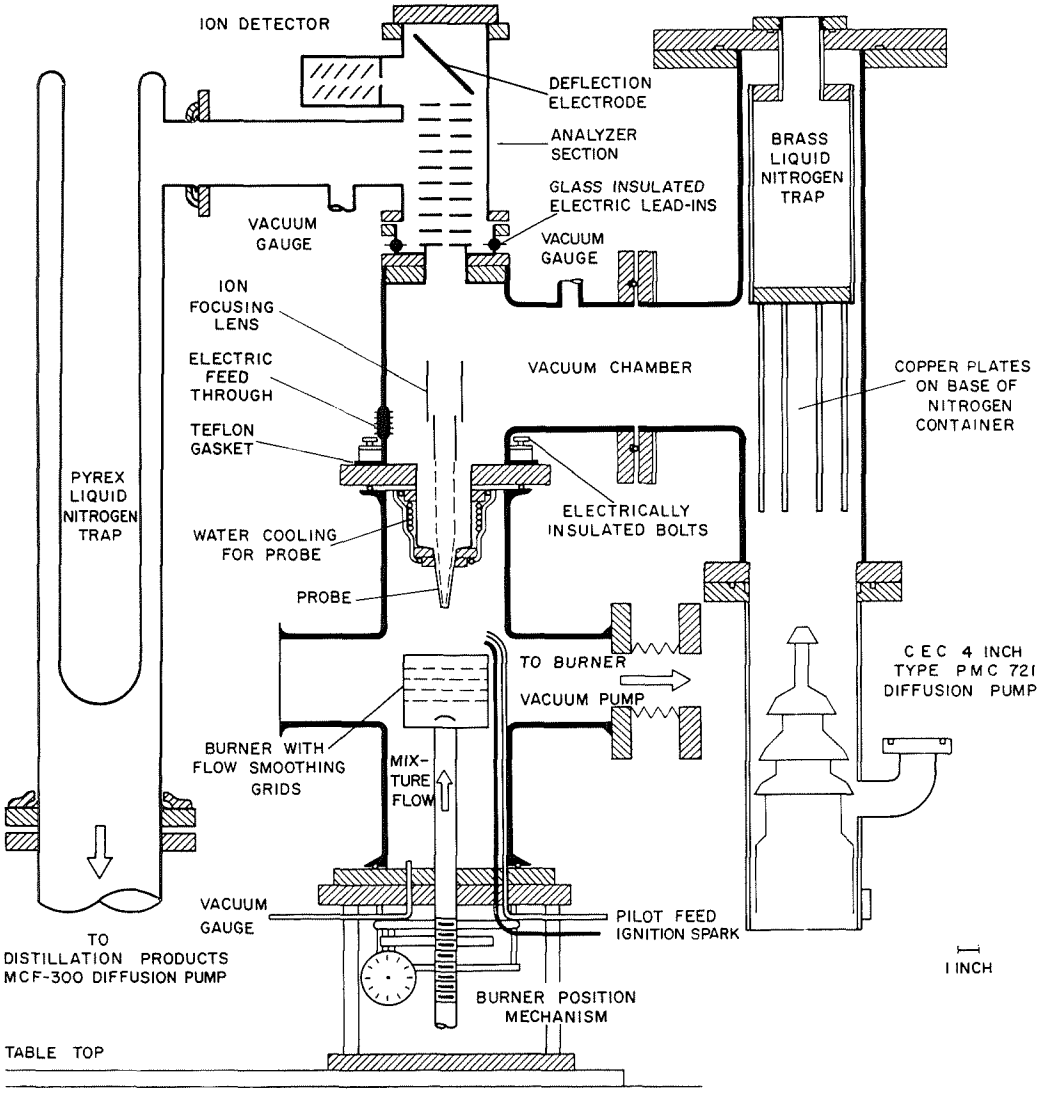

FIG. 6. Mass spectrometer system

because the sampling orifice was in a flat plate against which the flame played and they operated at relatively high pressures, 1 atm, and 10 to 40 mm Hg, respectively. We have developed techniques at lower pressures, 1 to 10 mm Hg,[24] which allows reasonably good spatial resolution. The techniques will be briefly described with some typical data, and the questions these detailed profiles raise will be discussed.

Mass Spectrometer

The instrument is shown in Figs. 5 and 6. It consists of a low pressure burner, a cone-shaped ion sampling probe, two vacuum systems for the mass spectrometer, an ion focusing section to focus the ions from the entrance orifice onto the first slit of the radio-frequency mass spectrometer, an ion multiplier tube to detect the ions, and an electrometer recording system.

Ion profiles are obtained by moving the flame across the orifice by adjusting the position of the 10 cm diameter flat flame burner. The cone-shaped sampling probe represents a compromise to give a minimum disturbance to the flame while allowing a maximum pumping speed in the mass spectrometer. The pressure inside the orifice is about 10^{-4} mm Hg, and in the analyzer section it is about 10^{-5} mm Hg. The entrance orifice is about 0.25 mm in diameter and 0.2 mm long. These dimensions are approximately equal to the mean free path of the ions in the flame, and thus ions pass through the orifice without colliding with the wall.

Ion profiles are obtained by sweeping the analyzer frequency and recording the ion current (measure of ion concentration) against the frequency (measure of ion mass). The frequency scale is calibrated in terms of mass by several means involving alkali metal ions and isotopes.

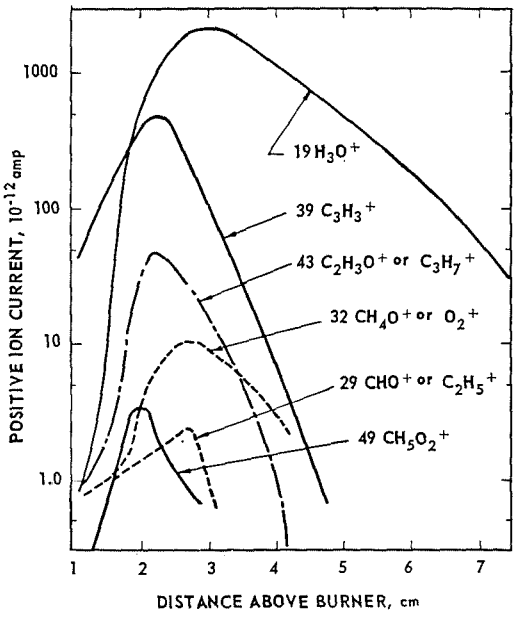

FIG. 7. Mass profiles for an acetylene–oxygen flame; pressure = 2.5 mm Hg; equivalence ratio = 0.66; total flow = 61 cc/sec.

Ion Profiles

Ion profiles are shown for a lean acetylene-oxygen flame at 2.5 mm Hg in Fig. 7. The $C_3H_3^+$ ion was identified by the addition of deuterated acetylene to the input gas; the other ions are probable identifications from the possibilities open to the system C, H, O. The general features of these results are consistent with other experiments with both acetylene–oxygen and ethylene–oxygen flames over a range of equivalence ratios.[24] A number of ionic species other than those noted in the figure also reach maximum concentrations at about 2 cm from the burner. These are:

Mass	Probable ion	Maximum current
42	$C_2H_2O^+$ or $C_3H_6^+$	80 × 10^{-12} amperes
53	$H_3O^+(OH)_2$	15
55	$H_3O^+(H_2O)_2$	7
27	$C_2H_3^+$	6
26	$C_2H_2^+$	5

Mass numbers: 15, 16, 21, 23, 28, 30, 31, 41, and 54 were also observed in very small concentrations.

The ion CHO^+ (mass 29), often considered as the primary ion produced from neutral species, appears in only small concentrations early in the flame. The ion has been observed in other flames but always in small concentrations. Van Tiggelen's group also observed mass 29 but only in small concentrations. This is as expected due to rapid proton charge transfer, but is unsatisfactory with regard to obtaining experimental verification of the first ion produced, because the concentrations are too low to accurately plot the CHO^+ profile. We are increasing the sensitivity of our equipment by a factor of about 100 and plan to study dilute hydrocarbon systems, various fuel systems, and the effect of additives as a means of seeking out the primary ion production mechanisms.

One of the most interesting results from this work has been the persistent appearance in large concentrations of $C_3H_3^+$ (mass 39) and the

consistency with which many ions, particularly masses 39 and 43, reach their maximum values at the same position in the flame—and ahead of H_3O^+. Many mechanisms for ion formation have been discussed (e.g., references 4 and 9), so it does not seem worthwhile belaboring the point here—more information is required before anything of consequence can be added. The problems associated with most of the previous proposals for the formation of $C_3H_3^+$ have already been presented.[24]

The fact that the ion concentrations all reach a maximum at about the same position in the flame indicates either that they are all formed from the same precursor or that they are all produced very rapidly after the generation of some single ionic specie.

The appearance of $C_3H_3^+$ in the flame front ahead of H_3O^+ does not necessarily mean that it is the precursor of H_3O^+, although it would be nice if the interpretation were so simple. Suppose, for example, that $C_3H_3^+$ were produced by the sequence of reactions:

$$CHO^+ + H_2O \rightarrow H_3O^+ + CO$$

$$H_3O^+ + C_3H_2 \rightarrow C_3H_3^+ + H_2O$$

The concentration of $C_3H_3^+$ would then be strongly dependent upon the concentration of C_3H_2, which must certainly be decreasing rapidly downstream from the flame front while the concentration of H_2O is steadily increasing. In fact, in a lean flame such as described in Fig. 7 it is difficult to understand the formation of any reasonable quantity of C_3H_2 or other hydrocarbon fragments of greater than two carbon atoms. Nevertheless, the relative concentrations of $C_3H_3^+$ and H_3O^+ differ very little in rich and lean flames. This again focuses attention on the need for more detailed profiles of as many facets, e.g., stable species, free radicals, and flame temperature, of the combustion wave as possible in order to choose between the possible explanations of ion production and subsequent reactions. With present information one is unable to make a unique choice.

Acknowledgments

Much of the experimental work was performed under Contract AF 04(647)–157 and interpreted under Contract NOw–62–0540–c. The work is continuing under Contract Nonr–3809(00).

The participation of James L. Reuter and Richard L. Revolinski in collecting the experimental results, and of Allan H. Schell who reduced the data, is gratefully acknowledged.

References

1. Calcote, H. F.: Combustion and Flame *1*, 385 (1957).
3. De Jaegere, J., Deckers, J., and Van Tiggelen, A.: *Eighth Symposium (International) on Combustion*, p. 155. Williams and Wilkins, 1962.
3. Knewstubb, P. F. and Sugden, T. M.: *Seventh Symposium (International) on Combustion*, p. 247. Butterworth, 1959.
4. Mukherjee, N. R., Fueno, T., Eyring, H., and Ree, T.: *Eighth Symposium (International) on Combustion*, p. 1. Williams and Wilkins, 1962.
5. Kinbara, T., Nakamura, J., and Ikegami, H.: Distribution of Ions in Low-Pressure Flames, *Seventh Symposium (International) on Combustion*, p. 263. Butterworth, 1959.
6. Bulewicz, E. M. and Padley, P. J.: Combustion and Flame *5*, 331 (1961).
7. Hand, C. W. and Kistiakowsky, G. B.: *The Ionization Accompanying the Acetylene–Oxygen Reaction in Shock Waves*. Gibbs Chemical Laboratory, Harvard University, Cambridge, March 1962. (To appear in J. Chem. Phys.)
8. Sternberg, J. C., Galloway, W. S., and Jones, T. L.: *The Mechanics of Response of Flame Ionization Detectors*. Pittsburgh Conference on Analytical Chemistry and Applied Spectroscopy, February 1961.
9. Calcote, H. F.: *Eighth Symposium (International) on Combustion*, p. 184. Williams and Wilkins, 1962.
10. Loeb, L. B.: *Basic Processes of Gaseous Electronics*, p. 201. University of California Press, Los Angeles, 1955.
11. Van Tiggelen, A.: *Experimental Investigation of Ionization Processes in Flames*. University of Louvain, ARL Report 68, May 1961.
12. Smith, F. T. and Gatz, C. R.: *Ionization in Afterburning Rocket Exhausts*. Stanford Research Institute, Technical Report BSD–TR–61–76, November 1961.
13. Bohm, D., Burhop, E. H. S., and Massey, H. S. W.: *The Characteristics of Electrical Discharges in Magnetic Fields*, Chap. 2, edited by A. Guthrie and R. K. Wakerling, McGraw-Hill, 1949.
14. Jeans, J.: *An Introduction to the Kinetic Theory of Gases*. University Press, 1959.
15. Hirschfelder, J. O., Curtiss, C. F., and Bird, R. B.: *Molecular Theory of Gases and Liquids*. J. Wiley and Sons, 1954.
16. Pauling, L.: *The Nature of the Chemical Bond*. Cornell University Press, 1944.
17. Altshuler, S.: Phys. Rev. *107*, 114 (1957).
18. Bulewicz, E. N.: J. Chem. Phys. *36*, 385 (1962).
19. Takeda, S. and Dougal, A. A.: J. Appl. Phys. *31*, 412 (1960).

20. HILL, R. M.: Abstracts Eleventh Gaseous Electronics Conference, N.Y., October 1958.
21. BURHOP, E. H. S. and MASSEY, H. S. W.: *Electronic and Ionic Impact Phenomena.* Oxford University Press, 1956.
22. KNEWSTUBB, P. F. and SUGDEN, T. M.: Proc. Roy. Soc. (London) *A255*, 520 (1960).
23. DECKERS, J. and VAN TIGGELEN, A.: *Seventh Symposium (International) on Combustion*, p. 254. Butterworth, 1959.
24. CALCOTE, H. F. and REUTER, J. L.: Mass Spectrometric Study of Ion Profiles in Low Pressure Flames, presented at the Fall Instrument-Automation Conference and Exhibit, Los Angeles, California, September 11–15, 1961, ISA Preprint No. 69–LA–61.
25. CALCOTE, H. F.: *Dynamics of Conducting Gases, Proceedings of the Third Bienneal Gas Dynamics Symposium*, p. 36. Northwestern University Press, Evanston, Illinois, March 1960.
26. PAGE, F. M.: Discussions Faraday Soc. *19*, 87 (1955).
27. SUGDEN, T. M.: *Fifth Symposium (International) on Combustion*, p. 406. Reinhold, 1955.
28. SCHNEIDER, J. and HOFFMAN, F. W.: Phys. Rev. *116*, 244 (1959).
29. BASU, S.: Phys. Fluids *3*, 456 (1960).
30. BELCHER, H. and SUGDEN, T. M.: Proc. Roy. Soc. (London) *A201*, 480 (1950).
31. DIBELIUS, M. R., LUEAKE, E. A., and MULLANEY, G. J.: Second Symposium on Engineering Aspects of MHD, March 9, 10, 1961.
32. BROWN, S. C. and ALLIS, W. P.: *American Institute of Physics Handbook*, sec. 5. McGraw-Hill Book Co., 1957.
33. SHKAROFSKY, I. P., BACHYNSKI, M. P., and JOHNSTON, T. W.: Collision Frequency Associated with High Temperature Air and Scattering Cross-Sections of the Constituents, RCA Victor Co. Ltd., Montreal, Canada, Report No. 7–801; presented at AFCRC Symposium on Plasma Sheath, Dec. 1959 (from compilation of literature values).

Discussion

DR. I. R. KING (*Texaco Experiment, Inc.*): Dr. Calcote is to be commended on the excellent work he has done and is still doing in the field of "Ions in Flames." His many papers, including the present one, have added much to our knowledge in this area. Calcote was, I believe, one of the first to postulate the CHO^+ ion as the parent or initial ion created in the combustion of hydrocarbon–air mixtures. This idea is rapidly gaining wide support, as evidenced at the present meeting.

I was particularly interested in Calcote's findings concerning the electron deficiency in flames. At Texaco Experiment, Incorporated, I have been interested in recombination processes in flames for some time and have been using both a probe and an electromagnetic attenuation technique in these studies. The probe measures positive ion concentrations while the attenuation technique measures the concentration of free electrons. Our results also show a deficiency of electrons. As Calcote has suggested, this is indicative of negative ion formation. Indeed, if we assume charge balance in the flame and obtain positive ion and electron concentration profiles downstream of the combustion zone, then by subtracting the two, we may obtain a negative ion profile. Second order recombination rates determined from the positive ion profile and from the negative ion profile give almost identical values. This is strongly suggestive of an ion–ion type recombination. The order of magnitude of the recombination coefficient is also indicative of an ion–ion process. Furthermore, the fact that recombination coefficients determined in a number of different hydrocarbon-air flames give almost identical values suggests that not only the same process is active in all these flames but the same species must be involved. Some typical results are shown in Table 1.

TABLE 1

Recombination in Flames of Several Fuels[a]

Fuel	Equivalence ratio[b]	Ambient pressure (atm)	Recombination coefficient (cm^3/sec)
Methane	1.08	0.087	2.5×10^{-7}
Propane	1.18	0.072	2.9×10^{-7}
Acetylene	1.15	0.026	2.8×10^{-7}

[a] Oxidizer, air. Platinum probe; radius, 0.007 cm.
[b] Equivalence ratio, ϕ, is the stoichiometric air-fuel ratio divided by the actual air-fuel ratio.

An examination of flame intermediates shows a number of species which are electronegative. Of these the OH radical seems to be the most likely to attach an electron and become a negative ion. Although there seems to be some disagreement as to the actual electron affinity of this radical, it does seem to be fairly high. Page and Sugden have suggested a value of 65 kcal/mole. If we assume this

value, a calculation of equilibrium concentrations shows that OH^- may actually outnumber the free electrons. Furthermore, all hydrocarbon-air flames contain fairly large amounts of OH. Thus OH^- seems the most likely candidate for the negative ion. In a recent article we suggested recombination in hydrocarbon-air flames probably occurs between the H_3O^+ ion, already identified in flames, and the OH^- ion. Although mass spectrometer studies have thus far failed to verify the presence of negative ions in these flames, it is extremely difficult to account for the observed electron deficiency in any other way.

Diffusive losses are undoubtedly responsible for some of the electron deficiency, especially at the lower pressures, but it is difficult to account for the entire loss in this manner. A dissociative recombination process, where the H_3O^+ ion picks up an electron and dissociates into H_2O and H, or similar products, has also been suggested. This process would also account for the loss of some electrons. However, under these conditions we would expect the positive ion and electron concentrations to be equal. This has not been found to be the case. Furthermore, the effects of temperature and pressure on recombination rates are not indicative of a dissociative process. Experimental results show that the recombination coefficient, α, varies inversely with pressure and shows a slight increase with increasing temperature. Theory says α should be independent of pressure and should vary approximately as $T^{-\frac{3}{2}}$. Also, according to Loeb, a dissociative process has only been observed in inert and pure nonelectron-attaching gases. Thus it seems rather unlikely that a dissociative recombination process is active in these flames.

All of the above evidence tends to verify the presence of negative ions in hydrocarbon–air flames. However, much remains to be done before a complete understanding of the ionization and recombination processes occurring in flames is obtained. Calcote has stressed the need for detailed profiles of ions, electrons, temperature, stable species, and intermediate species through the flame front of a number of different flames as a logical step in solving the riddle. Although this approach presents many problems, it does seem to be the most logical plan of attack for such a complicated system.

PROF. A. VAN TIGGELEN (*University of Louvain*): I would like to confirm the presence of OH^- ions in the hydrocarbon flames. We have recently identified a very weak peak at mass 17.

Concerning a primary process for ion formation I would suggest $CH + O_2 \rightarrow CO_2H^+ + e^-$ (±15 kcal?) as more probable. A lower apparent activation energy (as observed) would correspond to this process as compared to $CH + O \rightarrow COH^+ + e^-$. Furthermore, it is supported by the fact that the OH emission varies linearly with ion concentration as we have observed

$$CH + O_2 \begin{cases} \nearrow\ CO_2H^+ + e^- \\ \searrow\ CO + OH^* \end{cases}$$

Both processes occur simultaneously in an almost constant ratio.

DR. H. F. CALCOTE (*AeroChem Research Laboratories*): While I agree[1,2] with King's interpretation that the ion recombination process in flames may be an ion–ion recombination as opposed to an ion–electron recombination, I cannot agree with some of his arguments nor with his interpretation of Langmuir probe experiments.

He states that "the order of magnitude of the recombination coefficient is also indicative of an ion–ion process." True, three-body ion–ion recombination coefficients and mutual neutralization ion–ion recombination coefficients may be of the magnitude observed in flames, but so are ion–electron dissociative recombination coefficients (see reference 1 of this discussion for details).

When ambipolar diffusion is neglected, as King does, in computing the effect of pressure on recombination coefficients calculated from Langmuir prove curves, an inverse pressure relationship is obtained which is difficult to explain. When the correction for ambipolar diffusion is made the recombination coefficient is independent of pressure as the following data[2] shows:

Pressure (mm Hg)	Recombination coefficient (α, 10^{-7} cc/sec)
33	1.6
66	2.4
520	1.6
760	2
760 (Green and Sugden, this symposium)	2.2

Actually we agree that the recombination process is second order; this is consistent with a recombination coefficient which is *independent* of pressure. A pressure dependence of α for a second order process would require some explaining.

King further argues against a dissociative recombination process on the basis that his results for α show "a slight increase with increasing temperature" and he continues that "theory says α should be independent of pressure and should vary ap-

proximately as $T^{-\frac{3}{2}}$." It is a common error to interpret Bates' theory of dissociative recombination as giving a $T^{-\frac{3}{2}}$ dependence.[3,4] It may be this, or conceivably a positive temperature dependence. The theoretical treatment is hardly sufficient in its present state of development to eliminate from consideration a specific recombination as being dissociative because it does not conform to a particular temperature dependence. In fact the slight temperature dependence observed by King[5] may be dependent upon the means he uses to reduce his probe data or on his neglect of the diffusion correction.

The argument from Loeb's book published in 1955 is of little weight because most of the work on dissociative recombination has been done subsequent to the time that book was prepared.

Thus I see no reason, arising from the presence of negative ions, to abandon the dissociative recombination concept for ion losses in flames. In fact, the original proposal that the loss mechanism was dissociative recombination is completely consistent with negative ions. In reference 1 of this discussion it is stated: "The expected recombination process might be:

$$H_3O^+ + OH^- \rightarrow 2H_2O \qquad (1)$$

or

$$\rightarrow H_2O + OH + H \text{ etc.}$$

or

$$H_3O^+ + e^- \rightarrow H_2O + H \qquad (2)$$

or

$$\rightarrow OH + 2H".$$

The consistent observation of an excess of positive ions and negative ions over electrons and the observation that the electron-concentration–distance curves are relatively flat certainly favors reaction (1).

References

1. Calcote, H. F.: *Proceedings of the Third Biennial Gas Dynamics Symposium*, p. 36. Northwestern University Press, Evanston, Ill., 1960.
2. Calcote, H. F.: *Eighth Symposium (International) on Combustion*, p. 184. Williams and Wilkins, 1962.
3. Bates, D. R.: Phys. Rev. *78*, 492 (1950).
4. Bates, D. R. and Delgarno, A.: *Atomic and Molecular Processes*, p. 262, edited by D. R. Bates. Academic Press, 1962.
5. King, J. R.: J. Chem. Phys. *35*, 380 (1961).

Dr. P. F. Knewstubb (*University of Cambridge*): In view of the remarks which have been made regarding the occurrence of large numbers of negative ions in flames, I should like briefly to recount some experiments which we did, seeking to extract negative ions into our mass spectrometer and to analyze their masses.

Negative ions were not detected at all unless the flame was seeded with sodium or potassium to provide a considerable concentration of free electrons. When this was done, negative ions were readily detectable in the upper parts of the flame, but not in or near the reaction zone. Details of the numerous types detected are to be published. The suggestion is strong that the heavy negative ions are formed only in the cooled parts of the flame, and this is supported by the mobility experiments of Kinbara and Nakamura (Seventh Symposium on Combustion).

There is at first sight a possibility that the sampling of negative ions might be prevented by the retarding potential at the boundary of the plasma, until this falls with decreasing electron and flame temperatures. However, it was found that on introducing various amounts of iodine into the system, I^- ions could be found throughout the flame in concentrations satisfactorily close to those expected. Thus it does not seem that the sampling of negative ions from flames is seriously impeded by any wall potential in this apparatus.

Dr. P. J. Padley (*University of Cambridge*): Dr. Calcote mentions the difficulty of interpreting the observation in gas chromatography that the rate of ion formation in a hydrogen–air flame is directly proportional to the concentration of hydrocarbon introduced.

Flame ionization detectors are usually operated under such conditions that, once an ion is formed in the flame, it is drawn out and detected as a current reading. Thus the method unambiguously measures the rate of ion production directly, giving it, for this purpose, certain advantages over the mass spectrometric or cyclotron resonance type of observation presented at this Symposium which, at best, have to infer rates of ion production from steady state considerations and from rates of ion disappearance.

Now the work of Bulewicz and Padley (this Symposium) has shown that the concentration of single carbon atom species involved in the primary ionization step is directly proportional to the fuel concentration, for all hydrocarbon type fuels. An interpretation of the gas chromatography observation thus immediately follows.

We have interpreted our results (this Symposium) as implying an electron attachment process predominantly responsible for disappearance of electrons in both hydrocarbon–oxygen and cyanogen–oxygen flames; these may therefore lend support to the view that H_3O^+ probably reacts with an OH^- species rather than directly with an electron. How

ever, it seems rather unlikely that the observed discrepancy between positive ion concentration and electron concentration can be explained satisfactorily also in terms of this same species, OH^-. Taking a figure of 50 kcal/mole for the electron affinity of OH, the negative ion is most likely to be produced by direct attachment, in the pseudo-equilibrium

$$e + OH + X \rightleftharpoons OH^- + X$$

rather than by a process of the type

$$e + H_2O \rightleftharpoons OH^- + H.$$

Thus the Saha equation can still be used, even though both $[e^-]$ and [OH] are well out of equilibrium. Such calculations suggest that the observed discrepancy could, indeed, be accounted for in terms of OH^- at atmospheric pressure, but not, however, at lower pressures, since the ratio $[OH^-]/[e^-]$ decreases as the pressure decreases. The discrepancy does not seem to decrease as the pressure is reduced, and to account for it in the lowest pressure flames the flame gases would have to consist purely of OH.

DR. H. F. CALCOTE: Knewstubb has pointed out that he does not find OH^- with a mass spectrometer, although he has looked for it in 1 atm pressure flames. Padley has raised the question of equilibrium attachment of electrons to OH in low pressure flames and has pointed out that this would require an unreasonably large concentration of OH radicals. Both of these observations are inconsistent with our observation that $n_f > n_e$ and thus negative ions must be present in large concentrations. In spite of the uncertainties involved in electron determinations by Langmuir probes, it is difficult to concede that the probe results might be off by more than an order of magnitude which these two observations would require. Possibly Knewstubb has worked in different flames because in our 1 atmospheric flame (Table 3 of the paper) a reasonable excess of OH over the equilibrium value would account for the observed negative ion concentration. Such excesses of OH radicals have been reported by several authors in this and in previous symposia. I think the essential problem is the rate of attachment and we plan to address ourselves to this subject in the near future. Williams (Seventh and Eighth Combustion Symposia) has already shown that electron attachment rates are important in some flames.

I recognize the difficulty which Padley raises for low pressure flames; part of the explanation of low electron concentrations in these flames is certainly related to the high diffusion coefficient for electrons. We have already pointed out that diffusion is the dominant loss mechanism for both electrons and ions at low pressures (reference 25 of the paper). We are pursuing the problem of negative ion formation in flames further with both Langmuir probes and mass spectrometry; this paper represents only a progress report.

PROF. T. KINBARA (*Sophia University, Tokyo*): We must be very careful in applying the Langmuir probe method to the measurement of ion concentration in a flame. I would like to ask about these points.

1. A probe, except for its end, should be protected by a tube of some kind which is very resistive to the electric current through it. However, it is almost hopeless, I believe, to find a material which is completely resistive to an electric current at high temperatures in a flame. Such materials can be resistive but are porous and electrons can easily pass through them. The surface area of the protecting tube is quite large compared with that of the wire exposed to the flame, and this leakage current cannot be neglected. How does one correct the actually observed current and get the pure ion current which flows out the naked end of the probe wire?

2. I suppose platinum was used as a probe wire. Can one make sure that the catalytic action of platinum does not give any effect on the ion concentration in a flame?

3. In studying the ion concentration using a Langmuir probe wire of cylindrical form, it is necessary to know the surface area of the sheath around the probe wire. The area changes according to the current, and we need some assumptions for this relation. Results depend upon the assumption adopted. I would like to know how this problem was dealt with and I would like also to mention that the temperature of the probe is, in general, lower than that of the flame. This difference should be taken into account.

DR. H. F. CALCOTE: I certainly agree, the use of Langmuir probes in flames is fraught with difficulties. We tolerate its idiosyncracies because it is essentially the only means of obtaining local ion and electron concentrations through a flame front. In its defense, it should be pointed out that the rates of ion recombination and the mechanisms first deduced from probe measurements are being continually reconfirmed by other techniques as we have observed in this meeting.

In answer to the specific questions raised by Professor Kinbara.

1. We did not use only the end of the probe to measure currents but part of the cylindrical area. In some cases the probe was stretched completely across the flame so no insulators were involved. Data obtained by this technique and with the in-

sulated probe (Fig. 3 of the paper) gave the same result. Leakage current was maintained at a negligible level by the silver (or sometimes copper) cooling jacket.

2. Platinum–40% rhodium has been found to be the best probe material. Platinum is much more catalytic. Sometimes catalytic action, usually indicated by abnormal probe temperatures, effects the ion concentration but often it does not. Probes of different substances, e.g., rhodium, nickel, palladium, and stainless steel have been used at various times to verify the lack of influence of catalytic action.

3a. The difficulty of knowing the sheath area is avoided by extrapolating the positive ion current (at negative probe voltage) to the plasma potential where the sheath thickness is zero. Then the probe area is used. As can be seen in Fig. 1 of the paper this extrapolation is reasonable because the negative portion of the curve is essentially linear.

3b. The temperature of the probe is always lower than the flame temperature, the difference increasing with decreasing pressures because radiation cooling is independent of pressure and convective heating decreases with pressure. I do not believe this temperature difference is very important so long as small probes are used which do not greatly cool the surrounding gas. A quantitative analysis of this problem could be made by comparing the distance the probe cooling extends into the flame and the relaxation distance of the plasma properties as they diffuse through this cooled gas.

A CYCLOTRON RESONANCE STUDY OF IONIZATION IN LOW-PRESSURE FLAMES

E. M. BULEWICZ AND P. J. PADLEY

Electron concentrations and electron–molecule collision cross sections have been measured by the cyclotron resonance method in flames of hydrocarbons, alcohols, esters, ketones, and ethers, all at reduced pressure. The following summarizes the main observations made in the reaction zone:

1. The average electron-flame gas molecule collision cross section varies little from fuel to fuel.
2. The electron concentration in hydrocarbon flames is proportional to the total pressure.
3. A plot of the ratio of the electron concentration per molecule of fuel to the total burned flame gas concentration against the number of carbon atoms in the molecule shows the following regularities: points for saturated hydrocarbons lie on a smooth curve; those for unsaturated hydrocarbons lie on various smooth curves displaced upwards to greater ionization levels; if the fuel contains one oxygen atom the ionization is lowered by an approximately constant amount with respect to the corresponding saturated hydrocarbon; when two oxygen atoms are present the effect is doubled.
4. The effect of inert additives such as argon, and of nonhydrocarbon fuel additives such as hydrogen was studied.

The results are shown to suggest that a very important step in the process of ion production is the reaction $CH + O \rightarrow CHO^+ + e^-$. Polymerization reactions as a means of ion production appear to be of secondary importance.

Introduction

The understanding of the phenomenon of ionization in flames is a problem which has received increased attention in the last decade.[1–8] The experimental methods which have been used fall into three general groups: (a) measurements with probes,[1] giving quantitative information about the over-all ionization level; (b) studies of the effect of free electrons on the characteristics of microwave and radiofrequency circuits[2,3]; (c) recent, elegant applications of the mass spectrometer, by which the individual positive ions can be identified.[4–7]

Although it is well known that the ionization in the region of primary reaction in hydrocarbon flames is nonthermal, the process by which the ions are produced is still a subject for considerable speculation. This situation exists mainly because the rapidity of the initial combustion processes has so far precluded kinetic studies of the individual reactions. In general, the nature of the elementary processes must still be inferred from their over-all effect, on the level of ionization [methods (a) and (b)] and from the type of ions produced [method (c)]. So far, only the results of method (c) have led to any significant elucidation of the problem.

There has as yet been no systematic, quantitative study of the behavior of the over-all ionization level in a wide range of fuels under similar conditions with the view to understanding these processes in any detail. Such an attempt forms the basis of the present paper. The cyclotron resonance method used—essentially a type (b) method—is novel in its present application and will therefore be briefly outlined.

Theory of Method

The principle utilized here is that the cyclotron motion of free electrons, which takes place in an applied magnetic field, will cause power to be absorbed from a beam of electromagnetic radiation with its electric vector perpendicular to the field, provided that the radiation frequency is equal to that of the cyclotron motion. The product of power loss and line width at the resonance frequency can be related quantitatively to the concentration of electrons present in the flame. From the width of the resonance curve, electron–molecule collision frequencies can be calculated.[9–13]

The salient features of the theory of cyclotron resonance relevant to the present work are reproduced below.

The attenuation, β, in db, of the intensity of an electromagnetic wave passing through a partially ionized gas is related to the real part, σ', of the electric conductivity by the expression

$$\beta = 40\pi d\sigma'/c \cdot \log_{10} e \qquad (1)$$

where d is the path length in cm, and c the velocity of light. In a uniform magnetic field, parallel to the Z axis, the attenuation of a microwave beam travelling with E vector perpendicular to the field will be determined by the real part of the (transverse) component, σ_{xx}', of the conductivity, given by

$$\sigma_{xx}' = ne^2\{\nu/[\nu^2 + (\omega + \omega_c)^2] + \nu/[\nu^2 + (\omega - \omega_c)^2]\}/2m \qquad (2)$$

where n is the number of electrons/cc, ν the electron–molecule collision frequency, ω and ω_c the microwave and cyclotron frequencies, respectively, and e and m have their usual significance. When $\omega \gg \nu$, cyclotron resonance occurs near

$$\omega = \omega_c = eH/mc,$$

where H is the magnetic field strength in gauss.

From Eqs. (1) and (2) it can be shown that

$$n = \Delta H\sigma_{xx}'/ec = \Delta H\beta/40\pi ed \log_{10} e \qquad (3)$$

where ΔH is the cyclotron line width between the half conductivity points and β the attenuation at the center of the line.

Equation (3) holds provided that $\omega^2 \gg \omega_p^2 = ne^2/m\epsilon$, where ω_p is the plasma frequency and ϵ the dielectric constant. This condition is satisfied for values of n (1–5×10^{10} electrons/cc) and ω used in this work.

When the cyclotron line is sufficiently sharp, ν is given by

$$\Delta H/H_0 = 2\nu/\omega \qquad (4)$$

where H_0 is the value of the field at which maximum attenuation occurs. Hence the electron–molecule collision cross section, Q, can be obtained from

$$Q = \nu/N\bar{v} \qquad (5)$$

where $\bar{v}$ is the mean electron velocity

$$[\bar{v} = (8kT/\pi m)^{\frac{1}{2}}]$$

and N the concentration of neutral molecules. Rearrangement of this equation leads to

$$\frac{\Delta H}{p} = \left[\left(\frac{2k}{\pi m}\right)^{\frac{1}{2}} \frac{4 \cdot 273mcN_0}{760e}\right] \cdot \left(\frac{Q}{T^{\frac{1}{2}}}\right) \qquad (6)$$

where N_0 is Loschmidt's number and p is the pressure in mm Hg. Equation (6) reduces to

$$\Delta H/p = (6.8 \times 10^{17}) \cdot Q/T^{\frac{1}{2}} \qquad (7)$$

Experimental

The premixed flames were burned at pressures between 8 and 200 mm Hg inside a cylindrical Pyrex vessel, 20 mm in diameter on burner tubes 10–15 mm in diameter—an arrangement essentially similar to that described by Gaydon and Wolfhard.[14] The vessel was air-cooled. Gaseous fuels were obtained from the Matheson Gas Company, and all were stated to be at least 99 per cent pure. The gases were metered at atmospheric pressure with rotameters, after which they were sucked into the reduced pressure part of the apparatus through controlled leaks. Liquid fuels were introduced by bubbling a measured part of the oxygen supply through the thermostated fuel, contained in a saturator at atmospheric pressure. The total gas flow (at room temperature and atmospheric pressure) did not exceed 800 cc/min. The flame compositions were varied between $\lambda = 0.6$ and $\lambda = 2.0$ (λ, the mixture strength, = [oxygen present in unburned gases]/[oxygen present at stoichiometry]).

The flame vessel was arranged vertically in the 2.3 cm gap of a 12-inch, 20,000 gauss maximum, Varian Associates' electromagnet (field homogeneity over 1 cu inch volume at the center of the gap better than 1 part in 10^4). Radiation at 48 kMc/sec (obtained from a standard 2K33 Raytheon klystron combined with frequency multiplier), and modulated at 2 kc/sec, was passed horizontally through the flame in the vicinity of the reaction zone, i.e., the region of maximum electron concentration. The transmission across the flame was effected by two waveguide horns (I to K band transition sections) firmly clamped in a mount which surrounded tightly the flame vessel. The direction of flame propagation, the magnetic field and the E vector of the radiation were, therefore, all mutually perpendicular. After crystal detection and suitable amplification, the power transmitted through the flame was plotted automatically as a function of magnetic field strength, which was swept electrically over a range of about 3000 gauss in 2 minutes. This was sufficient to cover the whole of the resonance curve, the center of which lay near 17,000 gauss. Unless otherwise stated, all measurements were made in the reaction zone, which was several mm thick at the pressures used.

TABLE 1

Electron Molecule Collision Cross Sections in Different Fuels

C:H ratio	Fuel	$\Delta H/p$ observed (gauss/mm Hg)	Average Q (calc., A)	$Q \cdot p/\Delta H$
1:1	Acetylene	49	51.5	1.05
3:4	Methyl acetylene	50.5	54	1.07
2:3	Ethyl acetylene	52	55.5	1.07
1:2	Ethylene	55	58	1.05
3:7	*n*-Hexane	56	60	1.07
5:12	2-Methyl butane	58	60.5	1.03
2:5	Diethyl ether	54	61	1.13
3:8	Propane	57	61.5	1.08
1:3	Ethane	58	63	1.09
1:4	Methane	60	65.5	1.09

Results and Discussion

Average Electron–Molecule Collision Cross Sections

The third column in Table 1 lists observed $\Delta H/p$ values for a selection of stoichiometric fuel-oxygen flames; a more detailed list can be found elsewhere.[13] Q values are not given since the temperatures of all these flames are not known. However, since $T^{\frac{1}{2}}$ is hardly likely to vary greatly from one stoichiometric flame to another, the $\Delta H/p$ values should be approximately proportional to Q.

The fourth column in Table 1 lists the values of Q calculated for each fuel on the reasonable assumptions that only carbon dioxide and water contribute significantly to the over-all Q in stoichiometric mixtures, and that the values found for Q_{H_2O} and Q_{CO_2} in acetylene flames at 2000°K, i.e., 80 ± 4 Å^2, and 37 ± 2 Å^2, respectively,[11] are of general applicability. That these approximations are reasonable is illustrated by the fact that the values of $Q \cdot p/\Delta H$ (column 5) show no dependence on the carbon to hydrogen ratio. Further, the absence of significant deviations from the mean value of 1.06 (the closeness to unity is fortuitous) suggests that the temperature factor in Eq. (7) is, indeed, unimportant. Thus the average electron–molecule collision cross section for a flame can apparently be predicted with some certainty from known cross section values for its constituents.

Electron Concentration as a Function of Pressure

It has been previously found by King,[15] for propane–air flames between 100 mm Hg and 1 atmosphere, that the ratio of positive ion pressure to the total burned flame gas pressure is constant. In this work this relationship was tested at lower pressures (between 12 and 45 mm Hg) with other hydrocarbons. A typical plot of the electron concentration, n, against the total pressure, p, for an acetylene–oxygen flame is shown in Fig. 1. It is a good straight line (in agreement with King's observations at higher pressure) and appears to pass through the origin. Similar results are obtained at other mixture strengths and for other hydrocarbons—at least for those used in compiling Fig. 3. Thus R, the ratio of the electron pressure to the total burned gas pressure, is independent of the total pressure.

This suggests that the most important processes of electron production and decay are kinetically of the same order, because at the point of measurement (maximum electron concentration in the reaction zone) steady state conditions for electrons are presumed to exist. Since termolecular reactions in flames (at atmospheric pressure) are known to require of the order of 10 milliseconds to reach completion,[16] and since a

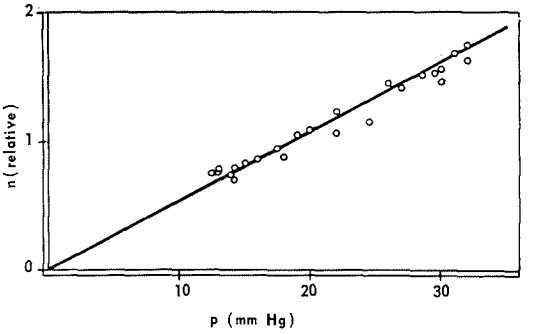

FIG. 1. Variation of electron concentration with total flame gas pressure in an acetylene–oxygen flame ($\lambda = 0.9$).

molecule passes through the reaction zone in about 50 microseconds, it is reasonable to conclude that bimolecular processes predominate.

Ionization in the Presence of Nonreactive Additives

The preburned mixtures were diluted with argon and nitrogen in such a manner that both the mixture strength, λ, and the total flow rate of unburned gases remained constant. Representative results for fuel-rich, stoichiometric, and fuel-lean acetylene–oxygen flames are shown in Fig. 2, which is a logarithmic plot of R (proportional to $n(T/p)$, where T is the measured flame temperature) against the mole fraction of acetylene present in the unburned gases. The features of interest are: firstly, all plots for nitrogen and argon addition have the same slope of two; secondly (again for nitrogen and argon) all points for $\lambda > 1.0$ lie on the same straight line; thirdly, if n is measured in pure acetylene–oxygen flames at various λ, and the same type of graph plotted, then for oxygen-rich flames the experimental points fall exactly on this same straight line.

Identical behavior is exhibited by all other hydrocarbons examined: Fig. 3 shows the results

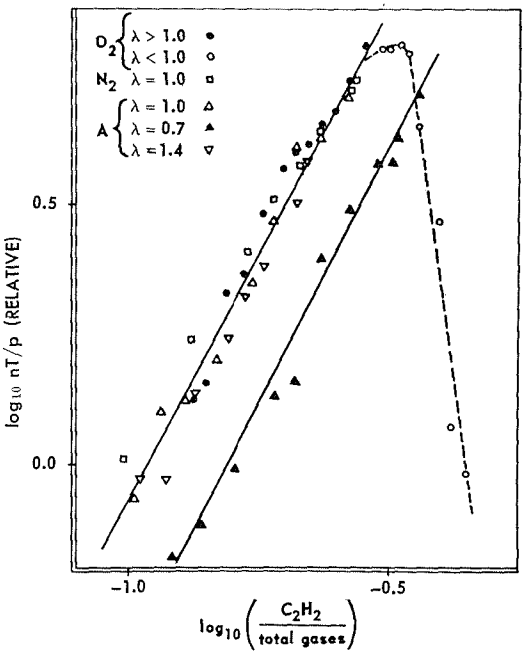

FIG. 2. Effect of inert diluents on ionization in acetylene flames. Plots of log (fuel fraction) against log (nT/p), where (nT/p) is proportional to R, the ratio of electron partial pressure to the total burned flame gas pressure.

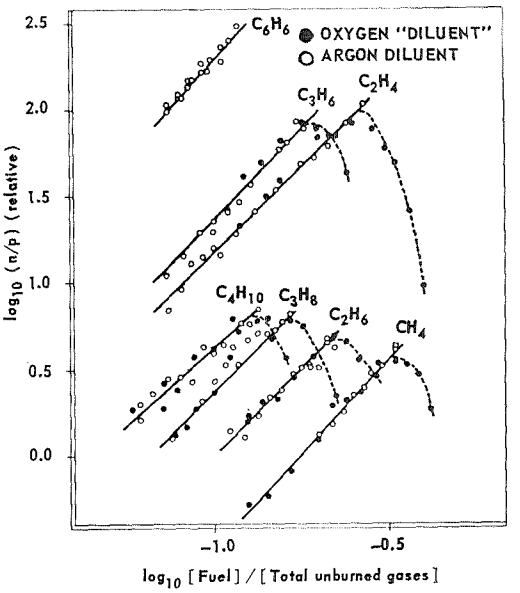

FIG. 3. Ionization as a function of fuel concentration. As for Fig. 2, but using other fuels.

for methane, ethane, propane, butane, ethylene, propylene, and benzene. Since the temperatures of these flames were not studied in detail, the quantity n/p was used to represent R; exclusion of the T factor, however, should not introduce more than about 20 per cent error over the dilution range examined. The dotted, curved portions on the right-hand side of each plot are obtained only when $\lambda < 1.0$; these will not be discussed here. These results confirm that the ionization is nonthermal, since flames containing the same proportions of nitrogen and argon differ in the temperature on account of the different specific heats of these two gases. Also, oxygen molecules in excess of those required for complete combustion of the fuel, in behaving in the same manner as an equivalent amount of either nitrogen or argon, apparently make no significant contribution to the primary ionization processes.

The consistent dependence of R on the square of the fraction of fuel in the unburned gases was an unexpected result. If the differences in ionization level in different hydrocarbons are related to the ability of the hydrocarbon firstly to form intermediate species (such as acetylene or an acetylenic fragment) and secondly for this species to polymerize and then produce ions, as has been supposed,[8] then some variation in the slopes of Fig. 3 might have been expected. As an example, since acetylene exhibits a much greater degree of ionization and more diverse spectrum of hydrocarbon ions than methane,[5] R for acetylene might have been expected to depend on a lower power

of the fuel fraction than R for methane, which molecule—on the polymerization theory—would presumably have to degrade and form unsaturated linkages before producing ions.

A reconciliation of the observed results with the polymerization theory would be possible if all hydrocarbons degraded to a single carbon atom species which could combine with another fragment also containing only one carbon atom, leading directly to ionization. Ferguson's observations on C_2 emission from acetylene flames, using C^{12} and C^{13} isotopes,[17] in demonstrating the carbon atoms comprising the C_2 to be randomized, have already suggested at least a limited breakdown of the fuel into single carbon atom species. This possibility will be examined shortly.

Ionization in the Presence of Nonhydrocarbon Fuel Additives

The fuels chosen were hydrogen, carbon monoxide, hydrogen sulfide and carbon disulfide. None of these, when burned alone with oxygen, gave measurable ionization (which, with our apparatus implies $n < 10^8$ electrons/cc, i.e., at least 3 orders of magnitude lower than in hydrocarbon flames). During the substitution of diluent fuel for hydrocarbon, both λ and the total rate of flow of unburned gases were kept constant, as in the previous section. Figure 4, a plot of relative R against hydrocarbon fuel fraction, illustrates typical results for a stoichiometric acetylene-oxygen-additive flame; points for argon, nitrogen, and oxygen additions are included for comparison.

The lowest curve (nitrogen, argon or oxygen) is known from Figs. 2 and 3 to correspond to R depending on the square of the fraction of fuel. Inspection of the curves for carbon monoxide and hydrogen shows that R now depends on a lower power of the fuel fraction. Furthermore, the value of the exponent varies with the flame composition—another difference from the behavior with inert diluents. For example, the exponents at λ 0.7, 1.0, 1.4, and 2.0 for acetylene–oxygen–hydrogen flames are approximately 1.4, 1.1, 0.85, and 0.85, respectively. Similar results are obtained for acetylene–oxygen–carbon monoxide flames, except that in this case the logarithmic plots are, in addition, slightly curved.

Low exponents are also obtained when either carbon disulfide or hydrogen sulfide are used (0.80 and 0.95, respectively, at $\lambda = 2.0$). These two cases are more complicated in that, for $\lambda < 1.5$, sulfur-containing fuels give rise to electron acceptors which modify considerably the free electron concentration.[18] For $\lambda > 1.5$, however, such interferences have been shown to be negligible.[18]

All these results are in broad agreement in the sense that they exhibit a pattern of behavior quite different from that found with "inert" additives.

It is very difficult to see how a polymerization theory—already a little strained in order to explain the observations with inert additives—can meet the additional requirement of interpreting the above results. However, it is still necessary to postulate that from the ionization viewpoint all hydrocarbons degrade to a single carbon atom species in order to explain the consistency of the slopes of the plots of Fig. 2 and 3. The new evidence provided by the present section is that these single carbon atom species must be reacting, not with themselves or some other carbon-containing fragment, but with a species which does not contain carbon, the concentration of which in the presence of a non-hydrocarbon fuel addi-

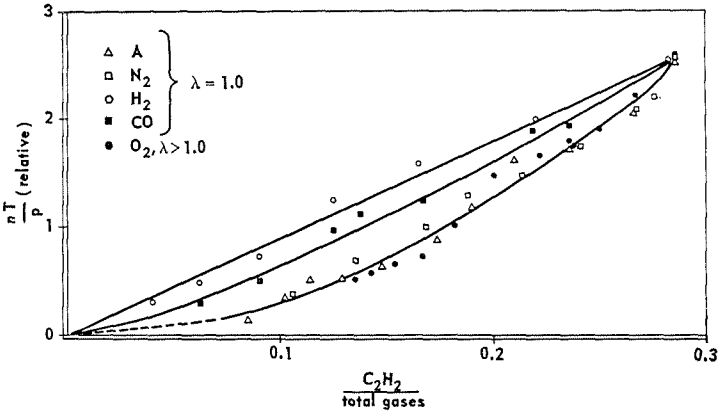

FIG. 4. Ionization in C_2H_2–O_2 flames in presence of diluents. As for Fig. 2 (but not plotted logarithmically), and including curves obtained with carbon monoxide and hydrogen as diluents. Note the difference between these curves and that obtained with argon and nitrogen diluents.

tive does not decrease so rapidly as when inert additives are used. Now the non-hydrocarbon fuels chosen for this study were selected so as to eliminate the possibility that the additive fuel itself, or its combustion products, were reacting with the single carbon atom species. Thus hydrogen molecules and atoms, water, hydroxyl radicals, carbon monoxide or carbon dioxide cannot be participants in the primary ionization reaction.

The only species left unconsidered are oxygen molecules and oxygen atoms. When an inert diluent is introduced into a hydrocarbon–oxygen mixture, not only the fuel concentration, but also the oxygen molecule and atom concentrations must necessarily decrease. On the other hand, it is in the nature of the experiments performed with nonhydrocarbon fuel additives that the oxygen molecule and atom concentrations need not be so affected. Indeed, depending on the diluting fuel and on the stoichiometry it is possible for the oxygen molecule and atom concentrations actually to increase: a quantitative analysis of this point would, of course, require experimentally measured values of $[O_2]$ and $[O]$. Now the effect of oxygen molecules can be discounted immediately, for it was shown in the preceding section that, when in excess of the number required for the stoichiometric reaction, oxygen molecules behave effectively as an inert diluent. Therefore it is inferred that the single carbon atom species is reacting with an oxygen atom.

The simplest explanation, then, of the observed square dependence of R on fuel fraction when inert diluents are used is that both the concentrations of the single carbon atom species and of oxygen atoms are proportional to the fraction of fuel present.

Ionization in Flames of Mixed Hydrogen–Nonhydrocarbon Fuels

Fuels containing carbon, but not hydrogen, such as carbon disulfide, carbon monoxide, and cyanogen, were mixed with various proportions of hydrogen and burned with oxygen. This was to test the possibility of producing reactions similar to those responsible for electron production in hydrocarbon-oxygen flames.

Mixtures with either carbon disulfide or carbon monoxide gave no measurable ionization at any composition (at a pressure of about 20 mm Hg, 10^8 electrons/cc would have been detectable). Mixtures with cyanogen gave a pronounced ionization peak at 10–20 per cent cyanogen in the fuel. The effect is, however, too complex for analysis here, and it is sufficient to note that the characteristics of this "induced" ionization are quite different from that found in hydrocarbon flames.

This negative evidence suggests the presence of the C–H bond in the original molecule to be an important prerequisite before any appreciable ionization can take place. In this case, the primary ionization process suggested by the results so far discussed is

$$CH_m + O \rightarrow R^+ + e^- + X \qquad (I)$$

where R^+ represents the positive ion produced and X may be a fragment split off in the reaction. If the simple interpretation of the slopes of Figs. 2 and 3 is correct, then the species CH_m cannot itself contain oxygen. The value of m remains, as yet, unspecified.

Relative Ionization in Flames of Different Carbon- and Hydrogen-Containing Fuels

The electron concentration was measured as a function of preburned fuel–oxygen composition for a wide range of fuels; the maximum values of

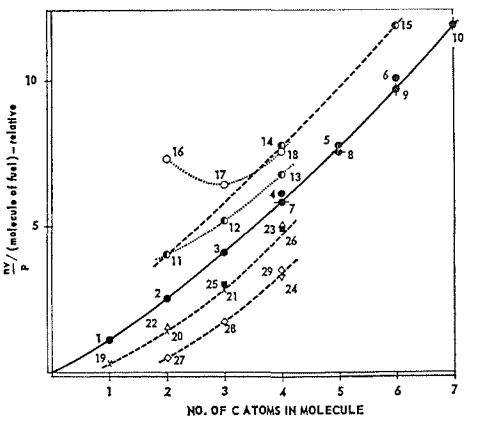

FIG. 5. Relative ionization in different fuels. Plot of relative nv/p (proportional to R) per molecule of fuel burned against the number of carbon atoms in the molecule. The points are identified as: (1) methane, (2) ethane, (3) propane, (4) butane, (5) n-pentane, (6) n-hexane, (7) isobutane, (8) 2-methyl butane, (9) cyclohexane, (10) methyl cyclohexane, (11) ethylene, (12) propylene, (13) 1-butene and also 2-butene, (14) butadiene, (15) benzene, (16) acetylene, (17) methyl acetylene, (18) ethyl acetylene, (19) methyl alcohol, (20) ethyl alcohol, (21) n-propyl alcohol, (22) dimethyl ether, (23) diethyl ether, (24) dioxane, (25) acetone, (26) 2-butanone, (27) methyl formate, (28) methyl acetate, (29) ethyl acetate. Of these fuels, 1–4, 7, 11–14, 16–18, and 22 are gases under normal laboratory conditions.

n so obtained (found in slightly fuel-rich flames) were then compared.

In Fig. 5 the value of *R per molecule of fuel burned* (given here the symbol EF) is plotted against the number of carbon atoms in the molecule: in this way the effect of molecular size and structure can be truly examined. Every point in Fig. 5 usually represents the mean of several determinations, each of which was accurate to about 10 per cent; and except for one or two of the least volatile compounds there was never any ambiguity in the EF value obtained.

Fuels investigated included: saturated hydrocarbons, normal 1–6 (see legend of Fig. 5 for the meaning of each number), isomeric 7, 8, and cyclic 9, 10; unsaturated hydrocarbons, 11–14, 16–18, and benzene 15; alcohols, 19–21; ethers, 22–24; ketones, 25, 26; esters, 27–29. The range of compounds examined was limited only by considerations of volatility.

Figure 5 shows a number of very striking regularities:

(a) Points for all saturated hydrocarbons containing up to seven carbon atoms lie on a smooth curve which appears to pass through the origin.

(b) If the fuel contains one oxygen atom, the ionization is lowered by an almost constant amount with respect to the corresponding hydrocarbon, apparently irrespective of the carbon-oxygen link.

(c) When two oxygen atoms are present the effect described in (b) is doubled.

(d) Points for unsaturated hydrocarbons lie on various smooth curves (depending on the type of unsaturation) displaced upwards to greater EF values.

The fact that the smooth plot obtained for hydrocarbons (points 1–10) is almost a straight line suggests that essentially the same process of electron production takes place in all these fuels; further, since the EF value for methane also lies on this curve, and not below it, this process probably involves mainly single carbon atom species. There is no determined gain or loss of the EF value if the hydrocarbon is cyclic or branched-chain rather than straight chain. A general rule, then, is that the level of ionization for saturated hydrocarbons depends only on the number of carbon atoms, and not in any detectable way on the molecular structure.

The plot also suggests that the value of m in CH_m cannot be greater than two, because if it were three or four the EF values would most probably tail off with increasing numbers of carbon atoms in the molecule. The cause of the slight upward curvature may be connected with the increasing carbon to hydrogen ratio as $CH_4 \rightarrow C_7H_{14}$, because this implies that the lower the hydrocarbon, the more advanced must the combustion process be before free CH_m can be released. On balance, then, the evidence of this section suggests that saturated carbon atoms behave predominantly as independent units.

The consistency of the effect of the presence of oxygen is remarkable. The presence of one oxygen atom (points 19–23, 25, 26), whether in alcohols, ethers or ketones, lowers the ionization compared to the corresponding hydrocarbon with the same number of carbon atoms by an approximately constant amount, irrespective of the number of carbon atoms in the molecule. If there are two oxygen atoms, as in esters or dioxane (points 24, 27–29), the lowering is doubled. Any difference between the effect of a double and a single C–O bond was too small to detect.

This provides strong confirmation of the conclusions already reached, i.e. that from the ionization viewpoint the fuel molecules are indeed shattered into single carbon atom fragments in passing through the reaction zone, and that the species CH_m most probably does not involve oxygen.

For unsaturated hydrocarbons (points 11–18), a less simple pattern of results is observed. The EF value, however, is certainly greater than that for the corresponding saturated hydrocarbon and, moreover, depends on the type of unsaturation involved. Simple manifestations of this effect, e.g., that an acetylene flame contains more ions than one of ethane, are already well known.[5] Sufficient data are presented in Fig. 5 to show three patterns of results: for olefins (points 11–13), for molecules in which each carbon atom makes at least one double bond (points 11, 14, 15), and for acetylenes (points 16–18).

These curves show that the property of the unsaturated bond responsible for enhanced ionization becomes impaired in the presence of saturated carbon atoms—the EF value for methylacetylene is found to be actually *lower* than that for acetylene itself. There appears to be no such impairing effect, however, when all carbon atoms in the molecule can exhibit the same unsaturated bond type: thus the EF values for ethylene, butadiene, and benzene all seem to lie on a good straight line passing through the origin. It is also interesting to note that the EF value for benzene, $(CH)_6$, is not three times that for acetylene, $(CH)_2$.

Since both benzene and acetylene exhibit very high ionization levels, the value of m in CH_m is therefore most likely less than the maximum value of two, previously suggested. A value of zero is improbable on several grounds; for example in view of the absence of detectable ionization in mixed fuels (preceding section),

and also since the ionization potential of carbon monoxide is 325 kcal/mole, whereas its dissociation energy is only 256 kcal/mole.[1,19] Thus the primary ionization step suggested by all these results is

$$CH + O \rightarrow CHO^+ + e^-, \qquad (II)$$

which is the reaction already proposed by Calcote.[20] The process is energetically feasible, for, taking the heat of dissociation of CH as +80 kcal/mole, the heats of formation of O, H, and CHO^+ as −58.6, −51.9, and +203 kcal/mole, respectively, and the high (170 kcal/mole) value for the latent heat of sublimation of carbon,[19,21] the heat of reaction (II) can be as large as +2 kcal/mole. The CHO^+ ion has been recently identified mass spectrometrically as a minor constituent in flames, by Bascombe, Green, and Sugden,[22] and kinetic calculations by the same authors have indicated the plausibility of a process such as reaction II.

Once such an ion is formed, other ions can be produced by proton exchange reactions. Thus, following Calcote[20]

$$CHO^+ + H_2O \rightarrow CO + H_3O^+ \qquad (III)$$

$$H_3O^+ + C_3H_2 \rightarrow C_3H_3^+ + H_2O \qquad (IV)$$

Vaidya's hydrocarbon bands have recently been shown to arise from excited CHO.[23] This species might be an intermediate in reaction (II)

$$CH + O \rightarrow CHO^* \rightarrow CHO^+ + e^- \qquad (V)$$

Now recent work by the authors[24] has indicated the possibility of a direct connection between the abnormally high electronic excitation temperatures measured in the reaction zones of hydrocarbon flames and the initial process of ionization. The simpler of two possible explanations was in terms of an unknown bimolecular process which had to be responsible for ion production, which also had to be capable of producing an excited species that could excite metal atoms by inelastic collision, and which furthermore had to be, apparently, at least 174 kcal/mole exothermic. It is perhaps, therefore, of interest to note that reaction (V) coupled with

$$CHO^* + M \rightarrow M^* + CO + H \qquad (VI)$$

where M is a metal atom introduced into the flame, would satisfy all these requirements.

Conclusions

1. From the ionization viewpoint the fuel molecules are predominantly shattered into species containing single carbon atoms.

2. If the fuel molecule is a saturated hydrocarbon, each carbon atom behaves almost as an independent unit, the ionization depending essentially on the number of carbon atoms and not in any measurable way on the molecular structure.

4. The primary ionization step suggested is

$$CH + O \rightarrow CHO^+ + e^- \qquad (II)$$

5. The effect of unsaturation in increasing the ionization level does not seem to arise from introduction of new charge producing reactions related to the appearance of ion polymers. If the effect is not simply one of modifying the concentrations of reactants in process II, then it could be related possibly to the ability of the uncharged polymer fragments to provide a wide spectrum of positive ions in which charge could be stored.

Acknowledgments

We would like to thank Dr. Walter Gordy for his continued interest in this work and for making available to us the facilities of his laboratory. We also wish to express our gratitude to Dr. T. M. Sugden, who read the draft of this paper and made many valuable comments.

This work was supported by the U.S. Air Force Office of Scientific Research of Air Research and Development Command.

References

1. Calcote, H. F.: Combustion and Flame *1*, 385 (1957).
2. Knewstubb, P. F. and Sugden, T. M.: Trans. Faraday Soc. *54*, 372 (1958).
3. Padley, P. J. and Sugden, T. M.: *Eighth Symposium (International) on Combustion.* Williams and Wilkins, 1962.
4. Deckers, J. and Van Tiggelen, A.: *Seventh Symposium (International) on Combustion*, p. 254. Butterworths, 1959.
5. Knewstubb, P. F. and Sugden, T. M.: *Seventh Symposium (International) on Combustion*, p. 247. Butterworths, 1959.
6. Knewstubb, P. F. and Sugden, T. M.: Proc. Roy. Soc. (London) *A255*, 520 (1960).
7. De Jaegere, S., Deckers, J., and Van Tiggelen, A.: *Eighth Symposium (Iniernational) on Combustion.* Williams and Wilkins, 1962.
8. *Eighth Symposium (International) on Combustion*: Discussions (ionization section). Williams and Wilkins, 1962.
9. Kelly, D. C., Margenau, H., and Brown, S. C.: Phys. Rev. *108*, 1367 (1957).
10. Schneider, J. and Hofmann, F. W.: Phys. Rev. *116*, 244 (1959).

11. Bulewicz, E. M.: J. Chem. Phys. *36*, 385 (1962).
12. Bulewicz, E. M. and Padley, P. J.: J. Chem. Phys. *35*, 1590 (1961).
13. Bulewicz, E. M. and Padley, P. J.: J. Chem. Phys. (in press).
14. Gaydon, A. G. and Wolfhard, H. G.: *Flames* (2nd ed.). Chapman and Hall, 1960.
15. King, I. R.: J. Chem. Phys. *31*, 855 (1959).
16. Bulewicz, E. M. and Sugden, T. M.: Trans. Faraday Soc. *54*, 1855 (1958).
17. Ferguson, R. E.: J. Chem. Phys. *23*, 2085 (1955).
18. Bulewicz, E. M. and Padley, P. J.: Unpublished data, 1961.
19. Gaydon, A. G.: *Dissociation Energies*. Chapman and Hall, 1953.
20. Calcote, H. F.: *Eighth Symposium (International) on Combustion*. Williams and Wilkins, 1962.
21. Field, F. M. and Franklin, J. L.: *Electron Impact Phenomena*. Academic Press Inc., 1957.
22. Bascombe, K. N., Green, J. L., and Sugden, T. M.: *Symposium on Mass Spectrometry*. Pergamon Press, 1961.
23. Vaidya, W. M.: *Eighth Symposium (International) on Combustion*. Williams and Wilkins, 1962.
24. Bulewicz, E. M. and Padley, P. J.: Combustion and Flame *5*, 331 (1961).

Discussion

Comments relevant to this paper will be found on pp. 654–658.

A STUDY OF IONIZATION IN CYANOGEN FLAMES AT REDUCED PRESSURES BY THE CYCLOTRON RESONANCE METHOD

E. M. BULEWICZ AND P. J. PADLEY

The ionization in the reaction zone of cyanogen–oxygen flames at reduced pressure was studied by the method of cyclotron resonance. Although the temperatures of these flames are sufficiently high for thermal ionization of nitric oxide to account for the observed free electron concentrations, other characteristics of the ionization are consistent only with the operation of nonthermal processes. These processes, however, appear to be different from those inferred to be taking place in hydrocarbon–oxygen flames, and seem to involve energetic three-body reactions. Some auxiliary spectral evidence is also presented.

When traces of hydrogen are added, the electron concentration decreases considerably—particularly for fuel-lean flames. As the concentration of cyanogen in the fuel is reduced to about 20 per cent, a second ionization maximum appears, associated with a greenish glow from the burned gases. It is shown that attempts to explain this effect simply in terms of reactions occurring in hydrocarbon–oxygen flames meet with difficulties which cannot be resolved at this stage.

Introduction

In spite of the potentialities of the cyanogen flame as a high energy spectroscopic source[1] (calculated maximum temperature about 4800°K), the fuel has so far received comparatively little attention. A study of the spectroscopy of the cyanogen–oxygen flame was made by Thomas, Gaydon, and Brewer,[2] but the few kinetic data so far available have been obtained in lower temperature, static systems.[3,4] CN and CN intermediates are frequently found in other gas reactions, e.g., when active nitrogen and other gas discharge products react with hydrocarbons, carbon monoxide, and carbon dioxide.[5–7] Apart from mass spectrometric observations carried out by van Tiggelen,[8] ionization processes appear not to have been studied at all.

The most easily ionizable component of cyanogen flame gases is NO (I.P. = 9.25 ev).[9] In fuel-rich flames at thermodynamic equilibrium, calculated [NO] is low—not greater than 10^{-2} per cent of the total gases (using equilibrium constants from Gaydon and Wolfhard[10] and an estimated flame temperature of 4000°K). In lean flames, however, [NO] can be of the order of 1 per cent of the burned gases. Thus, if the ionization is thermal, and if the Saha equation can be applied, a concentration of free electrons in the range 10^{10}–10^{11} electrons/cc is expected at the pressures (approx. 0.1 atmospheres) used in this study. Such concentrations should be readily detectable by the cyclotron resonance method.

Experimental

The cyclotron resonance method of measurement of free electron concentrations and of electron–molecule collision cross sections in burned flame gases under a variety of conditions has been described in earlier papers[11,12] and elsewhere at this symposium.[13]

A simple quarter-plate Hilger spectrograph was used to investigate qualitatively some of the spectral features of the flames under the same conditions as when the electron concentrations were measured. Photographs were taken on Kodak 103a–O and F plates. The emission was studied both in the reaction zone and in the burned gases; for this purpose the reaction vessel was fitted with plane quartz windows. A small grating monochromator was also used for visual observations.

Cyanogen was obtained from the American Cyanamid Co. It was prepared by the high temperature reaction of hydrogen cyanide and chlorine; drying of the gas was therefore considered unnecessary. Its toxicity only occasionally proved troublesome, as the flames were burned in a closed system and the components of the burned gases not removed by the pump traps were piped directly out of the building. Since the flame was not in direct contact with the vessel

walls, air-cooled Pyrex vessels used in previous studies were found to be adequate here. The flames were burned in the pressure range 50–200 mm Hg, above Pyrex tubes 10–15 mm in diameter. Measurements were made in the reaction zone, at the position of maximum attenuation, unless otherwise stated.

Results and Discussion

Cyanogen–Oxygen Flames

Electron Concentration and Electron–Molecule Collision Cross Section as a Function of Flame Composition. A typical cyclotron resonance line for a C_2N_2–O_2 flame at 60 mm Hg is shown in Fig. 1, with a line for a C_2H_2–O_2 flame at 10 mm Hg included for comparison. (The cause of the slight asymmetry of the lines is discussed elsewhere.[12])

It has been shown[13] that the observed cyclotron resonance line width, ΔH, in gauss, is related to the average electron molecule collision cross section Q and the total pressure p in mm Hg by the equation

$$\Delta H/p = 6.8 \times 10^{17} \times Q/T^{\frac{1}{2}}.$$

Allowing for the pressure difference between the two flames and for the fact that the temperatures of the cyanogen and acetylene flames were about 4000°K and 2000°K, respectively, it can be seen that if the average electron–molecule collision cross section were the same in both cases, the cyanogen line would be expected to be wider than observed by at least a factor of two. Evidently the average Q for cyanogen flames is considerably lower than the value of about 40 Å^2 found for near stoichiometric acetylene flames, due probably to the absence of H_2O from the burned gases for which $Q \simeq 80$ Å^2 under these conditions.[11]

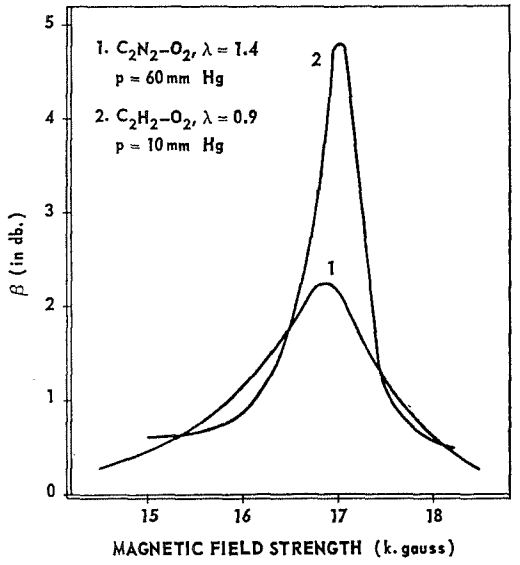

FIG. 1. Typical cyclotron resonance absorption lines: curve 1, C_2N_2–O_2, $\lambda = 1.4$, $p = 60$ mm Hg; curve 2, C_2H_2–O_2, $\lambda = 0.9$, $p = 10$ mm Hg.

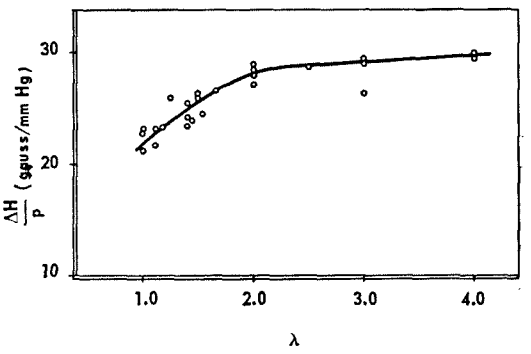

FIG. 2. Variation of $\Delta H/p$ with λ.

The variation of $\Delta H/p$ with λ {λ being defined as ([O_2] unburned)/([O_2] required for combustion to carbon monoxide and nitrogen)} is shown in Fig. 2. Absolute values of Q cannot be given since the temperatures of the flames have not been measured.

The electron concentration, n, is related to ΔH, (defined above) the attenuation at the center of the line, β (in db) and the thickness of the flame, d (in cm), by the expression[13]

$$n = \Delta H\beta/40\pi ed \log_{10} e = 3.87 \times 10^7 \Delta H\beta/d.$$

The flame described in Fig. 1, for which β, ΔH, and d were about 2.3 db, 1500 gauss, and 1.5 cm, respectively, contained close to 10^{11} electrons/cc, which is very similar to the electron concentration found in acetylene flames at about 15 mm Hg.

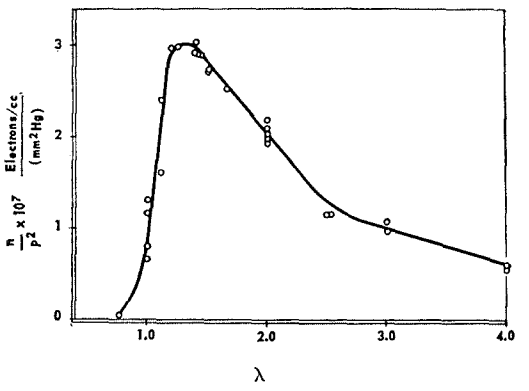

FIG. 3. Variation of n/p^2 with λ.

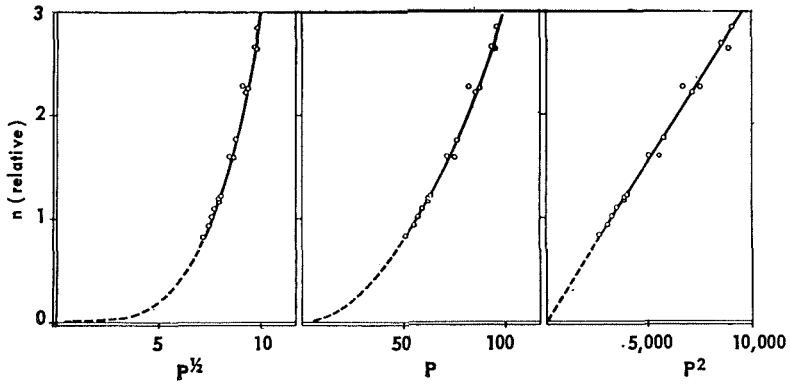

FIG. 4. Plots of n as a function of $p^{\frac{1}{2}}$, p, and p^2. p in mm Hg.

The dependence of the ionization on the flame composition is illustrated in Fig. 3, where n/p^2 has been plotted against λ (this type of plot was chosen for reasons to be discussed shortly). The sharp drop of n/p^2 on the fuel-rich side is not a result of the presence of several per cent of the electron acceptor CN, for even at a flame temperature as low as 3000°K, the formation of CN^- will reduce n by not more than about 20 per cent.[14] The only positive ion associated with the free electrons[8] is NO^+, contrasting sharply with the complexity of the ion spectra of hydrocarbon flames, in which H_3O^+, various hydrocarbon fragments and other ions appear.[15–17]

Since the temperatures of the flames used were not known (an attempt at measuring them, using a modification of the line reversal method[18] is to be made shortly), the equilibrium concentrations of all the species present could only be approximately estimated. For temperatures in the 4000–3000°K range, however, the ionization expected on the basis of equilibrium is comparable to that observed; in hydrocarbon flames, on the other hand, the ionization is known to be very considerably above the equilibrium level.[9] It is, therefore, of some interest to determine whether the ionization in cyanogen flames is, in fact, thermal.

On simple kinetic considerations this would seem unlikely, since it has been shown[19] that, for alkali metals, processes of the type

$$M + X \rightarrow M^+ + e + X$$

where X is a third body, require at least 1 msec for equilibration at atmospheric pressure, for activation energies greater than about 5 ev. For NO, with an ionization potential of 9.25 ev and with a binary collision frequency of about 2×10^8 sec^{-1} under flame gas conditions, it appears that the ionization could be produced in the time taken by the gases to travel through the reaction zone (ca 100 msec) only if these gases consisted of pure NO. In addition, it might be noted here that the introduction of NO into the preburned gases in quantities up to 5 per cent of the total volume has very little effect on the level of ionization other than that which can be attributed to a "dilution" effect. Thus the measured electron concentrations may be about two orders of magnitude too high.

Variation of n with Pressure. n was measured for cyanogen–oxygen mixtures burned at 50–200 mm Hg. Typical results are shown in Fig. 4 where n has been plotted against $p^{\frac{1}{2}}$, p, and p^2. If the ionization were thermal, the first plot should be a straight line. Since for cyanogen flames $n \propto p^2$, it is evident that the ionization is nonthermal, but different from that found in hydrocarbon flames for which $n \propto p$ (see Fig. 8). The quantity n/p^2 is therefore used throughout this paper in comparing ionization levels in different flames.

Ionization in Cyanogen–Oxygen Flames Containing Argon, Nitrogen, and Excess Oxygen. Figure 5 is a logarithmic plot of n/p^2 against r, where $r = [C_2N_2 + O_2]/[\text{total unburned volume}]$ for the addition of argon and nitrogen to a cyanogen flame. Reduction of r to about 0.5 results in a pressure rise from approx. 60 mm to 170 mm Hg, and an approximately threefold decrease in n, irrespective of which gas is added, although the nitrogen-containing flames are cooler than those with the same proportion of argon. Further, if r were reduced to 0.5 by nitrogen addition, an initial flame temperature of about 4500°K would fall to below 3000°K which, even neglecting any changes in [NO] would lead to at least 10^2-fold reduction in n as calculated from the Saha equation. This is about 10^2 times greater than the observed change. Thus nonthermal ionization is confirmed.

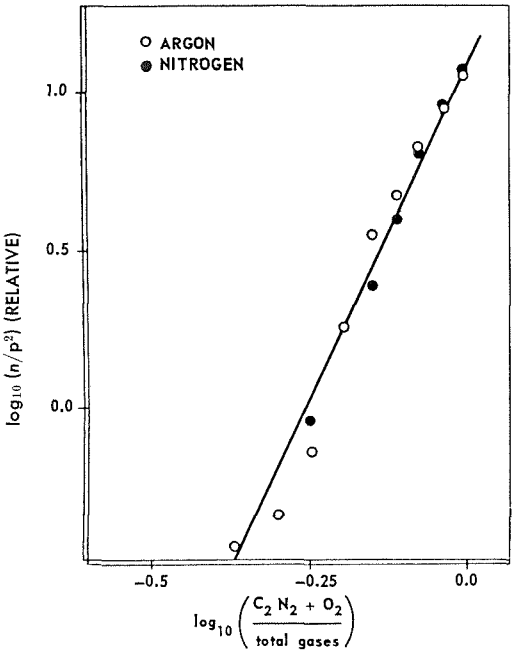

FIG. 5. Addition of argon (open circles) or nitrogen (closed circles) to a C_2N_2–O_2 ($\lambda = 1.4$) flame. (Both sets of results fall on the same line.)

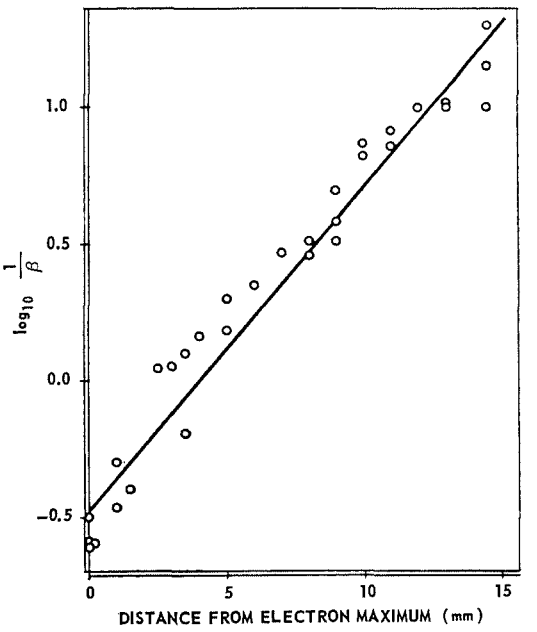

FIG. 6. Decay of ionization with time (proportional to height in the flame) after leaving the reaction zone. C_2N_2–O_2, $\lambda = 1.25$, $p = 55$ mm Hg.

The slope of the plot of Fig. 5 shows that, approximately n/p^2 appears to vary as r^4 (r is proportional to the fraction of fuel in the unburned gases)—this is true for flames with nitrogen or argon at all λ. For undiluted flames containing excess oxygen,

$$n/p^2 \propto ([C_2N_2]/[C_2N_2 + O_2])^2.$$

In contrast, for hydrocarbon flames $n/p \propto$ (fuel fraction)^2 for all flames with nitrogen, argon, or excess oxygen. This emphasizes again the marked difference between cyanogen and other fuels.

Decay of n Above the Reaction Zone. Figure 6 shows that the experimental points fit a first order decay plot reasonably well. There is slight curvature near the reaction zone itself, in the sense expected if there were some contribution from second order decay processes at very high electron concentrations.

Both Williams[20] and Calcote[21] have obtained similar plots for hydrocarbon-oxygen flames below about 30 mm Hg. Williams attributes this effect to electron attachment whereas Calcote ascribes it to ambipolar diffusion. Above about 30 mm Hg, second order recombination becomes of increasing importance in hydrocarbon–oxygen flames.[21] In cyanogen–oxygen flames, however, the present authors find that first order processes appear to persist up to at least 100 mm Hg (the highest pressure at which such measurements were made). Interpretation of such results as favoring electron attachment as the main process of electron decay must be made with caution, however, on account of changes of flame shape and temperature over the region of measurement, and on account of the thickness (approx. 3 mm) of flame sampled.

Spectral Features of Cyanogen–Oxygen Flames. The strongest features in the reaction zone of these flames were the CN red and violet systems and the C_2 Swan system. The γ–NO system and an unidentified system[2,5] at 3250–3300 Å appeared less strongly. The β–NO system was only just detectable—at atmospheric pressure it is reported to be strong.[2] The intensities of the CN and C_2 systems are greatest in fuel-rich flames, whereas the intensities of the γ–NO and the unidentified system are at a maximum in the $\lambda = 1.1$–1.5 range. Very fuel-rich cyanogen flames are brilliant white, and deposit carbon—in contrast to acetylene flames and cyanogen flames at atmospheric pressure.[2]

In the burned gases up to about 5 cm from the reaction zone all the above features are still observed, together with a strong continuum in the blue and ultraviolet (probably mainly due to the CO + O reaction[22]) and a greenish glow, which may arise from the NO + O reaction.[22]

The intensity of the glow, γ–NO, and the unidentified system all vary with flame composition rather like the electron concentration.

Addition of up to 5 per cent of NO to the burned gases weakens the CN and C_2 emission, possibly through reactions of the type

$$CN + NO \rightarrow N_2 + CO \qquad -144 \text{ kcal/mole}$$

$$C_2 + NO \rightarrow CN + CO \qquad -180 \text{ kcal/mole}$$

In the absence of precise photometric data it is not possible to give an unambiguous interpretation of all the ionization phenomena described. The following suggestions are, therefore, mainly tentative.

The explanation of the pressure dependence of n most probably lies in the production of ions in a reaction of a higher kinetic order than that by which they are destroyed, since at the point of measurement (maximum electron concentration) steady state conditions are presumed to exist. The simplest reactions energetically feasible for production of NO^+ are all termolecular, *viz.*,

$$CN + O + O \rightarrow CO + NO^+ + e^- \qquad -6 \text{ kcal/mole}$$

$$NO + N + N \rightarrow N_2 + NO^+ + e^- \qquad -12 \text{ kcal/mole}$$

$$NO + C + O \rightarrow CO + NO^+ + e^- \qquad -42 \text{ kcal/mole}$$

Of these the first could possibly proceed via CNO intermediate. The second has been proposed to explain the presence of free electrons in active nitrogen containing traces of oxygen.[23,24] The addition of NO to these flames has little effect on n, but this does not necessarily rule out the second reaction since extra NO can reduce [N] as well as produce NO^+.[25] For electron removal the simplest reaction to propose is the dissociative recombination process

$$NO^+ + e^- \rightarrow N + O$$

which can be up to 63 kcal/mole exothermic. This reaction has been recently shown to be the predominant process of electron decay in ionized NO.[26] The occurrence of such processes at the point of measurement in the reaction zone (where steady state conditions apply to n) would give

$$n = (k_{(A+B+C)}[A][B][C]/k_{(NO^+ + e^-)})^{\frac{1}{2}}$$

provided $[NO^+] = [e^-] = n$, and where A, B, and C represent the species involved in the ion production reaction. If [A], [B], and [C] are all proportional to (approximately) the first power of p, then a reasonable explanation of the pressure dependence is provided.

It is perhaps of interest to note that, if the predominant process of electron removal is electron attachment to a species X, with [X] proportional to p, then

$$n = k_{(A+B+C)}/k_{(X+e^-)} \times ([A][B][C])/[X]$$

and thus an exact fit with the observed pressure dependence could be obtained. Such an explanation—the simplest which gives exact agreement with the pressure dependence—would also provide an understanding of the apparently first order decay plot of Fig. 6. Similar arguments could be invoked to explain the more detailed evidence available for hydrocarbons.[13]

Cyanogen–Hydrogen–Oxygen Flames

Ionization in the Presence of Hydrogen. The effect of hydrogen on the ionization in cyanogen flames is different from that of any other additive, since, depending on its relative proportions it can either depress it markedly or enhance it.

The ionization in flames with hydrogen was investigated by replacing the cyanogen gradually

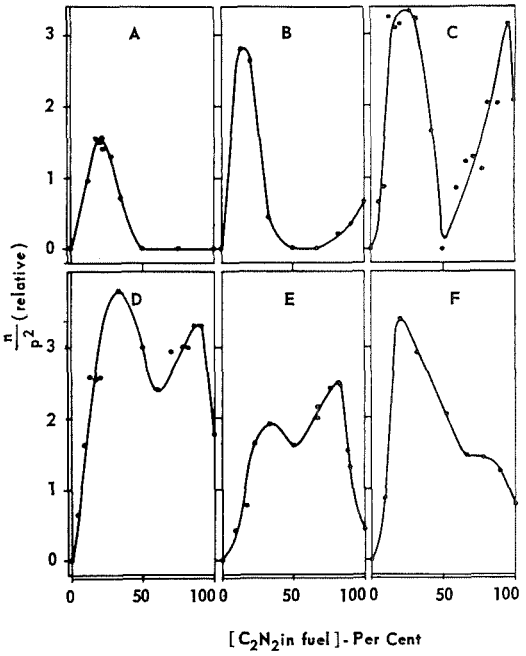

FIG. 7. Ionization in C_2N_2–O_2–H_2 flames, in terms of n/p^2, as a function of the percentage of cyanogen in the fuel. Curves A–E, λ = 0.625, 1.0, 1.5, 2.0, and 4.0, respectively. Curve F, λ = 1.5, with λ redefined in terms of combustion to N_2 and CO_2.

TABLE 1

Ionization in C_2N_2–H_2—O_2 Flames ($\lambda = 1.5$)

% C_2N_2 in fuel	0	9	17	27	42	60	71	83	95	100
p, mm Hg	25	23	20	18	19	27	36	44	44	70
$n(cc^{-1}) \times 10^9$	—	6.2	17	15	7.1	8.1	22	52	80	135
$n/p \times 10^8$	—	2.7	8.5	8.3	3.7	3.0	6.1	12	18	19
$n/p^2 \times 10^7$	—	1.2	4.3	4.6	2.0	1.1	1.7	2.7	4.1	28

by hydrogen while keeping both the total unburned volume and λ constant. Plots of n/p^2 against the percentage of cyanogen in the fuel are shown in Fig. 7, A–E, for λ between 0.625 and 4.0.

Although the flames with low $[C_2N_2]$ are cooler than those with high $[C_2N_2]$, these curves should reflect the true variation in the ionization level at all points to well within a factor of two. The most outstanding feature of the curves of Fig. 6 is the appearance of a maximum (the "second ionization maximum") at about 20 per cent of cyanogen; with all other additives used n/p^2 falls continuously from the value for the pure cyanogen flame. For $0.8 < \lambda < 1.5$ addition of only a trace of hydrogen causes a very sharp fall in n, and a rapid increase in the burning velocity of the mixture (as noted by a decrease in pressure at which the flame burns). Further addition of hydrogen produces a *rise* in n up to the second maximum—the burning velocity also goes through a maximum at that point—and then a decrease below the limit of measurement The results of a typical run are listed in Table 1

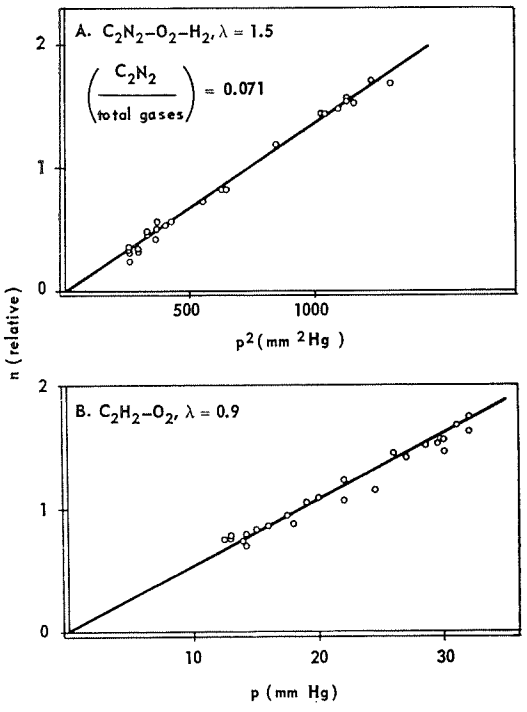

FIG. 8. A. Variation of n with p^2 in a C_2N_2–O_2–H_2 ($\lambda = 1.5$) flame. B. Variation of n with p in a C_2H_2–O_2 ($\lambda = 0.9$) flame.

The presence of the second ionization maximum is real, and is not due to changes in the cyclotron line width—the quantity $\Delta H/p$ increases continuously as cyanogen is replaced by hydrogen. Nor is it an effect of a play on the definition of λ, since the maximum in n/p^2 is hardly less pronounced when λ is defined in terms of combustion of the cyanogen to nitrogen and carbon dioxide, not carbon monoxide—see Fig. 7F, plotted for $\lambda = 1.5$ on the alternative definition. Figure 7F also shows that the appearance of yet another maximum in n/p^2 at high cyanogen content in oxygen-rich flames may be spurious.

These results have been plotted in terms of n/p^2 over the whole composition range, since the relationship $n \propto p^2$ is found to hold, even at the second ionization maximum. This is illustrated in Fig. 8, and suggests that the processes of ionization in cyanogen flames containing hydrogen are not analogous to those found in hydrocarbon–oxygen flames, for which $n \propto p$. The further facts that n at the second ionization maximum, in fuel-rich flames at least, is greater than the value found when the cyanogen is replaced by acetylene and that NO^+ is still the only positive ion,[8] support this view.

Spectral Features of Cyanogen–Hydrogen–Oxygen Flames. In the presence of hydrogen, systems due to NH, CH, and OH appear, their intensities being a function of λ and of the proportion of cyanogen in the fuel. The addition of even a trace of hydrogen reduces very markedly the intensities of the green glow, the γ–NO system, and the unidentified system in the ultraviolet, paralleling the behavior of the ionization level under the same conditions. The green glow is,

however, unique in one respect. While the intensities of the above systems decay smoothly to zero as the proportion of hydrogen is increased, the glow begins to be stronger again at low $[C_2N_2]$ (20–30%) and disappears only with complete removal of cyanogen. Thus the greenish glow appears to follow n under the same conditions, at all λ and at all proportions of hydrogen.

The addition of hydrogen results in the formation of H, OH, and H_2O, because of the operation of the rapidly balanced reactions[27]

$$H_2 + O = OH + H$$

$$H_2 + OH = H_2O + H$$

This causes a reduction in $[O]$ and lowering of the flame temperature. The pressure at which the flame burns decreases on account of the presence of new radicals through which the combustion process can proceed. These effects will, in general, be most marked in flames with less oxygen.

The production of NH can take place by, e.g.,

$$CN + OH \rightarrow CO + NH \qquad -51 \text{ kcal/mole}$$

CH can be produced by a number of reactions,

$$C_2 + OH \rightarrow CO + CH \qquad -120 \text{ kcal/mole}$$

$$C_2 + NH \rightarrow CN + CH \qquad -69 \text{ kcal/mole}$$

$$CN + NH \rightarrow N_2 + CH \qquad -32 \text{ kcal/mole}$$

The decrease of the intensities of the γ–NO system and the green glow can be explained in terms of the removal of O atoms and operation of the reaction[28]

$$NO + NH \rightarrow N_2 + OH \qquad -93 \text{ kcal/mole}$$

No satisfactory explanation of the ionization maximum observed at high $[H_2]$ can at present be put forward. The definite presence of CH in such flames makes it tempting to infer that the phenomenon arises simply through occurrence of reactions similar to those suggested to be taking place in hydrocarbon flames, viz.,

$$CH + O \rightarrow CHO^+ + e^-$$

$$CHO + H_2O \rightarrow H_3O^+ + e^-$$

$$H_3O^+ + NO \rightarrow NO^+ + H_2O + H$$

Knewstubb and Sugden[15] have suggested the third reaction to occur in hydrocarbon–oxygen systems containing added nitric oxide, and its operation could explain the limitation of the positive ion spectrum to NO^+. There are puzzling features of the phenomenon, however, such as the pressure dependence, which do not seem to fit with such a simple explanation. It is hoped that further insight may be provided by a quantitative photometric study of the spectral features described, and this is currently being undertaken.

ACKNOWLEDGMENTS

We would like to thank Dr. W. Gordy for the use of the facilities of his laboratory and are very grateful to Dr. T. M. Sugden for some valuable criticisms.

This work was supported by the U.S. Air Force Office of Scientific Research of Air Research and Development Command.

REFERENCES

1. BAKER, M. R. and VALLEE, B. L.: J. Opt. Soc. Am. *45*, 773 (1955).
2. THOMAS, N., GAYDON, A. G., and BREWER, L.: J. Chem. Phys. *20*, 369 (1952).
3. JAMES, H.: Rev. Inst. Franc. Petrole et Ann. Combustibles Liquides *13*, 83 (1958).
4. ROBERTSON, N. C. and PEASE, R. N.: J. Am. Chem. Soc. *64*, 1880 (1942).
5. JENNINGS, K. R. and LINNETT, J. W.: Trans. Faraday Soc. *56*, 1737 (1960).
6. BASS, A. M. and BROIDA, H. P.: J. Mol. Spectroscopy *2*, 42 (1958).
7. NICHOLLS, R. W. and KRISHNAMAHARI, S. L. N. G.: Can. J. Chem. *38*, 1652 (1960).
8. VAN TIGGELEN, A.: Private communication, Univ. de Louvain, Belgium, 1960.
9. CALCOTE, H. F.: Combustion and Flame *1*, 385 (1957).
10. GAYDON, A. G. and WOLFHARD, H. G.: Flames. Chapman and Hall, 1953.
11. BULEWICZ, E. M.: J. Chem. Phys. *36*, 385 (1962).
12. BULEWICZ, E. M. and PADLEY, P. J.: J. Chem. Phys. *35*, 1590 (1961).
13. BULEWICZ, E. M. and PADLEY, P. J.: This volume, p. 638.
14. BULEWICZ, E. M. and PADLEY, P. J.: Unpublished data, 1961.
15. KNEWSTUBB, P. F. and SUGDEN, T. M.: Proc. Roy. Soc. (London) *A255*, 520 (1960).
16. KNEWSTUBB, P. F. and SUGDEN, T. M.: *Seventh Symposium (International) on Combustion*, p. 247. Butterworths, 1958.
17. DE JAEGARE, S., DECKERS, J., and VAN TIGGELEN, A.: *Eighth Symposium (International) on Combustion*, p. 155. Williams and Wilkins, 1962.
18. KOHN, H.: Private communication, Duke University, Durham, N.C., 1960.
19. PADLEY, P. J. and SUGDEN, T. M.: *Eighth Symposium (International) on Combustion*, p. 164. Williams and Wilkins, 1962.
20. WILLIAMS, H.: *Eighth Symposium (International) on Combustion*, p. 179. Williams and Wilkins, 1962.

21. CALCOTE, H. F.: *Eighth Symposium (International) on Combustion*, p. 184. Williams and Wilkins, 1962.
22. GAYDON, A. G.: *The Spectroscopy of Flames*. John Wiley and Sons, 1957.
23. ULTEE, C. J.: J. Phys. Chem. *64*, 1873 (1960).
24. BROIDA, H. P. and TANAKA, I.: J. Chem. Phys. *36*, 236 (1962).
25. KAUFMAN, F.: J. Chem. Phys. *28*, 992 (1958).
26. DOEING, J. P. and MAHAN, B. H.: J. Chem. Phys. *36*, 569 (1962).
27. BULEWICZ, E. M., JAMES, C. G., and SUGDEN, T. M.: Proc. Roy. Soc. (London) *A235*, 89 (1956).
28. BULEWICZ, E. M. and SUGDEN, T. M.: Unpublished data, 1958.

Discussion

DR. E. P. GRAY (*APL/The Johns Hopkins University*): The comments which I want to make on the paper of Dr. Bulewicz and Dr. Padley, are concerned solely with the limitations inherent in, and the care required in using the cyclotron resonance method for probing the plasma constituting a flame; I shall not discuss the mechanism and chemistry of the flames inferred from the measured quantities, namely the average electron concentration and the collision frequency.

The main object of these comments is to point out that special care is required to keep the electron concentration of the flame being probed very low. Failure to do so will result in a broadening of the cyclotron resonance line by a mechanism unrelated to collision broadening, so that the collision frequency and the electron concentration are not obtainable from the line width. However, before proceeding any further I want to stress that the authors of this paper did take the requisite care, and that their results can not be criticized on those grounds. What I want to accomplish is to show how severe the requirements are, so as to help others who might want to use this method to avoid this trap.

The theory for the line width in terms of the collision frequency, upon which the interpretation of the measurements depends, was developed by Kelly, Margenau, and Brown[1] for resonance absorption by a *single particle* in a magnetic field. Only when the circular plasma frequency, $\omega_p = (4\pi ne^2/m)^{\frac{1}{2}}$ (where n is the electron concentration, e the electronic charge, and m the electron mass) is sufficiently smaller than the circular cyclotron frequency, $\omega_c = eB/mc$ (where B is the magnetic field and c, the velocity of light), is this single particle theory applicable.

An exact theory for cyclotron resonance absorption, which is valid even if $\omega_p > \omega_c$, has been developed by Buchsbaum, Mowrer, and Brown.[2] They compute the complex frequency shift, $\Delta f/f$, of the resonant frequencies of a cylindrical cavity filled with a uniform plasma subjected to an external axial magnetic field. The imaginary part of Δf is directly related to the real part of the transverse conductivity, and therefore to the line shape. Their calculation for the TE_{011} resonance is qualitatively applicable to Bulewicz and Padley's experiments, in that for both cases the external magnetic field, the direction of propagation of the microwaves, and the electric field vector are mutually perpendicular. The difference in geometry between the computed case of the cylindrical cavity and the actual experimental situation will make an accurate numerical comparison impossible, but should not affect the order of magnitude of the quantities involved.

The theory predicts that the complex frequency shift for the TE_{011} resonance is given by

$$\frac{\Delta f}{f} = \frac{x_{01}^2(R/a)^4}{16J_0^2(x_{01})}\,\alpha^2 \left\{\frac{[(1-\alpha^2)(1-\alpha^2-\beta^2)+\gamma^2]+j\gamma[(1-\alpha^2)^2+\beta^2+\gamma^2]}{(1-\beta^2-\gamma^2-\alpha^2)^2+\gamma^2(2-\alpha^2)^2}\right\},$$

where $x_{01} = 3.832$, the first root of $J_1(x) = 0$; R is the radius of the (uniform) plasma column; a is the radius of the cavity; $\alpha = \omega_p/\omega$; $\beta = \omega_c/\omega$; $\gamma = \nu/\omega$; ν is the collision frequency; and ω is the (circular) microwave frequency. From the imaginary part of $\Delta f/f$ the cyclotron resonance absorption has been obtained. This is shown in Fig. 1a, with the parameter $\nu/\omega = 0.01$, very close to the value of 0.015 used in Bulewicz and Padley's experiment. The most striking feature is a shift of the resonant frequency from $\omega = \omega_c$ to a new value, $\omega = (\omega_c^2 + \omega_p^2)^{\frac{1}{2}}$, but with a line width which does not change markedly until ω_p approaches ω. This phenomenon is caused by the absorption associated with an anomalous dispersion of the real part of $\Delta f/f$ (i.e., of the index of refraction), which has also been noted by Bulewicz and Padley.[3] If the plasma were uniform, therefore, the electron concentration and collision frequency could be obtained from the line width even for relatively large values of ω_p.

For the highly nonuniform plasma actually used, however, this conclusion changes drastically. In that case the observed line can be considered as an appropriate average over a group of these lines

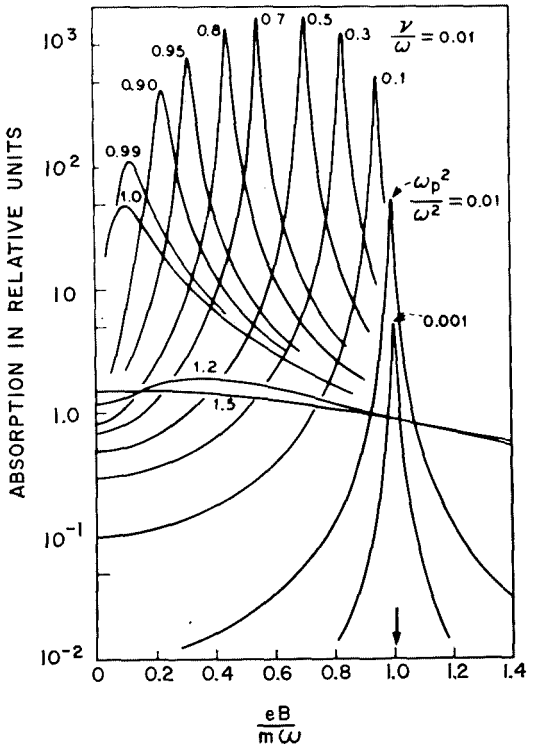

FIG. 1a. Absorption vs. magnetic field in a uniform plasma.

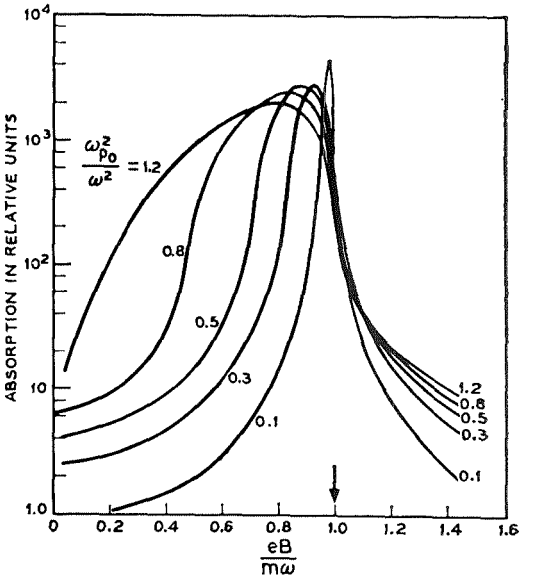

FIG. 1b. Absorption vs. magnetic field in a non-uniform plasma.

computed for the uniform plasma. Since each of these lines peaks at a different cyclotron frequency, the average will have a width that is governed by this frequency shift and not by the collision broadening which governs the width of the individual lines. The result of this averaging is shown in Fig. 1b, where the average has been computed over a

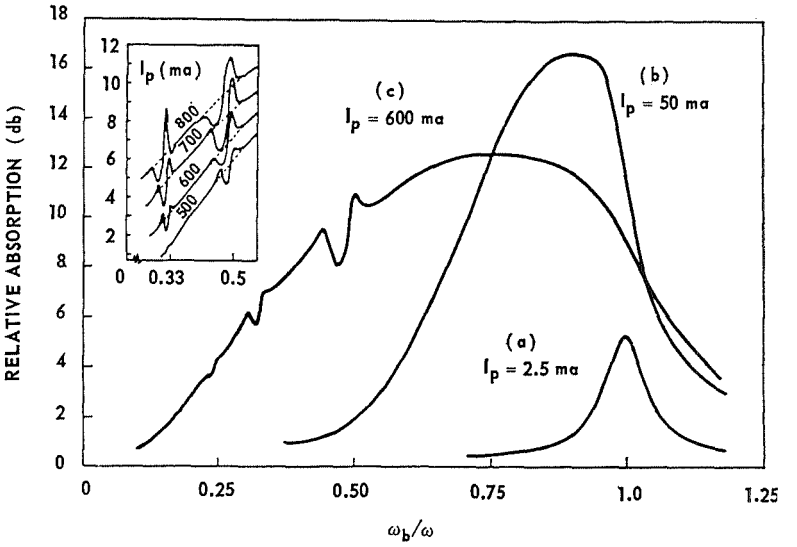

FIG. 2. Microwave power absorption in a cavity-plasma system as a function of magnetic field. The plasma is the positive column of a helium discharge at a pressure of 0.5 mm Hg.

plasma profile of the form $n/n_{max} = 1 - r^2/R^2$, where R is the radius of the plasma column. The values of ω_p shown correspond to the electron concentration on the axis. It is evident, therefore, that ω_p^2/ω^2 must be considerably below 0.1, the lowest value shown, in order that the line width be due to collision broadening. A sensible criterion would appear to be the requirement that the real part of the (circular) frequency shift, $\Delta\omega_c$, be considerably less than the line width. Such a criterion leads to the requirement that

$$(\omega_p/\omega)^2 \ll 4\nu/\omega.$$

These calculations have been confirmed experimentally by Bekefi, Coccoli, Hooper, and Buchsbaum.[4] Figure 2 shows the cyclotron absorption line for three different values of the current (corresponding to different ω_p). For case (b), ω_p^2/ω^2 is roughly 0.2, and the line is evidently broadened. For case (c), ω_p^2/ω^2 is about 0.01, and no broadening is evident. (I do not know the value of ν/ω, except that it lies between 10^{-4} and 10^{-1}.) These cases bracket the regime where noncollisional broadening could be troublesome.

In Bulewicz and Padley's experiment this restriction has been observed. For the highest value of electron concentration they mention, namely 5×10^{10} per cm^3, the parameter ω_p^2/ω^2 is approximately 0.002, as compared to a value for $4\nu/\omega$ of about 0.06. Their line widths, therefore, may certainly be interpreted on the basis of collision broadening.

In conclusion, I want to note that the qualitative features of this anomalous dispersion, and its effect on the asymmetry of the resonance line, have been pointed out previously by Bulewicz and Padley.[3] Only the application of Buchsbaum, Mowrer, and Brown's[2] detailed numerical calculations to the cyclotron resonance probing of flames is new. I also wish to acknowledge several useful conversations with Dr. Buchsbaum, and to thank him for providing me with a copy of some of his computed curves.

Dr. P. F. Knewstubb (*University of Cambridge*): In connection with the results shown in Fig. 7 of the paper by Bulewicz and Padley, I feel that it may be of interest to present a brief account of some measurements relating to the ionization of nitric oxide in flames. A premixed flame of acetylene-oxygen-nitrogen was formed, and 1% by volume of nitric oxide added to the mixture. The concentration of nitric oxide ion, measured by the mass spectrometer was found to reach a large maximum value just above the reaction zone, falling to lower values upstream, but to be everywhere many times greater than the level expected for thermal ionization. This, coupled with the rapid variation with distance, convinces us that the ion is produced by chemi-ionization. The observation that addition of nitric oxide causes also a large reduction of H_3O^+ ion concentration suggests strongly that the NO^+ is derived from the same source of chemical energy, at the expense of H_3O^+.

Accepting the scheme of chemi-ionization which is proposed by three papers in this Symposium, we may consider the interfering effect of nitric oxide in possible change exchange reactions:

$$CHO^+ + NO \rightarrow NO^+ + CHO \qquad (1)$$

$$H_3O^+ + NO \rightarrow NO^+ + H_2O + H. \qquad (2)$$

Examination of the quantities involved suggests that reaction (1) is unlikely to compete so successfully with the proton transfer reaction (3) as to produce the observed results

$$CHO^+ + H_2O \rightarrow H_3O^+ + CO. \qquad (3)$$

A suggestion of the importance of reaction (2) with which we are credited towards the end of this paper, was, I believe, made at a time when a high value of the heat of formation of H_3O^+ (of about 195 kcal/mole) seemed tenable. As a result of work published in the interim, a much lower value (of about 137 kcal/mole) is now favored for this quantity, and we would no longer support reaction (2) as likely to produce NO^+.

One suggestion may be made which seems to fit well all tests which we have been able to apply, as follows:

$$H + NO + M \rightarrow HNO + M \qquad (4)$$

$$HNO + H_3O \rightarrow NO^+H_2 + H_2O \qquad (5)$$

Details of the arguments leading to this will be given elsewhere. A scheme of this type, with the additional parameters thereby introduced, might be able to explain the results portrayed in Dr. Padley's Fig. 7.

Dr. P. J. Padley (*University of Cambridge*): *A priori*, a scheme along the lines suggested by Dr. Knewstubb appears to be highly plausible: for example, it gives a qualitative explanation of the shape of our Fig. 7. However, as we have pointed out, any such scheme involving "reactions similar to those taking place in hydrocarbon flames," i.e., where the primary ionization step is bimolecular, does not escape the difficulty presented by the pressure-dependence of the electron concentration in cyanogen–oxygen–hydrogen flames; the scheme of ion production must, apparently, involve a termolecular reaction, as in flames from which hydrogen is absent.

So far we have only thought of one mechanism satisfying this requirement and one, indeed, involving HNO, in an ion-producing scheme. This species, highly likely to be present in such flames and not, of course, present in pure cyanogen-oxygen flames

seems to be produced by a three-body reaction

$$H + NO + X \rightarrow HNO + X, \qquad (1)$$

where X is a third body. If this were to react with CHO* (vibrationally and electronically excited CHO), produced as an intermediate in the reaction

$$CH + O \rightarrow [CHO^*] \rightarrow CHO^+ + e^-, \qquad (2)$$

then ions could be produced by

$$CHO^* + HNO \rightarrow CO + H_2 + NO^+ + e^-. \qquad (3)$$

Such a scheme would be about 5 kcal/mole exothermic. We have already suggested (our paper, this Symposium) that a reaction of type (3), *viz.*,

$$CHO^* + M \rightarrow CO + H + M^*,$$

where M is an electronically excited metal atom, appears to satisfy well all observations so far made on metal atoms in the reaction zones of such flames. However, this scheme, (1)–(3), requires an almost impossibly high concentration of CHO* and will fail if reaction (2) is faster than reaction (3); thus we had not proposed it in our paper.

DR. A. FONTIJN (*AeroChem Research Laboratories*): Could Dr. Padley elaborate on the reasons why acetylene flames have a higher degree of ionization than the other flames studied?

DR. P. J. PADLEY: Comparing various hydrocarbon fuels, it appears quite possible that both [CH] and [O] could increase slightly as the hydrogen-to-carbon ratio decreases, whether or not there is a change in the degree of unsaturation in the original molecule. In C_2H_2–O_2 flames, for example, a smaller proportion of the combustion steps will involve processes similar to those in H_2–O_2 combustion than in, say, CH_4–O_2 flames, and this may well cause [O] to be higher. Again, the more hydrogen atom stripping that is necessary to produce CH from the original molecule, the later in the combustion is ionization likely to take place. This would certainly explain the slight upward curvature of the saturated hydrocarbons' plot. The picture is not necessarily complicated by the observation that the EF value for benzene is not three times that for acetylene.

The extraordinary behavior of the EF values for the acetylenic series would also be intelligible on this basis, when it is remembered that, from our results for mixed fuels, the presence of the CH bond in the original molecule appears to be a necessary condition for the production of ions by the CH + O mechanism. Methyl acetylene is the first member of the series to contain a carbon atom which does not make a CH bond; therefore, the EF value for this molecule can certainly be no greater than that for acetylene itself (the same should be true for allene, when compared to ethylene). In fact, it is observed to be somewhat less, which can be interpreted in terms of the slightly different over-all carbon to hydrogen ratios in these two molecules. From methyl acetylene onwards the series proceeds "normally," i.e., the increment in EF for each additional carbon atom is, to a good approximation, the same as for other hydrocarbons into which an additional CH group is introduced.

Those who have remarked on parallels between CH emission and degree of ionization (e.g., Professor Kistiakowsky's shock tube studies) may be oversimplifying the issue if such observations are suggested to support the CH + O → $CHO^+ + e^-$ ionization mechanism. For if traces of various hydrocarbons are introduced into hydrogen–oxygen–nitrogen flames, the CH emission intensity is found only in isolated cases (e.g., benzene and acetylene) to be approximately proportional to the fuel concentration; for most fuels a power dependence between 1.5 and 3.0 is observed. Since the proposed ionization mechanism requires CH ground state to be proportional to the fuel concentration, at least some CH emission must arise by processes other than by excitation of the ground state CH.

There are two important consequences of our observation that the electron concentration in hydrocarbon–oxygen flames is proportional to the pressure:

1. It is highly unlikely that the forward ionization step involves a third body. *A priori* the electrons could be produced in either a bimolecular or termolecular process; they could be destroyed by direct recombination with positive ion (either with or without a third body), by electron attachment or by diffusion to the walls. Thus eight simple steady state equations for the electron concentration can be set up, and of these only two satisfy the pressure dependence observation: termolecular electron production coupled with termolecular destruction, or bimolecular production coupled with bimolecular destruction. Now the recombination constant measured with positive ions, at 2×10^{-7} cm^3 sec^{-1} (King; Calcote; Green and Sugden; *vide* this Symposium) is rather fast for a termolecular process, and the fact that this recombination constant does not increase as the pressure decreases points to a bimolecular recombination process. Therefore the forward step, producing the ions, will be bimolecular.

2. Electron attachment is indicated as responsible for electron removal in our low-pressure system. Diffusion processes would imply an electron concentration proportional to the cube of the pressure, and seem therefore to be eliminated. A second order (in ions) recombination process is eliminated since this would predict the electron concentration proportional to the square root of the CH, or fuel, concentration, whereas our results indicate a direct proportionality. Thus one is only left with a bi-

molecular, first order (in electrons) process to consider, and this corresponds to electron attachment. It is perhaps significant that a similar analysis of the cyanogen-oxygen system, for which we observe a quite different pressure-dependence of the electron concentration, also leads to the same conclusion.

Thus in hydrocarbon-oxygen flames the recombination step could be

$$H_3O^+ + OH^- \rightarrow \text{products}$$

with the OH^- produced by electron attachment, and in cyanogen–oxygen flames,

$$NO^+ + CN^- \rightarrow N_2 + CO$$

with the CN^- produced by electron attachment. A slightly puzzling point is that our results imply the concentration of the attaching species not to vary significantly with flame composition, contrary to expectations. A more detailed answer must await the results of future work.

References

1. Kelly, D. C., Margenau, H., and Brown, S. C.: Phys. Rev. *108*, 1367 (1957).
2. Buchsbaum, S. J., Mowrer, L., and Brown, S. C.: Phys. Fluids *3*, 806 (1960).
3. Bulewicz, E. M. and Padley, P. J.: J. Chem. Phys. *35*, 1590 (1961).
4. Bekefi, G., Coccoli, J. D., Hooper, E. B., and Buchsbaum, S. J.: Phys. Rev. Letters *9*, 6 (1962).

FAST REACTIONS OF OH RADICALS

F. KAUFMAN AND F. P. DEL GRECO

The reversible, bimolecular reactions of OH radicals with OH, H_2, O, and H are discussed. New experimental data for the first three, in their forward direction, near 300°K, are obtained by measuring local OH concentrations in a discharge-flow system of high pumping speed in which the OH is produced by the fast reaction $H + NO_2 \rightarrow OH + NO$. For the reactions $2OH \rightarrow H_2O + O$, $OH + H_2 \rightarrow H_2O + H$, and $OH + O \rightarrow O_2 + H$ we measure rate constants of $1.5 \pm 0.4 \times 10^9$, $4.3 \pm 1.0 \times 10^6$, and $1.1 \pm 0.4 \times 10^{10}$ liter mole^{-1} sec^{-1}. The present status of the thermodynamic quantities ΔH° and ΔF° for the four equilibria is summarized and approximate expressions for the equilibrium constants are presented. Other recent work on these eight reactions is described and Arrhenius expressions are proposed for all the rate constants.

Introduction

Recent interest in the detailed understanding of combustion processes, in the reactions of the upper atmosphere, and in the fundamentals of reaction kinetics has greatly accelerated progress in atom and free radical reactions.

For the reactions of OH radicals with H, O, OH, and H_2, which are the topic of this paper, new experimental results come from four areas:

1. Flame photometry and sampling techniques in which the roughly isothermal approach of flame gases to equilibrium is measured;
2. Studies of the H_2–O_2 system at elevated temperatures near the explosion limit;
3. Shock tube studies involving the OH radical;
4. Studies of O and OH reactions in discharge-flow systems at low pressure.

While each of these techniques provides useful information, individual shortcomings must be kept in mind.

Flame techniques suffer from lack of specificity. At the high temperature and pressure of these experiments, several sets of fast, bimolecular reactions produce balanced steady states which, by rapidly distributing concentration changes among all species, mask the occurrence of particular, slow reactions. When flame methods are applied close to the reaction zone they require accurate knowledge of diffusion coefficients and temperature–distance plots, and may suffer from adverse effects due to the sampling probe or from deviations from an assumed one-dimensional flow.

The main shortcomings of gas-kinetic work near the explosion limit are the uncertain role of the surface and, more seriously, the limitations inherent in testing fairly elaborate mechanisms for their agreement with few experiments. This is equivalent to fitting data (usually over a small range of observables) to many-parameter expressions. As the complexity of the system increases, this approach may lose all meaning.

Shock tube studies suffer from the scatter of data due to a difficult experimental method, from uncertainty of the temperature and of one-dimensionality. It shares with the above two methods the difficulty of fitting elaborate kinetic models with limited experimental data.

The discharge-flow method suffers from incomplete knowledge of the discharge products, which may include electronically or vibrationally excited species; from the increased importance of surface reactions due to the low pressure; and from the intricacies of steady state, viscous flow which are usually disregarded.

It is a reassuring fact, however, that all of these methods have been used successfully to measure the rate constants of some OH radical reactions. Because of some of the limitations mentioned above, probable errors can not be expected to be less than ±10 to 20 per cent. One comment might be made which is generally applicable: Too often, in published work the emphasis is on the extraction of rate constants by fitting data to a proposed mechanistic scheme, but unless the scheme is clearly established, the uniqueness of this procedure is questionable. Therefore, the greatest effort should be expended towards demonstrating the correctness of the proposed mechanism by devising critical tests extending over a wide range of parameters.

In this paper, four reversible, bimolecular reactions of OH will be discussed. For three of them, (1), (2), (3), new experimental data ob-

tained by the discharge-flow method will be presented.

$$OH + OH \underset{k_{-1}}{\overset{k_1}{\rightleftharpoons}} H_2O + O \quad (1)$$

$$OH + H_2 \underset{k_{-2}}{\overset{k_2}{\rightleftharpoons}} H_2O + H \quad (2)$$

$$OH + O \underset{k_{-3}}{\overset{k_3}{\rightleftharpoons}} O_2 + H \quad (3)$$

$$OH + H \underset{k_{-4}}{\overset{k_4}{\rightleftharpoons}} H_2 + O \quad (4)$$

The equilibrium constants, K_1 to K_4, will be discussed briefly, and a general survey and discussion of the rate constants will follow.

Experimental

Though the apparatus has recently been described,[1] it is here reviewed briefly. As shown in Fig. 1 it consists of a quartz flow tube at whose upstream end there are four inlet tubes for the metered addition of gases, and of an optical-spectroscopic system for the measurement of OH by absorption spectrometry at any point along the quartz tube. A two-stage Roots pump (Consolidated Vacuum Corporation, Model VP-R-152A) backed by a mechanical pump (Cenco Hypervac 25) is able to produce linear average gas velocities up to 40 m/sec in the flow tube (3.0 cm inside diameter). The main discharge is excited by a microwave power generator (Raytheon PGM-100) and the auxiliary discharge by a magnetron oscillator at similar frequency (2450 mc/sec) but lower power (Microtherm, Model CMD-4).

The absorption measurement utilized a light source emitting OH radiation, quartz lenses, and front-surfaced mirrors which produced a light path traversing the flow tube three times perpendicular to the direction of flow, and a grating monochromator (Jarrell-Ash, Model 82–000) which isolated and recorded the intensity of particular lines of the (0, 0) or other bands of OH, $^2\Sigma^+ \rightarrow {}^2\Pi$, in the absence or presence of absorbing OH molecules. The entire light absorption apparatus was mounted on a platform movable along the full length of the flow tube. The three traversals across the tube gave a path length of 9 cm and were completely contained in an over-all width of 1.3 cm in the direction of flow, corresponding to a maximum time resolution of $\frac{1}{3}$ milliseconds under steady state conditions.

The light source was a microwave discharge in flowing Ar:H_2O mixtures with large excess Ar and at a pressure of 18 mm Hg. This discharge was operated at low power (Raytheon Microtherm, Model CMD-4) so as to emit OH radiation corresponding to low rotational (and translational) "temperature" and thereby of small Doppler line width. This is important because the monochromator, whose resolution at 3000 Å is about 0.2 Å, only isolates OH lines (Doppler width 0.01 Å), but does not resolve them and therefore integrates the emitted intensity over the entire line shape. The narrower the emission line compared to the absorbing line, the larger is the effective absorption coefficient. Since both emission and absorption line are of Doppler shape, the total absorption, $(I_0 - I)/I_0$, can be expressed in terms of $\alpha_0 l$ if the ratio of Doppler widths, $\beta \equiv \Delta\nu_E/\Delta\nu_A$, is known. Here, I_0 and I are recorded intensities with the monochromator set at the peak of a line, in the absence (I_0) or presence (I) of absorbing OH, α_0 is the true absorption coefficient at the center of the line, and l is the optical path length. It can also be shown that Beer's law is obeyed for $I_0/I \leq 1.5$ and that $\ln I_0/I = \alpha_0 l/(1 + \beta)^{\frac{1}{2}}$.

In this work, OH was generated by the very

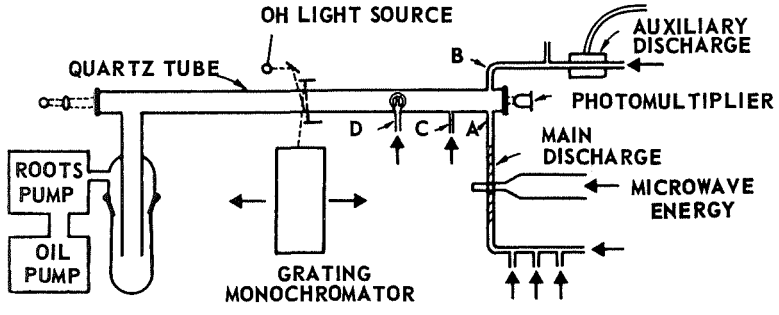

FIG. 1. Diagram of apparatus.

fast reaction

$$H + NO_2 \rightarrow OH + NO \qquad (5)$$

To a rapidly flowing He:H_2:H mixture containing 98 to 99 per cent He (or other inert diluents) NO_2 was added through a fast-mixing inlet (D) consisting of a ring of small Teflon tubing perforated with 31 small holes. Cylinder gases of best commercial grade were used.

Results

The Decay of OH *Radicals*

When OH was generated by adding NO_2 at D (Fig. 1) to a gas stream containing H atoms, strong light absorption was observed immediately downstream of D. By isolating various rotational lines from several branches of the (0, 0) band it was established that the absorber was OH in its ground vibrational state and with a distribution of rotational states corresponding to a temperature of 310° to 380°K, depending on the amount of NO_2 used (or OH formed). Such a temperature rise is reasonable since for reaction (5) $\Delta H_{298}^\circ = -29.18$ kcal/mole. It was also confirmed that this rotational "temperature" of the absorbing OH was approximately equal to the kinetic gas temperature in the mixing region by probing the region with glass-enclosed Pt, Pt–10 per cent Rh thermocouples.

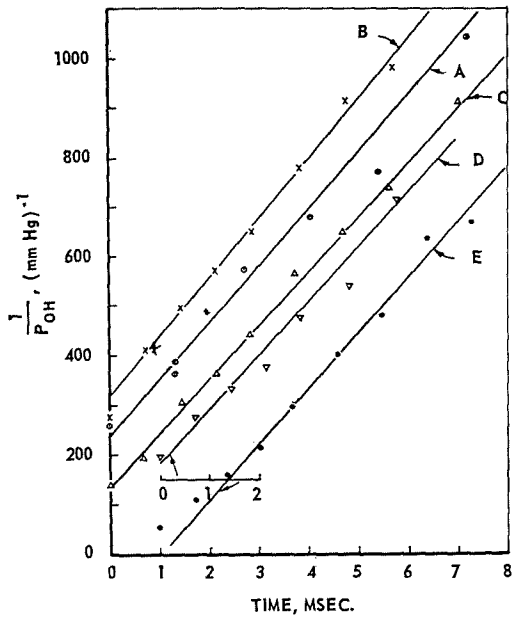

FIG. 2. Second order plots of OH decay. (Flows in moles/sec, pressures in mm Hg.) A: 0.041 H_2, 0.41 He; 0.52 mm Hg. B: 0.058 H_2, 6.26 He; 3.87 mm Hg. C: 0.042 H_2, 2.22 He (auxiliary discharge), 2.22 He (bypass); 2.70 mm Hg. D: 0.058 H_2, 6.26 He; 3.87 mm Hg. E: 0.032 H_2, 3.58 He; 2.08 mm Hg. B and D differ only in the amount of NO_2 added. D and E are displaced 1 msec for clarity.

As shown in Fig. 2, the OH decay downstream of the mixing region was of second order and could be followed over a tenfold decrease of initial OH concentration without change in rate constant. Two further results must be emphasized here: (1) Repeated searches for vibrationally excited OH in $v'' = 1$ and 2 in the mixing region and downstream were entirely unsuccessful and an upper limit of 0.02 can be set for the ratio of populations in $v'' = 1$ to $v'' = 0$. (2) The f-value for the electronic transition OH, $^2\Sigma^+ \rightarrow {}^2\Pi$, based on the stoichiometry of reaction (5) and on the assumption of thermally equilibrated OH ($^2\Pi$) is in good agreement with the best recent measurements. These two points are important, because they rule out energy transfer reactions of vibrationally excited OH as contributing to or masking the observed changes. These measured changes pertain to ground state OH ($^2\Pi$, $v'' = 0$) and they can not be explained in any way except by chemical reaction of OH. The interesting questions arising from the absence of vibrationally excited OH and the determination of the f-value will not be further discussed here.

The second-order decay of OH was found to be entirely reproducible, and the magnitude of its rate constant proves that earlier estimates[2,3] of the lifetime of OH were in error. The cause of this error (which amounts to about two orders of magnitude) lies in the method of production of OH. In the earlier investigations OH was made by electrical discharges in water vapor, and these are now known[4,5] to produce OH mainly by reactions of H and O_2 outside the discharge region throughout the flowing gas. This entirely falsifies the decay of OH, since it results in the slow disappearance of a steady state OH concentration which largely depends for its persistence on the long lifetime of H atoms. Entirely similar second order plots to those of Fig. 2 were recorded for He or Ar as diluent gas; at total pressures ranging from 0.5 to 3.9 mm Hg; at discharge power levels differing by a factor of 7; at ratios from 1:6 to 6:1 for gas flows through and bypassing the discharge; and for the following gases added bypassing the discharge, with fraction of total flow given in parentheses for each gas: N_2 (0.5), O_2 (0.05), NO (0.05), H_2O (0.05). Since the initial OH concentration corresponded to 0.002–0.02 of total flow, the above amounts represent 5- to 50-fold excess of added gas. The initial (OH) was controlled by the measured addition of NO_2 whose concentra-

tion was determined by light absorption at 4358 Å along the full length of the flow tube or by the weight loss of a bulb containing liquid NO_2–N_2O_4 in experiments of long duration. The ordinate in Fig. 2 is based on such measurements of NO_2 with the main discharge (Fig. 1) turned off, and on the equivalence of OH formed and NO_2 destroyed in the mixing region when the discharge was turned on. The H atom concentration produced by the discharge could be estimated by adding such flows of NO_2 (at D, Fig. 1) that a little NO_2 would persist. Normally, much lesser flows of NO_2 were used. The independence of the second order decay of OH on the amount of NO_2 used proves that reaction (4) can not be fast.

The decay was thus independent of initial OH concentration except at large $(OH)_0$ where deviations in and immediately beyond the mixing region can be ascribed to larger temperature rises, greater problems of good mixing, and the partial disappearance of OH within the mixing region due to its fast, second order reaction. The effective rate constant, k_b, was found to be 1.15×10^5 mm^{-1} sec^{-1} or 2.2×10^9 liter $mole^{-1}$ sec^{-1} with a probable error of ± 15 per cent, at 310°K.

Before we consider the mechanism of the reaction, the possible importance of surface reactions must be assessed. The reaction is clearly second order over a sufficient range of OH concentration that diffusion to the wall can not be rate-determining, i.e. must be faster than the surface reaction.

A solution of the diffusion equation

$$-dn/dt = D\nabla^2 n$$

at sufficiently long times for the contribution of higher modes to have become small, is the first order expression $-dn/dt = k_D n$ with $k_D = D/\Lambda^2$ where Λ is a characteristic dimension (diffusion length) and D is the diffusion coefficient of the diffusing species. For an infinitely long cylinder of radius r, $\Lambda = r/2.405$, and the effective first order rate constant, k_D, in our case ($r = 1.5$ cm) equals 2.60 D sec^{-1} where D has the units cm^2 sec^{-1}. Under typical experimental conditions, total pressure $P = 2.8$ mm Hg, and using $D = 540$ cm^2 sec^{-1} for OH in helium at 1 mm Hg,[6] $k_D = 500$ sec^{-1}. The corresponding k_D for dilution with argon ($D = 152$ cm^2 sec^{-1} at 1 mm Hg) is 178 sec^{-1}. These values must be compared with observed rates of OH disappearance which according to k_b, above, range from 600 to 1100 sec^{-1} at OH pressures of 0.005 to 0.01 mm Hg. It is clearly seen that diffusion is too slow to supply the surface with fresh OH molecules commensurate with the observed decay, and especially so for experiments with excess argon.

By collecting condensible reaction products at Dry Ice temperature in the large trap (Fig. 1) during experiments of long duration (30 to 120 minutes) it was shown that no H_2O_2 was produced, but that H_2O was a major reaction product. On the assumption that reaction (1) was followed by the still faster reaction (3), the yield of H_2O was nearly quantitative. This assumption is further justified below. The measured k_b then equals $\frac{3}{2}k_1$ and $k_1 = 1.5 \pm 0.4 \times 10^9$ liter $mole^{-1}$ sec^{-1}. The larger error range takes into account the fact that k_3 can not be very much greater than k_1. Experimental difficulties prevented a study of the temperature dependence of k_1, but since k_1 equals 1/80 of the gas-kinetic binary collision frequency of OH (assuming $\sigma_{OH} = 2.7$ Å) it is clear that reaction (1) can not have an activation energy of more than 1 to 2 kcal $mole^{-1}$.

The OH + H_2 *Reaction*

Whenever large flows of H_2 were used, either through or bypassing the discharge, the decay of OH was accelerated and no longer obeyed second order kinetics. The results of several experiments were fitted to the rate expression

$$-d(OH)/dt = k_b(OH)^2 + k_m(OH)$$

where the first order rate constant, $k_m = k_2(H_2)$. In integrated form,

$$\log \frac{(OH)_i}{(OH)_j} - \frac{k_m t_{ij}}{2.303} = \log \frac{k_m + k_b(OH)_i}{k_m + k_b(OH)_j}$$

where $(OH)_i$ and $(OH)_j$ are concentrations of OH at times i and j and t_{ij} is the time interval between i and j. Analysis of three experiments, two with 50 per cent H_2 and one with 100 per cent gave $k_2 = 4.3 \pm 1.0 \times 10^6$ liter $mole^{-1}$ sec^{-1} at an average temperature of 310°K.

The OH + O *Reaction*

Since O atoms are a product of the bimolecular reaction of OH radicals, it is important to have independent measurements of k_3. This was accomplished by mixing the discharged He–H_2 gas stream with one containing O atoms produced from nitrogen discharge products by the reaction $N + NO \rightarrow N_2 + O$. Since the recombination of H and O is a slow, termolecular reaction, and since the H + NO_2 reaction is much faster than the O + NO_2 reaction, it is possible to produce OH by reaction (5) in the presence of O atoms. When this is done, the decay of OH is seen to be greatly accelerated. As this acceleration dis-

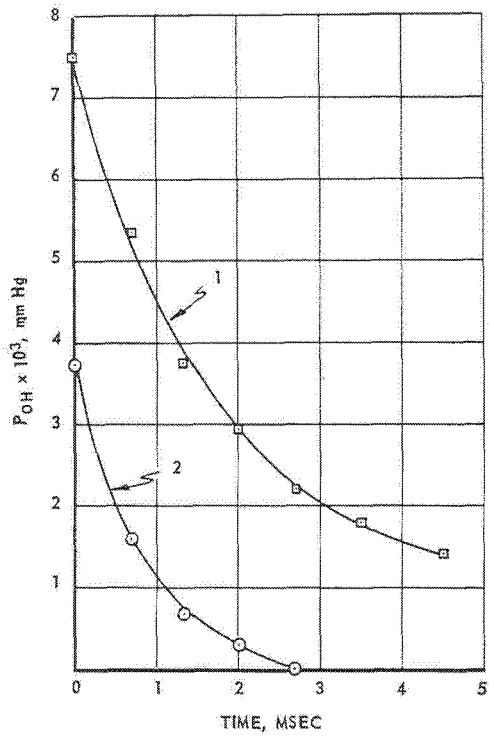

FIG. 3. OH decay in absence and presence of added O atoms. (Flows in moles/sec, pressures in mm Hg.) Curve 1: 0.042 H_2 and 2.25 He (auxiliary discharge), 1.04 N_2 and 1.12 He (main discharge off); 2.56 mm Hg. Curve 2: Same as 1 except main discharge on. O atoms (from N + NO) = 0.0091 mm Hg.

appears when the nitrogen discharge is turned off, it is reasonable to ascribe it to reaction (3). Quantitative treatment of the data is difficult, but was attempted in the following manner. As shown in Fig. 3, the addition of an initial concentration of atomic oxygen approximately equal to $(OH)_0$ brings about a very much faster decay (curve 2) than in the absence of O atoms (curve 1). $(O)_0$ was measured by the flow rate of NO necessary to produce extinction of the nitrogen afterglow and blue NO glow, and by NO_2 titration (at D, Fig. 1) of the O atoms produced. The rate of disappearance of OH and O are given by

$$-d(OH)/dt = k_1(OH)^2 + k_3(OH)(O)$$

$$-d(O)/dt = -\tfrac{1}{2}k_1(OH)^2 + k_3(OH)(O).$$

From the (OH) vs t plot in the presence of added O atoms, $-d(OH)/dt$ was read at several (OH), and since k_1 is known from our work, k_3 (OH) (O) was obtained by difference. Because reaction (1) makes O atoms, the concentrations of OH and O reacted away are not equal, as is best seen by subtracting the two rate expressions to give

$$d[(O) - (OH)]/dt = \tfrac{3}{2}k_1(OH)^2.$$

By graphical integration of $(OH)^2$ vs time we obtain

$$[(O) - (OH)]_0^t = \tfrac{3}{2}k_1\int_0^t (OH)^2\,dt$$

and thereby a better estimate of (O) at time t. Analysis of four experiments with added O atoms gave $k_3 = 1.1 \pm 0.4 \times 10^{10}$ liter mole^{-1} sec^{-1}.

Discussion

Thermodynamic Quantities

In the recent literature, there is a surprisingly large spread of values of ΔH and log K for reactions (1) to (4). The only quantity still of questionable accuracy is the bond strength of OH.[7] The data presented here are based on the JANAF Thermochemical Tables[8] which use ΔH_{298}° = 9.33 kcal mole^{-1} for the heat of formation of OH. Gray[9] prefers 8.88 kcal mole^{-1}. In Table 1 we give the values of ΔH° and ΔF° for the four reactions, at 300° and 1500°K, calculated from the JANAF tables.

The arbitrary choice of the two temperatures, 300° and 1500°K, makes ΔH° appear more temperature-independent than it really is. The ΔH° for reactions (1) and (2) is lowest at about 800°K (−17.15 and −15.30 kcal mole^{-1}) and above that temperature it becomes increasingly less negative. For reaction (3), ΔH° is lowest near 400°K (−16.81) and it rises fairly rapidly above 400°K. Reaction (4) has its highest (least negative) ΔH° near 700°K (−1.85) and it slowly becomes more negative with increasing temperature.

The following expressions for $K_{1\text{ to }4}$ reproduce the equilibrium constants with less than 3 per

TABLE 1

ΔH° and ΔF° for Reactions (1) to (4)

	ΔH° (kcal mole^{-1})		ΔF° (kcal mole^{-1})	
Reaction	300°K	1500°K	300°K	1500°K
(1)	−16.90	−16.96	−15.62	−9.93
(2)	−15.03	−15.03	−14.24	−10.48
(3)	−16.79	−15.96	−14.99	−8.22
(4)	−1.87	−1.93	−1.38	+0.55

cent error over the indicated temperature range:

$$K_1 = 0.092 \exp(17.06/RT) \quad (300° \text{ to } 2400°)$$

$$K_2 = 0.21 \exp(15.19/RT) \quad (300° \text{ to } 2200°)$$

$$K_3 = 3.33 \times 10^{-3} T^{0.372} \exp(17.13/RT) \quad (300° \text{ to } 2500°)$$

or

$$K_3 = 0.048 \exp(16.80/RT) \quad (300° \text{ to } 600°)$$

$$K_3 = 0.077 \exp(15.9/RT) \quad (1500° \text{ to } 1700°)$$

$$K_4 = 0.44 \exp(1.87/RT) \quad (300° \text{ to } 2500°)$$

Only K_3 requires a third parameter which is here given as a power of T. Two simplified, two-parameter expressions are also given, but they fit less well and over small ranges of temperature. The temperature change of $\Delta H°$ for this reaction is so large that large errors result if $\Delta H_0°$ is used at all temperatures.

The above expressions are based on reliable thermodynamic quantities for the species H_2, O_2, H, O, and H_2O. However, a change of 0.5 kcal mole^{-1} in the heat formation of OH would produce large changes in the K's. At 300°K, K_1 would change by a factor of 5, $K_{2 \text{ to } 4}$ by a factor of 2.3. At 2000°K, K_1 would change by 28 per cent, $K_{2 \text{ to } 4}$ by 13 per cent.

The Rate Constants for Reactions (1) *to* (4)

There appears to be little information on k_1 and k_{-1}. Schott[10] sets

$$k_1 = 3 \times 10^{11} \exp(-6.0/RT)$$

(all rate constants are given in the units liter mole^{-1} sec^{-1}, activation energies in kcal mole^{-1}) though in the earlier quoted paper, Duff[11] has $k_1 = 3 \times 10^{11} \exp(-2.5/RT)$ quoting a private communication by Davidson.

Voevodskii and Kondratiev[12] quote an activation energy E_{-1} of 18.0 ± 0.2 on the basis of preliminary results by Azatyan.

In flame studies, the concurrent reactions (2), (3), and (4) make direct observation of (1) impossible. Using $k_1 = 1.5 \times 10^9$ at 310°K as determined in this work and assuming $E_1 = 1.0$ (near 300°K, $E_1 = 1.5$ is an upper limit if $\sigma_{OH} = 2.7$ Å is used), we obtain $k_1 = 7.6 \times 10^9 \exp(-1.0/RT)$ and $k_{-1} = 8.3 \times 10^{10} \times \exp(-18.1/RT)$. E_{-1} is thus in good agreement with Azatyan's result. It must be remembered that k_1 is defined by the rate of disappearance of OH, and that k_{-1} therefore refers to ½ the rate of disappearance of O atoms.

Reaction (2) was investigated by Avramenko and Lorentso[13] in a discharge-flow system and by Fenimore and Jones[14] at 1300° to 1500°K by the addition of D_2O to rich H_2–air flames. More recently, Fenimore and Jones[15] in a summary of bimolecular rate constants have suggested $k_2 = 2.5 \times 10^{11} \exp(-10/RT)$. This expression gives $k_2 = 2.2 \times 10^4$ at 310°K whereas we find 4.3×10^6. If we assume the frequency factor to be 2.5×10^{11}, the activation energy E_2 is 6.8 kcal mole^{-1}. This difference of 3.2 kcal in E_2 amounts only to a factor of 3 in k_2 at 1500°K, but it rules out Avramenko's low temperature results. The tentative value of 2×10^7 at a temperature of 793°K which Baldwin[16] obtained from a study of the first explosion limit of the $H_2 + O_2$ reaction is also in poor agreement with the present results, but is in good agreement with Fenimore's[15] estimate of k_{-4}. Since Baldwin's interpretation suggests an identification of either k_2 or k_{-4} with his calculated rate constant, it now appears that he measured k_{-4}.

Clyne and Thrush[17] recently studied reaction (5) and, finding more NO_2 used per H atom in the presence of much H_2, ascribed this apparent occurrence of reaction (2) to vibrationally excited OH made in reaction (5). As we found[1] no vibrationally excited OH, but observed a faster decay of ground state ($v'' = 0$) OH when H_2 was added, evidently there is direct reaction between OH ($v'' = 0$) and H_2. If we fit an Arrhenius expression to a value of k_2 at 1500°K from Fenimore's suggested rate constant[15] and to our value 4.3×10^6 at 310°K, we obtain $k_2 = 6.3 \times 10^{10} \exp(-5.9/RT)$. From this, using the equilibrium constant K_2, $k_{-2} = 3.0 \times 10^{11} \exp(-21.1/RT)$. These last two expressions for k_2 and k_{-2} are to be preferred over those with $E_2 = 6.8$ because of their somewhat lower pre-exponential factor. With $E_2 = 6.8$, k_{-2} would be $1.2 \times 10^{12} \exp(-22.0/RT)$, but 1.2×10^{12} seems excessively high even for an H atom reaction.

Though little work has been done on reaction (3), much information is available on reaction (−3) which is, because of its endothermicity, the rate-determining step in the H_2–O_2 reaction. Thus, Karmilova, Nalbandyan, and Semenov[18] obtained k_{-3} from the slow oxidation of H_2 over the temperature interval 733° to 873°K and reported $k_{-3} = 5.7 \times 10^{10} \exp(-15.1/RT)$. Baldwin[16] reported $k_{-3} = 2.7 \times 10^6$ at 793°K and an activation energy E_{-3} of 15.2 which gives $k_{-3} = 4.2 \times 10^{10} \exp(-15.2/RT)$. Schott and Kinsey[19] studied the formation of OH during the induction period of the H_2–O_2 reaction in a shock tube, deduced a value of 1.4×10^9 at 1650°K from their experiments, and combined it with 5×10^6 at 793°K to yield $k_{-3} = 3 \times 10^{11} \times \exp[-(17.5 \pm 3)/RT]$. Fenimore and Jones[20]

obtained $k_{-3} = 1.5 \times 10^8$ at 1100°K and $E_{-3} = 18 \pm 3$ kcal mole^{-1} in H_2–air flames and thus reported[15] $k_{-3} = 6 \times 10^{11} \exp(-18/RT)$. Using the reflected shock technique, Strehlow and Cohen[21] reported $E_{-3} = 16.5$ over the temperature range 900° to 2000°K. It is seen that most of the quoted values of E_{-3} cluster around $\Delta H°$ for that reaction which is 16.8 to 16.0 at 500° to 1500°K. The values of 15.1 and 15.2 by Semenov and Baldwin are somewhat too low, since the reverse reaction is a bimolecular one which is unlikely to have a negative energy of activation.

Our experimental result, $k_3 = 1.1 \times 10^{10}$ at $T = 310°$, i.e., about 1/10 of the gas-kinetic collision frequency, can be combined with the equilibrium constant expression near 300°K to give $k_{-3} = 2.3 \times 10^{11} \exp(-16.8/RT)$ ($T = 300°$ to 600°K). For an estimate of k_{-3} at higher temperatures, some dependence of k_3 on temperature must be assumed. Two examples will be tiven. If k_3 is proportional to $T^{0.5}$, i.e., $k_3 = 6.3 \times 10^8 T^{0.5}$, $k_{-3} = 1.9 \times 10^{11} T^{0.13} \times \exp(-17.1/RT)$ ($T = 300°$ to 2500°). If $E_3 = 1$ kcal mole^{-1} is assumed, $k_3 = 5.6 \times 10^{10} \times \exp(-1.0/RT)$, and $k_{-3} = 1.2 \times 10^{12} \times \exp(-17.8/RT)$ ($T = 300°$ to 600°), $7.3 \times 10^{11} \exp(-16.9/RT)$ ($T = 1500°$ to 1700°), or $1.7 \times 10^{13} T^{-0.37} \exp(-18.1/RT)$ ($T = 300°$ to 2500°).

Our experiments showed that reaction (4) must have an appreciable activation energy, but we can not extract quantitative information. The presence or absence of excess H atoms did not influence the bimolecular decay of OH. From this we estimate an approximate lower limit for the activation $E_4 \geq 4$ kcal mole^{-1} if the preexponential factor is within a factor of ten of the gas-kinetic collision frequency. This is equivalent to $E_{-4} \geq 6$. There are three recent studies, however, which have presented quantitative data on k_{-4}. Clyne and Thrush[22] studied the O + H_2 reaction in a discharge-flow system at temperatures from 409° to 733°K. O atoms were produced from active nitrogen by the N + NO reaction (in the absence of O_2) and their decay was measured by the intensity of the air afterglow produced by known additions of NO. A value of $1.2 \times 10^{10} \exp(-9.2/RT)$ was obtained for k_{-4}. Fenimore and Jones[15] calculated k_{-4} to be 2.5×10^8 at 1660° and 3.0×10^8 at 1815°K from a study of composition and temperature traverses through low pressure flames. These rate constants are lower by a factor of three than those of Clyne and Thrush. Combining the flame work with Baldwin's[16] estimate of either k_2 or k_{-4} at 793°K, Fenimore and Jones report $k_{-4} = 2.5 \times 10^9 \exp(-7.7/RT)$. Azatyan, Voevodskii, and Nalbandyan[23] studied the explosion limits of CO–O_2 mixtures with small amounts of added H_2 at 840° to 930°K in vessels of high surface recombination efficiency and concluded $k_{-4} = 9 \times 10^{10} \exp(-12.1/RT)$. In its temperature range, this expression can not be reconciled with the other results, whereas the three other studies are in moderately good agreement with the rate expression of Fenimore and Jones. We therefore prefer $k_{-4} = 2.5 \times 10^9 \exp(-7.7/RT)$ and $k_4 = 5.7 \times 10^9 \exp(-5.8/RT)$.

TABLE 2

$\log_{10} A$ and E for Rate Constants k_i

$k_i = A_i \exp(-E_i/RT)$, $\quad i = \pm 1$ to ± 4

i =	$\log_{10} A$[a]	E[a]
+1	9.88 ± 0.3	1.0 ± 0.5
−1	10.92 ± 0.8	18.1 ± 1.0
+2	10.80 ± 0.7	5.9 ± 1.0
−2	11.48 ± 1.0	21.1 ± 1.5
+3	10.75 ± 0.3	1.0 ± 0.5
−3	12.08 ± 0.8[b]	17.8 ± 1.0[b]
−3	11.86 ± 0.8[c]	16.9 ± 1.0[c]
+4	9.76 ± 1.0	5.8 ± 1.5
−4	9.40 ± 0.7	7.7 ± 1.0

[a] All values are applicable over the range 300° to 2000°K, except where noted otherwise.
[b] $T = 300°$ to 600°K.
[c] $T = 1500°$ to 1700°K.

Table 2 presents a summary of recommended rate expressions. The simple form $k_i = A_i \times \exp(-E_i/RT)$ is retained, though, particularly for reaction (3), it is of doubtful validity.

ACKNOWLEDGMENTS

We would like to thank Dr. D. M. Golden for his assistance in the calculation of rotational temperature, f-value, and partition function of OH.

REFERENCES

1. DEL GRECO, F. P. and KAUFMAN, F.: Discussions Faraday Soc. *33*, 128 (1962).
2. OLDENBERG, O.: J. Chem. Phys. *3*, 266 (1935).
3. DOUSMANIS, G. C., SANDERS, T. M., and TOWNES, C. H.: Phys. Rev. *100*, 1735 (1955).
4. KAUFMAN, F. and DEL GRECO, F. P.: J. Chem. Phys. *35*, 1895 (1961).
5. FONER, S. N. and HUDSON, R. L.: J. Chem. Phys. *23*, 1974 (1955); *ibid. 25*, 602 (1956).
6. WESTENBERG, A. A.: Combustion and Flame *1*, 346 (1957).
7. BARROW, R. F.: Arkiv Fysik *11*, 281 (1956).

8. *JANAF Thermochemical Tables.* The Dow Chemical Company, Midland, Mich., 1960.
9. GRAY, P.: Trans. Faraday Soc. *55*, 408 (1959).
10. SCHOTT, G. L.: J. Chem. Phys. *32*, 710 (1960).
11. DUFF, R. E.: J. Chem. Phys. *28*, 1193 (1958).
12. VOEVODSKII, V. V. and KONDRATIEV: *Progress in Reaction Kinetics*, Chapter 2. Pergamon Press, 1961.
13. AVRAMENKO, L. I. and LORENTSO, R. V.: Zhur. Fiz. Khim. *24*, 207 (1950).
14. FENIMORE, C. P. and JONES, G. W.: J. Phys. Chem. *62*, 693 (1958).
15. FENIMORE, C. P. and JONES, G. W.: J. Phys. Chem. *65*, 993 (1961).
16. BALDWIN, R. R.: Trans. Faraday Soc. *52*, 1344 (1956).
17. CLYNE, M. A. A. and THRUSH, B. A.: Trans. Faraday Soc. *57*, 2176 (1961).
18. KARMILOVA, L. V., NALBANDYAN, A. B., and SEMENOV, N. N.: Zhur. Fiz. Khim. *32*, 1193 (1958).
19. SCHOTT, G. L. and KINSEY, J. L.: J. Chem. Phys. *29*, 1177 (1958).
20. FENIMORE, C. P. and JONES, G. W.: J. Phys. Chem. *63*, 1154 (1959).
21. STREHLOW, R. A. and COHEN, A.: Phys. Fluids *5*, 97 (1962).
22. CLYNE, M. A. A. and THRUSH, B. A.: Nature *189*, 135 (1961).
23. AZATYAN, V. V., VOEVODSKII, V. V., and NALBANDYAN, A. B.: Doklady Akad. Nauk S.S.S.R. *132*, 864 (1960).

Discussion

PROF. P. HARTECK (*Rensselaer Polytechnic Institute*): It may be interesting to recollect some historic points. Prompted by band spectroscopic investigations of W. Watson[1] and others, Bonhoeffer and Reichardt[2] in Haber's Institute showed that at high temperatures above 1000°C water vapor does not dissociate simply into oxygen and hydrogen, but also into hydrogen and two OH radicals. This was indeed of paramount importance because band spectroscopic data had for the first time helped to modify basic thermodynamic results which until then had been considered definite and complete.

1. Dr. Kaufman made his beautiful experiments with rather refined experimental tools: pumping velocities an order of magnitude faster than normally used, and concentration measurements via OH band absorption observed through a monochromator with a photomultiplier. This reminds me of an experiment which I made thirty years ago letting ozone and nitrogen dioxide react with hydrogen atoms and trying to get the OH absorption spectrum with the help of a hydrogen continuum and a Hilger quartz spectrograph. Obviously this arrangement was doomed to failure even though this was a good equipment for those times. But I also recall a very sensitive device for determining OH radicals which I didn't pursue because at that time I left Haber's Institute. This method was envisaged in discussions with Dr. F. G. Houtermans and I don't believe anyone is now using such a technique and therefore, I may be allowed to briefly mention it. Suppose we would interrupt the emission source as used by Dr. Kaufman and simply observe the fluorescent radiation which would also be intermittent. This intermittent fluorescence could be easily amplified and conveniently measured. This method would not give absolute OH concentrations, but could be calibrated similarly by the NO_2 with H atom reactions. This method I believe would extend the measurements to much lower concentrations.

2. I would like to show some results obtained by Dr. Reeves. The accompanying figure shows the OH flame with ozone and hydrogen atoms. The flame is T shaped because it impinges on the opposite glass wall. On the upper left side the flame is shown in the infrared. Using an ultraviolet filter a flame emitting the ultraviolet band at 3060 Å ($OH\ ^2\Sigma \rightarrow OH\ ^2\Pi$) of about the same shape can be seen as shown in the lower left. By adding O atoms to the H atoms it can be seen that both these flame intensities can be substantially increased in agreement with the high reaction rates for $OH + O \rightarrow O_2 + H$ as indicated by Dr. Kaufman which regenerates the H atoms, once more reforming the excited OH radicals via reaction with ozone. It is therefore of major interest, that $H + NO_2$ gives OH only in the vibrational ground state.

3. The rate coefficients given by Kaufman and Del Greco are of paramount importance for better understanding of the Meinel or OH bands observed from the night sky.[3] Since per square centimeter per second over 10^{12} OH photons are emitted by primarily formed OH vibrationally excited molecules produced by the H atom plus ozone reaction, the question arises how high the hydrogen atom concentration must be in the atmosphere. It was generally assumed that the hydrogen atoms were regenerated by the OH plus O atom reaction, and with the more precise results the necessary H atom concentration needed can be given with much smaller limits of error. It also shows that the OH concentration must be minor or the OH reaction with itself would destroy H atoms and the catalytic chain would become broken because the relatively stable H_2O molecule would become formed. This does not occur since the intensity of the OH is reasonably constant during the entire night.

4. In radiation chemistry there are two groups which have different ideas on the formation of hydrogen peroxide when liquid water is irradiated with ionizing radiation. In one case the H atom

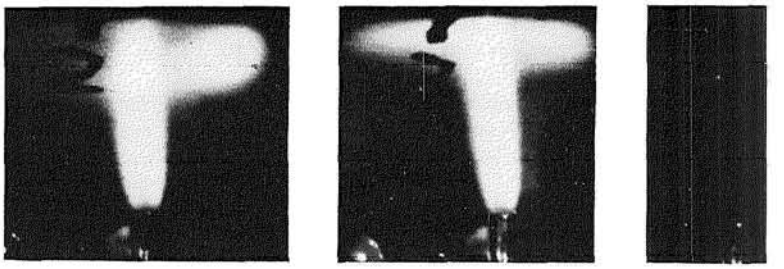

Infrared emission of OH bands from $O_3 + H \rightarrow O_2 + OH$

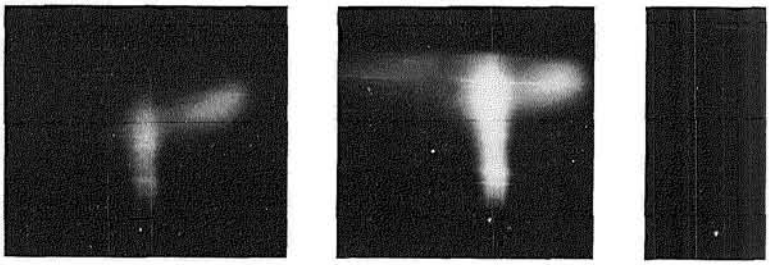

$O_3 + H$ $O_3 + H + O$ $O + H$

Ultraviolet emission of OH bands (identical conditions)

plus O_2 yields HO_2 and $2HO_2$ yields H_2O_2 plus O_2, a mechanism which is generally accepted. But the question arises if in the aqueous solution two OH molecules may recombine forming predominantly H_2O_2 or if they may form predominantly $H_2O + O$. I would like to ask Dr. Kaufman to comment on this and if he thinks it is possible that 2OH may recombine predominantly in aqueous solution to form H_2O_2.

Dr. R. R. Baldwin (*University of Hull*): One of the difficulties of using high temperature studies to obtain activation energies of free radical reactions is the low temperature coefficient involved. Thus even if an activation energy as high as 20 kcal/mole is determined by measuring the velocity constant at two temperatures 100°K apart and around 1000°K, an error of 10% in each k causes an error of 5 kcal/mole in E. For this reason, the value of 15.2 kcal/mole for E_{-3}, quoted from my paper by Kaufman and Del Greco, was never intended as an accurate estimate, but rather as confirmation that the relevant reaction involved was (−3)

$$H + O_2 = OH + O \qquad (-3)$$

The most accurate estimate of the activation of this reaction can probably be obtained by combining the following sets of values on a log k–$1/T$ plot:

1. The value of 1.5×10^9 liter mole^{-1} sec^{-1} at 1650°K obtained by Schott and Kinsey from measurements of the H_2/O_2 reaction in a shock tube.

2. The value of 1.5×10^8 at 1100°K given by Fenimore and Jones from studies of H_2–air flames.

3. The value of 0.6×10^7 at 813°K, given by Baldwin and Cowe[4] as the mean of values obtained by Baldwin from studies of the first limit of H_2/O_2 mixtures, by Semenov[5] from studies of the second limit, and by Baldwin and Cowe from studies of the inhibiting action of formaldehyde on the H_2/O_2 reaction.

4. The value of 0.334 at 310°K obtained by combining the value of 1.1×10^{10}, given by Kaufman and Del Greco for the reverse reaction, with their value for the equilibrium constant.

5. The value of 0.19 at 293°K obtained by combining the value of 3×10^{10}, given by Clyne for the reverse reaction, with the equilibrium constant given by Kaufman and Del Greco.

Assuming that these results follow an Arrhenius expression over the range 293°–1500°K, the parameters are given by: $E = 16.6 \pm 0.8$ kcal/mole, $\log_{10} A = 11.33 \pm 0.3$. The estimates of error are generous and allow a 50% error in both high and low temperature values. If the $T^{\frac{1}{2}}$ relation is preferred, then $k_{-3} = 4.2 \times 10^9\, T^{\frac{1}{2}} \exp(-15{,}900/RT)$.

Dr. B. A. Thrush (*University of Cambridge*): Dr. Clyne and I considered that the value of k_{-4} given in our paper

$$1.2 \times 10^{10} \exp[-(9200 \pm 600)/RT] \text{ liter mole}^{-1} \text{ sec}^{-1}$$

is preferable to that given by Kaufman and Del Greco for the following reasons:

1. Our data covers a greater range in $1/T$ than do the high temperature data.

2. Our pre-exponential factor is closer to that normally encountered in related reactions such as $Cl + H_2$.

3. If the data of Azatyan, Voevodskii, and Nalbandyan are included, our rate expression is a very good compromise between the three sets of high temperature data.

DR. R. R. BALDWIN: I should like to comment on the reaction

$$O + H_2 = OH + H, \qquad (-4)$$

discussed by Kaufman and Del Greco, in relation to the reaction

$$O + CO = CO_2. \qquad (23)$$

This latter reaction has recently been studied by Avramenko and Kolesnikova,[6] who give evidence that the reaction is bimolecular and give $k_{23} = 1.8 \times 10^6 T^{\frac{1}{2}} \exp(-3000/RT)$ liter mole^{-1} sec^{-1}. The ratio k_{-4}/k_{23} can be obtained from studies of the second limit of CO/O_2 mixtures sensitized by H_2. From results given in 1938 by Buckler and Norrish[7] and in 1953 by Dixon-Lewis and Linnett,[8] a ratio of 50–100 is obtained assuming that O + CO is bimolecular and that this reaction causes chain termination. The velocity constant for $O + H_2$ given by Azatyan, Nalbandyan, and Voevodskii, and referred to by Kaufman and Del Greco, was obtained by studying the first limit of CO/O_2 mixtures sensitized by traces of H_2. It was assumed that there was a competition between $O + H_2$ and O → surface; if the surface process is diffusion controlled, its rate can be calculated and hence k_{23} can be obtained. I have not been able to find any evidence in their papers that the competing process is surface dependent, and it is equally possible to interpret their results by assuming a competition between $O + H_2$ and the bimolecular reaction O + CO, in which case the ratio k_{-4}/k_{23} comes out as 60–70, in close agreement with the previous estimates. If this interpretation should be correct, it is not surprising that, as pointed out by Kaufman and Del Greco, the value of k_{-4} given by Azatyan *et al.* is inconsistent with other estimates.

However, the evidence on which O + CO is considered bimolecular also needs re-examination. If we combine the expression given by Kaufman and Del Greco ($k_{-4} = 2.5 \times 10^9 \exp(-7700/RT)$ with Avramenko and Kolesnikova's value for k_{23}, the ratio k_{-4}/k_{23} is about 3 at 540°C. This suggests that one or both of the expressions for k_{-4} and k_{23} may be in error, and since the values for k_{-4} obtained by different workers agree reasonably, k_{23} seems likely to be wrong. Once this is admitted, the evidence that O + CO is bimolecular becomes less convincing. The only alternative explanation is that the excited CO_2 from reaction (23) is capable of continuing the chain in the H_2/O_2 reaction about 19 times out of 20.

DR. H. WISE (*Stanford Research Institute*): Although the results suggest a minor contribution to the loss of OH radicals by heterogeneous recombination, I wonder whether an estimate could be made of the upper limit of the recombination coefficient of OH on the walls?

DR. F. KAUFMAN (*Ballistic Research Laboratories*): In reply to Prof. Harteck's comments, the use of OH fluorescence would probably not be a very sensitive method and it may suffer from the variable and efficient quenching of the upper electronic state by molecules such as O_2 or H_2O as was shown convincingly by Carrington.[9] It should be possible, however, to improve the sensitivity by using chopped double-beam operation with ac amplification as recently described by Oldenberg, Bills, and Carleton.[10] Regarding the formation of H_2O_2 from OH in aqueous solution I see no reason for excluding such a process. Even in the gas phase, Black and Porter[11] have recently shown that the reaction

$$OH + OH + M \rightarrow H_2O_2 + M$$

is fast enough to become rate-determining in the pressure range of 0.1 atm and above.

In reply to Dr. Wise, a very approximate upper limit of 10^{-1} to 10^{-2} can be estimated for the recombination coefficient of OH on the walls of our quartz tube.

REFERENCES

1. WATSON, W. W.: Astrophys. J. *60*, 145 (1924).
2. BONHOEFFER, K. F. and REICHARDT, H.: Z. physik. Chem. *A139*, 75 (1928).
3. HARTECK, P. and REEVES, R.: *Chemical Reactions in the Lower and Upper Atmosphere*, p. 219. Interscience, 1961.
4. BALDWIN, R. R. and COWE, D. W.: Trans. Faraday Soc. *58*, 1768 (1962).
5. SEMENOV, N. N.: Acta Physicochim. U.R.S.S. *20*, 290 (1942).
6. AVRAMENKO, L. I. and KOLESNIKOVA, R. V.: Izvest. Akad. Nauk S.S.S.R. Otdel. Khim. Nauk 1562 (1959); *ibid.* 561 (1960).
7. BUCKLER, E. J. and NORRISH, R. G. W.: Proc. Roy. Soc. (London) *A167*, 292 (1938).
8. DIXON-LEWIS, G. and LINNETT, J. W.: Trans. Faraday Soc. *49*, 756 (1953).
9. CARRINGTON, T.: J. Chem. Phys. *30*, 1087 (1959).
10. OLDENBERG, O., BILLS, D. G., and CARLETON, N. P.: J. Opt. Soc. Am. *51*, 526 (1961).
11. BLACK and PORTER: Proc. Roy. Soc. (London) *A266*, 185 (1962).

A STUDY OF THE REACTION OF POTASSIUM WITH CH_3Br IN CROSSED MOLECULAR BEAMS

M. ACKERMAN, E. F. GREENE, A. L. MOURSUND, AND J. ROSS

The reaction $K + CH_3Br \rightarrow KBr + CH_3$ has been studied by measurements on the scattering of a velocity selected K beam by a crossed thermal beam of CH_3Br. Although KBr could not be detected directly, information about the reaction could be obtained from the measurements of the elastic scattering in the reactive system. An analysis based on the assumption that the interaction of the reactants can be represented by a spherically symmetric potential led to: (1) potential parameters for an assumed analytic form of interaction; (2) the threshold of the reaction cross section, 0.24 kcal/mole; (3) the probability of reaction as a function of relative initial kinetic energy at the distance of closest approach; (4) the energy dependence of the total reaction cross section; and (5) an estimate of the absolute value of the total reaction cross section, 21 Å^2, at 1.93 kcal/mole.

Introduction

The usual approach to the study of the kinetics of a chemical reaction begins with measurements of the variation of the rate of the reaction with temperature and the concentrations of reactants and products. These experiments lead to an empirical rate law and are often very helpful in the postulation of a mechanism for the reaction. If the mechanism is simple, the reaction rate may be compared with predictions based on theoretical models. One of the most common of these models for bimolecular reactions is that of hard spheres which react if and only if the component of the relative kinetic energy along the line of centers at impact is greater than a minimum or threshold value, E^*. The temperature dependence of the rate coefficient, $k(T)$, predicted by this model is

$$k(T) \sim T^{\frac{1}{2}} \exp(-E^*/kT)$$

a relation obtained by averaging the total chemical reaction cross section as a function of energy over the Maxwellian distribution. Although the threshold energy may be obtained from measurements of this temperature dependence, comparison of theory and experiment usually can not be made with sufficient precision to serve as a reasonable test for the model.

The reason for using crossed molecular beams in studying the kinetics of reactions is that a significant part of the normal averaging over collisions can be avoided. Instead of examining the temperature dependence and postulating mechanisms, individual collisions between known species at known kinetic energies can be studied. The desirability of this approach has long been evident, but the number of molecules scattered in reactive collisions is so small that only recently have experimental techniques advanced sufficiently for meaningful studies to be made.

The present paper is concerned with a particular example of a reaction in crossed molecular beams of uncharged chemical species, namely potassium atoms and methyl bromide molecules. Reactions between ions and molecules have been studied much more extensively because electric and magnetic fields interact with the charge on the ion and provide a convenient way to produce collimated ion beams of known energy. These reactions are in a separate class and are not discussed here.

Very few reactions between neutral particles have been examined by crossed molecular beam techniques up to the present time. Brief mention of some of this earlier work illustrates the advantages and complications of the method.

1. The first detailed study of a chemical reaction in crossed beams was Taylor and Datz's examination of the scattering of K by HBr to produce KBr and H.[1] The experimental results have been reanalyzed by Datz, Herschbach, and Taylor.[2] This reaction was chosen for three principal reasons. Alkali metals and alkali halides can be detected conveniently and quantatively by surface ionization on hot platinum and tungsten.[3] Secondly, the activation energy is low enough so that a significant fraction of the collisions between molecules in thermal beams lead to reaction. Thirdly, the very unequal masses of the products and the small change in zero point energy for the reaction, $\Delta D_0^0 = -4.2 \pm 1$

kcal/mole,[4,5] require that the KBr stay close to the center of mass vector for the collision so that energy and momentum be conserved. This fact leads to a concentration of the flux of KBr in a small fraction of the available solid angle. The measured angular distribution of the KBr corresponded reasonably well to the calculated distribution of the center of mass vectors for the collisions, but the Maxwellian distribution of speeds in the beams and the range of beam intersection angles, due to the angular distribution of the HBr beam, prevented a clear-cut determination of the energy threshold for the reaction. The authors suggest a value of E^* between 2.5 and 3.0 kcal/mole.

2. Herschbach, Kwei, and Norris have studied the reaction of alkali metals with a series of alkyl iodides.[6] These reactions are similar to that of K with HBr except that the mass ratio of the products is much closer to unity. Thus, the alkali halide formed can leave the center of mass of the collision and measurement of the differential reaction cross section becomes possible. Herschbach *et al.* could vary the angle of intersection of their thermal beams of reactants and also move their detector above and below the plane of the crossed beams. They found that the variation in scattering angles of the products with changes in experimental parameters could be predicted by their analysis of the mechanics of the scattering. Their most intriguing result was the observation of an asymmetry in the detected distribution of the alkali iodide with respect to the center of mass vector. For the reaction of K with CH_3I this asymmetry indicated that: (a) 90 per cent or more of the detected KI returned within a few degrees of the direction from which the K had come, while the corresponding CH_3 must of necessity have continued in the original direction of the K. (b) Of the 25 kcal/mole energy of reaction only about 0–5 kcal/mole on the average appeared as relative kinetic energy of the detected products, while the rest was converted into internal energy of vibration and rotation. (c) The duration of the collision must have been small compared to the rotational period of the complex (about 3×10^{-12} sec). Thus, there is no evidence for "sticky" collisions in this case.

3. The first chemical reaction studied in some detail as a function of relative energy by crossed molecular beam techniques was that of K with HBr.[7] Measurements of the scattered KBr gave an indication of the energy dependence of the total chemical reaction cross section. This result depended on the angular distribution of the HBr beam which was not known precisely; however, it was concluded that the threshold of the chemical reaction is less than 0.4 kcal/mole and the cross section varies but little with energy above this value.

More detailed information on the reaction was obtained from measurements of the elastically scattered potassium and an analysis based on the theory of two-body collisions. By comparison of the elastic scattering in the reactive system with that of a nonreactive system it was possible to deduce the probability of reaction as a function of the energy and either the impact parameter or the potential energy at the distance of closest approach in the collision. For impact parameters below 3.5 Å, about 90 per cent of all collisions lead to reaction. The total chemical reaction cross section was estimated to be 34 Å^2 at $\bar{E} = 2.6$ kcal/mole. At a constant distance of closest approach, the probability of reaction was noted to decrease with increasing energy, and this variation was interpreted as a consequence of the conservation of angular momentum. Calculations showed that for large impact parameters the initial orbital angular momentum had to be converted essentially completely into angular momentum of rotation of KBr with rotational quantum numbers ranging up to $J = 200$. Finally, an analysis based on the two-body model led to a value of the size parameter $r_m = 4.5$ Å in the exp–six potential Eq. (5).

Apparatus

The apparatus has been described previously,[7,8] so only a very brief outline of the essential features will be given here. The important parts are shown in Fig. 1. The potassium beam is formed by effusion from a double-chambered Monel oven (A) located in the first of three separately pumped vacuum chambers. Those atoms moving in the right direction pass through slit (B) and meet the rotating velocity selector (E). The latter is an aluminum cylinder milled with 504 helical slots 0.5 mm wide and driven by a variable speed motor outside the vacuum chamber. The selector passes the fraction of the incident K atoms which have the appropriate speed. The transmitted distribution of speeds is triangular with a width at half-height 0.084 times the central speed v_1.

After emerging from the selector the K atoms pass through slit (G) into the reaction chamber and form a beam 0.5 mm wide by 3 mm high. The K beam then intersects the crossed beam of CH_3Br, effusing from oven (H), at right angles to its center line. The intensity of the scattering gas is found experimentally to have an angular distribution about its center line proportional to $\cos^8(\gamma - \frac{1}{2}\pi)$, where γ is the angle between the two beams. The high pumping speed necessary to maintain a vacuum of 10^{-6} mm in the presence

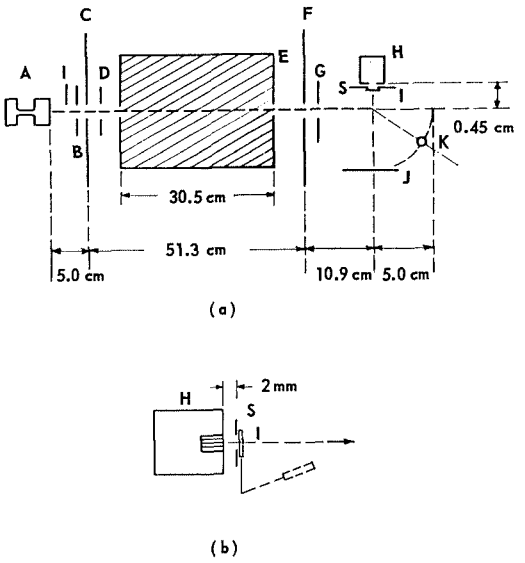

FIG. 1. Schematic diagram of apparatus. (a) Placement of components of molecular beam apparatus (top view); not to scale. (b) Detail of oven H with beam flag (side view).

of the large amount of CH_3Br is obtained by surrounding as much as possible of the scattering center by a $\frac{1}{8}$ inch thick copper shield cooled to the temperature of liquid nitrogen. A beam flag (I) can interrupt the flow of CH_3Br to the scattering region without changing the flow rate from the crossed beam oven (H) into the vacuum chamber. The scattering volume is defined by the region of overlap of the ribbon-shaped K beam with the diverging CH_3Br beam.

K and KBr may be detected by surface ionization on Pt, which is sensitive only to K, and on W, which is sensitive to both KBr and K.[3] The detector filaments used are ribbons 0.5 mm wide and 0.013 mm thick arranged vertically with a 6 mm central section exposed to the beam. The *W* ribbon is plated to 3 times its original thickness with *W* from the decomposition of $W(CO)_6$ in order to reduce the background noise from K atoms in the *W*.[9] The positive ions from the *Pt* or *W* filaments are collected at an electrode 30 V negative with respect to the filaments, and then the resulting current is amplified in a vibrating reed electrometer. The collector and the two filaments are 5 cm from the scattering center and can move in the plane of the two beams over the range $-5° < \beta < 115°$.

In a typical run the front and rear chambers of the K oven are at 710° and 580°K respectively corresponding to a K pressure of 0.35 mm. The CH_3Br oven is at 288°K and the gas is introduced from an external supply. The pressure is uncertain but may be checked for constancy by the attenuation of the K beam, which is typically 30 per cent. In use, the W and Pt filaments are heated to 1480°K and 1010°K, respectively, as determined with a Leeds and Northrup 8623-C optical pyrometer; the emissivities used are 0.3 and 0.65, respectively. At higher filament temperatures the CH_3Br beam impinging on either ribbon contributes excessively to the positive current.

The Reaction K with CH_3Br

Kinematics

Consider the collision of a potassium atom of speed v_1 with a CH_3Br molecule of speed v_2 and let the initial velocity vectors be perpendicular (Fig. 2). The relative velocity vector $\mathbf{v} = \mathbf{v}_1 - \mathbf{v}_2$ connects the two initial velocity vectors, and the center of mass motion vector (centroid) $(m_1 + m_2)\mathbf{v}_c = m_1\mathbf{v}_1 + m_2\mathbf{v}_2$, intercepts the relative velocity vector at a point determined by the equations

$$\mathbf{v}_1 = \mathbf{v}_c + [m_2/(m_1 + m_2)]\mathbf{v}$$

$$\mathbf{v}_2 = \mathbf{v}_c - [m_1/(m_1 + m_2)]\mathbf{v}.$$

The vector diagram in Fig. 2 is drawn to scale for the case of the highest experimental relative energy. This is the most favorable condition achievable in our experiments for the detection of KBr because the range of laboratory angles which must be scanned to detect KBr is then the smallest. The final relative velocity vector, $\mathbf{v}'$, may

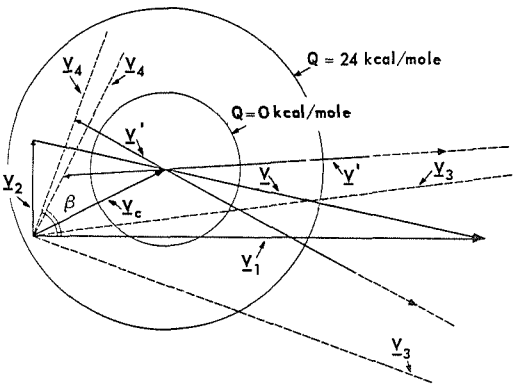

FIG. 2. Velocity vector diagram for beams of *K*, $\mathbf{v}_1$, and CH_3Br, $\mathbf{v}_2$, crossing at right angles. Two final relative velocity vectors, $\mathbf{v}'$, and two velocity vectors of KBr, $\mathbf{v}_4$, are drawn for a typical case, $Q = 5$ kcal/mole, corresponding to detection at laboratory angles β from $\mathbf{v}_1$.

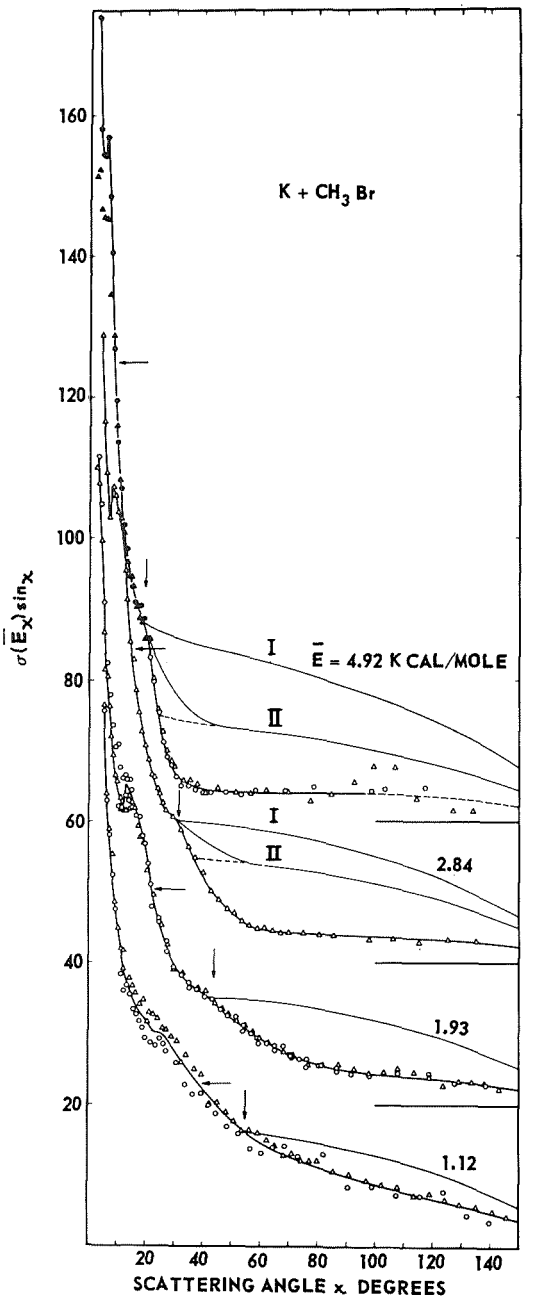

FIG. 3. Measured differential cross section multiplied by sin χ for K scattered by CH_3Br, $\sigma(\bar{E}\chi)$ sin χ, vs scattering angle χ in center of mass coordinates at four energies. Triangles denote measurements with the tungsten filament as a surface ionization detector; circles, platinum filament. Signals from the two filaments are normalized in the main K beam. The solid lines are calculated by two methods which lead to the same curves for the two lowest energies, and to the curves marked I and II for the two highest energies.

be drawn to pivot at the end of the centroid but the absolute magnitude (final relative speed) is unknown. Limits on the final relative kinetic energy E' may be obtained from the equation of conservation of energy

$$E + U = -\Delta D_0^\circ + E' + U', \qquad (1)$$

where U and U' are the internal energies of the reactants and products, respectively, and ΔD_0° is the difference in zero point energy, estimated to be -24 kcal/mole.[10] If the velocity of KBr is $\mathbf{v}_4$ and that of CH_3 is $\mathbf{v}_3$, then the product KBr appears at a laboratory angle β. If E' is so large that $v'm_3/(m_3 + m_4)$ extends to a circle including the origin 0, as may be the case in this reaction, then the product KBr may appear at all laboratory angles. The analysis of the distribution of products is further complicated if account is taken of the angular spread of the CH_3Br in the crossed beam, i.e., the distribution of beam intersection angles.

Measurements on KBr

A search for KBr in the horizontal plane in the quadrant containing the centroid indicates that the product flux at the detector was below the limit of detection. This limit varied from 2×10^{-16} amp at angles where there was not much scattered K to much larger values near the K beam. The absence of KBr is shown by the identical signals received by the W and Pt detectors at all scattering angles (Fig. 3). The signals of the two detectors are normalized at the main K beam. For the present reaction, unlike the reaction of K with HBr, no confinement of KBr to the centroid is required.

Measurements on Scattered Potassium

In collisions of reactive molecules the possibility of chemical reaction may be expected to alter the scattering pattern of unreacted molecules from that of a similar system in which chemical reaction does not occur. This difference may provide further information about the reaction. If a K atom collides with a CH_3Br molecule, not only is reaction possible but also elastic scattering and nonreactive inelastic scattering may occur. In our apparatus we cannot distinguish between the various types of nonreactive scattering. Elastic scattering is certainly much more probable than inelastic scattering resulting in translational-vibrational energy exchange. Although elastic scattering is also more probable than scattering resulting in translational–rotational energy exchange, there is some theoretical evidence that the two may differ by only a factor of two.[11] In principle, the scattering which would occur in the absence of chemical reaction

can be either estimated experimentally or calculated. We do not have measurements of the scattering of a satisfactory nonreactive analog of CH_3Br, and therefore we attempt a comparison with a theoretical calculation. For this we have to neglect the effects of nonreactive inelastic scattering as well as changes in the elastic scattering due to deviations from central forces.

Let a beam of K atoms with speed v_1 collide with a perpendicular beam of CH_3 Br atoms with the average speed of a Maxwellian distribution $\bar{v}_2$. The initial relative kinetic energy is thus $\bar{E} = (1/2)\mu(v_1^2 + \bar{v}_2^2)$, and the reduced mass is $\mu = m_1m_2/(m_1 + m_2)$. The number of K atoms, $I_k(\bar{E}\bar{q}\alpha\beta)$, arriving per unit time at the detector situated at given laboratory angles $(\alpha\beta)$ is proportional to

$$c\sigma(\bar{E}\alpha\beta)\sin\alpha\,\Delta\alpha\,\Delta\beta[1 + (m_1/m_2\bar{q})^2]^{\frac{1}{2}}N_1n_2, \quad (2)$$

where $\sigma(\bar{E}\alpha\beta)$ is the differential scattering cross section, c is a geometric factor, $\bar{q}$ is the ratio of momenta $(m_1v_1/m_2\bar{v}_2)$, N_1 is the flux of K atoms per unit area and unit time, n_2 is the density of CH_3Br in the source chamber, and $\sin\alpha\,\Delta\alpha\,\Delta\beta$ is the solid angle subtended by the detector. (For further details see reference 7.) From the relation of the differential scattering cross section in laboratory coordinates $(\alpha\beta)$ to that in relative coordinates $(\chi\Psi)$

$$\sigma(\bar{E}\alpha\beta)\sin\alpha\,d\alpha\,d\beta = \sigma(\bar{E}\chi)\sin\chi\,d\chi\,d\Psi, \quad (3)$$

it is seen that the differential scattering cross section, as a function of the relative scattering angle χ, is proportional to the flux of K; in the horizontal plane $(\alpha = \frac{1}{2}\pi)$ we have the equation

$$\sigma(\bar{E}\chi)\sin\chi = I_k(\bar{E}\bar{q}\beta)(d\alpha\,d\beta/d\chi\,d\Psi) \times\{cN_1n_2\,\Delta\alpha\,\Delta\beta[1+(m_1/m_2\bar{q})^2]^{\frac{1}{2}}\}^{-1}. \quad (4)$$

A plot of $\sigma(\bar{E}\chi)\sin\chi$ vs χ is shown in Fig. 3 for the system K and CH_3Br. The four curves illustrate the angular dependence of the elastic cross section for four relative energies. At small scattering angles each curve displays the maximum characteristic of the rainbow scattering phenomenon predicted for two-body collisions.[12,13]

If an analytical form is assumed for a spherically symmetric intermolecular potential energy $V(r)$ as a function of the reduced distance (r/r_m), say

$$V(r/r_m) = \frac{\epsilon}{[1 - (6/\alpha)]} \times\left\{\frac{6}{\alpha}\exp\left[\alpha\left(1 - \frac{r}{r_m}\right)\right] - \left(\frac{r_m}{r}\right)^6\right\}, \quad (5)$$

where ϵ is the value of the potential at its minimum and r_m is the intermolecular separation at that point, then it is possible to evaluate the parameter ϵ from the position of the rainbow angle (marked by horizontal arrows for each of the curves). For the exp-six potential, $\alpha = 15$, the parameter ϵ is found to be 0.32 kcal/mole (see Table 1) and these potential parameters are used in the interpretation of the experiment. For the exp-six potential with $\alpha = 12$ we find for ϵ and $V(y)$ at threshold 0.34 and 0.18 kcal/mole respectively; however, with these alternative parameters the rest of the interpretation is essentially unchanged.

TABLE 1

Parameters for the Scattering of K by CH_3Br[a]

$\bar{E}$	ϵ	$\chi_{threshold}$	y	$V(y)$
1.12	0.305	55.0	0.876	0.237
1.93	0.329	44.0	0.871	0.275
2.84	0.316	28.8	0.879	0.208
4.92	0.330	19.5	0.881	0.192

[a] For each of the four curves shown in Fig. 3 there is listed: the initial relative kinetic energy $\bar{E}$; the potential parameter ϵ determined from the angular position of the rainbow angle; $\chi_{threshold}$ the threshold angle (deg) at which a decrease of elastic scattering appears due to the onset of chemical reaction; the reduced distance of closest approach y for collisions resulting in scattering to the threshold angle; and $V(y)$, the potential energy at the distance of closest approach.

For comparison, the elastic scattering behavior of a nonreactive system, K + Kr, is shown in Fig. 4.[14,7] More pronounced rainbow scattering is observed, and the value of ϵ for this system is 0.18 kcal/mole ($\alpha = 12$). The important difference to be noted is the behavior of the cross section for scattering angles larger than the rainbow angle. The sharp decrease in scattered potassium for the case K + CH_3Br beyond threshold angles observable for three curves (vertical arrows, Fig. 3) is interpreted as an indication of the onset of chemical reaction. For a given relative kinetic energy and intermolecular potential of a two-body system the threshold angle of scattering is uniquely related to a given impact parameter or a given potential energy at the distance of closest approach, which constitutes the threshold energy or "activation energy" of the reaction. The vertical arrow for the curve of lowest energy is drawn to give a distance of closest approach at threshold which is the average of that for the three higher energies (see Table 1).

On the basis of the stated assumptions, the determination of ϵ and the threshold energy of the reaction proceeds straightforwardly from the

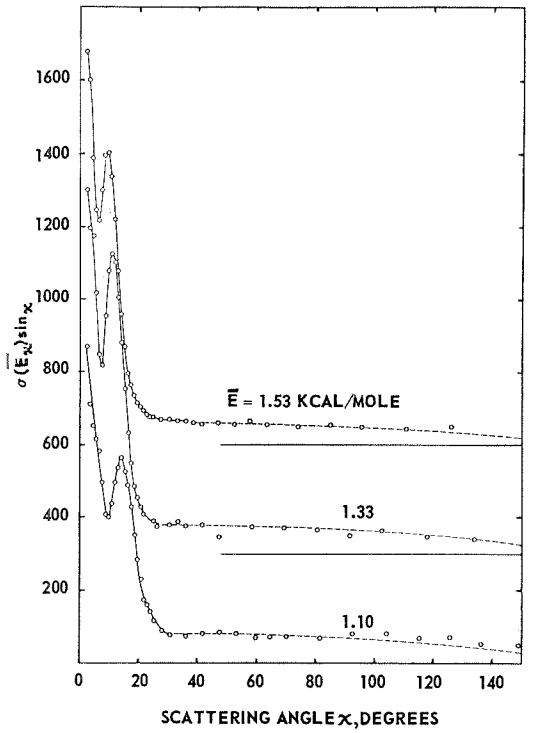

FIG. 4. Measured differential cross section in arbitrary units multiplied by sin χ for K scattered by Kr, $\sigma(\bar{E}\chi)$ sin χ, vs scattering angle in center of mass coordinates at three energies. The solid lines serve to connect the measured points. The dashed lines are calculated from classical two-body scattering theory [exp–six potential Eq. (5) with $\alpha = 12$, $\epsilon = 0.18$ kcal/mole] and fitted to the solid lines near $\chi = 40°$.

measured scattering curves. Next, we wish to evaluate the probability of reaction defined by the equation

$$P \equiv [\sigma_c(\bar{E}\chi) - \sigma(\bar{E}\chi)]/\sigma_c(\bar{E}\chi), \qquad (6)$$

where $\sigma_c(\bar{E}\chi)$ is the differential elastic cross section calculated for a nonreactive system with the potential Eq. (5) and the energy parameter determined above. The functions $\sigma_c(\bar{E}\chi)$ sin χ for the appropriate energies are fitted to the measured values at the threshold angles, Fig. 3, curves labelled I. However, this procedure does not conform to all the requirements of the model chosen for the representation of the nonreactive two-body scattering because the relative heights of the curves (I) differ from those predicted by the model. For this reason, a second set (II) of curves is drawn in Fig. 3 which do have the predicted relative heights. The curves for the lower two energies are identical for (I) and (II),

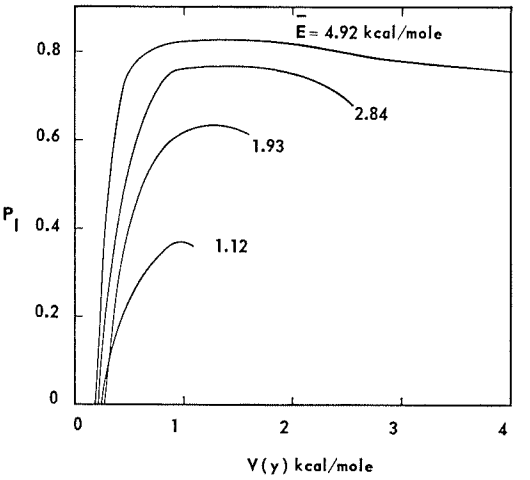

FIG. 5. Probability of reaction vs potential energy at distance of closest approach evaluated for each of the four energies with use of curves (I), Fig. 3.

but for the higher two energies the functions $\sigma_c(\bar{E}\chi)$ sin χ for curves (II) are drawn in arbitrarily at small angles to connect with the measured curves at the threshold angles. This second set of curves is shown to demonstrate the influence of the choice of theoretical nonreactive scattering curves on the interpretation of the data.

In Figs. 5 and 6 we plot the probability of reaction evaluated from Eq. (6) and the calculated curves I and II as a function of the potential energy at the reduced distance of closest approach $V(y)$ for the four experimental relative initial kinetic energies. There is not very much difference between the P_I and P_{II} curves so

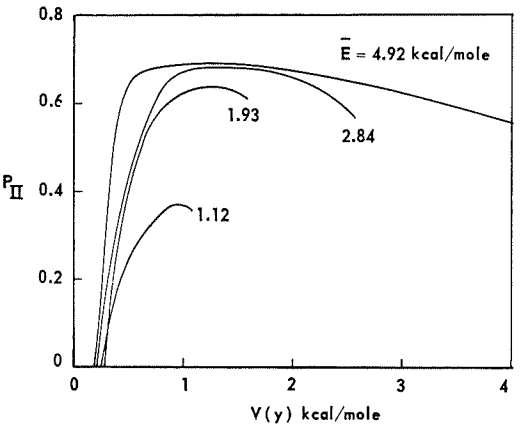

FIG. 6. Probability of reaction vs potential energy at distance of closest approach evaluated for each of the four energies with use of curves (II), Fig. 3.

that the probability of reaction appears to be relatively insensitive to the precise method of choosing the hypothetical scattering curve. The features of the curves of P vs $V(y)$ are the nearly constant threshold of reaction, 0.24 kcal/mole independent of $\bar{E}$, the rise to a maximum less than one, and the variation of the probability of reaction with the initial relative kinetic energy. The maximum value of P is reached at relatively large impact parameters ($b/r_m = 0.7$ at $V(y) = 1.17$ kcal/mole for $\bar{E} = 4.92$ kcal/mole) indicating that reaction may occur for a large range of impact parameters. It is possible that the variation of the probability of reaction with $\bar{E}$ is due to penetration of a barrier.

The total chemical reaction cross section $\sigma_R(\bar{E})$ can be shown to be related to $\sigma_c(\bar{E}, \chi)$ and $\sigma(\bar{E}\chi)$ by the equation

$$\sigma_R(\bar{E}) = 2\pi \int_0^{\pi} [\sigma_c(\bar{E}\chi) - \sigma(\bar{E}\chi)] \sin\chi \, d\chi, \tag{7}$$

which can be rewritten by use of Eq. (6) as a function of the impact parameter b,

$$\sigma_R(\bar{E}) = 2\pi r_m^2 \int_0^{b_{max}/r_m} P(b/r_m) \, d(b/r_m) \tag{8}$$

The total chemical reaction cross section can therefore be calculated as a function of energy either from Eq. (7) by graphical integrations of the appropriate areas on Fig. 3, or by graphical integrations of plots of Pb/r_m vs the reduced impact parameter b/r_m. The symbol b_{max} denotes the impact parameter at the threshold angle, i.e., the maximum impact parameter leading to reaction at a given $\bar{E}$. Figure 7 shows the curves for the variation of the chemical reaction cross section with initial relative kinetic energy based on the two sets of P vs $V(y)$ curves.

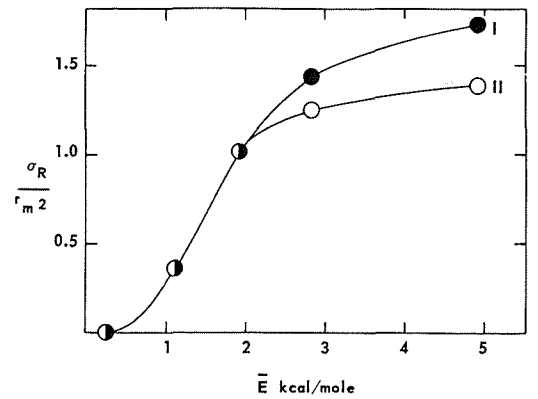

FIG. 7. Reduced total chemical reaction cross section vs. relative initial kinetic energy for K and CH_3Br evaluated by methods I and II.

In order to calculate absolute values of the total chemical reaction cross section from either Eq. (7) or (8) it is necessary to know the parameter r_m, Eq. (5). If we estimate its value to be the same as that of system K + HBr, then the total reaction cross section at 1.93 kcal/mol is 21 Å^2.

We realize the limitations of an analysis of the measurements based on the assumptions that the scattering behavior of the system K + CH_3Br follows that of a two-body system and is not influenced by nonreactive inelastic scattering. Evidence for and against these assumptions is available from measurements on other systems. In the system K + Kr we see rainbow maxima and curve shapes consistent with the theory but there is not enough evidence to compare the relative heights of the scattering at large angles with the predictions of the theory at different energies. For K + HCl we still see[15] rainbow maxima and there are ranges of angles between the maxima and the reaction threshold to which we can fit curves calculated from the theory of two-body collisions. The ratios of the functions $(\bar{E}\chi) \sin\chi$ in these ranges for different energies are not consistent with the theory but deviate in a way comparable to that for K + CH_3Br. For $K + Br_2$ no rainbow maxima are observed.[15] For K + CH_3Br there is enough resemblance to the scattering of a two-body system for an attempt at an interpretation based on these assumptions. There are enough differences to view the conclusions with caution.

In the absence of adequate theories of scattering of many body systems it may be better to estimate the probability of reaction by comparison of the elastic scattering of reactive species with elastic scattering of structurally similar non-reactive species, rather than with theoretical predictions.

ACKNOWLEDGMENT

This work was supported in part by a grant from the Atomic Energy Commission.

REFERENCES

1. TAYLOR, E. H. and DATZ, S.: J. Chem. Phys. *23*, 1711 (1955).
2. DATZ, S., HERSCHBACH, D. R., and TAYLOR, E. H.: J. Chem. Phys. *35*, 1549 (1961).
3. DATZ, S. and TAYLOR, E. H.: J. Chem. Phys. *25*, 389, 395 (1956).
4. HERZBERG, G.: *Spectra of Diatomic Molecules*, 2nd ed., p. 534. D. van Nostrand Co., 1950.

5. GAYDON, A. G.: *Dissociation Energies and Spectra of Diatomic Molecules*, 2nd ed., p. 225. Chapman and Hall, 1953.
6. HERSCHBACH, D. R., KWEI, G. H., and NORRIS, J. A.: J. Chem. Phys. *34*, 1842 (1961).
7. BECK, D., GREENE, E. F., and ROSS, J.: J. Chem. Phys. *37*, 2895 (1962).
8. ROBERTS, R. W.: Ph.D. thesis, Brown University, 1959.
9. GREENE, E. F.: Rev. Sci. Instr. *32*, 860 (1961).
10. COTTRELL, T. L.: *The Strengths of Chemical Bonds*, 2nd ed., pp. 277, 286. Butterworths, 1958.
11. BERNSTEIN, R. B.: Bull. Am. Phys. Soc. (II) *7*, 217 (1962).
12. MASON, E. A.: J. Chem. Phys. *26*, 667 (1957).
13. FORD, K. W. and WHEELER, J. A.: Ann. Phys. *7*, 259 (1959).
14. BECK, D.: J. Chem. Phys. *37*, 2884 (1962).
15. Unpublished.

Discussion

PROF. J. E. SCOTT (*University of Virginia*): It is generally recognized that the molecular collisions which lead to chemical reaction can be effectively studied by means of molecular beam experiments. Professor Greene and his colleagues at Brown University have taken another step in the actual demonstration of this fact as evidenced by their study of the reaction of K with CH_3Br in the crossed beam experiment which has just been described. Crossed beam experiments usually involve the measurement of the collision yield as a function of energy from which the total reaction cross section can be determined. In addition, the angular distribution of the products can often be interpreted in terms of the internal energy states of the reaction products and the dependence of reaction cross section on initial kinetic energy and molecular orientation. Greene *et al.* have taken a somewhat different approach in the use of the nonreactive scattering system for the determination of the "activation energy," the reaction probability, and the total reaction cross section. These results are based on a number of assumptions which must be made in connection with the scattering behavior of the system. Consequently, it should be emphasized that the validity of the reaction characteristics so determined may be limited by the assumptions required for the interpretation of the scattering data.

Continued emphasis should be placed on the examination of the internal energy states of the reaction products together with an investigation of the dependence of the reaction cross section on the internal energy states of the reacting partners. I am afraid, however, that these very worthy objectives are likely to require much diligence over a long time period prior to their attainment.

There are two questions which I would like to pose for Professor Greene:

1. Could he comment a little further on his proposed explanation of the variation of reaction probability with potential energy at the distance of closest approach? In particular, could he explain why these curves exhibit maxima?

2. Is the variation in potassium beam energy, resulting from the finite width of the selector slots, a serious shortcoming in the determination of the effective energy available in the collision system? Would not the effect of the divergence of the CH_3Br beam on the energy available in the center of mass system cause even more serious difficulties in the interpretation of the scattering data?

PROF. E. F. GREENE (*Brown University*): We believe that our curves of P_I and P_{II} vs. $V(y)$ give the general behavior of the actual probability of reaction. The curves are based on two approximations for the scattering curve to be expected in the absence of reaction. The use of these approximations and the existence of relatively large experimental errors in measurements at large angles mean that details of the structure such as the slight fall off at high energies may not be significant. The approximation of the K and CH_3Br velocities by delta function distributions is not likely to make any qualitative change in the conclusions, but a final decision must wait until a more detailed analysis is available.

DR. R. M. FRISTROM (*APL, The Johns Hopkins University*): I wonder if Prof. Greene would comment on what differences there would be in his analysis if the product were detected rather than the reactant and whether this approach would result in any simplifications.

PROF. E. F. GREENE: Measurements of reaction products would have permitted us to make an analysis similar to the one described by Herschbach, Kwei and Norris. However, we would not have been able to deduce the variation of the probability of reaction with impact parameter or potential energy at the distance of closest approach, since this type of analysis depends on a comparison of calculated and observed elastic scattering curves. The two approaches give different sorts of information and one is not necessarily less complex than the other.

DR. T. CARRINGTON (*National Bureau of Standards*): I would like to mention the matter of establishing a connection between the microscopic cross sections for interaction between molecules in specified quantum levels, on the one hand, and, on the other, the macroscopic behavior of chemical systems and the rate equations of conventional chemical kinetics. It is now clear that the "un-averaging" of conventional chemical kinetic rate constants to give detailed cross sections for interaction of molecules in specified quantum states is useless in practical cases. I would like to point out, however, that the reverse process, the averaging of the detailed cross sections to give over-all chemical behavior is also very difficult in cases where there are considerable departures from equilibrium. One must then use the detailed cross sections for molecules in specified quantum levels to calculate the actual distribution of molecules over internal states, and then use these distributions to calculate macroscopic behavior. The point I wish to emphasize is the difficulty of calculating nonequilibrium distributions from the measured detailed cross sections.

PROF. E. F. GREENE: Even though an exact determination of a rate constant from measured cross sections may still be very difficult, this problem is much more likely to be solved than is the reverse one of the determination of cross sections from measurements on rate constants. In addition, some features of the cross section, such as the threshold energy, should lead to a number of helpful deductions about special properties of the rate constant.

ATOMIC FLAME REACTIONS INVOLVING N ATOMS, H ATOMS AND OZONE

D. GARVIN AND H. P. BROIDA

Although no radiation is observable from the fast exothermic reaction

$$N + O_3 \rightarrow NO + O_2$$

the addition of H atoms produces a flame with ultraviolet and visible emission. The emitters in the flames are OH, NH, NO, N_2 and, under certain conditions, NH_2.

The characteristics of this prototype combustion system are:

(a) N atoms, H atoms and O_3 must all be present in the reaction zone.
(b) H atoms catalyze the consumption of ozone beyond that expected from $H + O_3 \rightarrow OH + O_2$.
(c) NO and NO_2 are not important intermediates.
(d) The nitrogen emission (1st positive bands) is not the result of the mechanism operating in the Lewis-Rayleigh nitrogen afterglow.
(e) Vibrationally excited OH radicals are important in the mechanism for forming NH and in the excitation of the emitters.

The rate constant for the reaction $N + OH \rightarrow NO + H$ is estimated to be greater than 10^{-11} cc/molecule-second.

Introduction

Emission spectra of ordinary flames and atomic reactions have long been used for the interpretation of combustion processes and to establish reaction mechanisms. The atomic flame technique in which a "fuel" molecule is reacted with an atom or a free radical has been particularly helpful in isolating elementary steps that occur in the more complex combustion processes and in providing detailed information about very rapid chemical reactions.

After noticing that the low pressure reaction of N atoms and ozone sometimes gave bright reaction zones, we began a more systematic examination of this emission. The reaction is of some interest because the process

$$N + O_3 \rightarrow NO + O_2 \qquad (1)$$

is highly exothermic, $\Delta H = -125$ kcal, and either product might be in an excited state. This energy, if concentrated in NO, could excite the $A\ ^2\Sigma^+$ state, from which the γ bands are emitted, or if concentrated in O_2 could lead to the emission of the Herzberg bands, as suggested by Barth and Kaplan.[1] Thus the reaction is one of a few bimolecular reactions that may serve as the source of chemiluminescence in combustion processes.

The kinetics of this reaction have been determined. It is first order in N and in O_3 and the initial products are as shown in reaction (1). The rate has been measured by Chen and Taylor ($k = 1.6 \times 10^{-14}$ cc/molecule sec)[2] and by Phillips and Schiff ($k = 5.7 \times 10^{-13}$ cc/molecule sec).[3]

One may predict the initial excitation. Both flash photolysis and atomic flame studies have shown that in exothermic reactions in which one atom is transferred there is preferential excitation of the product in which the new bond is formed. Several examples are[4–7]

$$O + NO_2 \rightarrow O_2^\dagger + NO$$

$$H + Cl_2 \rightarrow HCl^\dagger + Cl$$

$$NO + O_3 \rightarrow NO_2^* + O_2 \qquad (2)$$

$$H + O_3 \rightarrow OH^\dagger + O_2^*. \qquad (3)$$

(In these and subsequent equations a dagger (†) indicates vibrational excitation of the ground state and an asterisk (*) electronic excitation.) Thus in reaction (1) we would expect either the production of NO in a high vibrational level or in the $A\ ^2\Sigma^+$ electronic state but very little excitation of O_2.

It has turned out that it is the introduction of H atoms to the $N + O_3$ system that causes visible

flames. We have observed no radiation in the region 2200–7000 Å from N + O_3 without H atoms even when there was significant reaction. Also, H atoms have a markedly catalytic effect on the consumption of ozone. The effect is larger than that due to the H + O_3 reaction. It is observable at the trace impurity level of tank nitrogen and may be made large by deliberate addition of H atoms. Our examination of the published purification procedures used in the two kinetic studies leads us to believe that neither rate determination was made in a system entirely free from hydrogen.

Two different characteristic flames have been observed in mixtures of H atoms, N atoms, and ozone. At pressures below 1.5 mm Hg and with small amounts of H atoms and ozone a pink brush, filling a volume of 3 to 5 cc forms. With more hydrogen present and also at higher pressures (up to 10 mm Hg) a relatively bright white flame is found with a rather sharp zone no larger than 0.3 to 0.4 cc in volume. An intermediate regime can be established with a white flame surrounded by a pink halo.

In the spectral region from 2200 Å to 8900 Å the pink brush shows relatively strong emission from the 1st positive bands of N_2, including emission from $v' > 12$ and from the 3360 Å bands of NH. In addition there is weaker emission from the ultraviolet OH, the NO β and γ bands and, the 3240 Å NH system. The white flame is considerably brighter and shows the same emission systems plus strong emission from NH_2 (the α bands of ammonia)[8,9] and weak emission from the OH vibration–rotation bands. Moreover, the ultraviolet OH in the white flame is strong, as is NH. Except for the presence of N_2 1st positive and OH vibration bands, the white flame has a spectrum similar to the ammonia-oxygen atmospheric pressure flame[8] and the hydrazine O atom reaction.[10]

We have tested this system under various flow and pressure conditions and have examined a number of other atomic reactions that might be related to it. Our conclusions may be summarized as follows:

(a) N atoms, H atoms, and O_3 must all be present in the reaction zone.

(b) H atoms catalyze the rate of consumption of ozone.

(c) O atoms do not promote the phenomena we have observed.

(d) NO and NO_2 are not important intermediates (in macroscopic amounts).

(e) Vibrationally excited OH plays an important role.

(f) The first positive bands of nitrogen are not the result of the mechanism producing these bands in active nitrogen.

The experiments are described below and the discussion of likely steps in the mechanism is given.

Experimental

Reactor and Reagents

A low pressure (0.4 to 10 mm Hg) moderate throughput (5 to 15 cc/sec, STP) kinetic vacuum system was used. The reactor in which the reagents were mixed (Fig. 1) was constructed of Pyrex glass 25 mm in diameter and 150 mm long. It was fitted with quartz windows and two side arms each of which had a port (D) for admitting streams of partly atomized gas and nozzle (N) of adjustable length for ozone and other gases. Either pure or mixed gases could be supplied to any of these entry ports. The reagent gases, after purification and metering at pressures slightly above atmospheric, entered the glass system via stainless steel or nylon control valves. Stopcocks and semi-ball joints in the vacuum system were lubricated with "Apiezon" grease. The gas flow and purification system was glass and copper or stainless steel tubing (in the case of oxygen). Bourdon gages were used for pressure measurements with the exception that a Hg manometer was used for NO.

Tank oxygen (<1.5% N_2 + A) and nitrogen (<0.1% O_2 + A) were dried by passage through beds of calcium chloride, Ascarite (sodium hydroxide on asbestos), and magnesium perchlorate. Tank hydrogen was freed from oxygen by a "Deoxo" catalytic unit and dried as above. Tank nitric oxide was passed through a dry-ice-cooled trap prior to use. Nitrogen dioxide was prepared from nitric oxide and excess oxygen. The product used formed colorless crystals at 77°K. Ozone (less than 3% in oxygen) was made from purified oxygen in a Siemens type Pyrex ozonizer powered by a 25 kv transformer. For the studies of the N + O_3 reaction it was necessary to reduce further the residual impurities in the nitrogen with a liquid-nitrogen-cooled glass spiral in the low pressure system upstream of the discharge region. Nitrogen, oxygen, and hydrogen atoms were produced by passing these gases through an electrodeless discharge powered by a 24.5 kmc microwave generator. In all cases the discharged gases flowed more than 15 cm beyond the discharge region before reaching the mixing region in the reactor. At this point both nitrogen and oxygen showed only their typical afterglow emission and none of the spectral characteristics associated with the discharge.

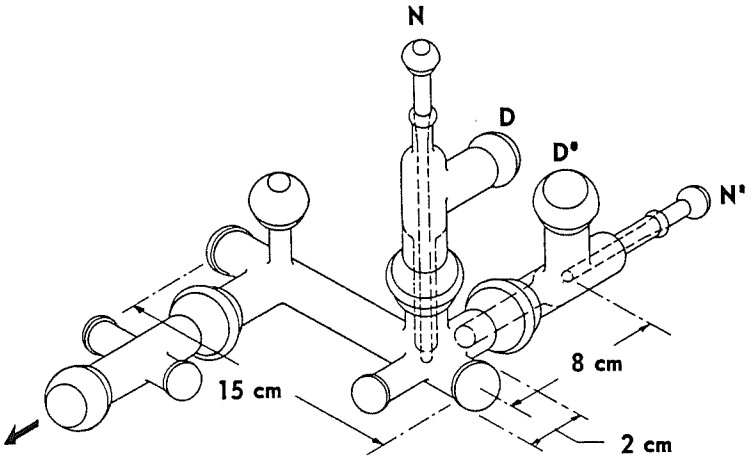

FIG. 1. Reactor for the low pressure H + N + O_3 and related reactions.

Spectrographic Arrangements

Several different spectroscopic instruments were used covering the region from 2200 to 8900 Å. Light absorption in the reactor was measured with an $f/8$ Ebert-Fastie[11] double pass monochromator using a Hg light source at 2537 Å for ozone and a low pressure discharge in air for detecting the NO (0, 0) γ-band at 2269 Å. Emission from the atomic flames was surveyed from 2200–7000 Å with the same instrument. Photographic spectra were obtained with an $f/4$ Cornu-type spectrograph with glass and quartz optics over the same range and with an $f/1.5$ Bass-Kessler[12] grating instrument from 4000–8900 Å. A limited range (4000–5000 Å) was photographed with a slower $f/12$ Cornu spectrograph (glass optics) in order to bring out more detail in some of the spectra. Several visible region spectrograms of very weak sources also were taken with an $f/0.8$ Auroral transmission grating spectrograph. Eastman Kodak films and plates Types 103aO, 103aF, and I–N were used.

Results

The characteristics of the three most closely related systems we have studied are described immediately below. Then details of the spectrographic analyses of the H + N + O_3 system are given, followed by a summary of the other diagnostic tests.

N + O_3

Active nitrogen produced from prepurified nitrogen (passed through a trap at 77°K) partially decomposed ozone but produced no emission spectra, other than the typical Lewis–Rayleigh active nitrogen afterglow (Fig. 3a), over the entire range studied. However, when water-pumped nitrogen was used for atom production a faint white emission zone, with an outer pink border, was observed at the end of the ozone nozzle. Purification of the nitrogen by trapping at 77°K eliminated the flame zone.

H + N + O_3

The weak white and pink emission noted above could be made much more intense by the addition of hydrogen atoms. Either the addition of hydrogen to the nitrogen before passage through the discharge or the separate addition of active (N atoms) nitrogen and active (H atoms) hydrogen to the reactor served the purpose. The appearance of the emission was markedly dependent upon the mixture ratios and upon the sequence of mixing. Two cases will serve as illustrations.

(a) When active nitrogen (6.0 cc/sec) and a trace of ozonized oxygen (0.1 cc/sec) were mixed in the horizontal side tube via D′ and N′ (Fig. 1) and then this mixture met a moderate flow of active hydrogen (0.45 cc/sec) from the vertical entry port, D, a bright pink brush was formed, extending out from the horizontal port. An increase in the hydrogen flow (or an increase in the power supplied to the hydrogen discharge unit) restricted the size of the brush. Further increase of H changed the color to white and restricted the emission to a conical region at the entry port. The pink brush could be obtained at pressures from 0.8 to 1.5 mm Hg and was brightest near 1.0 mm Hg.

(b) When mixed N_2 (5.6 cc/sec) and H_2 (0.25 cc/sec) passed through a discharge, D, and then encountered a coaxial flow of ozonized

TABLE 1

Consumption of Ozone

Flows (cc/sec, STP)			Pressure	$\Delta[O_3]$ (arbitrary units)		
H_2	N_2	O_2	(mm Hg)	$H + O_3$	$N + O_3$	White flame
0.23	4.7	2.45	1.8	7.4	7	35
0.20	4.7	2.45	1.8	6	5	36
0.84	4.7	2.45	1.8	25	11	40
1.77	8.1	4.6	2.3	13	0	27
0.21	8.1	4.6	5.0	4	19	80

oxygen (1.75 cc/sec) from nozzle N, the emission appeared white. Increase of the hydrogen content of the gas caused an intensity increase and a simultaneous contraction of this white flame. When hydrogen was varied from the trace level upward a progression from a pink emission to a pink bordered white flame to a well-defined white pencil-like flame was observed. White flames were obtained at pressures from 0.4 to 10 mm Hg and were brightest near 2 mm Hg.

$H + O_3$

This system, which produces vibrationally excited OH,[7] showed a dull red emission when H and O_3 were mixed coaxially. If this flame was first established on the vertical nozzle with a molecular nitrogen flow in from the side, and then the nitrogen was atomized, a white flame of roughly the same size replaced the red.

The sizes of the flame zones of either the red $H + O_3$ or the white $N + H + O_3$ reactions were pressure dependent. At pressures greater than about 2 mm Hg the flame zone became sharp and appeared somewhat like a Bunsen cone but at lower pressure the flame zone was quite diffuse. We interpret the above effects to mean that H atom diffusion controls the size of the reaction zone, that the $H + O_3$ (dull red) and $H + O_3 +$ N (white) processes are of comparable speed while the pink process is an order of magnitude slower.

Absorption Studies

Production of NO. In neither the $N + O_3$ nor the $H + N + O_3$ reaction was sufficient NO absorption found in a 15 cm path to permit photometry. The limit of sensitivity of our instrument for this path length was about 1 micron pressure of NO.

Consumption of O_3. The reagents were mixed together in the horizontal side tube using a short nozzle, while the absorption was measured in the main reactor. Total flows were maintained constant by admitting the nonatomized reagent through the vertical entry port. The ozone consumption is shown in Table 1. In each case the amount consumed in the $H + N + O_3$ flame exceeds the sum of the ozone disappearing in the individual cases. Coupled with the fact that the effective contact time prior to observation is shorter for the mixed system, this indicates catalysis of ozone consumption in the mixed system. Viewed as H atom catalysis of $N + O_3$, the effect is large. The mixing regime used in the absorption studies of $N + O_3$ was the same as that used for the pink brush emission. This shows the presence of ozone in the reaction zone of the latter.

Emission Spectra

Both similarities and marked differences occur in the emission spectra of the pink brush and white flame variants of the $H + N + O_3$ reaction. Their spectra are shown in Figs. 2 and 3 along with pertinent comparison spectra.

Briefly, the characteristics of the emissions are these. Both have essentially the same spectrum below 4000 Å: $NO\gamma(A\,^2\Sigma_u^+ \rightarrow X\,^2\Pi)$ and $\beta(B\,^2\Pi \rightarrow X\,^2\Pi)$ bands, $OH(^2\Sigma \rightarrow X\,^2\Pi)$ and $NH(^3\Pi \rightarrow {}^3\Sigma,\ c\,^2\Pi \rightarrow a\,^1\Delta)$. In the visible and near infrared region the pink brush shows only the N_2 first positive $(B\,^3\Pi \rightarrow A\,^3\Sigma_u^+)$ band while the white flame shows extensive NH_2 bands (α bands of ammonia), N_2 first positive bands and, weakly, several OH vibration–rotation bands. Details are discussed below.

In the ultraviolet region the pink brush was five or more times weaker than the white flame at comparable pressures based on NH emission. These relative intensities correlate with the ozone flows for the particular cases compared, but, generally less hydrogen and less ozone were needed for the pink brush than for the white

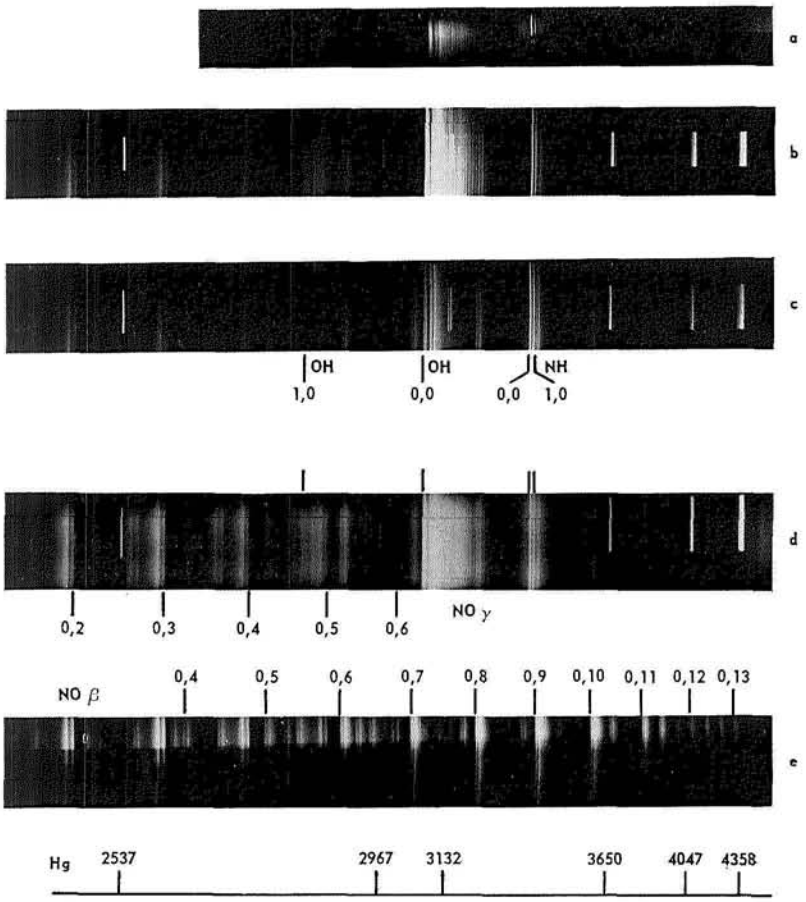

FIG. 2. Ultraviolet emission spectra. Except for (a) all spectra were taken on an $f/4$ Quartz Cornu Spectrograph using 103aO plates. (a) Ammonia–oxygen atmospheric pressure flame 103aF plate $f/12$ Quartz Cornu spectrograph. (b) H + N + O_3 white flame, 1.8 mm Hg, 103aO, 10 min exposure, 12 μ slit. (c) H + N + O_3 pink brush, 1.8 mm Hg, 45 min for comparison with (b). (d) H + N + O_3 white flame with pink border, 2 mm Hg, 7 min exposure, 30 μ slit. (e) NO emission bands from N + O, 2.2 mm Hg, 30 μ slit.

flame. The NO β bands were slightly more intense compared to NH in the pink brush than in the white flame while OH and the NOγ bands were weaker by factors of 5 and 2, respectively. Both NO band sequences are moderately strong in the white flame with the γ bands predominating at low pressure, <1 mm Hg, while above 3 mm Hg, the β bands become of comparable intensity.

The rotational intensity distribution of OH in the white flame was analyzed from photometric records. It is similar to that in a nonequilibrium hydrocarbon flame at 3000°K or to that in the H + O_3 reaction.[13] The rotational distribution changes only slightly with pressure increase, the higher levels having lower populations. NH shows a vibrational "temperature" exceeding the ammonia-oxygen atmospheric pressure flame and a nonequilibrium rotational distribution which populates high rotational levels.

In the visible and near infrared region the pink brush had the simpler spectrum. The N_2 first positive bands are extensive, each band having, qualitatively, a rotational distribution similar to that found in active nitrogen. That these bands are not merely those of the active nitrogen used in the experiments is apparent upon comparing Figs. 3a and 3c. The vibrational distributions in the upper state are different. Neither the intensity maxima at $v' = 11$ in active nitrogen are present, nor is the 6–3 band of abnormal intensity. In addition, faint bands originating in $v' > 12$ are present, i.e., at 5210 Å and 5185 Å corre-

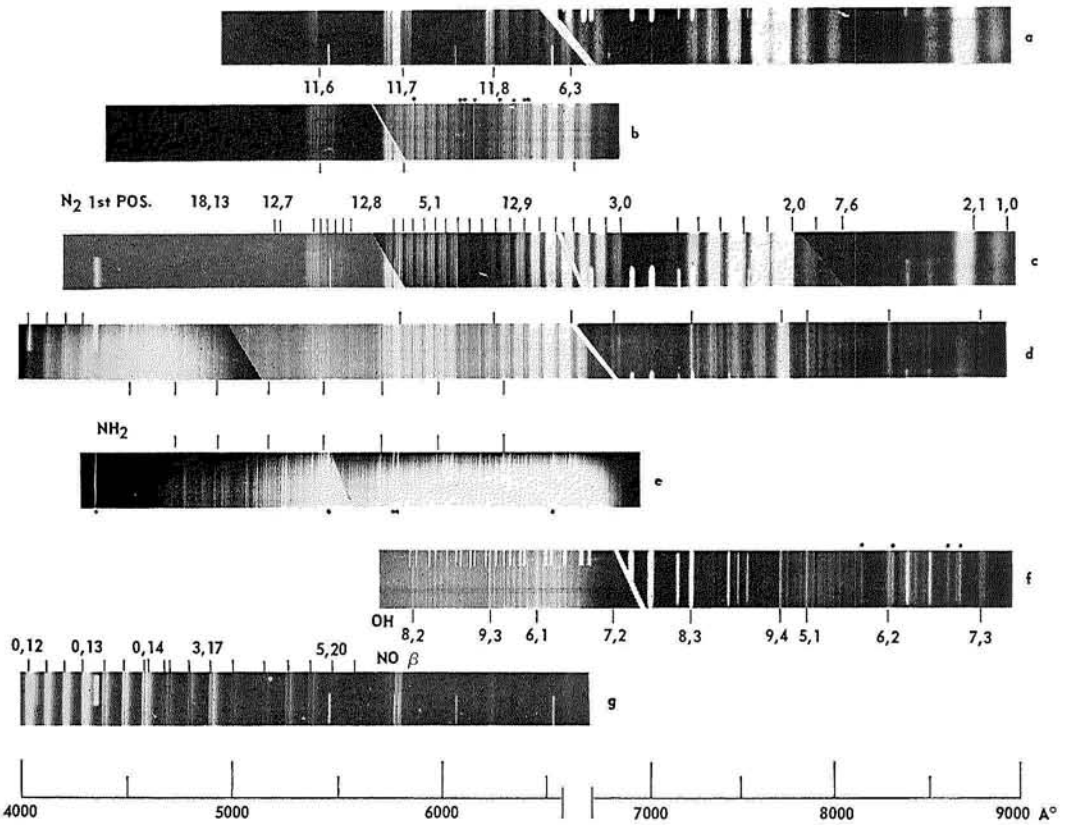

FIG. 3. Visible and near infrared emission spectra. All spectra taken on film with a $f/1.5$ Bass–Kessler Grating spectrograph. Above 6500 Å the first order was used; the rest are second order. Typical slit width was 20 μ but throughout the resolving power is limited by the emulsions. Comparison of intensities is feasible only for individual strips in the composite photographs. Spectral "cutoffs" at short and long wavelengths are due to exposure time, emulsion sensitivity, and filters except for (c) and (d). Obscure reference lines are indicated by dots. (a) Active nitrogen 10 mm Hg. Hg and Ne reference spectra. (b) Discharge through nitrogen, Ne reference spectrum. (c) H + N + O_3 pink brush. (d) H + N + O_3 white flame. (e) Ammonia–oxygen atmospheric pressure flame. (f) H + O_3 atomic flame. (g) Blue glow from N + O recombination.

sponding to 17,12 (5214 Å) and 18,13 (5184 Å).[14] The closest comparison is with the discharge through nitrogen (Fig. 3b) or the pink nitrogen afterglow.[15] We conclude that these bands are not a result of the reaction sequence in the usual active nitrogen afterglow.[16]

The most prominent visible feature of the white flame was the spectrum of NH_2. From 4300–5700 Å the correspondence with the ammonia–oxygen flame is striking (Figs. 3d and 3e). These bands extend farther into the red, but are less prominent than in the ammonia flame and are overlaid by weak N_2 first positive and by weak OH vibration–rotation bands. The OH bands are those expected from the H + O_3 reaction, with a similar non-equilibrium vibrational population distribution and a similar low rotational "temperature." [13] In comparative experiments the OH vibration–rotation band intensities were similar in the H + O_3 and H + N + O_3 flames. In the latter system the intensities paralleled the hydrogen content of the gas passed through the discharge.

The N_2 first positive bands in the white flame, as in the pink brush, did not show the same vibrational population distribution as does active nitrogen. Here again, emission from levels with $v' > 12$ probably occurs but because of the overlapping NH_2 bands the identification is uncertain. The vibrational distribution was somewhat similar to that of the pink brush with some indication of a superposition of active nitrogen. The rotational distribution seems to be markedly different from that in any of the comparison spectra. The long wavelength head, P_1, is weaker compared to the next (P_2) and the characteristic head near the middle of the band (Q_3) is sup-

pressed. Although the relative intensities are confused by the NH_2 spectrum in the same region the general appearance of these bands is consistent with a higher rotational temperature than in the discharge.

The relative intensities of the vibration–rotation bands of OH and its electronic bands merit mention. An earlier study[13] showed that the electronic bands vary in intensity with the square of the vibration–rotation band intensities. In a comparison using the 8–2 head (5870 Å) and the $^2\Sigma$–$^2\Pi$ Q head (3090 Å), a twofold increase (maximum) occurred in the vibration–rotation bands when N atoms were added to the H + O_3 flame while a 30-fold increase occurred in the electronic band. Clearly the H + O_3 reaction is not the major cause of the ultraviolet OH emission in the H + N + O_3 flame.

Tests of Other Systems

Oxygen Atoms

When O atoms were added to mixed N and H atoms the emission changed from that of active nitrogen to a blue glow (NO β and γ bands) which is associated with[17]

$$O + N + M \rightarrow NO^* + M \qquad (4)$$

and then to the green–white air afterglow attributed to the excited nitrogen dioxide formed in[18]

$$O + NO + M \rightarrow NO_2^* + M. \qquad (5)$$

No flame zones were formed. (Here and below third bodies are shown in recombination reactions. The three-body reactions probably are the predominate sources of product, but those products that emit may be formed in the competing two-body reaction.)

Nitric Oxide

NO is an expected product of N + O_3, but, although present in at least trace amounts in the pink and white flames, it does not appear to be a necessary intermediate. Coaxially mixed H + NO produced a red flame showing only the HNO bands. Other work has shown this to be a result of the primary reaction.[19,20]

$$H + NO + M \rightarrow HNO + M \qquad (6)$$

Addition of N atoms superimposed the air afterglow on this flame. The mechanism is[17]

$$N + NO \rightarrow N_2 + O \qquad (7)$$

followed by reaction (5). The H + NO reaction either with or without N atoms did not show any ultraviolet emission. In all probability, reaction (7), which is very fast, accounts for our failure to observe NO in absorption in the N + O_3 reaction.

NO + O_3 formed a dull red flame above 6 mm Hg. This emission has been shown[6] to be due to NO_2 formed in the reaction

$$NO + O_3 \rightarrow NO_2^* + O_2 \qquad (2)$$

Addition of H or N superimposed the air afterglow on the red flame but did not form a white flame.

Nitrogen Dioxide

The reaction of H atoms, with nitrogen dioxide[21,23]

$$H + NO_2 \rightarrow OH + NO \qquad (8)$$

produced no ultraviolet emission. Weak visible emission due to reaction (6) was found. The air afterglow also appeared when either the H atom concentration was high [reaction (5)] or when a large excess of NO_2 was used. This has been explained[22,23] in terms of

$$OH + OH \rightarrow H_2O + O \qquad (9)$$

followed by (5).

The systems H + N + NO_2 shows the same color changes as O + H + N and N + NO. Here the initial reaction probably is the formation of NO:

$$N + NO_2 \rightarrow NO + NO$$

The addition of O_3 to H + NO_2 also produced the air afterglow.

Well-defined flames were not formed in these NO_2 tests. This is interpreted to mean that the OH radicals produced in (8) do not support the "white" or "pink" H + N + O_3 flames. These OH radicals have been shown to be predominately in the $v = 0$ level of the ground state.[23]

Ozone

Several experiments on the H + O_3 system are pertinent. An H + O_3 red flame [reaction (3)] was established on the vertical nozzle (N, Fig. 1). A mixture of O_2 and N_2 passed through the horizontal discharge at (D') and into the reactor. When N atoms were present, as seen by either the active nitrogen or the blue NO glow [reaction (4)] the usual white flame was formed. When the air afterglow [reaction (5)] issued from (D′) the white flame vanished but the H + O_3 emission remained. The change was coincident with the appearance of the air afterglow. Oxygen atoms (and a trace of NO) are

present in the air afterglow but N atoms are not. We interpret these results to mean that N atoms are essential for the white flame and that neither O atoms nor trace quantities of NO interfere with it, or with the H + O_3 reaction. [Large quantities of NO, however, quenched the H + O_3 emission, replacing it with an air afterglow, probably by competition for H atoms and reaction (6) followed by (5).] The addition of NO_2 to a H + O_3 flame also quenched it for the same reason.

On the other hand, when a H + O_3 flame was established on nozzle (N′) in the side tube and the products then flowed to meet N atoms from (D) no flame occurred. This is interpreted to mean that the vibrationally excited OH produced in (3) are required in the pink and white flames. They must be formed *in situ* because they are quenched, on the average, in about 300 collisions.[24]

Ammonia and Hydrazine

Ammonia had little effect on a H + O_3 flame. Ammonia after passage through a discharge reduced the NH emission of a white flame while N + NH_3 showed little if any emission in the NH region. The flame of O atoms with hydrazine is known to produce NH, OH, NO, and NH_2 radiation,[10] but in our tests these emissions were weak compared to the white flame. Ozonized oxygen weakened the emission, possibly by dilution. The color of the well-defined flame is tan, or dirty yellow, like the ammonia–oxygen atmospheric pressure flame. The atmospheric NH_3–O_2 flame gave a spectrum very much like the white flame except that NO β and γ bands are very weak and the N_2 1st positive bands are not observed. Moreover, the rotational distribution for OH in the ammonia–oxygen flame is nearly thermal.[25] The reaction N + N_2H_4 produced no NH or other emission.

Discussion

Our main conclusions concerning the H + N + O_3 system have been summarized in the introduction. The bases for these have been stated in the presentation of the experimental results. We attempt here to interpret these conclusions in terms of likely elementary reactions.

Of prime importance are (a) the necessity for H + N + O_3 to be present in the reaction zone (or N + $OH^\dagger$) and (b) the catalytic effect of H atoms. The following sequence accounts for this by

$$H + O_3 \rightarrow OH^\dagger + O_2^*$$

$$k \geq 4 \times 10^{-12} \text{ cc/molecule sec} \qquad (3)[24]$$

$$N + OH \rightarrow NO + H \qquad (10)$$

providing a two-step catalytic cycle. The disappearance of NO and further production of H atoms are provided by

$$N + NO \rightarrow N_2O + O$$

$$k = 2.2 \times 10^{-11} \text{ cc/molecule sec} \qquad (7)[3]$$

$$O + OH \rightarrow O_2 + H$$

$$k = 3.3 \times 10^{-11} \text{ cc/molecule sec} \qquad (11)[22,23]$$

$$OH + OH \rightarrow H_2O + O$$

$$k = 2.5 \times 10^{-12} \text{ cc/molecule sec} \qquad (9)[23]$$

The rapid reactions (3), (7), (9), and (11) are two to three orders of magnitude faster than

$$N + O_3 \rightarrow NO + O_2 \qquad (1)$$

They are all sufficiently rapid to be consistent with the small sizes of the reaction zones observed here. Thus, for reaction (10) to be effective its rate constant must be of the order of $k_{10} = 10^{-11}$ cc/molecule-sec.

The reaction sequence above accounts for the negative results in the NO absorption studies [reaction (7)]. It also explains why the process is limited by the ozone supply as was found experimentally.

However it does not account for most of the emission bands. This is a common flaw in mechanisms for chemiluminescent flames. The main problem is to find reactions that are sufficiently exothermic to provide the excitation. Even the type of reaction is in question because of the limitations of emission spectroscopy. The reason is that it is not possible to tell whether the species that show nonequilibrium vibrational and rotational population distributions are formed directly in their excited electronic states or are formed in the ground state and are subsequently excited.

A particularly apt statement of this problem has been made by Wolfhard and Parker.[26] They suggested that all elementary reactions in combustion processes perturb the Maxwell-Boltzmann distribution, but whether or not these perturbations are observed depends on the reaction velocities and the temperature, i.e., on the time scale of the subsequent processes.

The problem is very troublesome when the excited species are present only in trace amounts, as is true here, but also remains when the emitters are major products. Only a combination of absorption spectroscopy (where possible) and emission studies would permit a decision between the two possible excitation routes.

We have not found suitable specific reactions for forming OH, NH, and NH_2 in their excited states. Several possible cases have been rejected.

The reaction

$$OH^{\dagger} + OH^{\dagger} \rightarrow OH^{*} + OH$$

has been shown to be too slow to account for the amount of OH* observed. The analogous reaction for NH would not be expected to be more efficient. The process

$$O + N + M \rightarrow NO^{*} + M \qquad (4)$$

is also too slow, being a three-body reaction, to serve in the white flame although it may contribute to the pink brush emission. Also, the reaction

$$N + H_2 + M \rightarrow NH_2^{*} + M \qquad \Delta H = -74 \text{ kcal}$$

may be ruled out for the same reason and because it is not observed in $N + H_2$ mixtures.

Thus we suggest that it is more likely that these species are formed in their ground states and then are excited. In our system the principal energy source is the recombination of nitrogen atoms. Either of these processes may apply

$$N + N + X \rightarrow N_2 + X^{*} \qquad (12)$$

or

$$N_2^{*\dagger} + X \rightarrow N_2 + X^{*} \qquad (13)$$

where $N_2^{*\dagger}$ represents any of the excited nitrogen molecules formed in the atom recombination, and X any of the species to be excited. The final reaction (13) should be favored slightly over (12) since these $N_2^{*\dagger}$ molecules need not be formed solely in the reaction zone but may come from the N atom recombination at all points downstream of the discharge in which atoms are formed.

Reactions (12) and (13) imply the formation of ground state NH in our system. Since this molecule has been observed (in emission) only when O_3 is present [and reaction (3) can occur], it may be formed by

$$N + OH^{\dagger} \rightarrow NH + O \qquad \Delta H = 14 - E \text{ kcal} \qquad (14)$$

where E represents the vibrational excitation of OH. For a thermally neutral or exothermic reaction E corresponds to OH in $v \geq 2$. Such excitation is readily available from reaction (3), but has not been observed in the $H + NO_2$ reaction. This is consistent with an absence of NH emission in our $N + H + NO_2$ studies. Reaction (14) would be likely to have a rate comparable to (10), the conversion being limited by the concentration of excited OH. Also, it could easily occur in high temperature processes where mildly excited OH could be present due to other processes or thermal excitation.

Experimentally the N_2 first positive bands in the pink brush also depend on the presence of ozone. Here a specific excitation process may apply

$$N\,(^4S) + N\,(^4S) + OH^{\dagger} \rightarrow N_2\,B(^3\Pi, v > 12) + OH. \qquad (15)$$

OH in $v' \geq 6$ would be sufficiently energetic to provide the maximum excitation. The third order nature of reaction (15) also is consistent with the pink brush reaction zone being larger than the white flame.

The essential feature of these excitation reactions (13, 15) is that a large amount of energy is transferred from one excited species to another. This implies a strong interaction or, in the language of chemical kinetics, a "sticky collision." The nonequilibrium populations observed for the upper states may be produced in these strong interactions, rather than be due to the specific exothermic chemical reactions that form the species in their ground states. Indeed, the study[13] of $H + O_3$ in which the OH* has been shown to have an entirely different rotational population distribution than the $OH^{\dagger}$ bears out this contention. The effect may be common and suggests that a search for specific excitation mechanisms must continue to be a major facet of the study of radiation from flames and other combustion processes.

Acknowledgments

We are indebted to Professor Schiff and to Dr. Clyne for making available to us information on their research prior to publication.

References

1. Barth, C. A. and Kaplan, J.: J. Chem. Phys. *26*, 506 (1957).
2. Chen, M. C. and Taylor, H. A.: J. Chem. Phys. *34*, 1344 (1961).
3. Phillips, L. F. and Schiff, H. I.: J. Chem. Phys. *36*, 1509 (1962).
4. Basco, N. and Norrish, R. G. W.: Can. J. Chem. *38*, 1769 (1960).
5. Cashion, J. K. and Polanyi, J. C.: Proc. Roy. Soc. (London) *A258*, 529 (1960).
6. Greaves, J. C. and Garvin, D.: J. Chem. Phys. *30*, 348 (1959).
7. Garvin, D.: J. Am. Chem. Soc. *81*, 3173 (1959); Garvin, D., Kostkowski, H. J., and Broida, H. P.: J. Chem. Phys. *32*, 880 (1960).
8. Rimmer, W. B.: Proc. Roy. Soc. (London) *A103*, 696 (1923).
9. Dressler, K. and Ramsay, D. A.: Phil. Trans. Roy. Soc. London *A251*, 553 (1959).
10. Moore, G. E., Shuler, K. E., Silverman, S.,

and HERMAN, R. C.: J. Phys. Chem. *60*, 813 (1956).
11. FASTIE, W. G.: J. Opt. Soc. Am. *42*, 641 (1952).
12. BASS, A. M. and KESSLER, K. G.: J. Opt. Soc. Am. *49*, 1223 (1959).
13. BROIDA, H. P.: J. Chem. Phys. *36*, 444 (1962).
14. TANAKA, Y. and JURSA, A. S.: J. Opt. Soc. Am. *51*, 1239 (1961).
15. BEALE, G. E., JR. and BROIDA, H. P.: J. Chem. Phys. *31*, 1030 (1959).
16. BAYES, K. D. and KISTIAKOWSKY, G. B.: J. Chem. Phys. *32*, 992 (1960).
17. KISTIAKOWSKY, G. B. and VOLPI, G. G.: J. Chem. Phys. *27*, 1141 (1957).
18. BROIDA, H. P., SCHIFF, H. I., and SUGDEN, T. M.: Trans. Faraday Soc. *57*, 259 (1961).
19. CASHION, J. K. and POLANYI, J. C.: J. Chem. Phys *30*, 317 (1959).
20. CLYNE, M. A. A. and THRUSH, B. A.: Discussions Faraday Soc. *33*, 139 (1962).
21. CLYNE, M. A. A. and THRUSH, B. A.: Trans. Faraday Soc. *57*, 2176 (1961).
22. CLYNE, M. A. A.: This volume, p. 211.
23. DEL GRECO, P. and KAUFMAN, F.: Discussions Faraday Soc. *33*, 128 (1962).
24. GARVIN, D. and MCKINLEY, J. D.: J. Chem. Phys. *24*, 1256 (1956).
25. GAYDON, A. G.: *The Spectroscopy of Flames*, p. 214. Chapman and Hall, 1957.
26. WOLFHARD, H. G. and PARKER, W. G.: *Fifth Symposium (International) on Combustion*, p. 718. Reinhold, 1955.

Discussion

DR. M. A. A. CLYNE (*University of Cambridge*): This paper poses the interesting problem of distinguishing emission by electronically excited molecules formed by third order combination processes from emission due to molecules produced by subsequent excitation of ground state molecules. In this work, the "pink brush" and "white flame" emission depend upon the simultaneous presence of N, H, and O_3 (or OH). The fairly rapid reaction (9),

$$OH + OH \rightarrow H_2O + O \qquad (9)$$

is the process responsible for removal of active species, and the size of the reaction zone is determined by the rate of this reaction (9). The emission of chemiluminescent phenomena occurs only within the reaction zone. However, one cannot therefore exclude on the grounds of their slowness a possible contribution to the emissions by third order combination processes (involving O, N, H or OH) which lead directly to the formation of electronically excited molecules. This is because removal of emission precursors is controlled not by the rate of the third order processes concerned but by the much more rapid reaction (9). It seems possible therefore that the NO γ ($A\,^2\Sigma_u^+ \rightarrow X\,^2\Pi$) and β ($B\,^2\Pi \rightarrow X\,^2\Pi$) bands observed in the white flame and pink brush are due to the formation of excited NO* molecules in the third order process (4),

$$N + O + M \rightarrow NO^* + M \qquad (4)$$

Guenebaut, Pannetier, and Goudmand[1] have observed the NH ($^3\Pi \rightarrow {}^3\Sigma$) emission band at 3360 A with moderate intensity in the reaction of N with H,

$$N + H + M \rightarrow NH^* + M,$$

and it may be that this reaction is a source of the NH emission observed in the present work. The authors suggest that ground state NH may be produced in the reaction of N with vibrationally excited ground state $OH^\dagger$,

$$N + OH^\dagger \rightarrow NH + O \quad E - 14 \text{ kcal/mole.}$$

NH* is then formed by excitation of this NH radical. However, the fact that products of the $H + O_3$ reaction do not give a flame with atomic nitrogen does not prove that vibrationally excited hydroxyl are necessary for the emission, since the concentration of OH would be expected to be near zero at the point of addition of nitrogen atoms on account of the rapid reaction (9).

The observations on ozone removal in the presence of N and H give clear support for the postulated mechanism, involving the regeneration of hydrogen atoms in a rapid chain process. The reaction

$$OH + H_2 \rightarrow H_2O + H \qquad (15)$$

should also be included in the chain reaction scheme, since its rate is quite appreciable even at 293°K.[2,3] I think it might be useful if the authors can indicate the approximate ambient temperatures of the $N + O_3$, $H + O_3$, and $N + H + O_3$ systems. The reason for this suggestion is that the occurrence of rather exothermic reactions in a short reaction zone could lead to a higher temperature for $H + N + O_3$ than for either $H + O_3$ or $N + O_3$. Reactions (1), (3), or (15) could have an activation energy of one or two kcal/mole, and an increase of temperature of a few tens of degrees could increase the reaction rate appreciably. More O_3 would then be consumed in $N + H + O_3$ than in the $H + O_3$ and $N + O_3$ systems together.

REFERENCES

1. GUENEBAUT, H., PANNETIER, G., and GOUDMAND, P.: J. de Chim. Physique *58*, 513 (1961).

2. CLYNE, M. A. A. and THRUSH, B. A.: Discussions Faraday Soc. *33*, 139 (1962).
3. DEL GRECO, F. P. and KAUFMAN, F.: Discussions Faraday Soc. *33*, 128 (1962).

DR. D. GARVIN (*National Bureau of Standards*): Dr. Clyne has made many worthwhile points that deserve consideration. I agree that the experiments with premixed H + O_3 do not show the importance of $OH^{\ddagger}$. They do show the need for OH. However, experiments in which OH was produced by H + $NO_2 \rightarrow$ OH + NO showed no excitation such as we have observed. Since the H + NO_2 reaction does not form excited OH, the two sets of experiments show the need for excited OH.

The ambient temperatures are unknown. Spectra suggest that they are low and similar for H + O_3 and the "pink" H + N + O_3. The evidence is that the OH rotational "temperatures" in the infrared bands are less than 450°K. Also the N_2 first positive bands have "low" temperature structures. The "white" flame, on the other hand, may be a high temperature phenomena.

I do not agree with the idea expressed by Dr. Clyne that three-body reactions are the primary means of excitation. The problem is this: our reaction zones are small, gas residence times are 1–5 milliseconds, while the three-body reactions would have 0.5–10 second half-lives in our system. This means that the intensity of radiation due to the three-body reactions would be very low.

DR. A. FONTIJN (*AeroChem Research Laboratories*): I would like to suggest a mechanism which could explain the formation of N_2 ($B\ ^3\Pi\ v > 12$) and which, contrary to reaction (14), fits into the mechanism of the usual nitrogen afterglow as given by Kistiakowsky and co-workers. The part of this mechanism, pertinent to this discussion is:

$$N\ (^4S) + N\ (^4S) + M \rightleftharpoons N_2\ (^5\Sigma) + M \qquad (A)$$

$$N_2\ (^5\Sigma) + M \rightarrow N_2\ (B\ ^3\Pi\ v = 12, 11, 10) + M \qquad (B)$$

Reaction (B) is a radiationless collision induced transition. If reaction (B) occurs with an excited OH radical, then it is conceivable that the $B\ ^3\Pi$ state gets formed with more than 12 vibrational quanta which is the number corresponding to the cross-over of the $^5\Sigma$ and $B\ ^3\Pi$ potential energy curves.

DR. D. GARVIN: I am in agreement with Dr. Fontijn's suggestion on the formation of excited nitrogen. Two reactions in sequence are entirely reasonable. The main point is that the source of the excitation energy is a very specific one

DR. R. REEVES and PROF. P. HARTECK (*Rensselaer Polytechnical Institute*): Some pictures of the reaction of active nitrogen atoms with ozone have been made in our laboratory. We have also observed a pink emission at the interface between the ozone and nitrogen stream as they come together. A photograph shows three different emission regions, one yellow for the nitrogen afterglow, an interface pink, and a third in blue is due to be the NO B-bands. Using a filter to eliminate the red and yellow, we observed the green portion of the emission from the nitrogen afterglow and the blue of the nitric oxide emission, but the interface was dark. We attributed this to mean that the pink was probably coming from the interaction which would quench the nitrogen afterflow. This isolated pink zone is only obtained under the appropriate physical arrangement. The spectral results which were not anywhere near as refined as those of Garvin and Broida, indicated emission of the sixth vibrational level of the nitrogen $B\ ^3\Pi g$ state causing the pink and therefore we thought the following mechanism was probable:

$$N_2\ (^5\Sigma_g^+) + O_3 \rightarrow N_2\ (B\ ^3\Pi g_{v=6}) + O_2 + O$$

The reaction of N + O_3 can yield an electronically excited O_2 molecule. We have observed the Herzberg emission from this molecule produced by surface catalysis where a trace of H atoms can yield the OH molecule electronically excited, via:

$$O_2\ (A\ ^3\Sigma_u^+) + H\ (^2S) \rightarrow OH\ (^2\Sigma) + O\ (^3P)$$

This could also be the origin of the OH electronically excited species in this case.

DR. D. GARVIN: The suggestions made by Reeves and Harteck concerning N_2 + O_3 are reasonable. We have not observed this effect which merely means that, in our system, the effect was slight compared to the one we studied. The suggestion that OH ($^2\Sigma$) is formed from $O_2\ A(^3\Sigma_u^+)$ is one with which I find it hard to agree. I cannot devise an efficient process for the formation of the excited oxygen.

A KINETIC STUDY OF HYDROCARBON–OXYGEN–NITROGEN FLAME SYSTEMS AND MOLECULAR WEIGHTS OF CHAIN CARRIERS

W. E. FALCONER AND A. VAN TIGGELEN

On the basis of three experimental properties which have been measured in *n*-butane, isobutane, and neopentane flames in mixtures with oxygen either at different stoichiometric ratios or at different preheating temperatures, two important parameters have been derived: the over-all activation energy E_r of the branching process and the mean molecular weight M of the chain carriers in such flames.

The results are respectively:

n-butane:	$M = 23$; $E_r = 33$ kcal
isobutane:	$M = 24$; $E_r = 31$ kcal
neopentane:	$M = 28$; $E_r = 38$ kcal.

These results are compared to analogous data obtained previously with other hydrocarbons and an interesting relation is observed between the bond energy CH and the activation energy of the branching process at least for saturated hydrocarbon compounds. Furthermore the rather low value of the mean molecular weight of the chain carriers constitutes an argument in favor of a rapid destruction of the alkyl radicals in their reaction with molecular oxygen; no peroxy radicals persist at the higher temperatures of the flame as compared to the temperature in slow oxidations.

Introduction

The complexity of most theories which attempt to correlate the basic principles of flame propagation restricts their practical application to the simplest systems. A general but very simple theory of stationary premixed flames has been developed in this laboratory.[1,2] It proposes that reaction is sustained by active centers which diffuse, against the gas flow, from the burned gas into the reaction zone. Chain branching compensates for radicals which are lost through terminating reactions, or by being swept away with the burned gases. A simple expression for the propagation of the combustion wave into the unburned gas is obtained from an analysis of this branched chain mechanism. The justification for this simplified approach lies in the ability of the theory to correlate all the experimental data relating to the different flame properties.

The burning velocity, V_0, relative to the unburned gases at the temperature T_0, at which gas flows are measured (room temperature), can be expressed as

$$V_0 = \frac{4T_0}{\pi}\left[\frac{2R}{3T_m M}\right]^{\frac{1}{2}}\left[\frac{(\mathrm{A})^a(\mathrm{B})^b}{P^i}\exp\left(-E/RT_m\right)\right]^{\frac{1}{2}} \qquad (1)$$

where P is the total pressure, (A) and (B) are the partial pressures of oxidant and fuel, respectively, R is the gas constant, M is the mean molecular weight of the chain-carrying species, and E is an over-all activation energy. T_m is the mean flame temperature for which the following relation has been proposed[1] as a first approximation:

$$T_m = T_i + 0.74(T_f - T_i) \qquad (2)$$

where T_i and T_f are, respectively, the initial temperature of the unburned gas, and the maximum flame temperature. Exponents a and b are the partial orders with respect to oxidant and fuel; their sum $a + b = i$, has been found to be unity for all flames studied to date,[2,3,4] except those of hydrogen.[5] Since the branching reaction is also first order with respect to radical concentration, the global order is $i + 1$; that is, two for the majority of flames.

An activation energy can be determined by observing the change in burning velocity with temperature, keeping all other parameters, notably concentration and pressure, constant. Thus if Eq. (1) in a logarithmic form,

$$\log V_0 + \tfrac{1}{2}\log T_m = \text{constant} - E\frac{\log e}{2RT_m} \qquad (3)$$

is applied to a series of flames with a given mixture composition and pressure but burning at different temperatures, a plot of $\log V_0 + \frac{1}{2}\log T_m$ against $1/T_m$ will give the over-all activation energy E of flame propagation. This activation energy will be principally that of the chain branching process, with smaller contributions from the propagating reactions. Such a series of experiments can be effected by preheating the gases which feed the burner. However, as the preheating temperature must not exceed that at which slow reactions begin, this method is at times restricted to a prohibitively small temperature range. Equation (1) may be written as follows:

$$V_0 = \frac{K_0 T_0}{T_m^{\frac{1}{2}}}\left[\frac{(\mathrm{A})^a(\mathrm{B})^b}{[(\mathrm{A})+(\mathrm{B})]^i}\, Y^i \cdot \exp\left(-E/RT_m\right)\right]^{\frac{1}{2}}$$

where $Y = [(\mathrm{A}) + (\mathrm{B})]/P$; that is, Y is the fraction of flammable mixture in the total gas volume. Then, if the logarithmic form of this equation

$$\log V_0 + \tfrac{1}{2}\log T_m - (i/2)\log Y = \text{constant} - E\frac{\log e}{2RT_m} \quad (5)$$

is applied to a series of flames with a constant oxidant-fuel ratio, burning at constant pressure, but with T_m varied by changing the value of Y, E can be obtained by plotting the left-hand side against $1/T_m$. The changes in Y are achieved by adding increasing amounts of an inert gas (N_2). This method makes a wide temperature range available for study, but requires the *a priori* knowledge of the global order of reaction. Fortunately, this can be deduced from a theoretical consideration of the branching mechanism. Excellent agreement has been found between these two methods for determining activation energies.

The partial orders with respect to oxidant and fuel, a and b, are not necessarily constant if the composition of the burning mixture is varied between wide limits, but the sum remains constant and equal to i. The variation of a and b when the fuel to oxidant ratio is modified can be shown from an analysis of flame velocities and temperatures if the activation energy is known from one of the methods described above. Equation (1) can be rearranged in the following form:

$$\frac{V_0 T_m^{\frac{1}{2}}}{K_0 T_0}\left[\exp\left(E/RT_m\right)\right]^{\frac{1}{2}} = \left[\frac{(\mathrm{A})^a(\mathrm{B})^b}{P^{(a+b)}}\right]^{\frac{1}{2}} \quad (6)$$

Since $a + b = i$, Eq. (6) can be transformed into the logarithmic form:

$$2\log V_0 + \log T_m + 0.4343(E/RT_m) - i\log[(\mathrm{B})/P] = 2\log K_0 T_0 + a\log[(\mathrm{A})/(\mathrm{B})] \quad (7)$$

A plot of the left-hand side of Eq. (7) against $\log (\mathrm{A})/(\mathrm{B})$ gives a curve, the slope of which at any point gives the partial order a with respect to oxidant for the particular composition (A)/(B). The corresponding order b with respect to fuel is obtained by subtracting a from i.

The chain is propagated by two radicals; X, which is formed from the fuel, B, and reacts with the oxidant, A; and Y, which is formed from a reaction with a fuel molecule, and in turn reacts with the oxidant. The mean molecular weight of the chain carriers M can be defined as follows:

$$M = \frac{M_X\tau_X + M_Y\tau_Y}{\tau} \quad (8)$$

where τ_X and τ_Y are the mean lifetimes of radicals X and Y; $\tau = \tau_X + \tau_Y$ and is the total duration of one complete chain link; M_X and M_Y are the actual molecular weights of radicals X and Y. The mean molecular weight can be calculated from the following equation[2]:

$$V_0/(T_m)^{\frac{1}{2}} = [(3.9 \times 10^{-2})/M^{\frac{1}{2}}] \cdot (1/X_0) \quad (9)$$

if the mean free path of the chain carriers under standard conditions is accepted as 10^{-5} cm. Here X_0 is the flame front thickness, which has been demonstrated experimentally to obey the following relationship,[5]

$$S = 4.7X_0$$

where S is the distance between the luminous and the schlieren cones of a flame. Thus M can be determined from a knowledge of V_0, T_m, and S, all of which are experimentally determinable. Flames propagating in mixtures of oxygen with such hydrogen-containing fuels as hydrogen itself, acetylene, methane, ethylene, ethane, propane, benzene, carbon monoxide contaminated with hydrogen, diethyl ether, and ammonia have been found to have a nearly common value for M. This is expected if: (a) M_X and M_Y are almost equal, e.g. such pairs as $CH_3\cdot$ and $OH\cdot$, or $NH_2\cdot$ and $OH\cdot$, or (b) one chain-propagating radical has a much longer life-time than the other [e.g., if $\tau_Y \gg \tau_X$, which implies that rate (X + A) $\gg$ rate (Y + B)]. The variety of fuels giving a single value for M suggests that one, at least, of the chain carriers is the same in each case. The chain carrier is most probably the radical OH, with $M = 17$. Its life-

time, τ_{OH}, would be expected, theoretically, to be greater than τ_X, because a hydrogen abstraction by OH from a hydrocarbon,[7] for example, will have an activation energy of 6–8 kcal mole^{-1}; whereas that for reaction of the resultant alkyl radical with oxygen[8] is unlikely to be greater than 0–1 kcal mole^{-1}. Furthermore, the two examples in case (a) for ammonia and methane flames will give a value of M near to 17 for all ratios of τ_X to τ_Y.

However, the tested hydrocarbons are such that they have either low molecular weights and/or strong C–H bonds, which properties would, if OH is to be accepted as one chain carrier, tend to lower the molecular weight of its alternate and/or reduce τ_X; both trends lead to values of M which will be experimentally indistinguishable from one hydrocarbon to another.

Isobutane has been selected for the present investigation because its corresponding alkyl radical has a molecular weight 3.3 times that of OH, and furthermore because the weaker tertiary C–H bond should give rise to a more stable alkyl radical than in previous cases. An augmented value for M might thus be found, if alkyl radicals are chain carriers complementary to OH in the flames. Also, these same properties might exert some influence on the activation energy of the branching process.

For comparison, and to distinguish between the effects of molecular size and of C–H bond strength, neopentane, containing only primary bonds, has also been investigated. The system *n*-butane-oxygen was chosen to complete the study because those effects attributable to bond strength should lie between the extremes found for isobutane and neopentane for such a substance which contains secondary C–H bonds.

Burning velocities, flame temperatures, and the distances between schlieren and luminous cones have therefore been determined for isobutane–oxygen mixtures, neopentane-oxygen mixtures, and *n*-butane-oxygen mixtures, all diluted with nitrogen, and the experimental results and their implications are presented in the following sections.

Experimental

Photographic images of the schlieren and luminous flames cones of approximately equal intensity were obtained as described previously.[6] Flame velocities were determined by the total area method applied to the outside edge of the schlieren cone for those flames in which the schlieren and luminous cones were distinguishable. At preheating temperatures above about 500°K, the previously observed coalescence of schlieren and luminous images[4] necessitated the calculation of flame velocities from the inner edge of the luminous cone. The surface of the cones was calculated from tenfold enlargements of the photographic images. Each velocity is the mean of three measurements, reproducible to within $\pm 2\%$.

The method of measurement of the distance between the schlieren and luminous cones is described in reference 6. Each distance reported is the mean of twelve measurements, four made on each of three films; reproducibility is $\pm 5\%$.

For unpreheated mixtures, 5 mm diameter waterjacketed conical burners, 100 cm in length, produced flames whose schlieren images approached perfect right cones. Preheating of the mixture by the burning flame did not exceed 5°K.

When the gases were to be preheated, isobutane and nitrogen were entrained together and passed through a 300 cm length of 4 mm stainless steel tube, wound in a spiral around a 60 cm length of 10 mm diameter steel tube. Oxygen passed through a similar spiraled tube, and all gases entered the central tube at its base. The central tube, which was long enough to insure thorough mixing and a laminar gas flow at the flow rates used, was fitted with a 5 mm diameter burner head to give a conical flame. An insulated heating coil was wound outside the two spirals, and the whole was insulated with asbestos to reduce heat loss to the atmosphere. By maintaining a constant current input to the heating coil, exit gas temperatures could be held constant to ± 2°K for an indefinite period.

The preheating temperature was measured immediately upon extinguishing a flame, after each series of photographs, with a single junction iron-constantan thermocouple inserted to a depth of 1 mm along the burner axis. No evidence of erroneously high temperatures due to catalytic effects on the thermocouple surface was found. At the maximum preheating temperatures, 635°K for isobutane mixtures, and 560°K for neopentane mixtures, neither carbon dioxide nor formaldehyde could be detected in the unignited gas stream. Mixtures containing *n*-butane were not preheated.

Flame temperatures were measured by the sodium line reversal method.[6] Flames were uniformly colored by heating a sodium borate bead formed on a small resistance coil placed in the nitrogen stream. The calibrated tungsten ribbon lamp was frequently checked against standard methane-oxygen-nitrogen flames, to detect possible misalignment of the optical system, or drifts in the lamp. Reproducibility of temperature measurement is ± 10°K.

All gases were commercial grade, purity about

TABLE 1

Preheated Isobutane–Oxygen–Nitrogen Flames; $R = 0.130$

N_2 (%)	T_i (°K)	T_f (°K)	T_m (°K)	V_0, cm/sec
66	300	2535	1954	90
	360	2564	1991	100
	426	2585	2024	104
	469	2600	2046	108
	531	2625	2080	114
	636	2650	2126	120
67	300	2473	1908	85
	360	2492	1938	90
67	424	2530	1982	96
	464	2552	2009	99
	528	2572	2041	105
	625	2590	2079	114
69	300	2397	1852	73
	361	2430	1890	77
	424	2457	1928	84
	466	2474	1952	87
	530	2506	1992	92
	623	2526	2031	97
71	303	2313	1790	59
	360	2345	1829	63
	422	2362	1858	69
	464	2378	1883	72
	528	2402	1915	76
	608	2430	1956	83
73	303	2219	1721	45
	361	2254	1762	49
	421	2278	1795	53
	465	2293	1818	57
	525	2317	1851	59
	599	2341	1888	65
75	300	2134	1657	33
	359	2165	1695	38
	417	2190	1729	41
	459	2200	1753	43
	512	2234	1786	45
	586	2260	1825	48

99%. Trace impurities cause negligible errors, as it has been shown[9] that changes in velocity and temperature, when a second fuel is added to a flammable mixture, are small, and as a first approximation, may be taken as a linear extrapolation of the values for the separate fuels.

Gas flows were measured against a constant counter pressure of 6 cm Hg, to compensate for any resistance in the preheating tubes or in the burner itself. Hydrocarbon flow rates were measured on capillary flow meters; oxygen and nitrogen flows on rotameters. The flowmeters were calibrated at frequent intervals against a standard wet test meter.

Results

The Isobutane–Oxygen–Nitrogen System

Preheated Mixtures. Flame velocities and temperatures of six mixtures where

$$R = \frac{(\text{iso-}C_4H_{10})}{(\text{iso-}C_4H_{10}) + (O_2)} = 0.130,$$

and the nitrogen content varied from 66 to 75 per cent, were measured over an initial temperature range of 300° to 635°K. Straight lines are obtained if the experimental values of T_f, T_m, and V_0 (presented in Table 1) are plotted against the initial temperature, T_i.

An activation energy of 30.0 ± 1.6 kcal mole^{-1} is found by plotting these data in accordance with Eq. (3), as has been done in Fig. 1. When the data for mixtures diluted with 66 to 73 per cent nitrogen are plotted in accordance with Eq. (5), a single line is found whose slope corresponds to an activation energy of 31.0 kcal mole^{-1} (Figs. 2 and 3). The inclusion of the more er-

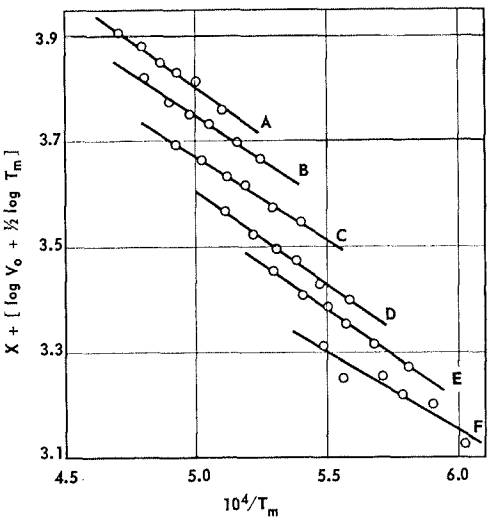

A: X = 0.15, E = 31.3, N_2 = 66% B: X = 0.10, E = 30.4, N_2 = 71%
C: X = 0.05, E = 27.7, N_2 = 67% D: X = 0 , E = 32.1, N_2 = 73%
E: X = 0 , E = 31.2 N_2 = 69% F: X = 0 , E = 27.5 N_2 = 75%

FIG. 1. Activation energy of isobutane–oxygen flames from preheating data.

TABLE 2

Unpreheated Isobutane–Oxygen–Nitrogen Flames

R	N_2 (%)	T_f (°K)	T_m (°K)	V_0, cm/sec	S, cm × 10^2
0.140	57.5	2718	2086	128	1.42
	60.7	2668	2049	110	1.54
	62.5	2620	2014	103	1.74
	65.0	2545	1958	96	1.91
	67.5	2454	1891	81	2.31
	70.0	2357	1819	69	2.34
	72.5	2240	1733	52	2.80
	75.0	2117	1642	38	3.62
	77.5	1980	1540	22	5.57
0.133	57.5	2775	2120	126	1.34
	60.0	2728	2090	115	1.49
	62.5	2660	2040	108	1.69
	65.0	2568	1975	94	2.00
	67.5	2475	1905	82	2.08
	70.0	2372	1825	68	2.46
	72.5	2260	1745	50	2.98
	75.0	2132	1650	37	3.91
	77.5	1995	1550	26	5.00
0.130	57.5	2723	2090	126	1.30
	60.7	2672	2050	110	1.42
	62.5	2620	2014	108	1.55
	65.0	2550	1962	95	1.80
	67.5	2465	1899	83	2.24
	70.0	2367	1827	71	2.25
	72.5	2262	1749	53	2.72
	75.0	2130	1651	39	3.56
	77.5	2005	1559	29	4.04
0.120	55.0	2740	2103	139	1.27
	57.5	2733	2095	123	1.26
	60.0	2647	2034	114	1.53
	62.5	2610	2005	102	1.68
	65.0	2532	1945	90	1.80
	67.5	2445	1880	80	2.00
	70.0	2360	1820	67	2.29
	72.5	2247	1735	53	2.62
	75.0	2147	1660	43	3.09
	77.5	2000	1550	29	4.17
	52.5	2713	2083	145	1.15
	55.0	2707	2078	137	1.21
	57.5	2657	2042	132	1.35
	60.0	2603	2000	111	1.47
	62.5	2567	1975	100	1.62
	65.0	2480	1910	89	1.88
	67.5	2392	1840	72	2.11
	70.0	2297	1770	63	2.32
	72.5	2215	1710	52	2.90
	75.0	2100	1625	43	3.19
	77.5	1968	1530	29	4.30

TABLE 2 (*continued*)

R	N_2 (%)	T_f (°K)	T_m (°K)	V_0, cm/sec	S, cm × 10^2
	50.0	2730	2097	151	0.97
	52.5	2693	2070	138	1.16
	55.0	2685	2060	123	—
	57.5	2609	2008	110	1.49
	60.0	2570	1975	104	1.49
	62.5	2500	1920	94	1.60
	65.0	2413	1860	79	1.91
	67.5	2335	1800	71	2.12
	70.0	2235	1730	60	2.43
	72.5	2152	1665	48	3.09
	75.0	2055	1595	38	3.44
	77.5	1905	1480	27	4.69

ratic data for slow propagation flames with 75 per cent nitrogen in the plot would increase this value by about 1 kcal mole^{-1}.

Unpreheated Mixtures. The results from experiments with unpreheated isobutane–oxygen mixtures are reported in Table 2. For six fuel–oxidant ratios, the dilution by nitrogen was varied over as wide a range as was practicable. The minimum nitrogen content was dictated by the maximum temperature that could be measured by the sodium line reversal apparatus; the

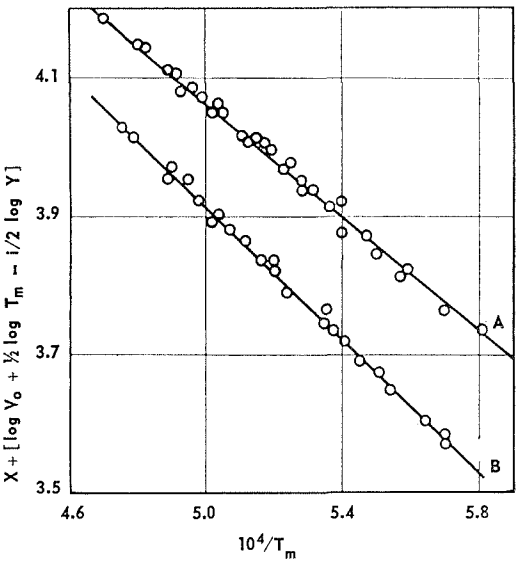

A: ISOBUTANE-OXYGEN FLAMES, X = 0.1, E = 31.0
B: NEOPENTANE-OXYGEN FLAMES X = 0, E = 36.7

FIG. 2. Activation energies from preheating data using dilution method of calculation.

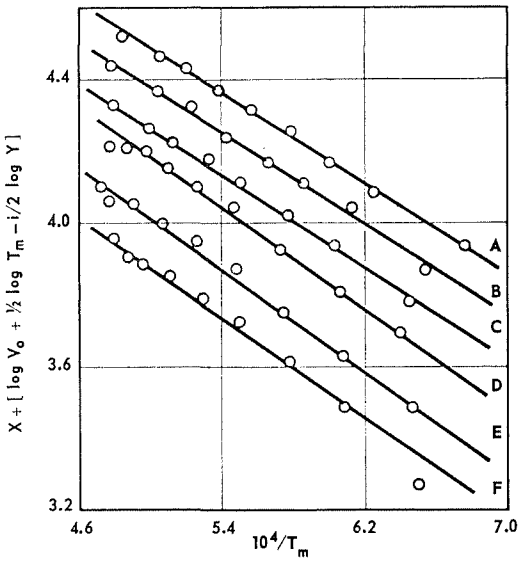

A: X = 0.6, R = 0.100, E = 29.6 B: X = 0.5, R = 0.110, E = 29.3
C: X = 0.4, R = 0.120, E = 29.7 D: X = 0.3, R = 0.130, E = 31.7
E: X = 0.15, R = 0.133, E = 32.6 F: X = 0 R = 0.140, E = 31.5

FIG. 3. Activation energy of isobutane–oxygen flames from dilution data; $i = 1$.

maximum dilution was that which still permitted the stabilization of conical flames on the burner.

Plots of flame velocity, V_0, and the reciprocal of the intercone distance, $1/S$, against the fraction of flammable mixture, Y, are straight lines within the experimental accuracy; plots of mean flame temperature, T_m, against Y are curved towards the concentration axis.

It is noteworthy that for mixtures burning with constant dilution, but with

$$R = \frac{(\text{iso-}C_4H_{10})}{(\text{iso-}C_4H_{10}) + (O_2)}$$

varied between 0.100 and 0.140, that the maximum of flame temperature and velocity shift towards lean mixtures when the dilution increases. This behavior has also been observed for H_2S flames burning in oxygen,[10] but it is opposite to the normal drift for fuel-oxygen systems.

An activation energy of 30.7 ± 1.2 kcal mole^{-1} is found when the data in Table 2 are plotted as in Fig. 3.

A plot of $V_0/(T_m)^{\frac{1}{2}}$ against $1/S$ for the six values of R studied, (Fig. 4) gives a single straight line whose slope yields a value of 24 for the mean molecular weight M of the chain carrying species. Lean mixtures tend to give a slightly higher value for M than stoichiometric or rich mixtures, but the difference is less than the experimental deviation, and it is doubtful if any significance can be assigned to this trend.

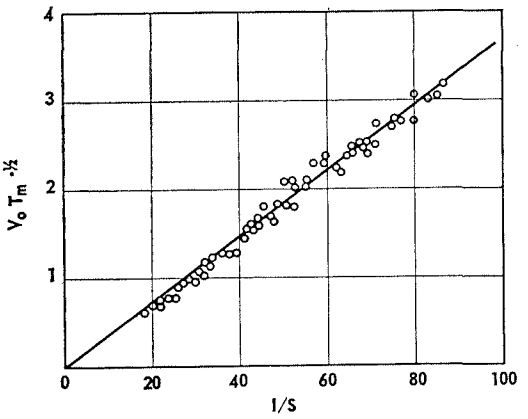

FIG. 4. Mean molecular weight of chain carriers for isobutane–oxygen flames.

In Fig. 5, the left-hand side of Eq. (7) is plotted against $\log [(O_2)/(\text{iso-}C_4H_{10})]$. In calculating these points, i was assumed to be unity, and a mean value of 30.5 kcal mole^{-1} was taken for the activation energy. Each point is the mean of between 30 and 40 measurements; the vertical lines indicate the mean deviation from the plotted values.

From the slope of this line, the partial order, a, with respect to oxygen is found to be constant, and equal to 1.5. Since i is unity, the partial order, b, with respect to fuel is also a constant, -0.5, over the concentration range investigated.

The Neopentane–Oxygen–Nitrogen System

Preheated Mixtures. Flame velocities, temperatures, and if possible, the distances between the

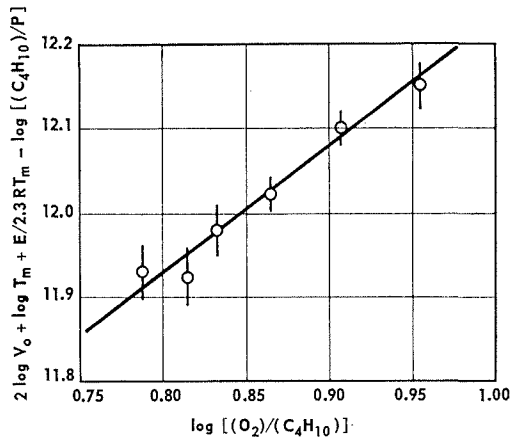

FIG. 5. Order of the branching reaction with respect to oxygen for isobutane–oxygen flames.

TABLE 3

Preheated Neopentane–Oxygen–Nitrogen Flames; $R = 0.111$

N_2 (%)	T_i (°K)	T_f (°K)	T_m (°K)	V_0, cm/sec	S, cm × 10^2
65	300	2569	1980	90	1.80
	355	2591	2009	95	—
	437	2607	2043	98	—
	530	2630	2085	108	—
	558	2642	2101	111	—
67	300	2490	1921	80	1.97
	354	2510	1957	85	1.84
	435	2533	1987	89	—
	524	2556	2027	99	—
	553	2563	2041	102	—
69	300	2423	1871	70	2.13
	352	2439	1896	71	1.97
	435	2462	1934	77	—
	520	2484	1974	84	—
	548	2495	1988	88	—
71	300	2333	1804	54	2.66
	347	2350	1830	57	2.46
	433	2378	1872	64	—
	512	2400	1909	69	—
	536	2411	1923	72	—
73	300	2260	1751	44	3.10
	344	2277	1774	48	2.66
	426	2300	1814	54	—
	501	2322	1849	58	—
	528	2328	1861	61	—

luminous and schlieren cones for five mixtures, where

$$R = \frac{(\text{neo-}C_5H_{12})}{(\text{neo-}C_5H_{12}) + (O_2)} = 0.111$$

and the nitrogen content varied from 65 to 73 per cent, were measured over an initial temperature range of 300° to 560°K. Straight lines are obtained if the experimental values of T_f, T_m, and V_0 (presented in Table 3) are plotted against T_i.

An activation energy of 39.3 ± 1.1 kcal mole^{-1} is found by plotting these data in accordance with Eq. (3), as has been done in Fig. 6. If these data are plotted in accordance with Eq. (5), a single line is found whose slope corresponds to an activation energy of 36.7 kcal mole^{-1} (Fig. 2B).

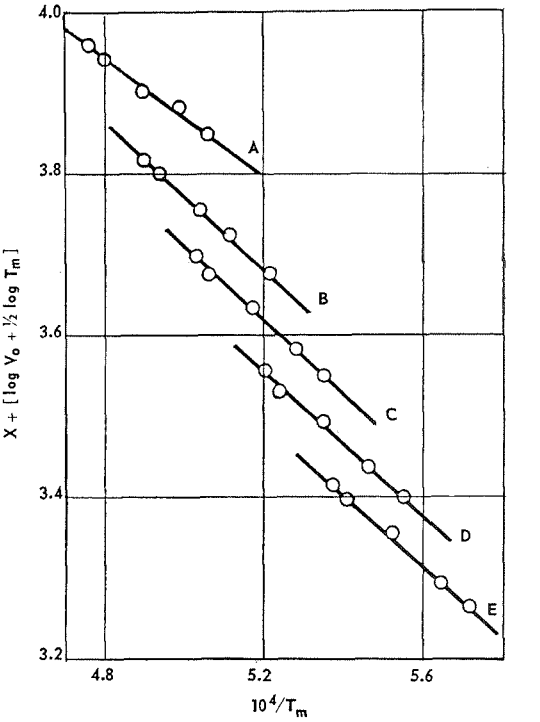

FIG. 6. Activation energy of neopentane–oxygen flames from preheating data.

A plot of $V_0/(T_m)^{\frac{1}{2}}$ against $1/S$ has been made in Fig. 7 using the data for those preheated mixtures in which S was measured combined with the data from unpreheated mixtures. A single straight line whose slope yields a value of 28 for

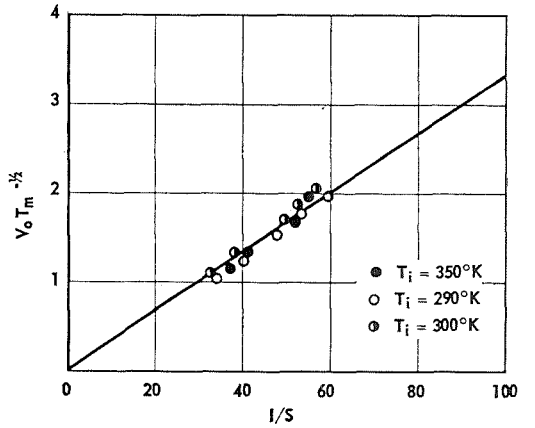

FIG. 7. Mean molecular weight of chain carriers for neopentane–oxygen flames.

TABLE 4

Unpreheated Neopentane–Oxygen–Nitrogen Flames; $R = 0.111$

N_2 (%)	T_f (°K)	T_m (°K)	V_0, cm/sec	S, cm × 10^2
65	2568	1976	88	1.68
67	2495	1922	76	1.93
69	2422	1867	66	2.16
71	2333	1804	53	2.50
73	2266	1752	43	2.95
75	2165	1675	35	3.55

the mean molecular weight of the chain carrying species is obtained.

Unpreheated Mixtures. The results from experiments with unpreheated neopentane-oxygen nitrogen mixtures are reported in Table 4. When these data are plotted in accordance with Eq. (5), as in Fig. 8, a straight line is obtained whose slope corresponds to an activation energy of 38.8 kcal mole^{-1}.

The n-Butane–Oxygen–Nitrogen System

Only unpreheated mixtures containing *n*-butane were investigated; the data are presented in Table 5. For two fuel-oxidant ratios, the dilution by nitrogen was varied between 59 and 73 per cent. Plots of flame velocity, V_0, and the reciprocal intercone distance, $1/S$, against the fraction of flammable mixture are linear. Plots of the mean flame temperature, T_m, against Y are concave towards the concentration axis.

TABLE 5

n-Butane–Oxygen–Nitrogen Flames

R	N_2 (%)	T_f (°K)	T_m (°K)	V_0, cm/sec	S, cm × 10^2
0.120	59	2697	2068	130	1.36
	61	2659	2040	120	1.48
	63	2618	2010	108	1.51
	65	2551	1961	100	1.63
	67	2496	1920	90	1.74
	69	2423	1867	78	2.04
	71	2355	1817	71	2.26
	73	2262	1758	57	2.59
0.133	59	2720	2087	129	1.45
	61	2675	2055	120	1.49
	63	2623	2017	109	1.59
	65	2574	1983	100	1.70
	67	2511	1933	90	1.99
	69	2450	1888	79	—
	71	2378	1835	67	2.43
	73	2280	1760	56	3.00

The data in Table 5 have been plotted according to Eq. (5) in Fig. 8, curves B and C. The slopes of the resulting lines correspond to an activation energy of 33.0 ± 0.3 kcal mole^{-1}.

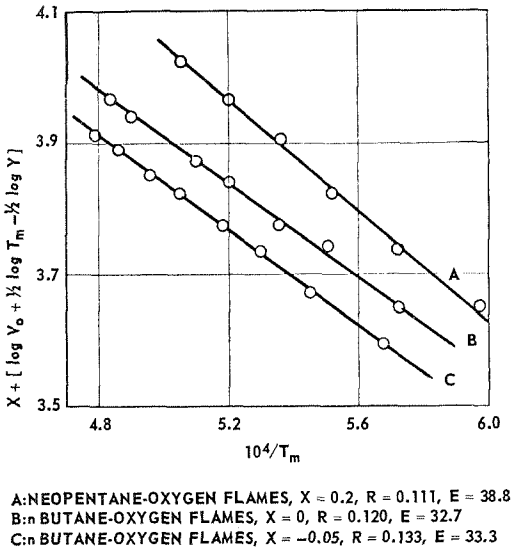

FIG. 8. Activation energies from dilutions data, $i = 1$.

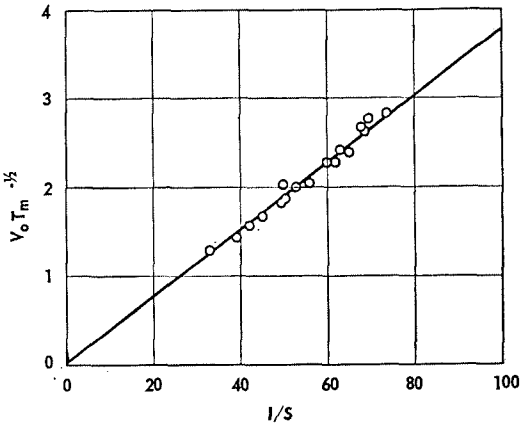

FIG. 9. Mean molecular weight of chain carriers for *n*-butane-Oxygen flames.

A plot of $V_0/(T_m)^{\frac{1}{2}}$ against $1/S$ gives a common straight line for both fuel-oxidant ratios studied (Fig. 9). The slope of this line yields a value of 23 for the mean molecular weight of the chain carriers.

Discussion

When the previously proposed mechanism[2] for the flame reaction is applied to isobutane-oxygen flames, two distinct possibilities exist, depending upon whether the isobutane is initially attacked at a primary or the tertiary position. Considering the propagation steps for attack on a primary H,

$$C_4H_{10} + OH \rightarrow (CH_3)_2CHCH_2\cdot + H_2O \quad (I)$$

or

$$C_4H_{10} + C_4H_9OO\cdot \rightarrow (CH_3)_2CHCH_2\cdot + C_4H_9OOH \quad (Ia)$$

followed by

$$(CH_3)_2CHCH_2\cdot + O_2 \rightarrow (CH_3)_2CHCH_2OO\cdot \rightarrow (CH_3)_2CHCHO + \dot{O}H \quad (II)$$

it is likely that the energy-rich isobutylperoxy radical will dissociate rapidly into OH and isobutylaldehyde. Thus the chain may be considered to propagate alternately by isobutyl and OH radicals. However, for tertiary attack, the propagating sequence is as follows:

$$C_4H_{10} + \dot{O}H \rightarrow (CH_3)_3C\cdot + H_2O \quad (III)$$

or

$$C_4H_{10} + C_4H_9OO\cdot \rightarrow (CH_3)_3C. + C_4H_9OOH \quad (IIIa)$$

followed by

$$(CH_3)_3C\cdot + O_2 \rightarrow (CH_3)_3COO\cdot \rightarrow ? \quad (IV)$$

Tertiary butyl radicals may be considered to be one of the chain carriers here, but the identity of the second is less clear. Tertiary butylperoxy radicals cannot undergo a simple decomposition to aldehyde and OH, analogous to reaction (II). Therefore, if OH is to be accepted as the second chain-carrying species, a decomposition yielding isobutene oxide or the biradical

$$(CH_3)_2{=}C(\cdot){-}O\cdot$$

as co-product with OH would have to take place. Alternatively, the peroxy radical itself might be the second species to propagate the chain.

Falconer, Knox, and Trotman-Dickenson have shown[11] that in slow oxidations hydrocarbon attack at the tertiary position is eleven times as probable as that at a primary C–H bond at 350°C. They found no appreciable activation energy difference between the reactions at these two positions. If a similar preference for tertiary attack of isobutane by the chain-propagating species, Y, is accepted for the flame reaction, then, due to the larger number of primary positions, reaction will follow the two paths (I–II) and (III–IV) in approximately equal proportions.

Two factors may thus contribute to the observed increase in molecular weight: First, if the two proposed mechanisms together constitute the propagation reactions and alkylperoxy radicals are important as chain carriers in one (or both) of the mechanisms, the large value of $M_{C_4H_9OO}$ would tend to elevate the mean molecular weight of the chain carriers. Second, if C_4H_9 has a reduced reaction efficiency due to possible steric hindrance in its subsequent reaction with oxygen, its lifetime would be increased, and the contribution of $M_{C_4H_9}$ to the mean molecular weight would be greater than that of less hindered alkyl radicals.

If peroxy radicals are neglected on the grounds that their lifetimes are short compared with OH and alkyl radicals, the mechanism for propagation simplifies to

$$C_4H_{10} + \dot{O}H \rightarrow C_4H_9\cdot + H_2O \quad (P)$$

$$C_4H_9\cdot + O_2 \rightarrow \dot{O}H + C_4H_8O \quad (P')$$

Then

$$\frac{\tau_{C_4H_9}}{\tau_{OH}} = f\frac{(C_4H_{10})}{(O_2)}\exp\left[-(E_P - E_{P'})/RT_m\right] \quad (10)$$

where f is the ratio of frequency factors for reactions of C_4H_9 and OH radicals. Inserting the known value of M into Eq. (8), $\tau_{C_4H_9}/\tau_{OH}$ is found to be 0.21. For the present series of experiments, $(C_4H_{10})/(O_2)$ is 0.10 to 0.15, and T_m varies between 1530° and 2120°K. $E_{P'}$ is zero[8] to a good approximation, and E_P is about 6 kcal mole^{-1} (reference 7). Then f in Eq. (10) is found to be about 9. That is, the collision efficiency of reaction (P') is about one-tenth that of reaction (P). As the orientation for an effective collision between a small reactive radical, such as OH, with a hydrocarbon is not critical, reaction (P) should have a high collision efficiency. However, an alkyl radical, such as isobutyl, must have a more specific spacial orientation to undergo an addition reaction with oxygen. Therefore, the lower collision efficiency observed for reaction (P') is in the expected direction. Any contribution of peroxy radicals to the mean

molecular weight of 24 of the chain carriers will necessarily lower $\tau_{C_4H_9}/\tau_{OH}$, and as a result, also lower the factor f.

For n-butane–oxygen flames, two possibilities again exist, as initial attack may be at a primary or secondary position. If a primary H is attacked, then

$$C_4H_{10} + \dot{O}H \rightarrow CH_3(CH_2)_2CH_2\cdot + H_2O \quad (V)$$

or

$$C_4H_{10} + C_4H_9OO\cdot \rightarrow CH_3(CH_2)_2CH_2\cdot + C_4H_9OOH \quad (Va)$$

followed by

$$CH_3(CH_2)_2CH_2\cdot + O_2 \rightarrow CH_3(CH_2)_2CH_2OO\cdot \rightarrow CH_3(CH_2)_2CHO + \dot{O}H \quad (VI)$$

The energy-rich butylperoxy radical formed in reaction (VI) will probably be dissociated rapidly into OH and butyraldehyde, and the chain may be considered to propagate alternately by n-butyl and OH radicals.

If attack occurs at the secondary position, then

$$C_4H_{10} + \dot{O}H \rightarrow C_2H_5\dot{C}HCH_3 + H_2O \quad (VII)$$

or

$$C_4H_{10} + C_4H_9OO\cdot \rightarrow C_2H_5\dot{C}HCH_3 + C_4H_9OOH \quad (VIIa)$$

followed by:

$$C_2H_5\dot{C}HCH_3 + O_2 \rightarrow C_2H_5(CH_3)CHOO\cdot \rightarrow C_2H_5(CH_3)CO + \dot{O}H \quad (VIII)$$

Here the secondary butylperoxy radical formed in reaction (VIII) will probably dissociate into OH and methyl ethyl ketone, and the chain thus propagates alternately by secondary butyl and OH radicals.

If secondary attack is accepted as being four times as probable as primary attack, as in slow oxidations,[11] the reaction will follow path (VII–VIII) about three times as often as path (V–VI).

The observed mean molecular weight of 23 can be explained in the same manner as for isobutane-oxygen flames. Either butylperoxy radicals may be important in the chain propagation, or the collision efficiency of reactions (VI) and (VIII) may be less than that of reactions (V) and (VII), or both factors may contribute. The enhanced stability of secondary butyl radicals over normal butyl radicals favors a longer lifetime for those radicals arising from secondary attack (tertiary butyl radicals should be again more stable).

If peroxy radicals are neglected as before, the relative collision efficiencies may be calculated. Inserting the value of $M = 23$ into Eq. (8), $\tau_{C_4H_9}/\tau_{OH}$ is found to be 0.18. From Eq. (10) a factor f of about 8 is found. These values are not unreasonable, for the same reasons as have been emphasized for the isobutane-oxygen flame reaction. Again, any contribution from peroxy radicals will lower $\tau_{C_4H_9}/\tau_{OH}$, and as a consequency lower f.

If neopentane undergoes an abstraction reaction similar to the butanes, only attack at primary C–H bonds is possible. The resulting neopentyl radical will not benefit from additional stabilization as do secondary and tertiary butyl radicals. Thus it should react rapidly with oxygen to yield 2,2-dimethyl propionaldehyde and OH,

$$(CH_3)_3CCH_2\cdot + O_2 \rightarrow (CH_3)_3CCH_2OO\cdot \rightarrow (CH_3)_3CCHO + \dot{O}H \quad (IX)$$

Peroxy radicals are no more likely to contribute to the mean molecular weight of the chain carriers than in ethane flames, where the mean molecular weight is 17. Neopentyl radicals and OH may be considered to be the alternate chain carriers.

Knowing that $M = 28$ for neopentane-oxygen flames, $\tau_{C_5H_{11}}/\tau_{OH}$ is found from Eq. (8) to be 0.25. The ratio $(C_5H_{12})/(O_2)$ is 0.125, and T_m is about 1800°K. Choosing $(E_P - E_{P'}) \simeq 6$, as before, then from Eq. (10), f is found to be about 11.

Thus the values of M observed for isobutane, n-butane, and neopentane can be explained by a sterically hindered reaction of the alkyl radical with oxygen. Alkylperoxy radicals, which may also contribute to the higher values found, need not have long lifetimes if the alkyl radicals themselves have lifetimes about one-quarter of those of OH radicals.

If steric hindrance alone were insufficient to reduce the collision efficiency of reaction (X),

$$R\cdot + O_2 \rightarrow RO_2\cdot \quad (X)$$

the factor f could also increase with increasing stability of the alkyl radical. Then f would be expected to be highest for isobutane, and lowest for neopentane, as the neopentyl radical is the least stable. However, if an entire methyl radical is abstracted in neopentane attack,

$$(CH_3)_3CCH_3 + \dot{O}H \rightarrow (CH_3)_3C\cdot + CH_3OH \quad (XI)$$

or

$$(CH_3)_3CCH_3 + ROO\cdot \rightarrow (CH_3)_3C\cdot + ROOCH_3 \quad (XIa)$$

then the more stable n-butyl radical will be formed. If reaction (XI) competes effectively

with the normal hydrogen abstraction reaction to form neopentyl radicals, then the concentration of *t*-butyl radicals could be higher in neopentane flames than in isobutane flames. In isobutane, only one-half of the alkyl radicals are formed from tertiary attack; the remainder will be isobutyl radicals.

The previously observed[11] formation of isobutane as an initial product in the slow oxidation of neopentane cannot be explained in an analogous manner to the formation of olefins as first products in most paraffin oxidations.

The following reaction sequence is suggested:

$$(CH_3)_3\dot{C}CH_3 + HO_2\cdot \rightarrow CH_3OOH + (CH_3)_3C\cdot \qquad \text{(XII)}$$

$$(CH_3)_2\dot{C}CH_3 + O_2 \rightarrow (CH_3)_2C{=}CH_2 + HO_2\cdot \qquad \text{(XIII)}$$

By analogy, reaction (XI) is not unreasonable.

The three possible explanations for the observed mean molecular weights of the chain-propagating radicals in isobutane, *n*-butane, and neopentane flames burning in oxygen are then:

1. Steric hindrance may decrease the collision efficiency of alkyl radicals reacting with oxygen.
2. Alkyl radical stability increases with decreasing strength of the C–H bond broken to form the radical; more stable radicals should have longer lifetimes, and tertiary radicals should be able to contribute more to the value of M than secondary, and secondary more than primary.
3. The lifetimes of alkylperoxy radicals may be long enough to effectively increase M. The effect should increase with the stability of the alkylperoxy radical, which probably parallels that of the alkyl radical from which it is formed.

The present experiments do not enable a choice to be made from these possibilities.

The activation energies derived by the two methods explained in the introduction give values in excellent accord. Activation energies of 30.5, 33.0, and 38.3 kcal mole^{-1} will be taken as representative for isobutane–, *n*-butane–, and neopentane–oxygen flames, respectively. They are compared in Table 6 with over-all activation energies of hydrocarbon-oxygen flames which have been investigated previously.

It can be seen from Fig. 10 that the activation energy for saturated hydrocarbon flames (diethylether and benzene flames can probably be included with those of alkanes in this grouping) decreases in an approximately linear fashion with the decreasing bond strength of the weakest carbon–hydrogen bond in the molecule. Ethylene and acetylene have activation energies much lower than this relationship would indicate.

The over-all activation energy determined experimentally is principally that of the branching reaction, with smaller contributions from the alternating propagating reactions. The differences in activation energy of about 8 kcal mole^{-1} observed between those saturated hydrocarbons containing only primary C–H bonds and isobutane, containing a tertiary C–H bond, cannot be attributed to differences in activation energies of the propagating reaction alone because, for radical–hydrocarbon reactions where absolute activation energies are small, activation energy differences when the substrate molecules are

TABLE 6

Activation Energies for Hydrocarbon–Oxygen Flames

Hydrocarbon	Weakest C–H bond (kcal mole^{-1})	Activation energy (kcal mole^{-1})
Methane	103.9 (14)	38 (4), 40 (5), 41 (15)
Ethane	98.3 (14)	39 (5)
Neopentane	99.3 (14)	38.3
n-Butane	94.6 (14)	33
Isobutane	91.4 (14)	30.5
Diethyl ether	95–100[a]	38.5 (10)
Benzene	101.8 (13)	40 (5)
Ethylene	102.5 (16), 105 (17)	36 (5)
Acetylene	121 (13)	32 (18, 19)
Hydrogen sulfide	90 (13)	26 (10)

[a] This value for D(C–H) in diethyl ether appears reasonable in light of the similarities in the nature of reactions of ethers and of saturated hydrocarbons.

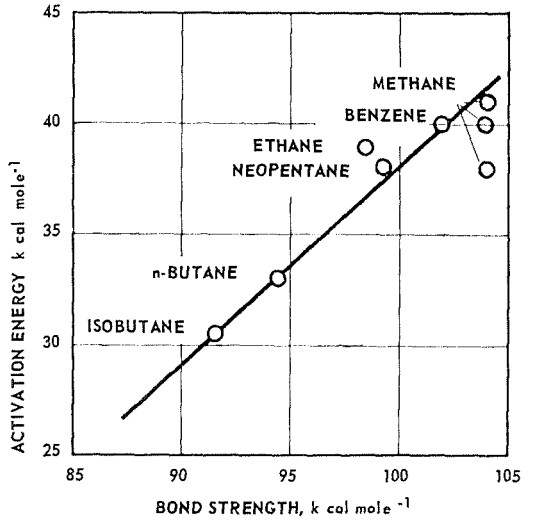

FIG. 10. Dependence of activation energy upon bond strength of weakest C–H bond.

changed are also small.[12] Therefore, the differences in activation energies must be assigned partly to the branching mechanism itself.

The observed parallelism between activation energy and bond strength suggests that those more stable radicals formed by the breaking of weak C–H bonds lead to a branching reaction with a lower activation energy in saturated hydrocarbon-oxygen flames, and that the activation energy is not greatly influenced by the molecular size. For unsaturated compounds, however, a reaction at the multiple bond must normally dictate the activation energy for subsequent branching. For an unsaturated hydrocarbon containing an easily abstracted hydrogen atom, as, for example, propylene, the reaction path having the lower activation energy would be expected to predominate in the chain branching. Thus by extrapolating Fig. 10, an activation energy of about 20 kcal mole^{-1} might be expected for propylene, based on a carbon–hydrogen bond strength of 77 kcal mole^{-1} in the paraffinic part of the molecule.[13]

The partial orders of 1.5 and −0.5 for oxygen and isobutane, respectively, are identical to those previously found by Vandenabeele, Corbeels, and A. Van Tiggelen[4] for methane-oxygen flames. From the observed orders, it is clear that chain branching must occur between an oxygen molecule and a chain-carrying radical that was also formed in a collision with oxygen. The most probable reaction[4,20,21] is one between the short livede nergy-rich alkylperoxy intermediate formed in reaction (X) and oxygen:

$$ROO\cdot + O_2 \rightarrow \text{branching} \qquad \text{(XIV)}$$

Although the exact form of reaction (XIV) is not easy to visualize, the reaction is certain to be highly exothermic, and this exothermicity coupled with the excess vibrational energy of formation possessed by the alkylperoxy radical could overcome to a large extent unfavorable molecular rearrangement in the reaction. However, a reaction such as

$$ROO\cdot + O_2 \rightarrow RO\cdot + O_3 \qquad \text{(XIVa)}$$

which has been proposed by Hanst and Calvert[22] for photosensitized hydrocarbon oxidations, provides branching with very little rearrangement.

As an alternative a possible branching reaction could be proposed according to the very general process:

$$\begin{matrix} & & R & & \\ & \diagdown & & & \\ R\text{—}CO_2\cdot & + & O_2 & \rightarrow & CO_2 + 2RO\cdot + R\cdot \\ & \diagup & & & \\ & & R & & \end{matrix}$$

where R represents either any alkyl radical or even a single hydrogen atom as in the simplest case:

$$CH_3O_2\cdot + O_2 \rightarrow CO_2 + 2\dot{O}H + H\cdot$$

ACKNOWLEDGMENTS

This research has been supported by the Directorate of Aeronautical Science, AFOSR, AFRD, of the Air Research and Development Command, USAF, monitored by the European Office of the Air Research and Development Command under Grant No. AF–EOARDC–61–23.

One of us (W.E.F.) is also indebted to NATO for a Postdoctoral Science Fellowship.

REFERENCES

1. VAN TIGGELEN, A.: Mem. Acad. Roy. Sc. Belg. (Cl. Sc.) *27*, 1 (1952).
2. VAN TIGGELEN, A. and DECKERS, J.: *Sixth Symposium (International) on Combustion*, p. 61. Reinhold, 1957.
3. VAN WONTERGHEM, J. and VAN TIGGELEN, A.: Bull. Soc. Chim. Belg. *64*, 780 (1955).
4. VANDENABEELE, H., CORBEELS, R., and VAN TIGGELEN, A.: Combustion and Flames *4*, 253 (1960).
5. VAN WONTERGHEM, J. and VAN TIGGELEN, A.: Bull. Soc. Chim. Belg. *64*, 99 (1955).
6. *Ibid. 63*, 235 (1954).
7. AVRAMENKO and LORENTSO: Doklady Akad. Nauk S.S.S.R. *67*, 867 (1949).
8. SLEPPY, W. C. and CALVERT, J. G.: J. Amer. Chem. Soc. *81*, 769 (1959); HOEY, G. R. and

KLUTSCHKE, K. O.: Can. J. Chem. *33*, 496 (1955); WENGER, F. and KUTSCHKE, K. O.: *ibid. 37*, 1546 (1959); MARCOTTE, F. B. and NOYES, W. A., JR.: Discussions Faraday Soc. *10*, 236 (1951).
9. LEASON, D. B.: *Fourth Symposium (International) on Combustion*, p. 369. Williams and Wilkins, 1953; CORBEELS, R. and VAN TIGGELEN, A.: Bull. Soc. Chim. Belg. *68*, 613 (1959).
10. VAN WONTERGHEM, J., SLOOTMAEKERS, P. J., and VAN TIGGELEN, A.: Bull. Soc. Chim. Belg. *65*, 899 (1956).
11. FALCONER, W. E., KNOX, J. H., and TROTMAN-DICKENSON, A. F.: J. Chem. Soc. *1961*, 782.
12. TROTMAN-DICKENSON, A. F.: *Free Radicals*, p. 65. Methuen, London, 1959.
13. COTTRELL, T. L.: *The Strengths of Chemical Bonds*. Butterworths, 1954.
14. FETTIS, G. C. and TROTMAN-DICKENSON, A. F.: J. Chem. Soc. *1961*, 3037.
15. FALCONER, W. E. and VAN TIGGELEN, A.: Unpublished results.
16. TROTMAN-DICKENSON, A. F. and VERBEKE, G. J. C.: J. Chem. Soc. *1961*, 2580.
17. HARRISON, A. G. and LOSSING, F. P.: J. Am. Chem. Soc. *82*, 519 (1960).
18. VAN WONTERGHEM, J. and VAN TIGGELEN, A.: *Fifth Symposium (International) on Combustion*, p. 637. Reinhold, 1955.
19. MORGAN, G. and KANE, W.: *Fourth Symposium (International) on Combustion*, p. 13. Williams and Wilkins, 1953.
20. WALSH, A. D.: Trans. Faraday Soc. *42*, 269 (1946).
21. SEMENOV, N. W.: *Some Problems in Chemical Kinetics and Reactivity*, pp. 71 and 163, translated by M. Boudart. Princeton University Press, 1958.
22. HANST, P. L. and CALVERT, J. G.: J. Phys. Chem. *63*, 71 (1959).

Discussion

DR. G. VON ELBE (*Atlantic Research Corporation*): It seems that correlations such as presented in this paper can be obtained by means of a simple formulation of the conservation equations together with a nonspecific chemical rate expression. For example, we may write

$$\bar{q}X_0 = cpV_0(T_f - T_i) \qquad (1)$$

where $\bar{q}$ is the average rate of chemical heat release per unit volume (cal/cm^3 sec), X_0 is the thickness of the reaction zone, and c and p are specific heat and density, respectively. The thickness of the reaction zone may be taken to be proportional to a characteristic length represented by the ratio of the thermal diffusivity K to the burning velocity V_0,

$$X_0 \sim K/V_0 \qquad (2)$$

whence $V_0 \sim \bar{q}^2$. The expression $\bar{q}$ presumably has an Arrhenius type temperature dependence, so that a plot of log V_0 vs. the reciprocal of a "mean" temperature T_m should yield straight line correlations and activation energies, such as obtained by the authors. Furthermore, since the observed intercone distances S are also $\sim K/V_0$, plots of V_0 vs. $1/S$ yield slopes proportional to the thermal diffusivity K, which in turn is proportional to $1/(M^{\frac{1}{2}})$, M representing an average molecular weight of the mixture. Correlations of this kind do not yield reaction-kinetic information except for "activation energies." The latter shed little light on the chemical mechanism and certainly provide no evidence concerning the branched chain character of the reaction, which the authors are postulating.

DR. W. E. FALCONER and DR. A. VAN TIGGELEN (*University of Louvain*): The straight line plots presented in the paper demonstrate that the temperature variation of the reaction rate, as reflected by the flame velocity, obeys an Arrhenius type law. It would not be surprising if $\bar{q}$, the average rate of heat release per unit volume as defined by Dr. von Elbe, followed an identical law, because $\bar{q}$ itself must be a direct measure of the reaction rate. Evidence that the flame process must be a branched chain reaction is given in references 1 and 2 of the paper. Because the mechanism is of the branched chain type, the over-all activation energy is ascribed mainly to the branching reaction, which initiates the chains, and to the propagating reactions which carry them. The later are known to have low activation energies, and therefore, to a good approximation, E (branching) $< E$ (over-all) $< E$ (branching) $+ E$ (propagating).

The experimental facts themselves best demonstrate that the proposed relationship between velocity and intercone distance gives useful information about the reaction kinetics. For fuels as heavy as benzene and diethyl ether, the value of M as defined by Eq. (9) remains equal to that for light fuels such as methane, ammonia, or even hydrogen itself. However, for the butanes, neopentane, and propylene[1] substantially increased values for M are found, as is to be expected from the increased stability of the alkyl radicals formed from these fuels. It appears that the phenomenon involved in fixing the intercone distance is not solely a diffusion of heat, in which all species are included, but in addition a "chemical diffusion" of reactive species to an im-

portant extent. It is this diffusion of active centers back into the unburned gases which provides the observed variations in slope in the plots of $V_0/(T_m)^{\frac{1}{2}}$ vs. $1/s$.

DR. F. J. WEINBERG (*Imperial College*): This question concerns the "flame thickness" used by the authors, which has been defined as proportional to the separation between the schlieren and the luminous zones of the flame.

The lower (schlieren) boundary has been shown to occur[2,3] at a temperature (AT_0) °K, where T_0 is the initial gas temperature (°K) and A is a constant depending on the variation of thermal conductivity of the reactant gas with temperature. If thermal conductivity increases with temperature, A is less than 2 and for most gases it is in the neighborhood of 1.5. In any case, the schlieren image occurs in a zone where temperature varies only gradually with distance, so that a small change in initial temperature will result in a very appreciable change in the thickness as defined above—a change which will lie almost entirely in the prereaction zone. Under these circumstances I find it difficult to understand how the variation of this thickness with initial temperature could convey any information of kinetic significance.

The low value of the temperature at which the schlieren image occurs is due entirely to the form of the dependence of refractive index on temperature—the variation decreasing rapidly as temperature rises. We could postulate a purely physical analogue in which gas at an initial temperature T_0 flows into a porous plate which is maintained at a higher temperature, T_p. A "thickness," defined in terms of the distance between the schlieren image and the plate, for instance, would be approximately inversely proportional to flow velocity. Yet there would be no kinetics to study! The schlieren image would coalesce with the plate when T_0 was raised to (T_p/A).

It can readily be shown[2,3] that the refractive index distributions in the two cases are virtually identical in the zone of the schlieren maximum.

DR. W. E. FALCONER and DR. A. VAN TIGGELEN: It appears that the point in question here is whether or not there is a kinetic significance to the flame front thickness as we have defined it.

Dr. Weinberg makes a comparison between the laminar flame and a heated porous plate towards which a gas is streaming at a constant velocity. In that case a schlieren image would be observed which he states would be located at a position which depends on the flow velocity, and, although not explicitly said in Weinberg's comment, the distance from the plate will also vary with the temperature of the plate. However, what Dr. Weinberg does not point out is that the equilibrium plate temperature will depend upon the energy input to the plate per unit time, that is, the *rate* of heating. Once a given temperature is assumed for the plate, and the schlieren image is located at a distance fixed by the flow velocity of the impinging gas stream, the rate of heating of the plate is also fixed.

The analogy with the flame lies in the fact that the rate of heating of the plate is equivalent to the rate of reaction in the flame front, which is of course flame kinetics.

We should also point out that the variation of flame front thickness with initial temperature is not the relationship we have used to obtain kinetic information, as Dr. Weinberg intimates. However, when the initial temperature was varied, the agreement among the various experimental parameters remained unchanged.

As Dr. Weinberg points out, the location of the schlieren image relative to the hot plate, or in our case, to the flame front, is very sensitive to small temperature changes in the region of the schlieren zone; however, the distance between this zone and the hot front is even more critically affected by the rate of heating of the fresh gases, which in turn is closely related to the ease of diffusion, and hence the size, of the chain propagating radicals. The measurement is thus a sensitive indicator of the quantity in question.

For these reasons, Dr. Weinberg's comments, instead of constituting an objection to our work, give further support to our own conclusions. The measurement of the distance between the schlieren and visual image of the flame indeed gives us direct information about the reaction kinetics. The theoretical equations needed to interpret the measurements have been derived in a previous work (reference 2 of our paper).

REFERENCES

1. VAN TIGGELEN, A.: University of Louvain, unpublished results.
2. WEINBERG, F. J.: Fuel *34*, S84 (1955); *ibid. 35*, 161 (1956).
3. WEINBERG, F. J.: "Geometric–Optical Techniques in Combustion Research," in *Progress in Combustion Science and Technology*. Pergamon Press, 1961.

717

COMBUSTION STUDIES OF SINGLE ALUMINUM PARTICLES

R. FRIEDMAN AND A. MAČEK

Our earlier work, both experimental and theoretical, on ignition and combustion of single aluminum particles at atmospheric pressure is briefly reviewed, and new experimental data, obtained by two methods, are presented. In the first method the aluminum particles are injected into the stream of hot gases generated by means of a flat-flame burner. In the second method the particles are burned in the combustion products of ammonium perchlorate flames with organic fuels added. In both cases aluminum is burned in an atmosphere of controlled temperature and composition. It is concluded that ignition occurs only upon melting of the oxide layer (m.p., 2300°K) which coats the particle. The process of ignition is not affected by the moisture content of the hot ambient gas and only slightly by its oxygen content. On the other hand, there are distinct effects of oxygen and of water vapor on combustion of the metal. Oxygen promotes vigorous combustion, and, if its concentration is sufficiently high, there is fragmentation of particles. In the virtual absence of water, diffusion and combustion take place freely in the gas phase, whereas in the presence of significant amounts of water, the process is impeded and confined to a small region, because the reactants must diffuse through a condensed oxide layer.

Description of the Problem

The general problem of droplet combustion is well known and an extensive literature exists. Burning aluminum droplets have properties, however, which make the previous body of work on other, generally more volatile, fuels almost irrelevant. Let us consider these properties.

Firstly, the combustion product, alumina, melts at 2303°K, and boils with decomposition at about 3800°K in the presence of one atm of the decomposition products (Al, AlO, Al_2O, Al_2O_2, O, O_2). Since there is insufficient combustion energy available to vaporize more than a fraction of the alumina formed, the maximum flame temperature will be governed by this pressure-dependent dissociative vaporization process. On the other hand, aluminum boils at about 2700°K at one atm. Thus, the phases in which reactants and products may exist in the combustion zone, as well as the possibility that a continuous molten oxide film may exist between fuel and oxidizer, become of dominant importance in determining the mechanism and rate of the process.

Secondly, the combination of very high flame temperature and high emissivity of a large or dense cloud of aluminum particles leads to such an intense radiant flux that this will become comparable with energy transfer by thermal conductivity through the gas during the combustion process. Accordingly, cooperative phenomena characteristic of a cloud of particles must be superimposed on single-particle characteristics for proper description of the process.

Thirdly, special factors enter when one becomes concerned with aluminum combustion under rocket motor conditions. The high pressures cause increases in the emissivity of the combustion products, the boiling point of aluminum, and the flame temperature. The oxidizing species may be water vapor and carbon dioxide rather than free oxygen. Halogen compounds may be present. In addition to these variables which may influence the ignition process and combustion rate, one must also be critically concerned with the particle size of the alumina formed, because of the effect on thermal and velocity lag in the nozzle expansion process.

The present research effort is based on the idea that single-particle combustion at atmospheric pressure should be thoroughly understood before the more difficult studies of cooperative effects at high pressures are undertaken.

Review of Past Work

Except for our earlier paper,[1] no detailed account of aluminum particle combustion has appeared in the open literature. Cassel and Liebman[2] failed to obtain ignition of aluminum particles in a furnace at 1400°C. Gordon,[3] Fassell *et al*,[4] and Wood,[5] have briefly described experiments involving observations of particle ignition induced by injection into nonmetallic flames. Fassell *et al.*[4] also describe hollow spheres

of metal oxide which may be recovered in the combustion products.

In the following paragraphs, the highlights of our earlier work[1] are reviewed.

The plan has been to inject single spherical aluminum particles of controlled sizes (10 to 74 microns) into hot product gases of propane–oxygen–nitrogen flames and to observe ignition and combustion behavior. A previously described[1] flat-flame burner of 4.25-cm diameter, operating at atmospheric pressure, was employed to produce a uniform laminar flow of combustion products of known and independently variable temperature and oxygen content. (A substantial water vapor content, 14–18 per cent, was always present, a fact which will later be seen to be significant.) Combustion behavior of injected particles was studied both by photographic and particle-recovery techniques.

It was found that injected particles would only ignite under certain conditions. Investigation of critical conditions for ignition showed that particle size and ambient oxygen content were relatively unimportant variables, but an ambient gas temperature of about 2300°K was the necessary condition for ignition. This coincides with the melting point of aluminum oxide. A detailed mathematical theory of the ignition limit was developed[1] which assumes that melting of the protective oxide layer causes a discontinuous increase in the surface reaction rate, leading to ignition.

An ignition delay time was measured in those cases in which ignition occurred. This time, which was found to vary with the square of particle diameter, was in agreement with a theoretical calculation of its magnitude. The calculation was based on the particle being heated from its initial state to the alumina melting point by conductive transfer from the hotter ambient gas. It was shown that the Nusselt number may be taken as two and that radiation may be neglected under the prevailing experimental conditions. The agreement between measurement and calculation shows that oxidative heating is negligible during this pre-ignition period.

Studies of the combustion mechanism of the ignited particles revealed a number of unexpected phenomena. When the ambient gases contained less than 28–38 per cent oxygen (depending on ambient temperature), a burning particle would appear as a sharp, straight, vertical track on an exposed photographic film. This mode of combustion is associated with growth of transparent alumina bubbles. The particles frequently burn on only one side, and may rotate at several thousand revolutions per second. The burning time is roughly proportional to the 1.5 power of particle diameter.

We believe that in the above mode of burning the aluminum starts to boil soon after ignition and inflates the surrounding alumina bubble asymmetrically, the not-yet-burned metal adhering to one side of the bubble. The combustion occurs at the bubble, as aluminum vapor meets oxygen. The bubble is an important diffusion barrier to reaction.

At ambient oxygen content above 28–38 per cent, another phenomenon, fragmentation, was observed. Particulate matter may be ejected in a random direction from the burning droplet. This may be preceded by ejection of a diffuse cloud from the burning particle, the cloud presumably being aluminum vapor burning to form colloidal alumina. The occurrence of droplet shattering greatly reduces burning time.

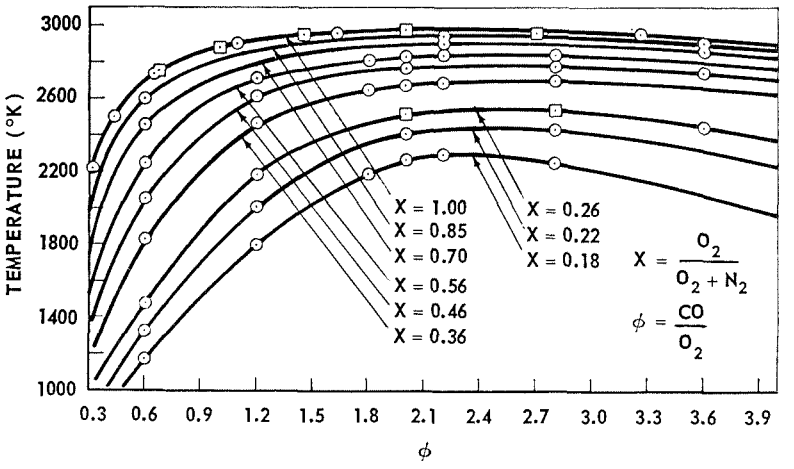

FIG. 1. Calculated adiabatic flame temperatures of $CO–O_2–N_2$ mixtures at 1 atm.

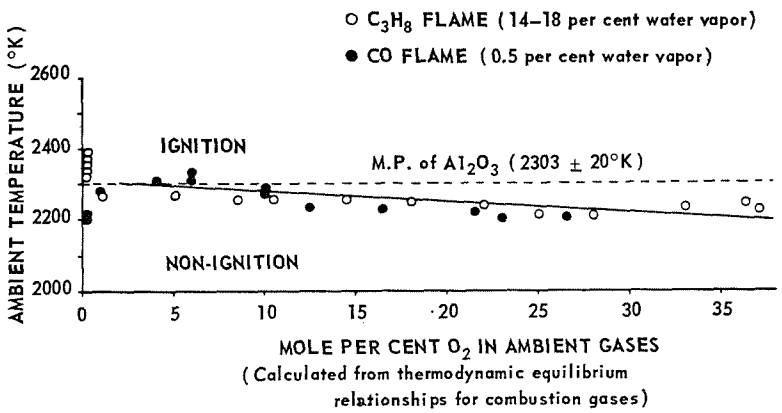

FIG. 2. Minimum ambient temperature for ignition of aluminum particle (Avg. particle diameter is 34 microns).

We believe that the higher reaction rates and metal flame temperatures associated with the higher oxygen content lead to more rapid boiling of the aluminum (superheating is possibly but not necessarily involved), resulting in rupture of the alumina bubble.

In the new work to be reported below, which is still in progress, emphasis is being placed on study of the variables governing transition between various modes of combustion. Effects of composition of ambient atmosphere and pressure are being sought in particular.

Combustion in Moisture-Free Gases

The hot gases produced by the propane-oxygen-nitrogen flames utilized in the above-described work had a rather high water vapor content, typically about 18 per cent. In order to assess the significance of this variable, experiments have been conducted with dry carbon monoxide-oxygen-nitrogen flames, stabilized on the same burner. In order to obtain a stable flat flame, it has been necessary to add a small proportion of hydrogen to the mixture, so that about 0.5 per cent water vapor is now present in the combustion products.

As in previous work,[1] the flame temperatures were computed by an IBM-704 program which assumes adiabatic equilibrium conditions, and takes into account all pertinent dissociation equilibria. Temperatures were then corrected for the heat loss to the water-cooled burner. Adiabatic temperatures for carbon monoxide flames are shown in Fig. 1.

The following experimental results on combustion of aluminum particles in low-moisture gases are similar to the results in high-moisture media:

a. Ignition is very abrupt at all ambient oxygen concentrations higher than about 2 per cent. The pre-ignition delays increase with the square of particle diameter as in the high-moisture gases.

b. The most important requirement for ignition, by far, is that the metal particle be heated to the melting point of alumina (2303 ± 20°K). As has been shown in the previously developed theory,[1] this occurs at ambient temperatures between 2200° and 2300°K, depending on the

TABLE 1

Some Ignition and Combustion Times

Avg. particle diameter (microns)	Ambient temp. (°K)	Per cent O_2	Per cent H_2O	Ignition time (t_i, msec)	Burning time (t_b, msec)	t_b/t_i
35	2510	5.8	18.1	7.6 ± 0.4	10.5 ± 0.5	1.4
49	2510	5.8	18.1	11.7 ± 0.7	≃19	1.6
35	2510	7.9	0.5	10.7 ± 1.0	6.6 ± 0.7	0.6
49	2510	7.9	0.5	16.5	≃12	0.7

amount of oxygen present. Figure 2 shows the minimum ignition temperatures as a function of oxygen content for particles of 34-micron average diameter both in high-moisture and low-moisture media. It can be seen that the linear relationship holds down to about 2 per cent of ambient oxygen. The relatively wide scatter of the data at very low oxygen content is due to the fact that in such oxygen-poor gases the ignition criteria are ill-defined.

Combustion of aluminum particles in low-moisture differs from that in high-moisture media in the following aspects:

a. While the striking feature of aluminum combustion in the presence of appreciable amounts of water vapor is the growth of a hollow shell of aluminum oxide attached to the unconsumed portion of the metal particle, the completely burned particle being a hollow sphere of translucent aluminum oxide of approximately the same size as the original aluminum, there is no evidence of such a process in low-moisture gases. Rather, the combustion is characterized by a steady diminution of the original particle; the oxide product consists of particles of irregular shapes and widely varying sizes smaller than the original particle. If, however, a significant amount of hydrogen is added to the carbon monoxide flame, the large translucent bubbles reappear. The amount of hydrogen necessary for this result is 5 to 10 per cent.

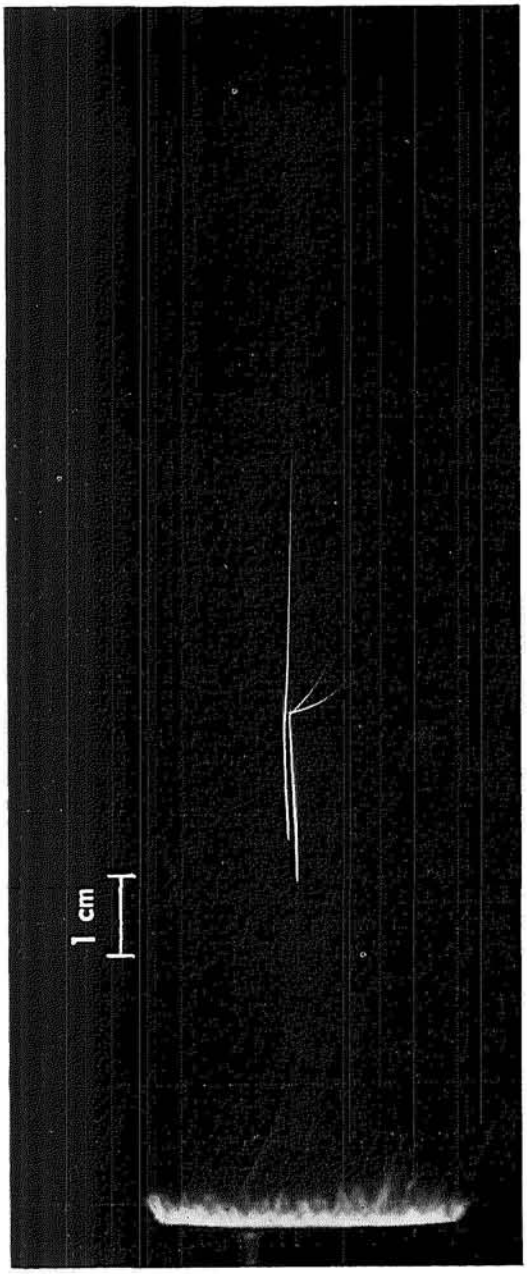

FIG. 3. Burning and fragmentation of 34-micron diameter particles. Ambient conditions: T = 2390°K, O_2 = 31.2%, H_2O = 17.0%.

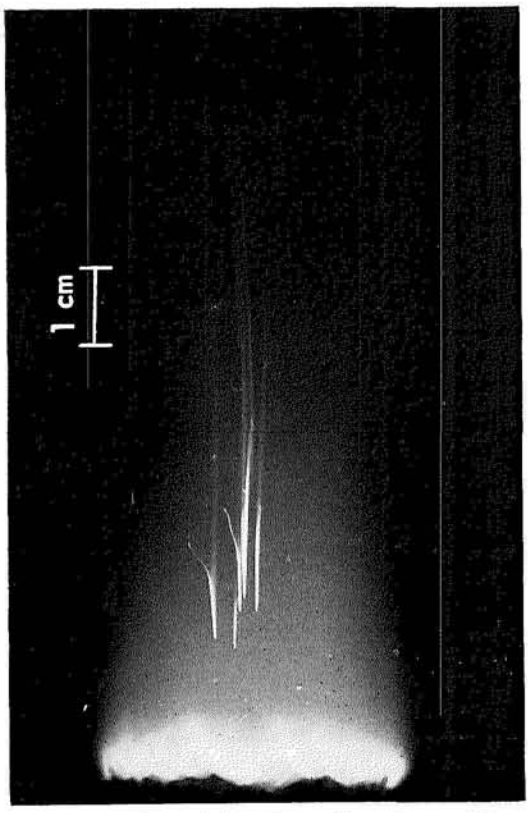

FIG. 4. Burning of 34-micron diameter particles. Ambient conditions: T = 2480°K, O_2 = 34%, H_2O = 0.5%.

b. Combustion of aluminum particles is considerably more rapid in low-moisture media than in the presence of appreciable amounts of water vapor. This can be seen from Table 1 which gives experimental preignition and combustion times for two particle sizes in two atmospheres which are similar except for widely different moisture contents.

c. While typical time-exposure photographs of burning particles in high-moisture gases show sharp tracks, there is much more diffuse luminosity in the low-moisture gases. This is illustrated by Figs. 3 and 4 which show photographs, taken at 1/50 sec, of burning particles in low-moisture and high-moisture media; the oxygen content in both cases is quite high. In the case of the high-moisture ambient gas, the tracks are sharp both before and after fragmentation which occurs after about 2 msec of burning. In the case of the low-moisture gas, large amounts of aluminum vapor appear adjacent to the particle. This appearance is often accompanied by sudden change in the direction of motion of the particle.

Combustion in Ammonium Perchlorate-Fuel Flames

While burning of aluminum particles on the flat-flame burner has given good results at atmospheric pressure, the method cannot be easily extended to higher pressures. A procedure is, therefore, being developed wherein aluminum particles are burned in the combustion products of ammonium perchlorate with fuels added. Combustion can take place either in the open or in a window bomb at pressures up to 2000 psi. Small amounts of spherical aluminum powder of controlled sizes are admixed to the combustible mixture, and burned either pressed into strands or in loosely tamped powder form. The latter method, employed by Arden, Powling and Smith,[6] appears somewhat more satisfactory. Our procedure has been to mix 0.05 or 0.1 per cent of aluminum powder of controlled size with a finely ground ammonium perchlorate-powdered organic fuel mixture which is tamped into cylindrical form (6.5 mm diam) surrounded by an annular "guard ring" of unaluminized perchlorate-fuel mixture of 17 mm diameter. Both trioxymethylene and plastisol-type polyvinyl chloride have been employed as fuels. The use of powdered fuels in a tamped or pressed composition rather than a polymeric binder system permits much greater latitude in fuel-oxidizer ratios and fuel type to obtain desired flame temperatures and combustion product compositions. Figure 5 shows calculated adiabatic flame temperatures as a function of pressure for the ammonium perchlorate-trioxymethylene system.

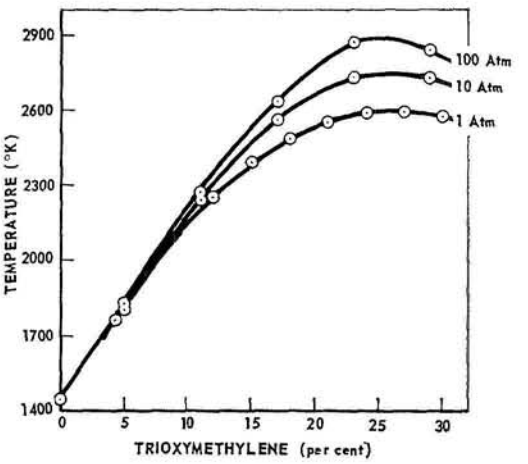

FIG. 5. Calculated adiabatic flame temperatures of ammonium perchlorate–trioxymethylene mixtures at several pressures.

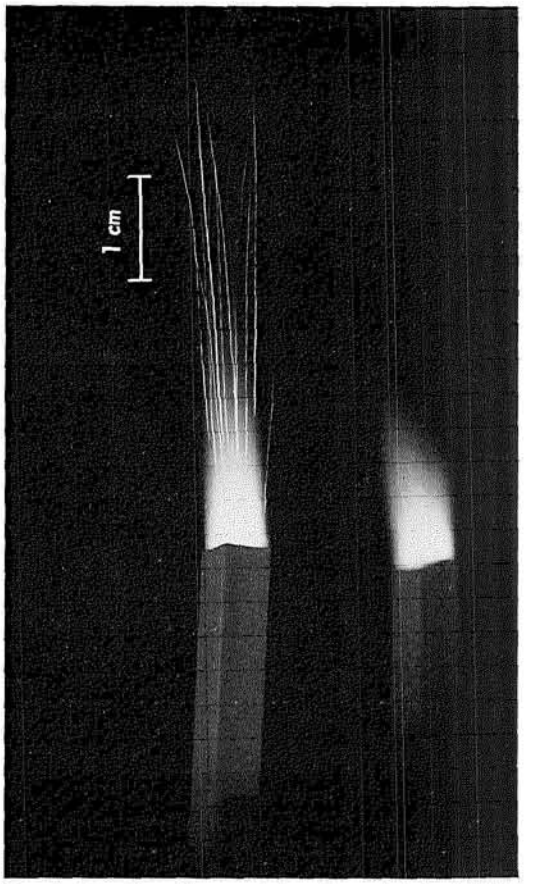

FIG. 6. Burning of pressed strands containing 78.7% ammonium perchlorate and 21.2% polyvinylchloride. Left: 0.1% aluminum (34-micron diameter) added. Right: no aluminum.

Experiments done so far have given the following results:

a. Aluminum does not ignite in the products of pure ammonium perchlorate flames at any pressure up to 2000 psi. In view of the fact that temperatures in such flames are far below the melting point of alumina, this result is most reasonable.

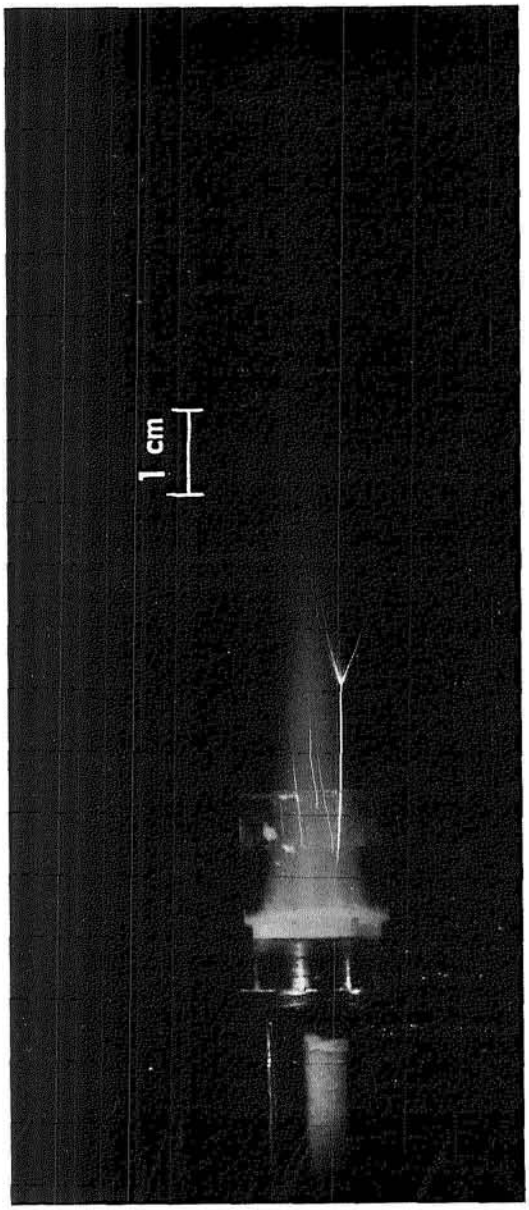

FIG. 7. Burning of a loose powder containing 84% ammonium perchlorate and 16% trioxymethylene; 0.05% aluminum (25-micron diameter) added. Ambient conditions: T = 2410°K, O_2 = 9.2%, H_2O = 43.2%.

b. Aluminum particles do ignite in mixtures which contain sufficient amounts of fuel both at atmospheric and at higher pressures. The minimum ambient temperature necessary for ignition at one atm is 2250–2300°K, in excellent agreement with the results obtained in the gas-burner work.

c. The ambient gases in these experiments generally contain about 40 per cent water vapor, and the combustion process follows the general pattern previously established for high-moisture media. The particle tracks in photographs are sharp. Combustion products have been collected at atmospheric pressure, and were found to contain translucent oxide bubbles. The particles fragment if there is sufficient oxygen in the hot ambient gases. Figure 6 shows two pressed strands of mixtures of ammonium perchlorate and polyvinyl chloride, one without aluminum, the other containing 0.1 per cent of aluminum powder, burning at atmospheric pressure; the product gas contains very little oxygen. Figure 7 illustrates the process of fragmentation as it occurs at atmospheric pressure in the flame products of a loose powder mixture of ammonium perchlorate and trioxymethylene. In view of the fact that the combustion gas in Fig. 7 contained only about 9 per cent of free oxygen, it appears probable that the fragmentation occurred upon contact with ambient air.

Discussion

The main topic requiring discussion is the pronounced difference in burning characteristics induced by the presence of water vapor in the combustion atmosphere. The discussion of this problem must be highly speculative, because very little is known of the alumina-water interaction at flame temperatures.

Brewer and Searcy[7] heated molten alumina in a Knudsen effusion cell and found the rate of volatilization to be the same in the presence and absence of one micron pressure of hydrogen. They presumed from this that no very stable gaseous aluminum subhydroxide species, such as AlOH or $HAlO_2$, exists. Also, Glemser and Volz,[8] studying volatility of solid alumina at 1700°C, found no significant change when one atm of water vapor was present. However, R. F. Walker *et al.*[9] have reported qualitative experiments with the solar furnace which indicate the volatility of molten alumina to be considerably enhanced by a pressure of 25 mm water vapor. They are continuing the study of this interaction.

It is clear that more definitive experiments of behavior of molten alumina in the presence of

water vapor must be carried out before our combustion results can be properly analyzed. However, we tentatively suggest at this time that our results are indicative of a chemical alteration of some property of molten alumina by water. For example, if a subhydroxide forms which is soluble in the molten alumina and changes its surface tension, or alternately forms early in the combustion process and decomposes again when the temperature has risen to a higher level, the bubble-forming property of the alumina to create a diffusion barrier to reaction could be influenced.

Conclusions

All experimental observations point to the conclusion that the ignition process is not affected by the moisture content of the hot ambient gas. The pre-ignition reaction is always controlled by diffusion through the oxide layer which coats the particle, and ignition occurs only when the layer melts, regardless of the composition of ambient gas. On the other hand, there is a distinct effect of water vapor on combustion of aluminum particles. In virtual absence of water, diffusion and combustion take place freely in the gas phase, whereas in the presence of significant amounts of water the process is impeded and confined to a smaller region, because the reactants must diffuse through a condensed oxide layer. Hence the qualitative and quantitative differences.

ACKNOWLEDGMENTS

The authors wish to thank Mr. J. M. Semple for valued experimental assistance in this work. The work was sponsored by Project SQUID which is supported by the Office of Naval Research, Department of the Navy, under Contract Nonr 1858(25) NR–098–038. Reproduction in full or in part is permitted for any purpose of the United States Government.

REFERENCES

1. FRIEDMAN, R. and MAČEK, A.: Combustion and Flame *6*, 9 (1962).
2. CASSEL, H. M. and LIEBMAN, I.: *Ibid. 3*, 467 (1959).
3. GORDON, D. A.: *Solid Propellant Rocket Research*, pp. 271–78. Academic Press, 1960.
4. FASSELL, W. M., PAPP, C. A., HILDENBRAND, D. L., and SERNKA, R. P.: *Ibid.*, pp. 259–69.
5. WOOD, W. A.: *Ibid.*, pp. 287–91.
6. ARDEN, E. A., POWLING, J., and SMITH, W. A. W.: Combustion and Flame *6*, 21 (1962).
7. BREWER, L. and SEARCY, A. W.: J. Am. Chem. Soc. *73*, 5308 (1951).
8. GLEMSER, O. and VOLZ, H. G.: *Third International Conference on the Reactivity of Solids*. Madrid, 1956.
9. WALKER, R. F., VICTOR, A. C., and EFIMENKO, J.: National Bureau of Standards Report 6297, p. 53, Jan. 1959, and subsequent private communication.

Discussion

PROF. I. GLASSMAN (*Princeton University*): In our spectroscopic investigation of burning aluminum wires in oxygen–inert gas mixtures, all bands and lines on the aluminum flame spectrograms are identifiable as Al, AlO, and impurities, and none can be attributed to Al_2O. The wavelength region covered was from the UV to 7400 Å (Fig. 1). Even time-resolved spectrograms synchronized with the ignition process show no unidentifiable bands which could possibly be Al_2O. Although Al_2O has been reported in very low pressure vaporization studies of Al_2O_3, there is no evidence to support its existence in aluminum flames. The only possibility that could resolve this disagreement would be for Al_2O to be present as a short-lived intermediate at the higher pressure at which aluminum flame experiments are carried out.

It is our belief that aluminum oxide hollow spheres are obtained not from a build-up of aluminum vapor pressure under a molten oxide, but from dissolved gas in the metal particle as initially suggested by Gordon.[1] Further, we believe that it is the burning rate, heat loss, and particle size which determine the type of product obtained, as shown in Fig. 2.[2] We would like to emphasize that in this scheme we showed the importance of having the surface temperature of the particle reach the oxide melting point in order to allow rapid combustion to be established. Also, the authors imply that the flame temperature increases with increasing oxygen content and that this factor as well can play a part in the type of products found. It is not apparent to us that the temperature of an aluminum particle diffusion flame could vary with the oxygen concentration, except at very low concentrations. The statement made is inconsistent with the fact that the flame temperature corresponds to the boiling point of the oxide.

In review of their past work the authors state that they find transparent alumina bubbles which they postulate are formed by metal vapor inflation. In their discussion of their new work they state that they find translucent spheres the size of the original particle. One must conclude then that the exhaust

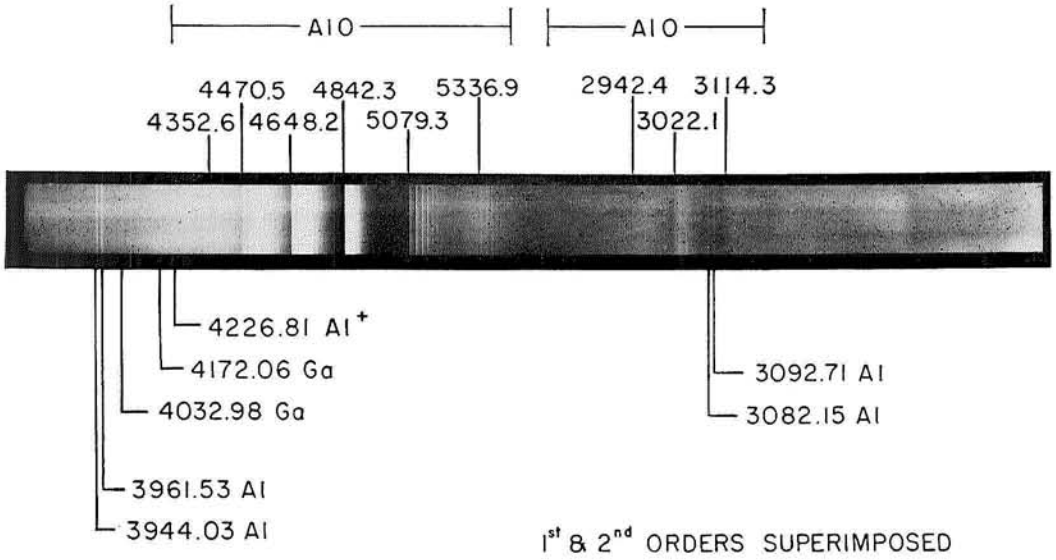

FIG. 1. Flame spectrum of aluminum wire burning in a mixture of oxygen and argon at 50 mm Hg. Oxygen 50%.

spheres are inflated to the size of the initial particle, which would be somewhat fortuitous.

In our work with aluminum wires burned in a certain regime of oxygen partial pressure and total pressure, we observe no change in the character of the aluminum flame or products with or without the presence of appreciable amounts of water vapor as shown in Figs. 3 and 4. In both cases vapor phase flames appear surrounding the lower ends of burning vertical wires. The appearance and spectrum of both flames are very similar. In the regime of operation given in Figs. 3 and 4, most of the products are small translucent spheres some of which are hollow. It may be interesting to note that we find hollow spheres for Zr and Ti when they are burned in a moisture-free oxygen atmosphere (Fig. 5). More im-

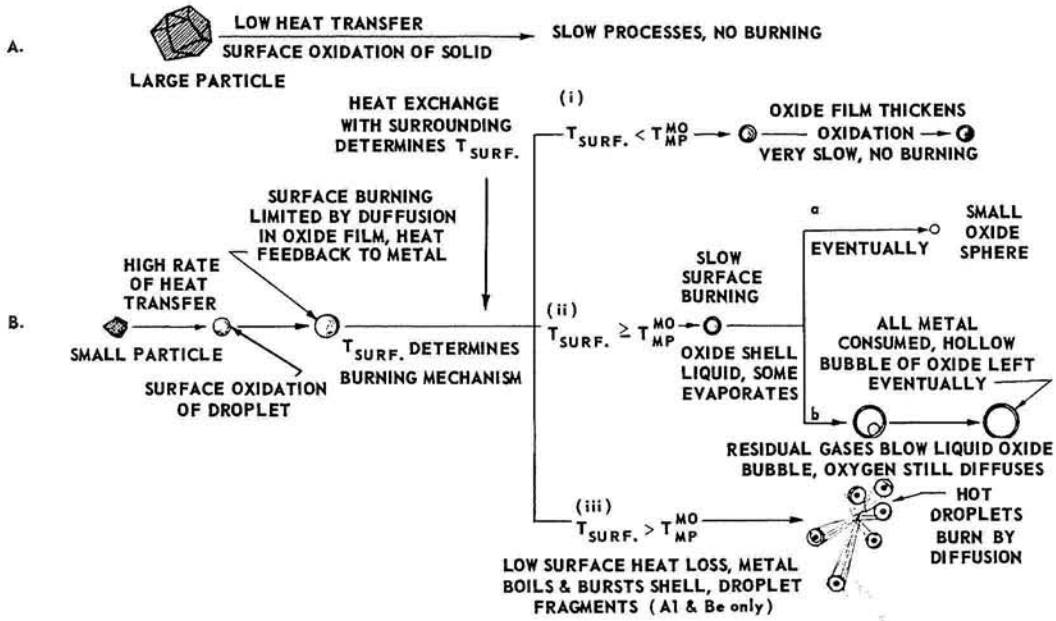

FIG. 2. Postulated explanation of observed burningmechanisms of aluminum powders (from reference 2).

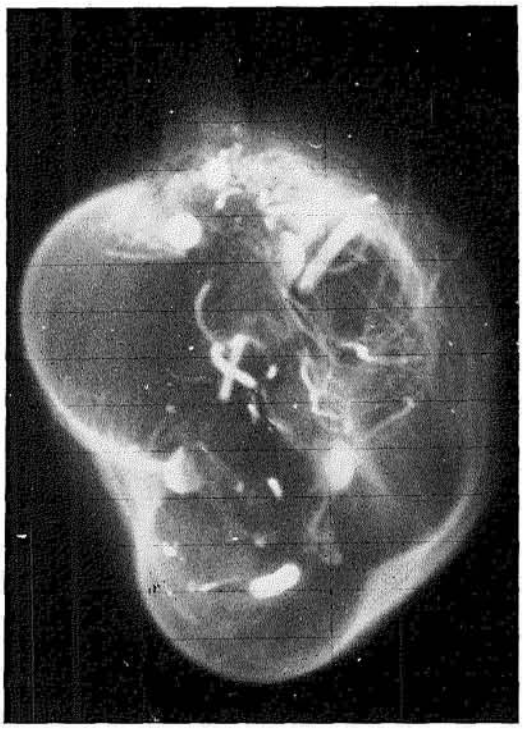

FIG. 3. Vapor-phase flame surrounding the lower end of a vertical aluminum wire. Pressure 50 mm Hg. Oxygen 50%; argon 50%. Wire diameter 0.9 mm.

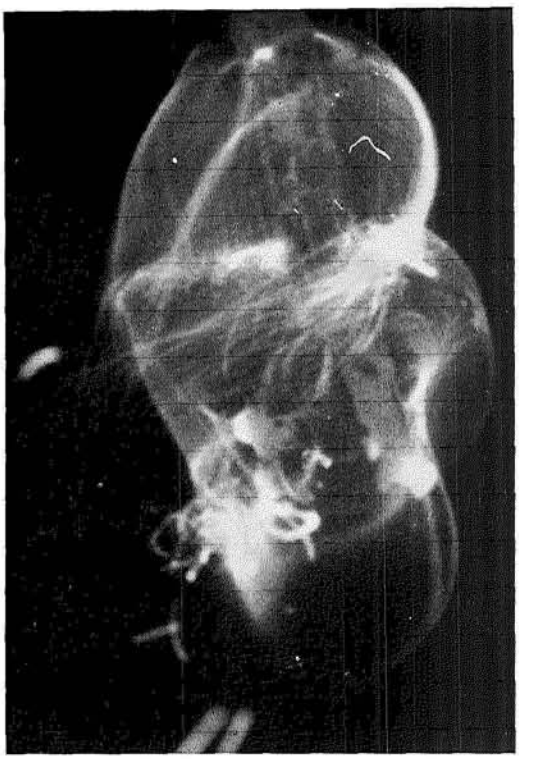

FIG. 4. Vapor-phase flame surrounding the lower end of a vertical aluminum wire. Pressure 50 mm Hg. Oxygen 50%; water vapor 50%. Wire diameter 0.9 mm.

portant to this point are our magnesium studies. A complete total pressure–oxygen partial pressure map of the burning characteristics of Mg wires in O_2–A (moisture-free) mixtures was made. Again, in a certain regime hollow MgO spheres were found. From photographs taken the spheres appear to form in the flame zone. The boundary of each product regime has been associated with a change in burning mechanism as established with corresponding spectrographic observations.

From these corollary pieces of evidence, it is our opinion that the presence of the metal oxide product as hollow spheres is due to a combination of burning mechanism, oxygen partial pressure, total pressure, heat loss, and particle size. The presence of water vapor can alter only the burning mechanism. Apparently the authors are near a regime boundary where a slight change of burning mechanism as altered by the presence of water vapor places them in another product regime.

REFERENCES

1. GORDON, D. A.: Stanford Research Institute, personal communication, 1960.
2. BRZUSTOWSKI, T. A. and GLASSMAN, I.: *Spectroscopic Investigation of Metal Combustion.* Bulletin of the 17th Meeting of the JANAF Solid Propellant Group, SPIA–APL, Johns Hopkins University, Silver Spring, Maryland, May 1961.

DR. F. J. WEINBERG (*Imperial College*): I should like to contribute some observations on the experimental study of combustion involving both radiative and molecular transport processes, in which the cooperative effects Friedman and Maček mention, become serious. This arises from the work on dust flames by Mr. W. S. Affleck and myself. We set out to stabilize a coal dust flame on a burner and, using the built-in particle tracks, deduce burning velocities, temperature changes across the flame zones, etc. If such information is to have any absolute value, the flame must "think that it is infinite," i.e., it must be very large by comparison with the mean free path of photons as well as of molecules. But this is incompatible with the attempted measurement; for if the cloud is so large that its center becomes a black body then, by definition, it is impossible to see those regions.

We are therefore making use of the large difference in the two kinds of mean free path. The dust

FIG. 5. Products of combustion of zirconium foil in oxygen (from reference 2).

cloud under study is small enough to be transparent, yet the cross section of the burner from which it issues is effectively infinite for molecular transport processes. It is viewed through an aperture in a radiating enclosure which surrounds it. The radiation from this enclosure corresponds to that of a black body at the (calculated) flame temperature of the cloud. A furnace would therefore not be adequate and a luminous annular diffusion flame of a hydrocarbon with oxygen (with some nitrogen, if necessary) is used. This is adjusted until pyrometric and calorimetric measurements indicate the desired radiation level. In this manner the cloud is in radiation equilibrium and, at the same time, is accessible to optical methods.

DR. H. SHANFIELD (*Aeronutronic*): The author has noted that a change occurs in the physical nature of the combustion products of aluminum where water vapor is present compared with the case where it is absent. It is worth noting that the presence of such a substantial amount of water vapor must result in a materially lower combustion temperature for the aluminum particle. On a diffusional basis, water will be principal reactant in the flame zone and the presence of the hydrogen will act as a diluent, leading to a reduced maximum temperature. In view of this, the surface temperature of the central particle may be considerably lower, favoring excessive condensation of product aluminum oxide on the particle. It is suggested that this be checked as a possible source of the differences observed.

DR. R. FRIEDMAN (*Atlantic Research Corporation*): Dr. Shanfield suggests a materially lower flame temperature when water vapor is present in the oxidizing atmosphere because of hydrogen diluent. The calculation of combustion temperature under the prevailing nonadiabatic two-phase diffusion-flame conditions is a formidable task and we have not attempted it. While there is a possibility that the point is valid, we feel that the lowering of temperature would probably be quite small unless new species such as AlOH and $HAlO_2$ form. Regardless of hydrogen, nitrogen is already present in substantial proportions as a diluent. Further, the high heat of vaporization of Al_2O_3, most of which remains unvaporized, makes the flame temperature relatively insensitive to diluents. Again, our experiments showed no influence of ambient oxidizer temperature on the combustion mode, and this should have had as much effect as diluent on combustion temperature.

THEORY OF TRANSPORT PROPERTIES OF GASES

E. A. MASON AND L. MONCHICK

This paper reviews recent theoretical work, some still in progress, on the transport properties of gases, with emphasis on those aspects which may be of importance in connection with flame processes. The classical Chapman-Enskog theory of gaseous transport properties is strictly valid only for molecules interacting with a single central force law, and undergoing only elastic collisions. Real gases can differ from this ideal model in at least three important respects: (1) Free radicals and valence-unsaturated atoms, such as occur in partially dissociated gases, can interact along a family of force laws rather than along a single force law, each force law corresponding to a different alignment of the electron spins as the atoms approach. (2) Real molecules usually have force laws which depend on the relative orientation of two molecules, and so are angular-dependent and not central forces. This is especially pronounced for polar gases. (3) Diatomic and polyatomic molecules can undergo inelastic collisions and interchange molecular energy. This affects the heat conductivity particularly strongly.

Recent modifications of the Chapman-Enskog theory which allow these effects to be taken into account (at least approximately) retain the general form of the Chapman-Enskog formulas, but some of the quantities in the formulas must be interpreted and calculated differently. In addition, a new quantity enters, the relaxation time for the transfer of internal molecular energy. The net result is that viscosities and diffusion coefficients are not affected much, but the heat conductivity is significantly affected. This should be taken into account in the estimation of commonly used dimensionless ratios such as the Lewis number and the Prandtl number.

Finally, there is discussed the peculiar special case of a dusty gas, which has also been treated earlier by Waldmann, using different methods. If the diameters of the dust particles are smaller than the mean free path of the gas molecules, the particles can be considered as giant molecules and treated by the present kinetic theory methods. Flames and rocket exhausts frequently contain very small suspended particles, and it is pointed out that the effective forces acting on these particles, owing to gradients of temperature and composition in the gas, can be very large.

Introduction

The purpose of this paper is to report on some recent theoretical work on the kinetic theory of transport properties of dilute gases, with emphasis on those aspects which may be important in connection with flame processes. The rigorous Chapman–Enskog kinetic theory of gases involves, among others, three important assumptions:

1. A pair of molecules interacts according to a single force law.
2. This force law is central; i.e., the force depends only on the distance of separation between the molecules.
3. Molecular collisions are elastic.

Thus the Chapman-Enskog theory strictly applies only to the noble gases, although it often gives a good account of the viscosity and diffusion properties of simple nonpolar polyatomic gases.[1,2] Real gases can often violate these three assumptions, as follows:

1. Free radicals and valence-unsaturated atoms, such as occur in partially dissociated gases, can interact according to a multiplicity of force laws rather than a single force law, each force law corresponding to a different alignment of the electron spins as the atoms approach. For instance, two hydrogen atoms will strongly attract each other if their electron spins are antiparallel (paired), or they will repel each other if their electron spins are parallel. These two situations correspond to the $^1\Sigma$ and $^3\Sigma$ spectroscopic states of H_2, respectively, and a collision of two hydrogen atoms will on the average follow the $^1\Sigma$ force law $\frac{1}{4}$ of the time and the $^3\Sigma$ force law $\frac{3}{4}$ of the time.

2. Real diatomic and polyatomic molecules usually have intermolecular forces which depend on the relative orientation of two molecules as well as on their distance apart. These forces are

thus angular-dependent and not central forces. In some cases this complication can be avoided by assuming that the molecules interact on the average according to an effective central force law, obtained by averaging the correct force law over all relative orientations. This assumption could hardly be expected to be satisfactory for polar molecules, however, for which the sign of the force at large separations (i.e., repulsion or attraction) depends on the relative orientation. In fact a simple unweighted average over all orientations causes the dipole–dipole force to vanish, and so such averaging artificially destroys the polar nature of the molecules.

3. Diatomic and polyatomic molecules can undergo inelastic collisions and interchange molecular internal and translational energy. Furthermore, polar molecules can often directly interchange a quantum of rotational energy on collision, without any change in the relative translational energy. These effects do not seem to have any important influence on viscosity and diffusion, but do strongly influence the heat conductivity.

Recent modifications and extensions of the Chapman–Enskog theory now allow us to take these effects into account, at least to a first approximation. This work is outlined in more detail in the following sections. Although some of the work is still in progress, the following general conclusions seem justified at this time. The Chapman–Enskog formulas retain their same general form, but some of the quantities in the formulas must be interpreted and calculated differently. In addition, some new quantities enter the formulas, which are essentially cross sections for the transfer of internal molecular energy. These are in some cases available experimentally from relaxation times determined by ultrasonic or shock tube techniques, but in other cases they must be estimated theoretically from the properties of the molecules themselves, or as a last resort treated as disposable parameters. The net result is that viscosities and diffusion coefficients are not affected much, but the heat conductivity is significantly affected in almost all cases. This should probably be taken into account in the estimation of commonly used dimensionless ratios such as the Lewis number and the Prandtl number.

We first consider multiple interaction curves, and the solution of this problem suggests an approximate treatment of orientation-dependent forces, which are considered next. Attempts to give a more mathematical expression to the physical arguments used to simplify the problem of orientation-dependent forces are discussed. These lead further to an approximate calculation of the effects of inelastic collisions, which are considered in the third section following. Finally, in the last section a peculiar special case is mentioned in which some of the molecules are extremely heavy and large (but not larger than the mean free path). This case is approximated in practice by a gas containing small suspended particles of dust or droplets of liquid. From the present point of view these are simply giant molecules. This special case of a dusty gas has been treated earlier by Waldmann by different methods than those used here, with essentially the same results. What is perhaps significant, however, is that flames and rocket exhausts frequently contain very small suspended particles, and it turns out that the effective forces acting on those particles, owing to temperature and composition gradients in the gas, can be very large.

Multiple Force Laws

To explain the effect of multiple force laws it is convenient to recall first the Chapman-Enskog results for a single force law, using the viscosity η as an illustration. For a pure gas composed of molecules of mass m at absolute temperature T, the viscosity is[1,2]

$$\eta = \tfrac{5}{16}[(\pi mkT)^{\frac{1}{2}}/\pi\sigma^2\Omega^{(2,2)*}], \qquad (1)$$

where k is Boltzmann's constant and σ is a molecular "size" or range-of-force parameter. The heart of the theory is contained in the reduced collision integral $\Omega^{(2,2)*}$, a dimensionless quantity which depends on the temperature and on the force law through the angle of deflection χ suffered in a binary molecular collision. The deflection angle is suitably averaged over all initial velocities g and impact parameters b to produce the collision integral, as follows:

$$\Omega^{(2,2)*} = \sigma^{-2}\int_0^\infty \gamma^7 \exp(-\gamma^2) \times \int_0^\infty [(1 - \cos^2\chi)\, b\, db]\, d\gamma, \qquad (2)$$

where $\gamma^2 = (m/4kT)g^2$. The details of this expression do not concern us here; what matters is that $\Omega^{(2,2)*}$ can be calculated straightforwardly by classical mechanics if the force law is given as a function of molecular separation. The definition of $\Omega^{(2,2)*}$ is such that it is equal to unity for rigid spheres of diameter σ, so that its deviations from unity as the temperature is changed can be considered as a rough measure of the "softness" of the intermolecular forces. Other collision integrals, involving somewhat different averaging over collisions than Eq. (2), arise for other

transport properties; of course the expressions for multicomponent mixtures are algebraically much more complicated than Eq. (1), but the basic computational procedure is always the same.

To allow for multiple force laws it is necessary to solve the whole kinetic theory problem over again from the very beginning. Somewhat surprisingly, the final result is quite simple and is valid to all degrees of the Chapman-Enskog approximation for mixtures of any complexity.[3] All the formulas retain exactly their original form, but each collision integral which appears must be replaced by a weighted mean over the different possible force laws. That is, for a given pair of colliding molecules we make the replacement,

$$\Omega^{(l,s)*} \longrightarrow \langle \Omega^{(l,s)*} \rangle \equiv \sum p_i \Omega_i^{(l,s)*}, \qquad (3)$$

where p_i is the statistical weight of the ith force law. For instance, in a gas composed of ground-state hydrogen atoms, the p_i take just the two values of $\frac{1}{4}$ and $\frac{3}{4}$ in Eq. (3). After $\langle \Omega^{(2,2)*} \rangle$ is formed, Eq. (1) can be used as it stands. In a gas composed of a mixture of ground-state hydrogen and nitrogen atoms, the p_i take the values of $\frac{1}{4}$ and $\frac{3}{4}$ for H–H collisions; for N–N collisions they take the values $\frac{1}{16}$, $\frac{3}{16}$, $\frac{5}{16}$, and $\frac{7}{16}$ corresponding to the four spectroscopic states of the N_2 molecule, and for N–H collisions they take the values $\frac{3}{8}$ and $\frac{5}{8}$ corresponding to the two spectroscopic states of the NH molecule. After the average collision integrals are formed, the rest of the calculation proceeds as for a binary mixture of inert gas atoms. (It is assumed in the foregoing that the same value of σ is chosen for all curves corresponding to a given binary encounter; otherwise it is the quantity $\sigma^2\Omega^{(l,s)*}$ that must be averaged.)

Orientation-Dependent Forces

Orientation-dependent forces produce two basic complications in the Chapman-Enskog theory. In the first place, they provide a mechanism for the interchange of rotational and translational energy, and so introduce all the traditional difficulties associated with inelastic collisions in kinetic theory. In the second place, the very complicated molecular collision trajectories associated with orientation-dependent forces make the mathematical computations necessary to obtain a collision integral almost impossibly difficult, even for a modern computing machine, and even if inelastic collisions are ignored. Fortunately, a little consideration of the basic physics of molecular collisions suggests two simplifying assumptions which make the problem mathematically tractable.[4]

Two Assumptions about Collisions

The first assumption is that the inelastic collisions, even though they may occur frequently, have little effect on the trajectories. Most inelastic collisions might be expected to involve the transfer of only one or two quanta of rotational energy. At ordinary temperatures, however, this amount of energy is much less than kT, but the average translational kinetic energy is of the order of kT. On energy grounds we thus expect rotational energy transfer to have only a small effect on the trajectories, and we neglect it. Evidence from the transport properties of nonpolar polyatomic gases also supports this assumption, since most of their transport properties can be described fairly well on the basis of a central field force law.[2] Thus the transport of momentum (viscosity) and of molecules (diffusion) are not much affected by inelastic collisions, and the very existence of molecular internal energy can largely be ignored for these properties. It cannot be ignored for any property which depends specifically on the transfer of internal energy, however, and this assumption is admittedly inadequate for the heat conductivity of polyatomic gases. Heat conductivity requires an entirely separate discussion, which is given in the next section.

The second assumption concerns the distortion of a collision trajectory by the orientation-dependent part of the intermolecular force. To at least a first approximation, the only feature of a collision which affects the transport properties is the angle of deflection χ in a collision, as illustrated by Eq. (2). Although the force acts along the whole trajectory, χ is determined primarily by the interaction in the vicinity of the distance of closest approach of the pair of colliding molecules. In more mathematical terms, the integral over the trajectory, which gives χ as a function of g and b, has its integrand sharply peaked in the region corresponding to the distance of closest approach. Over a small portion of the trajectory around the distance of closest approach it seems reasonable that the relative orientation of two colliding molecules does not have time to change much, so that χ is determined largely by only one relative orientation, rather than by all possible orientations assumed along the entire trajectory. We therefore assume that in a given collision only one relative orientation is effective, and for simplicity evaluate χ as if the orientation were fixed at one value throughout the whole collision, since the orientations away from the distance of closest approach have little effect on χ. Different collisions correspond to different fixed orientations, but in any one collision the force law is now effectively spherically symmetric. The col-

lision dynamics of this problem are soluble, so that the original insoluble problem has been converted to a different one which is soluble.

The approximation of a fixed relative orientation changes the emphasis of the problem from the collision dynamics to the kinetic theory. The kinetic theory problem now corresponds to a gas in which collisions follow not one intermolecular force law, but any one of a very large number of force laws, one for each relative orientation. Although we could not solve the original dynamical problem, we can solve this new kinetic theory problem—in fact, it is just the problem whose solution was discussed in the preceding section.

Polar Gases and Gas Mixtures

The foregoing approximations should be applicable to any angular-dependent force law, but the angular-dependent force of most practical interest is that between two dipoles, and this is the only case for which detailed numerical calculations have yet been made.[4] The simplest model which we can invent and which we may hope will mimic the main features of forces between two real polar molecules consists of a spherically symmetric force plus an angular-dependent force due to the two dipoles. For the spherical part it is reasonable to choose a form similar to that used for nonpolar molecules. A potential energy of interaction which has been very widely used for polar molecules is the Stockmayer potential,

$$\varphi = 4\epsilon_0[(\sigma_0/r)^{12} - (\sigma_0/r)^6] - (\mu_1\mu_2/r^3)\zeta, \quad (4)$$

where φ is the potential energy between two molecules at a given separation distance r and a given relative orientaiton, μ_1 and μ_2 are the molecular dipole moments, and ζ is the angle-dependent factor,

$$\zeta = 2\cos\theta_1\cos\theta_2 - \sin\theta_1\sin\theta_2\cos\phi,$$

in which θ_1, θ_2, and ϕ are the usual angles specifying the relative orientation of two dipoles. As μ_1 or μ_2 approaches zero, φ is just the Lennard-Jones (12–6) potential used for nonpolar gases, with a potential well depth of ϵ_0 and a "diameter" of σ_0.

According to our simplifying assumptions, collision integrals can be evaluated with ζ given a series of different fixed values, and then an average taken over the values of ζ. When this is done, the kinetic theory of polar gases looks just like the kinetic theory of nonpolar gases, but with a different set of collision integrals which still have to be calculated by numerical integration. We have carried out these calculations,[4] and used experimental viscosities and dipole moments of a number of polar gases to determine the parameters ϵ_0 and σ_0 of Eq. (4), which we then used to calculate other properties for comparison with experiment. The overall agreement, which is discussed in detail elsewhere,[4] is comparable to that obtained for nonpolar gases with the Lennard-Jones (12–6) model.

Although practically no measurements have been made on mixtures of two or more polar gases, many measurements are available on mixtures of a polar and a nonpolar gas. Our model can be easily extended to include mixtures,[5] with results for diffusion coefficients and viscosities which are generally of the order of experimental scatter (5 to 10% for diffusion and 1 to 2% for viscosity). Thermal diffusion results are potentially the most interesting, since they are very sensitive to the intermolecular forces, but experimental data are scanty. Our preliminary results look promising, nevertheless.[5]

Possible Further Applications

Although our treatment of orientation-dependent forces has been applied only to polar gases, it is applicable to any orientation-dependent force which falls off fairly rapidly with distance. It thus provides a mathematically tractable model for the investigation of the effect of molecular "shape" on gaseous transport properties. Although these "shape effects" are probably not of great importance in cases of interest in flame and combustion phenomena, the question has never been investigated in detail. It should now be possible to estimate these effects and see whether or not they need to be taken into account in fundamental flame processes.

Hornig and Hirschfelder[6] have given quantum-mechanical arguments for a similar treatment of collisions of molecules with angular-dependent forces. Essentially their argument amounts to the observation that the potential curves are functions only of r, the distance between the centers of mass of the two molecules, and the fact that in an impact parameter type of calculation the molecules will tend to follow one particular potential curve, although transitions between the various curves are possible. The results of a calculation along the lines proposed by these authors would be unambiguous only for large impact parameters, or if $\Delta\epsilon \ll 1$ in the notation of the next section. In an entirely different argument, Arthurs and Dalgarno[7] show that the classical limit of a distorted wave approximation for the collision of a linear rotator and an ion leads to an averaging procedure for the cross sections similar to that outlined in the previous section.

Inelastic Collisions

The arguments in the preceding section, about the effect of inelastic collisions, are plausible but not completely convincing. In particular, there is the implicit assumption that the *only* effect of inelastic collisions on viscosity and diffusion is a distortion of the collision trajectories, so that if this distortion is negligible, then the whole effect of inelastic collisions is also negligible. It is conceivable that inelastic collisions might influence these transport properties in other ways than through the trajectories, and it would be comforting to be able to investigate this point in more detail. Such an investigation requires as a starting point a comprehensive kinetic theory for polyatomic gases which includes the effects of inelastic collisions. Such a theory actually exists for a pure gas, developed over ten years ago by Wang Chang and Uhlenbeck[8] in a semiclassical approximation, and more recently by Taxman[9] for the classical limit. These theories formally solve the kinetic theory problem, but they appear almost unusable because the task of solving the dynamical problem of inelastic molecular collisions seems hopelessly complicated, even with modern computing facilities. However, when the formula for the viscosity is examined with the aim of providing a better justification for the approximations we have made, it becomes apparent that the terms referring to inelastic collisions can be sorted into several types, some of which can be reasonably neglected and some of which can be expressed in terms of other experimental quantities. This rather simple observation provided a key by which the effect of internal energy and inelastic collisions on the thermal conductivity could be handled by the existing formal theory.

In the first part of this section we illustrate this line of approach for pure gases. To proceed to mixtures we first need to develop a formal kinetic theory for multicomponent mixtures analogous to the theory of Wang Chang and Uhlenbeck and of Taxman for pure gases. This is straightforward in principle but very complicated and tedious in practice, and we are still in the process of working it out in collaboration with Dr. Kwang-Sik Yun. A few preliminary results are available, however, and these are discussed in the second part of this section.

Pure Gases

We first show how the formal theory can be handled for the comparatively simple properties of viscosity and diffusion, and then discuss the more complicated case of the thermal conductivity.[10]

Viscosity. The formal expression for the viscosity still looks like Eq. (1), but the collision integral is more complicated:

$$2\pi\sigma^2\Omega^{(2,2)*} = \Big[\sum_i \exp(-\epsilon_i)\Big]^{-2} \sum_{ijkl} \exp\,(-\epsilon_i - \epsilon_j) \times \int_0^\infty \gamma^3 \exp\,(-\gamma^2)\, d\gamma \int_0^\pi \sin\chi\, d\chi \times \int_0^{2\pi} \big[\gamma^4(1 - \cos^2\chi) + \tfrac{1}{3}(\Delta\epsilon)^2 - \tfrac{1}{2}(\Delta\epsilon)^2 \sin^2\chi\big] I_{ij}^{kl}\, d\phi, \quad (5)$$

where the internal quantum states of the molecules are denoted by the subscripts i, j, k, l, and $\epsilon_i = E_i/kT$, where E_i is the energy of the ith internal quantum state. A collision occurs between two molecules initially in internal quantum states i and j, which are scattered through the polar angle χ and the azimuth angle ϕ, and end up in states k and l. The differential cross section for this scattering process is $I_{ij}^{kl} = I_{ij}^{kl}(g, \chi, \phi)$, and $\Delta\epsilon = \epsilon_k + \epsilon_l - \epsilon_i - \epsilon_j = \gamma^2 - \gamma'^2$, where the prime refers to the relative kinetic energy after collision.

According to our assumptions, $\Delta\epsilon \ll \gamma^2$, and the terms in $\Delta\epsilon$ may be dropped from Eq. (5). The assumption of negligible distortion of the trajectory means that I_{ij}^{kl} can be replaced by the differential cross section for elastic scattering, I_{el}. The summation over internal states can be carried out because we assume the translational motion is independent of the internal states, and the integration over $d\phi$ yields 2π. Thus Eq. (5) reduces to

$$\sigma^2\Omega^{(2,2)*} = \int_0^\infty \gamma^7 \exp\,(-\gamma^2)\, d\gamma \times \int_0^\pi I_{el}(1 - \cos^2\chi) \sin\chi\, d\chi, \quad (6)$$

which is exactly equivalent to Eq. (2) in the classical limit, for which $I_{el} \sin\chi\, d\chi = b\, db$.[1,2]

We thus find that our approximations do indeed lead to a mathematically consistent result. We can even proceed to a higher approximation, since the terms involving $(\Delta\epsilon)^2$ are given by the theory in terms of a relaxation time τ:

$$\tau^{-1} = (2nk/c_{\text{int}})\,(kT/\pi m)^{\frac{1}{2}}\Big[\sum_i \exp\,(-\epsilon_i)\Big]^{-2} \times \sum_{ijkl} \exp\,(-\epsilon_i - \epsilon_j) \int_0^\infty \gamma^3 \exp\,(-\gamma^2)\, d\gamma \times \int_0^\pi \sin\chi\, d\chi \int_0^{2\pi} I_{ij}^{kl}\,(\Delta\epsilon)^2\, d\phi, \quad (7)$$

where n is the number of molecules per cc and c_{int} is the internal heat capacity per molecule. It is convenient to break the coupling between internal and translational motion which occurs in the term $(\Delta\epsilon)^2 \sin^2\chi$ of Eq. (5) by using some sort of average value for $\sin^2\chi$. This procedure yields

$$\eta^{-1} = \eta_{el}^{-1}\left[1 + \tfrac{4}{15}(\eta_{el}/p\tau)\,(c_{\text{int}}/k)\,(1 - \tfrac{3}{2}\,\overline{\sin^2\chi})\right] \tag{8}$$

where η_{el} is the elastic collision approximation obtained from Eq. (6). If we use for $\overline{\sin^2\chi}$ a value of $\frac{2}{3}$ corresponding to the rigid sphere model, we find the correction term vanishes. To a rough second approximation, then, the viscosity is not affected by inelastic collisions.

Diffusion. Diffusion is really a mixture property, even self-diffusion in pure gases, and the following result for the self-diffusion coefficient D_{11} is really a limiting case of the result in the second section:

$$D_{11} = (3/8\rho)\left[(\pi mkT)^{\frac{1}{2}}/\pi\sigma^2\Omega^{(1,1)*}\right], \tag{9}$$

where

$$\pi\sigma^2\Omega^{(1,1)*} = \left[\sum_i \exp(-\epsilon_i)\right]^{-2} \times \sum_{ijkl} \exp(-\epsilon_i - \epsilon_j) \int_0^\infty \gamma^3 \exp(-\gamma^2)\, d\gamma \times \int_0^\pi (\gamma^2 - \gamma\gamma' \cos\chi) \sin\chi\, d\chi \int_0^{2\pi} I_{ij}^{kl}\, d\phi, \tag{10}$$

where $\rho = nm$ is the gas density. If for a first approximation we entirely neglect inelastic collisions, we recover immediately the Chapman-Enskog expression. For a second approximation $\gamma\gamma'$ may be expanded as a series in $\Delta\epsilon$ and only the first two terms kept.[10] The first term gives us back the Chapman-Enskog expression; the second term is linear in $\Delta\epsilon$ and should integrate approximately to zero, since $\Delta\epsilon$ would be expected to be negative about as often as positive. To a rough second approximation, the self-diffusion coefficient is also not affected by inelastic collisions.

Thermal Conductivity. The traditional approximate approach initiated by Eucken has been to break up the transport of energy into two parts: one due to the translational energy of the molecules, which is taken to be the same as for the inert gases, and one due to the internal energy of the molecules, which is assumed to be transported by a diffusion mechanism. This approach leads to the following expression for the thermal conductivity λ:

$$\lambda m/\eta = \tfrac{5}{2}(\tfrac{3}{2}k) + (\rho D_{11}/\eta)\,(c_{\text{int}}), \tag{11}$$
$$= \lambda_{\text{tr}} m/\eta + \lambda_{\text{int}} m/\eta,$$

where the first term on the right is the translational contribution and the second term is the internal contribution.

The formal expression for λ given by Wang Chang and Uhlenbeck is quite complicated, and we shall not write it out; but when we neglect inelastic collisions and distortions of trajectories, we find to our surprise that Eq. (11) emerges directly. Although Eq. (11) has been derived many times by a variety of arguments, this is the first derivation by purely kinetic theory methods (for details see reference 10). Having established this much, we can now go one step further and include at least a first-order correction for the inelastic collisions. Instead of the factors $(\frac{5}{2})$ and $(\rho D_{11}/\eta)$ in Eq. (11) we get

$$\frac{5}{2} \rightarrow \frac{5}{2}\left[1 - \frac{5}{6}\left(1 - \frac{2}{5}\frac{\rho D_{\text{int}}}{\eta}\right)\left(\frac{c_{\text{int}}}{k}\right)\left(\frac{\eta}{p\tau}\right)\right] \tag{12}$$

$$\frac{\rho D_{11}}{\eta} \rightarrow \frac{\rho D_{\text{int}}}{\eta}\left[1 + \frac{5}{4}\left(1 - \frac{2}{5}\frac{\rho D_{\text{int}}}{\eta}\right)\left(\frac{\eta}{p\tau}\right)\right] \tag{13}$$

in which D_{int} is the diffusion coefficient for the diffusion of internal energy, and η is the true (experimental) viscosity, not just an approximation to it. For nonpolar polyatomic gases D_{int} should be essentially the same as D_{11}.

Equations (12) and (13) seem to give quite satisfactory agreement with experiment for nonpolar gases, as far as we have been able to test them,[10] and most of the previously noted anomalies in the ratio $f = \lambda M/\eta C_v$ are accounted for quantitatively. It turns out that the only significant contribution to τ under ordinary circumstances is that due to the interchange of rotational and translational energy. The decrease of λ_{tr} and the increase of λ_{int} with the onset of energy interchange between internal and translational energy are very likely universally true. This was deduced 20 years ago in an intuitive argument by Schäfer, Rating, and Eucken.[11] They observed that the rate of transport of translational energy in the absence of energy exchange is $\frac{5}{2}$ times as fast as the transport of internal energy (taking $\rho D_{11}/\eta = 1$ for simplicity). This is because the molecules with translational energy $\frac{1}{2}mv^2 > \frac{3}{2}kT$ travel faster than molecules with $\frac{1}{2}mv^2 = \frac{3}{2}kT$. When an average is taken over all velocities, the factor $\frac{1}{2}mv^2$ shifts the maximum of the velocity distribution and increases the net rate of transport of translational energy. When there is a possi-

bility of interchange of translational and internal energy, they argued, a molecule may travel with its energy in the form of translational energy part of the time and in the form of internal energy part of the time. The result will be a decrease in the net rate of transport of translational energy and an increase in the net rate of transport of internal energy.

For polar gases a second effect is often important in that a resonant exchange of rotational energy between two molecules is probable. Thus a glancing collision with exchange looks like a head-on collision without exchange, as far as the transport of the quantum of internal energy is concerned. This has the effect of reducing the value of D_{int} below that of D_{11}. This exchange effect can be calculated theoretically without too much trouble because of the resonance conditions, and nicely explains the fact that the thermal conductivity of some polar gases appears anomalously low.

Detailed numerical computations and comparisons with experimental results are given in reference 10.

Mixtures

The trick by which we have made the formal kinetic theory of pure polyatomic gases usable is to avoid trying to solve the difficult dynamical problem inherent in the differential cross sections $I_{ij}^{kl}(g, \chi, \phi)$, and instead to lump together the difficult parts and express them in terms of new experimental quantities, the relaxation times. We are, so to speak, letting the experiments evaluate the integrals for us. This can obviously be extended to mixtures, which are the cases of real interest in practical applications. Our work on this is still in progress, but we can at present report on the results for diffusion and viscosity.

Diffusion. Multicomponent diffusion is completely described by a set of binary diffusion coefficients,[2] so we need consider only these. The expression is

$$D_{12} = (3/8n)(\pi kT/2\mu)^{\frac{1}{2}}(\pi\sigma_{12}^2\Omega_{12}^{(1,1)*})^{-1},$$

where

$$\pi\sigma_{12}^2\Omega_{12}^{(1,1)*} = [\sum_i \exp(-\epsilon_i)]^{-2} \times \sum_{ijkl} \exp(-\epsilon_i - \epsilon_j) \int_0^\infty \gamma^3 \exp(-\gamma^2)\, d\gamma \times \int_0^\pi (\gamma^2 - \gamma\gamma' \cos\chi) \sin\chi\, d\chi \int_0^{2\pi} I_{ij}^{kl}\, d\phi, \tag{14}$$

where $\mu = m_1m_2/(m_1 + m_2)$ is the reduced mass of a pair of colliding molecules of species 1 and 2, and now $\gamma^2 = (\mu/2kT)g^2$. We can make exactly the same approximations as for D_{11}, and we find that to a rough second approximation the binary diffusion coefficient is not affected by internal energy and inelastic collisions.

Viscosity. The classical expression for the viscosity of a multicomponent mixture of gases with central forces and elastic collisions is[2]

$$\eta_{\text{mix}} = \frac{\begin{vmatrix} H_{11} & \cdots & H_{1\nu} & x_1 \\ \cdot & & \cdot & \cdot \\ \cdot & & \cdot & \cdot \\ \cdot & & \cdot & \cdot \\ H_{\nu 1} & \cdots & H_{\nu\nu} & x_\nu \\ x_1 & \cdots & x_\nu & 0 \end{vmatrix}}{\begin{vmatrix} H_{11} & \cdots & H_{1\nu} \\ \cdot & & \cdot \\ \cdot & & \cdot \\ \cdot & & \cdot \\ H_{\nu 1} & \cdots & H_{\nu\nu} \end{vmatrix}} \tag{15}$$

where x_i is the mole fraction of the ith component and

$$H_{ii} = \frac{x_i^2}{\eta_i} + \sum_{k=1,k\neq i}^{\nu} \frac{2x_ix_k}{(m_i + m_k)nD_{ik}} \times \left(1 + \frac{3}{5}\frac{m_k}{m_i} A_{ik}^*\right), \tag{16}$$

$$H_{ij}(i \neq j) = -\frac{2x_ix_j}{(m_i + m_j)nD_{ij}} (1 - \tfrac{3}{5}A_{ij}^*), \tag{17}$$

$$A_{ij}^* = \Omega_{ij}^{(2,2)*}/\Omega_{ij}^{(1,1)*}. \tag{18}$$

When we formally allow for inelastic collisions, we find that the results can be arranged to look exactly like Eqs. (15)–(17), with true (experimental) values of η_i and D_{ij} rather than elastic approximations, but that the collision integrals in the ratio A_{ij}^* are now given by Eqs. (5) and (14), with of course $2\mu_{ij}$ replacing m everywhere. In other words, the relation among experimental quantities is practically the same whether elastic collisions occur or not, and we can deposit the whole deviation from the relation in the quantity A_{ij}^*. But when we make our systematic approximations to evaluate the effect of inelastic collisions on A_{ij}^*, we find as before that there is no effect to at least a rough second approximation.

Equations (15)–(18) can be used to calculate diffusion coefficients from measurements on the viscosity of mixtures without the introduction of any specific information about intermolecular forces, other than through their very weak in-

fluence on A_{ij}^*. Very good agreement with direct measurements of diffusion coefficients has been obtained for mixtures of simple nonpolar gases.[12] The foregoing results now validate this useful procedure for mixtures involving polar molecules and complicated polyatomic molecules.

Other Transport Properties. The properties of most interest from the point of view of inelastic collisions are thermal conductivity and thermal diffusion. Unfortunately the results for these properties are extremely complicated when inelastic collisions are possible, and no final results have yet been obtained.

A Special Example: Dusty Gases

There is a peculiar special case, of some practical interest, which can be treated by the methods outlined in the preceding sections. It arises when one of the species in a gas mixture is present only as a trace (i.e., its mole fraction approaches zero), but the molecules of this species are much heavier and much larger than any other molecules in the mixture. Such a situation is closely approximated in practice by a gas mixture containing small suspended particles (dust, smoke, aerosols, etc.), the suspended particles acting like giant molecules. For brevity we refer to such a mixture as a dusty gas. It turns out that the effective forces on the dust particles, due to gradients of temperature, pressure, or composition in the gas, can be extremely large. For instance, a temperature difference of the order of a degree is sufficient to sweep almost all the dust out of the gradient region and into the colder boundary, if sufficient time is allowed to reach the steady state. The subject goes back at least to 1870, when Tyndall noticed a dust-free region (the "Tyndall dark space") in the gas space about a hot body,[13] but it is only in comparatively recent times that the subject has been viewed as merely a peculiar special case of the kinetic theory of gases. Since flames and rocket exhausts frequently contain very small suspended particles whose behavior may be of importance in understanding the flame processes, this special case may be of some interest in this symposium.

The dusty gas has been treated by Waldmann[14] by the procedure of adding up all the impulses transferred to a dust particle by the colliding gas molecules. Much the same procedure was carried through independently even earlier by Russian workers.[15] These momentum transfer calculations are much more difficult to carry through than the kinetic theory calculations (essentially because the difficult part of the calculation has already been completed in the kinetic theory), but the results are of course the same. The kinetic theory approach has been carried through by Mason and Chapman.[16]

The results depend to some extent on the nature of the collisions between gas molecules and dust particles. It is usually assumed that the dust particles can be taken as spheres and three scattering patterns are distinguished:

(a) Elastically specular scattering, in which the impinging molecule is reflected specularly from the sphere with no change in relative velocity. This corresponds to the classical Chapman–Enskog kinetic theory case, and leads to a collision integral for diffusion of dust particles of radius R of

$$\pi\sigma^2\Omega^{(1,1)*} = \pi R^2. \tag{19}$$

(b) Elastically diffuse scattering, in which the gas molecules rebound from the sphere with unchanged relative velocity, but in random directions. This corresponds to the multiplicity of interaction curves discussed in the second section, and gives a collision integral for diffusion of [16]

$$\pi\sigma^2\Omega^{(1,1)*} = (13/9)\pi R^2. \tag{20}$$

Usually specular and diffuse scattering are mixed, it being assumed that a fraction f rebounds diffusely and the remainder specularly. This yields $\Omega^{(1,1)*} = 1 + (4/9)f$.

(c) Thermally diffuse scattering, in which the gas molecules rebound from the sphere with a random distribution of directions and a random (Maxwellian) distribution of speeds. This corresponds to inelastic collisions and must be treated by the methods of the preceding section. The collision integral for diffusion found by Waldmann for this case is[14]

$$\pi\sigma^2\Omega^{(1,1)*} = [1 + (\pi/8)]\pi R^2. \tag{21}$$

If specular and thermally diffuse scattering are mixed by assuming that a fraction a rebounds diffusely and the remainder specularly, the result is $\Omega^{(1,1)*} = 1 + (\pi/8)a$.

Among the most interesting results for the dusty gas are the strong forces exerted on the dust by a temperature gradient. This corresponds to the kinetic theory phenomenon of thermal diffusion. The thermal diffusion factor α for the dusty gas, as worked out by the methods outlined earlier in the preceding section, can be written as

$$\alpha = (1/5)(6C_{12}^* - 5)(T\lambda_{tr}/pD_{12}) \tag{22}$$

where C_{12}^* is a collision integral ratio (analogous to A_{12}^*), λ_{tr} is the translational heat conductivity of the gas, and D_{12} is the diffusion coefficient

of the dust through the gas. For ordinary gas mixtures α is of the order of magnitude of unity or less. But for a dusty gas α is of the order of magnitude of 10^6 to 10^8.[14] This accounts for the tremendous effect of a very small temperature difference on suspended dust particles. Of course, D_{12} is reduced by a similar factor, so that the operation of thermal diffusion in a dusty gas is rather slow compared to that in an ordinary gas mixture, although much greater in magnitude.

For scattering patterns (a) and (b), the value of $(6C_{12}^* - 5)$ is unity, but for scattering pattern (c), Waldmann's results suggest that $(6C_{12}^* - 5) = [1 + (\pi/8)a]^{-1}$. The occurrence of λ_{tr} in Eq. (22) is particularly interesting. Usually one succeeds only in measuring the total thermal conductivity $\lambda = \lambda_{tr} + \lambda_{int}$. This suggests that it may be possible to make a direct measurement of λ_{tr} and so check individually the results given in Eqs. (12) and (13) for the effect of inelastic collisions on thermal conductivity.

Acknowledgments

The authors wish to thank Dr. Kwang-Sik Yun, who is collaborating with them on the investigation partially reported in the fourth section, and the National Aeronautics and Space Administration and the U. S. Navy for their support.

References

1. Chapman, S. and Cowling, T. G.: *The Mathematical Theory of Non-Uniform Gases*, 2nd ed. Cambridge Univ. Press, 1952.
2. Hirschfelder, J. O., Curtiss, C. F., and Bird, R. B.: *Molecular Theory of Gases and Liquids*. Wiley, 1954.
3. Mason, E. A., Vanderslice, J. T., and Yos, J. M.: Phys. Fluids *2*, 688 (1959).
4. Monchick, L. and Mason, E. A.: J. Chem. Phys. *35*, 1676 (1961).
5. Mason, E. A. and Monchick, L.: J. Chem. Phys. *36*, 2746 (1962).
6. Hornig, J. F. and Hirschfelder, J. O.: Phys. Rev. *103*, 908 (1956).
7. Arthurs, A. M. and Dalgarno, A.: Proc. Roy. Soc. (London) *A256*, 552 (1960).
8. Wang Chang, C. S. and Uhlenbeck, G. E.: *Transport Phenomena in Polyatomic Gases*. University of Michigan Engineering Research Report No. CM–681, 1951. See also reference 2, pp. 501–506.
9. Taxman, N.: Phys. Rev. *110*, 1235 (1958).
10. Mason, E. A. and Monchick, L.: J. Chem. Phys. *36*, 1622 (1962).
11. Schäfer, K., Rating, W., and Eucken, A.: Ann. Physik *42*, 176 (1942).
12. Weissman, S. and Mason, E. A.: J. Chem. Phys. *37*, 1289 (1962).
13. For a review of this and other early work see Rosenblatt, P. and La Mer, V. K.: Phys. Rev. *70*, 385 (1946).
14. Waldmann, L.: Z. Naturforsch. *14a*, 589 (1959).
15. A review of the earlier Russian work is given by Bakanov, S. P. and Derjaguin, B. V.: Discussions Faraday Soc. *30*, 130 (1960).
16. Mason, E. A. and Chapman, S.: J. Chem. Phys. *36*, 627 (1962).

Discussion

Dr. R. S. Brokaw (*NASA*): The thermal conductivities of highly polar gases (e.g., HF, H_2O, NH_3) appear to be anomalously low in relation to their viscosities. Mason and Monchick propose that this effect is largely due to a resonant exchange of rotational energy, which is probable on self-collisions of polar molecules.

We have made preliminary measurements on the relative thermal conductivities of H_2O and D_2O which we believe provide experimental verification of Mason and Monchick's postulate. In the absence of the resonant phenomenon we expect the thermal conductivity of H_2O to be somewhat larger than that of D_2O. This is a consequence of the smaller mass of ordinary water and also the smaller moments of inertia (which lead to larger rotational relaxation times for ordinary water). These factors are expected to outweigh the effect of the somewhat greater heat capacity of D_2O.

On the other hand, the resonance correction is inversely dependent on the moments of inertia and, hence, is larger for H_2O. From Mason and Monchick's equations [J. Chem. Phys. *36*, 1622 (1962)], we calculate that if the resonant exchange of rotational energy does indeed occur, it will outweigh all other effects and the thermal conductivity of H_2O should be smaller than that of D_2O.

We have used a Gow-Mac thermal conductivity analyzer to compare the conductivities of H_2O and D_2O at 215°C. The apparatus was calibrated using air, O_2, N_2, CO_2, H_2O, and Ar. Results may be summarized as follows:

	Theory	
	Nonresonant	Resonant
$\lambda H_2O/\lambda D_2O$	~1.05	0.92–0.99
	Experiment	
$\lambda H_2O/\lambda D_2O$	0.986	

Thus, experiment indicated that resonant exchange of rotational energy does indeed affect the thermal conductivities of polar gases. The calculation for resonant theory is uncertain to some extent because it was necessary to approximate the water molecule as a symmetric top, whereas it is in fact quite asymmetric. We plan to carry out more refined measurements which will include other isotopically substituted polar gases as well.

PROF. L. WALDMANN (*Max-Planck-Institut, Mainz*): Generally I should like to emphasize that one is very much impressed by the progress which Dr. Mason and Dr. Monchick have made in the theory of polyatomic gases. For the first time they have made detailed and realistic calculations on a sound kinetic theory basis and shown that an overall quantitative picture is possible.

Now there are some comments and questions.

Multiple Force Laws

The state of a gas, the molecules of which are capable of the degenerate internal eigenstates Ψ_M (different orientations), has exactly to be described by a distribution matrix $f(t, \mathbf{r}, \mathbf{c})_{MM'}$. The subscripts M and M' are magnetic quantum numbers running from $-J$ to J, and $\mathbf{c}$ means the molecular velocity. The uncorrelated distribution matrix of two molecules is given by

$$f_{MM_1,M'M_1'}(\mathbf{c}, \mathbf{c}') = f_{MM'}(\mathbf{c})f_{M_1M_1'}(\mathbf{c}_1)$$

or in short matrix notation

$$\mathfrak{f}(\mathbf{c}, \mathbf{c}_1) = \mathfrak{f}(\mathbf{c}) \times \mathfrak{f}(\mathbf{c}_1)$$

For the distribution matrix the following matrix Boltzmann equation is valid

$$[\partial \mathfrak{f}(\mathbf{c})/\partial t] + \mathbf{c}[\partial \mathfrak{f}(\mathbf{c})/\partial \mathbf{r}]$$

$$= \int \mathrm{tr}_1 \{\int \mathfrak{a}(\mathbf{e}, \mathbf{e}')\mathfrak{f}(\mathbf{c}', \mathbf{c}_1')\mathfrak{a}^+(\mathbf{e}', \mathbf{e})d\mathbf{e}'$$

$$- (2\pi/i)[\mathfrak{a}(\mathbf{e}, \mathbf{e})\mathfrak{f}(\mathbf{c}, \mathbf{c}_1) - \mathfrak{f}(\mathbf{c}, \mathbf{c}_1)\mathfrak{a}^+(\mathbf{e}, \mathbf{e})]\}g\, d\mathbf{c}_1/k^2$$

Here, $\mathfrak{a}$ means the matrix scattering amplitude for a binary collision of two molecules with relative velocity $\mathbf{g}' = g\mathbf{e}'$ before collision and $\mathbf{g} = g\mathbf{e}$ after collision and tr_1 means trace over the second of the pair of subscripts in those matrices like $\mathfrak{a}(\mathbf{e}, \mathbf{e}')$ or $\mathfrak{f}(\mathbf{c}, \mathbf{c}_1)$. The wave number is denoted by k.

From this matrix Boltzmann equation, which has been derived by the discussor[1] and independently in a subsequent paper by R. F. Snider,[2] the multiple force law formalism may be obtained by two steps.

(1) One assumes the scattering amplitude $\mathfrak{a}$ to be diagonal

$$a_{MM_1M'M_1'} = a_{MM_1}\delta_{MM'}\delta_{M_1M_1'}$$

(2) One assumes the distribution matrix $f(\mathbf{c})$ to be diagonal

$$f_{MM'}(\mathbf{c}) = f_M(\mathbf{c})\delta_{MM'}$$

at time $t = 0$. Then the latter is true at any time and the matrix Boltzmann equation turns out to be of the classical mixture type

$$\frac{\partial f_M(\mathbf{c})}{\partial t} + \cdots$$

$$= \sum_{M_1} \int\int [f_M(\mathbf{c}')f_{M_1}(\mathbf{c}_1') - f_M(\mathbf{c})f_{M_1}(\mathbf{c}_1)]$$

$$\times \sigma_{MM_1}(\chi)g\, d\mathbf{e}'\, d\mathbf{c}_1$$

with the scattering cross section

$$\sigma_{MM_1} = k^{-2} \mid a_{MM_1} \mid^2$$

Finally, isotropical orientation is assumed:

$$f_M(\mathbf{c}) = (2J + 1)^{-1} f(\mathbf{c})$$

By summing on M one obtains a classical Boltzmann equation of the pure gas type for the distribution function $f(\mathbf{c})$ with the effective differential cross section

$$\sigma = \frac{1}{(2J + 1)^2} \sum_{MM_1} \sigma_{MM_1}$$

This immediately yields Eq. (3) of the Mason–Monchick paper.

Fixed Orientation during Collision

There are phenomena which are not covered by this approximation. The assumption of fixed orientation means that the molecular moment of inertia should not influence the gas kinetic coefficients. However, one observes, e.g., with the mixtures of the hydrogen isotopes, a thermal diffusion factor according to the semi-empirical formula[3]

$$\alpha = 0.24 \frac{m_1 - m_2}{m_1 + m_2} + 0.20 \frac{\theta_1 - \theta_2}{\theta_1 + \theta_2}$$

(m, molecular mass, θ, molecular moment of inertia). Especially, one observes with the isobaric mixture D_2/HT a thermal diffusion factor, resulting solely from the difference in the moments of inertia, which is nearly as great as the thermal diffusion factor for DT/D_2. Physically one might say that a molecule with small θ is more easily turned around in a collision than a molecule of large θ and thus has effectively a smaller cross section, the molecules with smaller θ thus going to the hot side in a temperature gradient, as the small molecules do in the monatomic case. Obviously this effect cannot be understood if the orientation of the molecules is assumed to be fixed during collision (putting $\theta = \infty$, so to speak).

737

To study the effect of the moment of inertia, E. Trübenbacher[4] has calculated the thermal diffusion for a binary isobaric mixture of rough sphere molecules. The sign of α was in accordance with the D_2/HT experiments; the calculated absolute value, was however, much too small (by about a factor of 20).

Shape Effects

In support of the assumption that shape effects are small, one might refer to the viscosity and heat conductivity of *para* and *ortho* hydrogen at 20°K. Both coefficients are different by only 0.5% for both modifications.[5,6] The *para* molecules are not rotating; there is only one potential for them. The *ortho* molecules are rotating; they have a potential depending considerably on the orientation. Nevertheless, there is nearly no difference in viscosity and heat conductivity!

Inverse Collisions

The detailed balance relation for the cross section $I_{i'j'}{}^{ij}$ follows exactly from quantum mechanics and I should think that there are no intuitive elements in the derivation, as, e.g., given by the discussor in Handbuch der Physik.[7]

The argument briefly runs as follows. Let I_1', I_2' comprise the angular momentum and magnetic quantum numbers of two molecules before collision; and let $\mathrm{k}' = k'\mathrm{e}'$ be their relative momentum before collision. The asymptotic wave function depending on the relative coordinate $\mathbf{r}$ and the quantum numbers $I_1 I_2$ then is

$$\Psi \approx \exp(irk')\delta_{I_1'I_1}\delta_{I_2I_2'} + \frac{\exp irk}{r(kk')^{\frac{1}{2}}}\, a(\mathrm{e}I_1I_2,\ \mathrm{e}'I_1'I_2',\ E)$$

Here $\mathrm{e} = \mathbf{r}/r$ is a unit vector, E means the total energy in the center of mass system—this variable will be omitted in the following—and k is the wave number after collision. The incoming intensity is proportional to k'; the scattered intensity per unit solid angle is proportional to $k\cdot(kk')^{-1}\,|\,a\,|^2 = k'\cdot\,|\,a\,|^2k'^{-2}$. The cross section for an inelastic scattering process leading from the state $e'I_1'I_2'$ to the state $\mathrm{e}I_1I_2$ therefore is

$$\sigma(\mathrm{e}'I_1'I_2' \to \mathrm{e}I_1I_2) = |\,a(\mathrm{e}I_1I_2,\ \mathrm{e}'I_1'I_2')\,|^2k'^{-2}$$

From invariance of molecular dynamics under time reversal follows

$$a(\mathrm{e}I_1I_2,\ \mathrm{e}'I_1'I_2') = a(-\mathrm{e}' - I_1 - I_2,\ -\mathrm{e} - I_1\,I_2)$$

so that

$$k'\sigma(\mathrm{e}'I_1'I_2' \to \mathrm{e}I_1I_2) = k^2\sigma(-\mathrm{e} - I_1 - I_2 \to -\mathrm{e}' - I_1' - I_2')$$

Now, the sum may be taken on the magnetic quantum numbers contained in I_1, etc., on both sides of this relation. Then one is left with only the angular momentum quantum numbers which shall be denoted by ij and $i'j'$ respectively. The magnetic quantum number sum of the σ's may be denoted by I. Hence one finds the final detailed balance relation

$$k'^2I_{ij'}{}^{ij}(\mathfrak{a},\ E) = k^2I_{ij}{}^{i'j'}(\mathfrak{a},\ E)$$

This equation is also valid if by rearrangement of atoms the molecular masses are changed during collision (binary chemical reaction).

Determination of λ_{tr} by Observation of Dust Particles

The force $\mathbf{K}$ on a small spherical drop with radius r and velocity $\mathbf{v}^{(sph)}$ in a resting polyatomic gas with molecular mass m, pressure p, and translational heat conductivity λ_{tr} is given by Eq. (5.1) of reference (14)

$$\mathbf{K} = -\frac{8}{3}r^2\left(\frac{2\pi}{kT}\right)^{\frac{1}{2}}\left[\left(1+\frac{\pi}{8}\right)p\mathbf{v}^{(sph)} + \frac{1}{5}\lambda_{tr}\frac{\partial T}{\partial \mathbf{r}}\right]$$

in the two limiting cases in which (a) the rebounding molecules are translationally entirely accommodated to the temperature of the drop, but their internal energy is conserved, and (b) both energies, translational and internal, are fully accommodated in a collision with the drop surface. Hence, the observation of the motion of a small oil drop (or dust particle) in a heat conducting gas should indeed provide a good means for the determination of λ_{tr}.

This statement is easily inferred from the general formula for the force $d\mathbf{K}$ on a surface element dS with normal unit vector $\mathbf{e}$ directed into the gas

$$d\mathbf{K} = -\sum_i(\int_- m\mathbf{c}c_e f_i\, d^3c + \int_+ m\mathbf{c}c_e f_i^+\, d^3c)$$

Here, f_i means the distribution function of the molecules in the internal state i, $c_e = \mathbf{c}\cdot\mathbf{e}$ and the subscripts $-$ and $+$ on the integrals mean integration on the incoming or outgoing molecules, respectively, as in Eq. (1.1) of reference (14).

Now, in the above case (a), the distribution of the outgoing molecules is

$$f_i^+ = (n_i^+/n_i)f_i^{(0)}$$

where $f_i^{(0)}$ denotes an equilibrium distribution and where n_i^+ is determined by individual particle conservation:

$$\int_- c_e f_i\, d^3c + \int_+ c_e f_i^+\, d^3c = \sigma$$

This immediately yields $n_i^+/n_i = 2(\pi^{\frac{1}{2}})Z_i$ and

$$d\mathbf{K} = p\sum_i(n_i/n)[2\mathbf{Z}_i - (\pi^{\frac{1}{2}})Z_i\mathbf{e}]$$

where the integrals Z_i, $\mathbf{Z}_i$ are given by (6.1a,b) of reference (14). In the above case (b) one has

$$f_i^+ = (n^+/n)f_i^{(0)}$$

where n^+ is determined by over-all particle conservation

$$\Sigma(\int_- c_c f_i \, d^3c + \int c_c f_i^+ \, d^3c) = \sigma$$

This yields $n^+/n = 2(\pi^{\frac{1}{2}}) \, \Sigma_i^+ Z_i$ and thence the same formula for $d\mathbf{K}$ as in case (a).

Case (a) can be treated further along the same lines as the monatomic gas mixture in reference (14). Putting

$$f_i = f_i^{(0)} \cdot \left[1 + (\beta/n) \sum_r \int_{\frac{3}{2}}^{r} (\beta c^2) A_{i,r} \mathbf{c} \cdot \frac{\partial T}{T \partial \mathbf{r}} \right]$$

with $\beta = m/2kT$, S being the Sonine polynomials, and $A_{i,r}$ being series coefficients, one obtains for the temperature force in first approximation

$$\mathbf{K}^{(T)} \approx -\frac{2}{3} r^2 \left(\frac{2\pi m}{kT} \right)^{\frac{1}{2}} k \sum_i \frac{n_i}{n} A_{i,1} \frac{\partial T}{\partial \mathbf{r}}$$

The heat conductivity is exactly given by

$$\lambda = \frac{k}{2} \sum_i \frac{n_i}{n} \left(\frac{5}{2} A_{i,1} - \frac{E_i - \bar{E}_i}{kT} A_{i,0} \right)$$

E_i being the internal energy. From this expression, the translational heat conductivity is taken according to

$$\lambda_{tr} = \frac{5k}{4} \sum_i \frac{n_i}{n} A_{i,1}$$

and this now yields directly the formula for $\mathbf{K}$ stated at the beginning. Finally, in case (b), the same formula for $d\mathbf{K}$ being valid as in case (a), the result for $\mathbf{K}$ covers both limiting cases.

DR. L. MONCHICK (*APL/The Johns Hopkins University*): Professor Waldmann has gone into the fundamental theory deeper than we have: we have begun, essentially, where he has ended. I think that we are in substantial agreement in most things.

The fixed orientation approximation cannot explain all effects and for thermal diffusion ratios we would expect that inelastic effects would be important. This is a consequence of the well-known fact that, whereas most transport properties depend primarily on the existence of collisions, thermal diffusion depends primarily on their nature.

We re-evaluated the Wang Chang, Uhlenbeck formulas using the symmetry condition advocated by Professor Waldmann and found no change. Indeed, it seems that for ordinary processes kinetic theory seems to be independent of whether exact detailed balance or quasi-detailed balance is assumed.

REFERENCES

1. WALDMANN, L.: Z. Naturforsch. *12a*, 660 (1957); *ibid. 13a*, 609 (1958).
2. SNIDER, R. F.: J. Chem. Phys. *32*, 1051 (1960).
3. SCHIRDEWAHN, J., KLEMM, A., and WALDMANN, L.: Z. Naturforsch. *16a*, 133 (1961).
4. TRUBENBACHER, E.: Z. Naturforsch. *17a*, 363, 539 (1962).
5. BECKER, E. W. and STEHL, O.: Z. Physik *133*, 615 (1952).
6. HEINZINGER, K., KLEMM, A., and WALDMANN, L.: Z. Naturforsch. *16a*, 1338 (1961).
7. WALDMANN, L.: Handbuch der Physik *12*, 490 (1958).

ROTATIONAL RELAXATION AND THE RELATION BETWEEN THERMAL CONDUCTIVITY AND VISCOSITY FOR SOME NONPOLAR POLYATOMIC GASES

R. S. BROKAW AND C. O'NEAL, JR.

The dimensionless ratio $f = \lambda M/\eta C_v$ relating the thermal conductivity, molecular weight, viscosity, and constant volume molar heat capacity has been determined experimentally for oxygen, nitrogen, carbon dioxide, and acetylene (linear molecules), and also methane (nonlinear) in the neighborhood of room temperature (275°–290°K). The experimental method provides a direct determination of f by measurement of the subsonic temperature recovery factor. A recent theory of Mason and Monchick has been used to obtain collision numbers for rotational relaxation from the experimental data. A quantitative, but semiempirical analysis of the data on the linear molecules indicates that collision numbers for rotational relaxation for these molecules are determined by the following factors: (1) the molecular mass distribution, (2) the strength of the intermolecular attractive forces, and (3) the molecular asymmetry (characterized by the quadrupole moment). An empirical expression for collision number which involves these factors gives values for nitrogen, oxygen, and carbon dioxide which are nearly independent of temperature over the range which has been investigated experimentally. The data on methane show that a different expression is required for nonlinear molecules.

Introduction

Fundamental flame processes involve a complex wedding of transport properties and chemical kinetics. Thus a precise experimental and theoretical knowledge of the transport phenomena is basic to a detailed analysis and understanding of flames. This paper concerns an experimental investigation of the relation between thermal conductivity and viscosity. A theoretical analysis of the results yields information on rotational energy relaxation rates.

The fundamental equations of rigorous kinetic theory were established by Maxwell and Boltzmann, starting about a century ago, and in 1916–17 Chapman and Enskog independently obtained general solutions of these equations for the transport properties of monatomic gases.[1] However, it is only relatively recently that the necessary transport integrals (which must be evaluated numerically) have been computed for intermolecular potentials which approximate the forces between real molecules.[2–5]

Although the *rigorous* Chapman–Enskog theory is applicable strictly only to the noble gases, it provides a reasonable description of the viscosity and diffusion coefficients of nonpolar polyatomic gases and gas mixtures. This is presumably because the presence or absence of internal energy states has little effect on the transport of momentum or mass. On the other hand the internal degrees of freedom can make a substantial contribution to the energy flux, so that the theory must be modified to account for the thermal conductivity of polyatomic gases.

It is convenient to examine the thermal conductivity of a gas in terms of its relationship to the viscosity through the dimensionless ratio

$$f = \lambda M/\eta C_v.$$

Here λ is the thermal conductivity, and η is the viscosity; M is the molecular weight, while C_v is the constant-volume heat capacity. According to ultrasimplified kinetic theory,[6] $f = 1$. However, the Chapman-Enskog theory for monatomic gases predicts that f should be very nearly 5/2. This is due to the fact that the translational energy is related to the molecular velocity; the molecules possessing the most energy are the most rapid, have the longest mean free paths, and hence make an enhanced contribution to the heat transport. Indeed, it is found experimentally that f is about 2.5 for the noble gases.

For polyatomic gases, f is less than 2.5, being least for molecules with the most complex structures. In other words, f is smallest when the molar heat capacity is largest and originates mostly from internal energy modes. Consequently, Eucken[7] suggested that the transport of transla-

tional and internal energy be considered separately, and proposed

$$f = (f_{\text{trans}} C_{v\text{trans}} + f_{\text{int}} C_{v\text{int}})/C_v.$$

where $C_{v\text{trans}}$ and $C_{v\text{int}}$ are the translational and internal contributions to the total heat capacity C_v. Eucken assumed $f_{\text{trans}} = 5/2$, by analogy with the monatomic gases. However, because there should be little correlation between the velocity of a molecule and its internal energy, Eucken assumed $f_{\text{int}} = 1$, the result of the ultrasimple kinetic theory which does not account for the velocity–translational energy correlation.

Eucken's arguments are in no wise rigorous; the most obvious defect lies in setting $f_{\text{int}} = 1$. Ubbelohde[8] took the next important step. He considered molecules with excited internal energy states as belonging to different chemical species, and pointed out that the flow of internal energy can be regarded as energy transport due to diffusion of the excited states. This concept has been elaborated by Chapman and Cowling,[9] Schäfer,[10] and Hirschfelder[11]; it leads to the result

$$f_{\text{int}} = \rho D/\eta$$

where ρ is the density and D the self-diffusion coefficient. For many realistic intermolecular force laws $\rho D/\eta \approx 1.3$ over a large temperature range. Thus

$$f_{\text{modified Eucken}} = \frac{\rho D}{\eta} + \frac{3}{2}\left(\frac{5}{2} - \frac{\rho D}{\eta}\right)\frac{R}{C_v}. \quad (1)$$

Experimental values of f_{int}, calculated from experimental data by assuming $f_{\text{trans}} = 5/2$ seem to approach 1.3 for complex polyatomic molecules at high temperature.[12] However, for simpler molecules, where the internal energy is largely rotational (O_2, N_2, CO_2, CH_4), experimental f_{int} values are somewhat smaller.

Recently, Mason and Monchick[13] have derived explicit expressions for f_{trans} and f_{int} from the formal kinetic theory of polyatomic gases of Wang-Chang and Uhlenbeck[14] and of Taxman.[15] By systematically including terms involving inelastic collisions they derive the modified Eucken expression [Eq. (1)] as a first approximation, and, as a second approximation, an expression dependent on the relaxation times for the various internal degrees of freedom. For nonpolar gases their result may be written

$$f_{\text{Mason–Monchick}} = f_{\text{modified Eucken}} - \frac{1}{2}\left(\frac{5}{2} - \frac{\rho D}{\eta}\right)^2 \sum_k \frac{\eta}{P\tau_k}\frac{C_{vk}}{C_v}.$$

Here τ_k is the relaxation time for the kth internal energy mode and C_{vk} is the heat capacity of that mode, while P is the pressure.

It is convenient to express relaxation times in terms of a collision number

$$Z_k = \tau_k/\tau_{\text{coll}} = (4/\pi)(P\tau_k/\eta). \quad (2)$$

where $\tau_{\text{coll}} = (\pi/4)(\eta/P)$ is the mean time between collisions. Consequently,

$$f_{\text{Mason–Monchick}} = f_{\text{modified Eucken}} - \frac{2}{\pi C_v}\left(\frac{5}{2} - \frac{\rho D}{\eta}\right)^2 \sum_k \frac{C_{vk}}{Z_k}. \quad (3)$$

From Eq. (3) we see that deviations from the modified Eucken expression arise from internal energy modes with low collision numbers. In small polyatomic molecules these are the rotational modes, where Z_{rot} (with the exception of H_2) is generally less than 20 collisions. (Z_{vib} is usually the order of 10^3 to 10^7, so that the terms involving vibrational relaxation are negligible.)

In this paper we have used an experimental technique devised by Eckert and Irvine,[16] which is in essence a direct determination of f. Their method is based on the relation describing the adiabatic temperature attained by a flat plate in a high-velocity subsonic gas stream. This recovery temperature T_r is conveniently described in terms of a recovery factor

$$r \equiv (T_r - T_s)/(T_t - T_s), \quad (4)$$

where T_s is the static temperature of the stream at a sufficient distance from the plate, and T_t is the total temperature. (The total temperature is the temperature measured at a stagnation point.) Pohlhausen[17] calculated the recovery factor by integrating the laminar boundary layer equations, and found that r is a function of Prandtl number $C_p\eta/M\lambda$ only; for Prandtl numbers between 2/3 and 1 the approximation

$$r \cong (C_p\eta/M\lambda)^{\frac{1}{2}} = (C_p/fC_v)^{\frac{1}{2}} \quad (5)$$

reproduces numerical calculations to better than sixteen parts in ten thousand. Here C_p is the molar heat capacity at constant pressure.

In Eckert and Irvine's experiment the gas is expanded through a convergent nozzle; the pressure ratio is such that the issuing gas remains slightly subsonic. A butt-welded differential thermocouple is suspended along the nozzle axis with one junction upstream of the nozzle and the other junction just downstream of the nozzle exit. The upstream junction is in a low-velocity region, and senses the total temperature of the gas, while the downstream junction assumes the flat-plate recovery temperature. The static temperature T_s is not measured; rather it is computed from the pressure ratio across the nozzle and the isentropic flow relationship

$$T_s/T_t = (P_s/P_t)^{(R/C_p)}. \quad (6)$$

In a previous paper[18] we reported f values measured by this technique over the temperature range from 90°K to room temperature for helium, argon, nitrogen, oxygen, and hydrogen. The data on the noble gases were in close accord with rigorous kinetic theory for monatomic gases. Results for nitrogen, oxygen, hydrogen, as well as data for carbon dioxide[19] were analyzed in terms of Mason and Monchick's theory for polyatomic gases; for nitrogen and oxygen, the data yielded collision numbers for rotational relaxation in reasonable agreement with literature values. These collision numbers were nearly independent of temperature. The results confirmed the fact that the interchange of translational and rotational energy is unusually difficult for hydrogen.

This paper reports f values in the vicinity of room temperature for several nonpolar polyatomic molecules. Linear molecules included oxygen, nitrogen, carbon dioxide, and acetylene; methane was the only nonlinear molecule. Collision numbers for rotational relaxation have been computed using the theory of Mason and Monchick; these results give an insight as to the molecular parameters which determine rotational relaxation rates.

Experimental

We have described the apparatus and experimental procedure for measurement of recovery factor by Eckert and Irvine's technique previously.[18] The present determinations were all carried out at room temperature; hence temperature control was no problem. Furthermore, it was possible to work with fairly high flow rates so that the pressure ratios and differential thermocouple emfs could be read with greater accuracy. As a consequence the present measurements show considerably less scatter than our previous data.

In order to detect instrumental errors, 11 check determinations of the recovery factor of argon were interspersed throughout the course of this work. These values correspond to a temperature of about 275°K and yield a mean value of $f = 2.502$ with a standard error of 0.006. (The standard deviation of each datum was 0.019.) This is in excellent agreement with the theoretical value of $f = 2.5023$, and may be regarded as a calibration of the apparatus.

In the previous work, the gases investigated (He, Ar, H_2, N_2, O_2) had heat capacities which varied only slightly with temperature, so that there was little problem in selecting an appropriate heat capacity for use with Eq. (6). However, several of the gases considered in this paper have heat capacities which vary appreciably with temperature, so that it seemed worthwhile to reexamine the pressure–temperature relationship for the isentropic expansion, and to include deviations from the perfect gas law as well.

We wish to obtain the stream temperature from the total temperature and the pressure ratio by means of the relation

$$\ln (P_s/P_t) = \int_{T_t}^{T_s} (\partial \ln P/(\partial \ln T)_S \, d \ln T \quad (7)$$

where the subscript S indicates that the process considered is isentropic. For an ideal gas,

$$(\partial \ln P/\partial \ln T)_S = C_p/R,$$

and if the heat capacity is constant, Eq. (6) is obtained.

By straightforward thermodynamic methods we find that

$$\left(\frac{\partial \ln P}{\partial \ln T}\right)_S = \frac{T}{P} \frac{1}{\mu + (V/C_p)}, \quad (8)$$

where μ is the Joule–Thompson coefficient. This is a convenient expression because formulas for μ and C_p are often given explicitly for the various equations of state.

We have chosen to use the first two terms of the virial expansion,

$$PV/RT \cong 1 + (B/V),$$

where B, the second virial coefficient, is a function of temperature alone. In this event[20]

$$\mu \cong (B_1 - B)/C_{p0}$$

$$C_p \cong C_{p0} - RB_2/V,$$

where $B_1 \equiv (dB/d \ln T)$ and $B_2 \equiv T^2(d^2B/dT^2)$; C_{p0} is the zero pressure heat capacity. By substituting these expressions into Eq. (8) and eliminating terms of higher order involving B^2, BB_1, etc., we find

$$\left(\frac{\partial \ln P}{\partial \ln T}\right)_S = \frac{C_{p0}}{R}[1 - (B_1 + B_2R/C_{p0})/V]$$

The term involving volume is a small correction; hence ideal gas relationships may be used to eliminate volume in favor of temperature. Thus

$$\left(\frac{\partial \ln P}{\partial \ln T}\right)_S$$

$$= \frac{C_{p0}}{R}\left[1 - \left(B_1 + B_2 \frac{R}{C_{p0}}\right)\frac{P_t}{RT}\left(\frac{T}{T_t}\right)^{\bar{C}_{p0}/R}\right] \quad (9)$$

Here $\bar{C}_{p0}/R$ is a suitable mean value; it may be taken at a temperature midway between T and T_t. Equation (9) now contains only the temperature as a variable; therefore Eq. (7) can in principle be integrated numerically. In practice we

found that Eq. (9) varied by ten per cent or less over the temperature range of interest. Thus we merely used Eq. (9) to compute an effective value of R/C_p for use in Eq. (6); this value was taken at a temperature half way between the stream and total temperatures. A numerical integration revealed that this procedure introduced a maximum error of one part in four thousand or less.

Zero pressure heat capacities for oxygen and nitrogen were taken from reference 21, while values for the remaining molecules were calculated from suitable spectroscopic constants. Corrections for deviations from ideal gas behavior were made using B, B_1, and B_2 values computed assuming a Lennard-Jones (12–6) potential together with appropriate force constants.[22]

Results and Discussion

Experimental f values are presented in Table 1 together with corresponding temperatures. Also shown are values of Z^{-1}, the reciprocal of the collision number for rotational relaxation, as calculated from Eq. (3). Thus, for linear molecules

$$Z_l^{-1} = \tfrac{1}{2}\pi \frac{C_v}{R} \frac{f_{\text{modified Eucken}} - f_{\text{experiment}}}{[(5/2) - \rho(D/\eta)]^2}, \quad (10)$$

whereas for nonlinear molecules (methane)

$$Z_{nl}^{-1} = \tfrac{1}{3}\pi \frac{C_v}{R} \frac{f_{\text{modified Eucken}} - f_{\text{experiment}}}{[(5/2) - \rho(D/\eta)]^2}. \quad (11)$$

In order to calculate $f_{\text{modified Eucken}}$ from Eq. (1) and Z^{-1} from Eq. (10) or (11) it is necessary to evaluate $\rho D/\eta$. Values were computed from the relation $\rho D/\eta = (6/5)A^*$, where A^* is a very slowly varying function of the temperature.[23] A^* values were obtained by assuming either the exponental-6 or Lennard-Jones (12–6) potential and the ϵ/k values set forth in Table 2.

Mean values of Z^{-1} (which may be regarded as collision probabilities for rotational relaxation) are shown in Table 2. It is seen that the experimental errors in Z^{-1} are about the same size for the various molecules; therefore it is convenient to deal with Z^{-1} rather than Z. Note, however, that Z is in the range of 2–20 collisions. The collision numbers for nitrogen and especially oxygen differ somewhat from the values reported previously.[18] (For nitrogen we find 8.3 rather than 6.8 collisions, and for oxygen 13 rather than 6 collisions.) We believe our present results are the more reliable.

Brout[24] has calculated the rotational energy transition probability for homonuclear diatomic molecules. For molecules with molecular weight greater than 20 his result may be written as

$$Z_{\text{Brout}}^{-1} \cong \tfrac{1}{2}(4I/m\sigma_\eta^2). \quad (12)$$

Here I is the moment of inertia, m is the molecular mass, and σ_η is a kinetic theory collision diameter. The viscosity collision diameter is appropriate ($\sigma^2\Omega^{(2,2)*}$ in the notation of reference 6) because the collision number involves the viscosity [Eq. (2)].

Collision numbers for rotational relaxation can also be calculated for rough spheres. This model has been rigorously analyzed by classical kinetic theory,[25] and relaxation times (or bulk viscosities) have been evaluated.[26,14] Accordingly, for rough spheres

$$Z_{\text{rough sphere}} = \frac{5\pi}{12} \cdot \frac{(4I/m\sigma^2)}{1 + (13/6)(4I/m\sigma^2)}. \quad (13)$$

In Fig. 1 the experimental Z^{-1} values are plotted against the parameter $4I/m\sigma_\eta^2$; theoretical values from Eqs. (12) and (13) are shown as well. Viscosity collision diameters were computed using the force constants for the expo-

TABLE 1

Experimental Results

T	f	Z^{-1}	T	f	Z^{-1}
Oxygen			*Carbon Dioxide*		
276.1	1.988	0.076	282	1.724	0.454
276.8	1.991	0.069	282	1.723	0.457
277.3	2.001	0.041	283	1.732	0.420
277.3	1.971	0.124	283	1.731	0.425
278.2	2.003	0.036	284	1.732	0.417
278.3	1.978	0.105	284	1.740	0.388
278.3	1.982	0.093			
279.4	1.991	0.069	*Acetylene*		
279.5	1.995	0.058			
			283.6	1.662	0.394
Nitrogen			284.0	1.662	0.395
			284.9	1.660	0.399
274.3	1.977	0.122	285.0	1.661	0.395
274.3	1.963	0.160	289.1	1.651	0.426
275.4	1.974	0.129	290.7	1.656	0.395
275.6	1.974	0.129			
275.9	1.979	0.117	*Methane*		
276.4	1.978	0.118			
277.0	1.986	0.097	279	1.831	0.098
277.3	1.962	0.162	280	1.844	0.064
277.5	1.981	0.109	281	1.834	0.087
278.8	1.988	0.092	282	1.846	0.056
278.9	1.978	0.119	283	1.854	0.037
280.7	1.984	0.102	284	1.857	0.028

TABLE 2

Analysis of Data

	Oxygen	Nitrogen	Carbon dioxide	Acetylene	Methane
Molecular properties					
Type of potential	exp–6	exp–6	L-J 12–6	L-J 12–6	exp–6
Force constants:					
ϵ/k, °K	132	101.2	200	231.8	152.8
σ or r_m, Å	3.726	4.011	3.952	4.033	4.206
α	17.0	17.0	—	—	14.0
Moment of inertia, gm cm^2 × 10^{40}	19.3	14.01	71.47	23.65	5.341
Quadrupole moment, esu cm^2 × 10^{26}	0.19	1.49	3.07	5.28	0
Experimental data					
Temperature	278.0	277.0	283.0	286.0	281.0
Z^{-1} expt (mean)	0.075	0.121	0.427	0.401	0.062
Standard deviation	0.028	0.022	0.026	0.013	0.027
Standard error of the mean	0.010	0.006	0.011	0.005	0.011
Collision number, Z	13.0	8.3	2.3	2.5	16.0
Data analysis					
$Z_{expt}^{-1}/Z_{Brout}^{-1}$	1.35	2.83	4.60	8.53	(2.56)
$Z_{expt}^{-1}/Z_{l,a}^{-1}$	1.03	2.27	3.13	5.54	(1.88)
$(9/4)(Q^2/\sigma_\eta^5 kT)$	0.0034	0.177	0.267	0.60	0
$Z_{expt}^{-1}/Z_{l,a,q}^{-1}$	1.00	0.96	1.02	0.99	(1.88)
$Z_{l,a,q}^{-1}$ [calc. Eq. (15)]	0.075	0.126	0.417	0.407	(0.032)

nential–6 and Lennard-Jones (12–6) potentials listed in Table 2.

Figure 1 indicates little correlation with the experimental data—the oxygen data fall reasonably close to the Brout prediction, and the methane data lie close to the curve for rough spheres (which may perhaps apply to nonlinear molecules), but the results for nitrogen, carbon dioxide, and acetylene are widely scattered. Although Brout's expression was derived for homonuclear diatomic molecules, we might expect it to apply as well to symmetrical linear polyatomic molecules, such as carbon dioxide and acetylene. We would not expect Brout's expression to apply to nonlinear molecules such as methane, which possess three rather than two rotational degrees of freedom. Values of $Z_{expt}^{-1}/Z_{Brout}^{-1}$ presented in Table 2 differ considerably from unity—hence we conclude that other factors in addition to the molecular mass distribution must be involved. (The value for methane is shown parenthetically, since the Brout analysis is not expected to apply to this molecule.)

Both Brout's analysis and the rough sphere model consider only *repulsive* intermolecular forces, yet the interchange of rotational and translational energy occurs at close separations where attractive forces are important with real molecules. Schäfer[10] pointed out that the attractive forces increase the relative kinetic energy of the colliding molecules. Hence the relevant energy is of the order of $(3/2)kT + \epsilon$, where ϵ is the depth of attractive well of the intermolecular potential. We would expect this increase in kinetic energy to increase the transition probability, and lead to a correction factor of the type

$$(\tfrac{3}{2}kT + \epsilon)/\tfrac{3}{2}kT = 1 + \tfrac{2}{3}(\epsilon/kT).$$

Indeed, Parker[27] has calculated rotational relaxation for a two-dimensional model with attractive forces, and finds that relaxation times are dependent on ϵ/kT. (Parker's analysis predicts a considerable variation of collision number with temperature; this is not borne out by previous recovery factor determinations.[18]) Consequently the expression

$$Z_{\text{linear, attractive}}^{-1} = Z_{Brout}^{-1}[1 + \tfrac{2}{3}(\epsilon/kT)] \quad (14)$$

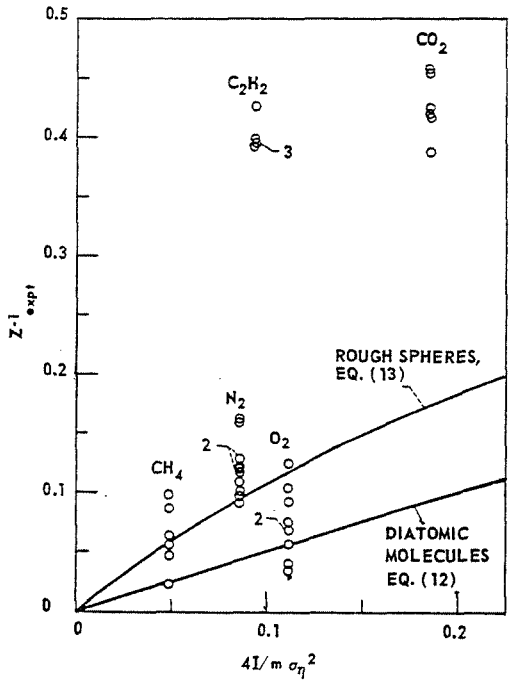

FIG. 1. Reciprocal collision number for rotational relaxation (calculated from experimental temperature recovery factor) as a function of mass distribution parameter.

might be expected to account for the intermolecular attractive forces; values of $Z_{expt}^{-1}/Z_{l,a}^{-1}$ are also shown in Table 2.

Equation (14) predicts the collision number for oxygen rather well, but fails for the other molecules. Especially surprising, at least at first glance, is the difference between oxygen and nitrogen, since these molecules have many similar physical properties: boiling point, molecular weight, moment of inertia, and collision diameter. However, oxygen and nitrogen do differ in one property which seems relevant: oxygen has almost no quadrupole moment whereas the quadrupole moment of nitrogen is appreciable. Furthermore, the quadrupole moments of carbon dioxide and acetylene are even larger; values derived from microwave collision diameters[28] are shown in Table 2. Indeed, the quadrupole moments parallel the values of $Z_{expt}^{-1}/Z_{l,a}^{-1}$.

The quadrupole interaction leads to an asymmetry in the intermolecular potential which may well be important in the interchange of rotational and translational energy. Let us now see if this variation in the potential is appreciable. The potential $\Phi^{(Q,\,Q)}$ between two identical cylindrically symmetric quadrupole moments, Q, is[29]

$$\Phi^{(Q,\,Q)} = \frac{3Q^2}{16r^5}[f(\theta_1, \theta_2, \phi_1 - \phi_2)].$$

Here r is the intermolecular distance and $f(\theta_1, \theta_2, \phi_1 - \phi_2)$ is a function of the angles $\theta_1, \theta_2, \phi_1, \phi_2$ which define all possible orientations of the two molecules—it ranges from -4 to $+8$. Hence the variation in the potential is

$$\Phi_{max}^{(Q,\,Q)} - \Phi_{min}^{(Q,\,Q)} = \Delta\Phi^{(Q,\,Q)} = \tfrac{9}{4}(Q^2/r^5)$$

We might reasonably regard the ratio $\Delta\Phi^{(Q,\,Q)}/kT$ at a distance of the order of the kinetic theory diameter as a rough measure of the importance of asymmetry due quadrupole interaction; values of this quantity are also shown in Table 2. Indeed it is found that the expression

$$Z_{l,\,a,\,Q}^{-1} = \frac{1}{2}\left(\frac{4I}{m\sigma_\eta^2}\right)\left(1 + \frac{2}{3}\frac{\epsilon}{kT}\right) \times \left(1 + 7.7\,\frac{9}{4}\frac{Q^2}{\sigma_\eta^5 kT}\right) \quad (15)$$

reproduces the experimental results. Thus values of $Z_{expt}^{-1}/Z_{l,\,a,\,Q}^{-1}$ differ from unity by only a few per cent. The final entries in Table 2, $Z_{l,\,a,\,Q}^{-1}$, are in excellent agreement with experiment (generally within the standard error of the mean). At first sight the empirical factor 7.7 might seem unduly large; however, the quadrupole moments of Table 2 are for rotating molecules and are roughly one-half the values for nonrotating molecules. Thus if the nonrotating quadrupole moments were available, the empirical factor would be reduced to about 2.

There remains another test for Eq. (15): Previous work suggested that collision numbers for carbon dioxide, nitrogen, and oxygen show little

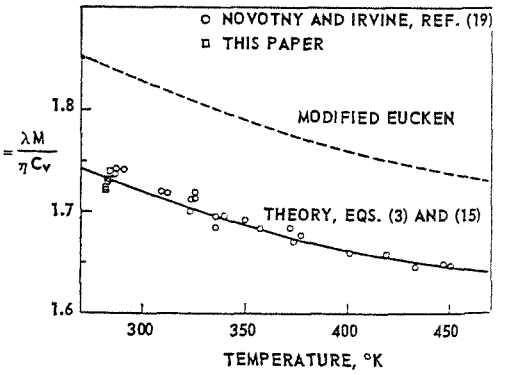

FIG. 2. Experimental and theoretical values of f for carbon dioxide.

variation with temperature.[18] Equation (15) meets this test over the experimental temperature ranges. This is illustrated in Fig. 2, where f for carbon dioxide is shown as a function of temperature. The experimental data are mainly from the work of Novotny and Irvine[19] but include the data of this paper as well. The solid curve has been computed from Eq. (3), with collision numbers from Eq. (15). The dashed curve represents the Modified Eucken expression, Eq. (1), and is the limiting value as $Z^{-1} \rightarrow 0$.

Thus Eq. (15) yields rotational collision numbers which, together with Eq. (3), describe the relationship between thermal conductivity and viscosity for linear nonpolar molecules (with the exception of hydrogen and deuterium). The data on methane show clearly that Eq. (15) is not applicable to nonlinear molecules; for methane $Z^{-1} = 0.061$ whereas Eq. (15) predicts a value only about one-half as large. This is scarcely surprising—there must obviously be a whole class of collisions which are effective in transferring energy between rotation and translation in three-dimensional molecules, which are not effective for linear molecules.

In conclusion, it must be emphasized that Eq. (15) has been deduced by qualitative arguments rather than a rigorous mathematical development—hence it must be regarded as tentative rather than proven. Nonetheless it appears that the following factors profoundly influence rotational relaxation rates for linear nonpolar molecules:

1. The mass distribution (characterized by the parameter $4I/m\sigma_\eta^2$).
2. The strength of the intermolecular attractive forces (characterized by ϵ/k).
3. The molecular asymmetry (characterized by the quadrupole moment).

It is hoped that this paper will provide the impetus as well as some guidelines for a renewed attack on the theory of rotational relaxation.

Acknowledgments

We are deeply indebted to Professor E. A. Mason for providing us with the manuscript of reference 13 prior to publication. This paper by Mason and Monchick provides the fundamental basis for interpreting the experimental results presented here. We also want to thank Bonnie McBride and Janet Ehlers of the Physical Chemistry Branch, Lewis Research Center, for providing the statistical mechanical heat capacity calculations for carbon dioxide, acetylene, and methane. Finally, we want to thank Virginia Renkel, also of the Lewis Research Center, for carrying out the numerical integrations which established the precision of Eq. (5) (the equation which relates the recovery factor to the Prandtl number).

References

1. Chapman, S. and Cowling, T. G.: *The Mathematical Theory of Non-Uniform Gases*, 2nd ed. Cambridge University Press, 1952.
2. Hirschfelder, J. O., Bird, R. B., and Spotz, E. L.: J. Chem. Phys. *16*, 968 (1948).
3. Mason, E. A.: J. Chem. Phys. *22*, 169 (1954).
4. Monchick, L.: Phys. Fluids *2*, 695 (1959).
5. Monchick, L. and Mason, E. A.: J. Chem. Phys. *35*, 1676 (1961).
6. Hirschfelder, J. O., Curtiss, C. F., and Bird, R. B.: *Molecular Theory of Gases and Liquids*, p. 13. Wiley, 1954.
7. Eucken, A.: Physik. Z. *14*, 324 (1913).
8. Ubbelohde, A. R.: J. Chem. Phys. *3*, 219 (1935).
9. Reference 1, p. 238.
10. Schäfer, K.: Z. physik. Chem. *B53*, 149 (1943).
11. Hirschfelder, J. O.: J. Chem. Phys. *26*, 282 (1957).
12. Vines, R. G. and Bennett, L. A.: J. Chem. Phys. *22*, 360 (1954).
13. Mason, E. A. and Monchick, L.: J. Chem. Phys. *36*, 1622 (1962).
14. Wang-Chang, C. S. and Uhlenbeck, G. E.: University of Michigan Engineering Research Rept. No. CM-681 (July 1951); also Reference 6, pp. 501–506.
15. Taxman, N.: Phys. Rev. *110*, 1235 (1958).
16. Eckert, E. R. G. and Irvine, T. F., Jr.: J. Appl. Mech. *24*, 25 (1957).
17. Pohlhausen, E.: Z. angew. Math. Mech. *1*, 115 (1921).
18. O'Neal, C., Jr. and Brokaw, R. S.: Phys. Fluids *5*, 567 (1962).
19. Novotny, J. L. and Irvine, T. F., Jr.: J. Heat Transfer *83*, 125 (1961).
20. Reference 6, Eqs. 3.B-5 and 3.B-6, pp. 231–2.
21. Hilsenrath, J., *et al.*: *Tables of Thermal Properties of Gases*. National Bureau of Standards Circular 564, Nov. 1955.
22. Reference 6, Tables I-A and I-B, pp. 1110–1115.
23. Reference 6, Eq. 8.2-48, p. 540.
24. Brout, R.: J. Chem. Phys. *22*, 1189 (1954).
25. Pidduck, F. B.: Proc. Roy. Soc. (London) *A101*, 101 (1922); Reference 1, pp. 199–217.
26. Kohler, M.: Z. Physik *125*, 715 (1949).
27. Parker, J. G.: Phys. Fluids *2*, 449 (1959).
28. Reference 6, Table 13.7-3, p. 1028.
29. Reference 6, Eq. 1.3-10, p. 27.

Discussion

DR. L. MONCHICK (*APL/The Johns Hopkins University*): This paper by Brokaw and O'Neal describes a very ingenious determination of the ratio f and yields some very interesting data. We found that we could correlate the values of NBS Circular 564 using the theory of J. G. Parker for the temperature variation of Z, the average number of collisions required for the rotational degrees of freedom to relax. But Brokaw and O'Neal find that their data seems to be correlated with a Z that is substantially temperature independent, which agrees with the theoretical calculation of Brout. I might cite a theoretical estimate by K. Takayanagi [Sci. Rep. Saitama Univ., Series A, *III*, 65 (1959)] that predicts yet a third temperature dependence, $Z \propto T^{-1}$. This would suggest the need for new work—theoretical and experimental—to determine the behavior of this new transport property.

HOMOGENEOUS AND HETEROGENEOUS REACTIONS OF FLAME INTERMEDIATES

H. WISE AND W. A. ROSSER

Studies of the homogeneous reaction kinetics of flame intermediates yield a reaction mechanism for the combustion of simple hydrocarbons. On the basis of such a mechanism the inhibition of flames by halogenated compounds and inorganic salts may be interpreted in terms of the removal of specific chain carriers as a result of: (1) their replacement by halogen atoms which no longer can lead to branching reactions, or (2) their homogeneous recombination catalyzed by alkali atoms.

The interaction of free radicals with solid surfaces may result in chemical reaction with the substrate and the formation of a volatile or nonvolatile product, or the reaction with the adsorbate. Measurements of the surface-catalyzed recombination of atoms have demonstrated the controlling effect of energy transfer to the solid in such exothermic heterogeneous reactions involving hydrogen or oxygen atoms. In the case of Pyrex glass and quartz a change in the order of the surface reaction with temperature has been noted. A number of tables are presented which summarize the available information on the catalytic efficiencies of various solids for atom recombination.

Introduction

During the past several years some advances have been made in our understanding of the kinetics and mechanism of flame reactions. Various experimental measurements have been carried out which have been aimed specifically at an elucidation of some of the reaction steps occurring in the gas phase and on surfaces of condensed materials. Some of the intermediates expected to occur in flames have been examined in an environment less complex than that prevalent in the high-temperature system. In general, the chemical composition of the reactants is simple since we are dealing predominantly with monatomic and diatomic species. However, their high reactivity and short lifetime require novel techniques with high time resolution, high sensitivity to constituents present at low concentrations, and preferably experimental determinations under time-invariant conditions. In the selection of topics for this paper several important aspects of flame kinetics have been ignored, such as the nonequilibrium distributions of the reaction intermediates and their reactivity in vibrationally, rotationally, and electronically excited states. Also the kinetics of charged particles has been neglected since it forms the subject matter of other papers in this discussion.

Homogeneous Reactions

Various optical and mass spectrometric studies[1–4] of premixed hydrocarbon–O_2 flames have revealed some features of the flame structure. In the case of CH_4–O_2 combustion the temperature and composition changes which occur during steady-state burning have been interpreted to some extent in terms of mechanisms of chemical change. This discussion of combustion reactions will be devoted primarily to CH_4 combustion, but with the understanding that some of the features may apply equally well to the combustion of other hydrocarbons. There is a strong family resemblance in all hydrocarbon flames and, by implication, a strong chemical similarity in the reactions which determine the rate of burning.

In general, a premixed CH_4–O_2-diluent flame may be divided into three zones: (1) a preheat zone extending from the cold boundary to the visible flame; (2) a reaction zone coinciding approximately with the visible flame; and (3) a recombination zone in which the excess concentration of H, O, and OH created in the flame zone are removed by recombination reactions. The transition between zones is not precise. Transport processes are important in all three zones, but from a kinetic viewpoint each zone differs markedly.

Reaction Zones

Very little of kinetic importance to combustion takes place in the preheat zone. The fuel-oxidizer mixture is heated by conduction to a rather high temperature, 1000° to 1500°K, depending on the circumstances. Simultaneously, a flux of reactive radicals from the downstream region of the flame, in conjunction with the high temperature,

results in a significant rate of reaction, and provides through the emission of radiation via secondary reactions an obvious transition from zone (1) to zone (2), the main reaction zone. The number of different reactions which take place in the reaction zone is undoubtedly very large. Many of these are secondary processes, dependent on but not affecting the main route of oxidation and the overall rate of combustion. The main reactions appear to be the following:

$$CH_4 + \left\{\begin{matrix} H \\ OH \\ O \end{matrix}\right\} \rightarrow CH_3 + \left\{\begin{matrix} H_2 \\ H_2O \\ OH \end{matrix}\right\} \quad \begin{matrix} (1a) \\ (1b) \\ (1c) \end{matrix}$$

$$CH_3 + O \rightarrow CH_2O + H \quad (2)$$

$$CH_2O + \left\{\begin{matrix} CH_3 \\ H \\ OH \\ O \end{matrix}\right\} \rightarrow CHO + \left\{\begin{matrix} CH_4 \\ H_2 \\ H_2O \\ OH \end{matrix}\right\} \quad \begin{matrix} (3a) \\ (3b) \\ (3c) \\ (3d) \end{matrix}$$

$$CHO \rightarrow CO + H \quad (4)$$

$$H + O_2 \rightarrow OH + O \quad (5)$$

$$OH + CO \rightarrow CO_2 + H \quad (6)$$

$$\left\{\begin{matrix} O \\ OH \end{matrix}\right\} + H_2 \rightarrow \left\{\begin{matrix} OH \\ H_2O \end{matrix}\right\} + H \quad \begin{matrix} (7a) \\ (7b) \end{matrix}$$

As shown, the initiating reactions (1a), (1b), and (1c) involve CH_4 and the three principal chain carriers H, O, and OH. A similar initiating reaction involving molecular oxygen is too slow to contribute significantly to the initial reaction.[4] The reactants shown in reaction (2) are indicated by results of a recent mass-spectrometric study.[5] The products are consistent with these two experimental facts: (a) CH_2O is a combustion intermediate,[1] and (b) reaction (2) leads ultimately[5] to CO. The stripping reactions (3a), (3b), (3c), and (3d) are assumed if the integrity of the carbon–oxygen bond is to be preserved in these and subsequent reactions. The decomposition of the HCO radical, reaction (4), is an automatic consequence of reaction (3) and of the weakness of the H–CO bond. Reaction (5) is the only reaction involving molecular oxygen. Its occurrence during hydrocarbon combustion is inescapable.[6] Reaction (6) is well verified as a kinetic feature of hydrocarbon combustion. The final pair of stripping reactions, (7a) and (7b), must occur because H_2, from reactions (1a) and (3b), is known to be a combustion intermediate.[1]

The reaction mechanism, reactions (1) through (7), represents the main path for oxidation of CH_4. Secondary reactions resulting ultimately in ions and electronically excited molecules are not included in the scheme. Most of the secondary features must ultimately be related to the CH_3 radicals produced by reaction (1). Methyl radicals may react, in ways not shown, to produce eventually a variety of carbon-containing molecules. In particular, CH_3 is subject to abstractive reactions in the same way as CH_4 and CH_2O. In principle, the complete sequence represented formally by reaction (8) is possible

$$CH_4 \xrightarrow{-H} CH_3 \xrightarrow{-H} CH_2 \xrightarrow{-H} CH \xrightarrow{-H} C \quad (8)$$

with a wealth of associated kinetic possibilities.

All the main reactions, (1) through (7), except (2) and (5) produce as many free valences as they consume. Reaction (2), however, consumes two free valences per reaction and would quickly use up the available supply if not sustained by the chain-branching reaction (5). Due to this branching reaction, the overall mechanism will produce two free valences for each molecule of CH_4 converted to carbon oxides. Consequently, CH_4 combustion, once initiated, will result in a rapid increase in the concentration of free radicals to an extent limited by the depletion of fuel and oxidizer, and by the recombination of chain carriers; these two influences jointly impose a ceiling on the concentration of radicals and therefore on the maximum and average rates of reaction.

Recombination Zone

The attainment of a maximum in both reaction rate and in radical concentration may be regarded as marking the transition from the main reaction zone to the recombination zone. The products leaving the reaction zone will usually include concentrations of H, O, and OH greater than those corresponding to thermal equilibrium,[1,4,7,8] and some unburned CO and H_2. The characteristic reactions in this zone are recombination reactions like those shown:

$$H + H \xrightarrow{M} H_2 \quad (9)$$

$$O + O \xrightarrow{M} O_2 \quad (10)$$

$$H + OH \xrightarrow{M} H_2O \quad (11)$$

As implied by the symbol M in reactions (9), (10), and (11), all three reactions require third-body stabilization for most experimental conditions. Because in flames reactions (9), (10), and (11) involve two scarce species and

require third-body stabilization, the rates of recombination are slow compared with possible bimolecular reactions. Consequently, reactions like (5), (6), (7a), and (7b) which go primarily to the right in the reaction zone can be approximately balanced by the opposing back reactions:

$$OH + O \rightarrow H + O_2 \quad (12)$$

$$H + CO_2 \rightarrow CO + OH \quad (13)$$

$$H + OH \rightarrow O + H_2 \quad (14)$$

$$H + H_2O \rightarrow OH + H_2 \quad (15)$$

The kinetic results are ratios H/O/OH determined by the local concentrations of H_2, CO, CO_2, H_2O, and O_2. These ratios in turn will determine the relative importance of the various possible recombination reactions. Simultaneously with the recombination of radicals, the excess of CO and H_2 is also consumed but at a rate governed by the rate of recombination.

Some but not all of the rate constants for the reaction scheme represented by reactions (1) through (15) are known. Those which are available are listed in Table 1.

Chemical Inhibition

The two important kinetic features of the reaction mechanism, linear chain-branching by a moderately endothermic reaction [reaction (5)], and quadratic chain termination [reactions (9), (10), and (11)] imply a sensitivity to kinetic inhibition. In fact, kinetic inhibition of the type and degree observed requires for sensible interpretation exactly those two features.

TABLE 1

Specific Reaction Rates of Elementary Reactions in Premixed CH_4–O_2-Diluent Flames[a]

Reaction	Rate constant	Footnote references	Remarks
2	2×10^{13} ml/mole sec	(a)	—
5	1.5×10^{11} ml/mole sec at 1100°K		—
	$E_a = 18 \pm 3$ kcal/mole	(b)	
6	$2.3 \times 10^{13} \exp(-10{,}300/RT)$ ml/mole sec	(b)	—
	$2.9 \times 10^{12} \exp(-5700/RT)$ ml/mole sec	(c)	
7a	$\sim 6 \times 10^{12} \exp(-6000/RT)$ ml/mole sec	(c)	—
7b	$1.3 \times 10^{14} \exp(-10{,}000/RT)$ ml/mole sec	(c), (d)	—
9	2×10^{16} ml^2/mole^2 sec	(e)	room T, $M = H_2$
	2×10^{16} ml^2/mole^2 sec	(f)	1600°K, $M = H_2O$
10	$\sim 7 \times 10^{14}$ ml^2/mole^2 sec	(g)	2000°K, $M = O_2$
11	5×10^{17} ml^2/mole^2 sec	(f)	1600°K, $M = H_2O$
	2×10^{17} ml^2/mole^2 sec	(h)	2000°K, $M = H_2O$
	1×10^{17} ml^2/mole^2 sec	(h)	2000°K, $M = CO_2$
	2×10^{16} ml^2/mole^2 sec	(h)	2000°K, $M = N_2$
13	$3 \times 10^{15} \exp(-33{,}000/RT)$ ml/mole sec	(b)	—
15	$1 \times 10^{15} \exp(-25{,}500/RT)$ ml/mole sec	(b)	—
16b	$8 \times 10^{11} T^{\frac{1}{2}} \exp(-1100/RT)$ ml/mole sec	(i)	—

[a] Some information also available for reactions (1a), (3a), and (3b), in reference j, below.

(a) FENIMORE, C. P. and JONES, G. W.: J. Chem. Phys. Chem. *65*, 1532 (1961).
(b) FENIMORE, C. P. and JONES, G. W.: J. Phys. Chem. *63*, 1834 (1959).
(c) KONDRATIEV, V. N.: *Seventh Symposium (International) on Combustion*, p. 41. Butterworths, 1959.
(d) FENIMORE, C. P. and JONES, G. W.: J. Phys. Chem. *62*, 693 (1958).
(e) WISE, H. and ABLOW, C. M.: J. Chem. Phys. *35*, 10 (1961).
(f) BULEWICZ, E. M. and SUGDEN, T. M.: Trans. Faraday Soc. *54*, 1855 (1958).
(g) KAUFMAN, F. and KELSO, J. R.: *Chemical Reactions in the Lower and Upper Atmosphere*, p. 255. Interscience, 1961.
(h) MCANDREW, R. and WHEELER, R.: J. Phys. Chem. *66*, 229 (1962).
(i) GILBERT, M. and ALTMAN, D.: *Sixth Symposium (International) on Combustion*, p. 222. Reinhold, 1957.
(j) STEACIE, E. W. R.: *Atomic and Free Radical Reactions*, 2nd ed. Reinhold, 1954.

Consider first the class of inhibitors represented by HBr.[9] By virtue of abstraction reactions such as (16a), (16b), and (16c)

$$\left.\begin{matrix}O\\H\\OH\end{matrix}\right\} + HBr \rightarrow \left\{\begin{matrix}OH\\H_2\\H_2O\end{matrix}\right\} + Br \qquad \begin{matrix}(16a)\\(16b)\\(16c)\end{matrix}$$

all three of the chain carriers H, O, and OH will be directly affected. Reactions (16a), (16b), and (16c) do not alter the supply of free valences, but rather replace H, O, and OH by Br atoms. The Br atoms may carry out, with regeneration of HBr, the abstraction function represented specifically by reactions (1), (3), and (7), or more generally by the sequence, reaction (8). However, Br atoms cannot substitute for H atoms in the branching reaction, nor for OH radicals in the oxidation of CO, nor for O atoms in the conversion of CH_3 to CH_2O. The net effect of replacing H, O, and OH by Br is then a reduction in the overall reaction rate and measurable changes in the properties which depend on reaction rate—flame speed, quenching distance, etc.

Inhibition of the type described is only effective because the critical link in the reaction chain, reaction (5), is an endothermic branching reaction. The branching insures a magnification of the effect of substituting Br for H and the endothermicity (about 20 kcal) permits reaction (16b) (an exothermic reaction) to be competitive with reaction (5) for large values of the ratio $(O_2)/(HBr)$. The substitution of Br for the other two chain carriers, O and OH, provides an additional contribution to inhibitor effectiveness in that the H atoms required for branching are supplied by reactions (2), (4), and (6).

Another class of inhibitors appears to affect the rate of combustion in a way quite different from that represented by reactions (16a), (16b), and (16c). Finely powdered materials, Na_2CO_3 for example, are strong inhibitors of hydrocarbon combustion in general and CH_4 combustion in particular.[10] Examination of this phenomenon revealed that the powder particles partially evaporate (possibly with decomposition) in the reaction zone and that the effective inhibitor in the case of Na_2CO_3 is the sodium atom. Various processes which might result in inhibition are possible. The most reasonable of these consistent with the reaction mechanism, reactions (1) through (7), involves the catalyzed recombination of chain carriers such as, for example:

$$OH + Na \xrightarrow{M} NaOH \qquad (17)$$

$$H + NaOH \longrightarrow Na + H_2O \qquad (18)$$

Other similar recombinations are possible, but the cited reaction pair, reactions (17) and (18), exemplify the main features.

Reaction (17), an exothermic recombination similar in nature to reactions (9), (10), and (11) will involve third-body stabilization of the product. Nevertheless, the specific sequence reactions (17) and (18) can significantly increase the overall rate of recombination of H and OH if the concentration of Na is comparable with or greater than the concentration of H. Because the concentration of chain carriers in the reaction zone is partly determined by the rate of carrier recombination, an increase in the rate of recombination will have obvious consequences. Chain branching, while not directly required by this type of inhibition mechanism, will provide an amplification factor in the same manner as it did in the case of halogen inhibitors.

Elements other than Na may presumably function in a similar manner, represented formally by the reaction pair

$$A + Z \xrightarrow{M} A - Z \qquad (19)$$

$$B + A - Z \longrightarrow AB + Z \qquad (20)$$

where A and B are chain carriers (e.g., OH and H) and Z is the inhibitor (e.g., Na). Effective inhibition can only be expected if two criteria are satisfied: (a) the bond strength of $A - Z$ must be great enough to insure stabilization of AZ until reaction with B; and (b) the strength of $A - Z$ should be no greater, and preferably much less, than the bond strength of the eventual product AB. These criteria are satisfied in the case of the reaction pair, reactions (17) and (18): D(Na–OH) $\approx$ 90 kcal, and D(H–OH) $\approx$ 120 kcal. Based on these criteria, a number of substances can be expected to affect hydrocarbon combustion in the manner described.

Heterogeneous Reactions

The property of a solid surface to catalyze the formation of reaction intermediates as well as their destruction has been recognized for some time. By suitable choice of experimental conditions some of the characteristics of the explosion limits in the thermal reaction of hydrogen–oxygen mixtures have been interpreted in terms of a surface reaction leading to the destruction of chain carriers.[11–13] Most of these experimental measurements were carried out in glass containers containing a coating of various salts such as KCl, $BaCl_2$, Na_2WO_4, $K_2B_4O_7$, etc. Although qualitatively such experiments demonstrate variation of the efficiency of removal of

the chain carriers by different surface coatings, few reliable measurements are available of the kinetics of such heterogeneous radical reactions and the specificity of various surface coatings for the destruction of chain carriers. Such a parameter may be conveniently expressed in terms of a surface reaction coefficient γ, which is defined as the ratio of the rate of effective surface collisions between the gaseous reactant and the solid to the total collision rate. In many of the published results on the relative efficiencies of various surfaces for radical or atom removal the temperature rise of the solid at a given point in the system is taken as an index of the catalytic properties.[14,15] However, as will be shown in the following section, such a calorimetric measurement by itself is not a satisfactory means to evaluate surface activity or free-radical density.

Measurement of Surface Activities for Atom Recombination

Of the various experimental techniques employed for the determination of the kinetics of free-radical reactions on solid surfaces, a steady state experiment based on diffusion flow of reactants inside a cylindrical enclosure has found application in our laboratory. The details of the measurements have been described.[16–20] Over a wide range of gas pressures and surface temperatures the kinetics has been found to be of first order with respect to the radical concentration.[16,20,21] However, more recently, surface reactions of second order have been observed.[22]

In our measurements the atoms are generated in an electrodeless discharge. They diffuse into a closed cylinder where they recombine on the walls of the tube and on the catalytically active filament employed to detect the residual atom concentration by microcalorimetry.[16] This probe can be moved axially inside the tube and the residual atom concentration determined at various distances from the atom source. From the atom-concentration profile so obtained the surface activity of the walls and of the filament may be evaluated. In addition, quantitative measurement of atom densities is accomplished by means of electron paramagnetic resonance spectroscopy. This tool has proved to be of high sensitivity and its applicability to problems related to the gas-phase and surface-catalyzed atom and free-radical reaction has been demonstrated by several workers.[23,24]

Experimental Results

Glass and Quartz. Because of the widespread use of glass in constructing experimental apparatus,

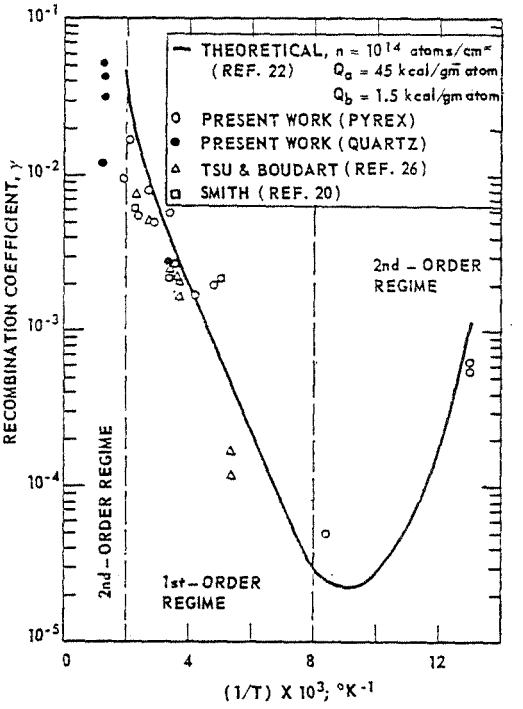

FIG. 1. Temperature dependence of rate of hydrogen atom recombination on Pyrex glass and fused quartz surfaces.

an understanding of its catalytic properties is desirable. A detailed study of the recombination rate of hydrogen atoms on Pyrex glass and fused quartz has been carried out over a temperature range from 70° to 1125°K. The glass and quartz surfaces used in the experiments were washed with concentrated nitric acid and rinsed in distilled water prior to use; no change in activity was noted. It was found that at temperatures above 550°K and less than 120°K a transition occurred from first- to second-order kinetics in the surface reaction. The results of our measurements are summarized in Fig. 1. In a temperature range from approximately 150° to 550°K the recombination coefficient of glass increases monotomically by a factor of 200. The observed kinetics may be interpreted in terms of two adsorption states with different binding energies.[25] Our results are in substantial agreement with the data obtained by Smith[20] and by Tsu and Boudart[26] over a smaller temperature interval. In a more recent publication[27] a value of $\gamma = 7 \times 10^{-6}$ has been reported for Pyrex glass treated with HF, compared with a value of $\gamma = 4 \times 10^{-3}$ for glass rinsed with HNO_3.

Numerous investigators added water vapor

to the hydrogen on the hypothesis that water acts as a surface poison.[28] Recent measurements question the inhibiting action of water although they suggest an increase in the production of hydrogen atoms in the presence of water vapor. Our measurements in the presence and absence of water vapor show a very small effect of the H_2O on the surface activity of Pyrex glass.[29] While for dry hydrogen $\gamma_H = 4 \times 10^{-3}$ was obtained in our measurements, the recombination coefficient in moist hydrogen was found to be $\gamma_H = 3 \times 10^{-3}$, which represents an insignificant change in the catalytic activity of glass. The enhancement in the concentration of H-atoms by the addition of water vapor to a hydrogen discharge is more likely due to phenomena in gas phase rather than inhibition of heterogeneous processes leading to atom destruction.[30,31]

A considerable amount of information has been accumulated on the kinetics of recombination of oxygen atoms on glass[32] and quartz. In general it is found that the recombination coefficient γ_O for oxygen atoms is smaller by approximately a factor of ten than γ_H under comparable conditions (Table 2). The values of γ_O of Pyrex glass appear to fall into two groups: one obtained at low pressures where the wall reaction predominates, the other at higher pressures where gas-phase atom recombination contributes to the loss of oxygen atoms. In the latter case, much lower recombination coefficients have been reported. The cause for this discrepancy is not apparent.

Certain analogies are apparent between the catalytic properties of glass for oxygen-atom and hydrogen-atom recombination. First of all, it is noted that water vapor has little if any effect[33] on the value of γ_O. Secondly, quartz and Pyrex glass appear to exhibit the same catalytic efficiencies for this process. Also the variation of γ_O with temperature[34] has certain characteristics observed in the case of the heterogeneous recombination of hydrogen atoms. The value of γ_O on glass rises from about 10^{-4} at 300°K to about 10^{-2} at 850°K. The flattening of the curve depicting the variation of log γ_O versus the reciprocal temperature suggests a complexity in the mechanism of the surface reaction which, as in the case of hydrogen, may be related to a change in the order of the reaction due to the presence of different adsorption states. It would be desirable to extend these measurements to higher and lower temperatures in order to examine in more detail the kinetics under such conditions.

For nitrogen atoms recombining on glass, the value of γ_N is still lower than that for hydrogen or oxygen atoms (Table 3). So far the nitrogen system has not been studied in great detail. For flames and related processes the role of nitrogen atoms is of less importance than that of H and O. In the case of alkyl radicals[35] the catalytic efficiency of glass is of the same magnitude as for hydrogen atoms (γ_{CH_3}, $\gamma_{C_2H_5} \sim 10^{-3}$). No reliable data are available on the kinetics of OH destruction by glass surfaces. In some early experiments, Smith[20] observed a large temperature rise on a KCl-coated glass surface when exposed to the products of a gas discharge through H_2–H_2O mixtures. However, no tem-

TABLE 2

Recombination Coefficient of Glass for Oxygen Atoms at Room Temperature

Surface	γ_O	Footnote reference
Pyrex glass	2.1×10^{-4}	Present work
Pyrex glass	1.3×10^{-4}	(a)
Pyrex glass	$<5 \times 10^{-5}$	(b)
Pyrex glass	7.7×10^{-5}	(c)
Soda glass	3.4×10^{-4}	(d)
Vitreosil	1.6×10^{-4}	(e)
Quartz (fused)	4×10^{-5}	(f)

(a) LINNETT, J. W. and MARSDEN, D. G. H.: Proc. Roy. Soc. (London) *A234*, 489 (1956).

(b) KRETSCHMER, C. B.: Private communication.

(c) ELIAS, L., OGRYZLO, E. A., and SCHIFF, H. I.: Can. J. Chem. *37*, 1680 (1959).

(d) GREAVES, J. C. and LINNETT, J. W.: Trans. Faraday Soc. *54*, 1323 (1958).

(e) GREAVES, J. C. and LINNETT, J. W.: Trans. Faraday Soc. *55*, 1355 (1959).

(f) HACKER, D. S., MARSHALL, S. A., and STEINBERG, M.: J. Chem. Phys. *35*, 1788 (1961).

TABLE 3

Recombination Coefficients of Various Surfaces for Nitrogen Atoms at Room Temperature

Surface	γ_N	Footnote reference
Pyrex glass	1.6×10^{-5}	(a)
Pyrex glass	3×10^{-5}	(b)

(a) HERRON, J. T., FRANKLIN, J. L., BRADT, P., and DIBELER, V. H.: J. Chem. Phys. *30*, 897 (1959).

(b) WENTINK, T., SULLIVAN, J. O., and WRAY, K. L.: J. Chem. Phys. *29*, 231 (1958).

perature increase was noted as a result of the interaction between KCl and hydrogen atoms. From such measurements γ_{OH} for Pyrex glass was evaluated. It ranged from $\gamma_{OH} = 10^{-4}$ at 400°K to about 6×10^{-2} at 800°K. It is not known whether the glass surface catalyzes the reaction H + OH, or OH + OH, or both, under these experimental conditions.

Metals. Numerous measurements of the catalytic properties of metals for atom recombination have been reported. The problem is complicated by the fact that, in addition to atom recombination, chemical reaction between the solid and the gas may occur with the formation of volatile oe nonvolatile products.[36-39] In this paper we shall not be concerned with these reactions; rather we shall confine our remarks to heterogeneous atom recombination.

In Table 4 the measured recombination coefficients[16] of a series of metals for hydrogen atoms are summarized. For each of these metals the kinetics exhibited first-order dependencey on gaseous atomic hydrogen concentration over a wide temperature range (for W the temperature was varied from 350° to 1100°K, for Ni from 300° to 900°K, for Pt from 350° to 1600°K). It is apparent that no correlation is to be found between the catalytic properties of these metals and the electron distribution in the valence band of the solid. As a matter of fact, some of the nontransition metals appear to have more favorable catalytic activity than the transition metals. However, it is to be remembered that in a system containing atomic hydrogen the formation of a chemisorbed layer can proceed readily without any activation energy. Such an adsorbate may cause changes in the electronic properties of the solid, such as filling of positive holes in the *d*-band, analogous to those produced by the formation of solid solution composed of transition and nontransition metals. Such an explanation may be offered in comparing the recombination coefficients of pure Pd with that of the Pd–Au alloy (Table 4). Also it would be expected that in the presence of atomic hydrogen the formation of a chemisorbed layer on gold would occur. As a result the formation of a hydrogen molecule by the Rideal mechanism, S—H + H → S + H_2 (where S—H is a surface-adsorbed atom), is feasible.

TABLE 4

Recombination Efficiencies γ_H of Various Solids for Hydrogen Atoms at Room Temperature

Metal	γ_H	θ_D
Titanium	0.38	430
Aluminum	0.27	375
Nickel	0.08	413
Copper	0.11	343
Gold[a]	0.08	164
Palladium	0.07	275
Tungsten	0.06	270
Platinum[a]	0.02	233
Alloy (38 atom % Pd, 62 atom % Au)	0.07	—
Carbon	0.009	—

[a] Material exhibits an activation energy for atom recombination: $E_a > 600$ cal/mole.

Some indication exists that the dissipation of the energy released in the heterogeneous reaction may play an important controlling role in this process. The normal mode-frequeney spectrum of a lattice has an upper limit at the Debye frequency. It may be expected that those solids which exhibit a high velocity of propagation of longitudinal and transverse waves will tend to have high recombination efficiencies. Indeed a correlation is found between catalytic activity and the Debye characteristic temperature of the solid, θ_D (Table 4). At the same time it is to be noted that in the collision between a gas atom and a solid, the transport of energy by phonons in the solid becomes less efficient above a critical value of the incident energy.[40,41] During a highly exothermic reaction on the surface of the solid similar limitations may prevail. As a result, partial accommodation of the energy released during heterogeneous atom recombinations may result in the formation of a molecule containing excess kinetic or internal energy. Recent observations have indicated the existence of electronically excited molecules formed presumably by reaction of atoms on a solid surface.[42]

We have carried out a series of experimental measurements in order to examine the coefficient of energy accommodation of various metals during atom recombination. For this purpose the atom flux incident upon the solid was determined by measuring the atom density with the electron paramagnetic resonance spectrometer. The energy released as a result of the recombination process was found simultaneously by evaluation of the difference in electric power required to maintain a catalytic metal filament at constant temperature (i.e., constant resistance) in the presence of the atomic species and in the presence of molecular hydrogen. From such experiments the product of the ac-

TABLE 5

Energy Accommodation by Solid during Hydrogen Atom Recombination at 400°K

Solid	α	γ^a	$\theta_D{}^b$
Ni	0.2	0.08	413
W	0.5	0.06	270
Pt	0.2	0.03	233

[a] WOOD, B. J. and WISE, H.: J. Phys. Chem. *65*, 1976 (1961).

[b] GRAY, D. E. (ed.): *American Institute of Physics Handbook*, McGraw-Hill, 1957.

commodation α and recombination coefficients γ may be obtained. For those metals for which the values of γ have previously been determined,[16] the energy accommodation coefficients may readily be computed (Table 5). It is to be noted that only a fraction of the energy released is transmitted to the solid.

On the basis of theoretical considerations for collisional energy transfer, the propagation of lattice waves from the point of impact may be expected to reach an upper limit at some frequency characteristic of the lattice. The quantity of energy that can be transferred would tend to decrease with increasing lattice-force constant, which in a one-dimensional lattice is related to the Debye characteristic temperature, θ_D (Table 5). From these considerations we may conclude that a solid may exhibit high efficiency for atom recombination, yet at the same time low-energy accommodation.

The nonequilibrium distribution of energy between the solid and the product molecule formed in the heterogeneous reaction must be taken into account in experiments in which a catalytic surface is employed for the quantitative detection of atoms by calorimetry. The energy released is related to the absolute atom density through the product of the two coefficients $\alpha \cdot \gamma$. Unless their magnitude is known, measurements of atom densities in flames by means of catalytic thermocouple probes[43,44] are difficult to interpret. Similar considerations apply to other systems containing free radicals and atoms

TABLE 6

Recombination Coefficients of Various Metal Oxides for Oxygen Atoms

Metal oxide	γ_O	$\theta_D{}^a$	Footnote references[c]
Arsenic	8.1×10^{-5}	120 (As_2O_3)	(a)
Chromium	2.5×10^{-4}	275 (Cr_2O_3)	(a)
Antimony	2.7×10^{-4}	—	(a)
Zinc	4.4×10^{-4}	275 (ZnO)	(a)
Vanadium	4.8×10^{-4}	200 (V_2O_5)	(a)
Lead	6.3×10^{-4}	—	(a)
Tin	1.0×10^{-3}	300 (SnO_2), 220 (SnO)	(a)
Molybdenum	1.0×10^{-3}	200 (MoO_3)	(a)
Calcium	1.6×10^{-3}	450 (CaO)	(a)
Cobalt	4.9×10^{-3}	—	(a)
Iron	5.2×10^{-3}	310 (FeO)	(a)
Nickel	8.9×10^{-3}	400 (NiO)	(a)
Manganese	1.3×10^{-2}	310 (MnO_2)	(a)
Magnesium	2.5×10^{-2}	530 (MgO)	(a)
Copper	4.3×10^{-2}	300 (CuO)	(a)
Magnesium[b]	6×10^{-2}	530 (MgO)	(b)
$ZnO \cdot Cr_2O_3$	1.0	—	(b)

[a] The Debye characteristic temperatures were estimated from specific heat data listed in footnote reference (c), below.

[b] T = 550°K.

[c] Footnote references:

(a) GREAVES, J. C. and LINNETT, J. W.: Trans. Faraday Soc. *55*, 1355 (1959).

(b) LAVROSKAYA, G. K. and VOEVODSKII, V. V.: Zhur. Fiz. Khim. *25*, 1050 (1951).

(c) KELLEY, K. K.: U. S. Department of Interior, Bulletin 477, 1950.

TABLE 7

Recombination Coefficients of Various Glass Coatings for Hydrogen Atoms at 300°K

Coating	Footnote reference[b]	Recombination coefficient (γ_H)
Al_2O_3	(a)	4.5×10^{-1a}
Na_3PO_4	(a)	$\geq 10^{-1}$
K_2CO_3	(a)	$\geq 10^{-1}$
KCl	(a)	2×10^{-5}
K_2SiO_3	(a)	7×10^{-2}
Pyrex glass	(a), (b)	4×10^{-3}

[a] Interpolated value.

[b] Footnote references:

(a) SMITH, W. V.: J. Chem. Phys. *11*, 110 (1943).

(b) WOOD, B. J. and WISE, H.: J. Phys. Chem. *66*, 1049 (1962).

In the case of oxygen- and nitrogen-atom recombination on metallic surfaces the experimental data are relatively meager. The catalytic properties of the solid are obscured by the chemical reaction these metallic surfaces undergo when exposed to the gaseous atoms. In the case of platinum catalyzing the recombination of oxygen atoms the results indicate that at $T > 1100°K$ the metal oxide is unstable.[45] At these temperatures we have measured a recombination coefficient of $\gamma_O = 0.04$.* At lower temperatures where the oxide is stable the measured value was $\gamma \simeq 0.01$. However, the oxide surface is not well defined. Work is in progress to examine the catalytic properties of metallic surfaces in the presence of nitrogen atoms. In the case of a nickel filament exposed to an atmosphere containing atomic nitrogen, a stable nitride Ni_3N was produced on the surface. Its recombination coefficient was found to be $\gamma_N = 0.1$ for a temperature range $350°K < T < 800°K$.

Metal Salts. Greaves and Linnett[34] have measured the efficiency of various metallic oxide coatings on glass for oxygen-atom recombination. Unfortunately, the metallic oxides present on the surface are not well defined and it is difficult to draw any quantitative conclusion from these results (Table 6) other than the fact that differences in activity were observed. However, analogous with observations for pure metals, the results for the metal oxides suggest that a high Debye characteristic temperature favors high catalytic activity. It is of interest that the efficiencies of the oxides reported are in qualitative agreement with the results obtained in studies of first explosion limits of hydrogen–oxygen mixtures[11] in glass vessels with various oxide coatings.

Various salt coatings on glass were examined for their catalytic properties toward hydrogen atoms. As shown in Table 7 most of the materials tested are superior to glass except for KCl.

Comparison of Homogeneous and Heterogeneous Reaction

The destruction of atoms by gas-phase reaction and by surface reaction proceeds by different mechanisms at widely different rates as shown in the preceding pages. It may be instructive to compare the loss rate of atoms by these two processes as a function of gas pressure, atom density, surface activity, and temperature. In a static cylindrical system the ratio of the gas-phase R_g and the surface reaction R_s rates is given by

$$(R_g/R_s) = \Phi = 4\,(\pi m/8RT)^{\frac{1}{2}}[X][M][k/\gamma(S/V)]$$

where $[X]$ is the concentration of atoms of mass m; T, the temperature of the gas and the cylinder walls (which are assumed to be equal); k, the rate constant for gas-phase atom recombination by three-body collisions; and (S/V), the surface-to-volume ratio of the cylinder.

In Fig. 2 a series of curves are drawn which show the magnitude of the ratio of reaction rates as a function of temperature for various values of the different parameters. In this calculation the rate constant for the gas-phase reaction was taken to be 10^{16} (gm atom/ml)$^{-2}$ sec^{-1} and independent of temperature. For an atom con-

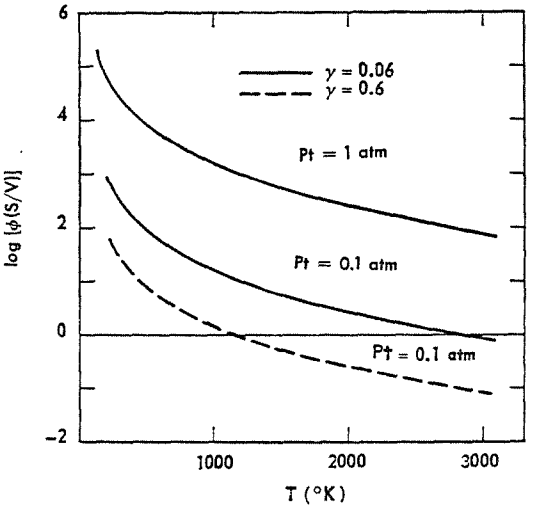

FIG. 2. Comparison of gas-phase and surface reaction kinetics; $[X] = 10^{-3}[M]$; $k_g = 10^{16}$ (gm atom/ml^{-2} sec^{-1}.

* A similar value for Pt has been reported at 900°K in reference 46.

centration of 0.1 volume percent of the total pressure, it will be noted that at $T < 1000°K$ the gas-phase reaction outweighs the surface reaction. As the total pressure is lowered from 1 atm to 0.1 atm in the presence of a highly catalytic surface (where $\gamma = 0.6$) the surf ce-reaction rate matches the gas-phase rate at about 1200°K for a surface-to-volume ratio of the cylinder equal to unity. For second-order, gas-phase reactions the relative influence of the wall may be more pronounced than shown by the theoretical curves in Fig. 2. Also it is to be expected that with increasing temperature the surface reaction becomes of second order with respect to the reactants.

ACKNOWLEDGMENT

This work was supported in part by Project SQUID, Office of Naval Research, Department of the Navy.

REFERENCES

1. FRISTROM, R. M., GRUNFELDER, C., and FAVIN, S.: J. Phys. Chem. *64*, 1386 (1960).
2. WESTENBERG, A. A. and FRISTROM, R. M.: J. Phys. Chem. *64*, 1393 (1960).
3. FRISTROM, R. M., GRUNFELDER, C., and FAVIN, S.: J. Phys. Chem. *65*, 587 (1961).
4. WESTENBERG, A. A. and FRISTROM, R. M.: J. Phys. Chem. *65*, 591 (1961).
5. FENIMORE, C. P. and JONES, G. W.: J. Phys. Chem. *65*, 1532 (1961).
6. FENIMORE, C. P. and JONES, G. W.: J. Phys. Chem. *63*, 1834 (1959).
7. FENIMORE, C. P. and JONES, G. W.: J. Phys. Chem. *62*, 178 (1958).
8. MCANDREW, R. and WHEELER, R.: J. Phys. Chem. *66*, 229 (1962).
9. ROSSER, W. A., WISE, H., and MILLER, J.: *Seventh Symposium (International) on Combustion*, p. 175. Butterworths, 1959.
10. ROSSER, W. A., JR., INAMI, S. H., and WISE, H.: Combustion and Flame (to be published).
11. WARREN, D. R. Trans. Faraday. Soc. *53*, 199 (1957).
12. LEWIS, B. and VON ELBE, G.: *Combustion, Flames and Explosion of Gases*, p. 22. Academic Press, 1961.
13. FROST, A. A. and ALYEA, H. N.: J. Am. Chem. Soc. *55*, 3227 (1933).
14. KATZ, S., KISTIAKOWSKY, G. B., and STEINER, R. F.: J. Am. Chem. Soc. *71*, 2258 (1949).
15. WARREN, D. R.: Trans. Faraday Soc. *53*, 206 (1957).
16. WOOD, B. J. and WISE, H.: J. Phys. Chem. *65*, 1976 (1961).
17. WISE, H. and ABLOW, C. M.: J. Chem. Phys. *29*, 634 (1958).
18. MOTZ, H. and WISE, H.: J. Chem. Phys. *32*, 1893 (1960).
19. WISE, H. and ABLOW, C. M.: J. Chem. Phys. *35*, 10 (1961).
20. SMITH, W. V.: J. Chem. Phys. *11*, 110 (1943).
21. LAIDLER, K. J.: J. Phys. Chem. *53*, 712 (1949).
22. WOOD, B. J. and WISE, H.: J. Phys. Chem. *66*, 1049 (1962).
23. KRONGELB, S. and STRANDBERG, M. W. P.: J. Chem. Phys. *31*, 1196 (1959).
24. HACKER, D. S., MARSHALL, S. A., and STEINBERG, M.: J. Chem. Phys. *35*, 1788 (1961).
25. HICKMOTT, T. W.: J. Appl. Phys. *31*, 128 (1960).
26. TSU, K. and BOUDART, M.: *Second International Congress on Catalysis*, p. 593. Technip, Paris, 1960.
27. COLLINS, R. L. and HUTCHINS, J. W.: Bull. Am. Phys. Soc. *7*, 114 (1962) Abstract C1.
28. WOOD, R. W.: Proc. Roy. Soc. (London) *A97*, 455 (1920).
29. SCHOTT, D. and WISE, H.: To be published.
30. COFFIN, F. D.: J. Chem. Phys. *30*, 593 (1954).
31. KAUFMAN, F. and DEL GRECO, F. P.: J. Chem. Phys. *35*, 1895 (1961).
32. GREAVES, J. C. and LINNETT, J. W.: Trans. Faraday Soc. *54*, 1323 (1958).
33. LINNETT, J. W. and MARSDEN, D. G. H.: Proc. Roy. Soc. (London) *A234*, 489 (1956).
34. GREAVES, J. C. and LINNETT, J. W.: Trans. Faraday Soc. *55*, 1355 (1958).
35. PANETH, F. and HERZFELD, K. F.: Z. Elektrochem. *37*, 577 (1931).
36. BONHEOFFER, K. F.: Z. physik. Chem. *113*, 199 (1924).
37. KING, B. J. and WISE, H.: J. Phys. Chem. (to be published).
38. BLACKWOOD, J. D. and MCTAGGART, F. K.: Australian J. Chem. *12*, 114 (1959); *ibid. 12*, 533 (1959).
39. STREZNEWSKI, J. and TURKEVICH, J.: *Proceedings of Third Symposium on Carbon*, p. 273. Pergamon, 1959.
40. CABRERA, N.: Discussions Faraday Soc. *28*, 16 (1959).
41. ZWANZIG, R. W.: J. Chem. Phys. *32*, 1173 (1960).
42. HARTECK, P., REEVES, R. R., and MANELLA, G.: Can. J. Chem. *38*, 1648 (1960).
43. KONDRATIEVA, H. and KONDRATIEV, V.: Acta Physicochim. U.R.S.S. *21*, 1 (1946).
44. KONDRATIEV, V.: Zhur. Fiz. Khim. *21*, 761 (1947).
45. FRYBURG, G. and PETRUS, H. M.: J. Chem. Phys. *32*, 622 (1960).
46. LAVROSKAYA, G. K. and VOEVODSKII, V. V.: Zhur. Fiz. Khim. *25*, 1050 (1951).

Discussion

DR. A. A. WESTENBERG (*APL/The Johns Hopkins University*): The present comments are restricted to the sections on heterogeneous atom recombination.

Very little about experimental research with free radicals and labile atoms lends itself to simple, unambiguous interpretation, and surface catalysis of atom recombination is certainly no exception. Thus the authors' comments on any or all of the following points would be helpful:

1. An interesting question has come up in connection with the Wood–Wise technique[1,2] for measuring atom recombination coefficients on the surface of the probe used as an atom detector, as described briefly in the paper. The first set of data[1] published using this technique for a series of metallic surfaces indicated that they all had nearly the same (within a factor of 2) catalytic activity for hydrogen atom recombination. This result, I must confess, did not strike me as particularly surprising at the time, since I doubt that we know enough about the details of such surface recombinations to say *a priori* whether various metals should act the same or differently. (If surface recombination occurs by reaction of an incoming atom with one in an absorbed layer completely covering the surface, perhaps all surfaces *would* act about the same, except for small effects due to differences in the surface forces extending beyond the adsorbed layer.) Apparently it did surprise some people, however, since Tsu and Boudart took the trouble to look into possible explanations in the technique itself, and published a paper[3] on it. Now a basic assumption of the theoretical model[4] used to interpret the probe experiments is that the atom concentration at the origin (i.e., in the discharge) is a constant independent of the position of the probe. Without going into mathematical details, which are simple enough, the essence of Tsu and Boudart's point was that if the presence of the probe (a partial atom sink) perturbs the atom concentration at the origin, and if this perturbation is taken into account, then the experimental data of relative concentration vs. probe position would depend on the catalytic efficiency of the tube walls, but not on that of the probe. Thus the apparent efficiencies of all probe materials might be expected to be about the same, as had been reported.

Obviously, the legitimate question raised by Tsu and Boudart required an answer. In a later paper[2] (from which Table 4 of the present paper was taken), Wood and Wise reported revised data on H atom recombination on metals taken with a coiled filament probe instead of the metal-coated, glass-enclosed thermocouple probe used earlier. The new data do show some variation in catalytic efficiency among metals. The authors also implicitly acknowledged the problem by noting some auxiliary experiments designed to show whether or not the probe perturbs the source concentration. Probably the most significant of these was an experiment with two side-arms containing "identical" platinum probes, in which they state that movement of one probe caused no "significant" steady state change in the relative concentration measured by the other (stationary) probe. This would seem to indicate that the basic objection about the probe perturbing the source may be unfounded. Apropos of this problem, it may be worth remarking that we have made some observations on the source concentration on a similar system used in connection with experiments for measuring the diffusion coefficient of the O–O_2 system. Monitoring of the O atom concentration was done by a photomultiplier which senses the glow (proportional to O concentration) given off when a trace of NO is added to the oxygen flow. With the photomultiplier at the junction of sidearm and main flow tube, there was indication of a drop in concentration when a nickel screen was closer than about 20 tube radii. These were rather crude experiments, however, and further checking of this point seems important, both for recombination experiments and others making use of similar discharge tube apparatus.

2. Another point about the probe experiments has occurred to me which seems worth bringing up, since if it is valid it would have fairly important bearing on the interpretation of the results. This has to do with the boundary condition at the probe when the latter is heated to obtain the dependence of the probe recombination coefficient on surface temperature. One can show (rigorously, as far as I can see, within the limits of Chapman–Enskog dilute gas theory) that, for atoms present at low concentrations, the concentration gradient at the probe surface ($x = L$) is given by

$$-d(N_1/N)/dx = (N_1/\delta' RN) + k_T\, d(\ln T)/dx \quad (1)$$

where N_1 is the atom concentration and N the total molar density, R is the side-arm radius, k_T is the thermal diffusion ratio for the atom-molecule pair, T is temperature, and

$$\delta' = [4D(1 - \gamma'/2)]/\gamma' cR \quad (2)$$

where D is the atom-molecule diffusion coefficient, c is the kinetic theory mean velocity of the atoms, and γ' is the probe recombination coefficient. The probe surface boundary condition used in the theoretical model for the Wood-Wise experiments [see Eq. (5) of reference 4 of this Discussion] was apparently obtained by neglecting the thermal diffusion term in Eq. (1) and regarding N as constant (i.e., assuming constant pressure and temperature throughout),

which gives simply

$$-(dN_1/dx)_L = (N_1)_L/\delta' R \qquad (3)$$

as one required boundary condition.

The neglect of thermal diffusion is certainly understandable since it makes the data analysis very complicated, if not impossible. It is obviously difficult to calculate the temperature gradient at the probe. I have made a very crude estimate of this gradient under typical conditions which, combined with the recent thermal diffusion recommendations of Weissman and Mason[5] for H–H_2, indicates that the thermal diffusion term in (1) may not be negligible. But aside from this complication, the thing that bothers me is that the authors apparently use values of D and c evaluated at the gas temperature to get γ' from the measured quantity δ' in Eq. (2), whereas it would seem that the probe surface temperature should be used. Aside from the so-called "temperature jump," the gas near the surface will be approximately at the surface temperature and not at that characteristic of the main tube (i.e., room temperature). For experiments where the probe was heated as high as 1100°K, as it was in certain cases (tungsten, platinum), this would be quite important.

If this is a valid point, it would seem that the temperature dependence of γ' should really be stronger than reported. Thus, from Eq. (2), and noting that $c \propto T^{0.5}$ and $D \propto T^{1.7}$ (roughly), we have $\gamma' \propto (T^{1.2}/\delta')$. This would mean that a metal like tungsten which was reported as being essentially independent of temperature might actually show $\gamma' \propto T^{1.2}$ under this interpretation, which in turn would imply an activation energy for recombination.

3. Further lack of agreement in this controversial field is revealed by the fact that in this paper the authors report practically no inhibiting effect of H_2O for the recombination of H atoms on Pyrex, while Boudart *et al.*[6] claim to have shown "unequivocally" (their word) that H_2O vapor lowers this recombination coefficient by a factor of 10^{-3}. The latter experiment was an entirely different one involving the first explosion limit of H_2–O_2 mixtures. As such it requires knowledge of certain elementary gas phase reaction rate constants to obtain a value for the surface recombination coefficient, a fact which should immediately give Wise *et al.* the offensive.

Another point of interest is that, while most results indicate an increase in surface recombination coefficients with temperature, at least one report[7] on the behavior of a AgO detector seems to show the reverse trend. It seems clear, therefore, that this area of research is still not completely settled.

DR. H. WISE (*Stanford Research Institute*): The first question concerns the perturbation of the atom source by the catalytic probe surface. Experimentally this problem was investigated with hydrogen atoms in two sets of measurements. In one set, a two-probe system was employed. The first probe (A) consisting of a small tungsten filament was located in a fixed position very near the atom source ($x = 0$), while the second probe (B), made of nickel wire was movable. In this way the distance between the two catalytic surfaces could be varied. During steady state conditions the atom density as detected[8] by probe A was examined while the position of probe B was varied. The results obtained at a total gas presence of 50×10^{-5} mm Hg are shown here in Table 1.

TABLE 1

Perturbation of Atom Source

Discharge power (watt)	Probe distance between A and B	Response of Probe A (arbitrary units)
24	0.3	0.415
	0.6	0.412
	0.9	0.412
	1.2	0.411
65	0.4	0.384
	0.9	0.384
	1.2	0.388

In the second type of measurement the hydrogen atom concentration profile in a quartz cylinder containing a movable catalytic probe was determined with the aid of an electron-paramagnetic resonance spectrometer (EPR). Since the catalytic activities of the tungsten probe and the quartz walls had previously been determined, a theoretical analysis[9] of the relative atom density at a given distance from the source as a function of the position of the tungsten probe was feasible. The excellent agreement obtained between the measured values of the atom concentration and the theoretical data suggests that the perturbation of the atom source is small under our experimental conditions.[10]

The next question concerns diffusion in a cylinder of finite length under nonisothermal conditions so that the differential equation is given by $\partial(D\,\partial n/\partial x)\,\partial x = 0$, rather than $D\,\partial^2 n/\partial x^2 = 0$. It can be shown that for the case of noncatalytic cylinder walls the relative atom density at the catalytic end plate[9] is given by

$$[(n_0/n) - 1]_{x=L} = L/\delta' R$$

(for terminology see text of main paper) under isothermal conditions. If the end plate is at a different temperature, T_s, from that of the gas, T_0, one

obtains instead

$$[(n_0/n) - 1]_{x=L} = \frac{L}{\delta' R}\left[\frac{3T_s^{1/2}(T_s - T_0)}{2(T_s^{3/2} - T_0^{3/2})}\right]$$

where the term in square brackets on the right-hand side of the equation represents a correction term due to the nonisothermal model. A Lewis number of unity was assumed for the nonisothermal case. It is of interest to compare the theoretical atom-concentration gradient at the catalytic filament surface as derived from the equation shown under isothermal and nonisothermal conditions (Table 2) for two probe locations. It may be concluded that the perturbation on the atom gradient is small when caused by the temperature difference between probe and gas. Consequently it appears more appropriate to employ the bulk gas temperature in the evaluation of the diffusive flux and the collision frequency rather than the probe surface temperature.

The inhibition effect of water on the recombination efficiency of Pyrex glass as deduced from indirect determinations is difficult to explain. Our direct measurements for hydrogen atoms and those of Linnett and co-workers for oxygen atoms[11] show no such poisoning of the walls for the atom-recombination reactions. Several authors have found pronounced effects of trace impurities in the gas phase on atom production caused either in the electrodeless discharge or by subsequent gas reactions downstream of the discharge. This problem merits further investigation.

As for the apparent negative temperature coefficient of silver oxide, a similar trend was observed for other metals in the case of oxygen-atom recombination.[12] Most likely this phenomenon is associated with phase and composition changes of the metal oxide film with temperature. For example in the case of platinum, the oxide formed at lower temperature tends to vaporize at high temperature. Experiments indicate that the oxygen atoms recombine on a platinum oxide at $T > 1000°K$ and on the metal surface at $T > 1000°K$. Such surface variations are accompanied by pronounced changes in the value of the recombination coefficient.

TABLE 2

Effect of Catalytic Filament Temperature on Atom Concentration Gradient[a]

	Relative atom concentration gradient at probe $(1/n_0)(dn/dx)$	
T_s (°K)	Probe distance = 1 radius	Probe distance = 10 radii
300[b]	0.167	0.066
400	0.164	0.064
600	0.162	0.060
800	0.161	0.058
1000	0.160	0.057

[a] These calculations are based on a surface activity corresponding to $\delta' = 5$ (cf. reference 2 of this discussion).

[b] Isothermal conditions.

DR. G. M. MARKSTEIN (*Cornell Aeronautical Laboratory*): I would like to ask whether any effects of condition of the surface on the recombination coefficient have been observed, and any change of the coefficient with time.

DR. R. S. BROKAW (*NASA, Cleveland*): The work of George Prok of the NASA Lewis Research Center on nitrogen atom recombination indicates that the method of surface preparation and prior history may profoundly influence catalytic activity. Thus the activity of a platinum surface increased from $\gamma = 0.012$ to $\gamma = 0.022$ over a period of two hours under nitrogen atom bombardment; similarly, the activity of a lithium chloride surface increased by more than two orders of magnitude after forty minutes of bombardment.[13] More recently, Prok has shown that the steady state activity of platinum varied by a factor of two, and the activity of copper varied by more than threefold, according to the method of surface preparation and cleaning.[14]

DR. D. E. ROSNER (*AeroChem Research Laboratory*): Wise and Rosser called attention to the fact that incomplete energy accommodation can cause large systematic errors in the use of calorimetric atom detectors, adding that unless the magnitude of $\alpha\gamma$ is known, atom concentration estimates in flames, such as those reported by Kondratieva and Kondratiev, are difficult to interpret. While many calorimetric techniques are unquestionably subject to this uncertainty, it may be interesting to note that a diffusion-controlled continuum catalytic detector (which the thermocouple device used by Kondratieva and Kondratiev approached) is a member of perhaps the only class of energy transfer atom detectors whose sensitivity can conceivably be independent of the magnitude of $\alpha\gamma$. As previously discussed[15] the active member of a differential probe will be diffusion-controlled for very large values of a parameter ζ which is of the order of γ/Kn_δ. Here γ is the conventionally defined heterogeneous atom recombination coefficient and Kn_δ is the Knudsen number based on the prevailing mean free path and diffusion boundary layer thickness, δ. In the extreme $\zeta \gg 1$ for the active member and $\zeta \ll 1$ for the inactive member, the differential probe output becomes independent of the magnitude of γ for

either surface, and the atom concentration (mass fraction) c_ϵ is obtained from a linear relation of the form

$$c_\epsilon = (c_p \cdot \Delta T)/(r_D \cdot Q) \qquad (1)$$

where ΔT is the differential temperature output, c_p is the mean specific heat of the prevailing gas mixture, Q is the effective heat of recombination and r_D is a "recovery factor for chemical energy" which depends principally on the ratio of the atom-mixture binary diffusion coefficient $D_{1-\text{mix}}$ to the thermal diffusivity α_{mix} of the gas mixture. This is essentially the same as the relation used in references 43 and 44 of the paper except that Kondratieva and Kondratiev took $r_D \approx 1$ for their quantitative estimates, whereas, in fact, values of r_D somewhat in excess of unity would be more realistic [$r_D \approx (D_{1-\text{mix}}/\alpha_{\text{mix}})^{2/3}$].

Now suppose that the energy accommodation referred to by Wise and Rosser is poor and the effective heat of recombination is less than the thermodynamic value appropriate to the catalyst surface temperature. If the latter is used in Eq. (1), are the values of c_ϵ so derived proportionately falsified? The answer to this question is likely to be no. Indeed, this process of surface catalyzed excitation (δCE) could possibly cause a negligible error in the inferred atom concentration. The reason is that in the diffusion controlled extreme excited molecules produced at the interface run the risk of being collisionally deactivated before proceeding very far into the boundary layer. If deactivated, their energy would, in fact, be released, but in the layers of gas near the interface instead of at the interface itself. Since ordinary heat conduction in the gas is available as an energy transport mechanism, Eq. (1) can remain correct; only the recovery factor r_D would undergo a small reduction reflecting the "roundaboutness" of the energy transfer mechanism to the solid. Now the number of binary collisions a molecule makes in escaping the diffusion boundary layer is of the order of $(Kn_\delta)^{-2}$. It can therefore be shown that the effect of surface catalyzed excitation would be negligible unless the desorbed molecules had an average collisional deactivation number Z^* approximately equal to, or much greater than $\zeta^2/\gamma\delta$. The parameter ζ is necessarily much larger than unity for the active member of a diffusion controlled detector and γ is, at most, of order unity. Thus, unless the desorbed molecules can survive some 10^4 or more binary collisions in the gas phase, poor energy accommodation at the surface could have a very minor effect on the output of such probes.

This argument leads one to conclude that the effect of a coefficient such as $\alpha\gamma$ on the output of an atom detector will depend greatly on the extent of diffusion control and should be negligible when the active probe member is diffusion controlled and the excited molecules (if any) formed at the surface are rapidly de-excited in the gas phase.

DR. H. WISE: In the double-probe experiment suggested by Rosner the differential temperature output will be affected by incomplete accommodation of the atom recombination energy even in the diffusion controlled regions. As a result of the heterogeneous formation of molecules with an excess of energy which are subsequently equilibrated by collisional deactivation, the total gas mixture (molecules and atoms) is raised in temperature. As pointed out by Rosner this process will tend to reduce the possible error introduced into this measurement so far as the catalytic probe is concerned. However, the noncatalytic probe will "see" a higher gas temperature than in the absence of the phenomenon of incomplete reaction energy accommodation and the differential temperature (ΔT) will be perturbed accordingly. Also changes in transport parameters may take place.

REFERENCES

1. WOOD, B. J. and WISE, H.: J. Chem. Phys. *29*, 1416 (1958).
2. WOOD, B. J. and WISE, H.: J. Phys. Chem. *65*, 1976 (1961).
3. TSU, K. and BOUDART, M.: Can. J. Chem. *39*, 1239 (1961).
4. WISE, H. and ABLOW, C. M.: J. Chem. Phys. *29*, 634 (1958).
5. WEISSMAN, S. and MASON, E. A.: J. Chem. Phys. *36*, 794 (1962).
6. NOWAK, E. J., KURZIUS, S., DECKERS, J., and BOUDART, M.: AFOSR-TN 60–1302, Princeton University.
7. ELIAS, L., OGRYZLO, E. A., and SCHIFF, H. I.: Can. J. Chem. *37*, 1680 (1959).
8. WOOD, B. J. and WISE, H.: J. Phys. Chem. *65*, 1976 (1961).
9. WISE, H. and ABLOW, C. M.: J. Chem. Phys. *29*, 634 (1958).
10. Project SQUID, Princeton University, Semiannual Progress Report, October 1962.
11. LINNETT, J. W. and GREAVES, J. C.: Trans. Faraday Soc. *55*, 1355 (1959).
12. WOOD, B. J. and WISE, H.: *Rarefied Gas Dynamics*, L. Talbot ed. Academic Press, 1961.
13. PROK, G. M.: Planetary and Space Science *3*, 38 (1961).
14. PROK, G. M.: NASA Technical Note D-1090, September 1961.
15. ROSNER, D. E.: ARS Journal *32*, 1065 (1962).

Colloquium on Chemical Reactions and Phase Changes in Supersonic Flow

(Organized by Prof. P. P. Wegener)
(Yale University)

Chairman: Prof. P. P. Wegener
(Yale University)

Vice Chairman: Dr. W. H. Jones
(Institute for Defense Analyses)

INTRODUCTION

PETER P. WEGENER

The field of chemical reactions and phase changes in supersonic flow is an extended one. Historically, the earliest work on the dynamics of such processes concerns the applications of chemical kinetics to rocketry. In recent years contributions from aeronautics have been added. From this viewpoint we find, for example, treatments of expansions of real gases in hypersonic nozzles, blunt body flows, boundary layer flows, wakes, trails, etc., all directed toward engineering solutions for hypersonic flight. Simultaneously, chemists turned to gasdynamic techniques to obtain information on mechanisms and rates of fast reactions. It is our hope for this colloquium to provide a broad meeting ground for individuals whose original work has been primarily associated with any one of the special fields mentioned. This is in keeping with the traditional spirit of the Combustion Symposium.

In order to reduce the coverage to manageable proportions we arranged a sequence of invited papers around the central ideal of flow of real gases in converging-diverging nozzles. A common basis to the treatment of such flows is the underlying chemistry to be discussed by S. W. Benson, with invited comments by S. H. Bauer. The paper by S. S. Penner, J. Porter, and R. Kushida brings us to the forefront of current problems in rocket nozzles. K. N. C. Bray presents his work on the calculation of flow parameters through hypersonic nozzles, a treatment which originated from the viewpoint of gasdynamics while assisting in the understanding of rocket nozzle flows as well. This discussion is extended by the paper of A. A. Westenberg and S. Favin who work in detail with some of the complex chemical reactions involved. Presentations closely related to these papers have been given by others notably in the paper by Dr. Eschenroeder *et al.* (see page 241).

Three additional aspects of nozzle flow are included in the colloquium. Condensation is discussed by W. G. Courtney who treats the "low temperature" expansions in nozzles. Not unlike the chemical kinetics problem, the high rate of cooling may lead to a metastable thermodynamic state of the vapors leading to spontaneous condensation delayed with respect to equilibrium. J. R. Kliegel investigated gaseous expansions with solid, inert particles distributed in the gas. This process may also introduce a lag problem resulting in detrimental effects, for example, on specific impulse. Finally, W. R. Sears, S. Rubin, and R. Seebass treat the fascinating flow processes occurring in nozzles if the fluid medium is an electrical conductor and moves in the presence of magnetic fields.

The papers present a wide spectrum of processes, most of which are of immediate technical importance. In scanning this picture it appears to the experimentalist that many of the problems discussed show a state of analytical development that has forged ahead of careful experimentation. For example, much experimental work needs to be done to improve our understanding of reaction mechanisms and rates of chemical reactions. Furthermore, it is not yet possible to predict the onset of condensation in the metastable state based on first principles alone. However, even experimental verification of some simpler condensation problems is not available. Effects such as those of the presence of solid particles on specific impulse have been measured. However, the details of the flow processes have not been studied. It is to be hoped that in two years hence, at the next symposium, we will have made experimental progress in these areas.

RATE AND RADIATIVE TRANSFER PROCESSES DURING FLOW IN DE LAVAL NOZZLES

S. S. PENNER, J. PORTER, AND R. KUSHIDA

Some of the important physical ideas that have been used in analyses of chemical changes in rocket nozzles are reviewed with particular reference to three-body recombination reactions. The conditions are specified under which the near-equilibrium flow criterion developed about 15 years ago leads to results that are substantially equivalent to estimates derived from the criterion of Bray, after the latter has been suitably corrected.

The problem of chemical changes during nozzle flow for interdependent, concurrent chemical reactions is examined. An explicit relation is presented for the rate of entropy production. A set of linear algebraic equations is derived for near-equilibrium flow in terms of the logarithm of the dimensionless ratio of the pressure quotient to the corresponding equilibrium constant.

Surface-catalyzed processes are likely to be important in determining atomic recombination rates in the nozzles of present-day solid-propellant rocket engines. The influence of radiative energy transfer on the effective thermal conductivity in two-phase nozzle flow (with chemical reactions) has been studied in the diffusion approximation.

Introduction

In the literature we find frequent reference to Lighthill's "ideal diatomic gas." This "ideal diatomic gas" refers to the classical harmonic oscillator-rigid rotator approximation[1] for diatomic molecules and includes only consideration of the electronic ground states for the atom A and for the molecule A_2 which participate in the homogeneous recombination reaction of the atoms. Lighthill noted that $[1 - \exp(-x)]x^{-\frac{1}{2}}$ is a slowly varying function of x and proposed to replace it by an effective mean value.[1-4] This "Lighthill approximation" is well justified for the range of values of $x = h\nu/kT$ (h = Planck's constant, ν = characteristic frequency, k = Boltzmann constant, T = temperature) actually encountered in some conventional rocket nozzles. It may be shown that the statement $[1 - \exp(-x)]x^{-\frac{1}{2}}$ = constant corresponds to the assumption that the vibrational energy of the molecule is half excited. The approximations involved in (a) neglecting the influence of excited electronic states, (b) assuming that the vibrational degrees of freedom are only half excited, (c) neglecting anharmonicity terms in the vibrational partition function, and (d) neglecting vibration-rotation interactions in the partition function for A_2, are all ultimately justified in view of the low accuracy inherent in nozzle-flow calculations because chemical reaction rates are usually not known to better than an order of magnitude.

Among the earliest studies of chemical reactions during flow through rocket nozzles are approximate numerical calculations by Penner and Altman,[5] the development of approximate procedures for defining "near-equilibrium" flow and "near-frozen" flow [cf. reference 1 (hereafter referred to as I) Chapter XXIII] by Penner[6] in which earlier work of Schäfer[7] was extended, and presumably exact numerical solutions of flow with recombination of hydrogen atoms by Krieger.[8] Actually Krieger made a slight error in his work since he treated the flow problem as isentropic. Revised calculations have been published recently.[9]

The near-equilibrium and near-frozen flow criteria (cf. I, Chapter XXIII) had as objective the determination of the point in a nozzle where effective freezing of chemical equilibria would occur. A serious difficulty arose in 1949 and 1950 because there existed at the time essentially no precise data which could be used in defining the absolute magnitudes not for conservative but rather for practical applications of the criteria. Owing to the concentration of effort in this field in recent years[2,10-14] we are now in a position to refine the method of application of the criteria. That this is indeed useful has been pointed out by Barrère[15] who showed that the near-equilibrium criterion could be made to yield substantially equivalent results to those of Bray[2,10] for Wegener's experimental data on the system $N_2 + 2NO_2 \rightleftharpoons N_2 + N_2O_4$.[14] Before proceeding with the quantitative studies, it appears ap-

propriate to note the slow convergence of a recently developed relaxation procedure,[9] Rudin's[11] reevaluation of the near-equilibrium criterion,[10] the very exacting calculations carried out particularly by Hall and his collaborators,[12,13] as well as the experimental work of Wegener.[14] Special mention should also be made of a review paper by Vincenti[15] and a demonstration by W. T. Yang* that Vincenti's expansion is equivalent to Penner's near-equilibrium criterion.

Bray's Approximate Criterion for Freezing and Penner's Criterion for Near-Equilibrium Flow

Barrère[15] has recently called attention to the fact that Bray's approximate criterion for freezing[10] and Penner's expression for near-equilibrium flow[1,6] are both useful in correlating Wegener's experimental results[14] for the system $N_2 + 2NO_2 \rightleftarrows N_2 + N_2O_4$. The same conclusion is reached from an examination of Wegener's 1960 paper for properly determined values of the important parameters (cf. Figs. 5, 7, and 9 in Wegener's paper). We shall verify Barrère's observation by an analytical comparison between the methods of Bray and Penner for the reaction

$$B + 2A \underset{k_D}{\overset{k_R}{\rightleftarrows}} B + A_2 \qquad (1)$$

where B represents an inert carrier that is present in vast excess.

Refinement of Bray's[10] Approximate Procedure

Bray's approximate procedure is well documented in the literature[10,14] but appears to involve a logical inconsistency which introduces a factor of one-half in the final expression for practical calculations. For this reason, we present now a detailed, appropriately modified, derivation in which we retain the physical ideas of Bray.

For the chemical reaction described in Eq. (1), it is readily shown that

$$-\frac{D\alpha}{Dt} = 2k_R\rho^2\alpha^2\frac{Y_B(Y_A)_0}{W_BW_A}\left(1-\frac{K}{K_e}\right) \equiv R\left(1-\frac{K}{K_e}\right) \qquad (2)$$

where k_R = specific reaction rate constant for the forward reaction, ρ = gas density, Y_X = mass fraction of species X, W_X = molecular weight of species X,

$$\alpha = \frac{Y_A}{Y_A + Y_{A_2}} = \frac{Y_A}{(Y_A)_0}, \qquad (3)$$

$$R = 2k_R\rho^2\alpha^2\frac{Y_B(Y_A)_0}{W_BW_A}\ (=\text{ recombination rate}) \qquad (4)$$

and

$$K = Y_{A_2}/Y_A^2, \qquad K_e = (Y_{A_2}/Y_A^2)_e, \qquad (5)$$

with the subscript e identifying local equilibrium conditions and the subscript 0 denoting initial (or nozzle entrance) conditions. Here we have also assumed that $(Y_{A_2})_0 = 0$ so that $Y_A + Y_{A_2} = (Y_A)_0$. Our analysis is now specifically applicable to the system $A = NO_2$.[14]

The deviations from local equilibrium are conveniently described through the parameter

$$r = \frac{Y_A}{(Y_A)_e} = \frac{Y_A/(Y_A)_0}{(Y_A)_e/(Y_A)_0} = \frac{\alpha}{\alpha_e} \geq 1. \qquad (6)$$

In terms of r and α_e, Eq. (5) becomes

$$K/K_e = (r^2)^{-1}[(1 - r\alpha_e)/(1 - \alpha_e)].$$

Similarly, Eq. (2) may be written in the form

$$-D\alpha/Dt = R\{1 - (r^2)^{-1}[(1 - r\alpha_e)/(1 - \alpha_e)]\} \equiv R - D \qquad (7)$$

where D represents the dissociation rate. For equilibrium flow, $r \equiv r_e = 1$, Eq. (7) becomes indeterminate and should be replaced by the law of mass action.

If R is sufficiently large, near-equilibrium flow obtains,

$$1 - (r^2)^{-1}[(1 - r\alpha_e)/(1 - \alpha_e)] \ll 1,$$

and, therefore,

$$-D\alpha/Dt \ll R(r^2)^{-1}[(1 - r\alpha_e)/(1 - \alpha_e)] \quad \text{for near-equilibrium flow.} \qquad (8)$$

On the other hand, when large deviations from equilibrium flow occur, $r = Y_A/(Y_A)_e$ becomes much larger than unity,

$$(r^2)^{-1}[(1 - r\alpha_e)/(1 - \alpha_e)] \ll 1,$$

and

$$-D\alpha/Dt \gg R\,(r^2)^{-1}[(1 - r\alpha_e)/(1 - \alpha_e)] \quad \text{for large deviations from equilibrium flow.} \qquad (9)$$

Comparison of Eqs. (8) and (9) shows that

$$-D\alpha/Dt = R(r^2)^{-1}[(1 - r\alpha_e)/(1 - \alpha_e)] \quad \text{between near-equilibrium flow and large deviations from near-equilibrium flow.} \qquad (10)$$

* Personal communication from Dr. P. P. Wegener; also ARS Journal *32*, 782 (1962)

We identify the spacial location where Eq. (10) is satisfied by the coordinate $x = x_0$.

If it is indeed true that a well-defined, narrow, spacial region exists in the nozzle where an abrupt transition occurs from near-equilibrium flow to near-frozen flow, then Eqs. (8) to (10) must all be satisfied in a small spacial region near x_0, i.e., Eq. (8) applies at $x = x_0 - \delta'$, Eq. (10) applies at $x = x_0$, and Eq. (9) applies at $x = x_0 + \delta''$. The hypothesis of Bray is equivalent to the assumption that $(x_0 - \delta')/x_0 \approx 1$, $(x_0 + \delta'')/x_0 \approx 1$. Bray now assumes that, in this case $r \simeq r_e \simeq 1$, $\alpha \simeq \alpha_e$, $-D\alpha/Dt \simeq -D\alpha_e/Dt$, and Eq. (10) therefore reduces directly to the expression

$$-D\alpha_e/Dt \simeq R_e \text{ (Bray's criterion)}.$$

However, it has been found by direct comparison with experiments,[14] that R_e should really be replaced by a factor of order $0.5R_e$ in Bray's criterion.

It appears more logical to use Eqs. (7) and (10) first to define conditions at x_0. Thus

$$\left[1 - (r^2)^{-1}\frac{(1 - r\alpha_e)}{(1 - \alpha_e)}\right]_{x_0} = \left[(r^2)^{-1}\frac{(1 - r\alpha_e)}{(1 - \alpha_e)}\right]_{x_0}$$

or

$$(D/R)_{x_0} \equiv \{(r^2)^{-1}[(1 - r\alpha_e)/(1 - \alpha_e)]\}_{x_0} = \tfrac{1}{2}. \tag{11}$$

Hence, again assuming that near-equilibrium flow is maintained to $x = x_0$, we find

$$-(D\alpha_e/Dt)_{x_0} \simeq (\tfrac{1}{2}R_e)_{x_0} \tag{12}$$

which is in better agreement with experimental findings[14] than is Bray's criterion. We shall refer to Eq. (12) as Bray's modified criterion in the following discussion.

Equation (11) may be used to obtain the value of r at x_0, *viz.*,

$$(r)_{x_0} = \frac{\alpha_e}{1 - \alpha_e}\left[\left(1 + \frac{2(1 - \alpha_e)}{\alpha_e^2}\right)^{\frac{1}{2}} - 1\right]. \tag{13}$$

Reference to Eq. (13) leads to the important conclusion that r at $x = x_0$ is not equal to unity but actually depends on the value of α_e at x_0. In fact, Eq. (12) cannot hold independently of α_e but rather depends on r being sufficiently close to unity even when Eq. (13) is satisfied. We have thus obtained an important criterion for checking the consistency of the idea that "sudden freezing" is possible: "sudden freezing" is possible, and Eq. (12) applies, only if the value of $(r)_{x_0}$ computed from Eq. (13) differs from unity by a negligibly small amount. Hence the modified Bray criterion must be used with circumspection and cannot be expected to hold, even for a given chemical system, when the boundary conditions (e.g., nozzle inlet and exit temperatures) are varied over wide limits. The precise meaning of the statement that $(r)_{x_0}$ must be "sufficiently close to unity" to justify the use of Eq. (12) is clearly ambiguous. What is required here is an honest perturbation calculation that is substantially equivalent to the precise solution of the problem. Nevertheless, the available[14] data for the recombination of NO_2 in the presence of N_2 suggest that the condition given in Eq. (12) is useful for determining the approximate location of x_0.

Comparison Between Bray's Modified Criterion and Penner's[1,6] Near-Equilibrium Criterion

Since

$$-D\alpha_e/Dt = -(\partial \ln \alpha_e/\partial \ln T)_S \alpha_e (D \ln T/Dt)$$

it follows that the modified criterion of Bray in Eq. (12) may be written in the form

$$\tfrac{1}{2} = [(\alpha_e/R_e)(D \ln T/Dt)(-\partial \ln \alpha_e/\partial \ln T)_S]_{x_0} \tag{14}$$

where the subscript S identifies isentropic flow. Barrère has noted that the right-hand side of Eq. (14) is essentially Damköhler's first similarity group D_I (cf. I, Chapter XXV) and that we may regard it as the ratio of a chemical time

$$(\tau_{ch})_B = (\alpha_e/R_e)(-\partial \ln \alpha_e/\partial \ln T)_S$$

to a convection time

$$\tau_{mech} = Dt/D \ln T.$$

This observation is of considerable value since we expect, on the basis of very general principles for reacting flow systems, that large deviations from equilibrium flow will occur for a specified value of this important similarity group.

Penner's approximate criterion for near-equilibrium flow is [cf. I, Eq. (9) on p. 299]

$$(T' - T)/T \simeq -(D \ln T/Dt)z \tag{15}$$

where [cf. I, Eq. (7) on p. 299]

$$(T' - T)/T \simeq [(K - K_e)/K_e](\partial \ln T/\partial \ln K_e)_S \tag{16}$$

and K and K_e have been defined in Eq. (5). The quantity z is a reaction time which becomes, for the chemical process described in Eq. (1) [cf. I, Eq. (10) on p. 300],

$$z = \left\{2 \Big/ R\left[\frac{2}{1 - \alpha} + \frac{4}{\alpha}\right]\right\}_e. \tag{17}$$

It is apparent that $(T' - T)/T$ again represents a form of Damköhler's first similarity group. We

shall assume that T' has the magnitude corresponding to a mass fraction Y_A which has deviated from the local equilibrium mass fraction $(Y_A)_e$ such that

$$r = Y_A/(Y_A)_e$$

at the point in the flow where effective freezing occurs.

From Eqs. (15), (16), and (17) we find that*

$$\frac{K - K_e}{K_e} = \frac{\alpha_e}{R_e}\left(\frac{D \ln T}{Dt}\right)\left(-\frac{\partial \ln K_e}{\partial \ln T}\right)_S \times \frac{1}{\{[\alpha_e/(1-\alpha_e)] + 2\}}. \quad (18)$$

But, using the definitions of K, K_e, r, α, and α_e,

$$\frac{K - K_e}{K_e} = \frac{1}{r^2}\frac{(1 - r\alpha_e)}{(1 - \alpha_e)} - 1. \quad (19)$$

Introducing Eq. (19) into Eq. (18) we finally obtain the result

$$1 - \frac{1}{r^2}\frac{(1 - r\alpha_e)}{(1 - \alpha_e)} \equiv \eta = \frac{\alpha_e}{R_e}\left(\frac{D \ln T}{Dt}\right)\left[-\frac{\partial \ln \alpha_e}{\partial \ln T}\right]_S \quad (20)$$

since

$$(\partial \ln K_e/\partial \ln T)_S = (-\partial \ln \alpha_e/\partial \ln T)_S \times \{2 + [\alpha_e/(1-\alpha_e)]\}.$$

Comparison of Eqs. (14) and (20) shows that the quantity η replaces $\frac{1}{2}$ in Bray's modified criterion. Thus Eqs. (14) and (20) are identical at the point in the flow where

$$(r^2)^{-1}[(1 - r\alpha_e)/(1 - \alpha_e)] = \tfrac{1}{2},$$

a condition which is precisely satisfied at the point $x = x_0$ as may be seen by reference to Eq. (11). Therefore, if we define $(T' - T)/T$ in such a way that Eq. (11) applies, then Bray's modified criterion and Penner's near-equilibrium criterion will necessarily yield identical results. The numerical value of the reduced temperature for $\eta = \frac{1}{2}$ is

$$(T' - T)/T \simeq -\tfrac{1}{2}(\partial \ln T/\partial \ln K_e)_S \quad (21)$$

at the point of significant departure from near-equilibrium flow. But, for Wegener's experiments,

$$(\partial \ln K_e/\partial \ln T)_S \simeq (\Delta H^\circ/RT) + \bar{\gamma}/(\bar{\gamma} - 1),$$

* Equation (18) is actually independent of the approximation implicit in the use of Eq. (15) since it represents simply a form of the continuity equation. However, the use of Eq. (11) in Eq. (15) does provide us with an unambiguous definition for $(T' - T)/T$.

where ΔH° is the standard molar heat of reaction, and $\bar{\gamma}$ is an effective value for the heat capacity ratio. Thus

$$T' - T \simeq \frac{-T/2}{(\Delta H^\circ/RT) + \bar{\gamma}/(\bar{\gamma} - 1)}. \quad (22)$$

For Wegener's experiments,[14] $\Delta H^\circ \simeq -13{,}000$ cal/mole, $\bar{\gamma} \simeq 1.3$, and $T \simeq 300°$K whence it follows that $T' - T \simeq 9°$K. This value is in good accord with the observed experimental results (cf. Wegener, 1960, ref. 14, Fig. 5).

Concurrent, Interdependent Reactions

Consider the case where there are ξ simultaneous (coupled) chemical reactions occurring in a gaseous mixture containing n chemical species formed from m elemental species. The rth reaction may be written formally as

$$\sum_{j=1}^{n} \nu_{jr}' M_j \rightleftarrows \sum_{j=1}^{n} \nu_{jr}'' M_j \qquad (r = 1, \cdots, \xi) \quad (23)$$

where M_j represents the jth chemical species and ν_{jr}' and ν_{jr}'' are the stoichiometric coefficients for species j in the rth reaction progressing in the forward and reverse directions, respectively.

For any mixture which contains all of the equilibrium species in nonzero concentration, we may write the quotient of partial pressures, K_{pr}, for the rth reaction as

$$\ln K_{pr} = \prod_{j=1}^{n} (\nu_{rj}'' - \nu_{rj}') \ln p_j \quad (24)$$

where p_j is the partial pressure of species j. In general, the mixture contains n distinct chemical species, $(n - m) > 0$ independent relations exist among the K_{pr}, and more than $n - m$ reactions are possible in the mixture. The condition for choosing a set of independent K_{pr} is a nonvanishing determinant of rank $n - m$ for the difference between the stoichiometric coefficients, $(\nu_{rj}'' - \nu_{rj}')$. If this condition cannot be met for the set of ξ reactions, then equilibrium is not possible and additional reactions must be included. We assume that a complete set of reactions has been included, at least during the initial part of the nozzle expansion process. We identify by the index q, where $q = 1, \cdots, n - m$, those reactions which have linearly independent values of $\ln K_{pr}$. The dependent K_{pr} may then be obtained from a set of equations of the form

$$\ln K_{pr} = \sum_{q=1}^{n-m} a_{qr} \ln K_{pq} \quad (r = n - m + 1, \cdots, \xi) \quad (25)$$

where the coefficients a_{qr} are constants. The equilibrium constants will have exactly the same

coefficients for corresponding terms, since $K_{pr} \to (K_{pr})_e$ at equilibrium, *viz.*,

$$\ln K_{pr}/(K_{pr})_e = \sum_{q=1}^{n-m} a_{qr} \ln K_{pq}/(K_{pq})_e \qquad (r = n - m + 1, \ldots, \xi). \quad (26)$$

The Nozzle Flow Equations in Terms of $K_{pq}/(K_{pq})_e$

The ratio of the partial pressure quotient, K_{pq}, to the equilibrium constant, $(K_{pq})_e$, is determined by the relation

$$\ln K_{pq}/(K_{pq})_e = \sum_{j=1}^{n} (\nu_{jq}'' - \nu_{jq}') \ln Y_j + \Delta n_q \ln \bar{W} + \Delta n_q \ln p - \sum_{j=1}^{n} (\nu_{jq}'' - \nu_{jq}') \ln W_j + (\Delta H_q^\circ/RT) - (\Delta S_q^\circ/R) \qquad (q = 1, \cdots, n - m) \quad (27)$$

where

$$\Delta n_q = \sum_{j=1}^{n} (\nu_{jq}'' - \nu_{jq}')$$

and

$$\bar{W} = \left[\sum_{j=1}^{n} (Y_j/W_j)\right]^{-1}$$

is the average molecular weight of the fluid mixture. Since the temperature always decreases monotonically in a supersonic nozzle without shocks, we may define a function $F(t)$ such that

$$\ln T = -F(t)$$

and

$$\dot{F} \equiv DF/Dt = -D \ln T/Dt.$$

Equation (27) may then be differentiated with respect to $\ln T$ to yield the relation

$$\frac{\partial \ln K_{pq}/(K_{pq})_e}{\partial \ln T} = -\sum_{j=1}^{n} \left[\frac{(\nu_{jq}'' - \nu_{jq}')}{Y_j \dot{F}} \frac{DY_j}{Dt}\right] + \Delta n_q \frac{\partial \ln \bar{W}}{\partial \ln T} + \Delta n_q \frac{\partial \ln p}{\partial \ln T} - \frac{\Delta H_q^\circ}{RT} \qquad (q = 1, \cdots, n - m). \quad (28)$$

From the one-dimensional nozzle flow equations (i.e., from the conservation equations for one-dimensional, inviscid, adiabatic flow combined with the ideal gas equation of state) for constant specific heat, we obtain

$$\frac{\partial \ln p}{\partial \ln T} = \frac{\bar{C}_p}{R} - \sum_{j=1}^{n} \frac{H_j^\circ}{RT} \frac{\bar{W}}{W_j} \frac{1}{\dot{F}} \frac{DY_j}{Dt} \quad (29)$$

whence it follows that

$$\frac{\partial \ln K_{pq}/(K_{pq})_e}{\partial \ln T} = -\sum_{j=1}^{n} \left\{\left[\frac{\nu_{jq}'' - \nu_{jq}'}{Y_j(\bar{W}/W_j)} - \Delta n_q + \frac{\Delta H_q^\circ}{RT}\right] \times \frac{\bar{W}}{W_j} \frac{DY_j}{Dt} \frac{1}{\dot{F}}\right\} - \frac{\Delta H_q^\circ}{RT} + \Delta n_q \frac{\bar{C}_p}{R}. \quad (30)$$

Here H_j° is the standard molar heat of formation of species j and C_p is an average molar heat capacity at constant pressure for the fluid mixture. The rate of change of the jth species produced by chemical reactions is given by

$$\frac{DY_j}{Dt} = \sum_{r=1}^{\xi} (\nu_{jr}'' - \nu_{jr}') \frac{W_j}{\bar{W}} R_r' \left[1 - \frac{K_{pr}}{(K_{pr})_e}\right] \quad (31)$$

where

$$R_r' = \bar{W} k_r' \rho^{\left(\sum_{i=1}^{n} \nu_{jr}' - 1\right)} \prod_{j=1}^{r} (Y_j/W_j)^{\nu_{jr}'}.$$

We finally obtain the following differential equation for $K_{pq}/(K_{pq})_e$:

$$\sum_{r=1}^{\xi} \left[\phi_{rq} - \Delta n_q \left(\frac{-\Delta H_r^\circ}{RT} + \Delta n_r\right)\right] \frac{R_r'}{\dot{F}} \times \left[1 - \frac{K_{pr}}{(K_{pr})_e}\right] = \frac{-\Delta H_q^\circ}{RT} + \Delta n_q \frac{\bar{C}_p}{R} - \frac{\partial \ln K_{pq}/(K_{pq})_e}{\partial \ln T} \quad (32)$$

where

$$\phi_{rq} = \sum_{j=1}^{n} \frac{(\nu_{jq}'' - \nu_{jq}')(\nu_{jr}'' - \nu_{jr}')}{Y_j(\bar{W}/W_j)}.$$

The term on the left-hand side of Eq. (32) may be identified with Damköhler's first similarity parameter, since it is the modified ratio of a characteristic convective flow time, $1/\dot{F}$, to the characteristic reaction time, $1/R_r'$. Equation (32), together with Eq. (31), may be used to solve for $K_{pq}/(K_{pq})_e$.

Rate of Entropy Increase in Nozzle Flow

In the absence of chemical reactions and for equilibrium flow, the usual ideal nozzle flow approximations are equivalent to the assumption of isentropic expansion. Explicit relations for entropy production may be obtained when chemical reactions occur in an otherwise ideal nozzle.

The entropy per unit mass of a mixture of perfect gases, $\bar{S}$, is

$$\bar{S} = \sum_{j=1}^{n} (Y_j/W_j)(S_j^\circ - R \ln p_j) \quad (33)$$

where S_j° is the standard molar entropy of species j. Taking the substantial derivatives of $\bar{S}$, we find that

$$\frac{D\bar{S}}{Dt} = \sum_{j=1}^{n} (S_j^\circ - R \ln p_j) \frac{1}{W_j} \frac{DY_j}{Dt} - \left(\frac{\bar{C}_p}{\bar{W}} - \frac{R}{\bar{W}} \frac{\partial \ln p}{\partial \ln T}\right) \dot{F}$$

where

$$p_j = p\bar{W}Y_j/W_j.$$

Combining the relation for $D\bar{S}/Dt$ with the nozzle flow relation [cf. Eq. (29)] and with the reaction rate expression [cf. Eq. (31)] we obtain

$$\frac{D\bar{S}}{Dt} = -\frac{R}{\bar{W}} \sum_{r=1}^{\xi} \left[\sum_{j=1}^{n} (\nu_{jr}'' - \nu_{jr}')\right] \times \left(\frac{H_j^\circ - TS_j^\circ}{RT} + \ln p_j\right) R_r' \left[1 - \frac{K_{pr}}{(K_{pr})_e}\right]. \quad (34)$$

But the first term in the bracket in Eq. (34), after the summation over j has been performed, is seen to be $\Delta F_r^\circ/RT$, where ΔF_r° is the standard Gibbs free energy change for the rth reaction; this quantity, in term, is related to the equilibrium constant $(K_{pr})_e$ by

$$-\ln (K_{pr})_e = \Delta F_r^\circ/RT.$$

The second term in the large braces is defined by Eq. (24) and is the quotient of partial pressures, $\ln K_{pr}$. Therefore,

$$\frac{D\bar{S}}{Dt} = -\frac{R}{\bar{W}} \sum_{r=1}^{\xi} R_r' \left[1 - \frac{K_{pr}}{(K_{pr})_e}\right] \ln \frac{K_{pr}}{(K_{pr})_e}; \quad (35)$$

for near-equilibrium flow,

$$\frac{D\bar{S}}{Dt} \simeq \frac{R}{\bar{W}} \sum_{r=1}^{\xi} R_r' \left[1 - \frac{K_{pr}}{(K_{pr})_e}\right]^2. \quad (35a)$$

Since R_r' is always positive, it is apparent from Eq. (35) that $D\bar{S}/Dt > 0$ for any positive value of $K_{pr}/(K_{pr})_e$. Also DS/Dt clearly vanishes for frozen flow ($R_r' = 0$). For equilibrium flow, it may be shown that $D\bar{S}/Dt$ must also vanish.*

* Reference to Eq. (31) indicates that the quantity $R_r'[1 - K_{pr}/(K_{pr})_e]$ is finite for a one-step reaction. Hence $D\bar{S}/DT$ in Eq. (35) must go to zero as K_{pr} approaches $(K_{pr})_e$ for a one-step reaction. This argument can be generalized to concurrent, interdependent reactions.

Near-Equilibrium Flow

Noting that Eq. (30) and the atomic species conservation laws are linear in DY_j/Dt, we may write formally an explicit equation for DY_j/Dt, *viz.*,

$$\frac{DY_j}{Dt} = \dot{F} \sum_{q=1}^{n-m} A_{qj} \left[\frac{-\Delta H_q^\circ}{RT} + \Delta n_q \frac{\bar{C}_p}{R} - \frac{\partial \ln K_{pq}/(K_{pq})_e}{\partial \ln T}\right] \quad (36)$$

where we need only $n - m$ terms on the right-hand side of Eq. (36) because the other cofactors in the species conservation law will necessarily vanish for $n - m$ independent equations. In general, the coefficient A_{qj} will not be zero. By definition, in equilibrium flow the ratio $K_{pq}/(K_{pq})_e$ is unity throughout the nozzle; hence the derivative of $K_{pq}/(K_{pq})_e$ vanishes. Therefore, even though $1 - K_{pq}/(K_{pq})_e$ vanishes in the rate law given in Eq. (31), it is evident from Eq. (36) that

$$\left(\frac{DY_j}{Dt}\right)_{eq} \equiv \lim_{\text{equilibrium}} \left(\frac{DY_j}{Dt}\right) = \dot{F} \sum_{q=1}^{n-m} A_{qj} \left(\frac{-\Delta H_q^\circ}{RT} + \Delta n_q \frac{\bar{C}_p}{R}\right)$$

is nonzero. It is plausible to assume, therefore, that in near-equilibrium flow, when $K_{pq}/(K_{pq})_e$ is close to unity, the rate of change DY_j/Dt is close to its equilibrium value. For frozen flow, $DY_j/Dt = 0$ whence it follows that (for $\dot{F} \neq 0$)

$$\left(\frac{\partial \ln K_{pq}/(K_{pq})_e}{\partial \ln T}\right)_{\text{frozen}} = \frac{-\Delta H_q^\circ}{RT} + \Delta n_q \frac{\bar{C}_p}{R}. \quad (37)$$

Equation (37) can be integrated without difficulty.

Application of the Near-Equilibrium Flow Approximation

The condition for near-equilibrium flow is that $1 - K_{pq}/(K_{pq})_e$ is small whereas

$$R_r'[1 - K_{pq}/(K_{pq})_e]$$

is not small. Then $\partial \ln K_{pq}/(K_{pq})_e/\partial \ln T$ is negligibly small in comparison with other terms in Eq. (32). Thus Eq. (32) becomes, in the near-equilibrium approximation,

$$-\sum_{r=1}^{\xi} \left[\phi_{rq} - \Delta n_q \left(\frac{-\Delta H_q^\circ}{RT} + \Delta n_r\right)\right] \frac{R_r'}{\dot{F}} \times \ln \frac{K_{pr}}{(K_{pr})_e} = -\frac{\Delta H_q^\circ}{RT} + \Delta n_q \frac{\bar{C}_p}{R} \quad (38)$$

which, together with Eq. (26), constitutes a set of linear algebraic equations in $\ln K_{pr}/(K_{pr})_e$. Once the $K_{pr}/(K_{pr})_e$ values are determined, a standard thermodynamic subroutine for computation of equilibrium composition in nozzle flow may be used with the difference that K_{pr} be substituted for $(K_{pr})_e$ as the equilibrium constant.

The present formulation permits starting solution of the exact differential equations at any point in the nozzle where near-equilibrium flow obtains ($\bar{S} \simeq S_{\text{initial}}$) since the basic expressions are completely algebraic. In this respect, the present procedure is superior to the expansion methods used by Hall[12] and by Vincenti.[16] The computational difficulty is, however, somewhat increased because it is necessary to solve iteratively for $K_{pr}/(K_{pr})_e$.

Equation (38) has been used for a quantitative analysis of the recombination rate of NO_2 in nozzle flow. Details concerning this work are described elsewhere by one of us (R. Kushida).

Influence of Surface-Catalyzed Processes on Atomic Recombination Rates in Rocket Nozzles[17]

In two-phase nozzle flow processes, it is of interest to consider the relative importance of a three-body gas-phase recombination reaction and a succession of heterogeneous two-body reactions.

We consider a uniform mixture of gaseous hydrogen and small liquid or solid particles. For the particle concentrations actually encountered in some rocket nozzles, the rate of heterogeneous two-body reactions may be equal to or larger than the rate of the three-body gas-phase recombination reaction. It is, therefore, clearly important to consider such heterogeneous two-body recombination reactions in quantitative rocket performance evaluation.

The following considerations are also of interest in connection with the development of experimental procedures for improving the performance of nuclear rockets using hydrogen as driving fluid. Finally, they may be modified to infer conditions under which the flow processes in hypersonic, air-breathing engines can be influenced by induced, heterogeneous chemical reactions.

The two assumed reaction paths for the recombination of hydrogen atoms are:

$$2\text{H} + \text{X} \xrightarrow{k_3} \text{H}_2 + \text{X} \qquad (39)$$

$$\text{H} + \text{Y} \xrightarrow{k_{2a}} \text{H---Y} \qquad (40a)$$

$$\text{H} + \text{H---Y} \xrightarrow{k_{2b}} \text{H}_2 + \text{Y}. \qquad (40b)$$

The quantities k_3, k_{2a}, k_{2b} denote appropriate specific reaction rate coefficients. X represents either H or H_2, Y is a small solid or liquid particle, and H—Y denotes a hydrogen atom adsorbed on the surface of Y.

The ratio

$$R^* \equiv \frac{-(dn_{\text{H}}/dt)_2}{-(dn_{\text{H}}/dt)_3} = \frac{N(k_{2a}n_{\text{H}}n_{\text{Y}} + k_{2b}n_{\text{H}}n_{\text{H---Y}})}{2k_3 n_{\text{H}}^2 n_{\text{X}}} \qquad (41)$$

is a measure of the relative importance of heterogeneous two-body to three-body processes in the removal of hydrogen atoms when n_{X} denotes the number of particles of species X per unit volume. We denote by α the fractional number of collisions that lead to adsorption in reaction (40a) and by β the fractional number of collisions leading to H_2 formation in reaction (40b). If the concentrations (H), (Y), and (H—Y) are small compared with (H_2), the $n_{\text{X}} \approx n_{\text{H}_2}$ and we obtain (17) for R^* the result

$$R^* = \left(\frac{2\pi kT}{m_{\text{H}}}\right)^{\frac{1}{2}} \frac{N^2\sigma_{\text{Y}}^2}{4k_3 n_{\text{H}_2}} \left(\frac{\alpha n_{\text{Y}} + \beta n_{\text{H---Y}}}{n_{\text{H}}}\right) \qquad (42)$$

where m_{H} = mass of the hydrogen atom, N = Avogadro number, σ_{Y} = collision diameter of the solid particle Y.

The ratio R^* has been calculated from Eq. (42) for the following numerical values: T = 1365°K, pressure = 5 atmos, $\sigma_{\text{Y}} = 3 \times 10^{-6}$ cm, and[20] $k_3 = 3 \times 10^{15}$ mole^{-2} (cm^3)^2 sec^{-1}. We find that

$$R^* \simeq (5 \times 10^6)(\alpha n_{\text{Y}} + \beta n_{\text{H---Y}})/n_{\text{H}}.$$

Therefore, the heterogeneous two-body processes will become of comparable importance with the three-body gas-phase collisions if

$$(\alpha n_{\text{Y}} + \beta n_{\text{H---Y}})/n_{\text{H}} \gtrsim 2 \times 10^{-7}$$

or

$$(n_{\text{Y}} + n_{\text{H---Y}})/n_{\text{H}} \gtrsim 2 \times 10^{-6}$$

for $\alpha \sim \beta \sim 1/10$. But, for a representative propellant system in two-phase nozzle flow, $(n_{\text{H}_2}) \simeq 10^{20}$ cm^{-3}, $(n_{\text{H}}) \simeq 10^{18}$ cm^{-3}, and $[(n_{\text{Y}}) + (n_{\text{H---Y}})] \simeq 10^{12}$ to 10^{15} cm^{-3}. Hence $(n_{\text{Y}} + n_{\text{H---Y}})/n_{\text{H}} \simeq 10^{-6}$ to 10^{-3}, i.e., the heterogeneous recombination processes may actually become dominant.

The product $\alpha\beta$ appears to be of the order of 10^{-2} for the conditions existing in representative rocket nozzles.[21,22]

The Influence of Radiant Energy Transfer on (Two-Phase) Nozzle Flow

The influence of radiant energy transfer[23–25] is not considered in conventional treatments of

(two-phase) nozzle flow. That the assumption that radiant energy transfer is unimportant is not obviously valid follows most simply from the fact that spectral absorption coefficients in homogeneous and in two-phase systems may become very large even at moderate optical depths. For example, carbon particles with diameters of the order of 0.05 μ are sensibly black in the visible and near-infrared regions of the spectrum for absorption and emission of radiation if about 10^{14} particles are present per unit volume and these particles are viewed in geometric lengths exceeding about 1 cm.

For very large and for very small values of the spectral absorption coefficients, it appears at first sight that radiant energy transfer will be unimportant for the following reasons:

a. For sufficiently large values of the absorption coefficient, the diffusion approximation applies, the Rosseland mean absorption coefficient is very large, and the radiant energy is essentially trapped locally.[26]

b. For sufficiently small values of the spectral absorption coefficient, the Planck mean may be used. In the limit of zero optical depth, radiant energy transfer will again be unimportant.[26]

It is apparent from the preceding considerations of the limiting cases that radiant energy transfer may well play an important role for intermediate values of the absorption coefficient. The quantitative importance of radiant energy transfer on nozzle flow processes cannot be estimated without actual solution of representative cases. A particularly interesting example concerns condensation processes in the nozzle for which the local values of the absorption coefficients may suddenly increase from relatively small values to very large values.

If photochemical processes are neglected, radiant energy transfer does not influence the species conservation equations.[23,24,26] Similarly, if radiation pressure is neglected, which is well justified at the temperatures that are of interest in two-phase nozzle flow, the momentum equation remains unchanged. However, radiative transfer can exert an important influence on the energy equation even at relatively low temperatures for systems with opacity values in the range expected for two-phase flow processes. For the following crude calculations, we shall assume that the diffusion approximation is applicable, i.e., that the radiation mean free path at all important wavelengths is small compared with the characteristic dimensions of the problem. In this special case it is readily shown[23,24,26] that the heat flux term involving the thermal conductivity,

$$\lambda_c \nabla T,$$

should be replaced by

$$(\lambda_c + \lambda_r) \nabla T \tag{43}$$

where

$$\lambda_r = 16\sigma T^3/3\bar{k}_{L,\mathrm{Ro}} \tag{44}$$

may be regarded as an effective conductivity associated with radiant energy transfer, σ represents the Stefan–Boltzmann constant, and $\bar{k}_{L,\mathrm{Ro}}$ is the Rosseland mean absorption coefficient per unit length. The Rosseland mean free path $\bar{\lambda}_{\mathrm{Ro}}$ equals the reciprocal of the Rosseland mean absorption coefficient $\bar{k}_{L,\mathrm{Ro}}$ and is defined by the relation

$$\bar{\lambda}_{\mathrm{Ro}} = (\bar{k}_{L,\mathrm{Ro}})^{-1} = (15/4\pi^4) \times \int_0^\infty (k_{L,\nu,T})^{-1}[x^4 e^x/(e^x - 1)^2]\, dx, \tag{45}$$

where $x = h\nu/kT$ and $k_{L,\nu,T}$ is the linear absorption coefficient [including the induced emission term $(1 - e^{-x})$] in the frequency interval between ν and $\nu + d\nu$ at the temperature T.

The fact that the present estimates must be regarded as highly approximate follows most obviously from the fact that Eqs. (43) and (44) are applicable only if $\bar{k}_{L,\mathrm{Ro}}$ is very large *at all important wavelengths* whereas λ_r can become large compared with λ_c only for small values of $\bar{k}_{L,\mathrm{Ro}}$. In two-phase nozzle flow problems it appears reasonable to assume that Eqs. (43) and (44) will lead to correct order-of-magnitude estimates if $\bar{\lambda}_{\mathrm{Ro}} \lesssim 3$ cm and that appropriate integral techniques must be used for larger values of the radiation mean free path.

Theoretical estimates of $k_{L,\nu,T}$ can be made, in principle, for all particles by using the Mie theory[27] provided the optical constants are available for the particle system. Unfortunately, this is not the case. For this reason, it is customary to assume that bulk properties (usually extrapolated from low-temperature measurements) may be used. Stull and Plass[28] have performed extensive calculations of absorption, scattering, and total cross sections and of spectral emissivities for carbon using (extrapolated) bulk properties and the Mie theory. We shall use the results obtained by Stull and Plass for the absorption cross section even though we recognize that this particular parameter will vary significantly from one solid material to another and that carbon is not representative of the solid phase in solid-rocket propellant exhausts.

The total cross section (σ_v in cm^2) is plotted as a function of wavelength in Fig. 1 for carbon particles with 200 Å radius and 987 Å radius using the data of Stull and Plass.[28] For these carbon particles, the scattering cross section is so small compared with the absorption cross section that the latter is practically identical

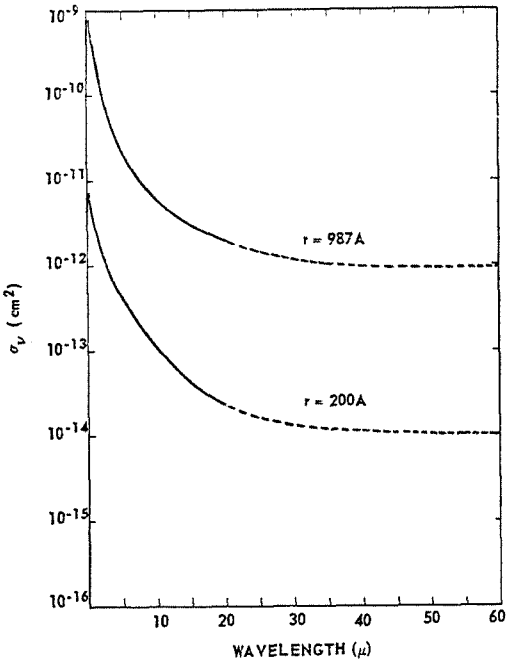

FIG. 1. The total absorption cross section (σ_ν) for spherical carbon particles with radius 200 Å and 987 Å as a function of wavelength (from Stull and Plass, reference 28). The dashed part of the curves is extrapolated.

with the total cross section. Furthermore, the optical constants (at least for carbon) are presumably only weakly dependent on temperature[28] so that we may use the data of Fig. 1 at all temperatures. The linear absorption coefficient is related to the absorption cross section through the expression

$$k_{L,\nu,T} = N\sigma_\nu(1 - e^{-x}) \qquad (46)$$

where N denotes the total number of particles per unit volume.

The quantity $G(x)/k_{L,\nu,T}$ where $G(x) = x^4e^x/(e^x - 1)^2$ is plotted as a function of x in Figs. 2 and 3 for the two selected particle radii at temperatures of 1000° and 2000°K and for a number density of 10^{12} particles/cm^3. The calculated Rosseland mean free paths are also indicated in Figs. 2 and 3. For 10^{12} particles/cm^3 with 200 Å radius, we find* $\bar{\lambda}_{Ro} \simeq 3$ cm at 1000°K and $\bar{\lambda}_{Ro} \simeq 1$ at 2000°K. Similarly, for the particles with 987 Å radius, we find $\bar{\lambda}_{Ro} \simeq 0.046$ cm at 1000°K and $\bar{\lambda}_{Ro} \simeq 0.014$ cm at 2000°K. Therefore, the diffusion approximation may be applicable for the assumed number density. On the other hand, for N less than about 10^{15} particles/cm^3, the effective thermal conductivity

* Note that $\bar{\lambda}_{Ro}$ is inversely proportional to the number density of carbon particles. We are indebted to L. D. Gray for performing the numerical calculations.

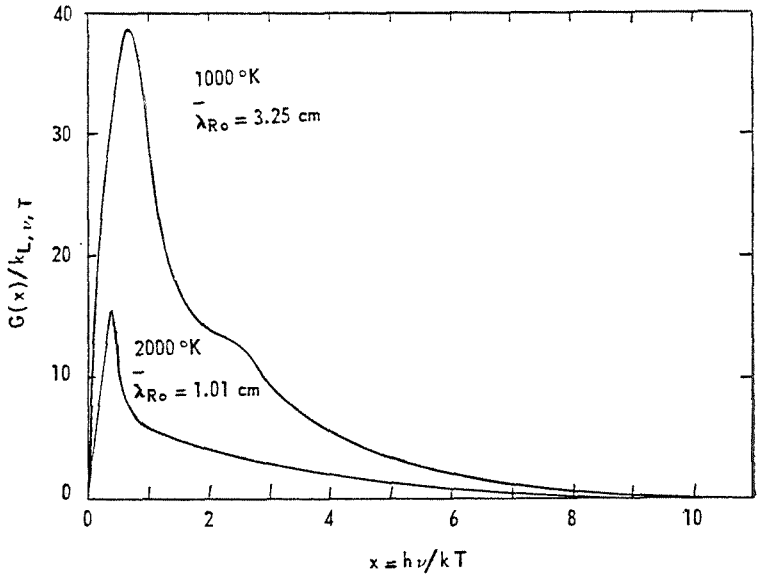

FIG. 2. The quantity $G(x)/k_{L,\nu,T}$ as a function of $x = h\nu/kT$ for carbon particles with radius 200 Å at 1000° and 2000°K for a number density of 10^{12} particles/cm^3.

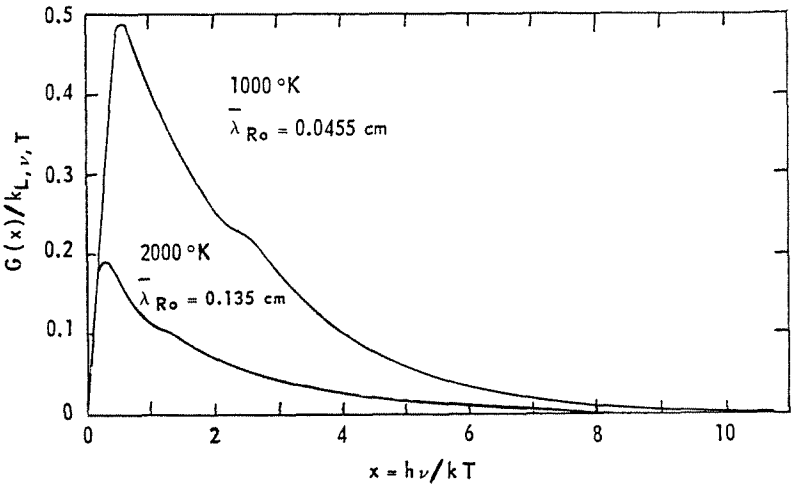

FIG. 3. The quantity $G(x)/k_{L,\nu,T}$ as a function of $x = h\nu/kT$ for carbon particles with radius 987 Å at 1000° and 2000°K for a number density of 10^{12} particles/cm^3.

λ_c is that of the gas phase. Thus we find for 10^{12} carbon particles/cm^3, that $\lambda_r/\lambda_c \simeq 270$, at 1000°K for 200 Å radius; $\lambda_r/\lambda_c \simeq 3.8$ at 1000°K for 987 Å radius; and $\lambda_r/\lambda_c \simeq 480$, at 2000°K for 200 Å radius; $\lambda_r/\lambda_c \simeq 6.5$ at 2000°K for 987 Å radius. Since the assumed number density for the carbon particles lies in the range of values encountered in some liquid-propellant systems, we conclude that, for these systems, radiative energy transfer between the particles is more important than gas-phase conductive heat transfer. Similarly, for solid-propellant engines with larger values of N and presumably smaller values of σ_ν and $k_{L,\nu,T}$ than for carbon, a similar conclusion may well be applicable.

The preceding considerations clearly require careful refinement before anything resembling a reasonable estimate for gas-phase to solid-phase heat transfer can be obtained in two-phase systems. Fortunately, the large uncertainties in the effective conductivity do not influence the observable performance parameters significantly.[29]

ACKNOWLEDGMENTS

Supported, in part, by the U. S. Army Research Office (Durham) under contract with the California Institute of Technology and, in part, by the Propulsion Laboratory, Aeronautical Systems Division, USAF, under contract with NESCO.

REFERENCES

1. PENNER, S. S.: *Chemistry Problems in Jet Propulsion*. Pergamon, 1957. This book is referred to in the text as I.
2. BRAY, K. N. C.: Aeronautical Research Council, Report 19,983, London, March, 1958.
3. LIGHTHILL, M. J.: J. Fluid Mech. *2*, 1 (1957).
4. FREEMAN, N. C.: J. Fluid Mech. *4*, 407 (1958).
5. PENNER, S. S and ALTMAN, D.: J. Franklin Inst. *245*, 421 (1948); ALTMAN, D. and PENNER, S. S.: J. Chem. Phys. *17*, 56 (1949).
6. PENNER, S. S.: J. Am. Chem. Soc. *71*, 788 (1949); J. Franklin Inst. *249*, 441 (1950); J. Chem. Phys. *19*, 877 (1951); *ibid. 20*, 341 (1952).
7. SCHÄFER, K.: On the Thermodynamics of Rocket Propulsion, I, Wright-Patterson Air Force Base, Dayton, Ohio, February, 1947.
8. KRIEGER, F. J.: ARS Journal *21*, 179 (1952).
9. REICHENBACH, R. and PENNER, S. S.: *Eighth Symposium (International) on Combustion*, p. 359. Williams and Wilkins, 1962.
10. BRAY, K. N. C.: J. Fluid Mech. *6*, 1 (1959); *Fourth AGARD Combustion and Propulsion Colloquium*, pp. 279–285. Pergamon, 1961.
11. RUDIN, M.: Phys. Fluids *1*, 1384 (1958).
12. HALL, J. G. and RUSSO, A. L.: AFOSR TN-59-1090, Cornell Aeronautical Lab., Inc., Buffalo, November, 1959.
13. ESCHENROEDER, A. Q., BOYER, D. W., and HALL, J. G.: Exact Solutions for Nonequilibrium Expansions of Air with Coupled Chemical Reactions, Report No. AF-1413-A-1, Contract No. AF 49(638)-892, Cornell Aeronautical Laboratory, Inc., Buffalo, May 1961.
14. WEGENER, P. P.: Phys. Fluids *2*, 264 (1959); ARS Journal *30*, 322 (1960); *Fourth AGARD Combustion and Propulsion Colloquium*, pp. 261–277. Pergamon, 1961.
15. BARRÈRE, M.: *Fourth AGARD Combustion and Propulsion Colloquium*, pp. 277–279. Pergamon, 1961.

16. VINCENTI, W. G.: Calculations of the One-Dimensional Nonequilibrium Flow of Air Through a Hypersonic Nozzle—Interim Report, Stanford University, Dept. of Aeron. Eng., Report No. 101, Palo Alto, Calif., January 1961.
17. PENNER, S. S. and PORTER, J.: Astronautica Acta *8*, (1962).
18. STEINER, W.: Trans. Faraday Soc. *31*, 623 (1935); AMDUR, I. and ROBINSON, A. L.: J. Am. Chem. Soc. *55*, 1395 (1933).
19. JEANS, J.: *Kinetic Theory of Gases*, p. 137. Cambridge Univ. Press, 1940.
20. GARDINER, W. C., JR. and KISTIAKOWSKY, G. B.: J. Chem. Phys. *35*, 1765 (1961).
21. HACKER, D. S., MARSHALL, S. A., and STEINBERG, M.: J. Chem. Phys. *35*, 1788 (1961).
22. WOOD, B. J. and WISE, H.: *Rarefied Gas Dynamics* (L. Talbot, ed.), pp. 51–59. Academic Press, 1961.
23. KOURGANOFF, V.: *Basic Methods in Transfer Problems*. Oxford, Clarendon Press, 1952.
24. CHANDRASEKHAR, S.: *An Introduction to the Study of Stellar Structure*. Univ. of Chicago Press, 1939.
25. GOULARD, R. and GOULARD, M.: Int. J. Heat and Mass Transfer *1*, 81 (1960).
26. For a simplified account of radiative transfer theory which is addressed to the non-specialist, see PENNER, S. S. and PATCH, R. W.: Radiative Transfer Studies and Opacity Calculations for Heated Gases, Technical Report No. 6, Contract AF 49(638)-984, California Institute of Technology, Pasadena, Calif., January 1962; see also "Papers Presented in Honor of Modesto Panetti" at the Politecnico di Torino (September 1962), Accademia Nazionale dei Lincei, Rome, Italy, 1962.
27. See, for example, STRATTON, J. A.: *Electromagnetic Theory*, p. 563 *et seq.* McGraw-Hill, 1941.
28. STULL, V. R. and PLASS, G. N.: J. Opt. Soc. Am. *50*, 121 (1959).
29. See, for example, the papers on two-phase flow in ARS Monograph No. 6 on *Detonations and Two-Phase Flow* (S. S. Penner and F. A. Williams, eds.). Academic Press, 1962.

Discussion

PROF. S. W. BENSON (*University of Southern California*): The treatment of H atom recombination via surface catalysis is extremely crude and ignores the details of the sorption process which involves the reverse process of desorption and the problem of surface saturation. These rates are not independent of the rate of surface H atom recombination but are rather coupled to this latter. It would not be very difficult for the authors to extend their analysis to the more complete system:

$$S + H \underset{2}{\overset{1}{\rightleftharpoons}} S\cdots H$$

$$S\cdots H + H \xrightarrow{3} S + H_2.$$

From the stoichiometry condition $S + S\cdots H = S_0$, the total number of active sites, and the usual steady state technique we find:

$$d(H_2)/dt = k_3(H)(S\cdots H)$$

$$= [k_3k_1(H)^2(S)]/[k_2 + k_3(H)]$$

$$= [k_1k_2(H)^2(S_0)]/[k_2 + k_1(H) + k_3(H)]$$

Under most conditions one would expect $k_1(H) > k_3(H) > k_2$ and the rate becomes: $d(H_2)/dt \sim k_3(H)(S_0)$. However, this could be very sensitive to the precise reaction conditions.

DR. R. KUSHIDA (*National Engineering Science Company*): The illustrative calculation of the paper neglects the back reaction

$$H\cdots Y \rightarrow H + Y$$

because we seek only orders of magnitude effects. To include it would require a slightly more elaborate treatment, which was not really justified in this upper limit estimate.

DR. A. Q. ESCHENROEDER (*Cornell Aeronautical Laboratory*): Dr. Kushida has raised some question in his paper regarding the uniformity of the freezing criterion as an approximation. J. A. Lordi at our laboratory has published recently [ARS Journal *32*, 1285 (1962)] a comparison between exact and approximate results for frozen atom fraction in nozzle expansions of singly dissociating gases. The approximately determined values never deviated more than 3 per cent from the results of exact numerical solutions. Reservoir pressure, reservoir temperature, and rate-geometry parameters were varied over wide ranges in this study. Based on these comparisons it appears as if the sudden freezing assumption gives a uniformly good approximation for cases characterized by true freezing to an asymptotically constant composition.

DR. R. KUSHIDA: For engineering approximation the freezing point analysis is an extremely handy

tool. Studies such as those of Lordi establish the validity and the range of usefulness of this criterion.

PROF. S. H. BAUER (*Cornell University*): Regarding the proposed computation of the entropy increase which occurs during the flow of a real gas through a supersonic nozzle, I call attention to three points:

a. No explicit formation was introduced for lagging vibrational equilibration, such that effectively two temperatures, one appropriate for translations and rotations and another for vibrations, must be included. The formalism could be appropriately generalized at the expense of additional complexity in the equations.

b. The entropy increase is based on a summation which must be taken over all kinetically active species. Thus ζ is a much larger number than is required for specification of the system near equilibrium conditions. Indeed, for any real case, such as the flow of combustion products from a solid propellant, the number of kinetic intermediates is staggering.

c. For cases where "sudden freezing" occurs, the introduction of an average rate of increase of entropy may not be meaningful. When the density decrease is small so that the reaction in question remains close to equilibrium, the flow is isentropic. Further, beyond the position of freezing, when the expansion had become very large, again the flow is essentially isentropic. The change in entropy is large and rather localized to the transition region. Of course, for different reactions, these transition regions may and do occur at different locations down the nozzle.

DR. R. KUSHIDA: There are innumerable complications that can be added to the rate processes in nozzles. At this time, we need to study these effects independently rather than to confound them all at once. In the present paper, we are concerned with several types of rate processes, each of which are treated in an approximate manner.

C-9

ENERGY TRANSFER PROCESSES AND CHEMICAL KINETICS AT HIGH TEMPERATURES

SIDNEY W. BENSON

Recent theoretical studies of the rates of recombination of atoms in gases are examined and discussed in terms of the experimental evidence available. Unfortunately most of the latter is of such low precision that many of the fine distinctions cannot be made. It does appear, however, that the recombination process must involve deactivation of nascent molecules by consecutive collisions rather than by large energy transfers.

The justification for a consecutive collision process is examined in terms of recent theoretical studies of the vibrational energy transfer process and shown to be quite strong. These studies yield two independent evidences supporting the belief that vibrational energy exchange occurs as a 1 quantum process for both ground level and highly excited oscillators.

Some recent studies on ionization processes in strong shocks will be examined briefly and mechanisms will be described for electronic excitation as well as ionization. It is shown that very low values for the ionization activation energy must be accompanied by such low Arrhenius A factors as to make the data implausible.

Finally some general considerations will be described governing the process of homogeneous catalysis of recombination at high temperatures and it will be shown that the recombination of H atoms can be accelerated by factors of 100-fold or more by the addition of small amounts (~1%) of suitable molecular species.

Introduction—Unimolecular Reactions

The unimolecular reaction of a molecular species, involving as it does the apparently isolatable event of spontaneous change, shares some of the mystery of comparable events such as the radioactive decay of metastable atomic nuclei. In principle we know that there are two requirements for such an event, activation and atomic rearrangement. The former must precede the latter since the rearrangement of an initially stable system will require energy.

These two processes are characterized by two quite different time scales. The rate of atomic rearrangement within a molecule could be expected to be of the order of atomic frequencies with a lifetime of about 10^{-13} seconds. On the other hand the process whereby a molecule in a dilute chemical system (i.e., gas) gains a large excess of internal energy relative to RT is one of molecular collision. At STP collisions occur at intervals of about 10^{-9} sec. As the pressure decreases, this time becomes correspondingly longer (10^{-6} sec at 1 mm Hg).

Such values would seem to imply that unimolecular reactions have rates which are controlled by the rates at which molecules may gain large amounts of internal energy and only exceptionally by the rates of internal rearrangement of atoms. We find however that this is true only of very simple molecules containing on the order of from 2 to 7 heavy atoms, i.e., O_2, O_3, N_2O_4, N_2O_5, cyclopropane, etc. For more complex molecules we find that the rate of unimolecular change is independent of the rate of energy transfer.

To account for such an observation we must invoke an additional process, that of internal energy migration, or the localization of energy within a molecule. If we picture the internal energy of an isolated molecule as consisting of a discrete number of units, let us say s quanta, and that these are distributed among n independent modes of internal motion (oscillators), then the simple probability that some very large number, m of these shall be localized in some specified way within the molecule is of the order of

$$(s - m + n - 1)!\, s!/(s + n - 1)!\,(n - m)!$$

$$\rightarrow (1 - m/s)^{n-1} \ll 1.$$

For very large values of n and s, this becomes such a sufficiently rare event (i.e., small fraction), that we can understand how strongly energized molecules can have lifetimes many powers of 10

in excess of the times of motion of their component atoms.

This very elementary version of the famous Rice-Ramsperger-Kassel Model of unimolecular reactions conceals another important concept, the transition state. That is, there must exist a configuration of the molecular system such that it demarcates reactant and product species. For computing rate events we must picture some transition structure through which all reactant species pass irreversibly on their way to products. The mathematical alternative to this (which has never been seriously explored) is a cradle-to-grave program in which we follow reactant(s) over its entire history to ground state product(s).

In the range of temperatures between 1000°K and 5000°K, the average energy content of molecules becomes so high that the rate of internal energy migration is sufficiently rapid to make collisional activation the rate-determining process for a unimolecular reaction. Thus even complex molecules like C_2H_6 or C_3H_8 will be expected to split into radicals at 2500°K at rates which are governed by second-order collisional activation.[1] Such processes which are termed, "energy-transfer processes" are then typical of the high temperatures of shocked gases.

It is the purpose of the present paper to review some simple energy-transfer processes from the point of view of the foregoing concepts and to examine the present kinetic evidence concerning them.

Recombination of Atoms—Experimental Studies

One of the most important chemical reactions occurring in shocked gases is the dissociation of diatomic molecules. In the subsequent expansion and cooling of the shocked gases the inverse processes of recombination of atoms to form diatomic molecules take a dominant role.

Experimental studies of both of these reactions are of relatively recent origin, dating back about three decades. The measurements of recombination have been done only once in a photostationary system by Rabinowitch and Wood.[2] Although potentially the most accurate method for these rate studies, the original studies gave very crude results and have not been repeated.

Studies of the recombination at room temperature by the photoflash technique have yielded the most reliable rate constants to date. They are believed accurate to within 10 to 20 per cent. The precision is limited by the accuracy of high speed spectrophotometry and a detailed knowledge of the behavior of metastable species.

Unfortunately no photoflash measurements have been made at sufficiently high temperatures to obtain reliable estimates of the temperature coefficient of the recombination rate constant. Instead the high temperature data have all come from shock tube studies of the rate of dissociation. The recombination rate constants have been deduced from these latter by means of the thermodynamic relation:

$$K_{eq} = k_d/k_r, \tag{1}$$

where K_{eq} is the precisely known equilibrium constant for the dissociation reaction, k_d is the second order dissociation rate constant, and k_r is the third order recombination rate constant.

The spread in rate constants measured by shock tube is usually within a factor of 2 to 10. The accuracy of shock tube rate constants is at present completely uncertain since there are few independent studies with which to compare them. If we take as an example the shock tube measurements of the rates of recombination[3] of O atoms in the range of 4000°–6000°K one finds that the results of 5 different laboratories cover a tenfold range.

The values of k_r calculated from Eq. (1) are subject to considerable uncertainty since K_{eq} and k_d are both very sensitive to temperature. Thus for O_2 at 3000°K, the critical ratio, E/RT is about 20 so that a 1 per cent error in temperature will lead to a 20 per cent error in either K_{eq} or k_d. Here E is the bond dissociation energy. This is not true of k_r and it is hoped that future shock tube work will turn to direct measures of k_r rather than k_d.

One further technique of measurement of k_r at room temperature has been made popular recently and this is the titration technique first reported by Harteck and co-workers.[4] Once again the accuracy of the method is still uncertain and there have been spreads of factors of 2 and 3 reported by different laboratories.[5] Here surface reactions and impurities can play an important role. In addition it is not quite certain that the metastable species produced in the initial discharge are without effect.

The result of the foregoing is that while it is generally believed that k_r decreases with increasing temperature, the magnitude of the effect is almost completely uncertain.

Microscopic Reversibility

A number of authors have questioned the validity of Eq. (1) for calculating the values of k_r and k_d. The basis on which these criticisms rest is that in a given experiment, there is a non-Maxwellian distribution of excited species.

If this energy distribution shifts with the relative concentration of atoms and molecules in the system, then, it is stated, there is no necessary relation between the mechanism far from equilibrium and near equilibrium. Hence there need be no simple relation such as Eq. (1) between a measured k_r (or k_d) and its inverse constant.

This argument is not correct. The application of microscopic reversibility can be readily justified if the system is in a stationary state, i.e., if there are no important concentrations of reactants tied up in intermediate states. Under these conditions it does not matter how non-Maxwellian the intermediate states; forward and back reactions will proceed through these at equal rates. Until there is some cogent experimental evidence indicating the contrary Eq. (1) may be considered to hold rigorously for kinetic studies.

The Collisional Deactivation Model for Recombination

We have recently proposed a modification[6] of the original Rice model for atom recombination which is the first to account for two anomalous features of this process. The first anomaly has to do with the fact that the Arrhenius factor of the inverse process, dissociation, is from 100 to 1000 times larger than collision frequencies, Z. This is in sharp contrast to the usual values of the Arrhenius factors for "normal" chemical, bimolecular rate constants which are all *smaller* than collision frequencies.

The anomalous value of A_d was explained by Rice[7] by invoking a pre-equilibrium between ground state molecules X_2 and a group of highly energized molecules, $X_2^{(n)}$ possessing energy on the average about RT below the dissociation threshold.

His dissociation mechanism is

$$\begin{aligned} &X_2 + M \underset{v}{\overset{a}{\rightleftharpoons}} X_2^{(n)} + M \\ &X_2^{(n)} + M \xrightarrow[c]{} 2X + M. \end{aligned} \tag{2}$$

If $k_v > k_c$ which seems reasonable, then the value of k_d is given by

$$k_d = k_c K^{(n)}, \tag{3}$$

where $K^{(n)}$ is the equilibrium constant for formation of $X_2^{(n)}$. Since the entropy of the $X_2^{(n)}$ species is very likely of the order of 8 to 13 eu, in excess of X_2, the value of A_d [which is given by $A_c \exp(\Delta S^{(n)}/R)$, with A_c of the order of the collision frequency Z] can readily exceed Z by two to three orders of magnitude.

It is important to note that the Rice model already implies the transfer of vibrational energy or collision in small increments. Any theory which proposes very large transfer of vibrational energy on collision will immediately lose the pre-equilibrium of X_2 with $X_2^{(n)}$ along with the favorable entropy involved. Such theories will therefore not be able to account for the very large values of A_d.

The second anomaly which required explanation is the weak decrease of k_r with increasing temperature which we have discussed briefly. If one uses (3) and (1) to calculate k_r one finds that k_r is not sensitive to temperature. Our modification of the Rice model which gives such an effect is to replace his pre-equilibrium by a stationary state so that k_v and k_c are not necessarily very different. From the point of view of recombination, the model looks like the following:

$$\begin{aligned} X + X &\rightleftharpoons X_2^* \\ X_2^* + M &\rightleftharpoons X_2^{(n)} + M \\ X_2^{(n)} + M &\rightleftharpoons X_2^{(n-1)} + M \\ \cdot \quad &\cdot \quad \cdot \quad \cdot \\ \cdot \quad &\cdot \quad \cdot \quad \cdot \\ \cdot \quad &\cdot \quad \cdot \quad \cdot \\ X_2^{(1)} + M &\rightleftharpoons X_2^{(0)} + M. \end{aligned} \tag{4}$$

$X_2^{(n)}$ is the highest, bound, vibrational state of X_2 while X_2^* is any pair of X atoms whose separation is less than some assignable distance r_m. Employing the usual steady state technigue which can be readily justified for this system it is possible to derive the following expression for k_r:

$$k_r = \lambda Z K^* G(T). \tag{5}$$

Here λ is the probability that a collision of X_2^* with M will lead to deactivation, K^* is the equilibrium constant for $2X \rightleftharpoons X_2^*$ while $G(T)$ is for all practical purposes the inverse of the number of vibrational states of X_2 within the energy range RT of the dissociation threshold.

The physical interpretation of this result [Eq. (5)] is that when 2X atoms come within bonding range of each other, a properly phased collision with a third body M can lead to the loss of sufficient energy so that a bound state of X_2 will be formed. The probability of such an occurrence per collision is given by the parameter λ. It is also assumed that the amount of energy lost by X_2^* in this collision will be of the order of RT so that one of the highest vibrational states of the species, $X_2^{(n)}$ will result. This highly excited species $X_2^{(n)}$ may however regain this energy in a further collision and be redissociated.

TABLE 1

Some Rate Constants for Atomic Recombination in Argon[a]

Atom	Temp (°K)	$k_r \times 10^{-9}$(l²/mole²-sec) Calc. Case IB	Calc. Case IIB	Obs.
H	300	13.5	3.8	9 ± 7(H_2=M)
	600	12.2	3.2	—
	1000	10.5	2.7	—
	2000	7.3	1.8	—
	6000	2.9	0.81	—
N	300	1.27	2.1	1.4
	600	1.12	1.6	—
	1000	0.96	1.3	—
	2000	0.67	0.79	—
O	300	1.14	2.0	1.0
	600	0.70	1.08	—
	1000	0.48	0.69	—
	2000	0.28	0.36	—
	3400	0.18	0.21	0.06
Br	300	2.32	6.4	3.1
	600	1.17	2.8	1.2
	1000	0.70	1.6	0.6
	2000	0.34	0.68	0.3
I	300	3.20	10.0	2.9
	600	1.35	3.7	1.2
	1000	0.75	1.9	0.6
	2000	0.34	0.76	—

[a] Reprinted in part from reference 6. IB is for Morse potential, IIB for Lennard–Jones potential.

As the temperature increases, the probability of redissociation increases and thus the total rate of recombination decreases.

In effect the group of highest vibrational states within RT of dissociation constitute an increasing barrier to recombination with increasing temperature. The net temperature dependence of k_r from this model approaches T^{-1} at high temperatures, i.e., temperatures of the order of $(h\nu/k)$.

Table 1 shows a comparison of some values of k_r calculated from Eq. (5), assuming $\lambda = 1$ and neglecting any contribution to recombination of upper excited electronic states. The values of K^* used here are calculated with a Sutherland correction to the viscosity diameters. The Sutherland is on the average about 10 to 20 per cent, thus almost negligible within the present uncertainties.

Within the imprecision of current data, Eq. (5) may be said to be in excellent agreement. It leaves unanswered a number of questions. One of the most interesting of these is why the upper electronic states of X_2 which are accessible to 2X atoms do not appear to contribute to recombination. The second concerns the correct value for λ. The third has to do with the proper potential function to use to describe X_2^* while the fourth has to do with the justification for small energy transfers occurring on collision.

The value of k_r is quite sensitive to the potential of interaction between X atoms at large distances. The Morse (Case IB) and the Lennard–Jones (Case IIB) potentials give results differing by factors of from 2 to 5. This is an unfortunate but real result. It is difficult to foresee any simple resolution of this problem other than an investigation of the X···X interaction potential at low energies and large distances.

On the question of the contribution of upper electronic states (such as $^1\Delta$ and $^1\Sigma$ for O_2) there is again no simple answer. One would expect contributions from such states, particularly at low temperatures. Their participation would imply values of λ of the order of 0.1 to 0.3 rather than unity as assumed. In addition they would be expected to contribute another source of negative temperature coefficient to k_r of the order of T^{-1}. Some independent studies of these states would appear to be well worth while.

On the question of small energy transfer we shall offer some evidence in the last section. First we shall present some aspects of an independent, homogeneous, catalytic mode for recombination.

Homogeneous, Catalytic Recombination of O Atoms

We have recently considered the general prospects for a homogeneous catalyst[8] for the recombination of atoms. Such considerations stem from the idea that if a species C forms a strong bond with an atom X and C has many internal degrees of freedom, then the nascent species, CX* formed in a bimolecular collision process may have a sufficiently long life to be able to be deactivated by collision. In such cases one can reasonably expect the following chain sequence for recombination:

$$\begin{aligned} &C + X \underset{2}{\overset{1}{\rightleftharpoons}} CX \\ &CX + X \xrightarrow[3]{} C + X_2. \end{aligned} \qquad (6)$$

Under the conditions that $k_3(X) > k_2$ so that dissociation of CX is negligible, and further that the reaction of C with X_2 (reverse of 3) is also negligible compared to the reaction of C with X, the rate of catalytic recombination R_c will be given by $k_1(C)(X)$. Comparing this with the termolecular process in which the third body M is X_2 we find

$$R_c/R_t = k_1/k_t(X) \times (C)/(X_2). \quad (7)$$

Now since k_1 may be expected to be of the order of 10^{10} l/mole-sec, while k_t is about 10^{10} l^2/mole^2-sec, we see that R_c/R_t will be of the order of 200 $(C)/(X_2)(X)$ at 2500°K with all concentrations expressed in atmospheres. Thus for $(X) = 0.001$ atm and $(C)/(X_2) = 0.01$ (i.e., 1 mole per cent) the catalytic rate can be 2000 times faster than the homogeneous, thermolecular rate. Under these conditions, the efficiency is still considerable when an appreciable fraction of CX redissociate via step 2 and there is appreciable back reaction of X_2 with C.

The corollary of all this of course is, that for such species C, one must be certain that they are not present as impurities in amounts of the order of 1 part in 100,000 or they will make an error of 100% in measurements of k_t.

The above mechanism, if applied to the very important problem of H atom recombination at very high temperatures and low pressures, suggest a number of possible catalysts approaching the above hypothetical efficiency. These are in descending order of utility, CH_4, C_2H_2, NH_3, and H_2O. A more detailed analysis of these molecules will be found in an independent paper (reference 8).

The chief requirements on C for high efficiency are that it contain at least three atoms and that the C—H bond strength be very large relative to RT. Both of these guarantee a long life for the nascent CX* species. Practical considerations of the method of utilization of C will dictate other requirements, not least of which is that C and CX be stable with respect to other kinetic processes in the regime and time of utilization. These we shall not be able to discuss here.

The possibility of finding efficient catalysts rests on the existence of species CX for which the rate of decomposition is controlled by internal energy migration. Under considerations where this is not the case, the decomposition of CX will be controlled by the rate of energy transfer and the lifetime of CX* may be too short to be of interest in the chain cycle, (6).

Ionization Rates in Hot Gases

At temperatures above 4000°K, ionization becomes an important phenomenon in hot gases and the process of dissociation into ions and electrons and the inverse recombination show many similarities with atom recombination. In recent years studies of the rates of ionization of rare gas atoms in shock tubes[9,10] have pointed to metastable states as being the chief precursor to ionization in the absence of impurities with low ionization potentials. The evidence adduced for this is that the activation energy for the rate of ion production has been considerably below the ionization potential of the rare gas in question. The mechanism for such a process is one of the two following:

Case A

$$M + X \underset{2}{\overset{1}{\rightleftharpoons}} X^* + M$$

$$X^* + M \underset{3}{\rightarrow} X^+ + e^- + M$$

Case B

$$M + X \underset{2}{\overset{1}{\rightleftharpoons}} X^* + M$$

$$X^* + X \underset{3'}{\rightarrow} X_2^+ + e^-.$$

If we apply steady state methods to X*, the metastable species, then we find for the rates:

$$\text{Rate}_A = [k_3k_1(M)(X)]/(k_2 + k_3) \quad (8)$$

$$\text{Rate}_B = [k_3'k_1(M)(X)^2]/[k_2(M) + k_3'(X)]. \quad (9)$$

When $(M) = (X)$ the two rate laws are indistinguishable. Let us consider the consequences of the fact that the ionization activation energy is very much less than the ionization potential.

Let it be first noted that mechanism A is inherently implausible relative to B if only by virtue of the fact that any second higher excited state of X produced by collision with M will dissociate its electron so rapidly (10^{-15} to 10^{-14} sec) that the product XM^+ will be effectively left behind. For this reason we shall consider only Case B even where the bond energy of XM^+ is very small.

In order for Rate_B to give an overall activation energy corresponding to step 1, $k_3' > k_2$ (assume $M = X$). However k_3' is not without activation energy of its own, namely the ionization potential of X* minus the bond dissociation energy of X_2^+. The former is of the order of 4–5 eV while the latter is about 1–2 ev. Thus k_3' should have an activation energy of the order of 3 ev. The only way in which the relation $k_2 < k_3'$ can be satisfied under these conditions is if the Arrhenius A factor for step 2 is much lower than that for step 3 (i.e., $A_2 \ll A_3'$).

The assignment of an activation energy to

step 2 is not a solution since the activation energy for step 1 would have to be raised by an identical amount in view of the relation $E_1 - E_2 = \Delta E^* =$ the excitation energy of X*.

But if k_2 has a very low Arrhenius A factor, so must k_1 since $R \ln (A_2/A_1) = \Delta S^* \sim 2$ (the entropy of excitation of X^*). However at the very high temperatures where the rates have been studied (7500°K), these inequalities are not very large. Thus an activation energy difference of 3 ev which will contribute a factor of 10^{-6} (at 2500°K) to the ratio of two rate constants, will contribute 10^{-3} at 5000°K and 10^{-2} at 7500°K. However the A factor for 3′, A_3' is already low. The standard entropy change in reaction 3′ is about 22 eu so that A_3' is about 10^5 smaller than A_4', the A factor for dissociative recombination. The latter however cannot exceed frequencies of about 10^{12} l/mole-sec so that $A_3' < 10^7$ l/mole-sec. This in turn implies that $A_2 < 10^5$ l/mole-sec which is then also the order of magnitude of A_1. There is no evidence at present to indicate that the Arrhenius factor for the ionization rate constant is so small.

An alternative mechanism has been presented by Petschek and Byron for the latter stages of ionization in shocked argon. They skip over the details of the process, assuming only that collisions of "colder" electrons with metastable Ar* are rate controlling. They further assume that Ar* are in equilibrium with electrons and not with Ar, ground state. But this assumes without evidence that the inelastic collision of $e^{-*} + \mathrm{Ar} \rightarrow \mathrm{Ar}^* + e^-$ is not reversible compared to the further excitation of $\mathrm{Ar}^* + e^- \rightarrow \mathrm{Ar}^+ + 2e^-$. This seems indefensible in terms of detailed balancing.[13]

It is my feeling that there is as yet very meager experimental evidence on which to base any detailed mechanism of ionization in shocks. What does appear to be well established is the difficulty of controlling impurity generated ionization.

Vibrational Energy Transfer

From the foregoing discussion it is perhaps evident that the inelastic transfer of energy between an internal oscillation in a complex molecule and the translation degrees of freedom is one of the keys to high temperature reaction rates. This problem has been under active investigation since the early 1930's[14] with results which are in about order of magnitude agreement with laboratory experiments.

There are two aspects of this work which have a direct bearing on the problems of chemical kinetics which it is of interest to discuss here. One has to do with the probability of collisional loss of a vibrational quantum by a highly excited oscillator (such as $X_2^{(n)}$ or X_2^*) while the other has to do with the relative probability of excitation of a lower energy oscillator to very high vibrational levels by an energetic collision.

We have recently at the Douglas Research Laboratories completed some computations of the classical, inelastic co-linear collisions of a diatomic molecule (harmonic oscillator) AB with an atom, C.[15] The computations were done on a machine (IBM 7090) and constituted a precise calculation of the mechanical trajectory of the collision over a broad range of the dynamical parameters of the system.

The interactions between the colliding species were represented by a Morse (or Lennard–Jones) potential with shallow minimum between atom B of the diatom AB and the atom C. For simplicity the collision was always between B and C. This is pretty much the model which has been examined by most previous investigators.

If l is taken as the range of the repulsive forces in the Morse potential

$$(V/V_0 = [1 - \exp(-\alpha(x - X_0))]^2 - 1) \quad (10)$$

with $l = 1/2\alpha$, V_0 the well depth and X_0 the equilibrium separation of B and C, then a hard-sphere, impulsive collision could be represented by setting $l \cong 0.01$ Å ($\alpha = 50$ Å^{-1}). These results could then be checked against the exact explicit solution which is available for the impulsive, hard sphere collision.[15] Some surprisingly interesting results came from this latter problem.

In Fig. 1a is shown a space–time diagram of the hard sphere collision. The straight lines through C represent the trajectories of C relative to A–B for different initial separations of C and A–B. The sinusoidal curve through B represents the harmonic trajectory of B relative to the center of mass of the oscillator (assumed fixed). All possible initial separations of C and A–B will be represented by a family of curves parallel to the lines through C.

What is most striking here is the fact that no intersection of the two trajectories can occur between the phases of oscillator motion represented by the region between the points P and Q! Between P and R, no collision can occur because B is moving faster than C and away from it while between R and Q the collision is prohibited by the prior collision at the preceding crest (e.g., P'). What this oversimplified model shows is that the collisions tend to be confined to oscillator phases corresponding to expansion which would on the average cause de-excitation.

Two extreme cases are represented in Fig. 1b and 1c. In Fig. 1b we see the result of a hard

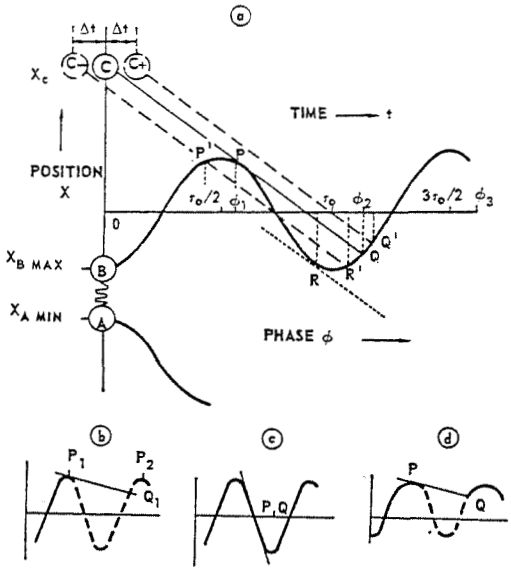

FIG. 1. Space–time trajectories for colliding hard spheres showing excluded phase angles.

sphere collision between a "cold" atom and a highly excited oscillator. This is the situation we envisage as the rate-determining step in atom recombinations. We see that the relative slopes are such as to favor collision near the peak of the oscillator separation where little kinetic energy is present for de-excitation. The effect of anharmonicity is shown in Fig. 1d. The result is to weight even more heavily the configurations of very large separation of the oscillator atoms and again make more probable the exchange of small amounts of kinetic energy. We believe that with all the limitations of the oversimplified model, this result added weight to our assumption that vibrational energy exchange takes place in small rather than large increments.

The other extreme situation where no oscillator configurations are excluded is shown in Fig. 1c representing the hard sphere collision of a "hot" atom C with a "cold" oscillator. There is now no longer any absolute restriction on phases but a further consideration appears.

This second consideration has to do with the observation that even in the completely classical system, the probability of excitation shows a sharp cutoff with collisional energy. This cutoff energy increases in magnitude with increasing softness of collision and is in fact a very sensitive function of the parameter α [Eq. (10)]. This is illustrated in Fig. 2 showing the de-excitation probability per collision, P_{1-0}, as a function of collisional energy and range α for a "soft" collision. The P_{1-0} curves go through a maximum

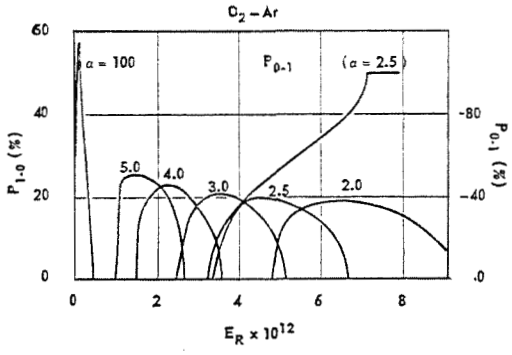

FIG. 2. Probability of excitation and de-excitation per collision from the first vibrational level to ground state.

and fall to zero with increasing energy. The reason for the maximum is that at higher collisional energies, excitation rather than deexcitation predominates (Fig. 1c).

If the excitation curves are examined (P_{0-1}) it is found that they exhibit a sharp decrease with increasing energy above their own cutoffs. This is due to the fact that with increasing collisional energy the probabilities of 2, 3, and higher quantum excitation becomes important. However, inspection of the curves shows that the cutoff for these higher order processes does not occur at an energy just $h\nu$ higher than the cutoff for the lower quantum jump. On the contrary, there is a considerably higher energy requirement.

What this implies is that if we consider the stepwise excitation of an oscillator (originally in the ground state) to any quantum level $nh\nu$, the stepwise rate will always be faster than the multiple quantum excitation. The kinetic reason for this arises from the steady state analysis of the system. For a 2-quantum process for example, the stepwise mechanism is

$$\mathrm{M} + \mathrm{X_2}^{(0)} \underset{2}{\overset{1}{\rightleftharpoons}} \mathrm{M} + \mathrm{X_2}^{(1)}$$

$$\mathrm{M} + \mathrm{X_2}^{(1)} \underset{4}{\overset{3}{\rightleftharpoons}} \mathrm{M} + \mathrm{X_2}^{(2)}, \qquad (11)$$

while that for the 2-quantum jump is:

$$\mathrm{M} + \mathrm{X_2}^{(0)} \underset{2'}{\overset{1'}{\rightleftharpoons}} \mathrm{M} + \mathrm{X_2}^{(2)}. \qquad (12)$$

The ratio of stationary rates for these processes, neglecting for the momement the deactivation rates 4 and 2', is:

$$R_{11}/R_{12} = k_1 k_3/[k_1'(k_2 + k_3)]. \qquad (13)$$

If $k_3 > k_2$ then $R_{11}/R_{12} \rightarrow k_1/k_1'$ while if as is much more likely $k_2 > k_3$, then $R_{11}/R_{12} \rightarrow$

$K_{1.2}k_3/k_1'$ where $K_{1.2}$ is the equilibrium constant for X_2[1] and has a temperature coefficient of precisely $h\nu$. It turns out however that the activation energy of k_3 is much less than that for k_2 so that process (11) is always faster than process (12). The exception to this is in the hard sphere case where the threshold energy is very close to the enthalpy change for excitation. Even in this case, however, there is a small, not inappreciable activation energy. This arises from the circumstance that if atom C were to transfer 100 per cent of the relative energy of the collision to vibration, it would be trapped as a motionless particle next to AB. On the next half-cycle of oscillation E would strike C and be de-excited.

A very crude analysis of the excess "activation" energy required in the classical, hard-sphere case yields a value of about 14% of the quantum excitation. That is, if C is to excite A–B by $nh\nu$, then the minimum relative collision energy of the system must be about 1.14 $nh\nu$. Substituting any such result in Ev. (13) yields the same conclusions, namely a more rapid stepwise excitation.

ACKNOWLEDGMENTS

This work has been supported in part by the Douglas Aircraft Co., Santa Monica, California, and by the National Science Foundation.

REFERENCES

1. BENSON, S. W.: *Developments in Mechanics*, Vol. 1, p. 554. Plenum Press, 1961. A brief discussion is present here.
2. RABINOWITCH, E. and WOOD, W. C.: Trans. Faraday Soc. *32*, 907 (1937); J. Chem. Phys. *4*, 487 (1936).
3. WILSON, J.: Thesis, Cornell Univ., 1962.
4. HARTECK, P., REEVES, R. R., and MANELLA, G.: J. Chem. Phys. *29*, 608 (1958).
5. HARTECK, P. and REEVES, R. R.: *Chemical Reactions in the Lower and Upper Atmosphere*, p. 219. Interscience, 1961. See this for comparisons of recent work.
6. BENSON, S. W. and FUENO, T.: J. Chem. Phys. *36*, 1597 (1962).
7. RICE, O. K.: J. Chem. Phys. *9*, 258 (1941).
8. BENSON, S. W.: In press.
9. JOHNSTON, H. L.: Paper presented at Spring Meeting of the American Chemical Society, Abstracts, April 1962.
10. PETSCHEK, H. and BYRON, S.: Ann. Phys. *1*, 270 (1957).
11. BIONDI, M. A.: *Chemical Reactions in the Lower and Upper Atmosphere*, p. 353. Interscience, 1961.
12. *Idem.*: Phys. Revs. *35*, 653 (1951). Values of A_2 reported here are about 10^7 l/mole-sec.
13. DOUGAL, A. A. and GOLDSTEIN, L.: Phys. Revs. *109*, 615 (1958). This shows that the equipartition of energy between atoms and electrons occurs extremely rapidly via coulombic collisions even at 0.001% ionization.
14. See HERZFELD, K. F.: *Thermodynamics and Physics of Matter*. Princeton Univ. Press, 1955.
15. BENSON, S. W., BEREND, G. C., and WU, J. C.: J. Chem. Phys. *38*, 25 (1963); *ibid. 37*, 1386 (1962).

Discussion

PROF. S. H. BAUER (*Cornell University*): For an audience which consists of a minority of chemical kineticists, it may be worthwhile to underscore that the notation and formalism of chemical kinetics is based on the assumption that each symbol is to be clearly identified with a distinct chemical species, the concentration of which could be measured, at least in principle. I should also remind you that the "rate constants" which chemical kineticists use to express probabilities of transformation of one such specie to others are *averaged* over many molecular parameters and states. If one is not on guard as to the significance of these hidden parameters, he will easily become confused.

The accepted formulation of a unimolecular process is:

$$A + X \underset{k_1}{\overset{k_2}{\rightleftharpoons}} A^* + X;$$

$$A^* \xrightarrow[k_3]{} \text{transition state} \longrightarrow \text{products.}$$

The "transition state" of the chemist is to the physicist a region of phase space which corresponds to the accumulation of a large amount of internal energy in a few (critical) vibrational modes. When these modes attain large amplitudes, the atoms are brought into a sequence of configurations required for the transformation of the reactant to the product. The "transition state" is that region of phase space which corresponds to the maximum of the potential energy surface along the minimum energy path (saddle point) in which the representative points are moving toward the configurations representative of the products; the correct vector quality is essential.

I must admit that I did not have the proper intuitive feeling for Prof. Benson's statement that at sufficiently high temperatures the rate of internal energy migration is sufficiently rapid to make collisional activation the rate-determining process for a unimolecular reaction. However, on the slide he

argued its validity by writing:

$$k_3 \approx \nu[(\bar{\epsilon} - \epsilon^*)/\bar{\epsilon}]^{n-1}.$$

Of course, if he chooses, he may introduce this dependence as an essential postulate; and then he will not obtain the usual Arrhenius temperature dependence of k_3. Generally, it has been assumed that

$$k_3 = \int_0^\infty k(\epsilon)D(\epsilon)\, d\epsilon,$$

where

$$k(\epsilon) = 0 \quad \text{for} \quad \epsilon < \epsilon^* = \nu[(\epsilon - \epsilon^*)/\epsilon]^{n-1} \quad \text{for} \quad \epsilon \geq \epsilon^*$$

and $D(\epsilon)$ is the distribution function over states. Then $k_3 = \nu \exp(-\epsilon^*/kt)$, and the unimolecular limit is maintained. Thus by performing the average over energies rather than over probabilities for reaction $[k(\epsilon)]$, Benson reached this rather unexpected conclusion, for which, as far as I know, there is no evidence.

The matter of notation arises again in the comparison of O. K. Rice's model for the dissociation of diatoms with that of Benson.

$$X_2 + M \underset{b}{\overset{a}{\leftrightarrows}} X_2^{(n)} + M$$

Prof. Benson treats $X_2^{(n)}$ as a distinct chemical species for which one may write a meaningful partition function, and thus deduce an equilibrium constant for the reaction, as written. Prof. Rice did not use this formalism because the $X_2^{(n)}$'s are nothing but X_2 molecules in their uppermost vibrational states which have already been included in the partition functions and equilibrium constants in the manner proposed. Now, the rate constant for dissociation may be simply written as the product of the normal collision number times the population of molecules in the states within kT of the dissociation limit.

$$k_d = Zn^* = Zg(D_0 - kT) \exp[-(D_0 - kT)/kT]$$

where $g(D_0 - kT)$ is the total number of states within kT of the dissociation limit. The last term assumes the essential attainment of a Boltzmann distribution for these states. Benson stated that his estimate of the population was obtained by solving for a steady state condition, with detailed balance among all the upper states. From the material presented it is not evident that his temperature dependence of the pre-exponential term could differ substantially from that of Rice. I strongly suspect that differences by a factor of $T^{1/2}$ or even T could be introduced by following different averaging paths. For example, a classical treatment of all the vibrational levels will give a different T dependence than one in which the lower levels are quantized.

I wish to counter to some extent the pessimism regarding diatom dissociation data as derived from shock tubes. If one considers all the published works, values for selected rate constants do differ by a factor of 10. However, values which appeared during the past 2–3 years are much more consistent; these range only over factors of 2–3. In particular, the rate constants for O_2 have settled down, and as was not admitted by Prof. Benson, Jack Wilson has shown that at 2800°K his directly measured recombination rate constant checks within 30% the value deduced from Skip Byron's measured dissociation rates.

Finally, with respect to the use of hydrocarbons such as CH_4 and C_2H_2 as catalysts for H atom recombination in nonequilibrium nozzle flow, attention is called to the paper by A. Q. Eschenroeder and J. A. Lordi (this volume, p. 241). They reported on a numerical analysis of the effect of introducing such species in the flow, and concluded that the loss in specific impulse due to the increase in average molecular weight is significant. The over-all gain is not dramatic.

PROF. S. W. BENSON (*University of Southern California*): In answer to Dr. Bauer's first point, that of the estimate of the half-life or rate constant of a critically energized species, this is done by a method indicated in my text "Foundations of Chemical Kinetics".[1] What is done is to set $\bar{\epsilon} = \epsilon^* + nkT$ on the crude assumption that the mean reactive molecule contains nkT excess internal energy beyond the barrier energy. There is considerable evidence for such an estimate.

In his second point Dr. Bauer confuses Rice's treatment and our own. Rice assumed that $X_2^{(n)}$ was in equilibrium with the ground states of X_2. We show on the contrary that $X_2^{(n)}$ is in a steady state whose concentration is less than equilibrium. Further this steady state concentration decreases with increasing temperature about like T^{-1}. It is this latter behavior which is responsible for the negative temperature dependence of the rate constant for termolecular recombination. I think it would be best on this score to refer to the original paper.[2]

On his last point concerning the rate of homogeneous catalysis I have not made an effort to calculate the performance gain in propulsion due to small amounts of CH_4 or C_2H_2. I did calculate the effects on the recombination rate of CH_4, C_2H_2, NH_3, and H_2O. They are in the order given with CH_4 about a factor of 10 more effective than C_2H_2. In view of the smaller molecular weight of CH_4 vs. C_2H_2 and the greater catalytic efficiency I would be surprised if it did not increase propulsion in the low thrust (low

chamber pressure) engines. But that is for the engineers to discover.

PROF. H. B. PALMER (*Pennsylvania State University*): Professor Benson has chosen as an example of shock tube kinetic results the case in which I believe the disagreement is the worst known from shock tube studies. In contrast I might cite the four independent studies that have been made of Br_2 dissociation, using differing tubes and differing inert gas dilution ratios. As I recall, the scatter in the entire collection of data is approximately a factor of two. As for checks of shock tube results by other methods, two examples with which I am familiar come to mind. At the last symposium, Deklau and I reported work on nitrosyl chloride decomposition in shock waves. Our scatter was large, but by using the kinetic results of Ashmore and of Waddington and Tolman at low temperatures, we were able to make a rate constant plot over a large temperature range. Dr. Ashmore has recently sent me a new result for nitrosyl chloride that falls almost perfectly on our best low T–high T line. Finally, in the case of CH_4 decomposition, T. J. Hirt and I have rate constant data, obtained from kinetic studies of carbon film formation, that agree extremely well with the best line through the shock tube data of Skinner and of Glick.

PROF. S. W. BENSON: In regard to the problem of the precision of shock tubery raised by Dr. Bauer and Dr. Palmer I must, of course, confess to playing devil's advocate in some measure. I would be very pleased to know that the precision of rate constants from shock tube studies was within a factor of 50% (spread of 2). This is certainly not true of the data with which I am currently acquainted. I think it is very important that Shock Tubers point out and emphasize the precision of their measurements. I hope that, in future work, independent checks of the type mentioned by Dr. Palmer will be available for comparison.

REFERENCES

1. BENSON, S. W.: *Foundations of Chemical Kinetics*, McGraw-Hill, 1960.
2. BENSON, S. W. and FUENO, T.: J. Chem. Phys. *36*, 1597 (1962).

CHEMICAL REACTIONS IN SUPERSONIC NOZZLE FLOWS

K. N. C. BRAY

Departures from thermochemical equilibrium involve energy withheld from the active degrees of freedom of the gas and may therefore cause a large loss of thrust in propulsive nozzles. Nonequilibrium effects are also important in the use of high enthalpy wind tunnels, where they may produce a test fluid whose composition and properties are very different from those of equilibrium air. Finally, freezing of the ionization level in a channel-type MHD electrical generator could lead to a useful increase in the dc conductivity of the gas.

The object of this paper is to provide a summary of the present state of knowledge concerning these problems. Basic assumptions which are made in theoretical studies of nonequilibrium flows are first reviewed. From the gas dynamic point of view, nozzle flows are well represented by the very simple, quasi-one-dimensional adiabatic flow approximation. All transport processes are neglected except in narrow boundary layers on the walls, whose only effect on the remainder of the flow is a small reduction in the effective cross-sectional area. Changes in chemical composition, ionization level, and vibrational excitation are assumed to occur through a finite number of supposedly elementary chemical reactions, and the rates of these reactions are obtained from experiments on simpler systems often under very different conditions. Large errors may result if the assumed reaction mechanisms are not in fact elementary or if an incorrect temperature dependence is assumed. Generalized computer programs exist which can solve nozzle flow problems in which an arbitrary set of relaxation processes is occurring. Results can continually be improved as more accurate kinetic data becomes available. At present, the accuracy of numerical results will often be severely limited by uncertainties in the kinetic data, so emphasis is placed on simple approximate solutions. A generalized sudden freezing method is presented for flows in which coupled chemical reactions are occurring. Each reaction is assumed to cease suddenly at a separate point in the flow. The inclusion of sudden freezing of vibrational energy is straightforward. Agreement with exact solutions is satisfactory.

Finally, the paper includes a brief survey of published experimental results. It is concluded that two types of experimental data are urgently required: experiments on simple chemical systems to determine rate constants applicable to nozzle flow problems, and experiments on flows where coupled chemical reactions are predicted to play a dominant role. Much effort is being invested in these problems and knowledge is likely to increase rapidly.

Introduction

The object of this paper is to provide a summary of the present state of knowledge on the subject of supersonic nozzle flows in which thermodynamic and chemical equilibrium is not always maintained. We are therefore concerned with a situation in which the characteristic times for various molecular relaxation processes may be comparable with the residence time during which particles pass through the nozzle flow. Processes which may depart significantly from equilibrium include chemical and ionizing reactions and adjustment of molecular vibrational energies. Rotational relaxation occurs too rapidly to depart significantly from equilibrium in nozzle flows.

The convergent–divergent de Laval nozzle is a device for accelerating a gas stream from subsonic to supersonic speed. In performing this function, it converts the thermal energy and potential energy (in the form of pressure) of the nearly stagnant, hot gas ahead of the nozzle, into the kinetic energy of the supersonic stream which emerges with lower temperature and pressure. If the ratio of exit area to throat area is large, most of the energy is converted into kinetic energy, and the pressure, density, and temperature at the exit are very much less than at the entrance to the nozzle. The nozzle then produces a hypersonic flow.

Consider a situation where a chemical reaction occurs in the accelerating gas as a result of the decreasing temperature and pressure. Energy released during the reaction will be in the form of thermal energy and the expanding nozzle will

convert some of this to kinetic energy. Both the exit velocity and the exit temperature will be higher than if the reaction had been too slow to occur within the nozzle. Most energy will be released, and the velocity and temperature will be highest, if the reaction is fast enough to remain essentially in equilibrium during expansion. The chemical kinetic and gas dynamic aspects of the problem are coupled together, because the rate of energy release affects not only the flow but also, through the temperature, the rate of the reaction. As the gas passes through the nozzle the density falls, so the rate of reaction is reduced and the composition tends to "freeze."

Departures from equilibrium are important in the design of propulsive nozzles. If combustion is not completed before the gas enters the exhaust nozzle, the combustion reactions may be too slow to reach completion within the nozzle. Also, the hot combustion products will be partly dissociated in the combustion chamber. The full chemical energy will only be available to the flow if recombination of dissociated products can occur as the temperature falls through the nozzle. If any of these reactions departs from equilibrium, or "freezes," energy is withheld from the active degrees of freedom of the gas. This frozen energy cannot be converted into kinetic energy by the nozzle and large losses in thrust can result. The hypersonic ramjet engine is particularly sensitive to nonequilibrium effects[1,2] and, at high Mach numbers, the thrust may go to zero if complete freezing occurs. Important losses in thrust can also occur as a result of freezing in rocket nozzles.[2]

Nonequilibrium nozzle problems also arise in the use of high enthalpy wind tunnels[3,4,5]. In this case, departure from equilibrium results in a test fluid which does not possess the composition and properties of equilibrium air, and may therefore give misleading experimental results. Wind tunnel experiments involving, for example, nonequilibrium flow past a body, or radio wave propagation through the ionized layer round such a body, may require detailed knowledge of the concentrations of all constituents of the test gas. This is obviously a much more rigorous requirement than in the case of the propulsive nozzle, where we are primarily interested in the gross properties which determine the thrust.

The design of magneto-hydrodynamic generators may also be significantly affected by nonequilibrium flow effects. As pointed out by Eschenroeder,[6] the freezing of reactions between ionized species may lead to a large increase in dc electrical conductivity in a supersonic nozzle flow, and this can perhaps be used to improve the efficiency of a channel-type generator.

Very similar problems also arise in computing the flow field past a hypersonic vehicle entering the earth's atmosphere, under conditions where nonequilibrium chemical reactions occur in the hot air surrounding the vehicle. Typical results are reported by Vaglio-Laurin and Bloom.[7]

Formulation of the Problem

In this selection we list and discuss the various gas dynamic and kinetic assumptions to be made in formulating the general problem of a flow with coupled chemical and ionizing reactions and simultaneous vibrational relaxation. Equations embodying these assumptions will be presented in the following section.

Gas Dynamics

As the overall accuracy of computed results is likely to be limited by the kinetic data, great sophistication would be out of place here. The quasi-one-dimensional approximation, in which all thermodynamic, chemical, and flow variables are assumed to depend only on the axial distance down the nozzle center line, has proved to be useful in many applications. To this approximation, velocity components and variations of properties in directions normal to the center line are ignored. Viscous, thermal conduction, and diffusion effects are confined to narrow boundary layers on the nozzle walls. These boundary layers are excluded from the region to be studied, it being assumed that their only effect on the main body of the flow is to produce a small displacement of the effective wall position. Consequently, friction, external heat transfer, and heterogeneous chemical reactions are all excluded from the region of interest, in which the flow is assumed to be steady, frictionless, and adiabatic and only gas phase reactions are considered. To this approximation, the gas dynamic side of the problem is very much simpler than in many cases of technical combustion, where diffusion and turbulent mixing processes predominate.

If conditions upstream of the nozzle are nonuniform and unsteady, as is often the case in propulsion applications, an exact solution of the flow problem becomes very difficult, and it is often necessary to apply empirical corrections to steady one-dimensional flow solutions. When the flow upstream of the nozzle is steady and uniform, the one-dimensional approximation leads to negligible errors under suitable conditions. The nozzle expansion angle must not be too large, the overall pressure ratio must be adjusted so that shock waves do not occur inside the nozzle and the Reynolds number must be sufficiently high for boundary layers to be thin. The last restriction is often the most serious, as very

thick boundary layers may be formed on the walls of large area-ratio nozzles.

Three-dimensional nozzle flow problems may be solved by the Method of Characteristics. However, it is again necessary to make empirical corrections for any nonuniformities that may exist in the flow ahead of the nozzle, as well as for boundary layer growth. These corrections may lead to large errors so that the solutions may, in fact, not be significantly more accurate than the much simpler quasi-one-dimensional results.

The Method of Characteristics must be used in order to predict the transverse gradients of concentrations and temperature, etc., which arise in a relaxing flow, because flow through different stream tubes will have different time histories (see, for example, reference 8). Calculations of this type have not been done for nozzle flows, and need to be carried out for a few cases in order to check that transverse gradients are small. However, the one-dimensional approximation should be adequate for the present purpose.

Vibrational Relaxation

The classical work of Landau and Teller[9] and many others has shown that the vibrational energy of a system of harmonic oscillators relaxes according to the equation

$$de_v/dt = k_{1,0}[1 - \exp(-h\nu/kT)][(e_v)_{eq} - e_v] = [(e_v)_{eq} - e_v]/\tau_v \quad (1)$$

where $k_{1,0}$ is the rate per second of transitions from state 1 to state 0, $(e_v)_{eq}$ is the equilibrium vibrational energy and τ_v is the vibrational relaxation time. This expression, with its attendant assumption that coupling between vibration and translation is weak, has been confirmed experimentally, but attempts to predict the numerical value of τ_v have not yet been completely successful. The best approach at the present time seems to be to use an empirical expression for τ_v based on experimental results. This can make use of a theoretical temperature dependence such as $\tau_v \sim \exp(T^{-\frac{1}{3}})$ as predicted by Landau and Teller. Also, because only binary collisions are important, $\tau_v \sim p^{-1}$ at fixed temperature.

A large amount of experimental data has been published (see, for example, references 10 and 11) concerning the vibrational relaxation of pure gases and simple mixtures. In applying such data to situations involving a complicated mixture of reacting species many additional effects must be ignored because of lack of quantitative information. For example:

(a) The many species present may have widely different efficiencies in promoting the relaxation of a particular molecular vibration.

(b) The vibrational energies of different species may be coupled together so that they do not relax independently.

(c) Molecular species produced in chemical reactions may not be formed with their vibrational energy in equilibrium with local conditions.[12] This could lead to the rapid equilibration of vibrational energy, or could accentuate vibrational nonequilibrium.

Fortunately, great accuracy is not required for the present purpose, because the fraction of the total flow energy which can be frozen into molecular vibrations is normally much less than that involved in chemical reactions.

Chemical Reactions

Only gas phase reactions will be considered here, as explained above. For an elementary, gas phase reaction of the form:

$$aA + bB \underset{k_b}{\overset{k_f}{\rightleftharpoons}} cC + dD + eE \quad (2)$$

where a, b,, etc., are stoichiometric coefficients, the rate equation is

$$\begin{aligned} &-a^{-1}[d(A)/dt] \\ &= -b^{-1}[d(B)/dt] = c^{-1}[d(C)/dt] \\ &= d^{-1}[d(D)/dt] = e^{-1}[d(E)/dt] \\ &= k_f(A)^a(B)^b - k_b(C)^c(D)^d(E)^e, \end{aligned} \quad (3)$$

where (A), (B), etc., are concentrations in moles/cc. The rate constants k_f and k_b cannot be predicted accurately from existing theories (see reference 13 for an up-to-date review) and must normally be obtained from experiments. For an elementary reaction they are functions of temperature only, and their ratio can therefore be obtained from the equilibrium constant

$$K(T) = k_f/k_b \quad (4)$$

even under conditions removed from equilibrium. The equilibrium concentrations $(A)_{eq}$, etc., are related through the equation

$$K(T) = (C)_{eq}^c(D)_{eq}^d(E)_{eq}^e/(A)_{eq}^a(B)_{eq}^b. \quad (5)$$

Is it justifiable to represent a complex reacting system by the sum of a limited number of supposedly elementary reactions obeying the above equations, and to determine the rates of these reactions from experiments on simpler systems under different conditions? This procedure has given a satisfactory explanation of the processes

occurring behind strong shock waves in air.[14] However, the rate constants used in this way represent a gross average over a number of elementary processes. For example, when air is heated by a sufficiently strong shock wave, dissociation and vibrational excitation of N_2 proceed at comparable rates. If, in these circumstances, dissociation is represented by single reaction of the form of Eq. (2), then the rate constant k_f describes an average rate of dissociation over a particular nonequilibrium distribution of vibrational energies. Clearly, this k_f cannot be used in Eq. (4) to predict the recombination rate constant k_b applicable to a nozzle expansion, where a different nonequilibrium vibrational energy distribution exists. Also, in many cases, it is difficult to find a set of elementary reactions which will provide a satisfactory explanation of observed phenomena.

Unfortunately, the majority of high temperature kinetic data must be obtained in shock tubes as rates of dissociation (see, for example, ref. 11), and the corresponding recombination rates must be obtained through use of Eq. (4). It is possible that this procedure may lead to significant errors. Also, dissociation rates are usually exponentially dependent on the temperature, and it is therefore very difficult to determine the much weaker temperature dependence of the recombination rate from an experiment in which the dissociation rate is measured. The many catalysts present in the system may have widely different efficiencies, and the temperature dependence of a reaction rate may also be affected by the catalyst. There is very little data on the efficiency of electrons as catalysts. Further information is also required on coupling between the relaxation rates of different internal energy modes and on the rates of photochemical processes.

Shortage of information about rate constants and their temperature dependence is still the most serious obstacle in the way of accurate nonequilibrium flow calculations. For the present application, a disturbing feature is the almost complete lack of kinetic data obtained in a recombining environment. However, many people are working on these problems and the situation is likely to improve rapidly.

Reactions Involving Ions and Electrons

Conventionally, the rates of ionizing and de-ionizing reactions are formally represented in terms of second order kinetics, independently of the order of the actual changes occurring. This convention will not be followed here, as it is more convenient to use the same formalism for reactions involving charged and neutral particles. Equations (2)–(5) may then be applied to ionizing reactions, and many of the comments made in the previous section still apply. However, additional complications may arise when free electrons are present. A very large number of alternative mechanisms must be considered[6] and there is very little data on reaction rates. The gas dynamic side of the problem may be complicated by ambipolar diffusion and charge separation effects. Also, because electrons are very much lighter than the other particles, a large number of collisions may be required to equilibrate the electron temperature with the translational temperature of the atoms and ions, particularly in inert gases. High electron temperatures have been measured in arc-heated wind tunnels employing argon.[15] It has been suggested[16] that at least part of this effect can be explained by assuming an electron–ion recombination mechanism in which an electron acts as a third body, so that the energy released during recombination raises the temperature of the electron gas.

General Equations

For steady, adiabatic, quasi-one-dimensional flow, the three conservation equations of gas dynamics are

$$\rho V A = \rho^* V^* A^* = \text{constant}, \tag{6}$$

$$\rho^{-1}(dp/dx) + V(dV/dx) = 0, \tag{7}$$

and

$$h + \tfrac{1}{2}V^2 = h_0 = \text{constant}, \tag{8}$$

where ρ is the density, V the velocity, A the nozzle cross-sectional area, p the pressure, and $h = e + p/\rho$ is the specific enthalpy, e being the specific internal energy; h_0 is the stagnation enthalpy and * represents conditions at the nozzle throat. The cross-sectional area is assumed to be given as a function of the distance x down the nozzle center line

$$A = A(x). \tag{9}$$

A notation similar to that of references 17 and 18 will be used in generalizing the equations of the section on Chemical Reactions. Let the total number of chemical species such as M_i be n, of which the first n_A are atomic and the remaining $n_M = n - n_A$ are diatomic and polyatomic molecules. The rth elementary reaction taking place in the mixture is formally written as

$$\sum_{i=1}^{n} \nu_i{}' M_i \underset{k_b{}^r}{\overset{k_f{}^r}{\rightleftharpoons}} \sum_{i=1}^{n} \nu_i{}'' M_i \tag{10}$$

where $r = 1, 2, \cdots, N$, N is the total number of reactions, $\nu_i{}'$ and $\nu_i{}''$ are the stoichiometric

coefficients of the forward and backward reactions and k_f^r and k_b^r are the rate parameters for the forward and backward changes in the rth reaction. Free electrons and ionized species are included in this formulation.

For a mixture of monatomic and diatomic perfect gases, the equations of state may be written

$$p = \sum_{i=1}^{n} p_i = \rho T R \sum_{i=1}^{n} \gamma_i \tag{11}$$

$$h/R = \sum_{i=1}^{n_A} \gamma_i \left[\tfrac{5}{2} T + \theta_i\right] + \sum_{i=n_A+1}^{n} \gamma_i \left[\tfrac{7}{2} T + (e_{vi}/R) + \theta_i\right] \tag{12}$$

where γ_i is the concentration of the ith species in moles/gm of mixture, $R\theta_i$ is the heat of formation of the ith species from a standard state, e_{vi} is the vibrational energy of the ith species (per mole of the ith species), and R is the universal gas constant.

If vibrational and translational energies are not in equilibrium, e_{vi} must be obtained from equations similar to Eq. (1)

$$V\, de_{vi}/dx = \left[(e_{vi})_{eq} - e_{vi}\right]/\tau_{vi}, \qquad i = (n_A + 1) \cdots n \tag{13}$$

where

$$(e_{vi})_{eq} = N_0 h\nu_i / \left[\exp(h\nu_i/kT) - 1\right]. \tag{14}$$

Here N_0 is Avogadro's number and ν_i is the frequency of the relevant vibrational mode.

Similarly, when chemical reactions depart from equilibrium, there are n_M differential equations expressing conservation of the n_M diatomic and polyatomic molecular species. These equations contain terms of the form of Eq. (3) for each contributing reaction, and are written here as:

$$d\gamma_i/dx = \sum_{r=1}^{N} a_i^r X^r, \quad i = (n_A + 1) \cdots n, \tag{15}$$

where

$$a_i^r = (\nu_i^{r''} - \nu_i^{r'})/\rho V$$

$$X^r = R_f^r - R_b^r$$

$$R_f^r = k_f^r \prod_{j=1}^{n} (\rho\gamma_j)^{\nu_j r'}$$

$$R_b^r = k_b^r \prod_{j=1}^{n} (\rho\gamma_j)^{\nu_j r''}$$

We may also write n_A equations expressing conservation of the n_A elements in both atomic and molecular forms. The ith of these is

$$\gamma_i + \sum_{q=n_A+1}^{n} S_{iq}\gamma_q = \Gamma_i, \quad i = 1, 2, \cdots, n_A \tag{16}$$

where Γ_i is the total concentration in moles/gm of mixture, of the ith element in both atomic and molecular forms, and is therefore constant. S_{iq} is the number of atoms of the ith element in the qth molecular species.

If the chemical kinetic data suggests that the rth reaction proceeds sufficiently fast to remain in chemical equilibrium, then the equilibrium Law of Mass Action:

$$R_f^r = R_b^r$$

or

$$k_f^r/k_b^r = K^r = \prod_{i=1}^{n} (\rho\gamma_i)^{\nu_i r'' - \nu_i r'} \tag{17}$$

may be used in place of one of Eqs. (15). If all the N reactions remain in equilibrium, then N Eqs. (17) may be written. It will be found that only n_M of these are independent, replacing the n_M Eqs. (15). In fact,[18] $N - n_M$ reactions can be arbitrarily slow, and the system can be kept in equilibrium by the remaining n_M independent reactions. However, as soon as the concentrations depart from their equilibrium values, any number of reactions may contribute, as is clearly illustrated by the kinetics of high temperature air.[14]

The general problem is described by the $(6 + n + n_M)$ equations: (6)–(9), (11)–(13), (15), and (16). The independent variable is x and the $(6 + n + n_M)$ dependent variables are: $p, \rho, T, h, V, A, \gamma_i (i = 1, 2, \cdots, n)$ and $e_{vi} (i = n_A + 1, \cdots, n)$.

Boundary conditions may be specified in several ways. If the flow is supersonic everywhere, a consistent set of initial values may be chosen at any station x. However, in the more usual case of a convergent–divergent nozzle, one boundary condition must ensure that the flow is choked, that is, that the mass flow rate is the maximum possible for given stagnation conditions. This will occur if the local flow velocity is equal to the "frozen" speed of sound[19]

$$c = \left[\partial p/\partial\rho\ (S, \gamma_i, e_{vi} = \text{const.})\right]^{\frac{1}{2}}, \tag{18}$$

at the "critical point" just downstream of the nozzle throat,[3] where the flow will exhibit sonic behavior. In Eq. (18) S is the specific entropy. The other boundary conditions for this case are a consistent set of dependent variables at any chosen station x. It is convenient to specify these far upstream of the throat where $V \to 0$, so that they become the "stagnation" values p_0, T_0, etc. which are related through the equilibrium relationships of Eqs. (14) and (17).

We then have a problem with two-point boundary conditions, which must be applied upstream of the throat, where $V \to 0$, and at the critical point x_c, where $V = c$. The exact location of x_c is not known *a priori*.

Equations (13) and (15) show that, with k_f^r, k_b^r, τ_{vi}, $d\gamma_i/dx$, and de_{vi}/dx all finite, departures from equilibrium must always occur. In other words, complete equilibrium cannot exist in a flow with finite gradients, unless all relaxation rates are infinite. Mathematically, the departure from equilibrium is a singular perturbation problem, because the equilibrium state is described by algebraic Eqs. (14) and (17) whereas the relaxing state requires differential Eqs. (13) and (15). A solution for the relaxing case therefore demands additional boundary conditions (the time history of the flow) which are not needed at equilibrium. Care is therefore required in carrying out a numerical integration in which the transition from an equilibrium to a nonequilibrium state occurs.

Whereas the flow strictly deviates from equilibrium as soon as nonzero concentration gradients exist, common sense and analysis both show that departures from equilibrium will be quite insignificant, numerically, if the reaction rates are sufficiently fast. In the nozzle problem, conditions very close to equilibrium will therefore exist at stations sufficiently far upstream, where the rates are fast. The equilibrium Laws of Mass Action may then be used, which may be written (Eqs. 15 and 17) in the form $R_f^r = R_b^r$. A useful criterion for the rth reaction to be close to equilibrium is therefore $R_f^r \approx R_b^r$ or [see Eq. (15)] $R_f^r \gg |X^r|$. It is convenient (reference 18) to define a quantity

$$B^r = R_f^r / |X^r|_{\text{eq}}, \tag{19}$$

where the suffix eq indicates that X^r is to be evaluated with the rth reaction in equilibrium. Under these conditions X^r is the small but finite difference between the two large numbers R_f^r and R_b^r. It must be calculated by differentiating the equilibrium law for the rth reaction [Eq. (17)] to find $d\gamma_i/dx$, substituting in Eq. (15) and solving for X^r (see reference 18).

Using this definition of B^r, the criterion for the rth reaction to be very close to equilibrium is simply $B^r \gg 1$. Under these conditions X^r is numerically indeterminate as the difference between R_f^r and R_b^r, and numerical difficulties will be experienced in integrating Eq. (15).

This criterion has been used by Appleton[20] to compute the minimum length of nozzle required to expand air to a given area ratio while maintaining conditions close to equilibrium. The results suggest that impossibly long nozzles are needed under many conditions of practical interest.

Methods of solution of the equations introduced in this section have been discussed by Bray and Appleton.[18]

Numerical Results

Exact Solutions

Exact step-by-step integration of the full set of equations listed above is quite possible with a high speed computing machine, and several generalized computer programs exist[5,21,22] which can solve nozzle flow problems in which an arbitrary set of relaxation processes is occurring. Special techniques, such as linearization of the governing equations about the infinite rate equilibrium solution,[5,23] are necessary during the initial departure from equilibrium ($B^r \gg 1$).

Results obtained in this way will be illustrated here from computations carried out at Cornell Aeronautical Laboratory, and reported by Eschenroeder, Boyer, and Hall.[5] These computations deal with air in vibrational equilibrium, with chemical changes represented by the following set of five reactions:

$$O_2 + M \rightleftharpoons O + O + M, \tag{20}$$

$$N_2 + M \rightleftharpoons N + N + M, \tag{21}$$

$$NO + M \rightleftharpoons N + O + M, \tag{22}$$

$$N + O_2 \rightleftharpoons NO + O, \tag{23}$$

$$O + N_2 \rightleftharpoons NO + N. \tag{24}$$

Results show that important deviations from equilibrium can occur when high temperature air expands through a nozzle, for a wide range of stagnation conditions. The large reduction in density which takes place as the gas passes through the nozzle reduces the rates of all the reactions and freezing tends to occur. As a consequence, energy is withheld from the active degrees of freedom of the gas and the temperature, pressure, and velocity are all reduced.

The fast nitric oxide exchange reactions, (23) and (24), play an important role in keeping the nitrogen atom concentration close to equilibrium long after the three-body recombination of reaction (21) has frozen. Over a range of conditions, most of the energy invested in nitrogen dissociation is recovered in this way, but the exchange reactions do not postpone the freezing of oxygen atom recombination. Figure 1 shows a typical computed result from reference 5. Composition is plotted against nozzle area ratio for a case where $p_0 = 100$ atmospheres and $T_0 = 8000°$K,

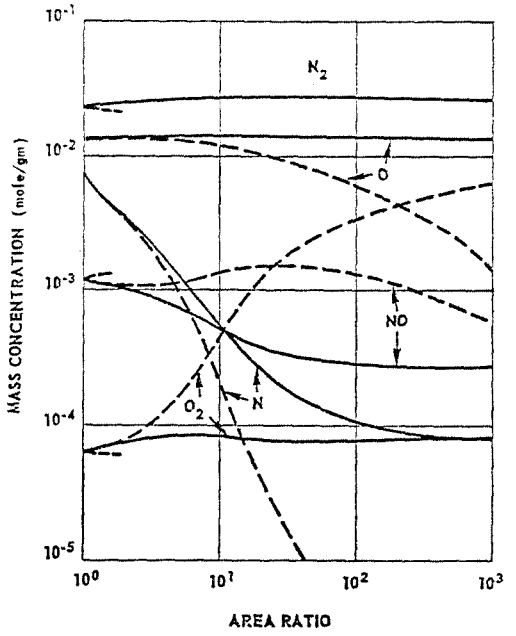

FIG. 1. Mass concentrations in moles per gram of mixture for air flow in hypersonic nozzle (from reference 5). T_0 = 8000°K; p_0 = 100 atmos; —— finite rate nonequilibrium; – – – infinite rate equilibrium.

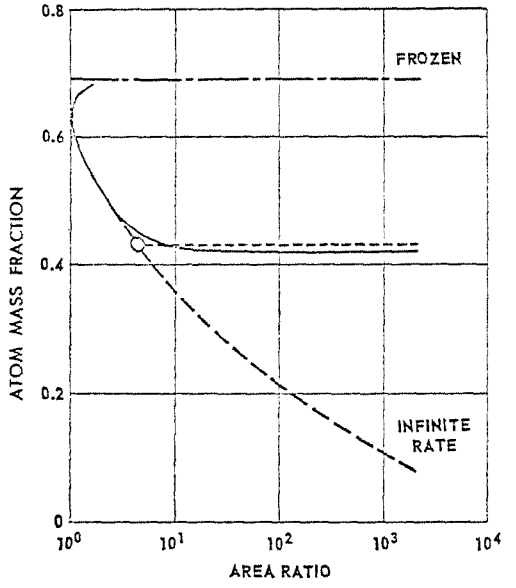

FIG. 2. Atom mass fraction for an ideal dissociating gas flowing in hypersonic nozzle (a typical result from reference 3); —— numerical solution for finite rate nonequilibrium; O – – – – sudden freezing approximation.

and infinite rate equilibrium values are also presented for comparison.

An important conclusion to be drawn from the work of reference 5 is that, at low temperatures, when oxygen dissociation is the only energetically significant process occurring, the kinetics of expanding air are well represented by Eq. (20) alone, but when nitrogen dissociation becomes significant a set of coupled reactions is required.

Numerical integrations where only one chemical reaction is considered[3,24] are useful, not only when one reaction actually dominates the chemistry, but also more generally, in throwing light on the coupling between flow and chemistry. Figure 2, taken from reference 3, illustrates the conclusions which can be drawn from simple calculations in which one dissociation–recombination reaction is considered. Three regions may be distinguished from Fig. 2.

(a) An upstream region of flow very close to equilibrium, in which $R_f \approx R_b$ so that the equilibrium Law of Mass Action is obeyed.

(b) A transition region in which significant departures from equilibrium become apparent. Energy is withheld from the active degrees of freedom of the gas, so the temperature falls below the infinite rate equilibrium value, as shown in Fig. 3. The falling temperature rapidly decreases R_f, because of the exponential temperature dependence of k_f, so that $d\gamma/dx \approx -aR_b$.

(c) A downstream region of nearly frozen flow, brought about by the large fall in density

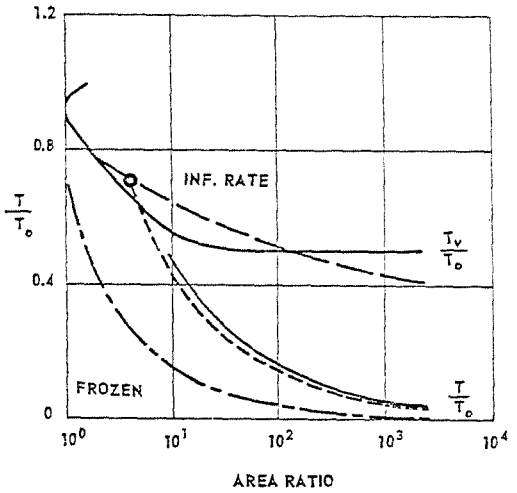

FIG. 3. Translational and vibrational temperatures for an ideal dissociating gas flowing in hypersonic nozzle (from references 3 and 30); —— numerical solutions for finite rate nonequilibrium; O – – – – sudden freezing approximation.

which has by now occurred, due to the expansion of the gas. Since $d\gamma/dx \approx -aR_b \sim \rho^2$, freezing is virtually complete in this region.

Figure 2 also shows that freezing occurs quite suddenly in this case, as the transition region (b) is small in comparison with regions (a) and (c). Physically, this is a consequence of the rapid decrease in the number of intermolecular collisions which results from the falling density. Also, the fraction of collisions that are effective in bringing about recombination is reduced as the gas passes through the nozzle. These observations have led to the introduction of the "sudden-freezing" approximation[3] which is described below.

Sudden-Freezing Analysis

In this method the transition region is shrunk to a point where the reaction is assumed suddenly to cease. Upstream of this point the infinite rate equilibrium solution is used while, downstream, the gas composition is frozen. The freezing point must be determined from an empirical criterion. In reference 3 this was chosen as the point at which the quantity B [Eq. (19)] was unity, but freezing was so sudden that the exact form of the criterion was not critical. Figures 2 and 3 show that the approximation gives reasonable agreement with numerical results.

Clearly, the best results will be obtained in applications involving large area-ratio nozzles, where the transition region can be a small part of the total flow. Also, freezing will be most rapid for three-body reactions, especially if the rate constant decreases as the temperature falls, and sudden freezing will be a good approximation in such cases. On the other hand, freezing will be much more gradual for two-body reactions and for reactions where the rate constant increases with falling temperature. In fact, Eschenroeder has shown[6] that, in extreme cases, it is not possible to define a sudden freezing point because the reaction continues at a significant rate throughout the nozzle.

A simple representation of the sudden freezing solution has been demonstrated by Bray[25] for a specified three-body recombination mechanism occurring in a given nozzle. If the sudden freezing points are plotted on a Mollier diagram for a wide variety of stagnation conditions, it is found that a single line can be drawn which accurately represents all the freezing points. It is then possible to make a Mollier diagram representation of the flow through a given nozzle, with equilibrium above this freezing line and constant composition below it. A diagram of this type is shown in Fig. 4[25] for air under conditions where

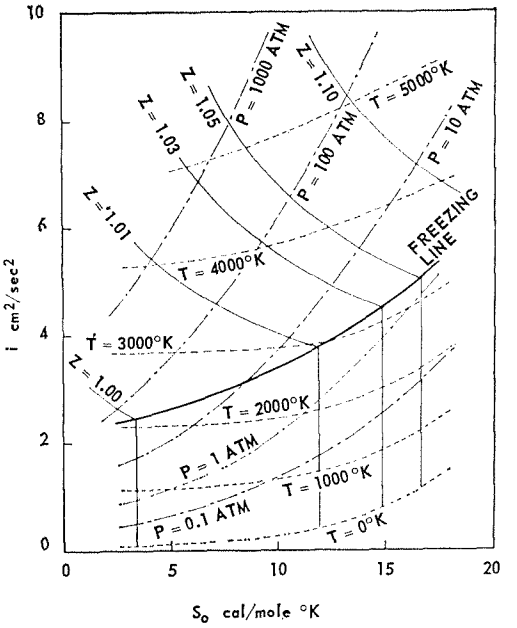

FIG. 4. Mollier-type diagram for air (from reference 25, using data from reference 26). The zero of entropy has been chosen arbitrarily.

oxygen recombination is the only significant process. The data for plotting Fig. 4 was taken from reference 26.

Another conclusion which may be drawn from simple nonequilibrium flow solutions[3] is the following. Many orders of magnitude in either recombination rate constant or in nozzle scale lie between solutions which approach the limiting cases of infinite rate equilibrium and frozen flow. Therefore, for many purposes, the recombination rate constant is not required with great accuracy. On the other hand, feasible increases in nozzle scale are not very effective in achieving equilibrium conditions. Because the recombination process involves three-body collisions, departures from equilibrium are very sensitive to the stagnation density or pressure, high pressure favoring equilibrium.

Many of the general conclusions obtained from single reaction flow systems apply also in cases where a set of coupled reactions are taking place. The rates of all chemical processes are reduced as the gas flows down the nozzle, because of the rapidly falling density. Particularly in large area-ratio, hypersonic nozzles, all processes may be expected to have effectively ceased before the nozzle exit where the density will be very low. This suggests that an extension of the sudden-freezing technique will apply in such cases. A method has been formulated by Bray and

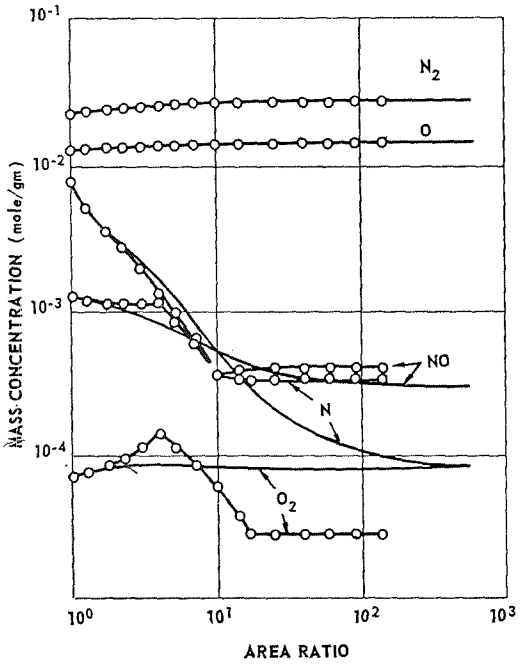

FIG. 5. Mass concentrations in moles per gram of mixture for air flow in a hypersonic nozzle: comparison of exact and sudden freezing solutions. $T_0 = 8000°K$; $p_0 = 100$ atmos; —— exact solution for finite rate nonequilibrium (from reference 5); O–O–O–O–O sudden freezing solution (from reference 27).

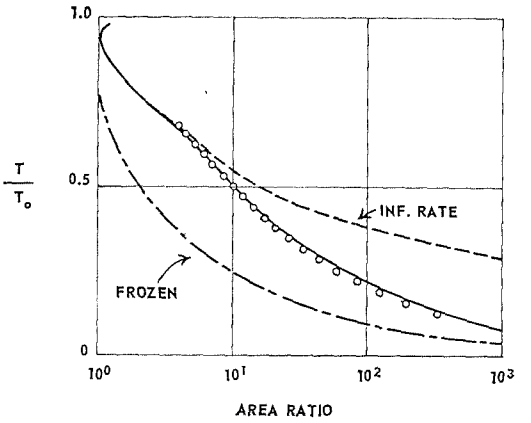

FIG. 6. Temperature distribution for air flow in a hypersonic nozzle: comparison of exact and sudden freezing solutions. $T_0 = 8000°K$, $p_0 = 100$ atmos; —— exact solution for finite rate nonequilibrium (from reference 5); O O O O O sudden freezing solution (from reference 27).

Appleton[18] in which each of the N reactions has its own sudden freezing point, is infinitely fast upstream of this point and ceases completely downstream. Examples have been worked out[27] by this technique for comparison with the exact numerical solutions of reference 5. For each reaction the sudden freezing point was determined from the empirical criterion used in reference 3, namely: $B^r = 1$ at the freezing point for the rth reaction.

Figure 5 shows concentrations computed by this method for the same air flow as that illustrated in Fig. 1. The three-body recombination reactions [Eqs. (20–22)] freeze first, while the exchange reactions (23, 24) remain in equilibrium until further downstream. The concentrations are not predicted as accurately as in the one-reaction case,[3] because reactions (23) and (24) involve two-body collisions. These reactions depart from equilibrium quite slowly because their rate is proportional to ρ instead of ρ^2. Better results could have been obtained using a freezing criterion: B^r = constant < 1 at the freezing points for these reactions. However, the concentrations have been predicted sufficiently accurately to determine the coupling between flow and chemistry, and accurate values of overall flow quantities are obtained. Figure 6 gives the temperature distribution calculated in this way.

Simple solutions such as the one described above, in which only algebraic equations are involved, do not compete with full numerical solutions such as those of reference 5. However, there are many cases in which the accuracy of the kinetic data at present available does not justify a full solution. In such cases, the approximate method may give results whose accuracy is limited by the kinetic data rather than by the analytical technique.

Vibrational Relaxation

The major uncertainty here is the degree of coupling between the rates of chemical and vibrational relaxation, as discussed in the section on Formulation of the Problem. Fortunately, the fraction of energy involved in vibration is not large, and for many purposes vibrational relaxation can probably be neglected.[23]

Numerical solutions by Lick and Li[28] and by Stollery[29] in which chemical relaxation effects are not included, and by Musgrove and Appleton[30] in which both chemical and vibrational rates are included but not coupled, all show that large deviations from vibrational equilibrium can occur under favorable circumstances. If vibrational energy is a small fraction of the stagnation enthalpy, the effect can be treated as a small perturbation on a previously determined flow.

A typical computed result is included in Fig. 3 from reference 20. It will be seen that relaxation can lead to an effective temperature for vibration, T_v, considerably in excess of the translational temperature. This could be important if the spectral line reversal technique[31] is used to measure temperature in an expanding flow, as this method tends to follow the vibrational temperature. The falling temperature and the falling pressure, as the gas passes through the nozzle, both tend to increase the vibrational relaxation time τ_v, so vibrational freezing occurs rapidly. For large area-ratio nozzles a sudden freezing approximation will represent T_v very well.

Electrons and Ions in Nozzle Flows

Most of the conclusions which have been drawn above apply also to reactions between charged particles, as these obey rate equations similar to those describing other reactions.

Eschenroeder[6] has studied electron–ion recombination in high temperature air flowing through a wind tunnel nozzle, and has also considered the effect of seeding the air with cesium. He concludes that, under some conditions, many parallel recombination mechanisms can be of comparable importance, but that for typical air operation of a hypersonic wind tunnel, the single reaction

$$NO^+ + e \rightarrow N + O \qquad (25)$$

will predominate. Departure from equilibrium is predicted to be gradual, and the reaction has not ceased at large downstream distances, so the sudden freezing approximation is not accurate. This arises because of the two-body mechanism, together with the assumed $T^{-\frac{3}{2}}$ temperature dependence of the rate constant, which keeps the recombination rate high in the expanded cold air. Eschenroeder introduces a modified sudden-freezing approximation employing an asymptotic form of the recombination rate expression in order to allow for this effect.

Bray and Wilson[16,32] have considered the flow of highly ionized argon through a hypersonic nozzle. The recombination mechanism which they assume is the inverse of the ionization process studied theoretically and experimentally by Petschek and Byron.[33] Recombination is assumed to take place via the first excited state of the atoms, leading to a recombination rate which increases exponentially as the electron temperature decreases. Electrons are assumed to act as third bodies in the recombination process, and the electron temperature is determined from a balance between energy gained in this manner and energy lost in elastic collisions with ions. Results indicate a gradual departure from equilibrium and no sudden freezing, because of the exponential temperature dependence of the rate constant. Electron temperatures are predicted which are considerably in excess of the temperature of atoms and ions.

In both of these examples departure from equilibrium is gradual and no sudden freezing occurs. This will be the case if two-body mechanisms and mechanisms with a large inverse temperature dependence predominate for the removal of electrons. If recombination occurs through a three-body reaction such as the Thomson mechanism, then freezing will be sudden.

Experimental Results

In this section some relevant experimental work is reviewed very briefly, with the objective of showing up areas where further experiments are required. Two types of experiment may be distinguished: those which study simple chemical systems in order to collect fundamental kinetic data and check relaxing flow theories, and experiments to determine departures from equilibrium in complex reacting mixtures for practical applications. No mention will be made here of the large amount of data that has been collected from experiments behind shock waves in conventional shock tubes, as this work has been reviewed elsewhere.[11,13,34]

The classical experiments of Wegener[35] on nozzle flows in which a reacting mixture of NO_2 and N_2O_4 was carried in inert N_2, have demonstrated the close agreement existing between relaxing gas flow theory and experiment in cases where the chemical kinetics is well understood. Wegener detected departures from equilibrium by means of light absorption and also from static pressure measurements. Results were in good agreement with numerical calculations, and departure from equilibrium was found to correlate with Eq. (19). A further series of experiments[36] confirmed the theoretical prediction[19] that weak waves in a reacting gas mixture propagate at the frozen sound speed.

A recent paper by Wilson[37] describes results of experiments to measure the recombination rate of oxygen. A small supersonic nozzle was set up in a shock tube. The oxygen, mixed with argon, was partly dissociated by the primary shock wave and the supersonic flow behind the shock wave passed through the nozzle. Oxygen molecule concentrations downstream of the nozzle were monitored by ultraviolet light absorption. Wilson deduces a value of the recombination rate

constant which is compatible, within the scatter of his data, with values calculated from the dissociation rate constant and the equilibrium constant, via Eq. (4).

An interesting technique for measuring temperature in a supersonic flow has been developed at the University of Toronto, and reported by Muntz.[38] A narrow beam of electrons is passed through a supersonic stream of nitrogen in the nozzle of an arc-heated wind tunnel. The path of the electron beam is luminous, and spectroscopic measurements on the emitted light yield the rotational and vibrational temperatures of the nitrogen. Muntz reports a rotational temperature of 890°K and a vibrational temperature of 1020°K at the nozzle center line where the Mach number was about 1.8. The experiment thus provides direct evidence of vibrational temperature lag in a nozzle.

The three experiments described above illustrate the close agreement that can be obtained between relaxing gas theory and experiment for simple reacting mixtures. They also show that nozzle flows are capable of providing valuable kinetic data on elementary reactions under conditions of practical interest. Much more work is needed along these lines in order to develop measuring techniques and to produce the necessary data.

Four more experiments, dealing with complex reacting mixtures, will be described briefly below. The first published experimental data on chemical relaxation in air during nozzle expansion is due to Nagamatsu *et al.*[39] Departures from equilibrium were detected from static pressure measurements on the nozzle wall. Hall *et al.*[23] have used the computer program mentioned above to calculate the static pressure under the conditions of these experiments for two typical cases. They found that, if they applied a suitable boundary layer correction to the theoretical results, these agreed with experimental pressures to within 8.6% and 1.5% for the two cases. The difference between equilibrium and frozen flow pressures is much greater than this.

It is worth noting that, according to the calculations,[23] oxygen recombination was the only energetically significant process occurring under the conditions of the experiments. Nitrogen dissociation was negligible, and the role of the nitric oxide exchange reactions [Eqs. (23) and (24)] in recombining nitrogen atoms was not therefore tested in comparing theory with experiment.

Preliminary results of microwave interferometer measurements of electron densities in the nozzle of a shock tunnel have recently been reported by Eschenroeder *et al.*[40] The results were in excellent agreement with theoretical predictions[6] in which the dissociative recombination rate constant for NO^+ [Eq. (25)] was obtained from Lin's ionization rate constant[41] for the inverse of Eq. (25). As the departure from equilibrium of neutral species concentrations was propably not large at the measuring station, the effect of coupled chemical reactions was again not tested critically in these experiments.

Nozzle experiments involving combustion products have been reported by Lezberg and Lancashire[42] and Lewis and Harrison.[43] The former authors used static pressure measurements and line reversal temperatures to study recombination in hydrogen-air combustion products. They carried out a sudden-freezing analysis assuming an overall reaction between hydrogen and oxygen, and predicted a sudden freezing point just downstream of the nozzle throat. Calculations assuming the flow to be frozen downstream of this point gave results which were generally in reasonable agreement with measured temperatures and pressures. Lewis and Harrison[43] used a gas sampling technique to study the combustion and recombination reactions occurring during the nozzle expansion process of a liquid propellant rocket engine. In this technique, the gas sample must be expanded rapidly, so that further reactions do not occur behind the shock waves which must exist when the supersonic flow is brought to rest in the probe. Reactions on the probe walls must also be avoided. Results indicated departures from equilibrium within the nozzle.

None of the above experiments has satisfactorily tested theoretical predictions under conditions where coupled chemical reactions are expected to play a dominant role. Further experimental work is urgently required.

Concluding Remarks

The following points seem to be worth emphasizing.

(a) Steady, quasi-one-dimensional nozzle flow equations can easily be formulated to take account of an arbitrarily complex system of coupled chemical reactions, ionization mechanisms, and internal energy relaxation processes. If rates are specified for all the processes to be considered then these equations can be solved on existing high-speed computers.[5,6,21,22] The quasi-one-dimensional flow approximation is adequate, except possibly in cases where very nonuniform flow exists upstream of the nozzle, or where very thick boundary layers form on the nozzle walls.

(b) Presently available chemical kinetic and

relaxation rate data is inadequate for many purposes. Further information is needed on the temperature dependence of recombination rate constants, and on the coupling between simultaneous relaxation processes, as well as data on mechanisms and rates in combustion products. Experimental data[11,37,40] has not contradicted the much used equation:

$$K = k_f/k_b,$$

but further work is needed on this subject.

(c) In view of the uncertainty of much of the available kinetic data, there are many applications where a full numerical solution of the problem may not be justified. In such cases, a simple sudden freezing analysis, either with a single freezing point[3,24,26,44] or with a separate freezing point for each reaction,[27] may yield results whose accuracy is limited by the kinetic data rather than by the method of analysis.

(d) Further experimental work is urgently required. Nozzle experiments on simple mixtures can yield much of the basic physicochemical data which is needed for practical applications. Experiments on more realistic flows are also required in order to check theoretical predictions concerning the effects of coupled chemical reactions.

Much effort is now being invested in these problems and knowledge is likely to increase rapidly.

References

1. Dugger, G. L.: Comparison of hypersonic ramjet engines with subsonic and supersonic combustion, in *Combustion and Propulsion—Fourth AGARD Colloquium* (Rothrock, Jaumotte, and Lefebvre, eds.), Pergamon, 1961.
2. Olsen, W. T.: Recombination and condensation in nozzles, Paper delivered at 2nd Int. Congress on Aero. Science, Zurich, 1960. *Advances in Aeronautical Sciences*, Vol. 4, p. 849. Pergamon, 1962.
3. Bray, K. N. C.: J. Fluid Mech. *6*, 1 (1959).
4. Heims, S. P.: Effect of oxygen recombination on one-dimensional flow at high Mach numbers, NACA TN 4144, 1958.
5. Eschenroeder, A. Q., Boyer, D. W., and Hall, J. G.: Exact solutions for non-equilibrium expansions of air with coupled chemical reactions, Cornell Aero. Lab. Rep. No. AF–1413–A–1, 1961.
6. Eschenroeder, A. Q.: ARS Journal *32*, 196 (1962).
7. Vaglio-Laurin, R. and Bloom, M. H.: Chemical effects in external hypersonic flows, in *Hypersonic Flow Research* (Riddell, ed.). Academic Press, 1962.
8. Appleton, J. P.: *The Structure of a Prandtl–Meyer expansion fan in an ideal dissociating gas*, Univ. of Southampton Report, U.S.A.A. 146, 1960.
9. Landau, L. and Teller, E.: Phys. Z. Sovjetunion *10*, 34 (1936).
10. Morris, J. F.: Physico-chemical reactions during nozzle flow, in *The Chemistry of Propellants* (Penner and Ducarme, eds.). Pergamon, 1960.
11. Ferri, A. (ed.): Fundamental Data obtained from Shock-tube Experiments, AGARDograph No. 41. Pergamon, 1961.
12. Lipscomb, F. J., Norrish, R. G. W., and Thrush, B. A.: Proc. Roy. Soc. (London) *A233*, 455 (1955–56).
13. Bauer, S. H.: Chemical Kinetics: A general introduction, in *Hypersonic Flow Research* (Riddell, ed.). Academic Press, 1962.
14. Lin, S. C., and Fyfe, W. I.: Phys. Fluids *4*, 238 (1961).
15. Clayden, W. A.: Recent research in the ARDE low density wind tunnel with a plasma jet heater in *Rarefied Gas Dynamics* (Talbot. ed.). Academic Press, 1961.
16. Bray, K. N. C.: Electron-ion recombination in Argon flowing through a supersonic nozzle, paper read at AGARD Meeting High Temperature aspects of hypersonic flow, Brussels, 1962. To be published by Pergamon Press. Also Univ. of Southampton Report A.A.S.U. No. 213, 1962.
17. Penner, S. S.: *Chemistry Problems in Jet Propulsion*. Pergamon, 1957.
18. Bray, K. N. C., and Appleton, J. P.: Atomic recombination in nozzles: Methods of analysis for flows with complicated chemistry, Univ. of Southampton Reports A.A.S.U. 166 and 178, 1961. Also Aero. Research Council Current Paper (to be published).
19. Chu, B. T.: Wave propagation in a reacting mixture, *1958 Heat Transfer and Fluid Mechanics Institute*. Stanford Univ. Press, 1958.
20. Appleton, J. P.: On the maintenance of chemical equilibrium during the expansion of reacting gas mixtures. The optimum nozzle design, Univ of Southampton Report A.A.S.U. 216, 1962. Also Proc. 2nd Rocket Symp., Col. of Aeronautics, April 1962.
21. Vincenti, W. G.: Calculations of the one-dimensional non-equilibrium flow of air through a hypersonic nozzle—interim report, Stanford University Report: Sudaer No. 101, 1961.
22. Momtchiloff, I. N., Taback, E. D., and Buswell, R. F.: This volume, p. 220.
23. Hall, J. G., Eschenroeder, A. Q., and Marrone, P. V.: Inviscid hypersonic airflows with coupled non-equilibrium processes, paper

presented at IAS 30th Annual Meeting, New York, Jan. 1962, IAS Paper No. 62–67.
24. Hall, J. G., and Russo, A. L.: Studies in chemical non-equilibrium in hypersonic nozzle flows, Cornell Aero. Lab. Report No. AD–1118–A–6, 1959.
25. Bray, K. N. C.: ARS Journal *31*, 831 (1961).
26. Boyer, D. W., Eschenroeder, A. Q., and Russo, A. L.: Approximate solutions for non-equilibrium airflow in hypersonic nozzles, Cornell Aero. Lab. Rep. No. AD–1345–W–3, 1960.
27. Bray, K. N. C.: Unpublished work.
28. Lick, W. J., and Li, T. Y.: Vibrational relaxation phenomena in a shock tunnel, Rensselaer Poly. Inst. TR AE 5704 (AFOSR TN–57–346, AD 132–419), 1957.
29. Stollery, J. L.: Nature *190*, 778 (1961).
30. Musgrove, P. J., and Appleton, J. P.: On molecular vibrational relaxation in the flow of a chemically reacting gas, Univ. of Southampton Report A.A.S.U. 183, 1961.
31. Clouston, J. G., Gaydon, A. G., and Glass, I. I.: Proc. Roy. Soc. (London) *A248*, 429 (1958).
32. Bray, K. N. C., and Wilson, J. A.: A preliminary study of ionic recombination of argon in wind tunnel nozzles, Univ. of Southampton reports U.S.A.A. 134 and A.A.S.U. 185, 1961. Also Aero. Research Council Current Papers (To be published).
33. Petschek, H., and Byron, S.: Ann. Phys. *1*, 270 (1957).
34. Wray, K. L.: Chemical kinetics of high temperature air, in *Hypersonic Flow Research* (Riddell, ed.). Academic Press, 1962.
35. Wegener, P. P.: ARS Journal *30*, 322 (1960).
36. Wegener, P. P.: A review of investigations of stationary supersonic nozzle flow with a reacting gas mixture, in *Combustion and Propulsion—Fourth AGARD Colloquium* (Rothrock, Jaumotte, and Lefebvre, eds.). Pergamon, 1961.
37. Wilson, J.: A measurement of the recombination rate of oxygen, paper presented at AGARD meeting High temperature aspects of hypersonic flow, Brussels, 1962. Pergamon, to be published.
38. Muntz, E. P.: Phys. Fluids *5*, 80 (1962).
39. Nagamatsu, H. T., Workman, J. B., and Sheer, R. E.: J. Aerospace Sciences *28*, 833 (1961).
40. Eschenroeder, A. Q., Daiber, J. W., Golian, T. C., and Hertzberg, A.: Shock tunnel studies of high-enthalpy ionized airflows, Paper presented at AGARD Meeting High temperature aspects of hypersonic flow, Brussels, 1962. Pergamon, to be published.
41. Lin, S. C., Neal, R. A., and Fyfe, W. I.: Rate of ionization behind shock waves in air, experimental results, Avco-Everett RR 105 (AFBMD TR–60–216), 1960.
42. Lezberg, E. A., and Lancashire, R. B.: Recombination of hydrogen–air combustion products in an exhaust nozzle, NASA TN D–1052, 1961.
43. Lewis, J. D., and Harrison, D.: A study of combustion and recombination reactions during the nozzle expansion process of a liquid propellant rocket engine, *Eighth Symposium (International) on Combustion*. Williams and Wilkins, 1962.
44. Yoshikawa, K. K., and Katzen, E. D.: Charts for air flow properties in equilibrium and frozen flows in hypervelocity nozzles, NACA TN D–693, 1961.

Discussion

Prof. Sidney W. Benson (*University of Southern California*): I don't see how one can ignore the details of the vibrational relaxation process when the initial conditions of the expansion usually prescribe very large quantities of atoms. These atoms form molecules (during recombination) in very high vibrational levels and one has to permit the decay of these very highly excited species or the recombination rate is itself affected. At the higher temperatures with large concentrations of atoms we have results which indicate that collisions of atoms with molecules are extremely efficient in relaxing vibrational energy. Because of this result, I would be in favor of assuming very rapid vibrational relaxations in systems with appreciable atom concentrations.

Prof. S. H. Bauer (*Cornell University*): Prof. Benson called attention to an important point. It is essential to introduce a coupling term between vibrational relaxation and dissociation. Failure to do so has led, in the past, to strange conclusions. For the temperature distribution in a normal shock such an omission resulted in a computed vibrational temperature which overshot that calculated for translation during the latter stages of the relaxation process. When a coupling term was introduced in

the machine program by Dr. C. E. Treanor (CAL) such a strange situation was no longer predicted.

Not only are the vibrational excitations coupled to dissociation but they are also coupled to a variety of scrambling reactions. Those which involve the oxides of nitrogen are clearly important at temperatures below 2500°K. In a forthcoming paper we have estimated half-times for scrambling reactions which are of importance at higher temperatures. These are best illustrated, but not limited to cases where isotopic labels are present:

$$O_2^{16}(v, \text{exc}) + O_2^{18}(v, \text{eq}) \rightleftharpoons 2O^{16}O^{18}(v, \text{relax}).$$

Any such atom switching process strongly couples vibrations to translations and serves as a highly effective path for vibrational relaxation. The above reaction has an estimated activation energy of 70 kcal, compared to 118 kcal required for dissociation. In computational programs such reactions must be specifically inserted; otherwise one is led to the conclusion that vibrational disequilibrium is maintained for too long a time.

Prof. K. N. C. Bray (*University of Southampton*): I fully agree with the comments made by Prof. Benson and Prof. Bauer and, in fact, I drew attention to the likelihood of coupling between chemical processes and vibrational relaxation in the written version of my paper. However, to the best of my knowledge, there is not yet sufficiently accurate information available to enable one to include such coupling effects in a machine program with any degree of confidence. It is not obvious to me that existing theories[1] for coupling dissociation and vibration rates are appropriate in the present context.

Dr. A. Q. Eschenroeder (*Cornell Aeronautical Laboratory*): First, I would like to congratulate Professor Bray for his very valuable documentation of not only the previous contributions, but also of the significant problem areas involved in carrying out the analyses. This should serve as an excellent paper for the newcomer to the field to gain insight into the problems and the methodology.

Second, in answer to Professor Bray's question regarding the existence of specific experimental results in the regime of coupled rate chemistry, I wish to describe some recent experimental work at the Cornell Aeronautical Lab. John Daiber is measuring electron densities and collision frequencies in a parallel flow portion of the 6-foot hypersonic shock tunnel nozzle. Since the presentation of the AGARD paper[2] we have obtained many more data for airflows over a range of 3500°K to something exceeding 7000°K reservoir temperature. Since the reservoir pressure range is from about 50 to 500 atmospheres, the measurements extend into a region of significant coupling involving N atoms and NO molecules. Chemical freezing occurs well upstream from the microwave test station while the deionization continues to follow a descending nonequilibrium trend. Because the rate constant for the $NO^+ + e^- \rightarrow N + O$ is least certain of all the values, the computing machine code described in reference 5 of the paper has been used to determine what value of this rate gives the best agreement with observations. Although final data reduction is incomplete, the results indicate that the rate constant giving best agreement is of the same order of magnitude as that deduced from the work of Lin *et al.* which was determined by an entirely different technique. The reporting of an actual rate value based on our measurements awaits a careful assessment of possible impurities effects.

Prof. K. N. C. Bray: I was very interested to hear about the experiments described by Dr. Eschenroeder, which provide much-needed evidence that the theoretical work on this problem is consistent with what actually happens.

Prof. P. Wegener (*Yale University*): We wish to give Dr. Rosner the opportunity to present some remarks at this time.

Dr. Daniel E. Rosner (*AeroChem Research Laboratories*): One may wish to pass to the limit of maximum simplicity in nonequilibrium flow problems because the corresponding results exhibit very useful similitude properties, i.e., an extremely large amount of information can be compressed onto a single piece of graph paper. In the course of a recent parametric study of the feasibility of magneto-hydrodynamic thrust vectoring of rocket motors[3] it was found that an accurate and compact representation of the rocket nozzle ionization problem was made possible by invoking a method equivalent to that first proposed by Smith.[4] The problem treated[5] is that in which small amounts of a single impurity or seed material present in the chamber, c, lead to an electron concentration n_e which decays within the nozzle but which may depart from equilibrium by a considerable amount at the nozzle exit section due to the rapidity of the expansion process.[4] In the nonequilibrium regime [i.e., where $n_e \gg (n_e)_{eq}$] a closed form asymptotic solution is readily obtainable. It can further be shown that the $n_e(x)$ distribution obtained by patching together the equilibrium solution and the appropriate asymptotic solution at their common point of tangency constitutes a maximum lower bound to the exact solution.

For a prescribed family of nozzles this allowed a single logarithmic plot to be made of the normalized local dc conductivity, σ/σ_e versus pressure ratio P_e/P, showing the various loci of "match" tangency points for fixed values of a nondimensional recom-

bination rate parameter. This fundamental scaling parameter is simply the ratio of the characteristic "flow" time D_t/c^* for the rocket, to the electron half-life in the chamber (where D_t is the throat diameter and c^* the characteristic velocity of the propellant). Using this plot one can immediately locate the match point conditions for a given electron–ion recombination mechanism and θ/T_c (ratio of characteristic ionization temperature to chamber temperature). This information, coupled with the asymptotic relation, allows a very rapid calculation of the remainder of the dc conductivity (or electron number density) curve. In practice this is further facilitated by providing certain tabulated functions of Mach number and γ alone, which appear in the asymptotic solution. Because of the universal character of these plots and functions they parallel the usual plots of thrust coefficient and related design parameters for constant γ isentropic nozzle expansions. As in the latter case, accurate results can be obtained in this way, and perhaps more important, the dominant trends are immediately perceived. Having generated just a few illustrative plots and tables of this type[3,5] on a desk calculator, one cannot help but feel that electronic computers would be useful here, too. The results generated are, of course, approximate, but so are the well subtabulated, constant γ, isentropic flow tables, the existence of which has been a blessing for some time now. In short, it seems to me that in the rush to generate very realistic results with virtually no generality, simple but useful nonequilibrium problems (which would require an insignificant amount of machine time) have been passed by. If carefully calculated and properly displayed this body of results would constitute a valuable addition to the literature.

DR. A. Q. ESCHENROEDER: An interesting feature of the dc conductivity profiles calculated by Dr. Bray is their reversal in slope. One of the promising applications which occurred to us when we noticed this reversal[6] was the use of a supersonic nozzle to supply a magnetohydrodynamic generator duct. This application had been rejected in the past on the grounds of insufficient equilibrium dc conductivities. The possible benefits are at least twofold: (1) Having converted a larger fraction of the internal energy of the working substance to directed kinetic energy, one can hope to remove a larger fraction of the total enthalpy in the form of electrical energy; and (2) the low static pressures which are possible with this mode of operation help alleviate the electrode heat transfer problems. The Parsons Company/Nuclear Research Centre at Newcastle-upon-Tyne is carrying out experimental evaluations of this application using cesium-seeded helium flows. The work there is under the direction of Dr. B. C. Lindley.

REFERENCES

1. HAMMERLING, P., TEARE, J. D., and KIVEL, B.: Phys. Fluids *2*, 422 (1959).
2. ESCHENROEDER, A. Q., DAIBER, J. W., GOLIAN, T. C., and HERTZBERG, A.: Shock Tunnel Studies of High Enthalpy Ionized Airflows, AGARD Specialist Meeting High Temperature Aspects of Hypersonic Flow, April 1962. To be published.
3. ROSNER, D. E.: AeroChem. TN–41, February 1962.
4. SMITH, F. T.: *Seventh Symposium (International) on Combustion*, pp. 93–97. Butterworths, 1959.
5. ROSNER, D. E.: AeroChem. TP–41, February 1962; ARS Journal *32*, 1602 (1962).
6. ESCHENROEDER, A. Q.: ARS Journal *32*, 196 (1962).

COMPLEX CHEMICAL KINETICS IN SUPERSONIC NOZZLE FLOW

A. A. WESTENBERG AND S. FAVIN

The subject to be discussed is that in which many elementary chemical reactions occur simultaneously in a gas undergoing laminar, steady, adiabatic flow through a supersonic expanzion nozzle. Some general comments on the techniques involved in the numerical analysis of this type of nonequilibrium flow with a high-speed digital computer will be given, but the emphasis throughout is on the chemical kinetic aspects of the problem. All internal degrees of freedom of the molecules are assumed to be in equilibrium with the local translational temperature everywhere. The flow is taken to be one dimensional in the usual fluid dynamic sense.

The interaction between chemical and fluid dynamic variables is illustrated by actual results on two types of mixtures. The first is characteristic of many ordinary solid or liquid rocket propellant exhaust gases and contains the species H_2, H_2O, CO, CO_2, H, and OH. The reasons for assuming that these take part in four elementary (reversible) reactions of importance are given. The second example considers a mixture containing the active species H_2, H_2O, O_2, H, OH, and O such as would be involved in a hydrogen-fueled ramjet, where eight elementary reactions are used. The relative significance of two-body and three-body reactions in influencing the gas composition and other flow variables is discussed. Some indication of the sensitivity of the results to the magnitudes assumed for the rate constants will be given. The degree of utility and validity of various popular approximations in this field is assessed, and some practical implications pointed out.

Introduction

The problem of calculating the flow of a chemically reacting gas through a supersonic nozzle has occupied the attention of a number of investigators in recent years. More than a decade has passed since the pioneer work of Penner[1] and Krieger[2] in this field. Later research by Wegener[3] was noteworthy in that it was the first to combine theory with a careful experimental program. The theoretical studies of Bray[4] and of Hall and Russo[5] added greatly to our knowledge of the details of such chemically reacting flow processes. All of the foregoing work was concerned with the simplest practical case, namely a flow in which a single reaction (generally of the atom recombination–molecule dissociation type) takes place. The general picture which emerged from these studies of such a flow expanding through a supersonic nozzle is that the mixture tends to follow more or less the composition characteristic of equilibrium at the local temperature and pressure until the reactions involved can no longer keep up even approximately with the rate of change of these variables. The gas then rapidly freezes to a fixed composition for the remainder of the flow.

Most real propellant and wind tunnel gas mixtures are more complicated than this insofar as their chemistry is concerned. With several chemical species present, there is the probability that several elementary reactions will occur to an appreciable extent. The qualitative and quantitative uncertainties surrounding the chemical kinetics in such cases, as well as the rather formidable numerical task of solving these complex flow problems, have meant that there has been relatively little work done on them until recently. Wider access to modern high-speed computers—a necessary tool in the thorough study of complex kinetic processes—has led to some progress in this field. Some calculations by Vincenti,[6] Eschenroeder, Boyer, and Hall,[7] and Westenberg and Favin,[8] have appeared, while Bray and Appleton[9] have discussed some general aspects of flows with complex chemistry. Other authors in this symposium have also attacked the problem, so that the field is opening up rapidly.

The present paper contains some remarks on the technique, its significance, and the limitations of complex kinetic flow computations, illustrated by actual results for a typical rocket exhaust and that of a possible hypersonic ramjet utilizing hydrogen as fuel.

Fundamentals

The basic assumptions we shall make for the calculations are that the flow is laminar, steady,

adiabatic, and one dimensional (in the usual fluid dynamic sense), and that effects due to diffusion, thermal conduction, viscosity, and external forces are negligible. These conditions are practically always assumed in studies of this kind. The first condition—that of laminarity of the flow—deserves some special comment, since it is not always stated explicitly and yet is an important restriction. It is a *necessary* restriction at the present time because we shall be using basic chemical kinetic data and concepts which are valid for molecular processes, and the latter are directly applicable only when the flow is laminar. If turbulence exists in the flow, as would be the case in many practical supersonic nozzles, the proper way to incorporate chemical kinetics into the problem remains essentially unknown. It is the perennial "turbulent flame" problem which, at least as far as the writers are concerned, is an entirely unsolved one, despite considerable attention at these Symposia over the years. Thus one should not forget to exercise some healthy skepticism toward reacting flow calculations when the turbulence complication exists.

In addition, we shall make another fundamental assumption, namely, that the internal degrees of freedom of the molecules present are in equilibrium with the local temperature at all times. If we compare first the transit time through the nozzle with rotational and vibrational relaxation times, the equilibrium assumption is questionable only for the latter. The effect of vibrational nonequilibrium can be included in the analysis[6] but is generally small in any case, and since the focus in this paper is more on chemical effects the above assumption is made. The influence of chemical reaction in disturbing local equilibrium of internal degrees of freedom is a much more difficult situation, and represents a basic, important problem in chemical kinetics at the present time. Since we have assumed such equilibrium, however, this implies that we may relate forward and reverse rate constants of a given elementary reaction by its equilibrium constant, as we shall see. Since there is usually experimental information on only one of the rate constants (if there is any at all), this relation is important.

Consider the gas to be composed of N chemical species each present at a concentration F_i (moles per unit mass of mixture). The usual flow variables are temperature T, density ρ, pressure P, and velocity v, making a total of $N + 4$ dependent variables. The axial distance z along the flow direction is the independent variable, and the cross-sectional area ratio A (relative to some reference—usually the minimum area) of the nozzle is assumed given as a function of z. The mass flow rate W per unit reference area is also assumed to have been chosen. Then the basic equations governing the flow are, first of all, the four fluid dynamic relations (summation over i means $i = 1, 2, \cdots, N$):

$$\rho v\, dv/dz + dP/dz = 0 \quad \text{(momentum)} \tag{1}$$

$$\sum_i [F_i\, dH_i/dz + H_i\, dF_i/dz] + (v/J)\, dv/dz = 0 \quad \text{(energy)} \tag{2}$$

$$\rho = P/(RT \sum_i F_i) \quad \text{(state)} \tag{3}$$

$$W = \rho v A \quad \text{(over-all continuity)} \tag{4}$$

where the H_i are absolute molar enthalpies. If there are L chemical elements represented in the mixture, and the number of atoms of an element e in a molecule of species i is called n_{ei}, there will be L element conservation equations of the form

$$\sum_i n_{ei} F_i = \text{Constant} \quad (e = 1, 2, \cdots, L) \tag{5}$$

To complete the necessary number of equations for the number of unknowns, $N + 4$, there will then be required $N - L$ species continuity relations of the form

$$dF_i/dz = (A/W) r_i \quad (i = 1, 2, \cdots, N - L) \tag{6}$$

where r_i is the net rate (moles per unit volume per unit time) of change in the concentration of species i due to all the chemical reactions in which it takes part. These equations introduce the chemical kinetics into the problem. The r_i will involve various concentration variables F_i, the density, and the temperature through the kinetic rate constants, as specific examples will show later.

The $N + 4$ equations, Eqs. (1)–(6), may easily be reduced to $N + 2$ equations by eliminating P and v as variables. Making use of the fact that for ideal gases the enthalpy H_i is a function only of T, so that $dH_i/dz = (dH_i/dT)(dT/dz) = C_i\,(dT/dz)$, where C_i is the molar heat capacity at constant pressure, it may be shown[8] that

$$dT/dz = \frac{J[(R\sum_i F_i)^{-1} - T\rho^2 A^2 W^{-2}] \sum_i H_i (dF_i/dz) + T[A^{-1}(dA/dz) - (\sum_i F_i)^{-1} \sum_i (dF_i/dz)]}{1 - J[(R\sum_i F_i)^{-1} - T\rho^2 A^2 W^{-2}] \sum_i F_i C_i} \tag{7}$$

and

$$d\rho/dz = \rho^3 A^2 W^{-2} \left\{ \frac{(dT/dz) - T[A^{-1}(dA/dz) - (\sum_i F_i)^{-1} \sum_i (dF_i/dz)]}{(R\sum_i F_i)^{-1} - T\rho^2 A^2 W^{-2}} \right\} - (\rho/A)\, dA/dz \tag{8}$$

Thus, for numerical solution, the equations are (5), (6), (7), and (8) for the $N + 2$ variables T, ρ, and the F_i.

Numerical Techniques

Solutions to actual problems in this work were obtained on an IBM–7090 computer. With all quantities known at some starting point $z = 0$, the machine was programmed to calculate the derivatives in Eqs. (6), (7), and (8). The derivatives were then fed to an available integration routine (IBM Share No. 602) for simultaneous, first-order differential equations which had a variable step-size feature for automatically doubling or halving the interval to satisfy a chosen precision index.

There are various practical aspects of a numerical nonequilibrium flow calculation which deserve some comment. Since it is usually assumed that the starting point is one where a state of chemical equilibrium exists, the static temperature, static pressure, and chemical composition are specified initially. The only remaining quantity to be established before proceeding with a numerical solution is the mass flow parameter W. How this is done depends on whether the solution is begun upstream of the throat of a convergent-divergent nozzle, or at the inlet to a divergent section with the flow assumed to be initially supersonic. In the former case, there is only one value of W which is allowed, i.e., which will give a monotonic decrease in temperature and density throughout the nozzle. This unique W for specified geometry, chemical kinetic behavior, and inlet conditions must be found by iteration until the solution satisfies the condition that the frozen Mach number is unity at a point somewhat downstream of the throat.[4] When the solution is begun supersonically at the entrance to a divergent section only, any supersonic value of W will allow a solution and no iteration is necessary. The examples to be reported here were done in this way, since most of the chemical interest is in the divergent portion of a nozzle anyway.

Starting a numerical solution from a state of equilibrium may give some trouble on occasion. This is because the dF_i/dz from Eq. (6) are (strictly, at least) zeros obtained from the differences of large numbers—the forward and reverse rates of the various elementary reactions—which tends to make the first few integration steps quite sensitive to truncation errors, etc. Formal perturbation schemes to solve this problem have been amply described in the literature.[5,6] The same thing can be accomplished in a less formal way by empirically adjusting the initial F_i slightly from their equilibrium values to make the derivatives approximately correct, since the subsequent solution is negligibly altered by small initial perturbations.[8] Actually, as a practical matter, smooth solutions were easily attainable simply by using directly the equilibrium initial conditions obtained from a separate, standard program[10] (which never gave exactly zero dF_i/dz to eight significant figures). After a negligibly small initial region (typically <0.05 cm) where the solution "found itself," the integration proceeded smoothly with no trouble.

A Carbon–Hydrogen–Oxygen Example

Many common solid propellants, or fuel-rich liquid hydrocarbon– oxygen systems, have an exhaust gas containing the stable species CO, CO_2, H_2, and H_2O, as well as various unstable atoms and radicals. The case chosen for study had the elemental mass fractions carbon = 0.25, hydrogen = 0.1, oxygen = 0.65, with static pressure and temperature at the inlet of a divergent section of $P_0 = 40$ atm, $T_0 = 3000°$K. A thermodynamic equilibrium calculation of the gas composition under these conditions yielded the following F_i values:

$$(F_{CO})_0 = 1.9254 \times 10^{-2};$$

$$(F_{CO_2})_0 = 1.5608 \times 10^{-3}$$

$$(F_{H_2})_0 = 3.0870 \times 10^{-2};$$

$$(F_{H_2O})_0 = 1.0841 \times 10^{-2}$$

$$(F_H)_0 = 1.1739 \times 10^{-3};$$

$$(F_{OH})_0 = 2.0817 \times 10^{-4}.$$

The only other species present in calculable amounts were O and O_2 which were two and three orders of magnitude, respectively, below OH, and were ignored. (Justification for this is given later.)

The elementary reactions which are likely to occur in such a mixture have been discussed elsewhere[8,11] in detail. It will be sufficient to say here that only atom and radical reactions are important, and that for these six species the only such reactions one can write (other than exchanges) are given below with the rate constants used:

$$CO + OH \underset{k_{-1}}{\overset{k_1}{\rightleftarrows}} CO_2 + H \qquad (I)^{11,12}$$

$k_1 = 10^{13} \exp(-10^4/RT)$ cm^3 mole^{-1} sec^{-1}

$$H_2O + H \underset{k_{-2}}{\overset{k_2}{\rightleftarrows}} H_2 + OH \qquad (II)^{13}$$

$k_2 = 10^{15} \exp(-2.5 \times 10^4/RT)$ cm^3 mole^{-1} sec^{-1}

$$H + H + M \underset{k_{-3}}{\overset{k_3}{\rightleftarrows}} H_2 + M \qquad \text{(III)}^{14-17}$$

$k_3 = 5 \times 10^{21}\, T^{-2}$ cm^6 mole^{-2} sec^{-1}

$$H + OH + M \underset{k_{-4}}{\overset{k_4}{\rightleftarrows}} H_2O + M \qquad \text{(IV)}^{18}$$

$k_4 = 10^{23}\, T^{-2}$ cm^6 mole^{-2} sec^{-1}

No distinction was made between the various third bodies M. The reverse rate constants were related to the forward rate constants by the equilibrium constant, e.g., $k_{-1} = k_1/K_1$. As previously mentioned, this is a questionable assumption in general, but justified here by the basic condition of local equilibrium assumed for the internal degrees of freedom. If separate data for the two rate constants were available (which they were not) they could just as well have been used. The T^{-2} dependence for (III) and (IV) is by no means established.

All calculations were done for a simple conical expansion section with total angle of 25° and inlet radius of 1 cm, i.e.,

$$A = (0.22169z + 1)^2$$

In the present example, the inlet flow was taken to be slightly supersonic at $W = 335.570$ g cm^{-2} sec^{-1}. Iteration for W was unnecessary in this case, and the exact supersonic value of W was immaterial for present purposes. Thermodynamic data were taken from an available tabulation.[19]

Since we are dealing with $N = 6$ chemical species involving $L = 3$ elements, there will be $N - L = 3$ rate expressions of the form of Eq. (6) required. If we use the major species CO, H_2, and H_2O, these equations are

$$dF_{CO}/dz = (A/W)\rho^2 K_1[-F_{CO}F_{OH} + F_{CO_2}F_H/K_1] \qquad (9)$$

$$dF_{H_2}/dz = (A/W)\rho^2[k_2(F_{H_2O}F_H - F_{H_2}F_{OH}/K_2) + k_3 \sum_i F_i(\rho F_H^2 - F_{H_2}/K_3RT)] \qquad (10)$$

$$dF_{H_2O}/dz = (A/W)\rho^2[k_2(-F_{H_2O}F_H + F_{H_2}F_{OH}/K_2) + k_4 \sum_i F_i(\rho F_H F_{OH} - F_{H_2O}/K_4RT)]. \qquad (11)$$

The other species are then obtained from the element conservation relations (5), i.e.,

$$F_{CO_2} = (F_{CO_2} + F_{CO})_0 - F_{CO}, \qquad (12)$$

$$F_{OH} = (F_{OH} + 2F_{CO_2} + F_{CO} + F_{H_2O})_0 - 2F_{CO_2} - F_{CO} - F_{H_2O}, \qquad (13)$$

$$F_H = (F_H + 2F_{H_2O} + 2F_{H_2} + F_{OH})_0 - 2F_{H_2O} - 2F_{H_2} - F_{OH}. \qquad (14)$$

Note that the number of elementary reactions has nothing to do with the number of rate equations necessary; each reaction simply contributes a pair of terms—one positive and one negative—to the quantity in brackets of the appropriate dF_i/dz equation.

Solution for chemically frozen flow was obtained from the same program simply by setting all the rate constants $k_1 - k_4$ equal to zero, while that for shifting chemical equilibrium ("equil") was calculated by a separate 7090 program.[10] The exact nonequilibrium solution (kinetic) required about 10 minutes of machine time to go a distance of about 35 cm down the nozzle. The temperature profiles for the three cases are given in Fig. 1, with the kinetic results occupying its expected position between the frozen and "equil" extremes. The difference between the latter two is not very great in this case because the concentrations of H and OH are rather small and, as we shall emphasize, it is the recombination of these which is the predominant influence on the gross flow variables such as temperature.

Of greater diagnostic value in analyzing the flow is the behavior of the composition variables F_i, of which three representatives are given in Fig. 2 (normalized to their inlet values) with their corresponding profiles for shifting equilibrium flow. The striking thing is the degree to which the actual gas composition deviates from

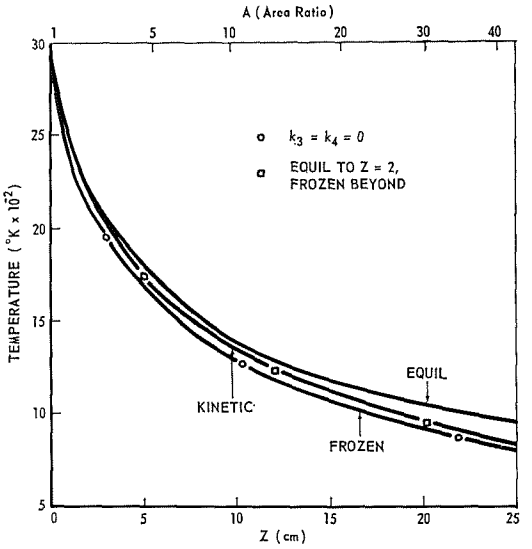

FIG. 1. Static temperature profiles in divergent nozzle for C—H—O example.

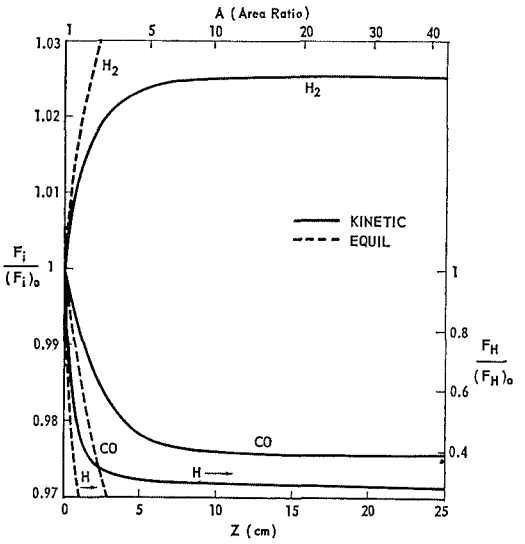

FIG. 2. Representative concentration profiles (normalized to inlet values) in divergent nozzle for C—H—O example.

equilibrium. While the latter curves are still changing sharply (off scale in the graph) throughout the nozzle length of practical interest, the kinetic solutions level out and "freeze" after the first few centimeters and relatively little composition change has occurred. Thus, the exact solution of a realistic, complex, reacting nozzle flow demonstrates the phenomenon of freezing like that first found by Bray[4] for a simple atom recombination case. With an inlet pressure as high as this (pressure effects are discussed more fully in the next section), the kinetic profiles follow the "equil" results for a short way and then rapidly deviate as freezing occurs.

The important difference between the freezing phenomenon in a complex flow and a simple flow involving one reaction (with its reverse) is that the former does not have a single freezing point but a separate one for each elementary reaction taking place. In the present case it is possible to determine these separate freezing points by proper application of the method devised by Bray[4] for a single reaction, and later extended to complex flows.[9] The Bray argument for a single recombination dissociation reaction is, in essence, that in the early stages of flow the reaction is nearly in equilibrium and the *net* rate must be small compared to either the recombination or dissociation rates, while far downstream where both temperature and pressure have dropped drastically, the *net* rate must be large compared to the dissociation rate with its exponential temperature dependence. Thus at some intermediate point the net rate and dissociation rate must be equal, and this may be defined as the freezing point (F. P.). This scheme was originally devised as a means of avoiding a complete, numerical nonequilibrium solution, since the assumption is made that chemical equilibrium exists up to the F.P. and equilibrium concentrations, temperature, and density may be used to compute the necessary rates.

For a complex flow, the difficulty is that the overall rate of change of concentration for a species as determined from the equilibrium solution will not be the net rate due to a specific reaction if the species is involved in more than one reaction. To apply the Bray method to each elementary reaction, the contribution of each to the overall net equilibrium rate of a species must be determined. In general, this is possible only when the number of reactions does not exceed $N - L$.* In the present case this condition is not met but seems to be an interesting exception in that CO appears only in reaction (I), so the method is directly applicable to it. This then furnishes a starting point to determine the other freezing points. (A rigorous proof of the validity of this procedure is not evident as yet and requires further study.) Figure 3 shows a section of the net rate $[dF_{CO}/dz]_{equil}$ obtained by graphical differentiation of the equilibrium solution, and also a section of the reverse rate term of reaction (I), i.e., referring to Eq. (9), the quantity $Q_I = A\rho^2 k_1 F_{CO_2} F_H / W K_1$, with all variables taken from the equilibrium solution. The intersection of these two curves defines the freezing point of (I).

To find the other freezing points we note that—at equilibrium—reactions (I) and (II) may be combined to give the water-gas reaction $CO + H_2O \rightleftarrows CO_2 + H_2$. Thus the change in F_{H_2O} due to reaction (II) is equal to the change in F_{CO} at any point, and the change in F_{H_2O} due to (IV) may be determined by subtracting that due to (II) from the total change in the equilibrium solution. The other net rates were found similarly to give the other three intersections shown in Fig. 3. The sequence of freezing points in the nozzle is thus noted to be reaction (III) first at $z \sim 0.4$ cm, followed by the other slow recombination reaction (IV), at $z \sim 1.2$. The slower of the two-body reactions, reaction (I), freezes next at

*Bray and Appleton[9] have used the criterion that the number of reactions must not exceed the number of molecules (i.e., diatomic or polyatomic species). The number of molecules equals $N - L$ only if all elements are present in the atomic state, which is not always the case as in the present example.

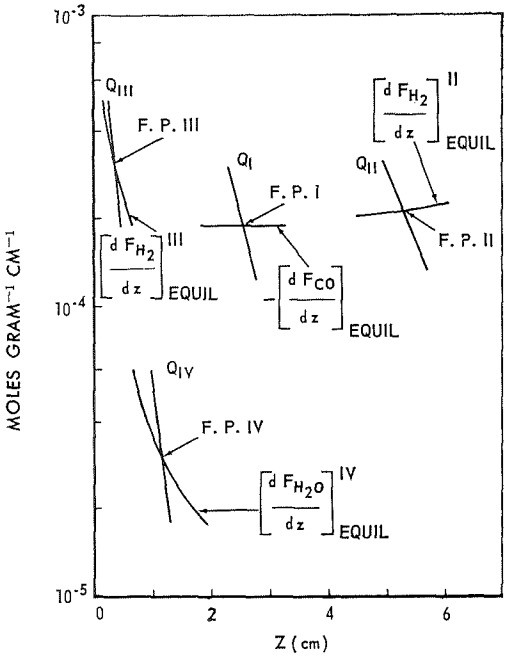

FIG. 3. Plots of rates defining separate freezing points (F.P.) of elementary reactions (I)–(IV), in C—H—O example.

$$Q_{\mathrm{I}} = A\rho^2 k_1 F_{\mathrm{CO_2}} F_{\mathrm{H}}/WK_1;$$

$$Q_{\mathrm{II}} = A\rho^2 k_2 F_{\mathrm{H_2}} F_{\mathrm{OH}}/WK_2;$$

$$Q_{\mathrm{III}} = A\rho^2 k_3 F_{\mathrm{H_2}} \Sigma_i F_i/WK_3RT;$$

$$Q_{\mathrm{IV}} = A\rho^2 k_4 F_{\mathrm{H_2O}} \Sigma_i F_i/WK_4RT$$

$z \sim 2.5$, while considerably later (II) freezes at $z \sim 5.3$.

Most of the energy release due to chemical reaction is associated with the recombinations (III) and (IV). This is clearly indicated by the fact that a kinetic solution with k_3 and k_4 set equal to zero, so that only the bimolecular steps (I) and (II) operate, follows nearly exactly the fully frozen solution in temperature (see Fig. 1), pressure, and the other overall flow variables (but not in composition, of course). Also, the net heat release due to (I) and (II) combined is about 10 kcal/mole, while (III) and (IV) each yield about 100 kcal/mole. Thus, even though the net mole change due to (I) and (II) is larger than that due to (III) and (IV), the latter account for most of the energy release affecting the flow. When (III) and (IV) are frozen, the whole flow is essentially frozen so far as temperature, pressure, etc., are concerned. Therefore, a good approximation to these flow variables could be attained by calculating an equilibrium solution to a point approximately at $z = 2$ and a frozen solution beyond. A few points plotted on the temperature profiles in Fig. 1 were obtained this way, and the agreement with the exact kinetic solution is good. That the gas composition is *not* really frozen beyond the recombination freezing points, however, is obvious from the profiles in Fig. 2. Appreciable changes continue owing to (I) and (II) for some distance beyond $z = 2$. Whether an approximate solution obtained this way is really worth while seems questionable. The kinetic information is necessary to calculate a reasonable freezing point anyway, so when high-speed computing facilities are available it would seem better to do the complete nonequilibrium problem. Furthermore, if the energetically important reactions should have appreciably different freezing points, assuming a single such point would be less satisfactory, nor is it possible to find the freezing points at all in more complex cases such as that which follows.

Hydrogen–Oxygen–Nitrogen Example

Basic Solutions. A more elaborate study has been carried out on mixtures which might be typical of those employed in hypersonic hydrogen-burning vehicles of various kinds. Hydrogen-air mixtures corresponding to stoichiometric equivalence ratio (E.R. = 1) and six times stoichiometric (E.R. = 6) at an equilibrium temperature of 3000°K and a range of pressures were considered. The calculated equilibrium concentrations of the six significant species (besides the inert N_2) H_2, H_2O, O_2, OH, H, and O are given in Table 1. The elementary reactions and rate constants used are as follows:

$$\mathrm{H_2O + H} \underset{k_{-1}}{\overset{k_1}{\rightleftarrows}} \mathrm{H_2 + OH} \qquad \text{(I)}^{13}$$

$k_1 = 10^{15} \exp(-2.5 \times 10^4/RT)$ cm³ mole⁻¹ sec⁻¹

$$\mathrm{O_2 + H} \underset{k_{-2}}{\overset{k_2}{\rightleftarrows}} \mathrm{OH + O} \qquad \text{(II)}^{20,21}$$

$k_2 = 5 \times 10^{14} \exp(-1.8 \times 10^4/RT)$ cm³ mole⁻¹ sec⁻¹

$$\mathrm{H_2 + O} \underset{k_{-3}}{\overset{k_3}{\rightleftarrows}} \mathrm{OH + H} \qquad \text{(III)}^{22,23}$$

$k_3 = 7 \times 10^{12} \exp(-8.5 \times 10^3/RT)$ cm³ mole⁻¹ sec⁻¹

$$\mathrm{H_2O + O} \underset{k_{-4}}{\overset{k_4}{\rightleftarrows}} \mathrm{OH + OH} \qquad \text{(IV)}$$

(No data on k_4. Assumed same as k_2.)

TABLE 1

Equilibrium Concentrations at 3000°K for H_2–Air Combustion Products at Nozzle Inlet[a]

Pressure (atm)	F_{H_2}	F_{H_2O}	F_{O_2}	F_{OH}	F_H	F_O	F_{N_2}
			E.R. = 1				
0.1	0.4111	0.4966	0.1539	0.2971	0.7157	0.3126	2.6600
1	0.2861	0.9396	0.1000	0.1998	0.1770	0.0747	2.6600
10	0.1541	1.1870	0.0522	0.1060	0.0400	0.0166	2.6600
100	0.0762	1.3075	0.0255	0.0520	0.0088	0.0036	2.6600
			E.R. = 6				
0.1	4.6056	0.8683	0.0088	0.2376	3.6675	0.1143	2.3281
1	5.6412	1.1415	0.0009	0.0837	1.2040	0.0108	2.3281
10	6.0110	1.2100	0.0001	0.0266	0.3845	0.0010	2.3281
100	6.1324	1.2293	0.0000	0.0084	0.1219	0.0001	2.3281

[a] All F_i have been multiplied by 10^2.

$$H + H + M \underset{k_{-5}}{\overset{k_5}{\rightleftarrows}} H_2 + M \qquad \text{(V)}^{14-17}$$

$k_5 = 2 \times 10^{18}\ T^{-1}$ cm^6 mole^{-2} sec^{-1}

$$O + O + M \underset{k_{-6}}{\overset{k_6}{\rightleftarrows}} O_2 + M \qquad \text{(VI)}^{24}$$

$k_6 = 2 \times 10^{18}\ T^{-1}$ cm^6 mole^{-2} sec^{-1}

$$H + O + M \underset{k_{-7}}{\overset{k_7}{\rightleftarrows}} OH + M \qquad \text{(VII)}$$

(No data on k_7. Assumed same as k_5 and k_6.)

$$H + OH + M \underset{k_{-8}}{\overset{k_8}{\rightleftarrows}} H_2O + M \qquad \text{(VIII)}^{18}$$

$k_8 = 3 \times 10^{19}\ T^{-1}$ cm^6 mole^{-2} sec^{-1}

No other reactions can be written for these six species except $OH + OH \rightleftarrows H_2 + O_2$ and $O + H_2O \rightleftarrows H_2 + O_2$, both of which were considered highly unlikely on steric grounds. Note that k_5–k_8 were given a T^{-1} dependence here instead as T^{-2} as in the recombination reactions of the previous example. Actually, variation in this temperature dependence was one of the things examined in this study, as will be shown. The nozzle geometry was the same as used previously. Inlet velocity was held constant at 5×10^5 cm/sec for all the cases treated, so that the mass flow parameter W varied for each case with the inlet density. This velocity corresponded to frozen inlet Mach numbers of roughly 3 and 4 for the E.R. = 6 and E.R. = 1 sets, respectively. Pressures of P_0 = 0.1, 1, 10, and 100 atm were used.

For this example, $N = 6$ species and $L = 2$ elements (excluding N_2), so four dF_i/dz relations were required, and were taken to be dF_{H_2}/dz, dF_{H_2O}/dz, dF_{O_2}/dz, and dF_{OH}/dz. These will not be reproduced here but were similar to Eqs. (9)–(11) of the previous example with appropriate terms for each of the reactions (I)–

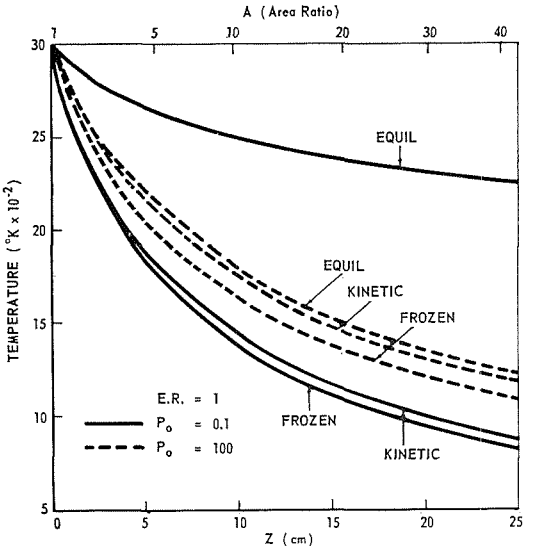

FIG. 4. Static temperature profiles in divergent nozzle for two inlet pressures in H—O—N example.

(VIII) in which a given species appears. Two element conservation equations analogous to (12)–(14) were then used.

Figure 4 shows samples of the "equil," frozen, and kinetic temperature profiles for two cases: E.R. = 1 at P_0 = 0.1 and 100 atm. The pronounced difference in the spread between the "equil" and frozen limits at the two pressures is clear. The lower pressure results in a much greater degree of dissociation for the given inlet temperature of 3000°K, and recovery of this dissociation energy in the "equil" flow keeps the static temperature much higher than in the high-pressure case. It is also clear that the actual kinetic profile follows the frozen profile much closer than the "equil" profile at the lower pressure, while the P_0 = 100 atm kinetic solution lies about midway between its two limits (similar to the previous C—H—O example). This is an indication of the direct effect of pressure on the reaction rates. That high pressure keeps the solution nearer equilibrium is also shown by the considerably increased computing time required, although the time for the 100 atm runs was not excessive (~15 min). The temperature profiles for the E.R. = 6 case showed similar behavior, except that at P_0 = 100 atm the kinetic and "equil" cases essentially coincided. The importance of pressure in maintaining equilibrium has been noted by Hall and Russo.[5]

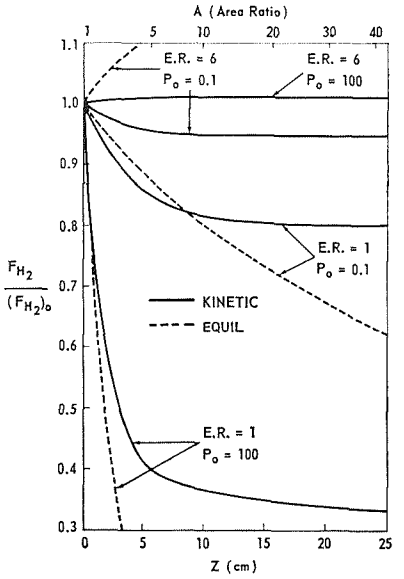

FIG. 5. H_2 concentration profiles (normalized to inlet values) in divergent nozzle for two equivalence ratios and two inlet pressures in H—O—N example. (Kinetic and equilibrium profiles for E.R. = 6, P_0 = 100 atm are indistinguishable on graph.)

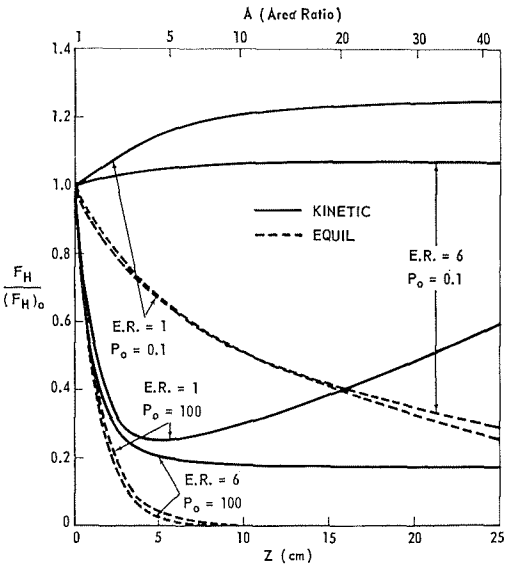

FIG. 6. H concentration profiles (normalized to inlet values) in divergent nozzle for two equivalence ratios and two inlet pressures in H—O—N example.

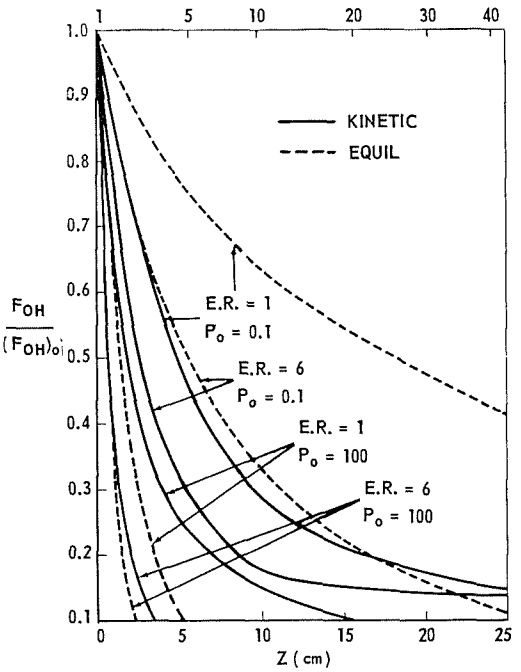

FIG. 7. OH concentration profiles (normalized to inlet values) in divergent nozzle for two equivalence ratios and two inlet pressures in H—O—N example.

Some representative concentration profiles at the extremes of pressure and for the two equivalence ratios are given in Figs. 5–7. These illustrate the complex behavior the gas composition can follow in certain cases. As is well-known by now, a reacting mixture can maintain itself nearly in chemical equilibrium with changing temperature and pressure only as long as the three-body recombination reactions follow fast enough. They are the controlling steps in the way that they are when a nonequilibrium mixture approaches the equilibrium state.[14] The two-body reactions merely exchange radicals back and forth, and may be individually nearly in equilibrium even though the mixture as a whole is not, owing to the slowness of the three-body reactions. This means that once the latter have frozen, large concentration changes can occur which may be opposite to that expected on the basis of full equilibrium calculations—and therefore surprising at first sight.

From the direction of shift in their equilibrium constants with decreasing temperature, the two-body reactions (I)–(IV) would tend toward the left as written while the recombinations (V)–(VIII) would tend toward the right. But the coupling of all these reactions, which determines the increase or decrease of each species down the nozzle, is obviously an impractically difficult (if not impossible) thing to predict *a priori*. Thus in Fig. 5 for H_2, the kinetic solution for E.R. = 1, P_0 = 100 atm, follows rather closely the rapidly dropping "equil" solution for a way and then deviates sharply as freezing sets in. This might be said to be the *"normal"* or expected behavior. At E.R. = 1, P_0 = 0.1 atm, however, the kinetic profile actually drops faster than the "equil" at first, presumably because the recombinations freeze very early in this low pressure case and H_2 is lost via reaction I faster than it is produced by (III). Eventually, the kinetic and "equil" curves cross as freezing of (I)–(IV) sets in. In the E.R. = 6, P_0 = 0.1 atm example, the kinetic and "equil" profiles proceed in opposite directions, while at P = 100 atm the two solutions coincide for all practical purposes, as has already been noted for the corresponding temperature profiles. In this very fuel-rich case at high pressure there is relatively little dissociation to begin with, and therefore little change in the major species like H_2 down the nozzle.

Interesting composition changes are demonstrated by the H profiles in Fig. 6. All the "equil" solutions predict decreasing concentrations of H atoms and the other radicals with distance (temperature), as would be expected. Note, however, that the P_0 = 0.1 atm kinetic solutions for both E.R. values show increasing H concentrations. At P_0 = 100 atm the recombination reactions are more effective in reducing H, but for E.R. = 1 the profile goes through a minimum and starts back up again as the recombinations freeze and the two-body reactions operate alone for a time. Effects like this would be practically impossible to predict without a complete numerical solution. The OH profiles in Fig. 7 are "normal" at P_0 = 100 atm, but at P_0 = 0.1 atm the kinetic results drop faster than "equil" for both E.R. values, showing the dominance of reactions (I)–(IV).

Rate Constant Variations. Since chemical rates are at the heart of nonequilibrium nozzle flows such as we are dealing with here, it is of interest to find out how sensitive the results are to the values assumed for the basic kinetic quantities—the elementary reaction rate constants. Experimental data on these are often questionable or completely lacking, as we have seen, and it is natural to ask how crucial our ignorance in this area might be expected to be. The kinetic solution was carried through (for E.R. = 1, P_0 = 1 atm) with various changes in the rate constants to shed some light on this question.

First, the three-body recombination rate constants were raised by a factor of 10 from the values originally used. The curves designated ($k_5 \cdots k_8$) × 10 in Figs. 8 and 9 resulted and are to be compared with the original results labeled "correct." The temperature profile in Fig. 8 was raised somewhat by raising the magnitude of k_5–k_8. Since these are the reactions releasing most of the energy, increasing their rates would be expected to affect the temperature in this way. The change is not great, how-

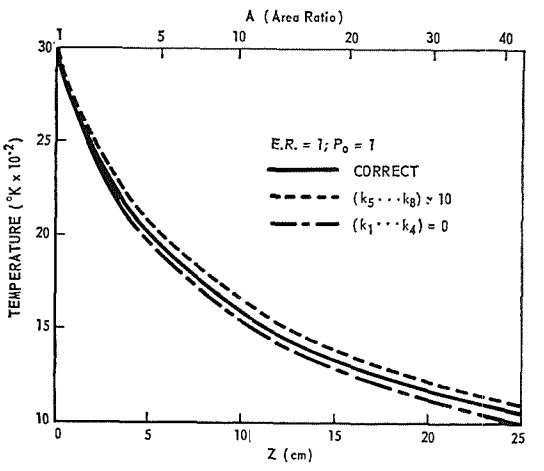

FIG. 8. Effect of rate constant variations on static temperature profile for a H—O—N example.

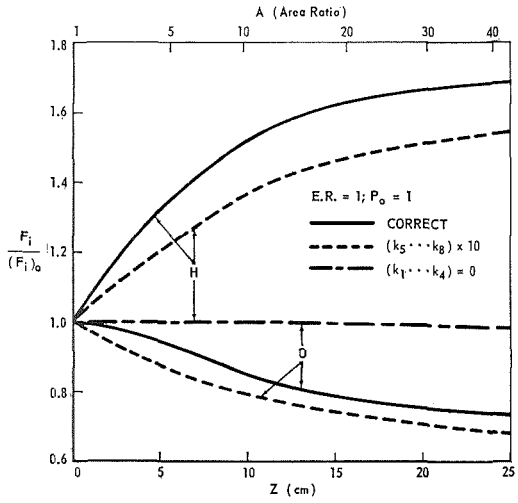

FIG. 9. Effect of rate constant variations on H and O profiles (normalized to inlet values) for a H—O—N example.

ever, and the variable of greatest importance for propulsion, i.e., velocity, is practically unaffected. The gas *composition* is appreciably altered, however, especially as far as the radicals are concerned. This is shown in Fig. 9 for two representative species. Both H and O are reduced by the increase in k_5–k_8 since they are more effectively removed in these recombination reactions.

Next, the three-body rate constants were made proportional to T^{-2} instead of T^{-1} as originally, but kept the same in absolute magnitude at the inlet temperature of 3000°K. This had no appreciable effect whatsoever on any of the profiles, indicating that at the lower pressures these reactions are unimportant by the time the difference in temperature can have any influence on the magnitude of the rate constants. At the higher pressure some small changes become noticeable, but the exponent of T used is generally quite irrelevant in this work. Hall and Russo[5] had similar experience.

Changes in the activation energies of some of the two-body reactions were tested by changing that of reaction (I) from 25 to 20 kcal/mole, and then that of reaction (III) from 8.5 to 5 kcal/mole. This amounts to altering their temperature dependences, of course, and neither change had any effect on the temperature solutions. This might be expected since these are not the main reactions energetically. The change in activation energy of (I) had a very slight effect on the composition beyond $z \sim 5$ cm, and the change in (III) none at all. Thus one would conclude that the two-body activation energies are not very critical within modest limits. Absolute magnitudes of the rate constants (i.e., pre-exponential factors) are somewhat more important.

When the two-body reactions are ignored entirely by setting $(k_1 \cdots k_4) = 0$, the temperature is lowered somewhat in Fig. 8 and the concentrations changed appreciably in Fig. 9. With only recombinations operating, all radicals decrease with distance. At the rather low pressure $P_0 = 1$ atm these reactions are slow, however, and the changes are slight—the difference between H and O not being enough to distinguish on the graph.

More informative perhaps was a series of runs in which the two-body reactions were eliminated one at a time, i.e., k_1, k_2, k_3, and k_4 were separately set equal to zero. This enabled the relative importance of these reactions to be assessed. Eliminating either (I) or (II) caused large composition changes, and small (but not negligible) changes in temperature, etc. Removing (IV) had no effect on temperature—presumably because the species involved (especially O) were present at low concentration—but some effect on concentrations. Removing (III) had no effect on anything. Qualitatively, the reason for these differences is that (I), (II), and (IV) all have roughly the same molar heat of reaction and rate of change of equilibrium constant with temperature, while (III) is much smaller in both these respects. Thus it would be expected that removing (III) from the reaction scheme would have the least effect on the results, as was the case.

As a final comment to this section, one should note that the results of these rate constant variations—and the general complexity of the kinetic processes in any real flow—are a good indication of the futility of trying to deduce anything reliable about kinetics from measurements only of gross flow properties such as temperature and/or pressure in a nozzle. These variables are rather insensitive to fairly large changes in rate constants, and meaningful interpretation of such data (difficult to obtain at best) *without good composition data in addition* seems practically impossible.

Two-Body Equilibrium. In view of the fact that the two-body rates are much faster than the three-body rates, an approximation which suggests itself is to assume that the former are equilibrated throughout the flow. (This has been referred to as the "partial equilibrium" state in the literature.[25]) Under this assumption, three of the four dF_i/dz kinetic relations required in the complete problem may be replaced by equilibrium constant relations for reactions (I)–

(IV); any three of the latter may be used, while the fourth is not an independent relation. Only one kinetic equation is then required, and this involves the nonequilibrium recombination reactions (V)–(VIII).

To calculate the flow history using this approximation, the following procedure was carried out: First, one may show rigorously by simple elimination of terms that the four species derivatives for the main dependent composition variables are related by

$$dF_{H_2}/dz + dF_{O_2}/dz + dF_{OH}/dz + 2(dF_{H_2O}/dz) = \frac{A\rho^2 \sum_i F_i}{W} \{k_5[\rho F_H^2 - (F_{H_2}/K_5RT)] + k_6[\rho F_O^2 - (F_{O_2}/K_6RT)] + k_7[\rho F_H F_O - (F_{OH}/K_7RT)] + k_8[\rho F_H F_{OH} - (F_{H_2O}/K_8RT)]\}. \quad (15)$$

The differentiated forms of the equilibrium constant relations for reactions (I), (II), and (III), together with the two (differentiated) element conservation relations provided five more equations, making six equations for the six species variables. In addition, differentiating the equilibrium relations introduced the derivative of the equilibrium constants with respect to distance. Since these are temperature functions only, one can write $dK_i/dz = (dK_i/dT)(dT/dz)$ and use dT/dz as a seventh variable by way of Eq. (7). dK_i/dT was obtained from a polynomial fit to the $K_i(T)$. Thus, a set of seven simultaneous equations was solved at each point (by a standard machine program) for the six dF_i/dz and dT/dz, and these derivatives fed to the regular integration scheme.

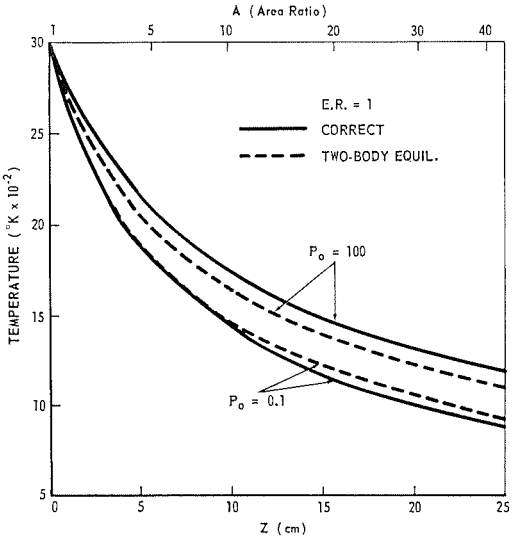

FIG. 10. Effect on static temperature profiles of assuming equilibrium of two-body reactions (I)–(IV) in two H—O—N examples.

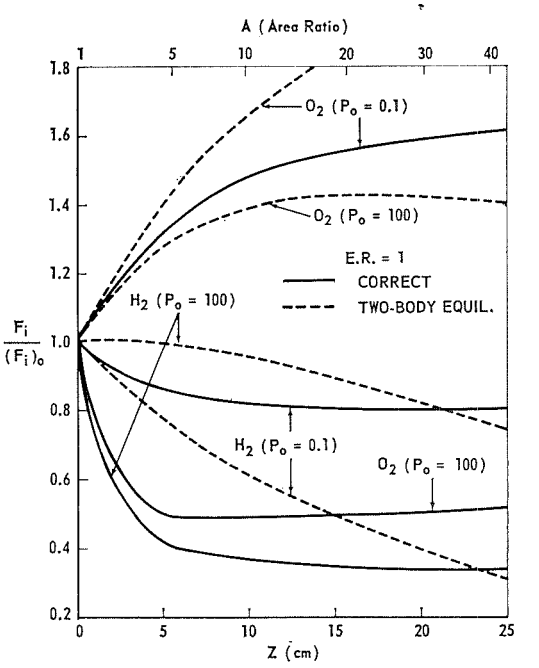

FIG. 11. Effect on H_2 and O_2 profiles (normalized to inlet values) of assuming equilibrium of two-body reactions (I)–(IV) in two H—O—N examples.

Figures 10 and 11 illustrate the results for two pressures at E.R. = 1. For $P_0 = 0.1$ atm, the two-body equilibrium temperature solution follows the full (correct) solution rather closely out to $z \sim 8$ cm before starting to deviate, while for $P_0 = 100$ atm the approximate solution is poor from the start. It is interesting that the two-body equilibrium curves deviate in opposite directions at two pressures. Figure 11 for H_2 and O_2 concentrations emphasize this behavior. The $P_0 = 0.1$ atm curves at least start out with the correct curves, while at $P_0 = 100$ atm even the directions are opposite—to say nothing of the gross differences in magnitude.

This effect of pressure should be expected. At low pressures the three-body reactions are quickly frozen and inoperative, so that the two-body equilibrium assumption ought to be qualitatively correct, and more or less quantitatively correct for a while until these reactions also freeze. At higher pressures where reactions (V)–(VIII) make significant contributions, however, the approximation can be very poor and—especially for composition—downright misleading.

Other Approximations. It is not possible to establish freezing points for the separate reactions in this example as was done in the C—H—O case. There are more reactions than can be handled to determine the individual contribution of each to the net change in concentration of a given species from the equilibrium solution.

It is perhaps worth noting that the classical steady state approximation often invoked in handling complex kinetic problems is not applicable here. The basic assumption necessary is that radical concentrations are small compared to major species and may be considered constant. This is patently not true in such cases as are dealt with here, nor would it introduce any real simplification even if it were. It should also be apparent that applying so-called "overall" kinetic expressions to complex flows like these is a very risky business. The effort involved in establishing that such an expression is really applicable to a given case might be better spent in analysis based on basic elementary reactions.

An approximation which may seem questionable at first sight is that of neglecting certain species in a kinetic calculation on the basis of low equilibrium inlet concentration, such as was done for O and O_2 in the C—H—O example. It would seem, however, that the only ways such neglect could lead to appreciable error are: (1) if the species were directly involved in reactions of great energetic importance so that small amounts could have an effect on the flow, or (2) if the species were involved in reactions of very high rate so that their concentration might increase down the nozzle to values which would affect either the energetics or the composition of the flow. In fact, neither of these possibilities is very likely. It is difficult to think of reactions which are so energetic or fast compared to the others occurring that they could affect conditions appreciably even though one or more of the participating species is initially two or more orders of magnitude below the others in concentration. Thus it would seem that elimination of species and their reactions on the basis of low equilibrium concentration should generally be a legitimate procedure. To check this, the C—H—O example was re-run with O and O_2 included, which necessitated adding reactions (II), (III), (IV), (VI), and (VII) of the H—O—N reaction scheme to the four reactions of the original C—H—O case. A comparison of some of the results is given in Table 2, and it is clear that the differences are entirely negligible. Even the sensitive radical concentrations are only slightly affected. Actually, once the equations are to be set up and programmed anyway, it is not much simpler to omit a few reactions. But in cases where there are a great many conceivable species and reactions, elimination of those at very low concentration can afford appreciable simplification.

TABLE 2

Comparison of Results for C—H—O Example with and without Inclusion of O_2 and O. Values are for $z = 20$ cm

	With O_2 and O	Without O_2 and O
T (°K)	960	960
F_{CO}	1.8784×10^{-2}	1.8786×10^{-2}
F_{H_2}	3.1643×10^{-2}	3.1649×10^{-2}
F_{H_2O}	1.7788×10^{-2}	1.7782×10^{-2}
F_H	3.4456×10^{-4}	3.4442×10^{-4}
F_{OH}	0.14×10^{-5}	0.15×10^{-5}

Practical Implications

The most important implication of the chemical kinetic behavior of nozzle gases from a practical point of view is probably in the area of propulsion. Whatever energy from a propellant goes into dissociating the gas and is not recovered by recombination in the nozzle cannot appear as directed kinetic energy of the exhaust, which is the quantity of propulsive interest. One way of presenting results to illustrate this behavior is by comparing the kinetic energy difference between nonequilibrium and frozen flow with the maximum kinetic energy difference obtainable from

TABLE 3

Approximate Values of Kinetic Energy Parameter (ϕ) in Nonequilibrium Flows

	ϕ (percent)	
	$Z = 10$ cm	$Z = 20$ cm
C—H—O example	70	55
H—O—N example:		
E.R. = 1, $P_0 = 0.1$ atm	5	5
E.R. = 1, $P_0 = 1$ atm	10	5
E.R. = 1, $P_0 = 10$ atm	40	25
E.R. = 1, $P_0 = 100$ atm	90	90
E.R. = 6, $P_0 = 0.1$ atm	5	5
E.R. = 6, $P_0 = 1$ atm	20	5
E.R. = 6, $P_0 = 10$ atm	25	20
E.R. = 6, $P_0 = 100$ atm	90	70

shifting equilibrium flow. Thus we define a kinetic energy parameter ϕ at any station in the nozzle by

$$\phi = [(v^2 - v_f^2)/(v_{eq}^2 - v_f^2)] \times 100, \quad (16)$$

where v, v_f, and v_{eq} are the velocities for the actual, frozen, and equilibrium flows, respectively, for given input conditions.

The examples studied in this work are compared in Table 3, using Eq. (16), for two different stations in the nozzle. The numbers are only approximate since they are quite sensitive to small interpolation errors, etc., depending as they do upon differences in squares of nearly equal velocities. The general trends are clear, however, and reflect what has been said about the importance of pressure in determining how far the flows deviate from equilibrium. The chemical energy recoveries at low pressure ($P_0 = 0.1$ and 1 atm) are very small indeed, and only at $P_0 = 100$ atm does it approach 100%. Once the flow has frozen, of course, no further energy release occurs, so the percentages tend to decrease with distance along the nozzle.

Whether such deviations from the equilibrium flow limit will be of real practical importance to an engine designer depends on circumstances. In a typical rocket, where the unburned propellant is essentially at room temperature and then burns to some high flame temperature, the fraction of the total chemical energy released which is tied up in dissociation (not to be confused with the quantity ϕ) is rather small, so that the difference between frozen and equilibrium specific impulse is usually a few percent at most. Furthermore, rocket chamber pressures tend to be high and area ratios low, which would favor fairly substantial values of ϕ. Thus, kinetic effects may be of minor—though perhaps not negligible—importance. In a high Mach number ramjet, however, the incoming air is typically diffused to a rather high static temperature before the fuel is injected. The combustion process may then result in very little actual temperature rise with a large part of the energy going into dissociation, and recovering this in the nozzle can become vital. The pressure will be an important factor here.

Aside from considerations of energy and propulsion, it seems likely that in certain types of combustion wind tunnels the kinetic behavior may be of interest simply because it determines the gas composition. As we have seen, large concentration changes can occur even after the flow is essentially frozen as far as energy effects (i.e., three-body recombinations) are concerned, because of the faster two-body steps. It may be important to know the gas composition in the test section, for example, regardless of overall energy effects—and a kinetic calculation could be of great assistance here.

Another practical matter may be mentioned in connection with gas sampling in reacting flows, such as has been extensively done in laminar flames.[11,12,14] The basis for using tiny uncooled probes for sampling in such systems is the assumption that rapid expansion through them (they are effectively small supersonic nozzles, with transition to free molecule flow) will quench, or freeze, the composition of the gas nearly at its inlet state—at least in regard to the major, stable species. Obviously, if large concentrations of atoms and radicals are present, such a sampling procedure will always be in error when used with ordinary gas analysis instruments such as mass spectrometers or gas chromatographs, since the radicals will recombine somewhere before reaching the end instrument (without very specialized techniques involving molecular beams, for example). Generally such large concentrations are not present, however, and kinetic analysis of such probe techniques would be very useful, although this has not been done as yet. It is clear that low pressure would be favored in this application, in which one desires as early freezing as possible.

References

1. Penner, S. S.: J. Am. Chem. Soc. *71*, 788 (1949).
2. Krieger, F. J.: ARS Journal *21*, 179 (1952).
3. Wegener, P. P.: Phys. Fluids *2*, 264 (1959).
4. Bray, K. N. C.: J. Fluid Mech. *6*, 1 (1959).
5. Hall, J. G. and Russo, A. L.: *Cornell Aero. Lab. Report AD-1118-A-6*, Nov., 1959.
6. Vincenti, W. G.: *AEDC-TN-61-65*, May, 1961.
7. Eschenroeder, A. Q., Boyer, D. W., and Hall, J. G.: *Cornell Aero. Lab. Report AF-1413-A-1*, May, 1961.
8. Westenberg, A. A. and Favin, S.: *The Johns Hopkins University, Applied Physics Lab. Report CM-1013*, March, 1962.
9. Bray, K. N. C. and Appleton, J. P.: *Univ. of Southampton Report A.A.S.U. 166*, April, 1961.
10. Brown, H. N. and Williams, M. M.: *U.S. N.O.T.S. (China Lake) NAVWEPS Report 7043*, June, 1960.
11. Westenberg, A. A. and Fristrom, R. M.: J. Phys. Chem. *65*, 591 (1961).
12. Fenimore, C. P. and Jones, G. W.: J. Phys. Chem. *62*, 1578 (1958).
13. Fenimore, C. P. and Jones, G. W.: J. Phys. Chem. *63*, 1834 (1959).
14. Bulewicz, E. M., James, C. G., and Sugden, T. M.: Proc. Roy. Soc. (London) *A235*, 89 (1956).

15. KASKAN, W. E.: Combustion and Flame *2*, 229 (1958).
16. SUTTON, E. A.: *Thesis, Cornell University*, 1961.
17. RINK, J. P.: J. Chem. Phys. *36*, 262 (1962).
18. BULEWICZ, E. M. and SUGDEN, T. M.: Trans. Faraday Soc. *54*, 1855 (1958).
19. WILLIAMS, M. M.: *U.S. N.O.T.S. (China Lake) NAVWEPS Report 7609*, Feb., 1961.
20. SCHOTT, G. L. and KINSEY, J. L.: J. Chem. Phys. *29*, 1177 (1958).
21. FENIMORE, C. P. and JONES, G. W.: J. Phys. Chem. *63*, 1154 (1959).
22. FENIMORE, C. P. and JONES, G. W.: J. Phys. Chem. *65*, 993 (1961).
23. CLYNE, M. A. A. and THRUSH, B. A.: Nature *189*, 135 (1961).
24. RINK, J. P., KNIGHT, H. T., and DUFF, R. E.: J. Chem. Phys. *34*, 1942 (1961).
25. SCHOTT, G. L.: J. Chem. Phys. *32*, 710 (1960).

CONDENSATION IN NOZZLES

WELBY G. COURTNEY

No definitive experimental work has been done with condensation via homogeneous nucleation and very little work apparently has been done with condensation in nozzle flow, where the complications of a dynamic system are added.

A review is given of the theories of homogeneous nucleation and of growth during condensation from the vapor phase. At the present time the usefulness of these theories remains uncertain or at least quite arguable. The principal current theoretical problems are the kinetic and thermodynamic behavior of ultra-small particles and particularly the accommodation coefficients for the growth of these particles and the possibility of non-Maxwellian vapor-particle collisions when growth is rapid.

A detailed theoretical analysis of condensation in nozzles requires solution of the differential equations of nozzle flow together with nucleation-growth kinetics. With rocket nozzles the influence of chemical reactions among the variety of vapor species on nozzle aerodynamics and particularly on nucleation and growth kinetics must be included. The mathematical equations relating nucleation kinetics to chemical reactions are briefly noted in this paper, but the relevant specific rate constants are unknown.

A semiquantitative insight into condensation in nozzles may be obtained by comparing supersaturations and the simple model of liquid-drop homogeneous nucleation and collision-frequency growth kinetics to the local residence times in the nozzle. This comparison suggests that nonsteady-state nucleation may be a bottleneck in certain cases and that even if particles are nucleated their subsequent growth may be too slow to permit appreciable condensation in the short times available in a nozzle. Clarification will require exact solution of the flow equations together with the 100 or so differential equations describing nonsteady-state nucleation [Eq. (2)] or an equation describing condensation [e.g., Eq. (28)].

Introduction

Condensation is encountered in many practical situations, such as the formation of metal oxide or halide particles in a combustion chamber or expansion nozzle in conventional rocket propulsion, the formation of zinc,[1] mercury,[1] or mercuric chloride particles[2] for use in electrostatic colloid propulsion, and the formation of water or liquid nitrogen drops in a supersonic wind tunnel. Condensation must be avoided completely for most wind tunnel applications, but the equilibrium amount of condensation is desired for most rocket and colloid propulsion applications. Also, thermal and mechanical slippage of particles in a nozzle or the plastering of particles onto the nozzle wall or turbine blades is intimately related to particle size and thus to condensation kinetics. This article reviews recent work on condensation and particularly examines the theoretical condensation behavior of representative systems in a nozzle.

Statement of the Problem

For the present purpose, nozzle flow involves cooling by expansion flow of a vapor mixture containing condensible components. If an equilibrated particle-vapor mixture is passed into the nozzle, the expansion cooling of the vapor will immediately cause the condensable vapor components to become supersaturated and to condense onto the particles. If an undersaturated homogeneous vapor mixture is passed into the nozzle, the vapor will become supersaturated, and particles will form, only at a certain position along the nozzle where the expansion is sufficiently drastic.

For example,[3] almost all rocket propellants which contain oxygen and aluminum or magnesium components should give a condensed oxide phase in the combustion chamber and pass a particle-vapor mixture into the nozzle. Most propellants containing boron and oxygen or lithium and fluorine compounds should form a condensed phase in the chamber, but a few formulations should give particles only in the nozzle and particularly only when expanded to less than 1 atm pressure. In a typical colloid generator being studied for heavy-particle electrostatic propulsion, the incoming vapor phase is saturated and immediately becomes supersaturated in the nozzle.

From a more fundamental viewpoint, the rate

TABLE 1

Metal-Containing Vapor Species in Typical Rocket Systems at Nozzle Entrance

System (moles)	T (°K)	P (atm)	Species (moles/mole metal atom) (100)																				
			Li	B	B_2	BH	LiF	BH_2	BH_3	$(LiF)_2$	B_2H_6	$(LiF)_3$	B_5H_9	HBO	HBO_2	Li_2	$(HBO_2)_3$	H_2BO_2	LiH	H_3BO_3	BO	$(BO)_2$	LiN	B_2O_3
$LiH+0.5N_2F_4$	3439	68	10				87			0.5		10^{-3}				10^{-2}			1			1	
$LiH+N_2F_4$	4598	68	3				96			10^{-2}		10^{-5}				10^{-2}			10^{-2}			0.4	
$B_5H_9+5H_2O_2$	3174	68		10^{-4}	10^{-10}	10^{-7}		10^{-3}	10^{-4}		10^{-12}		10^{-28}	17	63	10^{-4}		10^{-6}		10^{-2}	2	1		7
$B_5H_9+3.75H_2O_2$	2843	68		10^{-4}	10^{-9}	10^{-5}		10^{-2}	10^{-2}		10^{-10}		10^{-23}	31	34	10^{-3}		10^{-7}		10^{-2}	2	6		11
$B_5H_9+2.1N_2O_4$	3931	68		10^{-4}	10^{-7}	10^{-4}		10^{-3}	10^{-4}		10^{-13}		10^{-30}	19	42	10^{-5}		10^{-5}		10^{-2}	17	3		7

of condensation (i.e., the rate of disappearance of vapor molecules) and also the size and number distributions of the product particles involve the simultaneous kinetics of a sequence of nucleation, growth, and agglomeration reactions. Nucleation is defined as the formation of the least stable (thermodynamically or kinetically) cluster or particle of the new phase; nuclei contain less than 100 atoms (molecules, ions) in most cases and perhaps less than 10 atoms in some cases. Growth is the atom-by-atom deposition of new material onto the nucleus or larger particle. Agglomeration is the coalescence of two colliding particles to form a larger particle and includes a particle plastering onto a wall surface. Agglomeration kinetics was reviewed recently[4] and will be omitted here.

The kinetics of condensation will also depend upon whether the vapor phase contains only parent monomer molecules or whether it contains polymeric species or other species which must react chemically to give condensation. The condensation of H_2O or Hg vapor is simple because the vapor presumably contains only monomer molecules. However, condensation in rocket systems may be quite complex because the vapor contains a variety of chemical species; e.g., with a B—O—H propellant, the vapor phase includes HBO_2 and $(HBO_2)_3$ molecules which condense to form liquid B_2O_3 drops and H_2O vapor. Hereafter, the term "simple system" will be used to describe one in which condensation of only monomer vapor is involved. A "complex system" will refer to one in which condensation occurs from polymer and/or other chemical species. Table 1 lists the various metal-containing vapor species according to the JANAF thermodynamic tables[5] and their relative concentrations in typical LiH—N_2F_4, B_5H_9—H_2O_2, and B_5H_9—N_2O_4 rocket systems in order to outline the problem in those systems. A Li—H—F—N system includes 7 Li-containing species while a B—O—H system includes 15 B-containing species, and any or all of these species may be important in condensation.

In general, condensation may be considered to involve a set of chemical reactions of the type

$$P \rightarrow \mathbf{P}$$

$$1/n\ P_n \rightarrow \mathbf{P}$$

$$aA + bB \rightarrow \mathbf{P} + dD$$

where P is a vapor molecule which condenses to form **P**, P_n is a polymeric vapor molecule, and A and B are vapor molecules which react and condense to form **P** and D vapor with a, b and d denoting stoichiometry. The case when the

condensed phase is a mixture[6] is omitted here for simplicity.

The nozzle-condensation problem thus involves condensation kinetics via (1) simple nucleation and growth (wind tunnel and colloid propulsion), (2) complex nucleation and growth (a few rocket systems), or (3) merely complex growth (most rocket systems). The local "residence times" for condensation can be 3μ sec/cm (vapor velocity = 10,000 ft/sec) or less. In a combustion process, particle concentrations are about 10^9 to 10^{11} particles/cc and the end-product particles have diameters as low as 50 Å.[4]

Experimental

Condensation from ordinary impure vapor often occurs readily, but condensation from the pure vapor usually takes place only after an appreciable and moderately critical supersaturation is imposed. Since condensation readily occurs if large particles of the new phase are already present, nucleation is often a bottleneck in condensation—that is, the nucleation of particles is difficult compared to their subsequent growth.

Nucleation can be either homogeneous or heterogeneous. Heterogeneous nucleation occurs when the new phase initially deposits onto foreign impurities (e.g., dust, salt particles, ions) and thus bypasses the more difficult homogeneous nucleation step. Homogeneous nucleation occurs in the absence of such impurities. There is considerable uncertainty whether or not a true homogeneous nucleation ever does occur because the total absence of subtrace amounts of catalytic impurities is unlikely in nature and is difficult to prove even in a laboratory experiment.

Quantitative data on the rate of nucleation from the vapor phase is very limited. It is generally concluded[6,7] (however, see Mason[8] and this writer[9]) that the classical steady-state liquid-drop theory of the kinetics of homogeneous nucleation is in satisfactory qualitative agreement with "critical supersaturation" data obtained with water and various organic vapors in an expansion-type cloud chamber.[10] Some data with water and nitrogen have been obtained in supersonic wind tunnels.[11,12,13,14] Gilmore concluded that nonsteady-state nucleation problems in nozzles are unimportant compared to steady-state nucleation[15] (however, see Wilde[16]). There appears to be no quantitative data on the nucleation of materials occurring in rocket or colloid-generation nozzles.

Quantitative data on the rate of growth of the ultrasmall particles occurring in nozzle condensation and under radiation conditions[17] apparently are completely absent.

Theoretical

Nucleation

Nucleation involves the kinetics of a series of stepwise reactions where vapor molecules combine with a cluster of the daughter phase to form a larger cluster. Any one of these reactions or even a sequence of several reactions could be a bottleneck in a nucleation process. Furthermore, nucleation kinetics may be steady-state or nonsteady-state.

For a simple condensation where monomeric P vapor forms **P** particles (e.g., the condensation of H_2O or Hg vapor), nucleation involves a sequence of kinetic reactions of the type

$$\mathbf{P}_{g-1} + \mathrm{P} \underset{k_g{}^r}{\overset{k_{g-1}}{\rightleftharpoons}} \mathbf{P}_g \qquad (2 \leq g \leq G) \quad (1)$$

where P is a vapor molecule, $\mathbf{P}_g$ is a cluster containing g molecules of P vapor, k_{g-1} and $k_g{}^r$ are specific rate constants for the growth and dissociation reactions, respectively, and G is the number of molecules in a cluster which grows to form a particle. G is usually about 100 or so but can be as small as 40 for the condensation of H_2O at 233°K and as large as 1300 for the condensation of LiF at 2000°K.[18] The kinetics of simple nucleation therefore involve a series of 100 or so differential equations of the type

$$dc_g/dt = q_{g-1}c_{g-1} - r_g c_g + s_{g+1}c_{g+1} \quad (2)$$

where c and c_g are the concentrations of P and $\mathbf{P}_g$ in the system in, e.g., molecules or clusters/cc, $q_g = k_g c$, $s_g = k_g{}^r$, and $r_g = q_g + s_g$. The net flow between $\mathbf{P}_{g-1}$ and $\mathbf{P}_g$ is

$$I_g = q_{g-1}c_{g-1} - s_g c_g. \quad (3)$$

For the general case,[18] kinetic reactions of the type

$$\alpha\mathrm{A} + \beta\mathrm{B} + \mathbf{P}_{g-1} \underset{{}^A k_g{}^r}{\overset{{}^A k_{g-1}}{\rightleftharpoons}} \mathbf{P}_g + \delta\mathrm{D} \quad (4)$$

and

$$\mathrm{P}_2 + \mathbf{P}_{g-2} \underset{{}^2 k_g{}^r}{\overset{{}^2 k_{g-2}}{\rightleftharpoons}} \mathbf{P}_g \quad (5)$$

must also be included, where α, β, and δ denote the kinetic mechanisms, ${}^A k_{g-1}$ and ${}^A k_g{}^r$ are the specific rate constants for the forward and reverse reactions in Eq. (4), and ${}^2 k_{g-2}$ and ${}^2 k_g{}^r$ are the rate constants in Eq. (5). Assuming that the mechanism of the chemical reaction does not change with concentration or cluster size,

$$dc_g/dt = p'_{g-2}c_{g-2} + q'_{g-1}c_{g-1} - r'_g c_g + s'_{g+1}c_{g+1} + t'_{g+2}c_{g+2}, \quad (6)$$

where

$$p'_g = {}^2k_g c_2, \qquad q'_g = k_g c + {}^Ak_g c_A{}^\alpha c_B{}^\beta,$$
$$s'_g = k_g{}^r + {}^Ak_g{}^r c_D{}^\delta, \qquad t'_g = {}^2k_g{}^r,$$

and

$$r'_g = p'_g + q_g{}' + s'_g + t'_g.$$

Also,

$$I_g = p'_{g-2}c_{g-2} + q'_{g-1}c_{g-1} - (s'_g + t'_g)c_g. \quad (7)$$

Any theoretical approach to the kinetics of nucleation must deal with the batch of 100 or so interdependent differential equations in Eq. (2) or (3) for a simple system or Eq. (6) or (7) for a complex system. Even if the kinetic rate constants were known, the resulting mathematical problem obviously would be formidable. The various theoretical approaches assume different approximations in order to simplify the mathematical problem. Only a simple system has hitherto been examined with the single exception that condensation from a mixture of monomer and dimer vapor has been approximately treated by Frisch and Willis (see below).

Steady-State Nucleation (Simple)

In steady state the values of I_g in Eq. (3) are equal and can be replaced by I_g, the steady-state rate of formation of particles in, e.g., particles/cc. sec. Equation (3) can then be rearranged to give

$$I_s = \left(\sum_1^G \frac{1}{k_g c C_g (c/C)^g}\right)^{-1} = \left[\sum_1^G \frac{1}{k_g K_g (c)^{g+1}}\right]^{-1}, \quad (8)$$

where C and C_g are the equilibrium concentrations of P and $\mathbf{P}_g$ and K_g is the thermodynamic equilibrium constant

$$K_g = \frac{k_1 k_2 \cdots k_{g-1}}{k_2{}^r k_3{}^r \cdots k_g{}^r} = \frac{C_g}{(C)^g}. \quad (9)$$

Since $c \approx C$, each term in the denominator of Eq. (8) is directly related to the forward rate of a cluster reaction.

There are three general theories of simple steady-state nucleation wherein values for k_g and K_g are assumed and the sum in the denominator of Eq. (8) is then approximated.

Constant-Number Theory. The constant-number theory assumes that the concentration of a particular-size small cluster, $\mathbf{P}_n$, is always present in its equilibrium concentration because of kinetic or thermodynamic reasons. The number of molecules in the nucleus thus is essentially independent of temperature and supersaturation. The slow step in nucleation could be, for example, the initial formation of a two-atom cluster from monoatomic species because the recombination energy must be radiated or absorbed by a third-body collision; or perhaps it is the latter formation of a cluster containing less than about 10 atoms either because the equilibrium concentration of the P_n cluster is very low since its free energy is very high owing to excess energy reasons[9] or because k_n is very small. Equation (8) then becomes

$$(I_s)_{\text{radiation}} = k_r c_A c_B \quad (10)$$

$$(I_s)_{\text{recomb.}} = k_M c_A c_B c_M \quad (11)$$

$$(I_s)_{\text{excess energy}} = k_n c C_n = k_n K_n c^{n+1} \quad (12)$$

where k_r and k_M are the specific rate constants for the radiation and recombination reactions, c_A and c_B are the concentrations of the recombining species, and c_M is the concentration of the third body. Typically, k_r is about 10^{-15} cc/molecule·sec and k_M is about 10^{-33} cc^2/molecule^2·sec.[19] The radiation and recombination models do not appear to have been applied to nucleation but probably are unimportant (see later).

Liquid-Drop Theory. Most theories of nucleation are formulated in terms of the classical liquid-drop (LD) theory. The LD theory of the thermodynamics of cluster formation assumes that the equilibrium concentration of clusters can be calculated *a priori* in terms of the macroscopic volume and surface free energies of the vapor and condensed phases.

For a simple monomer vapor, the modified version[20] of the classical treatment gives

$$C_g = C_e \exp\{g \ln S - \mu g^{2/3}\} \quad (13)$$

where C_e is the concentration of monomer vapor in equilibrium with bulb condensed phase, S is supersaturation and is equal to c/C_e, $\mu = 4\pi(3m/4\pi\rho)^{2/3}\sigma/kT$, m is the mass of P, ρ is the macroscopic density and σ the macroscopic surface tension of the condensed phase, k is the Boltzmann constant, and T is absolute temperature. In the original version the pre-exponential factor was c. As g increases, C_g goes through a minimum value C_{g^*} given by

$$C_{g^*} = C_e \exp\{-16\pi\sigma^3 m^2/3\rho^2(kT)^3(\ln S)^2\}$$
$$= C_e \exp\{-\mu(g^*)^{2/3}/3\} \quad (14)$$

where g^* is the number of molecules in the cluster present in smallest concentration and is given by

$$g^* = (2\mu/3 \ln S)^3 \quad (15)$$

The $\mathbf{P}_{g^*}$ cluster is conventionally called the LD nucleus. The size of the LD nucleus decreases with increasing S or temperature.

The LD thermodynamic approach has limitations when it is applied to small clusters because σ decreases for small clusters, although this effect tends to be canceled by a similar decrease in ρ. The lower limit of applicability has been taken as a cluster containing 20 molecules,[21,22] 10 molecules,[15,23] and 2 molecules.[24]

The classical LD theories of steady-state nucleation kinetics assumed the Maxwellian mean collision frequency for k_g. Volmer[25] assumed the nucleus to be present in the equilibrium concentration; Becker and Döring[26] and Frenkel[27] derived a rate of nucleation by assuming that the steady-state kinetics of nucleation involved a sequence of similarly slow reactions localized around the nucleus. Becker and Döring took k_g as equal to k_1, while Frenkel took k_g as equal to the more realistic value of k_{g*}. Equation (8) was then converted to a continuous function of g and approximated by assuming $c = C$, substituting the original version of Eq. (13) for C_g, expanding the exponential factor about g (thus presuming C_g to have a sharp minimum at C_{g*}), using integral limits of $+\infty$ and $-\infty$, and evaluating the resulting error integral. Frenkel's result can be written as

$$(I_s)_{\text{Frenkel}} = \alpha_n c C_e (2m\sigma/\pi)^{1/2}(1/\rho) \times \exp\{-\mu(g^*)^{2/3}/3\} \quad (16)$$

where α_n is an accommodation coefficient for nucleation. The pre-exponential factors obtained by the three treatments differed, but the critical exponential factor was identical.

An exact mathematical evaluation[18] of the summation in Eq. (8) indicates the Frenkel I_s tends to be in error by a few per cent because of the mathematical approximations. This error is insignificant compared to experimental errors and uncertainties in α_n, ρ, and σ.

It will be noted that nucleation rates which involved CN kinetics would necessarily be less than nucleation rates predicted by the LD theory.

Statistical Mechanical Theories (Simple). Statistical mechanical techniques[28–31] have been used to predict equilibrium cluster concentrations; for example, the Cahn-Hilliard theory proposes that at high supersaturation the nucleus is larger than predicted by the LD theory. Also, quantum mechanical techniques were used by Taylor *et al.*[32] to predict cluster concentrations.

Steady-State Nucleation (Complex)

Nucleation kinetics in a rocket system probably involves a variety of chemical or polymeric species since appreciable quantities of such species exist in the parent vapor phase.

Frisch and Willis[33] examined nucleation kinetics when the vapor contained an equilibrated mixture of monomer and dimer and obtained

$$(I_s)_{\text{FW}} = \left(\sum_3^G \frac{1 - K'_g}{k'_g C_g}\right)^{-1}, \quad (17)$$

where $k'_g = k_g{}^r + {}^2k_{g-2}{}^r$ and K'_g is a complex alternating series of $k_g{}^r$ and k'_g. They neglected K'_g, approximated the sum at $g = g^*$, and concluded that an appreciable effect due to dinner reaction is found only when the monomer concentration is very small. An exact evaluation of Eq. (17) indicates that the dimer effect can be appreciable but probably still is negligible compared to the other errors.[18]

For the generalized system wherein reactions of the type in Eqs. (4) and (5) must be included, the equilibrium concentration of the $\mathbf{P}_g$ cluster is[18]

$$C_g = C_e \exp\{g \ln \mathbf{S} - \mu g^{2/3}\} \quad (18)$$

where

$$\mathbf{S} = S_1(S_2 S_3 \cdots S_N)^{1/N} \quad (19)$$

where S_1 is the supersaturation of monomer P vapor related to bulk $\mathbf{P}$ (i.e., is the previous S), S_i is the supersaturation of the ith reaction related to P vapor, and N is the number of independent reactions giving $\mathbf{P}$. N is equal to 7 for Li—H—F—N system and 15 for a B—O—H system according to the JANAF tables. For example, if S_2 is the supersaturation of the chemical reaction noted earlier, then

$$S_2 = \frac{c_A{}^a c_B{}^b / c_P c_D{}^d}{C_A{}^a C_B{}^b / C_P C_D{}^d} \quad (20)$$

where the numerator involves actual concentrations and the denominator involves equilibrium concentrations. Only the supersaturations of vapor species which are not in equilibrium with monomer must be included in $\mathbf{S}$. Equations (14) and (15) remain unchanged except that $\mathbf{S}$ replaces S.

Although only one of the variety of possible reactions usually will be rate-controlling in nucleation kinetics, the generalized steady-state rate of nucleation is[18]

$$(I_s)_{\text{general}} = U_g/V_g \quad (21)$$

where U_g and V_g are complicated functions of the rate of the dissociation reactions.

Nonsteady-State Nucleation (Simple)

Nonsteady-state nucleation kinetics are difficult to evaluate exactly, partly because of the mathematical complexity of solving the G

simultaneous differential equations in Eqs. (2) or (6) but mainly because of uncertainty in the kinetic and thermodynamic behavior of small clusters. Only the simple system has been examined although the complex system exemplified by Eq. (6) is readily amenable to computer solution.

Most authors used the kinetic and thermodynamic assumptions of the classical LD theory and approximated the mathematical problem by accepting Frenkel's conversion of the right-hand side of Eq. (2) to a continuous function of c_g and approximating the resulting mathematical expression in various ways.

Kantrowitz,[34] Probstein,[35] Collins,[36] and Wakeshima[37] assumed that only clusters in the vicinity of the nucleus were important. The result for the first three authors was

$$I_{g*} = (K/t)^{1/2} \times \exp\{-(2\pi m/kT)^{1/2} 4\pi\sigma/P_e S(\ln S)^2 t\}, \quad (22)$$

where I_{g*} is the net rate of nucleation at time t, K is a constant, and P_e is the vapor pressure of the bulk condensed phase in dynes/cm^2. The authors obtained different values for K, but all took the time lag for the establishment of steady state as the time when the exponential was unity. This time lag thus is the time for I_{g*} to be about $\frac{1}{4}$ of I_s. Wakeshima's time lag was smaller by 8π.

Christiansen[38] obtained an exact mathematical solution of a batch of four equations from Eq. (2) after assuming all k_g were equal, all k_g^r were equal, and $k_g c \gg k_g^r$. Gilmore[15] obtained semi-exact mathematical solutions of batches of 100 or more equations by numerical methods, but applied the LD theory to small clusters and used approximate values for k_g and k_g^r. He concluded that steady state in water vapor in air at 0°C was established in less than 0.1 μsec. Turnbull[39] solved batches of 4 and 25 of the differential equations on a computer using arbitrary numbers for k_g and k_g^r. This writer[22] solved batches of 100 and 200 of the equations on a computer, using collision-frequency kinetics and LD thermodynamics with the boundary conditions that the P_{19} cluster was at its equilibrium concentration and the concentrations of the P_{20}, P_{21}, etc., clusters were, e.g., zero at zero time. The physical usefulness of this approach must remain uncertain because the P_{19} cluster in a typical cloud-chamber experiment must increase from an initial value of 10^{-9} clusters/cc to an equilibrium value of 2 clusters/cc and the actual build-up time depends in part upon the particular experiment. The times required for e_{g*} to reach 95% of its steady-state value were a few microseconds for the condensation of water vapor at typical cloud-chamber conditions. The approximate time lag estimated by Eq. (22) was within 100% of the exact 95% time[18] and probably is sufficiently accurate for most purposes.

A serious limitation to the LD approach is that the time required for the dynamic surface energy to reach its steady-state static value has been neglected, although this time is reported to be about 1 millisec for water[40] and several minutes for mercury.[41,42]

Growth

The rate of growth of a particle depends upon the kinetics of a sequence of bulk diffusion (mass and heat), adsorption, surface and desorption reactions.

When the mean free path for vapor-vapor collisions is much larger than the particle radius, the vapor-particle collisions should resemble the discontinuous nature of vapor-vapor collisions. For a simple system where vapor diluted with inert gas is *slowly* condensing, the collisions between vapor and a particle should be Maxwellian. If temperature equilibration between the growing particle and vapor-inert gas mixture is also assumed, collision-frequency-controlled growth of a spherical particle gives[18]

$$dR/dt = (\alpha_g mc/4\rho)[(R_P/R) + 1]^2 \times \{(8\pi kT/m)[(m/m') + 1]\}^{1/2}, \quad (23)$$

where R is the radius of the growing particle at time t, α_g is the accommodation coefficient for growth (assumed constant) and is the probability that a molecule which hits the particle will be incorporated into it, m' is the mass of the particle, and R_p is the effective collision radius of the condensing vapor molecule. Equation (23) applies to a polydisperse colloid system. When the radius of the particle is much greater than that of the molecule, Eq. (23) reduces to a linear growth law

$$dR/dt = (\alpha_g/\rho)(mkT/2\pi)^{1/2} c. \quad (24)$$

When condensation is rapid, the collision frequency for vapor-particle collisions can become non-Maxwellian, particularly if a high heat of condensation is involved. Frisch and Collins[43] treated this case for a spherical particle in a monodisperse colloid and obtained

$$dR/dt = [4\pi R_\infty^3 D c_n/3(\gamma + R)][1 - (R/R_\infty]^3 \quad (25)$$

where R_∞ is the final particle radius, D is the

diffusion coefficient of P vapor, $\gamma = 2\langle s^2 \rangle / 3\langle s \rangle \alpha_0$ where $\langle s \rangle$ and $\langle s^2 \rangle$ are the mean jump length and mean square jump length for vapor-particle collisions, and c_n is the particle concentration. If $\gamma \gg R$ and $\langle s \rangle$ is Maxwellian, Eq. (25) reduces to Eq. (24). Frisch and Collins' corresponding equation for particle growth in a polydisperse colloid is unwieldy even if the particle-distribution function were known.

When the particle radius is much greater than the mean free path for vapor–vapor collisions, the parent vapor is essentially a continuous medium and Fick's diffusion equation should apply. Bulk-diffusion-controlled growth has no rigorous mathematical solution,[44] but approximate solution of Fick's equation for quasi-steady-state spherical diffusion of mass and heat (radiation neglected) in a simple system indicates parabolic growth kinetics for large single particles,[44–46] or

$$dR^2/dt = Kc, \qquad (26)$$

where K is a constant. Equation (25) reduces to (26) when $R \gg \gamma$ and then applies to isothermal mass-diffusion-controlled growth in a monodisperse colloid. Also, the particle radius raised to the third power vs. time has been proposed an approximation,[47] and a radius to the 4.4 power vs. time has been observed.[48] Oscillating growth rates could occur in diffusion-controlled growth if transient currents disrupt and quasi-steady-state diffusion gradient in the bulk phase.[49] The growth of a particle is fastest when limited by bulk diffusion disrupted by convection, is slower when limited by the quasi-steady-state diffusion gradient, and is slowest when limited by a surface reaction.

Particle growth in a complex system again should usually be controlled by the kinetics of a single species and thus would usually follow one of the above treatments. The kinetics of competing surface reactions has often been examined in the literature.[50]

The growth kinetics of a particle particularly depends upon the mechanism whereby new material deposits onto its surface. The surface of a liquid drop in contact with its vapor presumably is atomically rough or "melted," and a new molecule can deposit rapidly at almost any position on the surface. However, the surface of a solid particle in contact with its vapor is probably atomically smooth and a new molecule would only deposit either very slowly by a two-dimensional nucleation of an "island" on the surface or rapidly at kinks in the spiral surface steps generated by a screw-dislocation emerging from the surface of the imperfect particle.[51] Theoretically, a solid particle which is bound by nondislocated close-packed surfaces would not grow despite an appreciable supersaturation in the vapor phase. This has been experimentally observed in growth from aqueous solution.[52,53]

The principle current theoretical problems in growth kinetics are (a) the accommodation coefficient for particle growth and particularly for small particles, (b) the growth behavior of particles when the particle radius is much less than the mean free path for vapor-vapor collisions and when the particles may be undergoing non-Maxwellian collisions, and (c) radiation cooling.[17] When growth involves a chemical reaction, the accommodation coefficient must involve the usual activation energy and is probably less than one. The accommodation coefficient for simple condensation of a material onto an infinite liquid surface has been interpreted[54] in terms of the "free angle of rotation" in the liquid phase.[55] A vapor molecule must preserve its rotational energy during condensation and an adsorbed molecule would tend to re-evaporate if it must lose some of this rotational energy in order to fit into a restricted liquid lattice.

Condensation Kinetics

In a simple system, the rate of condensation at any time can be written in terms of a collision-frequency growth model as

$$-(\partial c/\partial t)_V = \alpha_0 \beta (c - C_e) S_t, \qquad (27)$$

where $-(\partial c/\partial t)_V$ is the rate of disappearance of vapor molecules at constant volume, β is the collision frequency per unit particle area and unit vapor concentration of vapor molecules against the particle, and S_t is the total surface area/cc in the system at time t. The rate of disappearance of vapor molecules due to nucleation is negligible compared to Eq. (27).

When a particle–vapor mixture is passed into the nozzle and only particle growth occurs, S_t depends upon the initial size distribution of the particles at the nozzle entrance and their subsequent growth in the nozzle. Very little is known about the initial particle-size distribution in combustion systems.

When a homogeneous vapor is passed into the nozzle, the rate of condensation can be written in terms of nucleation and growth kinetics. Assuming a simple constant-volume system and also classical steady-state LD nucleation of liquid nuclei, rapid freezing of these liquid nuclei, Maxwellian collision-frequency growth of spherical solid particles, and thermal equilibrium between vapor and particles, the concentration

of vapor at time t is[18]

$$c = c_0 - K_1 \int_0^t T^{3/2}(c - (C_e)_s) \times \left[\int_0^t c(C_e)_l \sigma_l^{1/2} \exp\{-K_2 \sigma_l^3 / T^3 (\ln[c/(C_e)_l])^2\} \right] \times \left[\int_{t'}^t (c - (C_e)_s)\, dt \right]^2 dt'\, dt, \quad (28)$$

where c_0 is the initial monomer concentration, $(C_e)_s$ and $(C_e)_l$ are the vapor concentrations in equilibrium with bulk solid and liquid, σ_l is the macroscopic surface tension of the bulk liquid, t' is the time when a particle was nucleated ($t - t'$ is the age of the particle), and

$$K_1 = 4\pi m^2 (\alpha^3 g / \rho_s^2 \rho_l)(k/2\pi m)^{3/2} \alpha_n (2m/\pi)^{1/2} \quad (29)$$

$$K_2 = 16\pi m^2 / 3\rho_l^2 k^3,$$

where ρ_s and ρ_l are the macroscopic densities of bulk solid and liquid. The temperature-dependent functions can in turn be related to supersaturation and t by the heat of condensation and heat capacity of the particular vapor mixture. Equation (28) can readily be solved by a computer after conversion of integrals to intervals. Also, Eq. (28) simplifies somewhat if condensation is isothermal and if nucleation and growth of only solid or liquid particles is assumed. Solution of Eq. (28) gives a sigmoidal c–t curve from which, for example, the time required to achieve 50% of condensation may be taken. Condensation involving nucleation and growth of liquid particles is faster than condensation involving only solid particles.[18]

Condensation from a complex vapor system requires use of S and inclusion of the more complicated variations of nucleation [Eq. (21)] and growth kinetics. However, if the condensation of monomer is slow compared to reactions involving the other vapor species, the nucleation and growth processes are simple and Eq. (28) applies.

Application

Condensation in a nozzle is occurring from a dynamic vapor system whose local temperature, pressure, and composition are continuously changing with time. An exact analysis of nozzle-condensation kinetics therefore requires a simultaneous solution of the differential equations which describe (a) the aerodynamics of nozzle flow, (b) a particular nozzle geometry, (c) any vapor-phase chemical reactions, and (d) nucleation-growth kinetics of the type in Eq. (28) or a

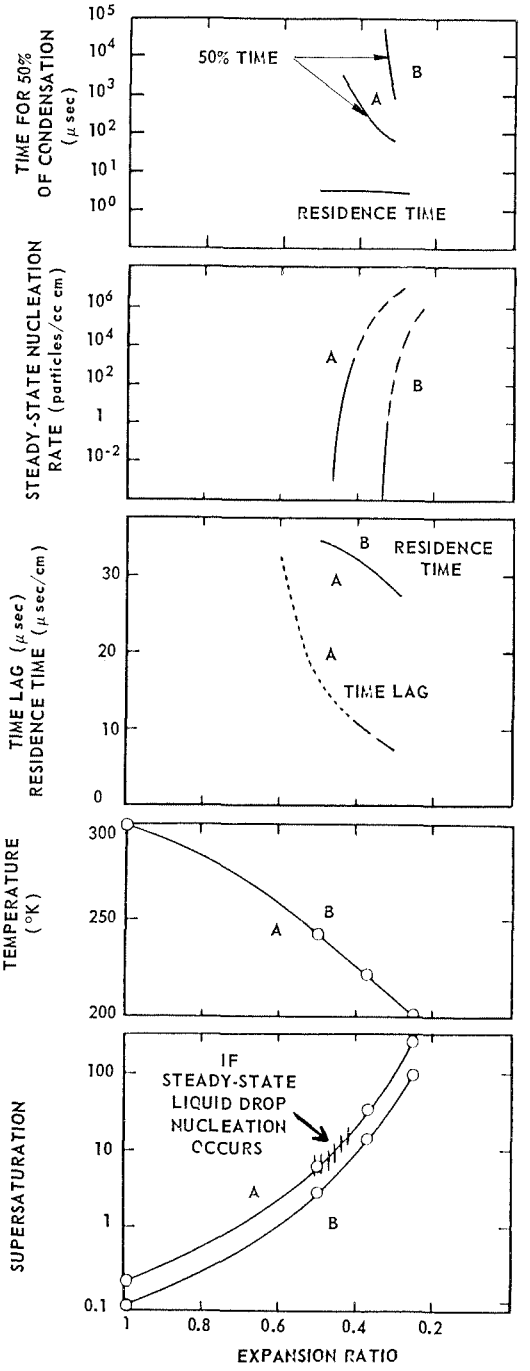

FIG. 1. Typical condensation conditions obtained with H_2O–N_2 in a nozzle. Initial conditions: (A) N_2 + 0.0061H_2O (saturated at 273°K, 1 atm, 298°K); (B) N_2 + 0.0028H_2O (saturated at 263°K, 1 atm, 298°K).

more complex variation. Simultaneous solution of these equations by a computer would give an exact solution to the mathematical problem of nozzle condensation. Unfortunately, the specific rate constants for the various vapor-cluster reactions are quite unknown and even the rate constants for the various vapor-vapor reactions in the complex systems are usually unknown.

However, a semi-quantitative insight into nozzle condensation can be obtained by calculating the degrees of supersaturation at successive positions along the nozzle when condensation arbitrarily is not permitted to occur, and comparing the theoretical LD nucleation rates and also condensation rates (assuming a simple system with $\alpha_g = 1$) at these supersaturations with the local residence times. These simple theoretical models serve as approximate upper limits for nucleation and condensation rates because in a simple system the LD nucleation rate is necessarily the upper limit, and in a

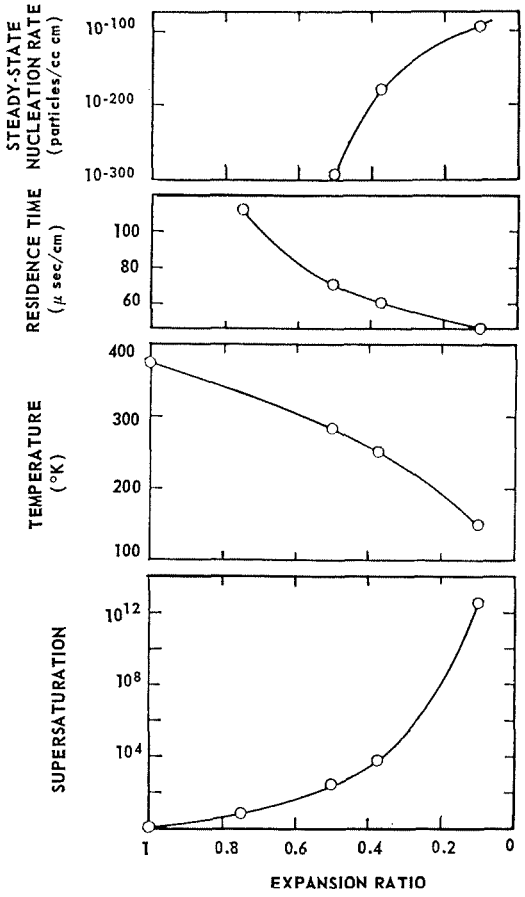

FIG. 2. Typical condensation conditions obtained with Hg vapor in a nozzle. Initial conditions: 3.59×10^{-4} atm, 373°K (saturated).

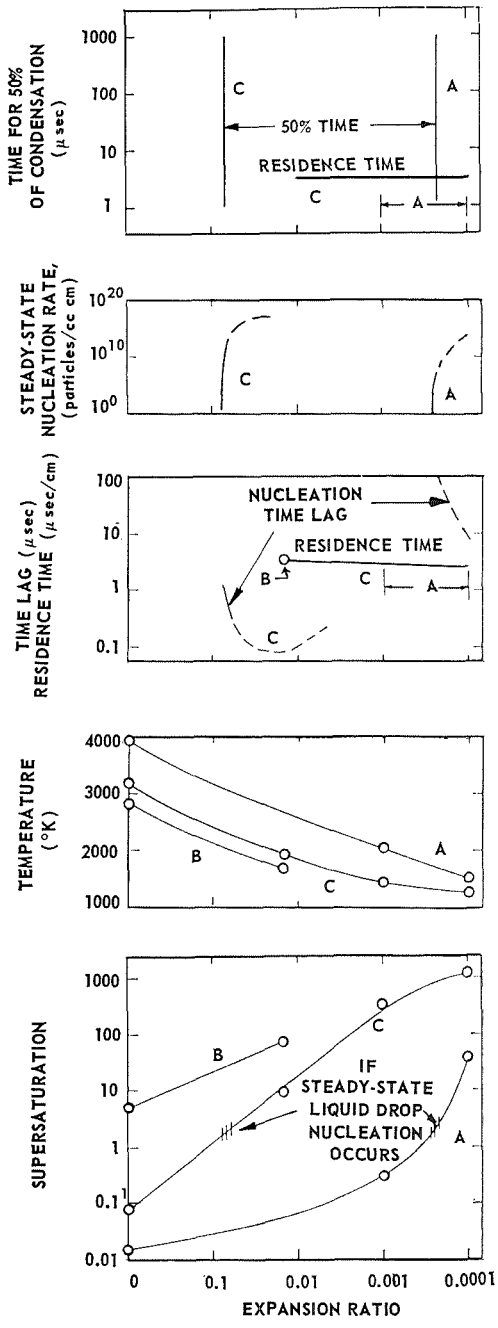

FIG. 3. Typical condensation conditions obtained with semishifting expansion of combustion products from B–O–H propellants. Initial nozzle conditions: (A) 3922°K, 68 atm (obtained from $B_5H_9 + 2.1N_2O_4$ at 298°K); (B) 2843°K, 68 atm (obtained from $B_5H_9 + 3.75H_2O_2$ at 298°K); (C) 3175°K, 68 atm (obtained from $B_5H_9 + 5H_2O_2$ at 298°K).

complex system the collision-frequency behaviors of the assumed simple vapor and the actual complex vapor will be similar but the actual α_g will be less than 1 since a chemical reaction is involved.

Figures 1 to 4 give typical local supersaturations, temperatures, residence times, theoretical time lags for nonsteady-state LD nucleation, and the theoretical 50% times required for condensation at constant volume which were obtained along an expansion nozzle for several systems. Semishifting expansion was assumed,

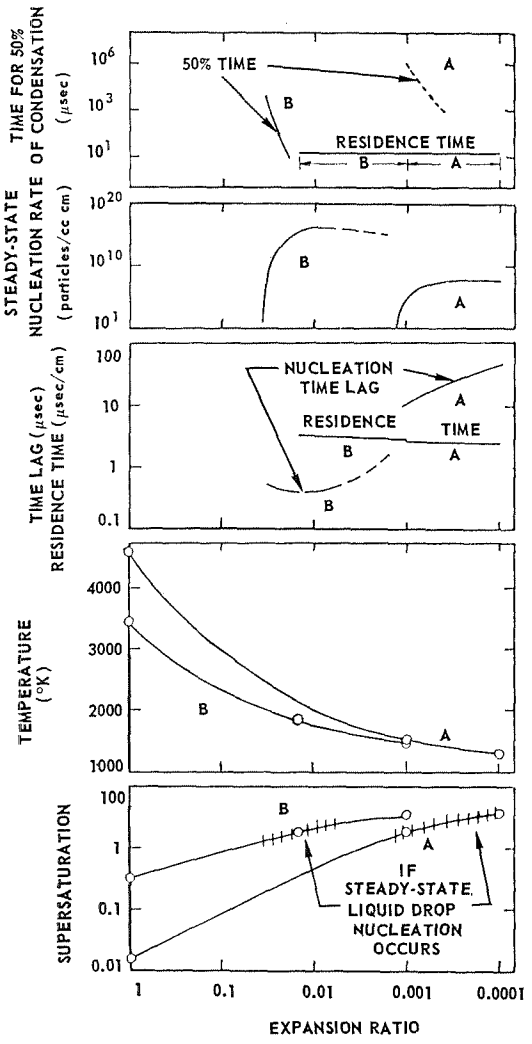

FIG. 4. Typical condensation conditions obtained with semishifting expansion of combustion products from Li–F propellants. Initial nozzle conditions: (A) 4598°K, 68 atm (obtained from LiH + $0.5N_2F_4$ at 298°K); (B) 3439°K, 68 atm (obtained from LiH + $0.25N_2F_4$ at 298°K).

wherein all vapor species were assumed to equilibrate with each other but no condensation was permitted. The expansion ratio is the final pressure divided by the initial pressure. JANAF data were used to calculate the rocket supersaturations, and supersaturations generally are somewhat questionable because of uncertainties in the thermodynamic data. The LD nucleation rates assumed a liquid condensed phase and also are often uncertain because the required data had to be extrapolated from other temperatures. The nucleation time lags were calculated for water from the exact Eq. (2) and for the other systems from the approximate Eq. (22). The steady-state nucleation rate *along the nozzle* was obtained by multiplying the nucleation rate from Eq. (16) (calculated as particles/cc·μsec) by the reciprocal of the linear gas velocity. Dashed lines indicate that the LD g^* is less than 20 molecules. Dotted lines indicate extrapolations. Details are given elsewhere.[18]

Supersaturations to 430 were encountered with H_2O, to 10^{12} with Hg, and to 3.5 in semishifting expansion and to 10^{36} in frozen expansion in the rocket systems.

It will be noted that the LD theories of nucleation apply to only short sections of the nozzle because at low supersaturations the steady-state rate of LD nucleation is negligible but at high supersaturations g^* becomes less than 20 and the LD theory becomes inapplicable.

A nonsteady-state kinetic problem should be expected when the time lag is similar to or greater than the local residence time. Similarly, a condensation problem would be expected if the time required for 50% of condensation (computed assuming steady-state LD nucleation and collision-frequency growth) is greater than the local residence time.

With H_2O vapor, computer solution of Eq. (2)[22] indicates a 95% time for the establishment of steady-state nucleation of 10 μsec when $S = 15$ at 233°K. The present wind-tunnel example in Fig. 1 has a local residence time of about 32 μsec at that temperature (case A, expansion ratio = 0.45). Since the residence time is appreciably greater than the time lag, steady-state nucleation probably is established in the present case. However, the local supersaturation increases from about 10 to only 20 as the temperature decreases from about 240 to 230°K. The steady-state rate of nucleation increases from about 1 to 100 particles/cc·μsec, or about 30 to 3000 particles/cc·cm along the nozzle. For comparison, the isothermal condensation of H_2O at 233°K and $S = 15$ theoretically requires about 10,000 μsec to achieve 50% of condensation.[9] Therefore, even though particles are nucleated,

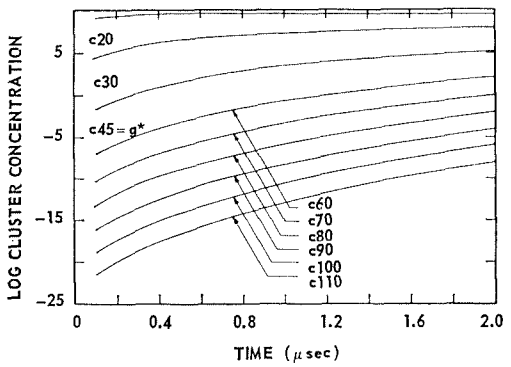

FIG. 5. Variation of concentrations of liquid B_2O_3 clusters with time at 1700°K and $S = 2$.

only a small amount of condensation should be expected in the available time.

Hg vapor has a negligible steady-state rate of LD nucleation because of the high surface tension of liquid Hg, and Hg vapor should not nucleate homogeneously under the noted conditions despite the high supersaturation.

The condensation problem in a B—O—H or Li—F nozzle system depends upon the particular system. Figures 3 and 4 show that with cases *A* the approximate nucleation time lags are appreciably greater than the local residence times, and nonsteady-state problems should be expected. The time lags for the other cases are less than the residence times, and steady-state nucleation should be approached. For example, monomeric LiF vapor at $S = 1.8$ establishes steady state in about 0.03 and 10 μsec at 1854° (case B) and 1521°K (case A), respectively, where the values for g^* are 27 and 105 molecules. The local residence times are only 3 μsec, and case A probably involves a nonsteady-state nucleation problem. With B_2O_3 vapor at 1700°K and $S = 2$, Fig. 5 shows that nucleation requires greater than 2 μsec to establish steady state according to computer solution of Eq. (2).[18] However, the local residence time in Fig. 3 is about 3 μsec for these conditions with case A. The times required for 50% of condensation are all less than the local residence times except for case A in the LiF system, and a condensation problem may be expected in that instance. It will be noted that with case A in the B_2O_3 system a nonsteady-state nucleation problem was anticipated and the predicted 50% time for condensation is invalid since this 50% time presumes steady-state nucleation. Results are summarized in Table 2.

It is perhaps of interest to note that the radiation and recombination aspects of the CN theory of nucleation do not apply to the present systems (excepting Hg) because the molecular species should already be present at the nozzle entrance in sufficient quantities to nucleate particles. It is generally difficult to decide about the excess-energy aspect of the CN theory. However, it will be noted (Table 1) that the Li–F systems already contain high concentrations of dimer and trimer molecules, e.g., the trimer concentration typically is 10^{11} trimers/cc after frozen expansion and 10^{15} trimers/cc after semishifting expansion. In either case, these concentrations would be sufficient to nucleate the 10^{10} or so particles/cc presumably required to achieve condensation. In any event, CN nucleation rates can be estimated by Eq. (12) assuming collision-frequency kinetics and JANAF thermodynamic data. Values of the mean collision frequency for monomer-dimer and monomer-trimer collisions for case A in Fig. 4 at $S = 1.8$ and 1521°K were about 10^{14} times the corresponding values of LD nucleation. Since it is unlikely that the accommodation coefficient would be as small as 10^{-14}, the LD theory predicts slower nucleation and would be applicable rather than the CN theory. However, the mean collision frequency for monomer-dimer and monomer-trimer collisions at $S = 1.8$ and 1854°K for case B in Fig. 4 is only 10-fold greater than $(I_s)_{LD}$, and the CN theory may be applicable if the accommodation coefficient is small.

TABLE 2

Summary of "Predicted" Condensation Behavior for Selected Nozzle Cases

Problem	Wind tunnel	Hg colloid generator	B–O–H propellants (A)	B–O–H propellants (C)	Li–F propellants (A)	Li–F propellants (B)
Nonsteady-state nucleation?	No	?	Yes	No	Yes	No
Rate of condensation?	Yes	Yes	(No)	No	Yes	No
Does condensation occur?	No	No	No	Yes	No	Yes

ACKNOWLEDGMENT

This work was supported by the Office of Naval Research.

REFERENCES

1. ANON.: Annual Report on Propellants for Electrical Propulsion Engines of the Contact or Bombardment Ion Type, Rocketdyne, ASD Tech. Rept. 61–150, March 15, 1961.
2. NORGREN, G. C.: Lewis Flight Research Center, Cleveland, personal communication.
3. DOBBINS, T. O.: Thermodynamics of Rocket Propulsion and Theoretical Evaluation of some Prototype Propellant Combinations, WADC TR–59–757, Wright Air Development Center, Dayton, December 1959.
4. COURTNEY, W. G.: ARS Journal *31*, 751 (1961).
5. JANAF Interim Thermochemical Tables, The Dow Chemical Company, Midland, Michigan, September 30, 1961.
6. REISS, H.: J. Chem. Phys. *18*, 840 (1950).
7. DUNNING, W. J.: Discussions Faraday Soc. *30*, 9 (1961); also, see reference 9.
8. MASON, B. J.: Discussions Faraday Soc. *30*, 20 (1961).
9. COURTNEY, W. G.: J. Chem. Phys. *36*, 2018 (1962).
10. VOLMER, M. and FLOOD, H.: Z. physik. Chem. *A170*, 273 (1934).
11. STEVER, H. G.: Condensation Phenomena in High Speed Flow, in *Fundamentals of Gas Dynamics*, Vol. III, p. 526. Princeton Univ. Press, 1958.
12. WEGENER, P. P. and MACK, L. M.: Condensation in Supersonic and Hypersonic Wind Tunnels, in *Advances in Applied Mechanics*, Vol. 5. Academic Press, 1958.
13. WILLMARTH, W. W. and NAGAMATSU, H. T.: J. Appl. Phys. *23*, 1089 (1952).
14. BOGDONOFF, S. M. and LEES, L.: Study of the Condensation of the Components in Air in Supersonic Wind Tunnels. Part 1. Absence of of Condensation and Tentative Explanation, Princeton Univ., Aeronautical Eng. Lab. Rept. No. 146, May 25, 1949.
15. GILMORE, F.: The Dynamics of Condensation and Vaporization, Ph.D. Thesis, California Institute of Technology, 1951.
16. WILDE, K. A.: J. Appl. Phys. *30*, 577 (1959).
17. FUCHS, N. A.: *Evaporation and Droplet Growth in Gaseous Media*, p. 14. Pergamon Press, 1959.
18. COURTNEY, W. G.: Kinetics of Condensation from the Vapor Phase, Texaco Experiment Inc. TM–1340, 1962.
19. ZINMAN, W. G.: ARS Journal *30*, 233 (1960).
20. COURTNEY, W. G.: J. Chem. Phys. *35*, 2249 (1961).
21. REISS, H.: Ind. Eng. Chem. *44*, 1284 (1952).
22. COURTNEY, W. G.: J. Chem. Phys. *36*, 2009 (1962).
23. BUCKLE, H. E.: Proc. Roy. Soc. (London) *A261*, 189 (1961).
24. FRISCH, H. L.: J. Chem. Phys. *27*, 90 (1957).
25. VOLMER, M.: *Kinetik der Phasenbildung*. Edward Brothers, 1945.
26. BECKER, R. and DÖRING, W.: Ann. Physik *24*, 719 (1935).
27. FRENKEL, J.: *Kinetic Theory of Liquids*. Dover, 1955.
28. MAYER, J. E.: J. Chem. Phys. *5*, 67 (1937).
29. YANG, C. N. and LEE, T. D.: Phys. Rev. *87*, 404 (1952).
30. REISS, H.: J. Chem. Phys. *20*, 1216 (1952).
31 CAHN, J. W. and HILLIARD, J. E.: J. Chem. Phys. *31*, 688 (1959).
32. TAYLOR, H. S., EYRING, H., and SHERMAN, A.: J. Chem. Phys. *1*, 68 (1935).
33. FRISCH, H. L. and WILLIS, C.: J. Chem. Phys. *22*, 243 (1954).
34. KANTROWITZ, A.: J. Chem. Phys. *19*, 1097 (1951).
35. PROBSTEIN, R. F.: J. Chem. Phys. *19*, 619 (1951).
36. COLLINS, F. C.: Z. Elektrochem. *59*, 404 (1955).
37. WAKESHIMA, H.: J. Chem. Phys. *22*, 1614 (1954).
38. CHRISTIANSEN, J. A.: Acta Chem. Scand. *8*, 909 (1954).
39. TURNBULL, D.: Metals Technol., p. 774. June 1948.
40. GÖRING, W.: Z. Elektrochem. *63*, 1069 (1959).
41. COOK, S. J.: Phys. Rev. *34*, 513 (1929).
42. LEMARCHANDS, M. and CONVERS, L.: J. Chem. Phys. *32*, 657 (1935).
43. FRISCH, H. L. and COLLINS, F. C.: J. Chem. Phys. *21*, 2158 (1953).
44. KIRKLADY, J. S.: Can. J. Phys. *36*, 446 (1958).
45. HAMM, F. S.: J. Appl. Phys. *30*, 1518 (1959).
46. MORRISON, J. A. and FRISCH, H. L.: J. Appl. Phys. *31*, 1621 (1960).
47. GREENWOOD, G. W.: Acta Met. *4*, 243 (1956).
48. LUBORSKY, F. E.: J. Phys. Chem. *61*, 77 (1957).
49. LAITINEN, H. A. and KOLTHOFF, I. M.: J. Am. Chem. Soc. *61*, 3344 (1939).
50. GLASSTONE, S., LAIDLER, K. J., and EYRING, H.: *The Theory of Rate Processes*. McGraw-Hill, 1941.
51. BURTON, W. K., CABRERA, N., and FRANK, F. C.: Phil. Trans. Roy. Soc. (London) *A243*, 299 (1951).
52. KRUEGER, G. C. and MILLER, C. W.: J. Chem. Phys. *21*, 2018 (1953).
53. COURTNEY, W. G.: J. Chem. Phys. *27*, 1349 (1957).
54. WYLLIE, G.: Proc. Roy. Soc. (London) *A197*, 383 (1949).
55. MORTENSEN, E. M. and EYRING, H.: J. Chem. Phys. *64*, 846 (1960).

GAS PARTICLE NOZZLE FLOWS

JAMES R. KLIEGEL

The equations governing the one-dimensional flow of gas-particle mixtures are discussed. It is shown that the sound velocity in the mixture is the frozen sound velocity in the gas alone and is unaffected by the presence of the particles unless the mixture is always in equilibrium. The equilibrium sound velocity in the mixture is derived and is shown to be lower than the frozen sound velocity. Shock waves in gas-particle mixtures are discussed and it is shown that two shock structures are possible. When the flow velocity in front of the shock is supersonic (based on the frozen speed of sound), the shock consists of a discontinuous shock front followed by a relaxation zone. When the flow velocity in front of the shock is greater than the equilibrium sound speed but less than the frozen sound speed, the shock is fully diffuse and consists of a relaxation zone in which both the gas and particle properties vary continuously. The frozen sound velocity is found to occur downstream of the nozzle throat for all gas-particle nozzle flows. It is shown that the throat conditions depend on the nozzle inlet geometry, and that the nozzle mass flow and performance are determined by the nozzle inlet geometry. Analytical and numerical solutions to the equations governing the one-dimensional flow of gas-particle mixtures through nozzles are presented. The particle velocity and thermal lags are found to be greatest at the nozzle throat and expressions are given for estimating these lags.

The equations governing axially symmetrical flows of gas-particle mixtures are briefly discussed. These equations are of hyperbolic type when the flow is supersonic (based on the frozen speed of sound in the gas) and can be solved by the method of characteristics. A sample nozzle calculation is given and compared with one-dimensional calculations. A summary is given of all gas-particle nozzle experiments and the results are compared to the calculated gas-particle nozzle flows. It is found that the calculations and experiments are in agreement within the accuracy of the experimental measurements. It is concluded that the flow of gas-particle mixtures can be accurately predicted by the present analysis.

Introduction

The use of propellants with metal additives has greatly increased in recent years. The exhaust products of these propellants contain a large fraction of condensed oxides and the expansion of such a gas-particle mixture through nozzles has been extensively studied in recent years. Engine firing experience has shown that the efficiency of metallized propellants (delivered impulse/theoretical impulse) is lower than the efficiency of nonmetallized propellants. This decreased efficiency has been observed to be approximately proportional to the particle mass fraction in the exhaust mixture. One can explain the above observations by postulating incomplete combustion of the metal additives. Chemical analysis of particles collected from the exhaust of such propellants has shown only trace amounts of unburned metal, however. These amounts (typically 0.2% of the total metal in the sample) correspond to performance losses much smaller than observed. This evidence suggests that the observed efficiency losses of metallized propellants are not primarily caused by incomplete combustion of the metal additives. It has also been observed that nozzle performance predictions based on treating the gas-particle exhaust of metallized propellants as an equivalent perfect gas can be seriously in error. In particular, large nozzle losses have been observed when optimum contoured nozzles (calculated assuming gas-particle equilibrium) were used with metallized propellants.

It would appear from the above observations that nonequilibrium effects are important in metallized propellant systems and should be considered in making performance predictions for these propellants. Early studies of gas-particle nozzle flows are summarized by Altman and Carter.[1] These studies placed bounds on the performance losses by examining the equilibrium and complete nonequilibrium cases and demonstrated that gas-particle velocity nonequilibrium had a much larger effect on performance than gas-particle thermal nonequilibrium. Gilbert,

Davis, and Altman[2] were the first to relate performance losses to particle size. They studied the velocity history of particles moving through a given gas flow in the nozzle and estimated performance losses from the gas-particle velocity lag at the nozzle exit plane. All of these early studies treated the nozzle expansion process as uncoupled since the particle velocity and thermal lags were considered independently, and the effect of the particles on the gas expansion was ignored.

The object of this paper is to summarize recent theoretical studies of gas-particle nozzle flows which include the most important coupling effects and to compare the results of these studies with experimental measurements. It will be shown that the behavior of gas-particle mixtures is quite similar to the behavior of chemically reacting gases.

One-Dimensional Gas-Particle Flow Equations

Let us consider the steady one-dimensional flow of a gas-particle mixture. The following assumptions will be made: (1) There are no mass or energy losses from the system; (2) there is no mass exchange between the phases; (3) the volume occupied by the particles is negligible; (4) the thermal (Brownian) motion of the particles is negligible; (5) the particles do not interact; (6) the gas is inviscid except for its interactions with the particles; (7) the gas is a perfect gas of constant composition; (8) the particle size distribution may be approximated by groups of different size spheres; (9) the internal temperature of the particles is uniform; (10) energy exchange occurs between the gas and particles only by convection; and (11) the heat capacity of the gas and particles are constant.

These assumptions have been used in previous[3–9] studies of gas-particle nozzle flows. It is easily verified[1,3] that they are reasonable for most gas-particle nozzle flows.

Using the above assumptions, the equations governing the steady one-dimensional flow of a gas-particle mixture are

$$\rho_g u_g A = \dot{w}_g \tag{1}$$

$$\rho_{pi} u_{pi} A = \dot{w}_{pi} \tag{2}$$

$$\dot{w}_g du_g + \sum_{i=1}^{N} \dot{w}_{pi} du_{pi} + A dP_g = 0 \tag{3}$$

$$\dot{w}_g\left[C_{pg}(T_g - T_{g0}) + \tfrac{1}{2}u_g^2\right] + \sum_{i=1}^{N} \dot{w}_{pi}\left[C_{pp}(T_{pi} - T_{g0}) + \tfrac{1}{2}u_{pi}^2\right] = 0 \tag{4}$$

$$P_g = \rho_g R T_g \tag{5}$$

$$u_{pi}(du_{pi}/dx) = \tfrac{9}{2}(\mu_g f_{pi} r^*/m_p r_{pi}^2)(u_g - u_{pi}) \tag{6}$$

$$u_{pi}(dT_{pi}/dx) = -3(\mu_g g_{pi} r^*/m_p r_{pi}^2)(C_{pg}/PrC_{pp})(T_{pi} - T_g) \tag{7}$$

The momentum and energy equations, Eqs. (3) and (4), are seen to contain terms coupling the gas and particle momentum and energy. Thus the coupling between the gas and particles will be very strong and any particle lags (either velocity or thermal) can be expected to have a large effect on the gas flow if the particle loading is appreciable. Since the particle mass fraction is typically 30% by weight of the exhaust of metallized propellants, gas-particle nonequilibrium effects can be anticipated if the characteristic relaxation distances for particle velocity and thermal lags are of the same order as a characteristic nozzle dimension. Equations (6) and (7) show that the characteristic relaxation lengths are of the same order for particle velocity and thermal lags and are proportional to the ratio of a characteristic nozzle dimension to the square of the particle size. The particle size will thus have a strong effect on the particle velocity and thermal lags and these lags will be approximately proportional to the square of the particle size.

For fixed chamber conditions, two gas-particle nozzle flows will be similar in geometrically similar nozzles if the ratio of the nozzle throat size to the square of the particle size is similar in both nozzles. Thus one can scale gas-particle nozzle flow only if the particle size can be scaled as the square root of the nozzle size. Since the particle size formed during propellant combustion is independent of any nozzle or engine characteristic dimension, the establishment of similarity through scaling is not possible in engine firings.

Sound Propagation

Let us examine the conditions under which an infinitesimal discontinuity may exist in a gas-particle flow. If P_g is eliminated from the momentum equation, Eq. (3), by use of Eqs. (1), (4), and (5), the momentum equation becomes

$$(M^2 - 1)\frac{du_g}{u_g} + \frac{1}{RT_g}\sum_{i=1}^{N}\frac{\dot{w}_{pi}}{\dot{w}_g} \times \left[\left(u_g - \frac{\gamma - 1}{\gamma}u_{pi}\right)du_{pi} - \frac{\gamma - 1}{\gamma}C_{pp}dT_{pi}\right] = dA/A. \tag{8}$$

The particle velocity and temperature will remain unchanged through a discontinuity since there is a finite relaxation time associated with changes in these particle properties. Since the flow area does not change across a discontinuity, the momentum equation across an infinitesimal discontinuity is

$$(M^2 - 1)(du_g/u_g) = 0 \qquad (8a)$$

Thus for an infinitesimal discontinuity to exist in a gas-particle flow, it must travel at the gas sonic speed, $(\gamma RT_g)^{\frac{1}{2}}$. The speed of sound in a gas-particle mixture is unaffected by the presence of the particles and the relaxation processes occurring in the flow, and is identical with the speed of sound in the gas alone. This result is similar to the situation found in reacting gas mixtures[10] where the speed of sound propagation is found to be independent of the chemical reactions occurring in the flow.

The above result is valid for the high-frequency sound propagation case (i.e., the time in which the disturbance occurs is much smaller than the relaxation time of the particles). The low-frequency sound propagation case in which the gas and particles remain essentially in equilibrium through the disturbance can be similarly treated. In the limit of complete gas-particle equilibrium the momentum equation across the disturbance is

$$(M_e^2 - 1)(du_g/u_g) = 0 \qquad (8b)$$

and the disturbance must travel at the equilibrium sound speed, $\{\gamma_e RT_g/[1 + (\dot{w}_p/\dot{w}_g)]\}^{\frac{1}{2}}$ where

$$\gamma_e = \frac{\gamma[1 + (\dot{w}_p/\dot{w}_g)(C_{pp}/C_{pg})]}{[1 + \gamma(\dot{w}_p/\dot{w}_g)(C_{pp}/C_{pg})]}.$$

Since $\gamma_e < \gamma$, the equilibrium speed of sound in a gas-particle mixture is less than the nonequilibrium (or frozen) speed of sound in the mixture. A similar result is found in studies of sound propagation in reacting gas mixtures.[10]

Shock Waves

Let us examine the conditions existant across a normal shock wave in a gas-particle mixture where upstream of the shock the gas and particles are in equilibrium ($u_{pi1} = u_{g1}$, $T_{pi1} = T_{g1}$) and far downstream of the shock the gas and particles are again in equilibrium ($u_{pi2} = u_{g2}$, $T_{pi2} = T_{g2}$). Across the shock wave the continuity, momentum, and energy equations become

$$\rho_{g1}u_{g1} = \rho_{g2}u_{g2} \qquad (9)$$

$$\rho_{pi1}u_{pi1} = \rho_{pi2}u_{pi2} \qquad (10)$$

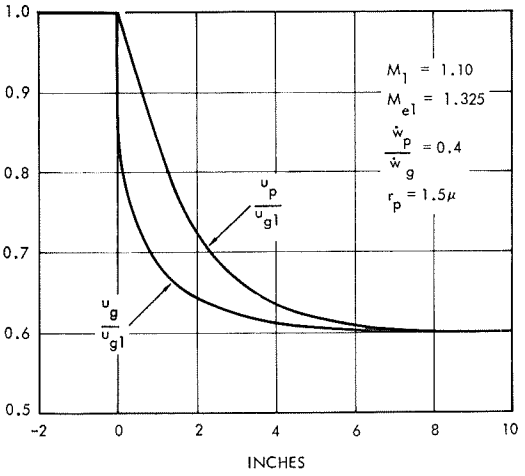

FIG. 1. Supersonic gas-particle shock wave velocity profile.

$$[1 + (\dot{w}_p/\dot{w}_g)](\rho_{g1}u_{g1}^2 - \rho_{g2}u_{g2}^2) + P_{g1} - P_{g2} = 0 \qquad (11)$$

$$\frac{\gamma}{\gamma - 1}\left(\frac{P_{g1}}{\rho_{g1}} - \frac{P_{g2}}{\rho_{g2}}\right) + \frac{1}{2}\left(\frac{1 + (\dot{w}_p/\dot{w}_g)}{1 + (\dot{w}_p/\dot{w}_g)(C_{pp}/C_{pg})}\right)(u_{g1}^2 - u_{g2}^2) = 0 \qquad (12)$$

where T_g has been eliminated through the use of the perfect gas law. Solving the above algebraic equations we find that[11]

$$P_{g2}/P_{g1} = 1 + [2\gamma_e/(\gamma_e + 1)](M_{e1}^2 - 1) \qquad (13)$$

$$\rho_{g2}/\rho_{g1} = [(\gamma_e + 1)M_{e1}^2]/[(\gamma_e - 1)M_{e1}^2 + 2] = u_{g1}/u_{g2} = \rho_{pi2}/\rho_{pi1}. \qquad (14)$$

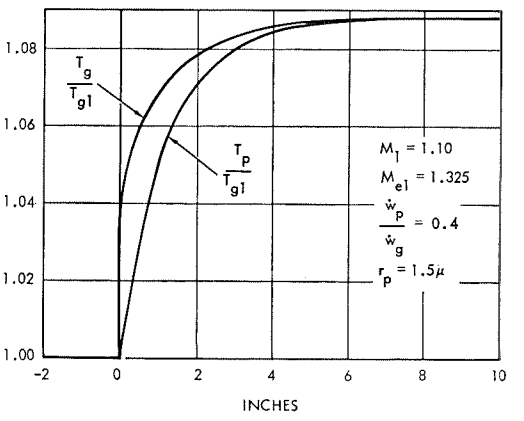

FIG. 2. Supersonic gas-particle shock wave temperature profile.

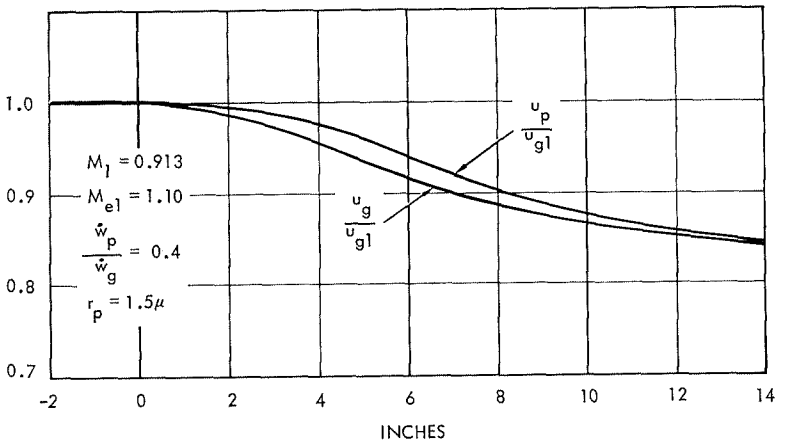

FIG. 3. Fully diffuse gas-particle shock wave velocity profile.

The above equations are the perfect gas normal shock relationships except that γ_e and M_e replace γ and M. With these modifications, gas tables can be used to obtain the final equilibrium flow conditions behind a normal shock in a gas-particle flow.

If the flow in front of the shock is supersonic ($M_1 > 1$), the shock will consist of a shock front several mean free paths thick followed by a relaxation zone.[3] Across the shock front the particle properties do not change and the gas properties can be obtained from the perfect gas normal shock relationships. Figures 1 and 2 show the velocity and temperature profiles in this type of gas-particle shock wave.[12] It is seen that the relaxation zone behind the shock front is quite thick, being many inches in length. The thickness of this relaxation zone decreases as the shock strength increases.[12] If the flow in front of the shock is not supersonic ($M_1 < 1$), a shock can still occur if $M_{e1} > 1$. In this case the shock wave will be fully diffuse and the gas and particle properties will vary continuously through the shock wave. Figures 3 and 4 show the velocity and temperature profiles in this type of gas-particle shock wave.[12] It is seen that the relaxation zone is very thick in these shocks and the shock structure is similar to those found in non-reacting gas mixtures.[13] Similar shock phenomena occur in reacting gas flows.[14,15]

Throat Conditions

The second term of Eq. (8) is always positive for accelerating flows. Thus the gas Mach number must always be less than 1 at the nozzle throat ($M^* < 1$) unless the axial gas velocity gradient is infinite at the throat. The sonic point in a gas-particle nozzle occurs downstream of the throat. At the sonic point

$$\frac{1}{RT_g}\sum_{i=1}^{N}\frac{\dot{w}_{pi}}{\dot{w}_g}\left[\left(u_g - \frac{\gamma-1}{\gamma}u_{pi}\right)\frac{du_{pi}}{dx} - \frac{\gamma-1}{\gamma}C_{pp}\frac{dT_{pi}}{dx}\right] = \frac{1}{A}\frac{dA}{dx}. \quad (15)$$

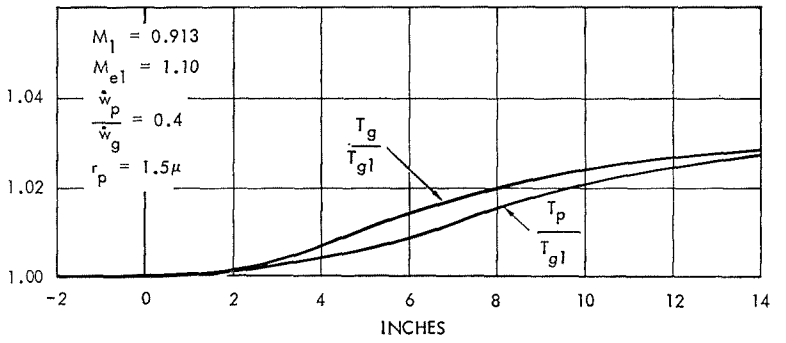

FIG. 4. Fully diffuse gas-particle shock wave temperature profile.

This condition determines the mass flow through the nozzle for a gas-particle system. Since the conditions at the sonic point depend on the particle lags at the sonic point, these conditions can be changed by changing the nozzle inlet and throat geometry. Thus the mass flow through the nozzle is not a unique function of throat size for a gas-particle system but also depends on the nozzle inlet and throat geometry. Similarly, the sonic point location depends on the nozzle geometry. The nozzle inlet and throat geometry will be of much greater importance for gas-particle nozzle flows than for pure gas nozzle flows. It is possible to significantly alter the performance of a gas-particle nozzle by changing only the nozzle inlet and throat geometry. Similar throat phenomena occur in reacting gas nozzle flows.

Constant Fractional Lag Nozzles

Let us now limit ourselves to flows in which the particles are always in Stokes' flow regime. In order to simplify the analysis and the interpretation of the results only one particle size will be considered present in the flow. It has been found[4] that there exists a family of solutions to the equations governing gas-particle flows in which

$$A^2/A^{*2} = (\bar{M}^2)^{-1} \times \{[2/(\bar{\gamma}+1)](1+\tfrac{1}{2}(\bar{\gamma}-1)\bar{M}^2)\}^{(\bar{\gamma}+1)/(\bar{\gamma}-1)} \quad (16)$$

$$P_{g0}/P_g = [1+\tfrac{1}{2}(\bar{\gamma}-1)\bar{M}^2]^{\bar{\gamma}/(\bar{\gamma}-1)} \quad (17)$$

$$\rho_{g0}/\rho_g = [1+\tfrac{1}{2}(\bar{\gamma}-1)\bar{M}^2]^{1/(\bar{\gamma}-1)} \quad (18)$$

$$T_{g0}/T_g = 1+\tfrac{1}{2}(\bar{\gamma}-1)\bar{M}^2 \quad (19)$$

$$u_g/(u_g)_{\max} = \{[(\bar{\gamma}-1)\bar{M}^2]/[2+(\bar{\gamma}-1)\bar{M}^2]\}^{\frac{1}{2}} \quad (20)$$

$$u_g = \tfrac{9}{2}(\mu_g r^*/m_p r_p^2)[(1-K)/K^2]x \quad (21)$$

$$u_p = Ku_g \quad (22)$$

$$\rho_p = (\dot{w}_p/\dot{w}_g)(\rho_g/K) \quad (23)$$

$$T_p = LT_g + (1-L)T_{g0} \quad (24)$$

where K and L are constants and

$$L = \left(1 + 3Pr\,\frac{C_{pp}}{C_{pg}}\,\frac{(1-K)}{K}\right)^{-1} \quad (25)$$

$$B = \frac{1+(\dot{w}_p/\dot{w}_g)K^2}{1+(\dot{w}_p/\dot{w}_g)(C_{pp}/C_{pg})L} \quad (26)$$

$$C = 1+(\dot{w}_p/\dot{w}_g)\{K[(1-K)\gamma+K] + (\gamma-1)(C_{pp}/C_{pg})BL\} \quad (27)$$

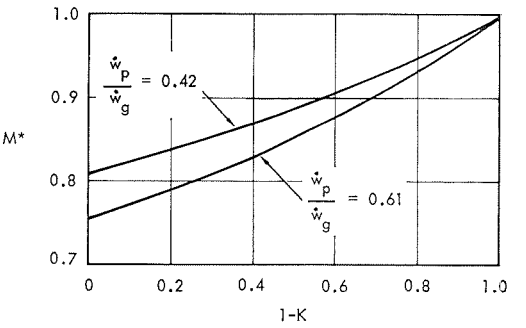

FIG. 5. Throat Mach number versus particle velocity lag in a constant fractional lag nozzle.

$$\bar{M} = C^{\frac{1}{2}}M \quad (28)$$

$$\bar{\gamma} = 1+(\gamma-1)(B/C) \quad (29)$$

$$(u_g)_{\max} = \left(\frac{2C_{pg}T_{g0}}{B}\right)^{\frac{1}{2}} \quad (30)$$

Equations (16) through (20) are the one-dimensional perfect gas flow relationships except that $\bar{\gamma}$ and $\bar{M}$ replace γ and M. With these modifications, gas tables can be used to predict the flow of a gas-particle system through a constant fractional lag nozzle. In equilibrium ($K = L = 1$), $\bar{\gamma}$ and $\bar{M}$ become equal to γ_e and M_e as expected.

In most cases of engineering interest, PrC_{pp}/C_{pg} is greater than $\frac{1}{3}$ so that L is less than K and the particle thermal lag $(1-L)$ is greater than the particle velocity lag $(1-K)$.

Equations (16), (27) and (28) show that $\bar{M}$ equals 1 at the throat of a constant fractional lag nozzle and $M^* < 1$ unless there is no particle flow. The throat conditions depend on the particle lags at the throat and hence on the nozzle inlet geometry as was shown earlier. Figure 5 is a plot of the throat Mach number in a constant fractional lag nozzle vs. particle velocity lag for typical metallized propellants. The throat Mach

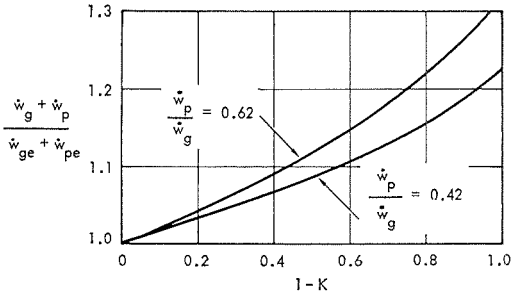

FIG. 6. Mass flow versus particle velocity lag in a constant fractional lag nozzle.

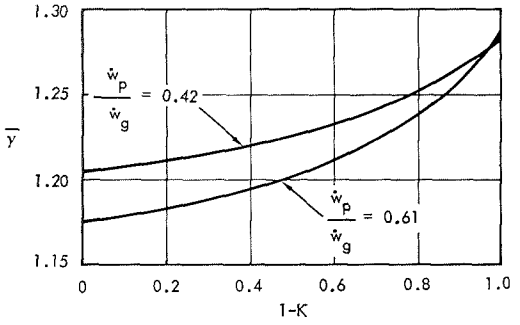

FIG. 7. Expansion coefficient versus particle velocity lag in a constant fractional lag nozzle.

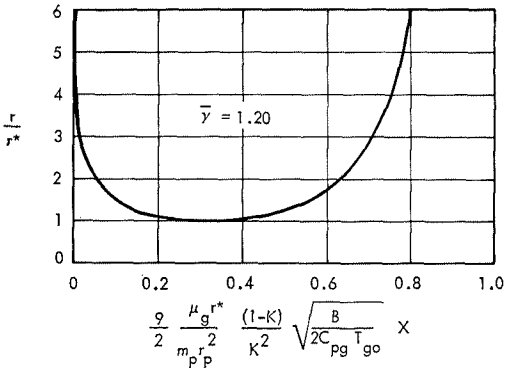

FIG. 8. Constant fractional lag nozzle profile.

number increases as the particle lags increase and is only slightly dependent on the particle mass fraction.

The mass flow through a constant fractional lag nozzle is easily obtained from the throat conditions and is found to depend on the particle lags at the throat and hence on the nozzle inlet geometry as was shown earlier. Figure 6 is a plot of nozzle mass flow (normalized with the equilibrium mass flow) vs. particle velocity lag in constant fractional lag nozzles for typical metallized propellants. The nozzle mass flow increases as the particle lags increase and is strongly effected by the particle lags.

Figure 7 is a plot of the effective expansion coefficient vs. particle velocity lag in constant fractional lag nozzles for typical metallized propellants. The effective expansion coefficient increases as the particle lags increase but is rather insensitive to particle lags for small particle lags.

Through use of Eqs. (20), (21), and (28) the area variation in constant fractional lag nozzles can be found as a function of the nondimensional distance

$$\frac{9}{2}\frac{\mu_g r^*}{m_p r_p^2}\frac{1-K}{K^2}\left(\frac{B}{2C_{pg}T_{g0}}\right)^{\frac{1}{2}}x.$$

Figure 8 illustrates the shape of an axially symmetric constant fractional lag nozzle. It is noted that these nozzles are trumpet shaped and are approximately symmetrical through the throat. Most of the length in these nozzles is in the throat section.

By relating the wall radius of curvature at the nozzle throat to the axial gas velocity gradient (and hence the particle lags), Kliegel[4] has extended Sauer's[16] throat relationships to gas-particle flows and found that

$$\frac{R^*}{r^*} = \frac{2}{\bar{\gamma}+1}\left[\frac{2}{9}\frac{m_p r_p^2}{\mu_g r^*}\frac{K}{1-K}u_g^*\right]^{\frac{1}{2}} \quad (31)$$

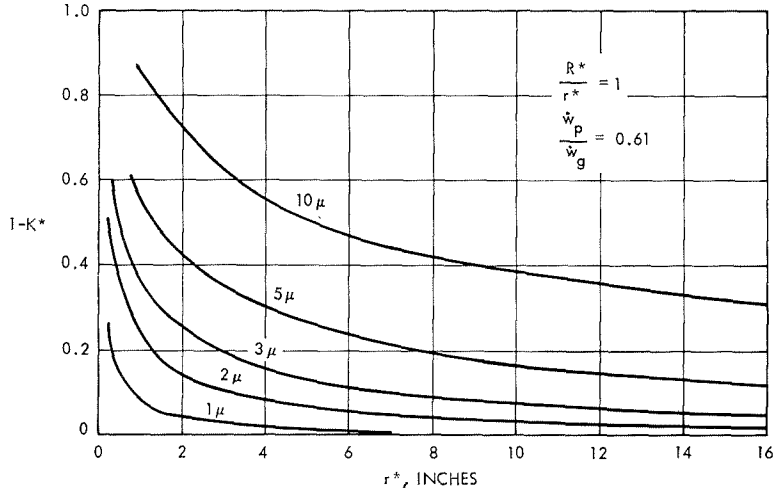

FIG. 9. Particle velocity lag versus throat size for constant fractional lag nozzles.

in axially symmetrical constant fractional lag nozzles.

Solving Eq. (31) for K, the relationship between particle lag and throat geometry in an axially symmetrical constant fractional lag nozzle is

$$K = \frac{9}{4}\frac{\mu_g^* r^*}{m_p r_p^2 u_g^*}\left[\frac{\bar{\gamma}+1}{2}\frac{R^*}{r^*}\right]^{\frac{1}{2}} \times \left\{\left[1+\frac{8}{9}\frac{m_p r_p^2 u_g^*}{\mu_g^* r^*}\left(\frac{\bar{\gamma}+1}{2}\frac{R^*}{r^*}\right)^{\frac{1}{2}}\right]^{\frac{1}{2}}-1\right\} \quad (32)$$

Figure 9 is a plot of particle lag vs. nozzle throat size for a typical gas-particle exhaust mixture flowing through an axially symmetrical constant fractional lag nozzle whose wall radius of curvature at the throat equals the throat radius. It is seen that 1 μ particles are essentially in equilibrium unless the nozzle is very small while 10 μ particles are essentially in equilibrium in only the largest nozzles. From Eq. (32) it is found that for small particle lags,

$$1 - K \simeq \frac{2}{9}\frac{m_p r_p^2 u_g^*}{\mu_g^* r^*}\left(\frac{2}{\bar{\gamma}+1}\frac{r^*}{R^*}\right)^{\frac{1}{2}}. \quad (33)$$

If the above dimensionless number is very small, gas-particle nonequilibrium effects will be negligible.

Equation (21) shows that the axial velocity gradient is constant in constant fractional lag nozzles. Since this condition is approximately true in the throat region of most nozzles of engineering interest, it would appear that the above results have general applicability. Gilbert[17] has recently shown that this conclusion is correct and extended the analysis to the case in which the particles do not remain in Stokes' flow regime. As Carrier[3] observed, the ratio $C_D Re/Nu$ is approximately 12 for spheres even outside Stokes' flow regime. With this assumption the relationship between the particle velocity and thermal lag is unchanged. The nozzle axial scale is changed since

$$du_g/dx = \tfrac{3}{2}(\mu_g f_p r^*/m_p r_p^2)[(1-K)/K^2] \quad (34)$$

when the particle is not in Stokes' flow regime. The particle velocity lag at the throat now becomes

$$K^* = \frac{9}{4}\frac{\mu_g^* f_p^* r^*}{m_p r_p^2 u_g^*}\left[\frac{\bar{\gamma}+1}{2}\frac{R^*}{r^*}\right]^{\frac{1}{2}} \times \left\{\left[1+\frac{8}{9}\frac{m_p r_p^2 u_g^*}{\mu_g^* f_p^* r^*}\left(\frac{\bar{\gamma}+1}{2}\frac{R^*}{r^*}\right)^{\frac{1}{2}}\right]^{\frac{1}{2}}-1\right\}. \quad (35)$$

In principle, the flow properties can be obtained during particle solidification in constant fractional lag nozzles.[4] It appears however that the required integrals cannot be expressed in closed form for the general case of arbitrary particle lag. For cases of engineering interest, appreciable particle solidification rarely occurs in rocket nozzles.

Nozzle Performance

One measure of nozzle performance is the specific impulse which for a fully expanded gas-particle nozzle is defined as

$$I_{sp} = \{g[1+(\dot{w}_p/\dot{w}_g)]\}^{-1}[u_g + (\dot{w}_p/\dot{w}_g)u_p]. \quad (36)$$

For a constant fractional lag nozzle in which the particles do not undergo a phase change,

$$I_{sp} = \frac{[1+(\dot{w}_p/\dot{w}_g)K]}{g[1+(\dot{w}_p/\dot{w}_g)]} \times \left[\left(\frac{1+(\dot{w}_p/\dot{w}_g)(C_{pp}/C_{pg})L}{1+(\dot{w}_p/\dot{w}_g)K^2}\right) \times 2C_{pg}(T_{g0}-T_{ge})\right]^{\frac{1}{2}}. \quad (37)$$

Altman and Carter[1] give expressions for the specific impulse of a gas-particle system for the special cases of complete kinetic and thermal equilibrium and nonequilibrium. The above expression for the specific impulse reduces to Altman and Carter's expressions for these cases.

Since most of the thrust of a nozzle results from the expansion which occurs between the chamber and the throat, it is of interest to estimate the efficiency of this expansion. The efficiency at the nozzle throat in a constant fractional lag nozzle is

$$\frac{I_{sp}}{I_{spe}} = \frac{u_g^*}{u_{ge}^*}\left[\frac{1+(\dot{w}_p/\dot{w}_g)K^* + (1/\gamma M^{*2})}{1+(\dot{w}_p/\dot{w}_g)+(1/\gamma M_e^{*2})}\right]. \quad (38)$$

For moderate lags ($K^* > 0.6$) the above expression can be approximated by

$$I_{sp}/I_{spe} \simeq 0.53[\dot{w}_p/(\dot{w}_g+\dot{w}_p)]\,K^*. \quad (39)$$

Comparison of the above two expressions as a function of K^* for various metallized propellants showed that the efficiency was accurately estimated by Eq. (39). Thus the efficiency loss in gas-particle nozzles is approximately proportional to the product of the particle mass fraction and the particle velocity lag.

To obtain optimum engine performance, one should optimize the propellant metal fraction and nozzle together since both have a large effect on the engine performance. For a given nozzle, the optimum metal fraction in the propellant will be less than the thermochemical optimum.

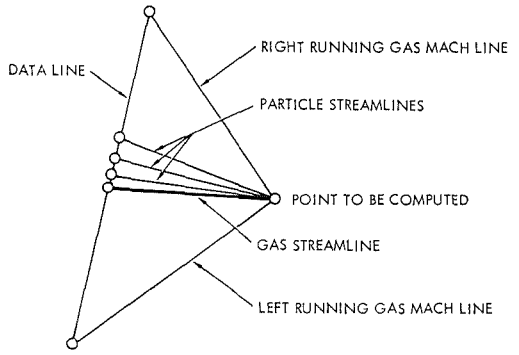

FIG. 10. Gas-particle characteristic mesh.

Characteristic Calculations

Using the same assumptions as above, the equations governing axially symmetrical gas-particle flows have been studied by Kliegel and Nickerson.[18,19] They find that all the characteristics of the equations governing the flow of gas-particle mixtures are real if the flow is supersonic ($M > 1$). Thus the supersonic flow of a gas-particle mixture can be computed using the method of characteristics. One of the characteristic directions of these equations is indentical with the gas Mach lines and is independent of presence of the particles. This result is similar to the situation found in reacting gas mixtures[20] in which one of the characteristic directions is also identical with the gas Mach lines and is independent of chemical reactions occurring in the flow. Figure 10 illustrates the characteristic mesh for gas-particle flows. The mesh calculations are quite similar to those employed in calculating rotational perfect gas flows with the additional complication that one must compute along both gas and particle streamlines.

In order to calculate the flow in a nozzle by the method of characteristics, one must know the flow properties in the throat region near the sonic line. For perfect gas flows, one can obtain transonic solutions to the flow equations by taking perturbations about the sonic velocity.[16,21] This method is applicable for perfect gas flows because the throat conditions are essentially determined by the nozzle geometry in the immediate neighborhood of the throat and are quite insensitive to the nozzle inlet geometry. This is not true for gas-particle flows as the throat conditions are determined by the nozzle inlet geometry. To obtain initial conditions to start a characteristic calculation for a gas-particle system, the complete subsonic and transonic flow field in the nozzle inlet and throat section must be solved. This is a formidable task and at the present time one must use approximate methods to obtain gas-particle flow properties in the nozzle throat region.

A qualitative description of the gas-particle flow in a nozzle throat can be obtained by considering the near-equilibrium case. In this case the gas properties in the throat region can be approximated by[4,16]

$$u_g/u_g^* \simeq 1 + \alpha(z/r^*) + (\gamma_e + 1)/8)\alpha^2(r^2/r^{*2}) \tag{40}$$

$$v_g/u_g^* \simeq (\gamma_e + 1/4)\alpha^2(zr/r^{*2}) + [(\gamma_e + 1)^2/16]\alpha^3(r^3/r^{*3}) \tag{41}$$

where

$$\alpha = \left[\left(\frac{2}{\gamma_e + 1}\right)\left(\frac{r^*}{R^*}\right)\right]^{\frac{1}{2}}$$

and the nozzle throat location is given by $z^*/r^* = -[(\gamma_e + 1)\alpha]/8$. To Sauer's[16] order of approximation is is found[18] that

$$\frac{u_p}{u_g^*} = K^*\left(1 + \alpha\frac{z}{r^*} + \frac{\gamma_e + 1}{8}\alpha^2\frac{r^2}{r^{*2}}\right) = K^*\frac{u_g}{u_g^*} \tag{42}$$

$$\frac{v_p}{u_g^*} \simeq \frac{\gamma_e + 1}{4}\alpha^2\left(\frac{z}{r^*} - \frac{1 - K}{K\alpha}\right)\frac{r}{r^*} + \frac{(\gamma_e + 1)^2}{16}\alpha^3\frac{r^3}{r^{*3}} \tag{43}$$

where K^* is given by Eq. (35). The particle and gas streamlines diverge in the throat region for all particle sizes even though the flow may be essentially in equilibrium. As shown in Fig. 11, the particles concentrate along the nozzle axis which greatly complicates calculation of the gas-particle flow properties in the nozzle throat region.

Equation (42) shows that the axial particle velocity is a constant fraction of the axial gas velocity in the throat region. Since the axial velocity is much larger than the radial velocity in the throat region, the gas-particle flow in a nozzle throat is approximately a constant fractional lag flow. Thus the gas properties in the

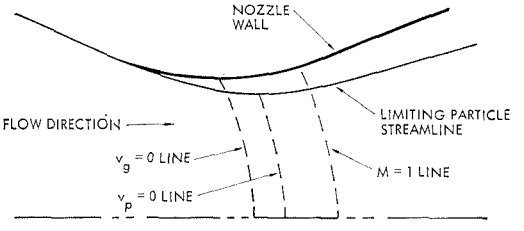

FIG. 11. Gas-particle flow in a nozzle throat.

throat region can be approximated by the perfect gas relationships [using the appropriate expansion coefficient, Eq. (31)] and the particle trajectories can be traced through the throat region to determine the particle properties along the initial data line. This method of obtaining the gas-particle flow properties in the throat region was used by Kliegel and Nickerson[18] in their study of gas-particle flows in axially symmetrical nozzles. The initial conditions thus determined are self-consistent since the characteristic calculations proceeded smoothly away from the initial line. Although the accuracy of the method has not been established, it is exact for equilibrium flows and one would expect that the flow properties predicted for near equilibrium flows would be substantially correct except possibly near the wall where the effect of the particles not following the gas streamlines will be largest.

Numerical Solutions

In addition to the physical properties of the combustion products, one needs the particle size distribution and particle drag and heat transfer coefficients in order to integrate the gas-particle flow equations. A discussion of numerical integration of these equations and of the accuracy with which these quantities are known has recently been given by Hogland.[22] Particle samples taken from the exhaust of various aluminized propellants[23,24] have been found to follow a logarithmic normal particle size distribution

$$\dot{w}_p(d_p)/\dot{w}_p = \left[(2\pi)^{\frac{1}{2}} d_p \ln \sigma_g\right]^{-1} \times \exp\left[-\frac{(\ln d_p - \ln \bar{d}_p)^2}{2 \ln^2 \sigma_g}\right] \quad (44)$$

where $\bar{d}_p = 3.5 \pm 1.0\ \mu$, $\sigma_g = 1.9 \pm 1.0\ \mu$.

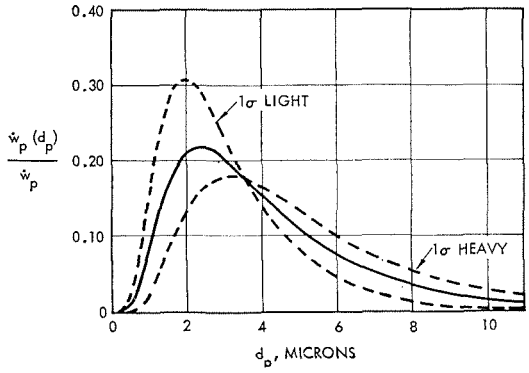

FIG. 12. Measured particle size distribution for aluminized propellants.

Figure 12 is a plot of this size distribution which was found to be independent of engine size and geometry, propellant composition, and chamber conditions for rather large engines. (There now exists experimental evidence[25] showing that in small test engines the particle size is dependent on the chamber pressure and/or geometry.) All particles collected were spherical and contained less than 0.2% by weight of unburned aluminum.[24]

In choosing the correct particle drag and heat transfer coefficients, rarefaction, compressibility, and free stream acceleration effects must be considered. A study of these effects for spheres showed that for the above particle size distribution only rarefaction effects are important in gas-particle nozzle flows of engineering interest. The rarefaction corrections used in the numerical calculations were[26]

$$C_D = C_D^{(0)} \cdot \left[\frac{(1 + 7.5Kn)(1 + 2Kn) + 1.91Kn^2}{(1 + 7.5Kn)(1 + 3Kn) + (2.29 + 5.16Kn)Kn^2}\right] \quad (45)$$

$$Nu = \frac{Nu^{(0)}}{1 + 2.72(Kn/\gamma^{\frac{1}{2}}Pr)\,Nu^{(0)}} \quad (46)$$

where $C_D^{(0)}$ and $Nu^{(0)}$ are the drag and heat transfer coefficient for spheres in the absence of rarefaction effects.[27,28]

Using the above particle size distribution and drag and heat transfer coefficients, the one-dimensional gas-particle flow equations have been numerically integrated for a large number of cases. Typical results are given in Figs. 14 through 19 for the conical nozzle shown in Fig. 13. The propellant exhaust mixture contained 38% by weight condensed oxides. For comparison purposes, the constant fractional lag predictions are also shown. The constant fractional lag predictions were calculated using Eq. (35) and the constant fractional lag relationships ignoring the fact that these solutions are valid only for linearly accelerating flows.

Figure 14 is a plot of the gas velocity profile in the nozzle. The flow is approximately a

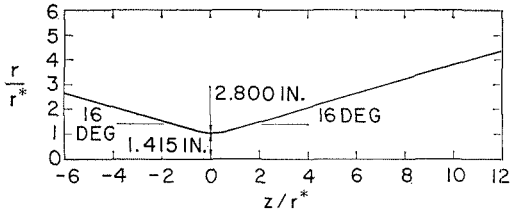

FIG. 13. Nozzle geometry used in numerical calculations.

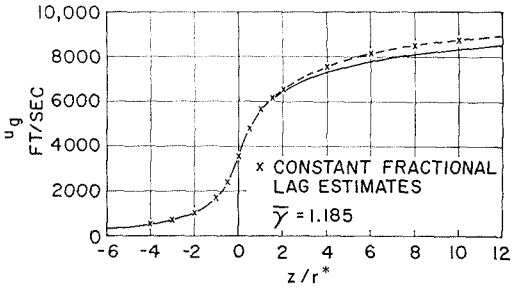

FIG. 14. One-dimensional gas velocity profile in nozzle shown in Fig. 13.

linearly accelerating flow in the nozzle throat section. The constant fractional lag estimate of the velocity in the throat and inlet sections is quite good. In the exit cone the constant fractional lag estimate is only fair, being in error by about 5% at the exit plane.

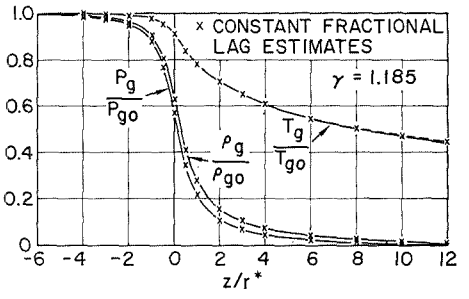

FIG. 15. One-dimensional gas temperature, pressure, and density profiles in nozzle shown in Fig. 13.

Figure 15 is a plot of the gas temperature, pressure, and density profiles in the nozzle. The constant fractional lag relationships accurately estimate these profiles in the nozzle throat and inlet sections. In the exit cone the constant fractional lag estimate of the temperature profile is fairly good, the error being less than 1%

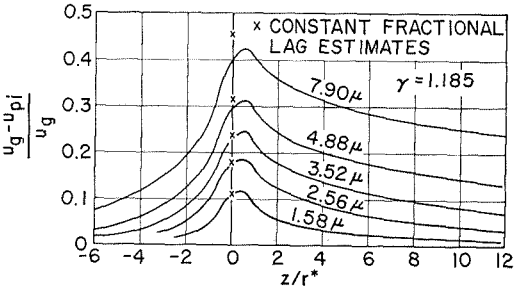

FIG. 16. One-dimensional particle velocity lags in nozzle shown in Fig. 13.

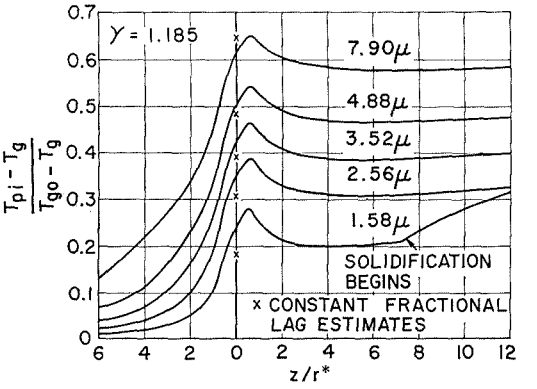

FIG. 17. One-dimensional particle temperature lags in nozzle shown in Fig. 13.

at the exit plane. The small values of the pressure and density ratios in the exit cone mask the fact that the error in the constant fractional lag estimates of these quantities is about 5% at the exit plane.

Figure 16 is a plot of the particle velocity lag through the nozzle for various size particles. It is seen that the particle velocity lag is greatest in the throat region and is reasonably well estimated by Eq. (45). The large effect of the particle size on the particle velocity lag is evident.

Figure 17 is a plot of the particle thermal lag in the nozzle for various size particles. The particle thermal lag is greatest in the throat section and is fairly well established at the throat by Eqs. (25) and (35). The particle size is seen to have a large effect on the particle thermal lag and the particle thermal lag is greater than the particle velocity lag as was shown earlier. Since only the smallest particle has begun to solidify in the nozzle, particle solidification has little effect on the nozzle flow and performance.

Figure 18 is a plot of the ratio of the particle density to the gas density in the nozzle. It is seen that the particle lags cause the concentra-

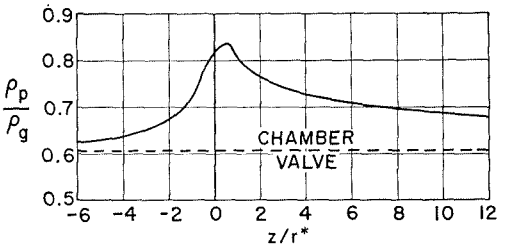

FIG. 18. One-dimensional particle-gas density ratio in nozzle shown in Fig. 13.

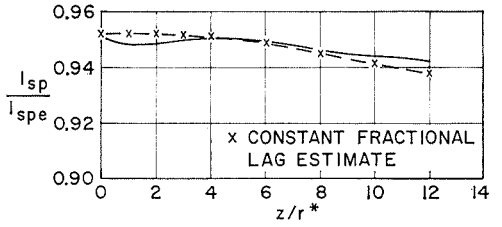

FIG. 19. One-dimensional nozzle efficiency in nozzle shown in Fig. 13.

tion of particles to increase in the nozzle, the ratio of the particle density to the gas density in the nozzle being everywhere larger than in the chamber. This increase in particle mass (compared to the gas mass) in the nozzle occurs during the nozzle starting transient.

Figure 19 is a plot of nozzle efficiency (delivered impulse/theoretical impulse) in the nozzle. It is seen that the particle lags cause an appreciable efficiency loss in the nozzle and that most of this loss occurs upstream of the nozzle throat (hence the large loss present at the throat). The constant fractional estimate of the nozzle efficiency is excellent at the throat and fairly good for the rest of the nozzle.

The major difference between one-dimensional and axially symmetrical gas-particle nozzle calculations is the change in the particle mass distribution in the nozzle due to the inability of the particles to follow the gas streamlines. Figures 20 through 25 are plots of the flow properties in the nozzle shown in Fig. 13 calculated by an axially symmetrical gas-particle characteristics program. The one-dimensional results are again given for comparison.

Figure 20 is a plot showing the limiting particle streamlines in the nozzle. These streamlines are those that originated at the wall in the nozzle inlet section. All particles of a given size will be located between the axis and its limiting streamline. It is seen that only the smallest particles follow the gas and that the largest particles are concentrated near the axis, filling only about a third of the nozzle area at the exit plane. The

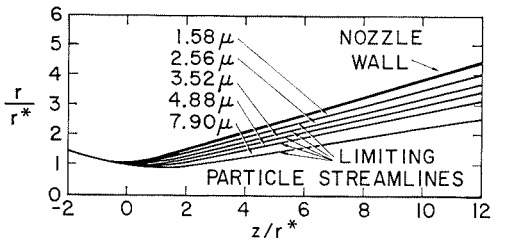

FIG. 20. Limiting particle streamlines in nozzle shown in Fig. 13.

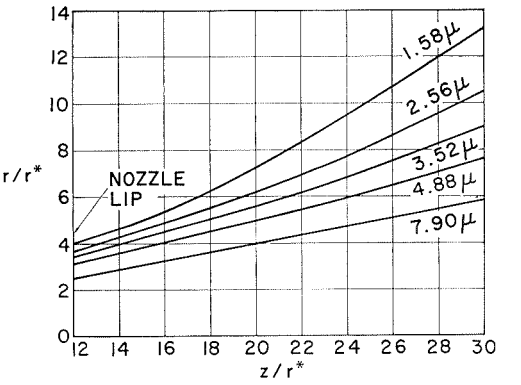

FIG. 21. Limiting particle streamlines in vacuum expansion plume outside nozzle shown in Fig. 13.

particles are turned in the throat section and although only the limiting particle streamlines are shown, all particle streamlines are straight lines in the exit cone. Characteristic calculations have shown that, even in contoured nozzles, the particle trajectories are essentially straight lines in the exit cone owing to the particles' high inertia. Thus the particle flow field in any nozzle exit cone is essentially conical and the particles' drag on the gas will force the gas flow field to be essentially conical also. The performance increases due to nozzle contouring are thus much lower for gas-particle systems than for pure gas systems since the particles cause the flow field to be essentially conical even though the nozzle wall is contoured. Figure 21 is a plot of the limiting

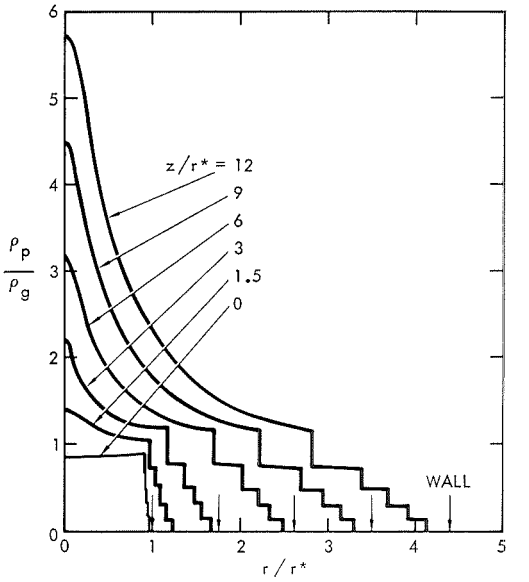

FIG. 22. Particle-gas density ratio at various stations in nozzle shown in Fig. 13.

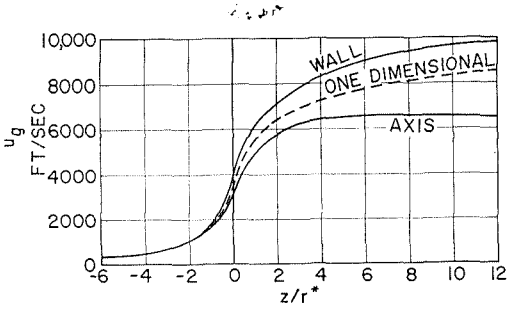

FIG. 23. Axis and wall gas velocity profiles in nozzle shown in Fig. 13.

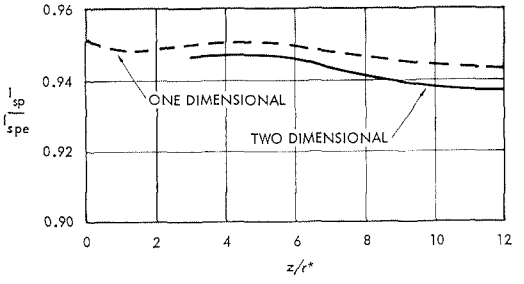

FIG. 25. Nozzle efficiency in nozzle shown in Fig. 13.

particle streamlines in the vacuum expansion plume outside the nozzle. It is seen that only the smallest particles are turned and even they are not greatly affected by the expansion outside the nozzle. All particle trajectories become straight lines shortly outside the nozzle (2 or 3 nozzle exit diameters) since the particle drag coefficients go to zero owing to rarefaction effects as the gas density drops outside the nozzle. The particle flow field outside the nozzle is conical and appears to originate from a source near the nozzle throat. Since the particle drag and heat transfer coefficients decrease to zero owing to rarefaction effects shortly outside the nozzle, the gas expansion is little effected by the particles.

Figure 22 is a plot of the ratio of the particle and gas densities at various stations in the nozzle, showing the concentration of the particles near the axis. This concentration at the nozzle axis is much larger than the one-dimensional estimate and near the nozzle wall the particle concentration is very low. Since there are no particles at the wall and the particle concentration near the wall is very small, the nozzle boundary layer can be treated by standard methods[29] without one having to consider particle effects. The steps in the figure occur at the limiting particle streamlines and are caused by considering the particle distribution to consist of five discrete sizes in the calculation.

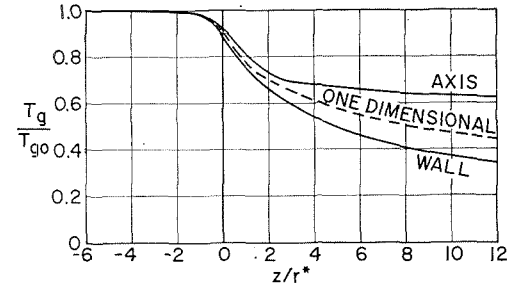

FIG. 24. Axis and wall gas temperature profiles in nozzle shown in Fig. 13.

Figure 23 is a plot of the gas velocity on the nozzle wall and axis. It is seen that the gas velocity on the nozzle wall is higher than the one-dimensional estimate while the gas velocity on the axis is lower than the one-dimensional estimate. Because of the high particle concentration on the nozzle axis (and hence high particle drag force on the gas) the gas velocity on the nozzle axis reaches a maximum in the nozzle and decreases slightly near the exit plane.

Figure 24 is a plot of the gas temperature along the nozzle wall and axis. It is seen that the gas temperature along the wall is lower than the one-dimensional estimate and the gas temperature along the nozzle axis is higher than the one-dimensional estimate. Because of the high particle concentration on the nozzle axis (and hence high particle heat transfer to the gas) the gas temperature on the axis remains essentially constant in the exit cone.

Figure 25 is a plot of the nozzle efficiency. It is seen that the efficiency is lower than the one-dimensional estimate. This efficiency difference is largely the result of the gas-particle mass separation which is not accounted for in the one-dimensional calculations. This difference is about 0.7 % in conic nozzles.[18]

Gas-Particle Nozzle Experiments

In recent years there have been many experimental studies of gas particle nozzle flows. Brown[6] has measured the particle velocity lag at the nozzle exit plane of small solid propellant engines using a high-speed framing camera which allowed him to photograph particle position as a function of time at the nozzle exit plane. The results of his study are summarized in Table I. The measured velocity lags are within those calculated to exist at the exit plane. Since the size of the particle tracked by the camera could not be determined, a quantitative interpretation of the results is impossible. Brown's study does demonstrate, however, that velocity lags of the order of those calculated do exist in

TABLE I

Measured Exit Particle Lag[6]

Motor	Nozzle length (inches)	Measured particle lag	Calculated Particle Lag[a]		
			1.58 μ	3.54 μ	7.90 μ
TPC	5.31	0.47	0.11	0.28	0.49
FPC	9.45	0.30	0.04	0.15	0.32
FPC–BT	8.27	0.05	0.04	0.15	0.32

[a] By author.

TABLE II

Comparison of Measured and Calculated Gas-Particle Expansion Losses in Conical Nozzles

ϵ	3.5	20	24	24	24	24
r^* (inches)	1.32	1.32	1.32	1.32	1.32	1.32
R^*/r^*	2	2	2	5	5	5
Cone angle, deg.	25.2	21.5	24	12	18	24
Calculated heat losses, %	0.6±0.2	0.8±0.2	0.9±0.3	1.3±0.4	1.1±0.3	1.0±0.3
Calculated friction losses, %	0.7±0.2	1.5±0.5	1.4±0.4	2.9±0.9	2.0±0.6	1.6±0.5
Measured engine efficiency, %	95.4±0.3	94.7±0.3	94.7±0.6	95.1±0.3	95.1±0.3	95.1±0.3
Measured expansion losses, %	3.3±0.7	3.0±1.0	3.0±1.3	0.7±1.6	1.8±1.2	2.3±1.1
Calculated expansion losses, %	5.0±1.0	4.8±1.0	4.9±1.0	3.5±1.0	4.1±1.0	4.6±1.0

nozzles. Carlson[30] recently measured the particle thermal lag of inert MgO particles in a research motor. The effective single particle size in Carlson's experiment was 1.9 μ and he found that the measured thermal lags agreed well with the thermal lags calculated for 2 μ particles. Carlson's study demonstrates that thermal lags of the order of those calculated do exist in nozzles.

Gilert *et al.*[31] have recently measured the mass flow variation as a function of particle mass fraction and nozzle inlet geometry in a carefully controlled experiment. They measured the difference in mass flow through two nozzles of the same throat area but differing throat geometries for a suspension of glass beads in nitrogen. Typical results from this experiment are shown in Fig. 26 which compares the predicted and measured differential mass flow through two nozzles as a function of particle mass fraction. It is seen that the measurements are in good agreement with the theoretical predictions.

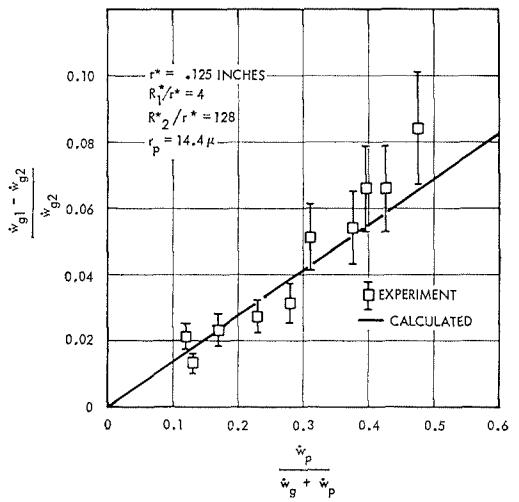

FIG. 26. Comparison of measured and calculated effects of nozzle throat geometry on nozzle mass flow.

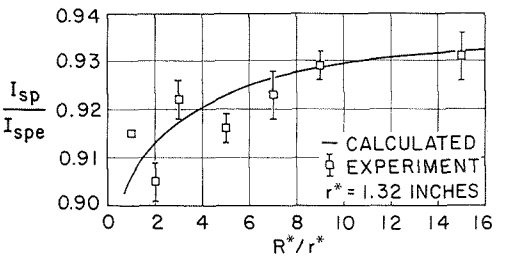

FIG. 27. Comparison of the measured and calculated effects of changes in nozzle throat geometry on nozzle efficiency.

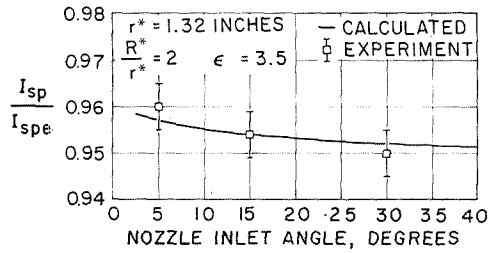

FIG. 28. Comparison of the measured and calculated effects of changes in nozzle inlet geometry on nozzle efficiency.

Kliegel and Nickerson[18] have presented a comprehensive comparison of calculated and measured gas-particle nozzle efficiencies in small solid propellant engines. Their results are summarized in Table II and Figs. 27 through 29. Table II summarizes the measured and calculated nozzle efficiencies of six conical nozzles. It is seen that the calculated heat, friction, and expansion loss reasonably account for the observed efficiency losses. Since these calculations were made assuming no combustion losses and the calculated losses slightly exceed the observed losses, it is concluded that the combustion losses in these firings were much smaller than the expansion losses due to particle lags in the nozzles.

Figure 27 compares the experimental and calculated effect of changes in nozzle inlet geometry. These nozzles consisted only of a convergent section. The nozzle inlet geometry was fixed and the wall radius of curvature upstream of the throat was varied. It is seen that the experimental results are in good agreement with the predicted efficiency decrease as the wall radius of curvature decreases.

Figure 28 is a comparison of the experimental and calculated effect of changing the nozzle inlet angle. These nozzles had identical throat and exit cone geometries and the wall inlet angle from the chamber wall was varied. It is seen that there is a slight efficiency increase as the nozzle inlet angle decreases which is well predicted by the calculations.

Figure 29 is a comparison of the experimental and calculated effects of nozzle contouring. The nozzles inlet and throat section were identical. The exit cones were the same length and had the same expansion ratio but different wall contours. It is seen that the efficiency gain from nozzle contouring is small and is accurately predicted by the calculations.

The above experimental results clearly demonstrate that the nozzle throat geometry has the largest effect on nozzle performance of all nozzle design parameters.

Conclusion

The experimental studies summarized above demonstrate that the expansion behavior of gas-particle mixtures in nozzles can be accurately predicted. Particle velocity and thermal lags have been measured in nozzles which are in substantial agreement with the calculated lags. The predicted mass flow increase with increasing particle concentration and particle lags in the throat section has been measured. The measured effects of changes in nozzle geometry are in good agreement with the predicted effects. It is concluded that the present analysis is capable of predicting the behavior of gas-particle mixture and their expansion through nozzles with good accuracy.

Nomenclature

A	Flow area
C_D	Particle drag coefficient
C_{pg}	Gas heat capacity

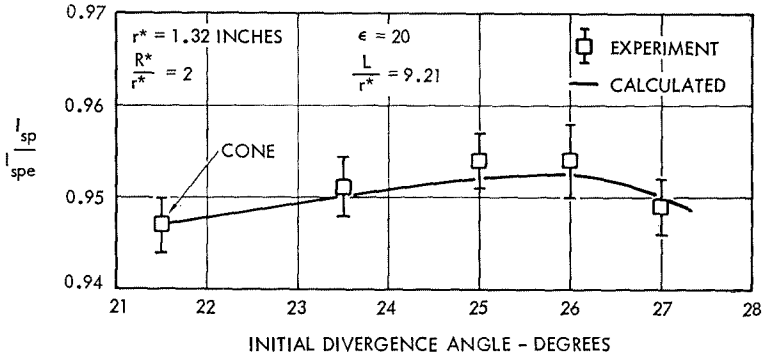

FIG. 29. Comparison of the measured and calculated effects of nozzle contouring on nozzle efficiency.

C_{pp}	Particle heat capacity
d_p	Particle diameter
f_p	Ratio $C_D Re/24$
g	Gravitational constant
g_p	Ratio $Nu/2$
h	Film heat transfer coefficient
I_{sp}	Vacuum specific impulse (unless noted in text)
K	Constant defining particle velocity lag
Kn	Knudsen number
k_g	Gas thermal conductivity
L	Constant defining particle thermal lag
$\bar{M}$	Modified Mach number for a gas-particle system
M	Gas Mach number
m_p	Particle density
Nu	Nusselt number, $2hr_{pi}/k_g$
P_g	Gas pressure
Pr	Gas Prandtl number $\mu_g C_{pg}/k_g$
R	Gas constant
Re	Particle Reynolds number, $2\rho_g r_{pi} \mid u_g - u_{pi} \mid /\mu_g$
R^*	Nozzle wall radius of curvature at nozzle throat
r	Radial coordinate
r_p	Particle radius
r^*	Nozzle throat radius
T_g	Gas temperature
T_p	Particle temperature
u_g	Axial gas velocity
u_p	Axial particle velocity
v_g	Radial gas velocity
v_p	Radial particle velocity
$\dot{w}_g$	Gas mass flow
$\dot{w}_p$	Particle mass flow
x	Normalized coordinate in flow direction
z	Axial coordinate
ϵ	Nozzle expansion ratio
γ	Gas adiabatic expansion coefficient
$\bar{\gamma}$	Expansion coefficient for gas-particle system
μ_g	Gas velocity coefficient
ρ_g	Gas density
ρ_p	Particle density in the gas (based on gas volume)

Subscripts

e	Refers to equilibrium or exit conditions
i	Refers to ith particle size
0	Refers to chamber reference conditions
1	Refers to conditions ahead of shock
2	Refers to conditions behind shock

Superscripts

*	Refers to throat conditions

ACKNOWLEDGMENT

This research was sponsored by Air Force Ballistic Missile Division Contract No. AF 04(694)-1.

REFERENCES

1. ALTMAN, D. and CARTER, J.: In *Combustion Processes* (B. Lewis, R. N. Pease, and H. S. Taylor, eds.). Princeton Univ. Press, 1956.
2. GILBERT, M., DAVIS, D., and ALTMAN, D.: Jet Propulsion *25*, 26 (1955).
3. CARRIER, G. F.: J. Fluid Mech. *4*, 376 (1958).
4. KLIEGEL, J. R.: One Dimensional Flow of a Gas-Particle System, Paper No. 60–S, IAS 28th Meeting, New York, January 1960.
5. BAILEY, W. S., NILSON, E. N., SERRA, R. A., and ZUPNICK, T. F.: ARS Journal *31*, 793 (1961).
6. BROWN, B.: In *Detonation and Two Phase Flow* (S. S. Penner and F. A. Williams, eds.). Academic Press, 1962.
7. MORGANTHALER, J. H.: In *Detonation and Two Phase Flow* (S. S. Penner and F. A. Williams, eds.). Academic Press, 1962.
8. RANNIE, W. D.: In *Detonation and Two Phase Flow* (S. S. Penner and F. A. Williams, eds.). Academic Press, 1962.
9. GLAUZ, R. D.: ARS Journal *32*, 773 (1962).
10. CHU, B. T.: In *1958 Heat Transfer and Fluid Mechanics Institute*. Stanford Univ. Press, 1958.
11. KRIEBEL, A. R.: Shock Waves in Particle Laden Gas, Technical Note 53/C–TN–9, Vidya Inc., Palo Alto, Calif., June 1961.
12. KRIEBEL, A. R.: Analysis of Normal Shock Waves in Particle Laden Gas, Technical Note 53/C–TN–19, Vidya Inc., Palo Alto, Calif., Oct. 1961.
13. SHERMAN, F. S.: J. Fluid Mech. *8*, 465 (1960).
14. WRAY, K. L.: In *Hypersonic Flow Research* (F. R. Riddell, ed.). Academic Press, 1962.
15. GRIFFITH, W. C. and KENNY, A.: J. Fluid Mech. *3*, 286 (1957).
16. SAUER, R.: General Characteristics of the Flow Through Nozzles at Near Critical Speeds, NACA TN 147, June 1947.
17. GILBERT, M., *et al.*: Dynamics of Two-Phase Flow in Rocket Nozzles, Second Quarterly Progress Report UTC 2005 QT2, United Technology Corp., Sunnyvale, Calif., Nov. 1961.
18. KLIEGEL, J. R. and NICKERSON, G. R.: In *Detonation and Two Phase Flow* (S. S. Penner and F. A. Williams, eds.). Academic Press, 1962.
19. NICKERSON, G. R. and KLIEGEL, J. R.: The Calculation of Supersonic Gas-Particle Flows in Axi-Symmetric Nozzles by the Method of Characteristics, Space Technology Laboratories Report 6120–8345–MU000, May 1962.
20. VINCENTI, W. G.: J. Fluid Mech. *4*, 376 (1958).
21. KLIEGEL, J. R.: Higher Order Approximations

to the Transonic Flow in a Nozzle Throat (to be published).
22. HOGLUND, R. F.: ARS Journal *32*, 662 (1962).
23. BROWN, B.: *Eighth Symposium (International) on Combustion*, p. 814. Williams and Wilkins, 1960.
24. Unpublished work performed at Space Technology Laboratories.
25. SEHGAL, R.: An Experimental Investigation of a Gas-Particle System, Jet Propulsion Laboratory Technical Report No. 32–238, March, 1962.
26. SCHAAF, S. A. and CHAMBRE, P. L.: In *Fundamentals of Gas Dynamics* (H. W. Emmons, ed.). Princeton Univ. Press, 1958.
27. GOLDSTEIN, S.: *Modern Developments in Fluid Mechanics*, vol. 1. Oxford Press, 1938.
28. MCADAMS, W. H.: *Heat Transmission*, McGraw-Hill, 1954.
29. BARTZ, D. R.: *Jet Propulsion 27*, 49 (1957).
30. CARLSON, D. J.: *ARS Journal 32*, 1107 (1962).
31. GILBERT, M., *et al.*: Dynamics of Two-Phase Flow in Rocket Nozzles, Third Quarterly Report UTC 2005 QT 3, United Technology Corp., Sunnyvale, Calif., March, 1962.

MAGNETO-FLUID-DYNAMIC NOZZLE FLOW

W. R. SEARS, A. R. SEEBASS, AND S. G. RUBIN

Studies are reported here of both crossed-fields and aligned-fields channel flows to ascertain whether and under what conditions the various transitions between elliptic and hyperbolic behavior can be crossed smoothly in steady flow and whether such nozzle and diffuser flows are stable to propagating disturbances.

Within the limits of various necessary approximations it is concluded (1) that smooth transitions occur in steady flow provided that choking at the speed of sound is avoided by meeting necessary design conditions, (2) that the resulting nozzle flows are stable to sufficiently small disturbances, (3) that aligned-field diffusers are unstable at the speed of sound and may also be unstable at the Alfvén speed, and (4) that crossed-field diffusers are generally unstable at a critical supersonic speed but may be stabilized by a divergence of area and the presence of a strong magnetic field.

Introduction

In conventional gas dynamics the most interesting features of nozzle and diffuser flows are related to passage through the speed of sound. There are, for example, the phenomenon of choking and the instability of decelerating, transonic, isentropic flow. It is therefore natural, when we examine the analogous magneto-gas-dynamic flows, to expect profound effects in the neighborhoods of the analogous "critical speeds" or "transitions."

What is especially interesting about magneto-gas-dynamic flows is that there is not just one such transition speed but several. Basically, this results because the propagation of small disturbances in a conducting gas in the presence of a magnetic field is anisotropic; the field direction is a preferred direction and the isotropy of conventional sound propagation is lost. (See, for example, references 1 and 2.) It has been pointed out[2,3,4] that this anisotropy leads to remarkable standing-wave phenomena in steady flow, the details depending on the geometry, and to the appearance in some cases, of several different transition speeds where conditions change from elliptic to hyperbolic or *vice versa*. Although a transition or critical speed is always the result of wave effects, it is important to notice that a critical speed is not always a wave-propagation speed.

The purpose of the present note is to report briefly on investigations of two different kinds:

1. Studies of steady channel flows, with particular attention to flow behaviors near the transitions from elliptic to hyperbolic conditions or *vice versa*.

2. Studies of the stability of such steady flows with respect to unsteady, propagating disturbances.

In both categories we report on two different types of channel flow, namely *crossed-fields* flow and *aligned-fields* flow. The former refers to flows in which the fluid moves across the magnetic lines of force, as for example in an accelerator or a generator; in general such motion induces an electric field. We treat here only the typical case wherein the applied magnetic field (in the absence of fluid motion) is directed essentially perpendicularly to the flow direction and the electric field is directed perpendicularly to both the flow and the magnetic field. The latter (aligned-fields flow) is atypical; it is the singular case wherein the flow velocity and the magnetic field are substantially parallel or antiparallel. In steady plane or axisymmetric aligned-fields motion no electric field occurs.

Crossed-fields flows, therefore, represent channel flows of considerable technical interest. Aligned-fields flows, on the contrary, are of more academic interest; they can easily be approximated in the laboratory by passing conducting fluid axially through a solenoid. They are also approximations to flows in which highly conducting fluids are guided through "magnetic nozzles" and similar devices.

Crossed-Fields Steady Flows

Channel flows of the crossed-fields category are usually treated in the approximations of quasi-one-dimensional gas dynamics. This approximation applies when the geometrical conditions, and also the configuration of applied fields,

vary only moderately along the length of the channel. It does not, as is sometimes erroneously supposed, imply that the dependent variables are independent of the cross-flow coordinates. Instead it is an approximation in which only the variations *along* the channel are involved.

This approximation was introduced in references 5, 6, and 7, and has been extended and applied in many subsequent papers and reports. In the present paper we wish only to emphasize certain conclusions that were drawn in references 6 and 7; namely:

1. *Choking*, i.e., the inability of a given channel to pass more than a certain maximum mass flow, occurs in general at the sonic speed ($M = 1$).
2. The occurrence of the sonic condition in such channels is divorced from the occurrence of a throat (minimum area) and is controlled by the interplay of electromagnetic effects, area variation, and the addition of heat.
3. For any channel, it is possible to pass through the sonic condition without choking by means of special variations of these variables. These special channels are the analogs of Laval nozzles but provide more generality, since, as emphasized above, there are such nozzles and diffusers for all choices of channel expansion or contraction. It is these channels, within the scope of certain further approximations, whose stability will be studied below.

Aligned-Fields Steady Flow

The most interesting aligned-fields flows are those of high electrical conductivity. In the limit of infinite Reynolds number and magnetic Reynolds number these are isentropic rotational flows. Their equations[2,4] display three distinct transition speeds as indicated in Fig. 1; these occur at the speed of sound a, at the speed of Alfvén-wave propagation α, and at the speed $(a^{-2}+\alpha^{-2})^{-\frac{1}{2}}$, as shown.

The curves "S = constant" in Fig. 1 are typical isentropes and therefore loci of A versus M for flows of this category. Note that the sequence of transition speeds—and the number of such speeds occurring—may be different for different isentropes. The isentrope for any given flow is determined by the ratio of static pressure to "magnetic pressure" $\mu H^2/8\pi$, i.e., by the relative strength of the magnetic field.

It seems pertinent to examine the ability of steady flow to pass smoothly through such critical speeds. Does the phenomenon of choking, for example, appear at one or more of these speeds?

This study has been made in reference 8. For isentropic plane flow it was found possible to adapt the technique of the *hodograph transformation*, i.e., transformation of the equations from the physical plane to one in which the velocity components are the coordinates. Thus linearization is avoided, as appears necessary in a study of trans-critical flows. Some results are presented in Figs. 2, 3, and 4; they may require some interpretation.

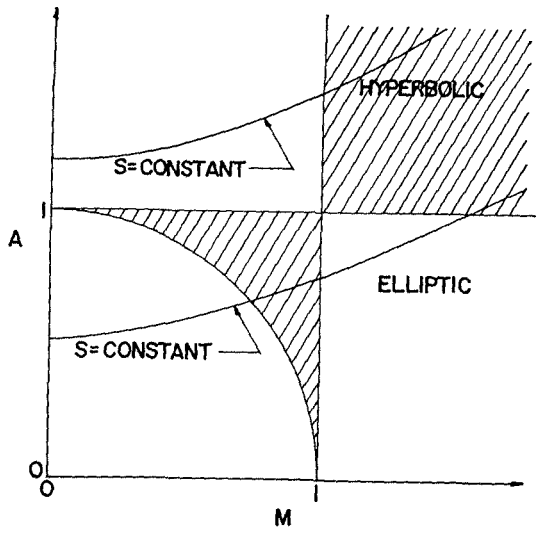

FIG. 1. Alfvén number A versus Mach number M for isentropic, aligned-fields, steady flow. The flow is elliptic (wave-free) in unshaded areas and hyperbolic in the cross-hatched areas. The curves S = constant are typical isentropes.

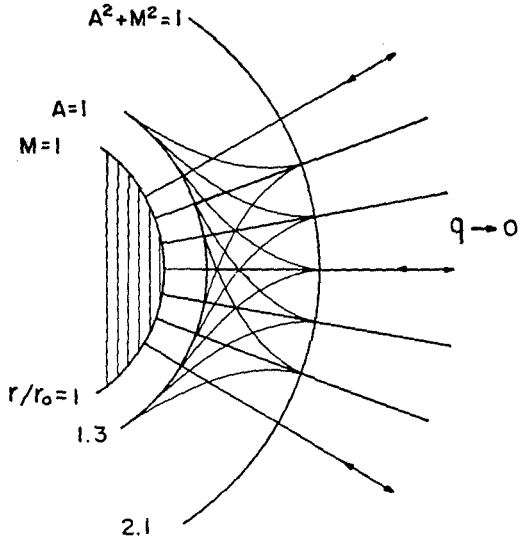

FIG. 2. Plane, steady, isentropic, subsonic, aligned-fields source or sink flow.

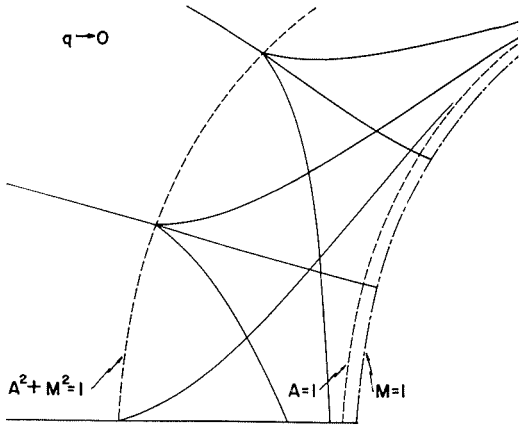

FIG. 3. An example of plane, steady, isentropic, aligned-fields flow that exhibits three transitions.

Figure 2 is a case of subsonic source or sink flow. It has previously been described in references 9, 10, and elsewhere. As is always the case with compressible source-sink flow, choking occurs at sonic speed ($M = 1$) because a throat is not provided there. In the case illustrated, the flow crosses the Alfvén speed ($A = 1$), thereby becoming hyperbolic in character, and then the speed $(a^{-2} + \alpha^{-2})^{-\frac{1}{2}}$, where it becomes elliptic again. Any two radii of Fig. 2 can be chosen to form a radial two-dimensional diffuser or nozzle.

Figure 3 shows a rather similar flow. This pattern is periodic in the vertical direction; slightly less than a half-cycle is shown. Here the three solid lines running from left to right (or the reverse) are typical streamlines, the dash lines are the transitions, and some typical characteristics are also shown. Like the sink flow of Fig. 2, this flow accelerates from rest at far left, becomes hyperbolic by crossing the transition $A^2 + M^2 = 1$, becomes elliptic again at the Alfvén speed, and proceeds to the sonic transition. What is essentially different about this particular flow is not visible in Fig. 3, but is theoretically important: this pattern actually becomes supersonic and hyperbolic to the right of the transonic transition, then encounters the mathematical phenomenon of the "limit line," and there reverses itself (not shown). The limit line is so close to the sonic line that it cannot be shown in the figure; nevertheless, the two curves are not identical (as they are in Fig. 2) but are separated by a small region of supersonic-hyperbolic flow, except at the lower right-hand point of Fig. 3, where they are tangent. Thus the flow of Fig. 3 crosses all three transitions. Furthermore, since a supersonic-hyperbolic flow can be truncated and patched to an infinity of downstream patterns, this flow could, in principle, be produced in an experiment.

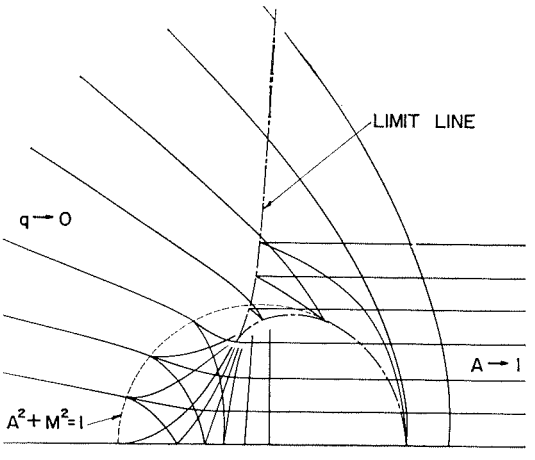

FIG. 4. An example of plane, steady, isentropic, aligned-fields flow that exhibits two transitions. Streamlines and limit lines of two distinct sheets are superimposed here.

Figure 4 was also presented in references 8 and 10. It is another flow derived from a simple solution in the hodograph plane as described in reference 8. It involves three distinct categories of streamlines:

1. Those running from rest at upper left, crossing the horizontal axis at lower right, and proceeding symmetrically to rest in the lower half plane (not shown). These are always subsonic-elliptic and therefore not of particular interest here.
2. Those running from rest at upper left, encountering two branches of limit lines, and finally running out to the right on a different sheet. These are not physically meaningful.
3. The lowest streamlines in Fig. 4, running from rest at far left, accelerating through the transition $A^2 + M^2 = 1$, and proceeding to far right where, at infinity, they reach the Alfvén speed. These do not encounter any limit lines; they appear to cross one (and also to cross the streamlines of category 1), but they are on a different surface.

Any two of these streamlines can be chosen to form the walls of a two-dimensional channel, i.e., a nozzle or diffuser. This flow is subsonic-hyperbolic everywhere to the right of the transition line, and again some typical characteristics are drawn; the flow speed rapidly attains a value close to $A = 1$ and so is nearly uniform and parallel in the lower right-hand part of the diagram. The flow of Fig. 4 is, of course, also reversible.

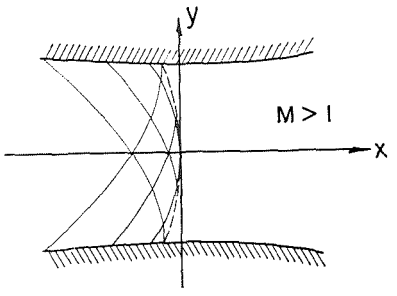

FIG. 5. Characteristics and streamline (channel-wall) configuration for small-perturbation sub-Alfvénic transition through the speed of sound.

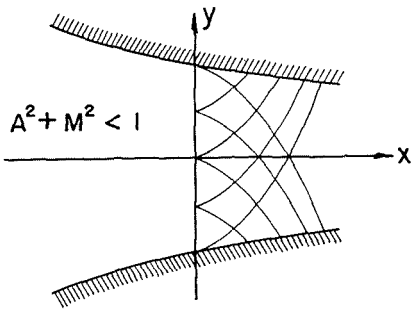

FIG. 7. Characteristics and streamline (channel-wall) configuration for small-perturbation transition through the critical speed $(a^{-2} + \alpha^{-2})^{-1/2}$.

A second technique for finding transition solutions of the aligned-fields equations, namely that of nonlinear small-perturbation theory, has also been used in reference 8. This is the technique by which the well-known von Kármán equation of transonic flow is derived. One assumes that the flow consists of small perturbations from the critical speed and simplifies the differential equations in a consistent manner; the result is a much simpler, but still nonlinear, equation. The process requires an analysis of the relative orders of magnitude in each case, and therefore an assumption of similitude or the equivalent.

This is carried out[8] for the cases of small perturbations from (a) sonic speed a, (b) Alfvén speed α, (c) the critical speed $(a^{-2} + \alpha^{-2})^{-\frac{1}{2}}$, and (d) the special case $a = \alpha$. The results, i.e., the small-perturbation equations and statements of orders of magnitude, will not be repeated here, but some simple flow patterns obtained by inspection from these equations in cases (a), (b), and (c) are shown in Figs. 5, 6, and 7. These are largely self-explanatory. In each case the only curves drawn are typical characteristics and the transition line.

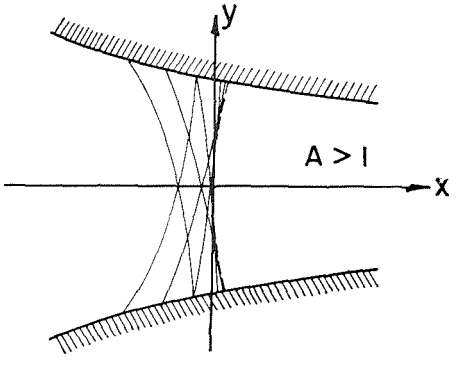

FIG. 6. Characteristics and streamline (channel-wall) configuration for small-perturbation subsonic transition through the Alfvén speed.

All of these flows are reversible. We expect all transition flows in magneto-gas-dynamics to be locally similar to these. Note that only the sonic transition (Fig. 5) occurs at a throat, as anticipated. The other two transitions also occur at locations determined solely by the channel area for any given isentrope of Fig. 1, in contrast to the crossed-fields case.

The conclusion that one may draw from these results is that aligned-fields channel flows that cross the various transitions smoothly can be found in both exact solutions of the isentropic equations and nonlinear small-perturbation descriptions. The sonic transition can be crossed only at a geometric throat. In the next section we discuss the stabilities of such flows.

Stability of Aligned-Fields Channel Flows

The question of stability of trans-critical channel flows is analogous to the question posed by transonic nozzles and diffusers in conventional gas dynamics. The latter was studied by Kantrowitz[11] and by Meyer.[12] The investigations reported here are generalizations of Meyer's work.

Briefly, Meyer's technique is to assume one-dimensional, steady, isentropic, transonic flow and to study the propagation of one-dimensional disturbances in such a steady flow. This study is accomplished by writing the differential equations of the disturbance in characteristic form and ascertaining thereby whether the disturbance grows or subsides as time goes on. The disturbances are assumed not to involve shock waves initially; thus the flow variables are taken to be continuous at the front of the disturbance. The growth criterion used by Meyer is the particle acceleration at the front; if it grows

without limit as time progresses, i.e., $t \rightarrow \infty$ the flow is deemed to be unstable.

The extension to magneto–gas–dynamic channel flows is carried out in reference 13. The differential equations for the unsteady isentropic disturbance in characteristic form display four propagation speeds; viz.,

$$v \pm a, \qquad \text{and} \qquad v \pm \alpha,$$

where v is the flow speed, a the speed of sound, and α the Alfvén-wave speed, as before.

Now, following Meyer, it can immediately be concluded that disturbances propagating at the speeds $v + a$ and $v + \alpha$ cannot produce instability, at least for finite-length channels and small enough disturbances, for they pass downstream through the channel in a finite length of time. Furthermore, channels that accelerate through the critical speed (a or α) cannot be unstable, for in such channels disturbances from upstream are carried downstream in finite time while disturbances from downstream cannot propagate upstream and never enter the channel. Thus *nozzles*, defined here as channels in which the flow accelerates through the sonic or Alfvénic speed, *can be said to be stable.*

The analysis of the sonic diffuser, however, is identical with Meyer's analysis for conventional gas dynamics. The characteristic equations disclose that any disturbance propagating with speed $v - a$ (or upstream with speed $a - v$) is trapped in the sonic region and grows without limit. *Thus sonic diffusers with aligned fields are unstable.*

It is still of interest to investigate the stability of a diffuser at $v = \alpha$, since it is clearly possible to produce a channel that crosses this critical speed, either subsonically or supersonically, and does not involve sonic diffusion. This analysis has been carried out and leads to the following remarkable conclusion: Instability occurs when the Alfvén speed is crossed from above.

Thus, a diffuser is always unstable at the Alfvén transition. But the nature of the disturbances that propagate at the speed $v \pm \alpha$ raises a question regarding the significance of this criterion. The polarization of these disturbances is such that their velocity increments are *across* the channel. It seems clear that such disturbances might occur in an annular channel, but their significance with respect to channels of rectangular or circular cross section is more difficult to judge.

Finally, there appears to be no danger of instability at the third transition speed

$$(a^{-2} + \alpha^{-2})^{-\frac{1}{2}}$$

since, as mentioned above, this is not actually a wave-propagation speed.

Stability of Crossed-Fields Channel Flows

The analogous analysis for crossed-fields channels is also carried out in reference 13.* It requires certain additional simplifications and some further explanation.

First, the analysis, like the steady-flow analysis discussed at the beginning of this paper, is limited to channels along which the geometry and applied fields, and therefore the steady-flow quantities, vary only slowly. Second, the analysis neglects the effects of both viscosity and electrical resistance; specifically, the diffusion of the magnetic field is neglected in writing Faraday's law of induction. It can be shown that this approximation requires that the electric-current density be small. Fortunately, this is a very good assumption for some of the nonchoking diffusers that we wish to investigate.

Within these approximations the Meyer analysis can now be undertaken for the crossed-fields case. The differential equations of propagating disturbances, in characteristic form, are somewhat more complicated than before but disclose that the propagation speeds are

$$v \pm c,$$

where

$$c = (a^2 + \alpha^2)^{\frac{1}{2}}$$

as is consistent with other analyses of magneto–gas–dynamic wave propagation, previously referred to.[1,2] But this propagation speed is not, in general, constant over a cross section of the channel, for both a and α vary across the section, even in a uniform or nearly uniform channel. The approximation of small current density, however, insures that this variation is small, so that the propagation speed can be considered to vary only with the time and the streamwise coordinate.

Once again *nozzles are stable* in the same sense and for the same reasons as explained above, but disturbances propagating with speed $v - c$ are trapped in a diffuser at the cross section where $v = c$, i.e., at a point upstream of the sonic point, and so there is a possibility of instability. The equations show that the condition for stability is

$$(v/c)' + (Q'/Q)(\alpha^2/c^2) > 0$$

at the point where $v = c = (a^2 + \alpha^2)^{\frac{1}{2}}$. Here the prime means differentiation with respect to the

* As explained here, an earlier analysis of this problem by J. Naze[14] is believed to be in error.

streamwise coordinate and Q is the channel cross section. *Thus a crossed-fields diffuser is necessarily unstable if it is untapered or convergent at the critical section, but it can be stable if it diverges and the magnetic field is strong.* We emphasize again that, in contrast to conventional gas dynamics, a diffuser may be convergent, untapered, or divergent.

Conclusions

On the basis of the quasi-one-dimensional gas–dynamic approximation we conclude that crossed-fields magneto–gas–dynamic nozzles and diffusers can be designed for steady flow. To avoid choking at Mach number equal to one, however, they must possess special properties at the sonic point. Convergent, untapered, and divergent nozzles and diffusers may be designed. A stability analysis for inviscid flow and small current density, however, discloses that whereas such nozzles are stable (to sufficiently small disturbances), diffusers are unstable unless an additional inequality is satisfied. This inequality requires that the diffuser be divergent at a certain critical supersonic point and that the magnetic-field strength be large.

In the category of aligned-fields flows at large Reynolds and magnetic-Reynolds numbers, nonlinear analysis of plane flow shows that nozzles and diffusers can be found that cross the three transition speeds smoothly. The sonic transition, however, requires a geometrical throat. Stability analysis discloses again that nozzles are stable with respect to small propagating disturbances. Diffusers are unstable at sonic speed. If a diffuser crosses the Alfvén speed α it is unstable to disturbances propagating with speed $v - \alpha$, but these disturbances involve cross-stream velocity perturbations, and it is not clear whether these must always be assumed to occur in diffusers of various cross sections.

Nomenclature

A	Alfvén number, v/α
a	Speed of sound, $(\gamma p/\rho)^{\frac{1}{2}}$
c	$(a^2 + \alpha^2)^{\frac{1}{2}}$
H	Magnetic-field strength
M	Mach number, v/a
p	Static pressure
Q	Cross-sectional area of channel
S	Entropy
t	Time
v	Fluid-flow speed
α	Alfvén-wave speed, $(\mu H^2/4\pi\rho)^{\frac{1}{2}}$
γ	Specific-heat ratio
μ	Permeability
ρ	Mass density

Acknowledgment

This study was supported by the Air Force Office of Scientific Research.

References

1. Friedrichs, K. O. and Kranzer, H.: Notes on Magneto-Hydrodynamics. VIII. Nonlinear Wave Motion. NYO–6486, Inst. Math. Sci. New York Univ., July, 1958.
2. McCune, J. E. and Resler, E. L., Jr.: J. Aero/Space Sci. *27*, 493 (1960).
3. Sears, W. R.: Revs. Mod. Phys. *32*, 701 (1960); reprinted in *Magneto-Fluid Dynamics* (F. N. Frenkiel and W. R. Sears, eds.), Nat. Acad. Sci., Nat. Res. Council Publ. No. 829, Washington, D. C., 1960.
4. Taniuti, T.: Progr. Theoret. Phys. (Kyoto) *19*, 749 (1958); *ibid. 21*, 606 (1959).
5. Rosa, R. J.: Engineering Magneto-Hydrodynamics, Ph.D. Thesis, Cornell Univ., June, 1956. Available from University Microfilms, Ann Arbor, Mich.
6. Resler, E. L., Jr. and Sears, W. R.: J. Aeronaut. Sci. *25*, 235, 258 (1958); *ibid. 26*, 318 (1959).
7. Resler, E. L., Jr. and Sears, W. R.: J. Appl. Math. and Phys. (ZAMP) *9b*, 509 (1958).
8. Seebass, A. R.: The Theory of Aligned-Fields Magnetogasdynamic Flows, Ph.D. Thesis, Cornell Univ., June, 1962. Available from University Microfilms, Ann Arbor, Michigan. Also AFOSR 2715.
9. Seebass, R.: Quarterly of Applied Mathematics *19*, 231 (1961).
10. Sears, W. R.: Some Paradoxes of Sub-Alfvénic Flow of a Compressible Conducting Fluid, in *Electromagnetics and Fluid Dynamics of Gaseous Plasma*, pp. 363–372. Polytechnic Press, 1962.
11. Kantrowitz, A.: The Formation and Stability of Normal Shock Waves in Channel Flow, N.A.C.A. Tech. Note No. 1225, 1947.
12. Meyer, R. E.: Quart. J. Mech. Appl. Math. *5*, 257 (1952).
13. Rubin, S. G.: On the Propagation of Disturbances in Magnetogasdynamic Channel Flows, Ph.D. Thesis, Cornell Univ., 1963. Available from University Microfilms, Ann Arbor, Michigan.
14. Naze, J.: Compt. rend. *246*, 3316 (1958).

Colloquium on Modeling Principles

(Arranged by Prof. D. B. Spalding)
(Imperial College, London)

Chairmen: Prof. H. C. Hottel
(Massachusetts Institute of Technology)
Prof. D. B. Spalding
(Imperial College, London)
Mr. S. L. Bragg
(Rolls Royce)

Vice Chairmen: Prof. A. H. Lefebvre
(Cranfield)
Prof. D. G. Shepherd
(Cornell University)
Dr. A. C. Scurlock
(Atlantic Research)

THE ART OF PARTIAL MODELING

D. B. SPALDING

The strict requirements of similarity theory are shown to be so numerous and restrictive that complete modeling of combustion processes is practically impossible; all successful modeling so far has involved deliberately ignoring many of the similarity rules. The paper reviews some of the more notable examples of this partial modeling, and mentions the physical facts which underlie their success. It is emphasized that every combustion-modeling technique represents a compromise between the requirements of cheapness and reliability.

Introduction

The Purpose and Nature of Modeling

The term "modeling" is here used to connote the practice of predicting the likely results of one experiment by way of the interpretation of the results of another experiment; if the technique used is a reliable one, only the second experiment needs actually to be performed. The first experiment is the one of main interest; it is usually described by the words: "full-scale," "prototype," "original," or "*Hauptausführung.*" The second is called the "model" experiment.

The technique of modeling is employed when the prototype experiment is prohibitively expensive of time, money, or material, or when its nature is such (e.g., short time, or high temperature) that certain desirable measurements are too difficult to make with sufficient accuracy. Satisfactory model experiments are correspondingly those which are cheap and quick to perform, or which permit the desired observations to be made with greater precision or leisure.

The practices which fall under the above definition are of many different kinds. In the present paper, modeling will be held to include the use of *analogs*, in which the physical or chemical processes of the model are of a different nature from those of the prototype. Perhaps arbitrarily, *mathematical* models, in which the experiment takes place in the mind of the analyst or within the circuits of a digital computer, will be excluded from consideration.

Our particular concern in the present colloquium is with the modeling techniques which are useful in the study of combustion, whether it be in connection with the control of a forest fire, the development of an engine, or the design of an industrial furnace. Such techniques have been widely used for many years, and it is impossible here to review the whole field or to name all the contributors. However, the following pioneers should be mentioned at the outset: Groume-Grjimailo,[7] who studied the flow in furnaces; Damköhler[5] who worked out the similarity rules for the modeling of chemical re-

actors; Rosin[15] who used models for research on open fires; Traustel[23] who worked out the theory of modeling applied to fuel beds; and Putnam and Jensen[13] who correlated the blow-off properties of gas flames by the use of dimensionless groups.

Set-up Rules and Interpretation Rules

The theory of modeling lays down the rules which must be obeyed, in setting up and in interpreting the results of the model experiment, if the prediction which is the aim of the exercise is to be reliable. These rules, which may be derived either by dimensional analysis or from study of the governing differential equations, mainly take the form of specifying which dimensionless groups of quantities must have the same value in the model as in the prototype. The groups referred to in the set-up rules contain only those quantities which may be chosen by the experimenter (e.g., equipment size, density and velocity of entering fluid); the interpretation rules refer to groups containing, in addition, quantities which are measured in the course of the experiment (e.g., shear stress on a wall, combustion efficiency).

Some of the dimensionless groups which are encountered in the modeling rules appropriate to combustion are collected in Table 1. There, each

TAB

Some Dimensionless Groups Rel

	Conduction	Diffusion	Viscous action	Buoyancy	Surface tension	Compressibility	Kinematics
Unit: $(\text{time})^{-1}$	$k/c\rho l^2$	D/l^2	$\mu g_0/\rho l^2$	$(\Delta\rho/\rho)^{1/2}(a_{grav}/l)^{1/2}$	$(sg_0/\rho l^3)^{1/2}$	$\frac{\{(\partial p/\partial\rho)_{isent}\, g_0\}^{1/2}}{l}$	V/l
Conduction	ζ	Dpc/k (Lewis)	$c\mu g_0/k$ (Prandtl)	$\left\{\frac{\rho a_{grav} l^3\,\Delta\rho}{(k/c)^2}\right\}^{1/2}$	$(sg_0c^2\rho l/k^2)^{1/2}$	$\frac{\{(\partial p/\partial\rho)_{isent} g_0\}^{1/2} c\rho l}{k}$	$c\rho Vl/k$ (Peclet)
Diffusion		ζ	$\mu g_0/D\rho$ (Schmidt)	$\left(\frac{a_{grav} l^3\,\Delta\rho}{D^2\rho}\right)^{1/2}$	$(sg_0l/D^2\rho)^{1/2}$	$\frac{\{(\partial p/\partial\rho)_{isent} g_0\}^{1/2} l}{D}$	Vl/D
Viscous action				$\left\{\frac{a_{grav}\rho l^3\Delta\rho}{(\mu g_0)^2}\right\}^{1/2}$	$\{s\rho l/\mu^2 g_0\}^{1/2}$	$\left\{\frac{(\partial p/\partial\rho)_{isent}}{g_0}\right\}^{1/2}\frac{\rho l}{\mu}$	$\rho Vl/\mu g_0$ (Reynolds)
Buoyancy				ζ	$(sg_0/\Delta\rho l^2 a_{grav})^{1/2}$	$\left\{\frac{(\partial p/\partial\rho)_{isent} g_0\rho}{a_{grav} l\,\Delta\rho}\right\}^{1/2}$	$(V^2/la_{grav})^{1/2}(\rho/\Delta\rho)^{1/2}$ (Froude)
Surface tension					ζ	$\left\{\frac{(\partial p/\partial\rho)_{isent} l\rho}{s}\right\}^{1/2}$	$(\rho lV^2/sg_0)^{1/2}$ (Weber)$^{1/2}$
Compressibility						ζ	$\frac{V}{\{g_0(\partial p/\partial\rho)_{isent}\}}$ (Mach)
Kinematics							ζ
Dynamics							
Homogeneous reaction							
Heterogeneous reaction							
Flame propagation							
Heat transfer to wall							
Mass transfer to wall							
Radiation							

column is headed by the name of a physical or chemical phenomenon; immediately beneath the heading is the symbol of a relevant physical or chemical quantity, associated with the symbols for length, density, specific heat at constant pressure, and the constant in Newton's Second Law, in such a way as to give the group the common dimension of $(\text{time})^{-1}$. The body of the table contains dimensionless groups of symbols formed by dividing the group at the head of the column by the group at the head of that column which lies immediately beyond the left-hand end of the row, as indicated by the arrow; thus the group $\rho Vl/\mu g_0$ is obtained by dividing V/l by $\mu g_0/\rho l^2$. Since several of the groups have been distinguished by the names of various research workers, these names have been inserted in the table where appropriate; the group just referred to is, of course, the Reynolds number. Although the table contains explicitly many of the groups which are commonly used, the existence of others is merely implied; for example, the length-free group characteristic of laminar flame propagation, $S_u\rho/(Z'''k/c)^{\frac{1}{2}}$, though absent itself, can be obtained by multiplying $S_u\rho/Z'''l$ by the group $(Z'''l^2c/k)^{\frac{1}{2}}$.

Most of the phenomena mentioned in the table play some part in nearly all combustion processes; it follows that the designer of a model experiment must maintain the constancy of a

LE I
evant to Combustion Modeling

Dynamics	Homogeneous reaction	Heterogeneous reaction	Flame propagation	Heat transfer to wall	Mass transfer to wall	Radiation	Particle disappearance
$(g_0\,\Delta p/\rho l^2)^{1/2}$	Z'''/ρ	$Z''/\rho l$	S_u/l	$\alpha/c\rho l$	$\dot{m}''/\rho l$	$\sigma T^3/c\rho l$	$(D/l^2)\ln(1+B)$
$\dfrac{(g_0\,\Delta p\rho)^{1/2}\,cl}{k}$	$Z'''l^2c/k$	$Z''lc/k$	$S_uc\rho l/k$	$\alpha l/k$ (Nusselt)	$\dot{m}''lc/k$	$\sigma T^3l/k$	$[D\rho/(k/c)]\times\ln(1+B)$
$(g_0\,\Delta p/\rho)^{1/2}l/D$	$Z'''l^2/D\rho$ (Damköhler II)	$Z''l/D\rho$	S_ul/D	$\alpha l/c\rho D$	$\dot{m}''l/\rho D$	$\sigma T^3l/cD\rho$	$\ln(1+B)$
$(\Delta p\rho/g_0)^{1/2}(l/\mu)$	$Z'''l^2/\mu g_0$	$Z''l/\mu g_0$	$S_u\rho l/\mu g_0$	$\alpha l/c\mu g_0$	$\dot{m}''l/\mu g_0$	$\sigma T^3l/c\mu g_0$	$(D\rho/\mu g_0)\times\ln(1+B)$
$\left(\dfrac{g_0\,\Delta p}{la_{grav}\,\Delta\rho}\right)^{1/2}$	$Z'''(l/\rho a_{grav}\,\Delta\rho)^{1/2}$	$Z''(\rho la_{grav}\,\Delta\rho)^{-1/2}$	$(S_u^2/la_{grav})^{1/2}(\rho/\Delta\rho)^{1/2}$	$\dfrac{\alpha/c}{(\rho la_{grav}\,\Delta\rho)^{1/2}}$	$\dfrac{\dot{m}''}{(\rho la_{grav}\,\Delta\rho)^{1/2}}$	$\dfrac{\sigma T^3/c}{(\rho la_{grav}\,\Delta\rho)^{1/2}}$	$\left(\dfrac{D^2\rho}{\beta\,\Delta\rho a_{grav}}\right)^{1/2}\times\ln(1+B)$
$(l\,\Delta p/s)^{1/2}$	$Z'''(l^3/\rho sg_0)^{1/2}$	$l^{1/2}Z''(\rho sg_0)^{-1/2}$	$(\rho lS_u^2/g_0s)^{1/2}$	$l^{1/2}\alpha(c^2sg_0\rho)^{-1/2}$	$l^{1/2}\dot{m}''(sg_0\rho)^{-1/2}$	$\sigma T^3l^{1/2}(c^2sg_0\rho)^{-1/2}$	$(D^2\rho/sg_0l)^{1/2}\times\ln(1+B)$
$\left\{\dfrac{\Delta p}{\rho}\Big/\left(\dfrac{\partial p}{\partial\rho}\right)_{isent}\right\}^{1/2}$	$\dfrac{Z'''l}{\rho\{(\partial p/\partial\rho)_{isent}g_0\}^{1/2}}$	$\dfrac{Z''}{\rho\{(\partial p/\partial\rho)_{isent}g_0\}^{1/2}}$	$\dfrac{S_u}{\{(\partial p/\partial\rho)_{isent}g_0\}^{1/2}}$	$\dfrac{\alpha/c\rho}{\{(\partial p/\partial\rho)_{isent}g_0\}^{1/2}}$	$\dfrac{\dot{m}''/\rho}{\{(\partial p/\partial\rho)_{isent}g_0\}^{1/2}}$	$\dfrac{\sigma T^3/c\rho}{\{(\partial p/\partial\rho)_{isent}g_0\}^{1/2}}$	$\dfrac{D/l}{\{(\partial p/\partial\rho)_{isent}g_0\}^{1/2}}\times\ln(1+B)$
$(g_0\,\Delta p/\rho V^2)^{\frac{1}{2}}$	$Z'''l/\rho V$ (Damköhler I) = ("Loading")$^{-1}$	$Z''/\rho V$	S_u/V	$\alpha/c\rho V$ (Stanton)	$\dot{m}''/\rho V$	$\sigma T^3/c\rho V$	$(D/Vl)\ln(1+B)$
↳	$\dfrac{Z'''l}{(g_0\rho\,\Delta p)^{1/2}}$	$\dfrac{Z''}{(g_0\rho\,\Delta p)^{1/2}}$	$\dfrac{S_u}{(g_0\,\Delta p/\rho)^{1/2}}$	$\dfrac{\alpha/c}{(g_0\rho\,\Delta p)^{1/2}}$	$\dfrac{\dot{m}''}{(g_0\rho\,\Delta p)^{1/2}}$	$\dfrac{\sigma T^3/c}{(g_0\rho\,\Delta p)^{1/2}}$	$\dfrac{D/l}{(g_0\,\Delta p/\rho)^{1/2}}\times\ln(1+B)$
	↳	$Z''/Z'''l$	$S_u\rho/Z'''l$	α/clZ'''	$\dot{m}''/lZ'''$	$\sigma T^3/clZ'''$	$(D\rho/Z'''l^2)\times\ln(1+B)$
		↳	$S_u\rho/Z''$	α/cZ''	$\dot{m}''/Z''$	$\sigma T^3/cZ''$	$(Dp/Z''l)\times\ln(1+B)$
			↳	$\alpha/c\rho S_u$	$\dot{m}''/\rho S_u$	$\sigma T^3/c\rho S_u$	$D/lS_u\ln(1+B)$
				↳	$c\dot{m}''/\alpha$	$\sigma T^3/\alpha$	$(D\rho c/\alpha l)\times\ln(1+B)$
					↳	$\sigma T^3/c\dot{m}''$	$(D\rho/\dot{m}''l)\times\ln(1+B)$
						↳	$(D\rho c/\sigma T^3l)\times\ln(1+B)$

large number of dimensionless groups, actually equal to the number of relevant columns minus one. However, the number of rules to be obeyed for correct modeling of a combustion process is even larger than that so computed, for the following reasons:

1. A dimensionless group of given kind may be represented in the set-up rules several times; for example, when two streams enter the combustion space, the velocity of each of them appears in a separate Reynolds number. Similarly each stream fluid has its own density, specific heat, and viscosity. It is usually convenient to consider one stream as providing the reference velocity, density, etc. for the formation of the groups of Table 1; then the similarity requirements for the other streams are expressed through dimensionless groups comprising velocity ratios, density ratios, etc.
2. In unsteady combustion processes, time itself must enter; correspondingly a further row of groups can be added to the table by multiplying the quantities in the top row by t. The first dimensionless group so formed would be $kt/c\rho l^2$, which is the reciprocal of the Fourier number.
3. There exist further set-up rules which are not easily expressed by means of dimensionless groups, namely those concerned with similarities of shape. The most obvious of this kind is the geometrical one: the boundaries of the model apparatus must be geometrically similar to those of the prototype. Others relate to functions; for example, when large temperature differences arise, the shape of the viscosity-temperature relationship appropriate to the model must be the same as that appropriate to the prototype.

The Central Problem of Combustion Modeling

The main practical consequence of the situation revealed above is that, except in rare cases, *combustion modeling is impossible*: already the number of set-up rules to be obeyed exceeds the degrees of freedom at the disposal of the experimenter; and, in addition, the requirements of cheapness, speed, and accuracy have to be met. How then is it possible that modeling techniques are used in combustion research, and that one can even hold a colloquium on the subject?

The answer to this question is that, though the theory of modeling requires that *all* the set-up and interpretation rules should be obeyed, experience has shown that flouting some of them does not entirely invalidate the prediction. Thus nearly all currently used combustion models* are examples of *partial modeling*, in which only a few of the rules are obeyed; the disregard of the others inevitably introduces some uncertainty about how the results of the experiments should be interpreted.

As a consequence, the mere enumeration of the dimensionless groups which must be held constant, though an easy and attractive task to theoreticians, has but slight value. *The central problem of partial modeling is to discern which modeling rules need not be obeyed*, and to estimate the resulting errors in the predictions which are made. There is no technique as mechanical and certain as dimensional analysis for the solution of this problem, which necessitates a high degree of physical insight and inspired guesswork on the part of the experimenter; it is for this reason that the word "art" has been included in the title of the present paper.

The art of partial modeling is rendered practicable by two main facts. The first is that it is never necessary to make a *complete* prediction about the outcome of a prototype experiment; often only a few pieces of information are desired, for example the overall pressure drop, the length of the flame, or its efficiency of combustion. The second is that, though many processes and input quantities influence the outcome of a given experiment, some influences are much weaker than others; it may therefore be permissible to observe only the modeling rules appropriate to the strong influences. The skill of the modeler, and his good fortune, are measured by the extent to which he is able to sort out the variables and phenomena with which he is concerned into semi-independent sets. Sometimes this separability is suggested by a study of the differential equations; more often its existence is perceived intuitively, or even assumed unthinkingly as a result of blissful ignorance. In the remainder of this paper, we consider some of the more successful or theoretically interesting examples of partial modeling applied to combustion.

Some Examples of Partial Modeling of Combustion Processes

The Case When Interest is Restricted to Fluid-Mechanical Features of the Process

Prototype Variables Which May Be Predicted. The interest of the experimenter in the outcome of a

* The same is true, perhaps to a lesser extent, of the modeling techniques used in other fields also, e.g., in marine engineering. The special difficulty about combustion modeling is that it involves chemical reactions; so of course do the scale-up techniques used for reactor design in the chemical industry.

combustion experiment is often, at least temporarily, restricted to certain fluid-mechanical quantities; for example, the designer of a gas-turbine combustor may wish to predict the pressure drop in the gas stream between entry and exit, or he may wish to observe the qualitative pattern of the flow within the combustor so that his experienced eye can assess its suitability for the maintenance of flame. Similarly, an early question asked by those who wish to predict the effect of very large city fires is: "How strong a wind will be generated, and how will it interact with the meteorological wind?" It is this restriction of interest which permits fairly reliable predictions to be made on the basis of model experiments which are superficially far from similar to the prototype in question.

*Modeling Rules Which May Be Neglected.** Experience has shown that, in many practical cases of the above kind, the experimenter may fairly safely ignore the dictates of similarity theory in the following ways:

1. If the Reynolds number is sufficiently large (e.g., $>10^5$ when formed from the largest V and l appearing anywhere in the problem), the Reynolds numbers of model and prototype need not be equal. This is particularly the case when the flow is of the "jet-mixing" type so common in furnaces.

2. If the Mach number is sufficiently low (e.g., 0.8 at the point of highest velocity), the Mach numbers of model and prototype need not be equal.

3. If the Froude number is sufficiently high, the Froude numbers of model and prototype need not be equal. This is the case for high-velocity flows, e.g., those in rocket motors, in which buoyancy effects are negligible; the flows in industrial furnaces have relatively low Froude numbers, however, so that this rule cannot always be safely ignored.

4. Two-phase flow effects (e.g., those associated with the presence of liquid-fuel sprays, clouds of coal particles, etc.) need not be simulated provided that the settling time of a particle is very much lower than the time of residence of the particle in the chamber.

5. If the density change associated with combustion is not too large, there is no need to maintain groups such as $Z'''l/\rho V$ equal for model and prototype; indeed there is no need for any chemical reaction to take place in the model. It is solely through the density change (and to a minor extent the viscosity change) that combustion has any fluid-mechanical influence; so, when the density variations due to combustion in the prototype are too large to be ignored, they can be produced in the model by any convenient technique, e.g., electrical heating.

6. While geometrical similarity is usually required between model and prototype in all gross features of the apparatus, minor departures from similarity are permissible and may even be advantageous. Thus, when the two fluids entering a model have a different density ratio from that appropriate to the prototype, it is better to distort the model injection system, so that the velocity ratio and the mass-flow-rate ratio have equal values in model and prototype, than to maintain the areas of the two streams in the same ratio for model and prototype. This procedure seems to have been first advocated by Thring and Newby,[21] following a suggestion of Squire and Trouncer.[20]

The Use of Water Models for the Study of Steady-Flow Combustion Systems. The relative unimportance of the modeling rules just referred to gives the designer of the experiment considerable freedom in the choice of apparatus size, operating pressure, nature of fluid, time scale, temperature level, etc. This freedom appears to have been first exploited by combustion workers in connection with steady-flow industrial furnaces of the open-hearth type.[3] Water has been widely used as the fluid of study, and the model has usually been much smaller than the prototype. Subsequently, the designers of gas-turbine combustion chambers have developed the water-model technique, often using models constructed from perspex (lucite) having the same linear dimensions as the original. Work of this kind is represented in the present colloquium by the paper of Clarke, Gerrard, and Holliday.[4] No attempt is made to maintain equality of Reynolds, Froude, or (of course) Mach numbers; and the density change resulting from combustion is not simulated at all. The flow is made visible by injection of air bubbles or other light-scattering particles. The users of the technique claim to have received great benefit from it, even though the results of the model experiments are often only interpreted qualitatively.

Accounting for the Effect of Combustion-Produced Density Variations. When the attempt is made to base quantitative predictions on water-model experiments, it is found that appreciable discrepancies exist between the prediction and the prototype results. The main reason is usually the absence in the water model of the density change which accompanies combustion. The marked effect which this density change can have, even

* The facts and suppositions described here were summed up in an earlier paper[16] as "the aerodynamic half-truth."

on the qualitative nature of the flow, is strikingly demonstrated by the work of Hern *et al.*[9] reported in the present colloquium; their technique of simulating the density variations occurring in liquid-propellant rocket combustion by the flash vaporization of liquid kerosene was originally suggested by Bragg.

Of course the technique in question might also be held to simulate the two-phase flow and vaporization effects of rocket motors. However, no attempt has been (or could easily be) made to obey the relevant set-up rules. If the flow patterns revealed in Hern's photographs are representative of rocket motors, it can only be by favor of the dispensation mentioned under (4) above. Further, the rates of phase change by "flashing" must be roughly those which keep the time of phase change in the same ratio to l/V for the model as for the prototype; this will only be fortuitously the case.

Another method of simulating combustion-produced density changes is to have a flame in the model also; this may sometimes eliminate the advantage of cheapness which the model experiment is supposed to possess, but not always. An example of the way in which flow patterns, even in premixed flames, seem sometimes to depend *only* on the density ratio is provided by the spread of a turbulent flame from a flame holder across a confined stream.[19]

The Case When Interest Is Concentrated on Mixing

Prototype Variables Which May Be Predicted. A mere knowledge of the velocity distribution in a combustion process does not usually suffice for the designer of equipment; he needs to know the corresponding flame length, the temperature distribution at the combustion-chamber outlet, and the distribution of fuel/oxidant ratio through the system. If a phase change takes place, knowledge may be required of the extent of its completion at various locations; as an example, it appears to be the vaporization of the injected droplets which controls the efficiency in liquid-propellant rockets.

Knowledge of the fuel/oxidant ratio is useful because, coupled with the assumption of thermodynamic equilibrium, it permits most of the mixture properties to be calculated*; the flame length and outlet temperature distribution therefore appear as deductions from the mixture-ratio distribution.

* This fact is expressed somewhat more precisely in the "thermodynamic half-truth,"[16] together with the accompanying corollaries and notes.

Modeling Rules Which May Be Neglected.† Since the distribution of fluid composition depends strongly on the fluid-mechanical aspects of the process (fortunately the reciprocal influence is incomparably weaker), it is clear that a model experiment in which mixing is of direct interest must satisfy the inescapable requirements of fluid-mechanical modeling in the first part of this section. Table 1 indicates some of the further rules which ought to be obeyed (see the columns headed "conduction," "diffusion," "heat transfer," "mass transfer," "radiation," "particle disappearance"); we here concentrate on the dispensations which are sometimes allowable from these requirements.

1. If the Reynolds number is sufficiently large, there is no need for the Prandtl and Schmidt numbers to be equal in model and prototype. This results from the unimportance of all molecular transport processes in such flows.
2. If the injected particles (oxidant droplets, coal-dust, smoke) are so small that their disappearance time is much less than the residence time of the fluid in the whole system, it may be permissible not to maintain equality of the dimensionless groups headed "particle disappearance" in Table 1.
3. If phase-change effects do have to be simulated, the similarity requirements are actually fewer than might be suggested by a straightforward application of dimensional analysis. For example, it suffices to maintain constancy of the so-called "transfer number" B[18]; so a mass-transfer process involving combustion may be simulated by one in which vaporization takes place without chemical reaction, or by artificially forcing an inert gas through a porous wall.

Model Experiments Using Tracers. The freedom to break the rules of strict modeling, implied in the above remarks, has been employed by many workers, particularly in the steel industry. The paper by Beer, Chigier, and Lee[2] in the present colloquium is an interesting development of a commonly used technique of this kind: a geometrically similar model of the furnace is used for the study of the mixing between the injected reactants and the recirculating combustion products, the latter being simulated by injecting helium as a tracer at a suitable point of the model.

Models using liquids are sometimes used. These give the possibility of making the mixing pattern visible by means of differences of color between the streams; the review paper by Hottel[10] at an

† Some aspects of this matter are discussed in reference 16 under the heading "the mixing half-truth."

earlier combustion symposium gives a good description of these. Of course, there is no need to restrict the technique to steady-flow systems, as witness the elegant work of Rizk[14] in modeling the inflow of fresh change to the cylinder of an internal-combustion engine.

Two-Phase Flow Models. The present colloquium also contains an example of the deduction of mixture ratio from a model experiment in which droplets of liquid are injected with a gas stream, as in so many combustion devices; this is the paper of Ellor,[6] who replaces a fuel (kerosene) by water, for the sake of experimental ease. It appears that experiments bear out the expectation that it is permissible to keep constant only the ratio of the entry velocities and the ratio between the mass flow rates; rate-of-vaporization effects appear negligible.

The Case When Interest Is Extended to the Gross Effects of Chemical Kinetics

The Importance of Chemical Kinetics. The techniques described in the previous subsection are useful because it can often be assumed that local departures from chemical equilibrium are small; this assumption holds fairly well for ground-level fires, for large industrial furnaces, for liquid-propellant rocket motors, and for gas-turbine combustion at low altitudes. In many circumstances, however, the rate constants of the chemical transformation are such that large departures from equilibrium can be found to exist; in extreme cases these lead to "flame extinction." Such departures occur particularly at high volumetric flow rates, at low pressures, and with the reaction zone in good thermal contact with cold surroundings. They may be found in ram-jet combustors at high altitude or in a small solid-fuel bed.

In addition to the above role of chemical kinetics in modifying a process which would still proceed at a finite rate if the rate constants of the reaction were infinite (i.e., a "physically controlled" process), there are several practically important combustion phenomena in which the chemical-kinetic constants exert a more direct influence. These include the propagation of flame across the combustion space of a gasoline engine, and the burning of a solid-propellant rocket motor, under either steady or transient conditions.

Prototype Variables Which May Be Predicted. The devising of modeling techniques for the above combustion phenomena would be impossible were it not for the fact that the experimenter's interest often extends merely to the gross features of the outcome of the prototype experiment: It is not necessary to be able to predict the distribution of OH radicals through the flame, but merely to decide whether the flame will be blown out; the combustion efficiency has to be estimated in terms of temperature rise, but the nature of the intermediate combustion products is not required; the engine designer wants to know the time between the passage of the spark and the completion of burning, not the thickness of the flame front. It is this restriction of interest which has permitted a relaxation of the strict requirements of similarity theory and has permitted modeling to throw light on kinetically influenced combustion also.

Modeling Rules Which May Be Neglected. The rate of chemical reaction at any point is of course greatly influenced by the fuel:oxidant ratio at that point; it follows that the rules for partial modeling of kinetically-influenced systems are based on those for partial modeling of mixing models, just as the latter were based on the rules for fluid-mechanical models. Further rules which ought to be obeyed are indicated in Table 1, whereby it should be remembered that the quantities Z''' and Z'' are reference values of the reaction rate; that there are as many of these quantities as there are chemical reactions which occur; that in addition most reactions are characterized by an activation energy E, so that E/RT_u is an important dimensionless group; and that even very simple combustion processes (e.g., the hydrogen–oxygen diffusion flame) represent the outcome of a large number of chemical reactions (between radicals and other intermediate products). It is evident that the experimenter must look with more hope to the rules which may be ignored than to those from which no departure is permissible. The former include:

1. Under some circumstances* it is possible for the reaction-kinetic constants of the combustion processes in the prototype model to be specified by a single set of numbers, just as though only one ("global") chemical reaction took place. There, if the exothermic process in the model is similarly specified, the requirements of similarity theory are met by causing a single dimensionless group (e.g., "Damköhler's first group," or the "chemical loading") to have the same value in both the model and the original. Actually, few experimenters can afford to inquire about whether the "certain circumstances" prevail in their particular case, but adopt a single

* These are detailed in reference 16, where the facts underlying this paragraph are expressed as "the chemical half-truth."

group nevertheless; though the resulting predictions are thereby rendered unreliable, the method has produced some useful results.

2. When a global homogeneous reaction is presumed, strict similarity requires its rate to be the same function of temperature for model and prototype. This requirement may be relaxed for flame-propagation problems if the reference value of Z''' is the value of Z''' averaged over the temperature range of the process; for flame-extinction problems, the *maximum* value of Z''' may form a more suitable reference. A similar relaxation may be presumed for heterogeneous reactions. However some error in the resulting prediction is inevitable.

3. Whenever the homogeneous reaction zone is very thin, and the Reynolds number is high, as when a turbulent flame can be regarded as a wrinkled laminar one, or when the chemical transformations occur only near the boundaries of the gas space, it is possible to ignore the dimensionless groups involving Z''' and Z'' and employ only those involving S_u, the laminar flame speed. Thus the gross features of a combustion process of this kind might depend only on the dimensionless groups S_u/V_{entry} and the density ratio between burned and unburned gases. This use of S_u is quite distinct from that in which groups involving S_u are used *in place of* groups involving Z''', without any reduction of the total number of modeling rules.*

4. With the shapes of reactor commonly used in the chemical engineering industry (tubes, packed beds), the requirement of geometrical similarity may be considerably relaxed, as was already recognized by Damköhler[5]; here the flow pattern is imagined as being essentially that of plug flow, with chemical transformations distributed uniformly across any cross section, and other fluid-mechanical factors only influential through the effect they have on the heat and mass transfer coefficients at the boundaries; of course the dimensionless groups involving these coefficients and the homogeneous and heterogeneous reaction-rate constants must have the same value for model and original. Some discussion of this type of modeling is given in the paper presented by Barkelew[1] in the present colloquium. Unfortunately combustion chambers are seldom of a suitable shape to permit the geometrical-similarity requirement to be ignored.

* Putnam and Jensen[13] happened to use dimensionless groups of the latter character rather than those involving Z'''. Since S_u, Z''' and the transport properties are connected via laminar flame theory, it is a simple matter to transform from one mode of expression to the other.

"pl Scaling." One of the most useful modeling techniques used in the development of air-breathing engines is that in which the only rules observed are that: there is geometrical similarity; fuel and air input velocities and temperatures are the same for both model and prototype; and the product of the absolute pressure and the linear dimension is also made equal for the two combustion chambers. The utility of this procedure derives from the fact that it preserves constancy of the Reynolds and Mach numbers (though variations in these numbers would actually be of minor importance) and also of the "global" chemical loading parameter (provided that Z''' is proportional to the square of the absolute pressure); it permits high-altitude combustion to be simulated by atmospheric-pressure tests on a smaller scale.

A study of the literature reveals that *"pl* scaling" was invented first by many different workers. One of them was Stewart[21] who contributes to the present coloquium. The method is implicit in Fig. 3 of Ellor's paper,[6] where the product of pressure and a linear dimension appears in the abscissa of a graph showing extinction conditions. Many other versions of the method are current. The paper by Hottel *et al.*[11] in the present colloquium contains, among other things, a critique of the validity of the method; these authors point, as others have done before, to the importance of the Reynolds and heat-loss parameters; they also draw attention to the role played by the Knudsen number at low pressures.

Water Injection. In *"pl* scaling" the reactants and their temperature levels remain constant from prototype to model, while the linear size changes. It is however possible to equal the chemical loading of a prototype chamber operating at low pressures by using as a model the identical chamber operating at atmospheric pressure; in this case the temperature or composition of the reactants must be modified so that the value of Z''' is appropriately decreased. A simple method of so reducing Z''' was described by Lefebvre and Halls[12] at the Seventh Combustion Symposium: They injected water into the air stream along with the fuel and considered Z''' to vary monotonically (though, of course, nonlinearly) with the easily measured kerosene/water ratio. Though not giving rise to quantitative predictions about low-pressure performance, and despite the fact that Reynolds number and other effects may be appreciable, this procedure appears to be useful to development engineers; it illustrates well the fact that the most successful technique is often that which

disregards the requirements of similarity most boldly.*

Simulation of Kinetically Influenced Combustion by Electrical Heating. A model technique which involves an even more drastic disregard of the rules of strict modeling is the "electrothermal analogue,"[18] in which the burning gas is simulated by a stream of air flowing through a space, throughout which are distributed electrical heater wires; the power dissipated in each heater is controlled by an external mechanism to have a relation to the local air temperature which is similar to the global-reaction-rate relation supposed to exist in the prototype. The reliability of the predictions afforded by this method, and by modifications of it, is discussed in the present symposium by Vortmeyer,[24] who concludes that, mainly because the density ratio of real flames is not simulated, the method is too unreliable to serve as a guide to development engineers even though its predictions are correct as to order of magnitude. Of course, this judgment may be considered too harsh when compared with the fact that the water-flow model, which equally fails to simulate density differences and provides no prediction at all about the stability or efficiency of the flame, is nevertheless highly regarded by designers; however, it is perhaps proper that the electrothermal analog, which is somewhat more difficult to construct and to understand than the water model, should be judged by higher standards.

Partial Modeling of Flame Propagation in Spark-Ignition Engines. As a final example of the modeling of a kinetically influenced combustion process, we consider one in which dispensation 3 (above) is exploited; this method was suggested by the present author for correlating data for the time of burning of the gases in a gasoline engine. If t_b is the time taken for the flame to spread from the spark throughout the gas, t_{str} is the time of an engine stroke, l is a typical dimension of the combustion space (e.g., piston diameter) and S_u is the laminar flame speed, dimensional analysis suggests that the experimental data for a given engine should obey the relation:

$$l/t_b S_u = f(l/S_u t_{str}, \text{Reynolds number}), \quad (1)$$

where $f(\ )$ is a function to be determined by experiment. The Reynolds number influence may, with good fortune, be fairly small.

This supposition has been put to the test by

* Of course a bold disregard of the rules is not a *sufficient* condition for success in modeling; care and intuition are equally necessary.

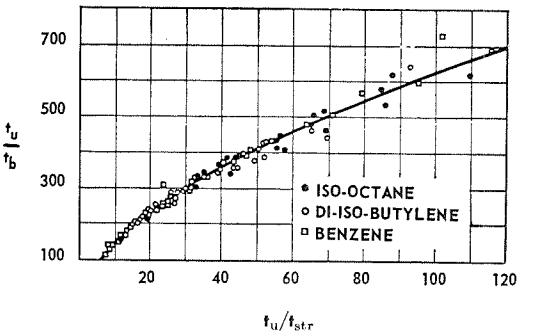

FIG. 1. Example of engine characteristic; see text for explanation.

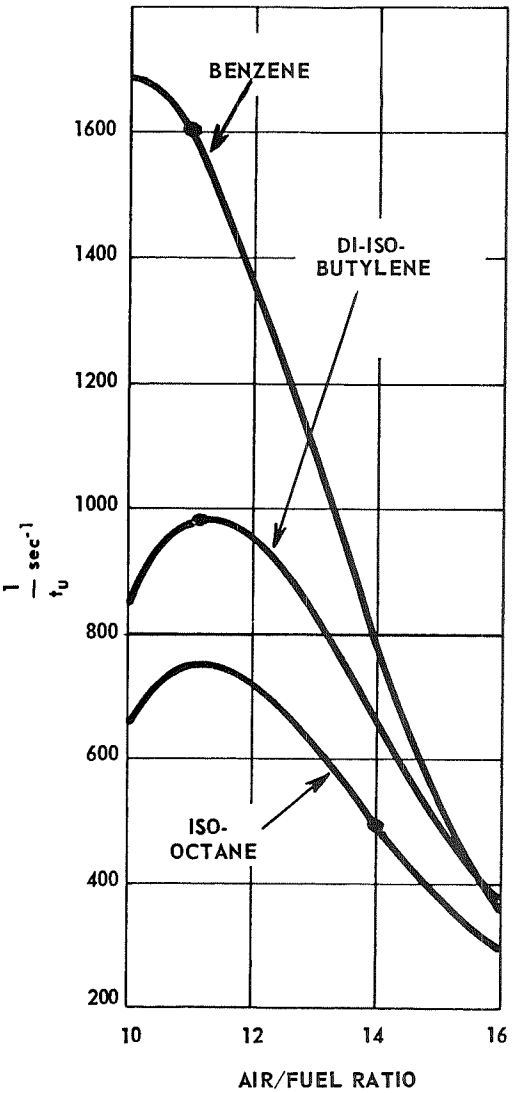

FIG. 2. Fuel characteristics, corresponding to Fig. 1.

Harrow and Orman[8] who measured the flame-travel time t_b on a Ricardo E 6 engine, using various fuels and fuel/air ratios. Since data for the laminar flame speeds S_u were not available for the conditions of pressure, temperature, and dilution with exhause products prevailing at the moment of ignition, curves of $1/t_b$ were plotted versus $1/t_{str}$; each curve related to a particular fuel and air/fuel ratio. Then a factor t_u was found for each curve which, when the ordinate and abscissa values for each point on the curve were multiplied by it, caused all the curves to coincide; the common curve of t_u/t_b versus t_u/t_{str} was regarded as the characteristic of the engine, while t_u was regarded as proportional to the reciprocal of S_u, a fuel characteristic.

Figure 1 contains the engine characteristic for the E 6 engine at full throttle, when the spark passed 15° before top dead center. Figure 2 contains corresponding fuel characteristics, $1/t_u$ versus air/fuel ratio, for three different fuels. The fact that the points on Fig. 1 can be caused to lie fairly close to a single curve, and that the $1/t_u$ curves are qualitatively similar in form to curves of S_u which prevail at atmospheric conditions, may be regarded as encouraging preliminary results.

Conclusions

The foregoing incomplete survey of the problems and practices of combustion modeling appears to suggest the following conclusions:

1. The strict requirements of similarity theory are so numerous that complete modeling of combustion processes is practically impossible. For this reason, only partial modeling is practicable.

2. Partial modeling gives useful results in combustion work mainly because the fluid-mechanical processes are not greatly influenced by mixing, and mixing is little influenced by chemical reaction. Success in modeling depends on the recognition and exploitation of such weak influences. One of the main functions of theory in combustion research is to facilitate this recognition.

3. No absolute or final decision can be made about the permissibility of a given modeling technique; the decision must always depend on the interests of the experimenter, the accuracy and urgency of the required prediction, and the availability of other techniques. Often the modeling technique which most flagrantly flouts the similarity rules is the most useful one in practice.

857

Nomenclature

a_{grav}	Gravitational acceleration [ft/hr²]
B	"Transfer number" or "driving force" for mass transfer
c	Specific heat at constant pressure [Btu/lb °F]
D	Diffusion coefficient [ft²/hr]
g_0	Constant in Newton's Second Law of Motion [lb ft/lb$_f$ hr²]
k	Thermal conductivity [Btu/ft hr °F]
l	Typical dimension of body [ft]
$\dot{m}''$	Mass-transfer rate across a phase interface [lb/ft² hr]
p	Pressure [lb$_f$/ft²]
s	Surface tension [lb$_f$/ft]
S_u	Laminar flame speed [ft/hr]
t	Time [hr]
t_b	Burning time in spark-ignition engine [hr]
t_u	Scale factor, proportional to reciprocal of laminar flame speed [hr]
T	Absolute temperature [°R]
Z''	Reference value of heterogeneous reaction rate [lb/ft² hr]
Z'''	Reference value of homogeneous reaction rate [lb/ft³ hr]
α	Surface heat transfer coefficient [Btu/ft² hr °F]
μ	Dynamic viscosity [lb$_f$ hr/ft²]
σ	Stefan-Boltzmann constant [Btu/ft² (°R)⁴]
ρ	Density [lb/ft³]
ρ_G	Density of gas phase [lb/ft³]
ρ_F	Density of particle [lb/ft³]
isent	Isentropic (subscript)

References

1. Barkelew, C. H.: This volume, p. 958.
2. Beer, J. M., Chigier, N. A., and Lee, K. B.: This volume, p. 892.
3. Chesters, J. H., Howes, R. S., Halliday, I. M. D., and Philip, A. R.: J. Iron and Steel Inst. *162*, 385 (1949).
4. Clarke, A. E., Gerrard, A. J., and Holliday, L. A.: This volume, p. 878.
5. Damköhler, G.: *Der Chemie-Ingenieur* (A. Eucken and M. Jakob, eds.), Band III, Teil 1. Akademische Verlag, 1937. Reprinted by VDI-Fachgruppe Verfahrenstechnik, Leverkusen, 1957.
6. Ellor, J. O.: This volume, p. 901.
7. Groume-Grjimailo, W. E.: *The Flow of Gases in Furnaces*. Wiley, 1923.
8. Harrow, G. A. and Orman, P. L. (Thornton Research Center, Shell Research): Private communication, 1962.
9. Hern, R. B., Siddal, R. G., and Thring, M. W.: This volume, p. 965.

10. HOTTEL, H. C.: *Fourth Symposium (International) on Combustion*, p. 97. Williams and Wilkins, 1953.
11. HOTTEL, H. C., WILLIAMS, G. C., JENSEN, W. P., and TOBEY, A. C.: This volume, p. 923.
12. LEFEBVRE, A. H. and HALLS, G. A.: *Seventh Symposium (International) on Combustion*, p. 654. Butterworths, 1959.
13. PUTNAM, A. A. and JENSEN, R. A.: *Third Symposium (International) on Combustion*. Williams and Wilkins, 1949.
14. RIZK, W.: Proc. Inst. Mech. Engrs. (London) *172*, 417 (1958).
15. ROSIN, P. O.: J. Inst. Fuel *12*, 198 (1939).
16. SPALDING, D. B.: *Third AGARD Colloquium*, pp. 269–306. Pergamon Press, 1958.
17. SPALDING, D. B.: *Some Fundamentals of Combustion*. Butterworths, 1955.
18. SPALDING, D. B.: Proc. Inst. Mech. Engrs. (London) *171*, 383 (1957).
19. SPALDING, D. B.: *Seventh Symposium (International) on Combustion*, pp. 595–603. Butterworths, 1959.
20. SQUIRE, H. B. and TROUNCER, J.: *ARC Tech. Rept. R. and M. No. 1974*, 1944.
21. STEWART, D. G.: *Selected Combustion Problems*, vol. 2, pp. 384–414. Butterworths, 1956.
22. THRING, M. W. and NEWBY, M. P.: *Fourth Symposium (International) on Combustion*, pp. 789–796. Williams and Wilkins, 1953.
23. TRAUSTEL, S.: *Modellgesetze der Vergasung und Verhüttung*. Akademie-Verlag, 1949.
24. VORTMEYER, D.: This volume, p. 936.

THE SIZE OF FLAMES FROM NATURAL FIRES

P. H. THOMAS

Uncontrolled fires produce flames where the initial momentum of the fuel is low compared with the momentum produced by buoyancy. The heights of such flames with wood as the fuel are examined and discussed in terms of both a dimensional analysis and the entrainment of air into the turbulent flame. They are then compared with other experiments on the flow of hot gases.

Some recent experiments on the effects of wind on such flames are also reported.

Introduction

This paper discusses one of the least studied features of natural fires—the length of the turbulent flames rising from the burning fuel.

Horizontal sources of fuel in still air are considered first either circular, square, or in the form of an infinite strip, each characterized by a single linear dimension D (diameter or width). The effects of wind are discussed later. The fuel is the gas or vapor generated by the heating of a solid or liquid. This heating is, of course, accomplished for large fires by the heat transfer from the flame zone itself. However, the solid or liquid fuel can be regarded as a burner of dimension D, and the mass rate of burning m is treated as an independent variable.

The fuel burns in a flame zone to a height L to produce a column of hot gases. At heights above the top of the flame this column may be considered as a thermal plume with constant convective heat flux. It is possible to correlate data on velocity and temperature in this plume for isothermal atmospheres by means of dimensionless variables deduced either from the appropriate differential equations or from elementary considerations of buoyancy and the conservation of convected heat. Because it will be shown that data on flames can be related approximately to data obtained in studies of nonreacting hot gases, reference will first be made to such dimensionless variables.

The temperature rise θ, at a height z, in the center of a plume of negligible initial momentum is determined by the convected heat flux H, the specific heat c, the density ρ, the coefficient of expansion of the gas $(1/T_0)$, the linear size of the source D, and the acceleration due to gravity g. Density is conventionally assumed constant in plumes and jets except where it affects local buoyancy. Considerations of the conservation of heat and the relation between momentum and buoyancy or a direct dimensional analysis of the above variables leads to the relationship for a plume

$$\Theta = \frac{\theta_c D^{5/3}}{(H^2 T_0/\rho_0^2 c^2 g)^{\frac{1}{3}}} = f(z/D). \qquad (1)$$

For a point source or for an extended source at values of z large compared with D, this correlation must become independent of D and the well known result is obtained

$$f(z/D) \propto (D/z)^{5/3},$$

i.e.,

$$\theta_c \propto H^{\frac{2}{3}}/z^{5/3}. \qquad (2)$$

For a line source, the correlation must similarly be independent of D except that H must only appear as the heat per unit length of the line source, i.e., in Eq. (1) H is replaced by $H'D$ and a function is found such that θ_c is independent of D. The well known result for the line source is then obtained

$$f(z/D) \propto D/z$$

i.e.,

$$\theta_c \propto H'^{\frac{2}{3}}/z \qquad (3)$$

Equation (1) is a general form for finite sources except that the unspecified function f depends on the shape of the source. Yokoi[1] has in fact presented correlations of this form for a variety of different shapes of source in horizontal and vertical planes. Lee and Emmons[2] have recently given a theoretical treatment of a strip source.

Where there are density differences between the two mixing fluids, the mixing, and consequently the expansion of the plume, can be related to the excess momentum.[3,4] However other difficulties arise in applying such arguments in detail to flames. Tall flames will be much taller than the potential core, but smaller flames will not necessarily be so. Heat is generated in flames so that the conservation of sensible heat in the

conventional treatments must be modified to allow for the progressive release of heat as a result of mixing with air. The application of theoretical analysis is also more difficult because the flame zone does not necessarily have the simple geometry associated with point or line sources. Arguments have previously been given[5,6] for assuming that for any one fuel the height of a turbulent diffusion flame is related to the volumetric flow rate of fuel Q_1 and the burner dimension D, as described by

$$L/D = f(Q_1^2/gD^5). \tag{4i}$$

For an infinite strip source Eq. (4i) is used in the form

$$L/D = f(Q_1'^2/gD^3) \tag{4ii}$$

or more generally

$$L/D = f(Q_1''^2/gD). \tag{4iii}$$

The variable quantities in these equations are similar to those in Eq. (1) if θ_c is regarded as constant at the flame tip or if Eq. (1) had been replaced by a similar equation involving concentration, and concentration were put as equal to a constant. The connection between the two equations is discussed below but a more direct derivation of Eqs. (4) follows immediately, which shows the physical basis more clearly. Some experimental results for the mean upward velocity of the gas in the flame zone are first discussed.

Velocity of Gases in the Flame Zone

Rasbash *et al.*[7] presented regression equations for the rate of increase of flame height during the course of the short pulsation of a flame. They found that the time of burning was a significant, though small, factor for petrol and kerosene but not for alcohol and benzole, despite the fact that the rate of burning varied with time most for benzole and alcohol and varied little for kerosene and petrol. However, plotting their original data averaged over all times of burning and introducing their values for the estimated flame temperature which varied between 921° and 1218°C for the four fuels, and assuming an ambient temperature of 15°C enables the upward velocity w_t to be plotted against $(2g\theta_{fl}z_t/T_0)^{\frac{1}{2}}$ (Fig. 1) which is the theoretical maximum velocity at a height z_t if the lateral transfer of momentum and friction are neglected. The straight line drawn in Fig. 1 is:

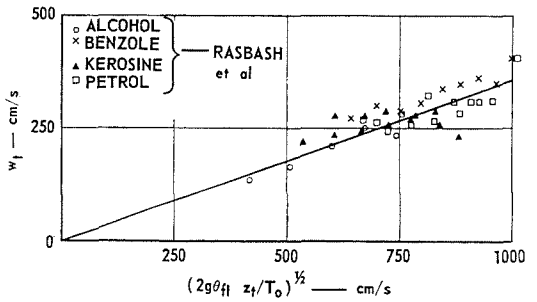

FIG. 1. Upward velocity of flame tip.

$$w_t = 0.36(2g\theta_{fl}z_t/T_0)^{\frac{1}{2}} \tag{5}$$

Rabash[8] recently presented his original data in the form

$$\rho_{fl}w^2 = 0.27z(\rho_1 - \rho_{fl})$$

which is virtually identical with Eq. (5).

The value z_t extended from about $\frac{1}{2}D$ for alcohol to $5D$ for the other fuels. If the flame zone is treated as a region of uniform temperature which is constant for a given fuel and a large enough fire, the characteristic mean upward velocity for similarly shaped flames where the injection velocity w_1 is small compared with $(gL)^{\frac{1}{2}}$ (where L is the mean flame height, i.e. the mean of z_t) will, from dimensional arguments, be of the form $(gL)^{\frac{1}{2}}$. For differently shaped flames the inclusion of a shape factor may be necessary and the mean velocity would then more generally be written as

$$\bar{w}_L \propto (gL)^{\frac{1}{2}}F(L/D), \tag{6}$$

where the bar denotes the mean value over the whole flame height.

The numerical value of $(gL)^{\frac{1}{2}}$ for flames say 200 cm high is about 450 cm/sec. The rate w_1, at which fuel gases leave a burning surface, for example a tank of fuel, is of the order of 1 cm/sec which explains why the velocities are correlated with buoyancy and not with the rate of burning or burner size.

Air Entrainment

Taylor[9] introduced the assumption, later used by Morton, Taylor, and Turner[10] that if air enters a rising column by entrainment, the entrainment velocity v is proportional to the local rising velocity w_z. The total flow into the rising plume may be then represented by:

$$Q_0 \propto \bar{v}G(L/D)D^2 \tag{7}$$

where G represents a shape factor for the envelope of the flame zone. For the two-dimensional flame from a strip source, Q_0' is considered instead of Q_0. The flame area per unit length of strip would be represented by $G(L/D)D$. From the above assumption regarding the proportionality between v and w_z, which is discussed in more

detail below, and with the total quantity of air Q_0 proportional to the quantity of fuel Q_1 the following relation is obtained from Eqs. (6) and (7),

$$Q_0 \propto Q_1 \propto (gL)^{\frac{1}{2}} F(L/D) G(L/D) D^2 \qquad (8)$$

from which Eq. (4) follows.

For turbulent flames in which the momentum of the injected fuel is significant compared with buoyancy, Eq. (6) must be generalized to

$$\bar{w}_L \propto (gL)^{\frac{1}{2}} f(L/D, Q_1^2/gD^5), \qquad (9)$$

where Q_1^2/gD^5 is the form of a Froude number expressing the ratio of the initial momentum to the buoyancy in terms of the characteristic dimension. Clearly this does not change the essential result of Eq. (4) except that it shows how Q_1 can have a double significance, one related to momentum the other to fuel and air quantity. A decrease in buoyancy relative to orifice momentum leads to a decrease in the velocity in the fuel stream and hence to a lower rate of entrainment and a larger flame. Thus L/D is an increasing function of Q_1^2/gD^5 and L/D should tend to an upper limit which has the value typical of a turbulent jet[11–14] where buoyancy is of minor importance and L/D cannot depend on g.

In Eq. (7) G is proportional to L/D for cylindrical flames and also for conical flames with the burner as the base and the flame top as the apex. It is proportioned to $(L/D)^2$ for long conical flames with the flame zone expanding upwards. Thus if

$$G(L/D) \propto (L/D)^q \qquad (10)$$

the index q might be expected to increase from 1 to 2 with increasing L/D.

If $\bar{v}$ is taken as proportional to $L^{\frac{1}{2}}$ and F constant, Eqs. (8) and (10) lead to

$$L/D \propto (Q_1^2/gD^5)^{1/(2q+1)} \qquad (11)$$

This equation shows that the L/D versus Q_1^2/gD^5 relation on a log–log basis is convex upwards. The index of Q_1^2/gD^5 thus varies from $\frac{1}{3}$ to $\frac{1}{5}$ as L/D increases, until at high values of Q_1^2/gD^5, when the effect of orifice momentum becomes significant, it tends to zero and L/D becomes constant. The value of q is 1 for strip sources when L/D is $\gg 1$, and the index of Q^2/gD^3 is $\frac{1}{3}$. Thus neither for long flames from finite burners nor from infinite line burners does theory suggest that L depends on D.

It will usually be necessary to employ m_1 (which is measured directly by weighing) instead of Q_1, and hence use will be made of the relations

$$m_1'' D^2 \propto m_1 \propto \rho_1 Q_1,$$

i.e.,

$$Q_1^2/gD^5 = m_1''^2/\rho_1^2 gD$$

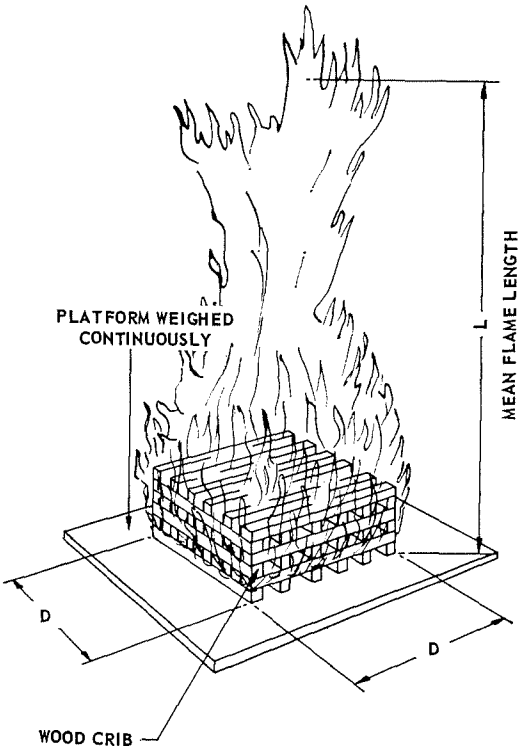

FIG. 2. Diagrammatic sketch of experimental arrangement.

Experimental

Cribs on Square Horizontal Base. Cribs of wood (spruce) sticks arranged on a square horizontal base of side D have been burned in the laboratory (Fig. 2). Varying the amount of wood and the design of the crib allowed a range of mass rates of burning, i.e., rates of weight loss m_1 could be obtained by direct weighing for a given value of D. The flame was photographed and the height measured from the base of the shallow crib.

The burning rate reached a maximum value which remained steady for a period; this and the mean height of the continuous flame zone corresponding to it were recorded as m_1, and L, respectively, the flame heights being averaged over a period considerably longer than the fraction of a second taken for a single fluctuation. In the period of steady burning it is mainly the volatiles from the wood that are involved. Apart from a small amount of carbonaceous residue burning at the crib edge, little carbon burned until the flames subsided and the gross rate of burning fell. The results are plotted in Fig. 3 as L/D in terms of $m''/\rho_0(gD)^{\frac{1}{2}}$. The viscosity of the volatiles μ_1 was assumed to be 10^{-4} cgs units and the density taken as 1.3×10^{-3} gram/cc, or the density of

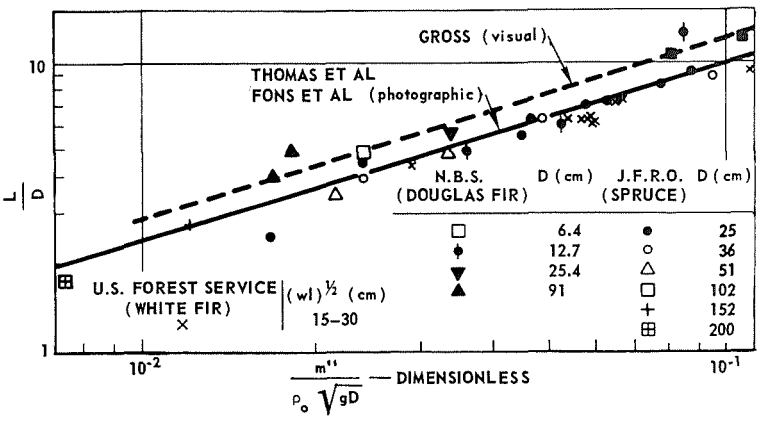

FIG. 3. Correlation of flame height data (still air—approximately radially symmetrical).

air. (Since the density of the wood volatiles is not properly known the value for air has been inserted solely to enable the order of magnitude of the dimensionless parameter to be seen.) Apart from one result of 1250, the Reynolds number Re at the orifice $(m_1/\mu_1 D)$ was over 2000 in all experiments, but in more than half it exceeded 10^4. Some unpublished data are also available.

Gross,[15] at the National Bureau of Standards, Washington, D.C. has burned sticks of Douglas fir of square section assembled in the form of cubical cribs. The Reynolds numbers based on 10^{-4} cgs units for μ_1 fell in the range 13 to 6400. Some of the results clearly referred to laminar flames, but all the data where the flames were less than 2 feet (50 cm) high have been excluded and the rest are plotted in Fig. 3. These results where the flame height was measured by eye follow the same trend as the others but are about 20 per cent higher. For these cubical cribs the crib height is also D, but a reduction of L/D by 0.5 on the assumption that the effective source is at the mid-height of the crib is not sufficient to explain the difference between the two sets of data. Some more recent comparisons suggest that this may be mainly a difference between visual and photographic measurement.

Use has also been made of some data given by Fons *et al.*[16] These refer to experiments on the spread of a burning zone along a crib of wood (white fir). Data obtained photographically from these experiments have been plotted using an equivalent square base defined by $D = (Wl)^{\frac{1}{2}}$, where W is the width of the crib and l the measured length of the flame zone in the direction of flame spread along the crib. The few results where the flame height was not greater than three times the larger of either W or l have been excluded because they cannot be regarded as approximately radially symmetrical. The remainder are shown in Fig. 3.

The best equation for the photographed flames in terms of the measured quantities is

$$L/D = 4.4(m_w^2 \times 10^6/D^5)^{0.30} \text{ (in cgs units)}. \qquad (12i)$$

In accordance with the notion of using air density for the purpose of plotting results on a dimensionless scale this equation may be written as

$$L/D = 42(m''/\rho_0(gD)^{\frac{1}{2}})^{0.61}. \qquad (12ii)$$

Rasbash has recently evaluated the flame height of a fire in a whisky warehouse and estimated the rate of burning from the thermal conditions in the fire. The result is shown in Fig. 4 where the data of Fig. 3 are also shown. Blinov and Khudiakov's[17] data are shown in Fig. 4 for tanks greater than 80 cm diameter. No attempt has been made to allow for the different character of these fuels.

There are in addition two "large-scale" wood fires reported in detail. These are the Camps Park fire, reported by Broido and McMasters[18] and the Trensacq test reported by Étienne[19] and Faure.[20] The results are plotted in Fig. 4 and lie below the extrapolation of the laboratory data. In the Camps Park fire the flames were reported as merged, for a short time, but because the fuel was in separated piles of timber the fire may not strictly be comparable with those in which fuel is spread over the whole "burner" area. The average rate of burning per unit area m_1'', was about 1 mgm cm^{-2} sec^{-1} which is about an order less than the values for the laboratory data given in Fig. 3. The fuel loading in Étienne's experiment was lower still giving a mean value of m_1'', of about

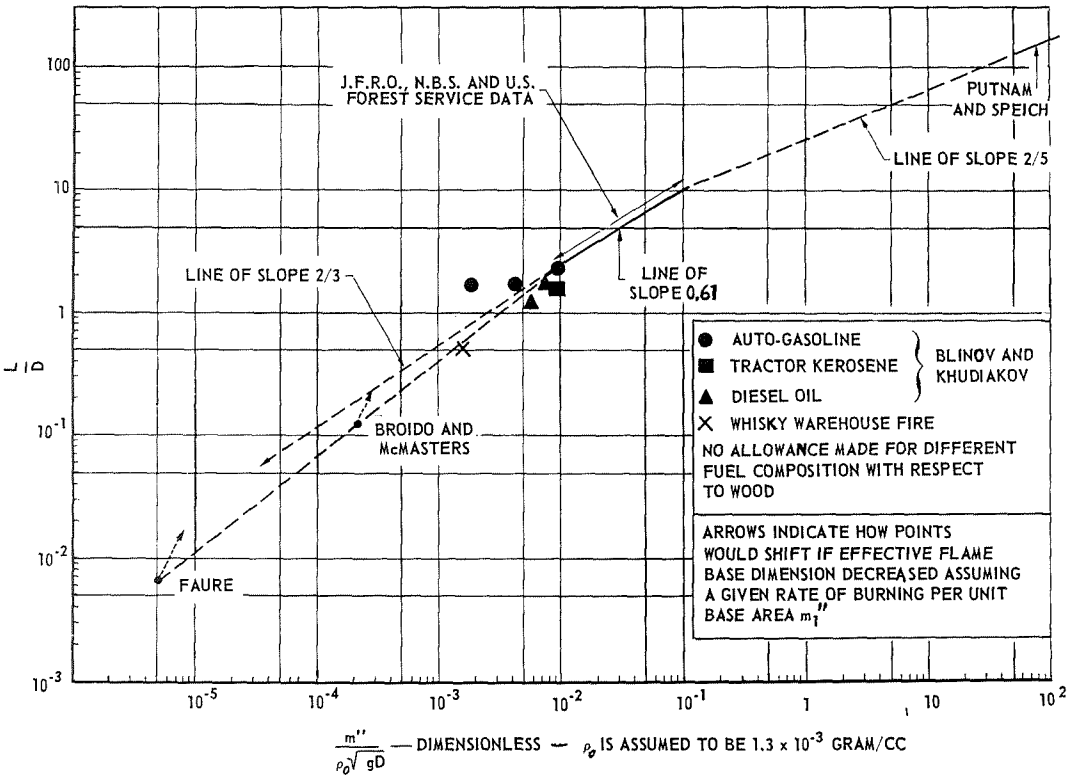

FIG. 4. Flame height correlation.

0.08 mgm cm^{-2} sec^{-1}. Clearly rates of burning per unit area comparable with the laboratory fires might lead to flames several hundred feet high. Under such conditions the properties of the atmosphere near the ground would presumably influence not only the plume of hot gases but the flame too.

For a very large fire area and rates of burning of the order found in a large fire, L/D may be so small that turbulence might be expected to break up the flame envelope. Therefore a large fire could not be considered as having a continuous envelope bounded by the fire area, but would tend to become a collection of fires of probable varying area and number. The flame height would therefore tend to be intermediate between that appropriate to an isolated fire of smaller size and that obtained by extrapolating the laboratory data assuming no break-up, i.e. assuming these fires are fully merged. This has the effect of reducing the value of L below that given by Eq. (12i) or (12ii). These results suggest that the index $1/(2q+1)$ in Eq. (11) increases above $\frac{1}{3}$ for small values of L/D. This may be due to the break-up of shallow flame envelopes: Fig. 4 shows how the position of the points would be affected by taking a smaller value of D. The suggestion given in a previous paper[6] as to how the index might increase above $\frac{1}{3}$ for small values of L/D is to some extent unsound as it considers total flame envelope area, not that projected vertically. But consideration might be given to the possibility of heavy cold air "falling" into the flame zone from above in between areas of rising fuel and combustion products.

Related Gas Experiments. Putnam and Speich's data[21] for city gas, which appears to be similar to methane, follow the law appropriate to a point source [Eqs. (10) and (11) with $q = 2$], and are represented by

$$L/D = 29(Q_1^2/gD^5)^{1/5} \qquad (13)$$

in the range $100 < L/D < 200$.

For the sake of presenting as much data on one graph as possible this correlation has been modified to make it comparable to the data for wood fires. This has been done on the assumption that the flame tip is defined approximately by a certain temperature rise and that in flames wholly controlled by buoyancy the only role of Q_1 or m_1 is to be a measure of the fuel supply. Hence for different fuels L has been assumed to be determined by the enthalpy supply and the modifica-

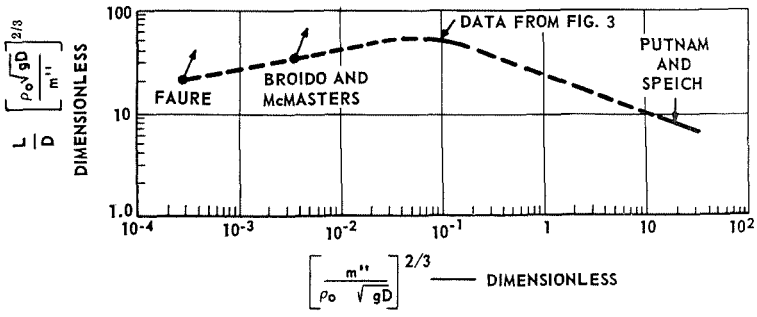

Arrows show effect of reducing D for a given m″

FIG. 5. Flame height correlation (modified scales).

tion based on the ratio of the calorific values of wood volatiles and city gas. Equation (13) may be written as

$$L = 140 m_1^{2/5}, \tag{14}$$

where 0.6×10^{-3} gram cm^{-3} was taken as the density of city gas.

Allowing for the difference in calorific values between wood and city gas the equation for wood volatiles would be

$$L = 90 m_w^{2/5}. \tag{15}$$

The lower calorific value of wood volatiles means that a higher volumetric flow (about three times) would be required to achieve the same flame length. But this higher flow and higher velocity could result in the initial momentum (increased about eight times) becoming significant so that Eq. (15) may well overestimate the flame length. With these reservations, Eq. (14) is used in Fig. 14 to show the extent of the range of interest and the limited parts of the range for which data are available. The data in Fig. 4 cover an immense range of $(m^2/\rho_0^2 g D^5)$ and it is desirable to adopt different dimensionless variables. X is accordingly defined as:

$$X = L/D(\rho_0(gD)^{\frac{1}{2}}/m'')^{2/3} \tag{16}$$

Figure 5 shows the data of Figs. 3 and 4 plotted as X with ρ taken as ρ_0 against $(m''/\rho_0(gD)^{\frac{1}{2}})^{\frac{2}{3}}$ for wood and city gas transformed as above to a wood basis.

Flames from Cubical Enclosures and Windows. The second experimental arrangement for which data on flame lengths are available is shown in Fig. 6. Varying amounts of wood (spruce) were burned inside a cubical enclosure having one side completely open. The mean rate of burning in the period when the burning was approximately constant and the corresponding mean flame height were measured, the latter visually. Some unpublished data of Webster and Smith of the Joint Fire Research Organization are included in addition to data previously published.[6] The results which cover a range of $\frac{1}{2}$-, 1-, and 2-inch sticks in cribs of heights varying from 4 to 16 inches in 2- and 3-foot cubes are plotted in Fig. 7. The Reynolds number $(m_1/\mu_1 D)$ with μ_1 equal to 10^{-4} cgs units varied from 2300 to 5400. These results also lie on a line of similar form to that for the open fires given in Fig. 3 but this correlation is relatively less well established in view of the small range of D.

As shown above, flames from an infinite strip source should follow Eq. (11) with $q = 1$ and Q replaced by $Q'D$ so that

$$L \propto Q'^{\frac{2}{3}}. \tag{17}$$

In the range of these experiments with cubical boxes the results do follow this law. However, departures from it might be expected when:

(a) The flames are short in comparison with the size of the wood crib and the box; and

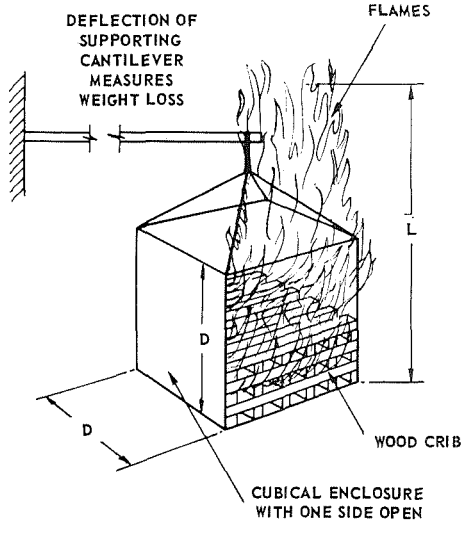

FIG. 6. Diagrammatic sketch of measurement of flames from windows.

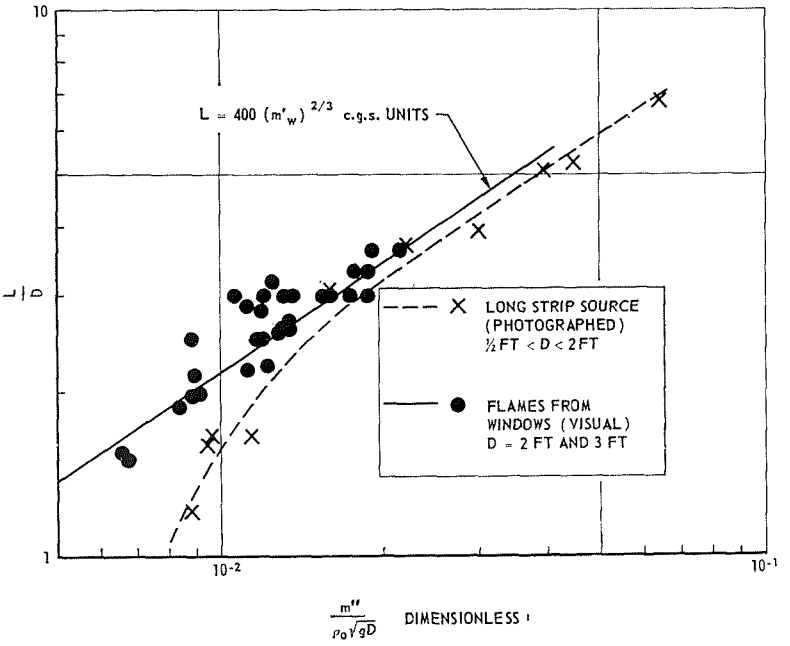

FIG. 7. Flames from long strips and windows.

(b) When the flame is very much longer than the width of the strip, in this case D, so that it is no longer two dimensional.

The equation to the line in Fig. 7 is

$$L = 400 m_w'^{\frac{2}{3}} \text{ cgs units} \qquad (18)$$

for $1.5 < L/D < 4$.

In an enclosure there is the added feature of entrainment in the horizontally moving stream under the "roof," but this might be expected to be small because of the relative difficulty of exchanging cold gas with lighter hot gas flowing over it.[22] Equation (18) should be increasingly close to the equation for a horizontal strip source as the ratio L/D increases.

Some experiments have been made by Thomas, Pickard, and Wraight[23] for wood fires on effectively infinite strips of width D. The results are shown in Fig. 7 together with Eq. (18). There is indeed a discrepancy for small values of L/D, but at higher values the two sets of data tend to a similar form. The discrepancy at small values of L/D arises from the difference in geometry between the two situations. The slight discrepancy at large values of L/D may well arise from the difference between visual and photographic assessments of L. It should be emphasized here that these results do not apply where there is a vertical "wall" above the opening though such results would be expected to be correlated by a relation of the same form. A one-sided flame could be regarded as having the same height as a two-sided flame burning twice the fuel.[1] From this argument it would be expected from Eq. (18) that a one-sided flame would be $2^{2/3}$, i.e., 1.6 times taller than a two-sided flame for the same value of m_1'.

Comparison with Calculations of Entrainment

It has been shown that flame lengths can be correlated by equations deduced from simple flow theory. These theoretical equations do not give the numerical value of flame length but only the form of the variation with m_1 and scale. However in the following sections the significance of the numerical results obtained experimentally will be discussed in the light of quantitative considerations of the entrainment of air with flames. These results will be compared with those from experiments on the flow of hot gases for which Yokoi[1] assumed the flame length to be the distance to the point where the rise in temperature falls to 500°C.

Entrainment into buoyant turbulent flames as opposed to plumes, where the density difference is small, has not so far been widely studied but it can be shown from the data of Rouse, Yih, and Humphries[24] that the horizontal velocity of entrainment v is 0.16 times the upward velocity w in the center of the plume at the same level. A momentum jet of local density ρ_θ entrains sur-

rounding fluid of density ρ_0 at a rate dependent on the excess momentum[3,4] and it can be shown that this implies that

$$v \propto w(\rho_\theta/\rho_0)^{\frac{1}{2}} \tag{19}$$

which will be here assumed to apply to flames. In a flame from an infinite strip source it is therefore assumed that

$$v \propto 0.16(\rho_{fl}/\rho_0)^{\frac{1}{2}}w, \tag{20}$$

and for a nominal temperature rise of 1000°C and T_0 equal to 290°K this becomes

$$v = 0.075\, w.$$

Because this discussion is only concerned with obtaining an approximate comparison it is assumed that Eq. (5) applies at all values of z less than z_t as well as at z_t itself and that it applies to line sources as well as radially symmetrical ones. Likewise Eq. (20) will be assumed to apply to radially symmetrical sources as well as to line sources. These approximations are sufficient for the immediate purpose of this paper; further experimental work in these fields is necessary before it is worth while undertaking more detailed analysis.

The mean mass rate of air entrainment per unit area in the vertical plane of the flame envelope is, from Eqs. (5) and (20), in cgs units

$$m_0'' \doteq \tfrac{2}{3} \times 1.3 \times 10^{-3} \times 0.16 \times 0.36 \times (gL)^{\frac{1}{2}}(2\theta_{fl}/T_{fl})^{\frac{1}{2}} \doteq 0.06_2 \times 10^{-3}(gL)^{\frac{1}{2}}.$$

Since m_0'' is proportional to $(\theta_{fl}/T_{fl})^{\frac{1}{2}}$ small variations in θ_{fl} are not important.

The total mass rate of air entrainment per unit length of strip is

$$m_0' \doteq 0.06_2 \times 10^{-3}(gL)^{\frac{1}{2}} \times 2L \quad \text{in cgs units.}$$

Eliminating L by means of Eq. (18) gives m_0'/m_w' as 31. If the nominal calorific value is taken as 2500 cal/gram (allowing for radiation loss) and the specific heat as 0.24 cal gram^{-1} °C^{-1}, the value of 31 gives an effective mean temperature rise of 320°C.

If it is assumed that the temperature distribution across a horizontal plume through the mean flame tip is the same as for a plume from a thermal line source, the data of Rouse, Yih, and Humphries can be employed to obtain the equivalent center line temperature.

The effective mean temperature is given by H/mc where m is the integrated mean mass flux. From the equations for velocity and temperature given by Rouse, Yih, and Humphries, the ratio of the maximum center-line temperature to H/mc can be evaluated as 1.47, giving the flame tip temperature rise as 470°C. This is of the same order but is less than the temperature at which a hot carbon particle is visible.

For a flame idealized in the form of a cone or a pyramid with the burner as base, the vertical projection of the flame envelope may be taken as $\pi DL/2$ for a circular base and $2DL$ for a square fire. The total rate of air entrainment for a square-based fire is therefore expected to be about

$$m_0 \doteq 0.06_2 \times 10^{-3}2DL(gL)^{\frac{1}{2}} \quad \text{(in cgs units)}.$$

If, instead of Eq. (12i) a line is drawn through the data of Fig. 3 having a slope of $\frac{1}{3}$, a slight distortion is introduced, but this makes the comparison between theory and experiment much easier. The best line of slope $\frac{1}{3}$ is

$$L/D = 420(m_w^2/D^5)^{\frac{1}{3}} \quad \text{(in cgs units)}. \tag{21}$$

Eliminating L by means of Eq. (21) gives the ratio of air to fuel (m_0/m_w) as 33.

For a radially symmetrical source the factor 1.47 is replaced by 1.67 as a result of applying the appropriate plume equations. It may then be shown that the air/fuel ratio 33 corresponds to a flame tip temperature rise of 510°C. In view of the assumptions and approximations made, these results can be regarded as satisfactory.

A Practical Application of Entrainment Calculations to Fire Protection within Buildings

An interesting practical problem arises in the control of fire spread in a building without a complete fire division wall. Consider a fire extending over that area of the floor beneath a part of the ceiling bounded by vertical curtains extending down from the ceiling (Fig. 8). Air enters the fire from four sides and hot gases are exhausted through a hole in the roof. It is assumed that the total inlet area is large enough in relation to the roof vent for the horizontal air flow to be given by Eq. (20). The value of the vent area A is sought for given values of building height h, curtain depth d, curtain perimeter p, and curtained area a. For θ_{fl} = 1000°C and T_0 = 290°K the application of Eqs. (5) and (20) gives the total air flow, neglecting effects at the corners, as

$$m_0 = 0.06_2 \times 10^{-3}[g(h-d)]^{\frac{1}{2}} \cdot p(h-d) \quad \text{(in cgs units)}.$$

The mass rate of fuel input is $m_1''a$. With 0.6 as the discharge coefficient for the roof vent, the discharge due solely to the buoyancy of hot gases

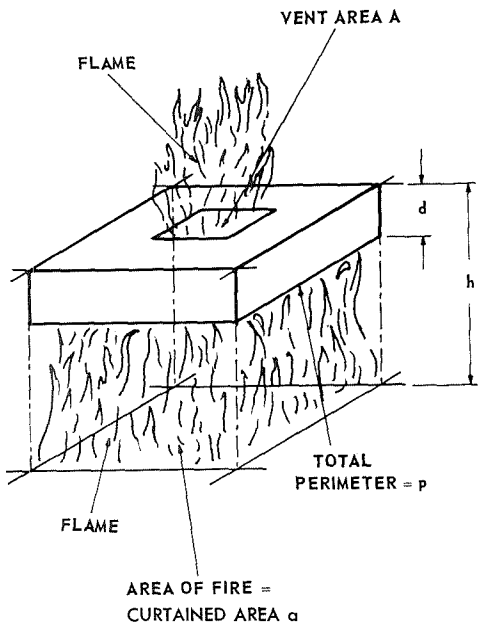

FIG. 8. Diagrammatic sketch of experiment simulating roof venting of a large fire.

of depth d is calculated as

$$0.6\rho_{fl}A(2g\theta_{fl}d/T_0)^{\frac{1}{2}}.$$

Combining these quantities and inserting numerical values

$$1.9_4 \times 10^{-3}p(h-d)^{3/2} + m''a = 0.015A(d^{\frac{1}{2}}) \quad \text{(in cgs units)}, \quad (22)$$

which is the theoretical relationship between A and $h - d$ for no flames or hot gases to emerge under the curtain. Some experiments were made with $a = 61$ cm^2, $d = 30$ cm, $p = 244$ cm, and $m''a = 6$ gram/sec of town gas. The measured and calculated results given in Table 1 agree satisfactorily. The calculations are for no spill of hot gas while the observations refer to no visible flame.

If this is the major part of the explanation for the slight difference, practical applications of this method will incorporate a safety factor.

Calculations for this kind of situation employing methods described by Fujita,[25] Kawagoe,[26] and Yokoi[27] lead to air flows approximately an order larger and consequently to much greater vents or deeper curtains than are in fact necessary. This discrepancy arises because the method used by the Japanese workers is applicable only to situations where there is a relatively slow movement of the hot gases within the enclosure. This allows the velocity head of the inlet and outlet flow to be calculated from pressure differences arising within the enclosure as in conventional "chimney theory." Such large pressure differences do not arise where there is a significant vertical acceleration.

TABLE 1

Heights of Opening to Prevent Flame Spillage

	Opening height $(h - d)$	
Vent area, A (cm^2)	Measured (cm)	Calculated (cm)
232	8	8.5
522	21	17
932	33	28

Comparison with Yokoi's Data

Yokoi[1] has measured temperatures at various heights above alcohol fires of different sizes and has employed the dimensionless parameters Θ and z/r appearing in Eq. (1) except that to make presumably a first approximation for the secondary effects of density in the "hot" part of the plume he has used the local density ρ instead of ρ_0. For different rectangular shapes of burning tray with sides W and l he took an equivalent radius

$$r \equiv (Wl/\pi)^{\frac{1}{2}}$$

instead of D, and a shape factor

$$n = W/l.$$

The range of H^2/r^5 which arises in Eq. (1) was relatively small (about 2:1), and although no data on flame heights are reported, only about 25 per cent variation in L/r would be expected on the basis of Eq. (12). The dimensionless relation similar to Eq. (1) was used by Yokoi to obtain flame heights taking a temperature rise of 500° or 550°C to define the limits of the radiating region which may for practical purposes be regarded as the visible flame tip. These results may now be compared with those described earlier in this paper using the criterion of 500°C which, as seen from above, is close to the values calculated from the entrainment of air into the flame.

Inserting the value Yokoi employs for c, the value of ρ at 500°C, 2500 cal/gram for the net convective calorific value of wood, and inserting $\theta_c = 500$°C, his correlation, which is the form of Eq. (1), can be redrawn as a relation between z/r and m_w^2/r^5 and a direct comparison made

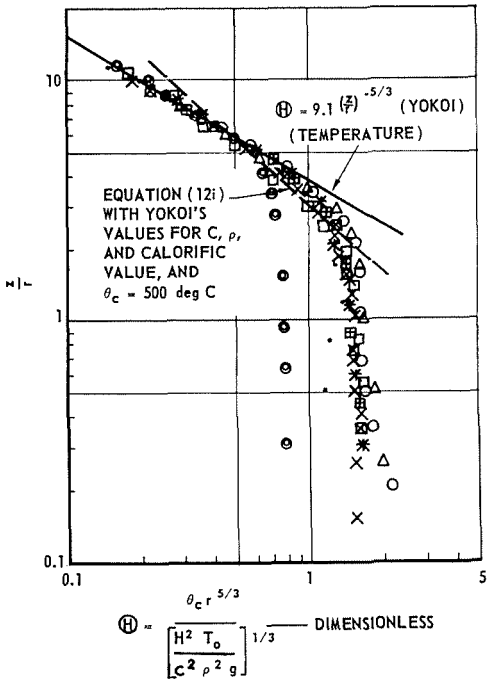

CONTINUOUS HEAT SOURCES

SYMBOL	r/cm
○	3.3
•	6
×	9.9
⊠	14.3
□	18.75
⊞	23.8
✳	37.5

DISCONTINUOUS HEAT SOURCE

SYMBOL	r/cm
△	16
○	20

FIG. 9. Correlation for horizontal circular and square heat sources.

with the correlations given in this paper. However, to retain his results in their original form the reverse procedure was adopted; namely, Eq. (12) has in effect been superimposed on Yokoi's results (Fig. 9). The discrepancy in trend between the two sets of data is a result of their different basis. However, the results agree in the region of z/r in the range 2 to 3 corresponding to the heights of the flames for Yokoi's experiments.

Yokoi gives data relating the temperature rise to s, the distance along the trajectory of hot gas emerging from windows, when there is no wall above them, a condition Yokoi refers to as "free space." He also gives data relating s to the corresponding vertical height z which is always less than s.

In comparing these data with corresponding data on flame height the following approximations and assumptions have been made:

(1) $z \doteq s$.

(2) In Eq. (18) m_w is the total rate of burning while in Yokoi's correlation H is the heat passing through the window. It has been assumed that the difference in origin is partially compensated for by using L from the base of the window in a manner analogous to s from the top of the window. The error entailed in this procedure tends to decrease at large values of L/D and z/r.

(3) Flame height and temperature depend on m' and H', respectively, not on m and H.

In the region of z/r and Θ, where the results follow the expected relation for a line source, i.e. $\Theta z/r$ is constant, it would be expected from this last assumption that $n^{\frac{1}{3}}\Theta z/r$ is constant.

Yokoi's data for different values of n do, in fact, follow this law as is seen in Fig. 10. The equation is

$$n^{\frac{1}{3}}\Theta z/r \doteq 1.0,$$

where he uses half the window height for l.

After substituting for n and r the expression becomes

$$z = 1.0(\pi T_0/\rho^2 c^2 g)^{\frac{1}{3}}(H'^{\frac{2}{3}}/\theta_c).$$

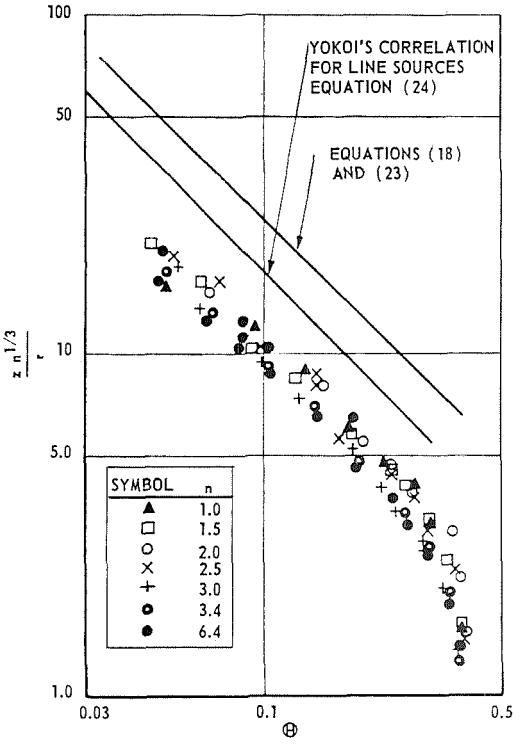

FIG. 10. Yokoi's data replotted as $zn^{1/3}/r$ (hot gases from windows).

With $T_0 = 290°K$, $c = 0.24$ cal gram^{-1} °C^{-1}; $\theta_c = 500°C$; $\rho = 0.000456$ gram/cc; and an effective calorific value of 2,500 cal/gram,

$$z = 160 m_w'^{\frac{2}{3}},$$

which may be compared with Eq. (18), which is also plotted in Fig. 10 in the equivalent form

$$n^{\frac{1}{3}}\Theta z/r = 2.5 \qquad (23)$$

For line sources on the ground Yokoi gives

$$n^{\frac{1}{3}}\Theta z/r = 1.76 \qquad (24)$$

also shown in Fig. 10.

The discrepancy between this latter set of temperature data and the flame length data is less. To get still better agreement a higher effective calorific value or a lower temperature criterion would have to be assumed. Some increase in the assumed calorific value is possible, of course, but not nearly enough to account for the discrepancy. A much lower temperature would not seem reasonable either. The use of the normal ambient density for air (1.3×10^{-3} gram/cc) makes the discrepancies greater.

There is, however, no real reason why there should be any close agreement although correlations exhibiting the same trends would be expected between the variables z and Θ. On the one hand there is a variation of a parameter through a region where conservation of heat obtains and on the other a variation determined by the limiting position of an extended region of heat generation. It will be shown in the next section that a similar comparison can be usefully made when there is the added influence of a wind.

Effect of Wind on Flame Length

Cribs of white-pine sticks were burned in a wind. The experimental arrangement is shown in Fig. 11. In order to vary the rate of burning independently of the over-all base dimensions of the cribs, sticks of square sections 1, $\frac{1}{2}$, and $\frac{1}{4}$ inch were used. The cribs were 3 feet wide with their sides parallel to the wind protected by noncombustible board. The length of the cribs in the direction of the wind was varied from 6 inches to 2 feet and the cribs were all less than 6 inches high. The moisture content of each crib was determined and in most of the experiments it was 11 per cent though in some it was as low as 9 or as high as 15 per cent. Each crib was mounted on noncombustible insulating board extending to the lee and the whole supported on a balance. Loss of wood from the crib was prevented by surrounding the lee side with wire netting. The

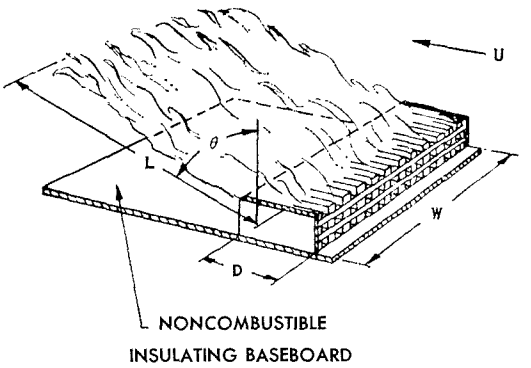

FIG. 11. Cribs burning in wind (diagrammatic sketch of experimental arrangement).

results of experiments in still air have been referred to previously.

The speed of the applied wind, which was in the 5–15 ft/sec range, was adjusted first to the required value using a vane anemometer. The crib was shielded and lit using a small quantity of kerosene and the shield removed after $1\frac{1}{2}$ min. The loss in weight of the crib was recorded and time-lapse photographs taken at 5-second intervals. The mass rate of burning was determined during the period when it was effectively constant and the ten or so photographs taken during that time were used to obtain average values of the flame length L to the tip of the continuous flame (Fig. 11).

Values of the inclination of the flame and the height above ground were also obtained. These will be reported elsewhere. In some of the early experiments the extension of the base board was very short. The results were studied to see if there was any noticeable difference but none was found to be significant when compared with the experimental variation. These results were therefore pooled with the others.

The results were analyzed statistically and the following equation was obtained:

$$L/D = 70(m''^2/\rho_0^2 gD)^{0.43}(U^2/gD)^{-0.11}, \qquad (25)$$

where, for the sake of presenting the results in dimensionless variables, the value of ρ for air ρ_0 was inserted. Had the cribs not been effectively infinite or had the Reynolds number been relevant there would have been a residual effect of D over and above that in the two variables m''^2/D and U^2/D. There was, in fact, a slight one, but it was not significant at the 5 per cent level. Its sign was positive, i.e., L/D increased slightly with D, and this probably corresponded to an effect of Reynolds number not of crib width. The range of Reynolds number (UD/ν) was 10^4

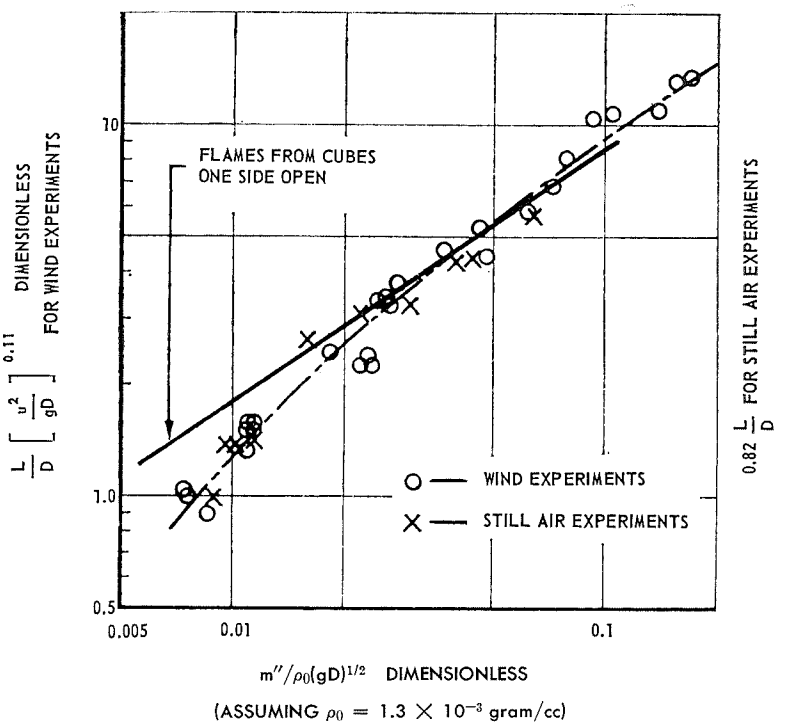

FIG. 12. Effect of wind speed and burning rate on flame length.

to 2×10^5. Over this range flame length varied as

$$L \propto \mathrm{Re}^{0.08}$$

for a given m''^2/D and U^2/D.

In some experiments the Reynolds number at the base of the flame was below 10^3, but there was no systematic effect on L; moreover, this is not regarded as a major criterion. The more relevant Grashof number based on the height of the top of the flame was in the range 10^8 to 5×10^{10}. It was disregarded because of the weakness and lack of statistical significance of the effect.

The results are shown graphically in Fig. 12 as $(L/D)\,(U^2/gD)^{0.11}$ plotted against $m''/[\rho_0(gD)^{\frac{1}{2}}]$. The range of values of U^2/gD was between 0.5 and 20. For comparison the data from Fig. 7 are also shown with $(U^2/gD)^{0.11}$ nominally constant at 0.82.

The standard deviation of the individual results about the regression line of Eq. (25) corresponded to ± 16 per cent and the overall correlation coefficient was 0.985. No part of this variation could be ascribed to the variation in moisture content. Further controlled experiments are being made to explore this factor.

There are two points of interest in Eq. (25) and Fig. 12. Firstly, the index 0.43 is somewhat larger than was found in any of the preceding correlations but the graphical plot in Fig. 12 shows that a power law is an approximation only and at large values of L/D the index is lower and the results lie closer to those for strip sources and windows in still air where the index is $\frac{1}{3}$.

Secondly the effect of wind speed on flame length is relatively small.

Over a range of 4.5 in $U/(gD)^{\frac{1}{2}}$, L varies by only 37 per cent. Other results yet to be published show that the height which the flame reaches above the ground is affected much more.

The reduction in flame length with increasing wind speed is presumably a result of better mixing.

Equation (25) can be rearranged with no loss of accuracy as

$$L(g\rho_0^2/m'^2)^{\frac{1}{3}} = 70[U\rho_0^{\frac{1}{3}}/(m'g)^{\frac{1}{3}}]^{-0.21}(m''^2/g\rho_0^2D)^{0.06},$$

where $m' = m''D$.

It may be noted in passing that the variable containing L is related to X as defined in Eq. (16).

To obtain the equation for a line source

$$L(g\rho_0^2/m'^2)^{\frac{1}{3}}(U\rho_0^{\frac{1}{3}}/(m'g)^{\frac{1}{3}})^{0.21}$$

was plotted linearly against D/m''^2 and extra polated to the zero value of D/m''^2.

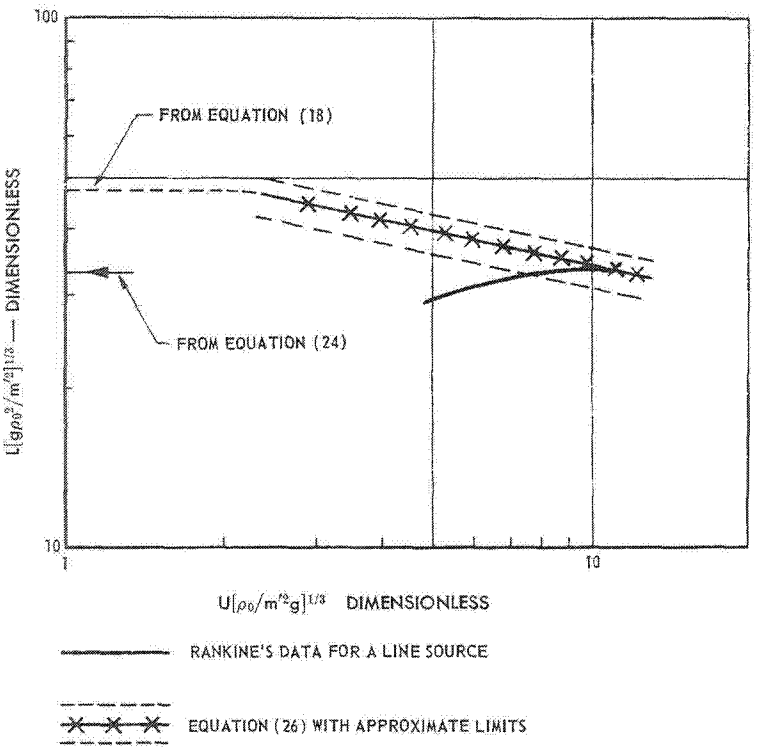

FIG. 13. Estimated correlation for a line source; ρ_0 was taken as 1.3×10^{-3} gram cc.

This gives a provisional equation for a line source as

$$L(g\rho_0^2/m'^2)^{\frac{1}{3}} = (55 \pm 5)\,(U\rho_0^{\frac{1}{3}}/(m'g)^{\frac{1}{3}})^{-0.21}. \quad (26)$$

This equation is shown in Fig. 13.

The results for strip sources tend, at large values of L/D, to approach Eq. (18) (Figs. 7 and 12) which corresponds to

$$L(g\rho_0^2/m'^2)^{\frac{1}{3}} = 47.$$

This may be taken as a limiting value for zero wind speed and is shown as such in Fig. 13.

In the same way as the data for flames in still air have been compared with Yokoi's temperature data, Eq. (26) can be compared with a dimensionless correlation obtained from Rankine's data.[23] This will be described in more detail elsewhere, but a brief outline of the comparison follows. Rankine measured velocities and the temperature rise (always less than 30°C) at various distances downwind and above ground from a line burner over a range of heat outputs from 3–35 cal cm^{-1} sec^{-1} and wind speeds of 45–150 cm/sec. Except near to the ground the temperature data would be expected on dimensional grounds to be correlated by

$$\Theta_x = \frac{\theta x}{(H'^2T_0/\rho^2c^2g)^{\frac{1}{3}}} = f(\Omega, z/x) \quad (27)$$

where $\Omega = (\rho c T_0/H'g)^{\frac{1}{3}}U$, and except near the ground where there is heat loss and the cool edges of the flow, correlation based on these variables is very good.

Rankines' own detailed heat balance suggests there is about a 5 per cent loss to the ground. This has been disregarded here, as have the small variations in density in calculating the dimensionless parameters. The maximum value of Θ_x occurred slightly above the ground (at z/x in the range 0.05 to 0.07). This maximum was evaluated for each of a range of values of Ω. The following values were then inserted into Θ_x and Ω, $T_0 = 290°K$, $\theta = 500°C$, $c = 0.24$, $\rho = (290/790)\rho_0$, $H' = 2500m_w'$, and $x = L$, where 2500 cal/gram was again taken as the effective calorific value of wood allowing for radiation loss, etc., and the flame tip has been assumed to be defined by a temperature rise of

500°C. The relation between the maximum Θ_x and Ω then appears as a relation between $(g\rho_0^2/m'^2)^{\frac{1}{3}}L$ and $U\rho_0^{\frac{1}{3}}/(m'g)^{\frac{1}{3}}$ which has been plotted in Fig. 13. Yokoi's data for line sources in still air [Eq. (24)] have similarly been used to obtain a limiting value of zero wind speed.

Unlike the results for flames, the trend is for dimensionless temperature to increase with wind speed though there is some sign that this increase is lower at higher wind speeds, but since small variations in heat loss might produce sufficient changes in Θ_x to make a weak trend reverse its direction, it is not possible to attach too much significance to this feature of the comparison without further analysis. What is interesting and from a practical point of view, useful, is that the actual values deduced for the dimensional flame length are comparable with the ones measured in what is in fact a very different experiment.

Conclusions

It has proved possible to apply a highly simplified dimensionless analysis to relating flame length to rate of burning and scale. Limitations to the accuracy of these experiments are not of much consequence to the type of practical application envisaged, but they preclude a discussion of some of the detailed aspects of the behavior. More experimental results are required, particularly for the effect of wind on flames, to pursue some of the questions involved. Nevertheless, reasonable quantitative agreement has been achieved in relating the concepts of entrainment in plumes to the determination of flame size and the work has been in part related to similar work on the scaling of flow of hot gases.

Nomenclature

A	Area of vent
D	Characteristic dimension, side of square, diameter, or width of infinite strip
F	Shape function of L/D affecting velocity of rising gases
G	Shape function of L/D affecting surface area of flame envelope
H	Convective heat flux
L	Flame length
Q	Volumetric rate of flow
T	Absolute temperature
U	Wind speed
W	Width of rectangular burning zone, width of window
X	Modified dimensionless flame length
a	Curtained area
c	Specific heat
d	Depth of curtain
f	A function of (general)
g	Gravitational acceleration
h	Height of building
l	Length of rectangular burning zone
m	Mass flow rate
n	Shape factor
p	Curtain perimeter
q	Index
r	Yokoi's characteristic dimension, effective radius
s	Distance along the trajectory
v	Sideways velocity of entrainment
w	Upward velocity on central vertical axis
x	Horizontal length
z	Height
μ	Viscosity
ρ	Density
ν	μ/ρ
θ	Temperature rise
Θ	Dimensionless temperature
Ω	Dimensionless wind speed
Re	Reynolds number

Subscripts

1	Fuel at burner
0	Surrounding air
c	Center-line of plume or flame
t	Flame tip—instantaneous
fl	Flame zone
w	Wood
$'$	Per unit length of line or strip
$''$	Per unit area

Acknowledgments

The work described in this paper is part of the program of the Joint Fire Research Organization of the Department of Scientific and Industrial Research and Fire Offices' Committee. The paper is published by permission of the Director of Fire Research.

References

1. Yokoi, S.: Japanese Ministry of Construction, Building Research Institute Report 34 (1960).
2. Lee, S.-L. and Emmons, H. W.: J. Fluid Mech. *11*, 353 (1961).
3. Thring, M. W. and Newby, M. P.: *Fourth Symposium (International) on Combustion*, p. 789. Williams and Wilkins, 1953.
4. Ricou, F. P. and Spalding, D. B.: J. Fluid Mech. *11*, 21 (1961).
5. Thomas, P. H.: Combustion and Flame *4*, 381 (1960).
6. Thomas, P. H., Webster, C. T., and Raftery, M. M.: Combustion and Flame *5*, 359 (1961).

7. Rasbash, D. J., Rogowski, Z. W., and Stark, G. W. V.: J. Inst. Fuel *35*, 94 (1956).
8. Rasbash, D. J : Fire Research Abstracts and Reviews *3*, 28 (1963).
9. Taylor, G. I.: U. S. Atomic Energy Commission. MDDC–919, 1945. LADC–276.
10. Morton, B. L., Taylor, G. I., and Turner, J. S.: Proc. Roy. Soc. (London) *A234*, 1 (1956).
11. Yagi, S.: J. Soc. Chem. Ind., Japan *46*, 608, 821, 873 (1943).
12. Yagi, S. and Saji, K.: *Fourth Symposium (International) on Combustion*, p. 771. Williams and Wilkins, 1953.
13. Hawthorne, W. R., Weddel, D. S., and Hottell, H. C.: *Third Symposium (International) on Combustion*, p. 282. Williams and Wilkins, 1949.
14. Wohl, K., Gazeley, C., and Kapp, N.: *ibid.* p. 288.
15. Gross, D.: J. Research Natl. Bur. Standards (Eng. and Inst.) *66C*, 99 (1962).
16. Fons, W. L. *et al.*: *Project Fire Model*, Summary Progress Report 1, Nov. 1958–60. U. S. Department of Agriculture, Forest Service, Pacific Southwest Forest and Range Experimental Station, Berkeley, California, 1960.
17. Blinov, V. I. and Khudiakov, G. N.: Doklady Akad. Nauk S.S.S.R. *113*, 1094 (1957).
18. Broido, A. and McMasters, A. W.: *Effects of Fires on Personnel in Shelters*. Pacific Southwest Forest and Range Experimental Station, Berkeley, California. Technical Paper 50 (1960).
19. Étienne, ——: *Rapport de Mission—Incineration de la lande de Trensacq*, April 13, 1955. Ministere de l'Intérieur, Paris, France.
20. Faure, J.: *International Symposium on the Use of Models in Fire Research*, p. 130. U. S. National Academy of Sciences, Pub. 786 (1961).
21. Putnam, A. A. and Speich, C. F.; *A Model Study of the Interacting Effects of Mass Fires*. Battelle Memorial Institute, Columbus, Ohio, Research Report, Nov. 9, 1961.
22. Richardson, L. F.: Proc. Roy. Soc. (London) *A97*, 354 (1920).
23. Thomas, P. H., Pickard, R. W., and Wraight, H. H.: To be published.
24. Rouse, H., Yih, C. S., and Humphreys, H. W.: Tellus *4*, 201 (1952).
25. Fujita, K.: Japan Ministry of Construction, Building Research Institute. Report 2(h).
26. Kawagoe, K.: *ibid.* Report No. 27, 1958.
27. Yokoi, S.: *ibid.* Report No. 29, 1959.
28. Rankine, A. O.: Proc. Phys. Soc. (London) *A63*, 417 (1950).

Discussion

Dr. A. F. Roberts (*Safety in Mines Research Establishment, England*): The relative importance of convection and radiation as heat feed-back mechanisms to a burning fuel was under discussion. Some experiments using high flash point alcohols were described in which the flame advanced across the liquid surface. Since the flame was nonluminous and the liquid was of low absorptivity, heat transfer by radiation from the flame to the liquid was negligible. Measured heat transfer rates were of the order of 2 to 3 cal/cm² sec; these were attributable mainly to intense recirculation of hot products of combustion in a small region at the base of the flame front. Such rates are ample for ignition of wood and are comparable with the heat flux from a black body at 500°C.

Dr. P. H. Thomas (*Fire Research Station, England*): Such a rate of heating could be very important locally, but the long range effect of radiation could be more important than a short range convection effect. It depends on the distribution of heat with distance. The relative importance of radiation and convection will no doubt vary with the conditions under which fire spread takes place. For example, we are concerned with flame spread up walls and across streets, etc., as well as through a bed of fuel and for some of these radiation would certainly play an important, if not decisive, role.

Dr. A. E. Pengelly (*United Steels Research*): All the papers concerned with natural fire propagation have treated rate of spread and scale but have considered mechanism in but summary form. Two connected points seem likely to have a bearing on the correlations:

Assuming temperatures of the order 1000°C and active plumes of reasonable height, a buoyancy force may be calculated and compared with other local forces—wind. Essentially they are comparable since buoyancy is clearly equivalent to velocities of about 20 fps when expressed kinetically. Has consideration been given to these effects and, particularly, the possibility that ignition of given sections dependent on available oxygen may be dependent on the balance between wind and entrainment forces?

Second and closely related—ignition depends on the achievement of a high fuel temperature by some heat transfer mechanism, and the simultaneous availability of oxygen. It seems possible, therefore, that in some cases spread may be critically de-

pendent on heat transfer while in others early mixing may be crucial. For example: fast spreading crown fires with plenty of air from below might be heat-transfer dependent while crib fires of close packed easily flammable material might depend on oxygen arrival. Could such a balance dictate the different slopes reported for correlations?

DR. P. H. THOMAS: The importance of wind effects lies precisely in this, that these typical wind speeds are comparable with the velocities of the gases in these flames.

Results are given in the paper for the effect of wind on flame length and these show that when $u^2/gD > 1$ the effect of wind is apparent, though the effect on deflection is greater than that on flame length, but these data have yet to be reported.

An attempt has been made in the paper to relate the results for flame length to the other parameters, burning rate R and size D for still air and it is hoped to extend this approach to consider the effect of wind.

This relation, for still air, treats m, the rate of burning, as an independent variable. The determination of m, even if it partially depends on flame length, will certainly involve a consideration of the factors described.

SCALE EFFECTS ON PROPAGATION RATE OF LABORATORY CRIB FIRES

W. L. FONS, H. B. CLEMENTS, AND P. M. GEORGE

This paper presents results of a laboratory-scale propagating flame model in which crib fires are used. The model permits establishment of a steady-state condition for the free burning of solid fuels in the form of wood cribs. The principal objectives are to evaluate quantitatively the effects of the properties of fuel and fuel bed on the many attributes of fire behavior and to establish relationships of the variables in terms of several dimensionless groups.

A dimensionless relationship of flame dimensions and modified Froude number is presented for data from a propagating flame model and is in close agreement with findings of other investigators using stationary flame models. Scale effects are also given for the fuel and fuel bed variables on burning time, propagating rate, and burning rate of laboratory crib fires.

The work led to the following conclusions: (1) Laboratory crib fires may be used to represent line fires; (2) scaling of fuel size to the 1.5 power for burning time is valid for loosely packed fuel beds; (3) same dimensionless groups may be used for correlation of data from propagating flame models and from stationary flame models.

Plans for future investigation include the use of crib fires to determine the effects of fuel spacing, wind, and slope on the burning characteristics.

Introduction

Research in the area of free-burning fires is relatively small and neglected when compared to the large and impressive effort in the field of combustion which is applicable to heat and power production. Combustion research has been motivated by useful rather than destructive applications, and consequently has contributed little to an understanding of free-burning urban and forest fires. Studies of fires under natural conditions over many years have produced mostly qualitative descriptions. This is understandable since free-burning fires are not only unplanned and unexpected but occur in many different and complicated situations. In other problems as complex as free-burning fires the basic research approach has led to great success. The Committee on Fire Research and the Fire Research Conference of the National Academy of Sciences, National Research Council, studied the present status of firefighting techniques and concluded that the ability to cope with large fires, both forest and urban, can be realized only through a major expansion of fundamental research.[1]

In the development of model laws for fire behavior in solid fuels, some attention has been given to the design and use of models representing uncontrolled fires. The reported work on models of free-burning fires includes studies under transient and steady-state conditions for stationary and propagating flames.[2-6]

This paper presents results of a propagating flame model in which wood crib fires were used. The experimental work was initiated early in 1959. The model used permits establishment of a steady-state condition for the free burning of solid fuels in the form of wood cribs.[2] The immediate objectives are to evaluate quantitatively the effects of the properties of fuel and fuel bed on the many attributes of fire behavior and to establish relationships of the variables in terms of dimensionless groups for laboratory-scale fires.[7,8]

A dimensionless relationship of flame dimensions and modified Froude number is presented for data from a propagating flame model. Scale effects of the fuel and fuel bed variables are also given for burning time, propagating rate, and burning rate.

Experimental

The essential elements of the model are: a wood fuel bed built in the form of a crib, a combustion table equipped to transport the fuel bed at a controlled rate, a base of inert material of known density, and sensing and recording instruments to measure specified variables.[2]

The fuel bed is a crib of wood sticks of square

cross section. The physical features of such a crib can be controlled; for example, the species, density, moisture content, and stick size, as well as width and height of the crib. The crib is formed by placing the sticks in tiers with a particular spacing between sticks. A drop of resorcinol–formaldehyde resin glue is placed on each junction to bond the crib into a rigid assembly. For several weeks before burning, the crib is conditioned to moisture equilibrium in an atmosphere of constant temperature and relative humidity.

The ignition device is a narrow, shallow trough containing an asbestos wick saturated with a liquid hydrocarbon fuel. To start the test, the ignition device is placed at one end of the crib, which is set on fire by ignition of the asbestos wick. The fire gradually spreads to the other end of the crib, reducing the wood to a residue of ash and charcoal.

The combustion table is equipped with a chain-belt mechanism which moves the crib and two heavy asbestos sheets, one on each side of the fire, in synchronism with the flame spread to simulate the relative movement of the fire front with the ground. The crib and its inert base rest on the chain-belt, which is moved manually by a gear drive in order to hold the flaming zone of the burning crib in a fixed position.

During the burning period, the combustion gases diluted by the entrained air are expelled from the room through a 2-foot diameter stack. Incoming conditioned air at the rate of about 5000 cubic feet per minute is supplied to the room through several louvered outlets in a continuous duct located near the ceiling around the room. The entrance to the stack is a hood 12 feet in diameter and located 12 feet above the combustion table.

Time-lapse cameras mounted on the wall photograph the test fires for subsequent measurements of flame depth and length. Three grids of thermocouples, suspended at different levels above the combustion table, measure temperatures of the convection column. A thermocouple and a Pitot tube mounted in the exhaust stack measure the temperature and velocity of combustion gases. Thermopile radiometers located at the front, rear, and side of the test fire measure radiation. The sensing elements are connected to recording instruments located in a control room adjacent to the combustion room.

Two important features of the model are: (1) The crib is made relatively long and a zone or band of fire travels the length of the crib. After an initial buildup, the rate of burning or spread reaches a constant value, which holds until near the end, and thus the difficulty of investigating a fire burning under transient conditions is avoided.

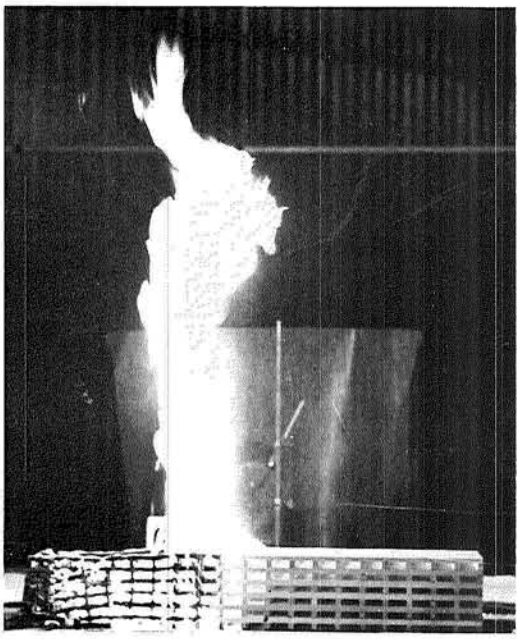

FIG. 1. A test fire during the steady-state burning period.

(2) The position of the flaming zone is held fixed in space by moving the fuel into the fire. This method permits a grid of thermocouples in the flame and convection column, radiometers surrounding the fire, and other sensing devices to be stationary. The rate of fire spread is equal to the rate the crib is moved to maintain the flame in a fixed position (Fig. 1).

The duration of the steady-state burning period is limited only by the buildup time and the length of the crib. The time for the burning to reach a steady-state condition after one end of the crib is ignited is dependent upon such factors as spacing, density, size, and moisture

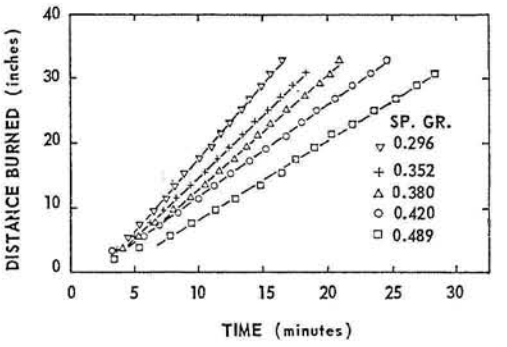

FIG. 2. Steady-state burning through cribs of white fir wood with different specific gravities.

content of the wood sticks. Typical curves for the spread of fire through cribs showing the steady-state periods for cribs of different wood density are presented in Fig. 2.

Results and Discussion

Influence of Specific Gravity and Moisture Content of Wood on Rate of Fire Spread. Six series of tests were made to determine the effect of specific gravity of wood on rate of fire spread for different levels of moisture content. The cribs for these tests were 5.5 inches high, 9.25 inches wide, and 35.5 inches long, and made from nominal $\frac{1}{2}$-inch square sticks of white fir (*Abies concolor*) with spacing of 1.25 inches between sticks in each tier. As shown in Fig. 3, the rate of spread increases rapidly with decreasing moisture for specific gravity less than 0.45 and moisture content less than 10 percent. Since litter, bark, moss, grass, leaves and partially decomposed wood have specific gravities somewhat less than 0.45 and are the fuels which mainly contribute to the spread of most forest fires, it is apparent that moisture content and specific gravity of these fuels are important in the spread of forest fires.

Flame Dimension Correlation. When buoyant combustible gases emerge from a burning fuel bed into an unconfined atmosphere where they burn as a flame, the rate of oxygen diffusion into the gaseous fuel stream determines the length of the flame. For free convection fires this diffusion of oxygen controls the rate of burning of the fuel per unit area of the burning zone. A detailed derivation of a simple dimensionless relationship among flame length, flame depth, and rate of burning for buoyant diffusion flames, including a discussion of the work of others, can be found in the paper by Thomas *et al.*[3]

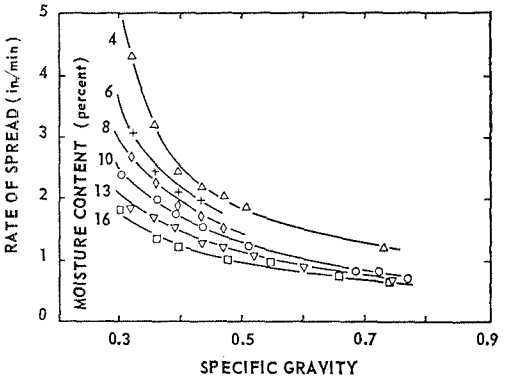

FIG. 3. Effect of specific gravity of wood on rate of fire spread through cribs at different moisture content.

The derived dimensionless relationship of the flame dimensions with the modified Froude number containing the combustion gas velocity V is

$$L/D = f(V^2/gD). \tag{1}$$

Assuming that the temperature of the combustion gases emerging from the fuel in the flaming zone is the same for the different fires and that it is equal to the flame temperature of 1650°F, then the velocity V of the gases is calculated by the relation

$$V = CG/\rho_g. \tag{2}$$

The term C is the weight of gas produced per unit weight of solid fuel. For conditions of complete combustion, no excess air, and gas temperature at 1650°F, $C = 6.13$ and $\rho_g = 0.019$ lb/ft^3.[9] The flame dimensions can be expressed in terms of the rate of burning per unit area G by combining Eqs. (1) and (2):

$$L/D = f(C^2G^2/\rho_g{}^2gD). \tag{3}$$

From time-lapse motion pictures taken during the steady-state burning period, measurements of length of flame L and depth of flaming zone D were made of 66 crib fires. These cribs were of varying width and height and contained wood of varying density, fuel size, and moisture content; but, in this flame dimension correlation, it is assumed that the fuel and fuel bed parameters are important only in their effect on G, the rate of burning per unit area of each crib, which was

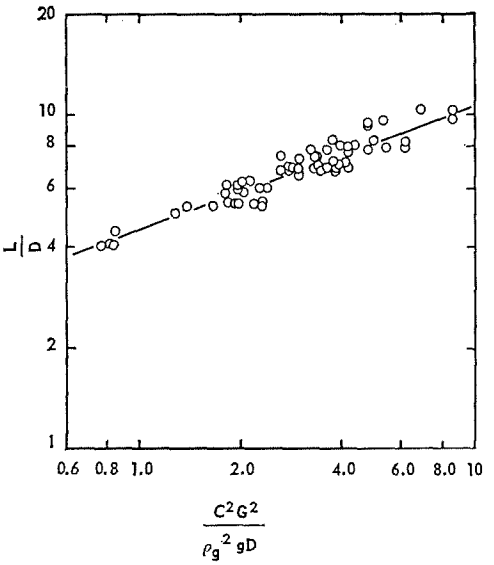

FIG. 4. Dimensionless correlation of flame dimensions and burning rate for crib fires (propagating flame model).

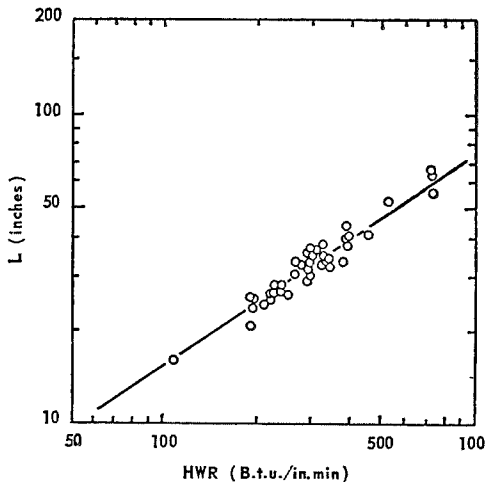

FIG. 5. Flame length as a function of rate of energy released per unit length of fire front.

calculated by the equation

$$G = WR/D. \tag{4}$$

Since the ratios of the flaming zone D to the width of the crib w_b for most of the fires burned were less than 1.0, i.e., $D/w_b < 1.0$, the advancing flaming zone for these fires may be considered, ideally, a semi-infinite strip or line fire. The results are shown in Fig. 4 and the equation for the line is

$$L/D = 4.5(C^2G^2/\rho_g{}^2gD)^{0.43}. \tag{5}$$

The exponent 0.43 in Eq. (5) is in agreement with the value found by Thomas[4] for line fires which were burned both with and without wind. This suggests that the functional power relationship between flame length and Froude number is independent of wind.

Data from fires with $D/w_b < 0.5$ were used to determine the relationship between the flame length L and the energy liberation rate per unit length of fire front HWR. Figure 5 shows that L is proportional to the two-thirds power of HWR. The value of $\frac{2}{3}$ is in agreement with that found by others for strip or line fires. The equation for the line is

$$L = 0.74(HWR)^{2/3}. \tag{6}$$

Burning Time Correlation. A flaming zone of depth D moving at a rate R through a fuel bed of solid fuel particles will require a time θ_r to pass a reference point in the fuel bed. During the time θ_r, a quantity of fuel W is burned at a rate G. Thus, by definition,

$$\theta_r = D/R = W/G. \tag{7}$$

If the position of a fuel particle is used as a reference point, then θ_r will be the time during which a fuel particle resides in the flaming zone and may be referred to as residence time. This fuel particle of initial thickness d_0 when ignited, is at the front of the flaming zone and is surrounded by a gas at temperature t_g. The gas is emitted by the burning particles spaced at regular intervals from each other. At ignition, the center of the particle is at temperature t_0, and its temperature increases with time until the particle reaches the rear of the flaming zone. It is assumed that when the particle arrives at the rear of the flaming zone all of its volatiles are released, and its center reaches the same temperature as that of the surrounding gas. The heat flow at the boundary between the gas and the burning particle is proportional to hd_0/k_g. Since the temperature of the surrounding gas is assumed to be constant, it follows then that the ratio h/k_g is effectively constant. The temperature t_g of the gas will depend on its heat capacity and the amount of heat transferred to it by the burning particles of the combustion zone less the losses by convection to the atmosphere. For steady-state conditions, it is assumed that the gas temperature t_g and density ρ_g remain constant and have the values of 1650°F, and 0.019 lb/ft^3, respectively.[9]

Consider a flaming zone moving through a fuel bed of height h_b and width w_b, and composed of fuel particles with initial thickness d_0, moisture content M_f, and density ρ_f. At the time θ, after the particle enters the flaming zone, the temperature t at the center of a particle may be determined by an equation which expresses the fuel and fuel bed parameters and the mass and energy transfer rates in terms of dimensionless groups. The equation is written as

$$(t - t_0)/(t_g - t_0) = f(\theta\alpha/d_0^2,\ L/D,\ k_g/hd_0,\ \rho_f/\rho_g,\ M_f,\ h_b/w_b,\ V_g/V_f,\ 4h_b/d_0,\ D/d_0). \tag{8}$$

The first two dimensionless groups on the right-hand-side of Eq. (8) are the Fourier number, and the ratio of the length and depth of flame, respectively; the latter is a function of Froude number as presented in the preceding section. Fourier number describes the heat transfer by conduction into a solid body from its surface and in this analysis it is assumed to be proportional to mass transfer.[10] Froude number, in this case, represents the natural convective heat and mass transfer from a source to the atmosphere. The third dimensionless group k_g/hd_0 is the reciprocal of Nusselt number which describes the heat transfer to the surface

TABLE 1

Range of Fuel and Fuel Bed Parameters

Source of data	No. of fires	ρ_f (lb/ft^3)	d_0 (in.)	h_b (in.)	w_b (in.)	M_f (per cent)	V_g/V_f
Ref. 8	84	19–47	0.25–1.25	2.72–12.7	5.75–16.2	2.5–16.7	1.2–4.1
Ref. 6	22	27	0.065–3.6	0.65–36	0.65–36	9.2	0.4–2.3

of the particle by the surrounding gas. The remaining six groups are ratios involving fuel and fuel bed parameters.

It follows that when $\theta = \theta_r$, then $t - t_0 = t_g - t_0$ and Eq. (8) may be written as

$$(\theta_r\alpha/d_0^2)\ (L/D) = f(k_g/hd_0,\ \rho_f/\rho_g,\ M_f,\ h_b/w_b,\ V_g/V_f,\ 4h_b/d_0,\ D/d_0). \quad (9)$$

In Eq. (9), if θ_r is replaced by D/R from Eq. (7), then the left side becomes $L\alpha/Rd_0^2$. Similarly, when θ_r is replaced with W/G in Eq. (9), the left side becomes $WL\alpha/GDd_0^2$. The product GD is the rate of burning per unit width of a line fire.

To determine the numerical value of the dimensionless group $\theta_r\alpha/d_0^2$, α is replaced by $k/\rho_f C_p$ and θ_r is replaced by D/R [Eq. (7)]. For each fire, measurements of the width of flaming zone D are taken from 3-second time-lapse motion pictures. Thermal diffusivity α is determined by using an empirical equation for thermal conductivity k expressed as a function of density ρ_f of bone-dry wood,[11] and a value of 0.327 is used for the specific heat C_p of bone-dry wood.[12] When ρ_f is expressed as lb/ft^3, the equation for α in units of in.^{2}/min becomes

$$\alpha = (0.100/\rho_f) + 0.0137. \quad (10)$$

Data from 106 fires, including 22 fires by Gross,[6] were analyzed to establish exponents for the dimensionless ratios on the right-hand side of Eq. (9). For fires by Gross, D/d_0 was held constant at a value of 10. For the propagating flame model in which the depth of the flaming zone was allowed to assume a natural value, data showed that the ratio D/d_0 for each fire was approximately 10.5. Since D/d_0 remained constant for the two types of models, this group was not considered in the analysis. In the dimensionless group k_g/hd_0, a value of unity was chosen for the ratio k_g/h. Table 1 shows the range of the fuel and fuel bed parameters for the fires used in the analysis. The fires by Gross were used to determine the exponent for V_g/V_f, because the ratios h_b/w_b and $4h_b/d_0$ for these cribs were constant and V_g/V_f was varied independently of fuel size.

Equation (9) with the exponents for the dimensionless groups becomes

$$(\theta_r\alpha/d_0^2)(L/D) = f[(k_g/hd_0)^{1.5}(\rho_f/\rho_g)M_f^{0.15}(h_b/w_b)^{0.1}(h_b/\lambda)^{0.65}], \quad (11)$$

where

$$\lambda = V_g d_0/4V_f.$$

Figures 6 and 7 show the correlation of data from the fires based on Eq. (11) with L/D values taken from the curve in Fig. 4 for calculated Froude numbers. Figure 7 shows that the curves for the stationary flame model[6] and the propagating flame model are almost superimposed and have a slope of unity.

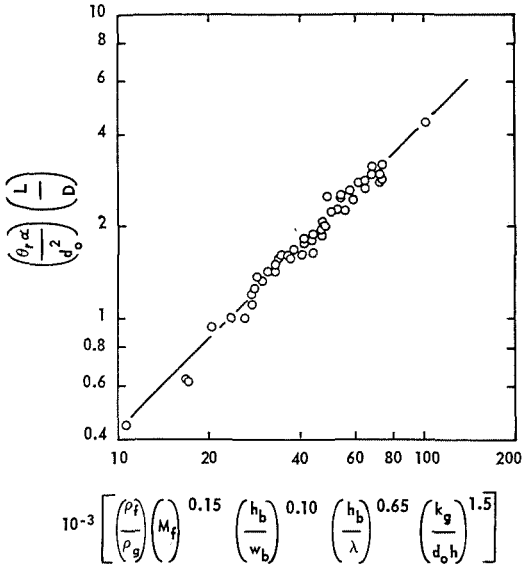

FIG. 6. Dimensionless correlation of heat and mass transfer with fuel and fuel bed parameters for laboratory crib fires (propagating flame model).

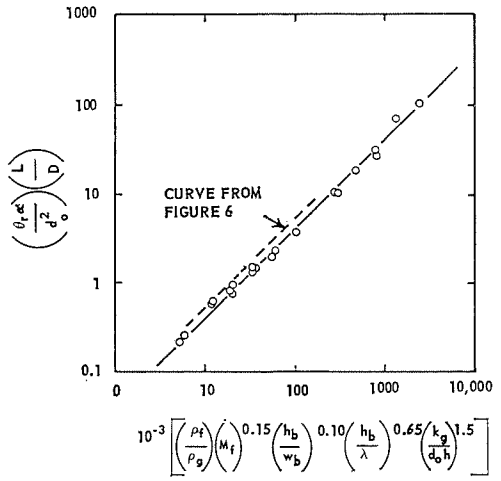

FIG. 7. Dimensionless correlation of heat and mass transfer with fuel and fuel bed parameters for laboratory crib fires (stationary flame model).

The ratio h_b/λ scales to the 0.65 power and its magnitude plays an important role in controlling the convective heat and mass transfer and the burning time. The 0.65 power compares favorably with the value of 0.50 reported for light forest fuels.[13]

Bryan[5] conducted experiments with a stationary flame model and concluded that burning time scales as the 1.5 power of the fuel size. However, no consideration was given to L/D and V_g/V_f in Bryan's experiments. Close observation suggests that for fires in fuel beds the burning time θ_r increases as gas/fuel-volume ratio V_g/V_f approaches zero. The fires burned by Gross[6] were in cribs with three different values of V_g/V_f (Table 1). Figure 8 shows burning time θ_r plotted against fuel size d_0 for different values of V_g/V_f. For cribs with $V_g/V_f = 2.3$ and $d_0 > 0.2$ inches, and for cribs with $V_g/V_f = 1.0$ and $d_0 > 0.6$ inches, fuel size scales to the 1.5 power. This agrees with the findings of Bryan[5] for cribs with $V_g/V_f = 1.3$ and for fuel sizes 1.3, 1.7, and 2.0 inches. Figure 8 illustrates that in the range of fuel size studied its scaling for burning time is dependent on both the ratio of V_g/V_f and the ratio of L/D.

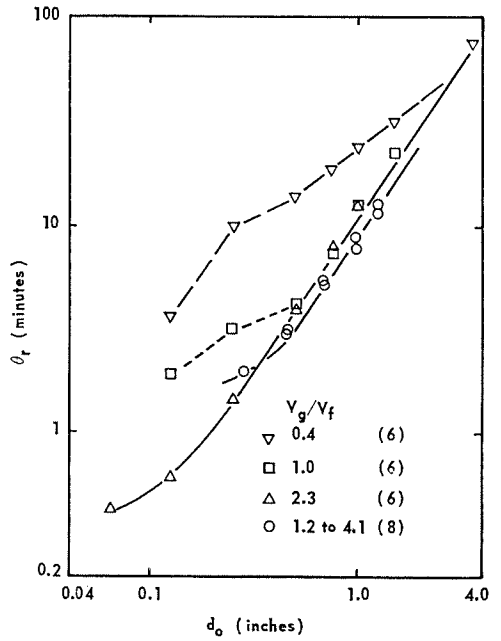

FIG. 8. Effect of fuel size on burning time for laboratory crib fires with different gas-to-fuel-volume ratios.

In summary, Eq. (11) gives the scale effects of the fuel and fuel bed variables on burning time, propagating rate, and burning rate for laboratory crib fires. With the exception of the gas/fuel-volume ratio, the range of fuel and fuel bed variables covered by the crib fires is comparable to that generally found in forest areas. For most forest fuel types, such as grass, litter, and brush, the gas/fuel-volume ratio (V_g/V_f) is greater than 4.0.[13] Equation (11) combined with Eq. (6), however, may be used to make quantitative estimates of flame length L, rate of propagation R, and rate of burning per unit width GD for line fires in forests.

Conclusions

1. Laboratory crib fires may be used to represent line fires providing the depth of flaming zone is less than the width of crib.
2. Dimensionless relationship of flame dimensions and modified Froude's number for the propagating flame model is in agreement with findings of other researchers using stationary flame models.
3. Individual effects of the various fuel and fuel bed parameters on the heat and mass transfer for laboratory crib fires can be determined independently.
4. Data from propagating flame models and stationary flame models can be correlated by the same dimensionless groups.
5. The scaling of fuel size to the 1.5 power for burning time is not valid for tightly packed fuel beds where $V_g/V_f < 1.0$.
6. The results obtained by the propagating flame model give certain guides to a better understanding of the behavior of wildfires and provide several relationships between the fuel and fuel bed parameters and the burning charac-

teristics for practical application in the field of fire suppression.

Plans for Future Work

Plans for future work include the use of crib fires to determine the effects of spacing, wind, and slope on the burning characteristics. The spacing in the vertical plane for cribs burned thus far was always equal to the thickness of the fuel particles. It is planned to burn cribs in which the vertical spacing of the fuel will be varied independently of fuel size. Since for most forest fuel types $V_g/V_f > 4.0$, cribs will be made and burned with values of V_g/V_f several times larger than used thus far. A low-speed wind tunnel will be used to evaluate the effect of wind speed on the flame dimensions and the burning rate of propagating and stationary fires in wood cribs. Cribs will be burned at different inclinations, simulating uphill and downhill burning, to determine the effects of slope on their burning characteristics. In addition, the scaling of fuel and fuel bed parameters established by laboratory crib fires will be applied to data collected on actual field fires or wildfires.

Nomenclature

C	Mass of combustion gas produced per unit mass of solid fuel
C_p	Specific heat of bone-dry wood
d_0	Initial thickness of fuel
D	Depth of flaming zone in direction of fire spread
g	Gravitational acceleration, 32.2 ft/sec^2
G	Rate of fuel burning, weight per unit area
h	Heat transfer coefficient
h_b	Height of fuel bed
H	Heat of combustion, low heat value
k	Thermal conductivity of bone-dry wood
k_g	Thermal conductivity of gas surrounding the particle
L	Flame length above top of crib
m	Mass of water in fuel
m_f	Mass of bone-dry fuel
M_f	100 m/m_f, percent fuel moisture content
R	Rate of fire propagation
t	Fuel temperature at time θ
t_g	Gas temperature in the flaming zone
t_0	Initial fuel temperature
V	Vertical velocity of combustion gases emerging from the flaming zone of the fuel bed
V_f	Volume of fuel in crib
V_g	Volume of gas or void in crib
w_b	Width of fuel bed
W	Weight of fuel burned per unit area
α	Thermal diffusivity of bone-dry fuel
θ	Time
θ_r	Burning time of fuel
ρ_g	Density of gas
ρ_f	Fuel density, bone dry
λ	Volume of voids per unit of fuel surface

Acknowledgments

The authors express their thanks to the Office of Civil Defense for providing financial support through contracts administered by the National Bureau of Standards, and to the Forest Research Council of the State of Georgia for making research facilities available.

References

1. The Committee on Fire Research: A proposed fire research program, Fire Research Abstracts and Reviews *1*, 1(1958).
2. Fons, W. L., Bruce, H. D., and Pong, W. Y.: A steady-state technique for studying the properties of free-burning wood fires, *The Use of Models in Fire Research*, No. 786, p. 219. National Academy of Sciences, National Research Council, Washington, D. C., 1959.
3. Thomas, P. H., Webster, C. T., and Raftery, M. M.: Combustion and Flame *5*, 359 (1961).
4. Thomas, P. H.: The Institution of Fire Engineers Quarterly *XXI*, 197 (1961).
5. Bryan, J.: *Scale Effects in the Burning of Timber*, Ministry of Home Security RC (F) *64*, 1943.
6. Gross, D.: J. Research Natl. Bur. Standards (C, Engineering and Instrumentation) 66C, 99 (1962).
7. Fons, W. L., Bruce, H. D., Pong, W. Y., and Richards, S. S.: *Project Fire Model, Summary Progress Report I*, Forest Service, U. S. Department of Agriculture, 1960.
8. Fons, W. L., Clements, H. B., Elliott, E. R., and George, P. M.: *Project Fire Model, Summary Progress Report, II*, Forest Service, U. S. Department of Agriculture, 1962.
9. Kawagoe, K.: *Fire Behaviour in Rooms*, Report of the Building Research Institute, No. 27. Japanese Ministry of Construction, 1958.
10. Spalding, D. B.: *Some Fundamentals of Combustion*, p. 107. Butterworths, 1955.
11. MacLean, J. D.: Heating, Piping, Air Conditioning *13*, 380 (1941).
12. Dunlap, F.: *The Specific Heat of Wood*. Bulletin 110, Forest Service, U. S. Department of Agriculture, 1912.
13. Fons, W. L.: J. Agric. Res. *72*, 93 (1946).

A MODEL STUDY OF THE INTERACTION OF MULTIPLE TURBULENT DIFFUSION FLAMES

A. A. PUTNAM AND C. F. SPEICH

This research program has shown that a valid model for studies of mass fires can be produced using multiple jets of gaseous fuels. The basic requirement is that the fuel jets produce turbulent diffusion flames which are buoyancy controlled. A specific operating range where this requirement is met was found for this model.

A number of flame arrays have been studied in which the dimensionless groups of (array-flame height/single-flame height), number of jets, source-shape factor, and [flame spacing/(fuel-flow rate)$^{2/5}$] were the important variables. Assuming the flame to be a series of point sources, only (array-flame height/single-flame height) and [flame-spacing/(fuel-flow rate)$^{2/5}$] showed a strong correlation. This correlation is shown to exist both analytically and experimentally, but not to the same extent. The experimental data showed no consistent effect of jet number or flame array. The difference between the analytical and experimental trends is accredited to a mutual aspirating effect of one flame upon another which decreases the effective spacing between the jets. A good correlation was also obtained, considering the flame as a continuous area fire, between the dimensionless flame height based on the extent of the fire area and the total fuel-flow rate.

Introduction

In recent years there has been interest in trying to model mass fires for the purpose of isolating those parameters which are most influential in determining the size, spread, and burning rate of such fires. A related problem is that of determining the parameters which are significant in the changeover or merging of a number of individual flames into a mass fire. Previous investigations have covered the flames produced by multiple sources of either liquid or solid fuels in close proximity. In these flames, the rate of fuel supply to the flame was determined by the strength of the back radiation which is the primary source of heat for vaporizing and pyrolizing the fuel. However, the difficulties encountered in modeling this radiant-energy transfer have greatly complicated the construction of a valid model for mass fires. One approach to the establishment of the desired modeling laws was to first use fires where radiation was not an important factor in controlling the fuel-flow rate and then consider the influence of radiation separately. A gaseous fuel, such as methane, would produce the type of flame desired for this study. The fuel-flow rate would be controlled by the investigator and thus would be an independent variable in the establishment of the modeling laws.

In liquid or solid-fueled fires where the fuel is stagnant, the physical transport of fuel, oxidant, and combustion gases occurs because of gradients set up by changes in density. For a gaseous fuel, however, the thrust of the fuel being injected into the ambient air can also affect these transport processes. Therefore, for this program, the condition was set that the fuel velocity and nozzle diameter be such that forces arising from buoyancy considerations always be controlling relative to forces arising from jet-thrust considerations. By holding to this condition, it was hoped that data using gaseous-fueled flames could eventually be correlated with data from flames of liquid and solid fuels. If such a flame could be established with a reasonable fuel-supply rate to the flame, then the second objective would be to investigate the influence of jet spacing, fuel-flow rate, and jet array geometry on the resulting flame configuration.

This paper is intended to report the preliminary findings of a study to establish modeling laws for partially and fully merged flames using gaseous fuels. The paper first discusses the efforts made to determine those flow conditions and nozzle diameters which produced single turbulent flames which were buoyancy controlled. Data for flames from different arrays of multiple jets are then presented and analyzed from two different viewpoints—considering the total flame source as a series of small or point sources of fuel, and considering the total flame source on an area basis. During the course of this initial program, both

analytical and experimental approaches were used to predict the important parameters affecting the merging phenomena. The analytical treatment, although admittedly unsophisticated in nature, has been of definite value in delineating the important parameters. An appendix is provided which briefly describes the apparatus used in this program.

Analytic Considerations

In the study of flames, particularly gaseous jets, one of the flame parameters which is of interest is the ratio of flame height to initial jet diameter (L/d_0). It is known that for thrust-controlled flames, this ratio is independent of fuel-flow rate. However, for buoyancy-controlled flames, this ratio is not independent of fuel-flow rate. Thus, the preliminary experimental and theoretical analyses of this program were concerned with the determination of the dimensionless height relationship and its dependence upon fuel-flow rate. Subsequently, the theoretical analysis was extended in an attempt to predict the flame height of multiple sources of fuel.

Single-Jet, Buoyancy-Controlled Turbulent Diffusion Flames

In order to obtain the type of flame believed necessary for this study, two relations between jet diameter and flow velocity had to be considered. For the first relation, a sufficiently high Reynolds number of the jet of fuel had to be achieved in order to assume turbulent flow for the flame. For this program, Reynolds numbers in excess of 5000 were always used. Since for a given flow rate the Reynolds number is inversely proportional to the diameter, small diameter jets for reasonable gas-flow rates would be desired. In addition, for the jets used in this study, the ratio of the buoyancy force to the thrust of the jet had to be sufficiently greater than unity so that the flame could be primarily buoyancy controlled. Some trivial manipulation shows this ratio is proportional to the Froude number to the $-2/5$ power for a given combusted fuel; thus, the second relation is concerned with a sufficiently low value of Froude number. In other words, for a given flow rate, a maximum nozzle diameter is desired.

To aid in the determination of actual values of flow rate and jet diameter which could be used in this study, the work of several investigators was studied. Since Spalding[2] and Ricou and Spalding[3] extended their relations for the mass flux induced by a buoyant jet to the case where jets of combustible material were burned in a diffusion flame, their approach was used in this study for a given fuel.

Figure 1 shows the data of Ricou and Spalding[3] in which they measured the amount of air aspirated within a given height for a convective jet or plume. These data were obtained by placing a porous cylinder around the flame and

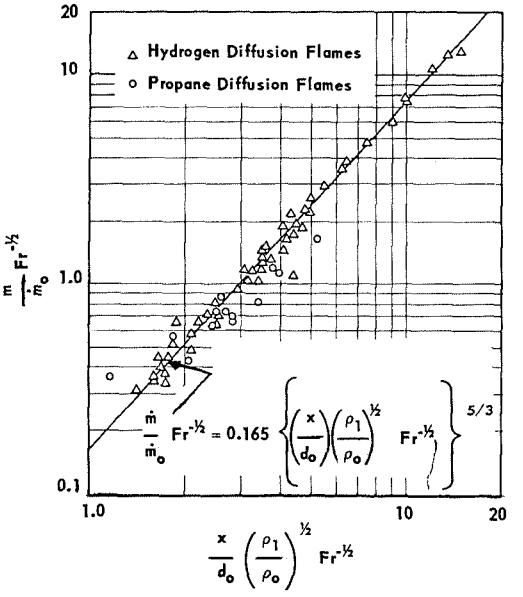

FIG. 1. Experimental data for turbulent diffusion flames (after Ricou and Spalding).

supplying sufficient air to cause a zero pressure difference between the region near the flame and the ambient. The symbol x which appears in the term used for the abscissa of Fig. 1 is not the flame height, but rather the height of the concentric cylinder used in the experiment. A well-fitting line through the data was found to have the equation

$$(\dot{m}/\dot{m}_0)\,\mathrm{Fr}^{-\frac{1}{2}} = 0.165\left[(x/d_0)(\rho_1/\rho_0)^{\frac{1}{2}}\,\mathrm{Fr}^{-\frac{1}{2}}\right]^{5/3}, \quad (1)$$

where Fr is a modified form of the Froude number. For a jet in which chemical reaction occurs, Ricou and Spalding[3] define the Froude number as

$$\mathrm{Fr} = \frac{C_1 T_1}{m_{fu} H + C_0(T_0 - T_1)}\left(\frac{U_0^2}{g d_0}\right)\left(\frac{\rho_1}{\rho_0}\right)^{\frac{1}{2}}. \quad (2)$$

Substituting Eq. (2) into Eq. (1) and reducing

$$\dot{m} = \dot{m}_0(x/d_0)^{5/3}(d_0^4U_0^2/gd_0^5)^{-1/3} \times \left[0.165(\rho_1/\rho_0)^{2/3}\left(\frac{C_1T_1}{m_{fu}H + C_0(T_0 - T_1)}\right)^{-1/3}\right]. \quad (3)$$

It is assumed that $\dot{m}/\dot{m}_0$ and the term within the brackets are constant at the end of the visible flame, where $x = L$. This assumption has implications with respect to: (a) the accuracy of the measured position of the flame tip, as related to the thickness of the region of a strong rate of change of luminosity relative to total flame length; (b) the accuracy of height measurement as related to a change in curvature of the flame tip from one type of flame to another; and (c) a chemical mechanism leading to production of a luminous flame. In the judgment of the authors, it is an acceptable assumption at this stage of progress. However, confirmation should and can only be found through experimental testing of the assumption by chemical composition measurements on several flames.

Proceeding on the basis that our assumption is valid

$$L/d_0 = K(Q_0^2/gd_0^5)^{1/5}, \quad (4)$$

or

$$L = K'Q_0^{2/5}.$$

Equation 4 suggests that data of flame height from buoyancy-controlled flames should fall along a line whose slope is 1/5 on log–log coordinates when plotted in terms of the parameters given in the equation. If, for a given flame, the flame height follows this relationship for low flow rates, but diverges from the line at higher flow rates, it can be assumed that the divergence occurs because the flame becomes thrust controlled. Figure 2 shows the variation in dimensionless flame height as a function of the term (Q_0^2/gd_0^5) as found for the experimental burners used in this research program. By following the datum points for specific diameters through increasing flow rates, it is seen that above certain values the datum points (as indicated by the box) do break away from the predicted trend and the flame height tends to remain constant.

Using only the points which follow the trend established for buoyancy-controlled flames, a value for the constant K in Eq. (4) can be established. Thus, Eq. (4) becomes

$$L/d = 29(Q_0^2/gd_0^5)^{1/5}. \quad (5)$$

Data of the type discussed above can also be used to establish an operating range over which the subsequent experiments can be run with some assurance of having flames which are

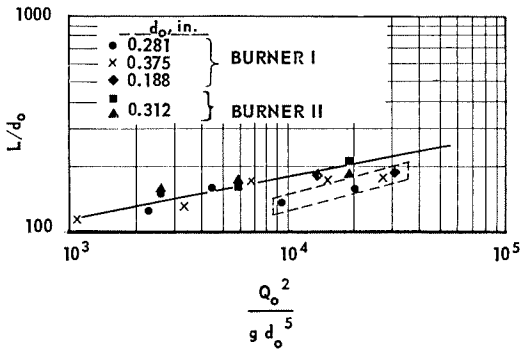

FIG. 2. Dimensionless flame height as a function of Q_0^2/gd_0^5 for single flames using experimental burners I and II.

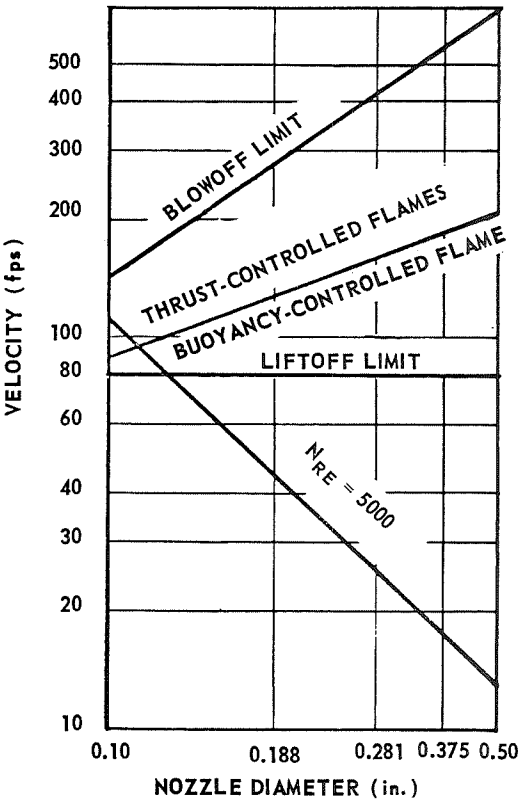

FIG. 3. Operating range of nozzle size and flow velocity.

turbulent and buoyancy controlled. Figure 3 shows the range of operation found for this experimental study in terms of the velocity of the fuel gas issuing from the nozzle and the nozzle diameter. The desired range is within the wedge formed by the limit line for which the Reynolds number is equal to or greater than 5000 and the limit line above which the flames are found to be thrust controlled.

It is interesting to note that somewhat below the lift-off limit the flame could be forced to lift off by passing a rod across the jet entrance. Pertinent to the approximation indicated in the analytical treatment was the observation that this lift-off did not change the shape or position of the upper portion of the flame, although it changed the luminosity of the lower portion.

Merging Effects in Arrays of Flames

The single jet study outlined above was for the case wherein the ratio of height of observation (or flame height in our case) to spud diameter is large. Furthermore, the remaining data discussed in this report are for the same condition. As a result, the diameter d_0, may be eliminated in the correlating relation. For the case wherein the ratio of observation height to the spud diameter (or puddle or fuel-array size in the many studies reported in the literature) is small, this ratio must remain as a second correlating dimensionless group. While this is not the case in the present study for an individual flame, it might be expected that arrays of large numbers of flames could act in a way similar to a continuous flame of large diameter relative to the height. This study is concerned, however, with the intermediate numbers of flame in arrays, and with flames which individually are tall compared with their base dimensions. Based on this stipulation, the upper limit in flame height of multiple jets can be obtained from an extension of Eq. (4).

If the multiple jets are very close together, relative to the height of the flame, it would be expected that the flame-array height will be given by the single-jet relation using the total flow rate. Thus, the flame-height relation

$$L = KQ_0^{2/5}$$

would be modified to

$$L' = K(nQ_0)^{2/5},$$

where L' is the flame height of the combined flame under the condition of close proximity and n is the number of jets, each with a flow rate of Q_0. If the height of a single isolated jet with the same fuel-flow rate is given by L^*, then

$$L'/L^* = n^{2/5}. \tag{6}$$

A more general case would be where the jets are spaced by a distance S. The flame interaction in this case is only partial. However, the height of the combined flame L', might be given by the relation,

$$L'/L^* = \text{function}\left[\text{source-shape factor}, n, S/(Q_0^2/g)^{1/5}\right], \tag{7}$$

where the source-shape factor is some function which describes the shape of the set of small or point sources. An alternate formulation, which has the advantage of having the limits of zero and one, is

$$\frac{(L'/L^*) - 1}{n^{2/5} - 1} = \text{function}\left[\text{source-shape factor}, n, S/(Q_0^2/g)^{1/5}\right]. \tag{8}$$

The disadvantage of this relation is that the term $(L'/L^*) - 1$ exaggerates small variations in the measurement of flame height.

With the limits of flame height determined, the next problem is to determine a relation for the height at intermediate jet spacings. In the derivations which will be discussed, three basic assumptions were made. In the first of these, a given jet was assumed to be shielded by all other jets in the array in that the path for the aspirated air for the given jet is partially blocked by the other jets. The blockage is assumed proportional to the diameter of the blockage jet as seen from the jet in question. Thus, it takes longer for the given jet to aspirate a specific mass flow of air when it is part of an array. The second assumption was that the rate of mass flux of aspirated air to mass flux of injected fuel $(\dot{m}/\dot{m}_0)$ at the flame tip is a constant for a jet, whether it is isolated or in close proximity to other jets. From these two assumptions, it would thus be expected that jets whose aspirated air supply is shielded will be taller than isolated jets where no shielding takes place. A third assumption was that there is no significant deviation of a jet from the

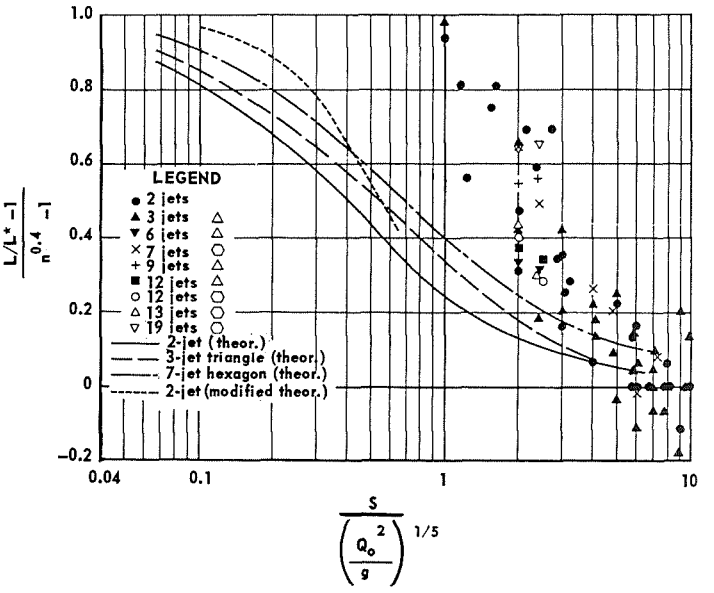

FIG. 4. Experimental and theoretical correlations of a dimensionless flame height as a function of $S/(Q_0^2/g)^{1/5}$ for the point source data.

vertical because of the mutual aspiration of adjacent jets. Such a "pulling together" of the flames would decrease the actual spacing between jets. This particular assumption, used in many combustion flow studies in the past, turns out to be a fatal flaw to the theory in this case, but its failure is quite illuminating and leads to a revised approach which will be discussed subsequently.

Using these assumptions, Eq. 3 was extended for the cases of: (a) two jets in close proximity; (b) three jets in an equilateral triangular pattern; (c) six and seven jets in a hexagonal pattern; and (d) three jets in a line. Some consideration was also given to the extension of the case of three jets in a line to many jets in a line. In no instance was a closed form of solution found. The resulting curves will be discussed in conjunction with the experimental results. The details of the analyses will be found in reference 1.

Discussion of the Experimental Results on Multiple Sources

Symmetric Flame Sources Treated As Point Sources

As shown by Eq. (7), the experimental data could be correlated by the dimensionless groups of

L'/L^*, number of jets, source-shape factor

and

$$\frac{S}{(Q_0^2/g)^{1/5}}.$$

In the correlations of data reported herein, L'/L^* has been plotted as a function of $S/(Q_0^2/g)^{1/5}$ with number of jets and source-shape factor as independent variables. Figure 4 shows a plotting of the experimental data as well as the predicted theoretical curves. Although the ordinate is expected to reduce all of the data to the range between 0 and 1, it has a tendency to accentuate experimental scatter, particularly at small values of the ordinate; this explains the points below zero. In future studies an individual flame will be run at the same time as an array flame, but outside its influence; this will eliminate one source of scatter.

The horizontal position of the theoretical curves, as compared with the data, is not significant; only the shape is important since a coefficient requiring experimental evaluation has been omitted.

It is of interest to note first that the theoretical curves show a strong correlation between (L'/L^*) and $S/(Q_0^2/g)^{1/5}$. In addition, there is a small effect of number of jets or source-shape factor, or both, which causes a displacement among the curves. It is not possible to distinguish which of the two factors, number or arrangement, is responsible for the shift.

It can be readily seen from Fig. 4 that the experimental data do not correlate with the theoretical curves but instead show a more rapid rate of change of flame height. There is considerable scatter in the data as evidenced by a comparison of data for similar configurations. Even so, the data do fall in a relatively narrow scatterband. In contrast to the results shown by the theoretical curves, there does not appear to be any consistent effect of jet number or source shape for the experimental data. Specific correlations which would delineate any such trends were also not effective in separating the effect of jet number. Also, a comparison of the two 12-jet arrays does not reveal any noticeable effect of source-shape factor.

Perhaps the most important difference between the experimental data and the theoretical curves is the trend in the data for decreasing values of $S/(Q_0^2/g)^{1/5}$. The vertical rise in the data at about 2 indicates that all of the arrays studied in the program show a similar rapid increase in flame height and are apparently almost fully merged. Since the theory outlined above accounted for the increase in flame height by the mutual blocking effect of jets on the aspired air supply, the further increase in the flame height must be accredited to some other mechanism. The most logical explanation is that at close spacings, the flame of each jet is aspirated by the adjacent jets, thus decreasing the effective spacing between the jets. That is, the third assumption used in the theoretical derivation is untenable. Thus, for a given array, the flame height will increase as the jets are spaced closer together until the flame aspirating effect becomes strong. Then large increases in flame height will occur with small further decreases in spacing as the flames merge. Further decreases in spacing seem to have little effect on the flame height. These trends can be seen by following the data for individual arrays.

To check on this explanation of the deviation, the third assumption related to vertical jets was dropped from the analytical treatment. The spacing between jets in a pair of jets was made a function of the height. The rate of change of spacing with height was considered to be a result of the unbalancing of momentum of the inflow due to the shielding on one side of each jet by the other jet. The result of this computation, as shown on Fig. 4, is seen to be that the two-jet curve rises more rapidly. While the rate of rise is still not quite as much as indicated by the experimental data (it should be recalled that the horizontal coordinate as far as this theory is concerned is relative and may be shifted), this may be the result of an arbitrary assumption that had to be made in assigning effective jet radii in the computation. Therefore, it is believed that mutual entrainment explains fully the rapid increase in flame height with a decrease in spacing, at the critical spacing distance.

Symmetric Flame Sources Treated as an Area Fire

The correlation as presented in Fig. 4 considers the merged flame as a set of point sources. The correlating functions are based on the flow rate and geometry of the individual jets which make up any given configuration. It is also possible to correlate these data in terms of an area fire in which the fuel-flow rate is the total fuel available for combustion and the principal dimention is some dimension indicative of the total area of the fuel source. This permits a

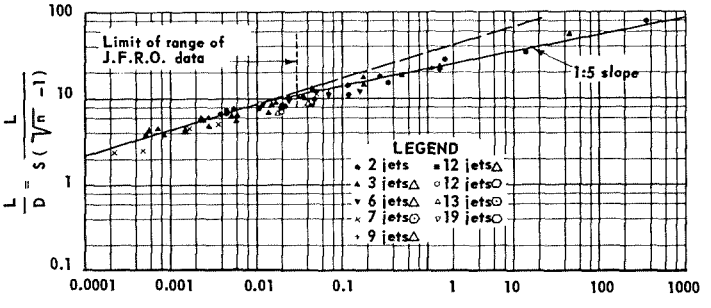

FIG. 5. Correlation of the data assuming an area source.

comparison with area fire data. The principal assumption which must be made concerns the "shape factor" for the array. In view of the small amount of data available, and the preliminary nature of this portion of the study, a very simple approach was used to determine an equivalent array size; it was assumed that the jets, regardless of their array pattern, are in a square array. With a spacing between jets of S, the principal dimension of the array then is equal to one side of the square or

$$D = S(n^{\frac{1}{2}} - 1)$$

where n is the number of sources in the array. This relation can now be used to obtain D from S and n for other than square arrays. One can now correlate the gaseous-fuel data obtained in this study in a form used by such investigations as Thomas[4] in his work on solid fuel fires.

Figure 5 shows a correlation of our jet data for gaseous fuels on an area source basis. The particular coordinates, a dimensionless flame height (L/D) and q^2/gD^5 where q is the total fuel-flow rate, were found by Thomas to give a good correlation. Specifically, the jet array to area conversion factors are

$$L/D = L/S(n^{\frac{1}{2}} - 1)$$

and

$$q^2/gD^5 = (Q_0^2/gd_0^5)[n^2d_0^5/(n^{\frac{1}{2}} - 1)^5S^5].$$

It is of interest to note that the data fall quite well along a line where the slope is 1/5. For comparison purposes, the best-fit line for the J.F.R.O. data on Fig. 10 of Thomas' paper have been superimposed on Fig. 5. This line has also been extrapolated beyond the range of data reported in his paper. Although there is a difference in slope between the two sets of data, it is not deemed necessary that a constant power relation exists over the wide range of data encompassed by these studies.[5] Furthermore, our data fare nicely into the referenced data at the lower coordinate values.

Line Fires

One of the arrays studied in the program was that of the line fire. Figure 6 shows a correlation for the data obtained with line fires of various lengths and two different fuel-flow rates. In a very elementary sense, it can be argued that increasing the number of fuel sources in a line fire should have a "marginal-return" effect on the over-all flame height of the array. Thus, an exponential-type equation might be expected to best fit the data. A curve, which has been found to pass through the data for all values of n used is given by

$$\tfrac{1}{29}[S/(Q_0^2/g)^{1/5}] - (S/L_n) = \tfrac{1}{67}[1 - \exp(-0.24(n-1)]. \quad (9)$$

From this equation, a maximum value of (L_n/S) would be

$$(L_n/S)_{\max} = \frac{29}{S/(Q_0^2/g)^{1/5} - (7/16)}. \quad (10)$$

It is of interest to note that the flame height for any given number of jets and spacing varies with

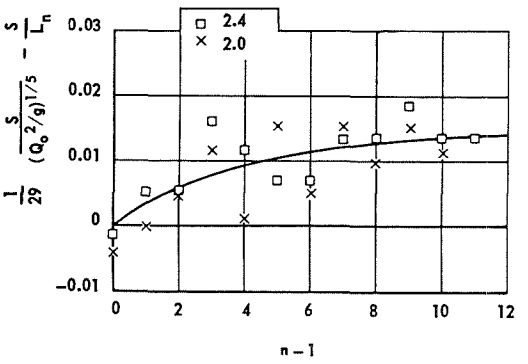

FIG. 6. Correlation of the finite line fire data using Eq. (3).

the fuel-flow rate to the 2/5 power instead of the 2/3 power as would be predicted from theoretical considerations of infinite line sources. Apparently, the jets were too widely spaced in the experimental studies reported herein with the results that the jets acted as individual point sources and not as a line source.

Conclusion

It appears that gaseous fuel jets in arrays can be used to study the merging of individually acting fires into mass fires. To satisfy the requirement of being a turbulent, buoyancy-controlled flame, the individual jets must exceed a critical Reynolds number, and be less than a

critical Froude number. Increasing the jet diameter increases the range over which this condition can be met. However, in modeling, there is a practical limit to the increase in single jet size that can be tolerated.

Providing these requirements are met, the ratio of flame height of the array of jet flames to single-jet flame height is a function of a dimensionless spacing, the number of jets, and source-shape factor. For roughly circular arrays, combining the height ratio and number of jets in such a manner as to give a range from zero to one permitted a correlation with the spacing factor that shows no further effect of source shape or number of jets. At a critical spacing factor of about two, the jet flames changed abruptly from acting as single jet flames to acting as a mass fire.

There is a strong indication that at a moderate number of jets, the exact number depending on the array pattern and the dimensionless spacing, the array may be treated as a single extended fire, giving results correlating with results on stacks of wood and similar fire sources.

In the study of the linear arrays, a gradual shift of the relation of flame height to flow rate from that observed for individual sources to that predicted for a pure line source was expected. This shift did not occur. Apparently the characteristic spacing for these studies was not made small enough to obtain this expected shift. A semi-empirical correlation of the array flame height indicated that flame height reaches a finite maximum as the number of jets in a line is increased.

Nomenclature

C	Specific heat at constant pressure
d_0	Nozzle port diameter
D	Principal dimension of an area fire
Fr	Froude number [defined Eq. (2)]
g	Gravitational constant
H	Heat of combustion
k, K, K'	Constants
L, L'	Height of the flame array
L^*	Height of a single, unmerged flame
L_n	Height of flame array made up of (n) jets
$\dot{m}$	Mass flux of the induced air
$\dot{m}_0$	Mass flux of the injected fluid
m_{fu}	Mass fraction of fuel in the injected fluid
n	Number of jets
q	Total fuel-flow rate
Q_0	Volume flux of injected fuel
S	Spacing between jet center lines
T	Absolute temperature
U_0	Injected-fuel-flow velocity
x	Distance above a reference plane
ρ	Mass density

Subscripts

0	Injected fluid
1	Ambient atmosphere

Acknowledgment

This paper is based on a program sponsored by the Office of Naval Research and the Office of Civil and Defense Mobilization through the Fire Research Section of the National Bureau of Standards.

References

1. Putnam, A. A. and Speich, C. F.: A Model Study of the Interacting Effects of Mass Fires, Battelle Summary Report to Fire Research Section, National Bureau of Standards, November 9, 1961.
2. Spalding, D. B.: The Theory of Turbulent Jets of Nonuniform Momentum, to be published.
3. Ricou, F. P. and Spalding, D. B.: J. Fluid Mech. *11*, 21 (1961).
4. Thomas, P. H.: Research on Fires Using Models. Institution of Fire Engineers Quarterly, *XXI*, 197 (1961).
5. Thomas, P. H.: Personal communication.

Appendix

Description of the Apparatus

Figure 7a is a photograph and Fig. 7b is a schematic sketch of the larger of two burners

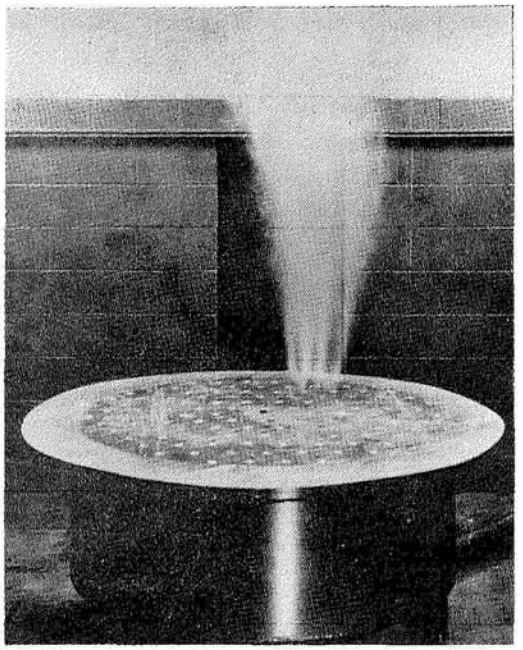

FIG. 7a. Experimental burner II photograph.

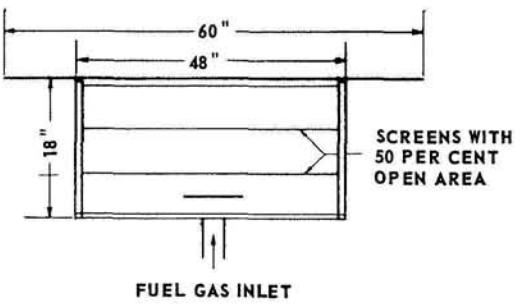

FIG. 7b. Experimental burner II schematic.

used for the multiple-flame studies. The burner face was 4 feet in diameter with an apron attached to increase the effective diameter to 5 feet. In contrast, the first burner was 10 inches in diameter with a 4-foot apron. Accommodations for 120 nozzles were available in the second burner, as contrasted to 7 in the first burner. A hexagonal pattern was used for the spud arrangement in both burners. However, a center-to-center nozzle spacing of 4 inches was used in the second burner as compared to a 2-inch space in the first burner.

Figure 8 is a line drawing of the gas nozzle used throughout this program. Each nozzle was

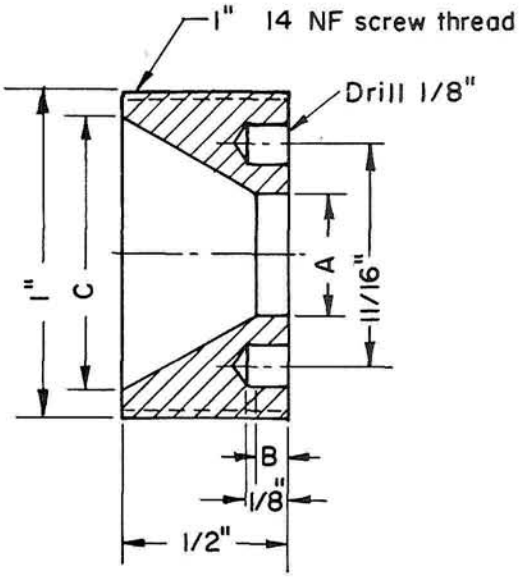

FIG. 8. Line drawing of nozzles.

calibrated to determine its discharge coefficient for at least one flow rate.

In the beginning of the program, sufficient nozzles were tested under various flow conditions in order to establish a curve of flow discharge coefficient as a function of Reynolds number. By using flow-visualization studies, it was established that no *vena contracta* existed downstream of the nozzle. Therefore, the discharge coefficient could be associated with velocity losses only.

When the larger burner was used with a number of gas nozzles firing, care was taken to use the nozzles with the same discharge coefficient throughout.

The principal task in the experimental phase of this research program was to record and measure the changes which occurred in the flame array with changes in the fuel-flow rate, spacing between jets, and/or the diameter of the jet. Photography served as the tool to make these flame-height measurements. For each flow condition or spacing of interest, a photograph was taken. The top of the flame was taken as the highest point where a flame image was recorded on the film.

Orthochromatic film (Kodak Royal Ortho) was selected and used consistently for most of the program. The slowest automatic speed on the camera used for this program was 1 second; this speed was used for the majority of the photographs.

Discussion

DR. D. G. STEWART (*Aeronautical Research Laboratory, Australia*): There has been some doubt expressed as to whether radiation is an important feature in the propagation of forest fires. It may be of interest that, in Australia, where such fires are unfortunately quite common, the vegetation consists mainly of tall Eucalyptus trees which have highly inflammable foliage located mainly at the top. Under these conditions, "crown fires" occur in which the foliage can definitely be ignited by radiation, ignition often occurring quite explosively. A knowledge of radiation effects is thus of great importance in the design of fire breaks.

DR. B. R. MORTON (*Manchester University*): I should like to add some comments on Professor Spalding's introduction to modeling, and to illustrate my points by particular reference to the papers presented by Dr. Fons and Mr. Putnam.

The technique of modeling serves as an important stage in our progress towards the understanding of any complicated physical system. Whether we proceed by theoretical argument, by experiment, or by the proper combination of the two, our aim is always to identify and concentrate our attention on the physical features which play a dominant role in our particular problem. These are the features which are important in our formulation of a theory, and over which we seek independent control in designing experiments. We do not expect that such theories will correspond exactly with nature, but rather that they will predict (within the general latitude of experimental error) the most significant aspects of behavior within some prescribed range of operating conditions. Nor need our model experiments reproduce exactly a natural situation, provided that we can infer from them what is likely to happen in practice. To put it very simply, particle dynamics provides a reasonably good model theory for the flight of a baseball from the hand of an inferior pitcher, because the inertia of the ball is about its only property that he uses. But the skilled pitcher will spin his ball so that it swerves in the air, and we can model experimentally the aerodynamic effects that he is using by mounting his actual ball on a rotating shaft in a wind tunnel and measuring the transverse force acting on it. (We did not ask our pitcher to step into the wind tunnel!)

The propagation of fire through a complex of wooden fuel is an extremely complicated situation. It certainly involves heat transfer by radiation, convection, and conduction, pyrolysis of the wood, combustion of solid and vapor fuel, and fluid flow and mixture in and around the flame. Moreover, most of these effects are interrelated, though the degree of coupling will change markedly according to the nature of the fire. Thus, for example, an increase in luminosity of the flame causes an increase in radiation which may affect the combustion balance, and also the pyrolysis rate and hence the supply of fuel vapor, and so on! If we are to model such a process effectively we must restrict our attention as narrowly as possible (without losing the problem altogether), or we may lose our way in the complexity of the problem. And, while we can neglect weak interactions, we must also try to simulate some of the strong interactions in such a way that we can exert an independent control over key features of the experiment. This breaking open to experimental control of tight, ill-understood couplings is one of the great benefits of experimental modeling.

Dr. Fons' crib burning experiments have the considerable advantage of reproducibility, but there are so many factors involved that for my own part I am very vague as to what he is reproducing. It seems to me that he does not have the sort of detailed internal control of his experiment that is so necessary; and in particular that he might learn more from his experiments if he were to decouple the processes of pyrolysis from those of fire spread, and by this I mean carrying out the pyrolysis and fire spread experiments quite separately so that he might have greater control over each. Indeed, I have never understood why it should be assumed so widely that wood is a suitable material for use in model experiments of fire spread, without any regard to the changes in time, length, and other scales involved. As Dr. Thomas has just observed: "Wood is an unhappy substance." Perhaps I can bring

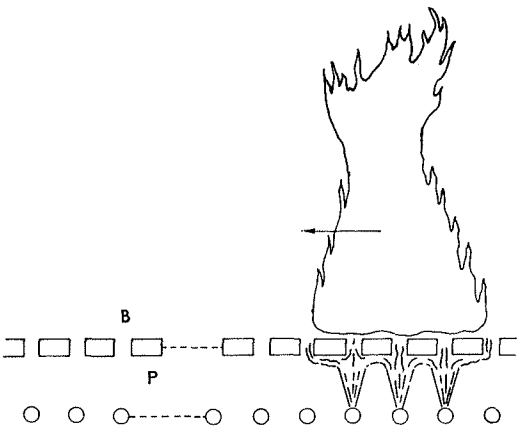

FIG. 1. Model of propagating fire.

out my ideas more clearly if I describe an alternative ideal propagation experiment for two-dimensional propagation. This consists of a series of metal bars (B) arranged with uniform spacing in a horizontal plane. As each bar is heated it expands and (in some way or other) opens a gas tap allowing gas to discharge from an associated underlying gas supply pipe (P). After a prearranged time (say) the supply of gas to P is shut off again. We now start a fire from one end of the system and observe its propagation. I am quite willing to concede that this experiment is mechanically naive, but I doubt that it is as naive scientifically; for we should be free to vary the properties of the fuel gas which in turn will govern the luminosity and other properties of the flame, we can introduce delay times and vary the rates of gas release, and we can select the sensitivity of the sensing bars (B) to radiation. Experiments with an apparatus of this general type might show up the relative importance of radiation and convection in flame propagation without confusion due to the peculiar properties of wood.

The experiment described by Mr. Putnam is not a case of fire but one of flame interaction. It has all the advantages of direct experimental control over the fuel supply, although they have not made full use of these yet. It could be extended into a study of fire if an arrangement were made to control the flow of gas according to the temperature of one or more thermal sensing elements placed on the upper surface of the loose plate, and this offers interesting experimental possibilities in view of the existing knowledge of pan fires. A disadvantage of working with such small numbers of jets is that the results show a major dependence on the source geometry; it appears that results with larger arrays which would not show this dependence might be more useful, and that these results should then be correlated in terms of mass, momentum, and buoyancy flow per unit area of base.

MR. A. A. PUTNAM (*Battelle Memorial Institute*): Dr. Morton's comments on our multiple gas-jet model are greatly appreciated. With regard to his suggestion for modeling a spreading flame, we should like to make the following observation. Such a flame model would require that a decision be made as to (1) the proper modeling relation between the back radiation in the vicinity of each fuel-supply nozzle and the consequent fuel-supply rate, and (2) the total (time integrated) radiation to the vicinity of the unactivated jets to be required to turn them on. The thermal radiation pattern of any gaseous flame array, as seen from the "ground," as well as any variations of the relative radiation pattern with fuel type for particular flame arrays and flame heights, can be determined experimentally. A decision on the relationship between the radiation and the fuel-supply rate would have to be based upon independent studies of the radiation effects on the combustible to be simulated. Once the decision is made, however, no further study of the type we are outlining appears necessary to accomplish Dr. Morton's aim, because each new set of jets ignited would merely result in a new array, for which static array rules would already be available. A similar argument can be used in relating the consumption of available fuel to the turning off of jets. Thus, we have, as Dr. Morton suggests, managed to break our interaction problem into separate parts.

Relative to the number of jets used, we have now used up to 29 jets at one time. For the larger numbers of jets, the exact number depending on the other dimensionless parameters involved, the performance appears to be equivalent of that from area fires.

SOME EXPERIENCES IN GAS TURBINE COMBUSTION CHAMBER PRACTICE USING WATER FLOW VISUALIZATION TECHNIQUES

A. E. CLARKE, A. J. GERRARD, AND L. A. HOLLIDAY

This paper presents a case study using a practical production-type of combustion chamber for an aircraft gas turbine, in which qualitative and quantitative data obtained using the water flow analogy are compared with corresponding data obtained when the chamber was operated under air flow, both isothermally and under combustion conditions, using a gaseous and a liquid fuel.

Introduction

The application of flow visualization techniques using the water flow analogy has received much attention over the past sixteen years in the diverse field of combustion research and practice, including ramjet and gas turbine engines, reciprocating engines, industrial furnaces, and domestic heating equipment.*

The water flow visualization technique provides a direct means of continuously observing detailed flow patterns by the use of transparent models, in which suitable tracers are introduced into the water flow at selected regions. The patterns are observed with the aid of a high intensity light source. In this way, an extremely useful means of analyzing the flow patterns in a complex fluid dynamic system is provided.

The advantages are obvious. The fulfillment of the aerodynamic design requirements can be assessed almost at a glance, and in a relatively short time any flow anomalies or undesirable patterns can be eliminated without resort to long and expensive combustion development programs, which in many cases are dependent upon *ad hoc* methods to obtain optimum performance. In addition, owing to the relatively low costs of operating a water flow model compared with testing full size equipment, which may require large quantities of compressed air as in the case of gas turbines, the overall cost of experimental work is considerably reduced.

There are, however, disadvantages. The use of an incompressible fluid to simulate the motion of a compressible gas flow is restricted, as is the choice of suitable tracers, which might be influenced by buoyancy, or inertial or gravitational effects. Again the expansion processes due to the evolution of heat cannot be simulated; hence in applications where pressure differences are small and convective flows weak, some reserve has to be placed on the interpretation from isothermal flow models. The superimposition of a fuel spray and the relative momenta between the fuel droplets and the local air flows are additional factors which might change the isothermal flow patterns.

The success of using water flow visualization techniques in combustion chamber practice has depended to a large extent on the qualitative correlation of flow patterns with the resulting combustion performance. For example, in the particular design of chamber described, it has been shown that optimum combustion performance in the primary zone is associated with a stable and orderly recirculatory flow pattern in the form of a toroid. In this connection, certain empirical relationships have been established which have enabled designers to fix a flame tube geometry such that the required flow pattern conditions and proportionate air/fuel ratios throughout the chamber are obtained in practice.

The use of water flow models has also been extended so that quantitative predictions can be made of the component pressure losses and flow distributions; and with the aid of a suitable chemical tracer it is also possible to predict the general pattern of the temperature distribution of the chamber exhaust.

Basic Requirements

The design of a gas turbine combustion chamber has to satisfy many stringent requirements. Not the least important is termed "combustion performance," which may broadly be subdivided into the following:

1. The attainment of a high rate of heat release for the minimum expenditure of pressure loss.

* References to flow visualization techniques and their application in combustion studies are listed in the Bibliography.

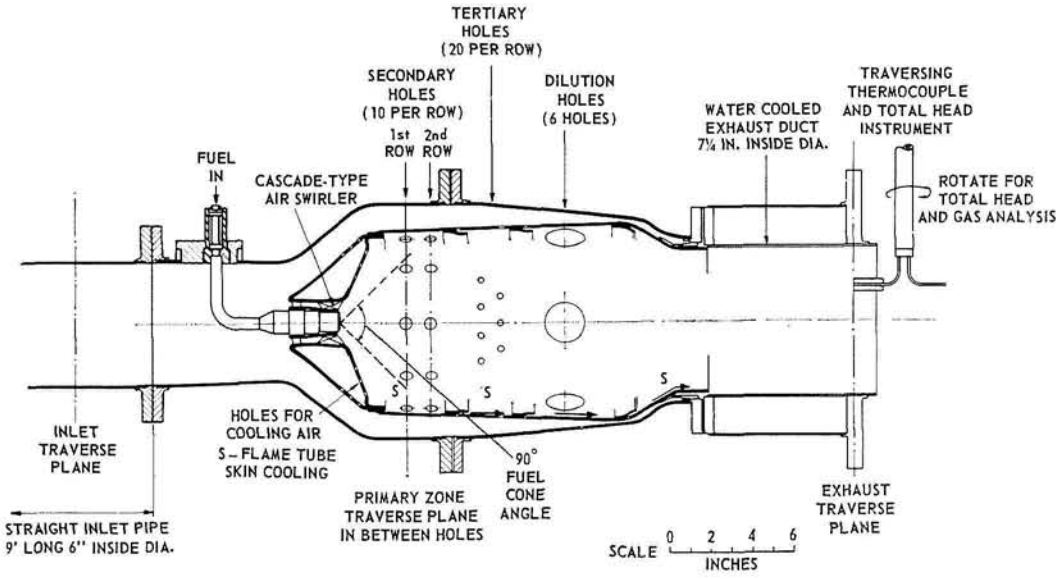

FIG. 1. Details of combustion chamber and instrument traverse planes.

2. A high combustion efficiency over a wide range of operating pressures and air and fuel flows.

3. A wide range of flame stability.

4. Ease of ignition and cross flame propagation under starting and arduous relight conditions.

5. The attainment of a specified temperature distribution at the chamber to match with the stressing of the turbine blades.

6. Stability and consistency throughout the range of operation.

Data obtained using water flow techniques have contributed in many ways to the ultimate achievement of the above performance requirements. However, the question has often been put as to how accurately the flow patterns observed, together with the quantitative information obtained under isothermal flow conditions, simulate the true combustion performance in an actual chamber, and to what extent the density changes due to the addition of heat might influence the basic isothermal patterns.

The studies described were confined to a practical chamber. Although they might be regarded as limited in scope they were nevertheless sufficiently comprehensive to satisfy the basic objects of the investigation.

The test conditions (Table 1) were such that the effects of compressibility under isothermal air flow were negligible and the type of liquid fuel injection also ensured that the atomization would be satisfactory.

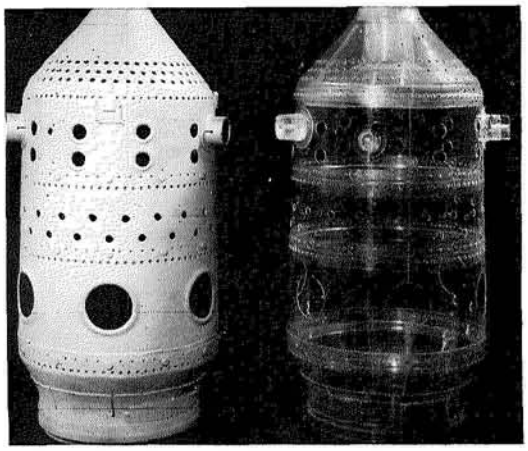

FIG. 2. Sheet metal and transparent flame tubes.

Description of the Combustion Chamber

Details of the combustion chamber used are shown in Fig. 1. Figure 2 is a photograph showing the sheet metal and transparent flame tubes. In describing the general design features, reference is made to the flow pattern sketched in Fig. 7.

The chamber is typical of Lucas practice, in which the primary zone flow pattern is characterized by the recirculatory flow of toroidal form. This flow is generated by the injection of air through the first of two rows of secondary holes, thus supplementing the primary air which passes

TABLE 1

Test Data

	Test									
	1	2	3	4	5	6	7	8	9	10
Unit	Perspex	Metal	Metal	Metal	Metal	Metal	Metal	Metal	Metal	Metal
Fluid	Water	Water	Water	Water	Air	Air	Air	Air	Air	Air
Mass flow, lb/sec, gpm	77.5, 465	77.5, 465	141,852	77.5, 465	1.52	2.98	3.96	1.52	1.52	1.52
Inlet pressure, atm	1	1	1	1	1	1	1	1	1	1
Inlet temperature, °C	15–25	15–25	15–25	15–25	46.3	45.6	49.7	41.9	39.8	37.6
Inlet Reynolds number	293,000	293,000	576,000	293,000	293,000	576,000	773,000	293,000	293,000	293,000
Inlet Mach Number	—	—	—	—	0.0927	0.183	0.244	0.0927	0.0927	0.0927
Fuel type	—	—	—	Chemical	—	—	—	Propane	Propane	Kerosene
Fuel flow, lb/sec	—	—	—	1.292	—	—	—	0.0253	0.0253	0.0253
Air/fuel ratio	—	—	—	60/1	—	—	—	60/1	60/1	60/1
Combustion	No	No	No	No	No	No	No	No	Yes	Yes
Fuel/air momentum ratio	—	—	—	0.0916/1	—	—	—	0.0895/1	0.0895/1	0.04125/1
Plot reference	△	○	○–	●	□	◇	▽	■	○|	○|

through the swirler. Additional combustion air, tertiary air, is injected through two rows of intermediate holes, followed by the admission of dilution air through a single row of six holes. Flame tube wall cooling is achieved by introducing air through rows of small diameter holes and thence deflecting the flow by rings which are riveted to the inside of the flame tube. The inner bore of the swirler locates the pressure-jet atomizer of nominal cone angle 90°. Both sheet metal and the transparent model were similar in size and geometry.

A further characteristic feature of the chamber is the control of helical swirl components in the primary zone flow pattern such that swirl is negligible compared with the two-dimensional nature of the flow across any diametral section of the toroidal flow pattern. This feature facilitated flow pattern observations and instrumentation for determining local velocities in the primary zone.

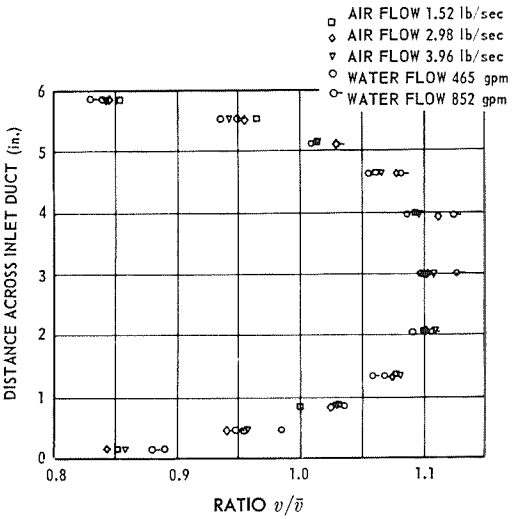

FIG. 4. Plot of weighted inlet velocity ratio $v/\bar{v}$ for air and water flow tests.

Techniques and Test Results

Inlet Flow Conditions

In any fluid dynamic exercise using model and simulation techniques, it is imperative to ensure that the inlet flow characteristics are identical to those in the practical equipment. It cannot be stressed too emphatically that failure to have the correct inlet flow conditions could lead to misleading data from a model. Experience in this field has shown that similarity of inlet flow and velocity distributions are more important than equality of Reynolds numbers, provided the latter are well into the turbulent flow regimes.

In the tests described, the transparent and actual combustion chambers were connected to the same length of inlet pipe, 9 ft in length, for all the studies. A typical inlet flow velocity distribution across a reference diameter is shown in Fig. 3; and a plot of weighted ratios of local velocity v, divided by mean velocity $\bar{v}$ for all the tests is shown in Fig. 4. The general scatter of the $v/\bar{v}$ values is within $\pm 2\%$, which was considered satisfactory.

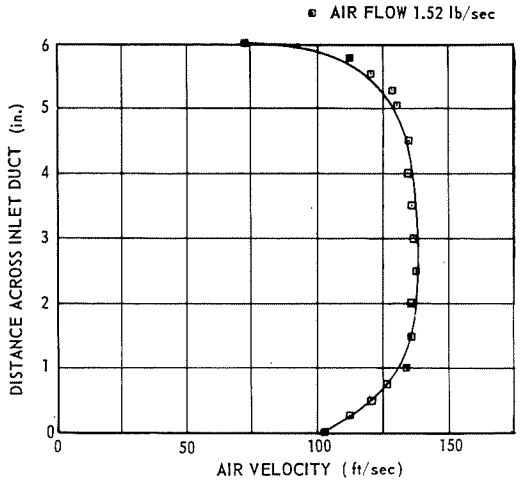

FIG. 3. Typical inlet velocity profile.

Flow Visualization Using Water

The isothermal flow patterns using water flow were obtained using the transparent model mounted with its axis vertically in a closed-circuit water tunnel. The patterns were observed by using small air bubbles as tracers, injected well upstream into the inlet pipe. Buoyancy effects were negligible at the flow conditions within the model, and air tracers were preferred simply because solid particles are difficult to remove from a closed-circuit system and they are also potential obstructions in pitot instruments.

Photographic reproductions of the flow patterns are shown in Figs. 5 and 6 and a diagram sketched from Fig. 5 is shown in Fig. 7.

In the authors' experience, the general observed flow pattern as a whole was stable throughout the

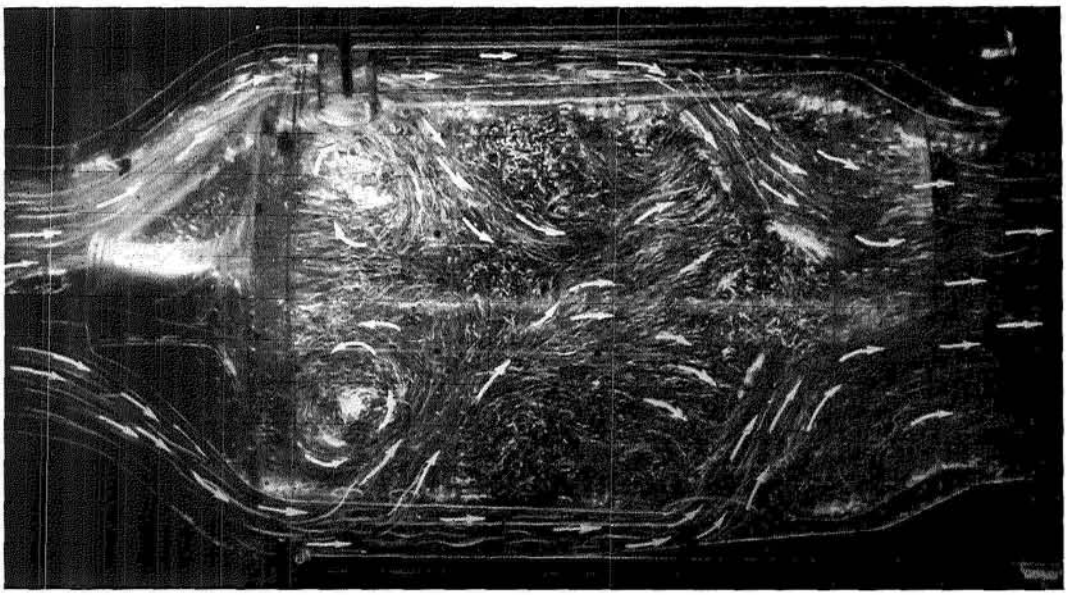

FIG. 5. Flow pattern in the axial plane through secondary and dilution holes.

flame tube, particularly with respect to the admission jets through the various flame tube holes, and in the intermediate, dilution, and exhaust regions. Some slight fluctuations in the shape of the primary zone recirculation were apparent, however, as a result of a small lateral or radial low-frequency oscillation of the "core" of the recirculatory flow, which probably accounts for certain differences experienced with the traverses shown in Figs. 8, 9, and 10.

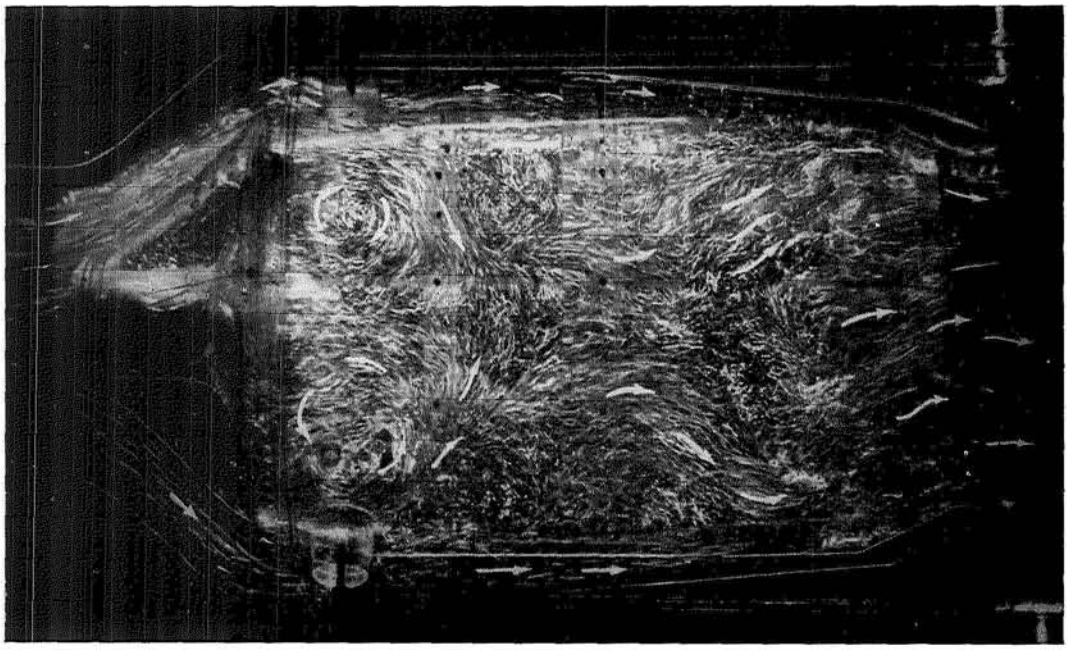

FIG. 6. Flow pattern in the axial plane between secondary and dilution holes.

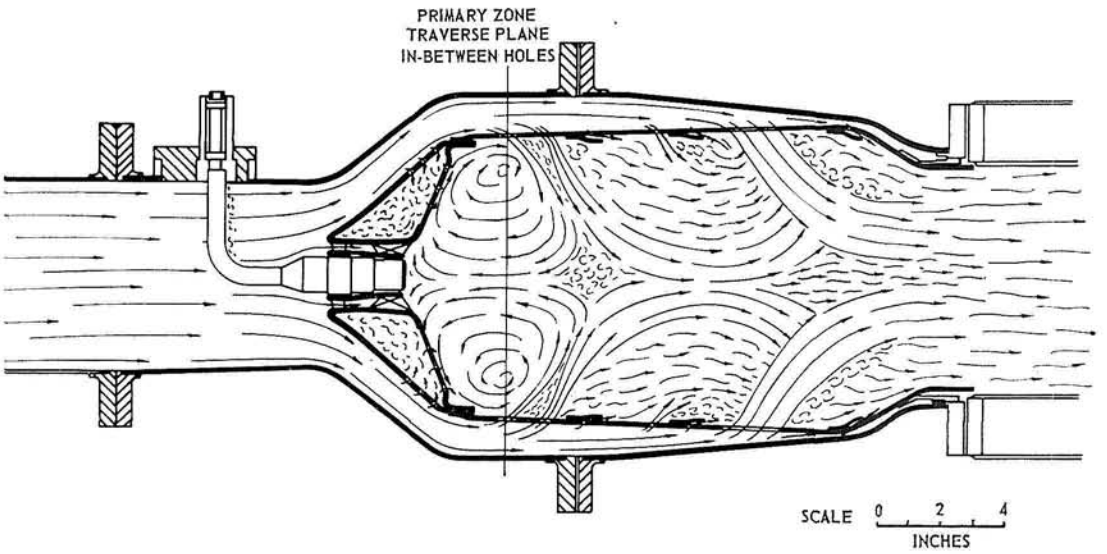

FIG. 7. Sketch of flow pattern in axial plane through secondary and dilution holes.

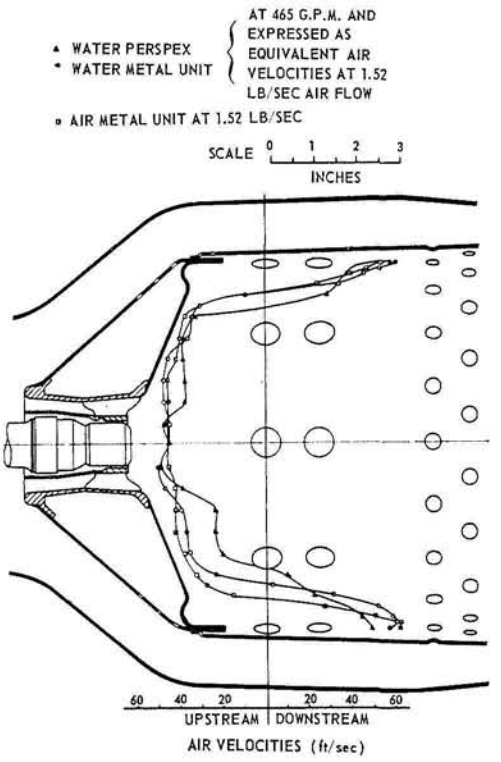

FIG. 8. Comparison of primary zone velocities using water and air flows.

The injection of gaseous fuel was simulated by injecting separately metered water such that the overall "air–fuel" ratio was 60/1, and the ratio of momentum of "fuel" to momentum of the inlet flow was maintained equal to that using gaseous propane fuel and air flow under both isothermal and combustion conditions. Details of the injector are given in the Appendix.

The effects of the "fuel" flow on the flow pattern were confined locally in the vicinity of the injector and in the flow in the outer boundaries of the recirculation, where the velocities were accelerated owing to the induced effects of the individual "fuel" jets. No further significant effects, however, were noticed on the general primary zone flow patterns. (See Fig. 9.)

Velocity Distribution Across the Primary Zone Toroidal Recirculation

The cylindrical-type pitot instrument used in the determination of velocities is simple in construction, and in water-cooled form facilitates traversing across a combustion zone. The directions of flow in the regimes explored, however, must be at approximately right angles to the axis of the instrument; hence care must be exercised in siting such instruments to ensure valid results. By traversing across a diameter through the axis of the toroidal recirculation under isothermal conditions as shown in Fig. 7, the limitations of the instrument were probably satisfied.

A comparison between the velocity profiles under water and isothermal air flow conditions,

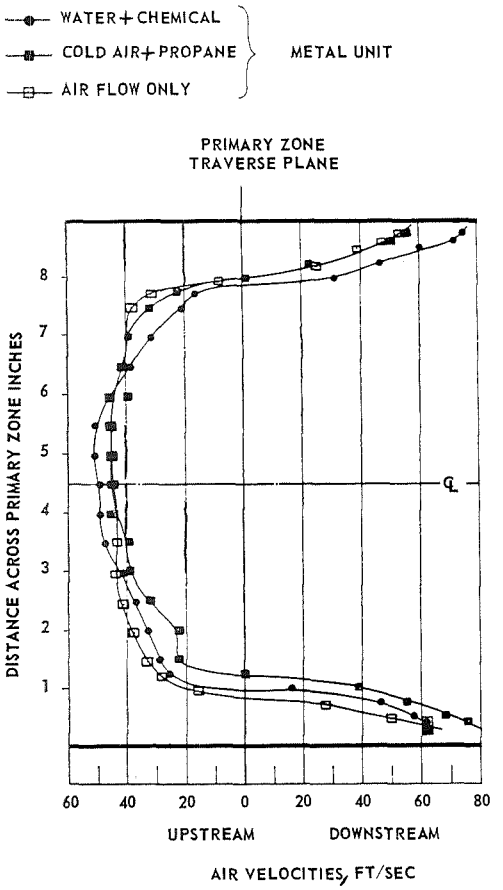

FIG. 9. Comparison of primary zone velocities using (1) water flow with chemical and (2) air flow with propane.

shown relative to the primary zone, are plotted in Fig. 8, from which it can be seen that, over the stable regions of the flow pattern, that is, in the vicinity of the axis of the flame tube and near the walls of the flame tube, the correlation for the metal unit was satisfactory. Away from the axis, the difference between the water and air results, where the velocity gradients are high, would probably be due to the displacement of the core, as already described in the preceding subsection.

In the transparent model the velocities in the axial and peripheral regions compared satisfactorily with the above results, although the differences within the recirculatory flow were more significant.

Chemical Tracer Technique

The use of a chemical tracer enhances water flow visualization studies so that mixing processes may be studied quantitatively. In the chamber investigated the chemical used was acidified ammonium ferrous sulphate, in solution with the water which simulated the "fuel" flow. The tests were on the sheet metal chamber fitted with the same injector and operated at the same conditions as in the subsection on Flow Visualization Using Water.

The test procedure was to inject the "fuel" at an overall air/fuel ratio of 60/1 and then to extract samples from the primary zone and the exhaust section respectively while discharging the outlet flow to waste. The iron content of the samples was thus measured quantitatively by adding thio-glycollic acid to give a purple coloration, which was assessed quantitatively using a Spekker absorptiometer. The results were then expressed in terms of equivalent air/fuel ratios.

A plot of the air/fuel ratios across the primary zone is shown in Fig. 11.

The exhaust concentrations were corrected to a mean overall air/fuel ratio of 60/1, to compensate for small experimental differences, and then, assuming combustion of gaseous propane fuel at a mean combustion efficiency of 100%, were expressed as equivalent gas temperatures.

A contour diagram showing the distribution of temperature at the exhaust plane using the chemical tracer technique in water is shown in Fig. 12A. The comparison between the contour

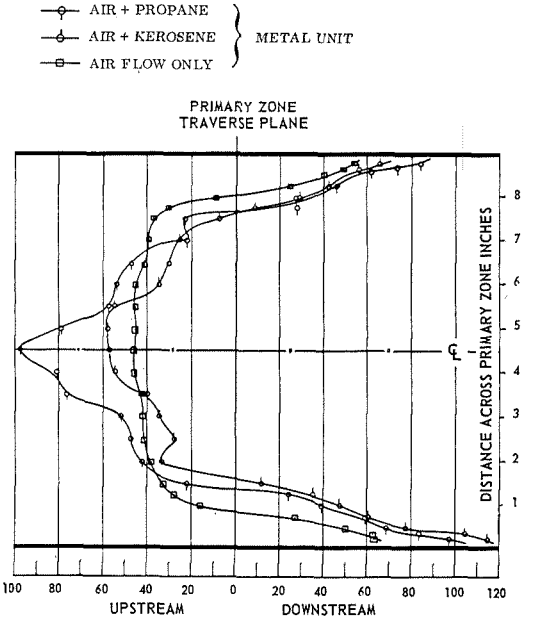

FIG. 10. Comparison of primary zone velocities with combustion using (1) air flow with propane and (2) air flow with kerosene.

diagrams shown in Fig. 12 is discussed in the following section.

The velocity distribution across the primary zone is shown in Fig. 9, where it can be seen that the correlation of the corresponding isothermal air conditions is satisfactory in the more stable regions of the recirculation; and that the effects of the "fuel" on the velocity distribution in the traverse plane were confined to the outer regions in which there was an apparent increase in velocity.

Isothermal Air Flow Using Gaseous Propane as a Tracer

Tests were repeated on the sheet metal chamber under isothermal air flow conditions at the same inlet plane Reynolds number as for the water flow. The requirement to maintain the same ratio of fuel momentum/inlet air momentum for both air and water flow necessitated a change in the size of injector holes. (See Appendix and Fig. 13.) Commercial propane gas was used, preheated to approximately 110°C at 114 psig for metering purposes and injected at a temperature and pressure of approximately 75°C, and $4\frac{1}{2}$ psig, respectively. The resulting propane–air mixture was subsequently burned in the ducting downstream of the exhaust plane of the chamber.

Samples of propane–air mixtures were obtained from the same cross section stations in the primary zone and the exhaust plane as before, and the concentrations were determined by gas analysis and expressed as equivalent air/fuel ratios. The primary zone air/fuel ratios are shown plotted in Fig. 11, from which both water and isothermal distribution may be compared.

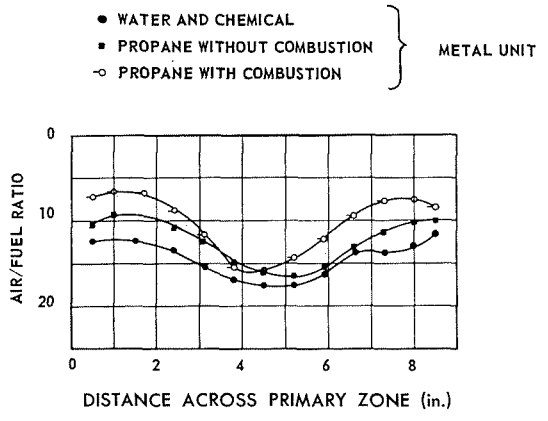

FIG. 11. Comparison of primary zone air/fuel ratio concentrations using (1) water flow and chemical, (2) air flow and propane without combustion, and (3) air flow and propane with combustion.

The exhaust concentrations were corrected to a mean overall air/fuel ratio of 60/1 and expressed as equivalent gas temperatures, assuming a combustion efficiency of 100%. The temperature contour diagram is shown in Fig. 12D.

Pressure and velocity determinations were also obtained across the inlet and outlet ducts, and also across the primary zone. In Fig. 9 the general similarity is shown together with the increased velocities in the outer regions due to the effects of the fuel injection.

Combustion Test Using Gaseous Propane Fuel

The above tests were repeated with combustion of the propane fuel. Air/fuel ratio concentrations in both the primary zone and exhaust planes were determined from gas analyses using a modified Orsat technique and the corresponding plot across the primary zone is shown in Fig. 11.

The exhaust concentrations were corrected to a mean overall air/fuel ratio of 60/1 and the equivalent gas temperatures computed, assuming a combustion efficiency of 100%. The temperature contour diagram is shown in Fig. 12E.

The actual temperature distribution across the exhaust plane was determined by traversing a shielded impact-type chromel-alumel thermocouple across the duct, in the same plane as for gas sampling and pressure determinations. The contour diagram of the temperatures, corrected to a mean overall air/fuel ratio of 60/1 and 100% combustion efficiency is shown in Fig. 12F.

Pressure and velocity traverses were also obtained across the inlet and the primary zone. Allowance was made for the density changes due to combustion in the latter when computing the actual velocities which are shown plotted in Fig. 10. The appropriate data are shown in the Appendix. It can be seen that in the center and outer regions the effects of combustion were to increase the local velocities, as would be expected, and also to change the shape of the plot over the whole region of the downstream flow. This may partly explain the increase in fuel richness in the primary zone under combustion conditions shown in Fig. 11, in that the increase in velocities adjacent to the flame tube wall would tend to reduce the angle of penetration and hence the coefficients of discharge of the first row of secondary holes. This would reduce the proportion of air flow into the primary zone recirculation. An additional factor is the slight change in chamber static pressure distribution under combustion conditions.

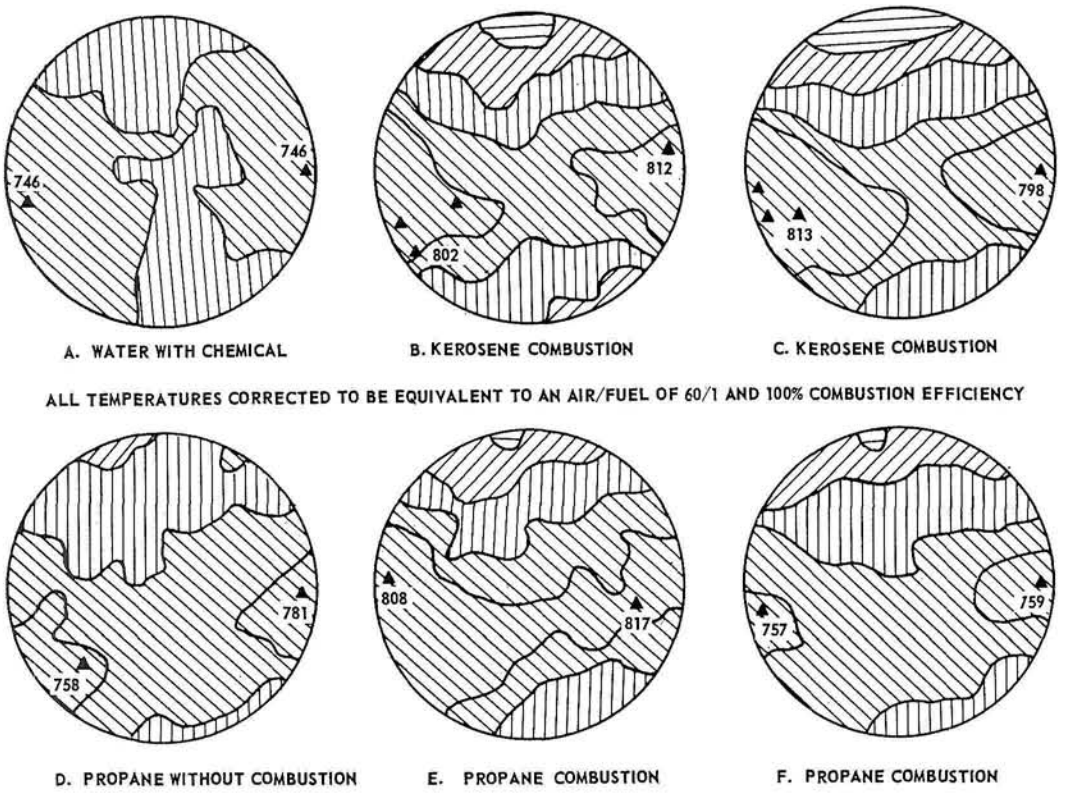

Diagram	*Conditions*	*Fuel*	*Details*
A	Water flow	Chemical	Temperatures from chemical concentrations
B	Air flow	Kerosene	Temperatures from gas analysis
C	Air flow	Kerosene	Temperatures from temperature traverse
D	Air flow	Propane	Without combustion, temperatures from gas analysis
E	Air flow	Propane	Temperatures from gas analysis
F	Air flow	Propane	Temperatures from temperature traverse

FIG. 12. Comparison of exhaust temperature distribution.

Combustion Test Using Liquid Kerosene Fuel

The tests were repeated using kerosene fuel which was injected through a conventional simplex-type pressure atomizer, of flow number 0.6, and cone angle 90°.

Pressure, velocities, air/fuel ratio concentrations, and exhaust temperatures were again determined, the results of which are shown, corrected to 60/1 and 100% combustion efficiency, plotted in Figs. 12B and 12C.

TABLE 2

Fluid	Mass flow (lb/sec)	Reynolds number at inlet	Inlet mean dynamic pressure $\rho v_i^2/2g$ (psi)	Overall loss in total pressure (LTP) (psi)	Pressure loss factor Φ_i
Water	77.5	293,000	0.27	0.59	2.18
Water	141.0	576,000	0.91	1.98	2.18
Air	1.52	293,000	0.096	0.20	2.08
Air	2.98	576,000	0.354	0.75	2.12
Air	3.96	773,000	0.627	1.36	2.17

Pressure Losses

The overall pressure losses, expressed as an "inlet" pressure loss factor

$$\Phi_i = \text{Loss in Total Pressure (LTP)}/(\rho v_i^2/2g),$$

where v_i represents the calculated mean velocity across the inlet plane, both for water and isothermal air flow, are shown in Table 2.

In Lucas practice it is customary to express the pressure loss factor in terms of the theoretical mean air velocity through the maximum cross sectional area in the plane of the primary zone, as follows:

Mean air casing velocity, v_c

$$= \frac{\text{total mass flow}}{\text{inlet density} \times \text{max. area}}$$

hence

$$\text{Pressure Loss Factor (PLF)} = \text{LTP}/(\rho v_c^2/2g).$$

Under combustion conditions the increase in pressure loss due to combustion depends upon the type of chamber and the operating conditions. Usually, the pressure loss factor under combustion is expressed as follows:

$$\text{PLF} = \text{LTP (hot)}/(\rho v_c^2/2g) = k_1 + k_2(\rho_r - 1),$$

where k_1 is the isothermal pressure loss factor; ρ_r is the ratio of density at inlet plane to density at outlet plane; and k_2 is the "hot loss factor," dependent upon the type of chamber; that is, $k_2 = 5$ for the design of pipe chamber investigated.

Generally, the difference in pressure between the inlet and outlet planes, together with the change in gas constant may be ignored, hence ρ_r may be substituted by T_r, where T_r represents the ratio

$$\frac{\text{mean outlet temperature}}{\text{mean inlet temperature}} = \frac{T_3}{T_2}$$

hence pressure loss factor $= k_1 + k_2(T_r - 1)$.

Prediction of pressure loss. For the chamber studies, the method of estimating pressure loss under combustion conditions from the data obtained under isothermal flow conditions using water is as follows:

Combustion conditions = Test 9, Table 1.
Air mass flow = 1.52 lb/sec.
Inlet air temperature = 312.8°K (39.8°C).
Outlet gas temperature = 971.3°K (698.3°C).

Maximum inside diameter of the air casing in the plane of the primary zone = $11\frac{1}{4}$ inches.

Calculated mean velocity of inlet air v_i = 109.5 ft/sec.

Calculated mean air casing velocity v_c = 31.7 ft/sec.

From the water flow tests the loss in total pressure under isothermal condition is therefore

$$\text{LTP} = 2.18 \times (\rho v_i^2/2g) = 0.199 \text{ psi}.$$

Measured LTP under isothermal air conditions = 0.198 psi. Now the isothermal casing PLF,

$$k_1 = 0.199/(\rho v_c^2/2g) = 26.1.$$

Hence PLF under combustion conditions = $26.1 + 5\{(971.3/312.8) - 1\} = 26.1 + 10.52 = 36.62$.

Therefore, predicted LTP under combustion conditions $= 36.62 \times (\rho v_c^2/2g) = 0.280$ psi.

Measured LTP under combustion conditions = 0.297 psi. In a similar way, the full load LTP can be obtained from knowledge of the operating conditions.

Discussion

The object of this paper was to present comparative data which would satisfy the question of how accurately the data obtained from isothermal water flow models simulate the actual combustion in a gas turbine combustion chamber.

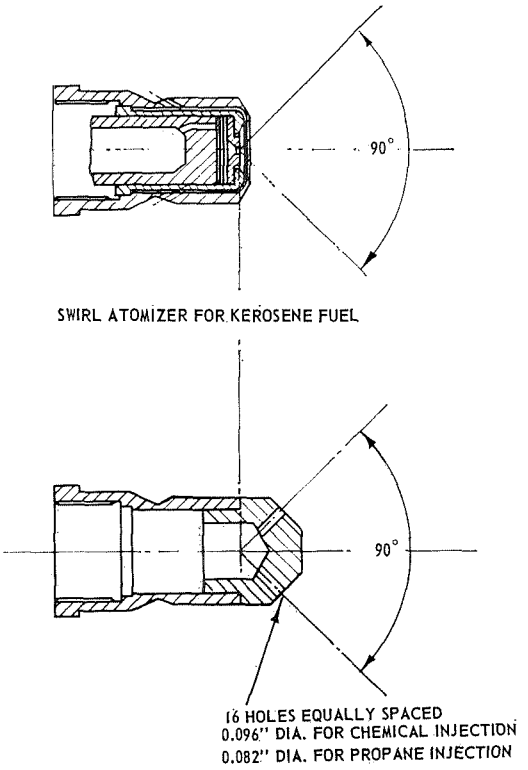

FIG. 13. Injector for gaseous fuel.

There appears little doubt that in the chamber studied the observed flow pattern using water correlates satisfactorily with the velocity distributions across the primary zone, obtained both under water flow and isothermal air flow respectively. Also, as would be anticipated, the cold pressure loss factors correlate well.

The data obtained using the chemical tracer technique in water also correlate well with that obtained using the propane gas tracer under isothermal air conditions, as can be seen in Figs. 11 and 9.

In comparing the results obtained under actual combustion conditions, the evidence in Fig. 10 shows that the recirculatory flow pattern in the primary zone remains generally similar. In Fig. 11 the changes in local mixture distribution under combustion are probably due to the combined effects of the increased gas velocities near the walls of the chamber which would reduce the angles of penetration of the secondary air jets and hence the amount of air entrained into the recirculation, and also an increase in chamber static pressure which would tend to reduce the proportion of secondary air injected through the holes.

Comparing the temperature distributions at the exhaust plane shown in Fig. 12, the general similarity shown by the diagrams is particularly encouraging. Although differences in levels of actual temperatures are apparent, the region of high temperature which extends across the section and the two cooler regions above and below are characteristic throughout. The similarities remain despite the two different types of fuel used and their mode of injection, which supports the hypothesis that the air flow pattern is the major controlling feature in this type of combustion chamber; and, provided the liquid fuel atomization is satisfactory, the fuel soon loses its identity and momentum in the flow pattern. The latter feature is supported by observations when the fuel injection is simulated under water flow conditions, and also by short duration tests in which liquid fuel is ignited in a transparent chamber and the resulting flame propagation observed and recorded by high speed photography.

Finally, although in some cases there might be certain technical objections to the use of the water flow simulation technique, there is no doubt that it is extremely valuable both qualitatively and quantitatively when supported by experience in its translation into practical combustion hardware.

Conclusions

As anticipated, there is a close similarity between water flow and isothermal air flow data with respect to relative velocity distributions (i.e., flow pattern) and pressure loss characteristics. Hence, if a hot loss factor for the particular type of unit is known, the overall pressure loss may be estimated.

Using a chemical tracer as "fuel" in water and a gaseous tracer in air under isothermal conditions gives similar concentration distributions in both the primary zone and exhaust planes.

Under combustion conditions, the flow pattern in the primary zone (as shown by velocity distribution) remains essentially similar to the water flow pattern, due allowance being made for density changes.

In the primary zone, the concentration distribution patterns are geometrically similar under combustion and water flow (with tracer as "fuel") conditions. In the combustion case the air/fuel ratios are slightly "richer," probably owing to small changes in static pressure and air jet angle of penetration.

The general similarity between the actual

TABLE 3

Primary Zone Velocities for Propane Combustion[a]

Station	Air/fuel ratio	Combustion efficiency (%)	Temperature T (°K)	Dynamic head[b] $h''(H_2O)$	Density ρ (lb/ft³)	Velocity[b] V (ft/sec)
1	7.3	43.5	754	0.86	0.0304	97.3
2	6.7	43.5	724	0.66	0.0316	83.6
3	6.1	43.5	704	0.46	0.0325	68.8
4	5.8	44.0	676	0.36	0.0339	59.6
5	5.6	44.0	666	0.16	0.0344	39.5
6	5.7	44.0	697	0.06	0.0330	24.7
7	6.0	45.0	832	−0.04	0.0276	−22.0
8	7.2	48.0	872	−0.14	0.0263	−42.2
9	9.0	52.0	1087	−0.14	0.0211	−47.1
10	11.1	61.5	1310	−0.14	0.0175	−51.8
11	14.1	75.0	1670	−0.24	0.0137	−76.6
12	15.7	83.0	1875	−0.24	0.0122	−81.1
13	15.6	84.0	1925	−0.34	0.0119	−97.8
14	14.5	77.5	1810	−0.24	0.0127	−79.6
15	13.0	71.5	1632	−0.14	0.0141	−57.8
16	11.5	65.0	1438	−0.14	0.0160	−54.2
17	9.3	54.0	1090	−0.14	0.0211	−47.1
18	7.8	48.7	890	−0.04	0.0257	−22.8
19	7.2	46.0	852	−0.04	0.0269	−22.3
20	7.0	45.5	852	0.06	0.0269	27.3
21	7.1	45.5	872	0.06	0.0263	27.6
22	7.5	46.2	882	0.16	0.0260	45.4
23	8.2	49.0	954	0.26	0.0230	61.6
24	9.0	52.0	984	0.36	0.0237	70.0
25	9.5	54.0	1075	0.46	0.0223	83.1

[a] Mean static pressure = 3.34 inches H_2O; barometric pressure = 29.83 inches Hg.
[b] Negative sign denotes upstream velocities.

exhaust temperature distributions and those derived from the isothermal studies with simulated fuel injection are particularly encouraging. Although differences in actual temperature levels are apparent, the hot and cooler regions remain similar throughout.

Nomenclature

A Area [sq inches]
A_e Effective area [sq inches]
k_1 Isothermal pressure loss factor
k_2 "Hot loss factor"
m Mass flow [lb/sec]
ΔP Loss in total pressure [lb/sq inch (psi)]
T_2 Mean inlet temperature [°K]
T_3 Mean outlet temperature [°K]
T_r T_3/T_2
v Velocity [ft/sec]
$\bar{v}$ Mean velocity [ft/sec]
ρ Density
ρ_r Density at inlet/density at outlet
Φ Pressure loss factor

Subscripts

a Air
f Fuel
i Inlet
s Fuel injector
w Water

Appendix

Fuel Injectors

Details of the fuel injectors are shown in Fig. 13. The momentum ratios of the gaseous fuel/air and the water-chemical/water injectors were cor-

TABLE 4

Primary Zone Velocities for Kerosene Combustion[a]

Station	Air/fuel ratio	Combustion efficiency (%)	Temperature T (°K)	Dynamic head[b] $h''(H_2O)$	Density ρ (lb/ft³)	Velocity[b] V (ft/sec)
1	15.6	56.0	1413	0.61	0.0155	114.8
2	14.8	47.0	1173	0.61	0.0187	104.6
3	12.5	42.8	953	0.41	0.0230	77.2
4	10.3	37.5	773	0.31	0.0284	60.5
5	7.6	33.0	715	0.21	0.0307	47.9
6	5.7	25.0	753	0.11	0.0291	35.6
7	4.4	20.0	853	0.01	0.0257	11.41
8	4.8	20.0	793	−0.19	0.0276	−33.03
9	5.9	29.0	543	−0.19	0.0407	−27.34
10	6.7	34.2	673	−0.19	0.0326	−44.2
11	7.9	42.0	853	−0.19	0.0257	−49.8
12	8.8	49.0	1012	−0.19	0.0217	−54.2
13	9.6	51.8	1123	−0.19	0.0200	−57.1
14	9.7	52.0	1163	−0.19	0.0189	−58.1
15	9.2	48.5	1036	−0.19	0.0212	−54.8
16	8.2	40.0	843	−0.09	0.0260	−34.1
17	6.8	31.0	653	−0.09	0.0336	−30.0
18	5.7	23.0	468	−0.09	0.0468	−25.4
19	5.1	19.0	413	−0.01	0.0531	−7.9
20	5.3	19.5	443	0.01	0.0495	8.25
21	5.7	21.0	493	0.11	0.0445	28.8
22	6.3	24.0	543	0.21	0.0404	41.8
23	7.3	27.4	598	0.31	0.0367	53.2
24	8.0	29.2	633	0.31	0.0346	54.8
25	8.1	32.0	673	0.41	0.0326	64.9

[a] Mean static pressure = 3.49 inches H_2O; barometric pressure = 29.55 inches Hg.
[b] Negative sign denotes upstream velocities.

related using the following relationship:

$$\frac{\text{momentum of fuel}}{\text{momentum of inlet air}} = \text{constant},$$

i.e.,

$$\frac{\text{mass flow of fuel} \times \text{theoretical injection velocity}}{\text{total mass of air} \times \text{mean inlet velocity}}$$

$$= \frac{m_f \times (m_f/\rho_f A_{e_s})}{m_a \times (m_a/\rho_a A_i)}$$

$$= [(m_f)^2/(m_a)^2](\rho_a/\rho_f)(A_i/A_{e_s}),$$

where A_{e_s} = effective area of the fuel injector; and A_i = area of cross section of inlet pipe.

The above relationship was satisfied by calibrating the injectors using water and propane respectively. The differences in density ratio ρ_a/ρ_f were mainly responsible for the change in the diameter of injector holes.

The above injectors were designed to ensure that the injection angle of fuel jets originated from the same point as that from the standard liquid fuel atomizer.

Primary Zone Gas Velocities Under Combustion Conditions

The effects of density changes due to combustion were taken into account as follows.

A/F ratios and combustion efficiencies, across the primary zone, were determined from gas samples and analyzed by a modified Orsat technique. By the use of theoretical temperature rise curves, the corresponding temperatures were computed.

The dynamic and static pressures across the primary zone were obtained by traversing the cylindrical pitot instrument and thence the density was derived using gas constants of 92.5

and 100 ft lb/lb °C for propane and kerosene combustion, respectively.

The corresponding values are shown in Tables 3 and 4.

ACKNOWLEDGMENTS

The authors would like to thank the directors of Joseph Lucas Ltd. for permission to publish this paper. Thanks are also due to members of the Burnley Combustion Laboratories and in particular to Mr. B. A. Coar, D.L.C.

BIBLIOGRAPHY

1. BACON, N. P.: Experiments with furnace models; *Joint Symposium on the Scaling-up of Chemical Plant and Processes*, The Institution of Chem. Engrs, 1957.
2. CHESTERS, J. H.:Chemistry and Industry *1951*, 448.
3. CHESTERS, J. H.: Iron Steel *27*, 7 (1954).
4. CHESTERS, J. H., HALLIDAY, I. M. D., and HOWES, R. S.: *Some Aspects of Fluid Flow (Conference)*, p. 176. Edward Arnold, 1961.
5. CHESTERS, J. H. and PHILIP, A. R.: J. Iron Steel Inst. *162*, 385 (1949).
6. CLARKE, A. E., HARRISON, A. J., and ODGERS, J.: *Seventh Symposium (International) on Combustion*, p. 664. Butterworths, 1959.
7. CLARKE, A. E., ODGERS, J., and RYAN, P. J.: *Eighth Symposium (International) on Combustion*, p. 982. Williams and Wilkins, 1962.
8. CLARKE, J. S.: The relation of specific heat release to pressure drop in aero–gasturbine combustion chambers, *Inst. Mech. Engrs.—A.S.M.E. Joint Conference on Combustion*, 1955.
9. CLARKE, J. S.: J. Roy. Aeronaut. Soc. *60*, 544 (1956).
10. CLARKE, J. S.: *Initiation and Some Controlling Parameters of Combustion in the Piston Engine.* Inst. Mech. Engrs, 1961.
11. CLARKE, J. S. and JACKSON, S. R.: General Considerations in the Design of Combustion Chambers for Aircraft and Industrial Gas Turbines, *1962 S.A.E. International Congress.*
12. COLLINS, R. D.: Instrument Practice, p. 39, Nov. 1952.
13. GERRARD, A. J. and MCAREAVEY, G.: Birmingham University Chemical Engineer *8*, 2 (1957).
14. GRAY, F. A. and ROBERTSON, A. D.: J. Inst. Fuel *29*, 189 (1956).
15. GROUME-GRIJMAILO, W. E.: Journal of the Russian Metallurgical Society, 1911 (Wiley).
16. HALLIDAY, I. M. D. and PHILIP, A. R.: J. Iron Steel Inst. *162*, 401 (1949).
17. HORN, G. and THRING, M. W.: J. Inst. Fuel *29*, 180 (1956).
18. HOWES, R. S. and PHILIP, A. R.: J. Iron Steel Inst. *162*, 4 (1949).
19. KNORRE, G. F.: Arch. f. Wärmewirtschaft und Dampfkesselwesen *13*, 9 (1932).
20. KUNUGI, M. and JINNO, H.: *Seventh Symposium (International) on Combustion.* Butterworths, 1959.
21. LANE, R. A., and MORRISON, E.: Trans. Am. Soc. Mech. Engrs. *71*, 941 (1949).
22. LEAF, W.: Mech. Eng. *67*, 586 (1945).
23. LLOYD, P.: Proc. Inst. Mech. Engrs. (London) *153*, W.E.12 (1945).
24. NEWBY, M. P.: Intl. Chem. Eng. *31*, 2 (1950).
25. NICHOLSON, H. M. and FIELDS, R. S.: *Third Symposium on Combustion Flame and Explosion Phenomena.* Williams and Wilkins, 1949.
26. POULSTON, B. V. and WINTER, E. F.: *Sixth Symposium (International) on Combustion.* Reinhold, 1956.
27. PUTNAM, A. A. and JENSEN, R. A.: Fuel *34*, 501 (1955).
28. RIZK, W.: Proc. Inst. Mech. Eng. (London) *172*, 417 (1959).
29. ROBERTS, A. G.: British Coal Utilisation Research Associated Monthly Bulletin *20*, 5 (1956).
30. ROSIN, P. O.: J. Inst. Fuel *9*, 287 (1936).
31. ROSIN, P. O.: J. Inst. Fuel *12*, 198 (1939).
32. THRING, M. W.: Birmingham University Chemical Engineer *8*, 3 (1957).
33. TRIEBNIGG, H.: MTZ. *13*, 10 (1952).
34. WATSON, E. A. and CLARKE, J. S.: *Combustion and Combustion Equipment for Aero–Gas–Turbines*, The Inst. of Fuel, October 1947.
35. WINTER, E. F. and DETERDING, J. H.: Brit. J. Appl. Phys. *7*, 247 (1956).
36. WINTER, E. F.: J. Royal Aeronaut. Soc. *62*, 568 (1958).

MODELING OF DOUBLE CONCENTRIC BURNING JETS

J. M. BEÉR, N. A. CHIGIER, AND K. B. LEE

The mixing in a furnace and cold model has been determined from measurements of gas concentrations and velocity distributions and the enclosed double jet has been reduced to its three component parts: the primary, secondary, and recirculated fluids, with the aid of tracer techniques.

Good agreement was found between the mixing patterns in the furnace and in the cold model when the nozzle diameters in the model were distorted according to the modified Thring–Newby similarity criterion. The similarity of mixing in the region close to the burner, however, required also that the mass ratio of the primary to the secondary fluids should be maintained the same in the model as in the furnace.

Buoyancy in the furnace was found to affect the mixing pattern near the burner when the gravitational forces were large compared with the inertia forces. Experimental evidence suggests that for these cases a dimensionless group, the Archimedes number, should be considered in addition to the abovementioned modeling criteria.

Introduction

The compound jets considered in this paper consist of a central primary jet, surrounded by a secondary annular jet. Both the primary and the secondary jets enter the combustion chamber with considerable momenta and mixing occurs between the two jets and also between the jets and the ambient fluid surrounding the jets in the combustion chamber.

Flames emerging from burners of the double concentric type represent a group between the extreme cases of the premixed flames and the pure diffusion flames. The primary jet usually transports the fuel in a rich mixture and the annular secondary jet supplies the rest of the combustion air. These burners are widely applied for combustion processes requiring a fuel-rich mixture at the flame front but a stoichiometric or lean mixing ratio further downstream so that complete combustion is obtained within the combustion chamber. Such a mixing program can be desirable for different reasons, such as to increase flame luminosity of hydrocarbon flames, to improve the stability of lean pulverized coal flames, or to avoid pre-ignition or explosion dangers inherent in premixed systems.

Modeling of single axial enclosed burning jets was considered by Thring and Newby[1] and the conclusion was reached that the similarity condition can be expressed by the dimensionless group:

$$\left(\frac{m_0}{m_a + m_0}\frac{L}{r_0}\right)_{\text{model}} = \left(\frac{(G_0\rho_F\pi)^{\frac{1}{2}}}{m_a + m_0}L\right)_{\text{hot system}} \quad (1)$$

In the present investigation mixing patterns in flames were compared with those in cold models when the above similarity criterion was used in a modified form for the case of the double concentric jet. The significance of describing the mixing pattern in the combustion chamber in terms of three components, the primary, the secondary, and the recirculated streams, was recognized from studies on the mechanism of ignition and of combustion. It was found for example that the entrainment of hot recirculated gases in the pre-ignition zone of the fuel jet was of great importance to flame stability. In the present investigation the three components have been distinguished by means of suitable tracer techniques.

Experimental

The Experimental Apparatus

Experiments were carried out with three different systems: The IJmuiden tunnel furnace with burning pulverized coal; the same furnace but used as a hot model with burning coke oven gas; the 1:5 scale cold model of the IJmuiden tunnel furnace.

The furnace and burners are shown schematically in Figs. 1 and 2. The pulverized coal, 105 kg/hr, mixed with 140 kg/hr primary air at 80°C, entered through the centrally arranged primary burner and the secondary air (1222 kg/hr), preheated to 500°C, entered the furnace through an annulus surrounding the primary

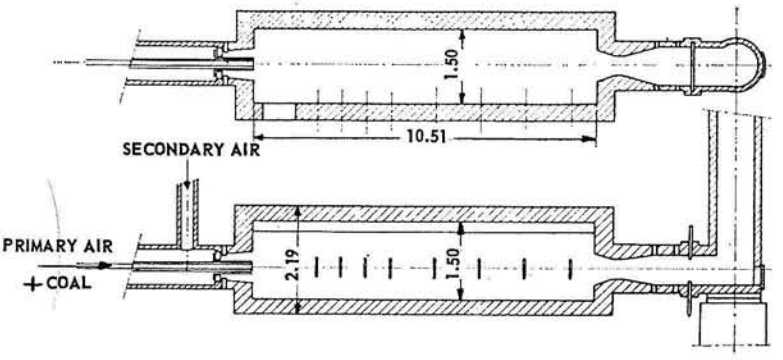

FIG. 1. Plan and sectional elevation of furnace.

burner. The range of variables is listed in Table 1. Helium was injected as a tracer far downstream from the burner into the jet and samples were collected between the burner and the point of helium injection. The samples were analyzed for helium by a gas phase chromatography apparatus. From the helium concentration of these samples the distribution of the recirculated fluid entrained by the jet was calculated. The measurements also included temperature, velocity, and solid and gas concentration traverses.

For the exploration of the region near the burner the same furnace arrangement as shown in Fig. 1 was used but no pulverized coal was supplied through the primary burner so that detailed measurements of concentration were possible close to the burner where otherwise the high solid concentration of the primary jet would have caused great experimental difficulties. Instead, a coke oven gas burner was placed on the furnace axis at a distance $3L$ from the burner.

In this way a nonisothermal system was obtained with conditions similar to those in the furnace under conditions of operation. The relatively cold double concentric jet was surrounded by hot recirculated combustion products, and the CO_2 concentration of the samples taken near the burner could be used as a tracer to calculate the concentration of the entrained recirculation within the boundaries of the jet.

In the 1:5 scale model the primary burner diameter was calculated from

$$(d_p)_m = (L_m/L_F)(d_p)_F(\rho_{p_F}/\rho_F)^{\frac{1}{2}} \quad (2)$$

and the annular cross section of the secondary

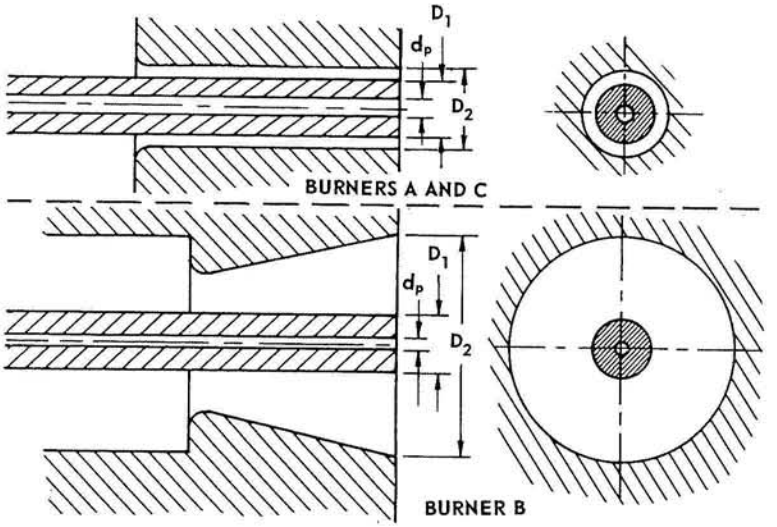

FIG. 2. Diagrammatic arrangement of burners.

TABLE 1

Input Conditions

a. Furnace burner

	A	B	C
d_p [m]	0.05	0.034	0.05
D_1 [m]	0.18	0.18	0.18
D_2 [m]	0.26	0.70	0.22
U_p [m sec^{-1}]	20	40	20
U_s [m sec^{-1}]	25	2	50
m_p [kg sec^{-1}]	0.04		
m_s [kg sec^{-1}]	0.34		
T_p [°C]	80		
T_s [°C]	500		
T_F [°C]	1500		

b. Cold model

	A'	B'	C'
d_p [m]	0.023	0.016	0.023
D_1 [m]	0.036	0.036	0.036
D_2 [m]	0.070	0.218	0.056
U_p [m sec^{-1}]	20	40	20
U_s [m sec^{-1}]	25	2	50
m_p [kg sec^{-1}]	0.010		
m_s [kg sec^{-1}]	0.088		

nozzle from

$$(A_s)_m = (L_m/L_F)^2(A_s)_F(\rho_{sF}/\rho_F). \quad (3)$$

The ratio between the primary and secondary mass flow rate was maintained constant in model and furnace, i.e;

$$(m_p/m_s)_m = (m_p/m_s)_F. \quad (4)$$

Under these conditions the exit Reynolds numbers of both primary and secondary jets were maintained well above the critical Reynolds number, and for all the burners considered in this paper the Reynolds numbers were within the range 10^4–10^5.

The Tracer Technique

It was found in the IJmuiden experiments[2] that both in the hot furnace and in the cold model the concentration of the recirculated gases surrounding the burner was practically the same as the concentration of the combustion products at the exit from the furnace when the burner radius was small compared to the width of the combustion chamber $r_0'/L < 0.1$. The tracer technique used was based on this property of enclosed jets. The tracer was introduced far downstream from the burner into the jet and was carried around by the recirculating stream. In this way it was possible to distinguish between the fractions of samples arriving at the point of sampling from the burner and from the recirculated fluid, respectively. A similar technique was used by Ibiricu[3] in his study of recirculation in enclosed jets.

When in addition to this the fuel in the primary jet was also considered as a tracer for the primary fluid, the concentrations of all three components. primary, secondary, and recirculating fluid, could be determined at any point inside the jet.[4]

Instead of the fuel, however, considerations based on the conservation of mass, heat, or momentum could also provide the second tracer required for a three component mixture. These considerations were applied, for example, in the evaluation of the cold model data discussed in this paper.

Experimental Results

Fully Developed Region. A mathematical analysis of the velocity distribution of double concentric jets[5] showed that at some distance downstream from the nozzle the two streams combine and the velocity distribution can be described at that point as a single Gaussian distribution. The jet was regarded as "fully developed" from this point downstream. Most of the following discussion concerns this region.

The total mass flow rate of gases within the boundaries of the combined jets was determined by integrating the measured velocity distribution at each section of the furnace.

The mass flow rate increased with distance from the burner owing to entrainment of recirculated gases until it reached a maximum at a position corresponding to the core of recirculation. After this maximum the mass flow rate decreased to the value of the input mass flow toward the exit from the furnace.

From the law of conservation of mass the difference between the total mass flow rate and the input mass flow rate at any section gave the mass flow rate of the recirculated gases at that section, i.e.,

$$M - (m_p + m_s) = m_r.$$

In Fig. 3 the ratio of the recirculated mass flow rate to input mass flow rate is plotted along the jet and hot furnace data are compared with those from the cold model. To enable comparison of different double concentric jets in both non-isothermal and constant density systems, the

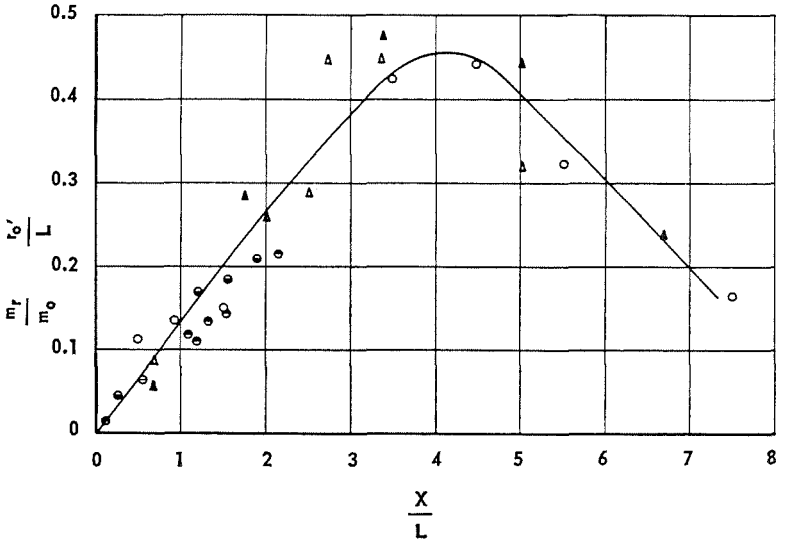

	PRIM. VEL. m/s	SEC. VEL. m/s	
○	20	25	COAL FLAME
●	25	25	GAS FLAME
●	25	50	GAS FLAME
△	20	25	COLD MODEL
▲	20	50	COLD MODEL

FIG. 3. Comparison of flow rate of recirculation in furnace with cold model.

ratio of m_r/m_0 has been multiplied by r_0'/L where the equivalent nozzle radius r_0' was calculated from the combined masses and momenta of the primary and secondary fluids as

$$r_0' = (m_p + m_s)/[(G_p + G_s)\rho_F \pi]^{\frac{1}{2}}. \quad (5)$$

The graph in Fig. 3 shows that the recirculated mass flow rate increased from the nozzle exit almost linearly with distance to reach a maximum and then decreased to zero toward the end of the furnace.

It is clear from Fig. 3 that there is agreement, both in form and magnitude, of the recirculation in furnace and cold model when the results are compared on the basis of the equivalent nozzle radius.

In Fig. 4 the ratio of the maximum of the recirculated mass flow to the input mass flow is plotted as a function of the inverse of the modified Thring–Newby criterion $1/\theta'$, as suggested by Cohen de Lara.[6]

Points on the graph of Fig. 4 originate from both hot furnace and cold model experiments. The hot furnace data are from IJmuiden oil and pulverized coal flames, respectively, and the cold model data from the 1:5 scale model at IJmuiden and also from experiments of Cohen de Lara *et al.*[6] with a circular cross section cold model.

The decay of the burner fluid concentration (primary and secondary) on the axis of the jet is plotted in Fig. 5 for the 1:5 scale cold model and hot furnace. In the hot furnace experiment the tracer technique described above was used with helium injection into a pulverized coal flame. Good similarity was found between the axial concentrations in the model and in the hot furnace.

Unlike in free jets there is no unique radial velocity and concentration distribution in enclosed jets but similarity can be shown by comparing radial concentration distributions of corresponding cross sections of model and hot furnace (Fig. 6). Here again the tracer technique was used in the hot furnace (coke oven gas burner) to determine the concentration distribution of the entrained recirculated fluid. The burner fluid concentration plotted in the graph was then calculated as

$$C_{bf} = 1 - C_{rec}.$$

In the model the burner fluid concentration is taken as the sum of the mole fractions of the primary and secondary nozzle fluids.

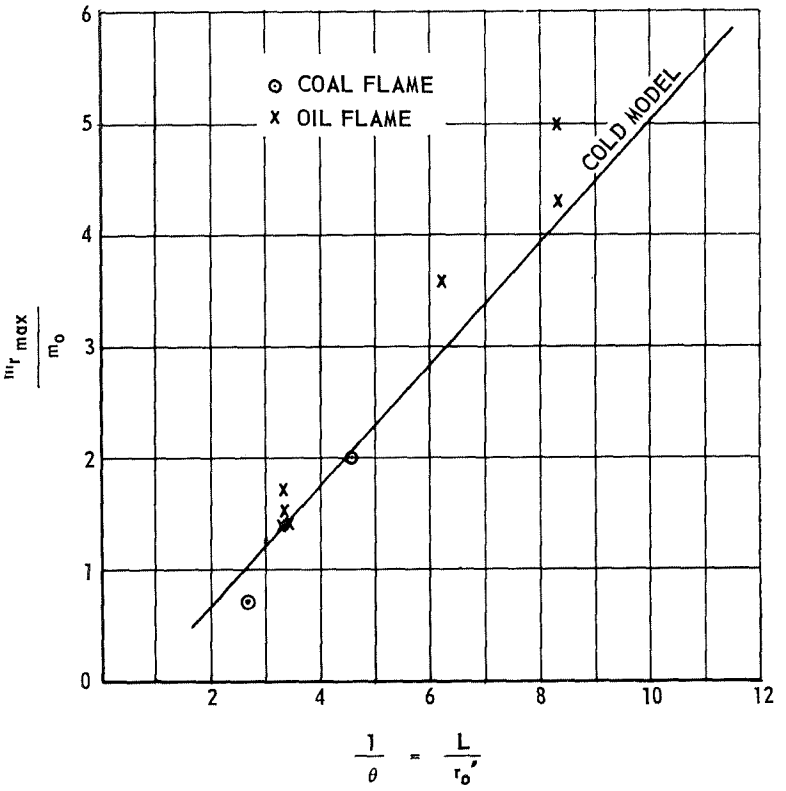

FIG. 4. Ratio of the maximum recirculated mass flow rate to the input mass rate as a function of the modified Thring–Newby criterion.

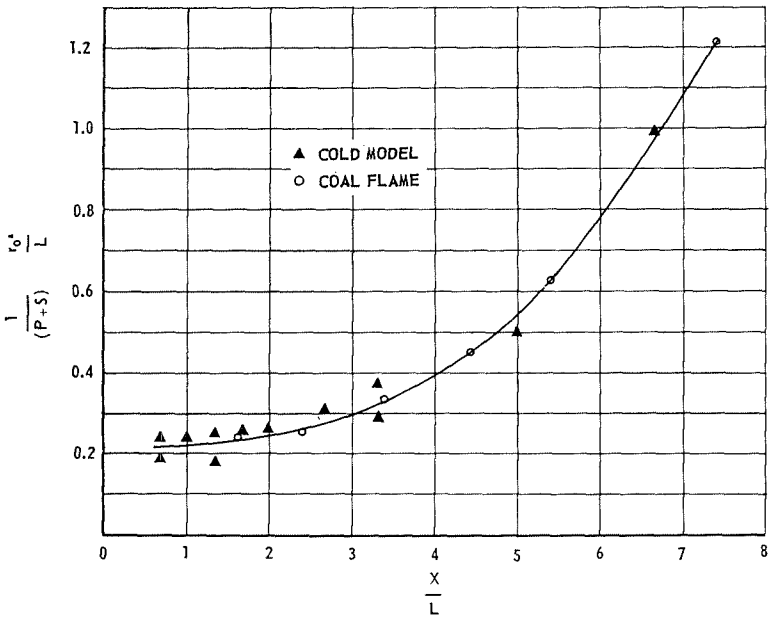

FIG. 5. Burner fluid concentration on the axis of the jet.

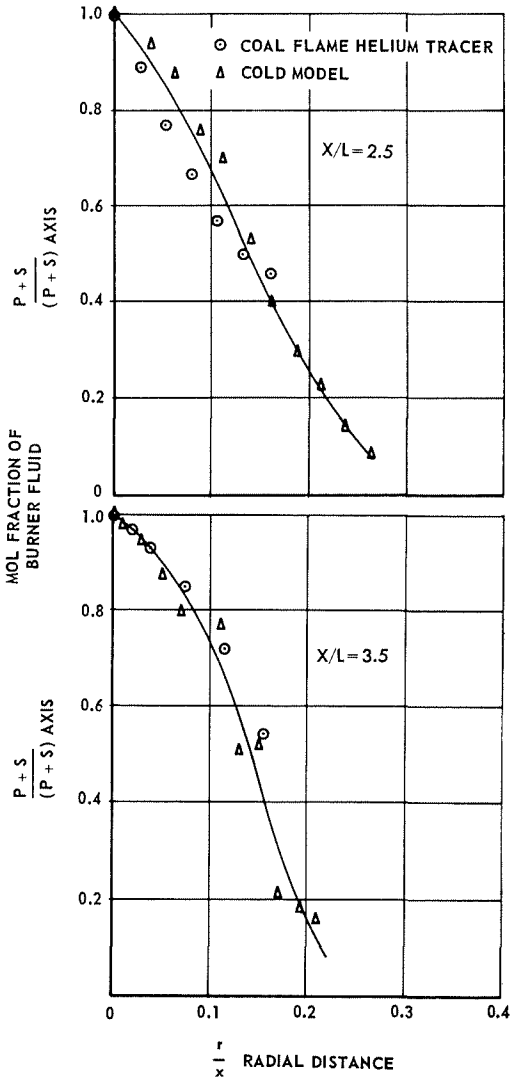

FIG. 6. Radial concentration distributions of burner fluid at two sections of the furnace and model (P = mole fraction of primary fluid; S = mole fraction of secondary fluid).

The Region Close to the Burner. In modeling double concentric jets it is of importance that the mixing between the two jet fluids, the primary and secondary, is also similar in the cold model and hot furnace. It was found that, when the primary and secondary burner cross sectional areas were corrected for the density differences according to Eqs. (2) and (3) and the mass ratios satisfied Eq. (4), reasonably good similarity of the mixing between the primary and the secondary fluids could be obtained as shown in Fig. 7.

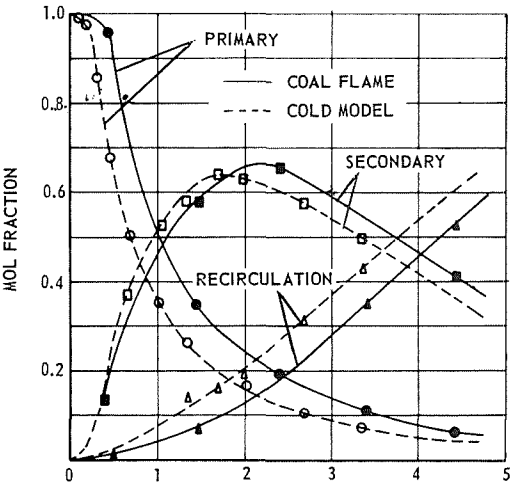

FIG. 7. Relative portions of primary, secondary, and recirculated fluid on the jet axis for furnace and model.

Experiments in the model furnace have shown that the mixing in the region near the burner depends on the mass ratio of the primary to secondary nozzle fluids. The concentration of the entrained recirculation, however, is independent of the mass ratio and depends on the ratio r_0'/L.

The effect is clearly shown in Fig. 8 where results of experiments are plotted in which the mass ratio m_p/m_s was varied in the range 0.03 to 0.7.

In the region close to the burner the mixing pattern can be distorted by buoyancy. The problem of the deflection of the axis of a single jet under the effect of buoyancy has been dealt with by several investigators (Horn[7] and Regenscheit[8]) but from the point of view of mixing between the primary and the secondary jet it is the effect of the buoyancy on the secondary jet which is of greater importance. It seems that when the gravitational forces are important owing to the density difference between the relatively cold secondary jet and the surrounding hot recirculated gases, compared with the inertia forces, i.e., the momentum of the secondary jet, the secondary fluid falls out of the jet to the bottom of the furnace and the primary jet is surrounded by a higher concentration of hot recirculated gases. This change in the density of the entrained mass in the early part of the jet was found to have a considerable stabilizing effect on pulverized coal flames.[9]

It is suggested that the Archimedes number (Ar) which expresses the ratio of the gravitational and inertia forces in a nonconstant density flow system be chosen to indicate the importance of the gravitational effect close to the burner.

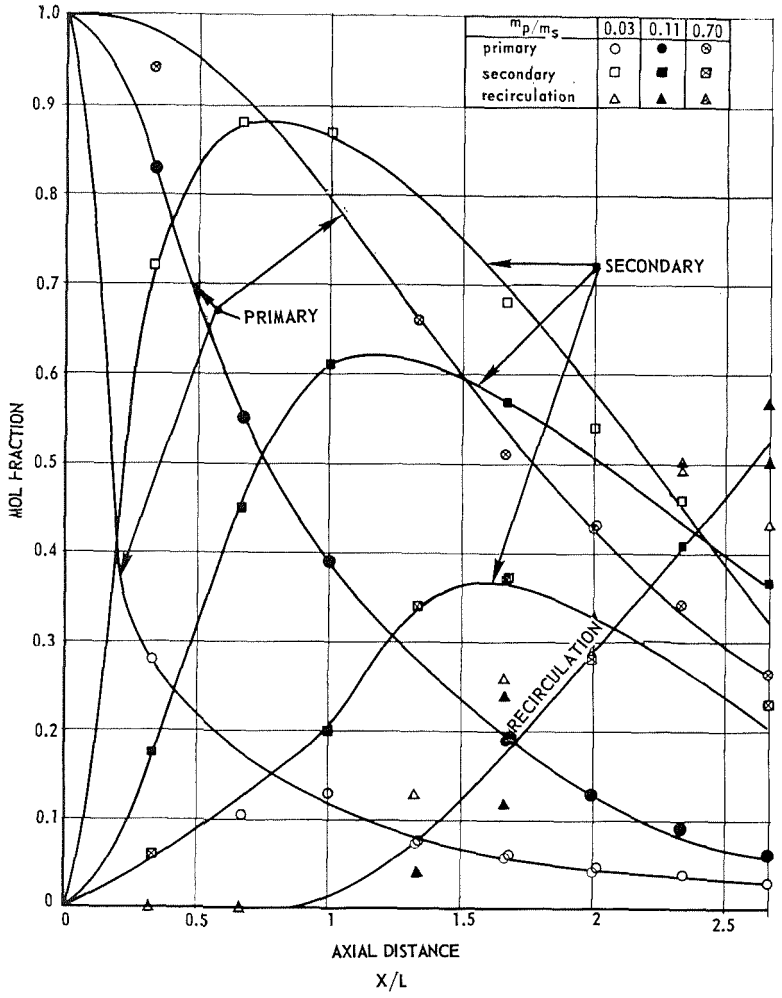

FIG. 8. Effect of varying the mass ratio of primary and secondary nozzle fluid on the axial concentration distribution (cold model—burner A).

The Archimedes number can be given in the form:

$$\mathrm{Ar} = (D_2 g\, \Delta T)/U_s^2 T_r, \qquad (6)$$

where D_2 = the diameter of the secondary burner; $\Delta T = T_r - T_s$; T_r is the recirculation temperature in °K; U_s = the secondary velocity; and g = the gravitational acceleration.

In Fig. 9 the concentration of the recirculated fluid is plotted along the flame axis in the form

$$C_{\mathrm{rec}}(r_0'/L) \text{ versus } (x/L).$$

The graph shows that in the case when the Archimedes number was low (burners A and C) the buoyancy did not affect the entrainment of the recirculated fluid into the jet. In contrast to this the concentration of the recirculation increased considerably on the jet axis when the secondary jet was affected by buoyancy, i.e., the Archimedes number was high.

Conclusions

An experimental tracer technique was developed in order to differentiate between fractions of samples arriving from the burner directly and from the recirculating fluid. The technique can be used in both the cold model and the hot furnace.

It is shown experimentally that the mixing between burner fluid and recirculated fluid in the fully developed region of enclosed double concentric jets depends only on the modified Thring–Newby criterion r_0'/L, where the equivalent burner radius r_0' is calculated from the

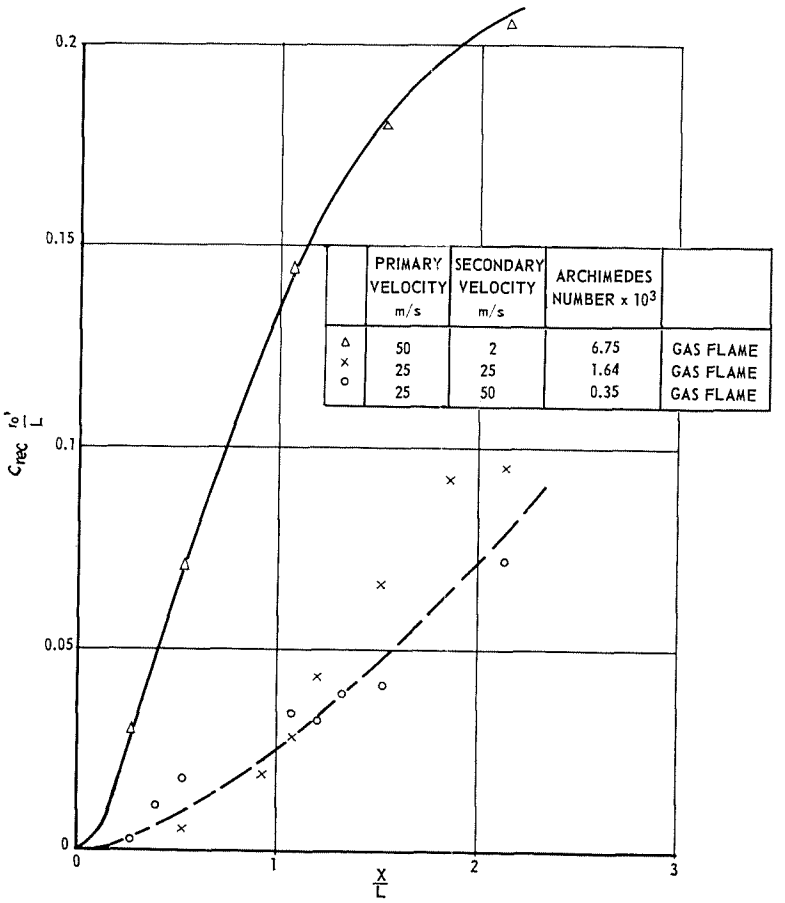

FIG. 9. Effect of buoyancy on the concentration of the recirculated fluid on the jet axis.

combined masses and momenta of the primary and secondary jets as

$$r_0' = (m_p + m_s)/[(G_p + G_s)\pi\rho_F]^{\frac{1}{2}}.$$

The mixing between the primary and secondary fluids in the region near the burner was found similar in the hot furnace and cold model when the primary burner was calculated as

$$(d_p)_m = (L_m/L_F)(d_p)_F(\rho_{pF}/\rho_F)^{\frac{1}{2}},$$

and the area of the secondary burner as

$$(A_s)_m = (L_m/L_F)^2(A_s)_F(\rho_{sF}/\rho_F).$$

The similarity required also that the ratio of the input mass flows of the primary and the secondary fluids be the same in the model as in the hot furnace.

$$(m_p/m_s)_m = (m_p/m_s)_F.$$

When the secondary velocity is low and the density of the secondary fluid is considerably higher than that of the recirculating fluid correspondingly more recirculation and less secondary air is entrained in the early part of the primary jet. This means that the fuel heats up faster—which has far-reaching effects on the stability of the flame.

The effect of the buoyancy near the burner can be characterized in terms of the Archimedes number which is the dimensionless ratio of the gravitational to inertial forces.

ACKNOWLEDGMENTS

The authors wish to thank members of the Staff of the Research Station for assistance in the experiments, and the members of the Joint Committee of the International Flame Research Foundation for permission to publish this paper.

Nomenclature

A_s	Cross sectional area of secondary annular burner [m^2]
C_{bf}	Burner fluid concentration ($P + S$)
C_{rec}	Concentration of recirculated fluid
d_p	Diameter of primary burner [m]
D_1	Internal diameter of secondary burner [m]
D_2	External diameter of secondary burner [m]
d_0'	Equivalent nozzle diameter [m]
G_0	Momentum flux through nozzle (Thring-Newby) [kg m sec^{-2}]
G_p, G_s	Momentum flux through primary and secondary burners respectively [kg m sec^{-2}]
L_m, L_F	Half-width of furnace in cold model and hot furnace respectively [m]
m_0,m_a	Mass flow rate of nozzle fluid and surrounding fluid respectively [kg sec^{-1}]
m_p, m_s, m_r	Mass flow rate of primary, secondary, and recirculated fluid respectively [kg sec^{-1}]
M	Mass flow rate within the combined jet boundaries [kg sec^{-1}]
P, S	Mole fractions of primary and secondary nozzle fluid respectively
r	Radial distance from the axis of the jet [m]
r_0	Equivalent nozzle radius for single jet (Thring–Newby) [m]
r_0'	Equivalent nozzle radius for double jet [m]
T_p, T_s	Burner exit temperature of primary and secondary fluids [°C]
T_F	Average temperature in the furnace past the flame front [°C]
U_p, U_s	Primary and secondary velocity at burner exit [m sec^{-1}]
ρ_{pF}, ρ_{sF}, ρ_F	Density of fluid based upon T_p, T_s, and T_F, respectively [kg m^{-3}]
θ	Thring–Newby criterion; $\theta = [(m_a + m_0)/m_0](r_0/L)$
θ'	Modified Thring-Newby criterion $\theta' = r_0'/L$

Subscripts

m	Cold model
F	Furnace

References

1. Thring, M. W. and Newby, M. P.: *Fourth Symposium (International) on Combustion*, p. 789. Williams and Wilkins, 1953.
2. Rivière, M.: Private communication.
3. Ibiricu, M. M.: Ph.D. thesis, University of Sheffield, 1962.
4. Lee, K. B.: International Flame Research Foundation, Document G 02/a/2, 1962.
5. Chigier, N. A. and Beér, J. M.: International Flame Research Foundation, Document G 02/a/1, 1962.
6. Cohen de Lara, G., Poux, J., and Perrin, R.: International Flame Research Foundation, Document Tb–F 61/bc/3, 1960; Hubbard, E. H.: J. Inst. Fuel *35*, 161 (1962).
7. Horn, G.: Ph.D. thesis, University of Sheffield, 1955.
8. Regenscheit, B.: Kältetechnik 11, 3 (1959).
9. Beér, J. M.: International Flame Research Foundation, Document K 20/a/1, 1962 (paper presented at the *Symposium on Flames in Industry*, June 1962, London, Institute of Fuel).

APPLICATION OF THE WATER TRAVERSE TECHNIQUE TO THE DEVELOPMENT OF AN AFTERBURNER

JAMES O. ELLOR

A technique was developed for assessing the fuel–air ratio distribution of a reheat burner with the engine run at design conditions, but without reheat in operation. Water is injected from the reheat burner fuel manifold, the associated drop in gas temperatures recorded by thermocouples in traverse planes around the burner being a measure of the water–air ratio distribution. Primary interest was in the radial and circumferential spread of the fuel at these planes, and the location of the jet core. By repeating the tests to cover the operational flow range of the burner, the local fuel–air ratio at the stabilizers can be expressed as a percentage of the total fuel–air ratio, at each condition.

The extinction limits of the burner having been established with reheat in operation in terms of total fuel-air ratio, the local stability limits of the flame stabilizers can be estimated. However, as the extinction limits generally occur at jet pipe conditions other than those at which the water traverse tests are carried out, appropriate similarity parameters must be used. These are compared quantitatively with the parameters affecting fuel penetration and dispersion in the literature.

A correlation has been done of the extinction limits of a series of different reheat burners from flight and test bed results using the water traverse technique.

Introduction

In developing an afterburner system for a jet engine it is essential to know the distribution of fuel produced by the various injection arrangements. However, not only is it difficult to construct accurate and reliable sampling gear for this purpose, but prolonged running at afterburner conditions is expensive while injecting fuel without lighting it is dangerous. Tests on small models tend to be unreliable because of scale effects.

We have therefore developed at Rolls-Royce a simple simulation technique for assessing the distribution of fuel in an afterburner system with the engine running at design conditions, but without afterburning in operation. Water is injected from the reheat burner fuel manifold, the resulting drop in gas temperatures, recorded by thermocouples in traverse planes around the burner, being a measure of the water:air ratio distribution. By taking account of the similarity parameter discussed later in the text, the water: air concentrations can be related to the fuel:air distribution of the afterburner. In a typical system the fuel is injected from a series of small holes in a circular manifold situated upstream of an annular V-gutter stabilizer. We are, of course, primarily interested in the radial and circumferential spread of the fuel at the burning zone and in the location of the "core" of the fuel jet. By repeating the tests to cover the operational flow range of the burner, the local fuel:air ratio at the stabilizers can be expressed as a percentage of the total fuel:air ratio at each condition.

Once the extinction limits of the burner have been established in terms of total fuel:air ratio with reheat in operation, the stability limits of the flame stabilizers can be estimated in terms of *local* fuel:air ratio using the results of the water tests. However, as the extinction limits generally occur at jet pipe conditions other than these at which the water traverse tests are carried out, appropriate similarity parameters must be used.

Principles

Assuming all the heat and mass transfer is by turbulent mixing alone, so that the local enthalpy is uniquely related to the concentration, an energy balance gives:

$$M_w\{L + (T_b - T_w) + C_{ps}(T_2 - T_b)\} = M_g C_{pg}(T_1 - T_2)$$

where M_w is the water flow past a point in the sampling plane, M_g the gas flow, L the latent heat of water, C_{ps}, C_{pg} the specific heats of steam and gas, respectively, and T_2 and T_1 the measured temperatures with and without water injection. T_w is the initial water temperature and T_b the boiling temperature of water at jet pipe pressure.

For a typical case in which $T_1 = 750°C$ and

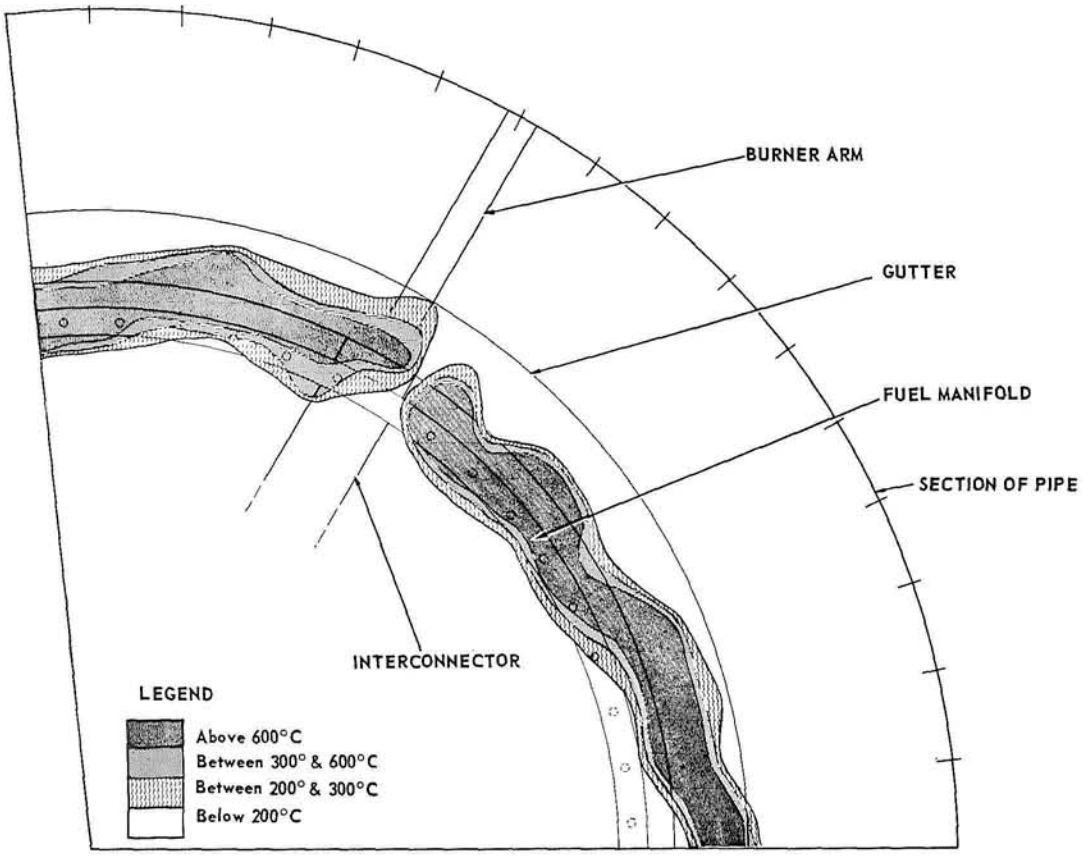

FIG. 1. Typical thermocouple traverse.

$M_w/M_g = 1/10$, we would have $T_1 - T_2 =$ 300°C which is easily measured to an accuracy of 1%. It is evidently not possible to measure a water:gas ratio much greater than twice this amount since all the water may not then be evaporated. This would result in the thermocouple recording T_w independently of the true mixture ratio.

Practice

Figure 1 shows a typical thermocouple transverse in the plane of the gutter, the results being expressed as the temperature difference between water off and water on conditions. It will be seen there are 17 thermocouple probes each traversing radially, the assembly covering a 100° sector. Readings have been taken at 0.25 in. and 0.5 in. radial increments over a 3 in. annulus in a pipe of 29.0 in. diameter. In some tests a larger range of probe penetration is required. The thermocouples are either the "stagnation" type or of "open head" construction, with chromel-alumel bimetal junctions. We have found these accurate enough in view of the comparative nature of the temperature measurement, even at low values of temperature drop. The gutter position is shown in Fig. 1, as is the location of one of the three radial arms supporting the burner. Since there is no fuel injection hole immediately behind the arm the fuel pattern is interrupted at this point.

The temperature drops are then averaged over an annulus of 0.25 inch radial depth, converted to a water:air ratio by energy balance as above, and plotted as shown in Fig. 2. A check is made that the integrated water:air distribution and airflow traverse in this 100° sector gives a total water flow in the correct proportion of the water feed to the manifold. It may be necessary to traverse other quadrants if the pattern is assymetrical. When as in this example, the fuel jets are closely pitched, the individual sprays fairly quickly form an annulus and it is not necessary to adopt a very close pitching of the radial traverse lines. In certain spoke injection systems, where the circumferential spacing is large, the fuel sprays must be

treated as separate cones, necessitating a greater number of radial traverses.

Figure 2 shows the water:air distribution 2.0 in. downstream of the stabilizer, at plane 2, in comparison with the distribution incident to the gutter at plane 1. As would be expected the patterns in plane 2 are similar to the two parts into which the gutter splits the distribution at plane 1. The further spread due to eddy diffusion between the planes has been more than offset by the acceleration of the flow, leading to a slightly narrower pattern at the downstream plane.

These particular tests are for downstream fuel injection where it was found that the jet "core" or locus of maximum concentration points followed a path midway between the injection direction and the airflow stream lines for 8 in. from the point of injection, thereafter following the gas flow. This was the case for both water and fuel injection and will be discussed under similarity parameters.

Although it is open to discussion as to which local fuel:air ratio controls gutter stability, we have assumed it to be the value at the gutter lips. In future tests we would only traverse in this plane.

Similarity Parameters

The Effect of Evaporation

Bahr[1] gives the following relation for the factors governing injectant evaporation:

$$N/(100 - N) = 52.5\,[(T_A)^{4.4}/(1000)] \cdot (V_A)^{0.8}/(100) \cdot 1/p_A{}^{1.2} \cdot P_f{}^{0.42} \cdot L^{0.8},$$

where N = evaporation as percentage; T_A = gas stream temperature; V_A = gas stream velocity (ft/sec); p_A = gas stream static pressure (in psi;) P_f = fuel stream pressure drop (in psi;) and L = distance from fuel injector in inches.

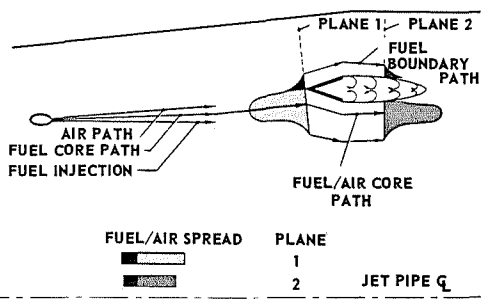

FIG. 2. Change of fuel/air spread with flow area.

The relation was based on tests with contra-stream fuel injection using iso-octane at stream temperatures not exceeding 200°C, the author stating the relation should apply to kerosene. Our results were with both kerosene or water with downstream injection at 750°C gas temperature. At this temperature, according to the equation kerosene will be 90% evaporated at 0.25 in. from the point of injection. For the same degree of evaporation a water spray will probably travel 1.5 in., based on the relative values of the heat necessary to evaporate the two fluids. These evaporation distances are small compared with the scale of the apparatus and thus the sprays of either water or kerosene may be treated effectively as vapor sprays. No similarity parameter based on evaporation is therefore required.

Factors Governing Fuel Dispersion with Downstream Injection

Beaton[2] and King[3] give expressions for the spread of a fuel spray caused by the eddy motion of the airstream, the tests being limited to an airstream temperature of 80°C.

Bahr[1] modifies the mathematical relation to include the effect of evaporation on dispersion, his formula being based on tests with airstream temperatures of up to 200°C. Interpreting the expression given:

$$f/f_{@r=0} = \exp\,(-r^2/M),$$

where f is the fuel:air ratio at a given radial distance (r) from the core; $f_{@r=0}$ is the peak fuel:air ratio in the core; and M is the spread index, which is related in the text to the relevant paramaters as follows:

$$M = 0.0598\phi + 0.00042,$$

where

$$\phi = \frac{[(T_A/1000)^{0.67} \cdot L^{0.76} \cdot P_f{}^{0.49} \cdot D^{0.79}]}{[(V_A/100)^{0.85} \cdot p_A{}^{0.57}]};$$

D is the diameter of the jet orifice in inches (the rest of the symbols have been defined earlier).

If the fuel spread radius is arbitrarily defined as that radius at which the local fuel:air ratio is 5% of the peak value, our results agree well with the above relation as shown in Appendix 1. We have defined dispersion as twice the fuel spread radius.

By comparing the results of references 2 and 3 with reference 1, it is found that evaporation appears to make very little difference to the dispersion. Comparative tests carried out by us at the same injectant flow with water and fuel have certainly given identical dispersion results. Thus the injectants used need not have a similar boiling point. Also if the above equation for ϕ is

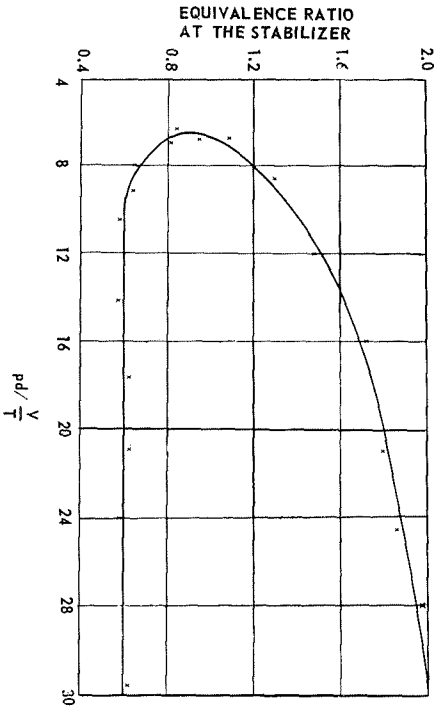

FIG. 3. Reheat stabilizer stability characteristics.

looked at carefully it will be seen to depend approximately on the ratio of fuel to air momentum, at a given distance from the injection point, and this parameter is kept constant between tests in any case.

Factors Affecting Dispersion and Penetration with 45° Downstream Injection

There appears to be no reference in the literature either to fuel spray dispersion or penetration when the fuel is injected at an angle to the airstream. However, the following penetration relation for normal to stream injection, suggested by Bragg[4] gives very good correlation with our results (see Appendix 2).

$$x/d = 0.7[P_f/(P - p)]\cdot \ln (L/d)$$

where x = cross stream penetration; d = jet orifice diameter; $P - p$ = gas stream dynamic head; P_f = fuel injection pressure drop; and L = downstream distance from injection point.

The ratio $P_f/(P - p)$ is essentially the fuel: air momentum ratio and as mentioned in reference 4 evaporation appears to have a negligible effect on the penetration, as the relation holds equally well for air temperatures below the above the injectant boiling point. The penetration observed with water jets inclined at 45° to the gas direction is given in Appendix 2.

Summarizing the above section, we conclude that the position of the core of the jet, i.e., the penetration, is determined by the liquid: gas momentum ratio, and this parameter must be kept constant for correct simulation. However, evaporation does not appear to be a significant factor in determining spread or penetration.

Correlation with Hot Tests

We have been successful in correlating the stabilizer extinction limits of a series of different reheat burners from flight and test-bed results using the fuel: air ratio at the stabilizer calculated from the results of the water traverses. The stability characteristic for plain gutters is given in Fig. 3, where the equivalence ratio at the gutter lip is plotted against the aerodynamic loading parameter $pd/(V/T)$. The symbols used are:

p = static pressure at the gutter lip (psi);
V = velocity at the gutter lip (ft/sec);
T = gas total temperature (°K);
d = stabilizer width (inches).

The curve shown is a mean line for a range of gutter widths from 1.0 in. to 2.0 in. over a pressure range of from 5 psi to 50 psi and for jet pipe temperatures from 500°C to 800°C.

It will be noted that:

(a) The aerodynamic loading is least when the local overall fuel: air ratio is 90% of the stoichiometric value, i.e., an equivalence ratio of 0.9.

(b) De Zubay's Law (ref. 5) holds very well at the "blow-off" point—0.9 equivalence ratio—and at equivalence ratios greater than this.

(c) It is surprising that the weak extinction fuel: air ratio is independent of the De Zubay number $pd/(V/T)$ over so large a range of it.

(d) A stabilizer is able to work over an equivalence ratio range of 0.60 to 2.0 at the value of $pd/(V/T)$ corresponding to the sea level static conditions of most of our jet engines.

Conclusions

The technique of simulating the fuel distribution of an afterburner by injecting water from the burner manifold is a useful development tool with the only proviso that the fuel: air momentum ratio must be the same in model test and prototype.

ACKNOWLEDGMENT

The tests and analysis of results in the paper have been conducted by the Reheat Development Department of Rolls-Royce.

REFERENCES

1. BAHR, D. W.: N.A.C.A., Evaporation and Spreading of Iso-Octane Sprays in High Velocity Air Streams, Report RM E.53114, November 16, 1962.
2. BEATON, A. B. P.: A Theoretical Expression for Point-Source Diffusion in Turbulent Flow (Unpublished MoA Report).
3. KING, C. N.: Fuel Distribution Experiments in a Turbulent Air Stream, (Unpublished MoA Report).
4. BRAGG, S. L.: Rolls-Royce Internal Report, April, 1955.
5. DEZUBAY, E. A.: Characteristics of Disc-Controlled Flame. Aero Digest, *61*, 54 (1950).

Appendix 1

Dispersion with Downstream Injection

With downstream injection we have found no change in the fuel dispersion of 3.0 in. width, when the water flow varies from 0.02 to 0.04 lb/sec per jet, the dispersion being measured 8.0 in. from the point of injection. This is in good agreement with reference 1, as the following table shows:

Gas velocity: 654 ft/sec;
Gas temperature: 760°C;
Gas pressure: 35 psi;
Gas mass flow: 160 lb/sec;
Jet diameter: 0.039 in.;
Jet flow No.: jet flow in imperial gal/hr per psi pressure drop.

Water flow jet (lb/sec)	Jet flow No.	Dispersion (in.)	Dispersion predicted from ref. 1 (in.)
0.02	1.75	3.0	2.8
0.04	1.75	3.0	3.2

Appendix 2

With 45° downstream injection, we found the dispersion and penetration varied with flow in the following manner, measurements again being referred to a plane 8.0 in. from injection point.

Gas velocity: 676 ft/sec;
Gas temperature: 750°C;
Gas pressure: 37.5 psi;
Mach No.: 0.30;
Gas mass flow: 160 lb/sec.;
Jet diameter: 0.039 in.

Water flow jet (lb/sec)	Jet flow No.	Dispersion (in.)	Penetration (in.)	Penetration predicted from ref. 4 (in.)
0.06	1.75	5.3	—	—
0.03	1.75	4.35	0.765	0.745
0.013	1.75	3.5	—	—

Discussion

DR. D. G. STEWART (*Aeronautical Research Laboratory, Australia*): The general success achieved with the water traverse technique is most encouraging. We have contemplated its use in ramjet scaling work but concluded that, at our air temperature (200°C), evaporation would be incomplete. The dependence of evaporation on (temperature)$^{4.4}$ quoted by Dr. Ellor explains the success obtained with temperature over 500°C.

The expression quoted for fuel distribution from downstream facing jets differs greatly from that of King for upstream facing jets and appears to lend itself more effectively to the achievement of similarity in scaling. This may be an argument in favor of the use of downstream jets when scaling is necessary.

Despite differences in the two expressions, it is, however, interesting that both tend to reduce in the simplest form to the approximate scaling law: $(\text{Injector diameter})^{\frac{1}{2}} \propto (\text{Chamber linear dimension})^{\frac{1}{2}}$.

MR. P. F. ORCHARD (*Bristol Siddeley Engines, Ltd.*): We have also used the water traverse technique to examine fuel distribution in reheat systems, but, while I agree that the peaks in the fuel/gas ratio can be traced quite adequately, I think the extension of the technique to predict quantitative values of fuel/gas ratio away from these peaks can be mis-

leading, for confirmatory checks made by taking gas samples of the same flame in a burning system have shown up significant discrepancies. This is especially important in high efficiency, high boost systems where fuel must be made to approach the wall of the liner as closely as possible without actually impinging on it.

DR. J. O. ELLOR (*Rolls-Royce, Ltd.*): We have not in fact applied the water traverse technique to the kind of reheat system referred to by Mr. Orchard. Because of this I cannot but accept this limitation of the technique. However, I should have thought the criticism restricted to the traverse method rather than to the injectant used, our experience being that water or fuel injectants give almost the same distribution under similar conditions. I would be interested to know from Orchard why the fuel distribution measured away from the peaks can give misleading results. While it is agreed that off-peak distributions are more difficult to measure, a reasonable accuracy of technique should give a satisfactory answer.

SIMILARITY AND SCALE EFFECT IN RAMJET COMBUSTORS

D. G. STEWART AND G. C. QUIGG

In view of the successful application of "pressure scaling" to gas turbine and reheat combustors, there is interest in using the technique for ramjets. However, as the fuel distribution process in typical ramjet combustors was suspected of causing scaling difficulties, the present work set out to determine the value of pressure scaling under these circumstances and to establish the appropriate fuel injector scaling criterion.

The work was carried out using a current design of practical ramjet combustor in sizes of approximately 3-, 5-, and 8-inch duct diameter. Besides direct scaling comparisons, it was found necessary to investigate the detailed performance of this type of combustor and to study the fuel distribution process, both from isolated injectors and within the actual combustor.

An important irregularity of combustor performance noted was the phenomenon of primary fuel penetration into the secondary zone, this giving rise to a high sensitivity of performance to fuel distribution effects. The injector scaling conditions necessary to preserve similarity of the penetration process under these circumstances have been determined in the form of an empirical law.

Assessment of the comparative performance of the three combustors shows that, under those operating conditions in which the above fuel penetration does not occur, combustion similarity is achieved by pressure scaling, broadly independent of fuel injector size. For conditions in which fuel penetration is marginal, use of the empirical law found for injector scaling results in reasonable similarity.

The only scale effect noted has been in the tendency of the primary zone stability limits to decrease in mixture strength as scale increases. This appears to be related to dissimilarity of air flow distribution, an effect which is being further investigated.

Introduction

The simple "PL" scaling law was first stated in 1951[1] when it was shown, by consideration of the component processes occurring in a combustion chamber, that similarity of those processes most likely to control the performance of the combustor could be achieved by "pressure scaling," i e., by:

1. Maintaining geometric similarity between model and full size unit;
2. Operating both at the same inlet temperature, inlet velocity, and fuel–air ratio;
3. Operating the model at a higher pressure than the full size unit, determined inversely as the ratio of linear dimensions. Hence the terms "PL" scaling or "pressure scaling."

The principle behind pressure scaling is easily understood by reference to a simplified combustion system whose performance is dependent only on the processes of mixing and reaction kinetics. The parameter controlling the former process is Reynolds number, constancy of which leads to

$$vLP = \text{constant}, \tag{1}$$

where temperature and composition are constant and the quantities v, L, P refer to velocity, length, and pressure, respectively. The latter process, requiring reaction time to be proportional to residence time leads, under the same circumstances to:

$$1/P \text{ proportional to } L/v,$$

i.e., to

$$PL/v = \text{constant}. \tag{2}$$

Equations (1) and (2) together give the familiar scaling requirements: PL = constant and v = constant.

Although the treatment of reference 1 is far more comprehensive than that above, the final simple result is the same. This treatment was later extended to cover atomization by swirl atomizers and other relatively minor refinements were introduced; a consolidated statement was presented at the 1955 AGARD Colloquium.[2] Experimental assessment of the theory commenced at Rolls-Royce in 1952 and work was later carried out at Lucas and N.G.T.E.[3] Other

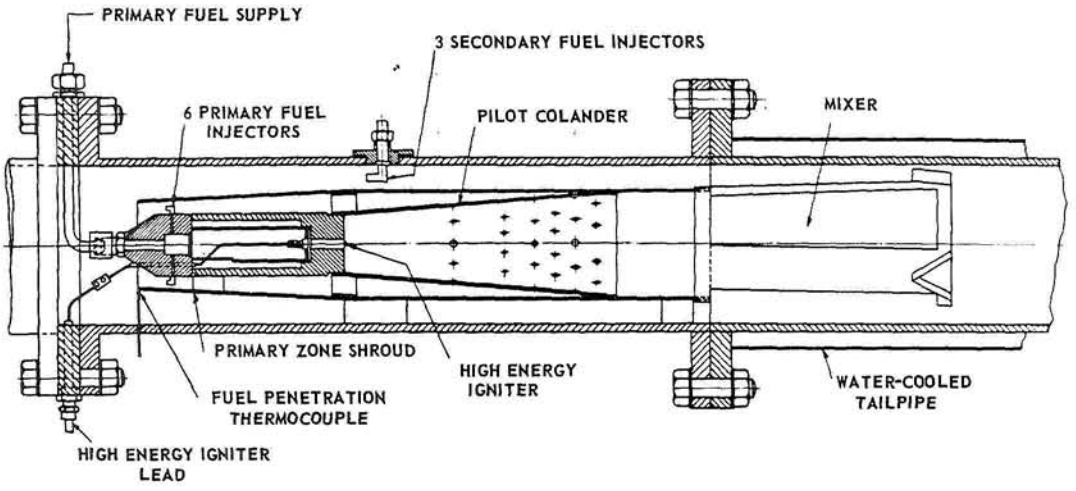

FIG. 1. N.G.T.E. "long colander" ramjet combustor.

contributions on scale effect appeared at the AGARD Colloquium, dealing with combustion in both jet engines[4–6] and rockets.[7,8] The present status of scaling techniques is reviewed by Lefebvre in reference 9.

It is now clear that "pressure scaling" is highly successful in relatively simple combustors such as those of reheat systems where the important component processes are essentially those of mixing and reaction kinetics. In less simple combustors, such as those fitted with swirl atomizers, pressure scaling is still effective provided similarity of the fuel injection process is maintained.[2,3] Essentially this involves maintaining the same fuel-air momentum ratio in both model and full size unit.

One second order departure from similarity found in pressure scaling is the scale effect in flame tube temperature dealt with in references 9 and 10. This arises essentially because, although convective heat transfer remains proportional to heat release, the ratio (heat absorbed by radiation)/(heat lost by convection) is proportional to L^2/vL^2P, i.e., to $1/vP$, and so larger units, operated at lower pressure, tend to run hotter.

As yet little has been published regarding the use of scaling techniques in ram jet combustors and it is this gap which the present investigation attempts to fill. Potentially, an effective scaling technique should be most useful for ram jets, as it is for reheat systems, because of the very large combustor sizes and testing plant capacity required. The major difficulty to be expected here is in effective scaling of the fuel injection and distribution processes since preliminary assessment of King's work on fuel distribution[11] has indicated scaling difficulties.

In carrying out this work, a current design of practical ram jet combustor, the N.G.T.E. "long colander" combustor[12,13] (Fig. 1) was chosen and practical operating conditions were closely simulated. The range of combustor operating conditions covered corresponds, according to the PL scaling law, to those of an 18-inch diameter ramjet operating at Mach number 2.5 at altitudes from 50,000 to 75,000 ft.

The objectives of the work were to assess the degree of similarity achieved by pressure scaling with this type of combustor, particularly under circumstances in which sensitivity to fuel distribution processes was apparent and to find, under these circumstances, what fuel distribution scaling criterion was necessary.

As a preliminary to the work it was found necessary to assess the performance of this type

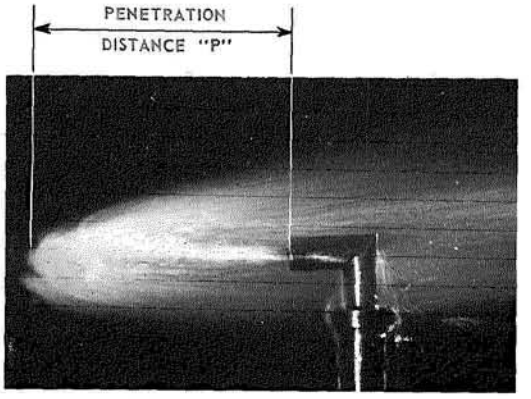

FIG. 2. Fuel distribution from upstream facing injector (air flow from left to right).

of combustor fairly thoroughly and this aspect is dealt with in an A.R.L. report to be published. The actual scaling investigation is recorded in a further A.R.L. report and the present paper forms a summary of those two reports.

Preliminary Consideration of Fuel Distribution

To place in correct perspective the problem of fuel distribution scaling, it is necessary to make some initial remarks concerning this process. The combustor of Fig. 1 employs simple upstream-facing tubular fuel injectors and the distribution of fuel from these may be observed qualitatively in the photograph of an isolated injector (Fig. 2). The fuel penetrates a distance p upstream and then diffuses laterally as it moves downstream towards the combustion region. To maintain similarly of this process during scaling it is clearly desirable that the fuel–air ratio distribution downstream of the injector should be the same in model and full size unit.

This process has been extensively studied by King[11] who found the lateral diffusion process to be essentially in agreement with the theory of diffusion from a point source as described in references 14 and 15 and that the effective point source was at the point of maximum upstream penetration. He further found empirical laws defining the penetration distance p and the effective diffusion coefficient.

Fuel distribution similarity implies similarity of both the diffusion and penetration processes. For the former, it can readily be deduced[11,14,15] that the parameter D/Lv is required to remain constant between scales, where D is the diffusion coefficient. For gaseous diffusion D/Lv is a function only of Reynolds number, but King's work showed empirically for spray diffusion

$$D/v \times 10^4 = 5.2(1 + 7.5Q_f) \qquad (3)$$

where D/v is in feet and Q_f, the fuel flow per injector, is in lb/sec. This latter expression, covering a limited range of variables, may however be misleading and more recent work at N.G.T.E. which, although inconclusive, did cover a range of duct sizes, indicates that more suitable empirical parameters in expression (3) might be D/Lv and Q_f/L. The first of these is the required similarity parameter and the second is effectively Reynolds number so that the requirement becomes similar to that for gaseous diffusion. It may thus be reasonably expected that constant Reynolds number, as maintained in pressure scaling, will achieve reasonable similarity of the diffusion process.

Regarding the penetration process, King found an empirical relation in the form:

$$p/d = k[(\rho_f v_f^2/\rho_a v_a^2)^n - 1], \qquad (4)$$

where p = upstream fuel penetration distance; d = injector inside diameter; ρ_f, ρ_a = fuel and air densities; and v_f, v_a = fuel and air velocities.

The term in the parentheses is, of course, the fuel/air momentum ratio, based on equal areas of fuel and air flow.

Applying to this the obvious scaling requirement (p/L = constant, PL = constant, v =

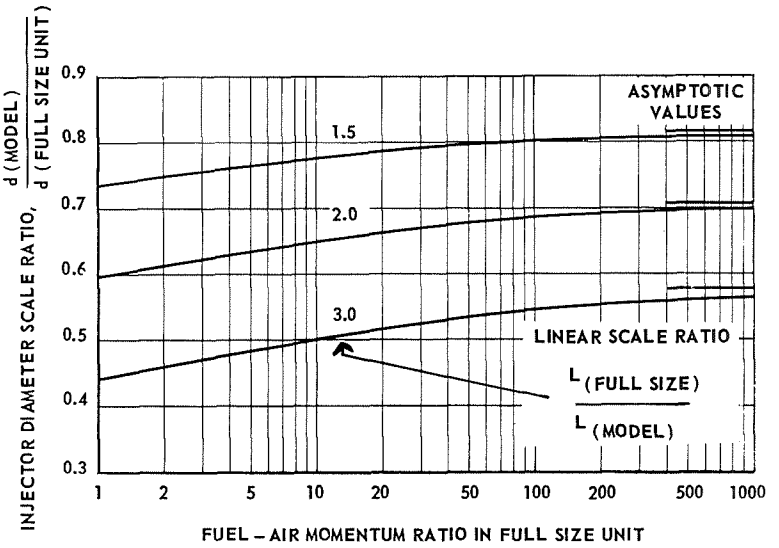

FIG. 3. Dependence of injector scaling on fuel–air momentum ratio (based on King's correlation).

constant, and the condition of constant fuel–air ratio) can be show to lead to:

$$\frac{d_1}{L_1}\left[\left(\frac{\rho_{f_1}v_{f_1}^2}{\rho_{a_1}v_{a_1}^2}\right)^n - 1\right] = \frac{d_2}{L_2}\left[\left(\frac{\rho_{f_1}v_{f_1}^2 d_1^4 L_2^3}{\rho_{a_1}v_{a_1}^2 d_2^4 L_1^3}\right)^n - 1\right], \tag{5}$$

where the suffixes 1 and 2 denote two scales of combustor.

If the momentum ratio is large compared with unity, this expression leads to:

$$d^{4n-1}/L^{3n-1} = \text{constant}. \tag{6}$$

Figure 3, based on Eq. (5), shows the dependence of injector scale ratio on fuel–air momentum ratio, for the case of $n = \frac{1}{2}$ (as found by King). It is apparent that, unless the momentum ratio is large compared with unity [in which case Eq. (6) applies] no one value of injector diameter is suitable for scaling over a range of momentum ratios. Thus it is inherently impossible to achieve similarity of fuel penetration using one fuel injector over a range of fuel flows. (This situation is very similar to that found for swirl atomizers in reference 3.)

The results of ref. 11 all correlated very well with expression (4) using $k = 31.0$ and $n = \frac{1}{2}$. However, other investigations at A.R.L. using isolated injectors show some variation. Some of these show $n = \frac{1}{2}$ but with k tending to decrease as turbulence level increases. Others show correlation to be best with $n = 3/4$ and with the p/d term modified to $(p/d)/\mathrm{Re}^{\frac{1}{4}}$ where the Reynolds number Re is based on air flow and jet outside diameter. Thus it appears that fuel penetration depends, not only on momentum ratio and jet size, but also on turbulence level, Reynolds number, and other factors not yet completely investigated. Equation (4) nevertheless forms a good first approximation to describing the process.

For approximate use in scaling the fuel penetration process, expression (6) reduces to:

$$d/L^{1/2} = \text{constant (if } n = \tfrac{1}{2}) \tag{7}$$

$$d/L^{5/8} = \text{constant (if } n = \tfrac{3}{4}) \tag{8}$$

An alternative expression, more applicable to conditions in the present combustor, is derived below.

Experimental

The N.G.T.E. combustor [12,13] (Fig. 1) consists essentially of a central pilot colander fed with fuel from six primary injectors and an annular passage fed with secondary fuel from three injectors. Mixing of the two streams is effected by a mixer having three fingers, on each of which is a small V-gutter, these being situated behind the three secondary injectors. Combustion is completed in a tail pipe section.

For the present investigations, three scales of

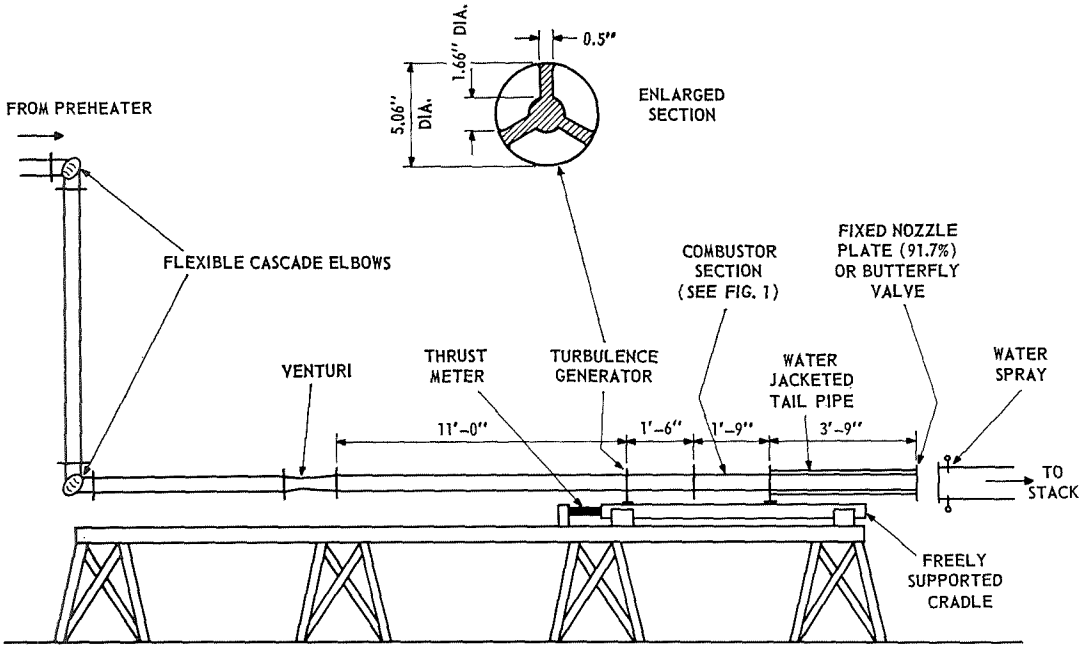

FIG. 4. Test rig (5-inch rig shown).

combustor were made, equivalent to duct inside diameters of 3.34, 5.06, and 7.75 inches (for convenience these are referred to as the 3, 5, and 8-inch scales). The smallest of these was considered the minimum desirable from the point of view of testing and manufacturing accuracy and the largest was set by the available plant capacity. Great care was taken in the manufacture of these to preserve true geometric similarity, even to the extent of scaling metal thickness proportional to linear dimension.

The general arrangement is shown diagramatically in Fig. 4, the dimensions shown being those for the 5-inch rig. The pipework was suspended on a floating thrust cradle and thrust measurements when required were made using a calibrated proving loop. A ball-jointed swinging link was used to supply air without introducing axial forces and, because of some air leakage at the ball joints, the air venturi was located after these. To ensure uniformity of fuel flow to the three secondary injectors, a distribution chamber was installed ahead of these. Arrangements for primary fuel injection and high energy ignition are shown in Fig. 1.

As shown in Fig. 4, a heavy turbulence generator was fitted upstream of the combustor to simulate practical combustor inlet conditions. At the exhaust end, a sharp-edged nozzle plate was used in most tests to provide 92% nozzling.

TABLE 1

Summary of Test Program

Rig size (L) (in.)	Secondary injector diam. (in.)	Primary injector				Type and number of observations				
						Penetration				
		No.	Diam. d (in.)	$(L)/(d)$	PL	Without comb.	With comb.	Primary stability	Overall stability	Thrust and efficiency
5.06	0.116	1	0.029	174	135	6	—	27	—	—
					200	7	—	43	—	—
					300	6	—	12	—	—
					400	—	—	12	—	—
		2	0.041	123	135	6	—	19	260	24
					200	8	—	48	580	50
					300	7	—	27	160	41
					400	—	—	24	80	33
3.34	0.094	5	0.020	167	135	6	—	9	—	—
					200	5	6	18	—	—
					300	—	—	—	—	—
		4	0.024	139	135	5	2	15	7	—
					200	12	6	29	8	—
					300	4	5	18	5	—
		3	0.033	101	135	7	—	7	27	28
					200	8	—	23	96	46
					300	6	—	—	39	54
					400	—	—	—	18	15
7.75	0.144	7	0.052	149	200	7	9	19	—	—
		9	0.060	130	200	8	5	5	—	—
					300	10	3	28	27	29
		8	0.073	106	200	8	—	23	—	—
					300	7	—	37	36	—

For tests of primary zone stability, requiring independent variation of chamber velocity, this was replaced by a water-cooled butterfly valve.

Three types of measurement were made as a basis of comparison of overall combustion performance of the three scales; these were primary zone stability, overall stability (in which primary and secondary fuel flows were independently varied), and combustion efficiency (determined by thrust measurement using a calibrated proving loop). Fuel penetration behavior in the combustor was investigated using the small thermocouple located as shown in Fig. 1 to detect the presence of primary fuel at the shroud edge.

Throughout this work, so as to facilitate comparison of the results of the three scales of combustor, standard values of combustor inlet total pressure were used, corresponding to values of PL of 135, 200, 300, and 400 where P is inlet pressure in p.s.i.a. and L is duct inside diameter in inches. If the PL scaling law applied, this would then result in performance dependent only on PL irrespective of scale and so comparison of scaling effects could be readily made. The range of PL chosen corresponds to an 18-inch diameter ramjet operating at Mach number 2.5 at altitudes from 50,000 to 75,000 ft, the appropriate inlet temperature of 200°C being achieved using a kerosene-fired preheater supplying vitiated air. Plant facilities allowed the 3- and 5-inch combustors to be tested at all these values of PL although operation of the 5-inch combustor at PL 135 resulted in the final nozzle being unchoked, and this fact must be considered in assessing the results. The 8-inch combustor could be tested completely only at PL 300 but lower values of PL were possible when the exhaust butterfly was used (i.e., when choking of the final nozzle was unnecessary).

A range of fuel injector sizes was used during this work. The basic 5-inch rig injectors (0.116-inch dia. secondary and .041-inch dia. primary) were designed to operator over the same range of fuel–air momentum ratios as occurred in the N.G.T.E. 6-inch high altitude combustors of refs. 12 and 13. The 3-inch and 8-inch rig secondary injectors were then derived from these using Eq. (7) and a range of primary injectors was used as discussed below. The full range of injectors, test conditions, and number of observations made is summarized in Table 1.

Comparison of Scaling Behavior

General Comments

Before making detailed comparison between the three scales of combustor, the general characteristics of this type of unit were examined using the 5-inch combustor.

In general, three particular characteristics of the combustor behavior were noted:

1. There is a tendency for "multiple" stability loops to occur—that is the curve of overall

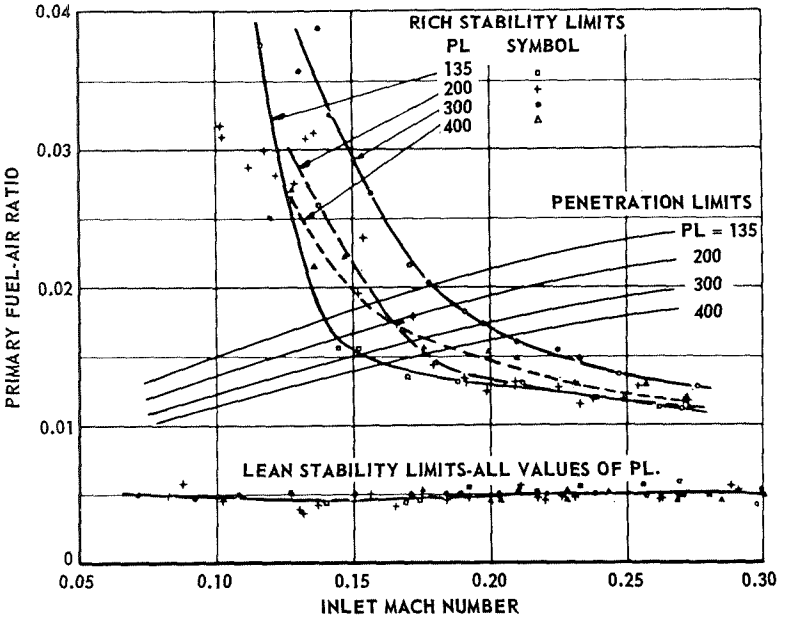

FIG. 5. Five-inch rig, primary zone stability.

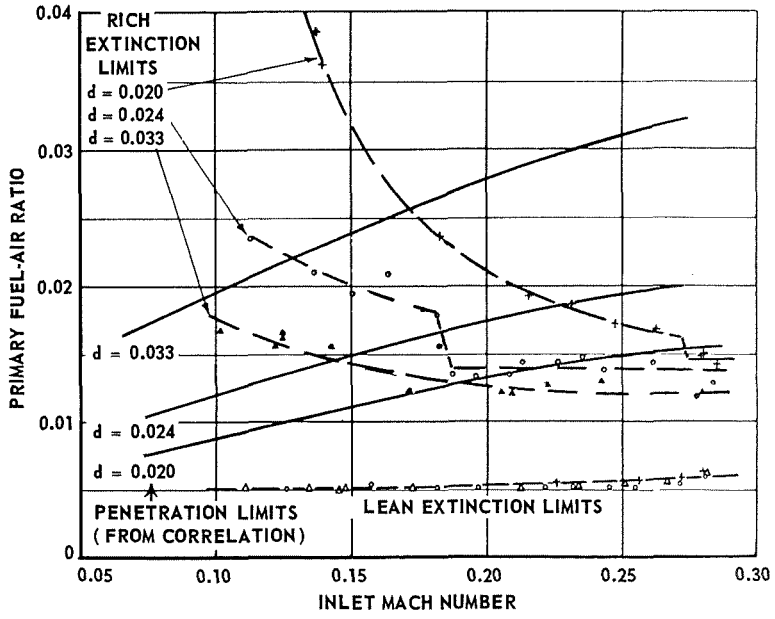

FIG. 6. Primary zone behavior—effect of injector size on stability (3-inch rig, PL = 200, d = 0.020, 0.024, 0.033).

stability can close at two or more distinct values of total fuel–air ratio (Fig. 8).

2. Under some circumstances, primary fuel may penetrate beyond the primary shroud and enter the secondary stream, causing a large effect on performance and thus great sensitivity to fuel distribution. (See for example, the marked effect of injector size in Fig. 6).

3. When such penetration does not occur, sensitivity of performance to primary fuel distribution is small.

Reference to these points will be made during discussion of the comparative results. In the following section the three aspects of performance, namely, primary zone stability, overall stability, and combustion efficiency, will be discussed by comparing the effect of varying scale at constant PL with that of varying PL at constant scale, the criterion of reasonable similarity being that the former effect is significantly less than the latter.

Primary Zone Stability

Figure 5 shows the 5-inch rig results over a range of values of PL. It is apparent that the lean stability limit is insensitive to PL but the rich limit generally shows the improvement to be expected as this quantity increases. (The relatively low values found at PL 400 were probably due to instability arising in the butterfly water-cooling system).

As noted earlier, it is possible for primary fuel to penetrate into the secondary region and the full significance of this will be discussed below. It is sufficient at the moment to note the curves in Fig. 5 indicating the mixture strengths above which this occurs.

Figure 7 shows the over-all comparison of the effect of scale on primary stability, illustrated for PL = 200 (results at other values of PL are very similar). Again, the fuel penetration limits are shown. Agreement between the three scales is generally quite good in the region in which fuel penetration does not occur, although there is a quite definite tendency for both lean and rich limits to increase in value as scale decreases.

In the region in which fuel penetration does occur there is a pronounced effect of scale, the reason for which will be will be clarified below.

Overall Stability

Figure 8 shows the complete results for the 5-inch combustor over the range of values of PL and illustrates both the degree of experimental accuracy achieved together with the occurrence of multiple stability loops mentioned above. The experimental scatter shown generally occurred in the form of differences between successive runs and, despite great care in ensuring reproducibility of hardware during repairs and

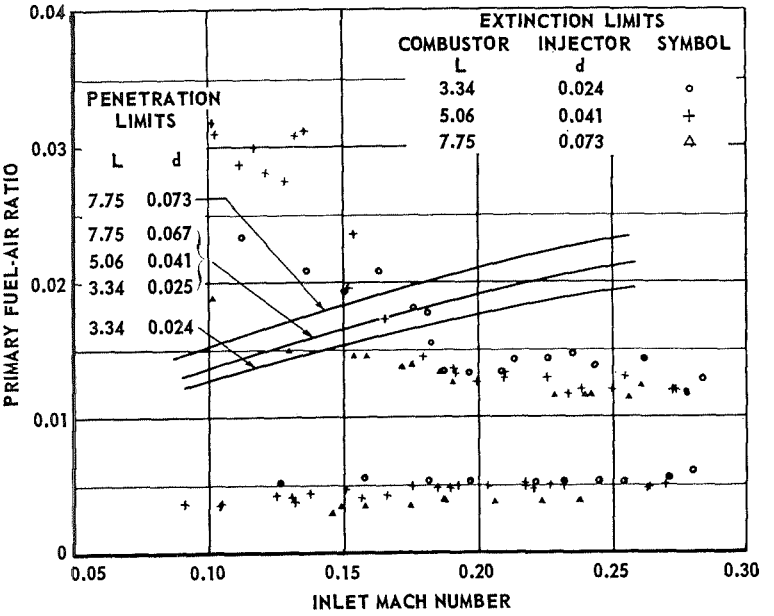

FIG. 7. Overall scaling comparison, primary zone stability. (PL = 200)

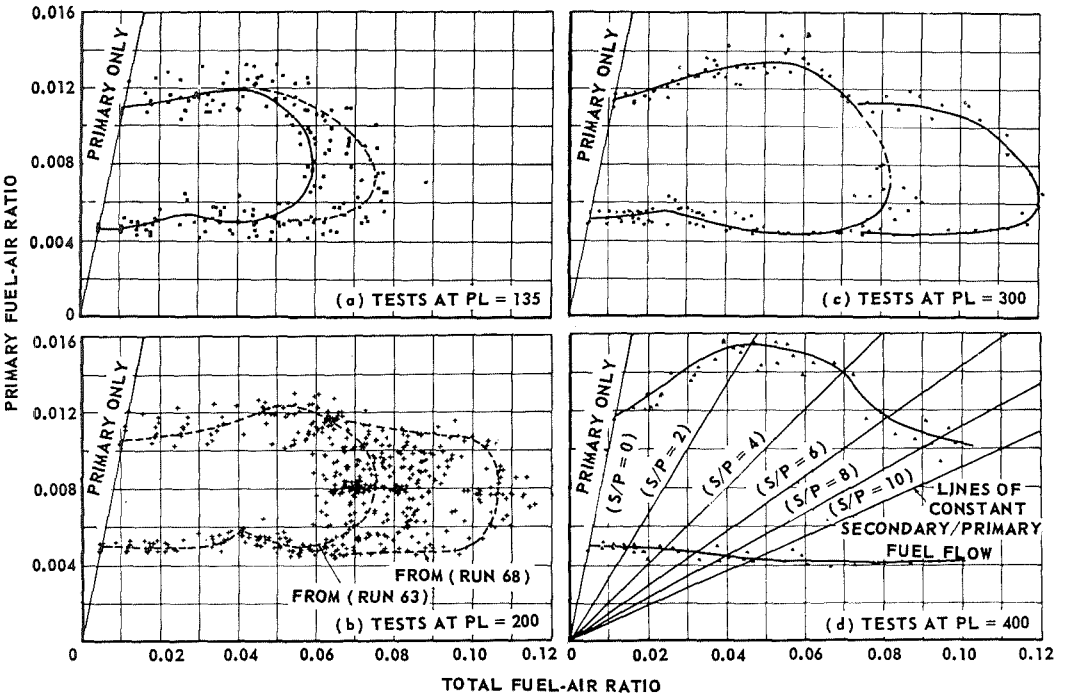

FIG. 8. Five-inch rig, overall stability (complete results).

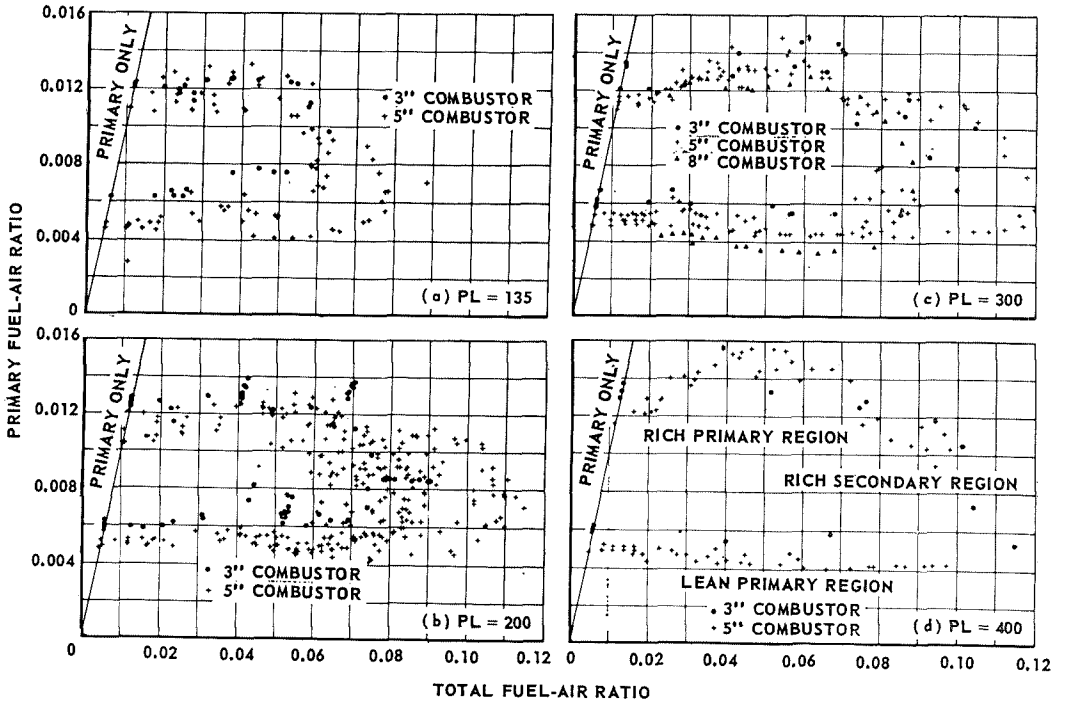

FIG. 9. Overall scaling comparison, overall stability.

in maintaining reproducible test conditions, no better accuracy could be achieved.

The phenomenon of multiple stability loops was carefully examined to see whether any extraneous influences could be responsible for these but the only significant conclusion drawn was that the "long" loop was generally associated with a low level of combustion noise. Extinction would usually occur at the "short" curve but under some circumstances (apparently those of low combustion noise level) this contributory cause of extinction was thus eliminated and stable burning would continue up to the "long" curve. Intermediate extinction points were also possible and this accounts for the large variation in the results at $PL = 200$. The two smooth curves shown on this figure refer to two typical individual runs giving rise to the "long" and "short" curve. For the purpose of the present scaling comparison it is necessary to accept this phenomenon as a characteristic of the combustor.

Figure 9 shows the overall comparison of the effect of scale at all values of PL (the 8-inch combustor could only be tested at $PL = 300$). The following observations may be made:

1. Within the limits of experimental accuracy there is quite good agreement in the region of rich primary mixtures (the regions referred to the indicated in Fig. 9d) although there is a slight tendency for extinction limit to increase as scale decreases.

2. In the lean primary region there is a definite scale effect with the limit increasing as scale decreases. This effect and that of 1, above are in the same direction as that observed with primary zone stability.

3. In the rich secondary region the 3- and 8-inch rig results agree well with the 5-inch rig "short" curves and there are also some 3-inch rig results at $PL = 300$ and 400 (and possibly 200) which indicate extinction on the "long" curve.

Thus, apart from the scale effect in primary zone mixture strength it may be generally concluded that similarity between scales is good. Certainly the effects of scale change are small compared with those caused by a change in PL. The question then arises as to whether similarity has been achieved by effective scaling of the fuel distribution process or whether, in fact, overall stability is relatively insensitive to fuel distribution. The result of Fig. 10 supports the latter view at least as regards primary fuel distribution; two different sizes of primary fuel injector have been used to give differing fuel distribution patterns and it is apparent that, except when fuel penetration takes place from primary to secondary region, overall stability remains unaffected. Other tests, as yet incom-

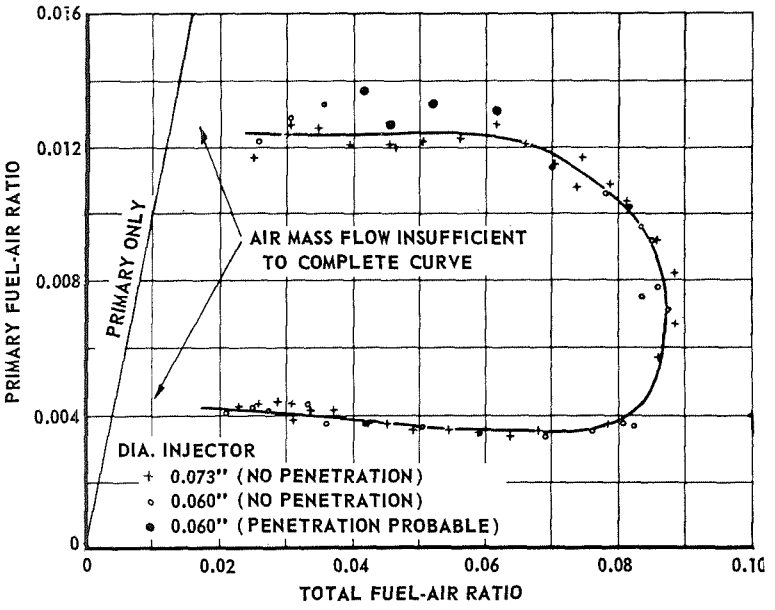

FIG. 10. Eight-inch rig—overall stability results. (PL = 300, d = 0.060, 0.073.)

pletely assessed, confirm the almost complete insensitivity of performance to primary fuel distribution under nonpenetrating conditions. These recent tests nevertheless show a reasonable sensitivity of performance to secondary fuel distribution.

Combustion Efficiency

Combustion efficiency, based on thrust measurement, was determined at constant values of secondary/primary fuel flow (i.e., by operation along the straight lines shown in Fig. 8d.) Typical

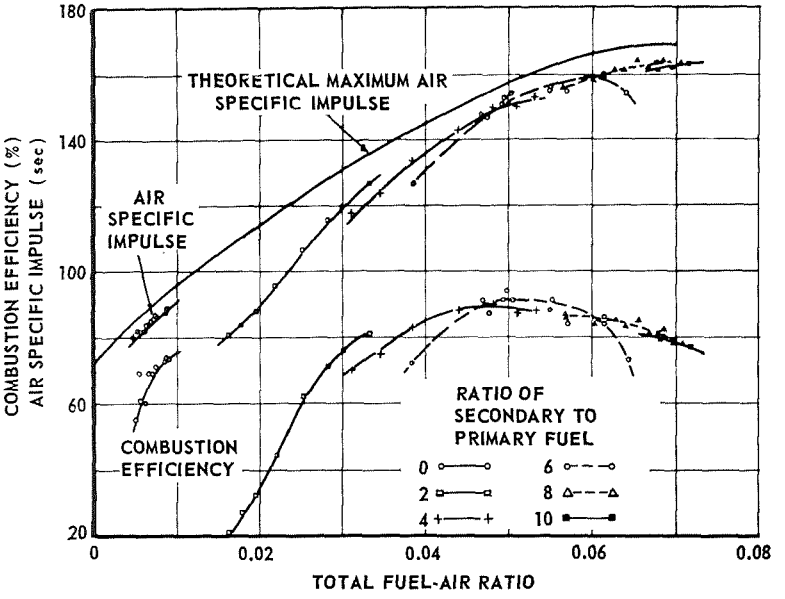

FIG. 11. Five-inch rig, air specific impulse and combustion efficiency. Effect of secondary/primary fuel flow ratio (PL = 200).

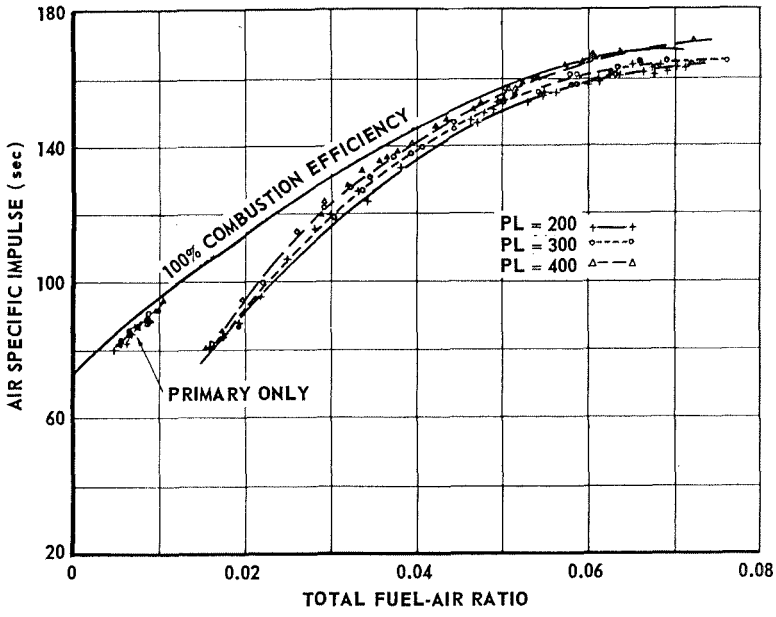

FIG. 12. Five-inch rig air specific impulse, effect of PL.

results (for the 5-inch rig at $PL = 200$) are shown in Fig. 11.

To facilitate overall comparison it is more convenient to deal with the envelope of the specific impulse curve and Fig. 12 expresses the effect of PL on the 5-inch rig results in this way. Figure 13 shows the comparison of results of the three scales at $PL = 200$, 300, and 400 (results at $PL = 135$ are omitted because the 5-inch rig final nozzle was barely choked at this condition).

In general Fig. 13 shows the agreement between scales to be very good at the lower fuel–air ratios and, although some divergence appears at richer mixtures (comparable with that caused by PL change in Fig. 12), the observation of some efficiencies over 100% indicates the divergence to be no worse than the experimental accuracy. It is also significant that the difference between 3-inch rig and 5-inch rig results at $PL = 200$ are in the opposite direction to those at $PL = 300$ and 400 so that no consistent scale effect is apparent.

Notes on Fuel Penetration Effects

The phenomenon of primary fuel penetration round the primary zone shroud was first noticed during preliminary running of the 5-inch rig when the primary injectors were initially made too small. As a result of this the injectors were redesigned on a basis of constant fuel–air momentum ratio as mentioned in the Experimental section.

Irregularities observed in many rich primary stability results can be explained on the basis of fuel penetration effects. For example, Fig. 14 shows a typical stability result together with observations of the condition at which primary fuel just starts to penetrate round the shroud (observed both with and without combustion). It is apparent that the rich extinction limit rises sharply when fuel starts to penetrate as it then burns in the secondary zone.

This behavior constitutes an important sensitivity of performance to fuel distribution which must be taken into account in scale testing. To investigate this further, a large number of observations of penetration limit were made under both burning and nonburning conditions. Although great experimental accuracy was probably not achieved in these tests, it was found possible to correlate all results empirically as shown in Fig. 15 by means of the formula:

$$Q_f = K(dQ_a/P^{1/2}L^2)^{3/2} \qquad (9)$$

where $K = 49.15$ for "cold" tests and 35.5 for "hot" tests. (See Nomenclature section for units.)

The use of the penetration limit correlation is illustrated in Fig. 6 to explain the observed dependence of primary rich stability limit on injector size. It is apparent that a sudden increase in stability occurs when the penetration limit curve meets the stability limit. (In the case

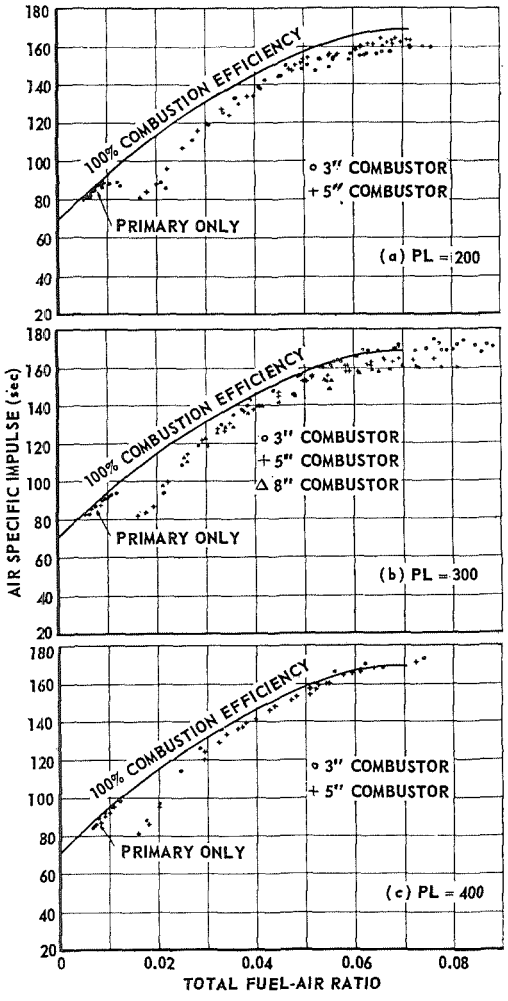

FIG. 13. Overall scaling comparison, specific impulse.

of the 0.033-inch dia. injector, no penetration occurred throughout the range of stability measurements.) A further example of the use of the penetration limit curve to explain the sudden increase in primary zone rich stability has already been quoted in Fig. 5.

The empirical penetration expression of Eq. (9) may be compared with the correlation for isolated injectors in Eq. (4). It can be shown that, using the units shown in the Nomenclature section, Eq. (9) reduces to

$$p/d = (122.0/K)(L^2P^{1/4}/d^{1/2}Q_a^{1/2}) \text{ (Momentum ratio)}^{1/2}, \quad (10)$$

so that the term in the second parentheses constitutes an empirical correction factor necessary to relate actual conditions in the practical combustor to those appropriate to a simple isolated injector. It has not yet been found possible to determine the dimensionless significance of this correction factor.

Regarding the significance of the penetration expression for scaling purposes, it can be shown that "pressure scaling" conditions together with the fundamental requirement, p/L = constant, lead, when applied to Eq. (10) to:

$$d/L^{7/6} = \text{constant}. \quad (11)$$

This leads to very different values of d from those determined by the earlier expression for isolated injectors [Eqs. (7) and (8)], where the exponent of L is $\frac{1}{2}$, or $\frac{5}{8}$, respectively.

It is now possible to assess more completely the effect of scale on primary zone stability shown in Fig. 7. Taking the 5-inch rig, 0.041-inch dia. primary injector as standard, Eq. (11) leads to .025- and .067-inch dia., respectively, for the 3- and 8-inch rig injectors necessary to preserve similarity of fuel penetration. In actual fact sizes of .024- and .073-inch dia., respectively, were used. Figure 7 shows the penetration limit curves for the ideal injectors and for those actually used. Although there is some scatter in the experimental stability limits in the penetration region, the 3-inch results (which used the .024-inch dia. injector, close to the ideal of .025-inch dia.) show some agreement with the 5-inch results. The 8-inch rig injectors were relatively too large (.073-inch dia. instead of .067-inch dia.) and so show a delayed penetration effect. (Results obtained subsequently using 8-inch rig injectors of .067-inch dia. show much better agreement with the 3- and 5-inch results.)

There is thus some indication that, despite the uncertainties of running in the penetration region (rough combustion and experimental inaccuracy usually occurred as a result of irregular combustion in the secondary region), some measure of combustion similarity can be achieved by correct scaling of the fuel penetration process.

Scale Effect in Primary Zone Performance

It has been noted that obvious scale effect exists in the primary zone stability limits (see Figs. 7 and 9) in the form of a progressive shift towards leaner mixtures (with both lean and rich extinctions) as scale size increases. In round figures the discrepancy between 3- and 5-inch rig and between 5- and 8-inch rig is about 20% for lean limits and 0–10% for rich limits.

When this effect was first encountered, the accuracy of fuel and air flow measurement was carefully checked and the total pressure profile ahead of the 3- and 8-inch combustors was cali-

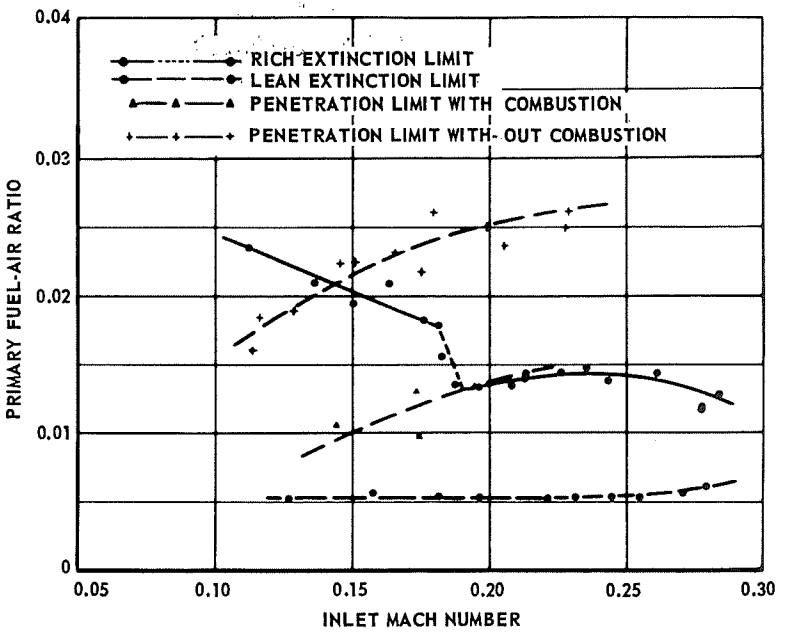

FIG. 14. Primary zone behavior, effect of fuel penetration on stability (3-inch rig, $PL = 200$, $d = 0.024$).

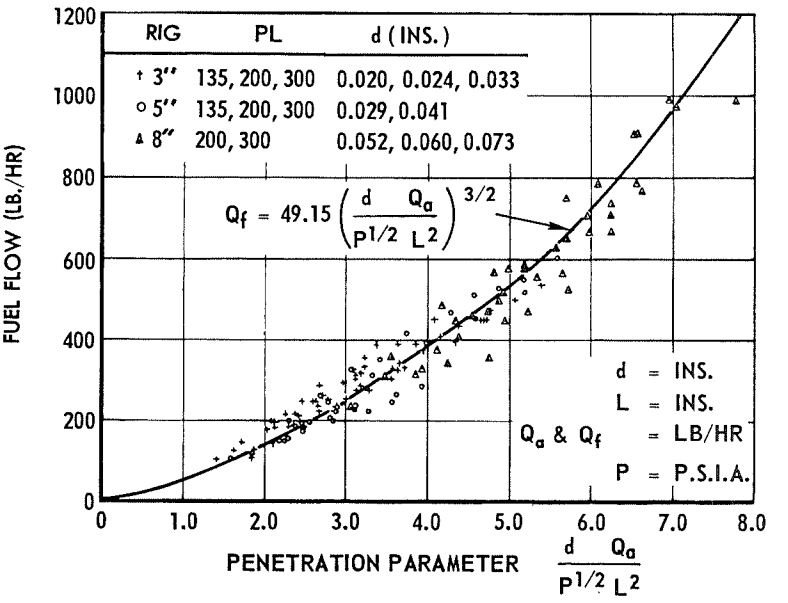

FIG. 15. Primary fuel penetration, correlation of results obtained without combustion.

brated. The latter calibration showed the difference in total pressure ahead of the primary and secondary regions to be less than 0.1% for both 3- and 8-inch rigs. As a further check the air mass flow–pressure loss relationship for the primary zones of the three combustors was calibrated under cold conditions, showing the relative mass flow of the 3- and 8-inch combustors to be about 5% high and 2½% low, respectively, compared with the 5-inch combustor. While this latter effect is in the right direction, it is insufficient to account for the observed variation in primary mixture strength.

These observations led to the belief that there was a genuine scale effect in combustion performance and the hypothesis was advanced that this was related to the increased colander metal temperatures which might be expected with increased scale.[9,10] The effect of this would be to generally widen the stability limits (see ref. 16) and also to reduce the primary air mass flow because of increased air temperature ahead of the colander metering holes. The interaction of these two influences would be to progressively lower the lean primary limit as scale increases while not greatly influencing the rich limit. This would thus be a possible explanation of the observed behavior.

More recently however, attempts have been made to measure the primary and secondary air mass flows under various operating conditions and, while great accuracy has not been achieved, there are indications that the proportion of primary air is greater in the 3-inch combustor than in the 8-inch combustor, even under nonburning conditions, and that the magnitude of this effect would be sufficient to account for the observed variation in lean stability limit.

The effect is consistent with the earlier measurements of pressure traverse and primary zone flow calibration, only if some dissimilarity exists in the secondary zone flow characteristics, and work is currently in progress to assess this. Although a firm conclusion must await completion of this work, the observations have stressed the need for accuracy of aerodynamic similarity as a prerequisite for combustion similarity.

Conclusions

The most important conclusion from this work is that pressure scaling results in reasonable combustion similarity in this type of ram jet combustor, certainly under conditions in which performance is relatively insensitive to fuel distribution. While this result is not unexpected, it is significant that even such an unpredictable effect as the existence of multiple stability loops shows similarity between scales.

The phenomenon of fuel penetration from primary to secondary zone results in marked sensitivity of performance to fuel distribution under some operating conditions. Even in these circumstances there is some indication that reasonable combustion similarity may be achieved when the required fuel penetration conditions are fulfilled (this is very nearly the case in Fig. 7).

The empirical relationship found to predict the phenomenon of primary fuel penetration in this combustor bears little resemblance to that found for ideal isolated injectors and it must be concluded that, pending further work, practical combustors must be individually investigated with respect to their fuel distribution behavior.

The only pronounced scale effect observed in this work is that in primary zone mixture strength and this appears to be related to dissimilarity of air flow distribution, an effect which is being further investigated.

Nomenclature

d	injector inside diameter [inches]
f	Fuel–air ratio, Q_f/Q_a
D	Diffusion coefficient [ft²/sec]
k	Constant
K	Constant
L	Linear dimension (typically combustor duct diameter) [inches]
n	Exponent in penetration expression
p	Penetration distance [inches]
P	Total pressure upstream of combustor [psia]
Q	Mass flow (of fuel or air) [lb/hr]
v	Velocity (of fuel or air) [ft/sec]
ρ	Density (of fuel or air) [lb/ft³]

$\rho_f v_f^2/\rho_a v_a^2$ is the fuel–air momentum ratio

[Total fuel (primary and secondary)]/(Total air) is the total fuel–air ratio

(Primary fuel)/(Total air) is the primary fuel air ratio

Subscripts

a	Air
f	Fuel

ACKNOWLEDGMENTS

The investigation reported here has been the subject of effort by a team of workers. The authors particularly wish to thank Messrs. M. V. Nesbitt and B. G. Catchpole, who appear as joint authors in the complete documentation on the work. They also wish to thank Mr. C. N. King, who carried out the early work on fuel distribution, for helpful advice and assistance on this subject and Mr. R. E. Broughton for current experimental work.

Thanks are also expressed to Messrs. F. T. Splatt and K. D. Riley for practical assistance with rig maintenance and operation and to Mrs. M. Cox and Mr. J. Purdy for computational effort.

Permission to publish this paper has been granted by the Chief Scientist, Australian Defence Scientific Service, Department of Supply, Australia, to whom appreciation is expressed.

REFERENCES

1. STEWART, D. G.: N.G.T.E. Memorandum M129, October 1951.
2. STEWART, D. G.: *Selected Combustion Problems II*, (*AGARD*) p. 384. Butterworths, 1956.
3. HERBERT, M. V. and BAMFORD, J. A.: N.G.T.E. Report R179, August 1955.
4. BRAGG, S. L. and HOLLIDAY, J. B.: *Selected Combustion Problems II*, (*AGARD*) p. 270. Butterworths, 1956.
5. WAY, S.: *Ibid.*, p. 296.
6. WELLER, A. E.: *Ibid.*, p. 371.
7. ROSS, C. C.: *Ibid.*, p. 444.
8. CROCCO, L.: *Ibid.*, p. 457.
9. LEFEBVRE, A. H. and HALLS, G. A.: *Advanced Aero Engine Testing*. Pergamon, 1959.
10. HERBERT, M. V. and LEFEBVRE, A. H.: N.G.T.E. Memorandum M324, February 1959.
11. KING, C. N.: N.G.T.E. Report R149, May 1954.
12. LEWIS, W. G. E. and DRABBLE, J. S.: N.G.T.E. Memorandum M264, June 1956.
13. DRABBLE, J. S.: N.G.T.E. Memorandum M310, January 1958.
14. LONGWELL, J. P. and WEISS, M. A.: Ind Eng. Chem. *45*, 667 (1953).
15. BEETON, A. B. P.: N.G.T.E. Report R154, March 1954.
16. WILLIAMS, G. C.: J. Aeronaut. Sci. *16*, 714 (1949).

Discussion

DR. M. G. PERRY (*Sheffield University, England*): Would the authors comment on the figure showing primary fuel/total air ratio against inlet Mach number for various injector sizes? It seems that if the step change in the curves is due to primary fuel leakage into the secondary zone, then this method of plotting is oversimplifying the picture, if we don't know the amount of leakage. If we do know it, then it ought to be possible to modify the primary fuel/total air ratio to allow for this, and so obtain a smooth curve.

DR. D. G. STEWART (*Aeronautical Research Laboratories, Australia*): It is true that if the amount of fuel leaking into the secondary zone were known, it would be possible to express the results in terms of effective primary fuel flow, and there is little doubt that a unique curve for all primary injector sizes would result.

However, our objective was to express the results in such a way that sensitivity to fuel distribution was made apparent, and the figure referred to, together with that showing the final scaling comparison, stress the sensitivity of performance to fuel distribution and indicate that if this process is correctly scaled, overall combustion similarity is achieved.

DR. J. O. ELLOR (*Rolls-Royce, England*): I am particularly interested in the weak extinction characteristic quoted by Stewart. It occurs at a primary fuel/total air ratio of .005 independent of the PL and M range investigated, at a vitiated temperature of 200°C.

Now, if the weak extinction is expressed in terms of primary fuel/primary air ratio, as it should be, the value will increase to 0.0334—the primary air being some 15 per cent of the total air flow. Adding to this the amount of fuel burned initially to raise the air temperature to 200°C (about 0.006 fuel/air ratio) gives an overall primary flow weak extinction of 0.04 which is 0.60 equivalence ratio.

This is, in fact, the same ratio weak extinction as that quoted in my paper for gutter stabilization at 700°C. We also found the weak extinction fuel/air ratio to be independent of gas conditions over about the same range as Stewart both in respect of M range and of pressure range (his minimum PL of

135 corresponds to 7.0 psi on the 18.0-inch full-scale combustor).

We appear independently to have found the fundamental local weak extinction characteristic of a kerosene–air mixture using very different geometries of burner and values of gas temperature.

DR. D. G. STEWART: The point raised by Dr. Ellor is most interesting. Although in our work precise determination of primary air mass flow is difficult, we have made preliminary observation of this quantity and find it to be 10–15% of the total air flow. Thus, the comparison quoted by Dr. Ellor is valid and does show a lean equivalence ratio of about 0.6 in his work and ours, independent of operating variables. This agreement, for two very different combustor types, gives promise of its general application to other combustors.

DR. A. J. GERRARD (*Lucas Gas Turbine Equipment, Ltd.*): In his paper Dr. Stewart correctly emphasizes the importance of fuel distribution in the scaling exercise. To spray a pencil-jet of fuel directly opposing an air stream requires precision setting of the injectors, even in Fig. 2 a slight asymmetry of the fuel plume can be observed; and in addition, fuel would be entrained in the aerodynamic wakes downstream of the injector stems. Could Dr. Stewart describe their limits of accuracy in positioning the injectors, and also could he comment as to what extent a small angle of yaw, say half a degree, would make to the resulting fuel distribution and combustion efficiency?

DR. D. G. STEWART: Realizing the importance of fuel injector alignment, reasonable care was used throughout in the positioning of fuel injectors. In the case of primary injectors, a special jig was used to position them, both as regards radial location and axial direction and the latter property was further checked by setting the assembled injector block vertically and flowing fuel upwards under static air conditions—a very sensitive test of flow alignment. It is estimated that setting accuracy of the order of $\pm 1/10$ degree would result.

In the case of secondary injectors, normal machining accuracy was used as the relatively smaller fuel penetrations in this case would be expected to make alignment less critical.

It is now felt that the setting accuracy in both cases was greater than necessary and that misalignments of about one degree would not show significant performance changes.

MODELING STUDIES OF BAFFLE-TYPE COMBUSTORS

H. C. HOTTEL, G. C. WILLIAMS, W. P. JENSEN, A. C. TOBEY, AND P. M. R. BURRAGE

Geometrically similar ramjet-type combustion chambers of 1.61, 4.026, and 6.065-inch diameter and lengths of 5.25D and 4.25D were operated at Reynolds numbers ranging from 24,000 to 230,000 and ambient pressure levels from 0.2 to 1.5 atmospheres, with propane fuel. Flameholders were annular V-gutters having a leading-edge included angle of 30° and producing 44% blockage of the combustor cross section. Excepting the wall thickness of some burners, all dimensions of burners, flameholders, upstream piping and mixing sections were scaled in proportion to burner inside diameters.

Analysis indicated the importance of keeping the following parameters constant if the model experiment was to reproduce prototype performance:

a. Reynolds number, $DU\rho/\mu$.
b. Chemical loading parameter, $k\rho^{n-1}D/U$.
c. Mach number, M U/C.
d. External heat-loss group, $\lambda_G/D[(L_w/\lambda_w) + (1/h_{c+r,0})]$.
e. Helmholtz resonator group $(D^3/V)^{\frac{1}{2}}/M$.

Analysis indicated the probable importance of group d above—the external heat-loss group—and a poorer performance to be expected of larger burners modeled by use of groups a and b alone, because of abnormally high external loss from large burners. An experimental study of the effect of wall losses, using emissivity control or radiation shielding, confirmed the analysis and explained some of the deviations in burner efficiency results of modeling based on groups a and b alone. This indicated the importance of including group d if the prototype walls run hot.

Longitudinal, tangential, or radial oscillations that may occur in modeled combustors are scaled only if the Mach number is kept constant. As indicated above, this is automatic with modeling based on Reynolds number and the chemical loading parameter if, but only if, the pressure exponent n is 2.

Introduction

The purpose of this work was to discover the chemical and flow parameters characterizing the modeling of ramjet-type burners. This work has been more fully described in reports of limited distribution.[1,2]

Interest in model studies is twofold, to improve understanding of combustion in turbulent flow (a process too complicated for rigorous mathematical analysis), and to save time and expense of propulsion engine development. Clearly the number of groups retained for the second interest may be less than for the first. Theoretical analyses of modeling for flow systems with combustion have been more numerous than experimental modeling programs. Among outstanding analytical papers in the field are those listed as references 3 to 11 inclusive. Noteworthy papers that report experimental similitude studies of air-breathing combustors are references 12 to 17 inclusive.

Depending upon the viewpoint of the analyst several different techniques have been used for finding the modeling parameters pertinent to given problems. The analysis used here was to write expressions for all the forces and transport processes conceived to be involved and combine these into parametric groups governing similitude between a prototype and its model. Some of the groups are mutually incompatible, and establishment of which groups can be neglected in characterizing performance must in some cases be done experimentally.

In operation of a ramjet-type combustor fed with a homogeneous gaseous fuel-air mixture the forces involved are:

1. Momentum, ρU^2D^2.
2. Viscous, $L^2(U/D)$.

3. Pressure-area, PD^2.
4. Buoyancy, $(\rho - \rho_a)gD^3$.

The terms which describe the mass conversion or transport are:

5. Feed rate, ρUD^2.
6. Gas diffusion, $D^2\mathfrak{D}\rho/D$.
7. Overall chemical reaction, $kD^3\rho^n$. (Consideration of chemical reaction is here limited to an overall result, with the same fuel, fuel/air ratio, and inlet temperature in all tests.)

Expressions for energy conversion or transport are:

8. Combustion, $UD^2\rho Q$, where Q is heat of combustion.
9. Convection, $UD^2\rho CT$.
10. Conduction, $\lambda_G D^2 T_0/D$.
11. Radiation from a gas volume to a boundary (gray system),[18]

$$q = 4E_B D^3 (d\epsilon_G/dx)_{x\to 0}$$

$$= 4KPD^3\sigma T_0^4 f_1(KPD, \epsilon\text{'s, shape}),$$

where K is the absorption coefficient for the gas, KPD is the dimensionless optical depth, and ϵ is the surface emissivity.

12. Radiation from a surface to a surface, $D^2\sigma T_0^4 f_2(KPD, \epsilon\text{'s, shape})$.
13. Rate of convective heat loss to wall,

$$h\,D^2(T_0 - T_a) = (\lambda_G/D) f_3(\mathrm{Re}, \mathrm{Pr})\, D^2(T_0 - T_a).$$

14. Rate of external heat loss,

$$(L_w/\lambda_w + 1/h_0)^{-1} D^2(T_0 - T_a)$$

where L_w is the wall thickness, not necessarily scaled to D.

All the quantitative statements concerning the combustion process can and must be built up from ratios formed within these groups, ratios formed from considering boundary conditions, and scale ratios which describe the geometry of the system. From the above groups twelve independent modeling parameters have been formed (counting ϵ's as one; and not counting the E/RT_0 term which appears in the kinetic constant nonlinearly and which is therefore in principle a thirteenth group). Some elimination is possible, however, including:

(a) The Schmidt number, ratio (5/6)/(1/2); and
(b) The Prandtl number, ratio (9/10)/(1/2), which may justifiably be assumed constant;
(c) The inside wall emissivities, which will be identical in model and prototype;
(d) The group formed of (8)/(9) and the group E/RT_0 because of restriction to a single fuel and fuel–air ratio;
(e) The group (13)/(9) since according to (d) the temperature ratio is modeled, allowing no new groups to appear in this parameter.

Of the remaining seven parameters, the modified Froude number, $U^2\rho/gD\,\Delta\rho$ will be so high that buoyancy effects may be neglected. The residual six parameters, most in dimensional form as a result of dropping physical properties and of taking ρ proportional to P, are:

From the Group	Parameter	
(1)/(2)	DUP	Reynolds number
(1)/(3)	M	Mach number
(5)/(7)	U/DP^{n-1}	Chemical loading
(11)/(9), (12)/(9)	PU PD	Basic radiation group Extinction coefficient group
(13)/(14)	$\left(\frac{\lambda_G/D}{\lambda_w/L_w} + \frac{\lambda_G/D}{h_0}\right)$ or $D^{-1}[(L_w/\lambda_w) + (1/h_0)]$	(wall + external)/(internal) thermal resistance ratio

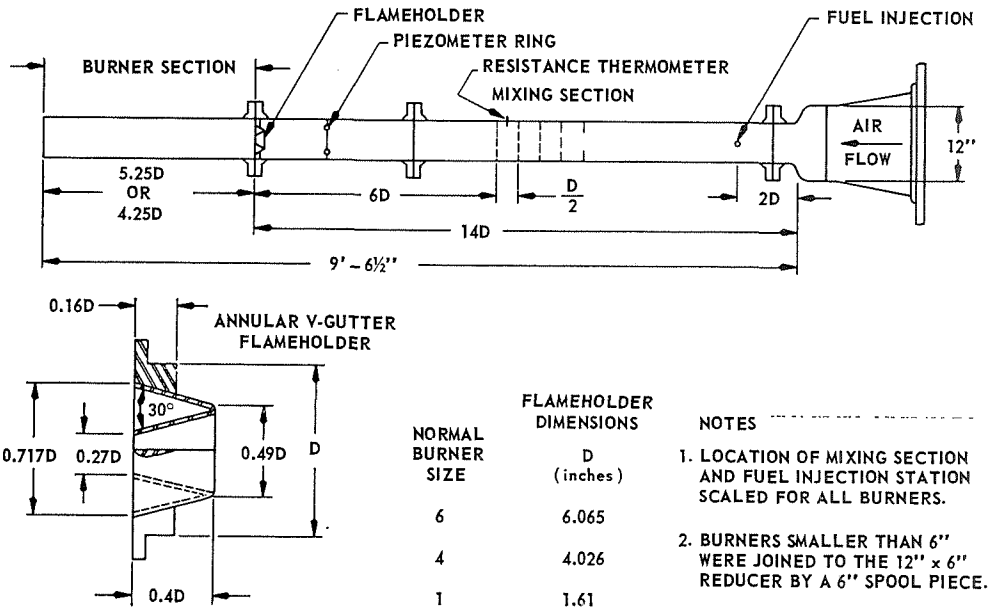

FIG. 1. Schematic of ramjet burner equipment.

Experience in this laboratory and elsewhere has shown that, for sub-atmospheric operation and combustor inlet Reynolds numbers between 20,000 and 200,000, both the Reynolds number and the chemical loading parameter are important, with their relative importance dependent mainly on the operating pressure level. NACA results[19] (not intended as modeling experiments) show convincingly the dependence on chemical kinetics at low pressures and the controlling influence of flame spreading (mixing), a function of Reynolds number, at higher pressures.

In most earlier work experimental results have been evaluated in terms of only two scaling parameters, the chemical loading group, proportional to $U/P^{n-1}D$, and the Reynolds number, (proportional to UPL with the assumptions and limitations outlined above). However, it is necessary to consider whether difficulty may arise if there is a range of velocities in which both Reynolds and Mach number are of some importance. The product of UPD and $U/P^{n-1}D$ indicates that for scaling, U^2/P^{n-2} must be constant from model to prototype. But the Mach number requires that U must also be constant. Thus, it is obvious that the Reynolds and Mach numbers are compatible scaling parameters only if the pressure exponent, n, is 2.0.

Assuming that either the Reynolds or the Mach number is influential, it and the chemical group should allow modeling, with all its implications, such as identity of temperature, velocity, and composition profiles at corresponding positions in model and prototype burners. This ideal situation is possible only (1) for a system in which radiant heat losses are of little importance since it is not possible to scale radiant heat loss from gas to walls by maintaining the Reynolds number constant; and (2) for a system in which the external and internal wall heat losses can be kept in step.

The primary interest here was to test modeling principles with ramjet type burners having symmetrical flameholders, over as wide as possible a range of the independent variables: velocity, pressure, and burner diameter. Combustion efficiency was the primary criterion of modeling. No attempt was made to set up experiments in which the heat-transfer parameters would be used quantitatively, but these were used qualitatively in the arrangement of experiments that appear to explain anomalies in the results obtained without consideration of heat losses.

Apparatus and Procedure

Figure 1 shows the burner apparatus schematically. Metered air was fed to the system through a silica-gel dryer and a preheater.

Natural-gas propane (about 96% propane, the rest mainly ethane and butane) was fed into the air stream through nine downstream-pointing holes in each of four tubes. The mixing section comprised five baffles, with successively finer scale openings. The flameholder was an annular V-gutter for which the leading-edge included angle of the V was 30°. Its projected area blocked 44% of the duct area. The flameholder was supported by four streamlined struts anchored between flanges that joined the burner and upstream piping. A spark igniter remained in place but not in operation after the burner had been lighted.

The burner inside diameters were 1.610 inch, 4.026 inch, and 6.065 inch. With the exception of flanges and in some cases wall thickness, all dimensions of the burners, flameholders, upstream piping, and mixing sections were scaled in proportion to burner inside diameters. Since nonexact scaling of the wall thickness made no detectable difference in results, some burners were used with wall thickness left larger than called for by scaling to the thickness of the 6-inch burner wall. Burners were either 5.25 or 4.25 diameters in length, measured from the flameholder leading edge to the tailpipe exist plane.

The 1.6 inch burner assembly was mounted vertically in a pressure vessel 3 feet in diameter by 8 feet high, and fitted at its upper end with valving which permitted pressure control above or below atmospheric. The flame was quenched by both dilution air and water sprays. Subsequently each of the three burner assemblies (1.6, 4, and 6 in.) was mounted in the 14 foot-long test section of an altitude chamber 4.5 feet in diameter and 50 feet long. The exit plane was kept in the same position for each burner (in line with an observation port) and dimensions were scaled from the tailpipe exit. The altitude chamber provided water quenching of the flame, and discharge of combustion products to absolute pressures between 0.05 and 1.0 atmospheres.

In all work the air was preheated to give a propane–air mixture temperature of about 250°F (710°R). Because of thermal inertia in the piping system the actual temperatures ranged between 700 and 730°R.

For efficiency measurements combustion products were sampled at the tailpipe exit plane, using a 6-point traverse (3 equal areas) for the 1.6 inch burner and 10-point traverses (5 equal areas) for the larger burners. Two water-cooled pitot-type sampling probes were used, one having a 0.040 inch bore, with the 1.6 inch burner, and one having 0.082 inch bore, with the 4 and 6 inch burners.

Combustion product samples were routinely analysed for oxygen with a paramagnetic oxygen analyzer. Conversion of these readings to local combustion efficiency was based on the assumptions that (a) products of fuel-lean combustion included only N_2, O_2, CO_2, H_2O vapor and unburned propane; (b) the sample remained unchanged chemically during sample quenching in the probe; (c) all water vapor was condensed or absorbed before the sample reached the oxygen meter; and (d) nitrogen was the only background gas in the analyzer. The effect of assuming all other gases to behave like nitrogen in the oxygen analyzer has been estimated to cause errors not exceeding 1% in the efficiency determination. A larger error (3–5%) was caused in some cases by the presence of an appreciable amount of carbon monoxide in the combustion products, the CO being disclosed by about a score of complete product analyses made with gas chromatography equipment.

Determination of a weighted arithmetic mean combustion efficiency and isokinetic sampling required measurement of local velocities. This was done using impact and static pressure measurements and a local total temperature calculated to correspond with the measured oxygen-consumption efficiency. A check on accuracy was obtained by comparing the mass flow so determined with that indicated by metering upstream of the burner. With due care to keep condensed moisture (in the probe) from spoiling the kinetic head measurements, the two mass-flow values agreed within about 5%.

Burner Stability Studies

Because of primary interest in efficiency studies, stability measurements were limited to the minimum necessary to establish the velocity range of stable operation and to check the reproducibility of burner operation.

Blowout velocity data are generally correlated by the expression

$$U_{BO}/P^a D^b T^c = F(f/a),$$

where U_{BO} is the burner-inlet velocity at blowout, f/a is the fuel/air ratio, and the other terms have their usual significance. Spalding,[20] DeZubay,[21] and Zukoski[22] have discussed the ways in which P, D, and T enter. Reasoning from the influence of pressure on flame speed, the exponent a should be, and usually is, near unity, although sometimes as low as 0.8 and as high as 2. The exponent b is generally between 0.5 and 1.0 and depends upon the flameholder configuration and blockage. (In a comment on the work of

Lefebvre and Halls,[17] Zukoski contends that this exponent is always unity if the flow is turbulent and if the "correct" characteristic dimension, the length of the recirculation zone, is used. We would observe that it is easier to know the dimension of the hardware than of a flame zone). On theoretical grounds one would expect c to be about 2.

Representative blowout velocity data for 4.25D burners are shown in Fig. 2. Here P_2 is the ambient pressure. In this work the inlet temperature varied somewhat with mass flow changes approaching blowout. In an early phase of this work[1] a temperature exponent of 2 satisfactorily correlated lean blowout limits when inlet temperature ranged from 560 to 710°R. Therefore lean limit velocities are adjusted here by the ratio $(710/T)^2$. For rich limits adjustment by the ratio $710/T$ gave better results. The significance of this finding may be that lean limits are more dependent on chemical kinetics, rich limits more on mixing.

Figure 2 shows that correlation on the basis of U_{BO}/P_2D is good for the 4 inch and 6 inch 4.25D burners for both rich and lean limits, with much less scatter than occurred with longer burners. Results with the 1.6 inch burner, however, show a shift to somewhat richer limits on both sides of the curve, as compared with the larger burners. Model analysis indicates that Reynolds number, as well as the chemical loading group, might be a factor in modeling blowoff. Examination of the data, however, gives no indication that the correlation would be significantly changed by including Reynolds number as a factor, above the minimum Re of 25,000 studied here.

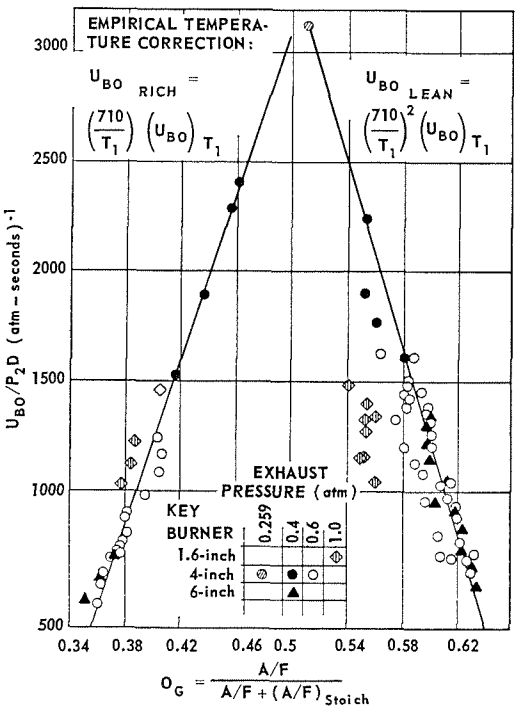

FIG. 2. Stability limits of 4.25D burners.

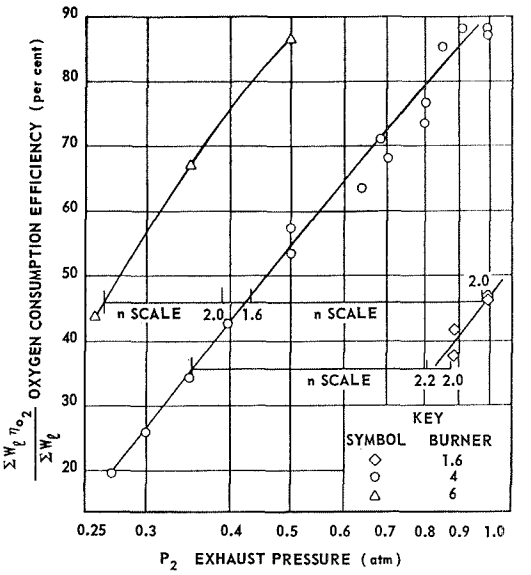

FIG. 3. Combustion efficiency of 1.6, 4, and 6 inch 4.25D burners at 108,000 Reynolds number.

Combustion Efficiency

In this study burner efficiency was defined as the attained fraction of the theoretically possible enthalpy increase due to combustion, and was approximated by an oxygen consumption efficiency, defined as:

$$\eta_{O_2} = \frac{O_2 \text{ required} - (O_2 \text{ measured} - O_2 \text{ excess})}{O_2 \text{ required}}.$$

In all of the efficiency studies the burner inlet temperature was approximately 720°R and the mixture ratio slightly leaner than stoichiometric, $O_G = 0.51$.

Although a loading group based on a second-order chemical reaction serves fairly well to model gas turbine combustors, it is appropriate first to consider the ramjet performance data in relation to reaction order n. Figures 3, 4, and 5 show results of experiments on burners of each of three diameters and two length/diameter ratios—all the data taken at a single Re of 108,000 to

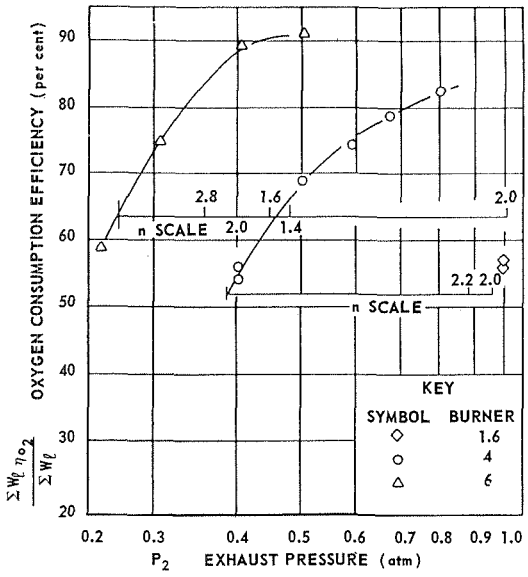

FIG. 4. Combustion efficiency of 1.6, 4, and 6 inch 5.25D burner at 108,000 Reynolds number.

eliminate possible effects of that variable. On the assumption that burner performance can be characterized by Reynolds number and loading factor alone, these data may be used to determine the value of the pressure exponent n which makes the loading factor, $U/P^{n-1}L$, constant for fixed efficiency and Reynolds number. Thus the curves for two values of L should differ only in the use of L as abscissa rather than $(U/P^{n-1}L)/(PUL)$ or P^nL^2; and a horizontal shift of the efficiency-pressure curve for apparatus of size L_1 by an amount equal to $(2/n)$ log L_2/L_1 should superimpose the curve onto that applicable for apparatus of size L_2. Visually the constancy of n is judged by whether a horizontal shift superimposes curves, and the value of n corresponds to the amount of the shift required. In each plot appears a horizontal n-scale applicable to the relative shift of data sets for two or three apparatus sizes, the scale being anchored in each case at its left end to the performance curve acting as standard.

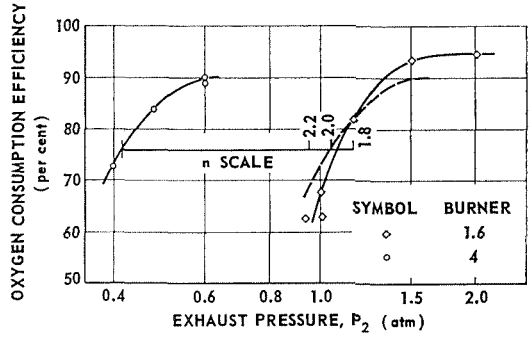

FIG. 5. Combustion efficiency of 1.6 and 4 inch long burners (early results) at 108,000 Reynolds number.

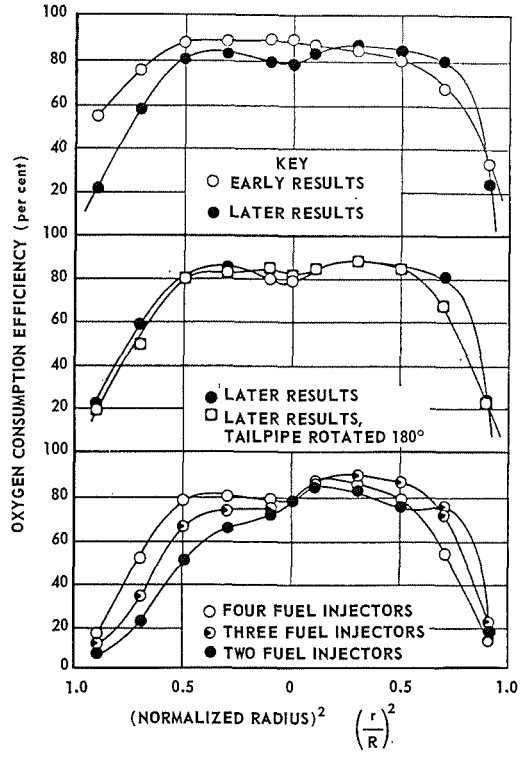

FIG. 6. Efficiency profiles for 4 inch, 5.25D burner at 108,000 Reynolds number and 0.4 atmosphere exhaust pressure; effect of mixing and fuel-injection distortions.

Consider first the "short" (4.25D) burners, Fig. 3. Comparing the 1.6 inch burner with the other two indicates an n between 1.9 and 2.1; comparing the two larger burners indicates an n of about 1.6. Performance of the "long" (5.25D) burners changed stepwise with time in an unexplained way (see later discussion). The more recent data appear in Fig. 4. They indicate an n of about 2 based on a comparison of the 1.6 inch and next larger burner, about 1.8 based on its comparison with the largest; but these data do not include a significant range of performance of the smallest burner. Comparison of the two

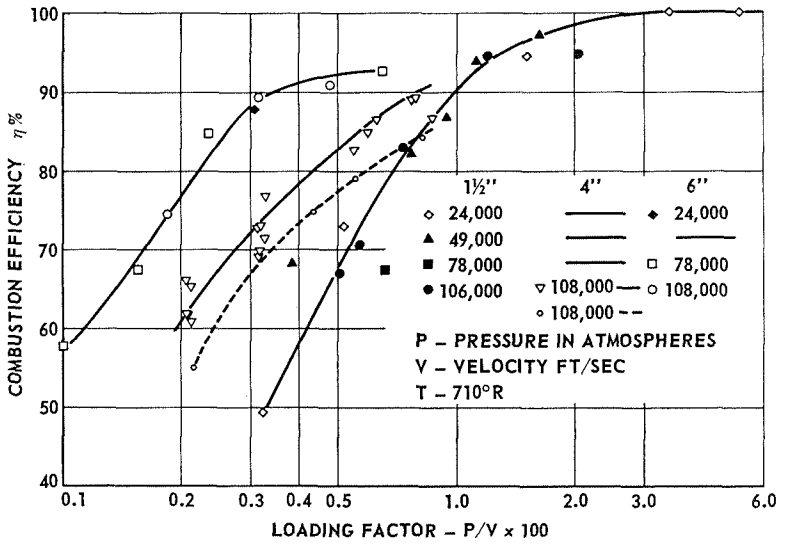

FIG. 7. Correlation of combustion efficiency against loading factor with $n = 2$.

larger burners indicates an n varying from about 1.6 at the lowest efficiency to 1.2 at the highest. Figure 5 shows earlier and more extensive data on the 1.6 inch burner for comparison with the 4 inch one; and n is seen to vary from 1.9 at low efficiency to 2.2 at 90%. The possible effects on n of failure to model external heat losses will be discussed later.

Difficulties in obtaining reproducible efficiency data are illustrated by distorted profiles of local efficiency, as in Fig. 6. Apparently the burner-flameholder combination was extremely sensitive to upstream variables or boundary-layer variables that were not reproduced from one period of use to another of the same apparatus. Figure 6 (top) shows that the flame failed to develop in the boundary layer on the left side, in the second running of a particular experiment. When the tailpipe was rotated 180° (Fig. 6, center) there was essentially no change, implying that the disturbing influence was upstream of the flameholder plane. To test the adequacy of upstream fuel-air mixing, experiments were made with the fuel injection pattern intentionally distorted. There was first a normal use of all four fuel injectors; next the same total fuel flow was put through only three injectors; and finally through only two injectors. The results (Fig. 6, bottom) indicate that distortion of the fuel injection pattern was indeed reflected downstream in distortions of the combustion efficiency profiles. These intentionally imposed distortions represented a radical extreme and a severe test of the mixing system, yet the resulting efficiency profiles were not more distorted than they had sometimes been with no known disturbing influence present.

Early results with a flat-cross flameholder on the effect of loading parameter on efficiency for different fixed Reynolds numbers indicated a downward trend of η with decreased Re. Later results on the V-gutter described here failed to substantiate the effect. If an n of 2 is accepted, η should then vary primarily with PD/V. Figure 7 shows the P/V relationship for the three burner sizes, with Reynolds numbers varying fourfold within each of two of the sizes. On the middle-sized burner great difficulty was experienced in reproducibility, and two curves are presented. No change was made except in tailpipe replacement between the two sets of data. If there is no Re effect, the curves should superimpose by horizontal displacement proportional to log D. This can be seen to be approximately the case at low values of η. A (6/1.5) displacement of the 6 inch curve to the right puts it on the 1.5 inch curve at its lower end but causes it to lie markedly below the 1.5 inch curve at high values of PD/V. As indicated later, this is to be expected when external losses are not modeled. Within the accuracy of the data, no Re effect is detectable, although there is every reason to expect an effect at lower values than investigated here, or in a chamber design more sensitive to mixing.

Deficiencies of Two-Parameter Modeling

As a rule of thumb for scale-up, the results of this modeling study indicate that scaling can be based on constancy of a loading factor based on an n of 2, provided Re is above the lowest value studied here (24,000). This conclusion is quite commonly given for turbojet and ramjet combustors. In this and other cases, however, it represents only a rough average of the experimental results. The most important qualification on loading-parameter modeling is that the pressure exponent, in any set of experiments, tends to vary with the factors that affect burner efficiency because it is left with the burden of making a single parameter suffice as the influence of others becomes increasingly significant. Among the factors believed to cause such variation of n are heat losses through burner walls, turbulence variations, acoustic instabilities and compressibility. Certain experiments were conducted to show the influence of these phenomena on burner modeling.

Heat Transfer Effects

Internal heat transfer from gases to walls is so dominantly due to convection as to justify concluding that radiation terms would have little importance in establishing internal modeling criteria. But the ratio of internal to external thermal resistance requires consideration. Heat loss by radiation from the burner walls to the surroundings becomes increasingly important as the surface temperature rises. External heat loss is not automatically scaled in geometrically similar systems. The ratio of wall-plus-external to internal thermal resistance, which must be kept constant from model to portotype to assure identical wall temperatures in the two, is:

$$\left(\frac{\lambda_G/D}{\lambda_w/L_w}+\frac{\lambda_G/D}{h_0}\right) \quad \text{or} \quad \frac{\lambda_G}{D}\left(\frac{L_w}{L_w}+\frac{1}{h_0}\right),$$

where L_w and λ_w refer to the thickness and thermal conductivity of the wall, and λ_G to conductivity of the gas. Since λ_G is not subject to change, it can be dropped; and h_0 can be expanded to indicate its representing convection plus radiation. The resulting dimensional group is

$$D^{-1}\left[(L_w/\lambda_w)+(h_{0,c}+4\sigma\epsilon_w T_{Av}^{3})^{-1}\right].$$

In this expression ϵ_w is the outside wall emissivity and T_{Av} is a mean temperature, approximately an arithmetic mean of wall and surroundings. Since T_{Av} varies along the wall, any means of keeping model and prototype rigorously in step must not involve use of different temperature levels for the two.

Consider now a model and prototype of dimensions D and $2D$. Assuming realistic values for the individual factors in the expression above, it appears that the first term in the parentheses is insignificant compared with the second. For the $2D$ prototype the second term must be doubled to keep the wall temperature constant, i.e., the group to be kept constant is $D(h_c+4\sigma\epsilon_w T_{Av}^{3})$. Strictly speaking the only remaining possibility is to halve both h_c and ϵ_w on the $2D$ prototype. In the experimental setup external convection was not controlled. On those parts of the wall running markedly hotter than 1200°R the radiation term became relatively more important; if the wall were hot enough it would suffice simply to halve ϵ_w. The conclusion is that, in general, it is impossible to scale without having control of the external h_c; that approximate compensation for lack of change in h_c may be made by making $\epsilon_{w,2}/\epsilon_{w,1}$ equal to

$$(D_1/D_2)+(h_c/h_{r_1})\left[(D_1/D_2)-1\right],$$

and that in the limit, as $h_r \gg h_c$, maintaining constancy of $D\epsilon_w$ fully satisfies the external heat transfer modeling criterion.

The conclusion that the external conductance of small equipment must be higher than that of its larger prototype appears to conflict with the widely used conclusion that pilot-plant operation of chemical processes must be watched to prevent excessive heat loss because of the abnormally high surface/volume ratio. There is no conflict; the present system, when small, is operated at an elevated pressure if it is to model a large one; and this is the source of the higher intensity reaction that necessitates increasing the specific surface losses to keep them in step with the burning rate. Thus the large low-pressure combustor tends to run colder than its small high-pressure model. On the other hand, for any given combustor the absence of external thermal modeling introduces increasing error as the pressure rises.

An experimental determination of the importance of heat loss from burner walls was made by the use of burners from which radiation was qualitatively controlled. In the first instance a 4 inch, $5.25D$ burner was gold-plated to a thickness of 0.0002 inch to reduce its emissivity from about 0.9 to about 0.04. The burner was operated at the same Reynolds number, 108,000, and the same range of pressures as had been used with an unplated stainless steel burner. The overall efficiency data (Fig. 8, bottom and middle

curves) show a marked improvement at the higher pressure for the plated burner, but not that corresponding to complete coverage with gold since the gold on the last diameter of tailpipe rapidly disappeared, presumably by infusion into the steel. In a second experiment the gold-plated burner was fitted with radiation shrouds, slipped over the tailpipe, with each shroud separated concentrically by 5/8 inch spacer rings placed at the ends and middle of the annuli. The burner was operated with and without the shrouds, and the overall efficiency data appear as the top curve in Fig. 8. The effect of shielding is primarily to increase combustion efficiency near the walls, an increase amounting to 10 to 45%. At a pressure level of 0.6 atm the gold-plated tailpipe was as effective as the shroud arrangement; the gold plating was still intact during that operation. The results show conclusively that unscaled external heat losses from geometrically scaled burners can seriously affect performance and prevent simple correlation of the data, and this effect should be accentuated by lengthening the burner and thereby producing a hotter tailpipe. The shapes of the left-hand curves of Figs. 5 and 7 are such that correction for unscaled external loss would reduce variation of n.

The question arises as to how far the modeling criteria established in this work are applicable to vehicles in flight in view of the enormously different external environment of the latter. If performance of a vehicle in flight is to be simulated, control and modeling of its external thermal resistance must be included. It is justifiable to conclude that if loading parameter and external-loss parameter are included and Reynolds number is above a critical minimum value, the model simulates the prototype. This section has served primarily to underline the conclusion that the external loss parameter, not mentioned in most discussions of modeling, can be important.

Turbulence Effect

Turbulence in a combustion system can cause marked increases in the rate of heat transfer, combustion intensity, and rate of flame spread. The increase of apparent flame speed is advantageous to efficiency and utilization of combustion space. An increase in the rate of heat transfer, on the other hand, may or may not be beneficial. Occurring at the walls it increases heat losses from the system and reduces combustion efficiency in gas layers near the walls. Too rapid mixing may cause rough burning and blowout.

It is generally accepted that turbulence in low Mach number flow is fully determined by the

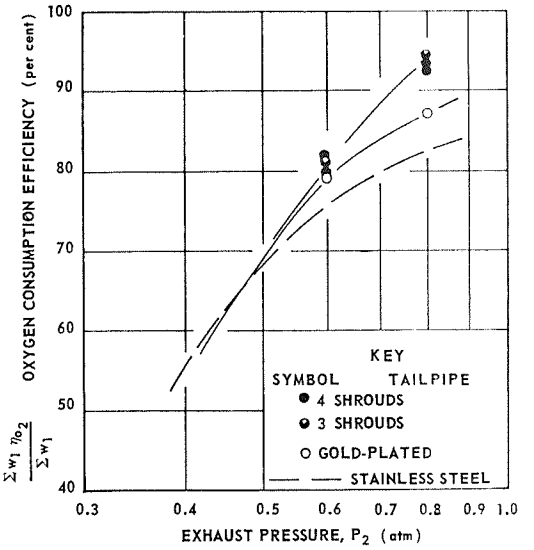

FIG. 8. Effect of radiation shielding on overall combustion efficiency of 4 inch burner at 108,000 Reynolds number.

Reynolds number, with no unique dependence upon pressure. Experimentally this view has been confirmed for pressures greater than about 0.25 atmospheres and the usual ambient temperatures. At higher Mach numbers turbulence is essentially independent of Reynolds number as well as pressure.

The idea that there may be an effect of pressure on turbulence intensity and scale, an effect which would appear at constant velocity or at constant Reynolds number, has been advanced by Khramtsov[23] in Russia, by Fine[24] of NACA, and Turano[25] of this laboratory. A pressure effect can be visualized if the molecular mean free path l is a significant variable, i.e., if it becomes comparable to a characteristic dimension of the flow. The flow condition near the wall for the case in which l is small but not negligible with respect to the body dimension L or the boundary layer thickness is called the slip-flow regime. In this case the Knudsen number, the ratio of l/L, is proportional to the ratio Mach number/Re, or M/Re. The ratio of interest here, however, is that of mean free path not to apparatus size but to an eddy scale, called the Kolmogoroff scale.

It is believed that the noncontinuum nature of the fluid motion associated with the smallest existing eddies influences turbulence intensity, that the Kolmogoroff scale is appropriate because it is characteristic of the eddy sizes responsible for the dissipation of turbulent energy in a flow

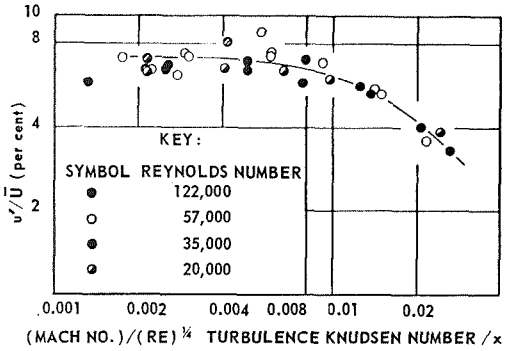

FIG. 9. Correlation of turbulence intensities by a turbulence Knudsen number (cold flow).

system; it represents the lower bound of eddy sizes. The ratio of mean free path to the Kolmogoroff scale is termed the "turbulence Knudsen number," Kn_t, which is proportional to $M/(\mathrm{Re})^{1/4}$.

Turano[25] has conducted an experimental study of rarefaction effects in low speed turbulence for the 6 inch model ramjet approach piping. Measurements were made with a hot-wire anemometer of the relative turbulence intensities in cold flow of air over a range of Reynolds numbers and at pressures between 0.04 and 1.0 atmosphere. The measurements were made at the center of the flameholder plane with the flameholder and tailpipe removed. For all Reynolds numbers at pressures less than about 0.2 atmosphere, the turbulence intensity was found to decrease with decreasing pressure and, at a fixed Knudsen number, to be a weak function of Re. When the Knudsen number was modified, as indicated above, to the "turbulence Knudsen number" $M/\mathrm{Re}^{1/4}$, turbulence intensity was found to depend on the latter only, and to be substantially constant below $M/\mathrm{Re}^{1/4} = 0.006$. Figure 9 shows the data.

Turano's findings imply that among burner modeling parameters either Kn or Kn_t should be included, to account for a rarefaction effect at low pressures. If loading factor (with $n = 2$) and Re are used as modeling parameters there is no problem because Kn_t is automatically fixed; and if Kn_t is small enough there is in any case no problem. If Re is eliminated and the resulting freedom is used to model the chemical loading group without changing the pressure, then at a constant loading group quadrupling D will quadruple U, multiply Re by 16, and Kn_t by $4/(16)^{1/4} = 2$. If the smaller device were operated at Kn_t of 0.01, the larger would be run at Kn_t of 0.02 and the turbulence intensity would fall from 6% to 4%, resulting in a failure to model turbulence.

The results of stability studies of the 6 inch burner with a flat-cross flameholder shown in Fig. 10 exhibit a marked influence of pressure, widening the rich limits as the pressure is decreased to 0.25 atm. with further widening at 0.2 atm. At 0.2 atm the burning was much smoother than at higher pressures, the flame appeared nearly laminar and the noise level was markedly reduced. The earlier work of Khramtsov and of Fine which had indicated the possible reduction of turbulence level as pressure was reduced and the anomalous effect noted above of pressure on stability led to the studies of Turano. Turano found that, for all Reynolds numbers studied, the turbulence intensity decreased with decreasing pressure below about 0.2 atm. The near concordance of the pressure level at which transition to smooth burning occurred and that at which the turbulence level in a cold system began to diminish with decrease in pressure level would at first appear to offer an explanation of the observed effect of lowered pressure level on the

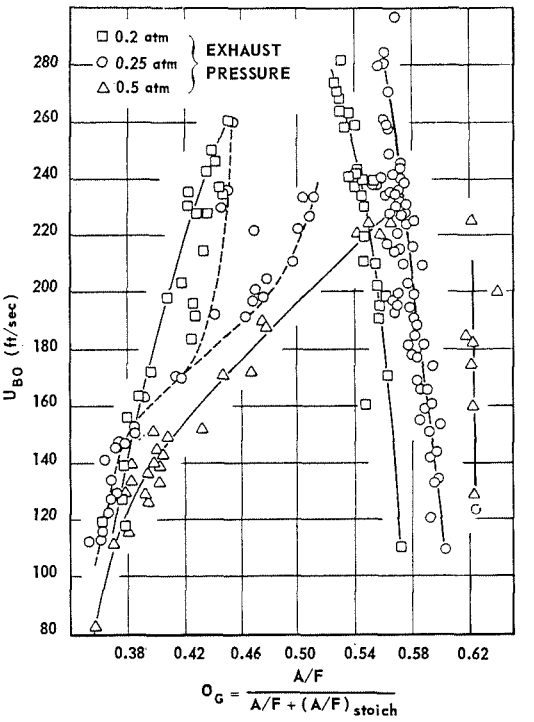

FIG. 10. Effect of pressure on stability limits of 6 inch burner (flat-cross flameholder).

rich stability limits. However, the stability limits of the smaller burners were measured at the same value of Kn_t as that at which the anomalous pressure effect was found for the 6-inch burner and no anomalous effect was observed. Thus, if one accepts the thesis that the turbulent Knudsen number is uniquely determined by Mach and Reynolds numbers, variation in turbulence level is not an explanation of the observed effect.

Oscillation Effects

Flame-driven or flame-amplified oscillations represent another uncontrolled effect that makes modeling difficult. The character of such oscillations depends primarily on the engine geometry, but may be modified in static tests by the geometry of the immediate environment. For example, acoustic coupling of a combustion chamber with an altitude test chamber may be described in terms of the Helmholtz resonator frequency

$$f = (C/2\pi)(A/VL)^{1/2},$$

where C = velocity of sound; A = burner cross-sectional area; V = volume of altitude test chamber; and L = burner length.

It is important now to consider how the various possible oscillatory phenomena may affect the modeling of geometrically similar combustion systems. All the more common frequencies (longitudinal, radial, tangential, or transverse) are expressible in the dimensional form: (sound velocity)/(characteristic dimension) times a dimensional constant. Multiplying by the residence time, proportional to L/U, one obtains as a dimensionless modeling parameter the Mach number. With modeling restricted to use of the same fuel and fuel/air ratio as in the prototype, and therefore to an identical temperature pattern, the only variable in the Mach number criterion is the approach velocity. It has already been pointed out that maintaining constancy of M between model and prototype is in conflict with holding Reynolds number and chemical loading group constant, unless the value of n in the latter is 2.

In the present studies both acoustic and nonacoustic oscillations usually were present in mild forms, but some modes gave rise to strong oscillations. Three types of vibrations were clearly discernible: First, the Helmholtz type; second, the fundamental closed organ pipe modes; and third, oscillations which occurred intermittently during steady combustion. The possible initiating and sustaining mechanisms for each of these modes may have been repetitive variations of heat release rate, or pressure perturbations across the combustor. The Helmholtz-type oscillations occurred in the small altitude chamber, thereby rendering questionable comparisons of these data with data taken in the large altitude chamber. The fundamental Helmholtz resonator frequency for the burner-chamber combination was 4 cps. The observed oscillations occurred at 3–5 cps. Some low-frequency oscillations occurred in the large altitude chamber but could not be correlated with any system dimensions. These were successfully eliminated by changing operating parameters of the chamber, in particular the quench water spray rate.

Strong oscillations occurred during blowout studies with the 4 inch $4.25D$ burner, causing data scatter at velocities above 180 fps. If one treats the combustor volume extending from the trailing edge of the flameholder to the tailpipe exit as a closed organ pipe, its fundamental frequency for the inlet temperature of 710°R is 230 cps; for an average combustion temperature of 3900°R it is 542 cps. These correspond closely to the observed frequencies.

During normal operating each size of burner had a characteristic frequency for each Reynolds number and pressure level of operation. At constant Reynolds number the sound intensity and frequency always decreased with decreasing pressure. At constant pressure the sound intensity and frequency decreased with decreasing Reynolds number.

Conclusions

1. For the modeling of high output combustion chambers, analysis indicated the probable importance of the following parameters: (a) Reynolds number, (b) chemical loading parameter, (c) Mach number, (d) external heat-loss group, (e) turbulence Knudsen number, (f) Helmholtz resonator group.

2. Experiments planned for study primarily of the first two parameters confirmed the importance of the chemical loading parameter, demonstrated a minor importance of the Reynolds number, and also indicated the occasional importance of one or more of the others.

3. Burner stability limits have been correlated quite well by the parameter U_{BO}/PD as a function of air/fuel ratio, implying dependence upon an over-all reaction order of 2. Difficulties sometimes found in reproducing stability data may be attributed to variation in mixing and burning

rates associated with uncontrolled oscillatory phenomena.

4. Based on combustion efficiency data geometrically scaled burners performed comparably when groups (a) and (b), with the pressure exponent in the latter at about 2 on the average, were each maintained constant with scale change, although there was some variation of n with the factors that affect efficiency.

5. Experiments which incorporated emissivity control or radiation shielding confirmed the need to include group (d) in modeling if the prototype walls run hot.

6. Reduction of the turbulence level as absolute pressure is reduced, while Reynolds number is maintained constant, has been demonstrated for cold flow at pressures below 0.2 atm. Where the effect of pressure on turbulence can be important the turbulence Knudsen number should be kept constant in burner modeling.

7. Longitudinal, tangential, or radial oscillations that may occur in modeled combustors are scaled only if the Mach number is held constant.

8. Helmholtz resonator oscillations cannot be scaled in operation of geometrically scaled apparatus without the generally unacceptable complication of scaling the altitude chamber to the burner.

ACKNOWLEDGMENT

This research was supported by the United States Air Force through the Aeronautical Research Laboratories of the Air Force Research Division under Contract Nos. AF33(616)–3037 and 5746.

REFERENCES

1. JENSEN, W. P., TOBEY, A. C., and RAYMOND, P. M.: Modeling Studies of Sub-Atmospheric Combustors, WADC Tech. Rept. 58–620, ASTIA NO. AD208857, December, 1958.
2. HOTTEL, H. C., *et al.*: Experimental Studies of Sub-Atmospheric Combustors, ARL Tech. Rept. 60–296, August, 1960.
3. DAMKÖHLER, G.: Z. Elektrochem. *42*, 846 (1936).
4. PENNER, S. S.: Similarity analysis and the scaling of liquid fuel rocket engines, *Combustion Researches and Reviews* (AGARD), Chapter 12. Butterworths, 1955.
5. WAY, S.: Jet Propulsion *27*, 162 (1957).
6. WAY, S.: *Selected Combustion Problems—II (AGARD)*, p. 269. Butterworths, 1956.
7. VON KARMAN, T.: *Ibid.*, p. 167.
8. WELLER, A. E.: *Ibid.*, p. 371.
9. ROSS, C. C.: *Ibid.*, p. 444.
10. STEWART, D. G.: *Ibid.*, p. 384.
11. ROSNER, D. E.: Similitude in Aerothermochemistry, Tech. Pub. No. 5, AeroChem Res. Labs., Inc., Princeton, New Jersey, July, 1958 (ASTIA No. AD200903).
12. WHITE, S. W. and LEWIS, W. G. E.: The Performance of a Multistage Combustion System, N.G.T.E. Rept. No. R165, May 1955.
13. LYALL, H. G.: Pilot Combustion Cans Employing a Large Scale Recirculation Flow Pattern, N.G.T.E. Memo No. M305, Sept. 1957.
14. GREENOUGH, V. W. and LEFEBVRE, A. H.: *Sixth Symposium (International) on Combustion*, p. 858. Reinhold, 1957.
15. WOODWARD, E. C.: *Ibid.*, p. 849.
16. WOODWARD, E. C.: ARS Journal *31*, 1401 (1961).
17. LEFEBVRE, A. H. and HALLS, G. A.: Some experiences in combustion scaling, in *Advanced Aero Engine Testing*, AGARDograph No. 37, p. 177. Pergamon Press, 1959.
18. HOTTEL, H. C.: Fire Modeling, in *International Symposium on the Use of Models in Fire Research*, Publication 786, National Academy of Sciences, National Research Council, Washington, D. C., 1961.
19. CHILDS, J. H., REYNOLDS, T. W., and GRAVES, C. C.: Relation of Turbojet and Ramjet Combustion Efficiency to Second Order Reaction Kinetics and Fundamental Flame Speed, NACA Rept. 1334, 1957.
20. SPALDING, D. B.: *Some Fundamentals of Combustion*, p. 188. Butterworths, 1955.
21. DEZUBAY, E. A.: Aero Digest *61*, 54 (1950).
22. ZUKOSKI, E. E. and MARBLE, F. E.: Experiments concerning the mechanism of flame blow-off from bluff bodies, *Gas Dynamics Symposium*, Northwestern U., Evanston, Illinois, August 22–24, 1955.
23. KHRAMTSOV, V. A.: *Seventh Symposium (International) on Combustion*, p. 609. Butterworths, 1959.
24. POTTER, A. E.: Personal communication (with W. P. Jensen) October 1958.
25. TURANO, A.: *Rarefaction Effects in Low Speed Turbulence*, Sc.D. Thesis in Chem. Eng., Mass. Inst. Technol. November 1959.

Discussion

DR. S. L. BRAGG (*Rolls-Royce, England*): One of Professor William's plots showed a linear relation between combustion efficiency and operating pressure. Was there any particular reason why such a relation should be expected?

Dr. Lefebvre, in his comments on this paper, had suggested the results at different Reynolds numbers could be correlated by plotting combustion efficiency against a loading parameter $p^2/\dot{m}$. I consider this form of loading parameter unsatisfactory as it is

difficult to extrapolate the results at low loading ($p^2/\dot{m}$ large) which are approaching asymptotically to a number rather near unity, at the same time that discrepancies are concealed by the large slope of the curve at high loadings ($p^2/\dot{m}$ small). If the inverse parameter ($\dot{m}/p^2$) is used these difficulties disappear and a reasonable near-linear curve of efficiency *versus* loading is obtained.

Furthermore, it is comparatively simple to extrapolate such a curve to very low loadings: If the efficiency is still below 100% at such points, it suggests that mechanisms other than chemical kinetics (e.g. fuel losses on the walls) are then responsible for combustion inefficiency.

PROF. G. C. WILLIAMS (*Massachusetts Institute of Technology*): There is plainly no theoretical reason to expect a linear relationship between combustion efficiency and either chemical loading group or its reciprocal. We agree with Dr. Bragg's viewpoint that extrapolation to low-output, high-efficiency operation is easier when the parameter ($\dot{m}/p^2$), equivalent to U/pL, is used instead of its reciprocal used by us.

EXAMINATION OF THE POSSIBILITY OF PREDICTING REACTION-RATE-CONTROLLED FLAME PHENOMENA BY THE USE OF COLD MODELS

D. VORTMEYER

The present paper is concerned with the application of modeling techniques to combustion processes in high-intensity premixed one-stream combustion chambers. The efficiency and extinction of these systems is regarded as solely determined by the interaction between the gas flow and the chemical reaction.

An analog for the simulation of these processes was proposed by D. B. Spalding in 1956.[1] Model and combustion chamber were geometrically similar, and the heat release was simulated by electrically heated coils. It was shown that the model of this type is capable of producing model flames of generally not more than 1° or 2°C above room temperature. The flames behaved similarly to real flames; for instance they were extinguished once the flow rate exceeded a certain critical value.

Do the extinction conditions of these model flames agree with those of real combustion systems? This paper answers this question for cylindrical and rectangular combustion chambers with geometrically simple flameholders in two-dimensional flows. Until now only a few measurements have been published. In the first paper on this subject[1] the results were presented of some measurements made on a prototype model for rectangular ducts with flat plates as flameholders. However at that time insufficient flame data were available for comparison. In another paper D. G. Martin and J. D. Webb[2] considered a special type of cylindrical combustion chamber. They report these to be in agreement qualitatively with flame results.

The analog method has been criticized because of the implicit assumption of similarity between flames and isothermal gas flows. For this reason, a part of this paper is devoted to summarizing the results of investigations concerning the question of similarity.

Introduction

The method of dimensional analysis has been applied to combustion processes by various authors.[3–8] From this work emerges the fact that under certain circumstances the performance of high-intensity one-stream premixed combustion systems can be presented by a single plot (Fig. 1) of efficiency η versus a nondimensional chemical loading factor L_V or L_d;

$$\eta = f(L_V) \qquad \text{or} \qquad \eta = f(L_d)$$

Because of the high gas velocities the effect of the Reynolds number becomes negligible. Spalding and Vortmeyer[9,10] give an example of how this relation can be obtained approximately by analytical methods if the gas-flow patterns are particularly simple and known. However, in more difficult cases the relation (Fig. 1) has to be found by other means, either by testing the actual combustion unit or, if possible, by cost-saving modeling work.

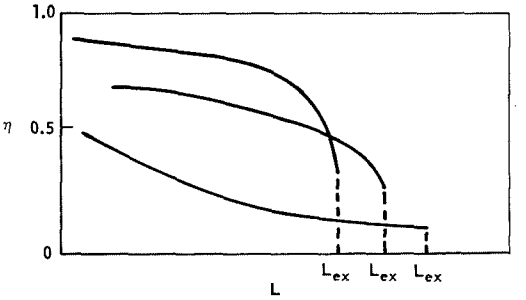

FIG. 1. Three characteristic η–L curves from reference 32.

The aim of this paper is to find out whether isothermal models are helpful in predicting important features of the combustion system. Particular importance is attached to the evaluation of the loading factor L_{ex} (Fig. 1) at the extinction point, since in this case the prediction can easily be checked against flame measurements.

Conditions for Similarity between Analog and Combustion Chamber

The analog discussed in this paper is designed to simulate the relatively complex process of interaction between gas flow and combustion processes. The success of this work naturally depends on the degree of similarity established between the practical combustion chamber and the isothermal cold model. The requirements for similarity are:

(1) The flow patterns in model and combustion chamber have to be similar.

(2) The heat release by the chemical reaction has to be simulated correctly in the model. In the case of appreciable heat losses from the walls of the combustion chamber this effect on the heat release has to be simulated as well.

These requirements can only be approximated in practice. In order to arrive at such approximations we follow Spalding[10] where, in the form of so-called "half truths," some rules are provided for this purpose. From this reference it follows that requirement (1) is satisfied best by designing a model of the same or similar geometrical shape (larger or smaller) and blowing air through it at such speeds that the Reynolds number is no longer of importance for the flow pattern.

Similarity condition (2) is fulfilled in the model by making use of the "half truth"[10] that in a premixed adiabatic one-stream conbustion chamber the heat release at each point of the chamber is a function of temperature only.

Figure 2 shows a typical reaction-rate curve[11] for stoichiometric gas mixtures in dimensionless coordinates ϕ and τ. Similarity between both systems requires the same rate curve for model and combustion chamber. For simplicity the reaction rate curve of Fig. 2 is approximated in the model by the single step-function, also shown in Fig. 2. Under these simplified conditions the model has to determine whether the temperature in a volume element is high enough to allow chemical conversion or not. The presentation of the heat release function as a function of the reactedness $\tilde{\tau}$ is only correct for a rather limited number of adiabatically conducted reactions,[11] namely, the single-step reaction and chain reactions under quasi-stationary conditions.

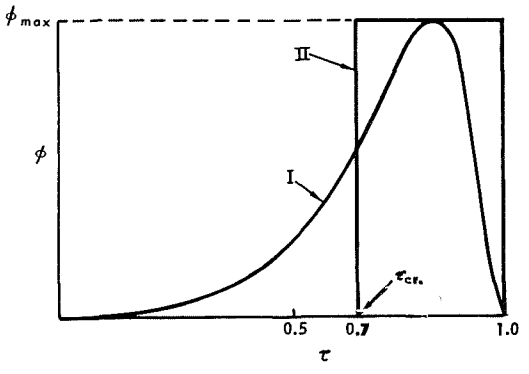

FIG. 2. I. Typical reaction rate function. II. Reaction rate function used in analog.

Probably neither of the two reaction schemes is followed by the hydrocarbon combustion in combustion chambers. Furthermore, heat losses from the combustion chamber may seriously affect the heat release function. These effects are not simulated by the model.

Qualitative Comparison of Hot and Cold Flow behind Flameholders

When it was recognized that the steady recirculating flow in the wake of the flameholders had a stabilizing effect on flames, the investigation of the reverse flow pattern aroused a good deal of interest. Since then it has become well known that the density changes consequent on combustion increase the length of the recirculation zone,[12–14] that the turbulent transition phenomenon is shifted to higher Reynolds numbers,[15] that the drag coefficients of the flameholder decrease,[16] and that the flame has a steadying effect on the reverse flow. It was pointed out by Scurlock[12] that for cylindrical rods the unsteady vortex shedding typical of isothermal flows was stabilized in the presence of flames, and thus the flow pattern became radically changed. Similar conclusions were drawn in a paper by Westenberg *et al.*[17] These authors injected helium through the downstream face of a flame-stabilizing cone. From the He-concentration profiles they concluded that the features of hot and cold flow patterns behind the cone were different, although a small recirculation zone was observed in the cold flow. The mixing process in the wake of flameholders appeared to be much more pronounced with flames than without.

For similar flameholders, Quick[18] investigated the cold reverse flow more quantitatively by taking velocity traverses. Unfortunately no comparisons were made with flows in the presence of flames. Based on some provisional test measurements Quick suggested that the total mass flow of recirculating gas under hot (with flames) and cold conditions might be the same.

This suggestion was recently tested by Winterfeld.[14] For disc baffles with blockage ratios $d/B \leq 0.1$ the reverse mass flows were approximately the same; however for larger blockage

ratios the reverse mass flow within flames increased considerably as compared to cold flow.

Measurements of residence times of gas particles in the region of recirculation were made by Bovina[19] and Winterfeld.[14] For comparison, both authors provide some additional data for cold flow under the same geometrical conditions. The residence times measured in flames were larger by factors between 1.5 and 3.7, indicating again that the mixing process in the wake of flameholders is appreciably affected by flames.

This short survey of literature indicates quantitative differences between "hot" and "cold" flows in respect of: the residence time of gas particles in the recirculation zones; the lengths of the recirculation zones; and the mass flow rates into the reverse flow region. However, none of the results describes the flow pattern in such detail that the information can be used for an evaluation of the extinction loading factor L_{ex}, defined as

$$\Gamma = L_{ex}\left[\frac{\dot{m}_{ex}c(T_{ad} - T_u)}{q_{max}V}\right].$$

A more detailed description of the recirculating flow is the main subject of the next section, where influence coefficients are defined and then measurements of them are presented.

Description of Flow Patterns by Influence Coefficients

The use of influence coefficients in the field of flame theory was first recommended in reference 10. In that paper, the influence coefficients β_{jk} were defined by the relation

$$\tau_j = \{1/\dot{m}c(T_{ad} - T_u)\}\int_v \beta_{jk}q(\tau_k)\,dV_k \quad (1)$$

where τ_j = dimensionless temperature or reactedness at j; q_k = volumetric heat release at point k; and dV_k = increment of volume associated with point k.

If the energy and material conservation equations are linear, the β's are functions of position alone for a given flow field. In the range of fully developed isothermal turbulent flow with relatively low Mach numbers (no compressibility effects) the β_{jk}'s are certainly independent of Re over a wide range of flow conditions.

Expressed in words, Eq. (1) states that the reactedness at any point in a steady flame is equal to a sum of terms, of which each is related by the $q(\tau)$ function to the reactedness prevalent at the point of the chamber that is represented by the term under consideration.

Once the coefficients β_{jk} are known, the set of j Eqs. (1) becomes solvable. Therefore the main importance of the influence coefficients rests in the fact that the unsolvable differential equations of mass and energy conservation (there exists at present no method to predict the flow pattern within a combustion chamber of complex geometry) become tractable in the form of Eq. (1) where the description of the flow pattern is replaced by experimental information. Some applications of influence coefficients to flame theory are contained in the references.[9,10,20]

Measurement of Influence Coefficients by Tiltman–Langley Ltd.[21]

For a closer investigation of the recirculating flow a tracer method similar to that employed by Westenberg *et al.*[17] was used. The tracer gas was argon. The recirculation zones behind a disc, cone, and hemisphere were subdivided into twelve symmetrically disposed volume elements as indicated by Fig. 3. The six inner elements (1–6) were of approximately cylindrical shape, the six outer ones of the shell type. For the sake of accuracy in concentration measurements, the shell volumes were further subdivided into six subvolumes of the same size. By regarding the recirculating flow as symmetrical to the axis of the burning system, the following procedure could be adopted for the measurement of influence coefficients:

While the sampling point was kept fixed in the centroid of one volume or subvolume element, the injection point was moved successively through all 42 partial volumes. Having thus finished one set of measurements the sampling point was moved to another volume element.

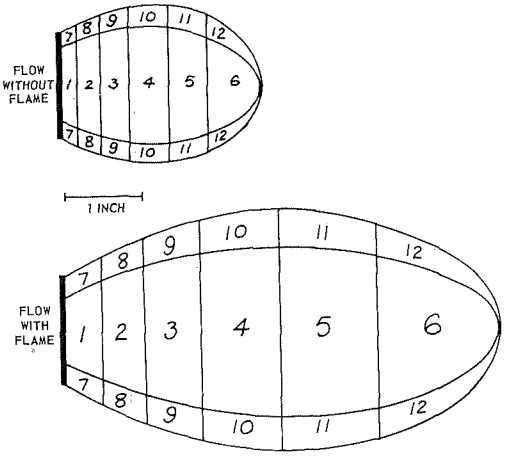

FIG. 3. Subdivision of the recirculation zone behind discs into 12 volume elements for hot and cold flow.

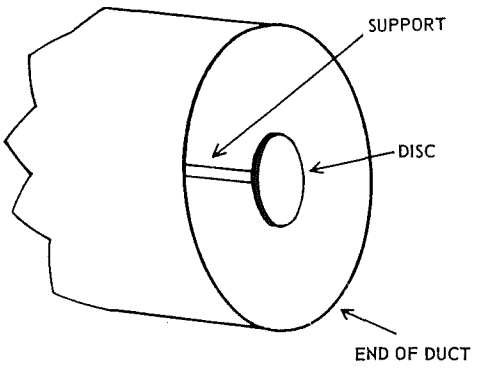

FIG. 4. Mounting of baffle at end of duct.

Because of the symmetry it was sufficient to adopt 12 different positions for the sampling point, and consequently $12 \times 42 = 504$ measurements were required for a complete survey of the flow pattern. Particular care was taken in those 12 cases for which the injection and sampling points were coincident in the element.

Then the concentration in that element was taken as the weighted mean of 16 readings in different parts of the elements. If the argon concentration $m_{\mathrm{Ar},j}$, the total mass flow $\dot{m}$ through the chamber, and the injection rate of argon, $\dot{m}_{\mathrm{Ar},k}$, are known, the influence coefficients can easily be worked out from the relation

$$\beta_{jk} = (\dot{m}/\dot{m}_{\mathrm{Ar},k})\, m_{\mathrm{Ar},j}. \qquad (2)$$

The measurements were carried out for flows with flames and for cold isothermal flows with the same burning system.

The experimental arrangement was such that the axially symmetrical flameholder (diameter $d = 1.38$ inches) was mounted at the open end of a tubular duct with the diameter $D = 2.87$ inches (Fig. 4). The ratio d/D was 0.48; the Reynolds number of the undisturbed duct flow was $\mathrm{Re} = 1.9 \times 10^5$.

Tables 1 and 2 contain measured influence coefficients for the recirculation zone behind a disc. The $\beta_{jk(\mathrm{hot})}$ are related to gas flow with flames and the $\beta_{jk(\mathrm{cold})}$ to the conditions of cold isothermal flow. Tables 3 and 4 present the ratios $\beta_{jk(\mathrm{hot})}/\beta_{jk(\mathrm{cold})}$ for disc and hemisphere.

The presentation of the actually measured influence coefficients for cone and hemisphere has been omitted since they do not reveal any new important features.

The following conclusions may be drawn:

1. A comparison of Tables 1 and 2 indicates that the influence coefficients increase by changing the conditions from cold to hot (flame) flow. The quantitative differences are considerable and are not constant from point to point.

2. For the investigated family of three axially symmetrical flameholders, in all cases the $\beta_{jk(\mathrm{hot})}$ show increases of the same order of magnitude (Tables 3, 4, and 5).

The results clearly indicate that appreciable quantitative differences exist between hot and cold flows and that there is nothing like a single constant multiplier by which a conversion of the $\beta_{jk(\mathrm{cold})}$-matrix to the hot one would be possible. The exchange of hot gas between two volume elements in the hot flow is stronger than between

TABLE 1

Measured Influence Coefficients $\beta_{j,k(\mathrm{cold})}$ in the Recirculation Zone Behind a Disc

		$k\rightarrow$											
		1	2	3	4	5	6	7	8	9	10	11	12
	1	47.0	16.6	9.1	10.5	13.6	9.1	5.6	9.4	5.0	6.9	8.8	7.6
	2	9.9	28.6	18.5	12.1	10.9	11.0	5.8	10.7	7.4	6.5	8.5	8.1
	3	7.1	10.8	13.1	18.5	13.8	14.6	5.5	7.1	7.6	8.9	11.8	13.3
	4	8.1	9.0	8.5	9.8	14.1	12.8	6.9	6.9	6.9	7.7	9.3	12.1
j	5	7.9	6.6	7.9	4.7	9.1	10.2	6.9	5.6	5.6	6.1	7.4	7.9
↓	6	4.2	4.4	3.4	3.2	2.9	8.6	3.7	4.4	4.1	3.4	2.4	13.0
	7	31.0	16.5	14.9	12.3	13.6	12.8	18.2	9.9	4.2	7.5	10.3	10.8
	8	17.3	17.3	15.2	11.6	15.6	11.0	26.2	12.8	6.9	7.6	10.5	8.9
	9	11.8	13.2	10.7	13.3	9.7	8.8	11.9	27.9	10.9	10.5	7.9	7.5
	10	13.7	9.8	9.5	10.0	7.4	7.6	11.6	9.1	14.4	7.9	6.6	6.0
	11	9.1	9.8	10.0	8.1	7.2	6.5	7.0	9.5	9.1	10.7	6.5	4.3
	12	6.2	6.1	5.0	5.0	4.8	0.4	5.8	3.8	4.6	5.6	7.1	4.8

TABLE 2

$\beta_{j,k(\text{hot})}$ for the Recirculation Zone Behind a Disc

		$k\rightarrow$											
		1	2	3	4	5	6	7	8	9	10	11	12
	1	166	73	49	32	33	28	7	11	13	13	20	20
	2	16	88	58	35	34	31	11	9	14	15	19	25
	3	12	24	50	45	41	35	13	12	14	15	22	28
	4	14	13	14	27	47	31	12	12	14	18	22	29
j	5	11	14	13	12	25	32	12	12	12	13	33	27
↓	6	9	10	13	12	13	21	7	9	11	12	12	24
	7	249	106	54	34	36	36	94	15	11	14	20	26
	8	30	82	66	40	29	37	45	75	14	11	18	27
	9	17	23	31	39	26	25	18	35	49	14	14	20
	10	13	19	21	22	22	19	15	25	47	22	10	13
	11	15	19	15	18	16	15	14	14	19	27	23	13
	12	11	13	10	13	12	11	9	10	12	15	12	29

TABLE 3

$\beta_{j,k(\text{hot})}/\beta_{j,k(\text{cold})}$ for a Disc Baffle

		$k\rightarrow$											
		1	2	3	4	5	6	7	8	9	10	11	12
	1	3.5	4.4	5.4	3.0	2.4	3.0	1.3	1.2	2.6	1.9	2.3	2.6
	1	1.6	3.1	3.1	2.9	3.1	2.8	2.0	1.0	1.9	2.3	2.2	3.0
	3	1.7	2.2	3.8	2.5	3.0	2.4	2.4	1.7	1.8	1.7	1.9	2.1
	4	1.7	1.4	1.7	2.7	3.3	2.4	1.7	1.7	2.0	2.3	2.4	2.4
j	5	1.4	1.8	1.6	2.5	2.8	2.2	1.7	2.1	2.1	2.1	4.5	3.4
↓	6	2.1	2.3	3.8	3.7	4.5	2.4	2.0	2.0	2.7	3.5	5.0	1.8
	7	8.0	6.4	3.5	2.8	2.6	2.8	5.1	1.5	2.6	1.9	2.0	2.4
	8	1.7	4.7	4.3	3.4	1.9	3.4	1.7	5.9	2.0	1.4	1.7	3.3
	9	1.4	1.7	2.9	2.9	2.7	2.8	1.5	1.3	4.5	1.3	1.8	2.7
	10	1.0	2.0	2.2	2.2	3.0	2.5	1.3	2.8	3.3	2.8	1.5	2.1
	11	1.6	2.0	1.5	2.2	2.2	2.3	2.0	1.5	2.1	2.5	3.5	3.0
	12	1.8	2.1	2.0	2.6	2.5	2.7	1.6	2.6	2.6	2.7	1.7	6.0

two similarly placed elements in the cold flow pattern; the exchange between the recirculating gas and the main stream is, however, weaker. This result, however, is already well established by the observation of Westenberg.[17]

Solution of Equation (1)

Each of the 144 influence coefficients of Tables 1 and 2 provides sufficient information on the flow pattern to permit the solution of Eq. (1) and the evaluation of the conditions for extinction. In order to do this we first reshape Eq. (1) by introducing a characteristic volume $V = Ad$, where A is the cross section of the duct, and d is the diameter of the flameholder. Further a term $q_{\max}$ is introduced that characterizes the maximum heat release. Then we may write instead of Eq. (1)

$$\tau_j = [\dot{m}c(T_{\text{ad}} - T_u)/q_{\max}V]^{-1} \times \int_{\text{recirculation zone}} \beta_{jk}\phi(\tau_k)\, dV_k/V. \quad (3)$$

Since in practice we are considering discrete volume V_k elements we approximate Eq. (3) by

TABLE 4

$\beta_{j,k(\text{hot})}/\beta_{j,k(\text{cold})}$ for a Hemisphere

		$k\rightarrow$											
		1	2	3	4	5	6	7	8	9	10	11	12
$j\downarrow$	1	1.7	2.6	2.8	3.3	2.9	2.0	1.3	2.2	3.0	3.3	2.0	0.7
	2	1.4	3.0	2.4	2.8	2.7	1.9	1.5	2.4	2.5	3.1	1.3	0.6
	3	1.3	1.5	2.4	2.0	3.0	2.7	1.1	1.5	3.3	2.3	1.5	0.6
	4	1.0	1.4	1.7	1.9	1.9	1.6	1.2	1.5	2.5	4.9	1.3	0.6
	5	1.15	1.5	1.7	1.7	2.7	3.6	1.2	1.7	2.5	3.0	3.3	1.1
	6	1.3	1.7	1.9	2.6	3.7	6.0	1.5	1.5	2.0	2.0	4.0	2.2
	7	3.5	2.8	2.9	2.4	2.9	1.5	1.6	2.1	2.6	2.5	1.0	0.3
	8	1.5	2.1	2.7	2.6	4.0	2.1	1.7	3.7	2.5	1.9	1.4	0.6
	9	1.2	2.1	3.0	3.1	2.7	1.3	1.3	2.4	2.7	2.0	1.2	0.6
	10	1.3	2.0	2.0	2.2	1.9	1.5	1.1	1.9	1.9	1.3	1.0	1.1
	11	1.0	1.2	1.0	1.6	2.0	1.4	1.1	1.4	1.6	3.3	1.3	0.6
	12	1.12	1.2	1.8	2.0	1.5	1.9	1.1	1.7	2.3	1.8	2.8	3.4

TABLE 5

Weighted Influence Coefficients $\alpha_{j,k(\text{cold})}$ for a Disc Baffle

		$k\rightarrow$											
		1	2	3	4	5	6	7	8	9	10	11	12
$j\downarrow$	1	1.27	0.62	0.58	0.93	1.01	0.45	0.15	0.35	0.32	0.61	0.66	0.38
	2	0.27	1.07	1.17	1.07	0.81	0.55	0.16	0.40	0.47	0.57	0.63	0.40
	3	0.19	0.40	0.83	1.63	1.03	0.73	0.15	0.26	0.48	0.78	0.88	0.66
	4	0.22	0.34	0.54	0.86	1.05	0.64	0.19	0.26	0.44	0.68	0.69	0.60
	5	0.21	0.25	0.50	0.41	0.68	0.51	0.19	0.21	0.35	0.54	0.55	0.39
	6	0.11	0.16	0.21	0.28	0.22	0.43	0.10	0.16	0.26	0.30	0.18	0.65
	7	0.84	0.62	0.94	1.08	1.01	0.64	0.49	0.37	0.27	0.66	0.77	0.54
	8	0.47	0.65	0.96	1.02	1.16	0.55	0.71	0.48	0.44	0.67	0.78	0.44
	9	0.32	0.49	0.68	1.17	0.72	0.44	0.32	1.08	0.69	0.93	0.59	0.37
	10	0.37	0.37	0.60	0.88	0.55	0.38	0.31	0.34	0.91	0.70	0.49	0.30
	11	0.25	0.37	0.63	0.71	0.54	0.32	0.19	0.35	0.58	0.94	0.48	0.21
	12	0.17	0.23	0.32	0.44	0.36	0.02	0.16	0.14	0.29	0.49	0.53	0.24

the sum

$$\tau_j = L^{-1} \sum_k \alpha_{jk}\phi(\tau_k), \qquad (4)$$

where α_{jk} are called the weighted influence coefficients, since they represent

$$\alpha_{jk} \equiv \beta_{jk}(\delta V_k/V). \qquad (5)$$

L has the meaning of a loading factor.

$$L = \frac{\dot{m}c(T_{\text{ad}} - T_u)}{q_{\max}V} = \frac{v\rho c_p(T_{\text{ad}} - T_u)}{q_{\max}d},$$

where v is an average linear gas velocity in the tubular duct. The α_{jk}'s are easily evaluated once the β_{jk}'s are known. Tables 6 and 7 show the β_{jk}'s of Tables 1 and 2 converted to α_{jk}'s. If in addition the $\phi(\tau)$ relation of Fig. 2 is known, the system of simple algebraic equations becomes solvable. This procedure is particularly simple since a netword analog computer[2] was especially designed for the solution of those equations.

By varying L in Eq. (3) we arrive at a critical L_{ex}, where the only possible solution of Eq. (4) becomes zero. At this point the flame has to be regarded as extinguished and L_{ex} therefore represents the required loading factor at the extinction point. Calculations of this kind were carried out for the disc, cone, and hemisphere

TABLE 6

Weighted Influence Coefficients $\alpha_{j,k(\text{hot})}$ for a Disc Baffle

		$k\rightarrow$											
		1	2	3	4	5	6	7	8	9	10	11	12
$j\downarrow$	1	10.5	7.0	10.2	11.7	16.8	7.2	0.4	1.1	2.7	4.8	10.2	5.1
	2	1.0	8.4	12.1	12.8	17.3	7.9	0.7	0.9	2.9	5.5	9.7	6.4
	3	0.8	2.3	10.4	16.5	20.9	9.0	0.8	1.2	2.9	5.5	11.2	7.2
	4	0.9	1.2	2.9	9.9	23.9	7.9	0.8	1.2	2.9	6.6	11.2	7.4
	5	0.7	1.3	2.7	4.4	12.7	8.2	0.8	1.2	2.5	4.8	16.8	6.9
	6	0.6	1.0	2.7	4.4	6.6	5.4	0.4	0.9	2.3	4.4	6.1	6.2
	7	15.7	10.2	11.3	12.4	18.3	9.2	5.9	1.4	2.3	5.1	10.2	6.7
	8	1.9	7.9	13.8	14.6	14.8	9.5	2.8	7.2	2.9	4.0	9.2	6.9
	9	1.1	2.2	6.5	14.3	13.2	6.4	1.1	3.4	10.2	5.1	7.1	5.1
	10	0.8	1.8	4.4	8.0	11.2	4.9	0.9	2.4	9.8	8.0	5.1	3.3
	11	0.9	1.8	3.1	6.6	8.2	3.8	0.9	1.3	4.0	9.9	11.7	3.3
	12	0.7	1.2	2.1	4.8	6.1	2.8	0.6	1.0	2.5	5.5	6.1	7.4

baffles with $\alpha_{jk(\text{hot})}$ and $\alpha_{jk(\text{cold})}$. Only the α's for a disc baffle are presented in Tables 5 and 6. Table 7 contains the L_{ex} values obtained in this way. It appears that the L_{ex} values, calculated from the "hot" influence coefficients are about an order of magnitude larger than those evaluated from the "cold" coefficients.

This increase in the loading factor by changing from cold to hot conditions is partly due to the increase in the volume of the recirculation zone (Fig. 3), partly due to the stronger exchange of mass between two points in the hot reverse flow pattern.

TABLE 7

Flameholder	$L_{ex(\text{cold})}$	$L_{ex(\text{hot})}$
Disc	4.93	47
Cone	4.4	54
Hemisphere	4.44	34

Summarizing the results of this section, we conclude that there are quantitative differences between the reverse flow pattern in "hot" and "cold" flow. Furthermore, it may be noted that the differences shown quantitatively by the influence coefficients should not be regarded as universally valid. For another family of flameholders with different geometry the matrices $\beta_{jk(\text{cold})}$ and $\beta_{jk(\text{hot})}$ may compare quite differently. The last point was first noted by Westenberg *et al.*[17]

Design of Models

Figures 5 and 6 show photographs of a rectangular and cylindrical model as they were used in modeling experiments. Both models were designed to deal either with axisymmetrical or with two-dimensional flow problems. The working section of the rectangular chamber was 0.194 m wide, 0.125 m high, and 0.25 m long. All four sides were of perspex. The 0.125 × 0.25 m faces of the working section were divided into a grid of 0.25 × 0.013 m rectangles, so that the whole working section was divided into 100 cells. Each cell contained a heater unit consisting of two parallel coils.

The coils were placed horizontally and perpendicularly to the approach flow. Furthermore each cell contained a copper–constantan thermocouple. Both heater and thermocouple could be operated individually by hand switches, which also could be replaced by an electronic device.

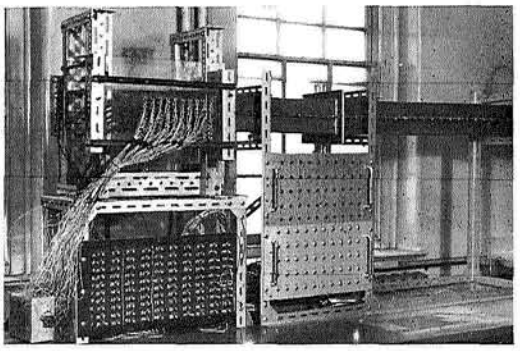

FIG. 5. Model of rectangular combustion chamber.

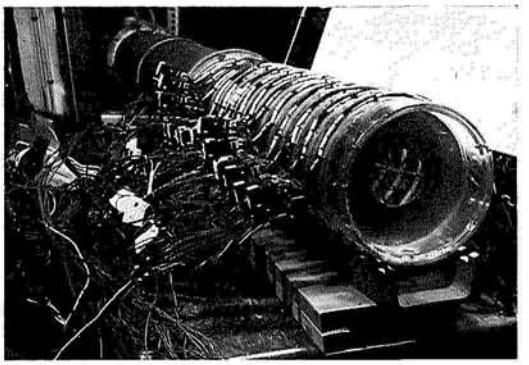

FIG. 6. Model of cylindrical combustion chamber.

The airflow was supplied by a blower. The maximum output of the blower was about 1100 kg/hr, but in all cases smaller flow rates were found to be sufficient. The pressure was atmospheric. The cylindrical model of Fig. 6 which was 0.80 m long and of 0.155 m inside diameter consisted of 16 elements with a length of 2 inches each. Each element incorporated six heaters and six thermocouples together with their supports. The heater wires were of nickel-chrome each with the resistance of 6.7 ohm. They were arranged in such a way as to divide each element into six cells of equal volume.

Experimental Procedure

The electric analog was operated as follows: After placing the baffle in position at the entrance of the working section, the air flow was switched on and a uniform voltage of 12 volts was supplied to all the heaters in the working section. The readings of the thermocouples were taken and an arbitrary temperature was chosen as a reference value. The heaters associated with the thermocouple readings below the reference temperature were switched off. In the wake of the baffle there remained a stable field of higher temperature readings; the reference temperature was increased.

This procedure was repeated, until a stable temperature field downstream from the flameholder no longer existed. Then the model flame could be regarded as blown off, and the reference temperature at this critical point (blow-off) was recorded and used for the calculation of the loading factors L_{ex} at the extinction point of the model.

$L_{ex,d}$, defined by the relation

$$L_{ex,d} = \frac{V_{ex}\rho c_p(T_{ad} - T_u)}{q_{max}d},$$

is easily evaluated from the data provided by the measurements.

V_{ex} = linear velocity of air at the blow-off point in the model.
c_p = specific heat at constant pressure.
ρ = density of air at room temperature.
$(T_{ad} - T_u) = (T_{cr} - T_u)/0.7$ (compare Fig. 2).
T_{cr} = the reference temperature at the blow-off point.
d = width or diameter of flameholder.
q_{max} = electric heat input per volume element.

Particular care was taken to ensure that the model was operated so that L_{ex} was independent of the Reynolds number and of the volumetric heat release rate. This was the case when the voltages applied at the heaters exceeded 9 volts.

Prediction of Extinction Loading factor by the Model

Loading factors obtained for the extinction point of flames by the methods described in the previous section were plotted as a function of the blockage d/B in Fig. 7 for a family of flameholders consisting of four differently shaped baffles—rectangular duct with flat plate, cylinder, semi-cylinder and 90° V-gutter. It is noticeable that with decreasing d/B the loading factors of the

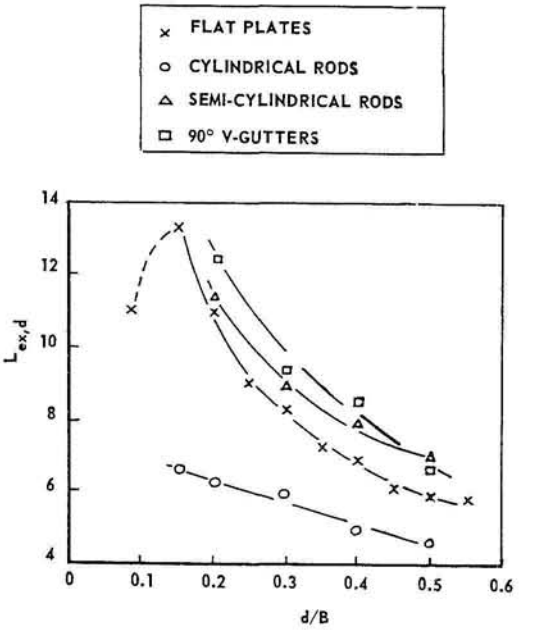

FIG. 7. Loading factors as predicted by model for rectangular chambers.

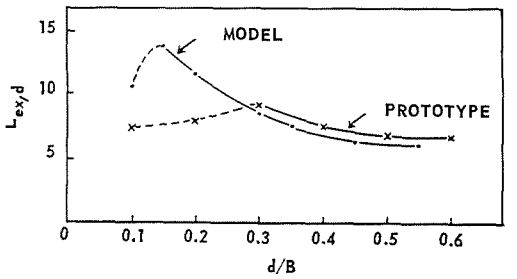

FIG. 8. Comparison of loading factors as measured in prototype and in final rectangular model.

four baffles show an increase. The values of L_{ex} lie between 4 and 14. Furthermore the graph shows that the model predicts the more stable flames for V-gutters, semicylinders, and flat plates. In the case of circular rods however, the loading factors drop to about half the value as measured for the three other baffles.

In Fig. 8 the loading factors for flat plates from Fig. 7 are compared with L_{ex} values that were obtained by D. B. Spalding in a prototype model.[1] At large blockage ratios both curves agree quite well. But at $d/B = 0.3$ Spalding's curve moves to lower values, while the more recent measurements show a further increase to $d/B = 0.15$. The different behavior of the two models is explained by the fact that the heater-coil diameter in the prototype was three times as large as the coil diameter of 0.25 inch in the new design. Both models were of the same height B. Since the simulation of flames requires the interaction of a number of heaters in the wake of the baffle it is certain that models with larger sized heaters can only give acceptable results with large blockage ratios.

A further conclusion of Fig. 7 is that the loading factors at large blockage are nearly independent of the coil diameter and that the blockages and the wakes which are caused by the electrical heaters do not influence the general flow pattern to a large extent.

Comparisons with Flame Data

A series of flame experiments in rectangular ducts using the same family of flameholders as previously in the model was carried out by Barrère and Mestre.[22] Summing up the results of these authors, the order of stabilizing ability of the two-dimensional stabilizers can be put as:

1. Flat plates (high stability).
2. 90° V-gutters.
3. Semicylinders.
4. Cylinders (low stability).

This order of sequence is not predicted by the model, where V-gutters and semicylinders produced larger loading factors than flat plates.

For quantitative comparisons the flame-stability measurements of various authors[13,23,24] were used to evaluate loading factors as a function of the blockage ratio d/B. The list of references is by no means exhaustive, as only those that contained measurements for blockage ratios $d/B \geq 0.15$ were of interest. The loading factor

$$L_{ex} = [V_{ex} c_p \rho (T_{ad} - T_u)]/q_{max} d$$

was calculated by inserting

V_{ex} = blow-off velocity at stoichiometric mixture ratio
$c_p\rho$ = specific heat and density of hot gas
$q_{max} = 740000 p^{1.8} (T_u/400)^{1.6}$ kcal/sec m³.

as measured by Longwell and Weiss for isooctane.[25,26] The Longwell–Weiss heat release rates were chosen as characteristic because they are the largest volumetric over-all combustion rates so far obtained in a turbulent premixed combustor, although this does not exclude the possibility of locally much higher rates in diffusion flames or premixed laminar flames (e.g., see the paper by Anagnostou and Potter[33]).

The same q_{max} value was taken as representa-

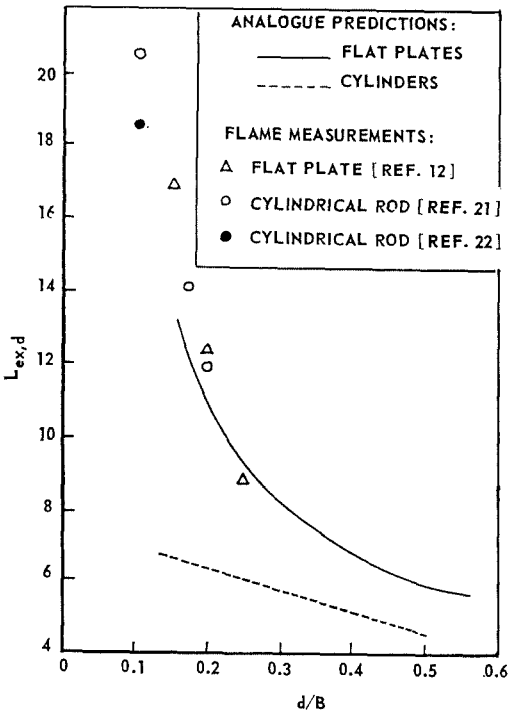

FIG. 9. Comparison between analog predictions and flame results for rectangular combustion chamber.

tive for other hydrocarbons too, an approximation which is supported by measurements of Clarke[27] *et al.*, who found a rather similar maximum heat release for propane. The dimensionless loading factors L_{ex} of the flames are plotted together with L_{ex} from the model in Fig. 9. It is noticed that only for a rather small range do the blockage ratios for both flame and model results overlap due to the constructional limitations of the model. Within this comparable range the following statements may be made:

(1) Model and flame loading factors increase with decreasing blockage ratios.

(2) Within the comparable range the agreement is quite good numerically for flat plates, however the predictions for cylindrical rods are only about half of the flame measurements.

(3) The large gap in performance between flat plates and cylinders as predicted by the model is not confirmed by flame measurements.

Cylindrical Models

Before discussion of the implications of the previous section, another set of analog results will be presented for cylindrical ducts. The flames were stabilized by circular discs, hemispheres, cones, and annular baffles.

The model extinction loading factors $L_{ex,d}$ and $L_{ex,V}$ in the case of annular baffles, are presented in Fig. 10 and Fig. 11. Figure 10 also contains the loading factors evaluated from cold influence coefficients as shown in Table 4. These values are lower by about 20–50%.

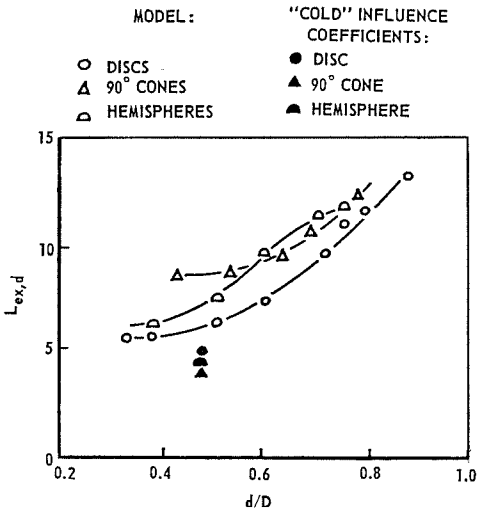

FIG. 10. Loading factors predicted by cylindrical model and evaluated from "cold" influence coefficients.

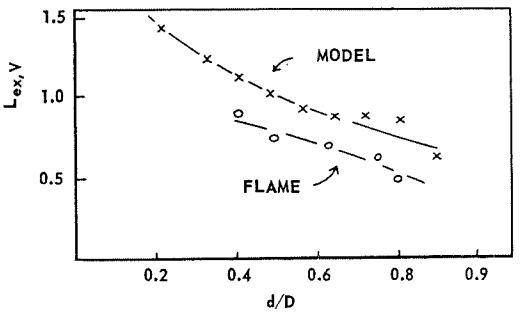

FIG. 11. Model predictions for annular baffles. Flame results of reference 28 are added for comparison.

By another series of experiments the influence of the cone apex angle ϵ on the stability limits was investigated. The results of those measurements are plotted in Fig. 12, indicating that with decreasing angle the stability limits increase. Although only relatively few flame data could be found for cylindrical chambers, the few available[16,28–30] suffice to check the model predictions. This is done in Figs. 11 and 13. Quantitatively the L_{ex} curves for flames and models both have rather similar slopes (Fig. 9 and Fig. 11); however, the relative position of the model predictions concerning the stabilizing ability of the baffles is not confirmed by flame experiments. From this emerges[17,22] that for a consistent series of flame experiments, the flames behind the most blunt bodies are always the more stable ones. Therefore the L_{ex} curve for discs in Fig. 13 should

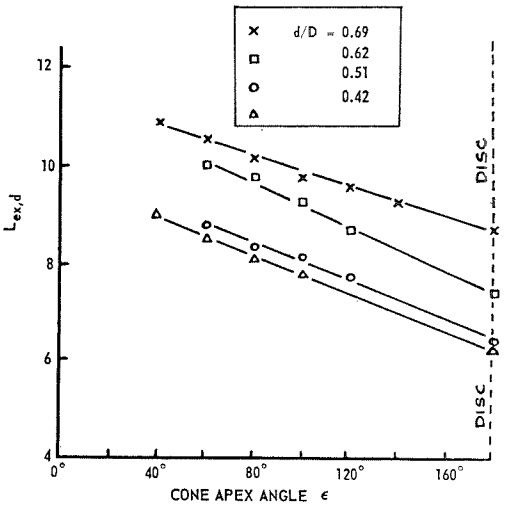

FIG. 12. Variation of extinction loading factors with cone apex angle ϵ (analog predictions).

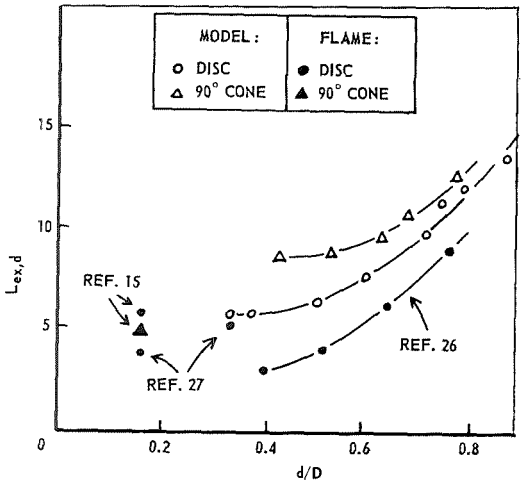

FIG. 13. Comparison of model predictions with flame data.

be above the other curves, and the slopes of the lines in Fig. 12 should be positive.

However, apart from those qualitative inaccuracies of the model predictions, the numerical values for the loading factors L_{ex} evaluated from flame measurements are remarkably close to the values predicted by the model (Figs. 11 and 13).

Discussion and Conclusions

If for a moment we concentrate on Figs. 11 and 13, where model predictions are compared with loading factors evaluated from flame measurements, the numerical agreement between these values is quite remarkable.

This result, however, becomes less understandable if we consider in addition the research on the flow pattern from the section dealing with influence coefficients. Then the position is the following one:

(1) There exists rough agreement between the loading factors L_{ex} predicted by the isothermal model and those evaluated from "cold" influence coefficients (Fig. 10). This is a result that one would expect, since both methods for the evaluation of L_{ex} are equivalent. The difference can be ascribed to the differing reaction rate functions as presented in Fig. 2.

(2) The loading factors predicted by the model are of the same order of magnitude as those evaluated from the actual combustion experiments (Figs. 9, 11, 13).

(3) The loading factors obtained by using the "hot" influence coefficients are about an order of magnitude larger than $L_{ex,flame}$ (Table 5 and Fig. 13). One should expect both to agree.

What are the reasons that the model predictions are in most of the cases in rough agreement with flame measurements, although a comparison of the loading factors obtained from "hot" and "cold" influence coefficients led to a quite different result?

The design of the model was based on so called "half-truths," one of them related to the flow pattern, the other based on some simplifications concerning the combustion process. We have already seen that quantitative differences do exist between the flow containing flames and cold isothermal flows in geometrically similar surroundings. Based on this result we had to expect model results and flame behavior to be different. This expectation was, however, based on the assumptions that the description of the combustion process as a temperature function only is right. Furthermore it was assumed for the evaluation of $L_{ex,flame}$, that the heat release rates within the combustion chamber reach the values of the Longwell-Weiss homogeneous reactor. This problem was investigated by Petrein *et al.*[31] These authors found that the average conversion or heat release rates were 6–8 times lower in a high-intensity combustion chamber than one would expect from the homogeneous data, although the possibility of homogeneous rates appearing locally is not excluded. Using these results for a rough check, we replace the q_{max} from homogeneous reactor experiments by $q_{max}/8$ for the evaluation of $L_{ex,flame}$. This procedure would in fact increase the loading factor $L_{ex,flame}$ by a factor of 8 and would make them comparable with those ones evaluated from "hot" influence coefficients. However this check can only be regarded as a guide as to the trend, since acceptance of the results of Petrein would mean abandoning the idea that reaction rate is a function of temperature only.

Final Remarks

The results and discussion of this paper have shown that the two assumed similarity criteria concerning flow and combustion process are questionable. The reasonable quantitative agreement between model predictions and flame experiments could only be explained by the fact that the errors introduced by the application of the two similarity criteria have the tendency to cancel one another instead of adding up.

Considering these results, the author could not use or recommend this method of isothermal modeling with confidence as a means of predicting the stability limits of new combustion chamber without confirmation by flame tests. The loading factors predicted by the model are difficult to explain and without investigations on the flow

patterns this interpretation would be too speculative to be of any value for the designer.

ACKNOWLEDGMENTS

The apparatus was made in the workshop of the Mechanical Engineering Department, Imperial College of Science and Technology. The author gratefully acknowledges the previous work done by Dr. A. A. El-Shirbini and Dr. A. A. K. El-Bahadli in designing the apparatus and in carrying out numerous experiments.

Nomenclature

A	Cross section of cylindrical or rectangular combustion chamber [m^2]
B	Width of rectangular chamber [m]
c	Specific heat at constant pressure [kcal/kg °C]
d	Diameter or width of baffle [m]
D	Diameter of cylindrical chamber [m]
L_d	$[v\rho c(T_{ad} - T_u)]/q_{max}d$, chemical loading factor
L_{ex}	$[\dot{m}_{ex}c(T_{ad} - T_u)]/q_{max}V$ or $[v_{ex}\rho c(T_{ad} - T_u)]/q_{max}d$, chemical loading factor at extinction point
L_V	$[\dot{m}c(T_{ad} - T_u)]/q_{max}V$, chemical loading factor
$\dot{m}$	Mass flow rate [kg/hr]
m_{Ar}	Mass fraction concentration, ρ_{Ar}/ρ_{total}
p	Pressure [atm]
q	Heat release per volume element [kcal/sec m^3]
q_{max}	Maximum heat release per volume element [kcal/sec m^3]
Re	$(v \cdot d)/\nu$, Reynolds number
T	Temperature [°K]
v	Linear velocity of gas [m/sec]
V	Characteristic volume [m^3]
α_{jk}	Weighted influence coefficient
β_{jk}	Influence coefficient
ϵ	Cone apex angle
δ_V	Volume element
ϕ	q/q_{max}, dimensionless combustion rate
τ	$(T - T_u)/(T_{ad} - T_u)$, dimensionless temperature
η	$(T_e - T_u)/T_{ad} - T_u)$, efficiency
ρ	Density [kg/m^3]
ν	Kinematic viscosity [m^2/sec]

Indices

Ar	Argon
ad	Adiabatic
cr	Critical
d	L_d, loading factor related to width of baffle
V	L_V, loading factor related to characteristic volume
e	Indicating conditions at the outlet of the combustion chamber
ex	At extinction point
j, k	Running indices
u	Unburned

REFERENCES

1. SPALDING, D. B.: Proc. Inst. Mech. Engrs. (London) *171*, 383 (1956).
2. MARTIN, D. G. and WEBB, J. D.: *Seventh Symposium (International) on Combustion*, p. 651. Butterworths, 1959.
3. DAMKÖHLER, G.: Z. Elektrochem. *42*, 846 (1936).
4. PENNER, S. S.: *Combustion Researches and Reviews*, p. 140. Pergamon, 1955.
5. STEWART, D. G.: *Selected Combustion Problems II*, p. 384. Pergamon, 1956.
6. BRAGG, S. L. and HOLIDAY, J. B.: *Selected Combustion Problems II*, p. 270. Pergamon, 1956.
7. ZUKOSKI, E. E. and MARBLE, F. E.: *Gasdynamics Symposium on Aerothermochemistry*, p. 205. Northwestern University, 1956.
8. SPALDING, D. B.: *Performance Criteria of Gas Turbine Combustion Chambers*. Aircraft Eng. Monograph. Bromhill Publ. London, 1956.
9. SPALDING, D. B. and VORTMEYER, D.: Brennstoff-Wärme-Kraft *13*, 259 (1961).
10. SPALDING, D. B.: *Third AGARD Colloquium, Combustion and Propulsion*, p. 219. Pergamon, 1958.
11. SPALDING, D. B.: Combustion and Flame *2*, 287 (1957).
12. SCURLOCK, A. C.: *M.I.T. Fuels Research Laboratories, Meteor Report No. 19*, 1948.
13. WRIGHT, F. H.: Combustion and Flame *3*, 319 (1959).
14. WINTERFIELD, G.: To be published.
15. ZUKOSKI, E. E. and MARBLE, F. E.: *Combustion Researches and Reviews*, p. 72. Pergamon, 1955.
16. MESTRE, A.: *Combustion Researches and Reviews*, p. 72. Pergamon, 1955.
17. WESTENBERG, A. A., BERL, W. G., and RICE, J. L.: *Gasdynamics Symposium on Aerothermochemistry*, p. 211. Northwestern University, 1956.
18. QUICK, A. W.: *D.V.L. Bericht No. 12*, Köln und Opladen, 1956.
19. BOVINA, T. A.: *Seventh Symposium (International) on Combustion*, p. 664. Butterworths, 1959.
20. SPALDING, D. B. and VORTMEYER, D.: Combustion and Flame *6*, 25 (1962).
21. TILTMAN-LANGLEY LTD.: Contract AF 61 (514)–1213 United States Air Force, Air Re-

search and Development Command, European Office, Brussels, Belgium, Technical Note No. 2, 1960.
22. Barrère, M. and Mestre, A.: *Selected Combustion Problems*, p. 426. Pergamon, 1954.
23. Williams, G. C., Hottel, H. C., and Scurlock, A. C.: *Third Symposium (International) on Combustion*, p. 21. Williams and Wilkins, 1959.
24. Fetting, F., Choudbury, A. P. P., and Wilhelm, R. W.: *Seventh Symposium (International) on Combustion*, p. 62. Butterworths, 1959.
25. Longwell, J. P. and Weiss, M. A.: Ind. Eng. Chem. *47*, 1634 (1955).
26. Weiss, M. A., Lang, R. J., and Longwell, J. P.: Ind. Eng. Chem. *50*, 257 (1958).
27. Clarke, A. E., Harrison, A. J., and Odgers, J.: *Seventh Symposium (International) on Combustion*, p. 664. Butterworths, 1959.
28. El-Bahadli, A. A. R.: Ph.D. Thesis, Imperial College, 1961.
29. De Zubay, A. E.: A.S.M.E. Preprint 54 S.A.–27 (1954).
30. Rushton, J. H.: Report, Imperial College, London, Dept. of Mech. Eng.
31. Petrein, R. J., Longwell, J. P., and Weiss, M. A.: Jet Propulsion *26*, 81 (1956).
32. Lyall, H. G.: National Gas Turbine Estab., Report M 305 (1957), Ministry of Supply, England.
33. Anagnostou, E. and Potter, A E.: This volume, p. 1.

SEMITHEORETICAL CONSIDERATION ON SCALING LAWS IN FLAME STABILIZATION

KARL-RICHARD LÖBLICH

With good approximation to reality the stability of flames on flameholders may be described with simple equations for heat and mass transfer. As a result of considerations with regard to a simple model a dimensionless number N_x is obtained, which is constant in the limiting case of large Reynolds numbers and small blockage ratios for all flameholders and gaseous fuels with a sufficiently high laminar flame speed. It combines the two stabilization laws found by Zukoski and Marble and by Putnam and Jensen, which were discussed further by Spalding. Regarding several deviations from the limit case we succeeded in finding adaptation functions from theoretical considerations or on an empirical basis. These were introduced into the stability equation, and permit comparison of seemingly very dissimilar systems.

A relationship between flame stability and flame flash back is pointed out as affected by transport mechanism and flame speed. In addition the combustion of heterogeneous mixtures is treated.

Introduction

The mechanism of any combustion process in technical equipment is so complex that an exact mathematical treatment is impossible. However, some important relations concerning stability and efficiency phenomena have been found empirically by several authors. Because the interpretations of the experimental facts are not always satisfactory, the purpose of this paper is to give a reasonable explanation of the experimental observations for the case of flame stabilization by bluff bodies. This is done by proposing a physical model which makes use of well known heat and mass transfer relations from other fields of transport processes. This model will reveal the similarity rules which are appropriate to the scaling of stability processes. Mainly, the combustion of homogeneous gas mixtures is considered.

Empirical Basic Concepts

Zukoski and Marble[1] found that the flame stability, represented by the blow-off velocity W, is strictly proportional to the length L of the recirculation zone behind the flameholder for constant laminar flame speed of the mixture and a sufficiently high Reynolds number. They defined a critical ignition time τ by the ratio L/W, and expressed their results by τ = constant. These authors considered that the wakes behind bluff bodies are similar in their stabilization properties, so that $L/W\tau$ = constant = S. While τ is a function of the laminar flame speed u of the mixture, the stability number S had been thought to be independent of u. However, this is only a limiting law, valid beyond $\mathrm{Re}_{Wd} = 5 \times 10^4$, where Re_{Wd} is the Reynolds number for the stability limit, which is evaluated from the blow-off velocity W, the kinematic viscosity ν of the approach stream, and the characteristic length d of the flameholder.

For $\mathrm{Re}_{Wd} > 10^4$ the boundary layer between the wake and main stream is turbulent over its entire length up to the separation point, whereas for $\mathrm{Re}_{Wd} < 10^3$ it is laminar over its entire length. In the transition interval between these limits the turbulence in the boundary layer increases with increasing Reynolds number, Re_{Wd} from downstream to upstream.[2] Because the stabilization properties of a recirculation zone behind a bluff body are influenced by the recirculation speed and the condition of the boundary layer between recirculation and main stream, the wakes cannot be considered to be similar if they are created by two different flameholders with the same Reynolds number or by flameholders with the same shape but different Reynolds numbers.[3] Thus, in the transition interval between $\mathrm{Re}_{Wd} = 10^3$ and 5×10^4, $L/W\tau$ becomes a function of the Reynolds number and the shape.

Under these circumstances, the concept of the ignition time $\tau = L/W$ is unsuitable, because it implies that the flow of fresh gas close to the wake edge has a velocity proportional to that of the main stream. Considerations about the fluid dynamics of the systems in the transition interval

show that this premise is not fulfilled but is only valid for $Re_{Wd} > 5 \times 10^4$, when the transition from the laminar to the turbulent state of the boundary layer has taken place.

Another relation governing the stability of a flame was found by Putnam and Jensen[4] showing that the blow-off velocity W for given flow conditions is proportional to the square of the laminar flame speed of the mixture. Spalding[5] has analyzed it more closely. To prove this relation experiments have been performed at constant pressure, constant initial temperature, and approximately equal values of Re_{Wd} (for cylindrical flameholder). The results show that the term $C^* = W/Lu^2$ is quite constant.[6] The thermal conductivity of the gas mixture, seems to have no greater influence than is already contained in u. On the other hand, the dimension of C^* points to an influence either of the kinematic viscosity $\nu[m^2\ sec^{-1}]$ or of the diffusivity $D[m^2\ sec^{-1}]$. But the diffusion influence does not exceed $Sc^{0.3}$, whereas ν is always given in fluid dynamic characteristic numbers.[6] Thus we obtain a dimensionless stability number N_x from C^* as a function of Re_{Wd} in the transition interval:

$$N_x = W\nu/Lu^2 = f(Re_{Wd}, F), \qquad (1)$$

where F represents the influence of the flameholder shape. N_x is formally the same as the group used by Bragg and Holliday.[7] However, these authors worked with the diameter of the stabilizer instead of the length of the recirculation zone as is done here. The introduction of L into the stability number N_x avoids dimensional difficulties if one goes from sharp-edged flameholders to cylinders.

Above the transition interval, $f(Re_{Wd}, F)$ approaches a limit, which follows from the relation found by Zukoski and Marble.[1] Below the transition interval another limit exists which does not have to be the same for stabilizers of different geometry according to our experiments.

A Stabilization Model

According to observations of several authors (e.g., Williams and Shipman[8]), the flame "tongs" which surround the wake (residual flames) are somewhat more stable than the flamefronts which extend downstream from the wake. It is therefore reasonable to regard the flame tongs at the edge of the wake as the initial flame which can only create the main flame under certain conditions. The author has shown reasons for the higher stability of the residual flame.[6]

The flow at the wake edge can formally be separated into two components, at least in time average. The outer part flows downstream with the main stream while the inner part is drawn into the recirculation. One can imagine a permeable border to separate the two regions. The beginning of the residual flame is on the wake side of this border. It is formed by transport of fuel and oxygen (at the first contact between wake and fresh gas) into the wake. These mix with the hot burned gas of the wake and begin to react. After a certain distance from the flameholder the flame crosses the imaginary border if the conditions necessary for this are fulfilled. Only then combustion takes place in the main stream (Fig. 1).

The residual flame changes into the main flame outside of the wake by crossing the imagi-

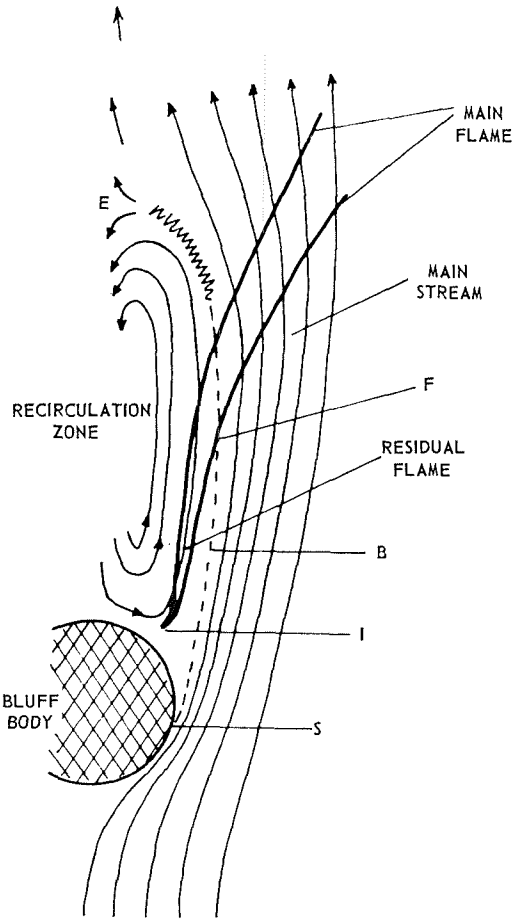

FIG. 1. The run-up stretch. At F the initial flame crosses the border B of the recirculation zone; $IF = \Lambda$, S is the separation point and I the ignition point. If the flow velocity w approaches the blow-off velocity W then F goes to the end E of the recirculation zone, i.e., $\Lambda \rightarrow \Lambda_{max}$)

nary border. The distance from the location of ignition to the crossover point can be designated by Λ ("run-up stretch"). Lowering of the stream velocity w is favorable for spreading of the initial flame into the main stream, i.e., Λ decreases. If one increases w, Λ increases while an increase of the burning velocity diminishes Λ. Λ cannot become larger than the distance between the ignition point and the downstream region of reversal of the recirculation flow. Although this stretch is curved it is, in most cases, nearly equal to the length of the recirculation zone, which is the distance between the downstream end of the bluff body and the point from which material is transported upstream. An exception is the ammonia flame, because the ignition point lies rather far downstream from the flameholder.[6] If Λ approaches L, then w approaches W, i.e., the stability limit is reached.

The temperature distribution through the flamefront is S-shaped. The inflection point of this curve lies where the heat production by combustion starts. Therefore, the initial flame can only cross the border between the recirculating stream of hot gases and the flowing fresh gas mixture where the inflection point lies outside of the border. Apart from the temperature difference, the heat flux from the hot to the cold gas is governed by the heat transfer coefficients α inside and outside the flame. Outside the flamefront (Index e), α_e is mainly a function of the Reynolds number whereas, inside the flamefront (i), α_i is additionally influenced by heat sources. The heat balance requires

$$(T_f - T_\omega)\alpha_i = (T_\omega - T)\alpha_e, \qquad (2)$$

where T_f is the flame temperature, T_ω the temperature at the inflection point, and T the temperature in the fresh gas flowing along the edge of the wake. Zukoski and Marble found that the temperature of the burned gas is not far from the adiabatic flame temperature, and nearly independent of the flow rate.[1] Assuming that the ratio $\vartheta = (T_f - T_\omega)/(T_\omega - T)$ is near 1 or constant, one obtains:

$$\alpha_e = c\alpha_i.$$

To arrive at a dimensionless form one substitutes for the heat transfer coefficients the corresponding Nusselt numbers which are given in an integrated form from the point of first meeting of hot and cold gas to the point Λ:

$$|\,\mathrm{Nu}_e\,|_0^\Lambda = c\,|\,\mathrm{Nu}_i\,|_0^\Lambda. \qquad (3)$$

It was shown earlier[6] that this formulation is also valid in the transition interval from the laminar to turbulent structure of the wake edge if it is split into two terms on both sides. Thus one can write, neglecting c:

$$|\,\xi_l\mathrm{Nu}_{e,l} + \xi_t\mathrm{Nu}_{e,t}\,|_0^\Lambda = |\,\xi_l\mathrm{Nu}_{i,l} + \xi_t\mathrm{Nu}_{i,t}\,|_0^\Lambda. \qquad (4)$$

The factors ξ_l and ξ_t have values between zero and one so that $\xi_l + \xi_t = 1$, according to the extent to which turbulence has reached upstream. The solution of this equation is first done for the limit cases $\xi_l = 1$; $\xi_t = 0$ and $\xi_l = 0$; $\xi_t = 1$, i.e., for the completely laminar and completely turbulent case, respectively. The general formulation of the Nusselt equations is

$$\mathrm{Nu} = k\,\mathrm{Re}^m f(\cdots), \qquad (5)$$

where $f(\cdots)$ stands for all the other groups which might have an influence on transport. On the reaction side of the flamefront border the Nusselt number is not only influenced by the flow, but also by the existence of heat sources, the energy flux of which may be considered as a function of the flame number (Fl) and of the Reynolds number. This must be added to the Nusselt equation for the inner side of the front. As characteristic length Λ is introduced into the characteristic numbers, for which Λ at the stability limit approaches L while w approaches W. Since the flow conditions inside and outside of the flamefront are dependent on the velocity of the main stream, the same value of the Reynolds number $\mathrm{Re}_{WL} = WL/\nu$ is taken for inside and outside. Differences in the boundary layer structures show up in the constants and exponents of the formulation; ν is a function of the temperature, $\nu = \nu(T)$, but this function is similar for all gases. Therefore one may calculate with the value for the initial temperature. Mistakes made in this way may be compensated for by adjusting the constants in the equations (see reference 6). The condition for the $\mathrm{Nu}_{e,t} = \mathrm{Nu}_{i,t}$ turbulent case leads to

$$k_1\,\mathrm{Re}_{WL}{}^m f_1(\cdots) = k_2\,\mathrm{Re}_{WL}{}^\alpha \mathrm{Fl}^\beta f_2(\cdots),$$

or

$$\mathrm{Re}_{WL} = (k_2/k_1)^{1/(m-\alpha)}\mathrm{Fl}^{\beta/(m-\alpha)}(f_2/f_1)^{1/(m-\alpha)}. \qquad (6)$$

Analogously, one obtains for the laminar case

$$\mathrm{Re}_{WL} = (k_4/k_3)^{1/(n-\gamma)}\mathrm{Fl}^{\delta/(n-\gamma)}(f_4/f_3)^{1/(n-\gamma)}. \qquad (7)$$

Because of the empirical relation (1) the expressions $\delta/(n-\gamma)$ and $\beta/(m-\alpha)$ have to assume the same value of 2. The quotients f_2/f_1 in Eq. (6) and f_4/f_3 in Eq. (7) are assumed to be approximately equal to 1. According to experimental

results[6] there is an influence of the diffusivity D in the mixture (because D has an influence upon the rate of heat release) which can be neglected for the turbulent case without making too large an error. The turbulent mass transfer processes are governed only by the fluid dynamics of the system contained in the functions with the Reynolds number. In the laminar case differences in the diffusion coefficients of fuel and oxygen greatly influence the equivalence ratio at the flamefront.[2] Instead of the Φ value (equivalence ratio fuel/oxidizer) in the main stream the value Φ^* fixes u in the characteristic number Fl in the laminar case. In the transition interval Fl is determined by Φ_{eff}. Introducing K' for $(k_2/k_1)^{1/(m-\alpha)}$ and K'' for $(k_4/k_3)^{1/(n-\gamma)}$ one now obtains for Eq. (4):

$$\text{Re}_{WL} = (\xi_1 K' + \xi_2 K'') \{\text{Fl}(\Phi_{\text{eff}})\}^2. \quad (8)$$

The derivation of Eq. (8) from Nusselt equations permits a better insight into the relation between fluid dynamics and chemical reaction implicit in u. The constants K' and K'' turn out to be functions of two k_x's which characterize the location of the temperature, concentration, and velocity profiles relative to each other inside and outside the flamefront. Any influence of the boundary layer profile will therefore also influence the value of the constants in Eq. (8). Through the formulation as a transport phenomenon, the formal relation between flame stability with flameholders and flashback in burner tubes[4] becomes even more lucid. The model used here differs from that of ref. 5.

Discussion

The discussion of Nusselt equations shows that a heat transfer equation, which has been obtained for a particular case, can only be applied to other cases if the profiles of the flow and temperature boundary layers as a function of the length l are similar too. This does not mean that all characteristic numbers which occur in the equation have to assume equal values (complete similarity) for reasonable scaling. But there must be an agreement in the functional relations of the dimensionless numbers, i.e., the heat transfer law must be the same. This law determines the constants and exponents in equations of the type of Eq. (5). If the boundary layer profiles are changed by any influences, the transfer law is also changed. Often a functional connection between these influences and the change of the transfer law can be calculated by theoretical considerations or can be obtained empirically. If one includes such an alteration function into the transfer equation, the transfer equation can be applied to all scaling problems with profile change, for which the alteration function is valid.

Actually the factor in Eq. (8) containing the ξ functions represents an alteration function for the transition from laminar to turbulent transport processes. This factor can be specified even further with regard to the constants K' and K''. Thus the profiles of laminar boundary layers at the edge of wakes, which are caused by rounded-off, elongated, or sharp-edged flameholders, show varying structure. This can be characterized by substituting K' by a constant K_1 multiplied by a form factor F. In the case of turbulent flow individual differences in the boundary layer structures are compensated after a very short run-up stretch. Thus the constant $K_2 = K''$ can be used for all flameholder shapes.

In the case of free flow around the body the locations of the profiles relative to each other belonging to K_1F and K_2 adjust themselves independently of the size d of the body. If the flow through the combustion chamber is confined the flow at the wake edge is influenced by the blockage ratio B (body diameter d/chamber width b). The contraction number ϵ is defined as $\epsilon = 1/(1 - B)$. In order to determine the influence of ϵ on the two terms in Eq. (8), experiments were performed by Baumgärtel[9] which led to the result that the laminar term increases at first in the interval $\epsilon = 1$ to $\epsilon = 2$ with increasing ϵ and then falls off again. The turbulent term steadily falls with increasing ϵ. Equation (8) can be written as

$$\text{Re}_{WL}[= \xi_1 K_1 F f_1(\epsilon) + \xi_2 K_2 f_2(\epsilon)][\text{Fl}(\Phi_{\text{eff}})]^2. \quad (9)$$

For practical purposes Eq. (9) can be written in the manner of Eq. (1) in abbreviated form after division by $f_2(\epsilon)$:

$$f(\epsilon) N_x(\Phi_{\text{eff}}) = \xi_1 K_1 F \pi(\epsilon) + \xi_2 K_2. \quad (10)$$

For the separate expressions one finds empirically:

$$K_1 = 0.18 \qquad K_2 = 0.27.$$

Form factor F for

cylinders	$F = 1.00$
V-gutters	1.08
plates	1.15

$$\xi_1 = \frac{16\,(\text{Re}_{Wd})^{1/2} + 4.94 \times 10^2}{\text{Re}_{Wd}} - 0.082[\text{Re}_{Wd}/(5 \times 10^4)]^2;$$

$$\xi_2 = 1 - \xi_1.$$

If $Re_{Wd} > 5 \times 10^4$, then $\xi_2 = 1$; compare also Fig. 4.

$$f(\epsilon) = 0.43\epsilon + 0.57$$

$$\pi(\epsilon) = [(\epsilon + 1)(\epsilon^2 - 1)^{1/2} + 1]/\epsilon^2.$$

The validity of $\pi(\epsilon)$ is limited by reaching the quenching distance. In $N_x(\Phi_{eff})$ is $u = u(\Phi_{eff})$.

For practical applications of Eq. (10) one has to estimate Re_{Wd}:

$$Re_{Wd} = 0.22(d/L)\,Fl^2. \qquad (11)$$

Equation (10) with estimated ξ functions will give an approximate value for N_x, the exactness of which can be increased by iteration. The calculation of Φ_{eff} will be shown later. Using Eq. (10), together with the adaptation functions, one has to keep in mind that the recirculation zone length L, is a function of ϵ, too. Values for $L = f(d, \epsilon)$ for several flameholder shapes are to be published by Baumgärtel.[9]

The adaption functions are valid for two-dimensional flow. The complete stability Eqs. (9) or (10) are valid for atmospheric pressure ($p_0 = 1$ atm) and room temperature ($T_0 = 293°K$). To transform the values to a different initial temperature and a different pressure one uses Eq. 12 (ref. 10, where similar stability relations are used):

$$(Re_{WL})_{T,p} = (Re_{WL})_0 (T/T_0)^{1.6} (p/p_0)^{0.7}. \qquad (12)$$

Because of the validity of the L–W relation in three-dimensional flow the type of Eq. (10) derived by use of data for two-dimensional flow does not change for its application to three-dimensional flow, and the exponents must be the same for both cases. The argument for this is given by dimensional theory. In contrast to the type of the Eqs. (9) or (10) the constants change in part with the transformation from a two-dimensional model to a combustion chamber with three-dimensional flow. To make possible calculations for combustion chamber design one has to determine the changes of the constants by experiments—one for each constant. However, the results of comparison measurements, e.g., concerning the influence of the burning properties of mixtures on the flame stability in a small model combustion chamber, are applicable to problems in large-scale combustion chambers without having to consider changes in the constants, when going from two- to three-dimensional flow.

The degree of turbulence of the stream ahead of the flameholder also has an influence on N_x in Eq. (10). Stronger initial turbulence distributes the heat flowing from the wake into the fresh gas faster onto a large stream cross section. The experiments performed by Williams *et al.*[11] show that N_x decreases with increasing degree of turbulence.

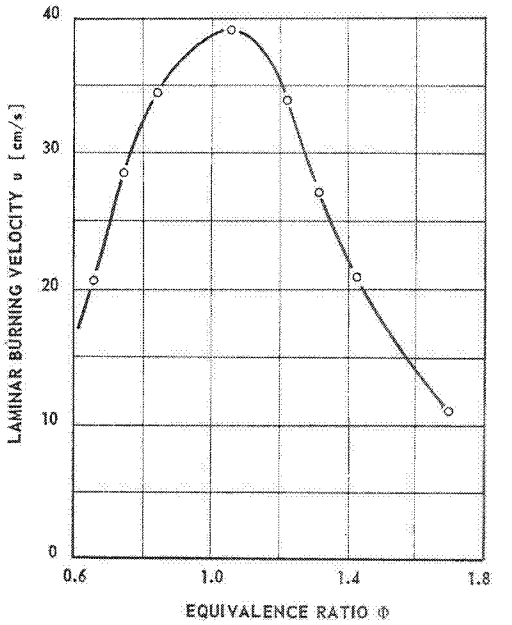

FIG. 2. Normal burning velocities of propane–air mixtures versus equivalence ratio Φ.

The effective values of Φ can be calculated by transfer equations. Starting from a laminar structure of the wake edge, one assumes that the reaction at the flamefront takes place so rapidly that the concentration of the basic masses is practically zero there. The ratio between fuel flow and oxygen flow is given by the quotient of the respective mass transfer equations:

$$Sh_j = \beta_j L/D_j = k\,Re^m\,Sc_j^n.$$

One obtains

$$\beta_f/\beta_{ox} = (D_f/D_{ox})^{1-n}. \qquad (13)$$

According to general experience with laminar mass transfer, the value 0.7 is to be expected for $(1 - n)$. Since a thermal diffusion influence arises because of the great temperature gradient, one finds approximately a value of 1 for the exponent for the results published by Zukoski and Marble.[2] The value of Φ^* at the flamefront is derived from the equivalence ratio Φ in the main stream by:

$$\Phi^* = \Phi(D_f/D_{ox}). \qquad (14)$$

In the case of fully developed turbulence, the

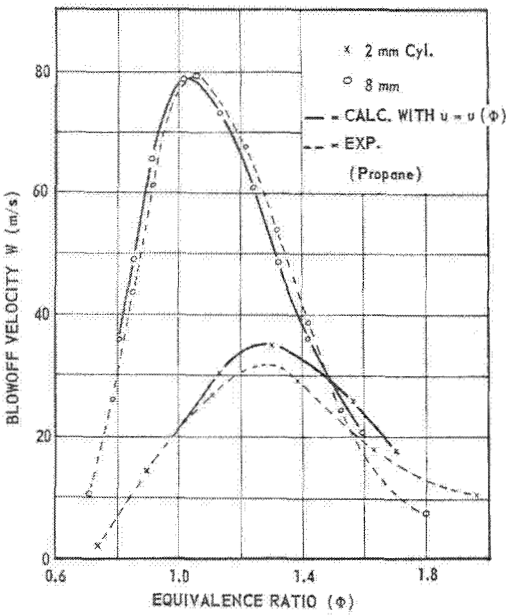

FIG. 3. Comparison of calculated with experimental stability curves (propane as fuel).

flamefront is torn apart, whereby fuel enters between the separate flame pockets. Therefore, Φ is just as large at the flamefront as in the main stream.

In the transition interval the effective value of Φ_{eff} at the flamefront is the sum of two parts:

$$\Phi_{\text{eff}} = \xi_1\Phi^* + \xi_2\Phi. \qquad (15)$$

The ξ functions in Eq. (15) are the same as in Eq. (10).

The equations derived so far are valid for homogeneous mixtures. The laminar flame speed curve,[12] $u = u(\Phi)$, of propane–air mixtures is plotted in Fig. 2 for checking the validity of Eq. (10) in connection with Eq. (15). Figure 3 and Table 1 show the accuracy of the stability Eq. (10). The recirculation zone lengths L of the two cylinders in the graph are 14.6 mm and 31.4 mm, respectively. The calculations of the maximum $W_{\max}$ of the blow-off velocities can be done with a high accuracy. The average error does not exceed $\pm 5\%$, the largest being 10 to 15%. Equation (10) fits the curves on the lean side of mixtures ($\Phi < 1$) better than on the rich side ($\Phi > 1$). For very lean or very rich mixtures the agreement is poor, which may be due to some additional gas effects.[13,14]

Equations (10) and (15) may be considered to be satisfactorily confirmed. They apply sufficiently well that one is able to determine laminar flame speeds by measuring blow-off velocities and calculating u by Eqs. (10) and (15) in the reverse way. They explain why small flameholders can stabilize a flame in rich mixtures of high molecular weight fuels relatively better than larger ones. This can be shown best by calculating the so-called reduced blow-off velocity $C = W/L$ (the reciprocal value of τ). The reduced blow-off velocity C decreased for $\Phi > 1$ with increasing diameter d of the flameholder in line with the behavior of the ξ functions with Re_{Wd} and the behavior of Eq. (15).

Practical Application

For practical purposes graphs are included which show the behavior of the ξ functions (Fig. 4) and of the stability number N_x as functions of the Reynolds number Re_{Wd} for the case $\epsilon = 1$ (Fig. 5). Figure 6 shows the ϵ-dependency of N_x for a Reynolds number $\text{Re}_{Wd} > 5 \times 10^4$. In agreement with Bragg and Holliday,[7] who used a similar dimensionless number, and with Zukoski and Marble's τ relation, $N_x(\text{Re}_{Wd})$ becomes constant if Re_{Wd} increases beyond 5×10^4. Below this limit there is a disagreement

TABLE 1

Comparison of Calculated with Measured Values of the Maximum Blow-Off Velocity, $W_{\max}$

Flameholders: cylinders. Fuel: propane.

Diam. d (mm)	Contraction number ϵ (dimensionless)	Max. blow-off velocity ($W_{\max}$) By Eq. (10) (m/sec)	Max. blow-off velocity ($W_{\max}$) Exptl. (m/sec)	Value of ratio $W_{\text{calc}}/W_{\text{exp}}$
2	1.05	35	32	1.09
8	1.23	78	80	0.98
8	1.31	71	75	0.95
8	1.42	58	62	0.93
8	1.53	54	53	1.02
12	1.58	69	76	0.91
12	1.74	67	66	1.02
20	1.87	82	77	1.07
8	1.89	44	46	0.96
25	2.39	91	82	1.11
12	3.40	46	51	0.91
				0.99 Average ratio

between the stability number used by Bragg and Holliday[7] and of N_x. This can be explained by the behavior of the relation between the bluff body diameter d and the recirculation zone length L as a function of the Reynolds number Re_{Wd}. Bragg et al. used d in their stability criterion whereas L is used in the present considerations. The different diffusion properties of the fuel and the oxidizer are better taken into account by using $N_x(\Phi_{\mathrm{eff}})$ in the case of premixed gases. The stability number N_x represents a

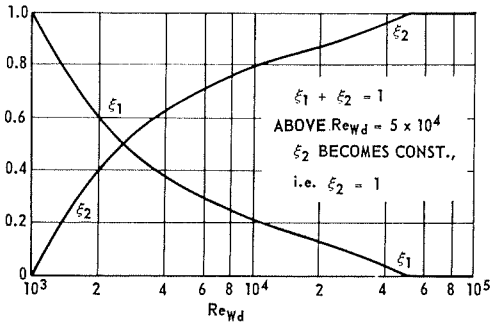

FIG. 4. The ξ functions in dependence on the Reynolds number Re_{Wd}. If $\mathrm{Re}_{Wd} < 10^3$, $\xi_1 = 1$, $\xi_2 = 0$. If $\mathrm{Re}_{Wd} > 5 \times 10^4$, $\xi_1 = 0$, $\xi_2 = 1$.

loading factor similar to that used by Spalding *et al.*[15]; but instead of the poorly known reaction rate it uses a function of the laminar flame speed.

Because the recirculation zone length L is the most important length in the flame stabilization mechanism it is possible to transfer results of experiments regarding fuel influence on flame stability from a small combustion chamber equipped with flameholders to a full-scale can type burner without special flameholders. Here, too, a recirculation is established. Its downstream length is given by the design of the can. If one knows the performance and the stability characteristics of a power plant for a particular fuel with or without premixing one can predict how the power plant will behave with a different fuel. Another application of Eq. (10) is in the determination of relative values of the effective laminar burning or ignition velocities of heterogeneous fuel–air mixtures. That is more easily carried out than with the Bunsen burner method used by Kaesche-Krischer and Zehr.[16] One does not obtain absolute values because of the inertia of the particles or droplets toward velocity changes in high speed flow. However, the accuracy of the comparison measurements should be good, if one pays attention to an approximate agreement of particle sizes and weights.

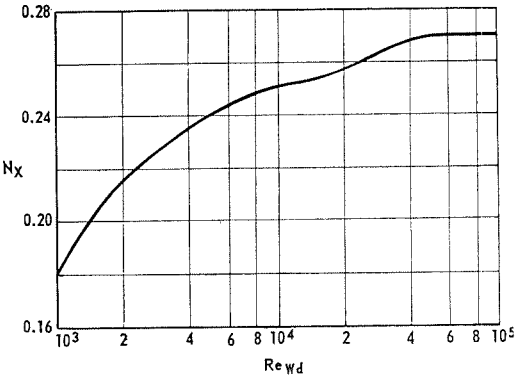

FIG. 5. The stability numbers $N_x = W\nu/L\alpha^2$ as a function of Re_{Wd} in the transition interval, drawn for the case $F = 1.00$ and $\epsilon = 1$. Beyond the limits of this interval N_x is constant.

Conclusion

All equations and considerations described above are derived for subsonic flow speeds. It appears possible to extend them by a simple manner for higher Mach numbers. On the other hand, the application of transport equations for the treatment of stability problems in premixed gases is limited, if the heat and mass transport rates in the flamefront have reached such high values that the mere chemical mechanism controls the effective reaction speed in the flamefront. This can only be the case if the turbulence pockets become so small that they are of the same dimension as the thickness of the thin

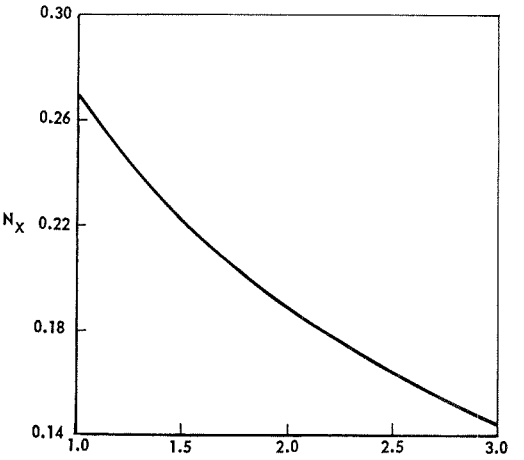

FIG. 6. The stability number N_x versus $\epsilon = 1/(1 - B)$, $\mathrm{Re}_{Wd} > 5 \times 10^4$.

luminous reacting layers which surround the individual flame pockets in the turbulent flame-front and if the time of their isolated existence is shorter than the ratio of the radius of a flame pocket to the laminar flame speed. As an estimate these conditions will be reached at flow rates about 1000 m/sec using saturated hydrocarbons and air. In heterogeneous fuel-oxidizer systems a limit is to be expected also for the applicability of the above equations.

The paper shows the possibility of solving some stability problems of high output combustion equipment by using small combustion chambers. This is easier than the prediction of the efficiency of large-scale combustors on the basis of experiments with small models because the efficiency is influenced by more variables. The results can also be applied to other flame stabilizations than by bluff bodies.

Nomenclature

b	Combustion chamber width
B	Blockage ratio
C	Reduced blow-off velocity
C^*	Stability parameter
d	Diameter of the flameholder
D	Diffusion coefficient
f	Symbolizes a function
F	Form factor
k	Constant
K	Constant
l	Characteristic length (in general case)
L	Recirculation zone length
p	Pressure
T	Temperature
u	Laminar flame speed (normal burning velocity)
w	Flow velocity (in general case)
W	Flow velocity at stability limit (blow-off velocity) both at chamber entrance

Characteristic Numbers

Fl	uL/ν, flame number
Nu	$\alpha l/\lambda$, Nusselt number
N_x	$W\nu/Lu^2$, stability number
Re	wl/ν, Reynolds number
Sc	ν/D, Schmidt number
Sh	$\beta l/D$, Sherwood number

Greek Symbols

α	Heat transfer coefficient
β	Mass transfer coefficient
ϵ	Contraction number
λ	Thermal conductivity
Λ	Run-up stretch
ν	Kinematic viscosity
ξ	Transition function
π	Symbolizes a function
Φ	Equivalence ratio

Indices

l	Laminar
t	Turbulent
W	Blow-off velocity
ω	Point of inflection

Acknowledgments

This work was carried out at the Institut für Technische Chemie (Director: Professor G. Schiemann), TH Hannover.

The author wishes to acknowledge the helpful discussions with Dr. F. Fetting. His thanks go to Mr. D. Stange too, whose help in experimental work and numerical calculations was very valuable.

References

1. Zukoski, E. E. and Marble, F. E.: *Gas Dynamics Symposium on Aerothermochemistry*, p. 205. Northwestern University, 1956.
2. Zukoski, E. E. and Marble, F. E.: *Combustion Researches and Reviews*, p. 167. Butterworths, 1954.
3. Löblich, K. R. and Fetting, F.: Paper presented at the *Ninth Symposium (International) on Combustion*, Cornell University, 1962. (Unpublished.)
4. Putnam, A. A. and Jensen, R. A.: *Third Symposium (International) on Combustion*, p. 89. Williams and Wilkins, 1949.
5. Spalding, D. B.: Aircraft Eng. *25*, 264 (1953).
6. Löblich, K. R.: Zur Kinetik der Stabilisierung turbulenter Flammen durch Flammenhalter. Dissertation, T. H. Hannover, 1961.
7. Bragg, S. L. and Holliday, J. B.: *Selected Combustion Problems II*, p. 270. Butterworths, 1956.
8. Williams, G. C. and Shipman, C. W.: *Fourth Symposium (International) on Combustion*, p. 733. Williams and Wilkins, 1953.
9. Baumgärtel, G.: Dissertation, T. H. Hannover (to be published).
10. Khitrin, L. N. and Goldenberg, S. A.: *Sixth Symposium (International) on Combustion*, pp. 443, 545. Reinhold, 1957.
11. Williams, G. C., Hottel, H. C., and Scurlock, A. C.: *Third Symposium (International)*

on Combustion, p. 21. Williams and Wilkins, 1949.

12. LEWIS, B. and VON ELBE, G.: *Combustion, Flames, and Explosion of Gases*. Academic Press, 1961.
13. FETTING, F., CHOUDHURY, A. F. R., and WILHELM, R. H.: *Seventh Symposium (International) on Combustion*, p. 621. Butterworths, 1959.
14. FILIPPI, F. and FABBROVICH-MAZZA, L.: *Eighth Symposium (International) on Combustion*, p. 956. Williams and Wilkins, 1962.
15. SPALDING, D. B.: *Performance Criteria of Gas Turbine Combustion Chambers*. Aircraft Eng. Monograph, Burnhill Publishers, 1956.
16. KAESCHE-KRISCHER, B. and ZEHR, F.: Z. physik. Chem. (N.F.) *14*, 384 (1958).

MODELING TECHNIQUES IN REACTOR DESIGN

C. H. BARKELEW

In many chemical operations for which large scale reactors must be designed, the rate of reaction is influenced by the fact that chemical and physical processes may proceed with comparable rates. This leads to considerable difficulty in constructing appropriate models for studying the behavior of reactors. In this paper, a few representative techniques which have been found useful are described, and compared with methods for modeling combustion chambers.

Introduction

In a chemical reactor we convert matter. In a combustion chamber we convert energy. Even though both types of conversion usually occur in both reactors and burners, it is this distinction in function that is important in discussing modeling techniques. There may be similarities between them and in some cases the same sort of reasoning can be used to model either, but there are many reactor properties which are not analogous to anything in the combustion field, and it is these which will be discussed here. In other words, if a technique has been found useful in modeling a combustion chamber, it is potentially useful in modeling a conceivable reactor. On the other hand, there are problems which arise in modeling reactors which are peculiar to reactors as defined above, and have not come to the attention of those who are interested in combustion. It is these that will be discussed in this paper.

The word "model" refers here to a piece of equipment rather than to a concept. A model of a reactor is a second reactor of different size, shape or function, which reproduces certain essential features of the prototype. I will not refer to a mathematical representation of the processes in a reactor as a "model," although I will refer to the use of these representations in deriving the characteristics of physical models.

A simple reactor problem is the following:

$$A + B \rightarrow C$$

$$C + B \rightarrow D$$

We want to make the product C, and to minimize the relative yield of D. Let us suppose that our reactor is to be a tank with a vigorous stirrer, into which we continuously feed A and B, and from which we continuously withdraw reaction mixture. A little reflection will show that there are just three variables which can influence the relative yields of C and D. They are the ratio of the feed rates of A and B, the "residence time" (i.e., the reactor volume divided by the combined feed rate), and the temperature in case the reaction rates depend differently on temperature. There are several simple models of this system. For example, a stirred beaker with provision for continuous addition and withdrawal will do. We simply run it over a range in each of the three independent variables. Then, knowing that in the full scale reactor the relative yields will not change, we can calculate the optimum conditions of operation. The technique is exactly equivalent to running experiments for determining the kinetics of the reaction, and then using those expressions to scale up the reactor.

Now a model of a reactor is not necessarily similar in operation to its prototype. We could get substantially the same information out of the beaker by removing the continuous feed and instead withdrawing samples for analysis at intervals. We could also get the necessary information from a totally different type of laboratory reactor. We could feed a mixture of A, B, and C into one end of a suitably designed pipe, and analyze what comes out the other end. Other arrangements can be suggested and used, all of which are quite simple and straightforward.

Let us look at a different type of reaction. Suppose we want to oxidize some impurity in water by blowing air through it. With most impurities we might find that the rate at which oxygen is consumed depends strongly on the way we put the air in. If we should stir vigorously the rate would increase, in most cases without an apparent limit. What about modeling in such a case? Here the practice of chemical engineering provides the answer. The system described is probably limited by mass transfer of oxygen, and the textbooks on unit operations tell us that mass transfer rate in gas-liquid systems correlates

strongly with the power input per unit volume and with very little else. An appropriate reactor model would be just a geometrically similar vessel, with the power applied to the stirrer in direct proportion to the volume.

In the first example, the rate of reaction was determined by the rates of chemical processes. In the second it was determined by the rate of a physical process. In both cases, the model and prototype were simply related. This is not true where physical processes and chemical processes proceed with comparable rates. We might find, for example, that the rate of oxygen absorption does not increase indefinitely with power input, but, "saturates" at some value which depends on the flow rate of the liquid. If the power required to reach this "level" is uneconomic, then there may be a real modeling problem. In a suitable operating range the reaction rate depends on both physical processes whose rates vary with size, and on chemical processes whose rates do not vary with size. The model is no longer obvious.

Reactor Types

There are many types of reactors which we use in the chemical process industry, and the design techniques are different for almost all. Listed below are a few of them, with some description of their characteristics.

The Continuous Stirred Tank

This is the simplest, and probably the most widely used reactor of all. If the reaction is exothermic, then possibly the rate at which heat can be removed from the system becomes comparable with the rate of reaction. This can lead to a situation where the rate processes interact to give instability, where the rate of reaction increases more strongly with temperature than does the rate of heat removal. If the reaction mixture has two phases then there may be a pronounced effect of coalescence of the dispersed phase. If the chemical processes are very fast, then the way in which reactants are mixed may have an important influence on the relative rates of competing reactions.

The Pipe Line

A typical example is a furnace coil, which might be used for the cracking of petroleum, for example. Very often pressure drop is high in such systems, particularly if more than one phase is involved, which makes modeling very difficult if not impossible. There is a particularly interesting feature of modeling such reactors which is caused by "Taylor Diffusion," the effect of nonuniform velocity on axial dispersion. This will be discussed in more detail later. Sometimes a pipe reactor is vertical, in which case it is referred to as a "tower."

The Packed Bed

This is a most interesting type of reactor to study. The reactor may be a vessel in which heat transfer is unimportant or it may be a heat exchanger, in which the tubes are packed with a solid for catalyzing a reaction in the fluid which passes through. "Runaway" reactions are possible if the system is exothermic. I will discuss this in detail later.

The Fluid Bed

A "fluid" reactor is a vessel in which a finely powdered solid, reactant or catalyst, is kept in continuous agitation by motion of a fluid through it. This type of reactor is widely used in the petroleum industry for catalytic cracking, however little useful has ever been published on what goes on in one. Their design is still somewhat of an art.

The "Batch" Reactor

Very often a reactor is just a stirred vessel into which reactants are placed, left for a fixed time, and then removed and processed. There are many gross mathematical similarities between batch and pipe line reactors, making it unnecessary to discuss batch processes separately.

Others

There are other classifications which might be listed, but they are relatively unimportant. We might try to carry out a reaction in a supersonic nozzle, for example. If so, we might even be able to work out a modeling technique. It would undoubtedly be specific to the system, however, and probably not of general utility. Notice that such a reactor would be similar to some combustion chambers.

Problems of Reactor Design

These classes constitute what someone in the chemical processing industry thinks of when he talks about reactors. Suppose an engineer must design one. What does he consider to be important when he specifies what sort of vessel is to be used in a plant?

First of all he must realize that the reactor is not isolated. Its operation and characteristics must be integrated with all other related operations. If, for example, the reactants are expensive, it might be important to get a high yield of the desired product per unit of feed consumed. If on the other hand, separation processes are expensive, it might be important to get a high concentration of the desired product in the reactor effluent. These two goals are not necessarily the same. If catalyst is expensive, it might be of extreme importance that runaways be avoided.

We will see that it is usually impossible to model a reactor completely. If the engineer decides to model his system, then his model will depend on what features of the reactor he considers to be important. It is usually in this economic stage that the type of reactor is selected.

Having determined what particular features of his reactor he wants to pay special attention to, the engineer begins to design it. If he is fortunate, he might have found that the reaction is entirely limited by mass transfer, or by chemical rates. In the first case his model is probably nothing but a geometrically similar vessel. He may want to try several. In the second case, his model is usually a piece of ordinary laboratory glassware. He needs only to run a few experiments to determine the kinetic properties of his reaction.

He may find that he does not know whether physical rates or chemical rates are important, and he must find out. This may be easy or difficult, depending on circumstances. For example, mass transfer rates and heat transfer rates can sometimes be estimated roughly from correlations. These estimates can be compared, in order of magnitude, with the observed rates. Chemical rates usually depend much more strongly on temperature than do physical rates (viscous effects in liquids excepted), hence a strong temperature dependence usually rules out the possibility of control by a physical process. Chemical rates do not depend on agitation, but mass transfer does. If varying the stirrer speed results in a varying rate of reaction, then he looks for mass transfer control (remembering that if two phases of different density are stirred together in a smooth-walled vessel, high stirrer speed may "centrifuge" the dense phase to the wall, giving a completely wrong indication of chemical control).

By the time this work is finished, the engineer knows something about his reaction. He knows, roughly, how its rate depends on the things which are likely to influence it. This is what he needs to know for design.

Although the above is somewhat off the subject of modeling, it is quite pertinent. It is only after having gone through such a sequence of reasoning that an engineer can decide whether or not he wants to study his reaction in a model of the prototype reactor. There are many things about a process which must be studied before it becomes commercially feasible. These studies are often made in a model process called a pilot plant, which contains the model reactor we have been talking about. This model reactor must behave like the prototype if the pilot plant study is to be successful, and this is where modeling technique comes in.

Now after this lengthy introduction, let us consider a few representative techniques.

Modeling Techniques

A commonly used modeling procedure is based on the suggestion that a good model of a reactor must preserve not only the mean residence time but also the way in which time spent in the reactor is distributed among "elements" of the fluid. Although this rule holds in certain linear systems, it is possible to construct cases in which it fails. In an isothermal system with two competing first order reactions, the rule could be used to make a model but it would not work if there were heat or other physical effects.

Consider a simple furnace tube through which is passed a gas, to be decomposed by heating. Suppose that it is important from process consideration that the model tell how pressure drop, tube wall temperature, heat input per unit of reactant, and degree of conversion depend on the conditions of operation. We would like these things to be independent of scale.

We know that the pressure drop is proportional to length over diameter, to the square of the velocity, and to the friction factor. The residence time, which is related to the degree of conversion, is just the length divided by the velocity. The heat input per unit of flow is proportional to the heat flux through the surface, and inversely proportional to the velocity. The three quantities are all different functions of the velocity and the dimensions. A little reflection will show that it is not possible to keep them all independent of the diameter, with only the velocity and length at our disposal. Thus this reactor cannot be modeled under the stated conditions. The engineer must find some restriction he is willing to relax. Perhaps it is pressure drop, because the reaction rate may not depend strongly on pressure. We can readily calculate the pressure drop in the real reactor, and hence we do not need to measure it.

The pilot plant compressors may be different from those in the large plant, but this is a minor difficulty. If we can relax the pressure drop requirement, then we can select a length and velocity to go with any given diameter which will preserve both the residence time and the rate of heat input. This is a model of the reactor.

Consider next a catalytic reaction taking place in the tubes of a heat exchanger. The engineer may have decided that it will be sufficient for his purposes to make a model consisting of a single packed tube. How many features of his reactor can be modeled in a tube of different diameter? He can vary the length, flow rate, and the size of his catalyst particles. Engineering correlations tell us how the rate of heat transport depends on the ratio of diameters of tube and catalyst, as well as on velocity. Diffusion theory[1] tells us how the apparent catalyst activity, and hence the rates of heat generation and reaction may depend on the size of the catalyst. Hence we should be able to choose a catalyst diameter and a flow velocity to go with each tube diameter, and thus the ratio of heat generation to heat removal can be specified. This will preserve the relationship between temperature and composition along the tube, and the desired conversion level can be obtained by selecting the proper length. Notice however that again we change the pressure drop. We may model it or the conversion, but not both. A more satisfactory model of this reactor might be a single tube of the same diameter and length as one of the process exchanger tubes. Then everything on the tube side would be modeled exactly. There may be hydrodynamic differences on the shell side, but this is not the point under discussion.

Next, consider again an empty tube with no heat transfer. It is well known that the flow is not uniform in a tube, varying from zero at the wall to a maximum velocity at the center. If an observer were moving with the average velocity, he would see material near the center gradually pulling ahead and material at the edge gradually lagging behind. At the same time, however, he would notice that the stream would mix somewhat due to the ordinary diffusion process. This would tend to cut down the spread relative to the observer, but would not eliminate it completely. This effect was first described by Taylor,[2] and has come to be known as "Taylor Diffusion." It has an important bearing on scaling of reactors. In general, the low conversion in the fast moving portion is not quite compensated by the higher conversion in the slow part. The result is that the conversion is not the same as though all the fluid were moving at a uniform velocity. It turns out that in large scale the effect is totally unimportant, effects on conversion are on the order of a fraction of one per cent. In laboratory-scale reactors, however, there may be differences of several per cent between plug flow and real flow. If we were to use such a recator as a model, we might be significantly in error. The effect has been described by Tichacek,[3] who gave rules for sizing of laboratory reactors to minimize the effect of this phenomenon.

Because of the relative inaccessibility of Tichacek's paper, I am including with his permission, a copy of the design chart (see Fig. 1).

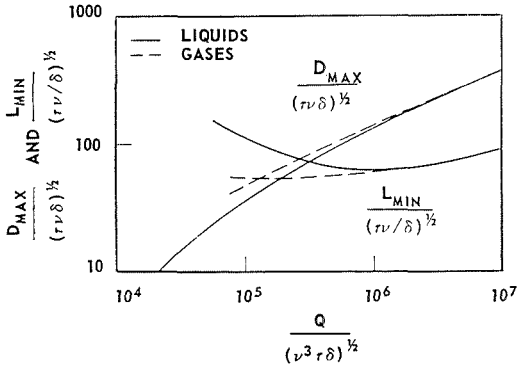

FIGURE 1.

He considered reactions in which the yield of a desired product has a maximum value somewhere in the tube, decreasing ultimately because of side reactions. He showed that axial mixing will flatten the peak, and that the relative loss in yield at or near the maximum is nearly independent of the type of reaction. He uses a parameter δ defined as the fractional yield loss which an experimenter is willing to accept. His figure (Fig. 1) shows two curves, giving the maximum diameter and minimum length for a laboratory tubular reactor as functions of δ. If these conditions are violated, the yield loss caused by Taylor diffusion will be too large. In the coordinates, τ is the mean residence time, ν is the kinematic viscosity, and Q is the volumetric flow rate.

So far I have discussed models which reproduce the steady state behavior of a prototype reactor. There is a noteworthy difference from the hydraulic models which are often useful in combustion research. We cannot conveniently vary the fluid properties, such as density and viscosity, because this might change the reaction rates in a complicated manner. We cannot dilute the fluid with inert material because it might change the heat capacity and hence the way in which

temperature and extent of reaction are related. These restrictions have led to the lack of faithfulness of models which were mentioned in the above examples. We must recognize that at most one or two characteristics of a reactor can be reproduced in a model, and plan experiments accordingly.

Dynamic Analysis

Next, let us look at some models for studying the dynamic characteristics of reactors. In some cases this is the most important part of reactor design.

Dynamic analysis of stirred reactors has been a popular subject in recent years.[4] I will not give a detailed literature review, but just touch briefly on the mathematical treatment, to show what dimensionless ratios are important. In a stirred vessel the heat and material balance relationships are:

$$V\,dx/dt = F(x_F - x) - VR(x, T)$$

$$Vc\,dT/dt = cF(T_F - T) + QR(x, T)V - hA(T - T_c),$$

where

V = volume
F = flow rate
x = concentration
R = reaction rate
c = heat capacity
T = temperature
t = time
Q = heat of reaction
h = heat transfer coefficient
A = heat transfer area
Subscript F refers to feed condition, and subscript c refers to coolant condition.

These equations are, of course, well known. In dimensionless form, they are:

$$d(x/x_F)/d(tF/V) = (1 - x/x_F) - RV/Fx_F,$$

$$d(T/T_F)/d(tF/V) = (1 - T/T_F) - QRV/FT_Fc - (hA/Fc)(T - T_c)/T_F;$$

x_F and T_F are not at our disposal for independent variations, since R depends on x and T, not x/x_F and T/T_F. Neither can the physical properties be changed. If a model is to be constructed, it thus must preserve V/Fx_F, QV/FT_Fc, and hA/Fc. In view of our requirement on physical properties, the first two are equivalent. The dynamic characteristics will thus be preserved if the residence time V/F, and the heat transfer rate per unit volume, are equal in model and prototype. This may be obvious when you think about it, but it is not always easy to accomplish experimentally because the quantity hA may vary strongly with scale. This may lead to a different internal configuration and hence to a different mixing pattern, and spoil the model. However with a little ingenuity, such problems can be handled and good dynamic models can be developed.

We are not nearly so lucky when it comes to tubular reactors, either packed or unpacked. These are what control engineers call "distributed parameter" systems, with spatial variation of conditions. They are described by partial rather than ordinary differential equations and hence the computation of "transfer functions" is not convenient, even if everything were to be made linear. Accordingly there is no reliable background literature on the dynamic properties of such systems, although some work has been reported.[5] It is quite likely that nothing exact can every be done except for numerical computation of transients in each specific case.

There is a way out of this difficulty, however, which has proved to be successful in application. This is the study of "parametric sensitivity." If you could watch the behavior of a catalytic exothermic reactor as you varied the rate of heat exchange, you would see the following sequence of events, assuming that the coolant temperature starts low and increases with time. First, the reactant temperature tends to drop from its feed value rapidly with distance to the temperature of the coolant. Next, this initial temperature drop decreases, until finally there appears a "hot spot," or maximum temperature, somewhere in the middle of the tube. The hot spot temperature increases slowly at first but then suddenly (in terms of the change in jacket temperature) jumps to a nearly adiabatic value. The suddenness of the jump depends on the way the reactor is run, the thermodynamic and kinetic properties of the system, and so on. In some cases it may never appear. But very often it is quite pronounced, and appears when all operating variables are traversed. It is a property of the steady state of the reactor, having nothing whatever to do with dynamics. The region of the jump is the region of parametric sensitivity. In most cases a reactor should not be operated in this region.

The calculation of the position of this region in parameter space is an important part of the study of dynamics of a reactor. It is done by

analyzing the differential equations:

$$QR - Ah(T - T_c) - cG\,dT/dZ = 0,$$

$$R + G\,dx/dZ = 0,$$

where the symbols G and Z mean mass velocity and length, respectively. It is convenient (but not necessary) to consider a particular form of R, namely $R = kx \exp[\gamma(T - T_c)]$. This is a first order reaction whose rate depends exponentially on the temperature. We can divide one equation by the other to eliminate Z, and write the result in dimensionless form as

$$-d\tau/dx = S - [N\tau \exp(-\tau)]/x,$$

where

$$S = Qx_0\gamma/c,$$
$$\tau \equiv \gamma(T - T_c), \text{ and}$$
$$N \equiv 2h/rck \exp(\gamma T_c),$$

r being the reactor radius. This equation contains all the operating parameters, and its solution can be used to determine the region of parametric sensitivity. All reactors which have the same values of the parameters N and S will be models insofar as parametric sensitivity is concerned. Maintaining these ratios can be as simple as making the heat transfer coefficient proportional to the diameter, since everything else is a reaction parameter. It can be more complicated. My own paper[6] covers the use of the method of parametric sensitivity in some detail.

Conclusion

One can get the distinct impression in reading the literature that most chemical reactors are designed in such a way that the rates of chemical processes limit the rate of reaction. In the same way, one gets the impression that in most combustion chambers the chemical processes are so fast that they can be considered to be instantaneous, and that models can be made by varying dimensions and physical properties. Neither of these impressions will stand up under a detailed inspection, but because they are broadly valid we see differences in the simplest modeling techniques. Thus, reactor designers often find concepts like "space velocity," and its reciprocal "residence time," to be useful. They do not find as much use for flow visualization and hydraulic models as does the combustion engineer. However, it is my thesis that such differences exist only in the simpler cases, and that we rely on fundamental reasoning when our systems become more complicated. This leads to considerations which vary enormously from one case to the next. The "spectrum" is indeed so broad that methods for modeling reactors and burners overlap to a significant extent.

Each problem in scaling reactors must be considered anew. We cannot make exact models which reproduce everything in detail, but rather must choose those features whose scale-up we regard as essential, whose effects we cannot calculate. Then we build our model in such a way that we reproduce the behavior we want to study, and calculate the rest as best as we know how.

For readers who might be interested in more detailed illustrations of how some of these procedures are used, an excellent reference is the chapter by Beek[7] in the recent volume of "Advances in Chemical Engineering."

References

1. Beek, J.: A.I.Ch.E. Journal *7*, 337 (1961).
2. Taylor, G. I.: Proc. Roy. Soc. (London) *A223*, 446 (1954).
3. Tichacek, L. J.: Paper presented at A.I.Ch.E. Meeting, Atlanta, Georgia, March 1960.
4. See, for example, Amundson, N. R. and coworkers in A.I.Ch.E. Journal and Ind. Eng. Chem.; e.g., Amundson, N. R. and Bilous, O.: A.I.Ch.E. Journal *1*, 513 (1955).
5. Amundson, N. R. and Bilous, O.: A.I.Ch.E. Journal *2*, 117 (1956).
6. Barkelew, C. H.: *Chemical Engineering Progress Symposium Series No. 25*, vol. 55, p. 38 (1954).
7. Beek, J.: Design of Packed Catalytic Reactors, in *Advances in Chemical Engineering*, Vol. III. Academic Press, 1962.

Discussion

Prof. T. Vermeulen (*University of California*): The models used in the chemical industry are usually "pilot plants" in which the desired reaction, itself, is studied at the temperature and the concentration or pressure level that will apply in the eventual full-scale plant. Dr. Barkelew's excellent analysis adopts this constraint, and appropriately so. However, it seems possible in principle—both for combustion and for chemical reactors—that we should be able to use different reaction conditions, or even different but analogous reactions, and still retain "chemical similitude" (as discussed, for instance, in the book by Johnstone and Thring).

Criteria for "chemical similitude" would appear

to be: (1) The same reaction order α and the same conversion, for the principal reaction; that is $K_0(c_0)^{\alpha-1}\tau$ = constant, with K_0 the rate coefficient at inlet temperature and τ the nominal residence time; (2) The same ratios of rates for competing reactions, relative to the principal reaction; and (3) The same effect of conversion (through temperature change) upon rate, indicated by

$$(\epsilon^{\ddagger}/R)[(1/T_0) - (1/T_{\text{final}})] = \text{constant}$$

Dr. C. H. Barkelew (*Shell Development Co.*): Dr. Vermeulen has suggested that modeling of a single chemical process, or perhaps two processes occurring simultaneously, can be achieved by scaling temperature, concentration, and time, or perhaps by choosing a different reaction system. This is certainly reasonable, provided that these changes do not cause changes in, or react with, important physical processes, such as heat transfer for example. Scaling of a system of simultaneous reactions, with different activation energies and reaction orders, would not seem possible by this procedure.

Prof. D. B. Spalding (*Imperial College*): Could you describe more precisely the relation Barkelew mentions between power input and mixing effectiveness? Would knowledge of this relation indicate whether mixing in a combustion chamber is more economically produced by a stirrer or by means of increased pressure drop?

Dr. C. H. Barkelew: I think that the relation between power input and mixing rate would apply strictly only if geometric scaling were preserved. This is so because we expect it to depend on the way the power is distributed in the vessel.

It should be possible to design a vessel which uses pressure drop in a highly efficient manner to promote mixing. We can certainly do it for stirred vessels. Now these two vessels are not necessarily the same, so the question to be answered is how does the "best" vessel using pressure drop compare with the "best" vessel using a stirrer.

I don't know the answer to this, but I recall that for blending liquids in large tanks [Fox, E. A. and Gex, V. E.: A.I.Ch.E. Journal *2*, 539 (1956)], jets and stirrers are about equivalent in mixing efficiency. Which would be more economical would depend on the specific application.

Perhaps the best general answer would be that if mixing is both important and difficult, then all feasible alternatives should be investigated.

FLOW PATTERNS IN A PHASE CHANGE ROCKET COMBUSTION MODEL

R. B. HERN, R. G. SIDDALL, AND M. W. THRING

A phase change giving a density change of the same order of magnitude as that which occurs between the injector face and the exit nozzle of an actual liquid rocket combustor is obtained by flashing hot kerosene in a vertical tube. With single jets flow patterns are identified and recorded photographically for different values of the inlet parameters and the physical dimensions. All flow patterns are symmetrical about the tube axis except for a swinging jet which may be produced under certain conditions. A pair of impinging jets and a pair of parallel jets are also investigated. It would appear that in the case of the impinging jets droplets from either jet may pass through the plane of impingement and out of the jet pair of the opposite side. These droplets are then observed in the recirculating vapor flow. By increasing jet momenta both the impinging and parallel jets can be made to produce flow patterns which are very similar.

In the model, evaporation is controlled by the kerosene vapor pressure exceeding the local static pressure. A residence time effect on the quantity of material evaporated is evident. The model does not permit quantitative relationships to be developed that can be used for rocket engine design but nevertheless permits the identification and recording of several flow regimes.

Introduction

Single phase models have been extensively used to simulate and predict the aerodynamic behavior of the enclosed turbulent jet diffusion flames which are used in the heating of conventional industrial furnaces.[1,2] In a rocket combustion chamber additional factors may have a significant effect on the mixing and combustion characteristics: no secondary fluid is supplied to satisfy the entrainment requirements of the primary jets, the drag effects between droplets and vapor phase material may cause substantial accelerations or decelerations in the initial region of the combustion chamber, a huge density change (somewhere in the range 200–1000 to 1) occurs in the flowing material between the injector face and the end of the combustion chamber. Normal single phase models cannot be used to simulate these effects and thus a two-phase model is necessary to represent some of the more important factors which control the aerodynamic behavior of rocket combustors.

The Phase Change Model

The simplest method of obtaining a density change of the same order of magnitude as that which occurs in a mono-liquid- or bi-liquid-fired rocket combustion chamber is to use a preheated liquid as the injector fluid. This liquid will then totally or partially evaporate within the chamber when the pressure is released, providing the necessary density change. Preheated Avcat kerosene is used as the injector fluid in the present model. The kerosene is passed through a single injector into a vertical cylindrical Pyrex tube. In order to avoid clouding of the walls by condensing kerosene is it necessary to heat the metal injector head and the tube walls. The use of a single jet is based upon the argument that if each injector in the actual showerhead has the same mass and momentum flow, then any jet in the central region of the showerhead will behave approximately as though it were surrounded by a cylindrical chamber of diameter equal to the distance between the axes of adjacent jets. Similarity of the single injector with the full-scale system will not be achieved if there is substantial imbalance between the jets in the actual showerhead.

The rate of flow of the vapor in the model is high enough to ensure that the system operates in the region of fully developed turbulent flow. The momentum of the liquid issuing from the injector is varied over a fairly wide range. Momentum values outside the range of those occurring in the practical system were used in some of the tests in order to investigate and record as wide a range of flow conditions as possible and to find the effect on the aerodynamic patterns of changes in jet momentum.

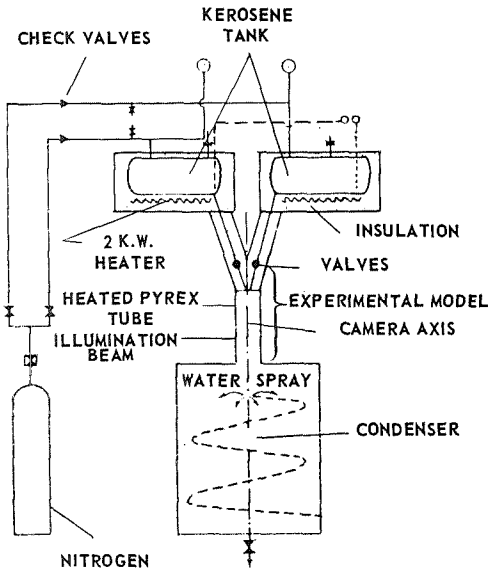

FIG. 1. Phase change model flow sheet.

The exit convergent–divergent nozzle of the practical system is omitted in the model. Since the mixing region in an actual chamber lies fairly close to the injector face, the omission of the nozzle should not lead to any serious distortions of the model mixing patterns.

The experimental set-up is illustrated in Fig. 1. A detailed description of the apparatus and the experimental procedure can be found in a previous paper.[3] The injected kerosene contains aluminum particles which assist in flow visualization. A light slice which passes through the tube in such a direction as to contain the tube axis is viewed against a background of black velvet. Light is reflected from both the aluminum particles and from liquid droplets. Flow patterns are recorded by a camera viewing approximately normal to the plane of the light slice.

Although a simple phase-change model as described here cannot achieve perfect similarity with the actual combustion process it helps to identify the record some of the different flow phenomena which might be expected to occur in the practical system.

Results for Single Jets

Flow Patterns with High Momentum Jets

The flow patterns of the high momentum jets differ according to the value of the parameter V_2/V_1, where V_2 is the average vapor velocity near to the station where the jet expands to the walls and V_1 is the injection velocity of the kerosene. In the model different values of C_2/V_1 are obtained principally by varying the ratio of the jet orifice area to the containing tube area.

For $V_2/V_1 > 1$ the potential core of the jet appears to influence the flow in such a way that a re-circulation zone containing vapor and fine droplets is established some distance from the plane of injection. Such a flow condition is illustrated in Figs. 2 and 3 for a case in which $V_2/V_1 = 1.84$.

As V_2/V_1 approaches unity the change in jet density is counteracted by the change in area to produce continuity of velocity, so that the flow pattern is similar to that of turbulent pipe flow. This condition is illustrated in Fig. 4.

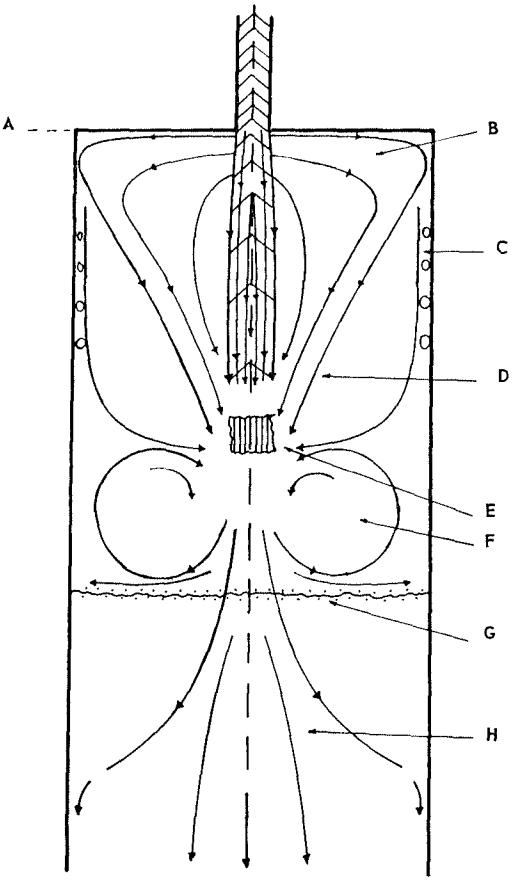

FIG. 2. Flow pattern of enclosed high momentum jet with $V_2/V_1 > 1$. A = P_1, B = radial spread of vapor, C = boundary layer eddies, D = vapor induction, E = Rayleigh zone, F = recirculation of vapor and fine drops, G = wall stagnation contour forming annular ring of droplets, H = turbulent flow of vapor and fine drops.

FIG. 3. Photograph of Fig. 2 flow pattern.

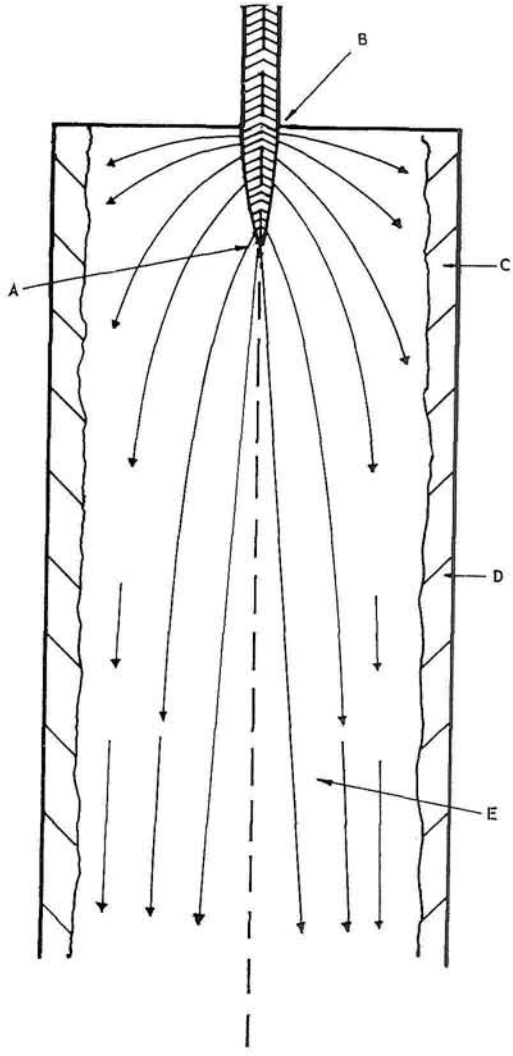

FIG. 4. Flow pattern of high momentum jet with $V_2/V_1 \simeq 1$. A = region of maximum evaporation, B = liquid potential core, C = turbulent boundary layer, D = boundary layer composed of vapor and fine drops, E = turbulent pipe flows.

For V_2/V_1 considerably less than unity the flow pattern is similar to that produced during constant density flow through a sudden enlargement. The jet expands to the tube walls fairly rapidly and recirculation vortices are established close to the injector face. This condition is illustrated in Fig. 5.

Flow Patterns with Low Momentum Jets

Low momentum jets exhibit different behavior from high momentum jets. The liquid stream issues from the orifice virtually intact and persists in liquid form, with very little spread, for some distance from the injector face. Sudden atomization then occurs. Such behavior is illustrated in Figs. 6 and 7. Recirculation of vapor occurs in the region of the point of breakup.

The Swinging Jet

If the jet momentum is held constant and the tube diameter gradually increased a point is reached at which the entrainment requirement of the jet cannot be satisfied by normal recirculation and the entire tail of the jet is induced to flow back up the tube, along the walls, in an attempt to satisfy its entrainment appetite. As the jet is drawn to one side, material is free to slip past downstream. A reverse static pressure gradient is thus set up and the jet is induced to

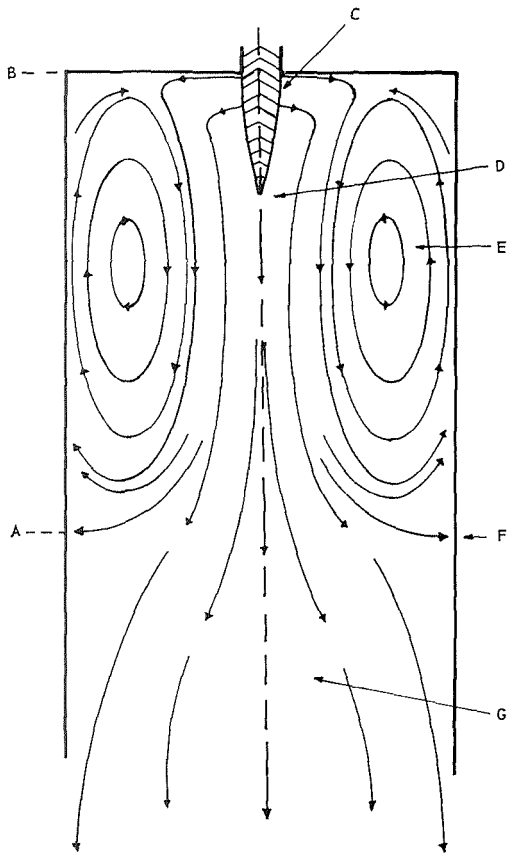

FIG. 5. Basic flow pattern of high momentum jet with $0.18 < V_2/V_1 < 1$. $A = P_2$, $B = P_1$, $C =$ potential core, $D =$ region of maximum evaporation rate, $E =$ torus of recirculation material, $F =$ stagnation point, $G =$ uniform turbulent pipe flow.

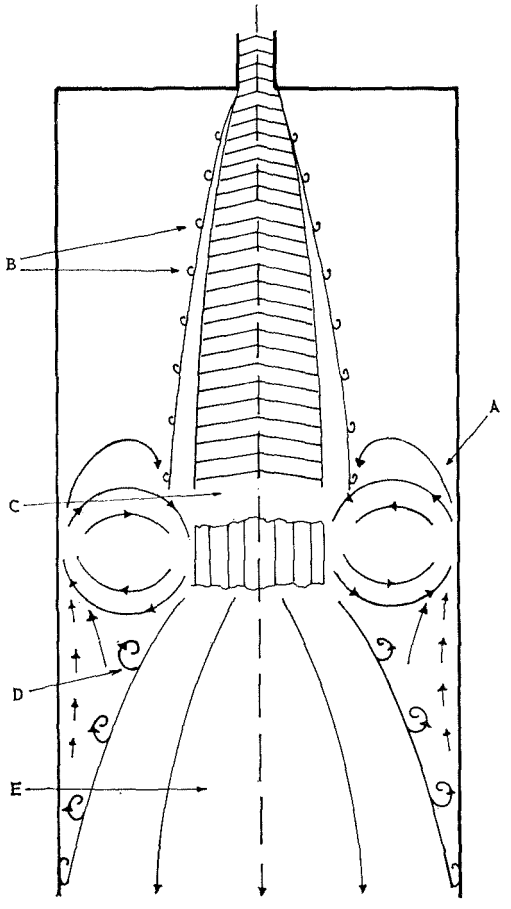

FIG. 6. Flow pattern on low momentum jet. $A =$ induced flow at Rayleigh point within evaporation zone, $B =$ eddy break away from vapor sheath, $C =$ zone of maximum evaporation, $D =$ shear stress eddies, $E =$ jet vapor section.

swing back across the tube and travel backwards along the diametrically opposite station. A cycle of movement is thus set in motion in which the jet swings periodically from wall to wall. The swinging jets is illustrated in Fig. 8.

Longitudinal Static Pressure Variation

The experimental results are well correlated by the expression

$$\frac{A_2(P_2 - P_1)}{(\rho_1 A_1 V_1^2/g)} = 1 - f(\rho_1 A_1/\rho_2 A_2)$$

$$= 1 - (V_2/V_1)$$

as is shown in Fig. 9, where A_1 is the orifice area, A_2 the cross-sectional area of the tube, P_1 the static pressure at the injector face, P_2 the static pressure at (or downstream) of the point where the jet spreads to the walls, ρ_1 the initial liquid density, ρ_2 the vapor density at the station where P_2 is measured, and f is the fraction of the original mass flow which is in vapor form at the downstream station. The derivation of the correlating expression is given in reference 3.

Impinging Jets

The flow patterns of two axisymmetrical like-on-like impinging jets, whose axes of symmetry lie in the same plane, show unequal recirculation zones. Greater spread of the combined flow is apparent in Fig. 10 which illustrates the flow pattern in the plane of the jet axes, than in Fig. 11 which illustrates the flow in the plane of

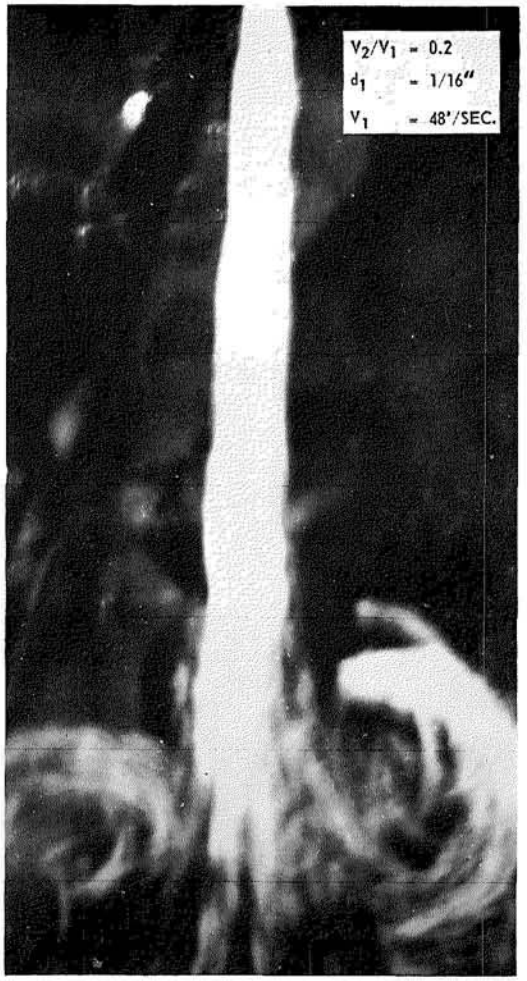

FIG. 7. Photograph of Fig. 6 flow pattern.

impingement. The stronger pair of vortices are associated with the greater spread in the plane of the jets, and the correspondingly short recirculation zones. It is probable that droplets passing through the plane of impingement and out of the jet pair on the opposite side from that at which they originated account for the greater apparent spread. The drag on the vapor phase material associated with these droplets may explain the stronger recirculation. Some of the droplets are turned by the vapor flow in the vortices and are observed in the recirculation flow. Less rapid spread of the jet pair is seen in the plane of impingement (Fig. 11) and the recirculation is correspondingly weaker. No droplets are observed in the recirculating flow in this plane; droplets which reach the tube wall are deposited on the stagnation contours of the weaker recirculation zones and appear as the

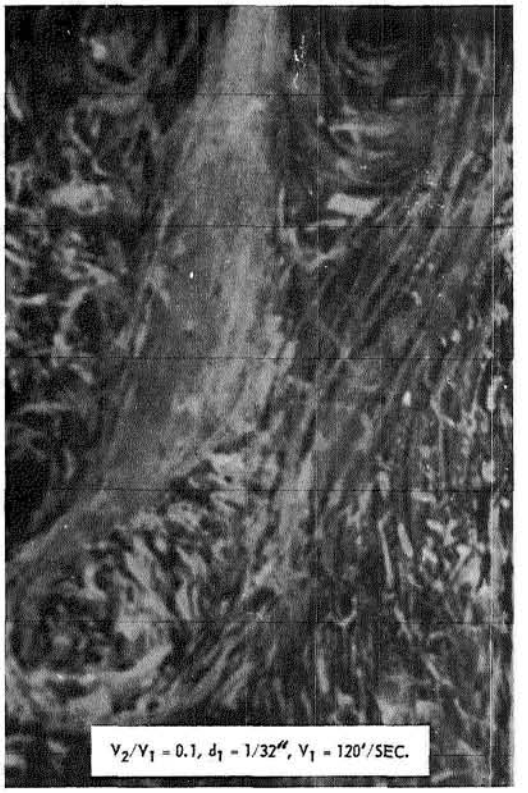

FIG. 8. Swinging jet.

black deposits on the tube wall which are apparent in Fig. 10. The contour of liquid appears black because it is interposed between the camera and the illumination slice. No such liquid

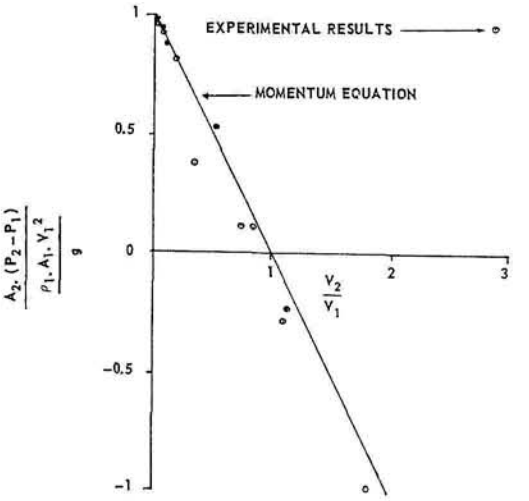

FIG. 9. Comparison of experimental static pressure results with predicted momentum equation.

FIG. 10. Flow pattern in plane of jets.

deposit is observed on the stagnation contours of the stronger recirculation zones (Fig. 11).

As can be seen in Fig. 10, the impinging jets quickly lose their individual identity and have the appearance of a single jet at a short distance from the injector face. Reducing the jet momenta or increasing the initial jet separation causes the point at which the jets merge to be displaced downstream, the individual character of each jet thus being apparent for a much greater distance.

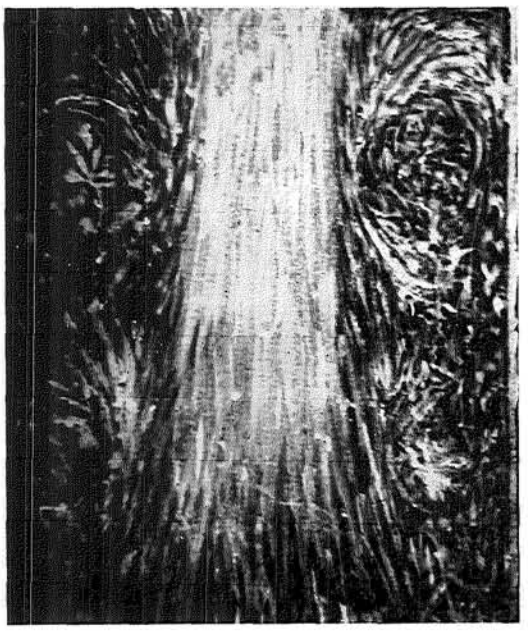

FIG. 11. Flow pattern in plane of impingement.

Parallel Jets

Figure 12 illustrates the flow pattern in the plane of the axis of two parallel jets. The jets have equal momentum and an exit velocity of 60 ft/sec and the axes are 1 inch apart. Under these conditions recirculation occurs between the jets as though a dividing wall were interposed. Increasing the jet momenta finally causes rapid merging and the individual identity of the two flows is no longer apparent. Recirculation zones at right angles to the plane of the axes are once again of different length from the pair in the plane of the axes.

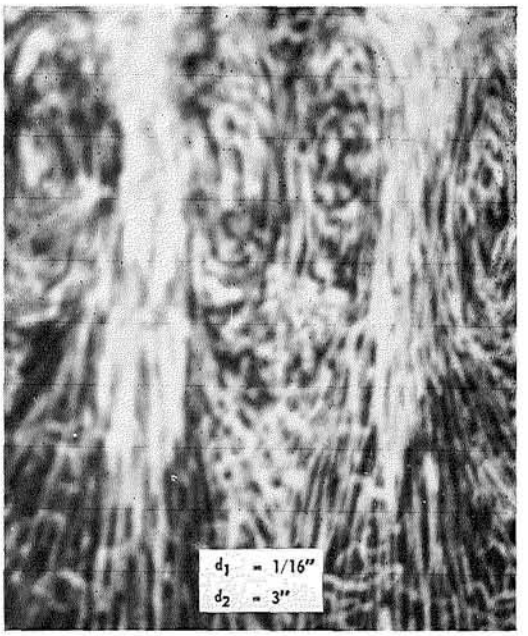

FIGURE 12. Flow pattern of two parallel jets.

Conclusions

The phase change model permits the identification and photographic recording of several flow regimes which may occur in enclosed mono-liquid or bi-liquid flames.

1. With high momentum single jets three regimes occur according to the value of parameter

$$f(\rho_1 A_1/\rho_2 A_2) = V_2/V_1.$$

For V_2/V_1 less than unity the static pressure at the tube wall rises from the injector face to the point where the jet strikes the walls. For V_2/V_1 approximately equal to unity the static pressure remains virtually constant, and for V_2/V_1 greater than unity the pressure falls from the injector face to the point where the jet strikes the walls. A simple formula is suggested which satisfactorily relates the static pressure change to the value of V_2/V_1.

2. Reducing the momentum of the fluid issuing from the orifice finally leads to a condition at which a liquid jet issues from the orifice and persists virtually unchanged for some distance downstream of the injector face. Sudden disintegration and vaporization then occurs.

3. Increasing the cross-sectional area of the tube surrounding the single jet, with fixed orifice conditions, eventually leads to a cyclic movement in which the tail of the jet is induced to travel backwards along the tube wall, alternating from one station to the diametrically opposite station at regular intervals.

4. With a pair of symmetrical placed impinging jets some droplets appear to cross the plane of impingement and out of the jet pair on the opposite side. Some of these droplets are then observed to be contained in the vigorous recirculating flow.

5. With a pair of parallel jets, symmetrically placed with respect to the axis of the tube, the jets each have an individual and identical flow pattern as though a solid wall had been placed between them. Increasing jet momenta or reducing the spacing between the jets finally produces the appearance of one large single jet at a short distance from the injector face.

A phase change model as described here does not represent the rate of change of density which is to be expected in an enclosed liquid fuel flame but it does give a density change of the same order of magnitude. The differences in the mechanisms of droplet evaporation in the two systems preclude the possibility of the numerical prediction of full scale combustor behavior from measured values on a phase change model of this type.

References

1. Chesters, J. H. and Philip, A. R.: J. Iron Steel Inst. *162*, 385, 494 (1949).
2. Thring, M. W.: J. Inst. Fuel (1961).
3. Hern, R. B., Siddall, R. G., and Thring, M. W.: *Second British Rocket Symposium, Cranfield, 27th April, 1962.*

Discussion

Dr. A. C. Tobey (*A. D. Little, Inc.*): Preliminary high-speed photographic observations under hot flow conditions indicate the presence of recirculation near the injector face of a constant area duct fed coaxially with gaseous methane and oxygen. The pattern was very similar to the authors' case in which the injection velocity was higher than the gas velocity within the chamber.

High-speed photos of cold flow impinging jets indicated that droplet recirculation may occur with velocities in the order of $\frac{1}{2}$ to $\frac{1}{4}$ of the injection velocity. Also, as the impingement angle increased the droplet density within the recirculation zone increases substantially.

In addition, for oscillations associated with start-up transients, the presence of recirculation initiated by the cold starting flow and its subsequent motion may play a dominant role as the triggering mechanism of instability phenomena within rocket engines.

Dr. R. S. Levine (*Rocketdyne*): Visually judging the spray fan angle formed by the authors' impinging jets, it seems that the streams, composed partially of vapor, do not form as broad a spray fan as, for instance, the liquid streams photographed by Lawhead in the 8th Symposium and hence do not model completely burning liquids. However, the character of Dr. Sidall's streams may well be pertinent for the starting transient of rocket thrust chamber using cryogenic propellants which become superheated before injection. The circulation generated at the start is probably quite important for smooth pressure rise and efficient performance during this period. Some thrust chambers proposed for space vehicles operate in a series of pulses, and the criteria the authors have developed should be especially valuable for their design.

The amount of material injected into the recirculation zone by a self-impinging injector with liquid streams has been estimated at about 2% of the total propellant flow in a recent NATO paper [see Combs, L. P., Lambiris, S., and Levine, R. S.: "Stable Combustion Processes in Liquid Propellant Rocket Engines," *Fifth AGARD Combustion and Propulsion Colloquium*, Braunschweig, 1962]. Again, visually it would appear that somewhat more of the material is recirculated by these partly gasified streams.

PROF. M. W. THRING (*University of Sheffield*): The word model is being used to describe three different things which I would call (1) complete physical model (equally scaled down or slice model of actual rocket combustion chamber); (2) partial physical model (equally isothermal aerodynamic model); (3) mathematical, numerical, or analog model based on simplifying assumptions.

There are three ways of solving a problem such as eliminating undesirable combustion oscillation:

(1) The fully empirical method of altering design variables until the problem is eventually solved (although it will be likely to recur in any new design).

(2) The fully fundamental methods of analyzing the problem into its fundamental processes, evaluating the differential equations governing the processes, making the necessary simplifying assumptions to give a mathematical model, solving the equations, and designing an improved system from the solution. This method requires exceptional insight in the choice of assumptions but gives maximum competence for large changes in design if it is successful.

(3) The intermediate method of using a hot model to give greater understanding of what occurs, a cold model with a wide range of geometrical changes to give the optimum flow pattern (our paper is concerned with such a cold model), then a modified hot model to test the new prepared system and finally the full size improved system. This is the method with a good chance of success and at the same time a good width of applicability of results.

MODELING TECHNIQUES FOR LIQUID PROPELLANT ROCKET COMBUSTION PROCESSES

R. B. LAWHEAD AND L. P. COMBS

A qualitative physical processes description of stable and unstable combustion in rockets is presented to establish the basis for choosing model hardware design criteria. It is concluded that it is not possible to scale rocket combustion processes in the usual sense of the term. The studies conducted at Rocketdyne have shown that model chambers which satisfactorily model the steady state behavior of large engines must be designed to maintain (1) the propellant injection density, and (2) the chamber to throat contraction ratio (hence chamber pressure). For studies of destructive acoustic modes of combustion instability a third parameter, the frequency, must also be maintained.

Introduction

Full-scale testing with large thrust rocket engines is an extremely costly and time consuming undertaking. Thus, to acquire the experimental information that is required for a realistic description of the physical processes of liquid propellant rocket combustion, it is necessary to resort to the use of model thrust chambers which can be operated at low thrust levels using relatively inexpensive hardware. In choosing a model configuration, care must be exercised to make sure that no processes or interactions among various processes have been accentuated or suppressed which will cause the model to behave differently, than the full scale chamber.

Test results from three types of model chambers are described and used to illustrate the reasoning leading to the choice of the above modelling criteria.

The use of model chamber results for building an analytical model of rocket combustion processes is described and discussed briefly.

Combustion Processes in a Bipropellant Liquid Rocket

Stable Combustion

As a prelude to the discussion of modeling criteria for liquid propellant rockets let us consider a qualitative description of the over-all processes which we are attempting to model. In this description it is convenient to separate the chamber into two major regions, one near the injector and one downstream from the injector.

The Region Near the Injector. Consider the injection of liquid propellants from a typical injector into a cylindrical thrust chamber as shown in Fig. 1. A pair of fuel or oxidizer streams impinge to form a "spray fan" inside which the liquid breaks into ligaments and, eventually, into small droplets. The spray fans of unlike propellants intersect and produce regions where both types of propellants are present. The injected streams, ligaments, and droplets in the spray-fan regions are enveloped by hot combustion gases which fill the remaining space near the injector face. The hot gases, in general being in a dissociated state, have the ability to (1) react with vapors from both propellants, (2) to transfer heat to the liquid propellants, thereby increasing their temperature and causing them to vaporize, and to (3) exert aerodynamic forces on the liquid fragments to increase their rates of atomization, vaporization, and axial velocities. Additional gases are produced as a result of the increasing interactions between the liquid propellants and hot gases. A portion of these gases recirculates toward the injector to keep the temperature and composition of the gases in this region at steady state conditions, while the rest flow toward the nozzles, increasing the axial gas velocity.

It is apparent that in the region near the injector there exist large gradients in all dimensions concerning the distribution and fragmentation of the liquids and, as a consequence, gradients in composition, temperature, and pressures for the gases surrounding them. Forces created by the interactions taking place in that region cause partial recirculation of the gases and, in general, tend to equalize these gradients. Therefore, in this region at steady state conditions, there exists a unique distribution of the liquid pro-

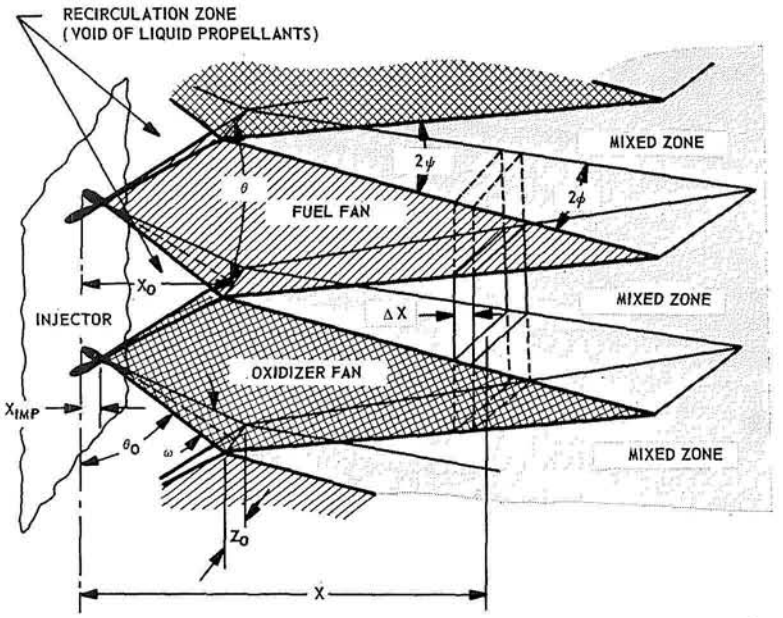

FIG. 1. Schematic representation of propellant distribution for a self-impinging doublet injector.

pellants and of the properties of the surrounding gases. This distribution is primarily imposed by the geometry of the injector-chamber configuration and the operating conditions—injection rate, chamber pressure, and over-all injection rate ratio for the propellants (mixture ratio). In general, atomization of streams, vaporization from ligaments and droplets, and vapor phase reactions (under conditions of high pressure, temperature, and gas flow velocities) are the processes which contribute to the establishment of quasi-steady state equilibrium distribution in that region. Because physical contact between the two propellants in their liquid state is possible in this region, liquid phase reactions could affect atomization and must be considered whenever applicable.

The Region Downstream from the Injector. The large transverse gradients, primarily caused by the distribution of the liquid propellants, diminish with increasing distance from the injector and, eventually, at some axial distance, become negligible. At this point, both propellants are completely atomized into well-mixed sprays so that the average concentration as well as the average weight ratio of the two propellants in a unit volume is nearly constant over the whole cross-sectional area of the chamber. The state of the gaseous phase is also uniform across each cross-sectional area.

Since the volumetric flow rate of liquids is a very small fraction of the volumetric flow rate of hot gases (approximately one per cent), the probability of droplet collision and interference is negligible. Therefore in this region there are droplets of both propellant types being accelerated by the flow of hot gases which completely surround each droplet. Heat is transferred from the hot gases to the droplets under prevailing conditions, causing them to vaporize; the resultant vapors interdiffuse and react with the surrounding gases to form additional gases which contribute to the axial gas flow. The aerodynamic flow forces imposed on the droplets, as a result of the accelerating gaesous flow, cause increasing deformation of their shape and, eventually overcoming the droplets' cohesive forces, may, in some cases, break them into smaller fragments. This process is designated as "secondary atomization" or droplet break-up. When all droplets are vaporized, the transformation of the two liquid propellants into hot gases is complete, and the problem of the subsequent flow is one of gas dynamics.

During steady state combustion in the region downstream from the injector, the rate of transformation of the liquid propellants into hot gases is generally controlled by heat and mass transfer processes under forced convection conditions. For some propellant combinations, the gaseous-phase chemical reaction may become a controlling process and should be considered when applicable.

The transition from the first to the second region is a gradual one, not sharply defined.

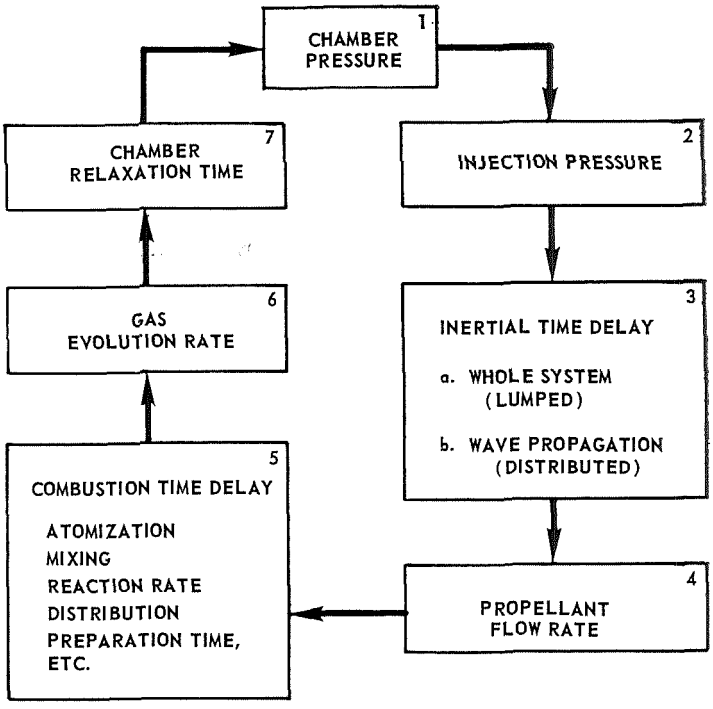

FIG. 2. Processes for flow fluctuation instabilities.

Even in a fixed-geometry, injector–chamber–nozzle assembly, the axial position where the "downstream" region effectively starts may very according to operating conditions such as chamber pressure, flow rates, etc.

Unstable Combustion

In the steady state combustion processes described above, there are always some fluctuations in the measured chamber pressure. These fluctuations are usually random in frequency and have peak-to-peak amplitudes much less than 10 per cent of the average chamber pressure. An engine is said to be experiencing combustion instability when high amplitude oscillations occur at discrete frequencies. The amplitude of the chamber pressure oscillations during unstable combustion may reach peak-to-peak values as great as two to three times the average chamber pressure. The frequency of the oscillations is determined by the particular type of instability encountered.

There are two major types of combustion instability which occur in our large thrust rocket engines, (1) flow fluctuation types in which there is a coupling between flow fluctuations in the supply system and chamber pressure oscillations, and (2) chamber resonance types in which the modes correspond with one of the normal acoustic modes of the chamber. The physical processes which act to sustain the various types of instability involve complex interactions between the combustion processes, the dynamics of the gas in the chamber and the hydrodynamics of the propellant supply system.

For the instabilities involving propellant flow fluctuations one can visualize some of the important interactions as shown in Fig. 2. Here a variation in chamber pressure reacts to change the injection pressure drop, which acts to change the propellant flow rate. The change in flow rate acts on the combustion processes, giving a change in the gas evolution rate. This in turn acts to change the chamber pressure in a manner determined by the gas dynamics of the chamber. There are characteristic times associated with boxes 3, 5, and 7 which can be considered as introducing time delays in the chain of events. If the proper phase relationships exist among all these processes the input and output pressures will be in phase and the system will oscillate. This loops is essentially the same for all types of flow fluctuation instabilities, the only difference being that high frequencies are obtained by considering the characteristic times in the combustion dynamic and hydrodynamic boxes as distributed rather than lumped parameters as is done for the low frequency oscillations.

An interaction loop for the acoustic modes of

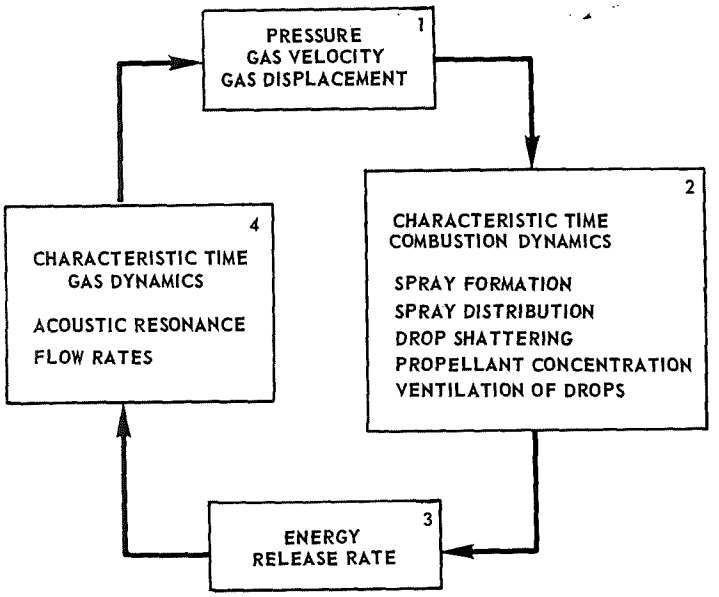

FIG. 3. Processes for "acoustic" modes of instability.

instabilities is shown in Fig. 3. Here the pressure, particle velocity, and particle displacements associated with the wave act on the combustion dynamics, which after a characteristic time determined by such processes as spray formation, spray distribution, droplet shattering, propellant concentration, ventilation of droplets, etc., acts to change the energy release rates, these in tern act on the gas dynamics which close the loop by affecting the pressure, velocities, and displacements.

Criteria for Model Thrust Chamber Design

To carry out research or development studies of combustion and combustion instability phenomena in full-scale thrust chambers is a costly and time consuming undertaking. Thus, basic process information as well as evaluation of new hardware designs, propellant combinations, etc., must be carried out in "low" thrust model chambers. (In our case the maximum thrust limitation is 20,000 to 30,000 lb thrust.) The major problem with using models for such studies is in making certain that the model preserves the important physical parameters so that the model will respond to changes in the same manner as the full-scale chamber. In the ensuing paragraphs we will describe and discuss the model criteria which have been evolved from studies at out laboratory.

Steady State Combustion

Basic Processes. The basic physical processes of combustion have been most effectively studied in a two-dimensional model thrust chamber in which combustion and flow are observed using both high speed motion picture and streak photographic techniques and these optical measurements correlated with pressure measurements at various positions in the system. In light of the discussion of the processes which must be taken into account it appears that two criteria for the model design can be set down immediately. These are (1) the model must operate at the same propellant injection density to maintain the interactions in the region near the injector face, and (2) the model must have the same contraction ratio to maintain the same aerodynamic interactions in both regions. These requirements immediately fix the same operating chamber pressure, P_c, if one is to operate at the same combustion efficiency since the quantities are related by the equation

$$C^* = \frac{P_c g}{r_c (W/A_c)} \qquad (1)$$

where C^* is the characteristic exhaust velocity (a measure of combustion efficiency), r_c is the contraction ratio chamber cross-section area divided by throat area, and (w/A_c) is the propellant injection density.

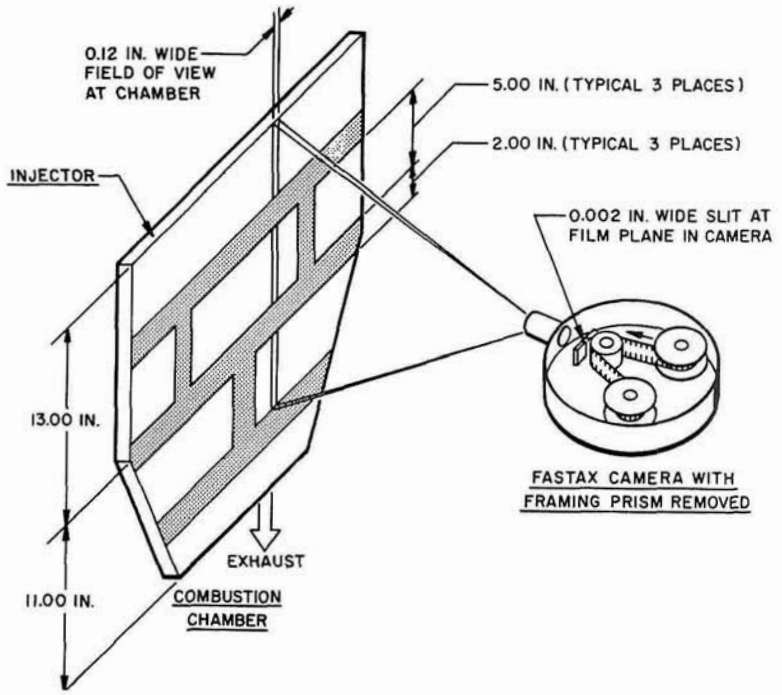

FIG. 4. Two-dimensional thrust chamber streak camera arrangement.

The chamber which has been used most effectively in our studies of the basic steady state processes is the transparent two-dimensional thrust chamber.[1,2] The chamber is a one-inch thick diametric "slice" of a typical large engine thrust chamber without the diverging section. Actually for the steady state studies the chamber width does not have to be as large as the 22 inches used here, however, since this chamber is also used for instability studies (as will be discussed later) the width is dictated by the instability portion of the program. The side walls of the chamber are made from Plexiglass 4 inches thick with 0.25-in. thick Pyrex linear protecting the Plexiglass from being burned by the hot combustion gases. A steel structural frame is designed to provide the required rigidity of the chamber so that operation to 1000 psi chamber pressure can be achieved. The combustion processes are visible over the whole chamber except for the small areas obscured by the structural members.

A self-impinging doublet injector is typical of the injectors used in the thrust chambers to be modeled. The two-dimensional design simulates a "slice" across the face of an 18 ring injector. Starting with fuel in the outer "ring," fuel and oxidizer are supplied to alternate rings. Shadow

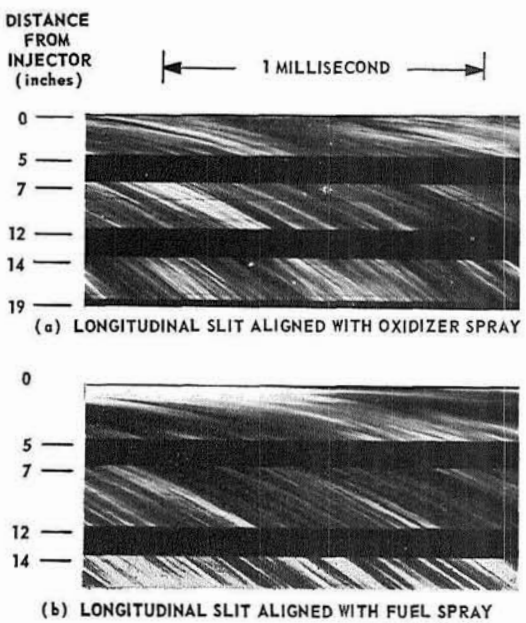

FIG. 5. Typical two-dimensional thrust chamber streak photos.

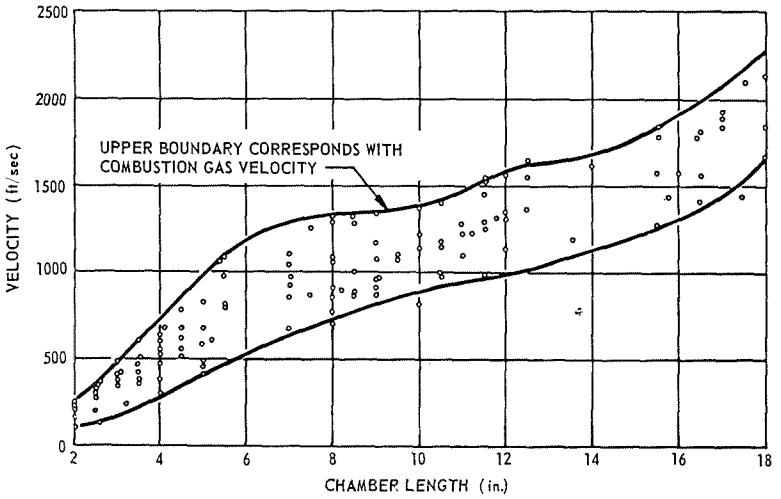

FIG. 6. Velocities derived from streak photos as a function of chamber length.

motion pictures show that the spray fans formed in the chamber at operating pressures are "flat" enough so that they do not wash the chamber side with propellant, thus the one-inch combustion chamber thickness appears to be sufficient to reduce any wall effects to a negligible level.

Normal steady state rocket engine test stand instrumentation is used to record chamber pressure, injection pressures, propellant flow rates, etc. In addition, several high frequency response photocon pressure transducers (capacitance type) are mounted in strategic locations in the chamber and propellant manifolds. The outputs of these transducers are recorded on magnetic tape.

Photographic instrumentation includes both high speed motion pictures and streak photographic records. Simultaneous motion and streak pictures are obtained by using internal slits in the streak cameras rather than the more conventional method of masking the chamber itself. Figure 4 shows schematically the arrangement for streak pictures. Figure 5 shows typical streak photos.

Each trace on the film is of approximate parabolic shape and describes the trajectory of a combustion element whose luminosity formed an image. The slope of such a trace represents the local axial velocity of the element as it moved along the length of the chamber. The velocities measured at various positions are shown in Fig. 6. It can be observed from these results that the measured velocities varied by as much as a factor of two at a given chamber position. A reasonable interpretation (and the one we use) of these traces is that the highest velocity streaks represent combustion gas velocities and the lower velocity streaks the velocities of burning propellant droplets. Accepting this interpretation, the experimental data from these model chambers can be used to evaluate the validity of mathematical models of the combustion processes. (It should be noted that fragmentary streak photo data which has been obtained from large thrust engines agree quantitatively within a few per cent with that obtained in the model thrust chambers.)

The analytical model of the steady state combustion processes that has been formulated has been discussed in detail.[1] The predicted gas and largest droplet velocity profiles using the analytical model and the experimental results from the two-dimensional chamber are shown in Fig. 7. The data shown is for a LOX–hydrocarbon system. Currently, studies are in progress which will extend the analytical description to other propellant combinations by modifying the physical process descriptions to fit experimental gas velocity and droplet velocity profiles obtained from model thrust chamber firings.

Performance Evaluation. Another steady state problem which makes use of model chambers is that of various injector types and propellant combinations. Here again our experience at Rocketdyne indicates that the same two criteria as mentioned in the basis processes section must be followed (i.e., propellant injection density and contraction ratio). Since evaluation tests are usually separate from the basic studies experiments, small diameter solid wall cylindrical combustion chambers operating at the 1000–5000 lb

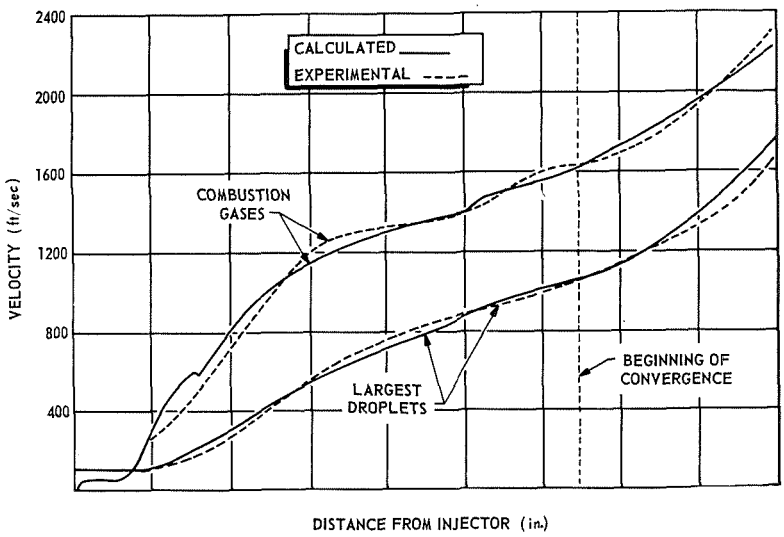

FIG. 7. Comparison of measured and computed velocities of gases and largest droplets.

thrust level are usually utilized since many more tests can be obtained per unit time with this type of hardware than with the transparent two-dimensional chambers. Also the hardware is usually cheaper to fabricate. The above criteria must be met if absolute values of performance are go be obtained. Experience has shown, however, that a qualitative screening of relative performance can be obtained from studies with a single cluster of orifices, typical of a given injector. (This requires a high contraction ratio to maintain P_c and hence aerodynamic interactions are not preserved and absolute performance is not obtained.)

Unstable Combustion

Destructive Acoustic Modes. Of the several different types of combustion instability which are encountered in liquid propellant rockets the most troublesome are the so called transverse acoustic modes, tangential and radial, which can cause burnout of an injector face in 200–300 msec.*

* There is a marked difference in the effects of longitudinal and transverse acoustic modes of instability and probably in the physical mechanisms which trigger and sustain them. The longitudinal modes do not cause as much physical damage to chamber as do the transverse modes, nor is there loss of performance. If the longitudinal mode frequency corresponds with that of one of the flow fluctuation modes, there are very large amplitude oscillations and a loss of performance which is directly proportional to the amplitude of the oscillations.

These oscillations have frequencies of oscillation closely approximating that given by classical acoustic theory

$$F_{1t} = 0.59(C/D) \qquad \text{(first tangential)} \qquad (2)$$

and

$$F_{1R} = 1.22(C/D) \qquad \text{(first radial)}, \qquad (3)$$

where C is the velocity of sound in the combustion chamber and D the diameter of the chamber. Although classical theory can be used to predict the frequencies of the oscillations, the instabilities are not linear phenomena since the amplitudes may range up to two to three times the average operating pressure.

Early in the studies of instability at this and other laboratories a trend was noted that shows that the tendency for a system to exhibit spontaneously triggered instability is directly proportional to the diameter of the chamber (or inversely proportional to the frequency).

High speed motion pictures of unstable combustion processes (described in detail in reference 2) have indicated that displacement of sidewise propellants by the oscillations was a reasonable process of setting up conditions which could trigger and sustain these types of instability. Assuming that as a first approximation the classical acoustic equations for particle velocity and particle displacement can be used to describe the "sound field" in the combustion chamber during instability, it is found that for a given amplitude of pressure perturbation the particle velocity is inversely proportional to the product of the sound velocity and gas density,

TABLE 1
Relative Stability Rating by Gas Flow Method

Fuel	"Barrel"	Two-dimensional	Full-scale
Isooctane	0.50	1.00	1.00
RP-1	1.00	1.00	1.00
DECH (diethylcyclohexane)	1.20	1.00	1.00

while the particle displacement is inversely proportional to the same factor multiplied by the angular frequency, i.e.

$$u = \Delta P/\rho c \quad \text{(velocity)} \tag{4}$$

and

$$\xi = \Delta P/w\rho c = \Delta P/2\pi f\rho c \quad \text{(displacement)}. \tag{5}$$

Thus the particle displacement has the same dependence on frequency as the observed occurrence of instability. Now on the basis of the above mentioned similarity of behavior, we have assumed that particle displacement is one of the important controlling factors for transverse instability. Thus to have comparable displacements for the same size of pressure disturbance in the model as in the full-scale chamber, the frequency of oscillation must be maintained. Also, as seen from Eq. (5) the chamber pressure (density) must be maintained. There are three convenient models in which these two parameters can be maintained. These are the "Barrel," the "Annular," and the already discussed two-dimensional chamber. Only the latter two maintain the propellant injection density and contration ratio mentioned in the earlier section on basic processes The importance of maintaining these other two criteria can be illustrated by considering a series of tests carried out with the "Barrel" chamber.

"Barrel" Chamber

A "Barrel" chamber has the same diameter as the full-scale chamber and models exactly the acoustic modes. This type of chamber must be operated at lower propellant injection densities (pounds of propellant per unit area of chamber cross section). Chambers tested at our laboratory have made use of injectors having annular distributions simulating two or three rings of a full-scale injector.

The tests were carried out to determine the effect of various hydrocarbon fuels (with liquid oxygen) on the stability of a system. To rate the relative stability with the different fuels a gas flow perturbation technique was utilized; with this technique normal stable operation at design conditions is established and then the system triggered into instability by a directed flow of an inert gas (in this case nitrogen). The magnitude of the gas flow required to trigger the instability is then used as a rating of the relative stability of the various systems.

About fifteen different fuels were utilized in the test series. The point which we wish to illustrate can be made by comparing the relative ratings of the two extreme types with the reference fuel, RP-1. The relative ratings obtained from the "Barrel" and an Atlas type booster thrust chamber rated in much the same manner are shown in Table 1.

In these tests the experimental accuracy was such that differences greater than ± 0.05 may be considered significant. It should also be noted here that in tests with the two-dimensional model (discussed in a previous section) the same relative ratings were obtained as were measured with the full-scale chamber. Thus, even though the "Barrel" model is showing up interesting differences in combustion behavior among different fuels, it does not model the behavior of the large engine with respect to gas-pulse-initiated stability.

Annular Chamber

The annular chamber which will maintain the same frequency as a full-scale cylindrical chamber has an outer diameter smaller than the cylindrical chamber, the exact dimensions depending on the relative size of the center body. The first tangential frequency is given by

$$F_{1t} = 2C/\pi(D_o + D_i),$$

where the subscripts refer to the inner and outer diameters respectively, of the annulus.

This chamber can be considered as a rolled up two-dimensional chamber, since to maintain the propellant injection densities at the research thrust levels it is necessary to limit the width of the annular combustion region to about one inch. This chamber has one advantage over the two-dimensional chamber in that it does have a continuous circumferential path such as that in full-scale chambers. Some critics of the two-dimensional chamber feel the reflection of the wave at each side wall changes the character fo the wave propagation effects in sustaining instability. Tests with this chamber have sbown that the relative rating of injectors as well as the occurrence of regions of spontaneous instability

are in good quantitative agreement with the results obtained with the two-dimensional chamber.

Two-Dimensional Chamber

The details of construction of the chamber have been outlined previously. The transverse mode in this chamber, whose frequency is given by

$$F = C/2L,$$

where L is the width of the chamber, has pressure, particle velocity, and particle displacement fields which only simulate the acoustic field in portions of the field of radical and tangential modes of cylindrical chambers.

In spite of all of its drawbacks, the two-dimensional chamber has proved to be the best all around chamber for the acoustic stability studies as well as the steady state basic studies.

Other Types of Instability. The other types of instability such as longitudinal acoustic modes, and the high and low frequency propellant flow fluctuation types ("buzz" and "chugging") have been noted at times in the three models described above as well as in other types of models. There is, however, too little data currently available on the correlation of the model results with large engine behavior to make it profitable to discuss these modes at length.

ACKNOWLEDGMENT

This work was supported under Air Force Contract AFO4(647)–672.

REFERENCES

1. LAMBIRIS, S., COMBS, L. P., and LEVINE, R. S.: Stable Combustion Processes in Liquid Propelland Rocket Engines, *Fifth Colloquium of Combustion and Propulsion Panel, Advisory Group for Aeronautical Research and Development (AGARD), Braunschweig, Germany, April 1962.*
2. LAWHEAD, R. B.: *Eighth Symposium (International) on Combustion,* p. 1140. Williams and Wilkins, 1962.

THEORETICAL AND EXPERIMENTAL MODELS FOR UNSTABLE ROCKET COMBUSTOR

RICHARD J. PRIEM

The three theoretical models of Damköhler and Penner, Crocco and Cheng, and Priem and Guentert are reviewed. Assumptions involved in each theory are described. The requirements for modeling combustion instability with each theory are also described. The three theoretical models are compared to show where they differ in their approach and how they solve the equations. Theoretical results obtained from solving the equations are then compared to show how the assumptions in each approach influence the results.

Six experimental combustors used to study combustion instability are described. Advantages and disadvantages of each combustor are given. Invariance of the theoretical similarity parameters with respect to full-scale combustors is discussed for each of the experimental combustors.

Combustion conditions in full-scale combustors are compared to those assumed for the theoretical models and those encountered in experimental combustors.

Introduction

In this paper, unstable combustion is considered to be that form of combustion which is accompanied by periodic pressure waves. There are many possible natural modes of acoustical oscillations within the combustor.[1] Only the traveling mode of the transverse wave in a cylindrical combustor will be considered herein, although the analyses are valid for all modes if the coordinate system and boundary conditions are modified to correspond to the mode of interest. The transverse mode is predominant in large-diameter combustors and is usually accompanied by high heat transfer rates which destroy the system. It is this aspect of the instability which requires that it be avoided.

The objective of this paper is to describe the various theoretical models and experimental combustors used in studying unstable combustion and the assumptions that were involved in each. There are numerous qualitative descriptions of combustion during instability and theories for variations in individual processes which can sustain instability. These descriptions and theories can be found in articles appearing in the bibliography at the end of this paper. The possibility of maintaining invariance with respect to the full-scale combustor of each of the theoretical parameters is compared for each of the experimental combustors.

Theoretical Models

A common method of modeling a physical system when only partial knowledge of the system is available is to use dimensional analysis. This avoids the problem of solving the equations that describe the system by determining certain necessary connections that must be satisfied by the solution.

Model of Damköhler and Penner

Damköhler[2] derived seven dimensionless groups from the conservation equations for reacting gases to scale a heterogeneous reactor. These seven groups are:

Reynolds number $\mathrm{Re} = \rho_0 v_g 2R/\mu$;
Schmidt number, $\mathrm{Sc} = \mu/\rho_0 D$;
Prandtl number, $\mathrm{Pr} = c_p/\mu D$;
Mach number, $M = (\rho_0 v_g^2/\gamma P_0)^{\frac{1}{2}}$;
Froude number, $\mathrm{Fr} = v_g^2/g2R$;
Damköhler's First Group, $\mathrm{D_I} = 2R/v_g t_i$; and
Damköhler's Third Group,

$$\mathrm{D_{III}} = q2R/v_g c_p T_0 t_i.$$

Penner[3] has added another similarity group for instability to maintain a constant ratio of chemical time t_i to wave time t_w or

$$\chi = t_i/t_w, \tag{1}$$

where

$$t_i = \rho Y_i/\omega. \tag{2}$$

This definition implies that the burning rate, ω, is proportional to the gas density and mass fraction of reacting species, Y_i. Penner states that the Froude number and Mach number can be neglected at low velocities with no acceleration effects. Furthermore, for the same propellant combination the Prandtl and Schmidt numbers are the same and Damköhler's Third Group is

equivalent to his First Group, resulting in three dimensionless groups required for similarity, Re, D_{III}, and χ. Thus, we see that Damköhler's heterogeneous reactor can be used to model combustion instability with very strict requirements that the model have the same Reynolds number, Damköhler's Third Similarity Group, and Penners chemical to wave time χ. Penner[7] also points out that the model studies should be performed at the same reaction frequency under invariant composition, pressure, and temperature conditions unless the reaction rate law is known.

Model of Priem and Guentert

To overcome some of these requirements an approach similar to that of Damköhler for the heterogeneous reactor was used[4] to obtain numerical results for instability limits in an annular combustor. The system can be expanded to a three-dimensional combustor. It was assumed that the propellants are uniformly introduced at the injector boundary and burn at some rate which depends on the position within the combustor. As the propellants burn, random disturbances can occur within the combustor. If a disturbance is large enough it will develop into a transverse wave traveling within the combustor. The problem is to determine for a given initial combustor condition the magnitude of disturbance which will lead to instability.

The conservation equations with mass and heat addition via a phase change are derived and nondimensionalized in reference 4. Five nondimensionalizing terms were required and the combustor radius and average steady state values of pressure, density, temperature, burning rate, and speed of sound in the gases were selected. The dimensional groups that were obtained are

$$R\omega_0/\rho_0 V_0 \qquad \text{and} \qquad \mu/\rho_0 R V_0.$$

These groups are comparable to Damköhler's third parameter and Reynolds number except that they are based on a sound velocity rather than a gas velocity. In terms appropriate to rocket technology the two groups become:

$$\mathfrak{L} \equiv Rm/\mathfrak{A}$$

$$\mathfrak{J} = \mu c^*/RP_0 g.$$

Two models were used in reference 4 to determine the local instantaneous burning rate. With one model the local instantaneous burning rate is assumed equal to the local vaporization rate. This implies that the mixing rate and chemical reaction rate are very rapid. Following reference 4 the burning rate expression for the vaporization model in a three-dimensional combustor with constant liquid velocity in the axial direction is

$$\omega^* = n_l \rho^{*\frac{1}{2}} (1 + |\mathbf{v}_g|^2/v_l^2)^{\frac{1}{2}}, \qquad (5)$$

where

$$n_l = 1 - \frac{\rho_0}{\rho_l N r_{30}{}^3} \mathfrak{L} f(\gamma) \int_{t^*=x/v_l}^{t^*} \omega^* \, d\theta. \qquad (6)$$

The last term determines the concentration of liquid at various positions in the chamber and is derived by assuming that the liquid injection rate is constant. The term $(\rho_0/\rho_l N r_{30}{}^3)$ is the mass ratio of gas to liquid in a unit volume near the injector. The n_l term was unity for the system investigated in reference 4.

The second model for the local instantaneous burning rate used in reference 4 assumed that the burning rate was equal to the chemical reaction rate as given by

$$\omega^* = a\rho^{*n} \exp\left[E/\mathfrak{R}T_0(1 - 1/T^*)\right], \qquad (7)$$

where

$$a = 1 + \frac{\mathfrak{L} f(\gamma)}{a_0} \int_{t^*=x/v_l}^{t^*} \left[\omega_{x0}{}^* - (\omega^*/\rho^*)\right] d\theta, \qquad (8)$$

and

$$a_0 = (\omega_0/\rho_0{}^{nk}) \exp\,(E/\mathfrak{R}T_0). \qquad (9)$$

This assumes that the supply rate of unburned gas was independent of time and varied with position, $(\omega_{x0}{}^*)$. The expression for $\omega_{x0}{}^*$ could be determined by the vaporization or mixing rate under steady state conditions.

While the three-dimensional combustor problem has not been solved numerically at this time results of the one-dimensional system[4] have illustrated the important parameters. The stability limits map of reference 4 (shown in Fig. 1) illustrates the fact that with low burning rate parameter, a model which assumes that the burning rate follows the chemical reaction rate is most susceptible to a disturbance. For large values of the burning rate parameter the vaporization

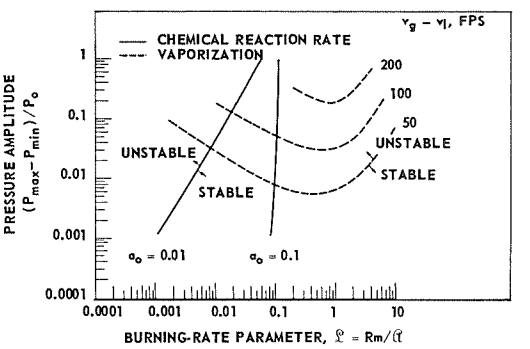

FIG. 1. Stability limits obtained by Priem–Guentert approach (see reference 4).

model requires the smaller disturbance to produce instability. It was also found that the order of reaction, activation energy, specific heat ratio, and gas velocity relative to the combustor wall had a negligible influence on the stability limits of the system. Therefore it may be assumed that they will also be unimportant in a three-dimensional system. For the chemical model the concentration of unburned propellants had an appreciable influence on the stability limits, while the velocity difference between liquid drops and the gas had a similar effect for the vaporization model.

Boundary conditions that did not appear in the annular model of reference 4 which could be encountered with a three-dimensional system, are the length to diameter ratio and the nozzle or combustor shape which would change the gas velocity profile. However, since gas velocity did not influence the results in reference 4, it is assumed that the nozzle or combustor shape would not influence the stability limits in a three-dimensional system.

The model of Priem and Guentert then is a system defined by two terms, a burning rate parameter and a viscous dissipation parameter and the concentration of unburned propellant (a_l or n_l for the two models) as well as the velocity difference between liquid and gas for the vaporization model. The importance of the geometric factor L/D has yet to be evaluated.

Model of Crocco and Cheng

The model used by Crocco and Cheng to attack the high-frequency instability problem[5] employed the equations of continuity and motion with an adiabatic gas law. The burning process is described by a time lag concept. The total time lag, τ_t, is made up of a pressure insensitive portion, τ_s, and a sensitive portion τ which is a measure of the response of the combustion process to a change in pressure.

$$\tau_t = \tau_s + \tau \tag{10}$$

and

$$\tau = \bar{\tau} - n_c \int_{t-\tau}^{t} (P'/P_0)\, d\theta \tag{11}$$

The perturbation of the burning rate from the average rate is then given by

$$\omega' = n_c(1 - e^{-s\tau})\,(P'/P_0)\rho_0\, dv_z/dz, \tag{12}$$

where n_c is the interaction index between burning rate and pressure. Thus the burning rate varies as P' varies with time and as the sensitive time lag τ varies with time. There are two independent parameters that must be determined from experimental data, $\bar{\tau}$ and n_c, the average sensitive time lag and the interaction index.

The numerical results of Crocco's and Cheng's analysis show that the stability map varies with the values of the sensitive time lag, interaction index, frequency of instability or diameter of combustor, nozzle shape, and concentration of burning. Experimental results[6] have shown that a stability map can be obtained for a combustor as a function of diameter and mixture ratio, from which the sensitive time lag and interaction index of the system can be determined. The experimental results have indicated that the interaction index and sensitive time lag are a function of the injector design and operating conditions.

The method of Crocco and Cheng can be used to model combustion instability with the requirements that the model have the same interaction index, sensitive time lag, chamber and nozzle geometry, and spatial distribution of combustion as the system of interest. The requirement of the same interaction index, sensitive time lag, and combustion distribution implies that the injector must produce the same burning characteristics.

Comparison of Theoretical Models

All of the theoretical approaches use the conservation equations in some form. The Priem–Guentert equations include terms in each equation for the addition of mass to the gas phase by a phase change with chemical reaction. The Damköhler–Penner equations do not include these terms nor do the early equations of Crocco. Recently Crocco has included these terms[6] in the conservation equations but drops them out by his linearizing approach whereby he assumes that all terms involving the square of the Mach number are unimportant. Crocco and Cheng[5] used an adiabatic gas law instead of the more genuine energy equation but in recent publications[6] the energy equation is used. Crocco and Cheng have not included viscous force terms in their equations which appear in both the Damköhler–Penner and Priem–Guentert equations. Damköhler and Penner included continuity equations for individual chemical species which are not considered in either of the other two theoretical models.

The physical models for determining burning rates are similar for the three approaches in that the combustion process is assumed to be sensitive to a pressure disturbance. Mathematically they differ in the method of characterizing the dependence on pressure. The Damköhler–Penner approach assumes that the burning rate is proportional to the density and mass fraction of reacting species and has a single mathematical propor-

tionality constant, t_i, which can be varied. The Crocco–Cheng approach uses a more complicated expression having two constants which assumes that the reaction rate is proportional to the pressure with a delay or time lag. The Priem-Guentert approach uses the steady state equations for a particular phenomenon which is part of the combustion process, thereby producing a specific relation between the burning rate and the pressure, density, temperature, and velocity perturbations.

The solution of the equations and the results obtained from the various approaches are quite different. Crocco and Cheng solve the equations in closed form by assuming that second order terms are unimportant and that terms involving the Mach number squared are also unimportant. This enables them to reduce the general equations to perturbation equations which are solvable. The solutions show that there is a stability map which is a function of these two parameters n_e and $\bar{\tau}$ for which a vanishingly small perturbation produces instability. The Priem–Guentert technique solves the equations using a numerical technique. This approach has required that the combustor geometry be a simplified annular ring of a full combustor although it is expected that results will eventually be obtained for the full combustor. To simplify the calculations the variables are grouped using dimensional analysis to produce the two similarity parameters mentioned above. The numerical results of the Priem–Guentert approach show that a finite amplitude disturbance is required to excite instability and that the amplitude is a function of the similarity parameters and the model assumed for the mechanism by which the burning rate varies with time. In the Damköhler–Penner technique the equations are not solved. Instead it is assumed that two systems with the same values of all similarity groups will exhibit the same degree of stability.

The approaches of Crocco–Cheng and Priem–Guentert are concomitant. In the Priem–Guentert analysis it is assumed that there is no time lag in the burning rate which Crocco shows will change the stability limits of the system. Similarly in the Crocco–Cheng approach it is assumed that the second order terms are unimportant, but in the Priem–Guentert approach these are shown to influence the stability limits of the system. Dropping second order terms and neglecting viscous forces by Crocco eliminates the two similarity terms obtained in the Damköhler–Penner and Priem–Guentert approach. Not including a term for the change from an unburned to burned state and the corresponding flow acceleration in the axial direction in the equations is responsible for the different numerical results obtained by the Crocco–Cheng approach and the Priem–Guentert approach. When the terms for the accelerations in the axial direction are omitted in the Priem–Guentert approach the numerical results indicate that a very small perturbation can excite instability which agrees with the results obtained by Crocco.

Experimental Combustors for Studying Combustion Instability

Several combustors have been used to study instability. These will be described in the following section to illustrate their advantages and disadvantages.

Small Thrust Combustor

Probably the simplest combustor used for studying instability is the small-scale device illustrated in Fig. 2(A). It is a miniature version of a large combustor. Because of its size, it is very adaptable to research installations. The injector characteristics can be designed to match those of large-scale combustors by using the same pattern, dimensions, flow density, etc. Because of its small size, however, the frequency of the instability is very high, requiring exceptionally high frequency-response equipment to study the phenomena. It is well suited for photographic studies of individual processes occurring during instability. Because of its high injection density the heat transfer rate during instability is very high and run duration must be short with instability.

Barrel Combustor

To eliminate the high-frequency problem of the small combustor the concept of a barrel combustor was devised [Fig. 2(B)]. For this design the diameter of the combustor is large (usually the same as the full-scale system) but the injection density is greatly reduced by using only a portion of the injector face (usually the outer edge). Usually this combustor is more complicated and larger than the small combustor, therefore it is not quite as adaptable to research-type studies. The reduced frequency is a great aid in eliminating many instrumentation problems. Similarly, because of the low injection density the velocity and heat transfer in the combustor is greatly reduced so that the combustor can usually be run for extended periods without damage to the combustor. The system lends itself to photographic studies and measurements involving average conditions within the combustor. Photographic measurements at a precise point or studies of individual processes

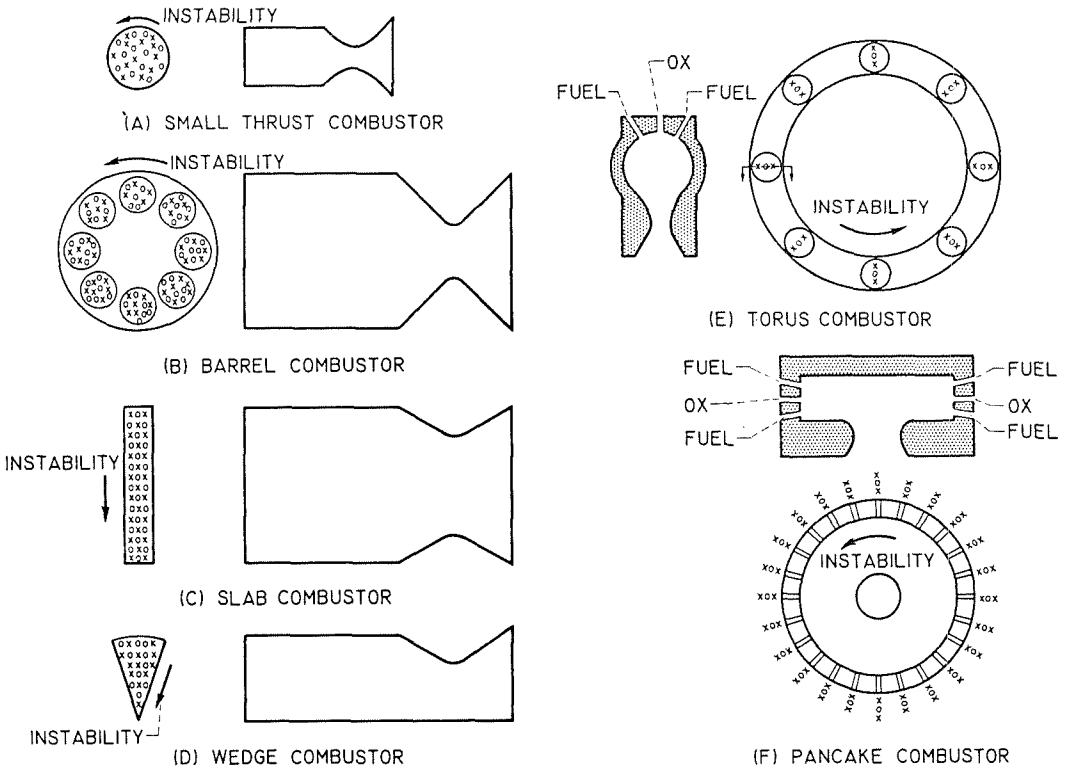

FIG. 2. Experimental combustors for model instability studies.

occurring during instability are difficult because of the large path length that is observed by a camera.

Slab Combustor

The slab combustor [Fig. 2(C)] is a segment of a large combustor. Usually it has the same diameter and length as the large combustor with a very small thickness, i.e., 1 or 2 inches. This achieves low frequency and high injection density. When one wall is replaced by a transparent window studies can be made of individual processes at a specific location. Because it has a high injection density the time during which instability can be studied without damaging the equipment is usually very short. Also, the mode of instability is changed from the traveling wave form with no pressure or velocity nodes to a transverse wave form with pressure and velocity nodes. Because of the physical limitation of 1- or 2-inch thicknesses with the large diameter the thrust of this combustor is quite large. For this reason, many research installations cannot use this combustor with the full diameter. Occasionally the width (or diameter) is reduced to obtain thrust levels that are usable in research installations, in which case it is often called a two-dimensional combustor.

Wedge Combustor

The wedge combustor [Fig. 2(D)] is very similar to the slab combustor in that it is a segment of a full-scale combustor. A sector of the full-scale hardware is used which has the same injection density and radius. By using a window for one side of the combustor, photographic studies at various points can be made. Like the slab combustor, its thrust is usually large for research installations and because of the high injection density and high heat transfer rate during instability, the run time during instability is very short. The normal mode of instability is also different from full-scale equipment in that the wave must travel in a radial direction or be reflected from the walls to produce a standing wave with nodes.

Torus Combustor

The torus combustor [Fig. 2(E)] is another system in which the frequency is maintained similar to the full-scale hardware by using a

combustor of the same diameter. The combustor is an annular ring so that the wave can travel around the combustor. The injection density can be much lower than the full-scale combustor if only a few injection points are used; this, however, produces a nonuniform injection pattern which is undesirable for modeling full-scale equipment. Thrust level is low so that the equipment is compatible with most research installations and because of the low injection density the heat transfer rate is low, permitting long duration runs with instability. It is readily adaptable to studying individual processes at a local point.

Pancake Combustor

The pancake combustor [Fig. 2(F)] uses radial injection and a very small combustor length. The diameter can be as large as full-scale hardware but because of fabrication problems and thrust size it is usually smaller than full-scale hardware. The injection density can be equal to or less than that used in full-scale equipment. The mode of instability is the transverse mode and one can observe or make measurements at local positions over the entire area. Because of the high injection density, run time with instability is limited. The combustion process is distributed along a radial line instead of the axis of the chamber as in a conventional combustor, similarly the combustion is not uniform throughout the area perpendicular to the axis.

Comparison of Values of Similarity Parameters of Experimental Combustors with Values for Full-Scale Combustors

The various experimental combustors for studying combustion instability in rocket engines can be compared with the full-scale combustor by determining the invariance with respect to a full-scale combustor of each of the theoretical parameters for each experimental combustor as shown in Table 1. For each combustor the values of the various parameters are compared to the full-scale hardware parameters and if they are invarient are marked "yes"; if not, they are marked "no." The slab model satisfies all parameters of all theoretical models except for the mode

TABLE 1

Invariance of Similarity Parameters Between Full-Scale Combustors and Experimental Combustors

Theoretical similarity parameters	Experimental combustor					
	Small	Barrel	Slab	Wedge	Torus	Pancake
D_{III}	No	No	Yes	Yes	Yes	Yes
Re	No	No	Yes	Yes	Yes	Yes
χ	No	Yes	Yes	No	No	Yes
t_i	Yes	No	Yes	Yes	No	Yes
$\mathfrak{L}$	No	No	Yes	Yes	Yes	Yes
$\mathfrak{J}$	No	No	Yes	Yes	Yes	Yes
a_l or n_l	Yes	No	Yes	Yes	No	No
L/D	Yes	Yes	Yes	Yes	No	No
$\bar{\tau}$	Yes	No	Yes	Yes	No	Yes
n	Yes	No	Yes	Yes	No	Yes
Freq.	No	Yes	Yes	No	Yes	Yes
	Yes	No	Yes	Yes	No	No
Burn. distr.	Yes	No	Yes	Yes	No	No
Mode	Yes	Yes	No	No	Yes	Yes
Comments	(1)	(2)	(3)	(3)	(2)	(4)

Comments:

(1) Small dimension does not allow simulating.
(2) Nonuniform injection and low injection density.
(3) Mode of instability is changed. Small thickness may give boundary layer effect.
(4) Direction of flow is changed. Small thickness may give boundary layer effect.

of instability. In decreasing order with respect to the number of parameters that are invariant the combustors may be listed: slab, wedge, pancake, small, torus, and then the barrel.

Except for the slab combustor the pancake combustor satisfies the most parameters for the Damköhler–Penner theoretical approach. Only the distribution of combustion with position $f(b)$ is different because of the axial flow. The wedge and slab combustors do not have the same mode of instability but can satisfy all the parameters in the Priem–Guentert approach. Except for the slab combustor the small-scale combustor is the best experimental model for the Crocco–Cheng approach as only the frequency is different from the full-scale combustor.

The data obtained with the various experimental combustors cannot be applied directly to full-scale engines. Since all of the parameters of the theoretical models are never satisfied, there always remains a question about the importance of the parameters which have not been simulated. Similarly, it is difficult to state which theoretical approach to modeling has the greatest merit from analysis of data from particular experimental combustors. This is due, again, to the fact that all parameters for all models are not completely satisfied. Therefore data from several different combustors are required to evaluate the influence of various parameters on combustion stability.

Discussion of Modeling Approaches

There are two unknowns in the theoretical and experimental modeling techniques described herein. One of these is the size of random disturbances which are present in all combustors and can trigger instability. The Priem–Guentert results indicate that a definite level of disturbance is required to initiate instability. This is in contrast to the small perturbation approach of Crocco–Cheng. Since data on sizes of disturbance required to initiate instability in full-scale or experimental models is limited and because data on disturbances in full-scale combustors are almost nonexistent, it is impossible to determine which theoretical model is most appropriate. It is also impossible to determine if experimental models are producing the same level and types of disturbances as full-scale equipment.

A second unknown which has not been considered in these models is the influence of turbulence on combustion stability. Experimental data on turbulence levels in combustors is very limited; it is difficult to estimate how important it might be in any of the models.

Selection of an experimental combustor to determine values of parameters in the theoretical approaches is very critical since some of the parameters in the experimental combustors are not invariant with full-scale equipment. For example, if the time lag, interaction index or characteristic conversion time were determined in a barrel or torus combustor they would not necessarily be the same in a full-scale combustor where the injection density is higher and the distribution of burning would be different. Similarly, the stability limits determined for a small or barrel combustor via the technique of the Priem–Guentert approach would not be the same limits as a full-scale combustor because the $\mathfrak{L}$ and $\mathfrak{J}$ parameter values are not invariant. Similarly, indiscriminate testing of the theoretical models with different combustors would not prove which approach is correct.

Nomenclature

A_c	Cross sectional area of combustor, sq in.
A_t	Throat area of combustor, sq in.
$\mathfrak{A}$	Combustor contraction ratio, A_c/A_t, dimensionless
a	Mole fraction of unburned gases, dimensionless
a_0	Average steady state mole fraction of unburned gases, dimensionless
c_p	Specific heat at constant pressure, Btu/(lb)(°F)
c_v	Specific heat at constant volume, Btu/(lb)(°F)
c^*	Characteristic exhaust velocity, in./sec
D	Molecular diffusion coefficient, sq in./sec
D_I	Damköhler's First Group $= 2Rv_g/t_i$, dimensionless
D_{III}	Damköhler's Third Group $= q2R/v_g c_p t_i$, dimensionless
E	Activation energy function in Arrhenius equation, (lb mole)/in. (lb force)
Fr	Froude number $= v_g^2/g2R$, dimensionless
$f(\gamma)$	Function of gamma $= \{[2/(\gamma+1)]^{(\gamma+1)/(\gamma-1)}\}^{\frac{1}{2}}$, dimensionless
g	Acceleration due to gravity, 386.09 in./sec^2
$\mathfrak{J}$	Viscous dissipation parameter, $\mu c^*/RP_0 g$, dimensionless
k	Exponential constant in Arrhenius equation, (cu in./lb)$^{n-1}$/sec
$\mathfrak{L}$	Burning rate parameter, $Rm/\mathfrak{A}$, dimensionless
M	Mach number $= (\rho_0 v_g^2/\gamma P_0)^{\frac{1}{2}}$
m	Burning rate, fraction/in.
N	Concentration of liquid drops, number/cu in.
n	Concentration exponent in Arrhenius equation, dimensionless

n_c Crocco's interaction index, dimensionless
n_l Concentration of liquid propellant, dimensionless
P Pressure, psi
P' Pressure perturbation, psi
Pr Prandtl number $= c_p/\mu D$
P_0 Average chamber pressure, psi
q Enthalpy difference between reactants and reaction products, Btu/lb
R Radius of combustor, in.
Re Reynolds number $= \rho_0 v_g 2R/\mu$, dimensionless
$\mathfrak{R}$ Gas constant, (in.) (lb force)/(°R) (lb mole)
r_{30} Volume mean liquid drop radius, in.
Sc Schmidt number $= \mu/D\rho_0$, dimensionless
s Generalized oscillation frequency, 1/sec
T Gas temperature, °R
T_0 Average steady state gas temperature, °R
T^* Reduced gas temperature $= T/T_0$, dimensionless
t Time, sec
t_i Characteristic conversion time, sec
t_w Wave time, sec
t^* Reduced time $= tV_0/R_0$, dimensionless
V_0 Speed of sound in gas, in./sec
v_l Velocity of unburned propellants, in./sec
v_g Gas velocity, in./sec
v_z Gas velocity in axial direction, in./sec.
Y_i Concentration of reacting gas, moles/mole

γ Specific heat ratio, c_p/c_v, dimensionless
λ Thermal conductivity of gases, Btu/(in.) (sec) (°F)
μ Average gas viscosity, lb/(in.) (sec)
ρ Gas density, lb/cu in.
ρ' Perturbation in gas density, lb/cu in.
ρ_l Density of liquid, lb/cu in.
ρ_0 Average steady state gas density, lb/cu in.
ρ^* Reduced density, ρ/ρ_0, dimensionless
τ Crocco's sensitive time lag, sec
$\bar{\tau}$ Average value of sensitive time lag, sec
τ_s Crocco's insensitive time lag, sec
τ_t Crocco's total time lag, sec
θ Dummy variable of integration
χ Penner's dimensionless time group $= t_i/t_w$, dimensionless
ω Burning rate, lb/sec cu in.
ω' Perturbation in the burning rate, lb/sec cu in.
ω_0 Average steady state burning rate, lb/sec cu in.
ω_{x0} Supply rate of unburned gas, lb/sec cu in.
ω^* Reduced burning rate, ω/ω_0, dimensionless

References

1. Smith, R. P. and Sprenger, D. F.: *Fourth Symporium (International) on Combustion.* Williams and Wilkins, 1953.
2. Damköhler, G.: Z. Elektrochem. *42*, 846 (1936).
3. Penner, S. S.: Jet Propulsion *27*, 156 (1957).
4. Priem, R. J. and Guentert, D. C.: *Combustion Instability Limits Determined by a Nonlinear Theory and a One-Dimensional Model.* NASA TN D-1409.
5. Crocco, L. and Cheng, Sin-I.: *Theory of Combustion Instability in Liquid Propellant Rocket Motors,* AGARDOGRAPH No. 9. Butterworths, 1956.
6. Crocco, L., Harrje, D. T., and Reardon, F. H.: *Transverse Combustion Instability in Liquid Propellant Rocket Motors.* ARS Paper No. 14, December 1960.
7. Penner, S. S.: Similarity Analysis for Chemical Reactors and the Scaling of Liquid Fuel Rocket Engines, *Combustion Researches and Reviews.* Butterworths, 1955.

Bibliography

Adler, J. and Spalding, D. B.: A One-Dimensional Theory of Liquid Fuel Rocket Combustion II: The Influence of Chemical Reaction. ARC 20,189 (1958).

Agoston, G. A., Rosser, W. A., and Wise, H.: Dynamic Factors Affecting the Combustion of Liquid Spheres, *Sixth Symposium (International) on Combustion,* p. 708. Reinhold, 1957.

Barker, L.-R. C.: Experiments Concerning the Occurrence and Mechanism of High Frequency Combustion Instability, California Institute of Technology, PR 20–356 (1958).

Barrère, M.: Les Instabilities de Combustion dans les Fusées a Propergol Liquide, Paper presented at Fifth Colloquium on High Temperature Problems Connected with Combustion and Propulsion, AGARD. Braunschweig, Germany, April, 1962.

Barrère, M., Moutet, A., and Sarrat, P.: Instabilities de la Combustion dans les Moteurs Fusées É'tude Experimentale. Office National D'É'tudes et de Recherches Aeronautiques, Publication, No. 82 (1956).

Berger, H.: A Non-linear Non-steady Aerothermochemical Analysis of Combustion Instability in a Rocket Chamber, AFOSR TN 59–702 (1959).

Bjerklie, J. W. and Bixon, L. L.: The Experimental Determination of Chemical Conversion Times in Liquid Fuel Rocket Engines, AFOSR TN 58–415 (1958).

Burstein, Samuel Z., Hammer, S., and Agosta, V. D.: A Spray Combustion Model with Droplet Breakup—Analytical and Experimental

Results, Paper 1719–61, presented at ARS meeting, Palm Beach, April 1961.

COAKLEY, J. L. and RICHARDSON, H. H : An Investigation of Combustion Instability in Liquid-Fuel Rocket Motors, MIT Rept. 96 (1960).

CONNAUGHTON, J. W., WHARTON, W. W., WILLIAMS, W. D., and ALLAN, B. D.: Experiments in Oscillatory Combustion, Bulletin of the Second Meeting of the Joint Army–Navy–Air Force Liquid Propellant Group, November 1960, p. 531.

CRAMER, F. B., WEBBER, W. T., and LAWHEAD, ROBERT B.: Research on the Basic Fluid Dynamic Phenomena Related to Rocket Combustion Instability, WADC Technical Note 57–426.

CROCCO, L., GREY, J., and HARRJE, D. T.: Theory of Liquid Propellant Rocket Combustion Instability and Its Experimental Verification, ARS Journal *30*, 159 (1960).

CULICK, F. E. C.: Stability of High Frequency Pressure Oscillations in Gas and Liquid Rocket Combustion Chambers, Massachusetts Institute of Technology TR 480 (1961).

DENISOV, YU N., TROSHIN, YA K., and SHCHELKIN, K. I.: On the Similarity Between Combustion in a Detonation Wave and in a Rocket Motor. Akademia Nauk SSSR, Izvestia Otdelenie Teknicheskikh Nauk, Energetika i Automatika, No. 6.

ELLIS, H. B. and PICKFORD, R. S.: High Frequency Combustion Instability, Aerojet General Report, TN 17, AFOSR TN–56–547 (1956).

GUNDER, D. F. and FRIANT, D. R.: Stability of Flow in a Rocket Motor, J. Appl. Mech. *17*, 327 (1950).

ILL 'YASHENKO, S. M.: Vaporization and Combustion of a Liquid One-Component Fuel in a Rocket Engine Chamber, Izvest. Vysskikh Ucheb. Zavedenii, Aviatsion. Tekh. *3*, No. 4 (1960).

IMBER, M.: Combustion Instability: Liquid Stream and Droplet Behavior. Part II. Estimating Primary Liquid Jet Breakup with Heat Transfer Considerations, WADC TR 59–720, Part II.

ISODA, H. and KUMAGAI, S.: Combustion of Fuel Droplets in a Vibrating Air Field, *Fifth Symposium (International) on Combustion*, p. 129. Reinhold, 1955.

KRIEG, H. C., JR.: The Tangential Mode of Combustion Instability, ARS Paper No. 1723–61 (1961).

KRIEG, H. C. and COULTAS, G. A.: Analytical Scaling Techniques, presented to the Combustion Institute, Paper 61–12, April 1960.

LAMBIRIS, S. and COMBS, L. P.: Steady State Combustion Measurements in a LOX/RP–1 Rocket Chamber and Related Spray Burning Analysis. ARS Paper No. 61–132–1826 (1961).

LAWHEAD, R. B.: Photographic Studies of Combustion Processes in Liquid Propellant Rockets, *Eighth Symposium (International) on Combustion*, p. 1140. Williams and Wilkins, 1962.

LAWHEAD, R. B.: Combustion Instability in Liquid Propellant Rockets, IAS 29th Annual Meeting, Paper 61–50 (1961).

MIESSE, C. C.: The Effect of Ambient Pressure Oscillations on the Disintegration and Dispersion of a Liquid Jet, Jet Propulsion *25*, 525 (1955).

MIRSKY, I.: The Behavior of Pressure Waves in a Pressure Dependent Combustion Field, AFOSR TN–975 (1961).

MORRELL, G.: Critical Conditions for Drop and Jet Shattering, NASA TN D–677.

MORRELL, G.: Breakup of Jets by Transverse Shocks, *Eighth Symposium (International) on Combustion*, p. 1059. Williams and Wilkins, 1962.

NAPHTALI, L. M. and BURSTEIN, S. Z.: *Evaporation and Breakup of Fuel Droplets in One-Dimensional Gas Flow in a Combustion Chamber.* To be published.

OSBORN, J. R. and BONNELL, J. M.: On the Importance of Chamber Geometry in High Frequency Oscillations in Rocket Motors, ARS Preprint No. 1108–60 or AFOSR TN 50–393 (1960).

OSBORN, J. R. and BONNELL, J. M.: On the Effect of Fuel Composition on High Frequency Oscillations in Rocket Motors Burning Premixed Hydrocarbon Gases and Air, ARS Paper 1489–60.

OSBORN, J. R. and PINCHARK, A. C.: Investigation of Aerothermodynamics Interaction Phenomena in Combustion Pressure Oscillations, Purdue University Report No. I–59–2 (1959).

PENNER, S. S.: Models in Aerothermochemistry, Paper presented before International Symposium on Models in Engineering, Venice, Italy, Oct. 1955.

PENNER, S. S. and BIXSON, L. L.: Overall Chemical Conversion Time for a Model Fuel Spray, AFOSR 156 (1960).

PEOPLES, R. G., BAKER, P. D., and KNOWLES, L. S.: High-Frequency Combustion Instability, Aerojet General Report No. 2126 (1961).

PICKFORD, R. S., KRIEG, H. C., JR., and ELLIS, H. B.: Basic Research on Combustion in Liquid Rocket Thrust Chambers, Aerojet General Report, No. 1193 (1957).

PICKFORD, R. S. and PEOPLES, R. G.: Inherent Stability of the Combustion Process, ARS Paper 1490–60 (1960).

PICKFORD, R. S., PEOPLES, R. G., and KRIEG, H. C.:

Analytical and Experimental Scaling of Thrust Chambers, ARS Paper 1436–60 (1960).

PRIEM, R. J. and MORRELL, G.: Application of Similarity Parameters for Correlating High-Frequency Instability Behavior of Liquid Propellant Combustors, ARS Paper 1721–61 (1961).

RABIN, E., SCHALLENMUELLER, A. R., and LAWHEAD, R. B.: Displacement and Shattering of Propellant Droplets, Final Summary Report AFOSR TR 60–75 (1960).

RAYLEIGH: *The Theory of Sound*, vol. II. Dover, 1955.

REBA, I. and BROSILOW, C.: Combustion Instability: Liquid Stream and Droplet Behavior Part III. The Response of Liquid Jets to Large Amplitude Sonic Oscillations. WADC Report 59–720, Part III.

ROSS, C. C.: Scaling of Liquid-Fuel Rocket Combustion Chambers. *Selected Combustion Problems II*. AGARDOGRAPH, Butterworths, 1956.

ROSS, C. C. and DATNER, P. P.: Combustion Instability in Liquid-Propellant Rocket Motors, *Selected Combustion Problems*, p. 352. Butterworths, 1954.

SCALA, S. M.: Transverse Wave and Entropy Wave Combustion Instability in Liquid Propellant Rockets, Princeton University (Ph.D. Thesis); Aero. Engineering Rept. 380 (1957).

SCHUYLER, F. L.: Combustion Instability: Liquid Stream and Droplet Behavior. Part I. Experimental and Theoretical Analysis of Evaporating Droplets, WADC TR 59–720 (1960).

SPALDING, D. B.: Some Thoughts on High-Frequency Oscillations in Rocket Motors, ARC 20, 868 (1959).

SPALDING, D. B.: A One-Dimensional Theory of Liquid-Fuel Rocket Combustion, ARC 20, 175 (1958).

SPALDING, D. B.: *Some Fundamentals of Combustion*. Butterworths, 1955.

SUMMERFIELD, M.: A Theory of Unstable Combustion in Liquid Propellant Rocket Systems, ARS Journal *21*, 108 (1951).

TORDA, P. T. and BURSTEIN, S. Z.: Nonlinear Theory of Combustion Instability, AFOSR TN 56–60 (1958).

THOMAS, N.: High-Frequency Instabilities and Scaling in Rocket Engines, Aerojet-General Corp., TN 27, AFOSR TN 58–1026 (1958).

TSIEN, H. S.: Servo-Stabilization of Combustion in Rocket Motors. ARS Journal *22*, 256 (1952).

WEBBER, W. T.: Spray Combustion in the Presence of Travelling Wave, *Eighth Symposium (International) on Combustion*. Williams and Wilkins, 1962.

WHARTON, W. W., CONNAUGHTON, J. W., ALLAN, B. D., and WILLIAMS, W. D.: The Effect of Sound Oscillations on Combustion and Heat Transfer, ARGMA TR 1C 36R (1959).

WIEBER, P. R. and MICKELSEN, W. R.: Effect of Transverse Acoustic Oscillations on the Vaporization of a Liquid-Fuel Droplet, NASA TN D–287 (1960).

WIGHT, H. M.: Study of Influence of Sound Waves on Chemical Reaction Rates, AFOSR TR 60–60 (1960).

WILLIAMS, F. A.: Detonations in Dilute Sprays, ARS Preprint 1704–61 (1961).

ZUCROW, M. J. and OSBORN, J. R.: An Experimental Study of High Frequency Combustion Pressure Oscillations. Jet Propulsion *28*, 654 (1958).

Discussion

DR. A. C. TOBEY (*Arthur D. Little, Inc.*): In view of the similarities that might exist (especially in the gaseous phase) between the instability phenomena of the solid and the liquid rocket, can the Priem–Guentert theory lend itself to the modeling of instabilities associated with solid propellant burning?

DR. R. J. PRIEM (*NASA*): The Priem–Guentert theory could be modified to determine instability parameters for solid propellants. The theory, however, would not account for any losses in the solid propellant grain which Dr. Hart discusses in his paper. The major modification would be in describing the burning rate used in the burning rate parameter. The burning rate in pounds of propellant per cubic inch per second, as used in the original burning rate parameter derived in reference 4 of the paper, would be a better parameter for solid propellant stability than the form described in the paper.

PROF. V. D. AGOSTA (*Polytechnic Institute of Brooklyn*): I would like to suggest an additional set of scaling parameters for modeling combustion instability which involves gas dynamics. These are the wave slope and velocity gradient in the direction of wave propagation. As it is known, a continuous wave steepens or broadens depending on the relative

magnitudes of the wave slope (i.e., the frequency-amplitude product), and the velocity gradient. Thus, when a source of perturbations, e.g., combustion-generated noise, is considered in a chamber, a selectivity can occur due to the relative amplification and/or attenuation of the waves comprising the noise spectrum. This in turn affects the rate of energy accumulation in the cavity. If a significant wave period corresponds to one of the acoustic characteristic time of the cavity, then resonance can occur in any of the acoustic modes of oscillation of the cavity. However, if there is an acoustic mismatch, and sufficient time (length) is allowed for wave development, then periodic behavior can occur which does not correspond to any of the acoustic modes of oscillation of the cavity. In view of the above-mentioned wave behavior, it is reasonable to assume that these parameters, i.e., wave slope and velocity gradient, be considered in scaling.

SCALING PROBLEMS ASSOCIATED WITH UNSTABLE BURNING IN SOLID PROPELLANT ROCKETS

R. W. HART AND J. F. BIRD

The general problem of acoustic instability was surveyed at a panel session of the Eighth International Symposium on Combustion. At that time emphasis was placed on the kinds of experimental measurements which would be necessary before our understanding of the phenomena could be put on a quantitative and practically useful basis. The nature of the role of theory in reaching for this goal was also considered.

Since that time much new research has been undertaken and much progress has been made. Accordingly, it seems to us that a re-examination of our status *vis-à-vis* the objective of a practical understanding could be valuable, particularly in focusing attention on essential unresolved problems, but also partly in enhancing a general awareness of recent progress and present activity. This re-examination is undertaken here within the restricted framework associated with scaling oscillatory instability.

It is not possible, in general, to determine the stability of a full scale motor by merely noting the stability of a scaled-down version. Nevertheless, it is possible to analyze the acoustic gains and losses via small scale tests, and one may hope thereby to evaluate the degree of stability of full scale motors. Of course it is possible to carry out this evaluation only to the extent that the important gain-loss parameters are known. Sample analyses are presented for such cases, and the limitations imposed by our present lack of knowledge are discussed.

Introduction

Unstable burning of solid propellant rocket motors has been a rather commonly occurring malfunction. One of the most troublesome kinds of unstable burning is characterized by the generation of acoustic fields within the motor cavity. Various undesirable effects may be produced by these acoustic fields. For example, the burning rate of the propellant is often sufficiently enhanced that severe overpressure occurs and the motor explodes.

Although much research has been devoted to acquiring a detailed understanding of this unstable burning,[1–4] the details are far from complete, and the translation of this understanding into engineering precepts useful in motor design has hardly begun. In fact, as the phenomena become better understood, one becomes increasingly impressed with the difficulty of that translation.

Since full scale testing tends to be prohibitively costly, the desirability of assuring the acoustic stability of a motor by means of small scale laboratory testing is quite apparent. But examination of the factors affecting this stability indicates that the possibility of rigorous scaling of motors as entities seems remote, although limited success has occasionally been achieved over limited regions with some motors.[3] Some of the difficulties are similar to those affecting the stability of liquid fuel motors while other problems arise which are unique to the solid motors. In spite of the general infeasibility of a gross scaling of the overall motor, it turns out that one may still hope to infer acoustic stability of large motors via small scale experiments. This expectation rests on a resolution of the factors influencing the stability such that each may be scaled individually. The stability of the motor itself may then be inferred by carefully considering the cooperative effect of these individually modeled factors. Of course, these ideas are not new. Many of the factors which will have to be known in order to determine motor stability were discussed at the Eighth Symposium on Combustion.[1]

In the present study, we wish to re-examine the status of this problem with particular emphasis on the problems of scaling. It will become apparent that much remains to be learned before the stability of full scale motors can be predicted confidently on the basis of small scale testing, although much valuable information is now becoming available. We hope that the discussion which follows will be of value to future research

in providing guide markers to aid in the delineation of areas which demand exploration, as well as in noting other regions where research is well under way.

The Criterion for Acoustic Stability

The Approach to the Problem

For the discussion of the question of acoustic stability or instability in a solid propellant motor, there are certain thoughts which should be fresh in the mind. The basic question is how the acoustic losses compare with the acoustic gains. Thus, it will be essential to specify the various mechanisms whereby acoustic energy may be gained or lost in the rocket motor.

What, then, are the sources of acoustic amplification and attenuation?

Consider the schematic representation of such a motor according to Fig. 1. Here, we view the motor as an acoustic cavity containing as an acoustic medium the solid propellant and the gas, note the variety of physicochemical factors influencing the growth or decay of sound, and pause for a moment to consider the magnitude of our task. One way to proceed would be to attempt to write down all of the equations describing the acoustic field and then attempt to solve them. A perhaps less difficult path to follow, and one adequate for modeling purposes, might be to avoid solving the partial differential equations by searching, instead, for *similarity principles*. It would serve no discernible purpose for us to attempt to follow either of these two courses here. The thought of attempting realistically to write down the equations describing the acoustic response of the chemical reactions, as well as those describing, in general, the frequency-dependent viscoelastic moduli of the solid propellant, is overwhelming. Thus, it is essential to forego the desire to model the motor as an entity. Instead, we shall assume that the relevant mechanisms may be studied experimentally, and then represented empirically in the analysis of stability. We must then evaluate the extent to which this approach will facilitate the assessment of acoustic stability via modeling.

The General Stability Criterion

To make the problem at all tractable, we shall consider in detail only the question of instability in the presence of arbitrarily small disturbances, with only occasional references to some of the more difficult but sometimes important finite amplitude aspects. For present purposes, then, we may restrict our attention to the question of whether an acoustic field, as described by the linearized fluid dynamic and viscoelastic equations, would tend to grow or decay. Several vital points appear:

(a) Throughout the chamber, the acoustic field will be described by the usual wave-equation,

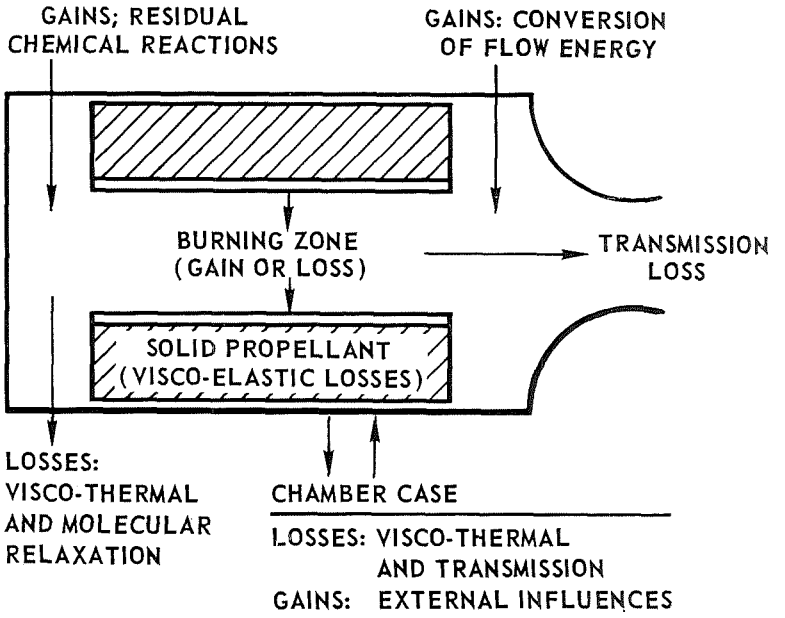

FIG. 1. Schematic diagram of motor showing acoustic sources and sinks

suitably modified by the steady flow of the burned propellant gas. In the typical case, acoustic losses and gains will be sufficiently small so that their effects can accurately be represented in terms of perturbations on the loss-free field.

(b) The various boundaries, insofar as they affect acoustic stability, will be characterized by acoustic admittances. Since the burning surface is very thin compared with sound wavelengths of interest, it will be collapsed and regarded, for purposes of acoustic stability, as a surface.

The condition for acoustic stability can be expressed symbolically in the following form[5]:

$$\oint_{\text{all boundary surfaces}} dS \{\text{Influx due to } [\text{mechanical work} + \text{convection}]\} - \int_{\text{gas and solid volume}} dV \{\text{volume dissipation (less gain)}\} < 0 \quad (1)$$

The overbar denotes time average, dS is the surface element, and dV is the volume element. The surface integral extends not only over the exterior surface but also over the surface bounding the burning zone. Both the gas and the solid will be assumed homogeneous insofar as their elastoacoustic properties are concerned. It is usually convenient to represent the volume dissipation or gain of acoustic energy by means of generalized viscosities. If amplification should be produced, by residual chemical reactions for example, the gas viscosity would be negative. For the solid dissipation it will be necessary, in general, to specify both the dilatational and the shear viscosities.

Equation (1) expresses the balance of acoustic gains and losses as a sum of contributions arising from each of the several surfaces, and from the volume of the gas and the solid. It is most important not to lose sight of the obvious but important fact that if the boundary conditions at the surfaces are specified in the usual way (in terms of admittance), and if the generalized viscoelastic constants of the media are known, then it becomes possible to assess the stability for any field by carrying out the indicated integrations. One should probably not be surprised that the acoustic field itself sometimes turns out to be readily scalable.

Thus the problem before us divides itself naturally into three distinct but interrelated parts:

(a) Specification of the acoustic field;
(b) Specification of the loss (or gain) components of the surface admittances; and
(c) Specification of the viscosities.

Each of these parts is susceptible to experimental determination under certain kinds of conditions, and in this way the stability of a motor may, in principle, be inferred from a study of the acoustic behavior of the propellant in a small scale test motor.

The Acoustic Field

As long as the pressure oscillations are small compared to the mean pressure, the sound field is determined by a linear partial differential equation with appropriate boundary conditions. If the losses (and gains) are relatively small, it is fruitful to consider them as producing perturbations in the field that would exist in their absence. The strengths of these sources and sinks of acoustic energy are then determined from this "zero-order" field, and the balance of gains and losses in turn decides the stability of the sound field. Let us consider the "zero-order" field equations.

The Acoustic Field in the Solid. To begin with, the field is complicated by the presence in the rocket chamber of two different media—the solid fuel and the product gas. If we confine our attention to a single frequency component, the displacement $\mathbf{S}$ characterizing the viscoelastic motion of the solid obeys the usual differential equation[6]

$$c_d^2 \operatorname{grad} \operatorname{div} \mathbf{S} - c_s^2 \operatorname{curl} \operatorname{curl} \mathbf{S} + \omega^2 \mathbf{S} = 0,$$

where c_d and c_s are dilatational and shear phase velocities determined by the elastic constants of the solid. (The time dependence $\exp(i\omega t)$ is assumed.) The familiar frequency vs length similarity principle obviously follows directly from this equation. This principle states that, for frequency-invariant boundary conditions and elastic constants, it would be possible to model the field by trading smaller dimensions for higher frequency. Unfortunately, in the rocket motor problem, both elastic constants and boundary conditions on the solid surfaces are frequency-dependent, so that such modeling does not apply in general. This is not necessarily a serious setback, however, because one of the things theory has accomplished with some rigor is the specification of acoustic fields, at least for regular geom-

etries, whenever the elastic constants of the media are known. Of course, propellants may exist which are sufficiently viscous to absorb whatever small fraction of incident acoustic energy might succeed in penetrating the solid–gas interface. In that event, the viscoelastic motion of the solid could legitimately be neglected in the determination of the zero-order acoustic field.

These considerations are intended mainly to emphasize the necessity for measurement of the viscoelastic moduli of solid propellants. Such data are now becoming available to us, and considerably more will soon be appearing.[7]

The Acoustic Field in the Gas. Although it is not possible entirely to separate consideration of the field in the gas from that in the solid, let us at least focus our attention for a moment on the gas-filled cavity. The immediate question is the determination of this field. Here, again, we would have a frequency-dimension similarity rule if it were not for the fact that again the boundary conditions are usually frequency-dependent and, in addition to this, the acoustic properties of the gas-filled medium are dimensionally dependent through the dependence of the mean flow field. The sonic nozzle continues to represent a fundamental difficulty, although some approximate theory presumably applicable to nontypical, very long nozzles has appeared recently.[8] It does seem significant, however, that in transverse modes the nozzle admittance may have a negative real part for some frequencies. This presumably indicates conversion to sound of energy transported into the nozzle via convection. Perhaps the familiar one-dimensional theory[9] will prove of value for the axial modes although it is based on the long nozzle approximation and mean flows which seem unrealistic for short nozzles.

In any event, it is still impossible to discuss with confidence the effect of nozzle scaling. For this reason it appears feasible at the present time to determine the acoustic field in the gas only for primarily transverse modes of long rockets where the nozzle effects may be ignorable, and for side nozzle test motors, where the effect of subsonic orifices has been treated for axial modes.[10] These "nozzles" are generally characterized by admittances having negative real parts.

Apart from the nozzle and the problems which arise from the head and tail cavities, there are other difficulties which arise from the mean flow of the gas. Qualitatively, these difficulties arise partly because sound travels faster downwind than it does upwind and partly because oscillatory energy transport in a mean flow can occur not only via sound waves but also via entropy waves propagating with the flow speed. At sufficiently high frequency, the entropy wave dissipates within a thin boundary layer near the burning surface where it is generated,[11] and its effect on the zero-order acoustic field can safely be ignored. At low frequencies, however, the entropy wave may persist throughout the chamber. In such a case, the fluid dynamic field is not properly represented in terms of sound waves alone. This introduces further complexities into the treatment of low frequency modes of small motors.

In summary, it should be clear that several basic problems in the determination of the acoustic field in solid propellant rocket motors remain inadequately treated from a theoretical point of view and inadequately explored from an experimental point of view.

Idealized Example. Having noted that many of the problems connected with the determination of even the loss-free—i.e., zero-order—acoustic field are still unsolved, let us attempt to gain some appreciation of what may be accomplished when the acoustic field is known by considering a highly idealized example adapted from ref. (3). Consider a long cylindrical motor without a head cavity, and restrict attention to the relatively high frequency, primarily transverse, modes. The solid propellant will be assumed to have a viscoelastic damping length that is short compared with the thickness of the grain. If the port-to-throat ratio is rather large, but the port Mach number small, it will seem reasonable to approximate the acoustic field in the propellant channel by neglecting the mean flow and regarding the port plane as an acoustic velocity node.* Then the acoustic pressure and velocity (in cylindrical coordinates r, ϕ, z) are approximated by the real parts of

$$p = \bar{P}p_0 \exp(i\omega t) \cos(m\phi) \cos(\pi hz/L) J_m(\alpha r) \tag{2}$$

and

$$\mathbf{u} = \frac{i}{\rho\omega} \operatorname{grad} p,$$

where $\alpha^2 \equiv (\omega^2/c^2) - (h\pi/L)^2$, and $c^2 = \gamma\bar{P}/\rho$. $(\bar{P}p_0)$ is the acoustic pressure amplitude, $\omega = 2\pi$ times frequency, ρ is the mean gas density, $\bar{P}$ is the mean pressure, m and h are the azimuthal and axial mode indices, and the frequency is determined by the condition that the propellant-gas interface correspond to an acoustic velocity

* For the conditions outlined here, the convective flow term in Eq. (1) can be neglected because the contributions from the propellant surface and the port plane tend to cancel.

node. In order to evaluate the stability criterion, as expressed by Eq. (1), it is necessary only to carry out the integrations indicated. This will, of course, require specification of the attenuation or amplification at boundaries and in the body of the gas, which will require the real part of the admittances of these boundaries and the acoustic damping length (or the generalized viscosity) of the burned gases. Accordingly, we turn now toward the specification of the sources and sinks of acoustic energy.

Surface Gains and Losses

We now wish to discuss the evaluation of the net efflux or influx of mechanical work at each boundary as indicated by the surface integral in Eq. (1). It is customary to specify the matching conditions at boundaries in terms of admittances, and our attention is therefore first directed toward the admittance of the burning surface, which is believed to be the most important source of amplification.

The Burning Zone. It is true, of course, that if the acoustic field were known, and if the acoustic admittance of the burning surface were also known, then the evaluation of the contribution of the burning surface to instability would be a mere formality. It is for this reason that much emphasis is placed on determination of the acoustic response of a burning propellant as measured by its admittance.

At the time of the Eighth International Combustion Symposium, only crude theoretical estimates of the properties and the order of magnitude of this admittance were available. Now, the first tentative measurements are becoming available, confirming the implication of the theory in general, but more importantly providing essential information pertinent to particular propellants.[12,13] Hopefully, other research directed toward this goal will also soon yield results.

Nevertheless, although the general stability question cannot be answered yet, considerable progress already can be made under some specific circumstances. In order to carry through the sample example begun in the previous section, we note that the mechanical work part of the surface integral extending over the propellant surface reduces (in terms of the admittance of the burning layer) to

$$\dot{E}_p \equiv -\int \overline{(\mathrm{Re}\ Y_b)\,|\,p\,|^2}\cdot dS, \qquad (3a)$$

where Y_b is the normal specific admittance associated with the burning zone, and $\dot{E}_p$ is the mean acoustic power flowing into the cavity through the burning surface.

A few comments seem in order, here. If the burning of the propellant were not influenced by the component of velocity parallel to the surface (erosion), the admittance would be a constant not dependent on the acoustic field itself, except through frequency, and thus could be removed from the integral sign. In general, however, this simplification must not be effected. For the illustrative example to be carried out here, however, we shall restrict our consideration to a configuration where the effect of erosion is believed to be negligible. For such a simple case, and for the field assumed in the previous section, Eq. (3a) reduces to[3]

$$\dot{E}_p = -\,\mathrm{Re}\,(Y_b)\,a\int_0^{2\pi} d\phi \int_0^L dz\,\overline{|\,\mathrm{Re}\,p(a)\,|^2} \qquad (3b)$$

$$= -\tfrac{1}{4}(\pi a L)\,(1+\delta_{m,0})\,(1+\delta_{h,0}) \times |\,p_0\,|^2 \bar{P}^2 J_m^{\,2}(\alpha a)\ \mathrm{Re}\,(Y_b). \qquad (3c)$$

We note that, if Re $Y_b < 0$, the burning propellant amplifies the sound field.

Volume Losses in the Gas. It is unfortunate that volume losses do not, in general, scale with volume of the rocket motor, but it is clear that the various attenuation mechanisms tend to be highly frequency-sensitive, and of course the mode frequencies are, in turn, functions of chamber volume.

There are several sources of acoustic attenuation in the body of the gas filling the propellant channel. Absorption occurs through ordinary gas viscosity and heat conduction, but more importantly from the relaxation of acoustic energy into internal energy of the molecular constituents.[3]

The relaxation loss of sound energy in the burned gases $\dot{E}_g$ can be expressed in terms of the corresponding attenuation constant α_g, by[3]

$$\dot{E}_g = -(\pi/4)\,La^2(1+\delta_{m,0})\,(1+\delta_{h,0}) \times |\,p_0\,|^2 J_m^{\,2}(\alpha a)\left[F_m(\alpha a) + \frac{\alpha c^2}{a\omega^2}\frac{J_m'(\alpha a)}{J_m(\alpha a)}\right]\frac{\bar{P}c}{\gamma}\,\alpha_g, \qquad (4a)$$

where

$$F_m(x) \equiv 1 - (m/x)^2 + [J_m'(x)/J_m(x)]^2. \qquad (4b)$$

It is unfortunate that no experimental information which bears directly on the relaxation loss in hot propellant gases is available. Here is another research area where the application of known techniques is required in the resolution of the rocket instability problem, but, so far as the authors are aware, no research directed explicitly toward this problem is now in progress. In order to assess the possible significance of such losses,

we shall have to resort to an idealized simple case, and use a crude order-of-magnitude estimate based on considering only the nitrogen component of the product gases (which is expected to become a much more effective absorber at rocket motor temperatures than it is at ordinary temperature). Assuming a 10% abundance of N_2, the attenuation constant has then been estimated from data presented in ref. (3) to be

$$\alpha_g \approx 7.3 \times 10^{-5}(f^2/\bar{P}) \qquad \text{for } 2500^\circ\text{K} \quad (4c)$$

where f is the frequency. It should perhaps be mentioned that relaxation loss can be extremely sensitive to chamber temperature, and this point should be kept in mind when we consider hotter propellants. Further, one should be cautioned that this type of relaxation can be very sensitive to the presence of small amounts of gases such as H_2, H_2O, etc. which are effective in energy transfer. The propellant gas is, of course, abundantly supplied with a variety of such species. The significance of this order-of-magnitude estimate is merely that it indicates that gas phase relaxation losses may well be important, and that they merit investigation.

At this point we should note that relaxations in chemical reactions could be included here by specifying an appropriate α_g for them. Relaxations in the shift of equilibrium would be expected to contribute a positive α_g (damping) while those related to incomplete reactions might result in either positive or negative values of α_g. There has been little research in this area pertinent to solid propellants.[14]

A further source of attenuation is the common presence of solid particles in the gas. The attenuation constant for small spherical particles (radius R, number density N) suspended in a gas has been calculated in reference 15. Loss arises both from heat transfer and momentum transfer. The major contribution arises from viscous damping and is expressed in terms of an attenuation constant given by

$$\alpha_p = \frac{3\pi R}{c}\frac{N}{\rho}\eta(1 + z_p) \times \left[\frac{16z_p^4}{16z_p^4 + 72z_p^3\delta + 81(2z_p^2 + 2z_p + 1)\delta^2}\right] \quad (5)$$

where $z_p = R(\omega\rho/2\eta)^{\frac{1}{2}}$, η is gas viscosity, and $\delta = \rho/\text{density of solid} \ll 1$. Replacing α_g by α_p in Eq. (4a) gives an expression for the power loss due to particle damping. (Note that for a distribution of particle sizes $N(R)dR$, α_p must be integrated over the distribution.)

Acoustic Loss at the Exterior Boundaries. Here, it is especially important to recognize that we are concerned with the possible build up of incipient disturbances, and that we therefore limit our attention to the usual linearized acoustic theory. It seems probable that the acoustic losses for finite amplitude will be very much greater than the small loss predicted by the linear theory, in view of the well-known severe enhancement of heat transfer rates which is often observed under severe oscillatory conditions. These considerations, however, presuppose that the mean temperature of the gas is equal to that of the wall, and that there is no mean flow of gas past the wall. In the rocket motor, both of these conditions are usually violated. Since the wall temperature is generally cooler than the gas temperature, the possibility of conversion of thermal energy into acoustic energy at the chamber wall must arise. In other words, we are not absolutely certain that the wall of the rocket motor is really an absorber rather than an amplifier of acoustic energy. Here is another area where both experimental and theoretical work would be of considerable importance to our problem.

For the simple illustrative example to be considered, however, we shall be primarily concerned with the head cavity in which the mean flow can be assumed to vanish. If the difference between wall temperature and gas temperature is neglected, the head wall loss may be estimated from the usual acoustic wall loss theory. One obtains[3]

$$\dot{E} = -(\pi/4)a^2(\eta/2\rho\omega)^{\frac{1}{2}} \mid p_0 \mid^2 J_m^2(\alpha a)(\bar{P}\omega/\gamma) \times (\alpha c/\omega)^2(1 + \delta_{m,0})\left[\left(1 + \frac{\gamma - 1}{\gamma^{\frac{1}{2}}}\frac{\omega^2}{\alpha^2 c^2}\right) \times F_m(\alpha a) + \frac{2}{\alpha a}\frac{J_m'(\alpha a)}{J_m(\alpha a)}\right]. \quad (6)$$

Order-of-magnitude calculations suggest that the losses at other exposed walls and through the outer wall of the rocket will ordinarily be negligible. There is, of course, the possibility of acoustic energy input at the outer walls at the aerodynamic screaming frequencies of the motor in flight, as has been noted by McClure.[16] The significance of this potential power source, which might go far toward explaining some differences in stability observed between missiles on the thrust stand and missiles in flight, has not yet been evaluated.

The importance of the nozzle as a sink of acoustic power has already been referred to in the discussion of the loss-free acoustic field, and will not be commented upon further here, except to note that the order of magnitude of the loss (or gain) component of the nozzle admittance as

obtained from long nozzle theory can be of the same order of magnitude as that characterizing the gain at the burning surface.[8,9] This fact, and experimental evidence, confirm that the nozzle can be an important constituent of the stability problem.

The Cold Propellant Region. The loss of acoustic energy in the body of the solid propellant should be expected to have a significant effect on the stability of the system. A completely general treatment of a solid absorptive medium seems unlikely to meet with success. Perturbation methods, however, have been used to handle two extreme cases, namely, the cases where the damping length in the solid is either long or short compared to the web thickness.

For the case of small viscous loss (long damping length) the solid must be treated as an acoustic medium bounded by gas medium. The motions of this two-medium system are calculated on a loss-free basis, and this result is then used to determine the losses which would ensue. Studies based on this standard perturbation treatment have been reported in previous papers.[17,18] Not unexpectedly, the effect of the solid turns out to be dominant from time to time during the course of burning for geometries in which the solid participates heavily in the motion, and this effect is a source of intermittency in the stability.[19]

When such is the case, the power loss due to solid damping can be represented by adding to the burning surface admittance Y_b [Eq. (3a)] the term Re $(i\omega S_r/-P_{rr})_{r=a}$, where S_r, P_{rr} are the radial components of displacement and stress on the grain. This term is awkward to write explicitly, but its general nature can be discerned from the characteristic solutions of the vector wave equation. Thus for specified physical properties (Lamé moduli, viscosities, and density), we have

$$\text{Re } (i\omega S_r/-P_{rr})_a = \text{function of } (m;\ hb,\ \omega b;\ a/b)$$

for the mode with frequency $\omega/2\pi$, azimuthal node number m, and axial wave number h. Hence some scaling of calculated or experimental data is possible. Calculations for azimuthal ($h = 0$) and for axial ($m = 0$) modes of a hypothetical propellant have been published.[17,18]

If, on the other hand, the damping length in the solid is quite short, the impedance mismatch at the solid-gas interface will be large. Consequently, nearly all of the acoustic energy incident on the solid surface will be reflected back into the gas, while the amount of energy which can be transmitted across the boundary will be dissipated. The solid then presents to the gas an admittance whose real part is

$$(\rho_s c_s')^{-1} = [\rho c/\rho_s c_s'](\rho c)^{-1} \qquad (\rho_s c_s' \gg \rho c), \quad (7)$$

where the subscript s refers to the solid (c_s' is the sound velocity in the solid appropriate to the modes under consideration). Thus the significance of the solid loss is determined by the relative magnitude of the real part of the admittance presented by the burning boundary, and that given by Eq. (7). As shown in reference 3, these two quantities will indeed tend to be of the same order of magnitude, and the amplifying ability can be expected to be somewhat reduced by losses in the solid. The frequency dependence of the solid propellant elastic constants is of considerable importance here, as is the fact that these constants tend to be very sensitive to temperature.

Sample Calculations

As we have tried to emphasize, many sources of gains and losses have not been quantitatively studied in connection with the question of the assessment of linear acoustic stability of solid propellant rockets via small scale tests. But it is important to consider whether or not these mechanisms are really vital to the problem, or whether they can be disposed of because their effects must be trivial. This poses a question which should be resolvable by a quantitative study. It is in this light that the crude sample calculations presented herein are to be viewed, because they are intended primarily to suggest the importance of certain loss mechanisms.

The attenuation or amplification arising from the various regions in Fig. 1 are conveniently expressed in terms of equivalent admittances at the burning surface by dividing the power by

$$[-(\pi/4)aL(1+\delta_{m,0})(1+\delta_{h,0}) \times |p_0|^2 \bar{P}^2 J_m^2(\alpha a)].$$

These (real) admittances are summarized in Table 1, where explicit expressions are given that hold for the field under the assumption that the solid surface is a velocity node for the zero-order acoustic field. We also indicate in the table the dependence of each gain or loss on the parameters describing the mode, the motor geometry, and the properties of the propellant and its product gas.

Finally, we can restate in admittance form the *criterion for stability*

$$-\text{Re } Y_b \leq \text{Re } (Y_s + Y_p + Y_g + Y_N + Y_W)$$

where the subscript s pertains to the solid, p to particles in the product gas, g to relaxation loss

TABLE 1

Equivalent* Admittances for Sample Calculation

REGION		CONTRIBUTION TO GAIN (–) OR LOSS (+) IN ADMITTANCE FORM (c.g.s. units)	PARAMETERS CHARACTERIZING THE SOURCE OR SINK
NON-BURNING SURFACES	HEAD-WALL	$\mathrm{Re}\ Y_W = \left[\frac{1}{1+\delta_{h,o}}\ \frac{a}{L}\ \frac{\omega}{\gamma \bar{P}}\sqrt{\frac{\eta}{2\rho\omega}}\right] \cdot \left(1-\frac{m^2}{a^2 a^2}\right)\left(\frac{a^2 c^2}{\omega^2}-\frac{\gamma-1}{\sqrt{\gamma}}\right)$	MODE + GEOMETRY $(m, \omega a, ha, \frac{a}{L}; a, h)$ GAS PHYSICALS (γ, c, ρ, η)
	NOZZLE PLANE	$\mathrm{Re}\ Y_N$ NO THEORY EXCEPT FOR LONG NOZZLES	MODE + GEOMETRY, FREQUENCY, BURNING RATE, SOUND VELOCITY, MEAN FLOW DISTRIBUTION
PRODUCT GAS	RELAXATION	$\mathrm{Re}\ Y_g = \frac{c}{\gamma \bar{P}}\left(1-\frac{m^2}{a^2 a^2}\right) a\, \alpha_g$ (cf. Eq. (4) for α_g)	MODE + GEOMETRY $(m, \omega a, ha, a)$ GAS PHYSICALS $(\gamma, c, \rho, \alpha_g$ (involves ω))
	PARTICLES	$\mathrm{Re}\ Y_p = \frac{c}{\gamma \bar{P}}\left(1-\frac{m^2}{a^2 a^2}\right) a\, \alpha_p$ (cf. Eq. (5) for α_p)	DITTO WITH $\alpha_g \to \alpha_p$ (α_p involves R, N(R), $\rho, \rho', c, \eta, \omega$)
COMBUSTION ZONE	ACOUSTIC LAYER / COMBUSTION LAYER	$\mathrm{Re}\ Y_b = \frac{-\bar{v}}{\bar{P}}\ \mathrm{Re}\left(\begin{matrix}\text{REDUCED}\\ \text{SPECIFIC}\\ \text{ADMITTANCE}\end{matrix}\right)$	MODE FREQUENCY ω STEADY STATE $\bar{v}, \bar{P}$ RESPONSE FUNCTION (GAS AND SOLID PHYSICO-CHEMICALS)
COLD PROPELLANT		$\mathrm{Re}\ Y_s = \mathrm{Re}\left(\frac{i\ \omega\ S_r}{-P_{rr}}\right)_a$ (low-loss); $= \frac{1}{\rho_s\ c_s'}$ (high-loss)	MODE + GEOMETRY $(m, \omega b, hb, \frac{a}{b})$ PROPELLANT PHYSICALS $(\lambda, \mu, \lambda', \eta, \rho_s)$

*(EACH ADMITTANCE IS NORMALIZED TO THE AREA OF THE BURNING SURFACE)

in the gas, N to the nozzle plane, W to the head wall, and b to the burning zone. The dependence on scale is only partly in evidence in Table 1 because the various elastic constants and damping lengths are, in general, functions of frequency which is a function of size and shape. Table 1 illustrates particularly how stability can be assessed when these parameters are known.

In order to display the possible significance of the various mechanisms for which we have made the order-of-magnitude estimates given in the preceding we shall consider each of them individually, pretending that each one, in turn, was dominant. Assuming a representative value of $-\frac{1}{5}(\bar{v}/\bar{P})$ for the net real part of the admittance of the burning zone ($\bar{v}$ is the mean velocity of the hot gas emerging from the burning zone), we find that the contours of neutral stability for this mode are as shown in Fig. 2, which is borrowed from reference 3, where its derivation is discussed in more detail. The relevant feature for the present discussion is that each of the gas phase damping mechanisms could very well influence stability. The relatively small exposed head wall area accounts for the fact that these losses are very small for the motor under discussion, so that they are not shown in the figure.

For the particular motor and mode under consideration, the curves of Fig. 2 constitute a set of similarity relations as summarized in Table 2 [which is taken from reference 3] where it is noted that the theoretical straight-line relation-

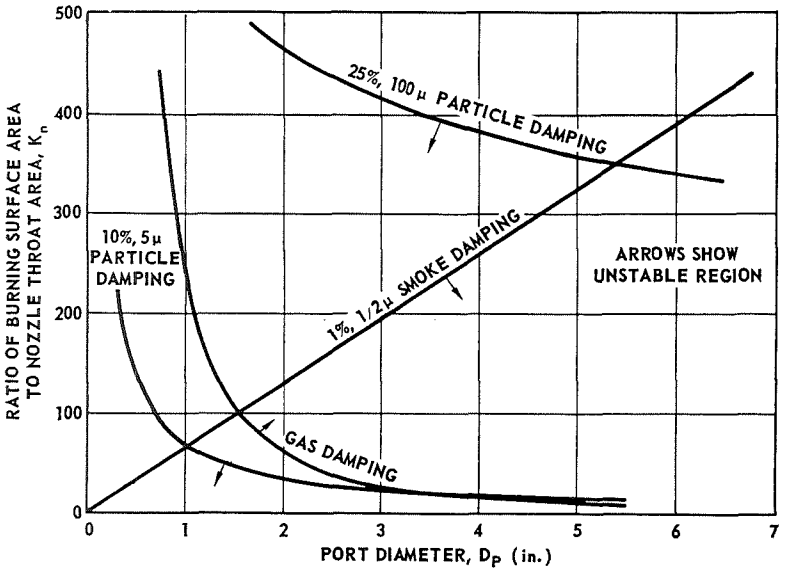

FIG. 2. Stability map showing stable and unstable operating regions characteristic of various kinds of gas phase losses. (The response of the burning surface has been assumed frequency-independent.)

ship for small particle damping is in excellent agreement with experimental data of Brownlee and Marble.[20]

In order to illustrate the varied stability behavior which occurs when motors are scaled, we have prepared Fig. 3. For this illustration, we have considered two sources of attenuation in the body of the gas, viz. molecular relaxation and particle damping, and adopted the numerical values used in reference 3. We will recall that, during burning, a given motor with a fixed nozzle area is represented by a diagonal line segment as indicated on the figure (an internal burning cylindrical charge is being considered). Since the burning area to throat area ratio (K_n) is dimensionless, the firing of a scale model of the motor is represented by shifting the line segment as shown in the figure (note the log scales). For the situation depicted, we can see that while the full scale motor should actually operate stably, tests on a scale model would indicate instability or stability depending on the degree of scaling. For example, the one-sixth scale motor should be unstable over almost its entire burning period, whereas the one-twelfth scale motor would be stable. This illustrates theoretically the well-known experimental fact that one cannot in general naively predict the stability or instability of a motor directly from the stability or instability of a scale model. Nevertheless, a careful analysis of scale model firings can give important information on the separate contributions of various mechanisms to the stability of the full scale engine.

TABLE 2

Scaling Rules*

LOSS MECHANISM	FORM OF THE STABILITY LINE	PORTION OF THE $K_n - D_p$ PLANE THAT IS UNSTABLE
SMALL PARTICLES IN THE GAS	$K_n \propto D_p$	LOWER – RIGHT
PARTICLES OF SIZE A FEW MICRONS	$K_n \propto D_p^{-1}$	LOWER – LEFT
PARTICLES OF SIZE A FEW TENS OF MICRONS	$K_n \propto D_p^{-2/7}$	
WALL DAMPING	$K_n \propto D_p^{-2}$	
MOLECULAR RELAXATION GAS DAMPING	$K_n \propto D_p^{-2}$	UPPER – RIGHT

* These rules pertain to the propellant of Fig. 2 having a burning rate pressure-exponent, $n = 1/3$. K_n is the ratio of burning propellant to nozzle throat area, and D_p is the port diameter.

Concluding Remarks

We have been considering the problem of determining the stability of a rocket motor against small pressure perturbations, by small scale, rather than full scale testing. It seems to be clear that such a determination should be possible, at least in large measure. What is required,

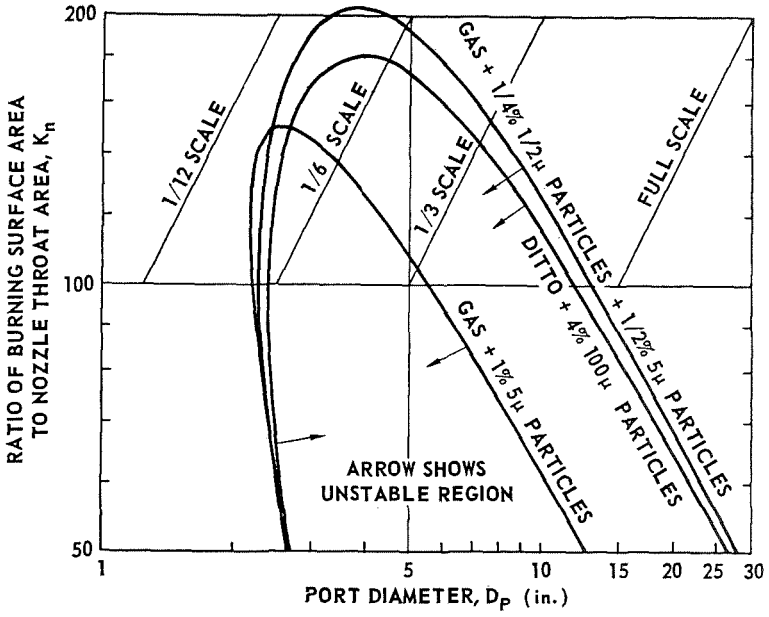

FIG. 3. The effect of scaling on the stability of the first tangential mode is shown for the values of gas phase damping parameters indicated. (The gas—i.e., relaxation—damping length is given in the text.) Quite different effects can be obtained in other modes and with other values of the admittance of the burning surface.

TABLE 3

Important Parameters Required for Stability Determination

QUANTITY	MECHANISM	FUNCTION OF	
ADMITTANCE OF BURNING LAYER	AMPLIFICATION OR ATTENUATION AT THE BURNING SURFACE	FREQUENCY, PRESSURE, PROPELLANT TEMPERATURE, EROSIVE VELOCITY	PROPELLANT COMPOSITION, CURING TIME, METHOD OF CURE, ETC.
GAS PHASE DAMPING LENGTH OR ATTENUATION COEFFICIENT	AMPLIFICATION OR ATTENUATION IN THE GAS PHASE	FREQUENCY, PRESSURE, PROPELLANT TEMPERATURE	DITTO THE ABOVE
SOLID PHASE VISCOELASTIC CONSTANTS	CONTRIBUTES TO DETERMINING MODE FREQUENCIES AND TO ATTENUATION IN THE SOLID PHASE	DITTO THE ABOVE	DITTO THE ABOVE
NOZZLE ADMITTANCE	CONTRIBUTES TO DETERMINING MODE FREQUENCIES AND TO GAIN OR LOSS AT THE NOZZLE PLANE	FREQUENCY, MODE, MEAN FLOW DISTRIBUTION, NOZZLE SIZE AND SHAPE, SOUND VELOCITY IN GAS, AND THE SOUND FIELD, ITSELF.	

OTHER PARAMETERS MAY OCCASIONALLY BE IMPORTANT ALSO, SUCH AS THOSE DESCRIBING WALL LOSSES, RESONANT ROD LOSSES, INPUTS DUE TO AERODYNAMIC SCREAMING, ETC.

however, is measurement of the parameters which are essential to characterizing the acoustic gains and losses. These will include at least those summarized in Table 3. We have attempted to indicate in the text the extent to which these parameters still constitute essentially virgin ground insofar as research in solid propellants is concerned. The extent of the untilled areas is quite impressive, at least to us.

There are other problems which we have avoided, such as those presented by irregular geometries, and by occasionally encountered oscillatory instability at very low frequencies not corresponding to the normal modes of the motor. These are among the incidental problems which should be susceptible, at least in principle, to the standard methods of attack, but which involve substantial new difficulties which have not been well explored. It is only natural that clarification in these areas should be delayed while the main interest lies in resolving the more commonly encountered problems.

A further complication which was discussed briefly ensues from the fact that at low frequencies the acoustic boundary layer may be so thick as to include within itself all or a substantial part of the motor cavity.[11] In that event the oscillatory field should not be represented by only the acoustic wave, but must include also the entropic wave, which is very sensitive to the mean flow distribution. It is not yet clear just how important these considerations will turn out to be in affecting the assessment of stability.

The effect of erosive velocity on the ability of the propellant to amplify or attenuate is another aspect of the stability problem which deserves both theoretical and experimental attention, as indicated both by crude theoretical assessment and by experiment.[4,12]

We would be in error, however, if we were to leave the implication that the stability determination will be settled once the question of linear stability has been answered. First of all there is the question of stability against finite amplitude disturbances. It has now been definitely established that solid propellant (like liquid propellant) motors will occasionally be encountered which remain stable only so long as they are not too seriously perturbed.[4] This problem is one of considerably greater difficulty from both the theoretical and experimental point of view, although it may be that measurement of the finite amplitude parameters indicated in Table 3 will go a long way toward resolving the finite amplitude question. There are further difficulties which appear, such as the fact that the solid propellant damping seems to be significantly altered after exposure to an oscillatory environment, and the question of the anomalous heat transfer rates which may also occur during severe oscillation. Thus, it would seem entirely premature to attempt to catalogue the status of the finite amplitude stability question.

Nomenclature

a	Inside radius of tubular grain ($= \frac{1}{2}D_p$)
b	Outside radius of tubular grain
c	Sound velocity in the chamber gas
c_s'	Sound velocity in the grain ($= c_d$ for dilatational wave, $= c_s$ for shear wave)
D_p	Port diameter ($= 2a$)
f	Circular frequency ($= \omega/2\pi$)
h	Axial index of acoustic mode [Eq. (2)]
J_m	Bessel function of first kind of order m
K_n	Ratio of burning surface area to nozzle throat area
L	Length of tubular grain
m	Azimuthal index of acoustic mode [Eq. (2)]
$N(R)$	Number density of particles of radius R in the gas
p	Acoustic pressure
$p_0\bar{P}$	Acoustic pressure amplitude
$\bar{P}$	Mean chamber pressure
P_{rr}	Radial component of stress in grain
r	Radial position in cylindrical coordinates
R	Radius of solid particles suspended in chamber gas
S_r	Radial component of displacement in grain
$\mathbf{u}$	Acoustic particle velocity
$\bar{v}$	Mean velocity of gas leaving burning zone
Y	Normal specific admittance
z	Axial position in cylindrical coordinates
α	Radial index of acoustic mode [Eq. (2)]
α_g	Attenuation constant due to gas relaxation
α_p	Attenuation constant due to particles in the gas
γ	Specific heat ratio of chamber gas
$\delta_{h,0}$	Kronecker delta symbol
$\delta_{m,0}$	Kronecker delta symbol
η	Shear viscosity
λ	Lamé modulus
λ'	Dilatational viscosity
μ	Lamé modulus
ρ	Density of chamber gas
ρ_s	Density of solid propellant
ρ'	Density of a solid particle in the chamber gas
ω	Angular frequency ($=2\pi f$)

ACKNOWLEDGMENT

The authors are especially grateful to Dr. F. T. McClure for many helpful discussions in connection with the preparation of this manuscript.

This work was supported by the Bureau of Naval Weapons, Department of the Navy, under NOw 62-0604-c.

REFERENCES

1. Panel Discussion, *Eighth Symposium (International) on Combustion*, p. 904. Williams and Wilkins, 1962.
2. McCLURE, F. T., HART, R. W., and BIRD, J. F.: *Solid Propellant Rocket Research*, p. 295. Academic Press, 1960.
3. BIRD, J. F., McCLURE, F. T., and HART, R. W.: *Proceedings of the Twelfth Annual International Astronautical Federation Congress*. To be published. Also available as The Johns Hopkins Univ. Applied Physics Laboratory Report TG 335-8, June 1961.
4. McCLURE, F. T., BIRD, J. F., and HART, R. W.: ARS Journal *32*, 374 (1962).
5. MORSE, P. M. and FESHBACH, H.: *Methods of Theoretical Physics*, p. 151. McGraw-Hill, 1953.
6. *Ibid.*, p. 142.
7. *Proceedings of the Second Meeting of the Technical Panel on Solid Propellant Combustion Instability*, The Johns Hopkins Univ. Applied Physics Laboratory Report TG 371-4a, May 1961.
8. CULICK, F. E. C.: Ph.D. Thesis. Massachusetts Institute of Technology, Technical Report No. 480 (1961).
9. CROCCO, L. and CHENG, S.: *Theory of Combustion Instability in Liquid Propellant Rocket Motors*. Butterworths, 1956.
10. McCLURE, F. T., HART, R. W., and CANTRELL, R. H.: To be published.
11. HART, R. W. and CANTRELL, R. H.: On Amplification and Attenuation of Sound by Burning Propellants. A.R.S. Journal (to be published). Also available as The Johns Hopkins Univ. Applied Physics Laboratory Report TG 335-11.
12. HORTON, M. D. and PRICE, E. W.: This volume, p. 303.
13. STRITTMATER, R., WATERMEIER, L., and PFAFF, S.: This volume, p. 311.
14. WIGHT, H. M.: AFOSR Report No. TR-60-60; also Aeronutronics Technical Report No. U-858, March, 1960.
15. EPSTEIN, P. and CARHART, R.: J. Acoust. Soc. Am. *25*, 553 (1953).
16. McCLURE, F. T.: Private communication, May, 1962.
17. McCLURE, F. T., HART, R. W., and BIRD, J. F.: J. Appl. Phys. *31*, 884 (1960); BIRD, J. F., HART, R. W., and McCLURE, F. T.: J. Acoust. Soc. Am. *32*, 1404 (1960).
18. DETERS, O. J.: ARS Journal *32*, 378 (1962).
19. RYAN, N. W., COATES, R. L., and BAER, A. D.: This volume, p. 328.
20. BROWNLEE, W. G. and MARBLE, F. E.: *Solid Propellant Rocket Research*, p. 455. Academic Press, 1960.

Discussion

MR. S. L. BRAGG (*Rolls-Royce*): Dr. Lawhead has shown that the modeling parameters can be kept constant, and the relative stability ratings of injector systems determined by tests on strip, annular, or segmental section models of liquid propellant rockets.

Could the same technique be applied to solid propellant motors? The frequency would be approximately correct if strip or annular chambers were used, and the extra wall damping might not be significant if the major part of the damping is in fact caused by the particles in the stream.

DR. R. W. HART (*APL/The Johns Hopkins University*): It is clear that the acoustic gain-loss balance is a function of quite a number of parameters and that modeling experiments in which one or perhaps a very few of these parameters were varied could be quite helpful. Of course, this would be particularly true if only one very significant quantity were varied. With respect to the experiments to which Dr. Bragg refers the steady state flow might be well reproduced in the model. The oscillation frequency which is known often to be an important quantity could also be held substantially fixed. The acoustic field, however, would then not be correctly modeled in all dimensions. I do not believe that it is yet known just how important this lack of fidelity in the model might be. There would be other varied quantities, however, such as the exposed motor wall area, and probably the acoustic loss at the orifice. These variable factors would be expected to influence the validity of the modeling to an extent which would have to be determined. Two important questions would appear to remain unilluminated, however. If the model proved to be stable, no information would seem forthcoming as to the margin of safety, and it would be difficult to infer finite amplitude properties from the model because the acoustic field would, in general, not be faithfully modeled.

Colloquium on Reciprocating Engine Combustion Research

(Organized by Prof. E. S. Starkman)
(*University of California*)

Chairmen: Prof. E. S. Starkman (*University of California*)
Dr. J. S. Clarke (*Lucas Ltd.*)
Vice Chairman: Prof. P. S. Myers (*University of Wisconsin*)

RECIPROCATING ENGINE COMBUSTION RESEARCH—A STATUS REPORT

E. S. STARKMAN

Depending upon one's point of view, strong argument can be made on either side of the proposition that real progress has been made during the last forty years in the field of research into reciprocating engine combustion. If one considers only whether the problems are being solved, the answer must be that progress has been remarkable. Control of combustion has been effected satisfactorily to date and to an extent that has allowed continual improvement in engine performance beyond the successive predictions of ultimate barriers. On the other hand, no agreement exists that there is a real understanding of the fundamentals applicable to reciprocating engine combustion. The solutions to combustion engine problems have been almost exclusively empirical, as has been the preponderance of research.

It was not the intent in assembling this introductory paper to the Colloquium on Reciprocating Engine Combustion Research to attempt either an exhaustive treatise nor to deal with history. Rather, what was in mind was to provide a framework within which more or less the 8 papers presented can be fit. Additionally this introduction was intended to provide a compendium of sources, primarily recent, from which one might glean a perhaps broader sense of the status of piston engine combustion research than is possible within the confines of a program as necessarily limited as this Colloquium must be. Thus this paper incorporates a large list of references, partly historical but mostly more recent than the last instance in which the subject was paid attention at a Combustion Symposium. In addition some of these references are intended to point to problem areas either recurrent or new which could well receive more attention. Please bear with the author if the references appearing herewith seem to be oriented in the literature of that language with which he is most conversant, and if some of the more recent references which should have been included have somehow been overlooked.

The Combustion Symposia are sporadic in their attention to the subject of reciprocating engine combustion *per se*. The first Symposium, in 1928, incorporated two papers[1,2] dealing with divergent subject matters. One paper recounted an early recognition that knock was related to mixture ratio as well as other factors[1] and the other, a disclosure that the progress of combustion reaction across an engine cylinder is a fuel-dependent variable.[2]

The Second Symposium in 1937 was approximately half given over to piston engine combustion phenomena. Included in the list of authors of the eleven papers[3–13] are many illustrious names. The program was admirably comprehensive in scope. Twenty-five years later, the subject matters of a majority of the papers are still pertinent and unfortunately still under study and even appear on the program of this, the Ninth Symposium.

The Third Symposium, in postwar 1948, incorporated only two strictly engine papers.[14,15]

One of these[15] was intended to settle once and for all the question of whether or not the phenomenon in the end zone is truly detonation, an argument which is still extant.

Only one engine paper[16] appeared on the program of the Fourth Symposium. The Fifth Symposium included seven[17–23]. It would appear that the program of the Fifth Symposium might have been assembled in a manner calculated to give a comprehensive picture of the problems and progress in engine combustion. Beyond two very good survey papers[21,23] however, the program seemed to fall somewhat short of this admirable goal. One might say that the papers in the Fifth Symposium were progress reports in selective areas.

The last of the Combustion Symposia preceding this in which engine combustion was considered was the Sixth. Three offerings appeared.[24,26] One of these[25] touched on a mushrooming area of concern—the source of unburned hydrocarbon in engine exhaust. Another[24] dealt with the continuing effort to correlate internal combustion phenomena with less complex systems. The third[26] was further in the argument, pro and con, on detonation.

No papers at all appeared on the subject of piston engine combustion as such in either the Seventh or Eighth Symposium. This does not mean that research and publication were not taking place. Nor does it mean that the subject matters of these symposia were not in part engine related. If anything, the compendium attached hereto is evidence to the contrary.

For the Ninth Symposium on Combustion it was decided it would be timely and appropriate to attempt a comprehensive Colloquium on Reciprocating Engine Combustion. In one respect, the program commemorates the 25th anniversary of the Second Symposium. It was originally intended that the subject matter be as comprehensive as possible and cover the presently pressing problems and the status of research principally on spark ignition engines. In small part it was also intended to include compression ignition combustion phenomena.

A reflection of the literature of the subject shows that the principal objective of piston engine combustion research is to determine the source and find a cure for the audible vibrations associated with combustion. These noises, in a variety of manifestations and however classified[27] and whether or not destructive of the piston engine, account for upwards of 90 per cent of research and development from 1920.[28] An excellent historical review up to 1950 may be had by resort to a combination of references, but mainly references 29 and 30. The variety, character, and classification of noises have not been simplified over the years. The kinds of problems and number of these have become more complex, and particularly as compression ratios have been raised, even though there have been large improvements in fuel antiknock quality and engine combustion chamber design.

Whereas octane number, until about the time of the Sixth Symposium, was a good yardstick by which to judge the mutual compatibility of fuel quality and engine compression ratio, a new phenomenon (or an old one reborn) has recently become sufficiently severe that compression ratio is not now limited by octane number but rather by pre-ignition, surface ignition, particle ignition, or precombustion reactions. Octane number in such instances is relatively a secondary factor in terms of combustion noises emanating from the engine. The character and source of some of these so-called abnormal combustion noises[31–36] can be related to combustion pressure rise rates. When the rate of pressure rise exceeds a given critical level, the power train, particularly the crankshaft, is set into vibration.[37–47] This phenomenon of induced mechanical vibration is in general identified by the names "rumble," "thudding," or "rough combustion." There is little difference in the resulting character of the phenomenon, whether it is attributed to exposure of the fuel–air mixture during compression to a hot surface, to deposits which have flaked from the surface, or, in the absence of deposits, to a preconditioning of the mixture to major exothermic reaction of any character prior to arrival of the spark initiated flame front.[48–75]

The phenomenon of so-called uncontrolled or pre-ignition combustion, taking place in the combustion chamber prior to, or occurring parallel with the spark ignited flame front is also encountered in high compression ratio engines while they are being cranked for starting.[76–78] This release of energy on compression obviously causes difficulty in engine starting. The cause of this type of pre-ignition is compounded from fuel reactivity characteristics, compression ratio, and time–temperature history of the charge.

The tendency for occurrence of the pre-ignition phenomena described above can be partially controlled, either through combustion chamber design, fuel composition, or through fuel additives.[79–81] Perhaps it is redundant to point out that the fundamental reasons for the action of additives, deposits, fuel composition, or engine design to influence the onset of this type of so-called abnormal combustion are not completely understood.

There is no question remaining today regarding whether the reactive mixture which feeds the

flame front, whether normal or abnormal, is the same material as that which entered the engine. By the time a flame is established the fuel has undergone varying extends of oxidation and decomposition. Depending upon the multitude of variables which exist, these precombustion reactions can lead to end result in either normal flame or a pre-ignition or a post-ignition problem.[82–94]

The question of whether the post-ignition engine noise, sometimes called detonation but more usually just called knock, is a true detonation has been touched on previously. The knock problem has been so extensively treated in other places and at other times that it will suffice here to call attention to a few more recent and seemingly pertinent publications on the phenomenon and its precursors[95–98] and upon some early,[99–100] later[101–103] and recent[104–105] efforts to photograph with high speed motion pictures the knocking combustion process in engines using windows in the combustion envelope.

Whether or not the flame progresses at a speed which is consistent with optimum performance is a matter of continuing study. So-called flame speed measurements are still being made[106–108] in part at least to aid in an explanation of phenomena such as rumble. Two papers in this Colloquium should aid in bringing the subject up to date.[109,110]

The fact that the flame front has passed through a combustion chamber unfortunately does not mean that combustion has been satisfactorily completed. The small amounts of unburned fuel and lubricant which pass out the exhaust valve along with oxides of nitrogen can be of a composition and quantity to cause concern with regard to air pollution.[111,112] Some legislative bodies have already taken action to restrict the emission of materials from piston engine exhaust.[113] Progress is being made, both on the mechanisms which lead to the production of the undesirable constituents and on means for at least partially reducing the amount of these materials which ultimately leave the engine or the exhause pipe.[114–123]

The problems of reciprocating engine combustion are not easy to study in an operating engine *per se*. It would be easier to study precombustion reactions and knock in more simple systems, but obviously some reasonable simulation of the time–temperature–pressure history is desirable. Over the past fifteen years the rapid compression machine has been used for just such purpose.[14,124–126] Further information on this type of investigation appears on this program.[127] More recently the shock tube has found a place in the study of precombustion reactions in a time–temperature–pressure environment closely akin to the reciprocating engine[128] and this subject also appears on the program.[129]

The part played by lead and other metal compounds in reducing knock tendency is also not yet generally agreed upon after 40 years of application. The activity in this area of research has decreased somewhat but is still at a level to occupy attention.[130] Tetramethyl lead appears to be coming into favor as a practical antiknock for present day motor gasolines.[131,132] A paper on this subject is on this Symposium program.[133]

It has also been a long-standing universal hope that a means may be found to predict fuel combustion characteristics in an engine from structural characteristics or chemical properties alone, and some progress has been made in this regard.[134,135] Part of this program deals with such effort toward a better understanding of how fuel structure or composition influence the combustion process.[136]

The other paper appearing on the Colloquium on Reciprocating Engine Combustion Research has to do with diesel engine combustion.[137] The diffusional flame, as a problem of reciprocating engine combustion may well be coming to a more prominent position with, in addition to the diesel engine itself, a tendency to reevaluate the spark ignition-fuel injection engine[138,139] in the form perhaps of a stratified charge configuration. The principles which apply to diesel engine combustion, while not directly parallel to spark ignition fuel injection are none the less pertinent.

The program of the Colloquium, while it is, as indicated, by no means either exhaustive or completely comprehensive, would be less so if mention was not made of at least another area or two in which there is presently new work under way. One of these is the calculation of and the measurement of the states of the gases in a reciprocating engine combustion chamber.[140–146] Progress can in large part be attributed to the more ready availability of high quality instrumentation and the advent of the high speed digital computer. Another area which should not be ignored by this author, at least, is that of the application to piston engines of unusual or non-hydrocarbon fuels.[147]

These papers, on the program and presented in other places, illustrate by example the state of recent theoretical and technological attacks on continuing problems of the reciprocating engine. There do not appear to be any earth-shaking discoveries or any complete solutions, but continued progress toward understanding of phenomena is surely apparent.

References

1. Campbell, J. M., Lovell, W. G., and Boyd, T. A.: Importance of Mixture Ratio in Rating Fuels for Knock, First Symposium on Combustion; Ind. Eng. Chem. *20*, 1045 (1928).
2. Maxwell, G. B. and Wheeler, R. V.: Some Flame Characteristics of Motor Fuels, First Symposium on Combustion; Ind. Eng. Chem. *20*, 1041 (1928).
3. Beatty, H. A.: Chemistry of Otto-Cycle Engine Combustion, Second Symposium on Combustion; Chem. Revs. *22*, 51 (1938).
4. Best, H. W.: The Knock Rating of Motor Fuels, Second Symposium on Combustion; Chem. Revs. *22*, 143 (1938).
5. Boerlage, G. D. and Broeze, J. J.: The Combustion Process in the Diesel Engine, Second Symposium on Combustion; Chem. Revs. *22*, 61 (1938).
6. Brown, G. G.: A Thermodynamic Analysis of the Rate of Pressure Rise in the Otto Cycle, Second Symposium on Combustion; Chem. Revs. *22*, 27 (1938).
7. Egloff, G., Hubner, W. H., and Van Arsdell: Fuels for Internal Combustion Engines, Second Symposium on Combustion; Chem. Revs. *22*, 175 (1938).
8. Hershey, A. E.: Flame Temperatures in Engines, Second Symposium on Combustion; Chem. Revs. *21*, 431 (1937).
9. Hottel, H. C. and Eberhardt, J. E.: A Mollier Diagram for the Internal Combustion Engine, Second Symposium on Combustion; Chem. Revs. *21*, 439 (1937).
10. Keith, P. C., Jr., Carey, J. S., and Ward, J. T.: Economics of Knock Ratings of Otto-cycle Engine Fuels, Second Symposium on Combustion; Chem. Revs. *22*, 281 (1938).
11. Lovell, W. G. and Campbell, J.: Molecular Structure of Hydrocarbons and Engine Knock, Second Symposium on Combustion; Chem. Revs. *22*, 159 (1938).
12. Rothrock, A. M. and Selden, R. F.: Factors Controlling Diesel Engine Performance, Second Symposium on Combustion; Chem. Revs. *22*, 89 (1938).
13. Schweitzer, P. H.: Methods of Rating Diesel Fuels, Second Symposium on Combustion; Chem. Revs. *22*, 107 (1938).
14. Jost, W.: Reactions of Adiabatically Compressed Hydrocarbon–Air Mixtures, *Third Symposium on Combustion, Flame and Explosion Phenomena*, p. 424, Williams and Wilkins, 1949.
15. Male, T.: Photographs at 500,000 Frames per Second of Combustion and Detonation in Reciprocating Engine, *Third Symposium on Combustion, Flame and Explosion Phenomena*, p. 721. Williams and Wilkins, 1949.
16. Yamazaki, Y. and Inumo, K.: Augmented Flames in an Engine Combustion Chamber, *Fourth Symposium (International) on Combustion*, p. 914. Williams and Wilkins, 1953.
17. Anzilotti, W. F. and Tomsic, J. V.: Combustion of Hydrogen and Carbon Monoxide as Related to Knock, *Fifth Symposium (International) on Combustion*, p. 356. Reinhold 1955.
18. Ball, G. A.: Photographic Studies of Cool Flames and Knock in an Engine, *Fifth Symposium on Combustion*, p. 366. Reinhold, 1955.
19. Levedahl, W. J.: Multistage Autoignition of Engine Fuels, *Fifth Symposium (International) on Combustion*, p. 372. Reinhold, 1955.
20. Livengood, J. C. and Wu, P. C.: Correlation of Autoignition Phenomena in Internal Combustion Engines and Rapid Compression Machines, *Fifth Symposium (International) on Combustion*, p. 347. Reinhold, 1955.
21. Lovell, W. G.: Combustion Problems in Internal Combustion Engines, *Fifth Symposium (International) on Combustion*, p. 1 Reinhold, 1955.
22. Malmberg, E. W., Smith, M. L., Bigler, J. E., and Babbitt, J. A.: A Study of Cool Flames and Associated Reactions in an Engine, *Fifth Symposium (International) on Combustion*, p. 385. Reinhold, 1955.
23. Schweitzer, P. H.: Combustion Problems in Diesel Engines, *Fifth Symposium (International) on Combustion*, p. 7. Reinhold, 1955.
24. Agnew, J. T., Agnew, W. G., and Wark, K, Jr.: Comparison of Emission Spectra of Low Temperature Combustion Reactions Produced in an Engine and in a Flat-Flame Burner, *Sixth Symposium (International) on Combustion*, p. 894. Reinhold, 1957.
25. Daniel, W. A.: Flame Quenching at the Walls of an Internal Combustion Engine, *Sixth Symposium (International) on Combustion*, p. 886. Reinhold, 1957.
26. Firey, J. C.: The Detonation Wave Theory of Gasoline Engine Knock, *Sixth Symposium (International) on Combustion*, p. 878. Reinhold, 1957.
27. Coordinating Research Council Report No. 278, Terms for Use in Otto Cycle Engine Combustion, New York, June 1954.
28. Midgley, T., Jr.: Combustion and Fuels in Internal-Combustion Engine, J. SAE *7*, 489 (1920).
29. Boyd, T. A.: Pathfinding in Fuels and Engines, SAE Quart. Trans. *4*, 182 (1950).
30. Rothrock, A. M.: Fuel Rating—Its Relation

to Engine Performance, SAE Trans. *48*, 51 (1941).

31. Echols, L. S., Yust, V. E., and Bame, J. L.: A Review of Research on Abnormal Combustion Phenomena in Internal Combustion Engines, *Proc. Fifth World Petroleum Congress*, VI, p. 159, 1959.
32. Goodger, E. M.: Fuel Additives, Automobile Engineer *51*, 56 (1961).
33. Massa, V. F.: A Study of the Normal and Abnormal Combustion Behavior of Gasolines, 1961 SAE International Congress and Exposition of Automotive Engineering, Detroit, Mich., Preprint No. 293C, Jan. 1961.
34. Perry, R. H., Jr., Gerard, P. L., and Heath, D. P.: The Influence of Gasoline Composition on Abnormal Combustion in Spark Ignition Engines, SAE National Fuels and Lubricants Meeting, Preprint No. 438A, Nov. 1961.
35. Sturgis, B. M.: Abnormal Combustion Problems in Gasoline Engines, 1961 SAE International Congress and Exposition of Automotive Engineering, Detroit, Mich., Preprint No. 293A, Jan. 1961.
36. Young, R. W.: Abnormal Combustion in High Compression Single-Cylinder Engines, SAE Fuels and Lubricants Meeting, Tulsa Okla., Preprint No. 105A, Nov. 1958.
37. Bame, J. L. and Tuell, R. G.: Engine Pounding—Its Cause and Control, SAE Trans. *67*, 148 (1959).
38. Bender, R. O., Mayer, G. D., and Pahnke, A. J.: Combustion Irregularities at High Compression Ratios, Div. Pet. Chem., ACS Preprints *3*(2), C-33 (1958).
39. Felt, A. E., Warren, J. A., and Hall, C. A.: Rumble—A Deposit Effect at High Compression Ratios, SAE Trans. *67*, 138 (1959).
40. Hostetler, H. F. and Tuuri, W. R.: Knock, Rumble and Ping, SAE Trans. *67*, 152 (1959).
41. Meagher, R., Johnson, R. L., and Parthemore, K. G.: Correlation of Engine Noises with Combustion Phenomena, SAE Trans. *63*, 481 (1955).
42. Morris, W. E. and Fariss, D. C.: Thudding in High Compression Ratio Engines, SAE Trans. *67*, 134 (1959).
43. Perry, R. H., Jr. and Lowther, H. V.: Knock Knock—Spark Knock, Wild Ping or Rumble? SAE Trans. *67*, 145 (1959).
44. Robison, J. A., Behrens, M. D., and Mosher, R. G.: Investigating Rumble in Single-Cylinder Engines, SAE Trans. *67*, 169 (1959).
45. Starkman, E. S. and Sytz, W. E.: The Identification and Characterization of Rumble and Thud, SAE Trans. *68*, 93 (1960).
46. Stebar, R. F., Wiese, W. M., and Everett, R. L.: Engine Rumble—A Barrier to Higher Compression Ratios? SAE Trans. *68*, 206 (1960).
47. Tupa, R. C.: Combustion Noise and Vibration, SAE Summer Meeting, Atlantic City, N. J., Preprint No. 78W, June 1959; SAE Jour. *67*, 80 (1959).
48. Bartleson, J. D. and Hughes, E. C.: Combustion Chamber Deposits as Related to the Carbon-forming Properties of Motor Oils, Ind. Eng. Chem. *45*, 1501 (1953).
49. Blaker, R. H.: The Surface Ignition of Fuels in Engines, *Literature of the Combustion of Petroleum* (No. 20 in Advances in Chemistry Series), p. 217, American Chemical Society, 1958.
50. Bowditch, F. W., Wilson, R. E., and Nebel, G. J.: Some Aspects of Particle Ignition, Proc. API *34*, 242 (1954).
51. Bowditch, F. W. and Yu, T. C.: A Consideration of the Deposit Ignition Mechanism, SAE Trans. *69*, 435 (1961).
52. Corzilius, M. W., Diggs, D. R., and Hoffman, R. A.: The Combustion-Chamber Deposit Problem in High-Compression-Ratio Engines, Proc. API *36*, 162 (1954).
53. Dumont, L. F.: Possible Mechanisms by Which Combustion Chamber Deposits Accumulate and Influence Knock, SAE Quart. Trans. *5*, 565 (1954).
54. Hirschler, D. A., McCullough, J. D., and Hall, C. A.: Deposit Induced Ignition, SAE Trans. *62*, 40 (1954).
55. Hopkins, S., Pecora, R. J., and Alpert, N.: Surface Ignition as Influenced by Engine Configuration and Fuels—A Consumer Type Study in Vehicles, SAE Summer Meeting, Atlantic City, N. J., Preprint No. 78V, June 1959; SAE Jour. *67*, 58 (1959).
56. Hundere, A and Bert, L. A.: Preignition and Its Deleterious Effects in Aircraft Engines, SAE Quart. Trans. *2*, 546 (1948).
57. Hyatt, K., Tomsic, V. J., and Mellinger, C. A.: Surface Ignition—A New Look with a New Instrument, SAE Summer Meeting, Atlantic City, N. J., Preprint No. 78V, June 1959; SAE Jour. *67*, 56 (1959).
58. LaCroix, L. D. and Kalinowski, M. L.: One Test Evaluates Motor Oil Contribution to Combustion Deposits, SAE Fuels and Lubricants Meeting, Chicago, Preprint No. 126U, Oct. 1959.
59. Landerl, H. P. and Sturgis, B. M.: Tetraethyl Radiolead Studies of Combustion Chamber Deposit Formation, Ind. Eng. Chem. *45*, 1744 (1953).
60. McNab, J. G., Moody, L. E., and Hakala, N. V.: The Effect of Lubricant Composition on

Combustion Chamber Deposits, SAE Trans. *62*, 228 (1954).

61. Melby, A. O., Diggs, D. R., and Sturgis, B. M., An Investigation of Preignition in Engines, SAE Trans. *62*, 32 (1954).
62. Mikita, J. J. and Sturgis, B. M.: The Chemistry of Combustion Chamber Deposits, *Proc. Fourth World Petroleum Congress*, VI, p. 357. Carlo Colombo, Rome, 1955.
63. Mrstik, A. V. and Payne, R. B.: The Interrelationship of Fuel Constituents, Combustion Chamber Deposits, and Automotive Engine Performance, SAE Fuels and Lubricants Meeting, Cleveland, Ohio, Preprint No. 257, November 1957.
64. Nebel, G. J. and Cramer, P. L.: Ignition Temperatures of Lead Compound–Carbon Mixtures, Ind. Eng. Chem. *47*, 2393 (1955).
65. Sabina, J. R., Mikita, J. J., and Campbell, H. H.: Preignition in Automotive Engines, Proc. API *33*, 137 (1953).
66. Shore, L. B. and Kunc, J. F., Jr.: The Effect of Simulated Surface Ignition on Engine Performance, SAE Summer Meeting, Atlantic City, N. J., Preprint No. 326, June 1954.
67. Shore, L. B. and Ockert, K. F.: Combustion Chamber Deposits—A Radiotracer Study, SAE Trans. *66*, 285 (1958).
68. Spindt, R. S., Wolfe, C. L., and Stevens, D. R.: Nitrogen Oxides, Combustion and Engine Deposits, SAE Trans. *64*, 797 (1956).
69. Sturgis, B. M., Cantwell, E. N., Morris, W. E., and Schultz, D. L.: The Preignition Resistance of Fuels, Proc. API *34*, 256 (1954).
70. Tomsic, V. J.: Surface Ignition Behavior of Fuels, SAE Annual Meeting, Detroit, Mich., Preprint No. 293E, Jan. 1961.
71. Williams, R. K. and Landis, J. R.: Some Effects of Fuels and Lubricants on Autoignition in Cars on the Road, SAE Trans. *62*, 56 (1954).
72. Wimmer, D. B.: Some Factors Involved in Surface Ignition in Spark-Ignition Engines, SAE Fuels and Lubricants Meeting, Tulsa, Okla., Preprint No. 872, Nov. 1956.
73. Winch, R. F.: The Occurrence of Preignition in Present Day Cars in Normal Service, SAE Trans. *62*, 50 (1954).
74. Winch, R. F. and Moyes, F. M.: A Method for Identifying Preignition, SAE Trans. *61*, 453 (1953).
75. Withrow, L. L. and Bowditch, F. W.: Flame Photographs of Autoignition Induced by Combustion Chamber Deposits, SAE Quart. Trans. *6*, 724 (1952).
76. Bowditch, F. W. and Stebar, R. F.: Autoignition Associated with Hot Starting, SAE Trans. *66*, 179 (1958).
77. Massa, V. R.: Starting and Stopping Modern Engines—New Combustion Problems, SAE Trans. *67*, 125 (1959).
78. Spindt, R. S. and O'Malley, D. R.: Abnormal Combustion at Engine Cranking Speeds, 1961 SAE International Congress and Exposition of Automotive Engineering, Detroit, Mich. Preprint No. 293B, Jan. 1961.
79. Burk, F. C., Test, L. J., and Jackson, H. R.: The Study of Fuel Additives to Reduce Preignition, Proc. API *34* (III), 270 (1954).
80. Burnham, H. D.: The Role of Tricresyl Phosphate in Gasoline for the Control of Ignition and Combustion Problems, Div. Pet. Chem., ACS Preprints *36*, 39 (1955).
81. Hughes, E. C., Fay, P. S., Szabo, L. S., and Tupa, R. C.: Effect of Boron Compounds on Combustion Processes, Ind. Eng. Chem. *48*, 1892 (1956).
82. Wiese, W. M.: If You Squeeze Them, Must They Scream? SAE Trans. *67*, 175 (1959).
83. Clarke, J. S.: Initiation and Some Controlling Parameters of Combustion in Piston Engines, Engineering *192*, 602 (1961).
84. Corzilius, M. W., Diggs, D. R., and Pastell, D. L.: Some Factors Affecting Precombustion Reactions in Engines, SAE Trans. *61*, 386 (1953).
85. Downs, D., Walsh, A. D., and Wheeler, R. W.: Study of Reactions that Lead to Knock in Spark Ignition Engine, Trans. Roy. Soc. (London) *A234*, 463 (1951).
86. Melby, A. O.: Effects of Fuel Additives on Precombustion Reactions of *n*-Heptane, J. Inst. Petrol. *38*, 965 (1952).
87. Pahnke, A. J.: Engine Studies of Preknock Reactions, *Literature of the Combustion of Petroleum* (No. 20 in Advances in Chemistry Series), p. 202. American Chemical Society, 1958.
88. Pahnke, A. J., Cohen, P. M., and Sturgis, B. M.: Preflame Oxidation of Hydrocarbons in a Motored Engine, Ind. Eng. Chem. *46*, 1024 (1954).
89. Pastell, D. L.: Precombustion Reactions in a Motored Engine, SAE Quart. Trans. *4*, 571 (1950).
90. Pipenberg, K. J. and Pahnke, A. J.: Spectrometric Investigations of *n*-Heptane Preflame Reactions in a Motored Engine, Ind. Eng. Chem. *49*, 2067 (1957).
91. Pipenberg, K. J., Pahnke, A. J., and Blaker, R. H.: Studies of the Chemical Reactions Which Occur in an Engine Prior to Knock, Proc. API *38*, 68 (1958).
92. Retailliau, E. R., Richards, H. A., Jr., and Jones, M. C. K.: Precombustion Reaction in the Spark-Ignition Engine, SAE Quart. Trans. *4*, 438 (1950).

93. WELLING, C. E., HALL, G. C., and STEPANSKI, J. S.: Concurrent Pyrolytic and Oxidative Reaction Mechanisms in Precombustion of Hydrocarbons, SAE Trans. *69*, 448 (1961).
94. WITHROW, L. L. and RASSWEILER, G. M.: Spectrographic Studies of Engine Combustion, Ind. Eng. Chem. *23*, 768 (1931).
95. BRINKLEY, S. R., JR. and LEWIS, B.: On the Transition from Deflagration to Detonation, *Seventh Symposium (International) on Combustion*, p. 807. Butterworths, 1958.
96. DIGGS, D. R.: The Effect of Combustion Time on Knock in a Spark Ignition Engine, SAE Trans. *61*, 402 (1953).
97. HOFFMAN, R. A.: A New Technique for Determining the Knocking Resistance of Fuels, SAE Annual Meeting, Detroit, Mich., Preprint No. 285C, Jan. 1961.
98. STURGIS, B. M.: Some Concepts of Knock and Antiknock Action, SAE Trans. *63*, 253 (1955).
99. RASSWEILER, G. M. and WITHROW, L. L.: Motion Pictures of Engine Flames Correlated with Pressure Cards, SAE Trans. *42*, 185 (1938).
100. WITHROW, L. L. and BOYD, T. A.: Photographic Flame Studies in the Gasoline Engine, Ind. Eng. Chem. *23*, 539 (1931).
101. MILLER, C. D.: Roles of Detonation Waves and Autoignition in Spark-Ignition Knock as Shown by Photographs Taken at 40,000 and 200,000 Frames per Second, SAE Quart. Trans. *1*, 98 (1947).
102. MILLER, C. D., OLSEN, H. L., LOGAN, W. O., JR., and OSTERSTROM, G. E.: Analysis of Spark Ignition Engine Knock as Seen in Photographs Taken as 200,000 Frames per Second, NACA TR 857, 1946.
103. OSTERSTROM, G. E.: Knocking Combustion Observed in a Spark Ignition Engine with Simultaneous Direct and Schlieren High-Speed Motion Pictures and Pressure Records, NACA TN 1614, 1948.
104. BOWDITCH, F. W.: Combustion Problems in Gasoline Engines, p. 119. FISITA Eighth Congress, The Hague, May 1960.
105. BOWDITCH, F. W.: A New Tool for Combustion Research. A Quartz Piston Engine, SAE Trans. *69*, 17 (1961).
106. CURRY, S.: A Three Dimensional Study of Flame Propagation in a Spark Ignition Engine, SAE Annual Meeting, Detroit, Mich., Preprint No. 452B, Jan. 1962.
107. MINTER, C. C.: Flame Movement and Pressure Development in Gasoline Engines, SAE Jour. *36*, 89 (1935).
108. STARKMAN, E. S., STRANGE, F. M., and DAHM, T. J.: Flame Speeds and Pressure Rise Rates in Spark Ignition Engines, SAE International West Coast Meeting, Vancouver, B. C., Preprint No. 83V, Aug. 1959.
109. CURRY, S.: Effect of Antiknocks on Flame Propagation in a Spark Ignition Engine, This volume, p. 1056.
110. KUMAGAI, S. and KUDO, Y.: Flame Studies by Means of Ionization Gap in a High-Speed Spark-Ignition Engine, This volume, p. 1083.
111. FAITH, W. L.: Ambient Air Quality, Ind. Wastes *5*, 44 (1960).
112. LARSON, G. P., CHIPMAN, J. C., and KAUPER, E. K.: A Study of Distribution and Effects of Automotive Exhaust Gas in Los Angeles, SAE Annual Meeting, Detroit, Mich., Preprint No. 420, March 1955.
113. MAGA, J. A. and HASS, G. C.: Development of Motor Vehicle Exhaust Emission Standards in California, J. Air Pollution Control Assn. *10*, 393 (1960).
114. BENNETT, P. A., JACKSON, M. W., MURPHY, C. K., and RANDALL, R. A.: Reduction of Air Pollution by Control of Emission from Automotive Crankcases, SAE Trans. *68*, 514 (1960).
115. CHANDLER, J. M., SMITH, A. M., and STRUCK, J. H.: Development of Concept of Non-Flame Exhaust Gas Reactors, SAE Automobile Meeting, Detroit, Mich., Preprint No. 486M, March 1962.
116. DANIEL, W. A. and WENTWORTH, J. T.: Exhaust Gas Hydrocarbons—Genesis and Exodus, SAE Automobile Meeting, Detroit, Mich., Preprint No. 486B, March 1962.
117. DAVIS, D. L. and ONISHI, G. E.: Catalytic Converter Development Problems, SAE Automobile Meeting, Detroit, Mich., Preprint No. 486F, March 1962.
118. HAGEN, D. F. and HOLIDAY, G. W.: Effects of Engine Operating and Design Variables on Exhaust Emissions, SAE Automobile Meeting, Detroit, Mich., Preprint No. 486C, March 1962.
119. HANSON, T. K. and EGERTON, A. C.: Nitrogen Oxides in Internal Combustion Engine Gases, Proc. Royal Soc. (London) *A163*, 90 (Nov. 1937).
120. JACKSON, M. W., WIESE, W. M., and WENTWORTH, J. T.: Influence of Air-Fuel Ratio, Spark Timing and Combustion Chamber Deposits on Exhaust Hydrocarbon Emissions, SAE Automobile Meeting, Detroit, Mich., Preprint No. 486A, March 1962.
121. RAYMOND, L.: Automotive Vehicles and Air Pollution, SAE Paper No. S323 (1962).
122. SCHNABEL, J. W., YINGST, J. E., HEINEN, C. M., and FAGLEY, W. S.: Development of Flame Type Afterburner, SAE Automobile Meeting, Detroit, Mich., Preprint No. 486G, March 1962.

123. STARKMAN, E. S.: A Radioactive Tracer Study of Lubricating Oil Consumption, SAE Trans. *69*, 86 (1961).
124. LEARY, W. A.: A Rapid Compression Machine Suitable for Studying Short Ignition Delays, NACA TN 1332, Feb. 1948.
125. RIFKIN, E. B. and WALCUTT, C.: A Basis for Understanding Antiknock Action, SAE Trans. *65*, 552 (1957).
126. TAYLOR, C. F., TAYLOR, E. S., LIVINGOOD, J. C., RUSSEL, W. A., and LEARY, W. A.: The Ignition of Fuels by Rapid Compression, SAE Quart. Trans. *4*, 232 (1950).
127. JOST, W.: Knock Reaction. This volume, p. 1013
128. GLICK, H. S., SQUIRE, W., and HERTZBERG, A.: A New Shock Tube Technique for the Study of High Temperature Gas Phase Reactions, *Fifth Symposium (International) on Combustion*, p. 393. Reinhold, 1955.
129. ORR, C. R.: Combustion of Hydrocarbons Behind a Shock Wave, This volume, p. 1034.
130. DOWNS, D., GRIFFITHS, S. T., and WHEELER, R. W.: The Part Played by the Preparational Stage in Determining Lead Antiknock Effectiveness, J. Inst. Petrol. *47*, 1 (1961).
131. PASTELL, D. L. and MORRIS, W. E.: Utility of Tetramethyl Lead in Gasoline, SAE Summer Meeting, Chicago, Preprint No. 207C, June 1960; SAE Jour. *68*, 38 (1960).
132. RICHARDSON, W. L., BARUSCH, M. R., KAUTSKY, G. J., and STEINKE, R. E.: Tetramethyl Lead—An Antiknock Agent for Modern Gasolines, Div. Petrol. Chem., ACS Preprints *5* (3), 37 (1960).
133. RICHARDSON, W. L., RYASON, P. R., KAUTSKY, G. J., and BARUSCH, M. R.: Organolead Anti-Knock Agents—Their Performance and Mode of Action, This volume, p. 1023.
134. CALCOTE, H. F., GREGORY, C. A., JR., BARNETT, C. M., and GILMER, R. B.: Spark Ignition—Effect of Molecular Structure, Ind. Eng. Chem. *44*, 2656 (1952).
135. VICHNIEVSKY, R.: Combustion in Petrol Engines, *Proceedings of the Joint Conference on Combustion*, p. 288. IME, ASME, London, 1955.
136. WALSH, A. D.: Knock Ratings of Fuels, This volume, p. 1046.
137. LYN, W. T.: Study of Burning Rate and Nature of Combustion in Diesel Engines, This volume, p. 1069.
138. BROCKHAUS, H., COWELL, T. F., and MASTERMAN, D. M. A.: Injection Versus Carburetion, A Comparison of Fuel Quality Requirements, p. 233. FISITA Eighth Congress, The Hague, 1960.
139. CONTA, L. D., DURBETAKI, P., and BACUNANA, J. L.: Stratified Charge Operation of Spark Ignition Engines, SAE Preprint No. 375B (1961).
140. AGNEW, W. G.: End Gas Temperature Measurement by a Two-Wavelength Infrared Radiation Method, SAE Trans. *69*, 495 (1961)
141. BURROWS, M. C., SHIMIZU, S., MYERS, P. S., and UYEHARA, O. A.: The Measurement of Unburned-Gas Temperatures in an Engine by an Infrared Radiation Pyrometer, SAE Trans. *69*, 514 (1961).
142. EDSON, M.: A Mathematical Model for Combustion, Ind. Eng. Chem. *52*, 1007 (1960).
143. GLUCKSTEIN, M. E. and WALCUTT, C.: End-Gas Temperature–Pressure Histories and Their Relation to Knock, SAE Trans. *69*, 529 (1961).
144. LIVINGOOD, J. C., TAYLOR, C. F., and WU, D. C.: Measurement of Gas Temperature in an Engine by the Velocity of Sound Method, SAE Trans. *66*, 683 (1958).
145. SIEGEL, B. R.: Use of Temperature-Density for Measuring Antiknock Quality, SAE Trans. *66*, 421 (1958).
146. STARKMAN, E. S., VICKLAND, C. W., STRANGE, F. M., and BELL, R. A.: A Consideration of the High Temperature Thermodynamics of Internal Combustion Engines, SAE Summer Meeting, St. Louis, Mo., Preprint No. 380A, 1961; SAE Trans. *70*, 785 (1962).
147. STARKMAN, E. S.: The Nitroparaffins as Potential Piston Engine Fuel, Ind. Eng. Chem. *51*, 1477 (1959).

KNOCK REACTION

W. JOST

Reaction in a rapid compression apparatus was followed by pressure recording, by photography, and by sampling and chemical analysis. It was possible to investigate the highly sensitive hydrogen-oxygen reaction with this equipment. Results obtained with this reaction make it highly improbable that any hot-point effects are present. Detailed results are presented for single or two-stage ignition of hydrocarbons with air.

Introduction

The method of adiabatic compression in the form of "pneumatic ignition" is of very old standing. As a method for quantitative measurements it was first used by Falk[2] at Nernst's suggestion, and later improved by Cassel. In a new and elegant form it was used by Tizard and Pye[4] for the investigation of hydrocarbon and other ignition reactions.

In the author's laboratory it has been used primarily for the investigation of hydrocarbon ignition since 1935. Attempts to use it for investigating the oxidation of carbon monoxide, hydrogen, etc., failed until about 1960 when we had sufficiently improved our method. This gave a check on the reliability of the hydrocarbon measurements.

The aim of our experiments was and is to investigate the kinetics of oxidation reactions, uninfluenced by wall effects. In order to achieve this, it proved necessary to extend the method by taking and analyzing gas samples during the induction time. A number of interesting results were obtained during the last two years, which, however, are not included in this report.

Special care in the experiments was taken to obtain completely homogeneous mixtures, by saturating gas streams with the vapor of pure components, and to ascertain that the last phase of compression, passing roughly a range of 50°C below reaction temperature, was sufficiently rapid to prevent reactions under uncontrolled conditions. As a consequence we avoided very short induction times, for which our time resolution was insufficient, the more so since the shock method is available for them. In order to achieve this, it was more important to maintain maximum piston speed up to the end of compression than to use extremely high piston speeds. At the same time this reduces the possibility of compression or shock wave formation.

The method has since been taken up in a number of laboratories (see, e.g., references 6, 13, 15, 16, 17, 18, and 19). Space does not permit a detailed comparison of the methods.

Experimental Results and Discussion

Table 1 gives a selection of so-called ignition temperatures of hydrocarbons and some other

TABLE 1

Ignition Temperatures of Organic Substances

Substance	Ignition temperature (°C)
n-Butane	430
n-Hexane	261
n-Heptane	244
n-Octane	240
n-Decane	231
i-Butane	540
i-Pentane	426
i-Octane	447
Cyclobutane	320
Cyclopentane	390
Cyclohexane	270
Benzene	595
Toluene	569
Methanol	400
Ethanol	425
n-Butanol	340
i-Propanol	400
Acetone	690
Diethylether	180

TABLE 2

Temperatures in the Unburned Mixture in an Engine

Initial temperature before compression, but including heat transfer and admixture of hot gases (°K)		313	333	353	373	393
Final compression temperature (°K) ($\gamma \approx 1.35$)						
Compression ratio						
6	(1)	584	618	656	693	731
8	(2)	648	686	728	769	811
10	(3)	698	742	787	832	879
Final temperature (°K) after compression by flame, if pressure rises by a factor 3 (*a*) or 5 (*b*)						
(1*a*)		784	830	880	930	981
(1*b*)		898	950	1008	1066	1124
(2*a*)		870	921	977	1032	1088
(2*b*)		996	1054	1119	1182	1247
(3*a*)		937	996	1056	1116	1180
(3*b*)		1073	1141	1210	1279	1352

organic compounds. The temperatures were determined in such a way as to represent the lowest temperatures where mixtures of these substances with air can ignite spontaneously. Many of these temperatures are remarkably low. While ignition temperatures are not independent of the method employed and vary with pressure they give, nevertheless the right order. We attempt to report the lowest temperature while avoiding wall influences.

Temperatures which may be reached in the unburned mixture in an Otto engine are listed for varying conditions and assumptions in Table 2. It is seen that these temperatures may be considerably higher than the ignition temperatures. Consequently, with almost any fuel there arises the question: How is a reliable engine combustion possible when the unburned mixture is heated far above its lowest ignition temperature? This suggests a refinement of the concept of ignition temperature. When determining ignition temperatures for questions of safety, one attempts to find the lowest possible values. This implies an extrapolation to "practically infinite" time lags. "Practically infinite" may mean times of the order of 1 to 10 seconds or more. Therefore, the first step must be to compare times available in engine combustion with time lags for ignition. One would expect considerably higher ignition temperatures if ignition is to occur within times of the order $\leq 10^{-2}$ sec, as is borne out by experiments.

If as a measure of reaction we introduce the relative amount of oxidation ξ varying from 0 to 1, then the magnitude of interest is

$$\xi_f = \int_{t_0}^{t_f} \dot{\xi}\, dt, \tag{1}$$

where the integration of the temperature-dependent relative reaction rate $\dot{\xi}$ is to be carried out along the actual path of temperature increase in the unburned mixture of an engine cylinder up to the final temperature T_f, reached at time t_f; $\tau = t_f - t_0$ is the time lag. The time t_f, when the maximum temperature of the unburned mixture is reached, is the same as that at which normal combustion is completed. Thus, conditions in an engine may be seen as a competition between combustion in a flame and spontaneous reaction in the unburned gas. As long as ξ_f is small compared to 1, spontaneous reaction is unimportant. If ξ_f approaches 1, a more detailed investigation must show how far the spontaneous reaction interferes with normal combustion and pressure rise in an engine.

One might consider a further improvement which, however, has not yet been tackled successfully, i.e., the interaction of the flame reaction in an engine and the spontaneous reaction in the unburned mixture. Here further experimental studies are necessary and might prove very valuable.

It will turn out that the reaction exhibits, at least in its first stage, all the characteristics of a

branching chain mechanism. As a consequence, an expression for ξ as in Eq. (1) is not completely determined by the concentration of stable products and the temperature, but depends also on the path by which this state has been reached. Thus, a method suggested by Teichmann deserves consideration: to simulate in kinetic investigations the change of temperature and pressure with time as it occurs in an engine. This type of an experiment resembles investigations with motored engines. It can be achieved, to a certain degree, by observing the reaction in a mixture adiabatically compressed by a moving, nonarrested piston. So far, we have not used this approach, because it is extremely difficult to evaluate experiments of this type kinetically. It seems worthwhile, however, to plan experiments of this type.

To study the reactions occurring in the unburned mixture of an engine under laboratory conditions we applied the method of rapid adiabatic compression (with Teichmann, Rögener, v. Weber, H. Gg. Wagner, Martinengo, Zunft, Hattwig, Karmann). The main features of the equipment in its final form are: compression cylinder of approx. 30 and 50 mm diameter, respectively, and approx. 1 m length; light-weight piston, with specially shaped and mounted Teflon rings, giving perfect fit without any lubricant; arresting of the piston moving at and above 20 m/sec in a distance of the order of 1/10 mm (during a time of the order of 10 μsec) by momentum transfer to a heavy mass, supported by springs of air. Reaction times of the order of 1 to 100 msec are accessible in this way. Shorter reaction times can be investigated if one allows for preliminary reactions during the last phase of compression or tries to correct for them. We extended the experiments to shorter induction times by means of shock tube experiments which agreed with the results of the adiabatic compression experiments.

The compression stroke in an engine, running at 3000 rpm takes 10 msec. Consequently, the time resolution obtained in our experiments is quite sufficient for comparison with engine conditions. The resolution is considerably better than the reaction time of about 1 msec which we consider roughly the limit for experiments undisturbed by reactions during compression.

It is a question of fundamental importance whether or not under conditions of adiabatic compression we may expect a homogeneous reaction. The walls of the compression cylinder and of the reaction chamber are never heated significantly above 100°C. Consequently from the point of view of reaction kinetics, they may be considered as "cool." There is no lubricant present. If the Teflon rings, gliding on steel, should get heated, they are separated from the reaction volume by a very narrow circular gap, preventing direct influence on the reaction.

A typical pressure record, obtained with a stoichiometric *i*-octane–air mixture is shown in Fig. 1. With an initial temperature of 80°C and atmospheric pressure, a compression temperature T_e of 700°K, and a compression pressure of 18.6 atmospheres are obtained. There is a very sharp break in the curve at the end of compression. The record shows a distinct two-stage ignition mechanism. A first induction period of 13.5 msec, counted up to the inflection point, corresponding to a maximum in reaction rate, is followed by a second induction time, with reaction rate dropping again to almost zero, and final ignition after a second induction time of 8.5

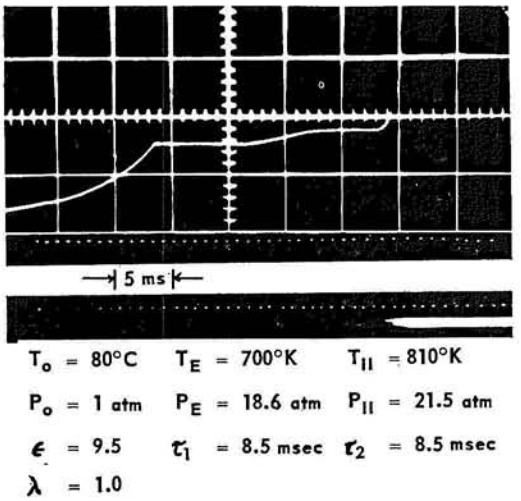

FIG. 1. Pressure record of stoichiometric *i*-octane–air mixture.

msec, corresponding to a total induction time of 22 msec.

In the second stage a pressure of 21.5 atmospheres and a temperature of 810°K are reached. The flame record, obtained with a rotating drum camera, is shown underneath the pressure record. This shows that ignition occurs within about 1 msec, but not quite homogeneously. Thus, a reaction rate derived from the pressure rise during the last phase gives only a lower bound to the actual value because flame propagation is included in the process. Flame propagation over a distance of 2.5 cm (half of the tube diameter) within 1 msec would correspond to a flame velocity of the order of 25 msec^{-1}, which is much higher than the flame velocity in a mixture at rest. With ignition lags of the order of 1 msec, flame velocities derived from pressure records are roughly 20 times higher. The most probable

explanation is that inhomogeneities due to boundary layer effects (perhaps of an indirect nature) cause local differences in reactivity. It should be emphasized that this experiment is not typical for engine conditions, the total induction time of 22 sec being much too long. For a total induction time of 1 msec 10 to 20 times the above flame speed would be obtained!

Ignition of Hydrogen–Oxygen Mixtures

We investigated the reaction of hydrogen and air or oxygen in the same apparatus. Owing to the lack of lubricants and the absence of other disturbances it was possible to measure reaction rates at and above the third explosion limit of hydrogen–air. A typical record of one-stage ignition is shown in Fig. 2. At a compression temperature of 960°K and a compression pressure of 3 atm ignition occurs within 1 msec. The rate of pressure rise at the end of the induction time is extremely fast. If these induction times, observed for varying temperatures and pressures, are extrapolated to (practically) infinite induction time, values for the third explosion limit are obtained (Fig. 3). Agreement between our values (for hydrogen + air) and those obtained from static reaction in a glass vessel (for $2H_2 + O_2$) is adequate, though not complete. If inhomogeneities, especially hot points in the compression apparatus, were responsible for the discrepancy, then the values obtained from adiabatic experiments should probably be lower than those from

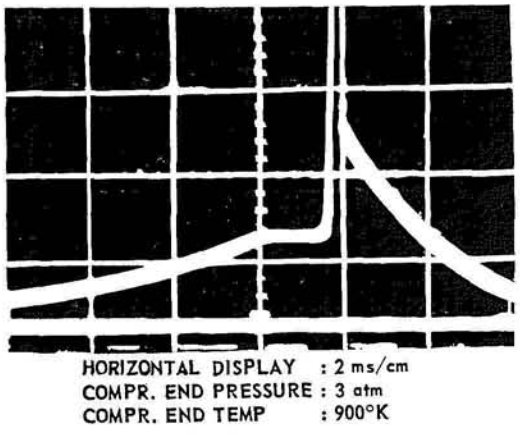

FIG. 2. Pressure record of hydrogen–air mixture.

static experiments. However, if there is a real difference, the contrary should be expected. Observed induction times are compatible with a bimolecular initiating reaction between H_2 and O_2, of the type

$$H_2 + O_2 \rightarrow 2OH$$

with an energy of activation between 60 and 65 kcal per mole, or some analogous bimolecular reaction followed by the usual branching chain

$$OH + H_2 \rightarrow H_2O + H$$

$$H + O_2 \rightarrow OH + O$$

$$O + H_2 \rightarrow OH + H, \text{ etc.,}$$

though the above reactions alone are insufficient to describe all details.

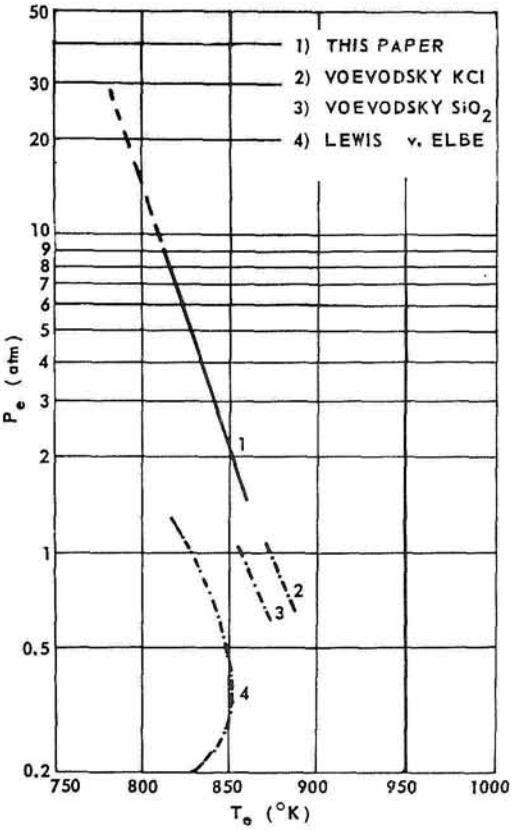

FIG. 3. Third explosion limit of hydrogen–air mixtures, derived from measurements by adiabatic compression (reference 1) compared with results from the literature (references 2, 3, and 4).

While not sufficient to prove the above mechanism, it shows that sufficiently fast reaction is possible without considering wall effects or impurities. Indeed, though a participation of impurities in chain initiation cannot be excluded definitely, it is difficult to conceive of an impurity present in sufficient concentration and a reaction of this impurity with sufficiently low energy of activation to cause initiation. These observations and considerations make it very improbable that in hydrocarbon oxidation under the conditions of adiabatic compression impuri-

ties or hot points play any role of importance, though inhomogeneities due to a boundary layer can never be totally excluded and may affect particularly the last stages of ignition.

Ignition of Hydrocarbon–Oxygen Mixtures

This section is a survey of results obtained with the two adiabatic compression machines which are at present in working condition.

In Figs. 4 to 7 we present records of four experiments with n-heptane and two with i-octane. In addition to the direct pressure record temperatures are plotted and time lags for the first (τ_1) and second (τ_2) reaction stage are given. The stoichiometric number λ is the ratio of the actual hydrocarbon concentration to that of the stoichiometric mixture ($\lambda < 1$ means lean, $\lambda > 1$ rich mixtures).

In Figs. 8 to 10 we give for comparison results for hydrogen–air mixtures.

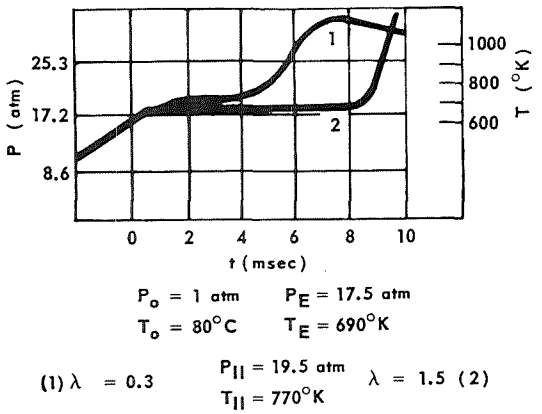

FIG. 4. Pressure records for two n-heptane–air mixtures. (λ = 0.3; 1.5)

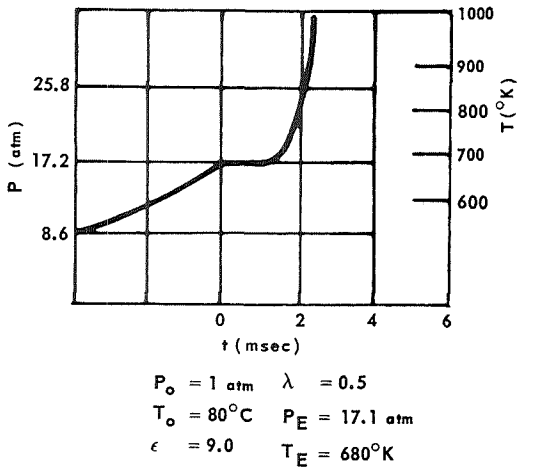

FIG. 5. Pressure record for n-heptane–air. (λ = 0.5)

Figures 11 to 14 give induction times τ_1, and τ_2, and $\tau = \tau_1 + \tau_2$, as defined above, for n-heptane, for other n-paraffins, and for i-octane.

Figures 15 to 17 give temperatures T_{II} of the second stage as a function of the original composition, for n-hexane and n-decane, induction times as function of T_{II}, and log τ_2 versus $1/T_{II}$.

Figures 18 to 21 give details of plots for θ_1, θ_2, and θ_r, as defined in Fig. 22.

Figure 23 gives the final rate of rise of pressure for several hydrocarbons and varied conditions. It is this magnitude which, in addition to the time lag, is of primary importance for fuel behavior in an engine. The maximum rate of pres-

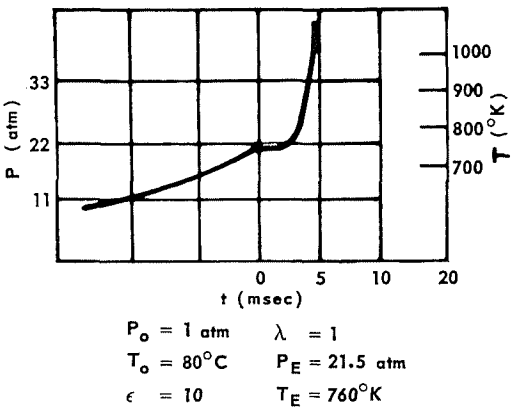

FIG. 6. Pressure record for n-heptane–air. (λ = 1.0)

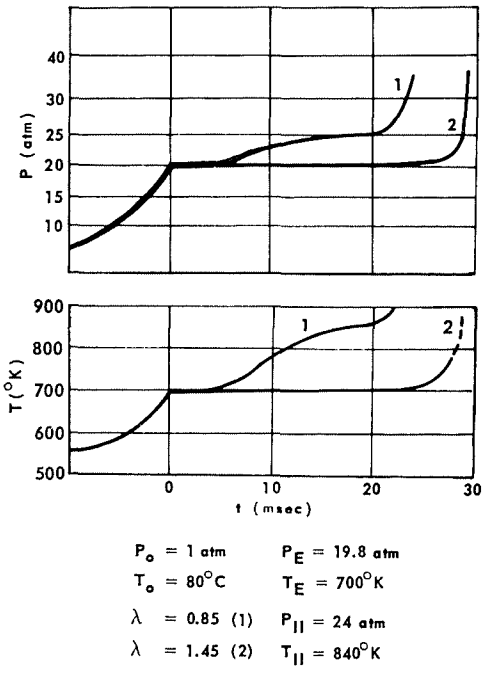

FIG. 7. Two records for i-octane–air. Top: pressure; bottom: temperature; both versus time.

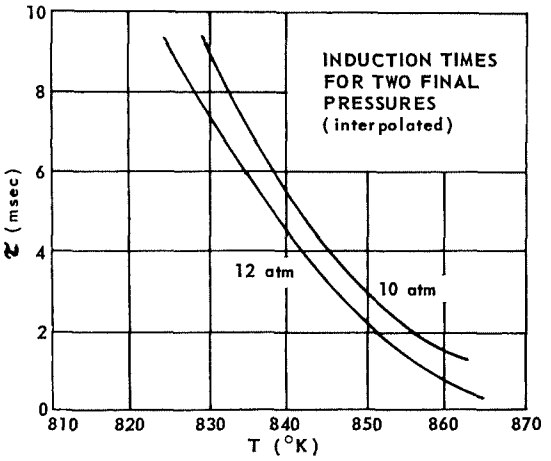

FIG. 8. Induction times for stoichiometric hydrogen–air mixtures. Parameter, pressure.

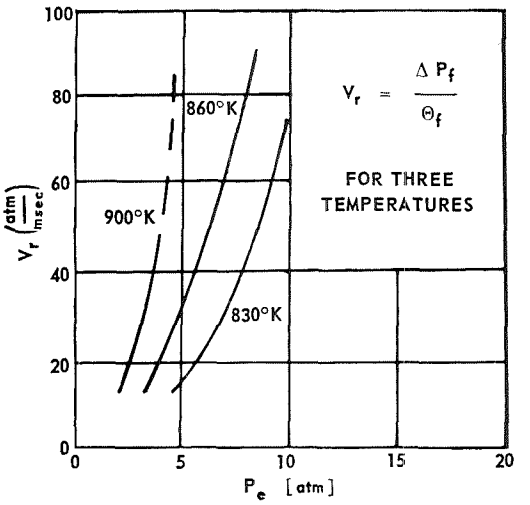

FIG. 10. Final rate of pressure rise, for hydrogen–air mixtures in atm/msec.

sure rise is of the order 10^3 to $>10^5$ atm/sec. This should be compared with the rate of pressure drop due to the propagation of rarefaction waves.

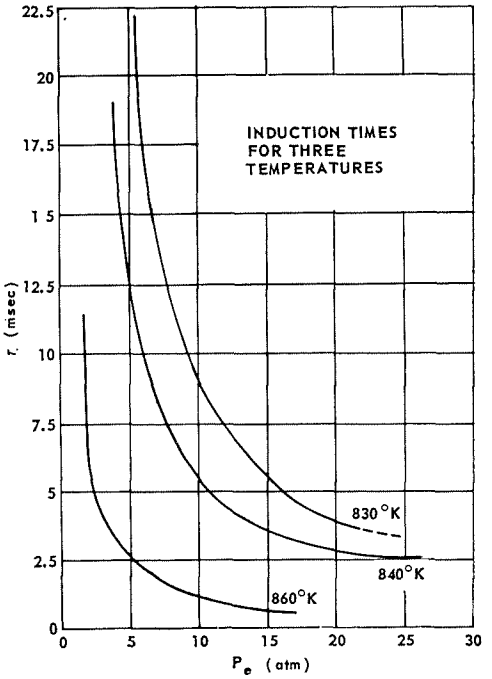

FIG. 9. Hydrogen–air mixtures. Parameter, temperature.

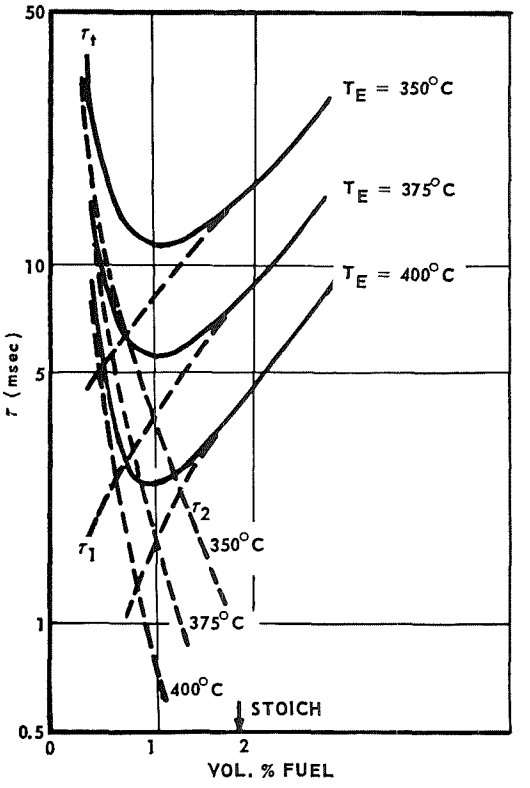

FIG. 11. Induction times for *n*-heptane–air mixtures.

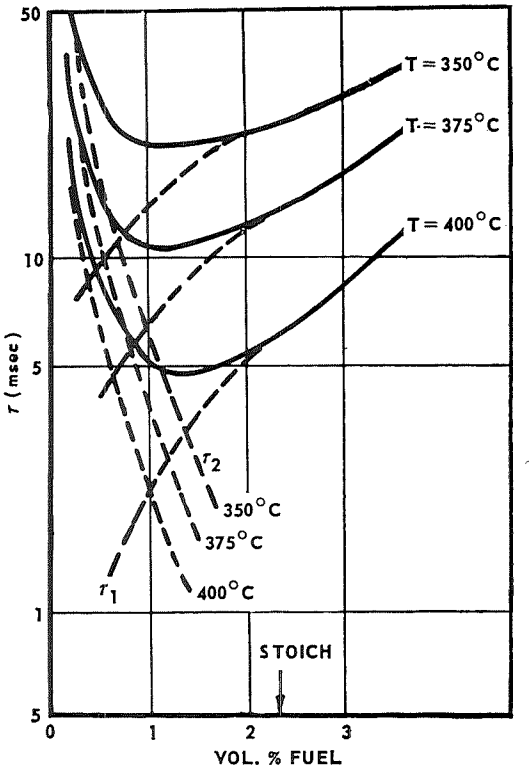

FIG. 12. Induction times for *n*-hexane–air.

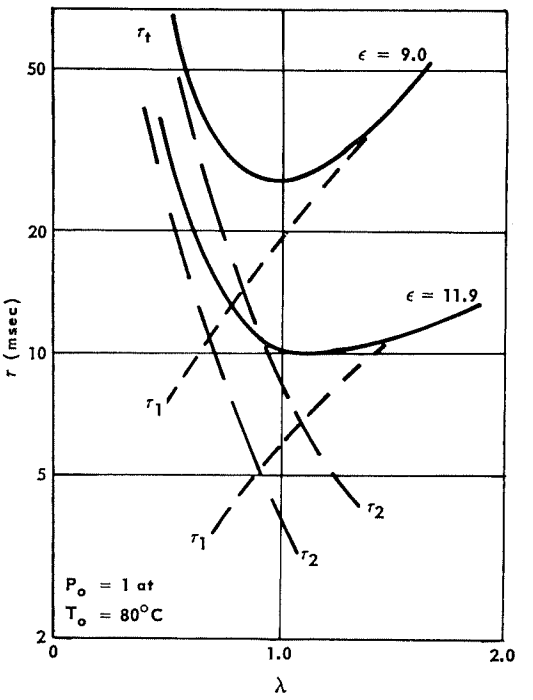

FIG. 14. Induction times for *i*-octane.

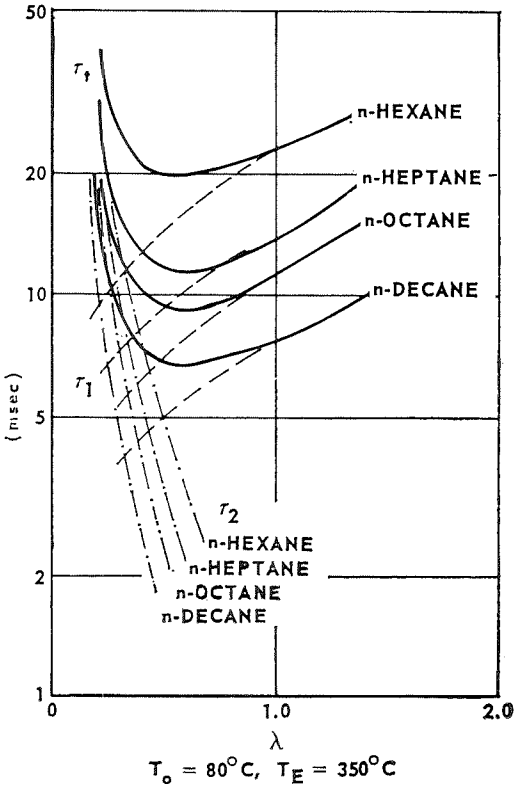

FIG. 13. Induction times for *n*-paraffins.

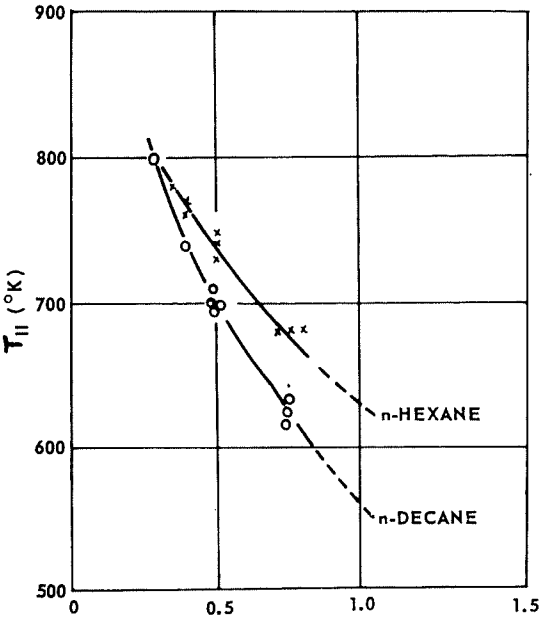

FIG. 15. Temperature T_{II} of second stage, for *n*-hexane and *n*-decane, as a function of mixture ratio.

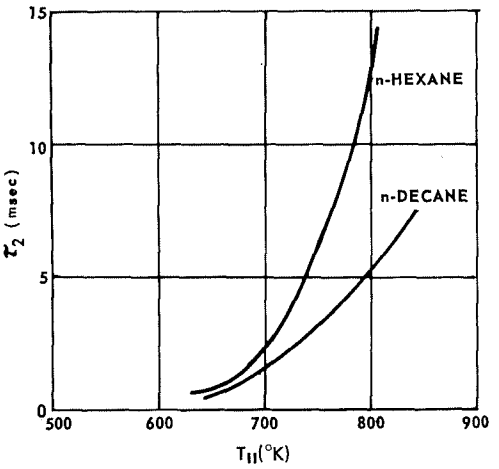

FIG. 16. Second induction time as function of T_{II}.

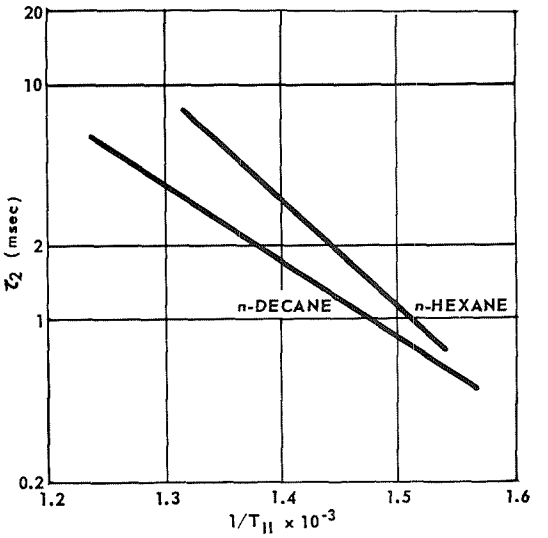

FIG. 17. Log τ_2 plotted versus $1/T_{II}$.

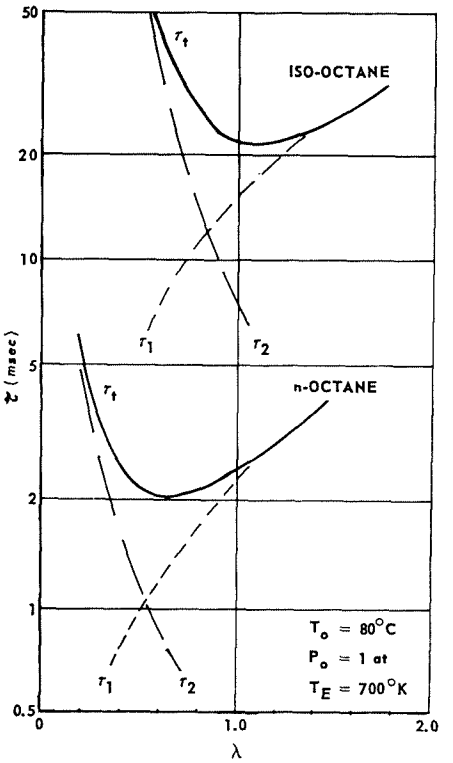

FIG. 18. Induction times for *i*-octane and *n*-octane.

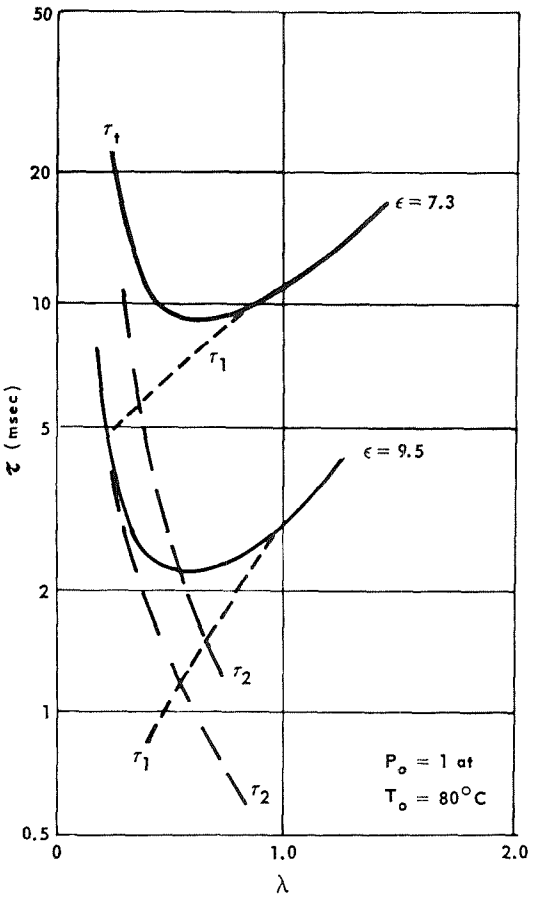

FIG. 19. Induction times for *n*-octane.

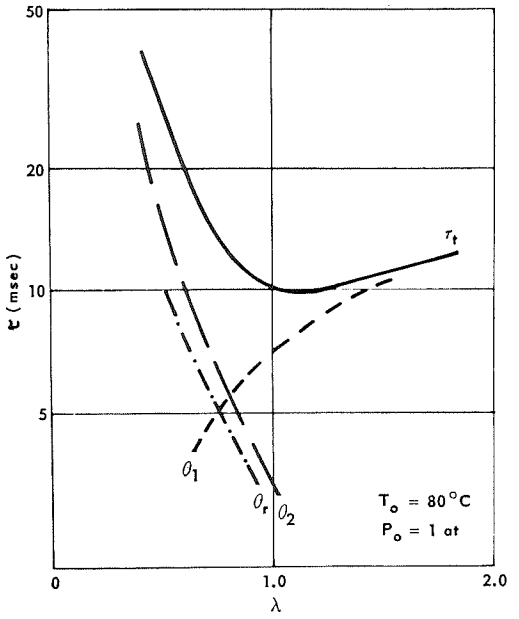

FIG. 20. Induction reaction times θ_1, θ_2, θ_r as defined by Fig. 22 for *i*-octane.

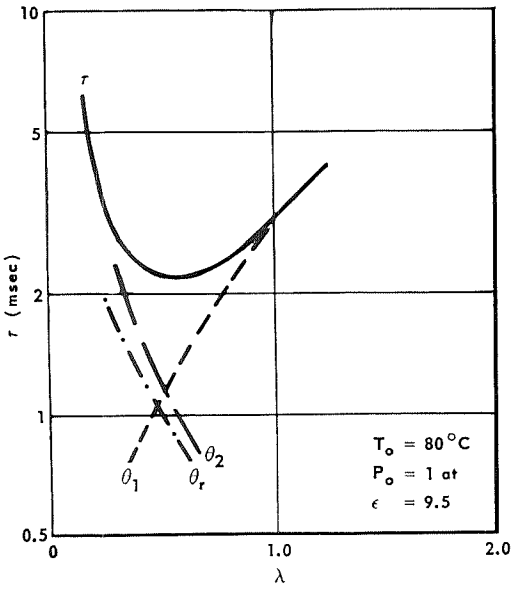

FIG. 21. Induction and reaction times θ_1, θ_2, θ_r for *n*-octane.

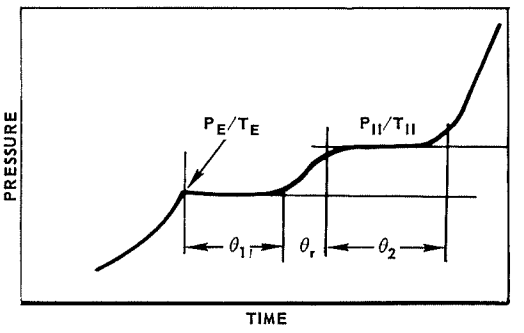

FIG. 22. Definition of induction times θ_1, θ_2, reaction time θ_r.

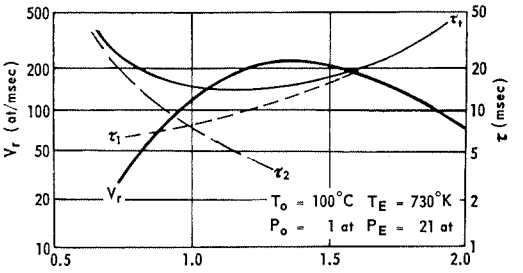

FIG. 23. Final rate of pressure rise, V_r, and induction times, τ_1, τ_2, and $\tau_t = \tau_1 + \tau_2$, for *i*-octane.

Nomenclature

τ_1	From end of compression to inflection point
τ_2	From inflection point to final pressure rise

Subscripts

0	Initial state
E	State at end of compression
II	State during second induction time

REFERENCES

1. FALK, K. G.: Ann. Physik *24*, 450 (1907).
2. FALK, K. G : J. Am. Chem. Soc. *29*, 1536 (1907).
3. DIXON, H. B., BRADSHAW, B., CAMPBELL, J.: J. Chem. Soc. *105*, 85 (1914).
4. TIZARD, H. T. and PYE, D. R.: Phil. Mag. *44*, 79 (1922).
5. JOST, W., MUFFLING, L. V.: Z. Elektrochem. *45*, 93 (1939).
6. WEBER, U. V.: Naturwiss. *27*, 164 (1939).
7. JOST, W.: Schrift. Deutsch. Akadem. Luftfahrtforsch. *9*, 133 (1939).
8. JOST, W. and TEICHMANN, H.: Naturwissenschaften *27*, 318 (1939).
9. TEICHMANN, H.: Z. Elektrochem. *47*, 297 (1941).

10. JOST, W. and RÖGENER, H.: Z Elektrochem. *47*, 307 (1941)
11. RÖGENER, H.: Z Elektrochem. *53*, 389 (1949).
12. JOST, W.: *Third Symposium (International) on Combustion*, p. 424. Williams and Wilkins, 1949.
13. LEARY, W. A., TAYLOR, E. S., and TAYLOR, C. F.: NACA-Rep. 1470 (1948).
14. JOST, W.: Forsch. Ing. Wes. *2*, 19 (1952).
15. LIVENGOOD, J. C. and LEARY, W. A.: Ind. Eng. Chem. *40*, 2797 (1954).
16. LEVEDAHL, W. J.: *Fifth Symposium (International) on Combustion*, p. 372. Reinhold, 1955.
17. LIVENGOOD, J. C. and WU, P. C.: *Fifth Symposium (International) on Combustion*, p. 347. Reinhold, 1955.
18. SCHMIDT, F. A. F.: Forsch. Ber. d. Landes Nordrh.-Westf. 1955.
19. LEVEDAHL, W. J. and HOWARD, F. L.: Ind. Eng. Chem. *43*, 2805 (1957).
20. KAESCHE-KRISCHER, B. and WAGNER, H. Gg.: Brennst.-Chem. *39*, 33 (1958).
21. BECKERS, A.: Diss. TH Aachen, 1958.
22. KRÖGER, C. and GONDERMANN, H.: Brennst.-Chem. *17/18*, 85 (1958).
23. MARTINENGO, A., WAGNER, H. Gg., and ZUNFT, D.: Z. physik. Chem. *22*, 292 (1959).
24. VOEVODSKY, V. V.: *Seventh Symposium (International) on Combustion*, p. 34. Butterworths, 1959.
25. MARTINENGO, A. and WAGNER, H. Gg.: Arbeitsschutz *11*, 254 (1959).
26. MARTINENGO, A. and WAGNER, H. Gg.: Forsch. Ing. Wes. *20*, 198 (1960).
27. HATTWIG, M.: Diplomarbeit, Göttingen 1962.
28. NABERT, K. and SCHÖN, G.: Sicherheitstechnische Kennzahlen brennbarer Gase und Dämpfe, Berlin 1953.

Discussion

DR. A. MARTINENGO (*Göttingen University*): When there is a "two-stage ignition" of adiabatically compressed hydrocarbon–air mixtures, one would like to know, how much fuel is consumed in the pre-reaction phase of combustion and what sort of reaction products have been built up during the induction periods τ_1 and τ_2.

Preliminary experiments show that the hydrocarbon concentration decreases from an initial 100% during the first induction period to 70% in the second induction period. Simultaneously there is a steady increase of CO (30% at the end of τ_2) while the concentrations of ethylene and aldehydes pass through maxima at the beginning of τ_2.

ORGANOLEAD ANTIKNOCK AGENTS—THEIR PERFORMANCE AND MODE OF ACTION

W. L. RICHARDSON, P. R. RYASON, G. J. KAUTSKY, AND M. R. BARUSCH

The effectiveness of various lead alkyls containing one or more methyl groups is compared. The response of many of these additives to lead extenders (agents which generate carboxylic acids in the combustion chamber) is described. A useful theory which explains the antiknock behavior of antidetonants and correlates their response to extenders is discussed.

Introduction

The initial commercial use of tetramethyl lead (TML) as an antiknock agent for gasoline occurred in the United States in early 1960. Since its introduction, the use of TML has spread; and it is now an ingredient of gasolines in more than 20 countries. The use of various mixtures of TML, tetraethyl lead (TEL), and the three mixed methyl ethyl lead alkyls followed the commercial introduction of TML. The application of mixtures of lead alkyls also appears to be spreading throughout the world.

The paper by Richardson *et al.*[1] compared the performance of TML with TEL in a variety of gasolines. TML was shown to be markedly superior to TEL in modern premium grade gasolines containing more than about 20% of aromatic hydrocarbons. The principal benefit obtained with TML was a gain of 1 to 2 Road octane numbers. A somewhat smaller increase in Motor method octane number was achieved when the TEL was replaced with TML. The two additives were shown to be about equivalent as octane number improvers as determined by the Research method.

Effectiveness of Methyl Ethyl Lead Alkyls

The increase in octane number obtained by replacing TEL with dimethyl diethyl lead, with trimethyl ethyl lead, and with TML in 11 experimental gasolines is summarized in Table 1. The gasolines employed were selected to represent the extremes of composition which would result from varying refining techniques. The compositions and some physical properties of all gasolines used in the work reported herein are summarized in Table 2. They are listed in order of increasing aromatic content. Nine of the gasolines are identical to the fuels used in the previous work.[1] When the data for TML in Table 1 are compared with the octane improvements reported in the previous paper, it is seen that the values do not precisely agree. The current comparisons of the dimethyl diethyl lead, trimethyl ethyl lead, TML, and TEL were obtained from a series of comparative measurements conducted at a different time from the data previously published. The small differences in reported values are due to the usual error of measuring octane numbers.

By the Research method, dimethyl diethyl lead shows little difference as an octane improver from TEL. In only one of the gasolines tested did it perform significantly differently from TEL; and when all the values for all the fuels were averaged together, its performance showed no difference from that of TEL. Both trimethyl ethyl lead and TML generally are somewhat more effective than TEL in Research ratings when employed in the highly aromatic gasolines used in this study. For all of the compounds, the differences are more marked when the octane number is determined by the Motor method. Of the three additives, TML has the greatest advantage over TEL as a Motor octane number improver. The substitution of TML for TEL produces a range of octane improvement of from 0.5 to 1.3 octane number, with an average Motor improvement in the 11 fuels of 0.95. Trimethyl ethyl lead approached TML in effectiveness as measured by the Motor method, with an average of 0.85 octane number improvement over TEL. The response to dimethyl diethyl lead was only slightly superior to that of TEL, with an average Motor octane number improvement of 0.15 octane number. Methyl triethyl lead was not included in this comparative study, as preliminary tests in a number of gasolines showed it to have no significant advantage over TEL.

Comparative Road octane data were obtained

TABLE 1

Antiknock Activity of Alkyl Lead Compounds

	Octane increase (alkyl lead compound minus TEL)[a]							
	Research method[b]			Motor method[b]			Road method[c]	
Fuel	DMDEL	TMEL	TML	DMDEL	TMEL	TML	TMEL	TML
1	0.7	0.8	−0.1	0.6	1.2	0.5	—	—
2	−0.2	0.4	0.5	0.1	0.5	1.2	—	—
3	—	0.2	0.3	0.1	0.8	1.1	1.0	1.0
4	−0.2	0.2	−0.1	−0.3	1.2	0.8	1.1[d]	1.1[d]
5	0.3	0.7	0.1	0.8	0.5	0.8	—	—
6	−0.1	0.3	0.3	0.4	1.0	0.8	—	—
8	0.0	0.1	0.1	−0.2	0.6	1.1	—	—
9	−0.4	0.0	0.1	0.0	0.7	0.8	—	—
10	—	0.4	0.0	−0.1	0.7	1.0	—	—
11	−0.2	0.7	0.6	−0.2	0.7	1.1	2.3	2.4
12	—	1.0	0.5	0.5	1.4	1.3	—	—
Average	0.00	0.44	0.21	0.15	0.85	0.95		

[a] 3.17 grams lead per gallon.

[b] Comparison of averages of quadruplicate determinations; 90% confidence interval is ±0.4 for Research method, ±0.5 for Motor method.

[c] Comparison of triplicate determinations (Modified Uniontown Procedure) in six cars; 90% confidence interval is ±0.2.

[d] Three cars only.

TABLE 2

Description of Test Gasolines

	Octane rating with TEL[a]		Hydrocarbon composition, volume %			Distillation[b] (°F at % evaporated)		
Fuel No.	Research	Motor	Aromatics	Olefins	Paraffins and naphthenes	10%	50%	90%
1	105.0	100.1	24	0	76	125	212	310
2	98.8	86.6	26	30	44	127	193	311
3	99.4	88.1	33	25	42	129	240	339
4	99.5	88.3	33	20	47	127	210	327
5	100.6	90.7	36	11	53	117	204	323
6	100.5	88.2	37	25	38	124	215	324
7	99.2	89.5	42	7	51	124	213	343
8	101.0	87.4	42	29	29	139	236	315
9	99.0	87.8	43	16	41	123	240	372
10	105.3	97.0	45	1	54	123	227	297
11	104.7	95.2	46	0	54	118	226	332
12	98.6	88.8	62	1	37			

[a] 3.17 grams lead per gallon. Octane data are averages of at least four determinations.

[b] ASTM Procedure D 86.

with trimethyl ethyl lead, TML, and TEL in only three of the gasolines. Previous data obtained in other fuels with dimethyl diethyl lead showed it to have no significant advantage over TEL in Road ratings, and it was not evaluated by the Road procedure in any of the fuels described in Table 2. TML and trimethyl ethyl lead show their greatest advantage over TEL in Road ratings. Extensive evaluation of these additives in other fuels supports this conclusion. In Road ratings, TML and trimethyl ethyl lead appear about equivalent. Octane increases over TEL varied from 1 to 2.4 road octane numbers. The Road values were obtained employing the same test fleet that was described in the previous paper.[1] All test automobiles were equipped with automatic transmissions. The evaluations were performed on a chassis dynamometer.

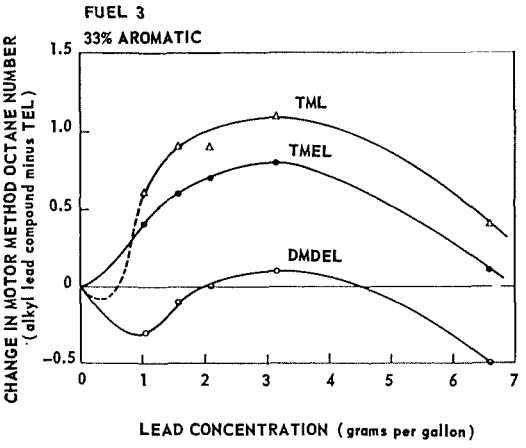

FIG. 1. Influence of lead concentration on antiknock effect.

Influence of Lead Concentration on the Relative Effect of Lead Alkyls

The molar concentrations of these lead alkyls have a pronounced influence on their effectiveness relative to TEL. Figure 1 presents a plot of the change in octane number obtained by substituting TML, trimethyl ethyl lead, and dimethyl diethyl lead for TEL as a function of lead concentration. The dotted portion of the curve for TML is drawn showing TML to be less effective than TEL at low concentrations. This effect was not observed in this fuel, as low concentrations of lead were not evaluated. A considerable amount of data in other fuels of similar composition supports the view that the curve for low concentrations of TML would be as shown. However, at concentrations of 1 gram of lead per gallon or higher, TML and trimethyl ethyl lead consistently are more effective than TEL in highly aromatic gasolines. Figure 2 shows a similar plot for a gasoline containing 62% aromatics. Between concentrations of 1 and 3 grams of lead per gallon, both dimethyl diethyl lead and trimethyl ethyl lead exhibited a constant

TABLE 3

Trimethyl Alkyl Lead Compounds Compared to TEL[a]

	Octane increase[b]					
	Test fuel 3		Test fuel 9		Test fuel 11	
	Research	Motor	Research	Motor	Research	Motor
Alkyl group						
Methyl	0.3	1.1	0.1	0.8	0.6	1.1
Ethyl	0.2	0.8	0.0	0.7	0.7	0.7
n-Propyl	−0.1	0.2	0.4	0.4	0.9	1.1
n-Butyl	0.0	0.5	0.1	0.9	0.9	0.8
n-Amyl	0.4	0.5	—	—	0.4	0.6
Vinyl	−0.2	1.0	—	—	—	—
Phenyl	0.0	1.4	—	—	0.9	1.1
Isopropyl	−0.6	0.0	−0.9	−0.1	0.2	0.6
t-Butyl	—	—	−1.5	−1.4	—	—
Allyl	−0.6	−0.5	—	—	—	—

[a] 3.17 grams lead per gallon.

[b] Comparison of averages of quadruplicate determinations.

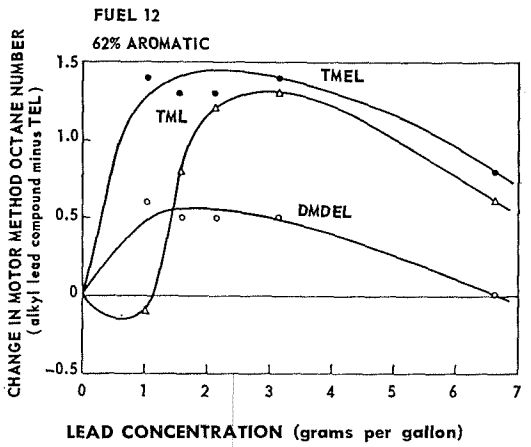

FIG. 2. Effect of lead concentration on highly aromatic fuel.

advantage in motor octane number compared to TEL. The response to TML was quite different in that small concentrations were less effective than TEL; whereas, at concentrations above about 1 gram of lead per gallon, TML was highly effective.

Evaluation of Various Trimethyl Lead Compounds

The exploratory evaluation of numerous organolead compounds of widely varying structures showed that most organolead compounds tested which contained three methyl groups were more effective than TEL in highly aromatic gasolines. This is illustrated by the data of Table 3. Here, it is seen that the replacement of one of the methyl groups of TML with the ethyl, *n*-propyl, *n*-butyl, *n*-amyl, vinyl, or phenyl group results in an antiknock agent having similar characteristics to TML. All of these lead alkyls were superior antiknock agents to TEL when added to aromatic gasolines, as evaluated by the Motor method. The replacement of one of the methyl substituents of TML with the isopropyl, *t*-butyl, or allyl group decreases the antiknock effectiveness.

Stability of Lead Alkyls

Although there is no general agreement and little evidence concerning the exact mechanism by which lead alkyls function as antiknock agents, most workers agree that the lead alkyls must first decompose before they can assert their knock-suppressing effect. In the earlier paper,[1] it was postulated that TML is a more effective antiknock agent than TEL in highly aromatic gasolines because it is more thermally stable and decomposes later in the engine cycle. An antiknock agent which decomposes too early forms relatively nonvolatile decomposition products which agglomerate with a corresponding loss in antiknock activity.

There are surprisingly few data in the literature on the kinetics of the decomposition of lead alkyls. The early work by Eltenton[2] and by Leermakers[3] actually indicates TEL to be more thermally stable than TML. However, these data were obtained under conditions of heterogeneous decomposition. Therefore, their significance in this context is open to question. The time scale in the gasoline engine is too short for wall reactions to be of major importance to the combustion process. More significant rates of decomposition were measured by Rifkin and Walcutt in a motored engine.[4] Still more recently, Rifkin[5] reported on the kinetics of decomposition of several other lead alkyls, including TML. These measurements also were conducted using a motored engine. They established that TML decomposes more slowly than does TEL over the entire temperature range investigated.

The thermal stabilities of all five of the methyl ethyl lead alkyls have now been measured under comparable conditions. In this work, a single pulse shock tube of the type first described by Hertzberg[6] was used. The thermal stabilities were determined in the temperature range 731–931°K. It is beyond the scope of this paper to present a detailed description of the experimental

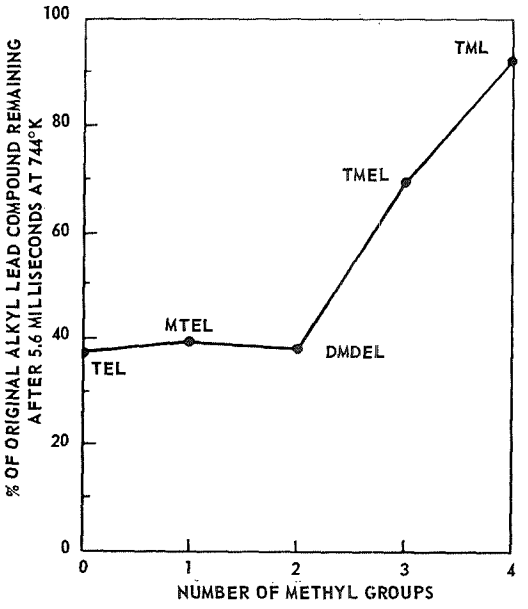

FIG. 3. Thermal stability of alkyl lead compounds.

techniques, the data, and their analysis. A separate publication discussing this work is in preparation.[7] The thermal stabilities of the lead alkyls that were obtained from the shock tube measurements parallel the performance of the lead alkyls as antiknock agents for aromatic gasolines. In Fig. 3, the decomposition of the various methyl ethyl lead alkyls is plotted as a function of the number of methyl groups in the molecule. The data shown represent the average results of the several determinations conducted at 744°K for 5.6 milliseconds. This condition was selected both because it is probably representative of a significant engine condition and because we have data for all five lead alkyls at this condition. More extensive data will be described in the forthcoming paper.

It was found that the TML was quite stable at this condition with less than 10% decomposed. About 30% of the trimethyl ethyl lead was destroyed. The stabilities of the tetraethyl lead, methyl triethyl lead, and dimethyl diethyl lead were shown to be nearly identical. These lead alkyls were nearly 60% decomposed under the conditions of the test.

In Fig. 4, the increase in Motor octane number obtained by substituting the methyl ethyl alkyls for TEL in aromatic gasolines is plotted against the number of methyl groups in the molecule. The octane number data used are the average Motor octane increases obtained in 11 of the gasolines listed in Table 2. It is clear that the relative effectiveness of the alkyls as antiknock agents parallels their thermal stabilities. Thus,

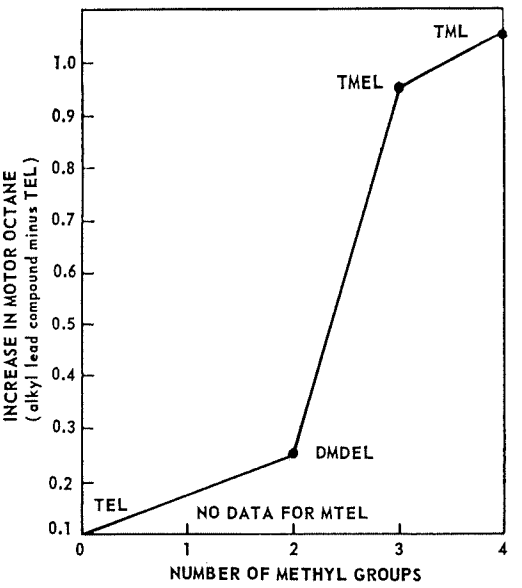

FIG. 4. Effect of structure on antiknock activity.

the findings are consistent with the previous postulate that tetramethyl lead is more effective than tetraethyl lead in aromatic fuels because of its increased thermal stability. Trimethyl ethyl lead approaches TML both in stability and in effectiveness as an antiknock additive. When fewer than three methyl groups are present in the molecule, the stabilities of the lead alkyls are nearly identical and their activities as octane improvers are similar.

TABLE 4

Antiknock Effect of *t*-Butyl Acetate with TEL and TML

Fuel	Octane increase[a]					
	Research method[b]		Motor method[b]		Road method[c]	
	TEL	TML	TEL	TML	TEL	TML
3	1.0	0.3	1.1	0.3	0.3	0.3
4	1.0	0.0	1.3	0.3	0.6	0.4
5	1.2	0.1	1.2	0.1	0.2	0.1
6	1.3	0.2	1.2	0.5	0.7	0.4
8	0.9	0.2	1.3	0.5	0.6	0.5
Five-fuel average	1.1	0.2	1.2	0.3	0.5	0.3

[a] Gasolines containing 3.17 grams of lead plus 1.0 weight per cent *t*-butyl acetate are compared to gasolines without *t*-butyl acetate.

[b] Comparison of averages of quadruplicate determinations.

[c] Comparison of averages of triplicate determinations in five automobiles.

Response of Lead Alkyls to Extenders

The addition of carboxylic acids, or compounds which will produce carboxylic acids in the combustion chamber of an engine, to aromatic leaded gasolines causes an increase in the octane rating of such fuels. This effect was reported independently by groups of researchers at the Texaco Laboratories[8] and the California Research Corporation.[9] The Texaco workers termed these compounds "lead appreciators"; whereas, the California Research group gave them the name "lead extenders."

As the concentration of extender in a leaded gasoline is increased, the octane number of the gasoline will increase to a maximum and then decline. Thus, for each gasoline there is an optimum quantity of extender which may be added for maximum effect. This optimum amount is dependent upon the quantity of TEL present in the gasoline. Increases in Research octane number of as much as 4 numbers were observed when extenders were added to a gasoline containing 6 ml of TEL per gallon. Gasolines containing TML do not respond as well to extenders as do the same gasolines containing TEL. This is shown by the data of Table 4. The effectiveness of *t*-butyl acetate as an extender for TEL and TML is compared in five fuels containing equal molar amounts of TEL and TML. It can be seen that with every fuel the Research method, the Motor method, and the Road rating all measured a smaller increase in octane number when the acetate was used in conjunction with TML than with TEL.

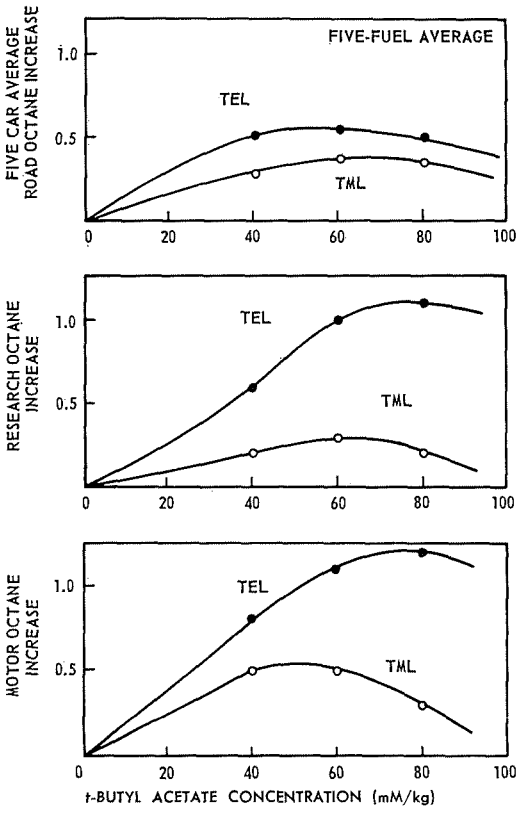

FIG. 5. Antiknock effect *t*-butyl acetate with TEL and TML (3.17 grams of lead per gallon).

Figure 5 compares the average increase in octane number obtained when various concentrations of *t*-butyl acetate were added to five gasolines containing 3 ml of TEL per gallon with the corresponding increase obtained with the molar equivalent of TML. It is seen that *t*-butyl acetate is somewhat less effective in enhancing the road octane number of gasolines containing TML than it is in the comparable gasoline containing TEL. This is true at all concentrations of the ester. The extender, *t*-butyl acetate, is also less effective in gasolines containing TML compared to the same fuels containing TEL, as evaluated in laboratory engines. These findings are considered to be consistent with the theory of the mechanism by which lead extenders function, which was previously presented.[9] It was there postulated that extenders interfere with the agglomeration of the active antiknock species, probably lead oxide. By interfering with the agglomeration, the extenders prolong the life of the antiknock species until a critical time in the engine cycle. This action is equivalent to increasing the concentration of the antiknock species at the time that it is needed. A possible reaction sequence whereby carboxylic acids could preserve the degree of dispersion of lead oxide particles was suggested. This was the reaction of the carboxylic acid with the lead oxide to form lead acetate and the subsequent decomposition of the lead acetate to regenerate the lead oxide. This hypothesis is, as yet, unproved. Alternatively, the extender may create a different antiknock species from the one normally present. The important postulate is that the extender somehow maintains the active antiknock species in a high degree of dispersion in the "end-gas."

There are similarities between the behavior of carboxylic acids as lead extenders and the effect obtained by substituting TML for TEL. Both methods of obtaining higher octane numbers only function in highly aromatic high-octane gasolines. The effectiveness of either method increases with aromatic content of the fuel and with increasing octane number. Thus, it appears that the substitution of TML for TEL delays the decomposition of the lead alkyl, giving a comparable effect to the antiknock improvement achieved by the extender, which preserves the

TABLE 5

Antiknock Effect and Extender Response of Alkyl Lead Compounds

Compound	Acetic acid concentration (mM/kg)	Octane increase due to lead[a]	Increase due to acetic acid	Total octane increase
Hexa-*p*-xylyl dilead	None	0.7	0	0.7
Hexamethyl dilead	80	2.9	1.8	4.7
Tetramethyl lead	80	3.7	1.6	5.3
Tetravinyl lead	80	3.6	2.0	5.6
Tetraethyl lead	80	3.6	2.5	6.1
Tetrapropyl lead	80	3.4	2.4	5.8
Dimethyldiethyl lead	80	3.6	1.8	5.4
Diethyldiisopropyl lead	100	1.6	3.7	5.3
Tetraisopropyl lead	100	1.9	3.0	4.9

[a] Research method, Fuel 9, 3.17 grams lead per gallon.

state of dispersion of the active antiknock species. Because TML decomposes later in the cycle than does TEL, the effect of the extender is less. This theory leads to the prediction that if the octane number of the gasoline is raised and the conditions of engine severity are increased eventually extenders should become more effective in gasolines containing TML.

The response of a number of other organolead antiknock agents to acetic acid has been measured. The resultant data are summarized in Table 5. The antiknock effects of nine different organolead compounds were measured in a single gasoline. Varying concentrations of acetic acid were added to the gasoline. Results of the increased antiknock effect obtained by adding the lead extender are reported for the optimum concentration of the acetic acid. These data are presented as a bar chart in Fig. 6. Unique in performance of these lead compounds is hexa-*p*-xylyl dilead. It caused an octane increase of only 0.7 number when present at 3.17 grams lead per gallon. Unlike any of the other compounds tested, its antiknock effect was not enhanced by the addition of acetic acid. This behavior can be explained by assuming the hexa-*p*-xylyl dilead has too great a thermal stability. If this additive shed all its aryl groups very late in the combustion cycle, it would not be a highly effective octane improver because the active antiknock species would not be available early enough for maximum effectiveness. It would not respond to a lead extender because the effect of agglomeration of the active antiknock species would not be important. It is planned to measure the stability of this additive in the future.

The hexamethyl dilead at the same molal concentration (3.17 grams lead per gallon) increases the research octane number by 2.9. Tetramethyl, tetravinyl, tetraethyl, tetrapropyl, and dimethyl diethyl lead are nearly identical in their effectiveness in increasing Research octane number. Gasolines containing these additives all exhibit a similar response to the acetic acid extender. Diethyl diisopropyl and tetraisopropyl lead are only about one-half as effective as these compounds for raising the research octane number. It is believed that the isopropyl group is relatively weakly bound to the lead, causing the lead alkyl to decompose so early in the cycle that agglomeration proceeds to the point that

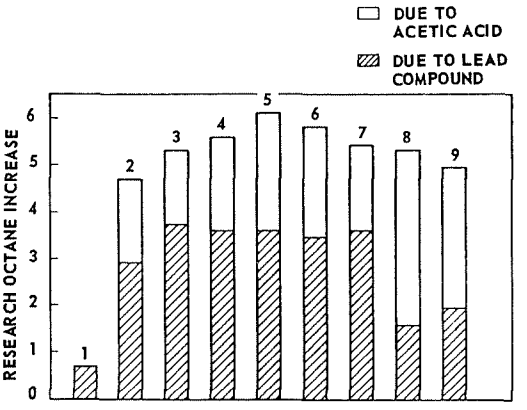

FIG. 6. Antiknock effect of lead compounds and acetic acid. 1. Hexa-*p*-xylyl dilead; 2. Hexamethyl dilead; 3. Tetramethyl lead; 4. Tetravinyl lead; 5. Tetraethyl lead; 6. Tetrapropyl lead; 7. Dimethyldiethyl lead; 8. Diethyldiisopropyl lead; 9. Tetraisopropyl lead.

TABLE 6

Performance of Extenders with Lead Naphthenate

	Extender concentration, wt. % 2-ethyl hexanoic acid	Octane increase		
		Research method[b]	Motor method[b]	Road method[c]
Lead naphthenate[a] alone	0	−0.7	0.9	−0.2
Naphthenate plus extender	0.72	2.7	2.4	0.0
Naphthenate plus extender	1.44	4.0	3.3	2.1

[a] Lead concentration equivalent to 6 ml TEL per gallon (6.35 grams Pb/gal) in Fuel 7.
[b] Comparison of averages of quadruplicate determinations.
[c] Comparison of averages of triplicate determinations; 90% confidence interval is ±1.1 using port injection 1957 Chevrolet.

considerable antiknock activity is lost. These isopropyl lead compounds show the greatest response to acetic acid. A 3.7 octane increase resulted from the addition of acetic acid to the gasoline containing diethyl diisopropyl lead. The isopropyl lead compounds are apparently so unstable that considerable agglomeration of the active antiknock species occurs prior to the time that the antiknock agent is needed for suppression of the knocking reactions. The entire results of Fig. 6 might be interpreted as showing that the use of a lead extender reduces the importance of the agglomeration process. Organolead compounds which are sufficiently thermally unstable to decompose prior to a critical point in the engine cycle provide nearly equivalent octane improvement in the presence of extenders.

There is other evidence in the literature that the state of agglomeration of the active antiknock species derived from a lead alkyl is more important in determining the antiknock effectiveness obtained from the additive. As early as 1927, Egerton and Gates showed that lead, introduced by an arc into the intake air of an operating gasoline engine, caused an appreciation in octane number.[10] This demonstrated that it was not necessary that the lead be in the form of an alkyl to obtain antiknock activity. However, Egerton's data showed the lead so introduced to be less effective than tetraethyl lead, probably because the lead agglomerated to a great extent prior to acting as an antiknock agent. Support is lent to this conclusion by the work of Rifkin,[11] who repeated Egerton's experiment, measuring particle sizes of the lead in the intake air stream.

It is well known that when lead salts are introduced into the gasoline engine little effect on octane numbers occurs. For example, the introduction of lead soaps has little or no effect on octane number. It has now been found that lead extenders can render such compounds of lead effective antiknock agents.

The data of Table 6 show the change in octane number resulting from the addition of a lead salt of naphthenic acid to an aromatic gasoline. The lead naphthenate had little effect on the octane number measured by either of the two laboratory engine methods or in road determinations. However, addition of an extender, 2-ethyl hexanoic acid, caused the lead naphthenate to be a markedly effective antiknock agent. As much as 4 research octane numbers were obtained by the combination of lead naphthenate plus 2-ethyl hexanoic acid.

When the gasoline containing the lead naphthenate evaporates, the lead naphthenate concentrates and finally forms relatively large particles of solid. The particle size obtained probably is a function of the size of the evaporating droplet from which it coalesced. These particles are so large that they have no influence on the knocking processes. The fact that the presence of an extender causes the solid to be an active antiknock agent suggests that the extender is dispersing the solid into very small particles. This supports the above-postulated theory that extenders function by interfering with the agglomeration of the active antiknock species and cause large aggregates to disperse.

Discussion

A lead alkyl must decompose in the engine before it can exert an antiknock effect. Probably the active antiknock agent is a lead oxide. There is considerable debate as to the state of subdivision of the antiknock species. Norrish has argued that it is present in the combustion cham-

ber in the form of vapor.[12] Walsh has vigorously advocated the view that it is in the form of a fine dispersion of solid particles.[13] In either case, the antiknock species must be finely dispersed in the combustion chamber so that adequate numbers of collisions of the critical reacting species with the antiknock agent will occur. It is logical to suppose that if the decomposition of the alkyls occurred sufficiently early in the engine cycle the inorganic lead compounds resulting might agglomerate to such an extent that loss in antiknock effectiveness would occur. This possibility has generally been ignored by previous investigators.

There is a considerable body of work in the literature which shows that the presence of lead tetraethyl in a hydrocarbon has no effect on the induction period preceding cool flame formation. This finding has supported the general belief that TEL exerts its effect as an antiknock agent following the cool flame reactions and has no effect during the τ_1 regime.[14] It has even been proposed that the heat of the precombustion reactions serves to promote the decomposition of TEL and thereby renders it effective as an antiknock agent.[15] Obviously, the lead alkyl exerts its most spectacular effect in extending the τ_2 induction period. However, the data of Pastell[16] and others[17] show that the presence of TEL can decrease the degree of cool flame reaction. To reduce the intensity of the cool flame reaction, the TEL must first decompose. If the compression ratio of an engine is raised, the temperatures and pressures to which the fuel and antiknock agent are exposed increase. Thus, the lead alkyl decomposes earlier in the cycle as compression ratios are increased. In this way, as compression ratios increase, the probability increases that agglomeration of the active antiknock species will proceed to too great a degree.

Just as compression ratios have been increasing over the years, the aromatic contents of gasolines have been increasing.[1] Benzene does not undergo cool flame reactions, and aromatic hydrocarbons generally are much more resistant to preflame reactions than are paraffinic hydrocarbons.[15] The degree of preflame reactions which occur in aromatics tends to be considerably less than in aliphatic fuels. Thus, it is certainly possible for lead alkyls to exert an antiknock effect earlier in the engine cycle when an aliphatic fuel is used than when an aromatic is employed. More of the chemical changes occur late in the engine cycle in aromatic fuels. Results in our laboratory show that as aromatic hydrocarbons are added to aliphatic gasolines the extent of cool flame reactions is reduced. In highly aromatic gasolines, the antiknock agent exerts most or all of its effect late in the engine cycle. This explains the observed fact that the more thermally stable lead alkyls are more effective antiknock agents in aromatic gasolines than the less thermally stable alkyls. For every engine fuel combination, there probably exists a lead alkyl which would decompose at about the correct time for optimum antiknock effectiveness.

There may exist an optimum particle size of the active antiknock species to give maximum antiknock effectiveness. This could be argued from Walsh's theory of the antiknock process. On the other hand, the Norrish theory states that the antiknock action is a homogeneous gas phase process. In either case, a high degree of dispersion of the antiknock agent is necessary for effective antiknock control. An agent that prevents agglomeration of the antiknock material should therefore enhance the effectiveness of unstable metal-containing antidetonants. The carboxylic acids appears to be such materials. In some manner, they retard agglomeration of the antiknock agent and preserve it in an effective form for a longer portion of the combustion cycle. They are less effective promoters for the more stable lead alkyls, such as TML, because the TML already possesses nearly optimum thermal stability for use in present-day premium gasolines. The extenders are more effective in promoting the activity of TEL in aromatic gasolines because the TEL decomposes so early in the cycle that agglomeration of the antiknock species destroys some of the antiknock activity.

As compression ratios, octane numbers, and aromatic contents of gasolines increase, the need for more stable lead alkyls and/or more effective extenders which will prevent agglomeration will also increase.

It is recognized that the arguments presented in this paper are, in the main, qualitative. As such, no exact mechanism for the antiknock process is proposed. At the present state of knowledge, no single detailed mechanistic scheme can be rigorously defended. However, the several striking parallelisms here recorded are probably not fortuitous. As such, they suggest that agglomeration is an important feature of any detailed mechanism explaining the process by which lead acts.

References

1. Richardson, W. L., Barusch, M. R., Kautsky, G. J., and Steinke, R. E.: J. Chem. Eng. Data *6*, 305 (1961); Ind. Eng. Chem. *53*, 305 (1961).
2. Eltenton, G. C.: J. Chem. Phys. *15*, 455 (1947).
3. Leermakers, J. A.: J. Am. Chem. Soc. *55*, 4508 (1933).

4. RIFKIN, E. B. and WALCUTT, C.: Ind. Eng. Chem. *48*, 1532 (1956).
5. RIFKIN, E. B.: Proc. Am Petrol. Inst. *38*, 60 (1958).
6. GLICK, H. S., SQUIRE, W., and HERTZBERG, A.: *Fifth Symposium (International) on Combustion*, p 393. Reinhold, 1955.
7. RYASON, P. R.: In preparation.
8. NEWMAN, S. R., DILLE, K. L., HEISLER, R. Y., and FONTAINE, M. F.: SAE Journal *68*, 42 (1960).
9. RICHARDSON, W. L., BARUSCH, M. R., STEWART, W. T., KAUTSKY, G. J., and STONE, R. K.: J. Chem. Eng. Data *6*, 309 (1961); Ind. Eng. Chem. *53*, 306 (1961).
10. EGERTON, A. and GATES, S. F.: J. Inst. Petrol. Technologists *13*, 244 (1927).
11. ROSS, A. and RIFKIN, E. B.: Ind. Eng. Chem. *48*, 1528 (1956).
12. ERHARD, K. H. L. and NORRISH, R. G. W.: Proc. Roy. Soc. (London) *A234*, 178 (1956).
13. CHEANEY, D. E, DAVIES, D. A., DAVIS, A., HOARE, D. E., PROTHEROE, J., and WALSH, A. D.: *Seventh Symposium (International) on Combustion*, p. 183. Butterworths, 1959.
14. LEWIS, B. and VON ELBE, G.: *Combustion, Flames, and Explosions of Gases*, 2nd ed., p. 138. Academic Press, 1961.
15. DOWNS, D., GRIFFITHS, S. T., and WHEELER, R. W.: J. Inst. Petrol. *47*, 1 (1961).
16. PASTELL, D. L.: SAE Quart. Trans. *4*, 571 (1950).
17. SYTZ, W. E.: Private communication (1962).

Discussion

DR. G. H. MEGUERIAN (*American Oil Company*): We would like to congratulate the authors from the California Research Corporation for their fruitful efforts to advance our knowledge of antiknock action in general. These efforts encouraged, a few years ago, the commercial use of tetramethyl lead.

This paper brings further evidence that a lead alkyl, to be an effective antiknock, must produce active lead oxide at the "right time" during the engine cycle. This "right time" varies with engine conditions, but is determined mainly by the precombustion properties of the fuel. An alkyl lead is not a good antiknock if it oxidizes to lead oxide when autoignition reactions are fully developed. Also, it is not an effective antiknock if it gives lead oxide long before the development of these reactions. In this case, the active lead oxide, produced early in the engine cycle, agglomerates under the influence of increasing pressure and temperature, and becomes inactive by the time its inhibitory action is needed.

One way of preventing lead oxide from agglomeration, and hence from deactivation, is by the use of extenders, as pointed out by the authors. We suggest that the prevention or postponement of agglomeration of lead oxide is possible because the acid from the extender, such as *tert*-butyl acetate, forms a lead salt which can exist in the engine in the gaseous or sublimed form. Evidence for this comes from our laboratory studies on the decomposition of *tert*-butyl acetate in the presence of TEL [HUGHES, F. J. and MEGUERIAN, G. H.: Preprint, 27th Midyear Meeting, Division of Refining, API, San Francisco, California, May 1962]. The results show that above 370°C *tert*-butyl acetate decomposes to acetic acid, which then reacts with lead oxide to give lead acetates. Between 370°C and 390°C lead acetates are in the gaseous or sublimed form. Above 390°C they decompose to lead oxide. When gaseous lead acetate decomposes, it should produce active lead oxide.

PROF. A. D. WALSH (*University of St. Andrews*): The ascription of the antiknock action of TEL to the surface properties of PbO particles has been objected to on the grounds of an assertion that there would not be time in an engine for the particles to grow to a sufficient size. On the theoretical side, Dr. P. G. Wright has shown in several recent papers that the objection is not necessarily valid. On the practical side a Tyndall beam effect occurring with a leaded fuel in the end-gas of an engine has been demonstrated and repeated by Downs and Griffith. Further demonstration that a fog of PbO particles can and does form inside an engine cylinder is probably not necessary; but the paper by Dr. Barusch and his colleagues does provide a third line of support. The explanation that is put forward and supported for the gain in "knock" ratings obtained by substituting TML for TEL and by adding "antiknock" extenders involves supposing that PbO molecules aggregate to growing particles in the end-gas; if it were impossible for particles to form, because of insufficient time, we shall be left with no understanding of the action of TML relative to TEL nor of the action of "antiknock" extenders.

DR. E. B. RIFKIN and DR. C. WALCUTT (*Ethyl Corp.*): The paper by Richardson and colleagues gives added support to the need for the proper timing between the decomposition of organolead antiknock agents and the onset of the knock-producing processes in the engine.

We view with considerable interest the use of a shock tube to determine the thermal stabilities of

these compounds and look forward to their forthcoming paper on this subject. It is reassuring to note that stabilities of TEL and TML as determined by the shock tube technique are in the same relationship as our work in a motored engine indicated. Our measurements of end gas temperatures in an engine by the velocity of sound technique indicate that considerably higher temperatures and shorter contact times than those the authors used would be preferable. We would recommend study of the effect of temperatures of about 1000° to 1100°K and contact times of the order of 1.0 millisecond.

The authors predict that with increase in engine compression ratio, end-gas temperatures will increase and the need for more stable lead alkyls or lead extenders will also increase. Our work in measuring end-gas temperature does not indicate that this will necessarily be true. We were able to demonstrate that an increase in compression ratio did not necessarily increase end-gas temperature. Our reasoning for this apparent anomaly was that as one goes to higher compression ratios, better quality fuels are required to maintain a fixed level of knock. As the fuel is improved, the heat produced by precombustion will probably decrease. Thus, the increased end-gas temperature expected from increased compression ratio may not be attained.

We have done considerable work concerning the antiknock effectiveness of inorganic lead particles. The best result we were able to achieve showed that lead, on a weight of metal basis, was only about one-third as effective as TEL. This was accomplished by decomposing TEL in a motored engine and taking the exhausted particles directly into the intake of a second engine. The lead oxide particles from the motored engine were 150 Angstroms in size. Apparently lead oxide particles of this size are larger and less effective than the particles formed *in situ* from the decomposition of TEL.

We wish to commend the authors for their finding that lead extenders are effective in improving the antiknock effectiveness of lead salts. This, clearly, is an added piece of information useful in extending our knowledge of the mechanism of antiknock action.

DR. M. R. BARUSCH (*California Research Corporation*): Rifkin and Walcutt recommend that the stabilities of lead alkyls be compared at 1000–1100°K, using contact times of the order of 1 millisecond. We do not consider such conditions to be as significant as the milder temperature range currently under study. It is our opinion that lead alkyls start to decompose relatively early in the engine cycle and that considerable agglomeration generally has occurred by the time the maximum temperatures of the end-gas are reached. As indicated in our paper, we also believe that the lead alkyls can exert antiknock effect prior to the time that the maximum end-gas temperatures are reached.

Had we measured the stabilities of the lead alkyls under the suggested conditions, we expect that all of the lead alkyls would have been decomposed so that no differences in stability would have been detected.

Rifkin and Walcutt report that increasing compression ratio does not necessarily result in increased end-gas temperature. However, it certainly must be the case that earlier in the cycle temperatures in the unburned gases increase with increasing compression ratio. This should cause the lead alkyls to decompose earlier in the cycle as compression ratio is increased.

COMBUSTION OF HYDROCARBONS BEHIND A SHOCK WAVE

C. R. ORR

The combustion of dilute fuel–oxygen mixtures in argon was studied by observing the infrared emissions of reactants, intermediates, and products. The combustion reactions were initiated by the incident shock wave in a simple two-section shock tube. Calibration data obtained on shock-heated samples containing known percentages of product gases do not agree with results from products generated by combustion because chemical reactions can impart considerable energy to the vibrational modes of a molecule. While quantitative calibration was not possible, emission of products formed from combustion presents a fair picture of product concentrations.

The rates of formation of products (H_2O, CO, and CO_2) from combustion of ethylene, acetylene, isooctane, *n*-heptane, benzene, and a mixture of hydrogen and CO were compared at two temperatures that were well above their minimum ignition temperature. Complete spectra (in frequency and time) were also obtained for the preflame region for isooctane, *n*-heptane, and benzene and for the entire low temperature flame region for *n*-heptane and benzene.

Isooctane and *n*-heptane showed extensive preflame activity. These fuels were completely degraded prior to the flame regardless of the length of the preflame region. The major products were ethylene, higher olefins, and carbonyl. Normal heptane produced acetylene in the flame while isooctane did not. Benzene was only 15–20 per cent degraded in the preflame region and produced much less intermediate material, aside from CO.

Of the hydrocarbons tested, *n*-heptane had the highest rate of combustion as indicated by rate of formation of CO_2 whereas isooctane had the lowest. Production of CO from benzene is considerably slower than from any other fuel. In respect to rate of heat release, as deduced from formation of products, the fuels are aligned in roughly the same order as their performance in reciprocating engines. The lack of correlation between CO and CO_2 emission indicates either that CO_2 may be formed in part by processes that do not involve CO, or that some species other than CO and oxygen is involved and it is a function of the original fuel.

Introduction

The primary objective in the combustion studies conducted in the shock tube is to expand our knowledge of combustion reactions by experimentally observing the appearance and disappearance of the various products and intermediates as they occur in the reaction. A shock tube[1–5] is particularly well suited for these studies because of its ability to produce a reaction that is sufficiently expanded in space for spectroscopic observation and is at the same time at temperatures that are comparable to those in practical combustion devices. This paper presents the results of our first efforts to identify the major species involved in the reaction.

Two temperature regions were studied. In the first, low temperature region, near minimum ignition temperature, intermediates, and products occurring in the preflame and low temperature flame were identified. In the second, high temperature region, well above minimum ignition temperature, the relative rates of formation of products (CO, CO_2, and H_2O) were determined. In preparing to analyze the data, an attempt was made to obtain calibration spectra of the products. At the same time, the effects of nonequilibrium energy distribution following a simple shock compression and a shock compression followed by combustion were also briefly explored.

Experimental Apparatus and Procedure

Tube design was based on published criteria[6–9] and the final apparatus resembled in some respects that of Windsor, Davidson, and Taylor.[10] Only the incident shock was used, not the reflected shock, however. The experiments were performed in a 3-inch square aluminum two-section shock tube, instrumented to give the shock velocity, the pressure versus time, visible light emission versus time, and the infrared emission versus time. Infrared emission was detected by a copper-doped germanium photoconductive element cooled to the temperature of

liquid helium and used in conjunction with the monochromator from a Beckman IR–7 Infrared Spectrometer. The detector was useful over the full range of the IR–7 and had a response time of about one microsecond.

Emission data were displayed on an oscilloscope as intensity–time records and were recorded photographically. Only one frequency of the emission may be observed during each experiment. In each case where spectra were required, they were obtained point by point in wave number from the emission–time records of a number of identical experiments. Spectra could then be constructed for any position or time after the shock wave.

The interval between points used in taking the infrared spectra was 100 cm^{-1}. Experience gained here indicates this was too large an interval, particularly in the low frequency regions. There did not appear to be much fine structure to the spectra under shock tube conditions; hence, the largest possible interval that does not completely overlook a band should be used. A better value to use in future work would be 50 cm^{-1}, at least in the low frequency region.

A slit width of 5.5 mm was used for the first fuels examined until it was discovered that order overlap occurred between the third and fourth orders. The slit width of 3 mm was used for the remainder of the fuels. Three millimeters has been satisfactory and gave better resolution than was warranted by the wave number interval used in obtaining spectra. A slightly larger slit may be used at low frequencies to improve signal strength.

The sample or channel gas consisted of the fuel to be studied, oxygen, and argon diluent. Argon was used to slow the reaction and, to the extent possible, produce isothermal combustion. The amount of dilution that could be used, however, was limited by sensitivity and signal-to-noise ratio of the infrared detector. The best compromise was about equivalent to 4 per cent of a stoichiometric mixture of ethylene and oxygen in argon.

All fuels, with the exception of hydrogen, were studied at a theoretical heating value of 3.3 kcal per mole of product (equivalent to 4 per cent ethylene plus oxygen), an equivalence ratio of 1, and a total sample pressure of 15 psia (Table 1).

TABLE I

Samples

Fuel	Concentration, per cent volume		
	Fuel[a]	Oxygen[a]	Argon[a]
Ethylene	1.06	3.18	95.7
Acetylene	1.09	2.72	96.2
Isooctane	0.275	3.45	96.2
n-Heptane	0.314	3.45	96.2
Benzene	0.441	3.32	96.2

[a] Theoretically equivalent fuel–oxygen ratios having a heating value of 3.3 kcal/mole product.

Calibration

Interpretation of the results is dependent upon calibration spectra (not shown) of the products. These were obtained pointwise for each product separately. The samples used in obtaining the spectra were made by mixing pure product gas (CO, CO_2, or water as the case may be) with argon. The samples were subjected to a series of identical shock waves and the emission recorded at a number of frequencies throughout the emission region of the product. An emission spectrum was also obtained from the water formed by combustion of hydrogen and oxygen behind a shock wave. The concentration of reactants was chosen to theoretically produce 6 per cent water which was equal to the concentration used for the CO and CO_2. The temperatures chosen were in the region of those used in the product formation studies, 3200°R.

These spectra were taken primarily to find frequencies that could be used to observe the formation of products (i.e., regions of minimum interference) and to obtain a quantitative calibration if possible. They were taken at constant slit width and were not corrected for efficiency of the monochromator or response of the detector.

Carbon dioxide emitted at 2300 cm^{-1} and 3650 cm^{-1}. The 2300 cm^{-1} band was the stronger by an order of magnitude but was very close to the CO emission region. At equal molar concentrations, however, the CO_2 band peak was about 35 times the CO contribution; hence, it can be used with an accuracy of about 3 per cent if no correction is made for the CO. The 3650 cm^{-1} region had strong interference from water and would not be useful without considerable correction. Carbon dioxide also has a band at about 670 cm^{-1} which was near the low frequency limit of the detector and was not recorded.

Carbon monoxide produced emission peaking at about 2200 cm^{-1} (2160 band). This was strongly overlapped by the CO_2 emission and was not suitable to use at its peak. The frequency in the CO band giving maximum total signal and minimum interference from CO_2 was about 2050 cm^{-1} in the second order of the monochromator. The second order was chosen

over the third to gain signal that results because of the larger effective slit size. Under the conditions of the spectrum (3200°R, 5.5 mm slit), CO_2 interference at 2050 cm^{-1} was about 10 per cent if the CO and CO_2 are present in equal concentrations. Interference can become appreciable when the concentration of CO is low and CO_2 is present in larger quantities.

Water produced emission at 1500 cm^{-1}, 1800 cm^{-1}, and 3500 cm^{-1}. The strongest was the 3500 cm^{-1} band but it had about 30 per cent interference from an equal concentration of CO_2. The 1500 cm^{-1} and 1800 cm^{-1} peaks had little product interference and were suitable for observing water.

The frequencies chosen to observe products are: 2300 cm^{-1} for CO_2, 2050 cm^{-1} for CO, and 1800 cm^{-1} for H_2O. The CO_2 and H_2O are relatively free from interference providing there are no products other than CO_2, H_2O, and CO. The CO emission at 2050 cm^{-1} is affected by CO_2 to an extent depending on the relative concentration of the two. Since CO_2 can be observed with little interference, the CO_2 contribution to the 2050 cm^{-1} emission can be subtracted providing an accurate CO_2 calibration is available for that frequency.

Relaxation Effects

In obtaining the calibration spectra, the problem of nonequilibrium energy distribution (vibrational and rotational relaxation) following shock compression became apparent. Relaxation effects must be considered in analyzing all the results, particularly those involving low mole weight polyatomic molecules. (Relaxation phenomena have considerable interest in themselves, as shown for instance by the number of papers on the subject at the Eighth Combustion Symposium.)

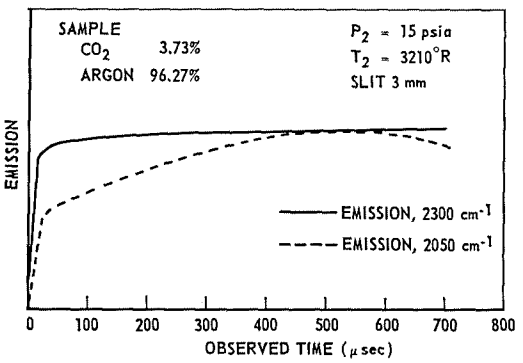

FIG. 1. Effect of frequency on observed emission from shock-heated CO.

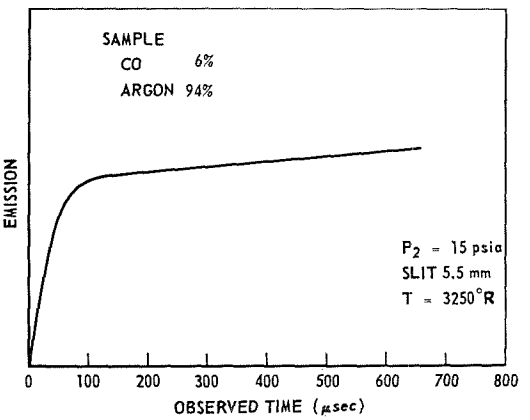

FIG. 2. Emission at 2050 cm^{-1} from CO heated by shock wave.

At 2300 cm^{-1} and 3210°R, CO_2 showed very rapid vibrational relaxation (Fig. 1). Emission rose rapidly in about 20 μsec, then remained relatively constant throughout the region behind the shock wave. There was a slight increase in emission with time that could be associated with the increase in pressure behind the shock wave (friction) or to a very slight relaxation effect. The 3650 cm^{-1} peak produced a similar picture. However, as emission was observed away from the peaks, particularly on the low frequency side, pronounced relaxation effects became apparent, for example, the emission at 2050 cm^{-1}.

Carbon monoxide required considerably more time for vibrational relaxation than CO_2 (Fig. 2). At 3250°R, 15 psia, and 6 per cent CO in argon, carbon monoxide required 100 μsec to rise to 85 per cent of its maximum value whereas CO_2 rose the same percentage in 20 μsec. The emission appeared to be similar at all frequencies.

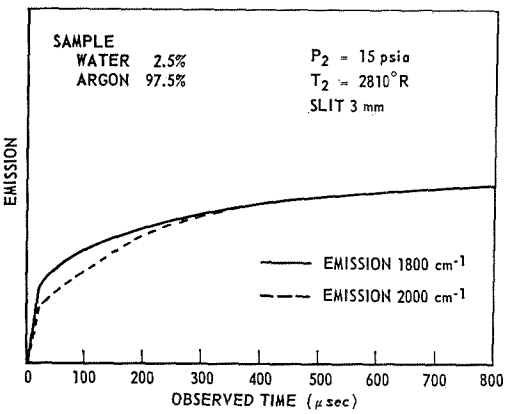

FIG. 3. Effect of frequency on observed emission of water heated by shock wave.

The emission from water heated by a shock wave rose rapidly (similar to CO_2) in the first 20 μsec, then after a very pronounced change in rate continued to increase at a decreasing rate throughout the remainder of the experiment (Fig. 3). At the peak frequencies, 1500 cm^{-1}, 1800 cm^{-1}, and 3500 cm^{-1}, the ratio of the initial rise to the maximum value attained at the end of the experiment was about 1:2.

At frequencies differing from the maxima, the initial rise became less and the ratio became more nearly 1:3. The overall effect of frequency appeared similar to that observed for CO_2. However, at the peaks, water exhibited a much more pronounced change with time.

The performance of the CO_2 and water suggests that the observed emission is affected by several relaxation phenomena with different time constants.

When complex relaxation effects (change in emission with time and frequency) are so evident from CO, CO_2, and water that are heated simply by a shock wave, a major question is raised whether these results are applicable to products generated from chemical reaction. Is a product that is produced by chemical reaction in vibrational and rotational equilibrium? What is the effect of a diluent in this case? Is CO_2 formed from decomposition of a carboxylic acid different from that formed from CO?

Some light can be shed on the problem by examining emission records for combustion of hydrogen and oxygen. The initial rise in emission from water formed by combustion was not as steep or rapid as that from shock-heated water; hence, the shape of the emission–time records appeared to be determined by rate of formation

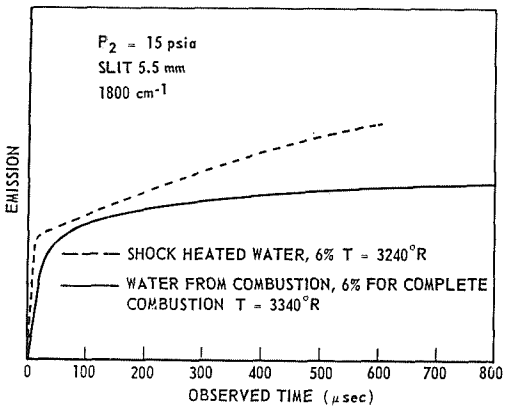

FIG. 4 Emission from water formed by combustion on hydrogen behind shock wave and shock-heated water (approximately equal temperature).

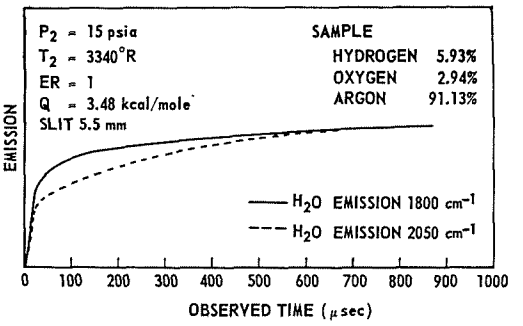

FIG. 5. Effect of frequency on observed emission of H_2O produced by combustion of hydrogen behind shock wave.

of water from the combustion process (Fig. 4) rather than relaxation effects. The rate of increase of emission at the longer times (>100 microseconds) was also much less and was very nearly zero at the end of the experimental time (Figs. 4 and 5). This indicated that the relaxation phenomenon that produced the gradual increase in emission with time was eliminated by the combustion process. However, the effect of frequency was still present (Fig. 5). Since this phenomenon was not affected by combustion, the frequency effect and the time effect must not be related. This can be explained by assuming that energy released by the combustion reaction is concentrated in vibrational modes and the increase in emission with time is a vibrational phenomenon that was eliminated in the combustion process. The change in emission with frequency appeared in both cases and is believed to be related to rotational relaxation.

A similar effect was observed in the CO emission from the combustion of *n*-heptane (Fig. 15). The CO emission following shock-initiated combustion increased more rapidly than emission of shock-heated CO; hence, it appears that vibrational energy was added in the formation process.

With the possible exception of CO_2 there is very little confidence in quantitative aspects of data obtained on the products. This is caused by differences in relaxation phenomena between shock-heated calibration samples and products generated by combustion. Before accurate quantitative data can be obtained, it will be necessary to have a thorough understanding of the relaxation processes of all the species involved in the reaction. These phenomena must also be considered in making a kinetic analysis. Emission of any one combustion-generated product that is observed over a period of time does appear to give a fair indication of the product history.

Low Temperature Combustion

To show appearance and disappearance of intermediates and products, spectra were constructed at several times in the preflame and low temperature flame regions. Fuels studied were *n*-heptane, benzene, and isooctane (Table 1). Isooctane was studied in the preflame region only.

Preflame data are presented as spectra of the emission immediately after the shock wave (shock region), immediately before the flame (preflame region), and about 300 μsec into the flame (flame region) when obtainable. Freehand sketches are given for emission of the reactant, intermediates, and products versus time. In many cases, the emission was very weak and subject to considerable interference so that identification was not positive.

Low temperature flame data are presented as spectra of the emission 150 μsec after the shock wave (near the beginning of the flame), 450 μsec after the shock (near the end of the flame), and 2400 μsec after the shock wave (near the end of the experiment).

The purpose of the sketches is to indicate the presence or possible presence of a compound or type of compound and to the extent possible to show its relationship to other compounds in all respects except concentration.

The preflame and low temperature flame regions required different techniques in operating the shock tube to produce the type of flow condition which was best suited for studying the particular region. Preflame reactions were studied at the minimum ignition temperature for the fuel. The resulting flow condition in the tube

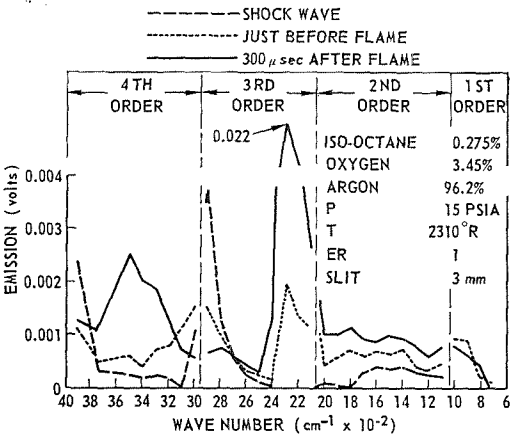

FIG. 6. Preflame region of isooctane (spectra).

just produced a flame in the last portion of sample to pass the observation station before arrival of the driver gas. Thus, most of the observation covers sample in various stages of preflame reaction. The flow in the tube becomes unsteady immediately after ignition and remains unsteady until the flame accelerates up to the shock wave. Thus, the condition used for preflame studies is on the verge of becoming unsteady, and if ignition occurs slightly before the observation station, it will appear unsteady. This operating condition was difficult to reproduce and often several attempts were required to obtain a satisfactory experiment.

Low temperature flame studies were conducted at the lowest stable flow above the minimum ig-

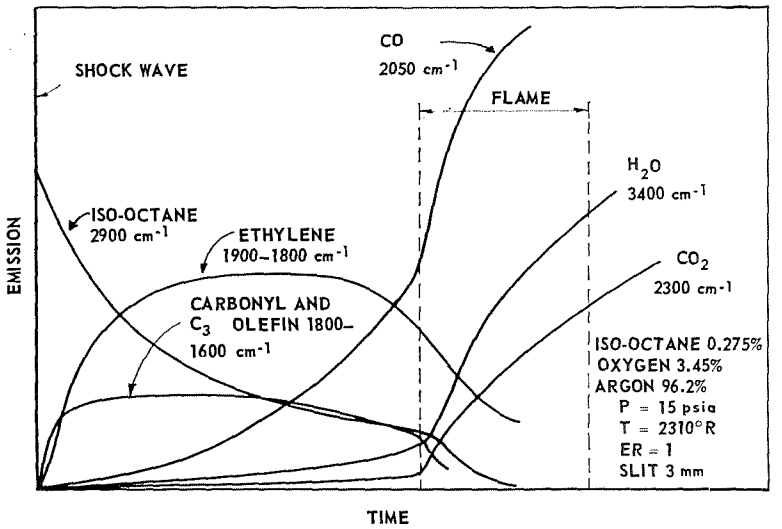

FIG. 7. Preflame region of isooctane (sketch of product history).

nition temperature. This flow was easily reproduced and did not present any particular experimental problems. Use of the lowest practical temperature insured the maximum expansion of the flame to facilitate analysis.

Preflame

Each fuel is discussed separately with respect to its particular or unusual features. In general, fuel was consumed in the region between the shock wave and the flame; the amount depended on the fuel. After the flame, fuel concentration dropped more rapidly. Carbon monoxide and water were formed at a gradually increasing rate in the region between the shock and the flame. At the flame, their rate of formation increased greatly and thereafter decreased with time. Carbon monoxide emission generally reached a maximum value near the end of the flame while water concentration continued to rise. Little or no carbon dioxide was formed in the preflame region. At the appearance of the flame, CO_2 emission rose sharply and continued to rise at a decreasing rate throughout the flame and following slow combustion region.

Isooctane. (Figures 6 and 7.) Isooctane concentration (2900 cm^{-1}) fell rapidly immediately after the shock wave, and after one-half the time to the flame, had dropped to considerably below 50 per cent of its original value. By the time of arrival of the flame, its concentration was very low. The spectrum of the region behind the shock wave showed very early formation of carbonyl and C_3 olefins emitting at 1950–1600 cm^{-1}.

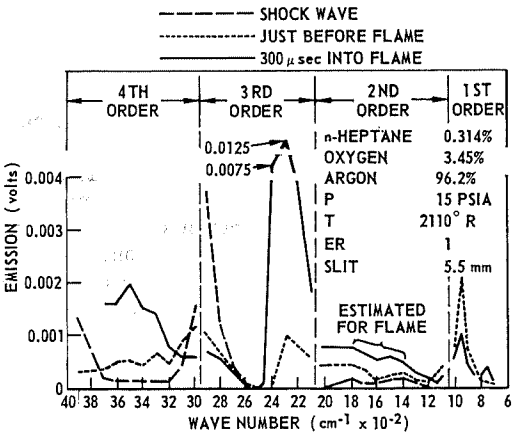

FIG. 8. Preflame region of *n*-heptane (spectra).

(Olefins were believed present here because of the emission at 1600 cm^{-1}.) The concentration of these products remained fairly constant through the preflame and early flame regions. Ethylene and higher olefins (1000–900 cm^{-1}) were formed in large amounts throughout the preflame region and the concentration appeared to be directly related to the amount of fuel consumed. The initial rate of formation was less than that of the carbonyl. No acetylene was formed in the preflame or early flame regions of isooctane. Carbon monoxide emission continued to rise throughout the flame, then became constant in the post flame region. Carbon dioxide did not appear until the flame arrived.

n-Heptane. (Figures 8 and 9.) Normal heptane (2900 cm^{-1}) concentration fell linearly through-

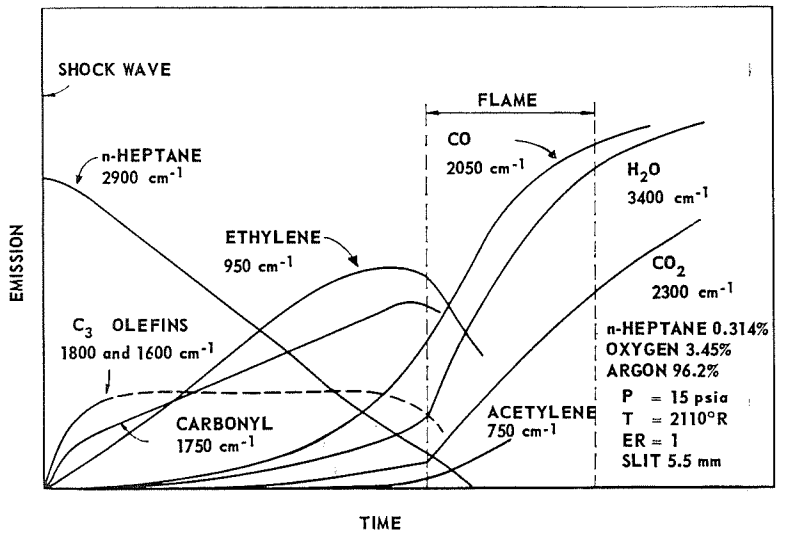

FIG. 9. Preflame region of *n*-heptane (sketch of product history).

out the preflame region and was very nearly zero by the time the flame arrived. Very early formation of carbonyl was indicated by emission at 1800–1600 cm^{-1} in the region immediately behind the shock wave. Less C_3 olefin was formed here than from the isooctane as indicated by the 1600 cm^{-1} emission, and this concentration appeared to be constant throughout the preflame region. Carbonyl concentration (1750 cm^{-1}) increased throughout the preflame region. Ethylene and higher olefin was formed in large concentrations but at a rate nearly constant throughout the preflame region, and was rapidly consumed after the flame. Acetylene was formed late in the flame and was not observed in the preflame region. Carbon monoxide increased throughout the flame as it did with isooctane. Carbon dioxide was formed at the flame.

Benzene. (Figures 10 and 11.) Benzene (3100 cm^{-1}) concentration was constant until the final portion of the preflame region, when concentration fell at an increasing rate to a value of about 80–85 per cent of initial at the flame. Benzene concentration then fell very rapidly in the flame to a value less than 50 per cent of initial, 300 microseconds after the flame. Phenol was formed at an increasing rate in the preflame region. After arrival of the flame, its concentration appeared to continue to increase more slowly; however, the picture was confused by interference from water.

Carbon monoxide was formed in the preflame region in large quantities. In contrast to isooctane and *n*-heptane, with benzene the CO emission reached its maximum well within the flame rather than near the end.

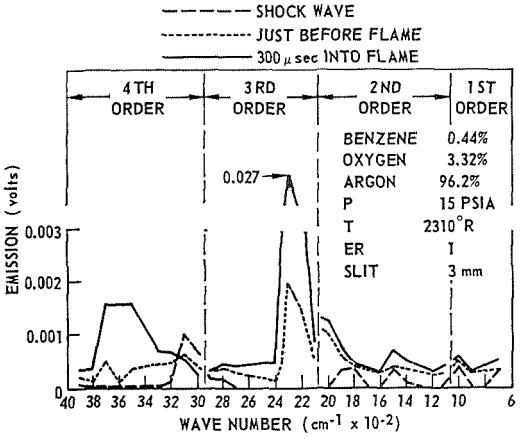

FIG. 10. Preflame region of benzene (spectra).

Low Temperature Flame

Flame spectra are difficult to analyze because of the very large concentration of water and carbon dioxide. In general, the spectra show the disappearance of the last portion of fuel or major intermediate and formation of large quantities of product. Carbon monoxide emission becomes very nearly constant near the end of the flame.

n-Heptane. (Figure 12.) Flame spectra of *n*-heptane showed considerable —CH (3000 cm^{-1}, not characteristic of the *n*-heptane) and CO present in the early portion of the flame. In fact, the early flame spectrum bears a close resemblance to the preflame spectrum. Normal heptane (2900 cm^{-1}) was consumed very rapidly in the earliest portion

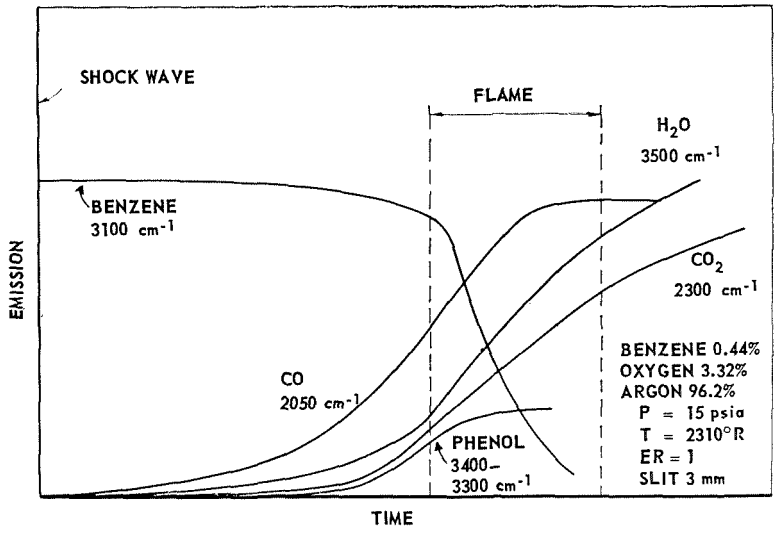

FIG. 11. Preflame region of benzene (sketch of product history).

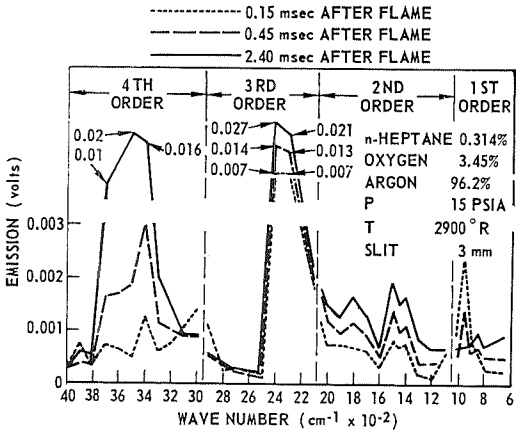

FIG. 12. Flame region of *n*-heptane (spectra).

of the flame or even before. Ethylene, other olefins, and perhaps carbonyl were formed in considerable amounts before arrival of the flame. These were completely consumed in the flame (indicated by the 950 cm^{-1} peak). As the intermediates were consumed, an unidentified product emitting at 850 cm^{-1} appeared.

Benzene. (Figure 13.) The benzene flame spectra appear quite simple. The major portion of the benzene persisted up to the flame and was then nearly all consumed. Carbon monoxide increased in the first portion of the flame, them remained constant, characteristic of the preflame emission. Carbon dioxide and water were formed rapidly in the flame and continued to increase slowly in the region beyond.

Summary

Two distinct types of preflame activity were observed; one was characteristic of the benzene and the other characteristic of the saturates isooctane and *n*-heptane. Benzene underwent very little preflame reaction. Under conditions designed to produce maximum preflame reaction (minimum ignition temperature), about 85 per cent of the fuel survived the preflame region and entered the flame zone. Concentration of CO increased in the first portion of the flame, then abruptly stopped increasing and remained constant through the remainder of the flame. The preflame product from benzene was predominantly CO, in contrast to other fuels.

Isooctane and *n*-heptane were completely consumed in the preflame region. In both fuels, the major preflame products were ethylene, C_3 olefins, and carbonyl although isooctane appeared to produce less. Even in experiments where the induction period was only a few microseconds, these fuels appeared to be consumed prior to the flame.

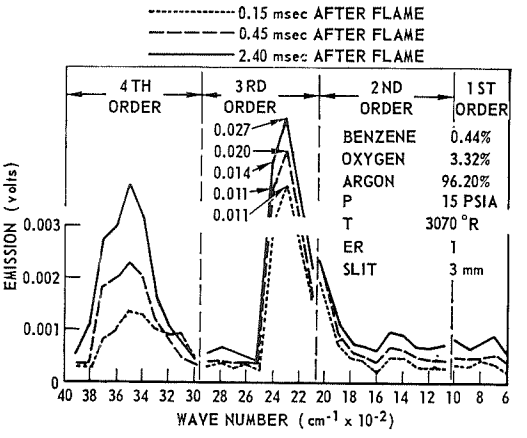

FIG. 13. Flame region of benzene (spectra).

High Temperature Combustion

The rate of formation of final products of a combustion reaction (H_2O, CO_2, and CO) is a measure of the heat release rate. Heat release

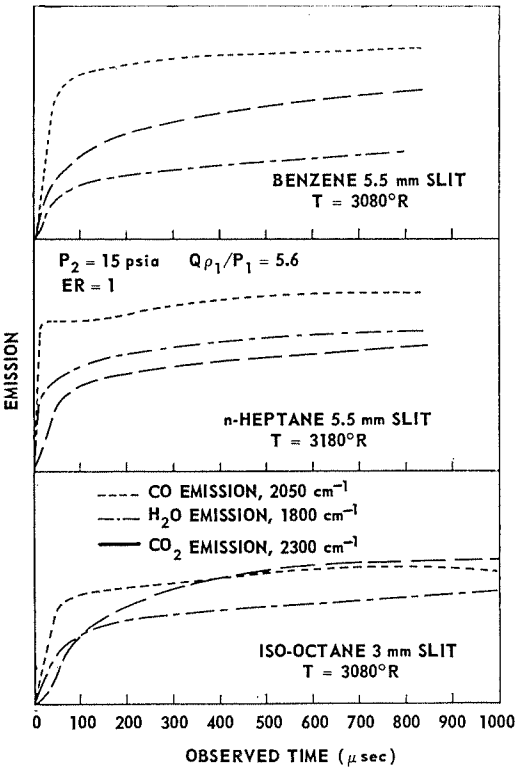

FIG. 14. Formation of products from combustion of hydrocarbons.

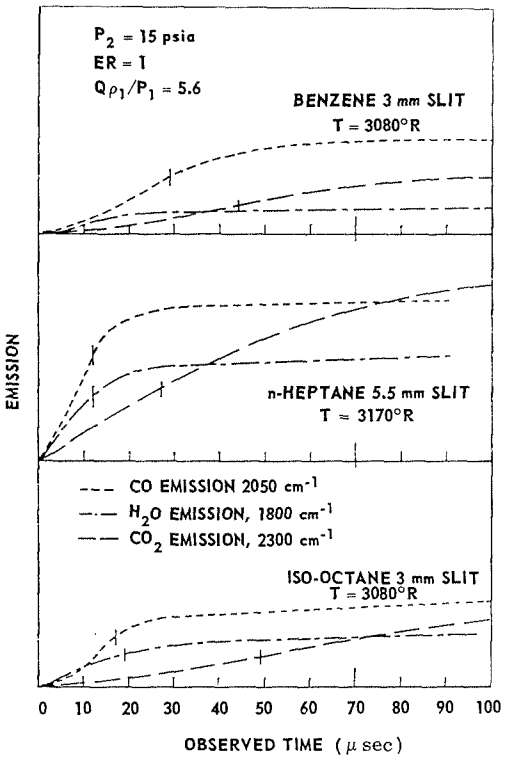

FIG. 15. Formation of products from combustion of hydrocarbons.

rate is of practical importance in continuous combustion devices in determining the size or length of combustion chamber required to realize a high combustion efficiency. In reciprocating engines, it greatly affects the rate of pressure rise from spontaneous ignition and to some extent the rate of pressure rise after a normal flame.

We observed the formation of H_2O, CO, and CO_2 from the combustion of ethylene, acetylene, *n*-heptane, isooctane, benzene, and a mixture of hydrogen and CO (Table 1). All the hydrocarbons were studied at least at two temperatures (about 3100°R and 3600°R) that were well above their minimum ignition temperature. Additional temperatures were used in showing temperature effects in detail. Hydrogen–CO mixtures were generally observed at lower temperatures to increase the time to produce products to a value compatible with the instrumentation and other data. The arrangement used here limited emission rise time to about 5 μsec. Shorter rise times (1 μsec) may be used when the signal-to-noise level is higher.

The following discussions of CO, CO_2, and H_2O emission refer to the total emission at 2050, 2300, and 1800 cm^{-1}, respectively. No correction was made for interference.

Product emission of the hydrocarbons followed a general pattern of very rapid increase in CO and water emission followed by CO_2 at a lower rate. After its initial rise, CO emission generally remained relatively constant for about 200 μsec, then showed the effect of the CO_2 interference. Carbon dioxide and water emissions rose gradually throughout the available time and indicated the occurrence of slow combustion throughout the entire region behind the flame.

An example of the hydrocarbon data is presented in Figs. 14 and 15. Two time scales were used: 100 μsec per division to show the general shape of the curves throughout the available time (Fig. 14) and 10 μsec per division to obtain an accurate impression of the production during the flame (Fig. 15).

Rates of formation of the products presented in this paper were compared on a time basis by letting the time at which the emission reaches 63.2 per cent of its value at 70 μsec serve as an inverse measure of the rate. These times are given in Table 2. At both high and low temperatures, the reaction temperature varied about 100°R but this was not sufficient to affect the results significantly. Water emission in the early stages was meaningless for benzene because of interference by the benzene. Water can also be affected by carbonyl or olefin if they are present in the post flame region.

TABLE 2

Time After Ignition to Produce 63.2 Per Cent of the Product Emission at an Observed Time of 70 Microseconds

Fuel	Time (microseconds) CO_2	H_2O	CO	Temperature (°R)
Isooctane	49	19	17	3080
n-Heptane	27	12	12	3170
Benzene	44	—	29	3080
Ethylene	38	12	15	3190
Acetylene	41	14	16	3180
Isooctane	31	11	3	3520
n-Heptane	19	4	4	3600
Benzene	26	—	10	3620
Ethylene	24	8	8	3530
Acetylene	25	9	9	3570

Effects of Fuel on Product Rates

Carbon Dioxide. Isooctane and *n*-heptane showed outstanding differences in their rate of formation of CO_2 and among the fuels studied represented the extremes. The rate of formation of CO_2 from *n*-heptane was about 1.8 times that of isooctane. Carbon dioxide formation from benzene was slightly faster than isooctane. Ethylene and acetylene reacted slightly more rapidly than benzene but are still more nearly equal to isooctane than *n*-heptane. This was true at both temperatures and it seems unusual that ethylene and acetylene should react so slowly when their minimum ignition temperatures are so much lower than either *n*-heptane or isooctane. This leads to the conclusion that rate of formation of CO_2, even at these high temperatures, is a function of the original fuel structure.

Water. The early stages of water emission from benzene were not obtained because of the interference with benzene. There is also the possibility of carbonyl interference in all the water data and this lowers confidence to the point that little can be said at this time except that CO and water appear to be closely parallel.

Carbon Monoxide. A comparison of the fuels on the basis of CO emission showed pronounced differences from the comparison on the basis of CO_2. With respect to CO formation, *n*-heptane was still very reactive. However, at 3600°R isooctane was equally or even slightly more reactive. The effect of increasing temperature on the rate of formation of CO from isooctane was much greater than for *n*-heptane. Benzene was outstanding, for its relatively low rate of formation of CO represented the low extreme at both temperatures. Acetylene and ethylene were intermediate between isooctane and *n*-heptane at 3100°R and between benzene and *n*-heptane at 3600°R.

In general, the fuels aligned themselves with respect to rate of formation of product in the same order as their performance in a reciprocating engine.

Hydrogen–CO Mixture

The formation of products, CO_2, and water, and disappearance of CO was observed in the combustion of the fuel mixture hydrogen–CO (Fig. 16). In general, these experiments were per-

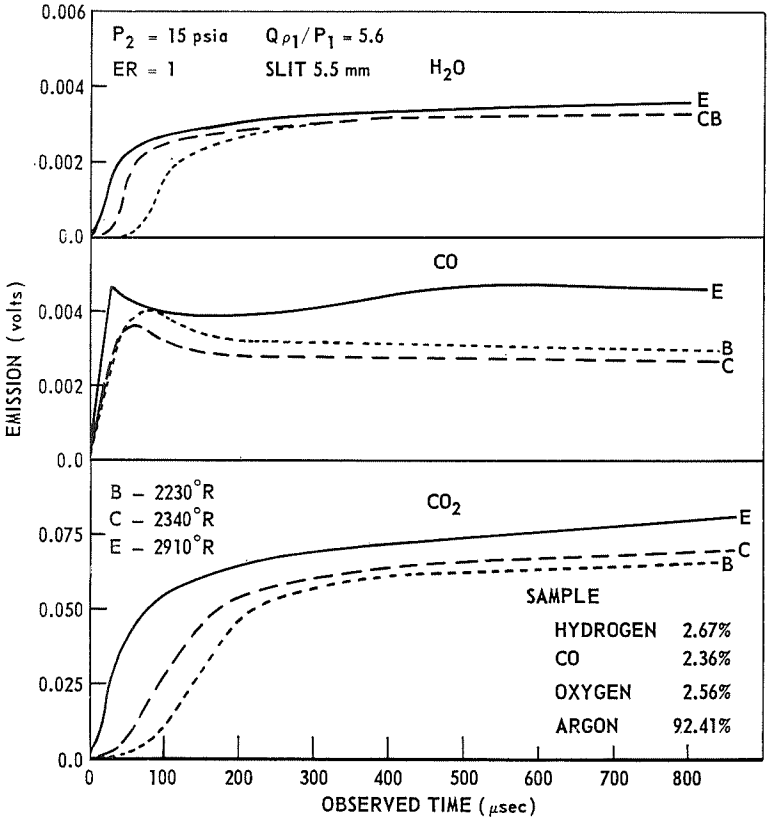

FIG. 16. Product emission from combustion of hydrogen and CO mixture.

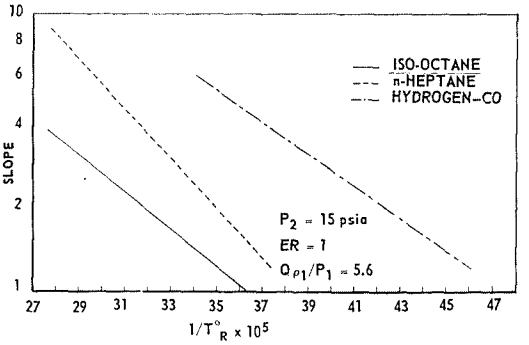

FIG. 17. Arrhenius plot for formation of CO_2 from *n*-heptane, isooctane and hydrogen and CO mixture.

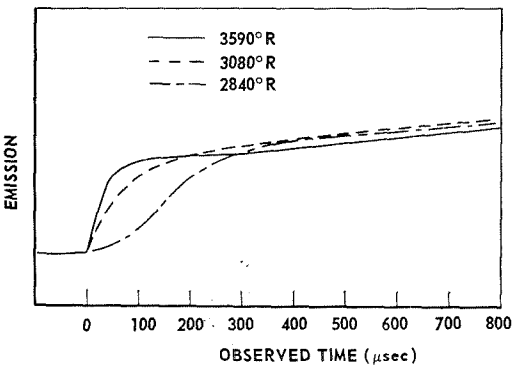

FIG. 18. Effect of temperature on rate of CO_2 formation in combustion of isooctane.

formed at lower temperatures because the fuel burned much more rapidly than the hydrocarbons. An Arrhenius plot of the CO_2 data (Fig. 17) indicates a lower activation energy than for the hydrocarbons; hence, the reaction rate for the hydrogen–CO mixture will not increase with temperature as rapidly as for the hydrocarbons and the fuels will become more similar with respect to heat release rate as temperature is increased.

Consumption of CO was never complete. The early portion of CO emission was influenced by relaxation effects which appeared to affect its initial rise while interference by the CO_2 was apparent at longer times. Carbon dioxide interference was most obvious in the 2910°R experiment (Fig. 16) and was similar to that observed with the hydrocarbons.

Effect of Temperature

The rate of formation of CO_2 from combustion of isooctane and *n*-heptane was studied at several temperatures in addition to those used in Table 2. These data are presented in Figs. 18 and 19 and also as an Arrhenius plot in Fig. 17. In preparing Fig. 17, maximum slopes of emission–time curves were used to indicate rate and the temperature of the induction region used for the temperature. Only three data points were available for isooctane; hence, accuracy of the Arrhenius plot is poor in this case.

The plot shows that the rate of CO_2 production for *n*-heptane increases more rapidly with temperature than isooctane and these fuels should appear relatively more dissimilar at higher temperatures. Hydrogen–CO is also included in the Arrhenius plot for comparison. Its slope is slightly less than that of the isooctane.

Conclusions

Interpretation of calibration spectra and their relationship to combustion-generated products is made difficult by nonequilibrium (relaxation) effects. Products generated from a combustion reaction undergo different relaxation processes than products heated by a shock wave. As a consequence, calibration spectra obtained from

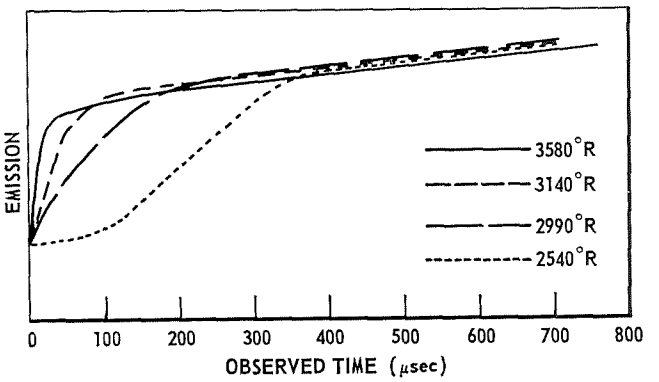

FIG. 19. Effect of temperature on rate of CO_2 formation in combustion of *n*-heptane.

samples heated simply by shock waves cannot be used to obtain quantitative information about combustion-generated products without a thorough understanding of the relaxation phenomena in both cases. Combustion tends to avoid relaxation problems.

Of the hydrocarbons tested, *n*-heptane had the highest rate of combustion as indicated by the rate of formation of CO_2. Isooctane had the lowest. Production of CO from benzene was considerably slower than from any other fuels. In respect to heat release, the fuels were aligned in roughly the same order as their performance in reciprocating engines. The lack of correlation between CO emission and CO_2 emission indicates either that CO_2 may be formed by processes that do not involve CO, or that some species other than CO and oxygen is involved and this molecule is characteristic of the original fuel.

The fuels that were studied in the preflame and low temperature flame regions fell into two general categories; those that underwent extensive preflame reaction and those that did not. Under all operating conditions isooctane and *n*-heptane were completely consumed before the flame. The principal intermediates were ethylene and higher olefins. Carbonyl was also found particularly in the region immediately behind the shock wave but its concentration was low. Only 15 to 20 per cent of the benzene was consumed in the preflame region and this was primarily in the region immediately before the flame.

References

1. Eisen, C. L., Gross, R. A., and Rivlin, T. J.: Combustion and Flame *4*, 137 (1960).
2. Dorrance, W. H.: J. Aerospace Sci. *28*, 43 (1961).
3. Gross, R. A. and Oppenheim, A.: ARS Journal *29*, 173 (1959).
4. Kistiakowsky, G.: Ind. Eng. Chem. *43*, 2794–97 (1951).
5. White, D. R.: Phys. Fluids *4*, 465 (1961).
6. Glass, I. I., Martin, W., and Patterson, G. N.: *A Theoretical and Experimental Study of the Shock Tube.* Institute of Aerophysics, University of Toronto, 1953.
7. Glass, I. I.: *Shock Tubes—Part I: Theory and Performance of Simple Shock Tubes.* Institute of Aerophysics, University of Toronto, 1958.
8. Hall, J. Gordon: *Shock Tubes—Part II: Production of Strong Shock Waves; Shock Tube Application Design and Instrumentation.* Institute of Aerophysics, University of Toronto, 1958.
9. Courant, R. and Friedrichs, K. O.: *Supersonic Flow and Shock Waves.* Interscience, 1948.
10. Windsor, M., Davidson, N., and Taylor, R.: *Seventh Symposium (International) on Combustion*, p. 80. Butterworths, 1958.
11. Polanyi, J. C.: J. Chem. Phys. *31*, 1338 (1959).

THE KNOCK RATINGS OF FUELS

A. D. WALSH

The purpose of this paper is to try to explain the relative knock ratings of fuels in terms of the chemical reaction steps that lead to knock. The problem is closely connected with the problems of explaining: (1) why some fuels have a "low" temperature portion of their ignition diagrams and others do not; (2) why some fuels have three lobes in the "low" temperature portions of their ignition diagrams, others only have two and others only have one; (3) why "low" temperature ignition is associated with the occurrence of cool flames; (4) the cause of the so-called "negative temperature coefficient" region observed in the ignition diagrams of most fuels.

It is concluded that isomerization of RO_2 radicals (where R is the original fuel molecule minus one H atom) plays an important part in the branching chain process that is needed to explain the formation of cool flames and "low" temperature ignition. The nature and consequences of this isomerization are discussed and its importance shown to offer some explanation of, *inter alia*: (1) the formation of various products, including dihydroperoxides and β-dicarbonyls; (2) the knock resistance of cyclohexane and cyclopentane and certain olefins relative to *n*-hexane and *n*-pentane; (3) why methane, alone among the paraffins, possesses no "low" temperature mode of branching and ignition and therefore has a very high knock rating; (4) the nature of the light emission from cool flames; (5) the decreasing knock resistance of *n*-paraffins with increasing chain length; (6) the occurrence of several lobes in "low" temperature ignition curves and why certain of these lobes are sometimes missing; (7) the connection of (6) with the knock ratings of branched-chain fuels and why fuels containing tertiary C–H bonds (which are particularly readily attacked by free radicals) may yet have high knock resistance.

Although various more or less striking generalizations concerning the relation of the comparative "knock" ratings of fuels to their molecular structures are well known, there is as yet little understanding of these generalizations. The purpose of the present paper is to try to explain some of them in terms of the chemical reaction steps that lead to knock.

Experimental Data

The experimental knock ratings have been excellently set out by Lovell,[1] whose review will be our main source of data. The ratings of course vary according to the engine conditions, test procedures, and rating scales employed. The relative ratings of fuels within the same chemical class (e.g., the paraffins, with which we shall be mainly concerned), however, fortunately do not usually change greatly when the test conditions are changed. Mostly, we shall be concerned only with qualitative statements concerning the relation of knock ratings and molecular structure.

Among the general statements that may be made are the following:

(1) Knock ratings are a very sensitive function of molecular structure. This is particularly seen in the enormous effect of isomerism: e.g , the various isomers of *n*-heptane have critical compression ratios which cover a very large range.

(2) Knock resistance decreases as the length of a molecular chain unbroken by branching increases, i.e., as the number of 2° C–H bonds increases. Among *n*-paraffins, the decrease with increasing molecular weight carries on to at least *n*-decane.[2]

(3) Knock resistance usually increases with number of methyl groups, i.e., as (a) 2° CH_2 groups are replaced by 3° CH groups, and as (b) the H atoms of 3° CH groups are replaced by methyl groups. The combined result of (a) and (b) is that the knock rating increases, fairly smoothly, with decrease in the number of 2° + 3° H atoms.[2]

(4) With the larger straight-chain paraffins and with the smaller branched-chain paraffins, change of a single bond to a double bond increases the knock resistance. With the smaller straight-chain paraffins, the reverse is true. With the larger branched-chain paraffins, either an increase or a decrease of knock resistance may occur on passage to a corresponding olefin, depending upon the paraffin and where the double

bond is inserted. The more central is the double bond within a straight-chain olefin molecule, the greater is the knock resistance.

(5) Cyclohexane and cyclopentane have much greater knock resistance than *n*-hexane and *n*-heptane, respectively, the increase being large for cyclohexane and extremely large for cyclopentane.

Discussion

It is well established[3] that with most fuels, including those in normal commercial use, knock occurs by the so-called "low" temperature process of ignition, i.e. it is associated with the occurrence of cool flames and is a two-stage process of ignition. Connected with this, it is also well known, from the work of Townend and others,[4,5] that the pressure corresponding to the tip of the envelope of the low temperature ignition peninsula, like knock ratings, varies very sensitively with fuel molecular structure; and indeed the higher the pressure of the tip (in ignition diagrams plotted under comparable conditions) the greater in general is the knock rating. It appears therefore that in order to understand knock ratings it is important always to bear in mind the relevant ignition diagrams—even though these refer to ignition irrespective of delay time, whereas knock is a process of ignition in a limited (and very short) time.

Now ignition curves of hydrocarbons, in addition to showing low and high temperature portions, show finer structure. Figure 1 shows clearly that the ignition curves for *n*-heptane and *n*-octane in the low temperature range (defined as the range within which cool flames arise) each consist of three regions or lobes—two prominent lobes at the lower temperatures and a less prominent lobe (but still distinct region) at the higher temperatures. The ignition curve for *n*-hexane (see Fig. 2) is also known to show three distinct low temperature regions. With other hydrocarbons all three lobes are not always present. Thus the plotted points of Fig. 1 show that, although for isooctane the uppermost of the three regions is present, it has below it only *one* prominent lobe—which seems clearly to correspond to the upper of the two prominent lobes for *n*-heptane and *n*-octane. The ignition curve for methane has all three regions absent; there is no low temperature portion of the ignition curve at all. Only one lobe is known in the ignition curve for ethane, which lobe—from the temperature range it covers—appears to correspond to the uppermost of the three lobes observed with *n*-paraffins such as *n*-heptane. Figure 2 shows that the low temperature ignition curve for cyclohexane shows two prominent lobes apparently corresponding to the two prominent lobes of the *n*-paraffin diagrams; but careful comparison of the cyclohexane curve with that for *n*-hexane (inset to Fig. 2) shows that in the former the uppermost of the three regions in the

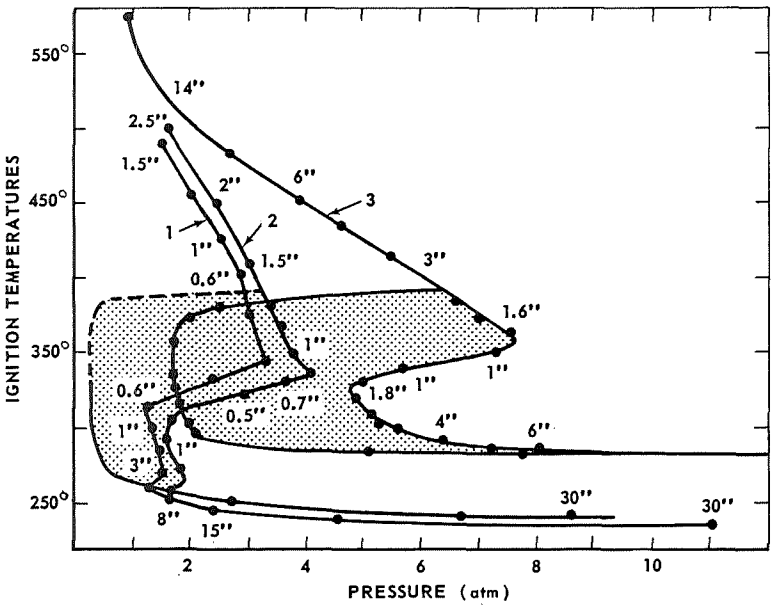

FIG. 1. Ignition curves for corresponding mixtures with air of (1) *n*-octane (2) *n*-heptane (3) *iso*-octane. (From Maccormac and Townend.[4] Courtesy, *J. Chem. Soc.*)

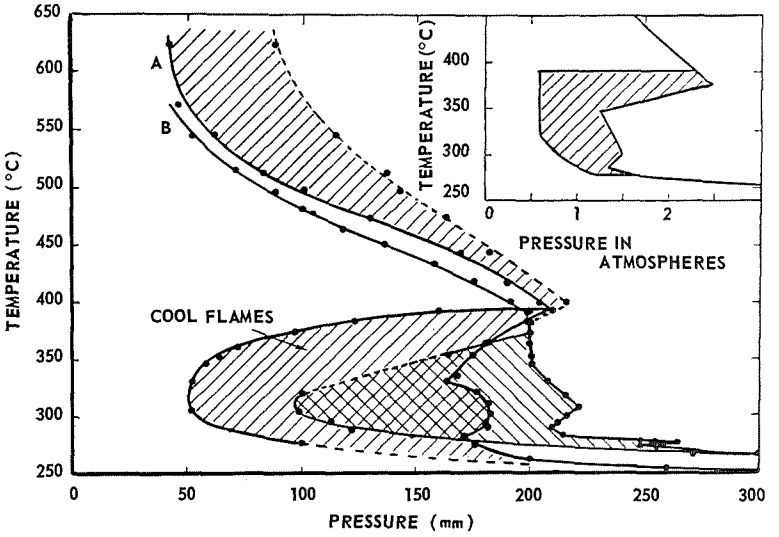

FIG. 2. Ignition diagrams for cyclohexane, cyclohexene and (inset) *n*-hexane
Curve A: cyclohexane. Curve B: cyclohexene. (From Burgoyne, Tang, and Newitt.[5] Courtesy, *Proc. Roy. Soc.*)

latter is missing. These facts are summarized in Table 1.

It is a pity that carefully plotted ignition curves are not available for many other fuels; for a full understanding of knock ratings must clearly include an understanding of why the low temperature ignition curves of the *n*-paraffins cited possess three distinct temperature regions and why some of these regions are missing with other fuels. Methane, for example, may be said to have a very high knock rating because its ignition curve includes none of the three regions revealed in the curves for the higher *n*-paraffins; as far as is known, methane is unique among the paraffins in possessing no low temperature ignition curve and so, perforce, knock with methane must be by the high temperature mode of ignition. Ethane may be said to have a high knock rating relative to the higher *n*-paraffins because its ignition curve has the two lowest temperature regions of the *n*-paraffin low temperature curves missing. The knock resistance of isooctane, relative to *n*-octane, must be at least partly due to the absence in the isooctane ignition curve of the lowest of the three temperature regions of the *n*-octane low temperature ignition curve.

In general, the lower the pressure corresponding to the tip of the envelope of the low temperature ignition peninsula, the lower appears to be also the minimum pressure required for a cool flame to appear. It is not therefore surprising that Barusch and Payne[6] have concluded, from

TABLE 1

Fine Structure of Low Temperature Ignition Curves

	Region 1 (lowest temperatures)	Region 2	Region 3 (highest temperatures)
CH_4	Absent	Absent	Absent
C_2H_6	Absent	Absent	Present
n-C_6H_{14}	Present	Present	Present
n-C_7H_{16}	Present	Present	Present
n-C_8H_{18}	Present	Present	Present
iso-C_8H_{18}	Absent	Present	Present
Cyclohexane	Present	Present	Absent

an experimental study of the formation of stationary cool flames, that the knock resistance of a fuel correlates with its resistance to cool flame formation. Further, it appears[7] that the composite nature of the low temperature ignition curves of fuels is a reflection of composite nature of the limiting pressure–temperature curves for cool flames to arise; and that in turn the composite nature of the cool flame limit curve is a reflection of lobes known to be present in a plot of the maximum rate of slow oxidation (at a constant pressure which is below the minimum pressure for cool flames to arise) against temperature. The probability is that cool flames only arise when the net branching factor (ϕ) of the reactions concerned is sufficiently great; and that the composite nature of the various curves referred to above is due to repeated waxings and wanings, as the temperature rises, of ϕ.

It seems, then, that to understand low temperature ignition we have to find in general not merely one branching chain reaction step and one reason for the dying away of this branching reaction as the temperature rises, but at least three branching chain reaction steps (presumably of successively higher activation energy), each having its own reason for waning in importance as the temperature rises. Each of these new branching processes must be associated with the characteristics (such as light emission) of low temperature combustion; presumably the different processes must be three forms of a single type of process which has these particular characteristics. We shall refer to the three subdivisions of the low temperature ignition process, in order of rising temperature, as L.1, L.2, and L.3.

We can distinguish two ways in which the knock resistance of two fuels may differ. The first is exemplified by *n*-heptane and *n*-octane. With these fuels all three presumed branching processes occur, but for some reason any one process is more difficult (requires a higher pressure) the less the number of CH_2 groups. The second way is exemplified by comparison of *n*-octane with isooctane or ethane; the branching process occurring at the lowest temperatures with *n*-octane for some reason cannot occur with isooctane and the branching processes occurring in the two lowest temperature regions with *n*-octane for some reason cannot occur with ethane. On the other hand, the branching process occurring with ethane cannot occur with cyclohexane.

Let us consider first the comparison of *n*-heptane and *n*-octane. We assume, plausibly, that knock with these fuels occurs by the L.1 mechanism of ignition. Since the L.1 mechanism does not occur with ethane, we deduce that the important L.1 reactions are ones that involve CH_2 rather than CH_3 groups. That the L.1 mechanism occurs with cyclohexane leads to the same conclusion. The apparently greater ease of branching with *n*-octane can hardly be due to a lower activation energy being required to abstract an H atom from the *n*-octane than from the *n*-heptane molecule, for both fuels ignite by the L.1 mechanism, i.e. at much the same temperature, and one would not expect the CH bond dissociation energies to differ appreciably in *n*-octane and *n*-heptane. Since the two fuels differ in the number of 2° CH bonds/molecule, it might perhaps be argued that the reaction

$$X + R—H \rightarrow X—H + R \qquad (1)$$

(which is undoubtedly the step which starts the oxidation of most of the fuel molecules), where X is some free radical and R—H represents a 2° C–H bond in the fuel molecule, will have a greater probability of occurring if R—H refers to *n*-octane rather than to *n*-heptane. But this reaction is not a branching step and, anyway, a similar argument might lead one to expect the knock ratings of fuels that contain only 1° C–H bonds to decrease as the number of such bonds/molecule increases; whereas 2,2-dimethylpropane and 2,2,3,3-tetramethylbutane show the opposite behavior very markedly. It seems much more probable that the explanation of the lowered knock resistance brought about by addition of an extra CH_2 group lies in a step subsequent to (1).

A further argument that this must be so lies in the fact that 3° C–H bonds are particularly readily attacked by free radicals and yet fuels containing 3° C–H bonds may have high knock resistance. It seems that knock resistance is not to be correlated with ease of production of R, but with some step or steps subsequent to the formation of R.

It is unlikely that there are big differences between the probabilities of attack on different CH_2 groups. R is therefore to be thought of as including all the free radicals which can be produced from R—H by removal of one 2° H atom. The unsatisfied valency will be the seat of the reactivity of R. Now, wherever this free valency is situated in the radical, since lengthening the chain of CH_2 groups decreases the knock resistance (i.e. causes the ignition curve to move to lower pressures) there must be some way in which events at the C atom possessing the free valency are influenced by a part of the radical which is apparently remote from that C atom. As Ubbelohde[8] puts it, there must be some way whereby any particular point in a paraffin molecule "knows what the rest of the molecule is doing. Otherwise, however much was attached

to the tail of a particular C–H bond would not affect the reactivity, apart from the collision probability of the molecule as a whole.... In other words, there must be some process whereby the head of the dog knows what the tail of the dog is doing." It is in fact easily seen that the decreased knock resistance in the series *n*-pentane, *n*-hexane, ···, *n*-decane implies that CH_2 groups in the β, γ, and even in the δ position to the C atom carrying the free valency are able to affect what happens at the site of the free valency.

In conjugated hydrocarbons it is well known that influences may be transmitted along a chain of C atoms; but the reasons for this have no application to paraffins. There seems only one way to account for the influence of an apparently remote group in a chain of CH_2 groups. That way is to realize that the remoteness may be apparent only. The structures of *n*-paraffin chains as commonly depicted in print are misleading. In fact, free rotation about C–C bonds can bring atoms that are linked to each other through three or more other atoms (thus forming a ring of five or more atoms) into sufficiently close proximity for strong interaction to occur. The possibility that molecular "crumpling and bunching" may be of importance to knock ratings has been particularly stressed by Ubbelohde.[8]

It seems then that the decreasing knock resistance of *n*-paraffins with chain length implies that low temperature oxidation involves an interaction between a formally "remote" CH_2 group and the point at which a hydrogen atom has been removed from the hydrocarbon molecule. It is difficult to see what form this interaction could take other than the transfer of an H atom from the remote CH_2 group to the free valency. If the interaction is supposed to take place in the radical R, it merely causes isomerization of the radical; and, since at low temperatures all possible secondary R radicals are presumably produced anyway by reaction (1), it is difficult to see why isomerization should be of any importance. Moreover, isomerization of R could hardly be an important process in *all* low temperature ignitions. It would, e.g. offer no explanation of the decreasing knock resistance from ethane to propane to *n*-butane. With ethane, propane and *n*-butane, transfer of an H atom to a free valency in R either makes no difference to R or involves interaction between H and C that are linked together through two or less intervening atoms; and intramolecular interaction between two atoms is only plausible if those atoms are linked through at least three other atoms (so forming a ring of at least five atoms). We conclude that the interaction does not take place in the radical R.

Since R has an unsatisfied valency and since the O_2 molecule may be thought of as having unsatisfied valencies, an important step subsequent to the formation of R is expected to be

$$R + O_2 \rightarrow RO_2. \qquad (2)$$

This reaction is expected to have zero activation energy and, for R larger than CH_3, to be second order (see Hoare and Walsh[9]). It will therefore be fast. The resulting RO_2 radical still has a free valency. If we suppose that lengthening the chain of CH_2 groups exerts its effect because of an interaction between a remote CH_2 group and the free valency in an RO_2 radical, the first of the above difficulties disappears. The interaction results in the transfer of an H atom from a CH_2 group to the free valency; it is an isomerization of RO_2. An —OOH group and a new free valency to which a second O_2 molecule readily attaches itself are thus created. A further isomerization may then take place and the process may be repeated. Alternatively, the radical containing four O atoms may decompose* or it may react with a fuel molecule to produce a dihydroperoxide which may subsequently decompose. There is indeed evidence of the formation of dihydroperoxides[10] and of products which can only have resulted from attack of O_2 at more than one C atom of the original hydrocarbon. The latter include β-dicarbonyls, e.g.,

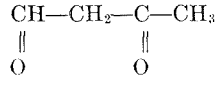

and

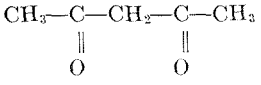

identified in the products of low temperature oxidation of *n*-butane and *n*-pentane, respectively.[11,12] Whatever happens, it is almost inevitable—having regard to the properties of hydroperoxides—that the original R radical gives rise to two or more radicals. Isomerization of RO_2 thus provides a possible identification of the branching process which occurs in low temperature oxidation.

The idea that hydroperoxides are concerned

* Much energy is liberated at each addition of O_2 and must in the first place be stored within the adduct. This energy, if it can flow along the carbon chain, will, via increased internal rotational and vibrational energy, facilitate interaction between formally "remote" points of the chain. RO_2 radicals are to be thought of as twisting and contorting somewhat vigorously. The possible importance of ease of energy flow has been stressed by Ubbelohde.[8]

in low temperature branching is an old one, but emphasis hitherto has always been placed on mono hydroperoxides formed intermolecularly. The new point is essentially that OOH groups may be formed intramolecularly in RO_2 radicals, with subsequent formation of RO_4 radicals possessing separate OOH and OO groups. Cartlidge and Tipper,[13] have expressed very similar views and have also applied them, briefly, to the knock ratings of fuels.

It is important to note that isomerization of RO_2 provides a method of branching which can apply to all fuels that ignite by the low temperature mechanism. The difficulty referred to above concerning the knock ratings of ethane, propane, and *n*-butane also disappears once we suppose isomerization of RO_2 rather than of R. Even with ethane, isomerization of RO_2 can take place as a result of interaction of an H atom with the free valency of an O atom that is linked to the H atom through three intervening atoms. Only with methane would isomerization of RO_2 involve transfer of an H atom to an O atom that was originally linked to the H atom through only two intervening atoms. It is likely that this is a much more difficult process (if it occurs at all) and it is possible that we have here the fundamental reason for the remarkable fact that methane, alone among the paraffins, possesses no low temperature mode of branching and ignition.

Moreover, isomerization of RO_2 provides a method of low temperature branching which can take more than one form, so accounting for the fine structure of the low temperature portions of ignition curves. The suggestion is that RO_2 isomerization via a 4-ring interaction does not occur in low temperature combustion, that RO_2 isomerization via 5-membered and larger rings does occur, but that isomerization via 5-membered rings (i.e. involving α C atoms) is more difficult (i.e. requires a greater degree of contortion and so a higher activation energy) than isomerization via 6-membered and larger rings. Isomerization via 6-, 7-, and 8-membered rings (i.e. involving β, γ, and δ C atoms) appears likely to have much the same ease. The study of models makes all these statements plausible. We thus arrive at the idea that with a fuel such as *n*-heptane the L.1 mechanism involves transfer of an H atom to a $\rangle$CHOO group from a β or more distant $\rangle CH_2$ group. We have already seen that the formation of dihydroperoxides and β-dicarbonyls at temperatures which almost certainly lie in the L.1 range provides direct evidence of β-transfer; and we have already argued (because of the ignition curves of ethane and cyclohexane) that the transfer must be from a 2° C atom. The decreasing minimum pressure required for ignition in the L.1 zone (and hence the decreasing knock resistance) as we pass from *n*-pentane to *n*-decane is ascribed to the increasing number of possible β-, γ-, or δ-transfers.

We may interpose here that RO_2 derived from cyclohexane, and particularly RO_2 derived from cyclopentane, have much less flexibility than RO_2 derived from *n*-hexane or *n*-pentane; so that the possibilities of H atom transfer must be fewer with cyclohexane and cyclopentane. We thus have an explanation of the striking facts that the knock ratings of cyclohexane and especially cyclopentane are much higher than those of *n*-hexane and *n*-pentane, respectively. It is difficult to see how we could explain these significant facts other than via the comparative rigidity of the cyclohexane and cyclopentane molecules. The effects of changing a single bond to a double bond may be explained similarly. The comparative rigidity of the C=C group reduces the likelihood of RO_2 isomerization; although reduction in dissociation energy of a C–H bond α to the C=C group, or the reactivity of the C=C group itself, provides an opposing effect. Two opposing effects are clearly needed to explain the data cited at the outset of this paper.

Arguing again from the ignition diagrams of ethane, cyclohexane and, say, *n*-hexane, the L.2 mode of ignition must also involve H transfer from CH_2 rather than CH_3 groups. We suggest that with, say, *n*-hexane the L.2 ignition involves branching via H transfer from an α $\rangle CH_2$ group to a $\rangle$CHOO group. That a higher temperature should be required for L.2 than for L.1 ignition is then understandable.

Arguing once again from the ignition diagrams of ethane, cyclohexane, and *n*-hexane, the L.3 mode of ignition presumably involves H transfer from CH_3 rather than CH_2 groups. That the L.3 branching process should require a higher temperature than the L.2 and L.1 processes is then

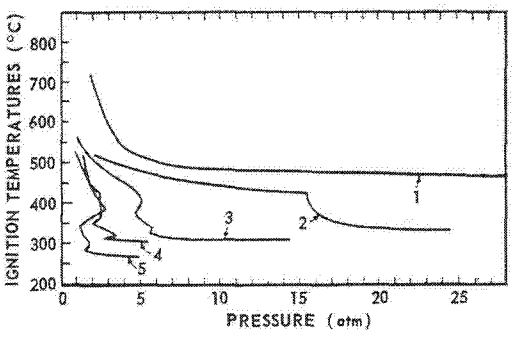

FIG. 3. Corresponding ignition diagrams for (1) methane; (2) ethane; (3) propane; (4) *n*-butane; and (5) *n*-hexane. (From Kane, Chamberlain and Townend.[14] Courtesy, *Proc. Roy. Soc.*)

understandable in view of the greater strength of a 1° than of a 2° C–H bond.

On these views, the fine structure of the low temperature portions of the ignition curves for propane and *n*-butane should not altogether correspond to the fine structure of, say, the *n*-heptane and *n*-octane curves; for with propane β transfer from a CH_2 group is impossible and with *n*-butane β-transfer from a CH_2 group is only possible if we suppose it occurs in the $CH_2(OO)\cdot CH_2\cdot CH_2\cdot CH_3$ radical. Experimentally, the ignition curves of propane and *n*-butane do appear to be somewhat anomalous in relation to the ignition curves of the higher *n*-paraffins (witness the close similarity of the ignition curves in Fig. 1 for *n*-heptane and *n*-octane and cf. Fig. 3); the lowest temperature lobe in the ignition curves for propane and *n*-butane lies at markedly higher temperatures than that in the ignition curves for the higher *n*-paraffins. β-Transfer of a 1° H atom is of course possible with both propane and *n*-butane, but involves supposing that with propane, reactions of the radical $CH_2(OO)\cdot CH_2\cdot CH_3$ are important in determining the ignition limits at the lowest temperatures; such transfer would be expected to occur at higher temperatures than for β-transfer of a 2° H atom. The ratio of 1° to 2° H atoms in propane of course favors formation of $CH_2(OO)\cdot CH_2\cdot CH_3$ as opposed to $CH_3\cdot CH(OO)\cdot CH_3$; with all higher *n*-paraffins, attack of O_2 at a 2° C atom may well be much more important than attack of O_2 at a 1° C atom.

Turning now to the second way in which the knock resistance of two fuels may differ (which way is exemplified by comparison of *n*-octane with isooctane) we note that with isooctane, unlike *n*-octane, β-transfer of an H other than 1° H is impossible at the lowest temperatures, provided (as is plausible) O_2 attack at these temperatures is confined to the 3° or 2° H atoms. α-Transfer of an H from a CH_2 group to a

group is possible. We thus have a possible explanation of why ignition of isooctane requires higher temperatures than that of *n*-octane and hence of the knock resistance of isooctane. With ethane, neither α- nor β-transfer of 2° H in RO_2 is possible, ignition requires markedly higher temperatures than are required for fuels which can ignite by the L.1 or L.2 processes, and the high knock resistance receives some explanation. *i*-Butane appears to be another fuel from whose ignition diagram (see ref. 15) the lowest temperature lobe is missing; with this fuel also, transfer of H from a β CH_2 group in an RO_2 radical cannot occur.

Presumably, transfer of 3° H is also possible within RO_2 radicals. Restriction of the RO_2 isomerization processes involved in L.1 and L.2 ignition to transfer of 2° or 3° H, however, offers an understanding in principle of why knock ratings are such a sensitive function of molecular structure; and in particular of why reduction in number of CH_2 or CH groups by further addition of CH_3 groups in general increases knock resistance. It appears to be significant that, of the eight paraffinic fuels cited by Lovell[1] as possessing a critical compression ratio >8 under standard conditions, none have a CH or CH_2 group β or γ to another CH or CH_2; that not until we pass below the critical compression ratio = 5 line do we find fuels with two CH_2 groups β to each other; that of the seven fuels having the lowest critical compression ratios all have two CH_2 groups β to each other; and that, with the exception of neopentane

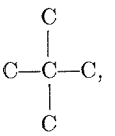

all fuels lying below the critical compression ratio = 5 line have either a CH or a CH_2 group lying β to another CH or CH_2 group.

It remains, however, to point out that to put stress on the ease or difficulty of RO_2 isomerization being an important factor in knock ratings is to imply that some process competes with the isomerization and does not lead to branching. Under conditions where surface chain-ending can be important, surface destruction of RO_2 may well supply the competing reaction in L.1 ignition of a fuel that so ignites. If the surface chain-ending is diffusion-controlled and if RO_2 isomerization requires an activation energy, the negative slope of the lower temperature boundary of the L.1 pressure–temperature ignition lobe would be explained. An alternative or additional competition of RO_2 isomerization with the reverse of reaction (2) would also be possible. Increasing oxygen pressure would then increase the concentration of RO_2 radicals and so favor the branching process—as would rise of temperature, supposing the reverse of (2) to require no activation energy. Further, competition of RO_2 isomerization with RO_2 decomposition to products other than $R + O_2$ is also probable. The most likely reaction step producing light emission (see reference 16) (i.e., producing electronically excited formaldehyde) is

$$CH_3O + X \rightarrow XH + CH_2O^*. \qquad (3)$$

RO_2 decomposition, if it occurs at the lowest temperatures will, according to the present ideas, occur at all low temperatures; it is plausibly the source of methoxy radicals required for reaction (3) to occur.

The upper temperature boundary of the L.1 ignition lobe implies the setting-in of a competition other than that involved along the lower temperature boundary. The positive slope of the upper temperature boundary on an ignition diagram implies competition of the branching process with another process which has both higher activation energy and lower order. The suggestion is that the competition

$$(\text{isomerized } RO_2)_1 + O_2 \rightarrow (RO_4)' \qquad (4)$$

$$(\text{isomerized } RO_2)_1 \rightarrow \text{decomposition} \qquad (5)$$

occurs. Reaction (4), but not (5), is expected to have zero activation energy and (5) has the required lower order. [The unimolecular decomposition (5) is expected to be first order.] At still higher temperatures, a new isomerization of RO_2 sets in and results, like the lower temperature isomerization, in a waxing of the net branching process. At still higher temperatures, the branching wanes again because of the inevitable setting-in of the competition

$$(\text{isomerized } RO_2)_2 + O_2 \rightarrow (RO_4)'' \qquad (6)$$

$$(\text{isomerized } RO_2)_2 \rightarrow \text{decomposition} \qquad (7)$$

At still higher temperatures, comes a third isomerization of RO_2, eventually dying away in importance (as the temperature rises), as a result of a third competition of the type (4)–(5) and (6)–(7). According to these views, each mode of RO_2 isomerization (leading to branching) carries with it its own nemesis at higher temperatures. Decomposition of each isomerized RO_2 leads to a radical plus a molecule and so to a straight-chain process distinct from the branching process whereby more than one radical is produced from one RO_2 radical. Decomposition of R (to radical + olefin) may, at the higher temperatures, compete with (2), also replacing the branching by a straight-chain process. Decomposition of RO_2 after transfer of H from an α C atom will produce an olefin + HO_2. Decomposition of RO_2 after transfer of H from a β C atom will presumably produce an aldehyde or ketone + an olefin + OH. There are thus plenty of possibilities for the competitions which are required both for the kinetic scheme and for explanation of the formation of the numerous oxidation products.

The present suggestions of factors involved in the knock ratings of fuels do not exclude of course additional effects due to further reactions of some of the molecular oxidation products. The correctness or otherwise of the various suggestions made here can only be settled by much more experimental work than is at present available, on the plotting of ignition curves in detail for a wide range of fuels under properly comparable conditions, and on product analysis that is carefully related to the various pressure–temperature features of the ignition curves. The present paper will have served its purpose if it acts as a stimulus to that needed new experimental work.

References

1. Lovell: Ind. Eng. Chem. *40*, 2388 (1948).
2. Cramer and Campbell: Ind. Eng. Chem. *43*, 893 (1951).
3. Downs, Walsh, and Wheeler: Phil. Trans. Roy. Soc. (London) *243*, 463 (1951).
4. Maccormac and Townend: J. Chem. Soc. *1938*, 238.
5. Burgoyne, Tang, and Newitt: Proc. Roy. Soc. (London) *A174*, 379 (1940).
6. Barusch and Payne: Ind. Eng. Chem. *43*, 2329 (1951).
7. Malherbe and Walsh: Trans. Faraday Soc. *46*, 824 (1950).
8. Ubbelohde: *Six Lectures on the Basic Combustion Process*. Ethyl Corporation, Detroit, 1954.
9. Hoare and Walsh: Special Publication Chem. Soc. No. 9, 17 (1958).
10. Cartlidge and Tipper: Proc. Chem. Soc. 190 (1959).
11. Barusch, Crandall, Neu, Payne, and Thomas: Ind. Eng. Chem. *43*, 2764, 2766 (1951).
12. Thomas and Crandall: Ind. Eng. Chem. *43*, 2761 (1951).
13. Cartlidge and Tipper: Combustion and Flame *5*, 87 (1961).
14. Kane, Chamberlain, and Townend: Proc. Roy. Soc. (London) *A160*, 174 (1937).
15. Townend, Cohen, and Manklekar: Proc. Roy. Soc. (London) *A146*, 113 (1934).
16. Walsh: Agardograph, in press.

Discussion

Dr. G. H. Meguerian (*American Oil Co.*): I would like to ask what the effect of pressure is on the formation of ignition lobes. Sometime ago Dr. Malenberg from Ohio State University studied product formation in engines and tubes and found that, although the intermolecular isomerization was pronounced in tubes, in the engine it was not.

Prof. A D. Walsh (*University of St. Andrews*): Dr. Malherbe and I found that while lobes or

breaks probably occurred in cool flame pressure–temperature limit diagrams they were commonly much more obvious in hot flame ignition curves (which of course lay at higher pressures); but I think a lot more study needs to be devoted to the factors that make the composite nature of low temperature ignition diagrams more or less obvious.

DR. M. R. BARUSCH (*California Research Corporation*): In our early work on preflame combustion products of hydrocarbons, we proposed that β-dicarbonyl compounds were formed by a mechanism involving an intramolecular proton transfer [BARUSCH, M. R., NEU, J. T., PAYNE, J. Q., and THOMAS, J. R.: Ind. Eng. Chem. *43*, 2766 (1951)]. This mechanism is identical with Professor Walsh's proposed isomerization of RO_2 radicals with subsequent formation of RO_4 radicals.

This proposed reaction scheme accounted for the fact that cyclopentane does not form β-dicarbonyls while a larger ring does. The reason is stereochemical. A molecular model of the peroxy radical of cyclopentane shows that the oxygen is not close enough to a β hydrogen to collide with it. In a larger ring such as cyclohexane, the oxygen appears to collide readily with the β hydrogen, thus permitting the introduction of oxygen atoms in the beta position.

Cyclohexane and cyclopentane usually exhibit similar chemical properties. However, it appears that for stereochemical reasons, cyclopentane peroxy radical cannot rearrange by β-hydrogen transfer whereas the cyclohexane peroxy radical does. It is suggested that this provides a most interesting test of Professor Walsh's theory explaining the lobes of the pressure-temperature diagram. Applying Professor Walsh's reasoning cyclopentane will not give a Region I lobe because the intramolecular rearrangement does not occur. As Walsh reports, cyclohexane does show a Region I lobe. Verification of the absence of the first lobe in cyclopentane oxidation would give considerable support to Professor Walsh's theory.

PROF. A. D. WALSH: I agree that a study ought to be made of the ignition curve for cyclopentane, which curve has, as far as I know, not yet been reported. I am not sure, however, whether β-transfer of an atom in RO_2 derived from cyclopentane should be regarded as impossible or merely difficult. Incidentally, an ignition curve for methyl cyclopentane has been reported [BURGOYNE, J. H. and SILK, J. A.: J. Chem. Soc. *1951*, 572] and clearly has at least two temperature regions of low temperature ignition.

DR. H. W. CARHART (*Naval Research Laboratory*): The tertiary hydrogen is preferentially removed from RH, hence RO_2 should be predominantly tertiary. How does this affect the appearance of lobes and internal isomerization and how does the negative temperature coefficient affect the various lobes of the ignition diagram?

DR. E. J. Y. SCOTT (*Socony Oil Co.*): Dr. Walsh mentioned that the ease of hydrogen atom abstraction by radicals from hydrocarbon molecules is in the inverse order of the corresponding C–H bond strengths, i.e., $3y > 2y > 1y$. Also, the ease with which knocking of hydrocarbon occurs is in the order: $2y \gg 3y > 1y$. In the past this difference has been explained by the ease with which aldehydes (formed by primary and secondary C—H attack) can generate branching chains compared with ketones (formed by tertiary C—H attack).

Dr. Walsh's theory suggests another interpretation. Initial abstraction of a hydrogen atom is no longer considered to be the determining step but rather abstraction in conjunction with isomerization of the RO_2 radical. Now the reaction (1)

$$\diagdown\!\diagup\!\text{C}\!\diagdown\!\diagup + \text{O}_2 \rightarrow \diagdown\!\diagup\!\text{C—O}_2\!\diagdown\!\diagup \qquad (1)$$

is exothermic to the extent of 30 to 40 kilocalories.

The exact value will depend on the strength of the C—O bond formed. The exothermicity of (1) will therefore decrease in the order: $1y > 2y > 3y$. This energy may be carried over to the isomerization reaction. If then, a further abstraction of the same type of hydrogen is considered, say, a β-secondary atom, the ease with which the over-all reaction (2) will occur

$$R_1\cdot + O_2 + R_2H \rightarrow R_1O_2H + R_2\cdot \qquad (2)$$

will be in the order $1y > 2y > 3y$.

In the case of intermolecular reaction the energy of reaction (1) would be most probably redistributed throughout the internal degrees of freedom of the RO_2 radical before the second hydrogen could be abstracted. However, when intramolecular reaction occurs, there is a possibility that the energy remains localized in the oxygen bond long enough to contribute to the second abstraction reaction. Thus although the ease of abstracting the initial hydrogen is in the order $3y > 2y > 1y$ the reverse order may apply to the second abstraction. The conflict between the two orders (which of course, apply to the same carbon atom) could therefore explain why attack at secondary C–H bonds appears to control the knock ratings of fuels. Does Professor Walsh think this is possible?

PROF. A. D. WALSH: In reply to the second of the two points raised by Dr. Carhart, if there are several lobes in the ignition diagram of a fuel then there are several temperature regions which may be described as possessing a "negative temperature coefficient of oxidation." I suggest that these result from com-

petitions of the type

(isomerized RO_2) + O_2 → (RO_4) and a branching chain

(isomerized RO_2) → decomposition and a straight chain.

The first of these competing reactions is expected to need zero activation energy and so to be overtaken by the second reaction (which is expected to require an activation energy) as the temperature is raised. There will be as many such competitions as there are types of isomerized RO_2 radicals. In addition, I suggest that the competition of isomerization and decomposition of (original) RO_2 occurs in all the temperature regions.

As regards Dr. Carhart's first query, I agree that R in RO_2 will particularly include tertiary alkyl radicals if the original fuel molecule contains tertiary C–H bonds; and have suggested that in the two lowest temperature regions RO_2 radicals derived from tertiary R isomerize only by internal transfer of an H atom from a secondary or tertiary C–H bond. Dr. Scott, however, makes an interesting point that may affect the relative importance of RO_2 radicals derived from tertiary and secondary R radicals in determining knock ratings. I think Dr. Scott must be right in the general point that energy factors must be taken into account in reaching a complete understanding of the processes leading to ignition at low temperatures.

In conversation, Dr. Scott has stressed to me a further observation that seems strongly to confirm the main point of my paper, *viz.*, the importance of intramolecular effects in determining ease of ignition and knock ratings. It is that *m*- and *p*-xylene have about the same knock resistance, but *o*-xylene is quite different and has a far lower knock rating. What explanation other than intramolecular interaction could be advanced for the large *o*-effect? One writes the sequence of reactions:

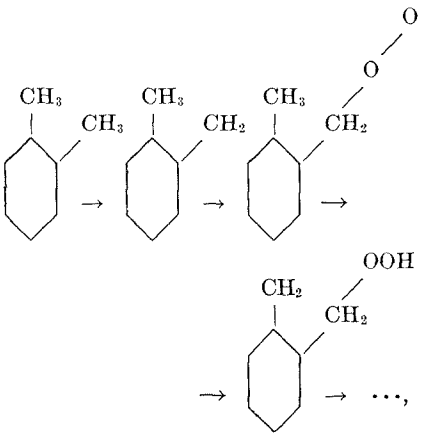

the last step written being very much more difficult for *m*- than for *o*-xylene and impossible for *p*-xylene. The point is similar to the stress on the high knock ratings of cyclohexane and cyclopentane relative to *n*-hexane and *n*-pentane, which ratings are all the more remarkable since the cyclohexane and cyclopentane molecules possess of course more CH_2 groups than the *n*-hexane and *n*-pentane molecules, respectively.

EFFECT OF ANTIKNOCKS ON FLAME PROPAGATION IN A SPARK IGNITION ENGINE

S. CURRY

Knock is normally accompanied by an acceleration of the primary flame to measured terminal velocities in the range of 300 to 1200 feet per second. The transition to these knock inducing flame propagation rates can occur over an extended period and the addition of tetraethyllead results in a significant reduction in the measured flame front velocities under knocking engine conditions. Tetraethyllead does not appear to affect flame propagation rates under nonknocking engine conditions.

Acceleration of the knock inducing flame fronts is believed to result from the formation of some critical concentration of active species produced during the course of the preflame reactions. It thus appears that tetraethyllead suppresses knock by deactivating or inhibiting the formation of these species.

The acceleration to knock inducing flame propagation rates can begin quite early in the combustion cycle and tetraethyllead can measurably suppress this acceleration.

Introduction

The ability of small quantities of antiknocks, such as the lead alkyls, to suppress or moderate knock in internal combustion engines is well known, but the exact mechanism by which antiknocks function is not completely understood. Although the fast rates of combustion which lead to knock and the effect of antiknocks on the combustion process have been the subject of extensive study, no single concept of knock and antiknock mechanism is sufficient to explain all of the various observations. The relationship between knocking combustion and antiknocks is such that an understanding of the events leading to knock should aid in the understanding and prediction of the effects of antiknocks on the combustion process.

Combustion in a spark ignition engine has been investigated in terms of flame development and subsequent propagation throughout the combustion chamber and the effect of tetraethyllead on the development of flame fronts associated with both knocking and nonknocking combustion has been studied. The results have led to a concept of knocking combustion which is consistent with the observed effects of antiknocks.

Experimental Equipment

The engine used was a Waukesha CFR engine with a split head combustion chamber mounted on an ASTM–CFR high speed crankcase and coupled to a variable speed dynamometer. A modified high compression ratio piston was used which allowed the compression ratio to be varied from 5:1 to 25:1. The progression of the flame front across the combustion chamber was detected by 49 ionization gaps, 27 mounted in the cylinder head and 22 on the surface of the piston. A sketch of the location of the ion gaps in the cylinder head is given in Fig. 1. The points indicated by letters on the sketch represent the positions at which flame front velocities were determined for many of the results presented here. A pressure sensing element was also used to determine the occurrence of knock, making possible the measurement of the time of knock as

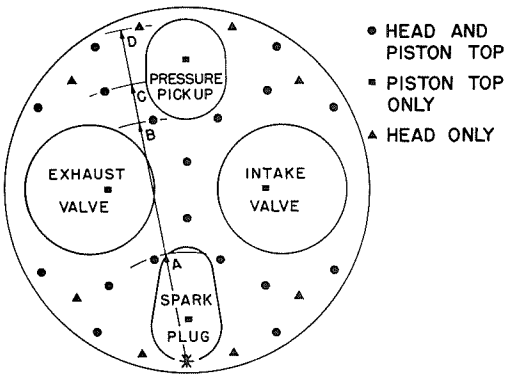

FIG. 1. Progression of the flame front was followed by multiple ionization gaps. An analysis of flame front velocities between points A, B,C, and D accurately describes the general trend.

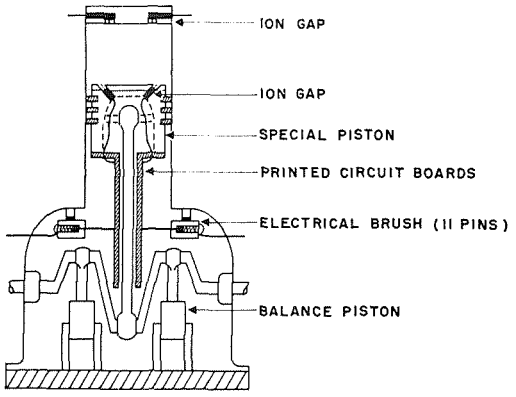

FIG. 2. Multiple ionization gaps were installed on both piston and cylinder head surfaces.

well as the time of peak pressure. A schematic cross section of the engine is shown in Fig. 2.

Because of the large amount of information available during each cycle, the instrumentation was designed to collect and store data at rates up to 100,000 events per minute with a time resolution of ten microseconds. A schematic diagram of the data handling facilities is shown in Fig. 3. The principle of operation may be described as follows: an ignition pulse ignites the charge and also starts, in a digital encoder, 28 binary counters which count at a frequency determined by an oscillator setting. When events of interest occur, pulses are produced by a synchronizer and transmitted to the digital encoder, stopping the counters. The time intervals recorded by the 28 counters are stored on a magnetic tape recorder during the exhaust stroke. The counters are then automatically reset to zero and this sequence is repeated for a predetermined number of firings. Information stored on the tape is processed by a digital computer and the information typed out at some convenient time.

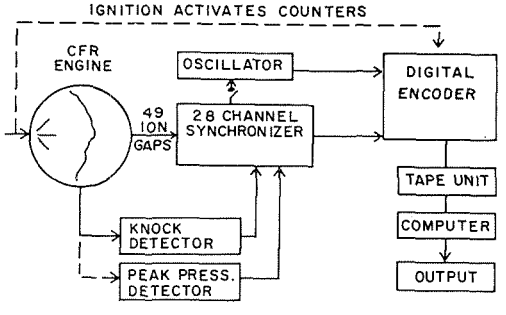

FIG. 3. The data handling facilities transmitted 28 channels of information from the engine to a tape recorder at rates up to 100,000 events per minute with a time resolution of 10 microseconds.

The 28 data points recorded represent the time interval from ignition to the time of the events. These times are then used to determine the flame propagation patterns and rates for consecutive single cycles or for the average of any preselected number of cycles.

A frequency switch signal was produced by the synchronizer and used at a selected time during the cycle to increase the oscillator frequency to a preselected high value, permitting very short time resolutions with a limited counter capacity. Low frequencies were used to follow the relatively slow moving flame front during the early phase of a cycle. The counting frequency was then switched to a higher value to follow the high flame speeds associated with knock.

A detailed description of the engine and modifications required to install the ionization gaps and of the instrumentation and data handling facilities is given in reference 1. Also discussed are the limitations inherent in the use of ionization gaps to detect the presence of a flame and the precautions taken to ensure that the measurements were as exact as possible. Although complete maps of the flame propagation patterns were obtained during this study, a point by point statement of the flame arrival times and propagation velocities will be used to describe the effects observed in this present work. This approach has been justified as a result of extensive analysis of flame propagation patterns in three dimensions on the basis of a single cycle and the average of many cycles. The work in three dimensions showed that a great deal of caution must be exercised in making a detailed analysis of a single cycle; however, the general trend can be described accurately by multicycle average data.

Concept of Knock

Before considering the influence of antiknock compounds on the development of knocking combustion, it is necessary to review the present concepts of the modes of combustion by which knock is induced. On the basis of earlier work, two predominant theories have prevailed—the autoignition theory and the detonation theory. The autoignition theory postulated that, owing to sensitization of the fuel-air charge of the end gas region by preflame reactions, several portions of the charge undergo virtually simultaneous autoignition and this high speed combustion results in a local pressure imbalance and the characteristic gas vibrations. The detonation theory postulates that, owing to shock waves or some other disturbance within the combustion chamber, a true detonation wave is established and propagates through the unburned portion of the charge at velocities in excess of sonic. Such a

detonation wave has associated with it a sharp pressure discontinuity which could give rise to the characteristic gas vibrations.

The initial results of the present work with these new facilities, presented in more detail in reference 1, have led to a concept of knocking combustion which is somewhat different from either of the two just discussed. This concept can be reviewed as follows: knock (engine noise and gas vibrations) can be induced as a result of a rapid rate of pressure rise associated with an acceleration of the primary spark ignited flame front to velocities on the order of 300 to 1200 feet per second. In other words, a single spark ignited flame can sweep through the gases at a rate sufficient to induce knock without either the occurrence of autoignition or the development of a true detonation wave.

Even at light levels of knock, the tendency of the flame front of a knocking cycle to accelerate to the high rates required to induce knock can be observed. The term "light knock" is applied to those conditions under which less than 100% of the cycles actually knock. Therefore, the reference to a 37% knock level would describe 100 consecutive engine firings in which there were 37 knocking cycles and 63 nonknocking cycles.

A typical example of the average flame propagation history for a 37% knock level is shown in Fig. 4. In this figure, the average times required for the flame to reach selected points on the cylinder head have been plotted for both knocking and nonknocking cycles. It can be observed that the knocking cycles are characterized by

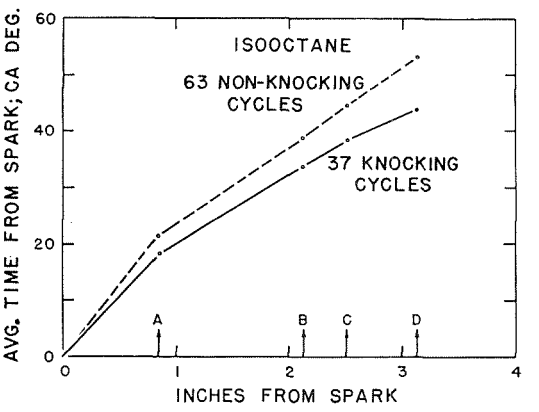

FIG. 4. The average flame propagation rate for knocking cycles was greater than for nonknocking cycles throughout the cycle. Fuel–isooctane; compression ratio—10.14; spark advance—20°btc; F/A ratio—0.0612; mixture temperature—200°F; map—30 inches Hg; Speed—1200 rpm; coolant temperature—212°F; per cent knock—37.

shorter burning times, and thus higher flame propagation rates, throughout the cycle. While analyses such as these leave no doubt that knock occurs on those cycles having the shortest end gas residence time, a study of the distribution of the flame arrival times of the selected points further demonstrates that knocking cycles are characterized by an acceleration of the primary flame front.

Histograms for the flame arrival times at

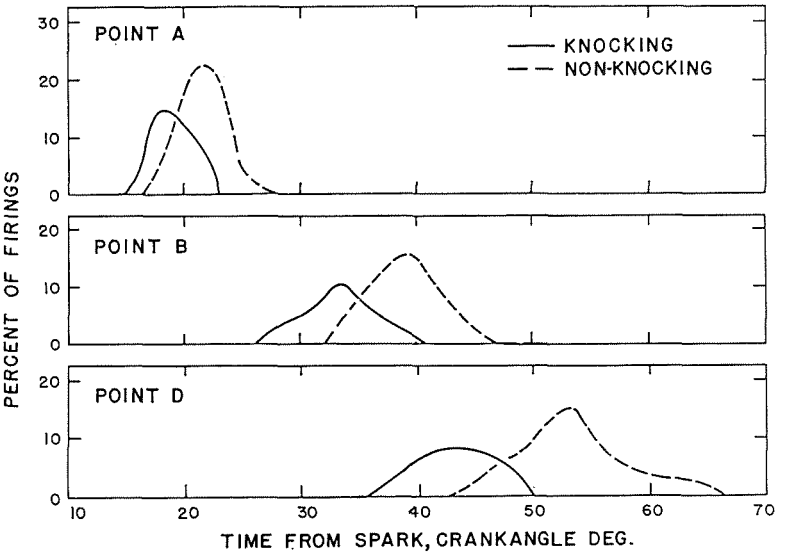

FIG. 5. The distribution of flame arrival times at the selected points depicts an increasing separation between knocking and nonknocking populations.

points A, B, and D were obtained and the envelopes which inscribe these histograms are shown in Fig. 5. The distributions for the knocking and nonknocking cycles were treated as separate populations. The spread between the two populations at point A is sufficiently small that it may be attributed to normal cycle-to-cycle variations. However, by the time the flame front reached point B, the spread between the two populations was sufficient that they must be regarded as two independent populations. Also, a distribution of this kind can no longer be attributed to normal cycle-to-cycle variation. By the time the flame has progressed to point D an almost complete separation has occurred as a result of the acceleration of flame fronts during those cycles which resulted in knock. In other words, it becomes possible later in the cycle to predict with increasing certainty the impending event of knock on the basis of flame propagation rate alone.

A complete separation of the two populations was not achieved at these light levels of knock because the ion gap at point D was not necessarily the last gap to fire and the method for detection of knock was not absolute. In spite of this, these data imply that, even under very light knocking conditions, the impending event of knock is accompanied by an acceleration of the primary flame front.

These accelerating flame fronts are more clearly depicted under heavy knock conditions, particularly with *n*-heptane. Studies of the flame propagation patterns of *n*-heptane under heavy knock conditions have resulted in velocity vector diagrams such as shown in Fig. 6. Under these

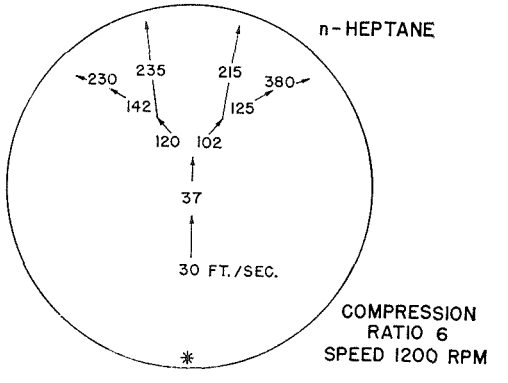

FIG. 6 With heavy knock the measured flame propagation rate increased to 10 to 20 times the normal velocity before knock occurred. Spark advance—15°btc; F/A ratio—0.073; mixture temperature—100°F; map—30 inches Hg; coolant temperature—212°F; speed—1200 rpm; 100% knock.

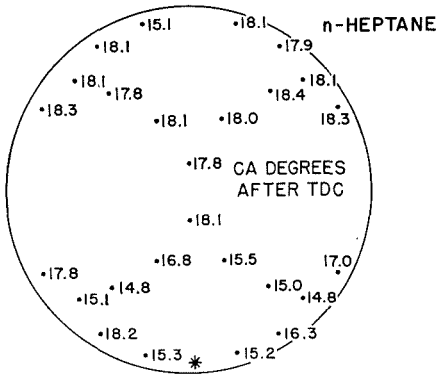

FIG. 7. The development of the combustion process resulting from pure autoignition is too complex for meaningful analysis. Fuel—*n*-heptane; compression ratio—7.54; spark time—none; F/A ratio—0.066; mixture temperature—100°F; speed—1200 rpm; map—30 inches Hg; coolant temperature—212°F.

conditions, the transition velocities have been increased to such an extent that statistical implications of the accelerating flame front are no longer necessary. Results such as these have shown that a spark ignited flame front can develop and accelerate across the combustion chamber reaching velocities sufficient to induce knock. The analysis of thousands of flame maps such as these has led to the conclusion that it is not necessary to have either autoignition in the end gas region or a true detonation wave to have knock. Thus, it appears that energy release rates associated with flame front speeds of 300 to 1200 fps are sufficient to produce knock.

These experiments indicate that knock is induced by the high rates of energy release associated with flame propagation rates 10 to 20 times normal and that even under conditions of light knock a detectable acceleration of the primary flame front occurs. Once we have established that one of the primary characteristics of a knocking cycle is a definite acceleration of the primary flame front, two important questions arise: (1) What factors cause the acceleration? and (2) Do antiknocks influence the development of the flame front under these conditions?

With regard to the first question, there are several possibilities. Certainly one important possibility is an autoignition process. While it is true that autoignition processes might, under heavy knock conditions, proceed in such a manner that they could give the appearance of a high speed flame front, it is not likely that they would account for the acceleration of the flame front with light knock. Attempts to study the development of the combustion process with pure autoignition resulted in flame maps such as

those shown in Fig. 7. Under these conditions, the development of the combustion process is so complex that the primary mode by which the charge is consumed cannot be ascertained. It can only be assumed that the final reactions were a result of autoignition. For the most part, these types of combustion patterns were not encountered in studies with spark ignited charges. Although autoignition was not uncommon, particularly with *n*-heptane, the development and acceleration of the primary flame was clearly evident even when average values for many consecutive cycles were used.

The two more likely reasons for acceleration of the flame front are an increasing temperature environment into which the flame is progressing and changes in the composition of the unburned gases. Such changes in composition would be likely to include active species formed during the preflame reactions.

It is known that preflame reactions occur in the unburned portion of the fuel-air charge ahead of the advancing flame and the rising temperatures resulting from compression tend to accelerate these reactions. The major products formed during the preflame reaction have been identified as hydrogen peroxide, formaldehyde, and the higher aldehydes. It is reasonable to assume that these products could have been formed from such simple radicals as OH and HO_2. Increasing concentrations of such mobile free radicals might increase the flame propagation velocity to a measurable extent. Under light knock conditions, normal cycle-to-cycle variations in the combustion process may give rise to higher than average burning rates and the higher temperatures and pressures associated with these faster burning cycles could result in higher than average concentrations of active species. This, in turn, could lead to even higher burning rates resulting in ever increasing concentrations of active species as the flame front progresses across the combustion chamber. These increasing concentrations might then increase the flame propagation velocity far above the normal flame velocity. The observations might also be explained on the basis of a thermal mechanism of flame propagation and thus it is difficult to separate temperature effects and the influence of composition; however, a study of the effect of antiknocks permits a more narrow interpretation.

Effect of Tetraethyllead on Flame Propagation

The second question raised as a result of the observed acceleration of the knock-inducing flame fronts is what effect, if any, do antiknocks exhibit on the development of the flame front. As

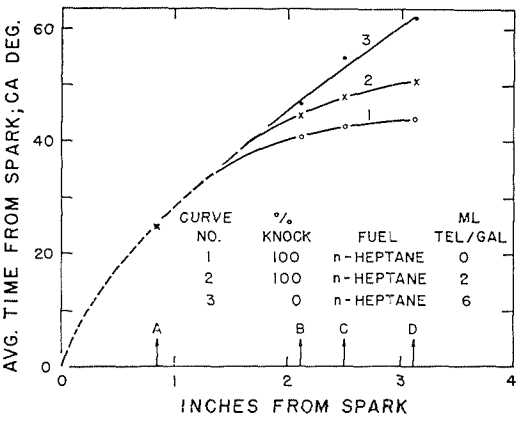

FIG. 8. The addition of tetraethyllead produces a marked increase in the average burning times required to reach the selected points under knocking conditions. Compression ratio—6.16; F/A ratio—0.066; spark advance—15°btc; mixture temperature—100°F; map—30 inches Hg; speed—1200 rpm; coolant temperature—212°F.

expected, the addition of tetraethyllead had no detectable effect on flame propagation rates during nonknocking combustion; however, its effect on flame propagation rates under knocking conditions was quite pronounced.

The most pronounced effects of tetraethyllead on flame propagation rates were obtained with *n*-heptane as the fuel. The results are presented in Fig. 8. The test conditions were such that the engine was operating at a compression ratio just below trace knock with *n*-heptane containing 6 ml of tetraethyllead per gallon. The data repre-

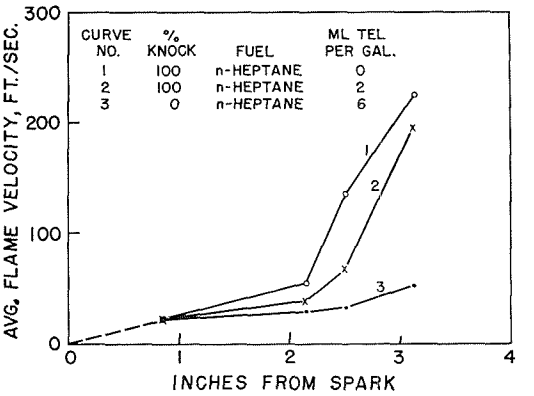

FIG. 9. The average flame front velocity undergoes a marked acceleration quite early in the cycle as tetraethyllead is removed and the knock intensity increased.

sent the average burning times required for the flame front to reach selected points in the combustion chamber. It can be seen that as the tetraethyllead concentration is reduced, and knock intensity increases, the burning time curve begins to depart from the nonknocking combustion curve quite early in the cycle.

An incremental velocity plot of these same data, shown in Fig. 9, provides a more graphic illustration of the transition in flame front velocities accompanying the knocking process. While it is recognized that these curves represent average data for 100 consecutive cycles, the averages clearly depict the trend which is also detectable on the basis of single cycle analysis. It can be observed that even with *n*-heptane + 6 ml tetraethyllead operating just below trace knock there is a detectable acceleration of the flame front in the end gas region. As knock intensity is increased by the removal of tetraethyllead, the average flame speed increases through most of the cycle. Conversely, then, it can be stated that the addition of tetraethyllead can suppress the acceleration of the flame front which precedes the occurrence of knock. On the basis of these data, it is evident that tetraethyllead can have a measurable effect on flame propagation rates in an internal combustion engine.

While these tests provide the first data which indicate that flame propagation rates in an engine can be reduced by metallic antiknocks, inhibition effects have been observed by other investigators outside of engines. Lask and Wagner[2] found that 0.015 volume percent of tetraethyllead decreased the flame velocity of a stoichiometric mixture of *n*-hexane and air by 30%. Bonne, Jost, and Wagner[3] found that as little as 0.01% of iron pentacarbonyl reduced the burning velocity of a stoichiometric methane-air mixture at atmospheric pressure by 25%. While the specific action of the additive was not determined, it was proposed that the inhibition effects resulted from an interaction with free hydroxyl radicals.

On the other hand, the ability of metal antiknocks to influence the transition of a deflagration to a detonation was demonstrated as early as 1937 by Shtsholkin and Sokolik.[4] While it has been shown that tetraethyllead does not affect the velocity of a detonation, Shtskolkin and Sokolik demonstrated that tetraethyllead could influence the predetonation path. Working with pentane, oxygen, and nitrogen mixtures, with initial pressures below atmospheric, they were able in some cases to increase the distance required for the detonation to form by a factor of two. However, these results were obtained at a very high tetraethyllead concentration (1.2%).

While all these results support the conclusion that metallic antiknocks can influence the propagation rate of a flame front, it still remains necessary to postulate a mechanism. Certainly the question remains as to whether acceleration of the flame fronts, which has been observed in this work, results from changes in the temperature or composition of the gas ahead of the flame. However, there are a number of facts which indicate that a purely thermal mechanism of flame propagation is not entirely responsible.

The work of Pastell[5] and Pahnke[6] showed that exothermic preflame reactions are not inhibited by tetraethyllead. In motored engine studies it was shown that the appearance of cool flames and the energy release associated with cool flames was not significantly affected by tetraethyllead. Further, it has been shown that for two fuels of the same octane level, one leaded and one unleaded, the leaded fuel will reach end gas temperatures several hundred degrees above the end gas temperature of the unleaded fuel before knocking combustion is encountered.[7] It thus appears from the results of reference 7 that two fuels of the same octane level can have entirely different temperature histories but the total combustion time of the leaded fuel, even though at higher temperature, is not much different from that of the unleaded fuel. These studies demonstrated that the main course of preflame reaction is not greatly altered by tetraethyllead. Therefore, it might seem logical to assume that development of the flame front as a result of temperature would not be greatly influenced by the presence or absence of tetraethyllead. However, this was not the case during combustion leading to knock.

Since the change in temperature of the gas into which the flame is advancing does not appear to be the primary cause for acceleration of the flame front, it is necessary to consider changing composition. A number of studies have shown that extensive decomposition of *n*-heptane can occur as part of the preflame reaction.[5,6,8,9] The major products of such reactions are formaldehyde and hydrogen peroxide which might result from reactions of simple radicals such as OH and HO_2. The influence of such active species and products of combustion on flame propagation rates has been demonstrated.[10,11] It appears entirely possible that the role of antiknocks may be very similar to that proposed by Bonne, Jost and Wagner;[3] namely, a deactivation of free radicals such as hydroxyl radicals. Therefore, it is believed that the acceleration of the flame front which has been observed results from the formation of high concentrations of mobile free radicals or atoms in the unburned portion of the fuel-air charge ahead of the flame front. The mechanism of antiknocks, such as tetraethyllead,

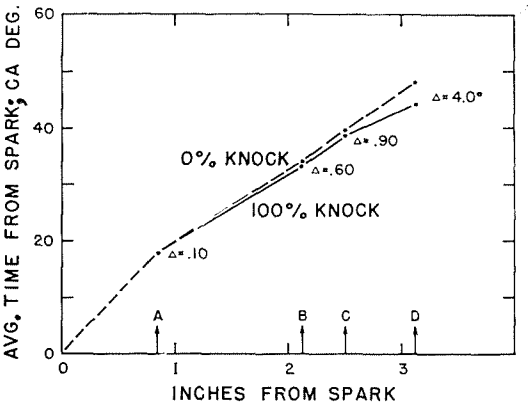

FIG. 10. The effect of tetraethyllead on the average flame propagation rate of isooctane is not so marked as in the case of *n*-heptane; however, the effect is still quite significant. Compression ratio—9.81; spark advance—20°btc; F/A ratio—0.061; mixture temperature 150°F; map—30 inches Hg; speed—1200 rpm; coolant temperature—212°F.

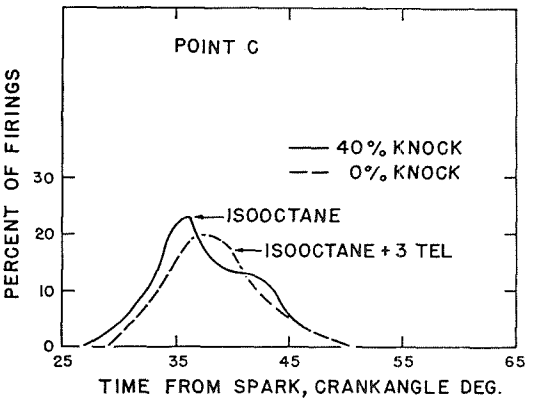

FIG. 12. The abnormality of the flame arrival distribution, as a result of knocking combustion, increases as the flame front progresses across the combustion chamber. Compression ratio—10.53; spark advance—15°btc; F/A ratio—0.071; mixture temperature—100°F; map—30 inches Hg; speed—1000 rpm; coolant temperature—212°F.

may then be one of destroying or suppressing the formation of such particles.

While the effect of tetraethyllead on flame propagation rates is quite detectable in *n*-heptane, the results are not so marked in high octane fuels such as isooctane. For example, when 100 knocking cycles for isooctane are compared with 100 nonknocking cycles, the results in Fig. 10 are obtained. Under these conditions there is no significant difference between the knocking and nonknocking cycles until about two-thirds of the volume has been burned. These results differ from the mixed knocking and nonknocking cycle data at light levels of knock in that the effect of normal cycle-to-cycle variations has been eliminated. Isooctane oxidizes more slowly and less extensively than *n*-heptane and thus produces critical concentrations of preflame reaction products later in the cycle, even though the region of reaction is at higher temperatures. Because of the delayed formation of active species which appear to cause knock, the effect of tetraethyllead on the average flame propagation rate is not detectable until later in the cycle. The effects observed, while small, are quite real and analysis of the flame arrival time distributions at points B and C, as given in Figs. 11 and 12, support this.

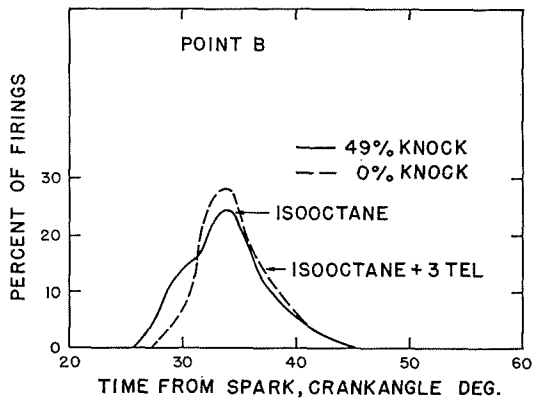

FIG. 11. The addition of tetraethyllead under knocking conditions reduces the average flame propagation rate and tends to normalize the distribution. Compression ratio—9.59; F/A ratio—0.070; spark advance—20°btc; mixture temperature—150°F; map—30 inches Hg; speed—1200 rpm.

Effect of Environmental Factors

Measurements obtained in a repetitive batch type reactor such as an engine are subject to changing environmental factors which might affect the results. Two such factors which might be of considerable importance are wall temperatures and exhaust gas dilution. To determine if these factors could account for the observations made, eight-cycle tests were conducted at very light knock levels. The eight-cycle tests were conducted by igniting the spark on every fourth revolution, with a fresh charge introduced into the cylinder every second revolution. In this manner the fresh charge could cool the cylinder and scavenge the burned gases.

Since the results obtained under eight-cycle

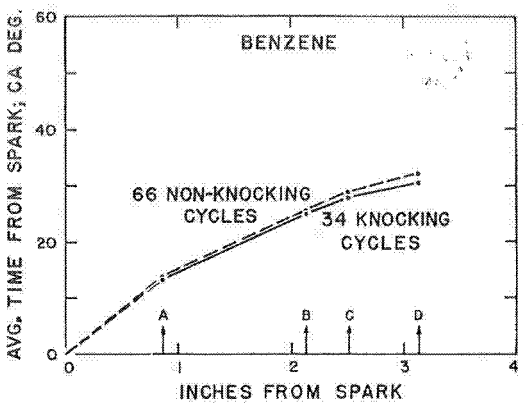

FIG. 13. The flame propagation rates for benzene are quite similar for knocking and nonknocking cycles at light knock. Fuel—benzene; compression ratio—11.43; spark advance—22°btc; F/A ratio—0.084; mixture temperature—300°F; speed—1200 rpm; map—30 inches Hg.

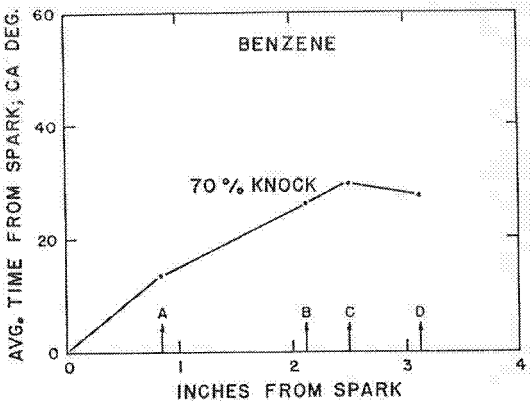

FIG. 15. The development of multiple flame fronts in the end gas is quite detectable even when average values are to be used. Fuel—benzene; compression ratio—11.43; spark advance—22°btc; F/A ratio—0.084; mixture temperature—300°F; map—30 inches Hg; speed—1200 rpm; per cent knock—70.

conditions were so similar to the four-cycle data, they will not be presented in detail. It is sufficient to state that under conditions of light knock the same conclusion concerning the effects of tetraethyllead can be drawn on the basis of data obtained under either eight-cycle or four-cycle engine conditions. It appears that wall temperatures and exhaust gas dilution are not primarily responsible for the effects observed with light knock.

This conclusion is further supported by results obtained with benzene. With benzene at a 34% knock level and four-cycle engine conditions, there was little difference between the knocking and nonknocking cycles, as shown in Fig. 13.

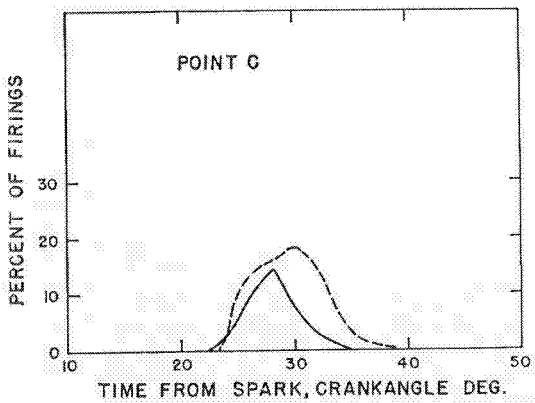

FIG. 14. The distribution of the flame arrival times at point C indicates that benzene does not undergo the acceleration to knock which is characteristic of the paraffinic fuels.

Even when the distributions were analyzed there was little evidence to indicate any unusual acceleration of the primary flame front of those cycles which produced knock. Such an analysis at point C is shown in Fig. 14. When benzene was stressed to higher knock levels, although less than 100 percent, the occurrence of multiple flame fronts was so pronounced that average values could not be used to describe the development of the flame fronts. Average burning times for benzene at a 70 percent knock level are presented in Fig. 15 and clearly depict the presence of multiple flame fronts.

The data presented in Figs. 14 and 15 suggest that knocking combustion develops in a manner quite different for benzene than for the paraffinic fuels. It is known that benzene does not undergo any significant preflame reaction of the type experienced with paraffinic fuels and for all practical purposes has no tetraethyllead response. Further, these data indicate that knocking combustion with benzene is not accompanied by the characteristic acceleration of the primary flame front observed with paraffinic fuels. This would suggest that knocking combustion in the case of benzene might proceed by autoignition.

The results obtained under eight-cycle engine conditions support the position that the accelerating characteristic of the knock inducing cycles of paraffinic fuels results from factors other than normal cycle-to-cycle variations. These results and the flame propagation characteristics of benzene under four-cycle engine conditions suggest that environmental factors are not primarily responsible for the differences between knocking and nonknocking combustion.

REFERENCES

1. CURRY, S.: SAE paper No. 452B, January 1962.
2. LASK, G. and WAGNER, H. G.: *Eighth Symposium (International) on Combustion*, p. 432–438. Williams and Wilkins, 1962
3. BONNE, U., JOST, W., and WAGNER, H. G.: Fire Research Abstracts and Reviews *4*, 6 (1962).
4. JOST, W.: *Explosion and Combustion Processes in Gases*, p. 191. McGraw-Hill, 1946; SHTSHOLKIN, K. and SOKOLIK, A.: Acta Physicochim. URSS *7*, 581 (1937).
5. PASTELL, D. L.: SAE Quart. Transactions *4*, 571 (1950).
6. PAHNKE, A. J.: Literature of the Combustion of Petroleum (No. 20 in Advances in Chemistry Series), p. 202. Am. Chem. Soc., 1958.
7. GLUCKSTEIN, M. E. and WALCUTT, C.: SAE Transactions *69*, 540 (1961).
8. LEVEDAHL, W. J.: *Fifth Symposium (International) on Combustion*, p. 372. Reinhold, 1955.
9. MALMBERG, E. W., SMITH, M. L., BIGLER, J. E., and BOBBITT, J. A.: *Fifth Symposium (International) on Combustion*, p. 385. Reinhold, 1955.
10. BASEVICH, V. YA., DEVISHEV, M. I., and KOGARKO, S. M.: ARS Journal Supplement, pp. 133–137, January (1962).
11. SIMON, D. M.: Ind. Eng. Chem. *43*, 2718 (1951).

Discussion

DR. L. S. ECHOLS (*Shell Oil Company*): Of the thought-provoking deductions made by the author it is clear that his conclusion that neither autoignition nor detonation are necessary for knock is the most noteworthy and questionable.

However, before discussing this, it is of some importance to point out several problems of measurement which require the exercise of caution in interpreting these data. First, will an ionization gap respond only to the passage of a hot flame? Our information suggests that ion gaps do not respond to cool flames, but it is not clear that signals may not result in the approach to autoignition conditions. For example, in Fig. 1 would the gas at Condition C be responsive? Second, the time lag of an ion gap may easily be 100 microseconds, and may be shorter at higher temperatures. Such successively shorter time lags would appear as an acceleration of the flame. Third, if the flame front approaches two ion gaps at an angle to a line connecting them, the calculated flame speed will be in error by a factor equal to the inverse sine of the included angle. This error may be large. Fourth, the proportion of the charge involved in light knock is small, because it is not uncommon for the knock event to occur after peak pressure. Even if as much as 10% of the charge is involved this would occupy only about 2% of the volume of the combustion chamber. It is unlikely that one, much less two, ion gaps are located in this volume. Hence, the observed speed of the flame in the knocking end gas will be lower than the true value. Finally, the flame velocities observed are the vector sums of the burning velocity and the transport velocity of the gas itself. The latter is a result of swirl and the expansion of the burned gas. Such expansion may account for velocities of the order of 50 ft/sec at the midpoint of the volume. These comments suggest that, although the flame may truly accelerate prior to knock, we must be careful in accepting the values found here, and we must seriously question the magnitudes of velocities quoted for the knock process itself.

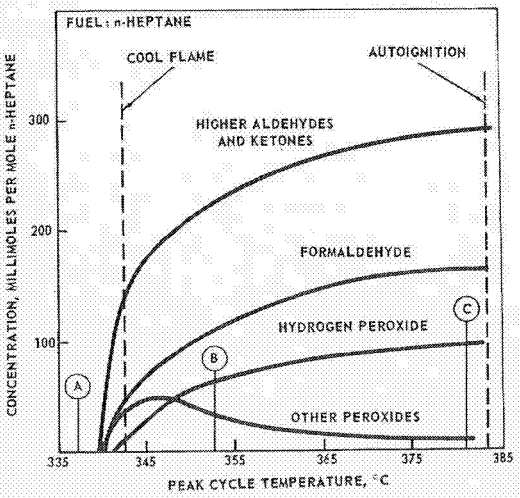

FIG. 1.

Is there reason to believe that the flame would move rapidly into gas which contains "active" species? In Fig. 1 the flame velocity at condition A would be the normal flame velocity. If, however, we bear in mind the fact that modern theory of autoignition requires that this is a degenerate explosion at T_i, the active species involved are probably unstable molecules such as formaldehyde and peroxides, not the hydrogen atoms and/or active free radicals responsible for propagation of the flame. It is not clear that these two major classes of active species would cooperate in accelerating the flame in prereacting gas. Direct measurements of flame velocities into, say, prereacting *n*-heptane/air mixtures would be interesting. If there is indeed cooperation between the molecules responsible for de-

generate chain branching and the atoms and free radicals of the flame then we would expect the flame velocity to increase greatly between states B and C of Fig. 1.

Are there no choices in knock theory other than detonation or simultaneous autoignition? A theory of knock based on the concept of a critical temperature gradient in the end gas just sufficient to produce autoignition of successive laminae giving a flame velocity approaching the velocity of sound has been proposed.[2] The velocity of this "gradient flame" is

$$(V_{fg})^{-1} = -K \exp(E/RT)(T^2)^{-1}(dT/dx),$$

where V_{fg} = the "gradient flame" velocity; E = the apparent activation energy for autoignition; R = the gas constant; T = the absolute temperature; and x = the distance of flame travel. The required gradients are of the order of a few degrees Centigrade per meter, and the results of this process alone, or of interaction with the pressure waves already present in the gas, are the high intensity pressure waves characteristic of knock. Detonation velocities may occur, but they are not a necessary consequence of this theory. The conclusions which may be drawn from the present work and from the work of Livengood and Wu[3] in their calculations of the critical conditions for knock based on end gas histories are consistent with the critical temperature gradient theory. Autoignition needs only to produce gradient flames having velocities approaching that of sound to result in the gas vibrations of knock.

DR. W. A. HERBST (*Esso Research and Engineering Co.*): The work Mr. Curry has reported is a fresh and imaginative approach to the old problem of the nature of combustion in spark-ignited internal combustion engines. It supplies another piece to the puzzle and helps to round out the overall picture. However, considering the complexity of the problem it is not surprising that it is easier to raise questions than to supply answers.

The data reported suggest that knock can be induced as a result of a rapid rate of pressure rise associated with an acceleration of the primary flame front to velocities in the order of 300 to 1200 fps. This is somewhat different from previous concepts of knock based on the occurrence of autoignition or a true detonation wave in the last part of the charge to burn. Before accepting the theory, however, a number of points need clarification:

Are the ionization gaps giving a true measure of what is occurring in the bulk of the charge? Flame velocities measured at the wall by the ion gaps may be low because of wall quenching effects and viscous resistance to flow. It may be that the flame velocities in the center of the charge are much higher than those reported. In this connection it might be instructive (but not conclusive) to determine whether the velocities as measured on the piston surface are different from those on the cylinder head. These may be different because of surface temperature difference. A study of the pressure-time diagrams would also be interesting. How do the pressure changes correlate with flame behavior as indicated by the ion gap elements?

Is it possible that the ion gaps are measuring the passage of an "ionization" wave but that knock results shortly thereafter from a rapid reaction of the ions and radicals thus formed?

Is it possible that a wave traveling at 300 fps can give rise to a noise having the frequency of

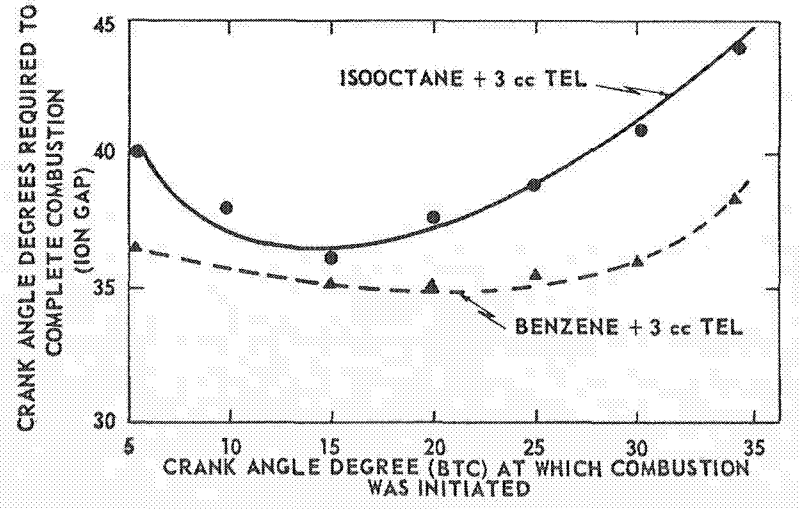

FIG. 2. Comparison ratio, 10/1; speed, 2000 rpm; throttle wide open.

knock, i.e., 3000 to 8500 cps? At 300 fps a wave will cross a 3.1 inch diameter chamber and return 583 times per second.

The differences in behavior between benzene and paraffinic fuels is interesting and is consistent with other data indicating benzene has a unique oxidation mechanism. In this connection Figure 2 may be of interest. It presents Esso Research data taken from a report by Massa.[4] It will be noted the time required to complete combustion for iso-octane with 3 cc TEL increases as ignition is started earlier in the cycle whereas benzene is relatively insensitive to this factor. It is believed this effect is due to the differences in precombustion reactions of the two fuels. At advanced ignition settings, iso-octane has less time in which to develop precombustion reactions; it therefore burns slower and takes longer for complete combustion. Benzene, on the other hand, is not prone to precombustion oxidation. It is therefore, relatively insensitive to ignition setting.

PROF. J. J. BROEZE (*Technical University of Delft*): The findings of the author concerning accelerating flame fronts in the case of *n*-heptane are most interesting, and call for some comments.

First, it is quite conceivable that in cases of very intense turbulence the very mechanism of flame propagation will embody elements of a self-ignition mechanism in isolated patches that are torn loose from the flaming mass. It should be clear that whereas most work in turbulent flow deals with turbulence intensities of the order of 5 to 15%, in the gasoline engine the incoming gas flow is converted 100% to turbulence.

Second, in distinguishing in the case of light knock between successive cycles that knock and that do not knock, there may be in actual fact a spread in the delay of flame spread which results in earlier or later combustion. Under borderline knock conditions, the early cycles will then knock, the late cycles not; in other words, the correlation may be the other way around.

Thus, there is usually a heat flow gradient in the combustion chamber in the direction of flame travel because: (1) The gases first burned are eventually the hottest from elementary thermodynamics; (2) they have the longest contact with the walls; and (3) the exhaust valve is usually in that area. This results in an inhomogeneous condition in the nonburned gas so that it will be nearer to self-ignition near the flame front than further away, and so a self-ignition may set up with a directional trend in the same way as the flame front.

Last, however, I would like to warn the author that in dealing with knock or detonation in engines he is dealing with engine pathology and should be careful to avoid the pitfalls of the psychiatrists who are all too likely to see their cases as normal. In particular, I take exception when he tends to call the case of *n*-heptane "normal." There is not a single gasoline pump in the world where it may be bought. The more normal case is that of iso-octane, being much nearer to the properties of commercial gasolines. So, normally, the flow front does not speed up appreciably.

DR. S. CURRY (*E. I. DuPont*): Dr. Herbst, Dr. Echols, and Prof. Broeze point out the many difficulties encountered in interpreting measurements associated with knocking combustion. However, the measurement limitations suggested by the discussors are not so extreme that valid conclusions cannot still be drawn if sufficient data are examined. A major point of concern pertains to the primary detection element of the instrumentation, namely, the ionization gap. It is asked whether ion gaps respond to cool flames and whether they give a true measure of what occurs in the bulk of the charge.

The answers to both questions depend upon the definition of a flame front—is it best defined by electron concentration, luminosity, or temperature? In any case, we agree with Echols that there is no information to suggest that ion gaps will respond to cool flames. The electron concentration required to activate an ionization gap is somewhere in excess of 10^7 ions per cubic centimeter and concentrations of this order appear to be found only in the highly reactive zone of the flame front. Attempts to correlate optical measurements with ionization gap measurements support this. Optical measurements using photoelectric cells were compared with signals simultaneously received from ionization gaps and, in general, no serious disagreement between the two measurements was observed. Also, the ion gap did not respond to visible cool flames. However, when one is working on a microsecond scale the slopes or rise times of the two signals assume increasing importance. It then becomes necessary to select a threshold of signal strength above which it will be stated whether a flame is or is not present. Under knocking conditions the discrepancy between the two measurements could be as much as 100 microseconds. However, this may be attributed primarily to flame curvature rather than lack of instrument sensitivity. In this work the flame front has been described as a function of the concentration of electrons sufficient to trigger the ionization gap. Using an instrument rise time of approximately 50 microseconds, the variations encountered were approximately ±20 microseconds under heavy knocking conditions. Thus it is believed that the velocities quoted for knocking combustion are representative and not greatly in error.

Herbst's question as to whether ionization gaps give a true measure of what is occurring in the bulk of the charge must be answered on the basis of preliminary data. To answer this question, the instrumentation has been extended to include pressure/

time measurements which are compatible in accuracy with the flame measurement data. Initial attempts to correlate the results have been made. For nonknocking or light knocking combustion, an excellent correlation between mass burned and volume burned has been obtained. The results of this work will be presented in the near future.

With regard to Herbst's question whether or not flames traveling at 300 fps can give rise to noise having the frequency of knock, it can only be stated that the frequencies associated with knock are present for many types of combustion which are normally classified as nonknocking combustion. There appears to be no absolute definition of knock and it is necessary to resort to a threshold technique whereby knocking combustion is classified as that type exciting the predominant frequencies above some threshold. Since the frequencies associated with the sonic pressure wave are present for many modes of combustion, there is no pressing reason to assume that a sonic flame front is required to excite the larger vibrations of knocking combustion.

In reference to the high flame propagation rates associated with knocking combustion, both Broeze and Echols have presented explanations for these rates based on a thermal mechanism. The autoignition across thermal gradients proposed by Echols and the self-ignition process near the flame front proposed by Broeze are quite similar but appear to be only logical extensions of a thermal mechanism of flame propagation. These concepts require the presence of an existing flame front to drive the accelerating reactions. It is quite difficult to distinguish, on this basis, between the concept of autoignition or self-ignition and the concept of thermal flame propagation. It appears that Broeze, Echols, and I are in quite good agreement as to the probability of knock resulting from the rapid acceleration of the primary flame front.

We also pointed out in our paper that a thermal mechanism may be sufficient to explain the results which were presented. However, the data obtained here and elsewhere by the use of antiknock additives such as tetraethyllead indicate that a thermal mechanism is not sufficient to account for the acceleration of the flame fronts. This would seem to be particularly true in the case of the accelerations observed with light knock.

We are in further agreement with Echols that the flame need only approach sonic velocity. Our work has simply gone a step further and defined the word approach as meaning velocities in the range from 300 to 1200 fps.

Broeze objects to the use of *n*-heptane as a fuel since this hydrocarbon cannot be purchased at the local gasoline pump. Yet, on the other hand, he seems to accept the data pertaining to iso-octane as being much more normal but to the best of my knowledge iso-octane is no closer to the commercial gas pump than is *n*-heptane. In any case his concern is valid and this work has been extended to include commercial fuels. The results obtained to date are generally the same as the results obtained with the pure hydrocarbons and will be presented in the near future.

Broeze seems to feel that an inverse relationship between flame propagation and the occurrence of light knock might be obtained by using some correlation between induction delay and knocking combustion. It is not clear what exact point is being made here. However, the term "induction delay" is by far the most arbitrary definition encountered in this type of work and, as we have shown in an earlier paper, the definition of this term will influence to a marked degree the conclusions which may be reached.

Another point of mutual concern is that of turbulence, gas whirl, and expansion of the burned gases. While it is agreed that these factors have a pronounced effect on propagation of the flame front, the effects observed with knocking combustion cannot be explained satisfactorily by these mechanisms. Certainly for the case of knocking combustion in which the higher flame propagation rates were observed, it would not seem likely that the induction of 3 to 6 ml of TEL would materially modify the direction of the swirl, the rate of expansion of the burned gases, or the degree of turbulence. Thus, while these points are certainly worthy of consideration, they do not, we believe, influence the conclusions drawn from these measurements.

It has been further pointed out by Echols that the mass of charge involved in light knock may be quite small and there is little likelihood of two or more ionization gaps being located in this volume. We agree with this and that is why we have not attempted to show a flame propagation rate associated with light levels of knock. For the case of light knock only, average burning times have been used to indicate the apparent trend; namely, acceleration of the flame front. However, in the case of heavy knock, flame propagation velocities have been presented which are believed representative of knocking combustion. In this case we are not dealing with a small fraction of charge, say 10%, as indicated by Echols; more probably 50–90% of the mass is involved. Even though this large a fraction of the mass may not be involved in the terminal velocities, it is certainly involved for velocities several times greater than normal. Thus, it is appropriate to consider these high velocity areas as being a portion of the knocking reactions. In this case, not one or two, but as many as 20 ionization gaps are located in the zone of knocking combustion.

Since the measurement of a velocity vector requires determination of a time increment between two discrete points, the final velocity measured is always the average. We can only speculate as to ve-

locities greater than those which we have recorded. There is little information in the literature which would indicate that flame propagation rates, regardless of the mechanism involved, have ever been recorded in excess of, say, 1000 fps in an internal combustion engine. Therefore, in view of our own data coupled with that available in the literature, no compelling reason exists to assume the presence of propagation rates in excess of those which have been measured.

Mr. Echols has raised the question as to whether there is sufficient reason to believe that active species can cause flames to move faster. We believe there is and the references quoted support this point. However, with respect to the exact nature of the species, our work is not sufficient in depth to provide an unqualified answer. We believe that our work with tetraethyllead, as well as the work of others, is sufficient to bring us to the conclusion already reached by many that a purely thermal mechanism of flame propagation is not sufficient.

References

1. Pahnke, A. J., Cohen, P. M., and Sturgis, B. M.: Ind. Eng. Chem. *46*, 1024 (1954).
2. Echols, L. S., Yust, V. E., and Bame, J. L.: *Proceedings of the Fifth World Petroleum Congress*, Section VI, Paper No. 11, 1959.
3. Livengood, J. C. and Wu, P. C.: *Fifth Symposium (International) on Combustion*, p. 347. Reinhold, 1955.
4. Massa, V. F.: *A Study of the Normal and Abnormal Combustion Behavior of Gasolines*. Soc. Automotive Engineers, January 9–13, 1961.

STUDY OF BURNING RATE AND NATURE OF COMBUSTION IN DIESEL ENGINES

W. T. LYN

In the present investigation the burning rates in diesel engines have been studied in some detail and the rate-controlling factors examined. Chemical kinetics based on activated collision could not play a part because otherwise the whole process would be very temperature sensitive, and this is not consistent with results from experimental investigation. The temperature drop during the expansion stroke would demand a drop in burning rate far greater than is shown by experiment, while the proportional increase in burning rate with engine speed could not be accounted for by the small increase in cycle temperature. Indeed the major factors affecting the burning rate are injection rate, engine speed, and combustion chamber design, all of which directly affect mixing. For a D.I. engine with central multihole nozzle, it is found that a relationship exists between the rate of injection and rate of burning. This relationship is independent of operating condition and therefore can be used to predict the rate of burning, and hence the cylinder pressure diagram from the rate of injection diagram.

While the mixing pattern of a specific combustion system may modify what follows to a certain extent the burning processes in a diesel engine generally proceed in three phases. During the first phase, in which the burning rate is the highest in a normal D.I. engine, the premixed part of the fuel jet burns with a nonluminous flame. This phase lasts only for 5° to 7° C.A. In the second phase, when the majority of the heat is released in about 40° C.A. there is a general decay of burning rate and the jet burns as a highly turbulent diffusion flame. In the third phase, which may last through the whole expansion stroke, the burning rate is quite low and the total heat released in this period accounts for 10 to 20% of the total heat input. The nature of the combustion in the third phase is not clear at present, but it appears to be an inherent and unavoidable part of the diesel combustion process.

Introduction

The burning rate of fuel is important in all reciprocating engines because it controls directly the cycle efficiency,[1] the noise emitted from the engine[2] and the peak pressure to which the engine components are subjected. Experience has shown that these requirements are often conflicting and the best design entails some logical compromise. A thorough understanding of the parameters which control rate of burning will have obvious advantages in the design and development of such engines.

In a premixed spark-ignition (petrol) engine, if the flame speed and the configuration of the combustion chamber are known, the rate of burning and heat release* can be calculated. This has been demonstrated by Lichty in his well-known text book[3] as early as the early 1930's, although there appears to be little subsequent work to follow up, due perhaps to the absence of flame speed data in engines. In the compression-ignition (diesel) engine field, although some spasmodic heat release patterns have been reported (e.g., see reference 4), even less work on the factors controlling burning rate is known to exist.

The present paper reviews some of the work carried out at the author's laboratory over several years on the study of burning rate and nature of combustion in the diesel engine. The primary aim of the investigation is to see to what extent the burning rate can be controlled by the rate of injection, but additionally a basic understanding of the nature of combustion in diesel engines is obviously desirable.

Method of Approach

In connection with this work two major experimental techniques have been employed. First, a normal engine is fully instrumented so that the rate of injection can be calculated from

* In this article ther term "burning" and "heat release" are used synonymously.

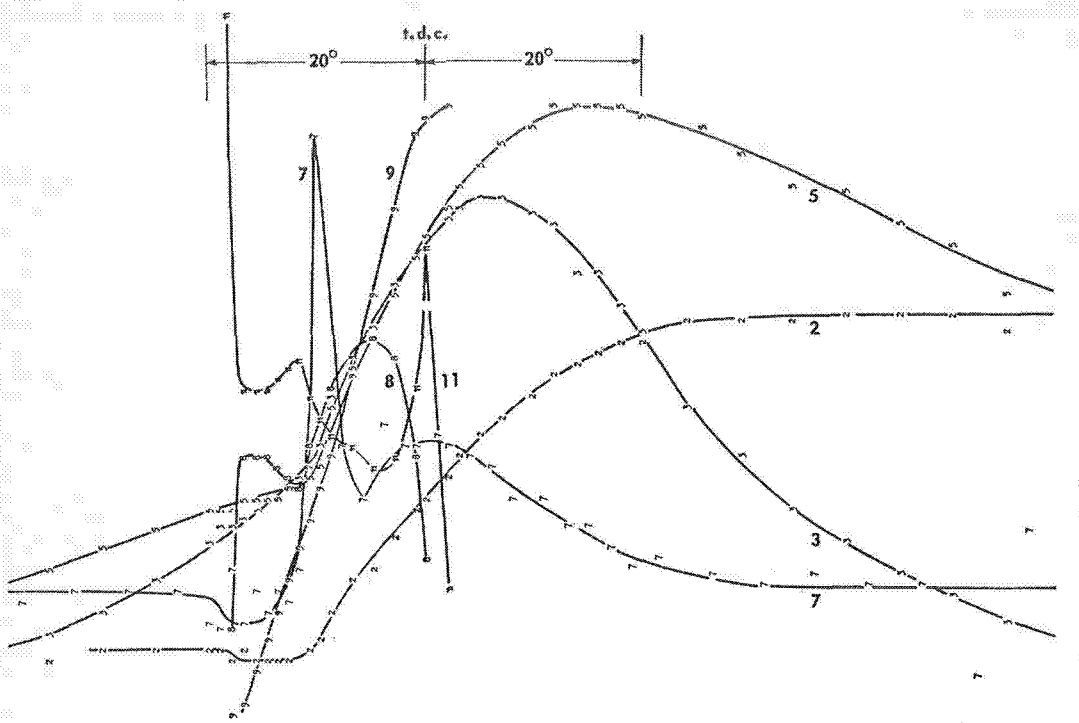

FIG. 1. Typical example of graphed output data from LEO computer. 2. Cumulative heat release. 3. Cylinder gas pressure. 5. Cylinder gas temperature. 7. Rate of heat release. 8. Rate of injection of fuel. 9. Cumulative fuel injected. 11. Sauter mean diameter (S.m.d.).

measurement of needle lift (orifice area) and nozzle and cylinder pressures (pressure drop across the orifice). The rate of burning can be calculated from measured cylinder pressure, mass flow, and volume (from known geometry of the engine), using published thermodynamic data.[5] In order to facilitate computation, a Leo II computer has been used and a typical computer output is shown in Fig. 1. Such analysis has been extended over a wide range of engine operating conditions both as regards speed and load, and also various designs of combustion system.

The second approach is to construct a special engine in which the physical processes of injection, evaporation, and mixing of fuel and air can be studied by high speed Schlieren photography. The details of this technique have been published elsewhere.[6] The object of this special engine is not to simulate a particular commercial combustion system (although a second smaller engine provides for this need), but to investigate the basic nature of the combustion processes within a controllable range of compression pressure and temperature, and to a certain extent air movement.

Burning Rate in a Small Direct Injection (D. I.) Engine

A fairly extensive analysis has been carried out in a small single cylinder direct injection (D.I.) chamber engine of $4\frac{1}{2}$ in. bore and $5\frac{1}{2}$ in. stroke, with speed range from 750 to 1500 rpm. The combustion chamber is of flat disc shape with central 4 hole nozzle. The results are shown in Figs. 2 to 4. Figures 2a–c show the rate of fuel injection (in terms of CHU/lb air/deg C.A.) against crank angle for (a) the variation of load at a fixed engine speed and injection timing, (b) the variation of engine speed at a fixed load and injection timing, and (c) the variation of injection timing at a given speed and load. The corresponding rate of burning diagrams (also in terms of CHU/lb air/deg C.A.) are shown in Figs. 3a–c and the cumulative heat release diagrams in Figs. 4 a–c.

It should be mentioned that the burning rate and the cumulative heat release shown in the above diagrams include only the heat in the form of internal energy of the cylinder gases and the work done on the piston. The difference between the sum of these two items and the total

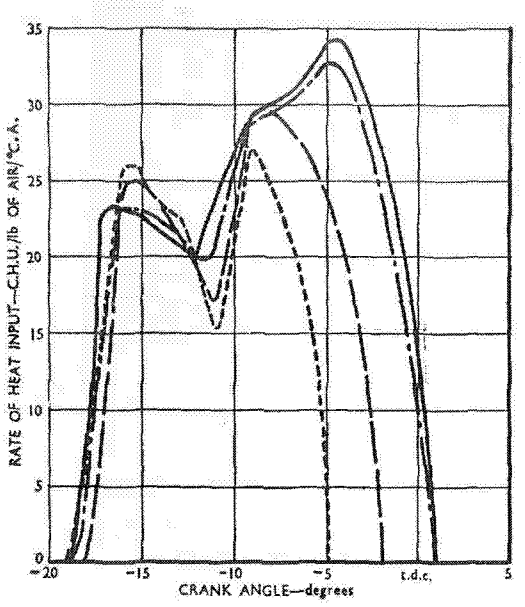

FIG. 2a. Injection characteristics: effects of varying load. —— 90.5 psi; —·— 80.4 psi; — — — 59.8 psi; ------ 39.6 psi. Speed, 1000 rpm. Timing, normal.

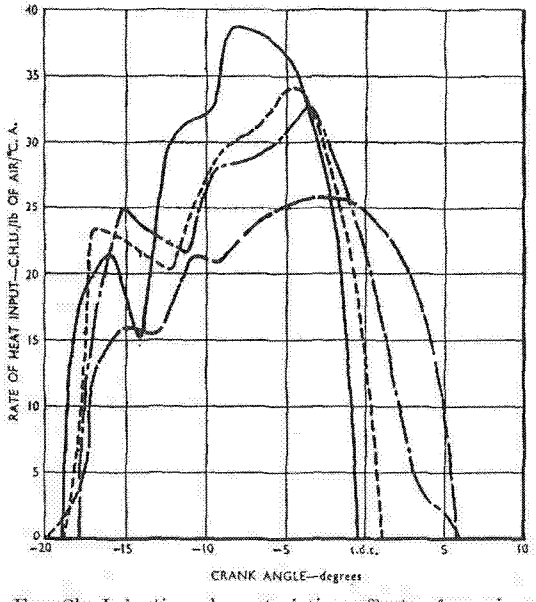

FIG. 2b. Injection characteristics: effects of varying speed. —— 762 rpm; ------ 1025 rpm; —·— 1280 rpm; — — — 1485 rpm. Timing, normal. Load, 90 psi b.m.e.p.

fuel input represents the heat loss to the cylinder wall since the amount of unburned found in the exhaust was negligible. The amount of heat loss to wall varies between 15 to 25% of the total heat (fuel) input according to operating condi-

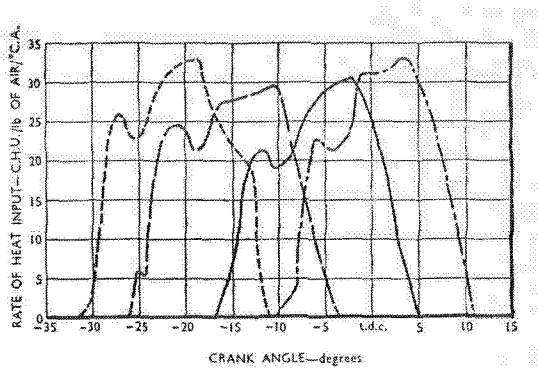

FIG. 2c. Injection characteristics: effects of varying injection timing. —·— 10° advance; —— 17° advance; — — — 26° advance; ------ 31° advance. Speed, 1000 rpm. Load, 80 psi b.m.e.p.

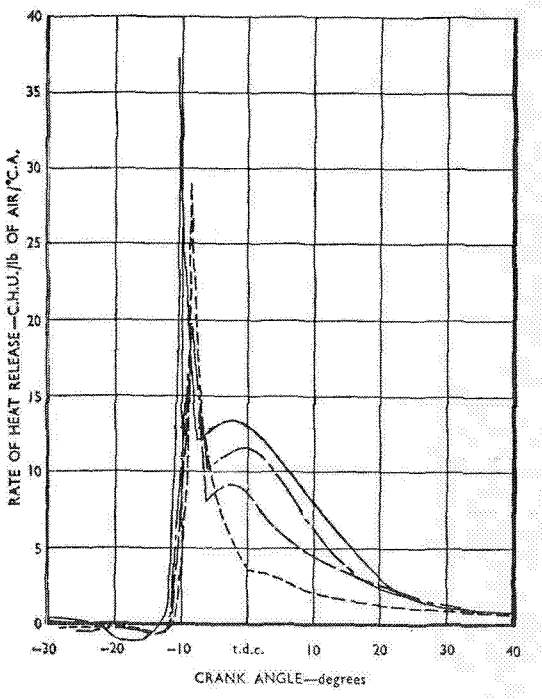

FIG. 3a. Analysis of heat release: effects of varying load. —— 90.5 psi; —·— 80.4 psi; — — — 59.8 psi; ------ 39.6 psi. Speed, 1000 rpm. Timing, normal.

tions. The actual rate of burning curve, of course, should include this heat loss to wall and hence depends on the variation of rate of heat loss with crank angle. However, since generally the rate of heat loss to wall is small compared with rate of heat release to the other two items, the general shape of both the rate of burning and the cumulative heat release diagram are not substantially changed by adding the heat loss. This is illus-

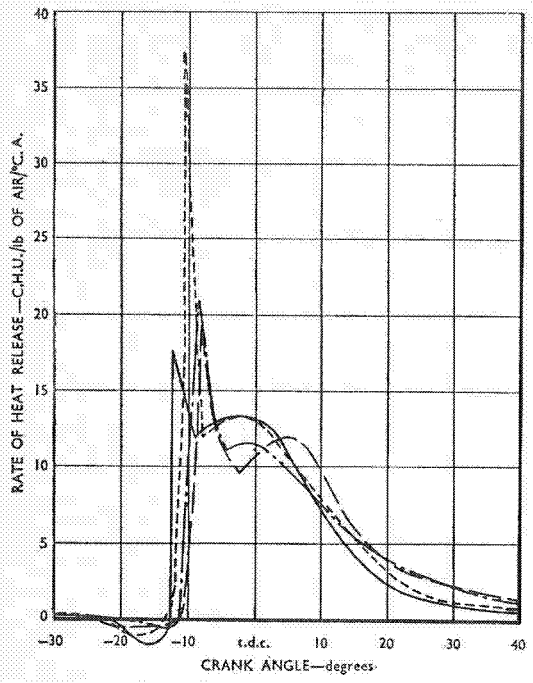

FIG. 3b. Analysis of heat release: effects of varying speed. —— 726 rpm; ------ 1025 rpm; —·— 1280 rpm; — — — 1485 rpm. Timing, normal. Load, 90 psi b.m.e.p.

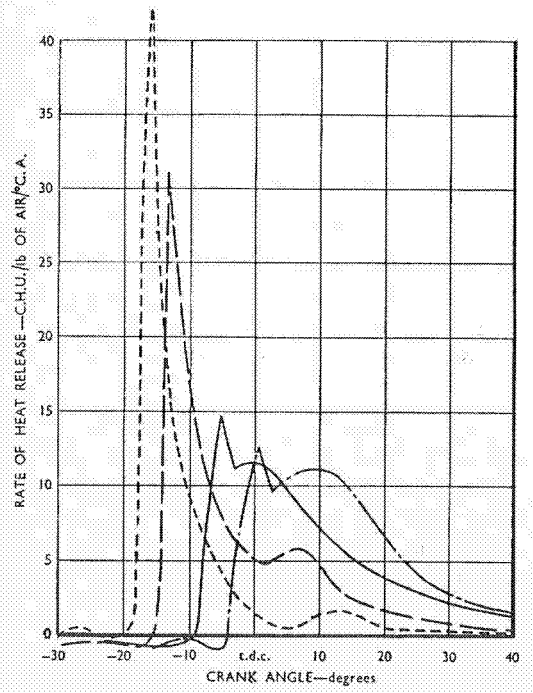

FIG. 3c. Analysis of heat release: effects of varying injection timing. —·— 10° advance; —— 17° advance; — — — 26° advance; ------ 31° advance. Speed, 1000 rpm. Load, 80 psi b.m.e.p.

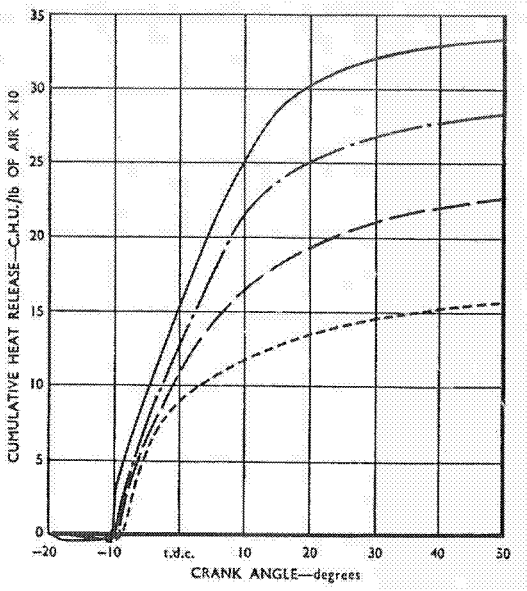

FIG. 4a. Analysis of heat release: effects of varying load. —— 90.5 psi; —·— 80.4 psi; — — — 59.8 psi; ------ 39.6 psi. Speed, 1000 rpm. Timing, normal.

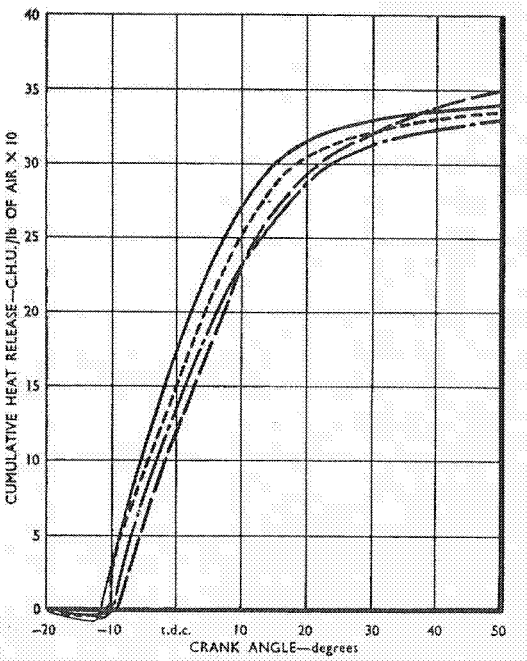

FIG. 4b. Analysis of heat release: effect of varying speeds. —— 762 rpm; ------ 1025 rpm; —·— 1280 rpm; — — — 1485 rpm. Timing, normal. Load, 90 psi b.m.e.p.

trated in Fig. 5 in which two vastly different rates of heat loss have been assumed: (a) a constant rate of heat loss and (b) a more realistic estimation, by determining the coefficients of

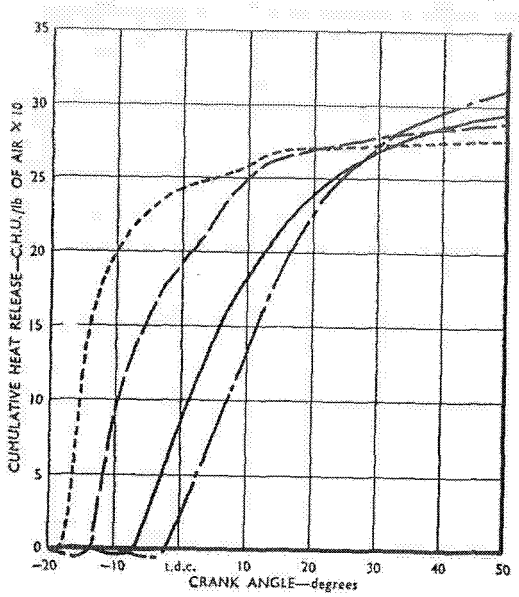

FIG. 4c. Analysis of heat release: effects of varying injection timing. —·— 10° advance; —— 17° advance; — — — 26° advance; ------ 31° advance. Speed, 1000 rpm. Load, 90 psi b.m.e.p.

heat transfer on the compression side of the cycle and assuming that the variation of this coefficient is symmetrical with respect to T.D.C. It will be noted that the essential features of these two curves and the uncorrected curve are quite similar.

Discussion of Burning Rate Diagrams in a D.I. Engine

It will be noticed from Figs. 3 and 4 that the general characteristics of the heat-release dia-

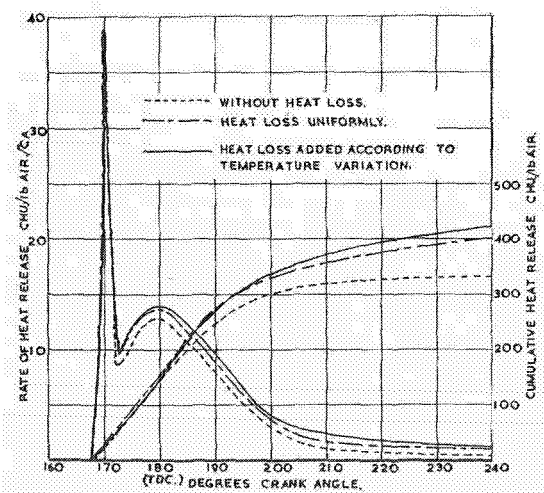

FIG. 5. Heat release with heat loss added.

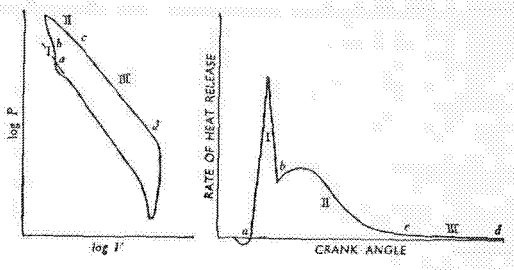

FIG. 6. Three phases of heat release

grams are very similar for all the test conditions. During the compression stroke, the rate of heat release is practically negligible until the injection of the fuel, at which point it shows a slight loss of heat throughout the delay period. This loss of heat is largely due to the evaporation of the injected fuel, but the accuracy with which it is estimated does not warrant any detailed analysis.

During the combustion period the burning proceeds in three distinguishable stages. In the first stage the rate of burning is generally very high and lasts for only three degrees crank angle. This corresponds to the period of rapid cylinder pressure rise. The second stage corresponds to a period of gradually decreasing rate of heat release and lasts about 40° C.A. This is the main heat-release period. Normally about 80% of the total heat is released in the first two periods. The third period corresponds to the "tail" of the rate of heat-release diagram in which a small but distinguishable rate of heat release persists throughout the expansion stroke. The heat release during this period amounts to about 20% of the total heat input.

It is interesting to define these three phases of burning in the log P–log V plot which is commonly used in determining the combustion time. Figure 6 shows schematically the rate-of-heat-release diagram side by side with the log P–log V plot. It is shown that the third phase corresponds to the straight line part in the log P–log V plot, the slope of which lies generally between 1.20 and 1.25, that is smaller than the mean adiabatic value of about 1.29. This means that heat is being released even without taking into account the heat loss to wall. In a petrol engine, the slope generally lies between 1.3 to 1.35 as compared with the mean adiabatic value of about 1.25.

Effect of Operating Variables on the Shape and Duration of the Injection and Heat-Release Diagrams

It is shown clearly in the rate-of-heat-release diagrams (Fig. 3) that during the third (final) stage of burning the rate of heat release is very small. The curves for various loads generally converge closely upon each other, and approach

the abscissa asymptotically. It is therefore difficult to determine the duration of heat release accurately. However, since the heat released in this part of the cycle is small the main heat-release period will be considered (that is, phases I and II) and the discussion on the shape and duration of the rate of heat release diagram must of necessity be qualitative.

Effect of Load. If the injection rate were constant the period of injection would be directly proportional to the amount of fuel injected, or roughly to i.m.e.p. But since, as can be seen, the injection rate generally increases until the pump spill port is uncovered, the duration of injection increases with increasing load rather less than proportionally to the quantity of fuel injected.

The total burning time also increases with increase of load to an extent about equal to the actual increase of injection period. Unlike the rate-of-injection curves, where for increasing load the fuel is added on at the end of the injection period the rate of heat release appears to increase generally uniformly throughout the main heat-release period. This is possible only when the burning time is long compared with injection time, and during most of the combustion period there is simultaneous burning of most of the fuel elements irrespective of their order of entering the chamber. There is also a noticeable tendency for the peak of the rate of heat release during the first stage of combustion to increase with reduction of load. This, as will be seen later, is related to the increase in delay period at light load.

Effect of Speed. At light loads, the injection period in terms of crank angle remains essentially constant when the speed is increased (750–1500 rpm). At high loads there is about 30% increase in injection period; the rate of injection, in terms of heat per unit crank angle, is therefore higher at lower engine speed.

The total burning period in terms of crank angle also increases with speed, and can be accounted for by the increase in injection period. This means that the actual burning time decreases with increase in engine speed and is almost inversely proportional to engine speed. The maximum rate of heat release (in terms of CHU/lb air/deg C.A.) which occurs in the first stage of combustion, increases slightly with increasing speed. This again is related to the increased delay period (in degrees crank angle) at high speed.

Effect of Injection Timing. The injection characteristics, as would be expected, are not altered when the timing is changed. Increasing the injection advance increases the delay period and with it the maximum rate of heat release. The total burning time is appreciably reduced with injection advance. If, however, the total time from the beginning of injection to the end of combustion is considered, then the reduction of this total time with injection advance is very much less. In other words, the reduction in burning time is largely due to the delay of the onset of combustion corresponding to the increase in delay period.

A Simple Model for Combustion in a D. I. Engine

The above discussion indicates that mixing is the main controlling factor of the burning rate in a diesel engine. Chemical kinetics based on activated collision does not seem to play a part because experimental results show that the burning rate is not temperature dependent. During the main heat release period, the variation in the rate of burning, if it is dependent on the logarithm power of absolute temperature, would be far greater than is observed. Likewise, the proportional increase of burning rate with engine speed can not be accounted for by the small increase in cycle temperature observed.

The three most significant observations between the rate of injection and rate of burning, as discussed in the above section, can be summarized as follows:

Firstly, the burning period is long in comparison with injection period. Secondly, the absolute burning rate increases proportionally with increasing engine speed so that in terms of crank angle basis the burning time remains essentially constant. Finally, the magnitude of initial peak of the burning rate diagram is associated with the ignition delay. These considerations, and the evidence of high speed photography to be discussed later, suggest the following model for combustion in a D.I. engine.

Referring to Fig. 7, which shows schematically the rate-of-injection and rate-of-burning diagram, the fuel injected is divided into elements according to the order in which they enter the chamber. The first element enters the chamber and mixes with the air and becomes "ready for burning" according to a certain law shown in the lower part of the diagram. The second and subsequent elements are likewise represented, and a total "ready for burning" diagram is obtained, the total area of the diagram being of course equal to that of the rate-of-injection diagram. Ignition, however, does not occur until after the lapse of the delay period. At the ignition point not all of the fuel injected up to that moment is ready for burning. The part which is mixed with air and ready for burning (indicated by shaded portion) is then added on to the total "ready for burning"

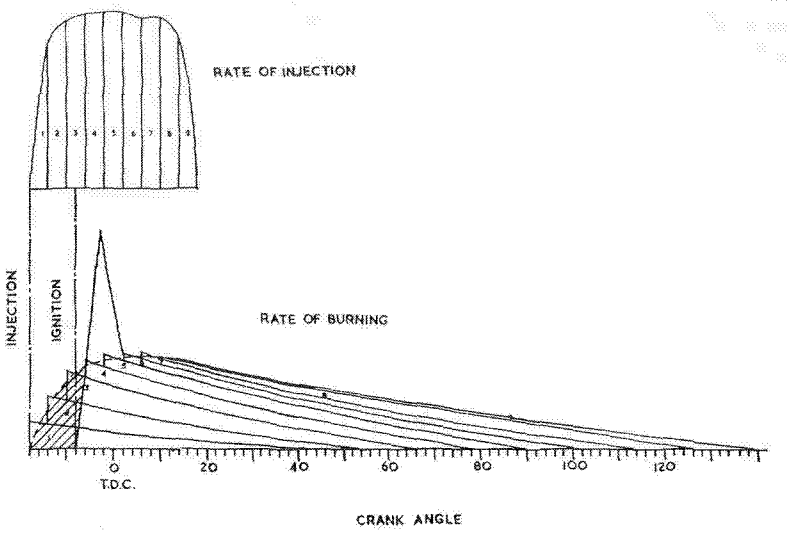

FIG. 7. Schematic relationship between rate of injection and rate of burning.

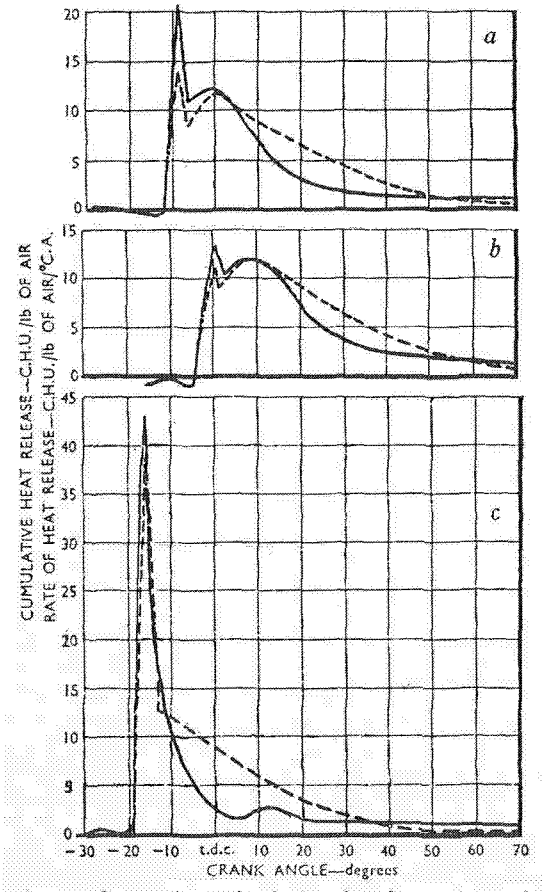

FIG. 8. Comparison of calculated and experimental rate of heat-release curves. Speed, 1000 rpm. Load, 80 psi b.m.e.p. —— Experimental curve; — — — Calculated curve. a Timing, normal. b Timing, 10° b.t.d.c. c Timing, 31° b.t.d.c.

diagram to give the high initial rate of burning generally observed in the engine. In this way the characteristics of the burning rate shown in Fig. 3 are all represented: There is simultaneous burning of most fuel elements as load is increased. The burning rate is expressed in terms of crank angle and hence independent of engine speed, and the longer the ignition delay, such as under light load and high speed, the higher is the initial rate of burning.

While a full theoretical treatment of the mixing of a jet of fuel droplets with air, particularly in the presence of cross wind, is not available, some simple empirical correlation has been found to relate the rate of burning to the rate of fuel injection.[7] Experience shows that the established burning rate of a single droplet in a free supply of air (rate proportional to diameter of droplet) does not fit into the present scheme. It has also been shown that with limited supply of air, as is the case in an engine, the rate of burning versus time curve is more like a triangle with the peak at the beginning of combustion. A scheme using the triangular burning rate, but with increasing burning time as injection proceeds gave a reasonable fit over the wide range of speed load and timing. The implication of this finding is that once this relationship between the rate of injection and rate of burning is found for one test condition, it can be used to predict engine behavior at others. It has been found that the prediction of burning rate is better under varying load and speed than under varying injection timing. Figure 8 compares the predicted (from rate-of-injection diagram) and measured (from cylinder pressure diagram) rate-of-burning diagrams at various timings and Fig. 9 compares the corresponding cylinder pressure diagrams,

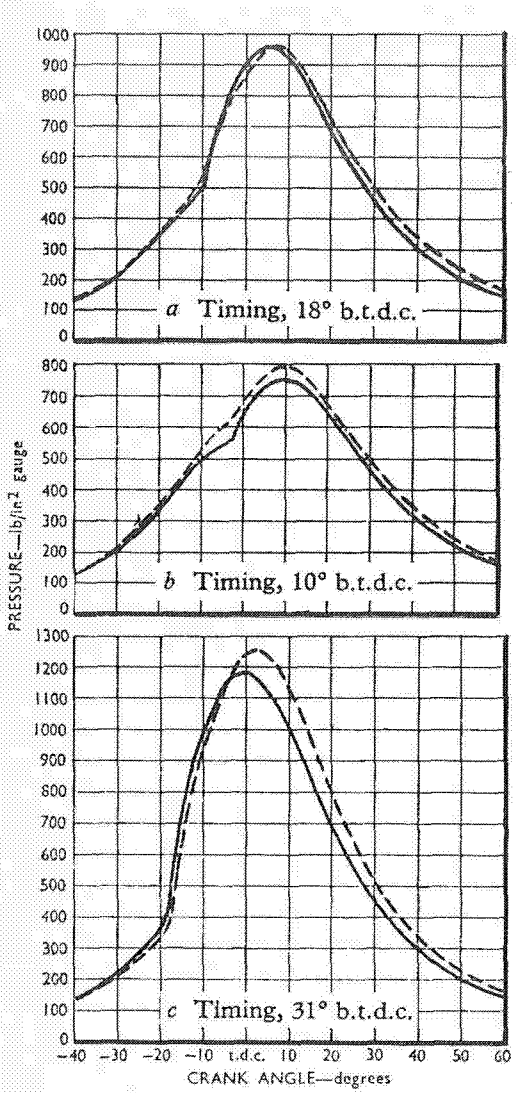

FIG. 9. Comparison of calculated and experimental cylinder-pressure diagrams. Speed, 1000 rpm. Load, 80 psi b.m.e.p. —— Experimental curve; — — — Calculated curve.

which is what matters as far as engine performance is concerned.

It will be noticed that the prediction of peak pressure is within 5%, the rate of pressure rise is almost exact, but the efficiency is only correct to 10%.

Correlation of High Speed Schlieren Photography with the Burning Rate Diagram (Fig. 10)

The simple model of combustion presented above appears to agree with the phenomena observed in an engine by high speed Schlieren photography. Although the combustion system of this special engine, which was fitted with quartz windows, is different from the one used in a normal engine, the essential features of the evaporation and burning of a liquid fuel jet are the same. Fuel injection commenced at 22° b.t.d.c. During the delay period the jet was swept round by the air swirl, and evaporation and mixing occurred at the fringe of the jet. Ignition occurred at about 13° b.t.d.c. and the rate of burning reached a peak at about 10° b.t.d.c. The flame, up to this crank angle position, was of very low luminosity because the burning was confined essentially to the premixed part of the jet. From a color transparency, the spreading of this bluish flame was estimated to attain a speed of the order of 50 m/sec. The first appearance of orange-colored luminosity occurs at 10° b.t.d.c., but does not spread to surround the tip of the jet until 7° b.t.d.c., at which point the rate of burning has already reduced considerably. The first peak of the rate of burning, which lasts for about 5° C.A., is therefore primarily a result of the premixed nonluminous flame. From this point onwards, the jet burns essentially as a turbulent diffusion flame, with high luminosity due to presence of carbon particles. This observation is in entire agreement with the infrared spectra taken in an earlier investigation.[8] The continuous, almost black body, radiation from a diesel flame is distinctly different from that of the flame of a petrol engine which shows mainly the 2.7 μ (water) and 4.3 μ (CO_2) peaks.

The Source of the Heat Released in the "Tail" of the Burning Rate Diagram

Engine thermodynamic consideration dictates that for high thermal efficiency the burning must take place early in the expansion stroke. The heat released during the third or "tail" phase of the burning rate diagram contributes little to the efficiency of the cycle.

As can be seen from Fig. 5, the major heat release period (phases I and II) is about 40° C.A. The amount of heat which appears in the "tail" depends of course on the accuracy of the estimation of heat loss distribution but probably lies between 10 to 20% of the total fuel input. It is estimated that if this heat could be released at t.d.c. a gain of 4 to 8% in efficiency would result. It is therefore of both practical and theoretical interest to look into the source of the heat released during this period.

The first possibility considered was unburned hydrocarbons. The earlier work of Egerton[9] and Garner[10] in which stroboscopic sampling was employed, showed no significant amount of either

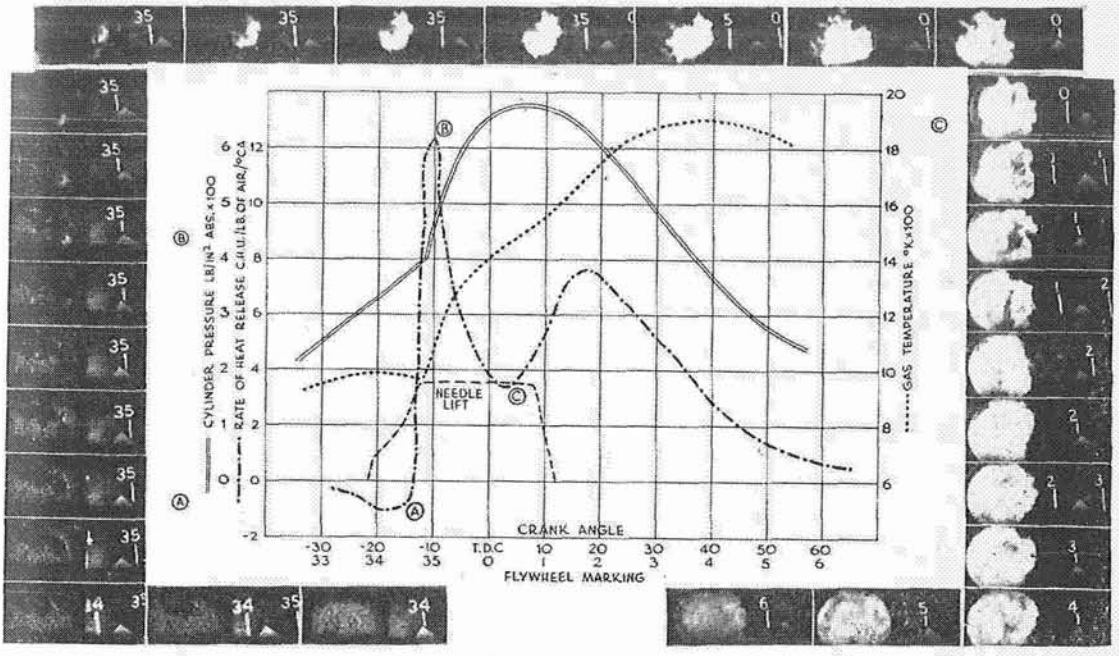

FIG. 10. Rate of heat release, cylinder temperature, cylinder pressure, and needle lift are shown with selected cine film stills.

unburned hydrocarbons or carbon monoxide so late in the expansion stroke. Ten per cent of the total heat applied corresponds to about 1.5% of CO or 0.5% of hydrocarbons. This should be easily detectable even with quite elementary analytical techniques. However, in these earlier investigations the sampling point was in the prechamber and so the possibility that the unburned fuel may exist in the main chamber cannot be excluded.

The second possibility is that the unreleased heat exists in the form of "carbon" or carbonaceous materials. Previous spectroscopic work[8] indicates that most of the liquid fuel may burn with the intermediate formation of carbonaceous material, which provides the continuous radiation. Garner *et al.*[10] also found a considerable amount of "soot" on their sampling probe. No determination of the amount of carbon at this period, however, has been made. It was therefore decided to repeat the earlier sampling work on a D.I. engine both for gaseous unburneds and for particulate matter (carbon). Figure 11 shows again the low concentration of the unburned (both the gas phase and the particulate materials) throughout the expansion stroke. In fact throughout the third phase of the heat release period the total unburned accounted for at the sampling point was no more than 1.5% of the total fuel input.

The analysis however, does show the inhomogeneity of the cylinder content for throughout the expansion stroke the sample fuel/air ratio was found nowhere equal to the mean value in the exhaust. The only way to settle this problem, it would appear, is to freeze and analyze for the *whole* cylinder content.

The third possibility is that the apparent heat release (or total pressure increase) is due to the mixing of the hot burned gases and the cold air at the same pressure.

The pressure increase due to mixing can be expressed as

$$P/P_m = 1 + (QRJ/V_mP)\,[(m_ac_a)^{-1} - (m_bc_b)^{-1}],$$

where P = pressure before mixing; P_m = pressure after mixing; Q = heat transferred during mixing; R = universal gas constant; J = mechanical heat equivalent; V_m = volume after mixing = total volume; m_a = molecular weight of air; c_a = specific heat of air; m_b = molecular weight of burned gases; and c_b = specific heat of burned gases.

Since the difference between the molecular weight of air and burned product is small but the specific heat of the burned products is a good deal higher than that of air, there will always be an increase in total pressure, or an apparent heat release, after mixing. Calculation shows that the apparent heat release due to this source is not more than 2% of the total fuel input or only

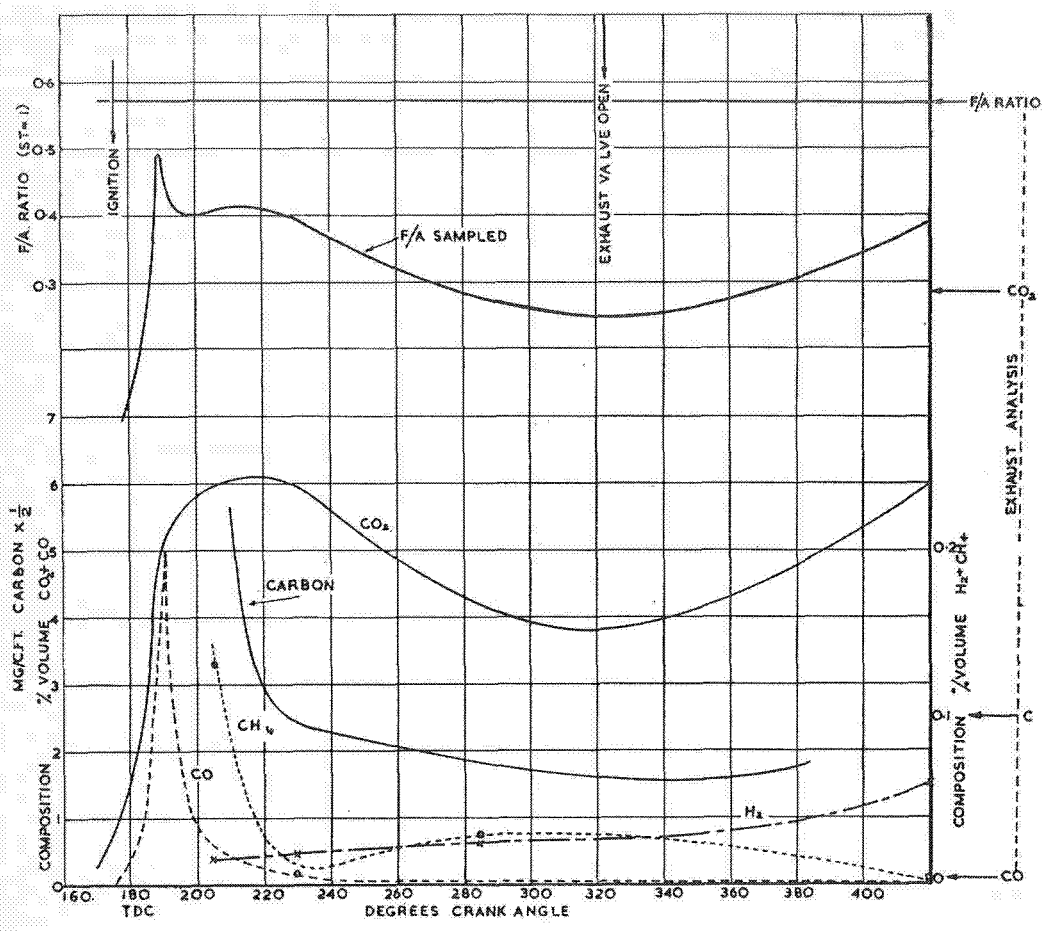

FIG. 11. Results of stroboscopic sampling.

about 10 to 20% of the heat release in the third phase.

Summarizing, it may be said that mixing of the burned products with the relatively cool air can account only for a minor part of the heat released during the "tail" period. Owing to the inhomogeneity of the cylinder content it has not been possible to establish whether the major heat released during this period is in the form of unburned hydrocarbons or "carbonaceous" materials. A complete analysis of the whole cylinder content might be decisive.

It may be mentioned here that, since physical mixing is shown to be the rate-controlling factor, the question of whether the heat released during the "tail" period comes from which particular form of unburned material is perhaps more of academic interest. From a physical point of view the most interesting question is the scale of unmixedness. The result from stroboscopic sampling work rather suggests that the scale must be quite large because the sampling period was as much as 8° C.A. during the latter part of the expansion stroke and average of a large number of cycles.

Effect of Combustion Chamber Design on the Rate of Burning Diagram

The model described in the section on the combustion model for the D.I. engine with bowl type chamber and central multihole nozzle was found not to be applicable if the fuel spray was directed tangentially to the chamber wall (such as the MAN M-system, the Ricardo Whirlpool type chamber and the Tangye chamber). This is to be expected if, as has been indicated above, mixing is the rate-controlling factor. Figure 12 shows the rate-of-injection and rate-of-burning diagram of the Meurer System for three engine speeds. If the D.I. model is applied to the M-system, where almost the whole of the fuel is injected before ignition occurs, the peak of the burning rate and hence rate of pressure rise would be very high.

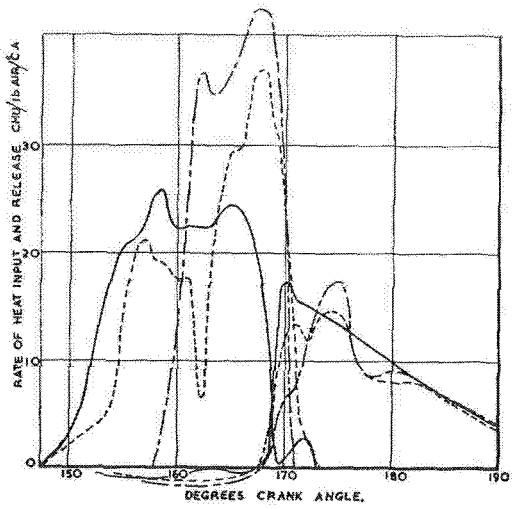

FIG. 12. Rate of heat input and release in M-system engines. —— 1750 rpm, 80 psi b.m.e.p.; ------ 1300 rpm, 80 psi b.m.e.p.; —·— 900 rpm, 80 psi b.m.e.p.

This obviously is not the case as shown in Fig. 12.

There are two possible reasons why this type of chamber should have a lower initial burning rate. Firstly the number of nozzle holes used is smaller, usually one or two against three or four for the normal D.I. engine. Secondly the direction of spray is generally tangential to the wall so that the free mixing surface of the jet cone is reduced. This, however, is not the whole story. For if this mixing rate is so slow that, in spite of the large quantity of fuel injected during the delay period, it only results in the rather low initial burning rate derived from analysis, then the burning time should be very much longer than that shown in Fig. 12. The obvious explanation is therefore that the mixing and hence burning speeds up once ignition takes place. This is possible since, the fuel being distributed initially near the wall, mixing is inhibited by the effect of the very high centrifugal forces on the fuel vapor which is of higher density than the air and so tends to remain near the wall. As soon as ignition takes place the hot burning mixture expands, decreases in density and is then removed rapidly towards the center of the chamber. This strong radial mixing is then the rate-determining process. This process can be clearly seen in the high speed Schlieren pictures which show the burned gases spiralling towards the center of the chamber quicker than the fuel vapor during the delay period.

An alternative and additional delaying mechanism is available if a significant quantity of fuel is deposited on the wall. The author's colleagues, Messrs. Knight and Fine have shown by calculation that at compression temperature the heat transferred from the cylinder gases to the film of fuel on the wall is too slow to account for the burning rate observed. Only after ignition takes place will the gas temperature be high enough to evaporate the fuel from the wall in a reasonable time.

The mixing process described above implies that the injection rate will have little effect on the subsequent mixing after ignition which will be largely controlled by the air swirl. This appears to be consistent with the result of the

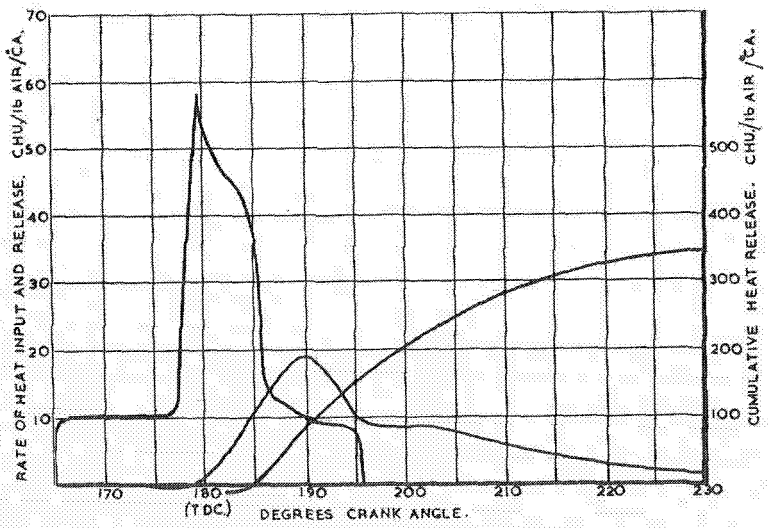

FIG. 13. Rate of heat input and release in swirl chamber engine.

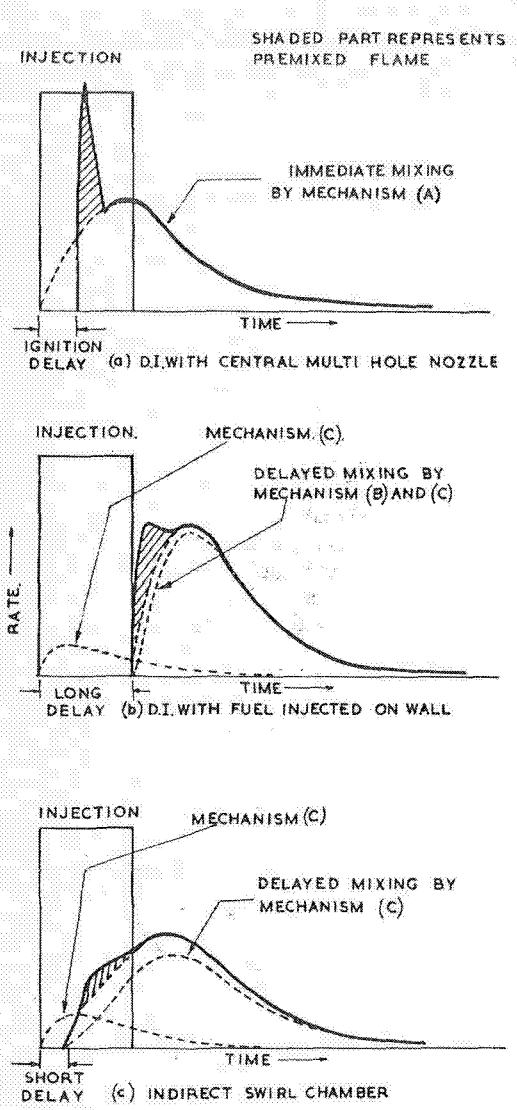

FIG. 14. Schematic injection rate and burning rate in three different engines.

analysis as shown in Fig. 12. Similar observations on the relationship between the inclusive angle of the fuel jet and chamber wall and the cumulative heat release have been made by Pischinger and Pischinger.[11]

In the case of a swirl chamber type engine, where the air in the main chamber is not immediately available for mixing, the dependence of burning rate on injection rate is again different. Figure 13 shows the rate of injection, rate of burning, and cumulative heat release of such an engine. It can be seen that the burning rate diagram is quite different from those shown previously for the D.I. engines, whether with central multihole nozzle or with fuel injected on the wall. The first peak is generally lower and extended over a longer duration than the conventional D.I. engine. The small size of the chamber, together with the associated high swirl rate, results in considerable fuel impingement on the wall. This, and the fact that the ignition delay is generally shorter in this type of engine due to the higher compression ratio used, account for the lower initial peak in the burning rate diagram. The rather delayed second peak may be due to the additional air made available as the piston descends from the top dead center position.

Summarizing the above discussion, a qualitative hypothesis may be put forward to explain the differences in the mixing patterns, and hence burning rates of the various engine types. Depending on the interaction between the fuel spray and air stream, the following three basic mixing and burning patterns may be postulated:

(A) Fuel injection across the chamber with considerable momentum—mixing proceeds immediately as it enters the chamber and is little affected by ignition.

(B) Fuel deposition on wall—negligible mixing during delay period due to limited evaporation. After ignition evaporation becomes rapid and rate is controlled by access of hot gases to the surface, radial mixing being induced by differential centrifugal force. Burning is therefore delayed by the ignition lag.

(C) Fuel distributed near the wall—mixing proceeds during delay, but at a rate smaller than (A). After ignition mixing is accelerated by the same mechanism as (B).

Figure 14 shows schematically the construction of the burning rate diagram from the same injection diagram for the three engine types discussed earlier.

In the case of a D.I. engine with central multihole nozzle, mechanism (A) is predominant and the injection and burning rate is shown schematically in Fig. 14(a). In the case of a D.I. engine with fuel spray tangential to the wall, mechanism (B) and (C) would be prevailing. The delayed mixing prevents excessive high initial burning rate. This is illustrated in Fig. 14(b). In the case of an indirect swirl type engine, the short delay period together with delay mixing (C) produces a gradual increase of the burning rate diagram as is shown in Fig. 14(c).

ACKNOWLEDGMENT

The author wishes to thank his many colleagues who participated in the investigation and in particular Dr. A. E. W. Austen, Director and Chief Engineer, for his interest and stimulating discussion.

Thanks are due to C.A.V. Ltd. for permission to publish.

References

1. Lyn, W. T.: Proc. Automotive Division, Inst. Mech. Eng. (London) *1*, 34 (1960–61).
2. Austen, A. E. W. and Priede, T.: *Symposium on Engine Noise and Noise Suppression*. Inst. Mech. Eng., London, 1958.
3. Lichty, L. C.: *Internal Combustion Engines*, McGraw-Hill, 1939.
4. Rothrock, A. M.: N.A.C.A. Report No. 401 (1931).
5. Gilchrist, J. M.: Proc. Inst. Mech. Eng. (London) *159*, 335 (1948).
6. Lyn, W. T. and Valdmanis, E.: J. Photographic Science (London) Mar/April (1962).
7. Austen, A. E. W. and Lyn, W. T.: Proc. Automobile Division, Inst. Mech. Eng. (London) *3*, 47 (1960–61).
8. Lyn, W. T.: J. Inst. Petroleum (London) *43*, 25 (1957).
9. Drinkwater, J. W. and Egerton, A. C. G.: Proc. Inst. Mech. Eng. (London) *138*, 415 (1938).
10. Garner, F. H., Morton, F., Nassan, A. H., Wright, E. P., Malpas, W. E., and Reid, W. D.: J. Inst. Petroleum (London) *38*, 301 (1952).
11. Pischinger, A. and Pischinger, F.: Motortechnische Zeitschrift. *20*, 1 (1959).

Discussion

Drs. W. L. Brown and J. E. Mitchell (*Caterpillar Tractor Company*): In Fig. 5, the author has indicated that heat transfer may be neglected due to the similar curve shapes with and without heat transfer. However, using the data presented it may be calculated that 95% of the total heat is released at 45° a.t.d.c. without heat transfer whereas only 80% is released at the same crank angle when heat transfer is considered. We would consider that significant.

The heat release rates used for Figs. 8 and 9 do provide reasonable accuracy from some viewpoints. However, the principal use of such a calculation would be in the choice of an optimum fuel injection pattern to provide the best compromise between maximum pressure and efficiency. The accuracy achieved does not seem good enough for that type of analysis.

The "tailing off" of burning rate or phase three burning seems to be accounted for by the inability of a fuel droplet to find usable oxygen after the main part of combustion is complete. Since the mixture is not homogeneous, this seems quite logical.

The paper states that heat release is not dependent on temperature or pressure but only on injection rate. We question this since the diffusion rate concept is rather fundamental and probably will have some influence. Have the authors any data on pressure-changed engines where this pressure and/or temperature change may be accented? The data presented do not indicate any such tests. Without this information we believe that it would be quite dangerous to apply the basic conclusion that heat release from one test condition may be used to calculate engine operation at another condition.

Prof. J. J. Broeze (*Technical University of Delft*): In commenting on this paper I would like to start by saying how gratified I am that our thirty year old teaching has found acceptance. I refer, of course, to the fact that combustion in a diesel engine may only be analyzed fruitfully against the background of the ideal heat input diagram derived from the injection characteristics (timing and quantity per degree crank angle) and assuming complete combustion of every drop of fuel as it enters the combustion chamber.

Our experiences, which have been reported on in several papers between 1936 and 1950, has shown that fuel properties may have a marked effect on the mixing and thereby on the efficiency of combustion. The most obvious one is viscosity with its corelated property of volatility, which helps to determine penetration and dispersion. The chemical properties, through the ignition delay, play a striking part which may result in considerable differences of efficiency at the extreme ends of the load curve.

Dr. W. T. Lyn (*C. A. V., London*): Regarding the question of heat loss raised by Drs. Brown and Mitchell, I think that they are at cross purposes in the discussion. In the text the general shape of the heat release diagram is discussed qualitatively. The substance of the discussion in the whole text would not be invalidated if in Figs. 3 and 4 the heat loss had been added. In discussing the unreleased heat in the "tail" part of the heat release diagram and in predicting the cylinder pressure diagram the heat loss was taken into consideration. This is why the 80% of heat released at 45° a.t.d.c. quoted by the discussors is in agreement with the text. It would be more proper, in the case where heat transfer is excluded, to refer the heat released at 45° a.t.d.c. as 31% of the total heat input, instead of 95% of the total heat released as quoted by the discussors.

I do not agree that the optimum fuel injection

pattern derived from the analyses will not provide an accurate enough compromise between peak pressure and efficiency. Disregarding the "tail" part of the heat release diagram, which is not controlled by the injection rate in any way, the difference in cycle efficiency between the predicted and measured heat release diagram in Fig. 8 is very small indeed, particularly when suitable timing is applied. The predicted peak pressure, as shown in Fig. 9 is accurate enough for most practical purposes. It should be emphasized, however, that the present investigation is not concerned with smoke. Thus, what is optimum for peak pressure and efficiency might not be optimum for smoke.

With regards to the effect of temperature and pressure for a given engine, the changes in temperature and pressure with operating condition would be quite small. Experience has shown that the same relationship between the rate-of-injection and rate-of-heat-release diagram holds over a wide range of operating conditions. Moreover, the same relation has been found to apply to engines of quite different compression ratios, but similar types of combustion chamber, i.e., D.I. with central multihole nozzles. With highly supercharged engines, up to say a pressure of some 40 atmospheres, the mixing rate may be different. But I have no practical data yet on this point.

I would like to point out that experience from high speed Schlieren photography and heat release analysis showed that fuel properties (viscosity and volatility) have little effect on the main mixing process and that the major difference in the heat release diagram, and hence peak pressure and cycle efficiency, is due to the difference in the delay period. In fact the same relationship between rate of injection and rate of heat release can be used for petrol and gas oil provided the difference in ignition delay is taken into consideration. This explains also why, generally, the specific consumption (based on calorific value) varies very little when different fuels are used.

FLAME STUDIES BY MEANS OF IONIZATION GAP IN A HIGH-SPEED SPARK-IGNITION ENGINE

S. KUMAGAI AND Y. KUDO

The time occupied by combustion in a super-high-speed engine is an extremely important factor. The designation "super-high-speed" will be used here to apply to engines which run at speeds above 10,000 rpm. Higher engine speeds, and resulting smaller size cylinders are favorable factors in increasing the output per unit of displacement volume. This paper describes studies associated with the ignition and combustion phenomena in four stroke cycle, small-scale spark-ignition engines in the super-high-speed classification.

Theoretical Background

Ignition and combustion phenomena in spark-ignition engines do not vary appreciably with speed even when the speed is raised to a very high value. However, certain factors affecting flame development may become important as engine speed is raised beyond the normal range. In a general way the following might be said about the progress of combustion in the spark-ignition reciprocating engine combustion chamber.

The time for a flame to complete travel across the engine cylinder after spark ignition can be divided roughly into three stages. The first of these is the so-called delay period in which no flame propagation is detectable. This delay period can, at first approximation, be considered independent of engine speed. Thus, the number of degrees of crank-angle rotation occupied by this period should increase proportionally with engine speed. The second stage is the initial phase of flame propagation extending only a small distance from the ignition point. During this period the flame apparently accelerates. The average flame speed increases less than proportionally with engine speed. This is evidently because the accelerating effect of turbulence is a minor item. The extent of crank-angle rotation occupied by this second period increases less than proportionally to engine speed. The third stage of flame travel may be considered to consist entirely of turbulent combustion. The average flame speed is usually a proportionate function of engine speed. The number of degrees of crank-angle rotation occupied by the third period seems to remain constant with speed.

In the high-speed engine of the type found in an automobile, the time occupied by flame travel is not influenced profoundly by the first and second stages of combustion and advancing the ignition timing can be used quite effectively to compensate for flame travel time as engine speed increases. With a super-high-speed engine having a small combustion chamber, the first and second stages of flame travel may occupy a disproportionate amount of flame travel time thus introducing difficulties in optimum utilization of the combustion process.

Ionization-Gap Technique

Ionization gaps, pressure indicators, and photography techniques are all familiar to those engaged in engine combustion research. Ionization gaps may be used for two purposes in engine combustion studies, either for indicating flame front position or for indicating extent of flame ionization current. Since ionization gaps are quite small, they are readily adaptable to small-sized engines, while pressure instrumentation might be difficult of application. The ionization gap, therefore, would serve not only to indicate the arrival of the flame front, but also to indicate the presence of pressure oscillations in the burned gases through the variable ion current accompanying knock. Generally, lower load resistances can be used for detecting flame fronts than for determining pressure oscillations in the burned gases.

Experimental Apparatus and Procedure

Experiments were conducted in a single-cylinder test engine designated as a 2K-001. This engine, essentially similar to a two-cylinder engine of the same size used by the Honda Re-

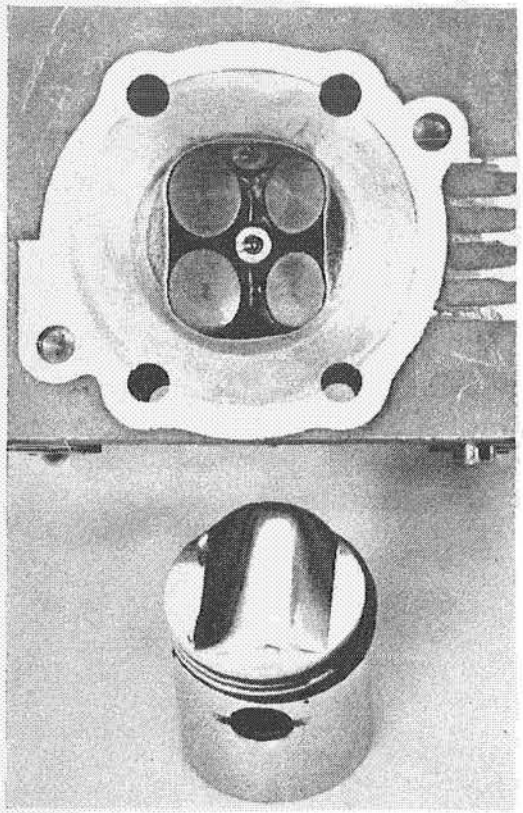

FIG. 1. Cylinder head and piston.

search and Development Co., has these specifications: cylinder bore, 44 mm; stroke, 41 mm; displacement volume, 62.4 cc; compression ratio, 10.2:1; two overhead inlet valves and two overhead exhaust valves; combustion chamber and piston of conoidal shape; and magneto ignition system.

Figure 1 shows the cylinder-head and piston of the engine. Two 10 mm spark plugs in addition to that normally located at the center of the combustion chamber were attached to the cylinder-head and used as ionization gaps. They were located 21.5 and 18.5 mm from the center plug.

The test engine was connected to a dc dynamometer. Intake pressures were kept constant at 760 mm Hg by regulating air flow to the engine. Air-flow rates were measured by an orifice installed between two surge tanks in the inlet system.

Figure 2 shows the electrical circuit used for amplification of the ion current. Timing marks were introduced into the record from the primary potential of the magneto.

The output of the ion-current amplifier was recorded at the rate of 60 inches per second and played back at 7.5 ips and reproduced therefrom on an oscillograph screen. Flame-travel times, as measured, fluctuated considerably from cycle to cycle. Mean values were obtained by averaging a dozen successive cycles.

Experimental Results and Discussions

Effect of Engine Speed. In the first series of experiments, the spark plug located at one edge of the combustion chamber was used for ignition and the other two plugs as ionization gaps. Figure 3 shows the resulting relationship between engine speed and flame travel time in degrees of crank rotation. These data were obtained under conditions of full throttle, maximum power mixture ratio, and with ignition timing set at 57° btc. The spark advance was that found to be optimum in previous performance testing of the engine. In Fig. 3, $\theta_{1,2}$ denotes the number of degrees of crank rotation occupied by flame travel from the spark plug to the ionization gap located

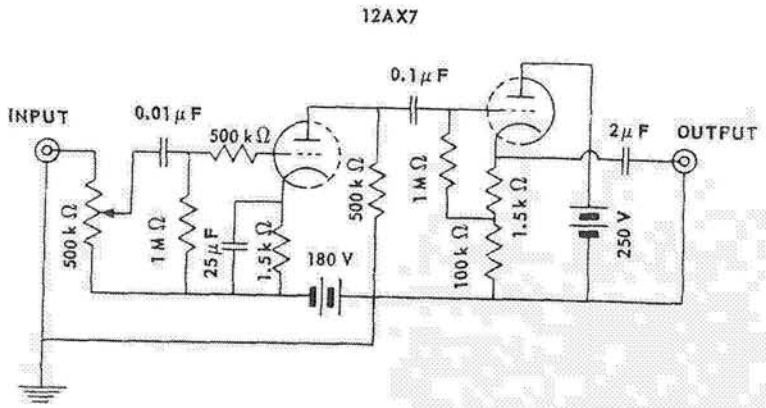

FIG. 2. Ion-current amplifier.

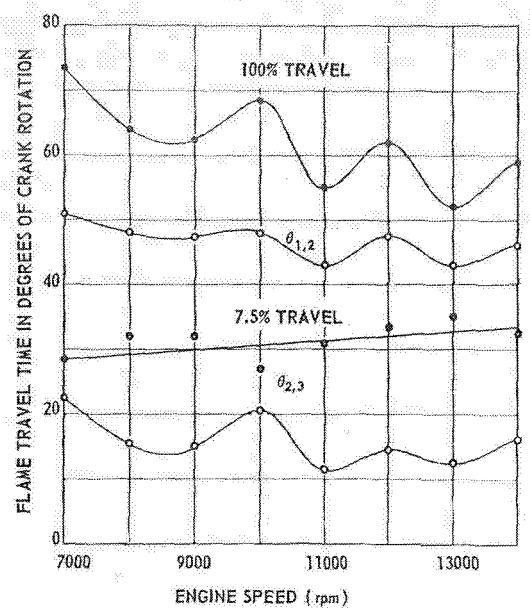

FIG. 3. Engine speed vs. flame travel time in degrees of crank rotation.

at the center of the cylinder. Similarly, $\theta_{2,3}$ represents the flame travel from the ionization gap at the center of the cylinder to that at the far side.

The periodic nature in the flame travel time versus engine speed plot is believed to have been caused by dynamic effects in the 225 mm long inlet pipe. The phenomenon is beyond the scope of this paper.

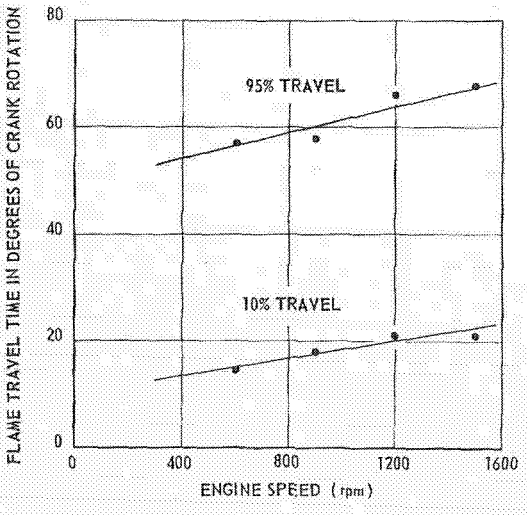

FIG. 4. Engine speed vs. flame travel time in degrees of crank rotation. (After Bouchard, Taylor, and Taylor.)

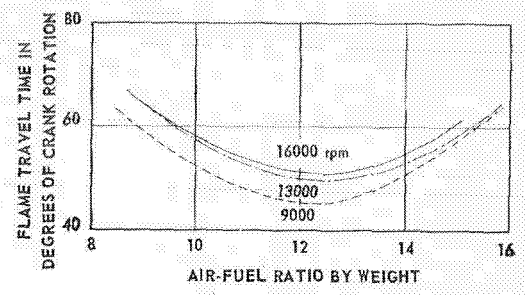

FIG. 5. Mixture ratio vs. flame travel time in degree of crank rotation.

For comparison, the experimental results of Bouchard, Taylor, and Taylor[1] obtained in a cylinder of larger size are reproduced in Fig. 4. Reference to both Figs. 3 and 4 shows that the time for the latter part of flame travel is much shorter than that for the first part of flame travel. A noteworthy difference is the effect of engine speed on the number of relative degrees of crank-angle rotation occupied by the total flame travel. These differences between flame development in low and in high-speed engines will be discussed later.

If $\theta_{1,2}$ can be considered to consist essentially of the delay period and the initial stages of flame development and turbulent flame propagation but in the same distance as that of $\theta_{2,3}$, the difference between them can be used to give an approximate estimate of the first 7.5 per cent of flame travel (21.5 minus 18.5 ÷ 21.5 plus 18.5 = 0.075).

Effect of Mixture Ratio. An investigation was made into the effect of mixture ratio on flame travel time in another series of experiments in which the spark plug at the center of the cylinder was used for ignition and the spark plug at the near edge was used as an ionization gap. Plotted

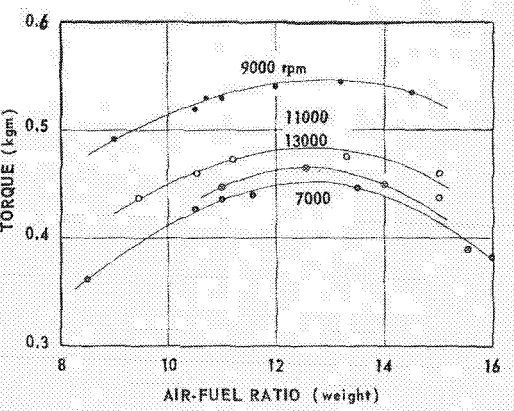

FIG. 6. Mixture ratio vs. engine torque.

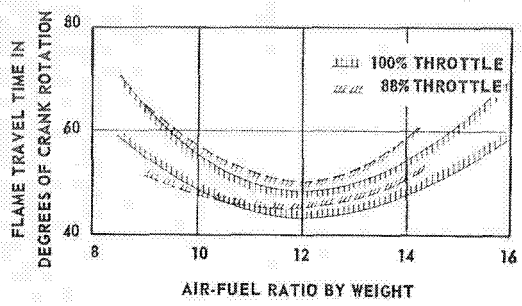

FIG. 7. Effect of throttling on flame travel time in degrees of crank rotation.

in Fig. 5 is the number of degrees of crank rotation occupied by combustion as a function of engine speed. In these experiments, the ignition timing was set at 47° btc and the engine was run at 100 per cent throttle. In Fig. 6 are shown the results of torque measurements under the same conditions. Both Figs. 5 and 6 indicate that the flame speed is fastest when the mixture ratio is that for maximum power.

Figure 7 illustrates the effect of part-throttle operation. The observed values of flame travel time are located in the cross-hatched area. The variation in flame-travel time appears not to be a strong function of throttle setting. The experiments of Bouchard, Taylor, and Taylor[1] by contrast, show a decrease in flame-travel time with decreasing inlet pressure.

Effect of Ignition Timing. Figure 8 illustrates the effect of advancing the spark on flame-travel time as a function of engine speed. The throttle setting was 100 per cent and air–fuel ratio was from 11.5 to 12.0. The flame travel went through

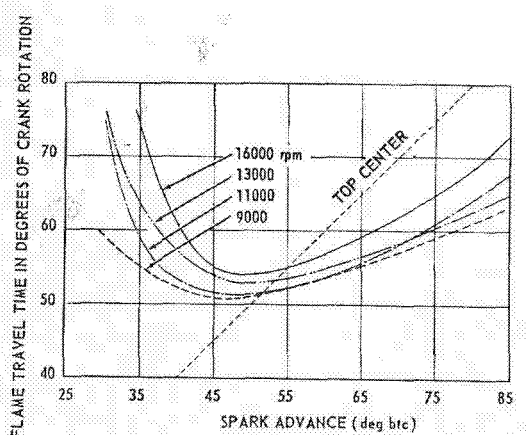

FIG. 8. Effect of spark advance on flame travel time in degrees of crank rotation.

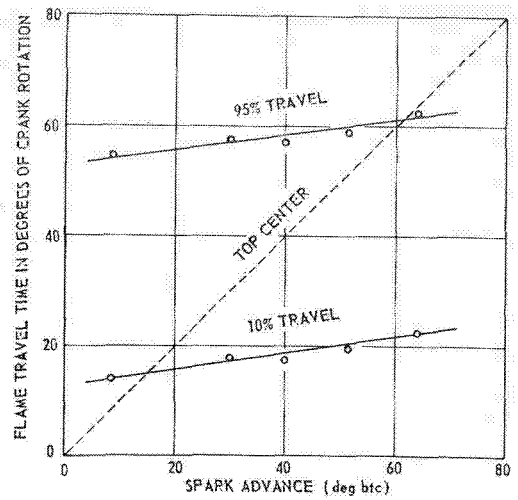

FIG. 9. Effect of spark advance on flame travel time in degrees of crank rotation. (After Bouchard, Taylor and Taylor.)

a minimum point as spark was advanced. For comparison, Fig. 9 shows the results of Bouchard, Taylor, and Taylor for the same variables. Again, the results differ.

Figure 10 shows the relationship between engine speed and optimum advance for a minimum flame-travel time together with the number of degrees of crank rotation for optimum spark advance setting. The lines have been faired through the data, ignoring the periodic changes in the observed values referred to previously. It will be noted that as engine speed increases, so does flame-travel time. Referring back to Fig. 3 it can be noted that flame-travel time decreases

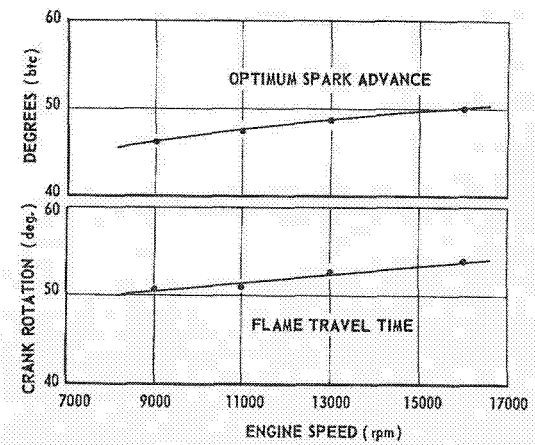

FIG. 10. Engine speed vs. optimum spark advance and corresponding flame travel time in degrees of crank rotation.

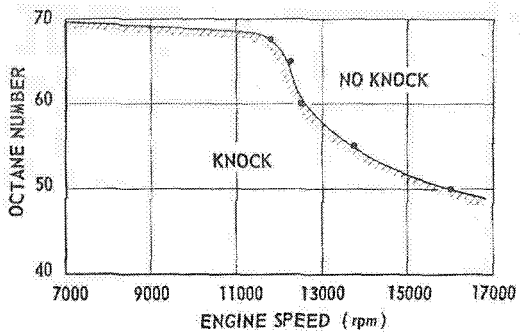

FIG. 11. Knock-limited engine speed vs. octane number of fuel.

with fixed spark advance as engine speed is increased.

Figure 10 shows, in correspondence to lower speed engine experiments, that flame-travel time in terms of degrees of crank rotation increases with increasing engine speed, even though ignition timing is fixed. Thus, the relationship between engine speed and total travel time as shown in Fig. 3 is not yet explainable.

There are several hypotheses as to why this apparent anomaly exists. It is possible that the third stage of flame propagation may be more than proportionally effected by engine speed, or that there is a change in air-fuel ratio with engine speed for which there has been thus far no accounting. In any event, further experimentation is needed to elucidate this phenomenon.

The dotted lines in Figs. 8 and 9 indicate the top dead center piston position. In Fig. 9 the middle of the combustion process is located very close to the top dead center piston position in the range of spark advances used. This may explain why combustion time is relatively unaffected by spark advance in lower speed engines. In high-speed engines the combustion process can shift radically from the top dead center position with the result that the first and second stages of flame travel can occupy this region.

Anti-Knock Characteristics. Further experiments were carried out in order to investigate the knock characteristics of small-sized high-speed spark-ignition engines. Ordinarily, fuels of approximately 100 octane number would be used in practical application. For this part of the investigation, fuels from 40 to 79 octane number were prepared by blending isooctane and normal heptane. In addition, a gasoline of 72 octane number was used. Ignition timing was fixed at 47° btc and jacket temperature regulated to a spark plug washer temperature between 170° and 180°C. In all cases, the throttle setting was 100 per cent and fuel supply set for best power. Engine speed was in each case gradually decreased from high rpm until knock was detected in the ionization current trace on the oscilloscope. As shown in Fig. 11 no knock was observed for 70 octane number fuel while knock was always observed for 40 octane number.

An attempt was made to operate the engine using normal heptane as fuel by accelerating the engine to high speed at no load and then increasing the load. This resulted in destruction of the engine due to cracks in the piston head.

Conclusions

In engines operating in the 15,000 rpm range, there is a disproportionate influence of the acceleration period and of the delay period in the combustion process as compared to engines running at normal speeds. The time for the initial phases of flame development thus is an extremely important item in small super-high-speed engines.

To shorten the delay as much as possible one might increase the spark gap to minimize the effects of quenching, intensify the spark to more than that necessary for marginal ignition, increase the inductance component or correspondingly decrease the capacity component of the spark.[2] Additionally, a straight capacity spark might possibly be a better source of ignition for the small high-speed engines than the normal inductive type spark because the delay period appears to be much shorter with such capacity-type sparks.

REFERENCES

1. BOUCHARD, C. L., TAYLOR, C. F., and TAYLOR, E. S.: SAE Journal *41*, 514 (1937).
2. KUMAGAI, S., SAKAI, T., and KIMURA, I.: J. Fac. Engng., Univ. Tokyo, *XXIV*, No. 1, 9 (1953).

CLASSIFICATION OF FUELS: THERMODYNAMIC AND REACTION KINETIC PROPERTIES IN OTTO ENGINES*

F. A. F. SCHMIDT

In order to describe fuels in regard to their potential specific performance and to the fuel consumption in Otto engines using different fuels, a new method of calculation is presented, based on an equational compilation of groups of hydrocarbons (paraffins, olefins, etc.), their chemical composition, and heats of combustion. The heat of combustion is divided into the heat of combustion of the elements forming the fuel and the molecular bond energies. Thus, the calorific properties of different fuels can be calculated in a simple manner and a precise relative prediction can be made of the effective performance and the effective fuel consumption for the operation of an engine with a fuel of arbitrary chemical composition.

Furthermore, a potential increase in performance and improvement in fuel consumption can be predicted by a suitable selection of hydrocarbons as fuel components with chemical compositions and molecular bonds.

The influence of chemical equilibrium and frozen flow on the performance and the fuel consumption of engines is considered. New comparative results are presented on the chemical reactions in Laval nozzles obtained in this Symposium (problems of frozen flow and equilibrium flow).

In order to classify the fuel properties relative to knock, the relation between self-ignition of the fuels and their engine operation are considered theoretically and experimentally. The results obtained in a compression apparatus are the basis for this consideration. A method is described which allows one to determine the laws for every phase of the ignition process by means of the values of the induction period. A method to calculate knock in the engine is presented, which uses the fuel constants of ignition delay.

In those cases in which the reaction process follows the same law during the entire ignition period a direct and reasonably exact calculation of the beginning of knock in engines can be carried out from thermodynamic considerations.

To specify the knock behavior of fuels two pieces of information are needed: (1) A value characterizing the level of the anti-knock quality at the mean operating condition of the engine; and (2) values characterizing the dependence of the self-ignition process on pressure and temperature.

---

* Due to late arrival of the main portion of the manuscript it was not possible to submit it to a regular editorial review and to include it in this volume. However, reprints of the entire paper can be obtained directly from Professor F. A. F. Schmidt, Technische Hochschule, Aachen, West Germany.

INDEX OF AUTHORS AND DISCUSSORS

(References in **boldface type** refer to authors of papers submitted for discussion)

INDEX OF AUTHORS AND DISCUSSORS